

# Comprehensive Coordination Chemistry II

**FROM BIOLOGY TO NANOTECHNOLOGY**

**EDITORS-IN-CHIEF**

**Jon A McCleverty  
Thomas J Meyer**

**Edited by  
M. Fujita, A. Powell, C. Creutz**

**Volume 7  
From the Molecular to the Nanoscale:  
Synthesis, Structure, and Properties**

# Introduction to Volume 7

In this volume recent progress in synthetic coordination chemistry, which has led to the production of materials displaying nanoscopic structural motifs, is described. The availability of increasingly powerful structure determination methods such as area detection for single-crystal X-ray diffraction and high-energy electron microscopies has been a key aspect to the development of this area. It is now possible to determine the structures of very large clusters, aggregates of metal ions, and coordination polymers to atomic resolution on a routine basis. For example, the field of coordination polymers has been explosively developed thanks to the advances in X-ray diffraction methods. The results of such structure determinations are fed back to the precise design of the structures and properties of coordination materials. For example, unique properties of coordination polymers (gas absorption, magnetism, etc.) have been explored through molecular-level designing.

The first eight chapters of this volume explore the emerging worlds of high nuclearity clusters, coordination polymers, and supramolecular systems. Naturally, some of these areas have points of overlap but it is convenient to consider the underlying structural motifs as defining the area of interest. Since the publication of the first edition of CCC (1987) these areas have become firmly established and the emerging importance of nanoscale structures has led to the development of synthetic strategies for producing materials based on coordination chemistry principles where the molecular entity builds up to a nanostructured material. The main aim of this volume is to illustrate this by considering the synthetic and structural aspects associated with this concept. In addition the aspects of the properties of such systems are discussed. These properties are often inexplicable in terms of simple molecular or macroscopic descriptions demanding considerable efforts in developing theoretical expressions to elucidate the observed behavior. Such unusual behavior points towards applications utilizing quantum effects and this aspect has been a major motivation for the huge synthetic efforts currently being applied to the area.

Active areas in coordination chemistry that are rapidly growing after CCC (1987) rely on the explosive development of nano science and technology in recent years. In contrast to the “top-down approach” from physical structures, the “bottom-up approach” from chemical components (i.e., molecules) has been showing remarkable potential for constructing well-defined, functional nanostructures. Coordination chemistry provides an ideal principle for the bottom-up design of molecules because metals and ligands naturally and spontaneously associate with each other through coordination interaction, giving rise to discrete and infinite structures in the nanoscopic region very efficiently. This approach produces not only nanosized structures but also nanoscopic functions, which is intrinsic to nanosized species due to the versatile properties latent in such transitions. This bottom-up approach to nanomolecules and materials is well documented in most of this volume.

Particularly noteworthy is the fact that the bottom-up approach has created new materials and functions which may open up commercial applications. For example, the gas-absorption property of nanoporous coordination materials, which are spontaneously formed from metals and relatively simple ligands in a very efficient fashion, has been explored only in recent years, and are becoming very promising candidates for hydrogen storage for fuel batteries.

In the first chapter the synthesis and structures of new heteropolyoxoanions and related systems are discussed. Such systems can enclose nanoscopic spaces and can be regarded as “nanoreactors”. Clusters containing fragments of the lattices of semiconducting materials such as CdSe provide a vivid illustration of the transition from molecular-based to extended solid properties and show how the properties in the nanoscale region differ from those at each extreme. These are described in the second chapter. A third physical property for which a bounded system

in the sub- to nanoscale regime can display unusual behavior is that of “molecular-based magnetism” and the synthetic and structural aspects of such open-shell systems are described in the third and fourth chapters on clusters and aggregates with paramagnetic centers.

The following chapters deal with supramolecular chemistry based on coordination chemistry. This area has been rapidly growing during the last decade of the twentieth century, making possible the facile production of nanoscopic materials by exploiting weak metal–ligand interactions. From structural aspects, infinite systems (e.g., coordination polymers) and finite systems (e.g., metallodendrimers) are discussed in Chapters 5 and 6. The infinite coordination systems is the most rapidly expanding area and the major interest in this field is shifting from structure to function. Accordingly, gas adsorption properties of nanoporous coordination networks are well discussed.

Templating and self-assembly, which are two major synthetic strategies of supramolecular coordination compounds, are focused upon in Chapters 7 and 8. Both methods have shown powerful potentials for the construction of well-defined nanoarchitecture with interesting properties. Although these methods were previously employed among organic chemists by using organic interactions (hydrogen bonding, van der Waals interactions, etc.), the coordination approach has recently been recognized to be the most efficient strategy for templating and self-assembly thanks to the variation of metal centers and their wide spectrum of coordination geometries. The dynamic properties of coordination assemblies are the current topic in this field, and switchable systems in which molecular motion and function can be controlled by the redox and photo activation of metal centers are focused upon.

In Chapter 9 two areas where single-crystal X-ray diffraction experiments cannot be used to explore the structures of the materials are reviewed. In effect, these are areas where coordination-based materials are processed to give new materials. Research into liquid crystals has burgeoned since CCC (1987) was published and the area of specific interest to coordination chemists, that of metallomesogens, has been developed in order to build in the advantages of incorporating metal centers into these phases. This is a rapidly expanding field which could lead to all sorts of “smart materials”, some of which might combine the sorts of systems discussed in the earlier chapters of the volume with mesogenic properties. Chapter 10 discusses another route to processing coordination compounds using sol-gel processing. This is another area new to CCCII with the possibility of producing materials with quite unusual features, such as thin films and glasses, which have potential applications in a variety of fields.

Whilst we have tried to present new research areas where molecular-based compounds extend to the nanometer-length scale in their overall structures, we were unfortunately not able to include one aspect of relevance to this idea, that of Biomineralization. This field has enjoyed considerable interest since the availability of powerful electron microscopes made it possible to look at the intricate details of the beautiful macroscopic architectures found in the mineralized structures of a variety of creatures at the nanoscale level. It has become clear through this research that much of the “crystal engineering” which is required to create phase- and function-specific structures, often with amazing control over the precise shape of the resulting biomineral, must utilize coordination chemistry principles with the idea put forward that various ligating species become involved during mineral formation to act as templates or growth inhibitors.

Although the vast majority of biomineral structures are composed of calcium carbonates and phosphates or silicate-based materials and therefore outside the scope of what we define as Coordination Chemistry, there are some very important transition metal-based systems, especially the iron oxides and oxyhydroxides, where the biominerals can provide important insights into the coordination chemistry approaches utilized by biological systems. The specific case of the iron(III) oxyhydroxide mineral utilized by organisms to store iron in ferritins is discussed in detail in Chapter 8.7 of Volume 8 of this series. In ferritin, the iron oxyhydroxide is stored inside a hollow spherical cavity of 7–8 nm diameter surrounded by 24 (or 12 dimeric) protein subunits. In this chapter, the general principles in the operation of controlling iron hydrolysis to create iron biominerals are discussed with reference to the coordinating species which can be involved in directing the phase and function of the mineral. Ferritins are also particularly relevant to the research discussed in our volume, since they consist of encapsulated nanoscopic particles where the “ligands” are still clearly visible (the protein shell of the system).

Although as has been stated above, most biominerals are based on what is readily available to organisms for forming structures, calcium and silicate-based systems, there are some very important lessons to be learned by coordination chemists aiming towards “new materials”. We need only think of the strength of rather light bones, which are some ten times stronger than ordinary concrete. When we consider that it is necessary to reinforce concrete with iron wires to achieve an

equivalent strength, and the disadvantages of this material in terms of weight, durability, and self-repair compared with our bones, we can appreciate that the composite material nature has come up with is far superior to anything we can currently create. The construction of calcium carbonate shells gives further insights into design principles we might wish to employ. As well as the different types of crystal growth to give different shapes, which can variously be described in terms of logarithmic growth, linear growth, concentric growth, and so on, there is also the creation of superstructures with careful layering of the mineral to reinforce a weak shear direction or else a change of phase on traveling from the inside of, say, an oyster shell, which is lined with mother-of-pearl (aragonite as nacre), to the tough outside made up of calcite.

In addition to such structural marvels, biomineral structures are used as sensors with some marine species displaying the structural motifs found in photonic crystals. As well as light sensing, calcium carbonate in the form of nanoparticles is used in the human ear as part of a gravity sensor and helps to keep us upright – it serves a similar purpose along the lateral line of fish. Perhaps most intriguing are the magnetic sensors, usually in the form of aligned and elongated nanocrystals of magnetite, found in the tissues of a variety of creatures including bacteria, bees, fish, and birds, which sense the Earth's magnetic field and help these creatures to orientate themselves.

In Chapter 11, Molecular Electron Transfer, the broad and deep field of electron-transfer reactions of metal complexes is surveyed and analyzed. In Chapter 12, Electron Transfer From the Molecular to the Nanoscale, the new issues arising for electron-transfer processes on the nanoscale are addressed; this chapter is less a review than a “toolbox” for approaching and analyzing new situations. In Chapter 13, Magnetism From the Molecular to the Nanoscale, the mechanisms and consequences of magnetic coupling in zero- and one-dimensional systems comprised of transition-metal complexes is surveyed. Related to the topics covered in this volume are a number addressed in other volumes. The techniques used to make the measurements are covered in Section I of Volume 2. Theoretical models, computational methods, and software are found in Volume 2, Sections II and III, while a number of the case studies presented in Section IV are pertinent to the articles in this chapter. Photochemical applications of metal complexes are considered in Volume 9, Chapters 11–16, 21 and 22.

In addition, subjects such as molecular photochemistry and photophysics and optical properties from the molecular to the nanoscale are closely related. Accordingly, a brief selection of lead-in references in these areas is provided. The organization and selection are strongly influenced by the interests of the author. Where possible review articles are cited rather than primary literature. At present the best consistent medium for review articles on inorganic photochemistry is *Coordination Chemistry Reviews*.

## 1. Molecular Photochemistry and Photophysics: General References

Vogler, A.; Kunkely, H. Luminescent metal complexes: diversity of excited states. In *Transition Metal and Rare Earth Compounds: Excited States, Transition, Interactions I*, Vol. 213; Yersin, H., Ed.; Springer: Berlin, 2001; pp 143–182.

Chen, P. Y.; Meyer, T. J. Medium effects on charge transfer in metal complexes. *Chem. Rev.* **1998**, *98*, 1439–1477.

Roundhill, D. M. *Photochemistry and Photophysics of Metal Complexes*; Plenum: New York, 1994.

Horvath, O.; Stevenson, K. L. *Charge Transfer Photochemistry of Coordination Compounds*; VCH: New York, 1993.

Adamson, A. W. Inorganic photochemistry – then and now. *Coord. Chem. Rev.* **1993**, *125*, 1–12.

Balzani, V.; Scandola, F. *Supramolecular Photochemistry*; Ellis Horwood: New York, 1991.

Ferraudi, G. J. *Elements of Inorganic Photochemistry*; Wiley: Chichester, UK, 1988.

Kutal, C.; Adamson, A. W. In *Comprehensive Coordination Chemistry*; Wilkinson, G., Ed.; Pergamon: Oxford, UK, 1987, Vol. 1, pp 385–414.

Zuckerman, J. J., Ed. *Inorganic Reactions and Methods*; VCH: Deerfield Beach, FL, 1986; Vol. 15.

Geoffroy, G. L.; Wrighton, M. S. *Organometallic Photochemistry*; Academic Press: New York. Adamson, A. W.; Fleischauer, P. D., Eds. *Concepts of Inorganic Photochemistry*; Wiley-Interscience: New York, 1975.

Balzani, V.; Carassiti, V. *Photochemistry of Coordination Compounds*; Academic Press, New York, 1970.

Rate constants for quenching of the excited states of metal complexes are available through the Notre Dame Radiation Laboratory DataBase <http://allen.rad.nd.edu/>

## 2. Metal-to-ligand Charge Transfer Excited States

### 2.1 $Ru(bpy)_3^{2+}$ and Other $d^6$ Metal Centers

Bhasikuttan, A. C.; Suzuki, M.; Nakashima, S.; Okada, T. Ultrafast fluorescence detection in tris(2,2'-bipyridine)ruthenium(II) complex in solution: relaxation dynamics involving higher excited states. *J. Am. Chem. Soc.* **2002**, *124*, 8398–8405.

Kelly, C. A.; Meyer, G. J. Excited state processes at sensitized nanocrystalline thin film semiconductor interfaces. *Coord. Chem. Rev.* **2001**, *211*, 295–315.

Qu, P.; Meyer, G. J. Dye sensitization of electrodes. In *Electron Transfer in Chemistry*; Balzani, V., Ed.; Wiley-VCH: New York, 2001; Vol. 4, Part 2, pp 354–411.

Scandola, F.; Chiorbelli, C.; Indelli, M. T.; Rampi, M. A. Covalently linked systems containing metal complexes. In *Electron Transfer in Chemistry*; Balzani, V., Ed.; Wiley-VCH: New York, 2001; Vol. 3, Part 2, pp 337–408.

Striplin, D. R.; Crosby, G. A. Photophysical investigations of rhenium(I)Cl(CO)<sub>3</sub>(phenanthroline) complexes. *Coord. Chem. Rev.* **2001**, *211*, 163–175.

Stufkens, D. J.; Vlcek, A. Ligand-dependent excited state behaviour of Re(I) and Ru(II) carbonyl–diimine complexes. *Coord. Chem. Rev.* **1998**, *177*, 127–179.

Damrauer, N. H.; McCusker, J. K. Ultrafast dynamics in the metal-to-ligand charge transfer excited-state evolution of Ru(4,4'-diphenyl-2,2'-bipyridine)<sub>3</sub> (2+). *J. Phys. Chem. A* **1999**, *103*, 8440–8446.

Sauvage, J. P.; Collin, J. P.; Chambron, J. C.; Guillerez, S.; Coudret, C.; Balzani, V.; Barigelletti, F.; Decola, L.; Flamigni, L. Ruthenium(II) and osmium(II) bis(terpyridine) complexes in covalently linked multicomponent systems – synthesis, electrochemical behavior, absorption spectra, and photochemical and photophysical properties. *Chem. Rev.* **1994**, *94*, 993–1019.

Schanze, K. S.; Macqueen, D. B.; Perkins, T. A.; Cabana, L. A. Studies of intramolecular electron and energy transfer using the fac-(diimine)ReI(CO)<sub>3</sub> chromophore. *Coord. Chem. Rev.* **1993**, *122*, 63–89.

Kalyanasundaram, K. *Photochemistry of Polypyridine and Porphyrin Complexes*; Academic Press: London, 1992.

Kalyanasundaram, K. Photophysics, photochemistry and solar energy conversion with tris(bipyridyl)ruthenium(II) and its analogues. *Coord. Chem. Rev.* **1982**, *46*, 159–244.

Sutin, N.; Creutz, C. Light-induced electron transfer reactions of metal complexes. *Pure Appl. Chem.* **1980**, *52*, 2717–2738.

### 2.2 Other Metal Centers

Vlcek, A. Mechanistic roles of metal-to-ligand charge-transfer excited states in organometallic photochemistry. *Coord. Chem. Rev.* **1998**, *177*, 219–256.

Vogler, A.; Kunkely, H. Photoreactivity of metal-to-ligand charge transfer excited states. *Coord. Chem. Rev.* **1998**, *177*, 81–96.

Scaltrito, D. V.; Thompson, D. W.; O'Callaghan, J. A.; Meyer, G. J. MLCT excited states of cuprous bis-phenanthroline coordination compounds. *Coord. Chem. Rev.* **2000**, *208*, 243–266.

Vogler, A.; Kunkely, H. A new type of MLCT transition relevant to oxidative additions:  $d \rightarrow \sigma^*$  excitation. *Coord. Chem. Rev.* **1998**, *171*, 399–406.

## 3. Ligand-to-metal Charge-transfer Excited States

Sima, J.; Brezova, V. Photochemistry of iodo iron(III) complexes. *Coord. Chem. Rev.* **2002**, *229*, 27–35.

Manson, J. L.; Buschmann, W. E.; Miller, J. S. Tetracyanomanganate(II) and its salts of divalent first-row transition metal ions. *Inorg. Chem.* **2001**, *40*, 1926–1935.

Stanislas, S.; Beauchamp, A. L.; Reber, C. The lowest-energy ligand-to-metal charge-transfer absorption band of trans-OsO<sub>2</sub>(malonate)<sub>2</sub> (2-). *Inorg. Chem.* **2000**, *39*, 2152–2155.

Villata, L. S.; Wolcan, E.; Feliz, M. R.; Capparelli, A. L. Competition between intraligand triplet excited state and LMCT on the thermal quenching in beta-diketonate complexes of europium(III). *J. Phys. Chem. A* **1999**, *103*, 5661–5666.

Yang, Y. S.; Hsu, W. Y.; Lee, H. F.; Huang, Y. C.; Yeh, C. S.; Hu, C. H. Experimental and theoretical studies of metal cation–pyridine complexes containing Cu and Ag. *J. Phys. Chem. A* **1999**, *103*, 11287–11292.

Kunkely, H.; Vogler, A. Photoreactivity of (HBpyrazolyl)<sub>3</sub>) TiCl<sub>3</sub> and (C<sub>5</sub>H<sub>5</sub>)TiCl<sub>3</sub> initiated by ligand-to-metal charge-transfer excitation. *J. Photochem. Photobiol. A-Chem.* **1998**, *119*, 187–190.

Stufkens, D. J.; Aarnts, M. P.; Rossenaar, B. D.; Vlcek, A. A new series of Re and Ru complexes having a lowest sigma pi\* excited state that varies from reactive to stable and long lived. *Pure Appl. Chem.* **1997**, *69*, 831–835.

Sima, J.; Makanova, J. Photochemistry of iron(III) complexes. *Coord. Chem. Rev.* **1997**, *160*, 161–189.

Kuma, K.; Nakabayashi, S.; Matsunaga, K. Photoreduction of Fe(III) by hydroxycarboxylic acids in seawater. *Water Res.* **1995**, *29*, 1559–1569.

Horvath, O.; Vogler, A. Photoredox chemistry of chloromercurate(II) complexes in acetonitrile. *Inorg. Chem.* **1993**, *32*, 5485–5489.

Kalyanasundaram, K.; Zakeeruddin, S. M.; Nazeeruddin, M. K. Ligand-to-metal charge-transfer transitions in Ru(III) and Os(III) complexes of substituted 2,2'-bipyridines. *Coord. Chem. Rev.* **1994**, *132*, 259–264.

Weit, S. K.; Ferraudi, G.; Grutsch, P. A.; Kutal, C. Charge-transfer spectroscopy and photochemistry of alkylamine cobalt(III) complexes. *Coord. Chem. Rev.* **1993**, *128*, 225–243.

Carlos, R. M.; Frink, M. E.; Tfouni, E.; Ford, P. C. Photochemical and spectral properties of the sulfite rhodium(III) complexes *trans*-Rh(NH<sub>3</sub>)<sub>4</sub>(SO<sub>3</sub>)CN and Na(*trans*-Rh(NH<sub>3</sub>)<sub>4</sub>(SO<sub>3</sub>)<sub>2</sub>). *Inorg. Chim. Acta* **1992**, *193*, 159–165.

Bergkamp, M. A.; Gütllich, P.; Netzel, T. L.; Sutin, N. Lifetimes of the ligand-to-metal charge-transfer excited states of iron(III) and osmium(III) polypyridine complexes. Effects of isotopic substitution and temperature. *J. Phys. Chem.* **1983**, *87*, 3877–3883.

#### 4. Polyoxometallates/ Metal Oxo Complexes

Texier, I.; Delouis, J. F.; Delaire, J. A.; Gionnotti, C.; Plaza, P.; Martin, M. M. Dynamics of the first excited state of the decatungstate anion studied by subpicosecond laser spectroscopy. *Chem. Phys. Lett.* **1999**, *311*, 139–145.

Duncan, D. C.; Fox, M. A. Early events in decatungstate photocatalyzed oxidations: a nanosecond laser transient absorbance reinvestigation. *J. Phys. Chem. A* **1998**, *102*, 4559–4567.

Ermolenko, L. P.; Delaire, J. A.; Giannotti, C. Laser flash photolysis study of the mechanism of photooxidation of alkanes catalyzed by decatungstate anion. *J. Chem. Soc. – Perkin Trans.* **1997**, *2*, 25–30.

Duncan, D. C.; Netzel, T. L.; Hill, C. L. Early-time dynamics and reactivity of polyoxometalate excited states – identification of a short-lived lmct excited-state and a reactive long-lived charge-transfer intermediate following picosecond flash excitation of W<sub>10</sub>O<sub>32</sub> (4-) in acetonitrile. *Inorg. Chem.* **1995**, *34*, 4640–4646.

Yamase, T.; Ohtaka, K. Photochemistry of polyoxovanadates. 1. Formation of the anion-encapsulated polyoxovanadate V<sub>15</sub>O<sub>36</sub>(Co<sub>3</sub>) (7-) and electron-spin polarization of alpha-hydroxyalkyl radicals in the presence of alcohols. *J. Chem. Soc. – Dalton Trans.* **1994**, 2599–2608.

Sattari, D.; Hill, C. Catalytic carbon–halogen bond cleavage chemistry by redox-active polyoxometalates. *J. Am. Chem. Soc.* **1993**, *115*, 4649–4657.

Yamase, T.; Sugeta, M. Charge-transfer photoluminescence of polyoxo-tungstates and polyoxo-molybdates. *J. Chem. Soc. – Dalton Trans.* **1993**, 759–765.

Winkler, J. R.; Gray, H. B. On the interpretation of the electronic spectra of complexes containing the molybdenyl ion. *Comments Inorg. Chem.* **1981**, *1*, 257–263.

#### 5. Metal-centered Excited States

##### 5.1 Ligand Field Excited States

Kirk, A. D. Photochemistry and photophysics of chromium(III) complexes. *Chem. Rev.* **1999**, *99*, 1607–1640.

Lees, A. J. Quantitative photochemistry of organometallic complexes: insight to their photo-physical and photoreactivity mechanisms. *Coord. Chem. Rev.* **2001**, *211*, 255–278.

Irwin, G.; Kirk, A. D. Intermediates in chromium(III) photochemistry. *Coord. Chem. Rev.* **2001**, *211*, 25–43.

##### 5.2 Excited States of $d^{10}$ and $s^2$ Systems

Vogler, A.; Kunkely, H. Photoreactivity of gold complexes. *Coord. Chem. Rev.* **2001**, *219*, 489–507.

Vitale, M.; Ford, P. C. Luminescent mixed ligand copper(I) clusters (CuI)(n)(L)(m) (L = pyridine, piperidine): thermodynamic control of molecular and supramolecular species. *Coord. Chem. Rev.* **2001**, *219*, 3–16.

Yam, V. W. W.; Chan, C. L.; Li, C. K.; Wong, K. M. C. Molecular design of luminescent dinuclear gold(I) thiolate complexes: from fundamentals to chemosensing. *Coord. Chem. Rev.* **2001**, *216*, 173–194.

Yam, V. W. W.; Lo, K. K. W. Luminescent polynuclear d(10) metal complexes. *Chem. Soc. Rev.* **1999**, *28*, 323–334.

Ford, P. C.; Cariati, E.; Bourassa, J. Photoluminescence properties of multinuclear copper(I) compounds. *Chem. Rev.* **1999**, *99*, 3625–3648.

Forward, J. M.; Bohmann, D.; J. P. Fackler, J.; Staples, R. J. Luminescence studies of gold(I) thiolate complexes. *Inorg. Chem.* **1995**, *34*, 6330–6336.

Ford, P. C.; Vogler, A. Photochemical and photophysical properties of tetranuclear and hexanuclear clusters of metals with  $d^{10}$  and  $s^2$  electronic configurations. *Acc. Chem. Res.* **1993**, *26*, 220–226.

Dossing, A.; Ryu, C. K.; Kudo, S.; Ford, P. C. Competitive bimolecular electron-transfer and energy-transfer quenching of the excited state(S) of the tetranuclear copper(I) cluster  $Cu_4i_4py_4$  – evidence for large reorganization energies in an excited-state electron-transfer. *J. Am. Chem. Soc.* **1993**, *115*, 5132–5137.

Stacey, E. M.; McMillin, D. R. Inorganic exciplexes revealed by temperature-dependent quenching studies. *Inorg. Chem.* **1990**, *29*, 393–396.

### 5.3 Excited States of $d^2 M\equiv N$ and MO Systems

Bailey, S. E.; Eikay, R. A.; Abu-Omar, M. M.; Zink, J. I. Excited-state distortions determined from structured luminescence of nitridorhenium(V) complexes. *Inorg. Chem.* **2002**, *41*, 1755–1760 and references therein.

Yam, V. W. W.; Pui, Y. L.; Wong, K. M. C.; Cheung, K. K. Synthesis, structural characterisation, photophysics, photochemistry and electrochemistry of nitrido- and *trans*- dioxorhenium(V) complexes with substituted dppe ligands (dppe=bis(diphenylphosphino)ethane). *Inorg. Chim. Acta* **2000**, *300*, 721–732.

Cheng, J. Y. K.; Cheung, K. K.; Che, C. M.; Lau, T. C. Photocatalytic and aerobic oxidation of saturated alkanes by a neutral luminescent *trans*-dioxoosmium(VI) complex  $OsO_2(CN)_2(dpphen)$ . *Chem. Commun.* **1997**, 1443–1444.

Kelly, C.; Szalda, D. J.; Creutz, C.; Schwarz, H. A.; Sutin, N. Electron transfer barriers for ground- and excited-state redox couples: *trans*-dioxo(1,4,8,11-tetramethyl-1,4,8,11-tetraazacyclotetradecane) osmium(VI)/osmium(V). *Inorg. Chim. Acta* **1996**, *243*, 39–45.

Yam, V. W. W.; Tam, K. K.; Lai, T. F. Syntheses, spectroscopy and electrochemistry of nitridorhenium(V) organometallics – X-ray crystal structure of  $ReVnme_2(Pph_3)_2$ . *J. Chem. Soc. – Dalton Trans.* **1993**, 651–652.

Schindler, S.; Castner, E. W., Jr.; Creutz, C.; Sutin, N. Reductive quenching of the emission of *trans*-dioxo(1,4,8,11-tetramethyl-1,4,8,11-tetraazacyclotetradecane)osmium(VI) in water. *Inorg. Chem.* **1993**, *32*, 4200–4208.

### 5.4 $s^2$ Metal Complexes

Vogler, A.; Nikol, H. The structures of  $s^2$  metal complexes in the ground and sp excited states. *Comments. Inorg. Chem.* **1993**, *14*, 245–261.

Vogler, A.; Nikol, H. Photochemistry and photophysics of the main group metals. *Pure Appl. Chem.* **1992**, *64*, 1311–1317.

### 5.5 $f^n$ Metal Complexes

Sabbatini, N.; Guardigli, M.; Lehn, J.-M. Luminescent lanthanide complexes as photochemical supramolecular devices. *Coord. Chem. Rev.* **1993**, *123*, 201–228.

## 6. Ligand-centered Excited States

Wang, X. Y.; Del Guerzo, A.; Schmehl, R. H. Preferential solvation of an ILCT excited state in bis(terpyridine-phenylene-vinylene) Zn(II) complexes. *Chem. Commun.* **2002**, 2344–2345.

Vlcek, A. Highlights of the spectroscopy, photochemistry and electrochemistry of  $M(CO)_4$ -( $\alpha$ -diimine) complexes,  $M = Cr, Mo, W$ . *Coord. Chem. Rev.* **2002**, *230*, 225–242.

Del Guerzo, A.; Leroy, S.; Fages, F.; Schmehl, R. H. Photophysics of Re(I) and Ru(II) diimine complexes covalently linked to pyrene: contributions from intra-ligand charge transfer states. *Inorg. Chem.* **2002**, *41*, 359–366.

Michalec, J. F.; Bejune, S. A.; Cuttell, D. G.; Summerton, G. C.; Gertenbach, J. A.; Field, J. S.; Haines, R. J.; McMillin, D. R. Long-lived emissions from 4'-substituted  $Pt(trpy)Cl^+$  complexes bearing aryl groups. Influence of orbital parentage. *Inorg. Chem.* **2001**, *40*, 2193–2200.

Yersin, H.; Donges, D.; Nagle, J. K.; Sitters, R.; Glasbeek, M. Intraligand charge transfer in the Pd(II) oxinate complex Pd(qol)(2). Site-selective emission, excitation, and optically detected magnetic resonance. *Inorg. Chem.* **2000**, *39*, 770–777.

van Slageren, J.; Hartl, F.; Stufkens, D. J.; Martino, D. M.; van Willigen, H. Changes in excited-state character of M(L-1)(L-2)(CO)(2)(alpha-diimine) (M = Ru, Os) induced by variation of L-1 and L-2. *Coord. Chem. Rev.* **2000**, *208*, 309–320.

Baba, A. I.; Shaw, J. R.; Simon, J. A.; Thummel, R. P.; Schmehl, R. H. The photophysical behavior of d<sup>6</sup> complexes having nearly isoenergetic MLCT and ligand localized excited states. *Coord. Chem. Rev.* **1998**, *171*, 43–59.

Kimachi, S.; Ikeda, S.; Miki, H.; Azumi, T.; Crosby, G. A. Spectroscopic and magnetic studies of complexes of d<sup>10</sup> closed-shell ions. *Coord. Chem. Rev.* **1994**, *132*, 43–50.

Watts, R. J.; Van Houten; J. The effect of energy gaps on multiple emissions in heterotriscchelated rhodium(III) complexes. *J. Am. Chem. Soc.* **1978**, *100*(6), 1718–1721.

## 7. Outer-sphere Charge Transfer in Ion Pairs

Electrostatic attraction between charged coordination compounds and oppositely charged counter ions in solution leads to ion pairing. The spectroscopic and photochemical properties of the ion pairs may markedly differ from those of the individual components. In some cases ion pair charge-transfer (IPCT) optical transitions may be observed and ion pairs may undergo energy transfer and photoinduced electron transfer.

Vogler, A.; Kunkely, H. Outer-sphere charge transfer in ion pairs with hydridic, carbanionic, sulfidic and peroxidic anions as electron donors – spectroscopy and photochemistry. *Coord. Chem. Rev.* **2002**, *229*, 147–152.

Billig, R. Optical and photoinduced electron transfer in ion pairs of coordination compounds. *Coord. Chem. Rev.* **1997**, *159*, 257–270.

Kunkely, H.; Vogler, A. Photoredox reaction of [Hg(cyclam)]<sup>2+</sup>[Co(CO)<sub>4</sub>]<sup>-</sup> induced by outer-sphere charge transfer excitation. *Z. Naturforsch.* **1993**, *48b*, 397–398.

## 8. Metal–Metal Bonded Species

Wong, K. M. C.; Hui, C. K.; Yu, K. L.; Yam, V. W. W. Luminescence studies of dinuclear platinum(II) alkynyl complexes and their mixed-metal platinum(II)–copper(I) and –silver(I) complexes. *Coord. Chem. Rev.* **2002**, *229*, 123–132.

Stufkens, D. J.; Aarnts, M. P.; Nijhoff, J.; Rossenaar, B. D.; Vlcek, A. Excited states of metal–metal bonded diimine complexes vary from extremely long lived to very reactive with formation of radicals or zwitterions. *Coord. Chem. Rev.* **1998**, *171*, 93–105.

Roundhill, D. M.; Gray, H. B.; Che, C.-M. Pyrophosphito-bridged diplatinum chemistry. *Acc. Chem. Res.* **1989**, *22*, 55–61.

## 9. Spectroscopy of Semiconductor Particles

Buhro, W. E.; Colvin, V. L. Semiconductor nanocrystals: shape matters. *Nature Mater.* **2003**, *2*, 138–139.

Khoudiakov, M.; Parise, A. R.; Brunshwig, B. S. Interfacial electron transfer in FeII(CN)<sub>6</sub><sup>4-</sup>-sensitized TiO<sub>2</sub> nanoparticles: a study of direct charge injection by electroabsorption spectroscopy. *J. Am. Chem. Soc.* **2003**, *125*, 4637–4642.

Brus, L. Model for carrier dynamics and photoluminescence quenching in wet and dry porous silicon thin films. *Phys. Rev. B* **1996**, *53*, 4649–4656.

Liu, H. J.; Hupp, J. T.; Ratner, M. A. Electronic structure and spectroscopy of cadmium thiolate clusters. *J. Phys. Chem.* **1996**, *100*, 12204–12213.

Turk, T.; Vogler, A.; Fox, M. A. Molecular models for semiconductor particles – luminescence studies of several inorganic anionic clusters. *Adv. Chem. Ser.* **1993**, 233–241.

Bawendi, M. G.; Steigerwald, M. L.; Brus, L. E. The quantum mechanics of larger semiconductor clusters (“quantum dots”). *Ann. Rev. Phys. Chem.* **1990**, *41*, 477–496.

Steigerwald, M. L.; Brus, L. E. Semiconductor crystallites: a class of large molecules. *Acc. Chem. Res.* **1990**, *23*, 183–188.

Brus, L. Electronic wave functions in semiconductor clusters: experiment and theory. *J. Phys. Chem.* **1986**, *90*, 2555–2560.

Brus, L. E. Electron–electron and electron–hole interactions in small semiconductor crystallites: the size dependence of the lowest excited electronic state. *J. Chem. Phys.* **1984**, *80*, 4403–4409.



## 10. Spectroscopy of Metal Particles

Kelly, K. L.; Coronado, E.; Zhao, L. L.; Schatz, G. C. The optical properties of metal nanoparticles: The influence of size, shape, and dielectric environment. *J. Phys. Chem. B* **2003**, *107*, 668–677.

Hu, M.; Hartland, G. V. Heat dissipation for Au particles in aqueous solution: relaxation time versus size. *J. Phys. Chem. B* **2002**, *106*, 7029–7033.

Link, S.; El-Sayed, M. A.; Schaaff, T. G.; Whetten, R. L. Transition from nanoparticle to molecular behavior: a femtosecond transient absorption study of a size-selected 28-atom gold cluster. *Chem. Phys. Lett.* **2002**, *356*, 240–246.

Link, S.; Beeby, A.; FitzGerald, S.; El-Sayed, M. A.; Schaaff, T. G.; Whetten, R. L. Visible to infrared luminescence from a 28-atom gold cluster. *J. Phys. Chem. B* **2002**, *106*, 3410–3415.

Hartland, G. V.; Hu, M.; Wilson, O.; Mulvaney, P.; Sader, J. E. Coherent excitation of vibrational modes in gold nanorods. *J. Phys. Chem. B* **2002**, *106*, 743–747.

El-Sayed, M. A. Some interesting properties of metals confined in time and nanometer space of different shapes. *Acc. Chem. Res.* **2001**, *34*, 257–264.

Link, S.; El-Sayed, M. A. Spectroscopic determination of the melting energy of a gold nanorod. *J. Chem. Phys.* **2001**, *114*, 2362–2368.

Mulvaney, P. Surface plasmon spectroscopy of nanosized metal particles. *Langmuir* **1996**, *12*, 788–800 and references therein.

Creighton, J. A.; Eadon, D. G. Ultraviolet-visible absorption spectra of the colloidal metallic elements. *J. Chem. Soc. Faraday Trans.* **1991**, *87*, 3881–3891.

M Fujita  
Nagoya, Japan  
July 2003

A Powell  
Karlsruhe, Germany  
July 2003

C Creutz  
Upton, USA  
May 2003



ELSEVIER



## COMPREHENSIVE COORDINATION CHEMISTRY II

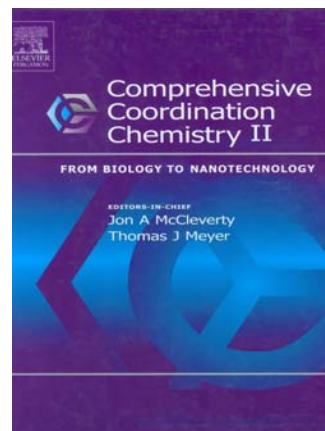
From Biology to Nanotechnology

Second Edition

Edited by

J.A. McCleverty, University of Bristol, UK

T.J. Meyer, Los Alamos National Laboratory, Los Alamos, USA



### Description

This is the sequel of what has become a classic in the field, Comprehensive Coordination Chemistry. The first edition, CCC-I, appeared in 1987 under the editorship of Sir Geoffrey Wilkinson (Editor-in-Chief), Robert D. Gillard and Jon A. McCleverty (Executive Editors). It was intended to give a contemporary overview of the field, providing both a convenient first source of information and a vehicle to stimulate further advances in the field. The second edition, CCC-II, builds on the first and will survey developments since 1980 authoritatively and critically with a greater emphasis on current trends in biology, materials science and other areas of contemporary scientific interest. Since the 1980s, an astonishing growth and specialisation of knowledge within coordination chemistry, including the rapid development of interdisciplinary fields has made it impossible to provide a totally comprehensive review. CCC-II provides its readers with reliable and informative background information in particular areas based on key primary and secondary references. It gives a clear overview of the state-of-the-art research findings in those areas that the International Advisory Board, the Volume Editors, and the Editors-in-Chief believed to be especially important to the field. CCC-II will provide researchers at all levels of sophistication, from academia, industry and national labs, with an unparalleled depth of coverage.

### Bibliographic Information

10-Volume Set - Comprehensive Coordination Chemistry II

Hardbound, ISBN: 0-08-043748-6, 9500 pages

Imprint: ELSEVIER

Price:

USD 5,975

EUR 6,274 Books and electronic products are priced in US dollars (USD) and euro (EUR). USD prices apply world-wide except in Europe and Japan. EUR prices apply in Europe and Japan. See also information about conditions of sale & ordering procedures -<http://www.elsevier.com/wps/find/bookconditionsofsale>.

[cws\\_home/622954/conditionsofsale](http://www.elsevier.com/wps/find/cws_home/622954/conditionsofsale), and links to our regional sales offices [http://www.elsevier.com/wps/find/contact.cws\\_home/regional](http://www.elsevier.com/wps/find/contact.cws_home/regional)

GBP 4,182.50

030/301

Last update: 10 Sep 2005

## Volumes

Volume 1: Fundamentals: Ligands, Complexes, Synthesis, Purification, and Structure

Volume 2: Fundamentals: Physical Methods, Theoretical Analysis, and Case Studies

Volume 3: Coordination Chemistry of the s, p, and f Metals

Volume 4: Transition Metal Groups 3 - 6

Volume 5: Transition Metal Groups 7 and 8

Volume 6: Transition Metal Groups 9 - 12

Volume 7: From the Molecular to the Nanoscale: Synthesis, Structure, and Properties

Volume 8: Bio-coordination Chemistry

Volume 9: Applications of Coordination Chemistry

Volume 10: Cumulative Subject Index

10-Volume Set: Comprehensive Coordination Chemistry II



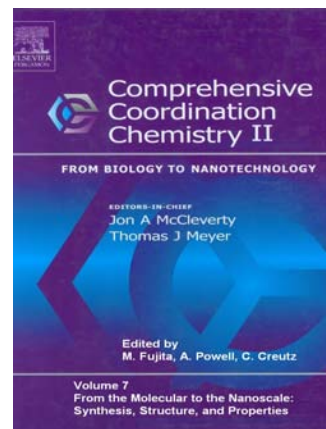
## COMPREHENSIVE COORDINATION CHEMISTRY II

### Volume 7:

### From the Molecular to the Nanoscale: Synthesis, Structure, and Properties

Edited by

**M. Fujita, A. Powell, C. Creutz**



#### Contents

- High nuclearity clusters: Iso and Heteropolyoxoanions and relatives (L. Cronin)
- High nuclearity clusters: clusters on the transition from semiconducting to metallic (J.F. Corrigan, M. de Groot)
- High nuclearity clusters: clusters and aggregates with paramagnetic centres: Oxygen and Nitrogen bridged systems (R.E.P. Winpenny)
- High nuclearity clusters: clusters and aggregates with paramagnetic centres: Cyano and Oxalato bridged systems (S. Decurtins, M. Pilkington)
- Coordination polymers: infinite systems (Susumu Kitagawa)
- Coordination polymers: discrete systems (E. Constable)
- Supramolecular systems: templating (J-P. Collin et al.)
- Supramolecular systems: self-assembly (K.N. Raymond)
- Metallomesogens (D.W. Bruce et al.)
- Sol-gel processing of metal compounds (U. Schubert)
- Molecular electron transfer (J.F. Endicott)
- Electron transfer from the molecular to the nanoscale (C. Creutz et al.)
- Magnetism from the molecular to the nanoscale (D. Gatteschi et al.)

# 7.1

## High Nuclearity Clusters: Iso and Heteropolyoxoanions and Relatives

L. CRONIN

*University of Glasgow, UK*

---

7.1.1	INTRODUCTION	2
7.1.1.1	Scope	2
7.1.1.2	Fundamental Units and Building Blocks	2
7.1.1.3	Basic Principles in Polyoxometalate Cluster Synthesis	3
7.1.2	VANADATES	4
7.1.2.1	{V <sub>12</sub> } Clusters	5
7.1.2.2	{V <sub>14</sub> } and {V <sub>15</sub> } Clusters	8
7.1.2.3	{V <sub>18</sub> }, {V <sub>22</sub> }, {V <sub>34</sub> } Clusters—Clusters Shaped by Encapsulated Templates	10
7.1.3	TUNGSTATES	15
7.1.3.1	Clusters Incorporating Monovacant Lacunary Fragments	18
7.1.3.1.1	{XW <sub>11</sub> } <sub>2</sub>	18
7.1.3.1.2	{XW <sub>11</sub> } <sub>2</sub> {Mo <sub>3</sub> S <sub>4</sub> } <sub>2</sub>	18
7.1.3.1.3	{XW <sub>11</sub> } <sub>3</sub>	19
7.1.3.2	Clusters Incorporating Different Types of Trivacant Lacunary Fragments	19
7.1.3.2.1	{X <sub>2</sub> W <sub>21</sub> }	19
7.1.3.2.2	{M <sub>9</sub> P <sub>5</sub> W <sub>27</sub> }	21
7.1.3.2.3	{XW <sub>9</sub> } <sub>1</sub> :{Eu <sub>3</sub> SbW <sub>24</sub> }	21
7.1.3.2.4	{XW <sub>9</sub> } <sub>2</sub> :{X <sub>2</sub> W <sub>21</sub> } {X <sub>2</sub> W <sub>22</sub> }	22
7.1.3.2.5	{XW <sub>9</sub> } <sub>3</sub>	22
7.1.3.2.6	{XW <sub>9</sub> } <sub>4</sub>	24
7.1.3.2.7	{XW <sub>9</sub> } <sub>11</sub>	24
7.1.3.3	Clusters Incorporating Hexavacant Lacunary Fragments	24
7.1.3.3.1	{P <sub>8</sub> W <sub>48</sub> }	24
7.1.3.3.2	{P <sub>5</sub> W <sub>30</sub> }	24
7.1.4	MOLYBDATES	26
7.1.4.1	From Keggin Ions to {Mo <sub>37</sub> } Clusters	27
7.1.4.2	From {Mo <sub>36</sub> } to {Mo <sub>57</sub> } Clusters—Two and Three Fragment Clusters Based on {Mo <sub>17</sub> } Units	27
7.1.4.3	{Mo <sub>154</sub> } Big Wheel Clusters	28
7.1.4.3.1	Construction of {Mo <sub>154</sub> }-type clusters	29
7.1.4.3.2	Determination of the molecular formula of {Mo <sub>154</sub> }-type clusters	30
7.1.4.4	Reactions of the {Mo <sub>154</sub> }-type Wheels	30
7.1.4.4.1	Formation of structural defects	30
7.1.4.4.2	Linking of wheels to chains and layers	32
7.1.4.4.3	Formation of host guest systems	32
7.1.4.4.4	Structural modifications of the big wheel clusters	36
7.1.4.5	{Mo <sub>176</sub> } Wheel and Derivatives	37
7.1.4.5.1	Comparison between the {Mo <sub>154</sub> } and {Mo <sub>176</sub> } big wheel clusters	37
7.1.4.5.2	Nucleation processes within a cluster cavity—from a {Mo <sub>176</sub> } to a {Mo <sub>248</sub> } cluster	38
7.1.4.5.3	Surface ligand exchange on the big wheel clusters	39
7.1.4.6	Synthesis of Wheels with Electrophiles	40
7.1.4.6.1	Synthesis of the big wheel-type clusters with Pr <sup>III</sup> salts	40
7.1.4.6.2	Synthesis of the big wheel clusters with Eu <sup>III</sup> salts	40
7.1.4.7	{Mo <sub>132</sub> } Big Ball Keplerate Clusters	42
7.1.4.7.1	Building block scheme for the Keplerate clusters	43
7.1.4.7.2	Construction of spherical species with icosahedral symmetry	44

7.1.4.7.3	Changing the bridging ligands in the Keplerate clusters	44
7.1.4.7.4	Structural derivatives: removing the lid of the Keplerate	45
7.1.4.7.5	From $\{Mo_{132}\}$ to $\{Mo_{72}M_{30}\}$ spherical clusters ( $M = Fe, Mo$ )	45
7.1.4.7.6	Formation of molecular barrels $\{Mo_{75}V_{20}\}$	46
7.1.4.7.7	Formation of solid-state structures with $\{Mo_{72}Fe_{30}\}$	47
7.1.4.7.8	Molecular hostages and networks of molecular hostages	48
7.1.4.8	$\{Mo_{368}\}$ Clusters: a Hybrid Between Wheel- and Ball-shaped clusters	49
7.1.4.9	Building Block Principles	51
7.1.5	OUTLOOK	52
7.1.6	REFERENCES	53

---

## 7.1.1 INTRODUCTION

Since the early 1980s the field of polyoxometalate chemistry has undergone a revolution. This has been characterized by the synthesis of ultra-large clusters that have nuclearities as high as 368 metal atoms in a single molecular cluster.<sup>1</sup> Of course, such discoveries have only been possible thanks to the advances of the instrumentation used to collect the diffraction data coupled with the advent of cheap and powerful computing power for structure solution and refinement. Much of the interest in these molecules has arisen because such clusters represent a paradigm in the discovery of systems that can be encouraged to grow from the molecular to the nanoscale. Polyoxometalates have also generated interest in areas as diverse as catalysis,<sup>2–13</sup> magnetism,<sup>14–23</sup> synthesis of molecular devices,<sup>24</sup> synthesis of new materials,<sup>25–51</sup> and have even found potential application as anti-viral agents.<sup>52–55</sup>

### 7.1.1.1 Scope

In this article the field of polyoxometalate chemistry will be reviewed and discussed as it has progressed from the 1980s to its position at the start of the new millennium. In embarking on this journey special attention will be given to the synthesis, structure, and properties of discrete polyoxometalate clusters with a nuclearity that is greater than 12 metal atoms. In nearly all cases the frameworks of these clusters are based upon V, Mo, and W. There is a rich chemistry with iso and heteropolyanions with nuclearities 12 and below (see also Chapters 4.10 and 4.11), but these will not be treated in this chapter unless they are used as fragments in the construction of larger clusters or have interesting physical properties.<sup>56,57</sup>

### 7.1.1.2 Fundamental Units and Building Blocks

Polyoxometalate cluster anions are comprised of aggregates of metal–oxygen units where the metal can be best visualized as adopting the center of a polyhedron and the oxygen ligands defining the vertices of this polyhedron. Therefore, the overall structures of the cluster can be represented by a set of polyhedra that have corner- or edge-sharing modes (face sharing is also possible but rarely seen), see Figure 1 for examples of corner- and edge-sharing polyhedra.

It is not surprising therefore that there are, at least theoretically, a bewildering number of structurally distinct clusters available for a given nuclearity. However, it will become evident that it is extremely useful, at least conceptually, to regard these metal-centered polyhedra and aggregates of these  $\{MO_x\}$  polyhedra as structural building blocks that can be used to help both understand and perhaps even manipulate the synthesis of cluster. The structures can then be considered to form via a self-assembly process involving the linking or aggregation of these polyhedra.<sup>58,59</sup> However, although such concepts will be widely considered here, care must be taken to distinguish between a structurally repeating building block and an experimentally available building block that can be proved to be present and incorporated during the construction of a given cluster.<sup>60</sup>

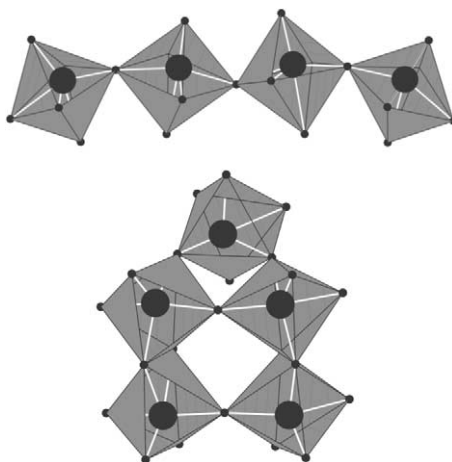


**Figure 1** A representation of corner- and edge-sharing polyhedra found in polyoxometalate clusters. The metal ions at the center of the open polyhedra are shown by the black spheres and the oxygen ligands at the vertexes of the polyhedra are shown by smaller black circles. The top image shows exclusively a corner-sharing mode whereas the bottom image shows a combination of edge and corner-sharing polyhedra.

### 7.1.1.3 Basic Principles in Polyoxometalate Cluster Synthesis

Before outlining the general approach to the synthesis of polyoxometalate clusters it is informative to consider the most useful synthetic results thus far discovered for derivatization and functionalization of fragments leading to a huge variety of structures. These are given below:

- The potential of the system to generate a versatile library of linkable units.
- The ability to generate groups (intermediates) with high free enthalpy to drive polymerization or growth processes, e.g., by formation of  $\text{H}_2\text{O}$ .
- The possibility for structural change in the building units or blocks.
- The ability to include hetero-metallic centers in the fragments.
- The possibility to form larger groups that can be linked in different ways.
- The ability to control the structure-forming processes using templates.
- The ability to generate structural defects in reaction intermediates (e.g., leading to lacunary structures) for example by removing building blocks from (large) intermediates due to the presence of appropriate reactants.
- The ability to localize and delocalize electrons in different ways in order to gain versatility.
- The ability to control and vary the charge of building parts (e.g., by protonation, electron transfer reactions, or substitution) and to limit growth by the presence of appropriate terminal ligands.
- The possibility of generating fragments with energetically low-lying unoccupied molecular orbitals.
- The ability to selectively derivatize both the outside and inside of clusters with sizable cavities.

Generally, the approaches used to produce high nuclearity polyoxometalate-based clusters are extremely simple, consisting of acidifying an aqueous solution containing the relevant metal oxide anions (molybdate, tungstate, and vanadate). In the case of the acidification of the metal oxide-containing solution (see Figure 2) for example, the acidification of a solution of sodium molybdate gives rise to fragments, which increase in nuclearity as the pH of the solution decreases (see Section 7.1.4).<sup>56,57</sup> These isopolyanions have been extremely well investigated in the case of molybdenum, vanadium, and tungsten. However the tungsten cases are limited due to the time required for the system to equilibrate, which is of the order of weeks.<sup>56</sup> Another class of cluster can be synthesized when hetero atoms are introduced, heteropolyanions (see Section 7.1.3) and these are extremely versatile. Indeed, heteroanions based on tungsten have been used in the assembly of extremely large clusters (see Section 7.1.3.2.7).<sup>61</sup> In the case of molybdenum the acidification of solutions of molybdate followed by its subsequent reduction yields new classes of clusters with interesting topologies and very large nuclearities (see Section 7.1.4).<sup>62,63</sup>

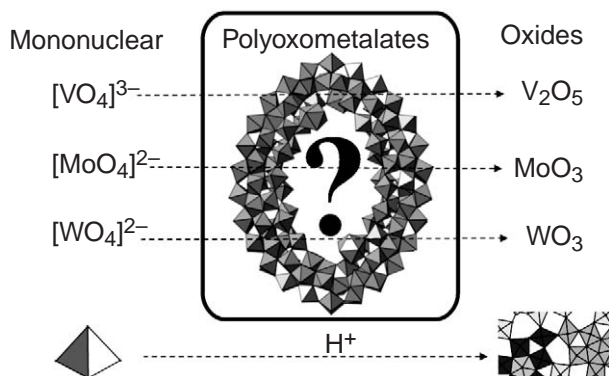


**Figure 2** Polyoxometalates are formed in experimental conditions that allow linking of polyhedra. Discrete structures are formed as long as the system is not driven all the way to the oxide. One such example, in this case a part of a  $\{\text{Mo}_{256}\text{Eu}_8\}$  cluster unit, is depicted in the square (see Section 7.1.4.6.2).

The synthetic variables of greatest importance in synthesizing such clusters may be outlined as follows:

- concentration/type of metal oxide anion;
- pH and type of acid;
- type and concentration of electrolyte;
- heteroatom concentration;
- possibility to introduce additional ligands (reducing ligands);
- reducing agent (in the case of the Mo systems);
- temperature; and
- solvent.

Often such syntheses are done in a single pot and this can mask the extraordinary complexity of the assembly event(s) leading to the high nuclearity cluster. Specific reaction variables and considerations will be discussed at the relevant points throughout this chapter.

## 7.1.2 VANADATES

The vanadates are structurally very flexible and as such can be based on a large number of different types of polyhedra  $\{\text{VO}_x\}$  where  $x = 4, 5, 6$  whereby the pyramidal  $\text{O}=\text{VO}_4$  polyhedra show a tendency to form cluster shells or cages which have topological similarities to the fullerenes and comprise aspects that are structurally analogous to the layers of  $\text{V}_2\text{O}_5$ .<sup>64,65</sup> The bulk of the polyoxovanadates reported so far possess a variable number of vanadium ions bridged by  $\mu_2$ -,  $\mu_3$ -oxo, and  $\mu$ -arseniato groups to yield complex structures ranging from approximate spherical to elliptical geometries.<sup>66,67</sup> The geometry around the vanadium ions can be square pyramidal, octahedral, or tetrahedral. In the tetrahedral case the ion is almost always vanadium(V), while in the square pyramidal/octahedral geometries the metal ion can either be in the +4 or +5 oxidation state. The resulting structures range from quite compact forms, for example, in the case of  $[\text{V}_{10}\text{O}_{28}]^{6-}$  to open ribbon, basket, shell, and cage-like host systems,<sup>64</sup> suitable for the uptake of neutral<sup>68,69</sup> and ionic guests.<sup>70–73</sup> In addition, two-dimensional layered materials,<sup>74,75</sup> as well as three-dimensional host structures,<sup>76</sup> have been described in recent years. Interestingly, simple vanadates have even been found useful to replace insulin in some mammals.<sup>77–79</sup>

The identification of the oxidation state of the square pyramidal vanadium ions is not always easy, especially when extensive electron delocalization is present. However valence bond summations can greatly aid the assignment in those cases where sufficiently high quality structural data have been obtained. Such assignments can be further checked by EPR and magnetic investigations. Indeed, one of the most exciting aspects of polyoxovanadate chemistry is the prospect of synthesizing topologically<sup>80–82</sup> interesting clusters that can behave as nanoscale magnets.<sup>19,83–88</sup> Such clusters are synthesized in aqueous solution with the appropriate precursor, anion templates and, in the case of the mixed valence species, reducing agents. However vanadates have also been synthesized under hydrothermal conditions,<sup>89</sup> and even in vanadium oxide sol–gel systems.<sup>30,90</sup>



### 7.1.2.1 $\{V_{12}\}$ Clusters

A number of heterotungstates and molybdates adopt either the Keggin ion structure or a structure derived from fragments of it.<sup>56,91</sup> However for heteropolyvanadates, the realization of the normal Keggin ion-type structure of the form  $XV_{12}O_{40}$  is limited by the generation of a high negative charge. The stabilization of such clusters appears to be facilitated by the incorporation of  $VO^{3+}$  or  $AsO^{3+}$  groups.

For example, the compound  $K_6[H_3KV_{12}As_3O_{39}(AsO_4)] \cdot 4H_2O$  (**1**)<sup>87,92</sup> is a good example of a mixed valence vanadium cluster with both localized and delocalized vanadium centers (Figure 3). Compound (**1**) is formally built up by nine  $VO_6$  octahedra, three  $VO_4$  tetrahedra, and four  $AsO_4$  tetrahedra, one of the latter being a central  $AsO_4^{3-}$  group. The terminal O atoms of each of the peripheral  $AsO_4$  groups are protonated and a potassium ion crowns the fragment. The number of vanadium(IV) centers, expected to be four, was confirmed by Barra *et al.* by manganometric titration.<sup>93</sup>

The identification of the vanadium(IV) centers in the structure is not a trivial endeavor. Bond valence sum (BVS) investigations<sup>94</sup> suggest that V10, V11, and V12 are localized vanadium(IV) centers, however the fourth vanadium(IV) ion is delocalized over the positions V1, V2, and V3, i.e., a  $\{V_{3+1}\}$  cluster, see Figure 3. The oxovanadium ions V10, V11, and V12 are connected by long O–As–O bridges and the delocalized vanadium(IV) spread on positions V1, V2, and V3 are connected by  $\mu_2$ -oxo bridges. The connection between the localized and delocalized vanadium(IV) ions are long and involve more atoms, so their interaction is negligible. The  $\{V_{3+1}\}$  electronic structure was also confirmed by magnetic measurements giving a room-temperature effective magnetic moment of  $3.17\mu_B$ , which corresponds to four unpaired electrons. The magnetic moment decreases smoothly with decreasing temperature giving a small plateau at  $2.36\mu_B$  in the range 10–20 K. This was modeled by including an exchange coupling constant,  $J$ , for the localized and  $J'$  for the localized–delocalized interaction. The best-fit values were reported as being  $J = 63\text{ cm}^{-1}$  and  $J' = 1.0\text{ cm}^{-1}$ . It would appear that this case provides useful information for the analysis of more complex systems, namely those in which there is ambiguity when judging the extent of delocalization vs. localization using the BVS approach. In addition the data indicate that the delocalization is extremely fast and thus one averaged coupling constant can be used.<sup>87,92</sup>

Synthesis of the isostructural clusters  $[V_{12}As_8O_{40}(KCO_2)]^{n-}$  (when  $n = 3$  (**2a**) the cations are  $2[HNET_3]^+$  and  $1[HNH_2Me]^+$  and when  $n = 5$  (**2b**) the cations are five sodium ions) gave an opportunity to compare two isostructural clusters that have different ratios of  $V^{IV}/V$  ions in the cluster framework, see Figure 4. (**2a**) contains six noninteracting and (**2b**) eight antiferromagnetically coupled  $V^{IV}$  ( $d^1$ ) centers.

Both cluster anions have  $D_{4h}$  symmetry and consist of 12 distorted tetragonal  $VO_5$  pyramids and four  $As_2O_5$  groups, which together link to form a hollow cavity that encapsulates a

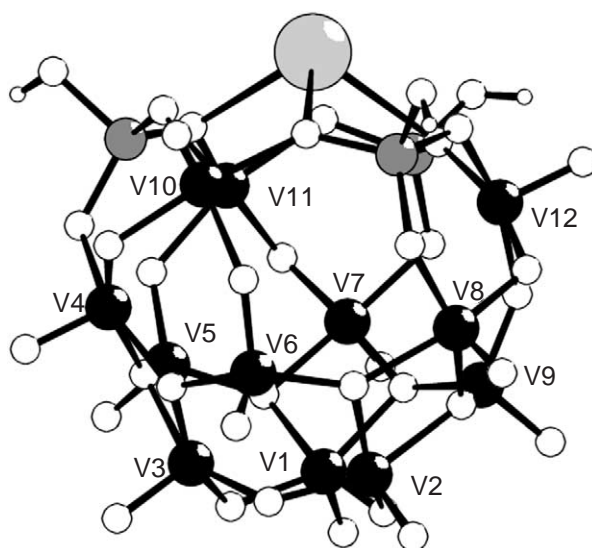


**Figure 3** A representation of the crystal structure of the  $\{V_{12}\}$  cluster (**1**). The vanadium ions are shown as black spheres, the arsenate ions by dark gray spheres and the potassium ion by the large light gray sphere. The small white spheres are oxygen atoms and the smaller white spheres are hydrogen atoms.

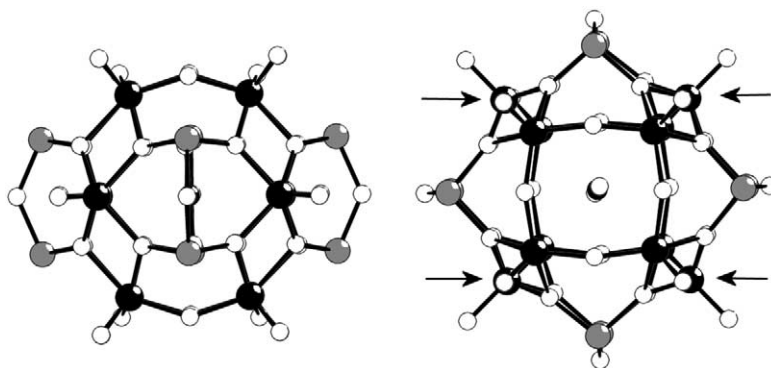


**Figure 4** Structure of the cluster (**2a**) and (**2b**) (left-hand side (LHS)=side view; right-hand side (RHS)=top view) with an encapsulated disordered formate ion (center of the RHS view). The trapped  $V^{IV}$  centers are shown by the arrows in the RHS view. The vanadium ions are shown as black spheres, the arsenate ions by dark gray spheres and the oxygen atoms as white spheres.

disordered formate ion.<sup>95,96</sup> The 12  $VO_5$  pyramids can be divided into two types that differ with respect to their position relative to the  $As_2O_5$  groups. The first consists of four pyramids that are bridged through edges by the  $As_2O_5$  groups forming the middle section of the anion where four  $V^{IV}$  centers are trapped, see **Figure 4**, while two  $V^{IV}$  centers in (**2a**) and four in (**2b**) are delocalized over eight sites, the remaining ions being formally  $V^V$  ions, i.e.,  $\{V_{4+2}\}$  and  $\{V_{4+4}\}$ , respectively. Although the magnetic analysis is quite complex it has been shown that the magnetic behavior correlates with the geometry and the topology of the cluster.<sup>96</sup> The four localized vanadium(IV) ions are bridged by  $\mu$ -O-As-O groups, while the delocalized sites are bridged by  $\mu$ -O and  $\mu$ -O-As-O groups, and the mixed localization sites are bridged by either double  $\mu_2$ -OAs or single  $\mu$ -O-As-O groups, see **Table 1**. The room-temperature effective magnetic moment of  $\{V_{4+2}\}$  is  $4.05\mu_B$  and the  $\{V_{4+4}\}$  is  $2.97\mu_B$ , indicating that in both cases there are many electrons with antiparallel spins. Overall, magnetic properties of  $\{V_{4+4}\}$  can be explained by assuming that the two vanadium(IV) ions in the delocalized sites are strongly antiferromagnetically coupled, so that the observed effective magnetic moment can be attributed to the four localized vanadium(IV) ions. Using this model the temperature dependence of the effective magnetic moment can be fitted with  $J = 10 \text{ cm}^{-1}$ . The magnetic properties of the  $\{V_{4+2}\}$  are more problematic as the data cannot be fitted with only antiferromagnetic coupling constants. However, if one constant is assumed to be ferromagnetic then a good fit is obtained, but the pathway that gives rise to this is difficult to assign.

**Table 1** Exchange pathways and coupling constants in some vanadates—see reference<sup>87</sup> for a more advanced and complete discussion.

Cluster	Atom 1	Atom 2	Bridge 1	Bridge 2	Distance	Coupl	Value
$\{V_{15}\}$ ( <b>7</b> )	$V_1$	$V_2$	$\mu_3$ -O	$\mu_3$ -O	2.87	$J$	556
	$V_1$	$V_2'$	$\mu_3$ -O	$\mu_2$ -OAs	3.05	$J'$	104
	$V_1$	$V_3$	$\mu_3$ -O	$\mu_2$ -OAs	3.02	$J_1$	104
	$V_2$	$V_2'$	$\mu_3$ -O		3.68	$J''$	208
	$V_2$	$V_3'$	$\mu_3$ -O		3.73	$J_2$	208
$\{V_{14}\}$ ( <b>8</b> )	$V_1$	$V_2$	$\mu_2$ -OAs	$\mu_2$ -OAs	3.06	$J_1$	19
	$V_3$	$V_4$	$\mu_3$ -O	$\mu_2$ -OAs	3.01	$J_2$	124
	$V_2$	$V_4$	$\mu_3$ -O	$\mu_3$ -O	2.84	$J$	507
	$V_2$	$V_3$	$\mu_3$ -O		3.60	$J_3$	55
$\{V_{3+1}\}$ ( <b>1</b> )	$V_{10}$	$V_{11}$	$\mu$ -OAsO		5.70	$J$	63
$\{V_{4+2}\}$ ( <b>2a</b> )	$V_{10}$	$V_{11}$	$\mu$ -OAsO	$\mu$ -OAsO	5.25	$J$	10
$\{V_{4+4}\}$ ( <b>2b</b> )	$V_{10}$	$V_8$	$\mu_2$ -OAsO	$\mu_2$ -OAs	3.16		
	$V_{10}$	$V_9$	$\mu_2$ -OAsO		5.28	$J'$	-12
	$V_8$	$V_9$	$\mu$	$\mu$	3.42		

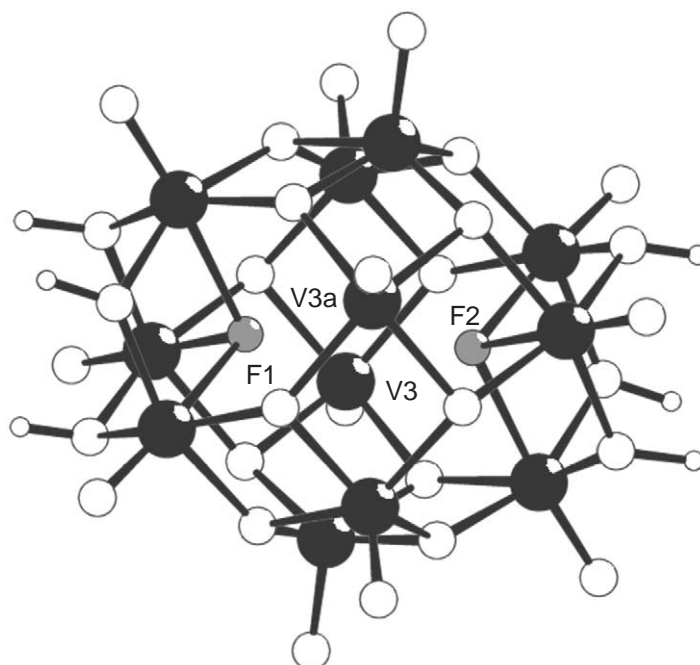


**Figure 5** Structure of the cluster anion  $[\text{H}_6\text{V}_{12}\text{O}_{30}\text{F}_2]^{6-}$ . The vanadium ions are shown as black spheres, the fluoride atoms by the gray spheres. The small white spheres are oxygen atoms and the smaller white spheres are hydrogen atoms.

The anionic cluster<sup>83,97</sup>  $[\text{H}_6\text{V}_{12}\text{O}_{30}\text{F}_2]^{6-}$  (**3**) contains 10  $\text{V}^{\text{IV}}$  and two localized  $\text{V}^{\text{V}}$  centers and as such, this compound offers another test for the validity of valence bond summations, which suggest all the charges are trapped. Standard BVS calculations clearly indicate that the localized  $\text{V}^{\text{V}}$  centers are those shown as V3 and V3a in Figure 5.

It is also possible to synthesize somewhat more open clusters. For example Klemperer *et al.* synthesized a topologically interesting vanadate, a  $[\text{V}_{12}\text{O}_{32}]^{4-}$  basket<sup>64,68</sup> (**4**) which comprises 12  $\text{V}^{\text{V}}$  ions. Interestingly the basket holds an acetonitrile molecule, see Figure 6.

This result was extended with the inclusion of  $\text{C}_6\text{H}_5\text{CN}$  in the molecular bowl (**5**), see Figure 7.<sup>98</sup> This result offers the possibility that vanadium oxide bowls could be used as molecular containers and may help capture and stabilize interesting molecules.

Indeed this approach was extended by Ozeki and Yagasaki<sup>99</sup> in 2000 when they managed to crystallize a  $\{\text{V}_{12}\}$  bowl (**6**) analogous to those reported before, but this time encapsulating a  $\text{NO}^-$  anion, see Figure 8.

This is the first example of the  $\text{NO}^-$  anion trapped in the solid phase and it is notable that the  $\text{NO}^-$  anion appears to rest deeper in the cavity than any of the previous guest molecules. This is of interest as an example of an anionic guest being isolated in an anionic host, but is by no means without precedent (see Section 7.1.4.4.3).

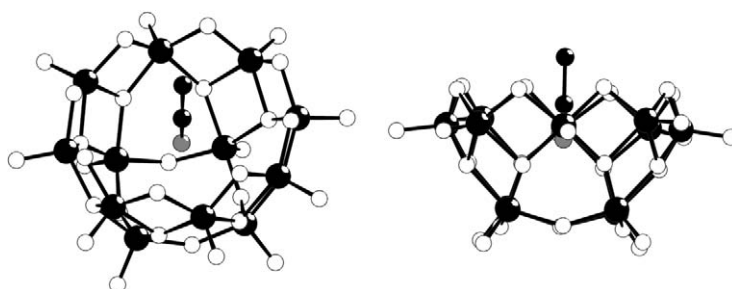


**Figure 6** Representation of the vanadate basket cluster,  $[\text{V}_{12}\text{O}_{32}]^{4-}$  (LHS = top view; RHS = side view). The acetonitrile solvent molecule can be seen in the center of the cavity. The vanadium ions are shown as black spheres and the white spheres are oxygen atoms.

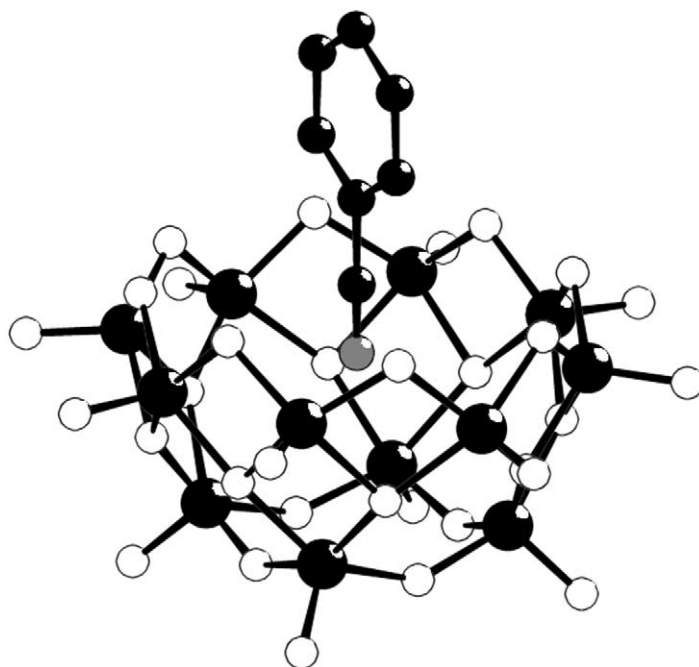


**Figure 7** A representation of the vanadate basket cluster,  $[V_{12}O_{32}]^{4-}$  including a  $C_6H_5CN$  molecule. The vanadium ions are shown as the large black spheres and the white spheres are oxygen atoms. The smaller black spheres and the gray sphere indicated the  $C_6H_5CN$  molecule.

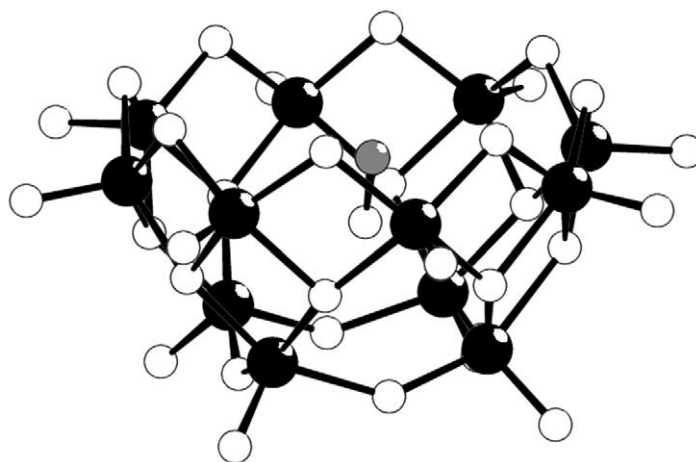


**Figure 8** A representation of the crystal structure of the  $NO^-$  anion in a vanadate-based molecular bowl. The vanadium ions are shown as the large black spheres and the white spheres are oxygen atoms. The  $NO^-$  molecule is shown as the linked gray and white sphere in the center of the cavity.

#### 7.1.2.2 $\{V_{14}\}$ and $\{V_{15}\}$ Clusters

One of the most interesting aspects of cluster synthesis is the possibility of engineering, by accident or design,<sup>100</sup> clusters with large but finite numbers of spins, which are coupled to each other. In this respect the cluster anion  $[V_{15}As_6O_{42}(H_2O)]^{6-}$  (7) comprising 15  $V^{IV}$  ions,<sup>87,101</sup> offers interesting possibilities.

The overall structure of (7) is shown in Figure 9, and the cluster has crystallographically imposed  $D_3$  symmetry. It consists of 15 distorted tetragonal  $VO_5$  pyramids and six trigonal  $AsO_3$  pyramids and it encapsulates a water molecule at the center of the quasi-spherical cluster sheath. The 15  $VO_5$  pyramids are linked to one another through vertices. Two  $AsO_3$  groups are joined to each other via an oxygen bridge forming a handle-like  $As_2O_5$  moiety.

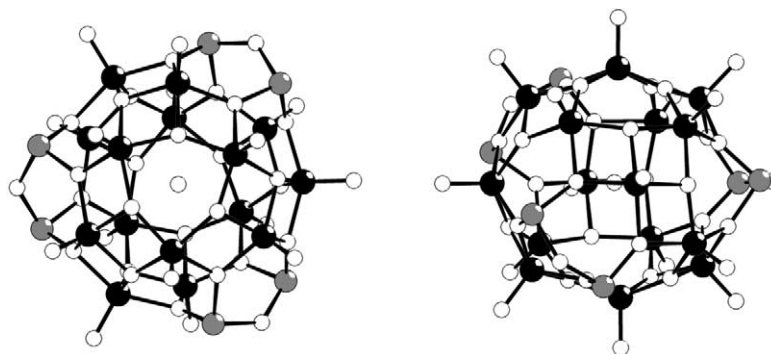


**Figure 9** A representation of the structure of (7) from the top (left) and the side (right) view respectively. The vanadium ions are shown as black spheres, the arsenate ions by dark gray spheres and the oxygen atoms as white spheres.

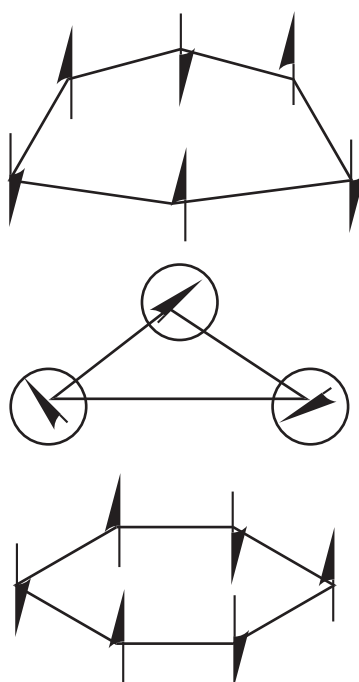


**Figure 10** Scheme of the magnetic layers in  $\{V_{15}\}$ .

The  $\{V_{15}\}$  cluster (7) has a room-temperature effective magnetic moment of  $4.0\mu_B$ , indicating strong antiferromagnetic coupling compared with the value for 15 uncoupled vanadium(IV) ions, which is  $6.7\mu_B$ . The effective magnetic moment decreases slowly on decreasing temperature and in the region of 100–20 K it tends to  $2.8\mu_B$ . Below 20 K  $\mu_{\text{eff}}$  decreases again reaching  $2.0\mu_B$  at 1.8 K. It would appear that the observation that the effective magnetic moment is essentially constant over a large range of temperatures is an indication that the strong antiferromagnetic coupling leaves at least three spins uncoupled at high temperature, i.e., a smaller antiferromagnetic exchange interaction couples the three spins together at low temperature, see Table 1 for details of bridging and coupling constants. Detailed analysis has shown this cluster to possess a unique multilayer magnetic structure.<sup>102,103</sup> Briefly, (7) can be considered as a small model of a multilayer structure with two external antiferromagnetic layers sandwiching an internal triangular planar layer, as schematically shown in Figure 10.

The cluster anion  $[V_{14}As_8O_{42}(SO_3)]^{6-}$  (8), which is shown in Figure 11, is also composed exclusively of  $V^{IV}$  ions. Of these, eight, which are connected by  $\mu_3\text{-O}$  and  $\mu_3\text{-OAs}$  groups, define an octagon, and then two sets of three  $V^{IV}$  ions connect diametrically opposed centers on the octagons. The room-temperature effective magnetic moment is  $4.45\mu_B$ , which is also smaller than expected for 14 uncoupled spins ( $6.48\mu_B$ ) clearly indicating the presence of antiferromagnetic coupling.<sup>102,103</sup>

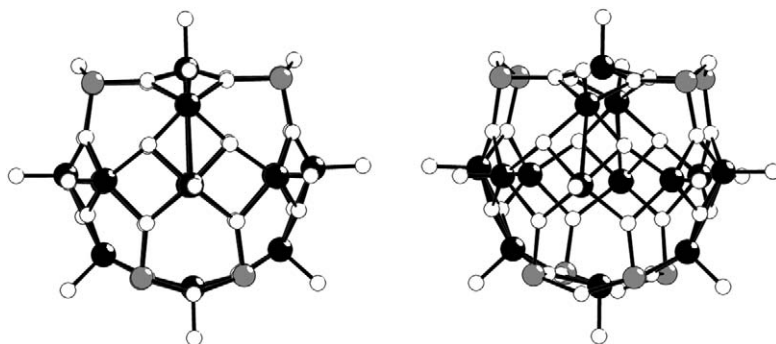


**Figure 11** A representation of the structure of the  $\{V_{14}\}$  cluster (**8**). The left view shows the central belt of vanadium ions and the caps above and below the belt. The right view shows that the central belt comprises eight vanadium ions and the caps of three vanadium ions above and below the central belt. The vanadium ions are shown as black spheres, the arsenate ions by dark gray spheres and the oxygen atoms as white spheres.

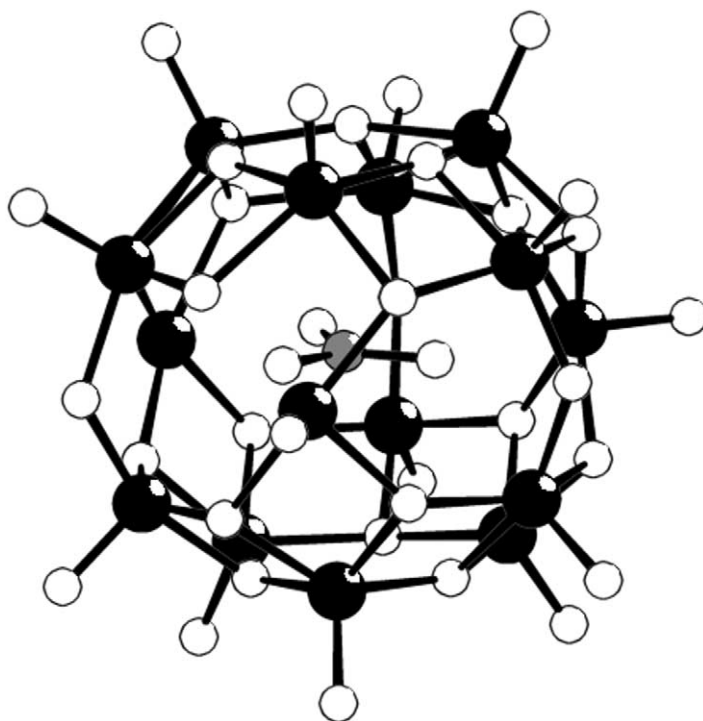


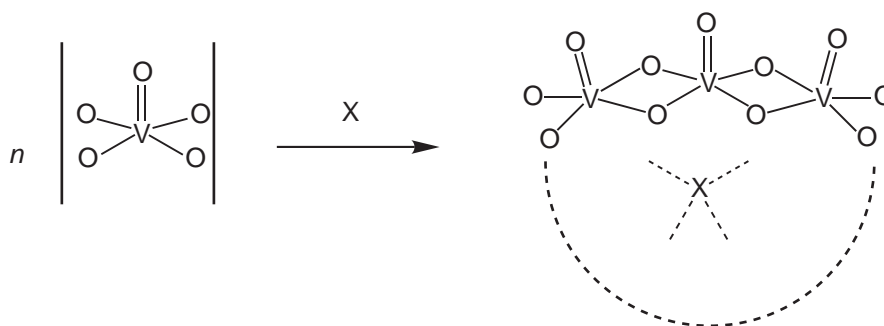
**Figure 12** A representation of the structure of the  $\{V_{15}\}$  (**9**) shell encapsulating a carbonate dianion. The vanadium ions are shown as black spheres and the oxygen atoms as white spheres. The carbon atom of the carbonate anion is shown as a gray sphere.

In studies by Yamase *et al.*<sup>104</sup> a  $\{V_{15}\}$  cluster encapsulating a  $CO_3^{2-}$  was synthesized and characterized, see **Figure 12**. The  $[V_{15}O_{36}(CO_3)]^{7-}$  anion (**9**) was synthesized by the photolysis of solutions of  $[V_4O_{12}]^{4-}$  at  $pH = 9$  adjusted by  $K_2CO_3$ . The resulting anion is a nearly spherical  $\{V_{15}O_{36}\}$  cluster shell encapsulating a  $CO_3^{2-}$  anion and formally contains eight  $V^{IV}$  and seven  $V^V$  centers. The structure of this cluster sheath is virtually identical to a  $\{V_{15}\}$  cluster (**9(a)**) synthesized by Müller in 1987 of the formula  $[V_{15}O_{36}Cl]^{6-}$ .<sup>105</sup>

### 7.1.2.3 $\{V_{18}\}$ , $\{V_{22}\}$ , $\{V_{34}\}$ Clusters—Clusters Shaped by Encapsulated Templates

It would appear that under certain reaction conditions, vanadate cluster shells can be generated by linking fragments that depend to a large extent on the size, shape, and charge of a template (in most cases the templates are anions) incorporated as a guest in the final structure. The cluster

cage...X interactions (where X is the anionic guest) appear to give a weakly repulsive surface around which the cluster can be formed (see Scheme 1), which is a schematic of the templating effect found with polyoxovanadate cluster synthesis whereby the templating molecule X helps to polymerize the  $\text{OVO}_4$  units around itself. These weakly repulsive interactions allow the encapsulation of anions in such a way that they can almost be observed to “hover” within the cavity. A further consideration is that these interactions can often give rise to very high coordination numbers; sometimes values as high as 24 have been observed, which can be compared to the highest conventional coordination number of 12. The possibility of including so many weak interactions appears to facilitate very subtle sculpting of the resulting cluster cage. For example, it is possible to synthesize structurally equivalent  $\{\text{V}_{18}\}$  cluster cages but with differing electron populations and guests encapsulated within the host.



Scheme 1

It has been shown by Müller *et al.* that the  $\{\text{V}_{18}\text{O}_{42}\}$  shell can exist in two different structural types.<sup>106</sup> The 24  $\mu_3$  oxygen atoms form either the edges of a distorted rhombicuboctahedron or a pseudorhombicuboctahedron (the “14th” Archimedean solid), see Figure 13.<sup>80,92</sup> The latter polyhedron can be generated by a  $45^\circ$  rotation of one-half of the rhombicuboctahedron around one of its  $S_4$  axes. Clusters corresponding to the rhombicuboctahedron can be regarded as being an enlarged Keggin ion, in which all the planes of the rhombicuboctahedron are spanned by 24 oxygen atoms and are capped by the  $\{\text{VO}\}$  units.

For example, the anion,  $[\text{H}_7\text{V}^{\text{IV}}_{16}\text{V}^{\text{V}}_2\text{O}_{42}(\text{VO}_4)]^{6-}$  (**10**) adopts  $T_d$  symmetry due to the highly charged, tetrahedral  $[\text{VO}_4]^{3-}$  “template” which seems to “force” the outer cluster shell to adopt the same symmetry, see Figure 14. This cluster is different from the other  $\{\text{V}_{18}\}$  clusters reported as the  $\{\text{VO}_4\}$  unit is actually bonded to the cluster shell, whereas in the other clusters guest molecules are merely included in the cluster as a nonbonded fragment.

In the case of the other guests (Table 2) such as  $\text{H}_2\text{O}$ ,  $\text{Cl}^-$ ,  $\text{Br}^-$ ,  $\text{I}^-$ ,  $\text{SH}^-$ ,  $\text{NO}_2^-$ ,  $\text{HCO}_2^-$  the cluster adopts the  $D_{4d}$  symmetry, see Figure 15.

Although only two structural types have been identified, within this structural classification there appear to be three types of redox states: (i)  $\text{V}^{\text{IV}}_{18}\text{O}_{42}$  (compounds **(11a)**–**(11d)**); (ii)  $\text{V}^{\text{IV}}_{16}\text{V}^{\text{V}}_2\text{O}_{42}$  (compound **(10)**); and (iii)  $\text{V}^{\text{IV}}_{10}\text{V}^{\text{V}}_8\text{O}_{42}$  (compound **(12)**) see Table 2.

Type (i) clusters are fully reduced anions with  $18\text{V}^{\text{IV}}$  centers and encapsulate either neutral or anionic guests; the nature of the guest is responsible for any structural variation. Compounds

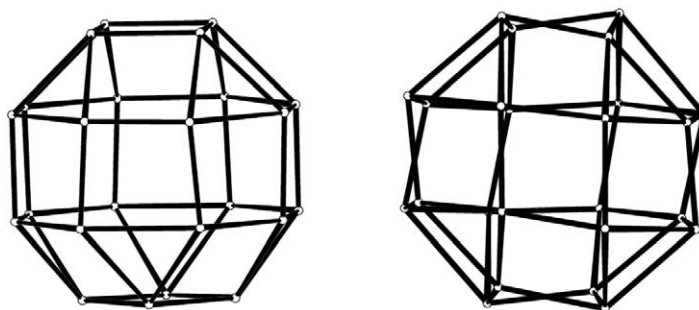


**Figure 13** A schematic of the two types of polyhedron formed by the  $\{\text{V}_{18}\}$  clusters. The  $T_d$  rhombicuboctahedron is shown on the LHS and the  $D_{4d}$  pseudorhombicuboctahedron is shown on the RHS.

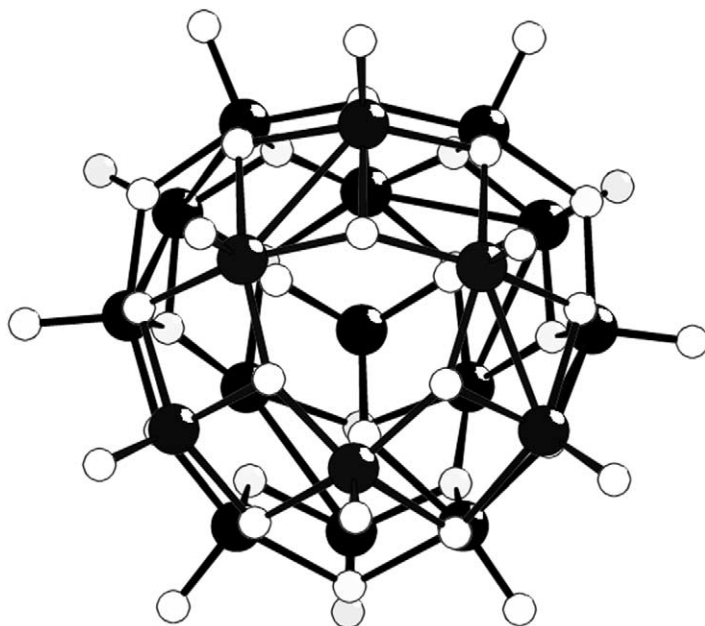


**Figure 14** A representation of the  $\{V_{18}+VO_4\}$  cluster (**10**), which includes a central  $\{VO_4\}$  unit that could be implicated as a template. The vanadium ions are shown as black spheres and the oxygen atoms as white spheres.

(**11a–c**) are synthesized under anaerobic conditions at high pH values (ca. 14) from aqueous vanadates solutions and under these conditions only water molecules are enclosed within the cluster shell. The incorporation of these anions in the fully reduced shell is facilitated by synthesizing the clusters at a lower pH and (ca. 10) by addition of the correct anion. Type (ii) clusters are mixed valence anions (type III according to the classification of Robin and Day)<sup>107</sup> with encapsulated anions. These compounds are synthesized under an inert atmosphere and at pH values 7–9. There is only one example of the type (iii) cluster (**12**) and this was synthesized from an existing<sup>108</sup>  $\{V_{18}\}$  cluster  $[V_{18}O_{42}(SO_4)]^{8-}$  by the addition of  $(NEt_4)I$  in air.

It is important to note that the differences in the electron population of  $\{V_{18}O_{42}\}$  were identified and confirmed structurally using BVS, EPR, and magnetochemistry.<sup>106</sup>

**Table 2** Summary of the shell types and the formulas of the clusters characterized in each shell type.<sup>106</sup>

Shell type	Compound formula
$V^{IV}_{18}O_{42}$	$Cs_{12}[V^{IV}_{18}O_{42}(H_2O)] \cdot 14H_2O$ ( <b>11a</b> ) $K_{12}[V^{IV}_{18}O_{42}(H_2O)] \cdot 16H_2O$ ( <b>11b</b> ) $Rb_{12}[V^{IV}_{18}O_{42}(H_2O)] \cdot 19H_2O$ ( <b>11c</b> ) $K_9[H_3V^{IV}_{18}O_{42}(H_2O)] \cdot 14H_2O \cdot 4N_2H_4$ ( <b>11d</b> ) $K_{11}[H_2V^{IV}_{18}O_{42}(Cl)] \cdot 13H_2O \cdot 2N_2H_4$ ( <b>13a</b> ) $K_9[H_4V^{IV}_{18}O_{42}(Br)] \cdot 14H_2O \cdot 4N_2H_4$ ( <b>13b</b> ) $K_9[H_4V^{IV}_{18}O_{42}(I)] \cdot 14H_2O \cdot 4N_2H_4$ ( <b>13c</b> ) $K_{10}[H_3V^{IV}_{18}O_{42}(Br)] \cdot 13H_2O \cdot 0.5N_2H_4$ ( <b>13d</b> ) $K_9[H_4V^{IV}_{18}O_{42}(NO_2)] \cdot 14H_2O \cdot 4N_2H_4$ ( <b>13e</b> ) $Cs_{11}[H_2V^{IV}_{18}O_{42}(SH)] \cdot 12H_2O$ ( <b>13f</b> )
$V^{IV}_{16}V^V_2O_{42}$	$K_{10}[HV^{IV}_{16}V^V_2O_{42}(Cl)] \cdot 16H_2O$ ( <b>14a</b> ) $Cs_9[H_2V^{IV}_{16}V^V_2O_{42}(Br)] \cdot 12H_2O$ ( <b>14b</b> ) $K_{10}[HV^{IV}_{16}V^V_2O_{42}(Br)] \cdot 16H_2O$ ( <b>14c</b> ) $Cs_9[H_2V^{IV}_{16}V^V_2O_{42}(I)] \cdot 12H_2O$ ( <b>14d</b> ) $K_{10}[HV^{IV}_{16}V^V_2O_{42}(I)] \cdot 16H_2O$ ( <b>14e</b> ) $K_{10}[HV^{IV}_{16}V^V_2O_{42}(HCOO)] \cdot 15H_2O$ ( <b>14f</b> )
$V^{IV}_{10}V^V_8O_{42}$	$Na_6[H_7V^{IV}_{10}V^V_8O_{42}(VO_4)] \cdot 21H_2O$ ( <b>10</b> ) $(NEt)_5[V^{IV}_{10}V^V_8O_{42}(I)]$ ( <b>12</b> )



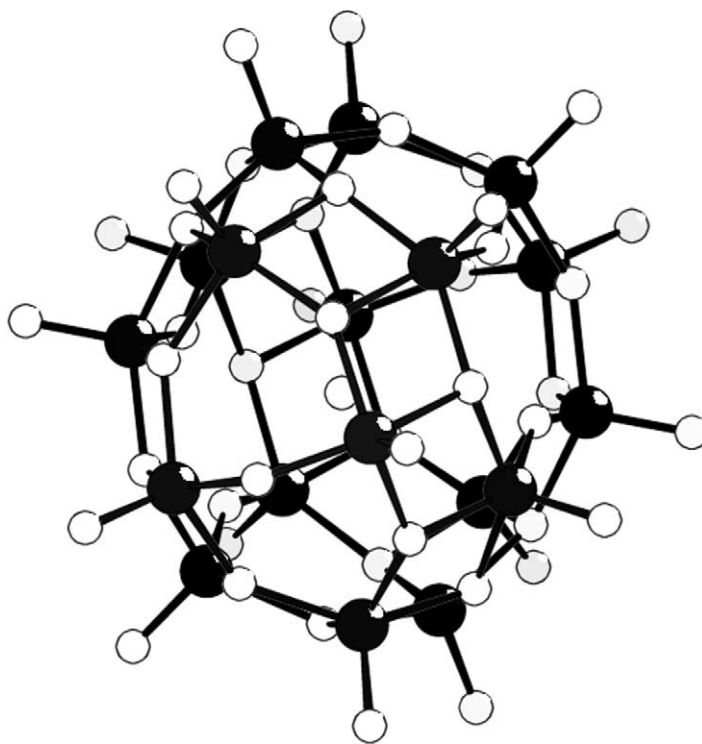


**Figure 15** A representation of the  $\{V_{18}\}$  cluster, which encapsulates weakly coordinated small molecules at its center (see Table 1). The vanadium ions are shown as black spheres and the oxygen atoms as white spheres.

This assembly principle can be extended to many types of anions. For example, the oxidation of  $[H_9V_{19}O_{50}]^{8-}$  in the presence of  $NEt_4X$  appears to generate vanadium clusters of differing nuclearity dictated by the size of the anion,  $X^-$ . As an illustration of this, when  $X$  is azide a  $\{V_{18}\}$  cluster results of the formula  $[H_2V_{18}O_{44}(N_3)]^{5-}$  (**15**) see Figure 16, for  $X$  is perchlorate a  $\{V_{22}\}$  cluster is produced,  $[HV_{22}O_{54}(ClO_4)]^{6-}$  (**16**) and when  $X$  is thiocyanate a  $\{V_{22}\}$  cluster is also produced,  $[HV_{22}O_{54}(SCN)]^{6-}$  (**17**), see Figure 17.

In an alternative synthetic procedure,<sup>97</sup> the reaction of an aqueous solution of  $KVO_3$  with  $N_2H_5OH$ , followed by the addition of acetic acid to a pH of ca. 8 with heating yields crystals of  $[H_2V_{22}O_{54}(OAc)]^{7-}$  (**18**). Changing the anion to  $NO_3^-$ , by acidifying with  $HNO_3$  instead of acetic acid, produces a  $\{V_{18}\}$  cluster encapsulating a  $NO_3^-$  (**19**) with the formula,  $[HV_{18}O_{44}(NO_3)]^{10-}$ , see Figure 18. In another approach, Yamase *et al.* have used a photochemical method<sup>109</sup> to synthesize some mixed valence  $\{V_{18}\}$  clusters with a large number of vanadium(IV) ions, and they have also chosen azide as a template,  $[V_{18}O_{44}(N_3)]^{14-}$  (**20**) and one example including phosphate,  $[V_{18}O_{42}(PO_4)]^{11-}$  (**21**) which exhibits the same type of super-Keggin structure as observed for (**10**),  $[H_7V^{IV}_{16}V^{V}O_{42}(VO_4)]^{6-}$ .

The cluster  $[H_2V_{18}O_{44}(N_3)]^{5-}$  (**15**) has approximate  $D_{2h}$  symmetry and the cluster is built from edge- and corner-sharing tetragonal  $O=VO_4$  pyramids. The azide ion rests in the cavity with the shortest  $N\cdots O$  distance being ca. 3.05 Å. The  $\{V_{22}\}$  clusters have very similar structures and are also comprised of tetragonal  $OVO_4$  pyramids with an overall  $D_{2d}$  symmetry. In the case of the perchlorate cluster the perchlorate anion rests in the cavity with the shortest  $O\cdots O$  distance being around 2.96 Å. However it appears that not only weakly bound anions can be incorporated into these cluster systems. It has also been possible to identify a  $[V_{34}O_{82}]^{10-}$  cluster anion (**22**) that appears to incorporate a bonded  $\{V_4O_4\}O_4$  cube within a cluster shell, see Figure 19. The overall cluster anion  $[V_{34}O_{82}]^{10-}$  has approximate  $D_{2d}$  symmetry and consists of an ellipsoid-shaped  $\{V_{30}O_{74}\}$  sheath, which is formed by linking 30 tetragonal  $VO_5$  pyramids, and a central  $V_4O_4$  cube. The sheath can be divided into two identical halves that are related by a  $90^\circ$  rotation with respect to each other as defined by the geometry of the central cube. Geometrically each half of the anion contains 20 of the 24 oxygen atoms of a  $O_{24}$  rhombicuboctahedron. One interesting observation is that the  $\{V_{18}\}$  sheath can be considered to be related to segments of a layer of vanadium pentoxide, see Figure 20.<sup>64,65</sup>

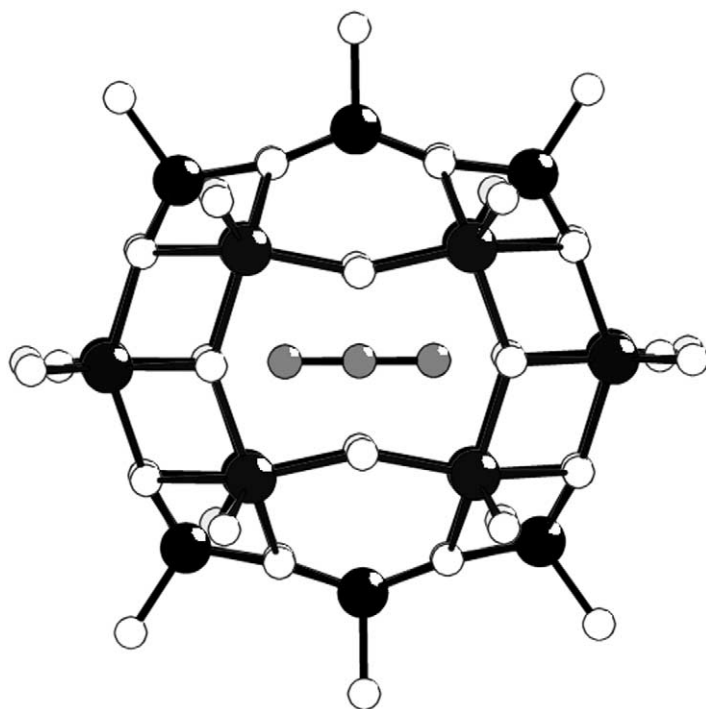


**Figure 16** Structure of  $\{V_{18}N_3\}$  (**20**).<sup>73</sup> The vanadium atoms are shown as black spheres and the oxygen atoms as white spheres, and the nitrogen atoms of the linear  $N_3^-$  anion are shown as gray spheres.

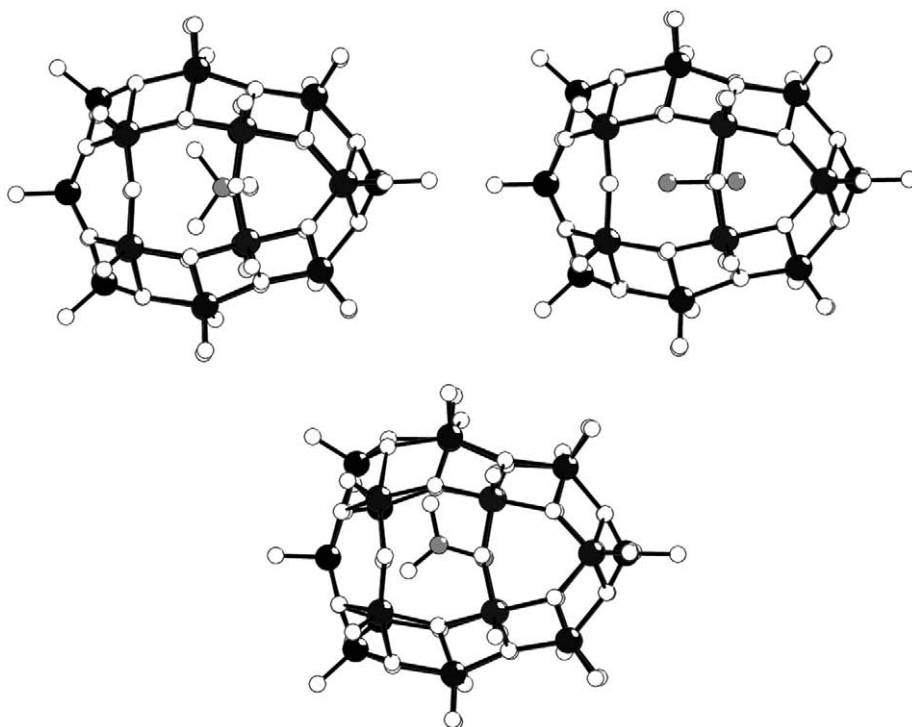


**Figure 17** Structures of the  $\{V_{22}ClO_4\}$  (top left), (**16**),<sup>73,97</sup>  $\{V_{22}NCS\}$  (disordered NCS) (top right), (**17**),<sup>97</sup>  $\{V_{22}OAc\}$ <sup>110</sup> (**18**) bottom center. The vanadium atoms are shown as black spheres and the oxygen atoms as white spheres, and the other nonoxygen atoms of the anion are shown as gray spheres.

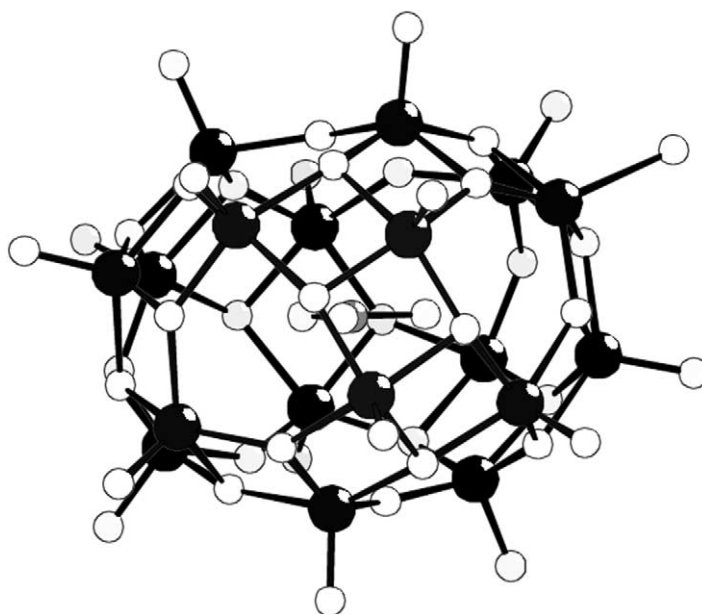


**Figure 18** The structure of the  $\{V_{18}NO_3\}$  cluster (19).<sup>111</sup> The vanadium atoms are shown as black spheres and the oxygen atoms as white spheres, and the non-oxygen atoms of the anion are shown as gray spheres.

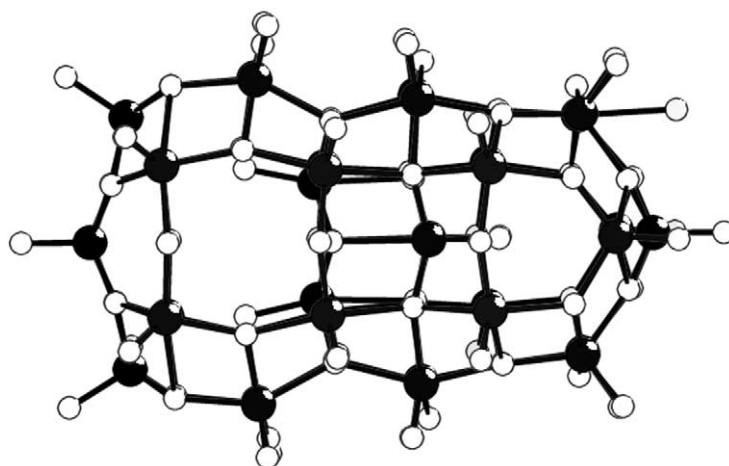


**Figure 19** The structure of the  $\{V_{34}\}$  cluster (22).<sup>112</sup> The vanadium atoms are shown as black spheres and the oxygen atoms as white spheres.

In summary it can be seen that linking  $VO_5$  units in the presence of anions and other templates gives rise to several structural types that appear to be critically dependent on the nature of the anion, and this is summarized in Figure 21.

### 7.1.3 TUNGSTATES

The structural features of large polytungstate clusters can be visualized in terms of subunits based on lacunary fragments of the Keggin ion. In such representations many of the fragments may not actually exist independently from the cluster containing these subunits. This also applies to the building blocks identified as part of the polyoxometallate clusters discussed in Sections 7.1.4 and 7.1.5.

The Keggin ion (Figure 22) can adopt up to five skeletal isomers ( $\alpha-\epsilon$ ),<sup>114</sup> and these isomers are related to each other by a rotation of one or more edge-shared  $\{W_3O_{13}\}$  groups by  $\pi/3$ .<sup>56</sup>

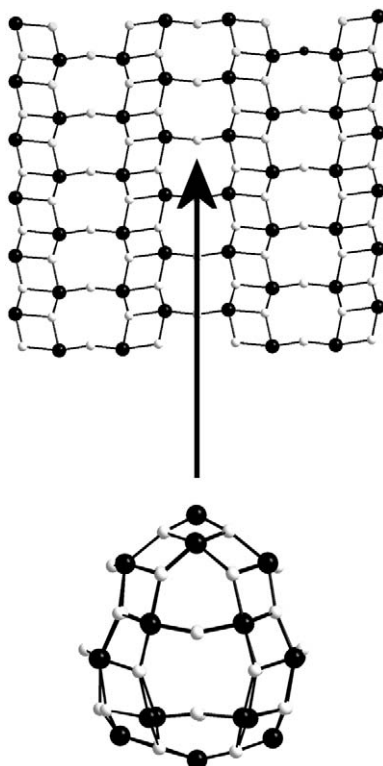


**Figure 20** View of a segment of a layer of  $V_2O_5$ <sup>113</sup> with the terminal atoms omitted for clarity. The  $\{V_{22}\}$  framework is shown below. The vanadium atoms are shown as black spheres and the oxygen atoms as white spheres.

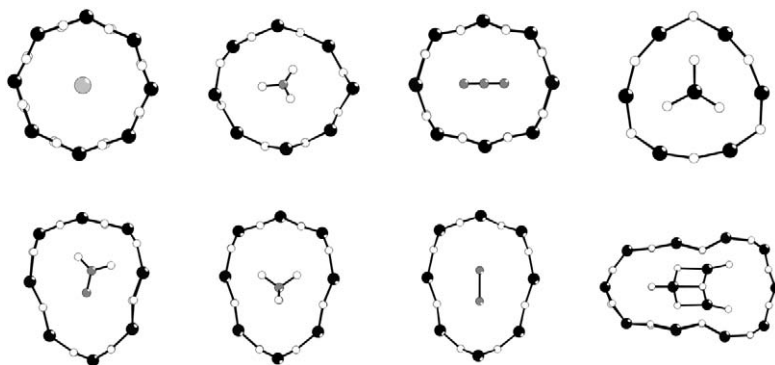


**Figure 21** A schematic showing the outer vanadium–oxygen frameworks (vanadium ion shown as black spheres and oxygen atoms by white spheres) and the encapsulated molecules. The clusters depicted from; left to right (top) are the  $\{V_{18}\text{-halide}\}$ ,  $\{V_{18}\text{-nitrate}\}$ ,  $\{V_{18}\text{-azide}\}$ ,  $\{V_{18}\text{-VO}_4\}$ ; left to right (bottom) are the  $\{V_{18}\text{-acetate}\}$ ,  $\{V_{18}\text{-perchlorate}\}$ ,  $\{V_{18}\text{-thiocyanate}\}$  (disordered NCS),  $\{V_{30}\text{-V}_4O_4\}$ .

The relative stability of the different skeletal isomers of the Keggin ion, and indeed the equilibria that can exist between difference isomers, have been the subject of much discussion in the literature.<sup>115,116</sup>

Lacunary versions of these clusters geometrically result from the removal of one or more W atoms. Examples of one monovacant and two divacant lacunary derivatives of the  $\alpha$ -Keggin ion are shown in Figure 23.

The two tri-vacant species in Figure 23 correspond to the loss of a corner-shared group of  $\{WO_6\}$  octahedral (A-type) or an edge-shared group (B-type). Furthermore it can be seen that in the B-type anion the central heteroatom has an unshared terminal oxygen atom; in this respect it is easy to imagine that B-type structures are observed when the central heteroatom has an unshared pair of electrons.

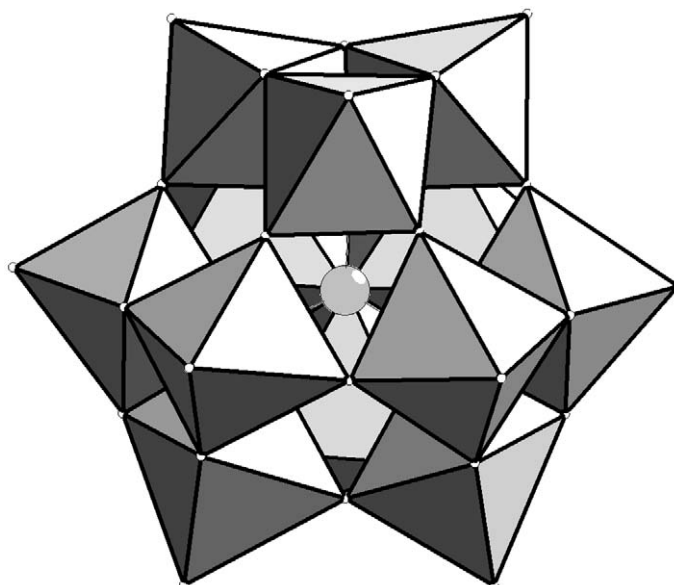


**Figure 22** Polyhedral representation of the  $\alpha$ -Keggin ion. The metal ions form the centers of the polyhedra and the oxygen atoms form the apexes of the polyhedra. The central heteroatom is shown as a gray sphere.

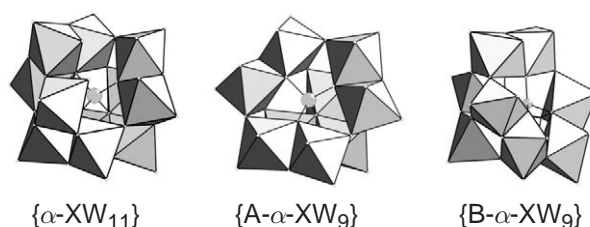


**Figure 23** Polyhedral representation of the Lacunary derivatives of the  $\alpha$ -Keggin ion; left— $\{\alpha\text{-XW}_{11}\}$ , middle— $\{\text{A-}\alpha\text{-XW}_9\}$ , right— $\{\text{B-}\alpha\text{-XW}_9\}$ . The metal ions form the centers of the polyhedra and the oxygen atoms form the apexes of the polyhedra. The central heteroatom is shown as a gray sphere.

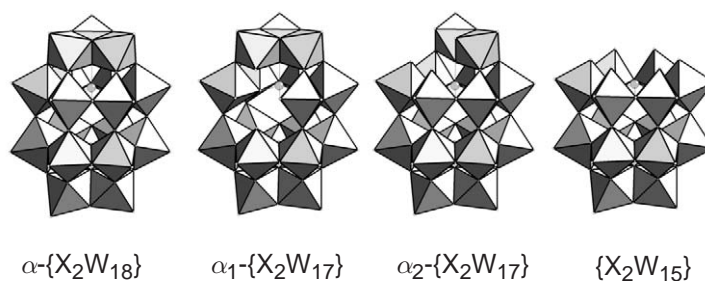


**Figure 24** Polyhedral representations of the  $\alpha$ -Dawson structure the associated three lacunary derivatives. The metal ions form the centers of the polyhedra and the oxygen atoms form the apexes of the polyhedra. The central heteroatom is shown as a gray sphere.

Linking of two  $[\text{A-PW}_9\text{O}_{34}]^{9-}$  clusters (**23**) generates a Wells–Dawson anion (**24**)  $[\text{P}_2\text{W}_{18}\text{O}_{62}]^{6-}$ . Six isomers of this anion are theoretically possible depending upon whether the half-units are derived from  $\alpha$  or  $\beta$ -Keggin species and also whether the fragments combined in a staggered (S) or eclipsed (E) fashion.<sup>114</sup> Four of these isomers have been observed for  $[\text{As}_2\text{W}_{18}\text{O}_{62}]^{6-}$  and three for  $[\text{P}_2\text{W}_{18}\text{O}_{62}]^{6-}$ .<sup>117</sup> As in the case of the Keggin ion, lacunary derivatives of the Wells–Dawson structure are also known. The most important of these are based on the most common isomer known as the  $\alpha$ -Dawson anion—see [Figure 24](#).

### 7.1.3.1 Clusters Incorporating Monovacant Lacunary Fragments

#### 7.1.3.1.1 $\{XW_{11}\}_2$

Monovacant lacunary anions (mla) of the type  $[PW_{11}O_{39}]^{7-}$  (**25**),  $[SiW_{11}O_{39}]^{8-}$  (**26**) and  $[P_2W_{17}O_{61}]^{10-}$  (**27**) form both 1:1 and 1:2 complexes with several metal cations. Such complexes were first reported by Peacock and Weakley<sup>118</sup> in 1971. Recently 1:1 complexes of  $[\alpha-SiW_{11}O_{39}]$  units have been shown to form polymers with lanthanide ions.<sup>119</sup> It was suggested that the heteropolyanion ligands were tetradentate, binding to the lanthanide center through the four oxygen atoms that surround the tungsten vacancy. In this way a quasi-square antiprismatic coordination sphere is provided for the metal ion. An examination of the literature reveals many types of mla have been extremely well exploited as ligands with many combinations of metal ion (see reference<sup>84</sup> for a further discussion of this point). Figure 25 gives a typical representation of one such  $[M(mla)_2]^{n-}$  complex (**28**), which adopts a *cis*-oid conformation with respect to the mla “ligands.” This is because the polyanionic ligand only has  $C_s$  symmetry and therefore there are four possible conformations for the complexes corresponding to *cis*-oid and *trans*-oid enantiomeric pairs.<sup>120</sup> It would appear that all the Keggin-derived complexes are *trans*-oid whereas  $[M(\alpha_2-P_2W_{17}O_{61})_2]^{(20-n)-}$  (**29**) (M = Ce<sup>IV</sup>, Lu<sup>III</sup>, U<sup>IV</sup>) are *cis*-oid. 1:1 and 2:2 complexes ( $\alpha_2-P_2W_{17}O_{61}$ ) linked by lanthanide ions have also been recently reported.<sup>121</sup>

#### 7.1.3.1.2 $\{XW_{11}\}_2\{Mo_3S_4\}_2$

It has been shown by Müller *et al.*<sup>122</sup> that the monovacant lacunary anion  $[SiW_{11}O_{39}]^{8-}$  (**30**) reacts as an electrophile towards the nucleophile  $[Mo_3S_4(H_2O)_9]^{4+}$  (**31**) to yield a bridged species  $\{(SiW_{11}O_{39})_2[Mo_3S_4(H_2O)_3]_2(\mu-OH)_2\}^{10-}$  (**32**). The resulting species has  $C_{2v}$  symmetry (see Figure 26). The two nucleophilic lacunary anions, of the Keggin type  $\{(SiW_{11}O_{39})^{8-}\}$  and of the Dawson type  $\{(P_2W_{17}O_{61})^{10-}\}$ , can be considered as negatively charged ligands which replace the coordinated water ligands of the electrophilic adduct. In this respect it has been suggested that the

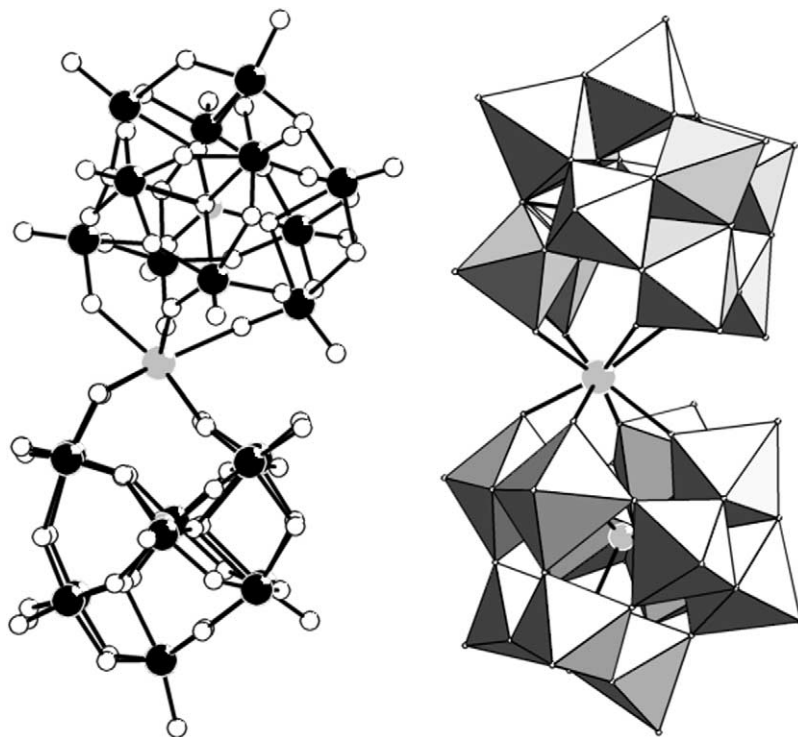


**Figure 25** Structure of  $[U(\alpha-GeW_{11}O_{39})_2]^{12-}$  (**28**). The ligands adopt a *trans*-oid conformation. A ball and stick representation is shown on the LHS (black spheres = W atoms, white spheres = O atoms and the visible gray sphere is the U atom). On the RHS the W atoms and the O atoms are represented as polyhedra.

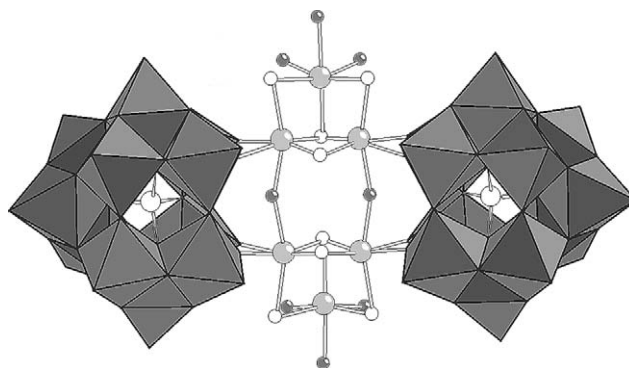


**Figure 26** View of the structure of  $\{(\text{SiW}_{11}\text{O}_{39})_2[\text{Mo}_3\text{S}_4(\text{H}_2\text{O})_3]_2(\mu\text{-OH})_2\}^{10-}$  (**32**). The lacunary Keggin-type fragments  $\{\alpha\text{-SiW}_{11}\}$  are shown as polyhedra, the  $\{\text{Mo}_3\text{S}_4\}$  units are in ball and stick representation.

monovacant lacunary anions with four oxygen donor atoms can be considered as an inorganic analogue of the porphyrin ligand.<sup>122</sup> The assembly of larger aggregates using this electronic complementarity is likely to become more significant in the drive to form “designer” solids.

### 7.1.3.1.3 $\{XW_{11}\}_3$

Tungstoboric acid yields two forms of crystalline product; a tetragonal form that contains a Keggin ion and a hexagonal form that comprises three lacunary  $\{\text{BW}_{11}\}$  anions linked by a central  $\{\text{W}_6\text{O}_{26}\}$  moiety (**33**). The overall structure has a  $C_{3h}$  symmetry, see Figure 27, and has the overall composition  $\text{H}_{21}[\text{B}_3\text{W}_{39}\text{P}_{132}]$  (**33**).<sup>123</sup>

## 7.1.3.2 Clusters Incorporating Different Types of Trivalent Lacunary Fragments

### 7.1.3.2.1 $\{X_2W_{21}\}$

The structure of the cluster anion  $[\text{P}_2\text{W}_{21}\text{O}_{71}]^{6-}$  (**34**)  $\{\text{P}_2\text{W}_{21}\}$  reveals a sandwich-like arrangement of two  $\{\text{PW}_9\}$  moieties around three  $\{\text{WO}_5(\text{H}_2\text{O})\}$ .<sup>124</sup> Close examination of the structure, Figure 28, reveals a threefold rotational disorder of the anion and that two positions can be modeled for the equatorial tungsten atoms. Solution studies of this cluster anion with NMR show that two of the tungsten atoms are displaced towards the threefold axis and that one tungsten atom is

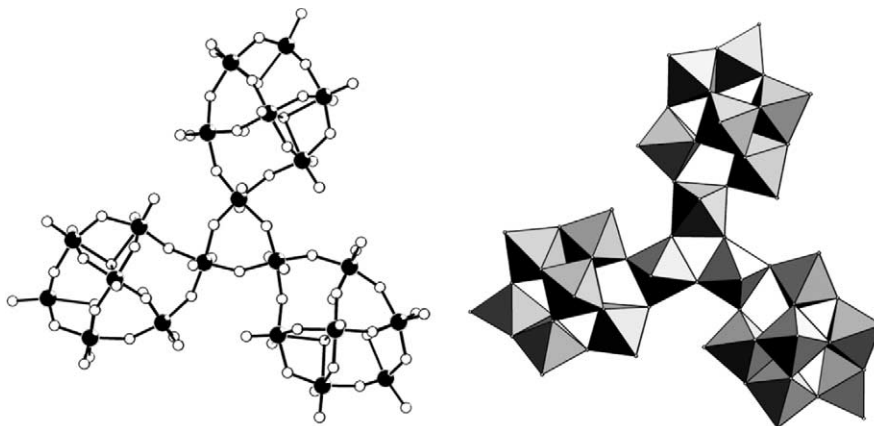


**Figure 27** A ball and stick (LHS) and a polyhedral (RHS) representation of the  $\text{H}_{21}[\text{B}_3\text{W}_{39}\text{P}_{132}]$  cluster (**33**). The W atoms are shown as black spheres and the oxygen atoms are shown as white spheres on the LHS. The W centers are shown as polyhedra on the RHS.

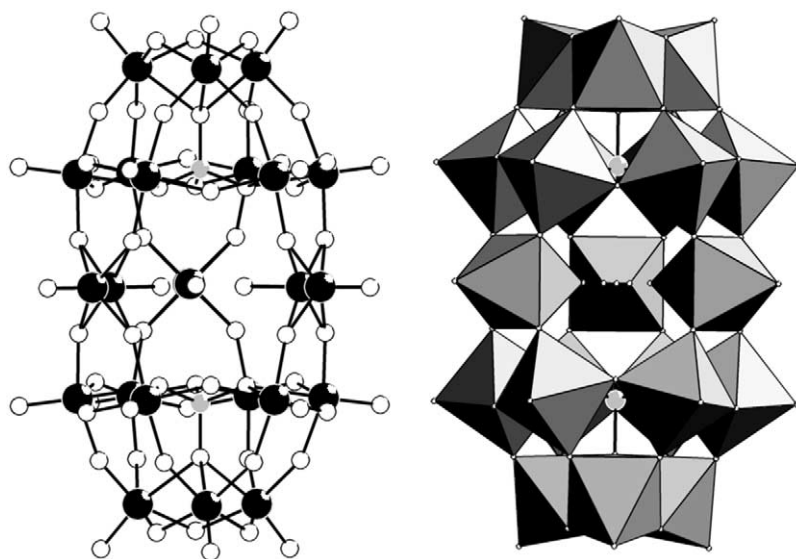


**Figure 28** Structure of  $[\text{P}_2\text{W}_{21}\text{O}_{71}]^{6-}$  (**34**)  $\{\text{P}_2\text{W}_{21}\}$  cluster. Again, a ball and stick representation (W atoms as black spheres, O atoms as white spheres) is shown on the LHS whereas a polyhedra representation is shown on the RHS. The P atoms are visible as gray spheres in both representations.

displaced away from this axis. The center of this cluster, therefore, encloses two “terminal” oxo oxygen atoms and a water molecule that is *trans* to the terminal atom of the third tungsten center. The central water ligand undergoes slow exchange with solvent water molecules.<sup>124</sup>

Cluster anion (**34**) is synthesized by the acidification of the lacunary species  $[\text{P}_2\text{W}_{11}\text{O}_{39}]^{7-}$ , whereas acidification of the potassium salt of the lacunary species leads to a lacunary derivative of (**34**).<sup>52</sup> An interesting anion  $\{\text{P}_2\text{W}_{20}\}$  incorporating potassium can be synthesized by the treatment of a heated suspension of  $[\text{K}_3\text{PW}_{12}\text{O}_{40}]$  with potassium carbonate and yields several products<sup>125</sup> one of which is  $\text{K}_{13}[\text{KP}_2\text{W}_{20}\text{O}_{72}] \cdot 30\text{H}_2\text{O}$   $\{\text{P}_2\text{W}_{20}\}$  (**35**). Similarly to  $\{\text{P}_2\text{W}_{21}\}$ , the anion comprises two A-type  $\{\alpha\text{-PW}_9\}$  units linked by two tungsten atoms, but now a potassium cation occupies a center of symmetry within the cluster, see **Figure 29**. Indeed, the cluster can almost be viewed as acting like a crown ether moiety ligating the potassium ion. Conversely, the potassium could act to provide a template for this cluster architecture.

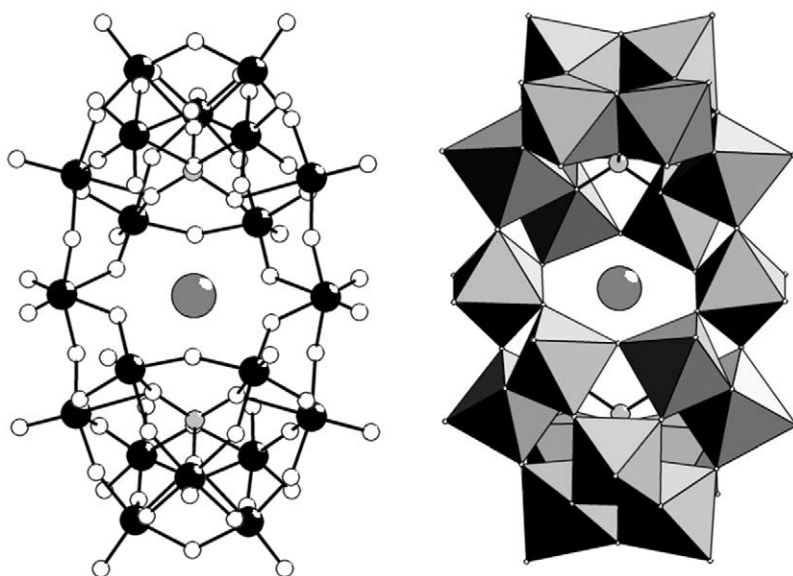


**Figure 29** The structure of the  $\text{K}_{13}[\text{KP}_2\text{W}_{20}\text{O}_{72}] \cdot 30\text{H}_2\text{O}$   $\{\text{P}_2\text{W}_{20}\}$  (**35**) cluster. A ball and stick representation is shown on the LHS and a polyhedral representation on the RHS. The central encapsulated potassium cation is shown in both representations as a large gray sphere.



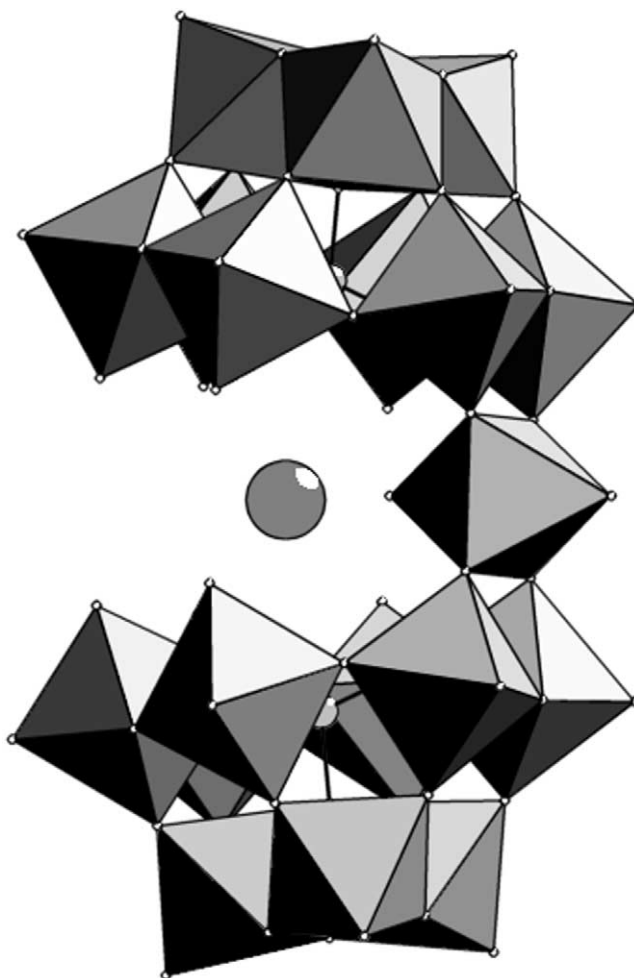


**Figure 30** A polyhedra representation of the structure of  $[\text{P}_2\text{W}_{19}\text{O}_{69}]^{14-}$  (**36**). The potassium cation ligated by the cleft formed by the cluster is shown as a large gray sphere.

A further derivative of  $\{\text{P}_2\text{W}_{21}\}$  is the cluster anion  $[\text{P}_2\text{W}_{19}\text{O}_{69}]^{14-}$  (**36**), see [Figure 30](#).<sup>126</sup> This anion appears to be quite unstable, but crystallizes readily in the presence of potassium cations, which occupy equatorial sites on the anion.

#### 7.1.3.2.2 $\{\text{M}_9\text{P}_5\text{W}_{27}\}$

The cluster anion,  $[\text{Co}_9(\text{OH})_3(\text{H}_2\text{O})_6(\text{HPO}_4)(\text{B-}\alpha\text{-PW}_9\text{O}_{34})_3]^{16-}$   $\{\text{Co}_9\text{P}_5\text{W}_{27}\}$  (**37**) was obtained as a by-product in the synthesis of  $[\text{Co}_4(\text{H}_2\text{O})_2(\text{PW}(\text{O}_{34}))]^{10-}$ . This anion has  $D_{3h}$  symmetry and comprises three Keggin units  $\{\alpha\text{-PW}_9\text{Co}_3\}$  linked by corner sharing  $\{\text{Co}_3\}$  triads with capping axial phosphate groups, see [Figure 31](#).<sup>127</sup> An analogous cluster incorporating nickel(II) instead of cobalt(II) has been synthesized and the magnetic properties of both have been studied.<sup>128,129</sup>

#### 7.1.3.2.3 $\{\text{XW}_9\}_4\{\text{Eu}_3\text{SbW}_{24}\}$

In 1990 an interesting europium-tungstoantimonate was reported by Yamase.<sup>130</sup> The cluster,  $[\text{Eu}_3(\text{H}_2\text{O})_3(\text{Sb}^{\text{III}}\text{W}_9\text{O}_{33})(\text{W}_5\text{O}_{18})_3]^{18-}$ ,  $\{\text{Eu}_3\text{SbW}_{24}\}$  (**38**) incorporates a  $\{\text{B-}\alpha\text{-SbW}_9\}$  and three  $\{\text{W}_5\}$  groups which are lacunary derivatives of  $[\text{W}_6\text{O}_{19}]^{2-}$ . The four units are arranged in an almost tetrahedral arrangement with respect to the central  $\{\text{Eu}_3\}$  unit see [Figure 32](#).

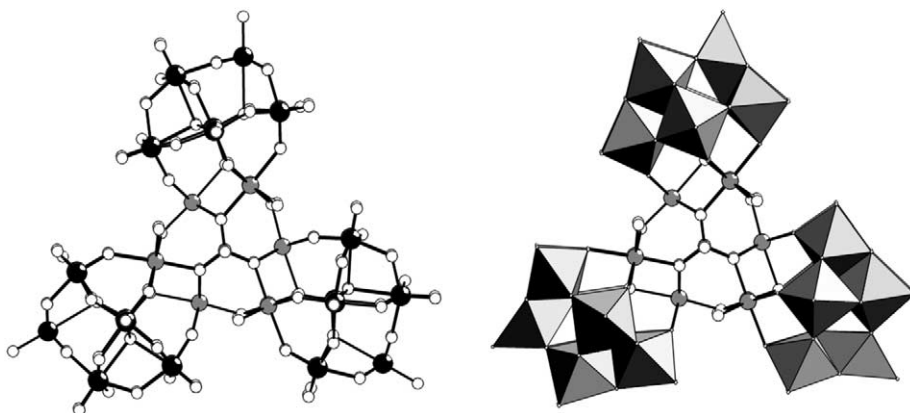


**Figure 31** Representations of the cluster anion  $[\text{Co}_9(\text{OH})_3(\text{H}_2\text{O})_6(\text{HPO}_4)(\text{B-}\alpha\text{-PW}_9\text{O}_{34})_3]^{16-}$   $\{\text{Co}_9\text{P}_5\text{W}_{27}\}$  (37). A ball and stick representation is shown on the LHS with the W atoms shown as black spheres, the oxygen atoms as white spheres, and the Co atoms as gray spheres. A polyhedral representation of the three  $\{\text{PW}_9\}$  units is shown on the RHS with the bridging units shown as ball and stick.

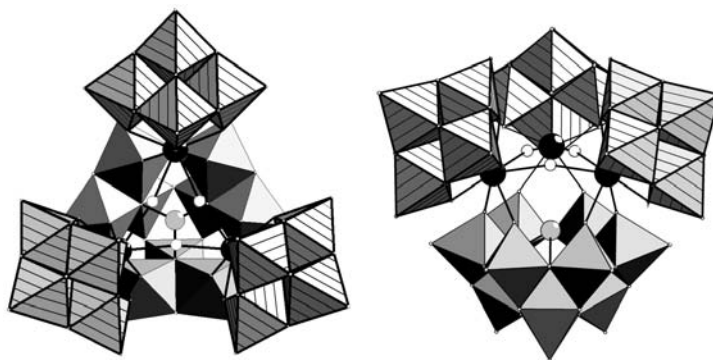


**Figure 32** The structure of the cluster anion  $[\text{Eu}_3(\text{H}_2\text{O})_3(\text{Sb}^{\text{III}}\text{W}_9\text{O}_{33})(\text{W}_5\text{O}_{18})_3]^{18-}$ ,  $\{\text{Eu}_3\text{SbW}_{24}\}$  (38). The Eu atoms are shown as large black spheres and the Sb atom as a gray sphere. The hatched polyhedra represent the  $\{\text{W}_5\}$  units whereas the gray polyhedra represent the  $\{\text{W}_9\}$  unit. A top view is shown on the LHS and the side view on the RHS.

#### 7.1.3.2.4 $\{\text{XW}_9\}_2:\{\text{X}_2\text{W}_{21}\}\{\text{X}_2\text{W}_{22}\}$

The structure of the anion  $[\text{As}_2\text{W}_{21}\text{O}_{69}(\text{H}_2\text{O})]^{6-}$   $\{\text{As}_2\text{W}_{21}\}$  (39) has been elucidated in the solid state by crystallography,<sup>131</sup> see Figure 33, and in the solution state by NMR.<sup>132</sup> The structure is analogous to  $\{\text{P}_2\text{W}_{21}\}$  (see Figure 34) but, due to the lone pair of electrons on  $\text{As}^{\text{III}}$ , the  $\{\text{AsW}_9\}$  units are of the B-type. The linking, equatorial tungsten atoms also adopt a different configuration with two  $\{\text{W}_{\text{out}}\}$  and one  $\{\text{W}_{\text{in}}\}$  due to the smaller available space.

Cluster anions, and their complexes with di- and trivalent transition metals thought to be based on  $\{\text{XW}_{11}\}$  have been shown to be dimeric, based on structural studies of the salts of  $[\text{Sb}_2\text{W}_{22}\text{O}_{74}(\text{OH})_2]^{12-}$  (40) and related species.<sup>133</sup> The structure of this anionic cluster is shown in Figure 34, and comprises two  $\{\text{B-}\beta\text{-XW}_9\}$  groups linked by two other tungsten atoms. Interestingly, two weakly bound tungsten atoms are bound to the periphery of the cluster and can be easily replaced by other transition metal ions.

#### 7.1.3.2.5 $\{\text{XW}_9\}_3$

The clusters  $\{\text{Ln}_2\text{As}_3\text{W}_{29}\}$  (41) and  $\{(\text{UO}_2)_3\text{As}_3\text{W}_{29}\}$  (42) result from the reaction of  $\{\text{B-XW}_9\}$  anions with lanthanide and actinide cations. For example the anion  $[\text{Ln}_2(\text{H}_2\text{O})_7\text{As}_3\text{W}_{29}\text{O}_{103}]^{17-}$  ( $\text{Ln}^{\text{III}} = \text{La}, \text{Ce}$ ) (41) contains three  $\{\text{AsW}_9\}$  fragments bridged by two additional tungsten atoms and two  $\text{Ln}^{\text{III}}$  cations. The stoichiometrically related derivative  $[(\text{UO}_2)_3(\text{H}_2\text{O})_5\text{As}_3\text{W}_{29}\text{O}_{104}]^{19-}$  also has a trimeric structure.<sup>84</sup>

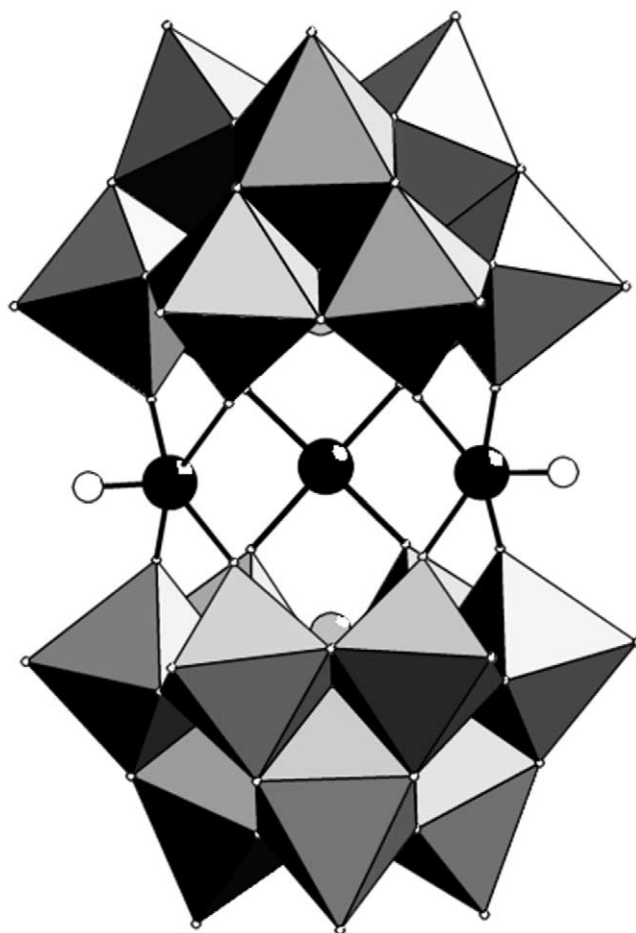


**Figure 33** The structure of the anion  $[\text{As}_2\text{W}_{21}\text{O}_{69}(\text{H}_2\text{O})]^{6-}$   $\{\text{As}_2\text{W}_{21}\}$  (39), the W atoms in the two  $\{\text{W}_9\}$  groups are shown in a polyhedra representation whereas the three linking W atoms are shown as black spheres and the associated oxygen atoms as white spheres.

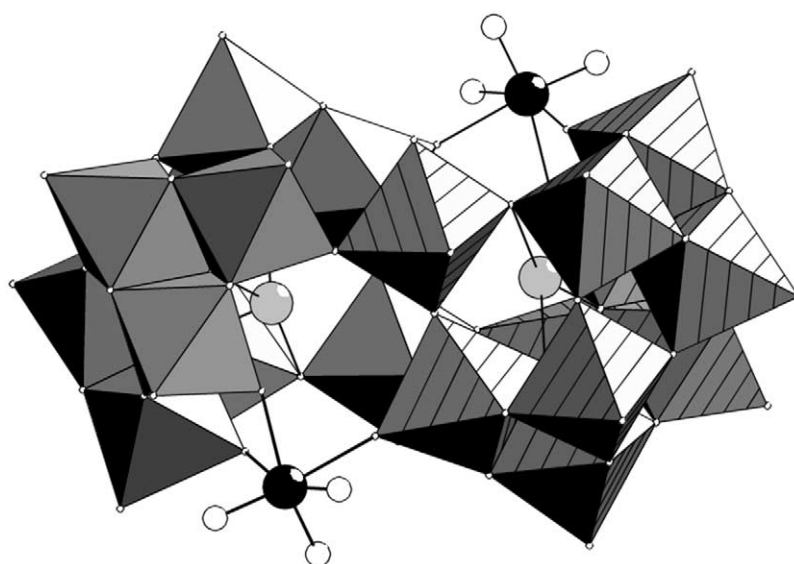


**Figure 34** Structure of  $[\text{Sb}_2\text{W}_{22}\text{O}_{74}(\text{OH})_2]^{12-}$  (40). The two  $\{\text{B-}\beta\text{-XW}_9\}$  groups are shown by the polyhedra and the Sb atoms are shown as gray spheres. The “additional” W atoms and associated oxygen ligands are shown by the black and white spheres, respectively.

### 7.1.3.2.6 $\{XW_9\}_4$

Clusters based on four linked  $\{XW_9\}$  have also been identified, see Figure 35. The cluster  $[As_4W_{40}O_{140}]^{28-}$  (**43**) is a cyclic anion, being composed of four  $\{\alpha\text{-}AsW_9\}$  units linked by additional tungsten atoms; the structure shown in Figure 35 is a dicobalt derivative.<sup>134</sup> Derivatives of (**43**) have also been produced with lanthanide cations.<sup>135</sup>

A further tetramer of  $\{XW_9\}$  has been reported<sup>133</sup> that has the composition  $[Na_2Sb_8W_{36}O_{132}(H_2O)_4]^{22-}$  (**44**). The top view, see Figure 36, seems similar to (**43**) shown in Figure 35 but the side view reveals the unique structure of this cluster. This is because the  $\{SbW_9\}$  groups have a  $\beta$  conformation and the bridging atoms are trigonal bipyramidally coordinated  $W^{VI}$  centers. Therefore the overall structure resembles that of a V-shaped cavity. The cavity contains two sodium ions and several water molecules.

### 7.1.3.2.7 $\{XW_9\}_{11}$

Recently, Pope *et al.* have synthesized a massive heteropolytungstate anion which is a dodecamer of the  $\{XW_9\}$  units,  $[Ln_{16}As_{12}W_{148}O_{524}(H_2O)_{36}]^{76-}$  (**45**).<sup>61</sup> The 12  $\{XW_9\}$  units are linked by  $Ln^{III}$  cations ( $Ln = La, Ce, Nd, Sm$ ) and additional tungsten atoms to produce a folded cyclic cluster with  $D_{2d}$  symmetry. The anion is completed by the four  $\{W_5O_{18}\}$  lacunary fragments and the structure is shown in Figure 37. This anion exhibits an interesting topology and exceptionally high nuclearity of metal ions.

## 7.1.3.3 Clusters Incorporating Hexavacant Lacunary Fragments

### 7.1.3.3.1 $\{P_8W_{48}\}$

One of the lacunary derivatives of the  $\alpha$ -Dawson anion forms crystals of composition,  $K_{28}Li_5H_7P_8W_{48}O_{184}\cdot 92H_2O$  ( $\{P_8W_{48}\}$ , (**46**)) with the cyclic structure shown in Figure 38.<sup>132,136</sup> A tetramer of  $\{P_2W_{12}\}$  groups leads to the  $D_{4h}$  symmetry of the structure of the  $\{P_8W_{48}\}$  anion. The crystal structure reveals that the central cavity of the anion contains a number of potassium cations.

### 7.1.3.3.2 $\{P_5W_{30}\}$

When sodium tungstate is boiled with an excess of phosphoric acid the main heteropolytungstate products are two isomers of the Wells–Dawson anions and a smaller amount of another species (**47**). Crystallographic analysis of this species showed the composition of this anion to be  $[NaP_5W_{30}O_{110}]^{14-}$  ( $\{P_5W_{30}\}$ , (**47**)) with the structure shown in Figure 39.<sup>132</sup>

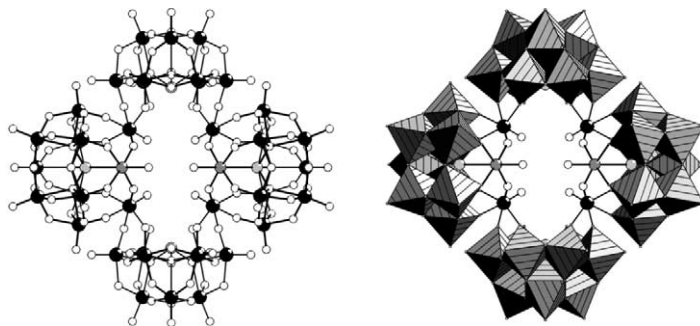


**Figure 35** The structure of the cyclic anion  $[As_4W_{40}O_{140}]^{28-}$  (**43**). A ball and stick representation is shown on the LHS and a polyhedral representation is shown on the RHS with the linking units shown in ball and stick. The W atoms are shown as black spheres, the As atoms as gray spheres and the O atoms as white spheres.

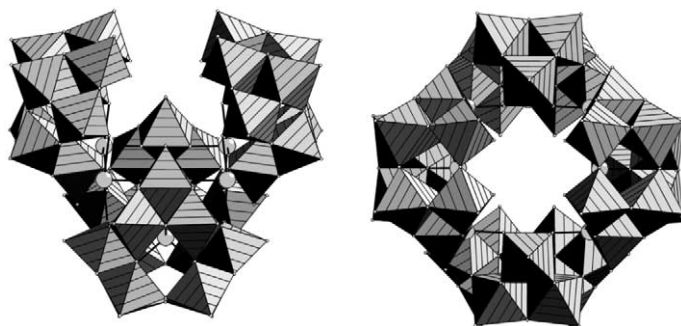


**Figure 36** Two polyhedral views of the cluster  $[\text{Na}_2\text{Sb}_8\text{W}_{36}\text{O}_{132}(\text{H}_2\text{O})_4]^{22-}$ . The W atoms are shown as polyhedra and the Sb atoms are shown as gray spheres.

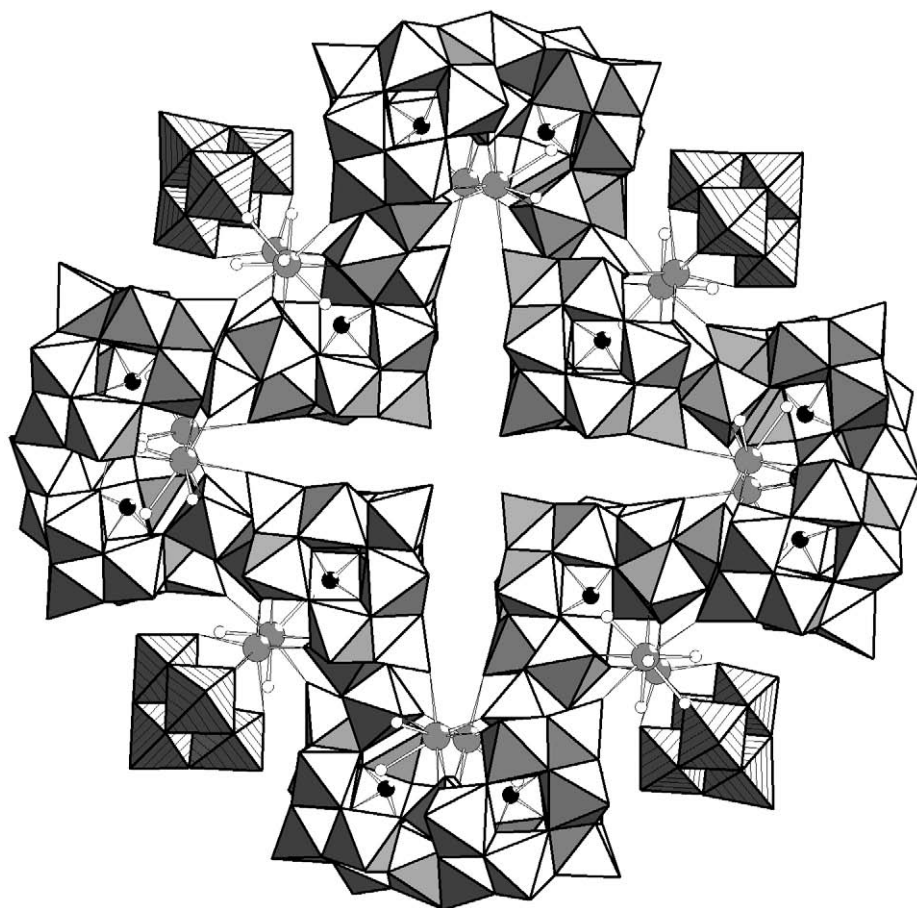


**Figure 37** Structure of the anion  $[\text{Ln}_{16}\text{As}_{12}\text{W}_{148}\text{O}_{524}(\text{H}_2\text{O})_{36}]^{76-}$  (45) as a folded cyclic assembly of 12  $\{\text{B}-\alpha\text{-AsW}_9\}$  groups linked by additional W centers, all shown as polyhedral representations and four  $\{\text{LnW}_5\}$  groups. Ce(La) centers as large gray spheres and As centers as small black spheres. Finally, the water ligands are shown as white spheres.

The fivefold symmetry of this anion is completed by the linkage of five  $\{\text{PW}_6\}$  groups and the central sodium ion lies in the center of a plane defined by the oxygen atoms of the phosphate groups. It appears that the kinetically inert (on the NMR timescale) sodium ion is essential for the construction of the cluster.<sup>137</sup> The presence of the sodium cation reduces the overall anion symmetry from  $D_{5h}$  to  $C_{5v}$ . The  $\{\text{P}_5\text{W}_{30}\}$  anion is even more robust than the  $\{\text{P}_8\text{W}_{48}\}$  one (pH stability range  $\sim 0$ – $10$ ). Under hydrothermal conditions the central  $\text{Na}^+$  can be replaced by other cations of similar size, e.g.,  $\text{Ca}^{2+}$ , most  $\text{Ln}^{\text{III}}$ , and  $\text{U}^{\text{IV}}$ .<sup>138–140</sup> Reduction of  $\text{Eu}^{\text{III}}$  to  $\text{Eu}^{\text{II}}$  in these complexes occurs within the potential range at which the polytungstate framework is reduced to

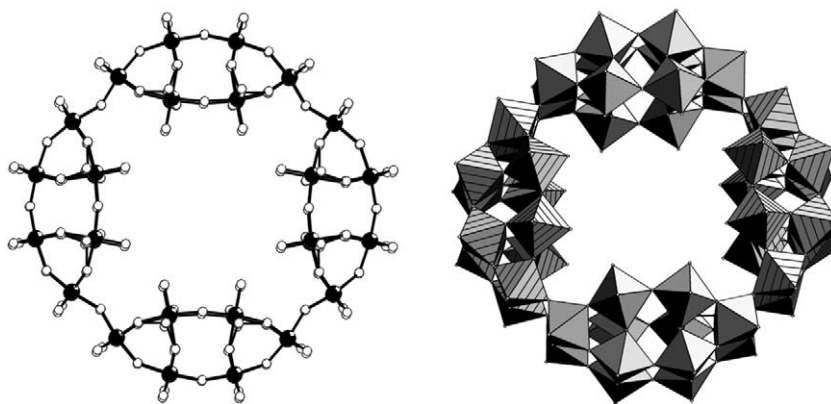


**Figure 38** Structure of the anion  $[P_8W_{48}O_{184}]^{40-}$ ,  $\{P_8W_{48}\}$  (**46**) as a cyclic assembly of four lacunary  $\{P_2W_{12}\}$  groups. A ball and stick representation is shown on the LHS and a polyhedral representation on the RHS.

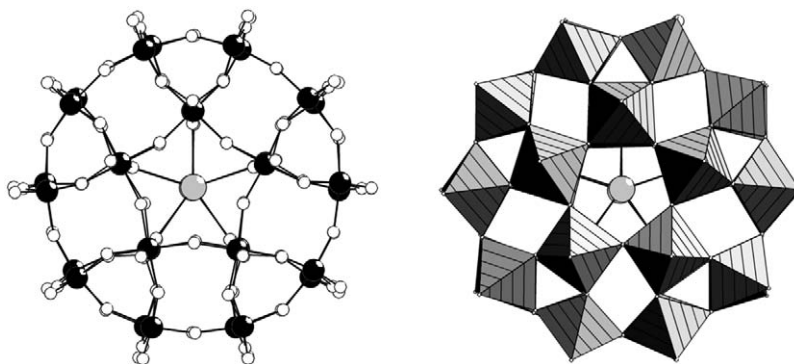


**Figure 39** Structure of the anion,  $[NaP_5W_{30}O_{110}]^{14-}$  ( $\{P_5W_{30}\}$ , **47**). A ball and stick representation is shown on the LHS and a polyhedral representation on the RHS. The central sodium ion is depicted as a large gray sphere.

heteropoly blues, and implies the possibility of generating an intermediate valence state compound.<sup>141,142</sup> Structures of the  $Eu^{III}$  and  $U^{IV}$  derivatives have been reported and show that these central cations are coordinated by a  $H_2O$  molecule that is enclosed in the central cavity.<sup>143</sup> The sodium derivative has been evaluated as a catalyst for the oxidation of  $H_2S$  to sulfur, and was the best of the polyoxometalates examined.<sup>144,145</sup>

### 7.1.4 MOLYBDATES

There is a rich chemistry of heteropolyoxomolybdates and polyoxomolybdates,<sup>56</sup> and it has been shown that the chemistry of these is extraordinarily versatile, which is directly related to the fact that it is very easy to reduce  $Mo^{VI}$  to  $Mo^V$  in aqueous solution. The generation of such “molybdenum blue” species adds a new dimension to polyoxometalate chemistry.

The history of soluble molybdenum blue (solid-state and heteropoly blues will not be considered here) dates back to Carl Wilhelm Scheele’s report from 1783.<sup>146</sup> Solutions of molybdenum blue are almost instantaneously obtained by the reduction of  $Mo^{VI}$ -type species in acid solutions ( $pH \leq 3$ ). Reducing agents may be metals (Al, Pb, Mo, Cu, Zn, Cd, Hg),  $B_2H_6$ ,  $NaBH_4$ ,  $N_2H_4$ ,  $NH_2OH$ ,  $H_2S$ ,  $SO_2$ ,  $SO_3^{2-}$ ,  $S_2O_4^{2-}$ ,  $S_2O_3^{2-}$ ,  $SnCl_2$ ,  $MoCl_5$ ,  $MoOCl_5^{2-}$ , formic acid, ethanol, ascorbic acid, and it appears that the term “molybdenum blue” refers to a wide range of products.<sup>56,147</sup> Under stronger reducing conditions, brown species are formed which in general show the presence of  $Mo^V$ - $Mo^V$  dumb-bells.<sup>148</sup> On adding electrolytes like ammonium chloride or other salts, polymerization and/or precipitation takes place. A straightforward fast identification of a molybdenum blue-type solution is possible by measuring the resonance Raman spectrum (with  $\lambda_e = 1064$  nm).

### 7.1.4.1 From Keggin Ions to $\{\text{Mo}_{37}\}$ Clusters

The cluster anion  $\{[\text{H}_{14}\text{Mo}_{37}\text{O}_{112}]^{14-}\}$  (**48**) represents a self-assembled molecular species that contains no symmetry elements, see Figure 40. The anion consists of a central  $\{\text{H}_6\text{Mo}_{12}^{\text{V}}\text{O}_{40}(\text{Mo}^{\text{V}}\text{O}_3)_4\}$  core and two similar but nonidentical coordinated ligands,  $\{\text{Mo}_{10}\}$  and  $\{\text{Mo}_{11}\}$  units. The ligands differ with respect to the number of Mo centers and the degree of reduction and protonation. The core is built up from a  $\{\text{Mo}_{12}^{\text{V}}\text{O}_{40}\}$   $\varepsilon$ -Keggin structure<sup>149</sup> which is capped by four  $\{\text{Mo}^{\text{V}}\text{O}_3\}$  groups.

The assembly of this anion occurs in an aqueous molybdate solution under reducing conditions and can be rationalized by assuming the initial formation of an  $\varepsilon$ -Keggin ion with  $T_d$  symmetry. Its reduction yields a highly nucleophilic  $\varepsilon$ -Keggin cluster that is stabilized by protonation and by the ligation of four electrophilic  $\{\text{Mo}^{\text{VI}}\text{O}_3\}$  groups, thereby forming the anion  $[\text{H}_x\text{Mo}_{12}^{\text{V}}\text{O}_{40}(\text{Mo}^{\text{VI}}\text{O}_3)_4]^{(20-x)-}$ , which has also been structurally characterized.<sup>150</sup> On further reduction the  $\{\text{Mo}^{\text{VI}}\text{O}_3\}$  groups on the surface of the cluster now become nucleophilic and can be regarded as adopting a templating function. In the next step the  $\{\text{Mo}_{10}\}$  and  $\{\text{Mo}_{11}\}$  groups are assembled on the surface of the central  $\varepsilon$ -Keggin-derived unit, see Figure 40.

### 7.1.4.2 From $\{\text{Mo}_{36}\}$ to $\{\text{Mo}_{57}\}$ Clusters—Two and Three Fragment Clusters Based on $\{\text{Mo}_{17}\}$ Units

The acidification of an aqueous solution of molybdate under ambient conditions has been shown to yield the  $\{\text{Mo}_{36}\}$ -type cluster ( $[\text{Mo}_{36}(\text{NO})_4\text{O}_{108}(\text{H}_2\text{O})_{16}]^{12-}$ ) (**49**) with two  $\{\text{Mo}_{17}\}$  groups linked by two  $\text{MoO}_2$  units.<sup>151</sup> It appears that this is the dominant species and the cluster crystallizes readily from solution, see Figure 41. The overall structure is best understood by realizing that the  $\{\text{Mo}_{17}\}$  unit can be further divided into two  $\{\text{Mo}_8\}$  units and one linking  $\{\text{Mo}_1\}$  unit.

If the acidified molybdate solution that forms the  $\{\text{Mo}_{36}\}$  cluster is then reduced in the presence of some divalent metal ions, a three fragment cluster of the form  $\{\text{Mo}_{57}\text{M}_6\}$  (**50**) type, for example,  $[\{\text{VO}(\text{H}_2\text{O})\}_6\{\text{Mo}_2(\mu\text{-H}_2\text{O})_2(\mu\text{-OH})\}_3\{\text{Mo}_{17}(\text{NO})_2\text{O}_{58}(\text{H}_2\text{O})_2\}_3]^{21-} = [\{\text{VO}(\text{H}_2\text{O})\}_6\{\text{Mo}_2'\}_3\{\text{Mo}_8\}_2\{\text{Mo}_1'\}_3]$  (Figure 6) is produced.<sup>151-154</sup> The  $\{\text{Mo}_{57}\text{M}_6\}$ -type cluster with three  $\{\text{Mo}_{17}\}$

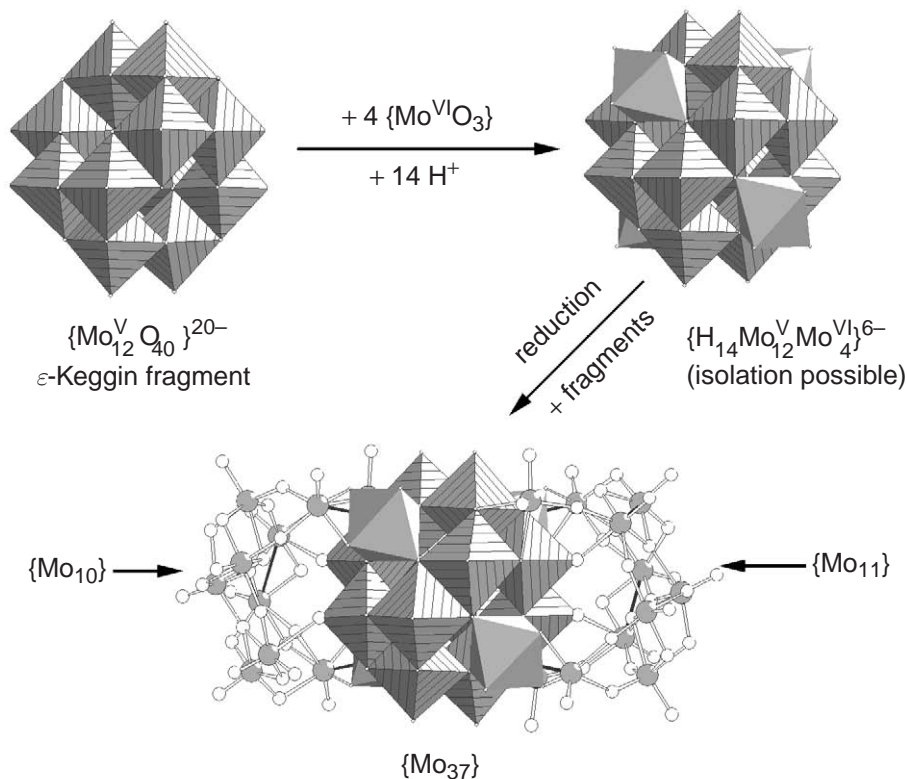


**Figure 40** Summary of the stepwise assembly of the  $\{\text{Mo}_{37}\}$  cluster. The  $\varepsilon$ -Keggin unit and the four added Mo units are shown as hatched and unhatched polyhedra respectively. The  $\{\text{Mo}_{10}\}$  and  $\{\text{Mo}_{11}\}$  units are shown in ball and stick with the Mo atoms as gray spheres and the oxygen atoms as white spheres.

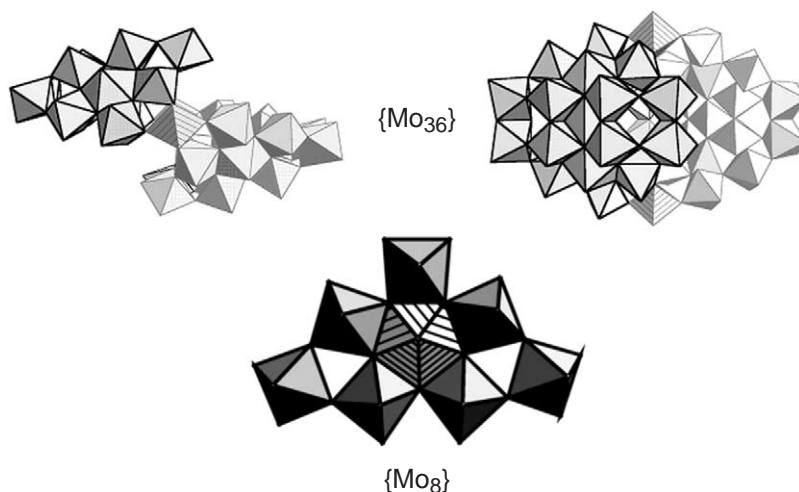


**Figure 41** Polyhedral representation of the cluster anion  $[\text{Mo}_{36}(\text{NO})_4\text{O}_{108}(\text{H}_2\text{O})_{16}]^{12-}$  ( $\{ \{ \text{MoO}_2 \}_2 \{ \text{H}_{12}\text{Mo}_{17}(\text{NO})_2\text{O}_{58}(\text{H}_2\text{O})_2 \}_2 \}^{12-} = [ \{ \text{Mo}_{17}^* \}_2 \{ \text{Mo}_8 \}_2 \{ \text{Mo}_{17}' \}_2 ]$ ). The  $\text{MoO}_6$  octahedra that are connecting the two  $\{ \text{Mo}_{17} \}$  units shown as hatched polyhedra. One of the two  $\{ \text{Mo}_8 \}$  building blocks that comprise the  $\{ \text{Mo}_{17} \}$  unit is also shown and the central pentagonal Mo atom is shown by the hatched polyhedron.

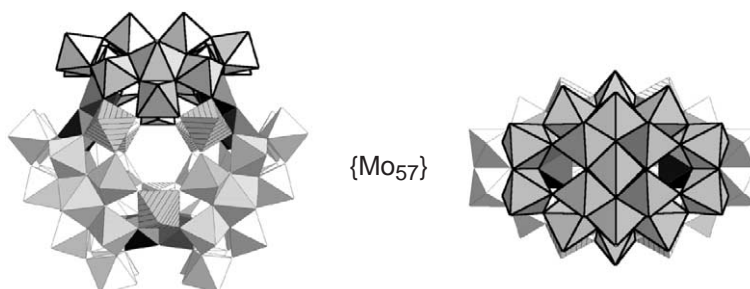


**Figure 42** A polyhedral representation of the  $\{ \text{Mo}_{57}\text{M}_6 \}$  cluster with one of the  $\{ \text{Mo}_8 \}$  units highlighted on the left and the  $\{ \text{Mo}_{17} \}$  unit on the right. The divalent TM ions are shown as hatched polyhedra.

groups (see Figure 42) is formed after adding, for instance, the strong electrophilic linker  $\text{V}^{\text{IV}}\text{O}^{2+}$  under reducing conditions, but other divalent metal ions can be included, e.g.,  $\text{Fe}^{2+}$ . In addition, different ratios of metal ions can be included, e.g.,  $\{ \text{Mo}_{57}\text{M}_x\text{M}_y \}$  where  $x + y = 6$ .<sup>155</sup> The  $\{ \text{Mo}_{57}\text{M}_6 \}$  cluster comprises six  $\{ \text{Mo}_8 \}$  units, three on each side with three  $\{ \text{Mo}_2' \}$  linking units and three  $\{ \text{Mo}_{17}' \}$  units which connect the two sides of the cluster together, see Figure 43. The divalent metal ions occupy three positions on the two inner rims of this cluster above and below the equator.

Another structural feature of the  $\{ \text{Mo}_{57}\text{M}_6 \}$  are the three gaps in each of the upper and lower rims of the cluster between the ends of the  $\{ \text{Mo}_8 \}$  units, see Figure 42. In studies by Müller *et al.*<sup>149</sup> it was shown that these six cavities are accessible to further coordination by the highly electrophilic  $\{ \text{MoO}_4 \}^{4+}$  groups. This can occur under reaction conditions in which the  $\{ \text{Mo}_{57}\text{M}_6 \}$  cluster is exposed to an excess of molybdate and gives rise to a stepwise growth process. This process allows the formation of the species  $\{ \text{Mo}_{57+x}\text{V}_6 \}$  where  $x$  can have values between 0 and 6. Each of the  $\{ \text{MoO}_4 \}^{4+}$  groups binds to three oxygen atoms (two terminal) of the  $\{ \text{Mo}_{57}\text{V}_6 \}$  core resulting in a tetrahedral coordination of the incorporated Mo atoms. The degree of occupation of the cavities can be correlated with the degree of reduction of the cluster. This is because the reduction process increases the nucleophilicity of the periphery of the cluster thereby enabling the cluster to take up further electrophiles. Furthermore, this process can be reversed by the oxidation of the system so that the electrophiles are then released, see Figure 43.

#### 7.1.4.3 $\{ \text{Mo}_{154} \}$ Big Wheel Clusters

In 1995 Müller *et al.* reported the synthesis and structural characterization of a very high nuclearity cluster  $\{ \text{Mo}_{154} \}$  that has a ring topology.<sup>62</sup> The interest generated by this result is partly due to its high nuclearity and partly because of the size of this cluster; with an outer diameter



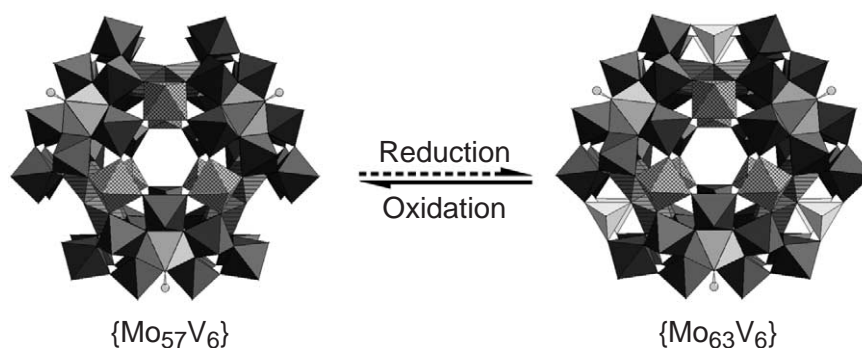


**Figure 43** Polyhedral representations of the cluster ligand on the LHS and then the result of metal uptake on the RHS (tetrahedral polyhedra). The hatched polyhedra are the divalent metal ions and the pentagonal Mo polyhedra that from the  $\{Mo_8\}$  units are clearly visible with the oxygen of the coordinating NO groups shown as a gray sphere.

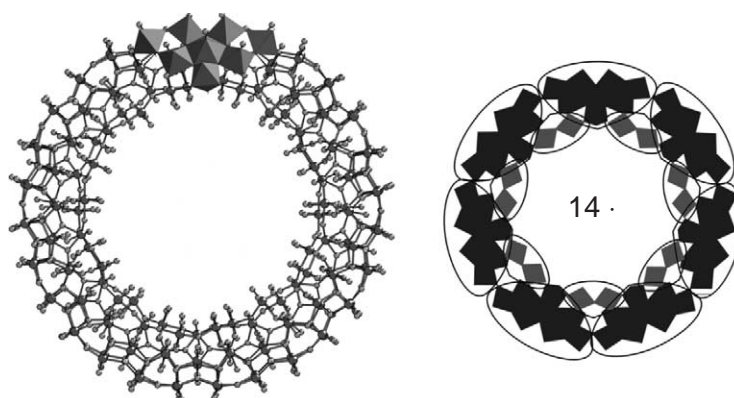


**Figure 44** LHS: a ball and stick representation of  $\{Mo_{154}\}$  big wheel cluster with one of the  $\{Mo_8\}$  building blocks highlighted with a polyhedral representation. RHS: a polyhedral representation of the top layer of the  $\{Mo_{154}\}$  cluster with the  $\{Mo_8\}$  (black units) and  $\{Mo_2\}$  (gray units) units clearly shown.

of ca. 34 Å, an inner diameter of 25 Å and a thickness of 14 Å it is a truly nanoscopic molecule. Using reaction conditions of pH  $\sim$  1, with a concentration of  $Na_2MoO_4$  of ca. 0.5 M and a degree of reduction of 1–20%, a solution is generated that yields “Giant-Wheel”-type cluster species, for example, comprising 154 Mo atoms of formula  $[Mo_{154}O_{462}H_{14}(H_2O)_{70}]^{14-}$  (**51**) see Figure 44 (this can be compared to the formula of the original structure of the Giant-Wheel cluster,  $[Mo_{154}(NO)_{14}O_{448}H_{28}(H_2O)_{70}]^{(25\pm 5)-}$ ; (**52**)—see Table 2). Amazingly, it is possible to synthesize gram quantities of (**51**) through a very simple “one-pot” reaction procedure in 24 hours.<sup>156,157</sup>

#### 7.1.4.3.1 Construction of $\{Mo_{154}\}$ -type clusters

Overall, the complete ring system consists of 140  $MoO_6$  octahedra and 14 pentagonal bipyramids of the type  $\{MoO_7\}$ , see Figure 45. The wheel can best be described as a tetradecamer comprising 14 basic  $\{Mo_8\}$  units with a central  $\{MoO_7\}$  group. This  $\{MoO_7\}$  unit is symmetrically connected to five  $\{MoO_6\}$  octahedral by edge sharing resulting in a  $\{Mo/Mo_5\}$  pentagon. It should be noted that any toroidal system, such as the ring-cluster discussed here, requires a fivefold symmetry element to form the overall toroidal or spherical geometry and this is also true for clusters with a spherical topology.<sup>58,59,63</sup> Four of the  $\{MoO_6\}$  octahedra are linked to further  $\{MoO_6\}$  octahedra via corners to form the  $\{Mo_8\}$  unit described above.

Continuing from the  $\{Mo_8\}$  unit the complete  $\{Mo_{154}\}$  cluster ring is built up as follows: (i) the two  $MoO_6$  octahedra that are not directly connected to the central  $MoO_7$  bipyramid are fused to neighboring  $\{Mo_8\}$  units through corners; (ii) neighboring  $\{Mo_8\}$  groups are additionally fused together by the  $\{Mo_2\}$  units, thereby completing the inner-ring parts of the upper and lower half of the ring structure; and (iii) the complete ring is constructed when the second half is rotated

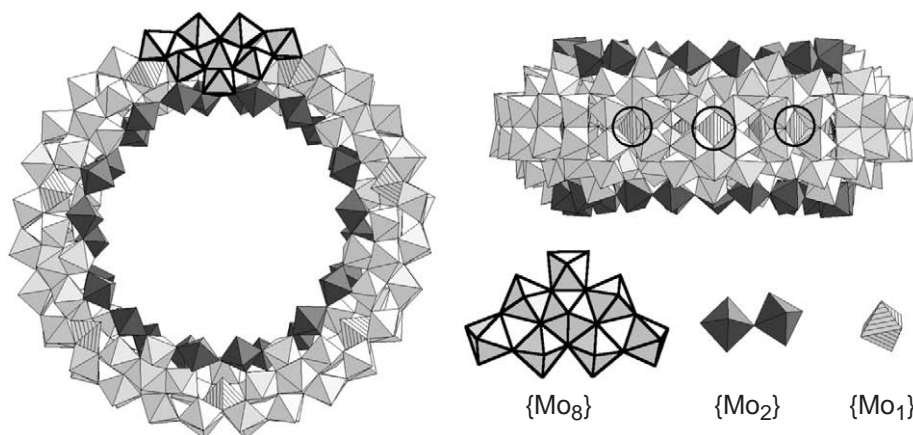


**Figure 45** A polyhedral representation of the  $\{\text{Mo}_{154}\}$  cluster with the component building blocks shown explicitly. The black polyhedra represent the  $\{\text{Mo}_2\}$  building blocks, the hatched polyhedra represent the  $\{\text{Mo}_1\}$  units that are positioned in the equator of the ring. One of the  $\{\text{Mo}_8\}$  units is highlighted in the top view of the ring (LHS) for clarity. The positions of the  $\{\text{Mo}_1\}$  groups are ringed on the side view of the ring (RHS) for clarity.

around  $360/14^\circ$  relative to the first and fused to it through the 14  $\{\text{Mo}_1\}$  groups, which are located at the equator of the complete ring, see Figure 45. Using the general architecture principle for the Giant-Wheel-type clusters the structural building blocks, e.g., for the  $\{\text{Mo}_{154}\}$ -type cluster, can be deduced from the formula,  $[\text{Mo}_{154}\text{O}_{462}\text{H}_{14}(\text{H}_2\text{O})_{70}]^{14-}$ , in terms of the three different building blocks as  $[\{\text{Mo}_2\}_{14}\{\text{Mo}_8\}_{14}\{\text{Mo}_1\}_{14}]^{14-}$ .

#### 7.1.4.3.2 Determination of the molecular formula of $\{\text{Mo}_{154}\}$ -type clusters

The deduction of the molecular formula (and the overall charge) for the first Giant-Wheel initially presented a tremendous problem. However, this information can now be routinely deduced from a combination of redox titrations, UV/Vis spectroscopy (the solution spectrum of the  $\{\text{Mo}_{154}\}$  cluster gives an absorption at ca. 750 nm with a  $\varepsilon \approx 6 \times 10^3 \text{ L mol}^{-1} \text{ cm}^{-1}/\text{Mo}^{\text{V}}$  center, corresponding to an intervalence charge transfer) and analyzing structural data by calculating the bond valence sums for the molybdenum centers.<sup>158</sup> There are  $n$  electronically practically independent  $\{\text{Mo}_5\text{O}_6\}$  compartments of incomplete double-cubane type, each of which carries two delocalized 4d electrons, a situation which is comparable to a so-called electronic necklace corresponding to an electron-storage system where the uncoupled storage elements are threaded like pearls on a string. These compartment-delocalized electrons are responsible for the intense blue color,<sup>146,158</sup> see Figure 46.

Using this information it has been found that the number of  $\{\text{Mo}_8\}$  or  $\{\text{Mo}_1\}$  units is equal to half the formal number of  $\text{Mo}^{\text{V}}$  centers and equal to the overall charge on the  $\{\text{Mo}_{154}\}$  cluster, except in the case of the first Giant-Wheel structure which also incorporated NO as a ligand. There are formally 28  $\text{Mo}^{\text{V}}$  centers corresponding to a charge of  $14^-$  for the  $\{\text{Mo}_{154}\}$  cluster  $\equiv [\{\text{Mo}_2\}_{14}\{\text{Mo}_8\}_{14}\{\text{Mo}_1\}_{14}]^{14-}$ .

At the time of discovery and publication, the  $\{\text{Mo}_{154}\}$  Giant-Wheel-type cluster represented the largest cluster to be structurally characterized by single crystal X-ray diffraction. In itself, the synthesis of this giant cluster generated enormous interest, even in the popular scientific media.<sup>159</sup> This is because the cluster is of nanoscopic dimensions, and as such, demonstrates potential to bridge the gap between the molecular world, characterized by small molecules or ions, and a world of macroscopic bulk compounds.

#### 7.1.4.4 Reactions of the $\{\text{Mo}_{154}\}$ -type Wheels

##### 7.1.4.4.1 Formation of structural defects

Under certain synthetic conditions it is possible to obtain Giant-Wheel clusters based on the  $\{\text{Mo}_{154}\}$  cluster that are structurally incomplete, i.e., there are defects when compared to

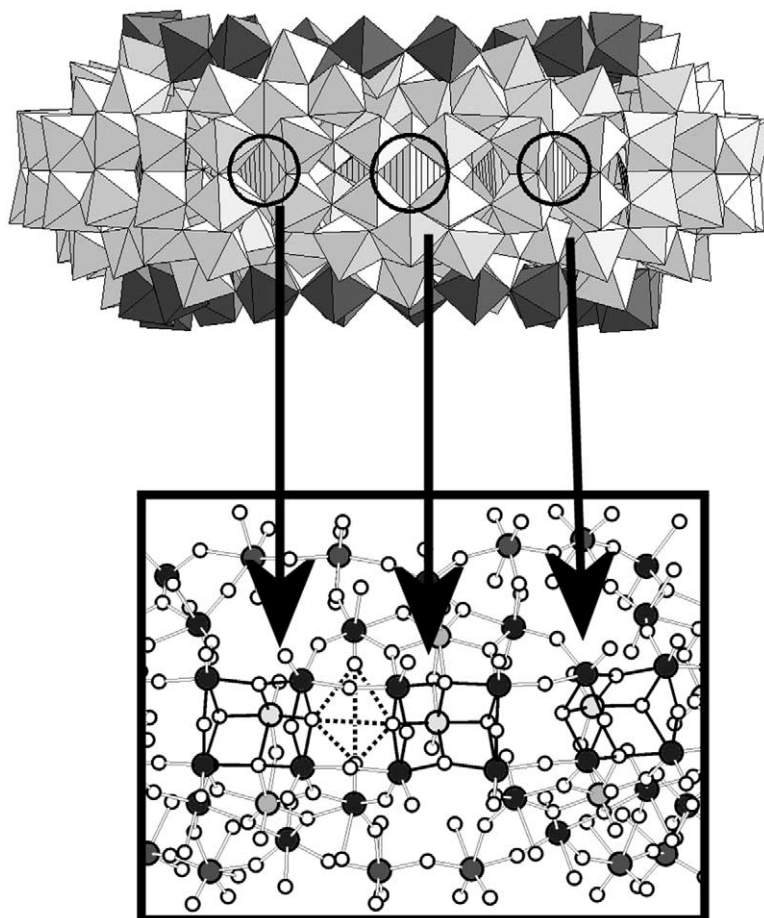


**Figure 46** Polyhedral representation of the equator of the tetradecameric  $\{\text{Mo}_{154}\}$ -type cluster with the  $\{\text{Mo}_1\}$  units that form the double-cubane-type compartments are circled. A zoom in ball and stick representation of these compartments is given below. This representation highlights (1) three of the 14 (incomplete) double-cubane-type compartments each of which is spanned by five Mo centers ( $\text{Mo}-\text{Mo} = 3.4-4.0 \text{ \AA}$ ) belonging to  $\{\text{Mo}_8\}$  as well as  $\{\text{Mo}_1\}$ -type groups and six O atoms (the lowered bond valence sum (BVS) values of the corresponding Mo atoms with an average value of 5.6 prove, besides other experimental data, that two 4d electrons are trapped in each compartment), and (2) one of the 14  $\{(\mu_3\text{-O})_2\text{O}_2\}$ -type compartments—indicated by dotted lines—which are located between two double-cubane-type compartments (the two characteristic  $\mu_3\text{-O}$  atoms (dark gray,  $\text{O}-\text{O} = 3.07 \text{ \AA}$ ) have an average BVS value of 1.2 proving protonation).

the original  $\{\text{Mo}_{154}\}$  cluster. These defects manifest themselves as missing  $\{\text{Mo}_2\}$  units, but statistically these defects can sometimes be seen as partially occupied  $\{\text{Mo}_2\}$  units when the distribution suffers from rotational disorder or translational disorder within the crystal structure. The most extreme case found to date has six defects, three on each side of the Giant-Wheel cluster and is a  $\{\text{Mo}_{142}\}$  cluster (**53**),<sup>156,157</sup> see Figure 47.

In this case the synthetic conditions needed to isolate the  $\{\text{Mo}_{142}\}$  required a very large concentration of electrolyte (in this case ca. 2 M sodium ions present) at the time of crystallization giving a compound of formula  $\text{Na}_{26}[\text{Mo}_{142}\text{O}_{432}(\text{H}_2\text{O})_{58}\text{H}_{14}] \equiv \{[\text{Mo}_2]_8\{\text{Mo}_8\}_{14}\{\text{Mo}_1\}_{14}\}^{26-}$  (**53**). This time the number of each type of building block is varied as six  $\{\text{Mo}_2\}^{2+}$  groups have been removed increasing the negative charge of the Giant-Wheel by 12. The increased charge, as a consequence of the defects, increases the number of sodium ions associated with each Giant-Wheel and it is not surprising that 12 positions were found in the crystal structure that were refined as partially occupied sodium ions (a total of 6.4 sodium ions were found over 12 positions).<sup>156,157</sup> It is interesting that the sodium ions were found to be ligated to the oxygen atoms of the remaining  $\{\text{Mo}_2\}$  units or ligated to the oxygen atoms present in the defect sites. In a recent study Yamase *et al.* also synthesized a similar species to the  $\{\text{Mo}_{142}\}$  cluster species but this time the synthesis was achieved via a photochemical reduction process.<sup>160</sup>

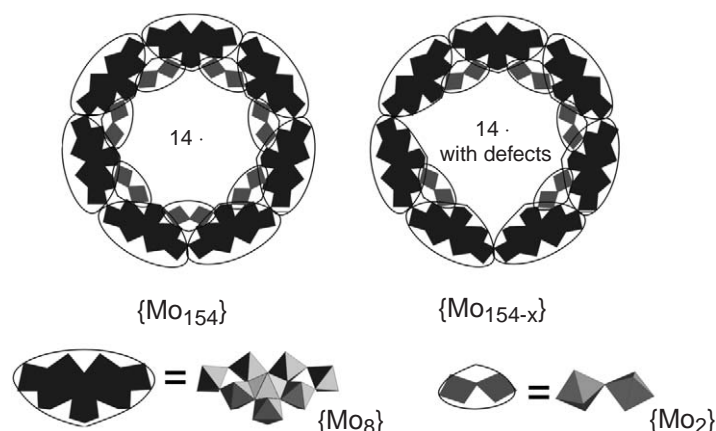


**Figure 47** A representation of the building blocks that comprise the top and bottom surfaces of the wheel cluster on the LHS. On the RHS the derivative with defects is shown; literally the removal of a number of the  $\{\text{Mo}_2\}$  results in a defect structure.

#### 7.1.4.4.2 Linking of wheels to chains and layers

As the introduction of defects increases the overall negative charge of the Giant-Wheel cluster,<sup>156–158,161</sup> the rings can be linked together into chains and layers (see Table 3). In general, the linking reactions occur through the condensation of the terminal  $\{\text{Mo}_2\}$ -based  $\text{H}_2\text{O}-\text{Mo}=\text{O}$  groups on the rings with the  $\text{H}_2\text{O}$  ligands on the  $\{\text{Mo}_2\}$  units,  $\text{O}=\text{Mo}-\text{L}$  ( $\text{L}=\text{H}_2\text{O}$ ) (see Figure 48).

For example a defect  $\{\text{Mo}_{144}\}$  cluster (**54**)<sup>161</sup> can be linked to chains (see Figure 49) and the other clusters  $\{\text{Mo}_{144}\}$  (**55**)<sup>156</sup> and  $\{\text{Mo}_{146}\}$  (**56**)<sup>156</sup> also form chains through defects. In addition to chains, a  $\{\text{Mo}_{152}\}$  defect cluster (**57**)<sup>158</sup> can be linked to form two-dimensional layers, as can a  $\{\text{Mo}_{154}\}$  (**58**) cluster derivatized with the  $(\text{H}_2\text{PO}_2)$  ligand on the inner rim, see Figure 50.<sup>158</sup>

The assembly of the chain shown in Figure 49 is thought to occur due to the increased negative charge resulting from the defects present in the ring, which results from the loss of  $\{\text{Mo}_2\}$  units. The existence of under-occupancy at the  $\{\text{Mo}_2\}$  sites is now well established<sup>156,157,161</sup> and has been found to be promoted by the addition of ligands which can abstract the  $\{\text{Mo}_2\}$  groups. For example the formate anion has been shown to extract the  $\{\text{Mo}_2\}$  units from the inner surface of the  $\{\text{Mo}_{154}\}$ -type cluster. This abstraction has the secondary effect of causing a higher nucleophilicity at the  $\text{O}=\text{Mo}(\text{H}_2\text{O})$  sites of the  $\{\text{Mo}_2\}$  units in the surrounding area. In the case of the layered compounds<sup>161,162</sup> the assembly to layers has, so far, been achieved with two approaches:

By producing defects that increase the nucleophilicity by increasing the local negative charge on the terminal oxygen ligand ( $\text{Mo}=\text{O}$ ) of the  $\{\text{Mo}_2\}$  units that are still present on the cluster. By introducing an electron withdrawing bidentate ligand e.g.,  $\text{H}_2\text{PO}_2^-$  (see Figure 48) to the  $\{\text{Mo}_2\}$  units to increase the nucleophilicity on the  $\{\text{Mo}_2\}$ -based  $\text{Mo}=\text{O}$  group. In this case the  $\text{H}_2\text{PO}_2^-$  acts as both the reducing agent (in the formation of the Giant-Wheel) as well as the bidentate ligand.

In the last process it can be considered that the reaction is facilitated by synergetically induced functional complementarity. Examination of the overall structure forms reveals the presence of a two-dimensional layer in which the cavities of the Giant-Wheel cluster stack up on each other to form nanotubes that are filled with  $\text{H}_2\text{O}$  molecules and sodium cations, see Figure 50.

#### 7.1.4.4.3 Formation of host guest systems

The ring-shaped  $\{\text{Mo}_{154}\}$ -type clusters linked into chains can also act as hosts for smaller polyoxometalate guest, such as the (nonreduced) two-fragment  $\{\text{Mo}_{36}\}$ -type cluster.<sup>58,59</sup> In this supramolecular system the interaction of the guest, which fits exactly into the cavity of the host, is

**Table 3** Giant-Wheel clusters and derivatives.

Compound	Building units	Structure	References
$\text{Na}_{15}\{0.5[\text{Mo}_{154}\text{O}_{462}\text{H}_{14}(\text{H}_2\text{O})_{70}] \cdot 0.5[\text{Mo}_{152}\text{O}_{457}\text{H}_{14}(\text{H}_2\text{O})_{68}]\}$	$\{\text{Mo}_2\}_{14}\{\text{Mo}_8\}_{14}\{\text{Mo}_1\}_{14} + \{\text{Mo}_2\}_{13}\{\text{Mo}_8\}_{14}\{\text{Mo}_1\}_{14}$	Two different discrete rings, one of which possesses a defect	156 51
$(\text{NH}_4)_{28}[\text{Mo}_{154}(\text{NO})_{14}\text{O}_{448}\text{H}_{14}(\text{H}_2\text{O})_{70}]$	$\{\text{Mo}_2\}_{14}\{\text{Mo}_8\}_{14}\{\text{Mo}_1\}_{14}$	Discrete rings	62 52
$\text{Na}_{36}[\text{Mo}_{142}\text{O}_{432}(\text{H}_2\text{O})_{58}\text{H}_{14}]$	$\{\text{Mo}_2\}_{18}\{\text{Mo}_8\}_{14}\{\text{Mo}_1\}_{14}$	Discrete rings	156 53
$\text{Na}_{24}[\text{Mo}_{144}\text{O}_{437}\text{H}_{14}(\text{H}_2\text{O})_{56}]$	$\{\text{Mo}_2\}_{19}\{\text{Mo}_8\}_{14}\{\text{Mo}_1\}_{14}$	Chains built up by rings with defects	164 54
$\text{Na}_{24}\{0.5[\text{Mo}_{144}\text{O}_{437}\text{H}_{14}(\text{H}_2\text{O})_{56}] \cdot 0.5[\text{Mo}_{144}\text{O}_{437}\text{H}_{14}(\text{H}_2\text{O})_{60}]\}$	$\{\text{Mo}_2\}_{19}\{\text{Mo}_8\}_{14}\{\text{Mo}_1\}_{14} + \{\text{Mo}_2\}_{19}\{\text{Mo}_8\}_{14}\{\text{Mo}_1\}_{14}$	Discrete rings with defects and chains built up by rings with defects	158 55
$\text{Na}_{22}[\text{Mo}_{146}\text{O}_{442}\text{H}_{14}(\text{H}_2\text{O})_{58}]$	$\{\text{Mo}_2\}_{10}\{\text{Mo}_8\}_{14}\{\text{Mo}_1\}_{14}$	Chains built up by rings with defects	156 56
$\text{Na}_{16}[\text{Mo}_{152}\text{O}_{457}\text{H}_{14}(\text{H}_2\text{O})_{66.5}]$	$\{\text{Mo}_2\}_{13}\{\text{Mo}_8\}_{14}\{\text{Mo}_1\}_{14}$	Layers built up by rings with defects	157 57
$\text{Na}_{21}[\text{Mo}_{154}\text{O}_{462}\text{H}_{14}(\text{H}_2\text{O})_{54}(\text{H}_2\text{PO}_2)_7]$	$\{\text{Mo}_2\}_{14}\{\text{Mo}_8\}_{14}\{\text{Mo}_1\}_{14}$	Layers with attached $\text{H}_2\text{PO}_2^-$ groups	158 58
$\text{Na}_{32}\{[\text{Mo}_{36}(\text{NO})_4\text{O}_{108}(\text{H}_2\text{O})_{16}] \subset [\text{Mo}_{148}\text{O}_{447}\text{H}_{14}(\text{H}_2\text{O})_{64}]\}$	$\{\text{Mo}_1^*\}_{2}\{\text{Mo}_8\}_{2}\{\text{Mo}_1^*\}_{2} \subset \{\text{Mo}_2\}_{11}\{\text{Mo}_8\}_{14}\{\text{Mo}_1\}_{14}$	$\{\text{Mo}_{36} \subset \text{Mo}_{148}\}$	58,59 59
$\text{Na}_3[\text{Mo}_{154}\text{O}_{462}\text{H}_{14}(\text{H}_2\text{O})_{48}(\text{L}^{2+})_{11}]$	$\{\text{Mo}_2\}_{14}\{\text{Mo}_8\}_{14}\{\text{Mo}_1\}_{14}$	Cysteine-derived ligands attached to the inner rim	162 60
$(\text{NH}_4)_{32}[\text{Mo}_{138}\text{O}_{416}\text{H}_6(\text{H}_2\text{O})_{58}(\text{CH}_3\text{CO}_2)_6]$	$\{\text{Mo}_2\}_{16}\{\text{Mo}_2\text{Ac}\}^*_2 \{\text{Mo}_8\}_{10} \{\text{Mo}_8\text{Ac}\}^*_4\{\text{Mo}_1\}_{10}$	Acetate ligands attached to the wheel	154 61
$(\text{NH}_4)_{26}[\text{Mo}_{142}(\text{H}_4\text{Cu}^{\text{II}})_3\text{O}_{432}(\text{H}_2\text{O})_{58}]$	$\{\text{Mo}_2\}_{18}\{\text{Mo}_8\}_{16}\{\text{Mo}_1\}_{16}$	Copper ions distributed around the equator	165 62
$\text{Li}_{16}[\text{Mo}_{176}\text{O}_{528}\text{H}_{16}(\text{H}_2\text{O})_{80}]$	$\{\text{Mo}_2\}_{16}\{\text{Mo}_8\}_{16}\{\text{Mo}_1\}_{16}$	Discrete rings	166,167 63
$\text{Na}_{16}[\text{Mo}_{248}\text{O}_{720}\text{H}_{16}(\text{H}_2\text{O})_{128}]$	$\{\text{Mo}_2\}_{16}\{\text{Mo}_8\}_{16}\{\text{Mo}_1\}_{16}\{\text{Mo}_{36}\}_2$	176 wheel with hub-caps	168 64
$\text{Na}_{14}[\text{Mo}_{154}\text{O}_{462}\text{H}_{14}(\text{CH}_3\text{OH})_8(\text{H}_2\text{O})_{62}]$	$\{\text{Mo}_2\}_{14}\{\text{Mo}_8\}_{14}\{\text{Mo}_1\}_{14}$	Discrete rings	170 65
$\text{Na}_{16}[\text{Mo}_{176}\text{O}_{528}\text{H}_{16}(\text{CH}_3\text{OH})_{17}(\text{H}_2\text{O})_{63}]$	$\{\text{Mo}_2\}_{16}\{\text{Mo}_8\}_{16}\{\text{Mo}_1\}_{16}$	Discrete rings	170 66
$\text{Na}_6[\text{Mo}_{120}\text{O}_{360}(\text{H}_2\text{O})_{60}\text{H}_{12}\{\text{Pr}(\text{H}_2\text{O})_5\}_6]$	$\{\text{Mo}_2\}_{18}\{\text{Mo}_8\}_{12}\{\text{Mo}_1\}_{12}$	Distorted ring with six $\text{Pr}^{3+}$ ions attached	171 67
$\text{Eu}_6\text{A}_2[\text{Mo}_{128}\text{Eu}_4\text{O}_{388}\text{H}_{10}(\text{H}_2\text{O})_{81}l_2 (2 \text{ A} = 2 \text{ H}^+ \text{ or } 2 \text{ K}^+)]$	$\{\text{Mo}_1\}_{12}\{\text{Mo}_2\}_{18}\{\text{Mo}_8\}_{14}\{\text{Mo}_7\}_{4}\{\text{Mo}_9\}_{4}\{\text{Mo}_2^*\}_2\text{Eu}_4$	Elliptical ring with four $\text{Eu}(\text{III})$ ions per ring	173 68

**Table 4** Keplerate clusters and derivatives.

Compound	Building units	Structure	References
$(\text{NH}_3)_{42}[\text{Mo}^{\text{VI}}_{72}\text{Mo}^{\text{V}}_{60}\text{O}_{372}(\text{OAc})_{30}(\text{H}_2\text{O})_{72}] = \{\text{Mo}132\}$	$\{\text{Mo}(\text{Mo})_5\}_{12} \{\text{Mo}_2\text{L}\}_{30}$ L = OAc	Discrete balls	63
$(\text{NH}_3)_{42}[\text{Mo}^{\text{VI}}_{72}\text{Mo}^{\text{V}}_{60}\text{O}_{372}(\text{HCO}_2)_{30}(\text{H}_2\text{O})_{72}] = \{\text{Mo}132\}$	$\{\text{Mo}(\text{Mo})_5\}_{12} \{\text{Mo}_2\text{L}\}_{30}$ L = HCO <sub>2</sub>	Discrete balls	177
$(\text{Na})_{46}[\text{Mo}^{\text{VI}}_{66}\text{Mo}^{\text{V}}_{50}\text{O}_{331}(\text{OAc})_{30}(\text{H}_2\text{O})_{56}] = \{\text{Mo}132\}$	$\{\text{Mo}(\text{Mo})_5\}_{11} \{\text{Mo}_2\text{L}\}_{25}$ L = OAc	Molecular basket	178
$[\text{Mo}^{\text{VI}}_{72}\text{Fe}^{\text{III}}_{30}\text{O}_{252}(\text{CH}_3\text{COO})_{10} \{\text{Mo}_2\text{O}_7(\text{H}_2\text{O})\} \{\text{H}_2\text{Mo}_2\text{O}_8(\text{H}_2\text{O})\}_3 (\text{H}_2\text{O})_{91}] = \{\text{Mo}72\text{Fe}30\}$	$\{\text{Mo}(\text{Mo})_5\}_{12} \{\text{Fe}\}_{30}$ (L) <sub>10</sub> C {Mo <sub>2</sub> } <sub>11</sub> {Mo <sub>2</sub> } <sub>3</sub> L = OAc	Discrete Fe-substituted ball	181
$[\text{Mo}_{102}\text{O}_{282}(\text{H}_2\text{O})_{78}(\text{CH}_3\text{CO}_2)_{12}] = \{\text{Mo}_{102}\}$	$\{\text{Mo}(\text{Mo})_5\}_{12} \{\text{Mo}\}_{30}$ (L) <sub>12</sub> L = OAc	Discrete balls	179
$\text{Na}_{20} \{ \text{Mo}^{\text{VI}}_{10}\text{O}_3(\text{H}_2\text{O})_{10} \{ \text{V}^{\text{IV}}\text{O}(\text{H}_2\text{O}) \}_{20} \{ \text{Mo}^{\text{VI}}_{5}\text{O}_2(\text{H}_2\text{O})_3 \}_{10} \{ \text{Mo}^{\text{VI}}_{5/2} \}_2 \{ \text{V} \}_{20} (\text{NaSO}_4)_5 \}$	$\{\text{Mo}(\text{Mo})_5\}_{10} \{\text{Mo}\}_{10} \{ \text{Mo}^{\text{VI}}_{5/2} \}_2 \{ \text{V} \}_{20} (\text{NaSO}_4)_5$	Barrel cluster	182
$[\text{H}_4\text{Mo}_{72}\text{Fe}_{30}\text{O}_{254}(\text{CH}_3\text{COO})_{10} \{\text{Mo}_2\text{O}_7(\text{H}_2\text{O})\} \{\text{H}_2\text{Mo}_2\text{O}_8(\text{H}_2\text{O})\}_3 (\text{H}_2\text{O})_{87}] = \{\text{Mo}72\text{Fe}30\}$ -linked	$\{\text{Mo}(\text{Mo})_5\}_{12} \{\text{Fe}\}_{30}$ (L) <sub>10</sub> C {Mo <sub>2</sub> } <sub>11</sub> {Mo <sub>2</sub> } <sub>3</sub> L = Oac	Balls linked to a 2d array	181
$[\text{PMo}_{12}\text{O}_{40} \subset \{(\text{Mo}^{\text{VI}})_{10}\text{Mo}^{\text{VI}}_{5}\}_{12}\text{Fe}^{\text{III}}\text{O}_{252}(\text{H}_2\text{O})_{102}(\text{CH}_3\text{COO})_{15}] = \{\text{PMo}_{12}\} \subset_{132}$	$\text{Mo}(\text{Mo})_5\}_{12} \{\text{Fe}\}_{30}$ (L) <sub>10</sub> C {PMo <sub>12</sub> } L = OAc	Discrete ball encapsulating Keggin ion	184
$[\text{PMo}_{12}\text{O}_{40} \subset \{(\text{Mo}^{\text{VI}})_{10}\text{Mo}^{\text{VI}}_{5}\}_{12}\text{Fe}^{\text{III}}\text{O}_{252}(\text{H}_2\text{O})_{102}(\text{H}_2\text{O})_{102} (\text{CH}_3\text{COO})_{15}] = \{\text{PMo}_{12}\} \subset_{132}$ -linked	$\text{Mo}(\text{Mo})_5\}_{12} \{\text{Fe}\}_{30}$ (L) <sub>12</sub> C {PMo <sub>12</sub> } L = OAc	Balls encapsulating Keggin ion linked to a 2d array	1
$\text{Na}_{48}[\text{H}_x\text{Mo}_{368}\text{O}_{1032}(\text{H}_2\text{O})_{240}(\text{SO}_4)_{48}] = \{\text{Mo}_{368}\}$	$[\text{H}_x \{ \text{Mo}(\text{Mo}_5) \}'_8 \{ \text{Mo}(\text{Mo}_5) \}''_{32} \{ \text{Mo}_2 \}'_{16} \{ \text{Mo}_2 \}''_{8} \{ \text{Mo}_2 \}'''_{8} \{ \text{Mo}_1 \}'_{64} ]$	Lemon cluster: ball wheel hybrid cluster	78

2d = two-dimensional.

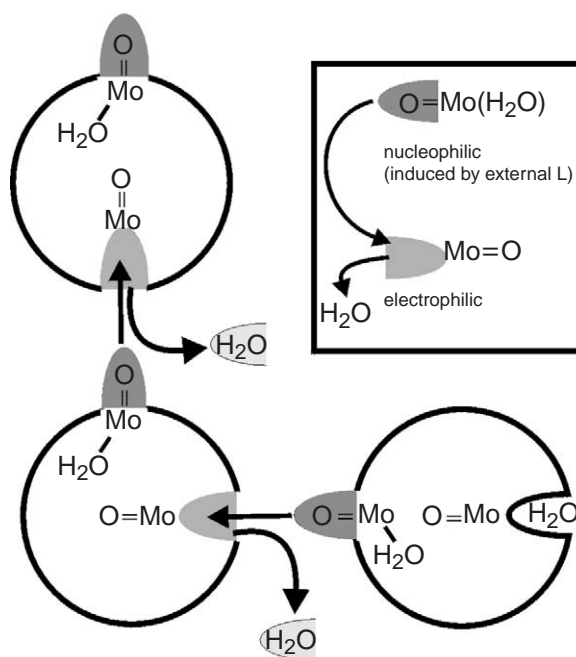


**Figure 48** Schematic representation of the basic assembly principle of the Giant-Wheel-shaped cluster units forming the networks and layers. The formation is based on the synergetically induced functional complementarity of the  $\{\text{Mo}_2\}$  units  $\text{O}=\text{Mo}(\text{L})$  (e.g.,  $\text{L} = \text{H}_2\text{O}, \text{H}_2\text{PO}_4^{2-}$ ) sites of their surfaces.

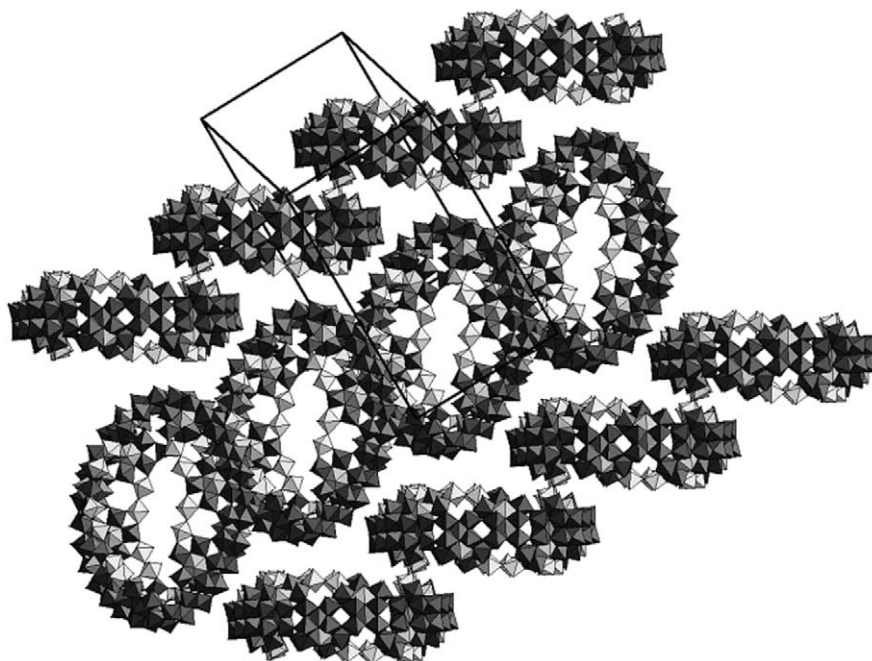


**Figure 49** A polyhedral representation of  $\{\text{Mo}_{144}\}$  (**54**) units linked to chains. The linking occurs via the  $\{\text{Mo}_2\}$  units (see Table 3).<sup>161</sup>

due to 16 hydrogen bonds as well as the Coulomb interaction mediated by four sodium cations located between the negatively charged host and negatively charged guest in the formation of  $\{\text{Mo}_{36} \subset \text{Mo}_{148}\}$  cluster (**59**), see Figure 51. This is an interesting system because a heavily reduced fragment has “captured” a nonreduced fragment. However, it has proved very difficult to reproduce and characterize this product further.

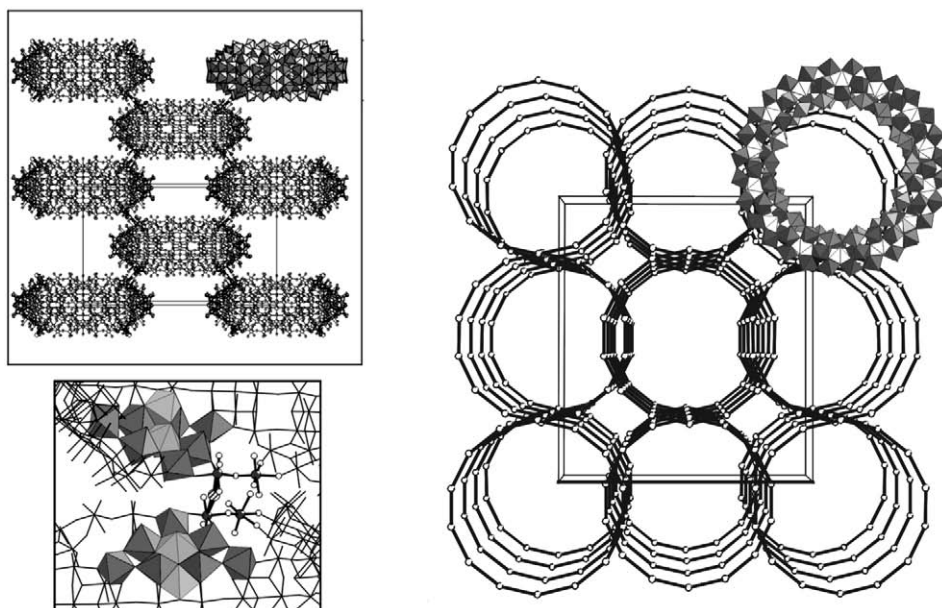


**Figure 50** Ball and stick representation of the “packing” of the linked rings (in the direction of the *b*-axis) linked in crystals of  $\text{Na}_{16}[\text{Mo}^{\text{VI}}_{124}\text{Mo}^{\text{V}}_{28}\text{O}_{429}(\mu_3\text{-O})_{28}\text{H}_{14}(\text{H}_2\text{O})_{66.5}] \cdot X\text{H}_2\text{O}$  ( $X \approx 300$ ) ( $\{\text{Mo}_{152}\}$ ) viewed along the crystallographic *b*-axis. Each ring is connected to surrounding rings via Mo—O—Mo bridges of the O=Mo—O—Mo—OH<sub>2</sub> units, thus forming layer networks parallel to the *ac* plane. One ring is shown as basic unit in polyhedral representation (LHS top). On the LHS, bottom, a detailed view of the bridging region between two cluster rings is shown. One {Mo<sub>8</sub>} unit of each ring along with one {Mo<sub>1</sub>} unit is shown in polyhedral representation and one {Mo<sub>2</sub>}<sup>2+</sup> (= {Mo<sup>VI</sup><sub>2</sub>O<sub>5</sub>(H<sub>2</sub>O)<sub>2</sub>)<sup>2+</sup>) unit per ring in ball and stick representation. On the RHS a perspective view along the crystallographic *c* showing the framework with nanotubes that are filled with H<sub>2</sub>O molecules and sodium cations. For clarity, only one ring is shown in a polyhedral representation. To represent the other rings only the equatorial {Mo<sub>1</sub>} units are given and connected in the remainder of the diagram.

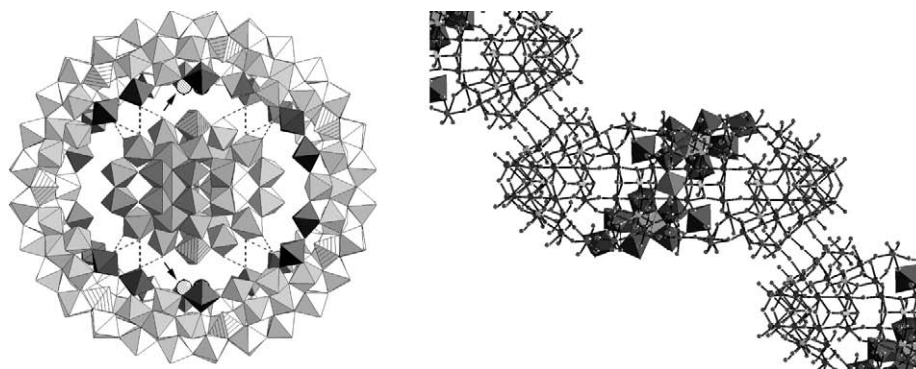


**Figure 51** Structural details of the {Mo<sub>36</sub> ⊂ Mo<sub>148</sub>} cluster system. RHS: part of the chain structure is shown, which is built up by linking ring-shaped cluster units {Mo<sub>148</sub>} (i.e., based on the {Mo<sub>154</sub>}-type with three missing {Mo<sub>2</sub>} groups). LHS: view perpendicular to RHS; the interaction between host and guest is due to 16 hydrogen bonds (dotted lines) and (at least) four sodium cations (indicated by arrow, only two Na positions are visible in this perspective view) situated between host and guest.

#### 7.1.4.4 Structural modifications of the big wheel clusters

In addition to the generation of cluster defects it has been possible to derivatize the isolated wheel clusters in other ways. For instance it has been possible to attach ligands to the inner rim of the cluster anion. This was achieved firstly by adopting reducing agents that could also act as ligands, for example cysteine,<sup>163</sup> which was inspired by the use of H<sub>2</sub>PO<sub>2</sub><sup>−</sup> as both a reducing agent and a ligand in the formation of the wheel layers.<sup>161,162</sup> In the presence of cysteine a wheel cluster forms that also ligates to 11 ligands derived from the oxidation of cysteine in the formation of the species {Mo<sub>154</sub>L<sub>11</sub>} (L = HO<sub>2</sub>C-(NH<sub>3</sub><sup>+</sup>)HC-CH<sub>2</sub>-S-S-CH<sub>2</sub>-CH(NH<sub>3</sub><sup>+</sup>)-CO<sub>2</sub><sup>−</sup>) (**60**) see Figure 52.



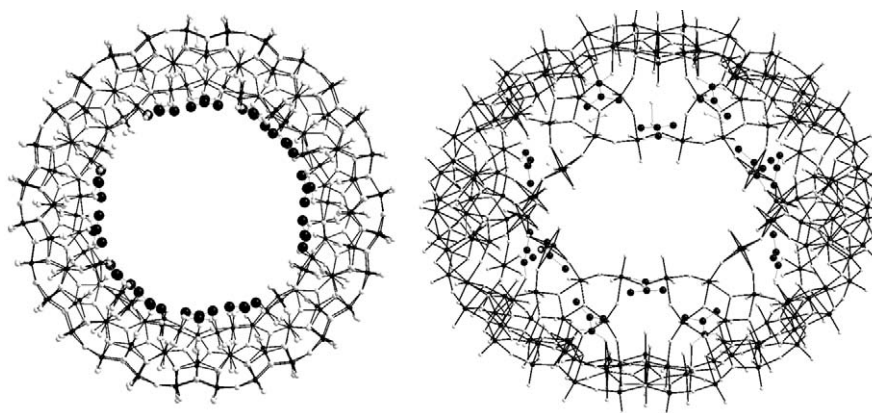


**Figure 52** Ball and stick representations of the modified big wheel cluster with the oxidized cysteine ligand. Only the positions of acetate groups of the ligand were crystallographically resolved and are shown as black spheres. The LHS shows a top view looking down on the  $\{\text{Mo}_{154}\}$  cluster and the RHS shows a view  $45^\circ$  inclined from the top view. The Mo—O framework is shown by small black and white spheres.

In an extension to this work the mixed valence cluster anion of the compound  $(\text{NH}_4)_{32}[\text{Mo}_8^{\text{VI}}_{110}\text{Mo}_6^{\text{V}}_{28}\text{O}_{416}\text{H}_6(\text{H}_2\text{O})_{58}(\text{CH}_3\text{CO}_2)_6] \cdot x\text{H}_2\text{O}$  (**1**) ( $x=250$ ) was synthesized under one-pot conditions. Structural analysis of this  $\{\text{Mo}_{138}\}$  (**61**) cluster demonstrated that it contains well-defined, different types of defects compared to the complete parent  $\{\text{Mo}_{154}\}$ -type cluster. However in addition to the defects the cluster also ligates six acetate anions.<sup>164</sup> In further studies other derivatives and variations of the  $\{\text{Mo}_{154}\}$  cluster includes the incorporation of  $\text{Cu}^{\text{II}}$  ions into a  $\{\text{Mo}_{142}\}$  wheel cluster of formula  $[(\text{H}_4\text{Cu}_5^{\text{II}})\text{Mo}_{28}^{\text{V}}\text{Mo}_{114}^{\text{VI}}\text{O}_{432}(\text{H}_2\text{O})_{58}]^{26-}$  (**62**).<sup>165</sup>

The crystal structure reveals the presence of the cluster anions  $[\{\text{Mo}_8^{\text{V/VI}}\text{O}_{26}(\mu_3\text{O})_2(\text{H}_4\text{Cu}_5)(\text{H}_2\text{O})_3\text{Mo}^{\text{V/VI}}\}_{14}\{\text{Mo}_2^{\text{VI}}\text{O}_5(\text{H}_2\text{O})_2\}_8]^{26-}$ , which are derivatives of the aforementioned tetradecameric  $\{\text{Mo}_{154}\} \equiv \{\text{Mo}_8\}_{14}\{\text{Mo}_1\}_{14}\{\text{Mo}_2\}_{14}$ -type species (**51**). In comparison to the  $\{\text{Mo}_{154}\}$  anion, (**62**) lacks six  $\{\text{Mo}_2\}$ -type building blocks and has the following structural additions. In the tetrahedral cavities spanned by four oxygen atoms (two  $\mu_3$  and two terminal, within the  $\{\text{Mo}_8\}$  building blocks) at well-defined sites on the cluster equator, five  $\text{Cu}^{2+}$  centers are incorporated but not uniformly distributed in the cavities, the largest occupation number being 0.73. These replace some of the 14 H atoms of the parent cluster (**52**), which are bonded to several of the  $\mu_3\text{-O}$  atoms that form the cavities. With high  $\text{H}^+$  ion concentrations the maximum 14-fold protonation of the tetradecameric cluster is achieved.

#### 7.1.4.5 $\{\text{Mo}_{176}\}$ Wheel and Derivatives

The synthesis of the  $\{\text{Mo}_{176}\}$ -type cluster can be related to that of the tetradecameric  $\{\text{Mo}_{154}\}$  cluster. The synthesis of this larger wheel-shaped cluster was achieved by the groups of Müller<sup>166</sup> and Zhang in 1998.<sup>167</sup> The most important change is that this requires reaction conditions with a pH lower than 1 and in the presence of an increased concentration of molybdate. The  $\{\text{Mo}_{176}\}$  cluster can be broadly described as a hexadecamer with two extra  $\{\text{Mo}_8\}$ ,  $\{\text{Mo}_2\}$  and  $\{\text{Mo}_1\}$  units respectively with a formula of  $[\text{Mo}_{176}\text{O}_{528}\text{H}_{16}(\text{H}_2\text{O})_{80}]^{16-}$  (**63**),<sup>166,167</sup> which, again, can be broken into the three types of building units,  $[\{\text{Mo}_2\}_{16}\{\text{Mo}_8\}_{16}\{\text{Mo}_1\}_{16}]^{16-}$ , see Figure 53.

##### 7.1.4.5.1 Comparison between the $\{\text{Mo}_{154}\}$ and $\{\text{Mo}_{176}\}$ big wheel clusters

As described in Section 7.1.4.3.1, the  $\{\text{Mo}_{154}\}$  Giant-Wheel cluster, with the formula,  $[\text{Mo}_{154}\text{O}_{462}\text{H}_{14}(\text{H}_2\text{O})_{70}]^{14-}$ , can be understood in terms of the three different building blocks as  $[\{\text{Mo}_2\}_{14}\{\text{Mo}_8\}_{14}\{\text{Mo}_1\}_{14}]^{14-}$ . It would appear the larger  $\{\text{Mo}_{176}\}$  wheel, with the formula,  $[\text{Mo}_{176}\text{O}_{528}\text{H}_{16}(\text{H}_2\text{O})_{80}]^{16-}$  (**63**),<sup>166,167</sup> can also be broken into the three types of building units,  $[\{\text{Mo}_2\}_{16}\{\text{Mo}_8\}_{16}\{\text{Mo}_1\}_{16}]^{16-}$ , see Figure 54. Therefore, it is easy to see that the  $\{\text{Mo}_{154}\}$  is a tetradecamer of these building blocks whilst the  $\{\text{Mo}_{176}\}$  wheel is a hexadecamer, see Figure 54.

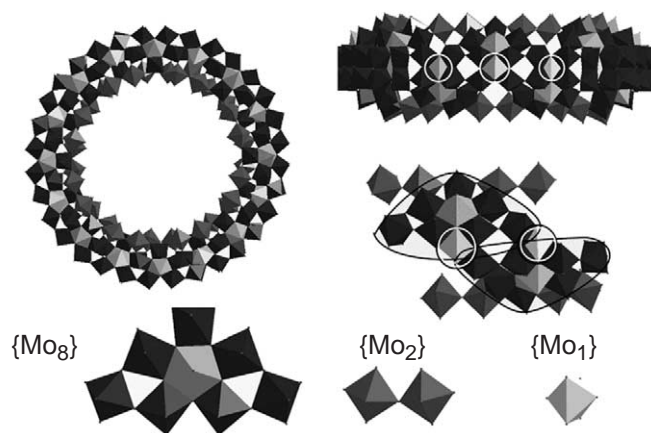


**Figure 53** Top (LHS) and side (RHS) polyhedral views of the hexameric  $\{\text{Mo}_{176}\}$  cluster. The  $\{\text{Mo}_8\}$ ,  $\{\text{Mo}_2\}$  and  $\{\text{Mo}_1\}$  building blocks are shown below and the positions of  $\{\text{Mo}_1\}$  units are ringed on the side view on the RHS.

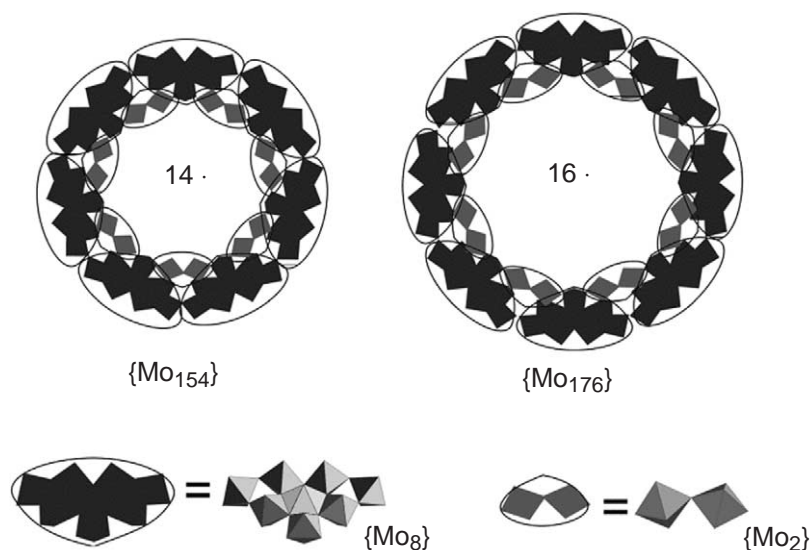


**Figure 54** Comparison between the  $\{\text{Mo}_{154}\}$  and  $\{\text{Mo}_{176}\}$  big wheel clusters. Only the top sections of the wheels are shown which comprise half of the total number of  $\{\text{Mo}_8\}$  and  $\{\text{Mo}_2\}$  building blocks. The equators which contain the  $\{\text{Mo}_1\}$  building blocks are omitted for clarity along with the base of the rings which contain the other  $\{\text{Mo}_8\}$  and  $\{\text{Mo}_2\}$  building blocks.

#### 7.1.4.5.2 Nucleation processes within a cluster cavity—from a $\{\text{Mo}_{176}\}$ to a $\{\text{Mo}_{248}\}$ cluster

To date, despite the increasing knowledge behind the reduction and synthesis of crystalline compounds containing Giant-Wheel clusters, it is interesting that all the diverse formulations of the  $\{\text{Mo}_{154}\}$ -type analogues have not been reproduced with the larger  $\{\text{Mo}_{176}\}$  ring structure. One possible explanation for this observation is that the  $\{\text{Mo}_2\}$  groups are more strained in the  $\{\text{Mo}_{154}\}$  than the  $\{\text{Mo}_{176}\}$  wheel due to the inclusion of more building groups. This is because the overall curvature in the  $\{\text{Mo}_{176}\}$  is less than in the  $\{\text{Mo}_{154}\}$  cluster. Therefore, any reactions that remove the  $\{\text{Mo}_2\}$  groups from the  $\{\text{Mo}_{176}\}$  cluster may be energetically unfavorable under the conditions that have been studied. This idea would also explain why no example of a defect or chain  $\{\text{Mo}_{176}\}$  cluster has been observed.

It is extraordinary, therefore, that under special types of reducing conditions, using ascorbic acid as a reducing agent,<sup>168</sup> the  $\{\text{Mo}_{176}\}$  cluster can be observed to grow. During this process a further two  $\{\text{Mo}_{36}\}$  units are added to each side of the cluster forming a spherical disk-shape cluster comprising 248 Mo atoms of the formula  $[\text{Mo}_{248}\text{O}_{720}\text{H}_{16}(\text{H}_2\text{O})_{128}]^{16-}$  (**64**), where the “hub-caps” were found to have a occupancy of 50%, see Figure 55. This appears to be a remarkable result when it is considered that the larger wheel cluster “cap”  $[\text{Mo}_{36}\text{O}_{96}(\text{H}_2\text{O})_{24}]$ -type

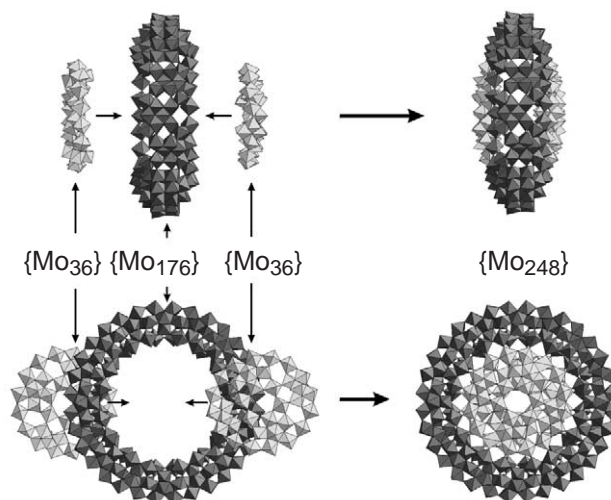


**Figure 55** A schematic representation of the growth process  $\{Mo_{176}\} \rightarrow \{Mo_{248}\}$ . The structure of one  $\{Mo_{248}\}$  cluster can formally be decomposed into one  $\{Mo_{176}\}$  ring and two  $\{Mo_{36}O_{96}(H_2O)_{24}\}$  hub-caps.

fragment is nearly identical to a segment of the solid-state structure of the compound  $\{Mo_5O_{14}\}$ .<sup>169</sup> This extraordinary structure offers the possibility to model crystal growth under boundary conditions, especially nucleation processes. Of particular note is that the growth event can be considered to start from the inner  $\{Mo_2\}$  groups, see Figure 55.

#### 7.1.4.5.3 Surface ligand exchange on the big wheel clusters

Both types of the Giant-Wheel clusters have a very large number of  $H_2O$  ligands present on the surface of the cluster; the  $\{Mo_{154}\}$  cluster supports 70  $H_2O$  ligands and the  $\{Mo_{176}\}$  cluster supports 80  $H_2O$  ligands. As a result, it appears possible to exchange these ligands by those with similar donor properties, for example,  $CH_3OH$ . In the presence of  $CH_3OH$  it has been found that the  $\{Mo_{154}\}$  and the  $\{Mo_{176}\}$  rings can take up eight and 17  $CH_3OH$  molecules, respectively, in the formation of  $\{Mo_{154} \cdot 8MeOH\}$  (**65**) and  $\{Mo_{176} \cdot 17MeOH\}$  (**66**), displacing  $H_2O$  ligands, as observed by single crystal X-ray crystallography (see Figure 56).<sup>170</sup> It is interesting to note that in both structures the  $CH_3OH$  ligands are only observed to replace the  $H_2O$  ligands that exist on one type of site, although the  $CH_3OH$  molecules were found to occupy only one type of site by X-ray crystallographic studies this does not rule out the possibility of disorder over other sites—both in solution and the solid state.<sup>170</sup> This site occurs on the  $\{Mo_8\}$  unit between the Mo polyhedra

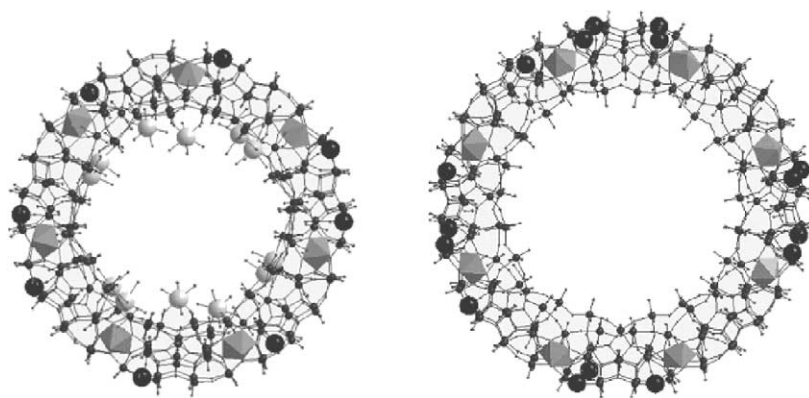


**Figure 56** Ball and stick representations of  $\{Mo_{154}\} \cdot 8MeOH$  (LHS) and  $\{Mo_{176}\} \cdot 17MeOH$  (RHS with surface exchanged methanol molecules shown in black and the central pentagonal unit of the  $\{Mo_8\}$  unit shown in polyhedra). The lower section shows a schematic showing the location of the methanol molecules on the  $\{Mo_8\}$  unit. The positions of the located sodium ions in the crystal structure of  $\{Mo_{154}\} \cdot 8MeOH$  are shown as gray spheres.

adjacent to the hole formed below the  $\{\text{Mo}_2\}$  units. Furthermore, in the case of the  $\{\text{Mo}_{154}\} \cdot 8\text{MeOH}$  several sodium ions were also located in the crystal structure. These are coordinated with 50% occupancy to the  $\{\text{Mo}_2\}$  units. These results have indicated that by modeling (pattern matching, donor matching) the sites amenable to surface exchange it should be possible to utilize ligands with more than one donor atom. For example, by functionalizing the ring with multi-donor ligands advantage of the chelate effect can be taken. Such derivatives can then be extended to incorporate amphiphilic ligands with the head part exchanging the  $\text{H}_2\text{O}$  ligands that can in turn allow the complexation of other species on to and into the wheel by the tail of the ligand.

#### 7.1.4.6 Synthesis of Wheels with Electrophiles

Formally, the removal of a  $\{\text{Mo}_2\}$  unit, introducing defects into the Giant-Wheel-type clusters, should result in the negative charge increasing by two providing a route to the specific derivatization of the inner side of the cluster (the defects only occur at the  $\{\text{Mo}_2\}$ -type sites on the inside of the cluster) and should allow the incorporation of electrophilic substrates.

##### 7.1.4.6.1 Synthesis of the big wheel-type clusters with $\text{Pr}^{\text{III}}$ salts

In a recent derivatization of the  $\{\text{Mo}_{154}\}$  cluster it has been shown that a smaller dodecameric cluster (rather than a tetradecameric cluster, as in the case of the  $\{\text{Mo}_{154}\}$ ) can be produced when the synthesis of the cluster is conducted in the presence of  $\text{Pr}^{\text{III}}$  ions of the formula  $[\text{Mo}_{120}\text{O}_{360}(\text{H}_2\text{O})_{60}\text{H}_{12}\{\text{Pr}(\text{H}_2\text{O})_5\}_6]^{6-}$  (67). However in the case of this smaller dodecameric cluster, six of the  $\{\text{Mo}_2\}$  groups are completely replaced by  $\{\text{Pr}(\text{H}_2\text{O})_5\}^{3+}$  moieties,<sup>171,172</sup> resulting in a  $\{\text{Mo}_{120}\text{Pr}_6\}$ -type Giant-Wheel cluster, see Table 3 and Figure 57.

The  $\{\text{Mo}_{120}\text{Pr}_6\}$ -type cluster consists of 12 sets of the three characteristic building blocks  $\{\text{Mo}_2\}$ ,  $\{\text{Mo}_8\}$ , and  $\{\text{Mo}_1\}$  corresponding to the formula of the dodecameric cluster. Therefore, the incorporation of  $\text{Pr}^{3+}$  into the ring system has resulted in a ring with increased curvature. The main consequence of the increased curvature is shown as a decreased average diameter and ring size, as the number of building blocks that can be incorporated is smaller than compared to the  $\{\text{Mo}_{154}\}$  Giant-Wheel cluster, see Table 3.

##### 7.1.4.6.2 Synthesis of the big wheel clusters with $\text{Eu}^{\text{III}}$ salts

Synthesis of the cluster in the presence of  $\text{Eu}^{\text{III}}$  rather than  $\text{Pr}^{\text{III}}$  salts instead results in a new type of elliptical cluster, see Figure 58.

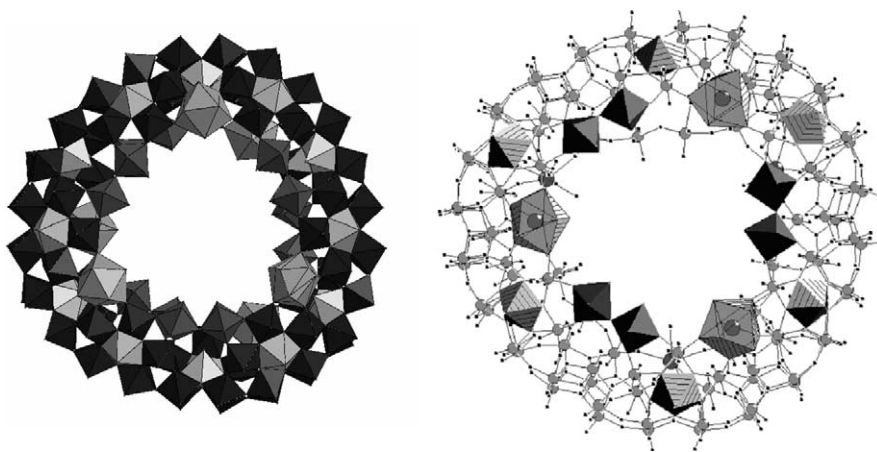


**Figure 57** A schematic showing the structure of  $\{\text{Mo}_{126}\text{Pr}_6\}$  Giant-Wheel cluster in polyhedral representation (LHS) and in ball and stick presentation (RHS) (view along the crystallographic  $a$ -axis). On the RHS, the  $\text{PrO}_9$  polyhedra (the Pr atoms are shown in the center of polyhedra with hatched sides and open faces), the pentagonal bipyramids (shown as hatched polyhedra) and the  $\{\text{Mo}_2\}$  units (shown as filled polyhedra) on the upper half of the wheel are shown in polyhedral representation.

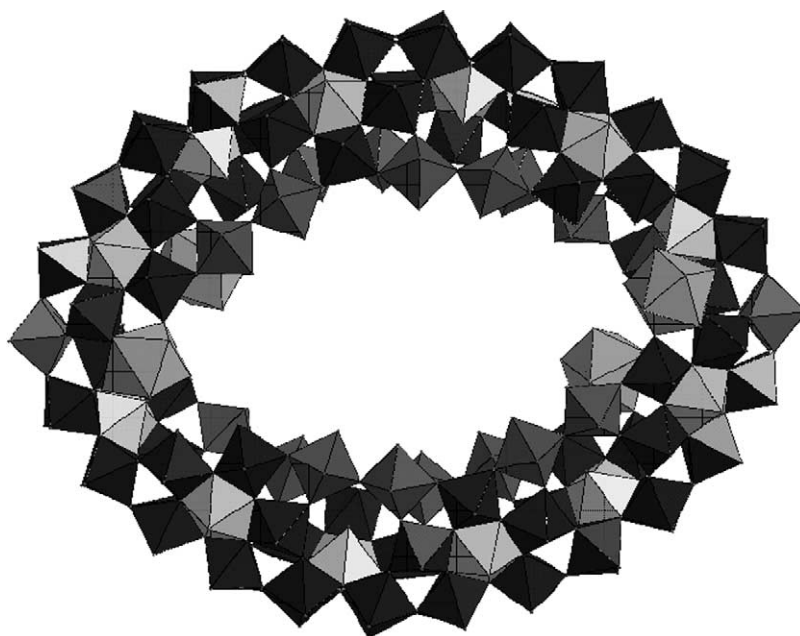


**Figure 58** Polyhedral representation of the structure of the  $\{\text{Mo}_{128}\text{Eu}_4\}$  cluster. The pentagonal centers in the  $\{\text{Mo}_8\}$  units are shown as the hatched polyhedra and the  $\text{Eu}^{\text{III}}$  ions are shown as hatched polyhedra.

This cluster was structurally characterized as dimer of two giant clusters with the formula  $\text{Eu}_6\text{A}_2[\text{Mo}_{128}\text{Eu}_4\text{O}_{388}\text{H}_{10}(\text{H}_2\text{O})_{81}]_2$  ( $2\text{A} = 2\text{H}^+$  or  $2\text{K}^+$ ) (**68**).<sup>173</sup> The dimer contains two elliptical molybdenum oxide-based units, linked together by two  $\text{Eu}-\text{O}-\text{Mo}$  bonds, each unit incorporates 128  $\text{Mo}^{\text{VI/V}}$  and four  $\text{Eu}^{\text{III}}$  centers and includes large fragments of the  $\{\text{Mo}_{154}\}$  “parent” cluster, see Figure 59. One explanation of this is that these dimers are formed by  $\text{Eu}^{\text{III}}$  centers acting as symmetry breakers which prevent the corresponding highly symmetrical parent-ring closure.<sup>146,173</sup> In addition, it is important to realize that such large fragments can, in principle, be used as synthons. The ability to connect or assemble clusters in

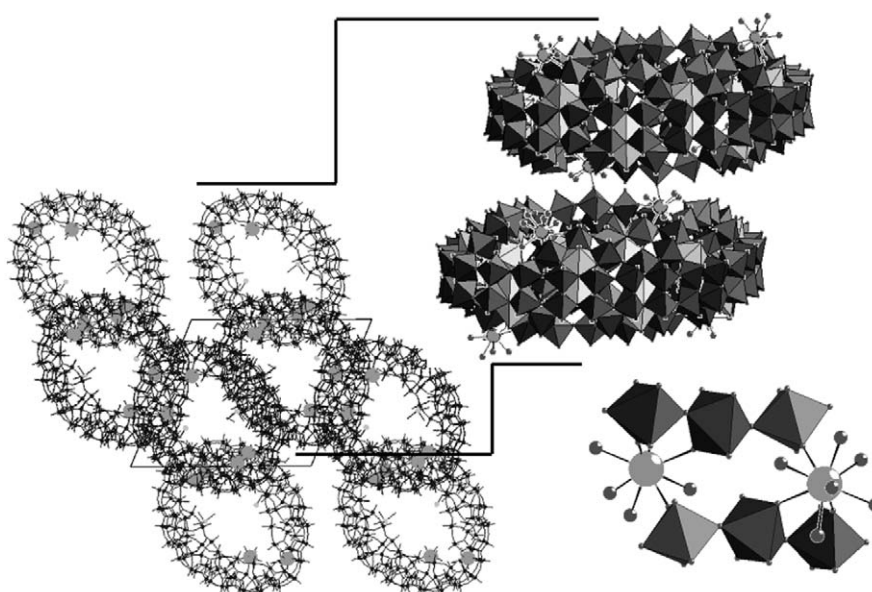


**Figure 59** On the left a packing diagram of the cluster units in ball and stick representation is shown looking down the “cavities” ( $\text{Eu}^{\text{III}}$  ions in gray). On the right a representation of the “dimeric” unit (**68**) is shown with the Mo-oxide-based units displayed as polyhedra ( $\{\text{Mo}_1\}$  units,  $\{\text{Mo}_2\}$  groups,  $\{\text{Mo}_8\}$  units with pentagonal units;  $\text{Eu}^{\text{III}}$  coordination spheres in ball and stick representation). An expanded view of the  $\text{Mo}-\text{O}-\text{Eu}$  groups linking the two cluster rings is also shown.

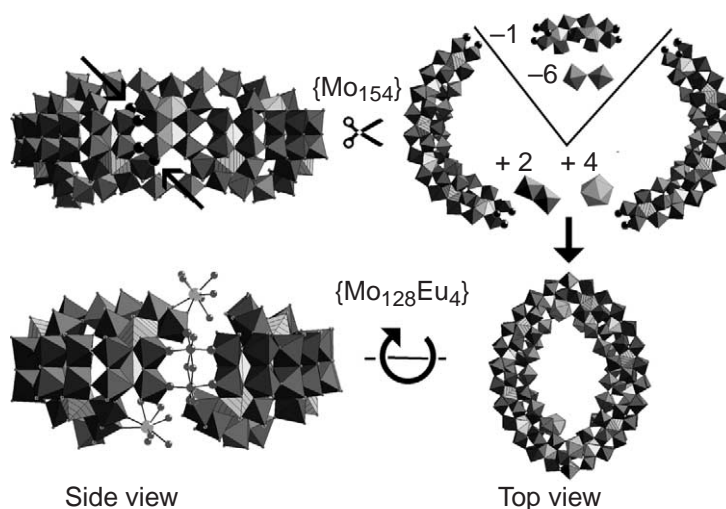


**Figure 60** Demonstration of a formal  $\{\text{Mo}_{128}\text{Eu}_4\}$  ring construction from a parent  $\{\text{Mo}_{154}\}$ -type cluster by a “cutting” process giving two large fragments. A side view of the  $\{\text{Mo}_{154}\}$  ring (top left) shows the cutting positions marked as large black spheres and the top right view those units which have to be removed from the  $\{\text{Mo}_{154}\}$  ring and those which have to be added to the resulting two large fragments (left and right) to generate the  $\{\text{Mo}_{128}\text{Eu}_4\}$  cluster unit which are shown in a side and top view at the bottom (the new  $\{\text{Mo}_2^*\}$  units are shown on the left side together with the  $\text{EuO}_9$  in ball and stick representation).

a predefined manner may allow for the design of nanoscopic devices using the “bottom up” approach.

The giant ring-shaped parent clusters (see above) obtained from molybdenum blue solutions are based on the three different building blocks  $\{\text{Mo}_1\}$ ,  $\{\text{Mo}_2\}$ , and  $\{\text{Mo}_8\}$ .<sup>146</sup> The remarkable feature in (68) is that this has undergone critical structural changes as a result of the incorporation of  $\text{Eu}^{\text{III}}$  (compare the  $\text{Pr}^{\text{III}}$  substituted cluster).<sup>171</sup> This situation could be explained in that the presence of  $\text{Eu}^{\text{III}}$  ions, which have a smaller ionic radius than  $\text{Pr}^{\text{III}}$  ions, prevent ring closure to the parent ring type as the accompanying increase of the curvature destabilizes the system.

The two ellipsoidal cluster entities of  $\text{Eu}_6\text{A}_2[\text{Mo}_{128}\text{Eu}_4\text{O}_{388}\text{H}_{10}(\text{H}_2\text{O})_{81}]_2 \cdot \text{ca. } 600 \text{ H}_2\text{O}$  ( $\text{A} = \text{H}^+$  or  $\text{K}^+$ ) can be approximately described by the building-block scheme used for the formation of the  $\{\text{Mo}_{154}\}$ - and  $\{\text{Mo}_{176}\}$ -type species, which comprise not only the building blocks  $\{\text{Mo}_1\}$ ,  $\{\text{Mo}_2\}$ , and  $\{\text{Mo}_8\}$ , but also the additional “new” units of the  $\{\text{Mo}_2^*\}$ ,  $\{\text{Mo}_7\}$ , and  $\{\text{Mo}_9\}$  type ( $\{\text{Mo}_2^*\}\{\text{Mo}_2^{\text{V/V}'}\text{O}_7(\text{H}_2\text{O})\}^{3-}$ ): the fragments are (formally) cut, as shown in Figure 60, from the  $\{\text{Mo}_{154}\}$ -type Giant-Wheel at four positions. The “cutting” process takes place between those polyhedra showing the least number of bonds. The large fragments obtained (Figure 60) have the composition  $[\{\text{Mo}_1\}_6\{\text{Mo}_2\}_4\{\text{Mo}_8\}_2\{\text{Mo}_7\}_2\{\text{Mo}_9\}_2]$ , that is, they include the two new  $\{\text{Mo}_7\}$  and  $\{\text{Mo}_9\}$  units, which are formally generated by “cutting” asymmetrically two neighboring  $\{\text{Mo}_8\}$  units at the above-mentioned positions to produce the two major parts of the new ellipsoidal ring. The complete ellipsoidal ring unit is formed when the two fragments are combined with two new  $\{\text{Mo}_2^*\}$  units and four  $\text{Eu}^{\text{III}}$  ions (Figure 60).

#### 7.1.4.7 $\{\text{Mo}_{132}\}$ Big Ball Keplerate Clusters

In 1998, Müller *et al.* synthesized and structurally characterized a polyoxometalate that can best be described as a molecular sphere with an outer diameter of 30 Å, and an inner diameter of 25 Å.<sup>63</sup> This molecular sphere, or inorganic super fullerene was given the name “Keplerate” corresponding to Kepler’s model of the cosmos and his concept of planetary motion, as described in his early opus *Mysterium Cosmographicum*.<sup>174</sup> In accordance with this speculative model, Kepler believed that the distances between the orbits of the planets could be explained if the ratios between the successive orbits were designed to be equivalent to the spheres successively circumscribed around and inscribed within the five Platonic solids. In analogy, the cluster correspondingly shows a spherical shell of terminal oxygen atoms in which an icosahedron spanned by the centers of the 12  $\{(\text{Mo})\text{Mo}_5\}$  pentagons—the Mo atoms of the central  $\text{MoO}_7$  bipyramids—is inscribed (see Figure 61).

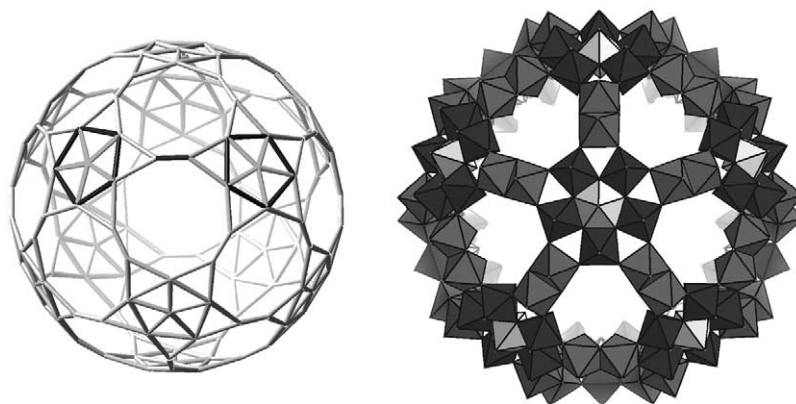


**Figure 61** Representations of the spherical Keplerate  $\{\text{Mo}_{132}\}$  cluster. LHS: schematic representation of the 132 molybdenum atom framework of the Keplerate cluster highlighting its spherical nature. Two pentagonal units  $\{(\text{Mo})\text{Mo}_5\}$  groups linked by an  $\{\text{Mo}^{\text{V}}-\text{Mo}^{\text{V}}\}$  bridge (red) are emphasized. RHS: polyhedral representation of the cluster. The pentagonal Mo centers are shown by the white polyhedra, the rest of the  $\{(\text{Mo})\text{Mo}_5\}$  groups are shown as the very dark (almost black) polyhedra and the  $\{\text{Mo}^{\text{V}}-\text{Mo}^{\text{V}}\}$  or  $\{\text{Mo}_2\}$  linker groups are shown as the lighter colored polyhedra.

#### 7.1.4.7.1 Building block scheme for the Keplerate clusters

The overall Keplerate clusters have the formula  $[\text{Mo}^{\text{VI}}_{72}\text{Mo}^{\text{V}}_{60}\text{O}_{372}(\text{MeCO}_2)_{30}(\text{H}_2\text{O})_{72}]^{42-}$  ( $\{\text{Mo}_{132}\}$ ) (**69**) and consist of two types of building block (Figure 61): 12 pentagonal  $\{\text{Mo}(\text{Mo})_5\}$  units and 30 linking  $\{\text{Mo}_2\}$  units, where this type of  $\{\text{Mo}_2\}$  unit can be formulated as  $\{\text{Mo}^{\text{V}}_2\text{O}_4(\text{OOR})^+\}$  ( $\text{R} = \text{CCH}_3, \text{CH}, \text{PO}_2$ ). In geometrical terms this type of cluster can be described as  $(\text{Pentagon})_{12}(\text{Linker})_{30}$ ;  $\text{Pentagon} = \{\text{Mo}(\text{Mo})_5\}$  and  $\text{Linker} = \{\text{Mo}^{\text{V}}_2\text{O}_4(\text{OOR})^+\}$ ,  $\{\text{OMo}(\text{H}_2\text{O})\}^{3+}$ ,  $\{\text{Fe}(\text{H}_2\text{O})_2\}^{3+}$ . Unlike the  $\{\text{Mo}_{154}\}$  cluster system, this cluster is synthesized at pH 4 (aqueous conditions) in an ammonia/acetate buffer using ammonium heptamolybdate with  $\text{N}_2\text{H}_4 \cdot \text{H}_2\text{SO}_4$  as a reducing agent. Sufficient reducing agent is used to reduce 45% of the total number of Mo centers from  $\text{Mo}^{\text{VI}}$  to  $\text{Mo}^{\text{V}}$ . Under these conditions crystals of the  $\{\text{Mo}_{132}\}$  cluster result in four days.

It is interesting that the  $\{\text{Mo}_2\}$  building unit can only be formed in the presence of stabilizing bidentate ligands and it is these units that are able to direct the formation of the  $\{(\text{Mo})(\text{Mo})_5\}$  pentagon, which does not exist as an independent unit. Furthermore the  $\{(\text{Mo})(\text{Mo})_5\}$  pentagon found in the Keplerate can be considered to be almost identical to the  $\{(\text{Mo})(\text{Mo})_5\}$  pentagons found in the  $\{\text{Mo}_8\}$  units, of which the  $\{\text{Mo}_{57}\}$  and Giant-Wheel clusters are comprised, Figure 62. In addition to the building units already mentioned it is possible to describe both the wheel and ball clusters in terms of  $\{\text{Mo}_{11}\}$  units.<sup>58,59</sup>

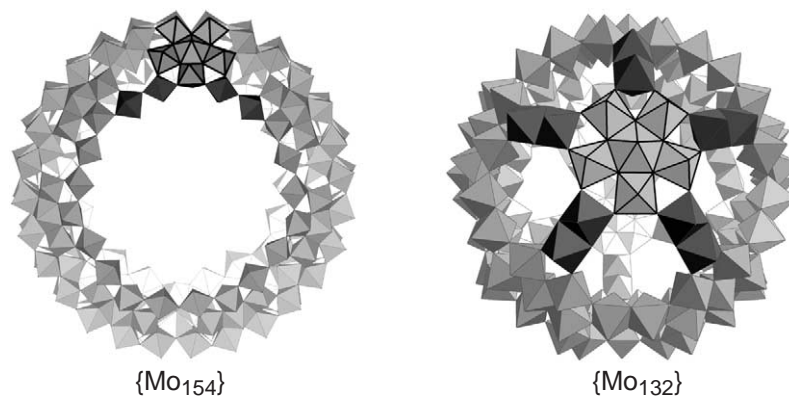


**Figure 62** Comparison of the polyhedral representations of the  $\{\text{Mo}_{132}\}$  Keplerate with the  $\{\text{Mo}_{154}\}$  cluster (not to scale) with the pentagonal  $\{\text{Mo}(\text{Mo})_5\}$  (in thick lines) and the adjacent  $\{\text{Mo}_2\}$  (dark gray) units emphasized in each. It is important to know, in the context of synthesis, that the  $\{\text{Mo}_2\}$  units have a different structure in each class of cluster, but it is only these units, which have been observed to be exchangeable for other metal ions.

### 7.1.4.7.2 Construction of spherical species with icosahedral symmetry

To synthesize giant molecular species the most obvious starting point appears to be in finding a reaction system in which pentagonal units<sup>60</sup> with  $C_5$  symmetry can first be generated, then become linked and be placed at the 12 corners of an icosahedron. In the case of polyoxomolybdates these pentagonal units ( $\{(Mo)Mo_5\}$  groups) can consist of a central pentagonal bipyramidal  $MoO_7$  unit-sharing edges with five  $MoO_6$  octahedra. As stated earlier, the  $\{(Mo)Mo_5\}$  unit is itself a constituent of the  $\{Mo_8\}$ -type unit abundant in many giant polyoxometalates (see Figure 62) in which two additional  $MoO_6$  octahedra are bound (sharing corners) to the  $\{(Mo)Mo_5\}$  unit. In the presence of linkers, units which are capable of bridging two (or more) building blocks, for instance those of the classical  $[Mo^V_2O_4]^{2+}$  type<sup>3</sup> (typically formed in reduced molybdate solutions in the presence of bidentate ligands), the icosahedral molecular system with 12 such pentagons and 30 such linkers is formed. When, for example, acetate anions act as bridging ligands for the  $Mo^V_2O_4^{2+}$  groups, the spherical cluster with the stoichiometry  $[Mo^{VI}_{72}Mo^{V}_{60}O_{372}(CH_3COO)_{30}(H_2O)_{72}]^{42-}$  ( $\{Mo_{132}\}$ ) results. The central Mo positions of the 12  $\{(Mo)Mo_5\}$  pentagons define the 12 corners, and the 30  $Mo^V_2O_4^{2+}$  groups the 30 edges of an icosahedron, in agreement with Euler's well-known formula. This corresponds to the formulation  $[\{(Mo)Mo_5O_{21}(H_2O)_6\}_{12}\{Mo^V_2O_4(CH_3COO)\}_{30}]^{42-}$ . Figure 63 describes the assembly, only in a geometrical sense, and this is vitally important if one is to both understand and design further spherical species.

### 7.1.4.7.3 Changing the bridging ligands in the Keplerate clusters

On substituting the bridging acetate ligands with formate groups this smaller ligand allows a special type of organization of the  $H_2O$  molecules encapsulated inside the cluster: a hydrogen-bonded water cluster as guest system with an "onion-type" structure which is induced by the peripheral spherical cluster shell, see Figure 64, in the synthesis of  $\{(H_2O)_n \subset Mo_{132}\}$  (70)

This type of inclusion compound is of particular interest in the study of the influence of the outer spherical shell (including the different types of coordinated ligands) on the organization of encapsulated, weakly bonded, guest molecules, in this case water molecules.<sup>175,176</sup> In addition to derivatives (69)  $\{Mo_{132}(OAc)_{30}\}$  and (70)<sup>177</sup>  $\{Mo_{132}(\text{formate})_{30}\}$  it is, in principle, possible to change the bidentate ligand that stabilizes the  $\{Mo_2^V\}$  group for other ligands as long as they will fit in the cavity created by the formation of the Keplerate. In addition it is possible to exchange the acetate ligands present in (69) with ligands like phosphate, hypophosphite, and partially for sulfate.<sup>178</sup>

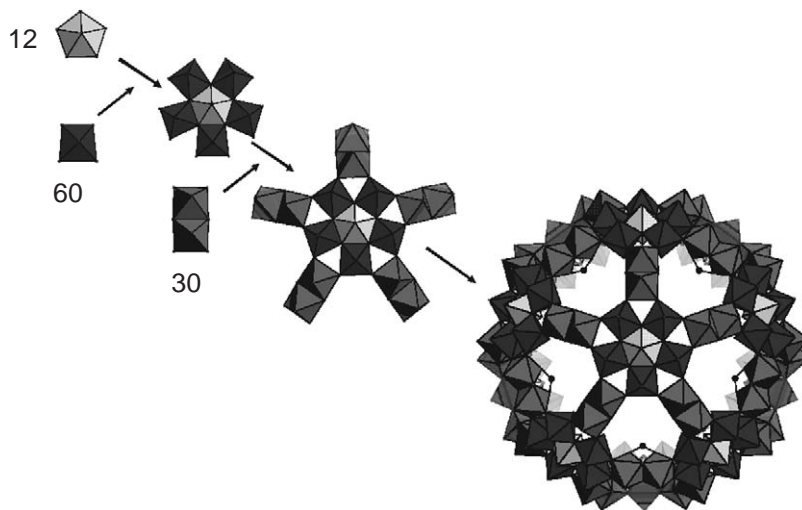


**Figure 63** A basic geometrical description of the construction of the spherical Keplerate. Going down the diagonal from the upper left to the bottom right: the pentagonal  $\{Mo\}$  unit is shown by the white polyhedra and the remaining five Mo groups are colored dark gray. The formation of one of 12  $\{(Mo)Mo_5\}$  building blocks is shown and then in the next step five  $\{Mo_2^V\}$  linkers are added (lighter gray polyhedra). In total 12  $\{(Mo)Mo_5\}$  units and 30  $\{Mo_2^V\}$  units combine to form the overall  $\{Mo_{132}\}$  cluster. NOTE this is not a mechanism for cluster formation, but a geometrical description.



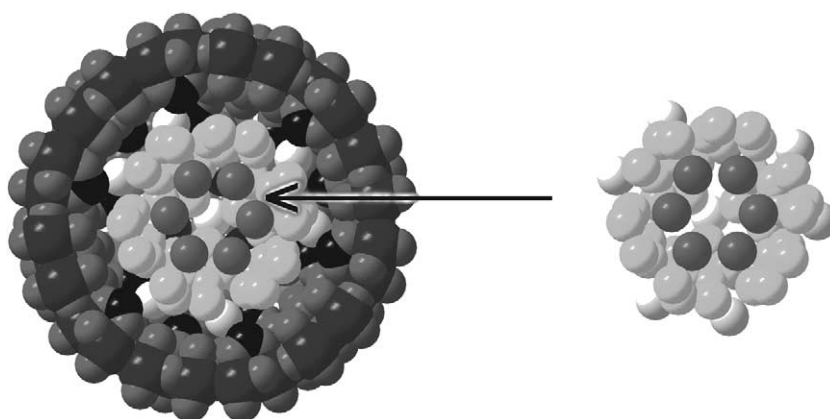


**Figure 64** Space filling representation of the cross-section of the cluster showing the central cavity with the organized water molecules inside. There are three shells of water molecules visible and these are depicted on the RHS. The framework of the cluster is depicted by the dark gray close-packed spheres on the LHS and the carbon atoms of the formate anions are shown by the black close-packed spheres.

#### 7.1.4.7.4 Structural derivatives: removing the lid of the Keplerate

In the same way as it is possible to form derivatives of the  $\{\text{Mo}_{154}\}$  wheel cluster with defects, it is possible to remove the “lid” from the  $\{\text{Mo}_{132}\}$  Keplerate cluster in the formation of a molecular basket, see Figure 65.<sup>178</sup>

This molecular basket has the composition  $[\text{Mo}_{116}\text{O}_{331}(\text{OAc})_{30}(\text{H}_2\text{O})_{56}]^{46-}$ , (71) and, by using the building block principle described earlier, the  $\{\text{Mo}_{132}\}$  cluster loses one  $\{\text{Mo}(\text{Mo})_5\}$  unit and five  $\{\text{Mo}_2\}$  units to yield the basket anion, see Figure 66. The  $\{\text{Mo}_{116}\}$  species comprises 66  $\text{Mo}^{\text{VI}}$  centers and 50  $\text{Mo}^{\text{V}}$  compared to 72  $\text{Mo}^{\text{VI}}$  and 60  $\text{Mo}^{\text{V}}$  species in the  $\{\text{Mo}_{132}\}$ . Therefore the reaction of  $\{\text{Mo}_{132}\}$  to the  $\{\text{Mo}_{116}\}$  cluster can be considered to be a partial oxidation. The reaction conditions for the synthesis of the  $\{\text{Mo}_{116}\}$  cluster are similar to that of the Keplerate species (69), but a very high concentration of NaCl is introduced into the reaction mixture and the solution is left to stand in air over a period of weeks.<sup>178</sup>

The reaction of  $\{\text{Mo}_{132}\}$  to the  $\{\text{Mo}_{116}\}$  presents some intriguing possibilities to remove the lid, deposit a guest molecule and then reseal the lid by careful reduction of the species to make a kind of “molecular hostage,” see Figure 66.

#### 7.1.4.7.5 From $\{\text{Mo}_{132}\}$ to $\{\text{Mo}_{72}\text{M}_{30}\}$ spherical clusters ( $M = \text{Fe}, \text{Mo}$ )

In an interesting extension to the chemistry of the  $\{\text{Mo}_{132}\}$  (69) Müller *et al.* have succeeded in exchanging the  $\{\text{Mo}_2\}$  groups present in the Keplerate species with  $\text{Fe}^{\text{III}}$  and  $\text{Mo}^{\text{V}}$  atoms in the formation of the neutral  $\{\text{Mo}_{72}\text{Fe}_{30}\}$  cluster (72)<sup>179</sup>  $[\text{Mo}_{72}\text{Fe}_{30}\text{O}_{252}(\text{CH}_3\text{COO})_{10}\{\text{Mo}_2\text{O}_7(\text{H}_2\text{O})\}]$

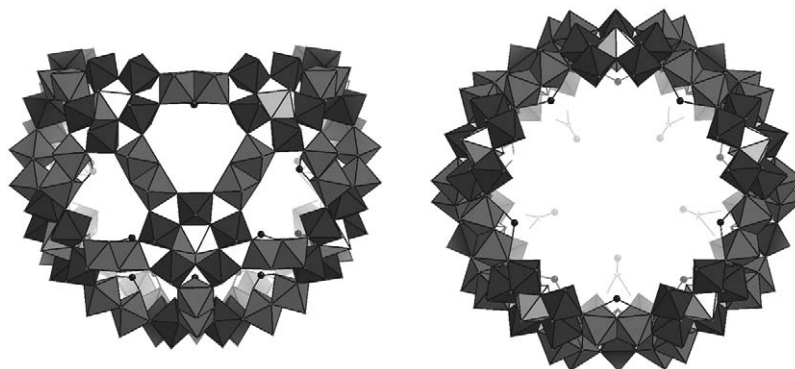


**Figure 65** Polyhedral representations of the basket-derived Keplerate  $\{\text{Mo}_{116}\}$  (71). A side view is shown on the LHS and the top view is shown on the RHS. The pentagonal centers of the  $\{\text{Mo}(\text{Mo})_5\}$  units are shown as white polyhedra whereas the appended Mo atoms are shown as very dark gray polyhedra. The  $\{\text{Mo}_2\}$  groups are shown by the lighter gray polyhedra.

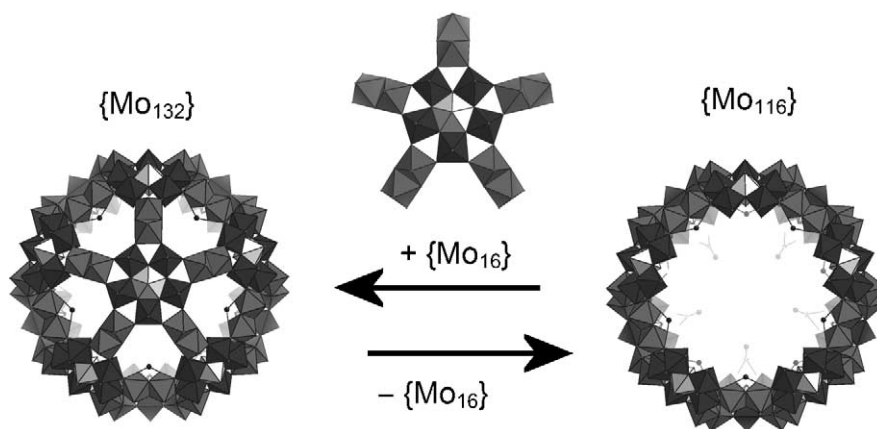


**Figure 66** A schematic representation of the loss of the lid to form the basket species. The  $\{\text{Mo}_{132}\}$  Keplerate cluster is shown on the LHS and the  $\{\text{Mo}_{116}\}$  is shown on the RHS. The pentagonal centers of the  $\{\text{Mo}(\text{Mo})_5\}$  units are shown as white polyhedra whereas the appended Mo atoms are shown as very dark gray polyhedra. The  $\{\text{Mo}_2\}$  groups are shown by the lighter gray polyhedra.

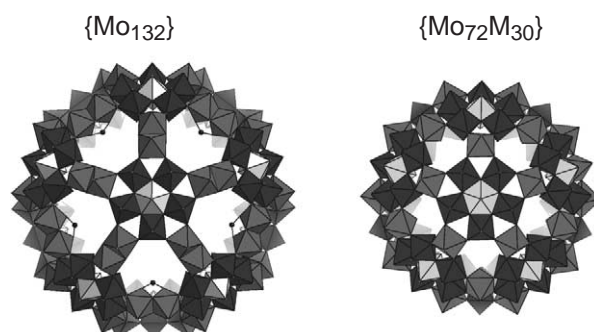


**Figure 67** A representation of the structure of the  $\{\text{Mo}_{72}\text{M}_{30}\}$  cluster on the RHS and a comparison with the  $\{\text{Mo}_{132}\}$  Keplerate cluster on the LHS. The pentagonal centers of the  $\{\text{Mo}(\text{Mo})_5\}$  units are shown as white polyhedra whereas the appended Mo atoms are shown as very dark gray polyhedra. The lighter gray polyhedra in the  $\{\text{Mo}_{132}\}$  refer to the  $\{\text{Mo}_2\}$  units whereas the lighter gray polyhedra in the  $\{\text{Mo}_{72}\text{M}_{30}\}$  refer to the  $\{\text{M}\}$  units.

$\{\text{H}_2\text{Mo}_2\text{O}_8(\text{H}_2\text{O})\}_3(\text{H}_2\text{O})_{91}]$  and a neutral  $\{\text{Mo}_{102}\}$  cluster (**73**)<sup>179</sup>  $[\text{Mo}_{102}\text{O}_{282}(\text{H}_2\text{O})_{78}(\text{CH}_3\text{CO}_2)_{12}]$ , respectively, see Figure 67. These spheres are smaller than the parent  $\{\text{Mo}_{132}\}$  with outer diameters of ca. 24 Å and inner diameters of ca. 18 Å. The  $\{\text{Mo}_{72}\text{Fe}_{30}\}$  cluster is comprised of only  $\text{Mo}^{\text{VI}}$  atoms whereas the  $\{\text{Mo}_{72}\text{Mo}_{30}\}$  cluster contains 36 reduced  $\text{Mo}^{\text{V}}$  centers where the 30 linking units are reduced and the remaining six centers are delocalized of the 12 pentagonal centers present in the cluster. It is, however, not possible to produce (**72**) in a one pot reaction and assemble the cluster from its constituent components. One must instead react the Keplerate cluster (**69**) with iron salts followed by heating and adjusting the pH to ca. 2.5. Similarly, the synthesis of (**73**) is achieved by acidification of a solution of the Keplerate cluster (**69**) with HCl followed by the addition of a large amount of NaCl. Crystals of (**73**) form after the solution is left for three days.

In essence the reaction of the  $\{\text{Mo}_{132}\}$  cluster to the  $\{\text{Mo}_{72}\text{Fe}_{30}\}$  species probably proceeds via a stepwise substitution of the  $\{\text{Mo}_2\}$  groups although no intermediates have been isolated. Remarkably, because it is possible to produce mono-anions of (**72**) and (**73**) it has even been possible to observe molecular ions of these species in the gas phase using MALDI mass spectrometry.<sup>180</sup> Such a result offers the interesting possibility that such a cluster can be “screened” with different guests included rather than resorting to full crystallographic analysis. Furthermore it may be possible to deposit such clusters from the gas phase to produce novel thin layer materials, perhaps with applications in molecular electronics, etc.<sup>36</sup>

#### 7.1.4.7.6 Formation of molecular barrels $\{\text{Mo}_{75}\text{V}_{20}\}$

If vanadyl sulfate is added to an acidified molybdate solution, the compound  $\text{Na}_{20}[\{\text{Mo}^{\text{VI}}\text{O}_3(\text{H}_2\text{O})\}_{10}\{\text{V}^{\text{IV}}\text{O}(\text{H}_2\text{O})\}_{20}\{\text{Mo}^{\text{VI}}/\text{Mo}^{\text{VI}}_5\text{O}_{21}\}(\text{H}_2\text{O})_3\}_{10}(\{\text{Mo}^{\text{VI}}\text{O}_2(\text{H}_2\text{O})_2\}_{5/2})_2(-\{\text{NaSO}_4\}_5)_2] \cdot x\text{H}_2\text{O}$

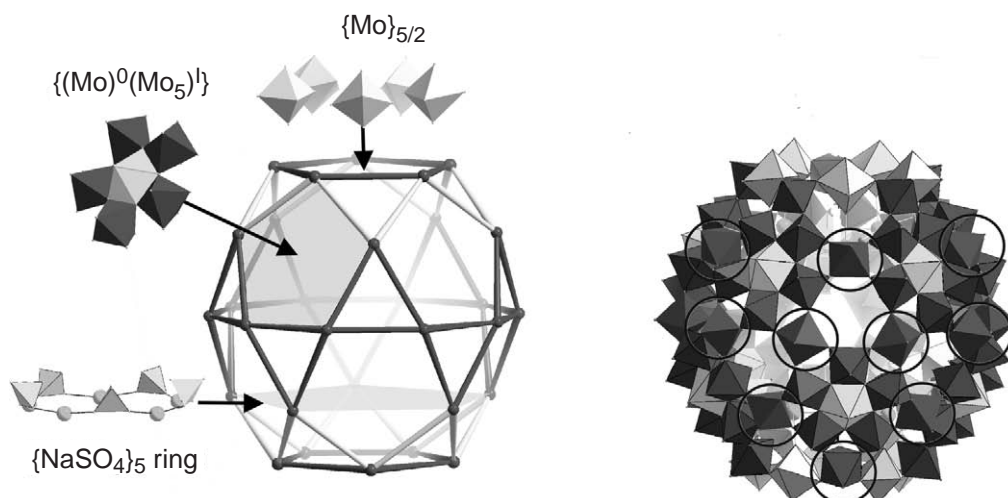


**Figure 68** The basic framework of (74) shown as a distorted icosidodecahedron with 20 triangles and 12 pentagons and the  $\{\text{Na}(\text{SO}_4)_5\}$  is also shown on the LHS. On the RHS a polyhedral representation of the overall cluster is shown. The vanadium centered polyhedra are shown by the black circles and the pentagonal centers of the  $\{\text{Mo}(\text{Mo})_5\}$  units are shown by the light gray polyhedra; the other polyhedra are the five appended Mo atoms of the  $\{\text{Mo}(\text{Mo})_5\}$  unit.

( $x = 70$ ) (74) precipitates when the electrolyte concentration is high enough. This anionic cluster has a barrel shape, being ca. 23 Å high and ca. 25 Å in diameter and is best described with reference to a distorted icosidodecahedron formed by 20 triangular and 12 pentagonal faces built up by  $\text{Mo}^{\text{VI}}$  and 20  $\text{V}^{\text{IV}}$  centers, see Figure 68. Ten triangles spanned by 20  $\text{V}^{\text{IV}}$  centers form an unusual equatorial magnetic ring shaped band. The remaining 10 triangles above and below this equatorial band, each formed by one  $\text{V}^{\text{IV}}$  and two  $\text{Mo}^{\text{VI}}$  centers, complete the (distorted) icosidodecahedron. Ten of the 12 pentagonal faces, each formed by one  $\text{Mo}^{\text{VI}}$  and four  $\text{V}^{\text{IV}}$  centers, are capped by a  $\{\text{Mo}(\text{Mo})_5\}$  pentagonal unit.<sup>182</sup>

#### 7.1.4.7.7 Formation of solid-state structures with $\{\text{Mo}_{72}\text{Fe}_{30}\}$

The solid-state chemistry based upon the spherically shaped Keplerate clusters is versatile. In crystals of the  $\{\text{Mo}_{132}\}$ -type species (space group  $Fm\bar{3}$ ), the spheres are ordered according to the cubic closed packing scheme.<sup>63</sup> This packing, similar to hard spheres, is simply due to the spherical shape of the cluster's van der Waals surface. In contrast, in the case of a monoclinic crystal modification of the functionalized Keplerate system  $\{\text{Mo}_{72}\text{Fe}_{30}\}$ ,<sup>181</sup> distinct solid-state reactions, i.e., the linking of these icosahedral spherical clusters to layers, can take place even at room temperature. During the dehydration process of crystals comprising  $\{\text{Mo}_{72}\text{Fe}_{30}\}$  units, crystal water molecules are expelled in a first, slow step and the cluster shells approach each other until a minimum distance between the  $\text{Fe}-\text{OH}_2\cdots\text{H}_2\text{O}-\text{Fe}$  groups (on adjacent clusters) is reached (Figure 69). This first step is followed by a second, faster one in which a condensation reaction takes place at four Fe sites on each cluster unit to produce a linked cluster, (75). This reaction mechanism is known for the formation of inorganic polycations at low activation energies.

This reaction finally results in a two-dimensional grid structure found in the compound  $[\text{H}_4\text{Mo}_{72}\text{Fe}_{30}\text{O}_{254}(\text{CH}_3\text{COO})_{10}\{\text{Mo}_2\text{O}_7(\text{H}_2\text{O})\}\{\text{H}_2\text{Mo}_2\text{O}_8(\text{H}_2\text{O})\}_3(\text{H}_2\text{O})_{87}] \cdot \text{ca. } 80 \text{ H}_2\text{O}$ . The four  $\text{Fe}-\text{O}-\text{Fe}$  links ( $\text{Fe}-\text{Fe} = 3.79 \text{ \AA}$ ) interconnect each cluster unit with four neighboring shells.<sup>42</sup> This also leads to a decrease of the effective magnetic moment from nearly 30 uncoupled  $\text{Fe}(\text{III})$  centers to approximately 26 uncoupled  $\text{Fe}(\text{III})$  centers as the iron centers of the nearly linear  $\text{Fe}-\text{O}-\text{Fe}$  groups are strongly coupled. This situation is typical for structurally similar (linear)  $(\mu\text{-O})\text{Fe}_2$  complexes.<sup>183</sup>

It is possible to isolate the intermediate compound containing the spherical clusters as discrete entities:  $[\text{Mo}_{72}\text{Fe}_{30}\text{O}_{252}(\text{CH}_3\text{COO})_{10}\{\text{Mo}_2\text{O}_7(\text{H}_2\text{O})\}\{\text{H}_2\text{Mo}_2\text{O}_8(\text{H}_2\text{O})\}_3(\text{H}_2\text{O})_{91}] \cdot \text{ca. } 100 \text{ H}_2\text{O}$  ( $\text{Fe}-\text{Fe} = 5.35 \text{ \AA}$ ), which crystallizes in the same space group ( $P2_1/n$ ) as the freshly prepared precipitated compound, before the dehydration (drying) process. In this compound the short



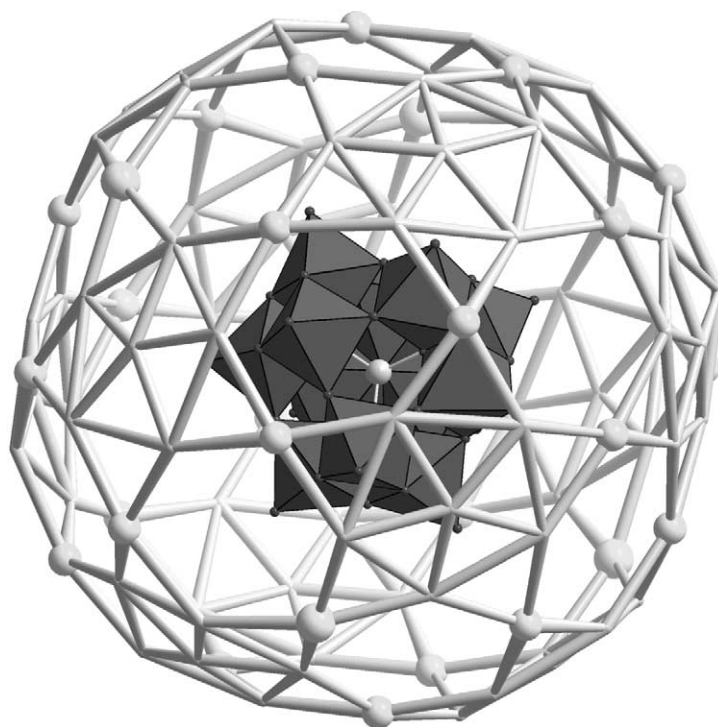


**Figure 70** A representation of the crystal structure of  $\{\text{PMo}_{12}\}_{\text{C}_{132}}$  (**76**). A wireframe representation of the  $\{\text{Mo}_{72}\text{Fe}_{30}\}$  cluster shell is shown with a polyhedral representation of the encapsulated Keggin ion.

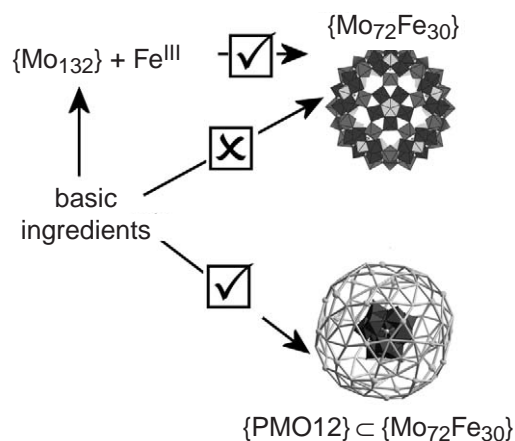


**Figure 71** A schematic showing the reaction processes leading to the  $\{\text{PMo}_{12}\}_{\text{C}_{132}}$  and  $\{\text{Mo}_{72}\text{Fe}_{30}\}$ . The molecular hostage complex can be synthesized directly from the most basic units but the empty  $\{\text{Mo}_{72}\text{Fe}_{30}\}$  cluster must be synthesized from the  $\{\text{Mo}_{132}\}$  cluster. These observations strongly suggest a role for the Keggin ion as a template to assemble the outer sphere.

#### 7.1.4.8 $\{\text{Mo}_{368}\}$ Clusters: a Hybrid Between Wheel- and Ball-shaped clusters

In a very recent result, Müller *et al.*<sup>1</sup> have reported the largest molecular cluster to be characterized by single crystal X-ray diffraction to date. In this case the molybdenum oxide based nanocluster is the size of hemoglobin, with an approximate diameter of 6 nm, and contains 368 metal (1,880 nonhydrogen) atoms formed by the linking of 64  $\{\text{Mo}_1\}$ -, 32  $\{\text{Mo}_2\}$ -, and 40  $\{\text{Mo}(\text{Mo}_5)\}$ -type units with the formula  $[\text{H}_x\text{Mo}_{368}\text{O}_{1032}(\text{H}_2\text{O})_{240}(\text{SO}_4)_{48}]^{48-}$  (**78**). Once again, the role of the pentagonal  $\{\text{Mo}(\text{Mo}_5)\}$  units in creating a curved surface cannot be overstated. The overall structure of the cluster is unprecedented, insofar as it incorporates two oppositely curved surfaces, i.e., a positive surface that goes through an inflexion point to a negative surface. The result is a cluster that resembles the shape of a lemon, see [Figure 73](#).

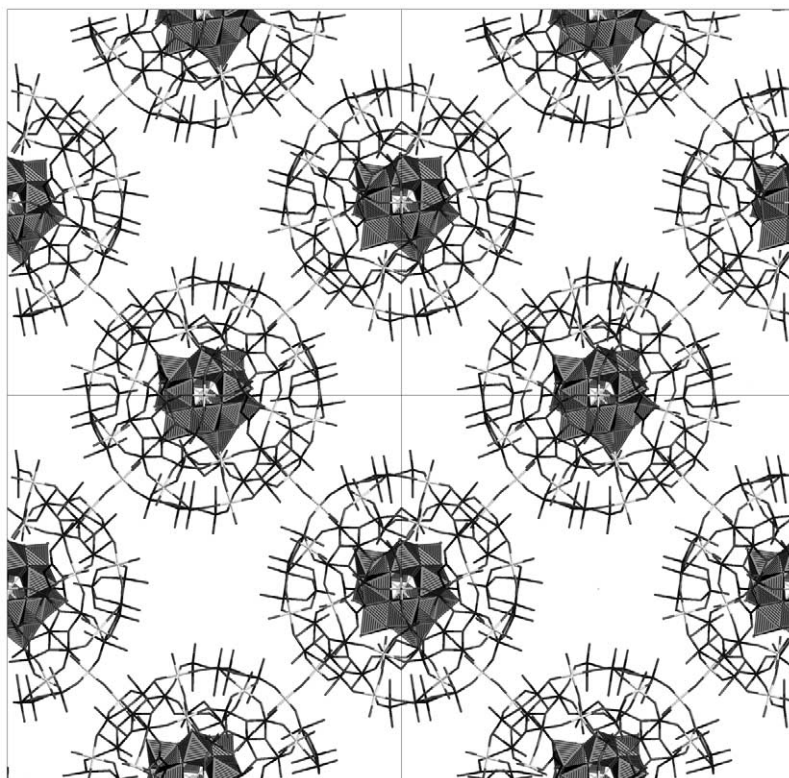


**Figure 72** Schematic structural representation of a layer of the two-dimensional network of (77) with the outer case,  $\{\text{Mo}_{72}\text{Fe}_{30}\}$  shown as a wire frame and the encapsulated Keggin ion shown as a polyhedral representation.

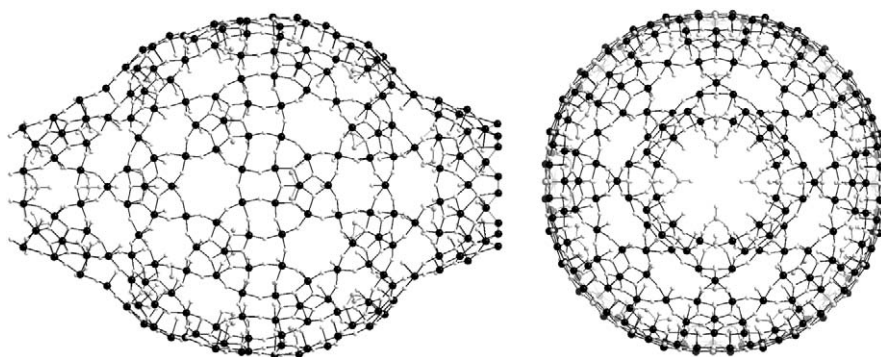


**Figure 73** A ball and stick representation of the structure of the  $\{\text{Mo}_{368}\}$  cluster; the molybdenum atoms are shown as black spheres, the oxygen atoms as white spheres and the sulfur atoms of the sulfate groups (inside the sphere) are shown as gray spheres. A side view is shown on the LHS, which shows the longest dimension of the cluster, being ca. 54 Å and a height of ca. 37 Å. A top view is shown on the RHS, which shows the opening at the top of the cluster of ca. 14 Å.

In terms of building blocks the  $\{\text{Mo}_{368}\}$  can be described as  $[\text{H}_x\{\text{Mo}(\text{Mo}_5)\}'_8\{\text{Mo}(\text{Mo}_5)\}''_{32}\{\text{Mo}_2\}'_{16}\{\text{Mo}_2\}''_8\{\text{Mo}_2\}'''_8\{\text{Mo}_1\}_{64}]^{48-}$  and has an approximate  $D_4$  symmetry with a central ball-shaped fragment,  $\{\text{Mo}_{288}\text{O}_{784}(\text{H}_2\text{O})_{192}(\text{SO}_4)_{32}\}$ , and two capping units,  $\{\text{Mo}_{40}\text{O}_{124}(\text{H}_2\text{O})_{24}(\text{SO}_4)_8\}$ , see Figure 74. Interestingly, there are three rather large areas, with different local symmetries:  $D_{8d}$  in the central part and  $C_{4v}$  in the two capping areas (Figure 74). The presence of the bidentate  $\text{SO}_4^{2-}$  appears to allow the construction of this cluster, the coordination type of the  $\text{SO}_4^{2-}$  ligands: 40 with  $\text{SO}_4^{2-}$  ligands and eight without located in the  $C_{4v}$  areas. The dinuclear units  $\{\text{Mo}_2\}$  not only differ with respect to the number of bidentate  $\text{SO}_4^{2-}$  ligands but also, for those at the ends of both caps, that is, the borderlines, both Mo centers have two terminal O

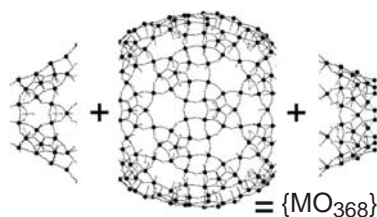


**Figure 74** Ball and stick representation of the  $\{\text{Mo}_{368}\}$  split into the three distinct units, the central cylinder and the two caps, all of which have different local symmetries.

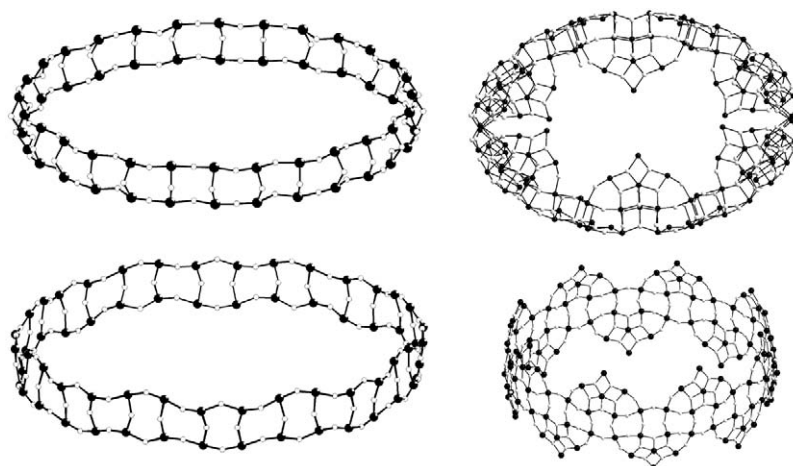


**Figure 75** Comparison of the equator frameworks of the  $\{\text{Mo}_{154}\}$  wheel (top section) and  $\{\text{Mo}_{368}\}$ -type clusters (bottom section). The equator associated with the  $\{\text{Mo}_{368}\}$  appears to be more corrugated than that of the wheel but the pentagonal units associated with the equator rim (bottom RHS) rise more closely to the vertical, perpendicular to the plane dissecting the equator than those of the wheel (top RHS).

atoms in a situation characteristic for stopping growth. The  $\{\text{Mo}_1\}$  units are of the classical type  $\{\text{OMo}^{\text{V}}(\text{H}_2\text{O})\}^{3+}$  and contribute correspondingly to the highly reduced state of (78). The other formally  $\text{Mo}^{\text{V}}$ -type centers are distributed over several parts of the cluster areas, which causes a widespread delocalization of the Mo 4d electrons.

The structure of (78) can be considered as a hybrid between the Giant-Wheel ( $\{\text{Mo}_{154}\}$ -type/ $\{\text{Mo}_{176}\}$ -type) and ball ( $\{\text{Mo}_{102}\}$ -type) clusters.<sup>187</sup> Examination of these two clusters and comparison with the  $\{\text{Mo}_{368}\}$  cluster is revealing; the  $\{\text{Mo}(\text{Mo}_5)\}$  and  $\{\text{Mo}_1\}$  units of the  $\{\text{Mo}_{102}\}$  ball-type cluster as well as  $\{\text{Mo}(\text{Mo}_5)\}$  and  $\{\text{Mo}_2\}$  units of the wheel-type species are all present in (78). In addition, this cluster has a definable equator, the framework of which can be compared to that of the wheel-shaped cluster, see Figure 75.

The high reduction state (ca. 112  $\text{Mo}^{\text{V}}$ , 256  $\text{Mo}^{\text{VI}}$ ), which is much higher than that in the wheel systems (e.g., 28  $\text{Mo}^{\text{V}}$ , 126  $\text{Mo}^{\text{VI}}$ ) seems to confirm the importance of  $\text{Mo}^{\text{V}}$  centers in the construction of clusters displaying extraordinary structural versatility. The  $\{\text{Mo}_{368}\}$  cluster is synthesized by reducing a solution of molybdate with  $\text{Na}_2\text{S}_2\text{O}_4$  acidified with  $\text{H}_2\text{SO}_4$ . It is important to note that this cluster appears to be constructed at higher reducing values, ca. 30%, i.e., 30% of the total number of the Mo centers in  $\{\text{Mo}_{368}\}$  cluster are  $\text{Mo}^{\text{V}}$  compared with 18–20% in the  $\{\text{Mo}_{154}/\text{Mo}_{176}\}$  clusters, 45% in the Keplerate  $\{\text{Mo}_{132}\}$ , and 35% in the  $\{\text{Mo}_{102}\}$  ball.

#### 7.1.4.9 Building Block Principles

In this section, high nuclearity clusters with sizes ranging from that of a normal molecule to a size approaching that of a small protein are described. A common theme that links all these systems is that almost all of these molecules can be synthesized under one-pot reaction conditions. Even more strikingly, these conditions need only to be adjusted in one or two respects to encourage

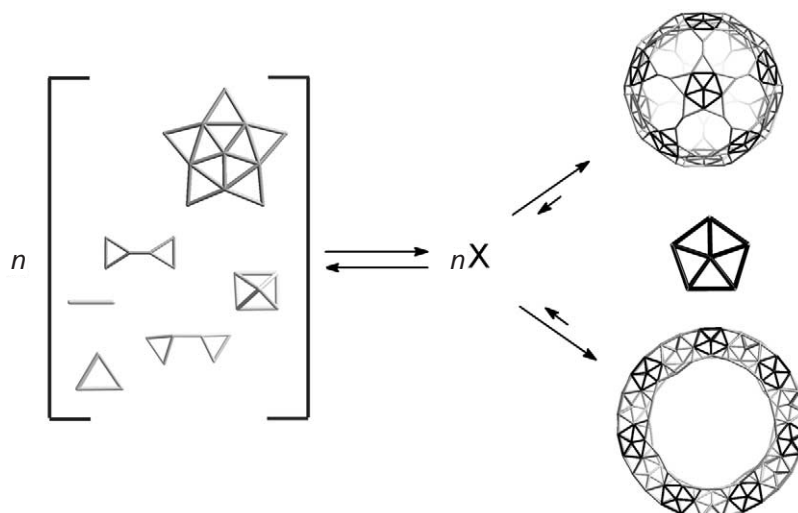


**Figure 76** A schematic showing the potential for many types of polyoxometalate building blocks in solution with the pentagon-based units forming closed units (and therefore more difficult to decompose, all things being equal, than a cluster system that had well defined edges and corners). On the LHS the vast number of hypothesized different building units present in solution, along with the pentagonal units are shown. Then our hypothesized equilibrium between these units and various clusters in solution is shown. Finally on the RHS the clusters with pentagonal building blocks with closed geometries are depicted with an equilibrium which is in favor of the close-spherical/ring-shaped cluster system.

growth of, for example, a  $\{\text{Mo}_{368}\}$  cluster rather than a  $\{\text{Mo}_{36}\}$  cluster (in this case the addition of reducing agent and a ligand). In the case of polyoxomolybdates chemistry, the use of pentagonal-type building groups, with different symmetries, plays a key role in the synthesis of these systems. This can be taken further by considering that edge-sharing (condensed) pentagons cannot be used to tile an infinite plane,<sup>188</sup> whereas exactly 12 pentagons are required, in connection with well-defined sets of hexagons, to construct spherical systems such as that observed in the truncated icosahedron—the most spherical Archimedean solid—in polyhedral viruses, or in the geodesic Buckminster–Fuller domes.<sup>189</sup> Therefore the use of pentagonal building blocks is absolutely essential in chemistry for the production of curved species—the paradigm of which is  $\text{C}_{60}$ .

However, the question of exactly why these cluster systems were discovered at all still remains. This can be highlighted by considering the simplicity of the constituent building blocks and, therefore, the literally hundreds, maybe thousands, of condensed metal oxygen fragments with varying charges and symmetries that could exist in a solution of partly reduced molybdate at certain pH values. To answer this question we must consider a solution with many hundreds of different types of linkable units present with smaller building block species in equilibrium with large species (it should be noted that in polyoxomolybdate chemistry this equilibrium is attained in a matter of minutes or hours).

Perhaps the answer can be found in the fact that the pentagonal unit facilitates the formation of a curved geometrical system with no edges. However, when one considers the formation of rigid pentagonal units in solution and the reaction through to the product, one can see that a closed cluster with no edges is uniformly reactive and, therefore, harder to decompose (if it is rigid) than a cluster with many edges and no rigidity. In summary, the combination of rigid units with pentagonal symmetry may result in many hundreds of species, but it is likely that only the structurally uniform, most stable species are likely to crystallize. In this way the equilibrium can be pushed towards the precipitation of closed geometrical systems with no edges, i.e., clusters with ring or spherical topology. This hypothesis is summarized in Figure 76.

### 7.1.5 OUTLOOK

In recent years there has been an unprecedented increase in the number of interesting polyoxometalate clusters that have been structurally characterized by single crystal X-ray crystallography and, of course, the absolute size of the molecules characterized. Indeed, the elucidation of the



structure of the  $\{\text{Mo}_{368}\}$  represents the largest nonbiologically derived macromolecule to be structurally characterized to date and there is no reason to suppose that the discoveries in this area will stop at this nuclearity.<sup>1</sup>

Polyoxometalates, with all their relevance to catalysis, reactivity, electronic structure, materials science, and medicine are set to become a paradigm for those working in nanoscience. This is because the polyoxometalate clusters described here are ideal candidates for the development of a new type of supramolecular chemistry based upon the building-block ideas already established. Using these ideas it should be possible to work towards designer nanomolecules of ever increasing size and complexity.<sup>190–192</sup> Such clusters, for instance, are being proposed for the design of molecular magnets<sup>17</sup> that could behave as super-paramagnets and electron storage devices that could be used in molecular electronics. Maybe such systems could be used to probe and even discover new physics at the quantum classical limit or examine molecular growth processes.<sup>168</sup> In addition, researchers could begin to answer the fundamental questions about the self-assembly processes that underpin the creation of such structures and ask what influence could our concept of building geometrical and real building blocks have in the design of these molecules.<sup>60</sup> If we are able to devise some rules for cluster design then it may be possible to design new types of molecular host-guest complexes that could be used in information storage or even in light-harvesting systems, as well as potential applications as robust sequestering agents. For example, there is the potential to design polyoxometalate clusters that can selectively assemble into a given structural type in the presence of the ion to be sequestered, e.g., actinide ions to give a system for sequestering radioactive elements. The design/discovery of polyoxometalate nanotubes and junctions would also be an important aspect and provide an interesting alternative to the carbon-based analogues.<sup>193</sup> Whatever the future, one thing is sure—that researchers will be captivated and motivated by the beauty and complexity of polyoxometalate structures that will be discovered during the coming years.

## ACKNOWLEDGMENTS

I would like to thank Professor A. Müller for introducing me to polyoxometalate chemistry and Dr. D. Long for proof-reading and helpful comments.

## 7.1.6 REFERENCES

1. Müller, A.; Beckmann, E.; Bögge, H.; Schmidtman, M.; Dress, A. *Angew. Chem., Int. Ed.* **2002**, *41*, 1162–1167.
2. Al-Zahrani, S. M.; Jibril, B. Y.; Abasaeed, A. E. *J. Mol. Catal. A, Chem.* **2001**, *175*, 259–265.
3. Comuzzi, C.; Dolcetti, G.; Trovarelli, A.; Cavani, F.; Trifiro, F.; Llorca, J.; Finke, R. G. *Catal. Lett.* **1996**, *36*, 75–79.
4. Hu, C. W.; He, Q. L.; Zhang, Y. H.; Liu, Y. Y.; Zhang, Y. F.; Tang, T. D.; Zhang, J. Y.; Wang, E. B. *Chem. Commun.* **1996**, 121–122.
5. Indovina, V.; Occhiuzzi, M.; Ciambelli, P.; Sannino, D.; Ghiotti, G.; Prinetto, F. *11th Int. Cong. Catal.—40th Ann., Parts A and B* **1996**, *101*, 691–700.
6. MoroOka, Y.; Ueda, W. *Adv. Catal.* **1994**, *40*, 233–273.
7. Pozniczek, J.; Bielanski, A.; Kulszewiczbajer, I.; Zagorska, M.; Kruczala, K.; Dyrek, K.; Pron, A. *J. Mol. Catal.* **1991**, *69*, 223–233.
8. Sadakane, M.; Steckhan, E. *J. Mol. Catal. A, Chem.* **1996**, *114*, 221–228.
9. Weiner, H.; Finke, R. G. *J. Am. Chem. Soc.* **1999**, *121*, 9831–9842.
10. Yang, X. Y.; Xia, X. Q.; Wu, N. Z. *Chin. J. Catal.* **2001**, *22*, 358–360.
11. Yang, Y. L.; Guo, Y. H.; Wang, Y. H.; Hu, C. W.; Wang, E. B.; Feng, S. H. *Prog. Nat. Sci.* **2002**, *12*, 153–157.
12. Zhang, X.; Sasaki, K.; Hill, C. L. *J. Am. Chem. Soc.* **1996**, *118*, 4809–4816.
13. Zhang, X. Y.; Pope, M. T. *J. Mol. Catal. A, Chem.* **1996**, *114*, 201–208.
14. Xiang, D. F.; Tan, X. S.; Zhang, S. W.; Han, Y.; Yu, K. B.; Tang, W. X. *Polyhedron* **1998**, *17*, 2095–2100.
15. Aebersold, M.; Andres, H. P.; Buttner, H.; BorrásAlmenar, J. J.; Clemente, J. M.; Coronado, E.; Gudel, H. U.; Kearley, D. *Physica B* **1997**, *234*, 764–765.
16. Chiorescu, I.; Wernsdorfer, W.; Müller, A.; Bögge, H.; Barbara, B. *J. Magn. Magn. Mater.* **2000**, *221*, 103–109.
17. Clemente-Juan, J. M.; Coronado, E. *Coord. Chem. Rev.* **1999**, *195*, 361–394.
18. Dhaussy, A. C.; Abraham, F.; Mentre, O.; Steinfink, H. *J. Solid State Chem.* **1996**, *126*, 328–335.
19. Gatteschi, D.; Pardi, L. *Mol. Cryst. Liq. Cryst.* **1993**, *232*, 577–590.
20. Müller, A.; Beugholt, C.; Kögerler, P.; Bögge, H.; Bud'ko, S.; Luban, M. *Inorg. Chem.* **2000**, *39*, 5176–5177.
21. Müller, A.; Kögerler, P.; Dress, A. W. M. *Coord. Chem. Rev.* **2001**, *222*, 193–218.
22. Müller, A.; Luban, M.; Schroder, C.; Modler, R.; Kögerler, P.; Axenovich, M.; Schnack, J.; Canfield, P.; Bud'ko, S.; Harrison, N. *Chem. Phys. Chem* **2001**, *2*, 517–520.
23. Wei, Y. G.; Zhang, S. W.; Shao, M. C.; Tang, Y. Q. *Polyhedron* **1997**, *16*, 1471–1475.
24. Volkmer, D.; Du Chesne, A.; Kurth, D. G.; Schnablegger, H.; Lehmann, P.; Koop, M. J.; Müller, A. *J. Am. Chem. Soc.* **2000**, *122*, 1995–1998.

25. Apblett, A. W.; Reinhardt, L. E. *Abstr. Pap. Am. Chem. Soc.* **1996**, 212, 259.
26. Coronado, E.; GalanMascaros, J. R.; GimenezSaiz, C.; GomezGarcia, C. J.; Laukhin, V. N. *Adv. Mater.* **1996**, 8, 801–811.
27. Evans, J.; Pillinger, M.; Zhang, J. J. *J. Chem. Soc., Dalton Trans.* **1996**, 2963–2974.
28. Nazar, L. F.; Koene, B. E.; Britten, J. F. *Chem. Mater.* **1996**, 8, 327–329.
29. Coronado, E.; Gomez-Garcia, C. J. *Chem. Rev.* **1998**, 98, 273–296.
30. Livage, J.; Bouhedja, L.; Bonhomme, C. J. *Sol-Gel Sci. Technol.* **1998**, 13, 65–70.
31. Vaidhyanathan, B.; Balaji, K.; Rao, K. J. *Chem. Mater.* **1998**, 10, 3400–3404.
32. Barton, T. J.; Bull, L. M.; Klemperer, W. G.; Loy, D. A.; McEnaney, B.; Misono, M.; Monson, P. A.; Pez, G.; Scherer, G. W.; Vartuli, J. C.; Yaghi, O. M. *Chem. Mater.* **1999**, 11, 2633–2656.
33. Duraisamy, T.; Ojha, N.; Ramanan, A.; Vittal, J. J. *Chem. Mater.* **1999**, 11, 2339–2349.
34. LaDuca, R. L.; Finn, R.; Zubieta, J. *Chem. Commun.* **1999**, 1669–1670.
35. Cronin, L.; Kögerler, P.; Müller, A. J. *Solid State Chem.* **2000**, 152, 57–67.
36. Kurth, D. G.; Lehmann, P.; Volkmer, D.; Müller, A.; Schwahn, D. *J. Chem. Soc., Dalton Trans.* **2000**, 3989–3998.
37. Kurth, D. G.; Volkmer, D.; Ruttorf, M.; Richter, B.; Müller, A. *Chem. Mater.* **2000**, 12, 2829–2832.
38. LaDuca, R. L.; Desciak, M.; Laskoski, M.; Rarig, R. S.; Zubieta, J. *J. Chem. Soc., Dalton Trans.* **2000**, 2255–2257.
39. Law, T. S. C.; Sung, H. H. Y.; Williams, I. D. *Inorg. Chem. Commun.* **2000**, 3, 420–423.
40. Mayer, C. R.; Thouvenot, R.; Lalot, T. *Chem. Mater.* **2000**, 12, 257–263.
41. Muhr, H. J.; Krumeich, F.; Schonholzer, U. P.; Bieri, F.; Niederberger, M.; Gauckler, L. J.; Nesper, R. *Adv. Mater.* **2000**, 12, 231–235.
42. Müller, A.; Das, S. K.; Krickemeyer, E.; Kögerler, P.; Booge, H.; Schmidtman, M. *Solid State Sci.* **2000**, 2, 847–854.
43. Zeng, H. D.; Newkome, G. R.; Hill, C. L. *Angew. Chem., Int. Ed.* **2000**, 39, 1772–1775.
44. Ito, T.; Inumaru, K.; Misono, M. *Chem. Mater.* **2001**, 13, 824–831.
45. Johnson, B. J. S.; Schroden, R. C.; Zhu, C. C.; Stein, A. *Inorg. Chem.* **2001**, 40, 5972–5978.
46. Liu, T. B.; Wan, Q.; Xie, Y.; Burger, C.; Liu, L. Z.; Chu, B. *J. Am. Chem. Soc.* **2001**, 123, 10966–10972.
47. Murakami, H.; Kozeki, T.; Suzuki, Y.; Ono, S.; Ohtake, H.; Sarukura, N.; Ishikawa, E.; Yamase, T. *Appl. Phys. Lett.* **2001**, 79, 3564–3566.
48. Cheng, L.; Cox, J. A. *Chem. Mater.* **2002**, 14, 6–10.
49. Devi, R. N.; Zubieta, J. *Inorg. Chim. Acta* **2002**, 332, 72–78.
50. Liu, S. Q.; Kurth, D. G.; Mohwald, H.; Volkmer, D. *Adv. Mater.* **2002**, 14, 225–230.
51. Wang, Y. H.; Wang, X. L.; Hu, C. W.; Shi, C. S. *J. Mater. Chem.* **2002**, 12, 703–707.
52. Tourne, G. F.; Tourne, C. M. In *Polyoxometalates: from Platonic Solids to Anti-retroviral Activity*; Pope, M. T., Müller A., Eds.; Kluwer: Dordrecht, The Netherlands, 1994, 1–414.
53. Fukuma, M.; Seto, Y.; Yamase, T. *Antiviral Res.* **1991**, 16, 327–339.
54. Judd, D. A.; Nettles, J. H.; Nevins, N.; Snyder, J. P.; Liotta, D. C.; Tang, J.; Ermolieff, J.; Schinazi, R. F.; Hill, C. L. *J. Am. Chem. Soc.* **2001**, 123, 886–897.
55. Pope, M. T.; Müller, A. *Angew. Chem., Int. Ed. Engl.* **1991**, 30, 34–48.
56. Pope, M. T. *Heteropoly and Isopoly Oxometalates*; Springer-Verlag: Berlin, 1983.
57. Pope, M. T. *Comprehensive Coordination Chemistry: Isopolyanions and Heteropolyanions*; Wilkinson, G., Gillard, R. D., McCleverty, J. A., Eds.; Pergamon Press, 1987; Vol. 3, 1023–1057.
58. Müller, A.; Kögerler, P.; Kuhlmann, C. *Chem. Commun.* **1999**, 1347–1358.
59. Müller, A.; Kögerler, P.; Bögge, H. *Mol. Self-assembly* **2000**, 96, 203–236.
60. Cronin, L. In *Inorganic Chemistry Highlights: The Potential of Pentagonal Building Blocks: From Giant Ring-shaped to Spherical Polyoxometallate Cluster*. Wiley: Weinheim, Germany 2002, 113–121.
61. Wassermann, K.; Dickman, M. H.; Pope, M. T. *Angew. Weinheim, Germany Chem., Int. Ed. Engl.* **1997**, 36, 1445–1448.
62. Müller, A.; Krickemeyer, E.; Meyer, J.; Bögge, H.; Peters, F.; Plass, W.; Diemann, E.; Dillinger, S.; Nonnenbruch, F.; Randerath, M.; Menke, C. *Angew. Chem., Int. Ed. Engl.* **1995**, 34, 2122–2124.
63. Müller, A.; Krickemeyer, E.; Bögge, H.; Schmidtman, M.; Peters, F. *Angew. Chem., Int. Ed.* **1998**, 37, 3360–3363.
64. Klemperer, W. G.; Marquart, T. A.; Yaghi, O. M. *Angew. Chem., Int. Ed. Engl.* **1992**, 31, 49–51.
65. Müller, A.; Reuter, H.; Dillinger, S. *Angew. Chem., Int. Ed. Engl.* **1995**, 34, 2328–2361.
66. Müller, A.; Penk, M.; Krickemeyer, E.; Bögge, H.; Walberg, H. J. *Angew. Chem., Int. Ed. Engl.* **1988**, 27, 1719–1721.
67. Hayashi, Y.; Fukuyama, K.; Takatera, T.; Uehara, A. *Chem. Lett.* **2000**, 770–771.
68. Day, V. W.; Klemperer, W. G.; Yaghi, O. M. *J. Am. Chem. Soc.* **1989**, 111, 5959–5961.
69. Khan, M. I.; Zubieta, J. *Angew. Chem., Int. Ed.* **1994**, 33, 760.
70. Priebisch, W.; Rehder, D.; von Oeynhausen, M. *Chem. Ber.* **1991**, 124, 761.
71. Huan, G.; Jacobsen, A. J.; Day, V. W. *Angew. Chem., Int. Ed.* **1991**, 30, 422.
72. Heinrich, D. D.; Foltling, K.; Streib, W. E.; Huffman, J. C.; Christou, G. *J. Chem. Soc., Chem. Commun.* **1989**, 1411.
73. Müller, A.; Krickemeyer, E.; Penk, M.; Rohlfing, R.; Armatage, A.; Bögge, H. *Angew. Chem., Int. Ed. Engl.* **1991**, 30, 1674–1677.
74. Khan, M. I.; Lee, Y. S.; O'Connor, C. J.; Haushalter, R. C.; Zubieta, J. *J. Am. Chem. Soc.* **1994**, 116, 4525.
75. Haushalter, R. C.; Wang, Z.; Thompson, M. E.; Zubieta, J.; O'Connor, C. J. *Inorg. Chem.* **1993**, 32, 3966.
76. Soghomonian, V.; Chen, Q.; Haushalter, R. C.; Zubieta, J. *Angew. Chem., Int. Ed. Engl.* **1993**, 32, 610.
77. Lonroth, P.; Eriksson, J. W.; Posner, B. I.; Smith, U. *Diabetologia* **1993**, 36, 113–116.
78. Goldfine, A. B.; Simonson, D. C.; Folli, F.; Patti, E.; Kahn, C. R. *Mol. Cell. Biochem.* **1995**, 153, 217–231.
79. Anonymous, *Chem. Br.* **1988**, 24, 754–755.
80. King, R. B. *Theochem, J. Mol. Struct.* **1995**, 336, 165–174.
81. Menke, C.; Diemann, E.; Müller, A. *J. Mol. Struct.* **1997**, 437, 35–47.
82. Müller, A.; Doring, J. Z. *Anorg. Allg. Chem.* **1991**, 595, 251–274.
83. Müller, A.; Rohlfing, R.; Barra, A. L.; Gatteschi, D. *Adv. Mater.* **1993**, 5, 915–917.
84. Müller, A.; Peters, F.; Pope, M. T.; Gatteschi, D. *Chem. Rev.* **1998**, 98, 239–271.
85. Ueda, Y. *Chem. Mater.* **1998**, 10, 2653–2664.
86. Chiang, M. H.; Huffman, J. C.; Streib, W. E.; Bollinger, J.; Christou, G. *Abstr. Pap. Am. Chem. Soc.* **1999**, 217, 290.

87. Gatteschi, D.; Pardi, L.; Barra, A. L.; Müller, A. *Mol. Eng.* **1993**, *3*, 157–169.
88. Gatteschi, D.; Tsukerblat, B. S.; Fainzilberg, V. E. *Appl. Magn. Reson.* **1996**, *10*, 217–249.
89. Lin, B. Z.; Liu, S. X. *J. Chem. Soc., Dalton Trans.* **2002**, 865–869.
90. Livage, J. *Coord. Chem. Rev.* **1998**, *180*, 999–1018.
91. Day, V. W.; Klemperer, W. G.; Yaghi, O. M. *Abstr. Pap. Am. Chem. Soc.* **1989**, *197*, 320.
92. Müller, A.; Penk, M.; Doring, J. *Inorg. Chem.* **1991**, *30*, 4935–4939.
93. Barra, A. L.; Gatteschi, D.; Tsukerblat, B. S.; Doring, J.; Müller, A.; Brunel, L. C. *Inorg. Chem.* **1992**, *31*, 5132–5134.
94. Brown, I. D.; Kang, K. W. *Acta Crystallogr. Sect. B, Struct. Commun.* **1976**, *B32*, 1957–1958.
95. Müller, A.; Doring, J.; Bögge, H. *J. Chem. Soc., Chem. Commun.* **1991**, 273–274.
96. Gatteschi, D.; Tsukerblat, B.; Barra, A. L.; Brunel, L. C.; Müller, A.; Doring, J. *Inorg. Chem.* **1993**, *32*, 2114–2117.
97. Müller, A.; Rohlfing, R.; Krickemeyer, E.; Bögge, H. *Angew. Chem., Int. Ed. Engl.* **1993**, *32*, 909–912.
98. Klemperer, W. G.; Marquart, T. A.; Yaghi, O. M. *Mater. Chem. Phys.* **1991**, *29*, 97–104.
99. Kawanami, N.; Ozeki, T.; Yagasaki, A. *J. Am. Chem. Soc.* **2000**, *122*, 1239–1240.
100. Winpenney, R. E. P. *J. Chem. Soc., Dalton Trans.* **2002**, 1–10.
101. Müller, A.; Doring, J. *Angew. Chem., Int. Ed. Engl.* **1988**, *27*, 1721–1721.
102. Barra, A. L.; Gatteschi, D.; Pardi, L.; Müller, A.; Doring, J. *J. Am. Chem. Soc.* **1992**, *114*, 8509–8514.
103. Gatteschi, D.; Pardi, L.; Barra, A. L.; Müller, A.; Doring, J. *Nature* **1991**, *354*, 463–465.
104. Yamase, T.; Ohtaka, K. *J. Chem. Soc., Dalton Trans.* **1994**, 2599–2608.
105. Müller, A.; Krickemeyer, E.; Penk, M.; Walberg, H. J.; Bögge, H. *Angew. Chem., Int. Ed. Engl.* **1987**, *26*, 1045–1046.
106. Müller, A.; Sessoli, R.; Krickemeyer, E.; Bögge, H.; Meyer, J.; Gatteschi, D.; Pardi, L.; Westphal, J.; Hovemeier, K.; Rohlfing, R.; Doring, J.; Hellweg, F.; Beugholt, C.; Schmidtman, M. *Inorg. Chem.* **1997**, *36*, 5239–5250.
107. Robin, M. B.; Day, P. *Adv. Inorg. Chem. Radiochem.* **1967**, *10*, 247–248.
108. Müller, A.; Doring, J.; Bögge, H.; Krickemeyer, E. *Chimia* **1988**, *42*, 300–301.
109. Yamase, T.; Suzuki, M.; Ohtaka, K. *J. Chem. Soc., Dalton Trans.* **1997**, 2463–2472.
110. Chirayil, T.; Zavalij, P. Y.; Whittingham, M. S. *Acta Crystallogr. Sect. C, Cryst. Struct. Commun.* **1998**, *54*, 1441–1444.
111. Müller, A. *Nature* **1991**, *352*, 115.
112. Müller, A.; Rohlfing, R.; Doring, J.; Penk, M. *Angew. Chem., Int. Ed. Engl.* **1991**, *30*, 588–590.
113. Shklover, V.; Haibach, T.; Ried, F.; Nesper, R.; Novak, P. *J. Solid State Chem.* **1996**, *123*, 317–323.
114. Baker, L. C. W.; Figgis, J. S. *J. Am. Chem. Soc.* **1970**, *92*, 3794–3795.
115. Weinstock, I. A.; Cowan, J.; Barbuzzi, E. M. G.; Zeng, H.; Hill, C. L. *J. Am. Chem. Soc.* **1999**, *121*, 4608–4617.
116. Teze, A.; Cadot, E.; Beraud, V.; Herve, G. *Inorg. Chem.* **2001**, *40*, 2000–2004.
117. Contant, R.; Thouvenot, R. *Inorg. Chim. Acta* **1993**, *212*, 41–50.
118. Peacock, R. D.; Weakley, T. J. R. *J. Chem. Soc.* **1971**, 1836–1838.
119. Sadakane, M.; Dickman, M. H.; Pope, M. T. *Angew. Chem., Int. Ed.* **2000**, *39*, 2914–2916.
120. Termes, S. C.; Pope, M. T. *Transit. Met. Chem.* **1978**, *3*, 103–105.
121. Sadakane, M.; Ostuni, A.; Pope, M. T. *J. Chem. Soc., Dalton Trans.* **2002**, 63.
122. Müller, A.; Fedin, V. P.; Kuhlmann, C.; Fenske, H. D.; Baum, G.; Bögge, H.; Hauptfleisch, B. *Chem. Commun.* **1999**, 1189–1190.
123. Herve, G.; Michelon, M.; Teze, A. *Inorg. Chem.* **1997**, *36*, 505–509.
124. Tourne, C. M.; Tourne, G. F.; Weakley, T. J. R. *J. Chem. Soc., Dalton Trans.* **1986**, 2237–2242.
125. Fuchs, J.; Palm, R. Z. *Naturforsch* **1984**, *39b*, 757–762.
126. Tourne, C. M.; Tourne, G. F. *J. Chem. Soc., Chem. Dalton Trans.* **1988**, 2411–2420.
127. Weakley, T. J. R. *J. Chem. Soc., Chem. Commun.* **1984**, 1406–1407.
128. Galan-Mascaros, J. R.; Gomez-Garcia, C. J.; Borrás-Almenar, J. J.; Coronado, E. *Adv. Mater.* **1994**, *6*, 221–223.
129. Coronado, E.; Gomez-Garcia, C. J. *Comments Inorg.* **1995**, *17*, 255–256.
130. Yamase, T.; Naruke, H.; Sasaki, Y. *J. Chem. Soc., Dalton Trans.* **1990**, 1687–1696.
131. Jeannin, Y.; Martin-Frere, J. *J. Am. Chem. Soc.* **1981**, *103*, 1664–1667.
132. Jeannin, Y. *J. Cluster Sci.* **1992**, *3*, 55–58.
133. Bosing, M.; Loose, I.; Pohlmann, H.; Krebs, B. *Chem. Eur. J.* **1997**, *3*, 1232–1237.
134. Herve, G.; Teze, A. *Inorg. Synth.* **1990**, *27*, 118–120.
135. Wassermann, K.; Pope, M. T. *Inorg. Chem.* **2001**, *40*, 2763–2768.
136. Contant, R.; Teze, A. *Inorg. Chem.* **1985**, *24*, 4610–4614.
137. Alizadeh, M. H.; Harmalkar, S. P.; Jeannin, Y.; Martin-Frere, J.; Pope, M. T. *J. Am. Chem. Soc.* **1985**, *107*, 2662–2669.
138. Creaser, I.; Heck, M. C.; Neitz, R. J.; Pope, M. T. *Inorg. Chem.* **1993**, *32*, 1573–1578.
139. Antonio, M. R.; Soderholm, L. *Inorg. Chem.* **1994**, *33*, 5988–5993.
140. Soderholm, L.; Liu, G. K.; Muntean, J.; J, M.; Antonio, M. R. *J. Phys. Chem.* **1995**, *99*, 9611–9616.
141. Antonio, M. R.; Soderholm, L. *J. Cluster Sci.* **1996**, *7*, 585–587.
142. Antonio, M. R.; Soderholm, L. *J. Alloys Compd.* **1997**, *250*, 541.
143. Dickman, M. H.; Gama, G. J.; Kim, K. C.; Pope, M. T. *J. Cluster Sci.* **1996**, *7*, 567–573.
144. Harrup, M. K.; Hill, C. L. *Inorg. Chem.* **1994**, *33*, 5448–5455.
145. Topsoe, H.; Clausen, B. S.; Topsoe, N. Y.; Pedersen, E.; Niemann, W.; Müller, A.; Bögge, H.; Lengeler, B. *J. Chem. Soc., Faraday Trans. 1* **1987**, *83*, 2157–2167.
146. Müller, A.; Serain, C. *Accounts Chem. Res.* **2000**, *33*, 2–10.
147. Müller, A.; Meyer, J.; Krickemeyer, E.; Diemann, E. *Angew. Chem., Int. Ed. Engl.* **1996**, *35*, 1206–1208.
148. Chae, H.; Klemperer, W. G.; Marquart, T. A. *Coord. Chem. Rev.* **1993**, *128*, 209–224.
149. Müller, A.; Meyer, J.; Krickemeyer, E.; Beugholt, C.; Bögge, H.; Peters, F.; Schmidtman, M.; Kögerler, P.; Koop, M. *J. Chem., Eur. J.* **1998**, *4*, 1000–1006.
150. Müller, A.; Dillinger, S.; Krickemeyer, E.; Bögge, H.; Plass, W.; Stammeler, A.; Haushalter, R. C. *Z. Naturforsch. (B)* **1997**, *52*, 1301–1306.
151. Müller, A.; Krickemeyer, E.; Dillinger, S.; Bögge, H.; Plass, W.; Proust, A.; Dloczik, L.; Menke, C.; Meyer, J.; Rohlfing, R. *Z. Anorg. Allg. Chem.* **1994**, *620*, 599–619.
152. Zhang, S.-W.; Huang, G.-Q.; Shao, M.-C.; Tang, Y.-Q. *J. Chem. Soc., Chem. Commun.* **1993**, 37–38.

153. Müller, A.; Krickemeyer, E.; Dillinger, S.; Bögge, H.; Proust, A.; Plass, W.; Rohlfing, R. *Naturwissenschaften* **1993**, *80*, 560–564.
154. Müller, A.; Bögge, H.; Krickemeyer, E.; Dillinger, S. *Bull. Pol. Acad. Sci., Chem.* **1994**, *42*, 291–298.
155. Müller, A.; Plass, W.; Krickemeyer, E.; Sessoli, R.; Gatteschi, D.; Meyer, J.; Bögge, H.; Krockel, M.; Trautwein, A. X. *Inorg. Chim. Acta* **1998**, *271*, 9–12.
156. Müller, A.; Das, S. K.; Fedin, V. P.; Krickemeyer, E.; Beugholt, C.; Bögge, H.; Schmidtman, M.; Hauptfleisch, B. *Z. Anorg. Allg. Chem.* **1999**, *625*, 1187–1192.
157. Müller, A.; Beugholt, C.; Koop, M.; Das, S. K.; Schmidtman, M.; Bögge, H. *Z. Anorg. Allg. Chem.* **1999**, *625*, 1960–1962.
158. Müller, A.; Krickemeyer, E.; Bögge, H.; Schmidtman, M.; Beugholt, C.; Das, S. K.; Peters, F. *Chem., Eur. J.* **1999**, *5*, 1496–1502.
159. Bradley, D. *News Scientist* **1995**, *18*, 18.
160. Yamase, T.; Prokop, P. V. *Angew. Chem., Int. Ed.* **2002**, *41*, 466–469.
161. Müller, A.; Krickemeyer, E.; Bögge, H.; Schmidtman, M.; Peters, F.; Menke, C.; Meyer, J. *Angew. Chem., Int. Ed. Engl.* **1997**, *36*, 484–486.
162. Müller, A.; Das, S. K.; Bögge, H.; Beugholt, C.; Schmidtman, M. *Chem. Commun.* **1999**, 1035–1036.
163. Müller, A.; Das, S. K.; Kuhlmann, C.; Bögge, H.; Schmidtman, M.; Diemann, E.; Krickemeyer, E.; Hormes, J.; Modrow, H.; Schindler, M. *Chem. Commun.* **2001**, 655–656.
164. Müller, A.; Maiti, R.; Schmidtman, M.; Bögge, H.; Das, S. K.; Zhang, W. J. *Chem. Commun.* **2001**, 2126–2127.
165. Müller, A.; Krickemeyer, E.; Bögge, H.; Schmidtman, M.; Kögerler, P.; Rosu, C.; Beckmann, E. *Angew. Chem., Int. Ed.* **2001**, *40*, 4034–4038.
166. Müller, A.; Krickemeyer, E.; Bögge, H.; Schmidtman, M.; Beugholt, C.; Kögerler, P.; Lu, C. Z. *Angew. Chem., Int. Ed.* **1998**, *37*, 1220–1223.
167. Jiang, C. C.; Wei, Y. G.; Liu, Q.; Zhang, S. W.; Shao, M. C.; Tang, Y. Q. *Chem. Commun.* **1998**, 1937–1938.
168. Müller, A.; Shah, S. Q. N.; Bögge, H.; Schmidtman, M. *Nature* **1999**, *397*, 48–50.
169. Cotton, F. A.; Wilkinson, G. *Advanced Inorganic Chemistry*; 4th ed.; John Wiley: New York, 1980.
170. Müller, A.; Koop, M.; Bögge, H.; Schmidtman, M.; Beugholt, C. *Chem. Commun.* **1998**, 1501–1502.
171. Müller, A.; Beugholt, C.; Bögge, H.; Schmidtman, M. *Inorg. Chem.* **2000**, *39*, 3112–3114.
172. Cronin, L.; Beugholt, C.; Müller, A. *J. Mol. Struct. Theochem* **2000**, *500*, 181–193.
173. Cronin, L.; Beugholt, C.; Krickemeyer, E.; Schmidtman, M.; Bögge, H.; Kögerler, P.; Luong, T. K. K.; Müller, A. *Angew. Chem., Int. Ed.* **2002**, *41*, 2805–2808.
174. Kemp, M. *Nature* **1998**, *393*, 123.
175. Viant, M. R.; Cruzan, J. D.; Lucas, D. D.; Brown, M. G.; Liu, K. J.; Saykally, R. J. *J. Phys. Chem. A.* **1997**, *101*, 9032–9041.
176. Ludwig, R.; Weinhold, F.; Farrar, T. C. *J. Chem. Phys.* **1997**, *107*, 499–507.
177. Müller, A.; Fedin, V. P.; Kuhlmann, C.; Bögge, H.; Schmidtman, M. *Chem. Commun.* **1999**, 927–928.
178. Müller, A.; Polarz, S.; Das, S. K.; Krickemeyer, E.; Bögge, H.; Schmidtman, M.; Hauptfleisch, B. *Angew. Chem., Int. Ed.* **1999**, *38*, 3241–3245.
179. Müller, A.; Shah, S. Q. N.; Bögge, H.; Schmidtman, M.; Kögerler, P.; Hauptfleisch, B.; Leiding, S.; Wittler, K. *Angew. Chem., Int. Ed.* **2000**, *39*, 1614–1616.
180. Müller, A.; Diemann, E.; Shah, S. Q. N.; Kuhlmann, C.; Letzel, M. C. *Chem. Commun.* **2002**, 440–441.
181. Müller, A.; Sarkar, S.; Shah, S. Q. N.; Bögge, H.; Schmidtman, M.; Kögerler, P.; Hauptfleisch, B.; Trautwein, A. X.; Schunemann, V. *Angew. Chem., Int. Ed.* **1999**, *38*, 3238–3241.
182. Müller, A.; Koop, M.; Bögge, H.; Schmidtman, M.; Peters, F.; Kögerler, P. *Chem. Commun.* **1999**, 1885–1886.
183. Müller, A.; Krickemeyer, E.; Das, S. K.; Kögerler, P.; Sarkar, S.; Bögge, H.; Schmidtman, M. *Angew. Chem., Int. Ed.* **2000**, *39*, 1612–1614.
184. Müller, A.; Das, S. K.; Bögge, H.; Schmidtman, M.; Botar, A.; Patrut, A. *Chem. Commun.* **2001**, 657–658.
185. Müller, A.; Das, S. K.; Kögerler, P.; Bögge, H.; Schmidtman, M.; Trautwein, A. X.; Schunemann, V.; Krickemeyer, E.; Preetz, W. *Angew. Chem., Int. Ed.* **2000**, *39*, 3414–3418.
186. Cronin, L.; Das, S. K.; Müller, A. *Unpublished results* **2000**.
187. Müller, A.; Kögerler, P.; Bögge, H. *Struct. Bonding* **2000**, *96*, 203–211.
188. Coxeter, H. S. M. *Introduction to Geometry* **1969**, Wiley: New York.
189. Kroto, H. W.; Heath, J. R.; O'Brien, S. C.; Curl, R. F.; Smalley, R. E. *Nature* **1985**, *318*, 162–163.
190. Müller, A.; Kögerler, P. *Bull. Pol. Acad. Sci., Chem.* **1998**, *46*, 207–219.
191. Müller, A.; Kögerler, P. *Coord. Chem. Rev.* **1999**, *182*, 3–17.
192. Müller, A.; Kögerler, P. *Coord. Chem. Rev.* **2000**, *199*, 335–341.
193. Cronin, L.; Yamase, T. *Personal communication* **2002**.

# 7.2

## High Nuclearity Clusters: Metal–Chalcogenide Polynuclear Complexes

M. W. DEGROOT and J. F. CORRIGAN

*The University of Western Ontario, London, ON, Canada*

---

7.2.1	INTRODUCTION	58
7.2.2	SYNTHETIC APPROACHES TO METAL CHALCOGEN CLUSTERS	58
7.2.2.1	Molecular Approaches	58
7.2.2.1.1	<i>Association of metal cations and chalcogenide or chalcogenolate anions (I)</i>	58
7.2.2.1.2	<i>Reduction of a chalcogen by <math>M(ER)_n</math> (II)</i>	59
7.2.2.1.3	<i>Phosphine chalcogenides as a source of E (III)</i>	59
7.2.2.1.4	<i>Insertion of chalcogen into M–R bonds (IV)</i>	60
7.2.2.1.5	<i>Silylated chalcogenide and chalcogenolate reagents (V)</i>	61
7.2.2.1.6	<i>Nucleophilic metal chalcogenide complexes (VI)</i>	62
7.2.2.1.7	<i>Cluster expansion/condensation by abstraction or induced elimination of a ligand (VII)</i>	63
7.2.2.1.8	<i>Excision of a molecular fragment from an extended solid (VIII)</i>	63
7.2.2.1.9	<i>Additional methods (IX)</i>	63
7.2.2.2	Solid-State and Solvothermal Approaches (X)	64
7.2.3	STRUCTURE AND BONDING	65
7.2.3.1	Chalcogen-containing Ligands	65
7.2.3.1.1	<i>Chalcogenide ligands</i>	65
7.2.3.1.2	<i>Organochalcogenolate ligands</i>	66
7.2.3.1.3	<i>Di- and polychalcogenide ligands</i>	66
7.2.3.2	Photophysics of Metal Chalcogen Clusters: Structure–Property Relationships	67
7.2.3.2.1	<i>Octahedral rhenium chalcogenide clusters</i>	67
7.2.3.2.2	<i>Group 11 metal–chalcogenolate clusters</i>	68
7.2.3.2.3	<i>Group 11 metal–chalcogenide clusters</i>	69
7.2.3.2.4	<i>Group 12 metal–chalcogenolate clusters</i>	70
7.2.4	COMMON STRUCTURAL TYPES IN METAL CLUSTER CHEMISTRY	71
7.2.4.1	Cubane-like Clusters	71
7.2.4.2	Clusters with Octahedral $M_6E_8$ Cores	72
7.2.4.3	Iron–Chalcogen Clusters Based on $Fe_2E_2$ Rhombs	74
7.2.4.4	Cubic Clusters	78
7.2.4.5	Clusters with Structures Based on Adamantane or Barrelene Cages and Related Fragments	78
7.2.5	DIVERSE STRUCTURES FROM WIDELY APPLICABLE SYNTHETIC ROUTES	81
7.2.5.1	Clusters from Silylated Chalcogen Reagents	81
7.2.5.1.1	<i>Early transition metal–chalcogenide clusters</i>	83
7.2.5.1.2	<i>Middle transition metal–chalcogenide clusters</i>	84
7.2.5.1.3	<i>Late transition metal–chalcogenide clusters</i>	84
7.2.5.2	Clusters from $E = PR_3$	95
7.2.5.3	Cluster Synthesis via Reactive Chalcogenometallates and Related Reagents	97
7.2.5.3.1	<i>Clusters synthesized from tetrachalcogenometallate anions <math>[ME_4]^{n-}</math></i>	97
7.2.5.3.2	<i>Related main group ligands</i>	102
7.2.5.3.3	<i>Clusters from polynuclear metalloligands</i>	104
7.2.5.4	Clusters Synthesized from Polychalcogenide Reagents	104
7.2.5.5	Chalcogen-bridged Clusters of the <i>f</i> -block Elements	106
7.2.6	NANOCLUSTERS	109

7.2.6.1	Copper Selenide and Silver Selenide “Megaclusters”	109
7.2.7.2	Quantum Confinement Effects	111
7.2.6.3	The Photophysical Properties of II–VI Nanoclusters	112
7.2.7	REFERENCES	114

---

## 7.2.1 INTRODUCTION

The past two decades have seen an explosion of growth in the area of polynuclear metal–chalcogenide chemistry, as highlighted by a number of timely and comprehensive reviews encompassing the areas of transition metal–chalcogen clusters,<sup>1–5</sup> the utility of sulfur,<sup>6,7</sup> selenium and tellurium-based ligands,<sup>8–10</sup> and clusters as structural analogues of solid-state materials<sup>11,12</sup> and biological systems.<sup>13–18</sup> There are almost as many driving forces behind the development of this area of research as there are structural motifs displayed by this interesting class of molecules. The early development of metal–sulfide clusters is often attributed to the structural relationships observed between discrete molecular models and those observed in biological systems.<sup>19–22</sup> The continued development of such model compounds has led to a greater understanding of the structure–property relationships of metalloproteins. These topics are thoroughly reviewed in Volume 4, Chapter 4.12; Volumes 5 and 6, in Volume 8, Chapter 8.2, Chapter 8.7, Chapter 8.17, and Chapter 8.23, and Volume 9, Chapter 9.22, and are thus outside the scope of this section.

Numerous advances in the development of new chalcogen reagents for the synthesis of metal–chalcogen clusters have further expanded metal–chalcogen chemistry. The inherent instability and toxicity of organoselenium and -tellurium complexes can be overcome via judicious ligand design. The resultant metal–chalcogenide clusters have also given rise to a materials-oriented focus due to the interesting physical properties often displayed by these polynuclear complexes. The wealth of chemistry exhibited by metal–chalcogen clusters containing four or more metals is such that a comprehensive listing of each is beyond the scope of this review. Our focus is to provide a detailed discussion of the reaction strategies that have been developed for structurally characterized groups IV–XII and lanthanide metals, and to summarize their structural and physical properties.

In this section, we endeavor to provide an overview of the development of metal–chalcogenide (S, Se, Te) cluster chemistry over the past two decades. We describe the common synthetic approaches used and the general bonding characteristics of M–E interactions that render the chalcogen-based ligands so effective in promoting and stabilizing polynuclear frameworks. The principal structural motifs of molecular  $M_4$ ,  $M_6$ ,  $M_8$ ,  $M_{10}$ , and  $M_{32}$  and larger clusters are described, including relationships to extended solids. Finally, the rich photophysical properties of metal–chalcogen clusters including the size-quantization effects observed in nanoclusters are reviewed. Literature from 1980 through the end of 2001 is cited.

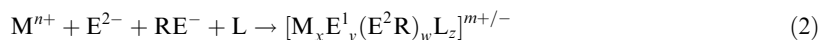
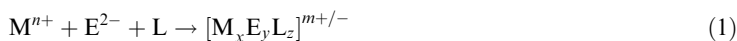
## 7.2.2 SYNTHETIC APPROACHES TO METAL CHALCOGEN CLUSTERS

### 7.2.2.1 Molecular Approaches

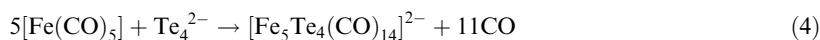
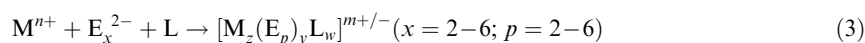
#### 7.2.2.1.1 Association of metal cations and chalcogenide or chalcogenolate anions(I)

The simplest approach to metal chalcogen cluster complexes involves the self-assembly of metal cations and chalcogen anions, usually in the presence of stabilizing ancillary ligands (Equation (1)). Chalcogenide anions,  $E^{2-}$ , can be generated *in situ* from  $H_2E$  in several ways including deprotonation in basic solution or via reaction with hydrated metal salts. While several examples of metal sulfide clusters synthesized using  $H_2S$  have been reported,<sup>23–39</sup> the use of  $H_2Se$  and  $H_2Te$  in cluster synthesis is much less common,<sup>33,40–42</sup> as these reagents, in addition to being very toxic, are difficult to handle, and often lead to a mixture of products. Soluble chalcogenide anions, of the formula  $A_2E_n$  ( $A = Li, Na, K$ ) represent a much more convenient source of chalcogenide. The mono-chalcogenide anions,  $A_2E$ , are efficient delivery agents of  $E^{2-}$  in metal chalcogen cluster synthesis, as they are relatively easy to handle, and react with a variety of metal salts (see Sections 7.2.4.1–7.2.4.4). Chalcogenolate anions  $RE^-$  can be introduced via similar reagents ( $RE-H$  or  $RE-A$ ), or formed *in situ* by the reduction of  $REER$ . These reagents are often used in conjunction

with chalcogenide anions to produce mixed chalcogenide/chalcogenolate clusters (Equation (2)). Ambitious design of chalcogenolate ligands with bulky substituents has led to a number of homoleptic metal chalcogenolate clusters;<sup>43–47</sup> however, in these systems there exists the competing factor of a preference for the formation of mononuclear metal chalcogenolate complexes:<sup>10</sup>

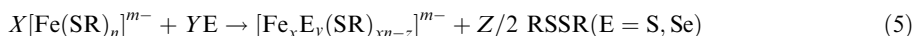


Polychalcogenides have also attracted much attention in cluster synthesis, due to the unique coordination modes adopted by these ligands.<sup>48</sup> Often denoted  $E_4^{2-}$ , polychalcogenides are known to exist in solution as a complex mixture of soluble anions,  $E_x^{2-}$ , where  $x = 2–6$ .<sup>49</sup> When reacted with metal salts, polychalcogenides undergo metathesis reactions, often resulting in polynuclear clusters containing several metal atoms (Equation (3)). The addition of polychalcogenides to metal carbonyl complexes promotes an internal redox reaction in which the chalcogenide chain is reduced by the metal center, resulting in oxidative decarbonylation of the metal.<sup>50</sup> The reaction of metal carbonyl complexes with polysulfides or polyselenides often results in the full decarbonylation of the metal center, and the formation of monomeric, metal–chalcogenide species.<sup>51,52</sup> Alternatively, polytellurides are inclined to promote only partial oxidation of the metal center, leading to the formation of clusters (e.g., Equation (4)).<sup>54</sup>



### 7.2.2.1.2 Reduction of a chalcogen by $M(ER)_n$ (II)

Metal thiolate complexes will reduce elemental sulfur or red selenium via the oxidative elimination of RSSR. In a similar manner, metal selenolate complexes can be used to reduce elemental selenium. The resulting  $E^{2-}$  ligands favor the formation of polynuclear cluster complexes, due to the greater tendency of  $E^{2-}$  (vs.  $RE^-$ ) to form bridging interactions between metal centers. Originally developed in the synthesis of  $[Fe_4 Se_4 (SPh)_4]$ ,<sup>54</sup> this method has been well utilized in the synthesis of a number of iron thiolate/sulfide clusters, as well as their selenide counterparts (Equation (5)).<sup>55–57</sup> More recently, sulfur- and selenium-containing lanthanide clusters (see Section 7.2.5.5) have been synthesized by the displacement of ER from  $Ln(ER)_3$ .<sup>58</sup>



An extension of this approach involves the synthesis of clusters containing  $E^{2-}$  ligands ( $E = S, Se$ ) from metal chalcogenolate cluster complexes. The replacement of  $RS^-$  ligands with  $E^{2-}$  can result in the formation of higher nuclearity clusters, as demonstrated in the synthesis of the clusters  $[M_{10} E_4^1 (E^2 R)_{16}]^{4-}$  (Equation (6)).<sup>59</sup> Metal chalcogenolates will not reduce elemental tellurium in this manner.<sup>1</sup> This can be attributed to the fact that tellurium, unlike its lighter congeners, does not exist in an  $E_8$  form, and as a result, is much less reactive:



### 7.2.2.1.3 Phosphine chalcogenides as a source of E (III)

Trialkylphosphine chalcogenides can be described as soluble, organometallic sources of elemental chalcogen. Despite being relatively stable, the selenide and (especially) telluride derivatives have sufficiently poor  $E=P$  orbital overlap, that they can act as transfer agents of zerovalent chalcogen.

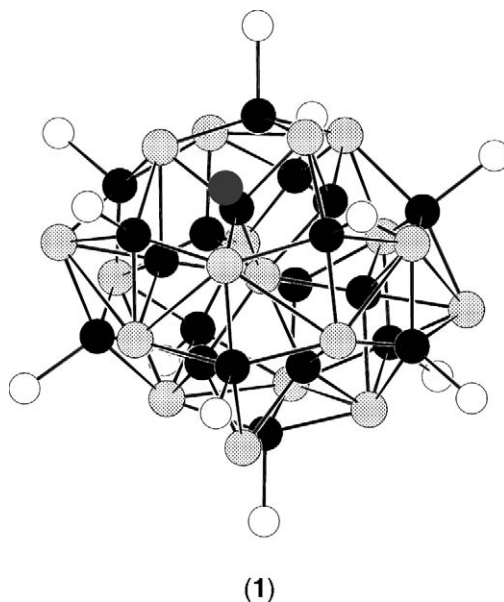
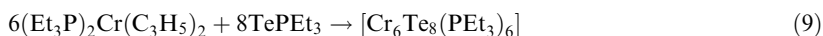


**Figure 1** Ball-and-stick representation of the cluster core of  $[\text{Ni}_{20}\text{Te}_{18}(\text{PEt}_3)_{12}]$  (1).

This is demonstrated by the ability of triethylphosphine telluride to reversibly undergo disproportionation to yield triethylphosphine and tellurium metal.<sup>60</sup> It has been recognized that these reagents can be used to transfer selenium or tellurium to metals with labile ligands. At high temperatures, these reactions typically result in the formation of bulk solid M/E materials.<sup>61–63</sup> At room temperature, intermediate cluster complexes can be isolated by the addition of stabilizing ancillary ligands.<sup>64</sup> Examples of these reactions are demonstrated in Equations (8)<sup>65</sup> and (9).<sup>66</sup> In some cases, tactical control of the reaction conditions can result in the isolation of different complexes. For example, the reaction of  $\text{TePEt}_3$  with  $\text{Ni}(\text{COD})_2$  ( $\text{COD} = \text{cyclooctadiene}$ ) and  $\text{PEt}_3$  in a 1:1:1 ratio yields the cluster  $[\text{Ni}_{20}\text{Te}_{18}(\text{PEt}_3)_{12}]$  (1) (Figure 1). The use of a half of an equivalent of  $\text{TePEt}_3$  and a large excess of phosphine results in the formation of  $[\text{Ni}_9\text{Te}_6(\text{PEt}_3)_8]$ .<sup>67</sup> Also notable are the numerous metal–selenide carbonyl clusters synthesized using phosphine selenide and related reagents.<sup>68</sup> Metal sulfide clusters are not generally accessible via this route owing to the strength of the  $\text{S}=\text{P}$  interaction, although a number of sulfide-bridged metal carbonyl clusters from  $\text{R}_3\text{P}=\text{S}$  reagents are known:<sup>69,70</sup>

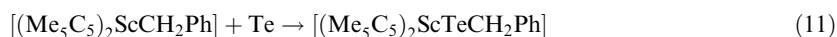


#### 7.2.2.1.4 Insertion of chalcogen into M–R bonds (IV)

The insertion of chalcogen atoms into a reactive metal–carbon bond is a common route in the synthesis of metal chalcogenolate complexes.<sup>10,71</sup> Typically, these reactions involve the addition of elemental chalcogen to an alkali (or alkaline earth) metal salt,<sup>72–76</sup> as demonstrated in Equation (10).<sup>71</sup> In fact, the preparation of many of the chalcogen-containing reagents described in this section involves chalcogen insertion reactions at some stage. Much less common are reactions involving the direct insertion of chalcogen atoms into transition metal–carbon bonds. The addition of sulfur to transition metal alkyls often results in the formation of metal polysulfide complexes,<sup>6,77,78</sup> however, the synthesis of several early transition metal selenolate and telluroolate complexes by this route have been reported<sup>79–84</sup> (e.g., Equation (11)).<sup>84</sup> These reactions generally involve coordinatively unsaturated metal starting reagents. In certain cases, chalcogen insertion has been used to produce polynuclear metal chalcogenolate complexes, as observed in the reaction



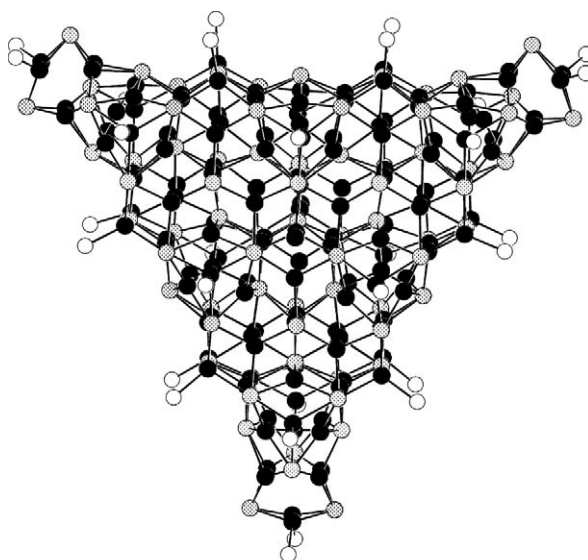
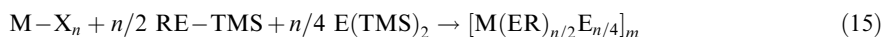
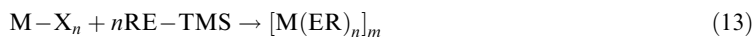
of  $\text{ZnEt}_2$  with sulfur (Equation (12)),<sup>85</sup> consistent with the well-developed strategy for synthesizing main group metal–chalcogen cluster molecules:<sup>86</sup>



### 7.2.2.1.5 Silylated chalcogenide and chalcogenolate reagents (V)

Substitution reactions involving silylated chalcogen reagents represent a powerful approach in metal–group-XVI cluster synthesis.<sup>2,87–89</sup> Compounds such as  $\text{E}(\text{TMS})_2$  and  $\text{RE-TMS}$  react readily with metal salts to form metal chalcogenide or chalcogenolate bonds (Equations (13)–(15)). The driving force for the reaction is the thermodynamically favorable formation of an  $\text{X-Si}$  bond and elimination of  $\text{X-TMS}$  (where  $\text{X} = \text{halide, OAc, etc.}$ ).

The generality of this approach is demonstrated by the ability of these main group complexes to react with a wide range of metal salts including those of early and late transition (see Section 7.2.5.1) and main group metals.<sup>90,91</sup> The products obtained are highly variable and are dependent upon the reaction conditions used. Extensive studies in the synthesis of XI–XVI clusters have demonstrated that careful control of the  $\text{M/E/PR}_3$  ratio, the nature of the phosphine, and the solvent system can have an incredible effect on the products formed,<sup>87</sup> which range from molecular clusters to the remarkable nanoparticles  $[\text{Cu}_{146}\text{Se}_{73}(\text{PPh}_3)_{30}]$  (**2**)<sup>92</sup> (Figure 2) and  $[\text{Ag}_{172}\text{Se}_{40}(\text{SeBu}^n)_9(\text{dppp})_4]$ <sup>93</sup> ( $\text{dppp} = 1,3\text{-bis}(\text{diphenylphosphino})\text{propane}$ ; see Section 7.2.6.1):



(2)

**Figure 2** Ball-and-stick representation of the cluster core of  $[\text{Cu}_{146}\text{Se}_{73}(\text{PPh}_3)_{30}]$  (**2**).

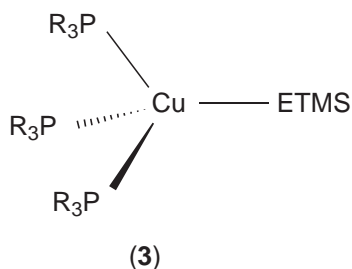
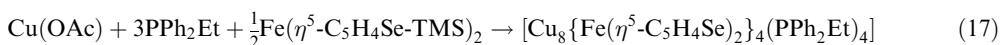
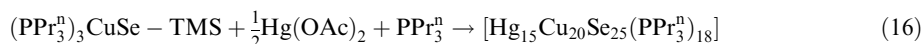


**Figure 3** Schematic representation of tris(trialkylphosphine)trimethylsilyl-chalcogenolate (3).

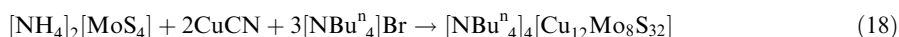
The ability to control product formation, the reproducibility of results, and the relatively mild conditions under which the reactions proceed, have made cluster syntheses by this method very attractive. Furthermore, the starting materials are themselves readily prepared and easily stored and handled. This is especially valuable in metal telluride chemistry, in which suitable reagents for cluster syntheses are often unstable and must be generated *in situ*, leading to complex mixtures of reaction products. The use of the silylated tellurium reagents  $\text{Te}(\text{TMS})_2$  and  $\text{RTe-TMS}$  has allowed access to a wealth of metal tellurium clusters with unique structures and properties.<sup>87,88,94,95</sup>

The approach of using  $\text{RE-TMS}$  reagents is readily adaptable to introduce specific chemical functionality in “R,” and has thus been extended to the synthesis of ternary  $\text{CuHg'E}$  nanoclusters via the use of silylated copperchalcogenolate complexes,  $[(\text{L})_3\text{Cu}(\text{E-TMS})]$  (3) ( $\text{E} = \text{S}, \text{Se}, \text{Te}$ ;  $\text{L} = \text{PPr}_3^n, \text{PEt}_3$ ) (Figure 3) as soluble delivery agents of  $\text{CuE}$  (Equation (16)).<sup>96</sup> Silylated ferrocenyl-selenolate reagents have also been used to introduce redox-active ferrocene units onto copper selenium cluster cores (Equation (17)).<sup>97</sup>

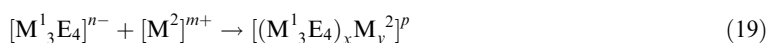


### 7.2.2.1.6 Nucleophilic metal chalcogenide complexes (VI)

Metal complexes containing chalcogenide or chalcogenolate ligands can themselves be used as a form of “metalloligand” in the synthesis of polynuclear complexes. Among these, the tetrachalcogenometallate anions,  $[\text{ME}_4]^{2-}$  ( $\text{M} = \text{V}, \text{Nb}, \text{Mo}, \text{W}, \text{Re}$ ) have been most widely used in cluster synthesis.<sup>98–101</sup> These complexes possess terminal chalcogenide ligands, which are rare in metal chalcogen chemistry. The addition of soft metal cations, such as  $\text{Cu}^+$  or  $\text{Ag}^+$ , results in bridge-forming reactions between the chalcogen atoms and the terminal chalcogenide ligands of the chalcogenometallate precursor (e.g., Equation (18)).<sup>102</sup> The vast number of  $\text{M-Cu}(\text{Ag})\text{-E}$  clusters that have been synthesized via  $[\text{ME}_4]^{n-}$  reagents are discussed in Section 7.2.5.3.1.

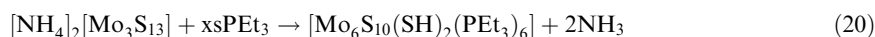


Polynuclear metal chalcogenide species have also found application as nucleophiles in cluster expansion reactions. The bridged iron-sulfur species  $\text{Fe}_2(\mu\text{-E})_2(\text{CO})_6$  reacts with metal cations to form heterometallic clusters of various nuclearities and structural types.<sup>103,104</sup> Similar studies involving other chalcogen-bridged transition metal species have produced a number of heterometallic cluster complexes (see Section 7.2.5.3.3). The “incomplete cubane” clusters,  $[\text{M}_3\text{E}_4]$ , whose structures are representative of a cubane with a “missing” metal vertex, can be used to synthesize heterometallic cubane-like clusters (Equation (19)).<sup>105–107</sup> The use of higher nuclearity precursors such as  $[\text{Nb}_6\text{S}_{17}]^{4-}$  and  $[\text{Fe}_6\text{S}_6\text{I}_6]^{3-}$  has also been demonstrated.<sup>108,109</sup>



### 7.2.2.1.7 Cluster expansion/condensation by abstraction or induced elimination of a ligand (VII)

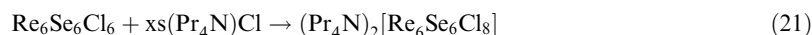
Most metal chalcogen clusters, especially those of the late transition elements, require ancillary ligands such as CO, phosphines, or even chalcogenolates (RE) to stabilize their metal chalcogenide cores. As a result, removal of one of these ligands should destabilize the cluster core, and in most cases it would be expected that such an action would result in degradation of the molecule. In some circumstances, however, these reactions result in the formation of larger clusters via condensation reactions. The addition of sulfur to a phosphine-stabilized cluster, in which cluster expansion is achieved via the generation and elimination of  $\text{S}=\text{PEt}_3$  is one method.<sup>110,111</sup> The same fundamental approach is involved in the reaction of  $\text{PR}_3$  with  $\text{Mo}_3\text{E}_7\text{Cl}_4$  ( $\text{E} = \text{S}, \text{Se}$ ), which involves the abstraction of  $\text{E}^{2-}$  to produce high nuclearity molybdenum chalcogenide clusters (Equation (20)).<sup>112,113</sup>



### 7.2.2.1.8 Excision of a molecular fragment from an extended solid (VIII)

There are several examples in solid-state chemistry of nonmolecular solids in which the primary building blocks are distinct cluster units,<sup>11</sup> and the isolation of these fragments as molecular species is an attractive goal. Unfortunately, many of these solids contain condensed structures in which the cluster components are connected via vertex-, edge-, or face-sharing interactions. For these systems, segregation of the independent units will not be possible, as rupture of these solid-state interactions will result in degradation of the cluster cores. If, however, the solid-state structure consists of discrete cluster units connected via bridging interactions then removal of the intact cluster core can be achieved by severing these linkages.<sup>11</sup>

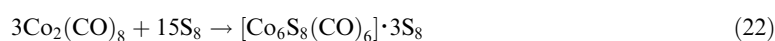
This approach has been fashioned in the pursuit of molecular rhenium chalcogenide clusters whose structures have not been accessible by conventional self-assembly techniques. The method, which has been termed “cluster excision,” involves the addition of a suitable ligand to the nonmolecular solid, such that the vacant sites on the metal centers will be occupied upon cleavage of the bridging interactions. Ligands that have been utilized in this approach include  $\text{Cl}^-$  and  $\text{CN}^-$ , affording molecular rhenium sulfide and selenide clusters (Equation (21)).<sup>114</sup> This method also allows access to previously known structures under milder synthetic conditions:



Until recently, this approach was useful only in the isolation of cluster units from one- or two-dimensional solids, as, except for a few reports<sup>115–117</sup> three-dimensional networks were generally inert to this type of treatment. To overcome this problem, the process of “dimensional reduction” was developed, in which the three-dimensional cluster framework is deconstructed by sequential addition of a reagent  $\text{A}-\text{X}$  ( $\text{A} = \text{Cs}, \text{Tl}$ ;  $\text{X} = \text{Cl}, \text{Br}$ ).<sup>118,119</sup> In each step, the anionic ligand,  $\text{X}$ , disrupts the bridging interactions in the nonmolecular solid, reducing the overall dimensionality of the framework (Figure 4). The cations,  $\text{A}^+$ , are added to preserve the electron count of the clusters by balancing the negative charge accumulated in each sequence.

### 7.2.2.1.9 Additional methods (IX)

In addition to the synthetic approaches described above, a number of alternative routes to polynuclear metal chalcogenide or chalcogenolate complexes have been described. Organometallic complexes will reduce elemental chalcogen, often resulting in the formation of clusters<sup>120–125</sup> (e.g., Equation (22)). Many other approaches involve the use of chalcogen reagents other than those described in the previous sections. A selection of these is summarized in Equations (22)–(25) below:<sup>120,126–128</sup>



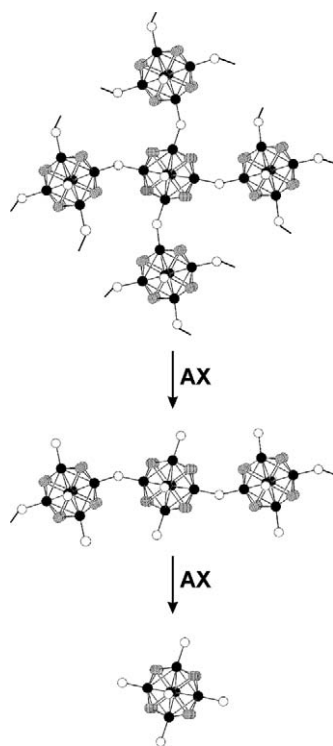
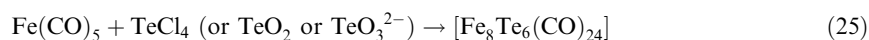
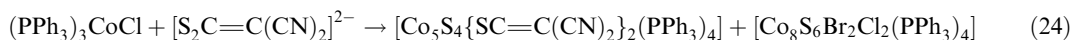
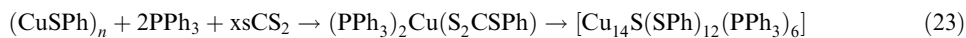


**Figure 4** The process of dimensional reduction (see text).



### 7.2.2.2 Solid-State and Solvothermal Approaches (X)

Direct reaction of elemental chalcogen and metal under ceramic conditions typically results in the formation of nonmolecular M/E solids (Equation (26)). Ancillary ligands may be included in the reaction mixture to aid in the stabilization and isolation of molecular complexes (Equation (27)). A variation of this method, termed the solvothermal approach, involves the use of a small amount of solvent in the synthesis to promote crystallization of the product. This approach was applied in the synthesis of the molybdenum polyselenide clusters  $[\text{Mo}_9\text{Se}_{40}]^{8-}$ <sup>129</sup> and  $[\text{Mo}_{12}\text{Se}_{56}]^{12-}$ ,<sup>130</sup> and has become a general route in the synthesis of clusters containing polychalcogenide ligands<sup>48</sup> (see also Table 17). Recently, this method has been utilized in the synthesis of three-dimensional framework solids containing supertetrahedral cluster units  $[\text{M}_4\text{In}_{16}\text{S}_{35-n}]$  (M = Mn, Co, Zn, Cd;  $n = 0, 2$ ).<sup>131,132</sup> The substitution of the metal and chalcogen elements for suitable metal chalcogenide reagents, such as tetrachalcogenometallates (Section 7.2.5.3.1) or other solids (Table 2) has been implemented in the synthesis of molecular clusters.



### 7.2.3 STRUCTURE AND BONDING

The extremely rich structural diversity in metal chalcogen cluster chemistry can be credited, in large part, to the flexibility of chalcogenide and chalcogenolate ligands. This is demonstrated in their ability to adopt several different coordination modes, their strong tendency to bridge metal centers, and to form stable bonds with most transition and post-transition metals. The tendency to adopt bridging coordination modes, of particular importance to the cluster chemist, can be attributed to the highly polarizable electrons and the anionic nature of these ligands. In contrast, neutral ligands such as  $H_2E$ ,  $R_2E$ , and  $REH$  form less stable complexes with metal centers, due to the lability of such ligands in both the terminal and bridging coordination modes.

#### 7.2.3.1 Chalcogen-containing Ligands

##### 7.2.3.1.1 Chalcogenide ligands

Chalcogenide ions ( $E^{2-}$ ) are the most electron rich ligands in this class. Consequently, terminal coordination of these ligands tends to occur in early transition metal complexes in their highest oxidation states. Examples of these include the tetrahedral polychalcogenometallate anions,  $ME_4^{n-}$  ( $M = V, Nb, Ta$ ;  $n = 3$ ;  $M = Mo, W$ ;  $n = 2$ )<sup>101,133</sup> and the cluster anions  $[M_6S_{17}]^{4-}$  ( $M = Nb$  (**4a**),  $Ta$  (**4b**)), depicted in Figure 5.<sup>134,135</sup> The latter complexes contain four differently coordinated sulfur atoms, including a  $\mu_6$ -S, demonstrating the flexibility of the sulfide ligands. Terminal chalcogenides are also observed in clusters of main group metals such as in  $[M_4E_{10}]^{4-}$  ( $M = Ga, E = S$  (**5a**);  $M = In, E = S$  (**5b**),  $Se$  (**5c**))<sup>136</sup> and  $[M_{10}S_{16}(SPh)_4]^{8-}$  ( $M = Ga$  (**6a**),  $In$  (**6b**))<sup>5</sup> (Figure 5). In these complexes, single metal chalcogenide bonds are observed, while the bonds in the transition metal species tend to be of higher order (1.5–2.0).

The above examples notwithstanding, chalcogenide ligands predominantly form bridging interactions with metal centers. As a result, binary metal chalcogenides are typically nonmolecular solids, with extensive bonding in one, two, or three dimensions. The synthesis of metal

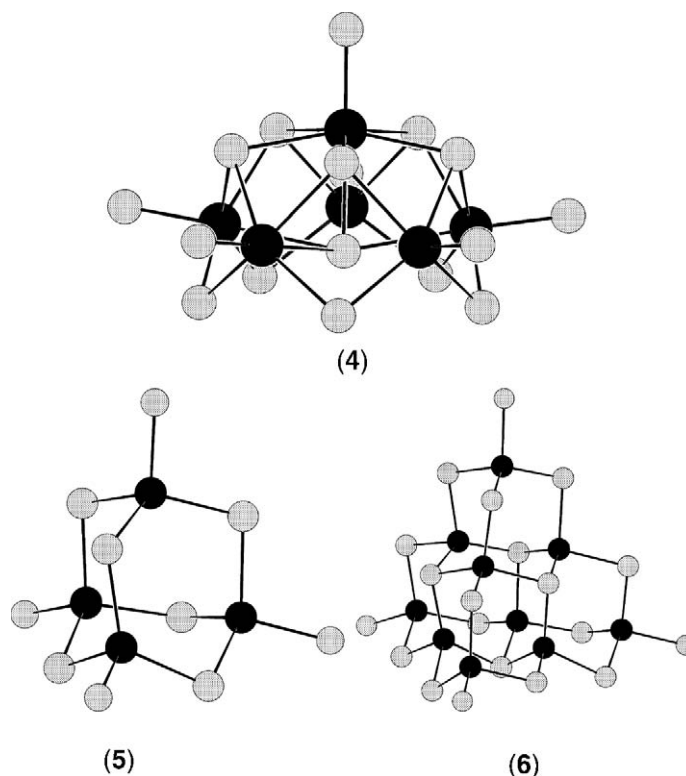


**Figure 5** Ball-and-stick representation of the cluster core of  $[M_6S_{17}]^{4-}$  (**4**),  $[M_4E_{10}]^{2-}$  (**5**), and  $[M_{10}S_{16}(SPh)_4]^{8-}$  (**6**).

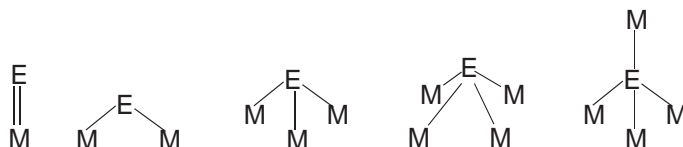


**Figure 6** Common bridging modes of chalcogenide ligands.

chalcogenide clusters, therefore, requires that these interactions be limited to “molecular” dimensions. This can be achieved via the use of heteroligands (most commonly halides, tertiary phosphines, or amines), organometallic ligands such as CO or  $C_5H_5^-$ , or organochalcogenolate anions ( $RE^-$ ), but other examples also exist. Regardless of their type, these ligands serve to stabilize the metal chalcogenide cluster core by bonding at the cluster surface, preventing further condensation to bulk materials. The nature of the ligands can have a profound effect on the structure of a cluster, and this matter will be addressed in subsequent sections.

The most typical bonding modes of chalcogenide ligands are the  $\mu_2$ -,  $\mu_3$ -, and  $\mu_4$ -bridging interactions (Figure 6); however, higher coordination is also observed. Of these, the doubly bridging ( $\mu_2$ -) interaction is the least stable. This is not surprising, as these ligands have readily available lone pairs of electrons, and thus provide an opportunity for further bridging interactions. Correspondingly (and similar to the terminal ligands), this type of interaction is most stable in clusters of main group metals or early transition metals. Nevertheless, there are many examples of this type of coordination in later transition metals, such as the iron chalcogenide “basket” clusters<sup>137–142</sup> and it has even been observed in group 10 metal clusters, such as  $[Pd_6Te_6(PEt_3)_8]$ .<sup>143</sup>

The three- and four-coordinate bridging modes are the most common for chalcogenide ligands. These ligands commonly act as capping atoms on  $M_3$  faces and this type of interaction is the foundation for the stability of the general  $M_4E_4$  (cubane)  $M_6E_8$  (octahedral) structural types (Sections 7.2.4.1 and 7.2.4.2). Four-coordinate chalcogenide ligands occur as capping atoms on  $M_4$  faces or as core atoms with (typically) tetrahedral geometry.

The ability to bridge metal centers increases going down the group from sulfur to tellurium, a characteristic that can be ascribed to the larger ionic radii, and thus larger polarizability of the heavier elements. Hence, higher bridging modes are more common for selenium and tellurium than for sulfur.

### 7.2.3.1.2 Organochalcogenolate ligands

Organochalcogenolate ligands ( $RE^-$ ) constitute a very important ligand type in metal cluster chemistry. Like their chalcogenide counterparts, they demonstrate a strong tendency to bridge metal centers. In contrast to chalcogenides, however, there exists the potential to modify the coordinating ability of these ligands by changing the organosubstituent (R), and in this sense they have been referred to as a “chalcogenide with a handle.”<sup>4</sup>

An important aspect of the coordination chemistry of chalcogenolates is the capacity of these ligands to adopt a terminal coordination mode on metal centers. As discussed above, this type of bonding mode is uncommon for the chalcogenide ligands. Several metal chalcogen clusters have been synthesized in which terminal positions on the cluster surface are occupied by chalcogenolate ligands. This, in effect, has allowed access to “binary” metal chalcogenide/chalcogenolate clusters with structures that are not available in metal chalcogenide chemistry.

Despite numerous examples of terminal coordination,<sup>4</sup> chalcogenolate ligands tend to favor bridging interactions between metal centers. The most common bonding mode is the doubly bridging ( $\mu_2$ ) type, which is observed in clusters with thiolate, selenolate, and tellurolate ligands. Doubly bridging chalcogenolate ligands possess a free lone pair of electrons that can be donated to a third metal atom to produce a third M–E bonding interaction. With respect to thiolates, this type of interaction is more common for selenolate and tellurolate ligands, again attributable to the larger size of the heavier chalcogens.

### 7.2.3.1.3 Di- and polychalcogenide ligands

One of the most interesting properties of chalcogens is the ease with which E–E bonds are broken and reformed, leading to an extraordinary ability to form rings or chains of different lengths.<sup>49</sup>

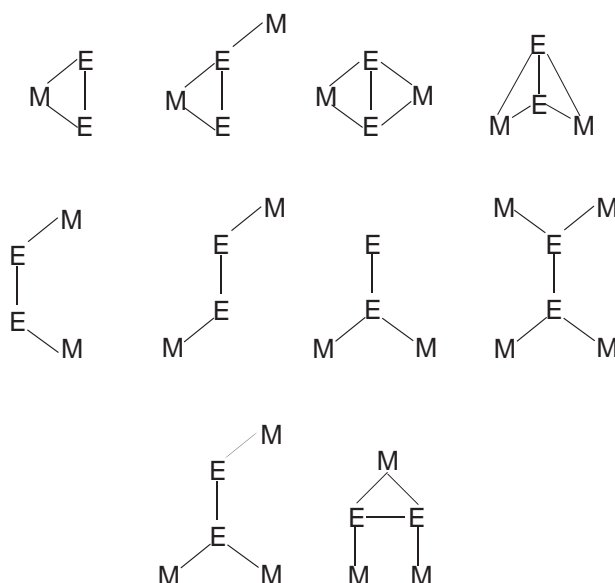


**Figure 7** Common bridging modes of dichalcogenide ligands.

Several of the anionic versions of these complexes ( $E_n^{2-}$ ) are excellent candidates to form bridging interactions between metal centers directed at the formation of polynuclear complexes.

The use of dichalcogenide ligands,  $E_2^{2-}$ , in the synthesis of metal chalcogenide clusters represents an active area of research. These ligands have the ability to form bridging interactions between two, three, or four metal centers in a variety of different coordination modes, as demonstrated in [Figure 7](#). As a result, clusters incorporating this type of ligand have structures not observed with chalcogenide or chalcogenolate ligands. Whereas  $S_2^{2-}$  and  $Se_2^{2-}$  are relatively common ligands, complexes containing  $Te_2^{2-}$  are often unstable, and usually require steric protection by bulky stabilizing groups.<sup>9</sup>

The polychalcogenide ligands,  $E_n^{2-}$  (where  $n = 3-6$ ), also find applications in metal chalcogenide cluster synthesis. Due to the negative charge associated with the terminal chalcogen atoms, coordination to metal centers by these ligands occurs, for the most part, by chelating to one metal center, or via a bidentate interaction between two metal centers. Clusters containing polychalcogenide ligands constitute a set of chalcogen-rich polynuclear complexes, and are interesting in terms of the unique structures observed. Some examples also include several different di- or polychalcogenide ligands in the same complex, such as is observed in  $[Hg_4Te_{12}]^{4-}$ <sup>144</sup> (**7**), and  $[Ni_4Se_{22}]^{4-}$ <sup>145</sup> (**8**) ([Figure 8](#)).

### 7.2.3.2 Photophysics of Metal Chalcogen Clusters: Structure–Property Relationships

In addition to the highly flexible bonding characteristics of chalcogenide and chalcogenolate ligands, investigations of the photophysical properties of metal chalcogen clusters are important not only in the development of new luminescent materials, but also in the establishment of structure–property relationships for such complexes. Exploration of the photophysics of soluble molecular species can provide valuable insight into the optical properties of related insoluble materials. There has been considerable interest in recent years in the photophysical properties of transition metal clusters, and in particular, numerous polynuclear  $d^{10}$  metal complexes have been shown to exhibit rich luminescent behavior.<sup>146,147</sup>

#### 7.2.3.2.1 Octahedral rhenium chalcogenide clusters

Theoretical investigations<sup>148,149</sup> have revealed that the electronic structure of the clusters  $[Re_6E_8X_6]^{4-}$  ( $E = S, Se$ ;  $X = Cl, I$ ) are analogous to those of the intensely luminescent  $[W_6X_8X'_6]^{2-}$  clusters.<sup>150,151</sup> Accordingly, the clusters  $[Re_6E_8X_6]^{4-}$  have also been shown to exhibit

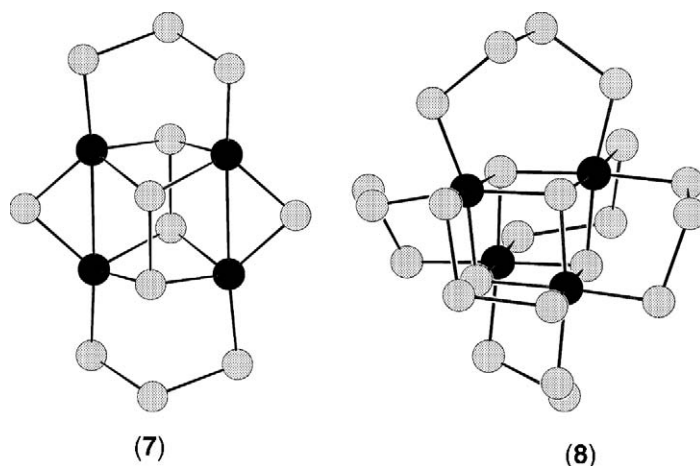


**Figure 8** Ball-and-stick representation of the molecular structure of  $[\text{Hg}_4\text{Te}_{12}]^{4-}$  (7) and  $[\text{Ni}_4\text{Se}_{22}]^{4-}$  (8).

rich photoluminescence both in solution and in the solid state. The LUMOs of these complexes are antibonding, with largely metallic character and some contribution from  $\text{E}^{2-}$  ligands, while the HOMOs reside primarily on the terminal halide ligands. Thus, the emitting excited state is presumably metal-localized. Several investigations have been carried out to probe the influence of ligand substitution of the terminal and capping ligands on the luminescence behavior. The absorption maxima of  $[\text{Re}_6\text{E}_8\text{X}_6]^{4-}$  shift to longer wavelength in the order  $\text{Cl} < \text{Br} < \text{I}$ ,<sup>119,152,153</sup> suggesting that a  $\text{X} \rightarrow \text{M}$  ligand-to-metal charge transfer (LMCT) process is involved. Interestingly, the absorption and emission properties of the paramagnetic complex  $[\text{Re}_6\text{S}_8\text{Cl}_6]^{3-}$  are rather different from those of the more reduced species, giving evidence of a substantial change in the electronic structure of the cluster upon oxidation.<sup>154</sup>

The emission maxima of the complexes  $[\text{Re}_6\text{E}_8(\text{CN})_6]^{4-}$  ( $\text{E} = \text{S}, \text{Se}, \text{Te}$ ) shifts to longer wavelength in the order  $\text{S} < \text{Se} < \text{Te}$ ; however, the luminescence quantum yield decreases in the unusual order  $\text{Se} \gg \text{S} > \text{Te}$ .<sup>155</sup> This is attributed to a competition between  $\pi$ -donation of the chalcogenide and  $\pi$ -backbonding to the  $\text{CN}^-$  ligands, which have an opposite effect on the emission characteristics of the clusters. A linear relationship between the nonradiative decay constant and the emission maxima for a series of  $\{\text{Re}_6\text{E}_8\text{L}_6\}$  clusters ( $\text{E} = \text{S}, \text{Se}$ ;  $\text{L} = \text{halide}, \text{PEt}_3, \text{solvent}$ ) demonstrates that the nature of the emitting species is not significantly affected by the identity of terminal or capping ligands.<sup>153</sup> Alternatively, an investigation of the emission properties of a number of  $[\text{Re}_6\text{S}_8\text{Cl}_4\text{L}_2]$  clusters (where  $\text{L} = \text{pyridine derivatives or pyrazine}$ ) was recently carried out.<sup>156</sup> It was found that the emission quantum yield was much greater for py and 4-methylpyridine (mpy) complexes, than for derivatives containing bipyridine, 4-cyanopyridine, or pyrazine. Different excited states were proposed for the two sets of complexes: the cluster-centered excited state was retained for the py and mpy derivatives, while emission from ligand  $\pi^*$ -orbitals were favored for the others.

#### 7.2.3.2.2 Group 11 metal–chalcogenolate clusters

The photophysical properties of the luminescent copper(I) and silver(I) thiolate clusters  $[\text{Cu}_6(\text{mtc})_6]$  (9),  $[\text{Ag}_6(\text{mtc})_6]$  (10a), and  $[\text{Ag}_6(\text{dte})_6]$  (10b) (mtc = di-*n*-propylmonothiocarbamate, dte = di-*n*-propyldithiocarbamate) have been investigated.<sup>157</sup> At 77 K, each of the complexes exhibits a strong single emission both in solution and the solid state ( $\lambda_{\text{em}}$  (9) solid = 767 nm;  $\lambda_{\text{em}}$  (10a) solid = 767 nm;  $\lambda_{\text{em}}$  (10b) solid = 545 nm). Strongly Stokes-shifted emission bands with respect to the excitation maxima indicate highly distorted excited state structures, likely due to enhanced metal–metal bonding. Emission lifetimes are quite long ( $>1 \mu\text{s}$ ), suggesting that the complexes emit from a spin-forbidden state. Emissions from these complexes in the visible region excludes the possibility that the excited states originate from an intraligand (IL)  $\pi-\pi^*$  (mtc<sup>-</sup> or dte<sup>-</sup>) transition. Similarly, the  $\pi^*$ -orbitals of the thiolate ligands are energetically too high to act as acceptor orbitals for low energy metal-to-ligand charge transfer (MLCT) transitions. Furthermore, the similar emission energies of (9) and (10a) rule out an MLCT assignment on the basis that  $\text{Cu}^{\text{I}}$  is much more readily oxidized than  $\text{Ag}^{\text{I}}$ . Based on the above considerations, as well as



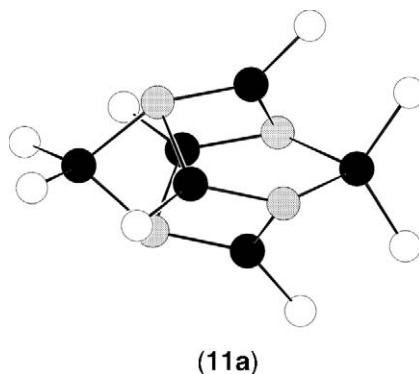


**Figure 9** Ball-and-stick representation of the cluster core of  $[\text{Cu}_6(\mu\text{-dppm})_4(\mu_3\text{-SePh})_4]^{2+}$  (**11a**).

experimental<sup>158</sup> and theoretical<sup>159</sup> investigations of copper(I) iodide clusters, the nature of the photoemissive state of these complexes was assigned to a triplet cluster-centered state with both  $d \rightarrow s$  and LMCT [ $\text{mtc}^-/\text{dtc}^- \rightarrow \text{M}_6$ ] character.

The ability to elucidate structure–property relationships from photophysical data was demonstrated in the investigations of the optical properties of trinuclear copper-arenethiolate complexes.<sup>160</sup> It was found that the orientation of the thiolate ligands played a crucial role in the excitation energy of different copper atoms. Lower energy transitions were assigned to copper atoms with thiolate ligands oriented such that the lone pairs on the sulfur atoms are aligned parallel to each other. This allows the formation of a three-electron two-center sulfur–sulfur bond in the excited state. For copper centers with the lone pairs of the thiolate ligands oriented perpendicular to each other, higher energy LMCT transitions were observed. More recently, the optical properties of a number of trinuclear copper(I) complexes with different thiolate ligands were reported.<sup>161</sup> A LMCT [ $\text{RS}^- \rightarrow \text{Cu}_3$ ] was favored in view of the fact that the emission energies were observed to be largely dependent on the electron-donating ability of the thiolate ligand. Two hexanuclear copper(I) selenolate complexes,  $[\text{Cu}_6(\mu\text{-dppm})_4(\mu_3\text{-SePh})_4]^{2+}$  (**11a**) and  $[\text{Cu}_6\{\mu\text{-}(\text{Ph}_2\text{P})_2\text{NH}\}(\mu_3\text{-SePh})_4]^{2+}$  (**11b**) (dppm = bis(diphenylphosphino)methane; Figure 9) were also synthesized. The similar emission energies of (**11a**) ( $\lambda_{\text{em}}$  acetone = 626 nm) and (**11b**) ( $\lambda_{\text{em}}$  acetone = 700 nm) precluded a ligand-to-ligand charge transfer (LLCT) [ $\text{PhSe}^- \rightarrow$  phosphine] assignment. Again, the origin of the emitting state was assigned to a triplet LMCT [ $\text{PhSe}^- \rightarrow \text{Cu}_6$ ], possibly mixed with a copper-centered  $d \rightarrow s$  state.

### 7.2.3.2.3 Group 11 metal–chalcogenide clusters

In order to examine the photophysical properties of group XI clusters with chalcogenide ( $\text{E}^{2-}$ ) ligands, a series of soluble tetranuclear cluster cations of the formula  $[\text{M}_4(\text{dppm})_4(\mu_4\text{-E})]^{2+}$  ( $\text{M} = \text{Cu}$ ,  $\text{E} = \text{S}$  (**12a**) or  $\text{Se}$  (**12b**);  $\text{M} = \text{Ag}$ ,  $\text{E} = \text{S}$  (**13a**),  $\text{Se}$  (**13b**), or  $\text{Te}$  (**13c**))<sup>162–165</sup> has been synthesized recently. These complexes are all structurally related, consisting of a distorted rectangular array of metal atoms bridged by a  $\mu_4$ -chalcogenide ligand (Figure 10). The clusters exhibit solid-state photoluminescence at room temperature, which, in regard to the strongly reducing nature of the chalcogenide ligands, has been assigned to an excited state with a high degree of LMCT [ $\text{E}^{2-} \rightarrow \text{M}_4$ ] character. The order of emission energies ((**12a**) > (**12b**)) and ((**13a**) > (**13b**) > (**13c**)) follows the same trend as the ionization energies of the chalcogens themselves, therefore supporting this assignment.

Although the  $\pi^*$ -orbitals of the phosphine ligands are sufficiently low in energy to allow a MLCT [ $\text{M}_4 \rightarrow$  phosphine] transition, comparable emission energies between (**12a**) and a dtpm (bis[bis(4-methylphenyl)phosphino]methane) analogue,<sup>166</sup> as well as between (**12a**) and (**13a**), exclude this assignment.

The assignment that the emissions arise from a LMCT [ $\text{E}^{2-} \rightarrow \text{M}_4$ ] excited state with mixing of a metal-centered ( $d \rightarrow s/d \rightarrow p$ ) state has been substantiated by *ab initio* and Fenske–Hall molecular orbital calculations performed for the silver(I) clusters.<sup>167–169</sup> These results revealed that the HOMOs of the clusters are principally Ag–E bonding orbitals, while the LUMOs are metal-localized orbitals with predominantly  $5s$  and  $5p$  character. Furthermore, the calculated HOMO–LUMO energy gaps decrease in the order (**13a**) > (**13b**) > (**13c**), consistent with the observed trend for the emission energies of the complexes.

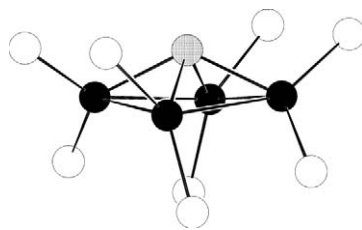


**Figure 10** Ball-and-stick representation of the cluster core of  $[M_4(dppm)_4(\mu_4-E)]^{2+}$  (**12**) and (**13**).

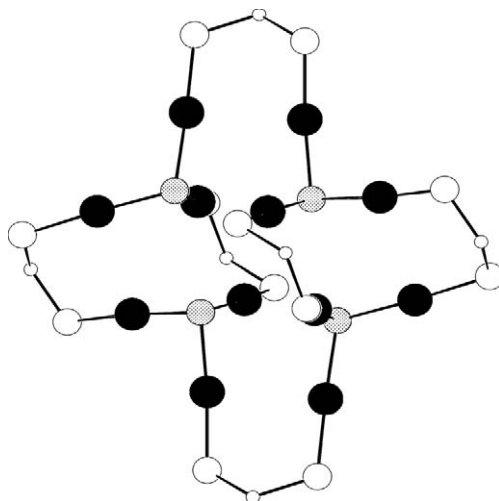


**Figure 11** Ball-and-stick representation of the cluster core of  $[Au_{12}(\mu-dppm)_6(\mu_3-S)_4]^{4+}$  (**14**).

The relativistic effects that cause a contraction of the  $ns$  orbital of  $d^{10}$  metal centers are greatest for gold(I),<sup>170</sup> and often lead to inter- and intramolecular gold–gold contacts, commonly referred to as auriphilic interactions.<sup>171</sup> As a result, polynuclear gold(I)-chalcogen complexes often demonstrate interesting luminescent behavior.<sup>172–175</sup> It has been shown for gold(I) thiolate complexes that emission behavior is influenced by gold(I)–gold(I) interactions and the nature of the thiolate ligand.<sup>176</sup> As an extension of the studies on the luminescent copper(I)- and silver(I)-chalcogenide clusters, a group of gold(I) sulfide clusters has been successfully prepared. The complexes  $[Au_{12}(\mu-dppm)_6(\mu_3-S)_4]^{4+}$  (**14**) (Figure 11),  $[Au_{10}\{\mu-Ph_2PN(Pr^i)PPh_2\}_4(\mu_3-S)_4]^{2+}$  (**15**), and  $[Au_6\{\mu-Ph_2PN(p-MeC_6H_4)PPh_2\}_3(\mu_3-S)_2]^{2+}$  (**16**) have been characterized structurally, and their photophysical properties investigated.<sup>37–39</sup>

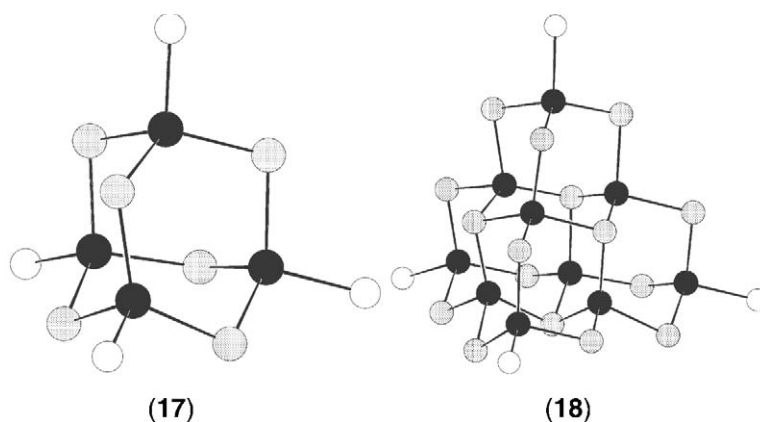
All three clusters exhibit long-lived luminescence in both the solid state and solution at room temperature. The data are summarized in Table 1. This is in contrast to the complex  $[S(AuPPh_3)_3]^+$  which only emits in the solid state at 77 K.<sup>177</sup> Based on considerations of the luminescence properties of clusters (**12a–b**) and (**13a–c**), the emitting states of (**14**)–(**16**) were tentatively assigned to originate from triplet LMCT  $[S^{2-} \rightarrow Au]$  transitions mixed with metal-centered ( $d \rightarrow s/d \rightarrow p$ ) states, modified by auriphilic  $Au^I \cdots Au^I$  contacts. An unusually large Stokes shift of the emission band with respect to the excitation maximum is observed for complex (**16**). This is indicative of a highly distorted excited state structure compared to that of the ground state. The Stokes shift is larger in the solution spectrum ( $\lambda_{em} = 810$  nm) than in that for the solid ( $\lambda_{em} = 635$  nm), suggesting that the distortion is greater in the former.

#### 7.2.3.2.4 Group 12 metal–chalcogenolate clusters

Due to many structural similarities to the solid-state structures, the soluble polynuclear complexes  $[Zn_4(SPh)_{10}]^{2-}$  (**17a**),  $[Cd_4(SPh)_{10}]^{2-}$  (**17b**), and  $[Cd_{10}S_4(SPh)_{16}]^{2-}$  (**18**) (Figure 12), may be considered as molecular models for the photophysical properties of the semiconductors ZnS and CdS.<sup>178,179</sup> Lowest energy bands in the absorption spectra have been assigned to LMCT transitions. These can be viewed as the molecular equivalents of the bandgap transition between the

**Table 1** Summary of the photophysical properties of the gold sulfide clusters (14)–(16).

Cluster	Medium (T K)	$\lambda_{abs}$ (nm)	$\lambda_{em}$ (nm)	$\tau_o$ ( $\mu$ s)
[Au <sub>6</sub> S <sub>2</sub> {Ph <sub>2</sub> PN(MeC <sub>6</sub> H <sub>4</sub> )PPh <sub>2</sub> } <sub>3</sub> ] [ClO <sub>4</sub> ] <sub>2</sub> (16)	CH <sub>2</sub> Cl <sub>2</sub> (298)	264,304,346	810	3.6
	CH <sub>2</sub> Cl <sub>2</sub> (77)		562	23.2,3.2
	MeOH (298)		808	3.1
	EtOH/MeOH (77)		564	37.6
	Solid (298)		635	14.3,2.5
	Solid (77)		603	–
[Au <sub>10</sub> S <sub>4</sub> {Ph <sub>2</sub> PN(Pr <sup>n</sup> )PPh <sub>2</sub> } <sub>4</sub> ][PF <sub>6</sub> ] <sub>2</sub> (15)	CH <sub>2</sub> Cl <sub>2</sub> (298)	268,336,400	510,759	0.10
	(Me) <sub>2</sub> CO (298)		509,768	0.11
	Solid (298)		522,657	0.23,1.28
	Solid (77)		526,662	3.77
[Au <sub>12</sub> ( $\mu$ -dppm) <sub>6</sub> ( $\mu_3$ -S) <sub>4</sub> ][PF <sub>6</sub> ] <sub>4</sub> (14)	MeCN (298)	266,332	546	0.25
	Solid (298)		648	2.7,0.3
	Solid (77)		634	–

**Figure 12** Ball-and-stick representation of the cluster core of [M<sub>4</sub>(SPh)<sub>10</sub>]<sup>2-</sup> (17) and [Cd<sub>10</sub>S<sub>4</sub>(SPh)<sub>16</sub>]<sup>2-</sup> (18).

filled S<sup>2-</sup> *np* orbitals of the valence band and the empty (*n* + 1)*s* M<sup>2+</sup> orbitals of the conduction band in the bulk semiconductor. Unlike the group 11 clusters described above, significant mixing of a metal-centered *d* → *s* state is not expected due to the stability of the *d*-orbitals in zinc and cadmium complexes. However, emission in related mercury(II) complexes, such as [Hg<sub>4</sub>(SPh)<sub>6</sub>(PPh<sub>3</sub>)<sub>4</sub>]<sup>2+</sup> has been proposed to occur from a mixed metal-centered *d* → *s*/LMCT excited state.<sup>180</sup> This is based on the similar energy separation between the relevant *nd*<sup>10</sup> and *nd*<sup>9</sup>(*n* + 1)*s*<sup>1</sup> configurations of Hg<sup>II</sup> (~43,000 cm<sup>-1</sup>) with respect to Ag<sup>I</sup> (~39,000 cm<sup>-1</sup>).

The luminescence spectra of the above complexes demonstrate substantial Stokes shifts with respect to their excitation maxima. Again, this can be attributed to a highly distorted excited state structure with increased metal–metal bonding interactions via population of a  $\sigma_{MM}$  bonding orbital. The absorption and emission energies of (18) are significantly red-shifted compared to those of (17b). This size dependence is related to the quantum confinement effects observed in larger nanoclusters and colloids. This topic will be described further in Sections 7.2.7.2. and 7.2.6.3.

## 7.2.4 COMMON STRUCTURAL TYPES IN METAL CLUSTER CHEMISTRY

### 7.2.4.1 Cubane-like Clusters

By far the most common structural type in metal chalcogen cluster chemistry is the M<sub>4</sub>E<sub>4</sub> cube-like structure in which a tetrahedral array of metal ions interpenetrates an inverted larger

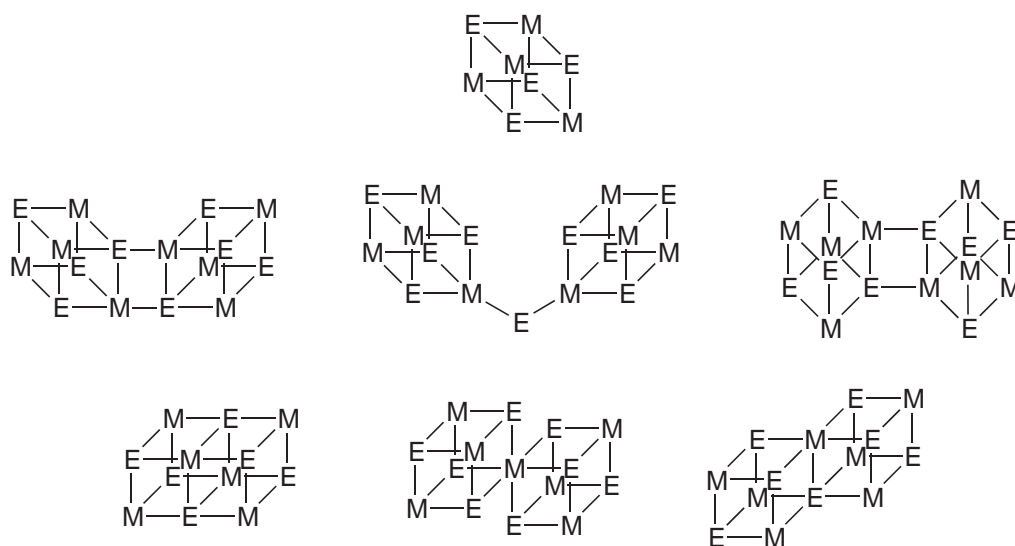


**Figure 13** Schematic representation of the single cubane cage (top) and various double cubane structures demonstrating some of the common bridging and vertex- and edge-sharing interactions.

tetrahedron of chalcogen atoms. Conversely, the structures can be viewed as an  $M_4$  tetrahedron, of which each triangular face is capped by a  $\mu_3$ -E ligand. The metal atoms are further coordinated to one, two, or three terminal ligands, which may be halides, chalcogenolates, organic groups, and many others. This group also includes the vast number of clusters whose structures are based on the fusion of two or more cubane units via vertex, edge, or face sharing interactions. A selection of these is depicted in Figure 13.

Interest in complexes of this type, especially those containing iron, molybdenum, and vanadium is based on their structural relationships to the  $M_4E_4$  clusters that occur in several biological systems.<sup>15,17,181,182</sup> These clusters play a central role in a variety of biological processes including photosynthesis, nitrogen fixation, and respiration. The role of metal clusters in biology is covered in Volume 8, Chapters 8.2, 8.7, 8.17, and 8.23.

#### 7.2.4.2 Clusters with Octahedral $M_6E_8$ Cores

The structural type displayed in hexanuclear clusters of the formula  $M_6E_8L_6$  is among the most abundant in metal chalcogen cluster chemistry. The structure of these complexes consists of six octahedrally disposed metal cations with triply bridging chalcogenide ( $E^{2-}$ ) ions capping the eight  $M_3$  faces, forming a pseudo-cube around the  $M_6$  octahedron. Six donor ligands ( $L = C_5H_5$ , CO,  $PR_3$ ,  $NR_3$ , X, solvent, etc.) occupy a terminal site at each metal center (Figure 14).

Much of the interest in clusters of this type arises from their structural similarity to the fundamental structural element of the superconducting Chevrel phases  $M_xMo_6E_8$  ( $M = Pb$ , Sn, Cu, etc.)<sup>183</sup> and more recently discovered rhenium–chalco–halide phases.<sup>184</sup> Although these solid-state compounds are known only for Mo and Re, molecular  $M_6E_8L_6$  clusters of Zr, V, Cr, Mo, W, Re, Fe, and Co have been reported (Table 2). The lone examples of octahedral zirconium- and vanadium-chalcogenide clusters are unique in that they also possess interstitial O and S atoms, respectively.<sup>185</sup> Evidence for interstitial H atoms in the clusters  $[Cr_6E_8(PEt_3)_6]$  ( $E = S$ , Se) has been presented.<sup>186</sup>

Typical synthetic approaches to group 6 octahedral clusters include the “reductive condensation” technique involving abstraction of chalcogen atoms from  $M_3E_7Cl_4$  ( $M = Mo$ , W;  $E = S$ , Se;  $M = W$ ;  $E = S$ ) by  $PEt_3$ , or ion association methods. Improved yields for  $W_6S_8$  clusters have been obtained by utilizing the isolated cluster  $W_6Cl_{14}$  in place of  $WCl_2$  (actually  $W_6Cl_{12}$ ).<sup>187</sup> Ion association reactions, along with a variety of other methods (see Table 2) have been used in the synthesis of octahedral iron- and cobalt-chalcogenide clusters. Many of these readily undergo reversible oxidation and reduction reactions, and clusters of similar composition display variable oxidation states in the synthesized products. The ability to undergo multisequential electron transfer reactions is most pronounced for the cluster  $[Fe_6S_8(PEt_3)_8]^n$ , for which four members

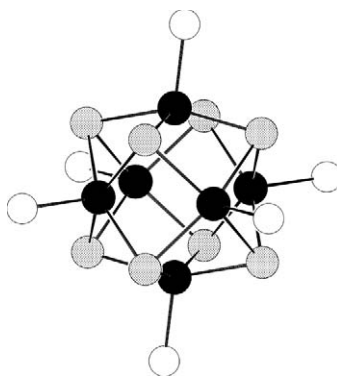


**Figure 14** Ball-and-stick representation of the cluster core of octahedral  $[M_6E_8L_6]$  complexes.

of the series ( $n=0-3$ ) have been isolated and structurally characterized. A fifth member ( $n=4$ ) has been obtained electrochemically; however, it has been suggested that the structural deformations required to stabilize this high oxidation state will preclude the prospect of isolating it as a stable complex.<sup>188</sup> The reduced forms of these complexes typically feature longer M–M bonds with respect to more oxidized species, indicating that the “extra” electron(s) occupies an antibonding orbital with respect to metal–metal bonding. This effect is much more pronounced for Fe and Co clusters than for those of Mo, indicating that the  $e_g$  MOs in the latter are only slightly antibonding.<sup>189</sup> In contrast, the shorter W–W bonds of the cluster  $[W_6Te_8(py)_6]^-$  relative to those in a neutral analogue  $[W_6Te_8(pip)_6]$  (pip = piperidine), suggests that the HOMO  $e_g$  orbitals of these clusters are metal–metal bonding in nature.<sup>190</sup>

Attempts to utilize  $M_6E_8$  clusters as low temperature precursors to the known molybdenum and elusive tungsten Chevrel phases have involved the thermolysis of clusters with (relatively) labile  $N$ -donor ligands. To this point, however, such endeavors have been unsuccessful, as only partial deligation of the terminal ligands is observed at lower temperatures, with disproportionation to  $MS_2$  and  $M$  occurring at higher temperatures.<sup>191,192</sup> Dimerization of  $[M_6S_8(PEt_3)_6]$  ( $M = Cr, Mo$ ) clusters has been achieved by removal of triethylphosphine by elemental sulfur to yield  $[M_{12}S_{16}(PEt_3)_{10}]$  ( $M = Cr$  (**19a**),  $Mo$  (**19b**))<sup>110,111</sup> (Figure 15). More recently, complexes of the formula  $[W_6S_8(PCy_3)_n(4-Bu^t\text{pyr})_{6-n}]$  ( $n = 1-6$ ) have been synthesized with the goal of using differences in thermal stabilities of the ligands in the directed synthesis of extended structures containing the  $W_6S_8$  unit.<sup>193</sup>

In contrast to the synthetic accessibility of the above complexes using solution approaches, the synthesis of octahedral rhenium chalcogenide clusters requires the implementation of high temperature solid-state reactions, or the conversion of cluster-containing solids into soluble molecular species by the methods of cluster excision or dimensional reduction (see Section 7.2.2.1.8). While cluster excision has produced the mixed sulfide(selenide)–chloride clusters  $[Re_6E_4+nCl_{10-2n}]^{6-n+}$  ( $n = 1-3$ ), the latter approach has led to the isolation of complexes with rhenium–chalcogenide cores  $[Re_6E_8X_6]^{4-}$  ( $E = S, Se; X = Cl, Br, I$ ).

An important facet of the chemistry of  $[Re_6E_8X_6]^{4-}$  clusters is the substitution-inert nature of the terminal halides on the  $Re^{III}$  centers. As a result, controlled substitution of the halide ligands for phosphines, amines, or solvent molecules yields a variety of clusters  $[Re_6E_8X_{6-n}(L)_n]^{(4-n)-}$  ( $n = 2-6$ ). The redox properties of these clusters have been found to be largely ligand-dependent. Clusters containing different combinations of substitution-inert phosphine and labile solvent ligands have been used to direct the synthesis of bridged-multiclusters by replacement of the solvent ligands with bridging amine ligands.<sup>194,195</sup> Thermolysis of similar clusters has resulted in the formation of condensed diclusters similar to those described for the  $Cr$  (**19a**) and  $Mo$  (**19b**) systems.<sup>196,197</sup> A condensed  $[Re_9Se_{11}Br_6]^{2-}$  (**20**) (Figure 16) cluster whose structure is comprised of two octahedral subunits sharing an  $\{Re_3\}$  face has been synthesized by solid-state synthesis.<sup>198</sup> Also reported is the synthesis of dendrimers based on the coordination of dendritic pyridyl-based ligands to the  $[Re_6Se_8]^{2+}$  cluster by the thermolytic replacement of  $MeCN$ .<sup>199</sup> Octahedral  $[Re_6E_8(CN)_6]^{4-}$  clusters have also been used in the synthesis of porous materials that are cluster-expanded analogues of a variety of metal–cyanide frameworks.<sup>200,201</sup> New materials containing these clusters include the Prussian blue analogues  $M_4[Re_6E_8(CN)_6]_3 \cdot xH_2O$  (**21**) ( $M = Ga, Fe; E = Se, Te$ )<sup>202</sup> (Figure 17) and chemical sensory materials containing  $Co^{2+}$  ions bridged by  $Re_6$  clusters.<sup>203</sup> Related  $Mo$  derivatives have been synthesized by the solid-state reaction of  $Mo/Se$  compounds in a  $KCN$  melt medium.<sup>204</sup>

**Table 2** Metal chalcogenide clusters based on octahedral  $M_6E_8$  ( $M = S, Se, Te$ ) cores.

Cluster	Synthetic approach(es)	References
$[Cp_6Ti_6Se_8]$	I	205
$[Cp_6Zr_6S_9]$	V	185
$[V_6Se_8O(PMe_3)_6]$	V	185
$[Cr_6S_8(PR_3)_6]$	I	186,206
$[Cr_6Se_8(PR_2R^2)_6]$	I	186,206
$[Cr_6Te_8(PET_3)_6]$	III	66
$[Cr_{12}S_{16}(PET_3)_{10}]$ ( <b>19a</b> )	VII	110
$[Mo_6S_8(PET_3)_6]^{n-}$ ( $n = 0, 1$ )	I, VII	189,191,207,208
$[Mo_6S_8(NO)(PET_3)_5]$	$[Mo_6S_8(PET_3)_6 + NOBF_4]$	209
$[Mo_6Se_8(PET_3)_6]^{n-}$ ( $n = 0, 1$ )	VII	189
$[Mo_{12}S_{16}(PET_3)_{10}]$ ( <b>19b</b> )	VII	111, 209
$[W_6S_8L_6]$ ( $L = PET_3, amine$ )	I, VII, ligand substitution	187,192,193,210,211
$[W_6Se_8L_6]$ ( $L = amine$ )	I	212
$[W_6Se_{8-x}Cl_x(PET_3)_6]^+$	I	213
$[W_6Te_8L_6]^{n-}$ ( $L = amine, n = 0, 1$ )	I	190,214
$[Re_6S_{4+n}Cl_{10-n}]^{n-}$ ( $n = 1-3$ )	VIII, X	215,216
$[Re_6S_6X_2(PPR^n)_3]^{n-}$ ( $X = As, P, NH, O, S$ )	V	217
$[Re_6Se_{4+n}Cl_{10-n}]^{n-}$ ( $n = 1-3$ )	VIII	114
$[Re_6E_5E(Cl_8)]^{2-}$ ( $E = S, Se;$ $E = O, S, Se, Te$ )	V	218
$[Re_6E_5(NR)Cl_8]^{2-}$ ( $E = S, Se$ )	V	219
$[Re_6S_8X_{6-n}L_n]^{(4-n)-}$ ( $X = Cl, Br, I$ CN; $L = PRt_3,$ $amine, solvent; n = 0-6$ )	VIII, ligand substitution	118,119,152-156,216,220,221
$[Re_6Se_8X_{6-n}L_n]^{(4-n)-}$ ( $X = Cl, Br, I, CN; L = H_2O, PR_3,$ $amine, solvent; n = 0-6$ )	VIII, ligand substitution	118,119,153,155,194,195, 197-199,222,223
$[Re_6Te_8(CN)_6]^{4-}$	VIII	155
$[Re_{6-n}Os_nSe_8Cl_6]^{n-}$ ( $n = 1-3$ )	VIII	224
$[Re_6Te_{8-n}Se_n(CN)_6]^{n-}$ ( $n = 1-8$ )	X	225
$Re_6Te_8(TeX_2)_6$ ( $X = Br, I$ )	X	226,227
$[(Re_6S_5OCl_7)_2O]^{4-}$	X	228
$[Re_9Se_{11}Br_6]^{2-}$ ( <b>20</b> )	XI	198
$[Re_{12}Se_{16}(PR_3)_{10}]$	VII	196,197
$[Re_{12}Se_{16}(PR_3)_{10}(L_2)_2]$	VII	194,195
$[Fe_6S_8(PET_3)_6]^{n-}$ ( $n = 0-4$ )	I	31,32,188,229-232
$[Fe_6Se_8(PET_3)_6]^+$	I	33
$[Co_6S_8L_6]^{n-}$ ( $L = PR_3, CO; n = 0, 1$ )	I, V, IX	34-36,120,233-240
$[Co_6S_7(\mu_3-H)(PET_3)_6]^+$	I	36
$[Co_{12}S_{14}(PET_3)_{10}]^{2-}$	I	241
$[Co_6Se_8L_6]$ ( $L = PR_3, CO$ )	I, V, IX	121,238,242,121
$[Co_6Te_8(PET_3)_6]^{n-}$ ( $n = 0-2$ )	III	243-245

### 7.2.4.3 Iron–Chalcogen Clusters Based on $Fe_2E_2$ Rhombs

Upon examination of the structures of iron chalcogen clusters, one feature that becomes apparent is that many of these complexes (Table 3) can be described in terms of vertex- or edge-sharing of  $Fe_2E_2$  rhombs. The simplest of these is the archetypal single planar rhomb structure found in the dimeric complexes  $[Fe_2S_2L_4]^{n-}$ .<sup>246,247</sup> Cuboidal  $[Fe_3S_4L_4]^{n-}$  and cubanoid  $[Fe_4S_4L_4]^{n-}$  (see Section 7.2.4.1) clusters are the most elementary examples of condensed structures based on these rhombohedral building units. The first examples of larger structures based on this structural motif were the “nest-like” clusters  $[Fe_6S_9(SR)_2]^{4-}$  (**22**).<sup>248-252</sup> Corresponding selenide–thiolate clusters have also been isolated.<sup>253</sup> The core of these complexes can be described in terms of eight fused  $Fe_2E_2$  units, two of which share all of their edges, while the other six each have two unshared edges (Figure 18). The  $[Fe_6S_9]^{2-}$  core is formally mixed valence, although there is no

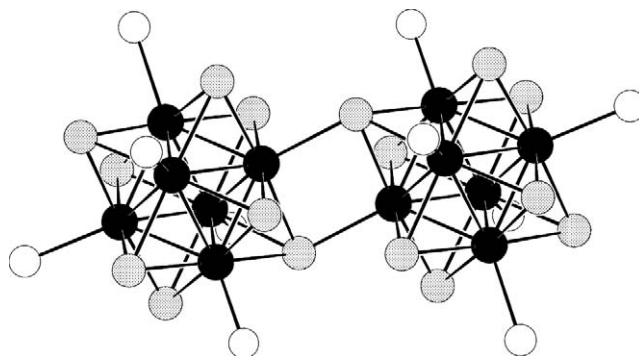


**Figure 15** Ball-and-stick representation of the cluster core of  $[M_{12}S_{16}(PEt_3)_{10}]$  (**19**) ( $M = Cr, Mo$ ).

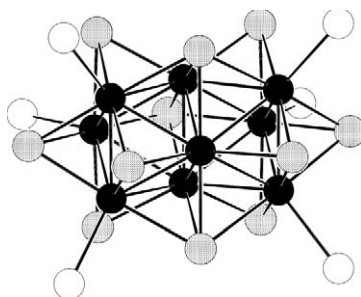


**Figure 16** Ball-and-stick representation of the cluster core of  $[Re_9Se_{11}Br_6]^{2-}$  (**20**).

localization of  $Fe^{II/III}$  positions. These clusters undergo reversible redox reactions, however attempts to isolate an  $[Fe_6S_9]^{2-}$  species resulted in cluster degradation.<sup>249</sup> Cluster degradation to  $[Fe_4S_4(SR)_4]^{2-}$  and  $[Fe_2S_2(SR)_4]^{2-}$  also occurs in the presence of excess thiolate, giving credence to the notion that the cluster is built up from such units. Further evidence is observed in the solid-state structure of  $[\{Fe_6S_9(SME)_2\}_2Na_2]^{6-}$ , which can be described in terms of condensed  $[Fe_3NaS_4]$  cubane subunits.<sup>251</sup>

A second structural type is observed in the prismane clusters  $[Fe_6S_6X_6]$  (**23**) ( $X = \text{halide, thiolate}$ ). The prismane structure consists of six  $Fe_2E_2$  units, but is probably better described as the fusion of two  $M_3E_3$  rings in a chair conformation, connected by  $M-E$  bonds (Figure 18). The structure can be derived from the more stable cubanoid by the addition of a  $Fe_2E_2$  unit to one of the faces. Coherent with this, one synthetic approach involves an oxidative cluster expansion reaction by the addition of  $Cp_2Fe^+$  to  $Fe_4S_4$ .<sup>254</sup> Upon heating, the cluster reverts back to a cubane complex.<sup>255</sup> Recently, the reaction of a diiron–diazanonane–dithiolate complex with  $[Fe_4S_4I_4]^{2-}$  resulted in the formation of the hexanuclear complex  $[\{Fe(\text{“Et}N_2S_2\text{”})\}_2Fe_4S_4I_2]$  (**24**) (“ $EtN_2S_2$ ” =  $N,N'$ -diethyl-3,7-diazanonane-1,9-dithiolate) with a unique “stair-like” configuration.<sup>252</sup> The structure is based on the fusion of seven  $Fe_2S_2$  rhombs arranged in an alternating horizontal–vertical fashion (Figure 18).

The synthesis of the clusters described above involves reaction systems containing halides or thiolates as the terminal ligands. The use of neutral terminal ligands such as tertiary phosphines has resulted in the formation of clusters with different structures. The mono-capped prismane cluster  $[Fe_7S_6(PEt_3)_6Cl_3]$  (**25**)<sup>140,256</sup> is an expanded version of the prismanes with an additional metal center coordinated to one of the  $M_3S_3$  faces (Figure 18). This structure has also been observed in cobalt sulfide clusters.<sup>235,257,258</sup> The basket-type structure is observed for more reduced derivatives  $[Fe_6S_6(PEt_3)_6]$  (**26a**) and  $[Fe_6S_6(PR_3)_4L_2]$  (**26b**) ( $L = \text{halide or thiolate}$ ) of the “ $Fe_6S_6$ ” series.<sup>137–142,259</sup> The selenide derivative  $[Fe_6Se_6(PR_3)_4Cl_2]$  (**26c**) has also been synthesized.<sup>138,140</sup> These complexes are topologically related to the prismane clusters in that they too are built up from six  $Fe_2S_2$  rhombs. The structure is not constructed *entirely* from these fragments, as a  $Fe-E-Fe$  unit serves as the basket “handle” (Figure 18). Furthermore, the structure contains a  $\mu_2-E$  or  $-SPh$ <sup>259</sup> (handle) as well as a  $\mu_4-E$  in its structure, as opposed to the prismane, which contains exclusively  $\mu_3-S$ .

Remarkable clusters in this series are the large ring-type structures comprised of  $[\mu_2-E]_n$  chains (Figure 19). The first of these are the  $[Na_2Fe_{18}S_{30}]^{8-}$  (**27**) clusters, which have been isolated as two

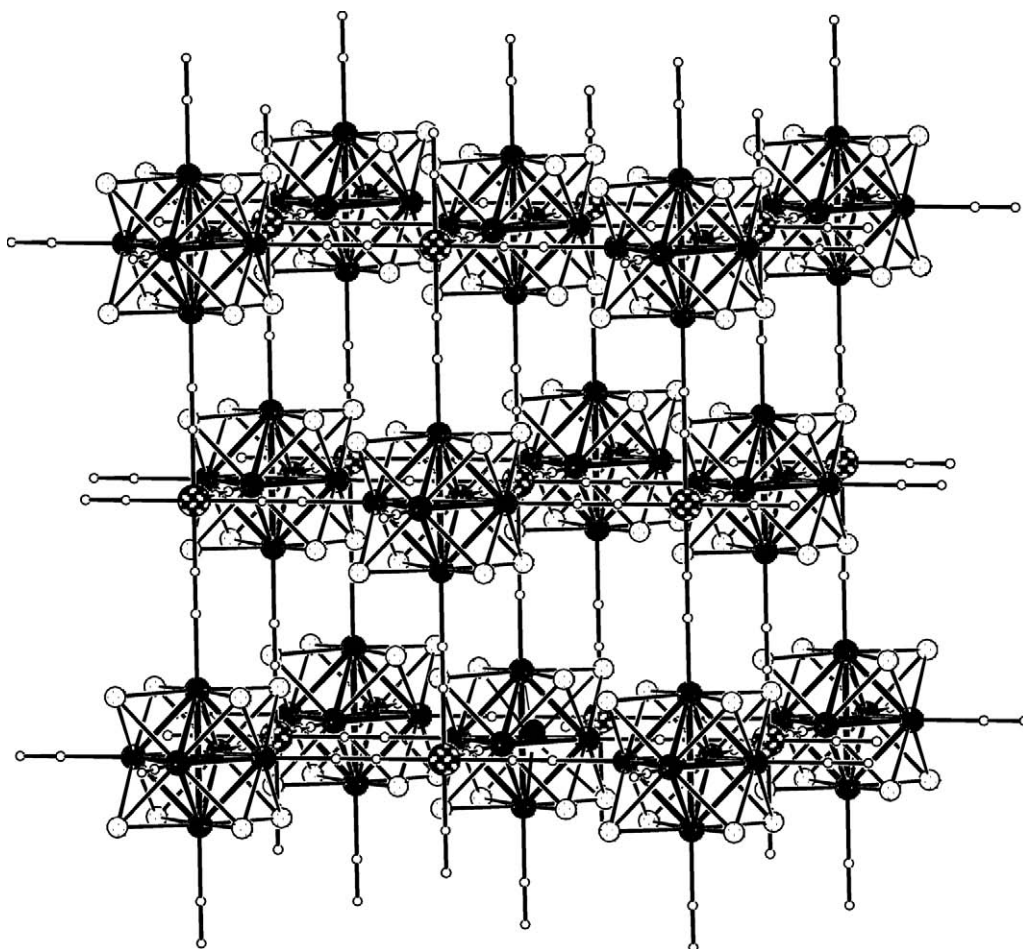


**Figure 17** Ball-and-stick representation of the Prussian blue analogue  $\text{Ga}_4[\text{Re}_6\text{E}_8(\text{CN})_6]_3 \cdot x\text{H}_2\text{O}$  (**21**).

**Table 3** Metal chalcogen clusters with structures based on  $\text{Fe}_2\text{E}_2$  rhombs.

Cluster	Synthetic approach(es)	Structure	References
$[\text{Fe}_6\text{S}_5(\mu\text{-SPh})(\text{PBu}^n_3)_4(\text{SPh})_2]$	VI	Basket	259
$[\text{Fe}_6\text{S}_6\text{X}_6]^{n-}$ ( $n = 2, 3$ ) ( <b>23</b> )	I, VI, ligand substitution	Prismane	254,255,264–270
$[\text{Fe}_6\text{S}_6(\text{PR}^1_2\text{R}^2)_4\text{X}_2]$ ( <b>26b</b> )	I, V, VI	Basket	137–140,259,271
$[\text{Fe}_6\text{S}_6(\text{PEt}_3)_6]^+$ ( <b>26a</b> )	I	Basket	140,141
$\{[\text{Fe}(\text{EtN}_2\text{S}_2)]\}_2\text{Fe}_4\text{S}_4\text{I}_2]$	VI	Stair-like	252
$\{[\text{Fe}(\text{EtN}_2\text{S}_2)]\}_2\text{Fe}_6\text{S}_5(\mu\text{-SR})_4]$	VI	Nest-like	252
$[\text{Fe}_6\text{S}_9(\text{SR})_2]^{4-}$ ( <b>22</b> )	I, II	Nest-like	248–251
$[\text{Fe}_6\text{Se}_6(\text{PR}^1_2\text{R}^2)_4\text{X}_2]$ ( <b>26c</b> )	V	Basket	138
$[\text{Fe}_6\text{Se}_9(\text{SR})_2]^{4-}$	I	Nest-like	253
$[\text{Fe}_6(\text{CO})_{12}(\text{TePh})_6]$ ( <b>30</b> )	V	Ring	263
$[\text{Fe}_7\text{S}_6(\text{PEt}_3)_4\text{Cl}_3]$ ( <b>25</b> )	V	Monocapped prismane	140,256,273
$\{[\text{Fe}_6\text{Se}_9(\text{SMe})_2\}_2\text{Na}_2]^{6-}$	II	Two prismanes joined by $\text{Na}^+$	251
$[\text{Fe}_{12}(\text{SePh})_{24}]$ ( <b>29</b> )	V	Ring	262
$[\text{Na}_2\text{Fe}_{18}\text{S}_{30}]^{8-}$ ( <b>27</b> )	I	See text	260,272
$[\text{Na}_9\text{Fe}_{20}\text{Se}_{38}]^{9-}$ ( <b>28</b> )	I	See text	260,261



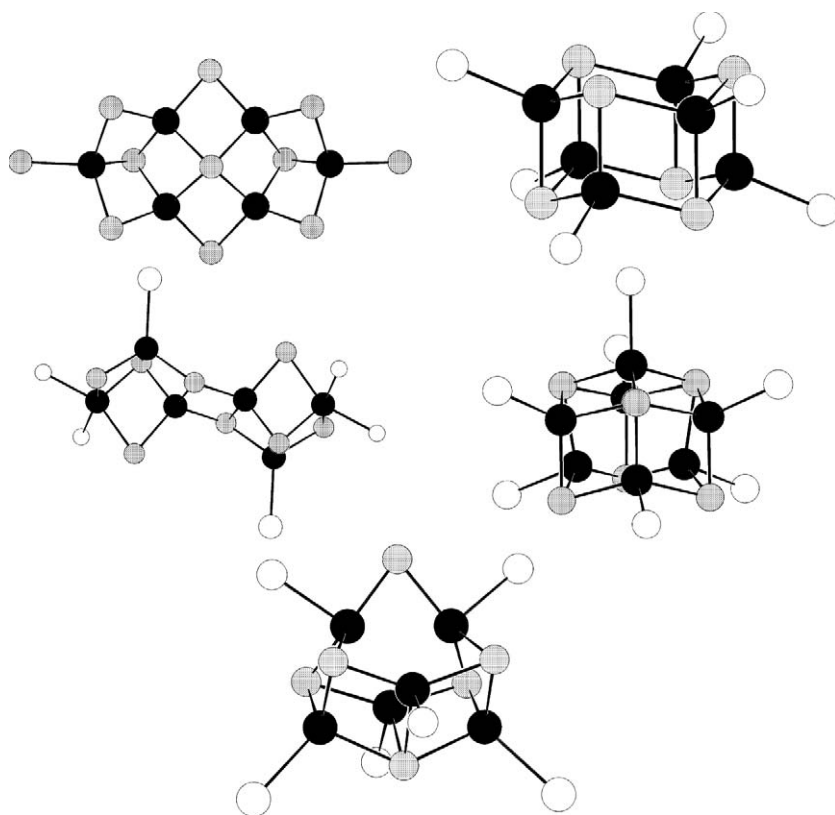


**Figure 18** Ball-and-stick representation of the cluster cores of iron chalcogenide clusters with structures based on  $\text{Fe}_2\text{E}_2$  rhombs.

isomers, designated the  $\alpha$ - and  $\beta$ -forms. The structure of the  $\alpha$ -isomer (**27a**) is constructed entirely from vertex- and edge-shared  $\text{Fe}_2\text{S}_2$  rhombs and can be viewed as a combination of two cuboidal  $\text{Fe}_3\text{S}_4$  and two  $\text{Fe}_6\text{S}_9$  units. Alternatively, the  $\beta$ -cluster (**27b**) consists of two  $\text{Fe}_2\text{S}_2$ , four  $\text{Fe}_3\text{S}_4$ , and two  $\text{FeS}_4$  fragments and contains two S atoms that cannot be viewed as being part of a  $\text{Fe}_2\text{S}_2$  rhomb. In the  $\alpha$ -form, the  $\text{Na}^+$  ions form bonding interactions with the S atoms in the cluster, and are thought to be essential in stabilizing the structure, while in the  $\beta$ -isomer, the  $\text{Na}^+$  ions are less tightly connected.<sup>260</sup> Replacement of  $\text{Li}_2\text{S}$  for  $\text{Li}_2\text{Se}$  in the self-assembly system of (**27**)

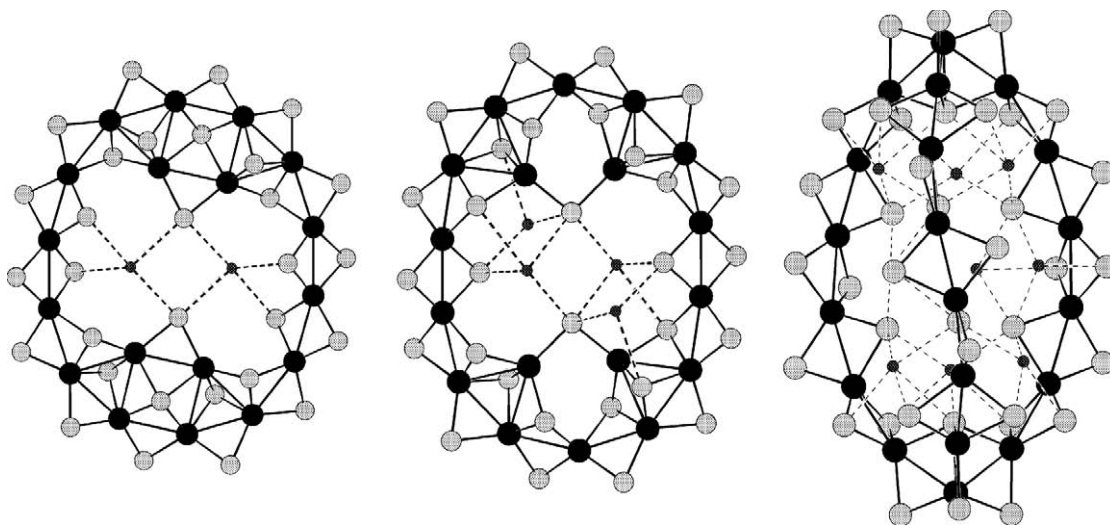


**Figure 19** Ball-and-stick representation of  $\alpha$ - $[\text{Na}_2\text{Fe}_{18}\text{S}_{30}]^{8-}$  (**27a**),  $\beta$ - $[\text{Na}_2\text{Fe}_{18}\text{S}_{30}]^{8-}$  (**27b**), and  $[\text{Na}_9\text{Fe}_{20}\text{Se}_{38}]^{9-}$  (**28**).

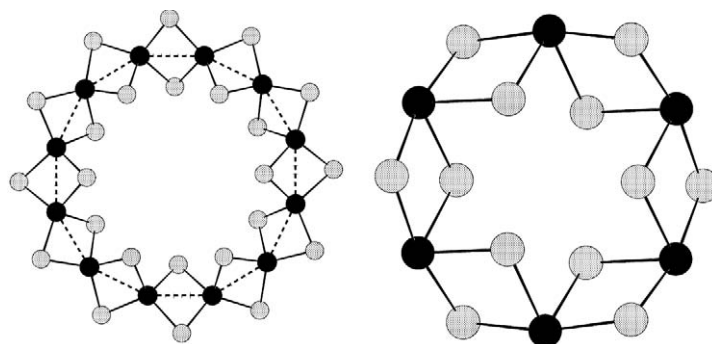


**Figure 20** Ball-and-stick representation of the cluster core of [Fe<sub>12</sub>(SePh)<sub>24</sub>] (**29**) and [Fe<sub>6</sub>(CO)<sub>12</sub>(TePh)<sub>12</sub>] (**30**).

resulted in the isolation of a selenide derivative [Na<sub>9</sub>Fe<sub>20</sub>Se<sub>38</sub>]<sup>9-</sup> (**28**).<sup>261</sup> The structure of this cluster is related to those of the sulfide counterparts in that it is constructed from 21 nonplanar Fe<sub>2</sub>Se<sub>2</sub> rhombs. It is also quite different in that it is a bicyclic structure, in which the two cycles are connected via μ<sub>4</sub>-Se bridges. Nine sodium ions are found encapsulated within the cavity of the cluster. This structure is unique in metal chalcogen cluster chemistry, and can be regarded as an inorganic cryptand. Extended Hückel calculations reveal a band-like structure and a small HOMO-LUMO gap, giving rise to antiferromagnetic properties.<sup>260</sup>

Similar ring-type structures have been observed for iron selenolate and tellurolate complexes synthesized from silylated chalcogen reagents. The clusters [Fe<sub>12</sub>(SePh)<sub>24</sub>] (**29**) and [Fe<sub>6</sub>(CO)<sub>12</sub>(TePh)<sub>12</sub>] (**30**) consist of 12 and six Fe<sub>2</sub>E<sub>2</sub> units, respectively, connected through vertex-sharing interactions (Figure 20).<sup>262,263</sup> All iron centers in the clusters are in the +2 oxidation state. This is in contrast to (**27**) and (**28**), which contain both Fe<sup>II</sup> and Fe<sup>III</sup>. Just as in (**27**) and (**28**), antiferromagnetic coupling is also observed for (**29**).

#### 7.2.4.4 Cubic Clusters

The organization of eight metal atoms in a cubic array, in which the six M<sub>4</sub> faces are capped by μ<sub>4</sub>-E ligands, is a fundamental unit in a number of mineral compounds including pentlandite,<sup>274</sup> bartonite,<sup>275</sup> and djerfisherite.<sup>11</sup> Thus, it is not surprising that this structural type (Figure 21) is observed in (albeit a small number of) molecular cluster complexes of iron, cobalt, and nickel (Table 4), as well as the lanthanide chalcogen clusters (see Section 7.2.5.5). The E-centered copper and silver cubes bridged by dichalcogenophosphate ligands (Section 7.2.5.3.2) may also be included in this group. An alternative E-centered structure is observed in the cluster [M<sub>14</sub>(μ-S)(SPh)<sub>12</sub>(PPh<sub>3</sub>)<sub>*n*</sub>] (M = Cu, *n* = 6 (**31a**), M = Ag, *n* = 8 (**31b**)), which consists of a Cu<sub>8</sub> cube encapsulated by an icosahedron of thiolate ligands.<sup>126,276</sup> The six additional Cu atoms form an octahedron that encapsulates the S<sub>12</sub> icosahedron (Figure 22). Extended Hückel calculations performed on a Ni-centered cube, as observed in [Ni<sub>9</sub>Te<sub>6</sub>(PEt<sub>3</sub>)<sub>6</sub>],<sup>67</sup> and a hypothetical Te-centered cube demonstrate that the latter is much more stable, owing to both Ni-Te and Te-Te interactions.<sup>277</sup> A unique M<sub>7</sub>E cube is observed in the large Zintl ion [Cu<sub>7</sub>As<sub>3</sub>Te<sub>13</sub>]<sup>4-</sup>.<sup>278</sup>

A different type of cube-like structure is observed for the clusters [M<sub>12</sub>E<sub>8</sub>]<sup>4-</sup> in which the chalcogen atoms form the eight vertices. The metal ions are located at the midpoints of the 12 edges of the cubes (Figure 21). The cluster [NaAu<sub>12</sub>Se<sub>8</sub>]<sup>3-</sup> is an inorganic cryptate in which the Na<sup>+</sup> ion is trapped inside the cube.<sup>279</sup> A similar complex, [KAu<sub>9</sub>Te<sub>7</sub>]<sup>4-</sup> with a “missing” Au<sub>3</sub>Te fragment can accommodate a larger (K<sup>+</sup>) ion.<sup>280</sup>

#### 7.2.4.5 Clusters with Structures Based on Adamantane or Barrelene Cages and Related Fragments

The single adamantane-like cage (Figure 12) is a fundamental structural type, frequently observed for chalcogen-bridged clusters containing a variety of metals adopting tetrahedral coordination geometry. The M<sub>4</sub>E<sub>6</sub> core of these complexes features a tetrahedral array of metal ions, the edges of which are bridged by six chalcogen ligands. The bridging ligands are generally chalcogenolates (RE<sup>-</sup>), with chalcogenide (E<sup>2-</sup>)-bridged species observed only for clusters of post-transition

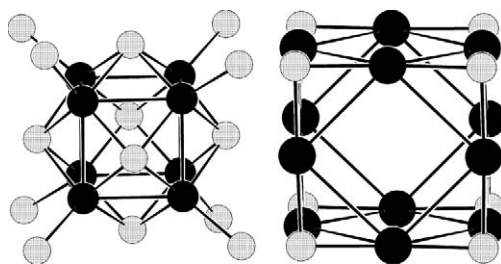


**Figure 21** Ball-and-stick representation of the cluster core of cubic  $[M_8E_6L_8]$  and  $[M_{12}E_8]^{4-}$ .

**Table 4** Metal chalcogen clusters with cubic core geometry.

<i>Cluster</i>	<i>Synthetic approach</i>	<i>References</i>
$[Nb_2O_2Se_6Cu_6(PMe_3)_6]$	VI	108
$[Mn_4Cu_4(SPr^t)_{12}S]^{2-}$	VI	281
$[Fe_8S_6I_8]^{3-}$	VI	282
$[Fe_8S_6(PCy_3)_4Cl_4]$	Decomposition of $[Fe_8S_8(PCy_3)_6]$ in $CHCl_3$	283
$[Fe_3Ni_5S_6I_8]^{3-}$	VI	109
$[Fe_4Ni_4S_6I_4(PMePh_2)_4]$	VI	284
$[Fe_6Ni_2S_6I_6(PMePh_2)_2]^{2-}$	VI	284
$[Co_8S_6Br_2Cl_2(PPh_3)_8]^{n-}$	IX	127
$[Co_8S_6(SPh)_8]^{n-}$ ( $n = 4, 5$ )	I	285,286
$[Cu_{14}S(SPh)_{12}(PPh_3)_6]$ ( <b>31a</b> )	IX	126
$[Ag_{14}S(SPh)_{12}(PPh_3)_8]$ ( <b>31b</b> )	IX	276
$[Ni_9Te_6(PEt_3)_8]$	III	67
$[Cu_7As_3Te_{13}]^{4-}$	X	278
$[Cu_{12}S_8]^{4-}$	I	287
$[Au_{12}S_8]^{4-}$	I	288
$[NaAu_{12}Se_8]^{3-}$	I	279
$[KAu_9Te_7]^{4-}$	I	280

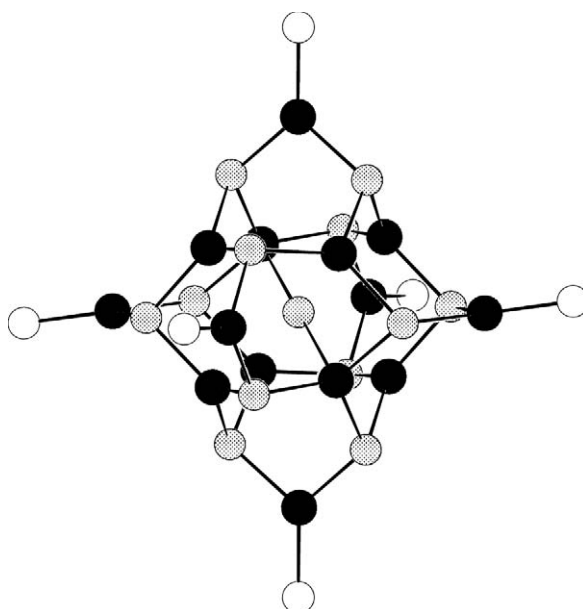


**Figure 22** Ball-and-stick representation of the cluster core of  $[Cu_{14}(\mu-S)(SPh)_{12}(PPh_3)_6]$  (**31a**).

metals. Each metal center is bonded to three  $\mu_2$ -bridging chalcogen ligands, and, with the exception of the  $\text{Cu}^{\text{I}}$  clusters  $[\text{Cu}_4(\mu\text{-ER})_6]^{2-}$  ( $\text{E} = \text{S}, \text{Se}$ ),<sup>289–294</sup> terminal ligands such as chalcogenides, chalcogenolates, halides, or tertiary phosphines, complete the tetrahedral coordination.

Of particular interest amongst complexes adopting this structural type are those containing the group 12 metals, Zn, Cd, and Hg. The adamantoid structure of these clusters is very similar to the basic structural unit of the cubic (sphalerite) phase of the corresponding bulk semiconductor (i.e., ZnS, CdSe, etc.),<sup>295</sup> and thus these complexes represent molecular models of the solid-state materials. In addition, several larger clusters, whose structures are based on the fusion of adamantane cages via edge-sharing interactions, have been synthesized, allowing investigation of the effects of cluster size on physical properties. Recently it has been demonstrated that the quantum confinement effects observed for colloidal CdSe nanoparticles can be extended to the molecular (albeit nanoscale) size regime<sup>296</sup> (see Section 7.2.6.3).

The fusion of four adamantoid cages results in the supertetrahedral structure (Figure 12) observed for the clusters  $[\text{E}^1_4\text{M}_{10}(\text{E}^2\text{R})_{12}\text{L}_4]^{n-}$  ( $\text{M} = \text{Zn}, \text{Cd}$ ;  $\text{E}^1, \text{E}^2 = \text{S}, \text{Se}, \text{Te}$ ;  $\text{L} = \text{E}^2\text{R}, \text{X}, \text{PR}_3$ ,  $n = 0, 4$ ). An expanded structure is observed for  $[\text{Cd}_{16}(\text{SePh})_{32}(\text{PPh}_3)_2]$  (32), where the four cages are separated by SePh bridges (Figure 23).<sup>297</sup> While it is possible to envision an endless series of clusters representing larger and larger sections of the sphalerite ME lattice, with the next members being  $[\text{M}_{20}\text{E}_{13}(\text{ER})_{22}]^{8-}$  and  $[\text{M}_{35}\text{E}_{28}(\text{ER})_{28}]^{12-}$  no such complexes have been structurally characterized, and it is suggested that the high charge of these clusters may preclude the isolation of such species.<sup>296</sup> Instead, larger tetrahedral clusters such as  $[\text{Cd}_{17}\text{E}_4(\text{EPh})_{28-n}\text{L}_n]$  ( $\text{E} = \text{S}, \text{L} = \text{SPh}$  (33a);  $\text{E} = \text{Se}, \text{L} = \text{PPh}_3$  (33b)),  $[\text{Cd}_{32}\text{E}_{14}(\text{ER})_{36}\text{L}_4]$  and  $[\text{Hg}_{32}\text{Se}_{14}(\text{SePh})_{36}]$  (34) (Figure 24) feature sphalerite-like core structures, with terminating barrelenoid cages residing at the four corners of the tetrahedron. The barrelenoid unit represents a cutout of the less thermodynamically stable hexagonal (wurtzite) phase of bulk II–VI semiconductors.<sup>295</sup> The interesting photophysical properties of these and other II–VI nanoclusters are discussed in Section 7.2.7.2. The reaction of  $\text{ZnEt}_2$  with sulfur produced the zinc–thiolate cluster,  $[\text{Zn}(\text{SEt})\text{Et}]_{10}$  (35) that resembled closely a portion of the wurtzite lattice of crystalline ZnS (Figure 25).<sup>85</sup> This complex is unique in regard to other  $[\text{Zn}(\text{SR}^1)\text{R}^2]_n$  clusters,<sup>298,299</sup> which do not resemble either the wurtzite or sphalerite phase of ZnS. A number of clusters containing a  $[\text{M}_8\text{E}_{13}]$  core have been isolated, and although their structures have been described recently as four very distorted barrelene cages,<sup>300</sup> they are not representative of the corresponding bulk hexagonal lattice.

There are few examples amongst II–VI clusters in which the basic structural unit is not related to the adamantane or barrelene cage, granting evidence to the thermodynamic stability of such structures. This is substantiated by the fact that similar structures are accessible via different synthetic routes (see Table 5). Nonadamantoid/barrelenoid structures usually consist of

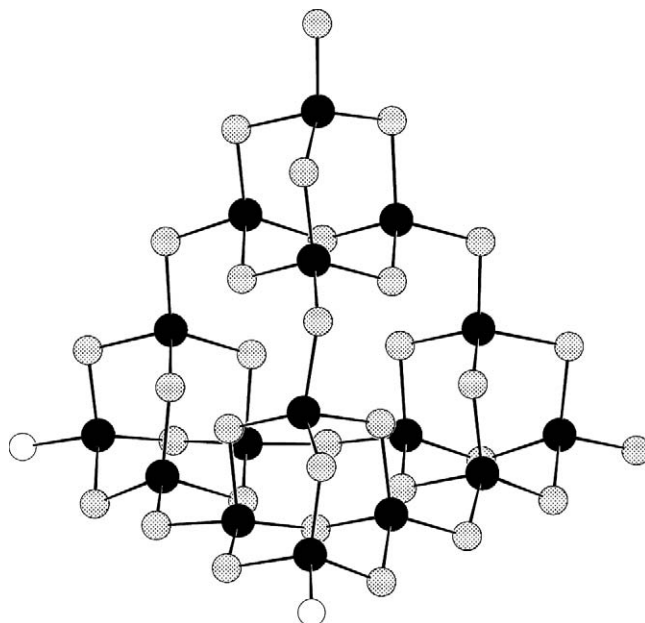
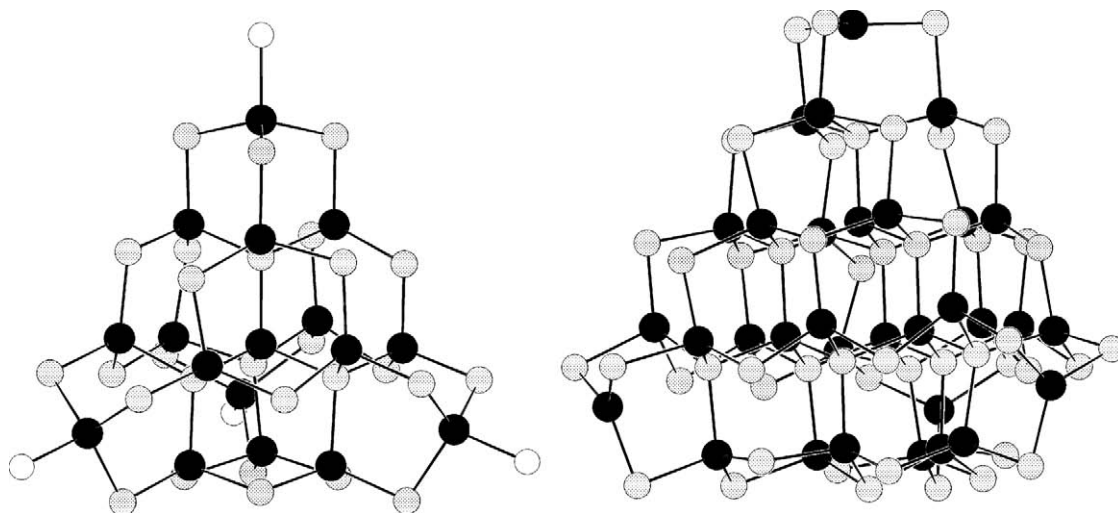
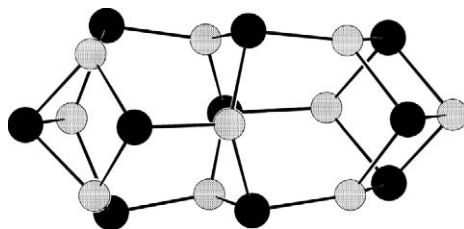


Figure 23 Ball-and-stick representation of the cluster core of  $[\text{Cd}_{16}(\text{SePh})_{32}(\text{PPh}_3)_2]$  (32).



**Figure 24** Ball-and-stick representation of the cluster core of  $[\text{Cd}_{17}\text{E}_4(\text{EPh})_{28}\text{L}_4]$  (33)  $[\text{Hg}_{32}\text{Se}_{14}(\text{SePh})_{36}]$  (34).



**Figure 25** Ball-and-stick representation of the cluster core of  $[\text{Zn}(\text{SEt})\text{Et}]_{10}$  (35).

multi-bridging or chelating ancillary ligands, which restrict the capacity of some of the metal centers to assume the customary tetrahedral configuration via metal–chalcogenolate bonding interactions. The cluster  $[\text{Zn}_{10}\text{S}_7(\text{py})_9(\text{SO}_4)_3]$ <sup>301</sup> contains a  $\text{Zn}_{10}\text{S}_7$  core which is capped by tridentate sulfate ligands, while a series of  $\text{ZnTe}$  clusters with chelating TMEDA or dpmm ligands has also been isolated recently.<sup>95</sup> The structures of these complexes are unique with respect to those observed for other II–VI clusters, and significant deviations from the ideal tetrahedral geometry of the Zn atoms are observed.

Structures based on fused adamantane-like units have also been observed in a selection of main group metal chalcogenide clusters.<sup>5,86,136</sup> Recently, ternary copper(I)–indium(III)–selenide clusters have been isolated from reactions of  $\text{InCl}_3$  and  $\text{CuCl}$  with silylated selenium reagents in the presence of phosphine ligands.<sup>302</sup> The clusters  $[\text{Cu}_6\text{In}_8\text{Se}_{13}\text{Cl}_4(\text{PPh}_3)_6(\text{THF})]$  and  $[\text{Cu}_6\text{In}_8\text{Se}_{13}\text{Cl}_4(\text{PPr}^n_2\text{Ph})_6]$  contain  $[\text{In}_8\text{Se}_{13}\text{Cl}_4]$  cores, analogous to those observed for corresponding II–VI complexes, but with  $\text{Cu}(\text{PR}^1_2\text{R}^2)_n$  units ( $n=1, 2$ ) coordinated to the external selenide ligands. The structure of the larger cluster  $[\text{Cu}_{11}\text{In}_{15}\text{Se}_{16}(\text{SePh})_{24}(\text{PPh}_3)_4]$  (36) (Figure 26) is derived from face-sharing interactions of adamantane and barrelene units containing copper, indium, and selenium atoms.

## 7.2.5 DIVERSE STRUCTURES FROM WIDELY APPLICABLE SYNTHETIC ROUTES

### 7.2.5.1 Clusters from Silylated Chalcogen Reagents

The use of silylated chalcogen reagents in the synthesis of chalcogen-bridged metal clusters has produced a remarkable number of complexes with a variety of structural types. The nuclearities and structures of these complexes can be highly dependent on the reaction conditions, the steric demands of the ancillary and/or chalcogenolate ligands, as well as the ratio M:E. Complexes

**Table 5** Metal chalcogen clusters with structures based on adamantane, barrelene and related structures.

Cluster	Synthetic approach(es)	References
$[\text{Mn}_4(\text{SR})_6\text{L}_4]^{2-}$ (L = SPh, Cl)	I, VI	303,304
$[\text{Mn}_4(\text{SePr}^t)_6\text{Br}_4]^{2-}$	VI	304
$[\text{Fe}_4(\text{SPh})_6\text{L}_4]^{2-}$ (L = SPh, Cl)	I	305–308
$[\text{Fe}_3\text{Cu}(\text{SPr}^t)_6\text{Cl}_3]^{2-}$	VI	309
$[\text{Fe}_3\text{Cu}(\text{SePr}^t)_6\text{Cl}_3]^{2-}$	VI	310
$[\text{Co}_4(\text{SPh})_{10}]^{2-}$	I	308,311,312
$[\text{Cu}_4(\text{SPh})_6]^{2-}$	I	289–292
$[\text{Cu}_4\{o\text{-(SCH}_2)_2\text{C}_6\text{H}_4\}_3]^{2-}$	I	293
$[\text{Cu}_4(\text{SePh})_6]^{2-}$	I	294
$[\text{Zn}_4(\text{SPh})_{10-n}\text{L}_n]^{2-}$ (L = SPh, Cl, Br; $n = 0, 1, 4$ ) ( <b>17a</b> )	I, II, ligand substitution	59,313–316
$[\text{Zn}_4(\text{SePh})_6\text{Cl}_4]^{2-}$	V	94
$[\text{Cd}_4(\text{SR})_{10-n}\text{L}_n]^{2-}$ (L = SPh, Cl, Br, PPh <sub>3</sub> , OClO <sub>3</sub> ; $n = 0, 2\text{--}4$ ) ( <b>17b</b> )	I, ligand substitution	59,315–320
$[\text{Cd}_4(\text{SePh})_6\text{L}_4]^{2-}$ (L = Cl, Br)	V	296,316
$[\text{Zn}_5(\text{SBU}^t)_5\text{Me}_5]$	I	298
$[\text{Hg}_6(\text{SePh})_{12}(\text{PBu}^t_3)_2]$	V	321
$[\text{Hg}_6(\text{SePh})_{14}]^{2-}$	V	321
$[\text{Zn}_8\text{Se}(\text{SePh})_{12+n}\text{L}_{4-n}]^{2-n-}$ (L = Cl, $n = 0$ ; L = PPr <sup>n</sup> <sub>3</sub> , $n = 2$ )	V	94
$[\text{Zn}_8\text{Te}(\text{TePh})_{12}\text{Cl}_4]^{2-}$	V	94
$[\text{XCd}_8(\text{SCH}_2\text{CH}_2\text{OH})_{12}\text{X}_3]$ (X = Cl, Br, I)	I	322
$[\text{ClCd}_8\{\text{SCH}(\text{CH}_2\text{CH}_2)_2\text{NHMe}\}_{16}]^{15+}$	I	323
$[\text{Cd}_8\text{S}(\text{SPh})_{16}]^{2-}$	I	324
$[\text{Cd}_8\text{Se}(\text{SPh})_{16}]^{2-}$	I	324
$[\text{Cd}_8\text{Se}(\text{SePh})_{16}]^{2-}$	I	324
$[\text{Cd}_8\text{Se}(\text{SePh})_{14-n}\text{L}_m]^{n-}$ (L = PPh <sub>3</sub> , Cl ( <b>84</b> ), DMF; $m = 2\text{--}4$ ; $n = 0, 2$ )	V	300
$[\text{Cd}_8\text{Te}(\text{SPh})_{16}]^{2-}$	I	324
$[\text{Cd}_8\text{Te}(\text{SePh})_{16}]^{2-}$	I	324
$[\text{Cd}_8\text{Te}(\text{TePh})_{14}(\text{PEt}_3)_3]$	V	300
$[\text{Cu}_6\text{In}_3(\text{SEt})_{16}]^{-}$	I	327
$[\text{Zn}_{10}(\text{SEt})_{10}\text{Et}_{10}]$ ( <b>35</b> )	IV	85
$[\text{Zn}_{10}\text{S}_4(\text{SPh})_{16-n}\text{L}_n]^{4-}$ (L = amine; $n = 0, 4$ )	I, II, IV	59,325,326
$[\text{Zn}_{10}\text{S}_7(\text{pyridine})_9(\text{SO}_4)_3]$	“Zn <sub>4</sub> S <sub>4</sub> (SPh) <sub>12</sub> ” + pyridine	301
$[\text{Zn}_{10}\text{Se}_4(\text{SPh})_{16}]^{4-}$	II	59
$[\text{Zn}_{10}\text{Te}_4(\text{TePh})_{12}(\text{PR}_3)_n]$ ( $n = 2, 4$ )	V	94,95
$[\text{Cd}_{10}\text{S}_4(\text{SPh})_{16}]^{4-}$ ( <b>18</b> )	I, II	59,325
$[\text{Cd}_{10}\text{S}_4(\text{SePh})_{16}]^{4-}$	II	59
$[\text{Cd}_{10}\text{Se}_4(\text{SPh})_{16}]^{4-}$	II	59
$[\text{Cd}_{10}\text{Se}_4(\text{SePh})_{12}(\text{PR}_3)_4]$ ( <b>85</b> )	V	296,297
$[\text{Zn}_{12}\text{Te}_9(\text{TeMes})_6(\text{dppm})_4]$	V	95
$[\text{Zn}_{14}\text{Te}_{13}\text{Cl}_2(\text{TMEDA})_6]$	V	95
$[\text{Zn}_{14}\text{Te}_{13}(\text{TMEDA})_6]^{2+}$	V	95
$[\text{Zn}_{14}\text{Te}_{13}(\text{TeMes})(\text{TMEDA})_6]^+$	V	95
$[\text{Cu}_6\text{In}_8\text{Se}_{13}\text{Cl}_4(\text{PPh}_3)_6(\text{C}_4\text{H}_8\text{O})]$ ( <b>36</b> )	V	302
$[\text{Cu}_6\text{In}_8\text{Se}_{13}\text{Cl}_4(\text{PPr}^n_2\text{Ph})_{12}]$	V	302
$[\text{Zn}_{16}\text{Te}_{13}(\text{TePh})_6(\text{TMEDA})_5]$	V	95
$[\text{Cd}_{16}(\text{SePh})_{32}(\text{PPh}_3)_2]$ ( <b>32</b> )	V	297
$[\text{Cd}_{17}\text{S}_4(\text{SPh})_{28}]^{2-}$ ( <b>33a</b> )	I	328
$[\text{Cd}_{17}\text{Se}_4(\text{SePh})_{24}(\text{PPh}_3)_4]^{2-}$ ( <b>33b</b> )	V	300
$[\text{Cu}_{11}\text{In}_{15}\text{Se}_{16}(\text{SePh})_{24}(\text{PPh}_3)_4]$	V	302
$[\text{Cd}_{32}\text{S}_{14}(\text{SR})_{36}\text{L}_4]$ (L = DMF ( <b>83a</b> ), H <sub>2</sub> O ( <b>83b</b> ))	I, Cd <sub>10</sub> S <sub>4</sub> (SPh) <sub>16</sub> + pyridine	329,330
$[\text{Cd}_{32}\text{Se}_{14}(\text{SePh})_{36}(\text{PPh}_3)_4]$ ( <b>83c</b> )	V	331
$[\text{Hg}_{32}\text{Se}_{14}(\text{SePh})_{36}]$ ( <b>34</b> )	V	331

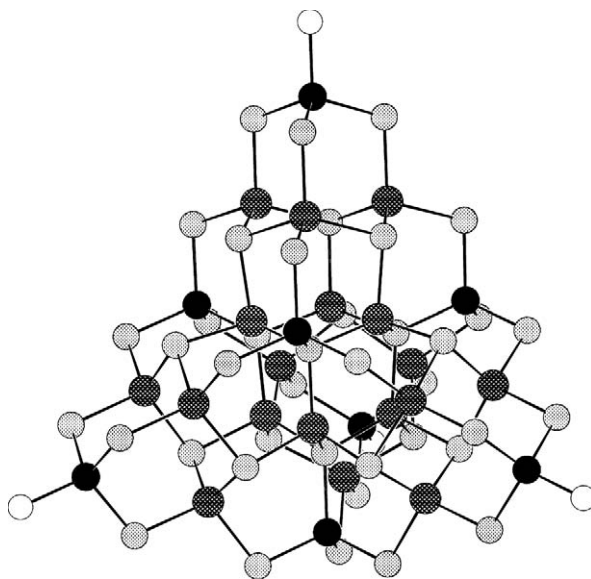


**Figure 26** Ball-and-stick representation of the cluster core of  $[\text{Cu}_{11}\text{In}_{15}\text{Se}_{16}(\text{SePh})_{24}(\text{PPh}_3)_4]$  (**36**).

ranging in size from truly molecular to the “giant” copper and silver selenide nanoclusters have been characterized structurally.

#### 7.2.5.1.1 Early transition metal–chalcogenide clusters

The relatively small number of early transition metal chalcogen clusters synthesized via this route (Table 6), includes the sulfur-rich clusters of Ta and Nb. The reaction of  $\text{CpTaCl}_4$  with  $\text{S}(\text{TMS})_2$  results in a mixture of polynuclear complexes including  $[\text{Cp}_4\text{Ta}_4\text{S}_{13}]$  and  $[\text{Cp}_8\text{Ta}_6\text{S}_{10}]$ .<sup>332</sup> The former is isostructural with  $[\text{Mo}_4(\text{NO})_4\text{S}_{13}]$ ,<sup>333</sup> consisting of a “butterfly” arrangement of Ta atoms, capped by two  $\mu_3\text{-S}$ , one  $\mu_4\text{-S}$ , and further bridged by four  $\mu_2\text{-S}_2$  ligands. In  $[\text{Cp}_4\text{Ta}_4\text{S}_{13}]$ , two  $\text{TaS}_6$  units are each connected to two  $\text{Cp}_2\text{Ta}$ , and to each other by  $\mu_2\text{-S}$  bridges. Perhaps the most remarkable structures in this group are observed for the hexanuclear complexes of the formula  $[\text{M}_6\text{S}_{17}]^{4-}$  (**4**) ( $\text{M} = \text{Ta}, \text{Nb}$ ).<sup>134,135</sup> The clusters are built up from 10 fused  $\text{M}_2\text{S}_2$  rhombs, resulting in a crown-type open cage structure as shown in Figure 5. Interestingly, these complexes contain four different types of coordinated sulfur atoms. Five  $\mu_3\text{-S}$  ligands connect the “apical” M atom to the other five metal atoms, which are linked to each other by  $\mu_2\text{-S}$  bridges. A central  $\mu_6\text{-S}$  ligand resides inside the cage, and each metal atom is additionally bonded to a terminal sulfur atom. The existence of four different types of sulfur atoms in the same complex is quite interesting, especially considering the wide range of coordination modes (terminal to  $\mu_6$ ) adopted by these ligands.

**Table 6** Early transition metal chalcogenide clusters synthesized using silylated chalcogen reagents.

Cluster	Structure	References
$[(\text{RC}_5\text{H}_4)\text{Ti}_4\text{S}_4]$	Cubane	334
$[\text{Cp}_4\text{Ti}_4\text{Se}_7\text{O}]$	O-centered $\text{Ti}_4\text{Se}_4$ cubane with one $\mu\text{-Se}$ and two $\mu\text{-Se}_2$	335
$[\text{Cp}_5\text{Ti}_5\text{S}_6]$	Distorted trigonal bipyramid of Ti capped by six $\mu_3\text{-S}$	336
$[\text{Cp}_6\text{Zr}_6\text{S}_9]$	S-centered octahedron	185
$[\text{V}_6\text{Se}_8\text{O}(\text{PMe}_3)_6]$	O-centered octahedron	185
$[\text{Nb}_6\text{S}_{17}]^{4-}$ ( <b>4a</b> )	See text	134,135
$[\text{Cp}_4\text{Ta}_4\text{S}_{13}]$	Two edge-sharing $\text{Ta}_3$ units bridged by one $\mu_4\text{-S}$ , two $\mu_3\text{-S}$ and five $\mu\text{-}\eta^2\text{-S}$	332
$[\text{Cp}_8\text{Ta}_6\text{S}_{10}]^{2+}$	Two $\text{Ta}_3(\mu\text{-S})_4$ units bridged by two $\mu\text{-S}$	332
$[\text{Ta}_6\text{S}_{17}]^{4-}$ ( <b>4b</b> )	Pentagonal pyramidal open cage	134,135

**Table 7** Middle transition metal chalcogen clusters synthesized using silylated chalcogen reagents.

Cluster	Structure	References
$[\text{Re}_6\text{E}^1_5\text{E}^2\text{Cl}_8]^{2-}$ ( $\text{E}^1 = \text{S, Se}$ ; $\text{E}^2 = \text{S, Se, Te}$ )	Octahedron	217,218
$[\text{Fe}_6\text{S}_6(\text{PET}_3)_4\text{X}_2]$ ( $\text{X} = \text{Cl, Br, I, SR}$ ( <b>26b</b> ))	Basket	138–140
$[\text{Fe}_6\text{Se}_6(\text{PET}_3)_4\text{Cl}_2]$ ( <b>26c</b> )	Basket	138
$[\text{Fe}_7\text{S}_6(\text{PET}_3)_4\text{Cl}_3]$ ( <b>25</b> )	Mono-capped prismane	140,256
$[\text{Fe}_6(\text{CO})_{12}(\text{TePh})_{12}]$ ( <b>30</b> )	$\text{Fe}_6$ planar ring bridged by 12 $\mu$ -TePh	263
$[\text{Fe}_{12}(\text{SePh})_{24}]$ ( <b>29</b> )	$\text{Fe}_{12}$ planar ring bridged by 24 $\mu$ -SePh	262
$[\text{Co}_4\text{Se}_4(\text{PR}_3)_4]$	Cubane	242
$[\text{Co}_6\text{S}_8(\text{PR}_3)_4]^n$ ( $n = 0, 1$ )	Octahedron	235
$[\text{Co}_6\text{Se}_8(\text{PR}_3)_4]^n$ ( $n = -1, 0, 1$ )	Octahedron	337
$[\text{Co}_7\text{S}_6\text{Cl}_2(\text{PPh}_3)_5]$ ( $\text{X} = \text{Cl, I}$ )	Mono-capped prismane	235,258
$[\text{Co}_8\text{Se}_8(\text{PPh}_3)_6]^n$ ( $n = 0, 1$ ) ( <b>38</b> )	See text	337
$[\text{Co}_9\text{Se}_{11}(\text{PPh}_3)_6]$ ( <b>37</b> )	See text	242

### 7.2.5.1.2 Middle transition metal–chalcogenide clusters

The two binary iron–chalcogenolate clusters<sup>262,263</sup> isolated from reactions of PhE-TMS ( $\text{E} = \text{Se, Te}$ ) with iron-containing salts have ring-type structures as described in Section 7.2.4.3. The reaction of  $\text{E}(\text{TMS})_2$  ( $\text{E} = \text{S, Se, Te}$ ) with  $(\text{PET}_3)_2\text{FeX}_2$  or  $(\text{PR}_3)_2\text{CoX}_2$  has produced several clusters with the frequently observed structures discussed in Sections 7.2.4.1–7.2.4.4 (Table 7). In addition, the complexes  $[\text{Co}_9\text{Se}_{11}(\text{PPh}_3)_6]$  (**37**)<sup>242</sup> and  $[\text{Co}_8\text{Se}_8(\text{PPh}_3)_6]^n$  (**38**) ( $n = 0, 1$ )<sup>337</sup> have been isolated. The structures of these clusters are related to the octahedral structures commonly observed in Co/E chemistry.  $[\text{Co}_9\text{Se}_{11}(\text{PPh}_3)_6]$  is constructed from two face-sharing  $\text{Co}_6$  octahedra, with eight  $\mu_3$ -Se atoms capping  $\text{Co}_3$  faces (Figure 27a). The three “butterfly-like” faces created by the fusion of the octahedral units are each capped by a  $\mu_4$ -Se ligand. The octanuclear clusters resemble edge-shared octahedra, except that a vertex is “missing” from the individual subunits (Figure 27b). Structures based on face-sharing octahedra are also common among nickel chalcogenide clusters (see Section 7.2.5.1.3(i)). Substitution reactions of face-capping chloride ligands for chalcogenides on octahedral  $\{\text{Re}_6\}$  clusters have been carried out using  $\text{E}(\text{TMS})_2$  ( $\text{E} = \text{S, Se, Te}$ ).<sup>217,218</sup> These clusters are described in Section 7.2.4.2.

### 7.2.5.1.3 Late transition metal–chalcogenide clusters

#### (i) Group 10 metal clusters

From a historical perspective, the application of this approach to the synthesis of chalcogen-bridged nickel clusters is of significance. First of all, it was in this system in which the ability to synthesize a wide variety of structural types by controlling the reaction conditions was first demonstrated. Ni–E clusters with nuclearities in the range of 3–34 have been isolated (Table 8). Secondly, the synthesis of the “giant” cluster  $[\text{Ni}_{34}\text{Se}_{22}(\text{PPh}_3)_{10}]$ , (**39**)<sup>242</sup> whose structure is described below, opened up a whole new domain in metal chalcogen cluster chemistry by confirming the existence of nanometer-sized “molecules” which could be structurally characterized.

The reaction of nickel phosphine halide complexes with  $\text{Se}(\text{TMS})_2$  always results in a mixture of products, in which trinuclear complexes of the formula  $[\text{Ni}_3(\mu_3\text{-Se})_2\text{X}_2(\text{PR}^1_2\text{R}^2)_4]$  ( $\text{X} = \text{Cl, Se-TMS}$ ) are inevitably present.<sup>338</sup> It is likely that the formation of larger clusters involves condensation of these complexes, as the structures of many can be viewed as being constructed from  $\text{Ni}_3$  triangular units. The strongest evidence for this route is observed in the structure of  $[\text{Ni}_{12}\text{Se}_{11}(\text{PPh}_3)_8\text{Cl}]^{2+}$  which appears to be a “frozen intermediate” between face-shared bioctahedral  $[\text{Ni}_9\text{Se}_9(\text{PPh}_3)_6]^{2+}$  and trioctahedral  $[\text{Ni}_{12}\text{Se}_{12}(\text{PPh}_3)_6]$  clusters (**40**) (Figure 28).<sup>339</sup> While the “ $\text{Ni}_9\text{Se}_9$ ” complex has not been isolated, its occurrence is suggested by the structure of  $[\text{Ni}_{12}\text{Se}_{11}(\text{PPh}_3)_8\text{Cl}]^{2+}$ , as well as the existence of a corresponding sulfide derivative,  $[\text{Ni}_9\text{S}_9(\text{PET}_3)_6]^{2+}$  (**41**).<sup>340</sup> Structures based on the condensation of octahedral  $\text{Ni}_6$  units are common among nickel chalcogenide clusters, although no “ $\text{Ni}_6\text{E}_8$ ” cluster has been isolated. Considering the “extra” electrons in the octahedral  $\text{Co}_6\text{E}_8(\text{PR}_3)_6$  clusters usually occupy Co–Co



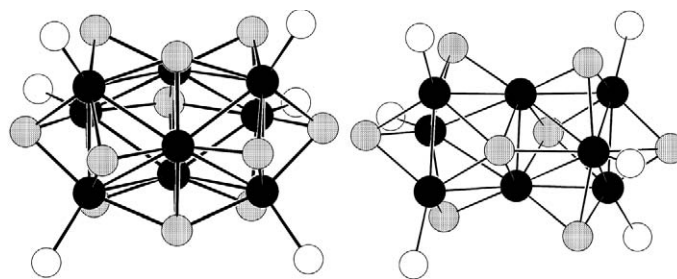


**Figure 27** Ball-and-stick representation of the cluster core of  $[\text{Co}_9\text{Se}_{11}(\text{PPh}_3)_6]$  (**37**) and  $[\text{Co}_8\text{Se}_8(\text{PPh}_3)_6]^n$  (**38**).

**Table 8** Group X metal chalcogenide clusters synthesized using silylated chalcogen reagents.

Cluster	References	Cluster	References
$[\text{Ni}_3\text{S}_2\text{Cl}_2(\text{PPh}_3)_4]$	343	$[\text{Ni}_{15}\text{Se}_{15}(\text{PPh}_3)_6]$	339
$[\text{Ni}_3\text{Se}_2(\text{Se-TMS})_2(\text{PPh}_3)_4]$	343	$[\text{Ni}_{20}\text{Se}_{12}(\text{SeMe})_{10}]^{2-}$ ( <b>42</b> )	262
$[\text{Ni}_4\text{Se}_2(\text{C}_5\text{H}_5)_4(\text{PPh}_3)_{2-n}]$ ( $n = 0, 2$ )	344	$[\text{Ni}_{21}\text{Se}_{14}(\text{PEt}_2\text{Ph})_{12}]$	338
$[\text{Ni}_4\text{Te}_2(\text{C}_5\text{H}_5)_4(\text{PPh}_3)_{2-n}]$ ( $n = 0, 2$ )	344	$[\text{Ni}_{34}\text{Se}_{22}(\text{PPh}_3)_{10}]$ ( <b>39</b> )	242
$[\text{Ni}_4\text{Se}_2(\text{CO})\text{BrCp}'_3]$	345	$[\text{Pd}_3\text{S}_2\text{Cl}_2(\text{PPh}_3)_4]$	343
$[\text{Ni}_4\text{Se}_3(\text{PPhe}_3)_5]$	338	$[\text{Pd}_3\text{Se}_2(\text{Se-TMS})_2(\text{PPh}_3)_4]$	343
$[\text{Ni}_5\text{Se}_4\text{Cl}_2(\text{PET}_2\text{Me})_6]$	338	$[\text{Pd}_4\text{NiS}_4\text{Cl}_2(\text{PPh}_3)_6]$	341
$[\text{Ni}_6\text{Se}_4(\text{C}_5\text{Me}_5)_5]$	345	$[\text{Pd}_5\text{Se}_4\text{Cl}_2(\text{PPh}_3)_6]$ ( <b>43</b> )	341
$[\text{Ni}_6\text{Se}_5(\text{PPh}_3)_6]$	339	$[\text{Pd}_5\text{Se}_5(\text{PPh}_3)_5]$	341
$[\text{Ni}_7\text{Se}_5(\text{PPr}'_3)_5]$	338	$(\eta^3\text{-C}_4\text{H}_7)_6\text{Pd}_6\text{Se}_3$ ( <b>44</b> )	342
$[\text{Ni}_8\text{S}_5(\text{PPh}_3)_7]$	335	$[\text{Pd}_6\text{Se}_4\text{Cl}_4(\text{PPh}_3)_6]$	341
$[\text{Ni}_8\text{S}_6\text{Cl}_{2-n}(\text{PPh}_3)_{6+n}]$ ( $n = 0, 2$ )	235,346	$[\text{Pd}_7\text{Se}_6(\text{SeH})\text{Cl}(\text{PPh}_3)_7]$	341
$[\text{Ni}_8\text{Se}_6(\text{PR}^1_2\text{R}^2)_{6-n}]$ ( $n = 0, 2$ )	338	$[\text{Pd}_8\text{Se}_8\text{Cl}_n(\text{PPh}_3)_8]^n$ ( $n = 0, 1$ )	341
$[\text{Ni}_{12}\text{Se}_{11}(\text{PPh}_3)_8\text{Cl}]^{2+}$	339	$[\text{Pt}_2\text{M}_2\text{Se}_2\text{Cl}_2(\text{PPh}_3)_4]$ ( $\text{M} = \text{Cu}, \text{Ag}$ )	347
$[\text{Ni}_{12}\text{Se}_{12}(\text{PET}_3)_6]$ ( <b>40</b> )	339	$[\text{Pd}_2\text{Au}_2\text{Se}_2\text{Cl}_2(\text{PPh}_3)_4]$	347
$[\text{Ni}_{15}\text{Se}_{10}\text{L}_3(\text{C}_5\text{Me}_5)_8]$	345		

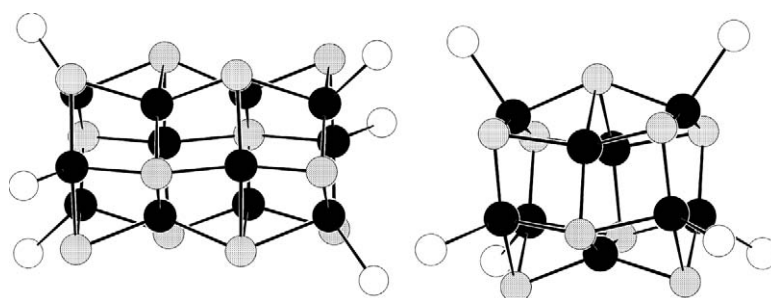


**Figure 28** Ball-and-stick representation of the cluster core of  $[\text{Ni}_{12}\text{Se}_{12}(\text{PPh}_3)_6]$  (**40**) and  $[\text{Ni}_9\text{S}_9(\text{PEt}_3)_6]^{2+}$  (**41**).

antibonding orbitals (see Section 7.2.4.2), the absence of related group 10 species can be explained in terms of electron counting arguments. The cubic  $\text{Ni}_8$  structures found for many nickel chalcogenide clusters (see Section 7.2.4.4) are also observed in this system. In the columnar structure of cluster  $[\text{Ni}_{21}\text{Se}_{14}(\text{PEt}_2\text{Ph})_{12}]$  two  $\text{Ni}_8$  cubes are fused to the basal faces of a Ni-centered,  $\text{Ni}_{12}$  cubeoctahedral core, with all square faces being capped by  $\mu_4$ -Se ligands.<sup>338</sup>

The structure of the largest structurally characterized nickel selenide cluster,  $[\text{Ni}_{34}\text{Se}_{22}(\text{PPh}_3)_{10}]$  (**39**) is unique with respect to other Ni/E clusters. The cluster has virtual fivefold symmetry, with layers of 5, 10, 10, and 5 nickel atoms (Figure 29). A  $\text{Ni}_4$  unit resides at the center of the molecule. The selenium atoms all act as  $\mu_4$ -capping ligands, save for the two  $\mu_5$ -Se that cap the top and bottom  $\text{Ni}_5$  pentagons. A similar arrangement is observed in the structure of the mixed selenide/selenolate cluster  $[\text{Ni}_{20}\text{Se}_{12}(\text{SeMe})_{10}]^{2-}$  (**42**) (Figure 29).<sup>262</sup> The formal oxidation number (1.7) of the Ni atoms in (**42**) suggests a mixing of valence states, which is quite common in Ni/E clusters.

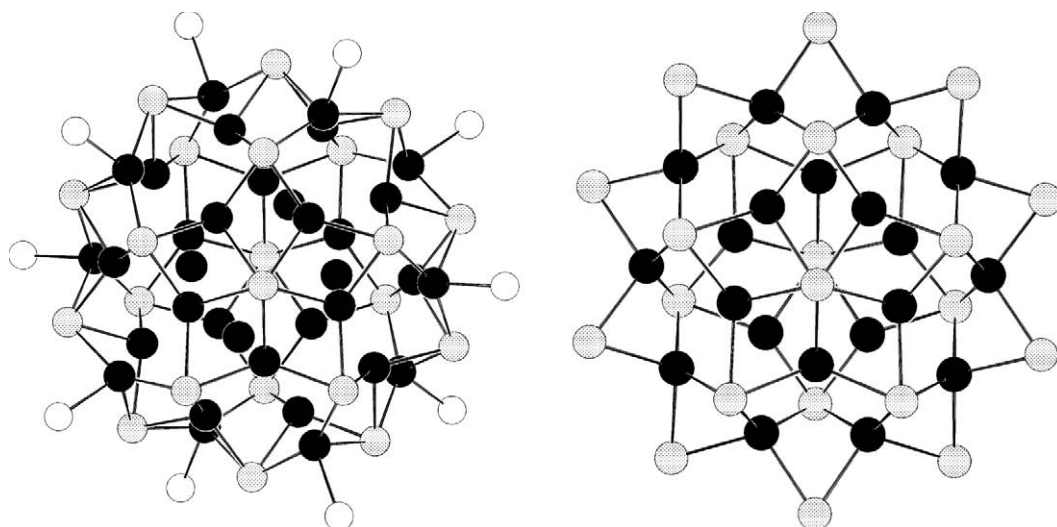


**Figure 29** Ball-and-stick representation of the cluster core of  $[\text{Ni}_{34}\text{Se}_{22}(\text{PPh}_3)_{10}]$  (39) and  $[\text{Ni}_{20}\text{Se}_{12}(\text{SeMe})_{10}]^{2-}$  (42).

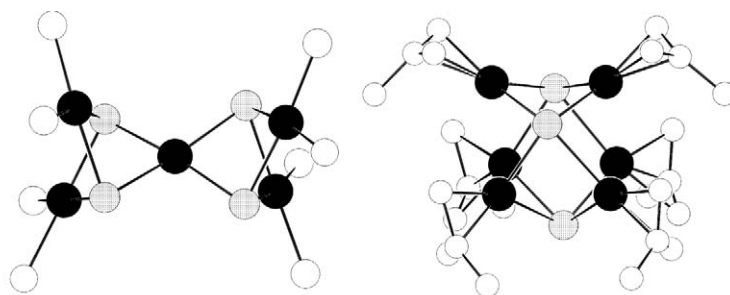


**Figure 30** Ball-and-stick representation of the cluster core of  $[\text{Pd}_5\text{Se}_4\text{Cl}_2(\text{PPh}_3)_6]$  (43) and  $[(\eta^3\text{-C}_4\text{H}_7)_6\text{Pd}_6\text{Se}_3]$  (44).

Complexes analogous to the trinuclear  $\text{Ni}_3\text{E}_2$  clusters described above are also prominent in reactions of  $\text{E}(\text{TMS})_2$  with palladium halide salts (Table 8). Higher Pd/E clusters can also be isolated, and although many of their structures can be described in terms of triangular  $\text{Pd}_3\text{E}_2$  units, these clusters show no structural relationships to the nickel clusters described above. While the structures of the latter tend to be more condensed, the Pd clusters are typically based on the linking of intact  $\text{Pd}_3\text{E}_2$  fragments through bridging or vertex-sharing interactions such as observed in  $[\text{Pd}_5\text{Se}_4\text{Cl}_2(\text{PPh}_3)_6]$  (43)<sup>341</sup> and  $[(\eta^3\text{-C}_4\text{H}_7)_6\text{Pd}_6\text{Se}_3]$  (44)<sup>342</sup> (Figure 30). The strong preference of  $\text{Pd}^{\text{II}}$  to adopt a square planar coordination geometry may prevent the formation of more spherical structures.

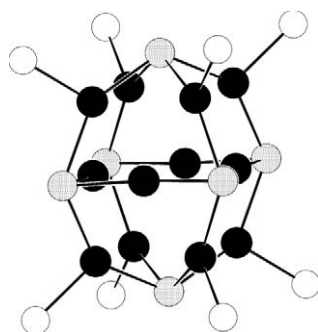
The reactive pendant —Se-TMS groups of the complex  $[\text{Pd}_2\text{Se}_2(\text{Se-TMS})_2(\text{PPh}_3)_4]$  have been exploited in the synthesis of a number of homo- and heterometallic clusters. The reaction of this complex with chloride salts of Pd, Pt, Ir, and Au have been reported to result in cluster expansion reactions via the elimination of Cl-TMS.<sup>2</sup> In certain cases the synthesis of heterometallic clusters is accompanied by the formation of Pd-only complexes. The clusters  $[\text{Pd}_3\text{Pt}_2\text{Cl}_2\text{Se}_4(\text{PPh}_3)_6]$  and  $[\text{Ir}_6\text{PdSe}_4(\text{COD})_6]$  feature spirocyclic structures, in which  $\text{Pt}_2\text{Pd}$  or  $\text{Ir}_3\text{Pd}$  units are joined at the Pd atom.<sup>2</sup> The individual units are capped by  $\mu_3\text{-E}$  and  $\mu_4\text{-E}$  ligands, respectively.

## (ii) Group 11 metal clusters

(a) *Copper clusters.* All copper sulfide clusters synthesized by this method to date<sup>349–351</sup> are neutral complexes whose Cu/S cores adhere strictly to the general formula  $[\text{Cu}_2\text{S}]_n$  (Table 9) observed in the bulk semiconductor.<sup>348</sup> The cluster cores of these complexes are roughly spherical, consisting of deltahedral  $\text{S}_n$  units, with  $2n$  Cu atoms coordinated on the edges and within the

**Table 9** Copper sulfide clusters synthesized using silylated chalcogen reagents.

Cluster	References
$[\text{Cu}_{12}\text{S}_6(\text{PR}^1_2\text{R}^2)_8]$ ( <b>45a</b> )	349,350
$[\text{Cu}_{20}\text{S}_{10}(\text{PR}^1_2\text{R}^2)_8]$	349,350
$[\text{Cu}_{24}\text{S}_{12}(\text{PPr}^i_2\text{Me})_{12}]$	351
$[\text{Cu}_{28}\text{S}_{14}(\text{PBu}^t_2\text{Me})_{12}]$ ( <b>47</b> )	351
$[\text{Cu}_{50}\text{S}_{25}(\text{PBu}^t_2\text{Me})_{16}]$ ( <b>46</b> )	351

**Figure 31** Ball-and-stick representation of the cluster core of  $[\text{Cu}_{12}\text{E}_6(\text{PR}^1_2\text{R}^2)_8]$  (**45**).

polyhedron. The most common structure is the dodecanuclear  $[\text{Cu}_{12}\text{S}_6(\text{PR}^1_2\text{R}^2)_8]$  (**45a**) (Figure 31), representing half the number of structurally characterized “ $\text{Cu}_2\text{S}$ ” clusters reported to date, accessed via this method.<sup>87</sup> The condensation of two spherical clusters, results in an overall “cylindrical” structure, such as that of the largest known copper sulfide complex  $[\text{Cu}_{50}\text{S}_{25}(\text{Pt-Bu}^t_2\text{Me})_{16}]$  (**46**), which can be described as arising from the condensation of two  $[\text{Cu}_{28}\text{S}_{14}(\text{Pt-Bu}^t_2\text{Me})_{12}]$  (**47**) units.<sup>351</sup> The structural relationship between (**46**) and (**47**) is demonstrated in Figure 32. Coordination environments of the copper atoms in Cu–S clusters approximate either trigonal planar or linear geometry, while sulfur atoms almost always act as  $\mu_4$  bridges. Additional bridging modes of the sulfur atoms, however, are observed in the larger derivatives (**47**) ( $\mu_3$ ,  $\mu_5$ ) and (**46**) ( $\mu_5$ ,  $\mu_6$ ). Although the higher coordination numbers in (**46**) are characteristic of  $\text{Cu}_2\text{S}$  phases,<sup>348</sup> its structure is not strongly related to that of the  $\text{Cu}_2\text{S}$  lattice.

While many of the metal sulfide clusters discussed to this point have selenide analogues, such congruence is not observed for the large Cu–Se clusters. Many copper selenide clusters, like their sulfide counterparts, display spherical structures; however,  $[\text{Cu}_{12}\text{E}_6(\text{PR}^1_2\text{R}^2)_8]$  (**45**) (E = S (**45a**); E = Se (**45b**)) represent the only topologically similar complexes between the two series. Structural differences can be attributed, in part, to the greater tendency of selenide ligands to adopt higher coordination modes compared with  $\text{S}^{2-}$ . This has led to a much larger structural diversity in the former, as well as the incidence of much larger species, including the  $\text{Cu}_2\text{Se}$  “megaclusters” whose structures are closely related to that of the bulk material (see Section 7.2.6.1). Coordination environments of the copper atoms vary from linear to trigonal to tetrahedral, with an inclination for higher geometries occurring in larger clusters. In addition to the majority of clusters with their strict obedience to the  $[\text{Cu}_2\text{Se}]_n$  formula (Table 10), nonstoichiometric species  $[\text{Cu}_{2x-y}\text{Se}_x(\text{PR}^1_2\text{R}^2)_m]$ , containing both  $\text{Cu}^{\text{I}}$  and  $\text{Cu}^{\text{II}}$  centers have also been isolated.

The structural diversity observed in copper selenide clusters has been expanded further via the use of alkyl- or arylselenolate reagents ( $\text{RSe-TMS}$ ). Due to the steric requirements of the organic substituent (R), these ligands are restricted to the surface of the clusters. As a result, clusters containing exclusively selenolate ligands are generally smaller than selenide derivatives. The presence of  $\text{RSe}^-$  surface ligands via the selenolate reagents, introduces an additional variable as to the structural type observed. Thus whereas only spherical frameworks are observed for copper–selenide clusters  $[(\text{Cu}_2\text{Se})_n(\text{PR}_3)_x]$  ( $n < 35$ ) such as  $[\text{Cu}_{52}\text{Se}_{26}(\text{PPh}_3)_{16}]$  (**48**),<sup>352</sup> mixed selenolato/selenide clusters yield both spherical (e.g.,  $[\text{Cu}_{58}\text{Se}_{16}(\text{SePh})_{24}(\text{dppa})_6]$  (**49**)<sup>353</sup> and layer-type structures such as  $[\text{Cu}_{32}\text{Se}_7(\text{SeBu}^n)_{18}(\text{PPr}^i_3)_6]$  (**50**)<sup>354</sup> (Table 10, Figure 33). The coordination modes of the  $\text{RSe}^-$  ligands in these clusters range from doubly to quadruply bridging. Higher connectivity is favored by the  $\text{Se}^{2-}$  ligands, and  $\mu_4$ – $\mu_8$  and even  $\mu_{12}$ -Se–Cu contacts are observed.

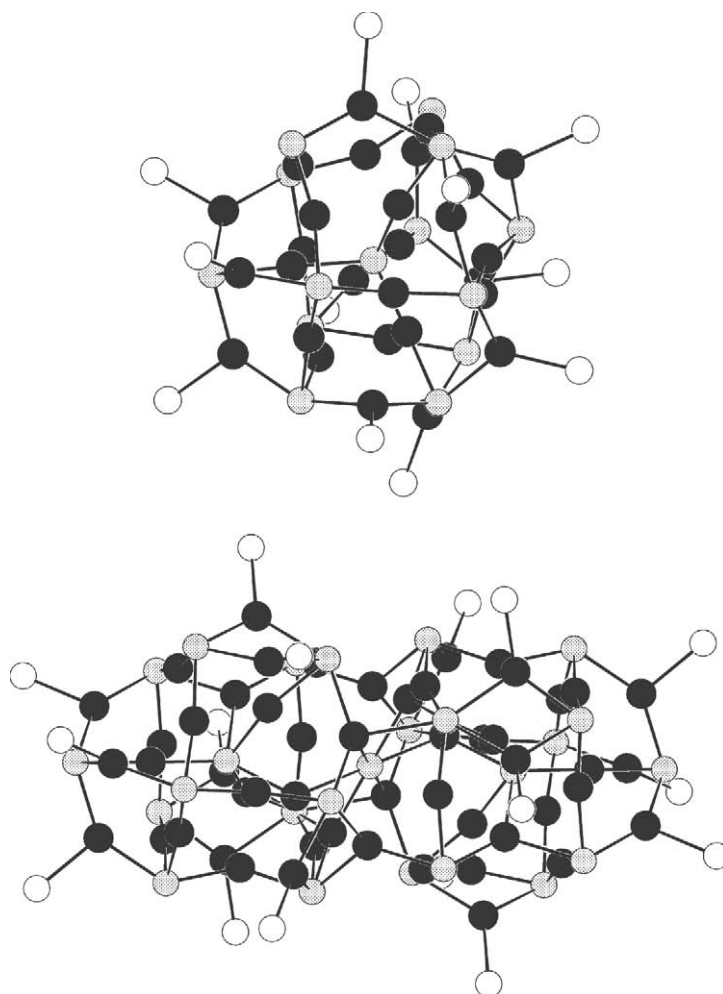


**Figure 32** Ball-and-stick representation of the cluster core of  $[\text{Cu}_{50}\text{S}_{25}(\text{PBu}^t\text{Me})_{16}]$  (**46**)  $[\text{Cu}_{28}\text{S}_{14}(\text{PBu}^t\text{Me})_{12}]$  (**47**).

Coordination numbers for Cu of two, three, or four are common with again, a tendency towards higher geometries in larger clusters. A five-coordinate copper atom is observed in the cluster  $[\text{Cu}_{25}\text{Se}_4(\text{SePh})_{18}(\text{dppp})_2]^-$ .<sup>353</sup> In the structure of (**50**) the 25 Se atoms comprise a triple-layer structure with a cubic close-packed arrangement, comparable to that observed in bulk  $\text{Cu}_2\text{Se}$ .<sup>355</sup> Similarly, silver selenium megaclusters with  $\text{Bu}^n\text{Se}^-$  ligands<sup>93</sup> show a strong structural relationship to nonmolecular  $\text{Ag}_2\text{Se}$ ,<sup>356</sup> suggesting that appropriate choice of surface groups may

**Table 10** Copper selenium clusters synthesized using silylated chalcogen reagents.

Cluster	References	Cluster	References
$[\text{Cu}_8\{\text{Fe}(\eta^5\text{-C}_5\text{H}_4\text{Se})_2\}_4(\text{PPh}_2\text{Et})_4]$ ( <b>51</b> )	97	$[\text{Cu}_{32}\text{Se}_7(\text{SeBu}^n)_{18}(\text{PPr}^i_3)_6]$ ( <b>50</b> )	354
$[\text{Cu}_{12}\text{Se}_6(\text{PR}^1_2\text{R}^2)_8]$ ( <b>45b</b> )	349	$[\text{Cu}_{36}\text{Se}_{18}(\text{PBu}^t_3)_{12}]$	360
$[\text{Cu}_{16}\text{Se}_4(\text{SePh})_8(\text{dppbe})_4]$	357	$[\text{Cu}_{36}\text{Se}_5(\text{SePh})_{26}(\text{dppa})_4]$	353
$[\text{Cu}_{20}\text{Se}_{13}(\text{PEt}_3)_{12}]$	358	$[\text{Cu}_{38}\text{Se}_{13}(\text{SePh})_{12}(\text{dppR})_6]$	353
$[\text{Cu}_{25}\text{Se}_4(\text{SePh})_{18}(\text{dppp})_2]^-$	353	$[\text{Cu}_{44}\text{Se}_{22}(\text{PR}^1_2\text{R}^2)_{18-n}]$ ( $n = 0, 6$ )	361
$[\text{Cu}_{26}\text{Se}_{13}(\text{PR}^1_2\text{R}^2)_{14-n}]$ ( $n = 0, 4$ )	359	$[\text{Cu}_{48}\text{Se}_{24}(\text{Me}_2\text{Ph})_{20}]$	350
$[\text{Cu}_{29}\text{Se}_{15}(\text{PPr}^i_3)_{12}]$	360	$[\text{Cu}_{50}\text{Se}_{20}(\text{SeBu}^t)_{10}(\text{PPr}^i_3)_{10}]$	354
$[\text{Cu}_{30}\text{Se}_{15}(\text{PR}^1_2\text{R}^2)_{12}]$ ( <b>82</b> )	360	$[\text{Cu}_{52}\text{Se}_{26}(\text{PPh}_3)_{16}]$ ( <b>48</b> )	352
$[\text{Cu}_{31}\text{Se}_{15}(\text{Se-TMS})(\text{PBu}^t\text{Me})_{12}]$	350	$[\text{Cu}_{58}\text{Se}_{16}(\text{SePh})_{24}(\text{dppa})_6]$ ( <b>49</b> )	353
$[\text{Cu}_{32}\text{Se}_{16}(\text{PPh}_3)_{12}]$	352	$[\text{Cu}_{59}\text{Se}_{30}(\text{PCy}_3)_{16}]$	359

dppbe = 1,4-bis(diphenylphosphino)benzene, dppa = bis(diphenylphosphino)acetylene.

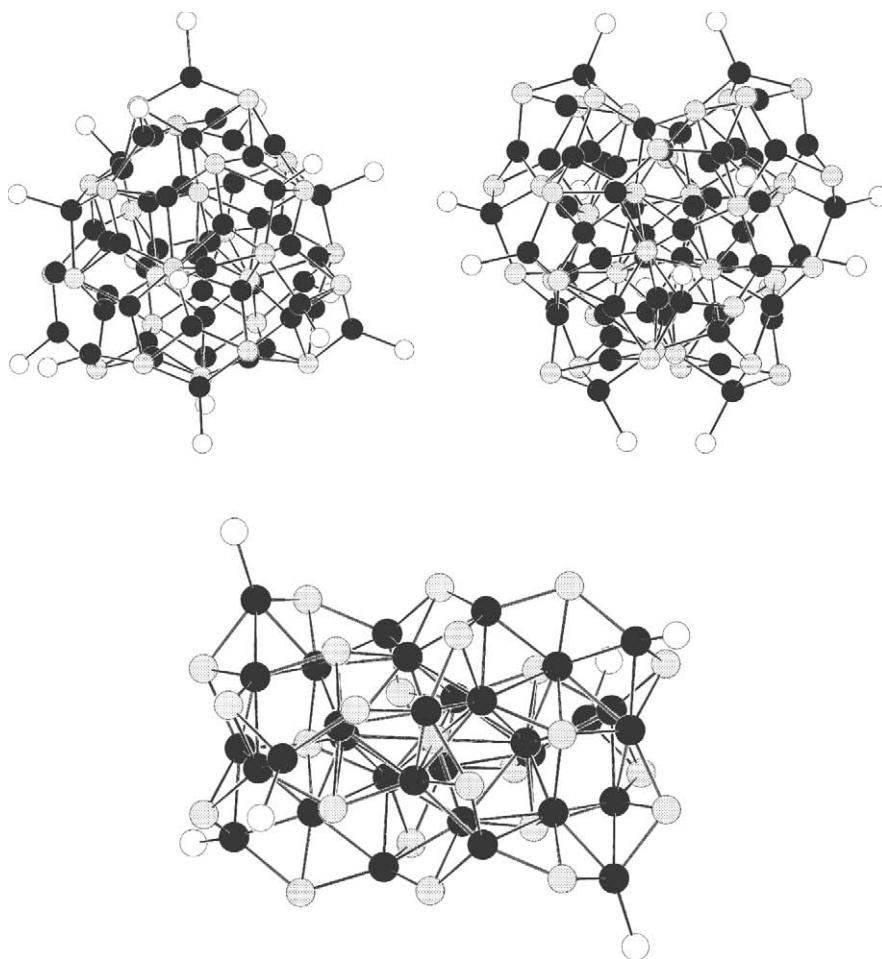


**Figure 33** Ball-and-stick representation of the cluster core of  $[\text{Cu}_{52}\text{Se}_{26}(\text{PPh}_3)_{16}]$  (**48**),  $[\text{Cu}_{58}\text{Se}_{16}(\text{SePh})_{24}(\text{dppa})_6]$  (**49**) and layer-type  $[\text{Cu}_{32}\text{Se}_7(\text{SeBu}^n)_{18}(\text{PPR}_3)_6]$  (**50**).

be important in the stabilization of nanometer sized fragments of the bulk lattice (see Section 7.2.6.1). The  $\text{Se}^{2-}$  ligands that occupy interstitial positions in the core of (**49**) and (**50**) are suggested to arise from Se–C scission reactions.<sup>353,354,357</sup>

The use of reaction mixtures containing a combination of RSe–TMS,  $\text{Se}(\text{TMS})_2$ , and monodentate phosphines, has also been investigated.<sup>354</sup> Curiously, mixed  $\text{RSe}^-/\text{Se}^{2-}/\text{Cu}^1$  complexes have only been produced when the phosphine employed is  $\text{PPr}_3$ . The use of other phosphine ligands ( $\text{PEt}_3$ ,  $\text{PBu}_3$ ) resulted only in the synthesis of  $[(\text{Cu}_2\text{Se})_n(\text{PR}_3)_m]$  clusters. The fact that these clusters contain relatively few (or no)  $\text{RSe}^-$  ligands with respect to  $\text{Se}^{2-}$  suggests that Se–C bond cleavage might also accompany cluster growth in these systems. The molecular formulae of such Cu/Se/RSe clusters are listed in Table 10.

This approach of using a combination of RSe–TMS and  $\text{Se}(\text{TMS})_2$  for cluster synthesis should allow for the tailored functionalization of semiconductor nanoparticles. Recently, the ability to functionalize the surface of  $\text{Cu}_2\text{Se}$  clusters has been demonstrated. The synthesis of 1,1'-bis(trimethylsilyl)ferrocene, and its consequent reaction with  $\text{CuOAc}$  and excess phosphine has produced the polynuclear copper selenide cluster  $[\text{Cu}_8\{\text{Fe}(\eta^5\text{-C}_5\text{H}_4\text{Se})_2\}_4(\text{PPh}_2\text{Et})_4]$  (**51**) with surface redox-active ferrocene units that are intimately coupled to the cluster core (Figure 34).<sup>97</sup>

Large deviations in structure and nuclearity notwithstanding, clusters synthesized via the reaction of  $\text{Cu}^1$  salts with  $\text{E}(\text{TMS})_2$  ( $\text{E} = \text{S}, \text{Se}$ ) have Cu:E ratios that invariably approach 2:1. This is a consequence of the (relatively) large discrepancies in ionization potentials, electron affinities, and electronegativities of the relevant ions. These differences are much smaller between  $\text{Cu}^+$  and  $\text{Te}^{2-}$ . Accordingly, this “rule” is not so stringently observed in the Cu/Te system, and nonstoichiometric “electron-rich” ( $\text{Cu}_{2+x}\text{Te}$ ) and “electron-deficient” ( $\text{Cu}_{2-x}\text{Te}$ ) complexes are frequently observed (Table 11). If a formal charge of 2– is assigned to the telluride ligands in these

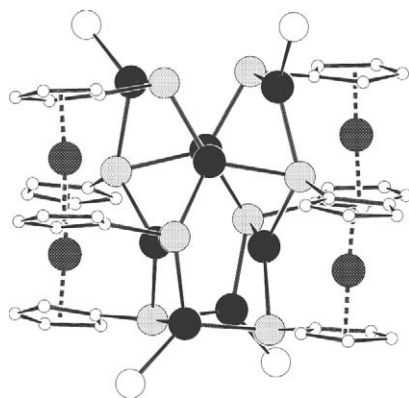


**Figure 34** Ball-and-stick representation of the cluster core of  $[\text{Cu}_8\{\text{Fe}(\eta^5\text{-C}_5\text{H}_4\text{Se})_2\}_4(\text{PPh}_2\text{Et})_4]$  (**51**), demonstrating the surface ferrocenyl selenolate ligands.

complexes, oxidation states of (+1 and +2) and (+1 and 0) respectively must be designated to the copper atoms. Theoretical studies have shown that in the latter case, as is observed in the cluster  $[\text{Cu}_{26}\text{Te}_{12}(\text{PEt}_2\text{Ph})_{12}]$ , localization of charge creating  $\text{Cu}^0$  centers is not possible.<sup>362</sup> Instead, the “extra” electrons are assigned to a valence band MO comprised of  $\text{Te}(5p)$  and  $\text{Cu}(4s)$  orbitals. Mixing of valences is also observed in certain nonmolecular  $(\text{Cu}_{2-x}\text{Te})$  phases,<sup>363–365</sup> as well as ternary alkali copper tellurides.<sup>366–369</sup> Despite this, close structural similarities between molecular species and bulk materials, such as those observed in the  $\text{Cu}_2\text{Se}$  system, are not found. Alternatively, strong correlations to the bulk structure for molecular  $[\text{Cu}_2\text{Se}]_n$  clusters does not occur until the number of copper atoms is greater than 59 (see Section 7.2.6.1). The largest copper telluride clusters characterized to date  $[\text{Cu}_{58}\text{Te}_{32}(\text{PR}^1_2\text{R}^2)_{16-n}]$  (**52**) ( $n = 0, 2$ )<sup>370,371</sup> do reveal a layered type structure for the 32 Te atoms (Figure 35), and the isolation of (as yet elusive) larger complexes may reveal more pronounced relationships.

As a result of the penchant for forming nonstoichiometric species, as well as the increased capacity for higher coordination of tellurium relative to its lighter congeners, tellurium-bridged copper clusters tend to be structurally disparate from those bridged by sulfur and selenium. Nevertheless, they still feature spherical, or shell-like construction, and a few smaller examples such as  $[\text{Cu}_{12}\text{Te}_6(\text{PPh}_3)_8]$ <sup>372</sup> (**45c**) do have structural analogues in the other systems (Figure 31). The distribution of tellurium atoms in copper telluride clusters can be described in terms of deltahedral frameworks, many of which are related to Frank–Kasper polyhedra.<sup>373</sup> The coordination numbers of  $\text{Te}^{2-}$  ligands vary from four to 12, with Cu atoms adopting three-coordinate ( $\text{PCuTe}_2$  or  $\text{CuTe}_3$ ) or four-coordinate ( $\text{PCuTe}_3$  or  $\text{CuTe}_4$ ) geometries. A small number of clusters containing ditelluride ( $\text{Te}_2^{2-}$ ) ligands have also been isolated from these reactions (Table 11).

**Table 11** Copper tellurium clusters synthesized using silylated chalcogen reagents.

Cluster	References	Cluster	References
$[\text{Cu}_4(\text{Te}_2)_2(\text{PPr}^1_3)_4]$	376	$[\text{Cu}_{23}\text{Te}_{13}(\text{PR}_3)_{12-n}]$ ( $n = 0, 2$ )	376,370,372,376
$[\text{Cu}_4(\text{TePh})_4(\text{PPr}^1_3)_3]$	375	$[\text{Cu}_{24}\text{Te}_{12}(\text{PPr}^1_3)_{12}]$	372
$[\text{Cu}_5(\text{TePh})_6(\text{PEt}_3)_3]^-$	375	$[\text{Cu}_{26}\text{Te}_{12}(\text{PEt}_2\text{Ph})_{12}]$	372
$[\text{Cu}_6(\text{TePh})_6(\text{PPh}_2\text{Et})_5]$	374	$[\text{Cu}_{26}\text{Te}_{10}(\text{Te}_2)_3(\text{PBu}^1_3)_{10}]$	376
$[\text{Cu}_{11}\text{Te}(\text{TeBu}^n)_9(\text{PPh}_3)_5]$	370	$[\text{Cu}_{27}\text{Te}_{15}(\text{PPr}^1_2\text{Me})_{12}]$	371
$[\text{Cu}_8\text{Te}_4(\text{PPh}_3)_7]$	372	$[\text{Cu}_{28}\text{Te}_{13}(\text{Te}_2)_2(\text{PEt}_2\text{Ph})_{10}]$	376
$[\text{Cu}_{12}\text{Te}_6(\text{PPh}_3)_8]$ ( <b>45c</b> )	372	$[\text{Cu}_{29}\text{Te}_{16}(\text{PPr}^1_3)_{12}]$	376
$[\text{Cu}_{12}\text{Te}_3(\text{TePh})_6(\text{PR}_3)_6]$	374,375	$[\text{Cu}_{29}\text{Te}_9(\text{TePh})_{12}(\text{PEt}_3)_8]^-$ ( <b>53</b> )	375
$[\text{Cu}_{16}\text{Te}_8(\text{PPr}^n_2\text{Ph})_{10}]$	372	$[\text{Cu}_{39}\text{Te}_{16}(\text{TePh})_{11}(\text{PEt}_3)_{13}]$	375
$[\text{Cu}_{16}\text{Te}_9(\text{PR}^1_2\text{R}^2)_8]$	372,376	$[\text{Cu}_{44}\text{Te}_{23}(\text{PR}^1_2\text{R}^2)_{15}]$	372
$[\text{Cu}_{18}\text{Te}_6(\text{TeBu})_6(\text{PR}^1_2\text{R}^2)_{8-n}]$ ( $n = 0, 1$ )	370,371	$[\text{Cu}_{50}\text{Te}_{17}(\text{TePh})_{20}(\text{PPh}_2\text{Et})_8]^{4-}$	374
$[\text{Cu}_{19}\text{Te}_6(\text{TeBu}^1)_7(\text{PEt}_3)_8]$	371	$[\text{Cu}_{58}\text{Te}_{32}(\text{PR}^1_2\text{R}^2)_{16-n}]$ ( $n = 0, 2$ ) ( <b>52</b> )	370,371

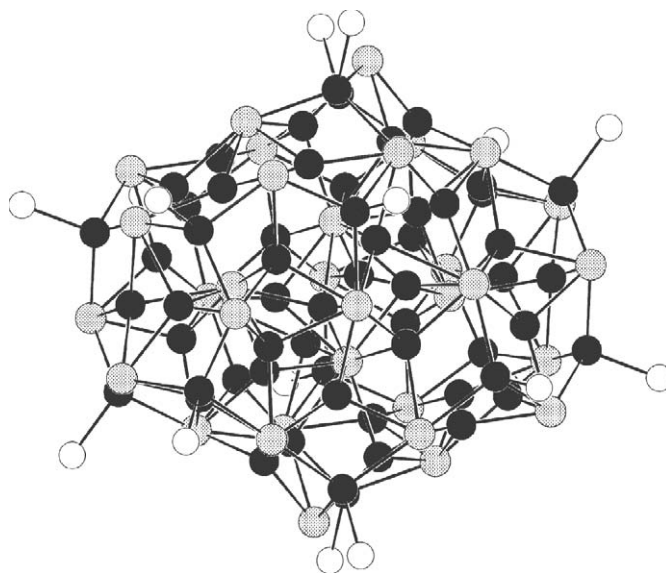


**Figure 35** Ball-and-stick representation of the cluster core of  $[\text{Cu}_{58}\text{Te}_{32}(\text{PR}^1_2\text{R}^2)_{16-n}]^-$  (**52**).

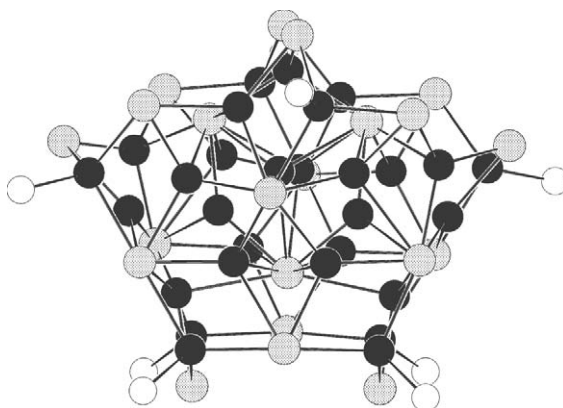


**Figure 36** Ball-and-stick representation of the cluster core of  $[\text{Cu}_{29}\text{Te}_9(\text{TePh})_{12}(\text{PEt}_3)_8]^-$  (**53**).

In reference to the Se–C scission that occurs in the production of Cu/Se clusters with mixed  $\text{Se}^{2-}/\text{RSe}^-$  ligands (*vide supra*), Te–C bond cleavage is even more facile. As a result, silylated organotelluroate complexes ( $\text{RTe-TMS}$ , where  $\text{R} = \text{Ph}, \text{Bu}^n, \text{Bu}^l$ ) represent good sources of both  $\text{RTe}^-$  and  $\text{Te}^{2-}$ . Indeed, the use of these reagents in cluster synthesis has resulted a variety of copper–telluroate, mixed telluroate/telluride, and telluride complexes (Table 11). It has also been demonstrated that “low-nuclearity” copper–telluroate complexes can be used in the formation of larger telluride-containing clusters via the elimination of  $\text{TePh}_2$ . The cluster  $[\text{Cu}_{50}(\text{TePh})_{20}\text{Te}_{17}(\text{PPh}_2\text{Et})_8]^{4-}$  is formed from solutions of  $[\text{Cu}_6(\text{TePh})_6(\text{PPh}_2\text{Et})_5]$ , with NMR evidence suggesting the presence of additional intermediate species.<sup>374</sup> Similarly, photolysis of a 2:1 mixture of  $[\text{Cu}_{12}\text{Te}_3(\text{TePh})_6(\text{PEt}_3)_6]^-$  and  $[\text{Cu}_5(\text{TePh})_6(\text{PEt}_3)_3]^-$  in THF produces the nanoclusters  $[\text{Cu}_{29}\text{Te}_9(\text{TePh})_{12}(\text{PEt}_3)_8]^-$  (**53**) (Figure 36) and  $[\text{Cu}_{39}\text{Te}_{16}(\text{TePh})_{11}(\text{PEt}_3)_{13}]^-$  via the generation and elimination of  $\text{TePh}_2$ .<sup>375</sup> The structures of these complexes are markedly different from those of triethylphosphine-stabilized clusters synthesized from  $\text{Bu}^n\text{-TMS}$  or  $\text{Bu}^l\text{-TMS}$ , demonstrating the dependence of product formation on the organo-substituent of the tellurium reagent. Neither of these condensation reactions occurs in the absence of light, indicating that the formation of  $\text{TePh}_2$  is photochemically induced.

In addition to the great number of binary copper chalcogenide clusters that has been isolated, silylated reagents have also been utilized in the synthesis of ternary clusters containing two different types of metal atoms. Ternary copper(I)–indium(III)–selenide clusters have been isolated from reactions of  $\text{InCl}_3$  and  $\text{CuCl}$  with silylated selenium reagents in the presence of phosphine ligands (see Section 7.2.4.5).<sup>302</sup> The ternary niobium–copper chalcogenide clusters

$[\text{Nb}_2\text{Cu}_6\text{S}_6\text{Cl}_5(\text{PEt}_3)_6]^-$  and  $[\text{NbCu}_6\text{Te}_3(\text{Te}_2)_2(\text{PEt}_3)_6]$  have been synthesized by the addition of  $\text{E}(\text{TMS})_2$  ( $\text{E} = \text{S}, \text{Te}$ ) to a mixture of  $\text{NbCl}_5$ ,  $\text{CuCl}$ , and  $\text{PEt}_3$ .<sup>377</sup> The structure of  $[\text{Nb}_2\text{Cu}_6\text{S}_6\text{Cl}_5(\text{PEt}_3)_6]^-$  consists of two  $\text{NbCu}_3\text{S}_3\text{Cl}$  cubane subunits connected via three  $\mu\text{-Cl}$  bridges, and is thus related to the fused cubane structures observed in tetrachalcogenometallate chemistry (see Section 7.2.5.3.1). The core of the telluride cluster features a Nb centered  $\text{Cu}_6$  trigonal prism, of which the two triangular faces, and one rectangular face are capped by  $\text{Te}^{2-}$  ligands. The remaining two rectangular faces are capped by  $\text{Te}_2^{2-}$ .

As part of the development of a general route to ternary  $\text{M}^1\text{M}^2\text{E}$  nanoclusters, a series of phosphine-stabilized copper chalcogenolate complexes,  $(\text{L})_3\text{CuE-TMS}$  (**3**) ( $\text{L} = \text{PEt}_3, \text{PPr}^n_3$ ;  $\text{E} = \text{S}, \text{Se}, \text{Te}$ ) has been synthesized.<sup>378</sup> These complexes contain a pendant trimethylsilyl moiety, and can be used as a source of “copperchalcogenolate” fragments. Their utility in ternary cluster synthesis has been demonstrated by reaction with mercuric acetate in the presence of excess phosphine to produce the nanoclusters  $[\text{Hg}_{15}\text{Cu}_{20}\text{E}_{25}(\text{PPr}^n_3)_{18}]$  (**54**) ( $\text{E} = \text{S}$  (**54a**),  $\text{Se}$  (**45b**)) in good yield.<sup>96</sup> The structure of the selenide derivative is depicted in Figure 37.

(b) *Silver clusters.* Despite the substantial success in the synthesis of copper–chalcogenide clusters using bis(silylated) chalcogenide reagents, similar efforts to extend this chemistry to silver–chalcogenide clusters have not yet proved successful. Instead, it is reported that the addition of  $\text{E}(\text{TMS})_2$  to silver(I) salts in the presence of phosphine results only in the precipitation of amorphous binary  $\text{Ag/E}$  solids.<sup>93</sup> Evidently, the phosphine ligands used to protect the  $\text{Cu/E}$  cluster cores are not able to stabilize molecular silver–chalcogenide complexes in a similar fashion. Alternatively, the use of monosilylated chalcogen reagents ( $\text{RE-TMS}$ ) has led to the isolation of crystalline products at low temperature whose structures could be determined.<sup>88,93</sup> In these complexes, the surface of the  $\text{Ag/E}$  cluster core is shielded by both phosphine ligands and the organic substituents of the chalcogenolate ligands, preventing condensation to bulk phases.

The addition of  $\text{RSe-TMS}$  ( $\text{R} = \text{Bu}^n, \text{Bu}^l$ ) to silver carboxylate salts at low temperatures has resulted in the isolation of a small number of silver–selenide/selenolate clusters. The two “smaller” clusters  $[\text{Ag}_{30}\text{Se}_8(\text{SeBu}^l)_{14}(\text{PPr}^n_3)_8]$  (**55**) and  $[\text{Ag}_{90}\text{Se}_{38}(\text{SeBu}^l)_{14}(\text{PEt}_3)_{22}]$  (**56**) are spherical, and show no structural relationship to bulk  $\text{Ag}_2\text{Se}$ .<sup>354</sup> Their structures can be described in terms of the selenium framework. Cluster (**55**) consists of three layers of selenium atoms, with top and bottom layers containing six Se atoms (four  $\text{Bu}^l\text{Se}^-$  and two  $\text{Se}^{2-}$ ) sandwiching a layer of 10 Se atoms (six  $\text{Bu}^l\text{Se}^-$  and four  $\text{Se}^{2-}$ ). The selenium atoms in cluster (**56**) constitute a “shell-like” framework with an outer shell consisting of both  $\text{Bu}^l\text{Se}^-$  and  $\text{Se}^{2-}$  ligands, and an inner shell comprised of only  $\text{Se}^{2-}$  (Figure 38). The coordination modes of the  $\text{Bu}^l\text{Se}^-$  ligands are either  $\mu_2$  or  $\mu_3$ , while the  $\text{Se}^{2-}$  ligands assume  $\mu_5\text{-}\mu_6$  (**55**) or  $\mu_4\text{-}\mu_8$  (**56**), with the higher coordination modes being adopted by the  $\text{Se}^{2-}$  atoms of the inner shell. The geometries of the silver atoms in these complexes are similar to those observed in the  $\text{Cu/Se}$  system, ranging from almost linear to trigonal planar and distorted tetrahedral. Larger complexes feature structures that show remarkable

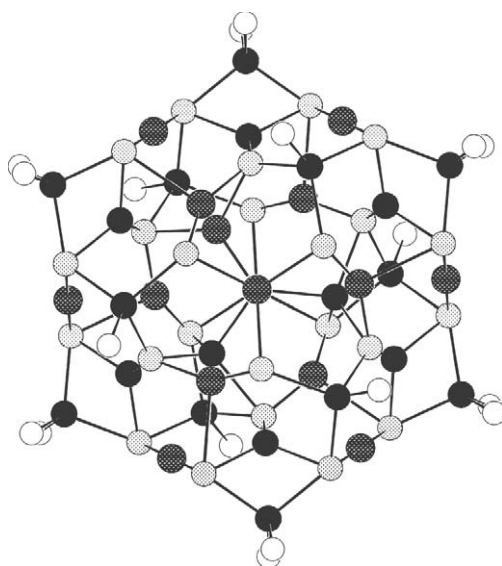
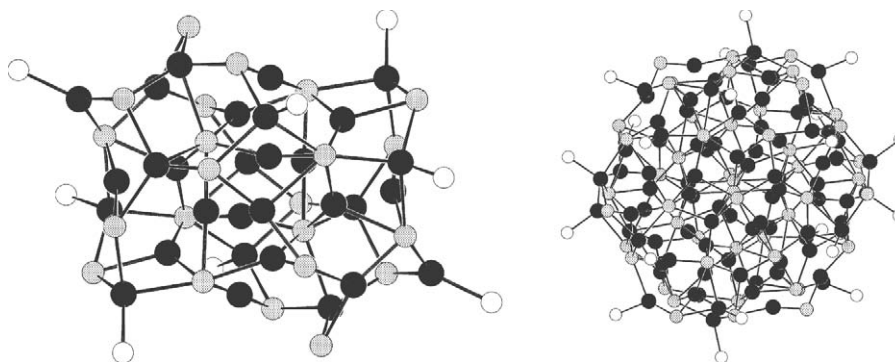


Figure 37 Ball-and-stick representation of the cluster core of  $[\text{Hg}_{15}\text{Cu}_{20}\text{E}_{25}(\text{PPr}^n_3)_{18}]$  (**54**).





**Figure 38** Ball-and-stick representation of the cluster core of  $[\text{Ag}_{30}\text{Se}_8(\text{SeBu}^{\text{I}})_{14}(\text{PPR}^{\text{n}})_3]$  (**55**) and  $[\text{Ag}_{90}\text{Se}_{38}-(\text{SeBu}^{\text{I}})_{14}(\text{PEt}_3)_{22}]$  (**56**).

similarities to bulk  $\text{Ag}_2\text{Se}$ , and these are discussed along with the  $\text{Cu}_2\text{Se}$  “megaclusters” in Section 7.2.6.1.

A number of tellurium-bridged silver clusters have also been synthesized using monosilylated organotellurolate reagents (Table 12). The only complex synthesized by this method containing exclusively butyltellurolate ligands (other than phosphine),  $[\text{Ag}_6(\mu_3\text{-TeBu}^{\text{n}})_4(\mu_2\text{-TeBu}^{\text{n}})_2(\text{PEt}_3)_4]$ <sup>379</sup> is also, not surprisingly, the smallest cluster characterized, with the telluride ligands occupying vertex positions of a nonbonded  $\text{Te}_6$  octahedron. In higher nuclearity clusters, silver atoms are held together by both  $\text{RTe}^-$  and  $\text{Te}^{2-}$ . One such structure,  $[\text{Ag}_{32}(\text{TeBu}^{\text{n}})_{18}\text{Te}_7(\text{PR}_3)_6]$  (**57**) can be synthesized using a variety of phosphines, suggesting an inherent stability for this  $\text{Ag}\text{—}\text{Te}$  framework. The largest  $\text{Ag}/\text{Te}$  cluster characterized to date  $[\text{Ag}_{48}(\text{TeBu}^{\text{n}})_{24}\text{Te}_{12}(\text{PEt}_3)_{14}]$ <sup>379</sup> (**58**) has also been synthesized using  $\text{Bu}^{\text{n}}\text{Te}\text{—}\text{TMS}$ , the structure of which can be viewed as a dimer of two  $\text{Ag}_{24}\text{Te}_{16}$  units, connected via four  $\mu_3\text{-TeBu}^{\text{n}}$  ligands (Figure 39). Unlike certain examples in other systems (e.g.,  $\text{Cu}/\text{S}$ ),<sup>351</sup> the corresponding “ $\text{Ag}_{24}\text{Te}_{16}$ ” subunit has not been isolated. The  $\text{Te}^{2-}$  ligands in these complexes may occur via the unavoidable presence of  $\text{Te}(\text{TMS})_2$  as an impurity produced in the synthesis of the butyltellurolate reagent. However, the inability to “target” the larger clusters using a mixture of  $\text{Bu}^{\text{n}}\text{Te}\text{—}\text{TMS}$  and  $\text{Te}(\text{TMS})_2$ , suggests that  $\text{Te}^{2-}$  may result from the facile  $\text{Te}\text{—}\text{C}$  bond cleavage of the butyltellurolate ligand, probably from intermediate cluster species such as  $[\text{Ag}_6(\mu_3\text{-TeBu}^{\text{n}})_4(\mu_2\text{-TeBu}^{\text{n}})_2(\text{PEt}_3)_4]$ .

The use of aryltellurolate reagents ( $\text{ArTe}\text{—}\text{TMS}$ , where  $\text{Ar} = \text{Ph}, \text{Mes}$ ) with silver(I) salts may be viewed as “milder,” resulting in the isolation of several  $\text{Ag}/\text{Te}$  complexes even at room temperature. “Low nuclearity” ( $\leq$ nine  $\text{Ag}$  atoms) complexes containing exclusively  $\text{ArTe}$  and  $\text{PR}_3$  ligands have structures consisting of three  $\text{Ag}\text{—}\text{Te}$  layers. Interestingly, the clusters  $[\text{Ag}_{14}(\text{TePh})_{12}(\mu_6\text{-Te})(\text{PR}_3)_8]$  ( $\text{PR}_3 = \text{PMe}_3$  (**59**);  $\text{PR}_3 = \text{PEt}_2\text{Ph}$  (**60**)) with identical  $\text{Ag}:\text{TePh}:\text{Te}:\text{PR}_3$  have distinctly different structures. While the  $\text{Te}_{13}$  framework of (**60**) represents a centered icosahedron, a monocapped centered octadecahedral construction is observed in (**59**). Once again, it is shown that the nature of the ancillary phosphine ligand can play a central role in the structure of a polynuclear complex. This is strongly emphasized with the structures of silver–telluride/tellurolate with bidentate phosphines,<sup>380</sup> which are markedly different than those with monodentate phosphine ligands. In contrast to the reaction chemistry of  $\text{Bu}^{\text{n}}\text{Te}\text{—}\text{TMS}$  described above, crystalline

**Table 12** Silver tellurium clusters synthesized using silylated chalcogen reagents.

Cluster	References
$[\text{Ag}_9(\text{TePh})_9(\text{PEt}_2\text{Ph})_6]$	382
$[\text{Ag}_{14}(\text{TePh})_{12}(\text{PMe}_3)_8]$ ( <b>59</b> )	382
$[\text{Ag}_{14}\text{Te}(\text{TePh})_{12}(\text{PEt}_2\text{Ph})_8]$ ( <b>60</b> )	382
$[\text{Ag}_{18}\text{Te}(\text{TePh})_{15}\{\text{Ph}_2\text{P}(\text{CH}_2)_3\text{PPh}_2\}_3\text{Cl}]$	380
$[\text{Ag}_{30}\text{Te}_9(\text{TePh})_{12}(\text{PEt}_2\text{R})_{12}]$	381
$[\text{Ag}_{32}\text{Te}_7(\text{TeBu}^{\text{n}})_{18}(\text{PEt}_3)_6]$ ( <b>57</b> )	379
$[\text{Ag}_{38}\text{Te}_{13}(\text{TeBu}^{\text{I}})_{12}\{\text{Ph}_2\text{P}(\text{CH}_2)_2\text{PPh}_2\}_3]$	380
$[\text{Ag}_{46}\text{Te}_{17}\{\text{Te}(\text{mes})\}_2(\text{PEt}_3)_{16}]$	381
$[\text{Ag}_{48}\text{Te}_{12}(\text{TeBu}^{\text{n}})_{24}(\text{PEt}_3)_{14}]$ ( <b>58</b> )	379

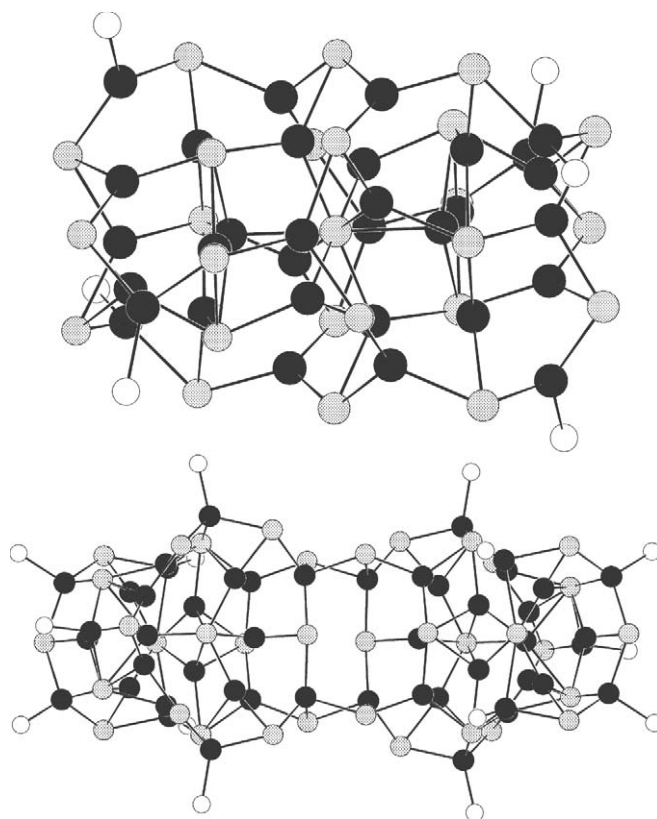


**Figure 39** Ball-and-stick representation of the cluster core of  $[\text{Ag}_{32}(\text{TeBu}^n)_{18}\text{Te}_7(\text{PR}_3)_6]$  (**57**) and  $[\text{Ag}_{48}(\text{TeBu}^n)_{24}\text{Te}_{12}(\text{PEt}_3)_{14}]$  (**58**).

products have been isolated from reactions employing a combination of  $\text{ArTe-TMS}$  and  $\text{Te}(\text{TMS})_2$ . The structure of  $[\text{Ag}_{30}(\text{TePh})_{12}\text{Te}_9(\text{PET}_3)_{12}]^{381}$  is very similar to that of the aforementioned Cu/Te cluster  $[\text{Cu}_{29}\text{Te}_9(\text{TePh})_{12}(\text{PET}_3)_8]^-$  (**53**). Despite the similar coordination geometries observed for the copper and silver atoms (trigonal planar and tetrahedral), this represents the only distinct structural relationship found between these two systems. Also absent from the Ag/Te series are mixed-valence complexes such as those observed in the Cu/Te system, attributable to the much higher oxidation potential of  $\text{Ag}^{\text{I}}$  with respect to  $\text{Cu}^{\text{I}}$ .

(c) *Gold clusters.* As was described in the previous sections, a wide variety of polynuclear complexes have been isolated from the reaction of  $\text{Cu}^{\text{I}}$  or  $\text{Ag}^{\text{I}}$  salts with silylated chalcogen reagents. Access to a similarly rich diversity for  $\text{Au}^{\text{I}}$  is expected, however, it has possibly been inhibited by the strong preference of monovalent gold to adopt linear coordination geometry. Nonetheless, the cationic clusters  $[\text{Au}_{10}\text{Se}_4(\text{dppm})_4]^{2+}$  (**61**) and  $[\text{Au}_{18}\text{Se}_8(\text{dppe})_6]^{2+}$  (**62**) have been synthesized from the reaction of  $\text{Se}(\text{TMS})_2$  with gold halide species stabilized by bidentate phosphine ligands.<sup>383</sup> Cluster (**61**) features a planar structure with eight phosphine-coordinated gold atoms forming an octagonal array, and two additional gold atoms at the center (Figure 40). The four  $\text{Se}^{2-}$  ligands act as  $\mu_3$ -capping ligands between two “outer” and one “inner” Au atom. The structure of cluster (**62**) is much different, consisting of an  $\text{Au}_6\text{Se}_2$  heterocubane unit, which is bonded by six “(dppe) $\text{Au}_2\text{Se}$ ” units. All gold atoms in complexes (**61**) and (**62**) are nearly linearly coordinated (P–Au–Se or Se–Au–Se). Noteworthy is that the use of monosilylated organoselenolate reagents invariably results in the formation of (**61**) (via Se–C scission), indicating the high stability associated with its structure.

### (iii) Group 12 metal clusters

Several chalcogen-bridged clusters of the group 12 metals (Zn, Cd, Hg) have been synthesized utilizing silylated reagents. Mostly, the structures of these complexes are based on adamantane-like cages, and are similar to II–VI clusters synthesized by other approaches, as described in

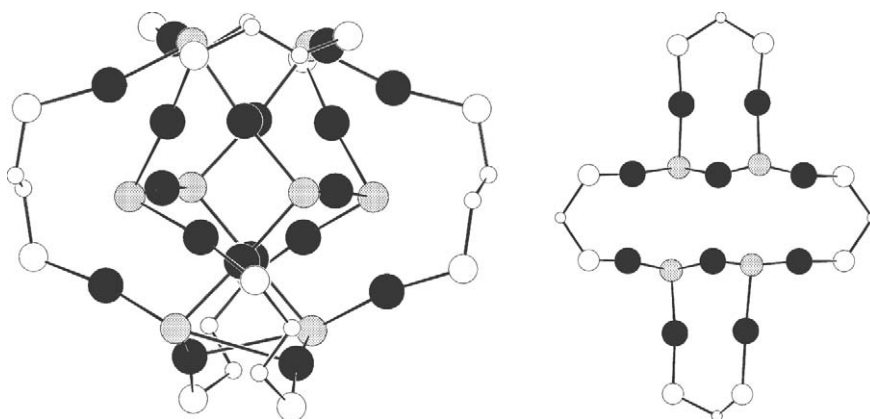


**Figure 40** Ball-and-stick representation of the cluster core of  $[\text{Au}_{10}\text{Se}_4(\text{dppm})_4]^{2+}$  (**61**) and  $[\text{Au}_{18}\text{Se}_8(\text{dppe})_6]^{2+}$  (**62**).

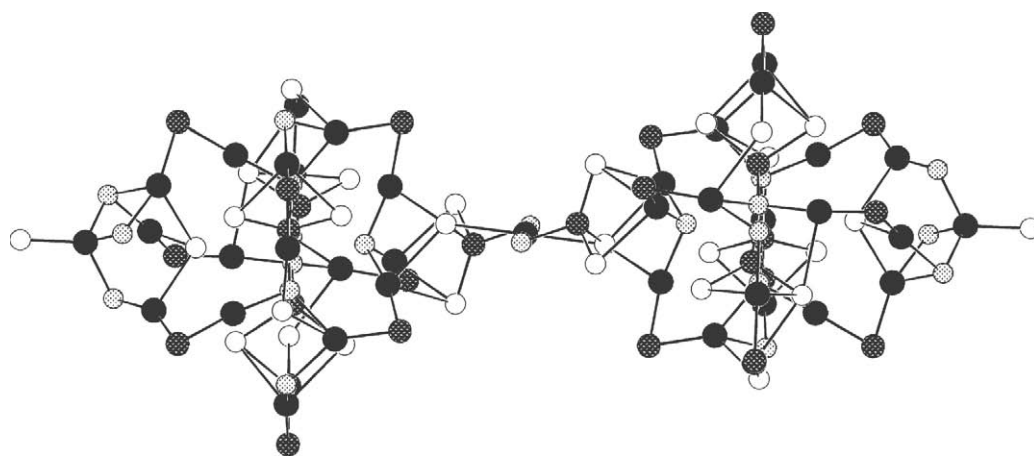


**Figure 41** Ball-and-stick representation of the cluster core of  $[\text{Hg}_{39}\text{Fe}_8\{\text{Fe}(\text{CO})_4\}_{18}\text{S}_8(\text{SBu}^t)_{14}\text{Br}_{28}]$  (**63**).

**Section 7.2.4.5.** Alternatively, the reaction of  $\text{Bu}^t\text{S-TMS}$  with the bimetallic complex  $[\text{Fe}(\text{CO})_4(\text{HgX})_2]$  ( $\text{X} = \text{Cl}, \text{Br}$ ) has produced a series of Hg–Fe clusters whose structures are not related to those of the II–VI complexes.<sup>384</sup> These clusters consist of Hg–Fe chains, which are bridged by sulfur and halide atoms. The structure of the largest cluster  $[\text{Hg}_{39}\text{Fe}_8\{\text{Fe}(\text{CO})_4\}_{18}\text{S}_8(\text{SBu}^t)_{14}\text{Br}_{28}]$  (**63**) is constructed from two  $\text{Hg}_{19}\text{Fe}_{13}$  clusters connected by a central Hg atom (Figure 41). In the center of the  $\text{Hg}_{19}\text{Fe}_{13}$  structure there exists an almost planar six-membered  $\text{Fe}_3\text{S}_3$  ring which is very similar to that observed for the iron thiolate complexes  $[\text{Fe}_3(\text{SR})_3\text{X}_6]$ .<sup>385</sup>

### 7.2.5.2 Clusters from $\text{E} = \text{PR}_3$

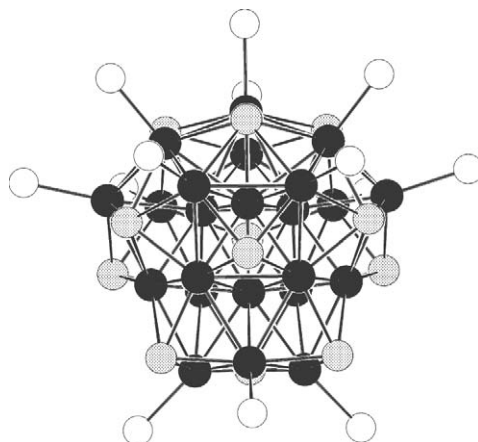
The endeavor to isolate cluster intermediates *en route* to solid-state materials is an attractive one, as these molecular species can provide insight into the mechanism of their formation, as well as the development of properties with particle size. To this end, the reaction system involving trialkylphosphine chalcogenide and low valent organometallics has been shown to produce molecular complexes under mild conditions (Table 13). In the  $\text{MnTe}$  and  $\text{FeTe}_x$  systems, the isolated molecular complexes are small, and bear no resemblance to the bulk lattice.<sup>62,63,386</sup> The reaction of  $\text{TePET}_3$  with  $\text{Co}_2(\text{CO})_8$  produces a series of small clusters which culminate with the octahedral cluster  $[\text{Co}_6\text{Te}_8(\text{PET}_3)_6]^{2-}$ <sup>243</sup> (Section 7.2.4.2). Thermolysis of the cluster in solution leads to the formation of  $\beta\text{-CoTe}$ , suggesting that this complex may be an intermediate in the formation of the solid. Similar results have shown that the octahedral Cr/Te cluster  $[\text{Cr}_6\text{Te}_8(\text{PET}_3)_6]^{6-}$  can be formed *en route* to bulk  $\text{Cr}_3\text{Te}_4$ .

**Table 13** Metal chalcogenide clusters synthesized using phosphine chalcogenide.

Cluster	References
[Cr <sub>6</sub> Te <sub>8</sub> (PEt <sub>3</sub> ) <sub>6</sub> ]	66
[Fe <sub>4</sub> Te <sub>4</sub> (PEt <sub>3</sub> ) <sub>4</sub> ]	386
[Co <sub>4</sub> Te <sub>2</sub> (PEt <sub>3</sub> ) <sub>4</sub> (CO) <sub>6</sub> ]	243
[Co <sub>6</sub> Te <sub>8</sub> (PEt <sub>3</sub> ) <sub>6</sub> ]	243
[Pd <sub>6</sub> Te <sub>6</sub> (PEt <sub>3</sub> ) <sub>8</sub> ]	143
[Ni <sub>9</sub> Te <sub>6</sub> (PEt <sub>3</sub> ) <sub>8</sub> ] ( <b>64</b> )	67
[Ni <sub>20</sub> Te <sub>18</sub> (PEt <sub>3</sub> ) <sub>12</sub> ] ( <b>1</b> )	67
[Ni <sub>23</sub> Se <sub>12</sub> (PEt <sub>3</sub> ) <sub>13</sub> ] ( <b>65</b> )	65

Cluster intermediates in what has been termed the “molecules-to-solids” pathway<sup>64</sup> have also been isolated from similar reactions involving Pd and Ni precursors. The structure of [Pd<sub>6</sub>Te<sub>6</sub>(PEt<sub>3</sub>)<sub>8</sub>]<sup>143</sup> can be described as μ<sub>2</sub>-Te bridged triangular Pd<sub>3</sub>Te<sub>2</sub> units, and in this sense it is closely related to that of other Pd/E clusters (see Section 7.2.5.1.3(i)). Thermolysis of this complex results in the formation of bulk PdTe. The same reaction that produces crystalline NiTe at high temperature yields the clusters [Ni<sub>9</sub>Te<sub>6</sub>(PEt<sub>3</sub>)<sub>8</sub>] (**64**) and [Ni<sub>20</sub>Te<sub>18</sub>(PEt<sub>3</sub>)<sub>12</sub>] (**1**) under milder conditions.<sup>67</sup> Cluster (**64**) converts to (**1**) upon standing at room temperature in toluene.<sup>387,388</sup> The structure of (**1**) is that of a Ni-centered cube capped by six Te ligands. Cluster (**1**) represents the largest structurally characterized Ni/Te cluster, with dimensions in the nanometer size regime. The structure can be described in terms of a twisted Ni<sub>6</sub> trigonal prism with a central Te, and capped by two additional Ni atoms (Figure 1). A similar fragment is present in the structure of Ni<sub>1+x</sub>Te.<sup>389</sup> It is also related to the structure of [Ni<sub>8</sub>S(SBu<sup>t</sup>)<sub>9</sub>],<sup>390</sup> which can be isolated from the reaction of NiCl<sub>2</sub> with NaSBu<sup>t</sup>. The other 12 Ni atoms are bonded to four Te<sup>2-</sup> ligands in an approximately square coordination, and further bonded to an ancillary phosphine ligand.

The reaction of Ni(COD)<sub>2</sub> and Se = PEt<sub>3</sub> in refluxing toluene results in a mixture of Ni<sub>3</sub>Se<sub>2</sub> and elemental nickel. Similar to the telluride system, a molecular intermediate has been isolated *en route* to the solid.<sup>65</sup> The structure of [Ni<sub>23</sub>Se<sub>12</sub>(PEt<sub>3</sub>)<sub>13</sub>] (**65**) can be divided into two identifiable fragments (Figure 42). The top of the cluster is a Se-rich Ni<sub>10</sub>Se<sub>9</sub> unit. Like many other Ni/Se clusters, the Se<sup>2-</sup> ligands are found on the surface of a nickel-only cluster core, acting as either μ<sub>4</sub>- or μ<sub>5</sub>-caps. The bottom of the cluster, however, is Ni-rich, being comprised of 13 nickel atoms and only three Se<sup>2-</sup> ligands. In this section, a central Ni atom makes bonding contacts with 12 other Ni. The Se<sup>2-</sup> ligands cap the bottom of the cluster. Noted resemblances of the top half to the structure of NiSe and that of the bottom half to elemental nickel suggest this cluster may result from an intergrowth of two different cluster types. Interestingly, thermolysis results in the formation of Ni<sub>3</sub>Se<sub>2</sub>, of which neither substructure is reminiscent.

**Figure 42** Ball-and-stick representation of the cluster core of [Ni<sub>23</sub>Se<sub>12</sub>(PEt<sub>3</sub>)<sub>13</sub>] (**65**).

### 7.2.5.3 Cluster Synthesis via Reactive Chalcogenometallates and Related Reagents

#### 7.2.5.3.1 Clusters synthesized from tetrachalcogenometallate anions $[\text{ME}_4]^{n-}$

The ability of tetrachalcogenometallates  $[\text{ME}_4]^{n-}$  ( $\text{M} = \text{V}, \text{Nb}, n = 3$ ;  $\text{M} = \text{Mo}, \text{W}, n = 2$ ;  $\text{M} = \text{Re}, n = 1$ ) to act as multidentate ligands to a variety of transition metals has been well documented.<sup>98–101</sup> As a result of this coordinative versatility, these complexes have been widely implemented in the synthesis of homometallic and heterometallic metal chalcogenide clusters with intact or altered  $[\text{ME}_4]^{n-}$  units. In particular, the synthesis of ternary polynuclear  $\text{M–Fe–E}$  and  $\text{M–Cu(Ag)–E}$  complexes has received much attention, due to their relevance to biological systems as well as interesting catalytic and physical properties.

##### (i) Ternary $\text{M}/\text{coinage}$ clusters

Early interest in the synthesis of  $\text{M–Cu(Ag)–E}$  clusters was stimulated by the phenomenon of  $\text{Cu–Mo}$  antagonism observed in biological systems.<sup>101</sup> More recently, several of these complexes have been shown to exhibit strong nonlinear optical behaviors such as optical limiting effects and third-order NLO susceptibilities that can be orders of magnitude greater than that of  $\text{C}_{60}$ .<sup>391</sup> Syntheses of these complexes using chalcogenometallate reagents have been carried out using both solution and solid-state approaches (see Table 14). The formation typically occurs via the sequential addition of  $\text{L}_n\text{Cu(Ag)}$  units to one or more of the six  $\text{E}\cdots\text{E}$  edges of the chalcogenometallate constituent. As a result, the tetrahedral coordination geometry of the  $\text{ME}_4^{n-}$  reagent is generally retained in the products  $\text{M}^1\text{M}_n^2$  (where  $n = 1–6$ ).

A common structural type in tetranuclear  $\text{M–Cu(Ag)–E}$  systems is the cubane-like assembly observed in clusters of the formula  $[(\mu_3\text{–M}^1\text{E}_4)(\text{M}^2\text{L})_3\text{X}]$  ( $\text{M}^1, \text{M}^2 = \text{Mo}, \text{W}$  or  $\text{Re}$ ;  $\text{E} = \text{S}, \text{Se}$ ). The structure of these complexes can be described as a distorted cube completed by three copper or silver atoms ( $\text{M}^2$ ) (each with a terminal halide, phosphine or arsine ligand, (L), a halide ligand (X), and a tridentate  $[\text{ME}_4]^{n-}$  unit, itself consisting of three bridging ( $\text{E}_b$ ) and one terminal ( $\text{E}_t$ ) chalcogenide ligands (Figure 43, left). The  $\text{M–E}_t$  bond distance is shorter than the  $\text{M–E}_b$  distances, and closer to that of the  $\text{M}=\text{E}$  double bond in  $[\text{ME}_4]^{n-}$ . If the starting material is  $\text{MOS}_3^{2-}$ , the O atom always adopts the terminal position. The large distortion in the cube is a consequence of the relatively weak interactions between the Cu or Ag atoms and the  $\mu_3$ -halide ligand. Although the coordination environment of the Cu or Ag atoms is formally tetrahedral, the geometry ranges from a strongly distorted tetrahedron to nearly trigonal planar, depending on the strength of the  $\text{Cu(Ag)–X}$  interactions.

A second structural type for clusters with a  $\{\text{M}_3^2\text{M}^1\text{E}_3\}$  core is the incomplete cubane arrangement. The structures are similar to those described above, except that the vertex occupied by the halide ligand is missing (Figure 43, middle). Addition of halide to these complexes yields the corresponding distorted cubane structure. Clusters with structures intermediate between those described above are referred to as “half-open” cubane-like complexes. The structure can be viewed as an incomplete cubane in which an open  $\text{M}^2\text{–M}^2$  edge is bridged by a ligand such as  $\text{Br}^-$ ,  $\text{I}^-$ , or  $\text{OAc}^-$  (Figure 43, right). Similar structures are observed for complexes in which the  $\text{Cu(Ag)}_3$  face is bridged by tridentate thiophosphate ligands. An interesting variation of this arrangement (Figure 44) is observed in the complex  $[\text{ReS}_4\text{Cu}_3\text{Cl}_5]^{3-}$  (**66**), synthesized by the addition of  $\text{CuCl}_2^-$  to  $\text{ReS}_4^-$ , the structure of which can be viewed as an incomplete cubane with an “extra” face.<sup>392</sup>

Other clusters with the tetrachalcogenolate unit are all based on the sequential addition of  $[\text{ML}_x]^+$  to the  $\text{E–E}$  edges of  $\text{ME}_4^{n-}$ . The addition of  $[\text{Cu}_2(\text{dppm})(\text{MeCN})_4]^{2+}$  to  $\text{MS}_4^{2-}$  ( $\text{M} = \text{Mo}, \text{W}$ ) has resulted in the formation of the “flywheel”-shaped clusters  $[\text{MS}_4\text{Cu}_3(\text{dppm})_3]^+$  (**67**) ( $\text{M} = \text{Mo}$  (**67a**);  $\text{M} = \text{W}$  (**67b**)).<sup>393–396</sup> The clusters consist of two different types of sulfur atoms. Three  $\mu_2$ -S ligands are bonded to the Mo(W) and one Cu, while the fourth S adopts a  $\mu_4$ -bridging mode and is bonded to the Mo(W) and all three Cu atoms, these Cu centers existing in a distorted tetrahedral environment.

Another structure featuring the coordination of  $\text{M}^2$  atoms to three  $\text{E}\cdots\text{E}$  edges of the chalcogenometallate ligand is seen in the open tetranuclear  $\text{M}^1\text{M}_3^2$  clusters (Figure 45). These clusters can effectively be described as T-shaped, with the four metal atoms essentially coplanar and  $\text{M}^2\text{–M}^1\text{–M}^2$  angles close to  $90^\circ$ . The  $\text{M}^2$  atoms adopt either a trigonal planar or tetrahedral geometry, depending on whether one or two ancillary ligands are attached. In clusters

**Table 14** Clusters synthesized via the reaction of tetrachalcogenometallate or related reagents with late transition metal salts.

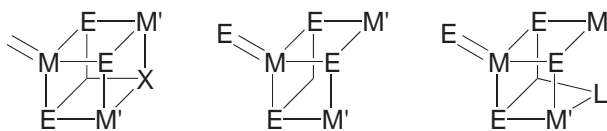
Cluster	Structure	References
[VS <sub>4</sub> Au <sub>3</sub> (PPh <sub>3</sub> ) <sub>3</sub> ]	T-shaped	424
[V <sub>2</sub> S <sub>4</sub> M <sup>2</sup> <sub>2</sub> L <sup>1</sup> <sub>2</sub> L <sup>2</sup> <sub>2</sub> ] <sup>2-</sup> (M <sup>2</sup> = Cu, Ag; L <sup>1</sup> = SPh, CS <sub>3</sub> ; L <sup>2</sup> = S <sub>2</sub> CN(OC <sub>4</sub> H <sub>8</sub> ), PPh <sub>3</sub> )	Cubane	425–427
[VS <sub>4</sub> Cu <sub>4</sub> (SPh) <sub>4-n</sub> (S <sub>2</sub> CNR) <sub>n</sub> ] <sup>3-</sup> (n = 0–3)	Planar	425,428
[VS <sub>4</sub> Cu <sub>6</sub> L <sub>5</sub> X <sub>3</sub> ] <sup>n-</sup> (L = PPh <sub>3</sub> , Cl; X = Cl, Br)	VS <sub>4</sub> bridging Cu <sub>6</sub> octahedron	55,56,58,55
[NbS <sub>3</sub> Cu <sub>3</sub> (PPh <sub>3</sub> ) <sub>3</sub> (DMF) <sub>3</sub> Br]	Cubane with X as one vertex	108
[NbS <sub>4</sub> Cu <sub>3</sub> (PPh <sub>3</sub> ) <sub>4</sub> ]	T-shaped	108
[NbSe <sub>3</sub> Cu <sub>3</sub> Cl <sub>3</sub> (DMF) <sub>3</sub> ]	Incomplete cubane	108
[NbSe <sub>4</sub> Au <sub>3</sub> (PPh <sub>3</sub> ) <sub>4</sub> ]	T-shaped	108
[Nb <sub>2</sub> Se <sub>4</sub> Au <sub>2</sub> Cl <sub>2</sub> (PMe <sub>3</sub> ) <sub>6</sub> ]	Cubane	108
[NbSe <sub>4</sub> Cu <sub>4</sub> (PR <sub>3</sub> ) <sub>4</sub> X <sub>n</sub> ] (X = Cl, SCN; n = 0, 1)	Planar	108,377
[NbSe <sub>4</sub> Cu <sub>5</sub> Cl <sub>2</sub> (dppm) <sub>2</sub> ]	Five CuL coordinated to NbSe <sub>4</sub>	108
[Nb <sub>2</sub> Se <sub>6</sub> Cu <sub>4</sub> (PMe <sub>3</sub> ) <sub>8</sub> ]	Two cubanes sharing a Nb <sub>2</sub> E <sub>2</sub> face	377
[Nb <sub>2</sub> O <sub>2</sub> Se <sub>6</sub> Cu <sub>6</sub> (PMe <sub>3</sub> ) <sub>6</sub> ]	Nb <sub>2</sub> Cu <sub>6</sub> cube	108
[Nb <sub>6</sub> Se <sub>12</sub> OCu <sub>4</sub> (PMe <sub>3</sub> ) <sub>4</sub> ] <sup>2+</sup>	O-centered Nb <sub>6</sub> octahedron with four faces capped with Se <sub>3</sub> Cu(PMe <sub>3</sub> )	377
[MoOS <sub>3</sub> Cu <sub>3</sub> X <sub>3</sub> L <sub>n</sub> ] <sup>2-</sup> (X = Cl, Br; L = NC <sub>5</sub> H <sub>4</sub> ; n = 0, 1)	Incomplete cubane	429–432
[MoOS <sub>3</sub> Cu <sub>3</sub> L <sup>1</sup> <sub>n</sub> L <sup>2</sup> <sub>m</sub> ] (L <sup>1</sup> = I, SCN; L <sup>2</sup> = amine; n = 1, 2; m = 1, 2, 5)	Incomplete cubane	433–435,470
[MoES <sub>3</sub> M <sup>2</sup> <sub>3</sub> L <sub>3</sub> X] <sup>n-</sup> (E = O, S; M <sup>2</sup> = Cu, Ag; L = PPh <sub>3</sub> , AsPPh <sub>3</sub> , Cl, Br, I; n = 0, 3)	Cubane with X as one vertex	432,436–440,471
[MoES <sub>3</sub> M <sup>2</sup> <sub>3</sub> (PPh <sub>3</sub> ) <sub>3</sub> {S <sub>2</sub> P(OR) <sub>2</sub> }] (E = O, S; M <sup>2</sup> = Cu, Ag)	Half-open cubane	441,474
[MoS <sub>4</sub> Cu <sub>3</sub> (dppm) <sub>3</sub> ] <sup>+</sup> ( <b>67a</b> ) [MoS <sub>4</sub> Re <sub>3</sub> (CO) <sub>9</sub> S]	“Flywheel” Cubane	393
[MoSe <sub>4</sub> Cu <sub>3</sub> (PPh <sub>3</sub> ) <sub>3</sub> ] <sup>+</sup>	Incomplete cubane	442
[MoSe <sub>4</sub> M <sup>2</sup> <sub>3</sub> (PPh <sub>3</sub> ) <sub>3</sub> X] (M <sup>2</sup> = Cu, Ag; X = Cl, Br, I)	Cubane with X as one vertex	442–447
[MoSe <sub>4</sub> Cu <sub>3</sub> (S <sub>2</sub> CNEt <sub>2</sub> ) <sub>3</sub> ] <sup>2-</sup>	T-shaped	448
[MoS <sub>4</sub> Cu <sub>4</sub> L <sub>4</sub> ] <sup>2+/-</sup> (L = PR <sub>2</sub> CH <sub>2</sub> PR <sub>2</sub> , S <sub>2</sub> CNEt <sub>2</sub> )	Planar	395,396,449,395
[MoS <sub>4</sub> Cu <sub>4</sub> X <sub>n</sub> L <sub>8-n</sub> ] <sup>m</sup> (X = Br, SCN; L = amine)	Planar	391,450,451,391
[MoS <sub>4</sub> Cu <sub>4</sub> Cl <sub>5</sub> ] <sup>3-</sup>	Cubane with an extra face	432
[MoSe <sub>4</sub> Cu <sub>4</sub> X <sub>2</sub> (NC <sub>5</sub> H <sub>4</sub> ) <sub>6</sub> ] (X = Cl, Br, CN)	Planar	442,449
[MoSe <sub>4</sub> Cu <sub>4</sub> (S <sub>2</sub> CNMe <sub>2</sub> ) <sub>3</sub> ] <sup>2-</sup>	Planar	448
[MoS <sub>4</sub> Cu <sub>5</sub> Cl <sub>7</sub> ] <sup>4-</sup>	MoS <sub>4</sub> bridging five CuCl <sub>n</sub>	452
[MoS <sub>4</sub> Cu <sub>6</sub> Cl <sub>9</sub> ] <sup>5-</sup>	MoS <sub>4</sub> bridging Cu <sub>6</sub> octahedron	409
[Mo <sub>2</sub> S <sub>8</sub> Ag <sub>4</sub> (PPh <sub>3</sub> ) <sub>4</sub> ] ( <b>69a</b> )	Hexagonal prism	414
[Mo <sub>2</sub> S <sub>8</sub> Cu <sub>5</sub> (S <sub>2</sub> CNMe <sub>2</sub> ) <sub>3</sub> ] <sup>2-</sup>	Two incomplete cubanes bridged by S <sub>2</sub> CNMe <sub>2</sub>	416
[Mo <sub>2</sub> E <sub>2</sub> S <sub>6</sub> Cu <sub>6</sub> X <sub>n</sub> ] <sup>4-</sup> (E = O, X = Br, I)	Two incomplete cubanes bridged by X	453,454
[(MoOS <sub>3</sub> ) <sub>4</sub> Cu <sub>4</sub> ] <sup>4-</sup>	Square M <sub>4</sub> Cu <sub>4</sub> bridged by S	417
[Mo <sub>2</sub> S <sub>4</sub> Pd <sub>6</sub> (dppm) <sub>2</sub> ] ( <b>73a</b> )	“Windmill”	423
[MoS <sub>4</sub> Cu <sub>10</sub> Cl <sub>12</sub> ] <sup>4-</sup> ( <b>68a</b> )	MoS <sub>4</sub> bridging Cu <sub>6</sub> octahedron with four additional Cu	411

Table 14 continued

Cluster	Structure	References
$[\text{MoSe}_4\text{Cu}_{10}(\text{SPh})_{12}]^{4-}$	$\text{MoSe}_4$ bridging $\text{Cu}_6$ octahedron with four additional Cu	448
$[(\text{MoOS}_3)_4\text{Cu}_8(\text{TMEDA})_4]$ (70a)	Planar $\text{M}_4\text{Cu}_4$ bridged by S with additional Cu(TMEDA) units	417
$[\text{Mo}_4\text{S}_{16}\text{Cu}_{10}\text{E}^1_2\text{E}^2]^{4-}$ ( $\text{E}^1, \text{E}^2 = \text{O}, \text{S}$ ) (71a)	Fused butterfly, incomplete cubane and triprism units	419,420
$[\text{Mo}_8\text{E}_4\text{S}_{28}\text{Cu}_{12}]^{4-}$ (72)	Cube	102,421
$[\text{WOS}_3\text{Cu}_3\text{Cl}_3]^{2-}$	Incomplete cubane	432
$[(\text{C}_5\text{H}_5)\text{WS}_3\text{Cu}_3(\text{PPh}_3)_3]^+$	Incomplete cubane	455
$[\text{WES}_3\text{M}^2_3\text{EL}_3\text{X}]^{n-}$ ( $\text{E} = \text{O}, \text{S}$ ; $\text{M}^2 = \text{Cu}, \text{Ag}$ ; $\text{L} = \text{PPh}_3, \text{AsPPh}_3, \text{Cl}, \text{Br}, \text{I}$ ; $n = 0, 3$ )	Cubane with X as one vertex	432,437,456,472,473
$[\text{WES}_3\text{M}^2_3(\text{PPh}_3)_3\{\text{S}_2\text{P}(\text{OR})_2\}]$ ( $\text{E} = \text{O}, \text{S}$ ; $\text{M}^2 = \text{Cu}, \text{Ag}$ )	Half-open cubane	457,475,476,457
$[\text{WS}_4\text{Cu}_3(\text{S}_2\text{CNC}_5\text{H}_{10})_3]^{2-}$	T-shaped	456
$[\text{WS}_4\text{Cu}_3\text{Br}_2(\text{dppm})_2]^{2-}$	T-shaped	395
$[\text{WS}_4\text{Cu}_3(\text{dppm})_3]^+$ (67b)	“Flywheel”	394–396
$[\text{WS}_4\text{Re}_3(\text{CO})_9\text{S}]$	Cubane	458
$[\text{WSe}_4\text{M}^2_3(\text{PR}^1_2\text{R}^2)_3\text{Cl}]$ ( $\text{M}^2 = \text{Cu}, \text{Ag}$ ; $\text{X} = \text{Cl}, \text{I}$ )	Cubane with X as one vertex	442,459–461
$[\text{WSe}_4\text{Cu}_3(\text{S}_2\text{CNET}_2)_3]^{2-}$	T-shaped	462
$[\text{WS}_4\text{Cu}_4(\text{PR}_2\text{CH}_2\text{PR}_2)_4]^{2+}$	Planar	395, 396
$[\text{WS}_4\text{Cu}_4]^{4-}$	Planar	439
$[\text{WS}_4\text{Cu}_4\text{X}_n\text{L}_{8-n}]^m$ ( $\text{X} = \text{Br}, \text{I}, \text{SCN}$ ; $\text{L} = \text{amine}$ )	Planar	391,450,451,463–465
$[\text{WS}_4\text{Cu}_4\text{Cl}_5]^{3-}$	Cubane with an extra face	432
$[\text{WSe}_4\text{Cu}_4\text{L}_4]^{2-}$ ( $\text{L} = \text{dppm}, \text{S}_2\text{CNET}_2$ )	Planar	401,462
$[\text{W}_2\text{Se}_4(\text{SeCH}_2)_2\text{Cu}_2(\text{Pcy}_3)_6]$	Cubane	466
$[\text{WS}_4\text{Cu}_5\text{X}_n]^{(n-3)-}$ ( $\text{X} = \text{Br}, \text{I}$ ; $n = 6, 7$ )	$\text{WS}_4$ bridging five $\text{CuCl}_n$	403–405
$[\text{W}_2\text{S}_8\text{Ag}_4(\text{AsPh}_3)_4]$ (69b)	Hexagonal prism	413
$[\{(\text{C}_5\text{H}_5)\text{WS}_3\}_2\text{Cu}_6\text{X}_6]^{2-}$ ( $\text{X} = \text{Br}, \text{SCN}$ )	Two incomplete cubanes bridged by X	467
$[\text{W}_2\text{S}_6\text{Cu}_5(\text{S}_2\text{CNMe}_2)_3]^{2-}$	Two incomplete cubanes bridged by $\text{S}_2\text{CNMe}_2$	415
$[(\text{LWS}_3)_4\text{Cu}_4]$ ( $\text{L} = \text{O}, \text{C}_5\text{H}_5$ ) (70b), (70c)	Square $\text{M}_4\text{Cu}_4$ bridged by S	417,418
$[\text{W}_2\text{S}_4\text{Pd}_6(\text{dppm})_2]$ (73b)	“Windmill”	423
$[\text{W}_2\text{Se}_4\text{Pd}_6(\text{dppm})_2]$ (73c)	“Windmill”	422
$[(\text{WSe}_4)_3\text{Se}_2\text{Cu}_6]^{4-}$	“Pinwheel”	461
$[\{(\text{C}_5\text{H}_5)\text{WSe}_3\}_3\text{Cu}_7(\text{MeCN})_9]$	Three incomplete corner-shared cubanes	468
$[\text{WS}_4\text{Cu}_{10}\text{Br}_{12}]^{4-}$ (68b)	$\text{WS}_4$ bridging $\text{Cu}_6$ octahedron with four additional Cu	411
$[(\text{WOS}_3)_4\text{Cu}_8(\text{TMEDA})_4]$	Planar $\text{M}_4\text{Cu}_4$ bridged by S with additional Cu(TMEDA) units	417
$[\text{W}_4\text{S}_{16}\text{Cu}_{10}\text{E}^1_2\text{E}^2]^{4-}$ ( $\text{E}^1, \text{E}^2 = \text{O}, \text{S}$ ) (71b)	Fused butterfly, incomplete cubane and triprism units	419,420
$[\text{Mo}_8\text{E}_4\text{S}_{28}\text{Cu}_{12}]^{4-}$	Cube	421
$[\text{ReS}_4\text{Cu}_3\text{Cl}_4]^{2-}$	Cubane with Cl as one vertex	392,469
$[\text{ReS}_4\text{Cu}_3\text{Cl}_5]^{3-}$ (66)	Incomplete cubane with an extra face	392

with bidentate ligands, such as dithiocarbamates, all  $\text{M}^2$  atoms attain a distorted tetrahedral geometry.

The only structural type known for pentanuclear  $\text{M}^1\text{M}^2_4$  clusters synthesized from chalcogenometallate anions is the open structure in which the  $\text{M}^1\text{E}_4^{2-}$  unit acts as a tetradentate ligand with a fourth



**Figure 43** Schematic representation of the structural types displayed by  $M^1M^2E$  cubane-like clusters synthesized via tetrachalcogenometallate reagents.

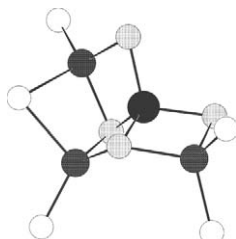


**Figure 44** Ball-and-stick representation of  $[ReS_4Cu_3Cl_5]^{3-}$  (66).

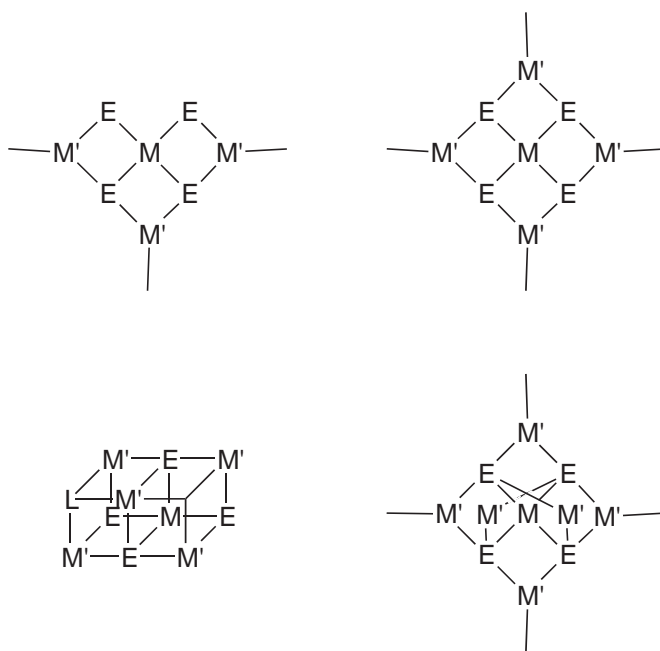


**Figure 45** Schematic representation of the structures of clusters synthesized via the sequential addition of  $M^2L_n$  units to tetrachalcogenometallate reagents.

$L_nCu$  coordinated on an  $E \cdots E$  edge (Figure 45). Due to the tendency of ancillary ligands such as halides and thiolates to partake in bridging interactions, many of these complexes occur as dimers, or as one-, two-, or three-dimensional aggregates in the solid state,<sup>397–401</sup> the dimensionality of which can be altered by changing the size of the counteranion.<sup>402</sup> Discrete molecular species have been isolated using bulky, chelating, and/or nonbridging ligands (Table 14). The four Cu atoms are typically coplanar, with the central tetrahedral M atom either part of the same plane, or very slightly displaced.

Clusters with higher nuclearity ( $n = 5$  or  $6$ ) can be achieved by coordination of  $M^2$  atoms to one or both of the remaining S–S edges of the  $M^1S_4^{2-}$  ligand. In the clusters  $[M^1S_4(CuL)_5X_2]$  (Figure 45) the five copper atoms constitute a distorted square pyramid in which the M atom lies on or just below the basal plane.<sup>403–405</sup> The structures may also be described as distorted double cubanes with elongated Cu–X bonds. The Cu atoms on the basal plane are tetrahedrally coordinated, while the “apical” Cu is three-coordinate. The sulfur atoms involved in face sharing interaction between the two pseudo-cubane units assume a  $\mu_4$ -bridging mode, while the other two adopt the more customary  $\mu_3$ -coordination.



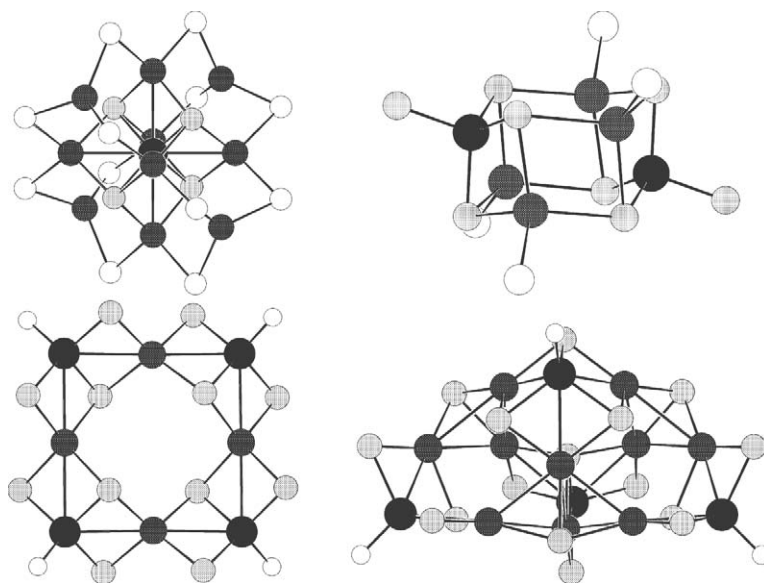


**Figure 46** Ball-and-stick representation of the cluster core of  $[\text{MS}_4\text{Cu}_{10}\text{X}_{12}]$  (**68**),  $[\text{M}^1_2\text{S}_6\text{E}_2\text{M}^2_4(\text{L})_4]$  (**69**),  $[\text{M}_4\text{Cu}_4\text{S}_{12}\text{O}_4]$  (**70**), and  $[\text{M}_4\text{S}_{16}\text{Cu}_{10}\text{E}^{12}\text{E}^2]^{4-}$  (**71**).

The ultimate degree of addition of copper(I) to the tetrathiomallate ligand is achieved in the complexes  $[\text{MS}_4(\text{CuL})_5\text{X}_2\text{CuX}]$  (Figure 45), in which all six  $\text{S}\cdots\text{S}$  edges are coordinated to a copper atom. The six copper atoms form a distorted octahedral array, which encapsulates the central  $\text{MS}_4$  unit. All four sulfur atoms are in a  $\mu_4$ -bridging mode, each connecting the central M atom to a triangular  $\text{Cu}_3$  face of the octahedron.<sup>406–409</sup> Notably, the metal–sulfide core of one such cluster  $[\text{VS}_4(\text{CuPPh}_3)_5(\text{CuCl})\text{Cl}_2]$  bears resemblance to the mineral sylvanite ( $\text{Cu}_3\text{VS}_4$ ), the structure of which is based on  $\text{VS}_4\text{Cu}_6$  clusters connected through  $\text{Cu}_3$  face-sharing interactions.<sup>410</sup> Increasing the Cu:MS<sub>4</sub> ratio has led to the isolation of the clusters  $[\text{MS}_4\text{Cu}_{10}\text{X}_{12}]$  (**68**) (M = Mo, X = Cl (**68a**); M = W, X = Br (**68b**)), which are extensions of these clusters with the addition of four copper atoms via Cu–Br–Cu bridging interactions (Figure 46, top left).<sup>411,412</sup>

A number of ternary M–Cu(Ag)–E clusters containing more than one intact  $\text{ME}_4^{n-}$  unit have also been isolated (Table 14). The formation of such complexes is proposed to result from the condensation of two or more of the various structures already described in this section. The hexanuclear clusters  $[\text{M}^1_2\text{S}_6\text{E}_2\text{M}^2_4(\text{L})_4]$  (**69**) ( $\text{M}^1 = \text{Mo}$ ,  $\text{M}^2 = \text{Cu}$ ,  $\text{L} = \text{PPh}_3$  (**69a**);  $\text{M}^1 = \text{W}$ ,  $\text{M}^2 = \text{Ag}$ ,  $\text{L} = \text{AsPh}_3$  (**69b**)) have been synthesized from  $\text{MS}_3\text{E}^{2-}$  starting materials both by solution and solid-state methods.<sup>413,414</sup> The clusters feature a cage structure in which two six-membered  $\{\text{M}^1_3\text{S}_3\}$  rings are connected via  $\text{M}^1\text{–S}$  and  $\text{M}^2\text{–S}$  linkages (Figure 46, top right). The structures may also be portrayed as a combination of two anti-parallel butterfly-shaped  $[\text{EM}^1\text{S}_3(\text{M}^2\text{L}_2)_2]$  units. The latter description may better reflect the process of formation, as evidenced by the significantly longer “interbutterfly”  $\text{M}^2\text{–S}$  bonds vs. the “intra-butterfly”  $\text{M}^1\text{–S}$  bonding interactions. The fusion of a butterfly ( $\text{EMS}_3\text{Cu}_2$ ) fragment with a nest-shaped ( $\text{SMS}_3\text{Cu}_3$ ) moiety yields the clusters  $[\text{M}_2\text{Cu}_5\text{S}_6\text{E}_2(\text{S}_2\text{R})_3]$  (M = Mo, W; E = O, S).<sup>415,416</sup> The units are linked via weak Cu–S bonds, as well as two bridging dithiocarbamate ( $\text{dte}^-$ ) ligands. The third  $\text{dte}^-$  ligand acts as a chelating ligand.

The few high-nuclearity M–Cu–E clusters in which the  $\text{ME}_4$  unit acts as a bidentate ligand include the octanuclear clusters  $[\text{M}_4\text{Cu}_4\text{S}_{12}\text{O}_4]$  (**70**) (M = Mo (**70a**); M = W (**70b**)) synthesized by the reduction of  $\text{Cu}(\text{NO}_3)_2$  by  $\text{BH}_4$  followed by subsequent additions of  $[\text{ME}_4]^{2-}$  and  $[\text{MO}_2\text{S}_2]^{2-}$ .<sup>417</sup> The clusters exhibit an approximately square array of metal atoms, of which the Mo(W) atoms occupy the four corners ( $\angle \text{M–Cu–M} \approx 180^\circ$ ;  $\angle \text{Cu–M–Cu} \approx 90^\circ$ ). Eight  $\mu_2\text{–S}$  atoms are found bridging the M–Cu linkages, while each Cu–M–Cu connection is bridged by a  $\mu_3\text{–S}$  ligand (Figure 46, bottom left). A similar structure is observed in the cluster  $[\{(\text{C}_5\text{H}_5)\text{WS}_3\}_4\text{Cu}_4]$  (**70c**).<sup>418</sup> The strategy of utilizing a source of sulfide ion ( $\text{Li}_2\text{S}$ ) to displace weakly “copper-philic” bromide ligands in reaction mixtures containing  $\text{MES}_3^{2-}$  (E = O, S) has led to the formation of new Mo/Cu complexes bridged exclusively by chalcogenide ligands.<sup>419,420</sup> The structure of the tetradecanuclear clusters  $[\text{M}_4\text{S}_{16}\text{Cu}_{10}\text{E}^{12}\text{E}^2]^{4-}$  (**71**) (M = Mo (**71a**); M = W (**71b**)) consist of two butterfly  $\{\text{ME}^1\text{S}_3\text{Cu}_2\}$  fragments, one incomplete cubane  $\{\text{ME}^2\text{S}_3\text{Cu}_3\}$ , and one triprism  $\{\text{MS}_4\text{Cu}_3\}$  unit (Figure 46, bottom right).

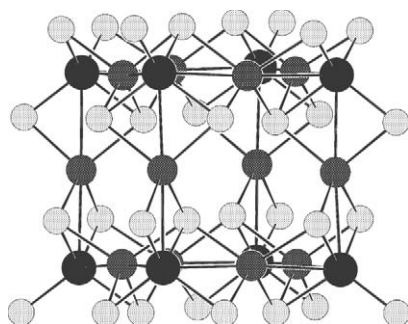


**Figure 47** Ball-and-stick representation of the cluster core of  $[M_8Cu_{12}S_{28}E_4]$  (**72**).

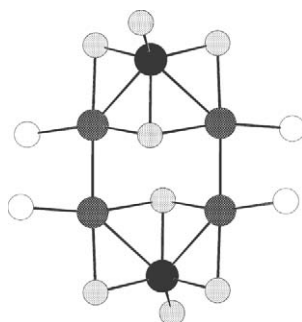


**Figure 48** Ball-and-stick representation of the cluster core of  $[M_2Pd_4E_8(dppm)_2]$  (**73**).

The largest clusters in the Mo–Cu(Ag)–E system to date are the icosanuclear clusters with the formula  $[M_8Cu_{12}S_{28}E_4]$  (**72**).<sup>102,421</sup> The overall arrangement can be described in terms of a large cubane in which the eight corners are occupied by M atoms, with Cu atoms occupying positions on each M–M edge (Figure 47). Each face consists of a  $M_4Cu_4S_{12}E_4$  unit, similar in structure to the octanuclear  $[M_4Cu_4S_{12}O_4]$  clusters (**70**). In  $[Cu_{12}Mo_8S_{32}]^{4-}$  (**72a**) there are four different types of sulfur centers, including terminal as well as  $\mu_2$ -S,  $\mu_3$ -S, and  $\mu_4$ -S bridging ligands. This is the only Mo–Cu–S cluster that contains all four of these types in the same cluster. The Mo atoms are tetrahedrally coordinated either by one terminal and three  $\mu_3$ -S, or by three  $\mu_2$ -S and one  $\mu_4$ -S. The two different types of Mo atom each occupy four nonadjacent positions in the cube. The Cu atoms are bonded to one  $\mu_2$ -S, two  $\mu_3$ -S, and one  $\mu_4$ -S in an approximate tetrahedral geometry.

Recently, related niobium reagents  $[NbE^1_3(E^2R)]^{2-}$  ( $E^1 = S, Se; E^2 = S, Se$ ) have been utilized in the synthesis of ternary NbCuE clusters.<sup>108,377</sup> While several of the products feature the structural types discussed above, a few of the clusters exhibit very different frameworks. The cluster  $[Nb_2O_2Se_6Cu_6(PMe_3)_6]$  consists of cubic  $Nb_2Cu_6$  arrangement, the faces of which are capped by  $\mu_4$ -Se ligands.<sup>108</sup> Palladium-containing clusters  $[M_2Pd_4E_8(dppm)_2]$  ( $M = Mo, E = S$  (**73a**);  $M = W, E = S$  (**73b**),  $Se$  (**73c**)) (**73**) have been synthesized by reaction of  $ME_4^{2-}$  with  $[Pd_2(\mu-dppm)_2Cl_2]$ .<sup>422,423</sup> These clusters exhibit a “windmill” shape, consisting of a planar  $Pd_4E_2$  unit that is bridged by two  $ME_4$  units and two dppm ligands (Figure 48).

#### (ii) Ternary M/Fe clusters

The reaction of  $ME_4^{n-}$  with iron salts has resulted in the formation of a number of heterometallic M/Fe clusters. Several of these complexes exhibit structural relationships to the FeMo-cofactor and P-cluster of the enzyme nitrogenase,<sup>477</sup> with research directed towards the synthesis of molecular models of this enzyme.<sup>16,18,478</sup>

#### 7.2.5.3.2 Related main group ligands

The ability to readily coordinate and bridge metal ions demonstrated by the  $ME_4^{n-}$  reagents is also observed for a variety of main group-based ligands which possess terminally bonded

**Table 15** Metal clusters with dichalcogenolate and related ligands.

Cluster	References	Cluster	References
[Mo <sub>4</sub> Cu <sub>8</sub> O <sub>4</sub> S <sub>12</sub> (Ph <sub>2</sub> PS) <sub>2</sub> N <sub>4</sub> ] <sup>4-</sup>	485	[Ag <sub>4</sub> {S <sub>2</sub> CC(CN) <sub>2</sub> ] <sub>4</sub> <sup>4-</sup>	479,493, 494,479
[Co <sub>5</sub> (CO) <sub>2</sub> S <sub>3</sub> (SC <sub>5</sub> H <sub>4</sub> N) <sub>7</sub> ]	486	[Ag <sub>6</sub> {S <sub>2</sub> CC(CN) <sub>2</sub> ] <sub>6</sub> <sup>6-</sup>	479,490, 491,479
[Co <sub>5</sub> S <sub>4</sub> {SC=C(CN) <sub>2</sub> }(PPh <sub>3</sub> ) <sub>4</sub> ]	127	[Ag <sub>6</sub> {S <sub>2</sub> P(OPr <sup>i</sup> ) <sub>2</sub> ] <sub>6</sub> ]	495
[Cu <sub>4</sub> (2-Se-NC <sub>5</sub> H <sub>4</sub> ) <sub>4</sub> ]	487	[Ag <sub>6</sub> {2-HS(C <sub>5</sub> H <sub>3</sub> N)CO <sub>2</sub> H} <sub>6</sub> ]	496
[Cu <sub>4</sub> (3-TMS-2-Se-NC <sub>5</sub> H <sub>4</sub> ) <sub>4</sub> ]	487	[Ag <sub>6</sub> {Se <sub>2</sub> P(OPr <sup>i</sup> ) <sub>2</sub> ] <sub>6</sub> ]	480
[Cu <sub>4</sub> {(Bu <sup>n</sup> )CS(NBu <sup>t</sup> ) <sub>4</sub> ]	488	[Ag <sub>8</sub> {S <sub>2</sub> CC(CN) <sub>2</sub> }(PPh <sub>3</sub> ) <sub>4</sub> ] <sup>4-</sup>	479,493, 494,479
[Cu <sub>4</sub> {S <sub>2</sub> CC(CN) <sub>2</sub> ] <sub>4</sub> <sup>4-</sup>	489	[Ag <sub>8</sub> S{S <sub>2</sub> P(OEt) <sub>2</sub> ] <sub>6</sub> ]	490
[Cu <sub>6</sub> S <sub>6</sub> {S <sub>2</sub> CC(CN) <sub>2</sub> ] <sub>6</sub> <sup>6-</sup>	479	[Ag <sub>8</sub> Se{Se <sub>2</sub> P(OPr <sup>i</sup> ) <sub>2</sub> ] <sub>6</sub> (74)	480
[Cu <sub>6</sub> {(Bu <sup>n</sup> )CS(NBu <sup>t</sup> ) <sub>6</sub> ]	488	[Ag <sub>9</sub> {S <sub>2</sub> CC(CN) <sub>2</sub> }(PPh <sub>3</sub> ) <sub>6</sub> ] <sup>3-</sup>	493
[Cu <sub>6</sub> {S <sub>2</sub> CC(CN) <sub>2</sub> ] <sub>6</sub> <sup>6-</sup>	489	[Ag <sub>11</sub> S(S <sub>2</sub> CNEt <sub>2</sub> ) <sub>9</sub> ]	497–499
[Cu <sub>6</sub> {S <sub>2</sub> P(OR) <sub>2</sub> ] <sub>6</sub> ]	479,490	[Ag <sub>11</sub> Se(Se <sub>2</sub> CNEt <sub>2</sub> ) <sub>9</sub> ]	498
[Cu <sub>8</sub> {S <sub>2</sub> CC(CN) <sub>2</sub> }(PPh <sub>3</sub> ) <sub>4</sub> ] <sup>4-</sup>	489	[Zn <sub>4</sub> Et <sub>4</sub> (OSCNEt <sub>2</sub> ) <sub>2</sub> (NEt <sub>2</sub> ) <sub>2</sub> ]	500
[Cu <sub>8</sub> {S <sub>2</sub> CC(CN) <sub>2</sub> ] <sub>8</sub> <sup>4-</sup>	479	[Zn <sub>4</sub> S(S <sub>2</sub> AsMe <sub>2</sub> ) <sub>6</sub> ]	501
[Cu <sub>8</sub> S{S <sub>2</sub> P(OR) <sub>2</sub> ] <sub>6</sub> ]	479,490,491	[Zn <sub>4</sub> S{S <sub>2</sub> P(OEt) <sub>2</sub> ] <sub>6</sub> ]	479
[Cu <sub>8</sub> S{S <sub>2</sub> P(OR) <sub>2</sub> ] <sub>6</sub> ]	503	[Cd <sub>4</sub> S(S <sub>2</sub> AsMe <sub>2</sub> ) <sub>6</sub> ]	501
[Cu <sub>11</sub> Se(Br) <sub>3</sub> {Se <sub>2</sub> P(OPr <sup>i</sup> ) <sub>2</sub> ] <sub>6</sub> ]	492	[Cd <sub>4</sub> (Se <sub>2</sub> ) <sub>2</sub> (PSe <sub>4</sub> ) <sub>4</sub> ] <sup>8-</sup>	502
[Cu <sub>12</sub> (P <sub>2</sub> Se <sub>6</sub> ) <sub>2</sub> {Se <sub>2</sub> P(OR) <sub>2</sub> ] <sub>8</sub> ]	481	[Hg <sub>4</sub> (Se <sub>2</sub> ) <sub>2</sub> (PSe <sub>4</sub> ) <sub>4</sub> ] <sup>8-</sup>	502

chalcogen atoms. Two such ligands that have been used extensively in cluster synthesis are dialkyldithiocarbamates, DTC (S<sub>2</sub>C=NR<sub>2</sub>N), and dichalcogenophosphates, DCP [E<sub>2</sub>P(OR)<sub>2</sub>]. Related ligands, such as chalcogenoamidates and ethylenethiolates, can bridge metal atoms through both hard (N, C) and soft (S) donor atoms. Like the metallachalcogenolate reagents, much of the success in the use of these ligands in cluster synthesis has been achieved by reaction with Cu<sup>I</sup> or Ag<sup>I</sup> sources (Table 15). Alternatively, in contrast to ME<sub>4</sub><sup>2-</sup> in which cluster formation is achieved via the coordination of metal ions across an E–E edge, these ligands typically act as bridging ligands between two metal atoms. The two chalcogen atoms of DTC or DCP ligands can coordinate to metal centers either in a terminal or μ<sub>2</sub>-bridging fashion. Thus, these ligands typically act as tridentate (μ<sub>2</sub>, μ<sub>1</sub>) or tetradentate (μ<sub>2</sub>, μ<sub>2</sub>) ligands resulting in clusters based on {ME<sub>3</sub>} and/or {ME<sub>4</sub>} units, respectively.

As a result of their limited bonding capabilities, clusters containing these ligands are restricted to a small number of geometrical arrangements.<sup>479</sup> The common structural types amongst these clusters include those based on tetrahedral, octahedral, or cubic arrangements of metal atoms, many of which contain central chalcogen atoms. Encapsulated chalcogenide anions are also observed in the structures of higher nuclearity clusters, which contain central E<sup>2-</sup> ligands in uncharacteristically high (μ<sub>5</sub>-S, μ<sub>9</sub>-Se) coordination modes. In several cases, multiple products can be isolated from the same reaction mixture, including the cocrystallization of [Ag<sub>8</sub>(μ<sub>8</sub>-Se){Se<sub>2</sub>P(OPr<sup>i</sup>)<sub>2</sub>]<sub>6</sub> (74) (Figure 49) and [Ag<sub>6</sub>{Se<sub>2</sub>P(OPr<sup>i</sup>)<sub>2</sub>]<sub>6</sub> with equal occupancies, which share a common [Ag<sub>6</sub>{Se<sub>2</sub>P(OPr<sup>i</sup>)<sub>2</sub>]<sub>6</sub> core.<sup>480</sup> Moreover, it has been demonstrated that tetrahedral or octahedral complexes can be converted to the corresponding cuboidal structures.

The addition of sulfur to a basic solution of [Cu<sub>4</sub>(*i*-MNT)<sub>4</sub>]<sup>4-</sup> or [Cu<sub>8</sub>(*i*-MNT)<sub>6</sub>]<sup>4-</sup> produces the hexanuclear cluster [Cu<sub>6</sub>S<sub>6</sub>(*i*-MNT)<sub>4</sub>]<sup>6-</sup> (*i*-MNT = [S<sub>2</sub>C=C(CN)<sub>2</sub>]<sup>2-</sup>). The structure of this complex consists of a planar hexagonal array of Cu atoms, connected by the S<sup>2-</sup> ligands.<sup>479</sup> Each *i*-MNT ligand forms an unusual chelate bridge between a Cu and a S atom. The addition of PPh<sub>3</sub> to the complex results in the abstraction of the S<sup>2-</sup> ligands (as S = PPh<sub>3</sub>), and a reversion back to the tetranuclear cluster. Another unusual structure is found in [Cu<sub>12</sub>(P<sub>2</sub>Se<sub>6</sub>){Se<sub>2</sub>P(OEt)<sub>2</sub>]<sub>6</sub>.<sup>481</sup> This complex contains a central P<sub>2</sub>Se<sub>6</sub><sup>4-</sup> ligand, which is produced from Se<sub>2</sub>P(OPr<sup>i</sup>)<sub>2</sub><sup>2-</sup> by an unknown mechanism. The ligand bridges eight copper atoms in a μ<sub>8</sub>-η<sup>3</sup>-η<sup>2</sup>-η<sup>2</sup>-η<sup>3</sup>-η<sup>2</sup>-η<sup>2</sup>-fashion. The other four Cu atoms are connected to the Cu<sub>8</sub> core by the bridging diselenophosphate ligands. Similar structural features are observed in the clusters which contain a central C<sub>2</sub>S<sub>6</sub><sup>2-</sup> moiety.<sup>482</sup> Related PS<sub>3</sub><sup>-</sup> and PS<sub>4</sub><sup>3-</sup> ligands are found in the clusters [Pd<sub>6</sub>(PS<sub>4</sub>)<sub>4</sub>(PPh<sub>3</sub>)<sub>6</sub>], [Cu<sub>4</sub>(P<sub>2</sub>S<sub>6</sub>)(PPh<sub>3</sub>)<sub>4</sub>], [Cu<sub>6</sub>(P<sub>2</sub>S<sub>6</sub>)Cl<sub>2</sub>(PPh<sub>3</sub>)<sub>4</sub>], and [Au<sub>4</sub>(P<sub>2</sub>S<sub>6</sub>)(PPh<sub>3</sub>)<sub>4</sub>], which have been synthesized using the silylated derivative of tetrathio phosphate, (S)P(S-TMS)<sub>3</sub>.<sup>483,484</sup>

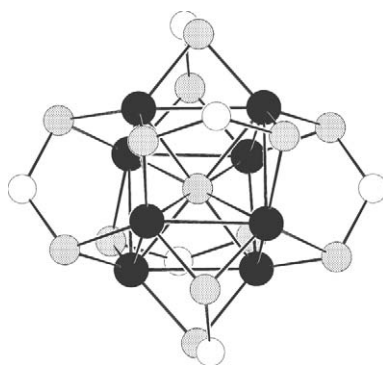


**Figure 49** Ball-and-stick representation of the cluster core of  $[\text{Ag}_8(\mu_8\text{-Se})\{\text{Se}_2\text{P}(\text{OPr}^i)_2\}_6]$  (**74**).

### 7.2.5.3.3 Clusters from polynuclear metalloligands

The use of polynuclear transition metal chalcogenide/chalcogenolate complexes as starting reagents for the synthesis of larger metal clusters has also been explored. The most common of these are the “butterfly-type” complexes bridged by two chalcogenide ligands, denoted by the general formula  $[\text{L}_n\text{M}_2(\mu_2\text{-E})_2]$ . Like the tetrachalcogenometallates, the available lone pairs of electrons on the chalcogenide ligands make these complexes versatile “metalloligands” for cluster synthesis. The addition of metal electrophiles to these reagents results in cluster expansion in which the “ $\text{M}_2\text{E}_2$ ” dimer may act as a monodentate, bridging, or chelating ligand. Amongst the most common of these reagents are the chalcogen-bridged iron carbonyl dimers  $[\text{Fe}_2(\mu_2\text{-E})_2(\text{CO})_2]$ . Typical cluster-forming reactions involve coordination of one or two metal ions to a planar or “butterfly” type  $[\text{Fe}_2(\mu_2\text{-E})_2(\text{CO})_2]$  unit. The largest example,  $[\text{Fe}_6\text{Cu}_5\text{S}_6(\text{CO})_{18}(\text{PPh}_3)_2]^-$ , can be viewed as an aggregate of three of these units surrounding a central  $\{\text{Cu}_5\}$ .<sup>504</sup> Many of the clusters synthesized using these and other related precursors are organometallic, and thus beyond the scope of this review. The reader is directed to a number of recent reports<sup>505–516</sup> and review articles<sup>103,517–519</sup> describing the synthesis and properties of these complexes. Related late transition metal dimers of the formula  $[\text{M}_2(\mu_2\text{-E})_n(\text{L})_m]$  have been used in the synthesis of polynuclear complexes containing up to seven metal centers (Table 16).<sup>102,520</sup> Very recently, a novel approach involving the reductive coupling of  $[(\text{Cl}_4\text{-cat})\text{MoOFeS}_2\text{Cl}_2]^{2-}$  and  $[\text{Fe}_2\text{S}_2\text{Cl}_4]^{2-}$  has been implemented in the synthesis of biologically relevant, higher nuclearity Mo/Fe/S clusters.<sup>271</sup>

Related chalcogenolate-bridged metal complexes  $[\text{M}_2(\text{EPr}^i)_6]^{2-}$  ( $\text{M} = \text{Mn}$ ,  $\text{E} = \text{S}$ ;  $\text{M} = \text{Fe}$ ,  $\text{E} = \text{S}$ ,  $\text{Se}$ ) have also been utilized in the synthesis of the heterometallic chalcogenolate clusters. The structure of  $[\text{Mn}_4\text{Cu}_4\text{S}(\text{SPr}^i)_{12}]^{2-}$  is based on a  $\text{Cu}_4\text{Mn}_4$  cube, which is occupied by an interstitial  $\mu_4\text{-S}$  atom bonded to the four Mn atoms<sup>281</sup> (see Section 7.2.4.4). The 12 thiolate ligands bridge the Mn–Cu edges of the cube. Reaction of the Fe derivatives with  $\text{Cu}^{\text{I}}$  have produced thiolate- and selenolate-bridged clusters with “truncated” adamantane-like structures (Section 7.2.4.5).<sup>309,310</sup>

A second series of polynuclear metalloligands used extensively in the synthesis of larger clusters are the incomplete cuboidal reagents,  $\text{L}_n\text{M}_3\text{E}_4$ , where M is often Mo. Since the bonding arrangements in these precursors bear much resemblance to those in cubane structures, the products of these reactions are typically single cubanes, corner-shared double cubanes, or edge-linked double cubanes (Figure 50), but some exceptions exist.<sup>105–107</sup> Heterometallic clusters containing group VI,<sup>545–547</sup> VII,<sup>548</sup> VIII,<sup>549</sup> IX,<sup>548,550–554</sup> X,<sup>555–567</sup> XI,<sup>443,554,569–575</sup> XII,<sup>553,560,564,576–579</sup> XIII,<sup>554,580–584</sup> XIV,<sup>585–598</sup> and XV<sup>538,599,600</sup> have been synthesized. Fenske–Hall molecular orbital calculations on a number of complexes of this type have been performed. The results demonstrate that the electronic structure of the corresponding cubane depends on the nature of  $\text{M}^2$ .<sup>601</sup> If  $\text{M}^2$  is a main group metal, the  $\text{M}^2$  atom is oxidized upon incorporation into the cubane, with no  $\text{M}^1\text{—M}^2$  bond formation occurring. Alternatively, the incorporation of a transition metal results in  $\text{M}^1\text{—M}^2$  bond formation, without oxidation of the heterometal atom.

### 7.2.5.4 Clusters Synthesized from Polychalcogenide Reagents

The chemistry of metal polychalcogenide clusters represents an area of increasing activity due to the structural diversity as well as the potential for the use of these clusters as precursors to new

**Table 16** Metal chalcogen clusters synthesized using dimeric metal–chalcogenide or –chalcogenolate precursors.

Cluster	$M_2E_n$ Precursor	References
$[(C_5H_5)_2Ti_2S_4Ru_2(C_5H_5)_2]$	$[(C_5H_5)_2TiS_2(\mu-S)_2]^{2-}$	521
$[(C_5H_5)_2Ti_2S_4M_2(cod)_2]$ (M = Rh, Ir)	$[(C_5H_5)_2TiS_2(\mu-S)_2]^{2-}$	521
$[(C_5H_5)_2Ti_2S_4Cu_2(PPh_3)_2]$	$[(C_5H_5)_2TiS_2(\mu-S)_2]^{2-}$	521
$[(C_5H_5)_2Mo_2S_4Cu_2Cl_2]$	$[(C_5H_5)_2TiS_2(\mu-S)_2]$	522
$[(S_2CNEt_2)_2Mo_2Cl_2S_4M_2(cod)_2]$ (M = Rh, Ir)	$[(S_2CNEt_2)_2Mo_2S_2(\mu-S)_2]^{2-}$	523
$[(S_2R)_2Mo_2S_4Cu_2L_2]$	$[(S_2R)_2Mo_2S_2(\mu-S)_2]^{2-}$	524, 525
$\{[MoCl_2(DMF)]\}_2[MoCl_2(L)]_2S_4Ir(C_5Me_5)_2$ (L = O, NNPhMe)	$[Mo_2O_2(\mu-S)_2(DMF)_6]^{2+}$ and $[(C_5Me_5)_2Ir_2Cl_2(\mu-SH)_2]$	526
$[(Cl_4-cat)_2Mo_2Fe_3S_5(PEt_3)_5]$ (Cl <sub>4</sub> -cat = tetrachlorocatechol)	$[(Cl_4-cat)_2MoOS_2FeCl_2]^{2-}$ and $[Fe_2S_2Cl_4]^{2-}$	271
$[(Cl_4-cat)_2Mo_2Fe_2S_3O(PEt_3)_3Cl]^{-}$	$[(Cl_4-cat)_2MoOS_2FeCl_2]^{2-}$	271
$[Mo_2Cu_2S_2(S_2)O_2(SC_2H_4S)_3]^{2-}$	$[Mo_2O_2(\mu-S)_2(SC_2H_4S)_2]^{2-}$	527, 528
$[Mo_2Cu_2S_2(Se_2)O_2(SC_2H_4S)_3]^{2-}$	$[Mo_2O_2(\mu-S)_2(SC_2H_4S)_2]^{2-}$	528
$[(SCH_2CH_2S)_2W_2S_4Cu_2(PPh_3)_2]$	$[(SCH_2CH_2S)_2W_2S_2(\mu-S)_2]^{2-}$	524
$[W_2Cu_2S_4(SCN)_8]^{4+}$	$[W_2S_2(\mu-S)_2(S_4)_2]^{2-}$	529
$[W_2Cu_2S_2(S_2)O_2(SC_2H_4S)_3]^{2-}$	$[W_2O_2(\mu-S)_2(SC_2H_4S)_2]^{2-}$	527
$[Mn_4(SPr^i)_6Cl_4]^{2-}$	$[Mn_2(SPr^i)_6]^{2-}$	304
$[Mn_4Cu_4(SPr^i)_{12}S]^{2-}$	$[Mn_2(SPr^i)_6]^{2-}$	281
$[Mn_4(SePr^i)_6Br_4]^{2-}$	$[Mn_2(SePr^i)_6]^{2-}$	304
$[Fe_3Cu(SPr^i)_6Cl_3]^{2-}$	$[Fe_2(SPr^i)_6]^{2-}$	309
$[Fe_3Cu(SePr^i)_6Cl_3]^{2-}$	$[Fe_2(SePr^i)_6]^{2-}$	310
$[Fe_2Cu_4(SePr^i)_8Cl_2]^{2-}$	$[Fe_2(SePr^i)_6]^{2-}$	310
$[Fe_6S_6(PR_3)_4Cl_2]$	$[Fe_2S_2Cl_4]^{2-}$	271
$[(Cl_4-cat)_2Mo_2Fe_6S_8(PR_3)_6]$	$[(Cl_4-cat)_2MoOS_2FeCl_2]^{2-}$ and $[Fe_2S_2Cl_4]^{2-}$	271
$[Pd_2(PPh_3)(SPr^i)]$ (u-SPr <sup>i</sup> ) <sub>2</sub> (C <sub>5</sub> Me <sub>5</sub> ) <sub>2</sub> Ru <sub>2</sub>	$[(C_5Me_5)_2Ru_2(\mu-S)_2(\mu-SPr^i)_2]$	530
$[(C_5Me_5)_4Rh_4S_4]$	$[(C_5Me_5)_2Rh_2Cl_2(\mu-SH)_2]$	531, 532
$[(C_5Me_5)_4Rh_4(S_2)_2(S_3)]^{2+}$	$[(C_5Me_5)_2Rh_2Cl_2(\mu-SH)_2]$	533
$[(C_5Me_5)_4Rh_4Se_4]$	$[(C_5Me_5)_2Rh_2Cl_2(\mu-SeH)_2]$	534
$[(C_5Me_5)_4Ir_4S_4]$	$[(C_5Me_5)_2Ir_2Cl_2(\mu-SH)_2]$	531, 532
$[(C_5Me_5)_4Ir_4S_4Fe]$	$[(C_5Me_5)_2Ir_2Cl_2(\mu-SH)_2]$	535
$[(C_5Me_5)_3Ir_3(S_2)_3(CuCl_2)]^+$	$[(C_5Me_5)_2Ir_2Cl_2(\mu-SH)_2]$	533
$[(C_5Me_5)_4Ir_4Se_4]$	$[(C_5Me_5)_2Ir_2Cl_2(\mu-SeH)_2]$	534
$[Pd_2S_2(PPh_3)_4Ag_2Cl_2]$	$[Pd_2(\mu-S)_2(PPh_3)_4]$	536
$\{[Pd_2Se_2(dppe)_2]_2M\}$ (M = Ni, Pd, Pt)	$[Pd_2(\mu-Se)_2(dppe)_2]$	537
$\{[Pd_2Te_2(dppe)_2]_2M\}^{2+}$ (M = Pt, Hg)	$[Pd_2(\mu-Te)_2(dppe)_2]$	538
$[Pt_2S_2(PPh_3)_4M_2Cl_2]$ (M = Ag, Au)	$[Pt_2(\mu-S)_2(PPh_3)_4]$	536
$[Pt_2S_2(dppy)_4Ag_2(dppm)]^{2+}$	$[Pt_2(\mu-S)_2(dppy)_2]$	539
$\{[Pt_2S_2(PPh_3)_4]_2Pd\}^{2+}$	$[Pt_2(\mu-S)_2(PPh_3)_4]$	540
$\{[Pt_2S_2(PPh_3)_4]_2Pd_2Cl_2\}^{2+}$	$[Pt_2(\mu-S)_2(PPh_3)_4]$	540
$\{[Pt_2S_2(PPh_3)_4]_2Cu\}^{2+}$	$[Pt_2(\mu-S)_2(PPh_3)_4]$	541
$\{[Pt_2S_2(dppe)_2]_2M\}^{n+}$ (M = Cu, Hg)	$[Pt_2(\mu-S)_2(dppe)_2]$	542
$\{[Pt_2Te_2(dppe)_2]_2M\}^{2+}$ (M = Pt, Pd)	$[Pt_2(\mu-Te)_2(dppe)_2]$	538
$\{[Pt_2S_2(PPh_3)_4Cu]_2(\mu-dppf)\}^{2+}$	$[Pt_2(\mu-S)_2(PPh_3)_4]$	536
$[Ag_2Pt_4S_4(PPh_3)_8]^{2+}$	$[Pt_2(\mu-S)_2(PPh_3)_4]$	543
$\{[Pt_2S_2(dppy)_4]_2Ag_3\}^{3+}$	$[Pt_2(\mu-S)_2(dppy)_2]$	539
$[S(AuPR^1_2R^2)_2(Au_2dppf)]^{2+}$	$[S(Au_2dppf)]$	544
$[Au\{S(Au_2dppf)\}_2]^+$	$[S(Au_2dppf)]$	544
$[(\mu-Au_2dppf)\{S(Au_2dppf)\}_2]^{2+}$	$[S(Au_2dppf)]$	544

dppf = 1,1'-bis(diphenylphosphino)ferrodine, dppy = 2-(diphenylphosphino)pyridine.

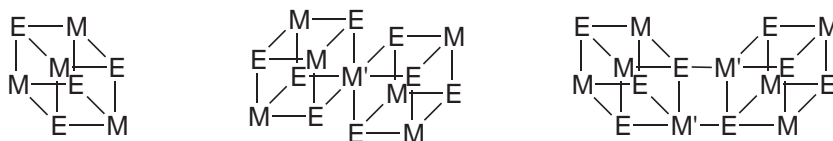


**Figure 50** Schematic representation of the structures of common heterometal cuboidal complexes with  $\text{Mo}_3\text{MS}_4$  cores.

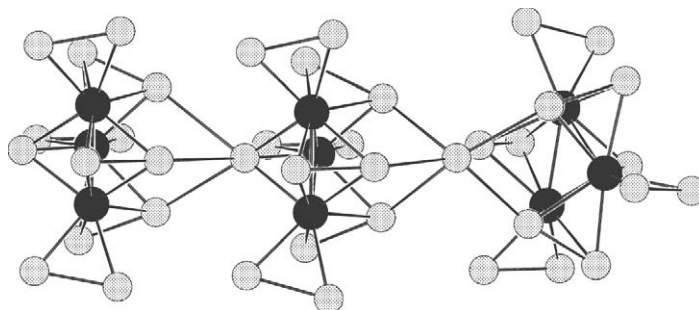


**Figure 51** Ball-and-stick representation of the cluster core of  $[\text{Mo}_9\text{Se}_{40}]^{8-}$  (75).

solid-state materials.<sup>8,9,48</sup> The wide variety of complexes obtained can be attributed to the unique and expansive coordination properties of polychalcogenide ligands,  $\text{E}_n^{2-}$  ( $n = 2-5$ ), as discussed in Section 7.2.3.1.3. In solution, these reagents exist as complex mixtures of anions, and thus several different species may be formed in a particular reaction. The isolated products may represent the most thermodynamically favorable option, or those that are most readily crystallized. The ability to delocalize the negative charge increases with increasing  $n$ . As a result, higher order polychalcogenide ligands ( $n = 3-5$ ) are better suited for stabilization of clusters containing late transition metals, while harder metals in higher oxidation states most often form complexes with  $\text{E}_2^{2-}$  ligands. That said, the single example of a lanthanide polychalcogenide cluster contains  $\text{Se}_3^{2-}$ ,  $\text{Se}_4^{2-}$ , and  $\text{Se}_5^{2-}$  ligands.<sup>602</sup>

The syntheses of polynuclear complexes of this type are typically carried out via ion association or solvothermal techniques (methods I and X in Section 7.2.2). For groups IV and V, these approaches almost exclusively lead to binary or ternary one-dimensional M/E solids, with isolated clusters remaining quite rare. All molybdenum polychalcogenide clusters isolated to this point have structures derived from triangular  $\text{Mo}_3$  units that are stabilized by bridging and chelating  $\text{E}_2^{2-}$  ligands. These include the interesting “clusters of clusters” in which  $\text{Mo}_3\text{E}_n$  subunits are linked together by  $\text{E}_n^{2-}$  bridges as observed in  $[\text{Mo}_{12}\text{Se}_{56}]$  and  $[\text{Mo}_9\text{Se}_{40}]^{8-}$  (75) (Figure 51).<sup>129,130</sup>

Polychalcogenide ligands will oxidatively decarbonylate transition metal complexes. If only partial oxidation/decarbonylation occurs, as is often the case for  $\text{Te}_n^{2-}$  and to a lesser extent  $\text{Se}_n^{2-}$ , polynuclear complexes may be formed. Because the reaction is associated with E–E bond cleavage of the polychalcogenide reagent, these clusters often contain exclusively  $\text{E}^{2-}$  ligands. Even so, the structures of the resultant metal carbonyl chalcogenide complexes are remarkably different compared with other  $\text{E}^{2-}$ -containing clusters.<sup>53,603–605</sup>

A list of clusters synthesized from polychalcogenide ligands is presented in Table 17. Complexes of this type are of relatively low nuclearity, and  $\text{M}_4$  structures predominate. Amongst these, complexes of the formula  $[\text{M}_4\text{E}^{1-}_4(\text{E}^{2-}_3)_{6-x}(\text{E}^{2-}_4)_x]$  seem to be particularly stable, which is not surprising considering they consist of the well-established  $\text{M}_4\text{E}_4$  core.

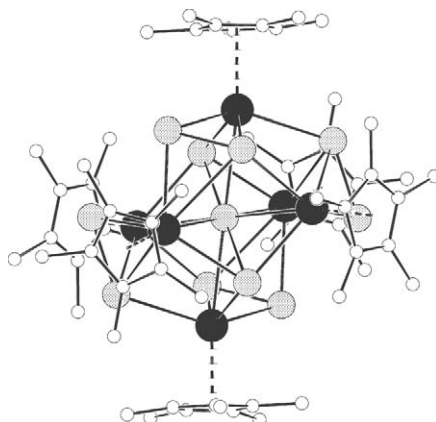
### 7.2.5.5 Chalcogen-bridged Clusters of the *f*-block Elements

Interest in complexes of this type arises from the potential use of solid-state lanthanide materials in optical applications,<sup>625–627</sup> as well as a fundamental interest in the nature of the Ln–E bond. The bonding in molecular lanthanide complexes is typically described as being ionic,<sup>628–630</sup> while covalent bonding arguments are used to describe solid-state Ln–E materials.<sup>631,632</sup> Accordingly, the study of polynuclear Ln–E complexes may be important in the development of structure–property relationships and an understanding of the change in physical properties in the transition from the molecular size regime to bulk  $\text{LnE}_x$  solids.<sup>633</sup>

**Table 17** Metal chalcogen clusters synthesized from polychalcogenide reagents.

Cluster	Synthetic approach(es)	References
[Ti <sub>6</sub> OS <sub>8</sub> (S <sub>2</sub> ) <sub>6</sub> ] <sup>6-</sup>	X	606
[MoS <sub>4</sub> Cu <sub>3</sub> (S <sub>5</sub> ) <sub>2</sub> ] <sup>3-</sup>	I	607
[{Mo <sub>3</sub> Se(Se <sub>2</sub> ) <sub>4</sub> (Se <sub>5</sub> ) <sub>3</sub> } <sub>2</sub> (Se <sub>4</sub> )]	X	608
[Mo <sub>9</sub> Se <sub>40</sub> ] <sup>8-</sup> ( <b>75</b> )	X	129
[Mo <sub>12</sub> Se <sub>56</sub> ] <sup>12-</sup>	X	130
[Re <sub>4</sub> S <sub>4</sub> (S <sub>3</sub> ) <sub>6</sub> ] <sup>4-</sup>	I	609,610
[Re <sub>4</sub> Se <sub>4</sub> (S <sub>3</sub> ) <sub>4</sub> (S <sub>4</sub> ) <sub>2</sub> ] <sup>4-</sup>	I	611
[Re <sub>4</sub> Te <sub>4</sub> (S <sub>3</sub> ) <sub>4</sub> (S <sub>4</sub> ) <sub>2</sub> ] <sup>4-</sup>	I	611
[Cp <sub>8</sub> Re <sub>8</sub> (Se <sub>3</sub> ) <sub>8</sub> (Se <sub>2</sub> ) <sub>8</sub> ]	I	612
[{Fe <sub>4</sub> Te <sub>4</sub> (CO) <sub>10</sub> } <sub>2</sub> (Te <sub>2</sub> )] <sup>2-</sup>	X	604
[Fe <sub>4</sub> (Te <sub>2</sub> ) <sub>2</sub> Te <sub>2</sub> (TeMe) <sub>2</sub> (CO) <sub>8</sub> ] <sup>2-</sup>	X	603
[Fe <sub>4</sub> Te <sub>6</sub> (TeEt) <sub>2</sub> (CO) <sub>8</sub> ] <sup>2-</sup>	X	605
[Fe <sub>5</sub> Te <sub>4</sub> (CO) <sub>14</sub> ] <sup>2-</sup>	I	53
[Fe <sub>6</sub> Te <sub>14</sub> (CO) <sub>12</sub> ] <sup>2-</sup>	X	605
[Fe <sub>8</sub> Te <sub>10</sub> (CO) <sub>20</sub> ] <sup>2-</sup>	I	53
[Ru <sub>4</sub> (Te <sub>2</sub> ) <sub>2</sub> Te <sub>2</sub> (TeMe) <sub>2</sub> (CO) <sub>8</sub> ] <sup>2-</sup>	X	603
[Ni <sub>4</sub> (S <sub>2</sub> )(SCH <sub>2</sub> CH <sub>2</sub> ) <sub>4</sub> ] <sup>2-</sup>	I	613
[Ni <sub>4</sub> Se <sub>4</sub> (Se <sub>3</sub> ) <sub>5</sub> (Se <sub>4</sub> )] <sup>4-</sup> ( <b>8</b> )	I	145,614
[Ni <sub>4</sub> Te <sub>4</sub> (Te <sub>2</sub> ) <sub>2</sub> (Te <sub>3</sub> ) <sub>4</sub> ] <sup>4-</sup>	I, III	614,615
[Pt <sub>4</sub> S <sub>4</sub> (S <sub>3</sub> ) <sub>6</sub> ] <sup>4-</sup>	X	616
[Pt <sub>4</sub> Te <sub>4</sub> (Te <sub>3</sub> ) <sub>6</sub> ] <sup>4-</sup>	I, III	615
[Cu <sub>4</sub> (S <sub>5</sub> ) <sub>2</sub> L <sub>4</sub> ] (L = amine)	I	617,618
[Cu <sub>4</sub> (S <sub>4</sub> ) <sub>2</sub> (S <sub>5</sub> )] <sup>4-</sup>	I	619
[Cu <sub>4</sub> (S <sub>4</sub> )(S <sub>5</sub> ) <sub>2</sub> ] <sup>4-</sup>	I	619
[Cu <sub>6</sub> (S <sub>4</sub> ) <sub>3</sub> (S <sub>5</sub> )] <sup>2-</sup>	I	620
[Cu <sub>4</sub> (Se <sub>4</sub> ) <sub>2.4</sub> (Se <sub>5</sub> ) <sub>0.6</sub> ] <sup>2-</sup>	I	621
[Cu <sub>4</sub> (SbTe <sub>5</sub> )(Te <sub>7</sub> )] <sup>3-</sup>	X	622
[Ag <sub>4</sub> (Se <sub>4</sub> ) <sub>2.1</sub> (Se <sub>5</sub> ) <sub>0.9</sub> ] <sup>2-</sup>	I	621
[Cd <sub>4</sub> Te <sub>2</sub> (Te <sub>2</sub> ) <sub>2</sub> (Te <sub>3</sub> ) <sub>2</sub> ] <sup>4-</sup>	I	623,624
[Hg <sub>4</sub> Te <sub>2</sub> (Te <sub>2</sub> ) <sub>2</sub> (Te <sub>3</sub> ) <sub>2</sub> ] <sup>4-</sup> ( <b>7</b> )	I, X	144,623
[Eu <sub>8</sub> (Se <sub>3</sub> )(Se <sub>4</sub> ) <sub>2</sub> (Se <sub>5</sub> ) <sub>2</sub> O(OH) <sub>12</sub> (DMF) <sub>13</sub> ]	I	602

The first structurally characterized lanthanide chalcogen clusters were isolated as decomposition products of monomeric or dimeric species. Trivalent telluroate complexes Ln[TeSi(TMS)<sub>3</sub>]<sub>3</sub> (Ln = Ce, La), which can only be isolated as dmpe derivatives, decompose in solution to yield polynuclear complexes.<sup>634,635</sup> The cerium derivative, Ce<sub>5</sub>Te<sub>3</sub>[TeSi(TMS)<sub>3</sub>], was structurally characterized. The cluster contains a central [(RTeCe)Te]<sub>3</sub> hexagonal ring, with a capping Ce(TeR)<sub>3</sub> group on each side of the ring. Similarly, the hexanuclear cluster [(C<sub>5</sub>Me<sub>5</sub>Sm)<sub>6</sub>Se<sub>11</sub>] (**76**) forms over several days from solutions of [(Cp\*Sm)<sub>2</sub>Se<sub>3</sub>] at room temperature.<sup>636</sup> The structure of (**76**) is unique (Figure 52), consisting of a distorted Sm<sub>6</sub> octahedron that envelops a central Se atom. The

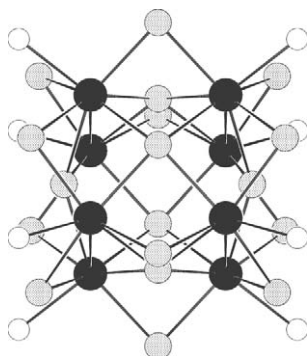
**Figure 52** Ball-and-stick representation of the cluster core of [(C<sub>5</sub>Me<sub>5</sub>Sm)<sub>6</sub>Se<sub>11</sub>] (**76**).

central Se is part of a linear  $\text{Se}_3^{4-}$ , in which the two peripheral Se atoms cap triangular  $\text{Sm}_3$  faces. Four  $\text{Se}_2^{2-}$  ligands encapsulate the octahedral core.

The realization that sterically hindering ancillary ligands are not requisite for the stabilization of molecular Ln–E complexes, coupled with a need for a more general approach to Ln–E clusters has led to the development of two general synthetic strategies for accessing such species.<sup>58</sup> Lanthanide chalcogenolate complexes,  $\text{Ln}(\text{EPh})_3$ , will reduce elemental E (E = S, Se) via the attendant elimination of PhEPh to generate polynuclear mixed chalcogenide/chalcogenolate clusters in good yields. A second approach involves the reductive cleavage of E–C bonds by low valent Ln ions. Identical products are often available by both synthetic routes, though yields may vary significantly. The most common structural type amongst lanthanide chalcogen clusters is observed for the octanuclear clusters  $[\text{L}_8\text{Ln}_8\text{E}^1_6(\text{E}^2\text{Ph})_{12}]$  (**77**) (L = Lewis base;  $\text{E}^1$ ,  $\text{E}^2 = \text{S}$ , Se).<sup>58,633,637,638</sup> A cubic array of eight Ln ions is capped at each face by a  $\mu_4$ -E ligand. Twelve  $\mu$ -EPh ligands bridge the edges of the cube (**Figure 53**). This basic structure is ubiquitous amongst the lanthanides from Ce–Er, with the exception of Eu and the radioactive Pm. The peculiar absence of the Eu derivative from this series may be explained by the relative instability of the trivalent oxidation state of Eu with respect to other Ln metals. Clusters with several different combinations of E, ER, and L have been synthesized (**Table 18**), and ligand displacement reactions have been carried out to produce heterochalcogen complexes. The ability to perform such reactions without decomposing the cluster core suggests an inherent stability for the  $\text{M}_8$  framework. The colors of most of the clusters are representative of that of the parent Ln ion, and thus assigned to forbidden  $f$ – $f$  transitions.<sup>638</sup> Clusters of the redox-active lanthanides, Ce and Sm are more deeply colored and absorptions in the latter have been assigned to  $\text{E}^{2-}$  to Sm charge transfer interactions.<sup>638</sup> Similar synthetic approaches involving the smaller lanthanides (Tm, Yb) have not yet produced octanuclear clusters. The cluster  $[(\text{py})_8\text{Yb}_4\text{Se}_4(\text{SePh})_4]$ <sup>639</sup> is an addition to the broad group of cubane-like complexes (see **Section 7.2.4.1**). An attempt to synthesize the sulfur derivative of this cluster produced  $[(\text{py})_{10}\text{Yb}_6\text{S}_6(\text{SPh})_6]$  whose structure is based on two “ $\text{Yb}_4\text{S}_4$ ” cubane units sharing a  $\text{Yb}_2\text{S}_2$  face.<sup>639</sup>

Modification of the procedures used to synthesize the octanuclear and cubane clusters has resulted in the isolation of tetranuclear  $[\text{Ln}_4\text{Se}(\text{SePh})_8]$  (**78**) clusters, albeit in modest yield.<sup>640</sup> Charge balance in these complexes requires two  $\text{Ln}^{2+}$  and two  $\text{Ln}^{3+}$  ions. Consequently, either redox active (Sm, Yb), or a combination of  $\text{Ln}^{\text{II}}/\text{Ln}^{\text{III}}$  metals can be used. Magnetic susceptibility results for the  $\text{Yb}_4$  derivative (**78a**) support the assignment of a 1:1 mixture of  $\text{Yb}^{3+}/\text{Yb}^{2+}$ . The structures of these complexes are based on a square arrangement of lanthanide ions, with a  $\mu_4$ -Se ligand capping one side of the  $\text{M}_4$  face and two  $\mu$ -SePh ligands bridging each  $\text{M}_2$  edge (**Figure 54**). The  $\text{Ln}_4\text{Se}$  unit is similar to a single face of the cubic  $\text{Ln}_8\text{E}^1_6(\text{E}^2\text{Ph})_{12}$  clusters (**77**), indicating that these complexes may represent intermediates in the formation of larger clusters and solid-state materials. However, in contrast to the octanuclear series, sulfur derivatives of the square clusters remain elusive.

Due to the EPh ligands present in the clusters described above, thermal decomposition of these complexes relies on E–C bond cleavage, and the associated elimination of RER. As a result, solid-state materials produced by the thermolysis of these clusters are contaminated with organic residues. The reduction of  $\text{I}_2$  and PhEPh by ytterbium metal and subsequent reaction with elemental sulfur produces the cluster  $[(\text{THF})_6\text{Yb}_4(\text{S}_2)_4(\mu_4\text{-S})]$ .<sup>641</sup> A  $\text{Yb}_4$  square is capped by a  $\mu_4$ -S ligand, with  $\text{S}_2^{2-}$  ligands bridging adjacent Yb atoms in a  $\mu$ - $\eta^2$ - $\eta^2$  fashion. Similar approaches have been used to synthesize square clusters containing  $\text{Se}^{2-}$ ,  $\text{Se}_2^{2-}$ , and  $\text{PhS}^-$  or  $\text{PhSe}_n\text{E}^-$  (E = Se, Te;  $n = 1$ –3) ligands.<sup>642</sup> These lanthanide clusters expand upon the structural chemistry of related  $\text{M}_4$  complexes

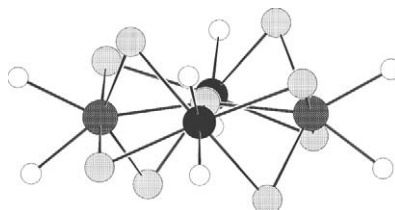


**Figure 53** Ball-and-stick representation of the cluster core of  $[\text{L}_8\text{Ln}_8\text{E}^1_6(\text{E}^2\text{Ph})_{12}]$  (**77**).



**Table 18** Chalcogen-bridged clusters of the *f*-block elements.

Cluster	References
$[(\text{NC}_5\text{H}_4)_3\text{Eu}(\text{SPh})_3\text{M}(\text{SPh})_2]$ (M = Zn, Cd, Hg)	643
$[(\text{THF})_3\text{Eu}(\text{SePh})_3\text{Hg}(\text{SePh})_2]$	644
$[(\text{THF})_6\text{Yb}_4\text{I}_2(\text{S}_2)_4\text{S}]$	641
$[(\text{pyridine})_8\text{Yb}_4\text{Se}_4(\text{SePh})_4]$	639
$[(\text{NC}_5\text{H}_4)_8\text{Yb}_4\text{Se}_2(\text{Se}_2)_2(\text{SPh})_4]$	642
$[(\text{NC}_5\text{H}_4)_9\text{Yb}_4\text{Se}(\text{Se}_2)_2(\text{SeSeTePhSeSePh})(\text{SeTePh})]$	642
$[(\text{DME})_4\text{Ln}_4\text{Se}(\text{SePh})_8]$ (Ln <sub>4</sub> = Sm <sub>4</sub> , Yb <sub>4</sub> , Sm <sub>2</sub> Yb <sub>2</sub> , Nd <sub>2</sub> Yb <sub>2</sub> ) ( <b>78</b> )	640,642
$[\text{Ce}_5\text{Te}_3\{\text{TeSi}(\text{TMS})_3\}_9]$	634,635
$(\text{NC}_5\text{H}_4)_{10}\text{Yb}_6\text{S}_6(\text{SPh})_6]$	639
$[(\text{C}_5\text{Me}_5)_6\text{Sm}_6\text{Se}_{11}]$ ( <b>76</b> )	636
$[\text{Sm}_7\text{S}_7(\text{SePh})_6(\text{DME})_7]^+$	58
$[(\text{THF})_8\text{Ln}_8\text{S}_6(\text{SPh})_{12}]$ (Ln = Ce, Pr, Nd, Sm, Gd, Tb, Dy, Ho, Er) ( <b>77</b> )	633,637,638,633
$[(\text{THF})_8\text{Nd}_8\text{Se}_6(\text{SePh})_{12}]$	633
$[(\text{THF})_8\text{Sm}_8\text{S}_6(\text{SePh})_{12}]$	633
$[(\text{THF})_8\text{Sm}_8\text{Se}_6(\text{SePh})_{12}]$ (L <sub>8</sub> Sm <sub>8</sub> Se <sub>6</sub> (SePh) <sub>12</sub> ) (L = THF, pyridine)	633 58,633

**Figure 54** Ball-and-stick representation of the cluster core of  $[\text{Ln}_4\text{Se}(\text{SePh})_8]$  (**78**) (Ln<sub>4</sub> = Sm<sub>4</sub>, Yb<sub>4</sub>, Sm<sub>2</sub>Yb<sub>2</sub>, Nd<sub>2</sub>Yb<sub>2</sub>).

of early transition metals.<sup>645,646</sup> The cluster  $[(\text{py})_8\text{Yb}_4\text{Se}(\text{SeSe})_3(\text{SeSeSePh})(\text{Se}_{0.38}\text{SePh})]$  can be converted to the cubane  $[(\text{py})_2\text{YbSe}(\text{SePh})_2]_4$  by reaction with  $(\text{py})_4\text{Yb}(\text{SePh})_2$ . The reverse reaction can be achieved by the addition of Se to  $(\text{py})_4\text{Yb}(\text{SePh})_2$ .<sup>642</sup>

## 7.2.6 NANOCLUSTERS

### 7.2.6.1 Copper Selenide and Silver Selenide “Megaclusters”

As described in Section 7.2.5.1.3, the use of silylated chalcogen reagents in cluster synthesis has resulted in the isolation of numerous copper or silver chalcogenide complexes encompassing a wealth of nuclearities and structural types. However, the spherical nature of most of these clusters precludes any substantial structural relationships to bulk M<sub>2</sub>E materials. Alternatively, above a certain number of metal atoms, an abrupt changeover to a layer-type arrangement of metal and chalcogen atoms resembling that of the bulk lattice can be observed. For copper selenide clusters, this “transition-point” appears to be somewhere between 60 and 70 copper atoms.<sup>87,648</sup> In the Ag/Se system, spherical structures are still observed for a cluster with 90 silver atoms, but larger complexes feature a more “bulk-like” construction.<sup>93</sup>

The structures of the copper selenide “megaclusters” are all related, adopting an overall trigonal prismatic shape. The Se atoms of these clusters are arranged into three planar layers resembling a hexagonal close-packed array. Structural differences between clusters of related size are quite nominal and occur, for the most part, on the corners of the cluster. For example,  $[\text{Cu}_{73}\text{Se}_{35}(\text{SePh})_3(\text{PPr}^i_3)_{21}]$ <sup>354</sup> consists of the identical  $\{\text{Cu}_{70}\text{Se}_{35}\}$  core as the clusters  $[\text{Cu}_{70}\text{Se}_{35}(\text{PR}^1_2\text{R}^2)_n]$  (**79**) ( $n = 21-24$ )<sup>351,358</sup> (Figure 55), but with three additional  $[\text{CuSePh}]$  units on three corners. Remarkably, this general hexagonal arrangement is observed in the 2.67 nm core in  $[\text{Cu}_{146}\text{Se}_{73}(\text{PPh}_3)_{30}]$  (**2**) (Figure 2).<sup>92</sup> Copper atoms are located in the holes of the selenium

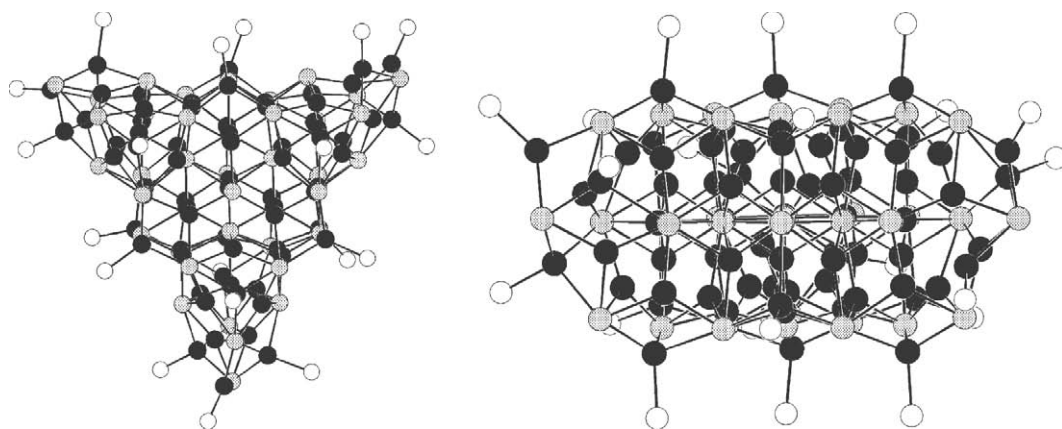


**Figure 55** Ball-and-stick representation of the cluster core of  $[\text{Cu}_{70}\text{Se}_{35}(\text{PEt}_3)_{21}]$  (**79**) demonstrating the prismatic shape of the cluster (left) and the layered arrangement of the Se atoms (right).

lattice, typically adopting trigonal or tetrahedral coordination. Similar assemblies are observed in binary  $\text{Cu}_2\text{Se}$  phases,<sup>355</sup> although the organization of Se atoms in these structures is based on a cubic close-packed arrangement. Nonetheless, these giant clusters can, in principle, be presumed to represent nanometer-sized fragments of the bulk semiconductor. Consistent with this, thermolysis of  $[\text{Cu}_{70}\text{Se}_{35}(\text{PET}_2\text{Ph})_{24}]$  results in a cleavage of the phosphine ligand shell, and the formation of bulk  $\alpha\text{-Cu}_2\text{Se}$ .<sup>649</sup> The factors controlling the selectivity of cluster formation using  $\text{E}(\text{TMS})_2$  at low temperatures are numerous, and small changes in reaction conditions can have a marked effect in product distribution. These factors have recently been reviewed.<sup>87</sup> A selection of the larger Cu/Ag–chalcogenide clusters obtained using silylated chalcogen reagents is listed in Table 19.

A selection of the giant Ag/Se nanoclusters that have been structurally characterized is shown in Figure 56. In these clusters, the Se framework is arranged in a distorted cubic-centered structure that is closely related to that of  $\text{Ag}_2\text{Se}$ .<sup>354</sup> The trigonal and tetrahedral coordination geometries favored by the Ag atoms in these clusters are also consistent with those observed in the bulk semiconductor. Furthermore, in the largest cluster,  $[\text{Ag}_{172}\text{Se}_{40}(\text{SeBu}^n)_{92}(\text{dppp})_4]$ ,<sup>93</sup> the  $\text{Ag}^+$  ions are highly disordered, as they are in bulk  $\text{Ag}_2\text{Se}$ . All of these nanoclusters were obtained from the reaction of phosphine-solublized  $\text{AgO}_2\text{CR}$  salts and  $\text{RSe-TMS}$  at low temperature, with the interstitial  $\text{Se}^{2-}$  ligands arising from Se–C scission reactions. The progression of increasing cluster size is highlighted with the structures of  $[\text{Ag}_{90}\text{Se}_{38}(\text{SeBu}^t)_{14}(\text{PET}_3)_{22}]$  (**56**),  $[\text{Ag}_{112}\text{Se}_{32}(\text{SeBu}^n)_{48}(\text{PBu}^t_3)_{12}]$  (**80**), and  $[\text{Ag}_{172}\text{Se}_{40}(\text{SeBu}^n)_{92}(\text{dppp})_4]$  (**81**) (Figure 56).<sup>93</sup>

**Table 19** Copper– and silver–chalcogen “megaclusters” (>50 Cu atoms) synthesized using silylated chalcogen reagents.

Cluster	References
$[\text{Cu}_{50}\text{S}_{25}(\text{PBu}^t_2\text{Me})_{16}]$	351
$[\text{Cu}_{50}\text{Se}_{20}(\text{SeBu}^t)_{10}(\text{PPR}^t_3)_{10}]$	354
$[\text{Cu}_{50}\text{Te}_{17}(\text{TePh})_{20}(\text{PPH}_2\text{Et})_8]^{4-}$	374
$[\text{Cu}_{52}\text{Se}_{26}(\text{PPh}_3)_{16}]$ ( <b>48</b> )	352
$[\text{Cu}_{58}\text{Se}_{16}(\text{SePh})_{24}(\text{dppa})_6]$ ( <b>49</b> )	353
$[\text{Cu}_{58}\text{Te}_{32}(\text{PR}^1_2\text{R}^2)_{16-n}]$ ( $n = 0, 2$ ) ( <b>52</b> )	370,371
$[\text{Cu}_{59}\text{Se}_{30}(\text{PCy}_3)_{15}]$	359
$[\text{Cu}_{70}\text{Se}_{35}(\text{PR}^1_2\text{R}^2)_{24-n}]$ ( $n = 0-3$ ) ( <b>79</b> )	87,351,358
$[\text{Cu}_{72}\text{Se}_{36}(\text{PPh}_3)_{20}]$	352
$[\text{Cu}_{73}\text{Se}_{35}(\text{SePh})_{24}(\text{dppa})_6]$	354
$[\text{Cu}_{74}\text{Se}_{38}(\text{PCy}_3)_{18}]$	87
$[\text{Cu}_{140}\text{Se}_{70}(\text{PR}^1_2\text{R}^2)_{36-n}]$ ( $n = 0, 2$ )	87,354
$[\text{Cu}_{146}\text{Se}_{73}(\text{PPh}_3)_{30}]$ ( <b>2</b> )	92
$[\text{Ag}_{90}\text{Se}_{38}(\text{SeBu}^t)_{14}(\text{PET}_3)_{22}]$ ( <b>56</b> )	93
$[\text{Ag}_{112}\text{Se}_{32}(\text{SeBu}^n)_{48}(\text{PBu}^t_3)_{12}]$ ( <b>80</b> )	93
$[\text{Ag}_{114}\text{Se}_{34}(\text{SeBu}^n)_{46}(\text{PBu}^t_3)_{14}]$	93
$[\text{Ag}_{172}\text{Se}_{40}(\text{SeBu}^n)_{92}(\text{dppp})_4]$ ( <b>81</b> )	93

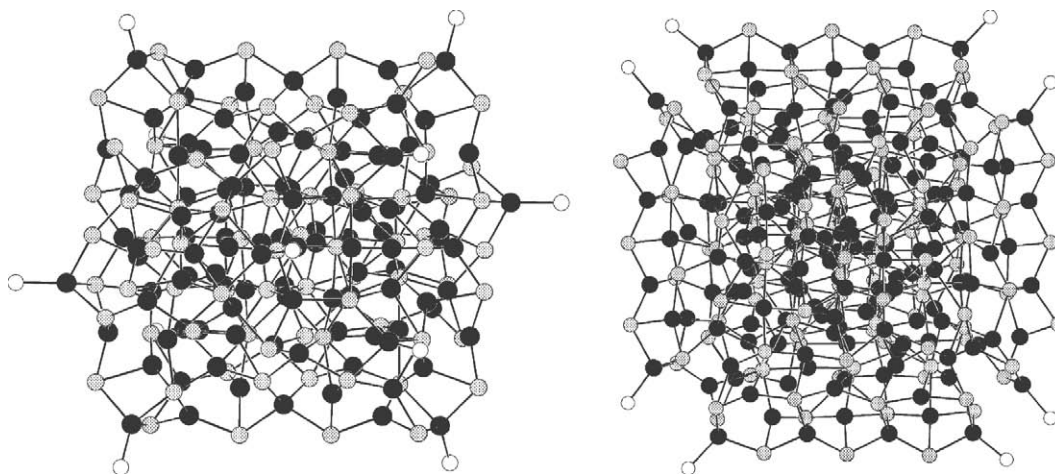


**Figure 56** Ball-and-stick representation of the cluster core of  $[\text{Ag}_{112}\text{Se}_{32}(\text{SeBu}^n)_{48}(\text{PBu}^1_3)_{12}]$  (**80**) and  $[\text{Ag}_{172}\text{Se}_{40}(\text{SeBu}^n)_{92}(\text{dppp})_4]$  (**81**).

In order to probe the electronic properties of Cu/Se nanoclusters, X-ray photoemission spectroscopy (XPS) studies have been carried out on the megaclusters  $[\text{Cu}_{146}\text{Se}_{73}(\text{PPh}_3)_{30}]$  (**2**) and  $[\text{Cu}_{70}\text{Se}_{35}(\text{PEt}_3)_{22}]$  (**79a**), as well as the smaller cluster  $[\text{Cu}_{30}\text{Se}_{15}(\text{PPr}^1_3)_{12}]$  (**82**), and compared to that of bulk  $\beta\text{-Cu}_2\text{Se}$ .<sup>650,651</sup> XPS binding energy can be related to the size of a semiconductor nanoparticle in the following way:<sup>652</sup> the photoemission process results in a core hole in the valence band. The cluster core compensates for this by drawing conduction electrons to screen the hole, which results in a Coulomb charge at the cluster surface. The final state energy is, as a result, increased by the Coulomb energy, which is equal to  $e^2/2r$  ( $r$  = radius of the cluster). This is observed as an increase in the binding energy in the XPS spectrum. XPS investigations of the  $\text{Cu}_2\text{Se}$  clusters revealed an increase in binding energy with respect to bulk  $\beta\text{-Cu}_2\text{Se}$ ; however, the anticipated increase with decreasing cluster size was not observed. The relative binding energy shift between the Cu  $2p_{3/2}$  and the Se  $3d$  spectra did however increase with decreasing size. This can be explained in the following manner: due to the effects of quantum confinement (see Section 7.2.7.2) the energy levels near the Fermi level will be more discrete in smaller clusters, and thus localization of the holes within the  $4p$  band will become more prominent. This valence hole localization results in a local polarization of the surroundings of the core hole. This effect results in a negative shift in the binding energy and this suggests that the smaller clusters exhibit a reduced conductivity because of a decrease in the efficiency of conduction-electron screening in core hole relaxation. In these cases, polarization of the surroundings of the core hole becomes a more significant factor. Thus, the positive binding energy shifts observed for these clusters are a result of the combination of a positive Coulomb charge effect and a negative polarization effect.

### 7.2.7.2 Quantum Confinement Effects

The electronic structure of a bulk semiconductor can be described in terms of the overlapping of atomic orbitals resulting in the formation of energy bands. A filled valence band and an empty conduction band are separated by an energy bandgap. This situation is depicted in Figure 57 (left). When an electron is excited into the conduction band, it becomes delocalized in three dimensions. This leaves a positively charged hole in the valence band, which is also delocalized throughout the semiconductor crystal. The free particles are delocalized over a distance much larger than the lattice constant, and thus the electronic properties are independent of the size of the crystal. On the opposite extreme lies the situation in a molecular crystal in which the linear combination of atomic orbitals leads to the formation of localized molecular orbitals (Figure 57, right). Intermolecular interactions are weak with respect to intramolecular bonding forces, so the electronic properties are essentially the sum of individual molecular contributions and are, again, independent of crystal size.

As the size of a semiconductor crystal is decreased to the nanometer size regime, the situation develops in which the particle size becomes on the order of, or even smaller than, the wavelength of the electron. In this circumstance, electrons must assume a state of higher kinetic energy

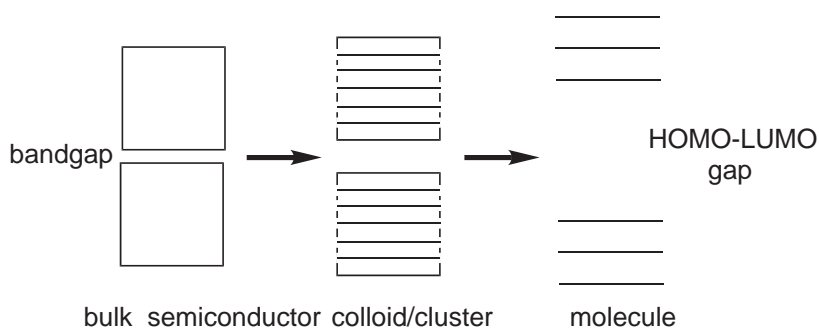


**Figure 57** Schematic representation of the electronic structure of bulk semiconductors (left), nanometer-sized clusters and colloids (middle), and molecular complexes (right).

(shorter wavelength) to “fit” into such a particle. The electrons thus abandon the delocalized state present in bulk semiconductors, and become trapped in what is said to be a “zero-dimensional” space. Electron-hole pairs are still freely mobile, as they are in the bulk state, but they also exhibit coulombic attraction, and are thus confined to the boundaries of the particle. This is known as the *quantum confinement effect*, and can be viewed as an experimental realization of the “particle-in-a-box” phenomenon.<sup>653–657</sup> The result is an increase in the size of the “bandgap” and the quantization of levels within the bands with decreasing size. In this size regime, the electronic density of states lies between the continuum observed in the band structure of a bulk solid and the discrete energy levels described by molecular orbital theory (Figure 57, middle). Consequently, the photophysical and electronic properties of nanometer-sized particles are also intermediate between those of molecules and bulk solids.

The effects of quantum confinement are more pronounced in semiconductor nanoparticles than those of metals. The development of a band structure upon increasing size from the molecular regime occurs first for the center of the band, followed by the band edges. In metals, the Fermi level lies at the center of a band, and, therefore, even small particles resemble the bulk metal in terms of electronic properties. Alternatively, the Fermi level in semiconductors lies within the bandgap. As a result, the “bandgap” remains relatively large, and the energy levels remain quantized (even at the band edges) even for particles as large as 10 nm.<sup>657</sup>

### 7.2.6.3 The Photophysical Properties of II–VI Nanoclusters

The study of the optical properties of semiconductor nanoclusters is attractive because the effects of polydispersity are removed, and because they allow the study of the development of bulk properties in the “molecular” size regime. In this sense, many II–VI nanoclusters represent ideal candidates for photophysical studies because their structures can be viewed as “cutouts” of the bulk semiconductor. Early examples of large II–VI nanoclusters were dominated by CdS.<sup>328–330</sup> The largest examples are the  $[\text{Cd}_{32}\text{S}_{14}(\text{SR})_{36} \cdot \text{sol}_4]$  (**83**) nanoclusters in which the cluster cores are nearly identical in structure and composition, the only differences lying in the nature of the SR groups, and the terminal solvent molecules (sol).<sup>329,330</sup> The structures of these clusters are related to that of the cluster  $[\text{Hg}_{32}\text{Se}_{14}(\text{SePh})_{36}]$  (**34**) (Figure 24),<sup>331</sup> except for the existence of terminal ancillary ligands coordinated at the four corners of the tetrahedral structure of the cadmium analogues. The nature of the thiolate ligand also plays an important role in the nature of packing of clusters within the crystal lattice. While the effect of quantum confinement in cadmium sulfide clusters is demonstrated by a blue shift in the lowest-lying transition with decreasing cluster size, unambiguous assignment of these to “excitonic” transitions in many cases is not possible. This is a result of the fact that CdS has a relatively wide bandgap (2.4 eV in the bulk) and thus, when the particle size is reduced to that of “molecular” clusters ( $\leq 1.2$  nm for known CdS clusters), the transitions of the first excited state become overshadowed by surface (SR) transitions. For example, in the  $\{\text{Cd}_{32}\text{S}_{50}\}$  clusters, when  $\text{R} = \text{Ph}$  and  $\text{sol} = \text{DMF}$  (**83a**), a  $\lambda_{\text{max}}$  of 358 nm is obtained.<sup>329</sup> If  $\text{R} = \text{CH}_2\text{CH}_2\text{OH}$  and  $\text{sol} = \text{H}_2\text{O}$  (**83b**), a blue shift of the first excitation is observed with  $\lambda_{\text{max}} = 325$  nm.<sup>330</sup> This inconsistency must be attributed to the different surface ligands on the clusters, and the “mixing” of intraligand transitions with the “bandgap” absorption. Similar problems have also been encountered in experimental<sup>501</sup> and theoretical<sup>1658</sup> studies of ZnS clusters, the bulk bandgap of which is 3.6 eV. Inhomogeneous broadening in the absorption

spectra was attributed to cluster–cluster interactions. A recent study on the photophysics of  $[\text{Cd}_{17}\text{S}_4(\text{SCH}_2\text{CH}_2\text{OH})_{26}]$  (**33a**) has demonstrated the importance of cluster interactions on photophysical properties. In the solid state, each cluster is bound covalently to its neighbors via sharing of a sulfide ligand at the corners of the tetrahedra, forming a “double-diamond superlattice.”<sup>328</sup> The reflectance spectrum of crystalline solid of (**33a**) exhibits a red-shift in the maximum with respect to that obtained in absorption spectra of nanocrystals in a dispersed solution.<sup>659</sup> The red-shift was attributed to stronger dipole–dipole interactions in the crystalline solid vs. those in solution.

In contrast to ZnS and CdS, the relatively narrow bandgap of CdSe suggests that surface ligand transitions are less likely to overshadow the “bandgap” excitation in the absorption spectra of nanoclusters of this type. Recent synthetic success<sup>297,300,331</sup> has allowed the study of the optical properties of a series of CdSe nanoclusters of different sizes.<sup>296,660,661</sup> The position of the first excitation is shifted to higher energy with decreasing core size for the clusters  $[\text{Cd}_{32}\text{Se}_{14}(\text{SePh})_{36}(\text{PPh}_3)_4]$  (**83c**),  $[\text{Cd}_{17}\text{Se}_4(\text{SePh})_{24}(\text{PPh}_2\text{Pr})_4]^{2+}$  (**33b**) (Figure 24),  $[\text{Cd}_8\text{Se}(\text{SePh})_{12}\text{Cl}_4]^{2-}$  (**84**), and  $[\text{Cd}_{10}\text{Se}_4(\text{SePh})_{12}(\text{PPR}_3)_4]$  (**85**) (Figure 12). Surprisingly, however, the absorption profiles of these clusters are relatively broad. If inhomogeneous broadening is a result of size distributions, then particles of a uniform size should negate this effect. The source of this broadening is unclear, however, it has been suggested that the cause may be the inhomogeneous distribution of surface coverage by phenyl ligands. It was also shown that the size dependence of the bandgap was an extension of those for previously prepared CdSe colloids, demonstrating that the effects of quantum confinement can be extended into the size regime of molecular clusters of II–VI semiconductors.

Because of their small size, the number of surface atoms in colloids and nanoclusters is a large fraction of the total atoms. As a result, the optical properties of these nanoparticles are greatly affected by the nature of the surface.<sup>662</sup> It has been demonstrated that surface ligand transitions can play a role in the overshadowing of bandgap absorptions and in the inhomogeneous broadening of absorption spectra, especially for nanoclusters in which the role of the surface is most profound. The greatest effect of surface states, however, can be observed in the emission spectra using photoluminescence (PL) spectroscopy.

The photoluminescence of II–VI nanoparticles can occur as two types; band edge PL and deep trap PL.<sup>663</sup> Band edge emission occurs due to the recombination of trapped charge carriers from shallow trap states within the particle. This type of emission results in a slight red shift with respect to the absorption due to the relaxation of the trapped charge carrier into lower lying energy states prior to recombination and usually has a narrow linewidth. In contrast, deep trap emission occurs via the recombination of trapped localized carriers from deep mid-gap trap states, which are usually hole traps at the surface of the colloid or cluster. Deep trap emission is characterized by a broad linewidth and is shifted significantly to the red of the excitonic absorption.

The effects of surface on the emission properties of II–VI materials is most pronounced for II–VI nanoclusters because of their small size. Thus, the PL spectra of the nanoclusters exhibit only trapped emission. The emission of the CdSe nanoclusters discussed above has been attributed to optically forbidden transitions involving surface ligands.<sup>296,660</sup> The clusters can be viewed as having an “imperfect” surface, which results in the generation of surface trap states. The trapped emission is independent of the size of the cluster, an effect that is also observed in colloidal samples. This indicates that the nature of the emitting state is similar for all species, also giving strength to the argument that surface states are responsible for this type of emission.

The effect of temperature on deep trap emission is similar to that observed for bandgap emission, with the intensity of the emission decreasing as the temperature increases. This can be explained by the involvement of nonradiative recombination processes dominating at higher temperature. Nonradiative relaxation in CdSe nanoclusters has been assigned to the involvement of a multiphonon relaxation mechanism mediated by a vibrational mode of the surface phenylselenolate ligands.<sup>296</sup>

Behavior similar to the fluorescence intermittency that occurs in II–VI colloids is also demonstrated in CdSe nanoclusters as photodarkening. Prolonged irradiation of a cluster sample at low temperature with a Xenon lamp coincides with the decreasing intensity of the emission over time. This can be viewed as a transfer of the clusters into a dark state caused by the trapping of a charge carrier in the ligand shell of the nanocluster, or the Nujol environment. When the samples were warmed from 2 K to 200 K in the dark the photoluminescence intensity of most samples was at least partially recovered, indicating that the photodarkening was not caused by photochemical degradation of the clusters.

## 7.2.7 REFERENCES

1. Dance, I.; Fisher, K. *Prog. Inorg. Chem.* **1994**, *41*, 637–803.
2. Fenske, D. *Clusters and Colloids, From Theory to Applications*; VCH: Weinheim, 1994; pp 217–297.
3. Saito, T. *Early Transition Metal Clusters with  $\pi$ -Donor Ligands*; VCH: New York, 1995; Chapter 3, pp 63–163.
4. Dance, I. G. *Polyhedron* **1986**, *5*, 1037–1104.
5. Krebs, B.; Henkel, G. *Angew. Chem., Int. Ed. Engl.* **1991**, *30*, 769–788.
6. Müller, A.; Diemann, E. *Comprehensive Coordination Chemistry*; Pergamon: Oxford, 1987; Vol. 2, Chapter 16.1, pp 515–558.
7. Müller, A.; Diemann, E. *Adv. Inorg. Chem.* **1987**, *31*, 89–122.
8. Roof, L. C.; Kolis, J. W. *Chem. Rev.* **1993**, *93*, 1037–1080.
9. Ansari, M. A.; Ibers, J. A. *Coord. Chem. Rev.* **1990**, *100*, 223–266.
10. Arnold, J. *Prog. Inorg. Chem.* **1995**, *43*, 353–417.
11. Lee, S. C.; Holm, R. H. *Angew. Chem., Int. Ed. Engl.* **1990**, *29*, 840–856.
12. Saito, T. *Adv. Inorg. Chem.* **1997**, *44*, 45–91.
13. Averill, B. *Metal Clusters in Proteins*; ACS Symposium Series 372, 1988; Chapter 13, pp 258–291.
14. Coucouvanis, D. *Metal Clusters in Proteins*, ACS Symposium Series 372, 1988; Chapter 19, pp 390–403.
15. Holm, R. H.; Ciurli, S.; Weigel, J. A. *Prog. Inorg. Chem.* **1990**, *38*, 1–74.
16. Malinak, S. M.; Coucouvanis, D. *Prog. Inorg. Chem.* **2001**, *49*, 599–662.
17. Holm, R. H. *Adv. Inorg. Chem.* **1992**, *38*, 1–71.
18. Coucouvanis, D. *Adv. Inorg. Biochem.* **1994**, *9*, 75–122.
19. Berg, J. M.; Holm, R. H. *Iron Sulfur Proteins*; Wiley-Interscience: New York, 1982; , Chapter 1, pp 1–66.
20. Holm, R. H. *Chem. Rev.* **1981**, *10*, 455–490.
21. Hughes, M. N. *Comprehensive Coordination Chemistry*; Pergamon: Oxford, 1987; Vol. 6, Chapter 62.1, pp 626–636.
22. Ibers, J. A.; Holm, R. H. *Science* **1980**, *209*, 223–235.
23. Ceconi, F.; Ghilardi, C. A.; Midollini, S.; Orlandini, A.; Vacca, A. *Inorg. Chem. Commun.* **2000**, *3*, 276–280.
24. Berti, E.; Ceconi, F.; Ghilardi, C. A.; Midollini, S.; Orlandini, A. *Inorg. Chem. Commun.* **1999**, *2*, 146–148.
25. Müller, A.; Schladerbeck, N. H.; Krickemeyer, E.; Bögge, H.; Schmitz, K.; Bill, E.; Trautwein, A. X. *Z. Anorg. Allg. Chem.* **1989**, *570*, 7–36.
26. Bottomley, F.; Day, R. W. *Can. J. Chem.* **1992**, *70*, 1250–1259.
27. Müller, A.; Schladerbeck, N. H. *Naturwissenschaften* **1986**, *73*, 669–670.
28. Müller, A.; Schladerbeck, N. H.; Bögge, H. *Chem. Commun.* **1987**, 35–36.
29. Bottomley, F.; Egharevba, G. O.; White, P. S. *J. Am. Chem. Soc.* **1985**, *107*, 4353–4354.
30. Müller, A.; Schladerbeck, N. H.; Bögge, H. *Chimia* **1985**, *39*, 24–25.
31. Ceconi, F.; Ghilardi, C. A.; Midollini, S.; Orlandini, A. *J. Chem. Soc., Dalton Trans.* **1987**, 831–835.
32. Goddard, C. A.; Long, J. R.; Holm, R. H. *Inorg. Chem.* **1996**, *35*, 4347–4354.
33. Ceconi, F.; Ghilardi, C. A.; Midollini, S.; Orlandini, A. *Inorg. Chim. Acta* **1997**, *254*, 387–389.
34. Ceconi, F.; Ghilardi, C. A.; Midollini, S.; Orlandini, A. *Inorg. Chim. Acta* **1982**, *64*, L47–L48.
35. Ceconi, F.; Ghilardi, C. A.; Midollini, S.; Orlandini, A. *Polyhedron* **1986**, *5*, 2021–2031.
36. Ceconi, F.; Ghilardi, C. A.; Midollini, S.; Orlandini, A.; Zanello, P.; Cinquantini, A.; Bencini, A.; Uytterhoeven, M. G.; Giorgi, G. *J. Chem. Soc., Dalton Trans.* **1995**, 3881–3889.
37. Yam, V. W. W.; Cheng, E. C. C.; Cheung, K. K. *Angew. Chem., Int. Ed. Engl.* **1999**, *38*, 197–199.
38. Yam, V. W. W.; Cheng, E. C. C.; Zhou, Z. Y. *Angew. Chem., Int. Ed. Engl.* **2000**, *39*, 1683–1685.
39. Yam, V. W. W.; Cheng, E. C. C.; Zhu, N. *Angew. Chem., Int. Ed. Engl.* **2001**, *40*, 1763–1765.
40. Bottomley, F.; Day, R. W. *Organometallics* **1996**, *15*, 809–813.
41. Herrmann, W. A.; Hecht, C.; Herdtweck, E.; Kneuper, H. J. *Angew. Chem., Int. Ed. Engl.* **1987**, *26*, 132–134.
42. Bottomley, F.; Day, R. W. *Organometallics* **1996**, *10*, 2560–2563.
43. Liu, C.; Wang, X.; Gong, Q.; Tang, K.; Jin, X. *Adv. Mater.* **2001**, *13*, 1687–1690.
44. Tang, K.; Jin, X.; Yan, H.; Xie, X.; Liu, C.; Gong, Q. *J. Chem. Soc., Dalton Trans.* **2001**, 1374–1377.
45. Tang, K.; Aslam, M.; Brock, E.; Nicholson, T.; Zubieta, J. *Inorg. Chem.* **1987**, *26*, 1488–1497.
46. Yang, Q.; Tang, K.; Liao, H.; Han, Y.; Chen, Z.; Tang, Y. *Chem. Commun.* **1987**, 1076–1077.
47. Bonasia, P. J.; Gindelberger, D. E.; Arnold, J. A. *Inorg. Chem.* **1993**, *32*, 5126–5131.
48. Kanatzidis, M. G. *Comments Inorg. Chem.* **1990**, *10*, 161–195.
49. Corbett, J. D. *Chem. Rev.* **1985**, *85*, 383–397.
50. Flomer, W. A.; O’Neal, S. C.; Jeter, D.; Kolis, J. W. *Inorg. Chem.* **1988**, *27*, 969–971.
51. O’Neal, S. C.; Kolis, J. W. *J. Am. Chem. Soc.* **1988**, *110*, 1971–1973.
52. O’Neal, S. C.; Kolis, J. W. *Inorg. Chem.* **1989**, *28*, 2780–2783.
53. Roof, L. C.; Pennington, W. C.; Kolis, J. W. *Angew. Chem., Int. Ed. Engl.* **1992**, *31*, 913–915.
54. Christou, G.; Ridge, B.; Rydon, H. N. *J. Chem. Soc., Dalton Trans.* **1978**, 1423–1425.
55. Christou, G.; Garner, C. D. *J. Chem. Soc., Dalton Trans.* **1979**, 1093–1094.
56. Hagen, K. S.; Holm, R. H. *J. Am. Chem. Soc.* **1982**, *104*, 5496–5497.
57. Hagen, K. S.; Reynolds, J. G.; Holm, R. H. *J. Am. Chem. Soc.* **1981**, *103*, 4054–4063.
58. Freedman, D.; Emge, T. J.; Brennan, J. G. *J. Am. Chem. Soc.* **1997**, *119*, 11112–11113.
59. Dance, I. G.; Choy, A.; Scudder, M. L. *J. Am. Chem. Soc.* **1984**, *106*, 6285–6295.
60. Zingaro, R. A.; Steeves, B. H.; Irgolic, K. J. *J. Organomet. Chem.* **1965**, *4*, 320–323.
61. Steigerwald, M. L.; Sprinkle, C. R. *Organometallics* **1988**, *7*, 245–246.
62. Steigerwald, M. L.; Rice, C. E. *J. Am. Chem. Soc.* **1988**, *110*, 4228–4231.
63. Steigerwald, M. L. *Chem. Mater.* **1989**, *1*, 52–57.
64. Steigerwald, M. L. *Polyhedron* **1994**, *13*, 1245–1252.
65. Brennan, J. G.; Siegrist, T.; Kwon, Y. U.; Stuczynski, S. M.; Steigerwald, M. L. *J. Am. Chem. Soc.* **1992**, *114*, 10334–10338.
66. Hessen, B.; Siegrist, T.; Palstra, T.; Tanzler, S. M.; Steigerwald, M. L. *Inorg. Chem.* **1993**, *32*, 5165–5169.
67. Brennan, J. G.; Siegrist, T.; Stuczynski, S. M.; Steigerwald, M. L. *J. Am. Chem. Soc.* **1989**, *111*, 9240–9241.

68. Cauzzi, D.; Graiff, C.; Predieri, G.; Tiripicchio, A. *Metal Clusters in Chemistry*; Wiley-VCH: Weinheim, 1999; Chapter 1.11, pp 193–208.
69. Imhof, W.; Huttner, G. *J. Organomet. Chem.* **1993**, *448*, 247–253.
70. Hogarth, G.; Taylor, N. J.; Carty, A. J.; Meyer, A. *Chem. Commun.* **1988**, 834–836.
71. Hope, E. G.; Levason, W. *Coord. Chem. Rev.* **1993**, *122*, 109–170.
72. Dabbousi, B. O.; Bonasia, P. J.; Arnold, J. *J. Am. Chem. Soc.* **1991**, *113*, 3186–3188.
73. Bonasia, P. J.; Gindlberger, B. O.; Dabbousi, B. O.; Arnold, J. *J. Am. Chem. Soc.* **1992**, *114*, 5209–5214.
74. Ball, J. M.; Boorman, P. M.; Fait, J. F.; Hinman, A. S. *Can. J. Chem.* **1989**, *67*, 751–758.
75. Lange, L.; du Mont, W. W. *J. Organomet. Chem.* **1985**, *286*, C1–C2.
76. Bonasia, P. J.; Arnold, J. *J. Organomet. Chem.* **1993**, *449*, 147–157.
77. Banda, R. M. H.; Dance, I. G.; Bailey, T. D.; Craig, D. C.; Scudder, M. L. *Inorg. Chem.* **1989**, *28*, 1862–1871.
78. Draganjac, M.; Rauchfuss, T. B. *Angew. Chem., Int. Ed. Engl.* **1985**, *24*, 742–757.
79. Coleman, A. P.; Dickson, R. S.; Deacon, G. B.; Fallon, G. D.; Ke, M.; McGregor, K.; West, B. O. *Polyhedron* **1994**, *13*, 1277–1290.
80. McGregor, K.; Deacon, G. B.; Dickson, R. S.; Fallon, G. D.; Rowe, R. S.; West, B. O. *Chem. Commun.* **1990**, 1293–1294.
81. Köpf, H.; Klapötke, T. *Chem. Commun.* **1980**, 1192–1193.
82. Klapötke, T. *Phosphorus, Sulfur Silicon, Relat. Elem.* **1989**, *41*, 105–111.
83. Piers, W. E. *Chem. Commun.* **1994**, 309–310.
84. Piers, W. E.; MacGillivray, L. R.; Zawortko, M. *Organometallics* **1993**, *12*, 4723–4725.
85. Zeng, D.; Hampden-Smith, M. J.; Duesler, E. N. *Inorg. Chem.* **1994**, *33*, 5376–5377.
86. Barron, A. R. *Comments Inorg. Chem.* **1993**, *14*, 123–153.
87. Dehnen, S.; Eichhöfer, A.; Fenske, D. *Eur. J. Inorg. Chem.* **2002**, 279–317.
88. Fenske, D.; Corrigan, J. F. *Metal Clusters in Chemistry*; Wiley-VCH: Weinheim, 1999; Vol. 3, Chapter 4.2, pp 1302–1324.
89. Fenske, D.; Ohmer, J.; Hachgenei, J.; Merzweiler, K. *Angew. Chem., Int. Ed. Engl.* **1988**, *27*, 1277–1296.
90. DeGroot, M. W.; Corrigan, J. F. *J. Chem. Soc., Dalton Trans.* **2000**, 1235–1236.
91. Wehnschulte, R. J.; Power, P. P. *J. Am. Chem. Soc.* **1997**, *119*, 9566–9567.
92. Krautscheid, H.; Fenske, D.; Baum, G.; Semmelmann, M. *Angew. Chem., Int. Ed. Engl.* **1993**, *32*, 1303–1305.
93. Fenske, D.; Zhu, N.; Langetepe, T. *Angew. Chem., Int. Ed. Engl.* **1998**, *37*, 2640–2644.
94. Eichhöfer, A.; Fenske, D.; Pfistner, H.; Wunder, M. *Z. Anorg. Allg. Chem.* **1998**, *624*, 1909–1914.
95. Pfistner, H.; Fenske, D. *Z. Anorg. Allg. Chem.* **2001**, *627*, 575–582.
96. Tran, D. T. T.; Taylor, N. J.; Corrigan, J. F. *Angew. Chem., Int. Ed. Engl.* **2000**, *39*, 935–937.
97. Wallbank, A. I.; Corrigan, J. F. *Chem. Commun.* **2001**, 377–378.
98. Hou, H. W.; Xin, X. Q.; Shi, S. *Coord. Chem. Rev.* **1996**, *153*, 25–56.
99. Laurie, S. H. *Eur. J. Inorg. Chem.* **2000**, 2443–2450.
100. Müller, A.; Diemann, E. *Comprehensive Coordination Chemistry*; Pergamon: Oxford, 1987; Vol.2, Chapter 16.3, pp 559–578.
101. Müller, A.; Diemann, E.; Jostes, R.; Bögge, H. *Angew. Chem., Int. Ed. Engl.* **1981**, *20*, 934–954.
102. Li, J.; Xin, X.; Zhou, Z.; Yu, K. *J. Chem. Soc., Chem. Commun.* **1991**, 249–250.
103. Okazaki, M.; Yuki, M.; Kuge, K.; Ogino, H. *Coord. Chem. Rev.* **2000**, *198*, 367–378.
104. Henkel, G.; Weißgräber, S. *Metal Clusters in Chemistry*; Wiley-VCH: Weinheim, 1999; Vol. 1, Chapter 1.10, pp 163–192.
105. Shibahara, T. *Coord. Chem. Rev.* **1993**, *123*, 73–147.
106. Shibahara, T. *Adv. Inorg. Chem.* **1991**, *37*, 143–173.
107. Sells, D. M.; Sykes, A. G. *J. Cluster Sci.* **1995**, *6*, 449–461.
108. Lorenz, A.; Fenske, D. *Z. Anorg. Allg. Chem.* **2001**, *627*, 2232–2248.
109. Saak, W.; Pohl, W. *Angew. Chem., Int. Ed. Engl.* **1991**, *30*, 881–882.
110. Kamiguchi, S.; Imoto, H.; Saito, T. *Chem. Lett.* **1996**, 555–556.
111. Amari, S.; Imoto, H.; Saito, T. *Chem. Lett.* **1997**, 967–968.
112. Tsuge, K.; Mita, S.; Fujita, H.; Imoto, H.; Saito, T. *J. Cluster Sci.* **1996**, *7*, 407–421.
113. Tsuge, K.; Imoto, H.; Saito, T. *Inorg. Chem.* **1992**, *31*, 4715–4716.
114. Yaghi, O. M.; Scott, M. J.; Holm, R. H. *Inorg. Chem.* **1992**, *31*, 4778–4784.
115. Stollmaier, F.; Simon, A. *Inorg. Chem.* **1985**, *24*, 168–171.
116. Rogel, F.; Corbett, J. D. *J. Am. Chem. Soc.* **1990**, *112*, 8198–8200.
117. Runyan, C. E.; Hughbanks, T. E. *J. Am. Chem. Soc.* **1994**, *116*, 7909–7910.
118. Long, J. R.; Williamson, A. L.; Holm, R. H. *Angew. Chem., Int. Ed. Engl.* **1995**, *34*, 226–229.
119. Long, J. R.; McCarty, L. S.; Holm, R. H. *J. Am. Chem. Soc.* **1996**, *118*, 4603–4616.
120. Diana, E.; Gervasio, G.; Rossetti, R.; Valdemarin, F.; Bor, G.; Stanghellini, P. L. *Inorg. Chem.* **1991**, *30*, 294–299.
121. Gervasio, G.; Kettle, S. F. A.; Musso, F.; Rossetti, R.; Stanghellini, P. L. *Inorg. Chem.* **1995**, *34*, 298–305.
122. Inomata, S.; Hiruma, T.; Ogino, H. *Chem. Lett.* **1998**, 309–310.
123. van den Berg, W.; Boot, L.; Joosen, H.; van der Linden, J. G. M.; Bosman, W. P.; Smits, J. M. M.; de Gelder, R.; Beurskens, P. T.; Heck, J.; Gal, A. W. *Inorg. Chem.* **1997**, *36*, 1821–1828.
124. van den Berg, W.; Boot, C. E.; van der Linden, J. G. M.; Bosman, W. P.; Smits, J. M. M.; Beurskens, P. T.; Heck, J. *Inorg. Chim. Acta.* **1994**, *216*, 1–3.
125. Ogino, H.; Tobita, H.; Yanagisawa, K.; Shimoi, M.; Kabuto, C. *J. Am. Chem. Soc.* **1987**, *109*, 5847–5848.
126. Tang, K.; Xia, T.; Jin, X.; Tang, Y. *Polyhedron* **1993**, *12*, 2895–2898.
127. Hong, M.; Su, W.; Cao, R.; Jiang, F.; Liu, H.; Lu, J. *Inorg. Chim. Acta* **1998**, *274*, 229–231.
128. Shieh, M.; Chen, P. F.; Tsai, Y. I.; Shieh, M. H.; Peng, S. M.; Lee, G. S. *Inorg. Chem.* **1995**, *34*, 2251–2254.
129. Liao, J. H.; Kanatzidis, M. G. *Inorg. Chem.* **1992**, *31*, 431–439.
130. Liao, J. H.; Kanatzidis, M. G. *J. Am. Chem. Soc.* **1990**, *112*, 7400–7402.
131. Li, H.; Kim, J.; Groy, T. L.; O’Keefe, M.; Yaghi, O. M. *J. Am. Chem. Soc.* **2001**, *123*, 4867–4868.
132. Wang, C.; Li, Y.; Bu, X.; Zheng, N.; Zivkovic, O.; Yang, C. S.; Feng, P. *J. Am. Chem. Soc.* **2001**, *123*, 11506–11507.

133. Coucouvanis, D. *Acc. Chem. Res.* **1981**, *14*, 201–209.
134. Sola, J.; Do, Y.; Berg, J. M.; Holm, R. H. *J. Am. Chem. Soc.* **1983**, *105*, 7784–7786.
135. Sola, J.; Do, Y.; Berg, J. M.; Holm, R. H. *Inorg. Chem.* **1985**, *24*, 1706–1713.
136. Krebs, B.; Voelker, D.; Stiller, K. O. *Inorg. Chim. Acta* **1982**, *65*, L101–L102.
137. Snyder, B. S.; Reynolds, M. S.; Noda, I.; Holm, R. H. *Inorg. Chem.* **1988**, *27*, 595–597.
138. Snyder, B. S.; Holm, R. H. *Inorg. Chem.* **1988**, *27*, 2339–2347.
139. Reynolds, M. S.; Holm, R. H. *Inorg. Chem.* **1988**, *27*, 4494–4499.
140. Snyder, B. S.; Reynolds, M. S.; Holm, R. H.; Papaefthymiou, G. C.; Frankel, R. B. *Polyhedron* **1991**, *10*, 203–213.
141. Snyder, B. S.; Holm, R. H. *Inorg. Chem.* **1990**, *29*, 274–279.
142. Harmjan, M.; Junghans, C.; Opitz, U. A.; Bahlmann, B.; Pohl, S. Z. *Naturforsch. B* **1996**, *51B*, 1040–1048.
143. Brennan, J. G.; Siegrist, T.; Stuczynski, S. M.; Steigerwald, M. L. *J. Am. Chem. Soc.* **1990**, *112*, 9233–9236.
144. Haushalter, R. C. *Angew. Chem., Int. Ed. Engl.* **1985**, *24*, 433–435.
145. McConnachie, J. M.; Ansari, M. A.; Ibers, J. A. *J. Am. Chem. Soc.* **1991**, *113*, 7078–7079.
146. Yam, V. W. W.; Lo, K. K. W. *Chem. Soc. Rev.* **1999**, *28*, 323–334.
147. Ford, P. C.; Vogler, A. *Acc. Chem. Res.* **1993**, *26*, 220–226.
148. Arratia-Pérez, R.; Hernández-Acevedo, L. *J. Chem. Phys.* **1999**, *110*, 2529–2532.
149. Arratia-Pérez, R.; Hernández-Acevedo, L. *J. Chem. Phys.* **1999**, *111*, 168–172.
150. Zietlow, T. C.; Nocera, D. G.; Gray, H. B. *Inorg. Chem.* **1986**, *25*, 1351–1353.
151. Jackson, J. A.; Turro, C.; Newsham, M. D.; Nocera, D. G. *J. Phys. Chem.* **1990**, *94*, 4500–4507.
152. Yoshimura, T.; Ishizaka, S.; Umakoshi, K.; Sasaki, Y.; Kim, H. B.; Kitamura, N. *Chem. Lett.* **1999**, 697–698.
153. Gray, T. G.; Rudzinski, C. M.; Nocera, D. G.; Holm, R. H. *Inorg. Chem.* **1999**, *38*, 5932–5933.
154. Guilbaud, C.; Deluzet, A.; Domercq, B.; Molinié, P.; Coulon, C.; Boubekeur, K.; Batail, P. *Chem. Commun.* **1999**, 1867–1868.
155. Yoshimura, T.; Ishizaka, S.; Umakoshi, K.; Sasaki, Y.; Kim, H. B.; Kitamura, N.; Naumov, N. G.; Sokolov, M. N.; Fedorov, V. E. *Chem. Lett.* **1999**, 1121–1122.
156. Yoshimura, T.; Umakoshi, K.; Sasaki, Y.; Ishizaka, S.; Kim, H. B.; Kitamura, N. *Inorg. Chem.* **2000**, *39*, 1765–1772.
157. Sabin, F.; Ryu, C. K.; Ford, P. C.; Vogler, A. *Inorg. Chem.* **1992**, *31*, 1941–1945.
158. Kyle, K. R.; Ryu, C. K.; Ford, P. C. *J. Am. Chem. Soc.* **1991**, *113*, 2954–2965.
159. Kyle, K. R.; Palke, W. E.; Ford, P. C. *Coord. Chem. Rev.* **1990**, *97*, 35–46.
160. Knotter, D. M.; Blasse, G.; van Vliet, J. P. M.; van Koten, G. *Inorg. Chem.* **1992**, *31*, 2196–2201.
161. Yam, V. W. W.; Lam, C. H.; Fung, W. K. M.; Cheung, K. K. *Inorg. Chem.* **2001**, *40*, 3435–3442.
162. Yam, V. W. W.; Lee, W. K.; Lai, T. F. *Chem. Commun.* **1993**, 1571–1573.
163. Yam, V. W. W.; Lo, K. K. W.; Cheung, K. K. *Inorg. Chem.* **1996**, *35*, 3459–3462.
164. Yam, V. W. W.; Lo, K. K. W.; Wang, C. R.; Cheung, K. K. *Inorg. Chem.* **1996**, *35*, 5116–5117.
165. Yam, V. W. W.; Lo, K. K. W. *Comments Inorg. Chem.* **1997**, *19*, 209–229.
166. Yam, V. W. W.; Lo, K. K. W.; Wang, C. R.; Cheung, K. K. *J. Phys. Chem. A* **1997**, *101*, 4666–4672.
167. Wang, C. R.; Lo, K. K. W.; Yam, V. W. W. *J. Chem. Soc., Dalton Trans.* **1997**, 227–229.
168. Wang, C. R.; Lo, K. K. W.; Yam, V. W. W. *Chem. Phys. Lett.* **1996**, *262*, 91–96.
169. Yam, V. W. W.; Lo, K. K. W.; Fung, W. K. M.; Wang, C. R. *Coord. Chem. Rev.* **1998**, *35*, 17–41.
170. Pykkö, P. *Chem. Rev.* **1988**, *88*, 563–594.
171. Schmidbaur, H. *Chem. Soc. Rev.* **1995**, *97*, 391–400.
172. Yam, V. W. W.; Chan, C. L.; Li, C. K.; Wong, K. M. C. *Coord. Chem. Rev.* **2001**, *216–217*, 173–194.
173. Yam, V. W. W.; Chan, C. L.; Cheung, C. K. *J. Chem. Soc., Dalton Trans.* **1996**, 4019–4022.
174. Jones, W. B.; Yuan, J.; Narayanaswamy, R.; Young, M. A.; Elder, R. C.; Bruce, A. E.; Bruce, M. R. M. *Inorg. Chem.* **1995**, *34*, 1996–2001.
175. Hanna, S. D.; Zink, J. I. *Inorg. Chem.* **1996**, *35*, 297–302.
176. Forward, J. M.; Bohmann, D.; Fackler, J. P., Jr.; Staples, R. J. *Inorg. Chem.* **1995**, *34*, 6330–6336.
177. Canales, F.; Gimeno, M. C.; Jones, P. G.; Laguna, A. *Angew. Chem., Int. Ed. Engl.* **1994**, *33*, 769–770.
178. Türk, T.; Resch, U.; Fox, M. A.; Vogler, A. *J. Phys. Chem.* **1992**, *96*, 3818–3822.
179. Türk, T.; Resch, U.; Fox, M. A.; Vogler, A. *Inorg. Chem.* **1992**, *31*, 1854–1857.
180. Kunkely, H.; Vogler, A. *Chem. Phys. Lett.* **1989**, *164*, 621–624.
181. Holm, R. H. *Pure Appl. Chem.* **1998**, *70*, 931–938.
182. Harris, S. *Polyhedron* **1989**, *8*, 2843–2882.
183. Chevrel, R.; Sergent, M. *Topics in Current Physics*; Springer-Verlag: Heidelberg; 1982, Vol. 32, Chapter 2.
184. Perrin, A.; Sergent, M. *New J. Chem.* **1988**, *12*, 337–356.
185. Fenske, D.; Grissinger, A.; Loos, M.; Magull, J. Z. *Anorg. Allg. Chem.* **1991**, *598–599*, 121–128.
186. Kamiguchi, S.; Imoto, H.; Saito, T.; Chihara, T. *Inorg. Chem.* **1998**, *37*, 6852–6857.
187. Venkataraman, D.; Rayburn, L. L.; Hill, L. I.; Jin, S.; Malik, A.; Turneau, K. J.; DiSalvo, F. J. *Inorg. Chem.* **1999**, *38*, 828–830.
188. Bencini, A.; Ghilardi, C. A.; Midollini, S.; Orlandini, A.; Russo, U.; Uytterhoeven, G.; Zanchini, C. *J. Chem. Soc. Dalton Trans.* **1995**, 963–974.
189. Saito, T.; Yamamoto, N.; Nagase, T.; Tsuboi, T.; Kobayashi, K.; Yamagata, T.; Imoto, H.; Unoura, K. *Inorg. Chem.* **1990**, *29*, 764–770.
190. Xie, X.; McCarley, R. E. *Inorg. Chem.* **1996**, *35*, 2713–2714.
191. Hilsenbeck, S. J.; McCarley, R. E.; Goldman, A. I. *Chem. Mater.* **1995**, *7*, 499–506.
192. Zhang, X.; McCarley, R. E. *Inorg. Chem.* **1995**, *34*, 2678–2683.
193. Jin, S.; Venkataraman, D.; DiSalvo, F. J. *Inorg. Chem.* **2000**, *39*, 2747–2757.
194. Zheng, Z.; Gray, T. G.; Holm, R. H. *J. Am. Chem. Soc.* **1999**, *38*, 4888–4895.
195. Selby, H. D.; Zheng, Z.; Gray, T. G.; Holm, R. H. *Inorg. Chim. Acta* **2001**, *312*, 205–209.
196. Zheng, Z.; Holm, R. H. *Inorg. Chem.* **1997**, *36*, 5173–5178.
197. Zheng, Z.; Long, J. R.; Holm, R. H. *J. Am. Chem. Soc.* **1997**, *119*, 2163–2171.
198. Fedorov, V. E.; Elsegood, M. R. J.; Yarovoi, S. S.; Mironov, Y. V. *Chem. Commun.* **1998**, 1861–1862.
199. Wang, R.; Zheng, Z. *J. Am. Chem. Soc.* **1999**, *121*, 3549–3550.



200. Beauvais, L. G.; Shores, M. P.; Long, J. R. *Chem. Mater.* **1998**, *10*, 3783–3786.
201. Shores, M. P.; Beauvais, L. G.; Long, J. R. *Inorg. Chem.* **1999**, *38*, 1648–1649.
202. Shores, M. P.; Beauvais, L. G.; Long, J. R. *J. Am. Chem. Soc.* **1999**, *121*, 775–779.
203. Beauvais, L. G.; Shores, M. P.; Long, J. R. *J. Am. Chem. Soc.* **2000**, *122*, 2763–2772.
204. Magliocchi, C.; Xie, X.; Hughbanks, T. *Inorg. Chem.* **2000**, *39*, 5000–5001.
205. Bottomley, F.; Chin, T. T.; Egharevba, G. O.; Kane, L. M.; Pataki, D. A.; White, P. S. *Organometallics* **1988**, *7*, 1214–1222.
206. Tsuge, K.; Imoto, H.; Saito, T. *Bull. Chem. Soc. Jpn.* **1996**, *69*, 627–636.
207. Saito, T.; Yamamoto, N.; Yamagata, T.; Imoto, H. *J. Am. Chem. Soc.* **1988**, *110*, 1646–1647.
208. Hilsenbeck, S. J.; Young, V. G.; McCarley, R. E. *Inorg. Chem.* **1994**, *33*, 1822–1832.
209. Mizutani, J.; Amari, S.; Imoto, H.; Saito, T. *J. Chem. Soc. Dalton Trans.* **1998**, 819–824.
210. Saito, T.; Yoshikawa, T.; Yamagata, T.; Imoto, H.; Unoura, K. *Inorg. Chem.* **1989**, *28*, 3588–3592.
211. Ehrlich, G. M.; Warren, C. J.; Vennos, D. A.; Ho, D. M.; Haushalter, R. C.; DiSalvo, F. J. *Inorg. Chem.* **1995**, *34*, 4454–4459.
212. Xie, X.; McCarley, R. E. *Inorg. Chem.* **1995**, *34*, 6124–6129.
213. Xie, X.; McCarley, R. E. *Inorg. Chem.* **1997**, *36*, 4011–4016.
214. Xie, X.; McCarley, R. E. *Inorg. Chem.* **1997**, *36*, 4665–4675.
215. Gabriel, J. C.; Boubekour, K.; Batail, P. *Inorg. Chem.* **1993**, *32*, 2894–2900.
216. Fedin, V. P.; Imoto, H.; Saito, T.; Fedorov, V. E.; Mironov, Y. V.; Yarovoi, S. S. *Polyhedron* **1996**, *15*, 1229–1233.
217. Decker, A.; Simon, F.; Boubekour, K.; Fenske, D.; Batail, P. *Z. Anorg. Allg. Chem.* **2000**, *626*, 309–313.
218. Uriel, S.; Boubekour, K.; Batail, P.; Orduna, J.; Canadell, E. *Inorg. Chem.* **1995**, *34*, 5307–5313.
219. Uriel, S.; Boubekour, K.; Batail, P.; Orduna, J. *Angew. Chem., Int. Ed. Engl.* **1996**, *35*, 1544–1547.
220. Willer, M. W.; Long, J. R.; McLauchlan, C. C.; Holm, R. H. *Inorg. Chem.* **1998**, *37*, 328–333.
221. Yoshimura, T.; Umakoshi, K.; Sasaki, Y.; Sykes, A. G. *Inorg. Chem.* **1999**, *38*, 5557–5564.
222. Zheng, Z.; Selby, H. D.; Roland, B. K. *Acta Crystallogr.* **2001**, *E57*, 1177–1179.
223. Chen, Z. N.; Yoshimura, T.; Abe, M.; Sasaki, Y.; Ishizaka, S.; Kim, H. B.; Kitamura, N. *Angew. Chem., Int. Ed. Engl.* **2001**, *40*, 239–242.
224. Tulskey, E. G.; Long, J. L. *Inorg. Chem.* **2001**, *40*, 6990–7002.
225. Mironov, Y. V.; Cody, J. A.; Albrecht-Smith, T. E.; Ibers, J. A. *J. Am. Chem. Soc.* **1997**, *119*, 493–498.
226. Mironov, Y. V.; Pell, M. A.; Ibers, J. A. *Inorg. Chem.* **1996**, *35*, 2709–2710.
227. Fedin, V. P.; Fedorov, V. E.; Imoto, H.; Saito, T. *Polyhedron* **1997**, *16*, 1615–1619.
228. Simon, F.; Boubekour, K.; Gabriel, J. C. P.; Batail, P. *Chem. Commun.* **1998**, 845–846.
229. Ceconi, F.; Ghilardi, C. A.; Midollini, S. *Chem. Commun.* **1981**, 640–641.
230. Del Giallo, F.; Pieralli, F.; Fiesoli, L.; Spina, G. *Phys. Lett.* **1983**, *96A*, 141–144.
231. Agresti, A.; Bacci, M.; Ceconi, F.; Ghilardi, C. A.; Midollini, S. *Inorg. Chem.* **1985**, *24*, 689–695.
232. Bencini, A.; Uytterhoeven, M. G.; Zanchini, C. *Int. J. Quantum Chem.* **1994**, *52*, 903–918.
233. Ceconi, F.; Ghilardi, C. A.; Midollini, S.; Orlandini, A. *Inorg. Chim. Acta* **1983**, *76*, L183–L184.
234. Gervasio, G.; Rossetti, R.; Stanghellini, P. L. *Inorg. Chim. Acta* **1984**, *83*, L9–L10.
235. Fenske, D.; Hachgenei, J.; Ohmer, J. *Angew. Chem., Int. Ed. Engl.* **1985**, *24*, 706–709.
236. Hong, M.; Huang, Z.; Lei, X.; Wei, G.; Kang, B.; Liu, H. *Inorg. Chim. Acta* **1989**, *159*, 1–2.
237. Bencini, A.; Ghilardi, C. A.; Midollini, S.; Orlandini, A.; Zanchini, C. *J. Am. Chem. Soc.* **1992**, *114*, 9898–9908.
238. Hong, M.; Huang, Z.; Lei, X.; Wei, G.; Kang, B.; Liu, H. *Polyhedron* **1991**, *10*, 927–934.
239. Jiang, F.; Huang, X.; Cao, R.; Hong, M.; Liu, H. *Acta Crystallogr.* **1995**, *C51*, 1275–1278.
240. Bencini, A.; Midollini, S.; Zanchini, C. *Inorg. Chem.* **1992**, *31*, 2132–2137.
241. Ceconi, F.; Ghilardi, C. A.; Midollini, S.; Orlandini, A. *Inorg. Chim. Acta* **1993**, *214*, 13–15.
242. Fenske, D.; Ohmer, J.; Hachgenei, J. *Angew. Chem., Int. Ed. Engl.* **1985**, *24*, 993–995.
243. Steigerwald, M. L.; Siegrist, T.; Stuczynski, S. M. *Inorg. Chem.* **1991**, *30*, 2256–2257.
244. Steigerwald, M. L.; Siegrist, T.; Stuczynski, S. M. *Inorg. Chem.* **1991**, *30*, 4940–4945.
245. Ceconi, F.; Ghilardi, C. A.; Midollini, S.; Orlandini, A.; Bencini, A. *J. Chem. Soc., Dalton Trans.* **1996**, 3991–3994.
246. Mayerle, J. J.; Denmark, S. E.; DePamphilis, B. V.; Ibers, J. A.; Holm, R. H. *J. Am. Chem. Soc.* **1975**, *97*, 1032–1045.
247. Bobrik, M. A.; Hodgson, K. O.; Holm, R. H. *Inorg. Chem.* **1977**, *16*, 1851–1858.
248. Christou, G.; Holm, R. H. *J. Am. Chem. Soc.* **1981**, *103*, 6269–6271.
249. Christou, G.; Sabat, M.; Ibers, J. A.; Holm, R. H. *Inorg. Chem.* **1982**, *21*, 3518–3526.
250. Hagen, K. S.; Watson, A. D.; Holm, R. H. *J. Am. Chem. Soc.* **1983**, *105*, 3905–3913.
251. Strasdeit, H.; Krebs, B.; Henkel, G. *Inorg. Chem.* **1984**, *23*, 1816–1825.
252. Osterloh, F.; Saak, W.; Pohl, S.; Kroeckel, M.; Meier, C.; Trautwein, A. X. *Inorg. Chem.* **1998**, *37*, 3581–3587.
253. Yu, S. B.; Papaefthymiou, G. C.; Holm, R. H. *Inorg. Chem.* **1991**, *30*, 3476–3485.
254. Coucouvanis, D.; Kanatzidis, M. G.; Dunham, W. R.; Hagen, W. R. *J. Am. Chem. Soc.* **1984**, *106*, 7998–7999.
255. Kanatzidis, M. G.; Dunham, W. R.; Hagen, W. R.; Coucouvanis, D. *Chem. Commun.* **1984**, 356–357.
256. Noda, I.; Snyder, B. S.; Holm, R. H. *Inorg. Chem.* **1986**, *25*, 3851–3853.
257. Jiang, F.; Huang, L.; Lei, X.; Liu, H.; Kang, B.; Huang, Z.; Hong, M. *Polyhedron* **1992**, *11*, 361–363.
258. Ceconi, F.; Ghilardi, C. A.; Midollini, S.; Orlandini, A. *Inorg. Chim. Acta* **1991**, *184*, 141–145.
259. Chen, C.; Cai, J.; Liu, Q.; Wu, D.; Lei, X.; Zhao, K.; Kang, B. *Inorg. Chem.* **1990**, *29*, 4878–4881.
260. You, J. F.; Papaefthymiou, G. C.; Holm, R. H. *J. Am. Chem. Soc.* **1992**, *114*, 2697–2710.
261. You, J. F.; Holm, R. H. *Inorg. Chem.* **1991**, *30*, 1431–1433.
262. Fenske, D.; Fischer, A. *Angew. Chem., Int. Ed. Engl.* **1995**, *34*, 307–309.
263. Bettenhausen, M.; Fenske, D. *Z. Anorg. Allg. Chem.* **1999**, *625*, 13–14.
264. Saak, W.; Henkel, G.; Pohl, S. *Angew. Chem., Int. Ed. Engl.* **1984**, *23*, 150–151.
265. Kanatzidis, M. G.; Salifoglou, A.; Coucouvanis, D. *J. Am. Chem. Soc.* **1985**, *107*, 3358–3360.
266. Kanatzidis, M. G.; Hagen, W. R.; Dunham, W. R.; Lester, R. K.; Coucouvanis, D. *J. Am. Chem. Soc.* **1985**, *107*, 953–961.
267. Saak, W.; Pohl, S. *Z. Naturforsch. B: Anorg. Chem., Org. Chem.* **1985**, *40B*, 1105–1112.
268. Kanatzidis, M. G.; Salifoglou, A.; Coucouvanis, D. *Inorg. Chem.* **1986**, *25*, 2460–2468.

269. Scott, M. J.; Holm, R. H. *Angew. Chem., Int. Ed. Engl.* **1993**, *32*, 564–566.
270. Evans, D. J.; Garcia, G.; Santana, M. D.; Torralba, M. C. *Inorg. Chim. Acta* **1999**, *284*, 296–299.
271. Han, J.; Koutmos, M.; Al Ahmad, S.; Coucouvanis, D. *Inorg. Chem.* **2001**, *40*, 5985–5999.
272. You, J. F.; Snyder, B. S.; Papaefthymiou, G. C.; Holm, R. H. *J. Am. Chem. Soc.* **1990**, *112*, 1067–1076.
273. Lewin, M.; Fisher, K.; Dance, I. *Chem. Commun.* **2000**, 947–948.
274. Rajamani, V.; Prewitt, C. T. *Can. Mineral.* **1973**, *12*, 178–187.
275. Evans, H. T. Jr.; Clark, J. R. *Am. Mineral.* **1981**, *66*, 376–384.
276. Jin, X.; Tang, K.; Liu, W.; Tang, Y. *Polyhedron* **1996**, *15*, 1207–1211.
277. Wheeler, R. A. *J. Am. Chem. Soc.* **1990**, *112*, 8737–8741.
278. Wang, C.; Haushalter, R. C. *Chem. Commun.* **1997**, 1457–1458.
279. Huang, S. P.; Kanatzidis, M. G. *Angew. Chem., Int. Ed. Engl.* **1992**, *31*, 787–789.
280. Haushalter, R. C. *Angew. Chem., Int. Ed. Engl.* **1985**, *24*, 432–433.
281. Stephan, H. O.; Kanatzidis, M. G.; Henkel, G. *Angew. Chem., Int. Ed. Engl.* **1996**, *35*, 2135–2137.
282. Pohl, S.; Saak, W. *Angew. Chem., Int. Ed. Engl.* **1984**, *23*, 907–908.
283. Goh, C.; Segal, B. M.; Huang, J.; Long, J. R.; Holm, R. H. *J. Am. Chem. Soc.* **1996**, *118*, 11844–11853.
284. Junghans, C.; Saak, W.; Pohl, S. *Chem. Commun.* **1994**, 2327–2328.
285. Christou, G.; Hagen, K. S.; Holm, R. H. *J. Am. Chem. Soc.* **1982**, *104*, 1744–1745.
286. Christou, G.; Hagen, K. S.; Bashkin, J. K.; Holm, R. H. *Inorg. Chem.* **1985**, *24*, 1010–1018.
287. Betz, P.; Krebs, B.; Henkel, G. *Angew. Chem., Int. Ed. Engl.* **1984**, *23*, 311–312.
288. Marbach, G.; Strähle, J. *Angew. Chem., Int. Ed. Engl.* **1984**, *23*, 715–716.
289. Coucouvanis, D.; Murphy, C. N.; Kanodia, S. K. *Inorg. Chem.* **1980**, *19*, 2993–2998.
290. Dance, I. G.; Calabrese, J. C. *Inorg. Chim. Acta* **1976**, *19*, L41–L42.
291. Dance, I. G.; Bowmaker, G. A.; Clark, R. G.; Seadon, J. K. *Polyhedron* **1983**, *2*, 1031–1043.
292. Baumgartner, M.; Bensch, W.; Hug, P.; Dubler, E. *Inorg. Chim. Acta* **1987**, *136*, 139–147.
293. Nicholson, J. R.; Abrahams, I. L.; Clegg, W.; Garner, C. D. *Inorg. Chem.* **1985**, *24*, 1092–1096.
294. Jin, X.; Tang, K.; Long, Y.; Tang, Y. *Acta Crystallogr.* **1999**, *C55*, 1799–1800.
295. Berger, L. I. *Semiconductor Materials*; CRC Press: New York, 1997; Chapter 5, pp 183–210.
296. Soloviev, V. N.; Eichhöfer, A.; Fenske, D.; Banin, U. *J. Am. Chem. Soc.* **2001**, *123*, 2354–2364.
297. Behrens, S.; Bettenhausen, M.; Eichhöfer, A.; Fenske, D. *Angew. Chem., Int. Ed. Engl.* **1997**, *36*, 2797–2798.
298. Adamson, G. W.; Bell, N. A.; Shearer, H. M. M. *Acta Crystallogr.* **1982**, *B38*, 462–465.
299. Adamson, G. W.; W.; Shearer, H. M. M. *Chem. Commun.* **1969**, 867–868.
300. Behrens, S.; Fenske, D. *Ber. Bunsenges. Phys. Chem.* **1997**, *101*, 1588–1592.
301. Ali, B.; Dance, I. G.; Craig, D. C.; Scudder, M. L. *J. Chem. Soc., Dalton Trans.* **1998**, 1661–1667.
302. Eichhöfer, A.; Fenske, D. *J. Chem. Soc., Dalton Trans.* **2000**, 941–944.
303. Costa, T.; Dorfman, J. R.; Hagen, K. S.; Holm, R. H. *Inorg. Chem.* **1983**, *22*, 4091–4099.
304. Stephan, H. O.; Henkel, G. *Polyhedron* **1996**, *15*, 501–511.
305. Hagen, K. S.; Berg, J. M.; Holm, R. H. *Inorg. Chim. Acta* **1980**, *45*, L17–L18.
306. Hagen, K. S.; Stephan, D. W.; Holm, R. H. *Inorg. Chem.* **1982**, *21*, 3928–3936.
307. Coucouvanis, D.; Kanatzidis, M.; Simhon, E.; Baenziger, N. C. *J. Am. Chem. Soc.* **1982**, *104*, 1874–1882.
308. Hagen, K. S.; Holm, R. H. *Inorg. Chem.* **1984**, *23*, 418–427.
309. Stephan, H. O.; Henkel, G.; Kanatzidis, M. G. *Chem. Commun.* **1997**, 67–68.
310. Lackmann, J.; Hauptmann, R.; Weißgräber, S.; Henkel, G. *Chem. Commun.* **1999**, 1995–1996.
311. Dance, I. G.; Calabrese, J. C. *Chem. Commun.* **1975**, 762–763.
312. Dance, I. G. *J. Am. Chem. Soc.* **1979**, *101*, 6264–6273.
313. Hencher, J. L.; Khan, M.; Said, F. F.; Tuck, D. G. *Inorg. Nucl. Chem. Lett.* **1981**, *17*, 287–290.
314. Dance, I. G. *Inorg. Chem.* **1981**, *20*, 2155–2160.
315. Hencher, J. L.; Khan, M.; Said, F. F.; Tuck, D. G. *Polyhedron* **1985**, *4*, 1263–1267.
316. Dean, P. A. W.; Vittal, J. J.; Payne, N. C. *Inorg. Chem.* **1987**, *26*, 1683–1689.
317. Hagen, K. S.; Holm, R. H. *Inorg. Chem.* **1983**, *2*, 3171–3174.
318. Dean, P. A. W.; Vittal, J. J.; Payne, N. C.; Wu, Y. *Inorg. Chem.* **1993**, *32*, 4632–4639.
319. Tang, K.; Xia, T.; Jin, X.; Tang, Y. *Polyhedron* **1994**, *21*, 3023–3026.
320. Adams, R. D.; Zhang, B.; Murphy, C. J.; Yeung, L. K. *Chem. Commun.* **1999**, 383–384.
321. Bettenhausen, M.; Fenske, D. *Z. Anorg. Allg. Chem.* **1998**, *624*, 1245–1246.
322. Dance, I. G.; Garbutt, R. G.; Craig, D. C. *Inorg. Chem.* **1987**, *26*, 3732–3740.
323. González-Duarte, P.; Clegg, W.; Casals, I.; Sola, J.; Rius, J. *J. Am. Chem. Soc.* **1998**, *120*, 1260–1266.
324. Lee, G. S.; Fisher, K. J.; Craig, D. C.; Scudder, M. L.; Bailey, T. D.; Dance, I. G. *J. Am. Chem. Soc.* **1990**, *112*, 6435–6437.
325. Choy, A.; Craig, D. C.; Dance, I. G.; Scudder, M. *Chem. Commun.* **1982**, 1246–1247.
326. Nyman, M. D.; Hampden-Smith, M. J.; Duesler, E. N. *Inorg. Chem.* **1996**, *35*, 802–803.
327. Hirpo, W.; Dhirga, S.; Kanatzidis, M. G. *Chem. Commun.* **1992**, 557–559.
328. Vossmeier, T.; Reck, G.; Katsikas, L.; Haupt, E. T. K.; Schulz, B.; Weller, H. *Science* **1995**, *267*, 1476–1479.
329. Herron, N.; Calabrese, J. C.; Farneth, W. E.; Wang, Y. *Science* **1993**, *259*, 1426–1428.
330. Vossmeier, T.; Reck, G.; Schulz, B.; Katsikas, L.; Weller, H. *J. Am. Chem. Soc.* **1995**, *117*, 12881–12882.
331. Behrens, S.; Bettenhausen, M.; Deveson, A. C.; Eichhöfer, A.; Fenske, D.; Lohde, H.; Woggon, U. *Angew. Chem. Int. Ed. Engl.* **1996**, *35*, 2215–2218.
332. Fenske, D.; Maué, P. G. *Z. Naturforsch.* **1989**, *44B*, 531–537.
333. Müller, A.; Eltzner, W.; Mohan, N. *Angew. Chem., Int. Ed. Engl.* **1979**, *18*, 168–169.
334. Darkwa, J.; Lockmeyer, J. R.; Boyd, P. D. W.; Rauchfuss, T. B.; Rheingold, A. L. *J. Am. Chem. Soc.* **1988**, *110*, 141.
335. Maue, P. G.; Fenske, D. *Z. Naturforsch.* **1988**, *43B*, 1213–1218.
336. Fenske, D.; Grissinger, A. *Z. Naturforsch.* **1990**, *45B*, 1309–1313.
337. Fenske, D.; Ohmer, J.; Merzweiler, K. *Z. Naturforsch.* **1987**, *42B*, 803–809.
338. Fenske, D.; Krautscheid, H.; Müller, M. *Angew. Chem., Int. Ed. Engl.* **1992**, *31*, 321–323.

339. Fenske, D.; Ohmer, J. *Angew. Chem., Int. Ed. Engl.* **1987**, *26*, 148–151.
340. Cecconi, F.; Ghilardi, C. A.; Midollini, S. *Inorg. Chem.* **1983**, *22*, 3802–3808.
341. Fenske, D.; Fleischer, H.; Krautscheid, H.; Magull, J. Z. *Naturforsch.* **1991**, *46B*, 1384–1394.
342. Fenske, D.; Hollnagel, A.; Merzweiler, K. Z. *Naturforsch.* **1988**, *43B*, 634–636.
343. Fenske, D.; Fleischer, H.; Krautscheid, H.; Magull, J. Z. *Naturforsch.* **1990**, *45B*, 127–133.
344. Fenske, D.; Hollnagel, A.; Merzweiler, K. *Angew. Chem., Int. Ed. Engl.* **1988**, *27*, 965–966.
345. Fenske, D.; Hollnagel, A. *Angew. Chem., Int. Ed. Engl.* **1989**, *28*, 1390–1392.
346. Fenske, D.; Magull, J. Z. *Naturforsch.* **1990**, *45B*, 121–126.
347. Harvey, P. D.; Eichhöfer, A.; Fenske, D. *J. Chem. Soc. Dalton Trans.* **1998**, 3901–3903.
348. Wells, A. F. *Structural Inorganic Chemistry*, 5th ed; Clarendon: Oxford, 1984; Chapter 25, pp 1142–1145.
349. Dehnen, S.; Schäfer, A.; Fenske, D.; Alrichs, R. *Angew. Chem. Int. Ed. Engl.* **1994**, *33*, 764–768.
350. Dehnen, S.; Fenske, D.; Deveson, A. C. *J. Cluster Sci.* **1996**, *7*, 351–369.
351. Dehnen, S.; Fenske, D. *Chem. Eur. J.* **1996**, *2*, 1407–1416.
352. Eichhöfer, A.; Fenske, D. *J. Chem. Soc., Dalton Trans.* **1998**, 2969–2972.
353. Bettenhausen, M.; Eichhöfer, A.; Fenske, D.; Semmelmann, M. Z. *Anorg. Allg. Chem.* **1999**, *625*, 593–601.
354. Zhu, N.; Fenske, D. *J. Chem. Soc., Dalton Trans.* **1999**, 1067–1075.
355. Heyding, R. D.; Murray, R. M. *Can. J. Chem.* **1975**, *54*, 841–848.
356. Wieggers, G. A. *Am. Mineral.* **1971**, *56*, 1882–1888.
357. Semmelmann, M.; Fenske, D.; Corrigan, J. F. *J. Chem. Soc., Dalton Trans.* **1998**, 2541–2546.
358. Fenske, D.; Krautscheid, H. *Angew. Chem., Int. Ed. Engl.* **1990**, *29*, 1452–1454.
359. Deveson, A.; Dehnen, S.; Fenske, D. *J. Chem. Soc., Dalton Trans.* **1997**, 4491–4498.
360. Fenske, D.; Krautscheid, H. *Angew. Chem., Int. Ed. Engl.* **1990**, *29*, 796–799.
361. Dehnen, S.; Fenske, D. *Angew. Chem., Int. Ed. Engl.* **1994**, *33*, 2287–2289.
362. Ahlrichs, R.; Besinger, J.; Eichhöfer, A.; Fenske, D.; Gbureck, A. *Angew. Chem., Int. Ed. Engl.* **2000**, *39*, 3929–3933.
363. Baranova, R. V.; Avilov, A. V.; Pinsker, Z. G. *Sov. Phys. Crystallogr.* **1974**, *18*, 736–740.
364. Blachnik, R.; Lasocka, M.; Walbrecht, U. *J. Solid State Chem.* **1983**, *48*, 431–438.
365. Lorenz, G.; Wagner, C. *J. Chem. Phys.* **1957**, *26*, 1607–1608.
366. Zhang, X.; Park, Y.; Hogan, T.; Schindler, J. L.; Kannewurf, C. R.; Seong, S.; Albright, T.; Kanatzidis, M. *J. Am. Chem. Soc.* **1995**, *117*, 10300–10310.
367. Park, Y.; Degroot, D. C.; Schindler, J.; Kannewurf, C. R.; Kanatzidis, M. G. *Angew. Chem., Int. Ed. Engl.* **1991**, *30*, 1325–1328.
368. Park, Y.; Kanatzidis, M. G. *Chem. Mater.* **1991**, *3*, 781–783.
369. Emirdag, M.; Schimek, G. L.; Kolis, J. W. *J. Chem. Soc., Dalton Trans.* **1999**, 1531–1532.
370. Corrigan, J. F.; Balter, S.; Fenske, D. *J. Chem. Soc., Dalton Trans.* **1996**, 729–738.
371. Fenske, D.; Zhu, N. *J. Cluster Sci.* **2000**, *11*, 135–151.
372. Eichhöfer, A.; Corrigan, J. F.; Fenske, D.; Tröster, E. Z. *Anorg. Allg. Chem.* **2000**, *626*, 338–348.
373. Frank, F. C.; Kasper, J. S. *Acta Crystallogr.* **1958**, *11*, 184–190.
374. Corrigan, J. F.; Fenske, D. *Angew. Chem., Int. Ed. Engl.* **1997**, *36*, 1981–1983.
375. DeGroot, M. W.; Cockburn, M. W.; Workentin, M. S.; Corrigan, J. F. *Inorg. Chem.* **2001**, *40*, 4678–4685.
376. Fenske, D.; Steck, J. C. *Angew. Chem., Int. Ed. Engl.* **1993**, *32*, 238–242.
377. Lorenz, A.; Fenske, D. *Angew. Chem., Int. Ed. Engl.* **2001**, *40*, 4402–4406.
378. Tran, D. T. T.; Corrigan, J. F. *Organometallics* **2000**, *19*, 5202–5208.
379. Corrigan, J. F.; Fenske, D. *Chem. Commun.* **1996**, 943–944.
380. Langetepe, T.; Fenske, D. Z. *Anorg. Allg. Chem.* **2001**, *627*, 820–826.
381. Corrigan, J. F.; Fenske, D. *Chem. Commun.* **1997**, 1837–1838.
382. Corrigan, J. F.; Fenske, D.; Power, W. P. *Angew. Chem., Int. Ed. Engl.* **1997**, *36*, 1176–1179.
383. Fenske, D.; Langetepe, T.; Kappes, M. M.; Hampe, O.; Weis, P. *Angew. Chem., Int. Ed. Engl.* **2000**, *39*, 1857–1860.
384. Fenske, D.; Bettenhausen, M. *Angew. Chem. Int. Ed. Engl.* **1998**, *37*, 1291–1294.
385. Whitener, M. A.; Baschkin, J. K.; Hagen, K. S.; Girerd, J. J.; Gamp, E.; Edelstein, N.; Holm, R. H. *J. Am. Chem. Soc.* **1986**, *108*, 5607–5620.
386. Steigerwald, M. L.; Siegrist, T.; Stuczynski, S. M.; Kwon, Y. U. *J. Am. Chem. Soc.* **1992**, *114*, 3155–3156.
387. Steigerwald, M. L.; Stuczynski, S. M.; Kwon, Y. U.; Vennos, D. A.; Brennan, J. G. *Inorg. Chim. Acta* **1993**, *212*, 219–224.
388. Nomikou, Z.; Schubert, B.; Hoffman, R.; Steigerwald, M. L. *Inorg. Chem.* **1992**, *31*, 2201–2209.
389. Barstad, J.; Gronvold, F.; Rost, E.; Vestersjo, E. *Acta Chem. Scand.* **1966**, *20*, 2865–2879.
390. Kruger, T.; Krebs, B.; Henkel, G. *Angew. Chem., Int. Ed. Engl.* **1989**, *28*, 61–62.
391. Song, Y.; Zhang, C.; Wang, Y.; Fang, G.; Jin, G.; Zhan, X.; Liu, S.; Chen, L.; Xin, X. *Mater. Lett.* **2000**, *46*, 49–52.
392. Simonnet-Jégat, C.; Halut, S.; Sécheresse, F. *J. Cluster Sci.* **1996**, *7*, 677–688.
393. Tan, W.; Zheng, H.; Jin, Q.; Jin, G.; Wei, J.; Long, D.; Xin, X. *Polyhedron* **2000**, 1545–1549.
394. Chan, C. K.; Guo, C. X.; Wang, R. J.; Mak, T. C. W.; Che, C. M. *J. Chem. Soc., Dalton Trans.* **1995**, 753–757.
395. Lang, J. P.; Tatsumi, K. *Inorg. Chem.* **1998**, *37*, 6308–6316.
396. Che, C. M.; Xia, B. H.; Huang, J. S.; Chan, C. K.; Zhou, Z. Y.; Cheung, K. K. *Chem. Eur. J.* **2001**, *7*, 3998–4006.
397. Zhang, C.; Jin, G.; Xu, Y.; Fun, H. K.; Xin, X. *Chem. Lett.* **2000**, 502–503.
398. Hou, H.; Fan, Y.; Du, C.; Zhu, Y.; Wang, W.; Xin, X.; Low, M. K. M.; Ji, W.; Ang, H. G. *Chem. Commun.* **1999**, 647–648.
399. Zhang, C.; Song, Y.; Xu, Y.; Fun, H.; Fang, G.; Wang, Y.; Xin, X. *J. Chem. Soc., Dalton Trans.* **2000**, 2823–2829.
400. Zhang, Q. F.; Leung, W. H.; Xin, X. Q.; Fun, H. F. *Inorg. Chem.* **2000**, *39*, 417–426.
401. Zhang, Q. F.; Raj, S. S.; Fun, H. K.; Xin, X. Q. *Chem. Lett.* **1999**, 619–620.
402. Sécheresse, F.; Bernès, S.; Robert, F.; Jeannin, Y. *J. Chem. Soc., Dalton Trans.* **1991**, 2875–2881.
403. Lang, J.; Zhou, W.; Xin, X.; Cai, J.; Kang, B.; Yu, K. *Polyhedron* **1993**, *12*, 1647–1653.
404. Sécheresse, F.; Bernès, S.; Robert, F.; Jeannin, Y. *Bull. Soc. Chim. Fr.* **1995**, *132*, 1029–1037.
405. Sécheresse, F.; Manoli, J. M.; Potvin, C.; Marzak, S. *J. Chem. Soc., Dalton Trans.* **1988**, 3055–3057.
406. Yu, X. F.; Zheng, F. K.; Huang, L. R. *Polyhedron* **1995**, *14*, 3599–3604.

407. Scattergood, C. D.; Bonney, P. G.; Slater, J. M.; Garner, C. D.; Clegg, W. *Chem. Commun.* **1987**, 1749–1751.
408. Chen, Z.; Cai, S. H.; Ye, J. L.; Huang, P. Q.; Zheng, F. K.; Huang, J. S. *Polyhedron* **1999**, *18*, 1339–1343.
409. Bernès, S.; Sécheresse, F.; Jeannin, Y. *Inorg. Chim. Acta* **1992**, *191*, 11–13.
410. Trojer, F. J. *Am. Mineral.* **1966**, *51*, 890–894.
411. Hong, M.; Wu, D.; Cao, R.; Lei, X.; Liu, H.; Lu, J. *Inorg. Chim. Acta* **1997**, *258*, 25–32.
412. Wu, D.; Hong, M.; Cao, R.; Liu, H. *Inorg. Chem.* **1996**, *35*, 1080–1082.
413. Sakane, G.; Shibahare, T.; Hou, H. W.; Xin, X. Q.; Shi, S. *Inorg. Chem.* **1995**, *34*, 4785–4789.
414. Müller, A.; Bögge, H.; Königer-Ahlborn, E.; Hellmann, W. *Inorg. Chem.* **1979**, *18*, 2301–2304.
415. Lei, X.; Huang, Z.; Hong, M.; Liu, Q.; Liu, H. *Inorg. Chim. Acta* **1989**, *164*, 119–121.
416. Lei, X.; Huang, Z.; Liu, Q.; Hong, M.; Liu, H. *Inorg. Chem.* **1989**, *28*, 4302–4304.
417. Huang, Q.; Wu, X.; Wang, Q.; Sheng, T.; Lu, J. *Inorg. Chem.* **1996**, *35*, 893–897.
418. Lang, J. P.; Tatsumi, K. *J. Organomet. Chem.* **1999**, *579*, 332–337.
419. Guo, J.; Sheng, T.; Zhang, W.; Wu, X.; Lin, P.; Wang, Q.; Lu, J. *Inorg. Chem.* **1998**, *37*, 3689–3697.
420. Guo, J.; Wu, X.; Zhang, W.; Sheng, T.; Huang, Q.; Lin, P.; Wang, Q.; Lu, J. *Angew. Chem., Int. Ed. Engl.* **1997**, *36*, 2464–2466.
421. Huang, Q.; Wu, Q.; Sheng, T.; Wang, Q. *Polyhedron* **1996**, *15*, 3405–3410.
422. Zhang, Q. F.; Raj, S. S. S.; Hong, M. C.; Cao, R.; Fun, H. K.; Xin, X. Q. *Inorg. Chem. Commun.* **1999**, 272–274.
423. Zheng, H.; Leung, W. H.; Tan, W.; Long, D.; Ji, W.; Chen, J.; Xin, F.; Xin, X. J. *Chem. Soc., Dalton Trans.* **2000**, 2145–2149.
424. Canales, F.; Gimeno, M. C.; Laguna, A. *Inorg. Chem.* **1998**, *37*, 5376–5377.
425. Liu, Q.; Yang, Y.; Huang, L.; Wu, D.; Kang, B.; Chen, C.; Deng, Y.; Lu, J. *Inorg. Chem.* **1995**, *34*, 1884–1893.
426. Zhu, H.; Liu, Q.; Huang, X.; Wen, T.; Chen, C.; Wu, D. *Inorg. Chem.* **1998**, *37*, 2678–2686.
427. Yang, Y.; Liu, Q.; Huang, L.; Kang, B.; Lu, J. *Chem. Commun.* **1992**, 1512–1514.
428. Yang, Y.; Liu, Q.; Wu, D.; Kang, B.; Lu, J. *Inorg. Chem.* **1993**, *32*, 5431–5432.
429. Hou, H. W.; Ye, X.; Xin, X.; Liu, J.; Chen, M.; Shi, S. *Chem. Mater.* **1995**, *7*, 472–476.
430. Müller, A.; Schimanski, U.; Schimanski, J. *Inorg. Chim. Acta* **1983**, *76*, L245–L246.
431. Hong, M.; Wu, M.; Huang, X.; Jiang, F.; Cao, R.; Liu, H.; Lu, J. *Inorg. Chim. Acta* **1997**, *260*, 73–76.
432. Jeannin, Y.; Sécheresse, F.; Bernès, S.; Robert, F. *Inorg. Chim. Acta* **1992**, 198–200, 493–505.
433. Hou, H.; Ang, H. G.; Ang, S. G.; Fan, Y.; Low, M. K. M.; Ji, W.; Lee, Y. W. *Phys. Chem. Chem. Phys.* **1999**, *1*, 3145–3149.
434. Hou, H.; Ang, H. G.; Ang, S. G.; Fan, Y.; Low, M. K. M.; Ji, W.; Lee, Y. W. *Inorg. Chim. Acta* **2001**, *299*, 147–154.
435. Zheng, H.; Chen, J.; Xin, X.; Leung, W. H.; Hong, M. *Synth. React. Inorg. Met.-Org. Chem.* **2000**, *30*, 761–775.
436. Hou, H.; Liu, Y.; Xin, X. *Synth. React. Inorg. Met.-Org. Chem.* **1995**, *25*, 1417–1427.
437. Müller, A.; Bögge, H.; Schimanski, U. *Inorg. Chim. Acta* **1983**, *69*, 5–16.
438. Zhu, N.; Wu, J.; Du, S.; Wu, X.; Lu, J. *Inorg. Chim. Acta* **1992**, *191*, 65–68.
439. Lang, J. P.; Bian, G. Q.; Cai, J. H.; Kang, B. S.; Xin, X. *Transition Met. Chem.* **1995**, *20*, 376–379.
440. Shi, S.; Ji, W.; Tang, S. H. *J. Am. Chem. Soc.* **1994**, *116*, 3615–3616.
441. Long, D. L.; Shi, S.; Xin, X. Q.; Luo, B. S.; Chen, L. R.; Huang, X. Y.; Kang, B. S. *J. Chem. Soc., Dalton Trans.* **1996**, 2617–2622.
442. Zhang, Q. F.; Zhang, C.; Song, Y. L.; Xin, X. Q. *J. Mol. Struct.* **2000**, *525*, 79–86.
443. Zhang, Q. F.; Xiong, Y. N.; Lai, T. S.; Ji, W.; Xin, X. Q. *J. Phys. Chem. B* **2000**, *104*, 3446–3449.
444. Zhang, Q. F.; Hong, M.; Su, W.; Cao, R.; Liu, H. *Polyhedron* **1997**, *16*, 1433–1437.
445. Zhang, Q.; Hong, M.; Liu, H. *Transition Met. Chem.* **1997**, *22*, 156–160.
446. Du, S.; Wu, X.; Lu, J. *Polyhedron* **1994**, *13*, 841–845.
447. Zhang, Q.; Cao, R.; Hong, M.; Wu, D.; Zhang, W.; Zhen, Y.; Liu, H. *Inorg. Chim. Acta* **1998**, *271*, 93–98.
448. Hong, M.; Zhang, Q.; Cao, R.; Wu, D.; Chen, J.; Zhang, W.; Liu, H.; Lu, J. *Inorg. Chem.* **1997**, *36*, 6251–6260.
449. Cao, R.; Zhang, Q.; Su, W.; Bao, M.; Zheng, Y.; Hong, M. *Polyhedron* **1999**, *18*, 333–339.
450. Zheng, H. G.; Tan, W. L.; Ji, W.; Leung, W. H.; Williams, I. D.; Long, D. L.; Huang, J. S.; Xin, X. Q. *Inorg. Chim. Acta* **1999**, *294*, 73–78.
451. Zhang, C.; Song, Y.; Jin, G.; Fang, G.; Wang, Y.; Raj, S. S. S.; Fun, H. K.; Xin, X. J. *Chem. Soc., Dalton Trans.* **2000**, 1317–1323.
452. Sécheresse, F.; Robert, F.; Marzak, S.; Manoli, J. M.; Potvin, C. *Inorg. Chim. Acta* **1991**, *182*, 221–228.
453. Hou, H. W.; Xin, X. Q.; Liu, J.; Chen, M. Q.; Shu, S. J. *Chem. Soc., Dalton Trans.* **1994**, 3211–3214.
454. Hou, H.; Long, D.; Xin, X.; Huang, X.; Kang, B.; Ge, P.; Ji, W.; Shi, S. *Inorg. Chem.* **1996**, *35*, 5363–5367.
455. Lang, J. P.; Kawaguchi, H.; Tatsumi, K. *J. Organomet. Chem.* **1998**, *569*, 109–119.
456. Huang, Z.; Lei, X.; Kang, B.; Liu, J. Liu Q.; Hong, M. *Inorg. Chim. Acta* **1990**, *169*, 25–29.
457. Zheng, H. G.; Tan, W. L.; Low, M. K. L.; Ji, W.; Long, D. L.; Wong, W. T.; Yu, K. B.; Xin, X. Q. *Polyhedron* **1999**, *18*, 3115–3121.
458. Hornung, F. N.; Klinkhammer, K. W.; Kaim, W. *Chem. Commun.* 2055–2056.
459. Christuk, C. C.; Ansari, M. A.; Ibers, J. A. *Inorg. Chem.* **1992**, *31*, 4365–4369.
460. Ansari, M. A.; Bollinger, J. C.; Christuk, C. C.; Ibers, J. A. *Acta Crystallogr.* **1994**, *C50*, 869–871.
461. Christuk, C. C.; Ansari, M. A.; Ibers, J. A. *Angew. Chem., Int. Ed. Engl.* **1992**, *31*, 1477–1478.
462. Zhang, Q. F.; Bao, M. T.; Hong, M. C.; Cao, R.; Song, Y. L.; Xin, X. Q. *J. Chem. Soc., Dalton Trans.* **2000**, 605–610.
463. Low, M. K. M.; Hou, H.; Zheng, H.; Wong, W.; Jin, G.; Xin, X.; Ji, W. *Chem. Commun.* **1998**, 505–506.
464. Fang, G.; Song, Y.; Wang, Y.; Zhang, X.; Li, C.; Zhang, C.; Xin, X. *Opt. Commun.* **2000**, *181*, 97–100.
465. Song, Y.; Zhang, C.; Zhao, X.; Wang, Y.; Fang, G.; Jin, G.; Qu, S.; Wu, S.; Xin, X.; Ye, H. *Chem. Lett.* **2000**, 1076–1077.
466. Zhang, Q. F.; Lau, K. K.; Wong, W. Y.; Leung, W. H. *Inorg. Chim. Acta* **2001**, *325*, 125–129.
467. Lang, J.; Kawaguchi, H.; Ohnishi, S.; Tatsumi, K. *Chem. Commun.* **1997**, 405–406.
468. Lang, J.; Kawaguchi, H.; Tatsumi, K. *Chem. Commun.* **1999**, 2315–2316.
469. Scattergood, C.; Garner, C. D.; Clegg, W. *Inorg. Chim. Acta* **1987**, *132*, 161–162.
470. Ji, W.; Ge, P.; Xie, W.; Tang, S. H.; Shi, S. *J. Lumin.* **1996**, *66–67*, 115–119.
471. Hoggard, P. E.; Hou, H. W.; Xin, X. Q.; Shi, S. *Chem. Mater.* **1996**, *8*, 2218–2222.
472. Shi, S.; Ji, W.; Lang, J. P.; Xin, X. Q. *J. Phys. Chem.* **1994**, *98*, 3570–3572.
473. Sakane, G.; Shibahara, T.; Hou, H.; Liu, Y.; Xin, X. *Transition Met. Chem.* **1996**, *21*, 398–400.
474. Zeng, D. X.; Ji, W.; Wong, W. T.; Wong, W. Y.; Xin, X. Q. *Inorg. Chim. Acta* **1998**, *279*, 172–177.
475. Chen, Z. R.; Hou, H. W.; Xin, X. Q.; Shi, S.; Yu, K. B. *J. Phys. Chem.* **1995**, *99*, 8717–8721.

476. Hou, H.; Liang, B.; Xin, X.; Yu, K.; Ge, P.; Ji, W.; Shi, S. *J. Chem. Soc., Faraday Trans.* **1996**, *92*, 2343–2346.
477. Chan, M. K.; Kim, J.; Rees, D. C. *Science* **1993**, *260*, 792–794.
478. Coucouvanis, D. *Acc. Chem. Res.* **1991**, *24*, 1–8.
479. Fackler, J. P., Jr.; Staples, R. J.; Liu, C. W.; Stubbs, R. T.; Lopez, C.; Pitts, J. T. *Pure Appl. Chem.* **1998**, *70*, 839–844.
480. Liu, C. W.; Shang, I. J.; Wang, J. C.; Keng, T. C. *Chem. Commun.* **1999**, 995–996.
481. Liu, C. W.; Chen, H. C.; Wang, J. C.; Keng, T. C. *Angew. Chem., Int. Ed. Engl.* **2001**, *40*, 2342–2344.
482. Kim, K. W.; Kanatzidis, M. L. *J. Am. Chem. Soc.* **1995**, *117*, 5606–5607.
483. Wirth, S.; Fenske, D. *Z. Anorg. Allg. Chem.* **1999**, *625*, 2064–2070.
484. Weigand, F.; Wirth, S.; Ahlrichs, R.; Fenske, D. *Chem. Eur. J.* **2000**, *6*, 545–551.
485. Niu, Y. Y.; Song, Y. L.; Zheng, H. G.; Long, D. L.; Fun, H. K. *New J. Chem.* **2001**, *25*, 945–948.
486. Zhuang, B.; Yu, P.; Huang, L.; He, L.; Pan, G. *Polyhedron* **1997**, *16*, 1425–1431.
487. Cheng, Y.; Emge, T. J.; Brennan, J. G. *Inorg. Chem.* **1996**, *35*, 7339–7344.
488. Chivers, T.; Downard, A.; Parvez, M.; Schatte, G. *Organometallics* **2001**, *20*, 727–733.
489. Liu, C. W.; Staples, R. J.; Fackler, J. P. Jr. *Coord. Chem. Rev.* **1998**, *174*, 147–177.
490. Matsumoto, K.; Tanaka, R.; Shimomura, R.; Nakao, Y. *Inorg. Chim. Acta* **2000**, *304*, 293–296.
491. Liu, C. W.; Stubbs, T.; Staples, R. J.; Fackler, J. P. Jr. *J. Am. Chem. Soc.* **1995**, *117*, 9778–9779.
492. Liu, C. W.; Hung, C. M.; Chen, H. C.; Wang, J. C.; Keng, T. C.; Guo, K. *Chem. Commun.* **2000**, 1897–1898.
493. Liu, C. W.; McNeal, C. J.; Fackler, J. P., Jr. *J. Cluster Sci.* **1996**, *7*, 385–406.
494. Birker, P. J. M. W. L.; Verschoor, G. C. *Chem. Commun.* **1981**, 322–324.
495. Liu, C. W.; Pitts, J. T.; Fackler, J. P., Jr. *Polyhedron* **1997**, *16*, 3899–3909.
496. Nomiyama, K.; Takahashi, S.; Noguchi, R. *J. Chem. Soc., Dalton Trans.* **2000**, 2091–2097.
497. Huang, Z.; Lei, X.; Hong, M.; Liu, H. *Inorg. Chem.* **1992**, *31*, 2990–2991.
498. Zhang, Q.; Cao, R.; Hong, M.; Su, W.; Liu, H. *Inorg. Chim. Acta* **1998**, *277*, 171–176.
499. Su, W.; Hong, M.; Jiang, F.; Liu, H. *Polyhedron* **1996**, *15*, 4047–4051.
500. Chunggaze, M.; Malik, M. A.; O'Brien, P.; White, A. J. P.; Williams, D. J. *J. Chem. Soc., Dalton Trans.* **1998**, 3839–3844.
501. Albinati, A.; Casarin, M.; Maccato, C.; Pandolfo, L.; Vittadini, A. *Inorg. Chem.* **1999**, *38*, 1145–1152.
502. Chondroudis, K.; Kanatzidis, M. G. *Chem. Commun.* **1997**, 401–402.
503. Liu, C. W.; Chen, H. C.; Wang, J. C.; Keng, T. C. *Chem. Commun.* **1998**, 1831–1832.
504. Zhuang, B.; Pan, B.; Huang, L.; Yu, P. *Inorg. Chim. Acta* **1994**, *227*, 119–127.
505. Mathur, P.; Trivedi, R.; Satyanarayana, C. V. V. *Organometallics* **1996**, *15*, 1062–1064.
506. Yuki, M.; Kuge, K.; Okazaki, M.; Mitsui, T.; Inomata, S.; Tobita, H.; Ogino, H. *Inorg. Chim. Acta* **1999**, *291*, 395–402.
507. Barber, D. E.; Sabat, M.; Sinn, E.; Averill, B. A. *Organometallics* **1995**, *14*, 3229–3237.
508. Curtis, M. D.; Williams, P. D.; Butler, W. M. *Inorg. Chem.* **1988**, *27*, 2853–2862.
509. Song, L. C.; Yang, J.; Hu, Q. M.; Wu, Q. J. *Organometallics* **2001**, *20*, 3293–3298.
510. Mathur, P.; Dash, A. K.; Hossain, M. M.; Satyanarayana, C. V. V.; Verghese, B. *J. Organomet. Chem.* **1996**, *506*, 307–312.
511. Liaw, W. F.; Lee, C. M.; Horng, L.; Lee, G. H.; Peng, S. M. *Organometallics* **1999**, *18*, 782–786.
512. Song, L. C.; Qin, X. D.; Hu, Q. M.; Huang, X. Y. *Organometallics* **1998**, *17*, 5437–5440.
513. Mathur, P.; Hossain, M. M.; Umbarkar, S. B.; Satyanarayana, C. V. V.; Rheigold, A. L.; Liable-Sands, L. M.; Yap, G. P. A. *Organometallics* **1996**, *15*, 1898–1904.
514. Albano, V. G.; Castellari, C.; Femoni, C.; Iapalucci, M. C.; Longoni, G.; Monari, M.; Rauccio, M.; Zacchini, S. *Inorg. Chim. Acta* **1999**, *291*, 372–379.
515. Calderoni, F.; Demartin, F.; Iapalucci, M. C.; Laschi, F.; Longoni, G.; Zanello, P. *Inorg. Chem.* **1996**, *35*, 898–905.
516. Mathur, P.; Ghose, S.; Hossain, M. M.; Satyanarayana, C. V. V.; Mahon, M. F. *J. Organomet. Chem.* **1997**, *543*, 189–199.
517. Shieh, M. *J. Cluster Sci.* **1999**, *10*, 3–36.
518. Kanatzidis, M. G.; Huang, S. P. *Coord. Chem. Rev.* **1994**, *130*, 509–621.
519. Mathur, P. *Adv. Organomet. Chem.* **1997**, *41*, 242–314.
520. Fong, S. W. A.; Hor, T. S. A. *J. Chem. Soc., Dalton Trans.* **1999**, 639–651.
521. Amemiya, T.; Kuwata, S.; Hidai, M. *Chem. Commun.* **1999**, 711–712.
522. Brunner, H.; GraBl, R.; Wachter, J.; Nuber, B.; Ziegler, M. L. *J. Organomet. Chem.* **1990**, *393*, 119–129.
523. Ikada, T.; Kuwata, S.; Mizobe, Y.; Hidai, M. *Inorg. Chem.* **1999**, *38*, 64–69.
524. Zhu, N.; Zheng, Y.; Wu, X. *Chem. Commun.* **1990**, 780–781.
525. Ikada, T.; Kuwata, S.; Mizobe, Y.; Hidai, M. *Inorg. Chem.* **1998**, *37*, 5793–5797.
526. Masumori, T.; Seino, H.; Mizobe, Y.; Hidai, M. *Inorg. Chem.* **2000**, *39*, 5002–5003.
527. Lin, P.; Wu, X.; Huang, Q.; Wang, Q.; Sheng, T.; Zhang, W.; Guo, J.; Lu, J. *Inorg. Chem.* **1998**, *37*, 5672–5674.
528. Lin, P.; Wu, X. T.; Chen, L.; Wu, L. M.; Du, W. X. *Polyhedron* **2000**, *19*, 2189–2193.
529. Jianhui, W.; Nianyong, Z.; Xiantao, X.; Jiayi, L. *Inorg. Chim. Acta* **1991**, *185*, 181–185.
530. Kuwata, S.; Mizobe, Y.; Hidai, M. *J. Am. Chem. Soc.* **1993**, *115*, 8499–8500.
531. Tang, Z.; Nomura, Y.; Ishii, Y.; Mizobe, Y.; Hidai, M. *Organometallics* **1997**, *16*, 151–154.
532. Tang, Z.; Nomura, Y.; Ishii, Y.; Mizobe, Y.; Hidai, M. *Inorg. Chim. Acta* **1998**, *267*, 73–79.
533. Kochi, T.; Tanabe, Y.; Tang, Z.; Ishii, Y.; Hidai, M. *Chem. Lett.* **1999**, 1279–1280.
534. Seino, H.; Mizobe, Y.; Hidai, M. *Organometallics* **2000**, *19*, 3631–3639.
535. Tang, Z.; Nomura, Y.; Kuwata, S.; Ishii, Y.; Mizobe, Y.; Hidai, M. *Inorg. Chem.* **1998**, *37*, 4909–4920.
536. Liu, H.; Tan, A. L.; Cheng, C. R.; Mok, K. F.; Hor, T. S. A. *Inorg. Chem.* **1997**, *36*, 2916–2918.
537. Matsumoto, K.; Kotoku, N.; Shizuka, T.; Tanaka, R.; Okeya, S. *Inorg. Chim. Acta* **2001**, *321*, 167–170.
538. Nishitani, C.; Shizuka, T.; Matsumoto, K.; Okeya, S.; Kimoto, H. *Inorg. Chem. Commun.* **1998**, 325–327.
539. Yam, V. W. W.; Yeung, P. K. Y.; Cheung, K. K. *Angew. Chem., Int. Ed. Engl.* **1996**, *35*, 739–740.
540. Briant, C. M.; Hor, T. S. A.; Howells, D.; Mingos, D. M. P. *Chem. Commun.* **1983**, 1118–1120.
541. Liu, H.; Tan, A. L.; Xu, Y.; Mok, K. F.; Hor, T. S. A. *Polyhedron* **1997**, *16*, 377–382.
542. Capdevila, M.; Carrasco, Y.; Clegg, W.; Coxall, R. A.; González-Duarte, P.; Lledós, Sola, J.; Ujaque, G. *Chem. Commun.* **1998**, 597–598.
543. Briant, C. M.; Hor, T. S. A.; Howells, D.; Mingos, D. M. P. *J. Organomet. Chem.* **1983**, *256*, C15–C18.
544. Canales, F.; Gimeno, M. C.; Laguna, A.; Jones, P. G. *J. Am. Chem. Soc.* **1996**, *118*, 4839–4845.
545. Routledge, C. A.; Humanes, M.; Li, Y. J.; Sykes, A. G. *J. Chem. Soc., Dalton Trans.* **1994**, 1275–1282.

546. Deeg, A.; Keck, H.; Kruse, A.; Kuchen, W.; Wunderlich, H. *Z. Naturforsch.* **1988**, *43B*, 1541–1546.
547. Rink, B.; Brorson, M.; Scowen, I. *J. Organometallics* **1999**, *18*, 2309–2313.
548. Finnegan, M. G.; Conover, R. C.; Park, J. B.; Zhou, Z. H.; Adams, M. W. W.; Johnson, M. K. *Inorg. Chem.* **1995**, *34*, 5358–5369.
549. Shibahara, T.; Akashi, H.; Kuroya, H. *J. Am. Chem. Soc.* **1986**, *108*, 1342–1343.
550. Moura, I.; Moura, J. J. G.; Münck, E.; Papaefthymiou, V.; LeGall, J. *J. Am. Chem. Soc.* **1986**, *108*, 349–351.
551. Shibahara, T.; Akashi, H.; Yamasaki, M.; Hashimoto, K. *Chem. Lett.* **1991**, 689–690.
552. Zhou, J.; Raebiger, J. W.; Crawford, C. A.; Holm, R. H. *J. Am. Chem. Soc.* **1997**, *119*, 6242–6250.
553. Moreno, C.; Macedo, A. L.; Moura, I.; LeGall, J.; Moura, J. J. G. *J. Inorg. Biochem.* **1994**, *53*, 219–234.
554. Curtis, M. D.; Riaz, U.; Curnow, O.; Kampf, J.; Rheigold, A.; Haggerty, B. *Organometallics* **1995**, *14*, 5337–5343.
555. Shibahara, T.; Yamasaki, M.; Akashi, H.; Katayama, T. *Inorg. Chem.* **1991**, *30*, 2693–2699.
556. Murata, T.; Gao, H.; Mizobe, Y.; Nakano, F.; Motomura, S.; Tanase, T.; Yano, S.; Hidai, M. *J. Am. Chem. Soc.* **1992**, *114*, 8287–8288.
557. Murata, T.; Mizobe, Y.; Gao, H.; Ishii, Y.; Wakabayashi, T.; Nakano, F.; Tanase, T.; Yano, S.; Hidai, M.; Echizen, I.; Nanikawa, H.; Motomura, S. *J. Am. Chem. Soc.* **1994**, *116*, 3389–3398.
558. Dimmock, P. W.; Lamprecht, G. J.; Sykes, A. G. *J. Chem. Soc., Dalton Trans.* **1991**, 955–960.
559. Conover, R. C.; Park, J. B.; Adams, M. W. W.; Johnson, M. K. *J. Am. Chem. Soc.* **1990**, *112*, 4562–4564.
560. Srivastava, K. K. P.; Surerus, K. K.; Conover, R. C.; Johnson, M. K. *Inorg. Chem.* **1993**, *32*, 927–936.
561. Shibahara, T.; Mochida, S.; Sakane, G. *Chem. Lett.* **1993**, 89–92.
562. Saysell, D. M.; Huang, Z. X.; Sykes, A. G. *J. Chem. Soc., Dalton Trans.* **1996**, 2623–2627.
563. Saysell, D. M.; Sykes, A. G. *Inorg. Chem.* **1997**, *36*, 2700–2701.
564. Lu, S. F.; Huang, J. Q.; Wu, Q. J.; Huang, X. Y.; Yu, R. M.; Zheng, Y.; Wu, D. X. *Inorg. Chim. Acta* **1997**, *261*, 201–209.
565. Masui, D.; Ishii, Y.; Hidai, M. *Bull. Chem. Soc. Jpn.* **2000**, *73*, 931–938.
566. Wu, B.; Zhang, W. J.; Yu, S. Y.; Sheng, T. L.; Wu, X. T. *J. Organomet. Chem.* **1997**, *545–546*, 587–589.
567. Schmidt, I.; Hyltoft, J.; Hjortkjaer, J.; Jacobsen, C. J. H. *Acta Chem. Scand.* **1996**, *50*, 871–874.
568. Nasreldin, M.; Li, Y. J.; Mabbs, F. E.; Sykes, A. G. *Inorg. Chem.* **1994**, *33*, 4283–4289.
569. Hegetschweiler, K.; Wörh, M.; Meienberger, M. D.; Nesper, R.; Schmalle, H. W.; Hancock, R. D. *Inorg. Chim. Acta* **1996**, *250*, 35–47.
570. Wu, X.; Lu, S.; Zu, L.; Wu, Q.; Lu, J. *Inorg. Chim. Acta* **1987**, *133*, 39–42.
571. Zhan, H.; Zheng, Y.; Wu, X.; Lu, J. *Inorg. Chim. Acta* **1989**, *156*, 277–280.
572. Llusar, R.; Uriel, S.; Vicent, C. *J. Chem. Soc., Dalton Trans.* **2001**, 2813–2818.
573. Nasreldin, M.; Routledge, C. A.; Sykes, A. G. *J. Chem. Soc., Dalton Trans.* **1994**, 2809–2814.
574. Shibahara, T.; Akashi, H.; Kuroya, H. *J. Am. Chem. Soc.* **1988**, *110*, 3313–3314.
575. Feliz, M.; Garriga, J. M.; Llusar, R.; Uriel, S.; Humphrey, M. G.; Lucas, N. T.; Samoc, M.; Luther-Davies, B. *Inorg. Chem.* **2001**, *40*, 6132–6138.
576. Butt, J. N.; Armstrong, F. A.; Breton, J.; George, S. J.; Thomson, A. J.; Hatchikian, E. C. *J. Am. Chem. Soc.* **1991**, *113*, 6663–6670.
577. Surerus, K. K.; Münck, E.; Moura, I.; Moura, J. J. G.; LeGall, J. *J. Am. Chem. Soc.* **1987**, *109*, 3805–3807.
578. Sokolov, M. N.; Virovets, A. V.; Dybtsev, D. N.; Gerasko, O. A.; Fedin, V. P.; Hernandez-Molina, R.; Clegg, W.; Sykes, A. G. *Angew. Chem., Int. Ed. Engl.* **2000**, *39*, 1659–1661.
579. Fedin, V. P.; Sokolov, M. N.; Lamprecht, G. J.; Hernandez-Molina, R.; Seo, M. S.; Virovets, A. V.; Clegg, W.; Sykes, A. G. *Inorg. Chem.* **2001**, *40*, 6598–6603.
580. Shibahara, T.; Kobayashi, S.; Tsuji, N.; Sakane, G.; Fukuhara, M. *Inorg. Chem.* **1997**, *36*, 1702–1706.
581. Sakane, G.; Shibahara, T. *Inorg. Chim. Acta* **1993**, *32*, 777–778.
582. Sakane, G.; Yao, Y. G.; Shibahara, T. *Inorg. Chim. Acta* **1994**, *216*, 13–14.
583. Varey, J. E.; Sykes, A. G. *Polyhedron* **1996**, *15*, 1887–1892.
584. Hernandez-Molina, R.; Fedin, V. P.; Sokolov, M. N.; Saysell, D. M.; Sykes, A. G. *Inorg. Chem.* **1998**, *37*, 4328–4334.
585. Akashi, H.; Shibahara, T. *Inorg. Chem.* **1989**, *28*, 2906–2907.
586. Varey, J. E.; Lamprecht, G. J.; Fedin, V. P.; Holder, A.; Clegg, W.; Elsegood, M. R. J.; Sykes, A. G. *Inorg. Chem.* **1996**, *35*, 5525–5530.
587. Müller, A.; Fedin, V. P.; Dimann, E.; Bögge, H.; Krickemeyer, E.; Söolter, D.; Giuliani, A. M.; Barbieri, R.; Adler, P. *Inorg. Chem.* **1994**, *33*, 2243–2247.
588. Keck, H.; Kruse, A.; Kuchen, W.; Mootz, D.; Wiskeman, R.; Wunderlich, H. *Z. Naturforsch.* **1989**, *45B*, 461–464.
589. Yu, R. M.; Lu, S. F.; Huang, J. Q.; Huang, X. Y.; Wu, Q. J.; Wu, D. X. *Inorg. Chem.* **2000**, *39*, 5348–5353.
590. Huang, J. Q.; Lu, S. F.; Huang, X. Y.; Wu, Q. J.; Yu, R. M. *J. Cluster Sci.* **1997**, *8*, 47–57.
591. Lu, S. F.; Huang, J. Q.; Huang, X. Y.; Wu, Q. J.; Yu, R. M. *Inorg. Chem.* **1999**, *38*, 3801–3805.
592. Lu, S. F.; Huang, J. Q.; Wu, Q. J.; Huang, X. Y.; Wu, D. X.; Zheng, Y.; Yu, R. M. *Polyhedron* **1998**, *18*, 281–287.
593. Yu, R. M.; Lu, S. F.; Huang, X. Y.; Wu, Q. J.; Huang, J. Q. *Inorg. Chem.* **1999**, *38*, 3313–3315.
594. Fedin, V. P.; Sokolov, M. N.; Sykes, A. G. *J. Chem. Soc., Dalton Trans.* **1996**, 4089–4092.
595. Sokolov, M. N.; Coichev, N.; Moya, H. D.; Hernandez-Molina, R.; Borman, C. D.; Sykes, A. G. *J. Chem. Soc., Dalton Trans.* **1997**, 1863–1869.
596. Saysell, D. M.; Fedin, V. P.; Lamprecht, G. J.; Sokolov, M. N.; Sykes, A. G. *Inorg. Chem.* **1997**, *36*, 2982–2987.
597. Hernandez-Molina, R.; Dybtsev, D. N.; Fedin, V. P.; Elsegood, M. R. J.; Clegg, W.; Sykes, A. G. *Inorg. Chem.* **1998**, *37*, 2995–3001.
598. Saysell, D. M.; Sykes, A. G. *J. Cluster Sci.* **1995**, *6*, 499–561.
599. Sakane, G.; Hashimoto, K.; Takahashi, M.; Takeda, M.; Shibahara, T. *Inorg. Chem.* **1998**, *37*, 4231–4234.
600. Saysell, D. M.; Sykes, A. G. *Inorg. Chem.* **1996**, *35*, 5536–5539.
601. Bahn, C. S.; Tan, A.; Harris, S. *Inorg. Chem.* **1998**, *37*, 2770–2778.
602. Pernin, C. G.; Ibers, J. A. *Inorg. Chem.* **1997**, *36*, 3802–3803.
603. Das, K. B.; Kanatzidis, M. G. *Inorg. Chem.* **1995**, *34*, 1011–1012.
604. Huang, S. P.; Kanatzidis, M. G. *Inorg. Chem.* **1993**, *32*, 821–825.
605. Das, K. B.; Kanatzidis, M. G. *Polyhedron* **2000**, *19*, 1995–2002.
606. Huang, F. Q.; Ibers, J. A. *Angew. Chem., Int. Ed. Engl.* **2001**, *40*, 2515–2516.

607. Guo, G. C.; Kwok, R. W. M.; Mak, T. C. W. *Inorg. Chem.* **1997**, *36*, 2475–2477.
608. Guo, G. C.; Mak, T. C. W. *J. Chem. Soc., Dalton Trans.* **1997**, 709–710.
609. Müller, A.; Krickemeyer, E.; Bögge, H. *Angew. Chem. Int. Ed. Engl.* **1986**, *25*, 272–273.
610. Müller, A.; Krickemeyer, E.; Bögge, H. *Z. Anorg. Allg. Chem.* **1987**, *554*, 61–78.
611. Mironov, Y. V. *Inorg. Chem.* **2001**, *40*, 5472–5474.
612. Jin, G. X.; Arikawa, Y.; Tatsumi, K. *J. Am. Chem. Soc.* **2001**, *123*, 735–736.
613. Tremel, W.; Henkel, G. *Inorg. Chem.* **1988**, *27*, 3896–3899.
614. McConnachie, J. M.; Ansari, M. A.; Ibers, J. A. *Inorg. Chim. Acta* **1992**, *198–200*, 85–93.
615. McConnachie, J. M.; Bolinger, J. C.; Ibers, J. A. *Inorg. Chem.* **1993**, *32*, 3923–3927.
616. Kim, K. W.; Kanatzidis, M. G. *Inorg. Chem.* **1993**, *32*, 4161–4163.
617. Hepp, A. F.; Richman, R. M.; Duraj, S. A.; Andras, M. T.; Moore, H. L.; Sabat, M.; Eckles, W. E.; Martuch, R. A. *J. Cluster Sci.* **1996**, *7*, 199–210.
618. Li, H.; Sheng, T.; Huang, Q.; Wu, X. *J. Cluster Sci.* **1995**, *6*, 403–410.
619. Müller, A.; Römer, M.; Krickemeyer, E.; Bögge, H. *Naturwissenschaften* **1984**, *71*, 43–44.
620. Müller, A.; Römer, M.; Bögge, H.; Krickemeyer, E.; Bergmann, D. *Chem. Commun.* **1984**, 348–349.
621. Cusick, J.; Scudder, M. L.; Craig, D. C.; Dance, I. G. *Polyhedron* **1989**, *8*, 1139–1141.
622. Dhingra, S. S.; Haushalter, R. C. *J. Am. Chem. Soc.* **1994**, *116*, 3651–3652.
623. Kim, K. W.; Kanatzidis, M. G. *Inorg. Chim. Acta* **1994**, *224*, 163–169.
624. Schreiner, B.; Dehnicke, K.; Fenske, D. *Z. Anorg. Allg. Chem.* **1993**, *619*, 1127–1131.
625. Choi, Y. G.; Kim, K. H.; Heo, J. *J. Appl. Phys.* **2000**, *88*, 3832–3839.
626. Shin, Y. B.; Heo, J.; Kim, H. S. *Chem. Phys. Lett.* **2000**, *317*, 637–641.
627. Furniss, D.; Seddon, A. B. *J. Mater. Sci. Lett.* **1998**, *17*, 1541–1542.
628. King, W. A.; Di Bella, S.; Marks, T. J. *J. Am. Chem. Soc.* **1996**, *118*, 627–635.
629. Anderson, D.; Cloke, F. G. N.; Cox, P.; Edelstein, N.; Green, J.; Pang, T.; Sameh, A.; Shalimoff, G. *Chem. Commun.* **1989**, 53–54.
630. Brennan, J.; Cloke, F. G. N.; Sameh, A.; Salkin, A. *Chem. Commun.* **1987**, 1668–1669.
631. Byrom, E.; Ellis, D. E.; Freeman, A. J. *Phys. Rev. B* **1976**, *14*, 3558–3568.
632. Zhukov, V. P.; Gubanov, V. A.; Weber, J. *J. Chem. Phys. Solids* **1981**, *42*, 631–639.
633. Freedman, D.; Emge, T. J.; Brennan, J. G. *Inorg. Chem.* **1999**, *38*, 4400–4404.
634. Cary, D. R.; Arnold, J. *J. Am. Chem. Soc.* **1993**, *115*, 2520–2521.
635. Cary, D. R.; Ball, G. A.; Arnold, J. *J. Am. Chem. Soc.* **1995**, *117*, 3492–3501.
636. Evans, W. J.; Rabe, G. W.; Ansari, M. A.; Ziller, J. W. *Angew. Chem., Int. Ed. Engl.* **1994**, *33*, 2110–2111.
637. Melman, J. H.; Emge, T. J.; Brennan, J. G. *Chem. Commun.* **1997**, 2269–2270.
638. Melman, J. H.; Emge, T. J.; Brennan, J. G. *Inorg. Chem.* **1999**, *38*, 2117–2122.
639. Freedman, D.; Melman, J. H.; Emge, T. J.; Brennan, J. G. *Inorg. Chem.* **1998**, *37*, 4162–4163.
640. Freedman, D.; Sayan, S.; Emge, T. J.; Croft, M.; Brennan, J. G. *J. Am. Chem. Soc.* **1999**, *121*, 11713–11719.
641. Melman, J. H.; Fitzgerald, M.; Freedman, D.; Emge, T. J.; Brennan, J. G. *J. Am. Chem. Soc.* **1999**, *121*, 10247–10248.
642. Kornienko, A. Y.; Emge, T. J.; Brennan, J. G. *Inorg. Chem.* **1998**, *37*, 11933–11939.
643. Brewer, M.; Lee, J.; Brennan, J. G. *Inorg. Chem.* **1995**, *34*, 5919–5924.
644. Berardini, M.; Emge, T. J.; Brennan, J. G. *J. Am. Chem. Soc.* **1994**, *116*, 6941–6942.
645. Seela, J. L.; Huffman, J. C.; Christou, G. *Chem. Commun.* **1987**, 1258–1260.
646. Babaiian-Kibala, E.; Cotton, F. A.; Kibala, P. A. *Polyhedron* **1990**, *9*, 1689–1694.
647. Zank, G. A.; Jones, C. A.; Rauchfuss, T. B.; Rheingold, A. L. *Inorg. Chem.* **1986**, *25*, 1886–1891.
648. Müller, A.; Fenske, D. *Curr. Opin. Solid State Mater. Sci.* **1999**, *4*, 141–153.
649. Eichhöfer, A.; Beckmann, E.; Fenske, D.; Herein, D.; Krautscheid, H.; Schlögl, R. *Israel J. Chem.* **2001**, *41*, 31–37.
650. van der Putten, D.; Zaroni, R. *Phys. Lett. A* **1995**, *208*, 351–355.
651. van der Putten, D.; Olevano, D.; Zaroni, R.; Krautscheid, H.; Fenske, D. *J. Electron Spectrosc. Relat. Phenom.* **1995**, *76*, 201–211.
652. van der Putten, D.; Zaroni, R. *Phys. Lett. A* **1995**, *208*, 345–350.
653. Goldstein, A. N.; Echer, C. M.; Alivasatos, A. P. *Science* **1992**, *256*, 1425–1427.
654. Weller, H. *Angew. Chem., Int. Ed. Engl.* **1993**, *32*, 41–53.
655. Wang, Y.; Herron, N. *J. Phys. Chem.* **1991**, *95*, 325–332.
656. Brus, L. E. *Appl. Phys. A* **1991**, *53*, 465–474.
657. Alivasatos, A. P. *J. Phys. Chem.* **1995**, *100*, 13226–13239.
658. Bertocello, R.; Bettinelli, M.; Casarin, M.; Maccato, C.; Pandolfo, L.; Vittadini, A. *Inorg. Chem.* **1997**, *36*, 4707–4716.
659. Döllefeld, H.; Weller, H.; Eychmüller, A. *Nano Lett.* **2001**, *1*, 267–269.
660. Soloviev, V. N.; Eichhöfer, A.; Fenske, D.; Banin, U. *J. Am. Chem. Soc.* **2000**, *122*, 2673–2674.
661. Soloviev, V. N.; Eichhöfer, A.; Fenske, D.; Banin, U. *Phys. Stat. Solid. B* **2001**, *224*, 285–289.
662. Tittel, J.; Gohde, W.; Koberling, F.; Mews, A.; Kornowski, A.; Weller, H.; Eychmüller, A.; Basche, T. *Ber. Bunsenges. Phys. Chem.* **1997**, *101*, 1626–1630.
663. Eychmüller, A.; Hasselbarth, A.; Katsikas, L.; Weller, H. *J. Lumin.* **1991**, 745–749.

## 7.3

# High Nuclearity Clusters: Clusters and Aggregates with Paramagnetic Centers: Oxygen and Nitrogen Bridged Systems

R. E. P. WINPENNY

*University of Manchester, UK*

---

7.3.1	INTRODUCTION	125
7.3.1.1	Explanation and Apology	125
7.3.1.2	Strategies for Making Polynuclear Cages	126
7.3.1.3	Serendipitous Assembly	126
7.3.1.4	Harris Notation	127
7.3.2	SURVEY OF THE 3d METALS	127
7.3.2.1	Vanadium	128
7.3.2.1.1	<i>Alkoxides</i>	128
7.3.2.1.2	<i>Phosphonates and arsonates</i>	130
7.3.2.1.3	<i>Other ligands</i>	131
7.3.2.2	Chromium	132
7.3.2.3	Manganese	134
7.3.2.4	Iron	145
7.3.2.5	Cobalt	151
7.3.2.6	Nickel	156
7.3.2.7	Copper	160
7.3.3	FAMILIES OF CAGES	166
7.3.3.1	Wheels and Metallocrowns	166
7.3.3.2	Cubanes	168
7.3.3.3	Trigonal Prisms	168
7.3.3.4	Planar Cages Based on Cadmium Iodide Cores	168
7.3.4	CONCLUSION	169
7.3.5	REFERENCES	171

---

### 7.3.1 INTRODUCTION

#### 7.3.1.1 Explanation and Apology

The area of polymetallic cage compounds has received much of its impetus from the fascinating magnetic properties many of these cages show. In particular, the observation of magnetic hysteresis of *molecular* origin reported by Christou, Hendrickson, and Gatteschi and co-workers<sup>1,2</sup> is an extraordinarily exciting phenomenon. This magnetic behavior, which has been termed single



molecule magnetism, is discussed elsewhere (see Chapter 7.13), and therefore this chapter concentrates on the structures displayed by these cage compounds.

The discussion is largely derived from a longer review article,<sup>3</sup> as are the figures. Self-plagiarising is not usually an acceptable practice; however, as the original article was intended to be a comprehensive account of the subject, removing or rewriting material would have produced a markedly worse review—which seems even less acceptable. The review has been edited—largely by removing detailed discussion of magnetic behavior or long discussions of results from the author's own group—and an attempt has been made to update the review to approximately the end of 2001. The extraordinary number of new compounds reported in 2002 and 2003 have, unfortunately, not been included.

### 7.3.1.2 Strategies for Making Polynuclear Cages

There are two broad synthetic strategies that are being pursued to make new cages that, ideally, will satisfy the criteria for a room-temperature single molecule magnet or SMM. One route uses ligands with predictable and controllable binding modes; this area is dominated by cyanide as the bridging ligand and is covered in Chapter 7.4.

The second strategy, discussed here, can be termed “serendipitous assembly” as there is much less element of strict design.<sup>4</sup> It is clear, however, that you cannot simply trust to luck in making such cages, there has to be considerable forethought in the ligands, metals, and conditions used for any significant progress to be made. Before reviewing the range of complexes that has been reported, it is perhaps worth considering some of the thought processes behind this approach. It is also worth commenting that there is no strict boundary between these two approaches, and that some of the results below are achieved by design, e.g., the many beautiful cages reported by Saalfrank and co-workers.

### 7.3.1.3 Serendipitous Assembly

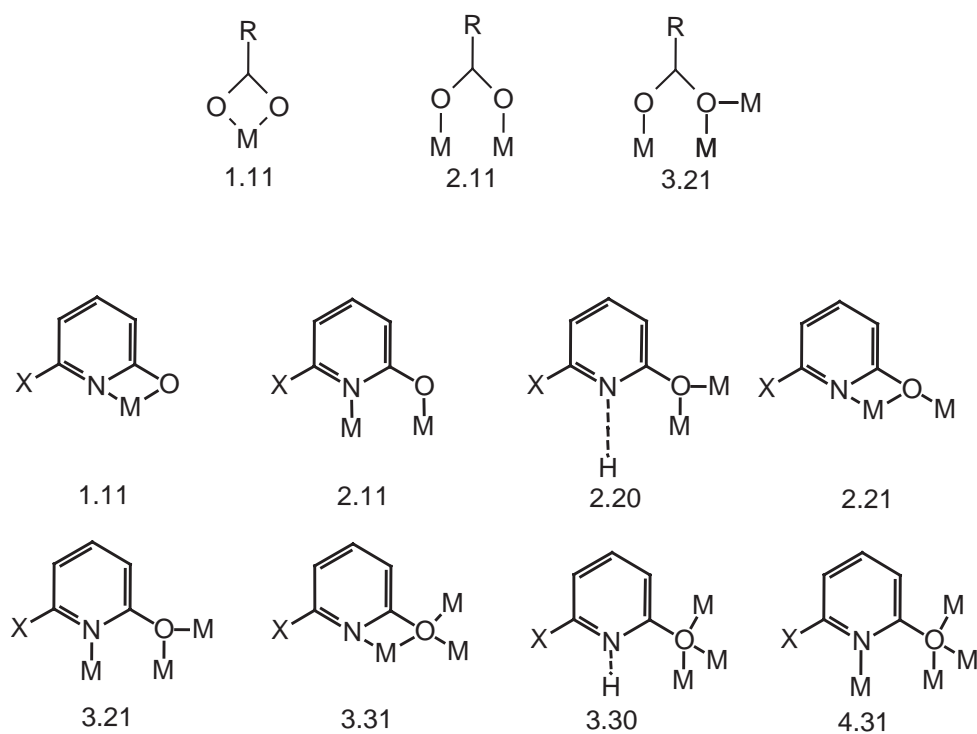
Serendipitous assembly often relies on creating a mismatch between the number or type of coordination sites available on a single metal site, and the donor set supplied by the ligand. This is perhaps best illustrated with two examples.

Carboxylates and pyridonates are frequently used as bridging ligands in this chemistry. They act as bridges because the alternative is for the two donor atoms present to chelate to one metal center, which creates a strained, four-membered chelate ring. For carboxylate ligands the end result is normally for the ligand to become 1,3 bridging (Scheme 1). For pyridonate ligands the behavior is more varied, and while the 1,3 bridging mode is observed, other modes where the two donor atoms bind to one metal and the oxygen binds to a second and sometimes third metal are also seen (Scheme 1). The M—O bond involving the metal to which the N atom is also bound is normally the longest. The oxygen of the pyridonate ligand is not coordinatively saturated by binding to one metal, and therefore acts as a bridge, which leads to the build-up of larger cages.

The second example involves the reaction of oxo-centered manganese carboxylate triangles with bidentate ligands, e.g., 2,2'-bipyridyl (bpy). The oxo-centered triangles have the general formula  $[\text{Mn}_3\text{O}(\text{O}_2\text{CR})_6\text{L}_3]^{0/+1}$  where L is a monodentate ligand, typically water or pyridine. Addition of a chelating ligand creates a mismatch, as there is only a monodentate site available for substitution *if* the triangular metal array is retained. Therefore, the structure is disrupted, and a larger  $\text{Mn}_4\text{O}_2$  butterfly is formed as the major product.<sup>5</sup> In this case it is possible to predict that addition of a chelating ligand will disrupt the initial structure, but it is not possible to predict the product that will result. This is a frequent observation in serendipitous assembly: you can predict there will be an effect, but cannot predict how that effect will be manifested.

The recognition that this synthetic approach generates unpredictable results should influence the choice of ligands. There is little point carrying out initial experiments with ligands that require considerable effort to make, as it cannot be foreseen whether they will have any utility. Secondly, as minor variations in the ligands may influence structure and solubility, ideally a series of related ligands should be explored. Thirdly, as a range of solvents will need to be used for crystallization of the cage compound, it is useful if the ligand has solubility in as many solvents as possible. One frustrating result, regularly encountered but rarely reported, is the formation of perfect, colorless crystals of ligand grown from intensely colored solutions of complexes.

The use of mixtures of organic ligands appears to lead to higher nuclearities than result from the use of single ligands. Examples of this are the octanuclear copper(II) complexes  $[\text{Cu}_8\text{O}_2(\text{O}_2\text{CR})_4(\text{chp})_8]$



Scheme 1

which feature both carboxylates and pyridonates.<sup>6</sup> Dinuclear complexes form when either of the ligands is present solely. It is unclear why the larger cage results from heteroleptic ligand arrays.

The choice of solvent for crystallization is important, but if a project is to make progress it is vital that a range of solvents is tested for every crystallization. The coordination of solvent molecules is frequently observed in structures of crystals grown from solutions of MeOH or MeCN. Sometimes changing to a non-coordinating solvent will lead to much larger cages because the absence of solvent molecules to complete the coordination sphere of metal sites can lead to greater bridging by the ligand(s). A specific example is the formation of  $[\text{Ni}_3(\text{chp})_4(\text{O}_2\text{CMe})_2(\text{MeOH})_6]$  from  $\text{Ni}(\text{O}_2\text{CMe})$  and Hchp (Hchp = 6-chloro-2-hydroxypyridine), crystallized from MeOH,<sup>7</sup> whereas the identical reaction crystallized from THF gives  $[\text{Ni}_{12}(\text{chp})_{12}(\text{O}_2\text{CMe})_{12}(\text{THF})_6(\text{H}_2\text{O})_6]$ .<sup>8</sup> The difference in the synthesis is that in the former cage six molecules of MeOH block coordination sites on the terminal Ni atoms, while in the latter cage the less strongly coordinating THF does not bind and thus allows growth of a wheel. More frequently, a change in solvent has a less easily rationalized influence.

#### 7.3.1.4 Harris Notation

The method currently used to describe the binding of polydentate ligands to multiple metal centers can seem clumsy—a mixture of Greek letters and sub- and super-scripts. An alternative is “Harris Notation”, developed in Edinburgh by Dr. S. G. Harris. Harris notation describes the binding mode as  $[\text{X}_1\text{Y}_2\text{Y}_3 \cdots \text{Y}_n]$ , where X is the overall number of metals bound by the whole ligand, and each value of Y refers to the number of metal atoms attached to the different donor atoms. Therefore, for a pyridonate, there will be two values for Y, while for  $\text{PhPO}_3^{2-}$  there will be three values of Y. The ordering of Y is listed by the Cahn–Ingold–Prelog priority rules, hence O before N. This notation is given in Scheme 1, and is used below in some examples.

#### 7.3.2 SURVEY OF THE 3d METALS

This review will proceed systematically across the 3d metals, beginning with vanadium and ending with copper. The other 3d metals are excluded, because their polynuclear cages are diamagnetic.

Discussion is restricted to N- and O-donor ligands for reasons of space. Finally, discussion will concentrate on cage compounds containing six or more metal centers. Literature searching has predominantly used the Cambridge Structural Database. Some examples will have been missed; for this I apologize.

### 7.3.2.1 Vanadium

Polynuclear vanadium chemistry is dominated by polyoxovanadates, and cages containing organic ligands are rare; the subject was authoritatively reviewed by Khan and Zubieta in 1995.<sup>9</sup> Two ligand types feature in most of these cages: alkoxides and phosphonates/arsonates. They lead to distinct structural types—for alkoxides the structures are clearly related to the polyoxovanadate cages, where some of the external oxygen centers are now part of a ligand—whereas for phosphonate ligands the P atom becomes part of the framework. Cages featuring other ligands are found, but they are the exceptions.

The most interesting cage from a magnetic viewpoint is a tetranuclear V<sup>III</sup> cage, [V<sub>4</sub>O<sub>2</sub>(O<sub>2</sub>CET)<sub>7</sub>(bpy)<sub>2</sub>](ClO<sub>4</sub>) (bpy = 2,2'-bipyridyl), reported by Christou and co-workers.<sup>10</sup> This has a “butterfly” structure, i.e., two V<sub>3</sub>O triangles sharing a V···V edge, and has an *S* = 3 spin ground state and is a SMM with an energy barrier of ca. 13.5 cm<sup>-1</sup> for reorientation of the magnetization. Other tetranuclear V<sup>III</sup> complexes have also been reported, but there are few examples of larger cages containing exclusively this oxidation state. One is a V<sup>III</sup> wheel, [V<sub>8</sub>(OH)<sub>4</sub>(OEt)<sub>8</sub>(O<sub>2</sub>CMe)<sub>12</sub>], reported by Kumagai and Kitagawa in 1996.<sup>11</sup> The eight vanadium centers within the wheel are alternately bridged by two carboxylates and a hydroxide, or by one carboxylate and two ethoxides. Both these bridging motifs are found in rings of other metals. No further studies have been reported on this cage.

#### 7.3.2.1.1 Alkoxides

With alkoxide ligands hexanuclear cages are found which are related to the [M<sub>6</sub>O<sub>19</sub>]<sup>8-</sup> core found for M = Nb, Ta, Mo, W. The central μ<sub>6</sub>-oxygen is surrounded by an octahedron of V atoms, with each edge of the octahedron bridged by a μ<sub>2</sub>-oxygen and with a single terminal oxygen attached to each vanadium. O atoms from alkoxide ligands replace some of the μ<sub>2</sub>-oxides. The series, [V<sub>6</sub>O<sub>19-3n</sub>{(OCH<sub>2</sub>)<sub>3</sub>CR}<sub>n</sub>]<sup>x-</sup> is known for *n* = 1–4, featuring tripodal alkoxides.<sup>12</sup> Different protonation and oxidation states of the *n* = 2 cage are known, i.e., [V<sub>6</sub>O<sub>13-x</sub>(OH)<sub>x</sub>{(OCH<sub>2</sub>)<sub>3</sub>CR}<sub>2</sub>]<sup>2-</sup> (R = Me, Et), where *x* = 0, 2, 3, 4, or 6 and the cage contains between zero and six V<sup>IV</sup> centers. In each case the unpaired electrons couple anti-ferromagnetically. Replacement of the μ<sub>2</sub>-oxides by monodentate alkoxides has also been observed—completely in [V<sub>6</sub>O<sub>7</sub>(OEt)<sub>12</sub>]<sup>13</sup> and partially in [V<sub>6</sub>O<sub>12</sub>(OMe)<sub>7</sub>]<sup>-</sup>.<sup>14</sup> The former is presumably mixed-valent. One cage [V<sub>6</sub>O<sub>13</sub>(OMe)<sub>3</sub>{(OCH<sub>2</sub>)<sub>3</sub>CET}]<sup>2-</sup> has been reported where both tris(alkoxide) and alkoxide ligands are present in place of bridging oxides.<sup>15</sup>

Not all the hexanuclear cages containing {(OCH<sub>2</sub>)<sub>3</sub>CR}<sup>3-</sup> ligands form octahedra. [V<sub>6</sub>O<sub>8</sub>{(OCH<sub>2</sub>)<sub>3</sub>CET}<sub>3</sub>{(OCH<sub>2</sub>)<sub>2</sub>C(CH<sub>2</sub>OH)R}<sub>4</sub>]<sup>2-</sup> contains a central {V<sub>4</sub>O<sub>16</sub>} core bound to two peripheral vanadium square pyramids via two μ<sub>2</sub> O atoms from the doubly deprotonated tripodal ligands.<sup>15</sup> The cage is again mixed valent, with a net four V<sup>V</sup> and two V<sup>IV</sup> sites, however the two d electrons are delocalized over four of the vanadium centers. In [H<sub>4</sub>V<sub>6</sub>O<sub>10</sub>-{(OCH<sub>2</sub>)<sub>3</sub>CCH<sub>2</sub>OH}<sub>2</sub>P<sub>4</sub>O<sub>4</sub>]<sup>6-</sup>, two V<sub>3</sub>O<sub>10</sub>{(OCH<sub>2</sub>)<sub>3</sub>CCH<sub>2</sub>OH} units, each containing a triangle of V<sup>IV</sup> centers, are linked by four {PO<sub>4</sub>} units.<sup>16</sup> The magnetochemistry of (6) confirms the presence of exclusively V<sup>IV</sup> and demonstrates that at low temperature one unpaired electron remains on each triangle, and that there is not a significant interaction between the two triangles.

A hexanuclear “metallocrown” [(VO)<sub>6</sub>{(OCH<sub>2</sub>)<sub>2</sub>N(OCH<sub>2</sub>OH)}Na]<sup>+</sup>, in which six vanadyl ions are bridged by the alkoxides, is derived from deprotonation of two arms of triethanolamine. The Na ion is encapsulated within the wheel, and is six coordinate. Magnetic studies suggest ferromagnetic exchange within this wheel.<sup>17</sup>

A variation of the triangular motif is found in [{V<sub>3</sub>O<sub>9</sub>F{(OCH<sub>2</sub>)<sub>3</sub>CCH<sub>2</sub>OH}(V<sub>4</sub>O<sub>7</sub>)]<sup>4-</sup>.<sup>16</sup> Here the triangular fragment, which contains a central fluoride, is linked by six corners to three {VO<sub>4</sub>} tetrahedra, which are further linked through corners to a fourth {VO<sub>4</sub>} tetrahedron so that the entire anion has C<sub>3v</sub> symmetry (discounting the terminal CH<sub>2</sub>OH group on the ligand). The four tetrahedra contain V<sup>V</sup> centers.

The octanuclear vanadium(IV) cage,  $[(VO)_8(OMe)_{16}(C_2O_4)]^{2-}$ , contains a  $\mu_8$ -oxalate within a cyclic  $\{(VO)(OMe)_2\}_8$  wheel.<sup>18</sup> Each  $V \cdots V$  edge is bridged by two methoxides, with every second edge further bridged by an O atom from the central oxalate.

The majority of decanuclear cages have the decavanadate core, i.e.,  $\{V_{10}O_{28}\}$ , with bridging oxides displaced by oxygen atoms from tripodal tris(alkoxide) ligands. Where the cage contains four such ligands both the oxidation and protonation state can change to give a family of cages of formula  $[V_{10}O_{16-x}(OH)_x\{(OCH_2)_3CR\}_4]^{n-}$  ( $x=0$ ,  $R=Et$ ,  $n=4$ ;  $x=0$ ,  $R=Me$  or  $Et$ ,  $n=2$ ;  $x=2$ ,  $R=CH_2OH$ ,  $n=2$ )<sup>19,20</sup> (Figure 1) while there is a unique cage,  $[V_{10}O_{13}\{(OCH_2)_3CEt\}_5]^{-}$ , containing five tris(alkoxides).<sup>20</sup> Magnetic studies of this family of cages reveal the anti-ferromagnetic exchange between spin centers. A tris(alkoxide) ligand also features in a further decanuclear cage,  $[\{V_3O_9F\{(OCH_2)_3CCH_2OH\}_2(V_4O_4)]$ , in which two  $\{V_3O_9F\{(OCH_2)_3CCH_2OH\}$  triangles are linked by four  $\{V(V)O_5\}$  pyramids.<sup>16</sup> The two  $V^{IV}$  centers in this mixed-valence cage are in the triangular fragments and the interaction between them is negligible.

A further example of  $\{V_3O_9F\{(OCH_2)_3CCH_2OH\}$  triangles linked by vanadium containing fragments is found in  $[\{V_3O_9F\{(OCH_2)_3CCH_2OH\}_2V_6O_6]^{6-}$ .<sup>16</sup> Here two triangles are linked by four  $\{V(IV)O_5\}$  and two  $\{V(V)O_5\}$  triangles. The connectivity was deduced by reference to the vanadate cage  $[H_6V_{12}O_{30}F_2]^{6-}$ . The magnetic behavior of both these cages shows strong anti-ferromagnetic exchange between the  $V^{IV}$  centers, but a resulting ground state that contains two uncorrelated unpaired electrons.

The alkoxide cage,  $[V_{16}O_{20}\{(OCH_2)_3CCH_2OH\}_8(H_2O)_4]$ ,<sup>21</sup> is related to the decavanadate structure, and the construction can be considered to involve four corner-sharing interactions between two  $\{V_8O_{24}\}$  cores which are derived from the decavanadate by removal of two adjacent  $\{VO_2\}$  caps (Figure 2). The synthesis is similar to that of  $[V_{10}O_{14}(OH)_2\{(OCH_2)_3CCH_2OH\}_4]^{2-}$ , with the major difference being that the solvothermal synthesis was performed at 170 °C, and at 150 °C to

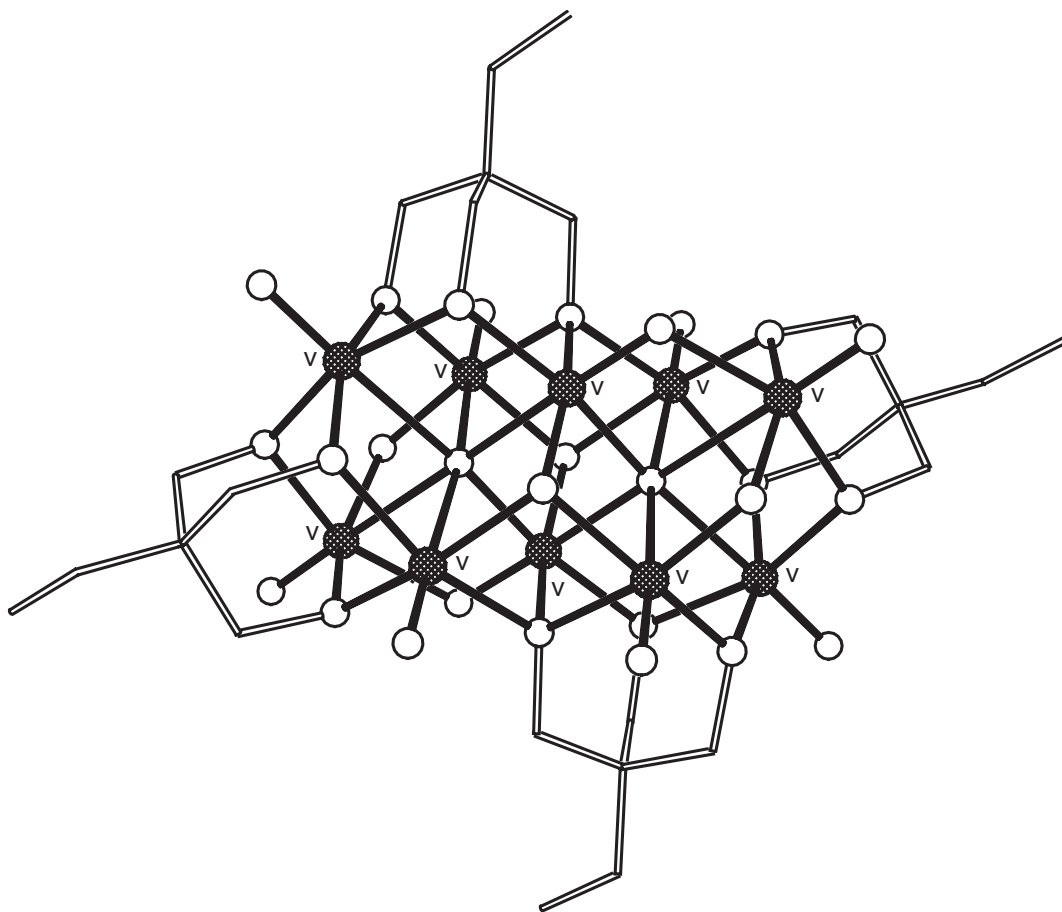


**Figure 1** The structure of  $[V_{10}O_{16-x}(OH)_x\{(OCH_2)_3CR\}_4]^{n-}$  (based on data from ref. 19) (shading: V, hatched circles; O, open circles; C, lines).

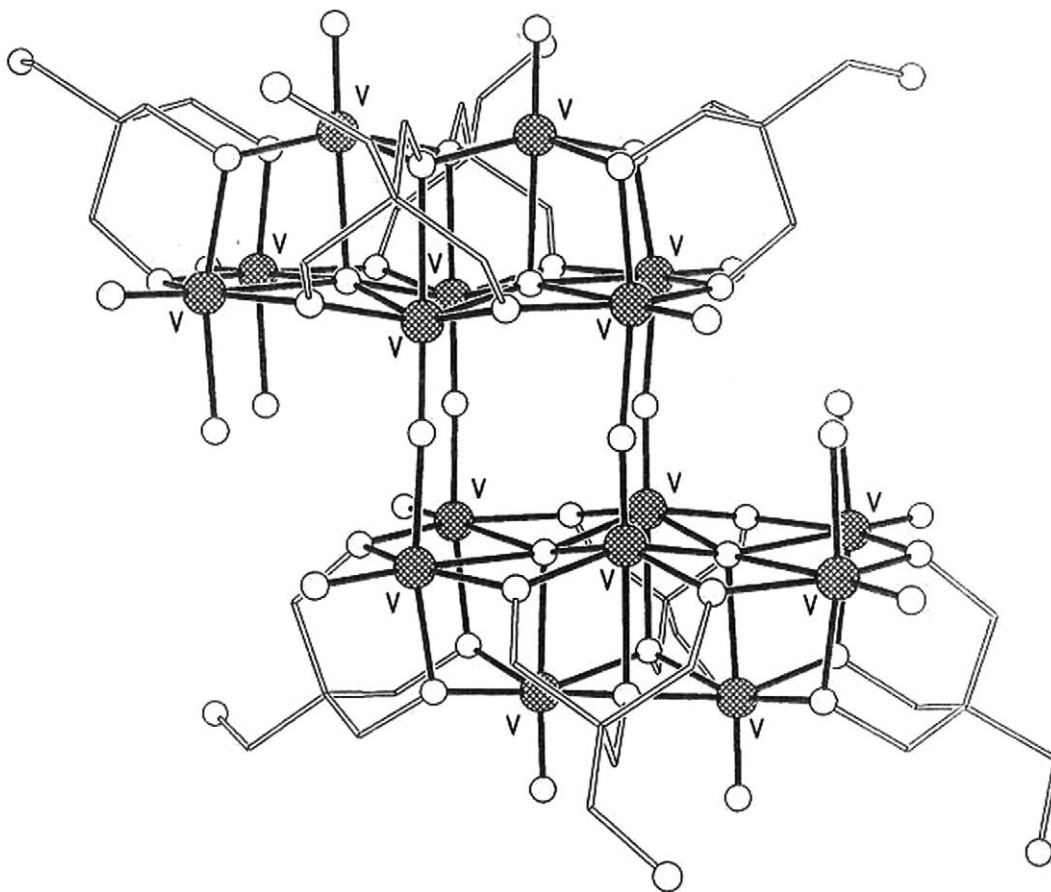


**Figure 2** The structure of  $[V_{16}O_{20}\{(OCH_2)_3CCH_2OH\}_8(H_2O)_4]^{21}$  (shading as Figure 1).

give the decanuclear cage. All the metal centers present are  $V^{IV}$ , and magnetic studies show anti-ferromagnetic exchange between these centers.

Nonadecanuclear  $[\{V_3O_{10}\{(OCH_2)_3CCH_2OH\}V_{16}O_{37}\}]^{7-}$ ,<sup>16</sup> is closely related to a naked vanadate cage,  $[H_{10}V_{19}O_{40}]^{7-}$ . Each contains two  $\{V_3O_{13}\}$  triangles, seven  $\{V(V)O_4\}$  tetrahedral and six  $\{V(IV)O_6\}$  octahedral, with the tris(alkoxide) ligand attached to one of the triangles. There are a net 12  $V^{IV}$  centers in the cage, and they couple anti-ferromagnetically. Larger vanadate cages are known which do not contain organic ligands.

### 7.3.2.1.2 Phosphonates and arsonates

In  $[(VO)_6(tBuPO_3)_8Cl]$  the six vanadium centers are arranged in an octahedron with each organophosphonate group capping a triangular face of the octahedron.<sup>22</sup> The chloride is encapsulated within the cage which has one  $V^{IV}$  and five  $V^V$  centers. A very similar cage can also be formed with the ligand  $Me_3SiOPO_3^-$ .<sup>23</sup>

An unusual hexanuclear cage is formed on reaction of  $[(tBupz)_4VO(H_2O)_2]Cl_2$  with  $Na(PhPO_3)$  ( $tBupz = 3\text{-tert-butylpyrazole}$ ).<sup>24</sup> The phosphonate displaces some of the pyrazole ligands, linking VO units together to give  $[(VO)_6(O_3PPh)_6(tBupz)_6(H_2O)_3]$ . This cage contains three pairs of vanadyl units, differing in the number of pyrazole ligands to which they are bound. The structure is a bicapped pentagonal prism, with alternately P and V centers at the vertices. Thus, in the 1:5:5:1 polyhedron, the first cap would be a vanadium, the first pentagon would contain two V and three P centers, the second pentagon three V and two P centers, and the final cap is a phosphorus.

The six vanadium centers in  $[H_2\{V_6O_{10}(O_3AsPh)_6\}]^{2-}$  are mixed valent (four  $V^V$  and two  $V^{IV}$ ) and arranged in a cyclic structure consisting of a twisted 24-membered ring  $\{V-O-As-O\}_6$  with additional intra-ring  $V-O-V$  and  $As-O-V$  bridges.<sup>25</sup>

$[(VO)_7O_5(O_3PPh)_6Cl]^{2-}$  is spherical and contains an encapsulated chloride ion.<sup>26</sup> The metal polyhedron is irregular—perhaps best described as an edge-capped octahedron. Four of the phosphonate ligands sit on triangular faces of the octahedron, while the remaining two phosphonates bind to the “edge-capping” site. All the metals are present in the +5 oxidation state.

$[V_{10}O_{24}(O_3AsC_6H_4NH_2)_3]^{4-}$  has a quite distinct structure, and exclusively  $V^V$  centers; however, it undergoes a reversible one-electron reduction to a paramagnetic compound.<sup>25</sup> The structure may be described as a  $[V_9O_{21}(O_3AsC_6H_4NH_2)_3]^{3-}$  toroid encapsulating a  $VO_3^-$  fragment. The toroid consists of  $\{V_3O_{13}\}$  triangular units linked through the arsonato groups.

Several dodecanuclear vanadium cages have been reported containing phenyl-phosphonates or -arsonates. The first,  $[\{VO(OH)\}_{12}(O_3PPh)_8]^{4-}$ , is mixed-valent, containing four  $V^{IV}$  and eight  $V^V$  ions.<sup>27</sup> The structure is best described as a pentagonal dodecahedron of V and P centers, with each  $V \cdots P$  edge bridged by one oxygen from a phosphonate, and each  $V \cdots V$  edge bridged by two hydroxides. The magnetic data reported show anti-ferromagnetic exchange between the  $V^{IV}$  centers.

Two further dodecanuclear cages containing phenylarsonate ligands have been reported. In  $[(MeOH)_2C V_{12}O_{14}(OH)_4(O_3AsPh)_{10}]^{4-}$  two MeOH molecules are encapsulated within a cavity created by the cage.<sup>28</sup> Two cages of very similar structure can also be isolated which contain 14 vanadium centers,  $[(MeCN)_2C V_{14}O_{22}(O_3PPh)_8]^{6-}$  and  $[(NH_4)_2Cl_2C V_{14}O_{22}(OH)_4(H_2O)_2(O_3PPh)_8]^{6-}$ , with the phosphonate or arsonate ligands playing identical roles in all the cages. Two of the AsPh units in the dodecanuclear cage are replaced by VO units in the larger cages.<sup>29</sup> The structures are complex. Increasing the ratio of phenylarsonic acid in the reaction produces another, structurally distinct dodecanuclear cage,  $[(H_2O)_2C V_{12}O_{12}(OH)_2(H_2O)_2(O_3AsPh)_{10}(HO_3AsPh)_4]^{2-}$ .<sup>28</sup> This structure is very hard to describe, but features vanadium-centered, square-based pyramids and octahedra, and organoarsonate tetrahedra and square pyramids.

The phosphonate cage,  $[H_6(VO_2)_{16}(O_3PMe)_8]^{8-}$ , resembles a tire with four  $(VO_2)_4$  tetramers spanning the “tread” and linked together along each “rim” by four  $O_3PMe^-$  ligands.<sup>30</sup> Redox titrations were used to confirm the presence of 14  $V^{IV}$  centers. No further studies of this cage have appeared in the open literature.

The octadecanuclear vanadium cage,  $[Cl_4C V_{18}O_{25}(H_2O)_2(O_3PPh)_{20}]^{4-}$ ,<sup>22</sup> contains four  $[V_4O_6(O_3PPh)_5]^{2-}$  clusters linked through P–O–V interactions to a central  $\{V_2O(H_2O)_2\}^{8+}$  unit. It is made in MeCN, however the same reaction in MeOH generates a structurally related pentanuclear cage,  $[V_5O_7(OMe)_2(O_3PPh)_5]^-$ . All the vanadium centers are  $V^V$ .

### 7.3.2.1.3 Other ligands

The cages  $[Cp_{6-x}V_6O_x(\mu_3-O)_8]_n$  ( $x = 0, n = 1$ ;  $x = 1, n = 1$  or  $2$ ) contain an octahedron of V centers with  $\mu_3$ -oxides on the faces of the octahedron and terminal cyclopentadienyl or oxide ligands.<sup>31</sup> All these cages are mixed-valent, e.g.,  $[Cp_6V_6(\mu_3-O)_8]$  must contain four  $V^{IV}$  and two  $V^{III}$  centers, and are paramagnetic at room temperature. Larger oligomers are known, and are related to other cyclopentadienyl metal oxides, an area which has been reviewed by Bottomley.<sup>31</sup>

In  $[V_6O_{10}(O_2CPh)_9]$  a cyclic array of five  $V^V$  and one  $V^{IV}$  centers are found, bridged by carboxylate and oxide groups in an irregular manner.<sup>33</sup> Three sequential edges are bridged by one oxide and one carboxylate, two edges are bridged by two carboxylates, and the final edge is bridged by one oxide and two carboxylates.

A nonanuclear mixed-valent vanadium complex,  $[(VO_4)\{V_2O_3(bdta)\}_4]^{7+}$  is known (bdta = butanediaminetetracetate).<sup>33</sup> The cage consists of a central  $\{V(V)O_4\}$  tetrahedron with each oxide bridging to a dinuclear  $\{V_2O_3(bdta)\}$  fragment. These dinuclear fragments are each mixed-valent with one  $V^{IV}$  and one  $V^V$  in each pair. Magnetic studies of this cage show anti-ferromagnetic exchange between the  $S = 1/2$  centers. A further nonanuclear cage,  $[V_9O_{19}(O_2CMe)_5]^{3-}$ , forms on reaction of  $[VOCl_4]^{2-}$  with silver acetate.<sup>34</sup> The cage is mixed-valent, with four  $V^V$  and five  $V^{IV}$  centers. The structure resembles a hemispherical bowl, with four acetates bridging along the edges of the bowl, and one acetate within the bowl. Magnetization data show the cage has an  $S = 3/2$  ground state.

A decanuclear cage,  $[H_6V_{10}O_{22}(O_2CMe)_6]^{2-}$  is known which contains two sets of four edge-sharing  $\{V(IV)O_6\}$  octahedral, linked through two  $\{V(V)O_4\}$  tetrahedral to form a double layer structure.<sup>35</sup> The six carboxylates bridge some of the  $V^{IV} \cdots V^{IV}$  edges on the exterior of the cage.

Use of squarate as a ligand has led to the largest coordination cage containing vanadium:  $[(VO)_{24}(C_4O_4)_{12}(OMe)_{32}]^{8-}$ .<sup>36</sup> The topology of this cage is fascinating. Eight  $[(VO)_3(OMe)_4]$

sub-units lie at the corners of a cube with the edges of the cube bridged by squarate. One methoxide within each sub-unit is  $\mu_3$  bridging, while the remaining three each bridge a single V···V edge.

The range and structural diversity of the vanadium cages is extraordinary. Reactions are sensitive to a wide range of variables—solvent, counter-cation, temperature, substitution pattern of organic ligands—in an unpredictable manner. There is no straightforward relationship between the larger clusters and any extended structure. The range of organic ligands used is small, with phosphonate/arsenate and alkoxide ligands dominant, and a limited number of cages known with carboxylate ligands. The remainder of the 3d-period shows a quite different use of ligands, with carboxylates extremely common and phosphonate/arsenate ligands very rare in cage complexes.

### 7.3.2.2 Chromium

Until 1990 polynuclear chromium chemistry was largely restricted to the oxo-centered metal triangles.<sup>37</sup> The lack of larger clusters appeared to be due to the stability of the oxo-centered triangles, and the unreactive nature of the Cr<sup>III</sup> ion, which meant that strategies that work with more substitutionally labile metals, e.g., Mn<sup>III</sup> or Fe<sup>III</sup>, simply failed. However, forcing conditions has recently led to a number of new cages, some of which have interesting magnetic properties. All the cages involve carboxylate ligands, and all of this chemistry has its origins in work from the group of G erb el e.

The cages can be broken into two groups. A series of chromium wheels has been reported, which feature a carboxylate and a second ligand that might be fluoride, hydroxide, or alkoxide. The first such cage is an octanuclear wheel [CrF(O<sub>2</sub>CCMe<sub>3</sub>)<sub>2</sub>]<sub>8</sub>.<sup>38</sup> This is made by reaction of chromium trifluoride with pivalic acid at around 130 °C. [CrF(O<sub>2</sub>CCMe<sub>3</sub>)<sub>2</sub>]<sub>8</sub> been the subject of extensive studies—both in its capacity to act as a guest for organic hosts<sup>39</sup> and for its magnetic properties.<sup>40</sup> Anti-ferromagnetic exchange is found giving an  $S = 0$  ground state in zero field, with a ground state crossover occurring as the external magnetic field is increased. A similar structure can be made with benzoate and hydroxide taking the place of pivalate and fluoride,<sup>41</sup> on this occasion by oligomerization of the oxo-centered triangle at 200 °C.

Oligomerization of oxo-centered triangles can also occur on heating in protic solvents. Refluxing basic chromium acetate in water for two hours produces a wheel of stoichiometry [Cr<sub>8</sub>(OH)<sub>12</sub>(O<sub>2</sub>CMe)<sub>12</sub>].<sup>42</sup> The Cr···Cr vectors are alternately bridged by two  $\mu$ -OH and one 1,3 bridging carboxylate or two 1,3-carboxylates and one  $\mu$ -OH. Again, anti-ferromagnetic exchange is found between Cr centers. McInnes and co-workers have reported a more complicated magnetic picture for a pair of “chromic wheels,” made by heating basic chromium acetate in MeOH or EtOH in an autoclave at 200 °C,<sup>43</sup> a piece of solvothermal chemistry reminiscent of the vanadium chemistry discussed above. These cages have the formula [Cr(O<sub>2</sub>CMe)(OR)<sub>2</sub>]<sub>10</sub> (where R = Me or Et), and the wheel is in each case symmetric, with each Cr···Cr vector bridged by one 1,3-carboxylate and two  $\mu$ -alkoxides. The wheels therefore contain the same metal topology as the older “ferric wheels” (see Sections 7.3.2.4 and 7.3.3.1). An oddity is that while the Cr···Cr exchange in the ethoxide wheel is found to be very weak (0.9 cm<sup>-1</sup>) and anti-ferromagnetic, the exchange for methoxide is weak (4.5 cm<sup>-1</sup>) but ferromagnetic with significant inter-wheel interactions. Each wheel in the latter case should therefore have an  $S = 15$  ground state, which is among the highest known.<sup>43</sup>

A final version of these chromium wheels can be made by addition of secondary amines to the reaction mixture that gave [CrF(O<sub>2</sub>CCMe<sub>3</sub>)<sub>2</sub>]<sub>8</sub>. A hydrogen-bonded assembly of cages can be formed of stoichiometry [(R<sub>2</sub>NH<sub>2</sub>)<sub>3</sub>{Cr<sub>6</sub>F<sub>11</sub>(O<sub>2</sub>CCMe<sub>3</sub>)<sub>10</sub>}(H<sub>2</sub>O)]<sub>2</sub> (R = *n*-propyl or *n*-pentyl).<sup>44</sup> The supramolecule consists of two symmetry-related [Cr<sub>6</sub>F<sub>11</sub>(O<sub>2</sub>CCMe<sub>3</sub>)<sub>10</sub>]<sup>3-</sup> “horseshoes,” held together by H bonds to protonated amines. Each [Cr<sub>6</sub>F<sub>11</sub>(O<sub>2</sub>CCMe<sub>3</sub>)<sub>10</sub>]<sup>3-</sup> horseshoe is derived from [CrF(O<sub>2</sub>CCMe<sub>3</sub>)<sub>2</sub>]<sub>8</sub> by removal of two of the Cr sites. Magnetic studies indicate anti-ferromagnetic exchange between the Cr centers within the molecule.

The second group of cages involves more compact structures—all of which have been made by thermal oligomerization of oxo-centered triangles. The original synthesis was of [Cr<sub>12</sub>O<sub>9</sub>(OH)<sub>3</sub>(O<sub>2</sub>CCMe<sub>3</sub>)<sub>15</sub>].<sup>45,46</sup> Sodium pivalate is added to an aqueous solution of chromium nitrate in the first step, producing a blue-green precipitate. In the second step this precipitate is heated to 400 °C under a stream of N<sub>2</sub>, leading to a color change to dark green. This green solid can be crystallized from isopropanol. The structure consists of a centered pentacapped trigonal prism (Figure 3). The ground state has  $S = 6$ , which is best shown by EPR spectroscopy<sup>46</sup> where the 12-line fine structure associated with this spin state can be observed. EPR spectroscopy also shows that the zero-field splitting parameter  $D = +0.085$  cm<sup>-1</sup>. The  $S = 6$  ground state was, at the

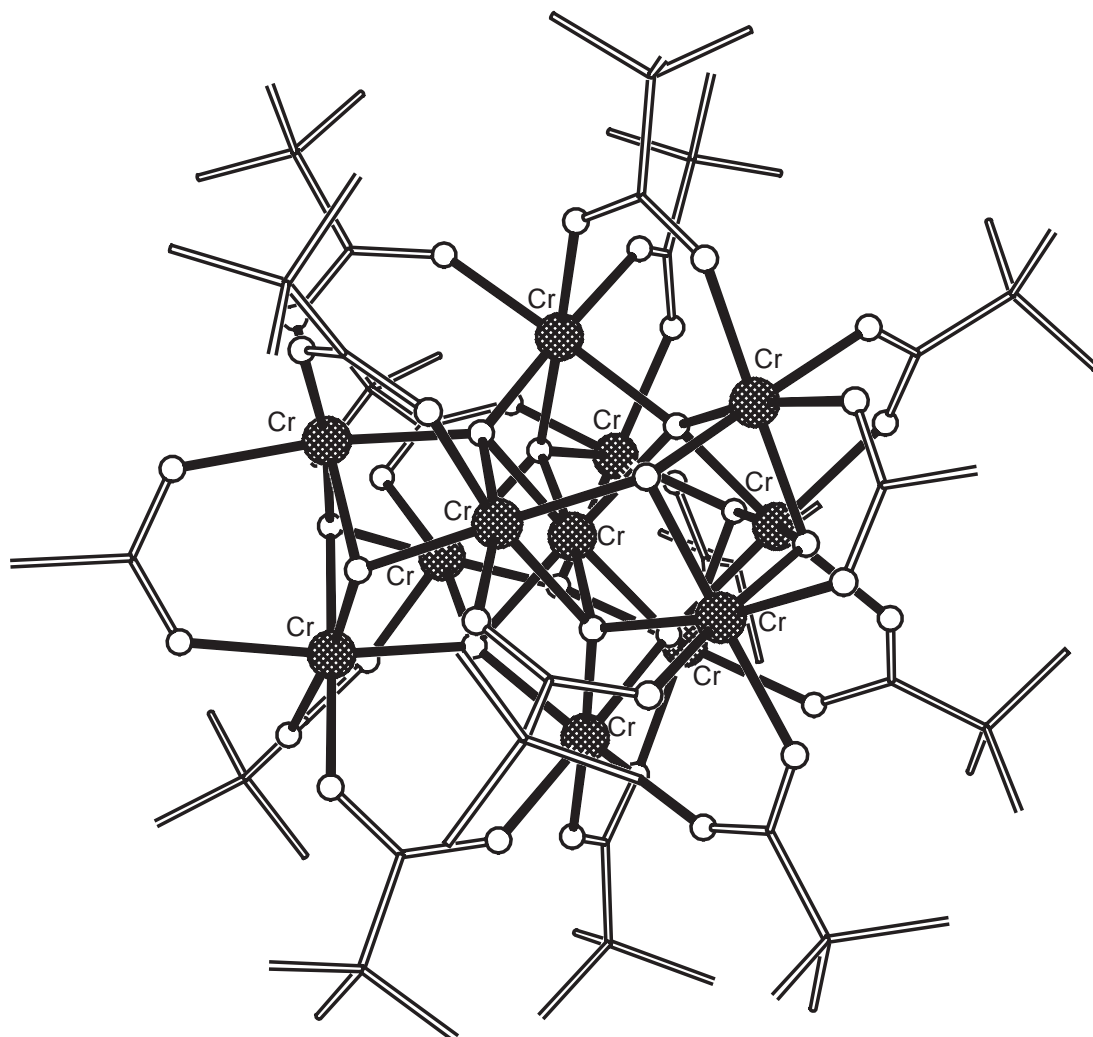


**Figure 3** The structure of  $[\text{Cr}_{12}\text{O}_9(\text{OH})_3(\text{O}_2\text{CCMe}_3)_{15}]^{46}$  (shading: Cr, cross-hatched; O, open; C, lines).

time, the equal highest for this metal, matching the ground state observed for  $[\text{Cr}_4\text{S}(\text{O}_2\text{CMe})_8(\text{H}_2\text{O})_4][\text{BF}_4]_2$  by Bino and co-workers.<sup>47</sup>

This high-temperature reaction can be varied productively. For benzoate at temperatures above 300 °C only water is lost in generating the cage  $[\text{Cr}_8\text{O}_4(\text{O}_2\text{CPh})_{16}]$ .<sup>41</sup> The structure contains a central  $\text{Cr}_4\text{O}_4$  heterocubane, with each oxygen center of the cube  $\mu_4$  bridging to an additional Cr cap. The benzoate ligands adopt two coordination modes, either 1,3 bridging between Cr atoms within the heterocubane and capping Cr centers, or chelating to the capping chromiums. The structure of the octanuclear capped heterocubane is closely related to a mixed-valent cobalt cubane  $[\text{Co}_8\text{O}_4(\text{O}_2\text{CPh})_{12}(\text{sol})_4]$  reported by Christou and co-workers prepared by oxidation of cobalt(II) benzoate in DMF or MeCN with  $\text{H}_2\text{O}_2$ .<sup>48</sup>

With isobutyrate as the carboxylate a further structural type forms at 400 °C. This has the stoichiometry  $[\text{Cr}_{12}(\mu_4\text{-O})_8(\text{OH})_4(\text{O}_2\text{CCHMe}_2)_{16}(\text{HO}_2\text{CCHMe}_2)_4]$ ,<sup>49</sup> illustrated in Figure 4. The cage consists of three face-sharing  $\text{Cr}_4\text{O}_4$  heterocubanes, with the two terminal cubanes capped by further chromium centers attached to the external  $\mu_4$ -oxides. The central cubane is held together exclusively through four  $\mu_4$ -oxides with an unusual “saw-horse” geometry rather than tetrahedral. The  $\mu_4$ -oxides involved in the external heterocubanes have a geometry approximating to tetrahedral. The structure is related to both  $[\text{Cr}_8\text{O}_4(\text{O}_2\text{CPh})_{16}]$  and other cubane cages. The nearest relation is an octanuclear triple-cubane containing mixed-valent cobalt(II)/(III), reported by Beattie and co-workers, which lacks the final four capping atoms.<sup>50</sup>

Including the carboxylate as the counter-ion of the oxo-centered triangle precursor can influence the amount of acid lost on heating. The reaction of  $[\text{Cr}_3\text{O}(\text{O}_2\text{CCMe}_3)_6(\text{H}_2\text{O})_3][\text{O}_2\text{CCMe}_3]$  at



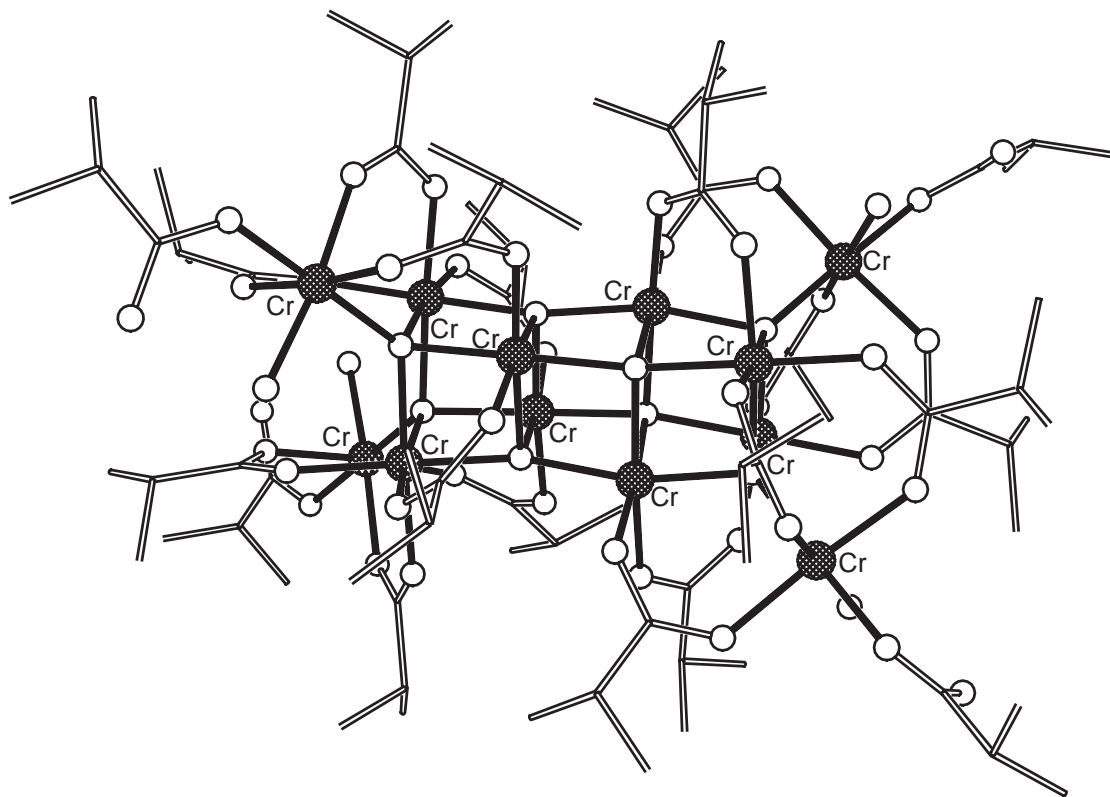


**Figure 4** The structure of  $[\text{Cr}_{12}(\mu_4\text{-O})_8(\text{OH})_4(\text{O}_2\text{CCHMe}_2)_{16}(\text{HO}_2\text{CCHMe}_2)_4]^{49}$  (shading: Cr, cross-hatched; O, open; C, lines).

300 °C is very different to the reaction of  $[\text{Cr}_3\text{O}(\text{O}_2\text{CCMe}_3)_6(\text{H}_2\text{O})_3][\text{NO}_3]$  or  $[\text{Cr}_3\text{O}(\text{O}_2\text{CCMe}_3)_6(\text{H}_2\text{O})_2(\text{OH})]$ .<sup>51</sup> Whereas the latter two complexes lose pivalate to give a  $\{\text{Cr}_{12}\}$  cage,  $[\text{Cr}_3\text{O}(\text{O}_2\text{CCMe}_3)_6(\text{H}_2\text{O})_3][\text{O}_2\text{CCMe}_3]$  loses less pivalate to give a hexanuclear complex of apparent stoichiometry  $[\text{Cr}_6\text{O}_4(\text{O}_2\text{CCMe}_3)_{11}]$ .<sup>51</sup> This again contains a heterocubane, but now only doubly capped on two  $\mu_4$ -oxo sites. If the remaining two  $\mu_3$ -oxygen sites are either both protonated or both deprotonated, the cage would be mixed-valent. However, electrospray mass spectrometry reveals one multiplet centered at  $m/z$  1,488 in the negative ion spectrum, while in the positive ion spectrum the multiplet is found at  $m/z$  1,490. These peaks match well for  $[\text{Cr}_6\text{O}_4(\text{O}_2\text{CCMe}_3)_{11}]^-$  and  $[\text{Cr}_6\text{O}_2(\text{OH})_2(\text{O}_2\text{CCMe}_3)_{11}]^+$ , respectively. Therefore, it appears that the crystals contain both these species, and presumably also the monoprotinated neutral complex.

Preliminary magnetic studies on these cages reveal that, other than in the cases noted above, anti-ferromagnetic exchange between chromium(III) centers leads to low-spin ground states.

### 7.3.2.3 Manganese

Work on manganese cages is dominated by work from the Christou/Hendrickson grouping, which in the main concentrates on carboxylate chemistry.<sup>5,52</sup>

The earliest hexanuclear manganese cage was reported by Thornton and co-workers in 1986.<sup>53</sup>  $[\text{Mn}_6\text{O}_2(\text{O}_2\text{CCMe}_3)_{10}(\text{HO}_2\text{CCMe}_3)_4]$  consists of an edge-sharing bitetrahedral cage, with each tetrahedron centered by a  $\mu_4$ -oxo ion. The cage is mixed-valent, containing four  $\text{Mn}^{\text{II}}$  and two  $\text{Mn}^{\text{III}}$  centers, with the  $\text{Mn}^{\text{III}}$  centers localized at the shared edge of the bitetrahedron. Several similar cages have been made,<sup>54–58</sup> differing in the terminal ligands, which include: pyridine, MeCN, EtOH,  $\text{H}_2\text{O}$ , acetone, THF; and in the bridging carboxylate which may be either pivalate, benzoate, or nitrobenzoate. The simplicity of the reaction, and moderate yields, makes these cages suitable starting materials for further synthesis. The magnetic properties have been studied for  $[\text{Mn}_6\text{O}_2(\text{O}_2\text{CPh})_{10}(\text{py})_2(\text{MeCN})_2]$ , and the cage has an  $S=0$  ground state.<sup>55</sup>

The second hexanuclear manganese cage reported is the first “high-spin cage”.<sup>59</sup> It is a cyclic molecule with a formula  $[\text{Mn}(\text{hfac})_2(\text{NITPh})_6]$  (hfac = hexafluoroacetyl-acetonate,

NITPh = 2-phenyl-4,4,5,5-tetramethyl-4,5-dihydro-1*H*-imidazolyl-1-oxyl-3-oxide—see Scheme 2), with each nitronyl–nitroxide ligand bound to two {Mn(hfac)<sub>2</sub>} fragments through the two oxygen atoms, giving a wheel which is homovalent (Figure 5). Synthesis involves mixing the two components in heptane. Magnetic studies show a value for  $\chi_m T$  at low temperature consistent with an  $S = 12$  ground state, which arises from anti-ferromagnetic exchange between the  $S = 1/2$  radicals, and the  $S = 5/2$  metal centers.

Hexanuclear cages with carbamate ligands have been reported for manganese, iron, and cobalt. The manganese cage, [Mn<sub>6</sub>(O<sub>2</sub>CNEt<sub>2</sub>)<sub>6</sub>], is made by addition of [Mn(Cp)<sub>2</sub>] to a solution of NHEt<sub>2</sub> in toluene, followed by reaction with carbon dioxide.<sup>60</sup> The structure consists of an edge-sharing bitetrahedron of manganese(II) centers. Both five- and six-coordinate Mn<sup>II</sup> sites are found, and the carbamate ligands show three different bridging modes: 1,1,1,1,3, and 1,1,3,3 bridges are found.

Further hexanuclear cages can be made with the pentadentate Schiff-base ligand, *N*-(*X*-substituted salicyclidene)-*N,N'*-bis(2-hydroxyethyl)ethylenediamine (*X* = 5-MeO, 5-Cl, 5-Br).<sup>61</sup> These cages contain exclusively Mn<sup>III</sup> centers, which are arranged in a planar array, bridged by two  $\mu_3$ -oxides, two  $\mu_3$ -methoxides, four  $\mu_2$ -methoxides, two  $\mu_2$ -acetates, and two ligands. Magnetic studies of the cages indicate anti-ferromagnetic exchange between the Mn<sup>III</sup> centers.

A series of hexanuclear cages featuring the anions of derivatives of dibenzoyl methane (Hdbm) have been made, and show  $S = 12$  ground states.<sup>62</sup> These cages have the general formula [Mn<sub>6</sub>O<sub>4</sub>X<sub>4</sub>(R<sub>2</sub>dbm)<sub>6</sub>] (*X* = Cl or Br, *R* = Me, Et). The structures consist of a Mn<sup>III</sup> octahedron with four nonadjacent faces bridged by  $\mu_3$ -oxides and the other four faces bridged by  $\mu_3$ -chlorides. A chelating R<sub>2</sub>dbm group is attached to each manganese center completing a

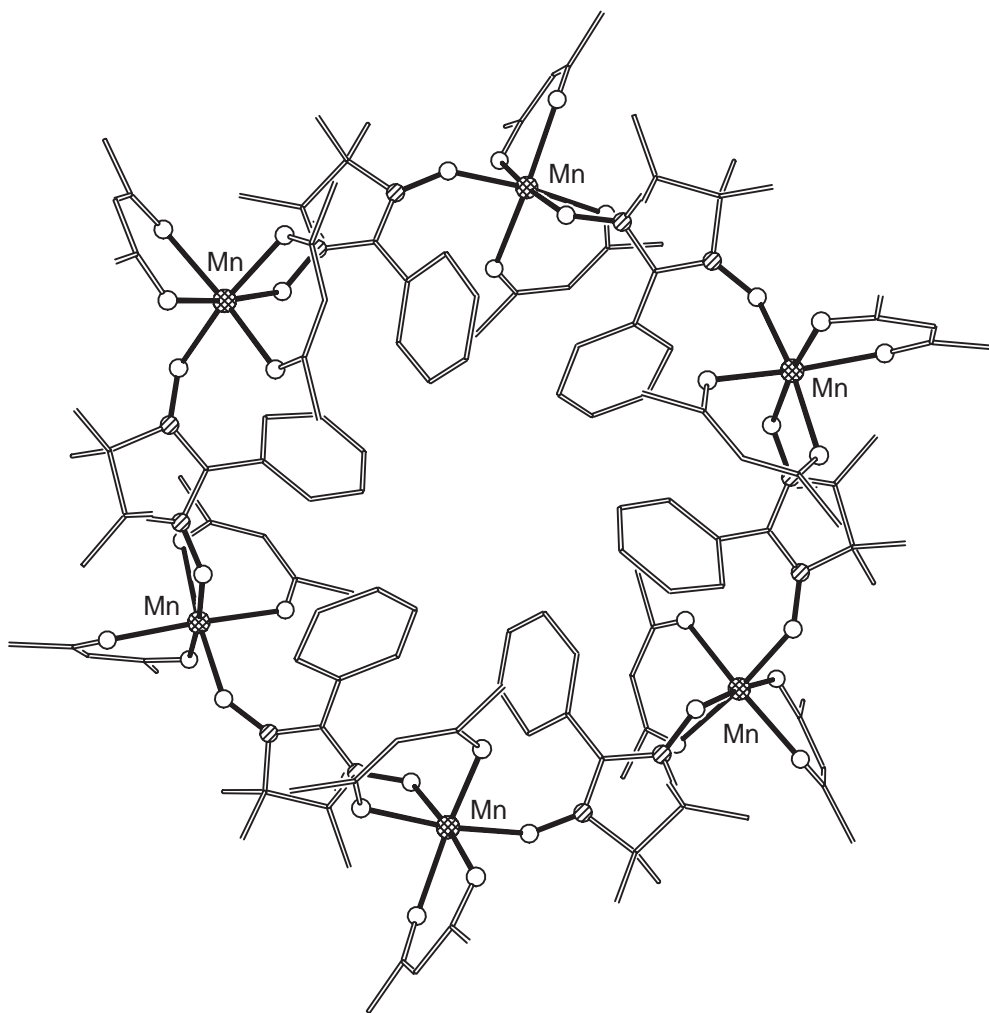
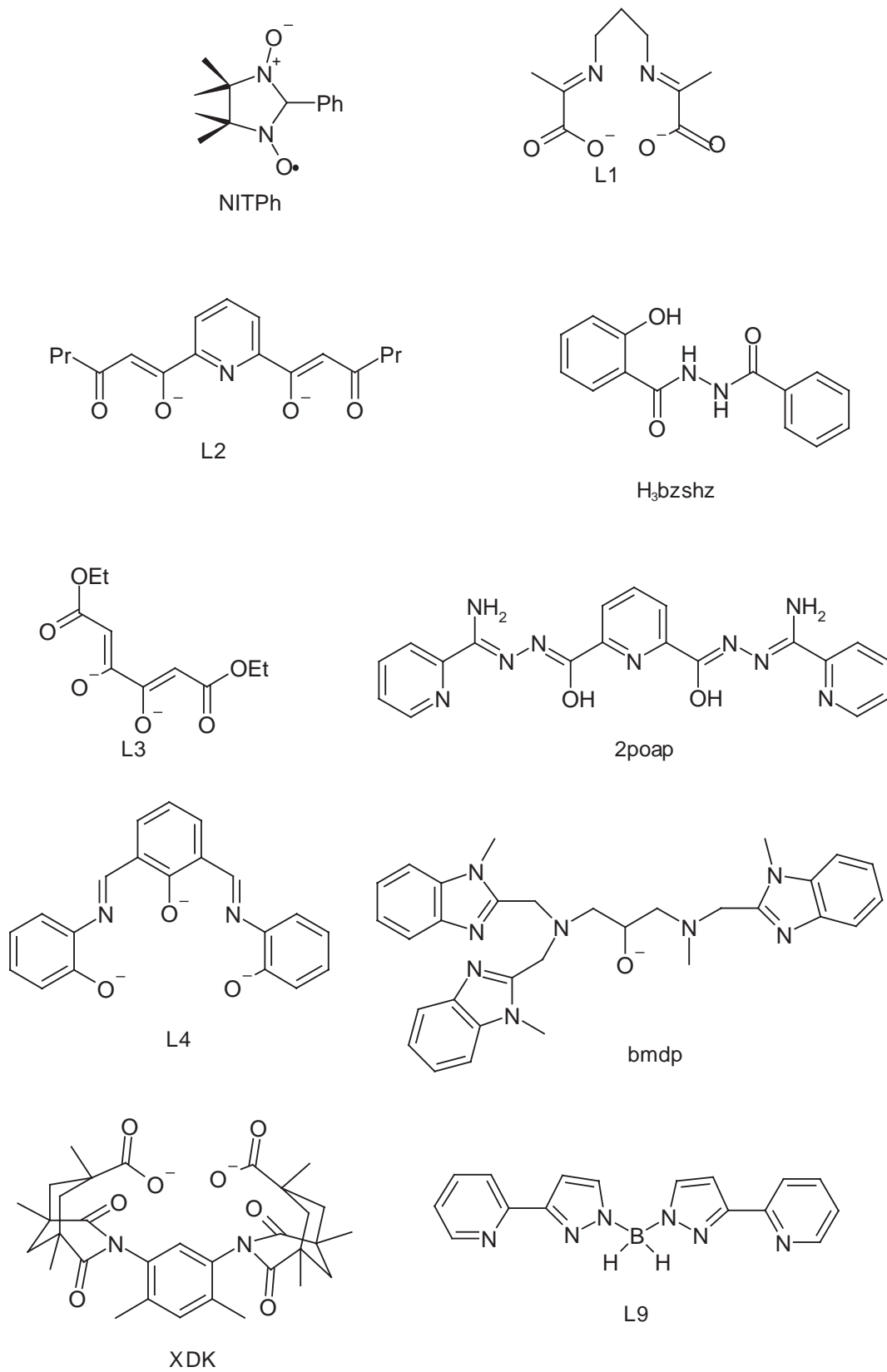
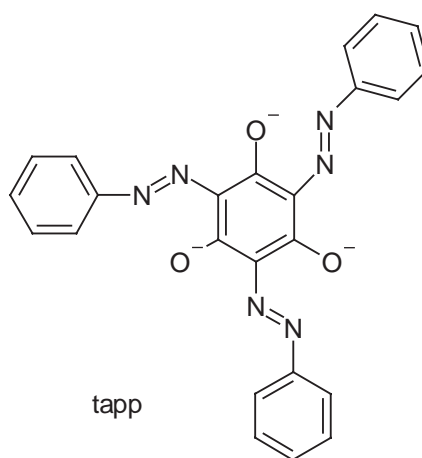
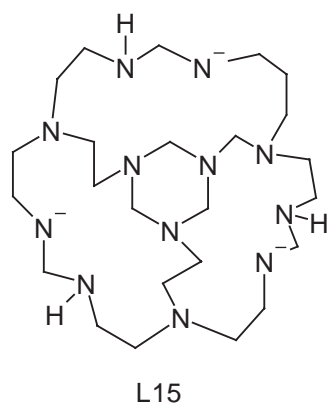
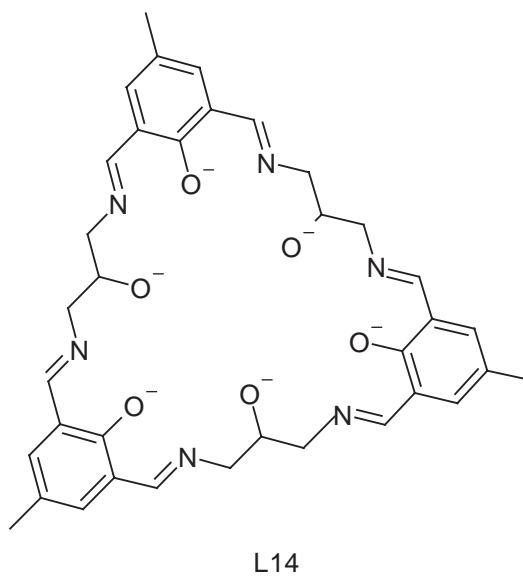
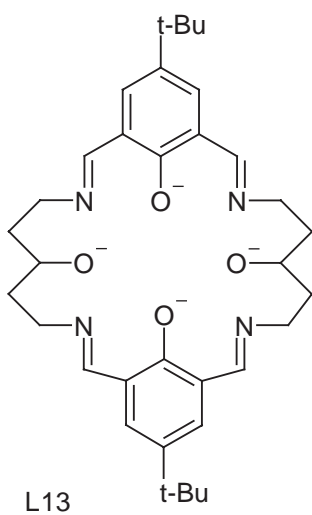
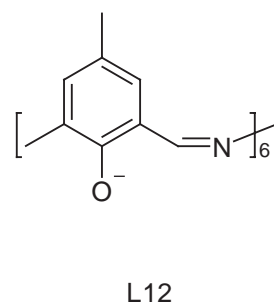
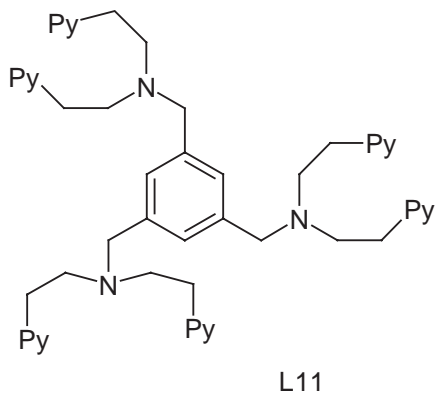
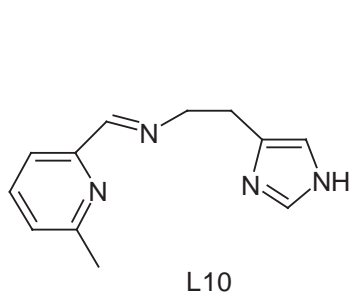


**Figure 5** The structure of [Mn(hfac)<sub>2</sub>(NITPh)<sub>6</sub>]<sup>59</sup> (shading: Mn, cross-hatched; O, open; N, diagonal lines; C, lines).



Scheme 2



Scheme 2 continued

Jahn–Teller distorted octahedral coordination sphere. The syntheses of these cages is by slow evaporation of solutions containing the mononuclear  $\text{Mn}^{\text{III}}$  complexes  $[\text{MnX}(\text{R}_2\text{dbm})_2]$ . Magnetic studies show an  $S = 12$  ground state and  $D = 0$ ; the latter is consistent with the  $T_d$  symmetry.

The hexanuclear cage,  $[\text{Mn}_6\{(\text{PhSiO}_2)_6\}_2\text{Cl}(\text{nBuOH})_6]^-$ , contains a  $\{\text{Mn}_6\text{Cl}\}$  plane sandwiched between two cyclohexasiloxanolate ligands,<sup>63</sup> as shown in Figure 6. The manganese centers are at the corners of a regular hexagon, with each Mn···Mn edge bridged by two O atoms from the cyclohexasiloxanolate ligands, creating an approximately square plane of O atoms about the Mn centers. The coordination geometry of each site is then completed by a coordinated alcohol molecule and by a long contact to the central chloride.

The compounds  $[\text{Mn}_6\text{O}_6(\text{O}_2\text{CR})_3(3,2,3\text{-tet})_4]^{5+}$  (3,2,3-tet = 1,5,8,12-tetraazadodecane; R = Me or Ph) were reported by Weatherburn and co-workers, and contain a planar, mixed-valent cage.<sup>64</sup> The structure consists of an approximately linear arrangement of four manganese ions, with each  $\text{Mn}\cdots\text{Mn}$  vector bridged by two oxides. The central two oxides also bind to the final two Mn centers in the structure. One of the three carboxylates spans the central  $\text{Mn}\cdots\text{Mn}$  contact, and the remaining two bridge from these Mn centers to the fifth and sixth Mn centers. The tetradentate amine ligands bind to the four external Mn sites. The two  $\text{Mn}^{\text{IV}}$  sites in the structure are assigned as the external manganese of the central linear portion of the structure, with the other four sites being  $\text{Mn}^{\text{III}}$ . No magnetic measurements are reported.

This group also synthesized the first heptanuclear manganese cage,  $[\text{Mn}_7\text{O}_4(\text{trien})_2(\text{dien})_2(\text{O}_2\text{CMe})_8]^{4+}$  (trien = triethylenetetramine, dien = diethylenetriamine) which also features both carboxylate and amine ligands.<sup>65</sup> The cage can be described as two mixed-valent  $\{\text{Mn}_4\text{O}_2\}$  butterflies, three  $\text{Mn}^{\text{III}}$ , and one  $\text{Mn}^{\text{II}}$ , sharing the  $\text{Mn}^{\text{II}}$  center. The cage is held together by the four oxides, which are each  $\mu_3$  bridging, and the carboxylate ligands, which all act as 1,3 bridges. The dien ligands act as chelating, terminal ligands while the trien ligands bind to both  $\text{Mn}^{\text{III}}$  centers which act as the body of the butterfly fragments. The synthetic procedure illustrates the redox-activity of manganese; the cage can be made from either  $\text{Mn}^{\text{II}}$  or  $\text{Mn}^{\text{III}}$  acetate with trien in air, and the dien found must result from oxidation of trien ligands during the reaction.

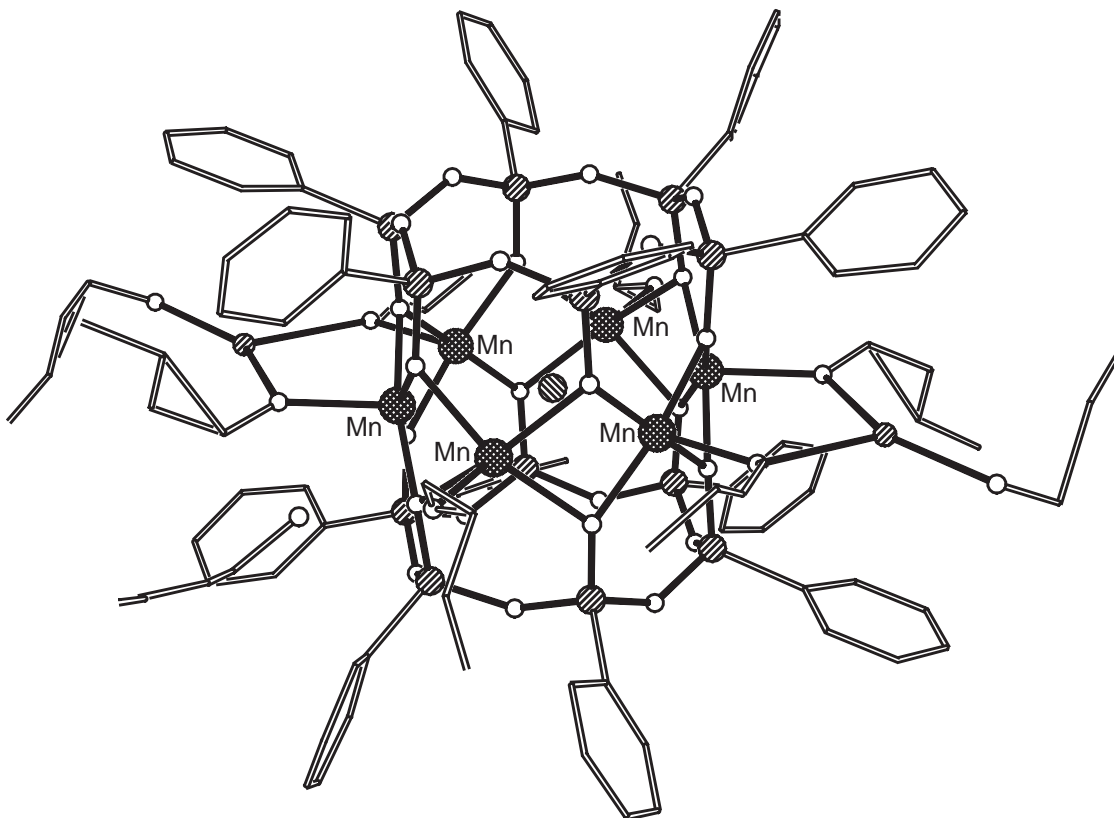


**Figure 6** The structure of  $[\text{Mn}_6\{(\text{PhSiO}_2)_6\}_2\text{Cl}(\text{ROH})_6]^{6-}$  (shading: Mn, hatched; O, open; Si, diagonal stripes top right bottom left; Cl, open; C, lines).

A similar arrangement of six manganese centers is found in  $[\text{Mn}_7\text{O}_4(\text{O}_2\text{CMe})_{10}(\text{dbm})_4]^-$  (dbm = the anion of dibenzoylmethane), which is homovalent.<sup>66</sup> The dbm ligands are found chelating to two of the four  $\text{Mn}^{\text{III}}$  centers which make up the “butterfly bodies.” Eight of the ten acetates adopt the 1,3-bonding mode, while the additional two acetates bridge in a 1,1,3 mode. The synthetic procedure is quite different, involving addition of  $\text{NEt}_4\text{Cl}$  to a tetranuclear manganese(III) butterfly,  $[\text{Mn}_4\text{O}_2(\text{O}_2\text{CMe})_6(\text{py})_2(\text{dbm})_2]$  in  $\text{CH}_2\text{Cl}_2$ . This transformation is solvent dependent; in MeCN the same reaction gives  $[\text{Mn}_4\text{O}_3\text{Cl}(\text{O}_2\text{CMe})_3(\text{dbm})_3]$ .<sup>67</sup> Magnetic measurements indicate a spin ground state of either  $S = 3$  or  $S = 4$ .<sup>66</sup>

A heptanuclear manganese(II) cage,  $[\text{Mn}_7\text{O}_6(\text{OEt})_{18}(\text{HOEt})_2]$ , has also been crystallized from the reaction of anhydrous  $\text{MnCl}_2$  with  $\text{NaSb}(\text{OEt})_4$  by controlled hydrolysis in toluene–ethanol.<sup>68</sup> The structure contains a central  $\text{Mn}^{\text{II}}$  center surrounded by a trigonal prism of six further  $\text{Mn}^{\text{II}}$  atoms, with the cage held together by  $\mu_5$ - and  $\mu_4$ -oxides, and  $\mu_3$ - and  $\mu_2$ -ethoxides.

The cationic species,  $[\text{Mn}\{\text{Mn}_6(\text{OH})_3\text{Cl}_3(\text{hmp})_9\}]^{2+}$ , is a mixed-valent “metallo-crown” (hmp = 2-hydroxymethylpyridine), with the metal centers within the crown alternating between  $\text{Mn}^{\text{II}}$  and  $\text{Mn}^{\text{III}}$ , while the encapsulated metal is  $\text{Mn}^{\text{II}}$ .<sup>69</sup> Magnetic studies indicate a high-spin ground state of either  $S = 10$  or  $S = 11$ . For either spin state, fit of reduced magnetization plots requires a negative  $D$ -value of either  $-0.15\text{ cm}^{-1}$  or  $-0.18\text{ cm}^{-1}$  respectively.

Similar cages can be formed by reacting  $\text{MnCl}_2$ ,  $\text{Na}(\text{OMe})$ , and Hdbm in MeOH, which gives  $[\text{Na}\{\text{Mn}_6(\text{dbm})_6(\text{OMe})_{12}\}]^+$ ,<sup>70</sup> and  $[\text{Mn}\{\text{Mn}_6(\text{dbm})_6(\text{OMe})_{12}\}]$ ;<sup>71</sup> the only difference in the synthetic procedure is that  $\text{Na}(\text{BPh}_4)$  is required for the former. The structures consist of a metallo-crown containing six Mn centers, each bound to one chelating dbm ligand, with each  $\text{Mn}\cdots\text{Mn}$  vector bridged by two  $\mu$ -OMe ligands. A seventh metal, either sodium or manganese, is encapsulated in the cavity. The magnetic properties of both cages are interesting. The Na-containing cage is homovalent, containing only  $\text{Mn}^{\text{III}}$  centers, and ferromagnetic exchange is observed between the metals, giving an  $S = 12$  ground state.<sup>70</sup>

The  $\{\text{Mn}_7\}$  metallo-crown is mixed-valent, and probably contains a net three  $\text{Mn}^{\text{II}}$  and four  $\text{Mn}^{\text{III}}$  centers.<sup>71</sup> The crystallographically imposed symmetry of the cage ( $S_6$ ) requires that there are only two independent Mn sites—the encapsulated manganese, which appears to be  $\text{Mn}^{\text{II}}$ , and the manganese sites which form part of the metallo-crown. These sites are therefore required to be  $1/3\text{ Mn}^{\text{II}}$  and  $2/3\text{ Mn}^{\text{III}}$ . Magnetization data are consistent with three sets of parameters: (a)  $S = 15/2$  ground state with  $g = 2.36$  and  $D = -0.34\text{ cm}^{-1}$ ; (b)  $S = 17/2$  ground state with  $g = 2.08$  and  $D = -0.27\text{ cm}^{-1}$ ; (c)  $S = 19/2$  ground state with  $g = 1.86$  and  $D = -0.21\text{ cm}^{-1}$ . The authors prefer the  $S = 17/2$  ground state, however it is not even clear that an isolated ground state will be found in such a complicated spin-frustrated system.

$[\text{Mn}\{\text{Mn}(\text{L}1)\}_6]^{2+}$  (for L1 see Scheme 2), takes the “metallo-crown” concept further towards “metallo-cryptands,” and contains a  $\text{Mn}^{\text{II}}$  center within a twisted trigonal prism of six further  $\text{Mn}^{\text{III}}$  centers.<sup>72</sup> The cage is stabilized by a tetradentate imino-carboxylate ligand, which binds to the equatorial sites of the manganese centers comprising the prism, with the second carboxylate oxygens either binding to axial sites of neighboring  $\text{Mn}^{\text{II}}$  centers of the prism, or binding to the encapsulated  $\text{Mn}^{\text{II}}$ . No magnetic data are reported for this cage.

The majority of octanuclear manganese cages are formed by dimerization of tetranuclear butterflies. For example,  $(^n\text{Bu}_4^{\text{N}})[\text{Mn}_4\text{O}_2(\text{O}_2\text{CMe})_7(\text{pic})_2]$  (pic = picolinate) reacts with one equivalent  $\text{Me}_3\text{SiCl}$ , with removal of one acetate per tetranuclear cage, followed by dimerization to give  $[\text{Mn}_8\text{O}_4(\text{O}_2\text{CMe})_{12}(\text{pic})_4]$ .<sup>73</sup> The tetranuclear butterfly structures are maintained, and the major change is that picolinate ligands, which are chelating via the ring N atom and one carboxylate oxygen in the tetranuclear cage, bridge to a second tetranuclear unit via the second carboxylate oxygen in the octanuclear cage. Alternatively, a bridging ligand can be added to replace the abstracted carboxylate, e.g.,  $(^n\text{Bu}_4^{\text{N}})[\text{Mn}_4\text{O}_2(\text{O}_2\text{CMe})_7(\text{dbm})_2]$  reacts with  $\text{Me}_3\text{SiCl}$  to give  $[\text{Mn}_4\text{O}_2(\text{O}_2\text{CMe})_6(\text{dbm})_2]$ , which can be linked through *trans*-1,2-bis(4-pyridyl)ethane (bpe) to give  $[\text{Mn}_4\text{O}_2(\text{O}_2\text{CMe})_6(\text{dbm})_2(\text{bpe})_2]$  in which two butterflies are linked through the diimine ligand.<sup>74</sup> A similar reaction with 4,4'-bipyridyl gives a polymer.<sup>74</sup>

Direct displacement of monocarboxylates by dicarboxylates can also lead to dimerization. Addition of 2,2-diethylmalonate ( $\text{Et}_2\text{mal}^{2-}$ ) to  $(^n\text{Bu}_4^{\text{N}})[\text{Mn}_4\text{O}_2(\text{O}_2\text{CMe})_9(\text{H}_2\text{O})]$  gives  $[\text{Mn}_8\text{O}_4(\text{O}_2\text{CMe})_{12}(\text{Et}_2\text{mal})_2(\text{H}_2\text{O})_2]^{2-}$ ,<sup>75</sup> where the dicarboxylates link the cages by chelating to a manganese site in one tetranuclear fragment through O atoms in differing carboxylates, making a six-membered chelate ring, and to a manganese in the other fragment through both O atoms of a single carboxylate, making a four-membered chelate ring. There is also a further bridging interaction provided by one of the oxide groups of the butterfly. The octanuclear cage is mixed-valent, containing six  $\text{Mn}^{\text{III}}$  and two  $\text{Mn}^{\text{II}}$  centers, whereas the precursor contains exclusively  $\text{Mn}^{\text{III}}$  ions. Magnetic studies suggest an  $S = 5/2$  ground state for each butterfly and no inter-butterfly coupling.<sup>75</sup>

If  $(^n\text{Bu}_4^{\text{N}})[\text{Mn}_4\text{O}_2(\text{O}_2\text{CPh})_9(\text{H}_2\text{O})]$  is treated with  $\text{Me}_3\text{SiCl}$  a homovalent octanuclear  $\text{Mn}^{\text{III}}$  cage is formed, but one which is not so clearly related to the tetranuclear precursor. The structure of  $(^n\text{Bu}_4^{\text{N}})[\text{Mn}_8\text{O}_6\text{Cl}_6(\text{O}_2\text{CPh})_7(\text{H}_2\text{O})_2]$ ,<sup>76</sup> contains an  $\{\text{Mn}_7\text{O}_6\text{Cl}_2\}$  core, related to two  $\{\text{Mn}_4\text{O}_3\text{Cl}\}$  cubes sharing an edge; however, there are two oxides in the shared edge rather than one. These two oxides bridge to the eighth manganese center in the cage. The benzoate ligands are all 1,3 bridging. Magnetic studies indicate an  $S=11$  ground state, with a very small negative  $D$ -value of  $-0.04\text{cm}^{-1}$ . This reaction should be compared with the designed synthesis that gave the other octanuclear manganese cages. It shows that disruption of the structure of a tetranuclear cage can be sufficient to generate a larger complex *without* addition of ligands designed to bridge the fragments. The element of design is lost, but the resulting cage has more interesting magnetic and electrochemical behavior.<sup>76</sup>

Work by Saalfrank and co-workers using polydentate ligands, L2 and L3 (see Scheme 2), has led to two strikingly beautiful octanuclear compounds.  $[\text{Mn}_8\text{O}_2(\text{L2})_6]$  contains a trigonal prism of  $\text{Mn}^{\text{II}}$  centers capped on the trigonal faces.<sup>77</sup> The six dianionic ligands each bind to three manganese centers. The result is a bis(triple-helicate) arrangement of ligands about the metal core.  $[\text{Mn}_8(\text{L3})_8(\text{HOPr})_4]$ , shown in Figure 7, contains two differently sized  $\text{Mn}^{\text{II}}$  squares with the same center and with the large square turned  $45^\circ$  relative to the small one.<sup>78</sup> The dianionic ligands again bridge three manganese centers. NMR studies of analogous zinc and cadmium cages indicate these structures are maintained in solution.

A further octanuclear manganese cage forms part of a study of heterometallic alkoxides.<sup>79</sup>  $[\text{Mn}_8\text{Sb}_4\text{O}_4(\text{OEt})_{20}]$  is made from reaction of  $\text{Na}(\text{OEt})$ ,  $\text{Sb}(\text{OEt})_3$ , and  $\text{MnCl}_2$  in toluene.

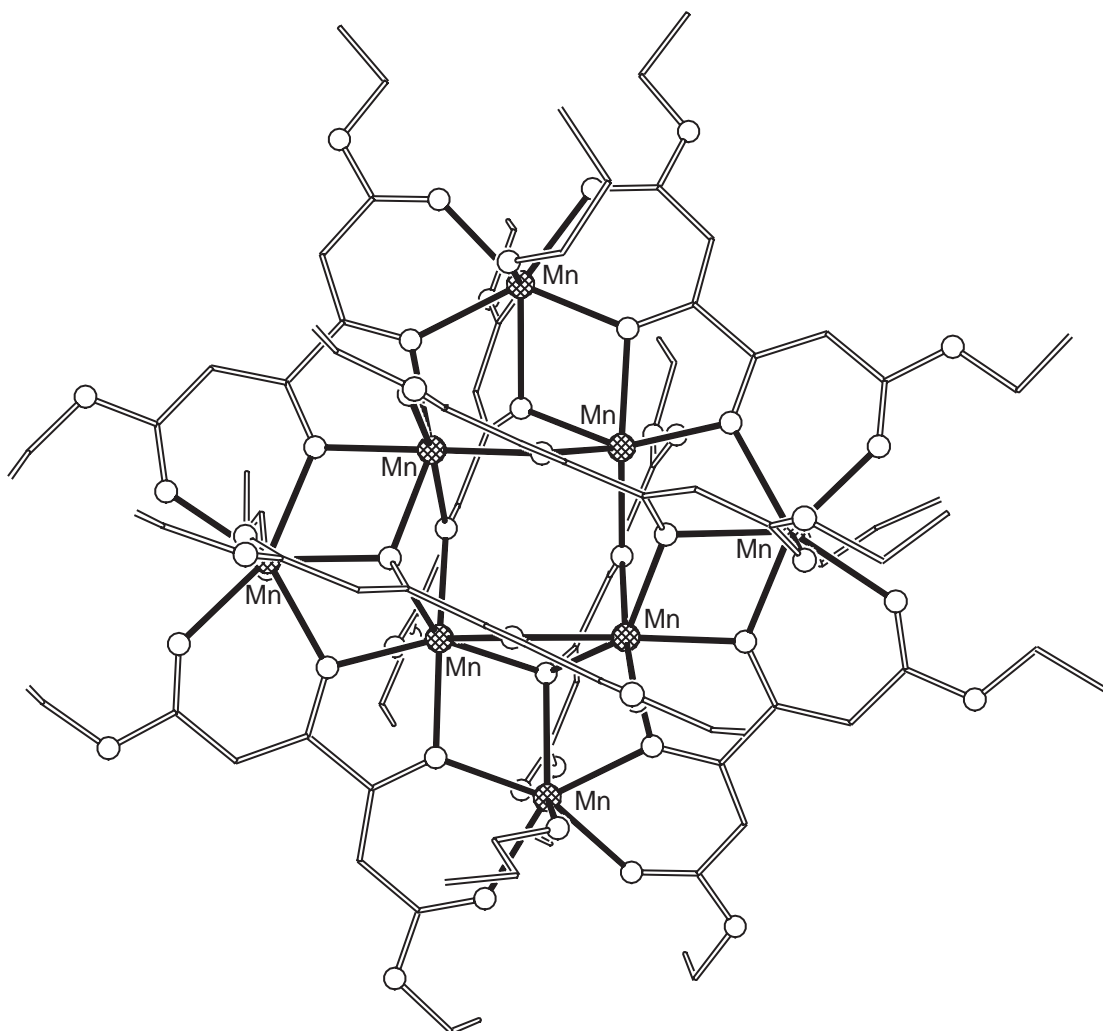


Figure 7 The structure of  $[\text{Mn}_8(\text{L3})_8(\text{HOPr})_4]$ <sup>78</sup> (shading: Mn, shaded; O, open; C, lines).

The oxides are all  $\mu_5$  bridging, while both  $\mu_3$ - and  $\mu_2$ -ethoxides are present. Three of the Mn<sup>II</sup> sites are six-coordinate with distorted octahedral geometries, and two are five-coordinate with square pyramidal geometries. The overall structure is perhaps best described as two {Mn<sub>6</sub>Sb<sub>2</sub>} square anti-prisms sharing a square face.

Wright and co-workers have reported an octanuclear Mn cage bridged by imido and amido ligands derived from 2-amino-4,6-dimethyl-pyrimidine via reaction of [Cp<sub>2</sub>Mn] with the parent ligand.<sup>80</sup> The structure contains a {Mn<sub>4</sub>N<sub>4</sub>} core, bridged to peripheral CpMn units, and is unusual. Even more interesting is this use of an organometallic approach to the synthesis of coordination cages, which is a path worth further exploration.

The nonanuclear cage [Mn<sub>9</sub>O<sub>4</sub>(O<sub>2</sub>CPh)<sub>8</sub>(sal)<sub>4</sub>(salH)<sub>2</sub>(py)<sub>4</sub>] (salH<sub>2</sub> = salicylic acid)<sup>81</sup> contains fragments which can be recognized as tetranuclear butterflies, containing a central {Mn(sal)<sub>4</sub>}<sup>6-</sup> fragment, with an eight-coordinate Mn<sup>II</sup> center bound to the oxygen centers of four chelating carboxylates. Each of these carboxylate oxygens then bridges to Mn centers of the tetranuclear {Mn<sub>4</sub>O<sub>2</sub>(O<sub>2</sub>CPh)<sub>4</sub>(salH)(py)}<sup>3+</sup> units which sandwich this central fragment. The tetranuclear units contain exclusively Mn<sup>III</sup> sites. The hydroxyl oxygens of the sal<sup>2-</sup> ligands also bind to metals within the tetranuclear units. The benzoate ligands act as 1,3 bridges within the butterflies. The magnetic data suggest an  $S = 3/2$  ground state.

The tetranuclear cage (<sup>n</sup>Bu<sub>4</sub><sup>N</sup>)[Mn<sub>4</sub>O<sub>2</sub>(O<sub>2</sub>CPh)<sub>9</sub>(H<sub>2</sub>O)] reacts with dibenzoyl peroxide to give a second nonanuclear cage, [Mn<sub>9</sub>Na<sub>2</sub>O<sub>7</sub>(O<sub>2</sub>CPh)<sub>15</sub>(MeCN)<sub>2</sub>].<sup>76</sup> Other cages containing this core have also been reported.<sup>58,82</sup> If the alkali metal cations present are included in the description, the polyhedron found in each case is very close to a centered icosahedron missing two vertices. Magnetic studies show the ground state to be  $S = 4$ .

A nonanuclear manganese(II) 3 × 3 grid has been reported. [Mn<sub>9</sub>(2poap)<sub>6</sub>] (for 2poap see Scheme 2) contains a polydentate N,O-donor with three “pockets” designed to bind to metal sites.<sup>83</sup> Six such ligands bridge to create the planar metal array. The magnetic ground state of the cage is  $S = 5/2$ . [Mn<sub>9</sub>(2poap)<sub>6</sub>] has an extremely rich electrochemistry, with five reversible redox waves found between +0.72 V and +1.58 V (vs. SCE). The first wave is a four-electron oxidation, while each of the following waves corresponds to a one-electron oxidation. The most oxidized cage therefore corresponds to one Mn<sup>II</sup> and eight Mn<sup>III</sup> centers.

The first decanuclear manganese cage reported was formed by aerial oxidation of a solution of Mn(CF<sub>3</sub>SO<sub>3</sub>)<sub>2</sub> and N(CH<sub>2</sub>CH<sub>2</sub>NH<sub>2</sub>)<sub>3</sub>(tren) in MeCN, which gives [Mn<sub>10</sub>O<sub>14</sub>(tren)<sub>6</sub>]<sup>8+</sup>,<sup>84</sup> which is mixed valent, containing four Mn<sup>III</sup> and six Mn<sup>IV</sup> centers. The cage consists of a planar core containing six octahedral Mn centers, with each octahedron sharing an edge with a neighbor. The 14 oxide ligands are found within this central raft. The four additional manganese centers are attached above and below the raft, and are bound to four of the six tren ligands, with the final two tren ligands bound to the terminal Mn atoms of the raft. No detailed magnetic studies have been reported.

The decanuclear cage, [Mn<sub>10</sub>O<sub>2</sub>Cl<sub>8</sub>{OCH<sub>2</sub>)}<sub>3</sub>CMe]<sub>6</sub><sup>2-</sup>,<sup>85</sup> reported by Zubieta and co-workers is a direct analog of the equivalent cages made with vanadium and has the {M<sub>10</sub>O<sub>28</sub>} decametallate core with 18 of the bridging oxide sites replaced by alkoxides from the tripodal ligand and the eight terminal oxides replaced by chlorides. The cluster is mixed valence, containing two Mn<sup>II</sup> and eight Mn<sup>III</sup> sites; the eight Mn<sup>III</sup> sites are those attached to the terminal chloride ligands. The room-temperature moment suggests anti-ferromagnetic exchange between the metal centers.

[Mn<sub>10</sub>O<sub>4</sub>(biphen)<sub>4</sub>X<sub>12</sub>]<sup>4-</sup> (biphen = 2,2'-biphenoxide; X = Cl or Br)<sup>86</sup> can be made from reaction of appropriate manganese(II) halide with 2,2'-biphenol in the presence of a base (either triethylamine or tetramethylammonium hydroxide). In each case the structure of the cage consists of a central {Mn<sub>6</sub>O<sub>4</sub>} adamantane structure, i.e., a tetrahedron of oxide ions with each edge containing a Mn center. Each oxide therefore binds to three Mn centers within the adamantane structure and also binds to a fourth Mn center, which creates a larger Mn<sub>4</sub> tetrahedron outside this central adamantane core. The 12 halide ions have three distinct structural roles; four are bound terminally to the Mn centers of the external tetrahedron, four are  $\mu_2$  bridging between an Mn atom of the adamantane and an Mn of the tetrahedron, and the final four are  $\mu_3$  bridging between Mn centers within the adamantane. The four biphen ligands each chelate to one Mn center of the adamantane, then each O atom bridges in a  $\mu_2$  fashion to an external Mn. The molecular structure therefore has  $D_{2d}$  symmetry. As is usual for Mn, both cages are mixed-valent. The four Mn<sup>III</sup> sites are the four metal centers within the adamantane which do not lie on the principal rotation axis; the remaining sites are Mn<sup>II</sup>. EPR measurements at 245 GHz support an assignment of an  $S = 12$  ground state with  $D$  around  $-0.04 \text{ cm}^{-1}$ .<sup>109</sup>

Two further decanuclear homovalent Mn<sup>III</sup> cages, [Mn<sub>10</sub>O<sub>8</sub>(O<sub>2</sub>CPh)<sub>6</sub>(pic)<sub>8</sub>] and [Mn<sub>10</sub>O<sub>8</sub>(O<sub>2</sub>CPh)<sub>6</sub>(pic)<sub>6</sub>(dbm)<sub>2</sub>],<sup>87</sup> can be made by dissolving the tetranuclear cage [Mn<sub>4</sub>O<sub>2</sub>(O<sub>2</sub>CMe)<sub>6</sub>(pic)<sub>2</sub>(MeCN)<sub>2</sub>]



in *N,N'*-dimethylacetamide, followed by dilution with  $\text{CH}_2\text{Cl}_2$ ; the difference in the two syntheses is that the latter compound requires addition of Hdbm to the reaction mixture. The metal cores of the two structures are identical, with an  $\{\text{Mn}_{10}\text{O}_8\}^{4+}$  core surrounded by the carboxylate ligands. The core can be described as two  $\{\text{Mn}_6\text{O}_4\}$  adamantanes sharing an  $\text{Mn}\cdots\text{Mn}$  edge. Susceptibility studies show both cages have diamagnetic ground states.

A decanuclear wheel,  $[\text{Mn}(\text{bzshz})(\text{MeOH})]_{10}$ , has been reported (for  $\text{H}_3\text{bzshz} = N$ -phenyl-salicylhydrazidate, see Scheme 2).<sup>88</sup> Each  $\text{Mn}^{\text{III}}$  is bound to three donors from one bzshz ligand, and two donors from a second bzshz, with the coordination geometry completed by a coordinated MeOH. Magnetic studies suggest antiferromagnetic exchange between the metals. The iron analog has also been described.<sup>88</sup>

The structure of  $[\text{Mn}_{11}\text{O}_{10}\text{Cl}_2(\text{O}_2\text{CMe})_{11}(\text{bpy})_2(\text{MeCN})_2(\text{H}_2\text{O})_2]^{2+}$  ( $\text{bpy} = 2,2'$ -bipyridyl) contains a linear, trinuclear manganese core which lies on a mirror plane and bridges between two  $\{\text{Mn}_4\text{O}_3\text{Cl}\}$  heterocubanes.<sup>89</sup> The bridges are provided by four  $\mu_3$  oxides, which each bind to two Mn centers of the trinuclear block and to one Mn from a cubane, and four carboxylates which bridge between the terminal Mn centers of the central fragment and Mn centers of the cubanes. The bpy ligands chelate to Mn centers within the cubanes.

A dodecanuclear manganese(II) cage,  $[\text{Mn}_{12}(\text{OH})_4(\text{L}4)_6(\text{O}_2\text{CMe})_2]$ , was reported by Tuchagues and co-workers in 1988,<sup>90</sup> using a binucleating Schiff-base ligand (L4, see Scheme 2). Each pentadentate L4 ligand binds to two  $\text{Mn}^{\text{II}}$  centers, with the phenol oxygens bridging to further  $\text{Mn}^{\text{II}}$  centers, generating a cyclic belt-like structure. Magnetic susceptibilities studies indicate antiferromagnetic coupling between the metal centers giving a diamagnetic ground state for the cage.

This very beautiful structure has been largely overlooked because of the fascinating magnetic behavior of the dodecanuclear cages with the general formula,  $[\text{Mn}_{12}\text{O}_{12}(\text{O}_2\text{CR})_{16}(\text{H}_2\text{O})_4]$ , shown in Figure 8.<sup>1,91–97</sup> Lis first reported this structure in 1980,<sup>91</sup> but significant work on these cages dates from a report in 1988 by Christou, Hendrickson, and co-workers.<sup>92</sup> The properties of this family of cages are discussed in detail in Chapter 7.13.

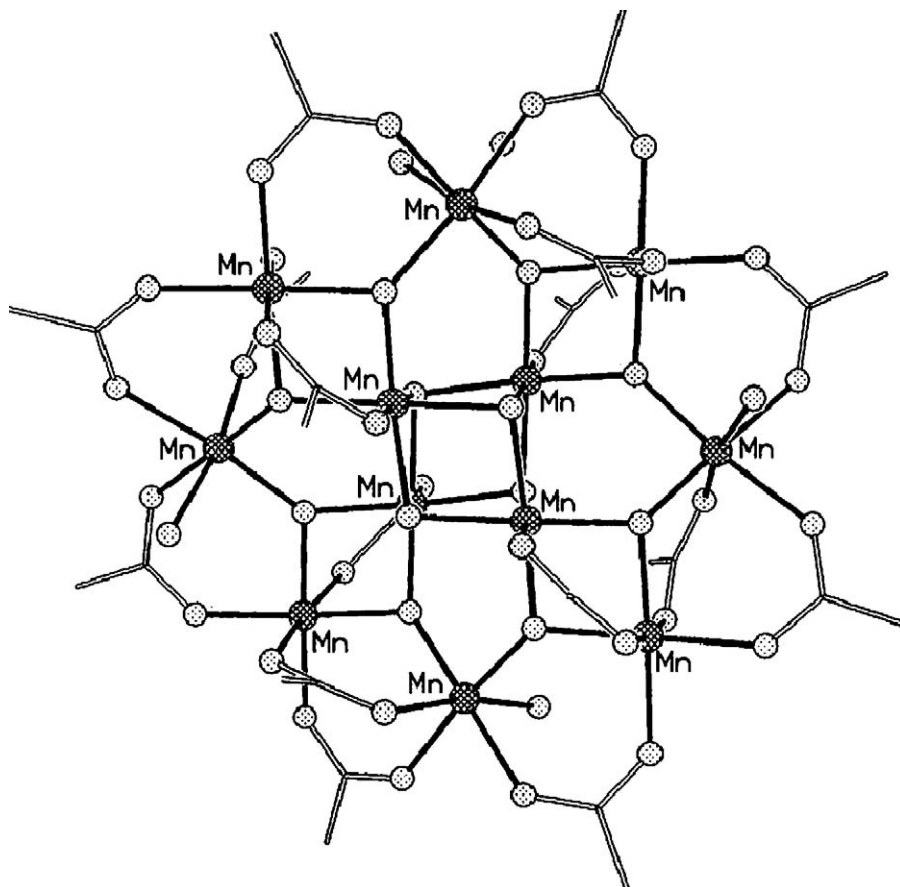


**Figure 8** The structure of  $[\text{Mn}_{12}\text{O}_{12}(\text{O}_2\text{CR})_{16}(\text{H}_2\text{O})_4]$ <sup>91</sup> (shading: Mn, hatched; O, dotted; C, lines).

The cages are known with a wide—and ever increasing—range of carboxylates.<sup>93</sup> Nitrate and phosphonate can also be incorporated.<sup>94,95</sup> The Christou and Hendrickson groups have also prepared, isolated, and studied the cages in three different oxidation states: neutral, mononegative<sup>96</sup> and dinegative,<sup>97</sup> and a heterometallic  $[\text{Fe}_4\text{Mn}_8\text{O}_{12}(\text{O}_2\text{CMe})_{16}(\text{H}_2\text{O})_4]$  cage.<sup>98</sup> While the majority of physical studies have concentrated on the neutral  $[\text{Mn}_{12}\text{O}_{12}(\text{O}_2\text{CMe})_{16}(\text{H}_2\text{O})_4]$  cage, the availability of other derivatives of this cage has given much insight into why this specific family of cages displays such unusual magnetic behavior.

The common structure for this family consists of a  $\{\text{Mn}_4\text{O}_4\}$  heterocubane surrounded by an octanuclear manganese wheel, bridged by carboxylates and oxide ligands. In the neutral molecules the central heterocubane contains exclusively  $\text{Mn}^{\text{IV}}$  sites, while the octanuclear wheel contains eight  $\text{Mn}^{\text{III}}$  sites. Where the cages are redox-active the reduction sites are the external  $\text{Mn}^{\text{III}}$  centers,<sup>96,97</sup> which means the mono- and di-negative cages contain three oxidation states— $\text{Mn}^{\text{II}}$ ,  $\text{Mn}^{\text{III}}$ , and  $\text{Mn}^{\text{IV}}$ . The octanuclear manganese wheel cannot be found in isolation for this metal, although it resembles the octanuclear vanadium and chromium wheels discussed above.

The compounds are remarkably straightforward to make. The parent acetate cage can be made in ca. 80% yield by reaction of manganese(II) acetate with potassium permanganate in acetic acid.<sup>1</sup> While other cages can be made directly by use of other manganese carboxylates in this comproportionation reaction, they are more easily made by simple ligand exchange of the acetates.

Most of these  $\{\text{Mn}_{12}\}$  cages have an  $S = 10$  ground state, which arises because the antiferromagnetic exchange between the  $\text{Mn}^{\text{III}}$  and  $\text{Mn}^{\text{IV}}$  centers is stronger than the antiferromagnetic exchange between either  $\text{Mn}^{\text{III}}-\text{Mn}^{\text{III}}$  or  $\text{Mn}^{\text{IV}}-\text{Mn}^{\text{IV}}$ . This leads to the spins on the metals of the central cubane being aligned parallel with each other, but anti-parallel to the spins on the metals of the wheel. The  $S = 10$  ground state is highly anisotropic, with  $D$ -values of around  $-0.5 \text{ cm}^{-1}$ . This leads to a significant energy barrier to reorientation of the magnetization. Therefore, the cage behaves as a “single molecule magnet” (SMM),<sup>1,2</sup> with very slow relaxation of magnetization in the absence of a field at sufficiently low temperatures.

The ability to vary the carboxylate in the  $\{\text{Mn}_{12}\}$  cages creates many possibilities for systematic study of these materials. The large anisotropy of the spin in the cages results in the main because the Jahn–Teller axes for all the  $\text{Mn}^{\text{III}}$  centers in the cage are aligned parallel. The Christou/Hendrickson groups have demonstrated that variation of carboxylate and even lattice solvation can change the relative orientations of these Jahn–Teller axes, producing cages with a lower energy barrier to reorientation of the magnetization.<sup>93</sup> Unfortunately it appears the original systems were optimized, and no *increase* in the energy barrier has yet been found, in these cages or in the other SMMs.

A further class of  $\{\text{Mn}_{12}\}$  SMMs have been reported,<sup>99</sup> involving 2-(hydroxymethyl)- or 2-(hydroxyethyl)-pyridine(hxp) in addition to the carboxylate.  $[\text{Mn}_{12}\text{O}_8\text{Cl}_4(\text{O}_2\text{CPh})_8(\text{hxp})_6]$  each contain three, incomplete, face-sharing double cubanes. The cage is mixed-valent, containing ten  $\text{Mn}^{\text{III}}$  and two  $\text{Mn}^{\text{II}}$  centers. Magnetic measurements suggest an  $S = 6$  or  $7$  ground state, with significant anisotropy.

Several larger manganese cages are known. A tridecanuclear cage,  $[\text{Mn}_{13}\text{O}_8(\text{OEt})_6(\text{O}_2\text{CPh})_{12}]$ , has perhaps the most appealing structure<sup>100</sup> which is shown in Figure 9. It is a “supercubane”, containing eight cubanes arranged in a cube. The central manganese site is a  $\text{Mn}^{\text{IV}}$  center, and is shared by all eight cubanes. The 12 surrounding Mn centers are half  $\text{Mn}^{\text{III}}$  and half  $\text{Mn}^{\text{II}}$ , and can be assigned because the  $\text{Mn}^{\text{III}}$  sites show a Jahn–Teller elongated coordination geometry. Six oxides are found at the centers of the faces of the cube, and are  $\mu_5$  bridging, while two oxides and six ethoxide oxygens are found  $\mu_3$  bridging at the corners of the supercubane. The 12 benzoates are all 1,3 bridging between pairs of Mn sites on the faces of the supercubane, with two carboxylates per face. The magnetic properties suggest an  $S = 15/2$  ground state with  $D = 0.33 \text{ cm}^{-1}$ .

Murray and co-workers have reported a  $\{\text{Mn}_{16}\}$  cage,<sup>101</sup> which is clearly related to the classic  $\{\text{Mn}_{12}\}$  cage.  $[\text{Mn}_{16}\text{O}_{16}(\text{OMe})_6(\text{O}_2\text{CMe})_{16}(\text{MeOH})_3(\text{H}_2\text{O})_3]$  contains a central  $\{\text{Mn}_6\text{O}_6(\text{OMe})_4\}^{8+}$  unit in which all sites are  $\text{Mn}^{\text{IV}}$ , surrounded by a ring of ten carboxylate- and methoxide-bridged  $\text{Mn}^{\text{III}}$  sites. Preliminary magnetic studies suggest many spin states are populated even at 1.8 K, but there are indications that this cage may be a SMM.

Three octadecanuclear cages have been reported. The earliest involves reaction of the butterfly cage  $(\text{NBu}_4)[\text{Mn}_4\text{O}_2(\text{O}_2\text{CPh})_9(\text{H}_2\text{O})]$  with the monopotassium salt of phthalic acid in MeCN. Phthalate (phth) displaces benzoate, and slow concentration of the solution gives  $[\text{Mn}_{18}\text{O}_{16}(\text{O}_2\text{CPh})_{22}(\text{phth})_2(\text{H}_2\text{O})_4]^{4-}$ .<sup>102</sup> The structure can be described as containing a central region of three  $\{\text{Mn}_4\text{O}_2\}$  butterflies sharing body vertices, which gives an  $\{\text{Mn}_{10}\text{O}_6\}$  “raft.” This

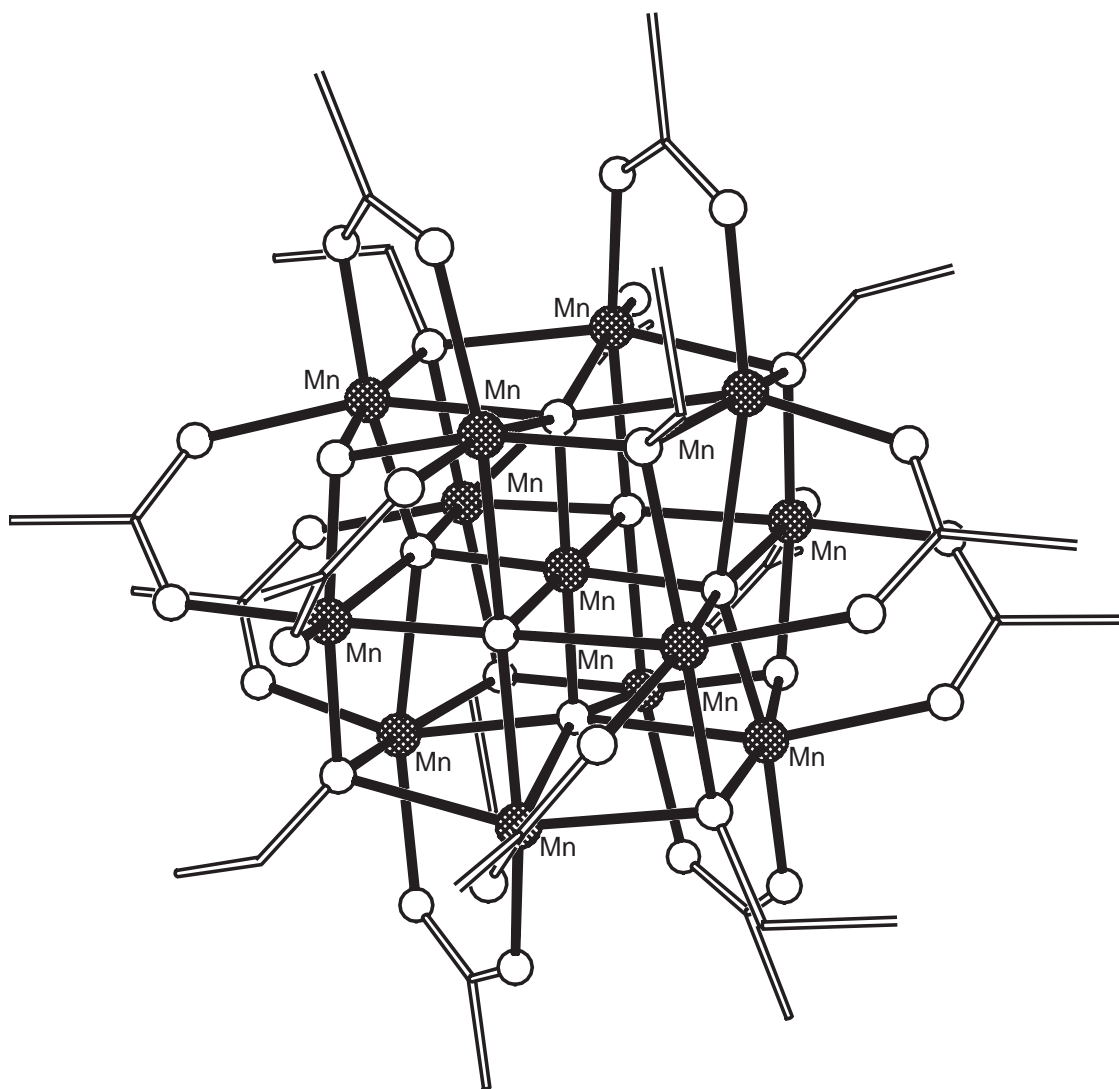


**Figure 9** The structure of  $[\text{Mn}_{13}\text{O}_8(\text{OEt})_6(\text{O}_2\text{CPh})_{12}]^{100}$  with phenyl groups excluded for clarity (shading: Mn, hatched; O, open; C, lines).

section links together two  $\{\text{Mn}_4\text{O}_3\}$  fragments where the Mn centers describe tetrahedra which are bridged on two faces by  $\mu_3$  oxides and on the opposite edge by one further oxide. This oxide binds to the wing-tip Mn site of the central  $\{\text{Mn}_4\text{O}_2\}$  butterfly of the raft, and is therefore also  $\mu_3$  bridging. The benzoates all act as 1,3 bridging ligands and the two phthalates are  $\mu_4$  bridging. All 16 oxides are  $\mu_3$  bridging. The cage has a diamagnetic ground state.

A second  $\{\text{Mn}_{18}\}$  cage has been reported by the Christou group.<sup>103</sup>  $[\text{Mn}_9\text{O}_7(\text{O}_2\text{CC}_6\text{H}_4\text{-}p\text{-}\text{OMe})_{13}(4,4'\text{-bpy})_2]$  contains two nonanuclear manganese cages linked by a 4,4-bipyridine(4,4'-bpy) ligands. The nonanuclear core is similar to other  $\{\text{Mn}_9\}$  carboxylates, and magnetic exchange is restricted to interactions within the individual  $\{\text{Mn}_9\}$  cages.

The third octadecanuclear cage,  $[\text{Mn}_{18}\text{O}_{14}(\text{OMe})_{14}(\text{O}_2\text{CCMe}_3)_8(\text{MeOH}_6)]$ , is mixed-valent, with a net 14  $\text{Mn}^{\text{III}}$  and four  $\text{Mn}^{\text{II}}$  sites.<sup>104</sup> The cage is made by mixing manganese(II) chloride, sodium pivalate, and Na(mhp) (mhp = the anion of 6-methyl-2-hydroxypyridine) in MeOH, followed by crystallization from hot MeOH. The structure consists of a central cubane capped on each face by a further cubane, generating a heptacubane  $\{\text{Mn}_{16}\text{O}_{14}(\text{OMe})_2\}$  core. Of the 14 oxides, four are  $\mu_6$ -, two  $\mu_4$ -, and eight  $\mu_3$  bridges while both methoxides are  $\mu_3$  bridges. Twelve of the metal sites show some form of Jahn–Teller distortion typical of  $\text{Mn}^{\text{III}}$ , while the remaining four sites need to be mixed-valent for charge balance considerations, and it appears they are a mixture of two  $\text{Mn}^{\text{II}}$  and two  $\text{Mn}^{\text{III}}$  sites. The two additional metal sites, which are attached to the heptacubane by  $\mu_4$  bridging oxides, are clearly  $\text{Mn}^{\text{II}}$ . The pivalate ligands all act as 1,3 bridges.

$[\text{Mn}_{19}\text{O}_{12}(\text{OCH}_2\text{CH}_2\text{OMe})_{14}(\text{HOCH}_2\text{CH}_2\text{OMe})_{10}]$  contains a central  $\{\text{Mn}_7\}$  core surrounded by 12 further Mn centers.<sup>105</sup> The structure of the cage is remarkably simple, with the core of the cage bridged by oxide while the periphery is bound to alkoxide ligands. The structure is strongly reminiscent of  $\{\text{Fe}_{19}\}$ <sup>106</sup> and  $\{\text{Co}_{24}\}$  cages.<sup>107</sup>

The largest manganese cage reported is  $[\text{Mn}_{30}\text{O}_{24}(\text{OH})_8(\text{O}_2\text{CCH}_2\text{CMe}_3)_{32}(\text{H}_2\text{O})_2(\text{MeNO}_2)_4]$ .<sup>108</sup> Unfortunately, little beyond a crystal structure has appeared, and even the structure is difficult to interpret as neither the figure nor the discussion is clear. The preparation is probably from a ligand exchange of  $\text{HO}_2\text{CCH}_2\text{CMe}_3$  with  $[\text{Mn}_{12}\text{O}_{12}(\text{O}_2\text{CMe})_{16}(\text{H}_2\text{O})_4]$  followed by crystallization from nitromethane. The influence of solvent here must be important—in almost all other cases this reaction produces a new form of  $\{\text{Mn}_{12}\}$ . The formation of  $\{\text{Mn}_{16}\}$ <sup>101</sup> and  $\{\text{Mn}_{30}\}$  cages<sup>108</sup> from reactions that were probably intended to give the well-known  $\{\text{Mn}_{12}\}$  cage suggests there remain many more large and curious manganese carboxylate clusters to discover.

### 7.3.2.4 Iron

The studies of high-nuclearity iron cages were originally motivated by a desire to understand biomineralization. As with manganese, a very broad range of structures has been found. Unlike manganese, the cages tend to be homovalent, containing  $\text{Fe}^{\text{III}}$  in the main.

The earliest hexanuclear iron complexes reported contain two  $\{\text{Fe}_3\text{O}\}$  carboxylate-bridged triangles linked by two  $\mu_2$ -hydroxide to form a planar  $\{\text{Fe}_6\text{O}_2(\text{OH})_2\}$  unit. G erb el eu and co-workers reported the derivative with pivalate ligands,<sup>109</sup> followed closely by a report by Micklitz and Lippard of the benzoate analog.<sup>110</sup> The benzoate analog has a diamagnetic ground state. Lippard and co-workers also demonstrated that oxo-centered iron triangles could be linked by a  $\mu_4$ -peroxide, to give a planar cage,  $[\text{Fe}_6(\text{O}_2)\text{O}_2(\text{O}_2\text{CPh})_{12}(\text{H}_2\text{O})_2]$ .<sup>111</sup> Pivalate and trifluoroacetate analogs of the peroxide-bridged cage have been prepared with a variety of monodentate ligands attached to the terminal Fe sites of the triangles.<sup>112</sup> These cages have been studied as mediators in the Gif-like oxygenation of organic substrates by  $\text{O}_2/\text{Zn}$ . Much more extraordinary is the trigonal prismatic cage,  $[\text{Fe}_6(\text{O}_2)_3\text{O}_2(\text{O}_2\text{CMe})_9]^-$ , made by reaction of hydrogen peroxide with basic iron acetate.<sup>113</sup> The cage contains two oxo-centered iron triangles arranged in a face-to-face fashion, forming a trigonal prism, with three  $\eta_2$ - $\mu_4$ -peroxides placed within each rectangular face of the prism (Figure 10). Each of the nine edges of the trigonal prism is bridged by a  $\mu_2$ -acetate. The magnetic data on this cage indicate an  $S = 1$  ground state for the cage.

Further hexanuclear cages have been reported using polydentate ligands featuring N-heterocycles. Reaction of 1,1-bis(*N*-methylimidazol-2-yl)-1-hydroxyethane(mimOH) with  $[\text{Fe}_3\text{O}(\text{O}_2\text{CMe})_6(\text{py})_3](\text{ClO}_4)$  in MeCN, followed by crystallization from  $\text{CH}_2\text{Cl}_2$  gives  $[\text{Fe}_6\text{O}_2(\text{OH})_2(\text{O}_2\text{CMe})_{10}(\text{mimO})_2]$ <sup>114</sup> where the hydroxy diimidazole ligand has displaced a terminal pyridine and a bridging carboxylate group from the original oxo-centered triangle, while two  $\mu_2$ -hydroxides and four 1,3 bridging carboxylates now bridge two triangles into a hexanuclear cage. A very similar cage,  $[\text{Fe}_6\text{O}_2(\text{OH})_2(\text{O}_2\text{CMe})_{10}(\text{mimO})_2]$ ,<sup>115</sup> results if 2-(*N*-methylimidazol-2-yl)-2-hydroxypropane(mimOH) is used in this reaction. Reaction of 2-hydroxymethylpyridine (Hhmp) with hydrated iron(III) chloride in MeCN gives a further hexanuclear cage,  $[\text{Fe}_6\text{O}_2(\text{hmp})_8\text{Cl}_4]$ .<sup>115</sup> This cage also has a core involving two bridged  $\{\text{Fe}_3\text{O}\}$  triangles. Magnetic studies of these cages illustrate the complexity that can result in such compounds. Whereas the earlier hexanuclear cages studied have diamagnetic ground states, the cages containing methylimidazole ligands have  $S = 5$  ground states while the cage with hmp has an  $S = 3$  ground state.<sup>115</sup>

Hegetschweiler and co-workers have made a series of octahedral iron(III) cages, based on the  $\{\text{M}_6\text{O}_{19}\}$  hexametallate core.  $[\text{Fe}_6\text{O}(\text{OMe})_{18}]^{2-}$  can be made by addition of sodium methoxide to a solution of anhydrous  $\text{FeCl}_3$  dissolved in MeOH,<sup>116</sup> while two cages are known with tripodal tris(alkoxide) ligands,  $[\text{Fe}_6\text{O}\{(\text{OCH}_2)_3\text{Et}\}_6]^{2-}$ <sup>117</sup> and  $[\text{Fe}_6\text{O}\{(\text{OCH}_2)_3\text{Et}\}_3(\text{OMe})_3\text{Cl}_6]^{2-}$ .<sup>118</sup> These cages are very similar to the hexavanadium cages reported by Zubietta (see Section 7.3.2.1.1), with a central  $\mu_6$ -oxide surrounded by an octahedron of iron(III) centers, with the remaining oxygen atoms of the hexametallate structure provided by the alkoxide or chloride ligands. Magnetic studies show diamagnetic ground states for these cages.<sup>118</sup>

Further octahedral iron cages result from reaction of oxo-centered iron(III) triangles with Hhmp in MeCN.  $[\text{Fe}_6\text{O}_2(\text{O}_2\text{CR})_6(\text{hmp})_6]^{2+}$  cages result for  $\text{R} = \text{Ph}$  and  $\text{CMe}_3$ .<sup>119</sup> Here, two  $\{\text{Fe}_3\text{O}(\text{O}_2\text{CR})_3\}$  triangles are linked by hmp ligands, with an oxygen of each hmp ligand  $\mu_2$  bridging each  $\text{Fe}\cdots\text{Fe}$  vector of the triangle while the pyridine nitrogen binds to an Fe atom in

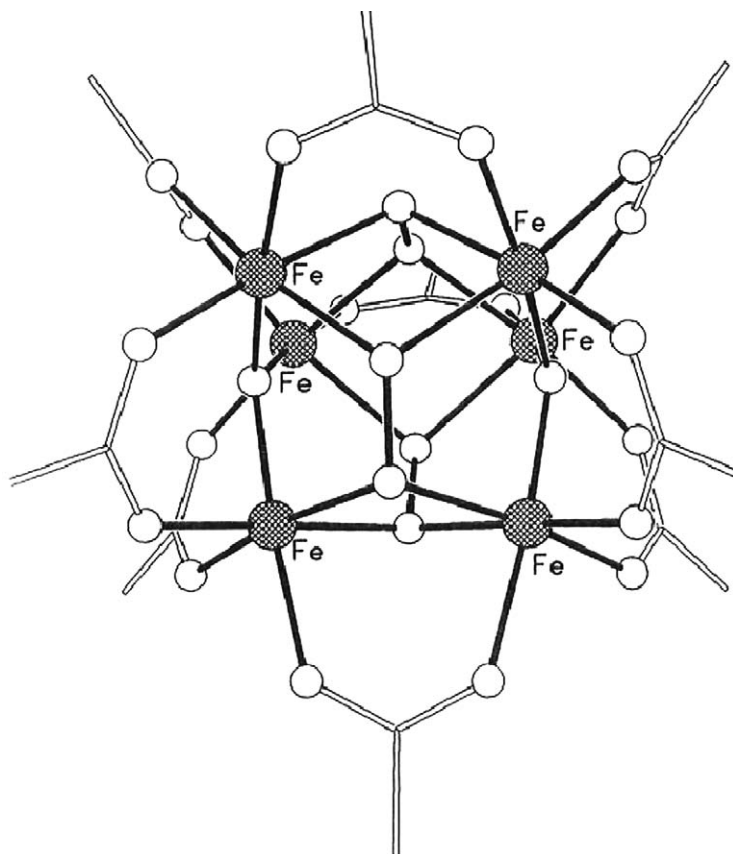


**Figure 10** The structure of  $[\text{Fe}_6(\text{O}_2)_3\text{O}_2(\text{O}_2\text{CMe})_9]^{13-}$  (shading: Fe, hatched; O, open; C, lines).

the second triangle. The cages, therefore, have noncrystallographic  $S_6$  symmetry. Magnetic studies of these octahedral Fe cages indicate that they have  $S=0$  ground states.

A rare example of a high-nuclearity  $\text{Fe}^{\text{II}}$  cage is formed when anhydrous iron(II) chloride is reacted with  $\text{NHEt}_2$  and  $\text{CO}_2$  in toluene.<sup>120</sup>  $[\text{Fe}(\text{O}_2\text{CNET}_2)_2]_6$  forms in good yield to give a structure with the six  $\text{Fe}^{\text{II}}$  centers arranged in an edge-sharing bitetrahedron; the structure is analogous to  $[\text{Mn}(\text{O}_2\text{CNET}_2)_2]_6$  (see Section 7.3.2.3). Hydrolysis of the isopropyl derivative gives an octanuclear  $\text{Fe}^{\text{II}}$  cage,  $[\text{Fe}_8\text{O}_2(\text{O}_2\text{CNiPr}_2)_{12}]$ .<sup>120</sup> This cage contains two oxo-centered  $\{\text{Fe}_4\}$  tetrahedra, bridged by carbamate ligands. The iron sites are either four- or five-coordinate, and the carbamate ligands show both the 1,3- and 1,1,3 bridging modes.

The hexanuclear cage  $[\text{NaFe}_6(\text{OMe})_{12}(\text{dbm})_6]^{+121}$  is a structural analog of the equivalent manganese metallocrown (see Section 7.3.2.3). The ground state is diamagnetic, however the  $S=1$  excited state can be studied, either by torque magnetometry or EPR spectroscopy.<sup>121</sup> Larger wheels involving  $\{\text{Fe}(\text{dbm})\}$  bridged by methoxide have also been reported when sodium is replaced by potassium or cesium.  $[\text{Fe}(\text{OMe})_2(\text{dbm})]_{12}$ <sup>122</sup> contains a twisted cyclic structure, which appears to be a compromise between the requirements of a regular dodecagon (where each  $\text{Fe}\cdots\text{Fe}\cdots\text{Fe}$  angle would be  $150^\circ$ ), and the preferred angle in edge-sharing octahedra ( $120^\circ$ ). Magnetic studies reveal an  $S=0$  ground state for both these cages. The dodecanuclear wheel reacts readily with sodium and lithium ions to form the hexanuclear metallocrown.<sup>123</sup>

Control of the size of metallocrowns has also been reported for cages made with the ligands triethanolamine and *N*-methyldiethanolamine. Reaction of the former ligand with  $\text{FeCl}_3$  in THF in the presence of either NaH or LiH gave  $[\text{MFe}_6\{\text{OCH}_2\text{CH}_2)_3\text{N}\}_6]\text{Cl}$  ( $\text{M} = \text{Li}$  or  $\text{Na}$ ).<sup>124</sup> The cage contains six iron centers at the corners of a regular hexagon, bridged by alkoxide oxygens from the tripodal ligand. Six of these oxygens line the inside of the cage, creating a cavity for incorporation of the alkali metal ion. Use of  $\text{Cs}_2\text{CO}_3$  leads to an octanuclear cage  $[\text{CsFe}_8\{\text{OCH}_2\text{CH}_2)_3\text{N}\}_8]\text{Cl}$ ,<sup>124</sup> which has an octagon of  $\text{Fe}^{\text{III}}$  centers in the metallocrown, encapsulating the larger Cs cation. Clearly, the alkali metal plays a templating role favoring the formation of one cage over another. With *N*-methyldiethanolamine, reaction with  $\text{FeCl}_3$  in

THF in the presence of  $\text{Cs}_2\text{CO}_3$  leads to an empty cage  $[\text{Fe}_6\text{Cl}_6\{\text{OCH}_2\text{CH}_2\}_2\text{NMe}\}_6]$ ,<sup>124</sup> with six terminal chloride ligands attached to the six Fe sites and no encapsulated alkali metal cation. Magnetic studies of the octanuclear crown have allowed some correlations to be made between magnetic exchange interactions and single-ion anisotropy.<sup>125</sup>

Use of a bis(bipyridine) ligand has generated a hexanuclear iron(III) cage,  $[\text{Fe}_6\text{O}_4\text{Cl}_4(\text{O}_2\text{CPh})_4(\text{L}6)_2]^{2+}$ ,<sup>126</sup> where  $\text{L}6 = 1,2\text{-bis}(2,2'\text{-bipyridyl-6-yl})\text{ethane}$ . This cage contains an  $\{\text{Fe}_4\text{O}_4\}$  ladder at its core, with two further  $\text{Fe}^{\text{III}}$  centers attached to the external oxides of the ladder. These final iron sites are tetrahedrally coordinated to two terminal chlorides, the bridging oxide and an oxygen from a 1,3 bridging carboxylate. The bis(bipyridine) ligands each bind to two iron centers of the ladder. This cage has a diamagnetic ground state.

A further hexanuclear cage has been reported simultaneously by two groups,<sup>127,128</sup> using *N*-(2-hydroxypropyl)imino-diacetic acid (hpida). The six  $\text{Fe}^{\text{III}}$  sites in  $[\text{NaFe}_6(\text{hpida})_6\text{O}_3]^+$  lie at the corners of a distorted trigonal prism. A carboxylate group bridges each edge of the triangles of the prism, while oxides bridge the edges linking the triangles. Carboxylate oxygen atoms also form a trigonal prismatic cavity where the sodium ion is encapsulated. Magnetic studies indicate the cage has a diamagnetic ground state.

A mixed-valent heptanuclear iron complex has been reported using the anion of bis(2-pyridyl-carbonyl)amine (bpca) as the chief ligand.<sup>129</sup> A mononuclear complex of this ligand,  $[\text{Fe}(\text{bpca})\text{Cl}_2(\text{EtOH})]$ , is reacted with NaOH to give a trinuclear anionic  $\text{Fe}^{\text{III}}$  cluster,  $[\text{Fe}_3\text{O}(\text{bpca})_2\text{Cl}_4(\text{EtO})_2]^-$ , in which a T-shaped iron array is bridged by a  $\mu_3$ -oxide and two  $\mu_2$ -ethoxides. Reaction of this cage with  $[\text{Fe}(\text{H}_2\text{O})_6]^{2+}$  gives a heptanuclear cage,  $[\text{Fe}\{\text{Fe}_3\text{O}(\text{bpca})_2\text{Cl}_4(\text{EtO})_2\}_2(\text{EtOH})_2]$ . Magnetization studies suggest an  $S = 6$  ground state.

$[\text{Fe}_7(\text{PDK})_2\text{Cl}_8(\text{H}_2\text{O})_2]$ <sup>130</sup> (PDK is a porphyrin substituted with Kemp's triacid imide) contains a pentanuclear Fe square-based pyramid, held together by chlorides and carboxylates which are derived from the PDK ligands. The final two Fe centers sit at the centers of the porphyrin rings. The cage is mixed valent, with two  $\text{Fe}^{\text{III}}$  and five  $\text{Fe}^{\text{II}}$  centers.

The oldest octanuclear  $\text{Fe}^{\text{III}}$  cage is also the iron cage with the most heavily studied magnetic properties; again, a detailed discussion of this molecule is given in Chapter 7.13.  $[\text{Fe}_8(\text{O})_2(\text{OH})_{12}(\text{tacn})_6]^{8+}$  ( $\text{tacn} = 1,4,7\text{-triazacyclononane}$ ), shown in Figure 11, was first reported

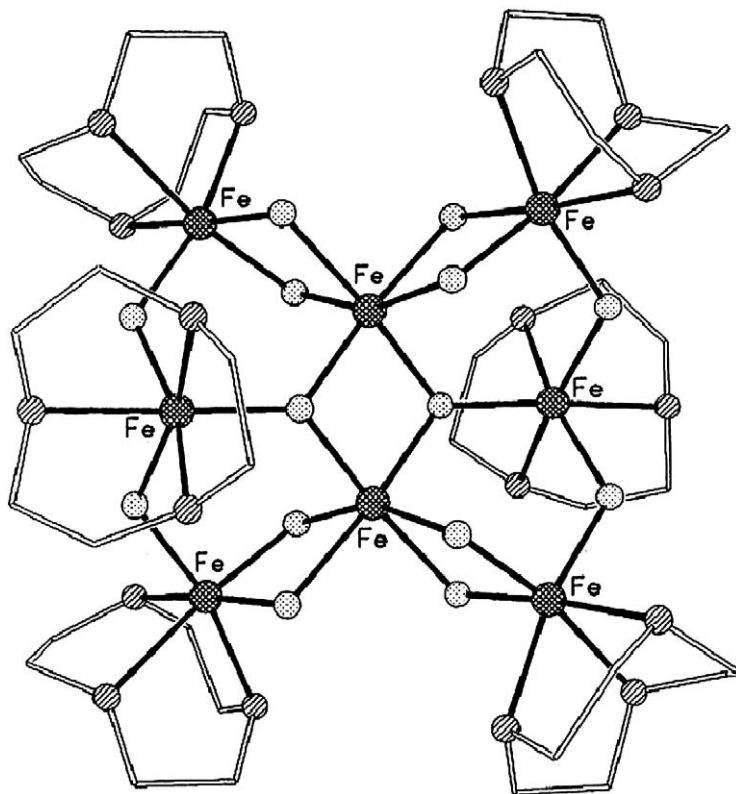


**Figure 11** The structure of  $[\text{Fe}_8(\text{O})_2(\text{OH})_{12}(\text{tacn})_6]^{8+}$ <sup>131</sup> (shading: Fe, hatched; O, dotted; N, striped; C, lines).

by Wieghardt and co-workers in 1984.<sup>131</sup> The cage was made by hydrolysis of  $[\text{FeCl}_3(\text{tacn})]$  at pH 9 in the presence of bromide. The structure consists of a planar octanuclear iron core bridged by two  $\mu_3$ -oxides and 12  $\mu_2$ -hydroxides. The iron atoms can be considered to be a central  $\{\text{Fe}_4\text{O}_2\}$  butterfly “capped” on each edge by a further  $\text{Fe}^{\text{III}}$  center. The six tacn ligands bind in a tridentate fashion to all the iron atoms except the two  $\text{Fe}^{\text{III}}$  atoms at the “body” of the butterfly. Magnetic studies indicate an  $S = 10$  ground state<sup>132</sup> with slow relaxation of the magnetization at low temperature<sup>133</sup> and is therefore a SMM.<sup>134</sup> The  $S = 10$  state arises because the spin on the two  $\text{Fe}^{\text{III}}$  sites at the “wing-tips” of the central butterfly are aligned anti-parallel to the spins at the other six  $\text{Fe}^{\text{III}}$  centers.

Replacement of the macrocyclic tridentate amine ligand, tacn, by the tripodal amine ligand tren leads to another octanuclear cage  $[\text{Fe}_8\text{O}_5(\text{O}_2\text{CMe})_8(\text{tren})_4]^{6+}$ .<sup>135</sup> The structure has noncrystallographic  $S_4$  symmetry. There is a central  $\{\text{Fe}_4\text{O}\}$  square, with each edge of the square bridged by an acetate ligand and an oxide, which alternate in being either above or below the plane of the square. The oxides bridge to the four further  $\text{Fe}^{\text{III}}$  centers, which are bound to the tridentate tren ligands. The final four acetates each bridge between one  $\text{Fe}^{\text{III}}$  of the square and an external  $\text{Fe}^{\text{III}}$  site. Preliminary magnetic studies indicate that anti-ferromagnetic exchange dominates, but that either the ground state or a low-lying excited state is paramagnetic. NMR studies reveal that the structure is maintained in solution.

A further cage with  $S_4$  symmetry, this time crystallographically imposed, is  $[\text{Fe}_8\text{O}_4(\text{bmdp})_4(\text{OH})_4(\text{O}_2\text{CMe})_4]^{136}$  (Hbmdp = *N,N,N'*-tris((*N*-methyl)-2-benzimidazolylmethyl)-*N'*-methyl-1,3-diamino-2-propanol, see Scheme 2). This cage was made by reaction of hydrated iron(III) nitrate with the polydentate ligand in water/acetone followed by addition of sodium acetate. This gives a tetranuclear tetracation. Metathesis of the anion with tetrafluoroborate leads to formation of the octanuclear cage. The  $\text{Fe}^{\text{III}}$  centers lie on a square, with four centers at the corners and four at the mid-points of the edges. The  $\text{Fe}\cdots\text{Fe}$  vectors are bridged alternately around the square by either a 1,3 bridging acetate and an alkoxide oxygen from bmdp, or by a  $\mu_2$ -oxide. No magnetic data have been reported for this cage.

A cage of still higher symmetry is formed from reaction of anhydrous  $\text{FeCl}_3$  with pyrazolate.  $[\text{Fe}_8\text{O}_4(\text{pz})_{12}\text{Cl}_4]^{137}$  (Hpz = pyrazole) has a central  $\{\text{Fe}_4\text{O}_4\}$  heterocubane core, with each oxide binding to an additional  $\text{Fe}^{\text{III}}$  center, the oxides are therefore  $\mu_4$  bridging and the additional Fe centers form a second Fe tetrahedron around the first. Each contact between an Fe within the cubane and an external iron is bridged by a pyrazolate ligand, and each external iron has a terminal chloride attached. The cage therefore has noncrystallographic  $T$ -symmetry. The cage shows three reversible reductions between  $-0.43$  V and  $-1.07$  V (vs. ferrocene/ferrocenium). A fourth reduction is irreversible at 285 K, but becomes quasi-reversible at lower temperatures.

$[\text{FeF}(\text{O}_2\text{CCMe}_3)_2]_8^{138}$  is an octanuclear wheel, isostructural with the chromium analog discussed above in Section 7.3.2.2. It has not been studied in as much detail as its chromium counterpart, nor the larger “ferric wheels.”

In  $[\text{Fe}_8\text{O}_4(\text{OCH}_2\text{CCMe}_3)_2(\text{O}_2\text{CPh})_{14}(\text{HOCH}_2\text{CCMe}_3)_2]^{139}$  the core is based on an edge-sharing bitetrahedron, bridged by oxide, alkoxide, and carboxylate ligands. The cage was made by reaction of the oxo-centered iron benzoate triangle with neopentanol in toluene. At the center of the cage six  $\text{Fe}^{\text{III}}$  centers are arranged in a bitetrahedron, with a  $\mu_4$ -oxide at the center of each tetrahedron. The two centers in each tetrahedron which are not in the shared edge are bridged by further oxides, which also bridge to the final iron centers in the polyhedron; these are therefore  $\mu_3$ -oxides. The carboxylates bridge in a typical 1,3-fashion, while the alkoxides are either  $\mu_2$ -bridging or terminal. Magnetic studies reveal antiferromagnetic exchange, leading to an  $S = 0$  ground state.

Reaction of  $\text{FeCl}_3$  with  $\text{Na}(\text{O}_2\text{CR})$  ( $\text{R} = \text{Ph}$  or  $\text{Me}$ ) and  $\text{Na}(\text{hmp})$  in  $\text{MeOH}$  gave further octanuclear cages,  $[\text{Fe}_8\text{O}_4(\text{O}_2\text{CPh})_{11}(\text{hmp})_5]$  and  $[\text{Fe}_8\text{O}_4(\text{O}_2\text{CMe})_{12}(\text{hmp})_4]^{118}$ . The two structures are clearly related, involving four  $\{\text{Fe}_3\text{O}\}$  triangles linked either through a single Fe atom or through a shared  $\text{Fe}_2$  edge. The shared edge is at the center of the cage, creating an  $\{\text{Fe}_4\text{O}_2\}$  butterfly. In the former cage the two terminal triangles are *anti* about the central butterfly, while in the latter cage they are *syn*. The carboxylates adopt their usual 1,3 bridging mode. The hmp groups all chelate to one Fe center, and bridge to a second via the O atom.

A nonanuclear iron cage,  $[\text{Fe}_9\text{O}(\text{cit})_8(\text{H}_2\text{O})_3]^{7-}$  (cit = citrate),<sup>140</sup> has been reported by Bino *et al.* from reaction of iron(III) nitrate, sodium citrate, and 2,9-dimethyl-1,10-phenanthroline in water. The structure consists of three parallel  $\{\text{Fe}_3\}$  units that form a slightly distorted trigonal prism. Each exterior plane is connected to the central fragment by three tetradentate  $\text{cit}^{4-}$  ligands, and is also capped by a further citrate. The central plane has a typical oxo-centered triangle structure, with a central  $\mu_3$ -oxo group surrounded by three  $\text{Fe}^{\text{III}}$  atoms, with each  $\text{Fe}\cdots\text{Fe}$  edge bridged by

two carboxylates from citrate groups. The external planes have  $\{\text{Fe}_3\text{O}_4\}$  cores, with the O atoms supplied by the alkoxide groups of the deprotonated citrates. The remaining coordination sites on the Fe atoms are occupied by terminal carboxylates. No magnetic data are reported.

The first decanuclear iron(III) cage reported was the “ferric wheel,” reported by the Lippard group and shown in Figure 12. This cage has the formula  $[\text{Fe}(\text{OME})_2(\text{O}_2\text{CCH}_2\text{Cl})]_{10}$ .<sup>141</sup> Similar cages have since been reported with other carboxylates: acetate<sup>142</sup> and 3-(4-methylbenzoyl)propionate.<sup>143</sup> The original preparation involves reaction of the oxo-centered triangle of chloroacetate and hydrated iron(III) nitrate in MeOH, however, latter reports suggest that direct reaction of iron(III) nitrate with the sodium salt of the carboxylate and sodium methoxide in MeOH can also be used. The structure consists of a decanuclear wheel, with each  $\text{Fe}\cdots\text{Fe}$  edge bridged by one 1,3 bridging carboxylate and two  $\mu_2$ -methoxides. Magnetic studies of these wheels all show an  $S=0$  ground state in zero field. However, detailed studies<sup>141</sup> show that at 4.6 T, a component of an  $S=1$  state becomes the ground state, then at higher field sequentially  $S=2, 3, 4, 5, 6, 7, 8,$  and 9 states.

$[\text{Fe}_{10}\text{O}_4(\text{OME})_{16}(\text{dbm})_6]$ <sup>144</sup> can be made from a very similar route to that which gives the metallocrown  $[\text{NaFe}_6(\text{OME})_{12}(\text{dbm})_6]^+$ : reaction of  $\text{FeCl}_3$  with Hdbm and  $\text{Na}(\text{OME})$  in MeOH. The structure consists of three layers of a cubic close-packed array of oxygen atoms, with five  $\text{Fe}^{\text{III}}$  ions occupying octahedral holes between each of the layers. The five  $\text{Fe}^{\text{III}}$  sites in each case describe a trapezium. The magnetic behavior indicates a low-spin, probably  $S=0$ , ground state. A very similar core structure is found in  $[\text{Fe}_{10}\text{Cl}_8\text{O}_4(\text{OME})_{14}(\text{MeOH})_6]$ ,<sup>145</sup> where chlorides and MeOH are found in terminal positions. The preparation of the latter cage is simple: addition of hydroxylamine to a MeOH solution of  $\text{FeCl}_2$ . No magnetic data are reported.

$[\text{Fe}_{10}\text{Na}_2\text{O}_6(\text{OH})_4(\text{O}_2\text{CPh})_{10}(\text{chp})_6(\text{H}_2\text{O})_2(\text{Me}_2\text{CO})_2]$  (chp = 6-chloro-2-pyridonate),<sup>142</sup> has a very-high-spin ground state of around  $S=11$ . It is made by reaction of  $[\text{Fe}_2\text{OCl}_6]^{2-}$  with  $\text{Na}(\text{chp})$  and  $\text{Na}(\text{O}_2\text{CPh})$  in MeCN, followed by crystallization from acetone/ether. The  $\{\text{Fe}_{10}\text{O}_{10}\}$  core is perhaps best described as two  $\{\text{Fe}_6\text{O}_6\}$  hexagonal prisms sharing a square face.

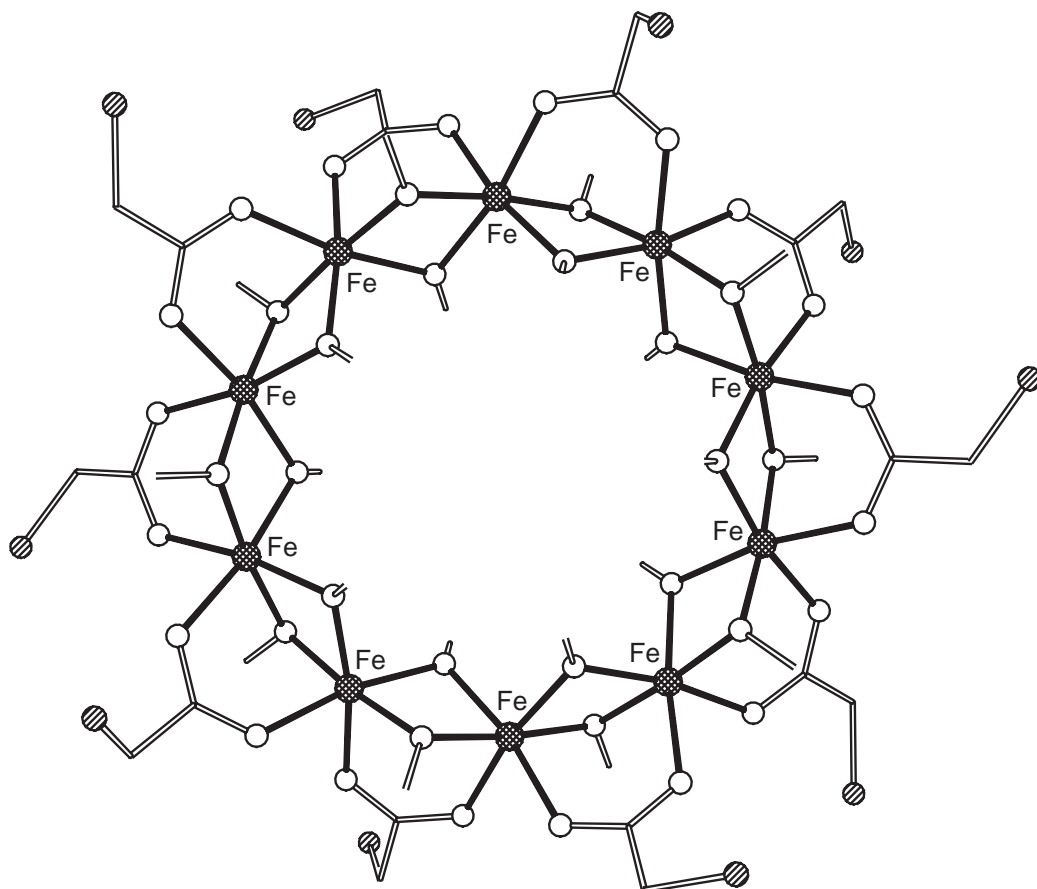


Figure 12 The structure of  $[\text{Fe}(\text{OME})_2(\text{O}_2\text{CCH}_2\text{Cl})]_{10}$ <sup>141</sup> (shading as Figure 10, plus Cl, open).



The complicated structure and mixture of bridging groups present make modeling the variable-temperature magnetic data difficult; however, Cano *et al.* have recently reported Monte Carlo studies which allow exchange parameters to be calculated.<sup>146</sup> AC susceptibility studies also reveal it is a SMM, with an energy barrier of 5.3 K to reorientation of the magnetization.<sup>146</sup>

The first undecanuclear iron cage,  $[\text{Fe}_{11}\text{O}_6(\text{OH})_6(\text{O}_2\text{CPh})_{15}]$ , was also reported by the Lippard group.<sup>147</sup> It is formed by controlled slow hydrolysis of a solution containing  $[\text{Fe}_2\text{OCl}_6]^{2-}$  and  $\text{Na}(\text{O}_2\text{CPh})$  in MeCN. The structure consists of a pentacapped trigonal prism of  $\text{Fe}^{\text{III}}$  centers, with six  $\mu_3$ -oxides inside the prism and six  $\mu_3$ -hydroxides on the exterior of the prism. The carboxylates bridge in a 1,3-fashion. Magnetic studies show a low-spin ground state, probably  $S=1/2$ ; however, there are clearly low-lying excited states of higher spin multiplicity. The presence of exterior hydroxides on this cage make this  $\{\text{Fe}_{11}\}$  core a good model for iron-oxyhydroxide surfaces, and a derivative has been made with the corrosion inhibitor for mild steel, 3-(4-methylbenzoyl)-propionate.<sup>143</sup> This keto-carboxylate shows the same carboxylate binding mode as benzoate; however, the ketone groups form hydrogen bonds to the  $\mu_3$ -hydroxides. It has been suggested that this H bond plays an important part in the utility of 3-(4-methylbenzoyl)-propionate as a surface-modifying agent.<sup>143</sup>

A mixed-valent dodecanuclear iron cage can be made from reaction of iron(II) acetate with lithium methoxide in MeOH, followed by careful addition of dry dioxygen.  $[\text{Fe}_{12}\text{O}_2(\text{OMe})_{18}(\text{O}_2\text{CMe})_6(\text{HOMe})_{4,67}]$ <sup>148</sup> contains four  $\text{Fe}^{\text{III}}$  and eight  $\text{Fe}^{\text{II}}$  centers arranged in a core which is related to the decametallates,  $\{\text{M}_{10}\text{O}_{28}\}$ , found for vanadium and manganese with two additional octahedral Fe sites attached to the decametallate core. The terminal groups are methoxides or acetates, without the “naked” oxygen centers typical of the vanadium cages. The four  $\text{Fe}^{\text{III}}$  sites are assigned as the four metal sites *trans* to the shared edge of a decametallate core. Magnetic studies show a diamagnetic ground state.

It has always been intriguing that the Keggin structure, so well known for  $d^0$  configurations, had not been reported for open-shell configurations. Work from Bino *et al.* has corrected this, with the structure of  $[\text{Fe}_{13}\text{O}_4\text{F}_{24}(\text{OMe})_{12}]^{5-}$ , which has the full  $T_d$  symmetry required by a Keggin ion.<sup>149</sup> The involvement of fluoride appears vital, and possibly this may be the trick to produce further polyoxometallate analogs; terminal  $\text{F}^-$  may function for middle 3d metals the way terminal  $\text{O}^{2-}$  functions for early metals.

Burger and Klüfers have reported a tetradecanuclear iron cluster stabilized by a deprotonated poly-ol ligand—*meso*-butane-1,2,3,4-tetraol (known as erythritol trivially).<sup>150</sup> The 14  $\text{Fe}^{\text{III}}$  centers form a hexacapped cube which is surrounded by  $\text{Ca}^{\text{II}}$  and poly-ol ligands.

A mixed-valent heptadecanuclear iron cage has also been reported by the Lippard group as part of a series of general formula  $[\text{Fe}_{16}\text{MO}_{10}(\text{OH})_{10}(\text{O}_2\text{CPh})_{20}]$  ( $\text{M} = \text{Fe}, \text{Mn}$  or  $\text{Co}$ ).<sup>151</sup> These cages are formed in low yield from reactions of the mixed-valent triangle  $[\text{Fe}_3\text{O}(\text{O}_2\text{CPh})_6(\text{H}_2\text{O})_2(\text{MeCN})]$ ; the  $\{\text{Fe}_{17}\}$  cage results from hydrolysis of a solution of the triangle in MeCN, while the cages containing Mn or Co involved reaction with suitable metal salts prior to crystallization. The structures of all three cages are virtually identical and complicated. The core is in each case a  $\{[\text{Fe}_3\text{O}_3(\text{OH})\text{M}]\}$  double cubane sharing a corner with the divalent ion  $[\text{Mn}^{\text{II}}, \text{Co}^{\text{II}}, \text{or } \text{Fe}^{\text{II}}]$  at the shared corner. This double cubane is surrounded by an  $\{\text{Fe}_{10}\text{O}_4(\text{OH})_4\}$  ring, with the surface coated with benzoate ligands. There are structural similarities to the undecanuclear cages reported by the same group.<sup>147</sup> Magnetic studies show low-spin ground states.

Another heptadecanuclear cage,  $[\text{Fe}_{17}\text{O}_{15}(\text{OH})_6(\text{chp})_{12}(\text{phen})_8(\text{OMe})_3]$ ,<sup>152</sup> can be formed by reaction of  $[\text{Fe}_2\text{OCl}_6]^{2-}$  with  $\text{Na}(\text{chp})$  and phen in MeCN, followed by crystallization from EtOAc—again with a poor yield. The structure is extremely irregular, which may be due to packing of the chelating phen ligands, which leads to “ridges” along the cage.

A further heptadecanuclear cage is found co-crystallized with a nonadecanuclear cage in work from Heath and Powell (Figure 13).<sup>106</sup> More recently, Goodwin *et al.* have isolated the pure nonadecanuclear cage by variation of the polydentate ligand used.<sup>153</sup> The original work used the ligand heidi,  $[\text{H}_3\text{heidi} = \text{N}(\text{CH}_2\text{COOH})_2(\text{CH}_2\text{CH}_2\text{OH})]$ , reacted with hydrated iron nitrate in water, with the pH controlled by addition of pyridine. The more recent work uses methyl or ethyl-substituted derivatives,  $\text{N}(\text{CH}_2\text{COOH})_2(\text{CHRCH}_2\text{OH})$  ( $\text{R} = \text{Me}, \text{metheidi}$  or  $\text{Et}, \text{etheidi}$ ), which traps exclusively the larger cluster. The structures contain a core which resembles a fragment of an  $\{\text{Fe}(\text{OH})_2\}$  lattice, surrounded by the tripodal ligands. The spin ground state for the cage  $[\text{Fe}_{19}(\text{metheidi})_{10}(\text{OH})_{14}\text{O}_6(\text{H}_2\text{O})_{12}(\text{NO}_3)]$  is  $S = 33/2$ , and a small negative zero-field splitting is present. This cage is therefore a SMM with one of the highest spin ground states known.<sup>153</sup>

The final iron cage discussed is the largest known “ferric wheel.” The octadecanuclear wheel,  $[\text{Fe}(\text{OH})(\text{XDK})\text{Fe}_2(\text{OMe})_4(\text{O}_2\text{CMe})_2]_6$ <sup>154</sup> (XDK = the dianion of *m*-xylylenediamine bis(Kemp’s triacid imide), see Scheme 2), shown in Figure 14, is made from reaction of the dinuclear iron

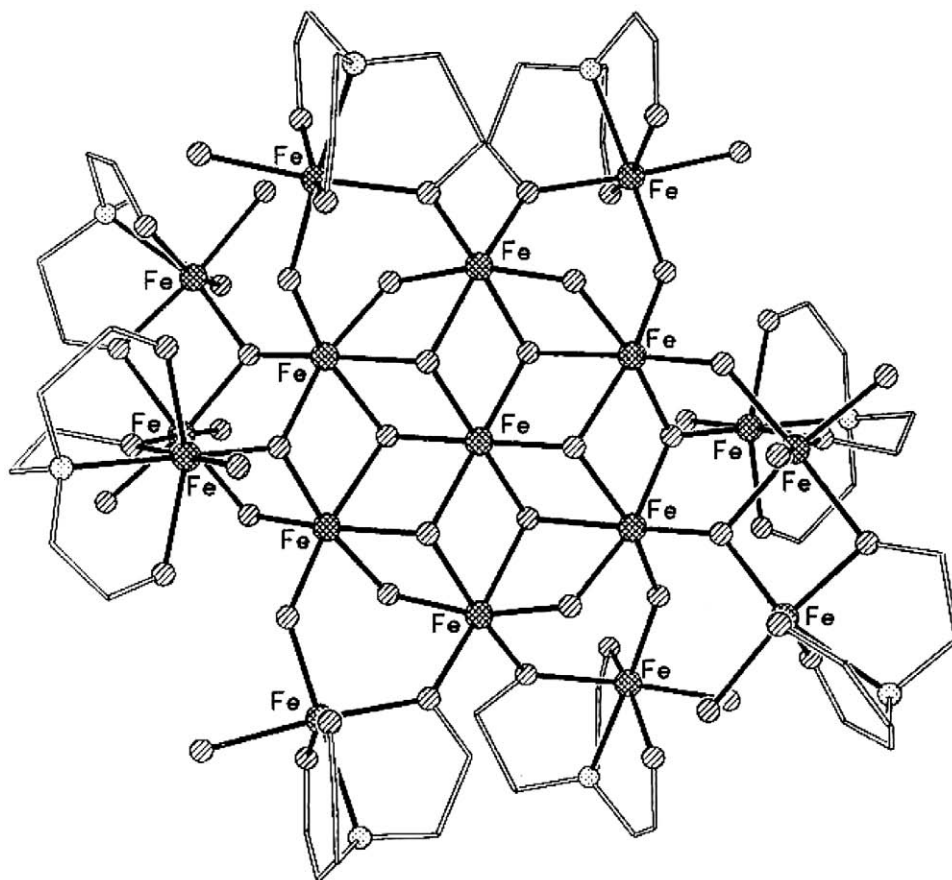


**Figure 13** The structure of  $[\text{Fe}_{17}\text{O}_4(\text{OH})_{16}(\text{heidi})_8(\text{H}_2\text{O})_{12}]^{+106}$  (shading: Fe, hatched; O, striped; C, lines).

complex of XDK with  $[\text{NEt}_4](\text{O}_2\text{CMe})$  in methanol, followed by addition of 1-methylimidazole. The dinuclear units of the precursor are retained, but these are linked by additional  $\text{Fe}^{\text{III}}$  centers which are bridged to the dinuclear units through two  $\mu_2\text{-OMe}$  and one acetate bridges. Magnetic studies reveal the usual anti-ferromagnetic exchange between  $\text{Fe}^{\text{III}}$  centers, resulting in a diamagnetic ground state.

### 7.3.2.5 Cobalt

There are far fewer high-nuclearity cages known for cobalt than for manganese or iron and their magnetic properties have not been well studied. Unless otherwise stated, magnetic data have not been reported for the following complexes.

The first hexanuclear cobalt(II) cage reported was  $[\text{Co}_6(\text{O}_2\text{CNET}_2)_{12}]$ ,<sup>155</sup> which has a similar structure to  $\text{Mn}^{\text{II}}$  and  $\text{Fe}^{\text{II}}$  complexes of the same ligand (see Sections 7.3.2.3 and 7.3.2.4 above).

A hexanuclear cobalt(II) metallocrown has been reported by Thornton and co-workers.<sup>156</sup> Reaction of  $\text{Na}(\text{OMe})$  with cobalt(II) acetate and Hmhp in MeOH apparently gives  $[\text{Co}_6\text{Na}(\text{mhp})_{12}]^+$ ; an anion was not located in a highly disordered crystal structure. A yield is not reported, and crystallization required a period of months. The structure contains six tetrahedral  $\text{Co}^{\text{II}}$  centers each bound to two N and two O donors from pyridonate ligands. Six of these oxygen atoms lie within the metallocycle, and form an ideal cavity for coordination of sodium. This cage is closely related to the previously reported hexanuclear copper metallocrown,  $[\text{Cu}_6\text{Na}(\text{mhp})_{12}]^+$ <sup>157</sup> (see Section 7.3.2.7 below).

A better-characterized cobalt wheel is made from the solvothermal reaction of hydrated cobalt nitrate with the tripodal ligand  $\text{N}(\text{CH}_2\text{PO}_3\text{H}_2)(\text{CH}_2\text{CO}_2\text{H})_2$  in the presence of KOH in MeOH.<sup>158</sup> Within  $\text{K}_2[\text{Co}\{\text{N}(\text{CH}_2\text{PO}_3)(\text{CH}_2\text{CO}_2)_2\}_6]$  each cobalt(II) center is five-coordinate, with a trigonal bipyramidal geometry. This compound shows a room-temperature magnetic moment consistent

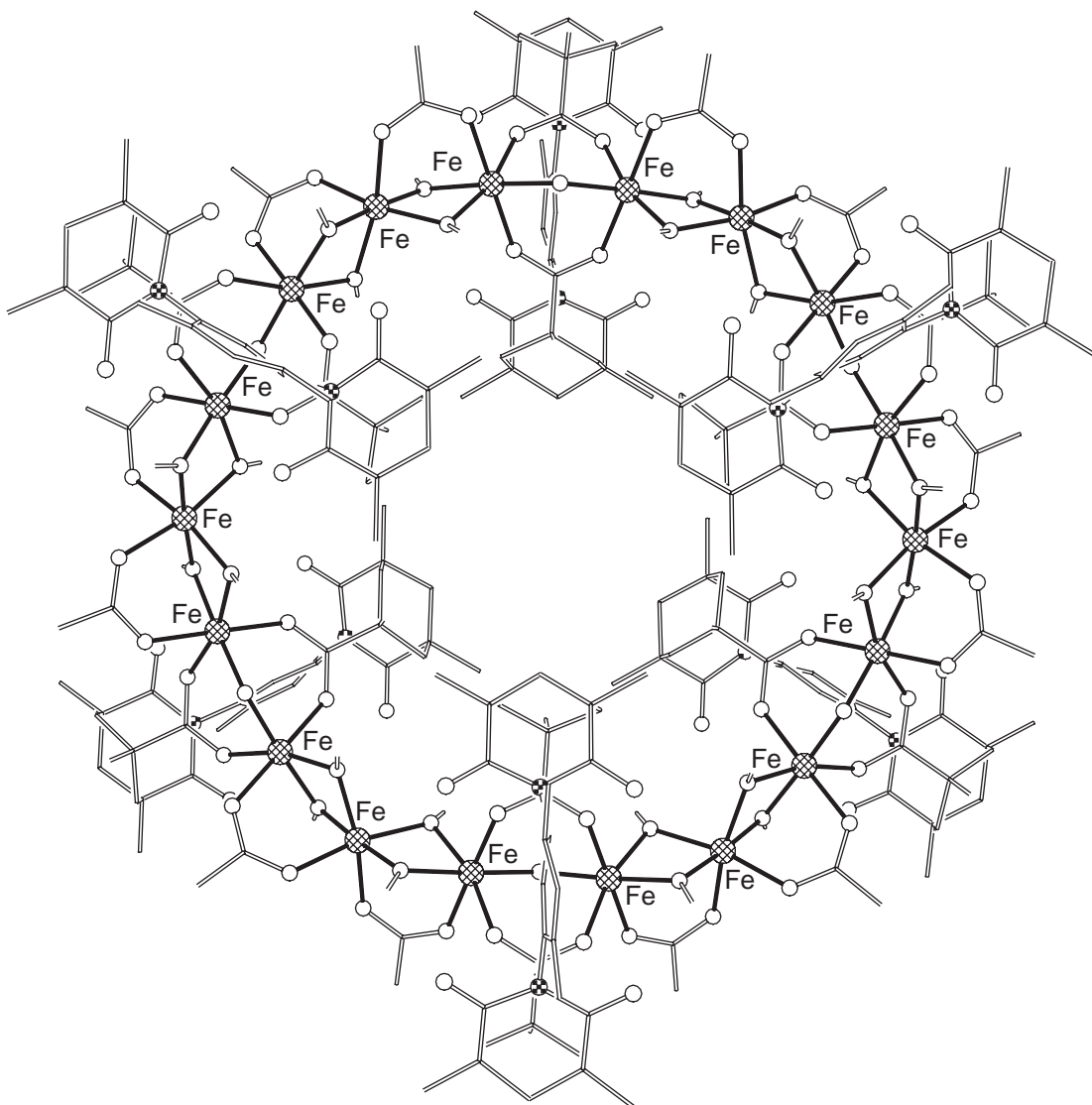


**Figure 14** The structure of  $[\text{Fe}(\text{OH})(\text{XDK})\text{Fe}_2(\text{OMe})_4(\text{O}_2\text{CMe})_2]_6$ <sup>154</sup> (shading: Fe, hatched; O, open; C, lines).

with noninteracting cobalt(II) centers; at 14 K there is a magnetic phase transition to a canted antiferromagnetic state.<sup>158</sup>

A planar hexanuclear cobalt cage,  $[\text{Co}_6\{(\text{PhSiO}_2)_6\}_2\text{Cl}(\text{solvent})_6]^-$ , which has the same metal core as a manganese(II) cage, has been reported.<sup>63</sup> The experimental details are so limited that it is difficult to identify the molecules attached in the axial positions of the six cobalt centers.

A further hexanuclear cobalt cage involves 6-(diethylamino)-2-hydroxo-4-sulfanyl-1,3,5-triazine- $(\text{H}_2\text{OSta})$  and a condensation product of this ligand.<sup>159</sup> The cage was formed in very poor yield by reaction of  $\text{Na}(\text{OSta})$  with cobalt(II) chloride and  $\text{Na}(\text{O}_2\text{CPh})$ . The complex has the formula  $[\text{Co}_6\text{NaO}(\text{OSta})_7(\text{L7})_2(\text{O}_2\text{CPh})_2(\text{H}_2\text{O})_2]$ , and a complicated array of two  $\text{Co}^{\text{III}}$  and four  $\text{Co}^{\text{II}}$  sites.

At the opposite extreme, the cage  $[\text{Co}(\text{hathc})]_6$ <sup>24-</sup> ( $\text{H}_6\text{hathc}$  = hexazatriphenylenehexacarboxylic acid) has a beautifully simple structure:<sup>160</sup> the  $\text{Co}^{\text{III}}$  centers are at six of the eight corners of a cube and ligands lie on each edge creating a chair conformation. The magnetic moment of this cage falls with temperature.

Six cobalt centers are also found in the mixed-metal cage  $[\text{Co}_6\text{Cu}_2(\text{OH})_4(\text{mhp})_2(\text{O}_2\text{CPh})_{10}(\text{mhp})_2(\text{Hmhp})_4(\text{H}_2\text{O})_2]$ ,<sup>161</sup> which is formed by reaction of a mixture of copper and cobalt benzoates with  $\text{Hmhp}$ , followed by crystallization from  $\text{EtOAc}$ . The structure is dominated by oxo-centered metal triangles. At the core of the cage is a  $\{\text{Co}_4\text{O}_2\}$  butterfly. The wing-tip cobalt sites are then each part of a further  $\{\text{Co}_2\text{CuO}\}$  triangle. All  $\text{Co}^{\text{II}}$  sites have octahedral

coordination geometry, while the two  $\text{Cu}^{\text{III}}$  are five-coordinate. The benzoate ligands show three different binding modes: two are bound through a single oxygen to a cobalt; two are 3.21 bridging; the remainder bridge in the conventional 2.11-fashion. The mhp ligands chelate to the copper sites, and bridge to a cobalt atom through the oxygen donor.

The equivalent reaction involving copper and cobalt acetates reacted with Hchp gives a non-nuclear cage,  $[\text{Co}_7\text{Cu}_2(\text{OH})_2(\text{chp})_{10}(\text{O}_2\text{CMe})_6]$ .<sup>161</sup> Here, the copper sites are both five-coordinate, while the cobalt atoms are found with either five or six ligands bound to them. The polyhedron defined by the metal sites is extremely irregular. The seven  $\text{Co}^{\text{II}}$  sites can be described as belonging to two  $\{\text{Co}_4\text{O}_2\}$  butterflies which share a body vertex. The two  $\text{Cu}^{\text{II}}$  atoms then cap opposite edges of this central  $\{\text{Co}_7\text{O}_4\}$  fragment. Magnetic studies indicate a spin ground state of at most  $S = 3/2$ .

A series of heptanuclear cobalt cages has been reported of general formula  $[\text{Co}_7(\text{OH})_2(\text{O}_2\text{CR})_4(\text{chp})_8(\text{solv})]$ ,<sup>162</sup> where  $\text{R} = \text{Ph}$  or  $\text{CMe}_3$  and  $\text{solv} = \text{MeCN}$  or  $0.69 \text{ Hchp}:0.31 \text{ MeCN}$  or  $0.75 \text{ Hchp}:0.25\text{H}_2\text{O}$ . The basic structure consists of a square-based pyramid of  $\text{Co}^{\text{II}}$  centers capped on one triangular face and on the adjacent edge of the square base by two further cobalt atoms. One of the  $\mu_3$ -hydroxides bridges between the capping atom on the edge and the two atoms within the edge, while the second  $\mu_3$ -hydroxide bridges the three Co centers in the triangular face opposite. The four carboxylates are all 2.11 bridging; however, the eight pyridonates show four different bonding modes.

The other heptanuclear cobalt(II) cage in the literature involves *o*-mercaptophenolate ligands.  $[\text{Co}_7\text{Na}_2(1,2\text{-OSC}_6\text{H}_4)_8(\text{DMF})_{12}]$ <sup>163</sup> is formed from reaction of  $\text{CoBr}(\text{PPh}_3)_3$  with sodium mercaptophenolate in DMF. The structure consists of an almost linear chain of five tetrahedrally coordinated  $\text{Co}^{\text{II}}$  and two sodium centers, with two further Co centers attached at the end of the chain. The room-temperature magnetic moment is a little lower than would be expected for seven cobalt(II) centers.

The octanuclear cobalt cages fall into two categories. A number of mixed-valence clusters based on cubane cores have been reported, and there are two cyclic structures known. The cubane cages have two distinct structures. The earlier structure, found in  $[\text{Co}_8\text{O}_4(\text{O}_2\text{CPh})_{12}(\text{solv})_3(\text{H}_2\text{O})]^{48}$  and ( $\text{solv} = \text{MeCN}$  or DMF), contains a central  $\{\text{Co}_4\text{O}_4\}$  heterocubane, with each oxide also bridging to a further cobalt site, and thus acting as a  $\mu_4$  bridge. These structures are therefore directly analogous to an octanuclear chromium cage (see Section 7.3.2.2 above). These cobalt cubanes are made from addition of hydrogen peroxide to cobalt(II) benzoate dissolved in either DMF or MeCN. Structural parameters indicate that the molecule is valence-trapped with the cobalt sites within the heterocubane being  $\text{Co}^{\text{III}}$  and the external sites  $\text{Co}^{\text{II}}$ . Each  $\text{Co}^{\text{III}}\cdots\text{Co}^{\text{II}}$  contact is bridged by a 2.11-bound benzoate. The external  $\text{Co}^{\text{II}}$  sites have trigonal bipyramidal coordination geometries, with the fifth coordination site occupied by a solvent molecule. Magnetic studies show a decline in magnetic moment with temperature; however, this decline is likely to be due to single ion effects of the five-coordinate  $\text{Co}^{\text{II}}$  sites, rather than as a result of antiferromagnetic exchange between them. These cages have interpretable <sup>1</sup>H-NMR spectra, which suggest the structures are maintained in solution.

The second cubane-related structure was originally found in  $[\text{Co}_8\text{O}_4(\text{OH})_4(\text{O}_2\text{CMe})_6(\text{L8})_2]^{2+}$  ( $\text{L8} = 1,2\text{-bis}(2,2'\text{-bipyridyl-6-yl})\text{ethane}$ ).<sup>164</sup> The cage forms from treatment of an ethanol solution of cobalt(II) acetate and L8 with hydrogen peroxide. The structure consists of a triple-cubane structure, with the central  $\{\text{Co}_4\text{O}_4\}$  heterocubane containing four  $\text{Co}^{\text{III}}$  centers and the four  $\text{Co}^{\text{II}}$  centers in the exterior sites of the cage. The four  $\mu_4$ -oxides have a "saw-horse" arrangement. There are also four  $\mu_3$ -hydroxides which bridge within the exterior cubanes. Each  $\text{Co}^{\text{II}}\cdots\text{Co}^{\text{II}}$  edge is bridged by a bis(bipyridyl) ligand while the carboxylate ligands bridge in a 1,3 fashion across six of the faces of the triple cubane. Magnetic studies again show a decline in magnetic moment with temperature. A very similar structure is found for  $[\text{Co}_8\text{O}_4(\text{O}_2\text{CMe})_6(\text{OMe})_4\text{-Cl}_4(\text{OH})_n]^{4-}$  ( $n = 1$  or  $2$ ),<sup>50</sup> which is formed by passing ozone through a solution of cobalt(II) acetate in acetic acid. The triple cubane and the bridging modes adopted by carboxylate and  $\mu_4$ -oxide ligands are identical to those in the former cage,<sup>164</sup> with the role of the  $\mu_3$ -hydroxides taken by  $\mu_3$ -methoxides. The formula as written suggests that at least six  $\text{Co}^{\text{III}}$  centers are present; however, the room-temperature magnetic moment reported is too high for this proposition to be correct.

The two known octanuclear cobalt(II) wheels contain very different ligands  $[\text{Co}_8(\text{L9})_{12}(\text{ClO}_4)]^{3+}$  ( $\text{L9} = \text{bis}\{3\text{-(2-pyridyl)pyrazol-1-yl}\}$  dihydroborate, see Scheme 2).<sup>165</sup> The eight  $\text{Co}^{\text{II}}$  centers are each bound to three ligands which act as bidentate ligands to individual centers, then bridge to a second. Either one or two L9 units bridge the  $\text{Co}\cdots\text{Co}$  edges of the octagon. A perchlorate anion is found at the center of the ring. Electrospray mass spectrometry indicates the structure is maintained in solution, including the encapsulated anion.

$[\text{Co}_8(\text{O}_2\text{CMe})_8(\text{OMe})_{16}]^{166}$  is a much more typical wheel, clearly related to the “ferric” and chromium wheels described above. The cage is formed by dissolution of cobalt(III) acetate in MeOH in the presence of  $\text{NH}_4\text{PF}_6$ . Each  $\text{Co}\cdots\text{Co}$  edge is bridged by two methoxides and one carboxylate. An ammonium cation is found at the center of the cage. As the cage contains exclusively  $\text{Co}^{\text{III}}$  centers it is diamagnetic.

The nonanuclear cobalt(II) cage  $[\text{Co}_9(\text{chp})_{18}]^{167}$  shown in Figure 15, is a rare example of a homoleptic paramagnetic cage. It is formed by reaction of freshly prepared cobalt hydroxide with Hchp at  $130^\circ\text{C}$ , followed by crystallization from EtOAc. The structure has crystallographic  $D_{3d}$  symmetry and contains four  $\{\text{Co}_4\text{O}_6\}$  adamantanes, sharing either  $\{\text{Co}_3\text{O}_3\}$  faces or a single cobalt vertex. The chp ligands each bind in a 2.21 fashion (Harris notation), i.e., chelating to one cobalt center through both N- and O-donors, and bridging to a second cobalt through the oxygen.

The nonanuclear cobalt(II) cage,  $[\text{Co}_9\{(\text{py})_2\text{CO}_2\}_4(\text{O}_2\text{CMe})_8(\text{OH})_2]^{168}$  shown in Figure 16, is formed by reaction of cobalt(II) acetate and di-2-pyridylketone,  $(\text{py})_2\text{CO}$ , in MeCN. This structure contains two  $\{\text{Co}_5\}$  square-based pyramids sharing a cobalt vertex. The two hydroxides bridge the four cobalt centers within the square bases while each of the eight acetates bridge an edge of the base. The two pyramids are bridged by the  $\{(\text{py})_2\text{CO}_2\}$  dianions which act as 5.3311 ligands (Harris notation). The central Co atom is bound to all eight oxygens from the four  $\{(\text{py})_2\text{CO}_2\}$  dianions. Magnetic studies reveal a fall in magnetic moment with temperature. Perlepes and co-workers have shown the hydroxide can be replaced by azide,<sup>169</sup> with a dramatic transformation of the magnetic behavior. The analogous nickel chemistry is equally exciting.<sup>170</sup>

The four decanuclear cobalt cages known all come from similar chemistry, which originally gave a dodecanuclear cage,  $[\text{Co}_{12}(\text{OH})_6(\text{mhp})_{12}(\text{O}_2\text{CMe})_6]^{171}$ . The dodecanuclear cage was reported by Garner and co-workers in 1983 from reaction of cobalt acetate with Hmhp. The structure contains a centered-pentacapped trigonal prism; however, while the dodecanuclear nickel analog has since been reported,<sup>172</sup> no further studies of the original  $\{\text{Co}_{12}\}$  have been possible. Two decanuclear cages,  $[\text{Co}_{10}(\text{OH})_6(\text{mhp})_6(\text{O}_2\text{CPh})_7(\text{Hmhp})_3\text{Cl}(\text{MeCN})]$  and  $[\text{Co}_{10}(\text{OH})_6(\text{mhp})_6(\text{O}_2\text{CCMe}_3)_7(\text{Hmhp})\text{Cl}(\text{MeCN})_3]$ , contain a similar core, but it is now a centered-tricapped-trigonal prism (ttp) missing the two caps on the trigonal face.<sup>172</sup>

$[\text{Co}_{10}(\text{OH})_4(\text{chp})_{10}(\text{O}_2\text{CCMe}_3)_6(\text{EtOH})_2]^{172}$  was made from a similar reaction, involving cobalt chloride, Na(chp), and  $\text{Na}(\text{O}_2\text{CCMe}_3)$  in MeOH, followed by crystallization from EtOH. Here, the pentacapped centered-trigonal prism in  $(\text{Co}_{12})$  is missing two metal centers from one edge of the prism.

$[\text{Co}_{10}(\text{OH})_6(\text{mhp})_6(\text{O}_2\text{CCPh}_3)_6(\text{Hmhp})_3(\text{HCO}_3)_3]^{173}$  is formed in very low yield from reaction of cobalt chloride with Na(mhp) and  $\text{Na}(\text{O}_2\text{CCPh}_3)$  in MeOH, followed by crystallization from

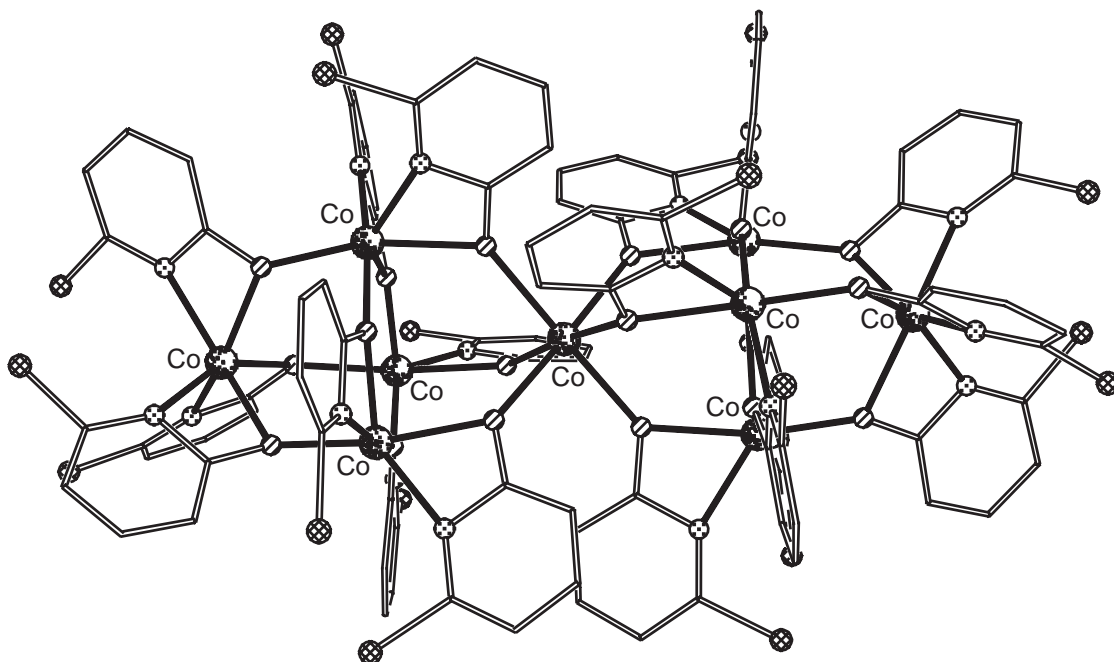
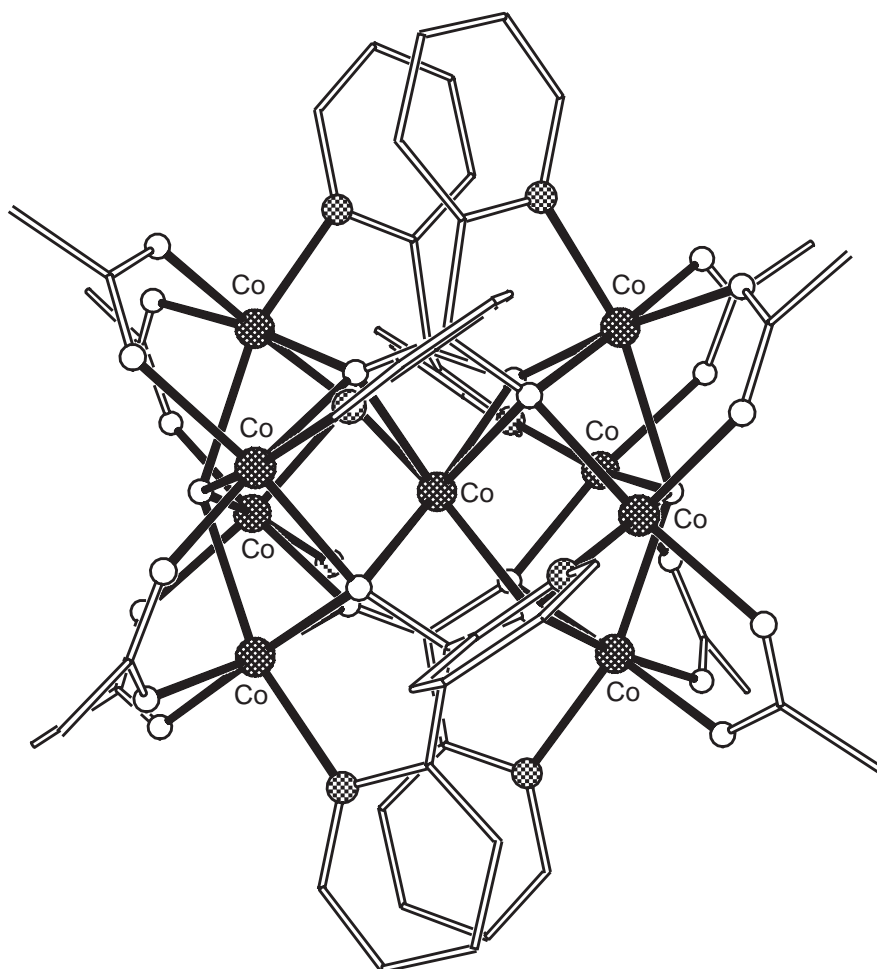


Figure 15 The structure of  $[\text{Co}_9(\text{chp})_{18}]^{167}$  (shading: Co, random shading; O, striped, N, dotted; C, lines).



**Figure 16** The structure of  $[\text{Co}_9\{(\text{py})_2\text{CO}_2\}_4(\text{O}_2\text{CMe})_8(\text{OH})_2]$ <sup>168</sup> (shading: Co, hatched; O, open; N, dotted; C, lines).

EtOAc. The structure contains a centered trigonal prism; however, this prism is capped on the midpoint of the edges of the prism. The central cobalt site is  $\text{Co}^{\text{III}}$ , rather than  $\text{Co}^{\text{II}}$  and is surrounded by six  $\mu_3$ -hydroxides, which each bridge to a cobalt at a vertex of the prism and a capping cobalt site. The triphenylacetate ligands bind in the 2.11 mode, while the mhp ligands each adopt the 2.21 mode. A curiosity of the structure is the apparent presence of coordinated hydrogen carbonate.

A second dodecanuclear cage,  $[\text{Co}_{12}(\text{chp})_{18}(\text{OH})_4\text{Cl}_2(\text{Hchp})_2(\text{MeOH})_2]$ , is known.<sup>174</sup> This cage is centrosymmetric, and contains two  $\{\text{Co}_4\text{O}_3\text{Cl}\}$  cubanes linked by a central eight-membered ring involving four  $\text{Co}^{\text{II}}$  centers and four O atoms from pyridonate ligands. The final cobalt sites are at the periphery of the cage and are attached to the cubanes through  $\mu_2$  oxygen atoms from chp ligands. The chp ligands show four different bonding modes.

A tridecanuclear cobalt cage,  $[\text{Co}_{13}(\text{chp})_{20}(\text{phth})_2(\text{OH})_2]$ ,<sup>162</sup> shown in Figure 17, can be made by the procedure which gives the heptanuclear cobalt pyridonate cages, but replacing the monocarboxylate ligand benzoate with the dicarboxylate ligand, phthalate. The structure contains an irregular, centrosymmetric cage, which can be considered to contain two square-based pyramids of  $\text{Co}^{\text{II}}$  centers arranged about a central cobalt, which lies on the crystallographic inversion center. Two further  $\text{Co}^{\text{II}}$  sites cap edges of the square bases of the pyramids. The two phthlate ligands are both bound to four metal centers, with a 4.1111 mode in Harris notation, while the 20 pyridonate ligands adopt three binding modes: 3.21, 2.21, and 3.31.<sup>162</sup>

The largest cobalt cage reported is  $[\text{Co}_{24}(\text{OH})_{18}(\text{OMe})_2\text{Cl}_6(\text{mhp})_{22}]$ .<sup>107</sup> This is formed by reaction of partially hydrated cobalt chloride with  $\text{Na}(\text{mhp})$  in MeOH, followed by evaporation to dryness and crystallization from EtOAc. The structure is based on the structure of cobalt hydroxide, with a central raft of  $\{\text{Co}_3(\text{OH})_4\}$  incomplete cubanes sharing edges, surrounded by mhp ligands. Ten of the cobalt(II) sites at the center of the cage have regular octahedral

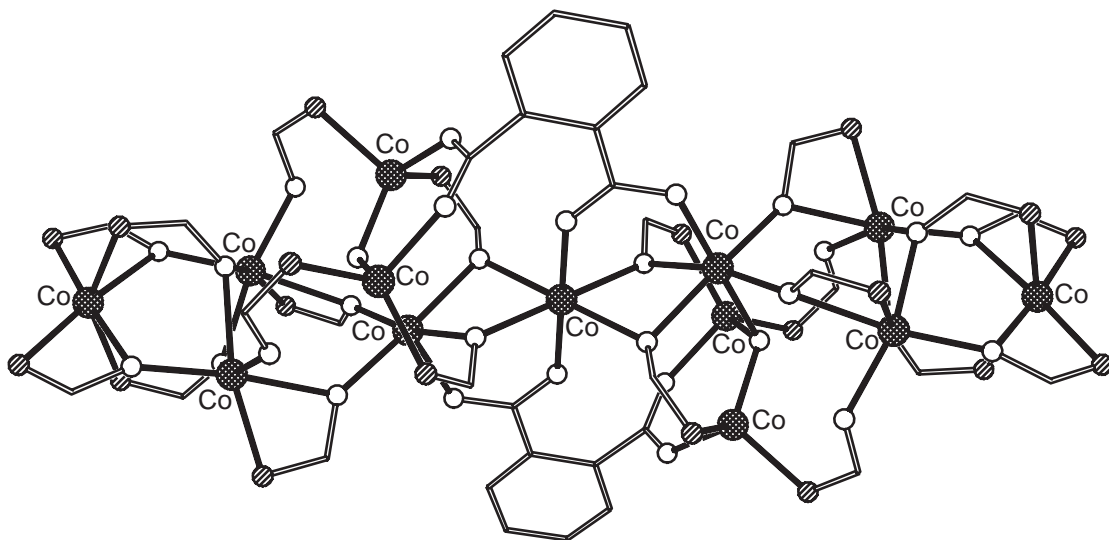


**Figure 17** The structure of  $[\text{Co}_{13}(\text{chp})_{20}(\text{phth})_2(\text{OH})_2]$ <sup>162</sup> with all C atoms of pyridonate ligands except C2 removed for clarity (shading: Co, hatched; O, open; N, striped; C, lines).

geometries, while the cobalt sites at the periphery have very distorted geometries. The mhp ligands adopt three binding modes: 2.11, 2.21, and 3.21. It is clear that the immense coordinative flexibility of the pyridonate ligands is important in stabilizing these large cobalt cages. The structure is clearly related to the  $\{\text{Fe}_{19}\}$  cages reported by Heath and Powell.<sup>106,153</sup>

### 7.3.2.6 Nickel

High-nuclearity cage complexes of nickel(II) with O- or N-donor ligands are rather rare, which is surprising as ferromagnetic exchange is frequently found for this metal in smaller cages, and hence high-spin ground states could be expected. Some of the chemistry is very similar to that of cobalt.<sup>161,167,170,172</sup>

A heterometallic cage,  $[\text{Ni}_6\text{Zn}_2\text{O}_2(\text{O}_2\text{CNiPr}_2)_{12}]$ , was made by addition of  $[\text{Ni}(\text{MeCN})_6][\text{ZiCl}_4]$  to a toluene solution of  $\text{HNiPr}_2$  which had been previously saturated with  $\text{CO}_2$ .<sup>175</sup> The structure is very similar to  $[\text{Fe}_8\text{O}_2(\text{O}_2\text{CNiPr}_2)_{12}]$ <sup>120</sup> and contains two oxo-centered  $\{\text{Ni}_3\text{Zn}\}$  tetrahedra, bridged by carbamate ligands. The nickel sites have trigonal bipyramidal geometries and the zinc sites are tetrahedral. No magnetic data were reported.

The hexanuclear cage  $[\text{Ni}_6\{\text{PhSiO}_2\}_6\text{Cl}(\text{ROH})_6]$  ( $\text{R} = \text{Et}$  or  $n\text{Bu}$ )<sup>176</sup> is very similar to Mn and Co cages with this ligand.<sup>63</sup> Magnetic studies show anti-ferromagnetic exchange between the nickel centers, leading to an  $S=0$  ground state.<sup>176</sup> A related octanuclear nickel cage has also been reported.<sup>177</sup>

Three further heterometallic cages containing six nickel centers have been reported. The first,  $[\text{Ni}_6\text{Cu}_2(\text{OH})_4(\text{mhp})_2(\text{O}_2\text{CPh})_{10}(\text{mhp})_2(\text{Hmhp})_4(\text{H}_2\text{O})_2]$ , is isostructural with the cobalt cage, and is made by an analogous procedure.<sup>161</sup> The other two contain central 4f ions surrounded by nickel-containing “complex ligands.” Yukawa and co-workers reported  $[\text{Sm}\{\text{Ni}(\text{pro})_2\}_6]^{3+}$  ( $\text{pro} = \text{L-proline}$ ) (Figure 18),<sup>178</sup> and the Schröder group reported  $[\text{La}\{\text{Ni}(\text{L1})\}_6]^{3+}$  (for L1 see Scheme 2),<sup>72</sup> very similar principles apply to both structures. A nickel(II) center is coordinated by two N- and two O-donors from the ligands, either two prolines or one L1 ligand, with a square geometry. Six of these units then coordinate to a lanthanoid ion, which has an icosahedral coordination geometry. Carboxylate oxygens from neighboring units bind to the apical positions of the nickel centers, making the nickel sites octahedral and hence paramagnetic. No magnetic data are reported for any of these heterometallic complexes. The complex ligand  $\{\text{Ni}(\text{L1})\}$  can also be used to construct a nonanuclear cage,  $[\text{Na}_4\{\text{Ni}(\text{L1})\}_9(\text{H}_2\text{O})(\text{MeOH})(\text{ClO}_4)]^{3+72}$  in which the Ni centers are arranged in a tricapped trigonal prism encapsulating the four sodium ions. This surprising change in nuclearity may be related to the size of the cavity of the metallocryptand; the icosahedral cavity formed in  $[\text{La}\{\text{Ni}(\text{L1})\}_6]^{3+}$  is probably too large for a single sodium center, but too small for two.



**Figure 18** The structure of  $[\text{Sm}\{\text{Ni}(\text{pro})_2\}_6]^{3+178}$  (shading: Ni, hatched; Sm, striped top-left bottom-right; O, striped top-right bottom-left; N, dotted; C, shaded).

$[\text{Ni}_7(\text{OH})_4(\text{NO}_2)_8(\text{OHpn})_2(\text{Opn})_2]$  (**89**) (OHpn = 1,3-diamino-2-propanol) was reported in 1996,<sup>179</sup> however without any description of the preparation. The structure consists of a distorted hexagon of  $\text{Ni}^{\text{II}}$  centers, with a seventh nickel at the center. Magnetic studies reveal antiferromagnetic exchange between the spin centers, giving a low-spin ground state, presumably  $S = 1$ .

$[\text{Ni}_7(\text{chp})_{12}\text{Cl}_2(\text{MeOH})_6]$  and  $[\text{Ni}_7(\text{chp})_{12}(\text{OH})_2(\text{MeOH})_6]$  are formed from reaction of freshly prepared nickel hydroxide or methoxide with Hchp at 130 °C.<sup>167</sup> Both cages contain  $\{\text{Ni}_4\text{O}_6\}$  adamantanes sharing a nickel vertex, and are therefore related to  $[\text{Co}_9(\text{chp})_{18}]$ .<sup>167</sup> The oxygen atoms on the  $\text{Ni}\cdots\text{Ni}$  edges are from chp ligands, which all adopt the 2.21 bonding mode. In the former  $\{\text{Ni}_7\}$  cage the adamantane cages are regular, and the vacant sites on the exterior triangular nickel faces are occupied by six MeOH ligands, which then H bond to two chloride counter-ions. In the latter this regularity is lost, as a  $\mu_3$  hydroxide is found at the center of each of these faces. A closely related nonanuclear cage,  $[\text{Ni}_9(\text{chp})_{16}(\text{OH})_2(\text{MeCN})_2]$ , has also been prepared.<sup>167</sup> This is an extension of the distorted  $\{\text{Ni}_7\}$ , but with two of the coordination sites on each triangular face occupied by O-donors from  $\{\text{Ni}(\text{chp})_3\}$ —“complex ligands”; the third O atom of this unit H bonds to the  $\mu_3$  hydroxide group. Magnetic studies are not reported.

$[\text{Ni}_7(\text{tepra})_4\text{Cl}_2]$  is made by reaction of nickel chloride with the ligand in refluxing naphthalene in the presence of *t*-butoxide as a base.<sup>180</sup> The structure has approximate  $D_4$  symmetry, with the linear  $\{\text{Ni}_7\}$  wire surrounded by four polydentate ligands. The inner five Ni centers have square planar geometries, disregarding  $\text{Ni}\cdots\text{Ni}$  contacts, and are therefore diamagnetic, while the outer



two Ni centers are square pyramidal. Anti-ferromagnetic exchange is found between these two paramagnetic centers.

An octanuclear nickel(II) cage,  $[\text{Ni}_4(\text{cit})_3(\text{OH})(\text{H}_2\text{O})]_2^{5-}$ , is formed from the reaction of nickel hydroxide and citric acid in water at pH 9.20.<sup>181</sup> The structure consists of two highly distorted tetrahedral  $\text{Ni}^{\text{II}}$  centers whose coordination sites are occupied in the main by oxygen donors from the citrate ligands. No magnetic data are reported. This work has been extended by Murrie *et al.*<sup>182</sup> who have produced  $\{\text{Ni}_7\}$  and  $\{\text{Ni}_{21}\}$  cages by varying the conditions reported. Control is achieved through pH variation and crystallization times.  $[\text{Ni}_7(\text{cit})_6(\text{H}_2\text{O})_2]^{10-}$  contains two O-centered Ni triangles linked via a seventh nickel. The citrates are tetradeprotonated and use all binding groups. Magnetic data suggest an  $S=7$  ground state, due to weak ferromagnetic exchange interactions.

An apparently mixed-valent nonanuclear nickel cage has been reported with trimethylacetate ligands.<sup>183</sup>  $[\text{Ni}_9\text{O}_3(\text{OH})_3(\text{O}_2\text{CCMe}_3)_{12}(\text{HO}_2\text{CCMe}_3)_4]$  can be made by reaction of nickel chloride with potassium pivalate in water, followed by extraction of the precipitate into  $\text{CH}_2\text{Cl}_2$ , benzene, or hexane. A mirror plane passes through the center of the molecule. Six of the Ni centers form a trigonal prism, with the three further nickel centers forming a  $\{\text{Ni}_3\text{O}\}$  oxo-centered triangle. A  $\mu_4$  oxygen links the two Ni atoms in one edge of the prism to two Ni atoms comprising one edge of the triangle. The exterior of the cage is then coated with carboxylate ligands, which show a range of binding modes, including 1,3 and 1,1,3 bridging and terminally bound through one O-donor. The authors suggest  $\text{Ni}^{\text{III}}$  is present in addition to  $\text{Ni}^{\text{II}}$ , however neither the synthesis nor the structural parameters for each Ni center support this proposition. It is more likely that additional protons are present, possibly attached to the "oxide" ligands. Magnetic data are reported down to 83 K, which suggest weak anti-ferromagnetic exchange between metal centers.

A further nonanuclear cage,  $[\text{Ni}_9(\text{CO}_3)(\text{OH})_6(\text{chp})_3(\text{Hchp})_3(\text{O}_2\text{CCH}_2\text{NMe}_3)_9\text{Cl}]^{6+}$ , is formed from the reaction of hydrated nickel chloride,  $\text{Na}(\text{chp})$ , and  $\text{O}_2\text{CCH}_2\text{NMe}_3$  in MeOH, followed by crystallization from EtOAc.<sup>173</sup> The yield is extremely poor. Two features dominate the structure. First, a central carbonate ion which is  $\mu_6$  bridging, leading to a planar hexagon of Ni centers. Secondly, the preference of the tertiary ammonium groups of the nine betaine ligands to lie as far apart as possible leads to a very open structure.

$[\text{Ni}_9\{(\text{py})_2\text{CO}_2\}_4(\text{O}_2\text{CMe})_8(\text{OH})_2]$  has been prepared, which has an analogous structure to the nonanuclear cobalt cage  $[\text{Co}_9\{(\text{py})_2\text{CO}_2\}_4(\text{O}_2\text{CMe})_8(\text{OH})_2]$ ,<sup>168</sup> discussed previously in Section 7.3.2.5 (see also Figure 16). This has an  $S=1$  ground state. Perlepes *et al.* have shown that this hydroxide can be replaced by azide, leading to an  $S=9$  ground state.<sup>170</sup> This is exciting chemistry, not only because of the dramatic transformation in the magnetic properties, but because it is a rare example of reaction chemistry taking place at a coordination cage with the structure remaining intact.

Decanuclear, undecanuclear, and dodecanuclear nickel cages can be made by similar chemistry to that employed for cobalt cages.<sup>172</sup> The decanuclear cages  $[\text{Ni}_{10}(\text{OH})_6(\text{mhp})_{6.5}(\text{O}_2\text{CCHMe}_2)_{6.5}(\text{Hmhp})_3\text{Cl}(\text{H}_2\text{O})]$  and  $[\text{Ni}_{10}(\text{OH})_6(\text{chp})_6(\text{O}_2\text{CCHPh}_2)_6(\text{Cl})_2(\text{Hchp})(\text{H}_2\text{O})_2(\text{MeOH})]$  both involve carboxylates with two substituents at the  $\alpha$  carbon, while the undecanuclear cages  $[\text{Ni}_{11}(\text{OH})_6(\text{mhp})_9(\text{O}_2\text{CMe})_6(\text{H}_2\text{O})_3]^+$  and  $[\text{Ni}_{11}(\text{OH})_6(\text{mhp})_9(\text{O}_2\text{CMe})_7(\text{Hmhp})_2]$  both involve acetate. The dodecanuclear cage  $[\text{Ni}_{12}(\text{OH})_6(\text{mhp})_{12}(\text{O}_2\text{CCH}_2\text{Cl})_6]$  involves chloracetate as the carboxylate. These subtle variations in carboxylate must in some way cause the differences in the nuclearity observed for the cages, but it is far from clear how. In the undecanuclear cages one of the Ni centers capping the trigonal face of the prism is missing when compared with the dodecanuclear cage; in the decanuclear cages both these trigonal caps are absent.<sup>172</sup>

Magnetic studies of these cages reveal a very complicated picture.<sup>172</sup> Considering only the trigonal prismatic core, the presence of six  $\mu_3$  hydroxides around the central  $\text{Ni}^{\text{II}}$  site creates a position where six distorted  $\{\text{Ni}_3(\text{OH})\}$  triangles intersect at this point. The relative magnitudes of the exchange interactions along the edges of these triangles decide the spin ground states for the cages. It appears that the ttp core of the  $\{\text{Ni}_{12}\}$  cage has an  $S=8$  ground state, while  $\{\text{Ni}_{11}\}$  has an  $S=4$  ground state and a  $\{\text{Ni}_{10}\}$  has an  $S=2$  ground state.

$[\text{Ni}_{10}(\text{OH})_4(\text{mhp})_{10}(\text{O}_2\text{CCMe}_3)_6(\text{MeOH})_2]$  and  $[\text{Ni}_{10}(\text{OH})_4(\text{mhp})_{10}(\text{O}_2\text{CCMe}_3)_6(\text{H}_2\text{O})_2]$  contain a pentacapped-centered trigonal prism missing an edge of the prism, and therefore have an analogous structure to decanuclear cobalt cages (see above).<sup>172</sup> No magnetic studies of these cages have been reported.

A further decanuclear nickel cage contains two fused pentanuclear nickel(II) metallocrowns.<sup>184</sup> The cage has the formula  $[\text{Ni}_2(\text{mcpa})_2][\text{Ni}_4(\text{shi})_2(\text{pko})_2(\text{MeOH})_2]$   $[\text{Ni}_4(\text{shi})_3(\text{pko})(\text{MeOH})(\text{H}_2\text{O})]$  (Hmcpa = 2-methyl-4-chlorophenoxyacetic acid, Hpko = di-(2-pyridyl)ketone oxime, H<sub>3</sub>shi = salicylhydroxamic acid). The cage was made in good yield by reaction of nickel chloride with

H<sub>3</sub>shi and Hpko and NaOH in MeOH, followed by addition of Na(mcpa). While other groups have frequently introduced two potential bridging ligands, this use of three different bridging ligands in one pot is unusual. The structure consists of two {Ni<sub>5</sub>} planes joined by Ni—O and Ni—N bonds between the two planes. The {Ni<sub>5</sub>} fragments contain a Ni square with a fifth nickel at the center. Magnetic studies show anti-ferromagnetic exchange between the nickel centers.

The undecanuclear cage [ $\{\text{Ni}_6(\text{OH})_6\}\{\text{Ni}(\text{mhp})_3\}_5(\text{Hmhp})\text{Cl}(\text{H}_2\text{O})_2$ ] can be made by reaction of nickel hydroxide with Hmhp at 160 °C, followed by crystallization from MeCN.<sup>104</sup> The {Ni<sub>6</sub>(OH)<sub>6</sub>} double-cubane core is bound to five {Ni(mhp)<sub>3</sub>}<sup>-</sup> complex ligands, using either three or two of the O atoms of the pyridones. All the nickel sites are six-coordinate, with terminal water, chloride, or Hmhp ligands completing the coordination environment of four of the nickel centers within the cubane. Magnetic studies show anti-ferromagnetic exchange between the metal centers.

[Ni<sub>12</sub>(chp)<sub>12</sub>(O<sub>2</sub>CMe)<sub>12</sub>(THF)<sub>6</sub>(H<sub>2</sub>O)<sub>6</sub>]<sup>8-</sup> is a cyclic molecule made from reaction of nickel acetate with Hchp, followed by crystallization from THF. The Ni···Ni contacts within the dodecanuclear wheel are each bridged by two μ<sub>2</sub> oxygens, derived from either a chp ligand, a water, or an acetate, and a 1,3 bridging carboxylate. Ferromagnetic exchange between the nickel(II) centers leads to an *S* = 12 ground spin state, however the exchange is weak and lower spin levels are still occupied at 1.8 K. The equivalent cage with 6-bromo-2-pyridonate can also be made. The *S* = 12 state has a small negative anisotropy, and the cage is a SMM.<sup>185</sup>

[Ni<sub>16</sub>Na<sub>6</sub>(chp)<sub>4</sub>(phth)<sub>10</sub>(Hphth)<sub>2</sub>(MeO)<sub>10</sub>(OH)<sub>2</sub>(MeOH)<sub>20</sub>]<sup>186</sup> shown in Figure 19, is made from reaction of nickel chloride with Na(chp) and Na<sub>2</sub>(phth) in MeOH. The structure consists of four nickel cubanes arrayed about a central sodium octahedron. The {Na<sub>6</sub>} octahedron provides the anchoring point for the structure; a phthalate ligand bridges from each face of this octahedron to one of the nickel cubanes. There are therefore two phthalate bridges between each cubane and the central octahedron. The Ni sites are all octahedral. Magnetic studies are consistent with an *S* = 2 ground state for each cubane, with immeasurably weak coupling between the cubanes.

The reaction from which [Ni<sub>7</sub>(cit)<sub>6</sub>(H<sub>2</sub>O)<sub>2</sub>]<sup>10-</sup> crystallizes produces crystals of [Ni<sub>21</sub>(cit)<sub>12</sub>(OH)<sub>10</sub>(H<sub>2</sub>O)<sub>10</sub>]<sup>16-</sup> when left.<sup>182</sup> The core—a {Ni<sub>7</sub>(OH)<sub>6</sub>} unit—matches the core of the {Fe<sub>19</sub>},<sup>106</sup> {Mn<sub>19</sub>},<sup>105</sup> and {Co<sub>24</sub>}<sup>107</sup> cages. At the periphery of the cage, however, the structure is far less regular. Magnetic studies on this cage suggest an *S* = 3 ground state.

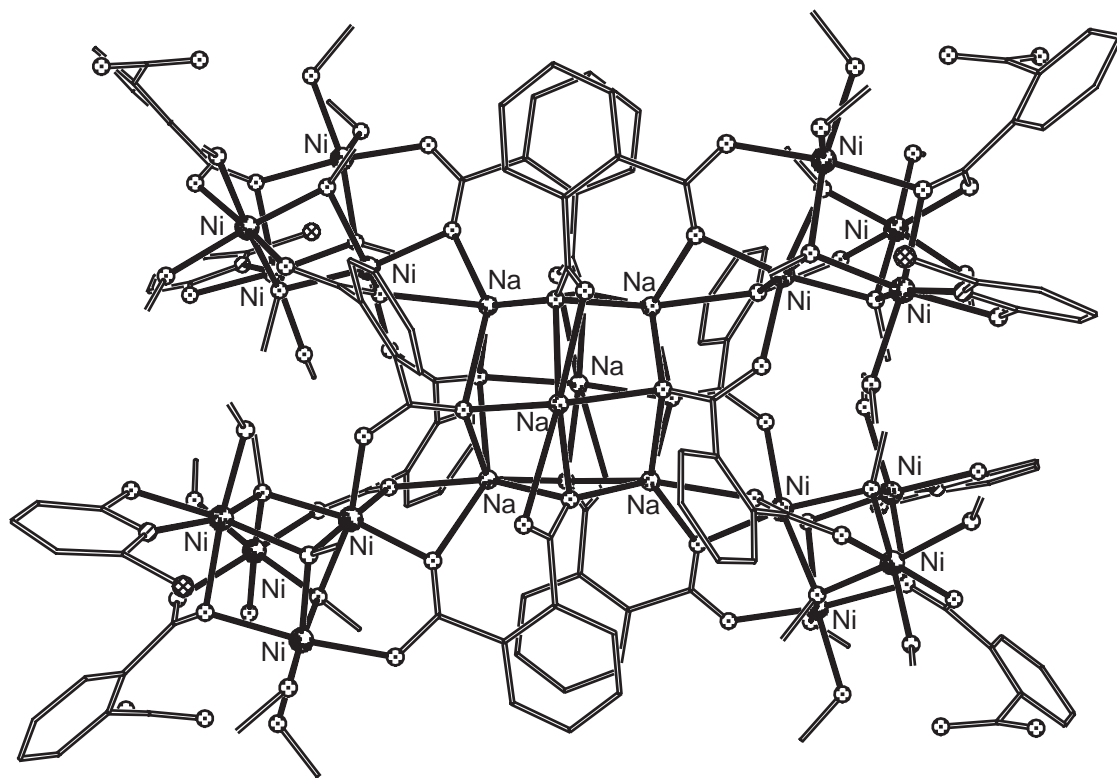


**Figure 19** The structure of [Ni<sub>16</sub>Na<sub>6</sub>(chp)<sub>4</sub>(phth)<sub>10</sub>(Hphth)<sub>2</sub>(MeO)<sub>10</sub>(OH)<sub>2</sub>(MeOH)<sub>20</sub>]<sup>186</sup> (shading: Ni, random shading; O, dotted; N, striped; Na, light shading; Cl, hatched; C, lines).

The largest nickel(II) cage known is  $[\text{Ni}_{24}(\text{OH})_8(\text{mpo})_{16}(\text{O}_2\text{CMe})_{24}(\text{Hmpo})_{16}]$  ( $\text{Hmpo} = 3\text{-methyl-3-pyrazolin-5-one}$ ),<sup>187</sup> which can be made from reaction of nickel acetate with Hmpo in MeOH, followed by crystallization of the green precipitate from MeCN. The structure consists of an octamer of chemically equivalent trinuclear building blocks  $\{\text{Ni}_3(\text{OH})(\text{mpo})_2(\text{O}_2\text{CMe})_3(\text{Hmpo})_2\}$ . Each Ni···Ni contact is bridged by a 1,3 carboxylate and two  $\mu_2$  oxygens, with the latter groups derived from mpo, acetate, and hydroxide groups. In addition to the metal–ligand bonding, the structure is stabilized by a large quantity of H bonding. The majority of these interactions arise from the proton on the second N atom within the pyrazolinone ligands. All the metal centers are six-coordinate, with approximately octahedral symmetry. Magnetic measurements indicate that while the magnetic behavior is dominated by anti-ferromagnetic exchange this is weak and many magnetic states remain populated at even very low temperatures.

### 7.3.2.7 Copper

The high-nuclearity cages reported for copper(II) contain a greater variety of ligands than for other 3d-metal cages. While cages of earlier 3d-metals tend to be stabilized by simple O-donor ligands, e.g., carboxylates, alkoxides, for copper polydentate and macrocyclic N-donor ligands are more common.

With carboxylates the “lantern” structure of copper(II) acetate is most commonly found, i.e., two copper centers bridged by four ligands. An exception is the hexanuclear cage formed by phenoxyacetate.<sup>188</sup>  $[\text{Cu}(\text{O}_2\text{CCH}_2\text{OPh})_2]_6$  contains a compressed trigonal anti-prism of copper centers bridged by phenoxyacetate ligands which adopt one of two binding modes. Six bridge in the conventional 1,3 fashion common for carboxylate ligands, while the remaining six use the ether oxygen to bond in addition to the carboxylate group, which binds in a 1,1,3 fashion. The ether oxygen bonds to one of the three  $\text{Cu}^{\text{II}}$  centers to which the carboxylate is bound, forming a five-membered chelate ring.

Addition of alcohols to dimeric copper carboxylates can also produce hexanuclear complexes. Dissolving copper(II) acetate in 2-diethylaminoethanol followed by addition of ether produces  $[\text{Cu}_6(\text{O}_2\text{CMe})_6(\text{OH})_2(\text{OCH}_2\text{CH}_2\text{NEt}_2)_4(\text{H}_2\text{O})]$ .<sup>189</sup> The structure is described as two distorted copper–oxygen heterocubanes sharing a common face. The oxygen vertices within the shared face come from aminoalkoxide ligands, while two hydroxides and two aminoalkoxide oxygens occupy the four external O sites of the dicubane. A very similar cage,  $[\text{Cu}_6(\text{O}_2\text{CCH}_2\text{Cl})_6(\text{OH})_2(\text{OCH}_2\text{CH}_2\text{NEt}_2)_4(\text{H}_2\text{O})]$ , is found for chloropropionate.<sup>190</sup> No magnetic data are reported for either compound.

$[\text{Cu}_6(\text{amp})_8](\text{ClO}_4)_4$  ( $\text{amp} = 2\text{-amino-2-methyl-1-propanolato}$ ) is formed from reaction of copper(II) perchlorate with Hamp in MeOH.<sup>191</sup> The structure consists of a bicapped  $\text{Cu}_4\text{O}_4$  heterocubane, with the four O atoms within the cubane derived from  $\mu_3$  O atoms from amp ligands and the remaining coordination sites of the copper centers occupied either by amino groups, or by  $\mu_2$  bridging oxygens from further amp ligands which attach the two capping Cu centers to the central cubane. The magnetic behavior of the cage shows a diamagnetic ground state.

With 1,3-bis(dimethylamino)-2-propanolato(bdmap), a hexanuclear copper cage  $[\text{Cu}_6(\text{bdmap})_3\text{Cl}_6(\text{O}_2\text{H})]$  with an elongated trigonal anti-prismatic structure is found.<sup>192</sup> The three bdmap ligands each chelate to two copper centers with the alkoxide oxygen shared between the two coppers. This creates the edges of the trigonal antiprism. The trigonal faces have a central oxygen atom, below the face of the  $\{\text{Cu}_3\}$  triangle with an  $\text{O}\cdots\text{O}$  separation of 2.45 Å; a H atom lies between these two O atoms forming a very strong H bond. The six chlorides are each terminally bound to a copper site. Magnetic studies show a diamagnetic ground state.

Reaction of copper(II) pivalate with sodium methoxide in ethanol (presumably a source of ethoxide not methoxide) produces a cyclic hexanuclear structure  $[\text{Cu}(\text{O}_2\text{CCMe}_3)(\text{OEt})]_6$ .<sup>193</sup> The  $\text{Cu}\cdots\text{Cu}$  vectors are alternately bridged by two 1,3 carboxylates or two  $\mu_2$  ethoxide oxygens. Magnetic studies show strong anti-ferromagnetic exchange between the  $\text{Cu}^{\text{II}}$  centers.

Two hexanuclear cages have been reported with oxime ligands,  $[\text{Cu}_3\text{O}(\text{dpmieo})_3(\text{ClO}_4)]_2$  ( $\text{dpmieo} = 1,2\text{-diphenyl-2-(methylimino)ethanone-1-oxime}$ )<sup>194</sup> and  $[\text{Cu}_3\text{O}(\text{bibo})_3(\text{ClO}_4)]_2$  ( $\text{bibo} = 3\text{-(benzylimino)butanone-2-oxime}$ ).<sup>195</sup> In both cases two triangular  $\{\text{Cu}_3\text{O}\}$  fragments are linked through Cu–O bonds to form the hexanuclear unit. Magnetic studies of the former cage indicate a diamagnetic ground state, while electrochemical studies of the latter indicate a reversible one-electron oxidation *per triangle* to a mixed-valent species.

Linked copper triangles are also found in  $[\text{Cu}_6(\text{OH})_2(\text{pz})_6(\text{NO}_3)_4(\text{Hpz})_6]$  ( $\text{Hpz} = \text{pyrazole}$ ).<sup>196</sup> Each triangle has a central hydroxide group, with each edge of the triangle bridged by a pyrazolate

ligand. The triangles are linked by two nitrate groups, which bridge in a 1,3 fashion. One further nitrate binds to the upper face of each triangle in a  $\mu_3\text{-}\eta_4$  fashion. The Hpz ligands bind through one N atom to a copper site.

$[\text{Cu}_2(\text{OMe})_2(\text{tftbd})_2]_3$  (tftbd = 4,4,4-trifluoro-1-(2-thienyl)-butane-1,3-dionate)<sup>197</sup> consists of three planar methoxo-bridged copper dimers, joined by out-of-plane copper–oxygen bonds involving either the methoxide or  $\beta$ -diketonate ligands. The former ligands are therefore present as both  $\mu_2$  and  $\mu_3$  bridges, and the latter ligands are either chelating or chelating and bridging within the structure. The molecule has a diamagnetic ground state.

Linked  $\beta$ -diketonates are found in  $[\text{K}\{\text{Cu}_3(\text{L}3)_3\}_2(\text{OMe})]^{198}$  which contains triangles of copper(II) centers, with each edge of the triangle bridged by a bis( $\beta$ -diketonate). The O atoms of six L9 ligands then form a cavity in which a single potassium ion is found. This cage is prepared by adding potassium hydroxide to a solution containing copper(II) chloride and  $\text{H}_2\text{L}9$  in MeOH. The analogous reaction with sodium generates  $[\text{Na}\{\text{Cu}_3(\text{L}3)_3\}(\text{X})_2]$  ( $\text{X} = \text{CuCl}_2$  or  $\text{BF}_4$ ) in which the Na centers sit within the copper triangles. A triple-decker cage,  $[\text{Na}\{\text{Cu}_3(\text{L}3)_3\}(\text{BF}_4)]_3$ , can also be made.<sup>78</sup> No magnetic data are reported for these cages.

Two hexanuclear copper(II) cages,  $[\text{Cu}_6\{(\text{PhSiO}_2)_6\}_2(\text{sol})_6]^-$  ( $\text{sol} = \text{EtOH}$  or DMF), related to Mn, Co, and Ni cages have been reported;<sup>63,199</sup> they differ from the cages of the other metals in lacking the central  $\mu_6$  chloride.

$[\text{Cu}_3(\text{OH})(\text{CO}_3)(\text{bipy})_5]_2^{6+}$  is a centro-symmetric hexanuclear copper(II) cage.<sup>200</sup> The center of the cage is a  $\{\text{Cu}_2(\text{OH})_2\}$  ring, with each five-coordinate Cu atom of this ring bound to one chelating bipy ligand. The apical site of the square pyramidal copper sites is occupied by an O atom from carbonate. These carbonate groups are  $\mu_3$  bridging, attaching the remaining copper sites to this central core. The external copper sites are each bound to two chelating bipy ligands. The cage is made from reaction of bipy with copper hydroxide in air, followed by addition of sodium perchlorate or hexafluorophosphate. The carbonate ions therefore come from fixing of atmospheric carbon dioxide. Magnetic studies of the cage show ferromagnetic exchange between the metal sites, and a resulting  $S = 3$  ground state.

$[\text{Cu}_6(\text{ox})_3(\text{N}_3)_2(\text{tmen})_6(\text{H}_2\text{O})_2]^{4+}$  also contains simple dimine ligands, in this case  $N,N,N',N'$ -tetramethylethane-1,2-diamine (tmen).<sup>201</sup> Six copper centers, to each of which is coordinated a chelating tmen ligand, are alternately bridged by oxalate or azide groups. The azide ligands bridge in a 1,3 fashion. Magnetic studies indicate a diamagnetic ground state.

The ligand, 2-(4-imidazolyl)-ethylimino-6-methylpyridine (HL10, see Scheme 2), contains four N donors, and can form a cyclic hexameric structure depending on the pH of the solution.<sup>202</sup> Reacting HL10 with copper(II) chloride in MeOH at high pH gives a cyclic hexamer,  $[\text{Cu}(\text{L}10)]_6(\text{ClO}_4)_6$ . Within the hexamer each copper site is four-coordinate, bound to the pyridine and imine N atoms and one imidazole N atom from one ligand, and the second imidazole N atom from the neighboring atom.

Several hexanuclear copper cages are known with more complicated ligands. With the tris-tridentate ligand L11 (see Scheme 2),  $[\text{Cu}_3(\text{OH})_2(\text{N}_3)(\text{L}11)]_2^{6+}$  forms in the presence of azide<sup>203</sup> and contains a central  $\{\text{Cu}_2(\text{OH})_2\}$  ring, with the remaining coordination sites on the central copper sites occupied by one tridentate unit from L11. The remaining tridentate binding sites bond to the four further copper(II) atoms. EPR spectroscopy suggests strong antiferromagnetic exchange is present within each dinuclear unit.

$[\text{Cu}_6(\text{tidah})_2\text{Cl}_{10}(\text{H}_2\text{O})_4]$  results from reaction of 1,1,6,6-tetrakis(imidazol-2-yl)-2,5-diazahexane (Htidah) with copper chloride in ethanol,<sup>204</sup> and contains an irregular array with a central copper(II) rectangle with opposite edges bridged by chloride or imidazolate groups. The additional two copper sites are attached to the rectangle by bridging chlorides that are approximately co-linear with the  $\text{Cu}\cdots\text{Cu}$  vector bridged by the imidazolate. Magnetic studies show a low-spin ground state.

Reaction of 2,6-bis(aminomethyl)-4-methylphenol monohydrochloride, 2,6-diformyl-4-methylphenol, copper(II) acetate, and  $(\text{NBu}_4)(\text{BF}_4)$  in boiling MeOH gives  $[\text{Cu}_6(\text{L}12)(\text{O}_2\text{CMe})_2(\text{OH})_2(\text{MeOH})_2(\text{H}_2\text{O})_2]^{2+}$  (L12, see Scheme 2).<sup>205</sup> The six copper centers have a cyclohexane-like boat configuration, with each  $\text{Cu}\cdots\text{Cu}$  vector bridged by a phenolate O atom from L12 and one further bridge. This is provided either by a  $\mu_2$  hydroxide or by a 1,1,3 bridging acetate ligand. No magnetic data are reported.

A similar reaction of 2,6-diformyl-4-methylphenol or 4-*tert*-butyl-2,6-diformylphenol with 1,5-diamino-3-hydroxypropane in MeOH in the presence of copper salts generates a series of tetranuclear cages.<sup>206</sup> Slow recrystallization of these tetranuclear cages from DMF–MeOH, or from dry MeOH in presence of a base generates octanuclear cages.  $[\text{Cu}_4\text{O}(\text{L}13)(\text{ClO}_4)]_2^{2+}$  (L13 shown in Scheme 2), contains a planar tetranuclear copper cage encapsulated within the Schiff base

macrocycle, with the four copper centers bound to a central oxide. This oxide bridges to a copper of the second tetranuclear fragment within the cage. The magnetic behavior of the cage indicates antiferromagnetic exchange between the Cu<sup>II</sup> centers.

A similar reaction involving 2,6-diformyl-4-methylphenol with 1,3-diamino-2-hydroxypropane in the presence of copper nitrate gives a second hexanuclear cage encapsulated within a macrocyclic ligand, L14 (see [Scheme 2](#)).<sup>207</sup> A difference is that in [Cu<sub>6</sub>(L14)(OH)<sub>3</sub>](NO<sub>3</sub>)<sub>6</sub> the planar hexanuclear cages “dimerize” via out-of-plane Cu—O bonds to create a dodecanuclear array. Within the hexanuclear cage Cu···Cu contacts are alternately bridged by a single phenolate oxygen or by a phenolate oxygen and an exogenous hydroxide. Two of the hydroxides also bridge to Cu centers in the second hexanuclear cage in the dimer. Magnetic properties show strong anti-ferromagnetic exchange between the Cu centers within the hexanuclear cage.

Several hexanuclear copper “metallocrowns” have been reported, formed from the solid state reaction of copper(II) nitrate with Na(mhp), followed by crystallization from CH<sub>2</sub>Cl<sub>2</sub>. [NaCu<sub>6</sub>(mhp)<sub>12</sub>](NO<sub>3</sub>)<sub>157</sub> is related to earlier metallocrowns, with six four-coordinate copper sites bridged by pyridonate ligands, which are 1,3 bridging with regard to Cu sites alone. Six of the mhp O atoms form a central cavity, in which the sodium ion is found. The analogous cage, [Cu<sub>6</sub>(mhp)<sub>12</sub>]<sup>2+</sup> with copper at the center has been reported.<sup>208</sup> No magnetic data have been reported for either of these metallocrowns.

Similar crowns have been formed using *N*-(2,5-dimethylbenzyl)iminodiethanol as the ligand.<sup>209</sup> These cages are related to hexanuclear iron crowns discussed in [Section 7.3.2.4](#) above. Both Na and Li can be coordinated to the O atoms of this cage, however they do not lie within the cavity but coordinate on an external face, i.e., they bind to three O donors per {Cu<sub>6</sub>} crown rather than six.

A further wheel has been reported where the copper centers are linked by organic radicals, 4-pyrimidinyl nitronyl nitroxide (PMM).<sup>210</sup> This chemistry is similar to that reported for manganese by Gatteschi *et al.* in 1988.<sup>59</sup>

Heterometallic cages containing six copper centers form when perchlorate salts of copper and lanthanoids are mixed in the presence of sodium iminodiacetate.<sup>211</sup> [LnCu<sub>6</sub>{(O<sub>2</sub>CCH<sub>2</sub>)<sub>2</sub>N}<sub>4</sub>(OH)<sub>3</sub>{(O<sub>2</sub>CCH<sub>2</sub>)N(HO<sub>2</sub>CCH<sub>2</sub>)<sub>2</sub>}<sub>2</sub>]<sup>2-</sup> forms for Ln = La and Tb, and contains a central lanthanoid surrounded by a trigonal prism of copper centers. Susceptibility measurements suggest anti-ferromagnetic exchange between metal centers.

A heptanuclear complex results from the reaction of Na(O<sub>2</sub>N<sub>2</sub>NEt<sub>2</sub>) with copper(II) chloride and Na(OMe) in MeOH.<sup>212</sup> The structure contains a central linear trinuclear copper unit, [Cu<sub>3</sub>(OMe)<sub>4</sub>(O<sub>2</sub>N<sub>2</sub>NEt<sub>2</sub>)<sub>2</sub>], in which the Cu···Cu contacts are each bridged by two methoxides with O<sub>2</sub>N<sub>2</sub>NEt<sub>2</sub> ligands chelating to the external copper sites. This trinuclear unit is bound through Cu···O(methoxide) contacts to two dinuclear [Cu<sub>2</sub>(OMe)<sub>2</sub>(O<sub>2</sub>N<sub>2</sub>NEt<sub>2</sub>)<sub>2</sub>] fragments. Preliminary magnetic measurements suggest strong anti-ferromagnetic exchange between the copper centers.

Crystals of a vertex-sharing double cubane, [Cu<sub>7</sub>(OH)<sub>8</sub>(bpym)<sub>6</sub>(H<sub>2</sub>O)<sub>2</sub>]<sup>6+</sup> (bpym = 2,2'-bipyridine) can be grown from slow evaporation of an aqueous solution of copper(II) nitrate, bpym, and sodium carbonate.<sup>213</sup> The central {Cu<sub>7</sub>(OH)<sub>8</sub>} double cubane is somewhat distorted, with two *trans* Cu—O bonds involving the shared copper vertex longer than other Cu—O bonds within the cubane ([Figure 20](#)). The bpym ligands chelate to the six copper vertices that are not shared. Magnetic studies show weak ferromagnetic exchange between the copper(II) centers, with an *S* = 7/2 ground state.<sup>213</sup>

Work from the Perlepes group has produced a series of copper cages using ligands derived from di-2-pyridyl ketone, (py)<sub>2</sub>CO. A heptanuclear cage, [Cu<sub>7</sub>{(py)<sub>2</sub>CO<sub>2</sub>}<sub>3</sub>(O<sub>2</sub>CMe)<sub>6</sub>(OH)<sub>2</sub>] and a dodecanuclear cage, [Cu<sub>12</sub>{(py)<sub>2</sub>CO<sub>2</sub>}<sub>6</sub>(O<sub>2</sub>CMe)<sub>12</sub>], result from reaction of copper(II) acetate with (py)<sub>2</sub>CO in hot MeCN.<sup>214</sup> The smaller cage forms green crystals, while the latter gives violet–blue crystals. The {Cu<sub>7</sub>} cage contains a highly distorted, vertex-sharing copper dicubane core. The (py)<sub>2</sub>CO<sub>2</sub><sup>2-</sup> gem-diolate ligands adopt two bridging modes, 3:2211 and 4:3211 (Harris notation) and lie at the center of the cage. This contrasts with the 5:3311 mode adopted in nonanuclear Co and Ni cages [M<sub>9</sub>{(py)<sub>2</sub>CO<sub>2</sub>}<sub>4</sub>(O<sub>2</sub>CMe)<sub>8</sub>(OH)<sub>2</sub>]<sup>168</sup> (see [Sections 7.3.2.5](#) and [7.3.2.6](#) above). The acetate groups bridge the external edges of the cage in the classic 1,3 mode (2.11 by Harris notation). Magnetic studies show an *S* = 1/2 ground state.

The minor product of the reaction is a dodecanuclear copper cage, which has a beautiful “flywheel” structure shown in [Figure 21](#).<sup>214</sup> Six internal Cu centers form a chair-shaped cluster, which lies within a second, larger, chair-shaped cluster consisting of the outer copper(II) sites. All the (py)<sub>2</sub>CO<sub>2</sub><sup>2-</sup> ligands adopt the 4:3211 bonding mode, bridging one outer and three inner copper sites. Six acetate ligands bridge between copper centers of the inner and outer chair in a 2.11 fashion, while the final six acetate ligands bind monodentately to exterior copper sites. No magnetic data are reported for this unique cluster.

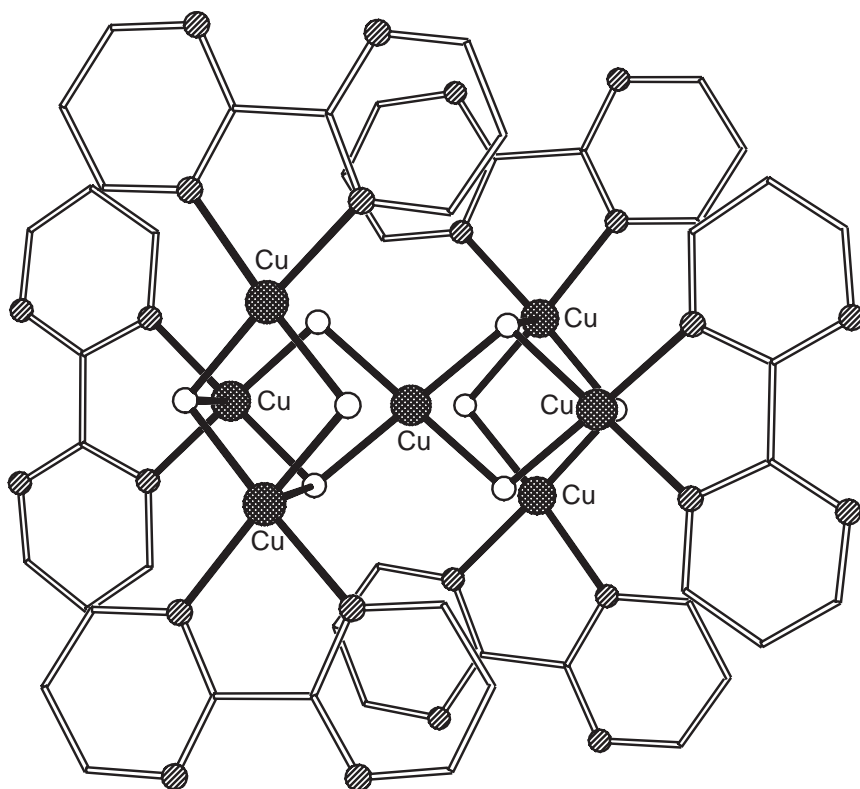


**Figure 20** The structure of  $[\text{Cu}_7(\text{OH})_8(\text{bpym})_6(\text{H}_2\text{O})_2]^{6+214}$  (shading: Cu, hatched; O, open; N, dotted; C, lines).

When copper(II) acetate and  $(\text{py})_2\text{CO}$  are mixed in water, followed by addition of sodium perchlorate and slow evaporation of the solution, an octanuclear copper cage,  $[\text{Cu}_8\{(\text{py})_2\text{CO}(\text{OH})\}_8(\text{O}_2\text{CMe})_4]^{4+}$  can be isolated.<sup>215</sup> This features two  $\{\text{Cu}_4\text{O}_4\}$  heterocubanes bridged by acetate ligands, with the oxo atom of the  $(\text{py})_2\text{CO}(\text{OH})^-$  ligands occupying the O atom vertices. The bonding mode of the ligand is therefore 3:3011, with the hydroxyl oxygen not bound to any metals. EPR studies suggest a spin triplet may be the ground state, but this is a tentative assignment.

$[\text{Cu}_8\{(\text{py})_2\text{CO}_2\}_4(\text{O}_2\text{CMe})_4(\text{Hhp})_4]^{4+}$  (Hhp = 2-hydroxypyridine)<sup>216</sup> is formed from reaction of copper acetate with  $(\text{py})_2\text{CO}$  in MeCN/ $\text{H}_2\text{O}$ , followed by addition of Hhp, sodium acetate, and sodium perchlorate. Here, the inner copper structure is a tetrahedron while the outer structure is a distinctly flattened tetrahedron. The  $(\text{py})_2\text{CO}_2^{2-}$  ligands adopt a new 4:2211 mode, while the acetate ligands are bridged in a 2.11 fashion and the Hhp ligands are attached through the exocyclic oxygen atom. Magnetic studies show a low-spin ground state. The cage also shows two quasi-reversible reduction processes.

The copper cage,  $\{[\text{Cu}_3\text{O}(\text{L15})]_2\text{Cu}\}$ , is mixed-valent, containing two oxo-centered copper(II) triangles, bridged by a single copper(I) center, bound to the two oxo groups.<sup>217</sup> The triangles are encapsulated in a polydentate N-donor ligand L15 (see Scheme 2). Magnetic studies show anti-ferromagnetic exchange between the  $\text{Cu}^{\text{II}}$  centers giving a diamagnetic ground state.

$[\text{Cu}_8(\text{urid})_8\text{Na}(\text{H}_2\text{O})_6]^{7-}$  (urid = uridine) contains copper centers bound to a pyrimidine nitrogen atom from one uridine, and ribose oxygen atoms from two different uridines.<sup>218</sup> The resulting cage has a square anti-prismatic array of copper centers, with the eight bridging uridine ligands forming a torus. A  $\{\text{Na}(\text{H}_2\text{O})_6\}^+$  cation is found at the center of the cage. No magnetic data are reported for this cage.

Reaction of polymeric copper(I)-3,5-dimethylpyrazolate (dmpz) suspended in wet  $\text{CH}_2\text{Cl}_2$  with dioxygen gives  $[\text{Cu}(\text{dmpz})(\text{OH})]_8$ .<sup>219</sup> The cage contains a planar ring of copper(II) centers, with each  $\text{Cu}\cdots\text{Cu}$  vector bridged by a dmpz and hydroxide. No magnetic data are reported for the compound.

Wang and co-workers have reported  $[\text{Y}_2\text{Cu}_8\text{O}_2(\text{hp})_{12}\text{Cl}_2(\text{NO}_3)_4(\text{H}_2\text{O})_2]$  and  $[\text{Nd}_2\text{Cu}_8\text{O}_2(\text{hp})_{12}\text{Cl}_2(\text{OMe})_4(\text{H}_2\text{O})_4]$ ,<sup>220</sup> which are made from reaction of copper methoxide with Hhp in MeOH, followed by addition of either yttrium nitrate or neodymium chloride. The metal core is similar in both compounds, with a central  $\{\text{M}_2\text{Cu}_4\}$  octahedron ( $\text{M} = \text{Y}$  or  $\text{Nd}$ ), with the

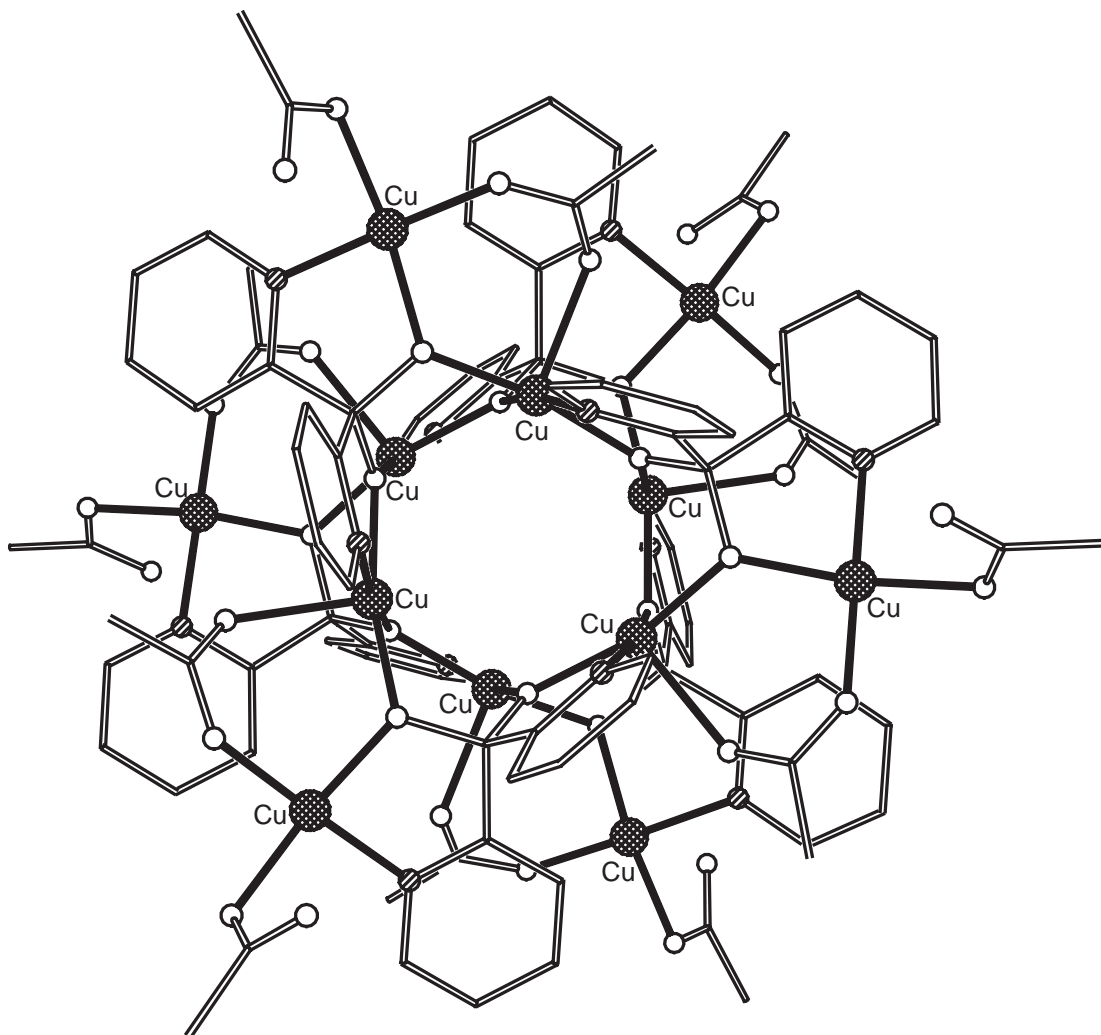


**Figure 21** The structure of  $[\text{Cu}_{12}\{(\text{py})_2\text{CO}_2\}_6(\text{O}_2\text{CMe})_{12}]^{215}$  (shading: Cu, hatched; O, open; N, dotted; C, lines).

heterometallic centers *trans* to one another. The final four copper(II) centers are then arranged in two pairs parallel to the  $\text{M}\cdots\text{M}$  axis. Two  $\mu_4$  oxides are found within the  $\{\text{M}_2\text{Cu}_4\}$  octahedra, while all the hp ligands adopt the 3.21 bridging mode. Antiferromagnetic exchange is found between the copper centers.

The homometallic cages,  $[\text{Cu}_8\text{O}_2(\text{O}_2\text{CR})_4(\text{xhp})_8]$  ( $\text{R} = \text{Me}$ ,  $\text{Ph}$  or  $\text{CF}_3$ ;  $\text{xhp} = 6\text{-chloro-}$ ,  $6\text{-bromo-}$  or  $6\text{-methyl-2-pyridonate}$ ),<sup>6</sup> can be prepared either from reaction of the copper carboxylate with the neutral ligands, or by reaction of the copper carboxylate with copper complexes of pyridonate ligands,  $[\text{Cu}_2(\text{chp})_4]^{221}$  or  $[\text{Cu}_6\text{Na}(\text{mhp})_{12}]^+$ .<sup>157</sup> The structures consist of a central edge-sharing, oxygen-centered bitetrahedron  $\{\text{Cu}_6\text{O}_2\}$ , surrounded by two  $\{\text{Cu}(\text{xhp})_4\}^{2-}$  “complex ligands”. Each carboxylate ligand bridges in a 2.11 fashion, while the pyridonate ligands adopt both the 2.11 and 3.21 binding modes. Magnetic studies of the cages show a decline in magnetic moment at low temperature, with either an  $S = 0$  or 1 ground state.

The ligand 6,6'-oxybis[1,4-bis(2'-pyridylamino)phthalazine] (obpp) binds to four copper centers, with the resulting cage linked through a nitrate group to give  $[\{\text{Cu}_4(\text{obpp})(\text{OH})_2(\text{NO}_3)_2(\text{H}_2\text{O})_7\}_2(\text{NO}_3)]^{7+}$ .<sup>222</sup> The ligand, obpp, contains two distinct cavities, in each of which is bound a  $\{\text{Cu}_2(\text{OH})\}$  fragment. In one cavity of the pair a nitrate ion bridges between the two copper centers, while in the second cavity the nitrate present bridges to a neighboring tetranuclear fragment, generating the complete octanuclear cation. The magnetic behavior of the compound could be modeled as a strongly antiferromagnetically coupled dimer.

The trianion of a pentadentate Schiff-base, 2-hydroxy-1,3-propanediyl bis(acetylacetonimine)- (hpbaa) reacts with copper(II) perchlorate in MeOH to give the octanuclear cage

$[\text{Cu}_8(\text{hpbaa})_4(\text{OH})_3]^+$ .<sup>223</sup> The cage has an unusual structure containing four dinuclear  $\{\text{Cu}_2(\text{hpbaa})\}$  units linked through hydroxides. No magnetic data are reported for the cage.

An octanuclear copper complex has been reported using azathioprine (aza) as a co-ligand with the  $\beta$ -diketonate 2,2,6,6-tetramethylheptane-3,5-dione (thd).<sup>224</sup>  $[\text{Cu}_4(\text{aza})_2(\text{thd})_5(\text{OH})_2]$  was made by reaction of  $[\text{Cu}(\text{thd})_2]$  with aza in MeCN. The cage contains  $\{\text{Cu}_3(\text{OH})\}$  fragments, with two edges of the triangles bridged by in a 1,3 fashion by aza ligands. The second N atom of the imidazole ring binds to further copper atoms, in one case binding a fourth copper center to the triangle and in the second case bridging to the second triangle within the octanuclear cage. Magnetic measurements indicate anti-ferromagnetic exchange between the copper centers within the triangle.

An octanuclear copper(II) cage has been reported with linked  $\beta$ -diketonate ligands.<sup>225</sup> The structure is of a  $4 \times 2$  parallelogram, with the central region linked by methoxide. The polydentate ligand encloses the metal cage. Susceptibility measurements show a diamagnetic ground state.

A nonanuclear cage,  $[\text{Cu}_9(\text{O}_2\text{CCHCl}_2)_{10}\{\text{OCH}_2\text{C}(\text{NH}_2)\text{Me}_2\}_6(\text{OH})_2]$ , can be made from reaction of copper(II) dichloroacetate with 2-dimethylaminoethanol in ethanol.<sup>226</sup> The structure consists of two distorted copper heterocubanes bridged, via carboxylate and hydroxide ligands, through a central ninth copper center. The carboxylates adopt both the conventional 2.11 bonding mode, and the less frequently found 3.21 mode. The aminoalkoxide ligands triply bridge through the O atom, with the N-donor bound to one of the three copper centers to which the O atom is bound—the 3.31 bonding mode in Harris notation. The magnetic behavior suggests a doublet ground state.

The nonanuclear cage  $[\text{Cu}_9(2\text{poap})_6]^{12+}$  has a structure<sup>227</sup> closely related to the equivalent manganese cage  $[\text{Mn}_9(2\text{poap})_6]$ ,<sup>83</sup> containing a  $3 \times 3$  grid of copper(II) centers bridged by the linear polydentate ligand (see Section 7.3.2.3). Magnetic studies support an assignment of an  $S = 7/2$  ground state cage due to predominant ferromagnetic exchange between the copper(II) centers.

The majority of cages containing 12 copper(II) centers are heterometallic. The first to be reported was  $[\text{Cu}_{12}\text{La}_8(\text{OH})_{24}(\text{NO}_3)_{21.2}(\text{Hmhp})_{13}(\text{H}_2\text{O})_{5.5}][\text{NO}_3]_{2.8}$ , which contains a cuboctahedron of copper(II) centers within a cube of eight lanthanums, with a  $\mu_3$ -hydroxide at the center of each  $\text{Cu}_2\text{La}$  triangle.<sup>157</sup> The remaining ligands are bound to the lanthanum sites, except for a central nitrate anion, which is encapsulated within the cage. No magnetic data have been reported for this cage.

A curious observation is that the same copper and hydroxide arrays are found in several other heterometallic cages, formed with betaine and carboxylate ligands. Thus,  $[\text{Cu}_{12}\text{M}_6(\text{OH})_{24}(\text{O}_2\text{CCH}_2\text{NC}_5\text{H}_5)_{12}(\text{H}_2\text{O})_{18}(\text{ClO}_4)](\text{ClO}_4)_{17}$  ( $\text{M} = \text{Y}, \text{Nd}, \text{or Gd}$ );<sup>228</sup>  $[\text{Cu}_{12}\text{M}_6(\text{O}-\text{H})_{24}(\text{O}_2\text{CCH}_2\text{CH}_2\text{NC}_5\text{H}_5)_{12}(\text{H}_2\text{O})_{16}(\text{ClO}_4)](\text{ClO}_4)_{17}$  ( $\text{M} = \text{Sm or Gd}$ );<sup>229</sup> and  $[\text{Cu}_{12}\text{M}_6(\text{OH})_{24}(\text{O}_2\text{CR})_{12}(\text{H}_2\text{O})_{18}(\text{ClO}_4)](\text{NO}_3)_4(\text{OH})$  ( $\text{R} = \text{CH}_2\text{Cl or CCl}_3$ ;  $\text{M} = \text{La or Nd}$ )<sup>230</sup> all contain a copper cuboctahedron, but in these cages the second metal forms an octahedron. The encapsulated perchlorate ions found in all these cages are  $\mu_{12}$  bridging. Magnetic studies<sup>228,230</sup> reveal anti-ferromagnetic exchange between copper(II) centers to be the dominant magnetic interaction in most cases.

A further dodecanuclear copper(II) cage also contains a cuboctahedron of copper centers. The ligand is the trianion of 2,4,6-triazophenyl-1,3,5-trihydroxybenzene (tapp, see Scheme 2), which acts as a tri-bidentate chelator.<sup>231</sup> The centroids of these ligands in  $[\text{Cu}_{12}(\text{tapp})_8]$  are at the corners of a cube, placing the copper centers at the mid-point of the edges of this cube, thus creating a cuboctahedron. No magnetic data are reported for this extraordinary complex that contains an approximately  $816 \text{ \AA}^3$  cavity.

Recently, a mixed-ligand cage has been reported, which also contains a dodecanuclear copper core.<sup>232</sup>  $[\text{Cu}_{12}\text{Cl}_6(\text{dmpz})_{10}(\text{O}_3\text{PtBu})_6(\text{HO}_3\text{PtBu})_2]$ , shown in Figure 22, contains an elaborate array of metal centers held together by  $\mu_3$  and  $\mu_4$  chlorides,  $\mu_2$  pyrazolates,  $\mu_3$  and  $\mu_2$  phosphonates, and  $\mu_2$  hydrogenphosphonates. The cage consists of two linked hexanuclear units. Within each unit there is a  $\{\text{Cu}_4\text{Cl}_2\}$  butterfly, with the two wing-tip copper sites linked by a third chloride. This chloride bridges to the fifth copper of the hexanuclear block, with one of the chlorides within the butterfly binding to the sixth copper. Magnetic measurements show weak anti-ferromagnetic exchange between copper centers.<sup>232</sup>

Two mixed-valent tetradecanuclear cages,  $[\text{Cu}(\text{II})_6\text{Cu}(\text{I})_8\{\text{SC}(\text{Me})_2\text{CH}_2\text{NH}_2\}_{12}]^{7+}$ <sup>233</sup> and  $[\text{Cu}(\text{II})_6\text{Cu}(\text{I})_8(\text{pen})_{12}\text{Cl}]^{5-}$   $\{\text{H}_2\text{pen} = D\text{-penicillamine}, \text{HSC}(\text{Me})_2\text{CH}(\text{CO}_2)\text{NH}_3\}$ ,<sup>234</sup> also contain mixtures of high-symmetry polyhedra, with  $\text{Cu}^{\text{I}}$  centers at the corners of a cube and the six  $\text{Cu}^{\text{II}}$  atoms at the corners of an octahedron. No magnetic data are reported, beyond a statement that the room-temperature value for the magnetic moment of these compounds is consistent with ca. 40% of the copper being present as copper(II).

The largest copper cage is a hexadecanuclear cage reported by Klüfers and Schumacher, which is stabilized by deprotonated sorbitol.<sup>235</sup> The structure contains a wheel of copper centers held together by alkoxides derived from the poly-ol. As with the  $\{\text{Fe}_{14}\}$  cage discussed in Section 7.3.2.4 above, this extraordinary structure has not led to a greater exploitation of poly-ols as ligands in this chemistry.



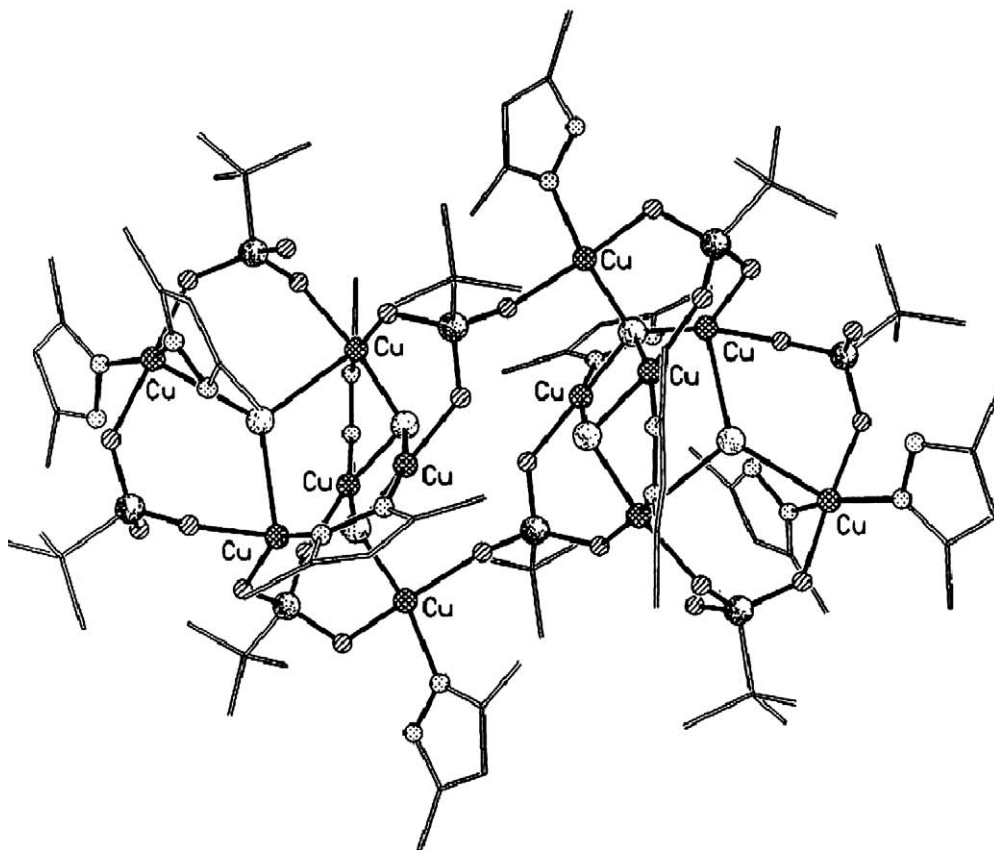


**Figure 22** The structure of  $[\text{Cu}_{12}\text{Cl}_6(\text{dmpz})_{10}(\text{O}_3\text{PtBu})_6(\text{HO}_3\text{PtBu})_2]^{232}$  (shading: Cu, hatched; O, striped; N, dotted; P, random shading; C, lines).

### 7.3.3 FAMILIES OF CAGES

The structures discussed above show an enormous range of structural types, and a frustration in this area is the inability to recognize any central organizing principle to describe and rationalize these structures. Several “families of cages” exist, however, where cages can be grouped by the metal polyhedron displayed. Four of these families of cages are discussed briefly below.

#### 7.3.3.1 Wheels and Metallocrowns

Cyclic structures have an enormous esthetic appeal. For cages ranging upward from hexanuclear in size, wheels (Table 1), which contain no central metal, are more common than the metallocrowns (Table 2), which contain a further metal encapsulated within the cyclic array. Pecoraro and co-workers have made many smaller metallocrowns, and have recently reviewed the area.<sup>236</sup>

An obvious observation concerning these larger cyclic structures is that they always contain an even number of metal centers within the backbone of the wheel or crown. There is no straightforward explanation for the absence of hepta- and nonanuclear wheels, especially as metallocrown analogs of 15-crown-5 are well known.<sup>236</sup> Hexa- and octa-nuclear wheels are known for most of the 3d metals—chromium is absent from hexanuclear wheels, while no octanuclear nickel wheels are known. An octanuclear titanium(IV) wheel has been included for completeness.<sup>237</sup> These cages involve a range of ligands that bridge the  $\text{M}\cdots\text{M}$  edges of the wheel in a variety of ways. For octanuclear cages, bridging by two 1,3 carboxylates and one further  $\mu_2$  bridge (fluoride, hydroxide, methoxide, or oxide) is the most common motif, but many other variants are known. For decanuclear wheels only one bridging type is seen, the bis- $\mu_2$  alkoxide and single 1,3carboxylate bridge originally seen for the “ferric wheel”.<sup>141</sup> This nuclearity is also only seen for the metal centers in the +3 oxidation state. The two cages with higher nuclearity both consist of repeating trinuclear units; the octadecanuclear  $\text{Fe}^{\text{III}}$  cage is a hexamer of trinuclear fragments,<sup>154</sup> while the

**Table 1** Metal wheels.

<i>Cage</i>	<i>References</i>
<i>Hexanuclear</i>	
[V <sub>6</sub> O <sub>10</sub> (O <sub>2</sub> CPh) <sub>9</sub> ]	32
[Mn(hfac) <sub>2</sub> (NITPh)] <sub>6</sub>	59
[Mn <sub>6</sub> {(PhSiO <sub>2</sub> ) <sub>6</sub> } <sub>2</sub> Cl(EtOH) <sub>6</sub> ] <sup>-</sup>	63
[Fe <sub>6</sub> Cl <sub>6</sub> {OCH <sub>2</sub> CH <sub>2</sub> ) <sub>2</sub> NMe} <sub>6</sub> ]	124
[Co{N(CH <sub>2</sub> PO <sub>3</sub> )(CH <sub>2</sub> CO <sub>2</sub> ) <sub>2</sub> } <sub>6</sub> ] <sup>2-</sup>	168
[Co <sub>6</sub> {(PhSiO <sub>2</sub> ) <sub>6</sub> } <sub>2</sub> Cl(solvent) <sub>6</sub> ] <sup>-</sup>	63
[Ni <sub>6</sub> {(PhSiO <sub>2</sub> ) <sub>6</sub> } <sub>2</sub> Cl(EtOH) <sub>6</sub> ]	176
[Cu(O <sub>2</sub> CMe <sub>3</sub> )(OEt)] <sub>6</sub>	193
[Cu <sub>6</sub> {(PhSiO <sub>2</sub> ) <sub>6</sub> } <sub>2</sub> (EtOH) <sub>6</sub> ] <sup>-</sup>	63
[Cu(L10)] <sub>6</sub>	202
[CuX <sub>2</sub> (PMM)] <sub>6</sub> (X = Cl or Br)	210
<i>Octanuclear</i>	
[TiO(O <sub>2</sub> CC <sub>6</sub> F <sub>5</sub> ) <sub>2</sub> ] <sub>8</sub>	237
[V <sub>8</sub> (OH) <sub>4</sub> (OEt) <sub>8</sub> (O <sub>2</sub> CMe) <sub>12</sub> ]	11
[(VO) <sub>8</sub> (OMe) <sub>16</sub> (C <sub>2</sub> O <sub>4</sub> ) <sup>2-</sup> ]	18
[CrF(O <sub>2</sub> CMe <sub>3</sub> ) <sub>2</sub> ] <sub>8</sub>	38
[Cr(OH)(O <sub>2</sub> CPh) <sub>2</sub> ] <sub>8</sub>	41
[FeF(O <sub>2</sub> CMe <sub>3</sub> ) <sub>2</sub> ] <sub>8</sub>	138
[Fe <sub>8</sub> O <sub>4</sub> (bmdp) <sub>4</sub> (OH) <sub>4</sub> (O <sub>2</sub> CMe) <sub>4</sub> ]	136
[Co <sub>8</sub> (L9) <sub>12</sub> (ClO <sub>4</sub> ) <sup>3+</sup> ]	165
[Co <sub>8</sub> (O <sub>2</sub> CMe) <sub>8</sub> (OMe) <sub>16</sub> ]	166
[Cu(dmpz)(OH)] <sub>8</sub>	220
<i>Decanuclear</i>	
[Cr(O <sub>2</sub> CMe)(OMe) <sub>2</sub> ] <sub>10</sub>	43
[Cr(O <sub>2</sub> CMe)(OEt) <sub>2</sub> ] <sub>10</sub>	43
[Mn(bzshz)(MeOH)] <sub>10</sub>	88
[Fe(OMe) <sub>2</sub> (O <sub>2</sub> CCH <sub>2</sub> Cl)] <sub>10</sub>	141
[Fe(OMe) <sub>2</sub> (O <sub>2</sub> CMe)] <sub>10</sub>	142
[Fe(OMe) <sub>2</sub> (O <sub>2</sub> CCH <sub>2</sub> CH <sub>2</sub> C(O)-C <sub>6</sub> H <sub>4</sub> Me)] <sub>10</sub>	143
[Fe(bzshz)(MeOH)] <sub>10</sub>	88
<i>Dodecanuclear</i>	
[(R <sub>2</sub> NH <sub>2</sub> ) <sub>3</sub> {Cr <sub>6</sub> F <sub>11</sub> (O <sub>2</sub> CMe <sub>3</sub> ) <sub>10</sub> }(H <sub>2</sub> O)] <sub>2</sub>	44
[Fe(OMe) <sub>2</sub> (dbm)] <sub>12</sub>	122
[Ni <sub>12</sub> (chp) <sub>12</sub> (O <sub>2</sub> CMe) <sub>12</sub> (THF) <sub>6</sub> (H <sub>2</sub> O) <sub>6</sub> ]	8
[Ni <sub>12</sub> (bhp) <sub>12</sub> (O <sub>2</sub> CMe) <sub>12</sub> (THF) <sub>6</sub> (H <sub>2</sub> O) <sub>6</sub> ]	185
<i>Higher nuclearities</i>	
[Fe(OH)(XDK)Fe <sub>2</sub> (OMe) <sub>4</sub> (O <sub>2</sub> CMe) <sub>2</sub> ] <sub>6</sub>	154
[Ni <sub>24</sub> (OH) <sub>8</sub> (mpo) <sub>16</sub> (O <sub>2</sub> CMe) <sub>24</sub> (Hmpo) <sub>16</sub> ]	187

**Table 2** Metallocrowns containing six or more metals.

<i>Cage</i>	<i>References</i>
<i>Hexanuclear</i>	
[Mn <sub>7</sub> Mn <sub>6</sub> (OH) <sub>3</sub> Cl <sub>3</sub> (hmp) <sub>9</sub> ] <sup>2+</sup>	69
[Na <sub>7</sub> Mn <sub>6</sub> (dbm) <sub>6</sub> (OMe) <sub>12</sub> ] <sup>+</sup>	70
[Mn <sub>7</sub> Mn <sub>6</sub> (dbm) <sub>6</sub> (OMe) <sub>12</sub> ]	71
[Na <sub>7</sub> Fe <sub>6</sub> (OMe) <sub>12</sub> (dbm) <sub>6</sub> ] <sup>+</sup>	121
[Li <sub>7</sub> Fe <sub>6</sub> {OCH <sub>2</sub> CH <sub>2</sub> ) <sub>3</sub> N} <sub>6</sub> ] <sup>+</sup>	124
[Na <sub>7</sub> Co <sub>6</sub> (mhp) <sub>12</sub> ] <sup>+</sup>	156
[Na <sub>7</sub> Cu <sub>6</sub> (mhp) <sub>12</sub> ] <sup>+</sup>	157
[Cu <sub>7</sub> Cu <sub>6</sub> (mhp) <sub>12</sub> ] <sup>2+</sup>	208
[(NaBr <sub>2</sub> ) <sub>2</sub> Cu <sub>6</sub> {(OCH <sub>2</sub> CH <sub>2</sub> ) <sub>2</sub> NCH <sub>2</sub> C <sub>6</sub> H <sub>3</sub> Me <sub>2</sub> } <sub>6</sub> ] <sup>2+</sup>	209
<i>Octanuclear</i>	
[Cs <sub>7</sub> Fe <sub>8</sub> {OCH <sub>2</sub> CH <sub>2</sub> ) <sub>3</sub> N} <sub>8</sub> ]	124

tetraicosanuclear Ni<sup>II</sup> cage is an octamer of trinuclear blocks.<sup>187</sup> Therefore, if still larger wheels are to be constructed, a design principle might be to look for either larger oligomers of trinuclear fragments, or oligomers of higher nuclearity building blocks.

Only one metallocrown containing more than six metals in the cyclic backbone has been reported.<sup>124</sup> This may be due to problems with templating larger metallocrowns. Where larger cations or more than one cation is encapsulated, spherical cages or “metallocryptands” tend to result; for example, in the nonanuclear cage [Na<sub>4</sub>{Ni(L1)<sub>9</sub>(H<sub>2</sub>O)(MeOH)(ClO<sub>4</sub>)<sup>3+</sup>} reported by Doble *et al.*<sup>72</sup> where four sodium ions lie within a tricapped trigonal prism of Ni<sup>II</sup> centers.

### 7.3.3.2 Cubanes

These are very common building blocks in larger cages. Inclusion of incomplete {M<sub>3</sub>O<sub>4</sub>} cubanes would increase the members of the family to include most of the planar structures described above. The structures listed in Table 3 contain only those with at least one complete {M<sub>4</sub>X<sub>4</sub>} cubane core.

There are several points worth noting. Face-sharing cubanes exist for dicubanes, tricubanes, heptacubanes, and octacubanes, with additional capping metal centers found for di-, tri-, and hepta-cubanes. The decavanadate core is described here as a “face-sharing dicubane, capped by four V centers”; each of these capping V centers is part of incomplete cubanes which share edges with the central dicubane. In the dodecanuclear iron cage, [Fe<sub>12</sub>O<sub>2</sub>(OMe)<sub>18</sub>(O<sub>2</sub>CMe)<sub>6</sub>(HOMe)<sub>4.67</sub>],<sup>148</sup> the presence of two additional iron centers completes these additional cubanes. Similarly, in the hexanuclear vanadium cage, [V<sub>16</sub>O<sub>20</sub>{(OCH<sub>2</sub>)<sub>3</sub>CCH<sub>2</sub>OH}<sub>8</sub>(H<sub>2</sub>O)<sub>4</sub>],<sup>21</sup> the additional centers are part of incomplete cubanes.

The capping atoms in the hexa-, octa-, dodeca-, and octadeca-nuclear structures listed in Table 3 all have the same disposition, i.e., they are attached to a μ<sub>4</sub> oxo group of the central cubane(s) to complete a tetrahedral coordination geometry about this site. This contrasts to the additional metal sites in the decanuclear cages, where they are attached to μ<sub>6</sub> oxo groups, which have octahedral geometries.

### 7.3.3.3 Trigonal Prisms

While examples of this polyhedron are formed for chromium, manganese, and iron, the majority of structures containing this core are formed for cobalt and nickel (Table 4). All nuclearities between hexa- and dodeca-nuclear are observed, differing in the presence of additional metal centers. Thus, simple hexanuclear trigonal prisms have been found for iron(III), and two-centered heptanuclear trigonal prisms for manganese(II). If only the trigonal faces of the prism are capped, an octanuclear manganese(II) cage is observed, while capping exclusively on the edges of the rectangular faces or on these faces themselves generates nonanuclear cages.

Decanuclear cages can be formed in three ways, but all require the presence of a central atom. They are found with caps on the edges of the rectangular faces, on the rectangular faces, and with caps on all faces of the prism but with one edge of the prism missing. Undecanuclear cages form two related polyhedra: capped on both trigonal and all three rectangular faces, but without the central metal site, and centered but lacking one cap on a trigonal face. The three dodecanuclear cages are all centered and capped on all five faces of the trigonal prism. No clear cut examples of linked trigonal prisms have been reported, although the heptanuclear [Fe<sub>16</sub>MO<sub>10</sub>(OH)<sub>10</sub>(O<sub>2</sub>CPh)<sub>20</sub>] cages can be related to the undecanuclear iron(III) cages.<sup>151</sup>

While the regular occurrence of cages based on cubane units can be easily rationalized as related to the sodium chloride structure, it is considerably more difficult to rationalize the regular occurrence of trigonal prisms. An attempt has been made to relate the cobalt and nickel structures to the structure of the M(OH)<sub>2</sub> hydroxide.<sup>162</sup>

### 7.3.3.4 Planar Cages Based on Cadmium Iodide Cores

Many of the largest cages known have central cores based on {M<sub>3</sub>O<sub>4</sub>} fragments sharing edges (Table 5). Whether this is coincidence is doubtful; more likely a fragment of a mineral is being trapped. The earliest of these cages is the {Fe<sub>8</sub>} cage reported by Wiegardt.<sup>131</sup> Larger cages containing this fragment are now known for all the metals from Mn to Ni.

Table 3 Cubanes.

Cage	Description	References
<i>Hexanuclear</i>		
$[\text{Cr}_6\text{O}_4(\text{O}_2\text{CCMe}_3)_{11}]^-$	Cubane, capped by two Cr centers	51
$[\text{Cr}_6\text{O}_2(\text{OH})_2(\text{O}_2\text{CCMe}_3)_{11}]^+$	Cubane, capped by two Cr centers	51
$[\text{Cu}_6(\text{O}_2\text{CMe})_6(\text{OH})_2(\text{OCH}_2\text{CH}_2\text{NEt}_2)_4(\text{H}_2\text{O})]$	Face-sharing dicubane	189
$[\text{Cu}_6(\text{O}_2\text{CCH}_2\text{Cl})_6(\text{OH})_2(\text{OCH}_2\text{CH}_2\text{NEt}_2)_4(\text{H}_2\text{O})]$	Face-sharing dicubane	190
$[\text{Cu}_7(\text{OH})_8(\text{bpym})_6(\text{H}_2\text{O})_2]^{6+}$	Vertex-sharing dicubane	214
$[\text{Cu}_7\{\text{(py)}_2\text{CO}_2\}_3(\text{O}_2\text{CMe})_6(\text{OH})_2]$	Vertex-sharing dicubane	215
<i>Octanuclear</i>		
$[\text{Cr}_8\text{O}_4(\text{O}_2\text{CPh})_{16}]$	Cubane, capped by four Cr centers	41
$[\text{Mn}_8\text{O}_6\text{Cl}_6(\text{O}_2\text{CPh})_7(\text{H}_2\text{O})_2]^-$	Dicubane, sharing an edge	76
$[\text{Fe}_8\text{O}_4(\text{pz})_{12}\text{Cl}_4]$	Cubane, capped by four Fe centers	137
$[\text{Co}_8\text{O}_4(\text{O}_2\text{CPh})_{12}(\text{solvent})_3(\text{H}_2\text{O})]$	Cubane, capped by four Co centers	48
$[\text{Co}_8\text{O}_4(\text{OH})_4(\text{O}_2\text{CMe})_6(\text{L}8)_2]^{2+}$	Triple cubane, sharing two faces	164
$[\text{Co}_8\text{O}_4(\text{O}_2\text{CMe})_6(\text{OMe})_4\text{Cl}_4(\text{OH})_4]$	Triple cubane, sharing two faces	50
$[\text{Cu}_8\{\text{(py)}_2\text{CO}(\text{OH})\}_8(\text{O}_2\text{CMe})_4]^{4+}$	Two linked cubanes	216
<i>Nonanuclear</i>		
$[\text{Cu}_9(\text{O}_2\text{CCHCl}_2)_{10}\{\text{OCH}_2\text{C}(\text{NH}_2)\text{Me}_2\}_6(\text{OH})_2]$	Two cubanes linked via a Cu center	226
<i>Decanuclear</i>		
$[\text{V}_{10}\text{O}_{16-x}(\text{OH})_x\{\text{(OCH}_2)_3\text{CR}\}_4]^{m-}$	Face-sharing dicubane, capped by four V centers	19,20
$[\text{Mn}_{10}\text{O}_2\text{Cl}_8\{\text{OCH}_2\}_3\text{CMe}\}_6]^{2-}$	Face-sharing dicubane, capped by four Mn centers	85
<i>Undecanuclear</i>		
$[\{\text{Ni}_6(\text{OH})_6\}\{\text{Ni}(\text{mhp})_3\}_5(\text{Hmhp})\text{Cl}(\text{H}_2\text{O})_2]$	Face-sharing dicubane, capped by five further Ni centers	104
<i>Dodecanuclear</i>		
$[\text{Cr}_{12}\text{O}_8(\text{OH})_4(\text{O}_2\text{CCHMe}_2)_{16}(\text{HO}_2\text{CCHMe}_2)_4]$	Face-sharing tricubane, capped by four Cr centers	49
$[\text{Mn}_{12}\text{O}_{12}(\text{O}_2\text{CR})_{16}(\text{H}_2\text{O})_4]$	Cubane surrounded by ring of eight Mn centers	1,91
$[\text{Fe}_{12}\text{O}_2(\text{OMe})_{18}(\text{O}_2\text{CMe})_6(\text{HOME})_{4,67}]$	Four cubanes, sharing one face and two edges	148
$[\text{Co}_{12}(\text{chp})_{18}(\text{OH})_4\text{Cl}_2(\text{Hchp})_2(\text{MeOH})_2]$	Two linked cubanes	174
<i>Higher nuclearities</i>		
$[\text{Mn}_{13}\text{O}_8(\text{OEt})_6(\text{O}_2\text{CPh})_{12}]$	Eight cubanes sharing faces, arranged in a cube	100
$[\text{V}_{16}\text{O}_{20}\{\text{(OCH}_2)_3\text{CCH}_2\text{OH}\}_8(\text{H}_2\text{O})_4]$	Two linked cubanes, each capped by four V centers	21
$[\text{Ni}_{16}\text{Na}_6(\text{chp})_4(\text{phth})_{10}(\text{Hphth})_2(\text{MeO})_{10}(\text{OH})_2(\text{MeOH})_{20}]$	Four linked cubanes	186
$[\text{Fe}_{16}\text{MO}_{10}(\text{OH})_{10}(\text{O}_2\text{CPh})_{20}]$	Double cubane sharing a vertex surrounded by ring of ten Fe centers	151
$[\text{Mn}_{18}\text{O}_{14}(\text{OMe})_{14}(\text{O}_2\text{CCMe}_3)_8(\text{MeOH})_6]$	Six cubanes arranged on the faces of a seventh cubane capped by two Mn centers	104

A further observation is that these cages can be simply related to the heterocubanes: they simply lack one metal vertex per  $\{\text{M}_3\text{O}_4\}$  block. The trigonal prismatic nickel and cobalt cages have also been related to the cadmium iodide structure.<sup>162</sup> Therefore, it is possible that these many diverse structures for Mn to Ni are beginning to fall into a common, albeit highly complex, pattern based on the ways  $\{\text{M}_3\text{O}_4\}$  blocks are linked.

### 7.3.4 CONCLUSION

The rate at which polynuclear cages are reported is accelerating. The diversity of structures is remarkable, and has prevented any guiding structural principles being proposed. The cages do not

**Table 4** Trigonal prisms.

<i>Cage</i>	<i>Description</i>	<i>References</i>
<i>Hexanuclear</i>		
[Fe <sub>6</sub> (O <sub>2</sub> ) <sub>3</sub> O <sub>2</sub> (O <sub>2</sub> CMe) <sub>9</sub> ] <sup>-</sup>		113
[NaFe <sub>6</sub> (hpid <sub>a</sub> ) <sub>6</sub> O <sub>3</sub> ] <sup>+</sup>		127,128
[LnCu <sub>6</sub> (OH) <sub>3</sub> (Hida) <sub>2</sub> (ida) <sub>4</sub> ] <sup>2+</sup>		211
<i>Heptanuclear</i>		
[Mn <sub>7</sub> O <sub>6</sub> (OEt) <sub>18</sub> (HOEt) <sub>2</sub> ]	Centered	68
[Mn{Mn(L1)} <sub>6</sub> ] <sup>2+</sup>	Centered	72
<i>Octanuclear</i>		
[Mn <sub>8</sub> O <sub>2</sub> (L2) <sub>6</sub> ]	Capped on trigonal faces	77
<i>Nonanuclear</i>		
[Fe <sub>9</sub> O(cit) <sub>8</sub> (H <sub>2</sub> O) <sub>3</sub> ] <sup>7-</sup>	Capped on edges linking triangles	140
[Na <sub>4</sub> {Ni(L1)} <sub>9</sub> (H <sub>2</sub> O)(MeOH)(ClO <sub>4</sub> ) <sub>3</sub> ] <sup>3+</sup>	Capped on rectangular faces	72
<i>Decanuclear</i>		
[Co <sub>10</sub> (OH) <sub>6</sub> (mhp) <sub>6</sub> (O <sub>2</sub> CPh) <sub>7</sub> (Hmhp) <sub>3</sub> Cl(MeCN)]	Capped on rectangular faces and centered	172
[Co <sub>10</sub> (OH) <sub>6</sub> (mhp) <sub>6</sub> (O <sub>2</sub> CCMe <sub>3</sub> ) <sub>7</sub> (Hmhp)Cl(MeCN) <sub>3</sub> ]	Capped on rectangular faces and centered	172
[Co <sub>10</sub> (OH) <sub>4</sub> (chp) <sub>10</sub> (O <sub>2</sub> CCMe <sub>3</sub> ) <sub>6</sub> (EtOH) <sub>2</sub> ]	Pentacapped, centered, missing one edge	172
[Co <sub>10</sub> (OH) <sub>6</sub> (mhp) <sub>6</sub> (O <sub>2</sub> CCH <sub>3</sub> ) <sub>6</sub> (Hmhp) <sub>3</sub> (HCO <sub>3</sub> ) <sub>3</sub> ]	Capped on edges linking triangles and centered	173
[Ni <sub>10</sub> (OH) <sub>6</sub> (mhp) <sub>6</sub> ·5(O <sub>2</sub> CCHMe <sub>2</sub> ) <sub>6</sub> ·5(Hmhp) <sub>3</sub> Cl(H <sub>2</sub> O)]	Capped on rectangular faces and centered	172
[Ni <sub>10</sub> (OH) <sub>6</sub> (chp) <sub>6</sub> (O <sub>2</sub> CCHPh <sub>2</sub> ) <sub>6</sub> (Cl) <sub>2</sub> (Hchp)(H <sub>2</sub> O) <sub>2</sub> (MeOH)]	Capped on rectangular faces and centered	172
[Ni <sub>10</sub> (OH) <sub>4</sub> (mhp) <sub>10</sub> (O <sub>2</sub> CCMe <sub>3</sub> ) <sub>6</sub> (MeOH) <sub>2</sub> ]	Pentacapped, centered, missing one edge	172
[Ni <sub>10</sub> (OH) <sub>4</sub> (mhp) <sub>10</sub> (O <sub>2</sub> CCMe <sub>3</sub> ) <sub>6</sub> (H <sub>2</sub> O) <sub>2</sub> ]	Pentacapped, centered, missing one edge	172
<i>Undecanuclear</i>		
[Fe <sub>11</sub> O <sub>6</sub> (OH) <sub>6</sub> (O <sub>2</sub> CPh) <sub>15</sub> ]	Pentacapped	147
[Fe <sub>11</sub> O <sub>6</sub> (OH) <sub>6</sub> (O <sub>2</sub> CCH <sub>2</sub> CH <sub>2</sub> C(O)C <sub>6</sub> H <sub>4</sub> Me) <sub>15</sub> ]	Pentacapped	143
[Ni <sub>11</sub> (OH) <sub>6</sub> (mhp) <sub>9</sub> (O <sub>2</sub> CMe) <sub>6</sub> (H <sub>2</sub> O) <sub>3</sub> ] <sup>+</sup>	Capped on rectangular faces and one trigonal face, centered	172
[Ni <sub>11</sub> (OH) <sub>6</sub> (mhp) <sub>9</sub> (O <sub>2</sub> CMe) <sub>7</sub> (Hmhp) <sub>2</sub> ]	Capped on rectangular faces and one trigonal face, centered	172
<i>Dodecanuclear</i>		
[Cr <sub>12</sub> O <sub>9</sub> (OH) <sub>3</sub> (O <sub>2</sub> CCMe <sub>3</sub> ) <sub>15</sub> ]	Pentacapped and centered	45,46
[Co <sub>12</sub> (OH) <sub>6</sub> (mhp) <sub>12</sub> (O <sub>2</sub> CMe) <sub>6</sub> ]	Pentacapped and centered	171
[Ni <sub>12</sub> (OH) <sub>6</sub> (mhp) <sub>12</sub> (O <sub>2</sub> CCH <sub>2</sub> Cl) <sub>6</sub> ]	Pentacapped and centered	172

**Table 5** Planar cages with “CdI<sub>2</sub>” cores.

<i>Cage</i>	<i>References</i>
[Fe <sub>8</sub> O <sub>2</sub> (OH) <sub>12</sub> (tacn) <sub>6</sub> ] <sup>8+</sup>	131
[Mn <sub>10</sub> O <sub>14</sub> (tren) <sub>6</sub> ] <sup>8+</sup>	84
[Fe <sub>17</sub> O <sub>4</sub> (OH) <sub>16</sub> (heidi) <sub>8</sub> (H <sub>2</sub> O) <sub>12</sub> ] <sup>+</sup>	106
[Fe <sub>19</sub> O <sub>6</sub> (OH) <sub>14</sub> (heidi) <sub>10</sub> (H <sub>2</sub> O) <sub>12</sub> ] <sup>+</sup>	106
[Fe <sub>19</sub> O <sub>6</sub> (OH) <sub>14</sub> (metheidi) <sub>10</sub> (H <sub>2</sub> O) <sub>12</sub> ] <sup>+</sup>	153
[Mn <sub>19</sub> O <sub>12</sub> (OCH <sub>2</sub> CH <sub>2</sub> OMe) <sub>14</sub> (HOCH <sub>2</sub> CH <sub>2</sub> OMe) <sub>10</sub> ]	105
[Ni <sub>21</sub> (cit) <sub>12</sub> (OH) <sub>10</sub> (H <sub>2</sub> O) <sub>10</sub> ] <sup>16-</sup>	182
[Co <sub>24</sub> (OH) <sub>18</sub> (OMe) <sub>2</sub> Cl <sub>6</sub> (mhp) <sub>22</sub> ]	107

correspond in a straightforward manner to fragments of common minerals, or to polyhedral archetypes, but display a richness of topologies and nuclearities that is unpredictable but intriguing.

There remain many gaps in this field. Ligands that are regularly applied to one metal may not feature at all in the cage chemistry of another metal. The tendency in the area is for O-donor ligands to be used with early 3d metals, with nitrogen donors becoming more common as the transition series is traversed. While this obeys the “hard-soft” principle, it is not clear whether

the absence of alkoxide cages of nickel or pyrazolate cages of chromium is because these cages cannot be made, or because no-one has yet looked. The recent paper by Chandrasekar and Kingsley<sup>232</sup> is a very rare example of a phosphonate ligand used with a 3d metal other than vanadium.

Heterometallic cages are rare, and, in the context of magnetic behavior, could be very interesting. This lack contrasts with the many heterometallic cyanide cages known (see Chapter 7.4). Application of rigid, polydentate ligands remains rare, other than the pioneering work of Saalfrank<sup>77,78</sup> and Thompson.<sup>83,228</sup> This approach could generate many exciting cages, with the advantage of control of structure. The drawback is the additional organic chemistry required to make the ligands.

The reaction chemistry of these cages is at present an impenetrable mystery. The paramagnetism makes NMR a technique of limited applicability, especially in cases where some ligands are weakly bound, creating additional problems of fluxionality. Vibrational and electronic spectra of such cages contain too many and too few spectroscopic handles respectively to be useful. Therefore, solution studies have been limited. The growing use of electrospray mass spectrometry suggests more will be known in the future.

### 7.3.5 REFERENCES

- Sessoli, R.; Tsai, H.-L.; Schake, A. R.; Wang, S.; Vincent, J. B.; Foltling, K.; Gatteschi, D.; Christou, G.; Hendrickson, D. N. *J. Am. Chem. Soc.* **1993**, *115*, 1804–1816.
- Sessoli, R.; Gatteschi, D.; Caneschi, A.; Novak, M. A. *Nature* **1993**, *365*, 141–142.
- Winpenny, R. E. P. *Adv. Inorg. Chem.* **2001**, *52*, 1–111.
- Winpenny, R. E. P. *Dalton Trans.* **2002**, 1–10.
- Christou, G. *Acc. Chem. Res.* **1989**, *22*, 328–335.
- Blake, A. J.; Grant, C. M.; Gregory, C. I.; Parsons, S.; Rawson, J. M.; Reed, D.; Winpenny, R. E. P. *J. Chem. Soc., Dalton Trans.* **1995**, 163–175.
- Blake, A. J.; Brechin, E. K.; Codron, A.; Gould, R. O.; Grant, C. M.; Parsons, S.; Rawson, J. M.; Winpenny, R. E. P. *J. Chem. Soc., Chem. Commun.* **1995**, 1983–1986.
- Blake, A. J.; Grant, C. M.; Parsons, S.; Rawson, J. M.; Winpenny, R. E. P. *J. Chem. Soc., Chem. Commun.* **1994**, 2363–2364.
- Khan, M. I.; Zubieta, J. *Prog. Inorg. Chem.* **1995**, *43*, 1–149.
- Castro, S. L.; Sun, Z.; Grant, C. M.; Bollinger, J. C.; Hendrickson, D. N.; Christou, G. *J. Am. Chem. Soc.* **1998**, *120*, 2365–2375.
- Kumagai, H.; Kitagawa, S. *Chem. Lett.* **1996**, 471–472.
- Khan, M. I.; Chen, Q.; Höpe, H.; Parkin, S.; O'Connor, C. J.; Zubieta, J. *Inorg. Chem.* **1993**, *32*, 2929–2937.
- Kessler, V. G.; Seisenbaeva, G. A. *Inorg. Chem. Comm.* **2000**, *3*, 203–204.
- Hou, D.; Kim, G.-S.; Hagen, K. S.; Hill, C. L. *Inorg. Chim. Acta* **1993**, *211*, 127–130.
- Chen, Q.; Zubieta, J. *J. Chem. Soc., Chem. Commun.* **1993**, 1180–1182.
- Müller, A.; Meyer, J.; Bögge, H.; Stammler, A.; Botar, A. *Chem. Eur. J.* **1998**, *4*, 1388–1397.
- Chen, Y.; Liu, Q.; Deng, Y.; Zhu, H.; Chen, C.; Fan, H.; Liao, D.; Gao, E. *Inorg. Chem.* **2001**, *40*, 3725–3733.
- Chen, Q.; Liu, S.; Zubieta, J. *Inorg. Chem.* **1989**, *28*, 4433–4434.
- Khan, M. I.; Chen, Q.; Goshorn, D. P.; Hope, H.; Parkin, S.; Zubieta, J. *J. Am. Chem. Soc.* **1992**, *114*, 3341–3346.
- Khan, M. I.; Chen, Q.; Goshorn, D. P.; Zubieta, J. *Inorg. Chem.* **1993**, *32*, 672–680.
- Khan, M. I.; Lee, Y.-S.; O'Connor, C. J.; Zubieta, J. *J. Am. Chem. Soc.* **1994**, *116*, 5001–5002.
- Salta, J.; Chen, Q.; Chang, Y.-D.; Zubieta, J. *Angew. Chem., Int. Ed. Engl.* **1994**, *33*, 757–760.
- Thorn, D. L.; Harlow, R. L.; Herron, N. *Inorg. Chem.* **1995**, *34*, 2629–2638.
- Mokry, L. M.; Thompson, J.; Bond, M. R.; Otieno, T.; Mohan, M.; Carrano, C. J. *Inorg. Chem.* **1994**, *33*, 2705–2706.
- Khan, M. I.; Chang, Y.; Chen, Q.; Hope, H.; Parkin, S.; Goshorn, D. P.; Zubieta, J. *Angew. Chem., Int. Ed. Engl.* **1992**, *31*, 1197–1199.
- Chang, Y.-D.; Salta, J.; Zubieta, J. *Angew. Chem., Int. Ed. Engl.* **1994**, *33*, 325–326.
- Huan, G.; Day, V. W.; Jacobson, A. J.; Goshorn, D. P. *J. Am. Chem. Soc.* **1991**, *113*, 3188–3189.
- Khan, M. I.; Zubieta, J. *Angew. Chem., Int. Ed. Engl.* **1994**, *33*, 760–762.
- Müller, A.; Hovemeier, K.; Rohlfling, R. *Angew. Chem., Int. Ed. Engl.* **1992**, *31*, 1192–1195.
- Huan, G.; Jacobson, A. J.; Day, V. W. *Angew. Chem., Int. Ed. Engl.* **1991**, *30*, 422–423.
- Bottomley, F. *Polyhedron* **1992**, *11*, 1707–1731.
- Rehder, D.; Priebsch, W.; von Oeynhausen, M. *Angew. Chem., Int. Ed. Engl.* **1989**, *28*, 1221–1222.
- Launay, J.-P.; Jeannin, Y.; Daoudi, M. *Inorg. Chem.* **1985**, *24*, 1052–1059.
- Karet, G. B.; Sun, Z.; Streib, W. E.; Bollinger, J. C.; Hendrickson, D. N.; Christou, G. *Chem. Commun.* **1999**, 2249–2250.
- Müller, A.; Rohlfling, R.; Krickemeyer, E.; Bögge, H. *Angew. Chem., Int. Ed. Engl.* **1993**, *32*, 909–912.
- Spandl, J.; Brüdgam, I.; Hartl, H. *Angew. Chem. Int. Ed.* **2001**, *40*, 4018–4020.
- Cannon, R. D.; White, R. P. *Prog. Inorg. Chem.* **1988**, *36*, 195–298.
- Gérbéléu, N. V.; Struchkov, Y. T.; Timco, G. A.; Batsanov, A. S.; Indrichan, K. M.; Popovich, G. A. *Dokl. Akad. Nauk. SSSR.* **1990**, *313*, 1459–1462.
- Overgaard, J.; Iversen, B. B.; Palić, S. P.; Timco, G. A.; Gérbéléu, N. V.; Larsen, F. K. *Chem. Eur. J.* **2002**, *8*, 2775–2786.
- van Slageren, J.; Sessoli, R.; Gatteschi, D.; Smith, A. A.; Helliwell, M.; Winpenny, R. E. P.; Cornia, A.; Barra, A.-L.; Jansen, A. G. M.; Timco, G. A.; Rentschler, E. *Chem. Eur. J.* **2002**, *8*, 277.

41. Atkinson, I. M.; Benelli, C.; Murrie, M.; Parsons, S.; Winpenny, R. E. P. *Chem. Commun.* **1999**, 285–286.
42. Eshel, M.; Bino, A.; Felner, I.; Johnston, D. C.; Luban, M.; Miller, L. L. *Inorg. Chem.* **2000**, *39*, 1376–1380.
43. McInnes, E. J. L.; Anson, C.; Powell, A. K.; Thomson, A. J.; Poussereau, S.; Sessoli, R. *Chem. Commun.* **2001**, 89–90.
44. Gérbéléu, N. V.; Parsons, S.; Smith, A. A.; Timco, G. A.; Winpenny, R. E. P. (unpublished results).
45. Batsanov, A. S.; Timco, G. A.; Struchkov, Y. T.; Gérbéléu, N. V.; Indrichan, K. M. *Koord. Khim.* **1991**, *17*, 662–669.
46. Mabbs, F. E.; McInnes, E. J. L.; Murrie, M.; Parsons, S.; Smith, G. M.; Wilson, C. C.; Winpenny, R. E. P. *Chem. Commun.* **1999**, 643–644.
47. Bino, A.; Johnston, D. C.; Goshorn, D. P.; Halbert, T. R.; Stiefel, E. I. *Science* **1988**, *241*, 1479–1481.
48. Dimitrou, K. Sun, J.-S.; Folting, K.; Christou, G. *Inorg. Chem.* **1995**, *34*, 4160–4166.
49. Parsons, S.; Smith, A. A.; Winpenny, R. E. P. *Chem. Commun.* **2000**, 579–580.
50. Beattie, J. K.; Hambley, T. W.; Kleptko, J. A.; Masters, A. F.; Turner, P. *Polyhedron* **1997**, *16*, 2109–2112.
51. Coxall, R. A.; Parkin, A.; Parsons, S.; Smith, A. A.; Timco, G. A.; Winpenny, R. E. P. *J. Sol. State. Chem.* **2001**, *159*, 321–327.
52. Aromi, G.; Aubin, S. M. J.; Bolcar, M. A.; Christou, G.; Eppley, H. J.; Folting, K.; Hendrickson, D. N.; Huffman, J. C.; Squire, R. C.; Tsai, H.-L.; Wang, S.; Wemple, M. W. *Polyhedron* **1998**, *17*, 3005–3020.
53. Baikie, A. R. E.; Howes, A. J.; Hursthouse, M. B.; Quick, A. B.; Thornton, P. *J. Chem. Soc., Chem. Commun.* **1986**, 1587–1588.
54. Batsanov, A. S.; Struchkov, Y. T.; Timco, G. A.; Gérbéléu, N. V.; Manole, O. S.; Grebenko, S. V. *Koord. Khim.* **1994**, *20*, 604–606.
55. Schake, A. R.; Vincent, J. B.; Li, Q.; Boyd, P. D. W.; Folting, K.; Huffman, J. C.; Hendrickson, D. N.; Christou, G. *Inorg. Chem.* **1989**, *28*, 1915–1923.
56. Blackman, A. G.; Huffman, J. C.; Lobkovsky, E. B.; Christou, G. *Polyhedron* **1992**, *11*, 251–255.
57. Halcrow, M. A.; Streib, W. E.; Folting, K.; Christou, G. *Acta Crystallogr., Sect. C* **1995**, *51*, 1263–1267.
58. Murrie, M.; Parsons, S.; Winpenny, R. E. P. *J. Chem. Soc., Dalton Trans.* **1998**, 1423–1424.
59. Caneschi, A.; Gatteschi, D.; Laugier, J.; Rey, P.; Sessoli, R.; Zanchini, C. *J. Am. Chem. Soc.* **1988**, *110*, 2795–2799.
60. Belforte, A.; Calderazzo, F.; Zanazzi, P. F. *J. Chem. Soc., Dalton Trans.* **1988**, 2921–2926.
61. Xia, X. P.; Verelst, M.; Daran, J. C.; Tuchagues, J. P. *J. Chem. Soc., Chem. Commun.* **1995**, 2155–2157.
62. Aromi, G.; Knapp, M. J.; Claude, J.-P.; Huffman, J. C.; Hendrickson, D. N.; Christou, G. *J. Am. Chem. Soc.* **1999**, *121*, 5489–5499.
63. Igonin, V. A.; Shegolikina, O. I.; Lindeman, S. V.; Levitsky, M. M.; Struchkov, Yu. T.; Zhdanov, A. A. *J. Organomet. Chem.* **1992**, *423*, 351–360.
64. Bhula, R.; Collier, S.; Robinson, W. T.; Weatherburn, D. C. *Inorg. Chem.* **1990**, *29*, 4027–4032.
65. Bhula, R.; Weatherburn, D. C. *Angew. Chem., Int. Ed. Engl.* **1991**, *30*, 688–689.
66. Wang, S.; Tsai, H.-L.; Streib, W. E.; Christou, G.; Hendrickson, D. N. *J. Chem. Soc., Chem. Commun.* **1992**, 677–679.
67. Wang, S.; Folting, K.; Streib, W. E.; Schmitt, E. A.; McCusker, J. K.; Hendrickson, D. N.; Christou, G. *Angew. Chem., Int. Ed. Engl.* **1991**, *30*, 305–306.
68. Bemm, U.; Norrestam, R.; Nygren, M.; Westin, G. *J. Sol. State Chem.* **1997**, *134*, 312–318.
69. Bolcar, M. A.; Aubin, S. M. J.; Folting, K.; Hendrickson, D. N.; Christou, G. *Chem. Commun.* **1997**, 1485–1486.
70. Abbati, G. L.; Cornia, A.; Fabretti, A. C.; Caneschi, A.; Gatteschi, D. *Inorg. Chem.* **1998**, *37*, 1430–1431.
71. Abbati, G. L.; Cornia, A.; Fabretti, A. C.; Caneschi, A.; Gatteschi, D. *Inorg. Chem.* **1998**, *37*, 3759–3766.
72. Doble, D. M. J.; Benison, C. H.; Blake, A. J.; Fenske, D.; Jackson, M. S.; Kay, R. D.; Li, W.-S.; Schröder, M. *Angew. Chem., Int. Ed. Engl.* **1999**, *38*, 1915–1918.
73. Libby, E.; Folting, K.; Huffman, J. C.; Christou, G. *J. Am. Chem. Soc.* **1990**, *112*, 5354–5356.
74. Wang, S.; Tsai, H.-L.; Folting, K.; Martin, J. D.; Hendrickson, D. N.; Christou, G. *J. Chem. Soc., Chem. Commun.* **1994**, 671–672.
75. Wemple, M. W.; Tsai, H.-L.; Streib, W. E.; Hendrickson, D. N.; Christou, G. *J. Chem. Soc., Chem. Commun.* **1994**, 1031–1033.
76. Tsai, H.-L.; Wang, S.; Folting, K.; Streib, W. E.; Hendrickson, D. N.; Christou, G. *J. Am. Chem. Soc.* **1995**, *117*, 2503–2514.
77. Saalfrank, R. W.; Löw, N.; Trummer, S.; Sheldrick, G. M.; Teichert, M.; Stalke, D. *Eur. J. Inorg. Chem.* **1998**, 559–563.
78. Saalfrank, R. W.; Löw, N.; Demleitner, B.; Stalke, D.; Teichert, M. *Chem. Eur. J.* **1998**, *4*, 1305–1311.
79. Bemm, U.; Norrestam, R.; Nygren, M.; Westin, G. *Inorg. Chem.* **1995**, *34*, 2367–2370.
80. Aluarez, C. S.; Bond, A. D.; Harron, E. A.; Layfield, R. A.; McAllister, J. A.; Pask, C. M.; Rawson, J. M.; Wright, D. S. *Organometallics* **2001**, *20*, 4135–4137.
81. Christmas, C.; Vincent, J. B.; Chang, H.-R.; Huffman, J. C.; Christou, G.; Hendrickson, D. N. *J. Am. Chem. Soc.* **1988**, *110*, 823–830.
82. Low, D. W.; Eichhorn, D. M.; Draganescu, A.; Armstrong, W. H. *Inorg. Chem.* **1991**, *30*, 878–880.
83. Zhao, L.; Matthews, C. J.; Thompson, L. K.; Heath, S. L. *Chem. Commun.* **2000**, 265–266.
84. Hagen, K. S.; Armstrong, W. H.; Olmstead, M. M. *J. Am. Chem. Soc.* **1989**, *111*, 774–775.
85. Cavaluzzo, M.; Chen, Q.; Zubieta, J. *J. Chem. Soc., Chem. Commun.* **1993**, 131–133.
86. Goldberg, D. P.; Caneschi, A.; Delfs, C. D.; Sessoli, R.; Lippard, S. J. *J. Am. Chem. Soc.* **1995**, *117*, 5789–5800.
87. Eppley, E. J.; Aubin, S. M. J.; Streib, W. E.; Bollinger, J. C.; Hendrickson, D. N.; Christou, G. *Inorg. Chem.* **1997**, *36*, 109–115.
88. Liu, S.-X.; Lin, S.; Lin, B.-Z.; Lin, C.-C.; Huang, J.-Q. *Angew. Chem. Int. Ed.* **2001**, *40*, 1084–1087.
89. Perlepes, S. P.; Huffman, J. C.; Christou, G. *J. Chem. Soc., Chem. Commun.* **1991**, 1657–1659.
90. Luneau, D.; Savariault, J.-M.; Tuchagues, J.-P. *Inorg. Chem.* **1988**, *27*, 3912–3918.
91. Lis, T. *Acta Crystallogr. Sect. B* **1980**, *36*, 2042–2045.
92. Boyd, P. D. W.; Li, Q.; Vincent, J. B.; Folting, K.; Chang, H.-R.; Streib, W. E.; Huffman, J. C.; Christou, G.; Hendrickson, D. N. *J. Am. Chem. Soc.* **1988**, *110*, 8537–8538.
93. Aubin, S. M. J.; Sun, Z.; Ruiz, D.; Eppley, H. J.; Rumberger, E.; Guzei, I. A.; Folting, K.; Gantzel, P. K.; Rheingold, A. L.; Christou, G.; Hendrickson, D. N. *Inorg. Chem.* **2001**, *40*, 2127–2146.
94. Artus, P.; Boskovic, C.; Yoo, J.; Streib, W. E.; Brunel, L.-C.; Hendrickson, D. N.; Christou, G. *Inorg. Chem.* **2001**, *40*, 4199–4210.

95. Boskovic, C.; Pink, M.; Huffman, J. C.; Hendrickson, D. N.; Christou, G. *J. Am. Chem. Soc.* **2001**, *123*, 9914–9915.
96. Aubin, S. M. J.; Sun, Z.; Pardi, L.; Krzystek, J.; Foltling, K.; Brunel, L.-C.; Rheingold, A. L.; Christou, G.; Hendrickson, D. N. *Inorg. Chem.* **1999**, *38*, 5329–5340.
97. Soler, M.; Chandra, S. K.; Ruiz, D.; Davidson, E. R.; Hendrickson, D. N.; Christou, G. *Chem. Commun.* **2000**, 2417–2418.
98. Schake, A. R.; Tsai, H.-L.; De Vries, N.; Webb, R. J.; Foltling, K.; Hendrickson, D. N.; Christou, G. *J. Chem. Soc., Chem. Commun.* **1992**, 181–183.
99. Boskovic, C.; Brechin, E. K.; Streib, W. E.; Foltling, K.; Bollinger, J. C.; Hendrickson, D. N.; Christou, G. *J. Am. Chem. Soc.* **2002**, *124*, 3725–3736.
100. Sun, Z.; Gantzel, P. K.; Hendrickson, D. N. *Inorg. Chem.* **1996**, *35*, 6640–6641.
101. Price, D. J.; Batten, S. R.; Moubaraki, B.; Murray, K. S. *Chem. Commun.* **2002**, 762–763.
102. Squire, R. C.; Aubin, S. M. J.; Foltling, K.; Streib, W. E.; Hendrickson, D. N.; Christou, G. *Angew. Chem., Int. Ed. Engl.* **1995**, *34*, 887–889.
103. Eppley, H. J.; deVries, N.; Wang, S.; Aubin, S. M.; Tsai, H.-L.; Foltling, K.; Hendrickson, D. N.; Christou, G. *Inorg. Chim. Acta* **1997**, *263*, 323–340.
104. Brechin, E. K.; Clegg, W.; Murrie, M.; Parsons, S.; Teat, S. J.; Winpenny, R. E. P. *J. Am. Chem. Soc.* **1998**, *120*, 7365–7366.
105. Pohl, I. A. M.; Westin, L. G.; Kritikos, M. *Chem. Eur. J.* **2001**, *7*, 3438–3445.
106. Powell, A. K.; Heath, S. L.; Gatteschi, D.; Pardi, L.; Sessoli, R.; Spina, G.; Del Giallo, F.; Pieralli, F. *J. Am. Chem. Soc.* **1995**, *117*, 2491–2502.
107. Brechin, E. K.; Harris, S. G.; Harrison, A.; Parsons, S.; Whittaker, A. G.; Winpenny, R. E. P. *Chem. Commun.* **1997**, 653–654.
108. Soler, M.; Rumberger, E.; Foltling, K.; Hendrickson, D. N.; Christou, G. *Polyhedron* **2001**, *20*, 1365–1369.
109. G rbel u, N. V.; Batsanov, A. S.; Timco, G. A.; Struchkov, Y. T.; Indrichan, K. M.; Popovich, G. A. *Dokl. Akad. Nauk SSSR* **1987**, *293*, 364–367.
110. Micklitz, W.; Lippard, S. J. *Inorg. Chem.* **1988**, *27*, 3067–3069.
111. Micklitz, W.; Bott, S. G.; Bentsen, J. G.; Lippard, S. J. *J. Am. Chem. Soc.* **1989**, *111*, 372–374.
112.  elenlilil- etin, R.; Staples, R. J.; Stavropoulos, P. *Inorg. Chem.* **2000**, *39*, 5838–5846.
113. Shweky, I.; Pence, L. E.; Papaefthymiou, G. C.; Sessoli, R.; Yun, J. W.; Bino, A.; Lippard, S. J. *J. Am. Chem. Soc.* **1997**, *119*, 1037–1042.
114. McCusker, J. K.; Christmas, C. A.; Hagen, P. M.; Chadhu, R. K.; Harvey, D. F.; Hendrickson, D. N. *J. Am. Chem. Soc.* **1991**, *113*, 6114–6124.
115. Christmas, C. A.; Tsai, H.-L.; Pardi, L.; Kesselman, J. M.; Gantzel, P. K.; Chadhu, R. K.; Gatteschi, D.; Harvey, D. F.; Hendrickson, D. N. *J. Am. Chem. Soc.* **1993**, *115*, 12483–12490.
116. Hegetschweiler, K.; Schmale, H. W.; Streit, H. M.; Gramlich, V.; Hund, H.-U.; Erni, I. *Inorg. Chem.* **1992**, *31*, 1299–1302.
117. Hegetschweiler, K.; Schmale, H. W.; Streit, H. M.; Schneider, W. *Inorg. Chem.* **1990**, *29*, 3625–3627.
118. Cornia, A.; Gatteschi, D.; Hegetschweiler, K.; Hausherr-Primo, L.; Gramlich, V. *Inorg. Chem.* **1996**, *35*, 4414–4419.
119. Brechin, E. K.; Knapp, M. J.; Huffman, J. C.; Hendrickson, D. N.; Christou, G. *Inorg. Chim. Acta* **2000**, *297*, 389–399.
120. Belli Dell'Amico, D.; Calderazzo, F.; Labella, L.; Maichle-M ssmer, C.; Str hle, J. *J. Chem. Soc., Chem. Commun.* **1994**, 1555–1556.
121. Abbati, G. L.; Brunel, L.-C.; Casalta, H.; Cornia, A.; Fabretti, A. C.; Gatteschi, D.; Hassan, A. K.; Jansen, A. G. M.; Maniero, A. L.; Pardi, L.; Paulsen, C.; Segre, U. *Chem. Eur. J.* **2001**, *7*, 1796–1807.
122. Caneschi, A.; Cornia, A.; Fabretti, A. C.; Gatteschi, D. *Angew. Chem., Int. Ed. Engl.* **1999**, *38*, 1295–1297.
123. Abbati, G. L.; Caneschi, A.; Cornia, A.; Fabretti, A. C.; Gatteschi, D. *Inorg. Chim. Acta* **2000**, *297*, 291–300.
124. Saalfrank, R. W.; Bernt, I.; Uller, E.; Hampel, F. *Angew. Chem., Int. Ed. Engl.* **1997**, *36*, 2482–2484.
125. Waldmann, O.; Koch, R.; Schromm, S.; Sch lein, J.; M ller, P.; Bernt, I.; Saalfrank, R. W.; Hampel, F.; Balthes, E. *Inorg. Chem.* **2001**, *40*, 2986–2995.
126. Grant, C. M.; Knapp, M. J.; Streib, W. E.; Huffman, J. C.; Hendrickson, D. N.; Christou, G. *Inorg. Chem.* **1998**, *37*, 6065–6070.
127. Goodwin, J. C.; Price, D. J.; Powell, A. K.; Heath, S. L. *Eur. J. Inorg. Chem.* **2000**, 1407–1410.
128. Scheppensieper, T.; Liehr, G.; van Eldik, R.; Ensling, J.; G tlich, P. *Inorg. Chem.* **2000**, *39*, 5565–5568.
129. Kajiwara, T.; Ito, T. *Angew. Chem., Int. Ed. Engl.* **2000**, *39*, 230–233.
130. Zhang, X.-X.; Lippard, S. J. *Inorg. Chem.* **2000**, *39*, 4388–4389.
131. Wieghardt, K.; Pohl, K.; Jibril, I.; Huttner, G. *Angew. Chem., Int. Ed. Engl.* **1984**, *23*, 77–78.
132. Delfs, C.; Gatteschi, D.; Pardi, L.; Sessoli, R.; Wieghardt, K. *Inorg. Chem.* **1993**, *32*, 3099–3103.
133. Sangregorio, C.; Ohm, T.; Paulsen, C.; Sessoli, R.; Gatteschi, D. *Phys. Rev. Lett.* **1997**, *78*, 4645–4648.
134. Gatteschi, D.; Sessoli, R.; Cornia, A. *Chem. Commun.* **2000**, 725–732.
135. Nair, V. S.; Hagen, K. S. *Inorg. Chem.* **1994**, *33*, 185–186.
136. Satcher, Jr., J. H.; Olmstead, M. M.; Droegge, M. W.; Parkin, S. R.; Noll, B. C.; May, L.; Balch, A. L. *Inorg. Chem.* **1998**, *37*, 6751–6758.
137. Raptis, R. G.; Georgakaki, I. P.; Hockless, D. C. R. *Angew. Chem., Int. Ed. Engl.* **1999**, *38*, 1632–1634.
138. G rbel u, N. V.; Struchkov, Y. T.; Timco, G. A.; Manole, O. S.; Batsanov, A. S. *Dokl. Akad. Nauk SSSR* **1990**, *331*, 184–186.
139. Ammala, P.; Cashion, J. D.; Kepert, C. M.; Moubaraki, B.; Murray, K. S.; Spiccia, L.; West, B. O. *Angew. Chem., Int. Ed. Engl.* **2000**, *39*, 1688–1690.
140. Bino, A.; Shweky, I.; Cohen, S.; Bauminger, E. R.; Lippard, S. J. *Inorg. Chem.* **1998**, *37*, 5168–5172.
141. Taft, K. L.; Delfs, C. D.; Papaefthymiou, G. C.; Foner, S.; Gatteschi, D.; Lippard, S. J. *J. Am. Chem. Soc.* **1994**, *116*, 823–832.
142. Benelli, C.; Parsons, S.; Solan, G. A.; Winpenny, R. E. P. *Angew. Chem., Int. Ed. Engl.* **1996**, *35*, 1825–1828.
143. Frey, M.; Harris, S. G.; Holmes, J. M.; Nation, D. A.; Parsons, S.; Tasker, P. A.; Winpenny, R. E. P. *Chem. Eur. J.* **2000**, *6*, 1407–1415.



144. Caneschi, A.; Cornia, A.; Fabretti, A. C.; Gatteschi, D. *Angew. Chem., Int. Ed. Engl.* **1995**, *34*, 2716–2718.
145. Asirvatham, S.; Khan, M. A.; Nicholas, K. M. *Inorg. Chem.* **2000**, *39*, 2006–2007.
146. Benelli, C.; Cano, J.; Journaux, Y.; Sessoli, R.; Solan, G. A.; Winpenny, R. E. P. *Inorg. Chem.* **2001**, *40*, 188–189.
147. Gorun, S. M.; Papaefthymiou, G. C.; Frankel, R. B.; Lippard, S. J. *J. Am. Chem. Soc.* **1987**, *109*, 3337–3348.
148. Taft, K. L.; Papaefthymiou, G. C.; Lippard, S. J. *Inorg. Chem.* **1994**, *33*, 1510–1520.
149. Bino, A.; Ardon, M.; Lee, D.; Spingler, B.; Lippard, S. J. *J. Am. Chem. Soc.* **2002**, *124*, 4578–4579.
150. Burger, J.; Klüfers, P. *Angew. Chem., Int. Ed. Engl.* **1997**, *36*, 776–779.
151. Micklitz, W.; McKee, V.; Rardin, R. L.; Pence, L. E.; Papaefthymiou, G. C.; Bott, S. G.; Lippard, S. J. *J. Am. Chem. Soc.* **1994**, *116*, 8061–8069.
152. Parson, S.; Solan, G. A.; Winpenny, R. E. P. *J. Chem. Soc., Chem. Commun.* **1995**, 1987–1988.
153. Goodwin, J. C.; Sessoli, R.; Gatteschi, D.; Wernsdorfer, W.; Powell, A. K.; Heath, S. L. *J. Chem. Soc., Dalton Trans.* **2000**, 1835–1840.
154. Watton, S. P.; Fuhrmann, P.; Pence, L. E.; Caneschi, A.; Cornia, A.; Abbati, G. L.; Lippard, S. L. *Angew. Chem., Int. Ed. Engl.* **1997**, *36*, 2774–2776.
155. Belli Dell'Amico, D.; Calderazzo, F.; Giovannitti, B.; Pelizzi, G. *J. Chem. Soc., Dalton Trans.* **1984**, 647–652.
156. McConnell, S.; Motevalli, M.; Thornton, P. *Polyhedron* **1995**, *14*, 459–462.
157. Blake, A. J.; Gould, R. O.; Milne, P. E. Y.; Winpenny, R. E. P. *J. Chem. Soc., Chem. Commun.* **1991**, 1453–1456.
158. Gutschke, S. O. H.; Price, D. J.; Powell, A. K.; Wood, P. T. *Angew. Chem., Int. Ed. Engl.* **1999**, *38*, 1088–1090.
159. Coxall, R. A.; Harris, S. G.; Henderson, D. K.; Parsons, S.; Tasker, P. A.; Winpenny, R. E. P. *J. Chem. Soc., Dalton Trans.* **2000**, 2349–2356.
160. Masaoka, S.; Furukawa, S.; Chang, H.-C.; Mizutani, T.; Kitagawa, S. *Angew. Chem. Int. Ed.* **2001**, *40*, 3817–3819.
161. Brechin, E. K.; Harris, S. G.; Parsons, S.; Winpenny, R. E. P. *J. Chem. Soc., Dalton Trans.* **1997**, 3403–3404.
162. Brechin, E. K.; Graham, A.; Parkin, A.; Parsons, S.; Seddon, A. M.; Winpenny, R. E. P. *J. Chem. Soc., Dalton Trans.* **2000**, 3243–3252.
163. Hong, M.; Jiang, F.; Huang, X.; Su, W.; Li, W.; Cao, R.; Liu, H. *Inorg. Chim. Acta* **1997**, *256*, 137–141.
164. Grillo, V. A.; Sun, Z.; Folting, K.; Hendrickson, D. N.; Christou, G. *Chem. Commun.* **1996**, 2233–2234.
165. Jones, P. L.; Byrom, K. J.; Jeffrey, J. C.; McCleverty, J. A.; Ward, M. D. *Chem. Commun.* **1997**, 1361–1362.
166. Beattie, J. K.; Hambley, T. W.; Klepetko, J. A.; Master, A. F.; Turner, P. *Chem. Commun.* **1998**, 45–46.
167. Brechin, E. K.; Harris, S. G.; Parsons, S.; Winpenny, R. E. P. *Angew. Chem., Int. Ed. Engl.* **1997**, *36*, 1967–1969.
168. Tsohos, A.; Dionyssopolou, S.; Raptopoulou, C. P.; Terzis, A.; Bakalbassis, E. G.; Perlepes, S. P. *Angew. Chem., Int. Ed. Engl.* **1999**, *38*, 983–985.
169. Papaefstathiou, G. S.; Perlepes, S. P.; Escuer, A.; Vicente, R.; Font-Bardia, M.; Solans, X. *Angew. Chem. Int. Ed.* **2001**, *40*, 884–886.
170. Papaefstathiou, G. S.; Escuer, A.; Vicente, R.; Font-Bardia, M.; Solans, X.; Perlepes, S. P. *Chem. Commun.* **2001**, 2414–2415.
171. Clegg, W.; Garner, C. D.; Al-Samman, M. H. *Inorg. Chem.* **1983**, *22*, 1534–1538.
172. Benelli, C.; Blake, A. J.; Brechin, E. K.; Coles, S. J.; Graham, A.; Harris, S. G.; Meier, S.; Parkin, A.; Parsons, S.; Seddon, A. M.; Winpenny, R. E. P. *Chem. Eur. J.* **2000**, *6*, 883–896.
173. Graham, A.; Meier, S.; Parsons, S.; Winpenny, R. E. P. *Chem. Commun.* **2000**, 811–812.
174. Brechin, E. K.; Harris, S. G.; Parsons, S.; Winpenny, R. E. P. *Chem. Commun.* **1996**, 1439–1440.
175. Bacchi, A.; Belli Dell'Amico, D.; Calderazzo, F.; Giurlani, U.; Pelizzi, G.; Rocchi, L. *Gazz. Chim. Ital.* **1992**, *122*, 429–435.
176. Cornia, A.; Fabretti, A. C.; Gatteschi, D.; Pályi, G.; Rentschler, E.; Shchegolikhina, O. I.; Zhdanov, A. A. *Inorg. Chem.* **1995**, *34*, 5383–5387.
177. Levitsky, M. M.; Shchegolikhina, O. I.; Zhdanov, A. A.; Igonin, V. A.; Ovchinniko, Yu. E.; Shklover, V. E.; Struchkov, Yu. T. *J. Organomet. Chem.* **1991**, *401*, 199–210.
178. Yukawa, Y.; Igarashi, S.; Yamano, A.; Sato, S. *Chem. Commun.* **1997**, 711–712.
179. El Fallah, M. S.; Rentschler, E.; Caneschi, A.; Sessoli, R.; Gatteschi, D. *Inorg. Chem.* **1996**, *35*, 3723–3724.
180. Lai, S.-Y.; Lin, T.-W.; Chen, Y.-H.; Wang, C.-C.; Lee, G.-H.; Yang, M.-H.; Leung, M.-K.; Peng, S.-M. *J. Am. Chem. Soc.* **1999**, *121*, 250–251.
181. Strouse, J.; Layten, S. W.; Strouse, C. E. *J. Am. Chem. Soc.* **1977**, *99*, 562–571.
182. Murrie, M.; Stoekli-Evans, H.; Güdel, H. U. *Angew. Chem., Int. Ed. Engl.* **2001**, *40*, 1957–1960.
183. Eremenko, I. L.; Golubnichaya, M. A.; Nefedov, S. E.; Sidorov, A. A.; Golovaneva, I. F.; Burkov, V. I.; Ellert, O. G.; Novotortsev, V. M.; Eremenko, L. T.; Sousa, A.; Bermejo, M. R. *Russ. Chem. Bull.* **1998**, *47*, 704–718.
184. Psomas, G.; Dendrinou-Samara, C.; Alexiou, M.; Tsohos, A.; Raptopoulou, C. P.; Terzis, A.; Kessissoglou, D. P. *Inorg. Chem.* **1998**, *37*, 6556–6557.
185. Cadiou, C.; Murrie, M.; Paulsen, C.; Villar, V.; Wernsdorfer, W.; Winpenny, R. E. P. *Chem. Commun.* **2001**, 2666–2667.
186. Brechin, E. K.; Gould, R. O.; Harris, S. G.; Parsons, S.; Winpenny, R. E. P. *J. Am. Chem. Soc.* **1996**, *118*, 11293–11294.
187. Dearden, A. L.; Parsons, S.; Winpenny, R. E. P. *Angew. Chem., Int. Ed. Engl.* **2001**, *40*, 151–154.
188. Carruthers, J. R.; Prout, K.; Rossotti, F. J. C. *Acta Cryst., Sect. B.* **1975**, *31*, 2044–2046.
189. Ahlgrén, M.; Turpeinen, U.; Smolander, K. *Acta Cryst., Sect. B.* **1980**, *36*, 1091–1095.
190. Smolander, K. *Acta Chem. Scand., Ser. A* **1983**, *37*, 5–13.
191. Muhonen, H.; Hatfield, W. E.; Helms, J. H. *Inorg. Chem.* **1986**, *25*, 800–805.
192. Wang, S.; Pang, Z.; Zheng, J.-C.; Wagner, M. J. *Inorg. Chem.* **1993**, *32*, 5975–5980.
193. Mikuriya, M.; Azuma, H.; Nukada, R.; Handa, M. *Chem. Lett.* **1999**, 57–58.
194. Butcher, R. J.; O'Connor, C. J.; Sinn, E. *Inorg. Chem.* **1981**, *20*, 537–545.
195. Agnus, Y.; Louis, R.; Metz, B.; Boudon, C.; Gisselbrecht, J. P.; Gross, M. *Inorg. Chem.* **1991**, *30*, 3155–3161.
196. Sakai, K.; Yamada, Y.; Tsubomura, T.; Yabuki, M.; Yamaguchi, M. *Inorg. Chem.* **1996**, *35*, 542–544.
197. Olejnik, Z.; Jezowska-Trzebiatowska, B.; Lis, T. *J. Chem. Soc., Dalton Trans.* **1986**, 97–101.
198. Saalfrank, R. W.; Löw, N.; Kareth, S.; Seitz, V.; Hampel, F.; Stalke, D.; Teichert, M. *Angew. Chem., Int. Ed. Engl.* **1998**, *37*, 172–175.

199. Lindeman, S. V.; Shchegolikhina, O. I.; Molodtsova, Y. A.; Zhdanov, A. A. *Acta Cryst., Sect. C* **1997**, *53*, 305–309.
200. Kruger, P. E.; Fallon, G. D.; Moubaraki, B.; Berry, K. J.; Murray, K. S. *Inorg. Chem.* **1995**, *34*, 4808–4814.
201. Vicente, R.; Escuer, A.; Solans, X.; Font-Bardia, M. *J. Chem. Soc., Dalton Trans.* **1996**, 1835–1838.
202. Matsumoto, N.; Mizuguchi, Y.; Mago, G.; Eguchi, S.; Miyasaka, H.; Nakashima, T.; Tuchagues, J.-P. *Angew. Chem., Int. Ed. Engl.* **1997**, *36*, 1860–1862.
203. Karlin, K. D.; Gan, Q.-F.; Farooq, A.; Liu, S.; Zubieta, J. *Inorg. Chem.* **1990**, *29*, 2549–2551.
204. Koolhaas, G. J. A. A.; Driessen, W. L.; van Koningsbruggen, P. J.; Reedijk, J.; Spek, A. L. *J. Chem. Soc., Dalton Trans.* **1993**, 3803–3807.
205. Hoskins, B. F.; Robson, R.; Smith, P. J. *J. Chem. Soc., Chem. Commun.* **1990**, 488–489.
206. McKee, V.; Tandon, S. S. *J. Chem. Soc., Dalton Trans.* **1991**, 221–229.
207. Tandon, S. S.; Thompson, L. K.; Bridson, J. N.; Benelli, C. *Inorg. Chem.* **1995**, *34*, 5507–5515.
208. Blake, A. J.; Gould, R. O.; Grant, C. M.; Milne, P. E. Y.; Reed, D.; Winpenny, R. E. P. *Angew. Chem., Int. Ed. Engl.* **1994**, *33*, 195–197.
209. Saalfrank, R. W.; Bernt, I.; Hampel, F. *Angew. Chem., Int. Ed. Engl.* **2001**, *40*, 1700–1703.
210. Omata, J.; Ishida, T.; Hashizume, D.; Iwasaki, F.; Nogami, T. *Inorg. Chem.* **2001**, *40*, 3954–3958.
211. Liu, Q.-D.; Gao, S.; Li, J.-R.; Zhou, Q.-Z.; Yu, K.-B.; Ma, B.-Q.; Zhang, S.-W.; Zhang, X.-X.; Jin, T.-Z. *Inorg. Chem.* **2000**, *39*, 2488–2492.
212. Christodoulou, D.; George, C.; Keefer, L. K. *J. Chem. Soc., Chem. Commun.* **1993**, 937–939.
213. Real, J. A.; De Munno, G.; Chiappeta, R.; Julve, M.; Lloret, F.; Journaux, Y.; Colin, J.-C.; Blondin, G. *Angew. Chem., Int. Ed. Engl.* **1994**, *33*, 1184–1186.
214. Tangoulis, V.; Raptopoulou, C. P.; Paschalidou, S.; Bakalbassis, E. G.; Perlepes, S. P.; Terzis, A. *Angew. Chem., Int. Ed. Engl.* **1997**, *36*, 1083–1085.
215. Tangoulis, V.; Raptopoulou, C. P.; Terzis, A.; Paschalidou, S.; Perlepes, S. P.; Bakalbassis, E. G. *Inorg. Chem.* **1997**, *36*, 3996–4006.
216. Tong, M.-L.; Lee, K. H.; Tong, Y.-X.; Chen, X.-M.; Mak, T. C. W. *Inorg. Chem.* **2000**, *39*, 4666–4669.
217. Han, M. Y.; Min, K. S.; Suh, M. P. *Inorg. Chem.* **1999**, *38*, 4374–4375.
218. Galy, J.; Mosset, A.; Grenthe, I.; Puigdomènech, I.; Sjöberg, B.; Hultén, F. *J. Am. Chem. Soc.* **1987**, *109*, 380–386.
219. Ardizzioia, G. A.; Angaroni, M. A.; La Monica, G.; Cariati, F.; Moret, M.; Masciocchi, N. *J. Chem. Soc., Chem. Commun.* **1990**, 1021–1023.
220. Wang, S.; Pang, Z.; Wagner, M. J. *Inorg. Chem.* **1992**, *31*, 5381–5388.
221. Blake, A. J.; Gould, R. O.; Milne, P. E. Y.; Winpenny, R. E. P. *J. Chem. Soc., Chem. Commun.* **1992**, 522–524.
222. Zhang, Y.; Thompson, L. K.; Bridson, J. N.; Bubenik, M. *Inorg. Chem.* **1995**, *34*, 5870–5877.
223. Geetha, K.; Nethaji, M.; Chakravarty, A. R. *Inorg. Chem.* **1997**, *36*, 6134–6137.
224. Zhu, F.-C.; Schmalte, H. W.; Fischer, B.; Dubler, E. *Inorg. Chem.* **1998**, *37*, 1161–1168.
225. Aromi, G.; Gamez, P.; Roubeau, O.; Kooijman, H.; Spek, A. L.; Driessen, W. L.; Reedijk, J. *Angew. Chem. Int. Ed. Engl.* **2002**, *41*, 1168–1170.
226. Turpeinen, U.; Hämäläinen, R.; Reedijk, J. *Inorg. Chim. Acta* **1987**, *134*, 87–93.
227. Zhao, L.; Xu, Z.; Thompson, L. K.; Heath, S. L.; Miller, D. O.; Ohba, M. *Angew. Chem., Int. Ed. Engl.* **2000**, *39*, 3114–3117.
228. Chen, X.-M.; Aubin, S. M. J.; Wu, Y.-L.; Yang, Y.-S.; Mak, T. C. W.; Hendrickson, D. N. *J. Am. Chem. Soc.* **1995**, *117*, 9600–9601.
229. Chen, X.-M.; Wu, Y.-L.; Tong, Y.-X.; Huang, X.-Y. *J. Chem. Soc., Dalton Trans.* **1996**, 2443–2448.
230. Cui, Y.; Chen, J.-T.; Huang, J.-S. *Inorg. Chim. Acta* **1999**, *293*, 129–139.
231. Abrahams, B. F.; Egan, S. J.; Robson, R. *J. Am. Chem. Soc.* **1999**, *121*, 3535–3536.
232. Chandrasekhar, V.; Kingsley, S. *Angew. Chem., Int. Ed. Engl.* **2000**, *39*, 2320–2322.
233. Schugar, H.; Ou, C.; Thich, G. A.; Potenza, J. A.; Lalancette, R. A.; Furey, W. Jr. *J. Am. Chem. Soc.* **1976**, *98*, 7357–7359.
234. Birker, P. J. M. W. L.; Freeman, H. C. *J. Am. Chem. Soc.* **1977**, *99*, 6890–6899.
235. Klüfers, P.; Schuhmacher, J. *Angew. Chem., Int. Ed. Engl.* **1995**, *34*, 2119–2121.
236. Pecoraro, V. L.; Stemmmer, A. J.; Gibney, B. R.; Bodwin, J. J.; Wang, H.; Kampf, J. W.; Barwinski, A. *Prog. Inorg. Chem.* **1997**, *45*, 83–117.
237. Burrow, H.; Brown, D. A.; Alcock, N. W.; Clase, H. J.; Wallbridge, M. G. H. *J. Chem. Soc., Chem. Commun.* **1995**, 1231–1232.

## 7.4

# High Nuclearity Clusters: Clusters and Aggregates with Paramagnetic Centers: Cyano and Oxalato bridged Systems

M. PILKINGTON and S. DECURTINS  
*University of Berne, Switzerland*

---

7.4.1	INTRODUCTION TO MOLECULAR MAGNETISM	178
7.4.2	TRANSITION METAL CYANIDE CHEMISTRY	179
7.4.3	MAGNETIC MATERIALS FROM CYANOMETALATE BUILDING BLOCKS	180
7.4.3.1	Prussian Blue	180
7.4.3.2	Prussian Blue Analogues	181
7.4.3.3	Photomagnetism	182
7.4.3.4	One-, Two-, and Three-dimensional Compounds from $[M(CN)_6]^{n-}$ Precursors	184
7.4.3.4.1	<i>One-dimensional compounds</i>	184
7.4.3.4.2	<i>Two-dimensional compounds</i>	185
7.4.3.4.3	<i>Three-dimensional compounds</i>	189
7.4.3.5	Single-molecule Magnets	193
7.4.3.6	Heptacyanometalate Building Blocks	197
7.4.3.7	Octacyanometalate Building Blocks	201
7.4.3.7.1	<i>High-spin clusters</i>	201
7.4.3.7.2	<i>One-dimensional compounds</i>	205
7.4.3.7.3	<i>Two-dimensional compounds</i>	209
7.4.3.7.4	<i>Three-dimensional networks</i>	210
7.4.4	OTHER CYANOMETALATE PRECURSORS CONTAINING PARAMAGNETIC CENTERS	213
7.4.4.1	Tetracyanometalates	213
7.4.4.2	Dicyanometalates	213
7.4.5	OXALATE-BASED TWO- AND THREE-DIMENSIONAL MAGNETS	214
7.4.5.1	Basic Principles of Specific Two- and Three-dimensional Network Configurations	214
7.4.5.2	Structural Studies on Two-dimensional Compounds	217
7.4.5.3	Magnetic Studies on Two-dimensional Compounds	218
7.4.5.4	Structural Studies on Three-dimensional Compounds	219
7.4.5.5	Magnetic Studies on Three-dimensional Compounds	222
7.4.6	ENANTIOSELECTIVE SYNTHESIS OF OXALATE-BASED MAGNETS	222
7.4.7	SPIN CROSSOVER PHENOMENON	223
7.4.7.1	Utilizing the Spin Crossover Phenomenon: From Rational Design to Functional Molecular Materials	223
7.4.7.2	Structural Changes in Oxalate-based Spin Crossover Systems	224
7.4.8	ONE-DIMENSIONAL OXALATE-BASED MAGNETS	225
7.4.9	MAGNETIC COMPOUNDS CONTAINING BOTH OXALATE AND CYANIDE BRIDGING LIGANDS	225
7.4.10	WORKING TOWARDS THE DESIGN OF DUAL ACTION MATERIALS	225
7.4.11	REFERENCES	226

---

### 7.4.1 INTRODUCTION TO MOLECULAR MAGNETISM

Since the early 1980s the field of molecular magnetism has had a large influence on the coordination chemistry of clusters and aggregates containing paramagnetic centers. As a consequence it would be inappropriate to discuss recent advances in this area of chemistry without first briefly introducing the reader to the field of molecular magnetism.<sup>1-5</sup>

Molecular magnetism can be considered to be supramolecular in nature, since it results from the collective features of components bearing free spins and on their arrangement in organized assemblies.<sup>1</sup> The engineering of molecular magnetic systems thus requires the search for paramagnetic species linked via organic ligands and their arrangement in suitable supramolecular architectures so as to induce spin coupling and alignment (Figure 1). In comparison with the more conventional metal/intermetallic and metal oxide magnets, molecule-based magnets offer the additional advantages of low density, transparency, electrical insulation, and low-temperature fabrication.

Since the early 1990s the intense efforts of several research groups worldwide has led to the discovery of several classes of molecule-based magnets.<sup>5</sup> The first reported molecular magnet composed of spins in isolated *d* orbitals was an Fe<sup>III</sup> complex of stoichiometry Fe<sup>III</sup>(S<sub>2</sub>CNET<sub>2</sub>)<sub>2</sub>Cl with an intermediate spin  $S = 3/2$ .<sup>6-9</sup> This compound orders ferromagnetically at 2.46 K, but does not exhibit the phenomenon of hysteresis. The next class of magnets prepared were the ferromagnetically ordered compounds [Cr<sup>III</sup>(NH<sub>3</sub>)<sub>6</sub>]<sup>3+</sup>[Fe<sup>III</sup>Cl<sub>6</sub>]<sup>3-</sup> ( $T_c = 0.66$  K)<sup>10</sup> and [Cr<sup>III</sup>(NH<sub>3</sub>)<sub>6</sub>]<sup>3+</sup>[Cr<sup>III</sup>(CN)<sub>6</sub>]<sup>3-</sup> ( $T_c = 2.85$  K).<sup>11</sup> These early studies led to the development of materials with *d* orbital spin sites connected via coordinate bonds using rational synthetic organic methodology. Like conventional magnets, such as Fe<sub>3</sub>O<sub>4</sub>, Co<sub>5</sub>Sm, or CrO<sub>2</sub>, they have an extended network linking the *d* orbital sites.

Following these discoveries, the detailed study of network-structured solids with free spins residing on adjacent sites being in orthogonal orbitals led to a ferromagnetic coupling arrangement, and ferromagnetic ordering evolved.<sup>12,13</sup> Molecule-based magnets exhibit a wide range of bonding and structural motifs. These include isolated molecules (0-D), as well as those with extended bonding within chains (1-D), within layers (2-D), and within (3-D) network structures. A favorable approach for the design of crystalline solids is to use preorganized molecules such as transition metal complexes, since a high structural organization can be ensured through the multiple binding of transition metal ions, giving rise to a variety of extended inorganic networks in one-, two-, or three-dimensions.<sup>14</sup> The aim of this chapter is to highlight how a rational design

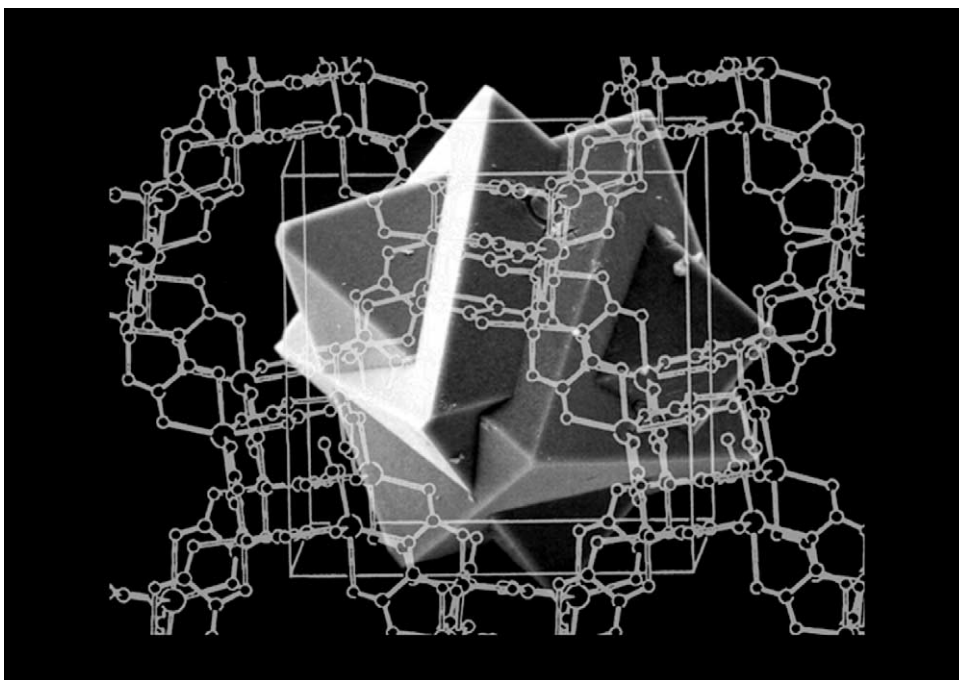


**Figure 1** Single crystal of a chiral three-dimensional molecular network compound with transition metals as spin carriers.<sup>14</sup>

strategy has been applied to cyanometalate and tris-oxalato transition metal building blocks incorporating paramagnetic centers, for the preparation of two classes of novel molecule-based materials displaying a range of interesting magnetic properties.

#### 7.4.2 TRANSITION METAL CYANIDE CHEMISTRY

The field of transition metal cyanide chemistry has a remarkable history that spans almost three centuries, dating back to the early eighteenth century.<sup>15</sup> The wide availability of transition metal cyanide complexes together with their diverse bonding and structural chemistry has led to their widespread applications in the field of materials chemistry. Several detailed reviews on metal cyanides describing their structures, reactivity, and physical properties have been published over the years.<sup>15–31</sup> A fully comprehensive review highlighting the most important advances in this area was written by Dunbar and Heintz in 1997.<sup>15</sup>

Cyanide is an efficient ligand for the stabilization of transition metals in either low or high oxidation states. This high electronic and coordinative versatility prompts its terminal coordination to almost all the transition metals, and permits a wide number of binding modes in cyanide-bridged complexes. By far the most commonly observed binding modes are the terminal C-bound mode (a) and the linear bridged arrangement (b); modes (d)–(h) are much less common (Figure 2). Significant deviations from linearity are frequently observed for the bridged geometry (c).

The charged nature of the cyanide ligand results in the formation of non-volatile salts that are only soluble in polar media. Water is usually the solvent of choice for most non-redox preparations of cyanide compounds, which involve the action of alkali metal cyanides on metal halides or other metal salts. This chemistry usually leads to complete substitution of all other ligands if an excess of cyanide ion is present. For low oxidation state transition metal cyanides, it is often easier to begin with higher oxidation states and carry out the reduction either chemically or electrochemically. Cyanide compounds are among the most stable transition metal complexes, tolerant on exposure to most reagents with the exception of strong acids. Nevertheless, CO, NO<sup>+</sup>, 2,2-bipyridine, and 1,10-phenanthroline ligands have all been observed to displace CN<sup>−</sup> under mild conditions.<sup>15</sup>

The versatility of the cyanide ligand results from its ability to act both as a  $\sigma$ -donor and a  $\pi$ -acceptor, combined with its negative charge and ambidentate nature. The ground state electronic structure of CN<sup>−</sup> is  $(1\sigma)^2(2\sigma)^2(3\sigma)^2(4\sigma)^2(1\pi)^4(5\sigma)^2$ , which corresponds to a triple bond between the C and N atoms. Calculations support the proposal that the negative charge is essentially evenly distributed over the two atoms.<sup>32</sup> The exact binding mode of CN<sup>−</sup> is not readily established by X-ray diffraction methods, which cannot distinguish the small differences in the scattering factors of the C and N atoms. In contrast, neutron diffraction<sup>33</sup> and IR investigations have provided compelling evidence to support the general consensus that monodentate cyanide ligands are bound through the carbon atoms.<sup>34</sup>

Carbon-bonded cyanide is at the high end of the spectrochemical series  $I^- < Br^- < Cl^- < F^- < [C_2O_4]^{2-} < H_2O < NH_3 < en < bpy < NO_2^- < CN^- \sim CO$ . Due to its ionic nature, cyanide is a stronger  $\sigma$ -donor than CO and a weaker  $\pi$ -acceptor than CO or NO<sup>+</sup>. The most compelling evidence for  $\pi$ -bonding comes from structural studies of the homologous series of metal ions

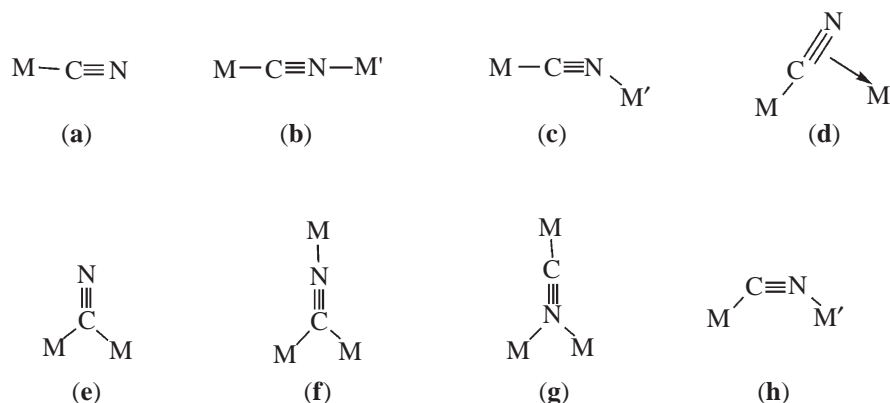


Figure 2 Observed binding modes for the cyanide ligand.

$[\text{M}^{\text{III}}(\text{CN})_6]^{3-}$  from Cr to Co where the M—C bond length steadily decreases from 2.08 Å to 1.89 Å, and from a comparison of the Fe—C bond distances, as well as the  $\nu(\text{Fe—C})$  and the  $\nu(\text{C}\equiv\text{N})$  frequencies in  $[\text{Fe}^{\text{II}}(\text{CN})_6]^{4-}$  and  $[\text{Fe}^{\text{III}}(\text{CN})_6]^{3-}$ . The infrared spectra of cyanide compounds have been well studied over the years; free cyanide exhibits a  $\nu(\text{C}\equiv\text{N})$  stretch at  $2,080\text{ cm}^{-1}$  in aqueous solution, and is often used as a reference. Terminal M—CN complexes generally exhibit sharp intense bands between  $2,000\text{ cm}^{-1}$  and  $2,200\text{ cm}^{-1}$ , which shift approximately  $50\text{--}100\text{ cm}^{-1}$  to higher frequencies upon additional ligation at the N atom.<sup>15</sup>

Transition metal cyanide compounds display a wide range of coordination numbers and geometries. Cyanide complexes of  $d^{10}$  metals, e.g.,  $[\text{M}(\text{CN})_2]^-$  (M = Ag, Au), generally exist as linear two-coordinate anions.<sup>24,35,36</sup> There are numerous four-coordinate transition metal complexes, among these are the isoelectronic tetrahedral anions of  $[\text{M}(\text{CN})_4]^{3-}$  (M = Cu or Ag)<sup>37</sup> and  $[\text{M}(\text{CN})_4]^{2-}$  (M = Zn, Cd or Hg),<sup>24</sup> containing  $d^{10}$  metals and the square planar  $d^8$  anions  $[\text{Au}(\text{CN})_4]^-$  and  $[\text{M}(\text{CN})_4]^{2-}$  (M = Ni, Pd, Pt).<sup>38–40</sup> The molecular structures of five-coordinated polycyano anions are generally based on distorted bipyramidal or square pyramidal geometries. Hexacyano anions of general formula  $[\text{M}(\text{CN})_6]^{4-}$ ,  $[\text{M}(\text{CN})_6]^{3-}$ , or  $[\text{M}(\text{CN})_6]^{2-}$  exhibit octahedral or distorted octahedral geometries for  $d^n$  configurations of six electrons or less. Many hexacyano-based structures contain a bridged —CN— moiety, similar to the well-known Prussian blue. The first heptacoordinated cyanide species was shown by X-ray crystallography to be a pentagonal bipyramidal complex. This geometry has also been established for  $\text{Mo}^{\text{II}}$ ,  $\text{W}^{\text{II}}$ , and  $\text{Re}^{\text{III}}$  in  $[\text{Mo}(\text{CN})_7]^{5-}$ ,<sup>41</sup>  $[\text{W}(\text{CN})_7]^{5-}$ ,<sup>42</sup> and  $[\text{Re}(\text{CN})_7]^{4-}$ .<sup>43</sup> Octacyanometalates are known for metals with  $d^1$  and  $d^2$  configurations; their structures most closely resemble the dodecahedron and square antiprism. The actual structure adopted in the solid state is often influenced by packing forces. The  $\text{Mo}^{\text{V}}$  analogue is dodecahedral in  $(\text{Bu}_4\text{N})_3[\text{Mo}(\text{CN})_8]$ ,<sup>44</sup> antiprismatic in  $\text{Na}_3[\text{Mo}(\text{CN})_8]$ ,<sup>45</sup> and approximately bicapped trigonal prismatic in  $\text{Cs}_3[\text{Mo}(\text{CN})_8]$ .<sup>46</sup> The analogous W compounds also exhibit isomers of these types. The niobium anions  $[\text{Nb}(\text{CN})_8]^{4-}$  and  $[\text{Nb}(\text{CN})_8]^{5-}$  are usually found to be dodecahedral.<sup>46–48</sup>

### 7.4.3 MAGNETIC MATERIALS FROM CYANOMETALATE BUILDING BLOCKS

A resurgence of inorganic research in the field of magnetism is centered on the use of transition metal coordination compounds for the synthesis of one-, two-, and three-dimensional materials with magnetic properties. In this respect, one class of interesting compounds are the novel architectures self-assembled from cyanide ligands and metallic centers that carry a magnetic moment. Since  $\mu$ -cyanide linkages permit an interaction between paramagnetic metal ions, cyanometalate building blocks have found useful applications in the field of molecule-based magnetism.<sup>3,15–18</sup>

#### 7.4.3.1 Prussian Blue

The use of octahedral building blocks is perhaps one of the most obvious and simplest strategies for the assembly of molecule-based three-dimensional solids.<sup>3,15,18</sup> In this context, an examination of suitable octahedral  $[\text{ML}_6]$  precursors reveals that some of the most inert are the hexacyanometalate anions  $[\text{M}^{\text{III}}(\text{CN})_6]^{3-}$  (M' = Cr, Mn, Fe, Co), which can be combined with divalent Lewis acids  $\text{M}^{\text{II}}$  (M = Cu, Ni, Co, Fe, Mn) to give face-centered cubic compounds closely related to Prussian blue (Figure 3).

Prussian blue appears to be the earliest recorded synthetic coordination compound reported in the chemical literature,<sup>49</sup> and owes its name to its color, since mixing together an aqueous solution of  $\text{K}_4[\text{Fe}(\text{CN})_6]$  with  $\text{Fe}^{\text{III}}$  chloride affords a beautiful deep blue color. The formula of Prussian blue itself is  $\text{Fe}^{\text{III}}_4[\text{Fe}^{\text{II}}(\text{CN})_6]_3 \cdot 15\text{H}_2\text{O}$  and the reaction leading to the neutral solid is a simple Lewis acid–base interaction. Prussian blue is considered as the archetype of mixed valence class II compounds according to the 1967 classification of Robin and Day.<sup>50</sup> Its molecular structure was first proposed by Keggin and Miles,<sup>51</sup> and then reformulated by Ludi and Güdel in the 1970s.<sup>25</sup> Essentially, the face-centered cubic structure of the earlier model, postulating the occurrence of interstitial  $\text{Fe}^{\text{III}}$  ions, was modified to a cubic lattice, with a random to more ordered arrangement of a stoichiometrically determined fraction of vacant lattice sites (Figure 3). Applying the revised structural model to Prussian blue, it becomes apparent that due to coordinated water molecules, the  $\text{Fe}^{\text{III}}$  ions are in an average  $\text{N}_{4.5}\text{O}_{1.5}$  coordination environment.

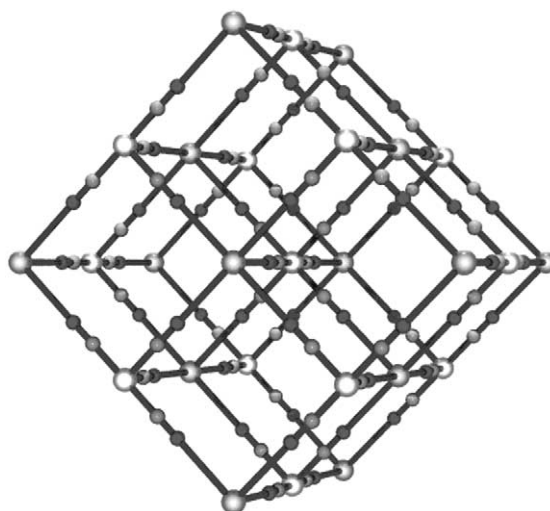


**Figure 3** Three-dimensional cubic structure of Prussian blue.

The appeal of Prussian blue itself lies both in its optical and magnetic properties. It displays long-range ferromagnetic ordering with  $T_c = 5.6$  K.<sup>52,53</sup> This critical temperature is low since only the high-spin  $d^5$   $\text{Fe}^{\text{III}}$  ( $S = 5/2$ ) sites carry a spin. The  $\text{Fe}^{\text{II}}$  centers are low spin and diamagnetic; hence the magnetic interactions occur between next-nearest metal ions through 10.6 Å long  $\text{Fe}^{\text{III}}\text{—NC—Fe}^{\text{II}}\text{—CN—Fe}^{\text{III}}$  linkages.<sup>54,55</sup> This propagation of magnetic interactions through extended bridging networks is due to the strong spin delocalization from the metal ion towards its nearest neighbors and seems to be specific to molecular compounds.

#### 7.4.3.2 Prussian Blue Analogues

The Prussian blue system has been reinvestigated with a view to engineering molecular solids.<sup>56</sup> As a consequence, substitution of  $\text{Fe}^{\text{II}}$  and  $\text{Fe}^{\text{III}}$  by other paramagnetic metal ions  $M$  and  $M'$  has afforded a series of Prussian blue analogues with face-centered cubic structures. The appealing character of the Prussian blue-like phases is related to (i) the possibilities for developing orbital interactions in three dimensions; (ii) the tolerance to host very different paramagnetic ions at will in the cubic lattice; (iii) the high symmetry of the cubic system, where the linear  $M\text{—CN—}M'$  enables the nature and amplification of the exchange interaction between the two paramagnetic metal centers to be tuned; and (iv) the possibilities for varying the number of magnetic neighbors ( $z$ ) around the metal centers  $M$  and  $M'$  with the stoichiometry, which in turn enables the Curie temperature to be varied.

The need for higher ordering temperatures has provided the driving force for several research teams to probe in detail the nature of the  $M\text{—CN—}M'$  interactions in this family of compounds. After the pioneering studies by Anderson and Bozworth in the 1950s,<sup>57,58</sup> and Lenze in the 1980s,<sup>59</sup> the results of Babel<sup>60,61</sup> led to the ferromagnetic compound  $\text{Cs}^{\text{I}}\text{Mn}^{\text{II}}[\text{Cr}^{\text{III}}(\text{CN})_6]$ ,<sup>60</sup> with a Curie temperature above liquid nitrogen,  $T_c = 90$  K. Kahn's orbital model<sup>1</sup> was then applied to these systems in order to address the challenge of obtaining materials that could easily be incorporated into devices. In 1995 this systematic approach paid off and Verdaguer and co-workers were able to increase the Curie temperature and overcome the room-temperature barrier with the mixed-valent Prussian blue  $\text{V}^{\text{II}}_{0.42}\text{V}^{\text{III}}_{0.58}[\text{Cr}(\text{CN})_6]_{0.86} \cdot 2.8\text{H}_2\text{O}$  which orders at  $T_c = 315$  K.<sup>62</sup> This compound represents a milestone in the field of molecule-based magnetism, since it one of the first rationally synthesized molecule-based magnets whose  $T_c$  is above room temperature. The ferrimagnetic properties displayed by this amorphous material directly arise from its mixed-valent  $\text{V}_3\text{Cr}_2$  stoichiometry. Following this discovery, it was suggested that the Curie temperature could be further increased by improving the crystallinity of the sample or by changing the stoichiometry to increase the number of magnetic neighbors. Adopting this strategy, several more complex, air-stable related materials with  $T_c$  values up to 372 K have also been prepared.<sup>63</sup> Holmes and Girolami were able to reach a  $T_c$  of 376 K,<sup>64</sup> which is above the boiling point of water and holds the world record in this series of Prussian blue analogues. A selection of Prussian blue-type compounds arranged according to their ordering temperatures  $T_c$  is provided in Table 1.

**Table 1** Magnetic properties of selected Prussian blue analogues.

Compound	Magnetic behavior	$T_c$ (K)	References
V[Cr(CN) <sub>6</sub> ]	Ferri	376	64
K <sub>0.58</sub> [V(CN) <sub>6</sub> ] <sub>0.79</sub> (SO <sub>4</sub> ) <sub>0.058</sub> ·0.93 H <sub>2</sub> O	Ferri	372	63
V[Cr(CN) <sub>6</sub> ] <sub>0.86</sub> ·2.8H <sub>2</sub> O	Ferri	315	62
[Cr <sub>5</sub> (CN) <sub>12</sub> ]·10H <sub>2</sub> O	Ferri	240	65
(Et <sub>4</sub> N) <sub>0.5</sub> Mn <sub>1.25</sub> [V(CN) <sub>5</sub> ]·2H <sub>2</sub> O	Ferri	230	66
Cs <sub>0.75</sub> [Cr <sub>2.125</sub> (CN) <sub>6</sub> ]·5H <sub>2</sub> O	Ferri	190	65
Cs <sub>2</sub> Mn[V(CN) <sub>6</sub> ]	Ferri	125	66
CsNi[Cr(CN) <sub>6</sub> ]·2H <sub>2</sub> O	Ferro	90	67
CsMn[Cr(CN) <sub>6</sub> ]	Ferri	90	61
Mn <sub>3</sub> [Cr(CN) <sub>6</sub> ] <sub>2</sub> ·12H <sub>2</sub> O	Ferri	63	68
(NMe <sub>4</sub> )Mn[Cr(CN) <sub>6</sub> ]	Ferri	59	61
Mn[Mn(CN) <sub>6</sub> ]	Ferri	48.7	69,70
CsMn[Mn(CN) <sub>6</sub> ]·0.5H <sub>2</sub> O	Ferri	41	71
(NMe <sub>4</sub> )Mn[Mn(CN) <sub>6</sub> ]	Ferri	28.5	45
Ni <sub>3</sub> [Fe(CN) <sub>6</sub> ] <sub>2</sub>	Ferri	23.6	72
Co <sub>3</sub> [Fe(CN) <sub>6</sub> ] <sub>2</sub>	Ferri	14	72
Cr <sub>2</sub> [Ni <sub>2</sub> (CN) <sub>4</sub> ] <sub>3</sub>	Ferri	12.4	73
Fe <sup>III</sup> <sub>4</sub> [Fe <sup>II</sup> (CN) <sub>6</sub> ] <sub>3</sub> ·15H <sub>2</sub> O	Ferro	5.6	52,53

One of the appealing aspects of magnetic studies dealing with Prussian blue phases clearly resides in the fact that it is now possible to predict the nature of the interaction and estimate the value of the critical temperature using simple theoretical models based on the symmetry of the singly occupied orbitals.<sup>1</sup>

Despite these advances, the cubic symmetry of the Prussian blue phases in the solid state does, however, introduce certain complications. The most common problem encountered during the course of these research efforts is the continuous struggle with amorphous or poorly crystalline compounds with peculiar stoichiometries. Decurtins *et al.*<sup>70</sup> have succeeded in growing air-stable single crystals of a transparent, colored, magnetically ordered Prussian blue analogue. This compound is particularly interesting since it crystallizes into a cubic lattice. Mixing together aqueous solutions of Mn(NO<sub>3</sub>)<sub>2</sub> and KCN in agar gel yielded a mixed valence Mn<sup>II</sup>/Mn<sup>III</sup> phase. Magnetic studies on this compound reveal that a long-range magnetic ordering transition occurs at  $T_c \approx 30$  K, proposing the onset of cooperative magnetic interactions. Further work to characterize the structural and magnetic properties of this compound fully is in progress.<sup>70</sup>

A further useful property of most Prussian blue analogues besides their high Curie temperatures is their optical transparency. This makes them potentially suitable candidates for magneto-optical recording. A prerequisite for this, however, is the deposition of the compound as a transparent layer. Prussian blue itself was deposited as a thin film in 1978, via an electrochemical procedure, and has been extensively studied since then.<sup>74</sup> Molecular-based ferromagnetic thin films incorporating mixed-valence chromium cyanides have been prepared by means of a simple electrochemical route.<sup>75</sup> A high critical temperature ( $T_c = 270$  K) was reported for Cr<sub>2.12</sub>(CN)<sub>6</sub>. The  $T_c$  values were controlled by changing the preparation conditions, and a reversible shift of  $T_c$  could be electrochemically induced which means that these cyanides could be switched reversibly back and forth between ferrimagnetism and paramagnetism. These magnets represent one of the first classes of molecule-based materials for which magnetic properties have been combined with electrical functions. Since molecule-based magnets are often colored compounds, the film type of transparent colored magnets is useful for the preparation of magneto-optical materials in the visible region. Hashimoto and co-workers have prepared magnetic thin films composed of M<sup>II</sup><sub>1.5</sub>[Cr<sup>III</sup>(CN)<sub>6</sub>]·2H<sub>2</sub>O (M<sup>II</sup> = Fe, Co, Ni or Cu) on the surface of a Nafion membrane. These films display several colors, e.g., orange (M = Fe), pink (M = Co), yellowish green (M = Ni), and green (M = Cu). They exhibit spontaneous magnetizations with  $T_c$  values of 22 K (M = Fe), 28 K (M = Co), 70 K (M = Ni), and 66 K (M = Cu).<sup>76,77</sup> Below  $T_c$ , these films show Faraday effects corresponding to their absorption spectra.<sup>78</sup>

### 7.4.3.3 Photomagnetism

As the limits of silicon-based electronics are approached, molecular electronics offers an alternative route to the design of materials for use not only at the macroscopic scale but also at the



molecular scale. Data could be stored, transmitted, and retrieved by means of molecules as in complex biological systems. Chemists are therefore looking both for suitable molecular systems as well as for a simple means to switch them between two available states.<sup>55</sup> In this respect, light is a very convenient and powerful way to induce molecular change. A new area in the field of molecule-based magnetism was opened up in 1996, when Hashimoto and co-workers reported that they had found a way to switch the long-range magnetic properties of a simple molecule-based system derived from Prussian blue with light of different wavelengths.<sup>79</sup> They were the first to observe an exciting photomagnetic effect in a Prussian blue analogue with stoichiometry close to  $\text{Co}^{\text{II}}_3[\text{Fe}^{\text{III}}(\text{CN})_6]_2 \cdot n\text{H}_2\text{O}$ . The Curie temperature of the initial system is low,  $T_c = 15\text{ K}$ , but a photoexcitation at the molecular level gives rise to a modification of the macroscopic properties of this material. Combining aqueous solutions of  $\text{Co}^{\text{II}}$  and hexacyanoferrate(III), Hashimoto *et al.* obtained a powder which exhibited a photoinduced enhancement of the magnetization at low temperature, together with an increase of the Curie temperature. The explanation for this effect was related to the presence of isolated  $\text{Co}^{\text{II}}\text{-Fe}^{\text{III}}$  diamagnetic pairs in the compound, otherwise built from  $\text{—Co}^{\text{III}}\text{—NC—Fe}^{\text{II}}\text{—}$  units, and a photoinduced electron transfer from  $\text{Fe}^{\text{II}}$  to  $\text{Co}^{\text{III}}$  through the cyanide bridge. Before the excitation, the iron and cobalt ions are low spin and diamagnetic and there is no interaction between them. The red light excitation induces spin on the ions (with CN surroundings,  $\text{Fe}^{\text{III}}$  is low spin ( $S = 1/2$ ), whereas  $\text{Co}^{\text{II}}$  becomes high spin ( $S = 3/2$ )) and a new interacting  $\text{Fe}^{\text{III}}\text{-Co}^{\text{II}}$  pair. The important point is that the local electron transfer at the molecular level switches on the interaction and allows the extension of the cooperative phenomenon throughout the network. It enhances the mean number of magnetic neighbors also enhancing the ordering temperature  $T_c$ . This increase is weak (4 K), but significant. An even more exciting observation is that the process can be partially reversed.<sup>75</sup> Changing the wavelength of the light is enough to go back to a state that looks like the initial one and to switch off some of the  $\text{Fe}^{\text{III}}\text{—CN—Co}^{\text{II}}$  interactions (Figure 4).

In subsequent years the preparation and study of related compounds has led to a better understanding of this phenomenon. It has now been established that the condition required to observe this effect is not only the presence of diamagnetic excitable pairs  $(\text{LS})\text{Co}^{\text{III}}\text{—}(\text{LS})\text{Fe}^{\text{II}}$ , but also the presence of a certain amount of defects in the cubic structure. This is due to the important expansion of the network that accompanies the photoinduced electron transfer. In a “perfect structure,” without vacant lattice sites, strain in the bulk would be so strong that only diamagnetic surface pairs would be transformed. In a structure with vacant lattice sites, however, the steric constraints are weaker, the network is more flexible, and the photoinduced metastable state is able to propagate in the bulk.<sup>18</sup> Although the initial phenomenon observed by Hashimoto *et al.* occurs over too low a temperature range and is too slow for practical applications, it demonstrates nevertheless that the tuning of long-range magnetic ordering is possible through a molecular excitation induced by photons, and is clearly one of the necessary steps towards the design of molecule-based magneto-optical devices. The study of this phenomenon, with the aim of incorporating photophysical properties into magnetic materials, is ongoing. The observations that magnetic ordering can be changed by photoinduced electron transfer through a molecular bridge are a significant contribution towards applying molecular magnetism to molecular electronics.<sup>80</sup>

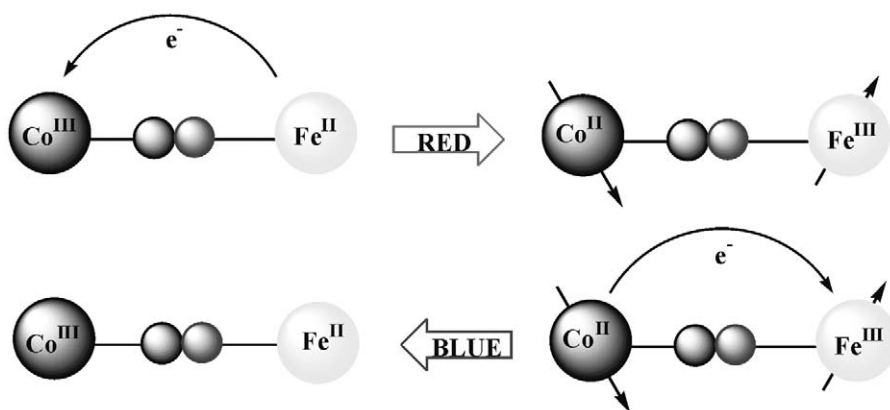


**Figure 4** Back and forth electron transfer induced by photons of different wavelengths through a molecular CN bridge, and the related magnetic changes.<sup>18,75</sup>

To summarize, the Prussian blues are not truly molecular but molecular based, at the border between molecular and solid-state chemistry. They present many vacancies and defects and are often mixtures. Nevertheless, it is inspiring that one of the oldest coordination compounds is providing such a “stir” in solid-state chemistry. Since the main features of the Prussian blue analogues are becoming increasingly understood, chemists have now begun to explore other directions.

#### 7.4.3.4 One-, Two-, and Three-dimensional Compounds from $[M(CN)_6]^{n-}$ Precursors

Since the early 1990s extending the approach to combine hexacyanometalate building blocks together with divalent transition metal complexes containing labile positions has afforded a wide range of one-, two-, and three-dimensional bimetallic, cyanide-bridged systems with very different physical properties from those of the face-centered cubic Prussian blues.<sup>15–18</sup> An overview of compounds prepared from hexacyanometalate building blocks is presented below. Since the magnetic properties of these materials are intimately related to their dimensionality, for clarity these compounds have been classed according to their structural topologies.

##### 7.4.3.4.1 One-dimensional compounds

Reaction of a 3:2 molar ratio of  $[Ni(en)_3]Cl_2$  and  $K_3[M^{III}(CN)_6]$  ( $M^{III} = Fe, Mn, Cr$ ) in aqueous solution afforded large single crystals of stoichiometry  $[Ni(en)_2]_2[M(CN)_6]_2 \cdot 2H_2O$ , which could be characterized by X-ray crystallography.<sup>81</sup> The asymmetric unit consists of one  $[M(CN)_6]^{3-}$  anion, one *cis*- $[Ni(en)_2]^{2+}$  cation, one half of a *trans*- $[Ni(en)_2]^{2+}$  cation, and a water molecule. A polymeric zigzag chain is formed via the alternating array of  $[M(CN)_6]^{3-}$  and *cis*- $[Ni(en)_2]^{2+}$  units, and two zigzag chains are combined by *trans*- $[Ni(en)_2]^{2+}$ , providing a one-dimensional rope ladder-type of chains running along the *c*-axis of the unit cell (Figure 5 (left)). In the lattice, the chains align along the diagonal line of the *ab* plane to form a pseudo two-dimensional sheet.

For the  $Fe^{III}$  analogue shown in Figure 5, the nearest  $Fe \cdots Fe$  and  $Ni \cdots Ni$  separations are 9.709 Å and 7.713 Å, respectively, and the nearest  $Ni \cdots Fe$  separation is 6.494 Å. This series of compounds can be classed as bimetallic one-dimensional assemblies and all display intramolecular ferromagnetic interactions as a consequence of the strict orthogonality of the  $t_{2g}$  ( $M^{III}$ ) and  $e_g$  ( $Ni^{II}$ ) orbitals. The exchange parameter  $J$  ( $16.8 \text{ cm}^{-1}$ ) has been estimated by Mallah *et al.*<sup>82</sup> for

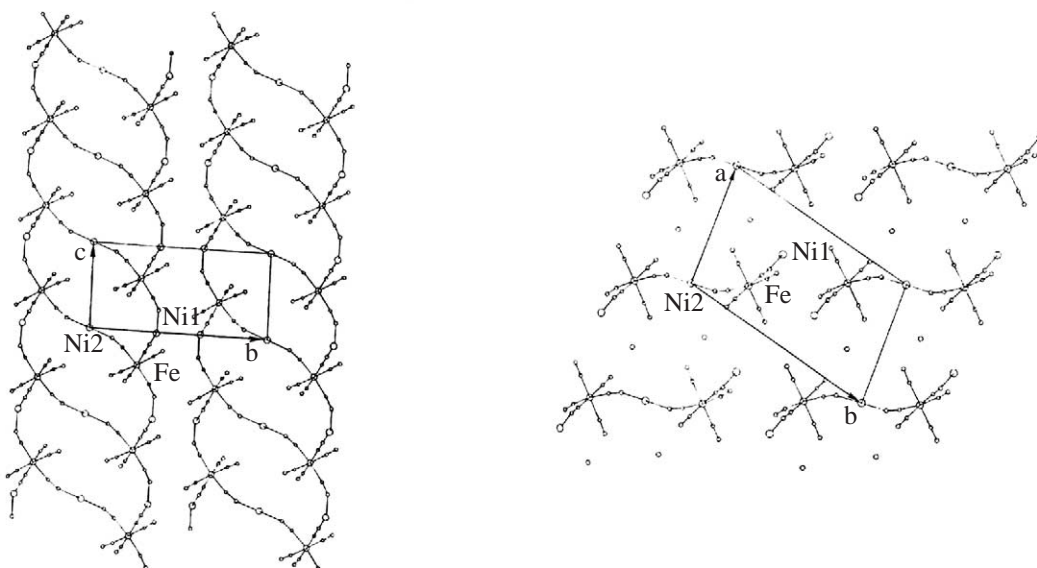


**Figure 5** Left: projection of the one-dimensional structure of  $[Ni(en)_2]_3[Fe(CN)_6]_2 \cdot 2H_2O$  onto the *bc* plane; right: projection of the polymeric structure onto the *ab* plane (the ethylenediamine molecules are omitted for clarity).<sup>81</sup>

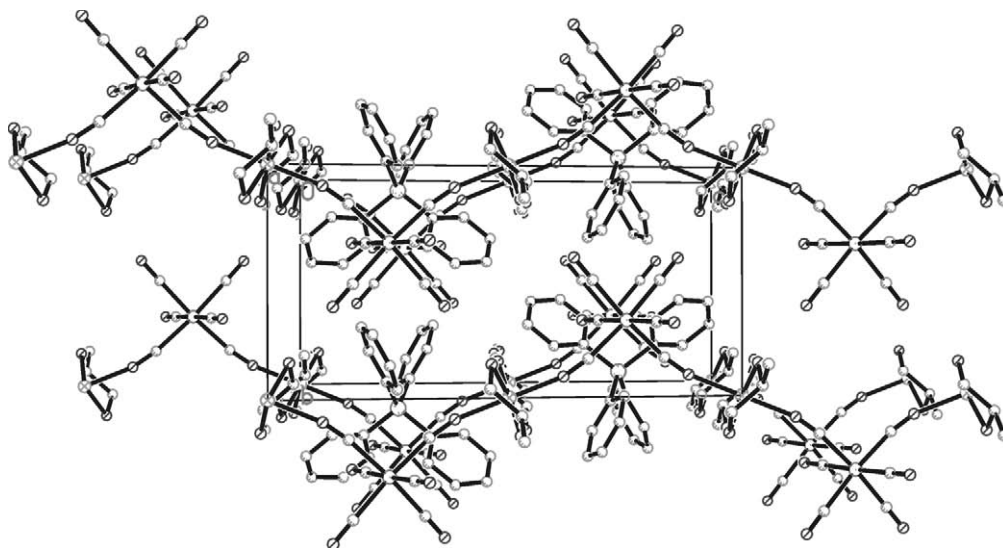


**Figure 6** Projection of the structure of  $\text{PPh}_4[\text{Ni}(\text{pn})_2][\text{Fe}(\text{CN})_6]_2 \cdot \text{H}_2\text{O}$  onto the  $bc$  plane.<sup>85,86</sup>

the heptanuclear complex  $[\text{Ni}(\text{tetren})_6][\text{Cr}(\text{CN})_6](\text{ClO}_4)_9$ . No net magnetic moment is exhibited by these compounds because of an antiferromagnetic intermolecular interaction between the pseudo two-dimensional sheets. A polycrystalline form of the  $\text{Fe}^{\text{III}}$  analogue has been prepared via a rapid precipitation method.<sup>83</sup> This compound displays metamagnetic behavior, which is thought to arise due to a structural disorder in the network, which provides quasi two- and three-dimensional domains. Different magnetic properties between a crystalline and polycrystalline sample have also been shown by Murray and co-workers for  $[\text{Ni}(\text{bpm})_2]_2[\text{Fe}(\text{CN})_6]_2 \cdot 7\text{H}_2\text{O}$ .<sup>84</sup> Another type of one-dimensional assembly has been prepared from the reaction of a 1:1:1 molar aqueous solution of  $[\text{Ni}(\text{pn})_3]\text{Cl}_2$ ,  $\text{K}_3[\text{M}(\text{CN})_6]$ , and  $\text{PPh}_4\text{Cl}$ .<sup>85,86</sup> The compounds of stoichiometry  $\text{PPh}_4[\text{Ni}(\text{pn})_2][\text{M}^{\text{III}}(\text{CN})_6] \cdot \text{H}_2\text{O}$  ( $\text{M}^{\text{III}} = \text{Cr}, \text{Fe}$  and  $\text{Co}$ ) have a one-dimensional zigzag chain structure (Figure 6).

The iron and chromium analogues both show a ferromagnetic interaction as a consequence of the strict orthogonality of the magnetic orbitals. The chromium analogue shows a tendency towards magnetic ordering, but this is overcome by an antiferromagnetic interchain interaction. The cobalt analogue is essentially paramagnetic within the one-dimensional chain, exhibiting only a weak antiferromagnetic interchain interaction. The use of  $[\text{Mn}(\text{acacen})\text{Cl}]^{3+}$  as the cationic constituent forms a one-dimensional linear chain of stoichiometry  $[\text{NEt}_4]_2[\text{Mn}(\text{acacen})][\text{Fe}(\text{CN})_6]$  that orders ferromagnetically due to the ferromagnetic coupling between the  $\text{Mn}^{\text{III}}$  and  $\text{Fe}^{\text{III}}$  ions.<sup>87</sup> The  $\text{Fe}^{\text{II}}\text{Fe}^{\text{III}}$  assembly  $[\text{Fe}(\text{cyclam})][\text{Fe}(\text{CN})_6] \cdot 6\text{H}_2\text{O}$  was prepared via the reaction of  $[\text{Fe}(\text{cyclam})](\text{ClO}_4)_2$  with an excess of  $\text{K}_3[\text{Fe}(\text{CN})_6]$ .<sup>88</sup> This compound also has a one-dimensional chain structure and shows a ferromagnetic intrachain interaction between nearest low-spin  $\text{Fe}^{\text{III}}$  ions, but no magnetic ordering in the bulk.

#### 7.4.3.4.2 Two-dimensional compounds

In contrast to the one-dimensional cyclam-containing compound  $[\text{Fe}(\text{cyclam})][\text{Fe}(\text{CN})_6] \cdot 6\text{H}_2\text{O}$  mentioned above, the  $\text{Ni}^{\text{II}}$  analogue of stoichiometry  $[\text{Ni}(\text{cyclam})]_3[\text{Fe}(\text{CN})_6]_2 \cdot 6\text{H}_2\text{O}$  prepared by Colacio *et al.* crystallizes in a two-dimensional honeycomb-like layered iron(III)–nickel(II) cyanide-bridged complex and exhibits ferromagnetic intralayer and antiferromagnetic interlayer interactions.<sup>89</sup> Above 3 K the magnetic properties of this compound are typical of a metamagnet with  $H_c = 5000$  G (0.5 T), whereas below 3 K, a canted structure is formed, leading to long-range ferromagnetic ordering. The isostructural substitution of  $[\text{Fe}(\text{CN})_6]^{3-}$  by  $[\text{Mn}(\text{CN})_6]^{3-}$  in the above compound afforded a second two-dimensional compound,  $[\text{Ni}(\text{cyclam})]_3[\text{Mn}(\text{CN})_6]_2 \cdot 16\text{H}_2\text{O}$ , which exhibits a metamagnetic behavior.<sup>89</sup>

Reaction of 3:2 molar aqueous solutions of  $[\text{Ni}(\text{N-men})_3]\text{Cl}_2$  and  $\text{K}_3[\text{M}^{\text{III}}(\text{CN})_6]$  ( $\text{M}^{\text{III}} = \text{Fe}, \text{Co}$ ) affords a two-dimensional bimetallic assembly of stoichiometry  $[\text{Ni}(\text{N-men})_3][\text{M}(\text{CN})_6]_2 \cdot \text{H}_2\text{O}$ .<sup>17</sup> X-ray crystallography reveals that this molecule also crystallizes in a two-dimensional honeycomb sheet structure. This work demonstrates that the introduction of a methyl substituent into the

ethylenediamine nitrogen gives rise to a drastic change in the network structure of this compound, from the one-dimensional zigzag chain when the ligand coordinated to the divalent metal is en, to the honeycomb sheet when the ligand is men. Three cyano nitrogens of  $[\text{M}(\text{CN})_6]^{n-}$  in the facial mode coordinate to the adjacent  $\text{trans}[\text{Ni}(\text{N-men})_2]^{2+}$  forming a hexagonal unit having  $\text{M}^{\text{III}}$  ions at each corner and  $\text{Ni}^{\text{II}}$  ions at the center of each edge.

The iron analogue exhibits ferromagnetic ordering below 10.8 K.<sup>17</sup> An inflection point is observed at 5 kG (0.5 T) in the magnetization curve which has been attributed to a disorder in the network due to a partial dehydration. The anhydrous sample was prepared by heating the above compound at 100 °C *in vacuo*. It shows a ferromagnetic interaction, but no spontaneous magnetization. Both the cobalt analogue and its anhydrous compound show a weak antiferromagnetic intersheet interaction. A related two-dimensional compound of stoichiometry  $[\text{Ni}(\text{cyclam})]_3[\text{Cr}(\text{CN})_6]_2 \cdot 20\text{H}_2\text{O}$  has also been reported by Verdaguer and co-workers.<sup>90</sup> It has a two-dimensional honeycomb structure with the nearest intersheet separations of  $\text{Cr} \cdots \text{Cr} = 9.06 \text{ \AA}$ ,  $\text{Ni} \cdots \text{Ni} = 9.06 \text{ \AA}$ , and  $\text{Ni} \cdots \text{Cr} = 8.06 \text{ \AA}$ . Magnetic studies on a powdered sample show a short-range ferromagnetic interaction between neighboring  $\text{Cr}^{\text{III}}$  and  $\text{Ni}^{\text{II}}$  ions, but no magnetic phase transition. Following this work, Mallah and co-workers have prepared and characterized the closely related compound  $[\text{Ni}(\text{tmc})]_3[\text{Cr}(\text{CN})_6]_2 \cdot 18\text{H}_2\text{O}$ <sup>91</sup> which adopts the same two-dimensional honeycomb structure as that of Verdaguer.<sup>90</sup> In the latter case, the tetradentate ligand cyclam has been used instead of tetramethylcyclam. Magnetic studies on this compound show interlayer ferromagnetic ordering. Below a critical temperature ( $T_c = 14 \text{ K}$ ) a bulk antiferromagnetic order is observed due to a small antiferromagnetic interaction between the layers. An antiferromagnetic to ferromagnetic phase transition occurs for an applied field of  $H_c = 1200 \text{ Oe}$  ( $9.5\% \cdot 10^4 \text{ A m}^{-1}$ ) as a consequence of the metamagnetic behavior of the compound. The phase diagram was constructed and the antiferromagnetic interlayer magnetic energy was estimated to be  $0.1 \text{ cm}^{-1}$ . In parallel studies, bimetallic assemblies of general formula  $[\text{Ni}(\text{L})_2]_2[\text{Fe}(\text{CN})_6] \cdot n\text{H}_2\text{O}$  ( $\text{L} = \text{en, pn, or 1,1-dmen}$ ) have been obtained with a range of counterions, e.g.,  $\text{X} = \text{ClO}_4^-, \text{BF}_4^-, \text{and PF}_6^-$ .<sup>81,92,93</sup> X-ray crystallographic studies on selected compounds have revealed a two-dimensional square sheet structure extended by  $\text{Fe}^{\text{III}}-\text{CN}-\text{Ni}^{\text{II}}-\text{NC}$  linkages. Four cyano nitrogens in a plane of  $[\text{Fe}(\text{CN})_6]^{3-}$  coordinate to adjacent  $\text{trans}[\text{Ni}(\text{L})_2]^{2+}$  units to form an octanuclear square unit with an  $\text{Fe}^{\text{III}}$  ion at each corner and a  $\text{Ni}^{\text{II}}$  ion at the center of each edge (Figure 7). The counterion resides in the square cavity. The two-dimensional sheet structures in the pn and 1,1-dmen compounds are essentially similar to each other; however, the intersheet separation is generally larger in the 1,1-dmen compounds because of the bulkiness of the diamine ligand.

These compounds in general exhibit ferromagnetic intrasheet interactions.<sup>17</sup> Metamagnetism appears when the intersheet separation is small enough ( $< 10 \text{ \AA}$ ) to cause an antiferromagnetic interaction between the sheets. Ferromagnetism occurs when the intersheet interaction is large ( $> 10 \text{ \AA}$ ) so that the intersheet magnetic interaction is negligible. Dehydration of the ferromagnetic compounds results in shortening the intersheet separation and, hence, metamagnetism. Analogous bimetallic assemblies have been reported by Liao and co-workers.<sup>94</sup> These compounds of stoichiometry  $[\text{Ni}(\text{L})_2]_2[\text{Fe}(\text{CN})_6]\text{NO}_3 \cdot n\text{H}_2\text{O}$  ( $\text{L} = \text{en or tn}$ ) have similar two-dimensional honeycomb network topologies with a short intersheet separation of  $8.9 \text{ \AA}$ . They show magnetic behavior very similar to that discussed above. Bimetallic assemblies of the general formula  $\text{A}[\text{Mn}(\text{L})_2][\text{M}(\text{CN})_6] \cdot n\text{H}_2\text{O}$  ( $\text{A} = \text{univalent cation: } \text{M}^{\text{III}} = \text{Cr, Mn, Fe, Co; } \text{L}^{2-} = \text{quadridentate Schiff bases}$ ) have been reported by Miyasaka *et al.*<sup>95–98</sup> These assemblies have a two-dimensional structure consisting of an octanuclear repeating unit  $(\text{Mn}-\text{NC}-\text{M}-\text{CN})_4$  with  $\text{M}^{\text{III}}$  ions at the corners and  $\text{Mn}^{\text{III}}$  ions on the edges of a deformed square. The magnetic properties of these compounds are ferromagnetic, antiferromagnetic, or metamagnetic, depending upon the  $\text{Mn}^{\text{III}}/\text{M}^{\text{III}}$  combination and the bulk structure.

An interesting cyano-bridged two-dimensional molecular complex of stoichiometry  $[\text{Ni}(\text{C}_6\text{H}_4\text{N}_2)]_3[\text{Fe}(\text{CN})_6]_2 \cdot 2\text{H}_2\text{O}$  has been reported by Coronado and co-workers.<sup>99</sup> The structure consists of a neutral network of bimetallic cyanide layers containing organic cyclohexane groups that project above and below the interlamellar region. This double layer of bulky diamine ligands imposes a large intersheet separation, with  $\text{Ni} \cdots \text{Ni}$  or  $\text{Fe} \cdots \text{Fe}$  interlayer distances equal to  $12.639 \text{ \AA}$  and a shorter  $\text{Ni} \cdots \text{Fe}$  interlayer distance of  $10.889 \text{ \AA}$  (Figure 8). The layers are composed of deformed rectangular grids of 12 octahedral metal sites in which alternating  $\text{trans}[\text{Ni}(\text{C}_6\text{H}_{14}\text{N}_2)_2]^{2+}$  cations and anions are linked via  $\text{CN}^-$  bridges (Figure 8 (center)).

The magnetic susceptibility of this compound in the temperature range 2–300 K follows the Curie–Weiss law above 50 K with a positive Weiss constant, indicating the presence of dominant

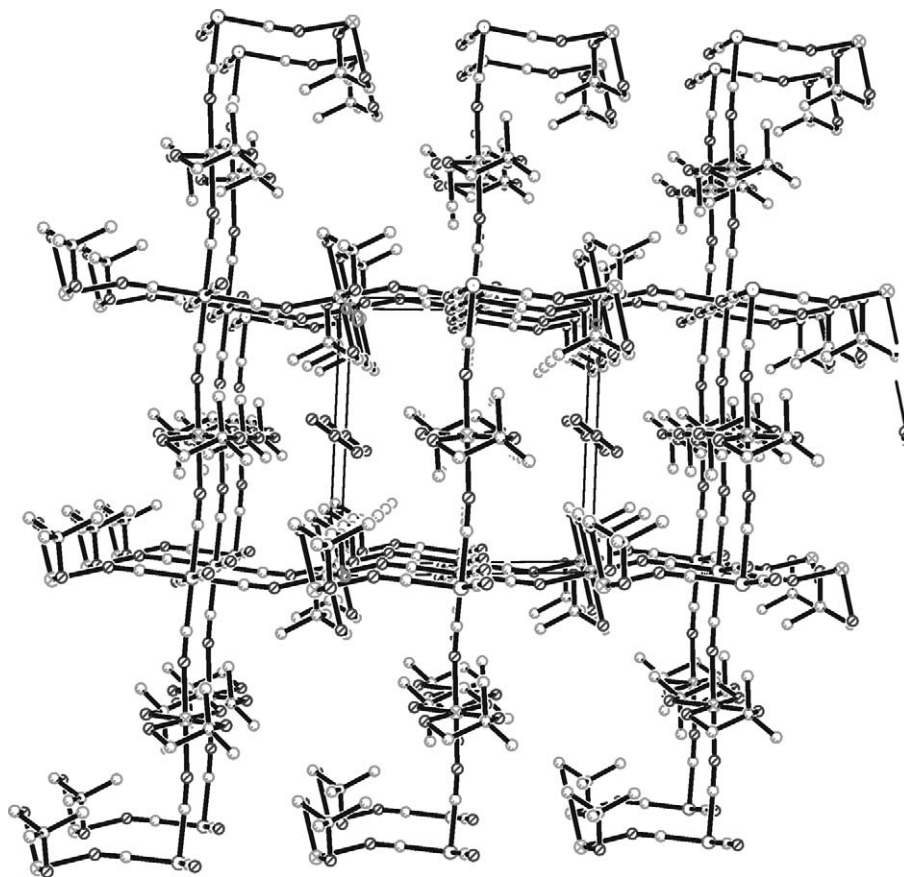


**Figure 7** Two-dimensional structure of  $[\text{Ni}(1,1\text{-dmen})_2][\text{Fe}(\text{CN})_6]\text{N}_3 \cdot 4\text{H}_2\text{O}$ .<sup>81,92,93</sup>

ferromagnetic interactions between neighboring  $\text{Fe}^{\text{III}}$  and  $\text{Ni}^{\text{II}}$  ions. Below 15 K,  $\chi_{\text{M}}$  increases sharply and saturates at low temperature. This behavior suggests the onset of a long-range ferromagnetic transition. The nature of this magnetic transition was confirmed by the field dependence of the isothermal magnetization performed at 2 K (Figure 9).

A rapid increase of the magnetization of approximately  $6.5 \mu_{\text{B}}$  is observed at 1 kOe ( $8.0 \% 10^4 \text{ A m}^{-1}$ ), and increases to  $7.7 \mu_{\text{B}}$  at 50 kOe ( $4.0 \% 10^6 \text{ A m}^{-1}$ ). This latter value is slightly smaller than, but close to,  $8 \mu_{\text{B}}$ , which is the expected value for a ferromagnetic alignment of the interacting spins in a  $\text{Ni}_3\text{Fe}_2$  unit. Hence, the compound behaves as a ferromagnet, although the lower than expected saturation value suggests the presence of some spin canting.

The bimetallic assembly  $[\text{Cu}(\text{dmen})_2][\text{Fe}(\text{CN})_6]$  (dmen = 2-dimethylaminoethylamine) prepared by Mitra and co-workers<sup>100</sup> crystallizes as a two-dimensional polymeric sheet with two different rings, the first a 4-membered square ring and the second a 12-membered hexagonal ring (Figure 10).

Each  $\text{Fe}^{\text{II}}$  has two free, two nearly linear bridging, and two end-on bridging cyanide groups. In the crystal, all the  $\text{Cu}^{\text{II}}$  ions have a distorted square-based pyramidal geometry. From magnetic susceptibility measurements, the complex was found to exhibit a weak ferromagnetic interaction between the nearest copper atoms.

Sieklucka *et al.*<sup>101</sup> turned their attention to the investigation of the chemistry of the geometrically anisotropic building block  $[\text{W}(\text{CN})_6\text{bpy}]^{2-}$ . In this case two coordination sites are occupied by a bipyridine ligand acting as a terminal coordinator that can also participate in  $\pi$ -stacking interactions. Reaction of  $[\text{Mn}(\text{H}_2\text{O})_6]^{2+}$  together with this complex resulted in the formation of  $[\text{fac}-(\text{H}_2\text{O})_3-(\mu\text{-NC})_3\text{-W}^{\text{IV}}(\text{CN})_3\text{bpy}] \cdot 4.5\text{H}_2\text{O}$  which crystallizes as an unusual basket weave-like, two-dimensional coordination polymer. In this case, face-to-face  $\pi$ -stacking interactions and hydrogen bonding interactions play an important role in stabilizing its molecular architecture. Since this compound possesses low-lying MLCT and LC  $\pi$ - $\pi^*$  excited states originating from the  $[\text{W}(\text{CN})_6\text{bpy}]^{2-}$  unit, it is an interesting candidate for the study of photomagnetic properties.

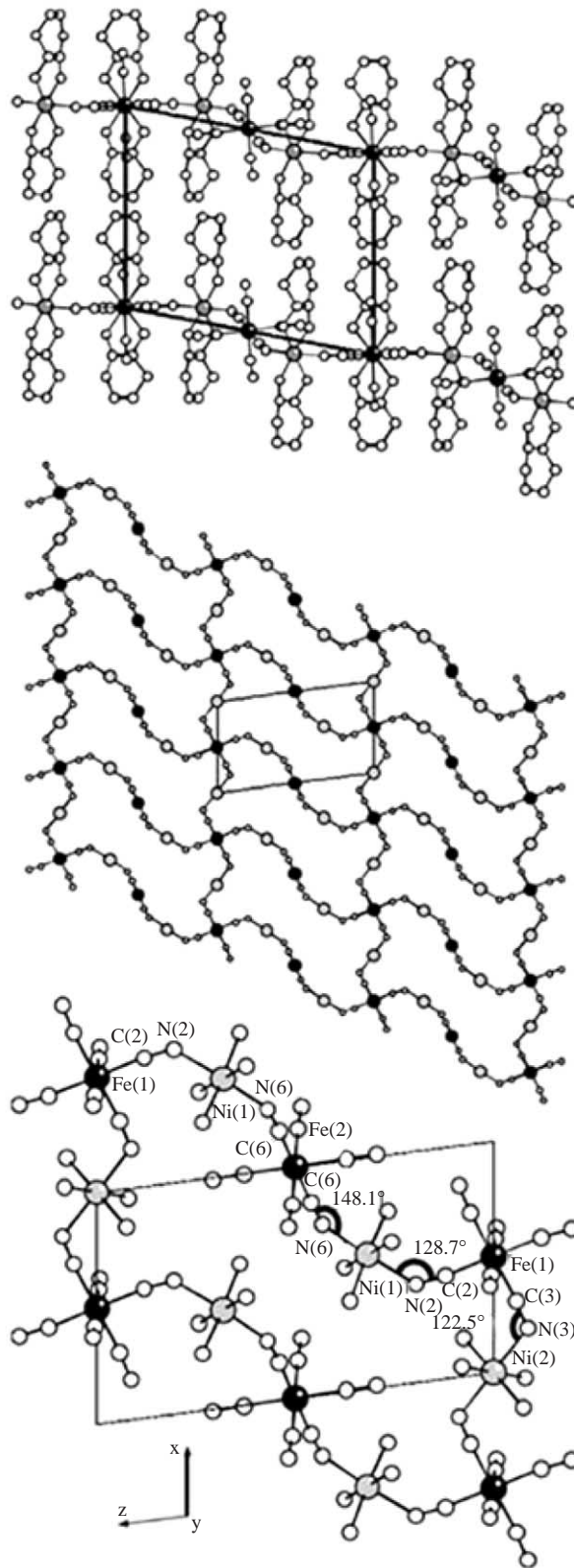


**Figure 8** Top: view of the structure of  $[\text{Ni}(\text{C}_6\text{H}_4\text{N}_2)]_3[\text{Fe}(\text{CN})_6]_2 \cdot 2\text{H}_2\text{O}$  showing the layers in the  $ac$  plane. Center: schematic view of the layers in the  $ab$  plane. Bottom: view of the  $\text{Fe}_6\text{Ni}_6$  ring showing the distortions in the bridging  $\text{Ni}-\text{N}-\text{C}$  bridges; the cyclohexane rings have been omitted for the sake of clarity (Fe atoms in black and Ni atoms in gray).<sup>99</sup>

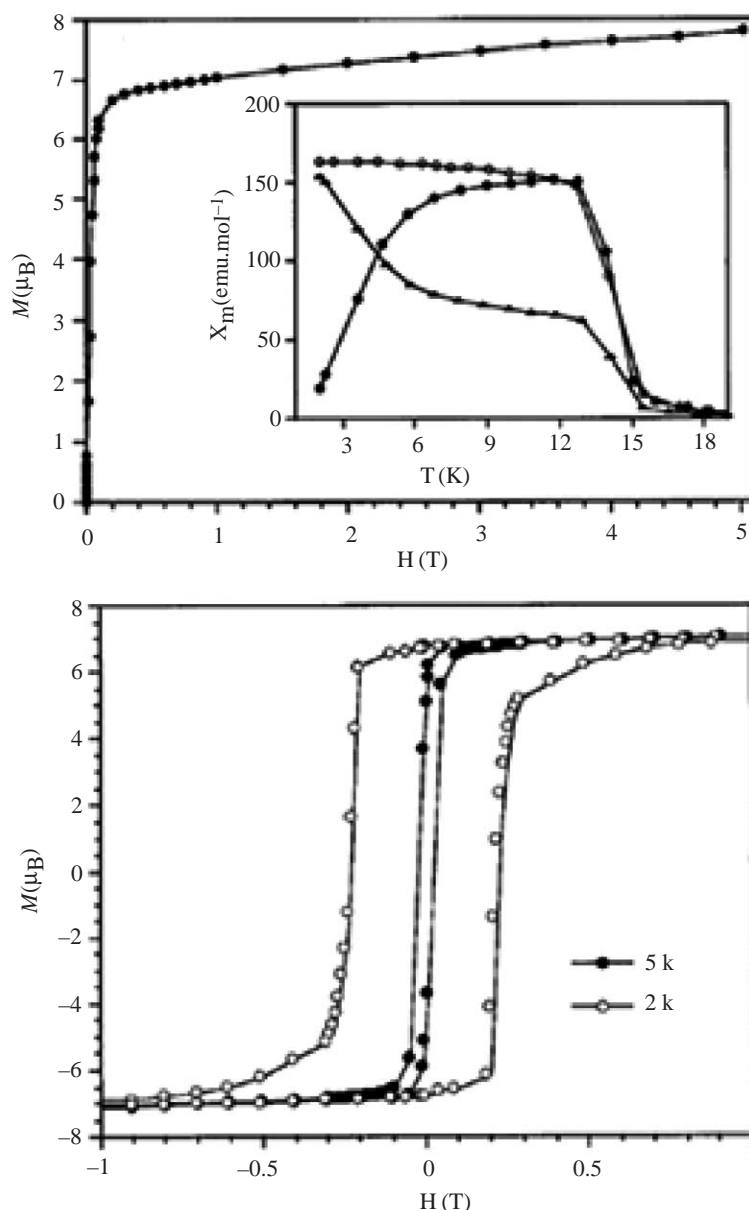


**Figure 9** Top: field dependence of the magnetization at 2 K for  $[\text{Ni}(\text{C}_6\text{H}_4\text{N}_2)_3][\text{Fe}(\text{CN})_6]_2 \cdot 2\text{H}_2\text{O}$  (inset shows zero-field cooled (filled circles) and field cooled (open circles) plots of the DC magnetic susceptibility at 1 G ( $10^{-4}$  T), and remnant magnetization (triangles)). Bottom: hysteresis loop for the compound at 2 K and 5 K.<sup>99</sup>

#### 7.4.3.4.3 Three-dimensional compounds

In order to construct a three-dimensional bimetallic network based on a  $[\text{M}(\text{CN})_6]^{n-}$  building block, the second metal complex as the connector must have at least three vacant sites for accepting cyanide nitrogens from adjacent  $[\text{M}(\text{CN})_6]^{n-}$  ions. These structural requirements are satisfied for the following compounds. Three-dimensional bimetallic assemblies with the general formula  $[\text{Ni}(\text{L})_2]_3[\text{Fe}^{\text{II}}(\text{CN})_6]\text{X}_2$  ( $\text{L} = \text{en}, \text{tn}; \text{X} = \text{PF}_6^-, \text{ClO}_4^-$ ) were obtained from the reaction of a 3:1 molar ratio of  $[\text{Ni}(\text{L})_3]\text{X}_2$  and  $\text{K}_4[\text{Fe}(\text{CN})_6]$ .<sup>102</sup> X-ray crystallography reveals a three-dimensional network structure extended by the  $\text{Fe}-\text{CN}-\text{Ni}-\text{NC}$  linkages, based on a  $\text{Fe}_8\text{Ni}_{12}$  cubic unit, with  $\text{Fe}^{\text{II}}$  ions at the corners and  $\text{Ni}^{\text{II}}$  ions at the middle edges (Figure 11). Two counterions reside in the cubic cavity and align along the diagonal axis.

Magnetic studies reveal a ferromagnetic interaction between nearest  $\text{Ni}^{\text{II}}$  ions through the diamagnetic  $\text{Fe}^{\text{II}}$  ion. No magnetic ordering occurs over the lattice down to 2 K due to the diamagnetic nature of  $[\text{Fe}^{\text{II}}(\text{CN})_6]^{4-}$ . Gatteschi and co-workers have reported a three-dimensional

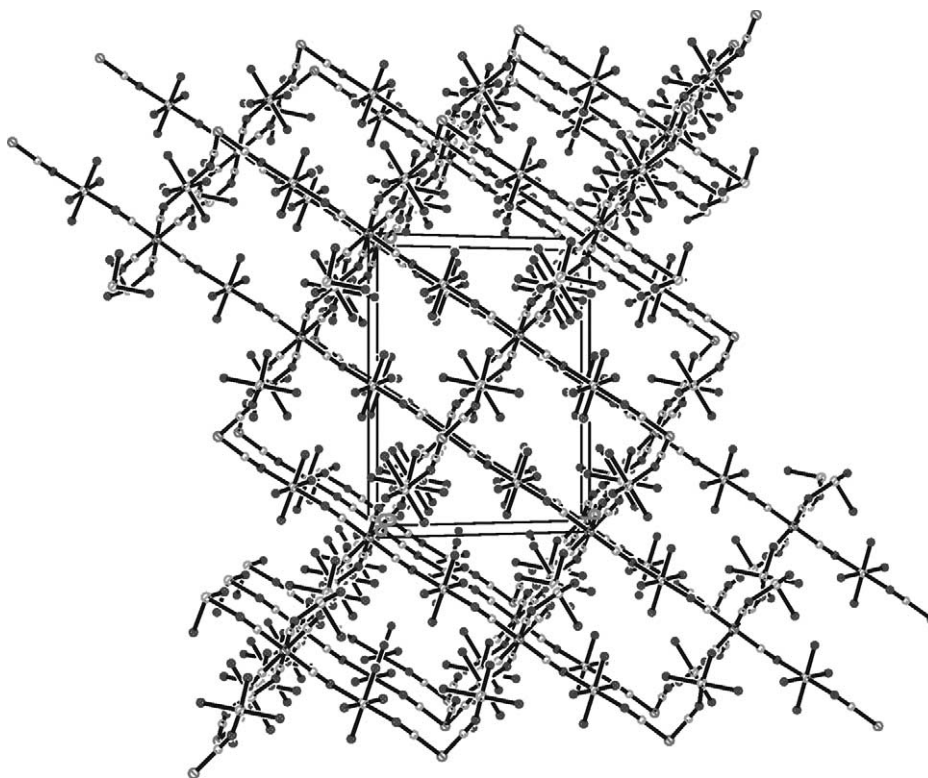


**Figure 10** Projection of the polymeric chain structure of  $[\text{Cu}(\text{dmen})]_2[\text{Fe}(\text{CN})_6]$  along the  $z$ -axis.<sup>100</sup>

bimetallic assembly of formula  $[\text{Ni}(\text{tren})]_3[\text{Fe}(\text{CN})_6] \cdot 6\text{H}_2\text{O}$ , which crystallizes in a complicated three-dimensional network and orders ferrimagnetically at 8 K.<sup>103</sup> Structural strain causes a weak antiferromagnetic interaction between the  $\text{Fe}^{\text{III}}$  and  $\text{Ni}^{\text{II}}$  ions on the intersections of the one-dimensional chains. A three-dimensional magnetic lattice then arises from the antiferromagnetically coupled one-dimensional ferromagnetic chains. A three-dimensional assembly of stoichiometry  $[\text{Mn}(\text{en})]_3[\text{Cr}(\text{CN})_6]_2 \cdot 4\text{H}_2\text{O}$  was obtained by Ohba *et al.*<sup>104</sup> Characterization by X-ray crystallography reveals that this network is formed by an alternating array of  $[\text{Cr}(\text{CN})_6]^{3-}$  and  $[\text{Mn}(\text{en})]^{2+}$  ions. The structure is also based on a defective cubane with three Cr atoms and four Mn atoms at the corners of the cube and eight Cr—CN—Mn edges. This compound has an overall ferromagnetic ordering temperature of 69 K based on a short-range antiferromagnetic interaction between  $\text{Mn}^{\text{II}}$  and  $\text{Cr}^{\text{III}}$  ions. The magnetic hysteresis loop at 2 K is typical of soft magnets showing a weak coercive field  $H_c = 28 \text{ G}$  ( $2.8\% \cdot 10^{-3} \text{ T}$ ). This compound can be compared with a Prussian blue-like phase where the  $[\text{M}(\text{H}_2\text{O})_2]^{2+}$  is simply replaced by  $[\text{M}(\text{en})]^{2+}$ . This strategy has been extended by Okawa and co-workers to prepare two cyanide-bridged three-dimensional bimetallic ferrimagnets of the type  $[\text{Mn}(\text{L})]_3[\text{Cr}(\text{CN})_6]_2 \cdot n\text{H}_2\text{O}$  ( $\text{L} = \text{ethylenediamine}$ ,  $n = 4$ ; or  $\text{L} = \text{glycine amide}$ ,  $n = 2.5$ ).<sup>68</sup> Once again X-ray crystallographic studies show that these compounds have a three-dimensional network structure based on a defective cubane unit. Magnetic studies demonstrate that both compounds are ferrimagnets with  $T_c$  values of 69 K and 71 K, respectively. These assemblies closely resemble the Prussian blue analogue  $\text{Mn}_3[\text{Cr}(\text{CN})_6] \cdot 12\text{H}_2\text{O}$  which is a ferrimagnet and orders at  $T_c = 63 \text{ K}$ .<sup>68</sup>

Many groups are following this strategy of using convergent precursors in order to lower the dimensionality of the Prussian blues into the molecular regime. In the late 1990s Long and co-workers also initiated experiments directed towards the preparation of molecular box clusters inherent to the Prussian blue-type structure.<sup>105</sup> The tridentate ligand 1,4,7-triazacyclononane (tacn) was employed to block a single face of each of the transition metal building blocks, preventing growth of the three-dimensional framework. Hence, reaction between  $[\text{Cr}(\text{H}_2\text{O})_3(\text{tacn})]^{3+}$  and  $[\text{Co}(\text{CN})_3(\text{tacn})]$  afforded the molecular cubes  $[\text{Cr}_4\text{Co}_4(\text{CN})_{12}(\text{tacn})_8]^{12+}$  and  $[\text{Co}_8(\text{CN})_{12}(\text{tacn})_8]^{12+}$  with core structures consisting of a single cubic unit excised from the Prussian blue-type framework. The structure of the cubic  $[\text{Co}_8(\text{CN})_{12}(\text{tacn})_8]^{12+}$  is shown in



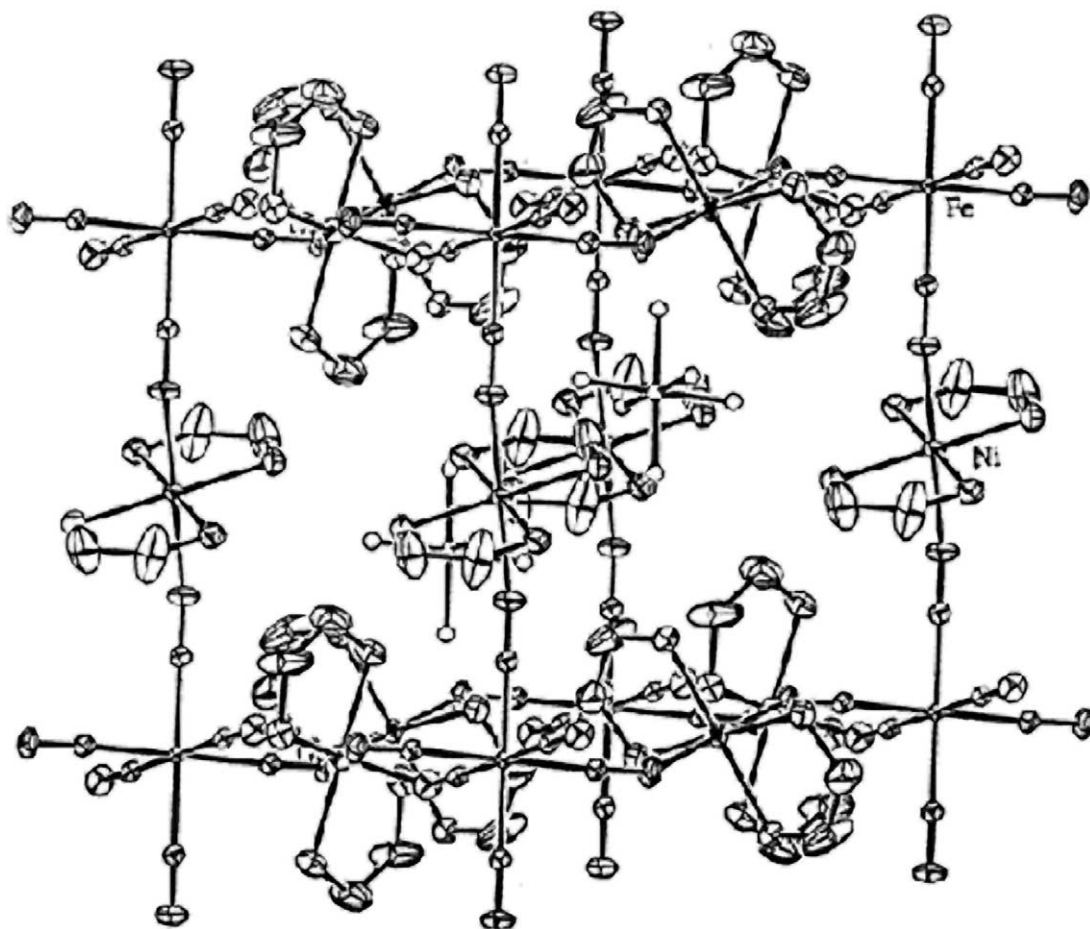
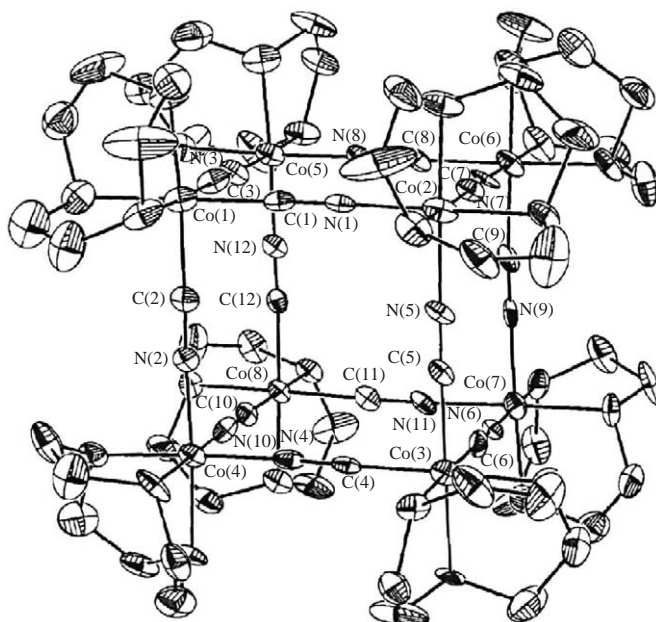


Figure 11 Structure of the  $\text{Fe}_8\text{Ni}_{12}$  cubic unit of  $[\text{Ni}(\text{en})_2][\text{Fe}(\text{CN})_6](\text{PF}_6)_2$ .<sup>102</sup>

Figure 12, and the space-filling model is shown in Figure 13, as viewed down a cube face. The structure of the  $[\text{Cr}_4\text{Co}_4(\text{CN})_{12}(\text{tacn})_8]^{12+}$  cube is similar with four  $\text{Cr}^{\text{III}}$  ions arranged in a tetrahedron over the cube vertices (replacing atoms Co(2), Co(4), Co(5), and Co(7) in Figure 12) and separated by intervening  $\text{Co}^{\text{III}}$  ions.

The temperature dependence of the magnetic susceptibility for the latter compound was measured. A fit of the data to the Curie–Weiss law gives an effective magnetic moment of  $7.5 \mu_{\text{B}}$  associated with a  $g$  value of 1.97 corresponding to four isolated  $S = 3/2$   $\text{Cr}^{\text{III}}$  ions per molecular cube.

Along these lines, with the aim of obtaining square units with octahedral metal ions at the vertices, Dunbar and co-workers have succeeded in capping four of the coordination sites with two bidentate ligands such as 2,2'-bipyridine or 1,10-phenanthroline.<sup>106</sup> This results in a  $90^\circ$  angle between the two unblocked sites. The air-sensitive complex  $\text{Mn}(\text{bpy})(\text{CN})_2$  has been prepared and its structure has been verified by X-ray crystallography. This strategy has been extended by the use of  $[\text{M}(\text{CN})_6]^{n-}$  anions to connect  $\text{cis-}[\text{M}(\text{L-L})_2]^{n+}$  units. Hexacyanometalate precursors can produce polymers via *trans* linkages, but there is also the possibility for the self-assembly of molecular squares through *cis*-cyano interactions. In order to investigate this, a series of transition metal complexes were reacted with  $[\text{Fe}(\text{CN})_6]^{3-}$ . Reaction of  $[\text{Mn}(2,2'\text{-bpym})_2(\text{H}_2\text{O})_2](\text{BF}_4)_2$  with  $\text{K}_3[\text{Fe}(\text{CN})_6]$  afforded the two-dimensional polymer  $[\text{Mn}(\text{H}_2\text{O})_2][\text{Mn}(2,2'\text{-bpym})(\text{H}_2\text{O})_2]_2[\text{Fe}(\text{CN})_6]_2$ .<sup>106</sup> This compound is obtained as a consequence of the loss of a 2,2'-bipyrimidine ligand and suggests that precursors with two bidentate “protecting” ligands are not always stable in the presence of cyanometalate anions. The 2,2'-bipyridine analogue of this compound was prepared in the same way and this compound is isostructural with the bipyrimidine compound. Both compounds are ferrimagnets with ordering temperatures of 11 K. In an attempt to favor the formation of discrete clusters over polymers, complexes of the type  $[\text{M}(\text{bpy})_3]^{2+}$  were used in reactions where the bpy ligands are lost slowly in favor of the nitrogen end of a cyanide ligand. Along these lines, reaction of  $[\text{Co}(\text{bpy})_3](\text{ClO}_4)_2$  with  $\text{K}_3[\text{Fe}(\text{CN})_6]$  afforded a trigonal bipyramidal



**Figure 12** Structure of the cubic  $[\text{Co}_8(\text{CN})_{12}(\text{tcn})_8]^{12+}$  cluster showing 30% ellipsoids and the core atom labeling scheme.<sup>105</sup>

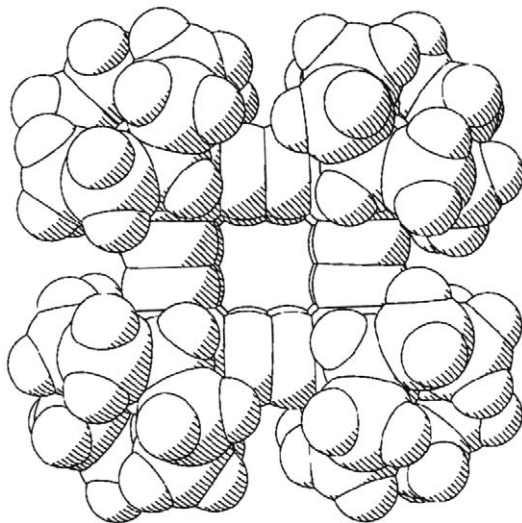


**Figure 13** Space-filling model of the  $[\text{Co}_8(\text{CN})_{12}(\text{tcn})_8]^{12+}$  cluster viewed down a cube face.<sup>105</sup>

(tbp) cluster of stoichiometry  $[\text{Co}(\text{bpy})_2]_3[\text{Fe}(\text{CN})_6]_2^+$ .<sup>106</sup> This cluster crystallizes in the chiral space group  $P6_322$ , and is formed via a spontaneous redox reaction. The compound is diamagnetic which supports the presence of LS  $\text{Fe}^{\text{II}}$  and  $\text{Co}^{\text{III}}$  ions. The formation of molecular squares was realized from the reaction of  $[\text{Zn}(\text{phen})_2(\text{H}_2\text{O})_2](\text{NO}_3)_2$  with  $[\text{Fe}(\text{CN})_6]^{3-}$  to afford the compound  $\{[\text{Zn}(\text{phen})_2(\text{H}_2\text{O})_2][\text{Fe}(\text{CN})_6]_2\}^{2-}$  whose structure has been confirmed by X-ray crystallography.<sup>106</sup> The molecular dianion is composed of two 1,10-phenanthroline-capped  $\text{Zn}^{\text{II}}$  ions linked by two *cis*-hexacyanoferrate units. The anion packing involves an intermolecular interaction between 1,10-phenanthroline ligands, which leads to a buckling of the CN ligands from an ideal  $180^\circ$  bonding angle. The magnetic properties of the cluster indicate the presence of two isolated non-interacting  $S = 1/2$   $\text{Fe}^{\text{III}}$  atoms. A pentamer of stoichiometry  $[\text{Ni}(\text{bpy})_2(\text{H}_2\text{O})][\text{Ni}(\text{bpy})_2]_2[\text{Fe}(\text{CN})_6]_2$  was prepared from the reaction of  $[\text{Ni}(\text{bpy})_2(\text{H}_2\text{O})](\text{OTf})_2$  with  $\text{K}_3[\text{Fe}(\text{CN})_6]$  in water.<sup>106</sup> The formation of the pentamer can be viewed as essentially the addition of an extra  $[\text{Ni}(\text{bpy})_2(\text{H}_2\text{O})]^{2-}$  unit to the square  $\{[\text{Ni}(\text{bpy})_2]_2[\text{Fe}(\text{CN})_6]_2\}^{2-}$ . The extra unit is stabilized by hydrogen bonding between the remaining water molecule and the nitrogen end of a nearby terminal cyanide corner

$[\text{Fe}(\text{CN})_6]^{3-}$  unit. The pentamer is neutral which accounts for its ease of isolation. This concept of adding additional building blocks to the central square can be extended to the formation of even larger molecules. For example, an unusual dcameric cluster of stoichiometry  $\{[\text{Zn}(\text{phen})_2][\text{Fe}(\text{CN})_6]\}_2\{\text{Zn}(\text{phen})_2\}[\text{Zn}(\text{phen})_2(\text{H}_2\text{O})][\text{Fe}(\text{CN})_6]\}_2$  has been isolated in this way.<sup>106</sup>

Preliminary magnetic data on the  $\text{Ni}_3\text{Fe}_2$  pentamer  $[\text{Ni}(\text{bpy})_2(\text{H}_2\text{O})][\text{Ni}(\text{bpy})_2]_2[\text{Fe}(\text{CN})_6]_2$  indicate that the ground state for this molecule is ferromagnetic  $S=4$ . More importantly, the cluster appears to behave as a single molecule magnet. AC magnetic susceptibility measurements on a batch of single crystals revealed a strong frequency dependence both in the  $\chi'$  (in-phase) and  $\chi''$  (out-of-phase) signals with a blocking temperature of  $\sim 2$  K. The fact that such a small cluster with only eight unpaired electrons can exhibit slow relaxation of the magnetization reversal hints at an appreciable anisotropy due, in part, to the presence of single-ion anisotropy (ZFS) as well as shape anisotropy. Following this strategy a variety of cluster geometries has been encountered including trigonal bipyramids, squares, pentamers, and decamers.<sup>106</sup> Molecular squares based on octahedral metal ions can in turn be used in a rational approach as building blocks for larger and highly unsymmetrical molecules. In parallel studies, Oshio and co-workers have also prepared a series of cyanide-bridged FeFe and FeCo molecular squares and the structures and electrochemistry of these compounds has been reported.<sup>107</sup>

Reaction of either  $[\text{Fe}(\text{CN})_6]^{3-}$  or  $[\text{Fe}(\text{CN})_6]^{4-}$  with a macrocyclic  $\text{Ni}^{\text{II}}$  complex leads to the same product, namely a novel three-dimensional iron(II)–nickel(II) cyanide-bridged bimetallic assembly of stoichiometry  $[\text{NiL}]_2[\text{Fe}(\text{CN})_6] \cdot 4\text{H}_2\text{O}$  ( $L = 3,10$ -bis(2-hydroxyethyl)-1,3,5,8,10,12-hexaazacyclotetradecane).<sup>108</sup> In the complex, each  $\text{Ni}^{\text{II}}$  ion is six coordinate with four nitrogen atoms from the macrocyclic ligand in the equatorial plane and two nitrogen atoms from the macrocyclic ligand in axial positions leading to a distorted octahedral geometry. Each  $[\text{Fe}(\text{CN})_6]^{4-}$  is coordinated to four  $[\text{NiL}]^{2+}$  cations through four cyano nitrogen atoms, in which two cyano nitrogen atoms coordinate with  $[\text{NiL}]^{2+}$  to form an  $\{[\text{Fe}(\text{CN})_6][\text{NiL}]\}_n$  chain; the other two cyano nitrogen atoms connect the adjacent chains through coordination with  $[\text{NiL}]^{2+}$ , forming a novel three-dimensional network with a vat-like structure. All of the water molecules are located within the lattice. The magnetic data are consistent with a weak ferromagnetic interaction between nearest  $\text{Ni}^{\text{II}}$  ions through the  $-\text{NC}-\text{Fe}-\text{CN}-$  bridge, and the ferromagnetic interaction is proposed to occur by a super exchange pathway between the nearest  $\text{Ni}^{\text{II}}$  ions through the empty  $d$  orbital of the  $\text{Fe}^{\text{II}}$  ion.

The choice of suitable organic ligands for the rational design of discrete molecular units has enabled Mallah and co-workers to tune finely the degree of delocalization and hence the optical properties of Prussian blue-like complexes.<sup>109</sup> Adopting a molecular stepwise approach, the reaction of  $\text{K}_4[\text{Fe}^{\text{II}}(\text{CN})_6]$  with six equivalents of  $[\text{Fe}^{\text{III}}(\text{L}_2)\text{Cl}]$ , where  $\text{HL}_2$  is the pentadentate ligand bis(3-salicylideneaminopropyl)methylamine, leads to the formation of a mixed-valence, mixed-spin heptanuclear complex  $[\text{Fe}^{\text{II}}\{\text{CN}\}_6\text{Fe}^{\text{III}}(\text{L}_2)]_6\text{Cl}_2$ , which reproduces all the electronic characteristics of Prussian blue.<sup>109</sup> Mallah and co-workers demonstrate that it is possible to tune the position of the intervalence band of Prussian blue-like molecules without changing the nature of the metal simply by adjusting the reduction potential of the peripheral  $\text{Fe}^{\text{III}}$  through a judicious choice of the organic ligand; the more easily reducible are the  $\text{Fe}^{\text{III}}$  ions, the lower in energy is the intervalence transition. Investigations are underway to study the relationship between the energy of the MMCT transition and the amplitude of the ferromagnetic coupling in these Prussian blue-type compounds.

### 7.4.3.5 Single-molecule Magnets

One of the exciting challenges facing chemists in the twenty-first century is to use nanoparticles or even single molecules as the ultimate size for magnetic information storage. There are several reported examples of particles in the 10–100 nm size range that exhibit the phenomenon of slow relaxation of magnetization below a critical temperature defined as the blocking temperature. Most of these nanomaterials are prepared from macroscopic samples by decreasing their sizes through a “top down” approach and are polydisperse. In order to achieve monodisperse systems, where the magnetic properties should be quantifiable and directly controllable, a “bottom up” approach is required. Since the properties of magnetic particles scale exponentially, it should be possible either to address the individual particles, or else ensembles of absolutely identical particles (monodisperse arrays) must be available. This has presented chemists with a formidable challenge, but an attractive solution has been found via the realization that molecules containing several transition metal ions can exhibit properties similar to nanoscale magnetic particles (nanomagnets).<sup>110</sup>

A new avenue in cyanide chemistry was opened up when it became apparent that under the right experimental conditions it is possible to crystallize high-nuclearity clusters from hexacyanometalates when the Lewis acid is a complex specifically designed to present more than one labile position, e.g.,  $[M^{II}L_5(H_2O)_3]$  ( $L_5$  is a pentadentate ligand). Under these conditions, the labile water can be substituted by one cyanide ion from  $[M(CN)_6]^{n-}$  (Figure 14).<sup>18</sup>

When the reaction is repeated  $n$  times, a polynuclear cluster is obtained, since the pentadentate ligand impedes the growth of the three-dimensional Prussian blue phase and the clusters possess a large ground state spin.<sup>18</sup> Following this strategy, Marvaud and co-workers have been successful in synthesizing and characterizing a range of high-spin molecules with ground states ranging from  $S=9/2$  for  $CrCu_6$ , to  $S=15/2$  for  $CrNi_6$ , to  $S=27/2$  for  $CrMn_6$  (Figure 15).<sup>18,110,111</sup> Initial work was carried out using tetra- and pentaamine ligands and preparing their corresponding mononuclear complexes, where the divalent metal ion = Cu, Ni, Co, or Mn. Reaction of these complexes with  $[M^{III}CN_6]^{3-}$  precursors afforded species with a large variety of symmetries induced by the flexibility of the cyanometalate coordination geometry (Figure 15). The ground state spin of these molecules can be predicted and tuned following Kahn's model of orbital interactions. These compounds display a range of ground state spins and diverse magnetic interactions.<sup>18</sup>

This approach follows a "bottom-up" strategy, and polynuclear transition metal complexes exhibiting superparamagnet-like properties are now referred to as single-molecule magnets (SMMs).<sup>112</sup> At low temperature the magnetic moments of these compounds orient in the direction of the magnetic field and stay aligned when the field is switched off. This property is due to an axial anisotropy caused by a zero field splitting (ZFS)  $D$  ( $D$  negative) of the ground state of the cluster, which gives rise to a potential energy barrier between the two degenerate  $\pm m_s$  states. The energy of this barrier is equal to  $DS_z^2$  for integer spins, with  $S_z$  being the projection of the spin of the ground state on the easy axis (Figure 16).<sup>110</sup>

The magnetic properties of SMMs are the subject of detailed investigations, and the presence of steps in the magnetic hysteresis loops, quantum tunneling, as well as quantum phase interference effects are now becoming better understood. Detailed aspects of this are discussed in Chapter 7.13.

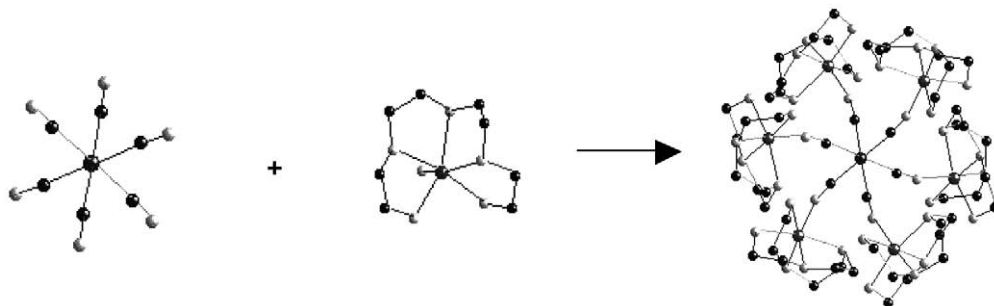


**Figure 14** Synthetic strategy for the preparation of high-nuclearity clusters from hexacyanometalates.<sup>18,110,111</sup>

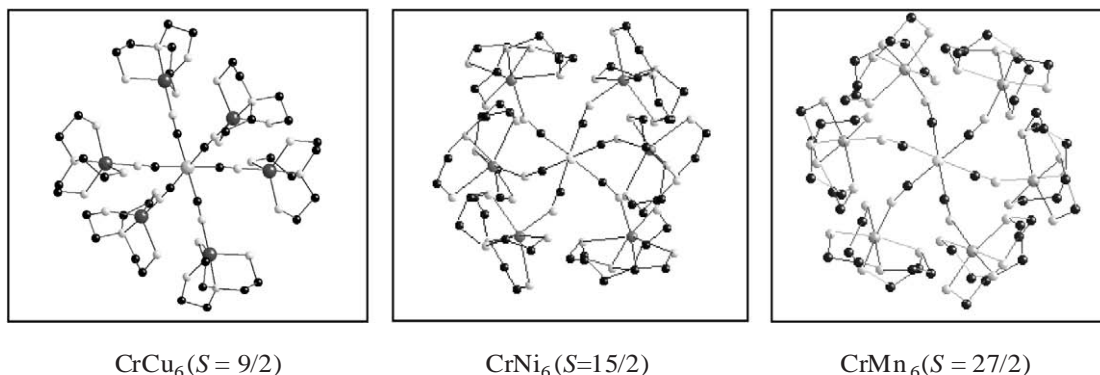


**Figure 15** Three examples of high-spin molecules prepared by Marvaud *et al.*<sup>18,110,111</sup>

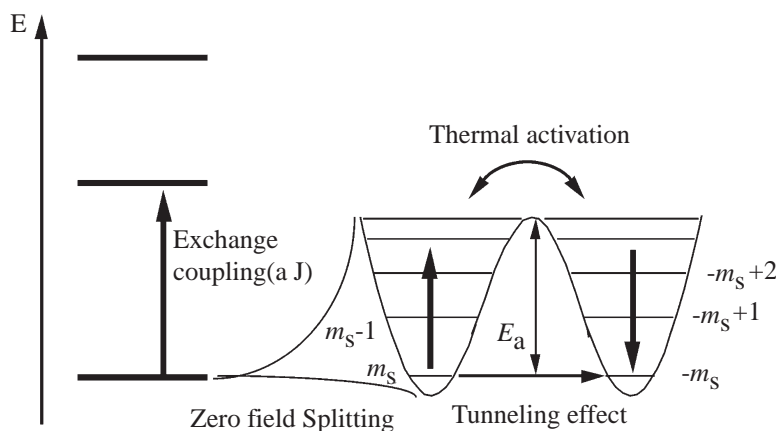


**Figure 16** Schematic plot of a single-molecule magnet experiencing axial zero field splitting.

To summarize briefly, working towards the design and assembly of novel SMMs, the major objectives of research groups are as follows.

- (i) Enhancement of the molecular spin, namely to make large clusters containing many transition metal ions with unpaired electrons. In this case the intent is to obtain a large ground state spin, well separated in energy from the first excited states. In the simplest case, separation is proportional to the exchange interaction  $J_{\text{intra}}$  between two neighboring spin carriers. The intramolecular  $J$  coupling constants must therefore be as high as possible.
- (ii) Improvement of the anisotropy of the system, since most of the interesting properties are related to the anisotropy barrier  $DS_z^2$ .

These two requirements are often difficult to satisfy at the same time, since high spin and anisotropy are often contradictory. Also playing an essential role are the intermolecular interactions between the polynuclear clusters, since for behavior based on a single molecule it is a prerequisite that these are negligible. Very few examples of clusters fulfilling all of the above criteria are available in the chemical literature. Concerning the spin value, in most cases serendipity has afforded several attractive high-spin clusters<sup>113</sup> (see also Chapter 7.3), but affords little or no effective control over the chemistry. As our level of understanding increases, there is an increasing need for the rational design of larger cluster geometries in which more paramagnetic centers are magnetically coupled. Long and co-workers have successfully applied a similar rational strategy for achieving higher nuclearities which involves the use of a blocking ligand on just one of the reaction components, thereby permitting cluster growth to propagate further before a closed structure forms.<sup>114</sup> In this way, reaction of  $\text{NiI}_2$  with  $[(\text{Me}_3\text{tacn})\text{Cr}(\text{CN})_3]$  in aqueous solution does not lead to the previously described face-centered cubic molecular square of stoichiometry  $[(\text{Me}_3\text{tacn})_8\text{Cr}_8\text{Ni}_6(\text{CN})_{24}]^{12+}$  obtained with chloride, bromide, nitrate, or perchlorate as counterions. Instead, crystallographic analysis of red-brown plates isolated from the reaction mixture revealed the compound was an open cage cluster of stoichiometry  $[(\text{Me}_3\text{tacn})_8\text{Cr}_8\text{Ni}_5(\text{CN})_{24}]\text{I}_{10}\cdot 27\text{H}_2\text{O}$ .<sup>115</sup> The core structure of this cluster most notably differs from face-centered cubic geometry by having a  $\text{Ni}^{\text{II}}$  ion missing from one of the cube faces (Figure 17).

The absence of this nickel atom leaves four terminal cyanide ligands retaining the  $\text{Cr}^{\text{III}}\text{--CN}$  connectivity, two of which are directed away from the center of the open cube face. A single iodine anion resides within the metal–cyanide cage of the cluster, as shown in Figure 17. The encapsulated ion is disordered over four positions in the crystal structure, each approaching an axial ligand site in a nickel center with a mean  $\text{Ni}\cdots\text{I}$  distance of 3.09 Å. Attempts to extract the central iodide ion by metathesis reactions are underway, with the intention of probing the host–guest chemistry of the cluster. In a surprising parallel,  $[\text{Ni}(\text{CN})_4]^{2-}$  reacts with the cyanide-rich  $[(\text{Me}_3\text{tacn})_8\text{Cr}_8\text{Ni}_5(\text{CN})_{24}]^{10+}$  cluster in aqueous solution to yield a compound that incorporates square pyramidal, trigonal pyramidal  $[\text{Ni}(\text{CN})_5]^{3-}$ , as well as square planar  $[\text{Ni}(\text{CN})_4]^{2-}$  units in a single cluster (Figure 18). The structure of this  $C_3$ -symmetric  $[(\text{Me}_3\text{tacn})_{10}\text{Cr}_{10}\text{Ni}_9(\text{CN})_{42}]^{6+}$  cluster bears no obvious relationship to its  $\text{Cr}_8\text{Ni}_5$  precursor and consists of a “barrel-shaped egg cage” enclosing a bound central  $[(\text{Me}_3\text{tacn})\text{Cr}(\text{NC})_3]$  moiety (Figures 18 and 19).

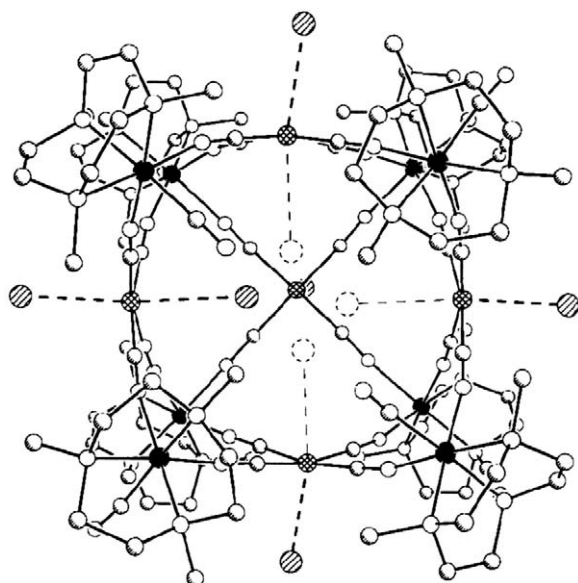


**Figure 17** Structure of the  $[(\text{Me}_3\text{tacn})_8\text{Cr}_8\text{Ni}_5(\text{CN})_{24}]^{10+}$  cluster and associated  $\text{I}^-$  anions. Black, cross-hatched, shaded, white, and hatched spheres represent Cr, Ni, C, N, and I atoms, respectively; H atoms are omitted for clarity. The cluster has maximal point group symmetry  $C_{2v}$ .<sup>115</sup>

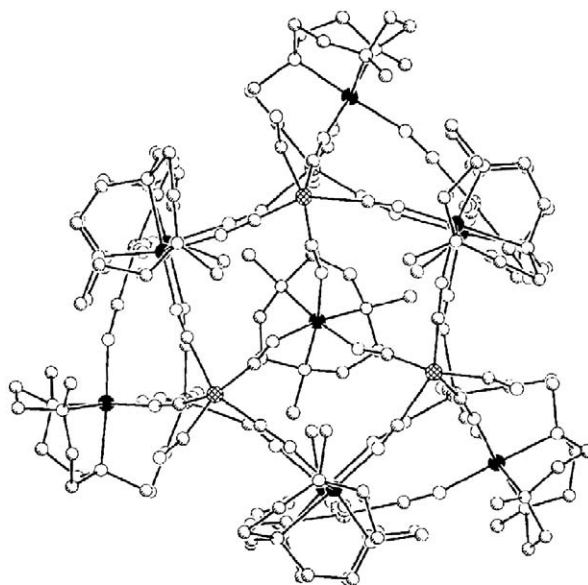


**Figure 18** Structure of the  $[(\text{Me}_3\text{tacn})_{10}\text{Cr}_{10}\text{Ni}_9(\text{CN})_{42}]^{6+}$  cluster viewed parallel (top) to the crystallographic  $6_3$  screw axis. Black, cross-hatched, shaded, and white spheres represent Cr, Ni, C, and N atoms, respectively; H atoms are omitted for clarity. The nickel centers adopting square planar (Ni(1)), square pyramidal (Ni(2)), and trigonal bipyramidal (Ni(3)) coordination geometries are located in the middle, lower, and upper tiers of the cluster, respectively.<sup>115</sup>

The surrounding cage framework is made up of three tiers each with six metal centers. The top and bottom tiers exhibit pseudo-hexagonal  $\text{Cr}_3\text{Ni}_3(\text{CN})_6$  rings, which are joined through cyanide bridges to three linear  $\text{CrNi}(\text{CN})_2$  units of the middle tier. Once again, a  $\text{Cr}^{\text{III}}\text{-NC-Ni}^{\text{II}}$  connectivity is adopted by all bridging cyanide ligands. The square planar nickel centers in the middle tier are each capped by a square planar  $[\text{Ni}(\text{CN})_4]^{2-}$  counterion through a weak  $\text{Ni}\cdots\text{Ni}$  bonding contact of 3.12 Å. As reflected in the magnetic properties of these two clusters, ligation by the strong field carbon end of cyanide results in exclusively diamagnetic  $\text{Ni}^{\text{II}}$  centers, eliminating the possibility of an exchange coupling directly between the cyanide bridges linking the metal sites. For both compounds the measured values of  $\chi_M T$  at temperatures above 30 K closely

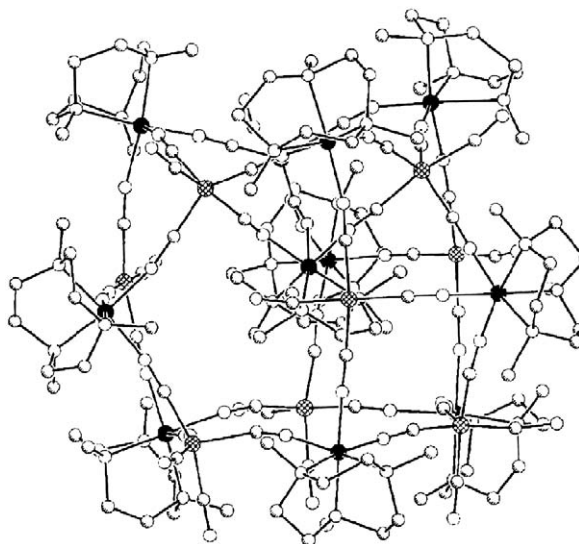


**Figure 19** Structure of the  $[(\text{Me}_3\text{tacn})_{10}\text{Cr}_{10}\text{Ni}_9(\text{CN})_{42}]^{6+}$  cluster perpendicular (bottom) to the crystallographic  $6_3$  screw axis.<sup>115</sup>

approximate to the predicted spin-only values of  $15 \text{ cm}^3 \text{ K mol}^{-1}$  and  $18.75 \text{ cm}^3 \text{ K mol}^{-1}$ , respectively, corresponding to 8 and 10 isolated  $S = 3/2$   $\text{Cr}^{\text{III}}$  ions per formula unit. In each case, a steady rise in  $\chi_{\text{M}}T$  below 30 K suggests the onset of weak ferromagnetic coupling between paramagnetic chromium centers. The minimum intercluster  $\text{Cr}\cdots\text{Cr}$  separations of 8.98 Å and 9.27 Å are significantly longer than the minimum intracluster  $\text{Cr}\cdots\text{Cr}$  separations of 6.64 Å and 6.92 Å, implying that the coupling more likely originates from superexchange within the clusters. The synthesis of related species utilizing paramagnetic cobalt(III) centers in place of nickel(II) is now being explored as a viable route for the preparation of new SMMs.<sup>115</sup>

#### 7.4.3.6 Heptacyanometalate Building Blocks

Although Prussian blue phases exhibit remarkable magnetic properties, their face-centered cubic structures mean that no magnetic anisotropy can be expected. To address this problem Kahn and co-workers turned their attention to an investigation of the versatility of  $[\text{M}(\text{CN})_7]^{n-}$  as a precursor. As for the Prussian blue phases, the presence of cyano ligands can lead to extended lattices, but in contrast, the heptacoordination of the precursor is not compatible with cubic symmetry. For compounds containing a heptacoordinated  $[\text{Mo}(\text{CN})_7]^{4-}$  precursor, the  $\text{Mo}^{\text{III}}$  ion is generally in a low-spin configuration and adopts a pentagonal bipyramidal coordination geometry. This means that the value of magnetization when applying a magnetic field strongly depends on the orientation of this field with respect to the five-fold axis of the pentagonal bipyramid.

Slow diffusion of two aqueous solutions containing  $\text{K}_4[\text{Mo}^{\text{III}}(\text{CN})_7] \cdot 2\text{H}_2\text{O}$  and a  $\text{Mn}^{\text{II}}$  salt afforded two cyano-bridged bimetallic phases with formulas  $[\text{Mn}_2(\text{H}_2\text{O})_5][\text{Mo}(\text{CN})_7] \cdot 4\text{H}_2\text{O}$  ( $\alpha$ -phase) and  $[\text{Mn}_2(\text{H}_2\text{O})_3][\text{Mo}(\text{CN})_7] \cdot 4.7\text{H}_2\text{O}$  ( $\beta$ -phase), respectively.<sup>116–118</sup> Single-crystal X-ray diffraction studies on these two phases reveal that both compounds crystallize in the monoclinic space group  $P2_1/c$ . The local environments of the metal sites are similar for both phases, but the three-dimensional organization is different. For both compounds, the unit cell contains one molybdenum site and two independent manganese sites. The molybdenum ion is surrounded by seven C—N—Mn linkages, and all cyano groups are bridging. The coordination polyhedron can be viewed as slightly distorted pentagonal bipyramidal. The two manganese ions are in distorted octahedral surroundings. The structure of the  $\alpha$ -phase is shown in Figure 20.

The three-dimensional structural arrangement of the  $\alpha$ -phase can be described as follows: edge-sharing lozenge motifs  $(\text{MoCNMnINC})_2$  form bent ladders running along the  $a$  direction. Each ladder is linked to four other ladders of the same type along the  $[011]$  and  $[0\bar{1}\bar{1}]$  directions through cyano bridges. These ladders are further connected by  $\text{Mn}_2(\text{CN})_3(\text{H}_2\text{O})_3$  groups. A Mn2 is linked to a Mo site of one of the ladders and to two Mo sites of an adjacent ladder. In the case of the  $\beta$ -phase, each ladder is made up of edge-sharing lozenge motifs that are surrounded by two instead of four

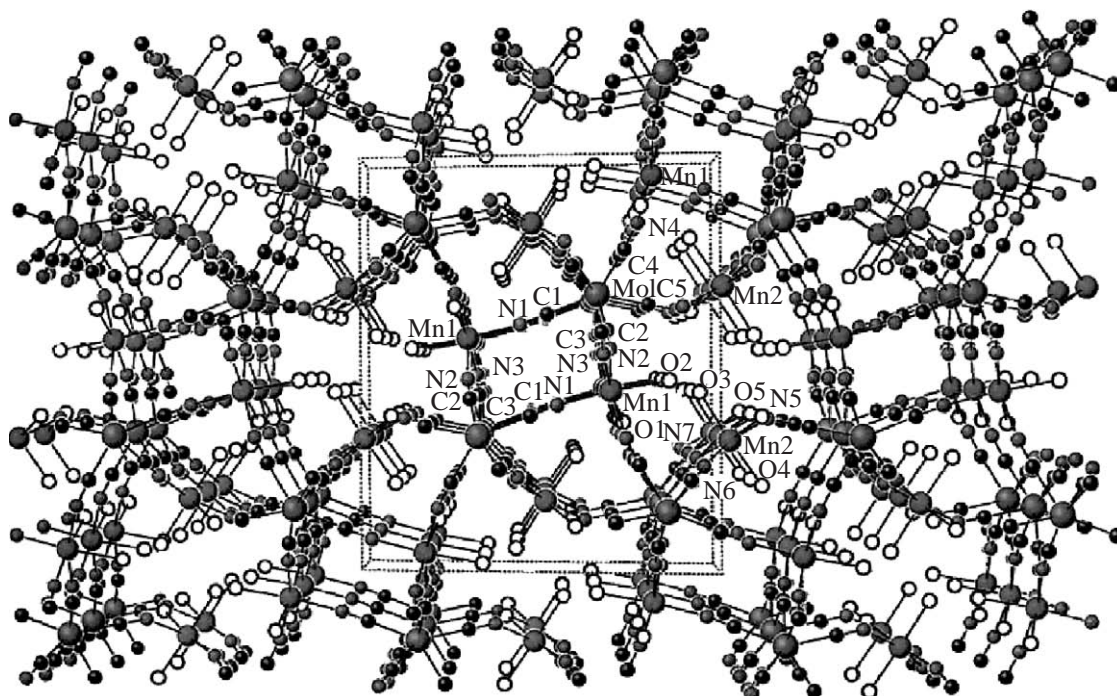


Figure 20 Crystal structure of  $\text{Mn}(\text{H}_2\text{O})_5\text{Mo}(\text{CN})_7 \cdot 4\text{H}_2\text{O}$  ( $\alpha$ -phase).<sup>121</sup>

identical ladders. Magnetic measurements reveal that both phases exhibit a long-range magnetic ordering at  $T_c = 51$  K, with a pronounced magnetic anisotropy in the magnetically ordered phase.

When the slow diffusion between aqueous solutions containing  $\text{K}_4[\text{Mo}^{\text{III}}(\text{CN})_7] \cdot 2\text{H}_2\text{O}$  and  $[\text{Mn}(\text{H}_2\text{O})_6](\text{NO}_3)_2$  was carried out in the presence of an excess of  $\text{K}^+$  ions, a new two-dimensional compound of formula  $\text{K}_2[\text{Mn}_3(\text{H}_2\text{O})_6][\text{Mo}(\text{CN})_7]_2 \cdot 6\text{H}_2\text{O}$  was obtained.<sup>119</sup> The two-dimensional structure has been characterized by single-crystal X-ray crystallography. Once again this compound contains one unique molybdenum site along with two manganese sites. Each molybdenum ion is surrounded by six  $-\text{C}-\text{N}-\text{Mn}$  linkages and a terminal CN ligand. The geometry may be described as a strongly distorted pentagonal bipyramid, as both the  $\text{Mo}-\text{CN}$  and  $\text{CN}-\text{Mn}$  bridging angles deviate significantly from  $180^\circ$ . In the case of the Mn ions, they are surrounded by four  $\text{NC}-\text{Mo}$  linkages, as well as two water molecules in a *trans* conformation. The two-dimensional structure is made of anionic double-sheet layers parallel to the *bc* plane.  $\text{K}^+$  ions and noncoordinated waters are found located between the layers. Each sheet is a type of grid in the *bc* plane made of edge-sharing lozenges of the type  $[\text{MoCNMn}_2\text{NC}]_2$ . Two parallel sheets of a layer are further connected by  $\text{Mn1}(\text{CN})_4(\text{H}_2\text{O})_2$  units situated between the sheets. Magnetic studies reveal that this compound exhibits ferromagnetic ordering at  $T_c = 39$  K, and that below  $T_c$  a field-induced spin reorientation occurs along the  $c^*$ -axis. No hysteresis was observed along *a* and *b*, while a narrow hysteresis of  $\sim 125$  Oe ( $9.95\% \cdot 10^3 \text{ A m}^{-1}$ ) was observed along  $c^*$  at 5 K. Kahn *et al.* have demonstrated that the magnetic properties of this compound can also be modified through partial dehydration.<sup>119</sup> After dehydration, the magnetic measurements strongly suggest that the crystallographic directions are retained. This compound once again exhibits ferromagnetic ordering; however, the critical temperature has been shifted to a higher temperature,  $T_c = 72$  K, compared to 39 K in the original hydrated sample. In order to investigate further the origin of the ferromagnetic coupling between the  $\text{Mn}^{\text{II}}$  and  $\text{Mo}^{\text{III}}$  ions through the cyano bridge in this compound a spin density study has been carried out. The nuclear structure at 50 K, just above the ordering temperature, has been determined from unpolarized neutron diffraction measurements.<sup>120</sup> The spin density maps were reconstructed and, surprisingly, opposite signs of the spin densities were observed on the metal ions, consistent with antiferromagnetic  $\text{Mn}^{\text{II}}\text{Mo}^{\text{III}}$  interactions through the cyanide bridge. Kahn *et al.* report that this contradiction with the previously reported magnetization measurements on this material, which suggest predominantly ferromagnetic interactions, may be due to the uncertainty of the sample mass. Low-temperature magnetic measurements are in progress to clarify this situation.<sup>120</sup>

In order to lower the symmetry of the lattice further, the macrocycle 2,13-dimethyl-3,6,9,12,18-pentaazabicyclo[12.3.1]octadeca-1(18),2,12,14,16-pentaene (L) has been utilized to impose



heptacoordination on the Mn<sup>II</sup> sites.<sup>121</sup> This macrocycle is known to adopt a planar conformation and can thus stabilize a heptacoordinated Mn<sup>II</sup> species of the type [MnL(H<sub>2</sub>O)<sub>2</sub>]<sup>2+</sup> with pentagonal bipyramidal geometry.

Reaction of [Mo(CN)<sub>7</sub>]<sup>4-</sup> with [MnL(H<sub>2</sub>O)<sub>2</sub>]<sup>2+</sup> did not give the expected compound, but afforded the compound [Mn<sup>II</sup>L]<sub>6</sub>[Mo<sup>III</sup>(CN)<sub>7</sub>][Mo<sup>IV</sup>(CN)<sub>8</sub>]<sub>2</sub>·19.5H<sub>2</sub>O, in which two-thirds of the [Mo<sup>III</sup>(CN)<sub>7</sub>]<sup>4-</sup> groups have been oxidized to [Mo<sup>IV</sup>(CN)<sub>8</sub>]<sup>4-</sup>.<sup>121</sup> This compound crystallizes in a two-dimensional arrangement of edge-sharing 48-membered rings (Figures 21 and 22). Each ring has a heart shape, and contains 16 metal sites: 2 Mo1 sites located on a two-fold axis together with 6 Mo2, 4 Mn1, and 4 Mn3 sites occupying general positions.

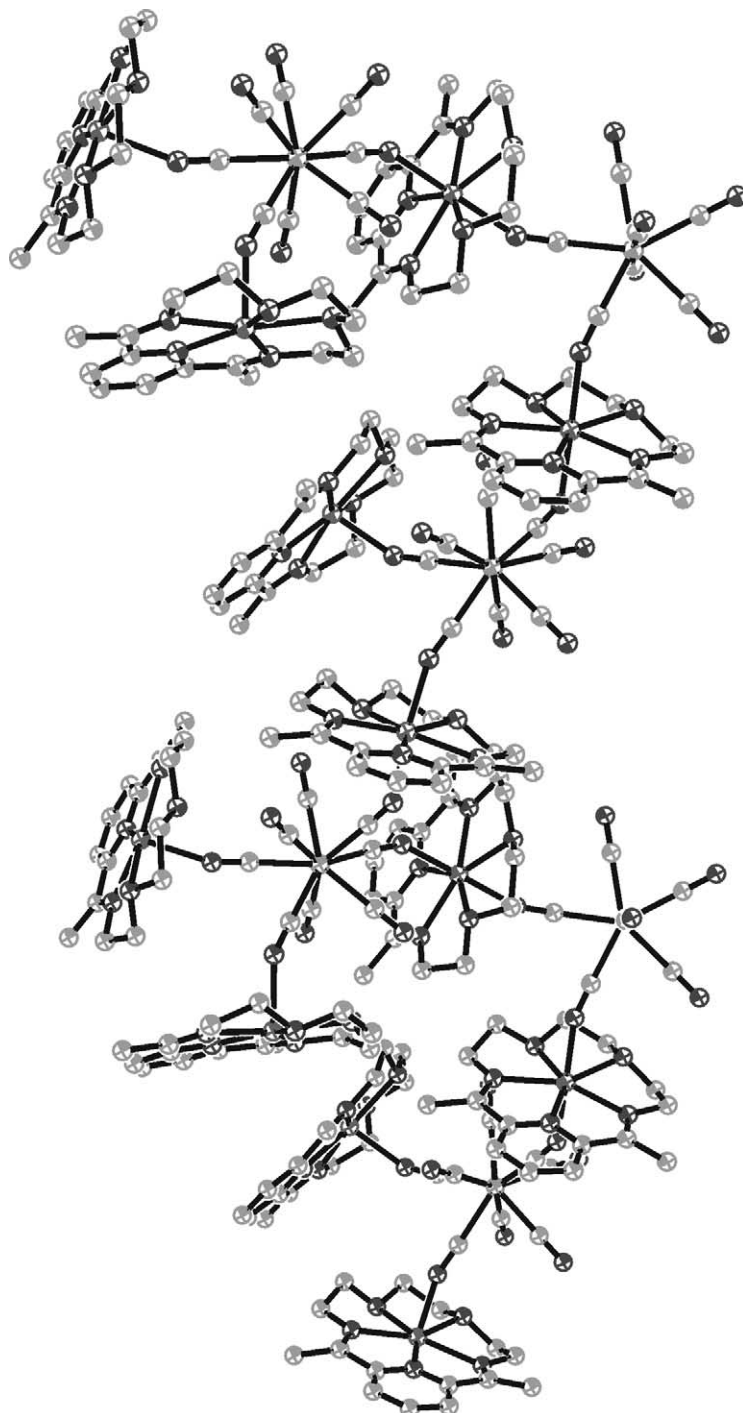


**Figure 21** Structure of a chain of stoichiometry [Mn<sup>II</sup>L]<sub>6</sub>[Mo<sup>III</sup>(CN)<sub>7</sub>][Mo<sup>IV</sup>(CN)<sub>8</sub>]<sub>2</sub>.<sup>121</sup>

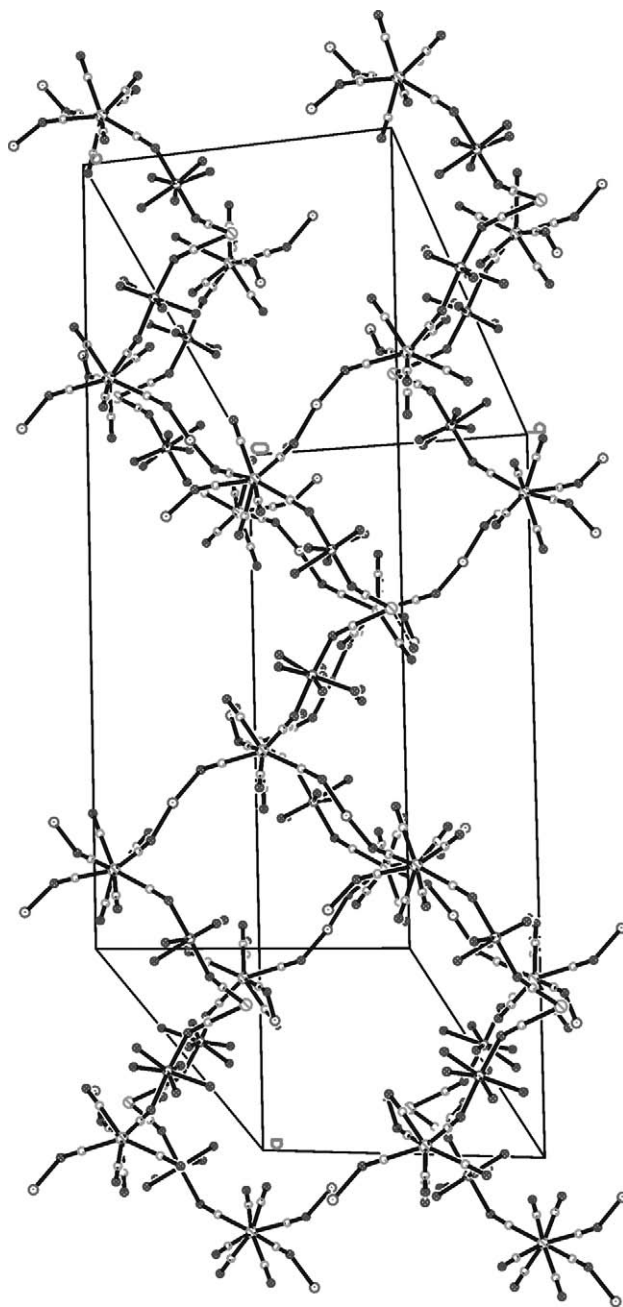


**Figure 22** Projection onto the  $ab$  plane for  $[\text{Mn}^{\text{II}}\text{L}]_6[\text{Mo}^{\text{III}}(\text{CN})_7][\text{Mo}^{\text{IV}}(\text{CN})_8]_2$ ; the macrocycles are omitted for clarity.

All of these sites are linked by cyano bridges: the carbon atoms being bound to the Mo ion and the nitrogen atoms to the manganese. The Mn2 site is linked to the Mo2 site through a cyano bridge, but is not directly involved in the ring. Noncoordinated water molecules occupy voids between the layers. The coordination sphere around the first molybdenum can be described as distorted pentagonal bipyramidal, whereas the second molybdenum has a lower symmetry closer to a square antiprism. All three manganese sites are surrounded by the five nitrogen atoms of the macrocycle in the equatorial plane. Two additional axial coordinating ligands complete a pentagonal bipyramidal geometry. Detailed magnetic studies indicate that this compound is a fully localized mixed-valence, mixed-spin species. The  $(\text{MnL})^{2+}$  groups are in three different crystallographic environments. In two cases, two axial  $N$ -coordinated cyano groups confer a low-spin state on the Mn1 and Mn3 ions. In the third case, one axial  $N$ -coordinated cyano group and an

axial water molecule confer a high-spin state on the Mn<sup>2+</sup> ion. Furthermore, the Mn<sup>2+</sup> ion is pulled out of the equatorial plane of the pentadentate ligand which diminishes the ligand field exerted by the macrocycle. It follows then that the local spins of the metal sites are  $S_{\text{Mo1}} = 1/2$ ,  $S_{\text{Mo2}} = 0$ ,  $S_{\text{Mn1}} = 1/2$ , and  $S_{\text{Mn}} = 5/2$ . Long-range ferromagnetic ordering is observed for this compound at 3 K. This low temperature is due to the fact that long-range ordering involves interactions not only through the cyano bridges, but also through the N—C—Mo<sup>IV</sup>—C—N bridging linkages that are very weak.

Reaction of  $[\text{Mo}(\text{CN})_7]^{4-}$  and Mn<sup>II</sup> ( $S = 5/2$ ) in the presence of a range of cations has afforded a series of new magnetic materials with stoichiometry  $(\text{cat})_2\text{Mn}_3(\text{H}_2\text{O})_3[\text{Mo}(\text{CN})_7]_2 \cdot n\text{H}_2\text{O}$  ( $\text{cat} = \text{K}^+$ ,  $\text{N}(\text{CH}_3)_4^+$ ,  $\text{Na}^+$ ,  $\text{NH}_4^+$ ).<sup>122</sup> A range of crystal structures displaying different magnetic properties has been obtained. One of the most interesting examples is the synthesis of  $[\text{N}(\text{CH}_3)_2\text{Mn}_3(\text{H}_2\text{O})_3[\text{Mo}(\text{CN})_7]_2 \cdot 2\text{H}_2\text{O}$  which exhibits the highest critical temperature, namely a ferromagnetic ordering at  $T_c = 86$  K, known for a structurally characterized compound assembled from Mn<sup>2+</sup> $[\text{Mo}(\text{CN})_7]^{4-}$  precursors.

#### 7.4.3.7 Octacyanometalate Building Blocks

Now that Prussian blue chemistry is enjoying an active revival, several independent groups are exploring the closely related octacyanometalate building block  $[\text{M}(\text{CN})_8]^{n-}$ , where M is a transition metal ion, for the self-assembly of novel supramolecular coordination compounds.<sup>123</sup> In each case, the information for the self-assembly of the entire structure is encoded into the individual building blocks due to their steric, topological, and intermolecular bonding capabilities. Furthermore, the inherent coordination preferences of the metal cation used in the assembly process are coupled together with the stereochemical flexibility of the octacyanometalate moiety. A survey of polytopal structures reveals that arrangements of three idealized eight-coordinate geometries, namely square antiprismatic, dodecahedron, and bicapped trigonal prismatic, are found to be essentially barrierless, hence transition among these structures occurs easily.<sup>101</sup>

##### 7.4.3.7.1 High-spin clusters

As previously highlighted, one of the most challenging issues in the field of molecule-based magnetism is the preparation of magnetic clusters with a designed topology and predictable properties. Along these lines, Decurtins and co-workers have structurally and magnetically characterized the novel cyano-bridged high-spin molecular cluster of stoichiometry  $[\text{Mn}^{\text{II}}\{\text{Mn}^{\text{II}}(\text{MeOH})_3\}_8(\mu\text{-CN})_{30}\{\text{Mo}^{\text{V}}(\text{CN})_3\}_6] \cdot 5\text{MeOH} \cdot 2\text{H}_2\text{O}$ , prepared by the self-assembly of  $[\text{Mo}^{\text{V}}(\text{CN})_8]^{3-}$  building blocks together with divalent metal ions (Figure 23).<sup>124</sup> The cluster is comprised of 15 cyano-bridged metal ions, namely 9 Mn<sup>II</sup> ions ( $S = 5/2$ ) and 6 Mo<sup>V</sup> ions ( $S = 1/2$ ), giving a total of 51 unpaired electrons within the cluster.

The Mo<sup>V</sup>—CN—Mn<sup>II</sup> geometry is such that the atoms are all linked to form an aesthetically pleasing topological pattern in which the polyhedron spanned by the peripheral metal ions is closest in geometry to a rhombic dodecahedron (Figure 24). Furthermore, in parallel studies Hashimoto and co-workers have also reported the synthesis of a Mn<sub>9</sub>W<sub>6</sub> cluster with an analogous structural topology.<sup>125</sup>

The magnetic properties of the Mn<sub>9</sub>Mo<sub>6</sub> cluster above 44 K are characterized by ferromagnetic intracluster coupling which finally leads to an  $S = 51/2$  ground state spin. In contrast to some high-spin clusters, this compound does not exhibit the typical phenomenon of molecular hysteresis and slow quantum tunneling at low temperatures. In this case, a competitive interplay of intra- and intercluster interactions leads to a very interesting magnetic regime. Unfortunately, a modeling of the magnetic data below 44 K, where bulk magnetic ordering seems to arrive, is not possible since this new situation has not been dealt with theoretically. Further experiments are needed before we can move forward in our understanding and interpretation of the magnetic data in the low-temperature regime. Interestingly, in contrast to these observations, antiferromagnetic intracluster interactions are reported for the Mn<sub>9</sub>W<sub>6</sub> cluster, which give rise to a smaller ground state spin value of  $S = 39/2$ .<sup>125</sup>

Although in both of the above cases the clusters exhibit large spin ground states, the magnetic anisotropy of these compounds is clearly too low. This has been assigned as being mainly due to the small anisotropy of the Mn<sup>II</sup> ions, together with the high symmetry of the cluster topology.

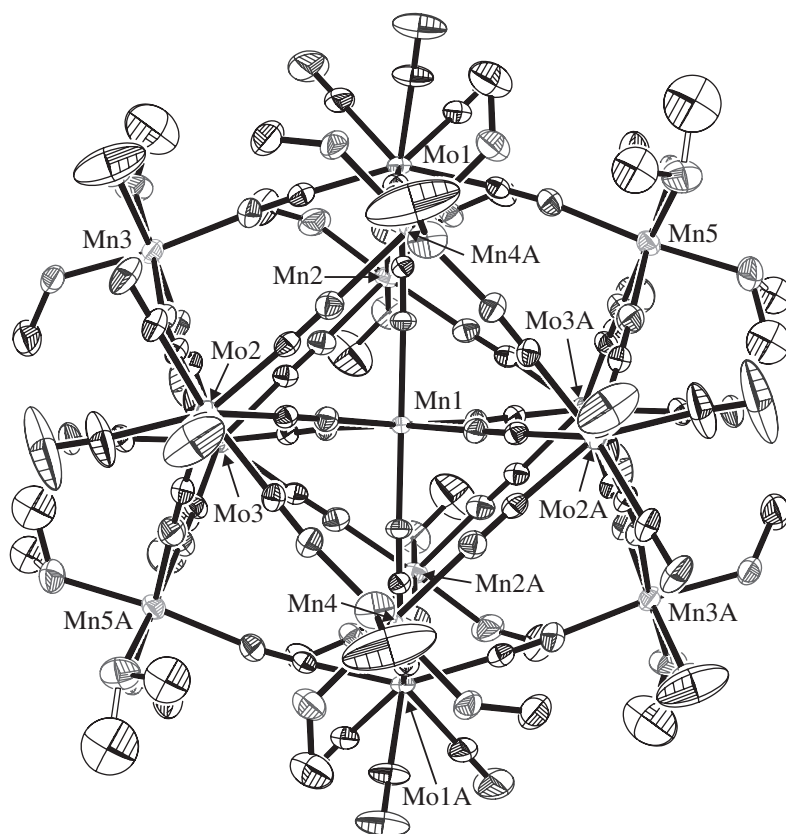


**Figure 23** ORTEP representation of the molecular structure of  $[\text{Mn}^{\text{II}}\{\text{Mn}^{\text{II}}(\text{MeOH})_3\}_8(\mu\text{-CN})_{30}\{\text{Mo}^{\text{V}}(\text{CN})_3\}_6]^{8-}$ ; for clarity only the  $\text{Mn}^{\text{II}}$  and  $\text{Mo}^{\text{V}}$  atoms are labeled and the H atoms are omitted.<sup>124</sup>

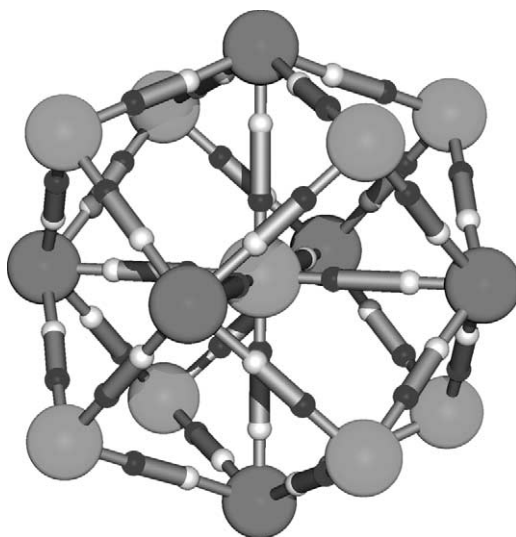


**Figure 24** Representation of an idealized  $[\text{Mn}^{\text{II}}_9(\mu\text{-CN})_{30}\text{-Mo}^{\text{V}}_6]$  cluster core. The light gray spheres represent  $\text{Mn}^{\text{II}}$  ions, the darker spheres represent  $\text{Mo}^{\text{V}}$  ions, and the bonds between them represent  $\mu$ -cyano ligands.<sup>124</sup>

As a consequence, these compounds do not behave as SMMs at temperatures down to 1.8 K. In order to address these problems this strategy has been extended, to replace Mn with Ni and prepare two new clusters of stoichiometry  $[\text{Ni}^{\text{II}}\{\text{Ni}^{\text{II}}(\text{MeOH})_3\}_8(\mu\text{-CN})_{30}\{\text{M}^{\text{V}}(\text{CN})_3\}_6]$ , where  $\text{M}^{\text{V}} = \text{Mo}$  or  $\text{W}$ .<sup>126</sup> These compounds are isostructural with the previously mentioned  $[\text{Mn}^{\text{II}}_9\text{-Mo}^{\text{V}}_6]$  cluster. Each cluster comprises 15 metal ions, 9  $\text{Ni}^{\text{II}}$  ions, and 6  $\text{M}^{\text{V}}$  ions, all linked by

$\mu$ -cyano ligands. Once again the compounds crystallize in the monoclinic  $C2/c$  space group, which means that the actual cluster has an overall  $C2$  symmetry with a crystallographic two-fold axis running through the central  $\text{Ni}^{\text{II}}$  ion. An extended intermolecular hydrogen bonded network connects each cluster to eight nearest neighbors. All the nearest-neighbor contacts between metal ions of different clusters are  $>7\text{\AA}$ . All terminal cyano and methanol ligands not involved in intercluster hydrogen bonding interactions take part in hydrogen bonding interactions to solvent molecules.

Magnetic susceptibilities and magnetization measurements on both single crystals as well as on the dissolved compounds indicate that the two clusters have an  $S=12$  ground state, originating from intracluster ferromagnetic exchange interactions between neighboring  $\mu$ -cyano-bridged  $\text{Ni}^{\text{II}}$  and  $\text{M}^{\text{V}}$  metal ions.<sup>126</sup> In AC magnetic susceptibility, no out-of-phase ( $\chi''_{\text{M}}$ ) signal in zero field down to 1.8 K was observed, indicating that the overall magnetic anisotropy in these compounds is still too low to class them as SMMs. These findings are also in accordance with the small uniaxial magnetic anisotropy value of  $D=0.015\text{ cm}^{-1}$ , estimated from high-field, high-frequency EPR measurements. From these observations it seems that the small single-ion magnetic anisotropy together with the highly symmetric arrangement of the metal ions in the cluster topology is still not favorable for the onset of SMM behavior.

In an attempt to change the solid-state structure of the cluster and perhaps reduce the crystal symmetry, Decurtins and co-workers have prepared an ethanol analogue of the  $\text{Mn}^{\text{II}}_9\text{Mo}^{\text{V}}_6$  cluster.<sup>127</sup> This new cluster has the stoichiometry  $[\text{Mn}^{\text{II}}\{\text{Mn}^{\text{II}}(\text{EtOH})_3\}_8(\mu\text{-CN})_{30}\{\text{Mo}^{\text{V}}(\text{CN})_3\}_6]\cdot 6\text{EtOH}\cdot\text{MeOH}$ , where larger ethanol molecules now complete the coordination sphere around the peripheral  $\text{Mn}^{\text{II}}$  ions. The molecular geometry of this compound has been determined by low-temperature single-crystal X-ray crystallography. The compound once again consists of cyanide-bridged  $\text{Mn}^{\text{II}}_9\text{Mo}^{\text{V}}_6$  units, with nine  $\text{Mn}^{\text{II}}$  ions defining a body-centered cube and six  $\text{Mo}^{\text{V}}$  ions constituting an octahedron. In contrast to the original cluster, this compound crystallizes in the triclinic space group  $P1$ , with a central  $\text{Mn}^{\text{II}}$  ion occupying each corner of the unit cell. Structurally, a slight change in the packing motif is observed which serves to better accommodate the more bulky ethanol molecules. In this case, each cluster is surrounded by six instead of eight nearest neighbors. This change in packing motif has had a subtle effect on the closest intercluster metal-metal contacts that are in the range 6.82–7.18  $\text{\AA}$  for  $\text{Mo}\cdots\text{Mn}$  and 7.36–8.23  $\text{\AA}$  for  $\text{Mn}\cdots\text{Mn}$ . Compared to the original cluster, the  $\text{Mo}\cdots\text{Mn}$  contacts are on average 0.4  $\text{\AA}$  shorter, whereas the  $\text{Mn}\cdots\text{Mn}$  interactions are 0.4  $\text{\AA}$  longer. The cluster-to-cluster distance (center-to-center) is found to be shorter for this compound, namely 17.2  $\text{\AA}$  compared to 17.5  $\text{\AA}$  for the first cluster. The intermolecular network of hydrogen bonding interactions has remained essentially intact; the ethanol ligands on neighboring clusters are simply not bulky enough to disturb these intercluster interactions. They are, in fact, well able to accommodate these interactions by twisting away from each other, thus minimizing steric interactions and enabling neighboring clusters to pack close together (Figure 25).

The shortest  $\text{O}\cdots\text{H}\cdots\text{N}$  contacts between adjacent clusters (2.74  $\text{\AA}$ ) are exactly within the range of hydrogen bonding interactions previously reported for the first cluster. Once again, each peripheral  $\text{Mn}^{\text{II}}$  ion in a cluster has one ethanol ligand that is involved in an intermolecular bond to the nitrogen of a cyano ligand in a neighboring cluster. All remaining terminal cyano and ethanol ligands are hydrogen bonded to solvent molecules. A detailed investigation of the magnetic properties of this cluster together with the preparation of new analogues is ongoing.

In parallel studies, Sieklucka and co-workers have also turned their attention to investigate the coordination architectures based on  $[\text{M}(\text{CN})_8]^{3-/4-}$  ( $\text{M}=\text{Mo}, \text{W}$ ) building blocks. The self-assembly of *cis*- $[\text{Mn}^{\text{II}}(\text{bpy})_2(\text{H}_2\text{O})_2]^{2+}$  together with  $[\text{W}^{\text{V}}(\text{CN})_8]^{3-}$  afforded the pentanuclear compound of stoichiometry  $[\text{Mn}^{\text{II}}(\text{bpy})_2][\text{Mn}^{\text{II}}(\text{bpy})_2(\text{H}_2\text{O})_2][\text{W}^{\text{V}}(\text{CN})_8]_2\cdot 7\text{H}_2\text{O}$ .<sup>128</sup> This pentanuclear molecule has a slightly distorted V-shape, with two  $\text{W}^{\text{V}}$  atoms linked by single cyano bridges to three  $\text{Mn}^{\text{II}}$  centers in the alternating sequence  $\text{Mn}-\text{W}-\text{Mn}-\text{W}-\text{Mn}$  (Figure 26). In the molecule, the central  $[\text{Mn}(\text{bpy})_2]^{2+}$  moiety is bound to two  $[\text{W}(\text{CN})_8]^{3-}$  ions through a single cyano bridge. Each of the  $[\text{W}(\text{CN})_8]^{3-}$  units is also coordinated to a terminal  $[\text{Mn}(\text{bpy})_2(\text{H}_2\text{O})]^{2+}$  moiety through a single cyano bridge. The Mn atoms are hexacoordinate and adopt a distorted octahedral geometry. In the crystal, the V-shaped molecules are packed into infinite columns due to head-to-head and arm-to-arm  $\pi-\pi$  stacking of the bipyridine rings of the terminal (“arms” of the pentamer) and the central (“head” of the pentamer) Mn atoms of neighboring molecules. Such an arrangement leads to a chain-like structure consisting of columns of pentamers clutched alternately with their “heads” and “arms” forming linear tubes, where  $\text{H}_2\text{O}$  molecules are located.<sup>128</sup> This compound exhibits intramolecular antiferromagnetic coupling between  $\text{Mn}^{\text{II}}$  and  $\text{W}^{\text{V}}$  centers consistent with a ground state spin of  $S=13/2$  and a ferromagnetic long-range transition at 0.66 K.

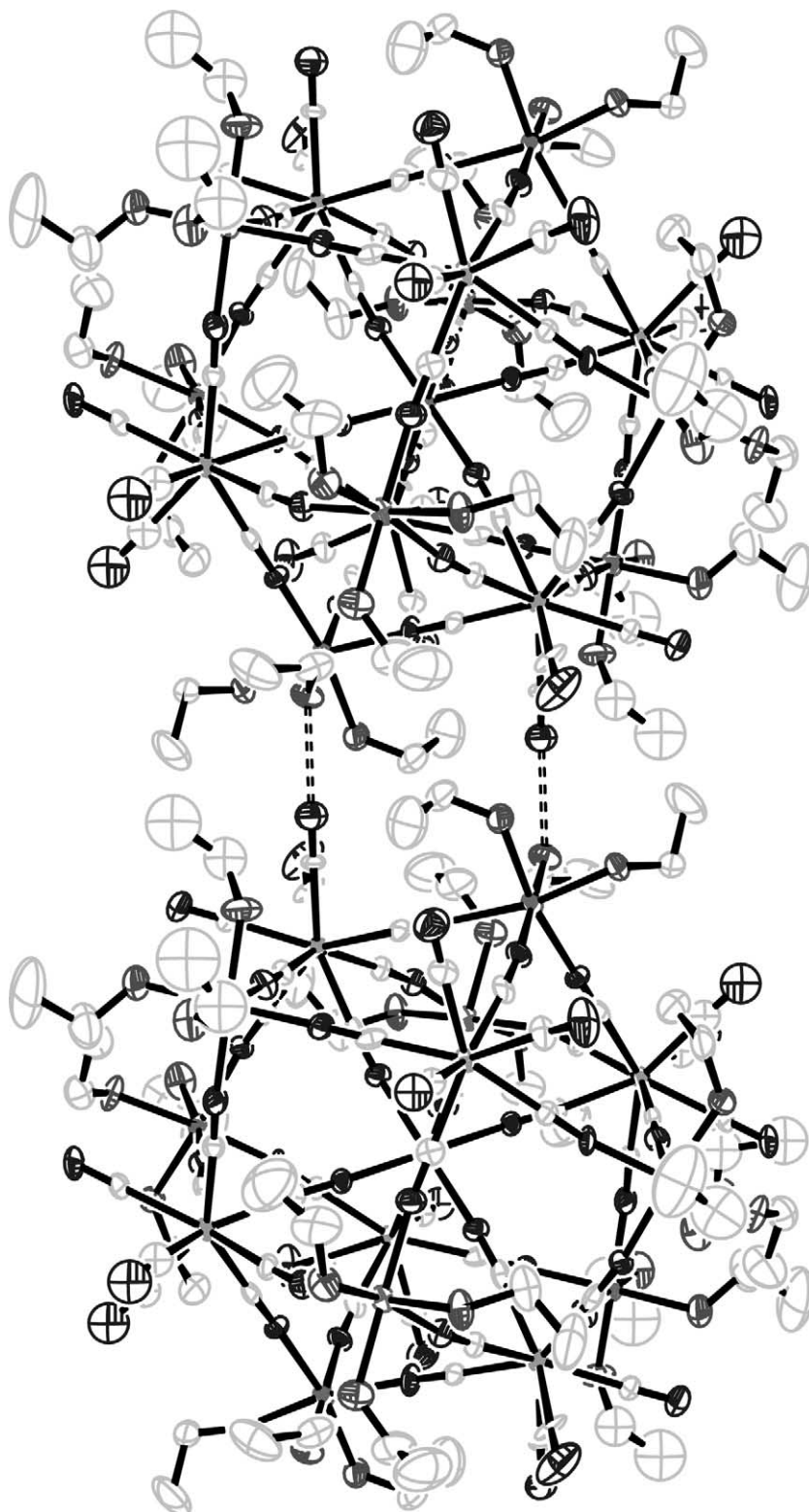


**Figure 25** ORTEP representation of two nearest-neighbor clusters with ethanol ligands on the outer  $\text{Mn}^{\text{II}}$  ions. H atoms are omitted for clarity. Dotted lines represent the shortest  $\text{O}-\text{H}\cdots\text{N}$  contacts (2.74 Å) between adjacent clusters.

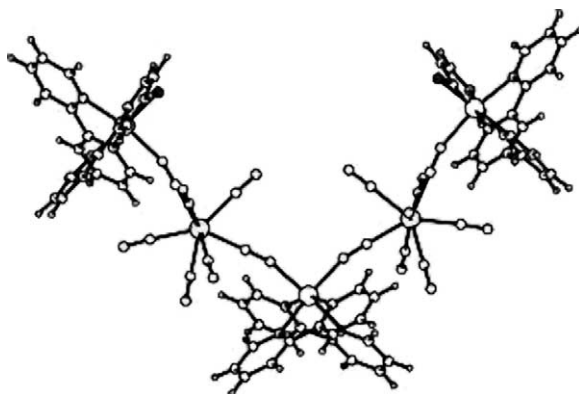


**Figure 26** View of  $[\text{Mn}^{\text{II}}(\text{bpy})_2][\text{Mn}^{\text{II}}(\text{bpy})_2(\text{H}_2\text{O})_2][\text{W}^{\text{V}}(\text{CN})_8]_2 \cdot 7\text{H}_2\text{O}$  along the  $a$ -axis.

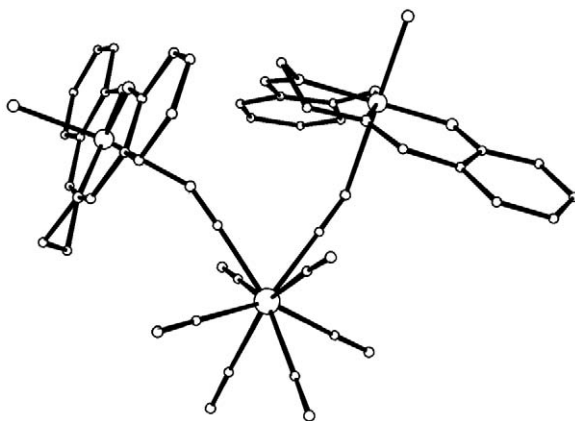


**Figure 27** Structure of the  $\{[\text{Mn}^{\text{III}}(\text{salen})\text{H}_2\text{O}]_2[\text{W}^{\text{V}}(\text{CN})_8]\}^-$  anion showing the bent cyano bridges.

Reaction of *trans*-directing  $[\text{Mn}^{\text{III}}(\text{salen})\text{H}_2\text{O}]^+$ , where  $\text{salenH}_2 = N,N'$ -bis(salicylidene)ethylenediamine, with  $[\text{W}^{\text{IV}}(\text{CN})_8]^{4-}$  resulted in the formation of a discrete  $[\text{Mn}^{\text{III}}(\text{salen})\text{H}_2\text{O}]_3[\text{W}^{\text{V}}(\text{CN})_8] \cdot \text{H}_2\text{O}$  species.<sup>101</sup> This complex consists of a trinuclear  $\{[\text{Mn}^{\text{III}}(\text{salen})\text{H}_2\text{O}]_2[\text{W}^{\text{V}}(\text{CN})_8]\}^-$  anion and a  $[\text{Mn}^{\text{III}}(\text{salen})\text{H}_2\text{O}]^+$  counteranion. Within the trinuclear unit, the W center adopts a distorted square antiprismatic geometry and has six terminal and two bridging cyano ligands, whereas the  $[\text{Mn}^{\text{III}}(\text{salen})\text{H}_2\text{O}(\text{NC})]^+$  units have a distorted octahedral geometry (Figure 27).

The W center is linked to two  $[\text{Mn}^{\text{III}}(\text{salen})\text{H}_2\text{O}]^+$  moieties through its two adjacent cyano corners of the triangular face of a square antiprism. The Mn—N—C linkages are exceptionally long and strongly bent. In the crystal the V-shaped trinuclear anions and isolated  $[\text{Mn}^{\text{III}}(\text{salen})\text{H}_2\text{O}]^+$  cations are packed separately into infinite columns stabilized by the face-to-face  $\pi$ – $\pi$  stacking of the salen rings. Such an arrangement leads to a broken wave-like structure (Figure 28).<sup>101</sup>

This compound exhibits intramolecular antiferromagnetic coupling between the  $\text{Mn}^{\text{III}}$  and  $\text{W}^{\text{V}}$  metal ions, consistent with a ground state spin  $S = 7/2$ , together with a ferromagnetic long-range transition at 6 K.

#### 7.4.3.7.2 One-dimensional compounds

A one-dimensional chain of stoichiometry  $[\text{Mn}^{\text{II}}_2(\text{L})_2(\text{H}_2\text{O})][\text{Mo}^{\text{IV}}(\text{CN})_8] \cdot 5\text{H}_2\text{O}$  (L is the macrocyclic ligand 2,13-dimethyl-3,6,9,12,18-pentaazabicyclo[12.3.1]octadeca-1(18),2,12,14,16-pentane) has been prepared from the reaction of  $\text{K}_4[\text{Mo}^{\text{IV}}(\text{CN})_8] \cdot 2\text{H}_2\text{O}$  with the complex  $[\text{Mn}^{\text{II}}\text{L}(\text{H}_2\text{O})_2]\text{Cl}_2 \cdot 4\text{H}_2\text{O}$ .<sup>129</sup> This compound has been structurally characterized by X-ray crystallography and its photomagnetic properties have been studied. The compound crystallizes as a polymeric arrangement of zigzag chains of alternating Mn(L) and  $\text{Mo}(\text{CN})_8$  units with an additional M(L) unit linked to the Mo as a pendent arm. This compound is paramagnetic, but shows important modifications of its magnetic properties under UV light irradiation, resulting in the formation of

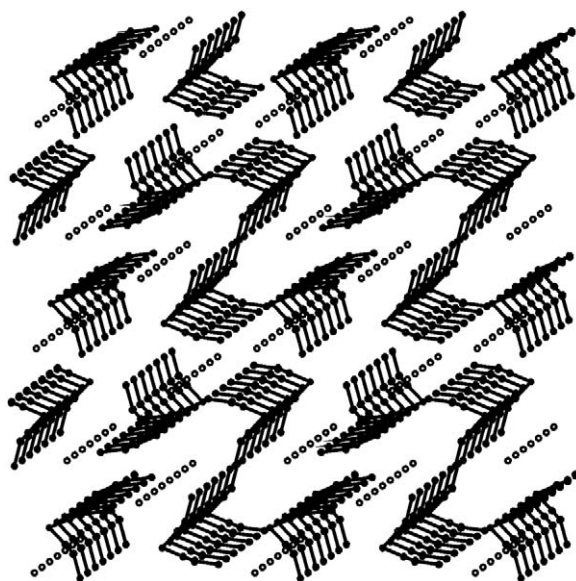


**Figure 28** Packing diagram of  $\{[\text{Mn}^{\text{II}}(\text{salen})\text{H}_2\text{O}]_2[\text{W}^{\text{V}}(\text{CN})_8]\cdot\text{H}_2\text{O}\}$  along the  $a$ -axis. For clarity only the skeleton of the  $\{[\text{Mn}^{\text{II}}(\text{salen})\text{H}_2\text{O}]_2[\text{W}^{\text{V}}(\text{CN})_8]\}^-$  and the Mn centers of the  $[\text{Mn}^{\text{II}}(\text{salen})(\text{H}_2\text{O})]^+$  counter-ions are shown.

ferrimagnetic chains. This nonreversible photomagnetic effect is thought to be caused by an internal photooxidation of a diamagnetic  $\text{Mo}^{\text{IV}}$  to a paramagnetic  $\text{Mo}^{\text{V}}$  ion. The crystallographic data indicate that the formation of hydrogen bonds between water molecules and neighboring nitrogen atoms of nonbridging cyano groups plays a key role in enabling the molybdenum photooxidation process to be observed.

The self-assembly of  $[\text{Cu}^{\text{II}}(\text{dien})(\text{H}_2\text{O})_2]^{2+}$  (dien = diethylenetriamine) and  $[\text{W}^{\text{V}}(\text{CN})_8]^{3-}$  in aqueous solution affords the one-dimensional chain of stoichiometry  $\{\text{W}^{\text{V}}[\text{CNCu}^{\text{II}}(\text{dien})\text{CN}]_4^{5+}\}_n$  whose 5+ charge is balanced by isolated  $[\text{W}(\text{CN})_8]^{3-}$  and  $\text{Na}^+$  counterions to give the compound of stoichiometry  $\text{Na}\{[\text{Cu}^{\text{II}}(\text{dien})]_4[\text{W}^{\text{V}}(\text{CN})_8]\}[\text{W}^{\text{V}}(\text{CN})_8]_2\cdot 8\text{H}_2\text{O}$ .<sup>101</sup> The core of the chain shown in Figure 29 is based on (i) square antiprismatic  $[\text{W}(\text{CN})_8]^{3-}$  units, with all cyano ligands involved in bridging to eight adjacent  $\text{Cu}^{\text{II}}$  sites, and (ii)  $[\text{Cu}(\text{dien})(\text{NC})_2]$  units of square pyramidal geometry, where N-bonded cyanides occupy the axial and equatorial sites.

The exact match of parallel squares of N-donors of the cyanides of  $\text{W}^{\text{V}}$  sites to the squares of  $\text{Cu}^{\text{II}}$  sites gives rise to a unique quadruple W-knotted cord-like pattern, formed by four bent threads of  $-\text{CN}-\text{Cu}(\text{dien})-\text{NC}-$  sequences knotted at the  $\text{W}^{\text{V}}$  centers. The geometry and orientation of copper centers limit the propagation of the polymer to one direction converging all threads to the neighboring tungsten node of the chain. Within the chain, the bridging  $[\text{W}(\text{CN})_8]^{3-}$  anion adopts a slightly distorted square antiprismatic geometry. The copper has a square pyramidal coordination, where the three nitrogen donors of the diene ligand occupy the equatorial positions. Two N donors of CN bridges from two neighboring W centers complete the pentacoordination sphere around the Cu ion. The cyanide groups have different bonding geometries: the equatorial bonds to the pyramidal copper are short, whereas the axial bonds are notably longer. These two sets of distances are related to the two different nonlinear geometries of the  $\text{W}-\text{CN}-\text{Cu}$  unit, being less bent in the equatorial shorter CN bridges and significantly more bent in the longer axial CN bridges. These two distinguishable types of  $\text{M}-\text{CN}-\text{Cu}$  ( $\text{M}=\text{nd}$

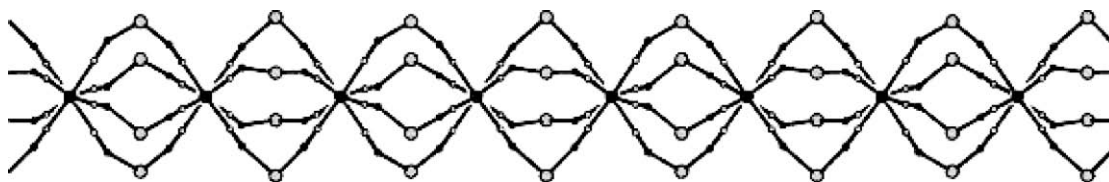


**Figure 29** Projection of the backbone of the chain  $\{\text{M}^{\text{V}}[-\text{CN}-\text{Cu}^{\text{II}}(\text{dien})-\text{CN}-]_4\}_n$  in  $\text{Na}\{[\text{Cu}^{\text{II}}(\text{dien})]_4[\text{M}^{\text{V}}(\text{CN})_8]\}[\text{M}^{\text{V}}(\text{CN})_8]_2\cdot 8\text{H}_2\text{O}$  ( $\text{M}=\text{Mo}, \text{W}$ ) along the  $b$ -axis.



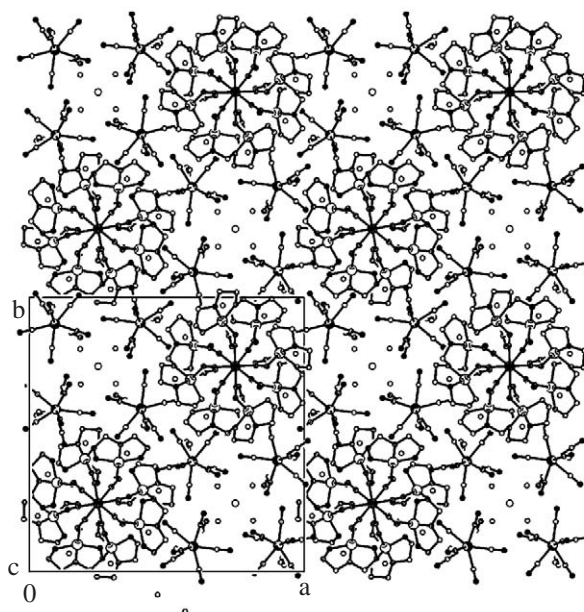


**Figure 30** Projection of the compound  $\text{Na}\{[\text{Cu}^{\text{II}}(\text{dien})_4][\text{M}^{\text{V}}(\text{CN})_8]\}[\text{M}^{\text{V}}(\text{CN})_8]_2 \cdot 8\text{H}_2\text{O}$  ( $\text{M} = \text{Mo}, \text{W}$ ) along the  $c$ -axis (parallel to the axis of the chain and perpendicular to the square planes of the bridging antiprismatic  $[\text{M}(\text{CN})_8]^{3-}$ ) showing the chain, nonbridging  $[\text{M}(\text{CN})_8]^{3-}$  anions,  $\text{Na}^+$  cations, and the lattice water molecules.

metal ion) linkages are fairly common for cyano-bridged assemblies based on square pyramidal copper complexes.<sup>130,131</sup> The projection of the molecular entity in the lattice is presented in Figure 30. The isolated  $[\text{W}(\text{CN})_8]^{3-}$  ions are distorted from an ideal square antiprismatic geometry.

The  $\text{Na}^+$  cations are located within the “cages” formed by the N atoms of isolated  $[\text{W}(\text{CN})_8]^{3-}$  units and the oxygen atoms of waters. Water molecules are located within the “tubes” formed by isolated  $[\text{W}(\text{CN})_8]^{3-}$  units, parallel to the  $c$ -axis, and are located around the tungsten knots of the chain. The molybdenum analogue of stoichiometry  $\text{Na}\{[\text{Cu}^{\text{II}}(\text{dien})_4][\text{Mo}^{\text{V}}(\text{CN})_8]\}[\text{Mo}^{\text{V}}(\text{CN})_8]_2 \cdot 8\text{H}_2\text{O}$  was found to be isomorphous.<sup>101</sup>

The magnetic behavior is consistent with two isolated paramagnetic  $[\text{W}^{\text{V}}(\text{CN})_8]^{3-}$  entities and  $\text{W}\text{Cu}_4$  pentanuclear units with a weak ferromagnetic intraunit interaction between the W and Cu metal ions, and a very weak antiferromagnetic interaction between neighboring  $\text{W}\text{Cu}_4$  units. The weak ferromagnetic interaction is due to the orthogonality of the  $\text{W}(d_{z^2})$  and  $\text{Cu}(d_{x^2-y^2})$  orbitals through the long  $\text{W}-\text{C}-\text{N}-\text{Cu}$  bridges, whereas the very weak antiferromagnetic coupling can be assigned to a weak overlap between the  $\text{W}(d_{z^2})$  and  $\text{Cu}(d_{x^2-y^2})$  magnetic orbitals over the shorter  $\text{W}-\text{C}-\text{N}-\text{Cu}$  pathway.

Reaction between  $[\text{Cu}(\text{tetren})]^{2+}$  and  $[\text{W}^{\text{V}}(\text{CN})_8]^{3-}$  precursors in a  $\text{Cu}:\text{W} = 3:2$  molar ratio in aqueous solution at pH 7.0 usually affords  $[\text{Cu}^{\text{II}}(\text{tetrenH}_2)]^{4+}$  precursors.<sup>101</sup> However, the actual product obtained in this case has the stoichiometry  $[\text{Cu}^{\text{II}}(\text{tetrenH}_2)]_4[\text{W}^{\text{IV}}(\text{CN})_8]_4 \cdot 10\text{H}_2\text{O}$  and contains a spontaneously reduced tungsten(IV) center. The structure of this compound comprises of cyano-bridged  $\text{W}_2\text{Cu}_2$  squares joined by single cyano bridges into an infinite one-dimensional polymer giving rise to a necklace pattern (Figure 31).<sup>132</sup>

There are two types of  $\text{W}_2\text{Cu}_2$  squares with alternating  $\text{W}-\text{Cu}$  corners. The first  $\text{W}_2\text{Cu}_2$  subunit contains W centers of distorted dodecahedral geometry with three bridging cyano ligands and pentacoordinated Cu centers, whereas the second consists of W centers with two bridging cyano ligands and hexacoordinated Cu centers. The blocking tetren ligand is coordinated by three central nitrogen donor atoms to Cu atoms in equatorial positions, while the remaining terminal nitrogens of the tetren ligand are protonated and uncoordinated. The  $[\text{Cu}^{\text{II}}(\text{tetrenH}_2)(\text{NC})_2]^{2+}$  units adopt a square pyramidal geometry with bent  $\text{N}$ -bonded cyanides occupying the axial and equatorial sites. The  $\text{mer}-[\text{Cu}^{\text{II}}(\text{tetrenH}_2)(\text{NC})_3]^+$  units adopt a distorted octahedral geometry, with almost linear equatorial and strongly bent axial cyano bridges. The terminal amino groups of the tetren ligand, terminal cyano ligands, and water molecules are involved in hydrogen bonds stabilizing the internal structure of the chain.

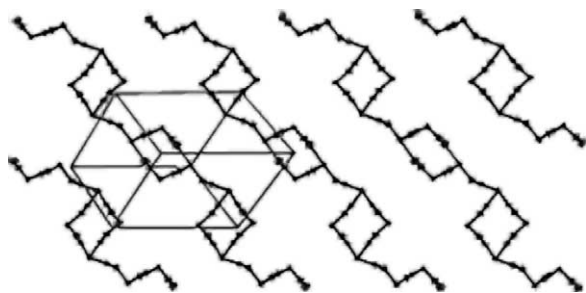


**Figure 31** Representation of the one-dimensional cyanide-bridged polymer of stoichiometry  $[\text{Cu}^{\text{II}}(\text{tetrenH}_2)_4][\text{W}^{\text{IV}}(\text{CN})_8]_4 \cdot 10\text{H}_2\text{O}$  (pH = 7). The structure is composed of  $\text{W}_2\text{Cu}_2$  squares joined through  $\text{CN}^-$  bridges. The lattice  $\text{H}_2\text{O}$  molecules are omitted for clarity.



**Figure 32** Representation of a one-dimensional cyanide-bridged polymer comprised of a long and short three-row wall pattern, for the compound of stoichiometry  $[\text{Cu}^{\text{II}}(\text{tetrenH}_2)_4][\text{W}^{\text{IV}}(\text{CN})_8]_4 \cdot 10\text{H}_2\text{O}$  (pH = 3.5).

The same molecular building blocks,  $[\text{Cu}^{\text{II}}(\text{tetrenH}_2)]^{4+}$  and either  $[\text{W}^{\text{V}}(\text{CN})_8]^{3-}$  or  $[\text{W}^{\text{IV}}(\text{CN})_8]^{4-}$  in a Cu:W = 3:2 molar ratio at pH 3.5, afford a second type of compound with stoichiometry  $[\text{Cu}^{\text{II}}(\text{tetrenH}_2)_4][\text{W}^{\text{IV}}(\text{CN})_8]_4 \cdot 10\text{H}_2\text{O}$  that crystallizes as a one-dimensional chain comprised of a long and short, three-row, brick wall-like pattern (Figure 32).<sup>132</sup>

The wall is comprised of fused  $\text{W}_2\text{Cu}_2$  squares forming the central row and  $\text{W}_3\text{Cu}_3$  distorted rectangles forming two external rows. There are two different types of W centers both with distorted square antiprismatic geometries; the first  $\text{W}_2\text{Cu}_2$  subunit contains W centers with four bridging cyano ligands, whereas the  $\text{W}_3\text{Cu}_3$  rectangle contains W centers with either four or two bridging cyano ligands. The Cu sites are bound to a *mer*-tetrenH<sub>2</sub> ligand and are hexacoordinate. The *mer*- $[\text{Cu}^{\text{II}}(\text{tetrenH}_2)(\text{NC})_3]^+$  in the  $\text{W}_2\text{Cu}_2$  subunit has one bent equatorial and two bent axial cyano bridges. The  $\text{W}_3\text{Cu}_3$  rectangle contains *mer*- $[\text{Cu}^{\text{II}}(\text{tetrenH}_2)(\text{NC})_3]^+$  units as well as a Cu site which is coordinated via one short and almost linear equatorial CN bridge, as well as two significantly bent axial bridges. The terminal cyano ligands of the  $[\text{W}(\text{CN})_8]^{4-}$  are involved in a network of hydrogen bonds linking parallel chains through the lattice water molecules.

Both compounds with the general formula  $[\text{Cu}^{\text{II}}(\text{tetrenH}_2)_4][\text{W}^{\text{IV}}(\text{CN})_8]_4 \cdot 10\text{H}_2\text{O}$ , obtained under different pH conditions, are examples of structural supramolecular isomers.<sup>133</sup> The components of the network remain the same, but they have a different superstructure and hence are effectively different compounds. The preference for one isomer over the other can be attributed to the substitutional reactivity of the  $[\text{Cu}(\text{tetren})]^{2+}$  precursor at different pH. Therefore, adjusting the pH of the reaction mixture can be an effective way of controlling the structural topology of these assemblies.

The assembly of  $[\text{W}(\text{CN})_8]^{3-}$  and  $[\text{Cu}(\text{tetren})]^{2+}$  building blocks in acidic aqueous conditions affords the compound of stoichiometry  $\{(\text{tetrenH}_5)_{0.8}\text{Cu}^{\text{II}}_4[\text{W}^{\text{V}}(\text{CN})_8]_4 \cdot 7.2\text{H}_2\text{O}\}_n$ .<sup>134</sup> This compound is comprised of anionic double layers of  $\{[\text{Cu}^{\text{II}}_4[\text{W}^{\text{V}}(\text{CN})_8]_4]^{4-}\}_n$  units, the charge of which is balanced by  $[\text{tetrenH}_5]^{5+}$  cations. Each  $[\text{W}(\text{CN})_8]^{3-}$  precursor adopts a bicapped trigonal prismatic geometry linked via CN bridges to five square pyramidal  $\text{Cu}^{\text{II}}$  centers. Four slightly bent equatorial cyanide bridges, Cu—N—C, give rise to the square-grid pattern of the single layer, while the practically linear axial—CN— bridge joins two layers and thus forms the double layer (Figure 33).

The double layer is thus formed by the two antiparallel stacked sheets of edge-sharing  $\text{Cu}(\text{NC}-\text{W})_5$  square pyramids. The cations and the water molecules lie in planes between the Cu—W double layers. The remaining three terminal CN ligands of the  $[\text{W}(\text{CN})_8]^{3-}$ , sticking out of the layer, are involved in an extensive network of hydrogen bonds that link parallel double layers through the lattice water molecules, stabilizing the overall structural topology. This compound exhibits soft ferromagnetic behavior with an ordering temperature  $T_c$  of 34 K. The ferromagnetic coupling can be rationalized in terms of the interactions of unpaired electrons originating from

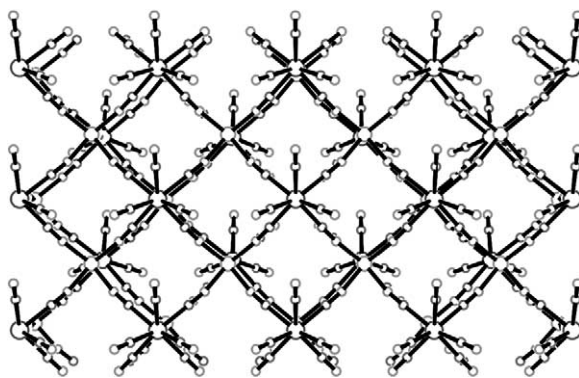


**Figure 33** Projection onto the *ac* crystallographic plane showing a square grid pattern of one double layer for the compound of stoichiometry  $\{(\text{tetrenH}_5)_{0.8}\text{Cu}^{\text{II}}[\text{W}^{\text{V}}(\text{CN})_8]_4 \cdot 7.2\text{H}_2\text{O}\}_n$ .

the mutually orthogonal  $3d_{x^2-y^2}$  orbital of the  $\text{Cu}^{\text{II}}$  together with the mixture of  $5d_{z^2}$  and  $5d_{x^2-y^2}$  ground state orbitals of the bicapped trigonal prismatic  $\text{W}^{\text{V}}$  center through both types of  $\text{Cu}-\text{NC}-\text{W}$  bridges.

#### 7.4.3.7.3 Two-dimensional compounds

Hashimoto and co-workers have prepared a novel cyano-bridged bimetallic complex composed of  $\text{Sm}(\text{H}_2\text{O})_5[\text{W}(\text{CN})_8]$  (Figure 34), showing, on cooling, rate dependent ferromagnetism.<sup>135</sup> The crystal structure of this compound consists of a two-dimensional cyanide-bridged network.

The neighboring sheets are in the same phase along the *c*-axis and the nearest sheet  $\text{Sm} \cdots \text{Sm}$  and  $\text{W} \cdots \text{W}$  separation is 7.329 Å. Variable temperature XRD spectra showed that at low temperature, the *a*- and *b*-axes increased by about 1%, and the *c*-axis decreased by about 5%. Moreover, a heat capacity anomaly was observed at 166 K. These results suggest that this compound undergoes a structural phase transition at 166 K. When the sample was slowly cooled from 300 K to 10 K at a rate of  $-1 \text{ K min}^{-1}$ , it showed antiferromagnetism with  $T_{\text{N}} = 3.0 \text{ K}$ . Conversely, when the sample was put directly into a sample chamber at 10 K, it showed ferromagnetism with  $T_{\text{c}} = 2.8 \text{ K}$  (Figure 35).

The self-assembly of  $[\text{Cu}^{\text{II}}(\text{dien})(\text{H}_2\text{O})_2]^{2+}$  and  $[\text{W}^{\text{IV}}(\text{CN})_8]^{4-}$  from an aqueous solution affords two-dimensional layers of stoichiometry  $\{[\text{Cu}^{\text{II}}(\text{dien})]_2[\text{W}^{\text{IV}}(\text{CN})_8] \cdot 4\text{H}_2\text{O}\}_n$ .<sup>101</sup> The crystal structure of this compound comprises tightly folded layers of a square grid-like topology (Figure 36).

Four tungsten centers are located at the corners and four Cu centers on the edges of the squares. Each  $[\text{W}^{\text{IV}}(\text{CN})_8]^{4-}$  adopts a square antiprismatic geometry and is linked to four Cu centers. The four cyano bridges are formed by  $\text{CN}^-$  groups occupying the corners of two adjacent triangular faces of a dodecahedron. The  $[\text{Cu}(\text{dien})(\text{CN})_2]$  units adopt a square pyramidal geometry, with N-bonded cyanides occupying one axial and one equatorial position. Similarly, as in  $\text{Na}\{[\text{Cu}^{\text{II}}(\text{dien})]_4[\text{W}^{\text{V}}(\text{CN})_8]\}[\text{W}^{\text{V}}(\text{CN})_8]_2 \cdot 8\text{H}_2\text{O}$ , the equatorial bridge is shorter and less bent than the axial one. The remaining four terminal  $\text{CN}^-$  ligands of  $[\text{W}^{\text{IV}}(\text{CN})_8]^{4-}$  that project out of the

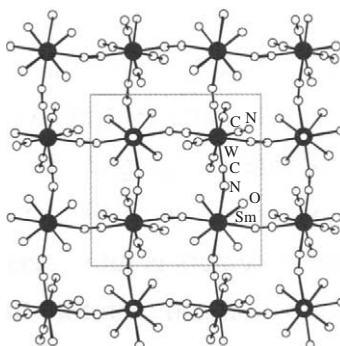


**Figure 34** Projection of the two-dimensional network  $\text{Sm}(\text{H}_2\text{O})_5[\text{W}(\text{CN})_8]$  on the *ab* plane.<sup>135</sup>

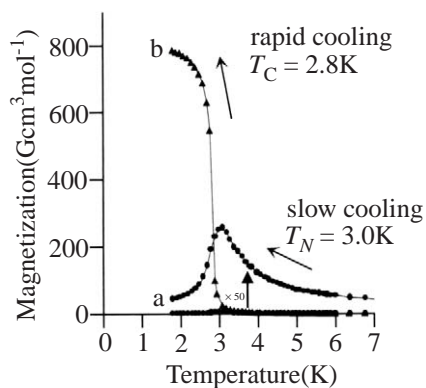


**Figure 35** FCM curves ( $H_0 = 10 \text{ G}$  ( $10^{-3} \text{ T}$ )) for the compound  $\text{Sm}(\text{H}_2\text{O})_5[\text{W}(\text{CN})_8]$ .

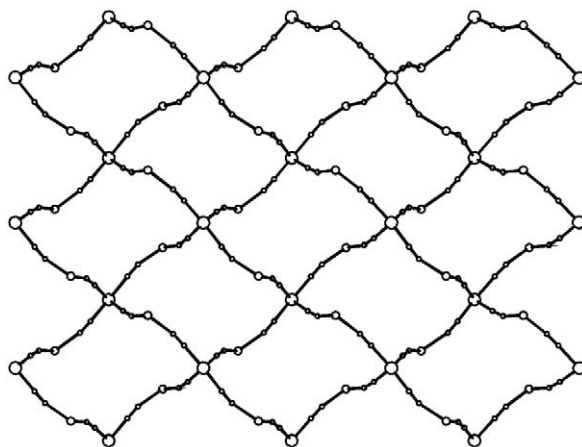


**Figure 36** View of the square grid pattern for the compound  $\{[\text{Cu}^{\text{II}}(\text{dien})]_2[\text{M}^{\text{IV}}(\text{CN})_8] \cdot 4\text{H}_2\text{O}\}_n$  ( $\text{M} = \text{Mo}, \text{W}$ ).

layer, together with the  $\text{RNH}_2$  groups from the diene ligand and the lattice water molecules are involved in an extensive network of hydrogen bonds that stabilize the structure. The molybdenum analogue  $[\text{Cu}^{\text{II}}(\text{dien})]_2[\text{Mo}^{\text{IV}}(\text{CN})_8] \cdot 4\text{H}_2\text{O}$  was found to be isomorphous.<sup>101</sup>

#### 7.4.3.7.4 Three-dimensional networks

One of the most interesting features of molecular-based materials is the way in which the magnetic properties may be transformed by quite small and subtle variations in the molecular chemistry. Working along these lines, Decurtins and co-workers have investigated the effects of changing the oxidation state of the metal in the octacyanometalate building block moving from  $\text{M}^{\text{V}}$  to  $\text{M}^{\text{IV}}$  ( $\text{M} = \text{Nb}, \text{Mo}, \text{W}$ ).<sup>136</sup> Hence, reaction of the appropriate octacyanometalate building block with an  $\text{M}^{\text{II}}$  salt afforded in all cases crystalline compounds which have been shown by single-crystal X-ray analysis to be cyano-bridged extended three-dimensional networks with a general stoichiometry of  $[\text{M}^{\text{IV}}\{(\mu\text{-CN})_4\text{M}^{\text{II}}(\text{H}_2\text{O})_2\}_2]$ . All compounds crystallize in the tetragonal space group  $I4/m$ , with one  $\text{M}^{\text{IV}}$  ion sitting on the crystallographic four-fold axis and a  $\text{M}^{\text{II}}$  ion, together with two coordinating water molecules occupying a crystallographic mirror plane. Figure 37 illustrates the molecular structure of the three-dimensional compound of stoichiometry  $[\text{W}^{\text{IV}}\{(\mu\text{-CN})_4\text{Fe}^{\text{II}}(\text{H}_2\text{O})_2\}_2]$ .<sup>137</sup>

The network comprises  $\text{W}^{\text{IV}}$  ions, which are connected to nearest-neighbor  $\text{Fe}^{\text{II}}$  ions through cyanide bridges in a three-dimensional grid-like arrangement. The  $\text{Fe}^{\text{II}}$  ions are in an octahedral environment, bonded to four nearest-neighbor  $\text{W}^{\text{IV}}$  ions; two axial water molecules complete the six-fold coordination.

Despite the structural similarities, the change in electronic ground state moving across the periodic table from  $\text{Nb}^{\text{IV}}$ , to  $\text{Mo}^{\text{IV}}$ , to  $\text{W}^{\text{IV}}$  confers two different classes of magnetic properties on

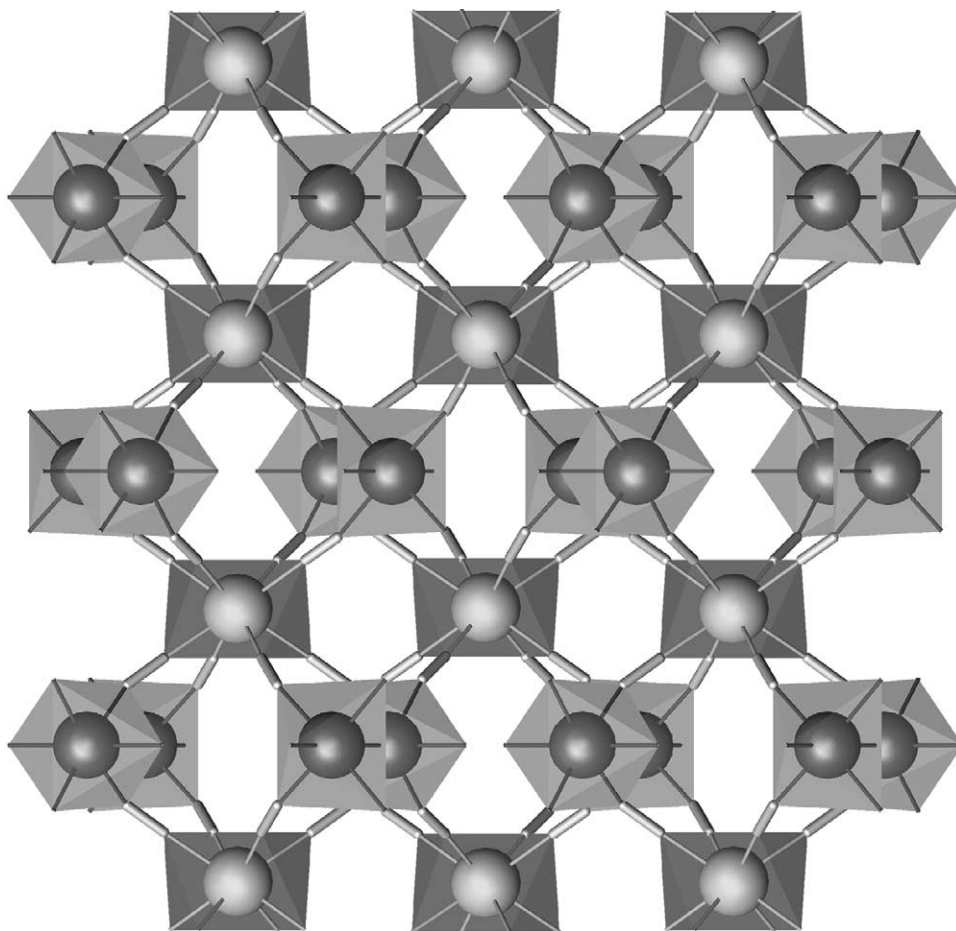


**Figure 37** View of the three-dimensional  $[\text{W}^{\text{IV}}\{(\mu\text{-CN})_4\text{Fe}^{\text{II}}(\text{H}_2\text{O})_2\}_2]$  network.<sup>137</sup>

these compounds. Due to the presence of the divalent metal ions, the networks incorporating the diamagnetic  $\text{Mo}^{\text{IV}}$  or  $\text{W}^{\text{IV}}$  metal ions are paramagnetic. However,  $\text{Nb}^{\text{IV}}$  has a  $d^1$  electronic configuration, hence a paramagnetic metal center and, accordingly, the three-dimensional networks which incorporate  $[\text{Nb}^{\text{IV}}(\text{CN})_8]^{4-}$  building blocks all show bulk magnetic behavior. Ongoing studies focus on the elucidation of the magnetic structures of this new class of three-dimensional materials, as well as detailed structural studies to develop a straightforward concept for the synthesis of new materials from cyanometalate building blocks, having a predictable structural order and a useful set of solid-state properties.

Hashimoto and co-workers have also turned their attention to characterizing the three-dimensional metal assemblies derived from  $[\text{M}(\text{CN})_8]^{3-}$  ( $\text{M} = \text{Mo}, \text{W}$ ) structurally and magnetically. The compound of stoichiometry  $[\text{Mn}^{\text{II}}_6(\text{H}_2\text{O})_9\{\text{W}^{\text{V}}(\text{CN})_8\}_4 \cdot 13\text{H}_2\text{O}]_n$  was synthesized from a hot aqueous solution containing octacyanotungstate,  $\text{Na}_3[\text{W}(\text{CN})_8] \cdot 3\text{H}_2\text{O}$  and  $\text{Mn}(\text{ClO}_4)_2 \cdot 6\text{H}_2\text{O}$ .<sup>138</sup> The compound crystallizes in the monoclinic space group  $P2_1/c$  and is comprised of a  $\text{W}^{\text{V}}\text{—CN—Mn}^{\text{II}}$  linked three-dimensional network (Figure 38).

There are two types of  $\text{W}^{\text{V}}$  sites: one is close to dodecahedral geometry with six bridging and two terminal CN ligands; the other is closer to a bicaeped trigonal prism with seven bridging and one terminal CN ligands. The field-cooled magnetization measurement showed that this compound exhibits a spontaneous magnetization below  $T_c = 54 \text{ K}$ . Further magnetization measurements on the field dependence indicate that it is a ferrimagnet where all of the  $\text{Mn}^{\text{II}}$  ions are antiparallel to all the  $\text{W}^{\text{V}}$  ions.

In parallel studies, reaction of  $\text{Fe}^{\text{II}}$  with the molybdenum octacyanide affords the  $\text{Fe}^{\text{II}}$ -based polycyanide  $[\text{Fe}_2(\text{H}_2\text{O})_4][\text{Mo}^{\text{IV}}(\text{CN})_8] \cdot 4\text{H}_2\text{O}$ .<sup>139</sup> This compound, although already known, has been structurally and magnetically characterized by Mathionière *et al.* The compound crystallizes in the tetragonal space group  $I422$ . There are two molybdenum sites in a distorted square antiprismatic arrangement, each site being surrounded by eight  $\text{CN—Fe}$  linkages. Four  $\text{NC—Mo}$  linkages and two axial water molecules give rise to a distorted octahedral coordination

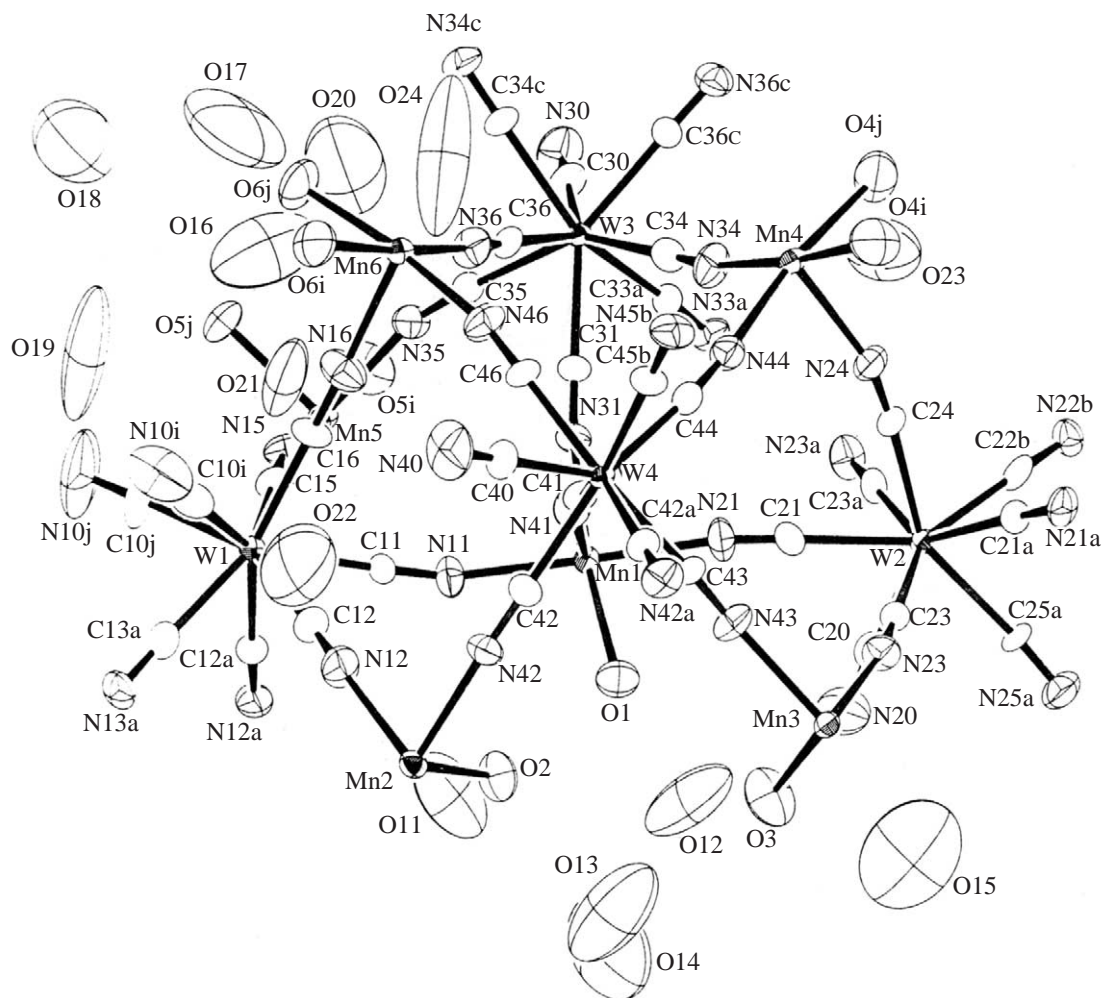


**Figure 38** Structure of  $\{\text{Mn}^{\text{II}}(\text{H}_2\text{O})\}_3\{\text{Mn}^{\text{II}}(\text{H}_2\text{O})_2\}_3\{\text{W}^{\text{V}}(\text{CN})_8\}_4 \cdot 13\text{H}_2\text{O}$ .<sup>138</sup>

geometry around the  $\text{Fe}^{\text{II}}$  ions. The structure is three-dimensional and highly symmetrical. This compound shows no evidence of long-range magnetic order, due to the diamagnetic  $\text{Mo}^{\text{IV}}$  ion, which suppresses the propagation of magnetic interactions between adjacent  $\text{Fe}^{\text{II}}$  ions through the CN bridges. These properties are in contrast to the  $\text{Fe}_2[\text{Mo}^{\text{III}}(\text{CN})_7] \cdot 8\text{H}_2\text{O}$  analogue which orders below 65 K as a ferrimagnet.<sup>139</sup> In other work Mathonière and co-workers have reported the structural and physical characterization of the compounds  $[\text{Cu}(\text{bipy})_2]_2\text{-}[\text{Mo}(\text{CN})_8] \cdot 5\text{H}_2\text{O} \cdot \text{CH}_3\text{OH}$  and  $\text{Cu}^{\text{I}}_2[\text{Mo}^{\text{IV}}(\text{CN})_8] \cdot 7.5\text{H}_2\text{O}$ .<sup>140</sup> The first compound crystallizes in the triclinic space group  $P\bar{1}$ . The structure consists of neutral trinuclear molecules in which a central  $[\text{Mo}(\text{CN})_8]^{4-}$  anion is linked to two  $[\text{Cu}(\text{bipy})_2]^{2+}$  cations through two cyanide bridges. Unfortunately, for the second compound the copper analogue crystallizes poorly so structural information was obtained via the wide-angle X-ray scattering (WAXS) technique. The compound crystallizes in an extended three-dimensional network for which the cyano groups act as bridges. An investigation of the magnetic properties reveals that both compounds behave as paramagnets. Under irradiation with light, they exhibit important modifications of their magnetic properties, with the appearance of magnetic interactions at low temperature. In the case of the first compound, the modifications are irreversible, whereas in the case of the second compound they are reversible. These photomagnetic effects are thought to be caused by the conversion of  $\text{Mo}^{\text{IV}}$  (diamagnetic) to  $\text{Mo}^{\text{V}}$  (paramagnetic) through a photooxidation mechanism for the first compound and a photoinduced electron transfer in the second. These results show that it is possible to apply a slightly different chemical strategy for the preparation of new photomagnetic extended systems using light-sensitive coordination compounds as molecular building blocks. To summarize, the choice of precursors must be guided by two criteria: first, their photoreactions must implicate a change in spin state; and second, they must contain bridging ligands.

Several other cyanometalate compounds for which the magnetic properties are switched between paramagnetism and ferromagnetism (or ferri magnetism) via photoirradiation have been reported by Hashimoto and co-workers.<sup>141</sup> In many cases detailed information with regard to the structural changes is not available as suitable single crystals could not be obtained. Nevertheless, single crystals of the compound  $\text{CsCoW}[(\text{CN})_8](3\text{-CNpy})_2$  (py = pyridine) have been obtained. This compound is paramagnetic, but switches to ferromagnetic below 30 K. The single-crystal X-ray structural analysis showed that this compound consists of a two-dimensional layer of cyanide-bridged cobalt(II)–tungstate(V), a  $\text{Cs}^{\text{I}}$  ion, and a  $\text{H}_2\text{O}$  molecule intercalated between the layers. The coordination geometries of the W and Co sites are bicapped trigonal prismatic and pseudooctahedral, respectively. This structure is preferred since the 3-cyanopyridine molecules cap the axial positions of the Co ion and hence only the equatorial positions are available for bridging with  $[\text{W}(\text{CN})_8]^{3-}$  units. Studies on the geometrical changes of this compound induced by photoirradiation are in progress.

#### 7.4.4 OTHER CYANOMETALATE PRECURSORS CONTAINING PARAMAGNETIC CENTERS

##### 7.4.4.1 Tetracyanometalates

The cyanide complex  $[\text{Mn}^{\text{II}}(\text{CN})_4]^{2-}$  prepared via the photochemical and thermal degradation of  $[\text{M}^{\text{IV}}(\text{CN})_6]^{2-}$  is the first member of a new class of paramagnetic, tetrahedral, coordinated cyanometalate building blocks.<sup>142–144</sup> The complex itself is fairly unusual since percyano complexes of first-row transition metals are well known to favor coordinatively saturated octahedral geometries. Occasionally, however, there are deviations from this trend. Several well-characterized nonoctahedral examples include  $[\text{V}^{\text{III}}(\text{CN})_7]^{4-}$ ,<sup>15,145,146</sup> the diamagnetic four-coordinate square planar  $d^8$   $[\text{M}^{\text{II}}(\text{CN})_4]^{2-}$  (M = Ni, Pd, Pt), and tetrahedral  $d^{10}$ , e.g., M =  $\text{Zn}^{\text{II}}$ ,  $\text{Cd}^{\text{II}}$ ,  $\text{Hg}^{\text{II}}$  complexes.<sup>22,29</sup> The rare  $d^7$  low-spin  $S = 1/2$  square planar  $[\text{Co}^{\text{II}}(\text{CN})_4]^{2-}$  complex provides a demonstration of the strong ligand field strength imposed by the cyanide ligand.<sup>146,147</sup>

It has been determined via magnetic susceptibility and EPR studies that the  $[\text{Mn}(\text{CN})_4]^{2-}$  precursor adopts a high ground state spin of  $S = 5/2$ , with an essentially temperature-independent moment of  $5.99 \mu_{\text{B}}$  and a Curie  $\theta$  value of 0 K. Miller and co-workers have exploited this compound as a building block for the assembly of new molecule-based materials.<sup>144</sup> The formation of this complex in both the solid state and solution has been studied. Due to dynamics and the lability of  $[\text{Mn}^{\text{II}}(\text{CN})_4]^{2-}$  in solution, its reaction with divalent first-row transition metal cations leads to the formation of lattice compounds with both tetrahedral and square planar local coordination geometries of the metal ions and multiple structural cyano-linkage isomers. The compound of stoichiometry  $\alpha\text{-Mn}^{\text{II}}[\text{Mn}^{\text{II}}(\text{CN})_4]$  has an interpenetrating sphalerite or diamond-like network structure, while a  $\beta$ -phase of this material has a noninterpenetrating disordered lattice containing tetrahedral  $[\text{Mn}^{\text{II}}(\text{CN})_4]^{2-}$ . Linkage isomerization or cyanide abstraction during formation results in  $\alpha\text{-Mn}^{\text{II}}[\text{Co}(\text{CN})_4]$  and  $[\text{Mn}^{\text{II}}(\text{Ni}^{\text{II}}(\text{CN})_4)]$  lattice compounds both containing square planar tetracyanometalate centres.  $\alpha\text{-Mn}^{\text{II}}[\text{Co}(\text{CN})_4]$  is irreversibly transformed to its  $\beta$ -phase in the solid state by heating to  $135^\circ\text{C}$ , which causes a geometric isomerization of  $[\text{Co}^{\text{II}}(\text{CN})_4]^{2-}$  from square planar ( $\nu_{\text{CN}} = 2,114 \text{ cm}^{-1}$ ,  $S = 1/2$ ) to tetrahedral ( $\nu_{\text{CN}} = 2,158 \text{ cm}^{-1}$ ,  $S = 3/2$ ) as evidenced by infrared and magnetic susceptibility measurements.  $\text{Mn}^{\text{II}}[\text{Ni}^{\text{II}}(\text{CN})_4]$  is the only phase formed with  $\text{Ni}^{\text{II}}$  due to the high thermodynamic stability of square planar  $[\text{Ni}^{\text{II}}(\text{CN})_4]^{2-}$ .<sup>144</sup>

##### 7.4.4.2 Dicyanometalates

The supramolecular chemistry of the dicyanoaurate  $[\text{Au}(\text{CN})_2]^-$  building block has been investigated by Leznoff and co-workers particularly in conjunction with paramagnetic transition metal cations.<sup>148</sup> This linear connecting unit forms polymers in a similar fashion to other anionic metal–cyanide precursors discussed in this chapter, but is unique in the respect that its central  $\text{Au}^{\text{I}}$  atom is prone to forming gold–gold bonds in the solid state. Although diamagnetic, the  $\text{Au}^{\text{I}}$  metal center is capable of propagating significant magnetic interactions, and, more importantly, can strongly influence the overall three-dimensional structure of compounds by forming aurophilic interactions. New inorganic coordination polymers of the form  $\text{M}(\text{pyrazine})[\text{Au}(\text{CN})_2]_2$  (M = Cu, Ni, Co) have been prepared.<sup>148</sup> The X-ray analysis of the  $\text{Cu}^{\text{II}}$  analogue revealed two

three-dimensional interpenetrating  $\alpha$ -polonium networks consisting of one-dimensional chains of Cu–pyrazine units connected by  $[\text{Au}(\text{CN})_2]$  bridges. The two networks are connected via weak aurophilic interactions ( $\text{Au}–\text{Au} = 3.4729(2) \text{ \AA}$ ). The cobalt and nickel analogues are reported to be isostructural to the copper one based on spectroscopic evidence. The magnetic susceptibility of the copper analogue shows a maximum in  $\chi_M$  at 5.0 K; these data could be fitted to the theoretical expressions for either a one- or a two-dimensional Heisenberg antiferromagnetic array ( $J = -2.74 \text{ cm}^{-1}$ ,  $g = 2.32$  and  $J = -3.25 \text{ cm}^{-1}$ ,  $g = 2.33$ , respectively). The magnetic susceptibility versus temperature data for the nickel and copper analogues showed effects primarily associated with single-ion zero field splitting; any weak antiferromagnetic coupling in these systems is very weak and, as a consequence, has not been quantified. In these cases the incorporation of  $[\text{Au}(\text{CN})_2]$  units does not significantly increase magnetic interactions.  $\text{Au} \cdots \text{Au}$  interactions between  $[\text{Au}(\text{CN})_2]$  units seem to be positive influences both for the formation of an interpenetrating structure and its subsequent stability, although unfortunately in this case, the interpenetrating nets do not interact magnetically.

#### 7.4.5 OXALATE-BASED TWO- AND THREE-DIMENSIONAL MAGNETS

The Decurtins group has shown that it is possible to develop a strategy for the self-assembly of supramolecular systems based on transition metal oxalates, which typically behave as host–guest compounds with different lattice dimensionalities.<sup>14,16,123,149,150</sup> All of these classes of structure are formally composed of metal–oxalate building blocks, and these compounds display a range of magnetic properties, since it is well known that the oxalate bridge is a good mediator of both antiferromagnetic and ferromagnetic interactions between paramagnetic metal ions.

##### 7.4.5.1 Basic Principles of Specific Two- and Three-dimensional Network Configurations

The multiple coordinating ability of the oxalate ion ( $\text{ox} = \text{C}_2\text{O}_4^{2-}$ ) has made it a useful and versatile choice as a bridging ligand for the design of two- and three-dimensional compounds. Indeed, the self-assembly of inorganic architectures incorporating oxalate ions as the bridging species has yielded various types of frameworks which include one-dimensional chains,<sup>151,152</sup> two-dimensional layers,<sup>153,154</sup> as well as three-dimensional networks.<sup>155</sup> All of these classes of structure are formally composed of  $[\text{M}^{z+}(\text{ox})_3]^{(6-z)-}$  building blocks, where each of these units represents a three-connected point (Figure 39).

As a consequence, it is the concept of connectivity that is important to address since it is the connectivity that defines the way in which a set of points are connected to construct a lattice which can be infinite in one, two, or three dimensions. In the following discussion, we focus on the fundamental ideas that are relevant to the formation of the two- and three-dimensional framework topologies.

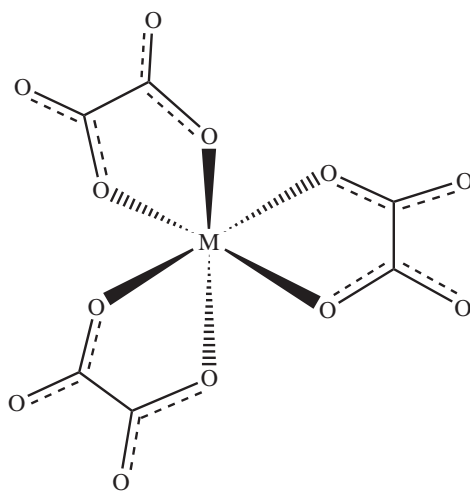


**Figure 39** Schematic representation of the chiral (the  $\Lambda$  isomer is shown) preorganized anionic coordination entity.



Oxalate building blocks can in principle polymerize in two ways. The first alternative leads to a two-dimensional honeycomb layered structure, whereas the second possible arrangement results in the formation of an infinite three-dimensional framework. In the former case, building blocks of opposite chirality are alternately linked which confines the bridged metal ions to lie within a plane (Figure 40(a)) and results in the formation of a two-dimensional layered motif (Figure 41). In contrast, an assembly of building blocks of the same chiral configuration (Figure 40(b)) leads to the three-dimensional framework shown in Figure 42.

After having considered the way in which the chirality of the subunits can influence the lattice dimensionality, it is then possible to apply a series of topological rules to define the number of building blocks that are needed to build closed circuits and, hence, extended framework motifs.

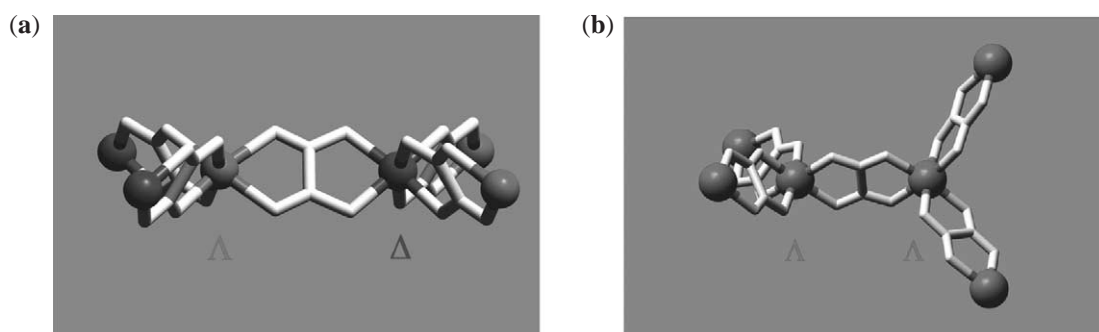


**Figure 40** Chiral  $[M^{z+}(ox)_3]^{(6-z)-}$  building blocks assembled with (a) alternating chiral configuration and (b) equal chiral configuration.

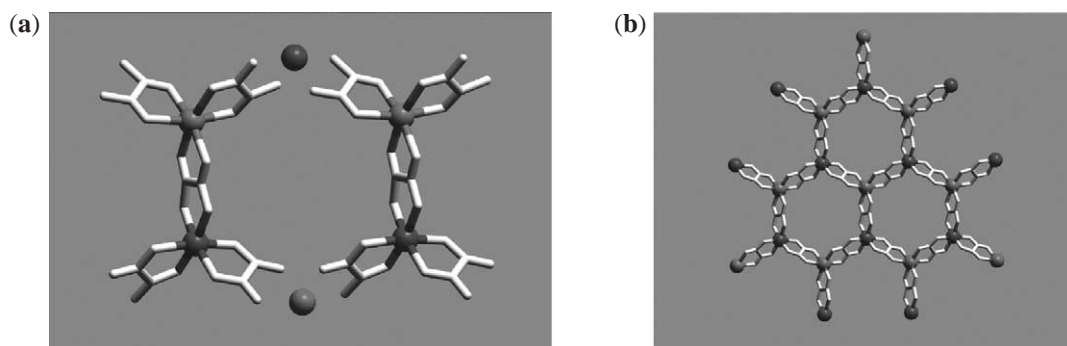


**Figure 41** (a) Two dimeric units of the alternating chirality type are necessary to form a closed hexagon ring; (b) the resulting planar network motif.

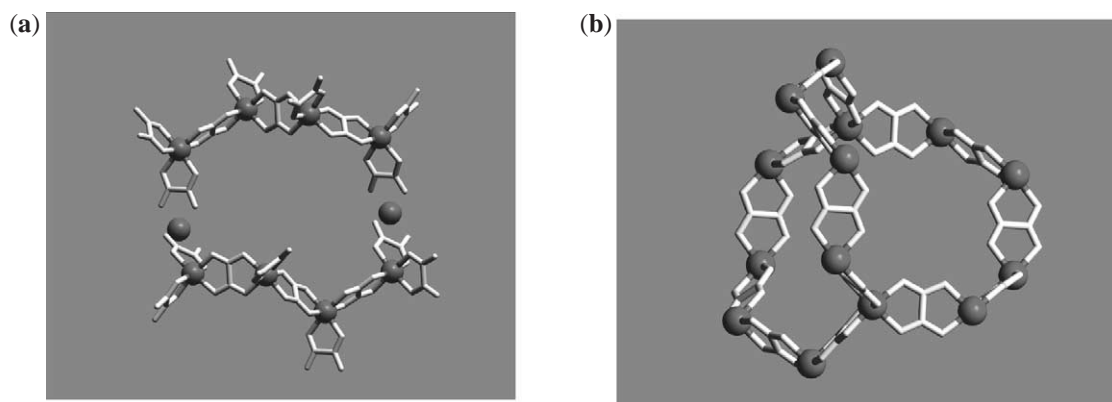


**Figure 42** (a) Two tetrameric units of the same chirality type are necessary to form a closed decagon ring; (b) a fragment of the three-dimensional chiral framework.

Generally, the formation of two-dimensionally linked assemblies affords subunits possessing either four-connected points or a combination of two three-connected points. Figure 41 illustrates the way in which two dimeric subunits may be combined to form a planar honeycomb network.

In an analogous manner, it can easily be seen that two tetrameric subunits are needed to build closed circuits composed of 10 metal centers, which in sum define a three-dimensional decagonal framework (Figure 42). Such tetrameric subunits are necessary, because only four three-connected points ( $Z=4$ ) combined together have the necessary number of six free links to build the three-dimensional net. Identically oriented links repeat at intervals of  $(Z+1)$  points, so that circuits of  $2\cdot(Z+1)$  points are formed. Thus, the structure represents a uniform net in the sense that the shortest path, starting from any point along any link and returning to that point along any other link, is a circuit of 10 points. In addition, the topological principle implies that for the three-dimensional case, only subunits of the same chirality are assembled. Consequently, the uniform anionic three-dimensional network type with a stoichiometry of  $[\text{M}^{\text{II}}_2(\text{ox})_3]_n^{2n-}$  or  $[\text{M}^{\text{I}}\text{M}^{\text{III}}(\text{ox})_3]_n^{2n-}$  ( $\text{M}^{\text{II/III}}$  = transition metal ions and  $\text{M}^{\text{I}}$  = Li, Na) is chiral, since it is composed of  $2n$  centers exhibiting the same kind of chirality. Naturally, this chiral topology is in line with the symmetry elements that are present in the crystalline state of these three-dimensional frameworks, which in sum constitute either one of the enantiomorphic cubic space groups  $P4_332$  or  $P4_132$  for the former and the cubic space group  $P2_13$  for the latter stoichiometry. Thereby, the  $2n$  metal ion centers occupy special sites with a three-fold symmetry axis. Figure 43 shows a view of this network topology.

Extended helical geometries are also encountered through the three-dimensional repetitive assembling of subunits with helical chirality. Thus, the framework structure may alternatively be seen as composed of either right-handed ( $\Delta$ -chirality) or left-handed ( $\Lambda$ -chirality) helices with a  $4_1$ ,  $4_3$ , or  $2_1$  arrangement, running in three perpendicular directions, while simultaneously being covalently bound to each other.

In contrast to the compounds that form chiral three-dimensional networks, the two-dimensional framework topology implies an assembly of coordination entities with alternating chirality between nearest neighboring centers. Finally, the discrimination between the formation and crystallization of either two-dimensional or three-dimensional frameworks with analogous network stoichiometries depends on the choice of the templating counterion. In particular,  $[\text{XR}_4]^+$ , ( $\text{X} = \text{N}, \text{P}$ ;  $\text{R} = \text{phenyl}, n\text{-alkyl}$ ) cations have been found to initiate the growth of two-dimensional

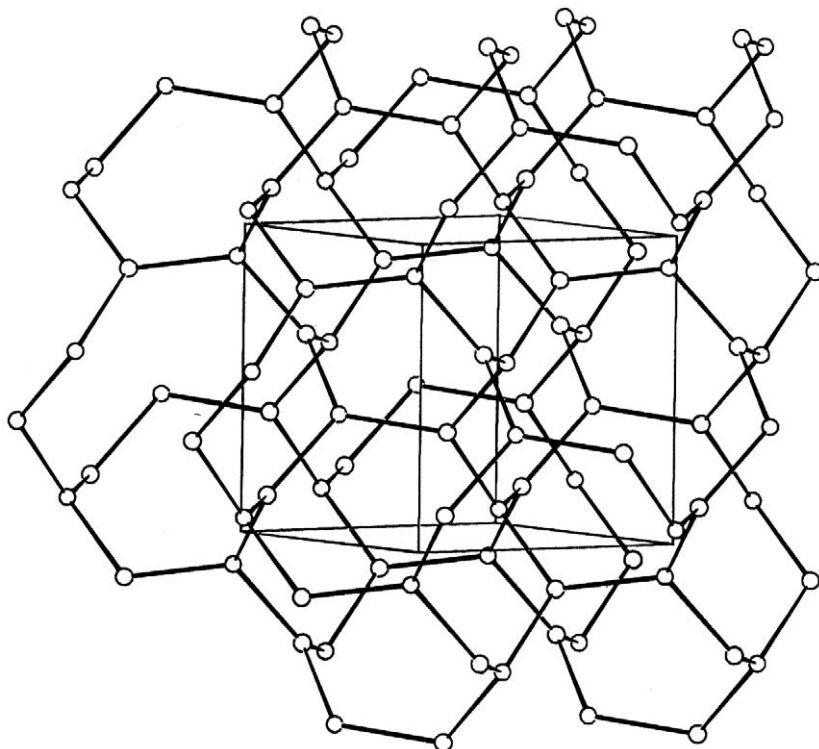


Figure 43 View of the three-connected decagon (10,3) network topology.

sheet structures containing  $[M^II M^III(ox)_3]_n$  network stoichiometries. Figure 44 shows a projection of a sector of a compound that crystallizes in two-dimensional honeycomb layers.

This thinking applies in particular when planning the design of a chiral three-dimensional supramolecular host-guest system, since the mutual interaction of the two distinct complementary molecular units or coordination entities is necessary. Examples of this methodology include the above described anionic, *tris*-chelated transition metal oxalato complexes  $[M^{2+}(ox)_3]^{(6-z)-}$  which form the host system together with the cationic, *tris*-chelated transition metal diimino complexes, e.g.,  $[M(bpy)_3]^{2+/3+}$  (*bpy* = 2,2'-bipyridine), which play the role of the guest compounds.

#### 7.4.5.2 Structural Studies on Two-dimensional Compounds

Several X-ray crystal structures of two-dimensional oxalato-bridged mixed-metal networks have been reported since 1993. The first structural information on two-dimensional oxalates was obtained by Atovmyan *et al.*<sup>153</sup> who succeeded in growing single crystals of the compound

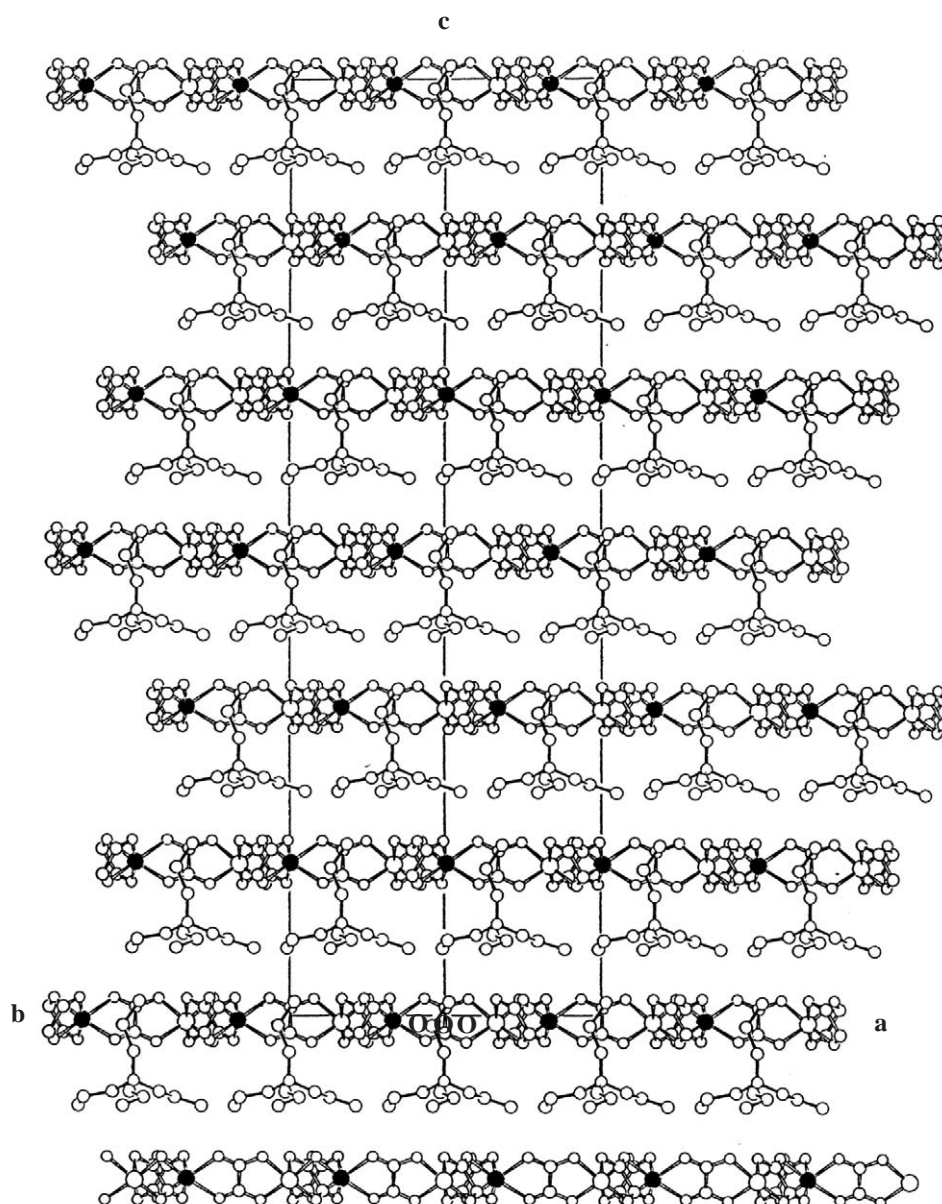


Figure 44 [110] projection of  $[N(n-C_3H_7)_4][Mn^II Cr^III(ox)_3]$ . Black spheres indicate  $Mn^II$  positions.<sup>150</sup>

[NBu<sub>4</sub>][Mn<sup>II</sup>Cr<sup>III</sup>(ox)<sub>3</sub>] by slow diffusion of aqueous solutions of a mixture of NBu<sub>4</sub>Br with K<sub>3</sub>[Cr(ox)<sub>3</sub>]·3H<sub>2</sub>O and MnCl<sub>2</sub> in an H-shaped tube. This structure revealed an anionic two-dimensional network consisting of  $\mu$ -oxalato-bridged Mn<sup>II</sup> and Cr<sup>III</sup> ions, with NBu<sub>4</sub><sup>+</sup> cations located between the layers. One of the butyl groups of the cations penetrates a void in the neighboring anionic layer and the separation between two adjacent anionic layers is 8.95 Å.

Shortly thereafter, Decurtins *et al.*<sup>155</sup> obtained single crystals of the compound [PPh<sub>4</sub>][Mn<sup>II</sup>-Cr<sup>III</sup>(ox)<sub>3</sub>], the structure of which is comparable to that obtained by Atovmyan *et al.* described above. It comprises an alternating assembly of the two types of chiral octahedron with  $\Delta$  and  $\Lambda$  configurations adopting a two-dimensional honeycombed layered structure with the network stoichiometry [Mn<sup>II</sup>Cr<sup>III</sup>(ox)<sub>3</sub>]<sub>n</sub>. There are six pairs of anionic and cationic layers per unit cell and the distance between two adjacent layers is reported to be 9.5 Å. Those phenyl groups of the cations that point vertically in the direction of the anionic layers just fit into the slightly ellipsoidal-shaped vacancies. In a subsequent communication<sup>150</sup> the single-crystal X-ray crystal structures of two additional compounds with stoichiometries [NPr<sub>4</sub>][Mn<sup>II</sup>Cr<sup>III</sup>(ox)<sub>3</sub>] and [NBu<sub>4</sub>][Mn<sup>II</sup>Fe<sup>III</sup>(ox)<sub>3</sub>] were also reported. Interestingly the compound with the latter stoichiometry crystallizes in the hexagonal space group *P6*<sub>3</sub>.

Day and co-workers<sup>156</sup> have carried out single-crystal X-ray crystallographic studies on the compound [N(*n*-C<sub>5</sub>H<sub>11</sub>)<sub>4</sub>][Mn<sup>II</sup>Fe<sup>III</sup>(ox)<sub>3</sub>] which exhibits a two-dimensional network connectivity pattern in accordance with the above findings. In this case, the special disposition of the organic cations interleaving the honeycombed anionic layers (whereby the cavities are occupied by two CH<sub>3</sub> groups approaching from opposite sides) leads to the molecule crystallizing in the orthorhombic space group *C222*<sub>1</sub>.

An alternative approach has been devised by Coronado and co-workers<sup>157,158</sup> which involves the combination of two magnetically active sublattices, namely the bimetallic oxalato-bridged honeycombed network [M<sup>II</sup>M<sup>III</sup>(ox)<sub>3</sub>] (M<sup>II</sup> = Mn, Fe, Co, Cr, Ni, Cu; M<sup>III</sup> = Cr, Fe) and the organometallic decamethylferrocenium cation. The crystal structure was solved for the Mn<sup>II</sup>Fe<sup>III</sup> derivative in the monoclinic space group *C2/m* and in this case the decamethylferrocenium cations intercalate the oxalato-bridged layers without penetrating into the vacancies. Day and co-workers<sup>159-161</sup> have reported detailed investigations of the synthesis and structural and magnetic characterization of a series of mixed-valent compounds with stoichiometries of the type [A][Cr<sup>II</sup>Cr<sup>III</sup>(ox)<sub>3</sub>] and [A][Fe<sup>II</sup>Fe<sup>III</sup>(ox)<sub>3</sub>], together with mixed-metal compounds of stoichiometry [A][Mn<sup>II</sup>Fe<sup>III</sup>(ox)<sub>3</sub>]. In this work, all of the phases prepared with a wide variety of organic template cations [A] were structurally characterized by X-ray powder diffraction, and the reflections indexed and unit cell constants refined on a hexagonal cell. All of these structures have been proved to be consistent with a two-dimensional honeycomb network. The systematic variation of [A] was aimed at modulating the separation between the layers and hence varying the physical properties.

Wood and co-workers investigated hydrothermal crystallization methods for the preparation of new molecule-based magnetic materials and succeeded in preparing a new two-dimensional oxalate network of stoichiometry Na<sub>2</sub>Co<sub>2</sub>(C<sub>2</sub>O<sub>4</sub>)<sub>3</sub>(H<sub>2</sub>O)<sub>2</sub>.<sup>162</sup> The X-ray crystal structure shows that the compound has a particularly interesting ladder topology of coupled cobalt(II) ions. The ladder frameworks run parallel to the *a*-axis and are held together by both hydrogen bonding and electrostatic interactions. Such structures are not very common, although there is much theoretical interest in their low-temperature quantum phase behavior. Unfortunately it appears that interladder exchange in this compound is large enough to cause the onset of a three-dimensional long-range ordering below 9 K. Nevertheless, for temperatures down to this transition, this compound may provide a real example of an *S* = 3/2 spin ladder.

### 7.4.5.3 Magnetic Studies on Two-dimensional Compounds

These two-dimensional polymeric materials all exhibit a wide range of magnetic behavior and ferro-, ferri, or antiferromagnetic long-range ordering processes have all been observed. Generally, the magnetic interactions and magnetic ordering in the [A][M<sup>II</sup>M<sup>III</sup>(ox)<sub>3</sub>] materials are strongly dependent on the character of the cations as well as the combination of M<sup>II</sup>M<sup>III</sup> metal ions.

In the early 1990s Okawa and co-workers<sup>163,164</sup> reported a synthetic and magnetic study on ferri- and ferromagnetic mixed-metal assemblies with the stoichiometry [NBu<sub>4</sub>][M<sup>II</sup>M<sup>III</sup>(ox)<sub>3</sub>] (M<sup>II</sup> = Mn, Fe, Co, Ni, Cu, Zn; M<sup>III</sup> = Cr, Fe). During this time these compounds were wrongly assumed to have a three-dimensional network structure, but in subsequent reports by Atovmyan

*et al.*<sup>153</sup> and Decurtins *et al.*<sup>154</sup> the verification of the two-dimensional class of structure has been proved. The series of Cr<sup>III</sup> derivatives shows a ferromagnetic phase transition with  $T_c < 14$  K and magnetic hysteresis loops with coercive fields  $H_c < 320$  G (0.032 T). The Fe<sup>III</sup> compounds with M<sup>II</sup> = Fe, Ni have been shown to behave as ferrimagnets with magnetic phase transition temperatures of 43 K and 28 K, respectively.<sup>163</sup>

In 1994 Day and co-workers<sup>160</sup> reported the results from a detailed investigation of the mixed-valent ferrimagnets [A][Fe<sup>II</sup>Fe<sup>III</sup>(ox)<sub>3</sub>] (A = quaternary ammonium or phosphonium). In a later communication, Nuttall and Day<sup>165</sup> presented a more comprehensive study on the temperature-dependent magnetization in these [A][Fe<sup>II</sup>Fe<sup>III</sup>(ox)<sub>3</sub>] layer compounds, and discussed the manifestation of Néel N and Q type ferrimagnetism. The major aim of these studies was to map and identify the reasons for the presence of negative magnetization at low temperature. According to Néel, the ground state of a ferrimagnet is determined by the saturation magnetizations of each magnetic sublattice and their relative ordering rates with respect to temperature. For the honeycomb lattice with alternating Fe<sup>II</sup> and Fe<sup>III</sup> ions, this situation corresponds to an initially steeper ordering on the Fe<sup>II</sup> sublattice.

The mixed-valent compound with stoichiometry [A][Cr<sup>II</sup>Cr<sup>III</sup>(ox)<sub>3</sub>] (A = NBu<sub>4</sub>, P(Ph)<sub>4</sub>) has also been synthesized and fully characterized structurally and magnetically.<sup>159</sup> Again, although short-range antiferromagnetic correlations are observed below 100 K, no transitions to a long-range ordered state were observed above 2 K.

For the network of stoichiometry [Mn<sup>II</sup>Fe<sup>III</sup>(ox)<sub>3</sub>], one encounters the rare situation of a bimetallic lattice in which both metal ions have the same electronic ground state, namely  $3d^5$ ,  $S = 5/2$ ,  $^6A_1$ . In this case, the compound has been found to mimic antiferromagnetic behavior. Thus the temperature dependence of the magnetic susceptibility is that of a classic two-dimensional antiferromagnet, reaching a broad maximum at 55 K. Definitive evidence for this behavior comes from a neutron powder diffraction study, which revealed a simple collinear antiferromagnetic alignment of Mn<sup>II</sup> and Fe<sup>III</sup> moments parallel to the *c*-axis, or in other words perpendicular to the layers.

The bimetallic two-dimensional tris-oxalato salts [*n*-C<sub>*n*</sub>H<sub>2*n*+1</sub>PPh<sub>3</sub>][M<sup>II</sup>Fe<sup>III</sup>(C<sub>2</sub>O<sub>4</sub>)<sub>3</sub>] (*n* = 3–7; M<sup>II</sup> = Mn, Fe) have been prepared by Day and co-workers.<sup>166</sup> These compounds behave as ferrimagnets, with magnetic parameters similar to the corresponding salts with symmetrical cations. In particular, the Mn<sup>II</sup>Fe<sup>III</sup> salts show spin canting below  $T_c$ , while the Fe<sup>II</sup>Fe<sup>III</sup> ones are Néel type N ferrimagnets with compensation temperatures and a negative low-temperature magnetization. Surprisingly, there is no clear correlation between the ordering temperatures and interlayer spacing in either series.

The first published work from neutron scattering studies on the magnetic structure of a layered bimetallic tris-oxalate was that of Decurtins *et al.*<sup>155</sup> and refers to a Mn<sup>II</sup>Cr<sup>III</sup> phase which orders ferromagnetically at  $T_c = 6$  K. The best agreement between the observed and calculated magnetic neutron intensities was achieved with a collinear ferromagnetic arrangement of both of the Mn<sup>II</sup> and Cr<sup>III</sup> spins along the *c*-axis. This picture is consistent with the results of a single-crystal magnetization experiment that showed the *c*-axis to be the easy axis of magnetization. In fact, the same conclusions had already been drawn by Atovmyan *et al.* in two earlier publications.<sup>153,167</sup>

#### 7.4.5.4 Structural Studies on Three-dimensional Compounds

The first structure of a three-dimensional transition metal network incorporating the oxalate ion was that of [Ni(phen)<sub>3</sub>][KCo<sup>III</sup>(ox)<sub>3</sub>]·2H<sub>2</sub>O (phen = 1,10-phenanthroline) reported by Snow and co-workers in 1971.<sup>168</sup> The true dimensionality of this compound, however, went unrecognized during this period, and the potential of oxalate ions to form three-dimensional networks was not fully realized until 1993, when Decurtins *et al.* published the crystal structure of the iron(II)-oxalato complex with tris(2,2'-bipyridine)iron(II) cations.<sup>155</sup> This compound has an overall stoichiometry of [Fe<sup>II</sup>(bipy)<sub>3</sub>]<sub>*n*</sub><sup>2+</sup>[Fe<sup>II</sup><sub>2</sub>(ox)<sub>3</sub>]<sub>*n*</sub><sup>2-</sup> and forms a three-dimensional anionic polymeric network that is best described with the three-connected decagon network topology. A view of this anionic network is shown in Figure 43.

The possibilities for linking paramagnetic metal ions via oxalate bridges in three-dimensional lattices and their possible applications in the field of molecule-based magnets have since provided the momentum for subsequent investigations into the self-assembly of three-dimensional oxalato-bridged metal complexes. Decurtins *et al.*<sup>169</sup> reported the structural characterization of three additional compounds, one homometallic with the same network stoichiometry, [Mn<sup>II</sup><sub>2</sub>(ox)<sub>3</sub>]<sub>2</sub><sup>2-</sup>, as the Fe<sup>II</sup> compound above, and two bimetallic with network stoichiometries of

$[\text{NaFe}^{\text{III}}(\text{ox})_3]_n^{2n-}$  and  $[\text{LiCr}^{\text{III}}(\text{ox})_3]_n^{2n-}$ , respectively. Both types of anionic networks form an analogous three-dimensional pattern, but their differences in stoichiometry result in them crystallizing in different space groups. The  $[\text{Mn}^{\text{II}}_2(\text{ox})_3]_2^{2n-}$  network is isostructural with the iron(II) compound and the structure of the two heterometallic compounds only differs in the respect that the overall space group symmetry is lowered to  $P2_13$ . According to the lower symmetry, the asymmetric unit contains a complete oxalate ligand, both metals of the network, and the complete bipyridine ligand. The planar oxalate ligands repeatedly bridge the metal ions in all three dimensions producing chiral left- or right-handed helical strands. Figure 45 shows the [100] projection of the  $[\text{LiCr}^{\text{III}}(\text{ox})_3]_n^{2n-}$  net. The tris-chelating  $[\text{M}^{\text{II}}(\text{bipy})_3]^{2+}$  cations occupy the vacancies within the network.

In 1996 a third related study was carried out by Decurtins *et al.*<sup>170</sup> the aim of which was to investigate the factors that contribute to the structural and chemical flexibility of this type of three-dimensional network. Since it had previously been established that the tris-chelated cations play an important role in initiating the formation and crystallization of the three-dimensional nets, the structural response towards varying the cations, i.e., using a  $[\text{M}^{\text{III}}(\text{bpy})_3]^{3+}$  ( $\text{M}^{\text{III}} = \text{Cr}, \text{Co}$ ) template or the bulkier  $[\text{Ni}^{\text{II}}(\text{phen})_3]^{2+}$  cations was investigated. In the former case, the system achieves this with an elaborate inclusion of an additional complex anion, while keeping the known three-dimensional topology (described above), crystal symmetry, and lattice parameters fixed. It does so by encapsulating these anions in cubic-shaped empty spaces formed by six of the planar bipyridine ligands from three adjacent cations. Figure 46 shows a view of the packing arrangement of three adjacent tris-chelated cations encapsulating a perchlorate anion. In the

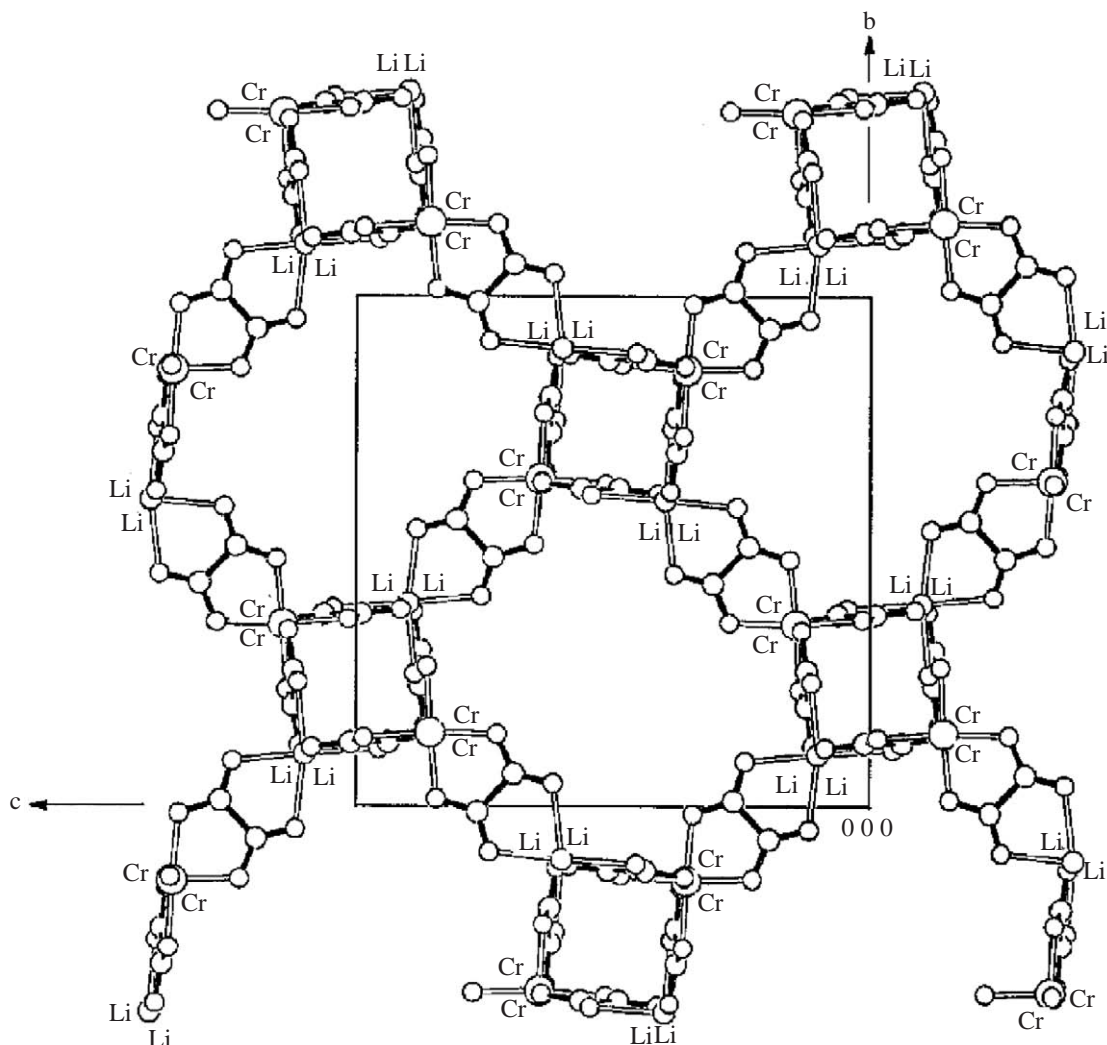
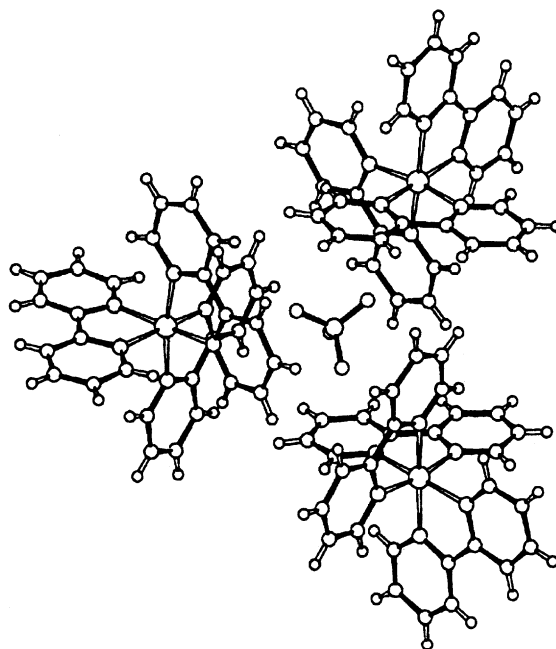


Figure 45 [100] projection of three-dimensional network of  $[\text{Fe}^{\text{II}}(\text{bipy})_3][\text{LiCr}^{\text{III}}(\text{ox})_3]$ .<sup>169</sup>



**Figure 46** View of three adjacent  $[\text{Cr}(\text{bipy})_3]^{3+}$  complexes exhibiting the cavity formed by three pairs of parallel-oriented bipyridine ligands. The center of the cage is occupied by a  $[\text{ClO}_4]^-$  anion.<sup>170</sup>

latter case, the framework demonstrates a marked flexibility in modifying both the shape and width of the cavities in order to accommodate the steric requirements of the bulky cations.

The possibility of using 1,2-dithiooxalate as an isosteric replacement to the oxalate bridging ligand has also been demonstrated, leading to the first reported example of a three-dimensional dithiooxalate-bridged compound. This compound with stoichiometry  $[\text{Ni}^{\text{II}}(\text{phen})_3][\text{NaCo}^{\text{III}}(\text{dto})_3]$  has a topology that is once again consistent with the chiral three-dimensional (10,3) network. In contrast to the previously reported structures, this compound crystallizes in the orthorhombic space group  $P2_12_12_1$  and, as a consequence, there is no longer a three-fold crystallographic axis imposed on the tris-chelated metal ions and the cations within the network. The 1,2-dithiooxalate ligands ( $\text{C}_2\text{O}_2\text{S}_2^{2-}$ ) are approximately planar, but one important structural difference worthy of comment is the discrimination in the coordination behavior of the bridging 1,2-dithiooxalate ligand, since bonding to cobalt(III) occurs through the sulfur atoms, whereas the sodium atoms bind to the oxygen ends of the bridging ligand. The interatomic Na—O distances with a mean value of 2.376(11) Å can be compared with the mean value of 2.319(3) Å in the oxalate-bridged network  $[\text{NaFe}^{\text{III}}(\text{ox})_3]_n^{2n-}$ .<sup>169</sup> The cation packing arrangement is similar to that in the cubic oxalate-bridged compounds, namely three adjacent cations with their V-shaped pockets form a sufficiently large cavity to accommodate additional molecules. These series of compounds clearly illustrate that the decagon framework is indeed flexible and can readily distort to account for changes in the nature of the ligand or the cations.

Decurtins *et al.*<sup>171,172</sup> have reported details regarding the crystal structures of several additional anionic three-dimensional polymeric networks. The crystals of the compound  $[\text{Fe}^{\text{II}}(\text{bipy})_3]_n^{2+}[\text{AgCr}^{\text{III}}(\text{ox})_3]_n^{2n-}$  have a regular tetrahedral morphology that is consistent with the cubic space group  $P2_13$ , and indeed this compound is isostructural with the previously described heterometallic  $[\text{M}^{\text{I}}\text{M}^{\text{III}}(\text{ox})_3]_n^{2n-}$  chiral three-dimensional polymeric networks. Furthermore, these authors have repeatedly demonstrated that it is possible to apply a straightforward series of topological rules to realize the same three-dimensional structural type for many different transition metal ions, an example being the compounds of stoichiometries  $[\text{Ru}^{\text{II}}(\text{bipy})_3]_n^{2+}[\text{NaM}^{\text{III}}(\text{ox})_3]_n^{2n-}$  with  $\text{M}^{\text{III}} = \text{Ru}^{\text{III}}, \text{Rh}^{\text{III}}$ . The study of these compounds was of particular interest for their photophysical properties.<sup>173</sup> Applying this methodology, Julve and co-workers have synthesized and reported the crystal structure of the chiral three-dimensional oxalato-bridged compound  $[\text{Co}^{\text{III}}(\text{bpy})_3][\text{Co}^{\text{II}}_2(\text{ox})_3]\text{ClO}_4$ .<sup>174</sup> As expected this compound is isostructural with the compounds of formula  $[\text{Cr}^{\text{III}}(\text{bpy})_3][\text{Mn}^{\text{II}}_2(\text{ox})_3]\text{ClO}_4$  and  $[\text{Cr}^{\text{III}}(\text{bipy})_3][\text{Mn}^{\text{II}}_2(\text{ox})_3]\text{BF}_4$  reported in 1996 by Decurtins *et al.*<sup>170</sup>

### 7.4.5.5 Magnetic Studies on Three-dimensional Compounds

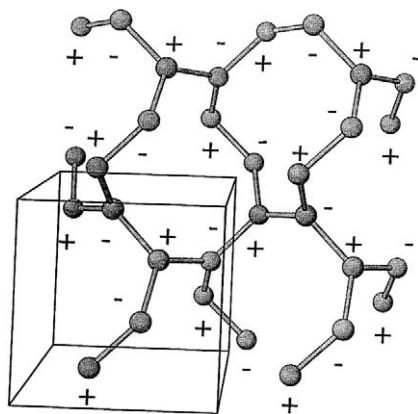
Three-dimensional homo- and heterometallic oxalate-bridged frameworks are examples of supra-molecular host-guest compounds which show long-range magnetic ordering behavior, as well as various kinds of photophysical properties.<sup>173,175</sup> The existence of a magnetically ordered phase was first deduced from magnetic susceptibility measurements on the three-dimensional compound  $[\text{Fe}^{\text{II}}(\text{bpy})_3][\text{Mn}^{\text{II}}_2(\text{ox})_3]$ .<sup>169</sup> The experimental data revealed a rounded maximum at about 20 K in the  $\chi_{\text{M}}$  versus  $T$  curve (thus  $T_{\text{N}} < 20$  K) as well as a Weiss constant  $\Theta$  of  $-33$  K in the  $1/\chi_{\text{M}}$  versus  $T$  plot. This long-range magnetic ordering originates from the exchange interactions between neighboring  $\text{Mn}^{\text{II}}$  ions, mediated by the bridging oxalate ligands. This compound was the first three-dimensional oxalato network for which the magnetic structure could be solved.<sup>176</sup> Neutron diffraction experiments were performed on a polycrystalline sample in the temperature range 30–1.8 K. As anticipated, the appearance of magnetic neutron intensities due to the long-range antiferromagnetic ordering of the spins of the  $\text{Mn}^{\text{II}}$  ions was detected.

Figure 47 depicts the pattern of the magnetic structure with the three-dimensional  $\text{Mn}^{\text{II}}$  network. Despite the three-dimensional helical character of the framework structure incorporating the magnetic ions, a two-sublattice antiferromagnetic spin arrangement has been proved; hence no helimagnetic structure is apparent and this behavior is in accordance with the typical isotropic character of the Heisenberg  $\text{Mn}^{\text{II}}$  ion.

Magnetic studies for the isostructural three-dimensional networks with stoichiometries  $[\text{Co}^{\text{III}}(\text{bpy})_3][\text{Co}^{\text{II}}_2(\text{ox})_3]\text{ClO}_4$  (1) and  $[\text{M}^{\text{II}}(\text{bpy})_3][\text{Co}^{\text{II}}_2(\text{ox})_3]$  ( $\text{M}^{\text{II}} = \text{Fe}$  (2) and  $\text{Ni}$  (3)) carried out by Julve and co-workers<sup>174</sup> show the occurrence of a weak ferromagnetism at low temperatures for compounds (1) ( $T_{\text{c}} = 9.0$  K) and (2) ( $T_{\text{c}} = 6.5$  K), whereas no magnetic ordering was observed for compound (3). This magnetic ordering at very low temperatures is attributed to the spin canting of the magnetic moments of the metal ions in the chiral three-dimensional oxalate-bridged cobalt(II) net. These results also suggest that the magnetic ordering of the three-dimensional  $[\text{Co}^{\text{II}}_2(\text{ox})_3]_n^{2n-}$  anionic framework is strongly dependent on the size and diamagnetic or paramagnetic character of the tris-chelated counterions used to achieve the electroneutrality. In this report, the influence of the size of the  $[\text{M}^{\text{II/III}}(\text{bpy})_3]^{2+/3+}$  complex on the spin canted magnetic structure is also discussed, but further work is needed to investigate these ideas in greater detail.

### 7.4.6 ENANTIOSELECTIVE SYNTHESIS OF OXALATE-BASED MAGNETS

All of the chiral three-dimensional structures described above were obtained from racemic starting materials. However, Verdaguer and co-workers<sup>177</sup> have applied this methodology to exploit the feasibility of the self-assembly of chiral two- and three-dimensional oxalato-bridged polymeric networks starting from homochiral subunits, namely resolved  $[\text{Cr}^{\text{III}}(\text{ox})_3]^{3-}$  and  $[\text{M}^{\text{II}}(\text{bpy})_3]^{2+}$  ( $\text{M}^{\text{II}} = \text{Ni}, \text{Ru}$ ) building blocks. Naturally, the topology of the three-dimensional systems is consistent with the chiral three-dimensional three-connected decagon (10,3) network configuration achieved from the enantiomeric mixture of the precursors. Solid-state circular dichroism (CD) measurements demonstrate the enantiomeric character of the resulting polymers. Following



**Figure 47** Scheme of antiferromagnetic collinear configuration of the magnetic moments originating from the  $\text{Mn}^{\text{II}}$  ions, which constitute the chiral three-dimensional network compound.<sup>176</sup>



these investigations, work in this area has continued. The feasibility of an enantioselective synthesis of optically active two- and three-dimensional oxalate-bridged polymers from resolved  $[\text{Cr}(\text{ox})_3]^{2-}$  and  $[\text{M}(\text{bpy})_3]^{2+}$  ( $\text{M} = \text{Ni}, \text{Ru}$ ) precursors has been investigated by Julve and co-workers who have reported a novel chiral three-dimensional  $\text{Fe}^{\text{III}}$  compound that orders at 40 K.<sup>178</sup>

In parallel studies, Coronado and co-workers have prepared molecule-based magnets comprised of bimetallic three-dimensional oxalate networks and chiral tris(bipyridyl) complex cations.<sup>179</sup> The compounds of stoichiometry  $[\text{A}^{\text{II}}(\text{bipy})_3][\text{ClO}_4][\text{M}^{\text{III}}\text{Cr}^{\text{III}}(\text{ox})_3]$  ( $\text{A}^{\text{II}} = \text{Ru}, \text{Fe}, \text{Co}, \text{Ni}$ ;  $\text{M}^{\text{III}} = \text{Mn}, \text{Fe}, \text{Co}, \text{Ni}, \text{Cu}, \text{Zn}$ ) are all isostructural and consist of a three-dimensional bimetallic network as previously described by Decurtins *et al.*<sup>155</sup> In contrast to the previous layered phases, in the three-dimensional phase, the two metal sites  $\text{M}^{\text{III}}$  and  $\text{M}^{\text{I}}$  have the same chirality. The network structure contains cavities in which the  $[\text{A}^{\text{II}}(\text{bipy})_3]^{2+}$  are located. These cavities have some flexibility and can also accommodate small monoanions such as  $\text{ClO}_4^-$ ,  $\text{BF}_4^-$ , or  $\text{PF}_6^-$ . This feature allows the range of compounds to be extended to include the formulas  $[\text{A}^{\text{III}}(\text{bipy})_3][\text{X}][\text{M}^{\text{I}}\text{M}^{\text{III}}(\text{ox})_3]$  and  $[\text{A}^{\text{III}}(\text{bipy})_3][\text{X}][\text{M}^{\text{II}}\text{M}^{\text{III}}(\text{ox})_3]$  ( $\text{A}^{\text{III}} = \text{Cr}, \text{Ru}$ ).<sup>179</sup> The photophysical properties of these paramagnetic compounds have been studied due to the presence of transition metal ions, e.g.,  $\text{Ru}^{\text{II}}$  and  $\text{Cr}^{\text{III}}$ , which give rise to energy transfer or electron transfer processes.<sup>170,180</sup> The series of three-dimensional oxalate compounds described above all behave as soft ferrimagnets. Since these compounds are chiral, in each single crystal the metallic centers possess the same configuration ( $\Delta$  or  $\Lambda$ ). Studies on the interplay between chirality and ferromagnetism can thus be performed on single crystals of these compounds. Such materials are of interest for the study of magnetochiral effects.

## 7.4.7 SPIN CROSSOVER PHENOMENON

The spin crossover phenomenon provides us with one of the most impressive examples of molecular bistability. It was first observed in the early 1930s, but it took nearly 50 years before researchers realized that spin crossover compounds could be used as active elements in memory devices. A spin crossover transition arises in molecular species containing an octahedral-coordinated transition metal ion with an electronic configuration ( $3 < n < 8$ ), which may “cross over” between a low-spin (LS) and a high-spin (HS) state. Scientists have been able to induce this crossover by varying temperature or pressure, or by irradiating the molecules with light. The origin of the spin crossover phenomenon is molecular, but the temperature dependence of the HS molar fraction  $\chi_{\text{HS}} = f(T)$  depends strongly on intermolecular interactions. The stronger these interactions are, the steeper the  $\chi_{\text{HS}} = f(T)$  curve around  $T_1$ . When the magnitude of these interactions overcomes a threshold value, the spin crossover may become cooperative; in other words, the crystal lattice as a whole is involved in the process. Thermally induced spin transitions between LS and HS states may not only be abrupt but may also occur with hysteresis; the temperature of the  $\text{LS} \rightarrow \text{HS}$  transition in the warming mode,  $T_{\text{c}\uparrow}$ , is higher than the temperature of the  $\text{HS} \rightarrow \text{LS}$  transition in the cooling mode,  $T_{\text{c}\downarrow}$ . Between  $T_{\text{c}\uparrow}$  and  $T_{\text{c}\downarrow}$  the system is bistable, and its electronic state, LS or HS, depends on its history, and hence on the information that the system stores. This chemical flexibility can be used to design complexes the critical temperature of which is tunable up to or above room temperature. As the color of the compound is determined by the electronic transitions implying  $d$  orbitals, the spin state change is frequently accompanied by a color change. Bistable molecules of this type have introduced a “new dimension” to molecular chemistry, namely memory. As a consequence, strategies that permit the rational design of molecule-based materials that can undergo a spin transition are very desirable.

### 7.4.7.1 Utilizing the Spin Crossover Phenomenon: From Rational Design to Functional Molecular Materials

As already highlighted, three-dimensional oxalate networks of the type  $[\text{M}^{\text{II}}(\text{bpy})_3][\text{M}^{\text{I}}\text{-M}^{\text{III}}(\text{ox})_3]$  possess an intriguing three-dimensional structure that contains perfect cavities for tris-bipyridyl complex cations. Hauser and co-workers<sup>181</sup> have taken advantage of these observations to induce a thermal spin crossover transition in a  $[\text{Co}(\text{bipy})_3]$  cation by adjusting the size of this cavity. In the three-dimensional oxalate networks, this can be achieved by variation of the metal ions of the oxalate backbone. In  $[\text{Co}(\text{bipy})_3][\text{NaCr}(\text{ox})_3]$ , the  $[\text{Co}(\text{bpy})_3]^{2+}$  complex is in its usual  ${}^4T_1(t_{2g}^5 e_g^2)$  high-spin ground state. Substituting  $\text{Na}^+$  by  $\text{Li}^+$  reduces the size of the cavity. The resulting

chemical pressure destabilizes the high-spin state of  $[\text{Co}(\text{bpy})_3]^{2+}$  to such an extent that the  ${}^2E(t_{2g}^6 e_g^1)$  low-spin state becomes the actual ground state. As a result,  $[\text{Co}(\text{bpy})_3][\text{LiCr}(\text{ox})_3]$  becomes a spin crossover system as shown by temperature-dependent magnetic susceptibility measurements, as well as from single-crystal X-ray crystallographic data measured at 290 K and 10 K.

#### 7.4.7.2 Structural Changes in Oxalate-based Spin Crossover Systems

The three-dimensional network crystallizes in the cubic space group  $P2_13$ ,  $Z=4$ . The general features of the crystal structure have been discussed earlier on in this chapter. As depicted in Figure 48, the structure is such that the three-dimensional oxalate backbone provides cavities which in terms of size and geometry provide a perfect fit for  $[\text{M}^{\text{II}}(\text{bpy})_3]^{2+}$  ions.

The site symmetry of both the tris-oxalate as well as the tris-bipyridyl complexes is  $C_3$ . Furthermore, the rather loose oxalate network is actively stabilized by the tris-bipyridyl complexes through electrostatic interactions from  $\pi$ -overlap between oxalate and bipyridine along the trigonal axis. Selected crystallographic data including relevant bond lengths and angles are presented in Table 2.

Comparing the bond lengths for the two temperature measurements, it is apparent that the  $\text{M}^{\text{I}}\text{—O}$  and  $\text{Cr—O}$  bond lengths are quite similar for the two temperatures. The  $\text{M}^{\text{II}}\text{—N}$  bond

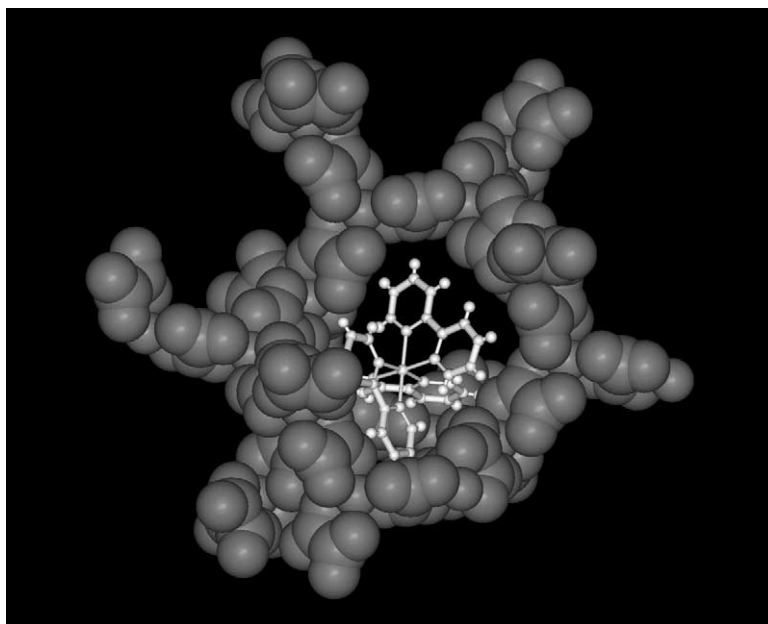


**Figure 48** Chiral three-dimensional host-guest compound of stoichiometry  $[\text{M}^{\text{II}}(\text{bpy})_3][\text{M}^{\text{I}}\text{M}^{\text{III}}(\text{C}_2\text{O}_4)_3]_n$ . Only one guest molecule is shown within the chiral framework.

**Table 2** Selected crystallographic data for oxalate complexes.<sup>181</sup>

Temperature	$[\text{Co}(\text{bpy})_3][\text{LiCr}(\text{ox})_3]$ at 293 K	$[\text{Co}(\text{bpy})_3][\text{LiCr}(\text{ox})_3]$ at 10 K
<i>Unit cell parameters</i>		
$A$ (Å)	15.3866(8)	15.2230(18)
$V$ (Å <sup>3</sup> )	3652.7	3527.8(7)
<i>Bond lengths (Å)</i>		
$\text{M}^{\text{II}}\text{—N1}$	2.096(2)	2.013(4)
$\text{M}^{\text{II}}\text{—N2}$	2.094(2)	2.015(3)
$\text{Cr—O1}$	1.978(2)	1.988(3)
$\text{Cr—O2}$	1.978(2)	1.981(3)
$\text{M}^{\text{I}}\text{—O3}$	2.143(6)	2.170(8)
$\text{M}^{\text{I}}\text{—O4}$	2.321(5)	2.222(7)

lengths, however, decrease from an average of 2.095 Å to 2.014 Å (i.e., by 0.081 Å) between 293 K and 10 K. This value is far too large to be due to thermal contraction alone and serves as a first indication that the  $[\text{Co}(\text{bpy})_3]^{2+}$  cation has become a spin crossover complex in this lattice.

#### 7.4.8 ONE-DIMENSIONAL OXALATE-BASED MAGNETS

Although, as already highlighted, the oxalate ion has allowed the construction of magnetic homo- and heterometallic two- and three-dimensional networks, a few examples of homometallic one-dimensional systems of formula  $(\text{M}(\mu\text{-ox})(\text{L})_x)_n$  (L = nitrogen donor or water) are known. Most of these are copper(II) systems whose magnetic studies reveal the occurrence of moderate<sup>182,183</sup> to weak<sup>154,184,185</sup> antiferromagnetic and even ferromagnetic intrachain couplings.<sup>186–188</sup> Examples of this class of compounds are the one-dimensional oxalato-bridged  $\text{Co}^{\text{II}}$ ,  $\text{Ni}^{\text{II}}$ , and  $\text{Cu}^{\text{II}}$  complexes with *n*-aminopyridine ( $n=2\text{--}4$ ) as the terminal ligand that have been prepared and characterized by Julve and co-workers<sup>189</sup>. All of these compounds are comprised of one-dimensional chains in which  $\text{M}(n\text{-ampy})^{2+}$  units are sequentially bridged by bis-bidentate oxalato ligands with  $\text{M}\cdots\text{M}$  intrachain distances in the range 5.34–5.66 Å. In all cases, the metal ions are six-coordinated to four oxygen atoms, belonging to two bridging oxalato ligands, and the endocyclic nitrogen atoms, from two *n*-ampy ligands, building distorted octahedral surroundings. The aromatic bases are bound to the metal atom in either *cis* or *trans* positions. Magnetic susceptibility measurements in the temperature range 2–300 K show the occurrence of antiferromagnetic intrachain interactions, with the exception of the copper analogue for which a weak ferromagnetic coupling is observed. The cobalt compound of stoichiometry  $\text{Co}(\mu\text{-ox})(4\text{-ampy})_2$  shows a spontaneous magnetization below 8 K, which corresponds to the presence of spin canted ferromagnetism. Julve and co-workers have also investigated the  $[\text{Cr}(\text{phen})\text{ox}]^{2-}$  complex as a versatile bis-oxalato building block for the design of heteropoly-metallic systems. Three new complexes have been prepared and studied displaying a range of structural and magnetic properties.<sup>190</sup>

#### 7.4.9 MAGNETIC COMPOUNDS CONTAINING BOTH OXALATE AND CYANIDE BRIDGING LIGANDS

The controlled assembly of inorganic building blocks is, as previously mentioned, one of the major goals in the field of molecular magnetism. As is apparent from the work discussed in this chapter much effort has been aimed at investigating the chemistry and associated magnetic properties of both cyanometalate and transition metal oxalate-based compounds. An approach adopted by the group of Zorilla has been to combine these two precursors and use  $[\text{M}(\text{CN})_n]^{p-}$  groups in conjunction with a transition metal ion oxalate complex.<sup>191</sup> In this way, the ability of both the cyano group as well as the bridging oxalate system can be exploited to connect various central atoms for the production of molecular assemblies with various dimensionalities. Initial work has been aimed at investigating the effect of peripheral ligands on the structural diversity and magnetic properties of oxalate-bridged compounds. Reaction of  $\{[\text{Ni}(\text{dien})(\text{H}_2\text{O})]_2(\mu\text{-oxo})\}(\text{PF}_6)_2 \cdot 2\text{H}_2\text{O}$  with  $\text{K}_2\text{Pd}(\text{CN})_4$  and  $\text{K}_2\text{Pt}(\text{CN})_4$  afforded the trimeric complexes  $\{[\text{Ni}(\text{dien})(\text{H}_2\text{O})]_2(\mu\text{-oxo})\{(\mu\text{-Pd}(\text{CN})_4)\}$  and  $\{[\text{Ni}(\text{dien})(\text{H}_2\text{O})]_2(\mu\text{-oxo})\{(\mu\text{-Pt}(\text{CN})_4)\}$ . The two compounds are isostructural. In both cases the two octahedrally coordinated Ni atoms are oxalate bridged and the coordination sphere of each Ni is completed by three nitrogen atoms from a diethylenetriamine ligand in a *fac*-arrangement and one nitrogen from a bridging cyanide ligands, which belongs to the corresponding square planar complexes  $[\text{M}(\text{CN})_4]^{2-}$ . These compounds display antiferromagnetic behavior. The magnetic coupling between the two nickel atoms might occur through both bridges, but the length of the exchange pathway through the bidentate tetracyanometalate ligands is large enough to predict that the magnetic interaction most likely takes place mainly through the oxalate ligand.

#### 7.4.10 WORKING TOWARDS THE DESIGN OF DUAL ACTION MATERIALS

One particularly attractive goal for chemists working in the area of molecule-based materials is the design of compounds combining two properties that would otherwise be difficult to achieve in

a conventional inorganic solid with a continuous lattice. This allows for the presence of two cooperative properties in the same crystal lattice which might also result in new physical phenomena and which in turn could lead to novel applications. A promising strategy for creating this type of bifunctionality targets hybrid organic–inorganic crystals comprising two functional sublattices exhibiting distinct properties. Along these lines, two groups have explored the possibilities of using the two-dimensional-type inorganic oxalate lattice to control the crystal packing of  $\pi$ -electron donor molecules.<sup>192,193</sup> In this way bis(ethylenedithio)tetrathiafulvalene (BEDT-TTF) and its derivatives, which form the basis of most known molecular conductors and superconductors, have been combined with two-dimensional oxalate anionic frameworks to yield a range of materials displaying magnetic as well as conducting, superconducting, and semiconducting properties. Following this approach, Coronado and co-workers have reported the first example of a molecule-based layered compound that is both magnetic as well as being an electrical conductor.<sup>177</sup> Single crystals of composition  $[\text{BEDT-TTF}]^+[\text{MnCr}(\text{C}_2\text{O}_4)_3]^-$  were grown via electrocrystallization methods. The partial crystal structure of this compound reveals that the organic layers, namely the BEDT-TTF cations, are found to be alternating with the honeycomb layers of the bimetallic oxalato complex. The BEDT-TTF cations are tilted with respect to the inorganic layer by an angle of  $45^\circ$ . All the donor molecules are related by translations, and adopt a pure two-dimensional pseudo-hexagonal  $\beta$ -type packing motif. The anionic oxalate-based bimetallic layer is crystallographically disordered and as a consequence the solvent molecules could not be located. Studies have shown that this compound is metallic down to 4 K and is ferromagnetic below 5.5 K. There is, however, no evident interplay between the two sublattices (ferromagnetic and conducting), which means that from an electronic point of view, the two lattices are quasi-independent. Nevertheless, these advances indicate that the design of molecule-based materials with dual properties is on the horizon. Consequently, one of the major challenges still to be realized in this field is the design of hybrid materials for which there is an interplay between at least two functional sublattices.

#### 7.4.11 REFERENCES

1. Kahn, O. *Molecular Magnetism*; Wiley VCH: Weinheim, Germany, 1993.
2. Miller, J. S.; Drillon, M., Eds. *Magnetism: Molecules to Materials II*; Wiley-VCH: New York, Vol. 2.
3. Verdager, M. *Polyhedron* **2001**, *20*, 1115.
4. Miller, J. S.; Epstein, A. J. *MRS Bull.* **2000**, *11*, 21.
5. Miller, J. S. *Inorg. Chem.* **2000**, *39*, 4392.
6. Wickman, H. H.; Trozzolo, A. M.; Williams, H. J.; Hull, G. W.; Merrett, F. R. *Phys. Rev.* **1967**, *155*, 563.
7. Wickman, H. H. *J. Chem. Phys.* **1972**, *56*, 976.
8. DeFohs, G. C.; Palacio, F.; O'Connor, C. J.; Bhaatia, S. N.; Carlin, R. L. *J. Am. Chem. Soc.* **1977**, *99*, 8314.
9. Arai, N.; Sorai, M.; Suga, H.; Seki, S. *J. Phys. Chem. Solids* **1977**, *36*, 1231.
10. Helms, J. H.; Hatfield, W. E.; Kwiecien, M. J.; Reiff, W. M. *J. Chem. Phys.* **1986**, *84*, 3993.
11. Bumel, R.; Casabo, J.; Pons, J.; Carnegie, Jr., D. E.; Carlin, R. L. *Physica* **1985**, *132B*, 185.
12. Kahn, O. *Struct. Bonding* **1987**, *68*, 89.
13. Kahn, O. *Angew. Chem., Int. Ed.* **1985**, *24*, 834.
14. Decurtins, S. *Chimia* **1988**, *10*, 539.
15. Dunbar, K. R.; Heintz, R. A. *Prog. Inorg. Chem.* **1997**, *45*, 283.
16. Pilkington, M.; Decurtins, S. *Crystal Design: Structure and Function*; Desiraju, G. R., Ed.; Wiley-VCH: New York, 2003; Chap. 7, p 275.
17. Ohba, M.; Okawa, H. *Coord. Chem. Rev.* **2000**, *198*, 313.
18. Verdager, M.; Bleuzen, A.; Marvaud, V.; Vaissermann, J.; Seuleiman, M.; Desplanches, C.; Sculler, A.; Train, C.; Garde, R.; Gelly, G.; Lamenech, C.; Rosenman, I.; Veillet, P.; Cartier, C.; Villain, F. *Coord. Chem. Rev.* **1999**, *1023*, 190.
19. El-Sayed, M. F. A.; Sheline, R. K. *J. Inorg. Nucl. Chem.* **1956**, *6*, 187.
20. Dows, D. A.; Haim, A.; Wilmarth, W. K. *J. Inorg. Nucl. Chem.* **1961**, *21*, 33.
21. Griffith, W. P. *Quart. Rev.* **1962**, *16*, 188.
22. Schriver, D. *Struct. Bonding* **1966**, *1*, 32.
23. Chadwick, B. M.; Sharpe, A. G. *Advances in Inorganic Chemistry and Radiochemistry*; Emel us, H. J.; Sharpe, A. G., Eds.; Academic Press: New York, 1966; Vol. 8, pp 83–176.
24. Britton, D. *Perspectives in Structural Chemistry*; Dunitz, J. D.; Ibers, J. A., Eds.; Wiley: New York, 1967; Vol. I, pp 109–171.
25. Ludi, A.; G udel, H. U. *Struct. Bonding* **1973**, *14*, 1.
26. Griffith, W. P. *Comprehensive Inorganic Chemistry*; Bailar, J. C., Jr.; Emel us, H. J.; Nyholm, R.; Trotman-Dickenson, A. F., Eds.; Pergamon: Oxford, UK, 1973; Vol. 4, pp 105–180.
27. Rigo, P.; Turco, A. *Coord. Chem. Rev.* **1974**, *13*, 133.
28. Griffith, W. P. *Coord. Chem. Rev.* **1975**, *17*, 177.
29. Sharpe, A. G. *The Chemistry of Cyano Complexes of the Transition Metals*; Maitlis, P. M.; Stone, F. G. A.; West, R., Eds.; Academic Press, New York, 1976.

30. Jones, L. H.; Swanson, B. I. *Acc. Chem. Res.* **1976**, *9*, 128.
31. Baranovski, I. B. *Russ. J. Inorg. Chem.* **1978**, *32*, 1429.
32. Boncarsi, R.; Petrongolo, C.; Scrocco, E.; Tomasi, J. *J. Chem. Phys.* **1968**, *48*, 1500.
33. Hibble, S. J.; Cheyne, S. M.; Hannon, A. C.; Everfield, S. G. *Inorg. Chem.* **2002**, *41*, 4990.
34. Golub, A. M.; Köhler, H. K. H.; Skopenko, V. V. In *Chemistry of the Pseudo Halides*, Monograph 21; Clark, R. J. H., Ed.; Elsevier: New York, 1986; p 77.
35. Hoard, J. L. *Z. Kristallogr.* **1933**, *84*, 231.
36. Rosenweig, A.; Cromer, D. T. *Acta Crystallogr.* **1959**, *12*, 709.
37. Sharpe, A. G. In *Comprehensive Coordination Chemistry*; Wilkinson, G.; McCleverty, J. A., Eds.; Pergamon: New York, 1987, Vol. 2, pp 7–14.
38. Krogmann, K.; Stephan, D. *Z. Anorg. Allg. Chem.* **1968**, *362*, 290.
39. Ledent, J. *Bull. Soc. R. Sci. Liege* **1972**, *41*, 537.
40. Ruegg, M.; Ludi, A. *Theor. Chim. Acta* **1971**, *20*, 147.
41. Drew, M. G. B.; Mitchell, P. C. H.; Pygall, C. F. *J. Chem. Soc., Dalton Trans.* **1977**, 1071.
42. Soares, A. M.; Kierman, P. M.; Cole-Hamilton, D. J.; Griffith, W. P. *J. Chem. Soc., Chem. Commun.* **1981**, 84.
43. Manoli, J.-M.; Potvin, C.; Bregeault, J.-M.; Griffith, W. P. *J. Chem. Soc., Dalton Trans.* **1980**, 192.
44. Corden, B. J.; Cunningham, J. A.; Eisenberg, R. *Inorg. Chem.* **1970**, *9*, 356.
45. Bok, L. D. C.; Leipoldt, J. G.; Basson, S. S. *Acta Crystallogr. B* **1970**, *26*, 684.
46. Basson, S. S.; Leipoldt, J. G.; Bok, L. D. C.; Vollenhoven, J. S.; van Cilliers, P. J. *Acta Crystallogr. B* **1980**, *36*, 1765.
47. Laing, M.; Gafner, G.; Griffith, W. P.; Kiernan, P. M. *Inorg. Chim. Acta* **1979**, *L119*, 33.
48. Hursthouse, M. B.; Galas, A. M.; Soares, A. M.; Griffith, W. P. *J. Chem. Soc., Chem. Commun.* **1980**, 1167.
49. *Misc. Berolinensia Incrementum Sci. Berlin* **1710**, *1*, 337.
50. Robin, M. B.; Day, P. *Adv. Inorg. Chem. Radiochem.* **1967**, *10*, 257.
51. Keggin, J. F.; Miles, J. F. *Nature* **1936**, *137*, 577.
52. Ito, A.; Suenaga, M.; Ono, K. *J. Chem. Phys.* **1968**, *48*, 3597.
53. Chappert, J.; Sawicka, B.; Sawicki, J. *Phys. Stat. Sol. B* **1975**, *72*, 139.
54. Mayoh, B.; Day, P. *J. Chem. Soc., Dalton Trans.* **1976**, 1483.
55. Verdaguer, M. *Science* **1996**, *272*, 698.
56. Kahn, O. *Nature* **1995**, *373*, 667.
57. Holden, A. N.; Matthias, B. T.; Anderson, P. W.; Lewis, H. W. *Phys. Rev.* **1956**, *102*, 1463.
58. Bozorth, R. M.; Williams, H. J.; Walsh, D. E. *Phys. Rev.* **1956**, *103*, 572.
59. Lenze, R. K.; Kanelloupolous, B.; Trageser, G.; Eysel, H. H. *J. Chem. Phys.* **1980**, *72*, 5819.
60. Geiebler, W. D.; Babel, D. *Z. Naturforsch.* **1982**, *87b*, 832.
61. Babel, D. *Comments Inorg. Chem.* **1986**, *5*, 285.
62. Ferley, S.; Mallah, T.; Ouahès, R.; Veillet, P.; Verdaguer, M. *Nature* **1995**, *378*, 701.
63. Hatlevic, O.; Buschmann, W. E.; Zhang, J.; Manson, J. L.; Miller, J. S. *Adv. Mater.* **1999**, *11*, 914.
64. Holmes, S.; Girolami, G. *J. Am. Chem. Soc.* **1999**, *121*, 5593.
65. Mallah, T.; Thiébaud, S.; Verdaguer, M.; Veillet, P. *Science* **1993**, *262*, 1554.
66. Entley, W. R.; Girolami, G. S. *Science* **1995**, *268*, 397.
67. Gadet, V.; Mallah, T.; Castro, I.; Verdaguer, M. *J. Am. Chem. Soc.* **1992**, *114*, 9213.
68. Usuki, N.; Yamada, M.; Ohba, M.; Okawa, H. *J. Solid. State Chem.* **2001**, *159*, 328.
69. Klenze, R.; Kanellakoupolous, B.; Trageser, G.; Eysel, H. H. *J. Chem. Phys.* **1980**, *72*, 5819.
70. Franz, P.; Stoeckli-Evans, H.; Decurtins, S. **2003**, in preparation.
71. Entley, W. R.; Girolami, G. S. *Inorg. Chem.* **1994**, *33*, 5165.
72. Juszczyk, S.; Johansson, C.; Hanson, M.; Ratuszna, A.; Malecki, G. *J. Phys. Condens. Matter* **1994**, *6*, 5697.
73. Juszczyk, S.; Johansson, C.; Hanson, M.; Malecki, G. *J. Magn. Mater.* **1994**, *136*, 5697.
74. Neff, V. *J. Electrochem. Soc.* **1978**, *125*, 886.
75. Sato, O.; Iyoda, T.; Fujishima, A.; Hashimoto, K. *Science* **1996**, *271*, 49.
76. Ohkoshi, S.; Fujishima, A.; Hashimoto, K. *J. Am. Chem. Soc.* **1998**, *120*, 5349.
77. Mizuno, M.; Ohkoshi, S.; Hashimoto, K. *Adv. Mater.* **1995**, *12*.
78. Ohkoshi, S.-I.; Hashimoto, K. *Electrochem. Soc. Interface* **2002**, 314.
79. Sato, O.; Iyoda, T.; Fujishima, A.; Hashimoto, K. *Science* **1996**, *272*, 704.
80. Verdaguer, M.; Galvez, N.; Garde, R.; Desplanches, C. *Electrochem. Soc. Interface* **2002**, 28.
81. Ohba, M.; Maruono, N.; Okawa, H.; Enoki, T.; Latour, J.-M. *J. Am. Chem. Soc.* **1994**, *116*, 11566.
82. Mallah, T.; Auberger, C.; Verdaguer, M.; Veillet, P. *J. Chem. Soc., Chem. Commun.* **1995**, 61.
83. Ohba, M.; Maruono, N.; Okawa, H.; Enoki, T.; Latour, J. M. *J. Am. Chem. Soc.* **1994**, *116*, 11566.
84. Parker, R. J.; Hockless, D. C. R.; Moubaraki, B.; Murray, K. S.; Spicia, L. *J. Chem. Soc., Chem. Commun.* **1996**, 2789.
85. Okawa, H.; Ohba, M.; Turnbull, M. M.; Sugimoto, T.; Thompson, L. K., Eds.; *Molecule-based Magnetic Materials*; ACS Symposium Series 644; American Chemical Society: Washington, DC, 1996; p 319.
86. Ohba, M.; Uski, N.; Fujita, N.; Okawa, H. *Inorg. Chem.* **1998**, *37*, 3349.
87. Re, N.; Gallo, E.; Floriani, C.; Miyasaka, H.; Matsumoto, N. *Inorg. Chem.* **1996**, *35*, 6004.
88. Colacio, E.; Dominguez-Vera, J. M.; Ghazi, M.; Kivekäs, R.; Klinga, M.; Moreno, J. M. *J. Chem. Soc., Chem. Commun.* **1998**, 1071.
89. Colacio, E.; Ghazi, M.; Stoeckli-Evans, H.; Lloret, F.; Moreno, J. M.; Pérez, C. *Inorg. Chem.* **2001**, *40*, 4876.
90. Ferlay, S.; Mallah, T.; Vaissermann, J.; Bartolome, F.; Veillet, P.; Verdaguer, M. *J. Chem. Soc., Chem. Commun.* **1996**, 2482.
91. Marvilliers, A.; Parsons, S.; Rivière, E.; Audière, J.-P.; Kurmoo, M.; Mallah, T. *Eur. J. Inorg. Chem.* **2001**, 1287.
92. Ohba, M.; Okawa, H.; Ito, T.; Ohto, A. *J. Chem. Soc., Chem. Commun.* **1995**, 1545.
93. Ohba, M.; Okawa, H. *Mol. Cryst. Liq. Cryst.* **1996**, *286*, 101.
94. Kou, H. Z.; Bu, W. M.; Liao, D. Z.; Jiang, Z. H.; Yan, S. P.; Fan, Y. G.; Wang, H. G. *J. Chem. Soc., Dalton Trans.* **1998**, 4161.
95. Miyasaka, H.; Matsumoto, N.; Re, N.; Gallo, E.; Floriani, C. *Angew. Chem., Int. Ed.* **1995**, *34*, 1446.
96. Miyasaka, H.; Matsumoto, N.; Okawa, H.; Re, N.; Gallo, E.; Floriani, C. *J. Am. Chem. Soc.* **1996**, *118*, 981.

97. Miyasaka, H.; Ieda, H.; Matsumoto, N.; Re, N.; Gallo, E.; Floriani, C. *Inorg. Chem.* **1988**, *37*, 255.
98. Miyasaka, H.; Okawa, H.; Miyazaki, A.; Enoki, T. *Inorg. Chem.* **1988**, *37*, 4878.
99. Belloud, F.; Clemente-León, M.; Coranado, E.; Galán-Mascarós, J. R.; Gómez-García, C. J.; Romero, F.; Dunbar, K. R. *Eur. J. Inorg. Chem.* **2002**, 1603.
100. Mondal, N.; Saha, M. K.; Bag, B.; Mitra, S.; Gramlich, V.; Ribas, J.; El Fallah, M. S. *J. Chem. Soc., Dalton Trans.* **2000**, 1601.
101. Sieklucka, B.; Podgajny, R.; Korzeniak, T.; Przychodźen, P.; Kania, R. *Compt. Rend. (Paris)*, in press.
102. Fukita, N.; Ohba, M.; Okawa, H.; Matsuda, K.; Iwamura, H. *Inorg. Chem.* **1998**, *37*, 842.
103. El Fallah, M. S.; Rentschler, E.; Caneschi, A.; Sessoli, R.; Gatteschi, D. *Angew. Chem., Int. Ed.* **1996**, *35*, 1947.
104. Ohba, M.; Usuki, N.; Fukita, N.; Okawa, H. *Angew. Chem., Int. Ed. Engl.* **1995**, *34*, 1446.
105. Heinrich, J. L.; Berseth, P. A.; Long, J. R. *J. Chem. Soc., Chem. Commun.* **1998**, 1231.
106. Smith, J. A.; Mascarós, J. R. G.; Clérac, R.; Sun, J.-S.; Ouyang, X.; Dunbar, K. R. *Polyhedron* **2001**, *20*, 1727.
107. Oshio, H.; Onadera, H.; Tamada, O.; Mizutani, H.; Hikichi, T.; Ito, T. *Chem. Eur. J.* **2000**, *6*, 2523.
108. Lu, T.; Xiang, H.; Su, C.; Cheng, P.; Mao, Z.; Ji, L. *New J. Chem.* **2001**, *25*, 216.
109. Røge, G.; Parsons, S.; Paulsen, C.; Villar, V.; Mallah, T. *Inorg. Chem.* **2001**, *40*, 3836.
110. Marvaud, V.; Herrera, J. M.; Barilero, T.; Tuyeras, F.; Garde, R.; Sculler, A.; Decroix, C.; Cantuel, M.; Desplanches, C.; Verdaguer, M. *Monatshefte für Chemie, Chemical Monthly* **2002**, in press.
111. Marvaud, V.; Decroix, C.; Sculler, A.; Guyard-Duhayon, C.; Vaissermann, J.; Gonnetb, F.; Verdaguer, M. *Chem. Eur. J.* **2002**, in press.
112. Christou, G.; Gatteschi, D.; Hendrickson, D. N.; Sessoli, R. *MRS Bull.* **2000**, *11*, 56.
113. Winpenny, R. E. P. *J. Chem. Soc., Dalton Trans.* **2002**, *1*, 1.
114. Berseth, P. A.; Sokol, J. J.; Shores, M. P.; Heinrich, J. L.; Long, J. R. *J. Am. Chem. Soc.* **2000**, *122*, 9655.
115. Sokol, J. J.; Shores, M. P.; Long, J. R. *Angew. Chem., Int. Ed.* **2001**, *49*, 236.
116. Larionova, J.; Sanchiz, J.; Golhen, S.; Ouahab, L.; Kahn, O. *J. Chem. Soc., Chem. Commun.* **1998**, 953.
117. Larionova, J.; Kahn, O.; Golhen, S.; Ouahab, L.; Clérac, R. *J. Am. Chem. Soc.* **1999**, *121*, 3349.
118. Larionova, J.; Clérac, R.; Sanchiz, J.; Kahn, O.; Golhen, S.; Ouahab, L. *Inorg. Chem.* **1999**, *38*, 3621.
119. Kahn, O.; Larionova, J.; Ouahab, L. *J. Chem. Soc., Chem. Commun.* **1999**, 945.
120. Strude, J.; Gillon, B.; Goukassov, A.; Larionova, J.; Clérac, R.; Kahn, O. *Magn. Supercond.* **2001**, 32.
121. Sra, A. K.; Andruh, M.; Kahn, O.; Golhen, S.; Ouahab, L.; Yakhmi, J. V. *Angew. Chem., Int. Ed.* **1999**, *38*, 2606.
122. Larionova, J.; Clérac, R.; Donnadiei, B.; Guerin, C. *Chem. Eur. J.* **2002**, in press.
123. Pilkington, M.; Decurtins, S. *Chimia* **2000**, *54*, 593.
124. Larionova, J.; Gross, M.; Pilkington, M.; Andres, H.-P.; Stoeckli-Evans, H.; Güdel, H. U.; Decurtins, S. *Angew. Chem., Int. Ed.* **2000**, *39*, 1605.
125. Zhong, Z. J.; Seino, H.; Mizobe, Y.; Hidai, M.; Fujishima, A.; Ohkoshi, S.; Hashimoto, K. *J. Am. Chem. Soc.* **2000**, *122*, 2952.
126. Bonadio, F.; Gross, M.; Stoeckli-Evans, H.; Decurtins, S. *Inorg. Chem.* **2002**, *22*, 5891.
127. Pilkington, M.; Gross, M.; Gilby, L.; Decurtins, S., in preparation.
128. Podgajny, R.; Desplanches, C.; Sieklucka, B.; Sessoli, R.; Villar, V.; Paulsen, C.; Wernsdorfer, W.; Dromzee, Y.; Verdaguer, M. *Inorg. Chem.* **2002**, *41*, 1323.
129. Rombaut, G.; Golhen, S.; Ouahab, L.; Mathionière, C.; Kahn, O. *J. Chem. Soc., Dalton Trans.* **2000**, 3609.
130. Kou, H. Z.; Liao, D. Z.; Cheng, P.; Jiang, Z. H.; Yan, S. P.; Wang, G. L.; Yao, X. K.; Wang, H. G. *J. Chem. Soc., Dalton Trans.* **1997**, 1503.
131. Fu, D. G.; Chen, J.; Tan, X. S.; Jiang, L. J.; Shang, S. W.; Zheng, P. J.; Tang, W. X. *Inorg. Chem.* **1996**, *26*, 220.
132. Korzeniak, T.; Podgajny, R.; Stadnicka, K.; Dromzee, Y.; Errington, W.; Kemp, T. J. Alcock, N. W.; Marvaud, V.; Sieklucka, B., in preparation.
133. Moulton, B.; Zaworotko, M. J. *Chem. Rev.* **2001**, *101*, 162.
134. Podgajny, R.; Korzeniak, T.; Baland, M.; Wasiutynski, T.; Errington, W.; Kemp, T. T.; Alcock, N. W.; Sieklucka, B. *J. Chem. Soc., Chem. Commun.* **2002**, 1138.
135. Ohkoshi, S.; Hozumi, T.; Hashimoto, K. *Phys. Rev. B* **2001**, *64*, 132404.
136. Franz, P.; Pilkington, M.; Decurtins, S.; Verdaguer, M.; Hashimoto, K. *Inorg. Chem.*, in preparation.
137. Pilkington, M.; Biner, M.; Decurtins, S.; Stoeckli-Evans, H., unpublished results.
138. Zhong, Z. J.; Seino, H.; Mizobe, Y.; Hidai, M.; Verdaguer, M.; Ohkoshi, S.-I.; Hashimoto, K. *Inorg. Chem.* **2000**, *39*, 5095.
139. Sra, A. K.; Rombaut, G.; Lahitète, F.; Golhen, S.; Ouahab, L.; Mathionière, C.; Yakhmi, J. V.; Kahn, O. *New J. Chem.* **2000**, *24*, 871.
140. Rombaut, G.; Verelst, M.; Golhen, S.; Ouahab, L.; Mathionière, C.; Kahn, O. *Inorg. Chem.* **2001**, *40*, 1151.
141. Hashimoto, K.; Ohkoshi, S.-I.; Arimoto, Y. *Phys. Rev. Lett.* **2001**, *65*, 64438.
142. Buschmann, W. E.; Vazquez, C.; McLean, R. S.; Ward, M. D.; Jones, N. C.; Miller, J. S. *J. Chem. Soc., Chem. Commun.* **1997**, 409.
143. Buschmann, W. E.; Arif, A. M.; Miller, J. S. *Angew. Chem., Int. Ed.* **1998**, *37*, 781.
144. Manson, J. L.; Buschmann, W. E.; Miller, J. S. *Inorg. Chem.* **2001**, *40*, 1926.
145. Wandner, K.-H.; Hoppe, R. Z. *Anorg. Allg. Chem.* **1988**, *557*, 153.
146. Meier, I. K.; Pearlsstein, R. M.; Ramprasad, D.; Pez, G. *Inorg. Chem.* **1997**, *36*, 1707.
147. Towns, R. L. R.; Levenson, R. A. *J. Am. Chem. Soc.* **1972**, *94*, 4345.
148. Leznoff, D. B.; Xue, B.-Y.; Stevens, C. L.; Storr, A.; Thompson, R. C.; Patrick, B. O. *Polyhedron* **2001**, *20*, 1247.
149. Pilkington, M.; Decurtins, S. *Magnetism: Molecules to Materials II*; Miller, J. S.; Drillon, M., Eds.; Wiley-VCH: New York, 2001; Chap. 10, p 239.
150. Pellaux, R. Schmalte H. W.; Huber, R.; Fischer, P.; Hauss, T.; Ouladdiaf, B.; Decurtins, S. *Inorg. Chem.* **1997**, *36*, 2301.
151. Girerd, J. J.; Kahn, O.; Verdaguer, M. *Inorg. Chem.* **1980**, *19*, 274.
152. Oshio, H.; Nagashima, U. *Inorg. Chem.* **1992**, *31*, 3295.
153. Atovmyan, L. O.; Shilov, G. V.; Lyubovskaya, R. N.; Zhilyaeva, E. I.; Ovanesyan, N. S.; Pirumova, S. I.; Gusakovskaya, I. G. *JETP Lett.* **1993**, *58*, 766.
154. Decurtins, S.; Schmalte, H. W.; Oswald, H. R.; Linden, A.; Ensling, J.; Gütllich, P.; Hauser, A. *Inorg. Chim. Acta* **1994**, *216*, 65.

155. Decurtins, S.; Schmalke, H. W.; Schneuwly, P.; Oswald, H. R. *Inorg. Chem.* **1993**, *32*, 1888.
156. Carling, S. G.; Mathonière, C.; Day, P.; Malik, K. M. A.; Coles, S. J.; Hursthouse, M. B. *J. Chem. Soc., Dalton Trans.* **1996**, 1839.
157. Clemente-Léon, M.; Coronado, E.; Galan-Mascaros, J.; Gomez-Garcia, C. *J. Chem. Soc., Chem. Commun.* **1997**, 1727.
158. Coronado, E.; Galan-Mascaros, J.; Gomez-Garcia, C.; Ensling, J.; Gütlich, P. *Chem. Eur. J.* **2000**, *6*, 552.
159. Nuttall, C. J.; Bellitto, C.; Day, P. *J. Chem. Soc., Chem. Commun.* **1995**, 1513.
160. Mathonière, C.; Carling, S. G.; Yusheng, D.; Day, P. *J. Chem. Soc., Chem. Commun.* **1994**, 1551.
161. Mathonière, C.; Nuttall, C. J.; Carling, S. G.; Day, P. *Inorg. Chem.* **1996**, *35*, 1201.
162. Price, D. J.; Powell, A. K.; Wood, P. T. *J. Chem. Soc., Dalton Trans.* **2000**, 3566.
163. Tamaki, H.; Mitsumi, M.; Nakamura, K.; Matsumoto, N.; Kida, S.; Okawa, H.; Ijima, S. *Chem. Lett.* **1992**, 1975.
164. Tamaki, H.; Zhong, Z. J.; Matsumoto, N.; Kida, S.; Koikawa, M.; Achiwa, N.; Hashimoto, Y.; Okawa, H. *J. Am. Chem. Soc.* **1992**, *114*, 6974.
165. Nuttall, C. J.; Day, P. *Chem. Mater.* **1998**, *10*, 3050.
166. Watts, I. D.; Carling, S. G.; Day, P. *J. Chem. Soc., Dalton Trans.* **2002**, 1429.
167. Atovmyan, L. O.; Shilov, G. V.; Ovanesyan, N. S.; Pyalling, A. A.; Lyubovskaya, R. N.; Zhilyaeva, E. I.; Morozov, Y. G. *Synth. Met.* **1995**, *71*, 1809.
168. Butler, K. R.; Snow, M. R. *J. Chem. Soc. A* **1971**, 565.
169. Decurtins, S.; Schmalke, H. W.; Schneuwly, P.; Ensling, J.; Gütlich, P. *J. Am. Chem. Soc.* **1994**, *116*, 9521.
170. Decurtins, S.; Schmalke, H. W.; Pellaux, R.; Schneuwly, P.; Hauser, A. *Inorg. Chem.* **1996**, *35*, 1451.
171. Schmalke, H. W.; Pellaux, R.; Decurtins, S. *Z. Kristallogr.* **1996**, *211*, 533.
172. Pellaux, R.; Decurtins, S.; Schmalke, H. W. *Acta Crystallogr. C* **1999**, *55*, 1057.
173. von Arx, M. E.; van Pieterse, L.; Burattini, E.; Hauser, A.; Pellaux, R.; Decurtins, S. *J. Phys. Chem. A* **2000**, *104/105*, 883.
174. Hernandez-Molina, M.; Lloret, F.; Ruiz, C.; Julve, M. *Inorg. Chem.* **1998**, *37*, 4031.
175. von Arx, M. E.; Hauser, A.; Riesen, H.; Pellaux, R.; Decurtins, S. *Phys. Rev. B* **1996**, *54*, 1500.
176. Decurtins, S.; Schmalke, H. W.; Pellaux, R.; Huber, R.; Fischer, P.; Ouladdiaf, B. *Adv. Mater.* **1996**, *8*, 647.
177. Andrés, R.; Gruselle, M.; Malézieux, B.; Verdager, M.; Vaissermann, J. *Inorg. Chem.* **1999**, *38*, 4637.
178. Armentano, D.; De Munno, G.; Lloret, F.; Pali, A. V.; Julve, M. *Inorg. Chem.* **2002**, *41*, 2007.
179. Coronado, E.; Galán-Mascaros, J. R.; Gómez-García, C. J.; Martínez-Agudo, J. M. *Inorg. Chem.* **2001**, *40*, 113.
180. Hauser, A.; Riesen, H.; Pellaux, R.; Decurtins, S. *Chem. Phys. Lett.* **1996**, *261*, 313.
181. Sieber, R.; Decurtins, S.; Stoeckli-Evans, H.; Wilson, C.; Yufit, D.; Howard, J. A. K.; Capelli, S. C.; Hauser, A. *Chem. Eur. J.* **2000**, *2*, 361.
182. Cavalca, L.; Chiesi-Villa, A.; Manfredotti, A.; Mabgia, A.; Tomlinson, A. A. G. *J. Chem. Soc., Dalton Trans.* **1972**, 391.
183. Michalowicz, A.; Gired, J. J.; Goulon, J. *Inorg. Chem.* **1979**, *18*, 3004.
184. Kitagawa, S.; Okubo, T.; Kawata, S.; Kondo, M.; Katada, M.; Kobayashi, H. *Inorg. Chem.* **1995**, *34*, 4790.
185. Garaj, J.; Lagfelderova, H.; Lundgren, J.; Gazo, J. *J. Collect. Czech. Chem. Commun.* **1972**, *37*, 3181.
186. Oshio, H.; Nagashima, U. *Inorg. Chem.* **1992**, *31*, 3295.
187. Suárez-Varela, J.; Domínguez-Vera, J. M.; Colacio, E.; Avila-Rosón, J. C.; Hidalgo, M. A.; Martín-Ramos, D. *J. Chem. Soc., Dalton Trans.* **1995**, 2143.
188. Gieser, U.; Ramakrishna, B. L.; Willet, R. D.; Hulsbergen, F. B.; Reedijk, J. *J. Inorg. Chem.* **1987**, *26*, 3750.
189. Castillo, O.; Luque, A.; Román, P.; Lloret, F.; Julve, M. *Inorg. Chem.* **2001**, *40*, 5526.
190. Marinescu, G.; Andruh, M.; Lescouezec, R.; Carmon-Munoz, M.; Cano, J.; Lloret, F.; Julve, M. *New J. Chem.* **2000**, *24*, 527.
191. Muga, I.; Gutiérrez-Zorilla, J. M.; Vitoria, P.; Roman, P.; Lloret, F. *Polyhedron* **2002**, *21*, 2631.
192. Rashid, S.; Turner, S. S.; Day, P.; Howard, J. A. K.; Guionneau, P.; McInnes, E. J. L.; Mabbs, F. E.; Clark, R. J. H.; Firth, S.; Biggs, T. *J. Mat. Chem.* **2001**, *11*, 2095.
193. Coronado, E.; Galan-Mascaros, J. R.; Gomez-Garcia, C. J.; Laukhin, V. *Nature* **2000**, *408*, 447.

# 7.5

## Coordination Polymers: Infinite Systems

S. KITAGAWA and S. NORO  
*Kyoto University, Japan*

---

7.5.1	STRUCTURE	231
7.5.1.1	Modules as Building Blocks	232
7.5.1.1.1	<i>Transition metal ions as connectors</i>	232
7.5.1.1.2	<i>Lanthanide ions as connectors</i>	232
7.5.1.1.3	<i>Metal clusters and polynuclear complexes as connectors</i>	233
7.5.1.1.4	<i>Mononuclear metal complexes as connectors</i>	234
7.5.1.1.5	<i>Inorganic ligands as linkers</i>	236
7.5.1.1.6	<i>Organic ligands as linkers</i>	237
7.5.1.1.7	<i>Metalloligands as linkers</i>	239
7.5.1.1.8	<i>Counteranions as linkers</i>	242
7.5.1.1.9	<i>Solvent molecules as templates</i>	243
7.5.1.2	Motifs for Infinite Structures	244
7.5.1.2.1	<i>One-dimensional structures</i>	244
7.5.1.2.2	<i>Two-dimensional structures</i>	244
7.5.1.2.3	<i>Three-dimensional structures</i>	244
7.5.1.2.4	<i>Interpenetration</i>	245
7.5.2	FUNCTIONS	245
7.5.2.1	Porous Function	245
7.5.2.2	Toward Coordination Polymer Magnets	250
7.5.2.3	Spin Cross-over Coordination Polymers	253
7.5.2.4	Chromism	253
7.5.2.5	Nonlinear Optical Properties	254
7.5.2.6	Redox Properties	254
7.5.2.7	Conductivity	255
7.5.3	NEW SYNTHESIS—BOTTOM-UP PREPARATION	255
7.5.3.1	Self-assembling	255
7.5.3.2	Usual Diffusion Method	255
7.5.3.3	Hydro(solvo)thermal Method	256
7.5.3.4	Microwave and Ultrasonic Methods	256
7.5.4	REFERENCES	256

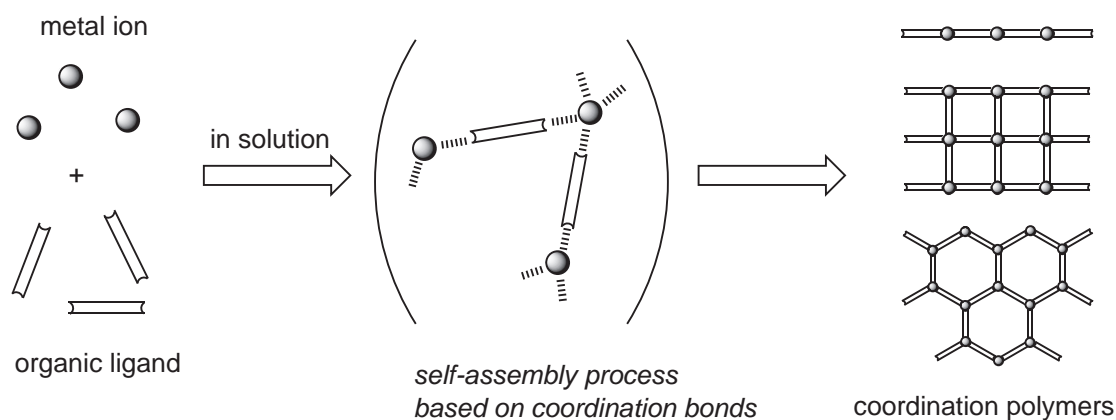
---

### 7.5.1 STRUCTURE

Coordination polymers have infinite frameworks constructed from metal ions and organic ligands (Scheme 1). Coordination bonds play an important role in the construction of extended structures as well as other weak chemical bonds such as hydrogen bonds, van der Waals interactions, etc. This synthetic chemistry is like playing with building blocks, where one can control the coordination frameworks by modifying the geometries of the components. Generally, the formation process proceeds automatically and, therefore, is called a self-assembly process. In particular, crystalline coordination polymers are of great use



because their structures can be exclusively determined by X-ray crystallographic methods, and have demonstrated that they have unique network motifs, structural diversity, and are available for physical and chemical properties ranging from magnetism, conductivity, and optical properties to porous functions such as adsorption, exchange, separation, and catalysis. The size and geometry of those components that control the topology and spatial dimensionality of networks, and the functionality of ligands determines the strength of coordination bonds, resulting in stable frameworks. Weakly coordinating anions influence not only the local structure of metal ions but also the overall framework, and so are regarded as framework regulators. It is worth noting that protic solvent molecules are involved in hydrogen bonding links in frameworks, forming a complementary linking network. In comparison to assemblies of discrete metal complexes, infinite coordination polymers have advantages for (i) the construction of a stable framework, which leads to microporous functions such as zeolites and activated carbons, (ii) a desirable arrangement of metal ions with spins, which is related to magnetostructural studies, and (iii) diverse framework motifs (chain, ladder, helix, fish-bone, square, rectangular, herringbone, bilayer, honeycomb, pillared-layer, diamondoid, octahedral net, etc.) and a control of overall crystal symmetry. These functions are tunable by combinations of reaction conditions (e.g., temperature, pressure, pH, and solvent), the selection of appropriate metal ions, and particular modifications of organic ligands.



Many reviews considering coordination polymers have been published.<sup>1–11</sup> In this chapter three areas are described; specific modules and motifs, functional coordination polymers, and developing synthetic methods.

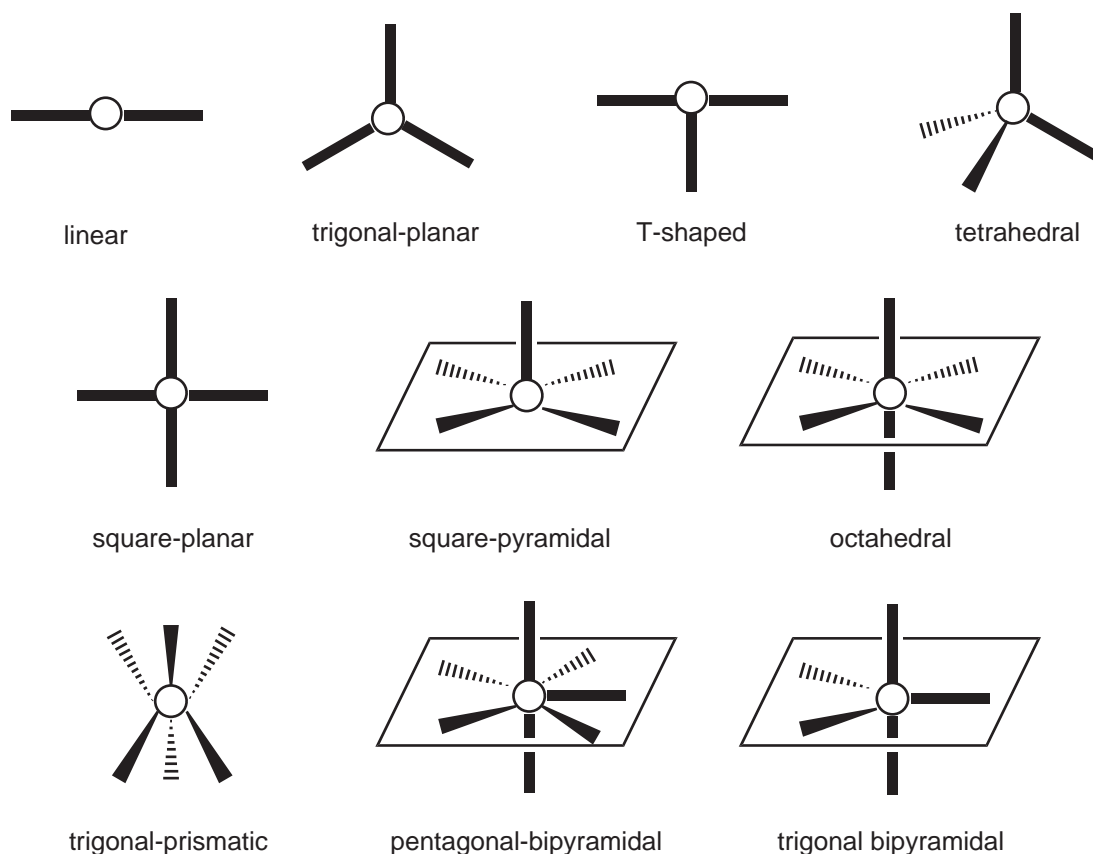
### 7.5.1.1 Modules as Building Blocks

#### 7.5.1.1.1 Transition metal ions as connectors

A transition metal ion is often utilized as a versatile connector in the construction of coordination polymers. Depending on the metal element and its valence, there can be various coordination geometries, e.g., linear, trigonal-planar, T-shaped, tetrahedral, square-planar, square-pyramidal, trigonal-bipyramidal, octahedral, trigonal-prismatic, pentagonal-bipyramidal, and their distorted forms, as shown in Scheme 2. For instance,  $\text{Ag}^{12}$  and  $\text{Cu}^{11}$  ions with  $d^{10}$  configurations possess various coordination environments in response to reaction conditions such as solvent, counteranions, ligands, etc. Therefore, they are considered to be useful connectors.

#### 7.5.1.1.2 Lanthanide ions as connectors

A large number of lanthanide-based frameworks have been synthesized utilizing polydentate ligands such as sulfoxides, carboxylates, nitriles, pyridones, and lactams.<sup>4,12–29</sup> In spite of the difficulty in controlling coordination mode, the high numbers (e.g., 7–10) encountered with

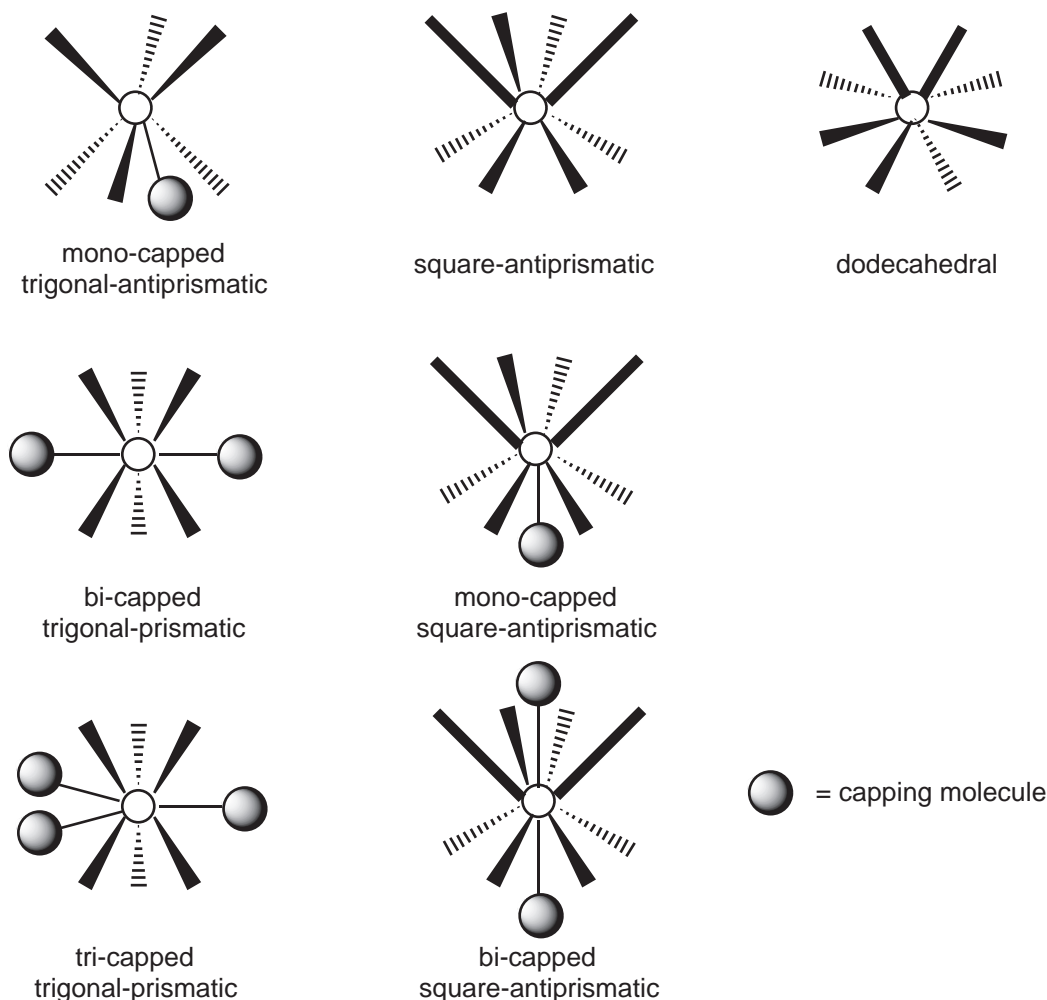


Scheme 2

lanthanide ions (Scheme 3) make them attractive for the discovery of new and unusual network topologies. In addition, the vacant binding sites on a lanthanide ion can be generated by removal of coordinated solvent molecules. The vacant sites could be used in chemical adsorption and heterogeneous catalysis. Furthermore, lanthanide ions have potential utility as luminescent and sensory materials. The crystal structure of  $\{[\text{Tb}_2(\text{EBP})_3(\text{NO}_3)_6] \cdot 5\text{MeCN}\}_n$  (EBP = *N,N'*-ethylenebis(pyridin-2-one)) shows that the EBP ligands bridge the  $\text{Tb}^{\text{III}}$  centers, whose geometry is distorted tri-capped trigonal-prismatic with the nitrate oxygen atoms at the capping atoms, forming sheets of contiguous 54-membered rings as illustrated in Figure 1 (two-dimensional(2-D) brick wall: Scheme 4e).<sup>15</sup> The representative examples of 1-D, 2-D, and 3-D coordination network motifs are mentioned in the following subsection and are shown schematically in Schemes 4–6. The coordination polymers with characteristic motifs are defined according to their schemes.

### 7.5.1.1.3 Metal clusters and polynuclear complexes as connectors

Multidentate linkers such as carboxylates provide rigid frameworks due to their ability to aggregate metal ions into M–O–C polynuclear units, which are referred to as secondary building units (SBUs).<sup>4,29–45</sup> The several cluster motifs are represented in Scheme 7. The SBUs are sufficiently rigid because the metal ions are locked into their positions by the carboxylates. Thus, instead of employing one transition metal ion at a network vertex (as is the case in metal-bipyridine compounds), the SBUs are available to produce extended frameworks of high structural stability. In several clusters with terminal ligands, their coordination sites may be opened to allow the study of metal site reactivity, which also occurs with lanthanide ions. The X-ray single crystal structure study of  $\{[\text{Cd}_3(\text{isonicotinate})_5(\text{EtOH})] \cdot \text{ClO}_4 \cdot \text{EtOH} \cdot 0.5(4\text{-nitro-aniline})\}_n$  shows a pillared-layer framework constructed from tricadmium carboxylate connector as illustrated in Figure 2.<sup>39</sup> The coordinated ethanol molecules can be removed by evacuation,



Scheme 3

providing coordinatively unsaturated metal centers. Dinuclear complexes of Mo, W, Re, Rh, and Ru are useful connectors for the design of infinite networks with the aid of other bridging ligands.<sup>46–54</sup> The X-ray crystallographic structure of  $[\{\text{Rh}_4(\text{CF}_3\text{CO}_2)_8(\text{TCNE})\} \cdot 2\text{benzene}]_n$  (TCNE = tetracyanoethylene) shows a 2-D sheet, in which the TCNE ligand acts as a tetradentate linker for Rh–Rh bimetallic unit.<sup>48</sup> One can envisage a variety of interesting phenomena that may be exhibited by materials composed of M–M connectors, including unusual optical, electronic, and magnetic properties.

#### 7.5.1.1.4 Mononuclear metal complexes as connectors

Metal complex connectors can control a joint angle. Surplus coordination sites can be blocked by chelating or macrocyclic ligands directly attached to a metal ion connector, and therefore, special sites are made available to the linker. This “ligand regulation” of a connector is quite useful. The  $[\text{Cu}(2,2'\text{-bpy})]^{2+}$  (bpy = bipyridyl) connector, that exhibits two *cis*-equatorial and two axial free-coordination sites, creates 1-D zigzag chain structures (Scheme 5b) with bipyridine derivatives.<sup>55</sup> Macrocyclic  $\text{Ni}^{\text{II}}$  complexes provide fixed numbers of coordination sites at axial positions.<sup>56–62</sup>  $[\{\text{Ni}(\text{C}_{12}\text{H}_{30}\text{N}_6\text{O}_2)(1,4\text{-BDC})\} \cdot 4\text{H}_2\text{O}]_n$  ( $\text{C}_{12}\text{H}_{30}\text{N}_6\text{O}_2$  = 1,8-(2-hydroxyethyl)-1,3,6,8,10,13-hexaazacyclotetradecane macrocyclic ligand; BDC = benzenedicarboxylate) possesses 1-D linear chains (Scheme 5a), in which axial sites for the Ni-macrocyclic connector are occupied by bridging 1,4-BDC ligands, and the chains are linked together by the hydrogen bonding interactions to afford a 3-D network (Figure 3).<sup>56</sup>

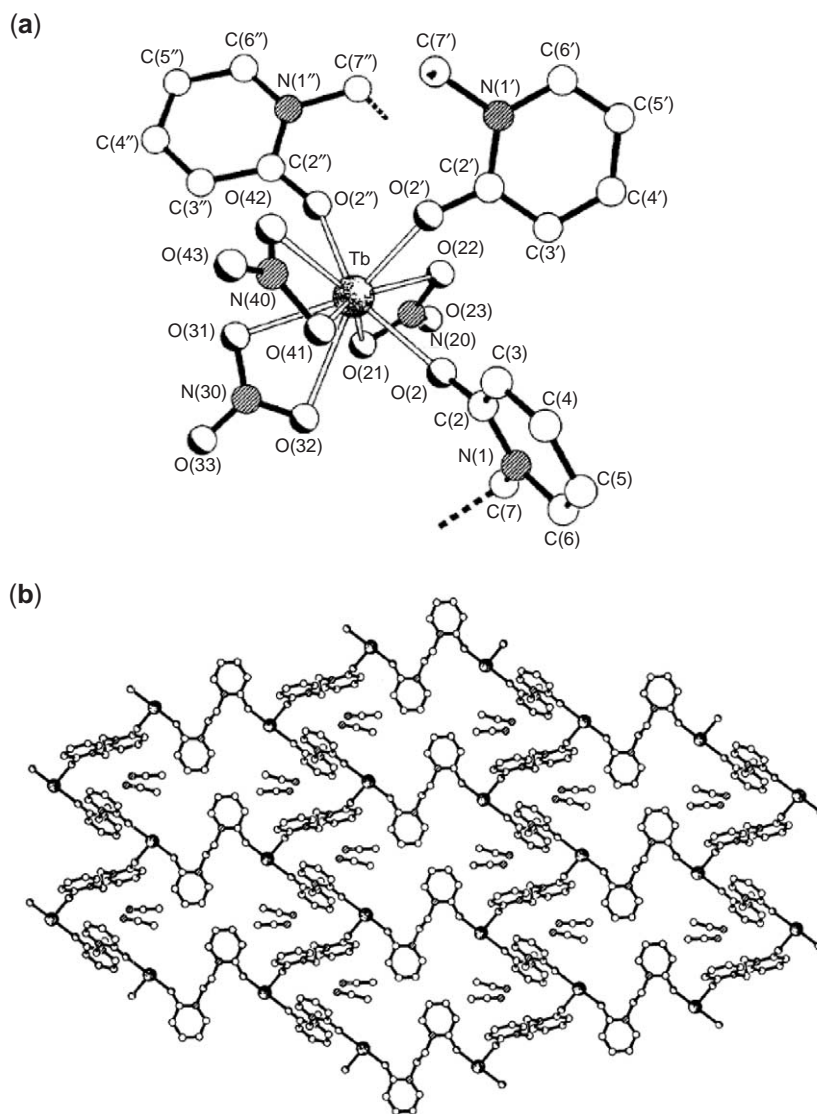
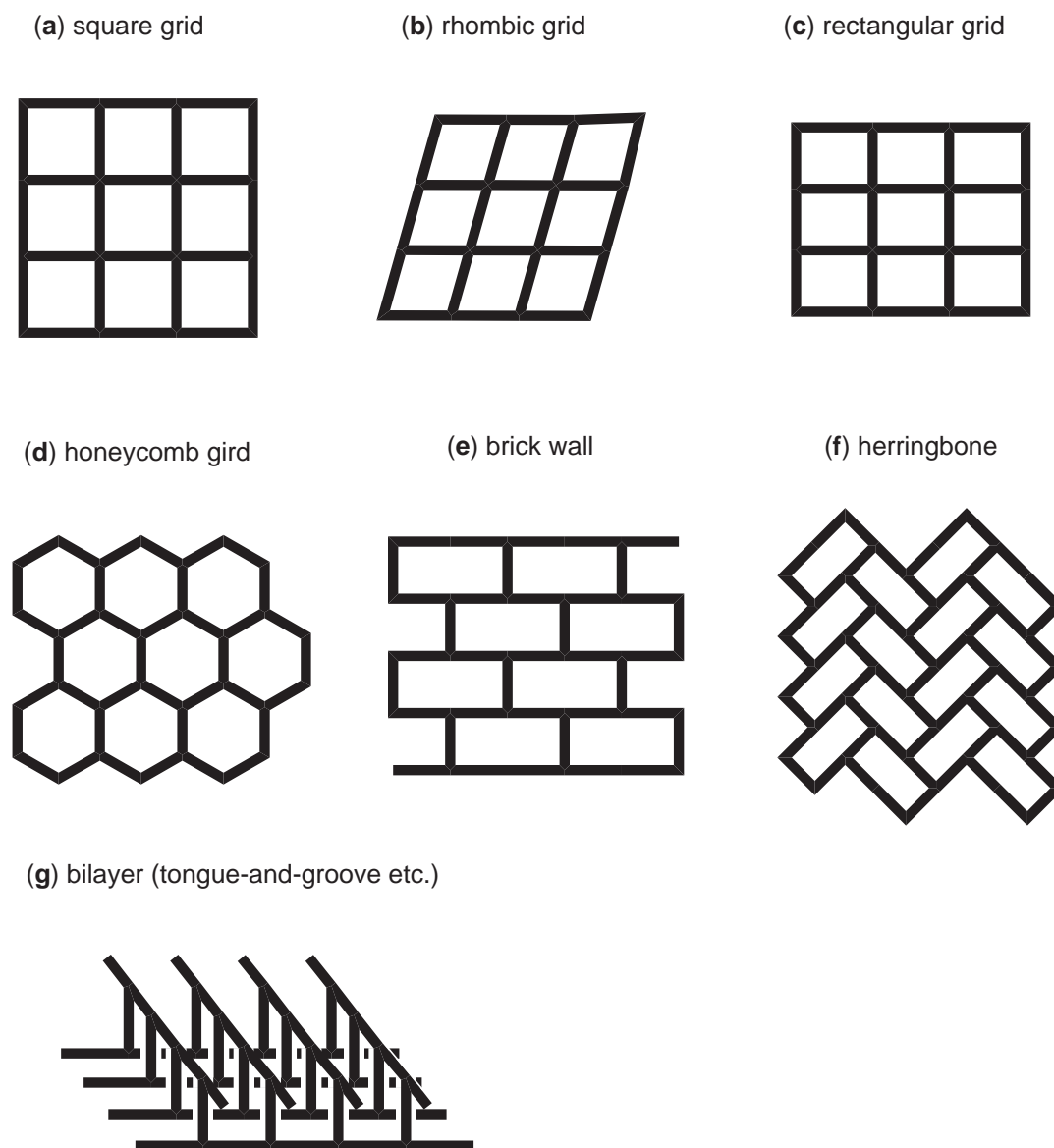


**Figure 1** (a) The coordination environment of the Tb<sup>III</sup> atom in the structure of  $[\{\text{Tb}_2(\text{EBP})_3(\text{NO}_3)_6\} \cdot 5\text{MeCN}]_n$ . Broken bonds indicate the linkage to the C-related portion of each independent ligand. (b) Part of the contiguous array of metallacyclic rings (reproduced by permission of Elsevier Science from *Inorg. Chim. Acta*, **1998**, 272, 131–140).

Complexes of  $[\text{Ni}^{\text{II}}(\text{diamine})_2]^{2+}$  (diamine = en, pn, tn, 1,1'-dmen, or 1,2-*trans*-chxn) (en = ethylenediamine; pn = 1,2-propanediamine; tn = trimethylenediamine; dmen = dimethylethylenediamine; chxn = cyclohexanediamine) which are employed mainly in magnetostructural studies, generate two *cis*- or *trans*-coordination sites depending on the synthetic condition.<sup>63–65</sup> The structure of  $[\{\text{Ni}(\text{tn})_2\}_2\{\text{Fe}(\text{CN})_6\} \cdot \text{NO}_3 \cdot 2\text{H}_2\text{O}]_n$  consists of a 2-D sheet of polycations containing Ni–N≡C–Fe linkages and  $\text{NO}_3^-$  anions (2-D square grid; Scheme 4a).<sup>65</sup> In the crystal the four  $\text{CN}^-$  ligands of  $\text{Fe}(\text{CN})_6^{3-}$  coordinate to the *trans*- $[\text{Ni}(\text{tn})_2]^{2+}$  cations in a bent fashion.  $[\text{M}^{\text{III}}(\text{salen})]^+$  and  $[\text{Mn}^{\text{III}}(\text{acacen})]^+$  (M = Fe or Mn; salen = *N,N'*-ethylenebis(salicylideneimine), acacen = *N,N'*-ethylenebis(acetylacetyloneimine)),<sup>66–70</sup>  $[\text{M}(\text{porphyrin})]^+$  (M = Mn, Fe), and their derivatives with free axial coordination sites are also utilized in magnetostructural chemistry.<sup>71–74</sup> The X-ray analysis of  $[\text{K}\{\text{Mn}(3\text{-MeOsalen})\}_2\{\text{Fe}(\text{CN})_6\} \cdot 2\text{DMF}]_n$  (3-MeOsalen = *N,N'*-ethylenebis(3-methoxysalicylideneimine)) reveals a 2-D network layer structure, in which a net unit is composed of a cyclic octanuclear structure  $(\cdots\text{Mn}-\text{NC}-\text{Fe}-\text{CN}\cdots)_4$  internally bridged by a sandwich structure as illustrated in Figure 4.<sup>66</sup> The combination of  $[\text{Fe}(\text{CN})_6]^{3-}$  with  $[\text{Ni}(\text{tren})]^{2+}$  (tren = tris(2-aminoethyl)amine) in which four coordination sites are obstructed and two *trans* sites are open creates the 3-D structure of  $[\{\text{Ni}(\text{tren})\}_3\{\text{Fe}(\text{CN})_6\}_2 \cdot 6\text{H}_2\text{O}]_n$ .<sup>75</sup> Two different metal

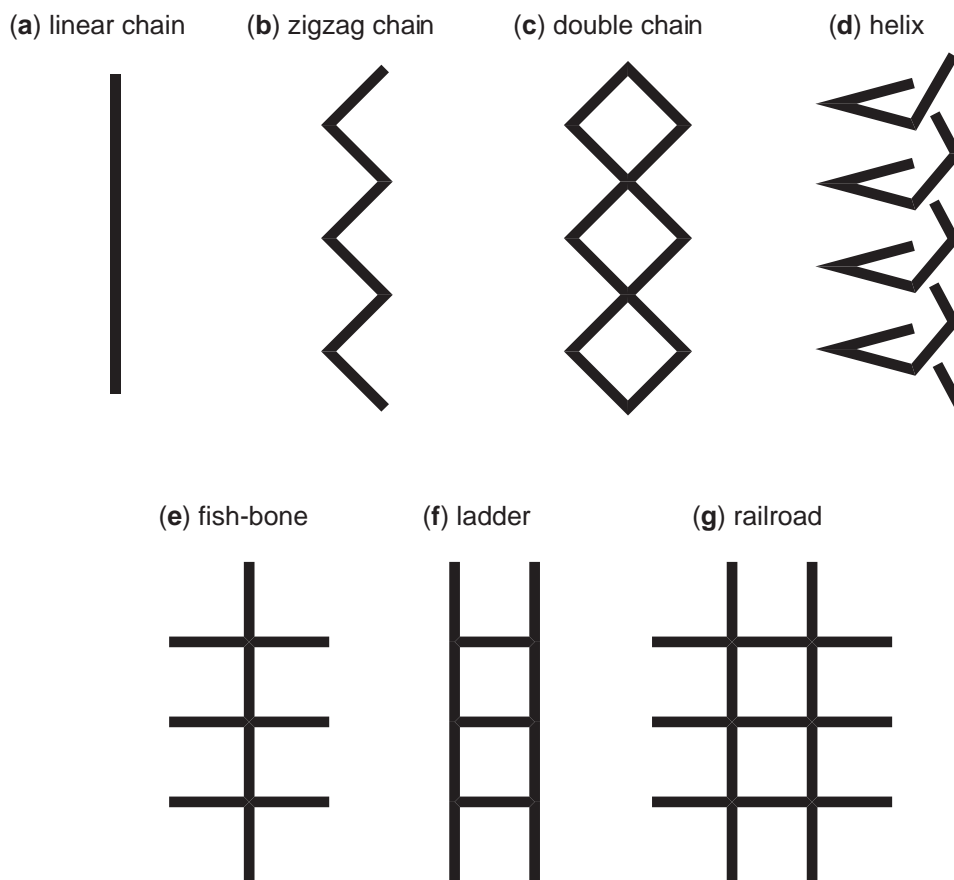


Scheme 4

complex connectors are incorporated in a 3-D framework of  $[\{\text{Cu}(\text{en})_2\}\{\text{Cu}(\text{en})\}\{\text{W}(\text{CN})_8\}\cdot 4\text{H}_2\text{O}]_n$  in which the W atom is coordinated by eight cyano groups in an irregular square antiprism.<sup>76</sup> Five of these act as linkers to form an infinite 3-D porous network containing a zigzag ladder structure.

#### 7.5.1.1.5 Inorganic ligands as linkers

Halides (F, Cl, Br, and I) are the smallest and simplest linkers of all bridging ligands. Quasi-1-D halogen-bridged mixed-valence compounds (MX chains) formulated as  $[\{\text{M}^{\text{II}}(\text{AA})_2\}\{\text{M}^{\text{IV}}(\text{AA})_2\text{X}_2\}\cdot 4\text{Y}]_n$  ( $\text{M}^{\text{II}}-\text{M}^{\text{IV}} = \text{Pt}^{\text{II}}-\text{Pt}^{\text{IV}}, \text{Pd}^{\text{II}}-\text{Pd}^{\text{IV}}, \text{Ni}^{\text{II}}-\text{Pt}^{\text{IV}}, \text{Pd}^{\text{II}}-\text{Pt}^{\text{IV}}, \text{Cu}^{\text{II}}-\text{Pt}^{\text{IV}}$ ; X = Cl, Br, I, and mixed halides; AA = en, 1,2-chxn, etc.; Y =  $\text{ClO}_4$ ,  $\text{BF}_4$ , halides, etc.) (1-D linear chain: [Scheme 5a](#)) have been investigated extensively in the last two decades because of their interesting physical properties.<sup>77,78</sup> A series of mixed-valence  $\text{Cu}^{\text{I}}/\text{Cu}^{\text{II}}-\text{X}$  (X = Cl, Br) chain compounds exhibit pinned charge density waves (1-D double chain: [Scheme 5a](#)).<sup>79</sup> In addition, halides can



Scheme 5

coexist in the coordination frameworks with neutral organic ligands.<sup>80–83</sup>  $\text{CN}^-$  and  $\text{SCN}^-$  have similar bridging ability to halides.<sup>84–87</sup>  $[\text{Cu}_2(\text{CN})_2(\text{quinoxaline})]_n$  affords undulating  $[\text{Cu}(\text{CN})]_n$  chains, which are linked through the quinoxaline ligands to generate a characteristic 2-D  $6^3$  net (2-D honeycomb layer: Scheme 4d).<sup>85</sup>

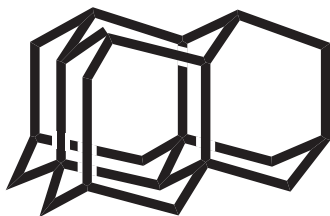
Cyanometallate anions show various geometries, e.g., linear, as in  $[\text{M}(\text{CN})_2]^-$  ( $\text{M} = \text{Au}^{88,89}$  and  $\text{Ag}^{90–92}$ ); trigonal, as in  $[\text{Cu}(\text{CN})_3]^{2-}$ ;<sup>93</sup> tetrahedral, as in  $[\text{Cd}(\text{CN})_4]^{2-}$ ;<sup>94–97</sup> square-planar, as in  $[\text{M}(\text{CN})_4]^{2-}$  ( $\text{M} = \text{Ni}^{98,99}$ ,  $\text{Pd}^{24,25,100}$  and  $\text{Pt}^{24,26}$ ); octahedral, as in  $[\text{M}(\text{CN})_6]^{3-}$  ( $\text{M} = \text{Fe}^{28,59,65,66,101}$ ,  $\text{Co}^{101–103}$ ,  $\text{Cr}^{27,61,104}$  and  $\text{Mn}^{105,106}$ ); and pentagonal bipyramidal, as in  $[\text{Mo}(\text{CN})_7]^{4-}$ .<sup>107–110</sup> In particular, octacyanometallates,  $[\text{M}(\text{CN})_8]^{7-}$  ( $\text{M} = \text{Mo}$  and  $\text{W}$ ), as one of these potential connectors, may show various geometrical structures, e.g., square-antiprism, dodecahedron, or bicapped trigonal-prism.<sup>109–112</sup> This diversity in structure makes cyanometallates as modules both useful and practical.

#### 7.5.1.1.6 Organic ligands as linkers

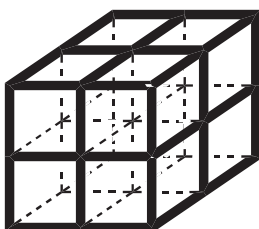
Typical organic ligands are shown in Scheme 8. The most well-known neutral organic ligands are pyrazine (pyz) and 4,4'-bpy.<sup>6–8,10</sup> Recent efforts have been devoted to using long bridging ligands with appropriate spaces.<sup>113–118</sup> For example, treatment of a long ligand  $\text{L} = 9,9$ -diethyl-2,7-bis(4-pyridylethynyl) fluorene with copper nitrate in ethanol leads to exceptionally large noninterpenetrating square-grid polymers of  $[\{\text{Cu}(\text{L})_2(\text{NO}_3)_2\} \cdot x(\text{solvent})]_n$  with grid dimensions of  $25 \text{ \AA} \times 25 \text{ \AA}$  (2-D square grid: Scheme 4a).<sup>118</sup>

Di-,<sup>4,119–121</sup> tri-,<sup>4,44,122</sup> tetra-,<sup>123,124</sup> and hexa-<sup>125,126</sup> carboxylate molecules are representative anionic linkers. Coordination polymers having nonsymmetric anionic ligands generally represented as pyridine-X-COO<sup>-</sup> (X = spacer) have been studied widely.<sup>5</sup>

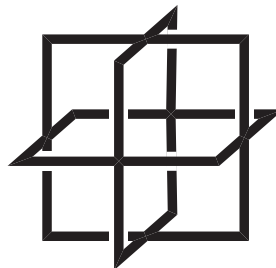
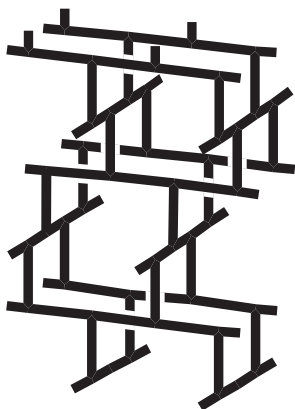
(a) diamondoid net



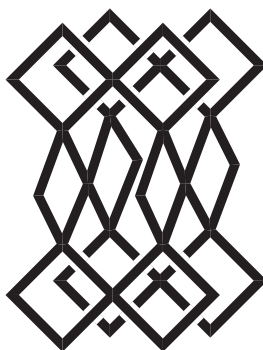
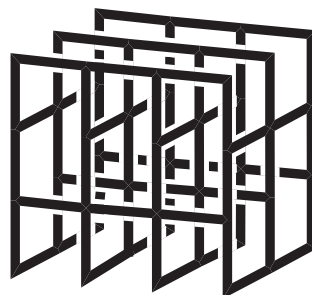
(b) octahedral net



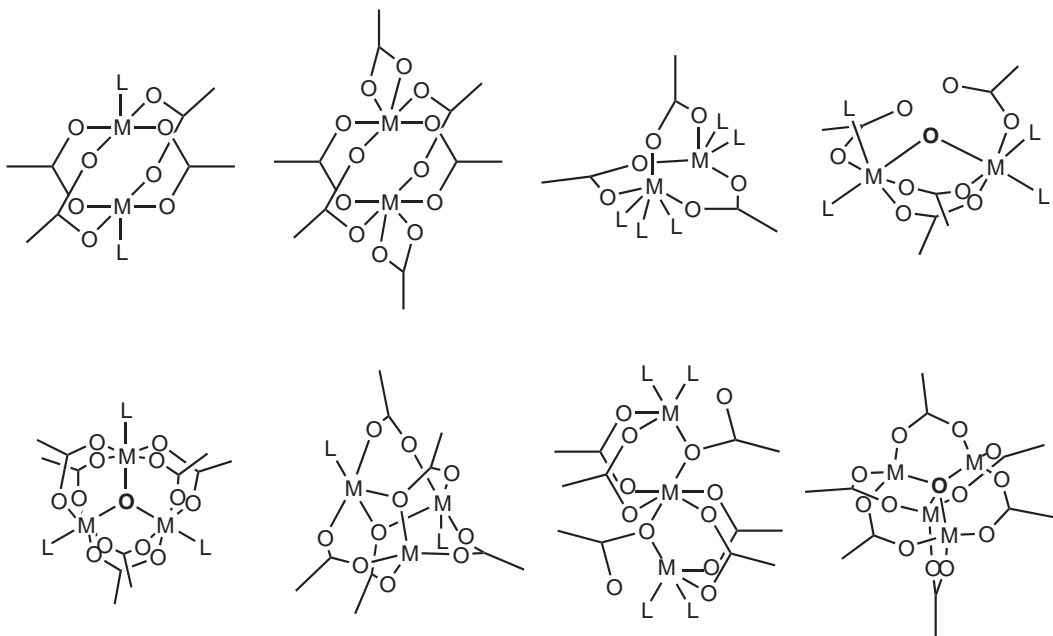
(c) NbO net

(d) ThSi<sub>2</sub> net

(e) PtS net

(f) CdSO<sub>4</sub> net

Scheme 6



Scheme 7

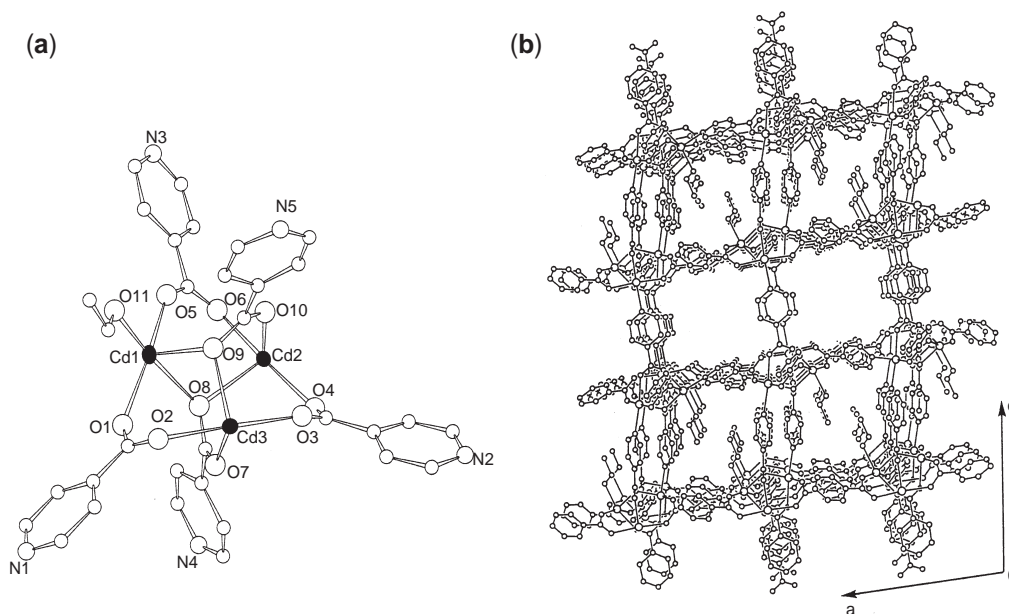


**Figure 2** (a) View of the asymmetric unit in  $[\{Cd_3(\text{isonicotinate})_5(\text{EtOH})\} \cdot ClO_4 \cdot \text{EtOH} \cdot 0.5(4\text{-nitroaniline})]_n$ . (b) View of the framework as viewed down the  $b$ -axis. Included ethanol and 4-nitroaniline molecules and perchlorate anions are omitted for clarity (reproduced by permission of the American Chemical Society from *Inorg. Chem.*, **2000**, *39*, 2189–2198).

1,4-Dihydroxy-2,5-benzoquinone and its derivatives provide a variety of frameworks in which this rigid group facilitated formation of coordination polymers.<sup>127</sup> The crystal structure of  $[\text{Cu}(\text{CA})(\text{pyz})]_n$  (CA = chloranilate) shows parallel sheets, which consist of rectangular arrays of  $\text{Cu}^{\text{II}}$  ions bridged by  $\text{CA}^{2-}$  and pyz linkers (2-D rectangular grid: [Scheme 4c](#)).<sup>128</sup>

There are almost no examples of coordination polymers with cationic organic ligands, this almost certainly being due to a very low coordination power for cationic metal ions. Novel cationic ligands based on  $N$ -aryl pyridiniums and viologen derivatives have been developed.<sup>129,130</sup> In  $[\{\text{Zn}[\text{di}(3\text{-pyridyl})\text{viologen}]_2(\text{MeCN})_2\} \cdot 6\text{ClO}_4]_n$ , one  $\text{Zn}^{\text{II}}$  atom is coordinated by four ligands and two acetonitrile molecules, and the opposing pyridyl moieties coordinate to neighboring  $\text{Zn}^{\text{II}}$  atoms forming a 2-D sheet-like structure (2-D rhombic grid: [Scheme 4b](#)).<sup>130</sup>

#### 7.5.1.1.7 Metalloligands as linkers

In order to functionalize micropores and/or microchannels and construct bimetallic compounds for molecular-based magnets, donor-type building blocks, composed of molecularly inorganic–organic hybrid bridging ligands (so-called metalloligands) have been developed.<sup>131–149</sup> A metalloligand has several advantages:

- Simple procedures to prepare multifunctional ligands. Organic bridging ligands having multifunctionalities require many intricate synthetic steps while metalloligands with multifunctionalities can be obtained from combination of simple connectors and linkers.
- Modification of coordination ability. Metalloligands are relevant for modifying coordination power of functional groups because of Lewis acidity and electrostatic effects of metal ions.
- Amphoteric properties. In addition to Lewis-basic coordination sites, metalloligands also provide Lewis-acidic sites associated with the metal ion.
- Two types of metal ions. Two roles of metal ions can be utilized: one to link connectors to afford a backbone of a framework, the other to make a branch for the backbone, and in a sense, to create novel chemical or physical properties. Both homometallic and heterometallic coordination polymers can be synthesized systematically.



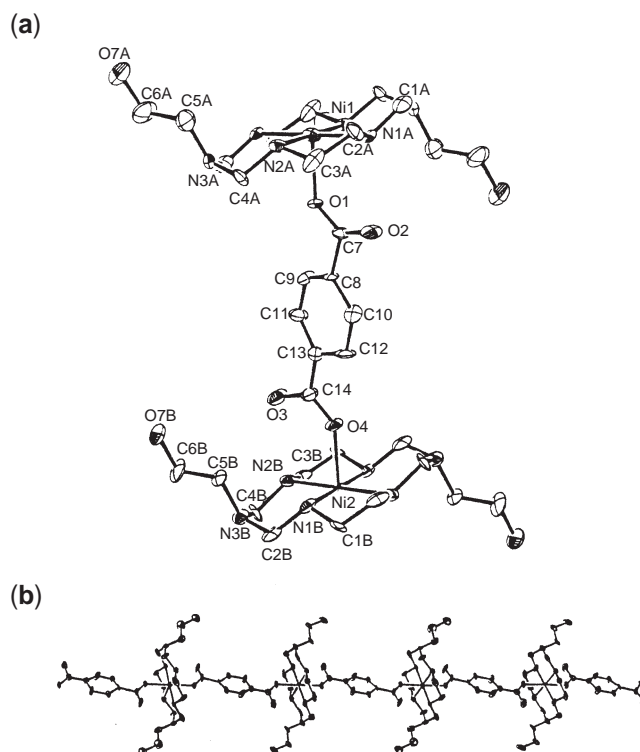


**Figure 3** (a) ORTEP drawing of the asymmetric unit of  $[\{\text{Ni}(\text{C}_{12}\text{H}_{30}\text{N}_6\text{O}_2)(1,4\text{-BDC})\}\cdot 4\text{H}_2\text{O}]_n$  with atomic numbering scheme. Thermal ellipsoids are drawn with 30% probability. (b) 1-D coordination polymer (reproduced by permission of the American Chemical Society from *Inorg. Chem.*, **1999**, 38, 6309–6312).

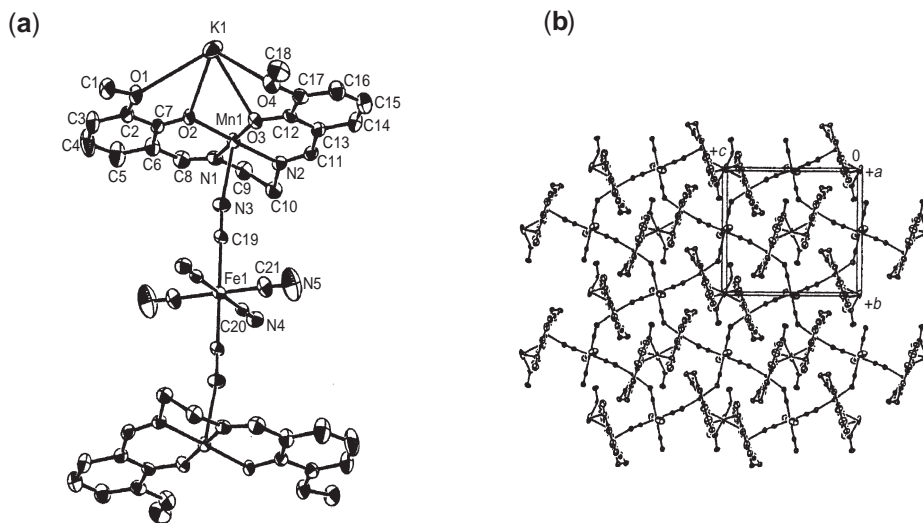


**Figure 4** (a) Structure of the trinuclear unit of  $[\text{K}\{\text{Mn}(3\text{-MeOsalen})\}_2\{\text{Fe}(\text{CN})_6\}\cdot 2\text{DMF}]_n$  (ORTEP drawing) with the numbering scheme of the unique atoms (50% probability ellipsoids). (b) Projection along the  $a$ -axis, showing a 2-D network structure, in which a net unit is composed of a cyclic, octanuclear structure ( $\cdots\text{Mn}-\text{NC}-\text{Fe}-\text{CN}\cdots$ ) and involves a sandwich structure (reproduced by permission of the American Chemical Society from *J. Am. Chem. Soc.*, **1996**, 118, 981–994).

Early reports of metalloligands include  $\text{Cu}^{\text{II}}$  complexes that contain oxamate, oxamide, benzoate, or propionate.<sup>131–133,150</sup> Utilization of the metalloligand,  $[\{\text{Cu}(2,4\text{-pydca})_2(\text{H}_2\text{O})\}\cdot 2\text{Et}_3\text{NH}]$  (pydca = pyridine-2,4-dicarboxylate) as a linker provides a porous coordination polymer,  $[\{\text{ZnCu}(2,4\text{-pydca})_2(\text{H}_2\text{O})_3(\text{DMF})\}\cdot \text{DMF}]_n$ , where  $\text{Zn}^{\text{II}}$  ion at the node of the network acts as a connector and the  $\text{Cu}^{\text{II}}$  ions in the channel walls are available for guest coordination, as illustrated in



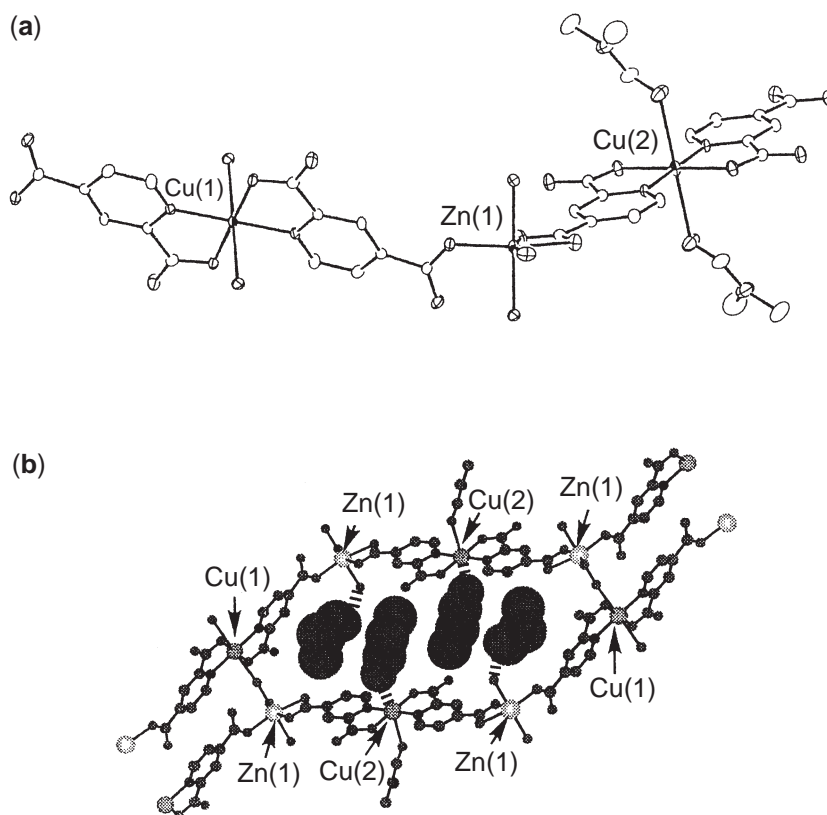


**Figure 5** (a) ORTEP drawing around metal centers of  $[\{ZnCu(2,4\text{-pydca})_2(H_2O)_3(DMF)\} \cdot DMF]_n$  at the 30% probability level. (b) View of one cavity. The guest DMF molecules are represented by a space-filling model (reproduced by permission of the Royal Society of Chemistry from *Chem. Commun.*, **2002**, 33, 222–223).

**Figure 5.**<sup>138</sup>  $[RuCl_2(py)_4]$ , which displays four equatorial *pyz* molecules with free *exo*-oriented N-donor atoms in a square-planar orientation, reacts with  $Ag^I$  salts to form 2-D and 3-D bimetallic networks.<sup>139</sup> Metalloporphyrins are widely used metalloligands.<sup>140,141,143</sup> They contain metal-ligating functions such as pyridine,<sup>141</sup> carboxylate,<sup>143</sup> and cyanide<sup>141</sup> on the periphery. The structural analysis of  $[Cu\{Cu(tpyp)\}]_n$  (*tpyp* = 5,10,15,20-tetra(4-pyridyl)-21H,23H-porphyrin) represents a PtS-related framework (Figure 6 and Scheme 6e).<sup>141</sup> This framework occupies less than half the volume of the crystal, the remaining space being comprised of highly disordered solvent molecules and anions.

The oxalate (*ox*)-bridged polymeric compounds of general formula,  $[cat\{M^I M^{III}(ox)_3\}]_n$  (2-D honeycomb grid: Scheme 4d) (*cat*<sup>+</sup>: monovalent cation;  $M^I$ : divalent metal ion;  $M^{III}$ : trivalent metal ion), are constructed from metalloligands  $[M^{III}(ox)_3]^{3-}$  ( $M^{III}$  = Cr,<sup>145</sup> Fe,<sup>147</sup> or Ru<sup>148</sup>). The similar metalloligand  $[Cr(dto)_3]^{3-}$  (*dto* = dithiooxalate) is used to create bimetallic assemblies  $[NPr_4\{M^{III}Cr(dto)_3\}]_n$  ( $M$  = Fe, Co, Ni, and Zn;  $NPr_4$  = tetrapropylammonium) (2-D honeycomb grid: Scheme 4d).<sup>149</sup>

#### 7.5.1.1.8 Counteranions as linkers

When neutral bridging ligands such as bipyridine derivatives are used as linkers, counteranions coexist in the framework due to requirement of overall charge neutrality. However, these anions can have other roles, e.g., as coordination and hydrogen bonding linkers, guests in vacant space, as such eventually acting as framework regulators.

$NO_3^-$ ,  $SO_4^{2-}$ , and  $SiF_6^{2-}$  anions are known to have the ability of bridging two metal centers. For instance,  $[\{M(SiF_6)(4,4'\text{-bpy})_2\} \cdot DMF]_n$  ( $M$  = Zn<sup>149</sup> and Cu<sup>152,153</sup>) gives a 3-D octahedral network (Scheme 6b), in which 2-D grids of  $[M(4,4'\text{-bpy})_2]_n$  are linked by F atoms of counter  $SiF_6^{2-}$  dianions.

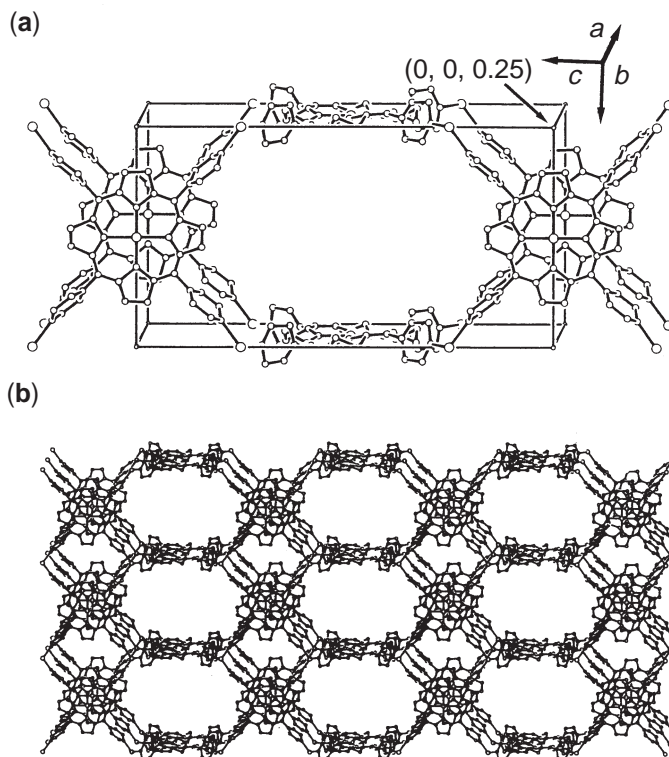


**Figure 6** (a) The tetragonal unit cell and (b) the extended structure of the  $[\text{Cu}\{\text{Cu}(\text{tpyp})\}]_n$  (reproduced by permission of the Nature Publishing Group from *Nature*, **1994**, 369, 727–729).

The structure of  $[\{\text{Cu}(\text{L})_2(\text{SO}_4)\} \cdot 0.5\text{H}_2\text{O} \cdot 0.5\text{CH}_2\text{Cl}_2]_n$  ( $\text{L} = (4,4'\text{-di}(3\text{-methyl pyridyl sulfide)})$ ) involves a 3-D noninterpenetrating network,  $\text{SO}_4^{2-}$  serving as a bridging ligand to connect two  $\text{Cu}^{\text{II}}$  ions, thereby forming in a rhombic box.<sup>154</sup>  $[\text{Ag}(\text{NO}_3)(4\text{-pytz})]_n$  ( $4\text{-pytz} = 3,6\text{-di}(4\text{-pyridyl})\text{-}1,2,4,5\text{-tetrazine}$ ) shows that the  $\text{NO}_3^-$  anions bridge adjacent linear chains of  $[\text{Ag}(4\text{-pytz})]_n$ , each of which is related to the next by a  $60^\circ$  rotation and by a step of 5.18 Å, thereby generating a helical staircase motif.<sup>155</sup>

Anions containing hydrogen-bonding sites such as O and F are useful for the construction of high-dimensional networks. In  $[\{\text{Cu}(\text{ClO}_4)_2(4,4'\text{-bpy})(\text{H}_2\text{O})_2\} \cdot 4,4'\text{-bpy}]_n$  (1-D linear chain: [Scheme 5a](#)),<sup>156</sup> the chains of  $[\text{Cu}(4,4'\text{-bpy})]_n$  are interconnected by hydrogen bonds between the coordinated  $\text{H}_2\text{O}$  and  $\text{ClO}_4^-$  molecules to form 2-D layers with cavities, each enclosing a free 4,4'-bpy molecule. The reaction of  $\text{Mn}(\text{NO}_3)_2 \cdot 6\text{H}_2\text{O}$  with 4,4'-azopyridine (azpy) affords  $[\{\text{Mn}(\text{NO}_3)_2(\text{azpy})(\text{H}_2\text{O})_2\} \cdot 2\text{EtOH}]_n$  (1-D linear chain: [Scheme 5a](#)),<sup>157</sup> whose network consists of 1-D chains of  $[\text{Mn}(\text{azpy})]_n$ . These are linked by hydrogen bonding between the coordinated  $\text{H}_2\text{O}$  and  $\text{NO}_3^-$  molecules thereby providing a logcabin-type 3-D structure.

Choice of counteranions is a major determinant of the architectural topology of coordination polymers.<sup>153,155,158–164</sup> These anions are framework regulators. Four complexes,  $[\{\text{Ag}(1,4\text{-dithiane})\} \cdot 2\text{anions}]_n$  (anions =  $\text{BF}_4^-$ ,  $\text{SCN}^-$ ,  $\text{NO}_2^-$ , and  $\text{CF}_3\text{SO}_3^-$ ), are all based on the same linker and connector, but the frameworks are different depending on the counteranion used.<sup>159</sup> Coordination polymers accommodating anions in their channels are capable of anion-exchange properties, described in the following subsection.

#### 7.5.1.1.9 Solvent molecules as templates

Various solvents are necessary to provide reaction media, but may also regulate framework topology.<sup>165–167</sup> Solvent molecules often occur in microspace formed by coordination polymer motifs. In other words, crystal structures of coordination polymers may be controlled by a template effect of solvent molecules. A vast number of compounds illustrate this effect. Copper compounds,  $[\text{Cu}_2\text{I}_2(\text{bpds})]_n$  ( $\text{bpds} = \text{bis}(4\text{-pyridyl})\text{disulfide}$ ) have either necklace (1-D double

chain: Scheme 5c) or tubular polymers, which are constructed from tetrahedral  $\text{Cu}_4\text{I}_4$  cubane connectors.<sup>166</sup> Three coordination polymers formed between CuI and bpds have shown a clear solvent-dependent topological isomerism.

### 7.5.1.2 Motifs for Infinite Structures

#### 7.5.1.2.1 One-dimensional structures

Representative examples of 1-D coordination polymer motifs are illustrated in Scheme 5. In these motifs, the helix remains quite rare in the context of coordination polymers, but there is additional interest because it is inherently chiral irrespective of the components.<sup>168–170</sup> The inherent chirality of this architecture comes from spatial disposition rather than the presence of chiral atoms.  $[\text{Ni}(4,4'\text{-bpy})(\text{benzoate})_2(\text{MeOH})_2]_n$  self-assembles as a helical architecture that is sustained by the linking of octahedral metal connectors with linear ligands (Scheme 5d).<sup>169</sup> The helical chains pack such that they are staggered, but align in a parallel fashion. Therefore, the bulk crystal is polar as every helix in an individual crystal is of the same handedness. Other examples of 1-D coordination polymers are listed in Table 1.<sup>155,169,171–175</sup>

#### 7.5.1.2.2 Two-dimensional structures

Scheme 4 illustrates some of the 2-D network motifs that have thus far been observed in coordination polymers. Square-grid networks (Scheme 4a) exemplify a particularly simple and commonly reported example of a predictable 2-D metal-organic network. Square-grid coordination polymers are based upon 1:2 metal:ligand complexes with linear bifunctional linkers. Grids with two types of linkers have also been reported, in which rectangular grids are formed (Scheme 4c).<sup>114,176,177</sup>

Other types of 2-D networks use a T-shape metal connector, which generates unique structural motifs, brick wall (Scheme 4e),<sup>117</sup> herringbone (Scheme 4f),<sup>178</sup> and bilayer (Scheme 4g).<sup>153,179</sup> To create such a T-shape module, chemists frequently utilize a  $\text{NO}_3^-$  anion, which blocks four coordination sites of hepta-coordinated metal ions such as  $\text{Cd}^{\text{II}}$  and  $\text{Co}^{\text{II}}$  in the chelating fashion. The remaining three coordination sites are bridged by bifunctional ligands, creating the T-shape module with a metal:ligand ratio of 1:1.5. The  $\text{Cu}^{\text{II}}$  center of  $[\{\text{Cu}_2(4,4'\text{-bpy})_3(\text{H}_2\text{O})_4\} \cdot \text{anions} \cdot 2\text{H}_2\text{O} \cdot 4\text{EtOH}]_n$  (anions =  $4\text{PF}_6^-$  and  $2\text{PF}_6^- + 2\text{ClO}_4^-$ ) has an octahedral environment with four nitrogen atoms of 4,4'-bpy ligands in the equatorial plane and two oxygen atoms of  $\text{H}_2\text{O}$  molecules at the axial sites. They, however, represent the bilayer motif (Scheme 4g) within the T-shape module, because one of four 4,4'-bpy ligands coordinated to the  $\text{Cu}^{\text{II}}$  ions is monodentate. Other representative examples with 2-D coordination networks are recorded in Table 2.<sup>117,176,178–182</sup>

#### 7.5.1.2.3 Three-dimensional structures

Diamondoid<sup>5,183,184</sup> and octahedral<sup>151,152,185,186</sup> networks (Schemes 6a and 6b), which contain tetrahedral and octahedral nodes, respectively, are well-known examples of the 3-D motif. Other new 3-D networks (e.g., Scheme 6c–6f) have been observed in recent years.<sup>30,187–192</sup>

**Table 1** Examples of the structures of 1-D coordination polymers.

Motif	Example (connector/linker/complex)	References
Linear chain	$\text{Ag}^{\text{I}}/4\text{-pytz}/[\{\text{Ag}(4\text{-pytz})\} \cdot \text{BF}_4]_n$	155
Zigzag chain	$\text{Cu}^{\text{II}}/4,4'\text{-bpy}/[\text{Cu}(\text{ClO}_4)_2(4,4'\text{-bpy})(2,2'\text{-bpy})]_n$	171
Double chain	$\text{Cu}^{\text{I}}/3,4'\text{-bpy}/[\text{CuBr}(3,4'\text{-bpy})]_n$	172
Helix	$\text{Ni}^{\text{II}}/4,4'\text{-bpy}/[\text{Ni}(4,4'\text{-bpy})(\text{benzoate})_2(\text{MeOH})_2]_n$	169
Fishbone	$\text{Cd}^{\text{II}}/4,4'\text{-bpy}/[\{\text{Cd}(4,4'\text{-bpy})_3(\text{H}_2\text{O})_2\} \cdot 2\text{ClO}_4 \cdot 2\text{H}_2\text{O}]_n$	173
Ladder	$\text{Ag}^{\text{I}}/\text{bpethy}^{\text{a}}/[\{\text{Ag}_2(\text{bpethy})_5\} \cdot 2\text{BF}_4]_n$	174
Railroad	$\text{Cu}^{\text{II}}/4,4'\text{-bpy}/[\{\text{Cu}_2(4,4'\text{-bpy})_3(\text{H}_2\text{O})_2(\text{phba})_2\} \cdot 2\text{NO}_3 \cdot 4\text{H}_2\text{O}]_n^{\text{b}}$	175

<sup>a</sup> bpethy = 1,2-bis(4-pyridyl)ethyne. <sup>b</sup> phba = 4-hydroxybenzoate.

**Table 2** Examples of the structures of 2-D coordination polymers.

Motif	Compound (connector/linker/complex)	References
Square grid	$\text{Cd}^{\text{II}}/4,4'\text{-bpy}/[\{\text{Cd}(\text{NO}_3)_2(4,4'\text{-bpy})_2\} \cdot 2\text{C}_6\text{H}_4\text{Br}_2]_n$	180
Rhombic grid	$\text{Zn}^{\text{II}}/4,4'\text{-bpy}/[\{\text{Zn}(4,4'\text{-bpy})_2(\text{H}_2\text{O})_2\} \cdot \text{SiF}_6]_n$	181
Rectangular grid	$\text{Cu}^{\text{II}}/4,4'\text{-bpy}, \text{pyz}/[\{\text{Cu}(4,4'\text{-bpy})(\text{pyz})(\text{H}_2\text{O})_2\} \cdot 2\text{PF}_6]_n$	176
Honeycomb grid	$\text{Cu}^{\text{I}}/\text{pyz}/[\{\text{Cu}_2(\text{pyz})_3\} \cdot \text{SiF}_6]_n$	182
Brick wall	$\text{Cd}^{\text{II}}/\text{L}/[\text{Cd}_2(\text{NO}_3)_4(\text{L})_3]_n^{\text{a}}$	117
Herringbone	$\text{Co}^{\text{II}}/\text{azpy}/[\{\text{Co}_2(\text{NO}_3)_4(\text{azpy})_3\} \cdot \text{CH}_2\text{Cl}_2]_n$	178
Bilayer	$\text{Co}^{\text{II}}/4,4'\text{-bpy}/[\{\text{Co}_2(\text{NO}_3)_4(4,4'\text{-bpy})_3\} \cdot 4\text{H}_2\text{O}]_n$	179

<sup>a</sup> L = 1,4-bis(4-pyridylmethyl)-2,3,5,6-tetrafluorobenzene.

**Table 3** Examples of the structures of 3-D coordination polymers.

Motif	Compound (connector/linker/complex)	References
Diamondoid net	$\text{Zn}^{\text{II}}/\text{L1}/[\text{Zn}(\text{L1})]_n^{\text{a}}$	193
Octahedral net	$\text{Cu}^{\text{II}}/4,4'\text{-bpy}, \text{SiF}_6/[\{\text{Cu}(\text{SiF}_6)(4,4'\text{-bpy})_2\} \cdot \text{DMF}]_n$	152
NbO	$\text{Cu}^{\text{II}}/\text{L2}/[\{\text{Cu}_2(\text{L2})_2(\text{H}_2\text{O})_2\} \cdot 8\text{DMF} \cdot 2\text{H}_2\text{O}]_n^{\text{b}}$	31
ThSi <sub>2</sub>	$\text{Ag}^{\text{I}}/4\text{-TEB}/[\text{Ag}(\text{CF}_3\text{SO}_3)(4\text{-TEB})]_n$	187
PtS	$\text{Cu}^{\text{II}}/\text{ATC}/[\{\text{Cu}_2(\text{ATC})\} \cdot 6\text{H}_2\text{O}]_n^{\text{c}}$	192
CdSO <sub>4</sub>	$\text{Cu}^{\text{II}}/\text{bpepha}/[\{\text{Cu}(\text{NO}_3)_2(\text{beptha})_2\} \cdot x(\text{guest})]_n$	188

<sup>a</sup> L1 = 4-[2-(4-pyridyl)ethenyl]benzoate. <sup>b</sup> L2 = 2-bromo-1,4-BDC. <sup>c</sup> ATC = 1,3,5,7-adamantanetetracarboxylate.

$[\{\text{Zn}(\text{nicotinate})_2\} \cdot \text{MeOH} \cdot 2\text{H}_2\text{O}]_n$  represents the first example of a 3-D coordination polymer that possesses a 4<sup>2</sup>.8<sup>4</sup> topology based solely upon square-planar nodes.<sup>190</sup> Further examples of some 3-D network motifs are listed in Table 3.<sup>30,152,187,188,192,193</sup>

### 7.5.1.2.4 Interpenetration

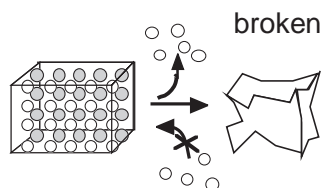
Interpenetration frequently occurs in coordination polymers with large grids or spaces. In some cases the frameworks generate spacious voids, cavities, and channels, which may account for more than half the volume of the crystal. These large spaces are usually occupied by highly disordered, essentially liquid, solvents. In other cases remarkable interpenetrating structures are formed in which the voids associated with one framework are occupied by one or more independent frameworks; an inherent feature of such entangled structures is that they can be disentangled only by breaking internal connections. Until recently examples were rare, but they are now being reported with ever increasing frequency. A detailed review has been published.<sup>11</sup> It is noteworthy that one of the first examples of coordination networks, reported many years ago, is a sixfold diamondoid net based on Cu<sup>I</sup> ions and the flexible bidentate adiponitrile (3-D diamondoid net: Scheme 6a).<sup>194</sup> The highest interpenetration (10-fold) diamondoid net based on only coordinative bonds (3-D diamondoid net: Scheme 6a) has recently been found in  $[\{\text{Ag}(1,12\text{-dodecanedinitrile})_2\} \cdot 2\text{NO}_3]_n$ .<sup>164</sup> Several coordination polymers with fluorinated ligands are not apt to be interpenetrated, due to weak intermolecular forces among fluorinated compounds.<sup>195</sup>

## 7.5.2 FUNCTIONS

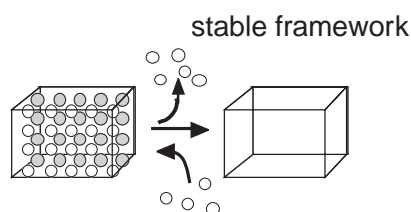
### 7.5.2.1 Porous Function

Porous coordination polymers are classified in three categories (Scheme 9). The first-generation compounds provide frameworks with microcavities and/or channels supported by guest molecules, which are collapsed by the removal of the guest molecules. The second-generation compounds have robust porous frameworks even after removal of guest molecules. The third-generation compounds bear dynamic frameworks, which change themselves responding to external physical stimuli, such as an electric or magnetic field or light, and chemical stimuli provided by guest molecules. Zeolites and activated carbons constructed from covalent bonds are

## First generation

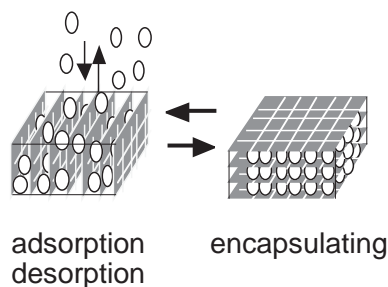


## Second generation



## Third generation

dynamic channels responding to stimuli



Scheme 9

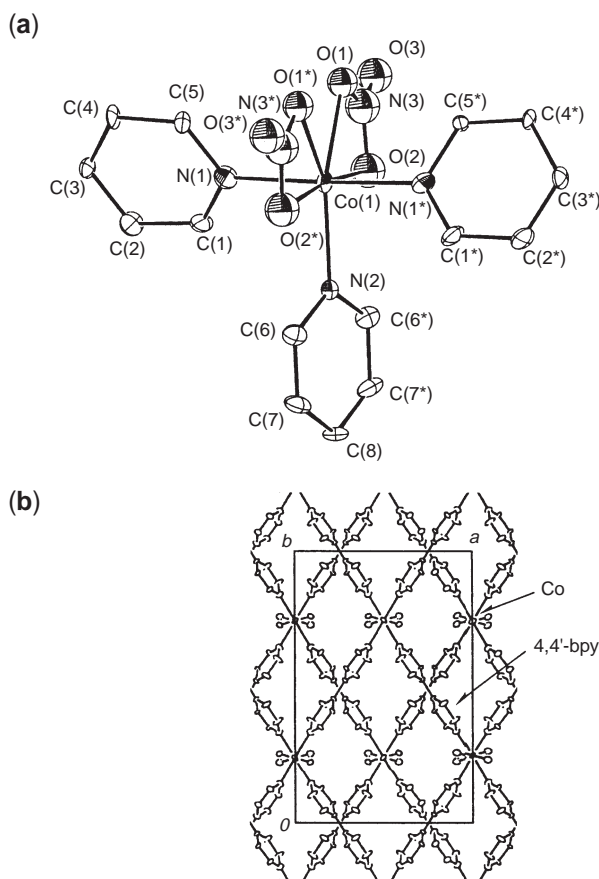
representative of porous solids and are often classified as second-generation compounds. Conversely, porous coordination polymers could afford not only stable second-generation compounds but also dynamic third-generation ones. The following discussion illustrates typical examples of second- and third-generation coordination polymers and their porous properties. Representative examples of coordination polymers with several porous functions are listed in Table 4.

Table 4 Representative examples of porous function.

	Function	Compound	Guests or substrates	Appeared in
Second generation compound	Adsorption (gas)	$[\text{Co}_2(\text{NO}_3)_4(4,4'\text{-bpy})_3]_n$	$\text{CH}_4$ , $\text{O}_2$ , $\text{N}_2$	1997 <sup>179</sup>
	Adsorption (vapor)	$[\text{Zn}_4\text{O}(1,4\text{-BDC})_3]_n$	$\text{CH}_2\text{Cl}_2$ , $\text{CCl}_4$ , $\text{C}_6\text{H}_{12}$ , etc.	1999 <sup>186</sup>
Third generation compound	Anion-exchange	$[\text{Cu}(\text{L1})]_n^{\text{a}}$	$\text{BF}_4^-$ , $\text{PF}_6^-$	1990 <sup>183</sup>
	Adsorption (gas)	$[\{\text{Cu}(\text{BF}_4)_2(4,4'\text{-bpy})(\text{H}_2\text{O})_2\} \cdot 4,4'\text{-bpy}]_n$	$\text{Ar}$ , $\text{N}_2$ , $\text{CO}_2$	2001 <sup>196</sup>
	Adsorption (vapor)	$[\text{Ag}(\text{CF}_3\text{SO}_3)(3\text{-TEB})]_n^{\text{b}}$	$\text{C}_6\text{H}_6$	1995 <sup>197</sup>
	Anion-exchange	$[\text{Ag}(\text{EDTPN})]_n^{\text{c}}$	$\text{NO}_3^-$ , $\text{CF}_3\text{SO}_3^-$ , $\text{ClO}_4^-$	2000 <sup>198</sup>
	Catalysis <sup>e</sup>	$[\text{Cd}(\text{NO}_3)_2(4,4'\text{-bpy})_2]_n$ $[\{\text{Zn}_3\text{O}(\text{L2})_6\} \cdot 2\text{H}_3\text{O} \cdot 12\text{H}_2\text{O}]_n^{\text{d}}$	Aldehydes and $\text{SiMe}_3\text{CN}$ Ester and alcohols	1994 <sup>180</sup> 2000 <sup>42</sup>

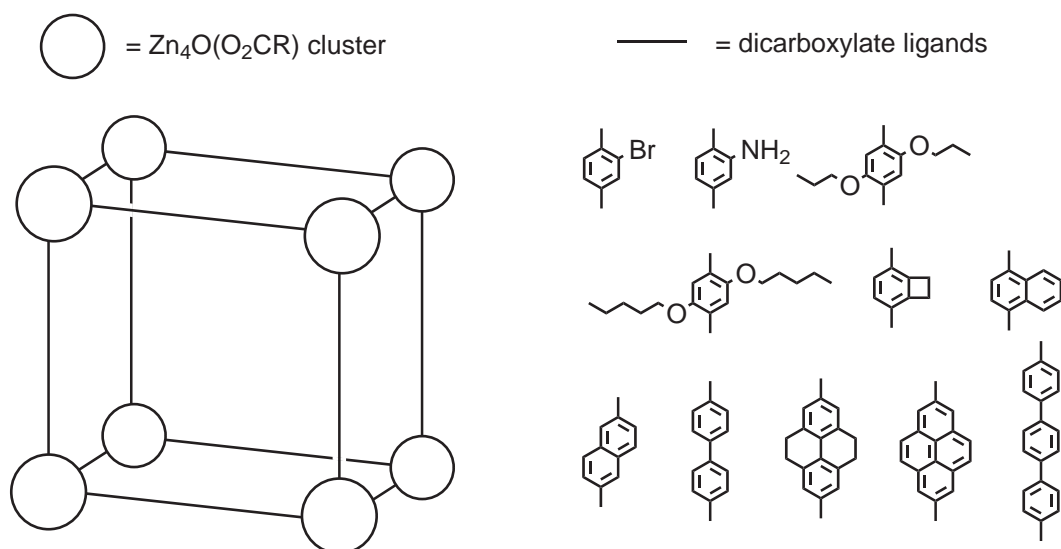
<sup>a</sup> L1 = 4,4',4'',4'''-tetracyanotetraphenylmethane. <sup>b</sup> 3-TEB = 1,3,5-tris(3-ethynylbenzotrile)benzene. <sup>c</sup> EDTPN = ethylenediamine-tetrapropionitrile. <sup>d</sup> L2 is chiral organic ligands. <sup>e</sup> The catalytic site including metal ions may be dynamic accompanying with bond formation/cleavage, and therefore, the pores could be classified in the third generation type. However, the dynamic behaviour of the framework was not observed for these compounds.

The adsorption of gases in porous solids is of great interest because of potential applications; e.g., storage and transport of natural gas. For the creation of suitable adsorbents research has been devoted to the synthesis of stable frameworks following the removal of guest molecules, viz second-generation compounds. The first report of gas adsorption properties involving porous coordination polymers at ambient temperature appeared in 1997. The framework is best described as a tongue-and-groove (bilayer) structure (2-D bilayer: Scheme 4g)  $[\{M_2(4,4'\text{-bpy})_3(\text{NO}_3)_4\} \cdot x\text{H}_2\text{O}]_n$  ( $M = \text{Co}$ ,  $x = 4$ ;  $\text{Ni}$ ,  $x = 4$ ;  $\text{Zn}$ ,  $x = 2$ ), formed from  $M(\text{NO}_3)_2$  and 4,4'-bpy.<sup>179</sup> The effective microchannel cross-section of a dried sample was obtained about  $3 \text{ \AA} \times 6 \text{ \AA}$  (after consideration of Van der Waals radii) as shown in Figure 7. This apohost reversibly adsorbs  $\text{CH}_4$ ,  $\text{N}_2$ , and  $\text{O}_2$  in the pressure range of 1–36 atm without collapse of the crystal framework. Similar coordination polymers capable of gas adsorption have been synthesized.<sup>31,152,153,157,196,199–206</sup> For example,  $[\{\text{Cu}(\text{AF}_6)(4,4'\text{-bpy})_2\} \cdot 8\text{H}_2\text{O}]_n$  ( $A = \text{Si}$  and  $\text{Ge}$ ) has a 3-D porous network, in which 2-D grid layers of  $[\text{Cu}(4,4'\text{-bpy})_2]_n$  are linked by pillar  $\text{AF}_6$  anions.<sup>152,153</sup> These complexes show high  $\text{CH}_4$  adsorption activity at room temperature and relatively low pressure (ca. 36 atm). In this century other types of complexes with high capacity have been synthesized successively.  $[\text{Zn}_4\text{O}(\text{L})_3]_n$  ( $L =$  several dicarboxylate ligands) with a  $\text{CH}_4$  adsorption property affords a 3-D cubic porous network, in which an oxide-centered  $\text{Zn}_4\text{O}$  tetrahedron connector is edge-bridged by six carboxylates to give the octahedron-shaped SBU (3-D octahedral net: Scheme 6b)<sup>31,186</sup> It should be noted that this 3-D porous system can be functionalized with the organic groups  $-\text{Br}$ ,  $-\text{NH}_2$ ,  $-\text{OC}_3\text{H}_7$ ,  $-\text{OC}_5\text{H}_{11}$ ,  $-\text{C}_2\text{H}_4$ , and  $-\text{C}_4\text{H}_4$  (Scheme 10) and that its pore size can be expanded by the long molecular struts biphenyl, tetrahydropyrene, pyrene, and terphenyl, while the original framework topology is retained (Scheme 10). To date, the highest surface area ( $3,265 \text{ m}^2 \text{ g}^{-1}$ ) is obtained in the 3-D coordination polymer,  $[\text{Cu}_2(4,4'\text{-biphenyldicarboxylate})_2(\text{DABCO})]_n$  ( $\text{DABCO} = 1,4\text{-diazabicyclo}[2.2.2]\text{octane}$ ) (3-D octahedral net: Scheme 6b).<sup>207</sup>



**Figure 7** (a) ORTEP drawing of  $[\{\text{Co}_2(4,4'\text{-bpy})_3(\text{NO}_3)_4\} \cdot 4\text{H}_2\text{O}]_n$  around the Co center (ellipsoids at 20% probability) (b) View of the crystal structure along the  $c$ -axis (reproduced by permission of Wiley-VCH Verlag GmbH from *Angew. Chem., Int. Ed. Engl.*, **1997**, 36, 1725–1727)





Scheme 10

Several third-generation compounds with flexible channels have been prepared. The compound  $[\{Cu(BF_4)_2(4,4'\text{-bpy})(H_2O)_2\} \cdot 4,4'\text{-bpy}]_n$  contains 1-D linear chains which are linked by metal-free 4,4'-bpy molecules via hydrogen bonds with coordinated  $H_2O$  molecules, thereby forming 2-D noninterpenetrated sheets (Figure 8) (1-D linear chain: Scheme 5a).<sup>208</sup> The adsorption of  $N_2$ , Ar, and  $CO_2$  suddenly begins at a certain relative pressure (gate pressure), therefore being of almost no adsorption below this gate pressure.<sup>196</sup> Such a unique adsorption phenomenon is associated with the hydrogen bond links. Third-generation compounds maybe described within three categories as shown in Scheme 11.<sup>209</sup>

- The “guest-induced crystal-to-amorphous transformation (CAT)” framework (type D): the framework in this species collapses due to close-packing force effective once the guest molecules have been removed. However, the structure is regenerated on reintroduction of the guest molecules.<sup>58,206,208,210</sup>

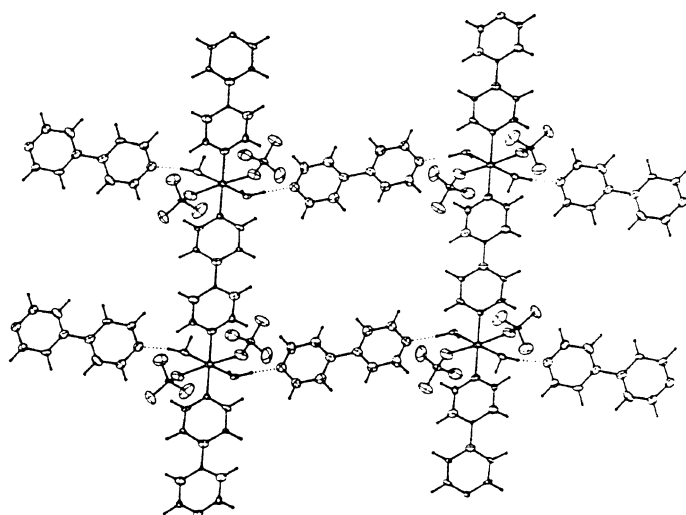
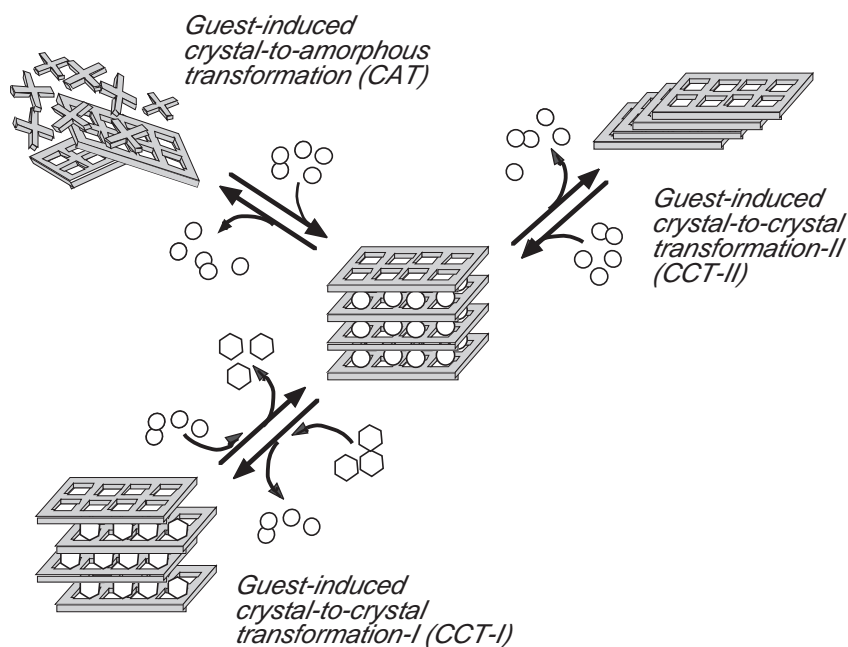


**Figure 8** 2-D architecture of the structure of  $[\{Cu(BF_4)_2(4,4'\text{-bpy})(H_2O)_2\} \cdot 4,4'\text{-bpy}]_n$  showing the Cu-4,4'-bpy-Cu (coordinated) and Cu- $OH_2 \cdots 4,4'\text{-bpy} \cdots H_2O$ -Cu (hydrogen bonded) 4,4'-bpy bridges (reproduced by permission of the Royal Society of Chemistry from *J. Chem. Soc., Dalton Trans.*, 1997, 913–914).



Scheme 11

- The “guest-induced crystal-to-crystal transformation-I (CCT-I)” framework (type II): this framework has the property that structural shifts in the network are induced by the simultaneous exchanging of guest molecules.<sup>152,198,211</sup>
- The “guest-induced crystal-to-crystal transformation-II (CCT-II)” framework (type III): this framework has the property that removal or addition of guest molecules causes a structural change in the network; however, it reverts to the original structure under the initial conditions.<sup>23,196,209,212,213</sup>

Interestingly, compounds of category II and III show “crystal-to-crystal transformation”. In a sense, this property results from the molecular inorganic–organic hybrid system.

Adsorption or exchange of volatile substances and small molecules by compounds of the third-generation type are extensively investigated.<sup>16,23,30,31,39,41,42,56–58,60,154,186,187,192,197,199,204,209,210,212–224</sup>

Properties such as guest removal and exchange within a host crystal are investigated using  $[\text{Ag}(\text{CF}_3\text{SO}_3)(4\text{-TEB})]_n$  (4-TEB = 1,3,5-tris(4-ethynylbenzotrile)benzene).<sup>214</sup> The nitrile moieties of the trigonal phenylalkyne ligand coordinate end-on to the trigonal-pyramidal silver cation to form a 3-D (3,3)-connected net topologically analogous to the inorganic structure type  $\text{ThSi}_2$  (3-D  $\text{ThSi}_2$  net: Scheme 6d). There are six interpenetrated  $\text{ThSi}_2$ -type networks with large channels with cross-sections of  $15 \text{ \AA} \times 22 \text{ \AA}$  in the final structure. Guest exchange of nonfunctionalized aliphatic and aromatic molecules leaves the original framework undisturbed. However, crystals containing aromatic alcohols can be indexed to a 2-D rectangular structure. On exposure to  $\text{H}_2\text{O}$  or MeOH vapor under pressure a hysteretic adsorption and desorption profile, accompanied by a transformation of the crystal structure, is observed for  $\{[\text{Cu}_2(\text{pzdc})_2(\text{dpyg})] \cdot 8\text{H}_2\text{O}\}_n$  (pzdc = pyz-2,3-dicarboxylate; dpyg = 1,2-di(4-pyridyl)glycol), which possesses a pillared-layer structure.<sup>213</sup> The size, shape, and substituent groups of organic molecules determine their adsorption characteristics and are highly significant with respect to the separation of mixtures.<sup>58,180,209,210,220,222</sup>

Structural diversity and easy modification of pore size in coordination polymers could give higher selectivities than those of zeolites or activated carbons.  $\{[\text{Co}(\text{HBTC})(\text{pyridine})_2] \cdot 2/3\text{pyridine}\}_n$  (BTC = 1,3,5-benzenetricarboxylate) (2-D honeycomb grid: Scheme 4d) selectively adsorbs aromatic molecules by  $\pi$ – $\pi$  interactions.<sup>222</sup> The selective uptake for guests with hydrogen bonding sites, in some cases, involving size and shape recognition, is also observed in several coordination polymers containing coordinatively unsaturated metal centers,<sup>210,220</sup> amide,<sup>209</sup> and both carboxylate and pyridine guest-binding sites.<sup>58</sup>

It is well known that porous zeolites show cation-exchange properties due to their anionic frameworks, while porous coordination polymers constructed from cationic metal ions and

neutral bridging ligands can exchange the counteranions that are included in the frameworks.<sup>153,183,198,211,225–227</sup> An anion-exchange property, which happens in a solid–liquid interface, was first reported in 1990.<sup>183</sup>  $[\{\text{Cu}(4,4',4'',4'''\text{-tetracyanotetraphenylmethane})\}\cdot\text{BF}_4\cdot x\text{C}_6\text{H}_5\text{NO}_2]_n$  contains a diamond-related cationic framework, which generates very large adamantane-like cavities occupied by disordered  $\text{C}_6\text{H}_5\text{NO}_2$  together with  $\text{BF}_4^-$  anions (3-D diamondoid net: Scheme 6a). This crystal readily undergoes anion-exchange with  $\text{PF}_6^-$ . Recently, the structural transformations in the crystalline state were observed concomitant with the anion-exchange.<sup>153,198,211</sup>

Porous coordination polymers that adsorb salts and metal complexes have been also found.<sup>42,58,60,206</sup> The X-ray crystal structure of  $[\{\text{Cu}(\text{pymo})_2\}\cdot\text{NH}_4\text{ClO}_4]_n$  (Hpymo = 2-hydroxypyrimidine) reveals that the combination of square-planar  $\text{Cu}^{\text{II}}$  ion with  $120^\circ$  bond angles provided by 2-hydroxypyrimidine generates a 3-D porous framework with  $\text{NH}_4^+$ ,  $\text{ClO}_4^-$ , and  $\text{H}_2\text{O}$  molecules included in the pores.<sup>206</sup> This complex reversibly and selectively sorbs  $\text{AClO}_4$  salts ( $\text{A} = \text{NH}_4, \text{Li}, \text{Na}, \text{K}, \text{Rb}$ ) when exposed to  $\text{AClO}_4$  aqueous solutions, giving highly crystalline  $[\{\text{Cu}(\text{pymo})_2\}\cdot\text{AClO}_4]_n$  clathrates. The X-ray structure of  $[\{\text{Ni}_3(\text{C}_{20}\text{H}_{32}\text{N}_8)_3(\text{CTC})_2\}\cdot 16\text{H}_2\text{O}]_n$  ( $\text{C}_{20}\text{H}_{32}\text{N}_8 = 1,8\text{-}(4\text{-pyridylmethyl})\text{-}1,3,6,8,10,13\text{-hexaazacyclotetradecane}$  macrocyclic ligand;  $\text{CTC} = \text{cis}, \text{cis}\text{-}1,3,5\text{-cyclohexanetricarboxylate}$ ) (2-D honeycomb grid: Scheme 4d) shows that each  $\text{Ni}^{\text{II}}$  macrocyclic unit binds two  $\text{CTC}^{3-}$  ions in the *trans* position and each  $\text{CTC}^{3-}$  ion coordinates three  $\text{Ni}^{\text{II}}$  macrocyclic complexes to form a 2-D layer, in which pendant pyridine rings are involved in the hydrogen bonding and the herringbone  $\pi\text{-}\pi$  interaction.<sup>58</sup> X-ray powder diffraction indicates that the framework is deformed upon removal of  $\text{H}_2\text{O}$  guests but is restored upon rebinding of  $\text{H}_2\text{O}$ . This host solid binds  $[\{\text{Cu}(\text{NH}_3)_4\}\cdot 2\text{ClO}_4]$  in MeCN.

Metal ions play key roles in organic transformations. Many investigators work with soluble species in a homogeneous solution. An advantage of heterogeneous catalysts is their ready recoverability, and they are important in industry. However, solid catalysts have so far been almost exclusively inorganic materials and microporous inorganic zeolites are especially useful. Despite much recent interest in metal-organic solids with zeolitic guest-binding properties, their catalytic activities are largely unexplored.<sup>16,42,180,223,228,229</sup>  $[\text{Cd}(\text{NO}_3)_2(4,4'\text{-bpy})_2]_n$ , which consists of 2-D networks (2-D square grid: Scheme 4a), shows with shape specificity catalytic activity for the cyanosilylation of aldehydes.<sup>180</sup> A homochiral open-framework solid, whose formula is given as  $[\{\text{Zn}_3\text{O}(\text{L})_6\}\cdot 2\text{H}_2\text{O}\cdot 12\text{H}_2\text{O}]_n$  ( $\text{L}$  is chiral organic ligands), reveals enantioselective catalytic activity for transesterification (2-D honeycomb grid: Scheme 4d).<sup>42</sup> Zr, Ti, and lanthanide complexes also show characteristic catalytic activities.<sup>16,223,229</sup> Utilization of a metalloligand as a building unit could provide a novel porous coordination polymer with high catalytic activity. This is because a coordinatively unsaturated metal center, which can function as activation sites in the heterogeneous process could be located in the channel wall which is less sterically hindered than the nodal position in an attack by organic molecules. Such a coordination polymer,  $[\{\text{ZnCu}(2,4\text{-pydca})_2(\text{H}_2\text{O})_3(\text{DMF})\}\cdot \text{DMF}]_n$ , in which some  $\text{Cu}^{\text{II}}$  ions are located in channel walls and their axial sites are capped by DMF molecules (Figure 5), has recently been synthesized.<sup>138</sup> This sort of architecture for catalytic pores is promising.

### 7.5.2.2 Toward Coordination Polymer Magnets

The field of molecular magnetism has shown quite spectacular advances in the last decade. For the design, the decrease in distance between spins and their 3-D interaction is of profound significance, and optimal design can lead to spontaneous magnetization at high temperature. Therefore, use of a short bridging ligand such as  $\text{CN}^-$ ,  $\text{N}_3^-$ , etc. can strengthen a spin–spin interaction between the metal ions. Another approach is to utilize an organic radical ligand which may serve not only as spin carriers but also as linkers to other magnetically active metal ions.

Hexacyanometalate ions  $[\text{M}(\text{CN})_6]^{n-}$  are often used as building blocks for bimetallic magnetic materials. Two types of bimetallic compounds have been derived from  $[\text{M}(\text{CN})_6]^{n-}$ : (i) the Prussian-Blue family constructed with a simple metal ion, and (ii) complex-based bimetallic assemblies constructed with a complex cation such as  $[\text{Ni}^{\text{II}}(\text{L})_2]^{2+}$  ( $\text{L} = \text{en}$  derivative),<sup>63–65</sup>  $[\text{Ni}^{\text{II}}(\text{L}')^{2+}$  ( $\text{L}' = \text{tren}$  and macrocyclic derivative),<sup>75,230–232</sup>  $[\text{Mn}^{\text{II}}(\text{L}'')^{2+}$  ( $\text{L}'' = \text{en}$  derivative),<sup>233,234</sup> and  $[\text{M}^{\text{III}}(\text{salen})]^+$  ( $\text{M} = \text{Fe}$  or  $\text{Mn}$ ).<sup>66–70</sup> The 3-D bimetallic assembly  $[\{\text{Mn}(\text{en})\}_3\{\text{Cr}(\text{CN})_6\}_2\cdot 4\text{H}_2\text{O}]_n$  reveals that all the cyanide groups of  $[\text{Cr}(\text{CN})_6]^{3-}$  are involved in coordination to adjacent  $\text{Mn}^{\text{II}}$  ions and shows magnetic ordering below 69 K, as illustrated in Figure 9.<sup>233</sup> To the best of the authors' knowledge, the magnetic phase-transition temperature  $T = 71$  K of a 3-D network  $[\{\text{Mn}(\text{glya})\}_3\{\text{Cr}(\text{CN})_6\}_2\cdot 2.5\text{H}_2\text{O}]_n$  ( $\text{glya} = \text{glycineamide}$ ) is the highest among the structurally characterized molecular-based magnets.<sup>235</sup>

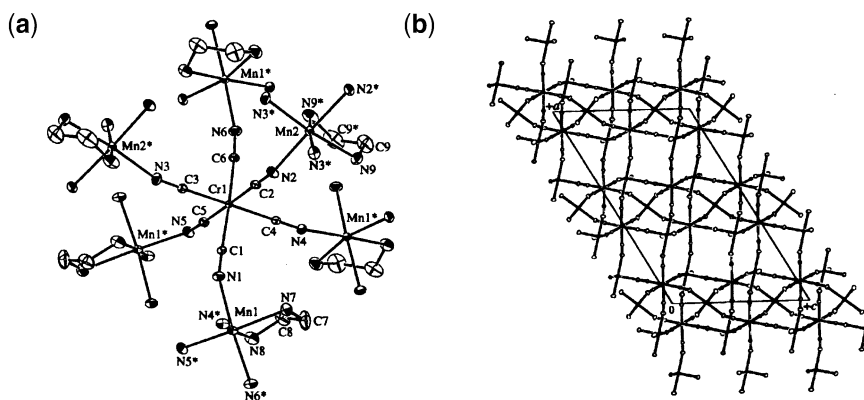


**Figure 9** (a) ORTEP drawing of the heptanuclear unit of  $[\{Mn(en)\}_3\{Cr(CN)_6\}_2 \cdot 4H_2O]_n$ . (b) Projection of the 3-D network structure onto the  $ac$  plane (reproduced by permission of Wiley-VCH Verlag GmbH from *Angew. Chem., Int. Ed. Engl.*, **1999**, *38*, 1795–1798).

The metalloligands are good candidate for the construction of novel bimetallic coordination polymers with spontaneous magnetization similar to hexacyanometalate ions. A series of Cu metalloligands have oxamate, oxamide, benzoate, and propionate components and bridge additional transition metal ions.<sup>131–133,150</sup> Ferromagnetically ordered  $[MnCu(pbaOH)(H_2O)_3]_n$  ( $pbaOH = 2$ -hydroxy-1,3-propylenebis(oxamato)) consists of ordered bimetallic chains running along the  $b$ -axis, with  $Mn^{II}$  and  $Cu^{II}$  ions bridged by oxamato groups (Figure 10) (1-D linear chain: Scheme 5a).<sup>150</sup> Ox- or dto-bridged polymeric compounds of general formula  $[cat \{M1^{II} M2^{III} \{L\}_3\}]_n$  contain the metalloligands  $[M2^{III} \{L\}_3]^{3-}$  ( $M2^{III} = Cr$ ,<sup>145</sup>  $Fe$ ,<sup>147</sup> and  $Ru$ <sup>148</sup>).

Polynuclear azide-bridged derivatives are a rich source of new magnetic systems where a variety of the coordination modes of the azido ligand;  $\mu_{1,3}$ - $N_3$  (end-to-end, EE, antiferromagnetic coupling),  $\mu_{1,1}$ - $N_3$  (end-on, EO, ferromagnetic coupling), or even in more exotic modes as  $\mu_{1,1,1}$ - $N_3$  or  $\mu_{1,1,3}$ - $N_3$ .<sup>236–241</sup> The compounds  $[Mn(N_3)_2(py)_2]_n$  ( $py = 3$ -methylpyridine and 3,4-dimethylpyridine) exhibiting a ferrimagnetic-like behavior show 1-D arrangement of double azido bridges between neighboring manganese atoms with the unprecedented  $-Mn-(\mu_{1,3}-N_3)_2-Mn-(\mu_{1,3}-N_3)_2-Mn-(\mu_{1,1}-N_3)_2-Mn-$  sequence (1-D double chain: Scheme 5c).<sup>238</sup>

Tricyanomethanide (tcm) and dicyanamide (dca) are small ligands that can bridge three metals and, due to their highly conjugated nature, can provide strong spin coupling between the metals.<sup>241–244</sup> The unsolvated  $\alpha$ - $[Mn(dca)_2]_n$ , with a rutile-like single network structure, is a spin-canted antiferromagnet (weak ferromagnet) with long-range magnetic ordering ( $T_N = 16$  K).<sup>244</sup>

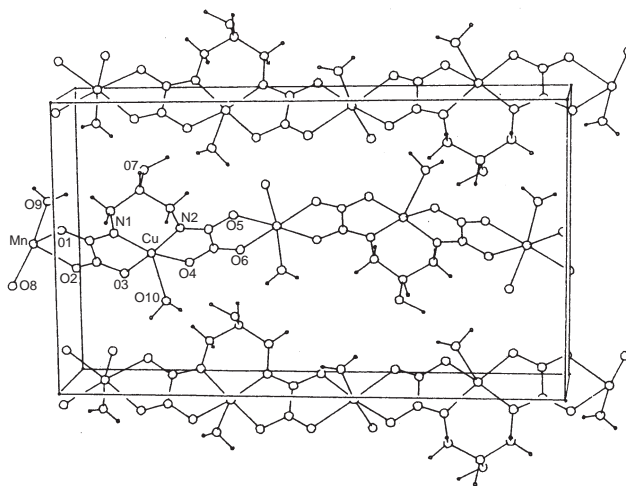


**Figure 10** Perspective view of three neighboring chains in  $[MnCu(pbaOH)(H_2O)_3]_n$ . The origin of the unit cell is in the upper left-hand corner; the  $a$ -axis runs top to bottom of page and the  $b$ -axis left to right (reproduced by permission of the American Chemical Society from *J. Am. Chem. Soc.*, **1988**, *110*, 782–789).

Three synthetic methods have been used to construct coordination polymer-based magnetic materials containing organic radical ligands:

- (i) utilization of an organic radical ligand for a direct linker
- (ii) generation of a radical on a linking ligand as a result of the formation reaction of the coordination polymer, i.e., a sort of redox process,
- (iii) production of a radical by light irradiation following the construction of coordination polymers.

A strategy for using  $\pi$ -conjugated polynitroxide radicals with high-spin ground states as bridging ligands for magnetic metal ions was applied to assemble and align spins on a macroscopic scale.<sup>245–247</sup> The X-ray crystal structure of the complex  $[\{Mn_3(hfac)_6(L)_2\} \cdot n-C_7H_{16}]_n$  ( $hfac$  = hexafluoroacetylacetonate;  $L$  = 1,3,5-tris[*p*-(*N*-*tert*-butyl-*N*-oxyamino)phenyl]benzene) reveals that six triradical molecules and six Mn ions make an extended honeycomb network (2-D honeycomb grid: Scheme 4d).<sup>246</sup>

Recently,  $[Co(hfac)_2(NITPhOMe)]_n$  (NITPhOMe = 4'-methoxy-phenyl-4,4,5,5-tetramethylimidazoline-1-oxyl-3-oxide) (1-D helix: Scheme 5d) was prepared, whose chains are magnetically isolated from each other. This is considered to be molecular magnetic nanowire.<sup>248</sup>

The crystal structure of the ferrimagnet  $[\{Mn(TPP)(TCNE)\} \cdot 2PhMe]_n$  (TPP = tetraphenylporphyrin) which was prepared by the electron-transfer reaction between  $[Mn^{II}(TPP)]$  and neutral TCNE, reveals that  $[TCNE]^-$  ( $S = 1/2$ ) is *trans*- $\mu_2$ -*N*- $\sigma$ -bound to  $Mn^{III}$  ( $S = 2$ ) forming 1-D  $\cdots D^+ A^- \cdots$  ( $D = MnTPP$ ;  $A = TCNE$ ) chains (Figure 11) (1-D linear chain: Scheme 5a).<sup>71,73</sup> Various chemical modifications of this compound have been carried out (the porphyrin ligand, solvent, acceptor molecule, and metal ion).<sup>74</sup>

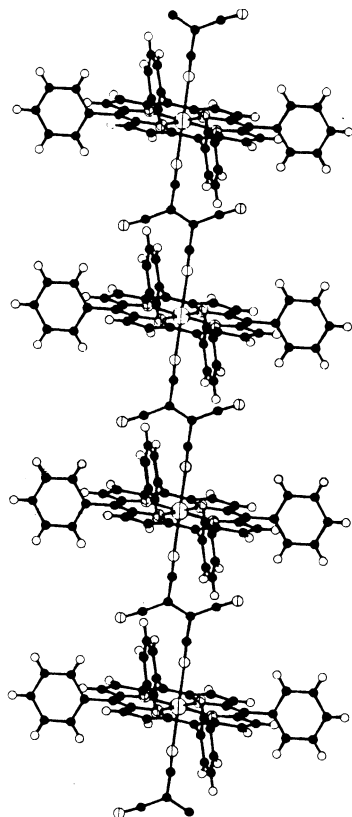


**Figure 11** Segment of an 1-D  $(\cdots D^+ A^- \cdots)$  chain ( $D = Mn(TPP)$ ;  $A = TCNE$ ) in  $[\{Mn(TPP)(TCNE)\} \cdot 2PhMe]_n$  (reproduced by permission of Wiley-VCH Verlag GmbH from *Adv. Mater.*, **1992**, *4*, 498–501).

The bridging ligands diazodi(4-pyridyl)methane and 5-trimethylsilyl-1,3-phenylenebis[diazo(4-pyridyl)methane] have two kinds of functional groups, two pyridyl nitrogens and a diazo group, which could be photolyzed thereby producing a carbene unit which could play a dual role of a triplet spin source and a magnetic coupling unit.<sup>249,250</sup> The complexes  $[\text{Mn}(\text{hfac})_2(\text{L})]_n$  ( $\text{L} = \text{diazodi}(4\text{-pyridyl})\text{methane}$ ), which form helical (1-D helix: Scheme 5d) and zigzag (1-D zigzag chain: Scheme 5b) infinite chains depending on the configuration modes of the ligands, show the characteristics of ferrimagnetic chains after light irradiation.<sup>249</sup>

### 7.5.2.3 Spin Cross-over Coordination Polymers

Some compounds containing  $\text{Fe}^{\text{II}}$  show a transition from the high-spin state (HS;  $S=2$ ) to the low-spin state (LS;  $S=0$ ) on cooling or upon increasing pressure, or conversely by light irradiation. This phenomenon is called “spin cross-over” (SC), which is also found in complexes of  $\text{Fe}^{\text{III}}$  and  $\text{Co}^{\text{II}}$ . One of the goals is to design new materials exhibiting SC behavior characterized by sharp spin transitions accompanied by thermal hysteresis, as well as an associated thermo-chromic effect. A straightforward strategy toward cooperative SC compounds is represented by the use of potential bridging ligands, which establish communication between the active SC sites.

In this regard, a number of 1-D,<sup>251–255</sup> 2-D,<sup>256–260</sup> and 3-D<sup>90,261,262</sup> compounds have been reported. Recently, thermal-, pressure-, and light-induced spin-transition behavior (light-induced excited spin-state trapping, LIESST) has been observed for the doubly interpenetrating 3-D bimetallic compounds  $[\text{Fe}(4,4'\text{-bpy})_2\{\text{Ag}(\text{CN})_2\}_2]_n$  and  $[\text{Fe}(\text{bpethe})_2\{\text{Ag}(\text{CN})_2\}_2]_n$  (bpethe = 1,2-bis(4-pyridyl)ethene).<sup>90</sup> The single crystals of the bpethe derivative undergo a spin transition with a large hysteresis loop at about 95 K. Interestingly, valence tautomeric coordination polymer of  $\text{Co}^{\text{II}}/\text{Co}^{\text{III}}$  with a quinone-like ligand,  $[\text{Co}(3,6\text{-DBQ})_2(\text{pyz})]_n$  (DBQ = di-*tert*-butyl-1,2-benzoquinone) shows chromic photo-induced mechanical oscillation (1-D linear chain: Scheme 5a).<sup>263</sup>

### 7.5.2.4 Chromism

There are three guiding points for modules which are used to construct coordination polymers exhibiting chromism. Each module must show chromic properties, either from (i) a metal complex connector, (ii) an organic ligand linker, or (iii) guest molecules in cavities. Chromic behavior generally occurs in (i) when the coordination environment of the metal ion changes by removal of coordinated guest molecules.<sup>41,209,212,218,264</sup> Coordination polymer of  $\text{Co}^{\text{II}}$ -containing face-capped octahedral clusters of the type  $[\text{Re}_6\text{Q}_8(\text{CN})_6]^{4-}$  ( $\text{Q} = \text{S}, \text{Se}$ ) (Figure 12), create a porous framework that displays dramatic color changes upon exposure to certain organic solvents. This is apparently caused by conversion of the  $\text{Co}^{\text{II}}$  centers from octahedral to tetrahedral coordination.<sup>212</sup>

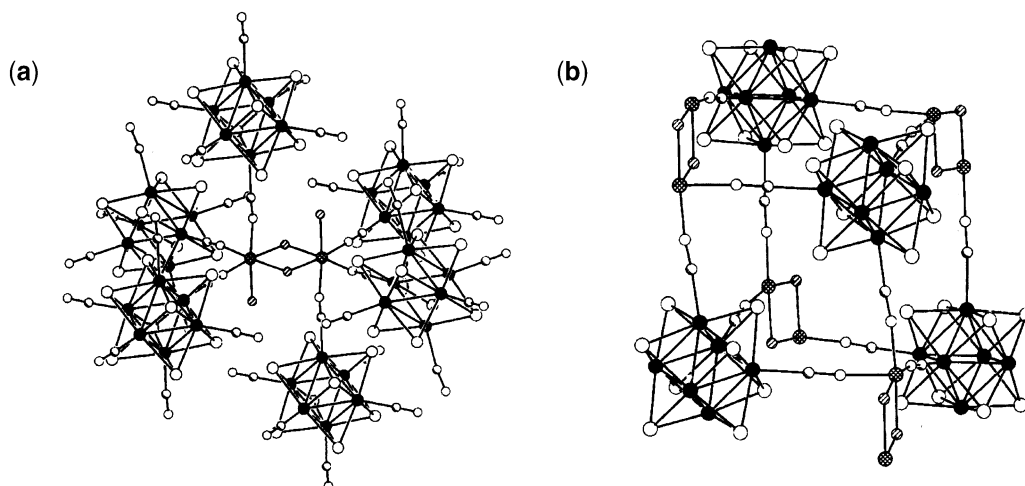


**Figure 12** (a) Local environment of the  $[\text{Co}_2(\text{H}_2\text{O})_4]^{4+}$  clusters in the structure of  $[\{\text{Co}_2(\text{H}_2\text{O})_4\}\{\text{Re}_6\text{S}_8(\text{CN})_6\}\cdot 12\text{H}_2\text{O}]_n$ . (b) Cube-like cage unit defining the cavities (reproduced by permission of the American Chemical Society from *J. Am. Chem. Soc.*, **2000**, *122*, 2763–2772).

Another approach is to introduce a chemically active molecule as a bridge or guest.<sup>129,265</sup> Polycyano-polycadmite host clathrates including a methylviologen dication ( $MV^{2+}$ ), which is a strong electron acceptor, show a color change from colorless to blue on UV irradiation, arising from the reduction of  $MV^{2+}$  to a methylviologen radical cation  $MV^{\cdot+}$ .<sup>265</sup>

### 7.5.2.5 Nonlinear Optical Properties

For synthesis, noncentrosymmetric arrangements of molecular chromophores are prerequisite, bulk second-order NLO susceptibility vanishing in a centrosymmetric environment. Conversely, recent success in the design and synthesis of novel materials based on metal-organic coordination networks has stimulated the use of supramolecular engineering of noncentrosymmetric solids for nonlinear optical effects by exploiting the strong and highly directional metal–ligand coordination bonds.

The polynitrile coordinated lanthanide complex  $\{[Eu(cda)_3(H_2O)_3] \cdot H_2O\}_n$  (cda = carbamoyldicyanomethanide) crystallized in the monoclinic space group  $Cc$ , affords a 2-D structure and exhibits a second harmonic generation (SHG) efficiency 16.8 times that of urea.<sup>21</sup> The compound  $\{[Cd[4-(4\text{-pyridyl})\text{benzoate}]_2] \cdot H_2O\}_n$ , which exhibits a powder SHG intensity of 310 relative to that of  $\alpha$ -quartz, adopts a sevenfold interpenetrated diamondoid structure (3-D diamondoid net: Scheme 6a) as illustrated in Figure 13.<sup>266</sup> The use of an unsymmetrical linking group introduces electronic asymmetry, and the rigidity of the bridging ligands facilitates good conjugation between the electron donors and acceptors.<sup>5</sup> These factors are necessary for second-order NLO effects.

Lattice inclusion of organic chromophores inside coordination polymers has also been used to achieve optical nonlinear effects. A SHG-active compound  $\{[Cd(4,4'\text{-bpy})_2(H_2O)_2] \cdot 4,4'\text{-bpy} \cdot 2(2\text{-nitroaniline}) \cdot 2ClO_4 \cdot H_2O\}_n$ , cocrystallized in the monoclinic space group  $Cc$ , has 2-D square grids (Scheme 4a) with 2-nitroaniline molecules, which is a NLO-active organic chromophore.<sup>173</sup>

Coordination polymers have also been investigated for third-order NLO properties.<sup>267-271</sup> Thus,  $[Co(NCS)_2(bpms)_2]_n$  (bpms = 1,2-bis(4-pyridylmethyl)disulfenyl) affords a 1-D double zigzag chain coordination polymer (1-D double chain: Scheme 5c) and shows significant third-order NLO properties.<sup>270</sup> Mn-4,4'-bpy polymers also show third-order NLO properties.<sup>267</sup> Recently, the 1-D quantum wire  $\{[Ni(1,2\text{-chxn})_2Br] \cdot 2Br\}_n$  (1-D linear chain: Scheme 5a) demonstrated gigantic third-order NLO activity.<sup>271</sup>

### 7.5.2.6 Redox Properties

Although redox properties of discrete coordination compounds are well investigated, the corresponding behavior of infinite coordination polymers has scarcely been investigated because of their insolubility.<sup>129,130,136,272</sup> The coordination polymer,  $\{[CuCl_2(BpyP)] \cdot 2Cl \cdot 11.275H_2O\}_n$

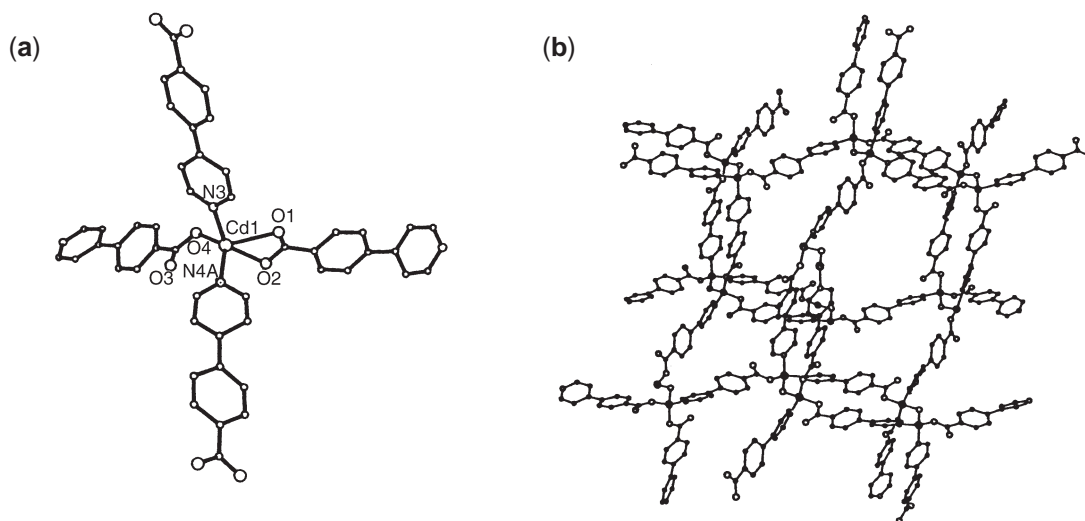


**Figure 13** Coordination environment (a) and diamondoid structure (b) of  $\{[Cd[4-(4\text{-pyridyl})\text{benzoate}]_2] \cdot H_2O\}_n$  (reproduced by permission of the American Chemical Society from *Chem. Mater.*, **2001**, *13*, 2705–2712).

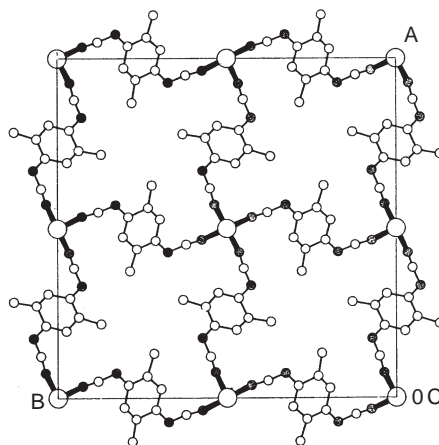


**Figure 14** *a,b*-Projection of the crystal structure of  $[\text{Cu}(2,5\text{-dimethyl-DCNQI})_2]_n$  (reproduced by permission of Wiley-VCH Verlag GmbH from *Angew. Chem., Int. Ed. Engl.*, **1986**, *25*, 740–741).

(BpyP = 3,6-bis(4'-pyridyl-1'-pyridinio) pyridazine) consists of 1-D infinite chains (1-D linear chain: Scheme 5a), in which photoelectron transfer from  $\text{Cl}^-$  to BPyP occurs, generating the pyridyl radical.<sup>129</sup> Solid state cyclic voltammograms of several 1-D coordination polymers containing ferrocene-based bidentate ligands (1-D linear chain: Scheme 5a) have been reported.<sup>136</sup>

### 7.5.2.7 Conductivity

Unusual behavior results from  $d\pi$ – $p\pi$  interactions between open-shell metal ions and organic radicals as illustrated by the family of 3-D metals  $[\text{Cu}(\text{R}^1, \text{R}^2\text{-DCNQI})_2]_n$  (DCNQI = *N,N'*-dicyanoquinonediimine) (Figure 14).<sup>273–277</sup> The halogen-bridged binuclear-metal mixed-valence complex,  $[\text{Pt}_2(\text{dta})_4\text{I}]_n$  (dta = dithioacetate) (1-D linear chain: Scheme 5a), exhibits metallic conduction above room temperature, representing the first example of a metallic halogen-bridged 1-D transition-metal complex.<sup>278</sup>

## 7.5.3 NEW SYNTHESIS—BOTTOM-UP PREPARATION

### 7.5.3.1 Self-assembling

Self-assembly is the most useful synthetic method. This is because: (i) it permits the realization of a wide variety of structures from simple building blocks of metal ions and organic ligands, (ii) it allows an easy and rational modification of organic ligands, (iii) several types of interactions such as coordination bonds, hydrogen bonds,  $\pi$ – $\pi$  interactions,  $\text{CH}$ – $\pi$  interactions,  $\text{M}$ – $\text{M}$  bonds, and van der Waals interactions can be incorporated and exploited, and (iv) there is the possibility of reaction control by temperature, pH, solvent, etc. For coordination polymers, recrystallization is unavailable due to their insolubility in most of solvents. Therefore, a new synthetic approach has been developed (*vide infra*).

### 7.5.3.2 Usual Diffusion Method

To avoid precipitation of powder, diffusion is frequently used to afford a single crystal of a coordination polymer suitable for an X-ray diffraction analysis. Various types of equipment for this procedure have been devised.



### 7.5.3.3 Hydro(solvo)thermal Method

The hydrothermal method, which is well established for the synthesis of zeolites, has been increasingly used to make coordination polymers. This method, typically carried out in the temperature range 120–260 °C under autogenous pressure, exploits the self-assembly of the product from soluble precursors. The reduced viscosity of water under these conditions enhances the diffusion processes so that solvent extraction of solids and crystal growth from solution are favored. Since differential solubility problems are minimized, a variety of simple precursors may be introduced, as well as a number of organic and/or inorganic structure-directing agents. Under such nonequilibrium crystallization conditions, metastable kinetic phases, namely unprecedented structural networks, rather than the thermodynamic phase are most likely to be isolated.

This synthetic technique has been applied extensively for a large number of metal-oxide-containing polymers.<sup>6</sup> Recent examples include  $[\text{Cu}(3,4'\text{-bpy})\text{MoO}_4]_n$ ,  $[\text{Cu}(3,3'\text{-bpy})_{0.5}\text{MoO}_4]_n$ , and  $\{[\text{Cu}(4,4'\text{-bpy})_{0.5}\text{MoO}_4] \cdot 1.5\text{H}_2\text{O}\}_n$ , which were prepared by heating at 120 °C for 72 hours, 180 °C for 75 hours, and 120 °C for 214 hours, respectively. These compounds have 3-D covalent frameworks, constructed from bimetallic oxide layers tethered by the dipodal organoimine ligands.<sup>279</sup>

Under hydro(solvo)thermal conditions,  $\text{Cd}^{\text{II}}$  and  $\text{Zn}^{\text{II}}$  coordination networks can be obtained by reactions of metal salts with cyanopyridine or pyridinecarboxaldehyde. Cyano-, carboxaldehyde-, and ester-substituents slowly hydrolyze to form corresponding carboxylic acid facilitating network formation.<sup>5</sup> For instance, bis[4-{2-(4-pyridyl)ethenyl}benzoato]- $\text{Zn}^{\text{II}}$  and  $\text{Cd}^{\text{II}}$  with eightfold diamondoid network structures were obtained by slow hydrolysis of (E)-4-(4-cyanos-tyryl)pyridine under hydro(solvo)thermal conditions (3-D diamondoid net: Scheme 6a).<sup>193</sup>

### 7.5.3.4 Microwave and Ultrasonic Methods

Microwave heating has been developed as a novel technique for the hydro(solvo)thermal synthesis of organic or inorganic solid-state materials. As a consequence, the reaction and crystallization time can be significantly reduced from days to minutes, and in some cases new materials, unreachable by conventional hydrothermal techniques, can be obtained. Examples of coordination polymers synthesized by the microwave method are still relatively rare.  $[\text{Ag}(\text{dpa})]_n$  (dpa = 2,2'-dipyridylamine) and metal-phosphate-4,4'-bpy coordination polymers were prepared in a microwave oven at 30 psi (corresponding ~120 °C in the phase diagram of water) for 40 minutes.<sup>280</sup>  $[\text{Cu}_2(\text{ox})_2(\text{pyz})_3]_n$ , which shows an extended sheet structure of  $\text{Cu}^{\text{II}}$  ions bridged by ox anions and pyz, was obtained by using a microwave oven operating at a frequency of 2.45 GHz and 500 W for 15 min.<sup>281</sup>

Ultrasonic techniques are expected to be useful but few instances have been reported for coordination polymers.

## 7.5.4 REFERENCES

1. Kitagawa, S.; Munakata, M. *Trends Inorg. Chem.* **1993**, 3, 437–462.
2. Munakata, M. *Adv. Inorg. Chem.* **1998**, 46, 173–303.
3. Blake, A. J.; Champness, N. R.; Hubberstey, P.; Li, W.-S.; Withersby, M. A.; Schröder, M. *Coord. Chem. Rev.* **1999**, 183, 117–138.
4. Eddaoudi, M.; Moler, D. B.; Li, H.; Chen, B.; Reineke, T. M.; O'Keeffe, M.; Yaghi, O. M. *Acc. Chem. Res.* **2001**, 34, 319–330.
5. Evans, O. R.; Lin, W. *Acc. Chem. Res.* **2002**, 35, 511–522.
6. Hagrman, P. J.; Hagrman, D.; Zubieta, J. *Angew. Chem., Int. Ed. Engl.* **1999**, 38, 2638–2684.
7. Kitagawa, S.; Kondo, M. *Bull. Chem. Soc. Jpn.* **1998**, 71, 1739–1753.
8. Moulton, B.; Zaworotko, M. J. *Chem. Rev.* **2001**, 101, 1629–1658.
9. Zaworotko, M. J. *Chem. Soc. Rev.* **1994**, 283–288.
10. Zaworotko, M. J. *Chem. Commun.* **2001**, 1–9.
11. Batten, S. R.; Robson, R. *Angew. Chem., Int. Ed. Engl.* **1998**, 37, 1460–1494.
12. Carrad, L. H.; Goodgame, D. M. L.; Hill, S. P. W.; Williams, D. J. *J. Chem. Soc., Dalton Trans.* **1993**, 1003–1008.
13. Doyle, G. A.; Goodgame, D. M. L.; Hill, S. P. W.; Williams, D. J. *Chem. Commun.* **1993**, 207–209.
14. Mao, J.-G.; Zhang, H.-J.; Ni, J.-Z.; Wang, S.-B.; Mak, T. C. W. *Polyhedron* **1999**, 18, 1519–1525.
15. Goodgame, D. M. L.; Hill, S. P. W.; Williams, D. J. *Inorg. Chim. Acta* **1998**, 272, 131–140.
16. Evans, O. R.; Ngo, H. L.; Lin, W. *J. Am. Chem. Soc.* **2001**, 123, 10395–10396.
17. Lee, E.; Heo, J.; Kim, K. *Angew. Chem., Int. Ed. Engl.* **2000**, 39, 2699–2701.

18. Liang, Y.; Hong, M.; Su, W.; Cao, R.; Zhang, W. *Inorg. Chem.* **2001**, *40*, 4574–4582.
19. Long, D.-L.; Blake, A. J.; Champness, N. R.; Wilson, C.; Schröder, M. *Chem. Eur. J.* **2002**, *8*, 2026–2033.
20. Pan, L.; Huang, X.; Li, J.; Wu, Y.; Zheng, N. *Angew. Chem., Int. Ed. Engl.* **2000**, *39*, 527–530.
21. Shi, J.-M.; Xu, W.; Liu, Q.-Y.; Liu, F.-L.; Huang, Z.-L.; Lei, H.; Yu, W.-T.; Fang, Q. *Chem. Commun.* **2002**, 756–757.
22. Wu, C.-D.; Lu, C.-Z.; Yang, W.-B.; Lu, S.-F.; Zhuang, H.-H.; Huang, J.-S. *Eur. J. Inorg. Chem.* **2002**, 797–800.
23. Kiritsis, V.; Michaelides, A.; Skoulika, S.; Golhen, S.; Ouahab, L. *Inorg. Chem.* **1998**, *37*, 3407–3410.
24. Knoepfel, D. W.; Liu, J.; Meyers, E. A.; Shore, S. G. *Inorg. Chem.* **1998**, *37*, 4828–4837.
25. Liu, J.; Meyers, E. A.; Shore, S. G. *Inorg. Chem.* **1998**, *37*, 5410–5411.
26. Du, B.; Meyers, E. A.; Shore, S. G. *Inorg. Chem.* **2001**, *40*, 4353–4360.
27. Figuerola, A.; Diaz, C.; Fallah, M. S. E.; Ribas, J.; Maestro, M.; Mahía, J. *Chem. Commun.* **2001**, 1204–1205.
28. Yan, B.; Wang, H.-D.; Chen, Z.-D. *Polyhedron* **2001**, *20*, 591–597.
29. Ma, B.-Q.; Zhang, D.-S.; Gao, S.; Jin, T.-Z.; Yan, C.-H.; Xu, G.-X. *Angew. Chem., Int. Ed. Engl.* **2000**, *39*, 3644–3646.
30. Eddaoudi, M.; Kim, J.; O’Keeffe, M.; Yaghi, O. M. *J. Am. Chem. Soc.* **2002**, *124*, 376–377.
31. Eddaoudi, M.; Kim, J.; Rosi, N.; Vodak, D.; Wachter, J.; O’Keeffe, M.; Yaghi, O. M. *Science* **2002**, *295*, 469–472.
32. Vodak, D. T.; Braun, M. E.; Kim, J.; Eddaoudi, M.; Yaghi, O. M. *Chem. Commun.* **2001**, 2534–2535.
33. Kim, J.; Chen, B.; Reineke, T. M.; Li, H.; Eddaoudi, M.; Moler, D. B.; O’Keeffe, M.; Yaghi, O. M. *J. Am. Chem. Soc.* **2001**, *123*, 8239–8247.
34. Eddaoudi, M.; Kim, J.; Wachter, J. B.; Chae, H. K.; O’Keeffe, M.; Yaghi, O. M. *J. Am. Chem. Soc.* **2001**, *123*, 4368–4369.
35. Braun, M. E.; Steffek, C. D.; Kim, J.; Rasmussen, P. G.; Yaghi, O. M. *Chem. Commun.* **2001**, 2532–2533.
36. Chae, H. K.; Eddaoudi, M.; Kim, J.; Hauck, S. I.; Hartwig, J. F.; O’Keeffe, M.; Yaghi, O. M. *J. Am. Chem. Soc.* **2001**, *123*, 11482–11483.
37. Yaghi, O. M.; Jernigan, R.; Li, H.; Davis, C. E.; Groy, T. L. *J. Chem. Soc., Dalton Trans.* **1997**, 2383–2384.
38. Kumagai, H.; Akita-Tanaka, M.; Inoue, K.; Kurmoo, M. *J. Mater. Chem.* **2001**, *11*, 2146–2151.
39. Evans, O. R.; Lin, W. *Inorg. Chem.* **2000**, *39*, 2189–2198.
40. Lin, W.; Wang, Z.; Ma, L. *J. Am. Chem. Soc.* **1999**, *121*, 11249–11250.
41. Gutschke, S. O. H.; Price, D. J.; Powell, A. K.; Wood, P. T. *Eur. J. Inorg. Chem.* **2001**, 2739–2741.
42. Seo, J. S.; Whang, D.; Lee, H.; Jun, S. I.; Oh, J.; Jeon, Y. J.; Kim, K. *Nature* **2000**, *404*, 982–986.
43. Bourne, S. A.; Lu, J.; Mondal, A.; Moulton, B.; Zaworotko, M. J. *Angew. Chem., Int. Ed. Engl.* **2001**, *40*, 2111–2113.
44. Gutschke, S. O. H.; Price, D. J.; Powell, A. K.; Wood, P. T. *Angew. Chem., Int. Ed. Engl.* **2001**, *40*, 1920–1923.
45. Tao, J.; Tong, M.-L.; Shi, J.-X.; Chen, X.-M.; Ng, S. W. *Chem. Commun.* **2000**, 2043–2044.
46. Aquino, M. A. S. *Coord. Chem. Rev.* **1998**, *170*, 141–202.
47. Barral, M. C.; Jiménez-Aparicio, R.; Pérez-Quintanilla, D.; Priego, J. L.; Royer, E. C.; Torres, M. R.; Urbanos, F. A. *Inorg. Chem.* **2000**, *39*, 65–70.
48. Cotton, F. A.; Kim, Y. *J. Am. Chem. Soc.* **1993**, *115*, 8511–8512.
49. Miyasaka, H.; Clérac, R.; Campos-Fernández, C. S.; Dunbar, K. R. *Inorg. Chem.* **2001**, *40*, 1663–1671.
50. Ouyang, X.; Campana, C.; Dunbar, K. R. *Inorg. Chem.* **1996**, *35*, 7188–7189.
51. Handa, M.; Yoshioka, D.; Yasuyoshi, S.; Shiomi, K.; Mikuriya, M.; Hiromitsu, I.; Kasuga, K. *Chem. Lett.* **1999**, 1033–1034.
52. Campana, C.; Dunbar, K. R.; Ouyang, X. *Chem. Commun.* **1996**, 2427–2428.
53. Lu, J.; Harrison, W. T. A.; Jacobson, A. J. *Chem. Commun.* **1996**, 399–400.
54. Cotton, F. A.; Kim, Y.; Lu, J. *Inorg. Chim. Acta* **1994**, *221*, 1–4.
55. Carlucci, L.; Ciani, G.; Gramaccioli, A.; Proserpio, D. M.; Rizzato, S. *Cryst. Eng. Comm.* **2000**, *29*, 1–10.
56. Choi, H. J.; Suh, M. P. *Inorg. Chem.* **1999**, *38*, 6309–6312.
57. Ko, J. W.; Min, K. S.; Suh, M. P. *Inorg. Chem.* **2002**, *41*, 2151–2157.
58. Min, K. S.; Suh, M. P. *Chem. Eur. J.* **2001**, *7*, 303–313.
59. Colacio, E.; Domínguez-Vera, J. M.; Chazi, M.; Kivekäs, R.; Klinga, M.; Moreno, J. M. *Chem. Commun.* **1998**, 1071–1072.
60. Choi, H. J.; Lee, T. S.; Suh, M. P. *J. Incl. Phenom.* **2001**, *41*, 155–162.
61. Marvilliers, A.; Parsons, S.; Rivière, E.; Audière, J.-P.; Kurmoo, M.; Mallah, T. *Eur. J. Inorg. Chem.* **2001**, 1287–1293.
62. Kou, H.-Z.; Gao, S.; Bai, O.; Wang, Z.-M. *Inorg. Chem.* **2001**, *40*, 6287–6294.
63. Ohba, M.; Usuki, N.; Fukita, N.; Okawa, H. *Inorg. Chem.* **1998**, *37*, 3349–3354.
64. Fukita, N.; Ohba, M.; Okawa, H. *Mol. Cryst. Liq. Cryst.* **2000**, *342*, 217–224.
65. Kou, H.-Z.; Bu, W.-M.; Liao, D.-Z.; Jiang, Z.-H.; Yan, S.-P.; Fan, Y.-G.; Wang, G.-L. *J. Chem. Soc., Dalton Trans.* **1998**, 4161–4164.
66. Miyasaka, H.; Matsumoto, N.; Okawa, H.; Re, N.; Gallo, E.; Floriani, C. *J. Am. Chem. Soc.* **1996**, *118*, 981–994.
67. Miyasaka, H.; Okawa, H.; Matsumoto, N. *Mol. Cryst. Liq. Cryst.* **1999**, *335*, 1015–1023.
68. Re, N.; Crescenzi, R.; Floriani, C.; Miyasaka, H.; Matsumoto, N. *Inorg. Chem.* **1998**, *37*, 2717–2722.
69. Miyasaka, H.; Okawa, H.; Miyazaki, A.; Enoki, T. *Inorg. Chem.* **1998**, *37*, 4878–4883.
70. Matsumoto, N.; Sunatsuki, Y.; Miyasaka, H.; Hashimoto, Y.; Luneau, D.; Tuchagues, J. P. *Angew. Chem., Int. Ed. Engl.* **1999**, 171–173.
71. Miller, J. S.; Epstein, A. J. *Chem. Commun.* **1998**, 1319–1325.
72. Hibbs, W.; Rittenberg, D. K.; Sugiura, K.; Burkhart, B. M.; Morin, B. G.; Arif, A. M.; Liable-Sands, L.; Rheingold, A. L.; Sundaralingam, M.; Epstein, A. J.; Miller, J. S. *Inorg. Chem.* **2001**, *40*, 1915–1925.
73. Miller, J. S.; Calabrese, J. C.; McLean, R. S.; Epstein, A. J. *Adv. Mater.* **1992**, *4*, 498–501.
74. Mikami, S.; Sugiura, K.; Maruta, T.; Maeda, Y.; Ohba, M.; Usuki, N.; Okawa, H.; Akutagawa, T.; Nisihara, S.; Nakamura, T.; Iwasaki, K.; Miyazaki, N.; Hino, S.; Asato, E.; Miller, J. S.; Sakata, Y. *J. Chem. Soc., Dalton Trans.* **2001**, 448–455.
75. Fallah, M. S. E.; Rentschler, E.; Caneschi, A.; Sessoli, R.; Gatteschi, D. *Angew. Chem., Int. Ed. Engl.* **1996**, *35*, 1947–1949.
76. Li, D.-F.; Okamura, T.; Sun, W.-Y.; Ueyama, N.; Tang, W.-X. *Acta Cryst.* **2002**, *C58*, m280–m282.
77. Okamoto, H.; Yamashita, M. *Bull. Chem. Soc. Jpn.* **1998**, *71*, 2023–2039.
78. Clark, R. J. H. *Chem. Soc. Rev.* **1990**, *19*, 107–131.

79. Scott, B.; Willett, R.; Porter, L.; Williams, J. *Inorg. Chem.* **1992**, *31*, 2483–2492.
80. Yaghi, O. M.; Li, G. *Angew. Chem., Int. Ed. Engl.* **1995**, *34*, 207–209.
81. Kawata, S.; Kitagawa, S.; Kumagai, H.; Iwabuchi, S.; Katada, M. *Inorg. Chim. Acta* **1998**, *267*, 143–145.
82. Blake, A. J.; Brooks, N. R.; Champness, N. R.; Cooke, P. A.; Deveson, A. M.; Fenske, D.; Hubberstey, P.; Li, W.-S.; Schröder, M. *J. Chem. Soc., Dalton Trans.* **1999**, 2103–2110.
83. Chesnut, D. J.; Kusnetzow, A.; Birge, R. R.; Zubieta, J. *Inorg. Chem.* **1999**, *38*, 2663–2671.
84. Ibrahim, A. M. A.; Siebel, E.; Fischer, R. D. *Inorg. Chem.* **1998**, *37*, 3521–3525.
85. Chesnut, D. J.; Plewak, D.; Zubieta, J. *J. Chem. Soc., Dalton Trans.* **2001**, 2567–2580.
86. Healy, P. C.; Pakawatchai, C. P.; Papisergio, R. I.; Patrick, V. A.; White, A. H. *Inorg. Chem.* **1984**, *23*, 3769–3776.
87. Blake, A. J.; Brooks, N. R.; Champness, N. R.; Crew, M.; Hanton, L. R.; Hubberstey, P.; Parsons, S.; Schröder, M. *J. Chem. Soc., Dalton Trans.* **1999**, 2813–2817.
88. Leznoff, D. B.; Xue, B.-Y.; Batchelor, R. J.; Einstein, F. W. B.; Patrick, B. O. *Inorg. Chem.* **2001**, *40*, 6026–6034.
89. Yeung, W.-F.; Wong, W.-T.; Zuo, J.-L.; Lau, T.-C. *J. Chem. Soc., Dalton Trans.* **2000**, 629–631.
90. Niel, V.; Muñoz, M. C.; Gaspar, A. B.; Galet, A.; Levchenko, G.; Real, J. A. *Chem. Eur. J.* **2002**, *8*, 2446–2453.
91. Iwamoto, T.; Soma, T. *Inorg. Chem.* **1996**, *35*, 1849–1856.
92. Bowmaker, G. A.; Effendy, Reid, J. C.; Rickard, C. E. F.; Skelton, B. W.; White, A. H. *J. Chem. Soc., Dalton Trans.* **1998**, 2139–2146.
93. Nishikiori, S. *J. Coord. Chem.* **1996**, *37*, 23–38.
94. Yun, S.-S.; Kim, Y.-P.; Kim, C.-H. *Acta Cryst.* **1999**, *C55*, 2026–2028.
95. Kitazawa, T.; Kikuyama, T.; Ugajin, H.; Takahashi, M.; Takeda, M. *J. Coord. Chem.* **1996**, *37*, 17–22.
96. Yuge, H.; Kim, C.-H.; Iwamoto, T.; Kitazawa, T. *Inorg. Chim. Acta* **1997**, *257*, 217–224.
97. Nishikiori, S.; Iwamoto, T. *J. Incl. Phenom.* **1985**, *3*, 283–295.
98. Iwamoto, T. *Inclusion Compounds*; (a) Oxford University Press, 1991, Vol. 5, Chapter 6, pp 172–212.
99. Iwamoto, T. *Inclusion Compounds*; Academic Press: London, 1984, Vol. 1, Chapter 2, pp 29–57.
100. Munakata, M.; Zhong, J. C.; Ino, I.; Kuroda-Sowa, T.; Maekawa, M.; Suenaga, Y.; Oiji, N. *Inorg. Chim. Acta* **2001**, *317*, 268–275.
101. Eriksen, J. O.; Hazell, A.; Jensen, A.; Jepsen, J.; Poulsen, R. D. *Acta Cryst.* **2000**, *C56*, 551–553.
102. Ferbinteanu, M.; Tanase, S.; Andruh, M.; Journaux, Y.; Cimpoesu, F.; Strenger, I.; Rivière, E. *Polyhedron* **1999**, *18*, 3019–3025.
103. Mondal, N.; Dey, D. K.; S, M.; Gramlich, V. *Polyhedron* **2001**, *20*, 607–613.
104. Kou, H.-Z.; Gao, S.; Zhang, J.; Wen, G.-H.; Su, G.; Zheng, R. K.; Zhang, X. X. *J. Am. Chem. Soc.* **2001**, *123*, 11809–11810.
105. Ziegler, B.; Witzel, M.; Schwarten, M.; Babel, D. *Z. Naturforsch.* **1999**, *54b*, 870–876.
106. Babel, D.; Kurtz, W. *Stud. Inorg. Chem.* **1982**, *3*, 593–596.
107. Larionova, J.; Kahn, O.; Golhen, S.; Ouahab, L.; Clérac, R. *Inorg. Chem.* **1999**, *38*, 3621–3627.
108. Kahn, O.; Larionova, J.; Ouahab, L. *Chem. Commun.* **1999**, 945–952.
109. Larionova, J.; Kahn, O.; Gohlen, S.; Ouahab, L.; Clérac, R. *J. Am. Chem. Soc.* **1999**, *121*, 3349–3356.
110. Sra, A. K.; Rombaut, G.; Lahitête, F.; Golhen, S.; Ouahab, L.; Mathonière, C.; Yakhmi, J. V.; Kahn, O. *New J. Chem.* **2000**, *24*, 871–876.
111. Zhong, Z. J.; Seino, H.; Mizobe, Y.; Hidai, M.; Verdagner, M.; Ohkoshi, S.; Hashimoto, K. *Inorg. Chem.* **2000**, *39*, 5095–5101.
112. Rombaut, G.; Golhen, S.; Ouahab, L.; Mathonière, C.; Kahn, O. *J. Chem. Soc., Dalton Trans.* **2000**, 3609–3614.
113. Banfi, S.; Carlucci, L.; Caruso, E.; Ciani, G.; Proserpio, D. M. *J. Chem. Soc., Dalton Trans.* **2002**, 2714–2721.
114. Biradha, K.; Fujita, M. *Chem. Commun.* **2001**, 15–16.
115. Withersby, M. A.; Blake, A. J.; Champness, N. R.; Cooke, P. A.; Hubberstey, P.; Schröder, M. *J. Am. Chem. Soc.* **2000**, *122*, 4044–4046.
116. Abrahams, B. F.; Hardie, M. J.; Hoskins, B. F.; Robson, R.; Sutherland, E. E. *Chem. Commun.* **1994**, 1049–1050.
117. Fujita, M.; Kwon, Y. J.; Sasaki, O.; Yamaguchi, K.; Ogura, K. *J. Am. Chem. Soc.* **1995**, *117*, 7287–7288.
118. Pschirer, N. G.; Ciurtin, D. M.; Smith, M. D.; Bunz, U. H.; zur Loye, H.-C. *Angew. Chem., Int. Ed. Engl.* **2002**, *41*, 583–585.
119. Choi, K.-Y.; Chun, K. M.; Suh, I.-H. *Polyhedron* **2001**, *20*, 57–65.
120. Zhang, H.-X.; Kang, B.-S.; Xu, A.-W.; Chen, Z.-N.; Zhou, Z.-Y.; Chan, A. S. C.; Yu, K.-B.; Ren, C. *J. Chem. Soc., Dalton Trans.* **2001**, 2559–2566.
121. Burrows, A. D.; Harrington, R. W.; Mahon, M. F.; Price, C. E. *J. Chem. Soc., Dalton Trans.* **2000**, 3845–3854.
122. Prior, T. J.; Rosseinsky, M. J. *Chem. Commun.* **2001**, 495–496.
123. Murugavel, R.; Krishnamurthy, D.; Sathiyendiran, M. *J. Chem. Soc., Dalton Trans.* **2002**, 34–39.
124. Kumagai, H.; Kepert, C. J.; Kurmoo, M. *Inorg. Chem.* **2002**, *41*, 3410–3422.
125. Endres, H.; Kniesner, A. *Acta Cryst.* **1984**, *C40*, 770–772.
126. Chui, S. S.-Y.; Siu, A.; Feng, X.; Zhang, Z. Y.; Mak, T. C. W.; Williams, I. D. *Inorg. Chem. Commun.* **2001**, *4*, 467–470.
127. Kitagawa, S.; Kawata, S. *Coord. Chem. Rev.* **2002**, *224*, 11–34.
128. Kawata, S.; Kitagawa, S.; Kondo, M.; Furuchi, I.; Munakata, M. *Angew. Chem., Int. Ed. Engl.* **1994**, *33*, 1759–1761.
129. Zhang, J.; Matsushita, M. M.; Kong, X. X.; Abe, J.; Iyoda, T. *J. Am. Chem. Soc.* **2001**, *123*, 12105–12106.
130. Matsushita, M. M.; Morikawa, M.; Kawai, T.; Iyoda, T. *Mol. Cryst. Liq. Cryst.* **2000**, *343*, 87–96.
131. Pei, Y.; Kahn, O.; Sletten, J.; Renard, J.-P.; Georges, R.; Gianduzzo, J.-C.; Curely, J.; Xu, Q. *Inorg. Chem.* **1988**, *27*, 47–53.
132. Baron, V.; Gillon, B.; Cousson, A.; Mathonière, C.; Kahn, O.; Grand, A.; Öhrström, L.; Delley, B.; Bonnet, M.; Boucherle, J.-X. *J. Am. Chem. Soc.* **1997**, *119*, 3500–3506.
133. Stumpf, H. O.; Ouahab, L.; Pei, Y.; Bergerat, P.; Kahn, O. *J. Am. Chem. Soc.* **1994**, *116*, 3866–3874.
134. Ciurtin, D. M.; Smith, M. D.; zur Loye, H.-C. *Chem. Commun.* **2002**, 74–75.
135. Dong, Y.-B.; Smith, M. D.; zur Loye, H.-C. *Inorg. Chem.* **2000**, *39*, 1943–1949.
136. Horikoshi, R.; Mochida, T.; Moriyama, H. *Inorg. Chem.* **2002**, *41*, 3017–3024.
137. Dong, G.; Hong, M.; Chun-ying, D.; Feng, L.; Qing-jin, M. *J. Chem. Soc., Dalton Trans.* **2002**, 2593–2594.

138. Noro, S.; Kitagawa, S.; Yamashita, M.; Wada, T. *Chem. Commun.* **2002**, 222–223.
139. Carlucci, L.; Ciani, G.; Porta, F.; Proserpio, D. M.; Santagostini, L. *Angew. Chem., Int. Ed. Engl.* **2002**, *41*, 1907–1911.
140. Goldberg, I. *Chem. Eur. J.* **2000**, *6*, 3863–3870.
141. Abrahams, B. F.; Hoskins, B. F.; Michail, D. M.; Robson, R. *Nature* **1994**, *369*, 727–729.
142. Sharma, C. V. K.; Broker, G. A.; Huddleston, J. G.; Baldwin, J. W.; Metzger, R. M.; Rogers, R. D. *J. Am. Chem. Soc.* **1999**, *121*, 1137–1144.
143. Diskin-Posner, Y.; Patra, G. K.; Goldberg, I. *Eur. J. Inorg. Chem.* **2001**, 2515–2523.
144. Zhong, Z. J.; Matsumoto, N.; Okawa, H.; Kida, S. *Chem. Lett.* **1990**, 87–90.
145. Tamaki, J.; Zhong, Z. J.; Matsumoto, N.; Kida, S.; Koikawa, M.; Achiwa, N.; Hashimoto, Y.; Okawa, H. *J. Am. Chem. Soc.* **1992**, *114*, 6974–6979.
146. Decurtins, S.; Schmalke, H. W.; Oswald, H. R.; Linden, A.; Ensling, J.; Glutlich, P.; Hauser, A. *Inorg. Chim. Acta* **1994**, *216*, 65–73.
147. Carling, S. G.; Mathonière, C.; Day, P.; Abdul Malik, K. M.; Coles, S. J.; Hursthouse, M. B. *J. Chem. Soc., Dalton Trans.* **1996**, 1839–1843.
148. Larionova, J.; Mombelli, B.; Sanchiz, J.; Kahn, O. *Inorg. Chem.* **1998**, *37*, 679–684.
149. Okawa, H.; Mitsumi, M.; Ohba, M.; Kodera, M.; Matsumoto, N. *Bull. Chem. Soc. Jpn.* **1994**, *67*, 2139–2144.
150. Kahn, O.; Pei, Y.; Verdager, M.; Renard, J. P.; Sletten, J. J. *J. Am. Chem. Soc.* **1988**, *110*, 782–789.
151. Subramanian, S.; Zaworotko, M. J. *Angew. Chem., Int. Ed. Engl.* **1995**, *34*, 2127–2129.
152. Noro, S.; Kitagawa, S.; Kondo, M.; Seki, K. *Angew. Chem., Int. Ed. Engl.* **2000**, *39*, 2082–2084.
153. Noro, S.; Kitaura, R.; Kondo, M.; Kitagawa, S.; Ishii, T.; Matsuzaka, H.; Yamashita, M. *J. Am. Chem. Soc.* **2002**, *124*, 2568–2583.
154. Su, X.-C.; Zhu, S.; Lin, H.-K.; Leng, X.-B.; Chen, Y.-T. *J. Chem. Soc., Dalton Trans.* **2001**, 3163–3168.
155. Withersby, M. A.; Blake, A. J.; Champness, N. R.; Hubberstey, P.; Li, W. S.; Schröder, M. *Angew. Chem., Int. Ed. Engl.* **1997**, *36*, 2327–2329.
156. Chen, X. M.; Tong, M.-L.; Luo, Y. J.; Chen, Z. N. *Aust. J. Chem.* **1996**, *49*, 835–838.
157. Kondo, M.; Shimamura, M.; Noro, S.; Minakoshi, S.; Asami, A.; Seki, K.; Kitagawa, S. *Chem. Mater.* **2000**, *12*, 1288–1299.
158. Blake, A. J.; Champness, N. R.; Cooke, P. A.; Nicolson, J. E. B.; Wilson, C. J. *J. Chem. Soc., Dalton Trans.* **2000**, 3811–3819.
159. Brooks, N. R.; Blake, A. J.; Champness, N. R.; Cunningham, J. W.; Hubberstey, P.; Teat, S. J.; Wilson, C.; Schröder, M. *J. Chem. Soc., Dalton Trans.* **2001**, 2530–2538.
160. Janiak, C.; Uehlin, L.; Wu, H.-P.; Klüfers, P.; Piotrowski, H.; Scharmann, T. G. *J. Chem. Soc., Dalton Trans.* **1999**, 3121–3131.
161. Wu, H.-P.; Janiak, C.; Rheinwald, G.; Hang, H. *J. Chem. Soc., Dalton Trans.* **1999**, 183–190.
162. Hirsch, K. A.; Wilson, S. R.; Moore, J. S. *Inorg. Chem.* **1997**, *36*, 2960–2968.
163. Horikoshi, R.; Mochida, T.; Maki, N.; Yamada, S.; Moriyama, H. *J. Chem. Soc., Dalton Trans.* **2002**, 28–33.
164. Carlucci, L.; Ciani, G.; Proserpio, D. M.; Rizzato, S. *Chem. Eur. J.* **2002**, *8*, 1520–1526.
165. Hennigar, T. L.; MacQuarrie, D. C.; Losier, P.; Rogers, R. D.; Zaworotko, M. J. *Angew. Chem., Int. Ed. Engl.* **1997**, *36*, 972–973.
166. Blake, A. J.; Brooks, N. R.; Champness, N. R.; Crew, M.; Deveson, A.; Fenske, D.; Gregory, D. H.; Hanton, L. R.; Hubberstey, P.; Schröder, M. *Chem. Commun.* **2001**, 1432–1433.
167. Withersby, M. A.; Blake, A. J.; Champness, N. R.; Cooke, P. A.; Hubberstey, P.; Li, W.-S.; Schröder, M. *Inorg. Chem.* **1999**, *38*, 2259–2266.
168. Hong, M.; Su, W.; Cao, R.; Fujita, M.; Lu, J. *Chem. Eur. J.* **2000**, *6*, 427–431.
169. Biradha, K.; Seward, C.; Zaworotko, M. J. *Angew. Chem., Int. Ed. Engl.* **1999**, *38*, 492–495.
170. Psillakis, E.; Jeffery, J. C.; McCleverty, J. A.; Ward, M. D. *J. Chem. Soc., Dalton Trans.* **1997**, 1645–1651.
171. Chen, C.; Xu, D.; Xu, Y.; Cheng, C.; Ling, R. *Acta Cryst.* **1992**, *C48*, 1231–1233.
172. Fun, H.-K.; Raj, S. S. S.; Xiong, R.-G.; Zuo, J.-L.; Yu, Z.; Zhu, X.-L.; You, X.-Z. *J. Chem. Soc., Dalton Trans.* **1999**, 1711–1712.
173. Huang, S. D.; Xiong, R.-G. *Polyhedron* **1997**, *16*, 3929–3939.
174. Carlucci, L.; Ciani, G.; Proserpio, D. M. *Chem. Commun.* **1999**, 449–450.
175. Tong, M.-L.; Chen, H.-J.; Chen, X.-M. *Inorg. Chem.* **2000**, *39*, 2235–2238.
176. Tong, M. L.; Chen, X. M.; Yu, X. L.; Mak, T. C. W. *J. Chem. Soc., Dalton Trans.* **1998**, 5–6.
177. MacGillivray, L. R.; Groeneman, R. H.; Atwood, J. L. *J. Am. Chem. Soc.* **1998**, *120*, 2676–2677.
178. Withersby, M. A.; Blake, A. J.; Champness, N. R.; Cooke, P. A.; Hubberstey, P.; Schröder, M. *New J. Chem.* **1999**, *23*, 573–575.
179. Kondo, M.; Yoshitomi, T.; Seki, K.; Matsuzaka, H.; Kitagawa, S. *Angew. Chem., Int. Ed. Engl.* **1997**, *36*, 1725–1727.
180. Fujita, M.; Kwon, Y. J.; Washizu, S.; Ogura, K. *J. Am. Chem. Soc.* **1994**, *116*, 1151–1152.
181. Gable, R. W.; Hoskins, B. F.; Robson, R. *Chem. Commun.* **1990**, 1667–1668.
182. MacGillivray, L. R. *Chem. Commun.* **1994**, 1325–1326.
183. Hoskins, B. F.; Robson, R. *J. Am. Chem. Soc.* **1990**, *112*, 1546–1554.
184. Otieno, T.; Rettig, S. J.; Thompson, R. C.; Trotter, J. *Inorg. Chem.* **1993**, *32*, 1607–1611.
185. Carlucci, L.; Ciani, G.; Proserpio, D. M.; Sironi, A. *Angew. Chem., Int. Ed. Engl.* **1995**, *34*, 1895–1898.
186. Li, H.; Eddaoudi, M.; O’Keeffe, M.; Yaghi, O. M. *Nature* **1999**, *402*, 276–279.
187. Gardner, G. B.; Venkataraman, D.; Moore, J. S.; Lee, S. *Nature* **1995**, *374*, 792–795.
188. Power, K. N.; Hennigar, T. L.; Zaworotko, M. J. *Chem. Commun.* **1998**, 595–596.
189. Carlucci, L.; Cozzi, N.; Ciani, G.; Moret, M.; Proserpio, D. M.; Rizzato, S. *Chem. Commun.* **2002**, 1354–1355.
190. Rather, B.; Moulton, B.; Walsh, R. D. B.; Zaworotko, M. J. *Chem. Commun.* **2002**, 694–695.
191. Gudbjartson, H.; Biradha, K.; Poirier, K. M.; Zaworotko, M. J. *J. Am. Chem. Soc.* **1999**, *121*, 2599–2600.
192. Chen, B.; Eddaoudi, M.; Reineke, T. M.; Kampf, J. W.; O’Keeffe, M.; Yaghi, O. M. *J. Am. Chem. Soc.* **2000**, *122*, 11559–11560.
193. Lin, W.; Ma, L.; Evans, O. R. *Chem. Commun.* **2000**, 2263–2264.

194. Kinoshita, Y.; Matsubara, I.; Higuchi, T.; Saito, Y. *Bull. Chem. Soc. Jpn.* **1959**, *32*, 1221–1226.
195. Kasai, K.; Aoyagi, M.; Fujita, M. *J. Am. Chem. Soc.* **2000**, *122*, 2140–2141.
196. Li, D.; Kaneko, K. *Chem. Phys. Lett.* **2001**, *335*, 50–56.
197. Venkataraman, D.; Gardner, G. B.; Lee, S.; Moore, J. S. *J. Am. Chem. Soc.* **1995**, *117*, 11600–11601.
198. Min, K. S.; Suh, M. P. *J. Am. Chem. Soc.* **2000**, *122*, 6834–6840.
199. Eddaoudi, M.; Li, H.; Yaghi, O. M. *J. Am. Chem. Soc.* **2000**, *122*, 1391–1397.
200. Mori, W.; Hoshino, H.; Nishimoto, Y.; Takamizawa, S. *Chem. Lett.* **1999**, 331–332.
201. Seki, K. *Phys. Chem. Chem. Phys.* **2002**, *4*, 1968–1971.
202. Barthelet, K.; Marrot, J.; Riou, D.; Férey, G. *Angew. Chem., Int. Ed. Engl.* **2002**, *41*, 281–284.
203. Li, D.; Kaneko, K. *J. Phys. Chem. B* **2000**, *104*, 8940.
204. Chui, S. S.-Y.; Lo, S. M.-F.; Charmant, J. P. H.; Orpen, A. G.; Williams, I. D. *Science* **1999**, *283*, 1148–1150.
205. Soldatov, D. V.; Ripmeester, J. A. *Chem. Mater.* **2000**, *12*, 1827–1839.
206. Tabares, L. C.; Navarro, J. A. R.; Salas, J. M. *J. Am. Chem. Soc.* **2001**, *123*, 383–387.
207. Seki, K.; Mori, W. *J. Phys. Chem. B* **2002**, *106*, 1380–1385.
208. Blake, A. J.; Hill, S. J.; Hubberstey, P.; Li, W. S. *J. Chem. Soc., Dalton Trans.* **1997**, 913–914.
209. Uemura, K.; Kitagawa, S.; Kondo, M.; Fukui, K.; Kitaura, R.; Chang, H.-C.; Mizutani, T. *Chem. Eur. J.* **2002**, *8*, 3587–3600.
210. Li, H.; Davis, C. E.; Groy, T. L.; Kelley, D. G.; Yaghi, O. M. *J. Am. Chem. Soc.* **1998**, *120*, 2186–2187.
211. Jung, O.-S.; Kim, Y. J.; Lee, Y.-A.; Park, J. K.; Chae, H. K. *J. Am. Chem. Soc.* **2000**, *122*, 9921–9925.
212. Beauvais, L. G.; Shores, M. P.; Long, J. R. *J. Am. Chem. Soc.* **2000**, *122*, 2763–2772.
213. Kitaura, R.; Fujimoto, K.; Noro, S.; Kondo, M.; Kitagawa, S. *Angew. Chem., Int. Ed. Engl.* **2002**, *41*, 133–135.
214. Gardner, G. B.; Kiang, Y.-H.; Lee, S.; Asgaonkar, A.; Venkataraman, D. *J. Am. Chem. Soc.* **1996**, *118*, 6946–6953.
215. Manakov, A. Y.; Soldatov, D. V.; Ripmeester, J. A.; Lipkowski, J. *J. Phys. Chem. B* **2000**, *104*, 12111–12118.
216. Carlucci, L.; Ciani, G.; Moret, M.; Proserpio, D. M.; Rizzato, S. *Angew. Chem., Int. Ed. Engl.* **2000**, *39*, 1506–1510.
217. Edgar, M.; Mitchell, R.; Slawin, A. M. Z.; Lightfoot, P.; Wright, P. A. *Chem. Eur. J.* **2001**, *7*, 5168–5175.
218. Forster, P. M.; Cheetham, A. K. *Angew. Chem., Int. Ed. Engl.* **2001**, *41*, 457–459.
219. Reineke, T. M.; Eddaoudi, M.; Fehr, M.; Kelley, D.; Yaghi, O. M. *J. Am. Chem. Soc.* **1999**, *121*, 1651–1657.
220. Yaghi, O. M.; Davis, C. E.; Li, G.; Li, H. *J. Am. Chem. Soc.* **1997**, *119*, 2861–2868.
221. Yaghi, O. M.; Li, H.; Groy, T. L. *J. Am. Chem. Soc.* **1996**, *118*, 9096–9101.
222. Yaghi, O. M.; Li, G.; Li, H. *Nature* **1995**, *378*, 703–706.
223. Sawaki, T.; Dewa, T.; Aoyama, Y. *J. Am. Chem. Soc.* **1998**, *120*, 8539–8640.
224. Lee, E.; Kim, J.; Heo, J.; Whang, D.; Kim, K. *Angew. Chem., Int. Ed. Engl.* **2001**, *40*, 399–402.
225. Yaghi, O. M.; Li, H.; Groy, T. L. *Inorg. Chem.* **1997**, *36*, 4292–4293.
226. Pan, L.; Woodlock, E. B.; Wang, X.; Lam, K.-C.; Rheingold, A. L. *Chem. Commun.* **2001**, 1762–1763.
227. Jung, O.-S.; Kim, Y. J.; Kim, K. M.; Lee, Y.-A. *J. Am. Chem. Soc.* **2002**, *124*, 7906–7907.
228. Naito, S.; Tanibe, T.; Saito, E.; Miyao, T.; Mori, W. *Chem. Lett.* **2001**, 1178–1179.
229. Sawaki, T.; Aoyama, Y. *J. Am. Chem. Soc.* **1999**, *121*, 4793–4798.
230. Ferlay, S.; Mallah, T.; Vaissermann, J.; Bartolomé, F.; Veillet, P.; Verdaguer, M. *Chem. Commun.* **1996**, 2481–2482.
231. Kou, H.-Z.; Gao, S.; Bu, W.-M.; Liao, D.-Z.; Ma, B.-Q.; Jiang, Z.-H.; Yan, S.-P.; Fan, Y.-G.; Wang, G.-L. *J. Chem. Soc., Dalton Trans.* **1999**, 2477–2480.
232. Xiang, H.; Gao, S.; Lu, T.-B.; Luck, R. L.; Mao, Z.-W.; Chen, X.-M.; Ji, L.-N. *New J. Chem.* **2001**, *25*, 875–878.
233. Ohba, M.; Usuki, N.; Fukita, N.; Okawa, H. *Angew. Chem., Int. Ed. Engl.* **1999**, *38*, 1795–1798.
234. Inoue, K.; Imai, H.; Ghalsasi, P. S.; Kikuchi, K.; Ohba, M.; Okawa, H.; Yakhmi, J. V. *Angew. Chem., Int. Ed. Engl.* **2001**, *40*, 4242–4245.
235. Usuki, N.; Yamada, M.; Ohba, M.; Okawa, H. *J. Solid. State Chem.* **2001**, *159*, 328–335.
236. Ribas, J.; Escuer, A.; Monfort, M.; Vicente, R.; Cortés, R.; Lezama, L.; Rojo, T. *Coord. Chem. Rev.* **1999**, *193–195*, 1027–1068.
237. Han, S.; Manson, J. L.; Kim, J.; Miller, J. S. *Inorg. Chem.* **2000**, *39*, 4182–4185.
238. Abu-Youssef, M. A. M.; Drillon, M.; Escuer, A.; Goher, M. A. S.; Mautner, F. A.; Vicente, R. *Inorg. Chem.* **2000**, *39*, 5022–5027.
239. Goher, M. A. S.; Cano, J.; Journaux, Y.; Abu-Youssef, M. A. M.; Mautner, F. A.; Escuer, A.; Vicente, R. *Chem. Eur. J.* **2000**, *6*, 778–784.
240. Hong, C. S.; Do, Y. *Angew. Chem., Int. Ed. Engl.* **1999**, *38*, 193–195.
241. Mautner, F. A.; Cortés, R.; Lezama, L.; Rojo, T. *Angew. Chem., Int. Ed. Engl.* **1996**, *35*, 78–80.
242. Miller, J. S.; Manson, J. L. *Acc. Chem. Res.* **2001**, *34*, 563–570.
243. Kurmoo, M. *Mol. Cryst. Liq. Cryst.* **2000**, *342*, 167–176.
244. Batten, S. R.; Jensen, P.; Kepert, C. J.; Kurmoo, M.; Moubaraki, B.; Murray, K. S.; Price, D. J. *J. Chem. Soc., Dalton Trans.* **1999**, 2987–2997.
245. Kumagai, H.; Inoue, K. *Angew. Chem., Int. Ed. Engl.* **1999**, *38*, 1601–1603.
246. Inoue, K.; Iwamura, H. *J. Am. Chem. Soc.* **1994**, *116*, 3173–3174.
247. Iwamura, H.; Inoue, K.; Koga, N. *New J. Chem.* **1998**, *22*, 201–210.
248. Caneschi, A.; Gatteschi, D.; Lalot, N.; Sangregorio, C.; Sessoli, R.; Venturi, G.; Vindigni, A.; Rettori, A.; Pini, M. G.; Novak, M. A. *Angew. Chem., Int. Ed. Engl.* **2001**, *40*, 1760–1763.
249. Karasawa, S.; Sano, Y.; Akita, T.; Koga, N.; Itoh, T.; Iwamura, H.; Rabu, P.; Drillon, M. *J. Am. Chem. Soc.* **1998**, *120*, 10080–10087.
250. Sano, Y.; Tanaka, M.; Koga, N.; Matsuda, K.; Iwamura, H.; Rabu, P.; Drillon, M. *J. Am. Chem. Soc.* **1997**, *119*, 8246–8252.
251. van Koningsbruggen, P. J.; Garcia, Y.; Kahn, O.; Fournès, L.; Kooijman, H.; Spek, A. L.; Haasnoot, J. G.; Moscovici, J.; Provost, K.; Michalowicz, A.; Renz, F.; Gütllich, P. *Inorg. Chem.* **2000**, *39*, 1891–1900.
252. Kahn, O.; Martinez, C. J. *Science* **1998**, *279*, 44–48.
253. Garcia, Y.; van Koningsbruggen, P. J.; Lapouyade, R.; Fournès, L.; Rabardel, L.; Kahn, O.; Ksenofontov, V.; Levchenko, G.; Gütllich, P. *Chem. Mater.* **1998**, *10*, 2426–2433.

254. Garcia, Y.; van Koningsbruggen, P. J.; Codjovi, E.; Lapouyade, R.; Kahn, O.; Rabardel, L. *J. Mater. Chem.* **1997**, *7*, 857–858.
255. Lavrenova, L. G.; Yudina, N. G.; Ikorskii, V. N.; Varmek, V. A.; Oglezneva, I. M.; Larionov, S. V. *Polyhedron* **1995**, *14*, 1333–1337.
256. Moliner, N.; Munõz, C.; Létard, S.; Solans, X.; Menéndez, N.; Goujon, A.; Varret, F.; Real, J. A. *Inorg. Chem.* **2000**, *39*, 5390–5393.
257. Real, J. A.; Andrés, E.; Munõz, C.; Julve, M.; Granier, T.; Bousseksou, A.; Varret, F. *Science* **1995**, *268*, 265–267.
258. Ozarowski, A.; Shunzhong, Y.; McGarvey, B. R.; Mislankar, A.; Drake, J. E. *Inorg. Chem.* **1991**, *30*, 3167–3174.
259. Vreugdenhil, W.; van Diemen, J. H.; de Graaff, R. A. G.; Haasnoot, J. G.; Reedijk, J.; van der Kraan, A. M.; Kahn, O.; Zarembowitch, J. *Polyhedron* **1990**, *9*, 2971–2979.
260. Kitazawa, T.; Gomi, Y.; Takahashi, M.; Takeda, M.; Enomoto, M.; Miyazaki, A.; Enoki, T. *J. Mater. Chem.* **1996**, *6*, 119–121.
261. van Koningsbruggen, P. J.; Garcia, Y.; Kooijman, H.; Spek, A. L.; Haasnoot, J. G.; Kahn, O.; Linares, J.; Codjovi, E.; Varret, F. *J. Chem. Soc., Dalton Trans.* **2001**, 466–471.
262. Garcia, Y.; Kahn, O.; Rabardel, L.; Chansou, B.; Salmon, L.; Tuchagues, J. P. *Inorg. Chem.* **1999**, *38*, 4663–4670.
263. Jung, O.-S.; Pierpont, C. G. *J. Am. Chem. Soc.* **1994**, *116*, 2229–2230.
264. Lu, J.; Paliwala, T.; Lim, S. C.; Yu, C.; Niu, T.; Jacobson, A. J. *Inorg. Chem.* **1997**, *36*, 923–929.
265. Yoshikawa, H.; Nishikiori, S.; Watanabe, T.; Ishida, T.; Watanabe, G.; Murakami, M.; Suwinska, K.; Luboradzki, R.; Lipkowski, J. *J. Chem. Soc., Dalton Trans.* **2002**, 1907–1917.
266. Evans, O. R.; Lin, W. *Chem. Mater.* **2001**, *13*, 2705–2712.
267. Hou, H.; Wei, Y.; Song, Y.; Zhu, Y.; Li, L.; Fan, Y. *J. Mater. Chem.* **2002**, *12*, 838–843.
268. Hou, H.; Meng, X.; Song, Y.; Fan, Y.; Zhu, Y.; Lu, H.; Du, C.; Shao, W. *Inorg. Chem.* **2002**, *41*, 4068–4075.
269. Hou, H.; Wei, Y.; Fan, Y.; Du, C.; Zhu, Y.; Song, Y.; Niu, Y.; Xin, X. *Inorg. Chim. Acta* **2001**, *319*, 212–218.
270. Hou, H.; Song, Y.; Fan, Y.; Zhang, L.; Du, C.; Zhu, Y. *Inorg. Chim. Acta* **2001**, *316*, 140–144.
271. Kishida, H.; Matsuzaki, H.; Okamoto, H.; Manabe, T.; Yamashita, M.; Taguchi, Y.; Tokura, Y. *Nature* **2000**, *405*, 929–932.
272. Noro, S.; Kondo, M.; Ishii, T.; Kitagawa, S.; Matsuzaka, H. *J. Chem. Soc., Dalton Trans.* **1999**, 1569–1574.
273. Sinzger, K.; Hünig, S.; Jopp, M.; Bauer, D.; Beitsch, W.; von Schütz, J. U.; Wolf, H. C.; Kremer, R. K.; Metzenthin, T.; Bau, R.; Khan, S. I.; Lindbaum, A.; Lengauer, C. L.; Tillmanns, E. *J. Am. Chem. Soc.* **1993**, *115*, 7696–7705.
274. Aumüller, A.; Erk, P.; Klebe, G.; Hünig, S.; von Schütz, J. U.; Werner, H.-P. *Angew. Chem., Int. Ed. Engl.* **1986**, *25*, 740–741.
275. Erk, P.; Gross, H.-J.; Hünig, U. L.; Meixner, H.; Werner, H.-P.; von Schütz, J. U.; Wolr, H. C. *Angew. Chem., Int. Ed. Engl.* **1989**, *28*, 1245–1246.
276. Kato, R.; Kobayashi, H.; Kobayashi, A. *J. Am. Chem. Soc.* **1989**, *111*, 5224–5232.
277. Aumüller, A.; Erk, P.; Hünig, S.; Hädicke, E.; Peters, K.; von Schnering, H. G. *Chem. Ber.* **1991**, *124*, 2001–2004.
278. Kitagawa, H.; Onodera, N.; Sonoyama, T.; Yamamoto, M.; Fukawa, T.; Mitani, T.; Seto, M.; Maeda, Y. *J. Am. Chem. Soc.* **1999**, *121*, 10068–10080.
279. Rarig, R. S. Jr.; Lam, R.; Zavalij, P. Y.; Ngala, J. K.; LaDuca, R. L. Jr.; Greedan, J. E.; Zubieta, J. *Inorg. Chem.* **2002**, *41*, 2124–2133.
280. Liao, J.-H.; Chen, P.-L.; Hsu, C.-C. *J. Phys. Chem. Solids* **2001**, *62*, 1629–1642.
281. Kitagawa, S.; Okubo, T.; Kawata, S.; Kondo, M.; Katada, M.; Kobayashi, H. *Inorg. Chem.* **1995**, *34*, 4790–4796.

# 7.6

## Coordination Polymers: Discrete Systems

E. C. CONSTABLE

*University of Basel, Switzerland*

---

7.6.1 INTRODUCTION AND SCOPE	263
7.6.2 METALLOSTARS AND METALLODENDRIMERS	263
7.6.2.1 Metallostars or Metallo dendrimers	263
7.6.3 STRUCTURAL AND SYNTHETIC CONSIDERATIONS	265
7.6.3.1 Sites of Metal Incorporation	265
7.6.4 SYNTHETIC STRATEGIES	266
7.6.5 METALLOSTARS	267
7.6.5.1 Metallostars Based Upon bpy and phen Domains	267
7.6.5.2 Metallostars Based Upon tpy Domains	279
7.6.5.3 Metallostars Based Upon Other Domains	282
7.6.6 METALLODENDRIMERS	284
7.6.6.1 Metallo dendrimers Based Upon bpy and phen Domains	284
7.6.6.2 Metallo dendrimers Based Upon tpy Domains	288
7.6.6.3 Metallo dendrimers and Metallostars Based Upon Other Domains	289
7.6.7 SURFACE DECORATION	291
7.6.8 METAL CORES DECORATED WITH DENDRITIC WEDGES	293
7.6.9 REFERENCES	297

---

### 7.6.1 INTRODUCTION AND SCOPE

This section deals with dendrimers and stars which incorporate metal centers into their framework or which have metal centers coordinated to donor sites at the surface, within or at the center of structure. This is an area of chemistry that had not been identified at the time that *Comprehensive Coordination Chemistry* (CCC, 1987) was published and which has developed rapidly since the early 1990s. The coverage will be limited in detail to well-defined systems in which the number and site of attached metal ions is known with reasonable certainty. Purely organometallic systems based upon metallocene and other arene metal motifs have been excluded from coverage in this chapter. Discretion has been used in the extent of coverage of compounds that contain metal-carbon bonds in addition to normal coordination interactions. Where metal ions are present within the structural core, the coverage is predominantly limited to kinetically inert systems but decoration at inner or surface sites with labile metal centers is discussed. The chapter does not intend to cover any aspects of the coordination chemistry of donor-functionalized polydispersed polymers or oligomers. The general area of dendrimer and metallo dendrimer chemistry has been reviewed in greater or lesser depth over the past few years and the reader is enthusiastically referred to these specialist publications. Relevant chapters have appeared in monographs devoted to dendrimer chemistry<sup>1-11</sup> as well as in the wider review literature.<sup>12-55</sup> Specific review articles dealing with synthetic aspects,<sup>14,25,37</sup> electrochemical and photophysical properties,<sup>3,15,52</sup> application as artificial photosynthetic systems,<sup>35,40,47,48</sup> applications to molecular electronics,<sup>10</sup> surface

decoration,<sup>18</sup> catalysis,<sup>9,24</sup> self-assembly,<sup>32,39</sup> stereochemistry,<sup>31,33</sup> and application to diagnostics<sup>6</sup> have appeared.

## 7.6.2 METALLOSTARS AND METALLODENDRIMERS

### 7.6.2.1 Metallostars or Metallo dendrimers

What are metallostars and metallo dendrimers? Dendrimers represent an aesthetically pleasing and increasingly useful structural motif that has grown in importance in the past 25 years. The name dendrimer refers to a tree-like structure and dendrimers are conveniently defined as “globular, highly branched, fractal-like polymers of well-defined three-dimensional shape, size and molecular weight that are constructed via iterative, or stepwise, procedures”.<sup>27</sup> The key feature is the multiple branching implied in the fractal structure and a prototype dendrimer is shown in Figure 1(a), which also introduces the key nomenclature, associated with the substructures and the

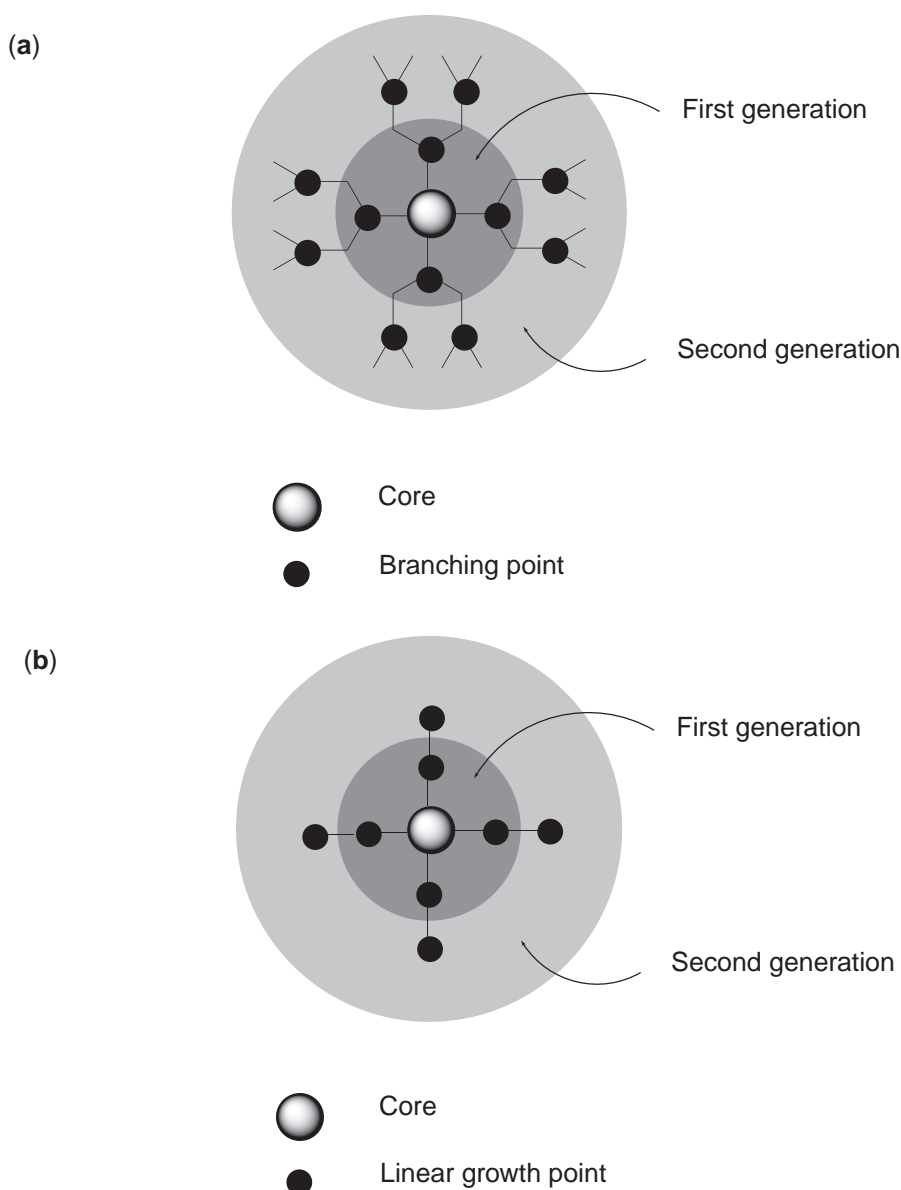


**Figure 1** The nomenclature of basic dendritic (a) and star (b) structures showing the core and two generations extending through a branching site of connectivity 2 in the case of the dendrimer.



concept of a core and subsequent generations. A key distinction needs to be drawn between dendrimers which are ideally single chemical species (*monodispersed* in the language of the polymer scientist) and the so-called *hyperbranched polymers*<sup>11</sup> which also contain multiple branching but which are prepared in a single assembly step and which are polydispersed (contain multiple chemical species). One of the principal problems facing the dendrimer chemist is convincing his or her colleagues that he or she is dealing with single molecular species rather than mixtures of polymers! A metallodendrimer is simply a dendrimer that incorporates metal center(s) at some site(s) within the overall structure. The possible sites of metal center incorporation are discussed in more detail in Section 7.6.3.1.

As indicated in Figure 1(a), a dendrimer develops radially from a core through multiply branched sites. Conceptually, the first step in this process is a structure with the core and the first generation of functionality. This is a first-generation dendrimer although the branching motif that defines the dendrimer may not necessarily be present. The nomenclature and formal classification of dendrimers has been discussed in detail elsewhere.<sup>56–58</sup> There is a large number of compounds which exhibit this structure which it is inappropriate on both conceptual and synthetic grounds to consider as dendrimers. In particular, it is possible to define systems in which the sole branching point is at the core and in which subsequent structural development through the generations is purely linear. These systems are described as stars and the obvious extension to metal-containing systems leads to the name metallostar (Figure 1(b)).

### 7.6.3 STRUCTURAL AND SYNTHETIC CONSIDERATIONS

The key structural motif present in a dendrimer is the repeated unit that gives rise to the branching and the dendritic structure. A very wide range of functional groups has been used in dendritic substructures and these have been reviewed in the general references discussed above. As far as metallodendrimers are concerned, there are a few other structural constraints that need to be considered in any design strategy. Firstly, the functionality present in the dendrimer must be compatible with the metal ion to be incorporated. In particular, easily hydrolyzed functionality should be avoided if Lewis acidic metal ions are to be incorporated in aqueous medium. Secondly, the metal-binding group that is incorporated to bind the metal centers should be unambiguous and commensurate with the desired metal ions, in terms of the number, type, and spatial arrangement of the donor atoms. Furthermore, consideration needs to be given to other functionality within the dendrimer such that it cannot offer alternative or better binding sites. This is a potential problem with amine and amide based metallodendrimers.

Another important factor relates to the kinetic lability or inertness of the metal center that is used. For robust molecules that can be unambiguously characterized as monodispersed systems kinetically inert metal centers have obvious advantages. Indeed, the majority of well-characterized metallodendrimers are based upon kinetically inert  $d^6$  and  $d^8$  metal centers. However, the use of these centers does have disadvantages; specifically, the rate of reaction in the key metal–ligand bond formation reactions may be prohibitively slow and competitive with degradative or scrambling processes. To a certain extent, this disadvantage may be circumvented by using reactions of ligands already coordinated to the inert center in the key metallation steps. In contrast, labile metal ions result in self-assembly processes in which the new metal–ligand bonds are formed rapidly and reversibly. The effect is to give thermodynamic products. In self-assembly processes with labile metal centers, particular care must be taken that alternative binding sites are not present within the dendrimer and that the degree of metallation is as high as theoretically anticipated.

#### 7.6.3.1 Sites of Metal Incorporation

Metal centers may be introduced into metallodendrimers and metallostars at a number of conceptually different sites. A convenient classification has been introduced by Balzani and co-workers and is used here in a slightly modified form.<sup>3,41</sup> Conceptually, the simplest site for metal ion incorporation is at the center of the complex. In principle, a mononuclear complex with dendron-functionalized ligands could be regarded as a metallodendrimer, although this chapter concentrates upon multinuclear systems.

The metal center(s) can play a structural role in the linear part of a dendrimer or a star compound in which it links together two components. Such systems are topologically linear and the metal is used as a convenient “molecular glue”.<sup>45</sup>

Alternatively, the metal center can be found at the branching point of the dendrimer in which case the connectivity and, possibly, the assembly of the dendrimer, are determined by the coordination number and geometry of the metal and the nature of the metal-binding domains.

Finally, the dendrimer or star may be surface or internally functionalized or decorated with metal-containing motifs. This type of dendrimer is widely investigated with a view to preparing novel catalytic systems in which a “dendritic effect” results in enhanced or modified catalytic properties with respect to a similar number of mononuclear complexes. As many of these species are strictly organometallic they do not fall properly within the scope of this volume.

#### 7.6.4 SYNTHETIC STRATEGIES

We will now briefly discuss the synthetic strategies that may be used for the preparation of metallostars and metallodendrimers. Clearly, different strategies will be appropriate to different sites of metal ion incorporation and the structural role of the metal center(s).

Fundamentally, there are two synthetic strategies that may be adopted—these are known as *divergent* and *convergent* approaches (Figure 2 where S is a spacer-group). The divergent approach is conceptually the most logical as it emphasizes the repeated branching of the structure within an iterative synthetic methodology. In the divergent method, a core structure  $CX_n$  with  $n$  reactive functional groups X is the starting point. In principle, this is simply reacted with a difunctional species  $ZRX_m$  that contains a reactive group Z that reacts specifically and in high yield with the functionality X. This would give a new branched species  $C(SRX_m)_n$  in which S represents the spacer resulting from the reaction of Z and X. The result is expansion of the core with  $n$  reactive X groups to a species with  $m \times n$  X groups. The difficulty arises because the Z functionality in  $ZRX_m$  can react just as well with the X groups of  $ZRX_m$  and  $C(SRX_m)_n$  as with  $CX_n$  and the result would be an uncontrolled mixture of oligomers and polymers. It is, thus, necessary to use an iterative protection–deprotection strategy using  $ZRX^*_m$  where  $X^*$  is a protected X group. The reaction of  $CX_n$  with  $ZRX^*_m$  is then specific and gives  $C(SRX^*_m)_n$ , which may then be deprotected to give  $C(SRX_m)_n$ . Subsequent reaction of  $C(SRX_m)_n$  with  $ZRX^*_m$  produces the next-generation dendrimer  $C(SR\{SRX^*_m\}_m)_n$  with  $m \times m \times n$   $X^*$  groups which may be deprotected and taken through to the next generation by reaction with  $ZRX^*_m$ . The very elegant protection–deprotection methods that have been developed are discussed in detail in the general references given above. The divergent approach has a number of advantages and

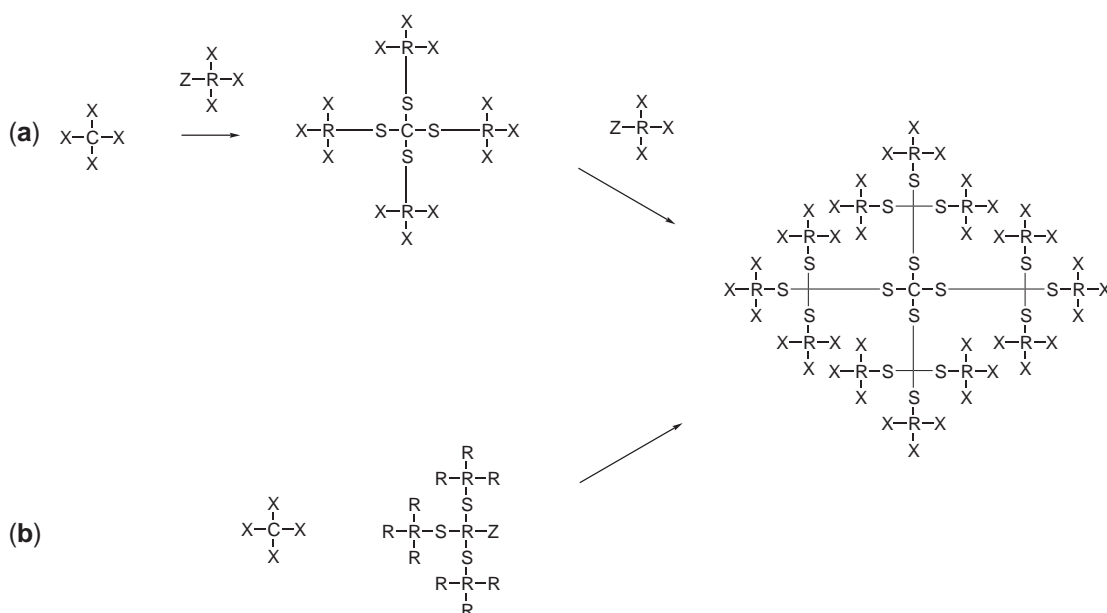


Figure 2 a) Divergent and b) convergent strategies for the synthesis of dendrimers.

disadvantages. Firstly, the strategy allows the synthetic process to be continued until a dendrimer of a generation with the desired properties is obtained. There is no *a priori* requirement to select a given generation as being the target at the beginning of the synthesis. The disadvantages are, however, significant. Firstly, it is essential to ensure that reaction of all the X sites at the surface in any given generation react in their entirety with the reagent  $ZRX^*_m$ . Consider a dendrimer with 32 X functional groups upon the surface reacting with  $ZRX^*_3$ . If only 31 react, the new compound produced with 93 X\* groups may not be easily separated or distinguished from the species in which all 32 sites have reacted and given 96 X\* groups. However, if we take the compound through to the next generation the problem is amplified. Even if we assume that all of the surface groups react in this step, the fully reacted species will give a compound with 288 X\* groups whereas the incompletely reacted species will give one with 279 X\*. The difference becomes increasingly significant as it is propagated through subsequent generations and gives rise to polydispersed species with surface voids and channels to the interior. Even if all the inner generation reactions are complete, there will eventually come a point at which the steric interactions at the surface are such that complete reaction of all the surface X groups is not possible. For a discussion of this effect, see Newkome *et al.*<sup>11</sup>

The convergent approach uses an alternative approach in which fragments (*dendritic wedges*) containing functionality to the desired generation are prepared and attached to the core in the final step of the reaction. This approach also has advantages and disadvantages. The principle advantage is that, until the final step, all of the molecular species are of low to medium molecular weight and can be fully characterized and purified by conventional chemical methods. Only in the final step is a high-molecular-weight species obtained. A more subtle advantage is seen when we consider the consequences of incomplete reaction of surface X functionality within the core. As we saw above in the divergent approach, incomplete reaction would result in errors being propagated through subsequent generations. Assuming that all of the dendritic wedges are pure (a reasonable assumption as these are conventional low-molecular-weight species), there will be no propagation effect. Furthermore, it will be immediately obvious if reaction is not complete. In the divergent approach, the difference in molecular mass between the completely and incompletely reacted species was simply the molecular mass of the small molecule  $ZRX^*_m$ , which is likely to be very small in comparison to dendrimer. In contrast, consider a convergent approach in which  $CX_4$  reacts with  $ZR\{SRX^*_m\}_m$ . Incomplete reaction will give  $XC\{SR\{SRX^*_m\}_m\}_3$  in addition to  $C\{SR\{SRX^*_m\}_m\}_4$  and these species will differ by approximately 25% in molecular weight. The major disadvantage in the convergent approach is the requirement to define the desired generation from the beginning of the reaction sequence. Different dendritic wedges are required for the preparation of dendrimers of different generations.

## 7.6.5 METALLOSTARS

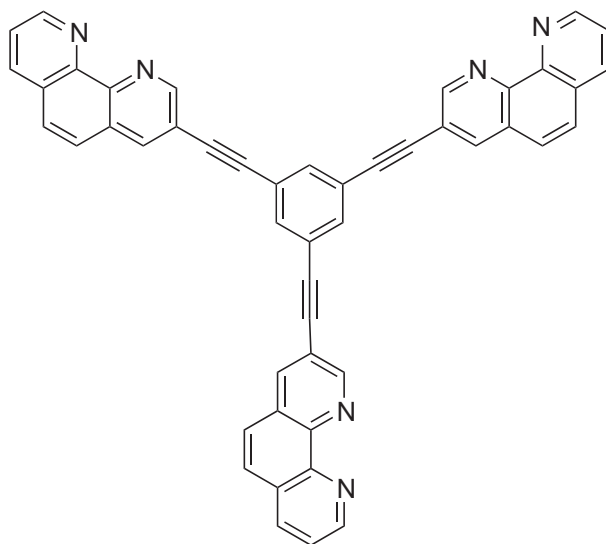
Although metallostars are by definition first-generation metallodendrimers, it is convenient to consider them as a separate class. In particular, the majority of compounds of this class have been specifically prepared as first-generation species without the structural development of the ligands that would be required for the preparation of a dendrimer. In the literature, the distinction between metallostars and metallodendrimers is not usually clearly made and many of these species are described as metallodendrimers. We will specifically consider metallostars with a core connectivity of three or greater; this excludes topologically linear dinuclear and trinuclear systems which are considered in chapters dealing with the appropriate metal.

### 7.6.5.1 Metallostars Based Upon bpy and phen Domains

The commonest metal-binding motif introduced into metallostars and metallodendrimers is probably the classical diimine  $N=C-C=N$  motif found in ligands such as bpy and phen. Although the majority of metallostars and metallodendrimers are based upon the bpy motif, a few examples incorporating phen metal-binding domains are known and these will be considered first.

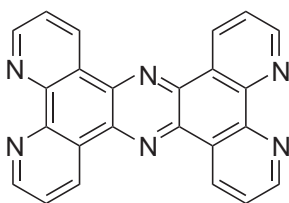
A convergent approach has been used for the preparation of the triruthena complex  $[(1)\{Ru(bpy)_2\}_3]^{6+}$  from palladium-catalyzed coupling of 1,3,5-triethynylbenzene and  $[Ru(bpy)_2(L)]^{2+}$  ( $L = 3\text{-Brphen}$ ). This is a very nice example in which the ligand in a kinetically

inert  $d^6$  complex is structurally elaborated in the key synthetic step. The metal centers in  $[(\mathbf{1})\{\text{Ru}(\text{bpy})_2\}_3]^{6+}$  are electronically isolated from one another.<sup>59</sup>

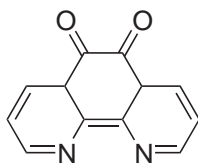


(1)

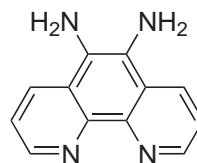
Another elegant use of ligand reactivity is seen in the convergent synthesis of the tetranuclear metallocentric species  $[\text{Ru}\{\mathbf{(2)}\text{Ru}(\text{phen})_2\}_3]^{8+}$  (**5**) from the condensation of  $[\text{Ru}(\mathbf{3})_3]^{2+}$  and  $[\text{Ru}(\mathbf{4})(\text{phen})_2]^{2+}$ . By using enantiomerically pure  $[\text{Ru}(\mathbf{3})_3]^{2+}$  and  $[\text{Ru}(\mathbf{4})(\text{phen})_2]^{2+}$  diastereomerically pure samples of  $\Delta\Lambda_3$ -**5**,  $\Delta\Delta_3$ -**5**,  $\Lambda\Lambda_3$ -**5**, and  $\Lambda\Delta_3$ -**5** were obtained.<sup>60–63</sup> The peripheral  $\{\text{Ru}^{\text{II}}(\mathbf{2})(\text{phen})_2\}$  centers are more readily oxidized than the core and two redox processes in a ratio of 3:1 at +1.36 V and +1.47 V (*versus* SCE) are observed.<sup>64</sup> The spectroscopic and photophysical properties of these metallostars have been studied in detail and it appears that the different diastereomers exhibit similar spectroscopic, photophysical, and redox properties which do not depend upon the relative spatial positioning of the components.<sup>64</sup>



(2)



(3)

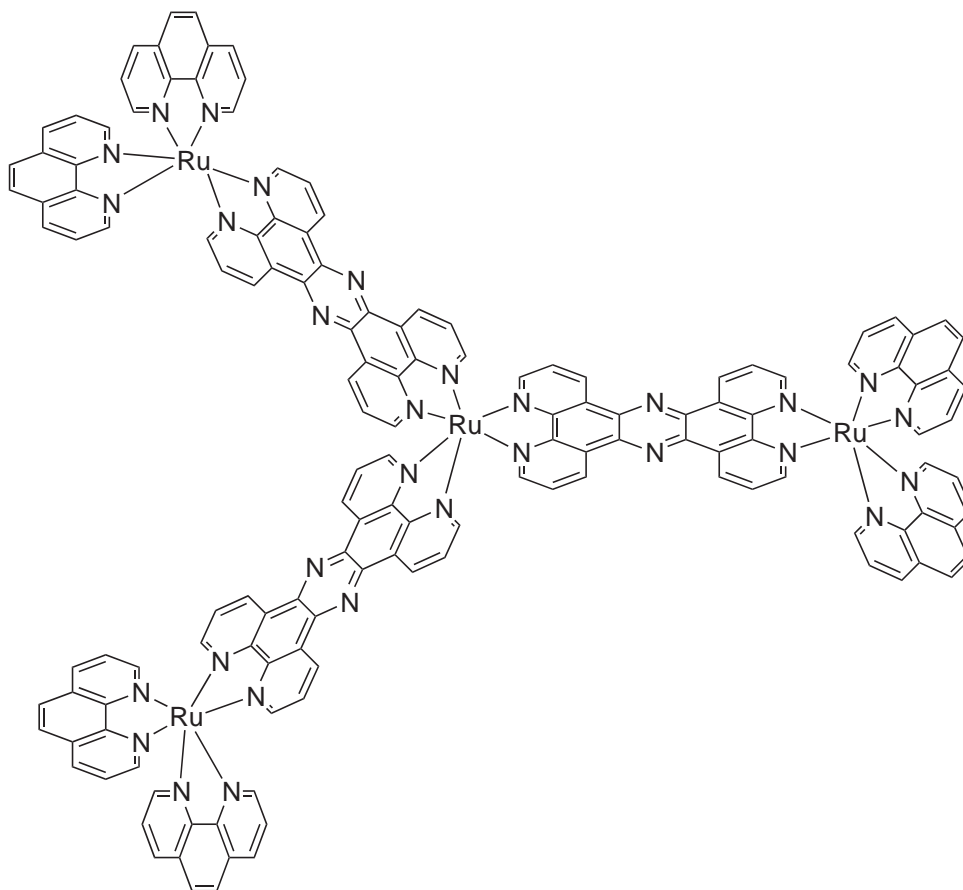


(4)

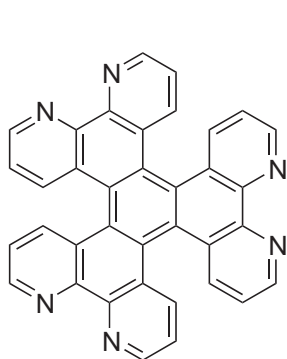
It is a simple extension of ligand **(2)** to trinucleating analogues that will provide the core for trinuclear metallostars and the best known examples of these are **(6)** and **(7)**. The ligand **(7)** was prepared by reaction of hexaaminobenzene with **(3)**, and converted to the diastereomerically pure complexes  $\Lambda_3$ - and  $\Delta_3$ - $[(\mathbf{7})\{\text{Ru}(\text{phen})_2\}_3]^{6+}$  by reaction with  $\Lambda$ - or  $\Delta$ - $[\text{Ru}(\text{phen})_2(\text{py})_2]^{2+}$  respectively.<sup>65</sup> The analogous complexes  $\Lambda_3$ - and  $\Delta_3$ - $[(\mathbf{7})\{\text{Ru}(\text{phen})_2\}_3]^{6+}$  were similarly prepared<sup>65</sup> following the earlier description of the preparation of a mixture of diastereomers.<sup>66</sup>

There are numerous examples of metallostars and metallodendrimers containing multiple bpy-like metal-binding domains and this section can only provide a brief introduction. An extremely useful review article collecting data for all ligands containing two or more 2,2'-bipyridine units appeared in 2000 and provides a good entry to the literature.<sup>67</sup> Unfortunately, fused systems are not explicitly included in the coverage.

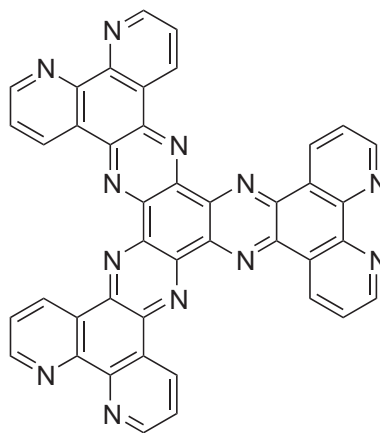
We start by considering systems with multiple “simple” bpy metal-binding domains. The majority of these ligands have been prepared with a view to encapsulating metal ions by binding some or all of the bpy domains to the same metal center. The ligand **(8)** gave of the complexes  $[(\mathbf{8})\{\text{Ru}(\text{bpy})_2\}_3]^{6+}$  and  $[(\mathbf{8})\{\text{ReCl}(\text{CO})_3\}_3]$  as mixtures of the diastereomers upon reaction with



(5)

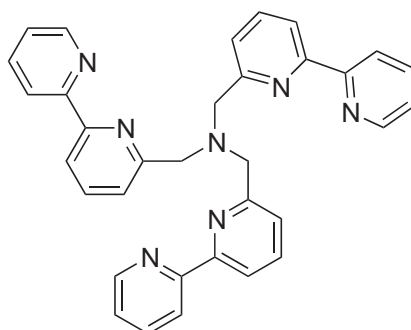


(6)

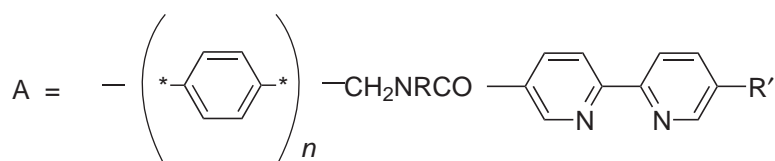
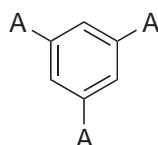


(7)

[Ru(bpy)<sub>2</sub>Cl<sub>2</sub>] or [ReCl(CO)<sub>3</sub>] respectively.<sup>68–70</sup> The complexes show typical luminescence behavior. A series of ligands bearing three pendant bpy domains at various distances from a 1,3,5-trisubstituted benzene core (9) has been prepared.<sup>71,72</sup> Homo- and heterometallic complexes with {Os<sup>II</sup>(bpy)<sub>2</sub>} and {Ru<sup>II</sup>(bpy)<sub>2</sub>} capping units have been prepared, and detailed electrochemical and photophysical studies reported. The metal-centered redox processes are independent of the structure of the ligand or the presence of a heterometallic center. The complexes exhibit Ru to Os energy transfer that decreases in efficiency with the length of the spacer.



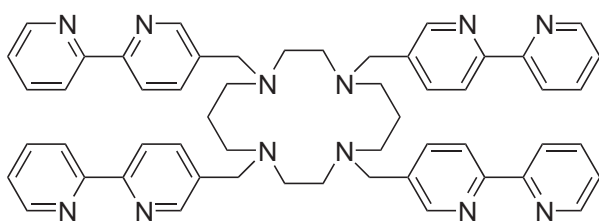
(8)



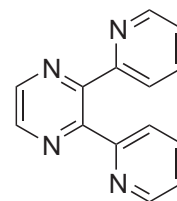
$$n = 0, 1, 2; R = \text{H, Bz}; R' = \text{H, CO}_2\text{Et, CO}_2\text{H}$$

(9)

A cyclam core bearing four pendant bpy metal-binding domains (**10**) has been prepared and the fluorescence quenching of the metallostar complex  $[(\mathbf{10})\{\text{Ru}(\text{bpy})_2\}_4]^{8+}$  has been used to quantify transition metal ion binding to the macrocyclic core.<sup>73</sup>



(10)



(11)

Some of the best known metallodendrimers and metallostars are based upon ligands that contain two bpy metal-binding domains fused within a single heterocycle. The prototypical ligands are the isomeric pyrazines (**11**) and (**12**), which each have two bpy domains spatially arranged such that they must bind two different metal centers rather than chelating a single site. Furthermore, the spatial arrangement is such that a divergent dinuclear complex will be obtained, as opposed to isomeric ligands such as the pyridazine (**13**), which has a convergent dinucleating

domain that leads to grids and ladders. The related quinoxaline (**14**) is also widely investigated. Complexes with these ligands have primarily been prepared as antenna systems for the collection and transfer of light energy and these applications together with the synthetic methodology have been extensively reviewed.<sup>3,12,14–17,21,23,25,26,34,37,41,43,46–48,52,54</sup> These metallostars differ from those considered earlier by having a metal ion at the center as opposed to an organic core structure. The core may best be viewed as an  $\{M(\mathbf{11})_3\}$  or  $\{M(\mathbf{12})_3\}$  moiety (Figure 3). A potential disadvantage of these ligands is seen in the diastereomeric diversity of the cores; not only is each mononuclear unit chiral, with both  $\Lambda$  and  $\Delta$ -enantiomers being possible but also *mer* and *fac* isomers could be formed. In general, ligand (**11**) is favored over (**12**) by the Balzani and Denti groups as it gives predominantly *meridional* complexes. The core complexes  $[Ru(\mathbf{11})_3]^{2+}$ ,<sup>74–80</sup>  $[Os(\mathbf{11})_3]^{2+}$ ,<sup>81,82</sup> and  $[Rh(\mathbf{11})_3]^{2+}$ <sup>83</sup> have been studied, and detailed spectroscopic and electrochemical properties reported. The homoleptic core complexes  $[Os(\mathbf{12})_3]^{2+}$ <sup>81</sup> and  $[Ru(\mathbf{12})_3]^{2+}$ <sup>85</sup> have also been described. Somewhat surprisingly, there does not appear to be a structurally characterized

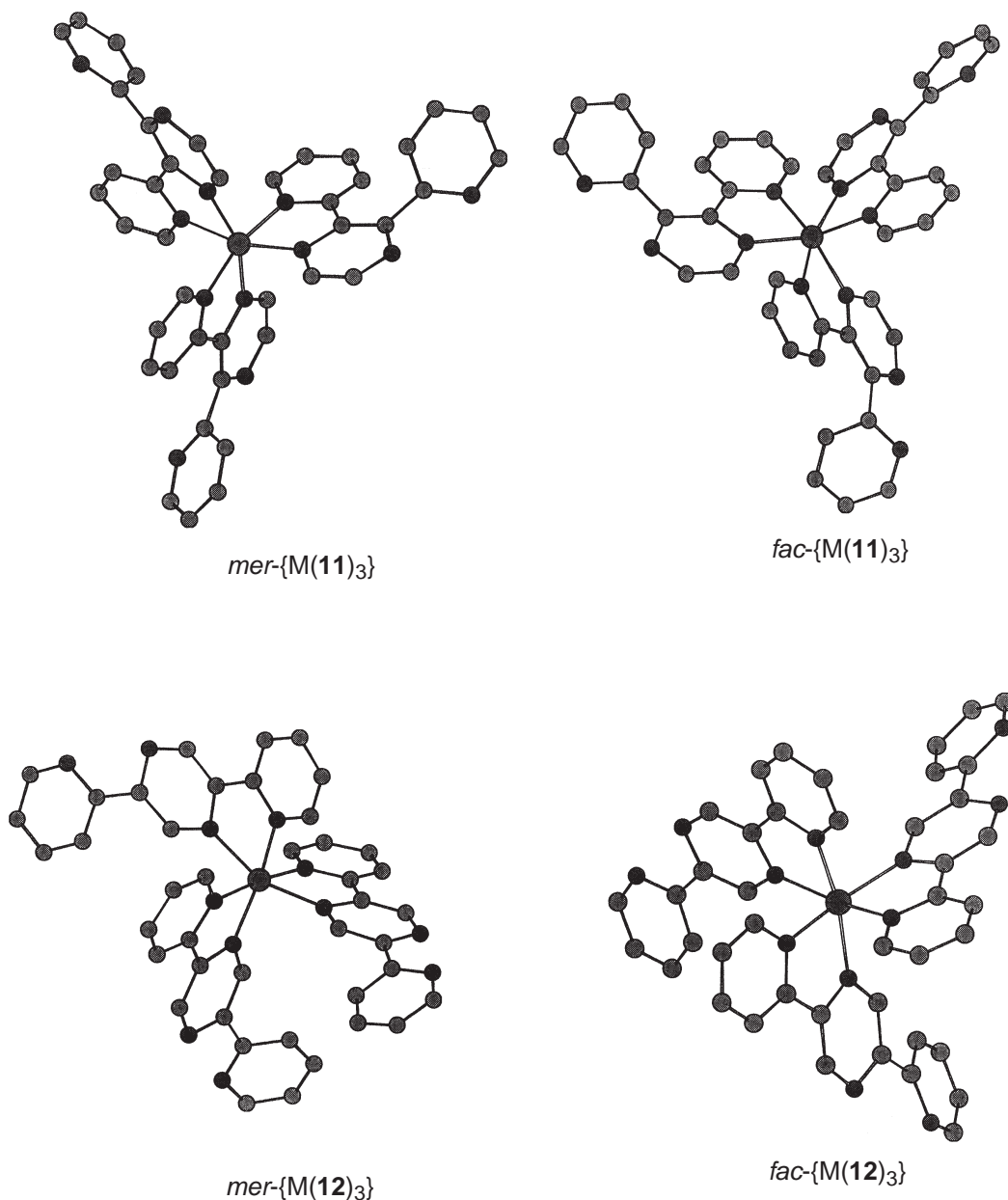
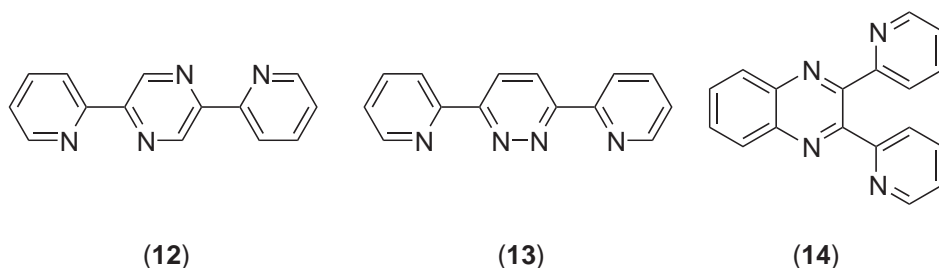


**Figure 3** Ligands **11** and **12** can build diastereomeric *mer* and *fac*  $ML_3$  complexes.

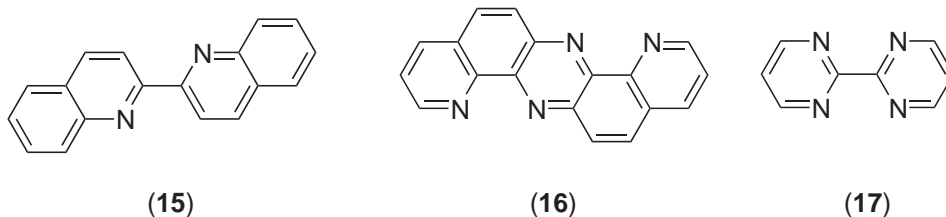
example of one of the mononuclear core complexes although the related complexes  $[\text{MLX}_2]^{n+}$  and  $[\text{ML}_2\text{X}]^{n+}$  ( $\text{L} = \mathbf{(11)}$  or  $\mathbf{(12)}$ ;  $\text{X} = \text{bpy}$  or  $\text{phen}$ ) are well known.



The simplest assembly methodology for metallostars and metal dendrimers of this type is divergent building out from the core complexes above, although this is not likely to have a high degree of diastereoselectivity unless enantiomerically pure  $[\text{ML}_2\text{X}_2]^{n+}$  ( $\text{L} = \text{bpy}$  or  $\text{phen}$  derivative,  $\text{X} = \text{labile ligand}$ ) species are used. In contrast, convergent approaches utilizing  $[\text{MLX}_2]$  ( $\text{L} = \mathbf{(11)}$  or  $\mathbf{(12)}$ ;  $\text{X} = \text{bpy}$  or  $\text{phen}$ ) can be made stereospecific as the mononuclear complexes can be obtained enantiomerically pure. The first-generation metallostars are tetranuclear with a central metal  $\text{M}$  and three outer-generation metals  $\text{M}'$ . To date, only complexes in which the outer three metal centers are the same have been reported; terminating ligands include  $\text{bpy}$  or  $\text{phen}$  and substituted derivatives and 2,2'-biquinoline ( $\mathbf{(15)}$ ). The parent tetranuclear homoleptic metallostar complexes  $[\text{Ru}\{\mathbf{(11)}(\text{RuL}_2)\}_3]^{8+}$  ( $\text{L} = \text{bpy}$ ,  $\text{phen}$ , or  $\mathbf{(15)}$ ) complexes have been prepared by the divergent reaction of  $[\text{Ru}(\mathbf{(11)})_3]^{2+}$  with  $[\text{RuL}_2\text{Cl}_2]$ .<sup>87,88</sup> Up to 18 ligand reduction processes in the complex have been determined and a detailed understanding of the electronic structure obtained.<sup>88</sup> The analogous tetranuclear metallostars  $[\text{Ru}\{\mathbf{(14)}(\text{RuL}_2)\}_3]^{8+}$  have also been prepared<sup>89</sup> as has the heterotetranuclear species  $[\text{Ru}\{\mathbf{(14)}(\text{PtL}_2)\}_3]^{2+,87}$ . The heteronuclear complexes  $[\text{Os}\{\mathbf{(11)}(\text{RuL}_2)\}_3]^{8+}$  have been obtained in a similar manner and the influence of the terminal ligands on the  $\text{Ru}$  to  $\text{Os}$  energy transfer processes investigated.<sup>90</sup> It is somewhat surprising that the convergent synthesis of heterotetranuclear species such as  $[\text{M}\{\mathbf{(11)}(\text{M}'\text{L}_2)\}_3]^{(3n+2)+}$  ( $\text{M} = \text{labile first row transition metal dication}$ ;  $\text{M}' = \text{nonlabile metal center}$ ) by the reaction of  $[\text{M}_2\text{L}_2(\mathbf{(11)})]^{n+}$  with a labile first row transition metal ion does not appear to have been described. The complex  $[\text{Ru}\{\mathbf{(12)}(\text{OsL}_2)\}_3]^{8+}$  has been prepared.<sup>85</sup> Peripheral functionalization of the surface ligands allows additional structural development of these star compounds, and the light-harvesting characteristics of the complexes  $[\text{Os}\{\mathbf{(11)}\text{RuL}_2\}_2]^{8+}$  ( $\text{L} = 4\text{-methyl-4'-[2-(1-pyrenyl)ethyl]-2,2'-bipyridine}$ ) have recently been described.<sup>84</sup>

The annelated ligand ( $\mathbf{(16)}$ ) is of interest as a rigid analogue of ( $\mathbf{(12)}$ ) and the tetranuclear metallostar  $[\text{Ru}\{\mathbf{(16)}(\text{Ru}(\text{phen})_2)\}_3]^{8+}$  has been prepared in a divergent reaction of  $[\text{Ru}(\mathbf{(16)})_3]^{2+}$  with  $[\text{Ru}(\text{phen})_2\text{Cl}_2]$ .<sup>91</sup>

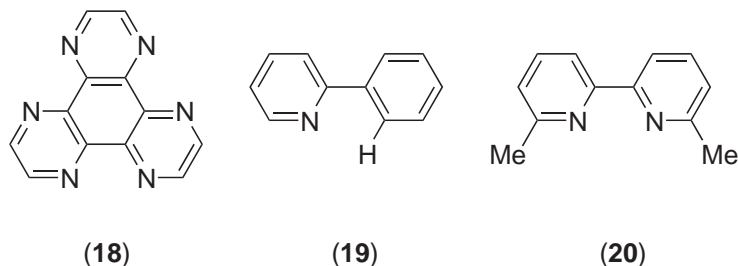
The parent metallostars of this series are probably best viewed as those derived from 2,2'-bipyridimine ( $\mathbf{(17)}$ ) and there is a well-developed literature dealing with these compounds. Specifically the core complexes  $[\text{M}(\mathbf{(17)})_3]^{n+}$  are well-characterized and are discussed elsewhere in this work. In contrast to the prototype structures involving the pyrazine ligands ( $\mathbf{(11)}$ ) and ( $\mathbf{(12)}$ ), a number of core mononuclear  $[\text{M}(\mathbf{(17)})_3]^{n+}$  species including  $[\text{Fe}(\mathbf{(17)})_3]^{2+,92-95}$  and  $[\text{Ru}(\mathbf{(17)})_3]^{2+,96}$  have been structurally characterized. Of more interest are the first-generation metallostars  $[\text{M}\{\mathbf{(17)}(\text{M}'\text{L}_2)\}_3]^{n+}$  that have generally been prepared in a divergent reaction of  $[\text{M}(\mathbf{(17)})_3]^{n+}$  with  $[\text{M}'\text{L}_2\text{Cl}_2]$ ; specifically electrochemical and photophysical investigations of the complexes  $[\text{Ru}\{\mathbf{(17)}(\text{Ru}(\text{bpy})_2)\}_3]^{8+,89}$  and  $[\text{Ru}\{\mathbf{(17)}(\text{Re}(\text{CO})_3\text{Cl})_3\}_3]^{2+,97}$  have been reported.



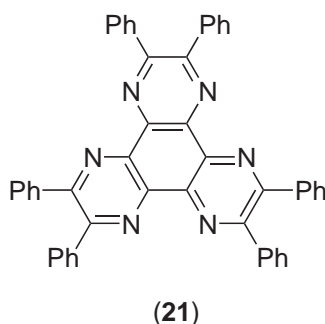
At this point, we return to the well-known trinucleating ligand 1,4,5,8,9,11-hexaazatriphenylene ( $\mathbf{(18)}$ ) which is related to compounds ( $\mathbf{(5)}$ )–( $\mathbf{(7)}$ ). This ligand can give rise to two series of metallostars. In the first, ligand ( $\mathbf{(18)}$ ) itself acts as a core and the first metal-containing generation comprises



three metal centers whilst in the second the core is a  $\{M(\mathbf{18})_3\}$  moiety and addition of the next metal-containing generation yields a heptanuclear metallostar or metallodendrimer with six metal centers in the outermost generation. The trinuclear complexes  $[(\mathbf{18})\{Ru(L)_2\}_3]^{6+}$  ( $L = \text{bpy}$  or  $\text{phen}$ ) have been prepared by the reaction of  $(\mathbf{18})$  with  $[RuL_2X_2]$  and detailed studies of the electrochemical and photophysical behavior together with mass spectrometric investigations have been reported.<sup>89,97–102</sup> The earlier studies are almost certainly on a mixture of diastereomers. The heterotrimetallic compounds  $\{[(\mathbf{19})\text{-H})_2Rh\}(\mathbf{18})\{Ru(\text{bpy})_2\}_2\}^{5+}$  and  $\{[(\mathbf{19})\text{-H})_2Rh\}_2\text{-}(\mathbf{18})\{Ru(\text{bpy})_2\}_2\}^{4+}$  containing the cyclometallated ligand  $(\mathbf{19})\text{-H}$  have been prepared by the reaction of  $\{[(\mathbf{18})\text{-H})_2Rh\}_2(\mu\text{-Cl})_2\}$  with  $[(\mathbf{18})\{Ru(\text{bpy})_2\}_2]^{4+}$  and  $[(\mathbf{18})\{Ru(\text{bpy})_2\}_2]^{2+}$ , respectively.<sup>100,103</sup> A  $^{99}\text{Ru}$  NMR investigation of  $[(\mathbf{18})\{Ru(\text{phen})_2\}_3]^{6+}$  has been reported.<sup>101</sup> In a series of elegant papers, Keene and co-workers have used enantiomerically pure precursors to prepare diastereomerically pure  $[(\mathbf{18})(ML_2)_n(M'L_2)_{3-n}]^{6+}$  ( $M, M' = \text{Ru, Os}$ ;  $L = \text{bpy, phen}$  or substituted derivative).<sup>104–107</sup>

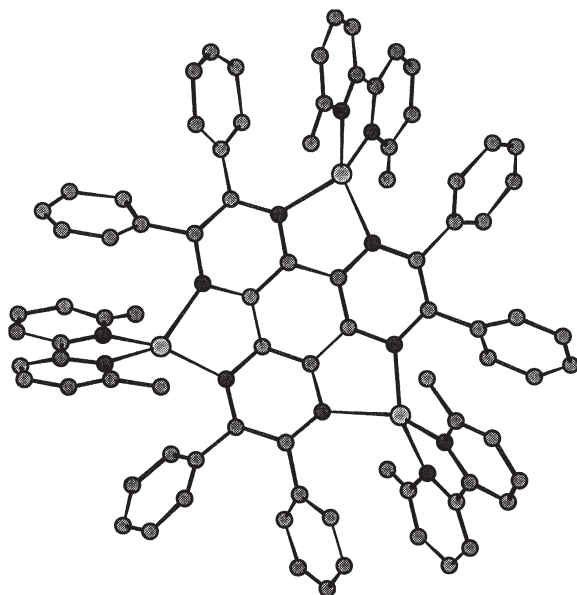


The multicomponent assembly of the tricopper(I) metallostar  $[(\mathbf{21})\{Cu(\mathbf{20})\}_3]^{3+}$  ( $\mathbf{22}$ ) from  $(\mathbf{21})$ ,  $(\mathbf{20})$  and  $[Cu(\text{MeCN})_4][\text{BF}_4]$  in  $\text{CH}_2\text{Cl}_2$  has been described by Lehn and Baxter.<sup>108</sup> This self-assembly process is the prototype reaction for the construction of a series of heteroleptic multinuclear cylindrical species. The related complex  $[(\mathbf{24})\{Cu(\text{dppe})\}_3]^{2+}$  has been reported and is of interest as in the reaction of copper(I) with  $(\mathbf{24})$ , the ligand is reduced to the radical anion  $(\mathbf{24}^-)$ .<sup>109</sup> The dicationic species  $(\mathbf{25})$  (only *ipso* carbon of the phenyl represented) comprises three copper(I) centers and a  $(\mathbf{24}^-)$  radical anion. The reaction of  $(\mathbf{18})$  with  $[\text{Cr}(\text{CO})_6]$  yields the trinuclear star  $[(\mathbf{18})\{\text{Cr}(\text{CO})_4\}_3]$  together with dinuclear and mononuclear species.<sup>110</sup> The trinuclear complex with terminal dicyanamide ligands  $[(\mathbf{18})\{\text{Co}(\text{N}(\text{CN})_2)_2\}_3]$  has also been reported and structurally characterized.<sup>111</sup>

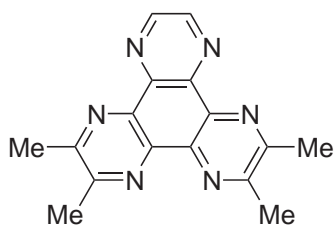


The core complexes  $[Ru(\mathbf{18})_3]^{2+}$ <sup>100</sup>,  $[Cu(\mathbf{18})_2]^{+}$ <sup>112</sup>,  $[Cu(\mathbf{21})_2]^{+}$ <sup>112</sup>,  $[Cu(\mathbf{23})_2]^{+}$ <sup>112</sup> have been described. The copper complexes have been used for the preparation of a series of interlaced heteroleptic species but no further structural elaboration to the metallostars appears to have been described. The complex  $[Ru(\mathbf{18})_3]^{2+}$  has been developed in a divergent sense to give the heptanuclear metallostar  $[Ru\{(\mathbf{18})(\text{Ru}(\text{phen})_2)_2\}_3]^{14+}$ .<sup>113–115</sup> STM methods have been used to obtain images of this heptanuclear complex on a graphite support.

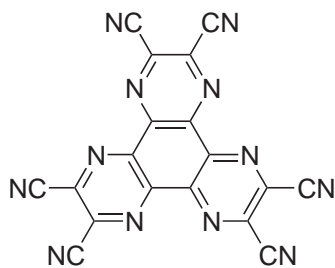
A series of heptanuclear metallostars based upon central  $\{M(\text{bpy})_3\}$  motifs and bearing pendant  $\{M'(\text{tpy})_2\}$  units has been prepared by Constable and co-workers making extensive use of the reactions of coordinated  $\text{bpy}$  and  $\text{tpy}$  ligands. The heterotopic mononuclear complex  $(\mathbf{26}^{2+})$  was prepared in good yield by the divergent reaction of  $[Ru(4,4'\text{-Cl}_2\text{bpy})_3]^{2+}$  with  $4'\text{-HOTpy}$ , but subsequent attempts to metallate the surface  $\text{tpy}$  domains to yield  $[(\mathbf{26})\{Ru(\text{tpy})\}_6]^{14+}$  were unsuccessful and mixtures were obtained. In a complementary convergent approach, the complex  $(\mathbf{27}^{4+})$  was obtained by the reaction of  $4,4'\text{-(HO)}_2\text{bpy}$  with  $[Ru(\text{tpy})(\mathbf{28})]^{2+}$ ;  $(\mathbf{27}^{4+})$  is a typical  $\text{bpy}$



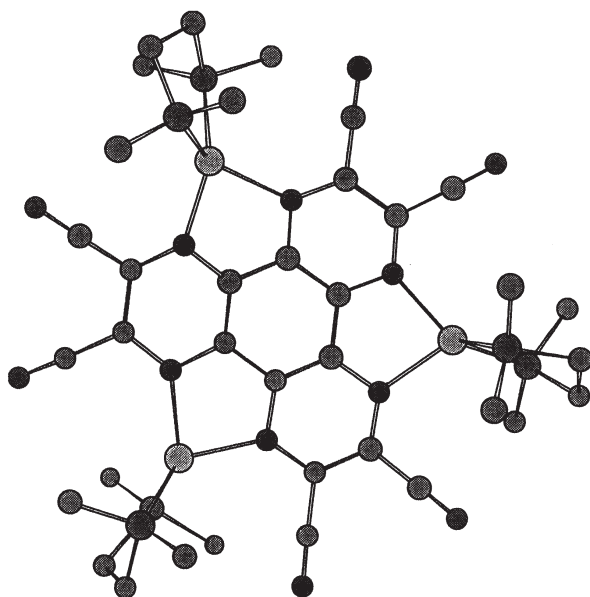
(22)



(23)

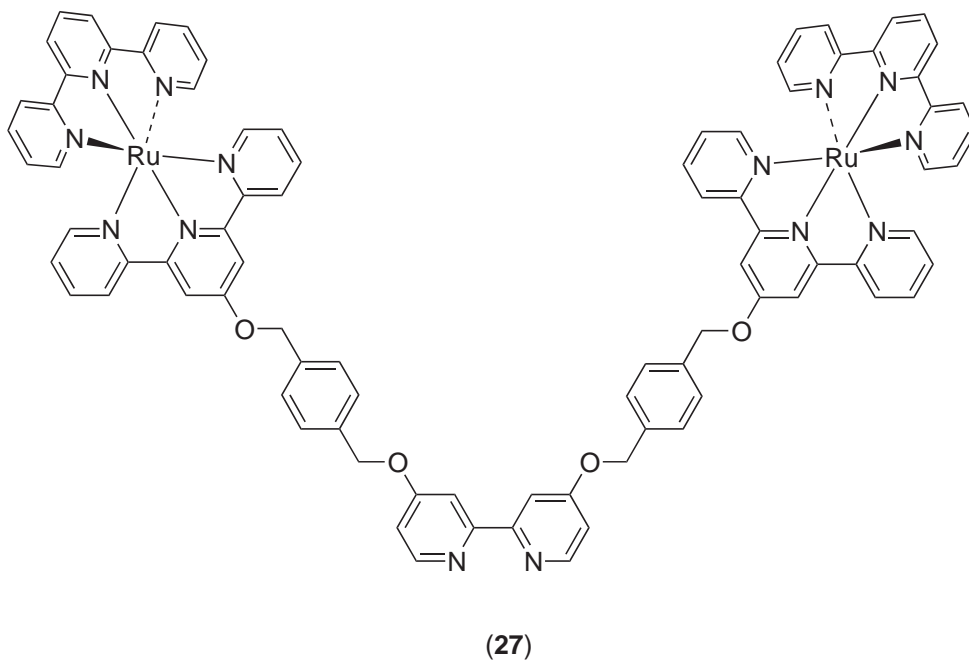
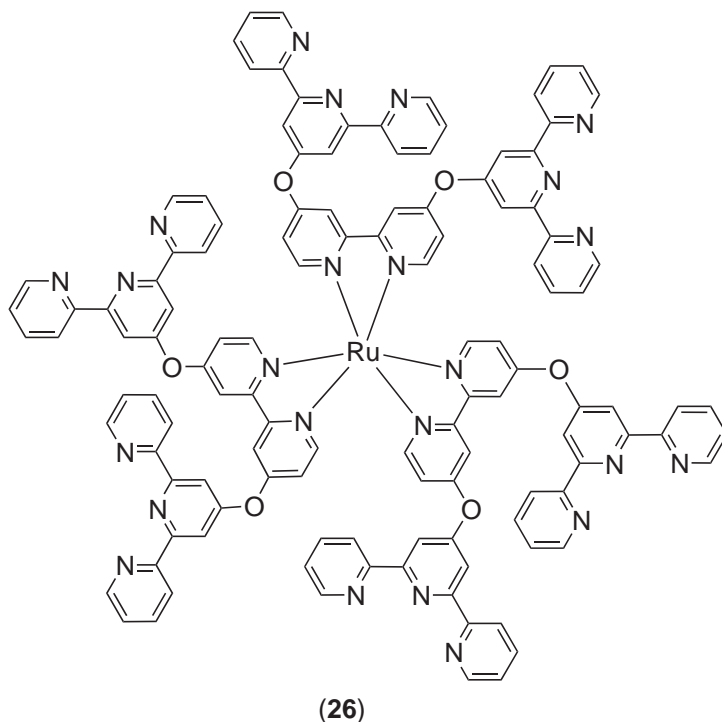


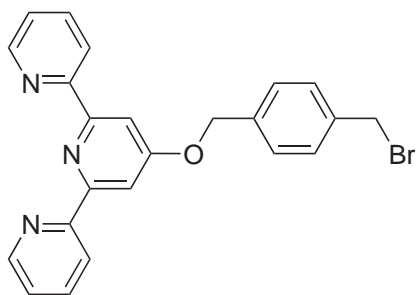
(24)



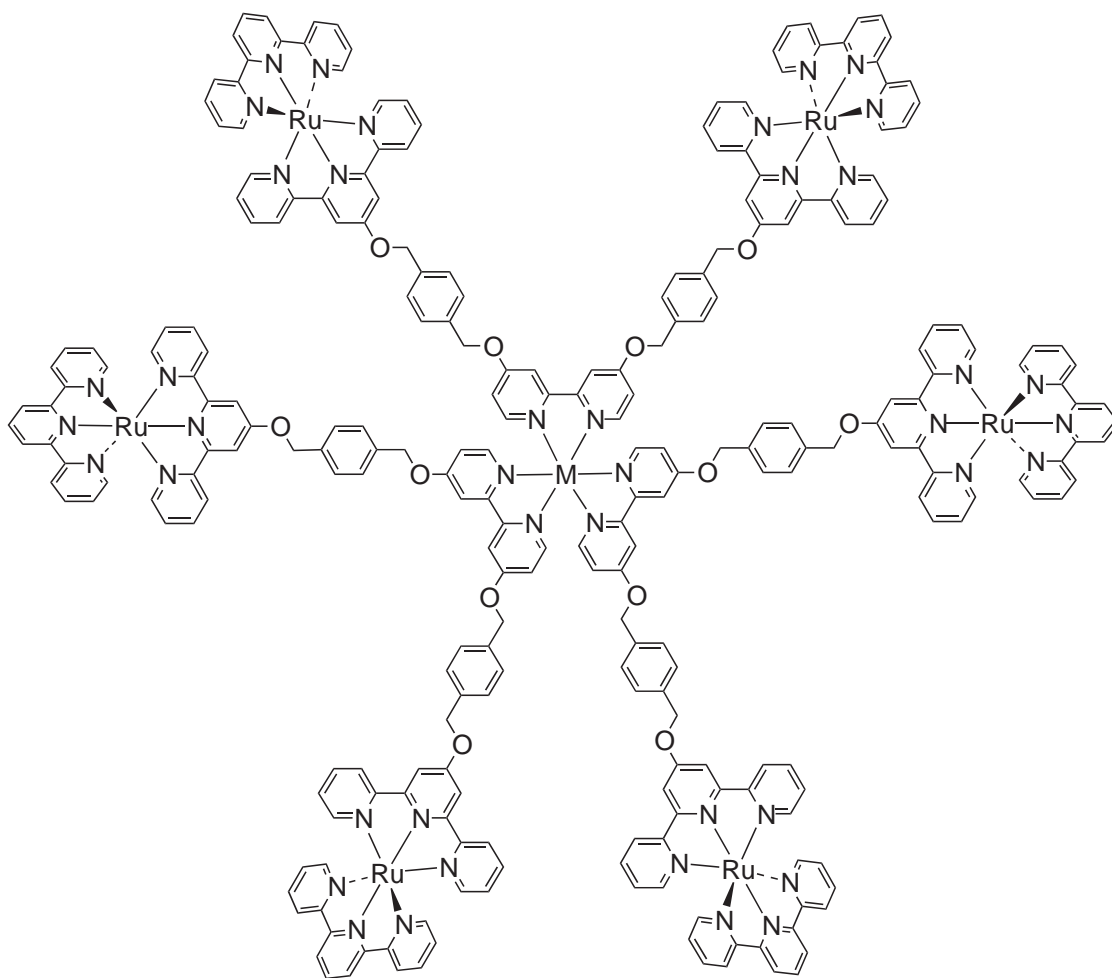
(25)

ligand and reaction with labile metal ions such as iron(II) or cobalt(II) results in the self-assembly of the heptanuclear complexes  $[M(27)_3]^{14+}$ , (29).<sup>116,117</sup> These studies have been extended to species related to (27) in which some of the ether links have been replaced by C—C bonds to give  $[M(30)_3]^{14+}$  which possesses significantly greater hydrolytic stability than (27).<sup>118,119</sup> A related series of heptanuclear metallostars incorporating polyalkyne spacers based upon the functionalized bpy ligands ( $31^{4+}$ ) have been prepared by coupling reactions of alkyne functionalized complexes.<sup>120</sup>

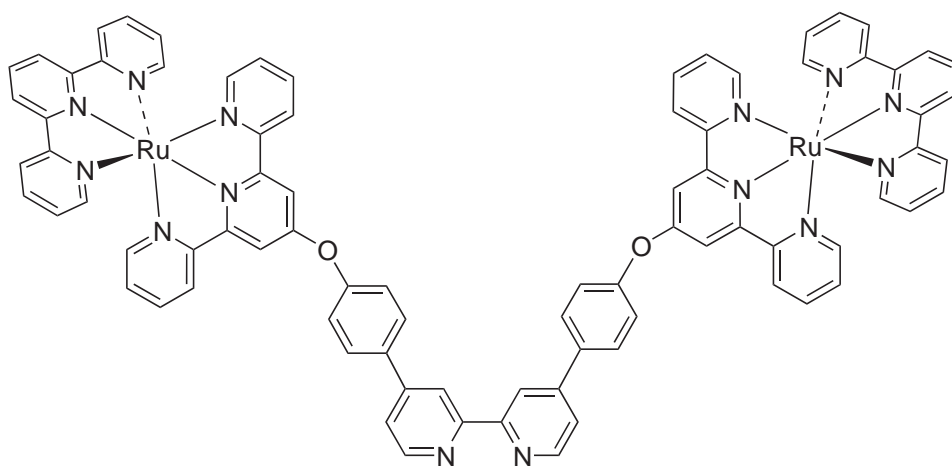




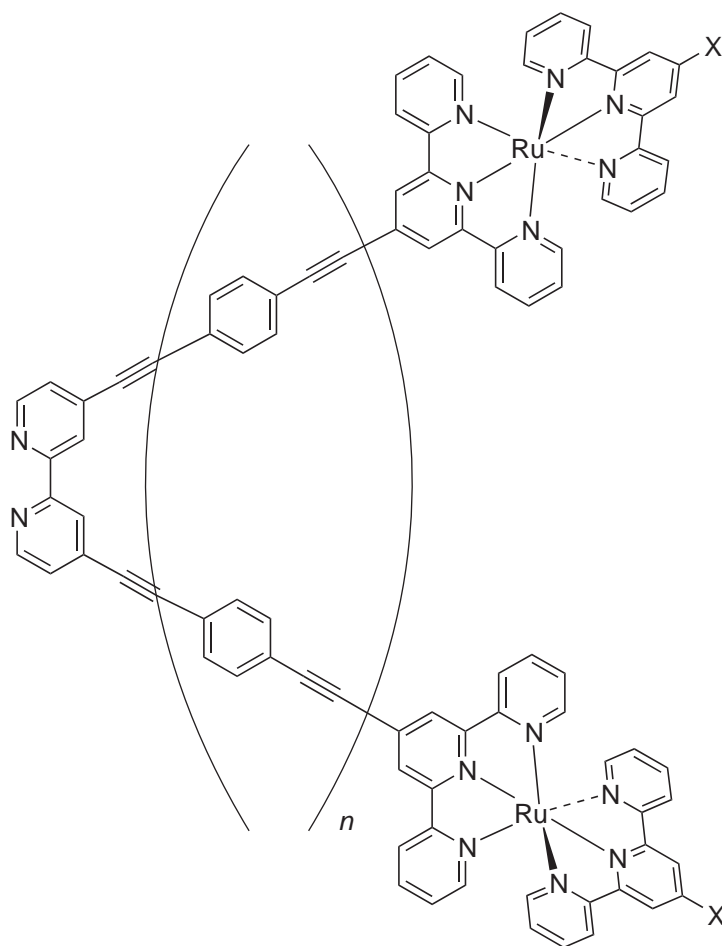
(28)



(29)

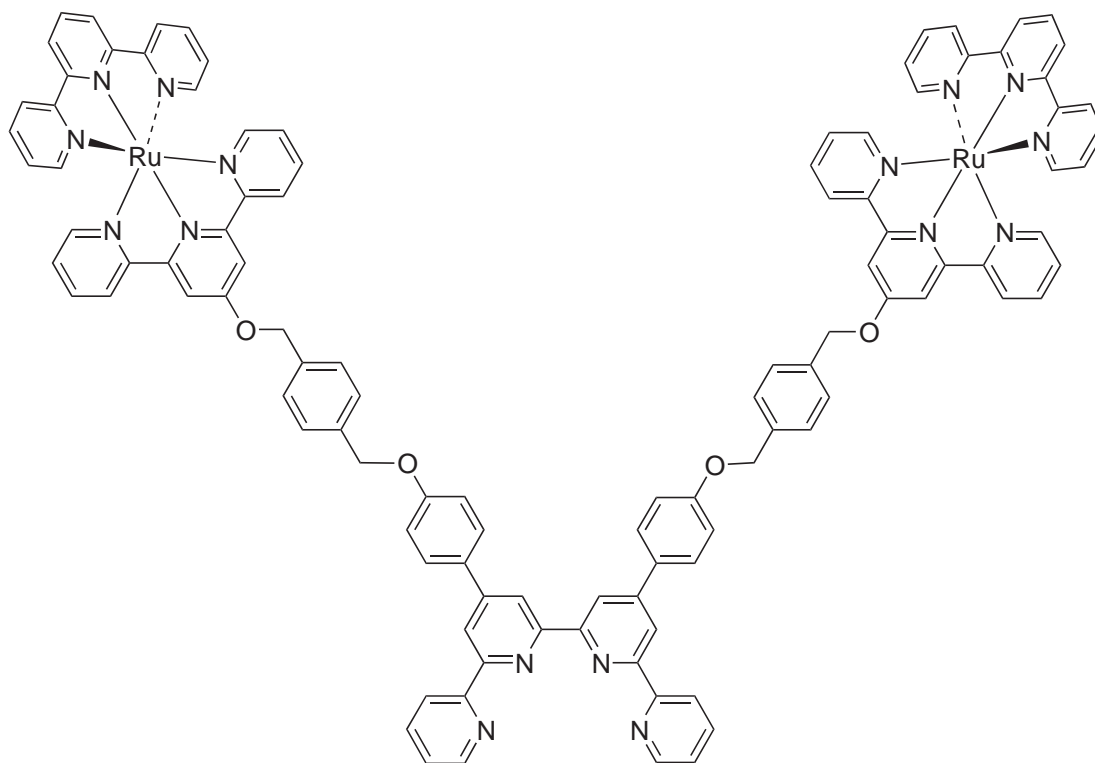


(30)



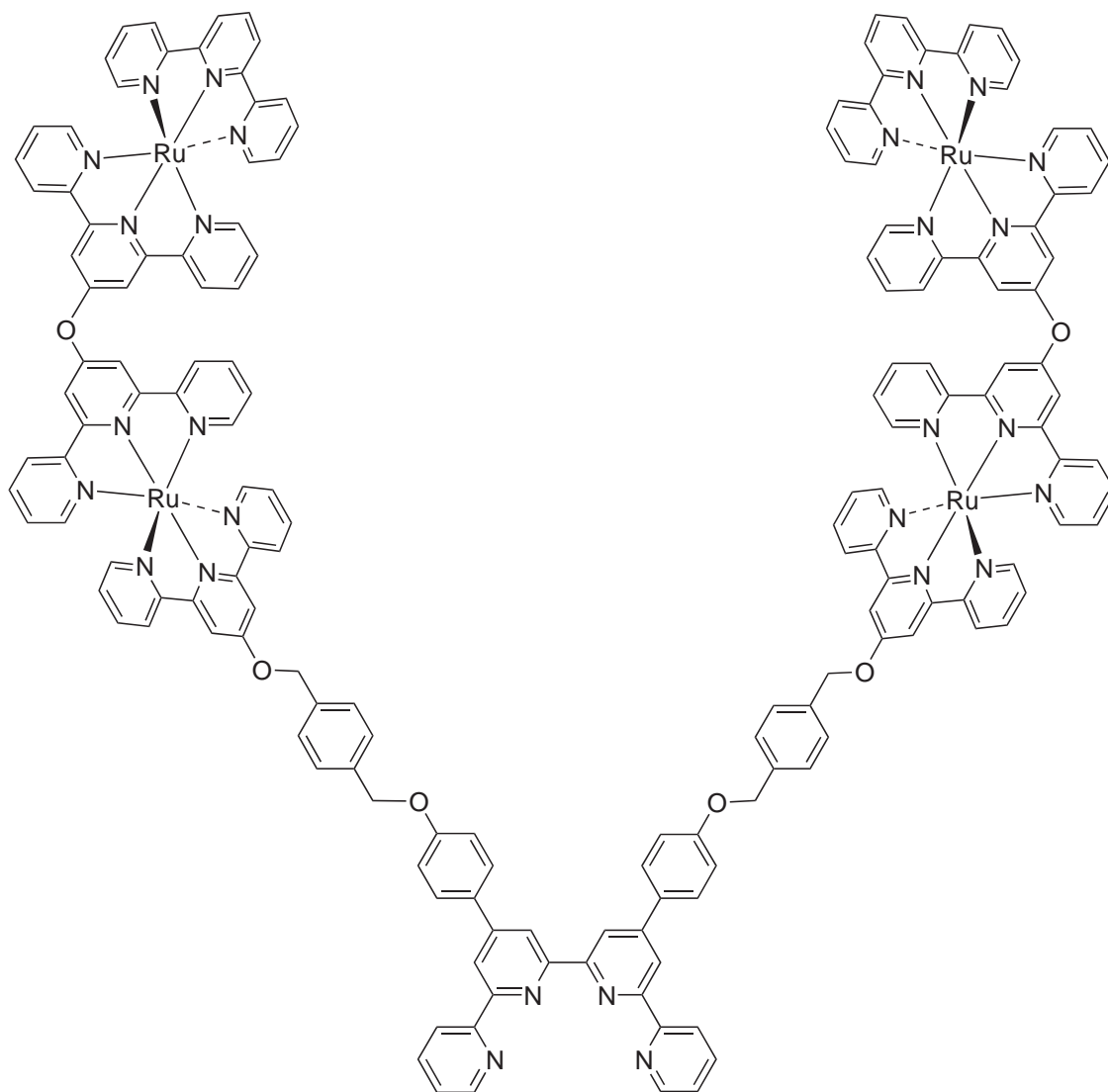
(31)

The use of self-assembled cores has been extended to systems (**32**<sup>4+</sup>) and (**33**<sup>8+</sup>) based upon qtpy metal-binding domains. Double helicates containing central {M<sub>2</sub>(qtpy)<sub>2</sub>} (M = Ag, Cu) are self-assembled upon reaction with copper(I) or silver(I) salts and the helicentric heteropenta- and heterodecanuclear complexes [M<sub>2</sub>(**32**)<sub>2</sub>]<sup>10+</sup> and [M<sub>2</sub>(**33**)<sub>2</sub>]<sup>18+</sup> (M = Ag or Cu) have been characterized.<sup>121</sup> A very recent paper has described the extension of the ligand reactivity method to the formation of complexes of bis(2,2'-bipyridin-4-yl) ether (L) and has investigated compounds including the metallostars [M{LRu(bpy)<sub>2</sub>}<sub>3</sub>]<sup>8+</sup> (M = Ru, Os).<sup>122,123</sup> The key synthetic step was the reaction of [M(4-Brbpy)<sub>3</sub>]<sup>2+</sup> with 4-HObpy to give the complex [ML<sub>3</sub>]<sup>2+</sup> with three noncoordinated bpy domains. Conceptually related metallostars [Ru{LRu(4,4'-X<sub>2</sub>bpy)<sub>2</sub>}<sub>3</sub>]<sup>8+</sup> (X = Me or EtCO<sub>2</sub>; L = 1,4-bis((4'-methyl-2,2'-bipyridin-4-yl)ethyl)benzene) have been prepared by the reaction of [Ru(4,4'-Me<sub>2</sub>bpy)<sub>2</sub>L]<sup>2+</sup> with ruthenium trichloride. The compound [Ru{LRu(4,4'-Me<sub>2</sub>bpy)<sub>2</sub>}<sub>3</sub>]<sup>8+</sup> shows a self-quenching of luminescence and provides an early example of the adsorption of a polynuclear system onto the electrodes in electrochemical studies.<sup>124</sup> The convergent self-assembly of the heterometallostar [Fe{L(Ru(bpy)<sub>2</sub>)<sub>3</sub>}]<sup>8+</sup> (L = 1,4-bis((4'-methyl-2,2'-bipyridin-4-yl)ethyl)benzene, 1,2-bis(4'-methyl-2,2'-bipyridin-4-yl)ethane, 1,5-bis(4'-methyl-2,2'-bipyridin-4-yl)pentane, or 1,12-bis(4'-methyl-2,2'-bipyridin-4-yl)dodecane) from the reaction of [Ru(bpy)<sub>2</sub>L]<sup>2+</sup> with iron(II) salts has been described; stability constants for the iron complexes are in the range 10<sup>13</sup> to 10<sup>15</sup> and the iron is an efficient internal quencher of the ruthenium emission.<sup>87</sup>



(32)

Finally, a diastereomeric mixture of tetranuclear metallostars [(**34**)<sub>4</sub>{Ru(bpy)<sub>2</sub>}<sub>4</sub>]<sup>8+</sup> has been obtained by the metallation of the tetrakis bpy ligand (**34**) with [Ru(bpy)<sub>2</sub>Cl<sub>2</sub>].<sup>125</sup>

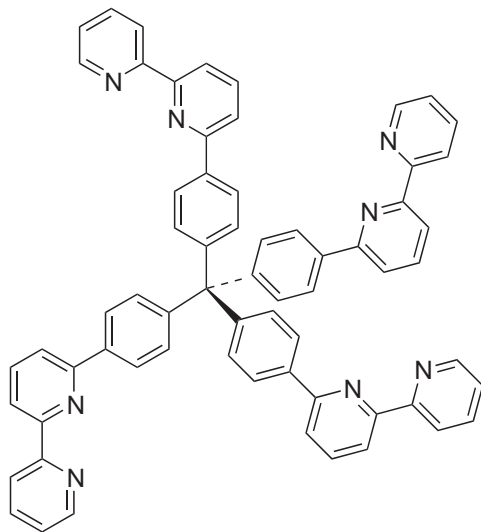


(33)

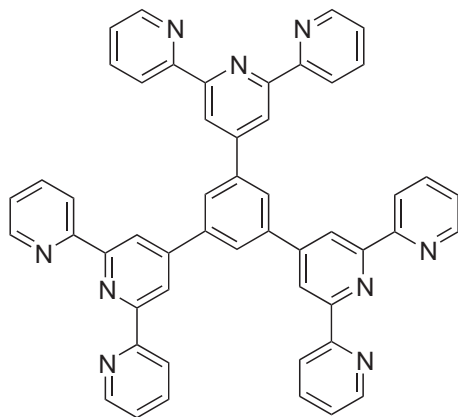
### 7.6.5.2 Metallostars Based Upon tpy Domains

The inherent chirality of the  $\{M(\text{bpy})_3\}$  motif is a disadvantage when it comes to multinuclear compounds as these will be formed as mixtures of diastereomers unless special conditions are used to optimize stereospecificity. In contrast,  $\{M(\text{tpy})_2\}$  units linked through the 4'-position are achiral and are an ideal motif for the linear extension of achiral metallostars. Metallostars based upon pentaerythritol units are discussed in detail in [Section 7.6.6.2](#).

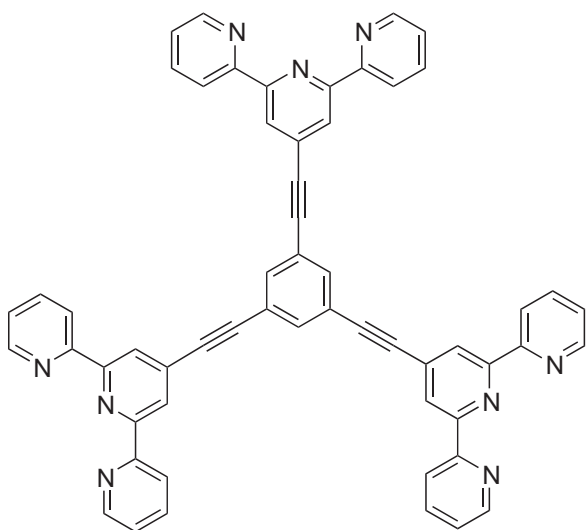
The ligand (35) has been prepared and the trinuclear metallostars  $[(35)\{Ru(\text{Xtpy})\}_3]^{6+}$  (Xtpy = tpy or substituted tpy) have been prepared. The tpy domains are thought to be near-orthogonal to the central benzene ring and there is no communication between metal centers.<sup>126,127</sup> Metallostars based on the related extended ligand (36) have been prepared by coupling reactions of preformed metal complexes.<sup>120</sup>



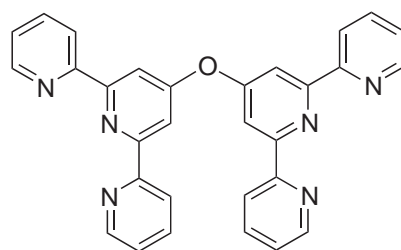
(34)



(35)



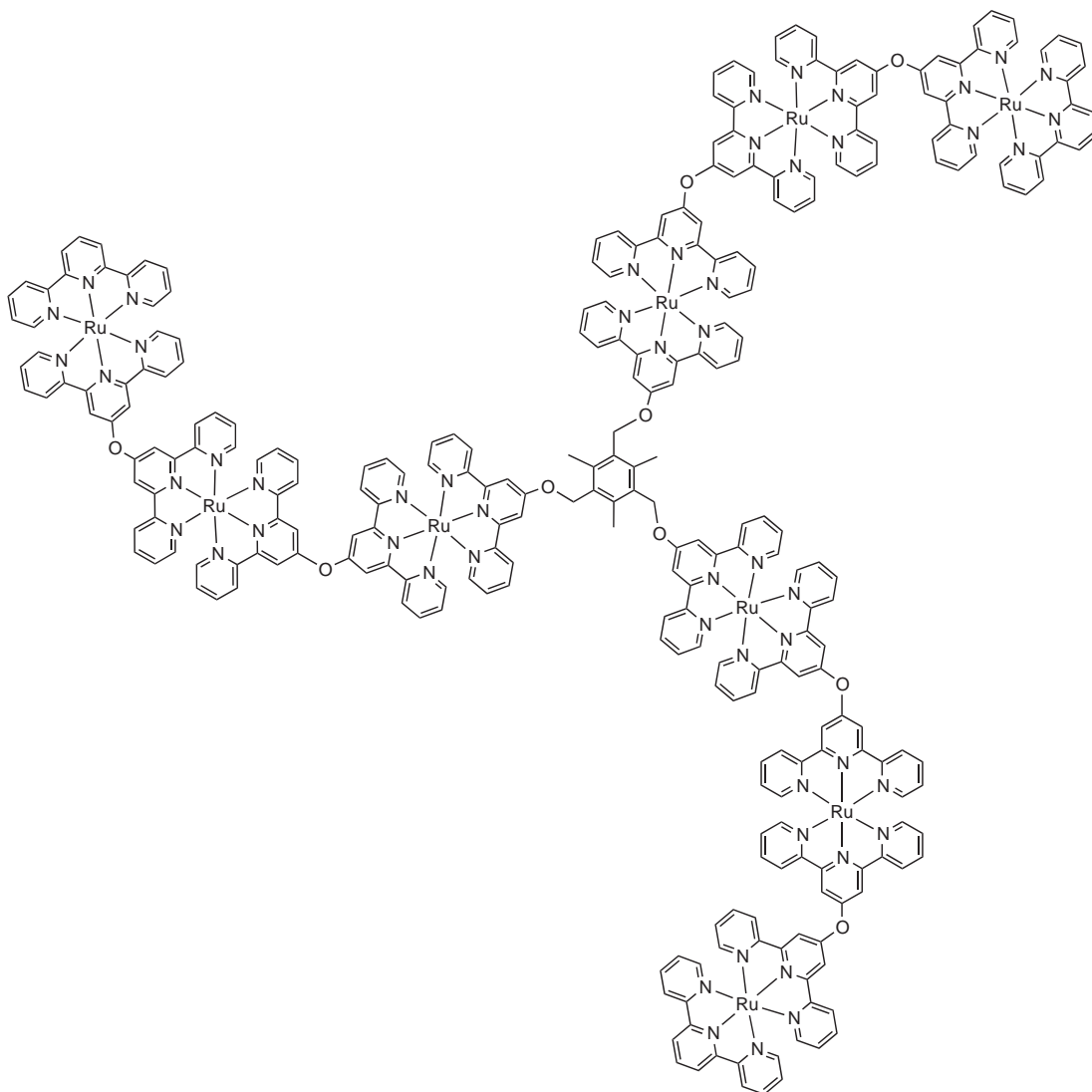
(36)



(37)

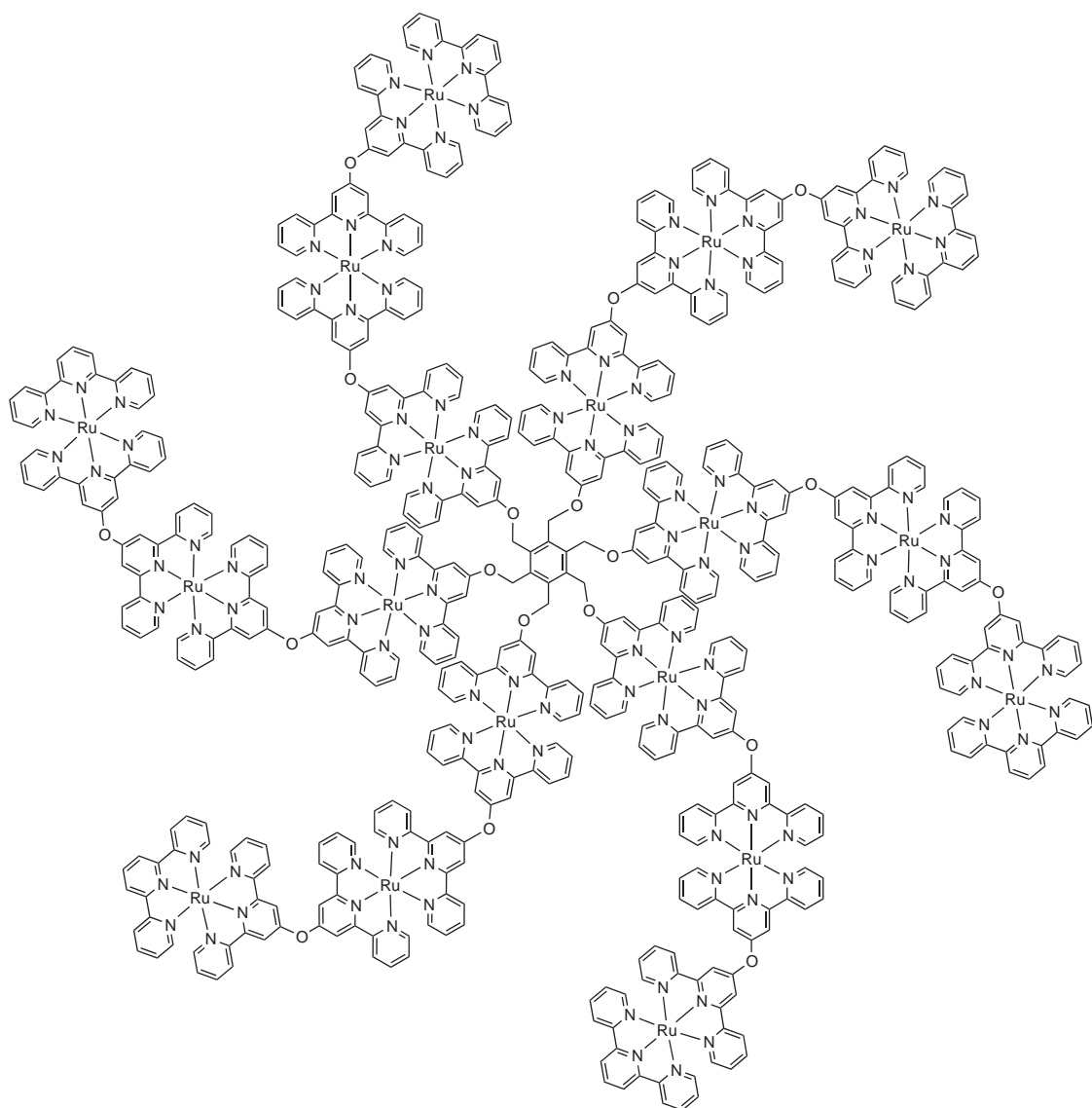


Reactions of coordinated ligands have been extensively used in the preparation of higher-generation star compounds based upon 1,3,5-trisubstituted benzene trifurcating and persubstituted benzene hexafurcating ligands. The key step in an overall convergent synthesis is the reaction of a 4'-HOTpy complex with electrophilic bromomethyl groups. Using this strategy and the trinuclear nucleophilic units  $[(4'\text{-HOTpy})\text{Ru}(\mathbf{37})\text{Ru}(\mathbf{37})\text{Ru}(\text{tpy})]^{6+}$ , reaction with 1,3,5-tris(bromomethyl)benzene or hexa(bromomethyl)benzene yielded the nona- $(\mathbf{38}^{18+})$  and octadecanuclear $(\mathbf{39}^{36+})$  metallostars.<sup>128,129</sup>



(38)

Astruc has utilized an elegant ligand reaction for the construction of the heptanuclear heterometallic stars  $[\text{CpFe}\{\mathbf{40}\}\{\text{Ru}(\text{bpy})_2\}_6]^{12+}$  and  $[\text{CpFe}\{\mathbf{41}\}\{\text{Ru}(\text{tpy})\}_6]^{12+}$ . The complex  $[\text{CpFe}(\text{Me}_6\text{C}_6)]^+$  is converted cleanly to the hexaol  $[\text{CpFe}\{\text{(HOCH}_2\text{CH}_2\text{CH}_2\text{CH}_2)_6\text{C}_6\}]^+$ , which may then be functionalized by reaction with 4-Brbpy or 4'-Cltpy to give a hexakis bpy or tpy functionalized ligands  $[\text{CpFe}(\mathbf{40})]^+$  and  $[\text{CpFe}(\mathbf{41})]^+$ , respectively. Subsequent reaction with  $[\text{Ru}(\text{bpy})_2\text{Cl}_2]$  or  $[\text{Ru}(\text{tpy})\text{Cl}_3]$  gave the desired heptanuclear species  $[\text{CpFe}\{\mathbf{40}\}\{\text{Ru}(\text{bpy})_2\}_6]^{12+}$  and  $[\text{CpFe}\{\mathbf{41}\}\{\text{Ru}(\text{tpy})\}_6]^{12+}$  respectively.<sup>130,131</sup>

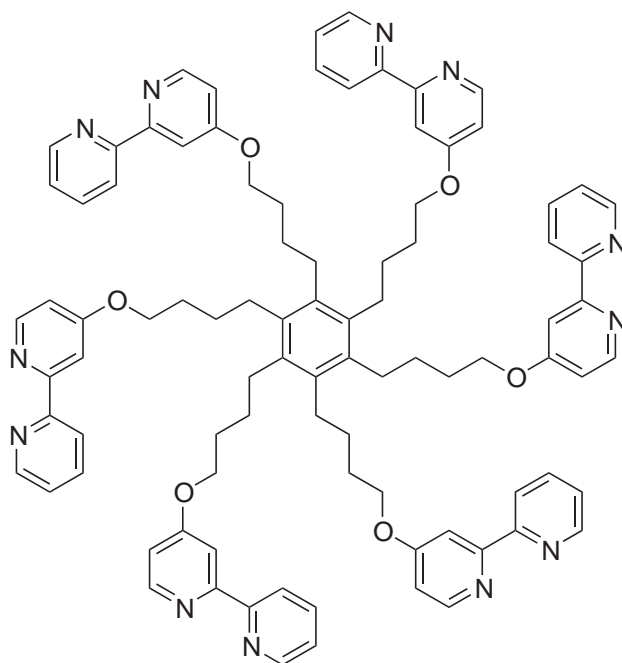


(39)

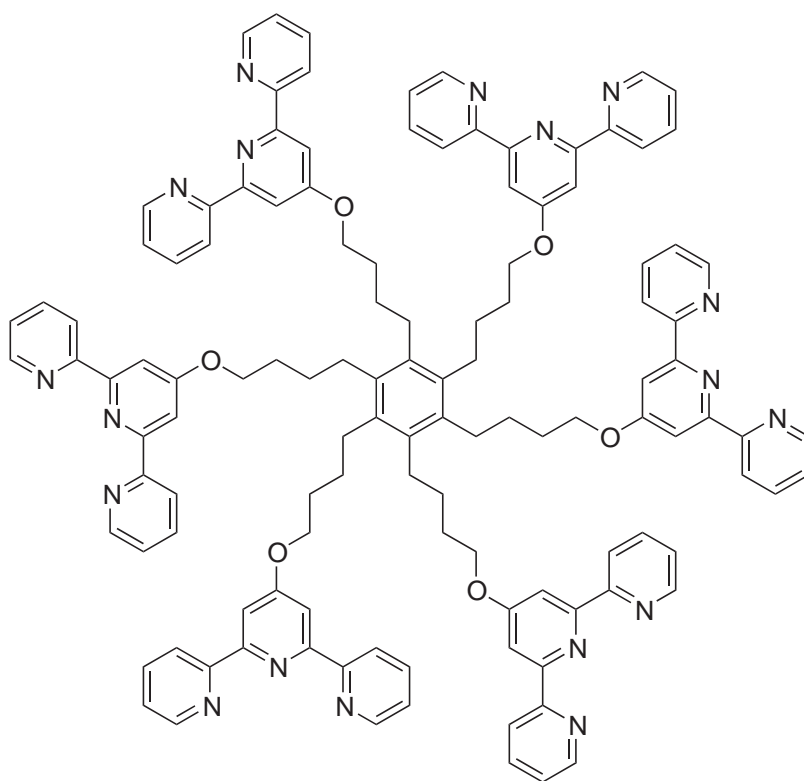
Ziessel has described the heterotopic heterotrinnuclear heptanuclear metallostars  $[\text{Fe}(\mathbf{42})_3]^{n+}$  in which alkynyl substituted bpy units are connected *via* C—Pt bonds. These complexes have interesting photophysical properties and are likely to lead to novel antenna systems.<sup>132</sup>

### 7.6.5.3 Metallostars Based Upon Other Domains

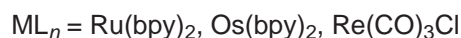
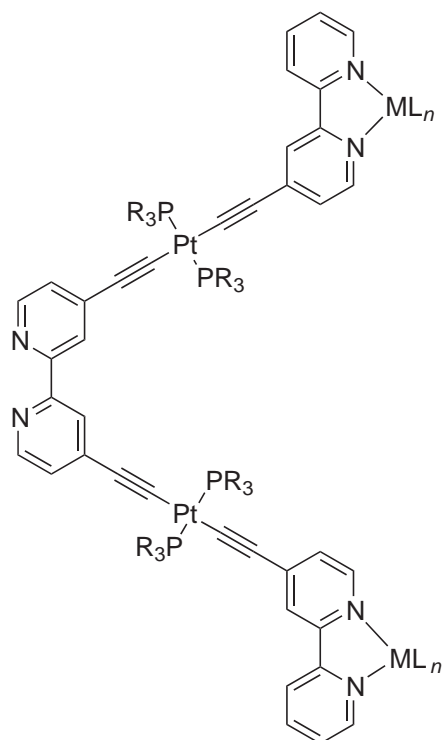
This class of compound is very widely dispersed in the chemical literature and any attempt at comprehensive coverage is bound to be deficient! These compounds are often synthetically and conceptually closely linked with the corresponding metallodendrimers or surface decorated dendrimers and are discussed in Sections 7.6.6.3 and 7.6.7.



(40)



(41)



(42)

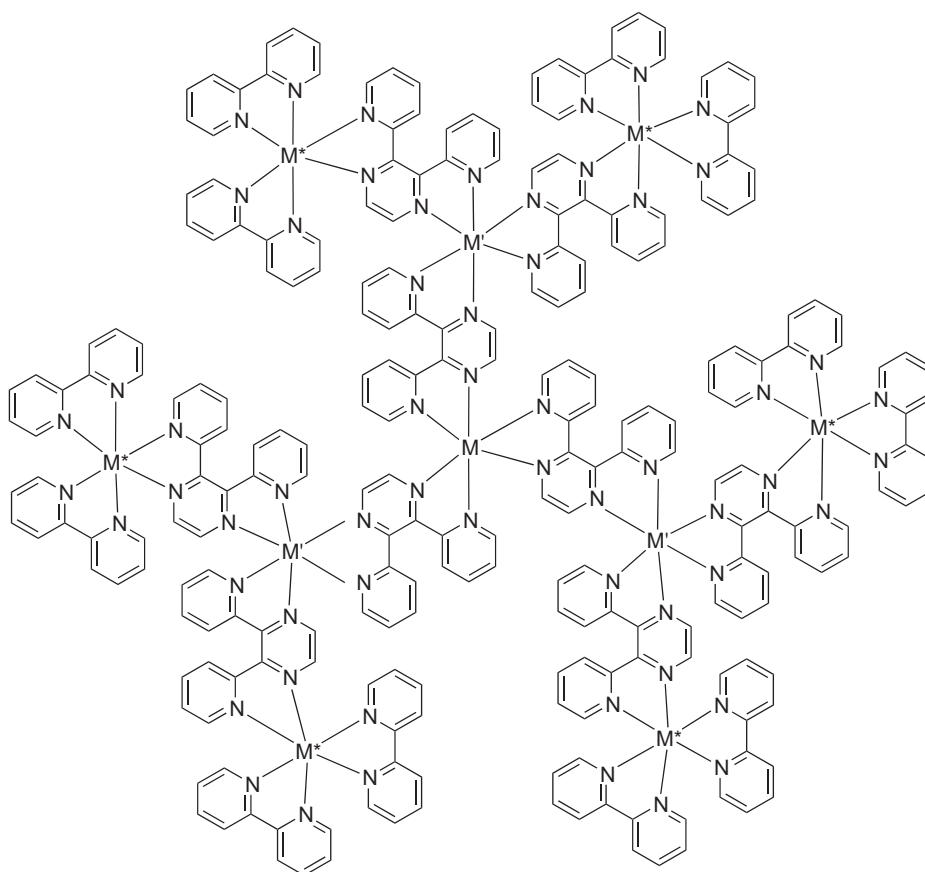
## 7.6.6 METALLODENDRIMERS

### 7.6.6.1 Metallo dendrimers Based Upon bpy and phen Domains

As discussed in Section 7.6.5.1, the earliest metallo dendrimers were based upon bpy metal-binding domains and were prepared as antenna systems for the vectorial transfer of energy or electrons following absorption of a photon. We commence with a discussion of the synthesis and properties of the Balzani and Denti systems based upon (**11**).<sup>133–154</sup> The general review literature is cited in Section 7.6.5.1.

The first bpy capped dendritic generation may be regarded as (**43**<sup>20+</sup>) and contains 10 metal centers. The strategy initially adopted can be regarded as convergent and the core complex  $[M(\mathbf{11})_3]^{2+}$  was reacted with the trinuclear complex  $[Cl_2\{M'(\mathbf{11})M^*L_2\}_2]^{4+}$  (L = bpy, phen, or derivative) to give (**43**<sup>20+</sup>) (Scheme 1). The choice of M, M', and M\* from Ru or Os allows a series of decanuclear species with preprogrammed directional energy transfer to be prepared. As generally presented, there is no diastereospecificity expected in this reaction unless the core and/or trinuclear units are enantiomerically or diastereomerically pure, respectively. In the heteronuclear complexes the direction of Ru to Os energy transfer (inside-to-outside or outside-to-inside) is controlled by the location of the various metal centers. The redox processes may be finely tuned because, even for a given metal center, the metal-centered processes for  $\{M(bpy)_2(\mathbf{11})\}$ ,  $\{M(phen)_2(\mathbf{11})\}$ ,  $\{M(biq)_2(\mathbf{11})\}$ , and  $\{M(\mathbf{11})_3\}$  units vary slightly. These processes have been discussed in detail for all of these systems. In general, the heterometallic systems show efficient energy transfer and only an osmium-centered emission. Detailed electrochemical studies have indicated that the reductions are localized on the ligands and in nonaqueous solvents, very large numbers of reduction processes have been observed.<sup>155,156</sup> With these relatively

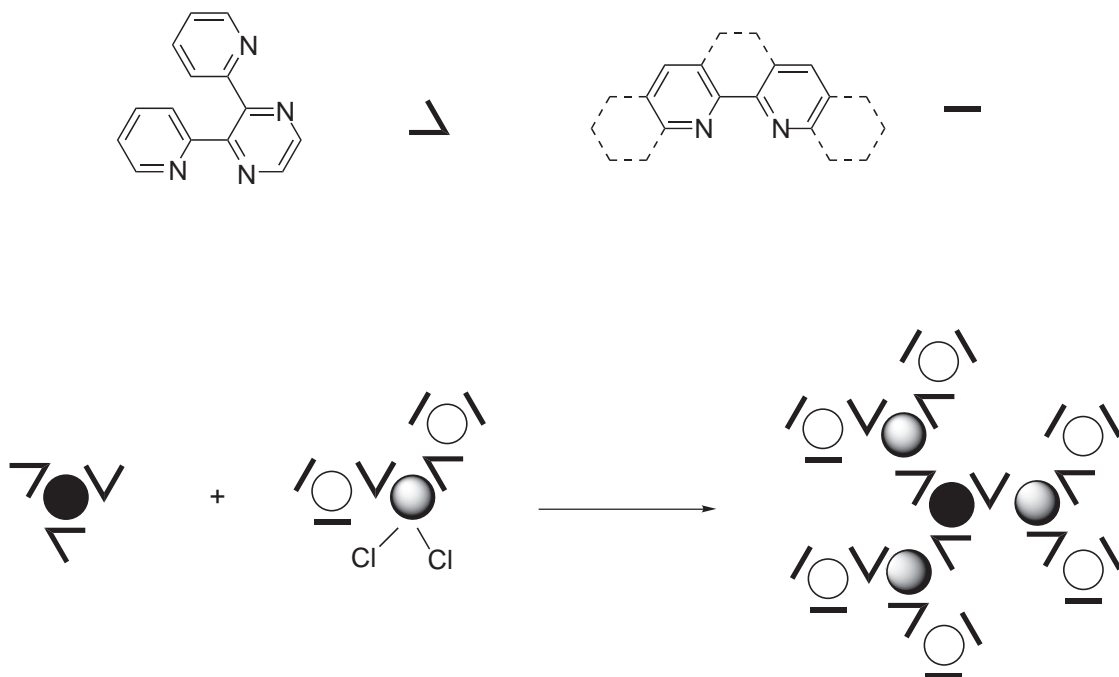
simple building blocks, a whole variety of species with nuclearities up to 22 metal centers have been prepared. An overview of the synthetic strategies is given in Schemes (1)–(2). Although the initial approach to the decanuclear complexes utilized a trinuclear species, it is not obvious how this approach can be extended to higher generations. In particular, this approach would require the use of progressively higher nuclearity dendritic wedges for the attachment of the arms. A more useful strategy involves the use of a tetranuclear core of the type  $[M\{(11)M^{\dagger}(11)_2\}_3]^{8+}$ , which has a total of six noncoordinated bpy metal-binding domains available for coordination (Scheme (2)). The reaction of this compound with  $[ML_2Cl_2]$  ( $L = \text{phen, bpy, or derivative}$ ) gives the decanuclear complexes ( $43^{20+}$ ). More usefully, reaction with the trinuclear species  $[Cl_2\{M'(11)M^*L_2\}_2]^{4+}$  results in the capping of each of the bpy domains with a trinuclear unit, incorporating another 18-metal  $M'_6M^*_{12}$  sphere. In the course of this work, a useful protection–deprotection methodology was developed involving the methylated ligand ( $44^+$ ). In this compound, only one of the two bpy domains is free for coordination to a metal ion and this allows the preparation of the key  $[M\{(11)M^{\dagger}(11)_2\}_3]^{8+}$  species as *N*-methylated derivatives, which are then deprotected before further coordination reactions at the surface. These studies have recently been extended to new types of bridging ligand including 3,5-bis(pyridyn-2-yl)-1,2,4-triazole.<sup>157,158</sup>



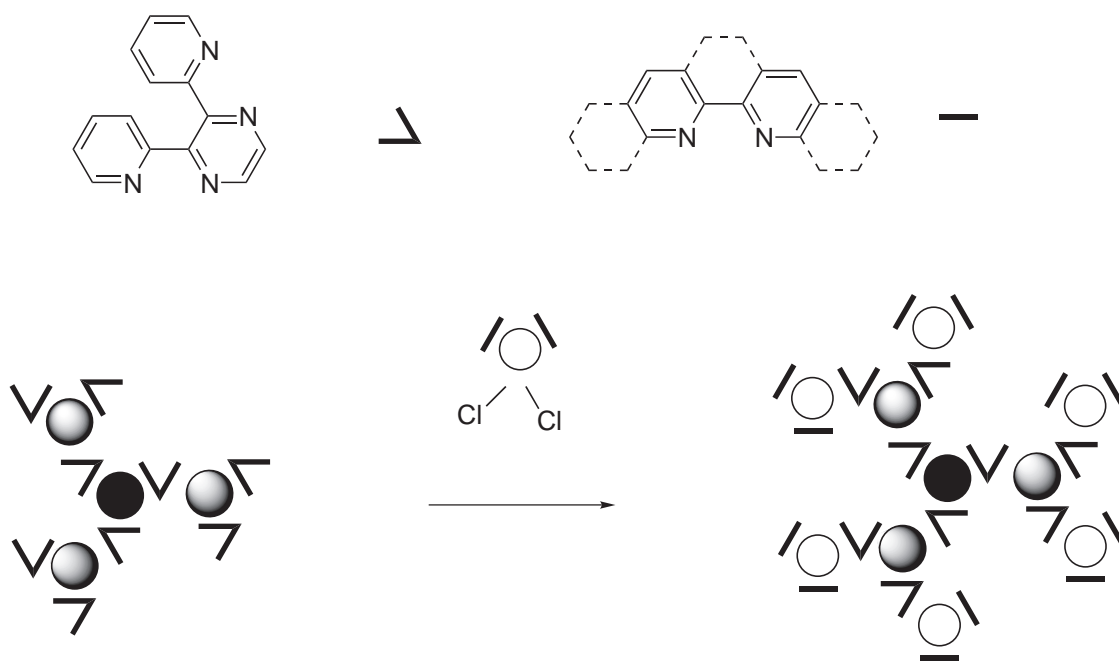
(43)

Puddephatt and co-workers have developed a very elegant method for the preparation of metallodendrimers based upon the oxidative addition of bromomethyl compounds to platinum(II) complexes to give kinetically inert platinum(IV) species. The prototype reaction is the addition of (45) to  $[LPt^{II}Me_2]$  ( $L = 4,4'$ -di(*tert*-butyl)-2,2'-bipyridine) to give (46). The compound (46) is simply a bpy ligand and can react with  $[Pt_2Me_4(\mu-SMe_2)_2]$  to give trinuclear  $[Pt(46)Me_2]$ , which is a homologue of  $[LPt^{II}Me_2]$ ; reaction with (45) then gives the hexanuclear platinum(IV) dendron (47). The dendron (47) can be metallated with  $[Pt_2Me_4(\mu-SMe_2)_2]$  to give heptanuclear  $[Pt(47)Me_2]$ . Dendrimers have been prepared in a convergent manner by the oxidative addition of 1,2,4,5-tetrakis(bromomethyl)benzene to  $[Pt(46)Me_2]$  to give a dodecanuclear compound or with

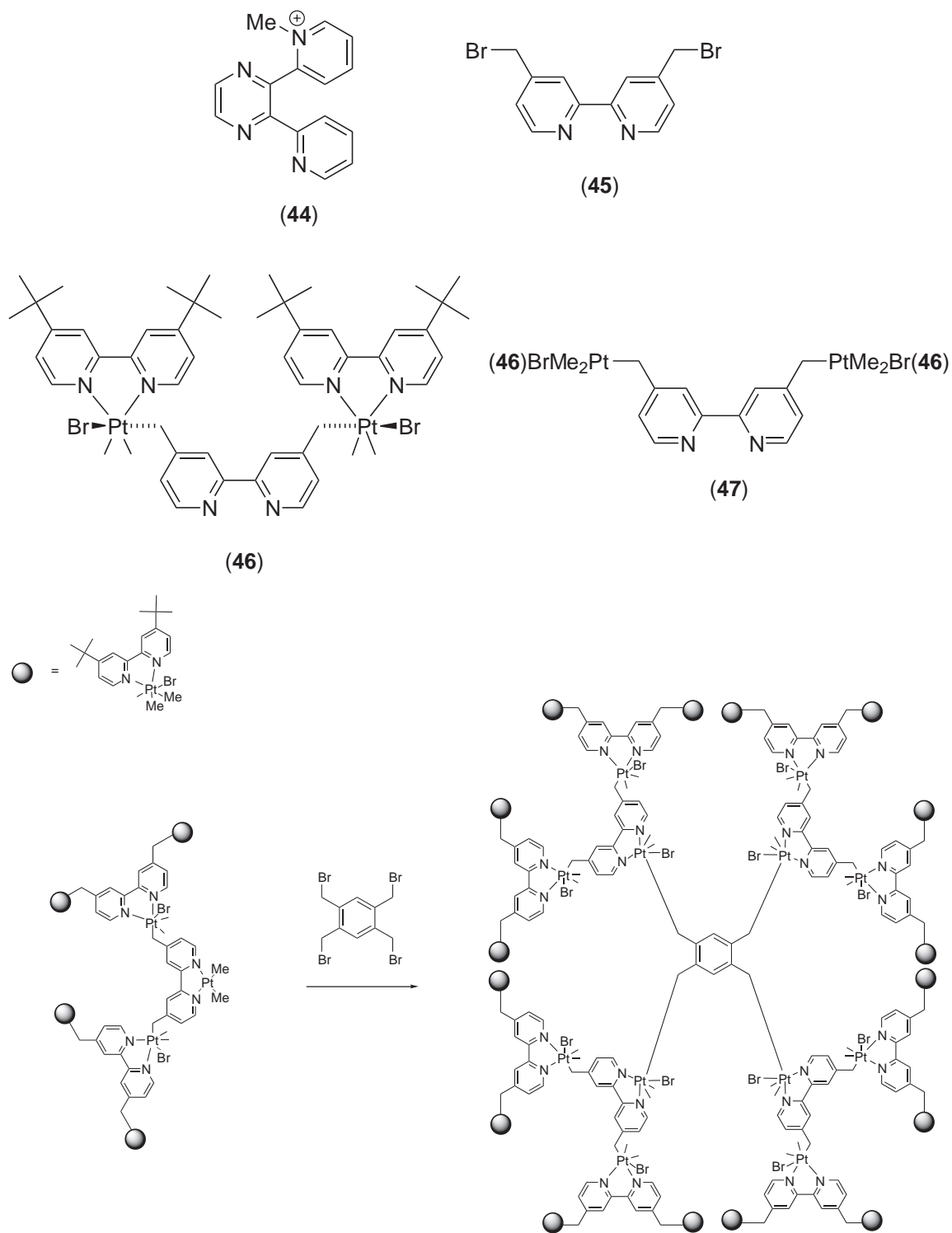
[Pt(**47**)Me<sub>2</sub>] to give a complex with 28 metal centers (Scheme 3).<sup>159–166</sup> Similar reactions with 1,4-bis(bromomethyl)-, 1,3,5-tris(bromomethyl)- and per(bromomethyl)benzene have been reported. By replacing the surface 4,4'-di(*tert*-butyl)-2,2'-bipyridine ligands by ferrocene-functionalized bpy ligands a series of surface redox functionalized systems has been prepared.<sup>159</sup> These studies have been extended to palladium and mixed-metal systems with varying degrees of success<sup>164</sup> and also developed into a divergent strategy.<sup>165</sup>



Scheme 1



Scheme 2



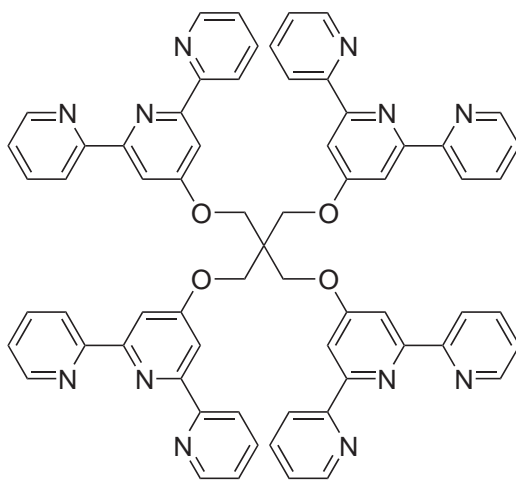
Scheme 3

The ligand reactivity strategy that was developed for the preparation of enantiopure metallostars based upon (2) has been developed into an elegant method for the preparation of dendritic systems. The key reaction step is the oxidation of peripheral phen ligands to the dione (3) and subsequent cyclization with  $[\text{Ru}(\text{phen})_2(4)]^{2+}$ . Thus, the dinuclear complex  $[(\text{phen})_2\text{Ru}(2)\text{Ru}(\text{phen})_2]^{4+}$  may be oxidized to  $[(3)_2\text{Ru}(2)\text{Ru}(3)_2]^{4+}$  and subsequently reacted

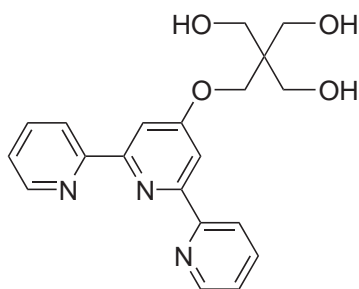
with  $[\text{Ru}(\text{phen})_2(\mathbf{4})]^{2+}$  to give the hexanuclear dendrimer  $[\{(\text{phen})_2\text{Ru}(\mathbf{2})\}_2\text{Ru}(\mathbf{2})\text{Ru}\{(\mathbf{2})\text{Ru}(\text{phen})_2\}_2]^{12+}$ . In a similar way,  $(\mathbf{5})$  can be oxidized to  $[\text{Ru}\{(\mathbf{2})\text{Ru}(\mathbf{3})_2\}_3]^{8+}$  and converted to decanuclear  $[\text{Ru}\{(\mathbf{2})\text{Ru}(\mathbf{2})\text{Ru}(\text{phen})_2\}_2\}_3]^{20+}$ .<sup>62,169</sup>

### 7.6.6.2 Metallo dendrimers Based Upon tpy Domains

As mentioned above, the stereogenic nature of the  $\{\text{M}(\text{bpy})_3\}$  motif makes systems based upon  $\{\text{M}(\text{tpy})_2\}$  units attractive synthetic targets. The tetrakis(tpy) ligand  $(\mathbf{48})$  is prepared from pentaerythritol and 4'-Cltpy, and has been converted to first-generation ruthenastars  $[(\mathbf{48})\{\text{Ru}(\text{tpy})\}_4]^{8+}$  by reaction with  $[\text{Ru}(\text{tpy})\text{Cl}_3]$ .<sup>170,171</sup> The reaction has been extended to 4'-functionalized tpy capping groups and the complex  $[(\mathbf{48})\{\text{Ru}(\text{Xtpy})\}_4]^{8+}$  with four 4'-(2-(*tert*-butyldimethylsilyl)-1,2-carba-boranyl)-2,2':6',2''-terpyridine (Xtpy) caps has been described.<sup>170,171</sup> The complementary ligand  $(\mathbf{49})$  has been prepared by the reaction of 4'-Cltpy with an excess of pentaerythritol and has been used for the preparation of the next-generation dendritic system. The reaction of  $(\mathbf{48})$  with  $[\text{Ru}(\mathbf{49})\text{Cl}_3]$  yields the tetra-ruthenium complex  $(\mathbf{50})$  (Scheme 4) with 12 pendant hydroxy groups. This complex is converted to the hexadecaruthenadendrimer  $(\mathbf{51})$  (Scheme 4) by reaction with  $[\text{Ru}(\text{tpy})(4'\text{-Cltpy})]^{2+}$  in basic conditions making use of the enhanced electrophilic character of the coordinated 4'-Cltpy ligand (Scheme 4).<sup>172</sup> The tetranuclear star complexes have been incorporated into carbon-based conducting composite electrodes and used as mediators for the oxidation of methionine<sup>173,174</sup> and cysteine<sup>173,174</sup> 5-hydroxytryptophan<sup>175</sup> and insulin.<sup>174</sup> Multilayered self-assemblies have been prepared by layer-by-layer deposition of  $[(\mathbf{48})\{\text{Ru}(\text{Xtpy})\}_4]^{8+}$  and the Dawson-type phosphatungstate,  $[\text{P}_2\text{W}_{18}\text{O}_6]^{26-}$  on a glassy carbon electrode to give multilayer films, which have been studied by spectrometry, cyclic voltammetry, and tapping mode AFM. The assemblies showed bifunctional electrocatalytic capability and mediated both iodate reduction and arsenite oxidation.<sup>176</sup> The adsorption of the higher nuclearity systems on metal oxide surfaces has been studied.<sup>178</sup>



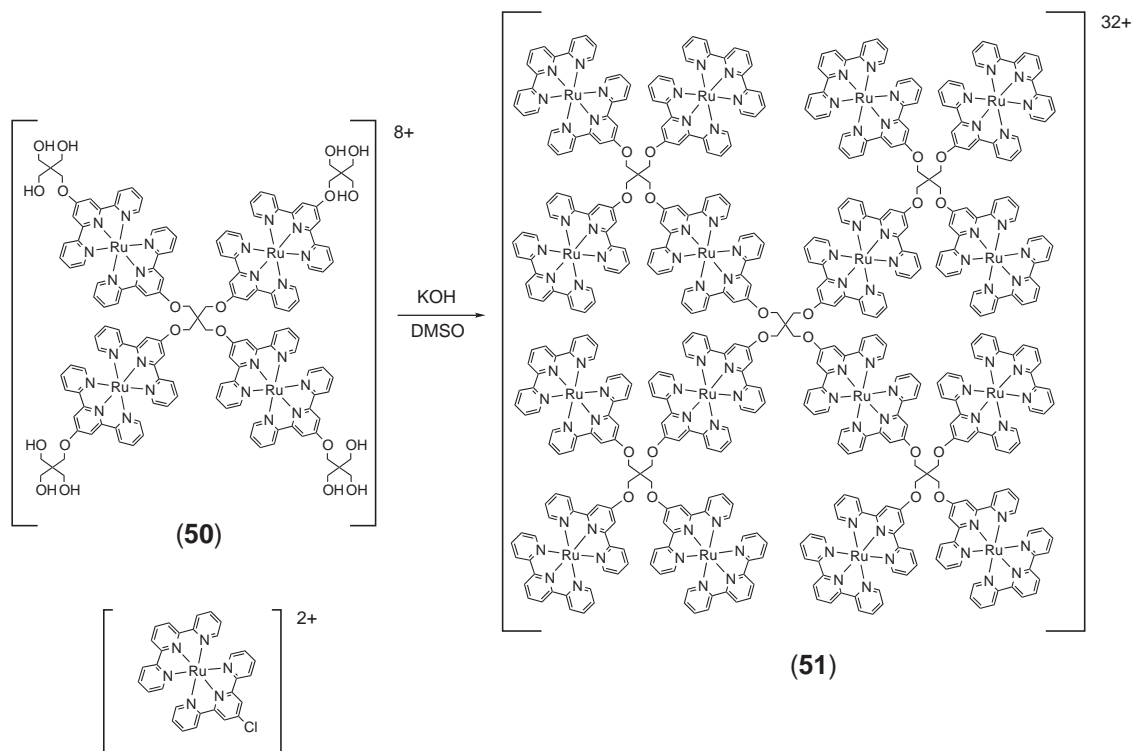
(48)



(49)



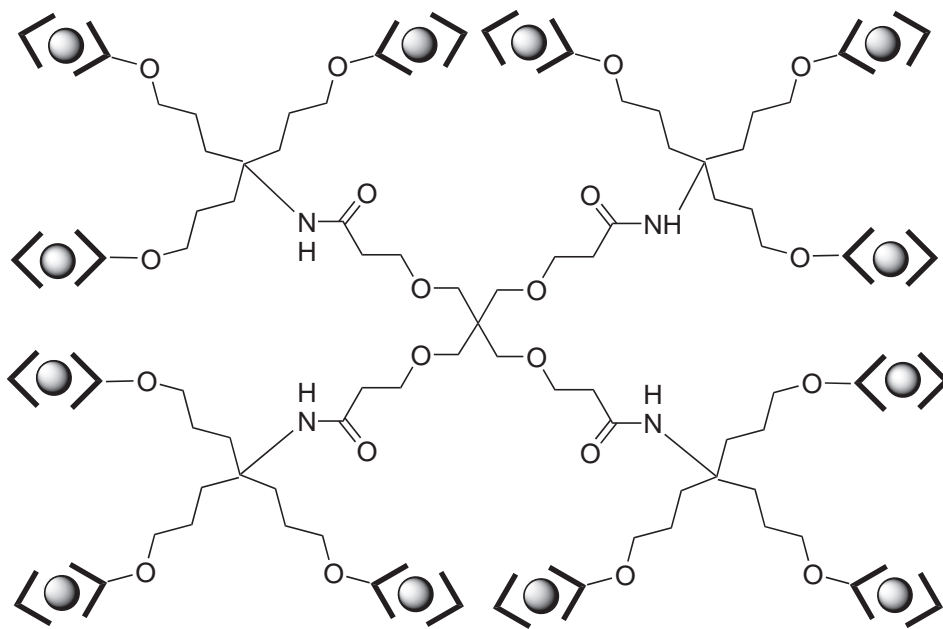
One of the first examples of a tpy metallodendrimer was based upon an expanded pentaerythritol core, and the dodecaruthena-species (**52**) was prepared by the reaction of  $[\text{Ru}(4'\text{-Rtpy})\text{Cl}_3]$  ( $\text{R} = \{\text{BzO}(\text{CH}_2)_3\}_3\text{C}(\text{CH}_2)_3\text{O}\}$ ) with the dodecatpy functionalized ligand  $\text{C}[(\text{CH}_2)_2\text{-CONHC}\{\text{C}(\text{CH}_2)_3\text{O-4'-tpy}\}_3]_4$ . The compound exhibited a single metal-centered redox process.<sup>177</sup> Newkome and co-workers have reported extensive studies upon related systems in which  $\{\text{Ru}(\text{tpy})_2\}$  motifs are used as assembly principles for high nuclearity metallodendrimers. In all of these studies, the emphasis is upon the careful design of the connector ligands and the stepwise assembly in a controlled manner.<sup>179–182</sup> A particularly elegant variation on the structural theme involves the incorporation of dicarboxylate spacers in the structure, such that the overall dendrimer is neutral.<sup>181–183</sup> These dendritic systems have been extensively reviewed elsewhere.<sup>1,11,27</sup>



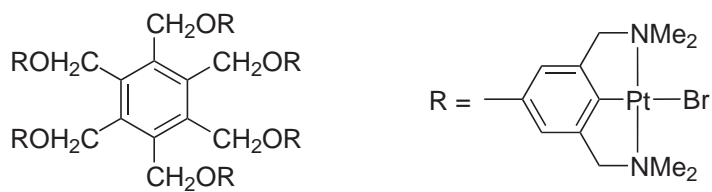
Scheme 4

### 7.6.6.3 Metallodendrimers and Metallostars Based Upon Other Domains

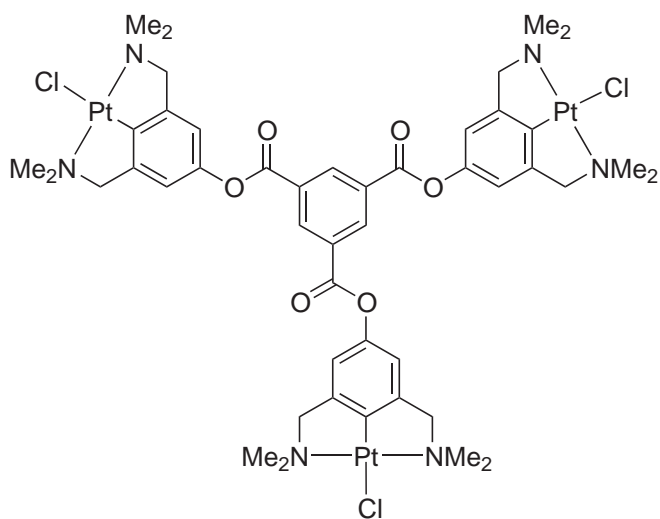
Systems based upon multiply linked porphyrins or phthalocyanines are discussed elsewhere in this work. van Koten and co-workers have reported a series of dendritic, decorated and star systems based upon *NCN* cyclometallated metal-binding motifs (**53–55**) and pendant phosphine donors.<sup>184–201</sup> These compounds have been shown to be effective in sensor devices for the detection of sulfur dioxide; the effectiveness of various generations and various nuclearities was assessed.<sup>184,185</sup> Related compounds in which the core metallated platinum center is functionalized with Frechet-type dendrimers of various generations are similarly effective in binding  $\text{SO}_2$ .<sup>186</sup> The synthetic studies have been extended to palladated and platinated systems with the *NCN* motif attached to carbosilane dendrimers (**55**).<sup>190–192,197</sup> The van Koten group has also been developing dendritic and star-shaped systems with surface aryl–nickel motifs that are effective in multisite catalysis.<sup>193–196,200</sup> The *PCP* donor ligands (**56**) and (**57**) have been prepared and converted to cyclopalladated star complexes.<sup>202–204</sup> Reinhoudt and other workers have extended these studies to dendritic and star systems containing *SNS* and *SCS* pincer donor sites.<sup>205–214</sup> The reader is referred to an excellent detailed review<sup>8</sup> for further details.



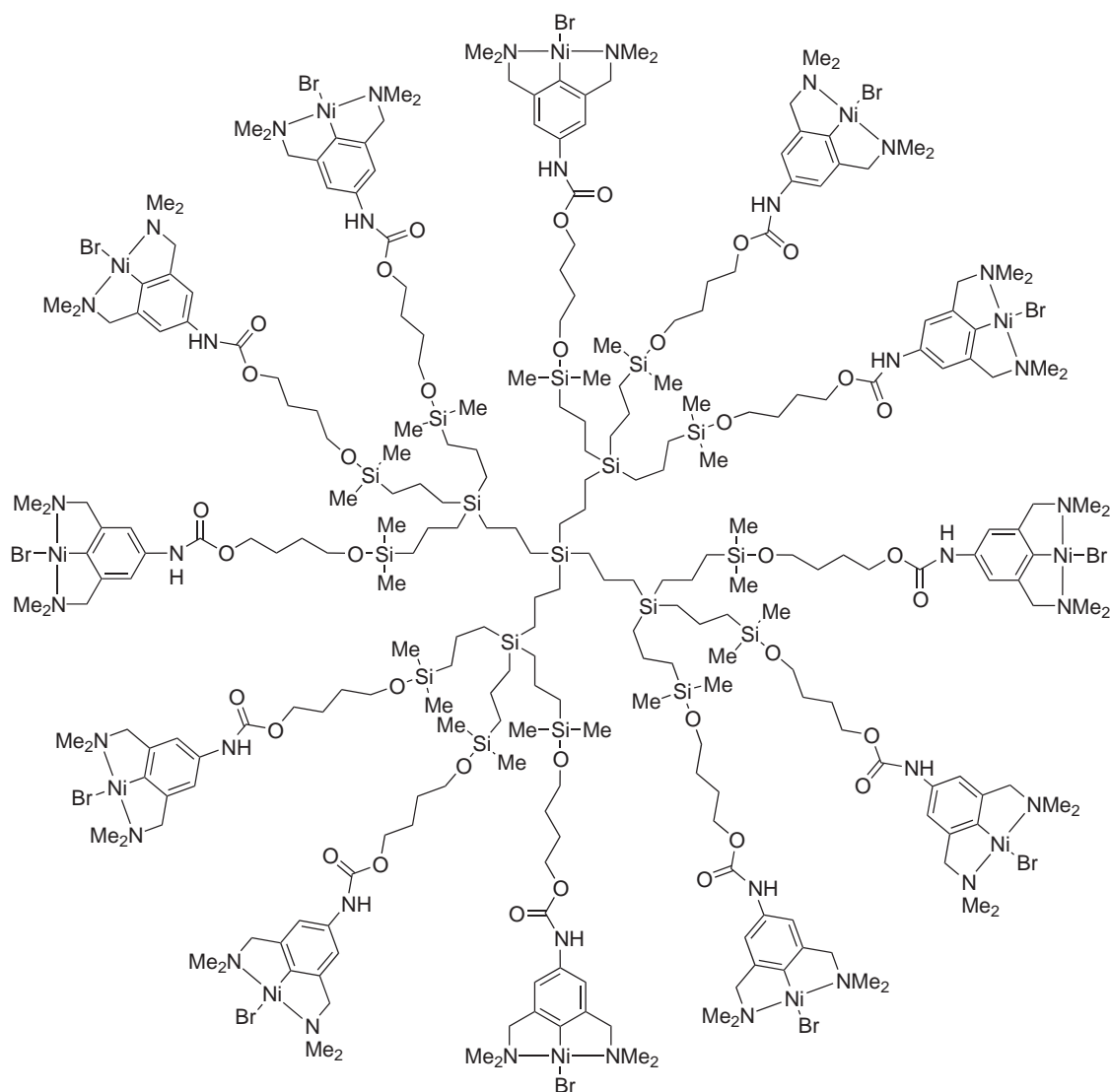
(52)



(53)



(54)



(55)

### 7.6.7 SURFACE DECORATION

The PAMAM core has been extensively used for the attachment of metal-containing surface units by Abruña and co-workers. PAMAM dendrimers of generation 0 to 4 bearing 4, 18, 16, 32, or 64 surface amino groups have been functionalized by amide formation reactions with 4-HO<sub>2</sub>CCH<sub>2</sub>CH<sub>2</sub>CH<sub>2</sub>-4'-Mebpy or 4'-HO<sub>2</sub>CCH<sub>2</sub>CH<sub>2</sub>tpy to give bpy or tpy surface-decorated species. Subsequent reaction with [Ru(bpy)<sub>2</sub>Cl<sub>2</sub>] or [Ru(tpy)Cl<sub>3</sub>] gave the metallodendrimers with surface {Ru<sup>II</sup>(bpy)<sub>3</sub>} or {Ru<sup>II</sup>(tpy)<sub>2</sub>} units.<sup>215</sup> The compounds exhibited the expected redox properties and absorbed onto platinum surfaces. The dynamics of electrochemically initiated changes in the adsorbed layers were investigated and the electrochemically determined surface coverages indicated that the dendrimers compressed upon absorption. As expected, the {Ru<sup>II</sup>(bpy)<sub>3</sub>} species were luminescent at room temperature whilst the {Ru<sup>II</sup>(tpy)<sub>2</sub>} functionalized dendrimers only showed an emission at low temperature in a rigid matrix.<sup>215,216</sup> It was subsequently shown that the tpy functionalized dendrimers of generations 0–3 assembled highly ordered polymeric films on graphite surfaces upon reaction with iron(II) or cobalt(II) salts. These were studied by STM and apparently consisted of one-dimensional polymeric strands. The electrochemical response of the film was typical for the appropriate {M(tpy)<sub>2</sub>} motif.<sup>217</sup> In a particularly elegant piece of work, Abruña has used ultrafast cyclic voltammetry in

combination with STM studies to conclude that the generation 4  $\{\text{Ru}^{\text{II}}(\text{tpy})_2\}$  decorated species are hemispherical when adsorbed in contrast to the expected solution spherical structures.<sup>218</sup> The corresponding generation 1 and 3 PAMAM species surface functionalized with  $\{\text{Co}^{\text{II}}(\text{tpy})_2\}$  units have also been reported and similar studies of monolayers described. It is possible that these species may be partially oxidized and contain some cobalt(III) centers.<sup>219</sup>

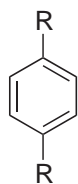
PAMAM dendrimers of generation 5 have also been functionalized with DOTA metal-binding domains and dysprosium complexes investigated as T2 contrast agents. Relaxivity measurements on the dysprosium complexes were interpreted in terms of an "inner sphere" Curie spin relaxation model with the large temperature dependence suggesting relaxation by a contact interaction effect, with the proton residence time as the primary time constant. The authors believe that it will be possible to create a new class of T2-selective contrast agents with systems of this type.<sup>220</sup>

A large number of papers have described the functionalization of dendrimers with DOTA and related metal-binding domains and subsequent studies of binding of lanthanoid and other paramagnetic centers with a view to designing novel agents for imaging or radiotherapy.<sup>6</sup> PAMAM dendrimers have been functionalized with DOTA and DTPA and linked to antibody fragments; initial studies indicate that  $^{90}\text{Y}$ ,  $^{111}\text{In}$ , and  $^{212}\text{Bi}$  complexes may be useful in radiotherapy and the Gd complexes for imaging.<sup>221</sup> Related PAMAM-based systems have been functionalized with diethylenetriaminepentaacetic acid units and the gadolinium complexes of the resultant ligand, containing up to 170 metal centers, have been shown to have a great potential in MR imaging.<sup>222</sup> Detailed studies of the vanadyl complexes of these ligands have given information about their solution dynamics.<sup>223</sup> Merbach has reported detailed studies of the solution behavior of a series of dendrimers modified with gadolinium macrocyclic complexes and has shown that the rotational correlation times for the dendrimers are four to eight times longer than for monomeric or dimeric Gd complexes.<sup>224</sup>

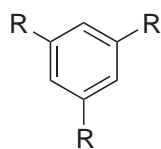
Surface decoration of dendrimers with groups that are catalytically active is a popular area of research.<sup>225</sup> The obvious technological advantages of multiple sites within a well-characterized macromolecule combine with the possibility of cooperative effects to make such compounds very exciting. The most popular surface functionalization is with phosphino groups, which bind low oxidation state or organometallic fragments.

Majoral has been active in the preparation of systems which not only have surface phosphorus coordination sites, but are also based upon inorganic phosphorus cores. A series of  $\text{Ph}_2\text{P}$ -terminated dendrimers radiating from a cyclotriphosphazene core have been prepared and functionalized with  $\text{Fe}(\text{CO})_4$ ,  $\text{W}(\text{CO})_5$ ,  $\text{RhCl}(\text{COD})$ , and  $\text{AuCl}$  surface functionality. Complexes have been prepared through to the fifth generation with up to 192 surface groups.<sup>18,226–230</sup> Schmidbauer has described the surface decoration of the star compounds bearing surface  $\text{PPh}_2$  groups with  $\text{AuCl}$  groups.<sup>231,232</sup>

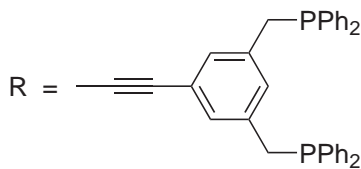
A series of dendrimers functionalized with binap domains has been prepared and shown to give effective hydrogenation catalysts.<sup>233</sup> Majoral has shown that metallodendrimers are efficient, recoverable catalysts for Stille couplings, Knoevenagel condensations, and Michael additions.<sup>234</sup> An exciting observation is the electrochemical reduction of  $\text{CO}_2$  catalyzed by palladated organophosphine dendrimers; the dendritic cores are derived from the iterative addition of vinylphosphonates to primary phosphines, followed by reduction to regenerate new surface primary phosphines.<sup>235</sup> Reetz has also reported the use of a series of phosphine and alkyne functionalized dendrimers as scaffolds for multisite catalysis.<sup>236–238</sup>



(56)



(57)



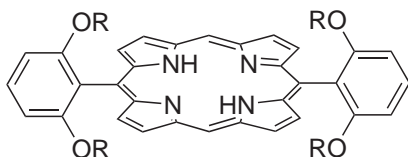
Carbosilane dendrimers have been functionalized with phosphine donors and a series of catalytic studies reported.<sup>239–241</sup> The core carbosilane dendrimers have also been utilized by van Koten and co-workers for the preparation of systems surface functionalized with organopalladium units.<sup>242,243</sup> A carbosilane dendrimer decorated with  $\{\text{Ru}(\text{bpy})_3\}$  units has been prepared and electrochemical studies reported.<sup>244</sup> Newkome has reported first-generation stars with surface polyoxometallate decoration.<sup>245</sup> A silsesquioxane core has been functionalized and a series of dendritic systems bearing Frechet-type dendritic wedges and pendant  $\{\text{Ru}(\text{tpy})(\text{bpy})_2\}$  decoration has been described. Up to 32 of these units containing didentate tpy ligands have been attached to the surface.<sup>246</sup>

### 7.6.8 METAL CORES DECORATED WITH DENDRITIC WEDGES

Considerable attention has been given to the synthesis of compounds in which a single mono- or multinuclear coordination unit is at the center of a dendrimer array. These systems have been prepared by the construction of ligands with pendant dendritic wedges with subsequent convergent assembly upon coordination of a metal ion at the center or by covalent synthesis of an appropriate dendrimer-functionalized macrocyclic core. The primary interest for the study of such compounds lies in the very unusual, usually hydrophobic, environment in which the metal(s) at the center find themselves. This environment has been likened to that at the active site of a metalloenzyme and numerous studies have dealt with the catalytic and biomimetic activity of such conjugates. A general introduction to the area and the concept of chemistry *within* dendrimers is available.<sup>123,247–250</sup> The term *dendrzyme* has been used to describe these systems.

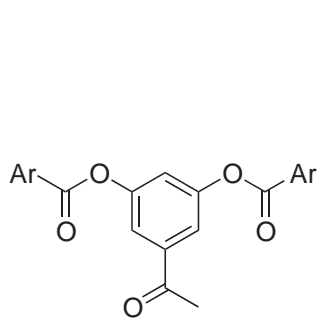
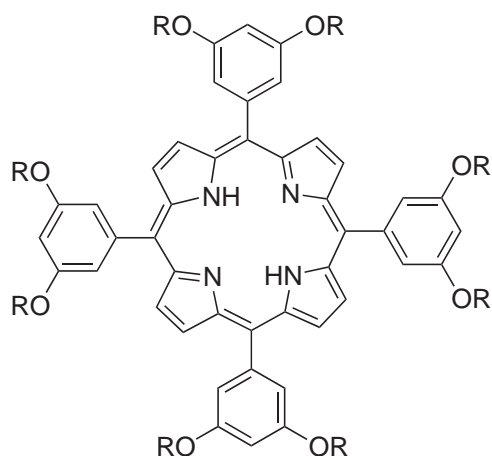
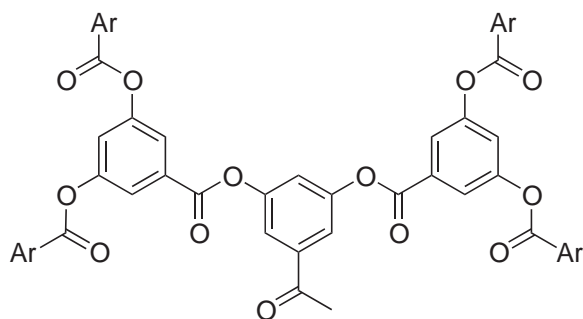
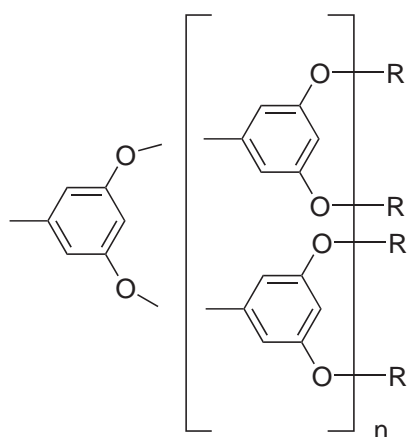
In view of the trend toward studying biomimetic reactions in these assemblies, it is not surprising that one of the most popular cores is the porphyrin ring system. This has the advantage of being readily functionalized with dendritic wedges of various generations to provide the peripheral dendritic substituents and giving a core with a very well established chemistry that binds the majority of metal ions. Diederich and co-workers have prepared a series of ligands based upon diarylporphyrins H<sub>2</sub>(**58**), H<sub>2</sub>(**59**) and H<sub>2</sub>(**60**) and have studied a series of biomimetic processes.<sup>251</sup> The polyoxyethylene chains render these species water soluble and they are proposed as models for globular enzymes. Both iron and zinc complexes have been prepared and the significant difference in iron(II)/(III) redox processes of 300 mV between [Fe<sup>III</sup>(**58**)Cl] and [Fe<sup>III</sup>(**59**)Cl] is taken as evidence for the encapsulation of the iron porphyrin in the second-generation complex [Fe<sup>III</sup>(**59**)Cl].<sup>252–254</sup> The complexes [Fe<sup>II</sup>(**58**)] and [Fe<sup>II</sup>(**59**)] reversibly bind dioxygen and CO in toluene solution in the presence of 1,2-dimethylimidazole and provide hemoglobin and myoglobin models.<sup>255</sup> A hydrogen-bonding interaction was thought to be important in stabilizing the dioxygen adducts. Analogues of these ligands have been investigated in which the imidazole is covalently linked via a spacer to one of the remaining *meso* positions of the porphyrin have also been investigated.<sup>256–259</sup> These compounds have proved to be effective catalysts for the epoxidation of olefins with iodobenzene as primary oxidant. Compounds with two imidazole ligands covalently attached to the ring, which can bind to both axial sites, have also been prepared.<sup>260</sup>

Suslick has prepared manganese complexes of first-generation H<sub>2</sub>(**61**) and second-generation H<sub>2</sub>(**62**) tetrafunctionalized *meso* porphyrin and these are effective selective epoxidation catalysts. The complexes [Mn(L)Cl] (L = (**61**), (**62**)) exhibit significantly higher selectivity than [Mn(TPP)(Cl)] but less than bis-pocket porphyrins.<sup>261–264</sup> Related tetra-substituted porphyrins H<sub>2</sub>(**63**) with dendritic wedges through to generation 5 have been prepared by Jiang and shown to form iron(II) complexes which form stable and long-lived dioxygen adducts.<sup>265,266</sup> Synthetic strategies for the Frechet-type systems H<sub>2</sub>(**64**) through to the fourth generation have been assessed and reliable methodologies developed. Attachment of dendritic wedges to the core porphyrin is probably the best strategy.<sup>267</sup> A detailed study of the electrochemical and photophysical properties of the [Zn(**64**)] complexes through to the fourth generation concluded that the substituents do not result in any significantly perturbation, in particular with respect to the quenching of fluorescence by viologens.<sup>268</sup>



R



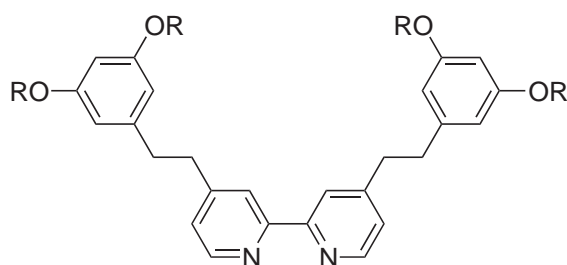
H<sub>2</sub>(61)H<sub>2</sub>(62)H<sub>2</sub>(63) R = MeH<sub>2</sub>(64) R = Bz

A *meso*-tetraaryl palladium porphyrin has been used as a core to which polyglutamate dendritic wedges of various generations have been attached to the 4- positions of the aryl substituents by a divergent approach. The compounds have surface carboxylate or ester groups. The compounds phosphoresce strongly ( $\lambda_{\max} = 690 \text{ nm}$ ) with lifetimes in the range of 0.5–1 ms; the phosphorescence is quenched by dioxygen and in water the quenching constants decreased with dendrimer generation. This was interpreted in terms of changes in the conformation of the dendrimer in various solvents, with an open conformation allowing oxygen diffusion towards the porphyrin core.<sup>269</sup>

Complexes of the type  $[\text{Ru}(\text{CO})\text{L}]$  ( $\text{L}$  = Frechet-functionalized *meso*-tetraphenylporphyrins) have been shown to be highly selective catalysts for epoxidation of alkenes with chemo- and diastereoselectivity increasing with the generation of the dendron.<sup>270</sup>

A few examples of dendron-functionalized phthalocyanines have also been recently reported<sup>271–276</sup> and the catalytic activity of some cobalt complexes investigated.<sup>273</sup>

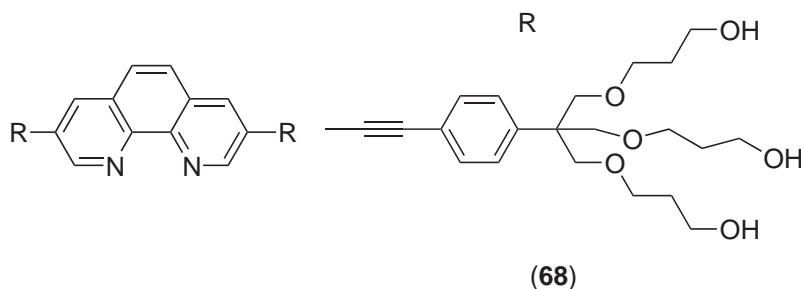
Not surprisingly, diimine ligands are popular core components for decoration with dendritic wedges and a variety of bpy, phen, and tpy systems have been reported. Vögtle and co-workers have described a series of Frechet-functionalized bpy ligands (**65**)–(**67**) and shown that both heteroleptic  $[\text{Ru}(\text{bpy})_2\text{L}]^{2+}$  and homoleptic  $[\text{RuL}_3]^{2+}$  ( $\text{L}$  = (**65**), (**66**) or (**67**)) are readily prepared.<sup>277</sup> The complexes are luminescent and it has been shown that the core is protected by the dendritic wedges and quenching by external quenchers is retarded. Similar studies with dendron-functionalized tpy ligands also confirm the isolated nature of the metal core, and redox processes at the metal center become less reversible with increasing generations of the dendron.<sup>278,279</sup>



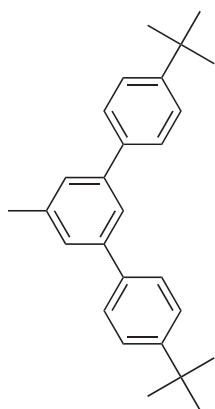
R

- (65) Bz  
 (66)  $\text{CH}_2\text{C}_6\text{H}_4(\text{OBz})_2$   
 (67)  $\text{CH}_2\text{C}_6\text{H}_4\{\text{OCH}_2\text{C}_6\text{H}_4(\text{OBz})_2\}_2$

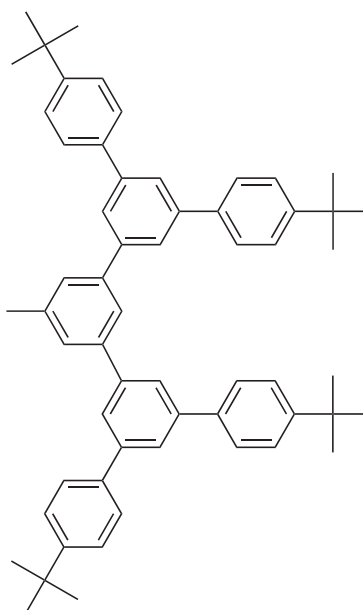
The dendron-functionalized phen ligand (**68**) forms the expected  $[\text{Fe}(\text{68})]^{2+}$  species, which have been investigated by Tor and co-workers.<sup>280</sup> More rigid analogues of these compounds have been prepared with polyaromatic dendritic wedges (**69**) and (**70**) and photophysical studies of metal complexes reported.<sup>281</sup> Related species with Frechet-type dendrimers attached to the 4- and 7- positions of phen ligands or the 4,4'- positions of bpy ligands have been prepared and detailed photophysical studies reported.<sup>282,283</sup> The excited-state lifetimes of the  $[\text{RuL}_3]^{2+}$  complexes are increased as a result of the shielding of the photocenter by the dendritic wedges.



(68)



(69)

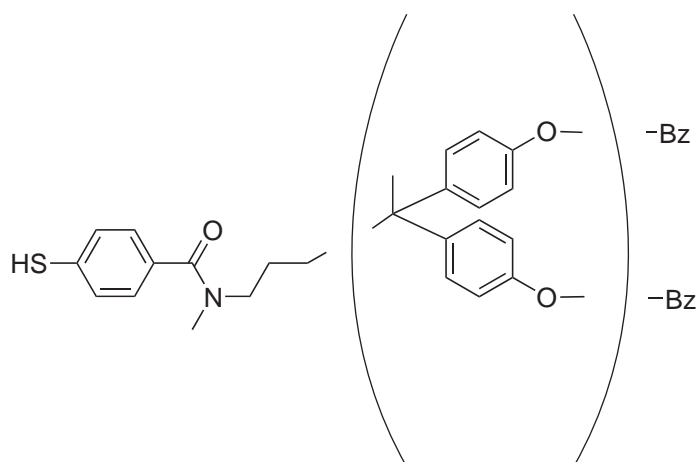


(70)

Nierengarten and co-workers have described a series of ligands based upon dendron functionalized phen ligands decorated with fullerenes such as and have reported detailed studies of energy and electron transfer processes in the  $[\text{CuL}_2]^+$  complexes.<sup>284,285</sup>

Multinuclear metal clusters are beginning to be used as cores for metal dendrimers and a number of key reports involving different types of cluster have recently appeared.

The biomimetic theme is well illustrated by the work of Gorman and co-workers, who have prepared a series of dendrimer-functionalized  $\{\text{Fe}_4\text{S}_4\}$  clusters out through the fourth generation. The compounds were prepared by ligand exchange of  $[\text{Fe}_4\text{S}_4(\text{SR})_4]^{2-}$  species with various types of thiolate functionalized dendritic wedges such as (71). The effect of dendrimer architecture on the redox properties of the encapsulated cluster core was investigated.<sup>36,38,286–290</sup> NMR spectroscopic studies have been used to obtain structural information about complexes with both paramagnetic and diamagnetic cores. It is hoped that these model systems will provide useful information about biological electron transfer systems based upon iron–sulfur clusters. Electron transfer rates depended upon the flexibility of the dendritic components.



(71)



These studies have been extended to systems containing  $\{\text{Mo}_6\text{Cl}_8\}^{291}$  and  $\{\text{Re}_6\text{Se}_8\}^{292}$  cores bearing six dendritic arms.

## 7.6.9 REFERENCES

1. Narayanan, V. V.; Newkome, G. R. In *Dendrimers. Supramolecular chemistry within dendritic structures*; Vögtle, F., Ed.; Springer-Verlag: Berlin, 1998, Vol. 197, pp 19–77.
2. Majoral, J. P.; Caminade, A. M. In *Dendrimers. Divergent approaches to phosphorus containing dendrimers*; Vögtle, F., Ed.; Springer-Verlag: Berlin, 1998, Vol. 197, pp 79–124.
3. Venturi, M.; Serroni, S.; Juris, A.; Campagna, S.; Balzani, V. In *Dendrimers. Electrochemical and photochemical properties of metal containing dendrimers*; Vögtle, F., Ed.; Springer-Verlag: Berlin, 1998, Vol. 197, pp 193–228.
4. Smith, D. K.; Diederich, F. In *Dendrimers II. Supramolecular dendrimer chemistry*; Vögtle, F., Ed.; Springer-Verlag: Berlin, 2000; pp 183–227.
5. Baars, M.; Meijer, E. W. In *Dendrimers II. Host-guest chemistry of dendritic molecules*; Vögtle, F., Ed.; Springer-Verlag: Berlin, 2000; Vol. 210, pp 131–182.
6. Krause, W.; Hackmann-Schlichter, N.; Maier, F. K.; Müller, R. In *Dendrimers II. Dendrimers in diagnostics*; Vögtle, F., Ed.; Springer-Verlag: Berlin, 2000, Vol. 210, pp 261–308.
7. Zimmerman, S. C.; Lawless, L. J. In *Dendrimers IV. Supramolecular chemistry of dendrimers*; Vögtle, F., Schalley, C. A., Ed.; Springer-Verlag: Berlin, 2001, Vol. 217, pp 95–120.
8. van Manen, H. J.; van Veggel, F.; Reinhoudt, D. N. In *Dendrimers IV. Non-covalent synthesis of metallo dendrimers*; Vögtle, F., Schalley, C. A., Ed.; Springer-Verlag: Berlin, 2001, Vol. 217, pp 121–162.
9. Kreiter, R.; Kleij, A. W.; Gebbink, R.; van Koten, G. In *Dendrimers IV, Dendritic catalysts*; Vögtle, F., Schalley, C. A., Ed.; Springer-Verlag: Berlin, 2001, Vol. 217, pp 163–199.
10. Crooks, R. M.; Lemon, B. I.; Sun, L.; Yeung, L. K.; Zhao, M. Q. In *Dendrimers III. Dendrimer encapsulated metals and semiconductors*; Vögtle, F., Schalley, C. A., Ed.; Springer-Verlag: Berlin, 2001, Vol. 212, pp 81–135.
11. Newkome, G. R.; Moorefield, C. N.; Vögtle, F. *Dendritic Molecules. Concepts, Syntheses, Perspectives* **1996**, VCH: Weinheim.
12. DeCola, L.; Barigelletti, F.; Balzani, V.; Belsler, P.; von Zelewsky, A.; Seel, C.; Frank, M.; Vögtle, F. *Coord. Chem. Rev.* **1991**, *111*, 255–260.
13. Archut, A.; Vögtle, F. *Chem. Soc. Rev.* **1998**, *27*, 233–240.
14. Balzani, V.; Campagna, S.; Denti, G.; Juris, A.; Serroni, S.; Venturi, M. *Coord. Chem. Rev.* **1994**, *132*, 1–13.
15. Balzani, V.; Juris, A.; Venturi, M.; Campagna, S.; Serroni, S. *Chem. Rev.* **1996**, *96*, 759–833.
16. Balzani, V.; Juris, A. *Coord. Chem. Rev.* **2001**, *211*, 97–115.
17. Balzani, V.; Ceroni, P.; Juris, A.; Venturi, M.; Campagna, S.; Puntoriero, F.; Serroni, S. *Coord. Chem. Rev.* **2001**, *219*, 545–572.
18. Caminade, A. M.; Laurent, R.; Chaudret, B.; Majoral, J. P. *Coord. Chem. Rev.* **1998**, *180*, 793–821.
19. Cuadrado, I.; Moran, M.; Casado, C. M.; Alonso, B.; Losada, J. *Coord. Chem. Rev.* **1999**, *195*, 395–445.
20. Grayson, S. K.; Frechet, J. M. J. *Chem. Rev.* **2001**, *101*, 3819–3867.
21. Denti, G.; Serroni, S.; Campagna, S.; Ricevuto, V.; Balzani, V. *Coord. Chem. Rev.* **1991**, *111*, 227–236.
22. Zeng, F. W.; Zimmerman, S. C. *Chem. Rev.* **1997**, *97*, 1681–1712.
23. Venturi, M.; Credi, A.; Balzani, V. *Coord. Chem. Rev.* **1999**, *186*, 233–256.
24. Twyman, L. J.; King, A. S. H.; Martin, I. K. *Chem. Soc. Rev.* **2002**, *31*, 69–82.
25. Serroni, S.; Campagna, S.; Puntoriero, F.; Di Pietro, C.; McClenaghan, N. D.; Loiseau, F. *Chem. Soc. Rev.* **2001**, *30*, 367–375.
26. Sauvage, J. P.; Collin, J. P.; Chambron, J. C.; Guillerez, S.; Coudret, C.; Balzani, V.; Barigelletti, F.; DeCola, L.; Flamigni, L. *Chem. Rev.* **1994**, *94*, 993–1019.
27. Newkome, G. R.; He, E. F.; Moorefield, C. N. *Chem. Rev.* **1999**, *99*, 1689–1746.
28. Moss, J. R. *Platinum Met. Rev.* **1995**, *39*, 33–36.
29. Majoral, J. P.; Caminade, A. M. *Chem. Rev.* **1999**, *99*, 845–880.
30. Majoral, J. P.; Larre, C.; Laurent, R.; Caminade, A. M. *Coord. Chem. Rev.* **1999**, *192*, 3–18.
31. MacDonnell, F. M.; Kim, M. J.; Bodige, S. *Coord. Chem. Rev.* **1999**, *186*, 535–549.
32. Lawrence, D. S.; Jiang, T.; Levett, M. *Chem. Rev.* **1995**, *95*, 2229–2260.
33. Keene, F. R. *Coord. Chem. Rev.* **1997**, *166*, 121–159.
34. Juris, A.; Balzani, V.; Barigelletti, F.; Campagna, S.; Belsler, P.; von Zelewsky, A. *Coord. Chem. Rev.* **1988**, *84*, 85–277.
35. Jiang, B. W.; Yang, S. W.; Bailey, S. L.; Hermans, L. G.; Niver, R. A.; Bolcar, M. A.; Jones, W. E. *Coord. Chem. Rev.* **1998**, *171*, 365–386.
36. Gorman, C. B.; Smith, J. C. *Acc. Chem. Res.* **2001**, *34*, 60–71.
37. Denti, G.; Serroni, S.; Campagna, S.; Juris, A.; Ciano, M.; Balzani, V. In *Perspectives in Coordination Chemistry, 'complexes as metals' and 'complexes as ligands'*; Williams, A. F., Floriani, C., Merbach, A. E., Eds.; VHC and VCH: Basel and Weinheim, 1992, pp 153–164.
38. Gorman, C. *Adv. Mater.* **1998**, *10*, 295–309.
39. Swiegers, G. F.; Malefsete, T. J. *Chem. Rev.* **2000**, *100*, 3483–3537.
40. Adronov, A.; Frechet, J. M. J. *Chem. Commun.* **2000**, 1701–1710.
41. Juris, A.; Venturi, M.; Ceroni, P.; Balzani, V.; Campagna, S.; Serroni, S. *Collect. Czech. Chem. Commun.* **2001**, *66*, 1–32.
42. Beer, P. D. *Adv. Inorg. Chem.* **1992**, *39* 79–157.
43. Serroni, S.; Campagna, S.; Denti, G.; Juris, A.; Venturi, M.; Balzani, V. In *Advances in Dendritic Macromolecules, Dendrimers based on metal complexes*; Newkome, G. R., Ed.; Jai Press: Greenwich, CT, 1996; Vol. 3; pp 61–113.
44. Stoddart, F. J.; Welton, T. *Polyhedron* **1999**, *18*, 3575–3591.
45. Constable, E. C. *Chem. Commun.* **1997**, 1073–1080.

46. Balzani, V.; Denti, G.; Serroni, S.; Campagna, S.; Ricevuto, V.; Juris, A. *Proc. Ind. Acad. Sci.—Chem. Sci.* **1993**, *105*, 421–434.
47. Balzani, V.; Campagna, S.; Denti, G.; Juris, A.; Serroni, S.; Venturi, M. *Sol. Energy Mater. Sol. Cells* **1995**, *38*, 159–173.
48. Balzani, V.; Campagna, S.; Denti, G.; Juris, A.; Serroni, S.; Venturi, M. *Acc. Chem. Res.* **1998**, *31*, 26–34.
49. Cuadrado, I.; Moran, M.; Losada, J.; Casado, C. M.; Pascual, C.; Alonso, B.; Lobete, F. In *Advances in Dendritic Macromolecules, Organometallic dendritic macromolecules: Organosilicon and organometallic entities as cores or building blocks*; Newkome, G. R., Ed.; Jai Press: Greenwich, CT, 1996; Vol. 3.
50. Hearshaw, M. A.; Moss, J. R. *Chem. Commun.* **1999**, 1–8.
51. Hearshaw, M. A.; Hutton, A. T.; Moss, J. R.; Naidoo, K. J. In *Advances in Dendritic Macromolecules, Organometallic dendrimers*; Newkome, G. R., Ed.; Jai Press: Stamford, CA, 1999, Vol. 4, 1–60.
52. Venturi, M.; Credi, A.; Balzani, V. *Coord. Chem. Rev.* **1999**, *186*, 233–256.
53. Vogtle, F.; Gestermann, S.; Hesse, R.; Schwierz, H.; Windisch, B. *Prog. Polym. Sci.* **2000**, *25*, 987–1041.
54. Serroni, S.; Denti, G.; Campagna, S.; Ciano, M.; Balzani, V. *J. Chem. Soc., Chem. Commun.* **1991**, 944–955.
55. Smith, D. K.; Diederich, F. *Chem. Eur. J.* **1998**, *4*, 1353–1361.
56. Wilks, E. S. *Macromol. Rapid Commun.* **1998**, *19*, U4–U9. *Macromol. Chem. Phys.* **1998**, *199*, U5–U10.
57. Newkome, G. R.; Baker, G. R.; Young, J. K.; Traynham, J. G. *J. Polym. Sci.*, **1993**, *31*, 641–651.
58. Baker, G. R.; Young, J. K. In *Advances in Dendritic Macromolecules, Vol 1, A systematic nomenclature for cascade (Dendritic) Polymers*; Newkome, G. R., Ed.; Jai Press: Greenwich, CT, 1994; Vol. 1, pp 641–651.
59. Tzalis, D.; Tor, Y. *Chem. Commun.* **1996**, 1043–1044.
60. Bodige, S.; Torres, A. S.; Maloney, D. J.; Tate, D.; Kinsel, G. R.; Walker, A. K.; MacDonnell, F. M. *J. Am. Chem. Soc.* **1997**, *119*, 10364–10369.
61. MacDonnell, F. M.; Ali, M. D. M.; Kim, M. J. *Comments Inorg. Chem.* **2000**, *22*, 203–225.
62. MacDonnell, F. M.; Kim, M. J.; Bodige, S. *Coord. Chem. Rev.* **1999**, *186*, 535–549.
63. Ishow, E.; Gourdon, A.; Launay, J. P.; Lecante, P.; Verelst, M.; Chiorboli, C.; Scandola, F.; Bignozzi, C. A. *Inorg. Chem.* **1998**, *37*, 3603–3609.
64. Campagna, S.; Serroni, S.; Bodige, S.; MacDonnell, F. M. *Inorg. Chem.* **1999**, *38*, 692–701.
65. Warnmark, K.; Heyke, O.; Thomas, J. A.; Lehn, J. M. *Chem Commun* **1996**, 2603–2604.
66. Jacquet, L.; Kirsch-De Mesmaeker, A. *J. Chem. Soc., Faraday Trans.* **1992**, *88*, 2471–2480.
67. Kaes, C.; Katz, A.; Hosseini, M. W. *Chem. Rev.* **2000**, *100*, 3553–3590.
68. Ziessel, R.; Lehn, J.-M. *Helv. Chim. Acta* **1990**, *73*, 1149–1162.
69. Lehn, J.-M.; Ziessel, R. *J. Chem. Soc., Chem. Commun.* **1987**, 1292–1294.
70. De Cola, L.; Belsler, P.; Ebmeyer, F.; Barigelletti, F.; Vogtle, F.; von Zelewsky, A.; Balzani, V. *Inorg. Chem.* **1990**, *29*, 495–499.
71. Grammenudi, S.; Vögtle, F. *Angew. Chem., Int. Ed. Engl.* **1986**, *25*, 1122–1125.
72. Belsler, P.; von Zelewsky, A.; Frank, M.; Seel, C.; Vogtle, F.; DeCola, L.; Barigelletti, F.; Balzani, V. *J. Am. Chem. Soc.* **1993**, *115*, 4076–4086.
73. Josceanu, A. M.; Moore, P.; Rawle, S. C.; Sheldon, P.; Smith, S. M. *Inorg. Chim. Acta* **1995**, *240*, 159–168.
74. Carlson, D. L.; Murphy, W. R. *Inorg. Chim. Acta* **1991**, *181*, 61–64.
75. Kalyanasundaram, K.; Nazeeruddin, M. K. *Inorg. Chem.* **1990**, *29*, 1888–1897.
76. Akasheh, T. S.; Elahmed, Z. M. *Chem. Phys. Lett.* **1988**, *152*, 414–418.
77. Brewer, K. J.; Murphy, W. R., Jr.; Spurlin, S. R.; Petersen, J. D. *Inorg. Chem.* **1986**, *25*, 882–884.
78. Roffia, S.; Marcaccio, M.; Paradisi, C.; Paolucci, F.; Balzani, V.; Denti, G.; Serroni, S.; Campagna, S. *Inorg. Chem.* **1993**, *32*, 3003–3009.
79. Anderson, P. A.; Anderson, R. F.; Furue, M.; Junk, P. C.; Keene, F. R.; Patterson, B. T.; Yeomans, B. D. *Inorg. Chem.* **2000**, *39*, 2721–2728.
80. Predieri, G.; Vignali, C.; Denti, G.; Serroni, S. *Inorg. Chim. Acta* **1993**, *205*, 145–148.
81. Denti, G.; Serroni, S.; Sabatino, L.; Ciano, M.; Ricevuto, V.; Campagna, S. *Gazz. Chim. Ital.* **1991**, *121*, 37–43.
82. Kalyanasundaram, K.; Nazeeruddin, M. K. *Inorg. Chim. Acta* **1990**, *171*, 213–216.
83. Tresoldi, G.; LoSchiavo, S.; Piraino, P. *Inorg. Chim. Acta* **1997**, *254*, 381–385.
84. McClenaghan, N. D.; Loiseau, F.; Puntoriero, F.; Serroni, S.; Campagna, S. *Chem. Commun.* **2001**, 2634–2635.
85. Juris, A.; Balzani, V.; Campagna, S.; Denti, G.; Serroni, S.; Frei, G.; Gudel, H. U. *Inorg. Chem.* **1994**, *33*, 1491–1496.
86. Denti, G.; Campagna, S.; Sabatino, L.; Serroni, S.; Ciano, M.; Balzani, V. *Inorg. Chem.* **1990**, *29*, 4750–4758.
87. Schmehl, R. H.; Auerbach, R. A.; Wacholtz, W. F.; Elliott, C. M.; Freitag, R. A.; Merkert, J. W. *Inorg. Chem.* **1986**, *25*, 2440–2445.
88. Marcaccio, M.; Paolucci, F.; Paradisi, C.; Roffia, S.; Fontanesi, C.; Yellowlees, L. J.; Serroni, S.; Campagna, S.; Denti, G.; Balzani, V. *J. Am. Chem. Soc.* **1999**, *121*, 10081–10091.
89. Sahai, R.; Morgan, L.; Rillema, D. P. *Inorg. Chem.* **1988**, *27*, 3495–3500.
90. Campagna, S.; Denti, G.; Sabatini, L.; Serroni, S.; Ciano, M.; Balzani, V. *J. Chem. Soc., Chem. Commun.* **1989**, 1500–1501.
91. Ruminski, R. R.; Deere, P. T.; Olive, M.; Serveiss, D. *Inorg. Chim. Acta* **1998**, *281*, 1–9.
92. De Munno, G.; Julve, M.; Real, J. A. *Inorg. Chim. Acta* **1997**, *255*, 185–188.
93. De Munno, G.; Poerio, T.; Viau, G.; Julve, M.; Lloret, F. *Angew. Chem. Int. Ed.* **1997**, *36*, 1459–1461.
94. Armentano, D.; De Munno, G.; Faus, J.; Lloret, F.; Julve, M. *Inorg. Chem.* **2001**, *40*, 655–660.
95. van Albada, G. A.; Smeets, W. J. J.; Spek, A. L.; Reedijk, J. *J. Chem. Crystallogr.* **2000**, *30*, 441–444.
96. Rillema, D. P.; Jones, D. S.; Woods, C.; Levy, H. A. *Inorg. Chem.* **1992**, *31*, 2935–2938.
97. Sahai, R.; Rillema, D. P.; Shaver, R.; van Wallendaal, S.; Jackman, D. C.; Boldaji, M. *Inorg. Chem.* **1989**, *28*, 1022–1028.
98. Kirsch-De Mesmaeker, A.; Lacquet, L.; Masschelein, A.; Vanhecke, F.; Heremans, K. *Inorg. Chem.* **1989**, *28*, 2465–2470.
99. Jacquet, L.; Kirsch-De Mesmaeker, A. *J. Chem. Soc., Faraday Trans.* **1992**, *88*, 2471–2480.
100. Didier, P.; Jacquet, L.; Kirsch-De Mesmaeker, A.; Hueber, R.; van Dorselaer, A. *Inorg. Chem.* **1992**, *31*, 4803–4809.
101. Orellana, G.; Kirsch-De Mesmaeker, A.; Turro, N. J. *Inorg. Chem.* **1990**, *29*, 882–885.

102. Masschelein, A.; Kirsch-De Mesmaeker, A.; Verhoeven, C.; Nasielski-Hinkens, R. *Inorg. Chim. Acta* **1987**, *129*, L13–L16.
103. Ortmans, L.; Didier, P.; Kirsch-De Mesmaeker, A. *Inorg. Chem.* **1995**, *34*, 3695–3704.
104. Rutherford, T. J.; Keene, F. R. *J. Chem. Soc., Dalton Trans.* **1998**, 1155–1162.
105. Rutherford, T. J.; Keene, F. R. *Inorg. Chem.* **1997**, *36*, 3580–3581.
106. Rutherford, T. J.; VanGijte, O.; Mesmaeker, A. K.; Keene, F. R. *Inorg. Chem.* **1997**, *36*, 4465–4474.
107. Keene, F. R. *Coord. Chem. Rev.* **1997**, *166*, 121–159.
108. Baxter, P.; Lehn, J.-M.; DeCian, A.; Fischer, J. *Angew. Chem.*; **1993**, *105*, 92–95.
109. Okubo, T.; Kitagawa, S.; Kondo, M.; Matsuzaka, H.; Ishii, T. *Angew. Chem., Int. Ed.* **1999**, *38*, 931–933.
110. Nasielski-Hinkens, R.; Benedek-Vamos, M.; Maetens, D.; Nasielski, J. *J. Organomet. Chem.* **1981**, *217*, 179–182.
111. Marshall, S. R.; Rheingold, A. L.; Dawe, L. N.; Shum, W. W.; Kitamura, C.; Miller, J. S. *Inorg. Chem.* **2002**, *41*, 3599–3601.
112. Moucheron, C.; Dietrich-Buchecker, C. O.; Sauvage, J.-P.; van Dorsselaer, A. *J. Chem. Soc., Dalton Trans.* **1994**, 885–894.
113. Latterini, L.; Pourtois, G.; Moucheron, C.; Lazzaroni, R.; Bredas, J. L.; Kirsch-De Mesmaeker, A.; De Schryver, F. C. *Chem. Eur. J.* **2000**, *6*, 1331–1336.
114. Latterini, L.; Schweitzer, G.; De Schryver, F. C.; Moucheron, C.; Kirsch-De Mesmaeker, A. *Chem. Phys. Lett.* **1997**, *281*, 267–271.
115. Moucheron, C.; Kirsch-De Mesmaeker, A.; Dupont-Gervais, A.; Leize, E.; van Dorsselaer, A. *J. Am. Chem. Soc.* **1996**, *118*, 12834–12835.
116. Constable, E. C.; Harverson, P.; Oberholzer, M. *Chem. Commun.* **1996**, 1821–1822.
117. Constable, E. C.; Harverson, P. *Polyhedron* **1999**, *18*, 1891–1901.
118. Constable, E. C.; Housecroft, C. E.; Poleschak, I. *Inorg. Chem. Commun.* **1999**, *2*, 565–568.
119. Constable, E. C.; Housecroft, C. E.; Neuburger, M.; Poleschak, I.; Zehnder, M. *Polyhedron* **2003**, *22*, 93–108.
120. Osawa, M.; Hoshino, M.; Horiuchi, S.; Wakatsuki, Y. *Organometallics* **1999**, *18*, 112–114.
121. Constable, E. C.; Harverson, P. *Polyhedron* **1999**, *18*, 3093–3106.
122. Borje, A.; Kothe, O.; Juris, A. *J. Chem. Soc., Dalton Trans.* **2002**, 843–848.
123. Borje, A.; Kothe, O.; Juris, A. *New J. Chem.* **2001**, *25*, 191–193.
124. Wacholtz, W. F.; Auerbach, R. A.; Schmehl, R. H. *Inorg. Chem.* **1987**, *26*, 2989–2994.
125. Constable, E. C.; Eich, O.; Housecroft, C. E.; Rees, D. C. *Inorg. Chim. Acta* **2000**, *300*, 158–168.
126. Constable, E. C.; Cargill Thompson, A. M. W. *J. Chem. Soc., Chem. Commun.* **1992**, 617–619.
127. Constable, E. C.; Thompson, A. M. W. *J. Chem. Soc., Dalton Trans.* **1992**, 3467–3475.
128. Constable, E. C.; Harverson, P. *Inorg. Chim. Acta* **1996**, *252*, 9–11.
129. Constable, E. C.; Harverson, P. *Chem. Commun.* **1996**, 33–34.
130. Marvaud, V.; Astruc, D. *Chem. Commun.* **1997**, 773–774.
131. Marvaud, V.; Astruc, D.; Leize, E.; van Dorsselaer, A.; Guittard, J.; Blais, J. C. *New J. Chem.* **1997**, *21*, 1309–1319.
132. Hissler, M.; Ziessel, R. *New J. Chem.* **1995**, *19*, 751–756.
133. Campagna, S.; Denti, G.; Serroni, S.; Ciano, M.; Balzani, V. *Inorg. Chem.* **1991**, *30*, 3728–3732.
134. Campagna, S.; Denti, G.; Serroni, S.; Ciano, M.; Juris, A.; Balzani, V. *Inorg. Chem.* **1992**, *31*, 2982–2984.
135. Campagna, S.; Denti, G.; Serroni, S.; Juris, A.; Venturi, M.; Ricevuto, V.; Balzani, V. *Chem. Eur. J.* **1995**, *1*, 211–221.
136. Campagna, S.; Serroni, S.; Juris, A.; Venturi, M.; Balzani, V. *New J. Chem.* **1996**, *20*, 773–780.
137. Denti, G.; Campagna, S.; Sabatino, L.; Serroni, S.; Ciano, M.; Balzani, V. *Inorg. Chem.* **1990**, *29*, 4750–4758.
138. Denti, G.; Campagna, S.; Sabatino, L.; Serroni, S.; Ciano, M.; Balzani, V. *Inorg. Chim. Acta* **1990**, *176*, 175–178.
139. Denti, G.; Campagna, S.; Serroni, S.; Ciano, M.; Balzani, V. *J. Am. Chem. Soc.* **1990**, *114*, 2944–2950.
140. Denti, G.; Serroni, S.; Campagna, S.; Ricevuto, V.; Balzani, V. *Inorg. Chim. Acta* **1991**, *182*, 127–129.
141. Denti, G.; Serroni, S.; Campagna, S.; Ricevuto, V.; Juris, A.; Ciano, M.; Balzani, V. *Inorg. Chim. Acta* **1992**, *200*, 507–512.
142. Denti, G.; Serroni, S.; Campagna, S.; Juris, A.; Balzani, V. *Mol. Cryst. Liq. Cryst. Sci. Technol., Sect. A: Mol. Cryst. Liq. Cryst.* **1993**, *234*, 79–88.
143. Juris, A.; Balzani, V.; Campagna, S.; Denti, G.; Serroni, S.; Frei, G.; Gudel, H. U. *Inorg. Chem.* **1994**, *33*, 1491–1496.
144. Juris, A.; Venturi, M.; Pontoni, L.; Resino, I. R.; Balzani, V.; Serroni, S.; Campagna, S.; Denti, G. *Can. J. Chem.* **1995**, *73*, 1875–1882.
145. Serroni, S.; Juris, A.; Venturi, M.; Campagna, S.; Resino, I. R.; Denti, G.; Credi, A.; Balzani, V. *J. Mater. Chem.* **1997**, *7*, 1227–1236.
146. Serroni, S.; Juris, A.; Campagna, S.; Venturi, M.; Denti, G.; Balzani, V. *J. Am. Chem. Soc.* **1994**, *116*, 9086–9091.
147. Serroni, S.; Denti, G.; Campagna, S.; Juris, A.; Ciano, M.; Balzani, V. *Angew. Chem. Int. Ed.* **1992**, *31*, 1493–1495.
148. Campagna, S.; Giannetto, A.; Serroni, S.; Denti, G.; Trusso, S.; Mallamace, F.; Micali, N. *J. Am. Chem. Soc.* **1995**, *117*, 1754–1758.
149. Serroni, S.; Campagna, S.; Denti, G.; Keyes, T. E.; Vos, J. G. *Inorg. Chem.* **1996**, *35*, 4513–4518.
150. Serroni, S.; Denti, G. *Inorg. Chem.* **1992**, *31*, 4251–4255.
151. Campagna, S.; Denti, G.; Serroni, S.; Juris, A.; Venturi, M.; Ricevuto, V.; Balzani, V. *Chem. Eur. J.* **1995**, *1*, 211–221.
152. Puntoriero, F.; Serroni, S.; Licciardello, A.; Venturi, M.; Juris, A.; Ricevuto, V.; Campagna, S. *J. Chem. Soc., Dalton Trans.* **2001**, 1035–1042.
153. Pink, M.; Sutra, P.; Balzani, V.; Venturi, M.; Campagna, S.; Serroni, S.; Juris, A. *Inorg. Chim. Acta* **2002**, *333*, 25–31.
154. Serroni, S.; Campagna, S.; Puntoriero, F.; Di Pietro, C.; McClenaghan, N. D.; Loiseau, F. *Chem. Soc. Rev.* **2001**, *30*, 367–375.
155. Carano, M.; Ceroni, P.; Fontanesi, C.; Marcaccio, M.; Paolucci, F.; Paradisi, C.; Roffia, S. *Electrochim. Acta* **2001**, *46*, 3199–3206.
156. Ceroni, P.; Paolucci, F.; Paradisi, C.; Juris, A.; Roffia, S.; Serroni, S.; Campagna, S.; Bard, A. J. *J. Am. Chem. Soc.* **1998**, *120*, 5480–5487.
157. Serroni, S.; Campagna, S.; Denti, G.; Keyes, T. E.; Vos, J. G. *Inorg. Chem.* **1996**, *35*, 4513–4518.
158. Lempers, H. E. B.; Haasnoot, J. G.; Reedijk, J.; Hage, R.; Weldon, F. M.; Vos, J. G. *Inorg. Chim. Acta* **1994**, *225*, 67–74.

159. Achar, S.; Vittal, J. J.; Puddephatt, R. J. *Organometallics* **1996**, *15*, 43–50.
160. Achar, S.; Puddephatt, R. J. *Organometallics* **1995**, *14*, 1681–1687.
161. Achar, S.; Puddephatt, R. J. *Chem. Commun.* **1994**, 1895–1896.
162. Achar, S.; Puddephatt, R. J. *Angew. Chem. Int. Ed.* **1994**, *33*, 847–849.
163. Achar, S.; Immoos, C. E.; Hill, M. G.; Catalano, V. J. *Inorg. Chem.* **1997**, *36*, 2314–2320.
164. Puddephatt, R. J. *Chem. Commun.* **1998**, 1055–1062.
165. Liu, G. X.; Puddephatt, R. J. *Organometallics* **1996**, *15*, 5257–5259.
166. Liu, G. X.; Puddephatt, R. J. *Inorg. Chim. Acta* **1996**, *251*, 319–323.
167. Sahai, R.; Rillema, D. P. *J. Chem. Soc., Chem. Commun.* **1986**, 1133–1134.
168. Murphy, Jr., W. R.; Brewer, K. J.; Gettliffe, G.; Petersen, J. D. *Inorg. Chem.* **1989**, *28*, 81–84.
169. Kim, M. J.; MacDonnell, F. M.; Gimion-Kinsel, M. E.; Du Bois, T.; Asgharian, N.; Griener, J. C. *Angew. Chem., Int. Ed.* **2000**, *39*, 615–619.
170. Armspach, D.; Cattalini, M.; Constable, E. C.; Housecroft, C. E.; Phillips, D. *Chem. Commun.* **1996**, 1823–1824.
171. Armspach, D.; Cattalini, M.; Constable, E. C.; Housecroft, C. E.; Neuburger M.; Zehnder, M. In *Advances in Boron Chemistry*; Siebert, W., Ed.; RSC, Cambridge, 1997.
172. Constable, E. C.; Housecroft, C. E.; Cattalini, M.; Phillips, D. *New J. Chem.* **1998**, *22*, 193–200.
173. Holmstrom, S. D.; Cox, J. A. *Anal. Chem.* **2000**, *72*, 3191–3195.
174. Cheng, L.; Pacey, G. E.; Cox, J. A. *Anal. Chem.* **2001**, *73*, 5607–5610.
175. Cohen, J. L.; Widera, J.; Cox, J. A. *Electroanalysis* **2002**, *14*, 231–234.
176. Cheng, L.; Cox, J. A. *Chem. Mat.* **2002**, *14*, 6–8.
177. Newkome, G. R.; Cardullo, F.; Constable, E. C.; Moorefield, C. N.; Thompson, A. *J. Chem. Soc., Chem. Commun* **1993**, *14*, 925–927.
178. Constable, E. C.; Harverson, P.; Ramsden, J. J. *Chem. Commun.* **1997**, 1683–1684.
179. Newkome, G. R.; He, E. F. *J. Mater. Chem.* **1997**, *7*, 1237–1244.
180. Newkome, G. R.; He, E. F.; Godinez, L. A. *Macromolecules* **1998**, *31*, 4382–4386.
181. Newkome, G. R.; He, E. F.; Godinez, L. A.; Baker, G. R. *Chem. Commun.* **1999**, 27–28.
182. Newkome, G. R.; He, E.; Godinez, L. A.; Baker, G. R. *J. Am. Chem. Soc.* **2000**, *122*, 9993–10006.
183. Newkome, G. R.; Guthrie, R.; Moorefield, C. N.; Cardullo, F.; Echevoyen, L.; Perez-Cordero, E.; Luftmann, H. *Angew. Chem. Int. Ed.* **1995**, *34*, 2023–2026.
184. Albrecht, M.; van Koten, G. *Adv. Mater.* **1999**, *11*, 171–174.
185. Albrecht, M.; Schlupp, M.; Bargon, J.; van Koten, G. *Chem. Commun.* **2001**, 1874–1875.
186. Albrecht, M.; Hovestad, N. J.; Boersma, J.; van Koten, G. *Chem. Eur. J.* **2001**, *7*, 1289–1294.
187. Albrecht, M.; Gossage, R. A.; Spek, A. L.; van Koten, G. *Chem. Commun.* **1998**, 1003–1004.
188. Albrecht, M.; Gossage, R. A.; Lutz, M.; Spek, A. L.; van Koten, G. *Chem. Eur. J.* **2000**, *6*, 1431–1445.
189. Rietveld, M. H. P.; Grove, D. M.; van Koten, G. *New J. Chem.* **1997**, *21*, 751–771.
190. Rodriguez, G.; Lutz, M.; Spek, A. L.; van Koten, G. *Chem. Eur. J.* **2002**, *8*, 46–57.
191. Kleij, A. W.; Gebbink, R.; Lutz, M.; Spek, A. L.; van Koten, G. *J. Organomet. Chem.* **2001**, *621*, 190–196.
192. Meijer, M. D.; Kleij, A. W.; Williams, B. S.; Ellis, D.; Lutz, M.; Spek, A. L.; van Klink, G. P. M.; van Koten, G. *Organometallics* **2002**, *21*, 264–271.
193. Knapen, J. W. J.; van Dermade, A. W.; Dewilde, J. C.; van Leeuwen, P.; Wijkens, P.; Grove, D. M.; van Koten, G. *Nature* **1994**, *372*, 659–663.
194. Kreiter, R.; Kleij, A. W.; Gebbink, R.; van Koten, G. In *Dendrimers IV Dendritic catalysts* **2001**, *217*, 163–200.
195. Gossage, R. A.; Jastrzebski, J. T. B. H.; van Ameijde, J.; Mulders, S. J. E.; Brouwer, A. J.; Liskamp, R. M. J.; van Koten, G. *Tetrahedron Lett.* **1999**, *40*, 1413–1416.
196. Kleij, A. W.; Gossage, R. A.; Gebbink, R.; Brinkmann, N.; Reijerse, E. J.; Kragl, U.; Lutz, M.; Spek, A. L.; van Koten, G. *J. Am. Chem. Soc.* **2000**, *122*, 12112–12124.
197. Kleij, A. W.; Gebbink, R.; van den Nieuwenhuijzen, P. A. J.; Kooijman, H.; Lutz, M.; Spek, A. L.; van Koten, G. *Organometallics* **2001**, *20*, 634–647.
198. Dijkstra, H. P.; Steenwinkel, P.; Grove, D. M.; Lutz, M.; Spek, A. L.; van Koten, G. *Angew. Chem. Int. Ed.* **1999**, *38*, 2186–2188.
199. Eggeling, E. B.; Hovestad, N. J.; Jastrzebski, J.; Vogt, D.; van Koten, G. *J. Org. Chem.* **2000**, *65*, 8857–8865.
200. Gossage, R. A.; van DeKuil, L. A.; van Koten, G. *Acc. Chem. Res.* **1998**, *31*, 423–431.
201. Davies, P. J.; Grove, D. M.; van Koten, G. *Organometallics* **1997**, *16*, 800–802.
202. Beletskaya, I. P.; Chuchurjukin, A. V.; Dijkstra, H. P.; van Klink, G. P. M.; van Koten, G. *Tetrahedron Lett.* **2000**, *41*, 1081–1085.
203. Huck, W. T. S.; Snellink-Ruel, B.; van Veggel, F. C. J. M.; Reinhoudt, D. N. *Organometallics* **1997**, *16*, 4287–4291.
204. Huck, W. T. S.; Prins, L. J.; Fokkens, R. H.; Nibbering, N. M. M.; van Veggel, F. C. J. M.; Reinhoudt, D. N. *J. Am. Chem. Soc.* **1998**, *120*, 6240–6246.
205. van Manen, H. J.; Fokkens, R. H.; Nibbering, N. M. M.; van Veggel, F.; Reinhoudt, D. N. *J. Org. Chem.* **2001**, *66*, 4643–4650.
206. van Manen, H. J.; Nakashima, K.; Shinkai, S.; Kooijman, H.; Spek, A. L.; van Veggel, F.; Reinhoudt, D. N. *Eur. J. Inorg. Chem.* **2000**, 2533–2540.
207. Chessa, G.; Canovese, L.; Gemelli, L.; Visentin, F.; Seraglia, R. *Tetrahedron* **2001**, *57*, 8875–8882.
208. van Veggel, F. C. J. M.; Huck, W. T. S.; Reinhoudt, D. N. *Macromol. Symp.* **1998**, *131*, 165–173.
209. Huisman, B. H.; Schonherr, H.; Huck, W. T. S.; Friggeri, A.; van Manen, H. J.; Menozzi, E.; Vancso, G. J.; van Veggel, F.; Reinhoudt, D. N. *Angew. Chem. Int. Ed.* **1999**, *38*, 2248–2251.
210. Huck, W. T. S.; van Veggel, F. C. J. M.; Sheiko, S. S.; Moller, M.; Reinhoudt, D. N. *J. Phys. Org. Chem.* **1998**, *11*, 540–545.
211. Huck, W. T. S.; Hulst, R.; Timmerman, P.; van Veggel, F. C. J. M.; Fokkens, R. H.; Reinhoudt, D. N. *Angew. Chem. Int. Ed.* **1997**, *36*, 1006–1008.
212. Huck, W. T. S.; van Veggel, F. C. J. M.; Reinhoudt, D. N. *J. Mater. Chem.* **1997**, *7*, 1213–1219.
213. Huck, W. T. S.; van Veggel, F. C. J. M.; Reinhoudt, D. N. *Angew. Chem. Int. Ed.* **1996**, *35*, 1213–1215.

214. Huck, W. T. S.; van Veggel, F. C. J. M.; Kropman, B. L.; Blank, D. H. A.; Keim, E. G.; Smithers, M. M. A.; Reinhoudt, D. N. *J. Am. Chem. Soc.* **1995**, *117*, 8293–8294.
215. Storrier, G. D.; Takada, K.; Abruna, H. D. *Langmuir* **1999**, *15*, 872–884.
216. Takada, K.; Storrier, G. D.; Moran, M.; Abruna, H. D. *Langmuir* **1999**, *15*, 7333–7339.
217. Diaz, D. J.; Storrier, G. D.; Bernhard, S.; Takada, K.; Abruna, H. D. *Langmuir* **1999**, *15*, 7351–7354.
218. Amatore, C.; Bouret, Y.; Maisonhaute, E.; Goldsmith, J. I.; Abruna, H. D. *Chem. Eur. J.* **2001**, *7*, 2206–2226.
219. Takada, K.; Storrier, G. D.; Goldsmith, J. I.; Abruna, H. D. *J. Phys. Chem. B* **2001**, *105*, 2404–2411.
220. Bulte, J. W. M.; Wu, C. C.; Brechbiel, M. W.; Brooks, R. A.; Vymazal, J.; Holla, M.; Frank, J. A. *Invest. Radiol.* **1998**, *33*, 841–845.
221. Wu, C. C.; Brechbiel, M. W.; Kozak, R. W.; Gansow, O. A. *Bioorg. Med. Chem. Lett.* **1994**, *4*, 449–454.
222. Wiener, E. C.; Brechbiel, M. W.; Brothers, H.; Magin, R. L.; Gansow, O. A.; Tomalia, D. A.; Lauterbur, P. C. *Magn. Reson. Med.* **1994**, *31*, 1–8.
223. Wiener, E. C.; Auteri, F. P.; Chen, J. W.; Brechbiel, M. W.; Gansow, O. A.; Schneider, D. S.; Belford, R. L.; Clarkson, R. B.; Lauterbur, P. C. *J. Am. Chem. Soc.* **1996**, *118*, 7774–7782.
224. Toth, E.; Pubanz, D.; Vauthey, S.; Helm, L.; Merbach, A. E. *Chem. Eur. J.* **1996**, *2*, 1607–1615.
225. Fodor, F.; Kolmschot, S. G. A.; Sheldon, R. A. *Enantiomer* **1999**, *4*, 497–511.
226. Bardaji, M.; Slany, M.; Lartigue, M. L.; Caminade, A. M.; Chaudret, B.; Majoral, J. P. *Main Group Chem.* **1997**, *2*, 133–140.
227. Slany, M.; Caminade, A. M.; Majoral, J. P. *Tetrahedron Lett.* **1996**, *37*, 9053–9056.
228. Slany, M.; Bardaji, M.; Casanove, M. J.; Caminade, A. M.; Majoral, J. P.; Chaudret, B. *J. Am. Chem. Soc.* **1995**, *117*, 9764–9765.
229. Slany, M.; Bardaji, M.; Caminade, A. M.; Chaudret, B.; Majoral, J. P. *Inorg. Chem.* **1997**, *36*, 1939–1945.
230. Bardaji, M.; Kustos, M.; Caminade, A. M.; Majoral, J. P.; Chaudret, B. *Organometallics* **1997**, *16*, 403–410.
231. Lange, P.; Schier, A.; Schmidbaur, H. *Inorg. Chim. Acta* **1995**, *235*, 263–272.
232. Lange, P.; Schier, A.; Schmidbaur, H. *Inorg. Chem.* **1996**, *35*, 637–642.
233. Fan, Q. H.; Chen, Y. M.; Chen, X. M.; Jiang, D. Z.; Xi, F.; Chan, A. S. C. *Chem. Commun.* **2000**, 789–790.
234. Maraval, V.; Laurent, R.; Caminade, A. M.; Majoral, J. P. *Organometallics* **2000**, *19*, 4025–4029.
235. Miedaner, A.; Curtis, C. J.; Barkley, R. M.; Dubois, D. L. *Inorg. Chem.* **1994**, *33*, 5482–5490.
236. Reetz, M. T. *Top. Catal.* **1997**, *4*, 187–200.
237. Reetz, M. T. *J. Heterocycl. Chem.* **1998**, *35*, 1065–1073.
238. Reetz, M. T.; Lohmer, G.; Schwickardi, R. *Angew. Chem. Int. Ed.* **1997**, *36*, 1526–1529.
239. Benito, M.; Rossell, O.; Seco, M.; Segales, G. *J. Organomet. Chem.* **2001**, *619*, 245–251.
240. de Groot, D.; Reek, J. N. H.; Kamer, P. C. J.; van Leeuwen, P. *Eur. J. Org. Chem.* **2002**, 1085–1095.
241. Garber, S. B.; Kingsbury, J. S.; Gray, B. L.; Hoveyda, A. H. *J. Am. Chem. Soc.* **2000**, *122*, 8168–8179.
242. Hovestad, N. J.; Hoare, J. L.; Jastrzebski, J.; Canty, A. J.; Smeets, W. J. J.; Spek, A. L.; van Koten, G. *Organometallics* **1999**, *18*, 2970–2980.
243. Hoare, J. L.; Lorenz, K.; Hovestad, N. J.; Smeets, W. J. J.; Spek, A. L.; Canty, A. J.; Frey, H.; vanKoten, G. *Organometallics* **1997**, *16*, 4167–4173.
244. Zhou, M.; Roovers, J. *Macromolecules* **2001**, *34*, 244–252.
245. Zeng, H. D.; Newkome, G. R.; Hill, C. L. *Angew. Chem., Int. Ed. Engl.* **2000**, *39*, 1771–1774.
246. Murfee, H. J.; Thoms, T. P. S.; Greaves, J.; Hong, B. *Inorg. Chem.* **2000**, *39*, 5209–5217.
247. Newkome, G. R. *Pure Appl. Chem.* **1998**, *70*, 2337–2343.
248. Smith, D. K.; Diederich, F. In *Dendrimers II; Supramolecular Dendrimer Chemistry – A Journey through the branched architecture*. Springer-Verlag: Berlin, 2000; Vol. 210, 183–228.
249. Hecht, S.; Frechet, J. M. J. *Angew. Chem. Int. Ed.* **2001**, *40*, 74–91.
250. Brunner, H. *J. Organomet. Chem.* **1995**, *500*, 39–46.
251. Diederich, F.; Felber, B. *Proc. Natl. Acad. Sci. USA* **2002**, *99*, 4778–4781.
252. Dandliker, P. J.; Diederich, F.; Gisselbrecht, J. P.; Louati, A.; Gross, M. *Angew. Chem. Int. Ed.* **1995**, *34*, 2725–2728.
253. Dandliker, P. J.; Diederich, F.; Gross, M.; Knobler, C. B.; Louati, A.; Sanford, E. M. *Angew. Chem., Int. Ed. Engl.* **1994**, *33*, 1739–1742.
254. Dandliker, P. J.; Diederich, F.; Zingg, A.; Gisselbrecht, J. P.; Gross, M.; Louati, A.; Sanford, E. *Helv. Chim. Acta* **1997**, *80*, 1773–1801.
255. Zingg, A.; Felber, B.; Gramlich, V.; Fu, L.; Collman, J. P.; Diederich, F. *Helv. Chim. Acta* **2002**, *85*, 333–351.
256. Weyermann, P.; Diederich, F. *Helv. Chim. Acta* **2002**, *85*, 599–617.
257. Weyermann, P.; Diederich, F.; Gisselbrecht, J. P.; Boudon, C.; Gross, M. *Helv. Chim. Acta* **2002**, *85*, 571–598.
258. Weyermann, P.; Diederich, F. *J. Chem. Soc., Perkin Trans. 1* **2000**, 4231–4233.
259. Collman, J. P.; Fu, L.; Zingg, A.; Diederich, F. *Chem. Commun.* **1997**, 193–194.
260. Weyermann, P.; Gisselbrecht, J. P.; Boudon, C.; Diederich, F.; Gross, M. *Angew. Chem. Int. Ed.* **1999**, *38*, 3215–3219.
261. Bhyrappa, P.; Young, J. K.; Moore, J. S.; Suslick, K. S. *J. Mol. Catal. A: Chem.* **1996**, *113*, 109–116.
262. Bhyrappa, P.; Young, J. K.; Moore, J. S.; Suslick, K. S. *J. Am. Chem. Soc.* **1996**, *118*, 5708–5711.
263. Bhyrappa, P.; Vijayanthimala, G.; Suslick, K. S. *J. Am. Chem. Soc.* **1999**, *121*, 262–263.
264. Sen, J.; Suslick, K. S. *J. Am. Chem. Soc.* **2000**, *122*, 11565–11566.
265. Jiang, D. L.; Aida, T. *Chem. Commun.* **1996**, 1523–1524.
266. Jiang, D. L.; Aida, T. *J. Macromol. Sci., Pure Appl. Chem.* **1997**, *34*, 2047–2055.
267. Pollak, K. W.; Sanford, E. M.; Frechet, J. M. J. *J. Mater. Chem.* **1998**, *8*, 519–527.
268. Pollak, K. W.; Leon, J. W.; Frechet, J. M. J.; Maskus, M.; Abruna, H. D. *Chem. Mater.* **1998**, *10*, 30–38.
269. Vinogradov, S. A.; Lo, L. W.; Wilson, D. F. *Chem. Eur. J.* **1999**, *5*, 1338–1347.
270. Zhang, J. L.; Zhou, H. B.; Huang, J. S.; Che, C. M. *Chem. Eur. J.* **2002**, *8*, 1554–1562.
271. Kimura, M.; Nakada, K.; Yamaguchi, Y.; Hanabusa, K.; Shirai, H.; Kobayashi, N. *Chem. Commun.* **1997**, 1215–1216.
272. Kraus, G. A.; van der Louw, S. *J. Org. Chem.* **1998**, *63*, 7520–7521.
273. Kimura, M.; Sugihara, Y.; Muto, T.; Hanabusa, K.; Shirai, H.; Kobayashi, N. *Chem. Eur. J.* **1999**, *5*, 3495–3500.
274. McKeown, N. B. *Adv. Mater.* **1999**, *11*, 67–69.

275. McKeown, N. B. *J. Mater. Chem.* **2000**, *10*, 1979–1995.
276. Sadamoto, R.; Tomioka, N.; Aida, T. *J. Am. Chem. Soc.* **1996**, *118*, 3978–3979.
277. Vögtle, F.; Plevoets, M.; Nieger, M.; Azzellini, G. C.; Credi, A.; De Cola, L.; De Marchis, V.; Venturi, M.; Balzani, V. *J. Am. Chem. Soc.* **1999**, *121*, 6290–6298.
278. Chow, H. F.; Chan, I. Y. K.; Fung, P. S.; Mong, T. K. K.; Nongrum, M. F. *Tetrahedron* **2001**, *57*, 1565–1572.
279. Hannon, M. J.; Mayers, P. C.; Taylor, P. C. *J. Chem. Soc., Perkin Trans. 1* **2001**, 1881–1889.
280. Tzalis, D.; Tor, Y. *Tetrahedron Lett.* **1996**, *37*, 8293–8296.
281. Kimura, M.; Shiba, T.; Muto, T.; Hanabusa, K.; Shirai, H. *Tetrahedron Lett.* **2000**, *41*, 6809–6813.
282. Serroni, S.; Campagna, S.; Juris, A.; Venturi, M.; Balzani, V. *Gazz. Chim. Ital.* **1994**, *124*, 423–427.
283. Issberner, J.; Vögtle, F.; De Cola, L.; Balzani, V. *Chem. Eur. J.* **1997**, *3*, 706–712.
284. Armaroli, N.; Boudon, C.; Felder, D.; Gisselbrecht, J. P.; Gross, M.; Marconi, G.; Nicoud, J. F.; Nierengarten, J. F.; Vicinelli, V. *Angew. Chem. Int. Ed.* **1999**, *38*, 3730–3733.
285. Nierengarten, J. F.; Felder, D.; Nicoud, J. F. *Tetrahedron Lett.* **1999**, *40*, 273–276.
286. Gorman, C. B. *Adv. Mater.* **1997**, *9*, 1117–1119.
287. Gorman, C. B.; Hager, M. W.; Parkhurst, B. L.; Smith, J. C. *Macromol.* **1998**, *31*, 815–822.
288. Gorman, C. B.; Smith, J. C.; Sachdeva, R.; Su, W. Y.; Jiang, H. W. *Macromol. Symp.* **2000**, *156*, 61–67.
289. Gorman, C. B.; Smith, J. C.; Hager, M. W.; Parkhurst, B. L.; Sierzputowska-Gracz, H.; Haney, C. A. *J. Am. Chem. Soc.* **1999**, *121*, 9958–9966.
290. Gorman, C. B.; Parkhurst, B. L.; Su, W. Y.; Chen, K. Y. *J. Am. Chem. Soc.* **1997**, *119*, 1141–1142.
291. Gorman, C. B.; Su, W. Y.; Jiang, H. W.; Watson, C. M.; Boyle, P. *Chem. Commun.* **1999**, 877–878.
292. Wang, R. Y.; Zheng, Z. P. *J. Am. Chem. Soc.* **1999**, *121*, 3549–3550.

# 7.7

## Supramolecular Systems: Templating

J.-P. COLLIN, C. DIETRICH-BUCHECKER, C. HAMANN,  
D. JOUVENOT, J.-M. KERN, P. MOBIAN, and J.-P. SAUVAGE  
*Université Louis Pasteur, Strasbourg, France*

---

7.7.1	INTRODUCTION	303
7.7.2	[2]CATENANES	304
7.7.2.1	Templated Syntheses of [2]Catenanes	304
7.7.2.2	<sup>1</sup> H NMR and Mass Spectrometries of Metal-free Catenane (1) and Copper [2]Catenane Cu(1) <sup>+</sup>	306
7.7.2.3	X-ray Structures of [2]Catenanes	307
7.7.3	[3]CATENANES AND MOLECULAR NECKLACES	310
7.7.3.1	The Eight-reacting-centers Approach	311
7.7.3.2	The Four-reacting-centers Approach	312
7.7.3.3	Molecular Necklaces	314
7.7.4	[2]CATENANES OBTAINED BY RING-CLOSING METATHESIS (RCM)	314
7.7.5	SYNTHESIS OF INTERLOCKING RINGS USING TWO DIFFERENT TRANSITION METALS AS TEMPLATING AND CONNECTING CENTERS: RuCu(20.4) <sup>3+</sup> , RuZn(20.4) <sup>4+</sup> , AND RuAg(20.4) <sup>3+</sup> CATENANES	318
7.7.6	TEMPLATE SYNTHESIS OF A 5-COORDINATE ZINC(II) CATENANE, THE CORRESPONDING CATENAND, AND RELATED COPPER(II) AND IRON(II) COMPLEXES	319
7.7.7	[2]CATENANE CONSTRUCTED AROUND A Ru(DIIMINE) <sub>3</sub> <sup>2+</sup> DERIVATIVE USED AS A TEMPLATE	322
7.7.8	CONCLUSION	322
7.7.9	REFERENCES	325

---

### 7.7.1 INTRODUCTION

A few decades ago, Schill and co-workers could make catenanes using very elegant but long synthetic routes.<sup>1</sup> Although their characterization techniques were fully convincing, with crucial mass spectroscopy experiments in particular,<sup>2</sup> the compounds could not, unfortunately, be characterized by X-ray structures. One of the [2]catenanes made was crystallized and a poor-quality X-ray diffraction pattern was obtained, leading to a low-quality structure which was never published.<sup>3</sup> In parallel with the important work done by the German group, Wasserman had detected catenanes, following a statistical strategy which obviously did not afford more than minute amounts.<sup>4</sup> This approach, published more than 40 years ago, was not efficient enough to allow the isolation of crystals, and X-ray structure studies were totally out of the scope of this contribution.

At the beginning of the 1980s, the situation changed dramatically when transition metals were proposed as templates to construct interlocking rings in an efficient way, following very short strategies.<sup>5,6</sup> Within a few years, the first X-ray structure was published, making these exotic species real molecules in the chemist's mind. This was the start of a second life for these compounds. Purely organic catenanes were made, thanks to the introduction of elegant routes

based on new templating principles (organic acceptor–donor interactions and hydrogen bonding).<sup>7–10</sup> Evidently the distance between Schill's work and the present situation, with virtually hundreds of catenanes described in the literature, is considerable. Not only has the synthesis of catenanes been dramatically improved by the many groups who have now joined the field, but numerous catenanes have been crystallized and studied by X-ray diffraction. In this respect, the work of Stoddart and his co-workers represents a particularly impressive contribution, also thanks to the associative work carried out with Williams and his group.<sup>11</sup>

The present chapter will be mostly concerned with the catenanes made in Strasbourg since about 1980. Some of the most important synthetic aspects will be discussed. A relatively large number of catenanes could be crystallized, and the structural features of these compounds will also be considered.

In the first section, we will mention the early work done in the authors' group, which led to a copper(I)-complexed [2]catenane in a preparative fashion and the corresponding ligand ("catenand"). A few X-ray structures (complexes and free catenane) will illustrate this section.

Multiring interlocking systems will be considered in the second section. Remarkable X-ray structures will be included, especially those of a free [3]catenane and of a dicopper(I) complex.

The third part will be devoted to the most recent synthetic developments based on Grubbs ring-closing metathesis (RCM) reaction. From various precursors bearing terminal olefins, interesting topologies could be obtained, and in particular interlocking-ring systems.

Transition metals have also been used to form the cyclic components of [2]catenanes. In this case, two different transition metals are used: (i) a gathering metal (copper(I)); and (ii) a "clipping" metal (divalent metal centre). This approach will be discussed in the fourth section.

The fifth and the sixth parts will be devoted to recent work based on templating metal centers other than copper(I). Five-coordinated systems constructed around  $Zn^{2+}$  will be considered in the fifth section, whereas the use of octahedral  $M(\text{diimine})_3^{2+}$  as templates will be the topic of the sixth and last chapter.

## 7.7.2 [2]CATENANES

### 7.7.2.1 Templated Syntheses of [2]Catenanes

Transition metals, with their ability to gather and dispose ligands in a given predictable geometry, can induce what is generally called a "template effect." This specific property has been widely used for the template synthesis of various macrocycles, one of the earliest examples probably being Reppe's cyclooctatetraene synthesis, in which a nickel atom is supposed to bring together four acetylene molecules around it prior to cyclotetramerization.<sup>12</sup> This section is devoted to the synthesis of the copper [2]catenane **Cu(1)**<sup>+</sup> by applying the 3-D template synthesis around a transition metal and to the corresponding metal-free assembly of two interlocked rings, the catenane (**1**) (Figure 1).<sup>5,6</sup>

To obtain interlocked rings, two strategies (Figure 2) are possible: both of them require that the ligands set around the metallic centre are adequate molecular threads which can be converted into rings in later stages. The straightforward strategy A involves simultaneous pairwise connection between eight reacting centres. Strategy B implies the preliminary synthesis of a chelating macrocycle, but the final cyclization step involves only the connection of four reacting centres.

Although strategy B is longer than strategy A, it offers the advantage of a step-by-step procedure, and this less risky route was tried first.<sup>5</sup> It is noteworthy that the first step of route B, i.e., the threading of a macrocycle by a linear molecule, is common for synthetic approaches leading either to metallo catenanes, and particularly to unsymmetrical catenanes<sup>13,14</sup> or to metallo rotaxanes.<sup>15</sup> The one-step procedure, method A, was nevertheless explored with real success in later experiments.<sup>6</sup> Most crucial is the choice of the different subunits: the nature of the coordinating fragment, the nature of the transition metal, the length of the link g–g. In the synthesis of **Cu(1)**<sup>+</sup> described here, and for most of the catenanes synthesized later in our group, the coordinating core is based on 2,9-diphenyl-1,10-phenanthroline (dpp). Combining  $Cu^I$  ions and dpp fragments proved to be an ideal association for a templated synthesis of catenanes. Indeed, in the presence of  $Cu^I$ , dpp forms a pseudotetrahedral complex of high stability<sup>16</sup> in which two dpp units fit in around the metal center.<sup>17</sup> The only additional requirement to use copper(I) complexes with such topography as building blocks was the possibility of functionalizing the ligands beyond their coordination sites. 2,9-dianisylphenanthroline (**2**) is easily converted



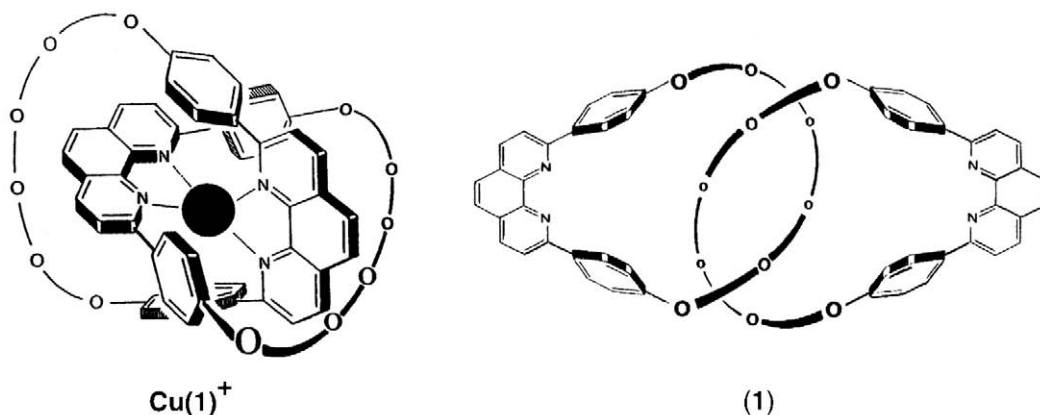


**Figure 1** Schematic representation of copper catenane  $\text{Cu}(\mathbf{1})^+$  and free catenane ( $\mathbf{1}$ ). In  $\text{Cu}(\mathbf{1})^+$  the two highly rigid coordinating subunits fit together while encaging the metal atom, leading to pronounced intramolecular  $\text{H}\cdots\text{H}$  interactions between the phen nucleus of a macrocycle subunit and one anisyl moiety of the other. In the free ligand ( $\mathbf{1}$ ), the two phen fragments are fully disentangled.

### Strategy A

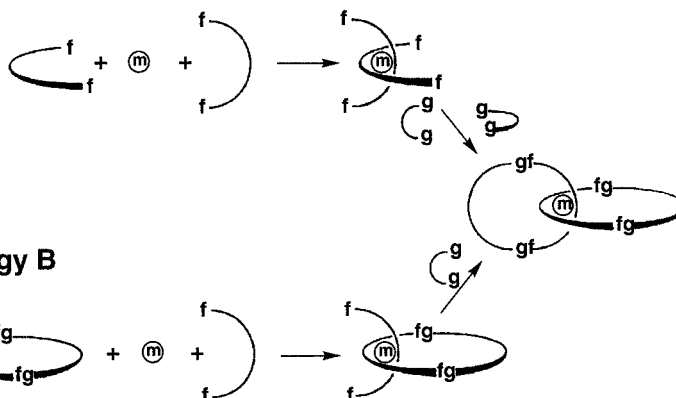


**Figure 2** Principle of the synthesis of interlocked ring systems. The strategy is based on a 3D-template effect induced by a transition metal. The molecular fragment f–f interacts with a transition metal (circle). f and g represent chemical functions able to react and form an f–g chemical bond.

to the nucleophilic 2,9-bis(*p*-hydroxyphenyl)-1,10-phenanthroline ( $\mathbf{3}$ ). Therefore ( $\mathbf{2}$ ) can be considered as the “universal precursor” of dpp-based copper catenanes (Figure 3).<sup>18</sup>

The archetype of the family of copper [2]catenanes,  $\text{Cu}(\mathbf{1})^+$  was thus synthesized using  $\text{Cu}^{\text{I}}$  as a 3-D template and 2,9-bis(*p*-hydroxyphenyl)-1,10-phenanthroline ( $\mathbf{3}$ ) as ligand. Strategy B implied the preparation of the preliminary 30-membered macrocycle ( $\mathbf{4}$ ). This was achieved by reacting ( $\mathbf{3}$ ) with the diiodo derivative of pentaethyleneglycol ( $\mathbf{5}$ ) (fragment g–g in Figure 2).<sup>5,18</sup> The threading of macrocycle ( $\mathbf{4}$ ) onto ( $\mathbf{3}$ ) was done quantitatively by mixing stoichiometric amounts of ( $\mathbf{3}$ ), ( $\mathbf{4}$ ), and  $\text{Cu}(\text{CH}_3\text{CN})_4\text{BF}_4$ . The resulting stable catenane precursor  $\text{Cu}(\mathbf{3.4})^+$  was reacted with the equivalent amount of the dihalide ( $\mathbf{5}$ ) in DMF containing a large excess of  $\text{Cs}_2\text{CO}_3$ . The copper catenane  $\text{Cu}(\mathbf{1})^+$  was obtained as nice red needles in a 42% yield with respect to ( $\mathbf{4}$ ).<sup>5</sup> Subsequently the same catenane was prepared following strategy A, i.e., the one-step procedure:<sup>6</sup>  $\text{Cu}(\mathbf{3})_2^+$  was here obtained quantitatively by mixing one equivalent of  $\text{Cu}(\text{CH}_3\text{CN})_4\text{BF}_4$  and two equivalents of ( $\mathbf{3}$ ). Reaction of  $\text{Cu}(\mathbf{3})_2^+$  with the same fragment g–g led to  $\text{Cu}(\mathbf{1})^+$  in 27% yield. At this stage, the first gram-scale preparation of a [2]catenane was achieved and the way was open to the access, by a directed strategy, to a fascinating new family of molecules.

Nevertheless, the reaction conditions required by strategy A, as well as strategy B, for the nucleophilic displacement of the halide ions in fragment g–g are a barrier to increasing spectacularly the yield of the catenation reaction. Indeed, the stability of the precatenane species  $\text{Cu}(\mathbf{3.4})^+$  or  $\text{Cu}(\mathbf{3})_2^+$  in basic medium is rather limited, especially at high temperature. A new approach was developed later, which utilizes a

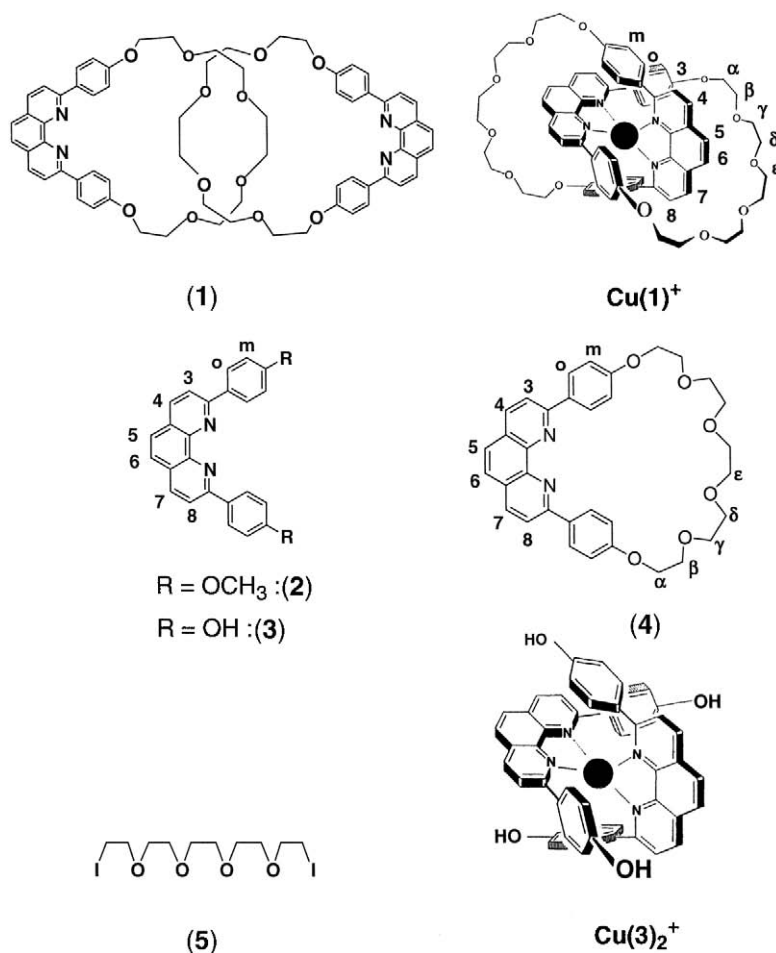


**Figure 3** Molecular representation of **Cu(1)<sup>+</sup>** and **(1)**, and of their precursors.

combination of the same transition-metal-based template strategy described above and the efficient approach to macrocyclic systems displayed by ring-closing metathesis (RCM). This spectacular enhancement of the efficiency of the catenation reaction, which allowed access to molecular systems of high topological complexity, will be described in the third section.

The metal free [2]catenane **(1)** was obtained quantitatively by treatment of **Cu(1)<sup>+</sup>** with tetramethylammonium cyanide in acetonitrile-water, or by potassium cyanide in dichloromethane-water.

### 7.7.2.2 <sup>1</sup>H NMR and Mass Spectrometries of Metal-free Catenane **(1)** and Copper [2]Catenane **Cu(1)<sup>+</sup>**

The highly characteristic mass spectrometry pattern of interlocked rings has already been described by Schill *et al.*<sup>2</sup> Except for the molecular ion peak, no fragmentation occurs until the molecular peak of the monomeric ring is reached. After the first fragmentation, the mechanical link between the two subunits no longer exists; the linear part is threaded out from the intact remaining ring, and both species undergo further fragmentations.

<sup>1</sup>H NMR studies clearly showed the entwined topography of **Cu(1)<sup>+</sup>** and also demonstrated that a complete conformational change occurs during the decomplexation process leading from the copper(I) catenane **Cu(1)<sup>+</sup>** to the metal-free catenane **(1)**: the two dpp fragments fit in together in **Cu(1)<sup>+</sup>**. Consequently, due to the ring current effect of the phenanthroline nucleus, the signals corresponding to protons H<sub>o</sub>, H<sub>m</sub>, and CH<sub>2α</sub> appear at a higher field (7.37, 6.02, and 3.62, respectively) than the corresponding protons in the free macrocycle **(4)**. After decomplexation, the two phenanthroline subunits separate and chemical shifts for H<sub>o</sub>, H<sub>m</sub>, and CH<sub>2α</sub> are close to those expected, i.e., to those of **(4)** (Figure 4).

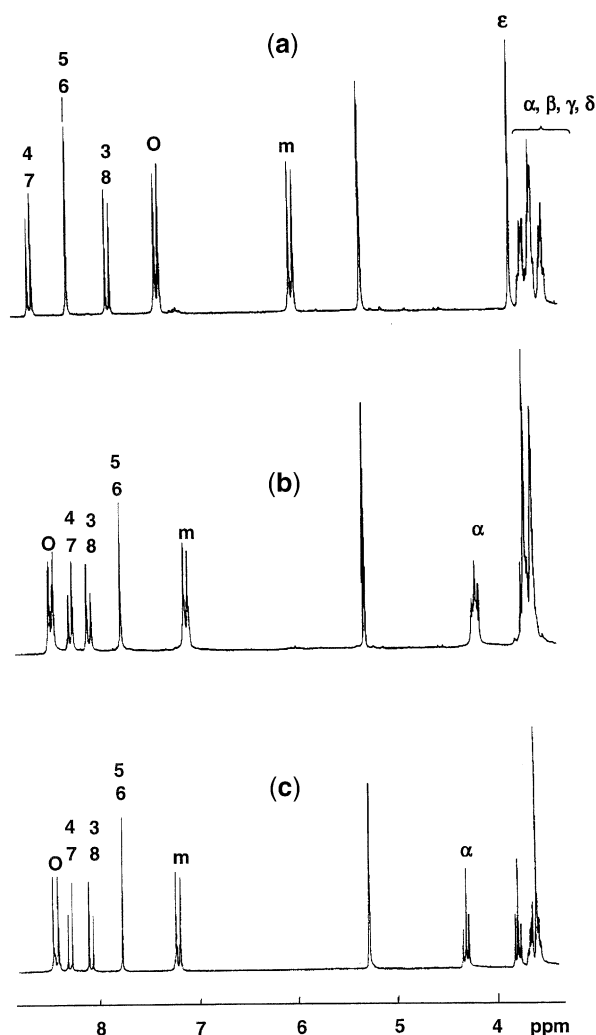


**Figure 4** 200 MHz  $^1\text{H}$  NMR spectra of (a) copper [2]catenane **Cu(1)** $^+$ ; (b) the free ligand (**1**); (c) the 30-membered macrocycle (**4**).

### 7.7.2.3 X-ray Structures of [2]Catenanes

The structural information displayed by  $^1\text{H}$  NMR and by X-ray studies is in perfect agreement. **Figure 5** represents the first X-ray structures of a metallo [2]catenane (**Figure 5a**) and a free [2]catenane (**Figure 5b**).<sup>19</sup> The interlocking of the two macrocycles in **Cu(1)** $^+$  is obvious in **Figure 5a**. The N–Cu distances range from 2.0 Å to 2.09 Å. The two phenanthroline nuclei are far from being perpendicular to one another, their dihedral angle being ca. 60°. The chelate bite angle of the phenanthroline ligand imposes two N–Cu–N angle values of ca. 83° to 136°. This pronounced distortion around the copper atom might originate from charge-transfer interactions between the phen nucleus of a macrocyclic subunit and one anisyl moiety of the other. Indeed (see **Figure 5**), each phen nucleus is almost parallel to one of the phenyl groups attached on the other phen nucleus. The corresponding dihedral angles are close to 7° and 11°, respectively. The phenanthroline ( $\pi$ -acceptor) to phenyl ( $\pi$ -donor) distance is ca. 3.35 Å: these interactions induce the noticeable up-field shift observed by  $^1\text{H}$  NMR for the protons of the phenyl groups (*vide supra*). In **Cu(1)** $^+$ , the two macrocycles are connected via the templating agent. Removal of this agent releases the two rings from each other and the molecular shape of the metal-free [2]catenane (**1**) becomes totally different (**Figure 5b**). The two phenanthroline fragments are fully disentangled and are ca. 11.2 Å apart. Each dpp subunit is almost planar, in contrast to the copper [2]catenane **Cu(1)** $^+$ . Aromatic nuclei intermolecular stacking interactions exist as in **Cu(1)** $^+$ , but only between free catenane (**1**) molecules related by inversion centres. The packing forces probably influence the molecular assembly within the crystal.<sup>19</sup>

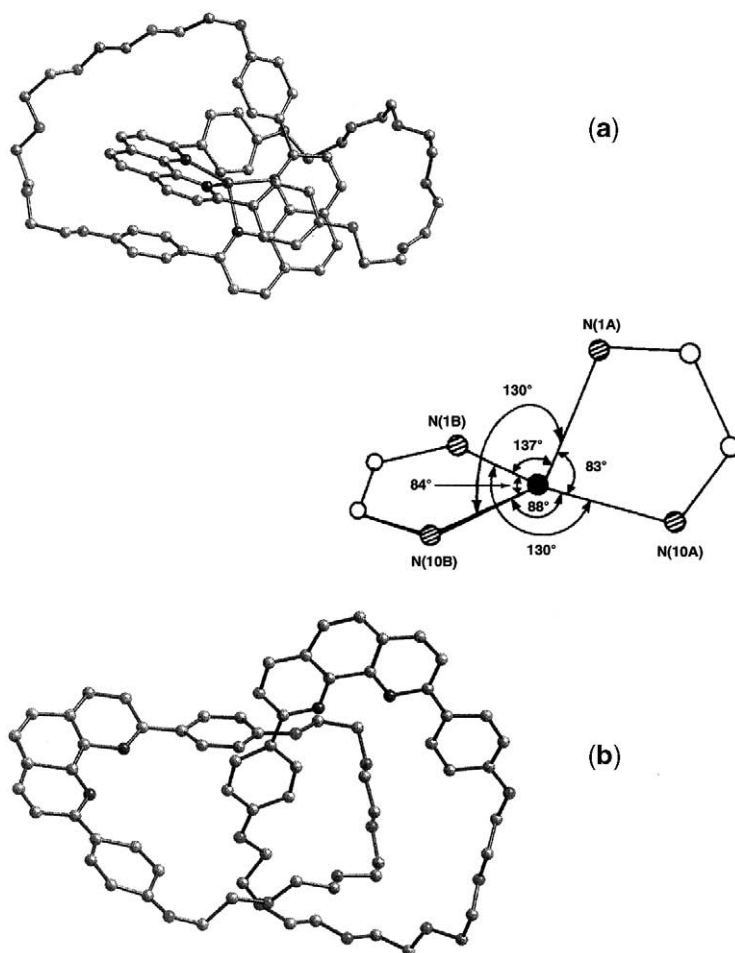


**Figure 5** (a) Molecular structure of the copper [2]catenane  $\text{Cu}(\mathbf{1})^+$  and the co-ordination polyhedron of  $\text{Cu}^+$ ; (b) Structure of the free catenane ( $\mathbf{1}$ ).

The recomplexation of the free [2]catenane ( $\mathbf{1}$ ) by copper(I) can be carried out quantitatively. This means that the rearrangement of the molecular geometry is reversible when going from the copper catenane, in which the two coordinated macrocycles are connected via the metal, to the assembly, in which the gliding of single interlocked rings is not prevented. It is noteworthy, in contrast to many complexing agents which are preorganized in a conformation appropriate to the interaction with a given substrate, that the [2]catenane ( $\mathbf{1}$ ) has no geometrical analogy with its corresponding complex, the metallo [2]catenane  $\text{Cu}(\mathbf{1})^+$ , although the stability<sup>16</sup> and the kinetic inertness<sup>20</sup> are extremely high. Due to the flexibility of ( $\mathbf{1}$ ), a series of metallo [2]catenanes could be synthesized.<sup>21</sup> In the particular case of nickel, it was possible to discriminate between the respective contributions of the metal and the ligand set to the overall structures of  $\text{Ni}(\mathbf{1})^+$  and  $\text{Ni}(\mathbf{1})^{2+}$ .<sup>22</sup> Indeed, nickel(I) and nickel(II) catenanes offer a nice example in which the geometry of the coordination polyhedron is governed either by the central atom [ $\text{Ni}^{\text{I}}$ ] or by internal charge-transfer interactions [ $\text{Ni}^{\text{II}}$ ]. Electrochemical measurements<sup>23</sup> evidenced a spectacular stabilization of the +1 oxidation state in  $\text{Ni}(\mathbf{1})^+$ , and X-ray structures showed noticeable differences in the arrangement of the macrocycles around the metals in  $\text{Ni}(\mathbf{1})^+$  and  $\text{Ni}(\mathbf{1})^{2+}$  (Figure 6).

The coordination polyhedron of  $\text{Ni}(\mathbf{1})^+$  is directly comparable to  $\text{Cu}(\mathbf{1})^+$ , with a dihedral angle between the two phenanthrolines of  $65^\circ$ . By contrast, the coordination polyhedron around  $\text{Ni}^{\text{I}}$  is significantly less distorted. For  $\text{Ni}(\mathbf{1})^+$ , whose  $d^9$  electronic configuration was confirmed by EPR,<sup>21,23</sup> no stacking interactions are observed and the aromatic rings attached to the phenanthroline nuclei are bent: the nickel(I) center imposes a tetrahedral geometry at the expense of the organic backbone. Conversely, electronic factors common to both the metal and the ligand set are involved in explaining the propensity of  $\text{Ni}(\mathbf{1})^{2+}$  to form intramolecular  $\pi$ - $\pi$  stacks: distortion of

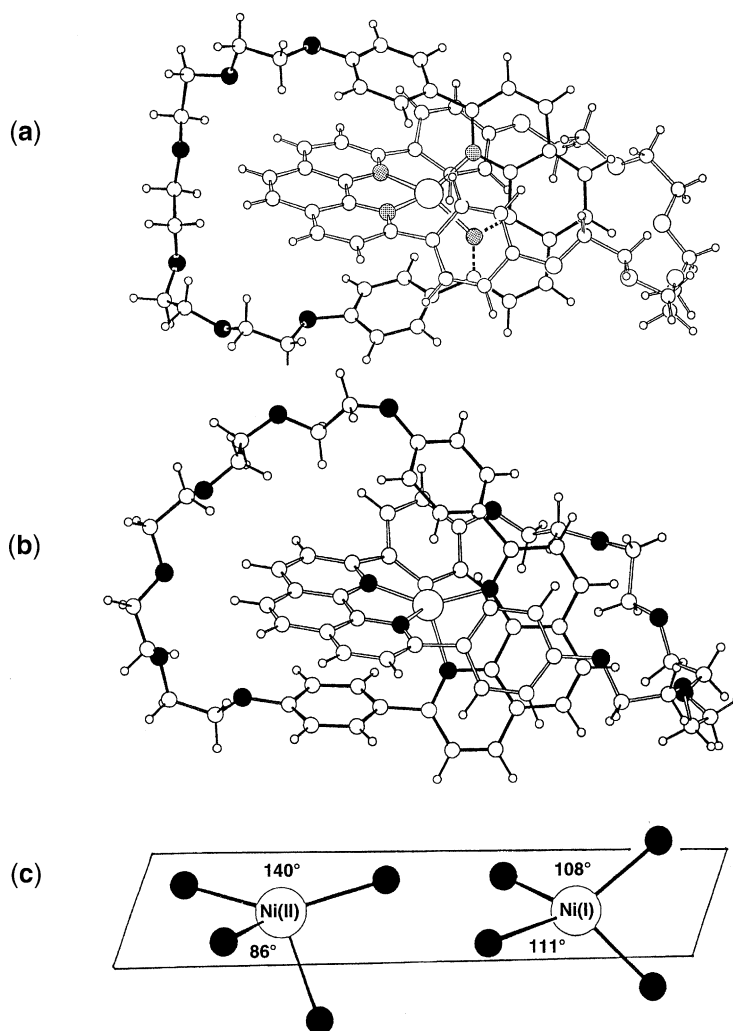


**Figure 6** (a) Ortep representation of the nickel(I) catenane; (b) Ortep representation of the nickel(II) catenane with the same orientation as for  $\text{Ni(1)}^+$  in Figure 6a; (c) Coordination around the metal center: (left) in divalent nickel catenane  $\text{Ni(1)}^{2+}$ , (right) in monovalent nickel catenane  $\text{Ni(1)}^+$ .

the tetrahedral coordination of the metal will stabilize  $\text{Ni}^{\text{II}}$ , simultaneously allowing intramolecular stacking interactions to take place between the anisyl-type nuclei and the phen units.

Monoprotonation of the free ligand (**1**) leads to a relative arrangement of the rings similar to that observed in  $\text{Cu(1)}^+$  or in  $\text{Ni(1)}^{2+}$ .<sup>24</sup> Here too, the two phenanthroline rings are facing each other with a dihedral angle of  $61^\circ$ , as illustrated in Figure 7.

A particular stacking is observed between a given phenanthroline ring and a phenyl group borne by the other phenanthroline: phen A and phen B are roughly parallel to ph2B and ph1A, respectively (dihedral angle  $25\text{--}10^\circ$ ). The internal stacking of the aromatic rings within  $\text{Cu(1)}^+$  and  $\text{H(1)}^+$  is also nearly the same, with very similar dihedral angles except for a larger deviation from parallelism in  $\text{H(1)}^+$  than in  $\text{Cu(1)}^+$ . This intramolecular interaction reflects the donor character of the phenyl groups but, moreover, it shows that by single protonation both phenanthroline nuclei become sufficiently electron accepting in nature to interact with the electron-donor phenyl rings.  $^1\text{H}$  NMR studies have been performed and showed that the solid-state structure of  $\text{H(1)}^+$  also corresponds to the geometry of the molecule in solution. In addition, these studies allowed the evaluation of the basicity of (**1**). Surprisingly, a great difference in basicity was observed between catenane (**1**) ( $\text{p}K_{\text{a}_1} = 8.5$ ) and (**2**) ( $\text{p}K_{\text{a}_1} = 5.1$ ), the open-chain analogue of (**1**), whereas (**1**) and (**2**) display the same electronic properties and have the same shape. Consequently, the high basicity of (**1**) originates mainly from the topology of the molecule: whereas  $\text{H(2)}^+$  is a normal phenanthroline ion,  $\text{H(1)}^+$  is highly stabilized by intramolecular stacking. Thus the acceptor–donor interaction occurring between the phenanthroline nuclei and the phenyl rings accounts for the

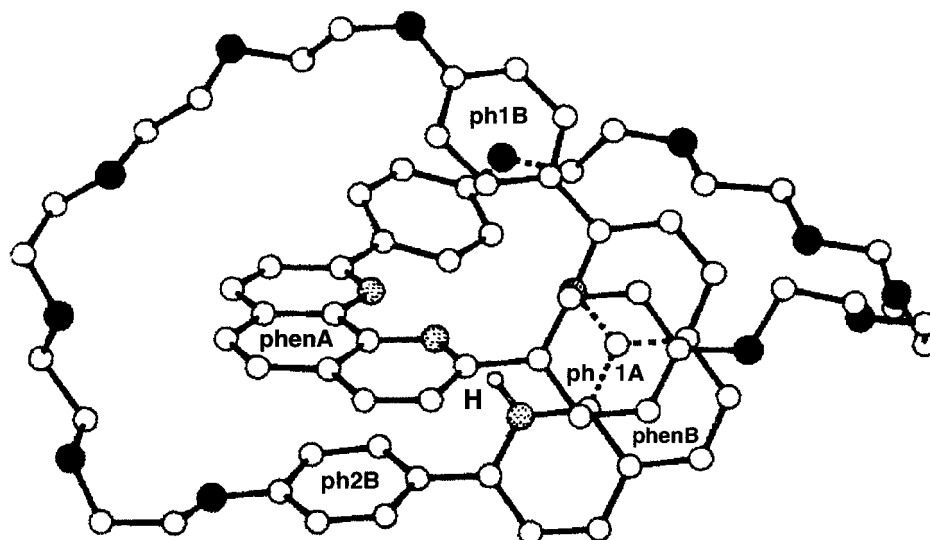


Figure 7 Molecular structure of the proton catenane  $\mathbf{H(1)^+}$ .

noticeable stabilization of  $\mathbf{H(1)^+}$  and of the dpp-based [2]catenanes in general. Moreover, second protonation of  $\mathbf{(1)}$  does not lead to the disentanglement of the two dpp units with subsequent formation of the catenane in which the two phenanthroline are each monoprotonated. This observation demonstrates that donor–acceptor interactions occurring in the monoprotonated catenane are strong enough to force the second proton to come close to the first one. The magnitude of such a stabilization effect was determined by comparing the acidity of the diprotonated catenane,  $\mathbf{HH(1)^{2+}}$  ( $pK_{a_2} \sim 1.5$ ), to that of the independent dpp fragment  $\mathbf{H(2)^+}$  ( $pK_a = 5.1$ ): the topological factor, i.e., the stabilization of the particular topography by interlocking the two rings of the proton catenane with respect to a second protonation, is thus  $\sim 5.4 \text{ kcal mol}^{-1}$ .

The above section describes the pioneering work which opened the route to the synthesis of interlocked rings, i.e., catenanes. The displayed X-ray structures of the prototypical free [2]catenane and of some metallo catenanes allow one to visualize the interlocking of the coordinating macrocycles, the intramolecular interactions responsible for the overall structures, and to understand their particular behavior (such as electrochemical properties, enhancement of basicity, etc.) due to their topography and to their topology.

### 7.7.3 [3]CATENANES AND MOLECULAR NECKLACES

After the syntheses of [2]catenanes based on one metal, the next most logical step was to prepare multiring interlocked systems containing several metal centers. Not only may these systems provide simple ways for building di- or polynuclear species with a strictly controlled arrangement of photo- and electroactive centers, suitable for long-range electron-transfer studies, but they were also highly challenging, topologically nontrivial molecular objects.

But if a [2]catenane is the simplest element of the family of compounds formed by interlocked rings, the complexity of the systems and the number of possibilities increase rapidly with the number of rings to be interlocked. For example, with three rings, there are already numerous combinations, the most accessible one being the [3]catenane (chain-like arrangement) which may simply be considered as the sum of two [2]catenanes. The synthesis of a chain made of three interlocked rings ([3]catenane) was first achieved by Schill and his co-workers in 1969.<sup>25</sup> More recently, Stoddart and co-workers could also obtain purely organic [3]catenanes by taking advantage of the template effect induced by organic acceptor–donor interactions. Their new templating principle allowed them even to have access to a [5]catenane, the most famous “olympiadane.”<sup>26,27</sup>

Considering the efficiency of the 3D-template effect induced by transition metals in the synthesis of [2]catenanes, we tried to generalize our concept for obtaining [3]catenanes. Still relying on the copper(I)/1,10-phenanthroline couple, we could develop two different strategies.

### 7.7.3.1 The Eight-reacting-centers Approach

The building principle given in Figure 8 clearly shows that dimerization leading to a [3]catenane may occur only if the linking fragment used in the cyclization step is too short to allow intramolecular ring formation. Such a prerequisite could be fulfilled by a short chain, such as the dibromo derivative of tetraethylene glycol. Reaction of precursor  $\text{Cu}(\mathbf{3.4})^+$  (obtained from a 1:1:1 mixture of the 30-membered macrocycle (**4**), diphenol (**3**), and  $\text{Cu}(\text{CH}_3\text{CN})_4^+$ ) with this short linker, under conditions similar to those used in the [2]catenane synthesis, afforded, although in a very poor 2% yield, the expected dinuclear [3]catenane  $\text{CuCu}(\mathbf{5})^{2+}$  (Figure 9).<sup>28</sup>

Demetalation of  $\text{CuCu}(\mathbf{5})^{2+}$  by KCN gave access to the free ligand (**6**), for which mass spectroscopy and  $^1\text{H}$  NMR studies first evidenced that it was indeed made of three rings: two peripheral 30-membered rings interlocked with a central 54-membered one. The assumed [3]catenane topology for ligand (**6**) was fully confirmed when its crystal structure could be determined by X-ray diffraction (Figure 10).<sup>29</sup>

Comparison between the information given by the NMR studies and the crystallographic studies showed a remarkable agreement between the conformation of the molecule in solution and its topography in the solid state. The intramolecular stacking interactions, clearly shown by the molecular structure of Figure 10, are approximately kept in solution ( $\text{CD}_2\text{Cl}_2$ ). In the crystal, the 1,10-phenanthroline subunits of the two lateral 30-membered rings are parallel and are stacked with a short interplane distance (3.34 Å). The large central ring adopts a chair-like conformation and the  $-(\text{CH}_2\text{CH}_2\text{O})_3-$  unit folds, forming two molecular hollows with the 30-membered rings in which  $\text{CH}_2\text{Cl}_2$  molecules (not represented on the figure) embed themselves.

Leading to the very first crystallographic structure of a [3]catenane, the eight-reacting-centers approach was successful, but nevertheless very disappointing because of the tedious purification processes and the very poor yields obtained, even by varying the length of the linker used in the last cyclization step: a maximum 6% yield could be obtained for the [3]catenane (30-48-30).<sup>28</sup> Therefore, the study of the specific electrochemical and photophysical properties of [3]catenanes being prohibited because of the small amounts available, we developed a more efficient procedure based on acetylenic oxidative coupling (Glaser reaction).<sup>30,31</sup>

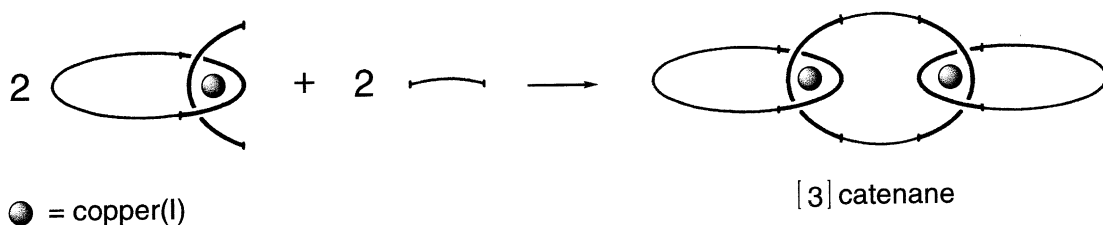


**Figure 8** Principle of template synthesis of a [3]catenane. Copper(I) holds the two coordination fragments (thick line) perpendicular to one another. The cyclization involves two additional short linear links (thin line) and requires the connection of eight reacting center.

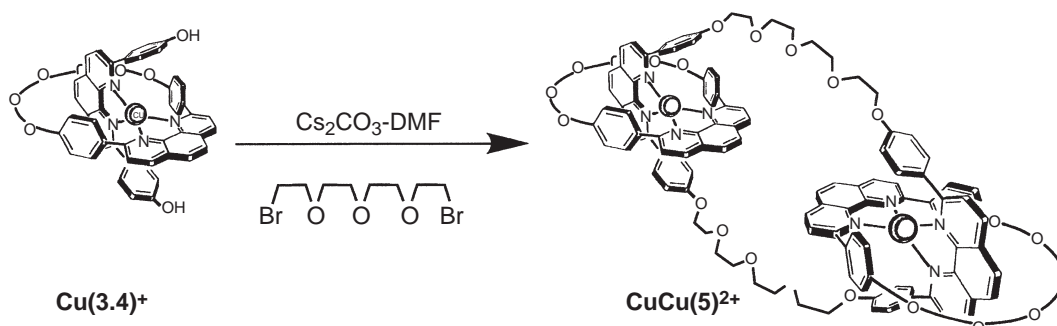


**Figure 9** Synthesis of catenane  $\text{CuCu}(\mathbf{5})^{2+}$  (30-54-30) from the diphenolic precursor  $\text{Cu}(\mathbf{3.4})^+$ .

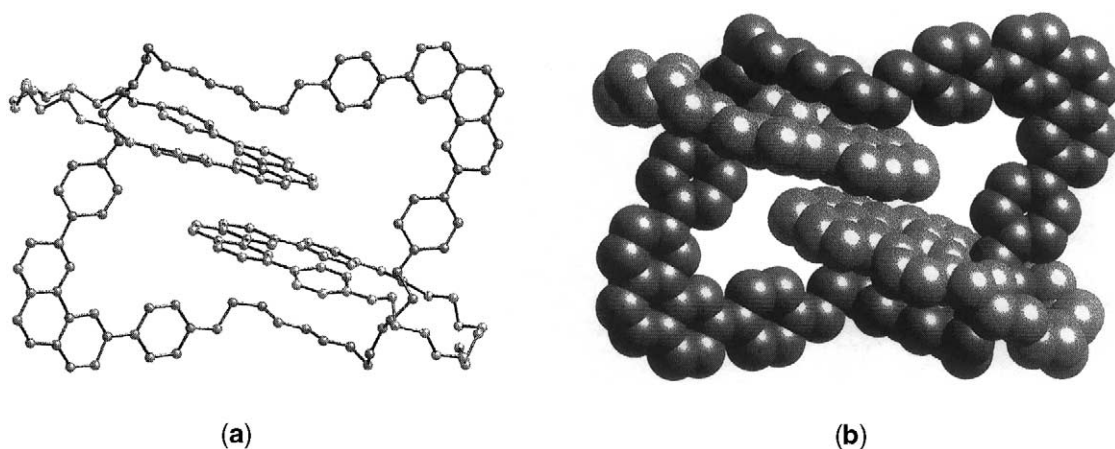


**Figure 10** Molecular structure of the metal-free [3]catenane (**6**), consisting of a central 54-membered ring and two 30-membered peripheral rings stacking via their aromatic parts.

### 7.7.3.2 The Four-reacting-centers Approach

This new approach, whose principle is depicted in **Figure 11**, corresponds to a true cyclodimerization involving four reacting centers only, in contrast to the above synthesis that required eight centers to be linked.

The precursors used and the reaction conditions are represented in **Figure 12**. Precursor complex **Cu(4.7)<sup>+</sup>** was obtained quantitatively by mixing stoichiometric amounts of the 30-membered macrocycle (**4**),  $\text{Cu}(\text{MeCN})_4^+\text{BF}_4^-$ , and a phenanthroline-based, open-chain diyne (**7**) in  $\text{CH}_2\text{Cl}_2\text{-MeCN}$ . The oxidative acetylenic coupling (Glaser reaction) performed in DMF at room temperature was surprisingly efficient. In its previous applications to the synthesis of macrocycles,<sup>32-35</sup> rigid paracyclophanes,<sup>36,37</sup> or cage-like compounds,<sup>38</sup> fine control of the experimental conditions was crucial, and this was also true in the present case. After the near 0% yield in the first attempt, the (30-44-30) [3]catenane **CuCu(8)<sup>2+</sup>** was finally obtained in 58% yield by careful control of solvent (dry DMF), temperature (ambient), amounts of copper(I) and copper(II) salts (140 and 25 equivalents respectively), presence of oxygen (compulsory), and concentration (1 mmol of **Cu(4.7)<sup>+</sup>** in 150 mL DMF). Besides **CuCu(8)<sup>2+</sup>**, another catenane was obtained in 22% yield. Based on <sup>1</sup>H NMR and mass spectroscopic studies, the latter compound could be identified as the trimetallic complex formed by cyclotrimerization of **Cu(4.7)<sup>+</sup>**, consisting of four interlocked rings: a central hexayne 66-membered ring, and three peripheral rings (**4**).<sup>39</sup>

The crystallographic study of **CuCu(8)<sup>2+</sup>** and the detailed <sup>1</sup>H NMR solution study, carried out in parallel, demonstrated that **CuCu(8)<sup>2+</sup>** has a geometry dramatically different from that given in **Figure 12**.<sup>40</sup>

As shown in **Figure 13**, the molecular shape of **CuCu(8)<sup>2+</sup>** is compacted and globular, with a distance of only 8.0 Å between the copper(I) centers, whereas in an expanded arrangement this distance would have been over 12 Å. The large central ring is folded up, bringing the 1,10-phenanthroline rings into a parallel arrangement, 7.7 Å apart. The diacetylenic chains are also parallel to one another and located 10.5 Å apart. The phenyl rings of the central cycle consist of two pairs of nearly parallel nuclei. The peripheral 30-membered rings are placed as bracelets in an approximately parallel fashion. Each aromatic ring of the molecular system is in close contact with another one (distance less than 3.5 Å), a rough parallelism being observed. All the phenyl rings are rotated around their link to their respective 1,10-phenanthroline nucleus, the average

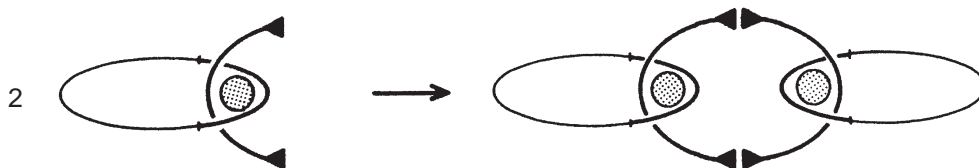


**Figure 11** Principle of the four-reacting centre approach to [3]catenanes. The black triangle represents a terminal acetylenic function able to react with itself in a Glaser oxidative coupling reaction.



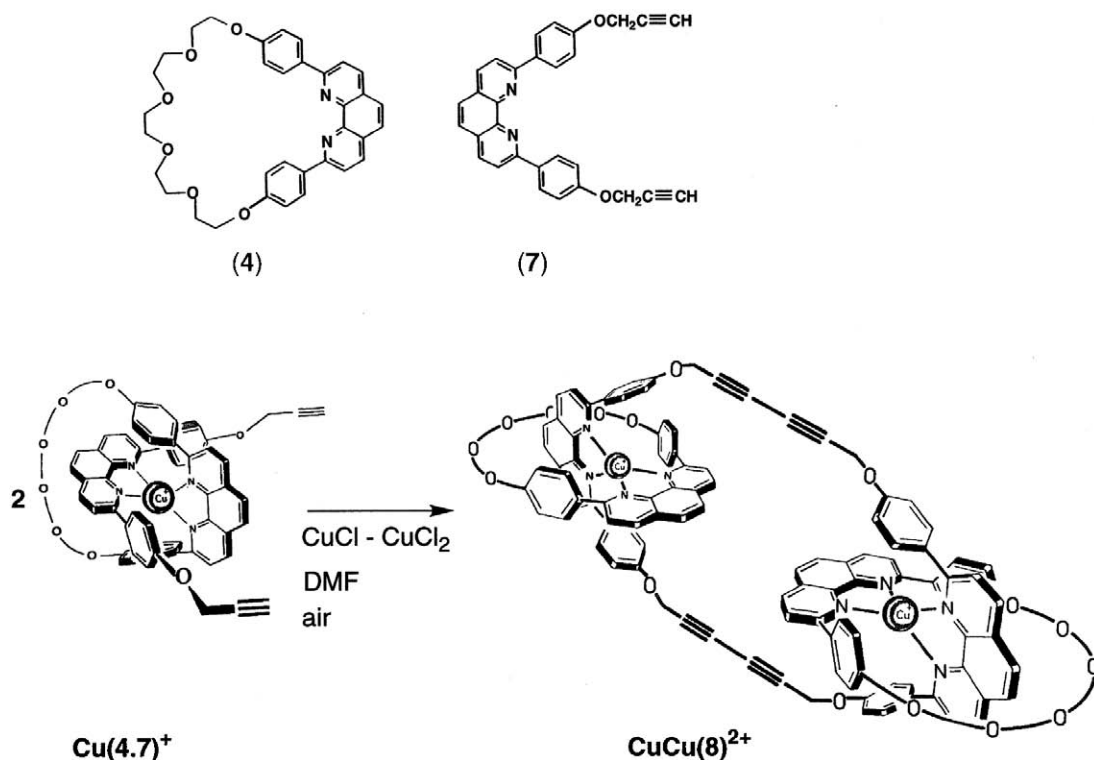


Figure 12 Precursors and reaction scheme leading to the [3]catenane **CuCu(8)<sup>2+</sup>** (30-44-30).

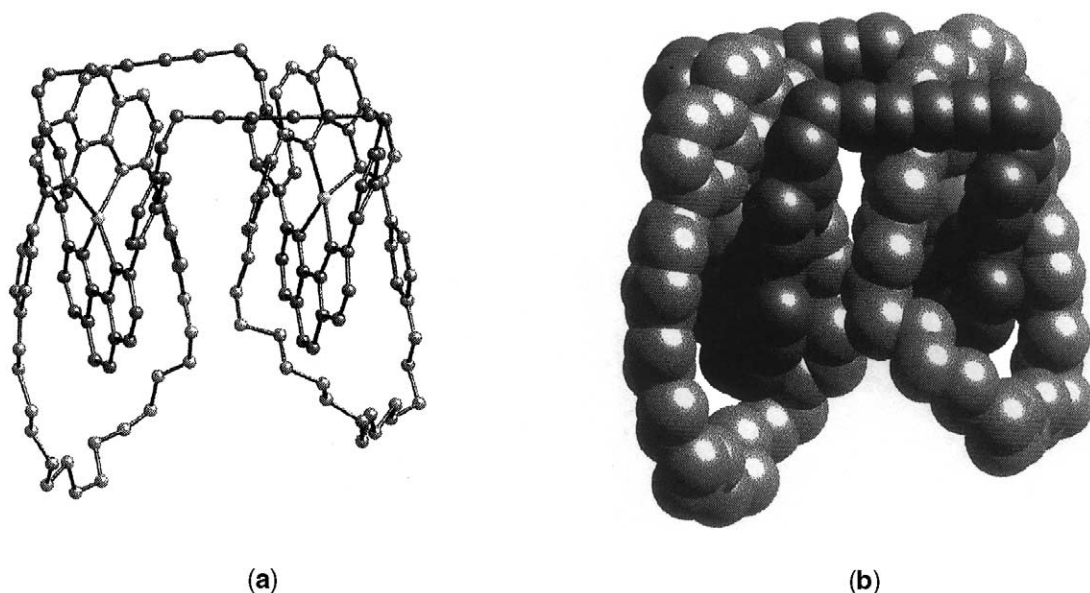


Figure 13 X-ray structure of the dicopper(I) [3]catenane **CuCu(8)<sup>2+</sup>** showing the folding of the large central 44-membered ring.

torsion angle being 43°. The curling up of **CuCu(8)<sup>2+</sup>** and the proximity of the two copper(I) complex subunits could also be detected by <sup>1</sup>H NMR solution measurements. In particular, the up-field shift of given H atoms as compared to the corresponding signals of the same fragments in the [2]catenane **Cu(1)<sup>+</sup>** could be explained only by a curled-up geometry. The analogy between the molecular shapes in the solid state and in solution was also confirmed by the observation of nuclear Overhauser effects (NOE) between certain protons of the 44-membered ring and the peripheral cycles. The folding up of the central ring and the subsequent globular shape of the

molecule might be explained by stabilizing  $\pi$ -interactions between the aromatic rings belonging to the two copper binding sites. It is noteworthy that the “ternary” structure of  $\text{CuCu}(\mathbf{8})^{2+}$  (by analogy to proteins) is stable enough to be maintained in solution.

The [3]catenane  $\text{CuCu}(\mathbf{8})^{2+}$  could be demetalated at room temperature by potassium cyanide, either completely or only partially, affording thus the free ligand ( $\mathbf{8}$ ) or the mononuclear complex  $\text{Cu}(\mathbf{8})^+$  containing a vacant site ready for coordination. Ligand ( $\mathbf{8}$ ) could be easily remetalated with various salts, giving thus access to the homodinuclear [3]catenanes  $\text{AgAg}(\mathbf{8})^{2+}$ ,  $\text{ZnZn}(\mathbf{8})^{4+}$ ,  $\text{CoCo}(\mathbf{8})^{4+}$ , and  $\text{NiNi}(\mathbf{8})^{4+}$ .<sup>41</sup> The 8.0 Å Cu–Cu distance found in the X-ray structure of  $\text{CuCu}(\mathbf{8})^{2+}$  being rather long, strong electronic interactions between the two metal centers were not expected. Nevertheless, since the space between the metal centers was filled up with stacking aromatic nuclei in the folded conformation, we thought that some interesting effects (of one complex subunit on the properties of the other) could be observed. This prompted us to study the electronic properties of the various symmetrical dimetallic [3]catenanes and to compare them with those previously obtained for the corresponding [2]catenanes designed by  $\text{M}(\mathbf{1})^{n+}$ . On the other hand, with the aim of inducing electron transfer from one site (MLCT excited state of one copper(I) subcomplex) to the other, we prepared the heterodinuclear [3]catenanes  $\text{CuAg}(\mathbf{8})^{2+}$ ,  $\text{CuCo}(\mathbf{8})^{3+}$ , and  $\text{CuZn}(\mathbf{8})^{2+}$ .<sup>42</sup>

Electrochemical studies showed that a long-range, ground-state, electrostatic interaction existed between the two subunits, whereas the photophysical studies could mainly show evidence of a dramatic luminescence quenching of one of the two moieties, mostly due either to an energy transfer or to an electron transfer.<sup>43</sup>

### 7.7.3.3 Molecular Necklaces

Having obtained a trimetallic complex, in addition to the expected cyclodimer  $\text{CuCu}(\mathbf{8})^{2+}$ , when applying the strategy of Figure 11 to the diyne precursor complex  $\text{Cu}(\mathbf{4.7})^+$ , suggested the formation of even higher homologues according to the general scheme given in Figure 14.

Multiple oxidative coupling of  $(n+1)$  precursors should lead to a whole family of cyclooligomers in which  $(n+1)$  peripheral rings are interlocked to a large polyacetylenic central cycle. Thanks to an extensive electrospray mass spectrometry (ESMS) study, such multiring systems—real molecular necklaces—could indeed be identified, the small peripheral rings being either 30-membered or 27-membered.<sup>44,45</sup> Both series gave almost similar results, so that the description of the various catenates observed (from  $n=1$  to  $n=5$ ) will be restricted in Figure 15a to the family containing 27-membered peripheral rings.

A chromatographic separation on silica gel afforded  $(\mathbf{9}^{2+})$ ,  $(\mathbf{10}^{3+})$ , and  $(\mathbf{11}^{4+})$  as pure isolated  $\text{BF}_4^-$  salts, whereas the higher homologues  $(\mathbf{12}^{5+})$  and  $(\mathbf{13}^{6+})$  could be identified only from a mixture. All these compounds are deep red, glassy solids which display very similar  $^1\text{H}$  NMR properties, identical elemental analyses, and thus could be distinguished from one another only by mass spectrometry. Yields and molecular weights are given in Figure 15a.

### 7.7.4 [2]CATENANES OBTAINED BY RING-CLOSING METATHESIS (RCM)

Since the development of template strategies based on transition metals, acceptor–donor organic complexes, and hydrogen-bonded precursors, interlocking rings became much more accessible, as testified by the many reports devoted to them since the mid-1980s. However, the ultimate cyclization reaction(s) affording the desired catenanes was often still a limiting step, leading to only moderate yields. So far, among the many cyclization reactions available, C–N and C–O bond

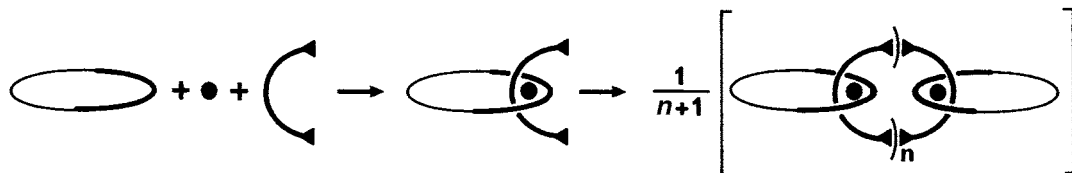
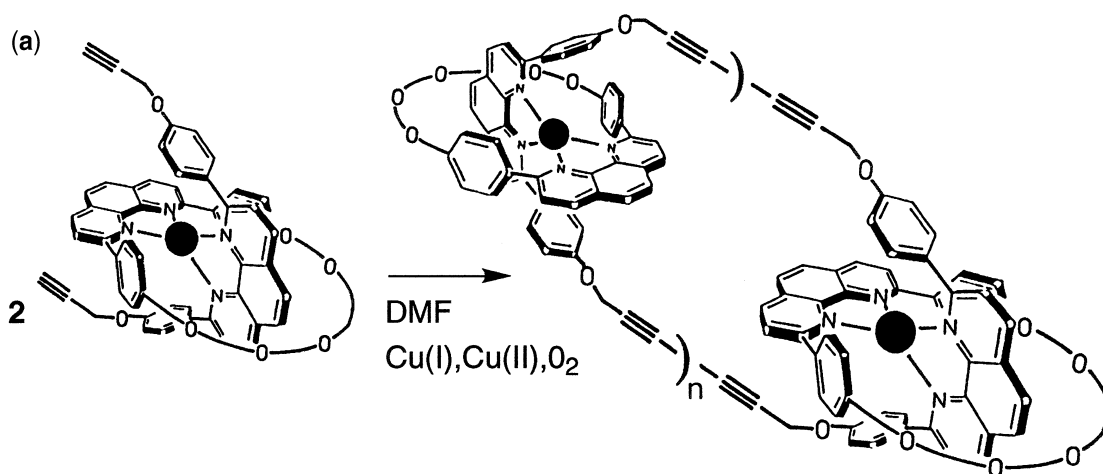


**Figure 14** Template synthesis of multiring catenanes. The coordination fragments are drawn in thick lines and the triangles represent the terminal acetylenic functions. The systems obtained are made of  $n+1$  peripheral rings interlocked to a large central ring resulting from a cyclooligomerization process.



	Compound	Yield	MW
$n = 1$	[3]catenane <b>9</b> <sup>2+</sup>	23%	2222.9
$n = 2$	[4]catenane <b>10</b> <sup>3+</sup>	23%	3333.3
$n = 3$	[5]catenane <b>11</b> <sup>4+</sup>	16%	4444.7
$n = 4$	[6]catenane <b>12</b> <sup>5+</sup>	13%	5557.2
$n = 5$	[7]catenane <b>13</b> <sup>6+</sup>	13%	6668.6

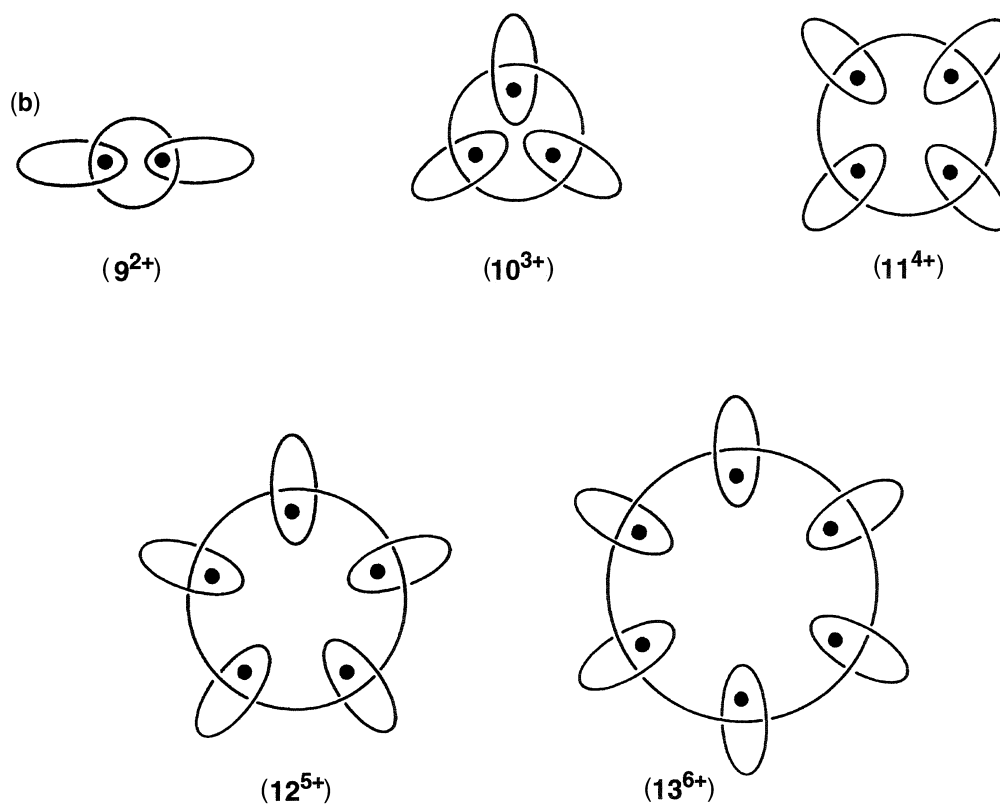


**Figure 15** (a) Precursor and reaction scheme leading to the multicatenanes (**9**<sup>2+</sup>) to (**13**<sup>6+</sup>); (b) Schematic diagrams of the molecular necklaces (**9**<sup>2+</sup>) to (**13**<sup>6+</sup>).

formations have been used in preference to C—C coupling reactions, even if they did not fully satisfy an essential requirement: ring-forming reactions should be mild enough to avoid any dissociation of the precursor complex. Ring-closing metathesis (RCM), which has been developed during the past decade as a particularly efficient methodology for making macrocyclic compounds by intramolecular formation of carbon–carbon double bonds in very mild conditions, appeared also to be very attractive for the obtaining of catenanes.<sup>46–51</sup> The ruthenium benzylidene catalyst—or Grubbs catalyst—which is easy to handle, tolerant to a large variety of chemical functions, and operative in neutral medium ( $\text{CH}_2\text{Cl}_2$ ) at room temperature, seemed particularly promising.

To test this new methodology, we used once more copper(I) as a gathering and orienting center, the molecular strings to be intertwined or threaded through a presynthesized macrocycle being end-functionalized by olefinic groups. The principle of this catenane synthesis is described in Figure 16, whereas the organic precursors and the compounds prepared by this methodology are depicted in Figure 17.<sup>52,53</sup>

By reacting the 30-membered macrocycle (**4**) with stoichiometric amounts of  $\text{Cu}(\text{CH}_3\text{CN})_4^+$ ,  $\text{PF}_6^-$ , and the coordinating open-chain unit (**14**) (obtained by reacting diphenol (**3**) in basic media successively with 2-(2-chloroethoxy)ethanol and allylbromide), the threaded system  $\text{Cu}(\mathbf{4.14})^+$  was formed quantitatively. Complex  $\text{Cu}(\mathbf{4.14})^+$  was submitted to intramolecular RCM with catalyst (**15**) ((**15**) =  $\text{Cl}_2(\text{PCy}_3)_2\text{Ru}=\text{CHPh}$ , Cy = Cyclohexyl, Ph = Phenyl) to afford the [2]catenane  $\text{Cu}(\mathbf{16})^+$  in extremely good yield (90%). The [2]catenane  $\text{Cu}(\mathbf{16})^+$  contains, besides the 30-membered ring, a 32-membered olefinic ring in which the newly formed double bond is mostly *trans*. It should be mentioned here that a similar excellent yield was obtained for the [2]catenane made of the 30-membered ring and a larger, 38-membered olefinic cycle. Demetalation of these copper[2]-catenanes with potassium cyanide afforded the free ligands (**18**) and (**19**) in almost quantitative yield.  $^1\text{H}$  NMR and FAB mass spectroscopy performed for all these compounds allowed their unambiguous characterization and confirmed their catenane topology.

Even more surprising was the efficiency of the one-pot synthesis represented in Figure 17b. The intertwined complex  $\text{Cu}(\mathbf{14.14})^+$  was formed quantitatively by reacting  $\text{Cu}(\text{CH}_3\text{CN})_4^+.\text{PF}_6^-$  with two equivalents of (**14**). A twofold RCM reaction in  $\text{Cu}(\mathbf{14.14})^+$  led exclusively to the [2]catenane  $\text{Cu}(\mathbf{17})^+$ , which contains two olefinic 32-membered rings (90% yield). Its demetalation afforded, in almost quantitative yield, the corresponding free ligand.

The remarkable efficiency of these RCM reactions pointed to this new cyclization methodology as an attractive and versatile approach for the synthesis of more complex catenanes and knots. Due to the very mild and highly preservative conditions in which RCM reactions occur, the latter compounds could be obtained by using much weaker templates (lithium or iron) than copper (I).<sup>54,55</sup>

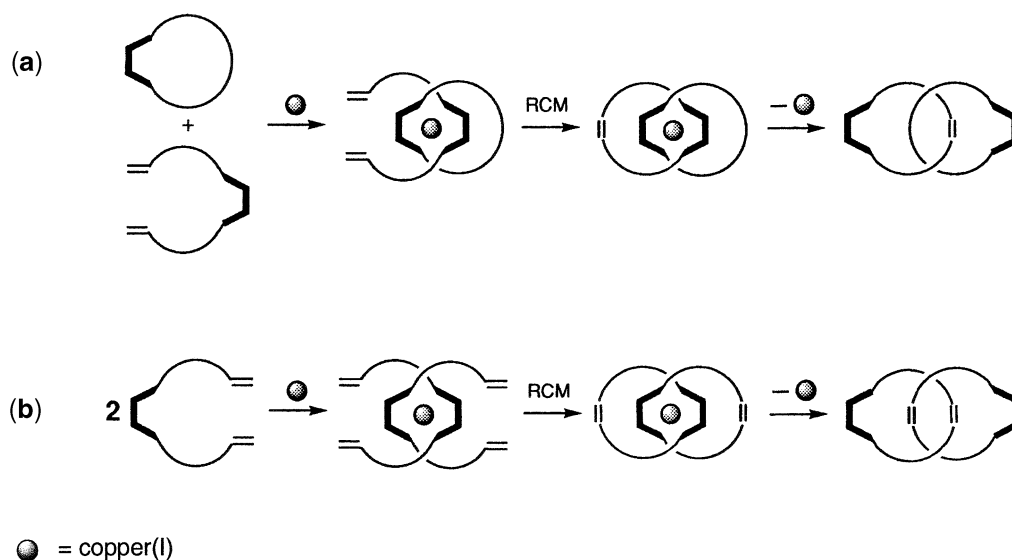


**Figure 16** Principle of [2]catenanes syntheses utilizing a transition-metal-based template strategy and RCM: (a) The two-step approach involving one RCM process; (b) The one-pot approach involving two simultaneous RCM processes.

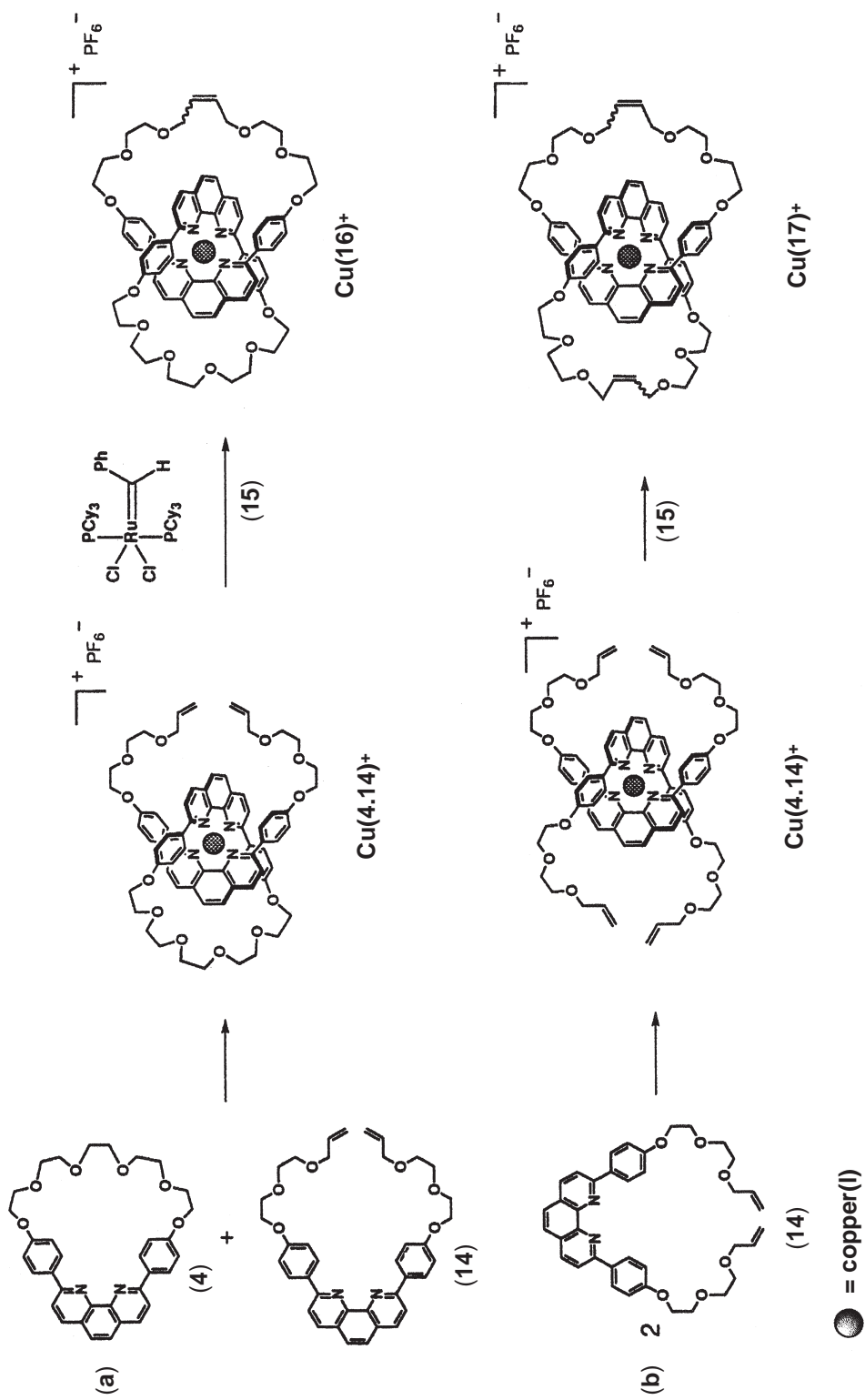


Figure 17 Syntheses of (a) [2]catenane Cu(16)<sup>+</sup> following the threading route; (b) [2]catenane Cu(17)<sup>+</sup> by the entwining strategy.

### 7.7.5 SYNTHESIS OF INTERLOCKING RINGS USING TWO DIFFERENT TRANSITION METALS AS TEMPLATING AND CONNECTING CENTERS: $\text{RuCu(20.4)}^{3+}$ , $\text{RuZn(20.4)}^{4+}$ , AND $\text{RuAg(20.4)}^{3+}$ CATENANES

The preparation of catenane  $\text{RuCu(20.4)}^{3+}$  containing two different types of transition metals is shown in Figure 18.

Copper(I) was used as a template to thread a polyfunctional string (20), containing a dpp moiety and two tpy ligands on its ends, into a dpp-containing, 30-membered macrocycle (4), while forming regioselectively a 4-coordinate pseudotetrahedral  $\text{Cu(dpp)}_2$  complex, the two dpp subunits adopting an intertwined structure.  $\text{Ru}^{\text{II}}$  was subsequently used to effect a macrocyclization (“clipping” reaction) on the intertwined precursor, by coordinating to the two free tpy moieties in a highly stable  $\text{Ru(tpy)}_2$  complex. Due to the different kinetic stability of both complexes, copper(I) could be selectively removed without affecting the Ru complex by reaction with KCN in  $\text{MeCN-H}_2\text{O}$ , leading to catenane  $\text{Ru(20.4)}^{2+}$  with a free tetrahedral coordination site.<sup>56</sup> The bimetallic complexes  $\text{RuZn(20.4)}^{4+}$  and  $\text{RuAg(20.4)}^{3+}$  were also easily made by mixing stoichiometric amounts of the appropriate metal salt and  $\text{Ru(DMSO)}_4\text{Cl}_2$ , followed by anion exchange with  $\text{KPF}_6$ . Both catenanes were obtained as red, crystalline solids. The ORTEP drawings for complexes  $\text{RuCu(20.4)}^{3+}$  and  $\text{RuAg(20.4)}^{3+}$  are depicted in Figures 19 and 20 respectively.

The  $\text{Ru(tpy)}_2^{2+}$  fragments show the usual distorted octahedral geometry. The observed bond distances and angles lie within the range usually shown by this type of complex,<sup>57,58</sup> which reflects the absence of distortion as compared to similar complexes, in spite of the geometrical restriction imposed by the inclusion of the complex in a macrocycle. This implies that the length of the spacers between the coordinating fragments is enough to allow the existence of a nondistorted, interlocked structure. The main differences between the two bimetallic complexes are observed in

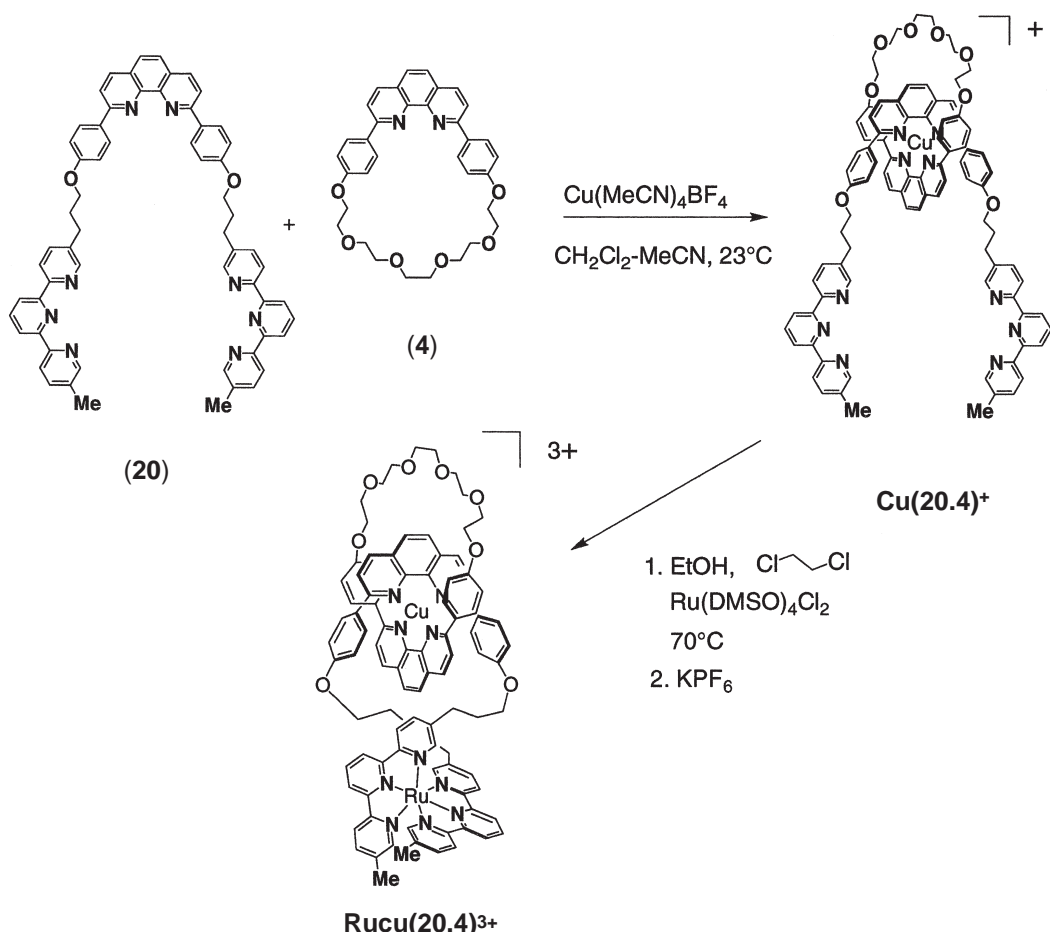
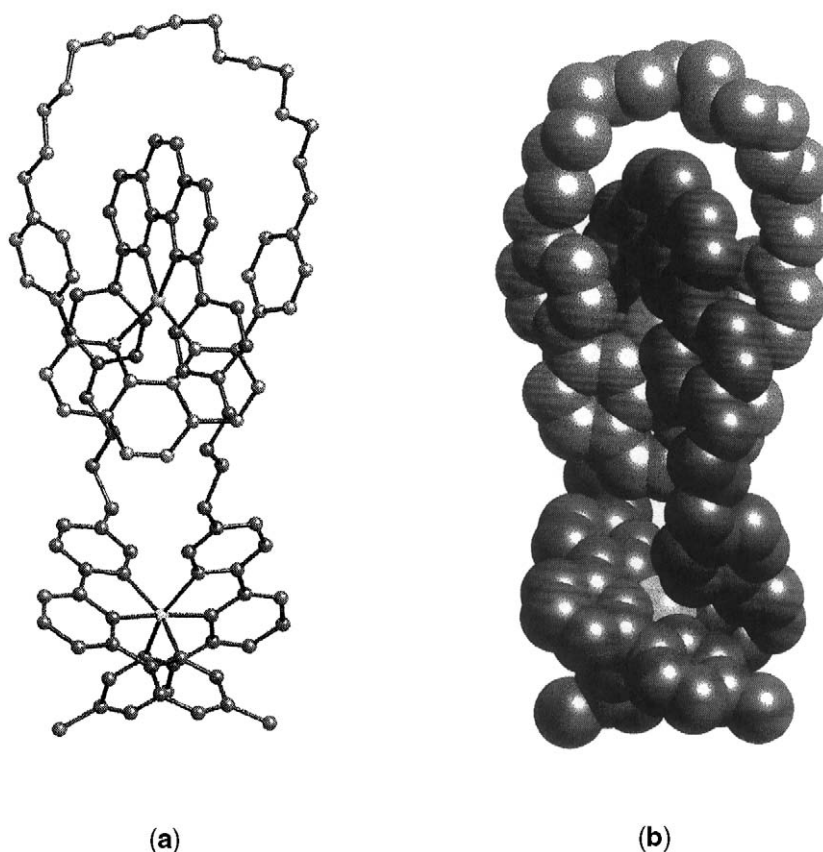


Figure 18 Synthesis of the catenane  $\text{RuCu(20.4)}^{3+}$  by a clipping coordination reaction.



**Figure 19** X-ray structure of the catenane **RuCu(20.4)<sup>3+</sup>**. (a) Balls and sticks representation; (b) Space-filling representation.

the  $M(dpp)_2^+$  fragment. In both cases distorted tetrahedral geometries around the metal centers are observed, but the degree of distortion is different according to the different radii of  $Cu^I$  and  $Ag^I$ .<sup>59</sup> As a consequence of the larger size of  $Ag^I$ , the angle  $N-Ag-N$  for  $N$  atoms belonging to the same  $dpp$  ligand ( $71.3(3)-73.3(3)^\circ$ ) is smaller than the corresponding bite angle of the  $Cu$  complex ( $81.9(2)^\circ$ ), and the dihedral angles between the mean planes of  $dap$  ligands are, respectively, equal to  $62.5(1)^\circ$  and  $85.9(1)^\circ$ . This has been observed when the crystal structures of  $Cu^I$  and  $Ag^I$  complexes of other phenanthroline-type ligands are compared.<sup>60,61</sup> The  $Cu-N$  bond distances ( $2.03-2.04 \text{ \AA}$ ) are similar to those observed for related complexes,<sup>62</sup> and smaller than the corresponding for the  $Ag^I$  derivative ( $2.316(7)-2.367(7) \text{ \AA}$ ). In both cases, the phenyl ring substituents of the phenanthroline units are oriented facing the other phenanthroline fragments, as was expected according to the high-field chemical shift observed for the aryl hydrogen atoms in the  $^1H$  NMR spectra.<sup>56</sup> The metal-metal distances in **RuCu(20.4)<sup>3+</sup>** and **RuAg(20.4)<sup>3+</sup>** are respectively  $10.400(1) \text{ \AA}$  and  $10.177(1) \text{ \AA}$  and preclude any metal-metal interaction. There are no unusual intermolecular contacts.

#### 7.7.6 TEMPLATE SYNTHESIS OF A 5-COORDINATE ZINC(II) CATENANE, THE CORRESPONDING CATENAND, AND RELATED COPPER(II) AND IRON(II) COMPLEXES

As described previously, copper(I) turned out to be particularly efficient as a gathering and templating metal for the construction of catenanes.

Five-coordinated metal centers have never been used as templates for synthesizing [2]catenanes. In order to make a 5-coordinated catenane, zinc(II) seemed to be an appropriate template. In fact, this cation forms stable pentacoordinated complexes with nitrogen-containing ligands. A terpy (terpy = 2,2':6',2''-terpyridine) and a phen (phen = 1,10-phenanthroline) form a convenient set of ligands.<sup>63</sup>

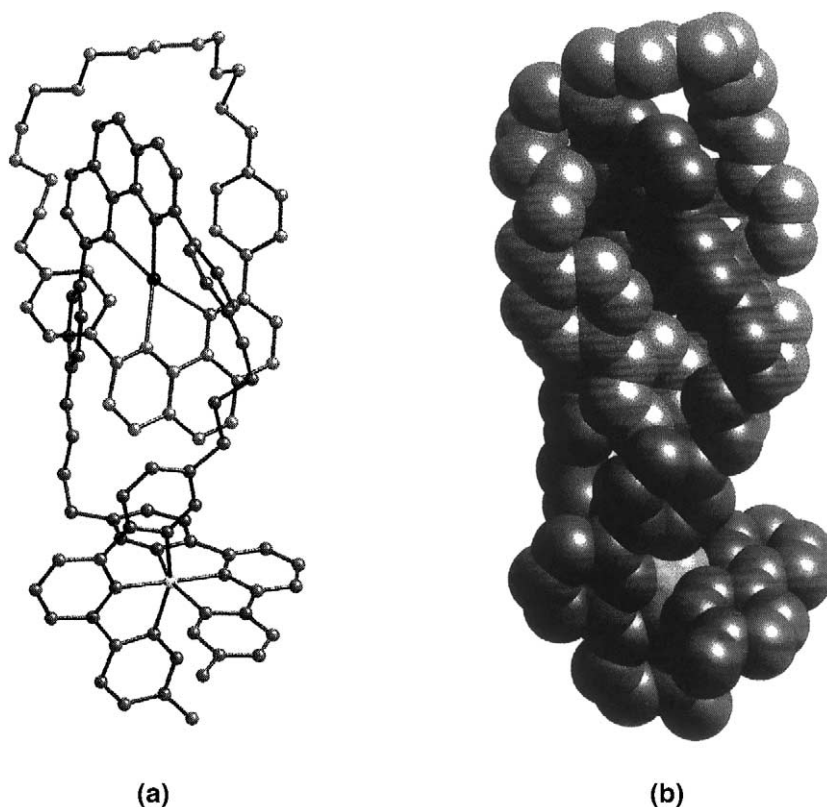


**Figure 20** X-ray structure of the catenane  $\text{RuAg}(\mathbf{20.4})^{3+}$ . (a) Balls and sticks representation; (b) Space-filling representation.

In order to avoid the formation of a 6-coordinated complex containing two terdentate ligands (i.e.,  $\text{Zn}(\text{terpy})_2^{2+}$ ),<sup>64,65</sup> it is compulsory to include the terpy fragment in a ring in an endotopic fashion. In principle, the use of bidentate chelates not belonging to a ring could lead to 4-coordinated complexes. This would be the case with copper(I), but the situation will be very different with zinc(II): formation of a 5-coordinated complex implies that the system be threaded. The preference of zinc(II) for 5-coordinated complexes is the driving force for the threading reaction. This principle is depicted in Figure 21.

The first terpyridine-containing ring (**21**), represented in Figure 22, was prepared separately, and subsequently zinc(II) was used as the gathering and threading element to pass the string-like component (**14**), incorporating a phenanthroline unit, through the ring.

This open-chain species bears two terminal olefins and the threaded species  $\text{Zn}(\mathbf{21.14})^{2+}$  was then subsequently subjected to ring-closing metathesis, using Grubbs first-generation catalyst to afford the desired catenane  $\text{Zn}(\mathbf{22})^{2+}$  (Figure 23a).<sup>46–51</sup> Hydrogenation of the double bond (Figure 23b) and then removal of the zinc(II) template in basic medium (Figure 23c) afforded the free pentacoordinating catenane (**24**). This free ligand (**24**) was thus obtained in 40% overall yield from the starting threaded species  $\text{Zn}(\mathbf{21.14})^{2+}$ .

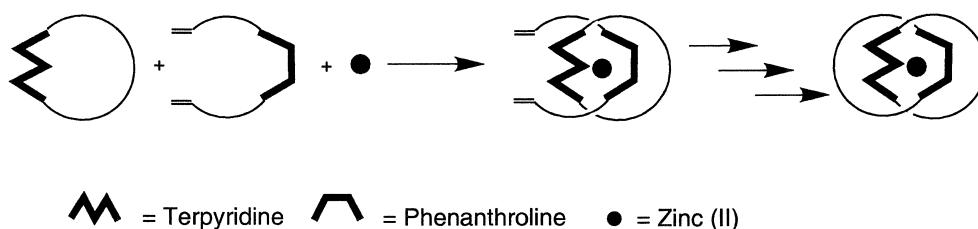


**Figure 21** Strategy used to prepare the [2]catenane  $\text{Zn}(\mathbf{23})^{2+}$ .



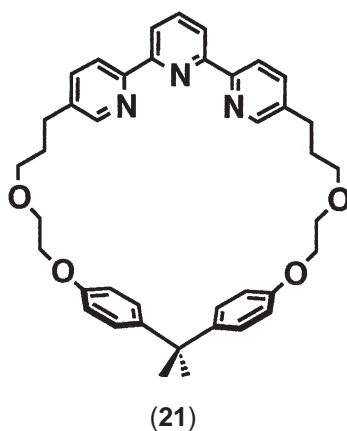


Figure 22 Terpyridine-containing precursor macrocycle (21).

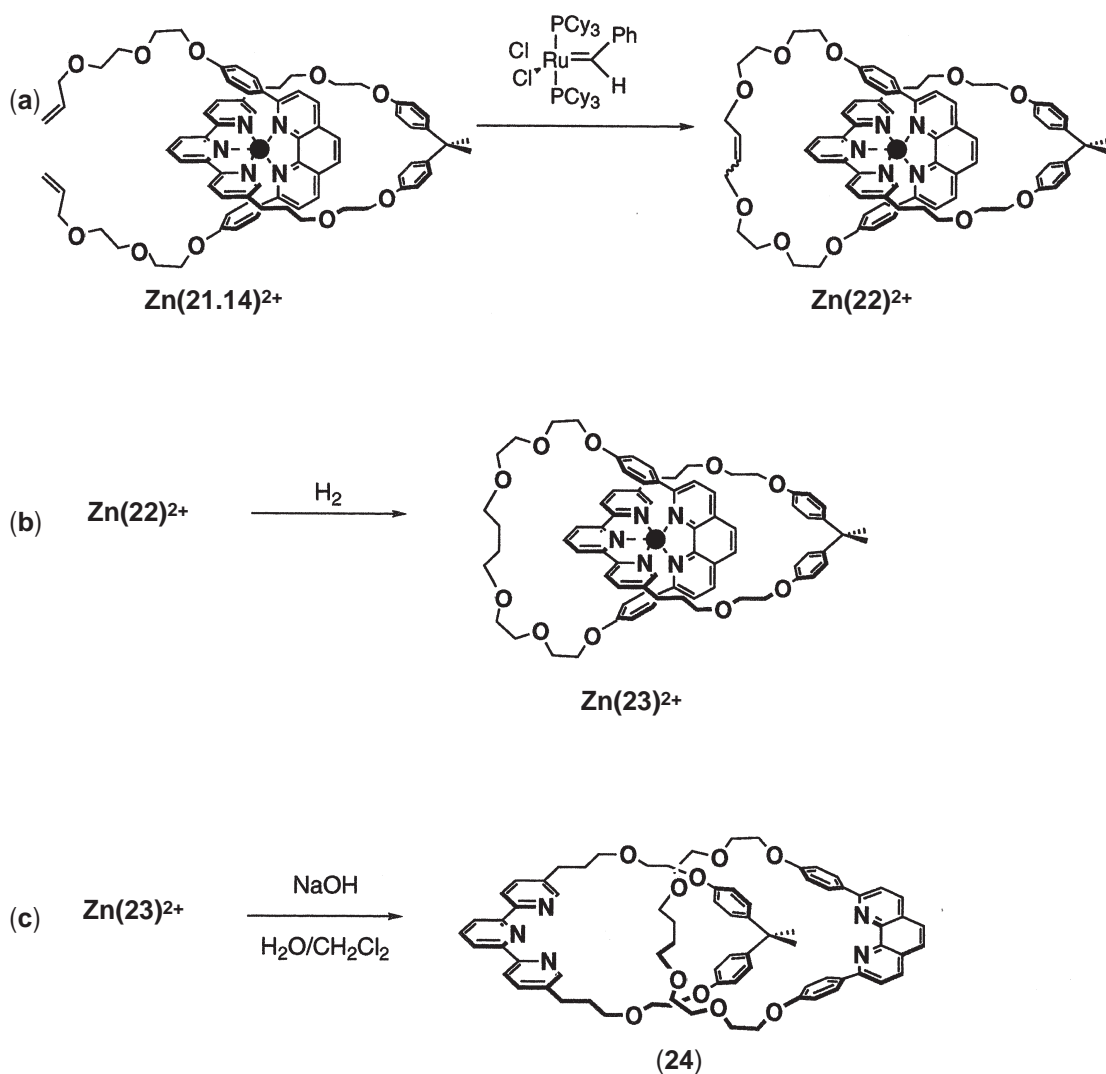


Figure 23 (a) Synthesis of the [2]catenane  $\text{Zn(22)}^{2+}$  by ring closing metathesis; (b) Subsequent hydrogenation of the double bond; (c) Demetallation affording the free catenane (24).

The ESMS and  $^1\text{H}$  NMR spectra afford clear evidence for the structure of this first pentacoordinating interlocking-ring system.

The free ligand was then remetalated with zinc(II), iron(II), and copper(II). The new 5-coordinated complexes,  $\text{Zn}(\mathbf{24})^{2+}$ ,  $\text{Fe}(\mathbf{24})^{2+}$ , and  $\text{Cu}(\mathbf{24})^{2+}$  were compared to their analogous 4-coordinated complexes with the  $\text{M}(\mathbf{1})^{n+}$  [2]catenanes previously discussed.<sup>21</sup>

Some electrochemical studies were performed by cyclic voltammetry. The most interesting observation is that the 5-coordinated complexes obtained are strongly stabilized: in fact, their reduction potentials are shifted towards cathodic values when going from the 4-coordinated species to  $\text{Zn}(\mathbf{24})^{2+}$ ,  $\text{Fe}(\mathbf{24})^{2+}$ , and  $\text{Cu}(\mathbf{24})^{2+}$ . For example, the reduction process of  $\text{Zn}(\mathbf{24})^{2+}$  occurs in two one-electron steps in dichloromethane at  $-1.19$  V/SCE and  $-1.44$  V/SCE. For its 4-coordinated analogous complex  $\text{Zn}(\mathbf{1})^{2+}$ , the redox potentials are  $-0.96$  V/SCE and  $-1.26$  V/SCE. In the case of the  $\text{Cu}^{\text{II}}/\text{Cu}^{\text{I}}$ , where the reduction occurs in a one-electron step, the potential is shifted to cathodic values by a difference of  $0.7$  V when going from the 4-coordinated species to  $\text{Cu}(\mathbf{24})^{2+}$ .

In conclusion, the presently reported [2]-catenane, consisting of a terdentate ligand inscribed in a cycle and a bidentate chelate incorporated in a ring, displays coordination properties which are markedly different from those of the classical 4-coordinated catenanes previously discussed. In particular, stable complexes with divalent metals could be prepared (zinc(II), copper(II), or iron(II)).

### 7.7.7 [2]CATENANE CONSTRUCTED AROUND A $\text{Ru}(\text{DIIMINE})_3^{2+}$ DERIVATIVE USED AS A TEMPLATE

Till now, octahedral transition-metal centers have been only rarely used as templates for synthesizing topologically nontrivial molecules such as catenanes. An early example deals with the use of a bis-terpy ruthenium(II) complex.<sup>66</sup> An alternative to the latter approach, which relies on two terdentate ligands, could be the use of three bidentate ligands coordinated to the ruthenium in an octahedral geometry.

A successful synthesis of a [2]catenane, based on a  $\text{Ru}(\text{diimine})_3^{2+}$  core, could indeed be achieved. The design of the system and the synthetic strategy are depicted in Figure 24. The main point of the design is the observation that it should be possible to incorporate two bidentate chelates of the octahedron in a ring, and subsequently to thread a fragment containing the third chelate through the ring. The threading process should be driven by coordination to the metal center.

Tetradentate ligands consisting of two separate bidentate ligands connected by an appropriate spacer and leading to  $C_2$ -symmetric complexes have already been reported. A particularly interesting example is that of von Zelewsky's chiragens,<sup>67</sup> consisting of two chiral bipy derivatives (bipy = 2,2'-bipyridine). Thus, relying on previous examples, we designed the large macrocycle (**25**) containing two phenanthroline units (Figure 25a). Due to its large size, it was supposed to lead to an octahedral complex in which the two phen fragments are disposed *cis* to one another in the metal coordination sphere. The synthesis of the large, 50-membered macrocycle (**25**) required ten steps.

The key step was the coordination reaction, supposed to lead to the cyclic precursor complex  $\text{Ru}[\mathbf{25}(\text{CH}_3\text{CN})_2]^{2+}$  (Figure 25b). This complex was formed by reacting (**25**) and  $\text{Ru}(\text{DMSO})_4\text{Cl}_2$  in refluxing 1,2-dichloromethane under high dilution conditions. The crude reaction mixture was heated under reflux in  $\text{CH}_3\text{CN}-\text{H}_2\text{O}$  (80–20) to afford  $\text{Ru}[\mathbf{25}(\text{CH}_3\text{CN})_2]^{2+}$  as an orange solid in 21% yield. The next step was carried out using the 2,2'-bipyridine derivative (**26**), analogous to a previously described example<sup>68,69</sup>, and the macrocyclic complex. The threading, performed under relatively harsh conditions (ethylene glycol,  $140^\circ\text{C}$ ), afforded the catenane precursor  $\text{Ru}(\mathbf{25.26})^{2+}$  in surprisingly good, 56% yield (Figure 26).

The final compound, catenane  $\text{Ru}(\mathbf{27})^{2+}$ , was prepared from  $\text{Ru}(\mathbf{25.26})^{2+}$  in 68% yield by ring-closing metathesis (RCM). The ESMS and  $^1\text{H}$  NMR spectra afford clear evidence for the structure of this first interlocking-ring system, built on a tris-bidentate chelate transition metal complex used as a template.

### 7.7.8 CONCLUSION

This chapter covers some synthetic and structural work, mostly done in Strasbourg since the early 1980s. From our first approach, based on the entwining of two coordinating fragments around a

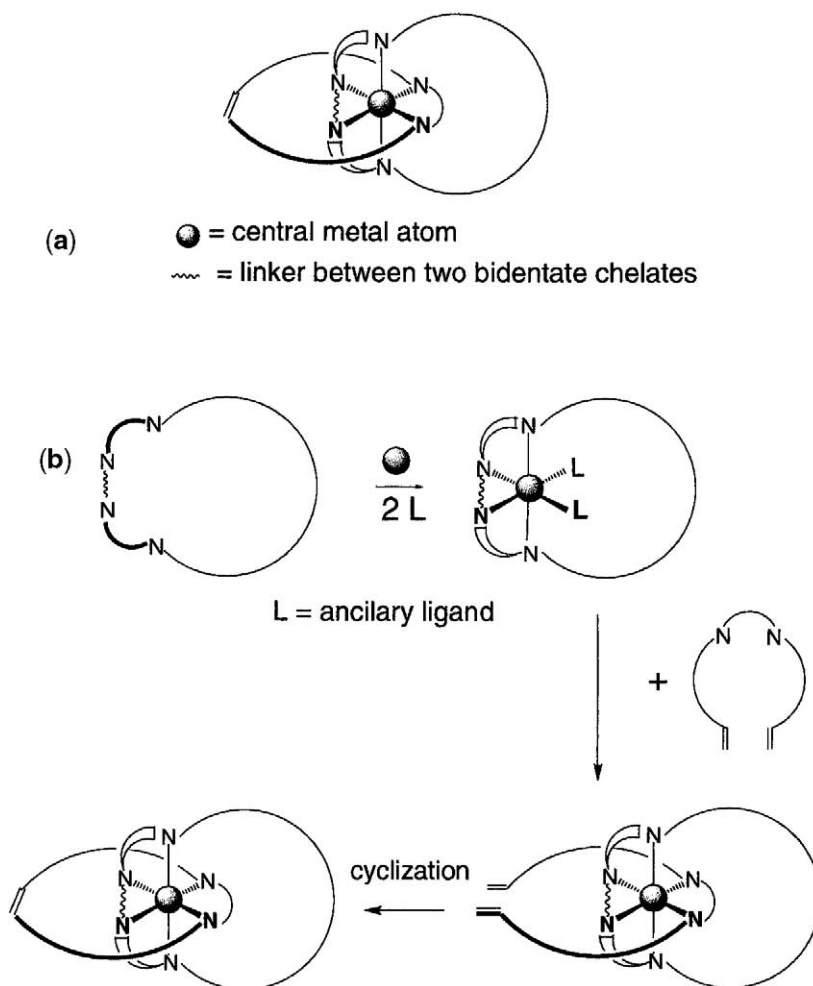


**Figure 24** (a) Schematic representation of a transition-metal-complexed [2]catenane containing two different rings. One of the macrocycles incorporates a bidentate chelate, whereas the other contains two bidentate coordinating fragments with a cis arrangement; (b) Synthetic strategy.

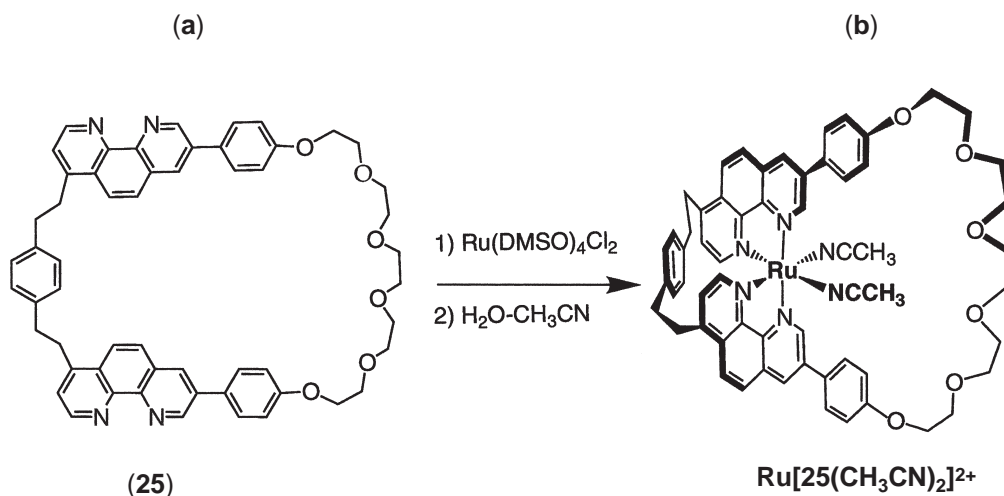


**Figure 25** Formation of the catenane precursor complex: (a) The large flexible 50-membered macrocycle (25) containing two phenanthroline units; (b) bis-bidentate macrocyclic octahedral  $\text{Ru}^{\text{II}}$  complex in which the two phen units adopt a cis-arrangement.

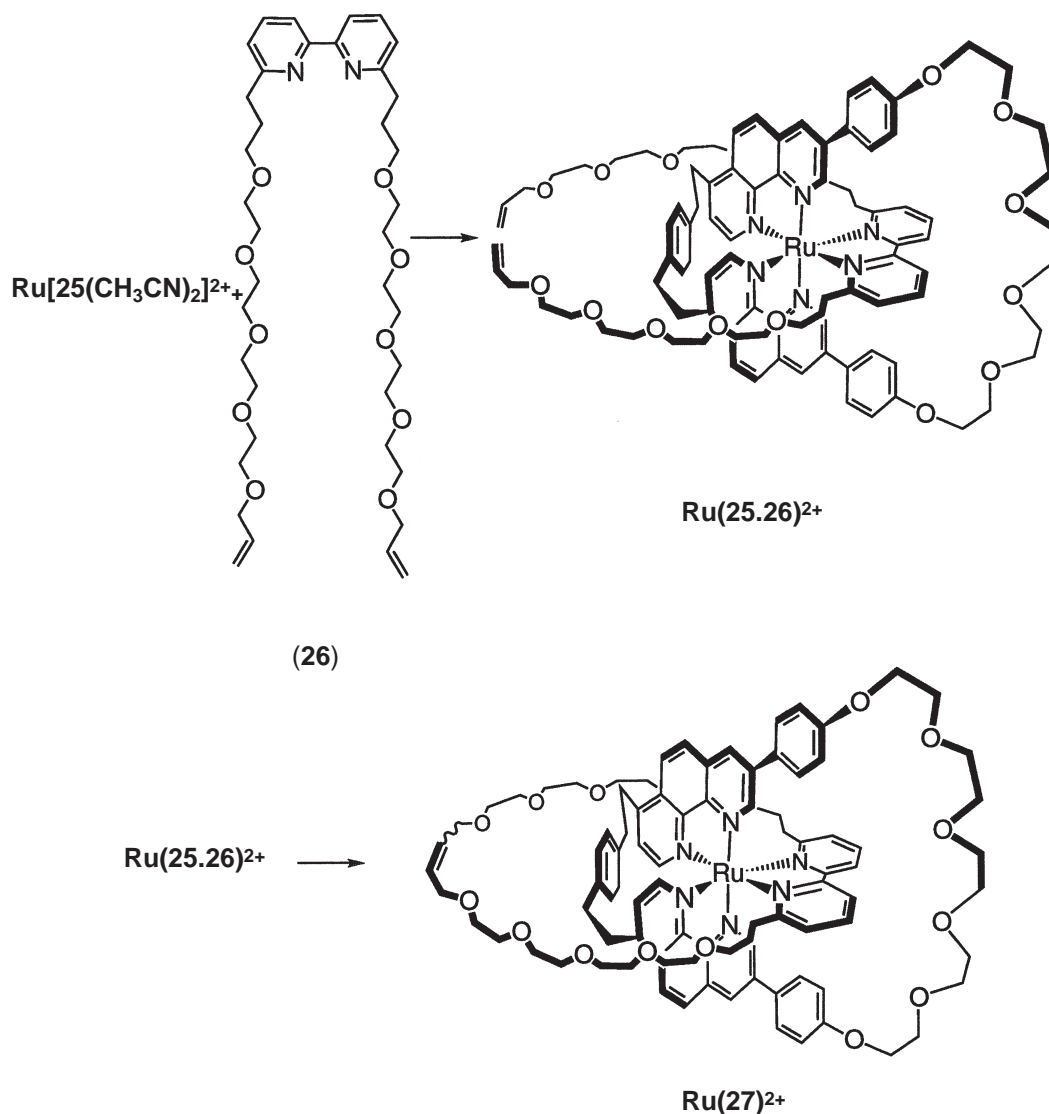


**Figure 26** Threading of the disubstituted bipyridine (26) leading to the complex  $\text{Ru(25.26)}^{2+}$  and subsequent cyclization by ring-closing metathesis.

copper(I) center followed by a double cyclization reaction, many extensions have been proposed. These new developments have been performed in several directions:

- (i) improving the synthesis of catenanes; in this respect, the use of the ring-closing metathesis reaction turned out to be particularly successful, since catenanes can now be prepared in yields exceeding 90%.
- (ii) increasing the topological complexity of the systems; the making of multiring systems is particularly significant in this respect, the record being the preparation of a [7]catenane of the “necklace” family.
- (iii) introducing novel functionality, so as to be able to envision the use of catenanes for elaborating interactive and responsive organic materials. The recent work on catenanes constructed around octahedral metals such as ruthenium(II) is particularly promising, in relation to future molecular “machines.”

We have particularly emphasized the structural aspects of the catenanes discussed in this chapter. The reasons for including several X-ray structures are twofold: (i) it was difficult to foresee in 1980 that so many catenanes would be crystallized and studied by X-ray

crystallography; and (ii) we believe that the structures of these interlocking molecules are particularly attractive from an aesthetic and topological viewpoint.

Whether catenanes will find applications some day as monomers to topologically novel polymers or molecular machines remains to be demonstrated. Nevertheless, this fascinating family of compounds has already triggered novel and exciting chemistry, covering many aspects of molecular science.

## 7.7.9 REFERENCES

- Schill, G. *Catenanes, Rotaxanes and Knot*; Academic Press: New York, 1971.
- Vetter, W.; Logemann, E.; Schill, G. *Org. Mass Spectrom.* **1977**, *12*, 351–369.
- Schill, G. personal communication.
- Wasserman, E. *J. Am. Chem. Soc.* **1960**, *82*, 4433–4434.
- Dietrich-Buchecker, C. O.; Sauvage, J.-P.; Kintzinger, J.-P. *Tetrahedron. Lett.* **1983**, *24*, 5095–5098.
- Dietrich-Buchecker, C. O.; Sauvage, J.-P.; Kern, J.-M. *J. Am. Chem. Soc.* **1984**, *106*, 3043–3045.
- Ortholand, J.-Y.; Slawin, A. M. Z.; Spencer, N.; Stoddart, J. F.; Williams, D. J. *Angew. Chem., Int. Ed. Engl.* **1989**, *28*, 1394–1395.
- Ashton, P. R.; Goodnow, T. T.; Kaifer, A. E.; Reddington, M. V.; Slawin, A. M. Z.; Spencer, N.; Stoddart, J. F.; Vicent, C.; Williams, D. J. *Angew. Chem., Int. Ed. Engl.* **1989**, *28*, 1396–1399.
- Hunter, C. A. *J. Am. Chem. Soc.* **1992**, *114*, 5303–5311.
- Vögtle, F.; Meier, S.; Hoss, R. *Angew. Chem., Int. Ed. Engl.* **1992**, *31*, 1619–1622.
- Amabilino, D. B.; Stoddart, J. F. *Chem. Rev.* **1995**, *95*, 2725–2828.
- Reppe, W.; Schlichting, O.; Klager, K.; Toepfel, T. *Liebigs Ann. Chem.* **1948**, *560*, 1–92.
- Dietrich-Buchecker, C. O.; Sauvage, J.-P.; Weiss, J. *Tetrahedron Lett.* **1986**, *27*, 2257–2260.
- Livoreil, A.; Dietrich-Buchecker, C. O.; Sauvage, J.-P. *J. Am. Chem. Soc.* **1994**, *116*, 9399–9400.
- Blanco, M.-J.; Jiménez, M.-C.; Chambron, J.-C.; Heitz, V.; Linke, M.; Sauvage, J.-P. *Chem. Soc. Rev.* **1999**, *28*, 293–305.
- Arnaud-Neu, F.; Marques, E.; Schwing-Weill, M.-J.; Dietrich-Buchecker, C. O.; Sauvage, J.-P.; Weiss, J. *New J. Chem.* **1988**, *12*, 15–20.
- Dietrich-Buchecker, C. O.; Marnot, P. A.; Sauvage, J.-P.; Kintzinger, J.-P.; Maltèse, P. *Nouveau J. Chim.* **1984**, *8*, 573–582.
- Dietrich-Buchecker, C. O.; Sauvage, J.-P. *Tetrahedron* **1990**, *46*, 503–512.
- Cesario, M.; Dietrich-Buchecker, C. O.; Guilhem, J.; Pascard, C.; Sauvage, J.-P. *J. Chem. Soc. Chem. Commun.* **1985**, 244–247.
- Albrech-Gary, A.-M.; Saad, Z.; Dietrich-Buchecker, C. O.; Sauvage, J.-P. *J. Am. Chem. Soc.* **1985**, *107*, 3205–3209.
- Dietrich-Buchecker, C. O.; Sauvage, J.-P.; Kern, J.-M. *J. Am. Chem. Soc.* **1989**, *111*, 7791–7800.
- Dietrich-Buchecker, C. O.; Guilhem, J.; Kern, J.-M.; Pascard, C.; Sauvage, J.-P. *Inorg. Chem.* **1994**, *33*, 3498–3502.
- Dietrich-Buchecker, C. O.; Kern, J.-M.; Sauvage, J.-P. *J. Chem. Soc. Chem. Commun* **1985**, 760–762.
- Cesario, M.; Dietrich-Buchecker, C. O.; Edel, A.; Guilhem, J.; Kintzinger, J.-P.; Pascard, C.; Sauvage, J.-P. *J. Am. Chem. Soc.* **1986**, *108*, 6250–6254.
- Schill, G.; Zürcher, C. *Angew. Chem.* **1969**, *81*, 996–997.
- Amabilino, D. B.; Ashton, P. R.; Reder, A. S.; Spencer, N.; Stoddart, J. F. *Angew. Chem., Int. Ed. Engl.* **1994**, *33*, 433–437.
- Amabilino, D. B.; Ashton, P. R.; Reder, A. S.; Spencer, N.; Stoddart, J. F. *Angew. Chem., Int. Ed. Engl.* **1994**, *33*, 1286–1290.
- Sauvage, J.-P.; Weiss, J. *J. Am. Chem. Soc.* **1985**, *107*, 6108–6110.
- Guilhem, J.; Pascard, C.; Sauvage, J.-P.; Weiss, J. *J. Am. Chem. Soc.* **1988**, *110*, 8711–8713.
- Glaser, C. *Ber. Deutsch. Chem. Ges.* **1869**, *2*, 422–424.
- Glasser, C. *Justus Liebigs Ann. Chem.* **1870**, *154*, 137–171.
- Eglinton, G.; Galbraith, A. R. *Chem. Ind. (London)* **1956**, 737–738.
- Eglinton, G.; Galbraith, A. R. *J. Chem. Soc.* **1959**, 889–896.
- Sondheimer, F.; Amiel, Y. *J. Am. Chem. Soc.* **1957**, *79*, 5815–5820.
- Sondheimer, F.; Amiel, Y.; Wolvsky, R. *J. Am. Chem. Soc.* **1957**, *79*, 6263–6267.
- Jarvi, E. T.; Whitlock, H. W., Jr. *J. Am. Chem. Soc.* **1980**, *102*, 657–662.
- Miller, S. P.; Whitlock, H. W., Jr. *J. Am. Chem. Soc.* **1984**, *106*, 1492–1494.
- O’Krongly, D.; Denmeade, S. R.; Chiang, M. Y.; Breslow, R. *J. Am. Chem. Soc.* **1985**, *107*, 5544–5545.
- Dietrich-Buchecker, C. O.; Khemiss, A.; Sauvage, J.-P. *J. Chem. Soc., Chem. Commun.* **1986**, 1376–1378.
- Dietrich-Buchecker, C. O.; Guilhem, J.; Khemiss, A.; Kintzinger, J.-P.; Pascard, C.; Sauvage, J.-P. *Angew. Chem.* **1987**, *99*, 711–714; *Angew. Chem., Int. Ed. Engl.* **1987**, *26*, 661–663.
- Dietrich-Buchecker, C. O.; Hemmert, C.; Khémis, A. K.; Sauvage, J.-P. *J. Am. Chem. Soc.* **1990**, *112*, 8002–8008.
- Dietrich-Buchecker, C. O.; Hemmert, C.; Sauvage, J.-P. *New J. Chem.* **1990**, *14*, 603–605.
- Armaroli, N.; Balzani, V.; Barigelletti, F.; De Cola, L.; Sauvage, J.-P.; Hemmert, C. *J. Am. Chem. Soc.* **1991**, *113*, 4033–4035.
- Bitsch, F.; Dietrich-Buchecker, C. O.; Khémis, A. K.; Sauvage, J.-P.; Van Dorsselaer, A. *J. Am. Chem. Soc.* **1991**, *113*, 4023–4025.
- Bitsch, F.; Hegy, G.; Dietrich-Buchecker, C. O.; Leize, E.; Sauvage, J.-P.; Van Dorsselaer, A. *New J. Chem.* **1994**, *184*, 801–807.
- Fürstner, A.; Kindler, N. *Tetrahedron Lett.* **1996**, *37*, 7005–7008.
- König, B.; Horn, C. *Synlett* **1996**, 1013–1014.
- Marsella, M. J.; Maynard, H. D.; Grubbs, R. H. *Angew. Chem., Int. Ed. Engl.* **1997**, *36*, 1101–1103.

49. Fu, G. C.; Grubbs, R. H. *J. Am. Chem. Soc.* **1992**, *114*, 5426–5427.
50. Schwab, P.; Grubbs, R. H.; Ziller, J. W. *J. Am. Chem. Soc.* **1996**, *118*, 100–110.
51. Dias, E. L.; Nguyen, S. T.; Grubbs, R. H. *J. Am. Chem. Soc.* **1997**, *119*, 3887–3897.
52. Mohr, B.; Sauvage, J.-P.; Grubbs, R. H. *Angew. Chem., Int. Ed. Engl.* **1997**, *36*, 1308–1310.
53. Mohr, B.; Sauvage, J.-P. *J. Org. Chem.* **1999**, *64*, 5463–5471.
54. Dietrich-Buchecker, C. O.; Sauvage, J.-P. *Chem. Commun.* **1999**, 615–616.
55. Dietrich-Buchecker, C. O.; Rapenne, G.; Sauvage, J.-P. *Chem. Commun.* **1997**, 2053–2054.
56. Cardenas, D. J.; Gavina, P.; Sauvage, J.-P. *J. Am. Chem. Soc.* **1997**, *119*, 2656–2664.
57. Beley, M.; Collin, J.-P.; Louis, R.; Metz, B.; Sauvage, J.-P. *J. Am. Chem. Soc.* **1991**, *113*, 8521–8522.
58. Thummel, R. P.; Jhang, Y. *Inorg. Chem.* **1986**, *25*, 2527–2534.
59. Shannon, R. D. *Acta Crystallogr.* **1976**, *A32*, 751–767.
60. Titze, C.; Kaim, W.; Zalis, S. *Inorg. Chem.* **1997**, *36*, 2505–2510.
61. Titze, C.; Kaim, W. *Z. Naturforsch.* **1996**, *51b*, 981–988.
62. Miller, M. T.; Gantzel, P. K.; Karpishin, T. B. *Angew. Chem., Int. Ed. Engl.* **1998**, *37*, 1556–1558.
63. Jiménez-Moléro, M. C.; Dietrich-Buchecker, C. O.; Sauvage, J.-P. *Angew. Chem., Int. Ed. Engl.* **2000**, *39*, 3284–3287.
64. Albano, G.; Balzani, V.; Constable, E. C.; Maestri, M.; Smith, D. R. *Inorg. Chim. Acta* **1998**, *277*, 225–231.
65. Loiseau, F.; Di Pietro, C.; Serroni, S.; Campagna, S.; Licciardello, A.; Manfredi, A.; Pozzi, G.; Quici, S. *Inorg. Chem.* **2001**, *40*, 6901–6909.
66. Sauvage, J.-P.; Ward, M. *Inorg. Chem.* **1991**, *30*, 3869–3874.
67. Hayoz, P.; von Zelewski, A.; Soteklli-Evans, H. *J. Am. Chem. Soc.* **1993**, *115*, 5111–5114.
68. Collin, J.-P.; Laemmel, A. C.; Sauvage, J.-P. *New J. Chem.* **2001**, *25*, 22–24.
69. A. C. Laemmel, Ph.D. Thesis, University Louis Pasteur, Strasbourg, France, 2000.

# 7.8

## Supramolecular Systems: Self-assembly

R. M. YEH, A. V. DAVIS, and K. N. RAYMOND  
*University of California, Berkeley, CA, USA*

---

7.8.1	INTRODUCTION	327
7.8.2	METAL-LIGAND SELF-ASSEMBLY	328
7.8.3	COORDINATION ASSEMBLIES	329
7.8.3.1	Assemblies with Two- and Three-coordinate Metal Ions	330
7.8.3.2	Assemblies with Four-coordinate Square-Planar Metal Ions	332
7.8.3.3	Assemblies with Four-coordinate Tetrahedral Metal Ions	338
7.8.3.4	Assemblies with Five-coordinate Metal Ions	340
7.8.3.5	Assemblies with Six-coordinate Octahedral Metal Ions	341
7.8.3.6	Assemblies with Higher Coordination Number (>6) Metal Ions	346
7.8.3.7	Assemblies with Eight-coordinate Dimetal Ions	348
7.8.4	PROPERTIES OF COORDINATION SUPRAMOLECULAR ASSEMBLIES	348
7.8.5	FUNCTION OF COORDINATION SUPRAMOLECULAR ASSEMBLIES	350
7.8.6	OUTLOOK	351
7.8.7	REFERENCES	351

---

### 7.8.1 INTRODUCTION

This chapter focuses on the application of coordination chemistry to the self-assembly of discrete, multinuclear structures with well-defined architectures. Self-assembly represents a powerful synthetic methodology for the synthesis of large and complex coordination structures. It is a key tenet of supramolecular chemistry—the broadly applied term describing the organization of molecules into larger structures through relatively weak and reversible *intermolecular* interactions, such as  $\pi$  stacking, van der Waals contact, and hydrogen bonding. Many metal-ligand coordination interactions exhibit reversibility (lability) which is an essential property for self-assembly. Therefore, self-assembled multinuclear coordination structures are considered supermolecules. Although a supermolecule has—in common with a covalently constructed molecule—well-defined molecular weight, formula, and connectivity, it has other properties that are unique to the assembly, and unattainable with the individual component molecules.

Lehn has described supramolecular chemistry as an “information science”: molecular subunits which contain the necessary information self-assemble into a larger specific structure.<sup>1</sup> Complementary and explicit interaction of individual components with the appropriate symmetry and geometry generates the product assembly. In terms of coordination chemistry, astute ligand design and judicious choice of metal center allow one to access complex self-assembled architectures, many in the nanometer regime.

Self-assembled coordination supramolecular structures encompass both discrete and polymeric types in a range of synthetic areas. Although coordination polymers, two- and three-dimensional coordination networks, polynuclear metal clusters (with primarily metal-metal or  $\mu$ -oxo or

similar type bridges), crystal engineering, metallo-dendrimers, mono-bridged dinuclear complexes, and metal templated topoisomers (rotaxane, pseudorotaxane, knots, and catenanes) are all relevant to the topic of metal–ligand self-assembly, they are excluded from this chapter and are discussed elsewhere in this volume.

## 7.8.2 METAL–LIGAND SELF-ASSEMBLY

Coordination bonds generally provide stronger and more directionally controllable interactions than either hydrogen bonds or van der Waals contacts, both of which are commonly utilized in supramolecular self-assembly. Therefore, compared to weaker interactions, the contact area and redundancy necessary to secure a persistent, predictable self-assembled structure decreases with the use of coordination bonds.

The knowledge of fundamental coordination chemistry is critical to the development of metal- and ligand-based supramolecular assemblies (also referred to as metallo-supramolecular assemblies). The late transition and main group metal ions are the most commonly used ions for the construction of coordination assemblies. These ions are characterized by predictable and well-defined coordination geometries, which facilitate the linkage of ligand components in a precise manner. Lability is critical to self-assembly, since reversible bond formation allows the system to achieve the thermodynamic product. Knowledge of the physical properties of metal ions allows one to target structures with desired functionality. For example, the metal ions used for self-assembly may be chosen for their electronic properties. While diamagnetic ions facilitate NMR characterization of assemblies, paramagnetic ions may lead to unique magnetic properties.

The formidable task of organizing molecular components into a well-ordered supermolecule continues to be a challenge. Several approaches have been developed toward the self-assembly of discrete multinuclear species. The two main approaches are based on either control of bonding vector direction among the building blocks or control of overall symmetry of interaction among the molecular components.<sup>2,3</sup> Newer developments such as the weak-link approach and dimetal building block approach allow for the formation of new structures with new ligand types and metal combinations.<sup>4,5</sup>

In the directional bonding approach, the “molecular library” strategy describes metal and ligand components as angular and linear pieces to be combined in the formation of two-dimensional polygons and three-dimensional polyhedra. Different combinations of these simplified elements provide a formula for the synthesis of an array of self-assembled architectures. An example from Fujita and co-workers is shown in Figure 1.<sup>6</sup> This strategy applies most clearly to systems with monodentate ligands.

The “incommensurate symmetry interaction” approach dissects a target assembly into its symmetry elements and considers the necessary geometric relationships among these elements.<sup>3</sup> For example, a tetrahedral assembly contains four  $C_3$  and six  $C_2$  axes (Figure 2). These incommensurate symmetry axes must be simultaneously satisfied to form a tetrahedral structure. The structure may be formed from the combination of four  $C_3$ -symmetric tris-bidentate chelated

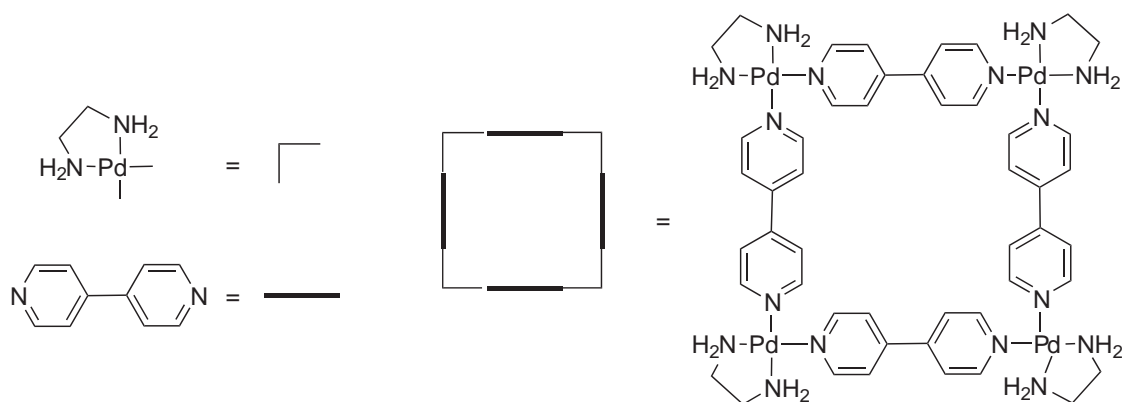


**Figure 1** Using a directional bonding approach, an  $M_4L_4$  square can be interpreted as the combination of linear and 90° components.<sup>6</sup>



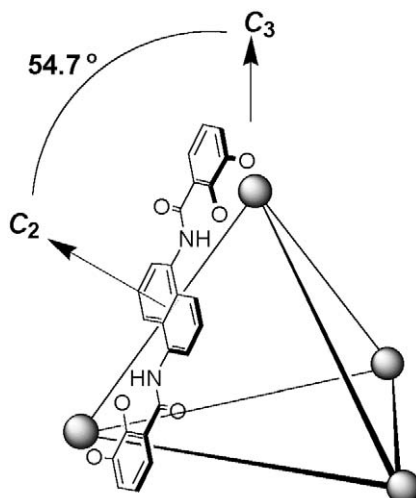


**Figure 2** In an  $M_4L_6$  tetrahedron tris-bidentate chelation of octahedral metal centers generates  $C_3$  axes, while the bis-bidentate ligands provide  $C_2$  axes. Precise arrangement of these symmetry axes is required for the formation the tetrahedral assembly.<sup>3</sup>

octahedral metal centers spanned by six  $C_2$ -symmetric bis-bidentate ligands. This approach places the metal ions at the vertices of the tetrahedron and the ligands on the edges. Not any combination of  $C_2$ -symmetric bis-bidentate ligands and octahedrally coordinated metal centers will generate a tetrahedron, however. The structure of the ligand is critical to achieving the correct orientation of symmetry elements in the target structure (e.g.,  $54.7^\circ$  between the  $C_2$  and  $C_3$  axes for a tetrahedron).

A diverse range of metallo-supramolecular architectures has been reported, and these coordination structures are often classified according to their architectural forms. The known structural motifs include one-dimensional linear structures such as helicates, two-dimensional polygons such as triangles and squares, and three-dimensional polyhedra such as cubes, tetrahedra, and octahedra. In this review, coordination number and geometry, as well as ligand structure and denticity, are highlighted in the presentation of representative structures. By focusing on the relationships between coordination chemistry and supramolecular architecture, a new perspective on this developing field may be gained. While this section attempts to cover many facets of coordination self-assembly, it cannot be comprehensive because of space constraints. For further details and examples we refer the reader to a number of recent reviews that pertain to this topic.<sup>2-5,7-12</sup>

### 7.8.3 COORDINATION ASSEMBLIES

A variety of metal and ligand components have been successfully employed in metallo-supramolecular chemistry. In reviewing this area of chemistry, it becomes clear that certain coordination motifs serve as staple components in assembly construction, while others rarely appear in supramolecular architectures. We will examine these trends both to enhance our understanding of design strategies, and to reveal untapped opportunities for new design.

Because of the importance of a well-defined stereochemistry, the transition metal and main group metal ions most commonly used in the self-assembly of discrete structures have either four-coordinate square-planar or six-coordinate octahedral configurations. If monodentate bridging ligands knit the structure together, capping ligands are used to inhibit oligomerization and maintain a discrete structure. Bridging ligands with chelating moieties often obviate the need for capping groups but can be more difficult to incorporate into certain architectures.

In addition to geometrical factors, lability is a critical parameter for self-assembly. While many reported structures contain labile ions, several ions that are normally not considered labile, such as  $Ti^{IV}$ ,  $Cr^{III}$ ,  $Co^{III}$ , and  $Pt^{II}$  have been successfully incorporated into elaborate multinuclear structures by forcing reaction conditions to reach thermodynamic equilibrium.

Beyond the metal ion stereochemistry, the design of ligands within a multinuclear coordination structure determines the overall architecture. A bridging ligand that ties several metal ions

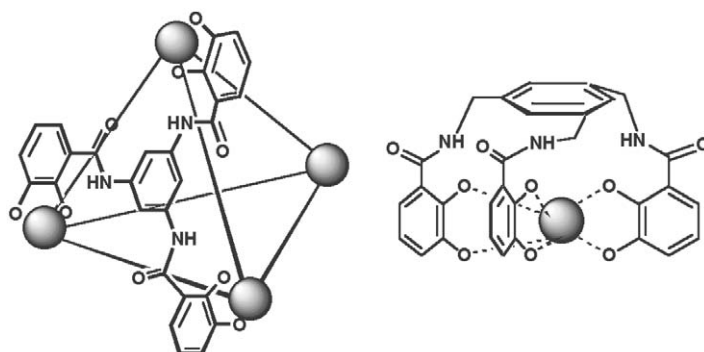


**Figure 3** Ligand structure is critical to assembly design. For example, an  $M_4L_4$  tetrahedral structure is formed with a rigid tris-bidentate ligand, whereas a mononuclear complex is formed with a more flexible tris-bidentate ligand.<sup>13–15</sup>

together in a well-defined configuration must be conformationally rigid. For example, compare the tris-bidentate ligands depicted in Figure 3. The only difference between the two ligands is the addition of flexible methylene bridges between the chelating groups and the central scaffold. When each one of these ligands is added to a solution of an octahedral metal ion in a 1:1 ratio, two distinct structures are formed. The flexible methylene bridged ligand forms a  $M_1L_1$  mononuclear complex with remarkably high stability owing to the pre-organized octahedral conformation of the three bidentate catecholate arms.<sup>13,14</sup> On the other hand, the rigid ligand forms exclusively a  $M_4L_4$  tetranuclear tetrahedron in which the four metal ions are located at the vertices and each ligand spans a face of the tetrahedron.<sup>15</sup> Therefore, although both ligands in this example contain  $C_3$ - and  $C_2$ - symmetry axes necessary for the formation of the  $M_4L_4$  tetrahedron, only the conformationally more rigid ligand forms the tetranuclear structure.

Clearly, other more subtle factors, which can exhibit strong influence over assembly configuration, must be considered in conjunction with metal coordination geometry and ligand structure. For example, secondary interactions contributed from host–guest chemistry in a particular metal–ligand system may cause a different structure to be favored in the presence of the guest than was favored in the absence of the guest.

In the following sections metal–ligand assemblies are organized in terms of metal coordination number and geometry. Within each subsection structures are discussed in the order of increasing nuclearity and complexity. Discussion of metallo-supramolecular assembly properties and development of function follows the review of synthesis and structure.

### 7.8.3.1 Assemblies with Two- and Three-coordinate Metal Ions

The use of lower coordinate (two or three) metal ions in the formation of supramolecular assemblies is limited by the linkages possible using such metal centers. Nonetheless, there are some notable examples.

A number of  $[Cu_2L_2]^{2+}$  structures with two-coordinate  $Cu^I$  have been synthesized. For example, a pyridine-linked bis-benzimidazol ligand forms a double stranded  $[Cu_2L_2]^{2+}$  helicate, with long-range pyridine–Cu interactions observed in the crystal structure.<sup>16</sup> Demonstrating the significance of the ligand backbone, the  $[Cu_2L_2]^{2+}$  structure in Figure 4 is a macrocycle with no helical topology.<sup>17</sup> Dinuclear  $M_2L_2$  macrocycles containing linear two-coordinate  $Ag^I$  have also been reported.<sup>18–20</sup>

An unusual double-stranded trinuclear structure incorporates one two-coordinate bent  $Ag^I$  and two four-coordinate tetrahedral  $Ag^I$  ions.<sup>21</sup> A double-stranded tetranuclear helicate,  $[Au_4L_2]^{4+}$ , employs two-coordinate  $Au^I$ .<sup>22</sup> The inner phosphorus atoms of this tetraphosphadecane ligand are chiral, but only three of the four possible stereoisomers were isolated. In each of these structures the two phosphorus atoms binding the same  $Au^I$  ion have the same chirality. Auophilic interactions are ascribed to the outer Au–Au pairs in each structure.

Two-coordinate metals can also be incorporated in capsule structures. In one example, three two-coordinate  $Ag^I$  ions stitch together two tris(imidazol-1-ylmethyl)-trimethyl benzene ligands to

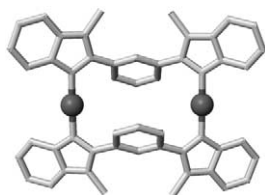


**Figure 4** Linear coordination of  $\text{Cu}^{\text{I}}$  by bis-benzimidazol ligands generates a  $[\text{Cu}_2\text{L}_2]^{2+}$  macrocycle.<sup>17</sup>

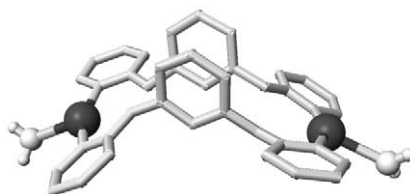


**Figure 5** Bis-pyridyloxybenzene and three-coordinate  $\text{Ag}^{\text{I}}$  form a  $[\text{Ag}_2\text{L}_2(\text{H}_2\text{O})_2]^{2+}$  macrocycle in which water serves as a capping type ligand.

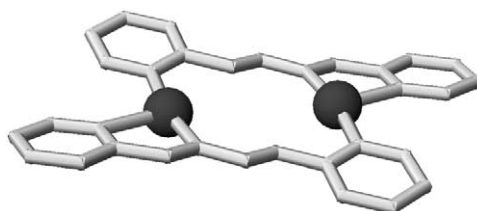


**Figure 6** Two bis-pyridylimine ligands saturate the coordination of three-coordinate  $\text{Ag}^{\text{I}}$  ions in a planar  $[\text{Ag}_2\text{L}_2]^{2+}$  structure.<sup>33</sup>

form a small capsule which encapsulates one  $\text{BF}_4^-$  anion.<sup>23</sup> Topologically similar  $[\text{Ag}_3\text{L}_2]^{2+}$  and  $[\text{Cu}_3\text{L}_2]^{2+}$  have been prepared from a tripodal tris(benzimidazolyl)trimethyl benzene ligand.<sup>24</sup> These structures encapsulated  $\text{BF}_4^-$  and  $\text{CuI}_3^-$ , respectively. Schmidbaur and co-workers have synthesized a  $[\text{Au}_3\text{L}_2]^{3+}$  capsule from the unexpected reaction of a hydrogen-bridged  $[\text{H}(\text{Ph}_2\text{PO})_2\text{Au}]_2$  dimer with  $\text{BF}_3$  which generated the assembly's tris(diphenylphosphinito) fluoroborate ligand.<sup>25</sup> Au–Au secondary interactions are implicated in structure, influencing deviations from linear two-coordinate  $\text{Au}^{\text{I}}$  coordination.

Gold(I) generally exhibits two-coordinate linear geometry and is thus a good candidate for the formation of low-coordinate self-assembled structures. However, auriphilic Au–Au interactions often play an important role in structure determination and stabilization.<sup>26–28</sup>

The construction of a number of structures containing three-coordinate metal ions is very similar to that of two-coordinate structures, as a terminal ligand occupies the third coordination site. Steel and co-workers have reported a series of  $\text{Ag}^{\text{I}}$  complexes of this type, including  $[\text{Ag}_2\text{L}_2(\text{H}_2\text{O})_2]^{2+}$  (Figure 5).<sup>29–31</sup> Water or  $\text{NO}_3^-$  serves as the terminal ligand to complete the distorted T-shaped coordination of each  $\text{Ag}^{\text{I}}$  ion. 1,4-Bis-(diphenylphosphino)butane (dppb) reacts with  $\text{Cu}^{\text{I}}$  to produce the  $[\text{Cu}_2(\text{dppb})_2(\text{ClO}_4)_2]$  macrocycle in which one perchlorate serves as a terminal monodentate ligand for each  $\text{Cu}^{\text{I}}$  ion.<sup>32</sup>

In other structures containing three-coordinate metal ions, the bridging ligands of the assembly provide all three donor atoms.<sup>21,33–35</sup> For example, three-coordinate  $\text{Ag}^{\text{I}}$  was reported in the formation of a  $[\text{Ag}_2\text{L}_2]^{2+}$  planar macrocycle, using a bis-pyridylimine ligand (Figure 6).<sup>33</sup> Long-range interaction with the oxygen atoms of the triflate anions on each face of the structure stabilizes the distorted T-shaped coordination geometry of the  $\text{Ag}^{\text{I}}$  metal ions. A  $[\text{Ag}_2\text{L}_3]^{2+}$  trigonal prism has been assembled with a bis-(benzimidazolyl)benzene ligand. The  $\text{Ag}^{\text{I}}$  ions are coordinated in a trigonal planar geometry and lie on the structure's threefold axis.<sup>36</sup>

### 7.8.3.2 Assemblies with Four-coordinate Square-Planar Metal Ions

Four-coordinate square-planar metal ions, particularly Pd<sup>II</sup> and Pt<sup>II</sup>, are prominent in metallo-supramolecular structures. Square-planar metal centers provide right angle or linear linkages for the supermolecule via either *cis* or *trans* coordination to the bridging ligands. *Cis* coordination can be enforced by capping adjacent metal binding sites with chelating ligands such as ethylenediamine or by having monodentate ligands such as triethylphosphine in *cis* configuration on the metal precursor. *Trans* coordination is achieved by using two monodentate ligands in *trans* positions. Structural motifs based on both are known, with most adopting the *cis*-coordination scheme. They include dinuclear macrocycles, square grids, triangles, squares, hexagons, rectangular and square boxes, cyclophane boxes, and adamantanoid boxes. Because of the linkage geometry, helicates based on square-planar four-coordinate metal ions are less common. Two examples are a dinuclear double-stranded helicate from Constable and a quadruple-stranded helicate reported by Steel and McMorran (Figure 7).<sup>37,38</sup>

Most dinuclear palladium and platinum macrocycles contain two bis-monodentate bridging ligands with nearly orthogonal binding units and *cis*-capping ligands on the metal centers. Fujita and co-workers have produced dinuclear macrocycles by utilizing nonlinear spacers between two pyridyl binding units and *cis*-capped Pd<sup>II</sup> ions.<sup>39–41</sup> When the simple phenylene scaffold ligand is used to form the macrocycle, catenation of the rings is observed due to  $\pi$  stacking. Analogous dinuclear ring structure and catenation phenomenon are observed in the platinum analog albeit with a higher energy barrier for catenation. The slower kinetics in the platinum system allowed the authors to isolate and confirm the catenane structure by X-ray crystallography. Several larger dinuclear macrocycles with aromatic, alkyl, and cyclic alkyl ligand scaffolds and Cu<sup>I</sup> and Pd<sup>II</sup> ions have also been reported.<sup>42–46</sup> Significant to the area of nano-machinery, some of these self-assembled macrocycles interlock reversibly to form complex topologies.

A series of bis-palladium and bis-platinum macrocycles that resemble molecular squares have been produced by incorporating iodonium as a vertex in the ligand (Figure 8).<sup>47–49</sup> The hyper-valent iodonium has pseudo-trigonal-pyramidal geometry that provides the 90° right angle critical to square geometry.<sup>50</sup> In addition, Stang and co-workers have introduced chiral binaphthalene groups to bis-phosphine capping ligands to form chiral dinuclear square macrocycles of different sizes.<sup>51</sup> This result shows that intramolecular asymmetric induction from groups such as binaphthalene moieties dictates the chirality of the self-assembly process, allowing only one of many possible diastereomers to form.

Diederich and co-workers incorporated a buckminsterfullerene into the ligand scaffold and thereby formed a bis-palladium macrocycle with two appended fullerenes (Figure 9).<sup>52</sup> The fullerene-containing macrocycle shows slight deviation from ideal square planar geometry for the metal ion. This example of integrating various chemical groups into the assembly is an important step towards functionalizing self-assembled structures.

The simplest of all polygons is the triangle. A small triangle with minimal ring strain was synthesized with 4,7-phenanthroline which has a 60° angle between the coordinate vectors.<sup>53</sup> Dinuclear *trans*-coordinating palladium units (Figure 10) are used because a single *trans*-coordinating palladium unit does not provide sufficient distance between the phenanthrolines.

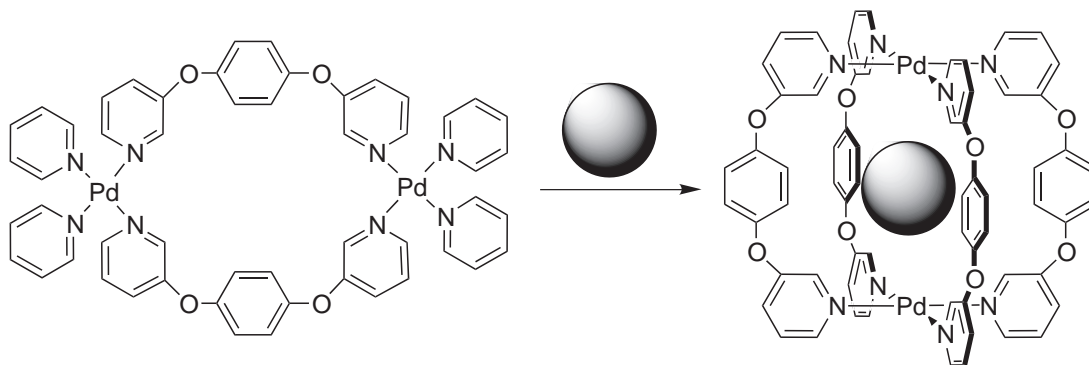


**Figure 7** A dinuclear Pd<sup>II</sup> macrocycle reorganizes into a quadruple-stranded helicate in the presence of hexafluorophosphate anion (represented by a sphere).<sup>38</sup>

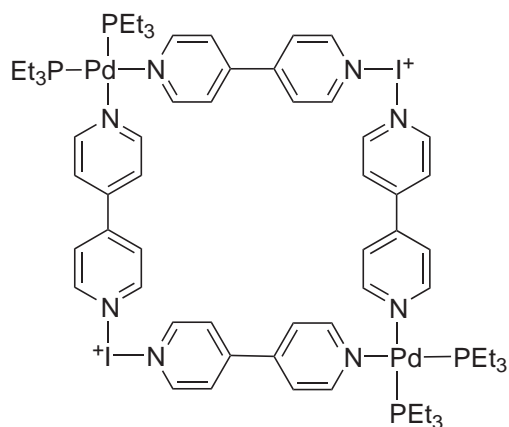


**Figure 8** Iodonium centers provide two of the 90° vertices of a dinuclear Pd<sup>II</sup> square, while *cis*-coordination of the metal centers creates the remaining 90° units.<sup>48</sup>

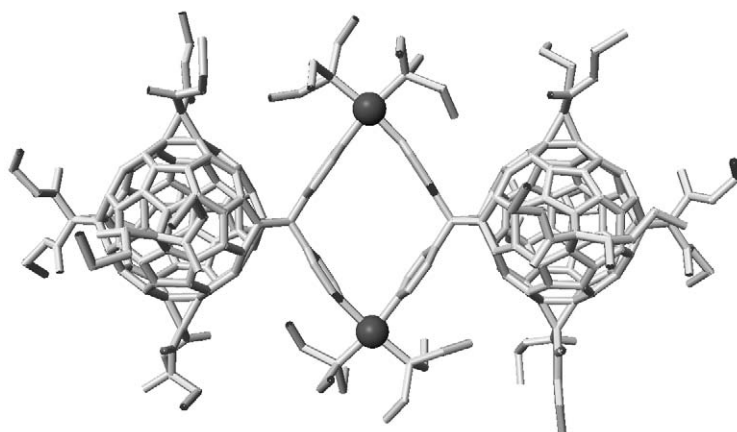


**Figure 9** Functionalization of a dinuclear Pd<sup>II</sup> macrocycle with fullerenes (C<sub>60</sub>) does not interfere with self-assembly of the structure.<sup>52</sup>

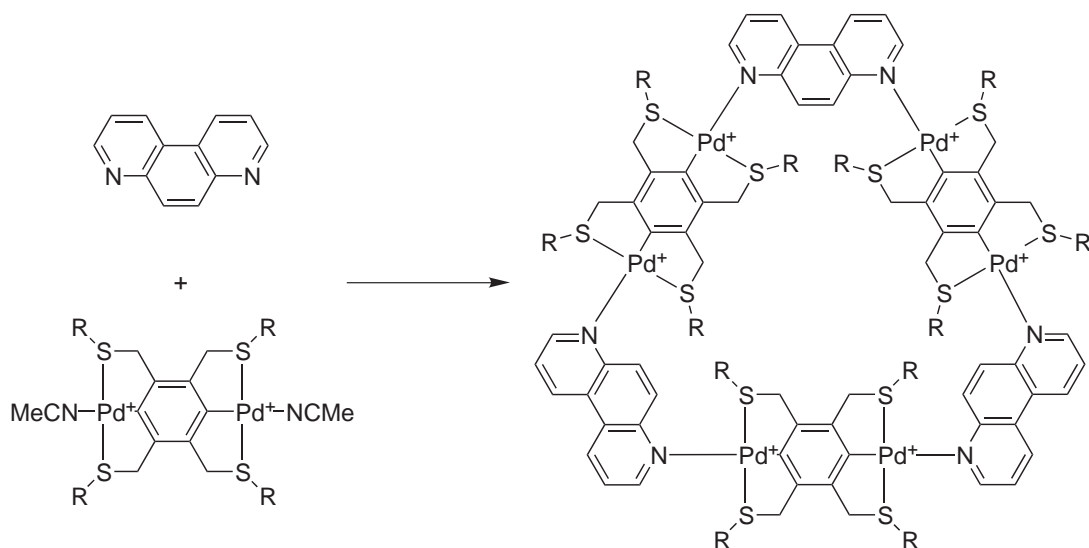


**Figure 10** A molecular triangle employs 4,7-phenanthroline to generate the requisite 60° angle between coordinate vectors. The dinuclear Pd<sup>II</sup> units allow for sufficient spacing between phenanthroline units.<sup>53</sup>

In yet another example with *trans*-coordinated platinum, a triangle was synthesized with benzimidazolone ligands.<sup>54</sup> While the majority of polygonal structures contain rigid and conformationally restricted ligands, a trinuclear triangle with very flexible aliphatic scaffold and *trans*-coordinated palladium centers was reported.<sup>55</sup>

A feature common to many triangles which contain *cis*-coordinated ions at the vertices is reversible conversion to the square structure. The energy difference between the triangle and square is often low enough such that a change in temperature, ligand, or metal concentration, or availability of a suitable guest molecule leads to structural conversion. The square is favored enthalpically due to lower macrocyclic ring strain whereas the smaller, simpler triangle is favored entropically. A number of such dynamic squares/triangles based on bis-*para*-pyridyl ligands have been synthesized (Figure 11).<sup>6,56</sup> In most cases the square is the major product strongly favored at higher concentrations. A triangle to square dynamic system shows not only concentration dependence behavior but also guest-induced equilibrium shift.<sup>57</sup> In another report, a trinuclear triangle that contains coordinatively unsaturated ligands is transformed into a hexanuclear calixarene-type structure when additional platinum ions are available to bind to the unsaturated ligand donors.<sup>58–60</sup>

The square is unquestionably the most common of all supramolecular structures with square-planar metal ions. There are numerous examples with linear bis-monodentate ligands and *cis*-capped palladium or platinum corner units. Fujita and co-workers observed near-quantitative assembly of a square from four *cis*-constrained palladium ions and four 4,4'-bipyridine ligands.<sup>6,56,61</sup> Interestingly, some squares recognize neutral aromatic guest molecules despite their 8+ cationic charge. Analogous squares were reported by Stang and co-workers utilizing phosphino rather than

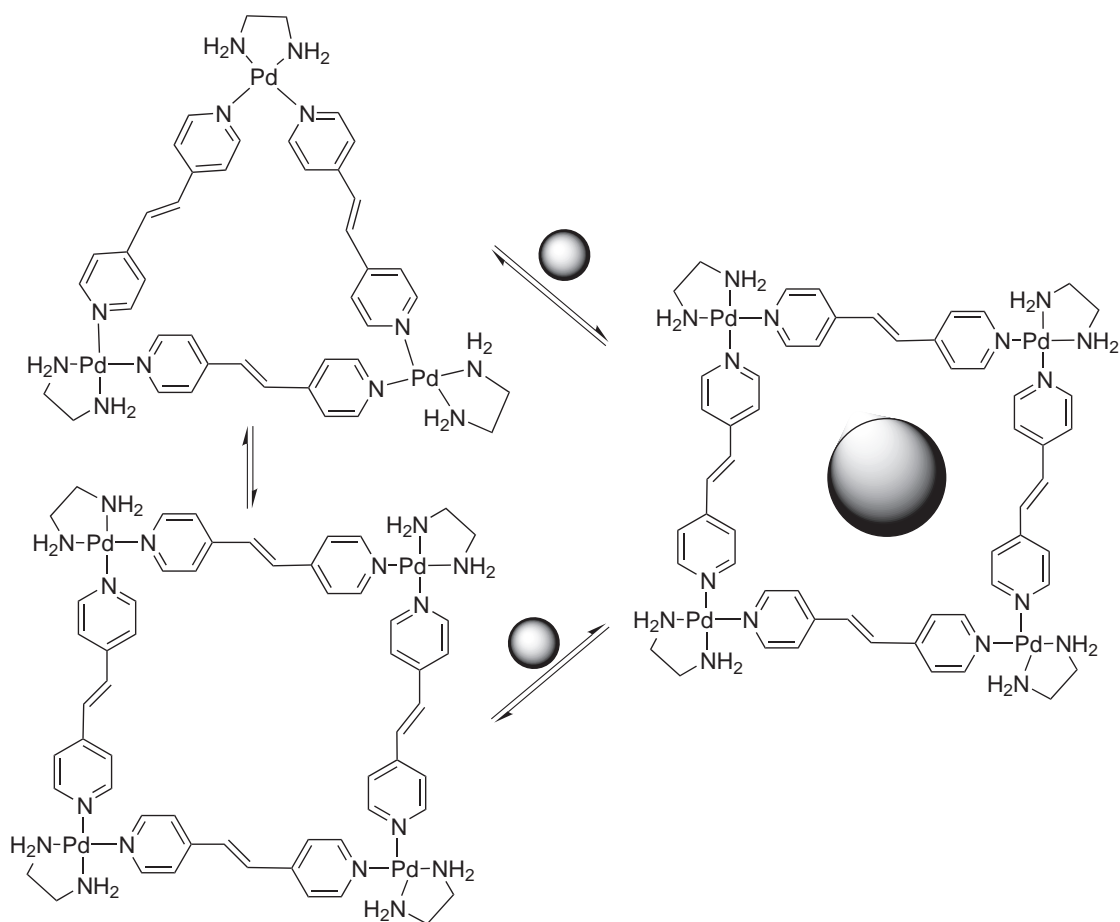


**Figure 11** The presence of a suitable guest molecule drives the triangle/square equilibrium towards the square.<sup>57</sup>

amino capping ligands.<sup>62–64</sup> Besides pyridyl donor ligands, supramolecular squares with palladium or platinum ions were also reported with uracil and other nucleobase derivatives as ligands.<sup>65</sup>

The capping ligands play an important role in determining the properties of the supramolecular square. In place of simple phosphine or amino *cis*-coordinating ligands, squares with calix-[4]-arene and crown ether modified bis-phosphine capping ligands were reported.<sup>66</sup> This creative combination of macrocyclic chemistry and supramolecular chemistry offers new possibilities in dual guest recognition. Chiral squares were obtained by appending binaphthalene groups onto the capping ligands akin to the dinuclear systems discussed earlier.<sup>67,68</sup> Furthermore, ferrocene moieties have been incorporated into capping ligands to produce organometallic/coordination square species.<sup>69</sup>

In a hybrid stepwise approach, mixed metal squares are self-assembled from precoordinated  $ML_2$  fragments and *cis*-coordinated  $M'$  ions. The metals in the  $ML_2$  fragment include titanium, rhenium, platinum, and palladium.<sup>70,71</sup> A rhenium-containing supramolecular square made using this approach exhibits luminescence which varies with different guest molecules.<sup>72</sup> Particularly interesting host–guest chemistry has been observed with assemblies in which acetylene units of the square coordinate to silver ions via the “ $\pi$  tweezers effect”.<sup>70,73</sup> The silver ions are bridged by guest molecules which contain two aromatic nitrogen atoms. This is an elegant example of post self-assembly modification (with the silver ions) followed by novel host–guest chemistry. Finally, very large supramolecular squares combines *cis*- and *trans*-coordinated platinum ions in a hybrid stepwise approach. The largest square in this family is estimated to be 3.4 nm long on each edge.<sup>74–76</sup>

Porphyrin-containing ligands are useful building blocks because of the predictable planar square conformation and well-known reaction chemistry. Porphyrins can be substituted with pyridine binding sites in either *cis* or *trans* positions. Coordination to either *cis* or *trans*  $Pd^{II}$  produces several square species (Figure 12).<sup>77–80</sup> The square supramolecular structure is observed regardless of whether the porphyrin is empty or contains a zinc ion. In an elegant demonstration of the “directed coordination vector” design principle, a discrete  $[Pd_{12}Cl_{24}L_4L'_4L''_4]$  square grid was synthesized in high yield.<sup>81</sup> In this grid structure the porphyrin units are the rigid scaffolds that support the pyridyl binding units on each ligand. A 4:4:1 ratio of the L, T, and + shaped bi-, tri-, and tetradentate ligands, along with *trans*  $Pd^{II}$  units provide all the necessary geometric pieces to create in a  $2 \times 2$  square grid.

Molecular pentagons and hexagons containing platinum bridges have been reported.<sup>82</sup> *Trans*-coordinated metal centers are bridged by ligands with  $120^\circ$  angle between the binding units (Figure 13). Due to flexibility and thermal distortion in all the bonds throughout each molecular component, the supramolecular assembly of multiple distorted pieces is capable of adopting both pentagonal and hexagonal structures.

The simplest supramolecular cage structures containing square–planar ions are morphologically analogous to dimerized cyclophanes. A series of tetragonal prisms of varying sizes was reported by Dalcanale and co-workers.<sup>83,84</sup> These supramolecular host structures have been grafted onto surfaces with the intention of allowing new applications.<sup>85</sup> In some cases, self-assembly of a cage must be induced by the presence of a suitable guest molecule. For example, trinuclear palladium cages which show strong formation dependence on the hydrophilicity of the templating guest molecule have been observed.<sup>86</sup>

Mixed palladium/tin and palladium/titanium cyclophane-type cages have been synthesized by combining ligands with both hard and soft donor groups that selectively recognize hard and soft metals in the self-assembly process.<sup>87,88</sup> A mixed  $Pd^{III}/Ni^{II}$  cage has been synthesized by Mingos and co-workers in which amidothiourea ligands discriminate between the two metal centers with nitrogen coordinated to the  $Ni^{II}$  and sulfur coordinated to the  $Pd^{III}$ .<sup>89</sup>

Several hexanuclear truncated tetrahedra have been reported.<sup>90–97</sup> Threefold symmetric ligands in combination with *cis*-coordinating palladium ions provide the requisite symmetry elements for a truncated tetrahedron. A structure reported by Steel and co-workers has idealized  $T_d$ -symmetry and forms spontaneously from the stoichiometric mixture of pyrazol-based ligands and  $Pd^{II}$  ions (Figure 14). Similarly, Fujita and co-workers have utilized ligands of various sizes to self-assemble truncated tetrahedral structures under ambient conditions with *cis*-capped  $Pd^{II}$  ions. High temperature and a guest template are necessary when synthesis of a  $Pt^{II}$  analog is desired. However, once the platinum structure is formed, it shows remarkable kinetic stability which allows the cage to be exploited as a pH-sensitive host for substrates such as *N,N*-dimethylaniline. (The  $Pd^{II}$  analog dissociates under similar conditions.) The large size of the host cavity allows encapsulation of multiple guest molecules. Due to its extensive host–guest chemistry, the hexanuclear palladium structure from Fujita and co-workers has become one of the most

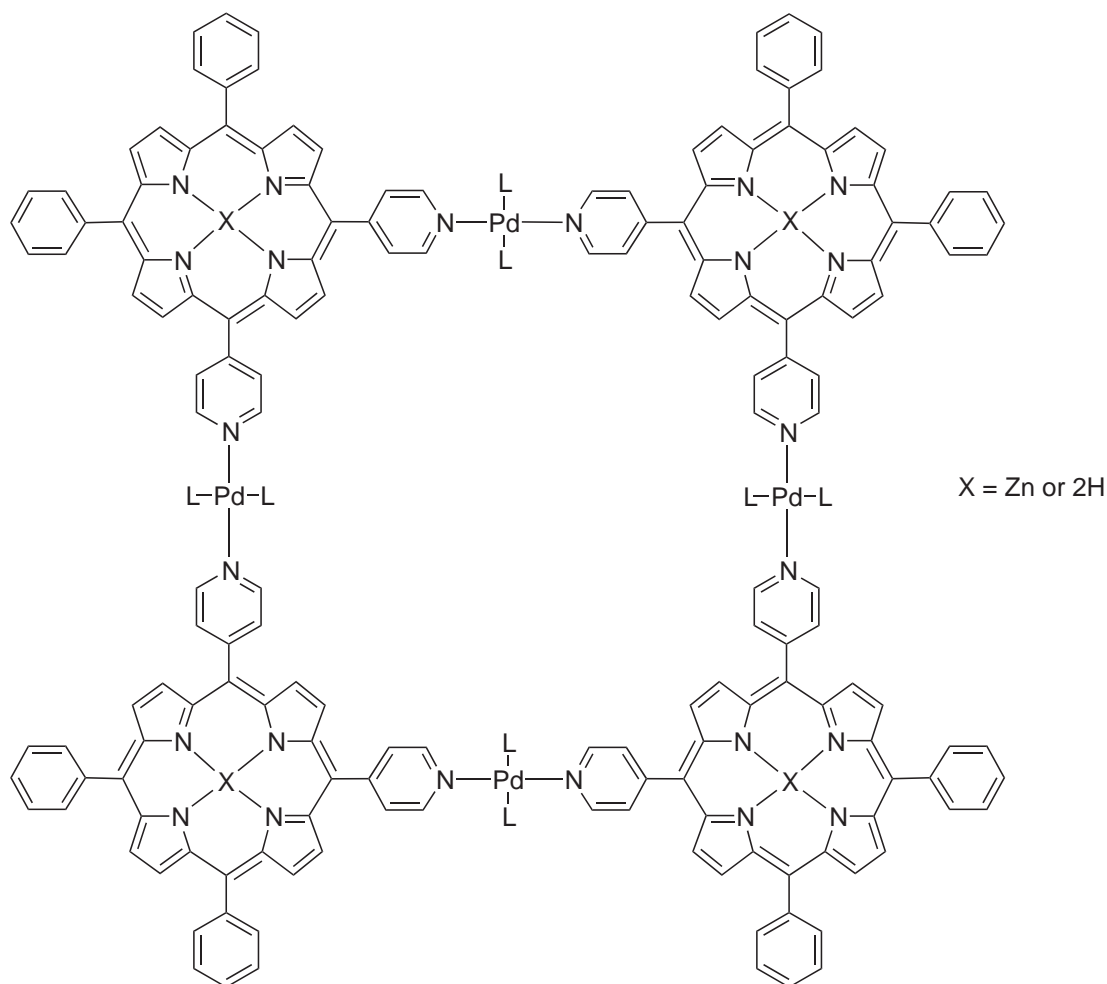


**Figure 12** A molecular square utilizes *cis*-substituted porphyrin as corner units and *trans*-coordinated Pd<sup>II</sup> units on the edges.<sup>78</sup>

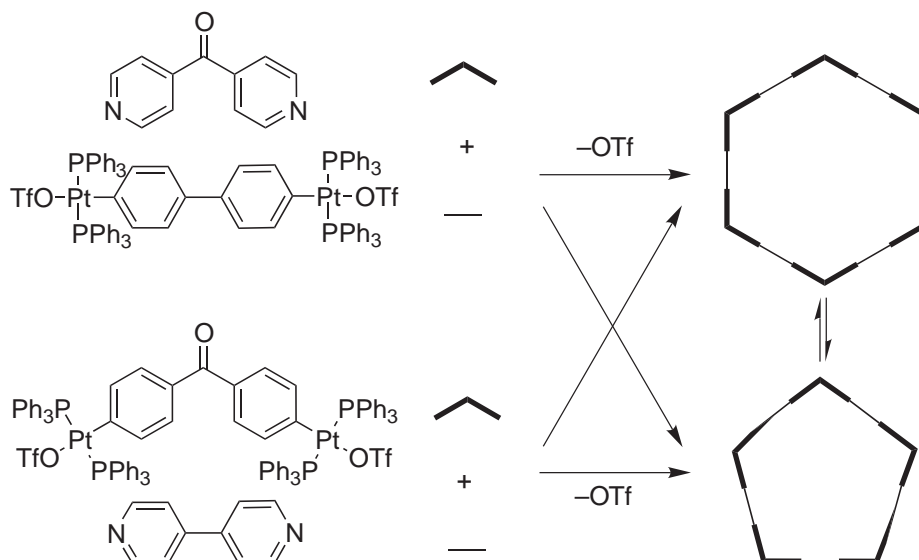


**Figure 13** The above systems are flexible enough so that the pentagonal and hexagonal structures exist in equilibrium.<sup>82</sup>



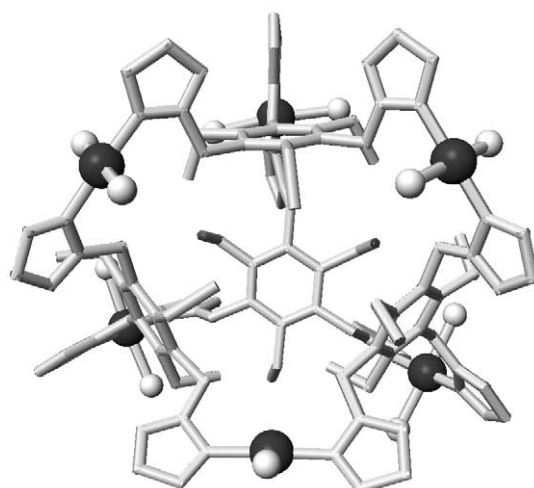


**Figure 14** Six *trans*-coordinated Pd<sup>II</sup> ions and four C<sub>3</sub>-symmetric tris-pyrazol create a truncated tetrahedron.<sup>96</sup>

important and extensively investigated of all supramolecular cage compounds (Figure 15). Chiral truncated tetrahedral structures have also been reported.<sup>97,98</sup>

Even larger supramolecular cage molecules have been created with platinum and palladium ions. Threefold symmetric tridentate and hexadentate ligands with pyridyl and pyrimidyl binding units were synthesized with the goal of forming octahedral and truncated octahedral structures.<sup>91,99–101</sup> A tridentate ligand self-assembles with *cis*-capped palladium ions to form a hexanuclear cage with *D*<sub>2h</sub> symmetry which exhibits rich host–guest chemistry.<sup>94,102,103</sup> In fact the robust structure of the cage has allowed detailed investigation of reaction chemistry inside the cavity, which is discussed later in detail.<sup>104,105</sup> A hexadentate ligand assembles in a 3–1 stoichiometry with Pd<sup>II</sup> to form a large truncated trigonal bipyramid with 18 Pd<sup>II</sup> metal (Figure 16).<sup>106</sup> Isolation of assembly intermediates implicated a stepwise formation mechanism.

Multinuclear Pd<sup>II</sup> and Pt<sup>II</sup> cage compounds have been shown to interpenetrate and form catenated species similar to catenation phenomenon observed in two-dimensional macrocyclic

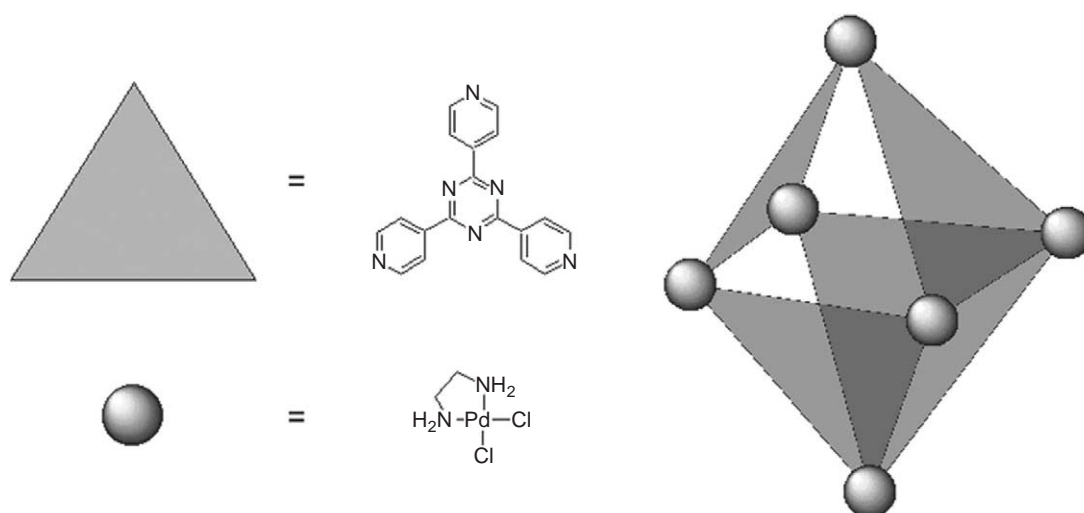


**Figure 15** A hexanuclear Pd<sup>II</sup> cage with threefold symmetric ligands partially paneling the surface of an octahedron is shown schematically.<sup>95</sup> Extensive host–guest chemistry has been reported using this [Pd<sub>6</sub>L<sub>4</sub>]<sup>12+</sup> cage.

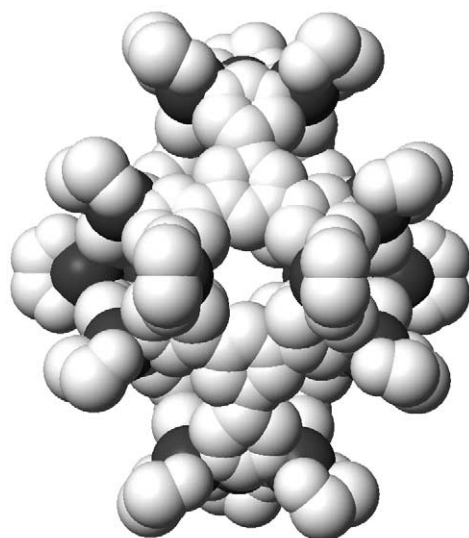


**Figure 16** Three Pd<sup>II</sup> ions connect three tris-pyrimidyl ligands at each of the two truncated axial vertices of this [Pd<sub>18</sub>L<sub>6</sub>]<sup>36+</sup> trigonal bipyramid, while four Pd<sup>II</sup> ions connect four ligands at each of the structure's three equatorial vertices.<sup>106</sup>

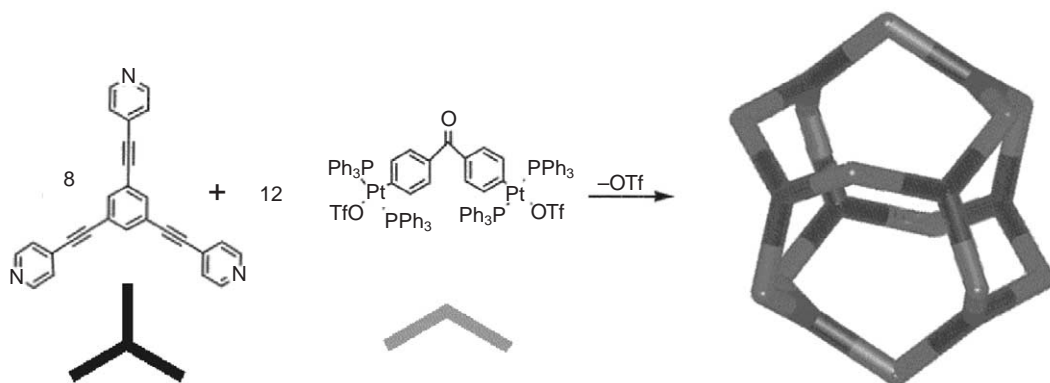


**Figure 17** A cubo octahedral Pt<sup>II</sup> cage.<sup>108</sup>

species described earlier.<sup>107</sup> The driving force for catenation is the strong and repeated  $\pi$  stacking interactions of the triazine scaffolds.

Large platinum supramolecular cubo-octahedra have been reported (Figure 17).<sup>108</sup> In an ambitious application of the “directed bonding vector” design principle, Stang and co-workers combined eight threefold symmetric planar tridentate ligands and twelve twofold symmetric ligands with 8 Pt<sup>II</sup> ions to spontaneously form the designed structures. These large structures were analyzed by pulse gradient spin echo (PGSE) NMR techniques and electrospray mass spectrometry. Structural characterization of large, complex, multi-component assemblies is a challenging issue that has been approached by the use of techniques commonly applied to biomolecules.

### 7.8.3.3 Assemblies with Four-coordinate Tetrahedral Metal Ions

As a result of tetrahedral coordination, ions such as Cu<sup>I</sup> and Ag<sup>I</sup> are amenable to helicate formation; bis-bidentate chelation around a tetrahedral metal center automatically leads to propeller-type chirality. In most cases, two bidentate chelating ligands complete the coordination

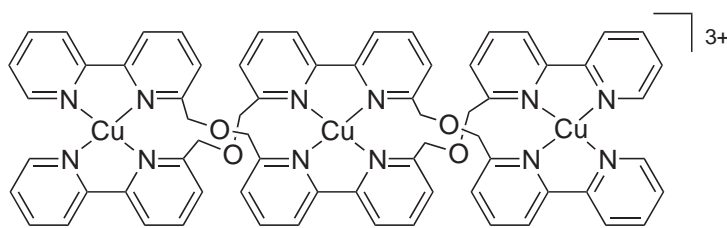


**Figure 18** An example of a trinuclear double-stranded helicate based on four-coordinate tetrahedral metal ions.<sup>10</sup>

sphere of a tetrahedral metal ion, therefore no capping ligands are necessary.  $\text{Cu}^{\text{I}}$  and  $\text{Ag}^{\text{I}}$  ions in combination with nitrogen donor ligands are the dominant metal–ligand combination for helicates. The term *double stranded helicate* was first introduced by Lehn in 1987 to describe discrete dinuclear and trinuclear copper double helices.<sup>109</sup>

A family of  $\text{Cu}^{\text{I}}$  and  $\text{Ag}^{\text{I}}$  double-stranded helicates with nuclearity ranging from 2 to 5 has been reported (Figure 18).<sup>10</sup> Each metal center is chelated by two bidentate units from different ligand strands in pseudotetrahedral geometry. The helicates exist as racemic mixtures of *P* and *M* isomers. The dinuclear racemates have a high racemization barrier of over 21 kcal mol<sup>-1</sup> for the copper species, with the higher nuclearity species expected to have even higher barriers.<sup>109</sup> The self-assembly process of the dinuclear helicates is highly cooperative because no intermediate species are isolable or observable in solution.<sup>110</sup> However, formation of the larger pentanuclear helicate takes place via a stepwise mechanism with intermediate dinuclear and trinuclear species detected by electrospray mass spectrometry.<sup>111</sup> Replacement of the ligand scaffold with larger moieties such as deoxyribonucleic acid residues or polyethylene glycol chains still yielded helicate structures.<sup>112,113</sup> Other soft bidentate chelators such as phenanthroline or thiophene have also been used to form helicates with tetrahedral ions.<sup>114–117</sup> Metal–ligand self-recognition was evidenced by the formation of nonmixed ligand helicates from a mixture of oligo-bipyridine ligands of varying lengths.<sup>118</sup> A different pool of ligands, however, generated mixed ligand helicates.<sup>119</sup> Appendage of enantiomerically pure stereocenters to the ligand induces formation of enantiomerically pure helicates; there are many examples of chiral induction in helicates.<sup>120,121</sup> Replacement of a bidentate chelator with a tridentate chelator and concurrent substitution of the tetrahedral ion with an octahedral six-coordinate ion such as  $\text{Fe}^{\text{II}}$  result in the formation of mixed-metal double-stranded helicates.<sup>122</sup> Wild and co-workers incorporated tetrahedrally coordinated  $\text{Ag}^{\text{I}}$  and  $\text{Au}^{\text{I}}$  ions with bis-bidentate phosphine ligands to produce double-stranded helicates.<sup>123,124</sup> An unusual example of a dinuclear quadruple-stranded copper cyclophane structure was reported in which hydrogen bonding of caged water molecules is integral to the structure.<sup>125</sup>

Von Zelewsky and co-workers have produced silver hexanuclear circular helicates with high enantiomeric purity by incorporating chiral pinene moieties on the bis-bipyridine ligands.<sup>126</sup> Matsumoto and co-workers have reported pH-dependent  $\text{Cu}^{\text{II}}$  circular helicate formation.<sup>127</sup> The cyclic hexameric structure dissociates to monomeric units when the imidazole nitrogen is protonated.

In addition to helical-type structures, simple dinuclear macrocycles composed of  $\text{Cu}^{\text{I}}$  and  $\text{Ag}^{\text{I}}$  with bridging ligands have been shown to exhibit guest recognition properties.<sup>128,129</sup> Larger structures such as a tetranuclear copper square have been synthesized with four  $\text{Cu}^{\text{I}}$  ions and four linear bis-bidentate ligands.<sup>130</sup> Silver and copper grids that show cooperativity during their formation have been observed.<sup>131,132</sup>

Pecoraro and co-workers have synthesized a large number of  $\text{Cu}^{\text{II}}$ ,  $\text{Ni}^{\text{II}}$ ,  $\text{Mn}^{\text{III}}$ , and mixed-metal metallacrown structures.<sup>133</sup> In these structures, generally four or five metal ions are bridged by nitrogen and oxygen donor ligands in a macrocyclic arrangement with a central cavity. The smaller metallacrowns exhibit alkali metal recognition properties akin to organic crown ethers, while the larger metallacrowns have been tailored for specific binding of large ions such as uranyl.<sup>134,135</sup>

In addition to their contributions to helicate chemistry, Lehn and co-workers have produced cage structures by combining linear oligo-pyridine ligands with threefold symmetric flat tris-bidentate ligands and copper or silver ions (Figure 19).<sup>136–139</sup> Multicompartmental trigonal cylinders of different lengths were produced by increasing the size of the linear ligands. The entire cylinder has a twist that is imposed by tetrahedral coordination of the copper centers. A large, complicated silver cage with pseudotetrahedral symmetry has been reported in which the



**Figure 19** Three tetrahedral  $\text{Cu}^{\text{I}}$  ions link each hexaazatriphenylene face to the bridging tetrapyridine sides of a trigonal capped cylinder.<sup>136</sup> Tetrahedral metal coordination imparts a helical twist to the structure.

triflate anions are critical to structural integrity.<sup>140</sup> An example of a copper-containing cage is a cuboctahedron composed of twelve  $\text{Cu}^{\text{II}}$  ions and eight tris-bidentate ligands which formed in high yield from one step (Figure 20).<sup>141</sup> The successful formation of this very large enclosed structure, composed of twenty components, exemplifies the importance of symmetry considerations in assembly design.

#### 7.8.3.4 Assemblies with Five-coordinate Metal Ions

While five-coordinate complexes are well known in mononuclear inorganic chemistry, they are unusual components in self-assembled metal–ligand structures because of the relative lack of stereoregularity in these geometries. Examples presented here include five-coordinate metal ions resulting from either the combination of terminal and bridging ligand coordination or from the exclusive interaction of bridging ligand donor atoms with the metal ions of the structure.

McCleverty, Ward and co-workers have characterized a  $[\text{Cu}_2\text{L}_2(\text{OAc})_2]^{2+}$  helicate based on square–pyramidal  $\text{Cu}^{\text{II}}$ .<sup>142</sup> One bidentate pyridyl/pyrazolyl chelate from each ligand and one monodentate terminal acetate ligand complete the copper coordination sphere.

A dynamic tetranuclear/hexanuclear assembly described by Lehn and co-workers also implicated five-coordinate  $\text{Cu}^{\text{II}}$ .<sup>143</sup> With a 1:1 ligand:metal stoichiometry,  $[\text{Cu}_4\text{L}_4]^{8+}$  species dominate

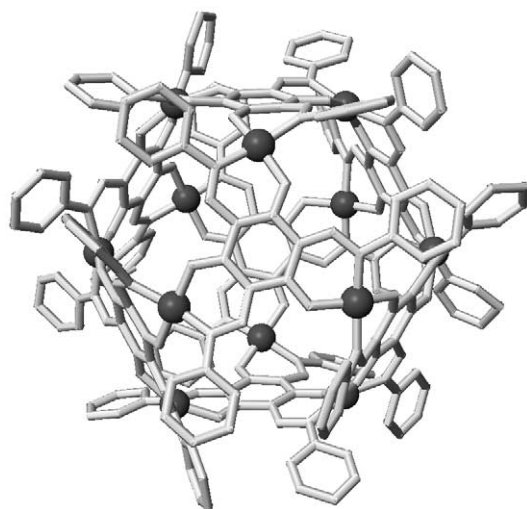


**Figure 20** This cuboctahedron contains twelve  $\text{Cu}^{\text{II}}$  ions bridged by eight threefold-symmetric triazophenyl–trihydroxybenzene ligands.<sup>141</sup> The structure is positioned to show the view down one  $C_3$  axis.

ES–MS spectra. With increasing  $\text{Cu}^{\text{II}}$  concentration, the  $[\text{Cu}_6\text{L}_6]^{12+}$  hexamer becomes the primary species in solution. Crystallographic characterization of the hexamer reveals five-coordinate metal ions, resulting from bis-bidentate coordination of adjacent ligands and monodentate coordination of acetonitrile, hydroxide, or triflate anion. In contrast, absorption spectroscopy and the solvent-dependent nature of the system indicate that the tetrameric structure contains four-coordinate tetrahedral  $\text{Cu}^{\text{II}}$ .

In their work with metal-linked resorcarenes, Beer and co-workers generated a unique hexanuclear zinc molecular loop.<sup>144</sup> Two bis-dithiocarbamate chelated  $\text{Zn}^{\text{II}}$  ions link adjacent resorcarenes, with a terminal pyridine completing the square–pyramidal coordination of each metal ion.

Self-assembled structures in which the bridging ligands saturate a five-coordinate metal ion have also been observed. Lehn and co-workers designed heteroduplex helicate systems specifically for pentacoordinate  $\text{Cu}^{\text{II}}$ : the metal ion acts to determine ligand pairing in  $[\text{Cu}_3\text{LL}']^{6+}$ -type structures. The structure of one  $[\text{Cu}_3\text{LL}']^{6+}$  helicate, in which pentacoordination brings together the tris-bidentate and tris-tridentate ligands, features a central trigonal bipyramidal  $\text{Cu}^{\text{II}}$  ion, flanked by two square pyramidal  $\text{Cu}^{\text{II}}$  ions (Figure 21).<sup>119</sup> In a related  $[\text{Cu}_3\text{LL}']^{6+}$  helicate, bidentate-bis-tridentate and tridentate-bis-bidentate ligands are also joined by  $\text{Cu}^{\text{II}}$  ions.<sup>122</sup>

### 7.8.3.5 Assemblies with Six-coordinate Octahedral Metal Ions

Whereas square–planar metal ions are incorporated most often into polygonal and polyhedral supermolecules, while tetrahedral ions are usually integrated into helical structures, six-coordinate octahedral metal ions allow facile access to many different architectures. The versatility of the octahedral metal ion derives from different modes of ligand interaction. The tris-bidentate chelation motif, which generates propeller-type chirality, lends itself to the self-assembly of helical structures as well as cages of tetrahedral symmetry. On the other hand, coordination of an octahedral ion with a tridentate facial capping ligand such as triazacyclononane leaves three orthogonal binding sites for incoming bridging ligands that correspond to the corner of a cube. Other octahedral coordination motifs such as bis-tridentate and equatorial porphyrin chelation have also been utilized in self-assembly.

A large number of helicates contain octahedrally coordinated ions such as  $\text{Fe}^{\text{II/III}}$ ,  $\text{Ti}^{\text{IV}}$ ,  $\text{Ni}^{\text{II}}$ ,  $\text{Ga}^{\text{III}}$ , and  $\text{Co}^{\text{II/III}}$ .<sup>109</sup> The use of bidentate chelators in the majority of these structures generates  $\Delta$  and  $\Lambda$  chirality at the metal centers, and arranges three ligand strands with a helical pitch. Tridentate chelators have been used to generate double-stranded helicates. For example, Lehn and co-workers have described the resolution of enantiomers of trinuclear double-stranded  $\text{Fe}^{\text{II}}$  and  $\text{Ni}^{\text{II}}$  helicates.<sup>145</sup>

Within a helicate, all of the metal centers are homoconfigurational. Intramolecular chiral induction through the incorporation of enantiomerically pure ligands effectively leads to enantiomerically pure helicates.<sup>146–150</sup> There have also been reports of the separation and enrichment of racemic helicates synthesized from achiral ligands. In a rare example, spontaneous resolution of trinuclear triple-stranded helicates was observed.<sup>151</sup> Williams and co-workers have produced helicates with labile  $\text{Co}^{\text{II}}$ , which allowed rapid racemization of the enantiomers. Subsequent oxidation of the metal centers to inert  $\text{Co}^{\text{III}}$  locked the helical twist and allowed for chiral

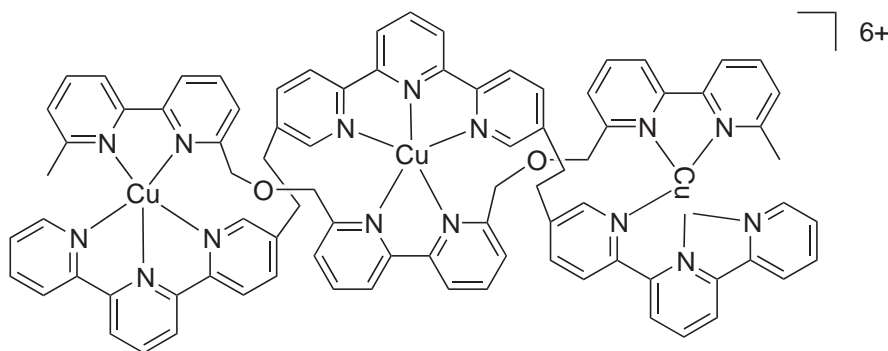


**Figure 21** A  $[\text{Cu}_3\text{LL}']^{6+}$  helicate uses five-coordinate  $\text{Cu}^{\text{II}}$  ions to link tris-bidentate and tris-tridentate ligands.<sup>119</sup>

separation and preservation of enantiomeric purity.<sup>152</sup> Efficient resolution of helicate enantiomers and asymmetric induction with a chiral counter ion has also been reported.<sup>153</sup> Intermolecular asymmetric induction in a labile dynamic helicate composed of achiral ligands has been observed.<sup>154</sup>

In some cases, the metal centers in a helicate adopt opposite chirality and produce a *meso* structure as opposed to the homoconfigurational helicate. The conversion of a chiral helicate to an achiral *meso* structure upon binding of water in its small cavity has been reported.<sup>155</sup> The sensitivity of  $M_2L_3$  assembly chirality to ligand structure has been investigated. In one system, formation of the *meso* structure was observed when the ligands have an odd number of methylene spacers, and the helicate an even number of methylene units.<sup>156,157</sup> Additional discussion of helicate chirality is provided in the section on supramolecular properties.

Self-recognition has been observed within a mixture of oligo-bipyridine ligands of varying lengths and  $Ni^{II}$  ions. Multinuclear helicates were formed with ligands of identical length.<sup>118</sup> Supramolecular self-recognition was also observed in another experiment where only homoleptic  $[Ga_2L_3]^{6-}$  helicates were observed despite a mixture of different bis-bidentate catecholamide ligands.<sup>158</sup>

Counterions are critical to the structural integrity of some helicates. Albrecht *et al.* have noted the significance of alkali cation interactions with some  $[Ti_2L_3]^{4-}$  helicate complexes.<sup>156,159</sup> In one case, the helicate forms only in the presence of  $Li^+$  or  $Na^+$ ; no discrete structure can be identified with  $K^+$ .<sup>160</sup> In another example, the helicate has a large enough cavity to bind two  $K^+$  ions (Figure 22).<sup>161</sup>

Conversion of the helicate to a more complex structure can be affected by changes to reaction conditions. A dinuclear triple-stranded helicate was isolated as a kinetic product *en route* to the formation of a pentanuclear circular helicate.<sup>162</sup> In another example, molecular modeling studies indicated that the  $M_2L_3$  helicate and  $M_4L_6$  tetrahedral structure for a certain metal–ligand system are energetically similar. Experimentally, strong host–guest interaction of the  $M_4L_6$  cavity-containing assembly was shown to shift the helicate–tetrahedron equilibrium to favor the larger structure (Figure 23).<sup>163</sup>

In addition to helicates, a number of polygonal structures have been reported with octahedral metal centers. One of the earliest molecular squares was synthesized serendipitously by Verkade and co-workers using chromium and tungsten as  $90^\circ$  corners of a square.<sup>164</sup> This example shows the strong directing effects of the carbonyl ligands that enforce *cis* coordination of the phosphorus bridging ligands.

When there are two types of binding sites on the ligand, the affinity of the sites must be orthogonal in order to have control over coordination specificity. In one example, the formation of a mixed-metal cyclophane-type cage was possible because of self-recognition between the silver and tin binding sites in the ligand (Figure 24).<sup>165</sup>

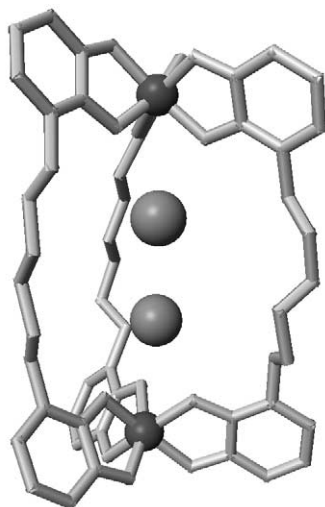


**Figure 22** Two  $K^+$  ions are located in the cavity of this  $[Ti_2L_3]^{4-}$  helicate, which is based on *bis*-catecholate ligands.<sup>162</sup> (Coordination of  $K^+$  is not shown.)

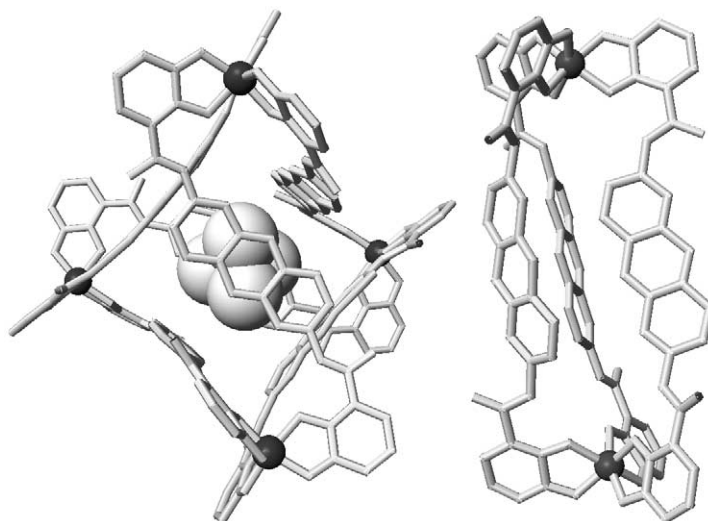


**Figure 23** A  $M_2L_3$  helicate rearranges into the  $M_4L_6$  tetrahedron in the presence of a suitable guest molecule, such as  $NMe_4^+$ .<sup>163</sup>

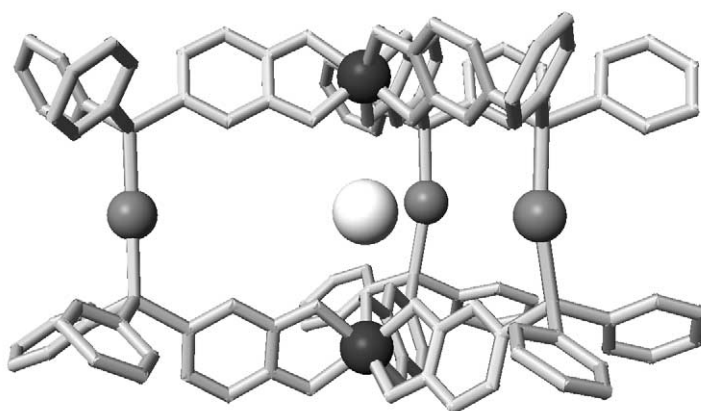


**Figure 24** In this mixed metal  $Ag^I/Sn^{IV}$  cage (with an encapsulated  $Cs^+$  ion) tris-bidentate chelation of  $Sn^{IV}$  by hard catecholate oxygen donor atoms creates threefold symmetry. Soft phosphine donor groups link the top and bottom halves of the  $D_3$ -symmetric structure through coordination of  $Ag^I$ , generating  $C_2$  elements.<sup>165</sup>

Self-assembly of a trinuclear iron triangle was reported containing a rigid alkyne-based ligand scaffold with  $60^\circ$  angle between the chelating groups.<sup>166</sup> Kajiwara and Ito have synthesized a large cavity-containing tetranuclear cobalt square from thiouracil-based ligands.<sup>167</sup> Tetranuclear ruthenium rectangles have also been synthesized.<sup>168</sup> The ruthenium ions were first chelated with oxalate bridges to form the short sides of the rectangle. The cymene half sandwich on the ruthenium acts as a *facial* cap that restricts the other coordination vectors to one quadrant and therefore directs the rectangle self-assembly. A number of tetranuclear grid structures have been reported.<sup>169–172</sup> The use of  $Fe^{II}$  and  $Co^{II}$  in many of the grid structures yields interesting magnetic and electrochemical properties. Cavity-containing rhodium cyclic hexamers have also been synthesized.<sup>173</sup>

In an unusual ligand scheme, a supramolecular triangle consisting of trimerized porphyrins was presented.<sup>174</sup> There are several other reports of utilizing the axial coordination sites of the zinc ions within porphyrin frameworks to build supramolecular squares and other structures.<sup>174–178</sup> Zinc-containing dinuclear macrocycles and helicates, which do not involve coordination to porphyrin ligands, have also been reported.<sup>179–181</sup>

Dynamic structure conversion can often be affected by the addition of a guest molecule that drives the system to form a new host assembly. Tetragonal, pentagonal, and hexagonal circular helicate structures with  $Fe^{II}$  have been produced from very similar or identical ligands.<sup>182</sup>

A large-anion ( $\text{SO}_4^{2-}$ ) template drives the formation of a hexagonal assembly while the smaller cavity of the pentagonal assembly is favored with a small anion ( $\text{Cl}^-$ ). With the insertion of an ether linkage to the tris-bipyridyl ligands, analogous tetranuclear circular helicate squares were reported (Figure 25).<sup>183</sup> These results highlight the sensitivity of final assembly structure to changes in ligand conformation and potential guest molecules.

While most examples of self-assembly involve labile metal ions, a racemic triangle/square mixture synthesized from inert  $\text{Co}^{\text{III}}$  ions has been isolated.<sup>184</sup> The triangles and squares, as well as the enantiomers of each respective structure, can be isolated because of kinetic inertness of the metal–ligand interaction. Formation of the square and triangle likely occurs via an irreversible self-assembly process in which the ratio of the triangle to square is kinetically determined. In this and other examples, inert ions have been used in self-assembly for the purpose of isolating kinetic products and potentially elucidating the self-assembly mechanism.

McCleverty, Ward, and co-workers have produced a number of multinuclear ring and cage structures.<sup>185–189</sup> An octanuclear  $\text{Co}^{\text{II}}$  circular helicate was shown to encapsulate an anionic guest in the central cavity.<sup>189</sup> A change to a larger scaffold with narrower coordinate vector angles on the ligands resulted in the formation of a tetrahedral cage. The  $[\text{Co}_4\text{L}_6]^{8+}$  cage encapsulates a  $\text{BF}_4^-$  anion in the cavity.<sup>185</sup> A remarkably large chiral truncated tetrahedral cage composed of 12  $\text{Co}^{\text{II}}$  and 18 bis-bidentate ligands was reported (Figure 26).<sup>186</sup> *Bis*-bidentate pyridyl–imine ligands have also been applied to the self-assembly of tetrahedral  $\text{M}_4\text{L}_6$  ( $\text{M} = \text{Zn}^{2+}, \text{Cu}^{2+}$ ) cages.<sup>190</sup>

Saalfrank and co-workers have described many multinuclear self-assembled rings and cages.<sup>191–198</sup> An early reported example of a tetranuclear adamantoid structure contained four  $\text{Mg}^{\text{II}}$  centers which are chelated by bis-bidentate malonate ligands (Figure 27).<sup>199</sup> A different adamantoid structure contains four  $\text{Fe}^{\text{III}}$  centers which do not show any electronic or magnetic communication within the cage framework.<sup>200</sup> In another system, a change in steric bulk and  $\pi$  stacking ability of the ligand scaffold, despite maintaining constant binding site positions, led to the formation of a  $[\text{Fe}_6\text{L}_6]$  trigonal anti-prismatic structure rather than a  $[\text{Fe}_4\text{L}_4]$  tetrahedral structure.<sup>201</sup> Many of the iron-containing structures reported by Saalfrank and co-workers have isostructural analogs containing magnesium, manganese, cobalt, cadmium, or nickel.<sup>195,198,202</sup> In reviewing his work, Saalfrank highlights the synergy between serendipity and rational design in the self-assembly of metallo-supramolecular complexes.<sup>197</sup>

Raymond and co-workers have generated a series of tetranuclear tetrahedra with  $\text{Ti}^{\text{IV}}$ ,  $\text{Fe}^{\text{III}}$ , and  $\text{Ga}^{\text{III}}$  using oxygen donor tris-bidentate chelation around the metal ions.<sup>3,15,203</sup> In an early demonstration of symmetry-based assembly design, a bis-hydroxamate ligand reacted with  $\text{Ga}^{\text{III}}$  to form the tetrahedral  $[\text{Ga}_4\text{L}_6]$  assembly (Figure 28).<sup>204</sup> The six ligands occupy the edges of the tetrahedron with the octahedrally coordinated metal centers located at the vertices. All three assembly diastereomers (having  $T$ ,  $C_3$ , and  $S_4$  symmetries) are present in solution.

On the other hand, all the metal centers in the  $T$ -symmetric  $[\text{Fe}_4\text{L}_6]^{12-}$  tetrahedron (Figure 2), containing naphthalene-bridged *bis*-catecholamide ligands, adopt identical configuration. Resolution of the racemic mixture of tetrahedra into  $\Delta\Delta\Delta\Delta$  and  $\Lambda\Lambda\Lambda\Lambda$  enantiomers has been reported.<sup>205</sup> In contrast to ligand self-recognition observed in helicates described earlier, assembly of mixed-ligand  $[\text{M}_4\text{L}^1_x\text{L}^2_{6-x}]^{12-}$  tetrahedra was observed due to the greater flexibility of the

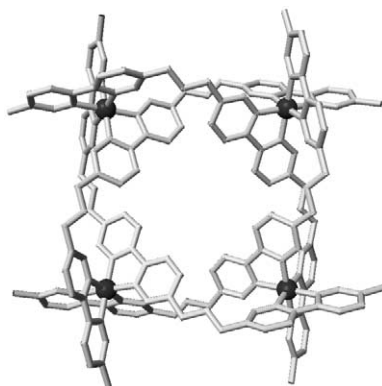


**Figure 25** The flexibility of an ether-linked tris-bipyridine ligand leads to formation of an  $[\text{Fe}_4\text{L}_4]^{8+}$  circular helicate.<sup>183</sup>



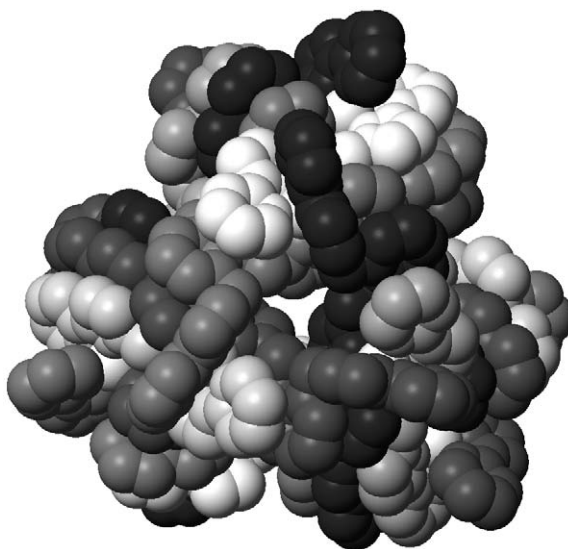


**Figure 26** An enormous chiral truncated tetrahedral cage self-assembles from 30 independent components.<sup>186</sup> The naphthy-bridged *bis*-pyrazolylpyridine ligand of this  $[\text{Co}_{12}\text{L}_{18}]^{24+}$  assembly is very slightly different in structure from a phenylene-bridged analog, which assembles a modest  $[\text{Co}_4\text{L}_6]^{8+}$  tetrahedron instead.

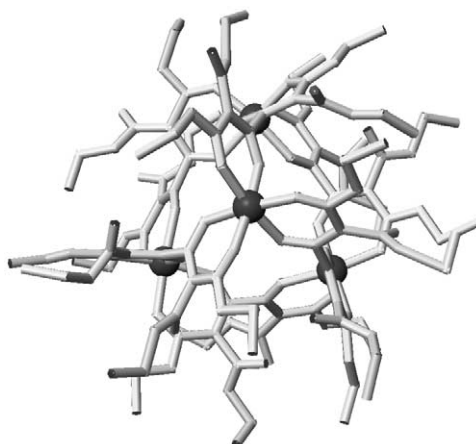


**Figure 27** Saalfrank and co-workers produced some of the earliest metallocsupramolecular cages. Here six *bis*-bidentate malonate ligands link four octahedrally coordinated  $\text{Mg}^{\text{II}}$  ions to form a tetrahedron.<sup>199</sup>

tetrahedral structure.<sup>206</sup> Enantiomerically pure  $\text{M}_4\text{L}_6$  tetrahedral structures have also been prepared by the use of chiral catecholamide ligands.<sup>207</sup>

In another example of the symmetry-based approach, a  $[\text{Ti}_4\text{L}_4]^{8-}$  tetrahedral assembly was synthesized from  $\text{C}_3$ -symmetric tris-catecholate ligands designed to occupy the faces of a tetrahedron (Figure 3).<sup>208</sup> However, the analogous  $\text{C}_3$ -symmetric tris-pyrazolone ligand did not form the anticipated  $[\text{Ga}_4\text{L}_4]$  assembly with  $\text{Ga}^{\text{III}}$  but instead produced a  $D_3$ -symmetric  $[\text{Ga}_6\text{L}_6]$  cylinder.<sup>209</sup>

Departing from tris-bidentate chelation of octahedral metal ions, a tetrahedral  $\text{Fe}^{\text{II}}$  cage was synthesized from a combination of tridentate *facial* capping phosphine ligands on each metal ion and bridging *bis*-monodentate ligands. The capping ligands direct the bridging ligands toward the orientation necessary for the tetrahedron (Figure 29).<sup>210</sup> A tetrafluoroborate anion was found inside the cavity of the tetrahedron and has been proposed as a template for cage formation.

Octanuclear cubic cages have been reported. Self-assembly of a ruthenium cube was found in which each ruthenium vertex of the cube is capped by a *facial* coordinating tridentate ligand and

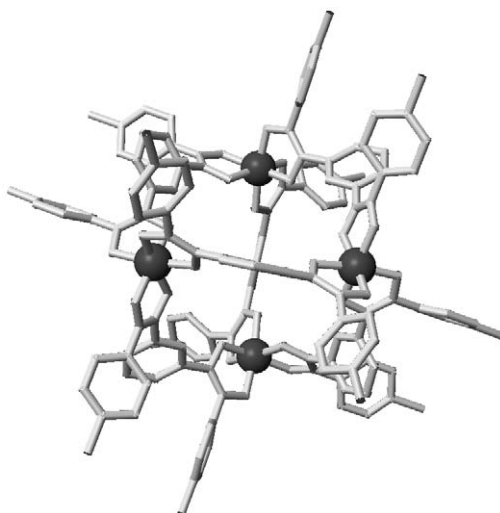


**Figure 28** Bis-bidentate hydroxamate ligands lie on the edges of a  $[Ga_4L_6]$  tetrahedron.<sup>204</sup> (View down the  $C_2$  axis.)

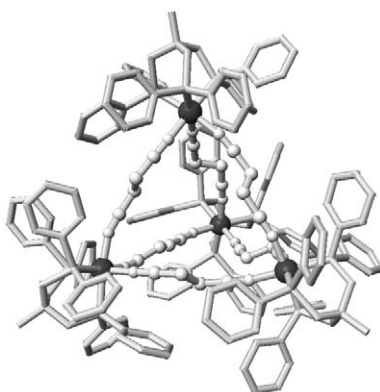


**Figure 29** This  $Fe^{II}$ -based tetrahedral cage is held together by ethylene *bis*-cyanide bridging ligands with tridentate *facial* capping ligands completing the octahedral coordination of the metal centers.<sup>210</sup>

connects to three orthogonal bridging ligands.<sup>211</sup> Long and co-workers have produced a number of discrete cubic cages with  $Co^{III}$ ,  $Cr^{III}$ , or  $Mo^{III}$  on the vertices, triazacyclononane as the capping ligand, and cyanide as the bridging ligands (Figure 30).<sup>212–216</sup> In some cases,  $Ni^{II}$  is incorporated into the faces of the cubes to produce mixed-metal assemblies. One of the goals for synthesizing these multinuclear cubes is to maximize their magnetic anisotropy in order to improve their potential as single-molecule magnets. Reversible encapsulation of solvent guest molecules has been observed. Other discrete Prussian blue analogs containing cobalt and rhodium have also been reported.<sup>217</sup> In addition, a mixed molybdenum/rhodium cube with cyanide bridging ligands and carbonyl capping ligands on the molybdenum has been synthesized.<sup>218</sup> Saalfrank and co-workers have also reported octanuclear zinc, manganese, and cadmium cages.<sup>202</sup>

### 7.8.3.6 Assemblies with Higher Coordination Number (>6) Metal Ions

Metal ions with higher (>6) coordination numbers, such as lanthanides and actinides, have less predictable coordination geometries than lower-coordination-number transition metal and main group ions. While it is difficult to incorporate these ions into rationally designed self-assembled supermolecules, a number of structures have been reported. The unique electronic properties of the *f*-elements have been exploited in supramolecular complexes to generate functional molecular devices.<sup>219</sup>

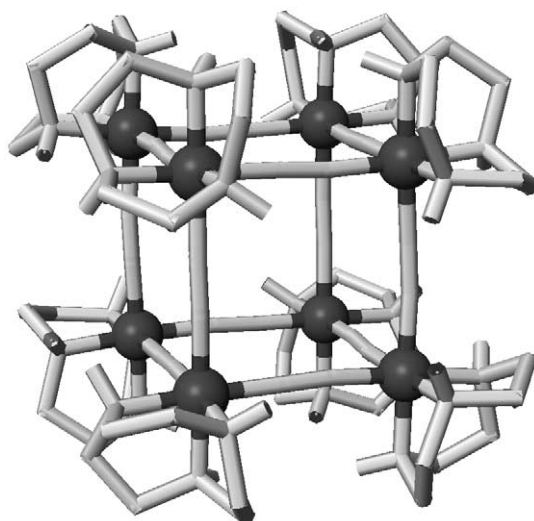


**Figure 30** *Facial* capping ligands limit this  $[\text{Co}_8(\text{CN})_{12}]^{12+}$  box to a molecular assembly by inhibiting formation of a three-dimensional network.<sup>212</sup>

The research groups of Piguet and Bünzli stand out as pioneers in the area of lanthanide helicates. They have focused on the development of predictable lanthanide–ligand coordination and its application to polynuclear structures with controllable photophysical properties.<sup>219,220</sup> They have produced homodinuclear helicates, which include the first lanthanide helicates,  $[\text{Ln}_2\text{L}_3]^{6+}$  ( $\text{Ln} = \text{La}, \text{Eu}, \text{Gd}, \text{Tb}, \text{Lu}$ ) (Figure 31).<sup>221,222</sup> These assemblies contain nine-coordinate tricapped trigonal prismatic metal centers linked by three bis-tridentate ligands with benzimidazole-based chelators. Development of carboxamide-containing ligands allowed for less water-sensitive luminescent  $[\text{Ln}_2\text{L}_3]^{6+}$  lanthanide helicates,<sup>223</sup> while the carboxylic acid-containing  $[\text{Ln}_2\text{L}_3]^{6+}$  structures self-assemble in water.<sup>224,225</sup> Piguet and Bünzli have also focused on the self-assembly of heterodinuclear structures, engineering thermodynamically differentiated binding sites. This has been accomplished with both *d-f* structures, such as  $[\text{EuZnL}_3]^{5+}$ , and with *f-f'* structures, such as  $[\text{LaEuL}_3]^{6+}$ .<sup>226,227</sup> These structures may allow access to new electronic properties.<sup>220,228</sup>

A series of water-stable  $[\text{Ln}_2\text{L}_3]$  helicates with dipicolinic acid-based ligands, which form nine-coordinate tris-tridentate  $\text{Ln}^{3+}$  complexes, has been reported. In the absence of crystal structures, a variety of spectroscopic experiments in combination with molecular modeling were performed to determine the structure.<sup>229</sup>

Dinuclear helicate-type structures in which the bridging ligands do not complete the coordination sphere of the metal ion have also been described. For example, three bidentate nitrate anions

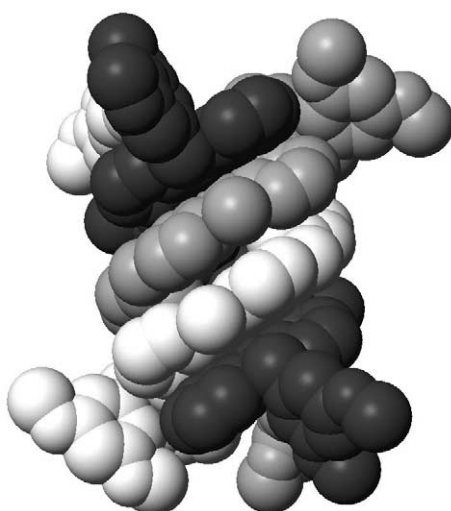


**Figure 31** Nine-coordinate  $\text{Ln}^{3+}$  ions combine with *bis*-tridentate ligands for form  $[\text{Ln}_2\text{L}_3]^{6+}$  helicates.<sup>221</sup>

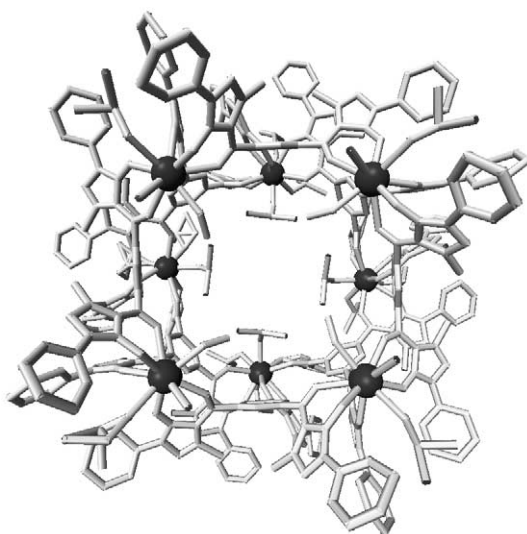


**Figure 32** A  $[La_8L_8]$  square antiprism is the product of the reaction of nine-coordinate  $La^{III}$  and tris-pyrazolone ligands.<sup>235</sup> Three tris-bidentate ligands chelate each  $La^{III}$ , with solvent molecules completing the coordination sphere.

fill the coordination sphere of  $Nd^{III}$  ions in a  $[Nd_2L_3(NO_3)_6]$  structure.<sup>230</sup> Several triply bridged  $[Ln_2L_3]^{6+}$  assemblies with  $Tb^{III}$ ,  $Sm^{III}$ , and  $Dy^{III}$  have been reported with bis-pyrazolone ligands.<sup>231–233</sup> These structures are eight-coordinate, with three bidentate pyrazolone chelates and two DMF molecules bound to each metal ion. The lanthanide ion coordination geometry was described as distorted square-pyramidal.

A hexanuclear  $(Cp^*SmCN)_6$  ring was reported as the unexpected product of hydrogenation of a mononuclear  $Sm^{III}$  imino-amido complex.<sup>234</sup>

A three-dimensional  $[La_8L_8]$  square-antiprism ( $D_{4d}$  symmetric) was created from nine-coordinate  $La^{III}$  ions and a  $C_3$ -symmetric tris-pyrazolone ligand (Figure 32).<sup>235</sup> Each  $La^{III}$  coordinates to three ligands and each tris-bidentate ligand coordinates to three  $La^{III}$  ions. Solvent molecules act as capping ligands and fill the residual coordination sites at each metal center. The chemistry of this ligand with  $Ga^{III}$  was discussed earlier.

Mazzanti and co-workers have synthesized several unique Ln-based supramolecular topologies. In the trinuclear  $[La_3L_2(OTf)_4(H_2O)_2]^{5+}$  complex each  $La^{III}$  is coordinated by one terpy moiety from each of the tris-tridentate ligands.<sup>236</sup> The  $La^{III}$  ion is 10-coordinate with triflate and water molecules completing the coordination sphere. A hexameric  $[Eu \subset Eu_6L_6]^{9+}$  ring was created from the tetradentate terpyridine carboxylic acid, which is able to bridge one  $Eu^{III}$  to another through a free carbonyl oxygen (Figure 33).<sup>237</sup> Each  $Eu^{III}$  has nine-coordinate distorted monocapped square-antiprismatic geometry, while the central  $Eu^{III}$  is coordinated by six free carbonyl oxygens in an octahedral geometry.

### 7.8.3.7 Assemblies with Eight-coordinate Dimetal Ions

A series of supramolecular assemblies based on dimolybdenum and dirhodium building blocks has been reported (Figure 34).<sup>238–242</sup> The dimetal unit functions as an eight-coordinate double-decker square-planar ion. Triangles and squares were produced and demonstrate the utility of dimetal units as building blocks for complex supramolecular architectures. In the solid state, stacking of the triangles and squares leads to large channels.

## 7.8.4 PROPERTIES OF COORDINATION SUPRAMOLECULAR ASSEMBLIES

The properties discussed in this section include the fundamental thermodynamic and kinetic parameters of self-assembly, the dynamic behavior of supramolecular ensembles and chirality at the supramolecular level.

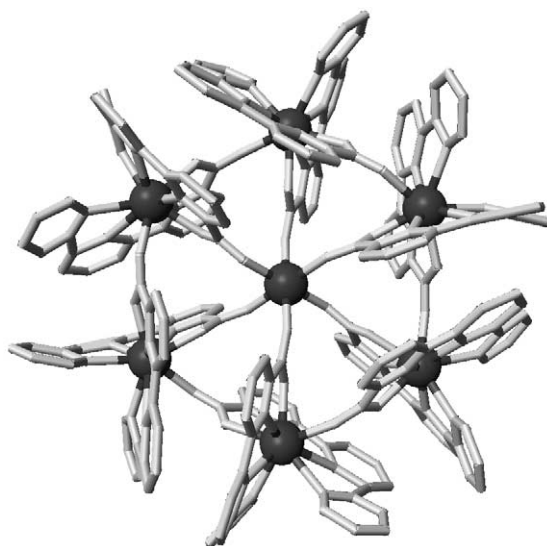


**Figure 33** Six nine-coordinate  $\text{Eu}^{\text{III}}$  ions form a  $[\text{Eu}_6\text{L}_{12}]^{6+}$  wheel which binds one six-coordinate  $\text{Eu}^{\text{III}}$ . Each of the ring  $\text{Eu}^{\text{III}}$  ions is coordinated by two tetradentate ligands, and each of these links to the next metal center through a free carbonyl oxygen.<sup>237</sup>

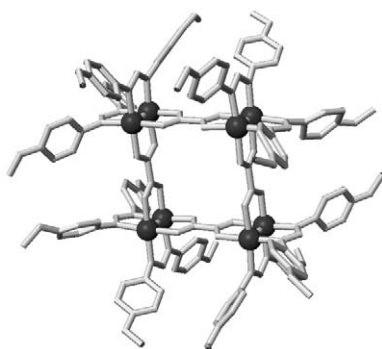


**Figure 34** Dimolybdenum units serve as the corners for a fumarate-linked square.<sup>242</sup>

A number of research groups have investigated the thermodynamics of metallo-supramolecular self-assembly, particularly for the assembly of helicate-type structures.<sup>243</sup> In some cases intermediate structures can be detected and stepwise formation constants can be determined. Lehn and co-workers first described the concept of positive cooperativity in such supramolecular systems.<sup>244,245</sup> They determined that an initial step in the assembly of a structure facilitates those that follow; sequential metal–ligand binding equilibria are thus nonlinear. Positive cooperativity is quantified with Scatchard and Hill-type analyses and is a clear demonstration of the molecular programming and self-organization of supramolecular assemblies.<sup>245–247</sup>

Solution dynamic study of mononuclear metal–ligand complexes is well established.<sup>248</sup> The description of self-assembly reaction dynamics presents new challenges in coordination chemistry.<sup>249</sup> The synthesis of assemblies from inert components produces a picture of stepwise complex formation.<sup>250</sup> However, it is unclear if self-assembly of labile components proceeds through a clean stepwise mechanism.

The dynamic assembly of some helicates have been investigated.<sup>251,252</sup> Spectrophotometric kinetic studies of tricuprous double-stranded helicates  $[\text{Cu}_3\text{L}_2]^{6+}$  indicated a stepwise mechanism, involving several kinetic intermediates.<sup>252</sup> These studies highlighted the rearrangement of misaligned components—structural self-correction—as an important mechanistic process.

In cavity-containing assemblies, addition of a guest template or a change in solution conditions may prompt the conversion of one structure to another, and in some cases these processes have been monitored. For example, conversion of a dinuclear triple-stranded helicate  $\text{M}_2\text{L}_3$  to a tetranuclear tetrahedron  $\text{M}_4\text{L}_6$  with the addition of an appropriate guest template was reported.<sup>253</sup>

The reaction was followed over 24 h at 70 °C, but no intermediate species were detected. The helicate might be considered as an intermediate in the formation of the tetrahedron, although it is not clear that the same mechanism of self-assembly is operable in the *de novo* formation of the tetrahedron from metal, ligand, and guest components.

The conversion of a triferrous linear triple helicate to a pentaferrous circular helicate with the addition of chloride as a guest for the larger structure has been observed.<sup>254</sup> In this system, the helicate is determined to be a kinetic product during circular helicate formation. The study highlights the role of kinetic control in self-assembly processes and the complexity of possible mechanistic interpretations.

Kinetic control was invoked in the study of  $[\text{Pt}_{30}\text{L}_{20}]^{60+}$  dodecahedron formation.<sup>255</sup> Initial formation of *syn* ring fragments (rings in which the growing ends extend in the same direction) facilitates further ring closures. Nucleation of the structure by initial ring formation seems to inhibit growth of unfavorable species.

Another area of supramolecular dynamics pertains to the racemization of chiral assemblies. There are numerous examples of chiral self-assembled coordination structures in which chirality is exhibited not only on the molecular level, but also on the supramolecular level. For example, helicates are inherently chiral even when assembled from achiral components. The *P* and *M* configurations of helicates are exclusively the properties of the supramolecular ensemble.

The racemization of dinuclear triple-stranded helicates has been studied.<sup>256</sup> These complexes adopt either  $\Delta\Delta$  or  $\Lambda\Lambda$  configurations arising from the tris-bidentate coordinated metal centers. A mononuclear tris-catecholate complex  $\text{ML}_3$  racemizes via a Bailar twist mechanism. Linked tris-catecholate metal centers would be expected to racemize at the same rate as that of the mononuclear complex in the absence of mechanical coupling. However, when two tris-catecholate complexes are linked in a helicate, the racemization of the  $\text{M}_2\text{L}_3$  structure (from  $\Delta\Delta$  to  $\Lambda\Lambda$ ) slows by a factor of one hundred,<sup>257</sup> while racemization of the four tris-catecholate metal centers in an  $\text{M}_4\text{L}_6$  tetrahedron  $\text{M}_4\text{L}_6$  is not observed.<sup>258</sup> Although the components of these assemblies are labile, the chiral tetrahedral structure displays structural inertness.

The effect of mechanical coupling on helicate racemization has also been investigated in a  $[\text{Co}_2\text{L}_3]^{4+}$  system. The authors attribute the slowing of  $\text{Co}^{\text{II}}$  racemization in the helicate (on the order of  $10^6$ ) to a dissociative mechanism.<sup>259,260</sup> The rigidity of their bis-benzimidazole-pyridine-based helicate prevents racemization without dissociation of one  $\text{Co}^{\text{II}}$  from the structure.

A more recent report describes the concerted inversion of a  $[\text{Mg}_4\text{L}_6]^{4+}$  tetrahedron from  $\Delta\Delta\Delta\Delta$  to  $\Lambda\Lambda\Lambda\Lambda$  configuration at the four metal centers.<sup>261</sup> The flexibility of the tetrahedral ligand scaffold permits sterically unhindered simultaneous atropenantiomerization of the six ligands. This motion leads to synchronized Bailar twisting at the four tris-bidentate chelated  $\text{Mg}^{2+}$  centers and the isomerization of the assembly.

Three general categories of chiral resolution or induction have been reported in supramolecular complexes. The first is the rare case of spontaneous resolution such as in the classic example of quartz.<sup>262</sup> Lehn and co-workers have reported a system in which helicates of the same twist direction spontaneous aggregate and separate from the opposite enantiomer.<sup>263,264</sup> A second category of chiral induction involves covalent attachment of a chiral center to the ligands of an assembly. The ligands can be either the bridging or capping type as long as the stereocenter communicates its chirality to the extended supramolecular structure. Many examples of this type have been described in the previous sections. Lastly, chiral resolution can be achieved via intermolecular asymmetric induction. Williams and co-workers resolved cobalt-based helicates by passing the racemic mixture of helicates through a chiral column. The helicates, locked into their respective configurations by the kinetically inert  $\text{Co}^{\text{III}}$  centers, cannot racemize once they exit the chiral column.<sup>153</sup> The  $\text{M}_4\text{L}_6$  tetrahedron presented in Figure 2 exists as a racemic mixture of homochiral enantiomers which are inert to racemization and has been separated by asymmetric ion pairing.<sup>205</sup>

### 7.8.5 FUNCTION OF COORDINATION SUPRAMOLECULAR ASSEMBLIES

Recent progress has been made in using cavity-containing supramolecular hosts to facilitate catalysis. The cavity provides a unique nano-environment isolated from bulk solvent, and achieves a high local concentration of reagents. For example, Fujita and co-workers reported heterogeneous Wacker oxidation of styrene in water within the cavity of a  $[\text{Pd}_6\text{L}_4]^{12}$  cage complex.<sup>104</sup> The nano-cavity acts as a phase transfer catalyst for styrene and product between hexane and

aqueous phases. No reaction occurs when styrene is treated with the catalyst in the absence of the nanovessel; the authors suggest this as strong evidence that the catalyzed reaction proceeds inside the cavity. The same cage complex is also able to effect the isomerization of allylbenzene to  $\beta$ -methylstyrene in 50% yield using a heterogeneous mixture.<sup>100</sup> Interestingly, the catalytic activity is inhibited by the presence of guest molecules that are bound more strongly than the reactants. Inter-molecular [2+2] photo-addition reactions are accelerated and stereo-regulated inside the confined cavity.<sup>265</sup> For example, acenaphthylene dimerizes inside the cage to form exclusively *syn* product. Fujita and co-workers have also reported the stabilization and synthesis of otherwise labile cyclic trimers of siloxanes within one of their nanocages.<sup>103,105</sup> The hydrophobic environment of the cavity allows the hydrophobic substrates to undergo reaction in aqueous media. Similarly, Raymond and co-workers have described the stabilization of a reactive ketone-phosphine adduct inside a hydrophobic cage cavity because of isolation from aqueous solvent.<sup>266</sup>

Another type of catalytic system being developed involves the tethering of a catalytically active metal center to the cavity of a supramolecular porphyrin square.<sup>267</sup> In this example, the square cavity serves as a protective barrier that significantly lengthens catalyst lifetime.

One route towards practical application involves attachment of the coordination structure to a surface. In one example, Reinhoudt, Dalcanale, and co-workers have appended palladium cyclophane cages to a gold surface.<sup>85</sup>

## 7.8.6 OUTLOOK

Self-assembly is a powerful synthetic tool for the formation of large, multifunctional metal-ligand complexes. As the numerous examples in this section illustrates, most metal ions can be incorporated into supramolecular coordination structures via self-assembly. New structures that further our understanding of structural design principles are routinely being reported. In addition, the mechanisms of self-assembly and host/guest chemistry of the self-assembled structures are increasingly being studied.

## 7.8.7 REFERENCES

1. Lehn, J. M. *Supramolecular Chemistry: Concepts and Perspectives* **1995**, VCH: Weinheim.
2. Leininger, S.; Olenyuk, B.; Stang, P. J. *Chem. Rev.* **2000**, *100*, 853–907.
3. Caulder, D. L.; Raymond, K. N. *J. Chem. Soc., Dalton Trans.* **1999**, 1185–1200.
4. Holliday, B. J.; Mirkin, C. A. *Angew. Chem., Int. Ed. Engl.* **2001**, *40*, 2022–2043.
5. Cotton, F. A.; Lin, C.; Murillo, C. A. *Proc. Natl. Acad. Sci. USA* **2002**, *99*, 4810–4813.
6. Fujita, M.; Sasaki, O.; Mitsuhashi, T.; Fujita, T.; Yazaki, J.; Yamaguchi, K.; Ogura, K. *Chem. Commun.* **1996**, 1535–1536.
7. Swiegers, G. F.; Malefetse, T. J. *Chem. Rev.* **2000**, *100*, 3483–3537.
8. Swiegers, G. F.; Malefetse, T. J. *Coord. Chem. Rev.* **2002**, *225*, 91–121.
9. Piguet, C.; Bernardinelli, G.; Hopfgartner, G. *Chem. Rev.* **1997**, *97*, 2005–2062.
10. Albrecht, M. *Chem. Rev.* **2001**, *101*, 3457–3497.
11. Johnson, D. W.; Raymond, K. N. *Supramol. Chem.* **2001**, *13*, 639–659.
12. Fujita, M. *Chem. Soc. Rev.* **1998**, *27*, 417–425.
13. Venuti, M. C.; Rastetter, W. H.; Neilands, J. B. *J. Med. Chem.* **1979**, *22*, 123–124.
14. Weitz, F. L.; Raymond, K. N. *J. Am. Chem. Soc.* **1979**, *101*, 2728–2731.
15. Caulder, D. L.; Bruckner, C.; Powers, R. E.; Konig, S.; Parac, T. N.; Leary, J. A.; Raymond, K. N. *J. Am. Chem. Soc.* **2001**, *123*, 8923–8938.
16. Piguet, C.; Bernardinelli, G.; Williams, A. F. *Inorg. Chem.* **1989**, *28*, 2920–2925.
17. Ruttimann, S.; Piguet, C.; Bernardinelli, G.; Bocquet, B.; Williams, A. F. *J. Am. Chem. Soc.* **1992**, *114*, 4230–4237.
18. Suzuki, T.; Kotsuki, H.; Isobe, K.; Moriya, N.; Nakagawa, Y.; Ochi, M. *Inorg. Chem.* **1995**, *34*, 530–531.
19. Schneider, R.; Hosseini, M. W.; Planeix, J. M.; DeCian, A.; Fischer, J. *Chem. Commun.* **1998**, 1625–1626.
20. Loi, M.; Hosseini, M. W.; Jouaiti, A.; De Cian, A.; Fischer, J. *Eur. J. Inorg. Chem.* **1999**, 1981–1985.
21. Caradoc-Davies, P. L.; Hanton, L. R.; Lee, K. *Chem. Commun.* **2000**, 783–784.
22. Schuh, W.; Kopacka, H.; Wurst, K.; Peringer, P. *Eur. J. Inorg. Chem.* **2002**, 2202–2206.
23. Sun, W. Y.; Fan, J.; Yu, K. B. *Acta Chim. Sin.* **2001**, *59*, 1102–1105.
24. Su, C.-Y.; Cai, Y.-P.; Chen, C.-L.; Lissner, F.; Kang, B.-S.; Kaim, W. *Angew. Chem., Int. Ed. Engl.* **2002**, *41*, 3371–3375.
25. Hollatz, C.; Schier, A.; Schmidbaur, H. *Inorg. Chem. Commun.* **1998**, *1*, 115–117.
26. Schmidbaur, H. *Chem. Soc. Rev.* **1995**, *24*, 391–400.
27. Schmidbaur, H. *Nature* **2001**, *413*, 31–33.
28. Pyykkö, P. *Chem. Rev.* **1997**, *97*, 597–636.
29. Hartshorn, C. M.; Steel, P. J. *Inorg. Chem.* **1996**, *35*, 6902–6903.
30. Hartshorn, C. M.; Steel, P. J. *J. Chem. Soc., Dalton Trans.* **1998**, 3935–3940.

31. Hartshorn, C. M.; Steel, P. J. *J. Chem. Soc., Dalton Trans.* **1998**, 3927–3933.
32. Kitagawa, S.; Kondo, M.; Kawata, S.; Wada, S.; Maekawa, M.; Munakata, M. *Inorg. Chem.* **1995**, *34*, 1455–1465.
33. Hamblin, J.; Jackson, A.; Alcock, N. W.; Hannon, M. J. *J. Chem. Soc., Dalton Trans.* **2002**, 1635–1641.
34. Habata, Y.; Yamashita, Y.; Akabori, S. *J. Chem. Soc., Dalton Trans.* **2001**, 966–968.
35. McMorran, D. A.; Pfadenhauer, S.; Steel, P. J. *Inorg. Chem. Commun.* **2002**, *5*, 449–451.
36. Su, C.-Y.; Cai, Y.-P.; Chen, C.-L.; Zhang, H.-X.; Kang, B.-S. *J. Chem. Soc., Dalton Trans.* **2001**, 359–361.
37. Constable, E. C.; Elder, S. M.; Healy, J.; Ward, M. D.; Tocher, D. A. *J. Am. Chem. Soc.* **1990**, *112*, 4590–4592.
38. McMorran, D. A.; Steel, P. J. *Angew. Chem., Int. Ed. Engl.* **1998**, *37*, 3295–3297.
39. Fujita, M.; Nagao, S.; Iida, M.; Ogata, K.; Ogura, K. *J. Am. Chem. Soc.* **1993**, *115*, 1574–1576.
40. Fujita, M.; Ibukuro, F.; Seki, H.; Kamo, O.; Imanari, M.; Ogura, K. *J. Am. Chem. Soc.* **1996**, *118*, 899–900.
41. Fujita, M.; Ibukuro, F.; Hagihara, H.; Ogura, K. *Nature* **1994**, *367*, 720–723.
42. Fujita, M. *Acc. Chem. Res.* **1999**, *32*, 53–61.
43. Fujita, M.; Ibukuro, F.; Yamaguchi, K.; Ogura, K. *J. Am. Chem. Soc.* **1995**, *117*, 4175–4176.
44. Fujita, M.; Aoyagi, M.; Ibukuro, F.; Ogura, K.; Yamaguchi, K. *J. Am. Chem. Soc.* **1998**, *120*, 611–612.
45. Ibukuro, F.; Fujita, M.; Yamaguchi, K.; Sauvage, J. P. *J. Am. Chem. Soc.* **1999**, *121*, 11014–11015.
46. Schneider, R.; Hosseini, M. W.; Planeix, J. M.; De Cian, A.; Fischer, J. *Chem. Commun.* **1998**, 1625–1626.
47. Stang, P. J.; Olenyuk, B.; Chen, K. C. *Synthesis-Stuttgart* **1995**, 937–938.
48. Stang, P. J.; Chen, K. C.; Arif, A. M. *J. Am. Chem. Soc.* **1995**, *117*, 8793–8797.
49. Stang, P. J.; Chen, K. C. *J. Am. Chem. Soc.* **1995**, *117*, 1667–1668.
50. Stang, P. J.; Zhdankin, V. V. *Chem. Rev.* **1996**, *96*, 1123–1178.
51. Olenyuk, B.; Whiteford, J. A.; Stang, P. J. *J. Am. Chem. Soc.* **1996**, *118*, 8221–8230.
52. Habicher, T.; Nierengarten, J. F.; Gramlich, V.; Diederich, F. *Angew. Chem., Int. Ed. Engl.* **1998**, *37*, 1916–1919.
53. Hall, J. R.; Loeb, S. J.; Shimizu, G. K. H.; Yap, G. P. A. *Angew. Chem., Int. Ed. Engl.* **1998**, *37*, 121–123.
54. Lai, S. W.; Chan, M. C. W.; Peng, S. M.; Che, C. M. *Angew. Chem., Int. Ed. Engl.* **1999**, *38*, 669–671.
55. Baker, A. T.; Crass, J. K.; Maniska, M.; Craig, D. C. *Inorg. Chim. Acta* **1995**, *230*, 225–229.
56. Fujita, M.; Ogura, G. *Bull. Chem. Soc. Jpn.* **1996**, *69*, 1471–1482.
57. Lee, S. B.; Hwang, S. G.; Chung, D. S.; Yun, H. S.; Hong, J. I. *Tetrahedron Lett* **1998**, *39*, 873–876.
58. Schnebeck, R. D.; Freisinger, E.; Glahe, F.; Lippert, B. *J. Am. Chem. Soc.* **2000**, *122*, 1381–1390.
59. Schnebeck, R. D.; Freisinger, E.; Lippert, B. *Angew. Chem., Int. Ed. Engl.* **1999**, *38*, 168–171.
60. Schnebeck, R. D.; Randaccio, L.; Zangrando, E.; Lippert, B. *Angew. Chem., Int. Ed. Engl.* **1998**, *37*, 119–121.
61. Fujita, M.; Yazaki, J.; Ogura, K. *J. Am. Chem. Soc.* **1990**, *112*, 5645–5647.
62. Cao, D. H.; Chen, K. C.; Fan, J.; Manna, J.; Olenyuk, B.; Whiteford, J. A.; Stang, P. J. *Pure Appl. Chem.* **1997**, *69*, 1979–1986.
63. Stang, P. J.; Cao, D. H. *J. Am. Chem. Soc.* **1994**, *116*, 4981–4982.
64. Stang, P. J.; Cao, D. H.; Saito, S.; Arif, A. M. *J. Am. Chem. Soc.* **1995**, *117*, 6273–6283.
65. Rauter, H.; Mutikainen, I.; Blomberg, M.; Lock, C. J. L.; Amochoa, P.; Freisinger, E.; Randaccio, L.; Zangrando, E.; Chiarparin, E.; Lippert, B. *Angew. Chem., Int. Ed. Engl.* **1997**, *36*, 1296–1301.
66. Stang, P. J.; Cao, D. H.; Chen, K. C.; Gray, G. M.; Muddiman, D. C.; Smith, R. D. *J. Am. Chem. Soc.* **1997**, *119*, 5163–5168.
67. Muller, C.; Whiteford, J. A.; Stang, P. J. *J. Am. Chem. Soc.* **1998**, *120*, 9827–9837.
68. Stang, P. J.; Olenyuk, B. *Angew. Chem., Int. Ed. Engl.* **1996**, *35*, 732–736.
69. Stang, P. J.; Olenyuk, B.; Fan, J.; Arif, A. M. *Organometallics* **1996**, *15*, 904–908.
70. Whiteford, J. A.; Lu, C. V.; Stang, P. J. *J. Am. Chem. Soc.* **1997**, *119*, 2524–2533.
71. Whiteford, J. A.; Rachlin, E. M.; Stang, P. J. *Angew. Chem., Int. Ed. Engl.* **1996**, *35*, 2524–2529.
72. Slone, R. V.; Yoon, D. I.; Calhoun, R. M.; Hupp, J. T. *J. Am. Chem. Soc.* **1995**, *117*, 11813–11814.
73. Whiteford, J. A.; Stang, P. J.; Huang, S. D. *Inorg. Chem.* **1998**, *37*, 5595–5601.
74. Manna, J.; Kuehl, C. J.; Whiteford, J. A.; Stang, P. J. *Organometallics* **1997**, *16*, 1897–1905.
75. Manna, J.; Kuehl, C. J.; Whiteford, J. A.; Stang, P. J.; Muddiman, D. C.; Hofstadler, S. A.; Smith, R. D. *J. Am. Chem. Soc.* **1997**, *119*, 11611–11619.
76. Manna, J.; Whiteford, J. A.; Stang, P. J.; Muddiman, D. C.; Smith, R. D. *J. Am. Chem. Soc.* **1996**, *118*, 8731–8732.
77. Stang, P. J.; Fan, J.; Olenyuk, B. *Chem. Commun.* **1997**, 1453–1454.
78. Drain, C. M.; Fischer, R.; Nolen, E. G.; Lehn, J. M. *J. Chem. Soc., Chem. Commun.* **1993**, 243–245.
79. Drain, C. M.; Batteas, J. D.; Flynn, G. W.; Milic, T.; Chi, N.; Yablon, D. G.; Sommers, H. *Proc. Natl. Acad. Sci. USA* **2002**, *99*, 6498–6502.
80. Fan, J.; Whiteford, J. A.; Olenyuk, B.; Levin, M. D.; Stang, P. J.; Fleischer, E. B. *J. Am. Chem. Soc.* **1999**, *121*, 2741–2752.
81. Drain, C. M.; Nifiatis, F.; Vasenko, A.; Batteas, J. D. *Angew. Chem., Int. Ed. Engl.* **1998**, *37*, 2344–2347.
82. Stang, P. J.; Persky, N. E.; Manna, J. *J. Am. Chem. Soc.* **1997**, *119*, 4777–4778.
83. Jacopozzi, P.; Dalcanale, E. *Angew. Chem., Int. Ed. Engl.* **1997**, *36*, 613–615.
84. Pirondini, L.; Bertolini, F.; Cantadori, B.; Ugozzoli, F.; Massera, C.; Dalcanale, E. *Proc. Natl. Acad. Sci. USA* **2002**, *99*, 4911–4915.
85. Levi, S. A.; Guatteri, P.; van Veggel, F. C. J. M.; Vancso, G. J.; Dalcanale, E.; Reinhoudt, D. N. *Angew. Chem., Int. Ed. Engl.* **2001**, *40*, 1892–1896.
86. Fujita, M.; Nagao, S.; Ogura, K. *J. Am. Chem. Soc.* **1995**, *117*, 1649–1650.
87. Sun, X. K.; Johnson, D. W.; Caulder, D. L.; Powers, R. E.; Raymond, K. N.; Wong, E. H. *Angew. Chem., Int. Ed. Engl.* **1999**, *38*, 1303–1307.
88. Sun, X. K.; Johnson, D. W.; Caulder, D. L.; Raymond, K. N.; Wong, E. H. *J. Am. Chem. Soc.* **2001**, *123*, 2752–2763.
89. Vilar, R.; Mingos, D. M. P.; White, A. J. P.; Williams, D. J. *Chem. Commun.* **1999**, 229–230.
90. Fujita, M.; Oguro, D.; Miyazawa, M.; Oka, H.; Yamaguchi, K.; Ogura, K. *Nature* **1995**, *378*, 469–471.
91. Fujita, M. *Struct. Bonding* **2000**, *96*, 177–201.
92. Ibukuro, F.; Kusukawa, T.; Fujita, M. *J. Am. Chem. Soc.* **1998**, *120*, 8561–8562.
93. Umemoto, K.; Yamaguchi, K.; Fujita, M. *J. Am. Chem. Soc.* **2000**, *122*, 7150–7151.
94. Kusukawa, T.; Fujita, M. *J. Am. Chem. Soc.* **1999**, *121*, 1397–1398.



95. Kusukawa, T.; Fujita, M. *Angew. Chem., Int. Ed. Engl.* **1998**, *37*, 3142–3144.
96. Hartshorn, C. M.; Steel, P. J. *Chem. Commun.* **1997**, 541–542.
97. Stang, P. J.; Olenyuk, B.; Muddiman, D. C.; Smith, R. D. *Organometallics* **1997**, *16*, 3094–3096.
98. Kubota, Y.; Biradha, K.; Fujita, M.; Sakamoto, S.; Yamaguchi, K. *Bull. Chem. Soc. Jpn.* **2002**, *75*, 559–565.
99. Umemoto, K.; Tsukui, H.; Kusukawa, T.; Biradha, K.; Fujita, M. *Angew. Chem., Int. Ed. Engl.* **2001**, *40*, 2620–2622.
100. Fujita, M.; Umemoto, K.; Yoshizawa, M.; Fujita, N.; Kusukawa, T.; Biradha, K. *Chem. Commun.* **2001**, 509–518.
101. Hong, M. C.; Zhao, Y. J.; Su, W. P.; Cao, R.; Fujita, M.; Zhou, Z. Y.; Chan, A. S. C. *J. Am. Chem. Soc.* **2000**, *122*, 4819–4820.
102. Kusukawa, T.; Yoshizawa, M.; Fujita, M. *Angew. Chem., Int. Ed. Engl.* **2001**, *40*, 1879–1884.
103. Yoshizawa, M.; Kusukawa, T.; Fujita, M.; Sakamoto, S.; Yamaguchi, K. *J. Am. Chem. Soc.* **2001**, *123*, 10454–10459.
104. Ito, H.; Kusukawa, T.; Fujita, M. *Chem. Lett.* **2000**, 598–599.
105. Yoshizawa, M.; Kusukawa, T.; Fujita, M.; Yamaguchi, K. *J. Am. Chem. Soc.* **2000**, *122*, 6311–6312.
106. Takeda, N.; Umemoto, K.; Yamaguchi, K.; Fujita, M. *Nature* **1999**, *398*, 794–796.
107. Fujita, M.; Fujita, N.; Ogura, K.; Yamaguchi, K. *Nature* **1999**, *400*, 52–55.
108. Olenyuk, B.; Whiteford, J. A.; Fechtenkotter, A.; Stang, P. J. *Nature* **1999**, *398*, 796–799.
109. Lehn, J. M.; Rigault, A.; Siegel, J.; Harrowfield, J.; Chevrier, B.; Moras, D. *Proc. Natl. Acad. Sci. USA* **1987**, *84*, 2565–2569.
110. Fatin-Rouge, N.; Blanc, S.; Pfeil, A.; Rigault, A.; Albrecht-Gary, A. M.; Lehn, J. M. *Helv. Chim. Acta* **2001**, *84*, 1694–1711.
111. MarquisRigault, A.; DupontGervais, A.; VanDorselaer, A.; Lehn, J. M. *Chem.-Eur. J.* **1996**, *2*, 1395–1398.
112. Harding, M. M.; Koert, U.; Lehn, J. M.; Marquisrigault, A.; Piguët, C.; Siegel, J. *Helv. Chim. Acta* **1991**, *74*, 594–610.
113. Eisenbach, C. D.; Schubert, U. S.; Baker, G. R.; Newkome, G. R. *J. Chem. Soc., Chem. Commun.* **1995**, 69–70.
114. Shaul, M.; Cohen, Y. *J. Org. Chem.* **1999**, *64*, 9358–9364.
115. Greenwald, M.; Wessely, D.; Katz, E.; Willner, I.; Cohen, Y. *J. Org. Chem.* **2000**, *65*, 1050–1058.
116. Greenwald, M.; Wessely, D.; Goldberg, I.; Cohen, Y. *New J. Chem.* **1999**, *23*, 337–344.
117. Greenwald, M.; Eassa, M.; Katz, E.; Willner, I.; Cohen, Y. *J. Electroanal. Chem.* **1997**, *434*, 77–82.
118. Kramer, R.; Lehn, J. M.; Marquisrigault, A. *Proc. Natl. Acad. Sci. USA* **1993**, *90*, 5394–5398.
119. Hasenknopf, B.; Lehn, J. M.; Baum, G.; Fenske, D. *Proc Nat Acad Sci USA* **1996**, *93*, 1397–1400.
120. Zarges, W.; Hall, J.; Lehn, J. M.; Bolm, C. *Helv. Chim. Acta* **1991**, *74*, 1843–1852.
121. Mamula, O.; von Zelewsky, A.; Bark, T.; Bernardinelli, G. *Angew. Chem., Int. Ed. Engl.* **1999**, *38*, 2945–2948.
122. Smith, V. C. M.; Lehn, J. M. *Chem. Commun.* **1996**, 2733–2734.
123. Airey, A. L.; Swiegers, G. F.; Willis, A. C.; Wild, S. B. *J. Chem. Soc., Chem. Commun.* **1995**, 695–696.
124. Airey, A. L.; Swiegers, G. F.; Willis, A. C.; Wild, S. B. *Inorg. Chem.* **1997**, *36*, 1588–1597.
125. Barbour, L. J.; Orr, G. W.; Atwood, J. L. *Nature* **1998**, *393*, 671–673.
126. Mamula, O.; von Zelewsky, A.; Bernardinelli, G. *Angew. Chem., Int. Ed. Engl.* **1998**, *37*, 290–293.
127. Matsumoto, N.; Motoda, Y.; Matsuo, T.; Nakashima, T.; Re, N.; Dahan, F.; Tuchagues, J. P. *Inorg. Chem.* **1999**, *38*, 1165–1173.
128. Maverick, A. W.; Buckingham, S. C.; Yao, Q.; Bradbury, J. R.; Stanley, G. G. *J. Am. Chem. Soc.* **1986**, *108*, 7430–7431.
129. Hartshorn, C. M.; Steel, P. J. *Angew. Chem., Int. Ed. Engl.* **1996**, *35*, 2655–2657.
130. Youinou, M. T.; Rahmouni, N.; Fischer, J.; Osborn, J. A. *Angew. Chem., Int. Ed. Engl.* **1992**, *31*, 733–735.
131. Marquis, A.; Kintzinger, J. P.; Graff, R.; Baxter, P. N. W.; Lehn, J. M. *Angew. Chem., Int. Ed. Engl.* **2002**, *41*, 2760–293.
132. Baxter, P. N. W.; Lehn, J. M.; Fischer, J.; Youinou, M. T. *Angew. Chem., Int. Ed. Engl.* **1994**, *33*, 2284–2287.
133. Bodwin, J. J.; Cutland, A. D.; Malkani, R. G.; Pecoraro, V. L. *Coord. Chem. Rev.* **2001**, *216*, 489–512.
134. Gibney, B. R.; Wang, H.; Kampf, J. W.; Pecoraro, V. L. *Inorg. Chem.* **1996**, *35*, 6184–6193.
135. Stemmler, A. J.; Kampf, J. W.; Pecoraro, V. L. *Angew. Chem., Int. Ed. Engl.* **1996**, *35*, 2841–2843.
136. Baxter, P.; Lehn, J. M.; Decian, A.; Fischer, J. *Angew. Chem., Int. Ed. Engl.* **1993**, *32*, 69–72.
137. Baxter, P. N. W.; Lehn, J. M.; Kneisel, B. O.; Baum, G.; Fenske, D. *Chem.-Eur. J.* **1999**, *5*, 113–120.
138. Baxter, P. N. W.; Lehn, J. M.; Baum, G.; Fenske, D. *Chem.-Eur. J.* **1999**, *5*, 102–112.
139. Baxter, P. N. W.; Lehn, J. M.; Baum, G.; Fenske, D. *Chem.-Eur. J.* **2000**, *6*, 4510–4517.
140. James, S. L.; Mingos, D. M. P.; White, A. J. P.; Williams, D. J. *Chem. Commun.* **1998**, 2323–2324.
141. Abrahams, B. F.; Egan, S. J.; Robson, R. *J. Am. Chem. Soc.* **1999**, *121*, 3535–3536.
142. Paul, R. L.; Couchman, S. M.; Jeffery, J. C.; McCleverty, J. A.; Reeves, Z. R.; Ward, M. D. *J. Chem. Soc., Dalton Trans.* **2000**, 845–851.
143. Baxter, P. N. W.; Khoury, R. G.; Lehn, J. M.; Baum, G.; Fenske, D. *Chem.-Eur. J.* **2000**, *6*, 4140–4148.
144. Fox, O. D.; Drew, M. G. B.; Beer, P. D. *Angew. Chem., Int. Ed. Engl.* **2000**, *39*, 136–140.
145. Hasenknopf, B.; Lehn, J. M. *Helv. Chim. Acta* **1996**, *79*, 1643–1650.
146. Prabakaran, R.; Fletcher, N. C.; Nieuwenhuyzen, M. *J. Chem. Soc., Dalton Trans.* **2002**, 602–608.
147. Murner, H.; von Zelewsky, A.; Hopfgartner, G. *Inorg Chim Acta* **1998**, *271*, 36–39.
148. Baret, P.; Gaude, D.; Gellon, G.; Pierre, J. L. *New J. Chem.* **1997**, *21*, 1255–1257.
149. Enemark, E. J.; Stack, T. D. P. *Angew. Chem., Int. Ed. Engl.* **1995**, *34*, 996–998.
150. Meyer, M.; Kersting, B.; Powers, R. E.; Raymond, K. N. *Inorg. Chem.* **1997**, *36*, 5179–5191.
151. Kramer, R.; Lehn, J. M.; Decian, A.; Fischer, J. *Angew. Chem., Int. Ed. Engl.* **1993**, *32*, 703–706.
152. Charbonniere, L. J.; Bernardinelli, G.; Piguët, C.; Sargeson, A. M.; Williams, A. F. *J. Chem. Soc., Chem. Commun.* **1994**, 1419–1420.
153. Jodry, J. J.; Lacour, J. *Chem.-Eur. J.* **2000**, *6*, 4297–4304.
154. Yeh, R. M.; Ziegler, M.; Johnson, D. W.; Terpin, A. J.; Raymond, K. N. *Inorg. Chem.* **2001**, *40*, 2216–2217.
155. Xu, J. D.; Parac, T. N.; Raymond, K. N. *Angew. Chem., Int. Ed. Engl.* **1999**, *38*, 2878–2882.
156. Albrecht, M. *Chem. Soc. Rev.* **1998**, *27*, 281–287.
157. Albrecht, M. *Chem. Eur. J.* **2000**, *6*, 3485–3489.

158. Caulder, D. L.; Raymond, K. N. *Angew. Chem., Int. Ed. Engl.* **1997**, *36*, 1440–1442.
159. Albrecht, M.; Schneider, M.; Rottele, H. *Angew. Chem. Int. Ed.* **1999**, *38*, 557–559.
160. Albrecht, M.; Kotila, S. *Chem. Commun.* **1996**, 2309–2310.
161. Albrecht, M.; Rottele, H.; Burger, P. *Chem. Eur. J.* **1996**, *2*, 1264–1268.
162. Hasenknopf, B.; Lehn, J. M.; Boumediene, N.; Leize, E.; Van Dorsselaer, A. *Angew. Chem., Int. Ed. Engl.* **1998**, *37*, 3265–3268.
163. Scherer, M.; Caulder, D. L.; Johnson, D. W.; Raymond, K. N. *Angew. Chem., Int. Ed. Engl.* **1999**, *38*, 1588–1592.
164. Stricklen, P. M.; Volcko, E. J.; Verkade, J. G. *J. Am. Chem. Soc.* **1983**, *105*, 2494–2495.
165. Sun, X.; Johnson, D. W.; Raymond, K. N.; Wong, E. H. *Inorg. Chem.* **2001**, *40*, 4504–4506.
166. Romero, F. M.; Ziesel, R.; DupontGervais, A.; VanDorsselaer, A. *Chem. Commun.* **1996**, 551–553.
167. Kajiwara, T.; Ito, T. *J. Chem. Soc., Chem. Commun.* **1994**, 1773–1774.
168. Yan, H.; SussFink, G.; Neels, A.; StoeckliEvans, H. *J. Chem. Soc., Dalton Trans.* **1997**, 4345–4350.
169. Bassani, D. M.; Lehn, J. M.; Fromm, K.; Fenske, D. *Angew. Chem., Int. Ed. Engl.* **1998**, *37*, 2364–2367.
170. Breuning, E.; Ruben, M.; Lehn, J. M.; Renz, F.; Garcia, Y.; Ksenofontov, V.; Gutlich, P.; Wegelius, E.; Rissanen, K. *Angew. Chem., Int. Ed. Engl.* **2000**, *39*, 2504–2507.
171. Ruben, M.; Breuning, E.; Gisselbrecht, J. P.; Lehn, J. M. *Angew. Chem., Int. Ed. Engl.* **2000**, *39*, 4139–4142.
172. Hanan, G. S.; Volkmer, D.; Schubert, U. S.; Lehn, J. M.; Baum, G.; Fenske, D. *Angew. Chem., Int. Ed. Engl.* **1997**, *36*, 1842–1844.
173. Yamanari, K.; Yamamoto, R.; Ito, R.; Kushi, Y.; Fuyuhiko, A.; Kubota, N.; Fukuo, T.; Arakawa, R. *Angew. Chem., Int. Ed. Engl.* **2001**, *40*, 2268–2271.
174. Wojaczynski, J.; LatosGrazynski, L.; Olmstead, M. M.; Balch, A. L. *Inorg. Chem.* **1997**, *36*, 4548–4554.
175. Wojaczynski, J.; Latosgrazynski, L. *Inorg. Chem.* **1995**, *34*, 1054–1062.
176. Wojaczynski, J.; Latos-Grazynski, L. *Coord. Chem. Rev.* **2000**, *204*, 113–171.
177. Chi, X. L.; Guerin, A. J.; Haycock, R. A.; Hunter, C. A.; Sarson, L. D. *J. Chem. Soc., Chem. Commun.* **1995**, 2567–2569.
178. Hunter, C. A.; Sarson, L. D. *Angew. Chem., Int. Ed. Engl.* **1994**, *33*, 2313–2316.
179. Houghton, M. A.; Bilyk, A.; Harding, M. M.; Turner, P.; Hambley, T. W. *J. Chem. Soc., Dalton Trans.* **1997**, 2725–2733.
180. Bilyk, A.; Harding, M. M.; Turner, P.; Hambley, T. W. *J. Chem. Soc., Dalton Trans.* **1994**, 2783–2790.
181. Bilyk, A.; Harding, M. M.; Turner, P.; Hambley, T. W. *J. Chem. Soc., Dalton Trans.* **1995**, 2549–2553.
182. Hasenknopf, B.; Lehn, J. M.; Kneisel, B. O.; Baum, G.; Fenske, D. *Angew. Chem., Int. Ed. Engl.* **1996**, *35*, 1838–1840.
183. Hasenknopf, B.; Lehn, J. M.; Boumediene, N.; DupontGervais, A.; VanDorsselaer, A.; Kneisel, B.; Fenske, D. *J. Am. Chem. Soc.* **1997**, *119*, 10956–10962.
184. Yamanari, K.; Fukuda, I.; Kawamoto, T.; Kushi, Y.; Fuyuhiko, A.; Kubota, N.; Fukuo, T.; Arakawa, R. *Inorg. Chem.* **1998**, *37*, 5611–5618.
185. Fleming, J. S.; Mann, K. L. V.; Carraz, C. A.; Psillakis, E.; Jeffery, J. C.; McCleverty, J. A.; Ward, M. D. *Angew. Chem., Int. Ed. Engl.* **1998**, *37*, 1279–1281.
186. Bell, Z. R.; Jeffery, J. C.; McCleverty, J. A.; Ward, M. D. *Angew. Chem., Int. Ed. Engl.* **2002**, *41*, 2515–2518.
187. Motson, G. R.; Mamula, O.; Jeffery, J. C.; McCleverty, J. A.; Ward, M. D.; von Zelewsky, A. *J. Chem. Soc., Dalton Trans.* **2001**, 1389–1391.
188. Ward, M. D.; McCleverty, J. A.; Jeffery, J. C. *Coord. Chem. Rev.* **2001**, *222*, 251–272.
189. Jones, P. L.; Byrom, K. J.; Jeffery, J. C.; McCleverty, J. A.; Ward, M. D. *Chem. Commun.* **1997**, 1361–1362.
190. He, C.; Wang, L. Y.; Wang, Z. M.; Liu, Y.; Liao, C. S.; Yan, C. H. *J. Chem. Soc., Dalton Trans.* **2002**, 134–135.
191. Saalfrank, R. W.; Dresel, A.; Seitz, V.; Trummer, S.; Hampel, F.; Teichert, M.; Stalke, D.; Stadler, C.; Daub, J.; Schunemann, V.; Trautwein, A. X. *Chem.-Eur. J.* **1997**, *3*, 2058–2062.
192. Saalfrank, R. W.; Low, N.; Kareth, S.; Seitz, V.; Hampel, F.; Stalke, D.; Teichert, M. *Angew. Chem., Int. Ed. Engl.* **1998**, *37*, 172–175.
193. Saalfrank, R. W.; Low, N.; Hampel, F.; Stachel, H. D. *Angew. Chem., Int. Ed. Engl.* **1996**, *35*, 2209–2210.
194. Saalfrank, R. W.; Bernt, I.; Uller, E.; Hampel, F. *Angew. Chem., Int. Ed. Engl.* **1997**, *36*, 2482–2485.
195. Saalfrank, R. W.; Burak, R.; Breit, A.; Stalke, D.; Herbstirmer, R.; Daub, J.; Porsch, M.; Bill, E.; Muther, M.; Trautwein, A. X. *Angew. Chem., Int. Ed. Engl.* **1994**, *33*, 1621–1623.
196. Saalfrank, R. W.; Bernt, I.; Chowdhry, M. M.; Hampel, F.; Vaughan, G. B. M. *Chem.-Eur. J.* **2001**, *7*, 2765–2769.
197. Saalfrank, R. W.; Uller, E.; Demleitner, B.; Bernt, I. *Struct. Bonding* **2000**, *96*, 149–175.
198. Saalfrank, R. W.; Bernt, I.; Hampel, F. *Chem.-Eur. J.* **2001**, *7*, 2770–2774.
199. Saalfrank, R. W.; Stark, A.; Peters, K.; Vonschering, H. G. *Angew. Chem., Int. Ed. Engl.* **1988**, *27*, 851–853.
200. Saalfrank, R. W.; Horner, B.; Stalke, D.; Salbeck, J. *Angew. Chem., Int. Ed. Engl.* **1993**, *32*, 1179–1182.
201. Saalfrank, R. W.; Glaser, H.; Demleitner, B.; Hampel, F.; Chowdhry, M. M.; Schunemann, V.; Trautwein, A. X.; Vaughan, G. B. M.; Yeh, R.; Davis, A. V.; Raymond, K. N. *Chem.-Eur. J.* **2002**, *8*, 493–497.
202. Saalfrank, R. W.; Low, N.; Trummer, S.; Sheldrick, G. M.; Teichert, M.; Stalke, D. *Eur. J. Inorg. Chem.* **1998**, 559–563.
203. Caulder, D. L.; Powers, R. E.; Parac, T. N.; Raymond, K. N. *Angew. Chem., Int. Ed. Engl.* **1998**, *37*, 1840–1843.
204. Beissel, T.; Powers, R. E.; Raymond, K. N. *Angew. Chem., Int. Ed. Engl.* **1996**, *35*, 1084–1086.
205. Terpin, A. J.; Ziegler, M.; Johnson, D. W.; Raymond, K. N. *Angew. Chem., Int. Ed. Engl.* **2001**, *40*, 157–160.
206. Ziegler, M.; Miranda, J. J.; Andersen, U. N.; Johnson, D. W.; Leary, J. A.; Raymond, K. N. *Angew. Chem., Int. Ed. Engl.* **2001**, *40*, 733–736.
207. Enemark, E. J.; Stack, T. D. P. *Angew. Chem., Int. Ed. Engl.* **1998**, *37*, 932–935.
208. Bruckner, C.; Powers, R. E.; Raymond, K. N. *Angew. Chem., Int. Ed. Engl.* **1998**, *37*, 1837–1839.
209. Johnson, D. W.; Xu, J. D.; Saalfrank, R. W.; Raymond, K. N. *Angew. Chem., Int. Ed. Engl.* **1999**, *38*, 2882–2885.
210. Mann, S.; Huttner, G.; Zsolnai, L.; Heinze, K. *Angew. Chem., Int. Ed. Engl.* **1996**, *35*, 2808–2809.
211. Roche, S.; Haslam, C.; Adams, H.; Heath, S. L.; Thomas, J. A. *Chem. Commun.* **1998**, 1681–1682.
212. Berseth, P. A.; Sokol, J. J.; Shores, M. P.; Heinrich, J. L.; Long, J. R. *J. Am. Chem. Soc.* **2000**, *122*, 9655–9662.
213. Sokol, J. J.; Shores, M. P.; Long, J. R. *Angew. Chem., Int. Ed. Engl.* **2001**, *40*, 236–239.
214. Sokol, J. J.; Shores, M. P.; Long, J. R. *Inorg. Chem.* **2002**, *41*, 3052–3054.

215. Shores, M. P.; Sokol, J. J.; Long, J. R. *J. Am. Chem. Soc.* **2002**, *124*, 2279–2292.
216. Sokol, J. J.; Hee, A. G.; Long, J. R. *J. Am. Chem. Soc.* **2002**, *124*, 7656–7657.
217. Klausmeyer, K. K.; Rauchfuss, T. B.; Wilson, S. R. *Angew. Chem., Int. Ed. Engl.* **1998**, *37*, 1694–1696.
218. Klausmeyer, K. K.; Wilson, S. R.; Rauchfuss, T. B. *J. Am. Chem. Soc.* **1999**, *121*, 2705–2711.
219. Bunzli, J. C. G.; Piguët, C. *Chem. Rev.* **2002**, *102*, 1897–1928.
220. Piguët, C.; Bunzli, J. C. G. *Chem. Soc. Rev.* **1999**, *28*, 347–358.
221. Bernardinelli, G.; Piguët, C.; Williams, A. F. *Angew. Chem., Int. Ed. Engl.* **1992**, *31*, 1622–1624.
222. Piguët, C.; Bunzli, J. C. G.; Bernardinelli, G.; Hopfgartner, G.; Williams, A. F. *J. Am. Chem. Soc.* **1993**, *115*, 8197–8206.
223. Martin, N.; Bunzli, J. C. G.; McKee, V.; Piguët, C.; Hopfgartner, G. *Inorg. Chem.* **1998**, *37*, 577–589.
224. Elhabiri, M.; Scopelliti, R.; Bunzli, J. C. G.; Piguët, C. *Chem. Commun.* **1998**, 2347–2348.
225. Elhabiri, M.; Scopelliti, R.; Bunzli, J. C. G.; Piguët, C. *J. Am. Chem. Soc.* **1999**, *121*, 10747–10762.
226. Edder, C.; Piguët, C.; Bernardinelli, G.; Mareda, J.; Bochet, C. G.; Bunzli, J. C. G.; Hopfgartner, G. *Inorg. Chem.* **2000**, *39*, 5059–5073.
227. Andre, N.; Scopelliti, R.; Hopfgartner, G.; Piguët, C.; Bunzli, J. C. G. *Chem. Commun.* **2002**, 214–215.
228. Piguët, C.; Edder, C.; Rigault, S.; Bernardinelli, G.; Bunzli, J. C. G.; Hopfgartner, G. *J. Chem. Soc., Dalton Trans.* **2000**, 3999–4006.
229. Lessmann, J. J.; Horrocks, W. D. *Inorg. Chem.* **2000**, *39*, 3114–3124.
230. Goodgame, D. M. L.; Hill, S. P. W.; Williams, D. J. *J. Chem. Soc. Chem. Commun.* **1993**, 1019–1021.
231. Yang, L.; Yang, R. *J. Coord. Chem.* **1994**, *33*, 303.
232. Yang, L.; Yang, R. *Polyhedron* **1995**, *14*, 507–510.
233. Yang, L.; Yang, R. *J. Mol. Struct.* **1996**, *380*, 75–84.
234. Obora, Y.; Ohta, T.; Stern, C. L.; Marks, T. J. *J. Am. Chem. Soc.* **1997**, *119*, 3745–3755.
235. Xu, J.; Raymond, K. N. *Angew. Chem., Int. Ed. Engl.* **2000**, *39*, 2745–2747.
236. Bretonniere, Y.; Mazzanti, M.; Wietzke, R.; Pecaut, J. *Chem. Commun.* **2000**, 1543–1544.
237. Bretonniere, Y.; Mazzanti, M.; Pecaut, J.; Olmstead, M. M. *J. Am. Chem. Soc.* **2002**, *124*, 9012–9013.
238. Cotton, F. A.; Donahue, J. P.; Lin, C.; Murillo, C. A. *Inorg. Chem.* **2001**, *40*, 1234–1244.
239. Cotton, F. A.; Donahue, J. P.; Murillo, C. A. *Inorg. Chem. Commun.* **2002**, *5*, 59–63.
240. Cotton, F. A.; Lin, C.; Murillo, C. A. *Chem. Commun.* **2001**, 11–12.
241. Cotton, F. A.; Lin, C.; Murillo, C. A. *Inorg. Chem.* **2001**, *40*, 6413–6417.
242. Cotton, F. A.; Lin, C.; Murillo, C. A. *Inorg. Chem.* **2001**, *40*, 478–484.
243. Piguët, C.; Bernardinelli, G.; Hopfgartner, G. *Chem. Rev.* **1997**, *97*, 2005–2062.
244. Garrett, T. M.; Koert, U.; Lehn, J. M. *J. Phys. Org. Chem.* **1992**, *5*, 529–532.
245. Pfeil, A.; Lehn, J. M. *J. Chem. Soc. Chem. Commun.* **1992**, 838–840.
246. Perlmutter-Hayman, B. *Acc. Chem. Res.* **1986**, *19*, 90–96.
247. Shinkai, S.; Ikeda, M.; Sugasaki, A.; Takeuchi, M. *Account. Chem. Res.* **2001**, *34*, 494–503.
248. Basolo, F.; Pearson, R. G. *Mechanisms of Inorganic Reactions* **1967**, Wiley: New York.
249. Davis, A. V.; Yeh, R. M.; Raymond, K. N. *Proc. Natl. Acad. Sci. USA* **2002**, *99*, 4793–4796.
250. Klausmeyer, K. K.; Rauchfuss, T. B.; Wilson, S. R. *Angew. Chem., Int. Ed. Engl.* **1998**, *37*, 1694–1696.
251. Fatin-Rouge, N.; Blanc, S.; Van Dorsselaer, A.; Baret, P.; Pierre, J.-L.; Albrecht-Gary, A.-M. *Inorg. Chem.* **2000**, *39*, 5771–5778.
252. Fatin-Rouge, N.; Blanc, S.; Pfeil, A.; Rigault, A.; Albrecht-Gary, A.-M.; Lehn, J.-M. *Helv. Chim. Acta* **2001**, *84*, 1694–1711.
253. Scherer, M.; Caulder, D. L.; Johnson, D. W.; Raymond, K. N. *Angew. Chem.-Int. Edit.* **1999**, *38*, 1588–1592.
254. Hasenknopf, B.; Lehn, J.-M.; Boumediene, N.; Dupont-Gervais, A.; Van Dorsselaer, A.; Kneisel, B.; Fenske, D. *Angew. Chem., Int. Ed.* **1998**, *37*, 3265–3268.
255. Levin, M. J.; Stang, P. J. *J. Am. Chem. Soc.* **2000**, *122*, 7428–7429.
256. Kersting, B.; Telford, J. R.; Meyer, M.; Raymond, K. N. *J. Am. Chem. Soc.* **1996**, *118*, 5712–5721.
257. Kersting, B.; Meyer, M.; Powers, R. E.; Raymond, K. N. *J. Am. Chem. Soc.* **1996**, *118*, 7221–7222.
258. Terpin, A. J.; Ziegler, M.; Johnson, D. W.; Raymond, K. N. *Angew. Chem., Int. Ed.* **2001**, *40*, 157–160.
259. Charbonniere, L. J.; Gilet, M.-F.; Bernauer, K.; Williams, A. F. *Chem. Commun.* **1996**, 39–40.
260. Charbonniere, L. J.; Williams, A. F.; Frey, U.; Merbach, A. E.; Kamalaprija, P.; Schaad, O. *J. Am. Chem. Soc.* **1997**, *119*, 2488–2496.
261. Saalfrank, R. W.; Demleitner, B.; Glaser, H.; Maid, H.; Bathelt, D.; Hampel, F.; Bauer, W.; Teichert, M. *Chem.-Eur. J.* **2002**, *8*, 2679–2683.
262. Natta, G.; Farina, M. In *Stereochemistry*; Natta, G.; Farina, M., Eds.; Trans Dempster, A.; Longman: London, 1972.
263. Suarez, M.; Branda, N.; Lehn, J. M.; Decian, A.; Fischer, J. *Helv. Chim. Acta* **1998**, *81*, 1–13.
264. Gulikkrzywicki, T.; Fouquey, C.; Lehn, J. M. *Proc. Natl. Acad. Sci. USA* **1993**, *90*, 163–167.
265. Yoshizawa, M.; Takeyama, Y.; Kusukawa, T.; Fujita, M. *Angew. Chem., Int. Ed. Engl.* **2002**, *41*, 1347–1349.
266. Ziegler, M.; Brumaghim, J. L.; Raymond, K. N. *Angew. Chem., Int. Ed. Engl.* **2000**, *39*, 4119–4121.
267. Merlau, M. L.; Mejia, M. D. P.; Nguyen, S. T.; Hupp, J. T. *Angew. Chem., Int. Ed. Engl.* **2001**, *40*, 4239–4242.

# 7.9

## Metallomesogens

B. DONNIO and D. GUILLON

*Institut de Physique et Chimie des Matériaux de Strasbourg, France*

R. DESCHENAUX

*Université de Neuchâtel, Switzerland*

and

D. W. BRUCE

*University of Exeter, UK*

---

7.9.1	PREAMBLE	359
7.9.2	GENERAL INTRODUCTION	359
7.9.3	THERMOTROPIC LIQUID CRYSTALS	360
7.9.3.1	Calamitic Mesogens	360
7.9.3.2	Mesophases of Calamitic Mesogens	361
7.9.3.2.1	<i>The nematic phase</i>	362
7.9.3.2.2	<i>The chiral nematic phase</i>	363
7.9.3.2.3	<i>The true smectic phases</i>	363
7.9.3.2.4	<i>The crystal smectic phases</i>	364
7.9.3.2.5	<i>Polymorphism</i>	365
7.9.3.3	Discotic Mesogens	365
7.9.3.4	Mesophases of Disk-like Mesogens	366
7.9.4	LYOTROPIC LIQUID CRYSTALS	366
7.9.5	PHYSICAL PROPERTIES OF LIQUID CRYSTALS	369
7.9.6	MESOPHASE CHARACTERIZATION	369
7.9.6.1	Polarized Optical Microscopy	370
7.9.6.2	Differential Scanning Calorimetry (DSC)	371
7.9.6.3	Small-angle X-ray Diffraction	372
7.9.7	MACROCYCLIC MESOGENS FORMING COLUMNAR PHASES	374
7.9.7.1	Phthalocyanines	374
7.9.7.1.1	<i>Peripherally octasubstituted phthalocyanines</i>	375
7.9.7.1.2	<i>Phthalocyanines with extended cores</i>	383
7.9.7.1.3	<i>Bis(phthalocyaninato)lanthanide complexes</i>	386
7.9.7.1.4	<i>Radially substituted phthalocyanines</i>	389
7.9.7.1.5	<i>2,3-Naphthalocyanines</i>	394
7.9.7.1.6	<i>Tetrapyrazinoporphyrazines</i>	394
7.9.7.2	Porphyryns	397
7.9.7.2.1	<i><math>\beta</math>-Octasubstituted metalloporphyryns</i>	397
7.9.7.2.2	<i>Meso-tetrasubstituted metalloporphyryns</i>	400
7.9.7.2.3	<i>Lanthanide complexes of porphyryns</i>	404
7.9.7.2.4	<i>Tetraazaporphyryns</i>	405
7.9.7.2.5	<i>Tetraazaporphyryns</i>	407
7.9.7.3	Triazolehemiporphyrazine and Triazolephthalocyanine Complexes	409
7.9.7.4	Tetraaza[14]annulenes	410
7.9.7.5	Tetraaza[14]cyclohexadecanes	411
7.9.7.6	Metallacrown Complexes	412
7.9.7.7	Macroheterocyclic Tetrametallo-organyls	414
7.9.7.8	Paracyclophanes	417

7.9.7.9	Metal Complexes of Azacrowns	418
7.9.7.10	Calix[4]arenes	420
7.9.8	DISCOTIC AND PSEUDO-DISCOTIC COMPOUNDS SHOWING COLUMNAR MESOPHASES	421
7.9.8.1	$\beta$ -diketonate Metal Complexes	421
7.9.8.1.1	<i>Bis[1-(substituted-phenyl)-3-alkyl-<math>\beta</math>-diketonato]metal complexes with two and four peripheral chains</i>	422
7.9.8.1.2	<i>Bis[1-(substituted-biphenyl)-3-substituted-<math>\beta</math>-diketonato]metal complexes with two and four peripheral chains</i>	422
7.9.8.1.3	<i>Bis[1,3-(substituted-phenyl)-<math>\beta</math>-diketonato]metal complexes</i>	426
7.9.8.1.4	<i>Mono-, tris-, and tetrakis-[1,3-substituted-phenyl-<math>\beta</math>-diketonato] metal complexes</i>	435
7.9.8.2	Copper Complexes of Anthraquinones	439
7.9.8.3	Mixed Phenylpyrimidine-1,3-(Substituted-Phenyl)- $\beta$ -diketonato)Metal Complexes	439
7.9.8.4	Triketonato and Tetraketonato Metal Complexes	440
7.9.8.5	Dithiolene Complexes	445
7.9.8.6	1,2-Dioxime Complexes	446
7.9.8.7	Dithiooxamide Complexes	450
7.9.8.8	Hydrazine Complexes	451
7.9.8.9	Benzalimines	452
7.9.8.10	Iminoketones	453
7.9.8.11	Complexes of Pyrazole-based Ligands	459
7.9.8.12	Metal Complexes Containing Triphenylene Units	459
7.9.9	METAL CARBOXYLATES	460
7.9.9.1	Carboxylates of Alkali Metals and Monovalent Metals	460
7.9.9.2	Alkali-earth and Divalent Metal Carboxylates	464
7.9.9.3	Transition Metal Alkanoates	466
7.9.9.3.1	<i>Tetra(alkanoato)dicopper(II) mesogens</i>	466
7.9.9.3.2	<i>Other tetraalkanoatedimetal complexes</i>	469
7.9.9.3.3	<i>Tetra(benzoato)dimetal complexes</i>	472
7.9.9.3.4	<i>Lanthanide carboxylates</i>	475
7.9.9.3.5	<i>Complexes of dithiocarboxylates and xanthates</i>	477
7.9.10	POLYCATENAR LIQUID CRYSTALS	477
7.9.10.1	Introduction	477
7.9.10.2	Simple Systems	480
7.9.10.3	Systems Based on Poly(alkoxy)stilbazole Ligands	482
7.9.10.3.1	<i>Complexes of group 10 metals</i>	482
7.9.10.3.2	<i>Complexes of silver(I)</i>	486
7.9.10.3.3	<i>Lyotropic mesomorphism of polycatenar complexes of silver(I)</i>	488
7.9.10.4	Systems Based on Other Types of Poly(alkoxy)substituted Ligands	489
7.9.10.5	Polycatenar Organometallic Complexes	490
7.9.10.6	Polycatenar Porphyrins	492
7.9.10.7	Salen Complexes	494
7.9.10.8	Other Polycatenar Metallomesogens	496
7.9.10.9	Wedge-shaped Complexes	500
7.9.11	METALLODENDRIMERS	502
7.9.12	TETRAHEDRAL COMPLEXES OF $\text{Cu}^{\text{I}}$ AND METALLOHELICATES	506
7.9.13	MISCELLANEOUS	506
7.9.14	CALAMITIC MATERIALS	508
7.9.14.1	Introduction	508
7.9.14.2	Ionic Metallomesogens	509
7.9.14.2.1	<i>Alkylammonium derivatives</i>	509
7.9.14.2.2	<i>Complexes of long-chain amines</i>	510
7.9.14.2.3	<i>Pyridinium and imidazolium salts</i>	511
7.9.14.2.4	<i>Thiolates</i>	513
7.9.14.2.5	<i>Dialkylphosphate salts</i>	514
7.9.14.3	Complexes of Monodentate Ligands	514
7.9.14.3.1	<i>Complexes of organophenylenes</i>	514
7.9.14.3.2	<i>Complexes of organonitriles</i>	515
7.9.14.3.3	<i>Complexes of organoisonitriles</i>	515
7.9.14.3.4	<i>Acetylide complexes</i>	522
7.9.14.3.5	<i>Carbene complexes</i>	523
7.9.14.3.6	<i>Complexes of substituted pyridines</i>	525
7.9.14.3.7	<i>Pyrazole complexes</i>	531
7.9.14.4	Physical Properties of Complexes of Monodentate Ligands	532
7.9.14.5	Mesomorphic Coordination Complexes of Bidentate Ligands	533
7.9.14.5.1	<i>Dithiolene complexes</i>	533
7.9.14.5.2	<i>Dithiobenzoate complexes</i>	533
7.9.14.5.3	<i>Dithiocarbamate complexes</i>	535
7.9.14.5.4	<i>Physical properties of mesogens with bidentate sulfur ligands</i>	536
7.9.14.5.5	<i>Benzoato complexes</i>	537
7.9.14.5.6	<i>Tropolone complexes</i>	537
7.9.14.5.7	<i>Complexes <math>\alpha</math>-substituted-<math>\beta</math>-dialdehydes and <math>\alpha</math>-substituted-<math>\beta</math>-diketones</i>	537
7.9.14.5.8	<i>Salicylaldehyde derivatives</i>	538

7.9.14.5.9	Complexes of bipyridine ligands	539
7.9.14.5.10	Complexes of diazabutadiene ligands	541
7.9.14.5.11	Complexes with N,O donor sets	541
7.9.14.5.12	N,N'-Disalicylidenealkylenediamine complexes	559
7.9.14.5.13	Bis(enaminoketonato) complexes	560
7.9.14.5.14	Other complexes with N,O donor sets	562
7.9.14.5.15	Complexes with N,N' donor sets	564
7.9.14.5.16	Ortho-metallated complexes	565
7.9.14.5.17	Oxo-bridged complexes	583
7.9.14.6	Organometallic Complexes	584
7.9.14.6.1	Tricarbonyliron(0) derivatives	584
7.9.14.6.2	$\eta^6$ -Benzene complexes	585
7.9.14.6.3	Ferrocene-containing thermotropic liquid crystals	585
7.9.14.7	Metalloporphyrins	594
7.9.14.8	Crown-ether Complexes	594
7.9.15	LYOTROPIC METALLOMESOGENS	598
7.9.15.1	Polymeric Systems	598
7.9.15.2	Amphiphilic Systems	600
7.9.15.2.1	Simple salts	600
7.9.15.2.2	Amphiphilic metal complexes	600
7.9.15.2.3	Schiff-base complexes	603
7.9.15.2.4	Concluding remarks	603
7.9.15.3	Columnar Systems	604
7.9.16	CONCLUSIONS AND ACKNOWLEDGMENTS	606
7.9.17	REFERENCES	607

---

## 7.9.1 PREAMBLE

The purpose of this chapter is to give an account of the types of metal complexes which will form liquid crystal mesophases and to describe the way these complexes are organized within the phases and the nature of the physical properties which are found. Since the subject began to develop apace in the mid 1980s, it has been covered by several reviews<sup>1-16</sup> and a book,<sup>17</sup> and these will inevitably provide the interested reader with different and, in many cases, more detailed perspectives. However, the aim of this chapter is to provide a self-contained introduction to the area of metallomesogens so that the first-time reader may gain a useful grasp of the subject and then be able to pursue it in more detail through the references given.

The division of the subject matter concentrates primarily on the type of liquid crystal phase formed and, to a large degree, this is a reflection of molecular shape, although as the reader will see this is not such a clear-cut distinction where polycatenar liquid crystals are concerned. However, within these broader classifications, material is then organized paying attention to the ligand types used to form the complexes. This is not a unique classification, but it does provide some sort of framework within which the field may be viewed.

The chapter starts with a discussion of the basics of liquid crystal phase behavior, the types of mesophase that are formed and methods for their characterization; those requiring more detail and/or breadth are directed to the volumes of reference.<sup>18</sup> This chapter does not cover all liquid crystals which might be considered as being somehow "inorganic" in origin, and so, for example, systems containing boron clusters, and the lyotropic mesophases of metal oxides,<sup>19-21</sup> etc., are omitted. Similarly, polymeric systems are not covered in any detail as since some earlier reviews,<sup>22,23</sup> there has been relatively little development in the field.

## 7.9.2 GENERAL INTRODUCTION

Matter is often considered as existing in one of three forms—solid, liquid, and gas. Yet there exists a state of matter between the solid and liquid states which possesses properties reminiscent of each, so that like a solid it has order, while like a liquid it is fluid. This true state of matter is the liquid crystal state and is generated in one of two ways. Thus, where a compound passes between the solid, liquid, and liquid crystal state as a primary function of temperature and in the absence of solvent, the liquid crystal behavior is termed *thermotropic*, while when the phase transitions are driven by the concentration of the liquid crystal in a solvent, the behavior is termed *lyotropic*.

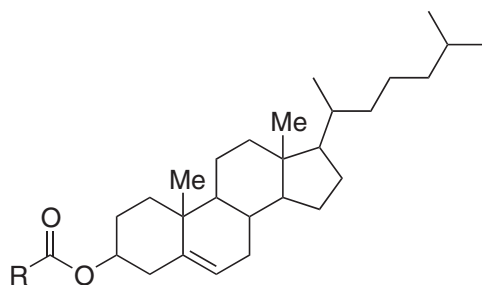


**Figure 1** Reinitzer's cholesteryl liquid-crystalline esters.

The recognition of the liquid crystal state is usually attributed to the work of Reinitzer<sup>24</sup> who, in 1888, published on the apparent two melting points of cholesteryl esters (Figure 1), although there is evidence of the recognition of what we now know to be liquid crystal properties in nerve myelin in the 1850s<sup>25</sup> and also in the behavior of magnesium soaps at about the same time.<sup>26</sup>

Since these initial discoveries, liquid crystals have become a major, multidisciplinary field of research which have impacted on society in a major way following the discovery of the cyanobiphenyl liquid crystals by Gray in the early 1970s, which led to the birth of the liquid crystal display industry, now worth >€15 billion/annum and ever increasing. This multidisciplinary nature is evidenced by the pervasive nature of liquid crystal science, extending from biology (the materials in cell membranes are liquid crystals), through chemistry to physics, mathematics, and electronic engineering. It is a constantly expanding and developing field with new applications constantly challenging the synthetic chemist and new phase types prompting physicists to see how they may be harnessed. Thus, despite being regarded as a "mature" discipline, liquid crystal research has probably never been so vibrant, and one of the significant developments since the mid 1980s has been that of metallomesogens—a term coined in the first review of the subject by Giroud-Godquin and Maitlis.<sup>1</sup>

Before proceeding further, it will be of use to introduce some of the terminology commonly associated with liquid crystals. A material which has liquid crystal properties is referred to as a *mesogen* and is said to exhibit *mesomorphism*; something which is "liquid crystal-like" is known as *mesogenic*, although something mesogenic is not necessarily mesomorphic. To avoid ambiguity, the (conventional) liquid state is referred to as the *isotropic* state. The temperature at which a material passes from the solid state into a mesophase is referred to as the *melting point*, while the temperature at which the mesophase transforms into an isotropic fluid is called the *clearing point*.

### 7.9.3 THERMOTROPIC LIQUID CRYSTALS

Thermotropic liquid crystals can be divided into three principal types through the mesophases they form; two of these will be introduced at this stage. This classification is based on the essential shape of the molecules and while, as will become evident, this taxonomy does not address all issues of physical properties and phase behavior, it does provide a framework by which we may begin to make sense of the observed behavior. The two types are the rod-like (calamitic) and the disk-like (discotic) liquid crystals.

As mentioned above, the liquid crystal state exists between the solid and liquid states and is stabilized by the presence of intermolecular, anisotropic dispersion forces which result from the anisotropic nature of the molecules which form the phases. Thus, rod-like molecules are much longer than they are broad and hence possess one unique, long axis. Similarly, disk-like molecules are rather flat and hence possess one, unique short axis (Figure 2).

#### 7.9.3.1 Calamitic Mesogens

A general structure of calamitic mesogens is often that given in Figure 3, which follows a design offered by Toyne.<sup>27</sup> If this figure is taken as indicative rather than prescriptive, then it forms a useful basis for the molecular design of calamitic mesogens.

What the model describes in general is an anisotropic molecule, normally, but by no means exclusively, composed of aromatic (or heteroaromatic) rings linked together in some way so that the overall anisotropy is maintained. In many cases there will be three or more rings and the linking group(s) (B) may preserve the conjugation of the system, although this is not necessary

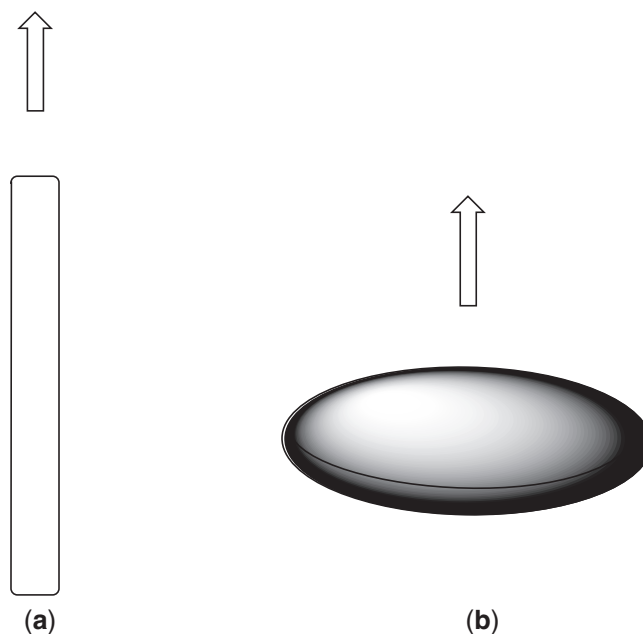


**Figure 2** The rod- (a) and disk-like (b) motifs of calamitic and discotic mesogens, respectively.

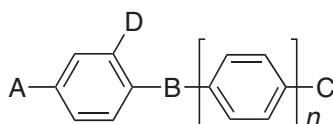


**Figure 3** A general molecular structure for calamitic mesogens.

(e.g.,  $-\text{CH}=\text{CH}-$ ,  $-\text{C}\equiv\text{C}-$ ,  $-\text{CH}=\text{N}-$ ,  $-\text{N}=\text{N}-$ ,  $-\text{CO}_2-$ ). The two terminal groups (A and C) can be the same or may be different, but in almost all cases one will be an alkyl (or alkyloxy) group which acts both to enhance the anisotropy of the molecule and also to reduce the melting point. Where the terminal groups are not the same, then in addition to an alkyl chain there will often be a small, dipolar group (e.g.,  $-\text{CN}$ ,  $-\text{NO}_2$ ,  $-\text{OMe}$ ). There are many thousands of liquid crystal molecules known and examples may be sought in Vill's remarkable database.<sup>28</sup> Occasionally, the molecule will possess a lateral group (D). In general, calamitic mesogens are none too tolerant of such lateral groups reducing, as they do, the structural anisotropy. However, used cleverly they can have profound and beneficial effects, the best example of which is the inclusion of lateral fluoro substituents, something beautifully described in a review.<sup>29</sup>

Some examples of "typical" calamitic mesogens are given in Figure 4. The cyanobiphenyls are included in this list due to their special position in the development of LCDs, but it should be noted that in so many ways they are not typical, their liquid crystal mesophases arising from antiparallel molecular correlations.

While such a general model is quite adequate to describe many known liquid crystal species, it is increasingly inadequate not because it is inaccurate, but rather because developments in the synthetic chemistry of liquid crystals have been such that, in reality, the usefulness of such general models might be called into question. Imagination has run wild! For example, a significant area of research is now with so-called bent-core (or banana) liquid crystals where the structural anisotropy "rules" given above simply do not hold and a  $120^\circ$  bend in the molecule is effectively a requirement.<sup>30</sup> Some other developments may be found elsewhere.<sup>31-33</sup>

### 7.9.3.2 Mesophases of Calamitic Mesogens

The true liquid crystal mesophases of calamitic mesogens are divided into two classes—the *nematic* and *smectic* phases—and these will be described in turn. There are, in addition, a series



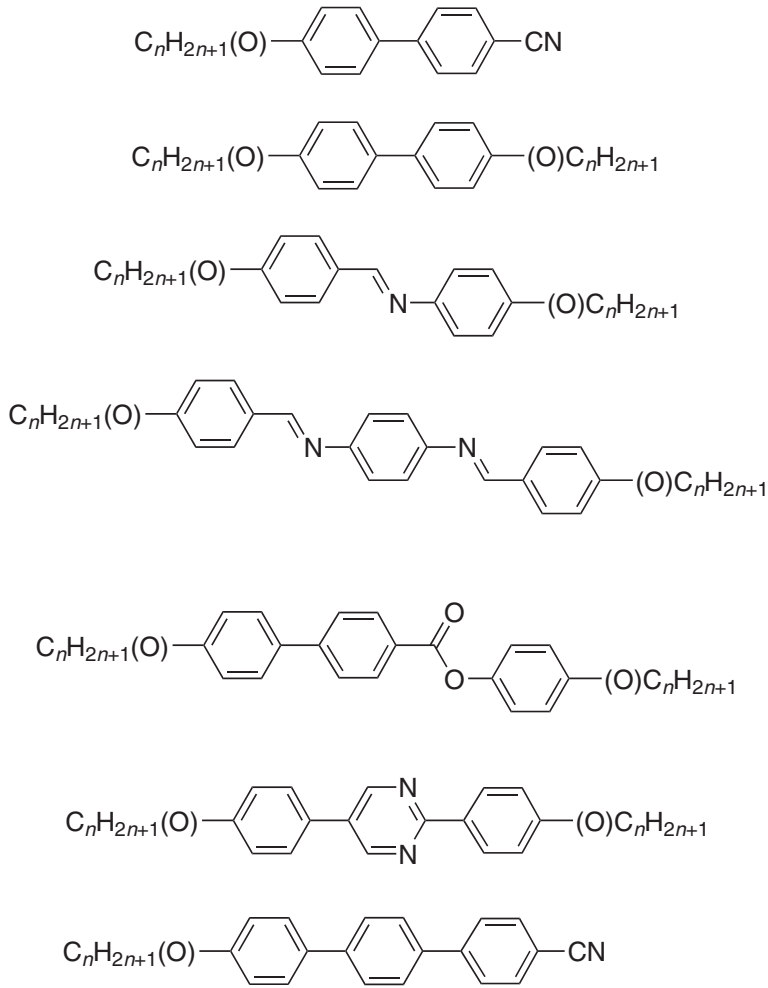


**Figure 4** Some typical calamitic mesogens.

of crystal smectic phases which are not really liquid crystal phases but which were for many years classified as such; these will be mentioned briefly below.

#### 7.9.3.2.1 The nematic phase

The nematic phase has the simplest structure of all of the mesophases, is very fluid, and is also the least ordered mesophase—it carries the abbreviation, N. The word nematic comes from the Greek *nematos* meaning thread-like—this arises from the observed optical texture of the phase between crossed polarizers (*vide infra*). The nematic phase is characterized by the one-dimensional orientational order of the molecules by virtue of correlations of the long molecular axes, although note that the orientational order is not polar. There is no translational order within the nematic phase. A schematic diagram of the nematic phase is found in [Figure 5](#).

The parameter known as the *director* ( $\hat{n}$ ) defines the average orientation of the molecules within the phase, while the degree of order within the phase is given by an order parameter,  $S$ , given by [Equation \(1\)](#):

$$S = \frac{1}{2} \langle 3 \cos^2 \theta - 1 \rangle \quad (1)$$

Here,  $\theta$  represents the angle between an individual molecule and the director and this is summed over all molecules. Typically for a nematic phase,  $0.7 > S > 0.4$ ; note that the transition from the

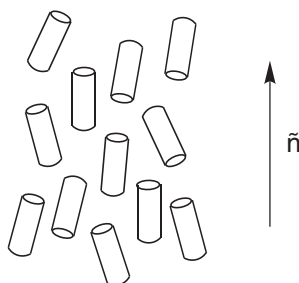


**Figure 5** Schematic representation of the molecular arrangement in the nematic phase.

isotropic liquid to the nematic phase is discontinuous and so at the transition,  $S$  will jump from a value of zero to about 0.3–0.4. While beyond the scope of this chapter, it is important to note that it is the nematic phase of liquid crystals which are the basis for almost all display applications.

#### 7.9.3.2.2 The chiral nematic phase

There exists a chiral version of the nematic phase which is found when a nematic phase is shown by a pure enantiomer, or by a mixture of enantiomers with one in excess or by a racemic or non-chiral compound doped with a chiral material at, say, 5–10%. This was the phase seen in cholesteryl benzoate by Reinitzer and so for many years (and still occasionally today) was known as the cholesteric phase, although the term “chiral nematic” is much preferred; it takes the abbreviation  $N^*$ . A compound will possess either a nematic phase or a chiral nematic phase, but only in the most exceptional circumstances of pitch inversion will it show both. Due to the packing constraints imposed by the materials being chiral, the molecules cannot simply align side by side in the phase and the long axis of one molecule will be slightly offset with respect to that of its neighbor. The net effect is for the director to precess through the phase (Figure 6), describing a helix which may be left- or right-handed depending on both the sense of the chirality and its position in the molecule;<sup>34</sup> two enantiomers of the same material will describe opposite twist senses for the helix.

The pitch ( $p$ ) of the helical twist is often of the order of the wavelength of visible light and is very sensitive to temperature. Coupled with the fact that the chiral nematic phase exhibits selective Bragg reflection of light of the wavelength equal to  $np$  (where  $n$  is the average refractive index of the material), then  $N^*$  materials appear to change color with temperature, making them useful as non-invasive thermometers. A more extensive description of the properties and applications of  $N^*$  materials may be found elsewhere.<sup>35</sup>

#### 7.9.3.2.3 The true smectic phases

The smectic phases<sup>36</sup> are more highly ordered than the nematic phase and are characterized by partial translational ordering of the molecules into layers, in addition to orientational correlations. The simplest smectic phase is the smectic A (SmA) phase, which is represented schematically

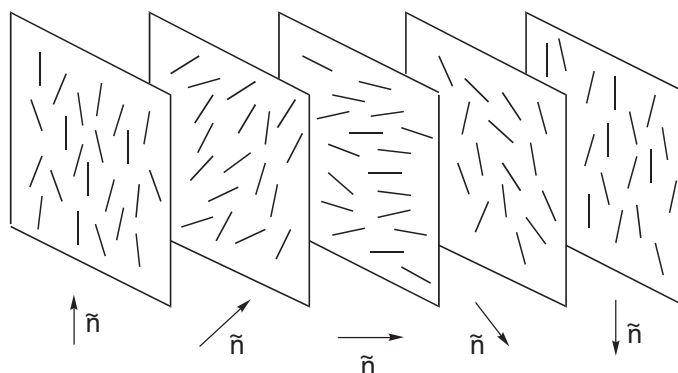


**Figure 6** Schematic diagram of the chiral nematic phase.

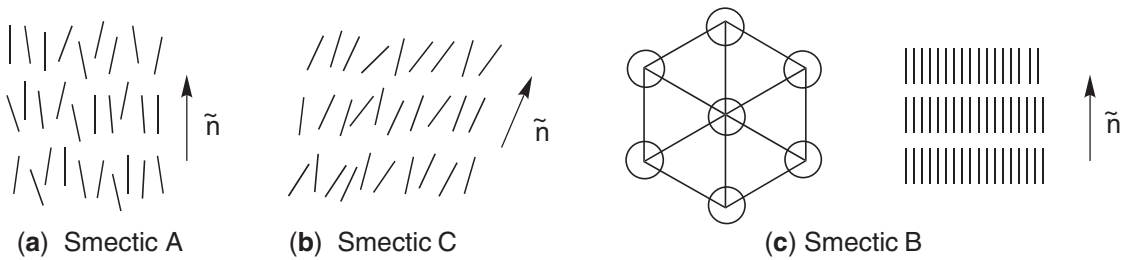


**Figure 7** Schematic representation of (a) the SmA, (b) SmC, and (c) SmB phases (viewed from above and from the side).

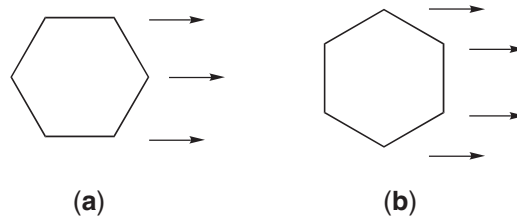


**Figure 8** Schematic representation of the (a) SmI and (b) SmF mesophases showing the directions of tilt.

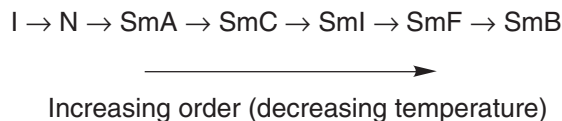
in Figure 7a. As in the nematic phase, the long axes of the molecules are oriented on average in the same direction but in addition, the molecules are loosely associated into layers, with the orientational direction perpendicular to the layer normal; diffusion between the layers occurs readily and the phase is fluid. In fact, this is a very idealized scheme and the layers in this (and the following phases) are much less well defined; a more precise description of the structure of the smectic phases may be found elsewhere.<sup>36,37</sup> If the SmA is modified slightly by tilting the molecules within the layer plane, then another smectic phase, the smectic C (SmC) is obtained, which is similarly fluid (Figure 7b).

Alternatively, the SmA may be modified by introducing hexagonal symmetry into the layer and increasing the order slightly so that the molecules sit at sites which describe a hexagonal net; this is the smectic B (SmB) phase (Figure 7c). As with all smectic phases, the SmB is fluid and interlayer diffusion of the molecules is facile, although rotation about the molecular long axes is concerted.

Two other smectic phases are obtained as tilted variations of the SmB, although both are more fluid. Thus, the smectic I (SmI) phase may be regarded as an SmB phase which is tilted towards a *vertex* of the hexagonal net, while the smectic F (SmF) phase may be regarded as an SmB phase which is tilted towards the *edge* of the hexagonal net (Figure 8).

These five phases are true smectic phases and in normal phase sequences would be expected to be found in the order shown in Scheme 1; the nematic and isotropic (I) phases are included for completeness.

In addition, the SmC, SmI, and the SmF may exist as chiral modifications (SmC\*, SmI\*, and SmF\*) either by doping with a chiral additive or by resolving a racemic material which shows one or more of the phases. Because of the low ( $C_2$ ) symmetry in these phases, the molecular dipoles align within the layers which are then ferroelectric. However, the chirality also requires that the direction of the ferroelectricity precesses through space from one layer to the next and so in the bulk sample, the ferroelectricity is lost unless the helix is unwound by the use of surface anchoring and thin cells.



**Scheme 1**

#### 7.9.3.2.4 The crystal smectic phases

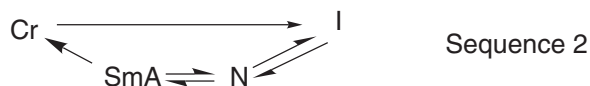
In addition to the true smectic phases, there is another class of mesophases, formerly also called smectic phases, which do possess extra positional order and which are derived from the true

smectics.<sup>37</sup> These phases are characterized by the appearance of inter-layer correlations and, in some cases, by the loss of molecular rotational freedom. Thus, the (crystal) B, G, and J phases are SmB, SmF, and SmI phases respectively with inter-layer correlations, while the E, H, and K phases are B, G, and J phases which have lost rotational freedom (note that, confusingly, there are both smectic and crystal B phases). These phases possess considerable disorder and are therefore properly intermediate between the solid and liquid states.

### 7.9.3.2.5 Polymorphism

The nature and number of any mesophases which are formed by a given material, and the temperatures at which they exist, must be determined experimentally, and require recourse to a selection of physical techniques, some of which are described below. However, it is helpful to know that, in most cases, the thermodynamic ordering of the various (fluid) mesophases maintains a fairly constant order which is given in [Scheme 1](#) (although note that “out-of-sequence” or *re-entrant* phases are known.<sup>38</sup> It is rather unlikely that a single material will show all of these phases and it is found empirically that certain combinations are more likely than others.<sup>37</sup>

In most cases, the observed mesophases are found on both heating and cooling a material, so that Sequence 1 in [Scheme 2](#) is fully reversible; such mesophases are termed *enantiotropic*. However, in some cases a particular mesophase may only appear on cooling a material and is therefore metastable (Sequence 2, [Scheme 2](#)); such phases are termed *monotropic*.



Scheme 2

### 7.9.3.3 Discotic Mesogens

Discotic liquid crystals came to prominence in the late 1970s when Chandrasekhar, Sadashiva, and Suresh reported the discovery of this new class of liquid-crystalline molecule which were found to form columnar phases.<sup>39</sup> The first of these, a hexaalkanoate of benzene, is shown in [Figure 9](#). There then followed a rather unfortunate confusion of nomenclature in which the phases formed by discotic molecules were themselves referred to as “discotic,” carrying the abbreviation “D.” A liquid crystal phase must be characterized by its symmetry and organization and not the shape of the molecules of which it is composed, and this is particularly important in columnar systems as many non-discotic molecules exhibit columnar phases. Indeed, columnar mesophases have been recognized for many years and studies date back to at least the 1960s with the work of Spegt and Skoulios with various metal soaps.<sup>40</sup> Columnar phases therefore take the abbreviation “Col” followed by some descriptor which describes the symmetry of the phase.

The important feature of discotic mesogens is that now the anisotropy is generated by the presence of a unique, *short* axis for, as their name suggests, the molecules are disk-like. Within

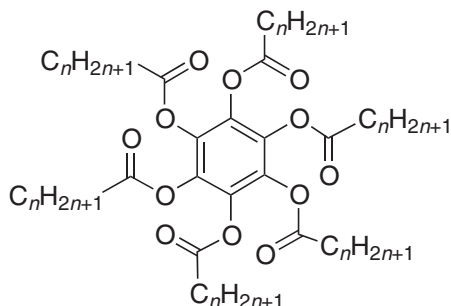


Figure 9 Discotic hexaalkanoates of benzene.

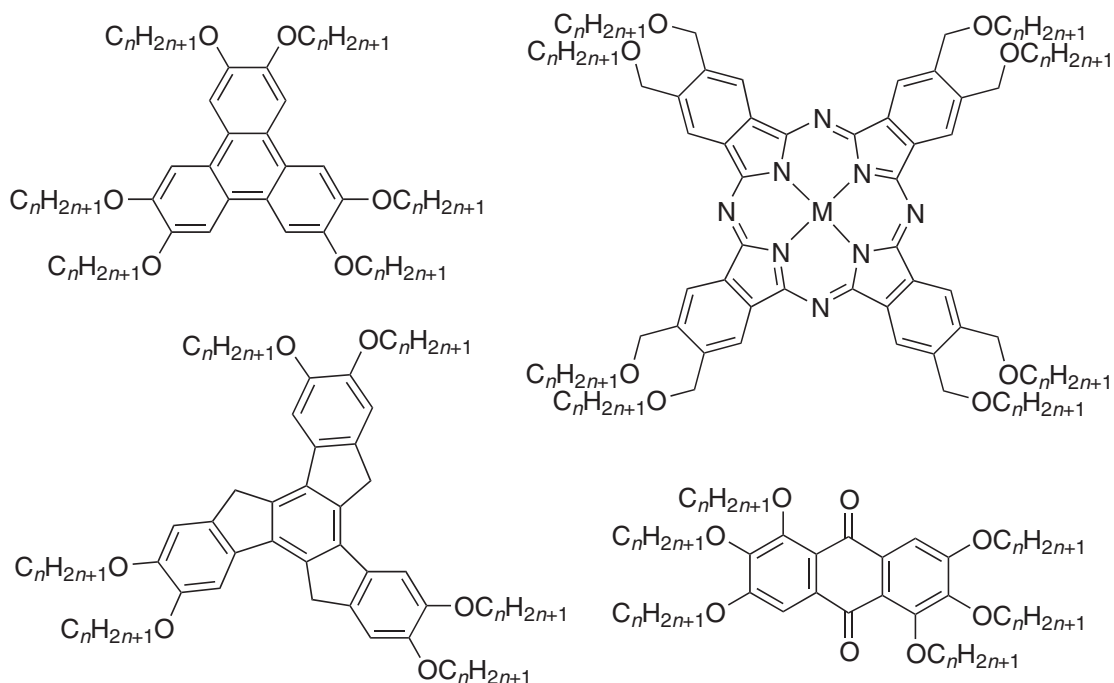


Figure 10 Representative examples of discotic materials.

reason, design of such mesogens is almost akin to choosing your favorite disk-like molecule and grafting at least six peripheral alkyl chains onto it. Importantly, this disk-like core does not need to be totally planar and, for example, hexaaza crown ethers have been shown to form columnar mesophases. Some examples of discotic mesogens are shown in Figure 10.

#### 7.9.3.4 Mesophases of Disk-like Mesogens

In contrast to calamitic phases, with discotic molecules,<sup>41</sup> it is the short axis which correlates and the simplest phase formed is a nematic phase which is usually abbreviated  $N_D$  and referred to as the discotic nematic phase, although for the reasons outlined above, this is somewhat unsatisfactory. In this nematic phase, there is again only orientational order as illustrated schematically in Figure 11a. Materials showing this phase are rather rare.

More common are the various columnar phases, which are characterized by the symmetry of the side-to-side molecular arrangement of columns formed by the stacking of the disk-like molecules. Figure 11b shows a side-on view of the columnar hexagonal phase ( $Col_h$ ) in which the molecules are arranged in columns which are further organized into a hexagonal array; within the columns there is some degree of liquid-like order. The common lattices of the columnar phases, namely hexagonal (a), oblique (b), and rectangular (c) and (d) are represented in Figure 12 as “aerial” views showing projections of the columns onto a two-dimensional plane; circles represent disks which are orthogonal within the columns, whereas ellipses represent disks which are tilted. Examples of so-called columnar nematic phases have been described by Praefcke<sup>42</sup> and by Ringsdorf;<sup>43</sup> these are nematic arrays of columnar stacks.

### 7.9.4 LYOTROPIC LIQUID CRYSTALS

If a surfactant molecule,<sup>44</sup> such as, for example, cetyltrimethylammonium bromide (CTAB), is dissolved in water at some specific concentration (known as the *critical micelle concentration—cmc*) the molecules will organize and form micelles. This formation of micelles (Figure 13) is caused by the hydrophobic effect,<sup>45</sup> which is entropically driven. Thus, in solutions of surfactant monomers, the hydrophobic chains are not molten and are surrounded by an organized layer of water; when the micelle forms, the water layer returns to the bulk and the chains become molten,

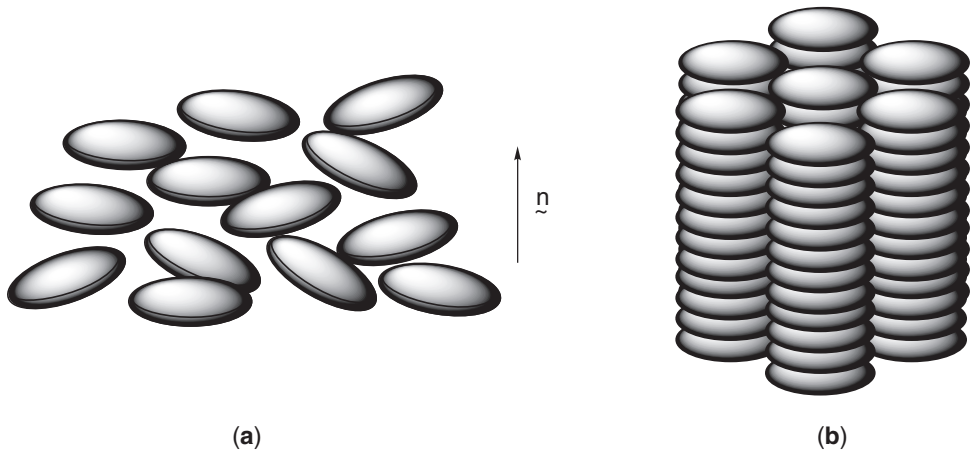


**Figure 11** Schematic structure of the (a)  $N_D$  phase and (b)  $Col_h$  phase.

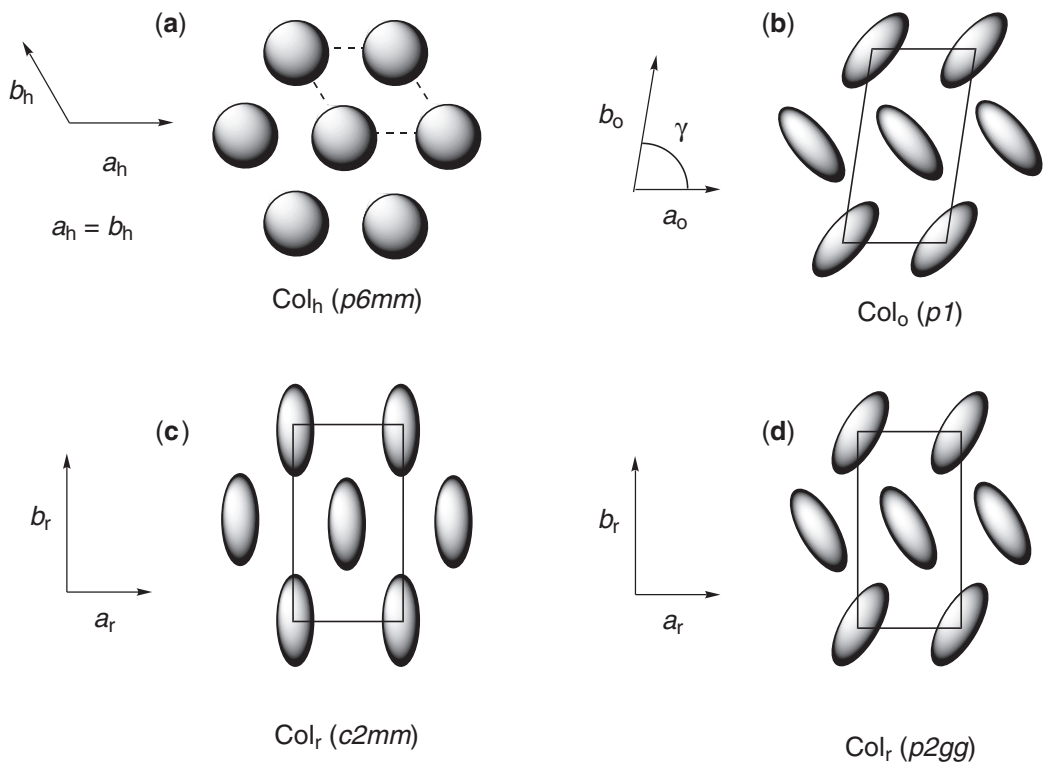


**Figure 12** Representations of the lattices of the (a) hexagonal, (b) oblique, and (c) and (d) rectangular columnar phases.

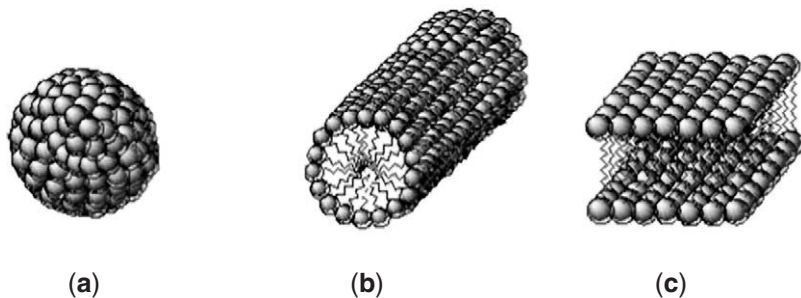


**Figure 13** Schematic representation of: (a) a “normal” cylindrical micelle, (b) a “normal” rod micelle, and (c) part of a plate-like micelle.

greatly increasing the disorder in the system. Micelles may be formed by cationic (e.g., CTAB), anionic (e.g.,  $C_{12}H_{25}OSO_3Na$ ), or non-ionic (e.g.,  $C_{12}H_{25}(OCH_2CH_2)_6OH$ ) surfactants, and solvents are not limited to water.

If more surfactant is added above the *cmc*, the concentration of micelles increases (rather than the concentration of free surfactant) until the micelle concentration becomes so high that they themselves organize to form ordered arrays of lyotropic liquid crystal phase. There are several well-characterized lyotropic liquid crystal phases and a host of so-called intermediate phases whose characterization is not unequivocal. While *cmc* values are found typically in the range  $10^{-5}$ – $10^{-3}$  mol dm<sup>-3</sup>, formation of lyotropic mesophases typically begins at around 20 wt.% of the surfactant in water.

As it is the aggregation of micelles which leads to the formation of lyotropic mesophases, then it is held to be true that the first mesophase formed is based on the micelles from which it is derived.<sup>46</sup> For example, spherical micelles give rise to micellar  $I_1$  cubic phases which may be regarded as cubic arrays of spherical micelles. (Note the subscript "1" refers to a so-called normal or oil-in-water phase, i.e., it is composed of micelles which have the hydrophobic chains on the interior and the polar headgroups on the surface. There are, in addition, type "2" phases which are inverse or water-in-oil phases where this arrangement is reversed; such phases tend to happen at rather high surfactant concentrations). Rod micelles give rise to hexagonal mesophases (termed  $H_1$ ), which consist of a hexagonal array of the rods, while disc micelles give rise to a lamellar phase ( $L_\alpha$ ), which is a solvent-separated bilayer phase.

A theoretical phase diagram for a lyotropic system is shown in Figure 14 and reveals, in addition, the  $V_1$  and  $V_2$  phases which are bicontinuous cubic phases (normal and reversed, respectively)<sup>47</sup> whose structure can be described by models involving interpenetrating rods<sup>48</sup> or periodic minimal surfaces.<sup>49,50</sup> Note also that each pair of phases is separated, at least in principle, by a cubic phase.

In addition to the lyotropic mesophases formed by surfactant amphiphiles, two other types are generally recognized, neither of which exhibits a *cmc*. The first of these are lyotropic phases of rigid-rod polymers which can form mesophases in both aqueous and non-aqueous solvents,<sup>51</sup> these mesophases being of the nematic or hexagonal type. Examples include polymeric metal acetylide complexes (*vide infra*) and DNA.<sup>52</sup> The other type is formed from usually flat and largely aromatic molecules which can stack to give lyotropic columnar phases, also referred to as chromonic phases.<sup>53,54</sup> This latter class are formed from systems with ionic or strongly hydrophilic peripheral functions and form mesophases in water, or by much more thermotropic-like systems which are surrounded by apolar alkyl chains and which form mesophases in apolar solvents such as alkanes.<sup>55</sup> Here, the stacks of molecules constitute the mesogenic unit which is known to organize into either a nematic phase where the stacks are well separated by water, or a hexagonal phase.

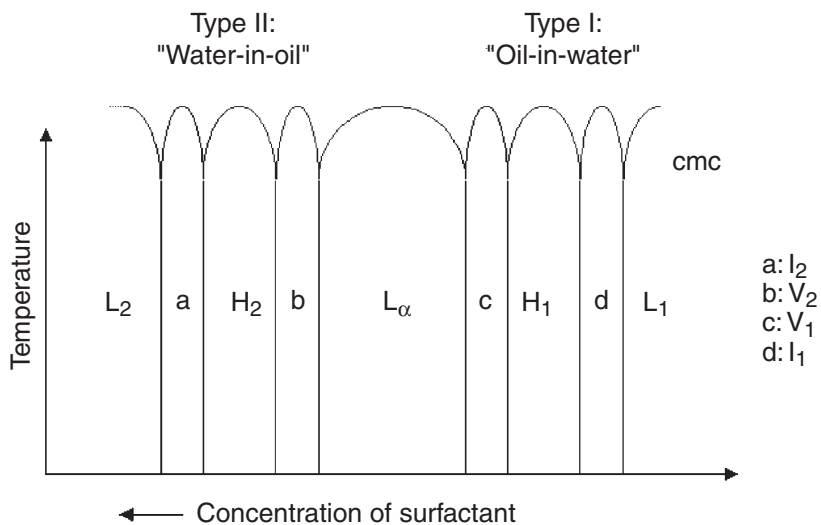


**Figure 14** Idealised, theoretical phase diagram for a binary surfactant/water system ( $L_1$  is a solution of micelles,  $L_2$  is a solution of reversed micelles).

### 7.9.5 PHYSICAL PROPERTIES OF LIQUID CRYSTALS

Probably the single most important thing about liquid crystal phases is that as fluids they are anisotropic; this means that their physical properties are likewise anisotropic and it is this feature which is the basis for the widespread application of the materials and also, in many cases, of their characterization. Consider, for example, the refractive indices of a nematic phase (Figure 15).

In the figure, it is assumed that the molecules have a greater polarizability along their long axis than along either of their two short axes, so that in case A, the electric vector of the light is coincident with the direction of greatest polarizability and so the light is retarded. However, in case B, the electric vector of the light is coincident with the direction of least polarizability and so the light is retarded little. The consequence is that the material has two refractive indices,  $n_{\parallel}$  (case A) and  $n_{\perp}$  (case B), and the difference between these ( $\Delta n = n_{\parallel} - n_{\perp}$ ) is termed the birefringence. (Note that as the nematic phase has  $D_{\infty h}$  symmetry, the two short axes are effectively equivalent and so the two possible  $n_{\perp}$  reduce to only one). Birefringence can either be positive ( $\Delta n > 0$ ) or negative ( $\Delta n < 0$ ).

This anisotropy as illustrated by refractive index extends to other properties, and common properties of interest would be the anisotropy in linear polarizability ( $\Delta\alpha$ ), dielectric permittivity ( $\Delta\epsilon$ ), and diamagnetism ( $\Delta\chi$ ). In the nematic phase, these properties are quite strongly temperature-dependent as the order parameter,  $S$ , increases as samples cool away from the N-I transition. This is illustrated in Figure 16 where it is also seen that the parallel component has the stronger temperature dependence as it is the orientational correlations which increase on cooling. Note that at the transition to the isotropic phase, there is a discontinuity as there is only a single component of each parameter in the isotropic state.

Such properties are determined primarily by molecular features and as such can be tuned at the molecular level. The values for the birefringence and dielectric anisotropy of the two-ringed cyano nematogens shown in Figure 17 illustrate this well, both quantities decreasing as the polarizability of the materials decrease (data from reference<sup>1</sup>).

### 7.9.6 MESOPHASE CHARACTERIZATION

Once a material is synthesized, it is necessary to establish which mesophases it forms and at what temperatures the transitions occur. Two techniques are used routinely in all laboratories for this purpose,

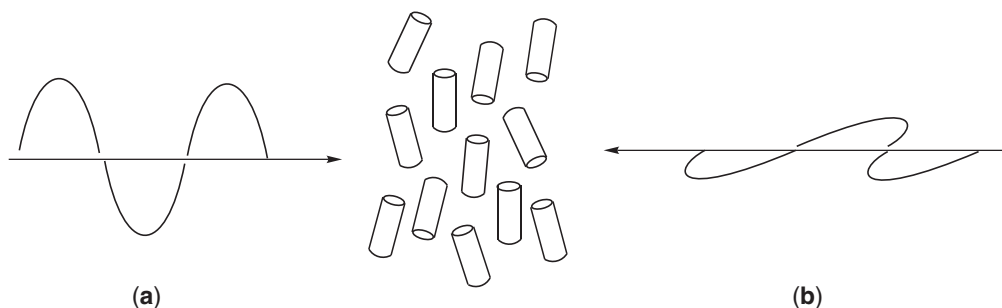


Figure 15 The interaction of polarized light with a nematic phase.

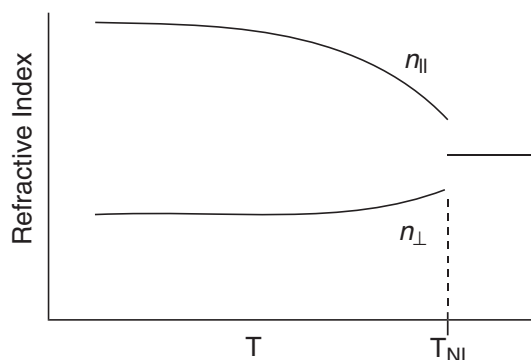
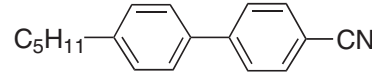
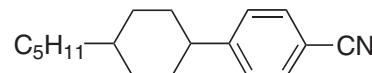
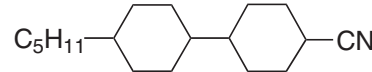


Figure 16 Variation of physical parameters in the nematic phase of liquid crystals.



	$\Delta n$	$\Delta \epsilon$
	0.18	11.5
	0.10	9.7
	0.06	4.4

**Figure 17** Birefringence and dielectric anisotropy as a function of molecular composition.

namely polarized optical microscopy and differential scanning calorimetry (DSC) and it is important that these are used in conjunction with one another. In addition, the technique of X-ray scattering is often used to give unequivocal phase identification when microscopy cannot so do, and also to provide additional insights into the structures adopted. These three primary techniques will now be described in more detail.

#### 7.9.6.1 Polarized Optical Microscopy

This is usually the first technique used to characterize the mesomorphism of a new material and is a relatively rapid way of gaining information. The microscope is arranged so that plane-polarized light impinges on the sample (ca. 1 mg between microscope cover slips) whose temperature may be controlled. The light which passes through then encounters another piece of polaroid (the analyzer) which is set with its polarization director at  $90^\circ$  to the first polarizer; light which passes through the analyzer is then observed (Figure 18).

Viewed through such a microscope, an isotropic liquid would appear black as the plane-polarized light would pass through unaffected and be absorbed by the analyzer. However, liquid crystals are anisotropic fluids and their birefringence causes the plane polarization to be lost, the light becoming elliptically polarized instead (i.e., there are two refracted rays). The observer then views an interference pattern (texture) whose appearance is determined by the symmetry of the mesophase and, hence, the phase can be identified. Occasionally, however, the molecules in certain mesophases (N, SmA, SmB, Col<sub>h</sub>) can arrange themselves so that the viewing of the

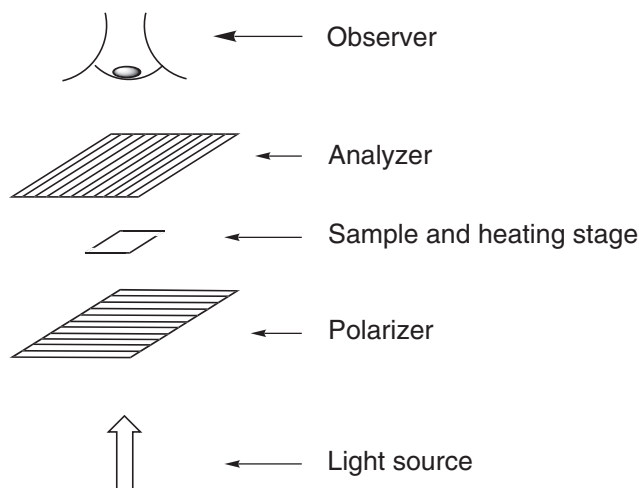


**Figure 18** Schematic view of a polarized, hot-stage microscope.

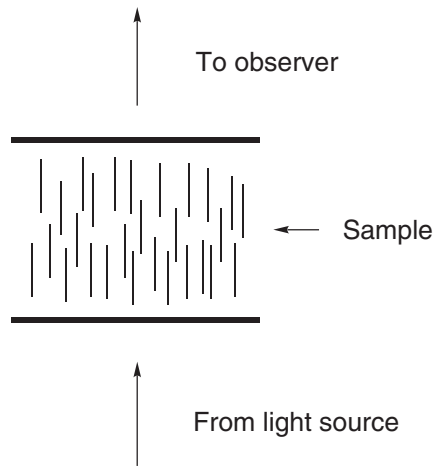


**Figure 19** Idealised figure showing the homeotropic alignment of a nematic phase.

sample is down its optic axis (Figure 19). In this case, the plane-polarized light experiences only one refractive index and so passes through the sample unchanged to appear black—this is the homeotropic texture. Textures are always best obtained on cooling a sample, the most diagnostic textures being obtained on cooling either directly from the isotropic liquid or from the homeotropic texture of a preceding phase.

A very useful method often used in conjunction with microscopy is miscibility. The simplest use of the technique is to bring two materials together on the cover slip in their mesophases in a contact preparation; the identity of the mesophase of one of the materials is already known. If the two materials are co-miscible, then both have the same mesophase (at the temperature in question) and this can then be a useful method of phase identification. Unfortunately, if the two materials are immiscible then no information is obtained as two materials in the same phase are not necessarily miscible (e.g., water and chloroform which are both isotropic!).

### 7.9.6.2 Differential Scanning Calorimetry (DSC)

Transitions between the solid and a mesophase, or between two mesophases, or between a mesophase and the isotropic liquid, are thermodynamic events and they are classified as either first- or second-order. In liquid crystals, transitions between phases are usually thought of as being weakly first order, although second-order transitions are not uncommon; the melting transition is, however, first order.

Thermodynamically, the term “first order” relates to the behavior of the free energy,  $G$ , with temperature. Thus, Equation (2) shows that the change in free energy with respect to temperature gives a measure of the entropy and it is the behavior of this function through a phase transition which determines its order. Thus, if the function shows a discontinuity through the phase transition, then that transition is first order. At the transition, it is assumed that  $\Delta G = 0$  and so there is an enthalpy of transition which is given by:  $\Delta H = T\Delta S$

$$\frac{\partial G}{\partial T_p} = -S \quad (2)$$

However, it is also possible that there is no change in entropy (and, hence, enthalpy) during the transition; rather, there is a discontinuity in the *second* derivative of the free energy with respect to temperature (the heat capacity—Equation (3)). Such transitions are termed second order:

$$\frac{\partial^2 G}{\partial T_p^2} = -\frac{C_p}{T} \quad (3)$$

Typical enthalpy changes between successive liquid crystal phases or between a liquid crystal phase and an isotropic liquid are typically small at around  $1 \text{ kJ mol}^{-1}$ , while transitions between a crystal and a liquid crystal phase are strongly first order and often in the range  $30\text{--}50 \text{ kJ mol}^{-1}$ . Transitions between phases of the same symmetry are always first order and, while all liquid crystal transitions can be first order, the SmC–SmA and SmA–N transitions are often second order.

In the DSC experiment, the change in heat capacity as a function of temperature is recorded, leading to a measure of the enthalpy change (and hence the entropy change) accompanying a phase transition. Information about the phase transition may therefore be derived from the relative magnitudes of the transition enthalpies, so that melting enthalpies are (obviously) much larger than those found for an N–I transition. While such information is informative, it does not allow generalizations to be made and the corresponding entropy changes are often considered more useful.

The technique needs to be regarded as strictly complementary to optical microscopy, as all changes in optical texture do not necessarily correspond to a change in mesophase type, while all phase changes do not always lead to an easily identifiable change in texture. Thus, DSC traces should always be compared with the results of the optical study to be sure of proper correspondence.

### 7.9.6.3 Small-angle X-ray Diffraction

Small-angle X-ray diffraction provides, in general, a definitive way to determine the structure of a liquid-crystalline phase, and has played a major role in the identification of mesomorphic phases and in the study of their transitions. Based on the Bragg law,  $2d\sin\theta = n\lambda$ , which states that X-rays are reflected from adjacent planes separated by a distance when the path difference between them is an integer multiple of the wavelength used, X-ray diffraction experiments provide information not only about the inter-planar distance, but also about the relative orientation and spatial orientational order of different sets of planes. Typically, layer thickness in smectic phases or intercolumnar distances in columnar mesophases are determined, along with the molecular organization within each layer or column, respectively.

X-Ray diffraction experiments on liquid crystals are much more difficult to perform than conventional experiments on single crystals, because of the small number of reflections obtained, because of other, special requirements such as temperature control and sample alignment. The latter is normally accomplished with the help of an external field, which is typically magnetic. Thus, on account of the diamagnetic anisotropy of the phase, calamitic mesogens are free to reorient in the nematic phase under the torque produced by the magnetic field and aligned, monodomain samples may be realized. By cooling down in the presence of the field, the orientation may then be kept in any subsequent smectic phases. For columnar mesophases, obtaining oriented samples is much more difficult to achieve, mainly because of the higher viscosity of the phases compared with those arising from calamitic materials. However, single domains of columnar mesophases can be obtained through a surface orientation process.<sup>57</sup> A typical X-ray diffraction experimental set-up is shown in Figure 20.

The experiment consists of a source of X-rays (S), a monochromator (M), a sample chamber (C) where the temperature may be controlled, followed by a detector (D). The most common

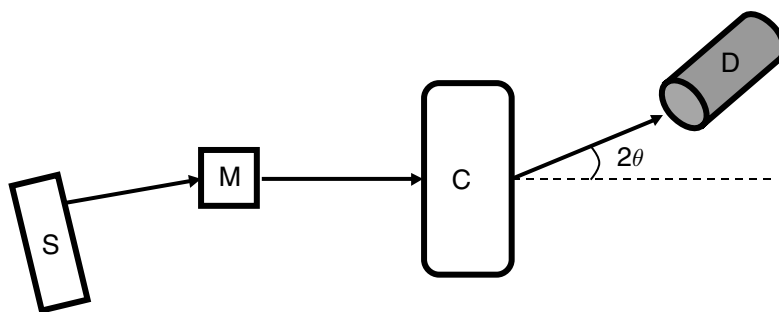


**Figure 20** Schematic of X-ray diffraction experimental setup. S is the source of X-rays, M the monochromator, C the sample chamber, and D the detector.  $\theta$  is the angle of diffraction.

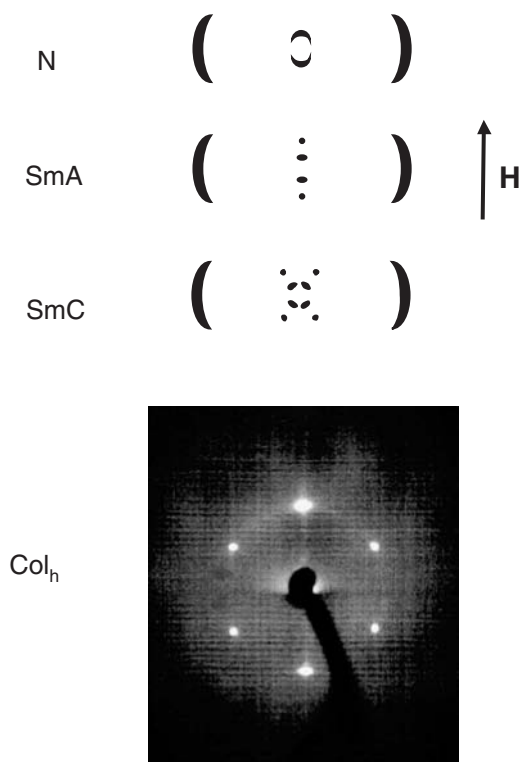


**Figure 21** Typical X-ray diffraction patterns of aligned samples of the nematic, smectic A, smectic C, and columnar hexagonal mesophases.

source of X-rays is a generator using a sealed tube, and the monochromator, made for example from a quartz crystal, is used to select a single wavelength from the polychromatic beam emerging from the source. The sample is placed in a chamber equipped with temperature control and facilities for alignment with a magnetic field. As for the detector, different choices can be made depending on the type of information sought. To obtain an overview of the diffraction pattern, a two-dimensional detector or an image plate (or even photographic film) are well suited. For quantitative information, a scintillation counter or a linear position-sensitive detector is essential.

Typical X-ray patterns of aligned liquid crystalline phases are shown in Figure 21. In the case of the nematic and smectic phases, the calamitic molecules are oriented parallel to the magnetic field and consequently a liquid-like peak (broad signal) corresponding to the length of the molecule appears along the direction of the field in the small-angle region (central part of the pattern). The diffuse peak arising from intermolecular distances is found in the direction perpendicular in the wide-angle region (side part of the pattern). In the smectic A phase, the diffuse peaks observed at small angles in the magnetically aligned nematic phase condense into sharp Bragg spots; in the wide-angle region, the diffuse peaks remain similar as in the nematic phase owing to the two-dimensional-like arrangement of the molecules within each smectic layer. As for the smectic C phase, the molecules are now tilted with respect to the layers. In this case, when the molecules are still oriented parallel to the magnetic field, the layers become tilted with respect to this direction, and the diffraction corresponding to the smectic layers gives rise to two pairs of reflections at small angles; the angle between these pairs being twice the molecular tilt angle. In the case of the columnar mesophase, the orientation is obtained using a preparation technique by which a small drop of the sample is heated on a cleaned glass plate up to the isotropic state and cooled down slowly to the temperature of investigation. Using this method, well-aligned monodomains are obtained by surface interaction. The incident X-ray beam is parallel to the glass plate and the scattered intensity is collected on a two-dimensional detector. The example given below clearly shows the two-dimensional hexagonal symmetry of the columnar phase. In circumstances where aligned samples cannot be obtained, the information content is slightly reduced and the spots “smear out” into rings which provide the same information on spacings, but a little less on properties such as tilt angles.

### 7.9.7 MACROCYCLIC MESOGENS FORMING COLUMNAR PHASES

As seen in the preceding part, structural anisotropy is essential in considering the specific intermolecular interactions that will promote or disfavor mesomorphism. Indeed, the formation of mesophases is a process of self-organization, and is influenced by the shape of the constituent mesogens. Calamitic mesogens tend to assemble into nematic and smectic phases, whereas columnar phases can be induced by discotic molecules. In both cases, the anisotropic order is produced by the specific arrangement of the rigid, mesogenic cores, and the fluidity is ensured by the molten aliphatic chains. It will be shown that the induction of columnar mesophases depend strongly on the mesogenic core and of the number and nature of the side chains. For these purposes, several types of mesophase have been identified and classified. Two nematic phases have been identified, namely the nematic discotic phase,  $N_D$ , and the columnar nematic phase,  $N_{Col}$ . The former is directly analogous to the nematic phase of calamitic molecules described earlier, while the latter consists of nematic ordering of small, columnar aggregates along a privileged direction, with the columnar axis taking the role of the unique molecular axis. Columnar mesophases result from the stacking of the disk-like mesogens into columns, and from the mutual arrangement of the latter into various two-dimensional lattices. The columns have either a cylindrical or an elliptical cross-section, depending of the molecular shape, the number and location of the side chains, and whether or not the molecules are tilted with respect to the columnar axis. Several columnar mesophases have now been identified, for which the two-dimensional symmetry can be hexagonal ( $Col_h$ ), rectangular ( $Col_r$ ), oblique ( $Col_o$ ), or tetragonal ( $Col_t$ ), some of them being further distinguished such as the  $Col_t-c2mm$  and  $Col_t-p2gg$ . In some cases, columnar aggregates of discoid molecules may arrange themselves into smectic layers, and depending on the long-range order of such organization, will be referred to as discotic lamellar,  $D_L$ , or lamellar discotic,  $L_D$ , or lamellar columnar,  $Col_L$ , phases; these are illustrated in Figure 22.

The most obvious family of compounds able to induce columnar phases is that constituted by the macrocyclic compounds which often possess a discoid molecular shape.<sup>58</sup> The ability of macrocyclic systems to stack and to self-assemble into columnar mesophases confers on these systems the properties required for potential utilization in molecular devices based on photonics, electronics, or low-dimensional ionic transport.<sup>59–65</sup> The search for new discotic mesogens is thus still of current interest, in order to improve their chemical, thermal, and photophysical stability, and new families of discogenic materials appear regularly.

#### 7.9.7.1 Phthalocyanines

Phthalocyanines represent a class of inherently disk-like molecules, and were the first, and are probably the most studied, type of discotic metallomesogens showing columnar mesophases. Their ability to form stable metal complexes with a wide variety of metal ions rendered the materials very attractive, as evidenced by the important systematic studies that will be described thereafter. The two hydrogen atoms in the central cavity can easily be replaced by metal ions and phthalocyanines can be regarded as weak, dibasic acids. When substituents were placed around the phthalocyanine ring, not only was the solubility of the compound increased—of essential importance in many aspects—but their tendency to self-assemble into columnar mesophases proved more efficient. One can distinguish two main classes of liquid crystalline phthalocyanines depending on the position of the side chains relative to the flat core: the mesogenic phthalocyanines substituted by eight flexible chains in the peripheral positions 2, 3, 9, 10, 16, 17, 23, 24, the most studied to date; and those functionalized in the non-peripheral positions, referred to in the following as the radial positions 1, 4, 8, 11, 15, 18, 22, 25. The free bases possess a  $D_{2h}$  molecular

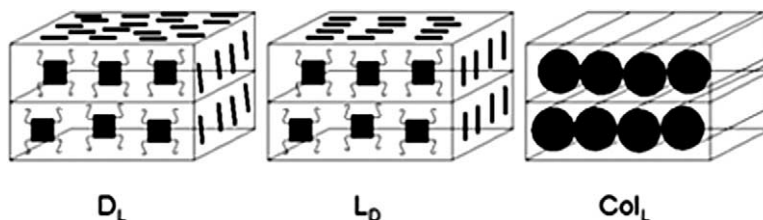
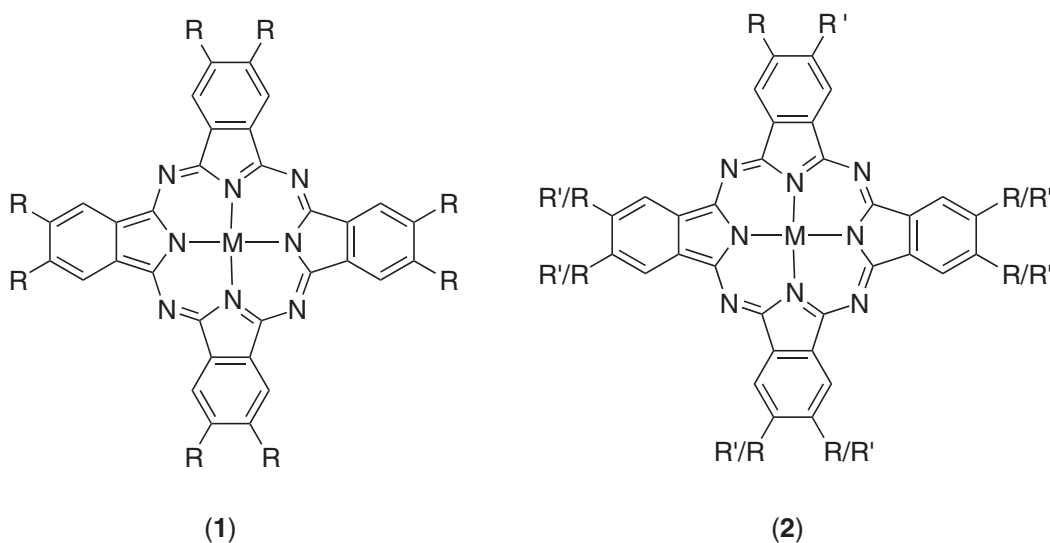


Figure 22 Structure of the  $D_L$ ,  $L_D$ , and  $Col_L$  phases.

symmetry, whereas on complexation to a transition metal, the molecular symmetry increases to  $D_{4h}$ , due to the equivalence of the pyrrolidine groups. They will be discussed separately. In some cases, phthalocyanines can be non-uniformly substituted: they can be either simply tetra- or octa-substituted but by two different components. In such cases, the synthetic method proceeds randomly, and generally a mixture of four different regio-isomers with different molecular symmetry are produced ( $C_{2v}$ ,  $C_{4h}$ ,  $D_{2h}$ ,  $C_s$ ) and the components separated.

### 7.9.7.1.1 Peripherally octasubstituted phthalocyanines

In 1982, Simon *et al.* reported the first liquid-crystalline copper(II) complex of phthalocyanine substituted with eight peripheral dodecyloxymethyl chains ((1):  $M = \text{Cu}$ , 2H,  $R = \text{CH}_2\text{OC}_{12}\text{H}_{25}$ ). The complex exhibited a  $\text{Col}_h$  phase from 53 °C up to 300 °C, at which temperature it started to decompose without clearing,<sup>66</sup> while the ligand possessed a  $\text{Col}_h$  phase over a slightly narrower temperature range.<sup>67–70</sup> Several other metal-containing octaalkoxymethyl-phthalocyanines ((1):  $M = \text{Cu}$ , Zn, Mn, Pb, Ni, Sn, Co,  $\text{Co}(\text{CN})_2$ ,  $R = \text{CH}_2\text{OC}_n\text{H}_{2n+1}$ )<sup>71–74</sup> were found to exhibit similar, wide-temperature-range  $\text{Col}_h$  phases. Some thermal data are collected in Table 1.



In general, mesophase stability increased upon complexation, generally due to a longer-range molecular stacking order. However, it appeared that depending on the nature of the divalent metal the transition temperatures and the arrangement in the columns were modified. The case of the lead(II) and tin(II) compounds are good examples of unusual arrangements into columns.

**Table 1** Transition temperatures of (1) with  $R = \text{CH}_2\text{OC}_n\text{H}_{2n+1}$ .

<i>M</i>	<i>n</i> = 8	<i>n</i> = 12
2H	Cr 66 $\text{Col}_h$ 322 I	Cr 79 $\text{Col}_h$ ~ 260 I
Cu	Cr 82 $\text{Col}_h$ > 300 dec.	Cr 53 $\text{Col}_h$ > 300 I
Zn	Cr 88 $\text{Col}_h$ > 300 dec.	Cr 78 $\text{Col}_h$ > 300 I
Pb	Cr -45 $\text{Col}_h$ 155 I / Cr 53 $\text{Col}_h$ > 300 I <sup>a</sup>	Cr-12 $\text{Col}_h$ 125 I
Ni	Cr 67.5 $\text{Col}_h$ > 300 I	Cr 58 $\text{Col}_h$ > 300 dec.
Co	Cr 72 $\text{Col}_h$ > 300 I	Cr 71 $\text{Col}_h$ > 300 dec.
Mn	–	Cr 44 $\text{Col}_h$ > 280 I
$\text{NaCo}(\text{CN})_2$	Cr 73 $\text{Col}_h$ > 300 I	Cr-7 $\text{Col}_h$ > 300 I
$\text{Si}(\text{OH})_2$		Cr 59 $\text{Col}_r$ 95 M 114 I
$\text{Sn}(\text{OH})_2$		(water loss + polymerization)

<sup>a</sup> The two sets of data arise from refs. 75 and 76, respectively. M: unidentified mesophase.

Indeed, due to their larger size, these metal ions cannot be accommodated in the cavity of the phthalocyanine, and they sat out of the plane of the resulting complexes ( $M = \text{Pb}$ ), or yielded the so-called super-phthalocyanines, i.e., made of five iminoisindoline units ( $M = \text{Sn}$ ). For the lead complexes,<sup>75,76</sup> a broad peak at ca. 7.4 Å was observed by X-ray diffraction, indicating pairs of molecules coupled in an antiferroelectric fashion; these dimers then stacked up into columns, and in order to preserve the hexagonal symmetry, each pair was tilted with respect to the columnar axis. This antiparallel stacking may explain the low melting points and thermal stability of the lead compound with respect to other divalent metal compounds. Note that the lead octyloxy-methyl phthalocyanine was prepared concomitantly by two different groups, and different transition temperatures were given. The tin phthalocyanine was unstable,<sup>77</sup> and became oxidized in air to a dihydroxytin(IV) species. It displayed both a  $\text{Col}_r$  and another birefringent mesophase before clearing to the isotropic liquid, this intermediate phase likely being associated to the departure of water. The isotropic liquid transformed slowly into a highly viscous, anisotropic phase, related to the formation of oxystannyl(IV) oligomeric linear chains as identified by spectroscopic analysis. The same polymerization process was observed with the polycondensation of siloxane<sup>78,79</sup> and cobalt compounds to form so-called *spinal* columnar liquid crystals. The effect of reducing the chain length has been investigated for the  $\text{Co}^{\text{II}}$  complexes ((1):  $M = \text{Co}$ ,  $R = \text{CH}_2\text{OC}_n\text{H}_{2n+1}$ ,  $n = 1-8$ )<sup>80</sup> and for chain length shorter than  $n = 8$ , liquid crystalline properties were inhibited, in contrast to the observations of Hanack.<sup>72</sup> Properties such as magnetic, conductive,<sup>81</sup> luminescent,<sup>82</sup> and other photophysical properties<sup>83-85</sup> were measured in the solid phase and in the mesophase, revealing the potential use of these metal complexes, and particularly the copper and zinc phthalocyanines, as one-dimensional conductors.

The influence of the nature of the chains on the transition temperatures and mesomorphism was then investigated systematically in order to try to find some correlations between the properties and the structure. This led to a broad study, where the alkoxymethyl chains of the above compounds were replaced by, for example, straight (or branched) alkyl chains, alkoxy chains, thioalkyl chains, octanoate chains, and ethylene oxide chains. The number of chains in the periphery has also been modified for the same purpose.

Some years ago, Nishi *et al.*<sup>86,87</sup> and Hanack *et al.*<sup>88</sup> prepared several octaalkyl metallophthalocyanines ((1):  $M = 2\text{H}$ ,  $\text{Cu}$ ,  $\text{Ni}$ ,  $R = \text{C}_n\text{H}_{2n+1}$ ,  $n = 5-14$ ,  $\text{CH}_2\text{CH}(\text{Et})\text{C}_4\text{H}_9$ ), and recently this range was increased to include zinc and cobalt complexes.<sup>74</sup> All the compounds were mesomorphic, with an increase in transition temperatures upon complexation, which was greater than that observed for the analogous alkoxymethyl complexes (Table 2). The mesophases were identified as  $\text{Col}_h$  phases for both metal-free and metal-containing systems. In most cases, even for long-chain-length derivatives, the clearing temperatures could not be determined either because the transition to the isotropic liquid occurred at too high a temperature and thus was not observable, or due to decomposition taking place in the mesophase. The melting temperatures were found to decrease quite rapidly on lengthening the chain. Branching the chains led to the complete suppression of mesomorphism ((1):  $M = 2\text{H}$ ,  $\text{Ni}$ ,  $R = \text{CH}_2\text{CH}(\text{Et})\text{C}_4\text{H}_9$ ), and both the free-base and the nickel compounds melted above 270 °C without showing mesophase. Compared with the analogous alkoxymethyl compounds, the result of this substitution was associated with a drastic increase in the transition temperatures. Note that related phthalocyanine complexes were also prepared, but with an oxotitanium(IV) fragment, which protruded out of one face of the macrocycle ((1):  $M = \text{TiO}$ ,  $R = \text{C}_n\text{H}_{2n+1}$ ,  $n = 3-5,7$ ).<sup>89,90</sup> These complexes were studied for purposes such as electronic and non-linear optical properties, but in spite of their mesogenic character, the authors did not provide information about their thermal behavior.

Several research groups concurrently prepared the same series of metal-free<sup>91,92</sup> and copper complexes<sup>93,94</sup> of octaalkoxy substituted phthalocyanines ((1):  $M = 2\text{H}$ ,  $\text{Cu}$ ,  $R = \text{OC}_n\text{H}_{2n+1}$ ,  $n = 5-14$ , 18; thermal data collected in Table 3). They observed mesomorphism for all the free-base

**Table 2** Mesomorphic properties of (1) with  $R = \text{C}_n\text{H}_{2n+1}$ .

<i>M</i>	$n = 8$	$n = 12$
2H	Cr 186 $\text{Col}_h$ 325 I	Cr 120 $\text{Col}_h$ 252 I
Cu	Cr 180 $\text{Col}_h > 380$ I	Cr 169 $\text{Col}_h$ 351 I
Ni	Cr 190 $\text{Col}_h$ 373 I	Cr 123 $\text{Col}_h > 300$ dec.
Zn	Cr 189 $\text{Col}_h > 325$ dec.	Cr 160 $\text{Col}_h > 325$ dec.
Co	Cr 158 $\text{Col}_h > 325$ dec.	Cr 112 $\text{Col}_h$ 290 I

**Table 3** Mesomorphic properties of (1) with  $R = OC_nH_{2n+1}$ .

<i>M</i>	<i>n</i> = 8	<i>n</i> = 10	<i>n</i> = 12	$R = OCH_2CH(Et)C_4H_9$
2H	Cr 94 Col <sub>h</sub> > 345 dec.	Cr 94 Col <sub>h</sub> > 345 I	Cr 83 Col <sub>h</sub> 309 I	Cr 170 Col <sub>t</sub> 223 N <sub>D</sub> 270 I
Cu	Cr 112 Col <sub>h</sub> > 345 dec.	Cr 104 Col <sub>h</sub> > 345 I	Cr 95 Col <sub>h</sub> > 345 I	Cr 204 Col <sub>t</sub> 242 N <sub>D</sub> 290 I
Ni	Cr 110 Col <sub>h</sub> > 300 dec.	Cr 87 M > 300 I	Cr 97 Col <sub>h</sub> 254 I	
Pd		Cr 90 M > 300 I		
Pt		Cr 64 M > 300 I	Cr 77 Col <sub>h</sub> > 345 I	Col <sub>o</sub> 205 I
Co	Cr 123 Col <sub>h</sub> > 300 dec.	Cr 111 Col <sub>h</sub> > 300 dec.	Cr 85 Col <sub>h</sub> 345 I	
Pb				Col <sub>t</sub> 79 M > 240 I
Zn	Cr 135 Col <sub>h</sub> > 300 dec.		Cr 99 Col <sub>h</sub> 375 I	
VO	Cr 63 Col <sub>r</sub> 250 dec.		Cr 51 Col <sub>r</sub> 250 dec.	

M: unidentified mesophase.

materials and their corresponding copper complexes, with overall reasonable agreement in results. For most of the complexes and free-base analogs, the mesophase was characterized as Col<sub>h</sub> by X-ray diffraction. To test whether the choice of the metal influenced these properties, nickel, palladium, platinum, cobalt, zinc, and lead complexes<sup>95–98</sup> were also prepared. On average, the transition temperatures were not modified to a great extent, remaining high, and in many cases, isotropization was not reached. The lowest melting transition was seen for the platinum complexes.

Some VO complexes were prepared recently ((1):  $M = VO$ ,  $R = OC_nH_{2n+1}$ ,  $n = 8, 12, 16$ )<sup>99</sup> and, while, in common with the lead complexes, they have a group (an oxo function) which protrudes from the phthalocyanine plane, they were found to display a Col<sub>r</sub> phase, at rather low temperature, with decomposition starting at temperatures higher than 250 °C. They were found to form antiparallel dimers by X-ray diffraction, which were stacked into columns, but with a tilt along the long dimer axis in order to preserve the rectangular symmetry. No tendency towards the change to a Col<sub>h</sub> phase was seen at higher temperatures.

Major effects were produced on the phthalocyanines having branched side chains ((1):  $M = 2H$ , Cu, Pb, Pt;  $R = OCH_2CH(Et)C_4H_9$ ).<sup>100–102</sup> The copper and free-base species exhibited two mesophases, a Col<sub>t</sub> and a N<sub>D</sub> phase at higher temperature. Such high melting was not expected, first by comparison with the linear-chain compounds, and secondly by the fact that they existed as a mixture of stereoisomers due to the stereogenic center in the 2-ethylhexyloxy chain (43 stereoisomers including 16 (+)/(-) pairs and 11 *meso* compounds). In contrast, both the platinum and lead compounds were room-temperature liquid crystals. The mesophase of the platinum complex was identified as Col<sub>o</sub>, while the lead homolog was found to have a Col<sub>t</sub> phase. The change of the two-dimensional symmetry can be understood by the presence of nonlinear chains that forbid a hexagonal arrangement of the columns on the basis of steric hindrance. However, the explanation for the absence of crystallization for these two complexes is not only due to the probable mixture of stereoisomers, but must also be a consequence of their original packing, i.e., the macrocycles were stacked in an antiferroelectric fashion in the crystalline phase as demonstrated recently for the platinum complex by EXAFS and XANES,<sup>103</sup> and previously for the lead complexes. For the platinum system, the origin of such stacking was due to the mesogenic core being not planar but concave instead.

Reducing the number of chains to four, i.e., half of the side groups were long chains and the other half were methoxy groups ((2):  $M = 2H$ , Cu,  $R = OC_nH_{2n+1}$ ,  $R' = OCH_3$ ,  $n = 12, 18$ ) did not suppress mesomorphism and gave mesophases at ca. 50–80 °C, but their nature was not identified.<sup>102</sup> The reduction of the mesophase stability was due to the presence of a mixture of four different molecular symmetries resulting from the statistical tetra-substitution.

In addition to the alkoxyethyl derivatives, dihydroxosilicon(IV) phthalocyanines bearing alkoxy peripheral groups were prepared ((1):  $M = Si(OH)_2$ ,  $R = OC_nH_{2n+1}$ ,  $n = 2, 4, 6, 8, 10, 12, 14, 16, 18$ ), and all displayed a Col<sub>h</sub> phase at low temperatures, with a decreasing mesophase stability due to the presence of axial hydroxyl groups.<sup>104–106</sup> Similar silicon and silicon-free phthalocyanines substituted by chiral (S)-citronellol were shown to form a Col<sub>h</sub> and, at higher temperatures, a Col<sub>r</sub> with a helicoidal structure.<sup>107,108</sup>

Moreover, the copper and nickel complexes substituted by eight<sup>109</sup> dodecyloxy chains displayed lyotropic N<sub>Col</sub> and Col<sub>h</sub> mesophases in contact preparations with organic solvents (linear alkanes, cyclohexane, benzene, chloroform). The lyomesophases were stable for the copper and nickel complexes, except for the binary mixture between the nickel complex and linear alkane, for which



the mesophases were monotropic. In all the binary phase diagrams, the  $N_{\text{Col}}$  phase was systematically the high-temperature mesophase, and was stable at high solvent concentrations. The  $\text{Col}$ - $N_{\text{Col}}$  transitions were first-order, exhibiting rather large biphasic regions.

Schouten *et al.*<sup>110,111</sup> showed that alkoxyphthalocyanines showed a blue shift of the  $Q$ -bands in the electronic absorption spectra, compared to that of the alkyl-substituted analogs, attributable to the strong electron-donating ability of the alkoxy chains. It was thus thought that the replacement by non-electron-donating groups, such as thioalkyl functions, would result in the red shift of the  $Q$ -band, i.e., to the reduction of the gap between the HOMO and LUMO, and accordingly to the increase in the electro-conductivity along the columns. With this in mind, and to understand further the role played by the linkage between the side chains and the disk-like core on the mesophase stability, a few phthalocyanines with eight thioalkyl chains were investigated. Zinc, copper,<sup>112,113</sup> cobalt,<sup>114</sup> nickel,<sup>115,116</sup> oxotitanium(IV),<sup>117,118</sup> and oxovanadium(IV)<sup>119</sup> octa(alkylthio)phthalocyanines were prepared ((1):  $M = 2\text{H}$ , Cu, Zn, Co, Ni, TiO, VO,  $R = \text{SC}_n\text{H}_{2n+1}$ ,  $n = 8, 10, 12, 16, 18$ ; thermal data in Table 4). All the copper complexes, as well as the free bases, exhibited an enantiotropic  $\text{Col}_h$  phase over large temperature ranges, irrespective of the metal ion. Again, mesophase stabilization was observed upon metal complexation. X-Ray diffraction further revealed, on both sides of the diffuse halo corresponding to the molten chains, two other diffuse scatterings, which were attributed to the presence of a mixture of monomers and dimers in the columns. Another explanation could be the result of a staggered stacking of the cores due to the large size of the sulfur atom. The cobalt complexes were also mesomorphic, probably showing the same mesophase, but they were not fully characterized ((1):  $M = \text{Co}$ ,  $n = 12$ ). Temperature-dependent electronic spectra of the UV–vis region were recorded, and indicated a red shift of the  $Q$ -band of the dodecylthio-substituted phthalocyanines ((1):  $M = 2\text{H}$ , Cu) in the  $\text{Col}_h$  phase compared to the dodecyl and dodecyloxy homologous compounds, i.e., an increase in the conductivity is thus expected for the former. The two metallophthalocyanines with a strong dipole moment perpendicular to the large rings also exhibited a  $\text{Col}_h$  phase over similar temperature ranges as the copper and free-base compounds. However, no signs which would correspond either to an antiferroelectric or ferroelectric stacking was detected by X-ray diffraction, suggesting a random distribution of the dipoles along the columns, maybe attributable to the greater van der Waals' radius of the sulfur atoms compared to the  $M=O$  groups.

The phthalocyanines of zinc and copper substituted with fewer than eight octylthio side groups displayed both thermotropic and lyotropic mesophases in hexadecane, the missing chains being replaced by chlorine atoms ((1):  $M = 2\text{H}$ , Cu, Zn,  $R = x\text{Cl} + (8-x)\text{SC}_8\text{H}_{17}$  with  $x = 0-7$ ).<sup>112</sup> A  $N_{\text{Col}}$  phase was seen at the boundary with the isotropic liquid, and a  $\text{Col}_h$  phase at lower solvent concentration, before the room-temperature thermotropic columnar phase of the neat sample. The extent of the molecular ordering (correlation length, intra- and inter-columnar orders) and the stability of the thermotropic mesophase were affected by the number of side chains and consequently by the existence of mixtures of isomers. The same was true for the lyotropic phase. Phase formation was greatly facilitated when the number of peripheral alkyl chains diminished due to the easier incorporation of the hydrocarbons such as hexadecane in the free volume close to the columnar cores. The fluid lyotropic mesophase of some of these phthalocyanines was easily aligned homeotropically when sandwiched between two untreated glass slides.<sup>120</sup> Similar results were obtained for the tetrathiododecyloxy copper phthalocyanines isomeric mixture<sup>121,109</sup> ((2):  $M = \text{Cu}$ ,  $R = \text{H}$ ,  $R' = \text{SC}_{10}\text{H}_{21}$ ) in linear alkanes, cyclohexane, benzene, and chloroform, which possessed  $N_{\text{Col}}$  and  $\text{Col}$  phases over a large domain with concentrations varying from 20 wt.% to 75 wt.% of complex.

Tetra- and octa-(13,17-dioxanonacosane-15-sulfanyl)-substituted, metal-free, and nickel phthalocyanines have been synthesized ((2):  $M = 2\text{H}$ , Ni,  $R = \text{H}$ ,  $R' = \text{SCH}(\text{CH}_2\text{OC}_{12}\text{H}_{25})_2$ , and

**Table 4** Mesomorphic properties of (1) with  $R = \text{SC}_n\text{H}_{2n+1}$ .

$n$	$M = 2\text{H}$	$M = \text{Cu}$	$M = \text{Ni}$
8	Cr 68 $\text{Col}_h > 340$ I	Cr 77 $\text{Col}_h$ 350 dec.	$n = 6$ : Cr 36 $\text{Col}_h$ 300 dec.
10	Cr 77 $\text{Col}_h > 340$ I	Cr 54 $\text{Col}_h$ 290 dec.	$n = 12$ : Cr 20 $\text{Col}_h$ 275 dec.
12	Cr 88 $\text{Col}_h$ 286 I	Cr 77.5 $\text{Col}_h$ 323 dec.	
16	Cr 95 $\text{Col}_h$ 228 I	Cr 26.5 $\text{Col}_h$ 262 I	
	$M = \text{TiO}$	$M = \text{VO}$	$M = \text{Co}$
18	Cr 59 $\text{Col}_h$ 68 $\text{Col}_h'$ 292 I	Cr 56 $\text{Col}_h$ 295 I	$n = 12$ : Cr 52 $\text{Col}$ 300 dec.

Col: unidentified columnar phase.

**Table 5** Mesomorphic properties of the free bases and metallophthalocyanines with four (**2**) and eight (**1**) biforked chains  $R/R' = \text{SCH}(\text{CH}_2\text{OC}_{12}\text{H}_{25})_2$ .

Type	R/R'	M	Mesomorphism
<b>2</b>	H/SCH(CH <sub>2</sub> OC <sub>12</sub> H <sub>25</sub> ) <sub>2</sub>	2H	Cr 13 Col <sub>h</sub> 141 I
<b>2</b>	H/SCH(CH <sub>2</sub> OC <sub>12</sub> H <sub>25</sub> ) <sub>2</sub>	Ni	Cr 9 Col <sub>h</sub> 171 I
<b>1</b>	SCH(CH <sub>2</sub> OC <sub>12</sub> H <sub>25</sub> ) <sub>2</sub>	2H	Col <sub>r</sub> 37 I
<b>1</b>	SCH(CH <sub>2</sub> OC <sub>12</sub> H <sub>25</sub> ) <sub>2</sub>	Ni	Col <sub>r</sub> 38 I

(**1**): M = 2H, Ni R = SCH(CH<sub>2</sub>OC<sub>12</sub>H<sub>25</sub>)<sub>2</sub>; thermal data are found in Table 5).<sup>122,123</sup> The tetra-substituted compounds showed accessible room-temperature Col<sub>h</sub> phase, with no significant difference due to the metal inclusion. The low temperature was due to the mixture of isomers as for all tetra-substituted systems in spite of the fact that these macrocycles possessed eight chains. The octa-substitution of such biforked chains led to a drastic depression in clearing temperatures, and to an important destabilization of the mesophases, which are room temperature over a few degrees. The mesophase symmetry was also reduced from Col<sub>h</sub> to Col<sub>r</sub>. This low-temperature behavior was due mainly to strong steric hindrance, and to the increase in the thermal fluctuations around the cores.

Very few phthalocyanines substituted by ester side chains have been reported so far. A dihydroxogermanium(IV) phthalocyanine ((**1**): M = 2H, Ge(OH)<sub>2</sub>, R = CO<sub>2</sub>C<sub>12</sub>H<sub>25</sub>) was found to exhibit a room-temperature Col<sub>h</sub> phase up to 171 °C,<sup>124</sup> at which temperature polycondensation occurred to yield the corresponding germoxane polymer; due to the in-phase polymerization, the clearing temperature could not be reached.<sup>125</sup> The high stability of the mesophase was attributed to the presence of the alkoxy carbonyl groups, as was the case for the corresponding metal-free phthalocyanines.<sup>126</sup> Note that octakis(dodecyloxycarboxylato)- and octakis(*N*-dodecylamido)-phthalocyanato)copper ((**1**): M = Cu, R = -CO<sub>2</sub>C<sub>12</sub>H<sub>25</sub>, -CONHC<sub>12</sub>H<sub>25</sub>) formed highly ordered films, but their thermal behavior was not mentioned.<sup>127</sup> Usol'tseva demonstrated, however, the amphitropic character of several tetra-alkoxycarbonylcopper(II) phthalocyanine complexes ((**2**): M = Cu, R = CO<sub>2</sub>C<sub>*n*</sub>H<sub>2*n*+1</sub>, R' = H; *n* = 1–4, 6, 7, 9–11, 16), and analogous tetracarboxyl tetraalkoxycarbonyl complexes ((**2**): M = Cu, R = CO<sub>2</sub>C<sub>*n*</sub>H<sub>2*n*+1</sub>, R' = CO<sub>2</sub>H; *n* = 4, 9, 11) for which selected thermal data are collected in Table 6.<sup>128</sup> In the first series, from the propyl ester onwards, a thermotropic columnar mesophase was seen at temperatures up to, and just above, 300 °C, where decomposition took place. The melting temperatures decreased rapidly (from 160 °C for *n* = 3 to 50 °C for *n* = 4) yielding room-temperature mesophases for chain length with *n* ≥ 6, which then rose once more with chain length (*n* = 16, Cr 80 Col > 300 I). The length of the side chains also affected the two-dimensional columnar order. Based on X-ray diffraction data, a two-dimensional square lattice (Col<sub>t</sub>) was found for compound with *n* = 7, while a hexagonal two-dimensional lattice (Col<sub>h</sub>) was determined for *n* = 11 and 16. At intermediate chain length (*n* = 9) both columnar mesophases co-existed. Lyotropic N<sub>Col</sub> and Col mesophases were also formed in binary mixtures with either chloroform or benzene and the tetraesters (*n* = 4, 7, 9, 16) at definite concentrations and temperatures. In alkane mixtures, the lyotropic behavior was dependent on the ratio between the number of methylene groups in the solvent and in the alkyl chains of the complex. For the other series having the free carboxyl groups, a thermotropic columnar mesophase was observed between ca. 100 °C and 300 °C for *n* = 9 and 11, while the butylcarboxyl derivative was not mesomorphic. Here again, induction and/or stabilization of mesophases was observed upon addition of solvent. A Col<sub>h</sub> phase (*M*-type in the nomenclature of chromonic

**Table 6** Mesomorphism of compounds (**2**) with R = CO<sub>2</sub>C<sub>*n*</sub>H<sub>2*n*+1</sub>, R' = H and R = CO<sub>2</sub>C<sub>*n*</sub>H<sub>2*n*+1</sub>, R' = CO<sub>2</sub>H.

<i>n</i>	<i>R</i> = CO <sub>2</sub> C <sub><i>n</i></sub> H <sub>2<i>n</i>+1</sub> , <i>R'</i> = H		<i>R</i> = CO <sub>2</sub> C <sub><i>n</i></sub> H <sub>2<i>n</i>+1</sub> , <i>R'</i> = CO <sub>2</sub> H			
	Thermotropic phase	Lyotropic mesophase	Thermotropic phase	Lyotropic mesophase		
		nonane CHCl <sub>3</sub> , C <sub>6</sub> H <sub>6</sub>	nonane	CHCl <sub>3</sub>	C <sub>6</sub> H <sub>6</sub>	DMF
4	Cr 50 Col <sub>t</sub> > 300 I	N <sub>Col</sub>	Cr > 300 dec.			Col
9	Col <sub>t</sub> 80 Col <sub>h</sub> > 300 I	N <sub>Col</sub>	Cr 130 Col > 300 I	Col	N <sub>Col</sub> , Col	
11	Cr 30.5 Col <sub>h</sub> > 300 I	N <sub>Col</sub>	Cr 100 Col > 300 I		N <sub>Col</sub> , Col	N <sub>Col</sub> , Col

Col: unidentified columnar phase.

**Table 7** Transition temperatures of (1) with  $R = \text{OCH}_2\text{CONR}^1\text{R}^2$ .

$R^1$	$R^2$	$M$	
$\text{C}_8\text{H}_{17}$	$\text{C}_8\text{H}_{17}$	2H	$\text{Col}_h$ 91 I
$\text{C}_8\text{H}_{17}$	$\text{C}_8\text{H}_{17}$	Cu	M 21 $\text{Col}_h$ 83 $\text{Col}_h$ 95 I
$\text{C}_8\text{H}_{17}$	$\text{C}_8\text{H}_{17}$	Ni	M 21 $\text{Col}_h$ 81 I
$\text{C}_8\text{H}_{17}$	H	2H	Cr > 250 dec.
$\text{C}_8\text{H}_{17}$	H	Cu	$\text{Col}_h$ > 250 I
$\text{C}_8\text{H}_{17}$	H	Ni	Cr 104 M 190 $\text{Col}_h$ > 250 I
$\text{C}_{12}\text{H}_{25}$	H	Cu	Cr > 250 dec.

M: unidentified mesophase.

systems) was induced for the butyl ester homolog ( $n = 4$ ) in dimethylformamide, while a nematic phase was induced for the longer-chain compounds ( $n = 9, 11$ ) in chloroform and benzene. Only the nonylester compound presented a columnar mesophase in alkane (nonane). The replacement of the four hydrogen atoms by four carboxyl groups contributed to a decreasing mesomorphic tendency caused by the decrease in micro-segregation forces, in that the polar core was extended and as such diminished the hydrophobic character and the capacity to incorporate apolar molecules. Note that here again, both series of compounds existed as mixtures of isomers. No studies on the metal-free compounds or with metallophthalocyanines with other metal ions have been undertaken to see if the metal played an essential role in the induction and stabilization of the mesophase.

Recently, the first examples of phthalocyanines substituted by long-chain amide groups ((1):  $M = 2\text{H}, \text{Cu}, \text{Ni}$ ,  $R = \text{OCH}_2\text{CONR}^1\text{R}^2$ ;  $R^1 = \text{C}_n\text{H}_{2n+1}$ ,  $R^2 = R^1$  or H; thermal data in Table 7) were reported.<sup>129</sup> Two distinct series were prepared, differing in the number of chains attached to the terminal amido groups. The sixteen-chain compounds displayed room-temperature mesomorphism consisting of a  $\text{Col}_h$  phase; all cleared into the isotropic liquid below 100 °C irrespective of the metal center. The eight-chain compounds behaved very differently. Only the copper and nickel complexes were mesomorphic, without showing a clearing behavior in the temperature range investigated. These differences in the mesomorphism were attributed to two main causes. The first one was the high number of aliphatic chains in the first series which, as shown above, played two roles, namely destabilizing the solid phase and mesophase. In contrast, however, they create sufficient disorder, and are able to fill the available space more efficiently. Secondly, in the second series, the free hydrogen atom left on the amide group is likely available for inter- and intra-molecular hydrogen bonding. This resulted in an increase in transition temperatures, and the strengthening of the columnar packing. The presence of a metal ion within the cavity of the mesogenic core, provided that the chains were not too long, appeared to balance such interactions, giving rise to mesophase, although at high temperatures for the nickel complex.

Cho and Lim<sup>130</sup> compared the effect of a variety of lateral substituents on the thermal behavior of peripherally octasubstituted, metal-free phthalocyanines and their copper complexes. Despite being an interesting study, the characterization of the mesophases was tentatively made by optical microscopy and thus some doubts concerning mesophase identification still persist. The results of this study are gathered in Table 8 along with some metal-free and copper complexes discussed above to allow comparison. The free base with a chiral chain exhibited a texture resembling that of the cholesteric phase, whereas that of the copper complex was not identified. Compounds substituted with chiral chains were room-temperature liquid crystals, whatever the length and number of asymmetric carbon atoms, and the columns described a helical twist.<sup>131,132</sup>

It is worth mentioning that some side-chain liquid crystal polymers<sup>(133)</sup> and liquid-crystalline networks ( $M = \text{Cu}, \text{Zn}, \text{Co}, \text{Ni}, \text{Pb}$ )<sup>134</sup> have also been prepared, usually preserving the properties of the monomeric discotic units. They may find some interesting applications in the field of one-dimensional conductors as well as applications using flexo- and piezo-electricity.

Amphiphilic systems, such as metal-free phthalocyanines substituted with ethylene oxide chains, have been found to exhibit thermotropic mesophases in their pure state and lyotropic mesophases in binary mixtures with organic solvents.<sup>71,135–137</sup> A few metallophthalocyanines substituted by such polar groups have also been prepared (Table 9). Octasubstituted phthalocyanines with alkoxy ethylene-oxide side chains ((1):  $M = 2\text{H}, \text{Cu}$ ,  $R = \text{O}(\text{CH}_2)_n\text{O}(\text{CH}_2\text{CH}_2\text{O})_3\text{Me}$ ) were reported. Both the short-chain-length compounds ( $n = 6$ ) displayed  $\text{Col}_h$  phases at room temperature, the phase being identified by microscopy.<sup>(138)</sup> The compound with the longer chain ( $n = 10$ ) was crystalline at room temperature, but displayed a  $\text{Col}_h$  phase at higher temperature.<sup>139</sup> Other groups reported tetra- and octa-substituted phthalocyanines with tri-3,6,9-oxadecyloxy<sup>140</sup>

**Table 8** Transition temperatures of free base and copper complexes of (1) with various lateral substituents.

<i>R</i>	<i>2H</i>	<i>Cu</i>
CH <sub>2</sub> SC <sub>12</sub> H <sub>25</sub>	Cr 95 Col <sub>r</sub> 267 I	Cr 108 Col <sub>r</sub> 304 I
CH <sub>2</sub> O(CH <sub>2</sub> ) <sub>2</sub> SC <sub>12</sub> H <sub>25</sub>	Cr 52 Col <sub>h</sub> 247 I	Cr 70 Col <sub>h</sub> 255 I
CH <sub>2</sub> OCH <sub>2</sub> C*HMeOC <sub>12</sub> H <sub>25</sub>	Cr 23 M* 158 I	Cr 29 M* 191 I
O <sub>2</sub> CC <sub>11</sub> H <sub>25</sub>	Cr 58 M 303 I	
CH <sub>2</sub> OC <sub>12</sub> H <sub>25</sub>	Cr 79 Col <sub>h</sub> ~ 260 I	Cr 53 Col <sub>h</sub> > 300 I
C <sub>10</sub> H <sub>21</sub>	Cr 163 Col <sub>h</sub> 282 I	Cr 169 Col <sub>h</sub> 351 I
OC <sub>12</sub> H <sub>25</sub>	Cr 83 Col <sub>h</sub> 309 I	Cr 95 Col <sub>h</sub> > 345 I
SC <sub>12</sub> H <sub>25</sub>	Cr 48 Col <sub>h</sub> 286 I	Cr 54 Col <sub>h</sub> 323 M 340 dec.
O(CH <sub>2</sub> ) <sub>2</sub> C*HMe(CH <sub>2</sub> ) <sub>3</sub> C*HMe <sub>2</sub>	<i>rac.</i> Cr 70 Col <sub>h</sub> 295 I	
	<i>chiral</i> M* 16 Col <sub>h</sub> 111 D 295 I	
O(CH <sub>2</sub> ) <sub>2</sub> C*HMe(CH <sub>2</sub> ) <sub>3</sub> C*HMe(CH <sub>2</sub> ) <sub>3</sub> CHMe <sub>2</sub>	Col <sub>h</sub> 34 Col <sub>h</sub> 173 Col <sub>x</sub> 185 I	

M, M\*: unidentified mesophases, and Col, D, Col<sub>x</sub>: unidentified columnar phases.

**Table 9** Mesomorphic properties of (1) with ethylene oxide chains.

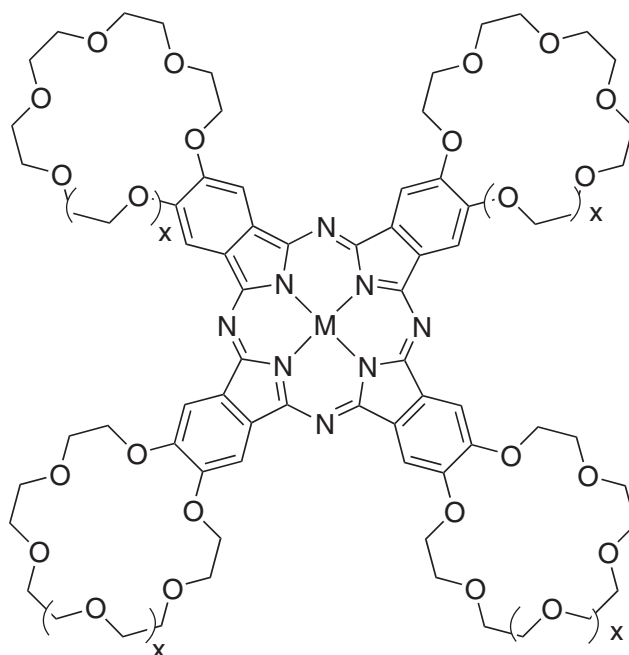
<i>R</i>	<i>M</i>	<i>Mesomorphism</i>
O(CH <sub>2</sub> ) <sub>6</sub> O(CH <sub>2</sub> CH <sub>2</sub> O) <sub>3</sub> Me	2H	Col <sub>h</sub> 140–160 I
O(CH <sub>2</sub> ) <sub>6</sub> O(CH <sub>2</sub> CH <sub>2</sub> O) <sub>3</sub> Me	Cu	Col <sub>h</sub> 210–225 I
O(CH <sub>2</sub> ) <sub>10</sub> O(CH <sub>2</sub> CH <sub>2</sub> O) <sub>3</sub> Me	Cu	Cr 136 Col <sub>h</sub> 220 I
O(CH <sub>2</sub> CH <sub>2</sub> O) <sub>3</sub> Me	2H	Col <sub>h</sub> 254 I
O(CH <sub>2</sub> CH <sub>2</sub> O) <sub>3</sub> Me	Zn	
O(CH <sub>2</sub> CH <sub>2</sub> O) <sub>3</sub> Me	Cu	Cr 62 Col <sub>h</sub> 260 dec.
S(CH <sub>2</sub> CH <sub>2</sub> O) <sub>3</sub> Me	2H	Cr 140 Col <sub>h</sub> > 250 dec.
S(CH <sub>2</sub> CH <sub>2</sub> O) <sub>3</sub> Me	Ni	Cr 80 Col <sub>h</sub> > 250 I dec.

((2): M = 2H, Zn, R = O(CH<sub>2</sub>CH<sub>2</sub>O)<sub>3</sub>Me, R' = H; 1: M = 2H, Zn, Cu, R = O(CH<sub>2</sub>CH<sub>2</sub>O)<sub>3</sub>Me), ((1): M = Cu, R = O(CH<sub>2</sub>CH<sub>2</sub>O)<sub>4</sub>Me), and tri-4,7,10-oxaundecan-1-sulfanyl<sup>(141)</sup> and the corresponding metal complexes ((2): M = 2H, Ni, R = S(CH<sub>2</sub>CH<sub>2</sub>O)<sub>3</sub>Me, R' = H; (1): M = 2H, Ni, R = S-(CH<sub>2</sub>CH<sub>2</sub>O)<sub>3</sub>Me). In the first series, with the oxygen link, only the octasubstituted free-base compound was mesomorphic at room temperature, while the tetrasubstituted analogs were crystalline solids and melted directly to the isotropic liquid. The copper compound<sup>(142)</sup> displayed a broad Col<sub>h</sub> phase. Interestingly, addition of triethylene glycol to the copper complex did not alter the mesophase, while at higher percentages of solvent, two mesophases were present, not yet identified, but probably the expected Col<sub>h</sub> and the N<sub>Col</sub> phases. Compounds with a sulfanyl linker exhibited a much richer mesomorphism, including both thermotropic and lyotropic properties. The four-chain nickel complex, as well as the free-base phthalocyanine, possessed a room-temperature Col<sub>h</sub> phase, such low-temperature behavior being explained by the existence of several structural isomers. The compounds with eight chains also displayed mesophases, but at higher temperatures. Additionally, lyomesophases were formed for all of them when mixed with various organic solvents (2-propanol, nitromethane, *n*-butyl acetate, diethyleneglycol monomethyl-ether, ethanol (95%), or ethylene glycol monomethylether acetate); these phases formed at room temperature. Compounds with four chains showed a N<sub>Col</sub> phase between the isotropic solution and the Col<sub>h</sub> phase, while those with eight chains exhibited only the Col<sub>h</sub> phase. This difference was rationalized by the deficit of peripheral chains in the former which allowed for an easier incorporation of the solvent near to the columnar core, filling the cavities before the loss of the two-dimensional intercolumnar interactions. On the basis of these few examples, the replacement of hydrocarbon chains with ethylene oxide chains of the same length leads to more conformational disorder in the side chains, which results in the substantial reduction in both the melting and clearing temperatures. However, this approach met its limits in that substitution by branched poly(ethyleneoxide) chains led to the suppression of the mesomorphism and yielded a room-temperature viscous oil ((1): M = Cu, Zn, R = CH<sub>2</sub>OCH[(CH<sub>2</sub>OCH<sub>2</sub>)<sub>2</sub>CH<sub>2</sub>OMe]<sub>2</sub>).<sup>143</sup> Finally, the case of free-base octakis((2-benzyloxy)ethoxy)phthalocyanine and the related copper complex ((1): M = 2H, Cu, R = O(CH<sub>2</sub>CH<sub>2</sub>OCH<sub>2</sub>C<sub>6</sub>H<sub>5</sub>), which were reported to show a Col<sub>h</sub> phase over large temperature ranges, is noted.<sup>144–146</sup>

The effect of chirality<sup>147</sup> has been investigated with copper and zinc phthalocyanines substituted with non-chiral and chiral polyhydroxy groups ((**1**): M = 2H, Cu, Zn, R = OCH<sub>2</sub>CH<sub>2</sub>CH(H)(OH)CH<sub>2</sub>OH).<sup>148</sup> While none of the compounds gave thermotropic mesophase, aqueous solutions of the copper complexes (racemic and chiral) formed fibrous assemblies of columns stabilized by  $\pi$ - $\pi$  interactions and hydrogen bonding, while the zinc complex did not aggregate. Moreover, the columns self-assembled into a columnar phase for the racemic copper complex, while for the optically active material, the columns arranged into lamellae (Col<sub>L</sub> phase). The left-handed helix induced in the latter columns was stabilized by an efficient and directional hydrogen-bonding network, which optimized preferentially in-plane interactions between neighboring columns. The nature of the metal was, therefore, a prerequisite for the formation of columns in these systems. However, the metal-free material was not synthesized, and thus it is not possible unequivocally to attribute the aggregation phenomenon to the simple presence of a metal.

An elegant variation on the phthalocyanine structure was the attachment of crown ether moieties at the periphery of the mesogenic core to produce compounds (**3**). These were made to form ordered ion channels, similar to those found in natural membranes ((**3**): M = 2H, Cu, Ni, Co, x = 0, 1, 2).<sup>149</sup> Most of the studies were concerned with the investigation of the aggregation properties and host-guest interactions of these systems with alkaline and alkaline-earth cations.<sup>150-152</sup> It is only during the study of their thermal stability that the copper complex of the phthalocyanine substituted with four benzo-15-crown-5 and the corresponding free base were found to exhibit a columnar mesophase with a two-dimensional square lattice, Col<sub>t</sub> ((**3**): M = 2H, Cu, x = 0).<sup>153</sup> Unlike the related derivatives with ethylene oxide chains, which have the ability to fill the space available between the columnar cores, the crown-ether moieties cannot occupy the voids in the same way due to conformational restrictions, justifying other modes of columnar packing and two-dimensional symmetries. On the basis of X-ray diffraction, both the copper and free-base compounds were self-assembled into an orthorhombic lattice, with a tilt in the molecular stacking in the solid phase. In the mesophase, the two-dimensional rectangular symmetry was transformed into a two-dimensional square lattice, and the molecules stacked without a tilt on top of each other, with the crown-ether moieties in a staggered conformation, and an intercrown distance of 8.2 Å. The potential mesomorphism of the closely related copper complexes of phthalocyanine substituted with 15-membered tetraazamacrocyclic has not been investigated.<sup>154</sup>

Thus, several types of substituent have been utilized for the uniformly peripherally substituted phthalocyanines. Overall, oxo and thioether links, as well as ester groups, provided ordered mesophases, in contrast to alkyl, alkoxy-methyl, and poly(ethyleneoxide) chains. The melting transition temperatures increased in the order ethyleneoxide < alkylthio < alkoxy-methyl



(3)

< alkoxy  $\ll$  alkyl, with the same tendency being found for the clearing temperatures. However, the diminution of the number of side chains from eight to four, the branching of the chains, and the use of some metal ions contributed substantially to the depression of both transition temperatures.

### 7.9.7.1.2 Phthalocyanines with extended cores

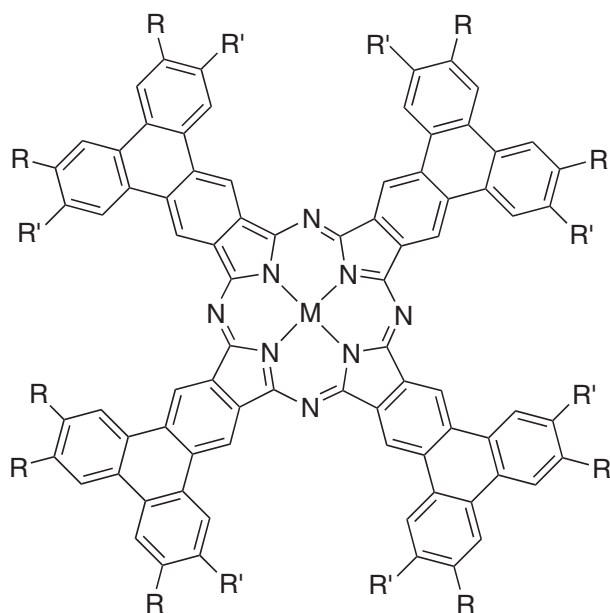
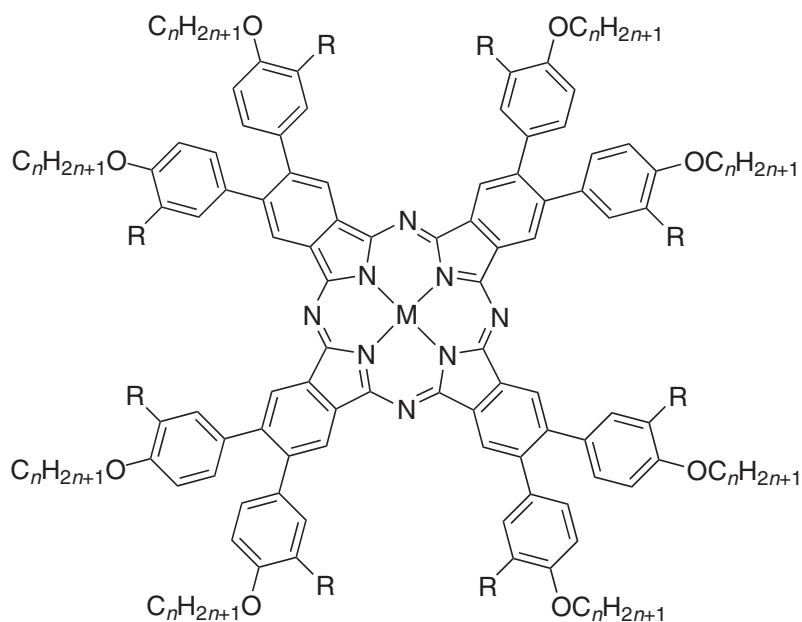
Two series of metal-containing liquid crystals based on expanded phthalocyanine cores have been reported, namely mono- and di-alkoxy substituted octaphenylphthalocyanines. They were obtained by replacing the peripheral chains with phenyl rings substituted by either one or two alkoxy chains. In these series, the phenyl groups provided rigid steric hindrance around the mesogenic core as they were unable to rotate freely. In the first series, with eight peripheral alkoxyphenyl ((4): M = 2H, Cu, R = OC<sub>n</sub>H<sub>2n+1</sub>, n = 8, 10, 12, 18, 2-ethylhexyl; thermal data in Table 10),<sup>155</sup> the thermal behavior of the free-base and copper complex were rather different. While the free-base compounds displayed a Col<sub>h</sub> phase, the copper complexes exhibited a Col<sub>r</sub> phase. The length of the side chains was an important parameter to be considered this time for mesophase induction, requiring a minimum of ten methylene groups per chain for observation of a Col<sub>h</sub> phase, while twelve carbon atoms were needed to observe a Col<sub>r</sub> phase. All the compounds decomposed at temperatures greater than 200 °C. This change in two-dimensional lattice was ascribed to the need of the copper ion to be coordinated axially with the *meso*-nitrogen atoms of the neighboring phthalocyanine molecules. In the series with sixteen peripheral alkoxy groups ((4): M = 2H, Ni Cu, R = OC<sub>n</sub>H<sub>2n+1</sub>, n = 10–12),<sup>156</sup> all the ligands and metal complexes were mesomorphic at room temperature. Moreover, the grafting of an additional chain at the *meta* position of the phenyl group prevented decomposition of the macrocycle at elevated temperature, and the isotropic liquid could be reached. No great differences were, however, observed between the ligands and the metal complexes, and all exhibited one or two Col<sub>r</sub> (Col<sub>r1</sub> and Col<sub>r2</sub>) phases, all with a *p2gg* plane group. Double clearing behavior was observed for the copper complexes and the ligand with dodecyloxy chains, and was attributed to the existence of several geometrical isomers (resulting from hindered rotations). The room-temperature phases were not identified (X), and not all the columnar phases were characterized further (Col<sub>x</sub>, Col<sub>1</sub>, Col<sub>2</sub>). The free-base 4-dodecyloxyphenyloxymethyl derivative, synthesized for comparison, did not show a phase transition from room temperature up to 300 °C. X-Ray diffraction carried out at 100 °C and 250 °C indicated the existence of a Col<sub>h</sub> phase. The increase in the mesophase stability was attributed to the coplanar arrangement of the phenyl ring with the macrocycle, which as such extended the central aromatic core.

The related triphenylenophthalocyanines, where two neighboring alkoxyphenyl groups were linked together oxidatively by a covalent bond, were found to be mesomorphic, too ((5): M = Zn, R, R' = H or OC<sub>6</sub>H<sub>13</sub>).<sup>157</sup> Preliminary investigations of their thermal behavior revealed that they all formed columnar mesophases, and that the isotropic liquid could not be reached; they were still liquid crystalline above 300 °C. The melting temperatures were dependent on the chain substitution pattern. The zinc complex with R = OC<sub>6</sub>H<sub>13</sub> and R' = H melted into a columnar phase at 270 °C, while its isomeric compound (R = H, R' = OC<sub>6</sub>H<sub>13</sub>) was mesomorphic at much lower temperature (Cr 185 Col). The most heavily substituted derivative (R = R' = OC<sub>6</sub>H<sub>13</sub>) was, however, liquid crystal at room temperature up to above 300 °C.

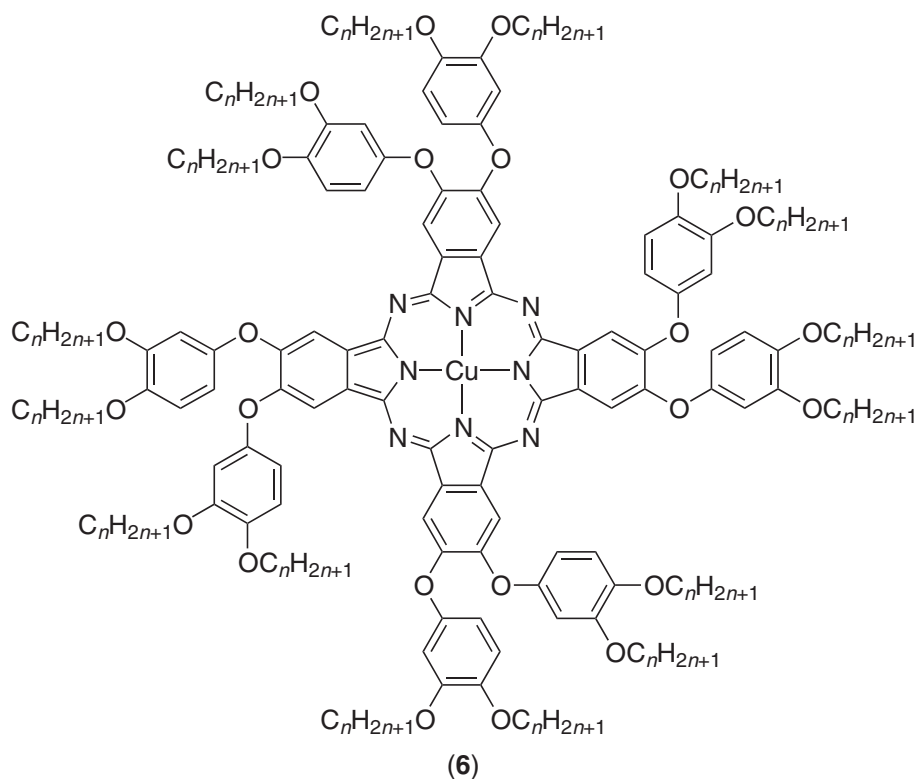
**Table 10** Transition temperatures of (4).

M	n	R = H	R = OC <sub>n</sub> H <sub>2n+1</sub>
2H	18	Cr 78 Col <sub>h</sub> 253 dec.	
Cu	18	Cr 82 Col <sub>r(c2mm)</sub> 220 dec.	
2H	12	Cr 192 Col <sub>h</sub> 261 dec.	Col 66 Col <sub>r</sub> 186 Col <sub>x</sub> 187 I
Cu	12	Cr 120 Col <sub>r(c2mm)</sub> 227 dec.	Col 72 Col <sub>r1</sub> 192 Col <sub>r2</sub> 197 I
2H	10	Cr 229 M 267 dec. <sup>a</sup>	X 56 Col <sub>1</sub> 106 Col <sub>2</sub> 184 I
Cu	10	Cr 222 dec.	Col 75 Col <sub>r1</sub> 196 Col <sub>r2</sub> 219 I
Ni	10		X 59 Col <sub>1</sub> 100 Col <sub>2</sub> 175 I

<sup>a</sup> M : unidentified mesophase. X : unidentified solid phase, and Col<sub>x</sub>, Col<sub>1</sub>, Col<sub>2</sub> : unidentified columnar phases.



Other expanded copper phthalocyanine complexes<sup>158</sup> ((6):  $n = 9$  to 14), differing from the previous ones in that the dialkoxyphenyl groups were linked to the phthalocyanine core by an ether linkage, yielded a rather rich mesomorphism including a low-temperature  $\text{Col}_h$  phase, three intermediate  $\text{Col}_r$  and/or one  $\text{Col}_t$  phases, and a high-temperature cubic (Cub) phase (Figure 23). The temperature ranges of the mesophases were quite large, and might be a direct consequence of the ether links, which forced the bulky side groups to expand within the macrocycle plane, extending as such the disk-like molecules. The results of these studies, however, raised important questions. First, the presence of the highly symmetrical  $\text{Col}_h$  phase below the less symmetrical  $\text{Col}_r$  and  $\text{Col}_t$  phases was surprising. Secondly, another unusual feature was the induction of a cubic phase in purely discotic materials. This rich mesomorphism was attributed to



the stepwise conformational changes and the mutual arrangement of the aryl groups. The latter proposition may explain the presence of the low-temperature  $\text{Col}_h$  phase due to less damaging thermal fluctuations.

Finally, several, novel, star-shaped octakis(stilbenoid phthalocyaninato) zinc complexes ((7):  $\text{R} = \text{R}^1$  or  $\text{R}^2$ ,  $n = 3, 6$ )<sup>159</sup> were synthesized. The thermal behavior of the twenty-four-chained complex was not studied ( $\text{R}^1$ ), but that with hexyloxy side chains ( $\text{R}^2$ ,  $n = 6$ ) was found to self-organize into a  $\text{Col}_h$  phase at room temperature up to 220 °C.

The dodecasubstituted bis(phthalocyanine) and its corresponding dinuclear copper complex ((8):  $\text{M} = \text{M}' = 2\text{H}$ ,  $\text{Cu}$ ,  $\text{R} = \text{CH}_2\text{CH}(\text{C}_2\text{H}_5)\text{C}_4\text{H}_9$ ) exhibited room-temperature mesophases which persisted up to 300 °C.<sup>160,161</sup> X-Ray diffraction indicated that the metal-free ligand exhibited two

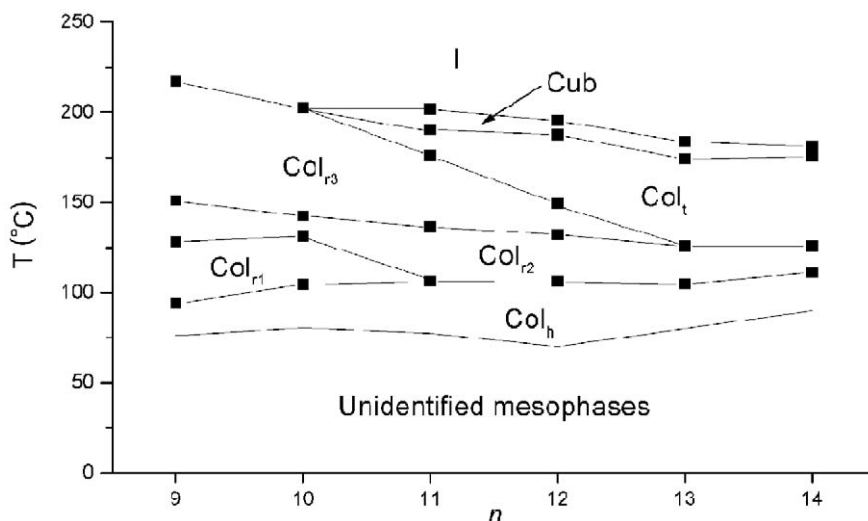
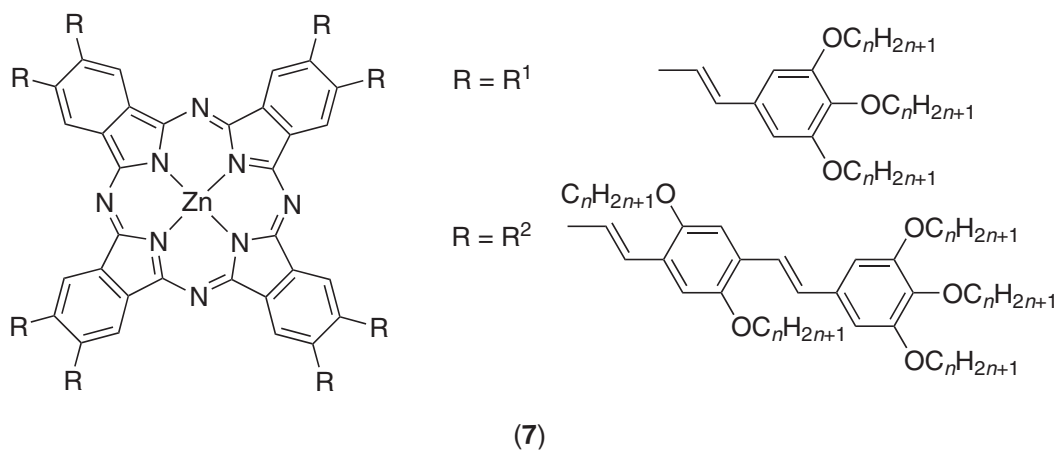
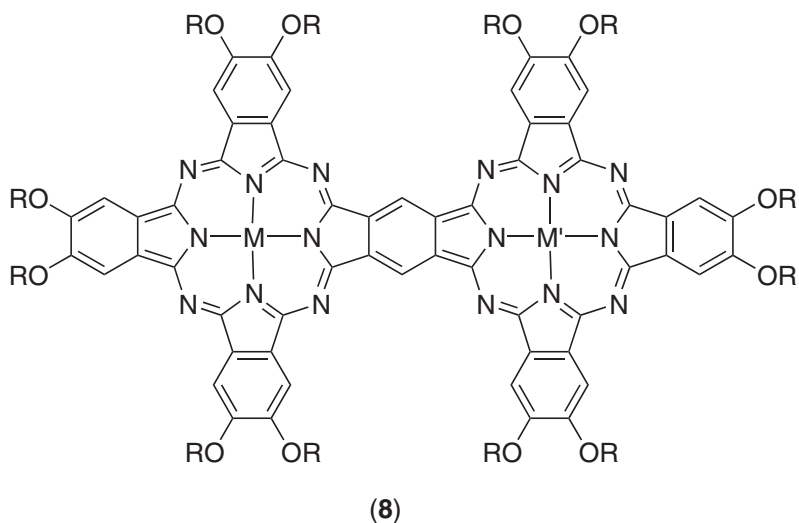


Figure 23 Thermal behavior of 6 as a function of chain length.





mesophases, with the transition not being detected by DSC: at room temperature and at 200 °C, a  $Col_r$  mesophase was identified, and another columnar mesophase with a two-dimensional square lattice ( $Col_t$ ) at 300 °C was found. Two compounds were, in fact, obtained during the preparation of the bis(phthalocyanine), as deduced from their absorption spectra. The metal-free compound described previously differed by the presence of two extra hydrogen atoms on the six-membered ring linking the phthalocyanine units. This protonated form showed a smectic phase with nematic order within the layers; the mesophase of the dicopper complex was not identified. Comparison with the related monomeric phthalocyanines showed a substantial decrease in the melting points and an increase in the clearing temperature, leading to the broadening of the mesomorphic temperature range. The nature of the mesophase was also modified, as the  $Col_t$  and  $N_D$  mesophases changed to  $Col_r$  and  $Col_t$  mesophases. The electronic structures of the metal-free and dicopper bis(phthalocyanines) have been determined by electronic absorption and magnetic circular dichroism, in good agreement with their hypothetical planar structures.<sup>162</sup>



### 7.9.7.1.3 Bis(phthalocyaninato)lanthanide complexes

Due to their large size, the inclusion of rare-earth metals into phthalocyanines leads to neutral, double-decker, bis(phthalocyaninato)lanthanide(III) complexes.<sup>163</sup> In these compounds, the trivalent lanthanide(III) ion is sandwiched between the two macrocyclic ligands, with the rings being rotated with respect to each other by 45°. The coordination polyhedron corresponds to a distorted square antiprism due to the non-equivalent bending deformations of both macrocycles

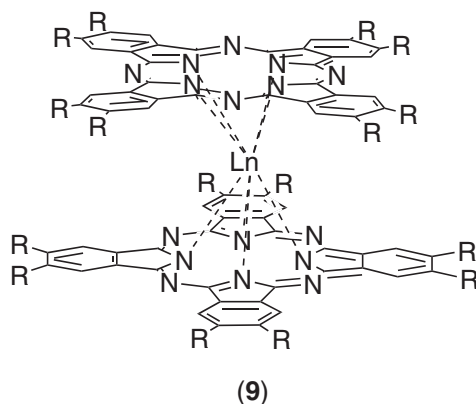


**Table 11** Transition temperatures of (9) with  $R = \text{CH}_2\text{OC}_n\text{H}_{2n+1}$ .

$Ln$	$R = \text{C}_8\text{H}_{17}\text{OCH}_2$	$R = \text{C}_{12}\text{H}_{25}\text{OCH}_2$	$R = \text{C}_{18}\text{H}_{37}\text{OCH}_2$
Lu	Cr 25 I	Cr 24 Col <sub>h</sub> 30 I	Cr 51 Col <sub>h</sub> 56 I
LuSbCl <sub>6</sub>	Cr -10 Col <sub>h</sub> 130 I	Cr 13 Col <sub>h</sub> 118 I	Cr 56 Col <sub>h</sub> 132 I

on complexation; the difference in the phthalocyanine ring distortions arises from the localization of the unpaired electron on the more distorted ring. Rare-earth phthalocyanine complexes are very stable, and are currently being studied due to their unique and intrinsic one-dimensional, semiconducting charge transport, and their electrochromic properties, features likely associated to the radical nature of the complexes  $[\text{Ln}]^{3+}[\text{M}_2]^{3-}$ .

The first liquid-crystalline lanthanides were the bis(octaalkoxymethyl-phthalocyaninato)lutetium(III) complexes ((9):  $\text{Ln} = \text{Lu}$ ,  $R = \text{CH}_2\text{OC}_n\text{H}_{2n+1}$ ,  $n = 8, 12, 18$ ) described by Simon and co-workers in 1985.<sup>164</sup> The lutetium complexes with dodecyl- and octadecyloxylethyl side chains displayed a Col<sub>h</sub> mesophase at rather low temperatures but over a very few degrees only. In contrast, the octyloxymethyl derivative was a room-temperature liquid. The mesophase structure was investigated by small-angle X-ray diffraction, and a series of five sharp Bragg reflections was observed, characteristic of a two-dimensional hexagonal lattice. The Lu–Lu spacing (intracolumnar distance) was ca. 7.3 Å, corresponding to about twice the thickness of one phthalocyanine molecule, and thus to a staggered arrangement of the macrocycles. The small mesophase stability range of the neutral forms was attributed to the deviation from planarity of the phthalocyanine macrocycles. Oxidation of the complexes greatly improved the mesophase stability ((9):  $\text{Ln} = \text{Lu}^{\text{III}}$   $[\text{SbCl}_6]^-$ ,  $R = \text{CH}_2\text{OC}_n\text{H}_{2n+1}$ ,  $n = 8, 12, 18$ ); data are collected in Table 11. Moreover, the melting temperatures were found to increase rapidly with the lengthening of the alkoxymethyl chains, and mesophase induction was observed for the octyloxymethyl derivative. Although the oxidized forms exhibited a mesophase over a much larger temperature range than the neutral forms, the complexes were relatively unstable, and after some heat–cool cycles, a mixture of both neutral and oxidized species was recovered. In addition, these complexes showed electrochromic behavior with two reversible redox systems (green/orange and green/blue)<sup>165</sup> and electronic conductivity along the columns was demonstrated.<sup>166</sup>

The alkoxy-substituted compounds formed more stable mesophases and with wider temperature ranges than the corresponding alkoxymethyl-substituted analogs. For instance, the dodecyloxy lutetium derivative ((9):  $\text{Ln} = \text{Lu}$ ,  $R = \text{OC}_{12}\text{H}_{25}$ ) exhibited a Col<sub>h</sub> phase between 85 °C and 189 °C, corresponding to an improvement of about 100 °C of the mesomorphic range with respect to the dodecyloxymethyl derivative complex.<sup>167</sup> The mesophase of the oxidized species ((9):  $\text{Ln} = \text{Lu}^{\text{III}}$   $[\text{BF}_4]^-$ ,  $R = \text{OC}_{12}\text{H}_{25}$ ) was even more stabilized than that of the neutral compound, being liquid crystalline from room temperature up to 253 °C. The mesophase stabilization in the ionic derivative was attributed to electrostatic contributions or to partial orbital overlap within the columns. The presence of a narrow peak at wide angles in the XRD patterns at about 3.3 Å implied a regular stacking periodicity for both compounds. The mesomorphic behavior of this compound was re-investigated some years later by van de Craats *et al.*<sup>168</sup> They found nearly the

**Table 12** Transition temperatures of (9)  $R = OC_nH_{2n+1}$ .

<i>Ln</i>	$R = OC_{12}H_{25}$	<i>n</i>	$Ln = Er$
Nd	Cr 57 Col <sub>h</sub> 167 I		
Eu	Cr 60 Col <sub>h</sub> 173 I	10	Cr 63 Col <sub>h</sub> 180 I
Er	Cr 54 Col <sub>h</sub> 174 I	12	Cr 60 Col <sub>h</sub> 173 I
Lu	Cr 85 Col <sub>h</sub> 189 I / Cr 45 Col <sub>r</sub> 90 Col <sub>h</sub> 196 I	18	Cr 61 Col <sub>h</sub> 154 I
LuBF <sub>4</sub>	Cr -3 Col <sub>h</sub> 253 I		

The two sets of data arise from refs. 167 and 169 respectively.

same transition temperatures as Belarbi *et al.* but reported the existence of an additional mesophase, below the Col<sub>h</sub>, later characterized as a Col<sub>r</sub> phase with a  $p2gg$  plane group.<sup>169</sup> No additional broad reflection was observed at 6–7 Å as would have been expected in the case of an orthogonal arrangement of the two macrocycles with respect to the lanthanide ion. This was also an indication of the equivalence of the phthalocyanine rings, which became planar. Steven *et al.*<sup>(170)</sup> reported a preliminary investigation on the mesomorphic behavior of a few more lanthanide complexes ((9): Ln = Nd, Eu, Er, Lu,  $R = OC_nH_{2n+1}$ ,  $n = 10, 12, 18$ ), and found a slight increase in both the melting and clearing temperatures over the lanthanide series from Ln = Nd, Eu, Er, and Lu (Table 12). The lengthening of the chains appeared to influence the clearing temperatures only slightly. The incorporation of the lanthanide ion resulted in the decrease in the mesomorphic range with respect to the metal-free ligand, while the opposite was observed with transition metals. Note that, europium, gadolinium,<sup>(171)</sup> yttrium,<sup>(172)</sup> and cerium<sup>(173)</sup> bis(octapentyloxyphthalocyanine) complexes, prepared previously for their spectroscopic and electrochemical properties, were not investigated with respect to their potential mesomorphic behavior. Higher conductivities were found for the sandwich compounds than for the corresponding free-base and complexes with transition metals.

Few alkyl derivatives were prepared,<sup>174</sup> and those that were showed liquid crystallinity, too ((9): Ln = Lu,  $R = C_nH_{2n+1}$ ,  $n = 8, 12, 18$ ). The octyl compound exhibited a Col<sub>h</sub> phase over a narrow temperature range (79–82 °C). The behavior was found to be slightly more complicated for the two other lutetium homologs, including double-clearing behavior. A virgin sample of the dodecyloxy complex showed a Col<sub>o</sub> phase at room temperature. On heating, the mesophase first cleared at 32 °C to an isotropic liquid, soon relaxing into an disordered Col<sub>h</sub> phase, then cleared again into the isotropic liquid at 44 °C. Rapidly cooled from the isotropic liquid, the disordered Col<sub>o</sub> phase was reformed, while slow cooling favored preferentially the formation of the Col<sub>h</sub> phase. Thus, the free energy of all of these phases was remarkably similar. The octadecyloxy compound behaved similarly, with similar transition temperatures, though this time the low-temperature mesophase was a discotic lamellar phase, D<sub>L</sub>. When the sample was cooled, a mixture of both D<sub>L</sub> and Col<sub>h</sub> phases was obtained.

The replacement of the eight peripheral chains by eight 4-octadecyloxyphenyl groups ((9): Ln = Lu,  $R = C_6H_4OC_{18}H_{37}$ ) modified the thermal behavior of the lutetium complex dramatically,<sup>175</sup> and it showed a room-temperature Col<sub>t</sub> phase, which transformed at 47 °C into a Col<sub>h</sub> phase, and cleared into the isotropic liquid at 242 °C. Decomposition of the isotropic liquid was observed at ca. 283 °C.

Some poly(oxyethylene)-substituted lutetium phthalocyanine complexes ((9): Ln = Lu,  $R = O(CH_2CH_2O)_nCH_3$ ,  $n = 1-4$ ) were prepared, but only one compound was mesomorphic ( $n = 3$ ), exhibiting a Col<sub>t</sub> phase between 53 °C and 58 °C.<sup>(142)</sup> The analogous compounds with shorter ( $n = 1, 2$ ) or longer ( $n = 4$ ) chain length did not show a mesophase; the most pronounced effect being the rapid decrease of the isotropization temperature on lengthening the chain (from 246 °C to 138 °C for  $n = 1, 2$  respectively) to yield a room-temperature liquid ( $n = 4$ ). No sign of a mesophase was found in the related crown-ether and mixed crown-ether-poly(ethyleneoxide) lutetium bisphthalocyanines.<sup>176-178</sup>

All the members of the octakis(alkylthio)-substituted series ((9): Ln = Eu, Tb, Lu,  $R = SC_nH_{2n+1}$ ,  $n = 8, 10, 12, 14, 16, 18$ ) exhibited a Col<sub>h</sub> phase over a broad temperature range (Figure 24).<sup>179</sup> A novel Col<sub>r</sub> phase with a pseudo-hexagonal, two-dimensional lattice ( $p2gg$ ) was induced for the homologs with the decylthio and dodecylthio chain (and also for the terbium(III) complex with the tetradecylthio chain). In the wide-angle region of the X-ray diffraction pattern, two broad peaks corresponding to two stacking periodicities were observed. One at ca. 7 Å corresponded to the double-decker structure of the complex, whereas that at ca. 3.5 Å related to the thickness of

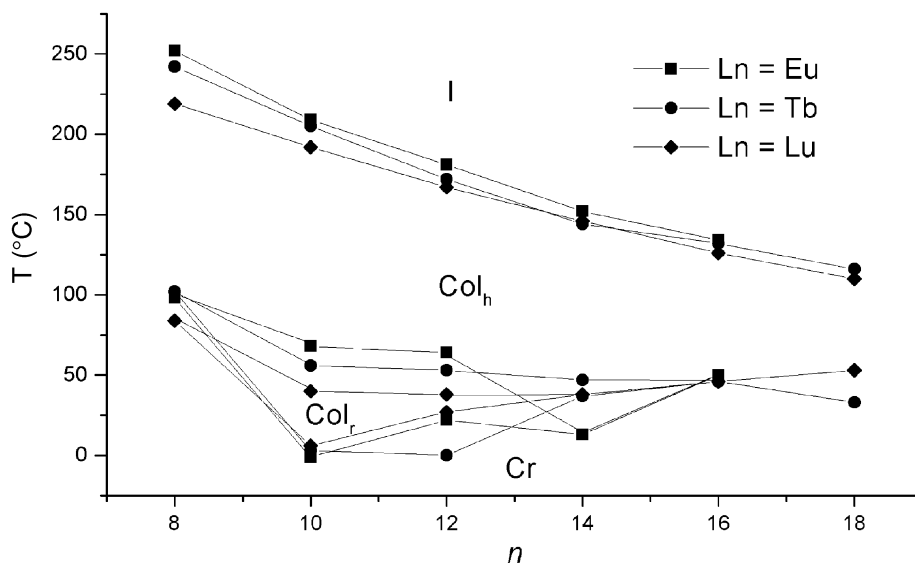


Figure 24 Thermal behavior of the octakis(alkylthio)-substituted series (9).

the macrocycle. The observation of these two scatterings was the result of thermal fluctuations causing trampoline-like movements of the phthalocyanine rings. A crystal structure was successfully obtained for the hexylthio lutetium complex.<sup>180</sup> It showed the anti-prismatic coordination of the lanthanide, with the two phthalocyanine rings being staggered by 42°; the molecule is, therefore, chiral assuming this arrangement persists into the mesophase. In the crystal state, the molecules were stacked into columns along the *a*-axis direction with a brick wall arrangement. The *Q*-band was red-shifted compared to the alkyl, alkoxy, and alkoxymethyl derivatives of the lutetium complexes.

Replacement of the alkoxy chains by alkylthio chains resulted in an increase of more than an order of magnitude in the intramolecular charge mobility to values in the range 0.15–0.3 cm<sup>2</sup> V<sup>-1</sup> s<sup>-1</sup>. The pronounced positive effect on the charge-transport properties of sulfur compared with oxygen as the group linking core and chains was attributed to the larger size of the sulfur atom which hindered rotational and translational displacements of the phthalocyanine macrocycles within the cores of the columns. Thus, whereas the alkoxy group is electron-donating to the phthalocyanine ring, the alkylthio group is, to a first approximation, neither electron-donating nor electron-withdrawing. Therefore, the HOMO–LUMO gap was smaller in the alkylthio-substituted compounds (red-shift of the *Q*-band), and hence the charge mobility was higher. The mobility remained high in the isotropic state, which indicated that a high degree of columnar order still existed and allowed charge transport to occur via intermolecular charge-transfer rather than by molecular ion diffusion. Because of the high charge mobility in the isotropic state, these compounds were considered to be the first liquid-phase, organic semiconducting materials. The photoconductivity of these complexes was also investigated and found to be very weak,<sup>181</sup> and non-radiative relaxations of the photoexcitations dominated. A significant enhancement of the photoconductivity was observed after doping with C<sub>60</sub>; for the lutetium(III) complex, the photoconductivity along the columns was two orders of magnitude larger than for the undoped material.

#### 7.9.7.1.4 Radially substituted phthalocyanines

As mentioned above, substitution of phthalocyanines can also be achieved in the eight radial (non-peripheral) positions of the mesogenic core, i.e., in the 1, 4, 8, 11, 15, 18, 22, and 25 positions. Cook and co-workers first demonstrated the mesomorphism of the metal-free and the copper octa-alkyl derivatives ((10): M = 2H, Cu, R = C<sub>n</sub>H<sub>2n+1</sub>, n = 4–10) in 1987.<sup>182,183</sup> Nickel ((10): M = Ni, R = C<sub>n</sub>H<sub>2n+1</sub>, n = 4–10), zinc ((10): M = Zn, R = C<sub>n</sub>H<sub>2n+1</sub>, n = 4–10, 12, 15, 18),<sup>184</sup> and cobalt ((10): M = Co, R = C<sub>n</sub>H<sub>2n+1</sub>, n = 4–10)<sup>185,186</sup> derivatives were also prepared to complete the study. Selected thermal data are collected in Table 13. All the compounds with side chains as short as hexyl (and pentyl for zinc) were mesomorphic, and showed a similar behavior. They exhibited a

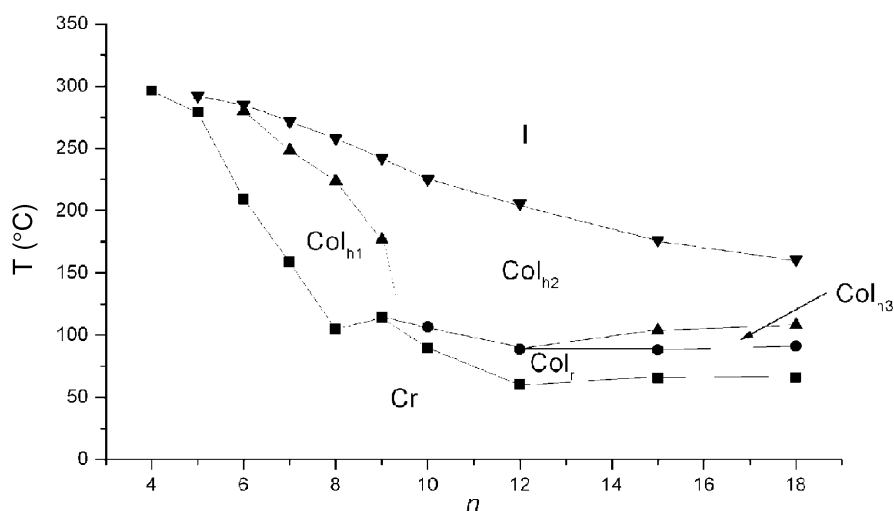
**Table 13** Thermotropic properties of (10) with  $R = C_nH_{2n+1}$ .

<i>M</i>	<i>n</i> = 4	<i>n</i> = 6	<i>n</i> = 8	<i>n</i> = 10
2H	Cr 230 I	Cr 161 Col <sub>h</sub> 171 I	Cr 84.5 (Col <sub>x</sub> 73) Col <sub>r</sub> 101 Col <sub>h</sub> 152 I	Cr 77.5 Col <sub>h</sub> 133 I
Cu	Cr 265 I	Cr 184 Col <sub>h1</sub> 235.5 Col <sub>h2</sub> 242 I	Cr 95.5 Col <sub>h1</sub> 156 Col <sub>h2</sub> 220 I	Cr 88 (Col <sub>r</sub> 69) Col <sub>h2</sub> 198 I
Zn	Cr 296 I	Cr 209 Col <sub>h1</sub> 280 Col <sub>h2</sub> 285 I	Cr 105 Col <sub>h1</sub> 224 Col <sub>h2</sub> 258 I	Cr 90 Col <sub>r</sub> 107 Col <sub>h2</sub> 225 I
Ni	Cr 245 I	Cr 145 Col <sub>h1</sub> 164 Col <sub>h2</sub> 169 I	Cr 66 (Col <sub>r</sub> 55) Col <sub>h2</sub> 153 I	Cr 64 Col <sub>h2</sub> 136 I
Co	Cr 300 I	Cr 177 Col 252 I	Cr 100 Col 220 I	Cr 74.5 Col 189 I

Col: unidentified columnar phase.

much richer mesomorphism than the isomeric materials described above, with mesophases occurring at lower temperature. In general, these compounds exhibited one or more mesophases, the highest temperature phase being assigned as Col<sub>h</sub>. At lower temperatures, some compounds developed either a second Col<sub>h</sub> phase, or a Col<sub>r</sub> phase, in addition to a monotropic behavior, detected for some compounds. The three mesophases were observed in one material for the long-chain zinc complexes only (Figure 25).<sup>187</sup> The low-temperature Col<sub>h</sub> mesophase was more ordered. From a structural point of view, the radial positions are more sterically demanding than the peripheral ones, and allow stronger interactions between the macrocycle and the core-chain linking group. This results in the lowering of the co-facial attraction of the aromatic units, and to the induction of mesophase with disordered stacking, and at low temperatures. As expected, increasing the chain length resulted in the depression of the transition temperatures, with a rapid drop in the melting temperatures and a linear fall in the clearing temperatures, leading to an overall increase in the mesophase stability. Relative to the metal-free derivatives, the nickel analogs showed lower transition temperatures. In contrast, these temperatures were raised in the zinc and copper complexes, while essentially the clearing temperature was increased in the cobalt compounds. Thus, zinc was the most effective metal for extending the mesomorphic temperature range, with the trend  $Zn > Co > Cu > Ni \approx 2H$ . The mesophase stabilization in the zinc compounds may be due to the extent of intermolecular metal-macrocycle interactions due to the propensity of the metal to five coordinate.

A crystal structure of the octahexylphthalocyanine complex of nickel<sup>188</sup> showed a striking resemblance to the crystal phase and the mesophases. In the crystalline phase, the molecules were stacked in a staggered fashion into columns, presumably to minimize the steric hindrance of the chains, with some tilt with respect to the axis, these columns being disposed into a pseudo-hexagonal array. In contrast to the unmetallated species,<sup>189</sup> the presence of the nickel has the

**Figure 25** Thermal behavior of the zinc(II) complex of series (10) as a function of *n*.

effect of increasing the attractive interactions with the  $\pi$ -systems of the molecules lying above and below, and to reduce the distance between aromatic planes.<sup>190</sup>

A few analogous derivatives with alkoxymethyl groups ((10): M = 2H, Cu, Zn, R = CH<sub>2</sub>OC<sub>7</sub>H<sub>15</sub>) were also prepared and showed mesophases, too.<sup>191,192</sup> Two mesophases were observed for the free-base compound (Cr 79 Col<sub>r</sub> 120 Col<sub>h</sub> > 300 dec.), while the Cu and Zn complexes showed only one as yet unidentified phase above 82 °C and 70 °C, respectively, until the materials decomposed above 300 °C.

Quite remarkably, none of the free-base, non-peripherally substituted octa(alkoxy)-phthalocyanines and their corresponding metal complexes ((10): M = 2H, Cu, Ni, R = OC<sub>n</sub>H<sub>2n+1</sub>) exhibited thermotropic mesophases on their own.<sup>193</sup> However, mesomorphism could be induced by contact preparations with the electron acceptor, TNF (trinitrofluorenone).<sup>194</sup> The mesophase, identified as lamello-columnar according to X-ray data, was stabilized over large TNF concentration (ca. 10 mol.% up to 80 mol.%), with the clearing temperature of the charge-transfer complex rising with TNF content, with a maximum of stabilization at 50–70 mol.%. Both the copper and nickel complexes showed the same behavior, and the metal ion did not affect the thermal stability of the complex. Contact preparations with benzene, chloroform, or alkanes were not efficient in inducing lyotropic phase behavior, either as the pure complex or as the charge-transfer complex, but rather probed the dissolution of the thermotropic mesophase of the electron donor–acceptor complexes in the solvents.

Several non-uniformly substituted, amphiphilic phthalocyanines were prepared as free-base materials and as metal complexes for their capability to form Langmuir and Langmuir–Blodgett films ((11): M = 2H, Cu, R = C<sub>n</sub>H<sub>2n+1</sub>, OC<sub>n</sub>H<sub>2n+1</sub>, R' = or ≠ R'' = O(CH<sub>2</sub>)<sub>m</sub>OH, O(CH<sub>2</sub>)<sub>m</sub>CO<sub>2</sub>H),<sup>195,196</sup> some were found to be mesomorphic.<sup>197,198</sup> Again, none of the alkoxy systems was found to be mesomorphic ((11): M = 2H, Cu, Ni, R = OC<sub>5</sub>H<sub>11</sub>, R' = R'' = O(CH<sub>2</sub>)<sub>3</sub>OH), but some of the alkyl derivatives displayed columnar mesophases ((11): M = 2H, Cu, Ni, R = C<sub>n</sub>H<sub>2n+1</sub>, R' = Me or R'', R'' = (CH<sub>2</sub>)<sub>m</sub>OH).<sup>199–201</sup> The mesomorphic properties were found to be intimately linked to the nature of the substituent and to the metal (Table 14). The most stable mesomorphic behavior was observed for the compounds having one methyl group. Moreover, desymmetrizing the alkyl and the hydroxyalkyl chain lengths led to a destabilization of the mesophase, which became monotropic, probably due to the distortion of the disk shape and the consequent disruption in the stacking.

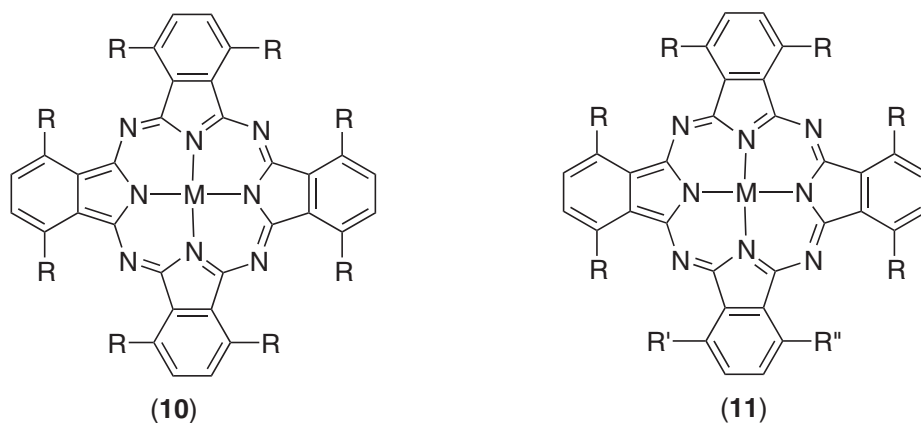


**Table 14** Mesomorphism of non-uniformly octasubstituted phthalocyanines (11).

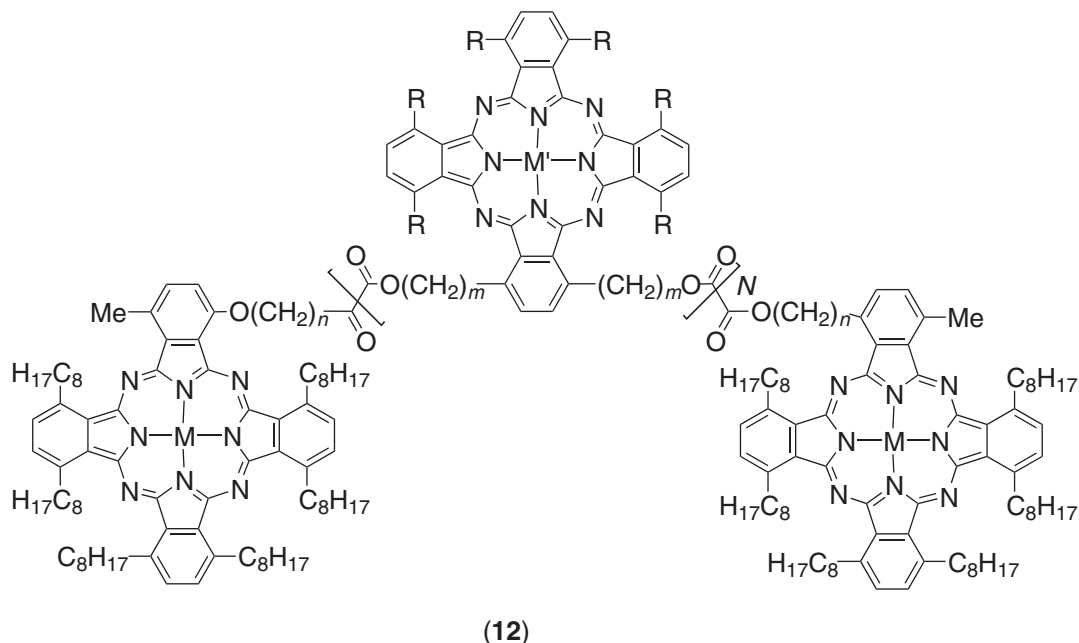
<i>R</i>	<i>R'</i>	<i>R''</i>	<i>M</i>	<i>Transition temperatures</i>
C <sub>8</sub> H <sub>17</sub>	Me	C <sub>5</sub> H <sub>10</sub> OH	2H	Cr 55 Col <sub>r</sub> 115 Col <sub>h</sub> 160 I
		C <sub>6</sub> H <sub>12</sub> OH	Cu	Cr 80 Col <sub>r</sub> 134 Col <sub>h</sub> 237 I
C <sub>8</sub> H <sub>17</sub>	C <sub>6</sub> H <sub>12</sub> OH	C <sub>6</sub> H <sub>12</sub> OH	2H	Cr 58 Col <sub>r</sub> 103 Col <sub>h</sub> 165 I
		C <sub>6</sub> H <sub>12</sub> OH	Cu	Cr 88 Col <sub>r</sub> 130 Col <sub>h</sub> 244 I
C <sub>9</sub> H <sub>19</sub>	C <sub>4</sub> H <sub>8</sub> OH	C <sub>4</sub> H <sub>8</sub> OH	2H	Cr 110 Col <sub>h</sub> 132 Col <sub>h</sub> 146 I
		C <sub>4</sub> H <sub>8</sub> OH	Cu	Cr 144 Col <sub>h</sub> 172 Col <sub>h</sub> 216 I
C <sub>10</sub> H <sub>21</sub>	C <sub>4</sub> H <sub>8</sub> OH	C <sub>4</sub> H <sub>8</sub> OH	2H	Cr 98 Col <sub>h</sub> 122 I
		C <sub>4</sub> H <sub>8</sub> OH	Cu	Cr 154 Col <sub>h</sub> 170 I
C <sub>10</sub> H <sub>21</sub>	C <sub>4</sub> H <sub>8</sub> OH	C <sub>4</sub> H <sub>8</sub> OH	Ni	Cr 95 Col <sub>h</sub> 123 I
		C <sub>4</sub> H <sub>8</sub> OH	2H	Cr 124 (Col <sub>h</sub> 77) I
			Cu	Cr 151 (Col <sub>h</sub> 136) I

**Table 15** Mesomorphism of the oligomeric phthalocyanines (**12**).

Dimer ( $N=0$ ) $n=5$		Trimer ( $N=1$ )					
$M$	Mesomorphism	$n$	$m$	$R$	$M$	$M'$	Mesomorphism
2H	(Col <sub>r</sub> 135) Col <sub>h</sub> 180 I	6	6	C <sub>8</sub> H <sub>17</sub>	2H	2H	Col <sub>h</sub> 177 I
Cu	(Col <sub>r</sub> 161) Col <sub>h</sub> 254 I	6	6	C <sub>8</sub> H <sub>17</sub>	Cu	Cu	Col <sub>h</sub> 252 I
		5	6	C <sub>7</sub> H <sub>15</sub>	Cu	2H	(Col <sub>r</sub> 125) Col <sub>h</sub> 222 I

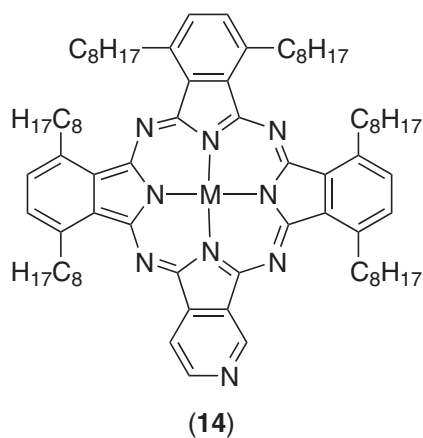
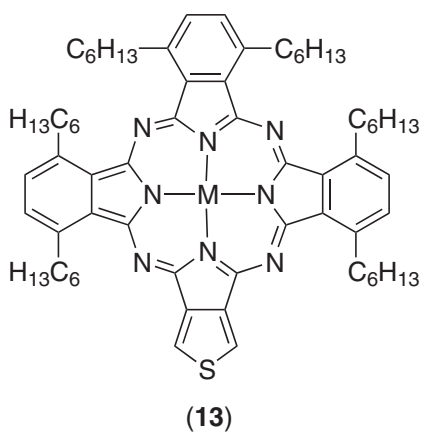
The attachment of the ferrocenyl moiety to the phthalocyanine core afforded a novel liquid-crystalline system ((**11**):  $M = 2H$ ,  $R = C_8H_{17}$ ,  $R' = Me$ ,  $R'' = (CH_2)_8OH$  or  $(CH_2)_{8-2}OC-Fc$  [ $Fc$  is the ferrocenyl group]).<sup>202</sup> The free-base compound displayed two columnar mesophases, Cr 56 Col<sub>r</sub> 62 Col<sub>h</sub> 170 I. As expected due to the bulky ferrocenyl group, the mesophase was destabilized, but not enough to be suppressed. The compound showed only one mesophase, Col<sub>h</sub>, between 60 °C and 133 °C.

The optimization of the synthetic procedure developed to prepare such non-uniformly substituted systems opened new perspectives in the area of mesogenic oligomeric<sup>203,204</sup> and polymeric phthalocyanines.<sup>205–207</sup> Thus, dimeric and trimeric materials were investigated as model compounds for main-chain liquid-crystalline polymers. The dimeric ((**12**):  $N=0$ ), and trimeric ((**12**):  $N=1$ ) phthalocyanines were prepared and were found to be liquid-crystalline at ambient temperature, and stable over broad temperature ranges (Table 15). The dimers showed the same mesophases as their monomeric precursors, although the stability of the Col<sub>h</sub> phase was enhanced at the expense of the Col<sub>r</sub> phase, which turned monotropic. Upon complexation, the mesophase range was extended by 74 °C. The trimers exhibited only the Col<sub>h</sub> phase, except the mixed copper-free-base compound, which showed a transient Col<sub>r</sub> phase on first heating. Similar temperature ranges were observed between both the dimer and trimer.



Following the encouraging results obtained with non-uniformly substituted phthalocyanines, Cook and Jafari-Fini investigated further the effects of chemical modification of the phthalocyanine ring on the physico-chemical and photophysical properties. Their approach consisted of the incorporation of heteroatomic rings into the phthalocyanine. Thus, two new metal-free and metal-containing mesogenic macrocycles, namely hexa-hexylthiopheno-tribenzoporphyrane ((**13**):  $M = 2H$ , Ni),<sup>208</sup> and hexa-octylpyridino[3,4]tribenzoporphyrane ((**14**):  $M = 2H$ , Ni, Zn),<sup>209</sup> were obtained by the replacement of one benzenoid ring of the phthalocyanine by a fused thiophene and a fused pyridine ring, respectively. Compounds (**13**) and (**14**) were obtained by reaction of the appropriate 3,4-dicyanothiophene or 3,4-dicyanopyridine with an excess of

3,6-dialkylphthalonitrile. In both series, the free-bases and the nickel complexes showed columnar phases, with greater mesophase stability and broader temperature ranges than the relative phthalocyanine derivatives. Complexation of nickel enhanced the mesomorphism, and additionally for **13**, induction of a novel phase was observed (Table 16). In solution, these already showed a great tendency to face-to-face type of aggregation, which became stronger with increasing concentration. The absence of the mesophase for the zinc complex was attributed to the formation of an edge-to-face complex through axial ligation of one molecule to the zinc ion of another in the solid and liquid phase, inhibiting the formation of a mesophase. The *Q*-band absorptions of the thiophenotribenzoporphyrazine compounds was red-shifted relative to the analogous phthalocyanine derivatives, indicating stronger intermolecular interactions, and their formulation as spin-coated film showed broad band absorption extended into the near infrared.



It is worth mentioning the case of an analogous heterocyclic phthalocyanine based on thiophene,<sup>73</sup> prepared as an alternative to the phthalocyanines discussed above. Such systems, (**15**), were investigated in an effort to improve the conductivity properties with respect to that of phthalocyanines. Note that the structure represented is one of four isomeric compounds (the isomerism is related to the relative orientation of the sulfur atoms of the thiophene rings). Both the free-base (Cr 48 Col<sub>h</sub> 223 I) and the metallated phthalocyanine (Cr 49 Col<sub>h</sub> 258 I) exhibited a stable mesomorphism, quite unaffected upon metal insertion. The free-base phthalocyanine with shorter chain length displayed additional transient Col<sub>r</sub> phases, which did not appear on cooling (Col<sub>r</sub> 36 Col<sub>r</sub> 75 Col<sub>h</sub> 278 I). The replacement of the benzene groups by thiophenes lowered the transition temperatures slightly, and caused a blue-shift in the UV-vis spectra.

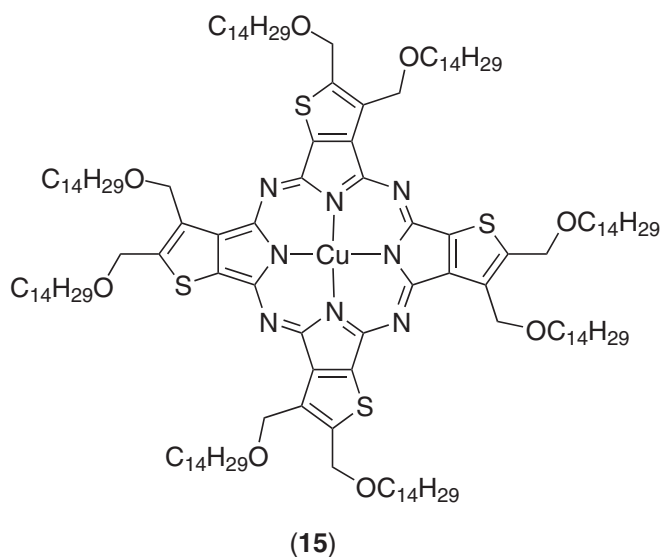




**Table 16** Mesomorphic properties of (13) and (14).

<i>Compound</i>	<i>Mesomorphism</i>
(13): M = 2H	Cr 158 Col <sub>h</sub> 231 I
(13): M = Ni	Cr 151 Col <sub>r</sub> 248 Col <sub>h</sub> 267 I
(14): M = 2H	Cr 142 Col <sub>x</sub> 156 Col <sub>h</sub> 237 I
(14): M = Ni	Cr 140 Col <sub>x</sub> 149 Col <sub>h</sub> 273 I
(14): M = Zn	Cr 181 I

Col<sub>x</sub>: unidentified columnar phase.

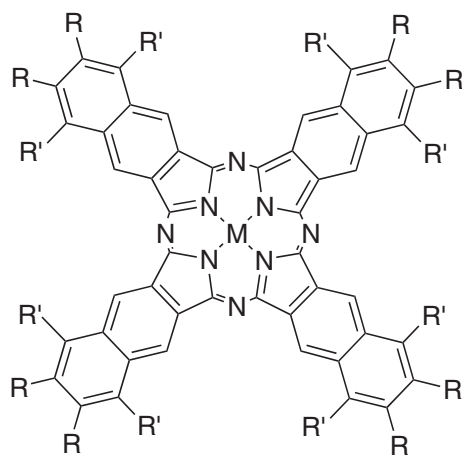
This study on phthalocyanines revealed several important features, which deserve comment. The first point concerns the usually high clearing temperatures, and the often-associated decomposition, which are two major drawbacks in the exploitation of phthalocyanine-based systems for various applications. However, important progress has been made in recent years in order to overcome these problems. Thus, it has been shown, for example, that the use of solvents allowed the formation of N<sub>Col</sub> phase, with can be more easily aligned without the need to go into the isotropic liquid, and thus advances in the processing of such materials are likely. Moreover, great efforts have been made in the chemistry, in particularly the synthesis of tetra-substituted systems, leading to materials with accessible transition temperatures without destroying the mesomorphism, providing that a minimum of structural conditions are still respected. The third point is related to the variety of side chains used, which have been found to influence not only the mesomorphic properties, but also other properties such as conductivity and photophysical properties. The systematic variation of the nature of the chains can allow for some property-tuning. The last point deals with the effect of the metal. Most divalent metals clearly did not affect the properties relative to the free-base phthalocyanines, or slightly improved the mesophase stability, seen more as disadvantageous than useful. However, some metals have shown interesting and exploitable feature such as those that are too large to fill the cavity of the macrocycle, metal fragments that induce a dipole, and metals having the ability to form sandwich complexes with phthalocyanine rings. Moreover, the film-forming and film-deposition tendencies were found to be affected by the mesogenic character of the phthalocyanines.

#### 7.9.7.1.5 2,3-Naphthalocyanines

New macrocyclic compounds based on the 2,3-naphthalocyanine core have been reported.<sup>210</sup> Only a limited number of mesogenic systems have been described, mainly due to the lack of convenient synthetic procedures leading to the di-substituted-2,3-dicyanonaphthalenes precursors. As for phthalocyanines, two positions of chain substitution are available, the peripheral ( $R' = H$ ), and the radial ( $R = H$ ). One peripherally octasubstituted zinc complex ((16): M = Zn, R = SC<sub>12</sub>H<sub>25</sub>, R' = H) was found to show a mesophase between 100 °C and 300 °C, at which temperature it decomposed. Due to absence of a well-developed texture, the nature of the mesophase was not given. Two other complexes with radial substitution ((16): M = Zn, R = H, R' = CH<sub>2</sub>OC<sub>6</sub>H<sub>13</sub> and CH<sub>2</sub>O(CH<sub>2</sub>CH<sub>2</sub>O)<sub>2</sub>C<sub>4</sub>H<sub>9</sub>) also showed a mesophase above 130 °C for the former and above 150 °C for the latter up to the decomposition point at 300 °C; one phase could be recognized by its texture, characteristic of a Col<sub>h</sub> phase. These are the first example of mesomorphic naphthalocyanines. Attempts to induce mesomorphism in octaalkyl- and octaalkoxy-2,3-naphthalocyaninato metal complexes failed, despite their disk-like structure and similarity to (1).<sup>211–213</sup>

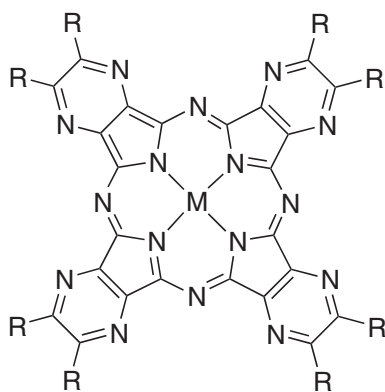
#### 7.9.7.1.6 Tetrapyrazinoporphyrazines

Tetrapyrazinoporphyrazines are phthalocyanine analogs, with nitrogen atoms replacing the carbon atoms in the peripheral rings. The starting material is the 2,3-dicyano-4,5-disubstituted pyrazine, and the procedure to form the macrocyclic compound is identical to that used for the preparation of the phthalocyanines. It was thus expected that they would be mesomorphic, too ((17): M = 2H, Cu, Ni and Co, R = C<sub>12</sub>H<sub>25</sub>), and indeed, the metal-free ligand was mesomorphic, forming a Col<sub>h</sub> phase,<sup>101,214</sup> although the isotropic liquid could not be reached due to decomposition. Upon complexation, the mesophase stability was slightly increased, though the



(16)

complexes decomposed before clearing, and the mesophase transformed from hexagonal to rectangular, irrespective of the metal. The  $Col_r$  phase was centered, showing the  $c2mm$  plane group. Thus, in this family of compounds the influence of the metal on the mesomorphism is more evident. UV-vis absorption spectra revealed a blue-shift of the  $Q$ -band compared to the analogous metallophthalocyanines. Another interesting comparison between the two macrocyclic compounds is that the pyrazinoporphyrazines were more easily reduced (by 0.5 V). Branching the chain did not suppress the mesomorphism ((17):  $M = 2H, Cu$ ,  $R = CH_2CH(Et)C_4H_9$ ), and stable compounds that did not decompose at elevated temperatures were obtained (Table 17).



(17)

In common with the phthalocyanines, metallomesogens based on extended pyrazino-porphyrzine cores have been prepared, namely substituted-octaphenyltetrapyrazino-porphyrzine ((18):  $M = Cu, Ni$ ,  $R = H$  or  $OC_nH_{2n+1}$ ),<sup>215</sup> and triphenylenopyrazinoporphyrazines (19),<sup>216</sup> and they have been reported to show mesophases over a wide range of temperatures (Table 18). In the first

Table 17 Mesomorphic properties of (17).

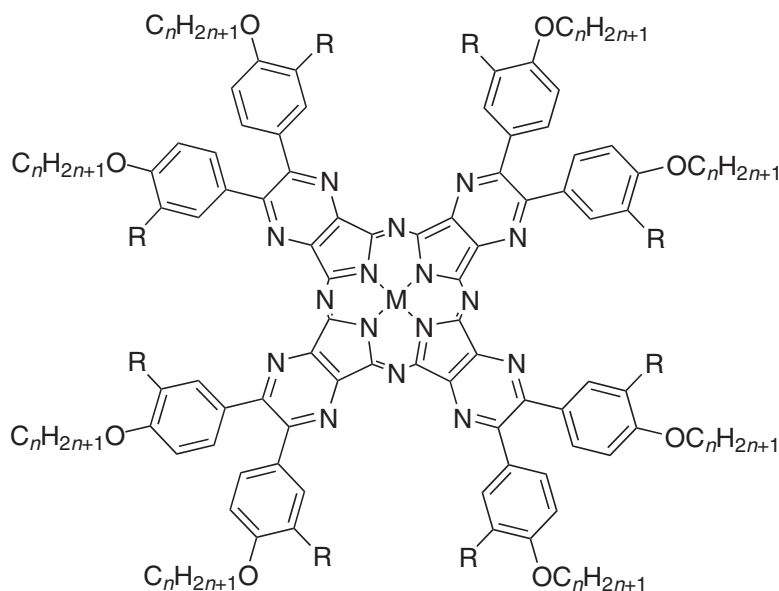
<i>M</i>	<i>R</i>	<i>Mesomorphism</i>
2H	$C_{12}H_{25}$	Cr 118 $Col_h$ 238 dec.
Cu	$C_{12}H_{25}$	Cr 114 $Col_r$ 288 dec.
Ni	$C_{12}H_{25}$	Cr. 118 $Col_r$ 264 dec.
Co	$C_{12}H_{25}$	Cr. 74 $Col_r$ 255 dec.
2H	$CH_2CH(Et)C_4H_9$	Cr 75 $Col_r$ 193 $Col_t$ 219 I
Cu	$CH_2CH(Et)C_4H_9$	Cr 90 $Col_r$ 232 I

**Table 18** Mesomorphism of compound (18).

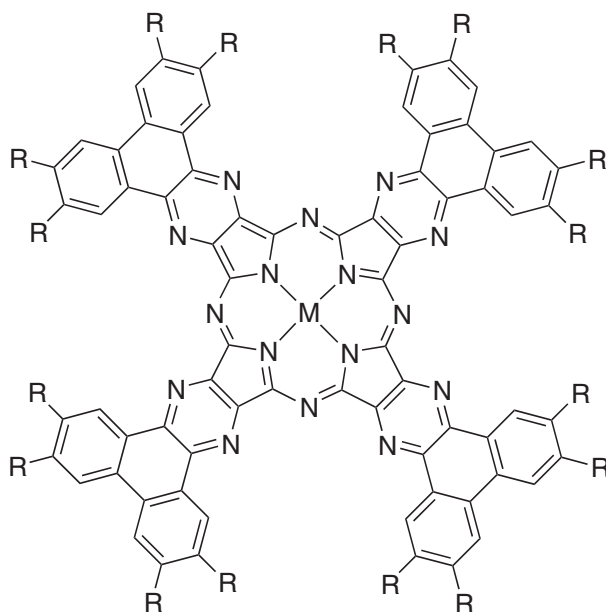
<i>M</i>	<i>n</i>	<i>R = H</i>	<i>R = OC<sub>n</sub>H<sub>2n+1</sub></i>
Cu	8		M -29~39 Col <sub>r1</sub> 247 Col <sub>r2</sub> 323 dec.
Ni	8		M -41~11 Col <sub>r1</sub> 226 Col <sub>r2</sub> 324 dec.
Cu	10	Col <sub>t</sub> 149 Col <sub>h</sub> 230 dec.	M -13~29 Col <sub>r1</sub> 221 Col <sub>r2</sub> 281 I + dec.
Ni	10	Col <sub>t</sub> 150 Col <sub>h</sub> 210 dec.	Col <sub>h</sub> 41 Col <sub>r1</sub> 214 Col <sub>r2</sub> 269 I + dec.
Cu	12	Col <sub>t</sub> 109 Col <sub>r(c2mm)</sub> 230 dec.	Col 14 Col <sub>h</sub> 44 Col <sub>r1</sub> 194 Col <sub>r2</sub> 241 I + dec.
Ni	12	Col <sub>t</sub> 109 Col <sub>r(c2mm)</sub> 230 dec.	Col <sub>h</sub> 40 Col <sub>r1</sub> 206 I + dec.

M: unidentified mesophase.

series, both octa- and hexadeca-substituted complexes showed a rich mesomorphism, including at least two different columnar phases. In the octasubstituted series ((18):  $R = H$ ), the high-temperature mesophase changed from Col<sub>h</sub> to Col<sub>r</sub> on lengthening the side chains, as observed in the relative, compound (4). However, whereas (4) were crystalline at room temperature, (18) showed a Col<sub>t</sub> phase. Thus, a rather small structural change led to quite dramatic modifications which were not really anticipated. Concerning the series with 16 side chains ((18):  $R = OC_nH_{2n+1}$ ), the same kind of polymorphism was observed, including transitions between mesophases of the same nature (Col<sub>r1</sub> and Col<sub>r2</sub> both have a  $c2mm$  plane group). One of the peculiarities, however, was the presence of the Col<sub>h</sub> mesophase, i.e., higher symmetry phase, at lower temperature than the Col<sub>r</sub> phase for some complexes. Such a transition can be explained by the tilting of the molecules with respect to the columnar axis with increasing temperature, thus losing the cylindrical geometry of the column and reducing the symmetry of the phase.

**(18)**

Both the copper and nickel complexes of triphenylenopyrazinoporphyrazine ((19):  $M = Cu, Ni$ ,  $R = OC_{10}H_{21}$ ) exhibited liquid crystalline behavior over the whole temperature range of investigation ( $-100^\circ C$  to  $300^\circ C$ ). The phase of both complexes was identified as Col<sub>t</sub> by X-ray diffraction, in which the complexes are likely stacked in a staggered arrangement deduced from the presence of the observed double periodicity in the columnar spacing. Thus, except for the mesophase of the related phthalocyanine, (5), which was not characterized, these extended discotic compounds behaved exactly the same way, possessing substantial mesomorphic ranges. The high clearing points are attributed to the extended  $\pi$ -system of the core and the consequently strong aggregation of the complexes, an argument supported by a substantial red-shift of the  $Q$ -bands with respect to the octaalkyl tetrapyrrolynes (17).



(19)

### 7.9.7.2 Porphyrins

Since the first report of a mesomorphic porphyrin by Goodby *et al.* in 1980,<sup>217</sup> in which a monotropic columnar phase was found in the octa(dodecyl) ester of uroporphyrin, there has been interest in the use of porphyrins for the formation of liquid crystals. Two categories of mesomorphic porphyrins can be distinguished depending on the location of the substituents around the core. Thus, the porphyrins are substituted either at the  $\beta$ -positions of the pyrrole rings, or they are functionalized at the *meso* positions. The small size of such discotic macrocycles was thought to bring about interesting features such as the decrease in the mesophase viscosity with respect to the larger phthalocyanine cycles, allowing for easier orientational and alignment properties.

#### 7.9.7.2.1 $\beta$ -Octasubstituted metalloporphyrins

The first mesogenic metalloporphyrins, described in 1987,<sup>218</sup> were substituted at the eight  $\beta$ -positions by chains linked through an ester function. The zinc and the free-base compounds ((20): M = 2H, Zn,  $n = 4, 6, 8$ ) were thought to exhibit one or two columnar mesophases depending on the chain length, but the mesophases were not identified. Indeed, it is only recently that a re-investigation permitted the full elucidation of the mesomorphic behavior of these octaesters. In addition, several new 2,3,7,8,12,13,17,18-octaacetatesporphyrins and their metal complexes were synthesized ((20): M = 2H, Zn,  $n = 3, 6, 8, 10-12, 14$ ; M = Cd, Cu, Ni, Pb, Pd, Pt,  $n = 10$ ).<sup>219</sup> Amongst the free-base and the zinc complexes, only those with a propyl chain ( $n = 3$ ) were not mesomorphic, all the others showing a single columnar phase identified by X-ray diffraction as Col<sub>r</sub>-*c2mm*, thus partly contradicting the first report, for which the authors claimed two different mesophases. Interestingly, the incorporation of the metal resulted in the increase in the mesomorphic range compared to the free-base compound, essentially due to the increase in the clearing temperatures, the melting points being identical for the zinc and free-base compounds (Figure 26).

The effect of the metal ion was investigated, too (Figure 27). Except for the lead complex, all complexes showed an enantiotropic, columnar mesophase characterized as Col<sub>r</sub> by miscibility studies with the zinc complex. As for the phthalocyanines, the lead ion was located out of the porphyrin plane but here, this distortion and the consequent disturbance of the  $\pi$  stacking led to total suppression of the mesophase. The transition temperatures were similar for all mesomorphic metal complexes, with a perceptible effect of the metal on the clearing temperatures, which

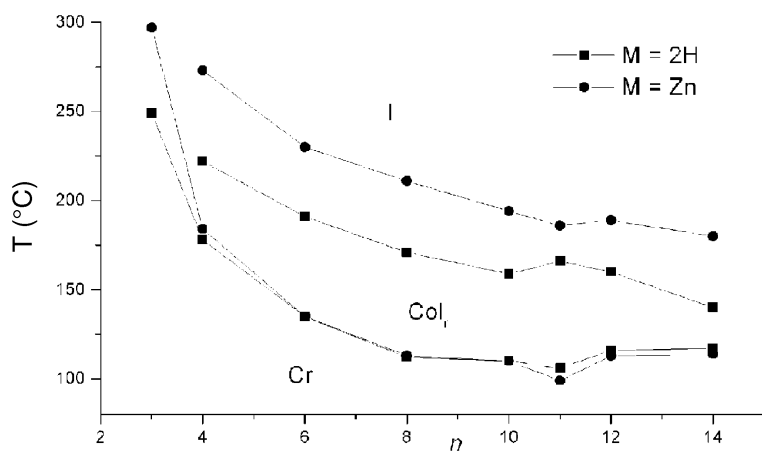
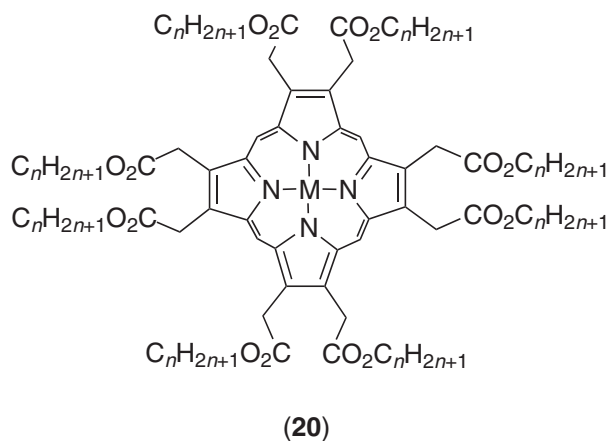


Figure 26 Thermal behavior of the free-base and zinc porphyrins (20).

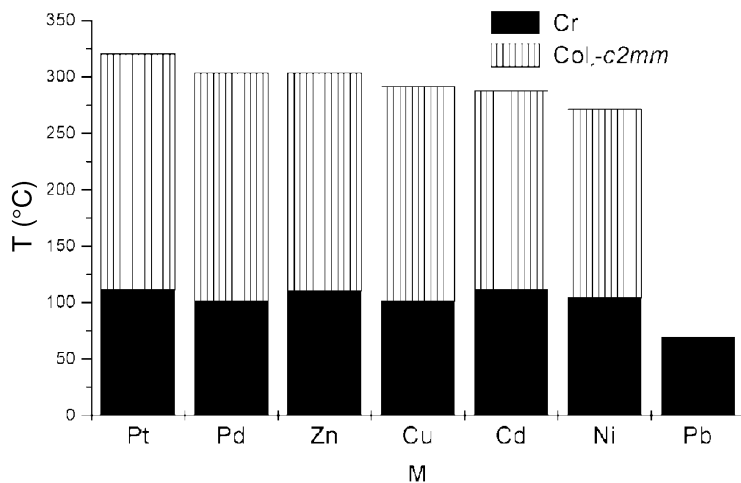
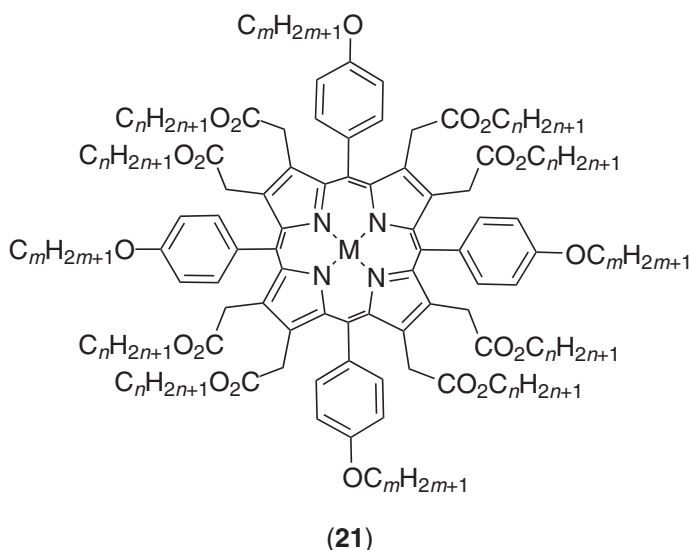


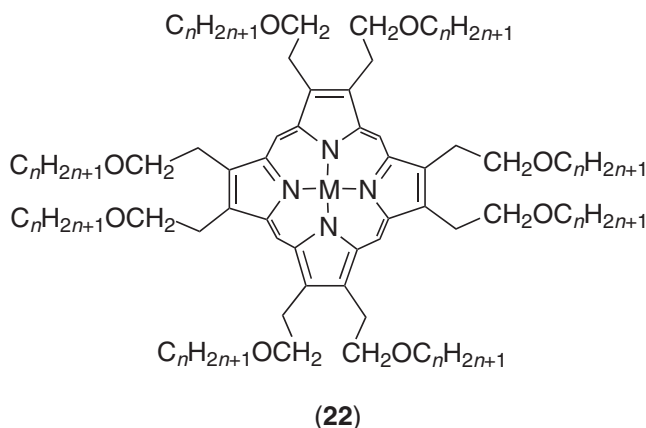
Figure 27 Effect of the metal on the mesophase stability of (20) ( $n = 10$ ).

decreased from platinum to nickel. In addition, some zinc and free-base porphyrins were found to form stable monolayers and Langmuir–Blodgett films.<sup>220,221</sup> The quality of the films was found to be connected to their tendency to self-organize into columnar mesophases, where an edge-on arrangement was favored.<sup>222</sup>

Note that the dodeca-substituted porphyrins functionalized in the eight  $\beta$  positions by ester chains, and in the four *meso* positions by alkoxyphenyl groups ((**21**): M = 2H, Zn, Cu,  $n = m = 8, 12$ ) were not mesomorphic despite the presence of twelve chains. The absence of mesophase was connected to a strong distortion from planarity of the porphyrin core.



The thermal behavior of an analogous series of octakis(alkoxyethyl)porphyrins was also investigated for comparison ((**22**): M = 2H, Zn, Cu, Pd, Cd,  $n = 4, 6, 8, 10$ ), and in order to decrease the viscosity, which was still high in the octaester systems. Thus, while only the free-base derivative with octyl chains was mesomorphic (Cr 84 Col 89 I), all the metal complexes were mesomorphic (Figure 28), the mesophase decreasing in stability as the chains were elongated.<sup>223,224</sup> In all cases, the fluid mesophase was identified by optical microscopy as columnar.



Here, the metal was central to the induction of mesomorphism, in contrast to the case with the octaester compounds. Mesophase stability was found to depend on the same electrostatic and geometric factors as for the octaester compounds, though the huge decrease in clearing temperatures was attributed to the absence of ester groups. Introduction of an electron acceptor (CN, NO<sub>2</sub>) in one of the *meso* positions depressed the transition temperatures (more for the nitro than for the cyano compound), and the authors also showed that reversing the ester linkage from CH<sub>2</sub>CO<sub>2</sub>R ((**20**)) to CH<sub>2</sub>CH<sub>2</sub>OCOR led to the suppression of the mesomorphism (isomer of (**20**): M = Zn, CH<sub>2</sub>CH<sub>2</sub>OCOC<sub>5</sub>H<sub>11</sub>, Cr 169 I). A zinc porphyrin has been found to be a fast charge

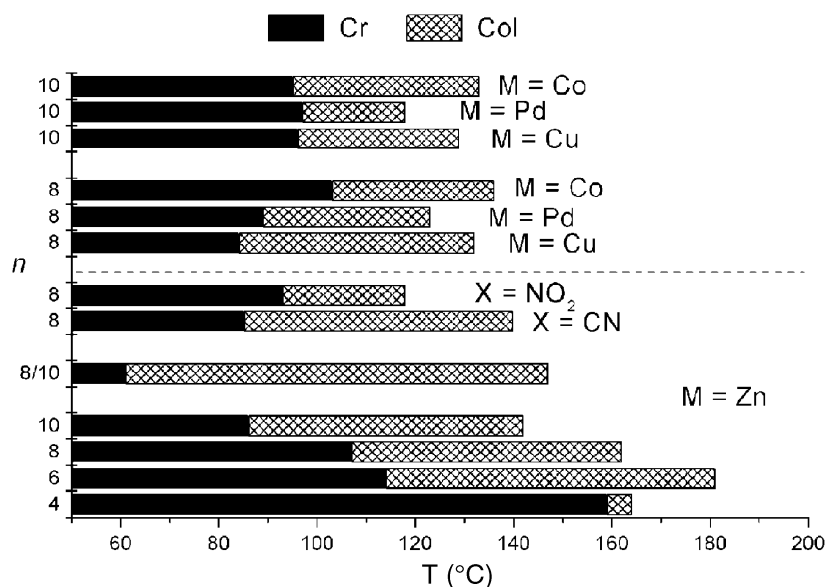


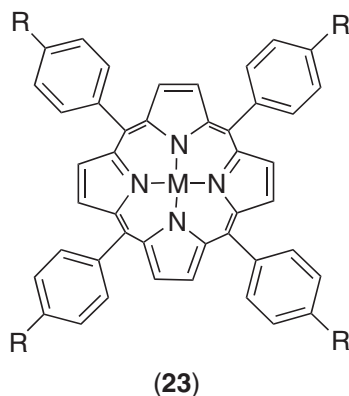
Figure 28 Mesomorphism of porphyrins (22).

carrier under irradiation<sup>225–227</sup> and an insulator in the dark, to exhibit interesting photoelectrochemical<sup>228,229</sup> properties, and to be efficient components in photovoltaic cells.<sup>(230)</sup>

Note that other, related octasubstituted porphyrins have been prepared but little information was given concerning their mesomorphism. The zinc  $\beta$ -octa(decyl)porphyrin (the eight chains were pure alkyl chains) was found to display a mesophase (probably columnar) between 117 °C and 177 °C, which is in the same temperature range as the ether analogs.<sup>(231)</sup> It also showed conductivity properties of the order of magnitude to that of (22). No mesomorphism was detected for porphyrins with eight alkoxy chains.<sup>232</sup>

#### 7.9.7.2.2 Meso-tetrasubstituted metalloporphyrins

Several tetraphenylporphyrins substituted in the four *meso* positions by various groups have also been investigated, and the induction and stability of mesomorphic properties were found to be dependent on the nature of the side chains. Simple alkyl chains directly connected in the four *meso* positions of metalloporphyrins ((23): M = Zn, Co, Cu, Ni, Pd) were not sufficient to induce mesophase.<sup>(231)</sup>



Free-base, zinc, and cobalt 5,10,15,20-tetrakis(decyloxyphenyl)porphyrins ((23): M = 2H, Zn, Co, R = OC<sub>10</sub>H<sub>21</sub>)<sup>233</sup>, and a manganese-tetracyanoethylene homolog with dodecyloxyphenyl groups ((23): M = Mn<sup>III</sup>TCNE (TCNE is tetracyanoethylene), R = OC<sub>12</sub>H<sub>25</sub>)<sup>234</sup> were claimed to be mesomorphic. The mesophase could not be identified in the former cases, and the high values of the

clearing enthalpy ( $\Delta H \sim 50 \text{ kJ mol}^{-1}$  to  $70 \text{ kJ mol}^{-1}$ ) suggested crystalline polymorphism instead. A  $\text{Col}_h$  phase, between  $108^\circ\text{C}$  and  $155^\circ\text{C}$ , was interpreted from a poorly resolved X-ray diffraction pattern for the last of these. The absence of mesomorphism in the free-base tetrakis(alkoxyphenyl)-porphyrins was later confirmed by X-ray diffraction ((**23**):  $\text{M} = 2\text{H}$ ,  $\text{R} = \text{OC}_n\text{H}_{2n+1}$ ,  $n = 5-14, 18$ ).<sup>235,236</sup> Comparing the enthalpy values of both metal-free and metal-containing systems, it can safely be advanced that the zinc and cobalt complexes were not mesomorphic either, and a recent report did mention the lack of mesomorphism in the zinc compound.<sup>(231)</sup> In contrast, the analogous free-base tetrakis(alkylphenyl)porphyrins<sup>236</sup> were reported to display mesophases from the hexyl homolog onwards ((**23**):  $\text{M} = 2\text{H}$ ,  $\text{R} = \text{C}_n\text{H}_{2n+1}$ ,  $n = 5-16$ ). One ( $6 \leq n \leq 10$ ) or two mesophases ( $n \geq 11$ ) were observed, both characterized as the  $\text{D}_L$  phase by X-ray diffraction. In this phase, the disk-like molecules are arranged with their short molecular axes perpendicular or at some angle with respect to the layer normal, forming a smectic-type organization. There is no positional order within the layer of the  $\text{D}_L$  phase, whereas for the  $\text{D}_L'$  phase, the molecules stacked into columns (with a staggered conformation), and these columns are arranged into layers. The aryl rings connected to the *meso* positions lie out of the porphyrin plane due to the steric effects, and, thus, the molecules are far from being totally planar.

Shimizu also tested the influence of the metal on tetrakis-*meso*-(dodecylphenyl)porphyrin, and undertook a broad, systematic study ((**23**):  $\text{M} = \text{Co}^{\text{II}}$ ,  $\text{Ni}^{\text{II}}$ ,  $\text{Cu}^{\text{II}}$ ,  $\text{Zn}^{\text{II}}$ ,  $\text{Pd}^{\text{II}}$ ,<sup>236</sup>  $\text{Al}^{\text{III}}\text{OH}$ ,<sup>237</sup>  $\text{Mo}^{\text{V}}\text{OCl}$ ,<sup>238</sup>  $\text{Mn}^{\text{III}}\text{Cl}$ ,  $\text{Mn}^{\text{III}}\text{TCNQ}^\ddagger$ ,<sup>239</sup>  $\text{Mo}^{\text{V}}\text{O}(\text{OH})$ ,  $\text{V}^{\text{IV}}\text{O}$ ,<sup>240</sup>  $\text{Si}^{\text{IV}}(\text{OH})_2$ ,  $\text{Si}^{\text{IV}}(\text{OMe})_2$ ,<sup>241</sup>  $\text{R} = \text{C}_{12}\text{H}_{25}$ ). The thermal behavior of these complexes is shown in Figure 29. Thus, complexes of divalent metals exhibited two  $\text{D}_L$  phases as did the free-base compound, with an apparent influence of the metallic ion on the clearing temperatures. The nickel complex alone showed a single  $\text{D}_L$  phase, and exhibited the lowest mesophase stability of the series. Complexes of the higher-valent metals all possessed axial groups, and were found to behave very differently, with the mesomorphism determined by the molecular geometry, specific intermolecular interaction, and steric hindrance. The hydroxoaluminium(III) complex displayed a  $\text{Col}_h$  phase, and once heated above the clearing point, the phase sequence changed to another type, indicating probably the formation of the  $\mu$ -oxo dimer, the formation of which was later confirmed by spectroscopic measurements.<sup>242</sup> The behavior of the dimer, prepared separately, was quite different to its monomer and several transitions were observed along with two  $\text{D}_L$  phases ( $\text{Cr} - 3\text{M10D}_{L1}69$   $\text{D}_{L2}148$  I). The  $\text{Mo}^{\text{V}}\text{OCl}$  complex, unique in the sense that it possessed two different axial groups, showed a  $\text{D}_L$  phase, too, over quite a broad temperature range.

The manganese complexes showed complicated thermal behavior, which was not reproducible beyond the first heat-cool cycle. Thus, both compounds showed a  $\text{D}_L$  phase, although heating the TCNQ (TCNQ is tetracyanoquinodimethane) compound at  $120^\circ\text{C}$  for several hours was necessary for mesophase formation. Among systems with specific interactions, the  $\text{V}^{\text{IV}}\text{O}$  complex and the  $\text{Mo}^{\text{V}}\text{O}(\text{OH})$  complex were thought to stabilize the columnar phase by means of dipole-dipole and hydrogen bonding interactions, respectively. While the  $\text{V}^{\text{IV}}\text{O}$  complex formed two  $\text{D}_L$  phases, the molybdenum complex exhibited a room-temperature  $\text{Col}_t$  phase. The absence of columns in the  $\text{V}^{\text{IV}}\text{O}$  complex was in agreement with the absence of significant VO interactions and the

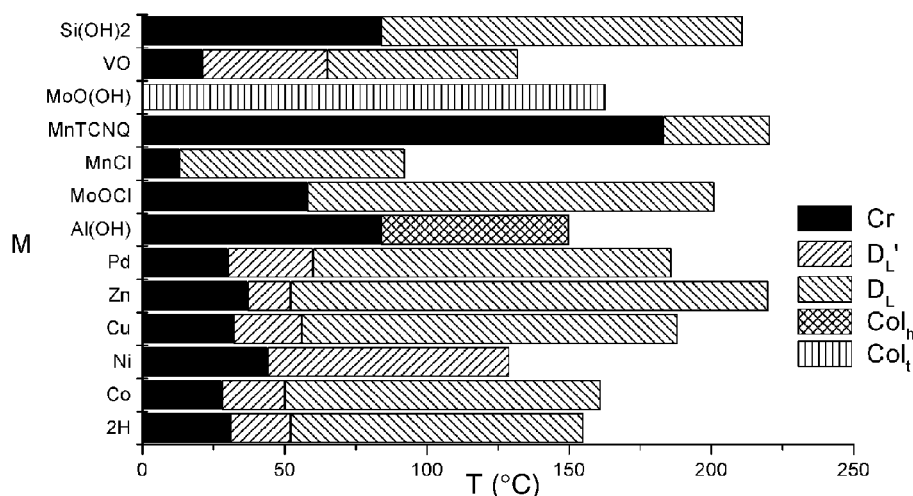


Figure 29 Mesomorphism of metal complexes of porphyrin (**23**).

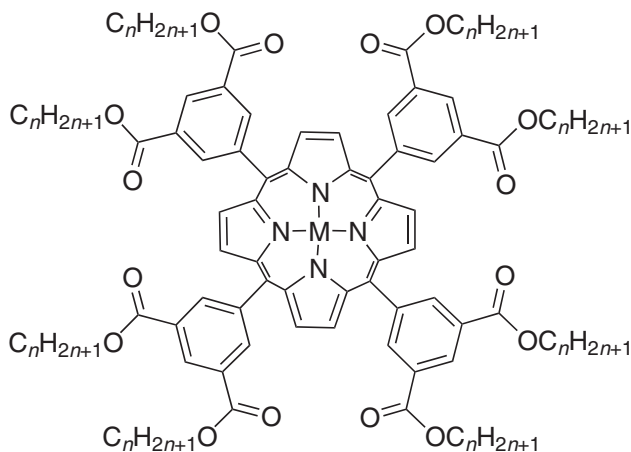


complexes showed behavior similar to that of the simple divalent metal complexes. However, it appeared that the  $\text{Col}_i$  phase of the  $\text{Mo}^{\text{VO}}(\text{OH})$  complex was stabilized by intermolecular hydrogen bonds, partially rigidifying the columnar backbone. The dihydroxysilicon(IV) porphyrin gave a discotic lamellar phase, probably  $\text{D}_{\text{L}}$ .

Increasing the chain length did not bring drastic modification to the thermal behavior of this family of compounds. Few were prepared, including the free-base,<sup>243-245</sup> nickel,<sup>246</sup> and oxovanadium<sup>247</sup> compounds bearing pentadecylphenyl side groups ((**23**):  $\text{R} = \text{C}_{15}\text{H}_{31}$ ;  $\text{M} = 2\text{H}$ , Cr 56  $\text{D}_{\text{L}}$ , 66  $\text{D}_{\text{L}}$  135 I;  $\text{M} = \text{Ni}$ , Cr 68  $\text{D}_{\text{L}}$  122 I;  $\text{M} = \text{VO}$ , Cr 51  $\text{D}_{\text{L}}$ , 82  $\text{D}_{\text{L}}$  140 I). On average, the clearing temperatures were found to be lowered by some few degrees only, but the nature of the mesophase was not modified. The photocurrent behavior of these compounds was also compared.<sup>248</sup> The mobility of charge carriers showed a tendency to disappear in the lamellar phase, which does not have the columnar structures found in the  $\text{D}_{\text{L}}$  phase. Photocurrent rectification was observed in the crystal and low-temperature lamellar phase ( $\text{D}_{\text{L}}$ ), and diminished at the  $\text{D}_{\text{L}}$ -to- $\text{D}_{\text{L}}$  phase transformation.

Substitution of the alkyl chains by oligo(ethyleneoxide) alkyl and alkoxy chains ((**23**):  $\text{M} = 2\text{H}$ , Zn,  $\text{R} = (\text{O})(\text{CH}_2)_n\text{O}(\text{C}_2\text{H}_4\text{O})_m\text{X}$ ,  $\text{X} = \text{H}$ , Me, Et) resulted in the complete suppression of the mesomorphism in both the free-base and zinc compounds, although the transition temperatures were reduced substantially.<sup>249</sup> Similarly, *meso*-tetrakis(alkylcarboxyphenyl)porphyrins and their metal complexes ((**23**):  $\text{M} = 2\text{H}$ , Zn, Cu,  $\text{R} = \text{CO}_2\text{C}_n\text{H}_{2n+1}$ ,  $n = 12, 16, 18$ )<sup>250</sup> appeared non-mesomorphic, with melting points in the range 100 to 140 °C.

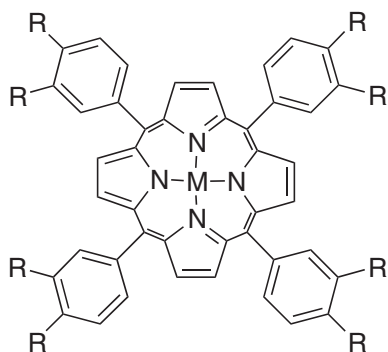
Patel and Suslick reported a homologous series of 5,10,15,20-tetrakis-(3,5-dialkylesterphenyl)porphyrins and one oxovanadium complex<sup>251</sup> which were mesomorphic ((**24**):  $\text{M} = 2\text{H}$ , VO,  $n = 8, 10, 12, 14, 16, 18, 20, 22$ ). In this case, the number of ester groups was double that found in the previously described structure. All of them were found to exhibit a  $\text{Col}_h$  mesophase from the decyl homolog onwards (identified by X-ray diffraction), with a narrowing of the mesomorphic range on increasing the chain length ( $\Delta T = 124^\circ\text{C}$ ,  $n = 10$ , to  $23^\circ\text{C}$ ,  $n = 22$ ), due to the increase in the melting point ( $-3^\circ\text{C}$  to  $78^\circ\text{C}$ ), and the depression of the clearing temperature ( $121^\circ\text{C}$  to  $101^\circ\text{C}$ ). The oxovanadyl ion strongly stabilized the mesophase (Cr 13  $\text{Col}_h$  233 I).



(24)

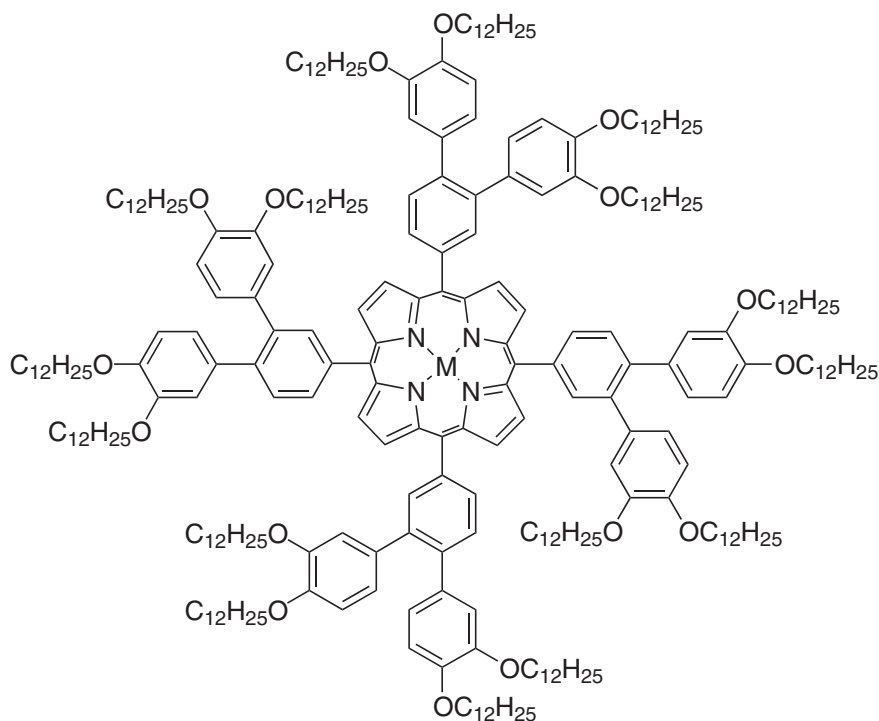
The relationships between molecular structure and mesophase structure of disk-like, porphyrin-based, liquid crystalline materials have led to the study of several series of porphyrins *meso* substituted by bulky groups. The first study concerned *meso*-tetrakis(3,4-dialkoxyphenyl)porphyrins and their copper complexes ((**25**):  $\text{M} = 2\text{H}$ , Cu,  $\text{R} = \text{OC}_n\text{H}_{2n+1}$ ,  $n = 4, 6, 8, 10, 12, 16, 18$ ).<sup>252</sup> Thus, liquid crystal properties were induced upon the grafting of an additional alkoxy chain in the *meta* positions of the side phenyl groups, contrasting with the non-mesomorphic nature of compound (**23**) ( $\text{R} = \text{alkoxy chain}$ ). Despite a rather complicated series of phase transitions, some of the free-base compounds ( $n = 12, 16, 18$ ), and one copper complex ( $n = 12$ ) exhibited a monotropic  $\text{D}_{\text{L}}$  phase below  $100^\circ\text{C}$  on cooling from the isotropic liquid. Similarly, free-base, copper, and nickel compounds based on *meso*-tetrakis(3,4-dialkylphenyl)porphyrins ((**25**):  $\text{M} = 2\text{H}$ , Cu, Ni,  $\text{R} = \text{C}_n\text{H}_{2n+1}$ ,  $n = 8, 12, 18$ ) were prepared.<sup>253</sup> Again, the thermal behavior consisted of a complicated thermodynamic melting and clearing behavior. However, the mesogenic character was depressed once compared to the analogous four-alkyl-chained derivatives which showed a

large domain of  $D_L$  phase ((23)). The octadecyl ( $n=18$ ) free-base, copper, and nickel compounds all behaved similarly, and exhibited a  $D_L$  phase at room temperature over a narrow temperature range, clearing at ca. 33–34°C. From this liquid, another mesophase,  $X_1$ , was formed, with unknown identity, which cleared at 58–63°C into a second liquid. Then, from this second liquid, another phase formed,  $X_2$ , which at last cleared into an isotropic liquid. This behavior appeared reversible for the three compounds, and seemed to be connected to the conformation of the side phenyl rings, which lie perpendicular to the aromatic core, disturbing the mesophase stability.



(25)

Tetra-substitution at the same *meso* positions of the porphyrin core by bulky *ortho*-terphenyl groups conferred to the macrocycle an overall macro-disk-like shape ((26):  $M=2H, Cu$ ).<sup>254</sup> In this case, both the free-base and the copper complex exhibited an enantiotropic  $Col_h$  phase from room temperature up to 59°C for the ligand and 57°C for the copper complex. The comparison between these macrocycles with the related phthalocyanine derivatives confirmed the perturbing role of the side groups on the stability of the  $Col_h$  phase, consequent to a disturbed molecular stacking. X-Ray diffraction suggested that the columns would be constituted by the stacking of dimer units, with a periodicity of about 9.5 Å.



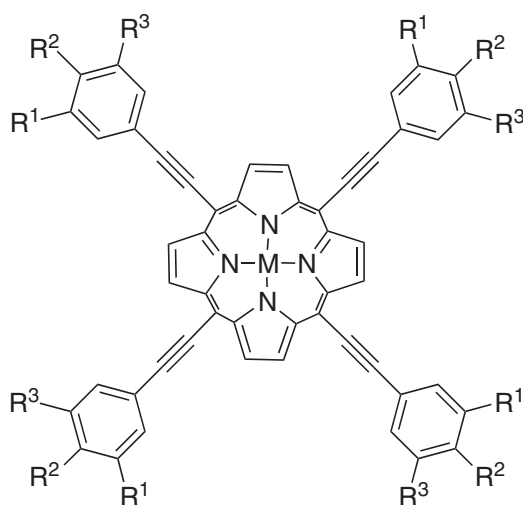
(26)

**Table 19** Mesomorphic properties of complexes (27).

Substituents	Mesomorphism
$R^1 = R^3 = H, R^2 = OC_9H_{19}$	Cr 149 M <sub>1</sub> 177 Col <sub>h</sub> 182 I
$R^1 = R^3 = OC_{10}H_{21}, R^2 = H$	Cr 107 M <sub>2</sub> 114 Col <sub>h</sub> > 250 dec.
$R^1 = R^2 = OC_{10}H_{21}, R^3 = H$	Cr 108 M <sub>3</sub> > 260 dec.

M<sub>1</sub>, M<sub>2</sub>, M<sub>3</sub>: unidentified mesophases.

Substituted 5,10,15,20-tetraarylethynylporphyrinatozinc complexes (Table 19) behaved as columnar discotic mesogens ((27): M = Zn,  $R^1, R^2, R^3 = OC_nH_{2n+1}$  or H).<sup>255</sup> The four-chain<sup>256</sup> and the eight-chain<sup>257</sup> compounds were synthesized prior to this investigation for their potential NLO activity due to the extended conjugation between the macrocycle and the aryl groups via the ethynyl bridges. The observation of a Col<sub>h</sub> phase for these systems was attributed to the presence of the ethynyl groups that confer planarity to the whole molecule, leading to some kind of macrodiscotic, flat molecules, able to stack on top of each other unlike the less planar alkylphenyl porphyrins described above.



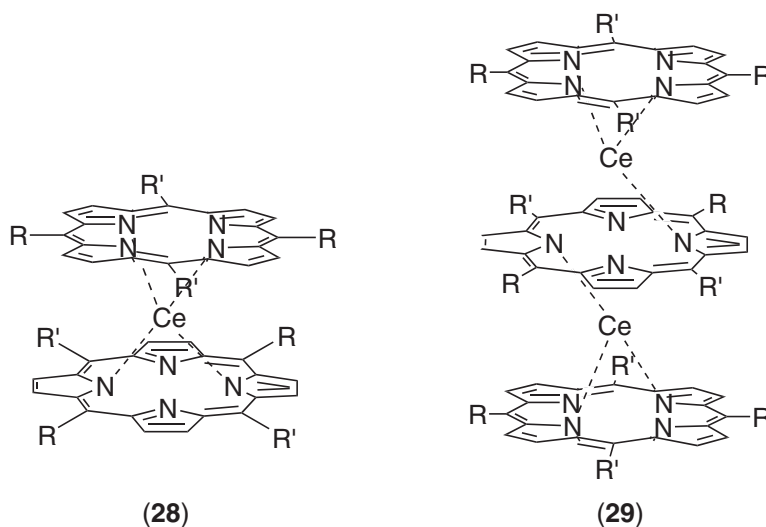
(27)

### 7.9.7.2.3 Lanthanide complexes of porphyrins

Selective complexation of di- and tetra-substituted porphyrins with cerium(III) ion led to novel double- and triple-decker sandwich complexes.<sup>258,259</sup> In such complexes, the two or three porphyrin macrocycles were rotated by ca. 20–45°. The various complexes were prepared by reaction of the parent porphyrins with cerium acetate.

Four different series of lanthanide compounds were prepared, and the progression of the mesomorphism from the free-base to the mononuclear and binuclear complexes was followed and analyzed. The first two series were concerned with 5,15-diarylporphyrins double-deckers ((28):  $R = C_6H_3(OC_nH_{2n+1})_2, R' = H$ ) and triple-deckers ((29):  $R = C_6H_3(OC_nH_{2n+1})_2/C_6H_3-(C_6H_4OC_{12}H_{25})_2/C_6H_3(C_6H_3(OC_nH_{2n+1})_2)_2, R' = H$ ). 5,15-Bis(dialkoxyphenyl) and 5,15-bis(dialkoxy-ortho-terphenyl) ligands showed lamello-columnar mesophases D<sub>L</sub> and D<sub>Lr</sub> respectively. The double-decker and triple-decker with the dialkoxyphenyl ligand still exhibited the D<sub>L</sub> phase, and both a D<sub>L</sub> and a Col<sub>r</sub>-p2gg mesophase (Table 20). The thermal behavior of the triple-decker complexes was investigated in more detail, and additional complexes were prepared, having ortho-terphenyl group. In such compounds, mesomorphism was either suppressed (di-alkoxy), or the Col<sub>r</sub> mesophase of the ligand transformed into Col<sub>h</sub> (tetra-alkoxy). 5,10,15,20-Tetrakis(dialkoxyphenyl)porphyrins displayed a D<sub>L</sub> phase, the double-deckers a Col<sub>r</sub> phase, whereas the triple-deckers were not mesomorphic (Table 20). All the mesophases were characterized by X-ray diffraction. The differences in mesomorphism were explained by differences in the steric hindrance

of the side chains for rotation along the axis connecting the center of the two or three porphyrins. Thus, in the di-substituted systems, complexation to cerium allowed for a mutual arrangement between the ligands to give an overall circular shape, developing a strong tendency to pack into columnar phases such as  $Col_r$  and  $Col_h$ , and, preferentially,  $D_L$  phases. However, this equilibrium was subtle since the aryl groups lay in perpendicular planes to the porphyrins. Appending additional bulky groups on the free *meso* positions ( $R'$ ) of the porphyrins allowed a stacking into  $Col_r$  for the double-deckers, but this arrangement was weakened in triple-decker, and mesomorphism suppressed (Table 20). Electrochemical and spectroscopic properties of the triple-decker complexes have also been reported.



Finally, the first mesomorphic lanthanide(III) monoporphyrin complex, i.e., hydroxy[5,10,15,20-tetra(*p*-decyloxy-*m*-methoxy)phenyl]porphyrin  $Yb^{III}$ , has recently been reported.<sup>260</sup> The complex was found to exhibit a  $Col_h$  phase between  $-11^\circ C$  and  $42^\circ C$ .

#### 7.9.7.2.4 Tetrabenzoporphyrins

A series of zinc benzoporphyrin complexes have been prepared and some of them were reported to be mesomorphic ((30):  $M = Zn$ ,  $R^1, R^2, R^3, R^4 = C_6H_4-OC_nH_{2n+1}$  or  $H$ ).<sup>261,262</sup> The structures of these benzoporphyrins were modified systematically by changing the substitution pattern at the *meso* positions of the macrocyclic ring. Thus, among all the tetra-5,10,15,20-, di-5,15-, tri-5,10,15-, di-5,10-, and mono-5-benzoporphyrinatozinc complexes prepared, only the tri-5,10,15-tris(alkoxy-phenyl)benzoporphyrin zinc complexes were found to be mesomorphic, although the mesophase was not identified: Cr 89 M 242 I for the decyloxy and Cr 41 M 229 I for the dodecyloxy derivatives.

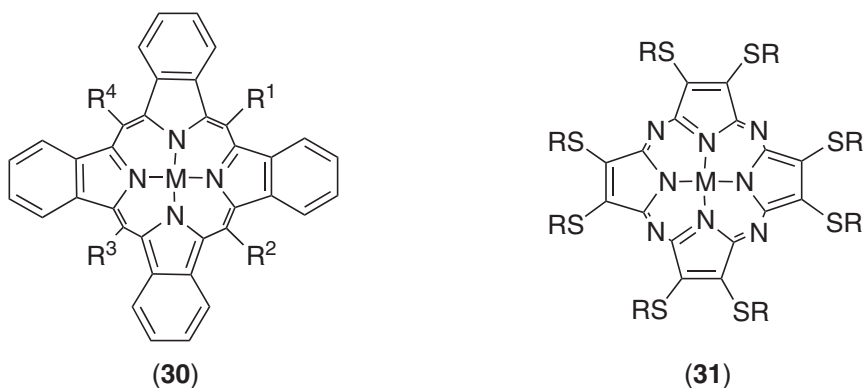


**Table 20** Transition temperatures of (28) and (29).

<i>R</i>	<i>R'</i>	Ligands <i>n</i> = 10	Double-deckers/28 <i>n</i> = 14	Triple-deckers/29 <i>n</i> = 10
	H	n = Cr 34 D <sub>L</sub> 214 I n = 12: Cr 60 D <sub>L</sub> 201 I n = 14: Cr 65 D <sub>L</sub> 183 I	n = 14: Cr 93 D <sub>L</sub> 106 I	n = 10: D <sub>L</sub> 104 Col, 148 I n = 12: D <sub>L</sub> 100 Col, 143 I n = 14: D <sub>L</sub> 106 Col, 136 I
	H	D <sub>Lr1</sub> 76 D <sub>Lr2</sub> 229 I		g 98 I
	H	n = 12: X 39 Col <sub>r</sub> 137 I n = 16: Col <sub>r1</sub> 70 Col <sub>r2</sub> 133 I		n = 12: g 104 Col <sub>h</sub> 158 I n = 16: Col <sub>h</sub> 49 Col <sub>h</sub> 127 I
		n = 8: Cr 126 I n = 10: Cr 111 I n = 12: Cr 100 (D <sub>L</sub> 67) I n = 16: Cr 93 (D <sub>L</sub> 44) I n = 18: Cr 99 (D <sub>L</sub> 55) I	n = 8: Col <sub>r</sub> 71 I n = 10: Col <sub>r</sub> 70 I n = 12: I n = 16: Col <sub>r</sub> 43.5 I n = 18: Col <sub>r</sub> 51 I	n = 10: I

X : unidentified solid phase.

## 7.9.7.2.5 Tetraazaporphyrins

It has been shown that small structural changes can have rather important effects on the physical and chemical properties of mesogenic compounds, and particularly on macrocyclic compounds (*vide supra*). Tetraazaporphyrins are one such macrocyclic compound, which can be regarded as porphyrins but where the methine bridges are replaced by aza bridges (*meso*-nitrogen atoms). They show excellent chemical, thermal, and photochemical stability, in addition to a rich coordination chemistry. The first liquid-crystalline metallotetraazaporphyrins were reported in 1990 by Doppelt.<sup>263</sup> Thus, copper, nickel, zinc, and cobalt 2,3,7,8,12,13,17,18-octakis-octylthiotetraazaporphyrins showed a  $\text{Col}_h$  phase, while the free-base compound was not mesomorphic. This result was soon confirmed by another group.<sup>264</sup> The study of the role of the chain length on the thermal behavior of four homologous series containing  $\text{Ni}^{\text{II}}$ ,  $\text{Cu}^{\text{II}}$ ,  $\text{Zn}^{\text{II}}$ , and  $\text{Co}^{\text{II}}$  was undertaken and revealed interesting features ((**31**):  $\text{M} = 2\text{H}$ ,  $\text{Ni}$ ,  $\text{Co}$ ,  $\text{Cu}$ ,  $\text{Zn}$ ,  $\text{R} = \text{C}_n\text{H}_{2n+1}$ ,  $n = 4, 6, 7, 8, 9, 10, 12$ ).<sup>265</sup> The starting product, 1,2-dicyano-1,2-bis(alkylthio)ethylene, was obtained by alkylation of the related sodium *cis*-1,2-dicyano-1,2-dithiolate species. The key step was the preparation of the macrocycle by a template reaction with  $\text{Mg}$ , which was then converted into the free base by treatment with trifluoroacetic acid. Metallacycles were obtained by complexation of the corresponding chloride salt. All the metalloporphyrins were mesomorphic, as well as only two free-bases, those with the shortest chain length ( $n = 4$  and  $6$ ). Metal complexation thus both induced and stabilized mesomorphism in this series of compounds, although the mesophase stability was decreasing on increasing the chain length, essentially due to the depression of the clearing temperatures, whatever the metal center. Within homologous series of metal complexes, the highest mesophase stability was found for the cobalt, followed by copper, zinc, and nickel complexes, i.e., the mesophase stability increased in relation to the capability of the metal ion to show axial coordination (Figure 30). The mesophase of the complexes was identified as  $\text{Col}_h$  for all complexes with  $n \geq 7$ , and for the  $\text{Ni}^{\text{II}}$ ,  $\text{Cu}^{\text{II}}$ ,  $\text{Zn}^{\text{II}}$  complexes with  $n = 6$ . For the shorter-length systems and the  $\text{Co}^{\text{II}}$  complex with  $n = 6$  (and the free bases), X-ray diffraction indicated that the columns were packed in a non-hexagonal fashion, the nature of which phase was not determined. The alignment of the columns in the liquid-crystalline phase of the decylthio derivatives has been investigated, and revealed an orientational behavior depending on the diamagnetic or paramagnetic nature of the metal ion.<sup>266</sup>

A series of related metallazaazaporphyrins has been studied which differ from the previous examples by the structure of the peripheral chains, which are alkenylsulfanyl groups ((**31**):  $\text{M} = 2\text{H}$ ,  $\text{Ni}$ ,  $\text{Co}$ ,  $\text{Cu}$ ,  $\text{R} = \text{C}_n\text{H}_{2n-1}$ ,  $n = 4-6, 7, 8$ ).<sup>267</sup> Thus, the presence of a terminal double bond in the peripheral chains did not preclude mesophase formation, as all the metal complexes exhibited mesomorphism, in addition to the free-base compounds with  $n = 4$  and  $5$  (Figure 31). Overall, the presence of the terminal double bond reduced the thermal range of the mesophase,

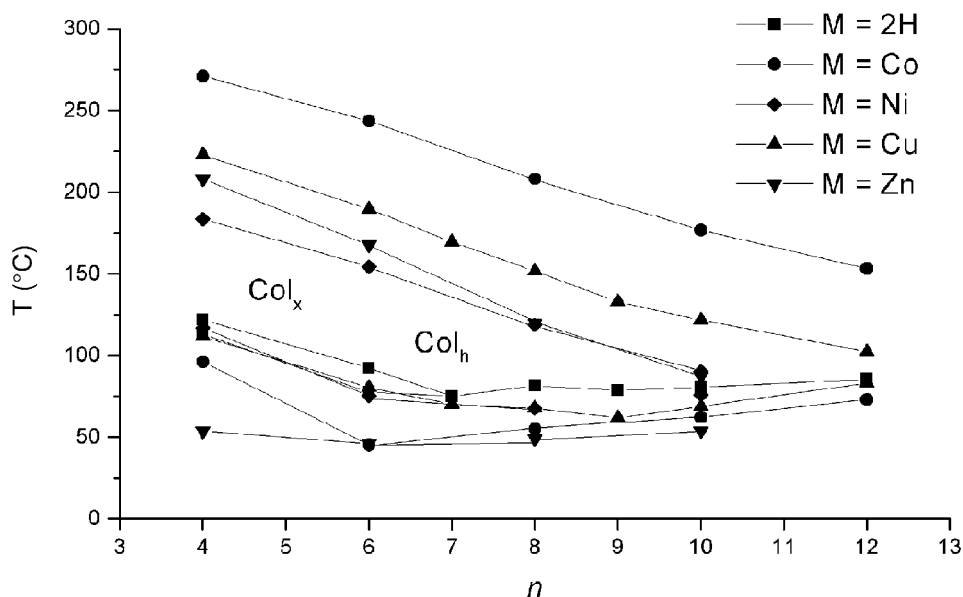


**Figure 30** Mesmorphism of the free-base, copper, nickel, zinc, and cobalt 2,3,7,8,12,13,17,18-octakis-octylthiotetraazaporphyrins (**31**).

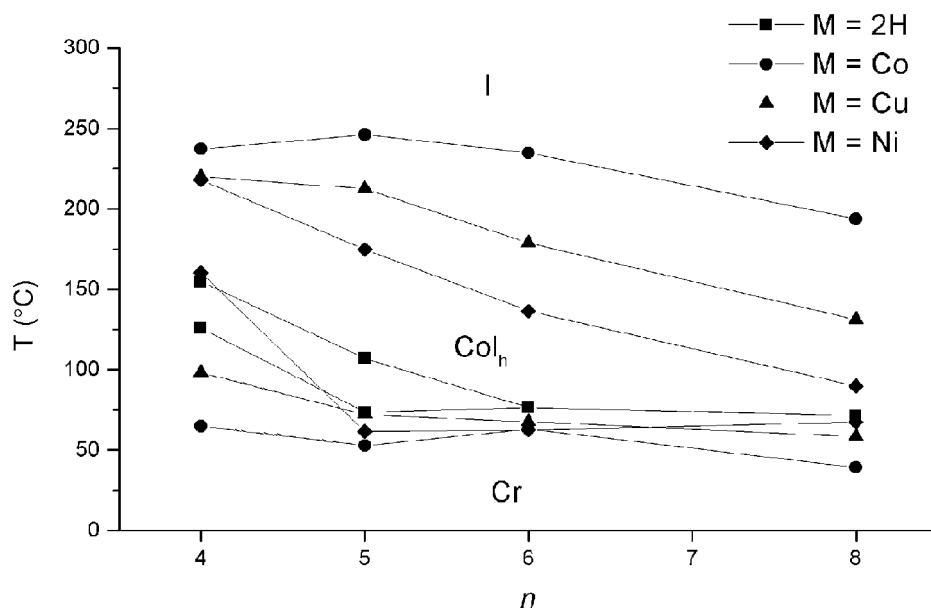


**Figure 31** Mesomorphism of the free-base, copper, nickel, and cobalt 2,3,7,8,12,13,17,18-octakis-alkenyl-sulfanyl tetraazaporphyrins (**31**).

particularly acting on the isotropization temperatures of the free-base macrocycles and the nickel and copper complexes. The same tendency concerning the relationships between metal and mesomorphic temperature range was found here when compared to the materials with saturated chains, although the higher thermal stability of the cobalt complexes was attributed (without any experimental evidence) to the possibility of intra-columnar cobalt–sulfur interactions between successive rings. The free-base compound exhibited what is probably a nematic discotic phase, on the basis of both the texture and the X-ray diffraction data. All the metal complexes showed a  $Col_h$  phase, and for the  $Cu^{II}$  complexes with  $n=4$  and 8, and for the  $Ni^{II}$  and  $Co^{II}$  with  $n=8$ , an additional mesophase was observed below the  $Col_h$  phase. The transition between these two mesophases was detected by optical microscopy and X-ray diffraction, but not by DSC.

Amphiphilic tetraazaporphyrins substituted by eight 3,6-dioxaheptylthio and 3,6,9-trioxaheptylthio chains and the corresponding metal complexes have recently been reported ((**31**):  $M = 2H, Co, Ni, Cu, Zn, R = S(CH_2CH_2O)_xCH_3$ ).<sup>268</sup> All the metal complexes except the  $Zn^{II}$  compounds were mesomorphic, showing a  $Col_h$  phase (Table 21). As expected from the previous systems described, the free-base porphyrins did not show mesomorphism either. The short-chain compounds were mesomorphic above room temperature, except for the  $Co^{II}$  complex, which was liquid crystal below 0 °C and over rather a large temperature range. Substantial destabilization of the mesophase was observed for the longer-chain homologs as evidenced by an important decrease in the clearing temperatures, as well as in the crystalline phase stability, since the complexes were mesomorphic below ambient temperature. Again, the cobalt complexes within each series had the highest mesophase stability. Note also that the long-chain compounds spontaneously aligned homeotropically between glass plates, while the shorter-chain-length homologs did not. At 30 °C, polar solvents such as dibutyl ether, 1,2-dimethoxyethane, and methanol, and the apolar  $CS_2$ , dissolved all the complexes to form isotropic solutions, while they were insoluble in decane and

**Table 21** Transition temperatures of (**31**).

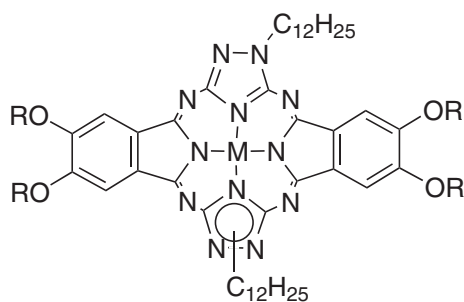
$M$	$R = S(CH_2CH_2O)_2CH_3$	$R = S(CH_2CH_2O)_3CH_3$
2H	Cr 55 I	Cr –34 I
Ni	Cr 44 ( $Col_x$ 35) $Col_h$ 115 I	Cr –33.5 $Col_x$ 10 $Col_h$ 170 I
Co	Cr –5.5 $Col_h$ 170 I	Cr –76 $Col$ 64 I
Cu	Cr 61 $Col_h$ 152 I	Cr –16 $Col_h$ 56 I
Zn	g –51 I	g –64 I

$Col_x$  : unidentified columnar phase.

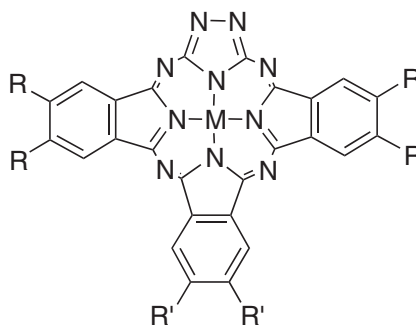
hexadecane. Water and ethylene glycol dissolved only the long-chain derivatives and, despite the formation of *H* aggregates, there was no formation of additional lyotropic mesophase before their complete dissolution in the solvent at higher temperature. Contact preparations of the short-chain  $\text{Co}^{\text{II}}$ ,  $\text{Ni}^{\text{II}}$ , and  $\text{Cu}^{\text{II}}$  complexes showed, however, that they can incorporate small amounts of hexadecane, decane, and ethylene glycol without changing the nature of the thermotropic mesophases, but with a drastic reduction of the clearing temperatures by about 50 °C. Despite the absence of novel mesophase induction, such as the columnar nematic phase, this approach nevertheless opens new opportunities for the processing of these materials. The film-forming properties of some derivatives has also been investigated by spin-coating and Langmuir–Blodgett techniques.

### 7.9.7.3 Triazolehemiporphyrazine and Triazolephthalocyanine Complexes

Novel, metal-free, and nickel and copper complexes of hexasubstituted triazolehemiporphyrazine have been reported.<sup>269</sup> Such macrocycles can be seen as a phthalocyanine analog in which two isoindole sub-units have been replaced by two 1,2,4-triazole moieties. Two series differing in the nature of the four side chains ((32):  $M = 2\text{H}$ ,  $\text{Cu}$ ,  $\text{Ni}$ ,  $R = \text{OC}_{12}\text{H}_{25}$  or  $\text{CH}_2\text{CON}(\text{C}_8\text{H}_{17})_2$ ) were prepared, and their thermal behavior compared. The synthesis of the metal-free macrocycles consisted of the condensation of 1-dodecyl-3,5-diamino-1,2,4-triazole with the corresponding 1,3-diiminoisoindoline. They were obtained as mixtures of the two regioisomers, *cis* and *trans*, due to the relative orientation of the dodecyl chain on the triazole moiety. In dilute conditions, one compound was obtained as the pure *trans* isomer. The compounds with four dodecyloxy side chains displayed a  $\text{Col}_h$  phase, demonstrated by X-ray diffraction, from just above room temperature up to 175 °C for the free-base derivative and up to 300 °C for the metal complexes (Table 22). The melting temperatures were relatively insensitive to the presence of the metal or its nature, while their incorporation into the center of the macrocycle raised the clearing temperature by about 150 °C. This enhancement of the mesophase stability was attributed to strong, intermolecular, dative associations that involve the metal. The UV–vis spectra of the  $\text{Cu}$  and particularly of the  $\text{Ni}$  complexes showed a substantial bathochromic shift of the highest wavelength band indicating a strong tendency to aggregate. Owing to the non-cylindrical shape of the compounds, the hexagonal symmetry of the mesophase implied an orthogonal stacking of the molecules (i.e., adjacent complexes are mutually rotated by 90°) or a rotationally averaged structure which induced an apparent circular molecular shape. Replacing the alkoxy groups by dialkylamide groups suppressed the mesomorphism totally, probably due to stronger steric demands which disrupted the regular stacking in columns (Table 22).



(32)



(33)

**Table 22** Transition temperatures of complexes (32).

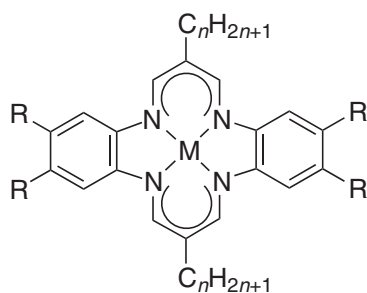
<i>M</i>	$R = \text{OC}_{12}\text{H}_{25}$	$R = \text{CH}_2\text{CON}(\text{C}_8\text{H}_{17})_2$
2H	Cr 39 $\text{Col}_h$ 165-175 I	Cr 157 I / Cr 177 I ( <i>trans</i> )
Cu	Cr 40.5 $\text{Col}_h$ 313 I	Cr 170 I
Ni	Cr 37 $\text{Col}_h$ 304 I	Cr 158 I



The closely related complexes based on the triazolephthalocyanine core were also found to be mesomorphic.<sup>270</sup> This macrocycle can be seen as a phthalocyanine analog in which one isoindole sub-unit has been replaced by a 1,2,4-triazole moiety. Both statistical and stepwise template syntheses were employed to prepare these compounds.<sup>271</sup> The hexa-alkoxy derivatives ((33):  $M = \text{Cu, Ni}$ ,  $R = R' = \text{OC}_8\text{H}_{17}$ ,  $\text{OC}_{12}\text{H}_{25}$ ) exhibited a very viscous, room-temperature mesophase characterized as  $\text{Col}_h$  by X-ray diffraction, and no change could be detected up to  $400^\circ\text{C}$ . The replacement of two alkoxy chains by dialkyl amide groups ((33):  $M = \text{Ni}$ ,  $R = \text{OC}_8\text{H}_{17}$ ,  $R' = \text{OCH}_2\text{CON}(\text{C}_8\text{H}_{17})_2$ ) did not alter the nature of the mesophase, but the clearing point could now be observed ( $200^\circ\text{C}$ ). However, complete substitution of the alkoxy chains by dialkyl-amide groups ((33):  $M = \text{Ni}$ ,  $R = R' = \text{OCH}_2\text{CON}(\text{C}_8\text{H}_{17})_2$ ) led to an important depression of the clearing temperature, in addition to the suppression of the mesomorphism, consistent with the above results.

#### 7.9.7.4 Tetraaza[14]annulenes

Metal complexes of disk-like or hexasubstituted annulenes ((34):  $M = \text{Co, Cu, Ni, Pd, Pt}$ ;  $n = 4, 6, 8, 10, 15$ ;  $R = \text{OC}_m\text{H}_{2m+1}$ ,  $m = 4, 6, 8, 10, 12, 14$ ), first synthesized in 1985 by Hunziker, were found to form columnar mesophases.<sup>272</sup> The various complexes showed a rather good thermal stability, and decomposition was not observed, even in the isotropic liquid. The thermal behavior of 33 new macrocyclic compounds was analyzed as a function of length and nature of the side chains, as well as the metal ions. The thermal behavior of some selected compounds is shown in Table 23. The mesophases belonged to the columnar type, and on average, increasing the dissymmetry between the alkyl and alkoxy side chain length resulted in the diminution of the transition temperatures, with reduction in mesophase stability, and even the total suppression of mesomorphism. The metal ion appeared to have some influence, too, mainly on the clearing temperatures. The mesomorphism was destabilized with the replacement of the four lateral alkoxy chains with alkyl chains ((34):  $M = \text{Ni}$ ;  $n = 6, 8$ ;  $R = \text{C}_9\text{H}_{19}$ ), or alkanoate chains ((34):  $M = \text{Ni}$ ;  $n = 8, 10$ ;  $R = \text{CO}_2\text{C}_8\text{H}_{17}$ ). When the R groups were ethylene oxide chains, the mesophase became metastable and were suppressed totally on increasing both the length of the alkyl and ethylene oxide chains ((34):  $M = \text{Ni}$ ;  $n = 6, 8, 10$ ;  $R = \text{OCH}_2\text{CH}_2\text{OC}_2\text{H}_5$ ,  $\text{O}[\text{CH}_2\text{CH}_2\text{O}]_2\text{CH}_3$ ).



Veber and co-workers have investigated the mesomorphic behavior of a related family of nickel(II) complexes of dibenzo[*b,i*] [1,4,8,11]tetraaza[14]annulenes (35), bearing four,<sup>273</sup> six, and eight<sup>274,275</sup> peripheral chains. The disk-like nickel complexes were prepared by a template reaction

**Table 23** Transition temperatures of complexes (34).

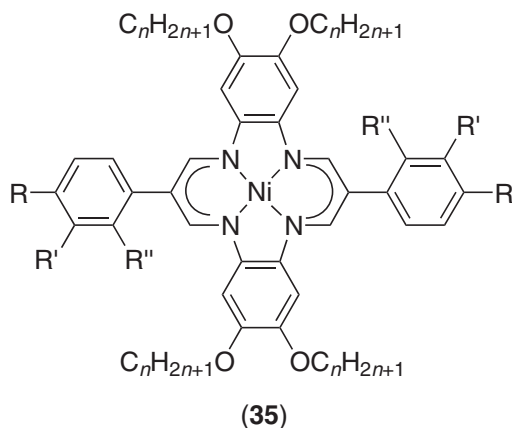
<i>M</i>	<i>n</i>	<i>R</i> = $\text{OC}_6\text{H}_{13}$	<i>n</i>	<i>M</i> = Ni, <i>R</i> = $\text{OC}_8\text{H}_{17}$	<i>n</i>	<i>M</i> = Ni, <i>R</i> = $\text{OC}_{12}\text{H}_{25}$
Ni	6	Cr 131 Col 204 I	4	Cr 146.5 Col 150 I	6	Cr 132 (Col 122) I
Pd	6	Cr 136 Col 239 I	6	Cr 132 Col 171 I	8	Cr 128 I
Pt	6	Cr 153 Col 213 I	8	Cr 137 Col 184 I	10	Cr 119 Col 139 I
Co	6	Cr 128 Col 216 I	10	Cr 118 Col 182 I		
Cu	6	Cr 123 Col 242 I				

Col : unidentified columnar phase.

**Table 24** Thermotropic behavior of (35).

$n$	$R = R' = R'' = H$	$R = OC_nH_{2n+1}, R' = R'' = H$	$R = R' = OC_nH_{2n+1}, R'' = H$
8	Cr 112 Col <sub>h</sub> 349.5 I	Cr 26 Col <sub>h</sub> 370 dec.	Col <sub>h</sub> > 200 I
10	Cr 107 Col <sub>h</sub> 340 dec.	Col <sub>h</sub> > 330 dec.	Col <sub>h</sub> 260 I
12	Cr 99 Col <sub>h</sub> 332 I	Cr 24 Col <sub>h</sub> > 300 dec.	Cr 18 Col <sub>h</sub> 250 I

of the corresponding vinamidinium salts, bis-(4,5-dialkoxy)orthophenylenediamine, in the presence of nickel acetate;<sup>276</sup> under non-template conditions, the free macrocycle could be isolated. All the nickel complexes prepared this way displayed a Col<sub>h</sub> mesophase over very broad temperature ranges. The ligand with four dodecyloxy chains was itself mesomorphic (Cr 97 Col<sub>h</sub> 209 I), and while the number of chains did not affect the type of mesophase, it modified the transition temperatures markedly. On increasing the number of side chains from four to eight (Table 24), both the melting and clearing points decreased gradually. While the six- and eight-chain compounds were room-temperature liquid-crystal materials ((35):  $R = OC_nH_{2n+1}, R' = R'' = H$  and  $R = R' = OC_nH_{2n+1}, R'' = H$ ), the melting temperatures of the four-chain systems ((35):  $R = R' = R'' = H$ ) first dropped rapidly (from 270 °C to 160 °C), and then smoothly for longer-chain derivatives (for  $n > 7$ , Cr 130 to 100 °C Col<sub>h</sub>). The clearing temperatures still remained high (>250 °C) irrespective of the number of aliphatic chains, and decomposition often occurred before reaching the isotropic liquid. Such high clearing temperatures, and consequently high mesophase stabilities, were due to very efficient  $\pi$ - $\pi$  stacking interactions between successive, extended, mesogenic cores in the columns as revealed by the systematic presence of a diffuse peak at around 3.5 Å in the X-ray pattern of each compound. In order to prove that such interactions were essential in promoting mesomorphism, a six-chain compound with two of the chains in the *ortho* position of the axial phenyl groups was synthesized ((35):  $R = R' = H, R'' = OC_{12}H_{25}, n = 12$ ), and, as expected, was not mesomorphic (Cr 122 I). This experiment clearly proved that the stacking was disturbed by the interpenetration of the lateral chains within the aromatic core area, resulting in the suppression of the mesomorphism and also in the reduction of the clearing temperature. An optical storage effect was also demonstrated successfully in one of the eight-chain compounds ((35):  $R = R' = OC_{10}H_{21}, n = 10$ ).<sup>277</sup>

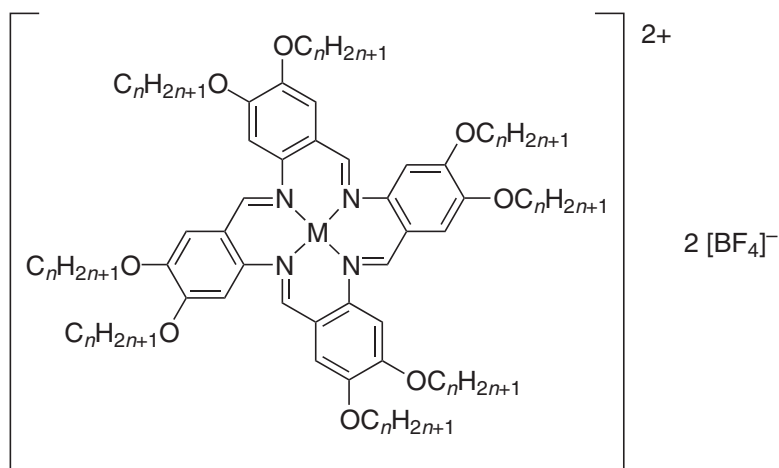


### 7.9.7.5 Tetraaza[14]cyclohexadecanes

Recently, another new family of ionic macrocycles<sup>278</sup> and their corresponding metal complexes<sup>279</sup> derived from tetrabenzo[*b,f,j,n*] [1,5,9,13]tetraazacyclohexadecane (36:  $M = Cu, Ni, Pd; n = 10, 12, 14, 16, 18$ ) have been reported. The tetrafluoroborate salt of the diprotonated octaalkoxy macrocycle was prepared by the self-condensation of 3,4-dialkoxy-2-aminobenzaldehydes in the presence of  $HBF_4$ , and the metal complexes were then obtained by reaction with the appropriate metal acetate. The metal-free macrocycles ((36):  $M = 2H, n = 8, 10, 12$ ) investigated previously by Kim *et al.* displayed a Col<sub>h</sub> phase from room temperature up to temperatures above 250 to 270 °C, depending on the chain length. The formation of columnar phases was, therefore, expected for the corresponding metal complexes. Indeed, they all showed an enantiotropic Col<sub>h</sub>

**Table 25** Thermotropic behavior of (36).

$n$	$M = Cu$	$M = Ni$	$M = Pd$
10	Col <sub>h</sub> 196 I	Col <sub>h</sub> 290 I	Col <sub>h</sub> 261 I
14	Cr 26 Col <sub>h</sub> 190 I	Cr 28 Col <sub>h</sub> 265 I	Col <sub>h</sub> 238 I
18	Cr 66 Col <sub>h</sub> 183 I	Cr 51.5 Col <sub>h</sub> 234 I	Cr 49 Col <sub>h</sub> 201 I



(36)

phase but with some alteration of the mesophase stability upon metallation. The mesophase occurred at or near room temperature ( $n = 10$  to 14) and at around 40–60° ( $n = 16, 18$ ) with clearing temperatures in the range 196–183 °C for the copper complexes, 290–234 °C for the nickel analogs, and 261–201 °C for the palladium congeners; these temperatures decreased as  $n$  increased from 10 to 18 (Table 25). The mesophase stability was thus reduced upon complexation to copper, was almost unchanged with palladium, and increased for nickel. Geometric arguments, such as the size of the metal ions, were used to try to rationalize these effects and the possibility of forming dative interactions between neighboring molecules cannot be excluded, nor can electrostatic interactions due to the charged nature of the mesogen. Whereas in the metal-free ligands a peak corresponding to regular stacking was observed by X-ray diffraction implying appreciable core-to-core interactions, this was absent in the metal complexes. Thus, mesophase stability seemed to be influenced by the ability of the anions to be located close to the central metal ion, or even to intercalate between the macrocycles to form ion pairs, in agreement with the increased separation between the mesogenic cores.

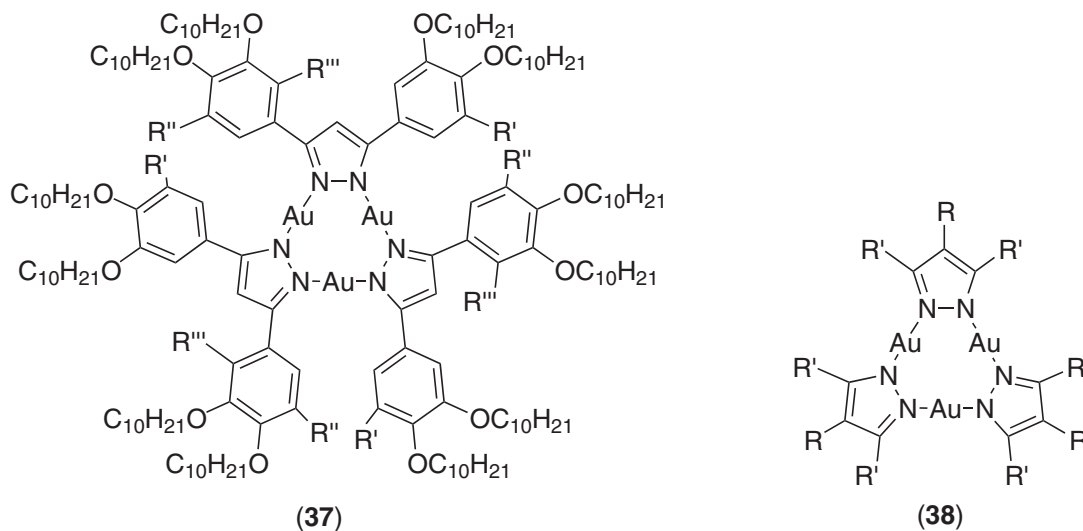
#### 7.9.7.6 Metallacrown Complexes

Metallacrowns,<sup>280</sup> rough analogs of organic crown ethers which contain a metal atom in the ring, represent a new genre of research in the field of metallomesogens. Oro and co-workers reported the first mesogenic metallacrowns in 1996, namely tri( $\mu$ -pyrazolato- $N,N'$ )trigold(I) complexes.<sup>281</sup> The design of such mesogenic species was based on the ability of group 11 metals to form trimers such as  $[ML]_3$  with pyrazolate ligands. The trinuclear gold complexes were prepared by reaction of  $[AuCl(tht)]$  with the appropriate pyrazolate ligand; the ligand was prepared *in situ* and was substituted by two aromatic rings, with a variable number of alkoxy chains.<sup>282</sup> Although the parent ligands were not mesomorphic, the four trinuclear gold complexes were, either at or near to room temperature ((37):  $N = 12$ :  $R' = R'' = R''' = H$ ;  $N = 15$ :  $R' = OC_{10}H_{21}$ ,  $R'' = R''' = H$ ;  $N = 18$ :  $R' = R''' = OC_{10}H_{21}$ ,  $R'' = H$  and  $R' = R'' = OC_{10}H_{21}$ ,  $R''' = H$ ; thermal data collected in Table 26). The complexes with 12 and 15 chains supercooled and crystallization took place only after several hours or sometimes weeks. The mesophase of the four metallacrowns was identified clearly by X-ray diffraction as Col<sub>h</sub>, with an average short-range correlation of 4.4 Å. Such a

**Table 26** Mesomorphic properties of compound (37).

		Number of chains ( <i>N</i> ) and molecular symmetry
$R' = R'' = R''' = H$	Cr 59 Col <sub>h</sub> 64 I	$N = 12, D_{3h}$
$R' = OC_{10}H_{21}, R'' = R''' = H$	Cr 36.5 Col <sub>h</sub> 59 I	$N = 15, C_{3h}$ and $C_s$
$R' = R''' = OC_{10}H_{21}, R'' = H$	Col <sub>h</sub> 22 I	$N = 18, C_{3h}$ and $C_s$
$R' = R'' = OC_{10}H_{21}, R''' = H$	Cr 35 Col <sub>h</sub> 58 I	$N = 18, D_{3h}$

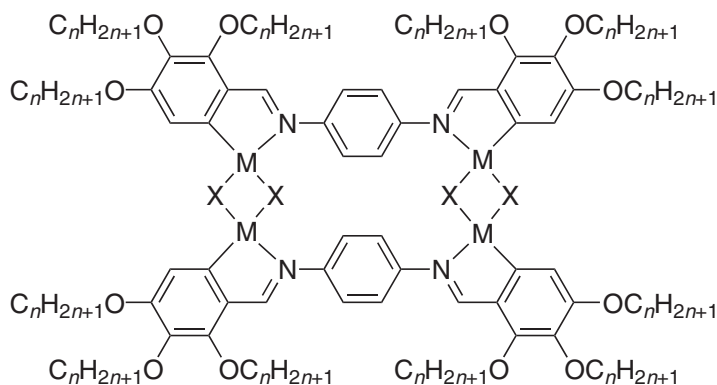
stacking distance indicated that the macrocycles were mutually rotated in such a way that the gold atoms interact with the pyrazole rings of neighboring macrocycles. A single-crystal X-ray structural analysis of the hexamethoxy derivative revealed that the supramolecular columnar arrangement existed in the crystalline state, with a repeat distance of 9.4 Å between complexes; the molecules crystallized in an orthorhombic cell. The comparison of the thermal behavior of the four complexes indicated that the increasing number of side chains ( $N = 12, 15,$  and  $18$ ) and the resulting off-plane distortion of the lateral groups with respect to the metallacrown was associated with reduction in both melting and clearing temperatures. The reduction in molecular symmetry by the non-equivalent chain substitution, and the consequent existence of regio isomers, also contributed to the mesophase destabilization. The unequally substituted complexes with  $N = 15$  and  $18$  were found to exist as a mixture of two geometric isomers ( $C_{3h}$  and  $C_s$ ) in 1:3 ratio as deduced from  $^1H$ -NMR studies, while the compounds with  $N = 12$  and  $18$  and with symmetrical substitution possessed a unique molecular symmetry,  $D_{3h}$ , and thus existed as single isomers. Therefore, for these unsymmetric compounds, the interactions between the molecules were probably more hindered and perturbed than for the symmetrical ones, leading to the reduction of the mesophase stability.



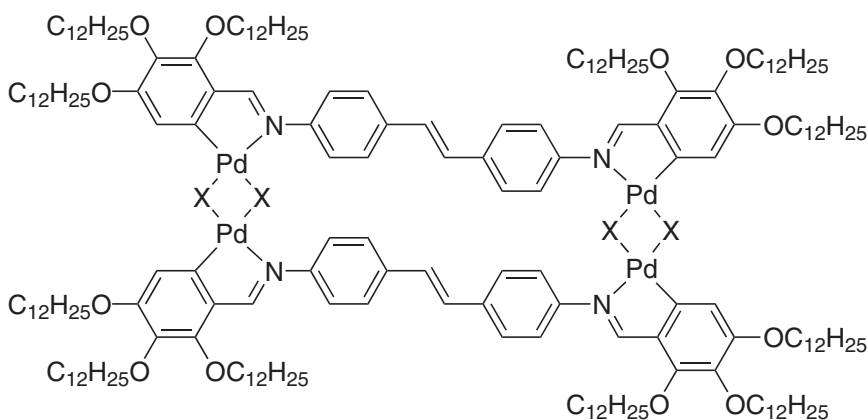
Mesomorphism could also be induced in less heavily substituted systems as evidenced by the report on other gold-pyrazone metallacrowns with only three long side chains ((38):  $R = C_nH_{2n+1}$ ,  $n = 7-9, 11$ ,  $R' = CH_3$ ), the one with six chains being non-mesomorphic ((38):  $R = H$ ,  $R' = C_8H_{17}$ ).<sup>283</sup> The compounds with the shortest chain length ( $n = 7, 8$ ) exhibited a monotropic, Col<sub>h</sub> phase (Cr 116 (Col<sub>h</sub> 112) I and Cr 112 (Col<sub>h</sub> 85) I respectively), while, and quite surprisingly, the other homologs with longer chains were not mesomorphic, clearing at 90 to 80 °C. A crystal structure of the six-chained octyl complex was obtained and revealed interesting features. It showed that the trinuclear gold complex formed a dimer, mainly through intermolecular Au–Au contacts (3.255 Å), and that the two macrocycles were in a staggered conformation. The molecular packing consisted of the stacking of this star-shaped dimer with six side chains, into columns, with a tilt with respect to the axis. In the mesophase the stack occurred without tilting, and the Col<sub>h</sub> phase was formed. It is likely that the dimers were kept within the mesophase, in which intermolecular Au–Au interactions may play an important role.

## 7.9.7.7 Macroheterocyclic Tetrametallo-organyls

Praefcke and co-workers have carried out important research on the tetrapalladium<sup>284–286</sup>, and tetraplatinum<sup>287,288</sup> organyls (**39**) and (**40**), derived from polycatenar bis(imine)phenylene, and the nematogenic<sup>289</sup> bis(imine)stilbenylene ligands. These  $[M_4(\mu^2-X)_4L_2]$  complexes were prepared by *ortho*-metallation of the appropriate diimine with palladium acetate or di- $\mu$ -chloro-bis- $[(\eta^3-2\text{-methylallyl})\text{platinum}]$ , followed by an acidic treatment to form the chloro-bridged compounds. The other complexes were obtained by ion-exchange reactions with the KBr, KI, and KSCN. The final structure of the complexes was confirmed by osmometry, single-crystal X-ray structure ((**39**): M = Pd, Pt, X = OAc, Cl, Br, I, SCN, N<sub>3</sub>; (**40**): X = Cl, Br, I, OAc, SCN), in addition to classical spectroscopic techniques. These large tetrametallaorganyls, with twelve alkoxy chains in the 2-, 3-, and 4-positions of each terminal ring, were thermotropic mesogens showing large-temperature-range columnar mesophases with either a rectangular or oblique lattice (Table 27).<sup>290,291</sup> The nature of the bridging group had some influence on these properties, as did the chain length and the length of the rigid spacer (phenylene, (**39**) or stilbenylene, (**40**) groups), whereas the metalion, Pd<sup>II</sup> or Pt<sup>II</sup>, appeared to have only minor effects. In the case of the benzylidene derivatives (**39**), the number of chains was reduced to eight by substituting in positions 2 and 3 ( $n = 12, 18$ ), or 2 and 4 ( $n = 12$ ). No change in the mesomorphism was detected and only changes in the transition temperature were observed (Cr 106 Col<sub>r</sub> 200 Col<sub>r</sub> 295 I, Cr 94 Col<sub>r</sub> 200 Col<sub>r</sub> 254 I, and Cr 93 Col<sub>r</sub> 257 I, respectively).



(39)



(40)

In addition to this thermotropic mesomorphism, the complexes formed lyotropic mesophases when dissolved in linear, lipophilic solvents such as alkanes, and in chloroform, benzene, octanol, octadecanol, and stearic acid.<sup>292–295</sup> In alkanes, the mesophases were stable over wide ranges of temperature and concentration. In general, at high complex concentration, a columnar phase was

**Table 27** Mesomorphic properties of the tetrametallo-organyls (**39**).

<i>M</i>	<i>n</i>	<i>X</i>	<i>Thermotropic phase</i>	<i>Lyotropic phase</i>
Pd	6	Cl	Cr 101 Col <sub>r</sub> ( <i>c2mm</i> ) 329 dec.	Col <sub>h</sub> , N in heptane, pentadecane, eicosane
		Br	Cr 103 Col <sub>o</sub> 306 dec.	Col <sub>h</sub> , N in heptane, pentadecane, eicosane
		I	Cr 123 Col <sub>o</sub> 306 dec.	Col <sub>h</sub> , N in heptane, pentadecane, eicosane
	8	Cl	Cr 76 Col <sub>r</sub> ( <i>c2mm</i> ) 320 dec.	No information
	10	Cl	Cr 55 Col <sub>o</sub> 220 M 316 I	Col <sub>h</sub> , N <sub>2</sub> in pentane, hexane, nonane Col <sub>h</sub> , N <sub>2</sub> , (N <sub>1</sub> ) in decane Col <sub>h</sub> , N <sub>2</sub> , N <sub>1</sub> in dodecane, tridecane, pentadecane, heptadecane
			Cr 70 Col <sub>r</sub> ( <i>c2mm</i> ) 298 dec.	Col <sub>h</sub> , N <sub>2</sub> in pentane, hexane, nonane, decane Col <sub>h</sub> , N <sub>2</sub> , (N <sub>1</sub> ) in dodecane Col <sub>h</sub> , N <sub>2</sub> , N <sub>1</sub> in pentadecane, heptadecane
	12	Cl	Cr 69 Col <sub>o</sub> 279 dec.	Col <sub>h</sub> , N <sub>1</sub> , N <sub>2</sub> in pentadecane, eicosane
			Cr 62 Col <sub>o</sub> 265 dec.	Col <sub>h</sub> in pentadecane, no N
			Cr 71 M <sub>1</sub> 114 M <sub>2</sub> 230 dec	No mesophase in alkane
			Cr 50 Col <sub>o</sub> 290 dec.	Col <sub>h</sub> , N in pentadecane
			Cr 60 M <sub>1</sub> 87 Col <sub>r</sub> 150 dec.	Col <sub>h</sub> in pentadecane, no N
	14	Cl	Cr 74 Col <sub>r</sub> ( <i>c2mm</i> ) 200 Col <sub>r</sub> ( <i>p2gg</i> ) 277 I	Col <sub>h</sub> , N <sub>2</sub> in pentane, hexane, nonane, decane, dodecane Col <sub>h</sub> , N <sub>2</sub> , (N <sub>1</sub> ) in pentadecane Col <sub>h</sub> , N <sub>2</sub> , N <sub>1</sub> in heptadecane
			Cr 81 Col <sub>r</sub> ( <i>c2mm</i> ) 265 I	No information
			Cr 95 Col <sub>r</sub> ( <i>c2mm</i> ) 200 Col <sub>r</sub> ( <i>p2gg</i> ) 249 I	No information
Pt	6	Cl	Cr 100 Col <sub>o</sub> 357 dec.	Col <sub>h</sub> , (N) in pentane, hexane, heptane
		Br	Cr 111 Col <sub>o</sub> 341 dec.	Col, N in alkane
		I	Cr 107 Col <sub>o</sub> 328 dec.	Col, N in alkane
		SCN	Cr 69 M 308 dec.	No information
	12	Cl	Cr 70 Col <sub>o</sub> 280 dec.	Col <sub>h</sub> , N <sub>2</sub> , (N <sub>1</sub> ) in dodecane Col <sub>h</sub> , N <sub>1</sub> , N <sub>2</sub> in pentadecane, octadecane
			Cr 68 Col <sub>o</sub> 292 dec.	No mesophase in alkane
			Cr 55 Col <sub>o</sub> 297 dec.	Col <sub>h</sub> , N <sub>1</sub> in pentadecane
			Cr 17 Col <sub>o</sub> 286 dec.	No information

M, M<sub>1</sub>, M<sub>2</sub> : unidentified mesophases.

observed, while at lower concentration, a nematic phase was usually induced. Here again, the mesophase behavior depended strongly on some intrinsic structural parameters, such as the type of bridges and the nature of the metal ions. Thus, while mesophases were not induced or stabilized in any of the  $\mu$ -acetato complexes, the metal appeared to have more influence on the lyotropic properties. For example, the columnar phase was retained and two nematic phases were induced for the bromopalladium complexes ((**39**): X = Br, M = Pd, *n* = 12)/pentadecane mixture, while the analogous mixture with the platinum analog was not mesomorphic. Similarly, a nematic phase (along with a columnar phase) was induced for the iodoplatinum complex ((**39**): X = I, M = Pt, *n* = 12) in pentadecane, while the palladium congener displayed a columnar phase only. The length of the rigid spacer, and consequently the dimensions of the complex, also played an important role in the nature of the lyomesophase (Tables 27 and 28). Particularly for the phenylene complexes with chloride and bromide bridges, an unexpected transition, reversible with temperature, between two lyotropic nematic phases was detected on the basis of abrupt

**Table 28** Mesomorphic properties of the tetrapalladium organyls (**40**).

<i>X</i>	<i>Thermotropic phase</i>	<i>Lyotropic phase in pentadecane</i>
Cl	Cr 126 Col <sub>o</sub> 248 M <sub>2</sub> 270 dec.	Col <sub>h</sub> , N
Br	Cr 126 Col <sub>o</sub> 252 dec.	Col <sub>h</sub> , no N
I	Cr 98 Col <sub>o</sub> 244 dec.	Col <sub>h</sub> , N
OAc	Cr 44 M <sub>1</sub> 75 M <sub>2</sub> 143 dec.	No mesophase
SCN	Cr 54 M <sub>1</sub> 240 dec.	Col <sub>h</sub> , M, no N

M<sub>1</sub>, M<sub>2</sub> : unidentified mesophases.

textural changes. In addition to the columnar phase, a single-nematic phase was induced for the thiocyanato-bridged complex (**39**), but not for the iodo- and azido-bridged members ((**39**):  $M = \text{Pd}$ ,  $X = \text{I}$ ,  $N_3$ ). The extension of the rigid spacer clearly diminished the tendency for nematic phase induction (no thermotropic nematic phase for (**40**)), and suppressed totally the nematic polymorphism (only one lyotropic nematic phase for some complexes (**40**)). The transition between two nematic phases, being a unique case, was investigated thoroughly, and particularly complexes (**39**) ( $M = \text{Pd}$ ,  $X = \text{Cl}$ ,  $n = 6, 10, 12, 14$ ) in various alkanes. While the high-temperature nematic phase,  $N_2$ , was present in all mixtures, the appearance of the low-temperature nematic phase,  $N_1$ , seemed to be dependent on the chain length of the alkane solvent and that of the complex's terminal chains. Indeed, this study revealed that  $N_1$  occurred enantiotropically for long-chain alkane solvent, monotropically for equal length of alkane and alkoxy groups, but did not form for short-chain paraffins. Evidence for the two nematic phases was also provided by measurement of the birefringence, which showed a substantial fall at the transition (e.g., (**39**) with  $M = \text{Pd}$ ,  $X = \text{Cl}$ ,  $n = 14$  in 40 wt.% of heptadecane,  $\Delta n = 0.012$  in  $N_1$  at 58 °C and 0.007 in  $N_2$  at 60 °C), and by the investigation of some orientational properties. When the transition between these two nematic phases took place, in most cases both the mesophases co-existed in a biphasic region suggesting, therefore, a first-order transition, although this was not confirmed by DSC as enthalpy changes were not detected. A model for these two nematic phases was proposed recently.<sup>296</sup> On the basis of UV/vis spectroscopy and small-angle X-ray diffraction, the columnar nature of both nematic phases was confirmed, with the solvent located between columnar aggregates rather than between the complexes. Due to swelling, the columns were arranged with only weak inter-columnar order. The correlation length of the columns was not given, but there was no long-range, intra-molecular ordering. The large, flat metallorganyls were stacked on top of each other, and arranged perpendicular to the axis of the columns forming the  $N_2$  phase. In the  $N_1$  phase, however, the complexes were tilted with respect to the columnar axis. If such a model were true, the  $N_1$  phase would be a further example of a lyotropic biaxial nematic phase,<sup>297</sup> the only case reported so far being found in the ternary phase diagram constituted by potassium laurate/decanol/ $\text{D}_2\text{O}$ .<sup>298</sup>

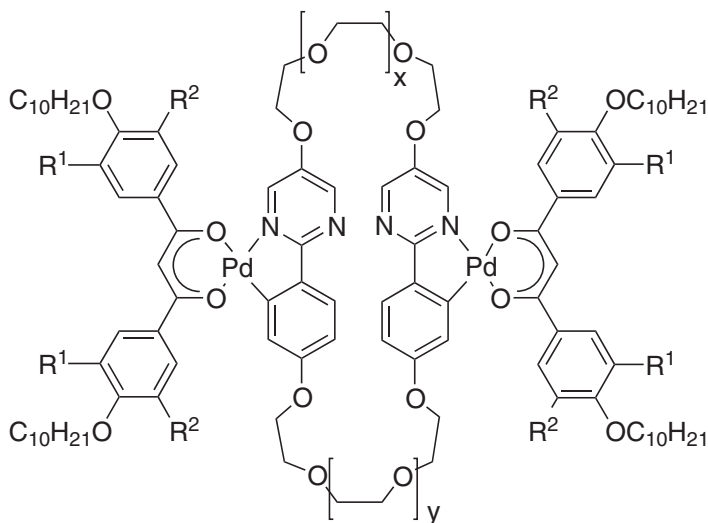
Thus, the extension of the aliphatic crown in these discotic metallomesogens by the incorporation of apolar aliphatic solvents enhanced the mesomorphic range by stabilizing the existing columnar phase, and favored the formation of more disordered mesophases such as the  $N_{\text{Col}}$  phase. The dependence of the mesomorphic properties on a combination of complex chain length and solvent chain length generated the idea of "internal" (i.e., complex chains) and "external" solvent (i.e., solvent chains)<sup>286</sup> and represents an interesting way of thinking about mesophase formation.

Formation of inclusion complexes caused by intercalation of small, electron-acceptor molecules, such as TNF (2,4,7-trinitro-9-fluorenone) and TAPA (2-(2,4,5,7-tetranitro-9-fluorenylidene-aminoxy)-propionic acid), between large, flat, electron-donor molecules has proved to be an original and effective means for mesophase induction, stabilization, and modification.<sup>299</sup> The stability of such charge-transfer complexes was connected to strong  $\pi$ - $\pi$  interactions between the donor and acceptor molecules, and has been shown to stabilize smectic phases by enhancing lateral interactions in calamitic systems, and columnar phases by improving columnar stacking in disk-like molecules. The tetrametallated organyls (**39**) and (**40**) discussed above, except those with an acetato bridge, also formed charge-transfer complexes with TNF, and gave rise to a viscous type of columnar phase on heating. X-Ray studies revealed a change from oblique/rectangular symmetry to a hexagonal lattice. The nematic lyomesophase stability was enhanced (higher clearing temperatures) in all systems, compared to the behavior of the pure complexes in pentadecane. One exception was found ((**40**):  $X = \text{SCN}$ ) which showed the same phase sequence as that observed in pentadecane in the absence of TNF. The columnar phase was still present in all cases. The structure of the different mesophases was characterized by X-ray diffraction, and confirmed the intercalation of TNF molecules in the columns formed by the planar complexes in both columnar phases. Induction of a chiral lyotropic nematic phase in a binary system composed of equimolar amounts of (**39**) and the chiral  $\pi$ -electron acceptor, TAPA (2'-(2,4,5,7-tetranitro-9-fluorenylidene-aminoxy)-propionic acid), in heptane, pentadecane, and eicosane, has been demonstrated.<sup>300</sup> As for non-chiral systems, the temperature range of the chiral nematic phase was found to increase concomitantly with the chain length of the solvent. Three different regions were separated: on decreasing the concentration of pentadecane, a biphasic N/I region was seen in dilute conditions, followed by a  $N^*/N$  biphasic region, and then by the  $N^*$  phase at lower solvent content. The chiral nematic phase existed over a large temperature range. Note that the helical pitch increased with increasing pentadecane content. This case study showed that charge-transfer interactions

with chiral electron acceptors is an efficient way to introduce chirality in lyotropic systems and opens new perspectives for producing chiral nematic phase in disk-like compounds.

### 7.9.7.8 Paracyclophanes

In order to create novel types of metallomesogens with new and unusual molecular shapes, Tschierske *et al.*<sup>301</sup> synthesized novel macrocyclic molecules combining two different molecular architectures; namely rod-like *para*-cyclophanes with two, half-disk-like 1,3- $\beta$ -diketonate units, fused together by *ortho*-palladation ((**41**):  $R^1, R^2 = \text{H}$  or  $\text{OC}_{10}\text{H}_{21}$ ;  $x, y = 1, 2, 3$ ). The macrocyclic cyclophane containing two phenylpyrimidine units were prepared using a standard, high-dilution, template-cyclization reaction. *Ortho*-palladation resulted in the formation of polymers, which were reacted with the appropriate Tl(I) 1,3- $\beta$ -diketonate to yield the final dinuclear complexes. The complexes were mesomorphic, with a smectic-to-columnar phase cross-over observed on increasing the chain number, concomitantly with an important decrease of the transition temperatures (Table 29). The paracyclophane units themselves were mesomorphic, but showed only monotropic mesophases, below 150–160 °C. The four-chain compound exhibited an SmA phase over a narrow temperature range, whereas those with twelve chains displayed an enantiotropic,  $\text{Col}_h$  phase, whatever the length of the polyether chains connecting the two central phenylpyrimidine moieties. While in this series the melting points were not changed, differences in the mesophase stability were observed as a function of the polyether chain length, particularly between the two isomeric compounds. Surprisingly, however, the compound with eight side chains was not mesomorphic. The two halves of the molecules were assumed planar, although due to the flexible connectors, the molecules can have an idealized planar conformation, but they can also adopt several conformations. The number of chains thus influenced the nature of the mesophase, while micro-segregation between the central polar cores and the aliphatic chains helped in stabilizing this arrangement (rather high transition temperatures) providing there was a required number of side chains.



(41)

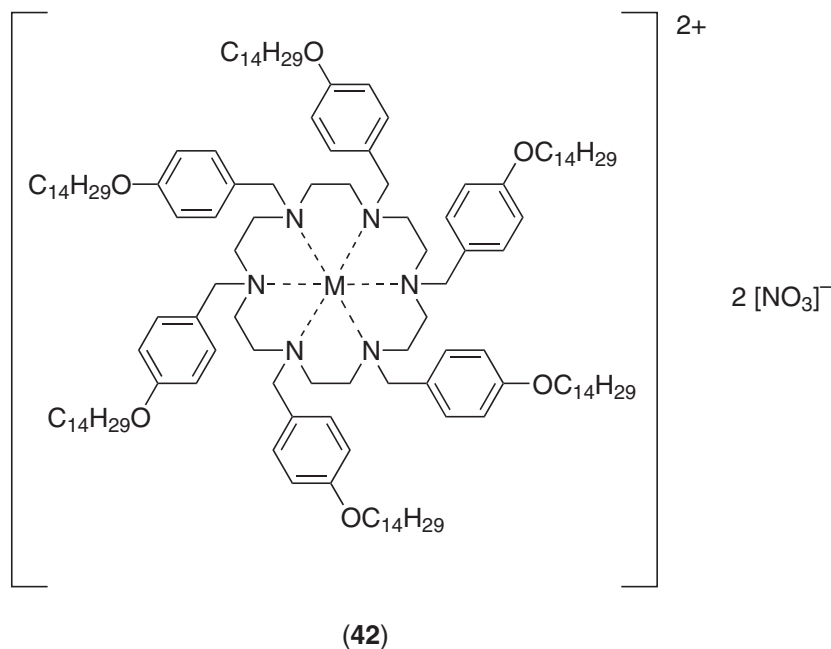
Table 29 Mesomorphic properties of (41).

$R^1$	$R^2$	$x$	$y$	Phase transitions
H	H	3	1	Cr 197 SmA 207 I
$\text{OC}_{10}\text{H}_{21}$	H	3	1	Cr 137 I
$\text{OC}_{10}\text{H}_{21}$	$\text{OC}_{10}\text{H}_{21}$	3	1	Cr 110 $\text{Col}_h$ 178 I
$\text{OC}_{10}\text{H}_{21}$	$\text{OC}_{10}\text{H}_{21}$	1	2	Cr 108 $\text{Col}_h$ 211 I
$\text{OC}_{10}\text{H}_{21}$	$\text{OC}_{10}\text{H}_{21}$	1	3	Cr 110 $\text{Col}_h$ 208 I

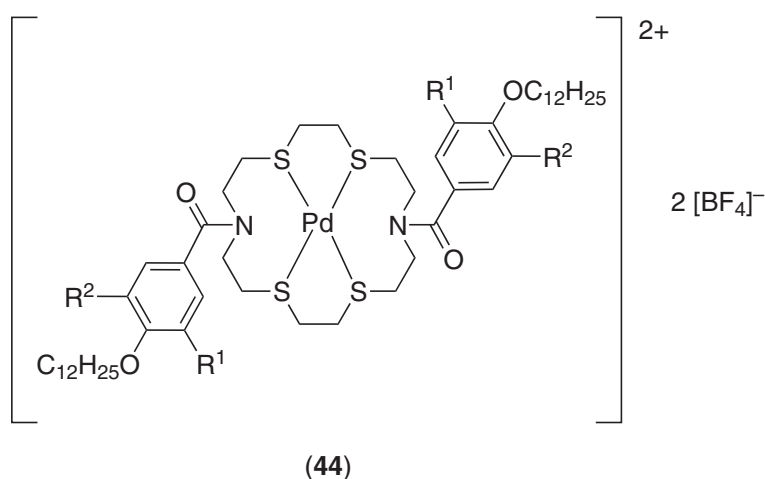
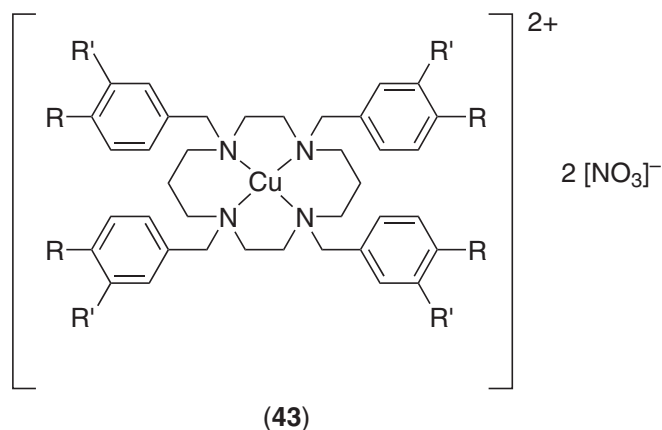


### 7.9.7.9 Metal Complexes of Azacrowns

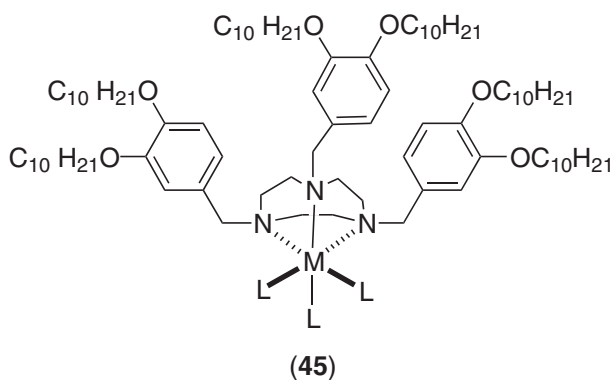
Large, macrocyclic polyamines substituted with alkoxybenzoyl groups have been reported by Lehn *et al.* to form columnar phases, referred to as “tubular” owing to the hollow structure of the columns formed by the stacking of the macrocycles.<sup>302,303</sup> The mesophase stability was found to decrease with increasing size of the crowns ring, which was attributed to the growing conformational flexibility of the molecule, and thus to the quite substantial deviation from a disk-like structure. Moreover, they were found to be highly hygroscopic, influencing the transition temperatures as well as modifying mesophase stability. A means to improve the mesophase stability was the formation of amide bonds between the macrocycle and the side groups. Another interesting approach consisted of stiffening the azacrown core moieties through metal coordination. Several new, non-mesomorphic azacrowns [18]aneN<sub>6</sub> ((**42**): M = Ni, Co) and [14]aneN<sub>4</sub> ((**43**): R = OC<sub>14</sub>H<sub>29</sub>, R' = H; R = R' = OC<sub>10</sub>H<sub>21</sub>) were prepared by Ringsdorf and co-workers.<sup>304</sup> Cobalt and nickel complexes of [18]aneN<sub>6</sub> exhibited mesophases, and the 2:1 (**42**)/Co(NO<sub>3</sub>)<sub>2</sub> “sandwich” compound displayed a columnar nematic phase (N<sub>CoI</sub>) between 30 °C and 60 °C, whereas the 1:1 (**42**)/Ni(NO<sub>3</sub>)<sub>2</sub> system showed an unidentified mesophase between 29 °C and 95 °C. During the complexation process of the cobalt ion to the azacrown [18]aneN<sub>6</sub>, oxidation of the central ion by atmospheric oxygen occurred, which appeared decisive in mesophase induction, the non-oxidized system being non-mesomorphic. Copper adduct (**43**) having four chains ((**43**): R = OC<sub>14</sub>H<sub>29</sub>, R' = H) also exhibited a broad mesophase from 18 °C up to 160 °C, preliminarily identified by X-ray methods as Col<sub>h</sub>; decomposition started to take place around 160 °C. In this case, not only the conformational rigidification of the system would appear to be essential for mesomorphism induction, but also the result of core-to-core interactions as indicated by susceptibility measurements, revealing a possible coupling between the metal ions. The structurally similar parent copper complex with eight chains was not mesomorphic, melting at 67 °C ((**43**): R = R' = OC<sub>10</sub>H<sub>21</sub>).<sup>305</sup>



Macrocycles containing an N<sub>2</sub>S<sub>4</sub> donor set have been obtained by acylation of 1,10-diaza-4,7,13,16-tetrathiacyclooctadecane, [18]aneN<sub>2</sub>S<sub>4</sub>.<sup>306</sup> Due to their conformational flexibility and disorder, none of the metal-free systems ((**44**): R<sup>1</sup>, R<sup>2</sup> = H or OC<sub>12</sub>H<sub>25</sub>) was mesomorphic, melting at 73 °C, 79 °C, and 101 °C for the two-, six-, and four-chain systems, respectively. However, induction of disordered smectic phases was observed for the palladium complexes, irrespective of the number of side chains. Both the four- and six-chain systems melted at ca. 160 °C into a mesophase; clearing temperatures were around 190–200 °C. The mesophases were transient in both cases, in that they did not reappear on cooling, and the only witnessed event was the formation of an anisotropic glass.



Lattermann and co-workers have also looked at a series of mesomorphic metal complexes, (45), with flexible, saturated tridentate ligands such as the non-mesogenic 1,4,7-tri-(3',4'-didecyloxy) benzyl-1,4,7-triazacyclononane. Due to the small diameter of the trisubstituted [9]aneN<sub>3</sub> ring, only monofacial coordination was possible. Upon complexation by Ni(NO<sub>3</sub>)<sub>2</sub>, the octahedral complex was found to be mesomorphic giving a Col<sub>r</sub> mesophase between 140 °C and 167 °C (Figure 32).<sup>307</sup> Then, in order to extend this study, other metal complex fragments such as group 6 tricarbonyls ((45): ML<sub>3</sub> = Cr(CO)<sub>3</sub>, Mo(CO)<sub>3</sub>, and W(CO)<sub>3</sub>)<sup>308</sup> and iron trichloride ((45): ML<sub>3</sub> = FeCl<sub>3</sub>)<sup>309</sup> were employed. All showed enantiotropic columnar mesophases (Figure 32). The chromium, molybdenum, and tungsten exhibited a wide temperature range, Col<sub>r</sub> phase, with no signs of decomposition being observed in the isotropic liquid. While the melting points remained almost the same for the three complexes (ca. 60 °C), the clearing temperatures increased steeply from the chromium to tungsten.



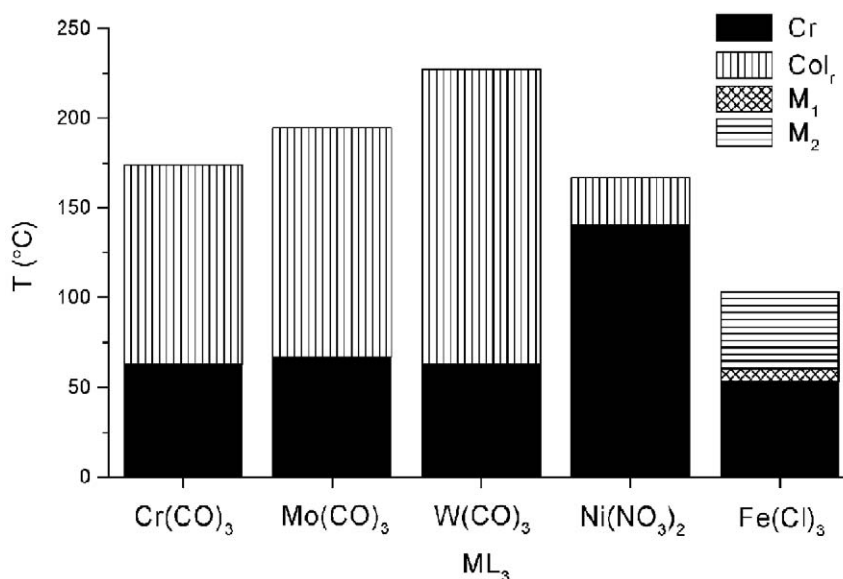


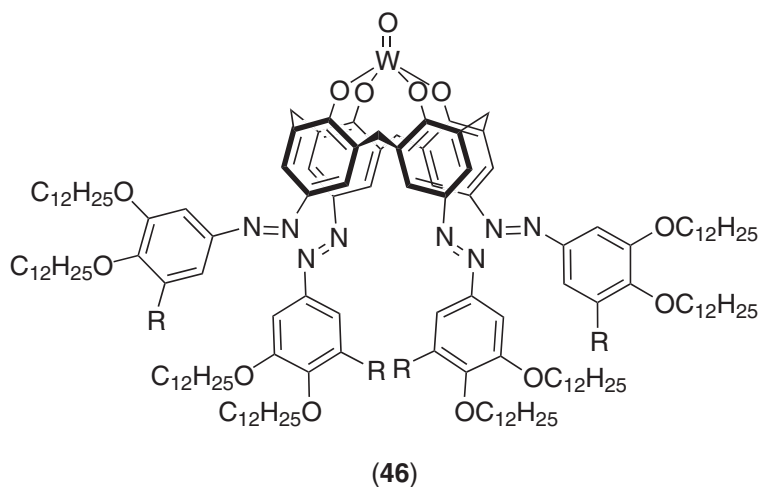
**Figure 32** Mesomorphic properties of the 1,4,7-tri-(3',4'-didecyloxy) benzyl-1,4,7-triazacyclononane metal complexes, (45). M<sub>1</sub>,M<sub>2</sub> : unidentified mesophases.

The case of the iron compound was more complicated. It displayed two mesophases, apparently columnar, the lower temperature phase of which was observed during the first heating cycle only, the other one above 70 °C but only after heating to 140 °C. Mössbauer and UV spectroscopy revealed that the peculiar thermal behavior of the iron complex was due to the existence of various octahedrally coordinated monomeric and dimeric species, as well as to reversible redox reactions. When coordinated to the metal, the triazacyclononane ring lost its flexibility and the inner part of the complex adopted the shape of a cone or pyramid. The formation of the columnar mesophase then presumably resulted from the stacking of such cones on top of one other, with thus a net polarization being expected in each column.

#### 7.9.7.10 Calix[4]arenes

When adequately and purposely designed, calixarenes were found to show liquid-crystalline properties.<sup>310</sup> An interesting advance in this field was described by Swager who reported the mesomorphism of azo-substituted calix[4]arene complexes of oxotungsten(VI)<sup>311,312</sup> ((46): R = H or OC<sub>12</sub>H<sub>25</sub>). The metal-free calixarene melted into an unidentified mesophase before clearing in the isotropic liquid; this phase was transient since it was observed only during the first heating cycle, and was lost on cooling from the isotropic liquid and during subsequent heat-cool cycles. This unusual behavior was explained by the presence of a mixture of several conformations in the liquid phase, preventing an easy return to the liquid-crystalline phase. Complexation with the oxotungsten(VI) group locked the conformation of the calixarene, and promoted the induction of enantiotropic columnar mesophases, which were stable over wide temperature ranges. Thus, the square pyramidal complex with eight terminal chains displayed a single mesophase before decomposition took place (Cr 136 Col 320 dec.), whereas that with twelve chains displayed two mesophases at lower temperatures (Cr 54 Col<sub>1</sub> 77 Col<sub>h</sub> 267 I). The ability to form 1:1 host-guest systems between the tungsten complexes and a Lewis base (L: DMF or pyridine) has been investigated. This resulted in the complete suppression of the mesomorphic behavior, the host-guest complexes clearing into the isotropic liquid at 115 °C and 84 °C for R = H and R = OC<sub>12</sub>H<sub>25</sub> respectively. However, further heating (200–250 °C) led to the dissociation of the Lewis bases, and the columnar phases reappeared. Likewise, complexes with pyridine guests showed the same thermal behavior and identical isotropization temperatures. A model suggested a head-to-tail arrangement of the bowl-like cores forming polar columns and the oxotungsten(VI) group of one molecule protruding into the empty cavity of its neighbor. Hence, these systems are other examples of materials exhibiting ferroelectric order within columns. The results of this study showed that a rigid bowl conformation consequent of the capping of the calixarene with the

tungsten-oxo moieties and the vacancy of the cavity are the necessary condition for mesophase induction in such systems, emphasizing once more the central role of the metal in this respect.



## 7.9.8 DISCOTIC AND *PSEUDO*-DISCOTIC COMPOUNDS SHOWING COLUMNAR MESOPHASES

### 7.9.8.1 $\beta$ -diketonate Metal Complexes

The ease of synthesis of  $\beta$ -diketonates, together with their potential use as ligands to generate mesomorphic metal complexes, have made this area quite fertile and has led to many interesting, and occasionally controversial, findings. The preparation of these chelating ligands consists of a straightforward Claisen condensation between the appropriate ketone and ester. They can readily form metal complexes of the type  $[ML_2]$  with a wide variety of metallic ions, and particularly with copper(II), nickel(II), and palladium(II) ions by the reaction of the ligand with the metal chloride, acetate, or sulfate.

In order to have a better overview of this important work, all  $\beta$ -diketonato complexes will be discussed together, irrespective of classifications based on molecular shape and mesomorphism. This is done as classical taxonomy does not work too well with these materials and also because it serves to illustrate the limitations of such taxonomy; indeed, it might be argued that some of the more interesting structure/property relationships exist at the limits of classification.

The general  $\beta$ -diketonate template has an overall lath-like structure, and subtle structural modifications can lead to crossover between smectic and columnar mesomorphism, or to structural change between discotic to calamitic shape, simply by changing the nature of the substituent  $R^1$  and  $R^2$  (Figure 33). This is an important aspect of this type of complex, which would not be appreciated fully and understood if discussed separately. For instance, symmetrical systems ( $R^1 = R^2$ ,  $D_{2h}$ ) can have either disk-like or X-shaped structures, whereas the unsymmetrical compounds ( $R^1 \neq R^2$ ) can possess either zigzag- or cross-shaped structures (Figure 33). For the latter, both *cis* ( $C_{2v}$ ) and *trans* ( $C_{2h}$ ) isomers are also possible, and it is reasonable to think that mixtures are always present and that *trans/cis* interconversion occurs at elevated temperatures. This study is clearly a textbook case in addition to being a perfect illustration of induction, modification, or suppression of mesomorphism on complexation.

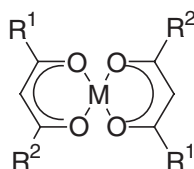
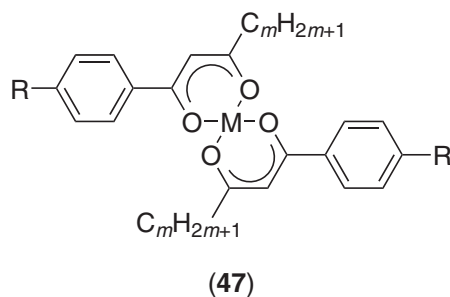


Figure 33 General motif of the bis- $\beta$ -diketonato metal complexes.

### 7.9.8.1.1 Bis[1-(substituted-phenyl)-3-alkyl- $\beta$ -diketonato]metal complexes with two and four peripheral chains

The first mesogenic complex based on  $\beta$ -diketonates was bis(1-octyloxyphenyl-1,3-butanedionato) palladium(II) ((47): M = Pd; R = OC<sub>8</sub>H<sub>17</sub>; m = 1) prepared in 1977,<sup>313</sup> but observations of any potential mesomorphism were limited by the darkening of the sample on heating above 170 °C due to decomposition. Then followed a series of articles by Ohta<sup>314–316</sup> on structurally related copper complexes ((47): M = Cu; R = C<sub>n</sub>H<sub>2n+1</sub>; n = 0–12, m = 1). All complexes were obtained as their *trans* isomers only and a complicated solid-state polymorphism was observed including various kinds of double melting behavior, but no liquid-crystalline behavior was detected. The origin of this complex polymorphism was studied by means of X-ray diffraction and IR spectroscopy,<sup>317</sup> and attributed to the difference in the packing of the alkyl chains rather than coordination change or *cis–trans* isomerization.



Liquid-crystalline  $\beta$ -diketonato complexes were first described by Giroud-Godquin and Billard in 1981 and are discussed below.

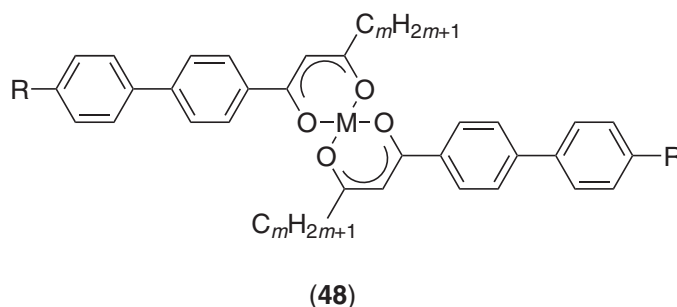
Copper complexes where R was an alkylcyclohexyl moiety ((47): M = Cu; R = C<sub>6</sub>H<sub>10</sub>–C<sub>n</sub>H<sub>2n+1</sub>, n = 3, 5, 7; m = 1–8) were found to show a monotropic nematic phase, except for those with m = 1, which were not mesomorphic. Only eight members of such bis[1-(4-*trans*-4-alkylcyclohexyl-phenyl)-alkylpropane-1,3-dionato]copper(II) complexes were synthesized but it turned out to be sufficient to rationalize their overall thermal behavior. Melting points were found to decrease very steeply with increasing m, suggesting that the lateral chains disrupted the efficiency of the molecular packing of the complexes in the crystal state. The crystal structures of two homologs ((47): M = Cu; R = C<sub>n</sub>H<sub>2n+1</sub>; n = 3; m = 1 and 8) showed the *trans* disposition of the ligands about the copper center and the planar nature of the complexes. Furthermore, the molecules were organized into layers in the crystalline phase, without specific intermolecular contacts.

Despite the disk-like nature of these complexes, smectic mesomorphism was observed for related vanadyl<sup>318</sup> and uranyl<sup>319</sup> complexes ((47) with long lateral chains (m). The square-pyramidal oxovanadium(IV) compounds ((47): M = VO; R = OC<sub>10</sub>H<sub>21</sub>; m = 7, 9, 11, 13, C<sub>6</sub>H<sub>10</sub>–C<sub>7</sub>H<sub>15</sub>) displayed monotropic SmA and SmC phases below 70 °C, while the octahedral dioxouranium(VI) complex ((47): M = UO<sub>2</sub>; R = OC<sub>10</sub>H<sub>21</sub>; m = 13) displayed an SmC phase between 59 and 75 °C, which supercooled to room temperature. The vanadyl complex ((47): M = VO; R = C<sub>6</sub>H<sub>10</sub>–C<sub>7</sub>H<sub>15</sub>; m = 8) and its fully saturated homolog ((47): R = C<sub>6</sub>H<sub>10</sub>C<sub>6</sub>H<sub>10</sub>–C<sub>7</sub>H<sub>15</sub>) were also mesomorphic at much lower temperatures than their copper analogs. The former showed two monotropic phases (N and SmA), while the latter exhibited a nematic phase between 108 °C and 128 °C and a monotropic SmA phase. The rather low melting temperatures was ascribed to the possible existence of a *cis–trans* mixture in the mesophase, to the long lateral chains, m, and to the absence of polymeric chains in the vanadyl compounds, although no evidence was presented to support the assertion of isomerism. Note that some ferrocenyl  $\beta$ -diketonatozinc(II) complexes (Figure 33, M = Zn; R<sup>1</sup> = ferrocene, R<sup>2</sup> = C<sub>n</sub>H<sub>2n+1</sub>) have also been described as mesomorphic materials below 100 °C, but without information concerning the nature of the mesophase.<sup>320</sup>

### 7.9.8.1.2 Bis[1-(substituted-biphenyl)-3-substituted- $\beta$ -diketonato]metal complexes with two and four peripheral chains

The elongation of the complexes of type (47) in one main direction can be achieved by introducing a biphenyl moiety in place of the phenyl unit. Thus, complexes of type (48) provide another

interesting case of structural modifications and mesomorphism cross-over. Despite their more rigid and linear structure, and the expected smectic mesomorphism (the ligand itself was mesomorphic, showing a crystal E and an SmA phase), the complexes displayed both columnar and nematic phases. The nature and the thermodynamic stability of the mesophases were influenced greatly by the length of the lateral chains. Columnar phases were found for all homologs having short lateral chains ((48): M = Cu; R = OC<sub>n</sub>H<sub>2n+1</sub>, n = 9 to 12, 16, 18; m = 1), the octyloxy derivative not being mesomorphic.<sup>321</sup> The mesophase range increased with increasing terminal chain length, due mainly to a strong reduction in the melting point (130–190 °C), isotropization taking place at around 200 °C, with some decomposition. The phase was identified as Col<sub>r</sub> by X-ray diffraction, with a *c2mm* plane group. The authors suggested that, owing to the small size of the lateral methyl groups, the complexes would be able to associate into dimers (also confirmed by X-ray diffraction) forming an overall discoid shape (X-shaped), suitable for the generation of a columnar phase. However, this model results in a large, unoccupied volume, which is not realistic in the mesophase. Another hypothesis would be to consider the breaking of the crystalline lamellae resulting from the strong undulations of the aliphatic sub-layers into finite ribbons of molecular clusters.

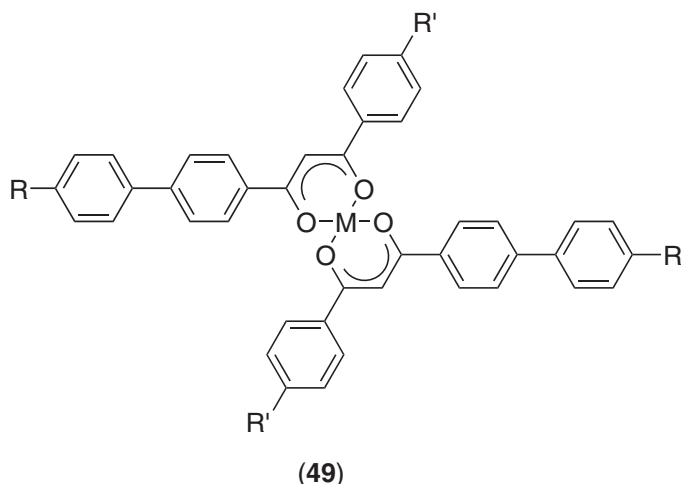


When fluorine groups were introduced in the 2- and 3-positions of the terminal aromatic ring of the biphenyl unit ((48): M = Cu; R = OC<sub>8</sub>H<sub>17</sub>; m = 1) no columnar phase was observed, but a monotropic nematic phase instead, probably due to the reduction of the molecular symmetry.<sup>322</sup> When the lateral chain was elongated, the columnar phase disappeared at the expense of an enantiotropic nematic phase ((48): M = Cu; R = OC<sub>n</sub>H<sub>2n+1</sub>, n = 6, 8, 10–12, 14 and m = 2; n = 12, m = 3; and n = 4, 8, m = 4), which became monotropic ((48): M = Cu, R = OC<sub>n</sub>H<sub>2n+1</sub>, n = 12, m = 4; n = 8, m = 8; and n = 12, m = 12.).<sup>323,324</sup> Furthermore, re-entrant (Section 7.9.3.2.5) nematic phases, between two crystalline phases, were also observed for the compounds in the series m = 2. Both the temperatures of the crystal-to-mesophase (163–219 °C) and mesophase-to-isotropic liquid (175–224 °C) decreased very rapidly with increasing m and n. The stability of the nematic mesophase was also found to depend on the bulkiness of the lateral chain. For instance, using a branched side group such as –CHMeEt did not suppress the monotropic phase but reduced the transition temperatures considerably.<sup>325</sup> The cross-over between the Col<sub>r</sub> and the nematic phase would then correspond to a decrease of the lateral interactions between molecules due to the steric hindrance of the chains.

Some compounds with alkyl chains attached to the biphenyl unit were also synthesized. The hexadecyl derivative ((48): M = Cu; R = C<sub>16</sub>H<sub>33</sub>; m = 1) showed a Col<sub>r</sub> phase which was slightly destabilized (reduction of the clearing temperature by 20 °C) with respect to the alkoxy homolog.<sup>326</sup> Surprisingly, however, none of the decyl homologs ((48): M = Cu; R = C<sub>10</sub>H<sub>21</sub>; m = 0, 1) was mesomorphic.<sup>327</sup> Quite different mesomorphism was obtained with four oxovanadyl complexes ((48): M = VO; R = C<sub>8</sub>H<sub>19</sub>, CH<sub>2</sub>C\*HMeEt; m = 8 and R = F; m = 9 or C<sub>7</sub>H<sub>15</sub>–C<sub>6</sub>H<sub>10</sub>–C<sub>6</sub>H<sub>10</sub>).<sup>318,327</sup> The non-chiral complex displayed monotropic phases (SmA and N), but the chiral variant showed a chiral nematic phase between 109 °C and 155 °C. The other two complexes possessed an enantiotropic nematic phase.

As a continuation of this structural study, Sadashiva *et al.* developed related diketonate complexes, preserving the same longitudinal motif found in (48), but elongating the rigid core in the lateral direction by means of substitution of the alkyl chain with a phenyl moiety (49). This new molecular structure, having a smaller length-to-width ratio than the previous one, could be seen as a structural intermediate between a rod and a disk. Most of the new diketonate ligands were mesomorphic, depending on the nature of both the longitudinal and the lateral substituent R and R' respectively, and on their combination within the structure. For instance, [1-(alkylbiphenyl)-3-(phenyl)propane]-1,3-diones (R = C<sub>n</sub>H<sub>2n+1</sub>, R' = H) exhibited SmA and monotropic N phases.<sup>328</sup>

The substitution of a methoxy group on the phenyl ring suppressed the mesophase, whereas a cyano group stabilized the SmA phase. When two long chains were grafted on both the biphenyl and phenyl cores ( $R = C_nH_{2n+1}$ ,  $R' = C_mH_{2m+1}$ ), mesomorphism was suppressed.



The copper and palladium complexes of ligands with various  $R'$  groups ((49):  $M = Cu, Pd$ ;  $R = C_nH_{2n+1}$ ;  $R' = H, Me, Et, OMe, OEt, OPr, Cl, Br, CN$ )<sup>329–332</sup> were mesomorphic showing a nematic phase and, in accordance with previous results, the mesophase was destabilized and occurred only on cooling from the isotropic liquid, the clearing temperatures being still rather high at ca. 180–250 °C (Table 30). No great differences (<10 °C) were observed between the transition temperatures of the palladium complexes (usually the highest) and those of the copper complexes. In general, the clearing temperatures decreased with increasing the chain length of the lateral substituent, but increased in the order  $Cl < Br < CN$  with complexes substituted by polar groups. As usual, the lengthening of the main chain provoked depression of both the crystal-to-isotropic and isotropic-to-nematic phase transitions. Substitution of the main alkyl chain by alkoxy chains ((49):  $M = Cu, Pd$ ;  $R = OC_nH_{2n+1}$ ;  $R' = H$ ) did not particularly improve the mesomorphic properties, which still occurred monotonically, but increased the transition temperatures considerably (200–260 °C). The same temperature increase was also observed for the ligands, which exhibited a broad enantiotropic SmA phase, but no N phase. The most stable N phase was obtained with a copper complex containing a cyclohexyl group ((49):  $M = Cu$ ;  $R = OMe$ ;  $R' = C_6H_{10}-C_7H_{15}$ ; Cr 247 N 280 I).<sup>333</sup> The calamitic nature of the nematic phase was previously confirmed by miscibility studies with the well-known nematogen 4''-pentyl-4-cyanoterphenyl

**Table 30** Transitions temperatures of complexes (49) and (50).

$R'$	$X$	$Y$	$M = Cu, R = C_{10}H_{21}$
H	H	H	Cr 198 (N 156) I
Me	H	H	Cr 221 (N 167) I
$C_2H_5$	H	H	Cr 181.5 (N 154) I
$C_3H_7$	H	H	Cr 173 (N 153) I
$C_nH_{2n+1}, n > 5$	H	H	Cr 176 to 188 I
OMe	H	H	Cr 192 (N 172) I
$OC_2H_5$	H	H	Cr 187 (N 166.5) I
$OC_3H_7$	H	H	Cr 183.5 (N 153.5) I
F	H	H	Cr 193 (N 175) I
Br	H	H	Cr 212 (SmA 182 N 183) I
$CF_3$	H	H	Cr 188 (SmA 131 N 132) I
CN	H	H	Cr 230 (N 202) I
Me	F	H	Cr 192 (N 146) I
OMe	F	H	Cr 178 (N 153) I
F	F	H	Cr 153 (N 141) I
H	H	Me	Cr 165 (N 138) I
H	H	OMe	Cr 195 (N 140) I

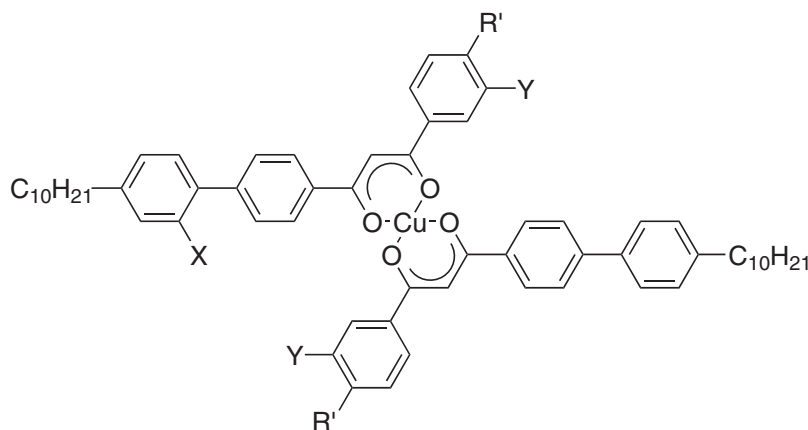
**Table 31** Transition temperatures for (51).

<i>R</i>	<i>X</i>	<i>Y</i>	<i>Z</i>	<i>Mesomorphism</i>
H	H	H	H	Cr 208 (N 195) I
Me	H	H	H	Cr 195 N 206 I
Et	H	H	H	Cr 226 N 228 I
C <sub>10</sub> H <sub>21</sub>	H	H	H	Cr 225 I
F	H	H	H	Cr 155 (SmC 122) SmA 250 I
Br	H	H	H	Cr 150 (SmC 141) SmA 260 I
CF <sub>3</sub>	H	H	H	Cr 228 (SmC 203) SmA 265 I
CN	H	H	H	Cr 259 N 273 I
H	H	H	F	Cr 176 SmA 209 I
H	H	F	H	Cr 180 (N 165) I
H	F	H	H	Cr 170 (SmC 150) SmA 179 N 188 I
H	H	F	F	Cr 172 I

(5CT). However, they later suggested that the nematic phase was of the biaxial type ( $N_b$ ) based on conoscopic observations of aligned samples,<sup>334–337</sup> miscibility studies, and X-ray studies.<sup>338</sup> (The biaxial nematic phase differs from the uniaxial phase in that in addition to the orientational order which characterizes the phase (see Figure 5), there is long-range order in the direction perpendicular to the main director, and the phase is optically biaxial (hence,  $N_b$ ). The phase remains to be demonstrated unequivocally in non-polymeric, thermotropic materials.) Further evidence was apparently provided by the observation of the phase sequence  $I-N_b-N_u$  ( $N_b$ ,  $N_u$ : biaxial and uniaxial nematic phases, respectively) in mixtures of complex (99.6%) and the nematogen 5CT (0.4%), although as the  $N_b$  phase is more ordered than  $N_u$ , this phase sequence is somewhat counter-intuitive. Despite these investigations, the existence of the  $N_b$  phase in these complexes remains to be widely accepted and, indeed, concerns have been expressed as to whether the biaxiality observed was induced by surface treatment and applied fields. The re-investigation of some of these compounds by another group led to the conclusions that the N phase was actually uniaxial.<sup>322</sup>

Two optically active oxovanadium(IV) complexes ((49):  $M=VO$ ;  $R=CH_2C^*HMeEt$ ;  $R'=OC_{10}H_{21}$ ,  $OC_{18}H_{37}$ ) were also prepared, and found to display a monotropic SmC\*.<sup>327</sup>

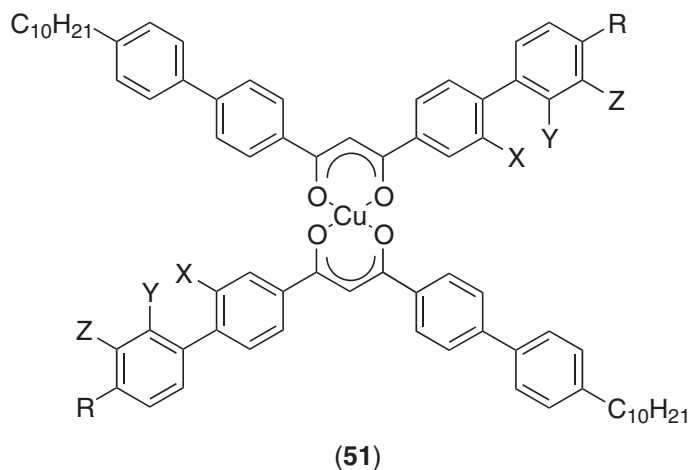
The effect of polarity was investigated in more detail by Thompson *et al.* on a series of copper complexes having the same mesogenic core (50).<sup>322,333,339</sup> From Table 30, one can see that the effect of incorporating polar groups within the structure did not lead to an improvement of the mesophase stability, nor to mesophase change, except for the compounds with a bromide or a trifluoromethyl groups which exhibited an additional monotropic SmA phase.

**(50)**

Stabilization of the mesophases was achieved by broadening the molecule through the elongation of the branches (51), leading to a cross-shaped molecular structure.<sup>322,333,339,340</sup> See (Table 31.) The difference in mesophase stability between complexes (49) and (50), and complexes 51 was attributed to the greater tendency of (51) to favor molecular associations via antiparallel

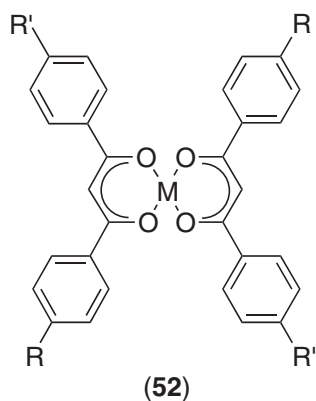


correlations. Additionally, they showed a greater ability to form smectic phases, despite the substantial deviation of the molecular structure from a rod shape. Lateral interactions appeared to be promoted when a polar substituent was located at the extremity of one biphenyl unit ((**51**): R = F, Br, CF<sub>3</sub>), i.e., when the dipole pointed away from the molecular core, the exception being with a cyano group, for which only a broad nematic phase was seen. To prove whether the formation of the smectic phases was connected to the direction of the dipole, the location of the fluoro substituent was varied along the arms. When the dipole pointed outwards the mesogenic core ((**51**): F in position Z or X), smectic mesomorphism was observed, though with a decrease of the mesophase stability when the dipole got closer to the core. However, when it pointed towards the core ((**51**): F in position Y), the smectic phase was not observed.



#### 7.9.8.1.3 Bis[1,3-(substituted-phenyl)- $\beta$ -diketonato]metal complexes

On account of the square-planar coordination around the metal ion, metal complexes with 1,3-(substituted-phenyl)- $\beta$ -diketonate (**52**) possess a more disk-like shape than the diketonate complexes described previously, and appeared therefore more promising candidates for the formation of columnar mesophases. Moreover, the versatility in the synthesis of the ligand has allowed the preparation of a wide variety of chemical structures for which the number of terminal aliphatic chains, as well as the position of substitution of these chains on the benzene rings, can easily be controlled. This has led to intensive activity in this area with relevant examples presented below.



##### (i) Complexes with four peripheral chains

In 1981, Giroud-Godquin and Billard reported an unidentified mesophase for the symmetrical copper complex with four decyl chains ((**52**): M = Cu; R = R' = C<sub>10</sub>H<sub>21</sub>).<sup>341</sup> This study was then extended to other diketonate ligands possessing different chain length and with other metal

**Table 32** Mesomorphism of some *bis*-diketonato complexes (**52**).

<i>M</i>	<i>R</i>	<i>R'</i>	<i>Mesomorphism</i>
Cu	C <sub>8</sub> H <sub>17</sub>	C <sub>8</sub> H <sub>17</sub>	Cr 76.1 L <sub>D1</sub> 117.2 L <sub>D2</sub> 142 I
	C <sub>10</sub> H <sub>21</sub>	C <sub>10</sub> H <sub>21</sub>	Cr 85.5 L <sub>D</sub> 128.5 I
	C <sub>12</sub> H <sub>25</sub>	C <sub>12</sub> H <sub>25</sub>	Cr 99 L <sub>D</sub> 120 I
Cu	C <sub>7</sub> H <sub>15</sub>	C <sub>13</sub> H <sub>27</sub>	Cr 71 L <sub>D</sub> 122 I
	OC <sub>8</sub> H <sub>17</sub>	OC <sub>8</sub> H <sub>17</sub>	Cr 82.5 D <sub>L</sub> 167 I
	OC <sub>10</sub> H <sub>21</sub>	OC <sub>10</sub> H <sub>21</sub>	Cr 82 D <sub>L</sub> 173 I
	OC <sub>12</sub> H <sub>25</sub>	OC <sub>12</sub> H <sub>25</sub>	Cr 74 D <sub>L</sub> 154 I
Cu	OC <sub>7</sub> H <sub>15</sub>	OC <sub>9</sub> H <sub>19</sub>	Cr 172 I
	C <sub>8</sub> H <sub>17</sub>	OC <sub>8</sub> H <sub>17</sub>	Cr 87 D <sub>L</sub> 144 I
	C <sub>10</sub> H <sub>21</sub>	OC <sub>10</sub> H <sub>21</sub>	Cr 94 D <sub>L</sub> 130.5 I
Ni	C <sub>12</sub> H <sub>25</sub>	OC <sub>12</sub> H <sub>25</sub>	Cr 81.5 D <sub>L</sub> 121 I
	C <sub>10</sub> H <sub>21</sub>	C <sub>10</sub> H <sub>21</sub>	Cr 83 I
Pd	C <sub>8</sub> H <sub>17</sub>	C <sub>8</sub> H <sub>17</sub>	Cr 99 L <sub>D1</sub> 121.5 L <sub>D2</sub> 138.5 I
	C <sub>10</sub> H <sub>21</sub>	C <sub>10</sub> H <sub>21</sub>	Cr 101.5 L <sub>D1</sub> 106 L <sub>D2</sub> 119 I
Pd	OC <sub>8</sub> H <sub>17</sub>	OC <sub>8</sub> H <sub>17</sub>	Cr 175 I
	OC <sub>10</sub> H <sub>21</sub>	OC <sub>10</sub> H <sub>21</sub>	Cr 168 (D <sub>L</sub> 87) I
	OC <sub>12</sub> H <sub>25</sub>	OC <sub>12</sub> H <sub>25</sub>	Cr 88 D <sub>L</sub> 159 I
	OC <sub>7</sub> H <sub>15</sub>	OC <sub>9</sub> H <sub>19</sub>	Cr 173 I
VO	OC <sub>8</sub> H <sub>17</sub>	OC <sub>8</sub> H <sub>17</sub>	Cr 168 (Col <sub>h</sub> 145) I
	OC <sub>10</sub> H <sub>21</sub>	OC <sub>10</sub> H <sub>21</sub>	Cr 165 (Col <sub>h</sub> 143) I
	OC <sub>12</sub> H <sub>25</sub>	OC <sub>12</sub> H <sub>25</sub>	Cr 145 (Col <sub>h</sub> 120) I
	OC <sub>7</sub> H <sub>15</sub>	OC <sub>9</sub> H <sub>19</sub>	Cr 167 (Col <sub>h</sub> 132) I
	OC <sub>8</sub> H <sub>17</sub>	OC <sub>12</sub> H <sub>25</sub>	Cr 160 (Col <sub>h</sub> 132) I

ions.<sup>342</sup> An unidentified mesophase was also observed for the homologous palladium complex,<sup>343</sup> while the nickel complex was not mesomorphic.<sup>342</sup> The increase in chain length was associated with a decrease of the mesomorphic range essentially due to the increasing melting point and decreasing clearing temperature. Reducing the symmetry of the complex by the use of different chain lengths ((**52**): *M* = Cu; *R* = C<sub>7</sub>H<sub>15</sub>; *R'* = C<sub>12</sub>H<sub>25</sub>) resulted in the slight lowering of the melting point (Table 32).

In the meantime, Ohta *et al.*<sup>344</sup> studied the complete series of symmetric copper complexes ((**53**): *M* = Cu; *R* = *R'* = C<sub>*n*</sub>H<sub>2*n*+1</sub>, *n* = 0 to 14), which confirmed the previous results. The ligand showed a crystal smectic E phase from the octyl derivative onwards as determined by miscibility studies. The first four complexes ((**53**): *M* = Cu; *R* = *R'* = C<sub>*n*</sub>H<sub>2*n*+1</sub>, *n* = 0 to 3) were not mesomorphic, then a monotropic phase was detected for *n* = 4, which became enantiotropic for *n* ≥ 5. Moreover, for *n* = 7 and 8, the copper complexes showed an additional mesophase, while the nonyl derivative exhibited two additional mesophases. Crystalline structures of some tetra-alkyl copper, palladium, and nickel complexes of β-diketonates<sup>345–349</sup> revealed that the flat molecular species were stacked into columns, the planes of the molecules forming a small tilt with respect to the columnar axis; these columns were further organized into layers. Variable-temperature ESR<sup>350,351</sup> and NMR<sup>352</sup> investigations performed on some copper complexes supported the evidence of a transition between a crystalline phase and a mesophase of the lamellar type. In the model proposed for the mesophase, the discoid molecules were thought to be stacked into columnar aggregates, these pseudo-columns being organized further into layers. Each layer was separated by insulating hydrocarbon regions, with the chains being aligned along the layer normal. The observations made by Billard using a polarizing microscope agreed well with such a model. Thus, the texture of the mesophase was found to contain cylindrical domains, a characteristic type of defect belonging both to columnar and lamellar structures.<sup>353</sup> This type of mesomorphic ordering was later referred to as lamellar discotic (L<sub>D</sub>) or discotic lamellar (D<sub>L</sub>) phase, depending on the correlation length within the columns, i.e., their size. Despite these rigorous studies, demonstration of the mesomorphic properties of the tetra-alkyl compounds still remains controversial. From a thermodynamic point of view, the transition enthalpy values were found too large for a mesophase-to-isotropic liquid transition ( $\Delta H \approx 30 \text{ kJ mol}^{-1}$ ) suggesting rather a mesophase with a very high degree of order. Moreover, the mesophases were extremely viscous. A detailed X-ray study performed in the mesophase of the tetra-decyl copper compound suggested that the molecular organization was not truly that of an ordered crystalline phase but possessed a lamellar structure with imperfect molecular organization (broad reflections) more closely related to the so-called

*condis* phase (conformationally disordered) or plastic crystal (orientationally disordered) than to a liquid-crystalline mesophase.<sup>354</sup> No detailed X-ray investigations were carried out in the mesophase of the other compounds of the series in order to prove their true liquid crystalline order.

Related systematic studies were performed with the analogous copper<sup>355–357</sup> and palladium<sup>358,359</sup> complexes bearing four alkoxy groups in the *para* positions of the benzene rings (note that the ligand itself displayed a crystal smectic phase for chain length with  $n=8$  onwards<sup>360</sup>). The complete series of symmetric tetra-alkoxy complexes of copper ((52):  $M = Cu$ ;  $R = R' = OC_nH_{2n+1}$ ,  $n=1-12, 14$ ) was synthesized, and only one enantiotropic mesophase was detected for each compound starting from  $n=3$ . The mesophase appeared more stable in this series than that of the alkyl compounds, in that the complexes melted and cleared on average at much higher temperatures (Table 32). The mesomorphic range was increased with chain length due to the destabilization of the crystalline phase, despite the decrease in the clearing temperature. X-Ray single-crystal structures of some of these copper discogens<sup>361–363</sup> revealed a crystalline arrangement made of layers of flat dimeric species. A lamellar mesophase was deduced from in-mesophase X-ray diffraction, with the molecules being tilted in each layer and positioned randomly within the layer<sup>364</sup> with absence of long-range columnar order. This mesophase was also referred to as discotic lamellar phase  $D_L$ . NMR and EPR studies confirmed this model, and the persistence of dimers with increasing temperature.<sup>365,366</sup> Magnetic measurements revealed a Curie-type behavior over the whole temperature range for the tetra-decyloxy copper complex, with no influence on the magnetic susceptibility and no long-range magnetic effects being detected at the different phase transitions.<sup>367</sup> Again, the mesophase was very viscous and the enthalpies of clearing too large for a mesophase ( $\Delta H \approx 60 \text{ kJ mol}^{-1}$ , higher than the crystal-to-mesophase transition!), suggesting a high degree of molecular organization and crystallinity, and questioning once more the liquid crystalline nature of the mesophases shown by such compounds. For the analogous palladium complexes, mesomorphism was observed for  $n \geq 10$ , occurring at much higher temperatures than for the copper complexes (Table 32). For the homologs with shorter chain lengths, decomposition took place on reaching the isotropic liquid. A discotic lamellar phase was also deduced from X-ray diffraction, although the mesophases of the copper and palladium series were not co-miscible. Note that none of the unsymmetrical copper and palladium complexes prepared ((52):  $M = Cu, Pd$ ;  $R = OC_7H_{15}$ ;  $R' = OC_9H_{19}, OC_{10}H_{21}$ ) possessed such thermal behavior and no mesophase was detected (Table 32).<sup>359</sup> Related copper complexes with branched chains ((52):  $M = Cu$ ;  $R = OC_{10}H_{21}$ ;  $R' = OCH(Me)C_4H_9$  or  $OCH(Me)C_6H_{13}$ ) were also not mesomorphic (m.pt.  $155^\circ\text{C}$  and  $133.5^\circ\text{C}$  respectively).<sup>368</sup>

The behavior of the unsymmetrical copper complexes having two alkyl and two alkoxy groups ((52):  $M = Cu$ ;  $R = C_nH_{2n+1}$ ;  $R' = OC_nH_{2n+1}$ ,  $n=4$  to 12), seen as intermediate between the two main series previously discussed above, was also investigated.<sup>369,370</sup> The first complex ( $n=4$ ) was not mesomorphic, and a monotropic phase was detected for the next three complexes of the series ( $n=5$  to 7). Higher homologs showed a stable mesophase between about  $80^\circ\text{C}$  and  $130^\circ\text{C}$ , similar to the transition temperatures observed for the tetra-alkyl complexes (Table 32). The enthalpies of clearing were smaller ( $\Delta H \approx 20 \text{ kJ mol}^{-1}$ ) than that of the symmetrical complexes, but it does seem that this phase is not truly liquid crystalline. The mesophase was found to be totally miscible with that of the tetra-alkoxy complexes confirming their isomorphism and therefore the same type of discotic lamellar phase. They were not co-miscible with the tetra-alkyl analogs. The crystalline structure of one compound ( $n=7$ ) showed the same characteristics described for the symmetrical complexes,<sup>371</sup> but additionally provided evidence for the *cis* arrangement of the chemically identical chains with respect to the central core. EPR spectra of the alkoxy and mixed alkyl-alkoxy systems were similar.<sup>372</sup> Note that a monotropic nematic phase, Cr 254 (N 212) I, was induced in one complex bearing a cyclohexyl group ((52):  $M = Cu$ ;  $R = C_6H_{10}C_7H_{15}$ ;  $R' = OMe$ ).<sup>333</sup>

A number of other copper complexes of type (52) bearing four terminal chains of different nature have also been synthesized. Ohta reported symmetric tetra-octylthio ((52):  $M = Cu$ ;  $R = R' = SC_8H_{17}$ ; mp:  $135^\circ\text{C}$ ) and mixed octylthio-octylsulfonyl ((52):  $M = Cu$ ;  $R = SC_8H_{17}$ ;  $R' = O_2SC_8H_{17}$ ; mp:  $208^\circ\text{C}$ ) complexes, but such modification suppressed the mesomorphic properties totally.<sup>373</sup> Copper complexes with oligo(ethylene oxide) groups were also prepared.<sup>374</sup> The symmetrical compound ((52):  $M = Cu$ ;  $R = R' = (OCH_2CH_2)_3H$ ; m.pt.  $122^\circ\text{C}$ ) was not mesomorphic, while the mixed analog ((52):  $M = Cu$ ;  $R = (OCH_2CH_2)_3H$ ;  $R' = OC_6H_{13}$ ) showed a mesophase between  $103^\circ\text{C}$  and  $146^\circ\text{C}$ , probably a discotic lamellar phase as suggested on the basis of X-ray diffraction. Conductivity measurements on the latter, doped with  $LiClO_4$  or iodine, showed an increase in the conductivity of two or three orders of magnitude when the sample was heated in the mesophase; this increase was sharp in the lithium-containing system, and continuous with that containing the iodine dopant.

As seen previously, complexation of oxovanadium(IV) to 1,3-bis(substituted-phenyl)- $\beta$ -diketonates resulted in the distortion of the square-planar geometry into a square-pyramidal coordination compound, giving rise to a discogen possessing a strong dipole moment along the small molecular axis, i.e., perpendicular to the molecular plane. The presence of such an axial dipole was expected to optimize the stacking of the compounds into columns and to favor the formation of columnar phases in preference to lamellar structures, by means of a polymeric chain induced by intermolecular V=O—V=O interactions. Thus, a series of twenty-eight  $\beta$ -diketonate complexes of oxovanadium(IV) were prepared in which the terminal chain length of the alkoxy groups was varied systematically to produce symmetrical and non-symmetrical species ((52): M=VO; R=OC<sub>n</sub>H<sub>2n+1</sub>, n=6–10, 12, 14; R'=OC<sub>m</sub>H<sub>2m+1</sub>, m=6–10, 12, 14; n= or  $\neq$  m).<sup>359,375,376</sup> With the exception of two symmetrical complexes with chain length n=m=6, 7, as well as the mixed hexyl–heptyl compound (n=6, m=7), which were not mesomorphic, all the other compounds showed a monotropic columnar phase. On the basis of their optical texture, miscibility studies with the hexagonal columnar phase of copper(II) tetradecanoate, and X-ray studies, the mesophase was assigned as columnar hexagonal, with a long-range order of the stacking periodicity. In accordance with this three-dimensional order, the enthalpies of clearing were indeed important ( $\Delta H = 50 \text{ kJ mol}^{-1}$ ). As a general trend, the transition temperatures were found to decrease with decreasing symmetry of both chain length R and R', i.e., where n and m were very different. The isotropic–mesophase transition temperatures were lower for the vanadyl than for the copper complexes by 25–30 °C. Infrared, X-ray, and EPR<sup>377</sup> analyses did not show evidence of the supposed strong V=O—V=O interactions along the columns, which may partly explain the lack of mesophase stability.

To conclude the discussion on X-shaped compounds, the effect of the polarity on mesomorphism should be mentioned.  $\beta$ -Diketonate ligands have been designed which carry a long chain on one ring, while the nature (polarity) of the substituent on the other ring was varied ((52): M=Cu; R=C<sub>6</sub>H<sub>13</sub>; R'=H, OMe, F, CF<sub>3</sub>, Br, CN).<sup>322</sup> They still possess a disk-like core, but were unsymmetrically substituted with two chains, reducing, in principle, the gap between discotic and calamitic structures. The melting points of the compounds were still high (130  $\leq$  m.pt.  $\leq$  200 °C). A monotropic nematic phase was observed for the fluoro compound and for the methoxy compound, whereas none of the other materials was mesogenic. It was thus quite remarkable that such small structural changes could lead to mesophase cross-over from a columnar (L<sub>D</sub>, D<sub>L</sub>, Col<sub>h</sub>) nematic phase type characteristic of calamitic liquid crystals. The transition temperatures of some selected complexes discussed in this part are gathered in Table 32.

### (ii) Complexes with eight peripheral chains

Given that all the 1,3-(substituted-phenyl)- $\beta$ -diketonate metal complexes with four peripheral chains gave highly ordered mesophases (or crystalline phases) irrespective of the metal ion, the nature of the chains, or the molecular symmetry, it was thought appropriate to increase the number of aliphatic chains on the diketonate ligands (i.e., increase the chain density) in order to promote mesophase formation. This proved to be a successful strategy, and the possibility of increasing the dissymmetry of the complexes by controlling the distribution of the chains around the rigid core appeared to be an additional useful tool in tuning mesomorphic properties.

This study began with systems having eight terminal chains grafted at the 3- and 4-positions of each benzene ring of the ligand. Giroud-Godquin reported the first copper complex of this type substituted by eight nonyloxy groups (53: M=Cu; n=m=9) which exhibited an enantiotropic columnar hexagonal phase (Col<sub>h</sub>) between 102 °C and 112 °C.<sup>378</sup> The mesophase was identified by optical microscopy, miscibility studies with a known material, and X-ray diffraction. A small clearing enthalpy was measured by DSC, confirming the liquid-like order of the mesophase. Magnetic susceptibility, electrical conductivity, NMR, and EPR measurements were also carried out on this compound in both the fluid phase and the gel phase formed in cyclohexane.<sup>379</sup>

Following this promising first result, a series of related copper complexes ((53): M=Cu, n=m=7–9, 11), as well as a few unsymmetric examples ((53): M=Cu; n=3, m=11; n=7, m=11; n=9, m=11) were prepared.<sup>380,381</sup> All the symmetric complexes were mesomorphic, showing a Col<sub>h</sub> mesophase, that of the heptyloxy derivative being monotropic (Table 33). “Double-melting” behavior was reported for the nonyloxy complex, and “double-clearing” was claimed for the octyloxy compound.<sup>381</sup> For the unsymmetrical complex, only that with the longest chain length was mesomorphic. Changing the ligand substitution pattern from the 3- and

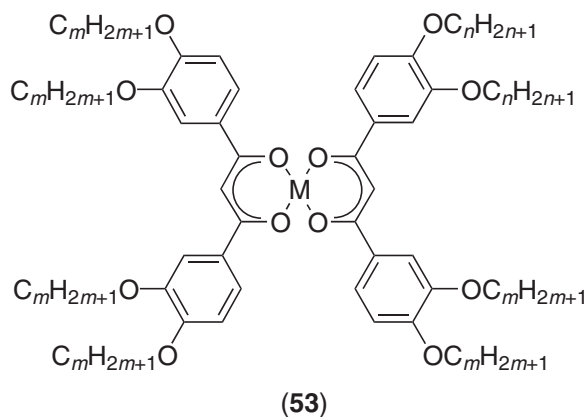


**Table 33** Mesomorphism of selected complexes (53) and (54).

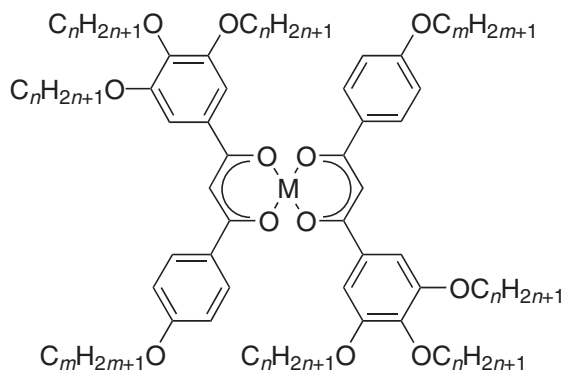
Complexes (53)				Complexes (54)			
<i>M</i>	<i>n</i>	<i>m</i>	Mesomorphism	<i>M</i>	<i>n</i>	<i>m</i>	Mesomorphism
Cu	7	7	Cr 119 (Col <sub>h</sub> 108) I	Cu	7	7	Cr 80 Col <sub>h</sub> 137 I
	8	8	Cr 111 Col <sub>h</sub> 113 I		8	8	Cr 83 Col <sub>h</sub> 140 I
	9	9	Cr 102 Col <sub>h</sub> 112 I		10	10	Cr 80.5 Col <sub>h</sub> 133 I
	11	11	Cr 103 Col <sub>h</sub> 108.5 I		12	12	Cr 80 Col <sub>h</sub> 127.5 I
	9	11	Cr 101 Col <sub>h</sub> 118 I		14	14	Cr 83 Col <sub>h</sub> 121 I
Pd	8	8	Cr 105 I	16	16	Cr 89.5 Col <sub>h</sub> 112 I	
	10	10	Cr 93 N <sub>D</sub> 97 I	8	8	Cr 77 Col <sub>h</sub> 144 I	
VO	8	8	Cr 99 (Col <sub>h</sub> 25) I	10	10	Cr 73 Col <sub>h</sub> 135 I	
	10	10	Cr 97 (Col <sub>h</sub> 32) I	12	12	Cr 71.5 Col <sub>h</sub> 130 I	

4-positions to the 3- and 5-positions,<sup>380</sup> or replacing the alkoxy chains by alkyl chains (i.e., octyl chains)<sup>381</sup> resulted in the complete suppression of the mesomorphism. On average, these copper complexes possessed higher melting and lower clearing temperatures than their four-chain analogs.

For this structural type, the metal appeared to influence the thermal behavior considerably. Liquid-crystalline properties were suppressed simply by the replacement of Cu<sup>II</sup> by Ni<sup>II</sup> ((53): M = Ni;  $n = m = 9$ : Cr 102 I),<sup>380</sup> while the palladium analogs melted directly to an isotropic phase (without decomposition) ((53): M = Pd;  $n = m = 6$  and 8) or, for  $n = m = 10$ , showed a narrow-range mesophase which, on account of its optical texture, was assigned as a discotic nematic phase, N<sub>D</sub> (Table 33)<sup>359</sup> In the case of the oxovanadium(IV) complexes, a complicated monotropic mesomorphism was observed for the octyloxy and decyloxy homologs.<sup>382</sup> The mesophases appeared only by super-cooling the isotropic liquid, and strongly depended on the thermal history, explaining why Poelsma *et al.* did not observe mesomorphism for the octyloxy derivative;<sup>359</sup> the mesophase was characterized tentatively as Col<sub>h</sub> by X-ray diffraction (Table 33). The X-ray structure determination of the butyloxy derivative revealed that the mesogenic cores were stacked with antiferroelectric order between successive vanadyl groups, and were tilted within the columnar structure, as in the case of some metallophthalocyanines (*vide supra*).

The bis- $\beta$ -diketonato complexes (54), isomeric with (53), were also studied, and the comparison of their mesomorphic properties was quite instructive. They differ in that one benzene ring of the ligand was substituted by three terminal chains in the 3-, 4-, and 5-positions respectively, while only one chain was attached to the other benzene ring in the *para* position. The molecular symmetry was thus reduced from  $D_{4h}$  (53) to  $D_{2h}$  (54). All the copper ((54): M = Cu;  $n = m = 5-8, 10, 12, 14, 16$ ) and palladium ((54): M = Pd;  $n = m = 8, 10, 12$ ) complexes thus prepared displayed enantiotropic Col<sub>h</sub> mesophases over much larger temperature ranges and at lower temperatures than their isomeric analogs (53) (Table 33).<sup>383,384</sup> The mesophases were characterized by powder X-ray diffraction, which showed small-angle reflections characteristic of a two-dimensional

hexagonal lattice, and a broad halo in the wide-angle region corresponding to the liquid-like correlations between the mesogenic cores. These results were in good agreement with a short-range stacking order, and consistent with the low clearing enthalpies. The palladium complexes had slightly more extended temperature ranges than their copper analogs, essentially due to their lower melting transition temperatures. The difference in the mesomorphic behavior between complexes of series (53) and those of series (54) was explained by the chain disposition around the rigid mesogenic core, and on the reduction of the molecular symmetry. In series (54), the molecular stacking was optimized through an alternating 90° rotation of neighboring complexes, and in such a way, the occupation of the available free volume was more efficient. In Table 33, the thermal behavior of some selected complexes of both series (53) and (54) are gathered for comparison.



(54)

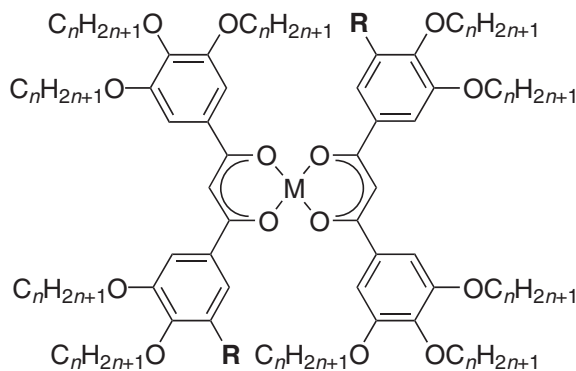
Replacing the single linear chain in copper complexes (54) by a branched chain modified the mesophase stability quite substantially.<sup>368</sup> Indeed, such copper complexes with a 1-methylbutyloxy chain ((54): M = Cu; OC<sub>m</sub>H<sub>2m+1</sub> = OCH(Me)C<sub>4</sub>H<sub>9</sub>, *n* = 8, 10, 12) were not mesomorphic, regardless of the alkoxy chain length, while those with 1-methylheptyloxy chain ((54): M = Cu; OC<sub>m</sub>H<sub>2m+1</sub> = OCH(Me)C<sub>6</sub>H<sub>13</sub>, *n* = 6–8, 10, 12) displayed a Col<sub>h</sub> phase. The mesophase stability depended on the alkoxy chain length, i.e., enantiotropic for *n* = 6, 8, and 10, and monotropic for *n* = 7, the dodecyloxy compound not being mesomorphic. The replacement of the single alkoxy chain by an alkanooate chain ((54): M = Cu, Pd; OC<sub>m</sub>H<sub>2m+1</sub> = -O<sub>2</sub>CC<sub>17</sub>H<sub>35</sub>, *n* = 10) resulted in a slight reduction in the transition temperatures, but still a large mesomorphic range was maintained ((54): M = Cu: Cr 60 Col<sub>h</sub> 116 I; M = Pd: Cr 53 Col<sub>h</sub> 120 I).<sup>385</sup> The dissymmetry of these complexes was increased by the substitution of the larger alkoxybenzoate group in place of the alkoxy chains ((54): M = Cu, Pd; OC<sub>m</sub>H<sub>2m+1</sub> = -O<sub>2</sub>CC<sub>6</sub>H<sub>4</sub>C<sub>17</sub>H<sub>35</sub>, *n* = 10), rendering the compounds more rod-like. Thus, this extension of the rigid core resulted in the reduction in the mesomorphic tendency, essentially associated to the better stability of the crystalline phases of the copper and palladium complexes, but the nature of the mesophase remained columnar ((54): M = Cu: Cr 78 Col<sub>h</sub> 106 I; M = Pd: Cr 91 Col<sub>h</sub> 115 I).

### (iii) Complexes with ten and twelve peripheral chains

The widest columnar mesophase temperature ranges were obtained for the bis-[1,3-di-(substituted-phenyl)-β-diketone] metal complexes bearing ten and twelve chains ((55): R = H or OC<sub>n</sub>H<sub>2n+1</sub>).<sup>382,386</sup> The ten-chain copper, palladium, and oxovanadium(IV) complexes ((55): M = Cu, Pd, VO; R = H, *n* = 6, 8, 10, 12, 14) were all mesomorphic and the enantiotropic mesophases were identified by optical texture and variable-temperature X-ray diffraction as columnar phases (Table 34). The copper and palladium complexes displayed a Col<sub>r</sub> phase for short chain length (*n* = 6, 8 for M = Cu; *n* = 6, 8, 10 for M = Pd), which transformed to a Col<sub>h</sub> phase as the chain length was increased. Surprisingly, no direct Col<sub>r</sub>-to-Col<sub>h</sub> phase transition was observed within the same compound, but weakly first-order Col<sub>r</sub>-to-Col<sub>r</sub> and Col<sub>h</sub>-to-Col<sub>h</sub> phase transitions were found for compounds with intermediate chain lengths. In contrast, the vanadium complexes exhibited only one Col<sub>r</sub> mesophase. Infrared studies indicated that the VO complexes possessed a linear V=O—V=O linear polymeric chain structure in the crystal phase, while no

**Table 34** Mesomorphic properties of *bis*-diketonato complexes (**55**).

<i>R</i>	<i>M</i> = Cu	<i>M</i> = Pd	<i>M</i> = VO
H, <i>n</i> = 8	Cr 78 Col <sub>r</sub> 142 Col <sub>r</sub> 149 I	Cr 36 Col <sub>r</sub> 158 I	Col <sub>r</sub> 141 I
H, <i>n</i> = 10	Cr 64 Col <sub>h</sub> 133 Col <sub>h</sub> 144 I	Cr 46 Col <sub>r</sub> 154 I	Col <sub>r</sub> 131 I
H, <i>n</i> = 12	Cr 69 Col <sub>h</sub> 104 Col <sub>h</sub> 135 I	Cr 44 Col <sub>h</sub> 134 Col <sub>h</sub> 146 I	Cr 24 Col <sub>r</sub> 122 I
OC <sub><i>n</i></sub> H <sub>2<i>n</i>+1</sub> , <i>n</i> = 8	Col <sub>h</sub> 68 (55 Col <sub>h</sub> 58 Col <sub>r</sub> 63 Col <sub>h</sub> 64) Col <sub>r</sub> 103 I	Col <sub>h</sub> 86 Col <sub>r</sub> 145 I	Cr 78 Col <sub>r</sub> 212 I
OC <sub><i>n</i></sub> H <sub>2<i>n</i>+1</sub> , <i>n</i> = 10	Col <sub>h</sub> 71 Col <sub>h</sub> 87 Col <sub>h</sub> 95 Col <sub>h</sub> 108 I	Col <sub>h</sub> 84 Col <sub>r</sub> 141 I	Cr 76 Col <sub>r</sub> 204 I
OC <sub><i>n</i></sub> H <sub>2<i>n</i>+1</sub> , <i>n</i> = 12	Cr 60 Col <sub>h</sub> 101.5 I	Col <sub>h</sub> 81 Col <sub>h</sub> 133 I	Cr 77 Col <sub>r</sub> 205 I

**(55)**

such polymeric association was detected for the other vanadyl complexes. Variable-temperature infrared experiments revealed that no such interactions were present in the mesophase.

In the series of complexes with twelve chains ((**55**): *M* = Cu, Pd, VO; *R* = OC<sub>*n*</sub>H<sub>2*n*+1</sub>, *n* = 6, 8, 10, 12, 14), an unusual phase sequence was observed (Table 34). The copper and palladium complexes displayed enantiotropic, disordered Col<sub>r</sub> and Col<sub>h</sub> phases, identified by their optical texture, and by X-ray diffraction. Quite uniquely, the Col<sub>h</sub> phase was systematically the lower-temperature mesophase, observed below the Col<sub>r</sub> phase. For the copper complexes, a Col<sub>r</sub> phase was seen for short-chain compounds with a transition to a Col<sub>h</sub> phase for *n* ≥ 10. The intermediate octyloxy derivative displayed an unusual, but reproducible, I–Col<sub>r</sub>–Col<sub>h</sub>–Col<sub>r</sub>–Col<sub>h</sub>–Col<sub>h</sub> phase sequence on cooling from the isotropic liquid, several of these transitions being weakly first order. The decyloxy analog displayed a Col<sub>h</sub>–Col<sub>h</sub>–Col<sub>h</sub>–Col<sub>h</sub> phase sequence, and the two next homologous compounds showed a single Col<sub>h</sub> phase. To have, supposedly, so many phases of apparently the same symmetry in a single material is most unusual and no explanation was offered to help understand the phenomenon. It is to be hoped that at some stage they may be subject to re-examination so that this exotic behavior may be properly understood.

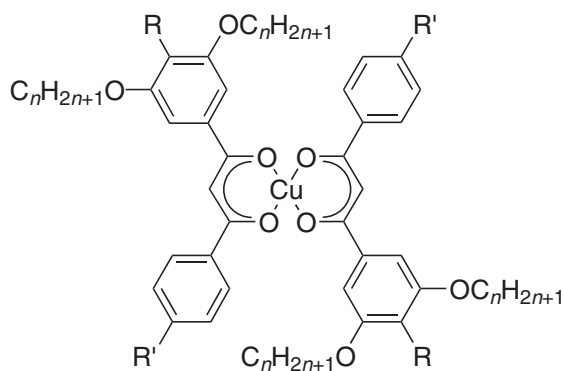
For the palladium complexes, more straightforward behavior was observed in that the shortest-chain homolog displayed a Col<sub>r</sub> phase, then a Col<sub>h</sub>–Col<sub>r</sub> phase sequence was seen at intermediate chain lengths (*n* = 8 and 10), and for *n* = 12 and 14, a Col<sub>h</sub>–Col<sub>h</sub> phase sequence was found (Table 34). The thermal behavior of the vanadyl complexes was more radically modified upon the increase of chain density. It was found that they had the highest clearing temperatures of all the twelve-chain compounds, while the opposite was true as far as the ten-chain complexes were concerned. While the hexyloxy homolog was crystalline, the octyloxy and decyloxy homologs displayed a crystalline rectangular phase, while the longest-chain complexes showed a Col<sub>r</sub> phase (Table 34). Results of the infrared investigations suggested the presence of weak, dative association in the mesophase.

Serrano and co-workers have investigated similar diketonato metal complexes bearing ten chiral aliphatic chains for potential uses as new types of ferroelectric discotic materials. The materials were obtained by replacement of the alkoxy chains of (**55**) by chiral chains derived from L-(–)-lactic acid (–<sub>2</sub>OCC\*H(Me)OC<sub>*n*</sub>H<sub>2*n*+1</sub>).<sup>387–389</sup> Six, new, ten-chain metal complexes were prepared ((**55**): *M* = Cu, Pd, VO; *R* = H, *n* = 6 and 7) and characterized fully. The NMR spectra

of the diamagnetic palladium complexes were consistent with the existence of the two *cis* and *trans* geometric isomers in the 1:1 ratio; infrared spectroscopy indicated the absence of polymeric chain structure for the vanadyl compounds. All the complexes were mesomorphic, showing an enantiotropic Col<sub>r</sub> mesophase from room temperature up to ~125 °C, ~130 °C, and ~150 °C for the VO, Cu, and Pd complexes, respectively. X-Ray diffraction revealed that the lattice of the Col<sub>r</sub> phase had a *pseudo*-hexagonal symmetry, with a *p2gg* plane group, and that the stacking periodicity was short range. An additional reflection was seen and attributed to the pitch of a helical superstructure. Such a superstructure was confirmed by circular dichroism and dielectric spectroscopy, and resulted from the stacking of tilted molecules whose tilt direction precessed along the columnar axis. Although the spontaneous polarization could not be evaluated due to the high conductivity of the materials, the electro-optical response was examined and found to be of the same magnitude to that of classical calamitic ferroelectric liquid crystals, and was in accordance with a strong molecular tilt with respect to the columnar axis. Note that such systems could find application in nonlinear optics applications.

(iv) Complexes with six peripheral chains

From the systematic study presented above, it was seen that the increase in chain density was correlated with the enhancement of the mesomorphic properties, and particularly of the columnar mesomorphism, with reductions in melting point increasing the mesomorphic range. These positive results allowed for practical physical measurements to be carried out, and for some properties to be investigated. However, the increase in aliphatic chains was usually accompanied by high viscosity, for example, slowing ferroelectric response times. Accounting for the empirical fact that at least a minimum of six chains are needed to obtain columnar mesophase, it was of interest to find out what was the most basic structural criteria with this type of material required to produce a columnar mesophase at accessible temperatures. Thus, Swager *et al.* synthesized several six-chained complexes ((**56**): R = OC<sub>n</sub>H<sub>2n+1</sub>; R' = H, n = 8, 12, 14).<sup>390</sup> This approach was successful in that these three complexes exhibited monotropic columnar hexagonal phases, contradicting another report<sup>383</sup> that the same copper complexes with decyloxy and dodecyloxy chains were not mesomorphic, and those with longer chain length (n = 14 and 16) exhibited an enantiotropic hexagonal columnar phase over narrow temperature ranges (n = 14: Cr 78 Col<sub>h</sub> 94 I; n = 16: Cr 79 Col<sub>h</sub> 91.5 I). The distribution of the chains around the mesogenic core was also studied and appeared to have dramatic effects in that the change of the chain substitution pattern ((**56**): R = H; R' = OC<sub>n</sub>H<sub>2n+1</sub>) led to the complete destruction of the mesomorphism in these isomeric compounds.<sup>368,383</sup>

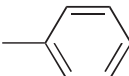
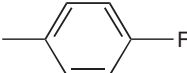
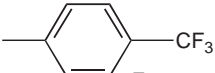
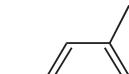
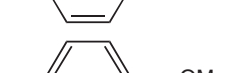
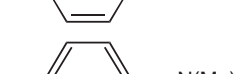
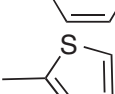


(**56**)

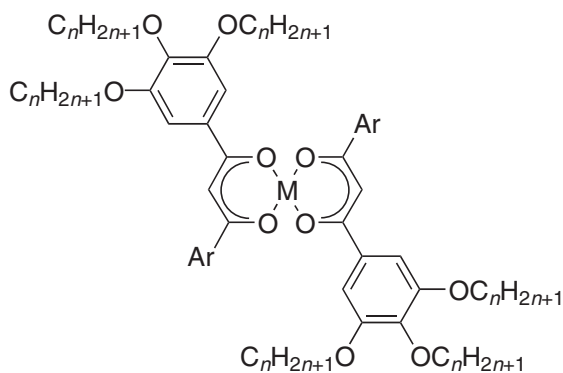
Stabilization of the mesomorphic properties of the six-chain  $\beta$ -diketonate complexes was nevertheless achieved by the replacement of the alkoxy phenyl group of (**56**) by substituted phenyl rings with polar groups (Ar) to yield complexes of type (**57**). Hence, enantiotropic, Col<sub>h</sub> mesophases were induced for the copper complexes (**57**) with Ar = *p*-C<sub>6</sub>H<sub>4</sub>F (n = 6, 8, 10, 12, 14), *p*-C<sub>6</sub>H<sub>4</sub>CF<sub>3</sub> (n = 12), *m*-C<sub>6</sub>H<sub>4</sub>F (n = 12), *p*-C<sub>6</sub>H<sub>4</sub>OMe (n = 12), thiophene (n = 8, 10, 12) (Table 35).<sup>390</sup> For the *para*-fluoro-substituted copper complexes, both the melting and clearing temperatures decreased when the chain length was increased, but a large mesomorphic range of ca. 60 °C was still preserved. On average, when the substituent was electron-withdrawing (e.g., F, CF<sub>3</sub>) the clearing temperatures were more elevated than



**Table 35** Mesomorphic properties of copper complexes (57) ( $n = 12$ ) with various R.

R	Mesomorphism
	Cr 82 (Col <sub>h</sub> 46) I
	Cr 60 Col <sub>h</sub> 115 I
	Cr 114 Col <sub>h</sub> 129 I
	Cr 80.5 Col <sub>h</sub> 108 I
	Cr 78 Col <sub>h</sub> 83 I
	Cr 127.5 I
	Cr 38 Col <sub>h</sub> 77 I

when it was electron-donating (e.g.,  $\text{OC}_n\text{H}_{2n+1}$ ). When Ar was a thiophene group, both melting and clearing temperatures were reduced (by ca.  $35^\circ\text{C}$  and  $65\text{--}75^\circ\text{C}$  respectively), but a minimum of eight methylene groups was found necessary to induce mesomorphism. For these non-discoid compounds, the mesophase formation resulted of the alternated stacking (rotation of  $90^\circ$ ) of nearest-neighbor molecules in order to generate a pseudo-circular, columnar core. Such molecular stacking was stabilized by the minimization of dipolar interactions. It is of interest to remark that related copper and palladium complexes with *p*- $\text{C}_6\text{H}_4\text{OH}$  ( $n = 10$ ) were not mesomorphic, probably due to the competitive formation of hydrogen bonding networks which do not favor the stacking of the compounds into disk-like dimeric units.<sup>385</sup>



(57)

Thus, this complete systematic study showed that mesomorphism in metal complexes of 1,3-bis(substituted-phenyl)- $\beta$ -diketonate was dependent on the metal and on the number and nature of terminal chains. To obtain columnar mesophases, a minimum of six chains was required. On average, the mesophase stability was found to increase with the number of chains, essentially due to a strong

**Table 36** Relationships between molecular structure and mesomorphism.

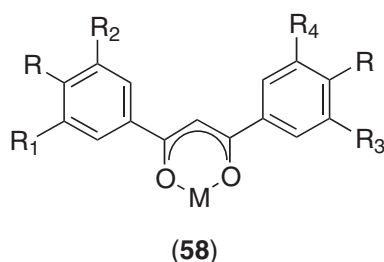
Complex chains	Number of Positions of chain substitution on the phenyl groups peripheral						Mesophases	Molecular symmetry and isomers
	3	4	5	3'	4'	5'		
(52)	2	•					Not LC	$C_{2h}$ , $C_{2v}$
(52)	4		•		•		$L_D$ , $D_L$ , $(Col_h)_h(N)$	$D_{2h}$ , $C_{2h}$ , $C_{2v}$
(56)	6	•		•	•		Not LC	$C_{2h}$ , $C_{2v}$
(56)	6	•	•	•			$Col_h$	$C_{2h}$ , $C_{2v}$
(53)	8	•	•		•	•	$Col_h$ , $N_D$	$D_{2h}$
(53)	8	•		•	•	•	Not LC	$D_{2h}$
(54)	8	•	•	•	•	•	$Col_h$	$C_{2h}$ , $C_{2v}$
(55)	10	•	•	•	•	•	$Col_h$ , $Col_r$	$C_{2h}$ , $C_{2v}$
(55)	12	•	•	•	•	•	$Col_h$ , $Col_r$	$D_{2h}$

decrease in the melting point. An important and influential parameter on these properties was the position of substitution of the chains, and the degree of dissymmetry. These relationships between mesomorphism and molecular structure have been summarized in Table 36.

#### 7.9.8.1.4 Mono-, tris-, and tetrakis-[1,3-substituted-phenyl- $\beta$ -diketonato] metal complexes

Other metals have been used to complex diketonato ligands to form mono-, tris-, and tetrakis-[1,3-di-(substituted-phenyl)- $\beta$ -diketonato] metallomesogens. Despite the fact that the molecular structures of such complexes diverge radically from a disk shape, most of them exhibited columnar mesophases.

Barberá *et al.* prepared a series of thallium(I) complexes, in which the position and number of side chains were changed systematically ((58):  $M = Tl$ ).<sup>391</sup> A minimum of four chains was required to induce mesomorphism in these systems (Table 37), and on the basis of X-ray diffraction, the monotropic mesophases were identified as  $Col_h$ . The formation of the columns was due to the association of these half-disk compounds into dimers, and to their subsequent stacking. The dimeric nature of these thallium(I) complexes was confirmed by the analysis of the single-crystal structure of the non-mesomorphic dimethoxy analog.<sup>392</sup> In the crystalline phase, the co-planar

**Table 37** Mesomorphism of complexes (58).

<i>M</i>	Substitution pattern	Mesomorphism
Tl	$R = OC_{10}H_{21}$ , $R_1 = R_2 = R_3 = R_4 = H$	Cr 85 I
Tl	$R = R_1 = R_3 = OC_{10}H_{21}$ , $R_2 = R_4 = H$	Cr 94 ( $Col_h$ 75) I
Tl	$R = H$ , $R_1 = R_2 = R_3 = R_4 = OC_{10}H_{21}$	Cr 65 I
Tl	$R = R_1 = R_2 = R_3 = OC_{10}H_{21}$ , $R_4 = H$	Cr 75 ( $Col_h$ 69) I
Rh(CO) <sub>2</sub>	$R = OC_8H_{17}$ , $R_1 = R_2 = R_3 = R_4 = H$	Not LC
Rh(CO) <sub>2</sub>	$R = R_1 = R_2 = OC_nH_{2n+1}$ , $R_3 = R_4 = H$	Not LC
Ir(CO) <sub>2</sub>	$R = R_1 = R_2 = OC_nH_{2n+1}$ , $R_3 = R_4 = H$	Not LC
Rh(CO) <sub>2</sub>	$R = R_1 = R_2 = R_3 = R_4 = OC_nH_{2n+1}$	$Col_h$
Ir(CO) <sub>2</sub>	$R = R_1 = R_2 = R_3 = R_4 = OC_nH_{2n+1}$	$Col_h$

dimer resulted from the strong Tl—Tl bonding interactions ( $\sim 3.75 \text{ \AA}$ ), and the stacking into columns was promoted by the axial Tl—O interactions between close neighbors. It is regarded as likely that these interactions persist into the mesophase.

Trzaska *et al.* reported the mesomorphic behavior of the two series of diketonato complexes of dicarbonyl-rhodium(I) and -iridium(I) ((58):  $M = \text{Ir}(\text{CO})_2, \text{Rh}(\text{CO})_2$ ;  $R = R_1 = R_2 = R_3 = R_4 = \text{OC}_n\text{H}_{2n+1}$ ,  $n = 4, 6, 8, 10, 12, 14, 16, 18$ ).<sup>393</sup> All the complexes exhibited a  $\text{Col}_h$  phase over large temperature ranges, and they were well characterized by X-ray diffraction. The mesophase stability was found to be dependent on the length of the chains, increasing chain length being correlated with a smooth decrease in the clearing temperature ( $129\text{--}73^\circ\text{C}$  for  $M = \text{Rh}$ ;  $143\text{--}93^\circ\text{C}$  for  $M = \text{Ir}$ ). The melting temperatures were high for the first homolog ( $n = 4$ ), then room-temperature mesophases were observed from the hexyloxy to the decyloxy homologs, and then for longer-chain complexes, the melting temperatures rose again, resulted in the narrowing of the mesomorphic range. X-Ray diffraction data suggested that the complexes stacked into columns in an antiparallel arrangement, consistent with the dipoles associated with the carbonyl groups preferentially aligning antiparallel, and to the strong steric effects of the chains which would favor a dimeric, disk-shaped unit. Reducing the number of chains led to non-mesomorphic compounds.<sup>394</sup>

As mentioned above, mesomorphism was also observed in some tris-[1,3-(substituted-phenyl)- $\beta$ -diketonato]metal complexes, obtained from metals with octahedral coordination geometry. In an attempt to obtain octahedral-based liquid crystal, Giroud-Godquin and Rassat<sup>395</sup> prepared the tris-[1,3-di-(*p*-dodecylphenyl)- $\beta$ -diketonato]iron(III) complex ((59):  $R = \text{C}_{12}\text{H}_{25}$ ;  $R_1 = R_2 = R_3 = R_4 = \text{H}$ ). The high viscosity of the phase, observed on both heating and cooling between  $-10^\circ\text{C}$  and  $51^\circ\text{C}$ , suggested a very ordered situation, also evidenced by strong supercooling of the isotropic liquid, and large clearing enthalpy; the nature of the phase has nevertheless not yet been elucidated. Ten years later, Swager and co-workers<sup>396–398</sup> re-investigated related complexes and prepared the dodecyloxy analogous to that reported by Giroud-Godquin. This complex also showed a highly viscous mesophase between  $82^\circ\text{C}$  and  $154^\circ\text{C}$ , at which temperature it melted into the isotropic liquid; X-ray diffraction studies revealed a highly ordered lamellar phase. They also prepared several series of tris-( $\beta$ -diketonato) complexes of iron(III), cobalt(III), manganese(III), and chromium(III), using more highly substituted ligands. In these systems, the ligand possessed either 4, 5, or 6 alkoxy chains, leading to complexes having twelve ( $N = 12$ ), fifteen ( $N = 15$ ), and eighteen ( $N = 18$ ) alkoxy chains on their periphery. All the complexes were mesomorphic, displaying columnar mesophases from room temperature to slightly above  $\sim 100^\circ\text{C}$  for  $N = 12$  ((59):  $R = R_1 = R_2 = \text{OC}_{12}\text{H}_{25}$ ;  $R_3 = R_4 = \text{H}$ ), around  $\sim 90^\circ\text{C}$  for  $N = 15$  ((59):  $R = R_1 = R_2 = R_3 = \text{OC}_{12}\text{H}_{25}$ ;  $R_4 = \text{H}$ ) and around  $\sim 70^\circ\text{C}$  for  $N = 18$  ((59):  $R = R_1 = R_2 = R_3 = R_4 = \text{OC}_{12}\text{H}_{25}$ ). This decrease in the clearing temperatures was attributed to the stronger dispersion forces arising from the greater number of chains. The number of chains also influenced the nature of the mesomorphism, sometime in conjunction with the metal (Figure 37). Thus, both series of complexes with  $N = 15$  and 18 exhibited a single  $\text{Col}_h$  phase, with very little influence of the metal and the chain density on the transition temperatures, presumably as the metal was well encapsulated within a dense aliphatic sphere. However, the three compounds with  $N = 12$ , and, therefore, with a less dense peripheral coverage of aliphatic groups, showed polymorphism, with a first-order  $\text{Col}_h$ -to- $\text{Col}_h$  phase transition for  $M = \text{Fe}$  and  $\text{Mn}$  (at ca.  $90^\circ\text{C}$  and  $60^\circ\text{C}$  respectively), and a  $\text{Col}_h$ - $\text{Col}_r$  phase transition for  $M = \text{Cr}$  and  $\text{Co}$  (at ca.  $60^\circ\text{C}$ ). The difference in mesophase stability and symmetry was likely due to the dynamics of the phenyl groups and the distortion of the octahedral arrangement around the metal ions (particularly for the fluxional, high-spin  $\text{Fe}^{\text{III}}$  and Jahn–Teller-distorted  $\text{Mn}^{\text{III}}$  species). A possible model for the structure of the columnar phases is sketched in Figure 34. These octahedral complexes have approximate  $D_3$  symmetry, and exist as two optical isomers  $\Delta$  and  $\Lambda$ . Since they should be present in a 50:50 ratio, they could be distributed randomly in a column, however with important mismatches in the structure. Another possibility that would give a more efficient packing is to consider a stacking of the complexes of identical absolute configuration about the metal center, in such a way that a net polarization is induced in the columnar axis direction (Figure 34). This would also mean that the complexes have the possibility to interconvert between the  $\Delta$  and  $\Lambda$  isomers (Figure 35), and that one species dominates over the other one. To support this idea, crystallographic analysis of a methoxy analogous complex indicates that the complexes were stacked into enantiomerically pure columns. In  $\text{Col}_h$  phase, the symmetry is such that the net dipole of every column cannot be cancelled out by the one of the neighboring column; that is, a perfectly antiferroelectric arrangement of the columns is precluded; the system is frustrated (Figure 36), and, thus, a net polarization must result in the columnar phase. In order to arrange enantiomerically pure columns onto a hexagonal

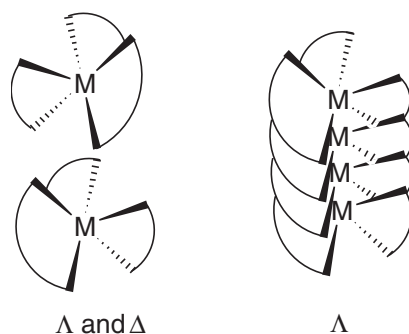


**Figure 34** The two stacking possibilities: equimolar amount of  $\Delta$  and  $\Lambda$  isomers or one pure enantiomeric column.

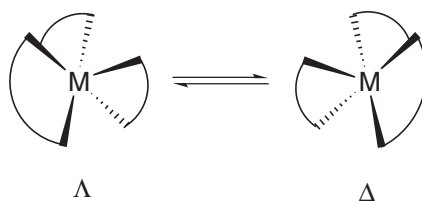


**Figure 35** Interconversion between  $\Delta$  and  $\Lambda$  isomers.

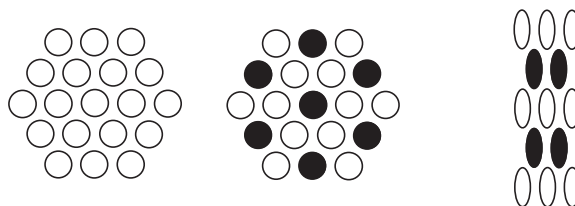


**Figure 36** Normal hexagonal lattice (uniform chirality), hexagonal superlattice (one chirality dominates), rectangular lattice (equal amount of each chirality).

lattice, one has to consider a superlattice where one chirality dominates. In the case of static chirality, i.e., conformationally locked complexes such as the  $\text{Cr}^{\text{III}}$  and  $\text{Co}^{\text{III}}$  species, a rectangular structure, which contains two columns in the lattice, can accommodate both  $\Delta$  and  $\Lambda$  isomers in equal amounts. This model was successfully verified by replacing the twelve alkoxy chains by twelve *R*- and *S*-chiral citronellyl side chain with both the iron and cobalt complexes ((**59**):  $\text{R} = \text{R}_1 = \text{R}_2 = R/S\text{-O}(\text{CH}_2)_2\text{C}^*\text{HMe}(\text{CH}_2)_3\text{CHMe}_2$ ;  $\text{R}_3 = \text{R}_4 = \text{H}$ ). Indeed, all these new complexes exhibited a single  $\text{Col}_h$  mesophase from room temperature to ca.  $80\text{--}90^\circ\text{C}$  (Figure 37). This revealed a strong, cooperative, chiral effect, and also showed that such molecules can resolve spontaneously into microdomains with a defined net chirality.

Finally, here, diketonate ligands have been used to form square-antiprismatic tetrakis-( $\beta$ -diketonato)zirconium(IV) complexes, (**60**).<sup>399</sup> These new and original structures are best described as a sandwich of two pairs of  $\beta$ -diketonate ligands bound to the zirconium ion, quite similar to the bis(phthalocyaninato)lanthanide complexes discussed above. However, the two *pseudo*-disk-like pairs of ligands are rotated with each other in a staggered conformation. The complexes with 24 chains ((**60**):  $\text{R}_1 = \text{R}_2 = \text{OC}_n\text{H}_{2n+1}$ ) displayed a room-temperature  $\text{Col}_h$  phase to  $49^\circ\text{C}$  ( $n = 8$ ) and  $45^\circ\text{C}$  ( $n = 10$ ), while that with 16 chains was not mesomorphic ((**60**):  $\text{R}_1 = \text{OC}_8\text{H}_{17}$ ;  $\text{R}_2 = \text{H}$ ), melting to the isotropic liquid at  $97^\circ\text{C}$ . The strong reduction in mesophase stability as compared to the analogous square-planar complexes with twelve chains was attributed to the important deviation from planarity of the ligands and to the fluxional nature of the zirconium(IV) center (Figure 38). Dramatic effects were observed when the linear chains were replaced by branched aliphatic tails ((**60**):  $\text{R}_1 = \text{R}_2 = R/S\text{-O}(\text{CH}_2)_2\text{C}^*\text{HMe}(\text{CH}_2)_3\text{CHMe}_2$ ). Indeed, mesomorphism was preserved, even stabilized as evidence of the increase of the clearing temperatures by approximately  $20^\circ\text{C}$  and the phase changed (X-ray evidence) from hexagonal to oblique (*R*-compound:  $\text{Col}_o$  68.5 I; *S*-compound:  $\text{Col}_o$  71.5 I).

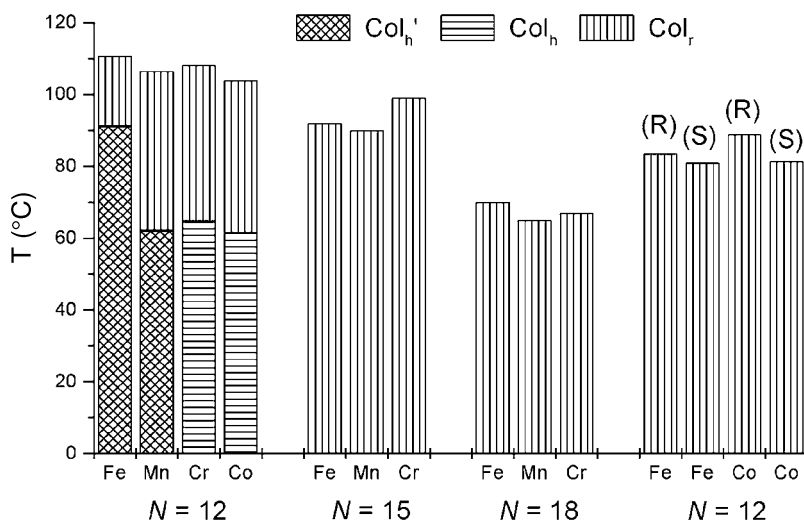
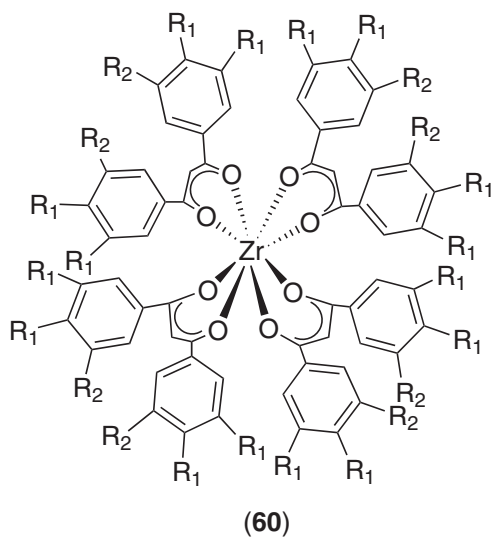
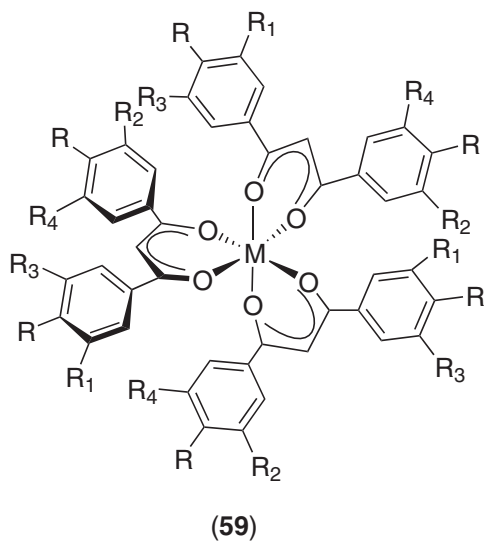


Figure 37 Relationships between molecular structure and mesomorphism.



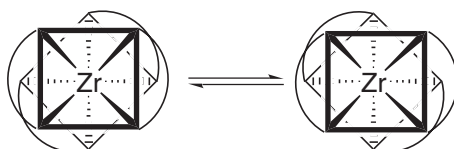
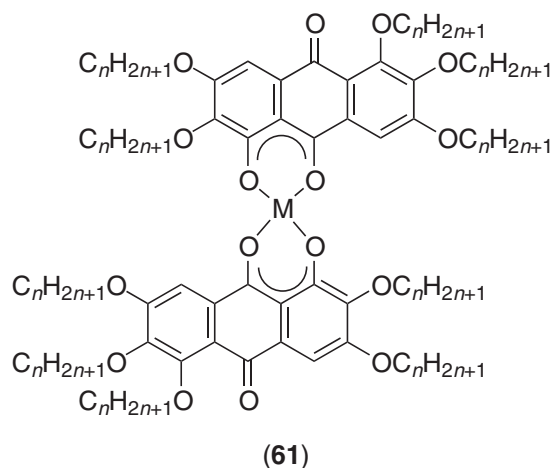


Figure 38 Fluxionality in square anti-prismatic complexes of zirconium(IV).

### 7.9.8.2 Copper Complexes of Anthraquinones

Due to the similarity between 1-hydroxy-2,3,5,6,7-pentakis(alkoxy)-9,10-anthraquinone and the  $\beta$ -diketone systems, it is expected that the rich chemistry that has been developed to the latter can be applied to the former, and, thus, the potential to develop a new family of metallomesogens can be envisaged. This idea has been tested recently by Kumar *et al.*<sup>400,401</sup> who prepared 1-hydroxy-2,3,5,6,7-pentakis(alkoxy)-9,10-anthraquinone, and the corresponding copper and palladium complexes ((**61**): M = Cu, Pd,  $n = 6, 12$ ). The ligand was prepared from 1,2,3,5,6,7-hexahydroxy-anthraquinone (rufigallol), which was then converted in three steps to the pentakis (alkoxy)-monoacetoxyanthraquinone, and then hydrolyzed to the desired monofunctionalized anthraquinone derivative. The ligands showed a monotropic columnar phase. Treatment of such anthraquinones with copper(II) acetate or palladium(II) acetate led to the desired complexes, (**61**). Complexes of both metals with dodecyloxy chains exhibited two mesophases, identified as Col<sub>r</sub> and Col<sub>h</sub> from their optical texture (M = Cu: Cr 72 Col<sub>r</sub> 121 Col<sub>h</sub> 146 I; M = Pd: Cr 68 Col<sub>r</sub> 138 Col<sub>h</sub> 168 I); the palladium complex decomposed in the isotropic liquid. Complexation of the ligand with hexyloxy chains to copper(II) gave a material which was not mesomorphic, melting at 171 °C. However, doped with an equimolar amount of the electron-acceptor TNF, the viscous 1:1 charge-transfer complex exhibited a columnar mesophase up to 232 °C, at which temperature it cleared. Again, the mesophase remained stable down to ambient temperature. These first interesting results opened new possibilities in designing metallomesogens containing anthraquinone cores with various substitution patterns and mixed with other ligands.



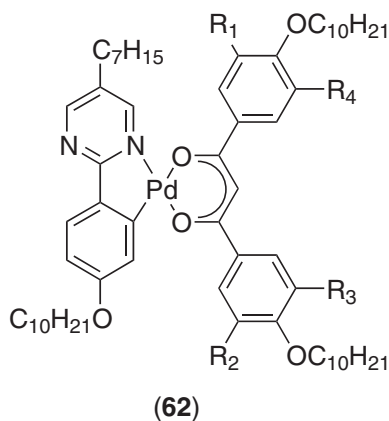
### 7.9.8.3 Mixed Phenylpyrimidine-1,3-(Substituted-Phenyl)- $\beta$ -diketonato)Metal Complexes

Hegmann *et al.* described an interesting concept for controlling the mesophase structure of novel molecules close to the calamitic/discotic cross-over point by combining a calamitic sub-unit, namely disubstituted 2-phenylpyrimidine, and a half-discotic moiety, i.e., substituted 1,3-diketonate, via *ortho*-palladation. The number of side chains on the diketonate fragment was increased step by step so that the overall molecular structure changed stepwise to a disk-like molecular shape. This type of study is important, in that with such molecular structures, mesophase transformation may occur through several intermediate mesophases including Cub, D<sub>L</sub>, L<sub>D</sub>, L<sub>Col</sub>, Col<sub>r</sub>, and N<sub>b</sub> phases, allowing for a better understanding of the intimate relationships between these different mesophases. This led to a novel series of liquid-crystalline, mononuclear *ortho*-palladated complexes ((**62**): R<sub>1</sub>, R<sub>2</sub>, R<sub>3</sub>, R<sub>4</sub> = H or OC<sub>10</sub>H<sub>21</sub>)<sup>402</sup> for which a discontinuous change from smectic to columnar mesophases was witnessed with increasing number of chains

**Table 38** Transitions temperatures of (62).

$R_1$	$R_2$	$R_3$	$R_4$	Pure compounds	Charge-transfer complexes
H	H	H	H	Cr 113 SmC 117 SmA 133 I	SmA <sub>b</sub> 178 Col 210 I
OC <sub>10</sub> H <sub>21</sub>	H	H	H	Cr 117 (SmA 101) I	SmA <sub>b</sub> 162 Col 179 I
OC <sub>10</sub> H <sub>21</sub>	OC <sub>10</sub> H <sub>21</sub>	H	H	Cr 115 I	SmA <sub>b</sub> 128 Col 165 I
OC <sub>10</sub> H <sub>21</sub>	OC <sub>10</sub> H <sub>21</sub>	OC <sub>10</sub> H <sub>21</sub>	H	Cr 72 Col <sub>h</sub> 134 I	
OC <sub>10</sub> H <sub>21</sub>	OC <sub>10</sub> H <sub>21</sub>	OC <sub>10</sub> H <sub>21</sub>	OC <sub>10</sub> H <sub>21</sub>	Cr 79 Col <sub>h</sub> 163 I	

(Table 38). Thus, the first compound of the series with a total number of four chains showed both SmC and SmA phases. Increasing the number of chains to five led to destabilization of the mesophase, and monotropic behavior, whereas with six chains, the mesomorphism was suppressed totally. Mesomorphism was then regenerated with the further increase in the number of chains, and Col<sub>h</sub> phases were formed. Moreover, the mesophase stability was enhanced on increasing the number of chains from seven to eight. The decrease in the mesophase stability of both the unsymmetrically compounds (five- and seven-chained compounds) relative to the corresponding symmetrical analogs (four- and eight-chained compounds) was attributed to the fact that the former were obtained as a *cis/trans* isomeric mixtures with respect to the pyrimidine ring, and in a 1:1 ratio as deduced from NMR. The reasons for the absence of mesomorphism in the six-chained compound are not yet understood. Interestingly, a binary phase diagram between the two unsymmetrical compounds revealed the induction of another birefringent mesophase at the contact region, with the destabilization of both mesophases of the pure compounds.



The existence of the biaxial SmA phase (SmA<sub>b</sub>)<sup>403</sup>, also known as the McMillan phase, has recently been demonstrated in some charge-transfer complexes formed with the metallomesogens (62) and TNF by textural observations and X-ray investigations (Like the biaxial nematic phase mentioned earlier, the SmA<sub>b</sub> phase has additional long-range order in a direction perpendicular to the principal director, (Figure 7a)). Two novel mesophases were induced systematically (Table 38). At low TNF concentration, an ill-defined mesophase with a structure different to that of the pure compound was formed, which remained stable at high temperature and up to high concentration of TNF (ca. 60 mol.%). X-Ray diffraction and optical textures suggested a columnar type of mesophase. At higher concentration of TNF, i.e., upwards from 20 mol.%, the three charge-transfer complexes formed the SmA<sub>b</sub> phase. By X-ray diffraction, the charge-transfer complexes self-organized into layers, with the flat molecules arranged parallel to each other, and orthogonal to the layers, with a long-range face-to-face organization, and short side-by-side correlations. This face-to-face interactions considerably hindered the molecular rotation around the long axis, reducing the symmetry and hence the phase is biaxial.

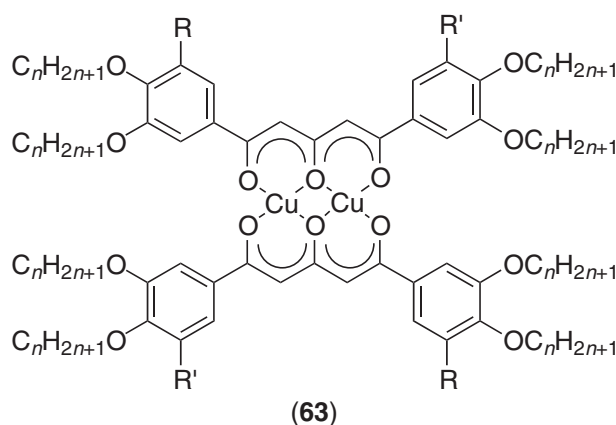
#### 7.9.8.4 Triketonato and Tetraketonato Metal Complexes

Swager has also conducted an interesting and innovative study on discotic bimetallic complexes based on 1,3,5-triketonoate and 1,3,5,7-tetraketonate ligands (63–66).<sup>404,405</sup> All the polyketonate

**Table 39** Mesomorphism of (63) and (64).

63	<i>n</i>	Mesomorphism	
R = R' = H	10	Cr 151.5 Col <sub>h</sub> 231 dec.	
	16	Cr 135 Col <sub>h</sub> 187 I	
	R = OC <sub>n</sub> H <sub>2n+1</sub> , R' = H	10	Cr 120.5 Col <sub>h</sub> 192 I
		6	Cr 98 Col <sub>r</sub> 218 I
	R = R' = OC <sub>n</sub> H <sub>2n+1</sub>	8	Cr 72 Col <sub>r</sub> 190 I
		10	Cr 67 Col <sub>r</sub> 181 I
		12	Cr 55.5 Col <sub>h</sub> 164 I
		14	Cr 65 Col <sub>h</sub> 148 I
		16	Cr 73 Col <sub>h</sub> 140.5 I
		(64)	6
	10	Cr 125.5 Col <sub>h</sub> 193 I	
	12	Cr 74 Col <sub>h</sub> 159 I	

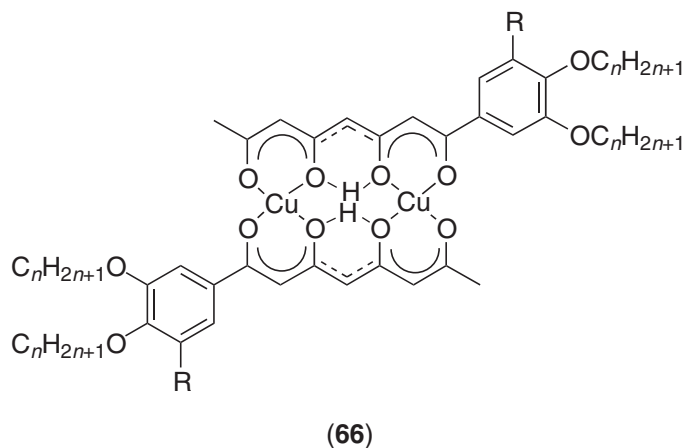
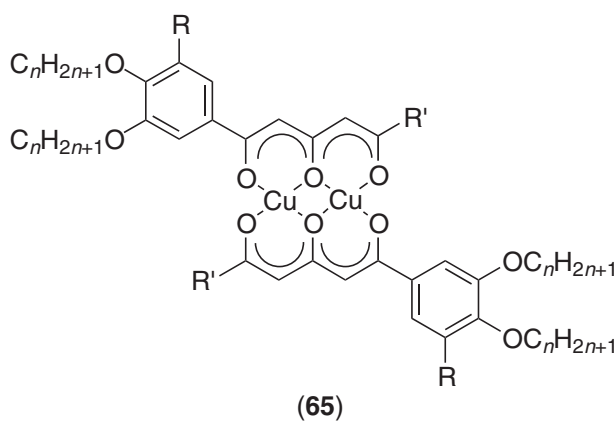
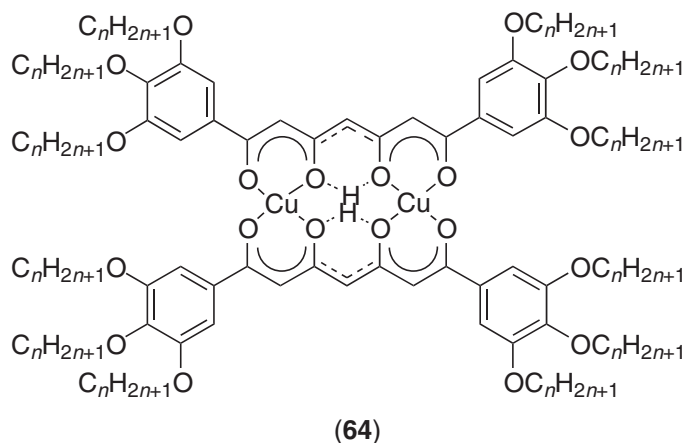
ligands were prepared using cross-Claisen condensation reactions, and the dicopper complexes were obtained directly by ligand exchange between the appropriate polyketonate and an excess of copper(II) acetate; all these complexes existed as *trans*-regioisomers as determined by infrared spectroscopy. Again, none of the new ligands was mesomorphic, but as expected due to their extended rigid core, most of the dicopper complexes were found to exhibit columnar mesophases (Table 39). Three series of complexes of type (63) having an almost disk-like shape were prepared, and the mesomorphism was found to depend on the number of chains. Complexes (63) with twelve chains ((63): R = R' = OC<sub>n</sub>H<sub>2n+1</sub>) displayed a Col<sub>r</sub> mesophase (*c2mm*) for shorter-chain-length ( $n \leq 10$ ), and a Col<sub>h</sub> phase for the longer-chain-length homologous compounds ( $n \geq 12$ ). The change in the two-dimensional mesophase symmetry was ascribed to the greater molecular anisotropy of the shorter side chain homologs (more elliptical) than the longer side chain complexes. The reduction of the number of chains to ten ((63): R = OC<sub>n</sub>H<sub>2n+1</sub>; R' = H) and eight ((63): R = R' = H) respectively did not suppress the mesomorphic properties – a Col<sub>h</sub> phase was observed in all cases – but resulted in an increase in both the crystal-to-mesophase and mesophase-to-isotropic liquid transition temperatures with respect to the twelve-chain parent compounds. For the latter two series, X-ray diffraction also revealed an additional halo in the wide-angle region (at ca. 3.4 Å), suggesting a more tight and regular packing of the flat rigid cores, in agreement with the higher mesophase stability.



The disk-like tetraketone derivatives (64), having twelve chains, displayed a single Col<sub>h</sub> mesophase over a wide temperature range whatever the chain length, and despite their larger core, the transition temperatures were similar to those of the related triketonate complexes (Table 39). On average, the mesophase stability and temperature range have been enhanced substantially when compared to the related monometallic *bis*(diketonato)copper(II) complexes discussed above, suggesting stronger intermolecular interactions consistent with the increase in the extent of the mesogenic cores.

Providing that the number of peripheral chains was appropriate (at least six), the non-discoid triketonate, (65), and tetraketone, (66), displayed a Col<sub>h</sub> phase (Table 40), with a more regular





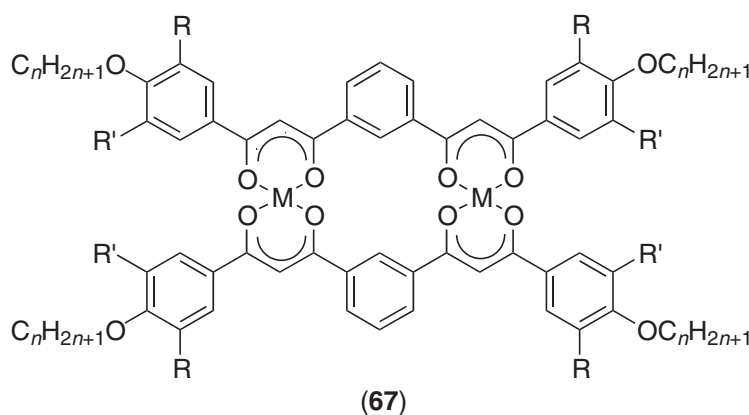
packing of the flat rigid cores for **(65)** (second halo at ca. 3.3 Å) than for **(66)**. Compounds **(65)** exhibited rather high clearing temperatures, and decomposition often occurred before reaching the isotropic phase. The mesomorphic range, as well as the transition temperatures, were found to decrease with increasing chain length. The most dramatic effect on these properties was observed with the nature of the R' substituent (**(65)**: R' = Me or CF<sub>3</sub>). Indeed, the substitution of the methyl group by the electron-withdrawing CF<sub>3</sub> group resulted in a considerable increase in melting point, although the increase was much less pronounced in its effect on the clearing point. The structurally related complex **(66)**, having a larger central core, was also mesomorphic when it possessed six chains, exhibiting a Col<sub>h</sub> phase at much lower temperature than its analog **(65)**. In order to explain

**Table 40** Mesomorphism of (65) and (66).

Compound	$R, R'$	$n$	Mesomorphism	
(65)	$R = H, R' = Me$	16	Cr 159 I	
	$R = OC_nH_{2n+1}, R' = Me$	6	Cr 139 Col <sub>h</sub> 247 dec.	
		8	Cr 129 Col <sub>h</sub> 237 dec.	
		10	Cr 102 Col <sub>h</sub> 220 I	
		12	Cr 95 Col <sub>h</sub> 205 I	
		14	Cr 88 Col <sub>h</sub> 192 I	
		16	Cr 91.5 Col <sub>h</sub> 178 I	
(66)	$R = OC_nH_{2n+1}, R' = CF_3$	10	Cr 156 Col <sub>h</sub> 221.5 I	
		14	Cr 123 Col <sub>h</sub> 205 I	
		12	Cr 173 I	
		$R = H$	12	Cr 57 Col <sub>h</sub> 165 I
			12	
			12	

the formation of a columnar mesophase in these systems, one has to consider the existence of a highly correlated structure in the mesophase, as in complexes of type (58) described above. Hence, complexes (65) and (66) adopt a disk-like shape through time-averaged structures with nearest neighbors rotated by 90°. This model was supported by the diameters of the columns of compounds (63) and (64) which have almost identical values to those of compounds (65) and (66). Finally, it is interesting to note that all the tetraketonates have lower transition temperatures than the respective triketonate analogs. This may be explained by the greater flexibility of the former systems (bending and twisting deformations), and the consequent greater fluctuations in the mesophase.

Other bimetallic tetraketonato complexes (67), similar to (63) and (64), were reported in a short communication, in which the two metal centers were not in close proximity but remote from each other.<sup>406</sup> These bimetallic complexes were obtained in high yields using the standard complexation methods. The dicopper complexes with eight and twelve chains ((67):  $R = OC_nH_{2n+1}, R' = H$ ;  $R = R' = OC_nH_{2n+1}$ ) were mesomorphic (Table 41), showing a Col<sub>h</sub> mesophase, providing that the chains contained at least ten methylene groups. The transition temperatures, as well as the mesomorphic ranges, were reduced upon the grafting of additional chains. The increase and the stiffening of the mesogenic cores yielded materials with greater mesophase stability than the related, less rigid dicopper complexes (63) and (64). As far as the divanadyl compounds were concerned, only those with twelve chains ( $n \geq 10$ ) were mesomorphic; again, a Col<sub>h</sub> phase was identified by X-ray diffraction (Table 41). In these materials, the Col<sub>h</sub> phase occurred at much lower temperature than for the dicopper complexes. This difference in mesophase stability may be attributed to the non-planarity and to the geometry of the divanadyl centers which can be either *syn* or *anti*, and to the consequent steric hindrance which reduces the packing efficiency.

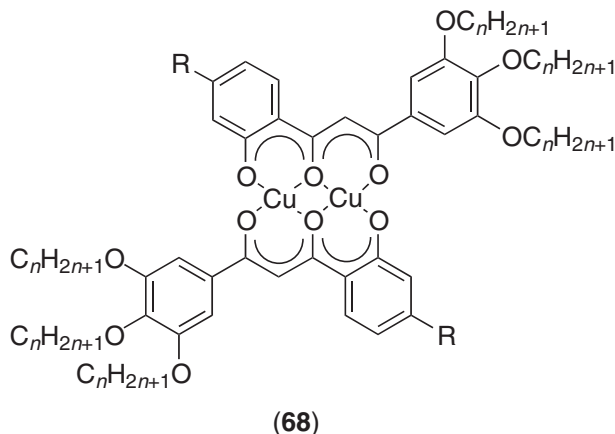


The latest developments in this class of metal complexes were concerned with the structural modification of the triketone ligands to the  $\beta, \delta$ -type. Two series of dicopper complexes were obtained with six and eight peripheral chains respectively ((68):  $R = H$  or  $OC_nH_{2n+1}$ ).<sup>407</sup> Not surprising, they all showed a Col<sub>h</sub> phase, the complexes with eight chains having lower transition

**Table 41** Thermal behavior of (67).

<i>M</i>	<i>R</i>	<i>R'</i>	<i>n</i>	<i>Mesomorphism</i>
Cu	H	H	12,18	Cr 250 to 300 I
	OC <sub><i>n</i></sub> H <sub>2<i>n</i>+1</sub>	H	12	Cr 132 Col <sub>h</sub> 254 I
			14	Cr 127 Col <sub>h</sub> 233 I
			16	Cr 123.5 Col <sub>h</sub> 219 I
			10	Cr 108 Col <sub>h</sub> 236 I
	OC <sub><i>n</i></sub> H <sub>2<i>n</i>+1</sub>	OC <sub><i>n</i></sub> H <sub>2<i>n</i>+1</sub>	12	Cr 100 Col <sub>h</sub> 193 I
14			Cr 91 Col <sub>h</sub> 169 I	
VO	H	H	12	Not LC
	OC <sub><i>n</i></sub> H <sub>2<i>n</i>+1</sub>	H	10,12,16	Not LC
			10	Cr 78.5 Col <sub>h</sub> 224 I
	OC <sub><i>n</i></sub> H <sub>2<i>n</i>+1</sub>	OC <sub><i>n</i></sub> H <sub>2<i>n</i>+1</sub>	12	Cr 60.5 Col <sub>h</sub> 188 I
			14	Cr 49 Col <sub>h</sub> 159.5 I

temperatures and mesomorphic temperature ranges than those with six chains (Table 42). This is likely due to the flexible bulky side chain, which disturbs the optimization of the intermolecular interactions and the efficiency of the stacking into columns. The complexes with six chains are more rod-like in shape than those with eight, and thus, in order to form columns, the molecules must stack in an alternating fashion (rotation of 90° between nearest neighbors). The authors also mentioned that the thermal behavior was dependent on the chain density of the phenyl ring. Indeed, liquid crystallinity was suppressed totally in derivatives substituted by 4-alkoxyphenyl (having a total of four peripheral alkoxy chains) and 3,4-dialkoxyphenyl (eight peripheral chains).

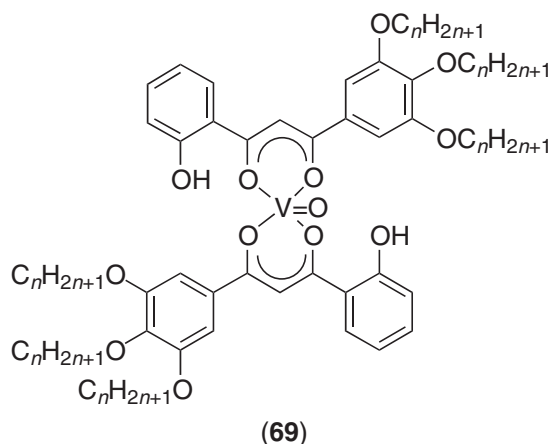


However, all attempts to generate the structurally related divanadyl complexes of (68) failed.<sup>408</sup> Indeed, only the mononuclear species (69) could be obtained, as confirmed by EPR studies and crystal and molecular structures, leaving the phenolic oxygen atom unbound. All the complexes with six chains ( $n \geq 5$ ) were mesomorphic displaying a Col<sub>h</sub> mesophase, as demonstrated unambiguously by X-ray diffraction. The clearing temperatures decreased almost linearly between ca. 200 °C to 160 °C on lengthening the chains, while the melting points first decreased steeply (from 180 to 18 °C with  $n=5$  to 10), and then gently rose afterwards ( $n \geq 10$ ); the mesomorphic temperature range was maximum for the decyloxy compound. X-Ray diffraction revealed the

**Table 42** Mesomorphism of (68).

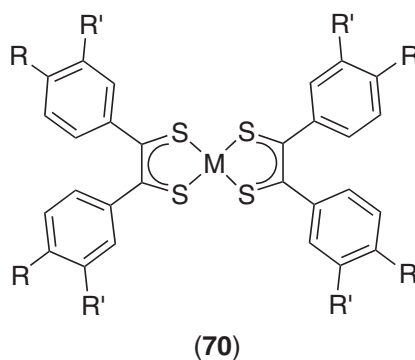
<i>R</i>	<i>n</i>	<i>Transition temperatures</i>	<i>R</i>	<i>n</i>	<i>Transition temperatures</i>
H	6	Cr 180 Col <sub>h</sub> 233 I	OC <sub><i>n</i></sub> H <sub>2<i>n</i>+1</sub>	6	Cr 80 Col <sub>h</sub> 137 I
	8	Cr 129 Col <sub>h</sub> 223.5 I		8	Cr 83 Col <sub>h</sub> 140 I
	10	Cr 101 Col <sub>h</sub> 219 I		10	Cr 80.5 Col <sub>h</sub> 133 I
	12	Cr 83 Col <sub>h</sub> 202 I			
	14	Cr 76 Col <sub>h</sub> 190.5 I			

presence of an additional weak peak in the wide angle region (at ca. 3.7 Å) near the diffuse halo associated to the molten chains. This weak peak corresponds to the core–core correlation and is consistent with a regular molecular stacking along the columnar axis. Variable-temperature infrared spectroscopy did indicate the presence of a polymeric linear structure in the mesophase and crystalline phase.



### 7.9.8.5 Dithiolene Complexes

Another interesting piece of work is concerned with metal *bis*(dithiolene) complexes substituted peripherally with four or eight aliphatic chains ((70):  $R = OC_nH_{2n+1}$ ,  $R' = H$ ;  $R = R' = OC_nH_{2n+1}$ ). Structurally similar to the metal  $\beta$ -diketonate complexes discussed above, it was expected that such complexes would exhibit columnar mesophases on the basis of their disk-like shape. Furthermore, combined with their  $\pi$ -acceptor properties, such discogens could find potential applications as low-dimensional conductors. The complexes were synthesized in a one-pot procedure: the appropriately substituted benzoin or benzil ( $\alpha$ -diketone derivative) was treated with  $P_4S_{10}$ , and complexation was carried out *in situ* with the metal chloride salt.



Veber *et al.*<sup>409</sup> and later Ohta *et al.*<sup>410,411</sup> reported the existence of a columnar mesophase in some bis-[1,2-(dialkoxyphenyl)ethane-1,2-dithiolene] nickel complexes ((70):  $M = Ni$ ;  $R' = H$ ;  $R = OC_nH_{2n+1}$ ,  $n = 9, 11, 12$ ), which was later assigned as discotic lamellar ( $D_L$ ). However, the rather large enthalpy of the mesophase-to-isotropic liquid transition suggested a more ordered mesophase instead. Indeed, X-ray investigations carried out on these three compounds by Veber *et al.*<sup>412</sup> revealed that the so-called  $D_L$  mesophase observed for these materials was in fact a lamellar crystalline phase with some degree of disorder along the crystallographic  $b$ -axis. More recently, Horie *et al.*<sup>413</sup> reported the synthesis of the complete alkoxy series ((70):  $M = Ni$ ;  $R' = H$ ;  $R = OC_nH_{2n+1}$ ,  $n = 1-12, 14, 16, 18$ ) as well as the tetra-alkyl-substituted series ((70):  $M = Ni$ ;  $R' = H$ ;  $R = C_nH_{2n+1}$ ,  $n = 1-12$ ) in order to establish their mesomorphic, thermochromic, and  $\pi$ -electron-acceptor properties. None of the new alkyl complexes was found to be mesomorphic,

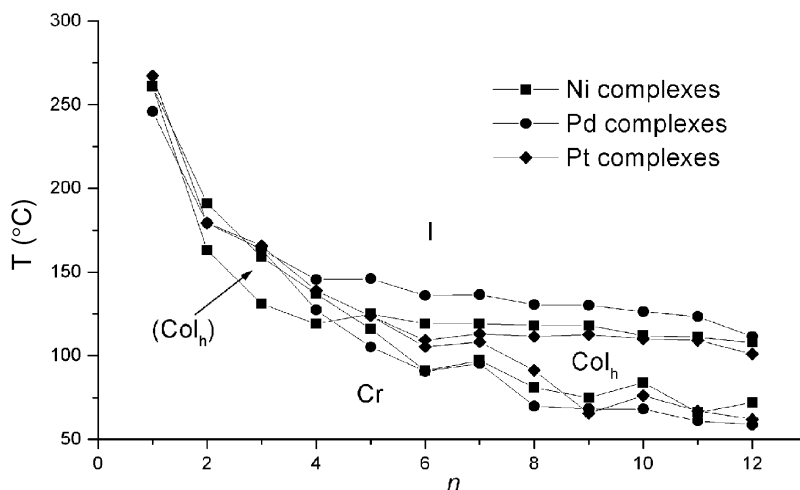


Figure 39 Mesomorphism of the octaalkoxy dithiolene complexes, (70).

but the authors claimed that most of the tetra-alkoxy complexes were! Nevertheless, both series of materials possessed interesting thermochromic properties and the measurements of half-wave reduction potential obtained by cyclic voltammetry proved that they were efficient  $\pi$ -acceptor materials.

Columnar mesophases were eventually obtained for some octasubstituted dithiolene complexes.<sup>414–416</sup> Thus, the nickel complexes with eight peripheral alkoxy chains ((70):  $M = \text{Ni}$ ;  $R = R' = \text{OC}_n\text{H}_{2n+1}$ ,  $n = 1–12$ ) turned out to be mesomorphic, showing a monotropic phase for the short-chain-length homologs ( $n = 2–4$ ), which became enantiotropic for  $n \geq 5$ . The identity of the mesophase was unequivocally determined by X-ray diffraction to be  $\text{Col}_h$ . The mesomorphic range increased slightly upon the elongation of the chains (Figure 39). The existence of the mesomorphic properties was found to depend on the nature of the substituent. Indeed, none of the alkyl systems prepared ((70):  $M = \text{Ni}$ ;  $R = R' = \text{C}_n\text{H}_{2n+1}$ ,  $n = 6, 8$ ) showed a mesophase, but were liquids at room temperature. Electrochemical measurements indicated half-wave reduction potentials in the range of  $-0.055 \pm 0.005$  V (versus SCE in  $\text{CH}_2\text{Cl}_2$ ) irrespective of the length of the alkoxy groups, slightly less positive than the corresponding unsubstituted dithiolene nickel compound. This study was extended in order to investigate the effect of the metal ion on these properties.<sup>417</sup> Thus, two series were successfully prepared by the same procedure used for the nickel complexes ((70):  $M = \text{Pd}, \text{Pt}$ ;  $R = R' = \text{OC}_n\text{H}_{2n+1}$ ,  $n = 1–12$ ). The same  $\text{Col}_h$  mesophase was still present in the two new series, but appeared at slightly longer chain length ( $n = 4$  for the Pd complexes,  $n = 6$  for the Pt complexes). From Figure 39, one can see that the mesomorphic range decreased as  $\text{Pd} > \text{Ni} > \text{Pt}$ , the palladium complexes having the highest clearing temperatures and the lowest melting point. The mesophase of essentially all the complexes were characterized by X-ray diffraction. As for the nickel complexes, a more or less diffuse scattering was systematically present at ca.  $3.6–3.7$  Å besides the broad halo of the molten chains (at  $4.5$  Å); on increasing the chain, this peak becomes broader and smaller, i.e., the intermolecular stacking is more regular and the columnar correlation length longer for the short-chain-length materials. The lattice parameter of the  $\text{Col}_h$  phase was independent of the central metal species and grew almost linearly with the number of methylene groups. Measurement of the reduction potentials by cyclic voltammetry (versus SCE in  $\text{CH}_2\text{Cl}_2$ ) revealed that the best  $\pi$ -acceptors were the Pd complexes ( $0.00 \pm 0.01$  V), the platinum complexes being worst ( $-0.09 \pm 0.01$  V).

#### 7.9.8.6 1,2-Dioxime Complexes

The  $\alpha$ -diketone precursors used to prepare the dithiolene complexes discussed above can be used for the preparation of other potential ligands such as dioximes. Such ligands are directly obtained by the reaction of the corresponding benzil species with hydroxylamine chloride. Dioximate complexes with  $d^8$  metals crystallize in columnar stacks with the formation of a chain of metals orthogonal to the molecular planes, and as such are potentially interesting candidates for the design of discotic systems with low-dimensional semiconducting properties. Ohta *et al.* reported a

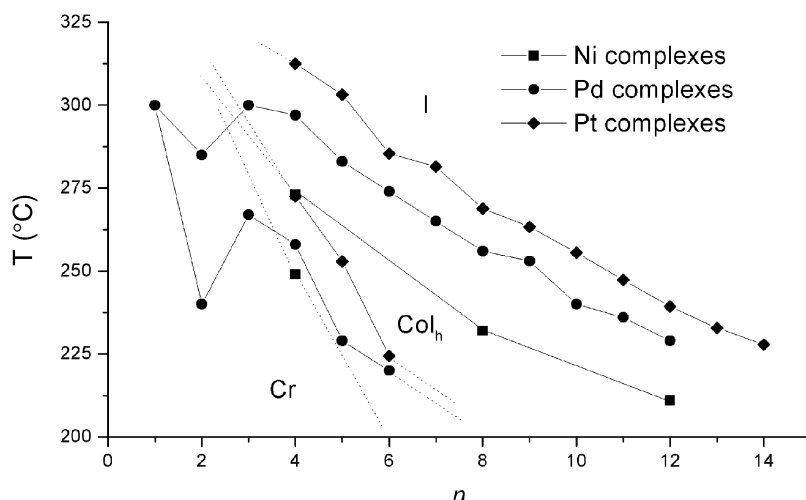
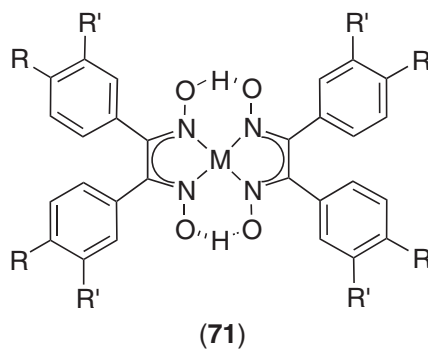


**Figure 40** Mesomorphism of the dioxime complexes, (71).

substantial study on discotic nickel,<sup>418</sup> palladium,<sup>419</sup> and platinum<sup>420</sup> complexes derived from di-(3,4-dialkoxyphenyl)ethane-1,2-dioximes ((71): M = Ni, Pd, Pt; R = R' = OC<sub>n</sub>H<sub>2m+1</sub>). The complexes were obtained by the reaction of an alcoholic solution of the metal chloride salt with the appropriate dioximes. All the complexes ((71): M = Ni, n = 4, 8, 12; M = Pd, n = 2–12; M = Pt, n = 4–14) exhibited enantiotropic, Col<sub>h</sub> phases with wide mesomorphic ranges. Above a certain chain length, the mesophases existed at room temperature (n ≥ 8 for Ni, n ≥ 7 for Pd and Pt). From the phase diagram (Figure 40), one can see clearly the effect of the metal on the clearing temperatures, which decreased in the order Pt > Pd > Ni, and consequently, the breadth of the mesomorphic domains followed the same order. The high clearing temperatures when compared to the related complexes (70) may be due to the possibility of intermolecular hydrogen bonds between neighboring species, which necessarily contribute both to the rigidity of the mesogenic cores and to a more efficient stacking into columns. Note that only the *anti*-isomers (or *E,E*-isomers referring to the relative conformation of the oxime groups in the ligands and the complexes) were obtained, and that this conformation enhanced the stability of the discotic shape of the metal complexes.



In addition to these mesomorphic properties, all complexes were found to possess thermo-chromic and solvatochromic properties. With increasing temperature, the nickel complexes turned gradually from red to yellow,<sup>421</sup> the palladium complexes from orange to yellow,<sup>422</sup> and the platinum compounds from green to yellow but with sharp color changes for the last of these. The platinum complexes exhibited the largest blue-shift rate, and the nickel complexes the smallest. Such a blue shift has several origins and can be attributed to the enlargement of band gap between the filled  $nd_z^2$  valence band and the empty  $(n+1)p_z$  conduction band of the central metal ion, to a metal-ligand charge transfer transition (MLCT band), and/or to the  $\pi-\pi^*$  transition in the ligand. The shift was found to be very sensitive to the monotonic increase in the metal-metal distance with temperature, i.e., the increase in the stacking periodicity between the discogens in the columnar structure. The one-dimensional metal structure is thus an essential

prerequisite for this thermochromism. Additionally, studies of the aggregation behavior of the nickel and palladium complexes in various solvents revealed solvatochromic properties and that the color change was sensitive to the polarity of the solvent (red in apolar solvents, and yellow in polar solvents), and thus to their aggregation behavior in these solvents. Interestingly, too, gel formation was observed in hexane solutions for the Ni<sup>II</sup><sup>421</sup> and Pd<sup>II</sup> complexes.<sup>423</sup> For the palladium complex, the gel appeared anisotropic, and by microscopy displayed a texture similar to that of the lyotropic H<sub>II</sub> phase found in some amphiphilic systems. X-Ray studies confirmed the two-dimensional hexagonal structure of the gel, and UV studies supported a similar structure in both dilute hexane solutions (lyotropic phase) and gel state.

The effect of the nature of chains has also been investigated. The substitution of the alkoxy groups by alkyl chains had dramatic effects on the mesomorphic, thermochromic, and solvatochromic properties. Indeed, the palladium complex with eight hexyl groups ((71): M = Pd; R = R' = C<sub>6</sub>H<sub>13</sub>)<sup>422</sup> displayed a Col<sub>h</sub> phase at lower temperature and over a narrow range (between 123 °C and 146 °C), an identical thermochromic behavior (blue shift in the liquid crystalline state), but did not exhibit solvatochromism. The nickel complex with eight dodecyl chains ((71): M = Ni; R = R' = C<sub>12</sub>H<sub>25</sub>)<sup>416</sup> showed a more varied mesomorphic behavior than the octyloxy homologous compound (the palladium and platinum complexes could not be isolated). Hence, from room temperature to 32 °C, a Col<sub>r</sub> phase (*p2/a*) was first identified, followed by the transition to a Col<sub>h</sub> phase up to 82 °C. In both complexes, the decrease in the clearing temperatures and the reduction of the mesomorphic range were due to the less electron-donating nature of the alkyl groups, and consequently to the decrease of the intermolecular interactions between the mesogenic cores.

Ohta *et al.* pursued this interesting structural study on the nickel dioxime complexes (71) in order to understand the effect of some critical molecular parameters on the mesophase structure, and particularly on the columnar-to-discotic lamellar phase transformation.<sup>424</sup> To do so, he adopted an original approach consisting of keeping the length of the four chains in the *p*-position (R) constant as dodecyloxy groups, and shortening stepwise the other four chains in the *m*-position (R') in order that the overall structure of the nickel dioxime complex was gradually modified from the perfectly discoid structure with eight chains to a more lath-like structure with four chains. As such, it was thought to be possible to locate precisely the transition between the columnar and the discotic lamellar structures and to identify the corresponding molecular parameters influencing this phase transformation. Thus, two new series of complexes with non symmetrical chain length were prepared ((71): R = OC<sub>12</sub>H<sub>25</sub>, R' = OC<sub>*n*</sub>H<sub>2*n*+1</sub> with *n* = 6 to 1; R = OC<sub>12</sub>H<sub>25</sub>, R' = C<sub>*n*</sub>H<sub>2*n*+1</sub> with *n* = 3 to 1). The mesomorphism was not modified to a great extent in that the first series (eight alkoxy chains) presented a room-temperature Col<sub>h</sub> phase with a regular stacking along the column, and with a linear decrease in the clearing temperatures from 297 °C for *n* = 1 to 188 °C for *n* = 6. Note that the compound with *n* = 3 displayed a transition between two Col<sub>h</sub> phases. Similar observations were made for the mixed-chain series with four dodecyloxy and four alkyl chains, which displayed a Col<sub>h</sub> phase over large temperature ranges (melting occurred at or slightly above ambient, and the clearing points were above 200 °C). Thus, even with a strong dissymmetry of chain substitution, the Col<sub>h</sub> phase was still preserved. Three more families of compounds were therefore synthesized, namely tetraalkoxy derivatives ((71): R = OC<sub>*n*</sub>H<sub>2*n*+1</sub>, *n* = 10, 12, 14; R' = H), one tetraalkyl derivative ((71): R = C<sub>12</sub>H<sub>25</sub>; R' = H), and a tetraalkoxy derivative with four hydroxyl groups ((71): R = OC<sub>*n*</sub>H<sub>2*n*+1</sub>; R' = OH, *n* = 8, 12, 16). All the complexes with long alkoxy chains in the *p*-position, except that with *n* = 8, exhibited a particular type of lamellar phase (Table 43), whereas the tetradodecyl analog possessed a columnar phase with two-dimensional, tetragonal symmetry (Col<sub>t</sub>). The liquid-crystallinity in these systems was demonstrated by X-ray diffraction for which the diffuse halo associated with the molten chains was systematically observed. It was proposed that the lamellar mesophase consisted of an arrangement of the flat, disk-like mesogenic cores parallel to the layer planes separated by sublayers of aliphatic chains; the chains lay normal to both the core complex and the layers. Moreover, the mesogenic cores

**Table 43** Mesomorphic properties of tetrasubstituted complexes (71).

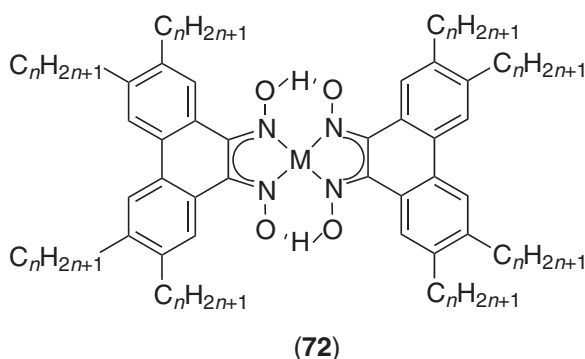
$R = OC_nH_{2n+1}, R' = H$	$R = OC_nH_{2n+1}, R' = OH$	$R = C_{12}H_{25}, R' = H$
$n = 10$ : Cr 70 D <sub>Lr</sub> ( <i>p2<sub>1</sub>2<sub>1</sub></i> ) 160 I	$n = 8$ : Cr 176 I	Cr 115 Col <sub>t</sub> 120.5 I
$n = 12$ : Cr 69 D <sub>Lr</sub> ( <i>p2<sub>1</sub>2<sub>1</sub></i> ) 149 I	$n = 12$ : Cr 105 D <sub>Lr</sub> ( <i>p2<sub>1</sub>1</i> ) 170 I	
$n = 14$ : Cr 77 D <sub>Lr</sub> ( <i>p2<sub>1</sub>2<sub>1</sub></i> ) 141 I	$n = 16$ : Cr 56 D <sub>Lr</sub> ( <i>p2<sub>1</sub>1</i> ) 164.5 I	

**Table 44** Thermotropic properties of complexes (72).

<i>M</i>	<i>n</i> = 6	<i>n</i> = 10
Ni	Cr 167 Col <sub>r</sub> 228 Col <sub>h</sub> 253 I	Cr 130.5 Col <sub>h</sub> 214 I
Pd	Cr 163 Col <sub>r</sub> 227 Col <sub>h</sub> 255 dec.	Cr 128 Col <sub>h</sub> 214 I
Pt	Cr 166 Col <sub>r</sub> 227.5 Col <sub>h</sub> 250 dec.	Cr 126 Col <sub>h</sub> 216 I

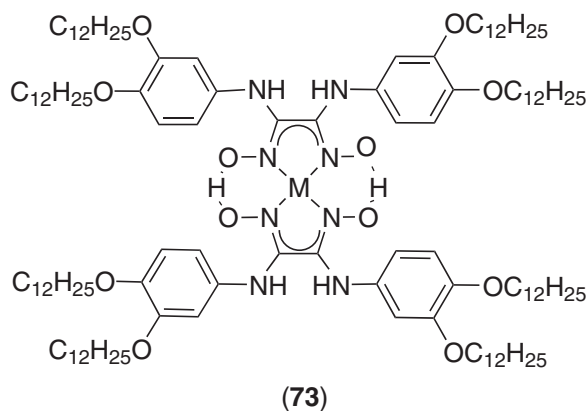
within the layers were arranged into different, two-dimensional rectangular lattices, the symmetry of which depended on the R' group (H or OH and possibility of intermolecular hydrogen bonds), i.e., with different positional and orientational correlations between adjacent layers. Such mesophases represent a new class of liquid-crystalline phases, described as laminated phases, and extend considerably the possibilities for molecular design.

To address similar issues, two other series of structurally related dioximato metal compounds were prepared. The first series was concerned with the octaalkyl substituted *bis*(phenanthrene-9,10-dionedioximato) complexes of nickel, palladium, and platinum ((72): M = Ni, Pd, Pt; *n* = 6, 10) (Table 44).<sup>425</sup> Both the *anti*- and *amphi*-isomers of (72) could be prepared and isolated, depending on the reaction conditions employed. However, the *amphi*-materials isomerized by thermal treatment or under acidic conditions into the *anti*-form, except for the nickel compounds for which both forms were stable under these conditions. Thus, all the *anti*-complexes exhibited enantiotropic columnar mesophases, Col<sub>r</sub> and Col<sub>h</sub> for the hexyl compounds, and a single Col<sub>h</sub> phase for the decyl compounds; the nickel *amphi*-isomers were not liquid crystals. As for compounds (71), they cleared into the isotropic liquid at rather elevated temperatures, and possessed fairly extended mesomorphic domains, which depend strongly on the peripheral chains. The metal, however, did not influence the transition temperatures drastically. The significant difference was the presence of the additional Col<sub>r</sub> mesophase at short chain lengths. This may be a direct consequence of the rigidity of the phenanthrene core, and the inhibition of the rotation of the substituted aromatic groups compared to (71), which favored the tilt of the molecular plane within the columns. The tilt arrangement in the columns was also confirmed by the absence of thermochromism (blue shift) in the electronic spectra. The octaalkoxy substituted homologs have been prepared and showed similar behavior, with larger mesomorphic ranges (ca. 50 °C).<sup>426,427</sup>



The second series of related materials was based on the (3,4-didodecyloxyphenyl)diaminodioxime derivative (73).<sup>428</sup> Vicinal dioximes are capable of coordinating through *N,N* or *N,O* sites of the oxime groups. Upon the complexation, the ligands fold back, and the transition metal complexes are *N,N*-coordinated with a square-planar structure. Both isomeric forms were selectively isolated for the nickel complexes, but only the *anti*-isomer for the palladium complex. The two *anti*-complexes exhibited a Col<sub>h</sub> phase ((73): M = Ni: Cr 78 Col<sub>h</sub> 117 I; M = Pd: Cr 80 Col<sub>h</sub> 131 I). Most astonishing, however, was the observation of a Col<sub>h</sub> phase for the isomeric *amphi*-nickel complex (*E,Z*-isomer), between 66 °C and 145 °C. Not only was the existence of mesomorphism surprising and unexpected, but the mesophase stability also increased with respect to the *anti*-complex.



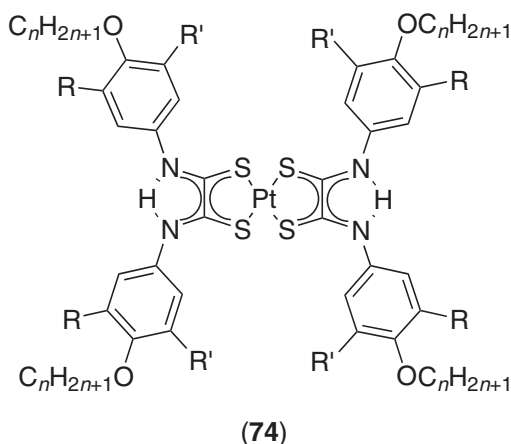


### 7.9.8.7 Dithiooxamide Complexes

The complexation of several, non-mesomorphic substituted dithiooxamide ligands to platinum(II) has yielded to a new family of discotic metallomesogens.<sup>429,430</sup> Upon complexation, the ligand locks into a more rigid conformation, and possesses a more extended flat core, and as such these systems were expected to show columnar mesophases. The dithiooxamides ligands were obtained from the corresponding bisamides after treatment with  $P_4S_{10}$ , and the complexes by their reaction with  $[PtCl_2(dmsO)_2]$ . Mesomorphism was observed for complexes with eight ((74):  $R = OC_nH_{2n+1}$ ;  $R' = H$ ) and twelve chains ((74):  $R = R' = OC_nH_{2n+1}$ ), but not with those with only four chains ((74):  $R = R' = H$ ) as it could have been anticipated from the results described above (Table 45). All the other complexes displayed an enantiotropic  $Col_h$  phase depending on the chain length. For the eight-chained complexes, the mesophase first appeared for  $n \geq 12$ , over narrow temperature ranges, whereas for the twelve-chained analogs, the mesophase was observed at lower chain length and over slightly larger temperature ranges. The addition of four supplementary chains thus modified the transition temperatures and the mesophase stability profoundly, and the lack of mesomorphism for the compound with  $n = 16$  was attributed to the faster decrease in the clearing point than the melting point.

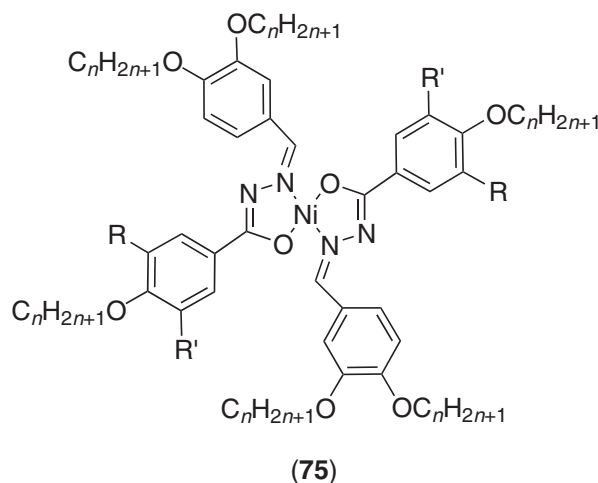
**Table 45** Thermotropic properties of complexes (74).

$n$	$R = OC_nH_{2n+1}$ , $R' = H$	$n$	$R = R' = OC_nH_{2n+1}$
8	Cr 107 I	8	Cr 83 $Col_h$ 125 I
12	Cr 111 $Col_h$ 116 I	11	Cr 55 $Col_h$ 103 I
13	Cr 113 $Col_h$ 119 I	13	Cr 42 $Col_h$ 59 I
14	Cr 110 $Col_h$ 119 I		
15	Cr 115 $Col_h$ 118 I		
16	Cr 106 $Col_h$ 114 I	16	Cr 39 I

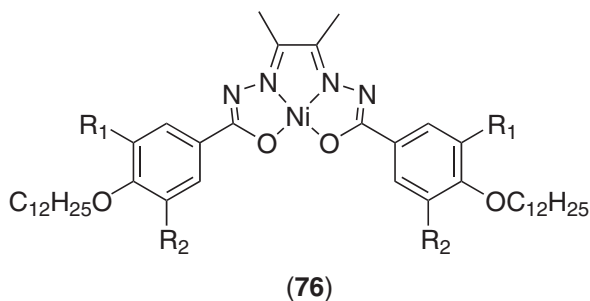


### 7.9.8.8 Hydrazine Complexes

A quite similar ligand conformation change was observed upon the complexation of polycatenar hydrazines with nickel. Once locked in a more rigid conformation, the complexes exhibited a disk-like shape, and a columnar mesomorphism.<sup>431</sup> The three-, four-, and five-chain aroylhydrazone derivatives were obtained by the condensation of the corresponding substituted benzoylhydrazines with 3,4-dialkoxybenzaldehyde. In principle, two types of complexes could be prepared and isolated, with a square-planar or octahedral geometry, depending on the nickel salt used, Ni(OAc)<sub>2</sub> or NiCl<sub>2</sub>, respectively. In this study, only the square-planar complexes were prepared. The formation, type, and stability of the columnar phases was found to depend on the length and number of chains. All the ten-chain complexes ((75): R = R' = OC<sub>n</sub>H<sub>2n+1</sub>, n = 5–8, 10, 12, 14) were mesomorphic. Complexes with shorter carbon chain lengths (n = 5 to 8) exhibited a monotropic Col<sub>f</sub> phase below the isotropic liquid (217–224 °C) down to room temperature, while longer-chain-length homologs showed a Col<sub>h</sub> phase, monotropic for the decyloxy compound (Cr 203.5 (Col<sub>h</sub> 201) I), and enantiotropic thereafter between ca. 78 and 174–190 °C (n = 12, 14). Decreasing the number of lateral chains led to the narrowing or complete suppression of the mesophase. The eight-chain compound ((75): R = H; R' = OC<sub>14</sub>H<sub>29</sub>) exhibited a Col<sub>h</sub> mesophase at higher temperature and over a narrower temperature range than its ten-chain homolog (Cr 132 Col<sub>h</sub> 158), whereas that with six chains ((75): R = R' = H) melted into the isotropic liquid at 116 °C.



Bis(mono-, di-, and trialkoxy substituted benzoylhydrazines) and their corresponding nickel complexes have also been prepared ((76): R<sub>1</sub>, R<sub>2</sub> = H or OC<sub>12</sub>H<sub>25</sub>).<sup>432</sup> Upon complexation, the ligand lost its linear shape to adopt a bent shape, which, with the adequate substitution, will have an overall half-disk shape. Thus, none of the ligands was mesomorphic, and only the nickel complexes with six chains showed a mesophase between 52 °C and 105 °C, characterized by X-ray diffraction as Col<sub>h</sub>. Both the crystal structure of the derivative with methoxy groups and the wide-angle X-ray pattern were in agreement with the antiparallel stacking of the complex into columns.

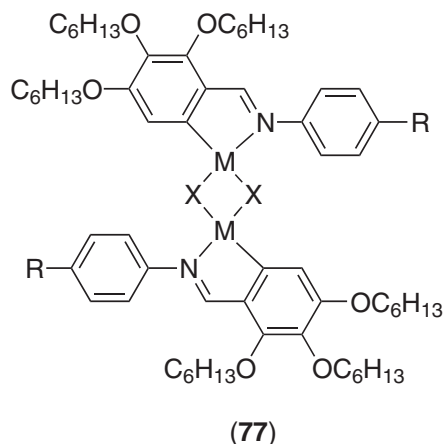


Very few discogenic complexes with a hydrazone moiety have been so far studied. One nickel complex based on 2,6-diacetylpyridinebis(3,4,5-tridodecyloxybenzoylhydrazone) has been previously reported by Battistini *et al.* as a potential columnar metallomesogen.<sup>433</sup> The mononuclear complex showed an apparently unidentified mesophase during the first heating which was not

re-observed afterwards, suggesting that perhaps the materials is not, after all, mesomorphic. The complex converted upon further heating into the more stable, but non-mesomorphic, paramagnetic discrete dimeric corresponding form.

### 7.9.8.9 Benzalimines

Praefcke and co-workers reported a series of disk-shaped, dinuclear *ortho*-palladated benzalimine complexes, (77), which were the first example of organometallic complexes showing the nematic phase of disk-like molecules,  $N_D$ .<sup>434</sup>



The chloro-bridged palladium complex was prepared by reacting the imine ligand with palladium acetate, followed by treatment with HCl, and the other complexes by ion-exchange reactions with KBr, KI, and KSCN. The flat, dinuclear halogeno- and thiocyanato-bridged complexes ((77): M = Pd; X = Cl, Br, I, SCN; R = C<sub>6</sub>H<sub>13</sub>) exhibited a monotropic  $N_D$  phase, whereas the acetato-bridged complex (X = OAc) was not mesomorphic, a consequence of its open-book structure (Table 46). The peculiar clearing process of the thiocyanato complex was caused by the composition of the nematogen, in that the thiocyanate moiety can be bridged parallel or anti-parallel to one other, leading to two structural isomers in the ratio 17:83. The structurally related chloro-bridged platinum complex ((77): M = Pt; X = Cl; R = C<sub>6</sub>H<sub>13</sub>), prepared by the reaction of the amine with di- $\mu$ -chloro-bis[( $\eta^3$ -2-methylallyl)platinum], also showed the  $N_D$  phase on cooling, although it melted at much higher temperature than the palladium congener.<sup>435</sup> The thiocyanato-bridged<sup>436</sup> platinum complex ((77): M = Pt; X = SCN; R = C<sub>6</sub>H<sub>13</sub>) was not mesomorphic and the bromo and iodo derivatives were not prepared.<sup>437</sup> Interestingly, unlike the chloro-bridged palladium complexes, the platinum complex existed as an isomeric mixture *syn/anti* (in the ratio 17:83) in solution, and attempts to separate the two isomers were unsuccessful because of decomposition

Table 46 Mesomorphism of (77).

Metal	R	X	Mesomorphism of pure 77	Mesomorphism of 77/TNF
Pd	C <sub>6</sub> H <sub>13</sub>	Cl	Cr 79 ( $N_D$ 43.5) I	Cr 94 Col <sub>h</sub> 188 I (50 mol%)
			Cr 73 ( $N_D$ 28) I	Cr 99 Col <sub>h</sub> 142.5 I (50 mol%)
			Cr 97 ( $N_D$ 27) I	Cr 85 Col <sub>h</sub> 96 I (35 mol%)
		OAc	Cr 56 I	No mesophase induction
			Cr 96 ( $N_D$ 50) I	Cr 85 $N_D$ 112 I (50 mol%)
Pt	C <sub>6</sub> H <sub>13</sub>	Cl	Cr 92 ( $N_D$ 54.5) I	Col <sub>h</sub> 195 I
		SCN	Cr 86 I	$N_D$ 98 I
Pd	(S)- $\beta$ -citronellol	Cl	Cr 65 I	Col <sub>h</sub> 145 I
		Br	Cr 67 I	Col <sub>h</sub> 86 I
		SCN	Cr 99 I	$N^*$ + $N$ 79 I
Pt	(S)-2-methylbutyloxy	Cl	Cr 90 ( $N^*$ 72) I	Col <sub>h</sub> 189 I

processes; the thiocyanato platinum complex was obtained as a single antiparallel isomer. The molecular geometry and the number of peripheral chains thus appeared crucial in determining the type of mesophase observed, since the related *ortho*-metallated imine complexes with four alkoxy chains exhibited exclusively calamitic mesomorphism, mostly SmA phases (*vide supra*). All these compounds also formed charge-transfer complexes when doped with strong electron acceptors such as 2,4,7-trinitrofluorenone (TNF) as indicated by a change of color.<sup>438,439</sup> The bridging group was found to influence strongly the type of induced mesophases (Table 46). Thus, enantiotropic Col<sub>h</sub> phases were induced in the binary mixtures of chloro- and bromo-bridged complexes with TNF respectively, with the suppression of the N<sub>D</sub> phase above 10% of TNF. The iodo-bridged palladium complex showed both the Col<sub>h</sub> and N<sub>D</sub> phases but at various TNF concentrations, i.e., above 45 mol.% TNF, a monotropic N<sub>D</sub> was induced. The N<sub>D</sub> phase became stabilized for the thiocyanato-bridged complex and, once more, the acetato-bridged complex did not show an induced mesophase in such mixtures. Contact preparations of the chloro-bridged platinum complex with TNF also resulted in an induced Col<sub>h</sub> phase, with a higher thermal stability than its palladium analog, and an induced N<sub>D</sub> phase for the thiocyanato compound (Table 46). The structure of the different mesophases was characterized by X-ray methods, and confirmed intercalation of TNF molecules between successive planar complexes in the columnar phases, while no such stacking was evidenced in the case of the nematic phase. The differences in the mesomorphism observed for the pure compounds and in the binary mixtures were explained from unequal core dimensions caused by the bridging groups, as well as space-filling (steric) and electronic effects.

Four chiral homologous complexes were also prepared.<sup>440</sup> None of the palladium complexes showed mesomorphic properties, whereas a monotropic chiral discotic nematic phase was observed for the platinum complex (Table 46). The absence of mesomorphism for the dinuclear palladium complexes may be due to the chiral chain used, which differed from that used for the platinum system. All of them form charge-transfer complexes with TNF. A Col<sub>h</sub> phase was induced for the two halo-bridged palladium complexes and for the platinum complex, as was observed for their non-chiral analogs. However, the chiral nematic phase of the platinum compound was suppressed. At low TNF content, a chiral N<sub>D</sub>\* phase was stabilized for the thiocyanato-bridged compound along with a non-chiral N<sub>D</sub> phase at higher concentration.

### 7.9.8.10 Iminoketones

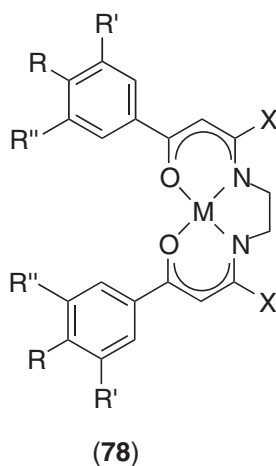
To further explore the complementary shape approach developed by Swager and co-workers (*vide supra*), several hemi-disk-shaped compounds, related structurally to the diketonato metal complexes (58) discussed above in which two ketonate ligands are connected through a diamino link, have been prepared. Systematic modifications of the chemical structures were carried out in order to understand some structure–property relationships, and the extension of the validity of such concepts. Such  $\beta$ -enaminoketonato ligands were, however, promising systems for columnar mesophase induction due to their better planarity compared to the  $\beta$ -diketonato structures.

A series of coordination complexes of the 1,3-diketonato Schiff-base ligands ((78): M = Ni, Cu, Pd, VO; X = Me; R = R' = R'' = OC<sub>n</sub>H<sub>2n+1</sub>, n = 10, 12, 16) was investigated.<sup>441</sup> Nickel, palladium, and copper iminoketone complexes were found to display a Col<sub>h</sub> phase over a 40–50 °C temperature range, although the square–pyramidal vanadyl compounds were not mesomorphic (Table 47). Both melting and clearing temperatures increased in the order Ni < Cu < Pd, with little influence from the chain length; a diffuse halo at 7.2 Å, corresponding to twice the inter-core distance, was detected by X-ray diffraction. This doubling of the periodicity along the columnar axis revealed that the columns were formed by arranging the mesogens in a shape-complementary

Table 47 Mesomorphism of (78).

$X = Me$		$X = H/R = R' = OC_nH_{2n+1} R'' = H$			
$M$	$R = R' = R'' = OC_{12}H_{25}$	$n = 8$	$n = 10$	$n = 12$	$n = 16$
Ni	Cr 44.5 Col <sub>h</sub> 91 I		Cr 110 I	Cr 58 Col <sub>h</sub> 108.5 I	Cr 67 Col <sub>h</sub> 100.5 I
Cu	Cr 44 Col <sub>h</sub> 103.5 I		Cr 94 I	Cr 90 I	Cr 89 I
Pd	Cr 78 Col <sub>h</sub> 116 I				
VO	Cr 94 I	Cr 88 Col <sub>h</sub> 160 I	Col <sub>h</sub> 156 I	Col <sub>h</sub> 158 I	Cr 55 Col <sub>h</sub> 150 I
Co		Cr 113 I		Cr 61 Col <sub>h</sub> 103 I	Cr 67 Col <sub>h</sub> 100 I

fashion so that, in effect, they were stacked in an antiparallel fashion. Lai and co-workers investigated some related iminoaldehyde-derived analogs, and looked thoroughly at the effect on the mesomorphism of the number of chains and the metal ion ((78):  $M = \text{Ni}, \text{Cu},^{442} \text{Co}, \text{VO};^{443}$   $X = \text{H}; R, R', R'' = \text{H}$  or  $\text{OC}_n\text{H}_{2n+1}$ ,  $n = 8, 10, 12, 14, 16, 18$ ). As expected from previous results, none of the nickel, copper, and cobalt complexes with two chains ((78):  $R = \text{OC}_n\text{H}_{2n+1}$ ,  $n = 8, 12, 16; R' = R'' = \text{H}$ ) was mesomorphic, all clearing into the isotropic liquid at temperatures around 100–120 °C. Only the vanadyl compounds were liquid crystals for which a  $\text{Col}_h$  phase was characterized between ca. 60 °C and 150 °C for those with chain length of 12 or more carbon atoms. The chain-length dependence was relatively small, although doubling the number of chains ((78):  $R = R' = \text{OC}_n\text{H}_{2n+1}; R'' = \text{H}$ ) appeared to be beneficial overall in inducing and stabilizing the  $\text{Col}_h$  phase. The nickel and cobalt complexes possessed very similar transition temperatures, whereas the vanadyl complexes showed the highest mesophase stability (Table 47). The decrease in the mesophase stability for the nickel and cobalt complexes relative to the oxovanadyl derivatives was attributed to a slight deviation from molecular planarity and to weaker intermolecular interactions for the former. Surprisingly, the copper complexes were not mesomorphic.



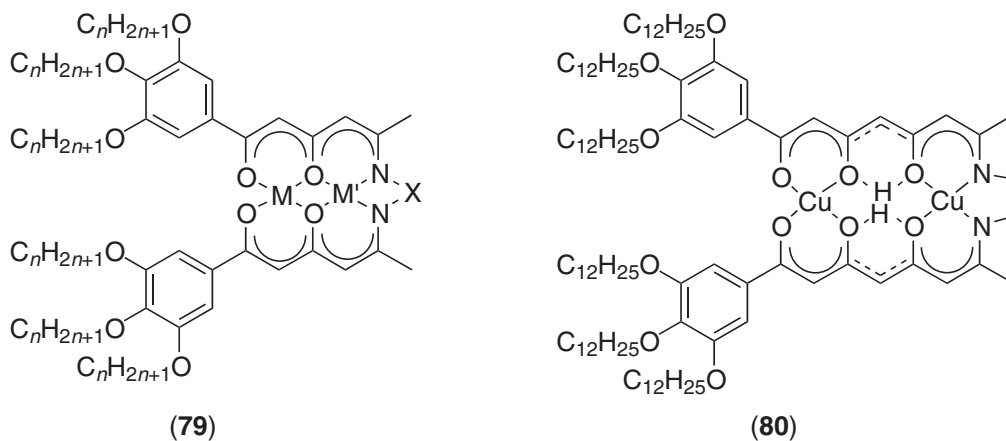
Among the three-chained complexes investigated ((78):  $M = \text{Cu}, \text{Ni}; R = R' = R'' = \text{OC}_n\text{H}_{2n+1}$ ,  $n = 14, 16$ ), only the nickel derivatives exhibited a  $\text{Col}_h$  phase above about 65–70 °C, existing for about 5 °C only, while again the copper complexes were not liquid crystals. Here, the reduction in the mesophase stability most probably resulted from steric factors. These results somehow contradicted those obtained for the iminoketone compounds ( $X = \text{Me}$ ), for which the presence of the methyl groups was expected to destabilize the mesomorphism and reduce the transition temperatures instead of enhancing the mesomorphic properties.

Interested by the effect of other structural modifications on the thermal behavior, and the possibility to combine several metal centers within the same compound, Swager and co-workers pursued this research, and reported series of homo-dinuclear, hetero-dinuclear 1,3,5-triketoneate (79), and 1,3,5,7-tetraketoneate Schiff-base complexes (80).<sup>404,405</sup> Providing a minimum of at least six lateral chains and short diamine spacers ((79):  $M, M' = \text{Cu}, \text{Ni}, \text{Mn}, \text{Pd}, \text{Co}; X = \text{C}_2\text{H}_4, \text{C}_3\text{H}_6$ ), complexes (79) displayed  $\text{Col}_h$  mesophases, being as such the first heterodinuclear metallomesogens (Table 48). The mesophase existed over broader temperature ranges than those of the related

Table 48 Mesomorphism of (79).

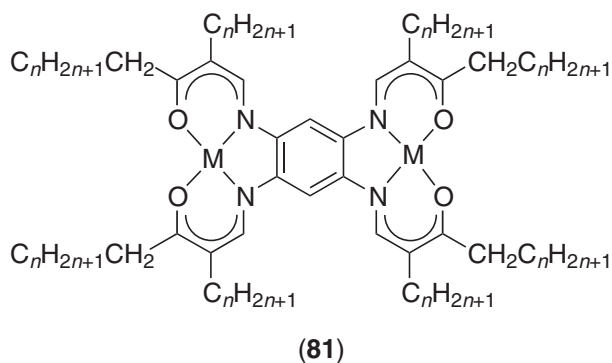
<i>n</i>	<i>M = M' = Cu</i>		<i>X = C<sub>2</sub>H<sub>4</sub>, n = 14</i>	
	<i>X = C<sub>2</sub>H<sub>4</sub></i>	<i>X = C<sub>3</sub>H<sub>6</sub></i>	<i>M/M'</i>	
6	Cr 131.5 $\text{Col}_h$ 245 dec.	Cr 183 $\text{Col}_h$ 246 dec.	Cu/Cu	Cr 81 $\text{Col}_h$ 248 dec.
8	Cr 96 $\text{Col}_h$ 248 dec.	Cr 108 $\text{Col}_h$ 203 dec.	Ni/Cu	Cr 97 $\text{Col}_h$ 226dec.
10	Cr 81 $\text{Col}_h$ 245 dec.	Cr 60 $\text{Col}_h$ 230 dec.	Ni/Pd	Cr 105 $\text{Col}_h$ 232 dec.
12	Cr 81 $\text{Col}_h$ 237dec.	Cr 52 $\text{Col}_h$ 228 dec.	Ni/Ni	Cr 48 I
14	Cr 81 $\text{Col}_h$ 248 dec.	Cr 64 $\text{Col}_h$ 200 I	Ni/Mn	Cr 50 I
16	Cr 76 $\text{Col}_h$ 205 I		Ni/Co	Cr 43 I

iminoketonato and iminoaldehyde complexes described previously. This was clearly related to the extension of the mesogenic cores, and hence the possibility of greater intermolecular interactions. Note that those complexes with four chains or with bulky spacers were, however, not liquid crystalline ((79): X = *cis*-1,2-cyclohexyl,  $\text{CH}_2\text{C}(\text{Me})_2\text{CH}_2$ ). As for the triketonato Schiff base, the dinuclear copper(II) complex ((80) also formed a  $\text{Col}_h$  phase between 61 °C and 174 °C. Mesophase formation was dependent on the various metal combinations, although this was partly attributed to the fact that some members retained axially coordinated methanol, reducing the tendency to mesophase formation.

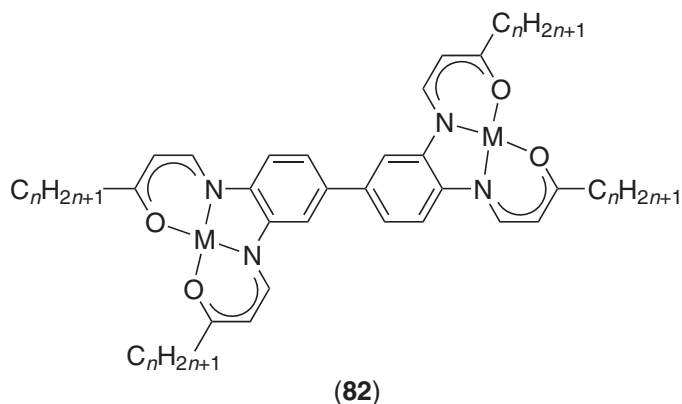


The bi- and trinuclear bis- and tris-*cis*-enaminoketonato complexes investigated by Pyzuk *et al.* also represent an interesting approach in designing new molecular species forming liquid crystals, with a perfect control of the location of active sites within the mesophase, thus allowing for specific interactions to take place. The choice of enaminoketonone as template ligands was dictated by their relative ease of synthesis, formation of chemically stable mesomorphic complexes (*vide supra*), and facile shape modification.

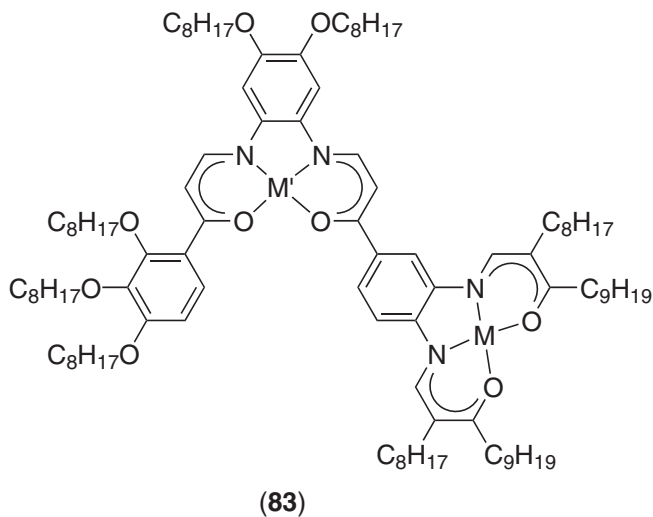
Several homodinuclear copper(II) and nickel(II) complexes based on large, flat, bis-enaminoketonone ligands were shown to exhibit enantiotropic columnar mesophases. The first series of ligands was obtained by the condensation of tetraaminobenzene with the corresponding dialkylketone.<sup>444</sup> As expected from their discoid molecular shape and their eight chains, the nickel ((81): M = Ni; *n* = 5) and the copper complexes ((81): M = Cu; *n* = 8, 10, 12) assembled into columnar phases assigned as  $\text{Col}_h$ . Despite the large number of aliphatic chains, the phases occurred at quite high temperatures, i.e., between 197 °C and 231 °C for the nickel complex, and between 179 °C, 164 °C, 149 °C, and 200 °C, 183 °C, and 166 °C for the copper complexes (*n* = 8, 10, 12 respectively).

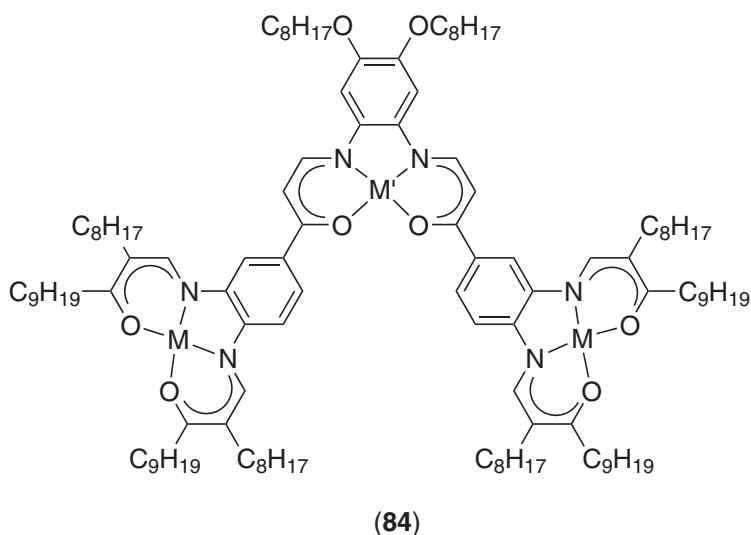


The second series of ligands was obtained with the same procedure as above, but starting from tetraaminobiphenyl. The binuclear metal complexes ((82): M = Ni, Cu; *n* = 5–11)<sup>445</sup> possessed a more elongated shape than (81) and, despite of having only four chains, the nickel and copper complexes exhibited  $\text{Col}_r$  mesophases above 150 °C and up to 250 °C. X-Ray diffraction studies of the thermally more stable nickel complexes revealed a lattice with the *p2gg* plane group, the elongated shape of the complexes implying that they had assembled into dimers as a prerequisite to column formation.



In the following study, the same group reported the synthesis of multinuclear (binuclear, **(83)** and trinuclear, **(84)**)<sup>446</sup> enamino-ketone complexes with a variety of different and controlled molecular symmetry. The overall ligands consisted of two and three chelating, tetradentate moieties joined together by single bonds. The synthesis of these sophisticated organic structures involved a straightforward condensation reaction between the sodium salt of the formyl ketone metal complex with the appropriate aromatic amine or diamine; the incorporation of the second metal ion was accomplished during this condensation. This led to two series of multinuclear complexes having different molecular symmetries depending on the various combinations of nickel, copper, or vanadyl ions employed. For instance, binuclear complexes containing copper or nickel have molecular  $C_s$  symmetry, whereas that containing vanadyl ions have  $C_1$  symmetry. For the trinuclear structures, the symmetry changes from  $C_{2v}$  to  $C_s$  depending on the relative orientation of the  $V=O$  groups. All the complexes synthesized were mesomorphic at room temperature. The mesophases of all the complexes **(83)** and **(84)** containing  $V=O$  were characterized as  $Col_h$ , whereas complexes **(84)** with other metals showed a  $Col_r$  phase (Table 49). In the first series, the various metal-pair combinations appeared to have no influence on the nature of the mesophase, and affected only the transition to the isotropic liquid, i.e., the mesophase stability. The divanadyl compounds consisted of a diastereomeric mixture of two forms,  $\alpha$  and  $\beta$ , related to the disposition of the oxygen atoms with the coordination planes (same or opposite sides). However, while separable by chromatography and stable at room temperature, the  $\alpha$  and  $\beta$  forms isomerized at elevated temperatures to give the diastereoisomeric mixture once more. The trinuclear complexes displayed both a  $Col_h$  and  $Col_r$  phase, except for the vanadyl-containing species which showed a  $Col_h$  phase only. NMR and ESR probed the potential existence of super-exchange coupling between the paramagnetic centers of the binuclear complexes. The long distance between the metals suggests that exchange operated through the conjugated,  $\pi$ -electron system. No indication about the ferro- and antiferro-magnetic character of the investigated compounds was given.



**Table 49** Mesomorphism of (83) and (84).

<i>M</i>	<i>M'</i>	Mesomorphism of dinuclear complexes <b>83</b>	<i>M</i>	<i>M'</i>	Mesomorphism of trinuclear complexes <b>84</b>
Ni	Ni	Col <sub>h</sub> 101 I	Ni	Ni	Col <sub>r</sub> 106 Col <sub>h</sub> 162 I
Cu	Cu	Col <sub>h</sub> 137 I	Cu	Cu	Col <sub>r</sub> 124 Col <sub>h</sub> 197 I
Ni	Cu	Col <sub>h</sub> 125 I	Ni	Cu	Col <sub>r</sub> 100 Col <sub>h</sub> 161 I
Cu	Ni	Col <sub>h</sub> 117 I	Cu	Ni	Col <sub>r</sub> 130 Col <sub>h</sub> 190 I
VO	VO(α)	Col <sub>h</sub> 80 I	Ni	VO	Col <sub>h</sub> 162.5 I
VO	VO(β)	Col <sub>h</sub> 120 I	Cu	VO	Col <sub>h</sub> 172-178 I
Cu	VO	Col <sub>h</sub> 155 I			
Ni	VO	Col <sub>h</sub> 147 I			

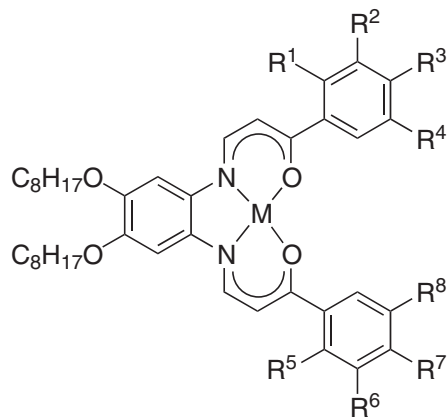
The related triangular, mononuclear species, (**85**), exhibited smectic or columnar phases depending on the substitution pattern chosen, but the change from smectic to columnar behavior was found to be discontinuous.<sup>447,448</sup> Thus, nickel complexes with four, five, and six aliphatic chains showed monotropic smectic phases or no mesophase, those with seven chains were not mesomorphic, whereas most of the eight-chained complexes showed Col<sub>h</sub> mesophases at room temperature (Table 50). Note that additional copper and cobalt complexes with six chains ((**85**): M = Cu, Co; R<sup>1</sup> = R<sup>2</sup> = R<sup>3</sup> = OC<sub>*n*</sub>H<sub>2*n*+1</sub>; R<sup>5</sup> = R<sup>6</sup> = R<sup>7</sup> = OC<sub>*m*</sub>H<sub>2*m*+1</sub>; *n* = *m* = 8, 10; *n* = 8, *m* = 10) showed the same mesomorphism as the nickel complexes, with the mesophase stability depending first on the metal and then on the chain length; the clearing temperatures, and thus the range of mesophase, were found to decrease slightly in the order Cu > Co > Ni.

**Table 50** Mesomorphism of (85).

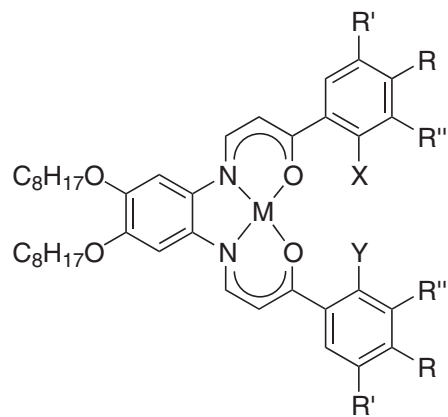
<i>R</i> <sup>1</sup>	<i>R</i> <sup>2</sup>	<i>R</i> <sup>3</sup>	<i>R</i> <sup>4</sup>	<i>R</i> <sup>5</sup>	<i>R</i> <sup>6</sup>	<i>R</i> <sup>7</sup>	<i>R</i> <sup>8</sup>	
H	H	OC <sub>8</sub> H <sub>17</sub>	H	H	H	OC <sub>8</sub> H <sub>17</sub>	H	Cr 137 (SmA 122) I
OC <sub>8</sub> H <sub>17</sub>	H	OC <sub>8</sub> H <sub>17</sub>	H	H	H	OC <sub>8</sub> H <sub>17</sub>	H	Cr 144 I
OC <sub>8</sub> H <sub>17</sub>	H	H	OC <sub>8</sub> H <sub>17</sub>	H	H	OC <sub>8</sub> H <sub>17</sub>	H	Cr 125 (SmA 116) I
OC <sub>8</sub> H <sub>17</sub>	H	OC <sub>8</sub> H <sub>17</sub>	H	OC <sub>8</sub> H <sub>17</sub>	H	OC <sub>8</sub> H <sub>17</sub>	H	Cr 104 (SmA 100) I
H	OC <sub>8</sub> H <sub>17</sub>	OC <sub>8</sub> H <sub>17</sub>	H	H	OC <sub>8</sub> H <sub>17</sub>	OC <sub>8</sub> H <sub>17</sub>	H	Cr 115 I
OC <sub>8</sub> H <sub>17</sub>	OC <sub>8</sub> H <sub>17</sub>	OC <sub>8</sub> H <sub>17</sub>	H	OC <sub>8</sub> H <sub>17</sub>	H	OC <sub>8</sub> H <sub>17</sub>	H	Cr 62 I
OC <sub>8</sub> H <sub>17</sub>	OC <sub>8</sub> H <sub>17</sub>	OC <sub>8</sub> H <sub>17</sub>	H	H	OC <sub>8</sub> H <sub>17</sub>	OC <sub>8</sub> H <sub>17</sub>	H	Cr 104 I
OC <sub>8</sub> H <sub>17</sub>	H	OC <sub>8</sub> H <sub>17</sub>	OC <sub>8</sub> H <sub>17</sub>	OC <sub>8</sub> H <sub>17</sub>	H	OC <sub>8</sub> H <sub>17</sub>	OC <sub>8</sub> H <sub>17</sub>	Cr 88 I
OC <sub>8</sub> H <sub>17</sub>	OC <sub>8</sub> H <sub>17</sub>	OC <sub>8</sub> H <sub>17</sub>	H	OC <sub>8</sub> H <sub>17</sub>	OC <sub>8</sub> H <sub>17</sub>	OC <sub>8</sub> H <sub>17</sub>	H	Col <sub>h</sub> 68 I
OC <sub>10</sub> H <sub>21</sub>	OC <sub>10</sub> H <sub>21</sub>	OC <sub>10</sub> H <sub>21</sub>	H	OC <sub>10</sub> H <sub>21</sub>	OC <sub>10</sub> H <sub>21</sub>	OC <sub>10</sub> H <sub>21</sub>	H	Col <sub>h</sub> 54 I



Three series of related four-chain ((86):  $R = OC_8H_{17}$ ;  $R' = R'' = H$ ;  $X, Y = H, OH, OMe, OC_8H_{17}$ ), six-chain ((86):  $R = R' = OC_8H_{17}$ ;  $R'' = H$ ;  $X = OH, Y = OH, OC_8H_{17}$ ), and their isomeric congeners ((86):  $R = R'' = OC_nH_{2n+1}$ ;  $R' = H$ ;  $X, Y = H, OH, OMe, OC_8H_{17}$ ) nickel complexes were also prepared and studied.<sup>448</sup> In the first series, the mesomorphism displayed was of the smectic type (SmA and SmC), all the mesophase being monotropic (below 130 °C) with a reduction in the mesophase stability on increasing the size of the groups X and Y. Note that for one four-chained dihydroxy compound ((86):  $R' = OC_8H_{17}$ ;  $R = R'' = H$ ;  $X, Y = OH$ ), i.e., without chains at the *para*-positions, a broad Col<sub>h</sub> phase was induced from room temperature up to 190 °C. In the second series, the smectic mesomorphism was suppressed, and the dihydroxy compound showed a broad Col<sub>h</sub> mesophase from ambient to ca. 210 °C. The enhancement of the mesophase stability was connected strongly to the formation of intra-molecular hydrogen bonds which stiffened and broadened the mesogenic core. The range of the Col<sub>h</sub> phase was reduced strongly when one of the OH group was substituted by an octyloxy chain (Cr 100 Col<sub>h</sub> 137 I), probably due to the hindered rotation of one of the arms. Only the dihydroxy compound of the last series was mesomorphic, while none of those with combination of H, OH, and OMe groups were liquid crystals. Thus, the dihydroxy compound ((86):  $R = R'' = OC_nH_{2n+1}$ ;  $R' = H$ ;  $X, Y = OH$ ) displayed the most unusual phase sequence, with a re-entrant isotropic liquid, an enantiotropic Col<sub>h</sub> phase and a monotropic SmA phase: Cr 102 (SmA 78) I 95 Col<sub>h</sub> 197.5 I,  $n = 8$ . Similar phase behavior was obtained with the  $n = 10$  homolog or with the mixture 25% ( $n = 8$ ), 25% ( $n = 10$ ) and 50% of the mixed octyloxy-decyloxy compound. From X-ray diffraction, it was deduced that the molecules arranged in an alternating fashion in both SmA and Col<sub>h</sub> phases; thus, the SmA phase is of a monolayer type.



(85)



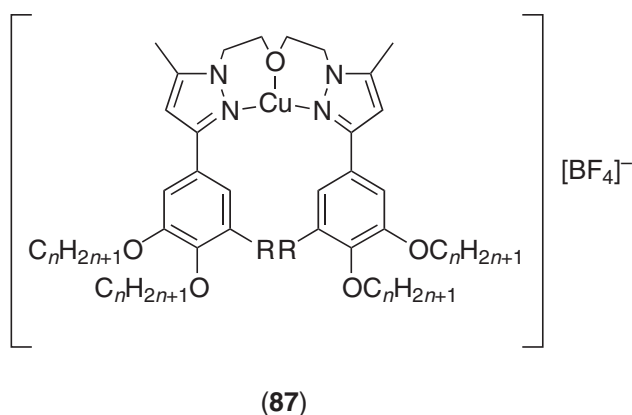
(86)

The unusual phase sequence Col<sub>h</sub>-I-SmA was supposed to arise from the difference in chain conformation. Thus, in the Col<sub>h</sub> phase, the molecules rotate around their short axis, and the chains are distributed homogeneously around the mesogenic core, whereas in the SmA phase, the rotation

occurs around the long molecular axis, and the chains are distributed anisotropically along this axis. The re-entrant isotropic liquid would, therefore, arise due to rotation around both axes.

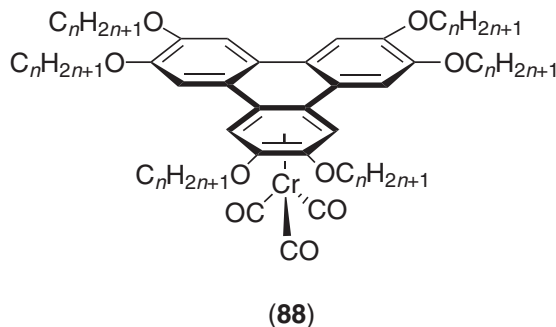
### 7.9.8.11 Complexes of Pyrazole-based Ligands

As seen earlier, half-disk-shaped metal complexes are not incompatible with the formation of stable columnar mesophases through the formation of correlated columns resulting from the alternating stacking of the molecular species along the columnar axis. Several novel examples have recently been provided, such as a copper(I) system based on bis(2-[3'-(substituted phenyl)-5'-methyl-1'-pyrazolyl]-ethyl) ethers, (**87**), reported by Lin *et al.*<sup>449</sup> In such systems, the Cu<sup>I</sup> center is unusually three-coordinate and is found within a T-shaped environment, apparently due to steric constraints. Thus, four- ((**87**): R = H,  $n = 8, 10, 12, 14, 16$ ) and six-chain ((**87**):  $n = 8, 10, 12, 14, 16$ ) copper(I) tetrafluoroborate complexes were prepared, and found to form enantiotropic Col<sub>h</sub> phases, with little dependence on chain length and number of chains. The melting and clearing temperature were found between 45–55 and 100–110 °C, respectively. In addition, the stability of the Cu<sup>I</sup> oxidation state was enhanced by the *N,O* bonding environment provided by the pyrazolyethyl ethers.

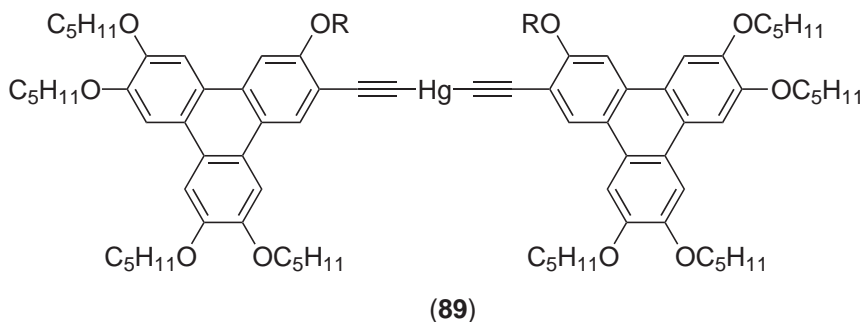


### 7.9.8.12 Metal Complexes Containing Triphenylene Units

Recently, original metallomesogens containing triphenylene sub-units have been reported. A series of ( $\eta^6$ -hexaalkoxytriphenylene)tricarbonylchromium(0) complexes (**88**) were obtained by refluxing the triphenylene, well known as a mesogen forming columnar phases, with [Cr(CO)<sub>6</sub>].<sup>450</sup> The chromium tricarbonyl moiety was attached exclusively to one of the peripheral, disubstituted rings as deduced from spectroscopic methods ((**88**):  $n = 5-10$ ). Upon complexation, the columnar stacking was severely disturbed by the bulky metallic fragment, and mesomorphism was either suppressed ( $n = 5-8$ ), unidentified ( $n = 10$ ), or modified ( $n = 9$ ). Thus, the authors claimed observation of a nematic phase for the related chromium complex (Cr 37 N<sub>D</sub> 58 I) with nonyloxy chains. The non-mesomorphic complexes cleared at temperatures close to that of the free triphenylenes, with a stronger destabilization of their crystalline phase on increasing chain length with respect to the corresponding free triphenylenes.



Another group reported the synthesis of discotic, mercury-bridged, triphenylene dimers ((**89**):  $R = OC_5H_{11}$ ,  $O(CH_2)_2CHMe(CH_2)_3CHMe_2$ ).<sup>451</sup> The bis(2,3,6,7,10-pentapentyloxytriphenylene-11-ethynyl)mercury(II) complex exhibited a highly viscous mesophase between 150 °C and 210 °C, and extensive decomposition precluded its identification. One of the pentyloxy chains was then replaced by the branched citronellyl chain, hoping to reduce the transition temperatures. This new complex cleared into the isotropic liquid at 186 °C, but on cooling a monotropic mesophase appeared at 185 °C, which transformed into a crystalline phase at 180 °C. On the basis of its *schlieren* texture, the mesophase was identified as  $N_D$ .

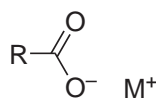


## 7.9.9 METAL CARBOXYLATES

It is now certain that metal carboxylates were the first metal-containing liquid crystals, reported in 1855 with Heinz's work on magnesium tetradecanoate.<sup>452</sup> Then, many other mesomorphic mono-, di-, and tri-valent carboxylate complexes, with the general formula  $[M(O_2CC_nH_{2n+1})_x]$  ( $x = 1, 2, 3$ ) or  $[M_2(O_2CC_nH_{2n+1})_4]$  were prepared. Some of them were described in 1910 by Vorländer.<sup>453</sup> These materials may show thermotropic nematic, smectic, cubic, and columnar mesophases, but also, when dissolved in water or alkanes, lyotropic mesophases. While not all of the compounds described in this section show columnar phases, it was decided to keep these materials together.

### 7.9.9.1 Carboxylates of Alkali Metals and Monovalent Metals

A systematic investigation of sodium salts as a function of temperature and of the acid chain length ( $n \geq 7$ ) ((**90**):  $M = Na$ ;  $R = C_nH_{2n+1}$ ) revealed that these compounds exhibit what the authors called *sub-waxy*, *waxy*, *super-waxy*, *sub-neat*, and *neat* phases.<sup>454–456</sup> The structures of the first four phases have been shown to be consistent with a two-dimensional, centered rectangular lattice of ribbons, whereas that of the last is lamellar. The two-dimensional arrangement of ribbons corresponds to the first thermotropic columnar mesophases observed, and the lamellar structure of the neat phase corresponds to a smectic phase. In the columnar mesophases, the polar groups are localized within the ribbons in such a way that their organization is crystalline, at least to a first approximation, whereas gradual disorder is established along the aliphatic chains, this disorder increasing with the distance from the ribbons. The equilibrium between the thermal agitation of the partially molten chains and the cohesion of the crystalline ribbons govern their width. By comparison, in the smectic phase the structure of the polar layers is disordered as in a two-dimensional liquid, and the conformation of the aliphatic chains is random along their entire length.



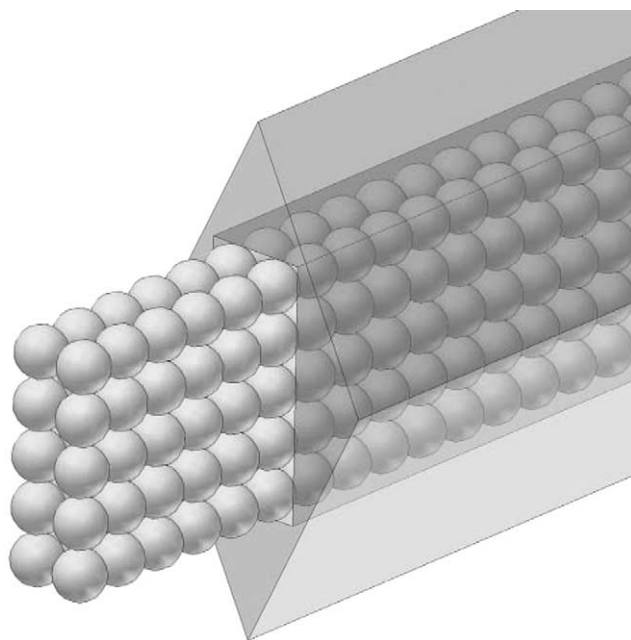


**Figure 41** Arrangement of polar groups (spheres) within ribbon phases.

The thermal behavior of these compounds is described as corresponding to a partial and continuous loss of order with increasing temperature. At low temperature, the structure is crystalline with a regular molecular arrangement. At a given temperature (above 100 °C), the organization within the aliphatic chains begins to break down, resulting in a breaking of the crystalline lamellae into ribbons (Figure 41), the width of which is determined by the equilibrium between the thermal motion of the chains and the extent of organization of the polar heads. The width of the ribbons becomes smaller and smaller with increasing temperature since the chains become more and more disorganized, until at high temperature the ribbons become so narrow that they collapse and the structure transforms from a columnar phase to a smectic phase.

Smectic and columnar mesophases have also been observed with lithium,<sup>457,458</sup> potassium,<sup>459–461</sup> rubidium,<sup>462,463</sup> and caesium<sup>464,465</sup> alkanooates ((90): M = Li, K, Rb, Cs; R = C<sub>n</sub>H<sub>2n+1</sub>). The case of lithium alkanooates, which has since been reinvestigated, confirms the original structural interpretation given by Skoulios *et al.*<sup>455,466</sup> At low temperature, a lamellar crystalline phase is characterized by double sheets of ionic groups alternated with layers of hydrocarbon chains in the all-*trans* conformation. At higher temperature, another lamellar phase has been tentatively described as being analogous to a rotator (plastic crystal) phase of linear paraffins. At even higher temperatures, a two-dimensional rectangular mesophase is found to be formed of ionic groups organized in ribbon-like double sheets of indefinite length with the hydrocarbons chains around in a liquid-like state.

Ubbelohde *et al.*<sup>467</sup> were the first to report on the liquid-crystalline behavior of alkali metal salts of short-chain alkanooates, in particular in the case of sodium butanoate and isovalerate. These compounds are particularly interesting because of the presence of a high electrostatic charge concentration and the absence of any pronounced anisometry. It was shown that there is a relationship between the mesophase formation and the radius and charge of the cation, as well as the chain length of the alkanooate anion.<sup>468</sup> Smectic mesophases have been found in binary mixtures of lithium and caesium acetates, propionates, and butyrates, which are themselves non-mesomorphic.<sup>469</sup> Ionic interactions in these molten systems give rise to electrostatic charge redistribution and the formation of new complex ions or ensemble of ions which create micro-ordering in the salt melt and ensure the appearance of a liquid-crystalline phase. Thus, the existence of a mesophase is not due to an anisotropy of the molecular shape but to an anisotropy of the distribution of the Coulombic charges. Binary ionic systems appear, therefore, able to provide additional possibilities for producing new liquid-crystalline phases as a consequence of the high sensitivity of the salt mesophase to the nature of its component ions. In contrast to classical smectic phases, ionic liquid-crystalline phases should show optical sensitivity with respect

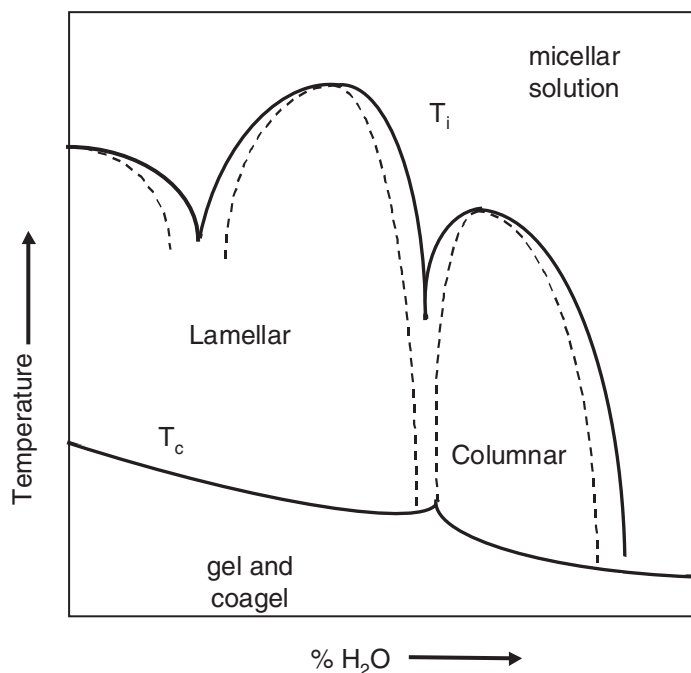


**Figure 42** Schematic phase diagram of the amphiphile–water binary system.

to even weak, alternating electric fields due to the high values of the components of the dielectric tensor of the ionic melt and the anisotropy of the electrical conductivity.

In an excellent review dealing with the supramolecular structures formed in concentrated aqueous solutions of alkali metal soaps, Skoulios described the different types of organization occurring as a function of the temperature and concentration and considered the influence of the electric interactions of the ionized polar groups on the structural parameters.<sup>470,471</sup> Three regions can be defined in the phase diagrams of soap/water binary mixtures (Figure 42). A micellar phase exists below  $T_i$ ; this phase is fluid, optically isotropic, and without any well-developed periodic structure. Between  $T_c$  and  $T_i$  exist birefringent mesophases with well-developed periodic structures. Finally, gel (transparent lamellar phase) and coagel (opaque phase resulting from demixing between the anhydrous alkaline soap and the aqueous solution) structures are formed below  $T_c$ , while lamellar, columnar, and even cubic phases can be found between  $T_c$  and  $T_i$ . The common feature of all these lyotropic phases is the disorganized state of the aliphatic chains of the soaps. The lamellar phase is formed by the stacking of alternated layers of soap molecules and water. The hydrophobic moieties are disordered whereas the hydrophilic ones are localized within the aqueous layers ((90):  $M = K^{472-474}$ ,  $Na^{475,476}$ ,  $Li$ ,  $Rb$ ,  $Cs^{477,478}$ ). The columnar mesophase results from a two-dimensional arrangement of indefinite cylinders formed by the soap molecules and separated by water molecules.<sup>474,476</sup> The hydrophobic chains are in a liquid-like state and the polar groups cover the surface of the cylinders. Mesophases were also observed in various sodium alkanoate–alkane binary mixtures.<sup>479</sup>

As far as the cubic phase is concerned, the structural element should have a polyhedral shape to be compatible with the symmetry of the lattice. Taking into account the size of the cubic cell with respect to that of the polar groups, the polyhedral shape can be considered as a sphere to a good approximation, and the structure of the cubic phase is thus described as resulting from the organization of water spheres localized in an aliphatic medium.<sup>480</sup> In all these phases where the polar groups are ionized and the aliphatic chains in a liquid-like state, the only important parameter is the specific area which is imposed by the electrical interactions within the aqueous regions. The specific area increases with temperature, and the dielectric constant of the system is small. The binary mixture adopts the type of structure (lamellar, columnar, or cubic) which best fits a good space-filling of the liquid aliphatic chains.

Below  $T_c$ , the gel phase is lamellar, but with ordered aliphatic chains. Soap molecules are parallel with one another and oriented perpendicular to the smectic planes, forming a single layer with the polar groups oriented alternately on each side of the aliphatic layer (Figure 43).

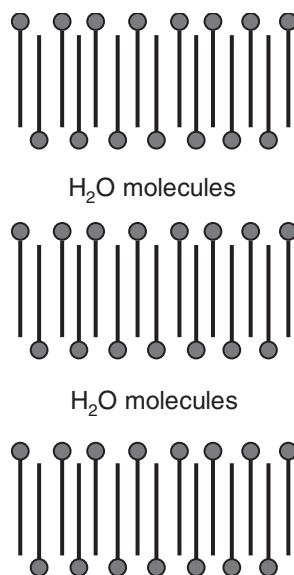


**Figure 43** Schematic of the gel phase of group 1 carboxylates.

The aliphatic chains are crystallized and are organized according to a hexagonal or rectangular lattice within each smectic layer. Water molecules are localized between the soap layers. In the present case, the structure should satisfy two contradictory tendencies, namely that the polar groups are disorganized and thus spread out, and the aliphatic chains are crystallized and thus the distance between them is well defined.

It is interesting to mention at this point the case of caesium perfluorooctanoate  $\text{Cs}(\text{O}_2\text{CC}_7\text{F}_{15})$  which provides a rare example of fluorinated surfactant coupled with unusual mesomorphic properties. In aqueous solution the molecules self-assemble into a nematic phase (micellar discotic nematic phase) over a large concentration range (0.25–0.65 weight fraction of surfactant) and temperature (11–77 °C); the phase is located between the isotropic micellar solution at higher temperatures/lower concentrations and the lamellar phase at lower temperatures/higher concentrations.<sup>481–483</sup> The aggregates were shown to adopt the shape of discrete discoid micelles, their size increasing with rising surfactant concentration, and coalescing eventually into an infinite bilayer structure. No other type of aggregation was detected over the entire concentration range. The rigidity and strong hydrophobicity of the fluorocarbon chain is responsible for the stability of the discoid micelles in a nematic arrangement over such a range. This is in contrast with the behavior of  $\text{Li}(\text{O}_2\text{CC}_7\text{F}_{15})$ ,<sup>484</sup> which aggregates in water into cylindrical micelles, which then self-assemble into a hexagonal  $\text{H}_1$  phase. The authors argued that the difference in aggregation behavior between these two salts can be explained by the hydration energy of the cations, lower for caesium ion than for lithium ion. The surface area and volume of the polar head of the latter is, therefore, increased with respect to chains, and the curvature of the hydrophilic/hydrophobic interface leads preferentially to the formation of cylindrical micelles.

As far as other monovalent metal carboxylates are concerned, only the thallium complexes have been studied ((**90**):  $\text{M} = \text{Tl}$ ;  $\text{R} = \text{C}_n\text{H}_{2n+1}$ ). Anhydrous thallium(I) alcanoates<sup>485,486</sup> have been shown to exhibit a liquid-crystalline lamellar mesophase, in which the layer thickness is less than twice the length of the fully extended molecule but greater than the length of one molecule. There is a head-to-head arrangement of the molecules within the layers, and both the headgroup and the hydrocarbon regions are in a disorganized state. The thermotropic behavior of anhydrous thallium(I) salts of branched aliphatic chains has also been investigated.<sup>487</sup> The salts of  $\alpha$ -branched acids do not show any smectic phase, whereas salts with alkyl chains substituted in the  $\beta$  and higher positions do show stable smectic phases.

Lamellar  $\text{L}_\alpha$  lyotropic phases were also induced in binary systems of  $\text{Tl}(\text{O}_2\text{CC}_n\text{H}_{2n+1})$  with their analogous free acids  $[\text{HO}_2\text{CC}_n\text{H}_{2n+1}]$ . All the binary mixtures from  $n = 3$  to  $n = 14$  were investigated and the lamellar phase was observed systematically.<sup>488</sup> Detailed temperature–composition phase diagrams of the  $n = 7$ <sup>489</sup> and  $n = 10$ <sup>490</sup>

Derivatives  $(x[\text{Tl}(\text{O}_2\text{CC}_n\text{H}_{2n+1})] + (1-x)[\text{HO}_2\text{CC}_n\text{H}_{2n+1}])$  revealed interesting features, similar for both, such as a eutectic reaction between the salt and the acid at very low mole-fractions of

salt ( $x$  ca. 0.1), a 1:1 acid–soap molecular compound (peritectic point), and the formation of a lamellar lyotropic mesophase in the high-temperature and salt-rich region (ca.  $x > 2/3$ , and  $T \approx 100^\circ\text{C}$ ).

### 7.9.9.2 Alkali-earth and Divalent Metal Carboxylates

In a systematic study of different alkali-earth carboxylates ((**91**):  $\text{M}(\text{O}_2\text{CC}_n\text{H}_{2n+1})_2$ ;  $\text{M} = \text{Mg}$ ,<sup>491</sup>  $\text{Cd}$ ,<sup>492</sup>  $\text{Ca}$ ,<sup>493,494</sup>  $\text{Sr}$ ,<sup>495</sup> and  $\text{Ba}$ <sup>496</sup>) as a function of temperature, Spelt and Skoulios showed that these compounds all exhibit a lamellar crystalline structure at room temperature and then paracrystalline and mesomorphic structures at higher temperatures until the complete melting.<sup>497</sup> These structures can be divided into two main classes. In the first one, the structural component is a disk formed by the polar groups of the molecules and surrounded by the aliphatic chains (Figure 44). In the second one, the structural component is a cylinder formed by the polar groups with the aliphatic chains being spread around. The common feature of the two classes of structure is the disorganized state of the hydrocarbon chains and the compact assembly of the polar groups. The number of metallic ions per unit length in a cylinder does not depend on the aliphatic chain length, nor on the temperature within one given cylindrical hexagonal mesophase, similar to the case of the ribbon phases described previously for anhydrous sodium soaps.<sup>455</sup> This implies that the arrangement of the polar groups is determined by the nature of the cation and by the geometry of its coordination.<sup>498</sup> The presence of a second hexagonal mesophase formed with cylinders occurs only with soaps with long aliphatic chains, the only difference between the two hexagonal phases lying in the values of the lattice parameters, which supports strongly the quasi-crystalline arrangement of the polar groups. Indeed, since the aliphatic chains are fully disorganized, the transition between the two hexagonal mesophases is related to a sudden change in the rearrangement of the polar groups, similar to the case of a polymorphic transformation. Note that the zinc and mercury<sup>499</sup> alkanooates of group 12 do not exhibit any liquid-crystalline mesomorphism ((**91**):  $\text{M} = \text{Zn}^{\text{II}}$ ,  $\text{Hg}^{\text{II}}$ ); this behavior can be attributed to insufficient cohesion between the polar groups to stabilize a mesophase.

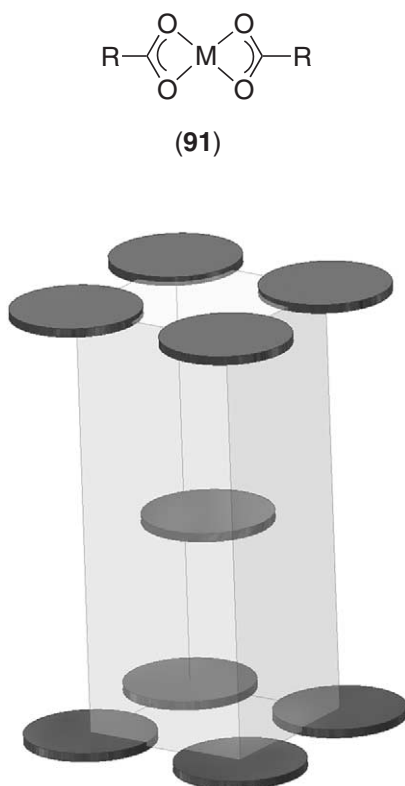


**Figure 44** Schematic of disks organized according to a three-dimensional, centered, rectangular lattice.

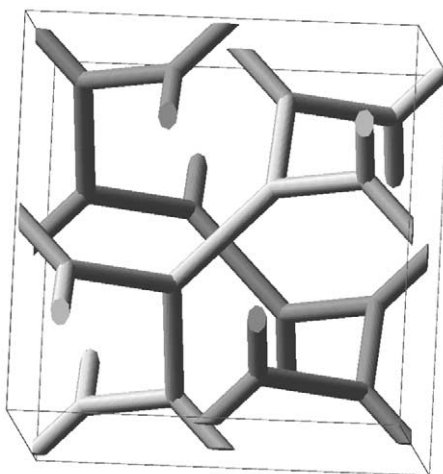


**Figure 45** Interwoven rod network of the cubic phase.

As a function of temperature, and up to 350 °C in some cases, magnesium and cadmium soaps exhibit only one or two cylindrical structures, whereas calcium soaps present both different successive structures with disk and cylinders. These two classes of structure are found also in strontium and barium soaps, with, in addition, a body-centered cubic structure.<sup>500</sup> These cubic phases have interesting features in that the polar groups are present on rods of finite length which belong to two, interwoven, infinite three-dimensional networks and the hydrocarbon chains constitute a continuous, paraffinic matrix (Figure 45).

It is interesting to note that most of the phases described so far for the alkaline and alkaline-earth carboxylates are formed by structural elements whose symmetry is analogous to that of the lattice found, namely planar sheets for the one-dimensional lamellar lattice, circular cylinders for the two-dimensional hexagonal lattice, rectangular prisms for the two-dimensional rectangular lattice and spheres for the face-centered cubic lattice. The body-centered cubic mesophase found at high temperature in strontium soaps does not belong to this category, since the structural element is a rod.

Mixtures of alkanooates and alkaline-earth metals have been investigated<sup>501,502</sup> with a view to preparing anisotropic two-dimensionally ordered ionic glasses. For example, binary mixtures of barium and sodium butanoates, or sodium butanoate with calcium and strontium butanoates, revealed the presence of a vitreous, anisotropic mesophase, which could be interesting for its physical and optical properties. The study of other systems obtained by mixing thallium butanoate with a divalent-metal butanoate (calcium, magnesium, zinc) has shown that the addition of the divalent metal soap causes thallium butanoate to express its latent liquid-crystalline properties.<sup>503</sup> Increasing the divalent cation content reduces the thermal stability of the induced mesophase to the point where it disappears. The smaller the radius of the divalent metal cation, the narrower the concentration range of the existence of the induced mesophase.

**Table 51** Mesomorphism of complexes (91)  $R = C_nH_{2n+1}$ ,  $n = 17$ .

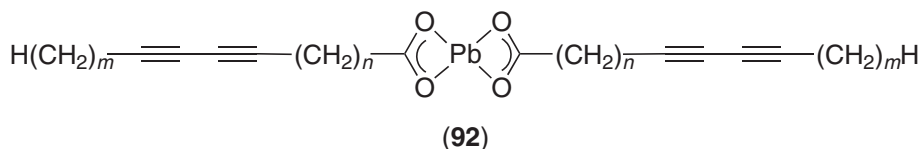
$M^{II}$	Mesomorphism <sup>a</sup>
Mg	Cr 110 Col <sub>h</sub> > 200 dec.
Ca	Cr 123 S 195 Col <sub>h</sub> > 350 dec.
Sr	Cr 220 Cub 275 Col <sub>h</sub> > 300 dec.
Ba	Cr 150 M 220 I
Cd	Cr 100 Col <sub>h</sub> > 230 dec.
Hg	Cr 115 I
Pb	Cr 111 S 115 I
Zn	Cr ~ 100 I

<sup>a</sup> S: non-identified smectic phase. M: unidentified mesophase.



Lead(II) carboxylates ((91): M = Pb) were investigated by several authors in the late 1980s.<sup>504–506</sup> In particular, detailed experimental data obtained by X-ray diffraction, DSC, optical observations with polarized light, and infrared, Raman,<sup>507</sup> and NMR<sup>508,509</sup> spectroscopic studies have permitted the reassignment of the thermotropic mesophases reported in 1976.<sup>510</sup> Thus, it appears that melting of the even-chain-length lead(II) carboxylates proceeds in more than one step. Heating from the initial lamellar crystalline phase results in a transition to another highly ordered lamellar phase characterized by partial disorder of the alkyl chains in the form of additional gauche conformations and decreased lateral interactions. The three-dimensional order is imposed by a kind of framework of ionic layers formed by strong ionic interactions. The alkyl chains sandwiched between the ionic layers are constrained to remain largely extended. This phase has also been described as condic crystal.<sup>511</sup> Further heating results in a transition directly to the isotropic phase for the longer-chain carboxylates. For the octanoate to the dodecanoate, complete melting proceeds via a disordered lamellar phase identified as smectic A, where the alkyl chains are completely disordered and where the remaining ionic interactions no longer impose three-dimensional order but still allow formation of a layer structure in two dimensions. A somewhat different view is also reported where the smectic phase is described as being of C type, although this is felt to be unlikely.<sup>512,513</sup> It should be noted that even in the isotropic liquid, the overall degree of dissociation of the lead carboxylate bond is small.

Lead(II) alkanediynoates (92), liquid-crystalline precursors to poly(diacetylenes), have also been investigated,<sup>514</sup> and are found to form highly ordered smectic structures with thermodynamic data similar to those of saturated lead(II) alkanooates ((91): M = Pb). In addition, they appear to form glassy mesophases at low temperatures, and thus the smectic structures can be observed at room temperature.



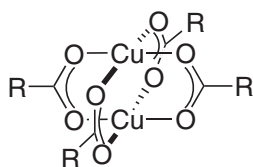
A number of studies have been reported concerning the solution behavior of some divalent carboxylate complexes ((91): M = Zn, Mn, Pb, Hg, Cd).<sup>515,516</sup> Krafft points (the Krafft point is the temperature at which micelles become soluble) and critical micelle concentration (cmc) were determined in a variety of long-chain alcohols, and for different carboxylate chain lengths. However, the demonstration of their lyotropic mesomorphism was not clear and it appeared that lamellar phases were induced, although over small ranges of temperature and concentration.

As in the case of the monovalent alkanooates of Tl<sup>I</sup>, binary mixtures of Pb<sup>II</sup> alkanooates [Pb(O<sub>2</sub>CC<sub>n</sub>H<sub>2n+1</sub>)<sub>2</sub>] with their acids were also investigated.<sup>517</sup> The detailed study of the binary mixture ( $x$ [Pb(O<sub>2</sub>CC<sub>13</sub>H<sub>27</sub>)<sub>2</sub>] + (1- $x$ )[HO<sub>2</sub>CC<sub>13</sub>H<sub>27</sub>])<sup>518</sup> revealed a surfactant-in-water-like behavior in that the solubility of the metal salt in the acid increased dramatically above a given concentration, a fact explained by the possible formation of micellar aggregates in the isotropic solution. At higher surfactant mole fractions ( $x > 0.33$ ), a cubic mesophase was thought to be induced, as concluded using polarized optical microscopy and the presence of large regions of total extinction. No molecular acid–soap association of any kind was found in the phase diagram. Since the anhydrous sample exhibits a lamellar mesophase, the acid likely inserts in the monolayer, forcing the apolar–polar interface to curve. In this case, the cubic phase would probably be bicontinuous, although X-ray diffraction studies are necessary to ascertain the true nature of the mesophase.

### 7.9.9.3 Transition Metal Alkanooates

#### 7.9.9.3.1 Tetra(alkanoato)dicopper(II) mesogens

Dicopper tetraalkanoates (93) have been known for many years for their “lantern” structures in the crystal state where two copper atoms are bridged by four carboxylate groups.<sup>519–522</sup> The copper–copper distance in the dimer is 2.58 Å, while between two dimers it is 3.22 Å. These materials have also been investigated thoroughly as a function of temperature since the early 1980s and have been shown to give rise to liquid crystal behavior, and in particular to columnar mesophases.



(93)

Indeed, all the copper alkananoates ((93):  $R = C_nH_{2n+1}$ ) from  $n = 2$  to  $n = 22$ , exhibit a mesophase at about  $120^\circ\text{C}$ ; the transition to the isotropic liquid occurs above  $200^\circ\text{C}$  with extensive decomposition. Inserting carbon-carbon double bonds in the carboxylate ligands or using a branched chain carboxylic acid results, however, in a significant decrease in the crystal-to-mesophase transition and, thus, to the occurrence of mesomorphic behavior near,<sup>523</sup> or even below,<sup>524</sup> room temperature. Copper octadecanoate was first reported to be a thermotropic liquid crystal in 1978 and its mesophase was assigned as SmC!<sup>525</sup> However, we now know that by retaining the binuclear units in the mesophase, as proved by EXAFS investigations,<sup>526-528</sup> the polar cores of the soap molecules are stacked to form columns of indefinite length, surrounded by the paraffinic chains with disordered conformations. The dimeric species are coordinated in axial positions by oxygen atoms of neighboring molecules, thus giving rise to pseudo-polymeric chains in which each copper atom is surrounded by five oxygen atoms in a square-pyramidal environment. Thus, the Cu atoms show square-planar coordination with four oxygen atoms, and form a weak, axial, intermolecular bond with one oxygen atom of the neighboring molecule (Figure 46).<sup>529</sup> Oriented parallel to each other, the columns are assembled into a two-dimensional, hexagonal lattice.<sup>530-533</sup> The transition from the crystal to the columnar mesophase is characterized by a change in the repeat distance of the binuclear cores along the pseudo-polymeric axis. In the crystalline phase, these cores are all oriented in the same direction with a repeat distance of  $5.2\text{ \AA}$ , while in the columnar mesophase, the polar cores are perpendicular to the columnar axis and superposed in a four-fold, helicoidal fashion, at least on a local scale, with a repeat distance of  $4.7\text{ \AA}$ . It is important to point out here that adjacent dicopper tetracarboxylate cores along a column are randomly shifted along the four possible metal-oxygen directions, perpendicular to that axis which allows interdimer bonding. The dynamic nature of this random disorder has been confirmed later on by neutron and NMR studies as we will see below. Note also that highly oriented fibers of copper dodecanoate obtained by melt-spinning of its columnar mesophase have been obtained. Examination by scanning electron microscopy and X-ray diffraction showed a high degree of orientation of the spun fibers in the solid state as well as in the columnar mesophase.<sup>534</sup>

X-ray diffraction experiments performed under pressure show that the area of the two-dimensional lattice decreases with increasing pressure and, at sufficiently high pressure, the columnar mesophase transforms into a crystalline lamellar phase. By combining Pressure-Volume-Temperature and X-ray diffraction measurements as a function of pressure, it was shown that the stacking period of the binuclear cores increases as a function of increasing pressure,<sup>535</sup> contrary to the lateral distance between columns which decreases, thus leading to a stretching of the columnar

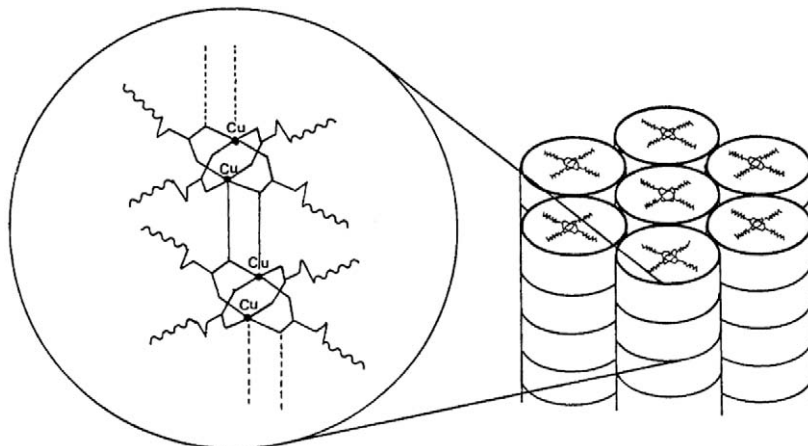
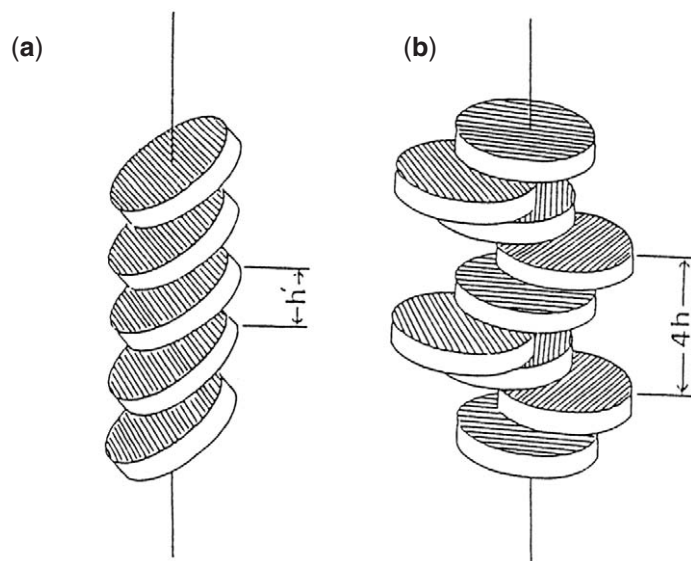


Figure 46 Organization of copper(II) alkananoates in the columnar hexagonal mesophase.



**Figure 47** Schematic representation of the stacking of the polar head groups of the soaps in (a) the crystalline, and (b) the columnar mesomorphic state.

cores. Starting from  $4.65 \text{ \AA}$  at ambient pressure, with the polar cores oriented perpendicular to the columnar axes, the stacking period increases to about  $4.8 \text{ \AA}$  at a pressure of 800 bar, a significant increase towards the distance found in the crystal ( $5.2 \text{ \AA}$ ). This stretching of the columns occurs concurrently with a tilting of the molecules and, thus, the action of pressure acts to bring the stacking mode of the polar heads nearer to that found in the crystal. This is achieved through a modification of the sequence of the oxygen atoms involved in the axial ligation, and a progressive tilting of the polar cores with respect to the columnar axis (Figure 47).

Different attempts to lock-in the long-range orientational order of the mesophases of the copper(II) carboxylates have been reported. One of them consisted of replacing the alkanolic acid moiety with a diacetylenic acid, namely, pentacos-10,12-diyonic acid, to lead to a new mesogenic material which can then be polymerized.<sup>536</sup> The copper complexes formed exhibited a mesophase with a lamello-columnar order, which has been processed into highly ordered crystalline fibers which were polymerized by UV radiation without disruption of the mesomorphic order. The combination of fiber morphology, order, and the presence of oriented polydiacetylene networks suggest that these systems could be of some interest as optically non-linear media.

Another attempt was to complex the copper(II) carboxylates with difunctional ligands such as pyrazine or bis-pyridine derivatives in order to form covalent, polymeric species consisting of stacks of the dinuclear complexes with the pyrazine or the bipyridyl as bridging ligand. However, the mesophases which have been found with such materials have not been elucidated to date. Some metallomesogenic polymers consisting of flexible aliphatic side chains with copper carboxylate complexes have been synthesized via addition reactions with polysiloxanes, with a view to applications in capillary gas chromatography analysis of phthalate esters.<sup>537,538</sup> These polymers are described as showing columnar mesophases. A recent study reports some copper(II) carboxylates with nicotinamide, which form mesophases in which the dimers are believed to be connected via hydrogen bonding to form a network.<sup>539</sup> This assumption was supported by the absence of mesomorphic properties in the related tetrakis- $\mu$ -carboxylatobis(dodecylnicotinato)dicopper(II) complexes.<sup>540</sup> Finally, there are a few copper carboxylates with the terminal chains modified by various groups (phenyl, esters, heterocycles, etc.) prepared in order to avoid thermal degradation occurring before clearing. This approach was found successful, and could be an interesting strategy for the design of thermally stable materials.<sup>541</sup>

With the aim of elaborating polymers with an anisotropic columnar structure and containing a quantitative ratio of metal centers incorporated to study their optical properties, *in situ* polymerization of reactive low-molar-mass liquid crystals oriented in their mesophase has been developed.  $\text{Cu}^{\text{II}}$ ,  $\text{Mg}^{\text{II}}$ , and  $\text{Zn}^{\text{II}}$  carboxylates bearing terminal acrylate functions and their subsequent

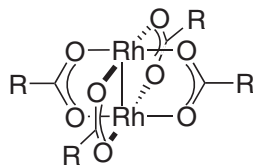
photo-polymerization were investigated.<sup>542</sup> This study revealed that the polymerization process is inhibited by copper(II) centers, whereas the close-shell Mg<sup>II</sup> and Zn<sup>II</sup> complexes could be polymerized as efficiently as other organic diacrylate monomers. Moreover, the hexagonal columnar structure of the mesomorphic monomer is retained in the polymer, giving rise to a material with a locally anisotropic structure.

The columnar hexagonal structure of the copper(II) alkanooates can be transformed into a nematic phase when these compounds are mixed with various hydrocarbon solvents.<sup>543,544</sup> Without perturbing the internal structure of the columnar cores, the solvent molecules are located among the disordered chains of the soap and lead the hexagonal lattice to expand in proportion to their amount in the mixture. Having lost their long-range, lateral positional order, but still aligned parallel to each other along the nematic director, their polar cores remain qualitatively unchanged. An alternative manner to induce the columnar-to-nematic transition in these systems is based on the introduction of geometrical disorder in the columnar mesophase by mixing copper(II) alkanooates of different chain lengths ( $x\%[\text{Cu}_2(\text{O}_2\text{CC}_n\text{H}_{2n+1})_4] + (1-x\%)-[\text{Cu}_2(\text{O}_2\text{CC}_m\text{H}_{2m+1})_4]; n \neq m$ ).<sup>545</sup> Viscoelastic organogels of copper complexes can also be formed in cyclohexane.<sup>546</sup>

Magnetic susceptibility studies of the copper alkanooates have proved to be very useful in probing the structural rearrangements upon the transition from the crystalline to the columnar phase.<sup>547</sup> Infrared studies indicated that it should be possible to follow phase changes by monitoring the position of the methylene frequency.<sup>548</sup> In particular, they concluded that a slight reorganization of the coordination shell, which retains the binuclear structure of the complex, occurs at the solid-phase transition;<sup>549</sup> this result was confirmed by dilatometry experiments.<sup>550</sup> The dynamic behavior of alkyl chains in a series of copper(II) alkanooate complexes was studied by incoherent quasidelectron neutron scattering, both in the crystalline and liquid-crystalline state.<sup>551,552</sup> It was concluded that large motions occur not only in the high-temperature columnar phase, but also in the crystalline phase; this is in accord with the large values of the temperature factors found in the X-ray crystallographic studies reported above. Moreover, the mean amplitude of the motion was observed to increase continuously with increasing length of the alkyl chains, and the part of the chain close to the columnar core moving in the same manner irrespective of the chain length. It was also suggested from these studies that a folding of the alkyl chains occurs in the mesomorphic phase which would facilitate the rotation of the whole molecule about the Cu–Cu axis. Further studies performed on oriented fibers of copper dodecanoate using neutron backscattering technique have shown that the motions of the methylene groups take place preferably in the equatorial plane of the copper dodecanoate molecules in their columnar phase.<sup>553</sup> This result is obviously related to the stereochemistry of the molecules and to their close axial packing in the columnar structure. With only four peripheral alkyl chains for each binuclear complex, there is more space available in the equatorial plane between the chains than in the direction of the columnar axis for the motions of the hydrogen atoms of the chains.

#### 7.9.9.3.2 Other tetraalkanoatedimetal complexes

Subsequently, related dimeric tetracarboxylates, but containing single and multiple metal–metal bonds, were prepared and found to be mesomorphic. The first examples of this type were the dirhodium(II) complexes ((94):  $\text{R} = \text{C}_n\text{H}_{2n+1}$ ) with a Rh–Rh single bond, which formed Col<sub>h</sub> mesophases between 100 °C and 200 °C, at which temperature they decomposed.<sup>554,555</sup> The columnar hexagonal mesophases were structurally identical to those of the copper tetracarboxylates.<sup>556</sup>

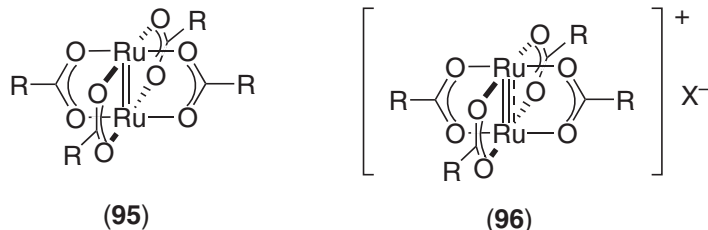


(94)

High-resolution <sup>13</sup>C NMR spectroscopic studies of dirhodium tetracarboxylates in their crystal and liquid-crystalline phases have provided a direct probe of the local symmetry and dynamics of the columnar mesophase of these complexes.<sup>557</sup> In particular, it has shown that the dimetallic

cores undergo fast axial bond exchange; moreover, among the two types of possible molecular motions of the dimers (horizontal shift and  $C_4$  rotation) which can result in statistical interdimer bonding, the rotation seems the more consistent with the NMR results, in agreement with the results obtained by neutron scattering on copper soaps (see above).

Diruthenium tetracarboxylates ((95):  $R = C_nH_{2n+1}$ ) containing a  $Ru^{II}=Ru^{II}$  double bond, and the paramagnetic, mixed-valence ((96):  $R = C_nH_{2n+1}$ ,  $X = O_2CC_nH_{2n+1}$ ) analogs, also formed columnar mesophases.<sup>558,559</sup> X-ray diffraction suggested the same model for the molecular organization of the  $Ru^{II}/Ru^{II}$  complexes in the columnar phase as that proposed for their isostructural copper and rhodium alkanoates, although for the  $Ru^{II}/Ru^{III}$  complexes, the intermolecular  $Ru-O$  interactions are not present as the anionic group acts as a spacer between  $Ru_2$  dimer units.



The  $Ru^{II}/Ru^{II}$  complexes substituted with linear alkyl chains (from  $R = C_4H_9$  to  $R = C_{19}H_{39}$ ) or unsaturated chains ( $R = CH_2=CH(CH_2)_8-$  and  $(CH_3)_2C=CHCH_2CH_2CH(CH_3)CH_2-$ ) showed a columnar hexagonal mesophase above  $100^\circ C$  (Table 52), although the isotropic liquid could not be reached due to decomposition.<sup>560</sup> It should be noted here that, as in the case of copper(II) and rhodium(II) carboxylates, unsaturation in the peripheral alkyl chains contributes strongly to the depression of the transition temperatures to the liquid-crystalline phase (Table 52). It can readily be seen from Table 52 that this transition temperature is also quite dependent upon chain length in the case of the linear carboxylates, decreasing from  $160^\circ C$  for  $n = 3$  to  $96^\circ C$  for  $n = 8$ , and remains relatively constant from  $n = 9$  to  $n = 19$  at around  $100^\circ C$ . For the complexes with short aliphatic chains, the cohesion of the metallic cores is preponderant and governs the stability of the crystal phase. However, this cohesion is disturbed when the chains get longer, and then the crystal stability is affected by the packing and interactions of the long fatty chains, leading to a somewhat constant value of the melting point.<sup>561</sup> In spite of the close proximity of the metallic centers and of the uni-dimensional character of the structure, no long-range magnetic interactions could be detected in these systems. Pyrazine adducts were not mesomorphic.

**Table 52** Transition temperatures of some dinuclear carboxylates (93 and 95 to 97) with branched, unsaturated and fluorinated chains.

<i>R</i>	<i>Mesomorphism</i>
-C*H(Et)C <sub>4</sub> H <sub>9</sub>	M = Cu <sup>II</sup> : Cr 101 Col <sub>h</sub> dec.
-CH <sub>2</sub> CH(C <sub>9</sub> H <sub>19</sub> ) <sub>2</sub>	M = Cu <sup>II</sup> : Cr 75 Col <sub>h</sub> dec.
-CH(C <sub>8</sub> H <sub>17</sub> ) <sub>2</sub>	M = Cu <sup>II</sup> : Col <sub>h</sub> 214 dec.
-(CH <sub>2</sub> ) <sub>3</sub> -C <sub>6</sub> H <sub>5</sub>	M = Cu <sup>II</sup> : Cr 155 M 235 I
-(CH <sub>2</sub> ) <sub>2</sub> CO <sub>2</sub> C <sub>10</sub> H <sub>21</sub>	M = Cu <sup>II</sup> : Cr 111 I
-(CH <sub>2</sub> ) <sub>8</sub> CH=CH <sub>2</sub>	M = Cu <sup>II</sup> : Cr 44 Col <sub>h</sub> > 200 dec. M = Ru <sup>II</sup> /Ru <sup>II</sup> : Cr 53 Col <sub>h</sub> > 200 dec.
-CH <sub>2</sub> CH(Me)(CH <sub>2</sub> ) <sub>2</sub> CH=CM <sub>e</sub> <sub>2</sub>	M = Cu <sup>II</sup> : Cr 70 Col <sub>h</sub> > 200 dec. M = Ru <sup>II</sup> /Ru <sup>II</sup> : Cr 79 Col <sub>h</sub> > 200 dec.
-(CH <sub>2</sub> ) <sub>11</sub> CH=CHC <sub>8</sub> H <sub>17</sub>	M = Cu <sup>II</sup> : Cr 63 M 190 I
-(CH <sub>2</sub> ) <sub>7</sub> CH=CHC <sub>8</sub> H <sub>17</sub>	M = Cu <sup>II</sup> : Cr 33 Col <sub>h</sub> > 200 dec.
-(CH <sub>2</sub> ) <sub>7</sub> CH=CHC <sub>6</sub> H <sub>13</sub>	M = Ru <sup>II</sup> /Ru <sup>III</sup> (O <sub>2</sub> CCR): Cr 128 Col <sub>h</sub> > 300 dec.
-(CH <sub>2</sub> ) <sub>8</sub> C-C≡C-C≡C-C <sub>12</sub> H <sub>25</sub>	M = Cu <sup>II</sup> : Cr 85 D <sub>L</sub> 210 dec.
-(CH <sub>2</sub> ) <sub>2</sub> C*H(Me)C <sub>5</sub> H <sub>11</sub>	M = Mo <sup>IV</sup> : Cr 35 Col 130 I
-C <sub>7</sub> F <sub>15</sub>	M = Ru <sup>II</sup> /Ru <sup>II</sup> : Not LC
	M = Cr <sup>IV</sup> : Cr 160 I
	M = Mo <sup>IV</sup> : Cr 165 Col 200 I
	M = W <sup>IV</sup> : Cr 25 I

M: unidentified mesophase, Col: unidentified columnar phase.

The mixed-valent Ru<sup>II</sup>/Ru<sup>III</sup> carboxylates are of interest because of their significantly greater air stability (decomposition does not occur before 190 °C)<sup>562,563</sup> compared to the isostructural Ru<sup>II</sup>/Ru<sup>II</sup> complexes, and also because of their unique magnetic and electronic properties (each dimer has three unpaired electrons). Different series of these tetracarboxylates (**96**) containing different combinations of equatorial carboxylates (RCO<sub>2</sub><sup>-</sup>) have been reported.<sup>564</sup> In the case of the series derived from linear, aliphatic carboxylates, the nature of the counter-ion affects the appearance of the liquid-crystalline order strongly. Thus, the chloro complexes ((**96**): X = Cl) are not mesomorphic, whereas the complexes with carboxylate or dodecyl sulfate as counter-anion ((**96**): X = O<sub>2</sub>CC<sub>n</sub>H<sub>2n+1</sub>, *n* = 5 to 15; X = O<sub>3</sub>SOC<sub>12</sub>H<sub>25</sub>, i.e., DOS) exhibit a columnar hexagonal mesophase above ca. 150 °C. From the X-ray diffraction data, it has been found that the columnar area is approximately three times larger than that calculated for the Ru<sup>II</sup>/Ru<sup>II</sup> (**95**) analogs corresponding to the same chain length. To understand the molecular arrangement in the mesophase of these mixed-valent complexes, it is reasonable to assume that the polymeric chains which exist in the crystalline phase<sup>565</sup> are retained in the columnar phase as has been suggested in several spectroscopic and magnetic studies. But to take into account the large parameter of the hexagonal mesophase, the structural model implies that each column of the hexagonal array is made up of four polymeric chains of dinuclear carboxylates entangled and axially shifted by half a dimer, as schematically represented in Figure 48.

Magnetic properties of several of these mixed-valent, long-chain, diruthenium carboxylates have been investigated.<sup>566</sup> Such studies provide important information about the electronic structure and the interdimer interactions present in these materials, showing in particular that the magnetic features of the [Ru<sub>2</sub>(μ<sup>2</sup>-O<sub>2</sub>CR)<sub>4</sub>]<sup>+</sup> moiety are essentially independent of the carboxylate substituent. Some axially coordinated anions can mediate antiferromagnetic interactions between neighboring ruthenium dimers. The interdimer exchange is negligible in the case of the dodecylsulfate anion (DOS), whereas in the chloride series the magnitude of this interaction can be important and is dependent on the Ru–Cl–Ru angle.<sup>567</sup> These studies also indicate that no significant structural change occurs at the crystal–liquid crystal transition in these metallomesogens.

Chisholm and co-workers prepared liquid-crystalline dimetallic carboxylates containing quadrupole bonds ((**97**): M = Mo<sup>II</sup>, Cr<sup>II</sup>, W<sup>II</sup>; R = C<sub>n</sub>H<sub>2n+1</sub>) which exhibited Col<sub>h</sub> mesophases.<sup>568–570</sup> The molybdenum alkanoates were mesomorphic from *n* = 3 to *n* = 9, and were thermally stable up to 250 °C. The melting points decreased rapidly from *n* = 3 (152 °C) to *n* = 4 (108 °C), and then remained almost constant, whereas the clearing temperatures decreased almost linearly with increasing *n*, resulting in the loss of the mesophase from *n* ≥ 10. The chromium complexes ((**97**): M = Cr) behaved very much like their ruthenium analogs, while the tungsten complexes ((**97**): M = W) were not mesomorphic. The similarity of the enthalpies of the crystal-to-columnar phase transition and of the melting point for all the metal carboxylates of identical chain length implies that dimeric interactions, and thus, axial metal–oxygen interactions are preserved in each system independent of the metal. Hence, the same model as that proposed for the copper complexes can be applied for Mo and Cr complexes. Furthermore, the differences in the thermal behavior and in the clearing points are in agreement with the strength of the axial ligation, which follows the order Cr ≫ Mo > W, and Cu, Rh, Ru ≫ Mo. For M = Mo, the axial interactions are weak enough to be overcome at temperatures before decomposition but strong enough to allow access to the mesophase, whereas for M = Cr, the axial interactions are comparable to those in the late

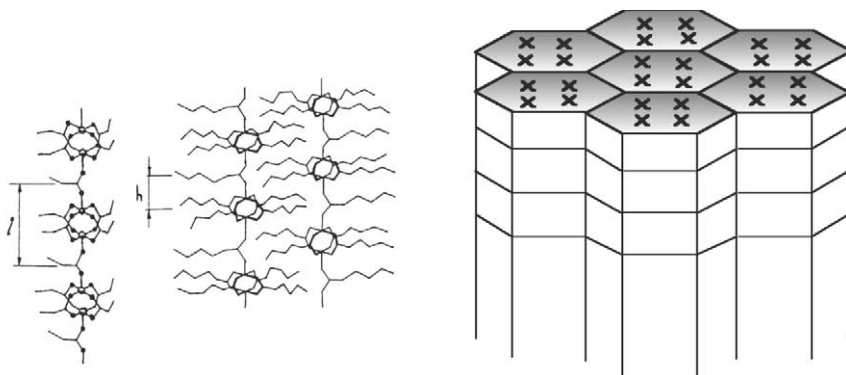


**Figure 48** Packing of dinuclear ruthenium carboxylates in the Col<sub>h</sub> phase.

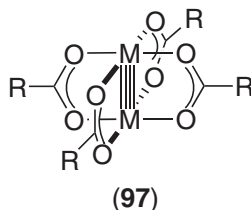


**Table 53** Comparison of the mesomorphism of complexes (93) to (97).

<i>M</i>	Bond multiplicity	<i>X</i>	$C_7H_{15}$	R $C_{11}H_{23}$	$C_{17}H_{35}$
$Cu^{II}$	0		Cr 85 Col <sub>h</sub> > 200 dec.	Cr 107 Col <sub>h</sub> > 200 dec.	Cr 116 Col <sub>h</sub> > 200 dec.
$Rh^{II}$	1		Cr 95 Col <sub>h</sub> > 220 dec.	Cr 100 Col <sub>h</sub> > 220 dec.	
$Ru^{II}$	2		Cr 103 Col <sub>h</sub> > 290 dec.	Cr 99 Col <sub>h</sub> > 290 dec.	Cr 103 Col <sub>h</sub> > 240 dec.
$Ru^{II}/Ru^{III}$	2.5	Cl	Cr > 260 dec.	Cr > 260 dec.	
$Ru^{II}/Ru^{III}$	2.5	$O_2CC_nH_{2n+1}$	Cr 156 Col <sub>h</sub> > dec.	Cr 150 Col <sub>h</sub> > dec.	
$Ru^{II}/Ru^{III}$	2.5	$C_{12}H_{25}OSO_3$	Cr 121 Col <sub>h</sub> ~ 200 dec.	Cr 152 Col <sub>h</sub> ~ 200 dec.	Cr 143 Col <sub>h</sub> ~ 200 dec.
$Mo^{IV}$	4		Cr 100 Col <sub>h</sub> 147 I	Cr 111 I	Cr 112 I
$Cr^{IV}$	4		Cr 99 Col <sub>h</sub> > 300 dec.	Cr 98 Col <sub>h</sub> > 320 dec.	Cr 107 Col <sub>h</sub> > 240 dec.
$W^{IV}$	4		Cr 90 I		

transition-metal tetracarboxylates and thus, the liquid-crystalline phase does not clear before the complex decomposes. When thiocarboxylates are used, replacing the  $M_2 \cdots O$  by  $M_2 \cdots S$  interactions, no mesophase is observed.

The rheology of dimolybdenum and dicopper octanoates was studied in their liquid-crystalline state and was found to be similar to that of conventional viscoelastic polymers such as polyethylene or polypropylene.<sup>571</sup> This strongly supports the observation that these metallomesogens form polymeric chains in their columnar mesophases, and thus can be processed in a way similar to that of conventional polymers to form films and fibers. Note, however, that the chains are believed to be dynamic, constantly being formed and re-formed due to the weak nature of the axial, intermolecular  $M \cdots O$  interactions.

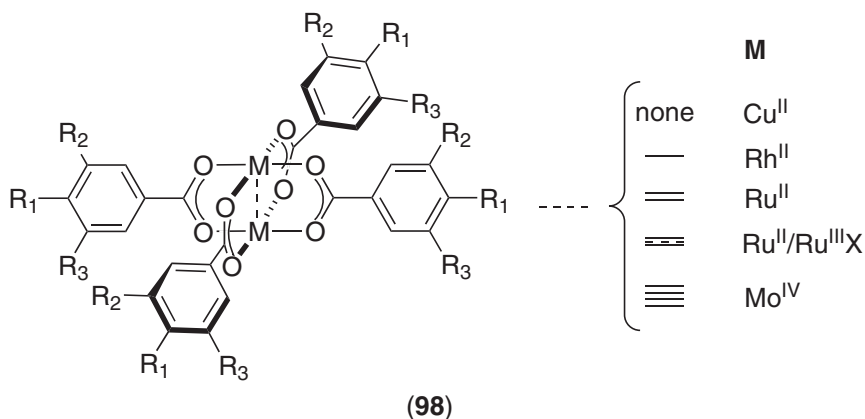
Induction and enhancement of mesophase stability were also observed through the use of mixtures of molybdenum complexes having alkyl chains with different length ( $[Mo_2(O_2CC_nH_{2n+1})_{4-x}Mo(O_2CC_mH_{2m+1})_x]$ ,  $n = 7, m = 8; n = 8, m = 11$ ) or chemical nature ( $[Mo_2(O_2CC_7H_{15})_{4-x}Mo(O_2CC_7F_{15})_x]$ ).<sup>572</sup>

In Table 53, the mesomorphic properties of dimetal carboxylates are compared as a function of both the metal ion and chain length.

### 7.9.9.3.3 Tetra(benzoato)dimetal complexes

A series of tetra(benzoato)dirhodium(II) complexes ((98):  $M = Rh$ ), substituted with different numbers of aliphatic chains, was prepared by Barberá *et al.*<sup>573</sup> and Rusjan *et al.*<sup>574</sup> These molecules contain four aromatic rings attached to the dinuclear benzoate unit, leading to a larger central core.

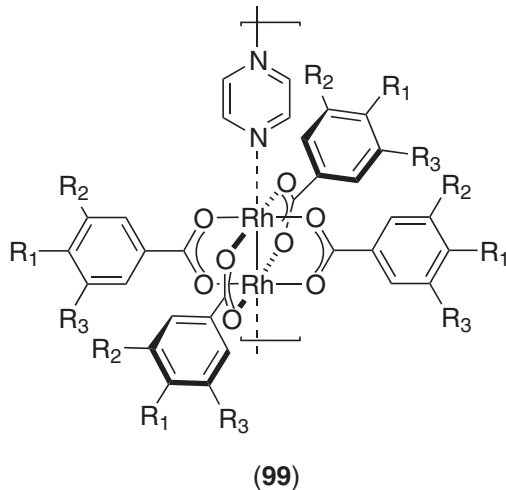
These complexes were also shown to display columnar mesophases, the symmetry of which depended on the number of peripheral chains attached to the phenyl rings. With four chains in total, the columnar mesophase has a rectangular symmetry and a regular intracolumnar stacking with the chains oriented in one preferred direction instead of surrounding the central core. With eight chains, the columnar mesophase has a rectangular symmetry at room temperature and a hexagonal symmetry at higher temperature. With twelve decyloxy chains, the rhodium complexes exhibit a crystalline phase at room temperature and a hexagonal columnar mesophase at higher temperature (see Table 54). The larger size of the rigid core in the benzoate derivatives in comparison with that in alkanooates precludes the formation of the hexagonal mesophase when only four alkoxy chains are present. The small number of chains is not sufficient to fill efficiently the space around the tetrabenzoate cores, and therefore the chains tend to align in one main direction giving rise to a rectangular columnar mesophase. On the contrary, twelve chains contribute to stabilize the hexagonal columnar mesophase with a good space filling around the



core. The mesomorphic behavior of the binuclear  $\text{Rh}^{\text{II}}$  complexes with eight chains is intermediate with the appearance of a rectangular mesophase at low temperature and a hexagonal mesophase at higher temperature, due to a stronger thermal conformational disorder allowing space-filling facilities of the alkoxy chains around the central core. It is clear from this study that the ratio of the volume occupied by the rigid core to the volume occupied by the flexible peripheral chains is the predominant factor in the type of symmetry of the mesophases displayed by these materials.

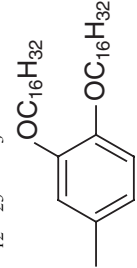
These electron-rich, bimetallic carboxylates with a "lantern" structure are powerful building blocks for one-dimensional coordination polymers, and a suitable ligand often used to bridge the metallic centers is pyrazine (pz). Indeed, much effort has been directed towards the synthesis of such one-dimensional polymers ( $[\text{M}_2(\mu^2\text{-O}_2\text{CR})_4(\text{pz})]_{\infty}$ ). Unfortunately, all the compounds obtained, namely  $[\text{Cu}_2(\mu^2\text{-O}_2\text{CC}_n\text{H}_{2n+1})_4(\text{pz})]$  ( $n=9,15$ ),  $[\text{Ru}_2(\mu^2\text{-O}_2\text{CC}_{11}\text{H}_{23})_4(\text{pz})]$ , and  $[\text{Rh}_2(\mu^2\text{-O}_2\text{CC}_6\text{H}_4\text{OC}_8\text{H}_{17})_4(\text{pz})]$  were not mesomorphic; copper derivatives polymerized by 4,4'-bipyridine were similarly not mesomorphic. The only compound that appeared promising was a branched-chain carboxylate complex of copper, although a detailed characterization of its mesophase was not reported.

The absence of mesomorphism in these compounds was explained on the basis of space-filling requirements. Thus, the intercalation of pyrazine between the binuclear units creates free volume which needs to be filled to obtain a stable, condensed phase; when the carboxylates bear only one chain, the interdimeric space is likely filled by the aliphatic chains belonging to a different polymeric chain, giving rise to a crossed structure which prevents the formation of a columnar mesophase. However, as will be seen later, liquid-crystalline behavior was induced in the case of mixed-valence diruthenium(II,III) carboxylate complexes with bulky equatorial ligands bearing two and three aliphatic chains; as with such ligands, it was possible to fill the interdimeric space and thus to induce a thermotropic columnar mesophase. Very recently, the synthesis, characterization, and mesomorphic properties of pyrazine-polymerized divalent rhodium benzoates have also been reported (99).<sup>574</sup> Most of these compounds exhibit columnar ( $\text{Col}_h$ ,  $\text{Col}_r$ ,  $\text{Col}_N$ ) and cubic mesophases with melting transition temperatures close to, or even below, room temperature.





**Table 54** Mesomorphism of complexes (98).

<i>M</i>	<i>n</i>	<i>X</i>	<i>Chain substitution</i>		
			$R_1 = OC_nH_{2n+1}$ $R_2 = R_3 = H$	$R_1 = R_2 = OC_nH_{2n+1}$ $R_3 = H$	$R_2 = R_3 = OC_nH_{2n+1}$ $R_1 = H$
Cu <sup>II</sup>	8		Cr 175 S dec.		Cr 80 Col <sub>h</sub> 130 I
	12				Cr 85 Cub 113 I
Rh <sup>III</sup>	18				Cr 55 Col <sub>h</sub> 189 I
	10		Cr 156 Col <sub>r</sub> 203 I	Col <sub>r</sub> 138 Col <sub>h</sub> > 235 dec. Cr 57 Col <sub>r</sub> 109 Col <sub>h</sub> 175 I	Cr 45 Col <sub>h</sub> 90 I
Ru <sup>III</sup> Ru <sup>III</sup>	18			Cr ~50 S 157 Col <sub>h</sub> dec. Cr 90 S 140 Col <sub>h</sub> 306 I	Col <sub>h</sub> > 220 dec. Cr 30 Col <sub>h</sub> 285 I
	12	Cl			Cr 58 Col <sub>h</sub> > 220 dec.
Ru <sup>III</sup> Ru <sup>III</sup>	14	Cl			
	18	Cl			
Ru <sup>III</sup> Ru <sup>III</sup>	16	C <sub>12</sub> H <sub>25</sub> OSO <sub>3</sub>		Cr 41 M 160 I	
	16			Col <sub>ho</sub> 48 Col <sub>h</sub> > 260 dec.	
Cr <sup>IV</sup>	7				
Mo <sup>IV</sup>	7		Cr 260 Col 270 I		
			Cr 250 dec.		

<sup>a</sup> M: unidentified mesophase. S: unidentified smectic phase. Col: unidentified columnar phase.

Thus, it is possible to obtain polymeric metallomesogens in which the electron-rich metal centers are connected by communicating ligands, giving rise to structures which might eventually act as molecular wires.

In the case of the ruthenium series ((98):  $M = \text{Ru}^{\text{II}}$ ) derived from benzoates possessing several aliphatic chains (namely the 3,4-dialkoxybenzoates), the formation of mesophases was enhanced, even with a small anion, such as chlorine, in contrast to the non-mesomorphic character of the linear aliphatic analogs. Furthermore, the transition from the crystalline to the liquid-crystalline phase of the penta-benzoates ((98):  $\text{Ru}^{\text{II}}/\text{Ru}^{\text{III}}$ ,  $X = \text{O}_2\text{CC}_6\text{H}_4(\text{OC}_n\text{H}_{2n+1})_2$ ) was lowered considerably using this type of ligand, and indeed, room-temperature liquid crystals were obtained. These results indicate that the key parameter which can be tuned in order to enhance the mesomorphic behavior of these materials is an efficient filling of space around a rigid "skeleton" of stacked, polar cores within a columnar structure.

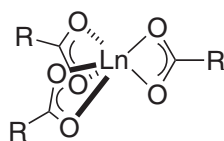
More recently, binuclear complexes derived from long-chain 3,4,5-trialkoxybenzoates with chlorine were prepared<sup>575</sup> ((98):  $M = \text{Ru}^{\text{II}}/\text{Ru}^{\text{III}}$ ,  $X = \text{Cl}$ ) and showed a low-temperature  $\text{Col}_h$  phase, with in particular, room-temperature mesophases for the decyloxy and dodecyloxy homologs. Diruthenium(II,III) 3,4-di- 3,5-di- and 3,4,5-tri-(tetradecyloxy)benzoates also exhibited lyotropic mesophases in dodecane.<sup>576</sup> They all behave similarly, in that the  $\text{Col}_h$  phase is seen at concentrations below 40–55 wt.% of solvent. Above this concentration, and up to 60–70 wt.% of solvent, the 3,5-di- and 3,4,5-trialkoxy compounds exhibited an additional  $\text{Col}_N$  phase.

The related trialkoxybenzoate copper complexes ((98):  $M = \text{Cu}$ ) was also mesomorphic, between 75 and 85 °C and 110 and 130 °C, but the most intriguing feature was the change of the  $\text{Col}_h$  phase ( $n = 10, 12, 14$ ) into a  $\text{Cub}$  phase ( $n = 16, 18$ ) with increasing chain length. The cubic phase was found to exist in the space  $\text{Im}\bar{3}\text{m}$  group, but whether the phase is bicontinuous or micellar has yet to be established.

#### 7.9.9.3.4 Lanthanide carboxylates

The molecular design of liquid crystals containing lanthanide ions led to metallomesogens where the coordination number is higher than 6, since the coordination number of these trivalent ions is typically 8 or 9<sup>577</sup> (see in particular the crystal structure of lanthanum(III) butanoate monohydrate).<sup>578</sup> The main driving forces for the development of lanthanide-containing liquid crystals were essentially due to the unique physical properties of lanthanide ions, such as a very intense photo- or electro-luminescence and the paramagnetism due to the unfilled 4f subshell. However, this molecular design is a challenge: indeed, because of the high coordination number of trivalent lanthanide ions in complexes, it is rather difficult to obtain complexes which show a sufficient structural anisotropy to induce stable mesophases.

Infrared spectroscopic and conductometric studies were performed on some lanthanide octanoates in 1995, but with no mention of any particular thermal behavior.<sup>579</sup> However, some years later, mesomorphism of lanthanide carboxylates was reported in a series of cerium(III) alkanates ((100):  $\text{Ln} = \text{Ce}$ ;  $\text{R} = \text{C}_n\text{H}_{2n+1}$ ).<sup>580</sup> It was found that for the tetradecanoate and longer-chain-length soaps, only one mesophase was observed, tentatively assigned as a smectic A phase. For the shorter-chain soaps, a more gradual melting behavior was observed, involving two or more intermediate phases between the lamellar crystalline phase and the isotropic liquid. From DSC experiments, it was deduced that electrostatic interactions in the polar regions played an important role in the melting process and that an incomplete melting of the chains induced the presence of molecular aggregates. These cerium(III) alkanates were re-investigated more recently with the support of X-ray diffraction,<sup>581</sup> and it was found that all the compounds from the tris(hexanoate) to the tris(octadodecanoate) exhibited a smectic A phase characterized by a lamellar structure where the polar groups were localized in infinite, parallel, and equidistant planes separated from each other by a bilayer of alkyl chains. Another mesophase, M, is present for the shorter homologs, but was not identified (Figure 49).



(100)

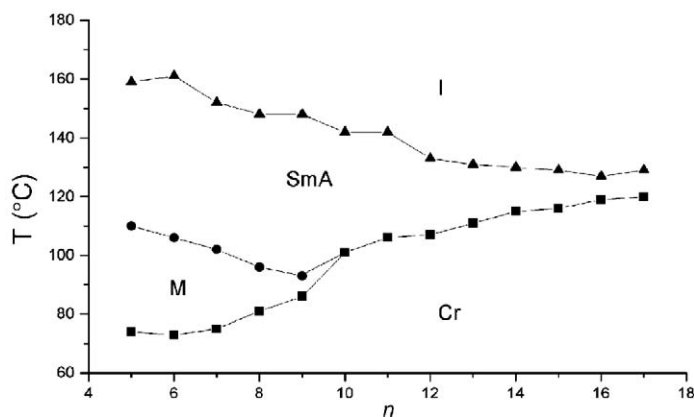


Figure 49 Phase diagram of the compounds  $\text{Ce}(\text{O}_2\text{C}-\text{C}_{n-1}\text{H}_{2n-1})_3$ .

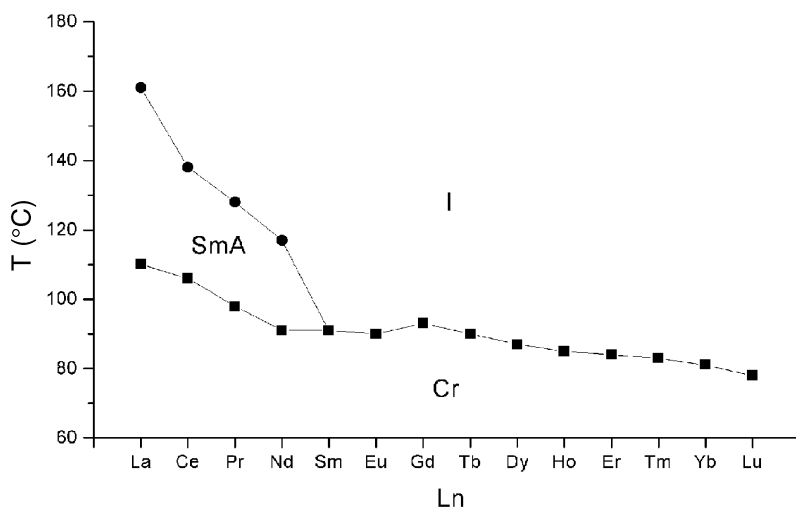


Figure 50 Phase diagram of the compounds  $\text{Ln}(\text{O}_2\text{C}-\text{C}_{11}\text{H}_{23})_3$ .

A similar structure had been reported before for the smectic A phase of lanthanum(III) tetradecanoate ((100):  $\text{Ln} = \text{La}$ ;  $\text{R} = \text{C}_{13}\text{H}_{27}$ ), where the lanthanum ions are arranged in parallel planes in close contact with a sufficient number of carboxylate groups separated by molten aliphatic chains.<sup>582</sup> A systematic study of lanthanide(III) dodecanoates<sup>583</sup> ((100):  $\text{Ln} = \text{La}, \text{Ce}, \text{Pr}, \text{Nd}, \text{Sm}, \text{Eu}, \text{Gd}, \text{Tb}, \text{Dy}, \text{Ho}, \text{Er}, \text{Tm}, \text{Yb}, \text{Lu}$ ;  $\text{R} = \text{C}_{11}\text{H}_{23}$ ) has shown that these compounds have a lamellar bilayer structure in the crystalline phase, with the alkyl chains in an all-*trans* conformation normal to the ionic sublayer. The size of the trivalent lanthanide ion proved to be a critical factor for the existence of mesophases, and thus, it was found that a smectic A phase could only be obtained with the lighter lanthanide ions having larger ionic radii, i.e.,  $\text{La}^{\text{III}}$ ,  $\text{Ce}^{\text{III}}$ ,  $\text{Pr}^{\text{III}}$ , and  $\text{Nd}^{\text{III}}$ , and the mesophase stability range decreased rapidly on traversing the lanthanide series (Figure 50). No mesomorphic behavior was observed for samarium(III) dodecanoate, nor dodecanoates of heavier lanthanides. Interestingly, the yttrium(III) alkanoates ((100):  $\text{M} = \text{Y}$ ), for which  $\text{Y}^{\text{III}}$  has the same ionic radius as  $\text{Ho}^{\text{III}}$ , was not mesomorphic either. The difference in thermal behavior between the dodecanoates of light and heavy lanthanides has been interpreted in terms of a model that takes into account the size of the lanthanide ions and the electrostatic interactions between the carboxylate groups. The alkyl chain length was found also to have an influence on the thermal behavior and, for example, in the case of the  $\text{Nd}^{\text{III}}$  compounds ((100):  $\text{Ln} = \text{Nd}$ ;  $\text{R} = \text{C}_n\text{H}_{2n+1}$ ), a smectic A phase was identified for the homologous series ( $n = 4-14$ ), but no mesophase was observed for the  $\text{Nd}^{\text{III}}$  pentadecanoate or higher homologs (Figure 51).<sup>584</sup> The compounds of the series with  $n = 4-10$  showed an additional mesophase between the crystalline and the smectic A phases. Similar behavior was observed for the  $\text{La}^{\text{III}}$  ((100):  $\text{Ln} = \text{La}$ ;  $\text{R} = \text{C}_n\text{H}_{2n+1}$ ,  $n = 4-19$ : SmA;  $n = 4-9$ : M),<sup>585</sup> and  $\text{Pr}^{\text{III}}$  ((100):  $\text{Ln} = \text{Pr}$ ;  $\text{R} = \text{C}_n\text{H}_{2n+1}$ ,  $n = 5-19$ :

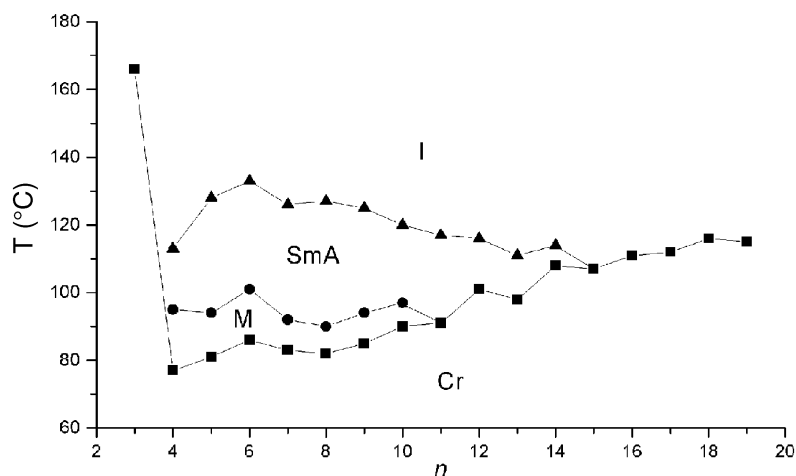


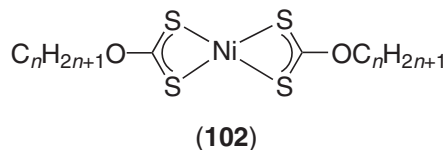
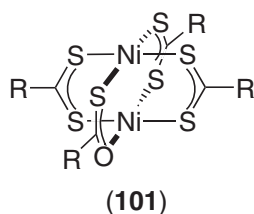
Figure 51 Phase diagram of the compounds  $\text{Nd}(\text{O}_2\text{C}-\text{C}_{n-1}\text{H}_{2n-1})_3$ .

SmA;  $n=5-8$ : M)<sup>586</sup> alkanooates. Within the mesomorphic carboxylate complexes, the lanthanum carboxylates possess the highest transition temperatures and the widest mesomorphic temperature range, which decreases in the order  $\text{La} > \text{Ce} > \text{Pr} > \text{Nd}$ . Mesophase could nevertheless be induced in mixtures of samarium(III) or heavy lanthanide ion dodecanoate with  $\text{La}^{\text{III}}$ ,  $\text{Ce}^{\text{III}}$ ,  $\text{Pr}^{\text{III}}$ , or  $\text{Nd}^{\text{III}}$  dodecanoates.<sup>587</sup>

It is interesting to note that the mesomorphic behavior of these lanthanides carboxylates is much closer to the behavior of alkaline and alkaline earth soaps than to the transition metal soaps described above. However, it is less complex since only one smectic A mesophase is observed, although sometimes a second mesophase, which has not been identified by X-ray diffraction, is present for the short-chain homologs. Such a simple behavior has been attributed to the high carboxylate-to-metal ratio, which makes the ionic layer more rigid.

#### 7.9.9.3.5 Complexes of dithiocarboxylates and xanthates

Dithiolate compounds are similar to the carboxylates, with sulfur atoms taking the place of the oxygen atoms in the polar head. Each of the tetrakis(alkyldithiolato)nickel(II) complexes ((**101**):  $\text{R} = \text{C}_n\text{H}_{2n+1}$ ,  $n=4-11$ ) shows a monotropic lamellar mesophase between 80 °C and 90 °C, which has been described as discotic lamellar ( $\text{D}_L$ ) phase (see Figure 22).<sup>588</sup> In the case where R is a branched chain, an enantiotropic  $\text{Co}_h$  and a monotropic  $\text{D}_L$  mesophases have been found for tetrakis(1-ethylpentylthiolato)nickel(II) complex.<sup>589</sup>



The bis(alkylxanthato)nickel(II) complexes (**102**) exhibited double melting behavior, with a monotropic lamellar mesophase being detected for the nonyl, undecyl, and dodecyl homologs.

## 7.9.10 POLYCATENAR LIQUID CRYSTALS

### 7.9.10.1 Introduction

While it is in discotic liquid crystals that the formation of columnar phases is most readily recognized (*vide supra*), there exists a family of non-disk-like mesogens, the *polycatenar* liquid

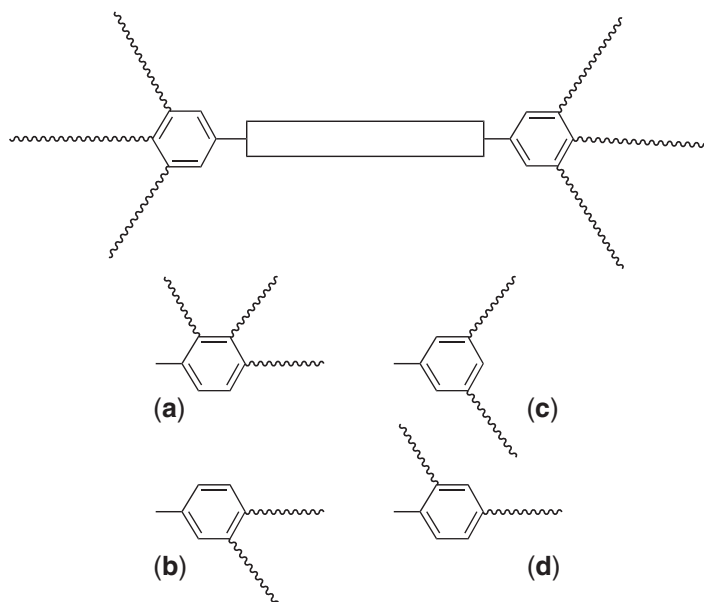


**Figure 52** Schematic representation of polycatenar mesogens showing different potential terminal ring configurations.

crystals, where these mesophases are also formed extensively. As will be seen from their shape, discussed below, this observation is of some interest, but it is the fact that certain of these polycatenar materials can, within a homologous series, show the mesomorphism characteristic of both rod-like and disk-like mesogens, which makes them particularly interesting.

Polycatenar mesogens<sup>590,591</sup> are based on a calamitic motif (Figure 52), having a rather extended, central core which terminates in several alkoxy chains, hence giving rise to the name polycatenar (literally many-tailed). As a rule-of-thumb, it is said that there needs to be at least as many chains as rings if mesomorphism is to result. The nomenclature of polycatenar systems depends on the number of terminal chains, so that those with four chains are termed *tetracatenar*, those with six chains *hexacatenar*, and so on. Another aspect of the structure of polycatenar systems is that for a given number of chains, there can be more than one possible arrangement. For example, the central part of Figure 52 and Figure 52a show two different ways in which three terminal chains may be arranged, while Figure 52b–d shows three possible arrangements for two terminal chains. There is a nomenclature associated with this which would indicate that a tetracatenar mesogen where each terminal ring was of type c in Figure 52 would be designated tetracatenar (2mm) + (2mm) (*o*, *m*, and *p* here refer to the *ortho*-, *meta*-, and *para*- positions of the terminal phenyl ring). Of course, terminal substitution patterns need not be symmetric, so that a tetracatenar (2mm) + (2mp) mesogen would have terminal functions b and c in Figure 52.

The number and arrangement of the chains has a profound effect on the mesomorphism and, while it is not the intention here to describe this in too much detail, some explanation is required. The mesomorphism of most isomers, is, in fact, rather straightforward as they form columnar phases. This is true for hexa-, penta-catenar systems, and tetracatenar (2mm) + (2mm) systems and the phases observed are normally either of hexagonal and/or rectangular (e.g., *c2mm* or *p2gg*). Tricatenar (2mp) + (p) species tend to form smectic (usually SmC) and nematic phases, while tricatenar (3mpm) mesogens often form cubic phases. However, by far the most interesting are the tetracatenar (2mp) + (2mp) mesogens and their mesomorphism will be described in a little more detail.

The reason for the interest is that in these systems, short-chain-length homologs show nematic and/or SmC phases, while longer-chain homologs show columnar phases – that is to say, the mesomorphism of rods and disks is combined into a single homologous series. When the chain length is short, the materials resemble calamitic materials and so N or smectic phases are expected. With these systems it is always the tilted SmC phase which is observed, however, due to the fact that at the interface between the rigid core and the chains, the cross-sectional area of the chains is greater than that of the core and so to fill space efficiently, the cores must tilt (Figure 53).<sup>592</sup>

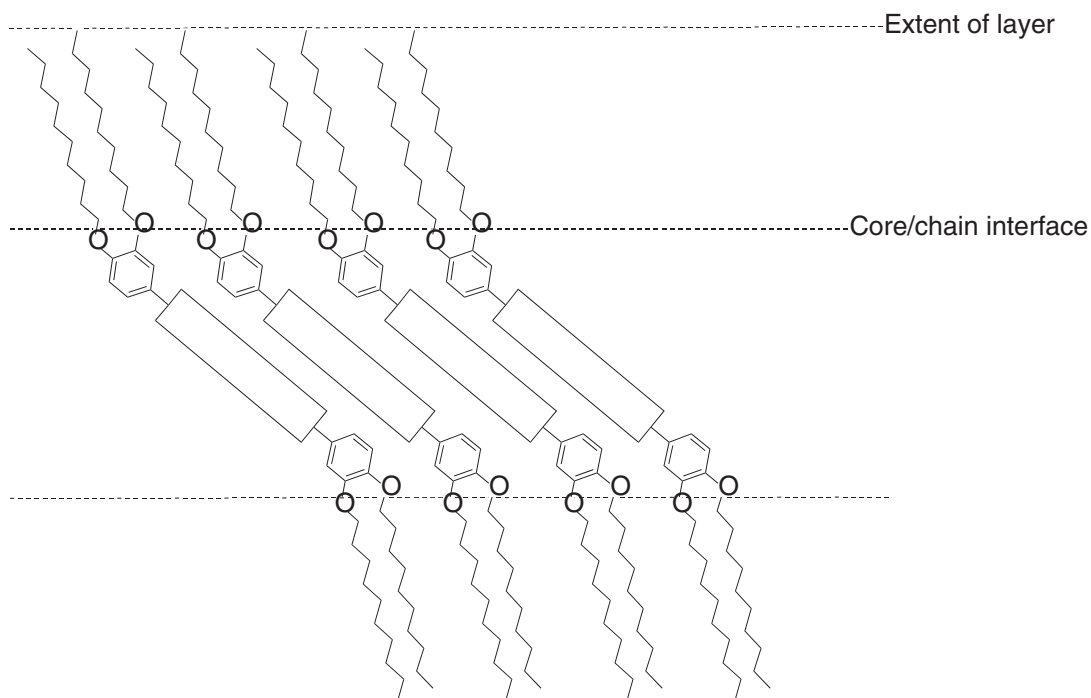


**Figure 53** SmC phase of tetracatenar mesogens.

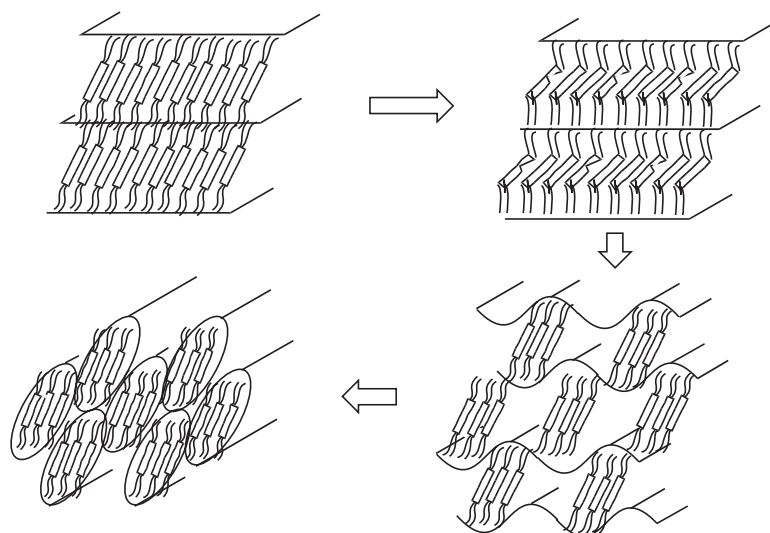
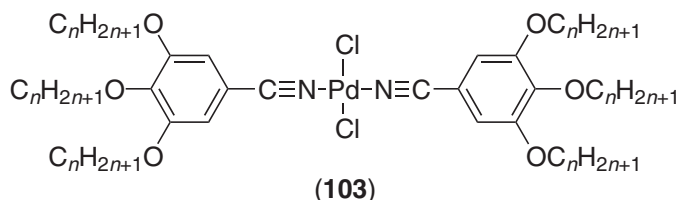


**Figure 54** Schematic showing the transition from SmC to columnar phase.

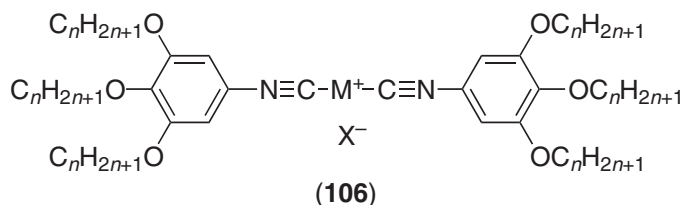
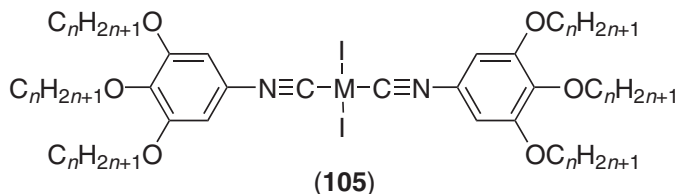
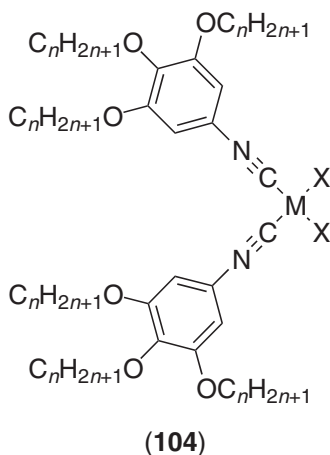
However, as the chains grow in length and/or as the temperature increases, the chains begin to occupy a greater volume and, in order to accommodate this additional volume requirement, the chains tilt even further. However, this can only go so far and eventually the situation is reached where the smectic layers can no longer hold together and they break up, leading to the formation of a columnar phase (Figure 54). Passage from the SmC to the columnar phase normally takes place gradually (e.g., one or two compounds showing both phases) or via the intermediacy of another phase often, but not always, of cubic symmetry.<sup>593</sup> As Figure 54 suggests, experimental data infer that the repeat unit in the columnar phases of these, and in fact other, polycatenar mesogens is constituted of more than one molecule, typically three or four.

## 7.9.10.2 Simple Systems

Some of the simplest systems reported actually challenge the model presented above in containing few rings and it is perhaps a point of semantics as to whether these are, in fact, polycatenar in nature or perhaps ought more properly to be described as discotic. The first of these (**103**) was based simply on the coordination of 3,4,5-trialkoxybenzonitriles to Pd<sup>II</sup>,<sup>594</sup> following a motif which was described some years earlier for the formation of simple, calamitic systems.<sup>595</sup> Only two compounds with different chain lengths were studied ( $n = 10, 18$ ). The ligands were themselves not mesomorphic, but on complexation, a Col<sub>h</sub> phase was observed over small temperature ranges, i.e., 73–91 °C for the complex with six tridecyloxy chains, and between 58 °C and 80 °C for that with six octadecyloxy chains.



This structural motif was then used by Espinet and co-workers for the synthesis of a series of isocyanide complexes of group 10<sup>596</sup> (**(104)**: M = Pd, Pt, X = Cl, Br,  $n = 4, 6, 8, 10$ ; **(105)**: M = Pd, Pt,  $n = 4, 6, 8, 10$ ) and 11<sup>597</sup> (**(106)**: M = Ag, Au, X = BF<sub>4</sub>, PF<sub>6</sub>, NO<sub>3</sub>) metals. Again, none of the free isocyanides were found to be mesomorphic, but columnar mesophases were induced for the corresponding organometallic complexes.



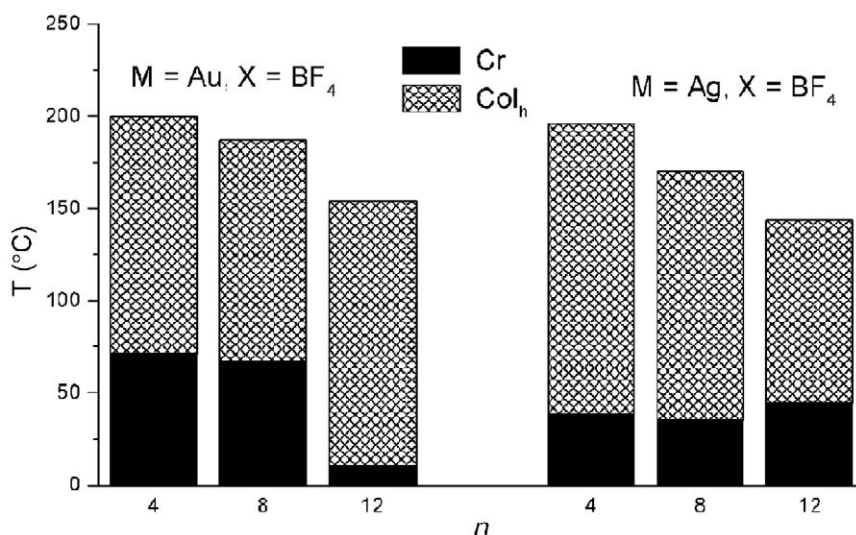
In the neutral, group 10 complexes (**104**, **105**), most of the complexes exhibited Col<sub>h</sub> phase, sometime from the ambient up to temperatures greater than 200 °C. The mesophase stability was found to depend predominantly on the type of halide groups and chain length, the clearing temperatures decreasing in the order Cl > Br > I, and with increasing  $n$ . On average, the transition temperatures, and particularly that of the Col<sub>h</sub>-to-I transitions, of the platinum complexes were higher than those of their palladium congeners (Table 55). All the chlorides and bromides were showing wide-range, enantiotropic Col<sub>h</sub> phases, whereas the iodides with butyloxy were not mesomorphic, and those with longer chain length displayed both monotropic (**(105)**: M = Pd,  $n = 6, 8, 10$ ; M = Pt,  $n = 6$ ) and enantiotropic Col<sub>h</sub> phases (**(105)**: M = Pt,  $n = 8, 10$ ). None of

**Table 55** Mesomorphism of Complexes **(104)** (*cis*) and **(105)** (*trans*).

<i>X</i>	<i>n</i>	<i>Pd</i>	<i>Pt</i>
Cl	4	Cr 70 Col <sub>h</sub> 220 I	Cr 73 Col <sub>h</sub> 248 I
Cl	8	Col <sub>h</sub> 184 I	Col <sub>h</sub> 170 I
Br	4	Cr 77 Col <sub>h</sub> 147 I	Cr 67 Col <sub>h</sub> 220 I
Br	8	Cr 42 Col <sub>h</sub> 143 I	Col <sub>h</sub> 200 I
I	4	Cr 138 I	Cr 133 I
I	8	Cr 45 (Col <sub>h</sub> 27) I	Cr 32 Col <sub>h</sub> 41 I

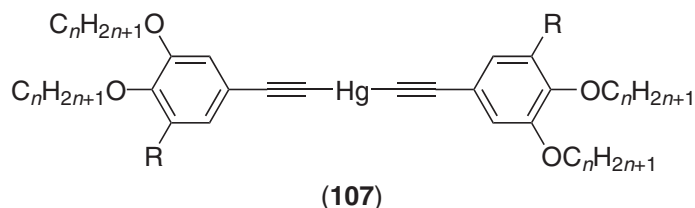
these complexes crystallized on cooling, and the Col<sub>h</sub> phase was found to be stable on further heat-cool cycles. Interestingly, the chloro- and bromo-palladium and platinum complexes (**(104)**) were obtained as *cis*-isomers, and thus exhibited a net dipolar moment, while the iodides were all *trans* compounds, and therefore apolar. This can explain the poorest tendency of the iodo complexes to give large mesomorphic domains, and stable mesophases. By means of X-ray investigation, it was deduced that the columnar phase results from the antiparallel arrangement of the *cis* isomers with the energetically favorable dipole-dipole interactions, and orthogonal stacking for the *trans* derivatives. Note that the mesophase stability was greatly enhanced in the isonitrile palladium complexes (**(104)**) compared to the benzonitrile isomeric coordination compounds (**(103)**).

In a similar way, the mesomorphism of the ionic group 11 complexes (**(106)**: M = Au, X = PF<sub>6</sub>, BF<sub>4</sub>, NO<sub>3</sub>, *n* = 4, 8, 12; M = Ag, X = BF<sub>4</sub>, NO<sub>3</sub>, *n* = 4, 8, 12) depended upon the nature of the anion (X) and, of course, the metal. Thus, with gold, for *n* = 8 and 12, the PF<sub>6</sub><sup>-</sup> salts gave room-temperature Col<sub>h</sub> phases which cleared just above 100 °C; only the butyloxy homolog was not mesomorphic. However, with BF<sub>4</sub><sup>-</sup> as counter-anion, homologs with *n* = 4, 8, and 12 were all mesomorphic showing a Col<sub>h</sub> phase: the melting points dropped from 71 °C to 10 °C with increasing chain length, and the clearing temperatures similarly fell from 200 °C to 154 °C. The related nitrates (*n* = 8) were, however, thermally unstable and decomposition was observed in the columnar phase at about 50 °C. For the silver compounds, the PF<sub>6</sub><sup>-</sup> salts were not reported but both the BF<sub>4</sub><sup>-</sup> and NO<sub>3</sub><sup>-</sup> salts were mesomorphic forming Col<sub>h</sub> phases, the latter now showing greater thermal stability and clearing around 110–120 °C, albeit with decomposition. The nitrates melted at similar temperatures to their BF<sub>4</sub><sup>-</sup> analog, on average around 30 to 40 °C, except the first member of the series which melted at 87.5 °C. The clearing points of the tetrafluoroborate salts were falling from 196 °C to 144 °C with increasing *n*. Thus, in both silver and gold complexes, the tetrafluoroborate gave the widest range of mesophase (120–160 °C). The influence of the metals on the properties is not dramatic, as can be seen from the phase diagram (Figure 55) representing the thermal behavior of both the gold and silver tetrafluoroborate salts.

**Figure 55** Mesomorphism of complexes **(106)**.



Two mesomorphic tetracatenar and one hexacatenar  $\text{Hg}^{\text{II}}$  acetylides have been reported ((107):  $\text{R} = \text{H}$  or  $\text{C}_n\text{H}_{2n+1}$ ).<sup>598</sup> The two tetracatenar complexes ( $n = 5, 12$ ) exhibited a columnar phase between  $73^\circ\text{C}$  and  $125^\circ\text{C}$  for the short-chain-length compound, and from room temperature up to  $106^\circ\text{C}$  for the longer-chain derivative. The hexacatenar ( $n = 5$ ) displayed an unidentified phase, though probably columnar due to the structural similarity with the previous compounds, between  $70^\circ\text{C}$  and  $122^\circ\text{C}$ . These mesophase assignments were performed by microscopy only, and thus need to be confirmed.



In all the two ring-systems discussed above, each elementary repeat unit is constituted of one molecule only, similar to pure discotic materials, and as such differ from true polycatenar materials. Indeed, for the latter, the internal structure of the columns is completely changed upon the elongation of the rigid cores, and the repeat unit is constituted of several molecular species which aggregate together into clusters, these clusters stacking into columns. These systems will be discussed below.

### 7.9.10.3 Systems Based on Poly(alkoxy)stilbazole Ligands

#### 7.9.10.3.1 Complexes of group 10 metals

This work is predominantly an extension of studies carried out by Bruce and co-workers on 4-(mono)alkoxystilbazoles<sup>599</sup> and their complexes with metal of groups 9, 10, and 11. The ligands examined are shown in Figure 56 and are a variety of isomers of di- and tri-alkoxystilbazoles. Because the chain substitution pattern in these ligands is varied systematically and because they have been complexed to a range of  $\text{MX}_2$  fragments for Pd and Pt, and also to a range of  $\text{AgX}$

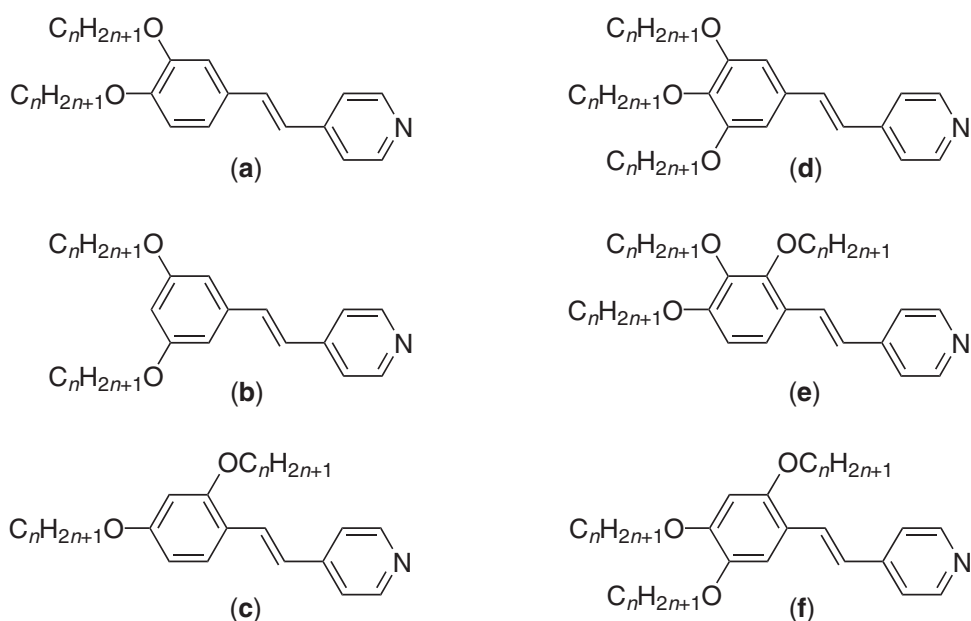
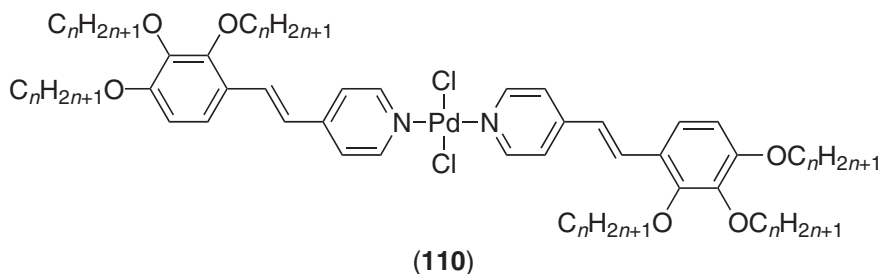
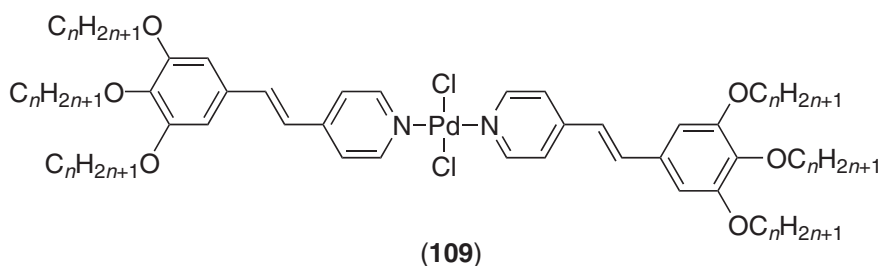
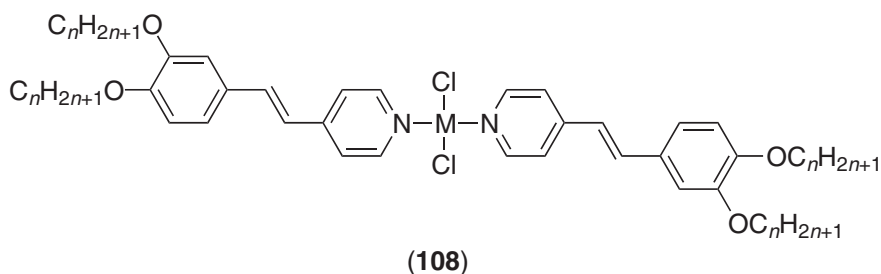


Figure 56 Di- and tri-alkoxy stilbazoles.

fragments, it is possible to gain a rather clear view of how metal and ligand interplay with one another to vary the mesomorphism. Note also here that none of the ligands is itself mesomorphic and that mesomorphism is induced on coordination.

Binding a number of these stilbazoles to  $\text{Ir}^{\text{I}}$  gave the square-planar complexes *cis*-[ $\text{IrCl}(\text{CO})_2$  (stilbazole)], none of which was liquid crystalline (*vide infra*). However, complexes with  $\text{PdCl}_2$  and  $\text{PtCl}_2$  were readily formed ((108) to (110):  $\text{M} = \text{Pd}, \text{Pt}$ ) for these ligands with the  $\text{Pd}^{\text{II}}$  congeners being, in general, studied in more detail.<sup>600</sup>



Of the hexacatenar complexes formed from ligands **d** to **f**, those derived from the 2,4,5-trialkoxystilbazoles **f** were non-mesomorphic, while columnar phases were observed when **d** and **e** were used (109, 110). The thermal behavior is summarized in Figure 57. The hexacatenar (3mpm) + (3mpm) complexes (109) were mesomorphic for  $n \geq 9$  and had mesomorphic ranges of some  $50^\circ\text{C}$ , clearing just above  $100^\circ\text{C}$ . The mesophase was originally reported as  $\text{Col}_h$  and, while this phase does exist in these materials, a  $\text{Col}_r$  phase was found at lower temperature by X-ray methods and was assigned the  $c2mn$  plane symmetry.<sup>601</sup> The (3omp) + (3omp) isomers (110) were mesomorphic for  $n \geq 8$  and formed what were reported to be an unassigned columnar phase and a second, unidentified mesophase. Melting points were around  $60\text{--}70^\circ\text{C}$ , while clearing was observed between  $140^\circ\text{C}$  and  $150^\circ\text{C}$ . Later work using X-ray diffraction showed<sup>601</sup> that the upper phase was  $\text{Col}_h$  while once more, the lower phase was  $\text{Col}_r$ , only this time with the  $p2gg$  plane symmetry. It is interesting to note here that, contrary to the assertion in the introduction to this section that as many rings as chains were required to realize mesomorphism in polycatenar systems, here we are considering four-ring systems with readily accessible mesophases. Why this should be the case here is not entirely clear.

Tetracatenar mesogens formed from ligand **c** were found to be non-mesomorphic, while for ligand **b**, an unidentified mesophase was reported for  $n = 14$ . However, the tetracatenar (2mp) + (2mp) complexes (108) derived from ligand **a** were much more interesting and were

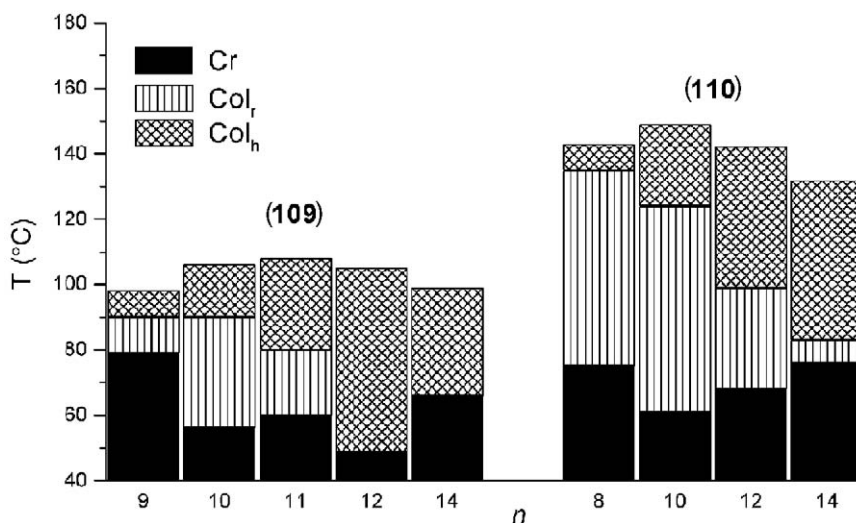
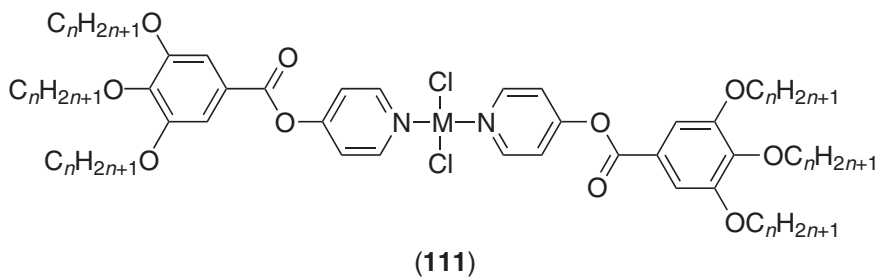


Figure 57 Mesomorphism of (96) and (97).

studied for both palladium and platinum. For Pd ((108): M=Pd), homologs for which  $4 \leq n \leq 12$  were found to show an SmC phase, whereas it was reported that for longer chain lengths a Col<sub>h</sub> phase was found. Similar behavior was reported for the Pt congeners ((108): M=Pt), although as all homologs were not synthesized, the point at which the SmC phase gave way to the Col<sub>h</sub> was not so precisely known. As was indicated in the introduction to polycatenar mesogens, it is normally the case that the changeover from the lamellar SmC phase to a Col<sub>h</sub> phase happens either via the intermediacy of another phase (Cub or Col<sub>r</sub> phase) or by one or two compounds showing both phases as the SmC phase become destabilized at the expense of the columnar phase. As this was not the case with the Pd complexes, they were studied in some detail using X-ray methods, leading to a re-interpretation of the phase behavior.<sup>593</sup> Thus, it was confirmed that for  $4 \leq n \leq 12$ , an SmC phase exists and that for  $n=17, 18$ , a Col<sub>h</sub> phase is found. However, for  $13 \leq n \leq 16$ , through a combination of X-ray and optical microscopy, it was shown that the phase was still lamellar, although not an SmC phase. The precise nature of this phase is not yet elucidated, although it was felt that, given its proximity to a Col<sub>h</sub> phase and the ease with which this phase was induced in mixtures, it was probably some sort of lamello-columnar phase.

Some related complexes were described in which the vinyl group at the center of the stilbazole was replaced by an ester ((111): M = Pd, Pt) giving rise to a series of hexacatenar Pd and Pt materials.<sup>602</sup> The complexes showed a Col<sub>h</sub> phase, confirmed by X-ray methods, and for M = Pt, it was observed (Figure 58) that the melting point decreased steadily as  $n$  increased, while the clearing point increased rather steeply. For M = Pd, such trends were much less obvious.



There has also been an isolated report of a single, and rather elongated, hexacatenar palladium mesogen<sup>603</sup> based on an elongated phenylenevinylene (112) which showed a Col<sub>h</sub> phase between 164 °C and 234 °C.

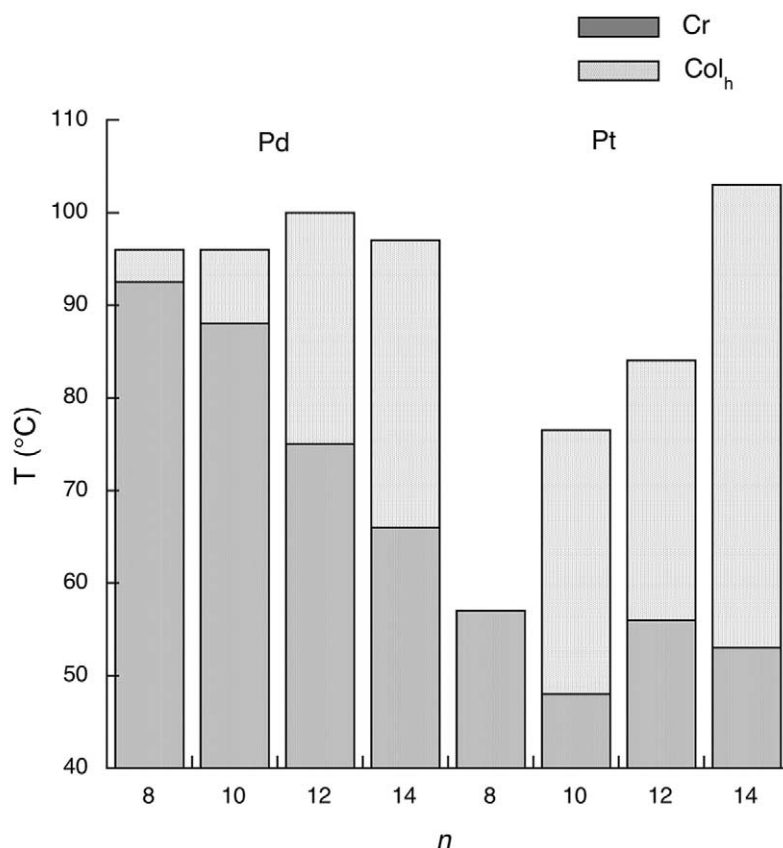
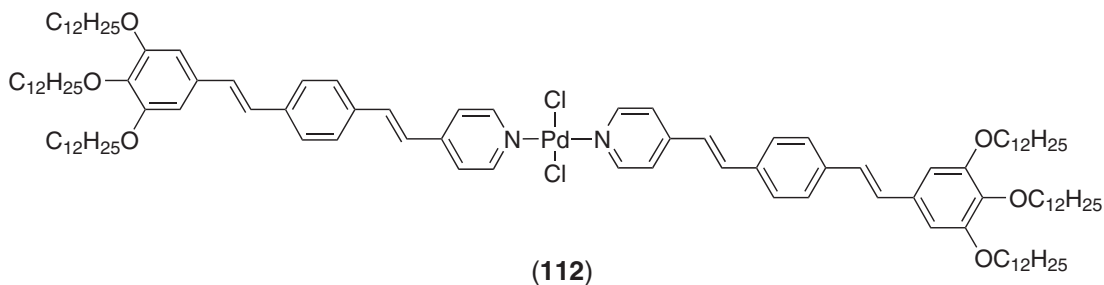
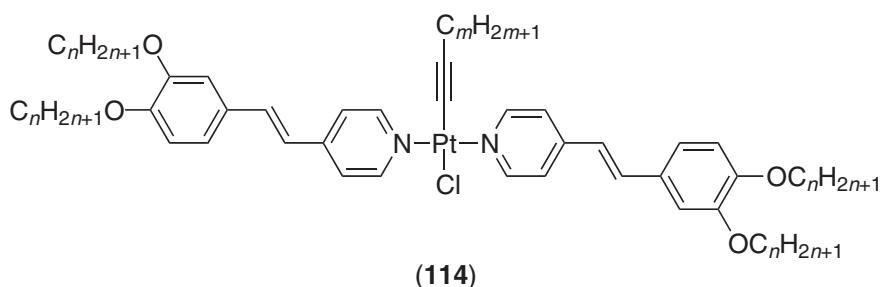
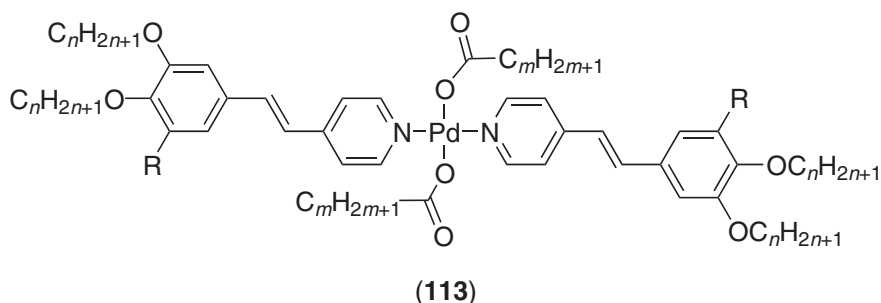


Figure 58 Mesomorphism of hexacatenar stilbazole ester complexes (111).



Results were also described from studies which introduced lateral substituents into these complexes and in one paper the effect of introducing lateral alkanooate groups was reported (113).<sup>604</sup> The use of lateral alkanooates had been described previously by Maitlis and co-workers<sup>605</sup> in palladium complexes of 4-alkoxystilbazoles (Section 7.9.14.3.6(iv)) and had been shown to induce the formation of liquid crystal nematic phases. In the present situation where the complex was polycatenar, it was not clear whether the chains would act to increase the volume of the core of the polycatenar mesogen or simply as extra chains, so rendering the complex more classically discotic. In fact, the answer was “neither” and at all chain lengths ( $n$  and  $m$ ) and degrees of substitution ( $R = H$  or  $OC_nH_{2n+1}$ ) where mesomorphism was observed, a nematic phase was seen at or near room temperature. This behavior was somewhat puzzling and is so far without explanation.

The acetylide complexes (114) were synthesized on Pt rather than on Pd, due to the lability of the latter metal which precluded isolation of such species on other than Pt. These species were accessed as neutral analogs of related  $Ag^I$  complexes (*vide infra*) in order to try to delineate the effect on the mesomorphism of the charge on the silver complexes and how this might relate to the stability of the cubic phase seen extensively in the silver complexes.<sup>606</sup> The Pt-acetylide

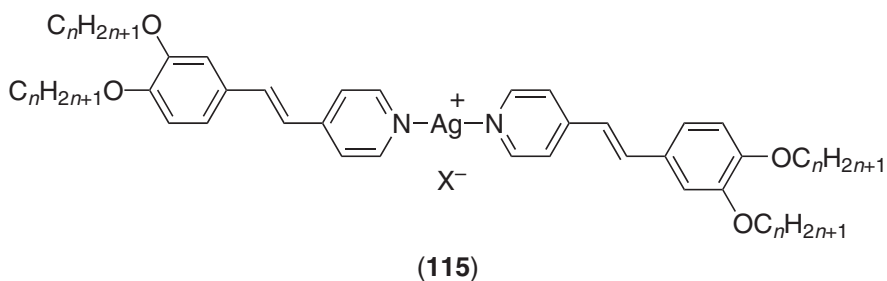


complexes turned out<sup>607</sup> to be predominantly nematic in their phase behavior and the consequences in relation to cubic phase behavior were discussed. Curiously, however, the complexes did, in addition, show an SmC phase. It is almost universally true that liquid crystals bearing lateral chains show only nematic phases,<sup>608</sup> and so this aspect of the behavior of the Pt complexes still requires explanation.

#### 7.9.10.3.2 Complexes of silver(I)

The mesomorphism of silver(I) complexes of poly(alkoxy)stilbazoles has been reviewed recently.<sup>609</sup> However, it is appropriate to cover this work here in order to see the effect of an anion on mesomorphism in cationic complexes and to allow some comparison to be made with the complexes described in the preceding section. In these studies, there were two main variables, namely the substitution pattern of the stilbazole used and the nature of the anion. The former was varied in the same way as for the palladium and platinum complexes just described, while the latter was either triflate or an alkylsulfate whose chain length was varied.

Complexes of 3,4-dialkoxy stilbazole with silver dodecylsulfate ((115):  $X = C_{12}H_{25}OSO_3^-$ ; AgDOS) behaved in many ways as rather typical tetracatenar mesogens and exhibited a cubic and a columnar phase as shown in Figure 59, although no SmC phase was seen at shorter chain lengths, almost certainly due to the presence of the lateral dodecylsulfate chain.<sup>610</sup> While it was not possible to establish the symmetry of the cubic phase by X-ray methods, employing freeze-fracture techniques enabled it to be identified as  $Ia\bar{3}d$ .<sup>611</sup> Further, through the careful application of X-ray and dilatometry, a model was proposed for the transition between the columnar and cubic phases.<sup>612</sup>



One of the factors considered as being important in determining the mesomorphism of these tetracatenar silver complexes with lateral, alkylsulfate chains is the extent to which the chain extends beyond the rigid core of the complex, and this will be discussed later (Section 7.9.14.3.6)

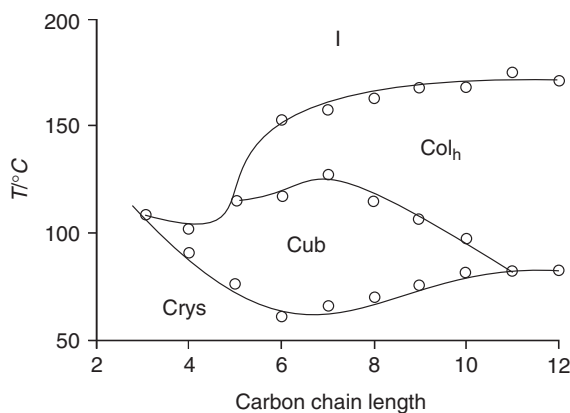


**Figure 59** Phase diagram for 3,4-dialkoxystilbazole complexes of AgDOS, (**115**).

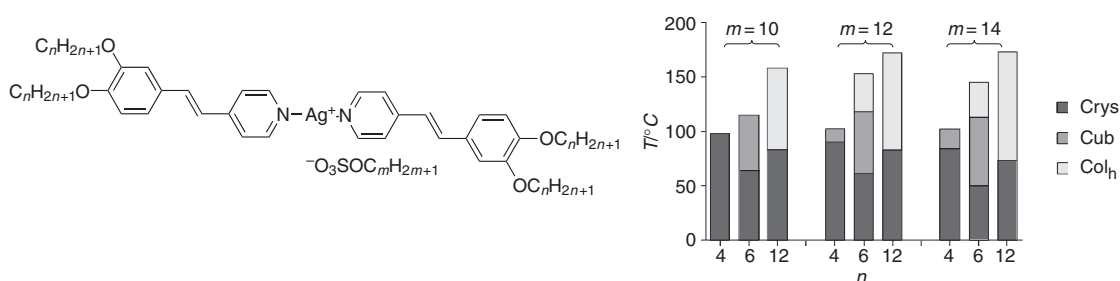


**Figure 60** The dependence of the mesomorphism of tetracatenar AgDOS (**115**) complexes on both ligand and anion chain length.

in relation to the calamitic complexes. This effect was investigated in these tetracatenar complexes ((**115**):  $X = O_3SOC_mH_{2m+1}$ ) where the mesomorphism was evaluated as a function of both ligand and anion chain lengths,<sup>613,614</sup> and some of the results are summarized in Figure 60. It was found that only cubic and columnar phases appeared as a function of the ligand and alkylsulfate chain lengths, and for the didodecyloxystilbazole ligands, only a columnar phase was formed whatever the alkylsulfate chain length ((**115**):  $n = 12$ ;  $m = 10, 12, 14$ ), whereas for the dihexyloxystilbazole ligands ((**115**):  $n = 6$ ;  $m = 10, 12, 14$ ), a cubic phase was seen, too, with the columnar phase being absent with the decylsulfate anion; dibutyloxystilbazole gave either a cubic phase or no mesophase at all ((**115**):  $n = 4$ ;  $m = 10, 12, 14$ ). Note here that as the ligand chain length increases, the stability of the phases also increases. This is consistent with the ideas discussed later (Section 7.9.14.3.6) that the mesomorphism is affected profoundly when the lateral alkylsulfate chain extends beyond the core of the molecule and that in such cases it contributes, in effect, to the space occupied by the terminal chains.

This view was further reinforced when the mesomorphism of the triflate complexes ((**115**):  $X = CF_3SO_3$ ) was studied. Thus, while the mesomorphism was broadly similar to that of the DOS salts (Figure 61), the columnar phase appeared only at much longer chain lengths as now the lateral group does not extend past the core of the molecule and does not contribute to the terminal chain volume.

In addition to the tetracatenar systems based on 3,4-dialkoxystilbazoles, those derived from the 3,5-dialkoxy isomer were also studied (**116**).<sup>615</sup> In this case, a  $Col_h$  phase was found (Figure 62) and at rather low temperature. The remarkable thing here was the fact that so many of the complexes were mesomorphic for, while mesomorphic tetracatenar (2mm) + (2mm) mesogens are known, mesomorphism is normally observed only in the longest-chain homologs and at longer core lengths. The reason for such extensive mesomorphism in the present systems is still not entirely clear.

In addition, the mesomorphism of some hexacatenar (3mpm) + (3mpm) derivatives was investigated and the phase diagram for the DOS salts ((**117**):  $X = C_{12}H_{25}OSO_3$ ) is shown in Figure 63. As expected, the mesomorphism is entirely that of a  $Col_h$  phase which melts from the crystal phase very close to room temperature. However, with a triflate anion ((**117**):  $X = CF_3SO_3$ ), it was found that a cubic phase was seen at shorter chain lengths ( $6 \leq n \leq 8$ ), with the columnar phase appearing for  $n \geq 8$ .

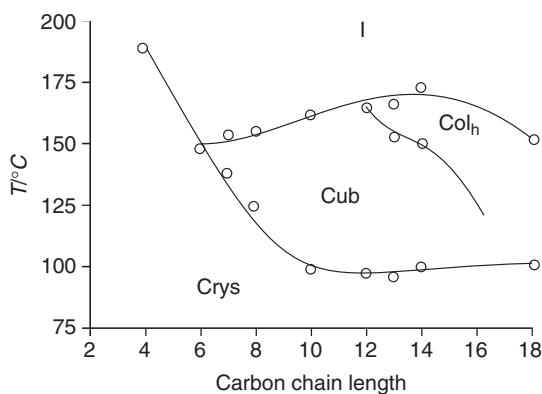


**Figure 61** Phase diagram for the silver triflate complexes of 3,4-dialkoxystilbazoles ((115), X = OTf).

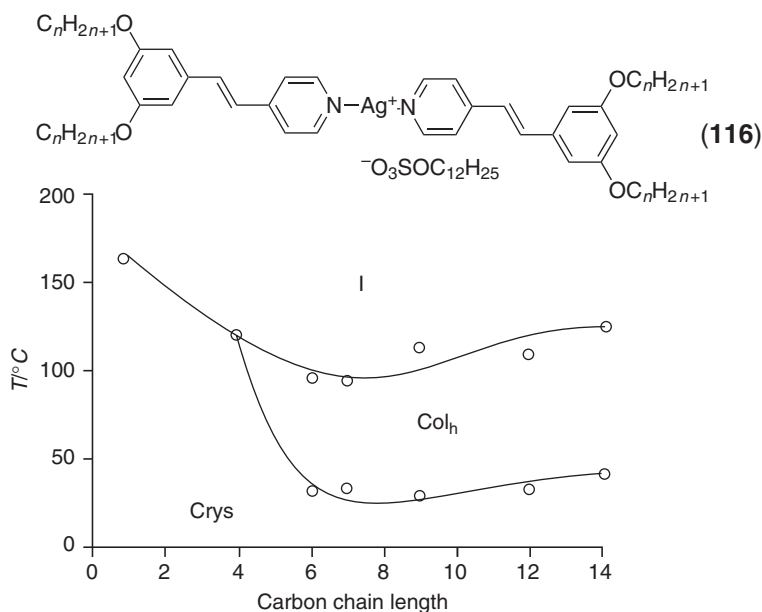


**Figure 62** Phase diagram for the AgDOS complexes of 3,5-dialkoxystilbazoles, (116).

### 7.9.10.3.3 Lyotropic mesomorphism of polycatenar complexes of silver(I)

As seen in the previous section, the thermotropic mesomorphism of polycatenar silver stilbazole complexes has been investigated thoroughly, but it is only recently that attention has turned to lyotropic properties. This work is included here as the arguments advanced to interpret the observed phase behavior relate to the preceding discussion. Thus, Smirnova and Bruce investigated the solution behavior of some tetracatenar silver complexes ((115): X = O<sub>3</sub>SOC<sub>m</sub>H<sub>2m+1</sub>)<sup>616</sup> in order to test the idea of whether the addition of *external solvent* would have a pronounced effect on the mesomorphic properties. This approach has been proved fruitful, and interesting results were obtained with the three silver complexes with four classes of solvent, namely linear alcohols, linear alkanes, cyclic hydrocarbons, and small, polar, aprotic solvents. Binary mixtures with small polar solvents induce the formation of lamellar mesophases at low solvent concentrations without suppressing the existing mesophases (*vide supra*). A two-component phase diagram between (115) and DMSO showed that the columnar phase vanished at 10 wt.% of solvent, and that between 10 and 90 wt.% of DMSO, the form of the phase diagram was constant, showing a large-range lamellar phase and a narrow-range cubic phase, separated by the biphasic region. The induction of lamellar phases suggests that the small solvent molecules were located near the polar, rigid core of the complexes, and as such contributed to an increase in the core area with respect to chain area, the latter of which remained unchanged. Lyomesophases were also induced in protic solvents, but their nature depended on the length of the alcohol used. Thus, short-chain alcohols

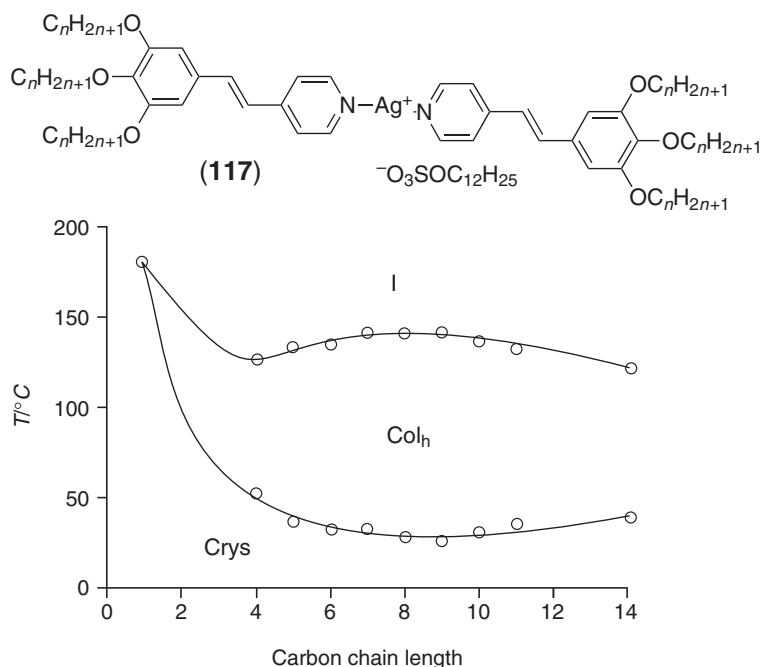


**Figure 63** Phase diagram for the AgDOS complexes of 3,4,5-trialkoxy stilbazoles, (117).

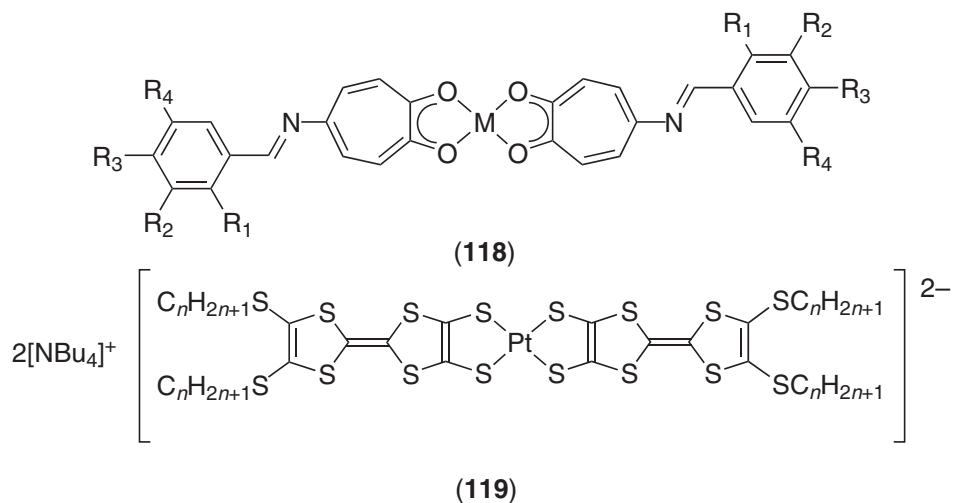
induced a nematic and the tetragonal phase,  $S_4$ , along with the existing thermotropic mesophases. With longer chain length, cubic and hexagonal phases were either induced or stabilized. In the former case, the solvent may have contributed to both the core and the chain, but the chain area becomes greater, and the interface curves. Monotropic cubic phases were induced for (115) in alkane and other hydrocarbon solvents.

#### 7.9.10.4 Systems Based on Other Types of Poly(alkoxy)substituted Ligands

Another example of crossover between lamellar and columnar mesophases was observed with the polycatenar bis[5-(dialkoxybenzylidene)aminotropolonato]copper(II) complexes (118). Tropolones show complexing ability akin to that of  $\beta$ -diketones, and are the core of certain natural products having strong bio-activity. The ligands were prepared by condensation of the appropriate substituted benzaldehydes with 5-aminotropolone, and the complexes were obtained by reacting the ligands with copper(II) acetate. Three series of polycatenar mesogens were prepared.<sup>617,618</sup> In the first series, with alkoxy chains in the *ortho* and *para* positions ((118):  $M = \text{Cu, Ni, Zn}$ ;  $R_1 = \text{OC}_m\text{H}_{2m+1}$ ,  $m = 12, 16$ ;  $R_3 = \text{OC}_n\text{H}_{2n+1}$ ,  $n = 6, 10, 16$ ;  $m = n$  or  $m \neq n$ ;  $R_2 = R_4 = \text{H}$ ), mesomorphic materials did not result in accordance with the results obtained for the palladium complexes of similarly substituted stilbazole. Lengthening the chains or replacing copper with nickel or zinc affected the melting temperatures slightly. However, the copper complexes with ligand chains in the *meta* and *para* positions ((118):  $M = \text{Cu}$ ;  $R_2 = R_3 = \text{OC}_n\text{H}_{2n+1}$ ,  $n = 8-16$ ;  $R_1 = R_4 = \text{H}$ ) showed  $\text{SmC}$  ( $n = 8-12$ ), and  $\text{Col}_h$  ( $n = 13-16$ ) phases, although none of the complexes exhibited both phases together. The melting into the mesophase occurred at rather elevated temperatures (150 to 200 °C) and isotropization was above 200 °C. Since both temperatures decreased almost linearly with increasing chain length, the mesomorphic temperature range was quite similar along the whole series (ca. 40–50 °C). One tetracatenar copper complex with hexadecyloxy chains in the four *meta* positions ((118):  $M = \text{Cu}$ ;  $R_2 = R_4 = \text{OC}_{16}\text{H}_{33}$ ;  $R_1 = R_3 = \text{H}$ ) produced an accessible  $\text{Col}_h$  phase between 40 and 127 °C. Due to the similarity of these tropolonato complexes with those of stilbazole discussed previously, it is realistic to consider similar self-organization and self-assembling processes.

Dianionic platinum(II) complexes ((119):  $n = 10, 14, 18$ ) with sulfur-rich dithiolato ligands based on tetrathiafulvalene have been reported.<sup>619</sup> These potentially interesting complexes for their unique electronic properties, having a polycatenar structure unfortunately did not form a mesophase. The absence of mesomorphism may be simply due to the bulkiness of the counter ion,





tetrabutyl ammonium, and it would be of interest to try other cations to see whether such structures may be compatible with the induction of mesomorphic properties.

#### 7.9.10.5 Polycatenar Organometallic Complexes

Polycatenar complexes containing the  $\text{Fe}(\text{CO})_3$  fragment bound in an  $\eta^4$  fashion to a 1,4-disubstituted butadiene (**120**) were reported<sup>620</sup> and, as might be expected for polycatenar complexes, nematic ( $n=6, 10,$  and  $11$ ), SmC ( $n=10$  and  $11$ ), and  $\text{Col}_h$  ( $n=12-16$ ) phases were obtained (Table 56). The melting temperatures first decreased from  $100^\circ\text{C}$  ( $n=6$ ) to ca.  $60^\circ\text{C}$  ( $n=12-14$ ), then rose again to  $85^\circ\text{C}$  ( $n \geq 15$ ). The clearing temperatures decreased almost linearly with  $n$  ( $144-100^\circ\text{C}$ ). Resolution of the pure enantiomers gave rise to the corresponding chiral mesophases for the short-chain homologs ( $\text{N}^*$  and  $\text{SmC}^*$ ), although it was not clear whether the  $\text{Col}_h$  phase was chiral. Some small temperature changes were observed, though a sort of odd-even effect could be observed for the clearing temperatures. Small spontaneous polarizations were also measured.

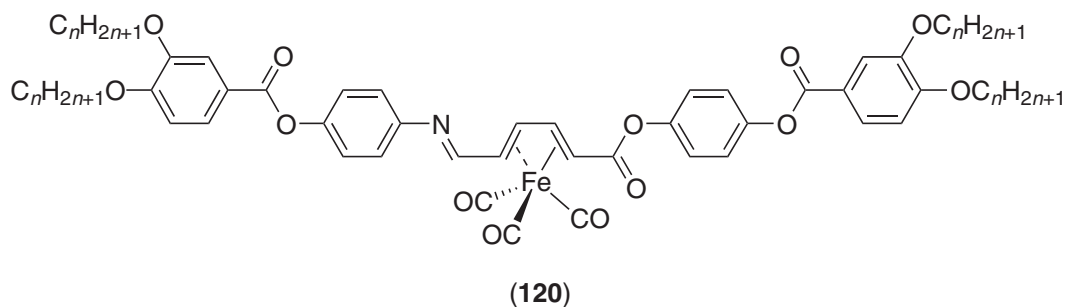


**Table 56** Mesomorphism of polycatenar complexes of  $\text{Fe}^0$ , (**120**).

$n$	Racemates ( $\pm$ )	Enantiomers <sup>a</sup>
6	Cr 101.5 N 144.5 I	Cr 84 N* 139 I
10	Cr 72 SmC 104.5 N 124 I	Cr 73.5 SmC* 109 N* 127 I
12	Cr 59 $\text{Col}_h$ 110 I	Cr 60.5 $\text{Col}_h$ 112.5 I
16	Cr 85 $\text{Col}_h$ 111 I	Cr 89.5 $\text{Col}_h$ 103.5 I

<sup>a</sup> (+) for  $n=6$ , (-) for  $n=7-16$ .

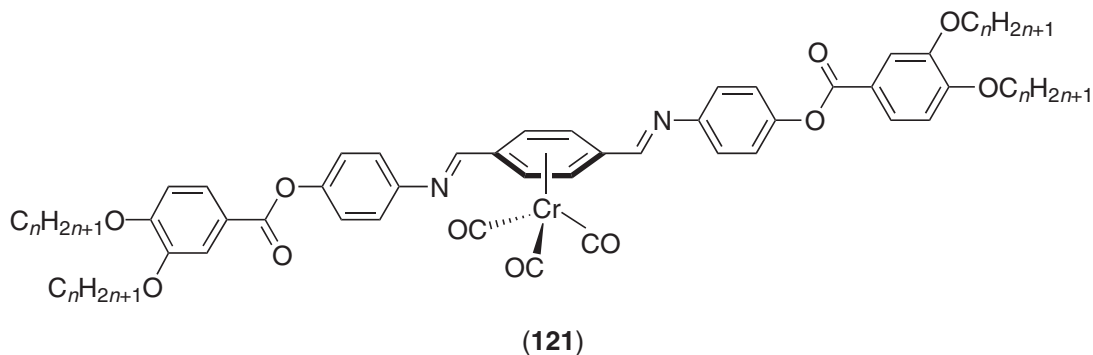
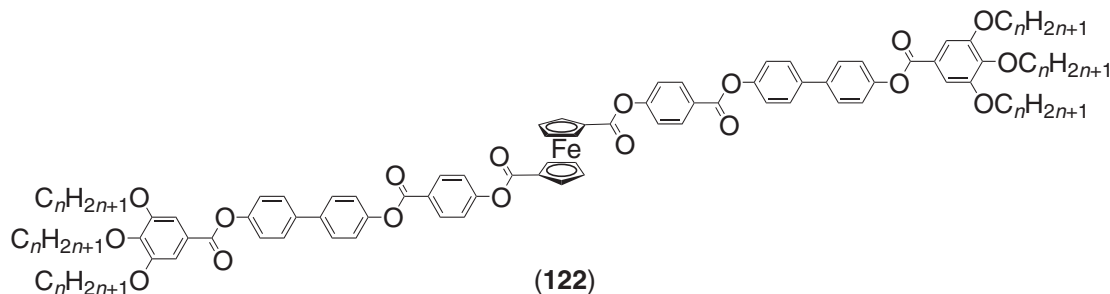


**Table 57** Mesomorphism of polycatenar complexes of Cr<sup>0</sup>, (121).

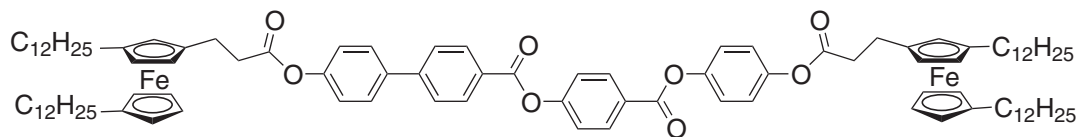
<i>n</i>	Ligand	Complex
8	Cr 137 SmC 198.5 N 206.5 I	Cr 95 SmC 102 N 140 I
10	Cr 125 SmC 185 I	Cr 94 SmC 110 N 131 I
12	Cr 127.5 SmC 128.5 Col <sub>o</sub> 161 Col <sub>h</sub> 186 I	Cr 92 SmC 118 I
14	Cr 123 Col <sub>h</sub> 176 I	Cr 95 SmC 99 I

The ( $\eta^6$ -arene)tricarbonylchromium complexes (121) were reported by Campillos *et al.*<sup>621</sup> and the uncomplexed ligands showed a mesomorphism typical of polycatenar mesogens, progressing from N and SmC phases at shorter chain lengths to Col<sub>o</sub> and Col<sub>h</sub> phases at longer chain lengths. Upon complexation, the columnar mesophase was suppressed entirely, the nematic range was extended for the first two derivatives, and the SmC phase was now present for all homologs (Table 57). An important observation was the rather rapid decrease in the mesophase temperature range as the alkoxy chain length was increased, essentially due to a huge reduction in the clearing temperature of the complexes, the melting point being almost invariant (ca. 90 °C). Compared to the structurally related butadienetricarbonyliron(0) complexes (120), the disappearance of the columnar mesophases was rather surprising. X-Ray studies showed that the SmC spacings were smaller for the free ligand than for the complexes and this was interpreted in terms of a variation in the ligand conformation. However, this observation is entirely consistent with the “core” of the complex possessing a larger cross section at the aliphatic–aromatic interface than the free ligand, reducing the mismatch with the two terminal chains leading to a much smaller tilt. This would, in turn, greatly reduce the driving force for columnar phase formation.

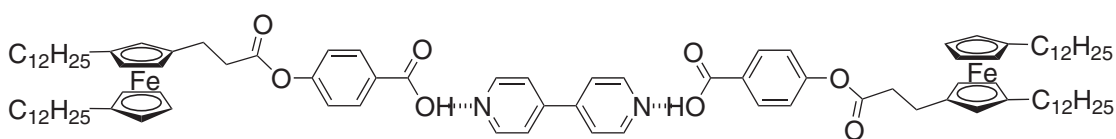
Very extended, hexacatenar ferrocenes, (122), were reported by Seo *et al.*<sup>622</sup> who prepared the even-numbered homologs from  $6 \leq n \leq 20$ . On account of their extended size, the melting points were quite high (ca. 120 °C for all *n*, except for *n*=8 at 163 °C) considering that they are hexacatenar materials, and clearing at ca. 170–175 °C. The first homolog, *n*=6, was not mesomorphic (m.pt. 200 °C). For *n*=8 and 10, an *Ia3d* cubic phase was identified by X-ray methods (*a* = 136.7 Å), while longer-chain homologs gave a Col<sub>h</sub> phase (*n*=12, 14, 16, 18). Curiously, the complex with *n*=20 was reported as non-mesomorphic clearing at 118.5 °C, when the Col<sub>h</sub>–I transition temperatures of the previous homologs were all around 179 °C, and a mesomorphic temperature range of ca. 50 °C. While the columnar phase is not at all unexpected, the cubic phase is somewhat noteworthy as its observation is rare in hexacatenar mesogens.



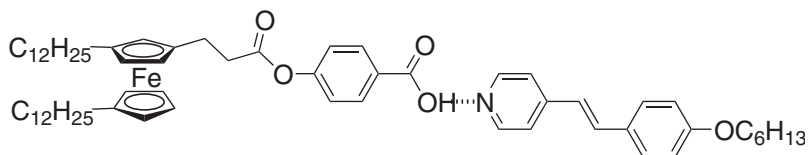
Some rather unconventional polycatenar mesogens were described by Deschenaux *et al.*<sup>623</sup> in which the terminal chains are found not as part of phenyl rings, but rather as substituents on the  $\eta^6$  cyclopentadienyl rings of ferrocene (**123** to **125**). Despite this unconventional geometry, the two tetracatenar complexes showed a  $\text{Col}_h$  phase, between 52 and 84 °C for the covalently linked compound (**123**), and in the range 66 to 72 °C for the tris-adduct (**124**), while the tricatenaer material (**125**) showed an SmC and an SmA phase (Cr 55 SmC 84 SmA 101 I) the latter not normally being found in “conventional” tricatenaer mesogens.



(123)



(124)



(125)

### 7.9.10.6 Polycatenar Porphyrins

A small number of polycatenar metalloporphyrin derivatives have been reported, based on 5,15-disubstituted systems (Figure 64). Wang and Bruce had first reported<sup>624</sup> the tetracatenar compound (**126**) in which they had shown that the “fly-over” chains disrupted attractive, intermolecular porphyrin interactions and gave materials whose melting and clearing points decreased markedly over those which did not possess these extra chains.<sup>625</sup> Tetra- and hexacatenar porphyrins were then synthesized both without (**127** to **128**) and with (**129** to **130**) the “fly-over” chains<sup>626</sup> and it was shown that without the extra chains, the tetracatenar mesogen showed an SmC and N phase at temperatures between ca. 275 °C and 320 °C (**127**), while the hexacatenar analog gave a columnar phase between 188 °C and 288 °C (**128**). However, on introduction of the “fly-over” chains, the mesomorphism of both changed to show only a nematic phase, with the tetracatenar compound (**129**) being nematic between 133 °C and 169 °C, while the hexacatenar material (**130**) melted at 50 °C, clearing at 153 °C. Note that to produce mesomorphic materials, the number of aromatic rings had to increase concomitantly with the number of peripheral aliphatic chains.

Other 5,15-disubstituted porphyrins were described by Ohta and co-workers,<sup>254</sup> but most do not fit the label “polycatenar” and are described in the section on discotic materials (Section 7.9.7.2). However, one derivative did possess a more conventional tetracatenar structure (**131**) and was reported as showing the so-called discotic lamellar phase. While it does not contain a central metal, it is included here for completeness.

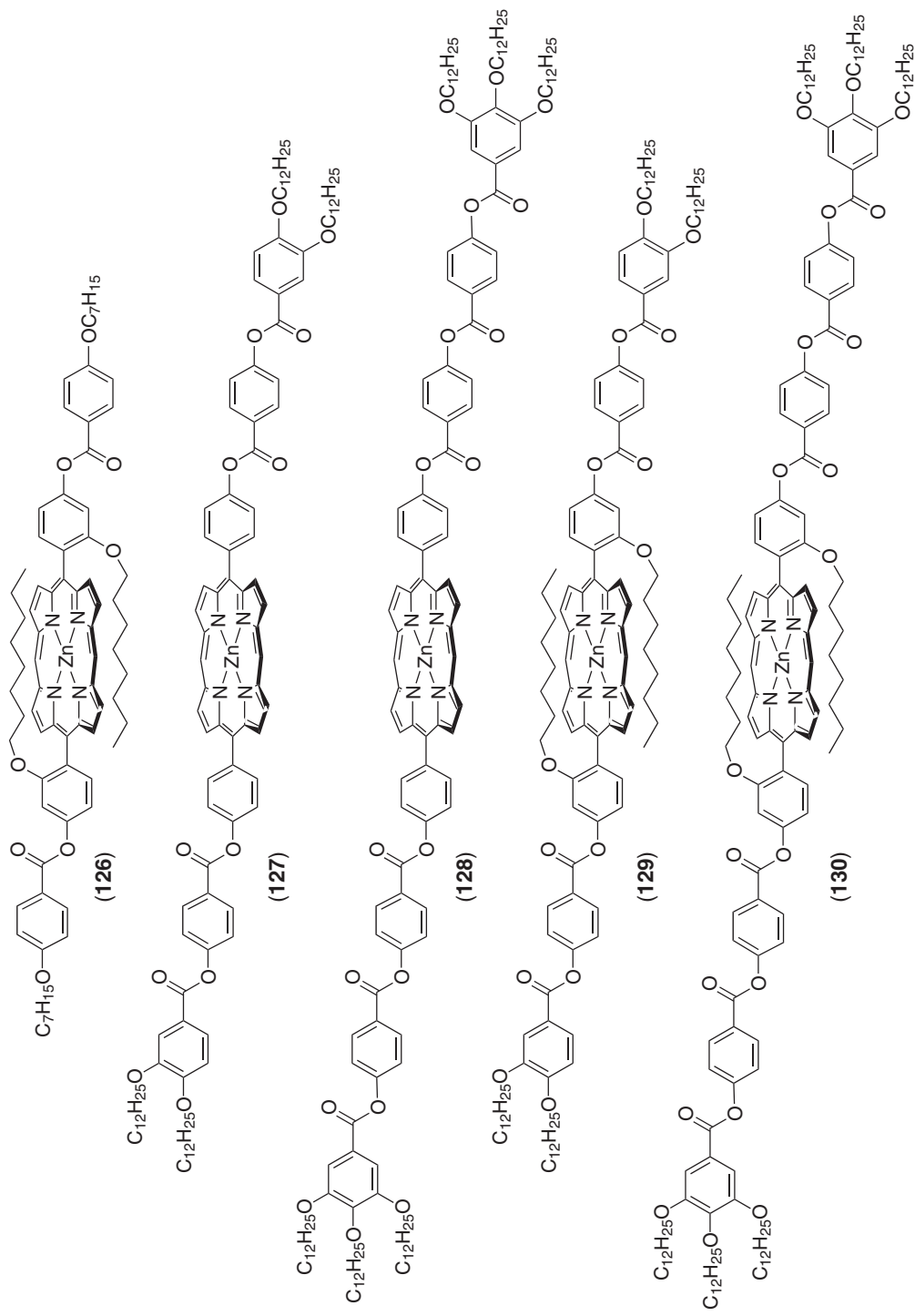
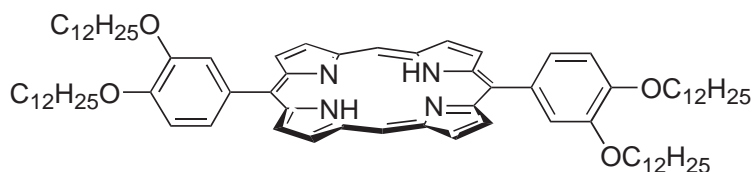


**Figure 64** Extended, polycatenar porphyrins (127) to (130).



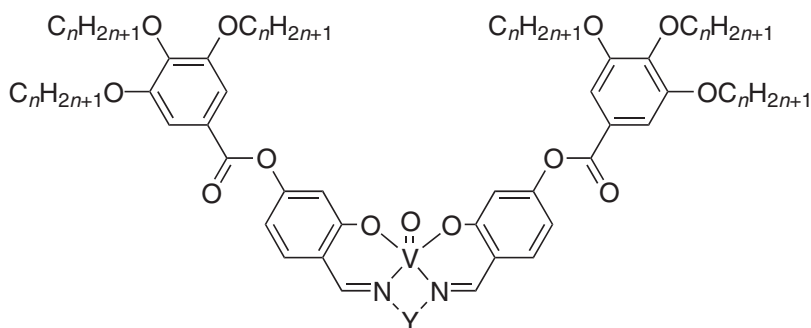
### 7.9.10.7 Salen Complexes

Swager and co-workers reported the rich columnar polymorphism of two series of hexacatenar vanadyl Schiff-base complexes (**132**) and (**133**). The ligands were of the salen type, and the spacer, Y, as well as the position of anchorage of the trialkoxy benzoate groups were varied systematically, ((**132**), (**133**): Y = CH<sub>2</sub>CH<sub>2</sub>, CH<sub>2</sub>CH<sub>2</sub>CH<sub>2</sub>, CH<sub>2</sub>C(Me)<sub>2</sub>CH<sub>2</sub>).<sup>627</sup> As such, the molecular shape and the relative strength of the dative interactions between vanadyl groups could be easily monitored: (**132**) thus adopted a slightly bent structure, whereas (**133**) possessed a more conventional elongated hexacatenar structure. All the materials were monomeric in the isotropic state, i.e., the frequency of the V=O stretching mode was found at ca. 990 cm<sup>-1</sup>. However, in the crystal and liquid crystal states, the situation differed depending on the spacer type. The formation of structures containing V=O—V=O interactions was demonstrated for the complexes with trimethylene spacer (Y = CH<sub>2</sub>CH<sub>2</sub>CH<sub>2</sub>), which exhibited the strongest intermolecular vanadium–oxygen interactions ( $\nu_{\text{V}=\text{O}}$  ca. 850–860 cm<sup>-1</sup>), and for the complexes with the bulky CH<sub>2</sub>C(Me)<sub>2</sub>CH<sub>2</sub> spacer ( $\nu_{\text{V}=\text{O}}$  ca. 870–910 cm<sup>-1</sup>), but not for those with dimethylene spacer ( $\nu_{\text{V}=\text{O}}$  ca. 990 cm<sup>-1</sup>). Consequently, the monomeric species ((**132**), (**133**): Y = CH<sub>2</sub>CH<sub>2</sub>) exhibited only a single room-temperature Col<sub>h</sub> phase, with almost the same mesophase stability for both compounds, whereas the linear-chain derivatives displayed a number of columnar mesophases (Table 58). For the bent compounds (**132**) the authors claimed that they observed up to four different Col<sub>h</sub> mesophases within the same compound, whatever the nature of the spacer, while a Col<sub>r</sub>–to–Col<sub>h</sub> transition was observed for the elongated complex (**133**) with Y = CH<sub>2</sub>CH<sub>2</sub>CH<sub>2</sub>, and an unidentified mesophase for the complex (**133**) with Y = CH<sub>2</sub>C(Me)<sub>2</sub>CH<sub>2</sub>. However, additional X-ray studies required revision of some earlier assignments of the mesophases, particularly those of the bent complexes ((**132**): Y = CH<sub>2</sub>CH<sub>2</sub>CH<sub>2</sub>).<sup>628,629</sup> In fact, these complexes also exhibited the same Col<sub>r</sub>–to–Col<sub>h</sub> phase sequence as found in the isomeric derivatives (**133**). On the basis of these X-ray data, the bent compounds were thought to stack in an antiparallel fashion, whereas (**133**) were believed to stack orthogonally to one another. The columnar superstructures were stabilized by intermolecular, dative interactions, and the resulting polar order produced highly organized structures in which the mesogens were held in tight register. The slightly higher mesophase stability of (**132**) with respect to (**133**) was mainly due to steric constraints, and to a better occupation of the free space available. Dielectric studies carried out on (**132**) ((**132**): Y = CH<sub>2</sub>CH<sub>2</sub>CH<sub>2</sub>) revealed enhanced conductivity and low-frequency dielectric absorption in the mesophases. Moreover, the low-temperature Col<sub>r</sub> mesophases seemed to possess an antiparallel ordering of dipolar chains, this long-range dipolar order breaking down on heating, and being lost totally in the Col<sub>h</sub> mesophase.

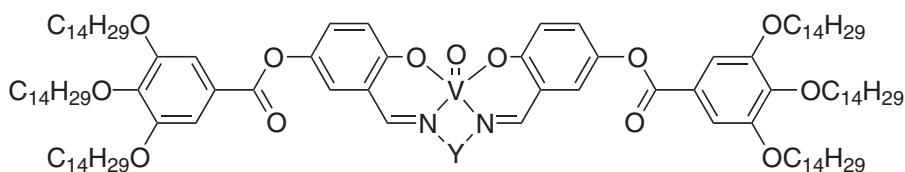
**Table 58** Mesomorphism of compounds (**132**) and (**133**).

Y	–CH <sub>2</sub> CH <sub>2</sub> –	–CH <sub>2</sub> CH <sub>2</sub> CH <sub>2</sub> –	–CH <sub>2</sub> C(Me) <sub>2</sub> CH <sub>2</sub> –
( <b>132</b> ) n = 14:	Col <sub>h</sub> 150 I	n = 10: Cr 85 Cr <sub>X</sub> 120 Col <sub>r</sub> 153 Col <sub>r</sub> 172 Col <sub>h</sub>	n = 14: Cr 28 Col <sub>h</sub> 67 Col <sub>h</sub> 91 Col <sub>h</sub>
		181 I	147 I
		n = 12: Cr 68 Cr <sub>X</sub> 97 Col <sub>r</sub> 141 Col <sub>r</sub> 158 Col <sub>h</sub>	
		182 I	
		n = 14: Cr 82 Cr <sub>X</sub> 90 Col <sub>r</sub> 135 Col <sub>h</sub> 188 I	
( <b>133</b> ) Col <sub>h</sub> 156 I		n = 14: Cr 62 Col <sub>r</sub> 107 Col <sub>h</sub> 170 I	Cr 78 M <sup>T</sup> 115 I

M<sup>T</sup> is a transient mesophase seen during the first heating only. Cr<sub>X</sub> is an orientationally disordered crystalline phase.

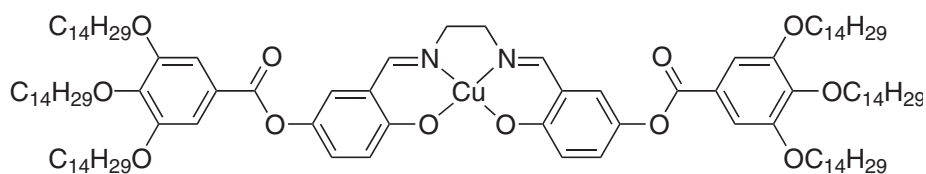


(132)

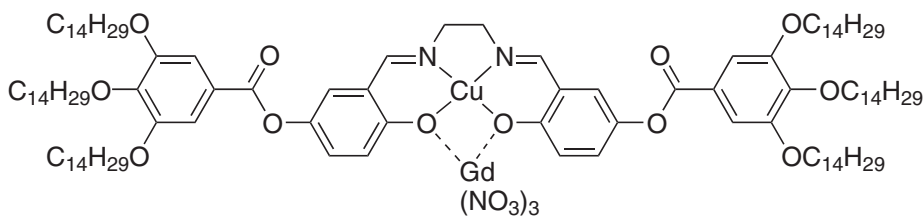


(133)

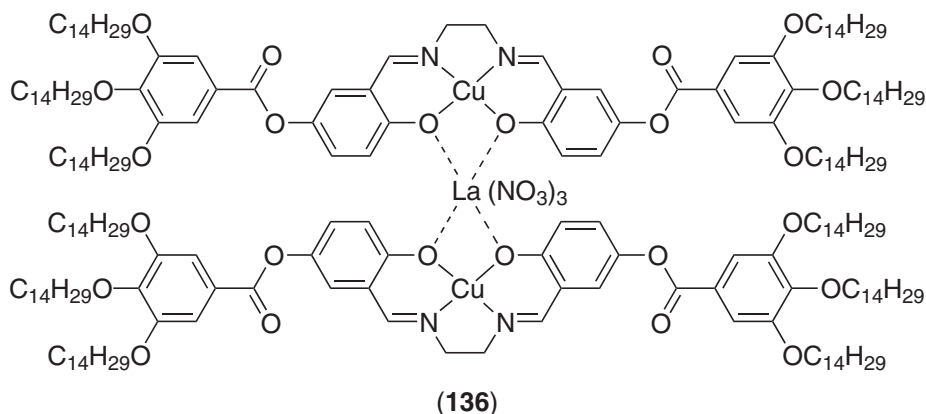
Some mixed f-d heteropolynuclear metallomesogens have been synthesized with the same type of ligand as those in series (133) and their mesomorphism studied.<sup>630</sup> Such mixed f-d metallomesogens represent an interesting new class of materials, as they may combine specific magnetic interactions of f-d coordination compounds (such as magnetic exchange interactions) with the properties of liquid crystals. The copper-lanthanum complex (136) and the copper-gadolinium complex (135) were obtained by reaction of copper complex (134) with the corresponding lanthanide nitrate. Two different stoichiometries were found depending on the lanthanide ions: the adduct of lanthanide(III) nitrate with the copper complex yielded a heterotrimeric compound (136), whereas for gadolinium, a heterobinuclear complex (135) was formed. The three complexes exhibited a wide-temperature-range  $Col_h$  mesophase as determined by DSC and X-ray diffraction. The mesophase stability was considerably enhanced in both lanthanide-copper adducts with respect to the copper complex: (134) melted into the  $Col_h$  at 58 °C and cleared at 159 °C, whereas the dinuclear (135) and the trinuclear (136) adducts melted in the mesophase at 77 °C and 95 °C respectively. However, for the mixed complexes, the clearing temperatures could not be reached as they both decomposed above 220 °C. Both (134) and (135) were found to assemble in pairs in order to achieve a pseudo-discoid shape (not necessary for (136)) and they all stacked in an alternating fashion to form the columns.



(134)

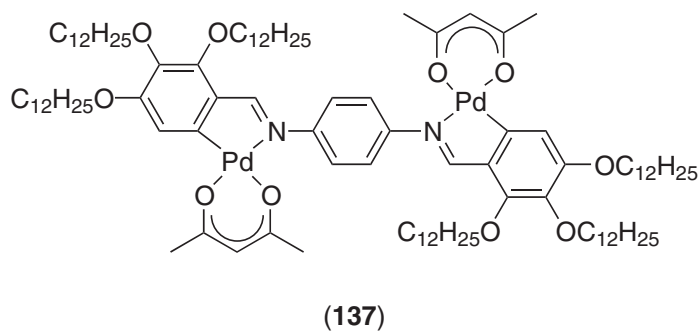


(135)



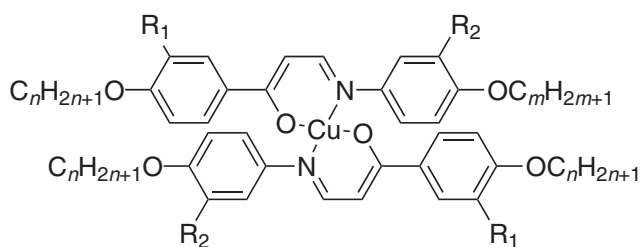
### 7.9.10.8 Other Polycatenar Metallomesogens

The dipalladium organyl (**137**), derived from (**39**) ( $X = \text{Cl}$ ) by ligand exchange reaction between the bridging group and acetylacetonate, was not mesomorphic in its pure state nor in binary mixtures with pure alkanes. However, it formed a charge-transfer complex with TNF as indicated by a change in color. This association was found to induce a thermotropic mesophase, with a two-dimensional arrangement of columns, with a maximum clearing temperature at ca. 60 mol.% of TNF. Moreover, contact preparation with heptane, pentadecane, eicosane, and with eicosane/pentadecane mixtures (molar ratios 1:1, 2:1, and 1:2)<sup>292</sup> revealed induced lyotropic behavior for the charge-transfer complex. Several compositions were investigated with different donor-acceptor ratios (70:30 mol.% to 30:70 mol.%) and two columnar phases with hexagonal and nematic symmetry were induced. The  $N_{\text{Col}}$  phase was monotropic in mixtures of up to 50 mol.% of TNF, and above this concentration became enantiotropic.



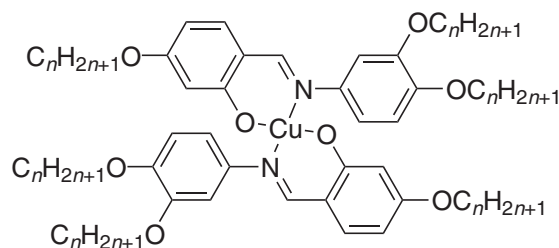
Krówczynski *et al.* studied the effect of the chain substitution pattern on the mesomorphism of some disk-like copper complexes of enaminketones, (**138**).<sup>631</sup> Four types of such complex were prepared, differing from each other by the number and/or the position of the alkoxy chains. In the series with four chains only ((**138**):  $R_1 = R_2 = \text{H}$ ;  $n = m = 8$ ), the complex showed an SmC phase at rather elevated temperatures (Cr 164 SmC 203 I), whereas that possessing eight chains was not mesomorphic ((**138**):  $R_1 = R_2 = \text{OC}_8\text{H}_{17}$ ;  $n = m = 8$ ), melting into the isotropic liquid at 105 °C. The thermal behavior of the complexes with six side chains depended considerably on the position of substitution,  $R_1$  and  $R_2$ , with respect to the iminoketone moiety. For the first series of isomers ((**138**):  $R_1 = \text{OC}_8\text{H}_{17}$ ;  $R_2 = \text{H}$ ;  $n = 8$ ,  $m = 8, 10, 12$ ), only the first compound ( $m = 8$ ) was mesomorphic displaying monotropic SmC and SmA phases (Cr 108 (SmC 73 SmA 80) I). Concerning the other series of isomeric compounds, the mesomorphism was enhanced slightly ((**138**):  $R_2 = \text{OC}_8\text{H}_{17}$ ;  $R_1 = \text{H}$ ;  $n = 8$ ,  $n = 6, 8, 10$ ). The shortest homolog of the series ( $m = 6$ ), showed monotropic SmC and N phases (Cr 86 (SmC 82 N 84) I), whereas the phases became enantiotropic for the other two ( $m = 8$ : Cr 74 SmC 84 N 85 I;  $m = 10$ : Cr 74 SmC 84 N 85 I), although the nematic phase existed over a very narrow temperature range ( $\approx 1^\circ\text{C}$ ). Thus, in this system, the substitution pattern influenced the mesomorphism in a very unusual manner, destabilizing the

mesophases upon addition of lateral chains. This can be seen as the consequence of the relative position of the two aromatic rings of each ligand with respect to the chelating system. Thus, the aniline rings lie perpendicular to the rest of the complex and so the chains attached to the two phenyls lie in perpendicular planes. Optical microscopy experiments (conoscopy) suggested that the nematic phase was uniaxial.



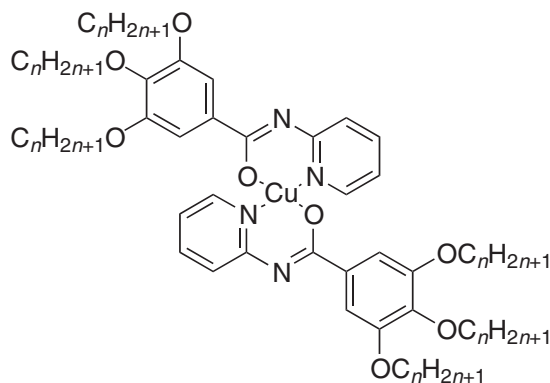
(138)

Quite interestingly, some copper complexes of bis(*N*-3',4'-dialkoxyphenyl)-4-alkoxysalicylaldiminato) ((139):  $n = 8, 10, 12, 14, 16$ )<sup>632</sup> were reported to exhibit a very broad-range  $\text{Col}_h$  phase between  $136^\circ\text{C}$  and  $179^\circ\text{C}$ , and  $253^\circ\text{C}$  and  $325^\circ\text{C}$ , the temperature range of the mesophase decreasing from  $150^\circ\text{C}$  to  $120^\circ\text{C}$  with the lengthening of the chains, as did the melting and clearing temperatures. The free Schiff-base ligands were not mesomorphic. This was rather surprising following the disappointing results obtained for the iminoketone complexes (138) having the same substitution pattern. In such complexes, the structure of the mesogenic core influences the thermal behavior drastically.



(139)

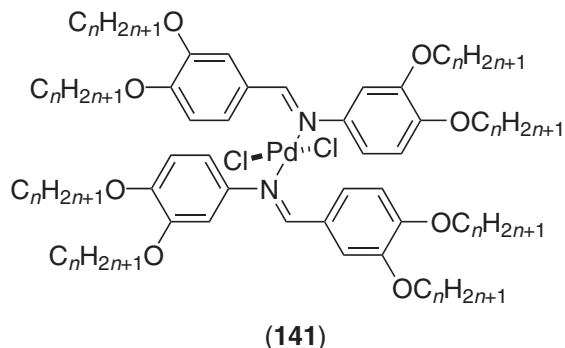
The influence of the core structure was shown again in copper(II) complexes of 2-phenylazomethinopyridine derivatives ((140):  $n = 12, 14, 16, 18$ )<sup>633</sup>. The formation of a mesophase was found to be sensitive to both chain length and chain number. The compounds with long chains exhibited  $\text{Col}_h$  mesophases at relatively elevated temperatures and over a few degrees only ( $n = 16$ : Cr  $177^\circ\text{C}$   $\text{Col}_h$   $179^\circ\text{C}$ ;  $n = 18$ : Cr  $161^\circ\text{C}$   $\text{Col}_h$   $180^\circ\text{C}$ ), the other compounds being isotropic liquids at  $197^\circ\text{C}$  and  $185^\circ\text{C}$  respectively for  $n = 12$  and  $14$ . None of the two- and four-chained compounds was mesomorphic.



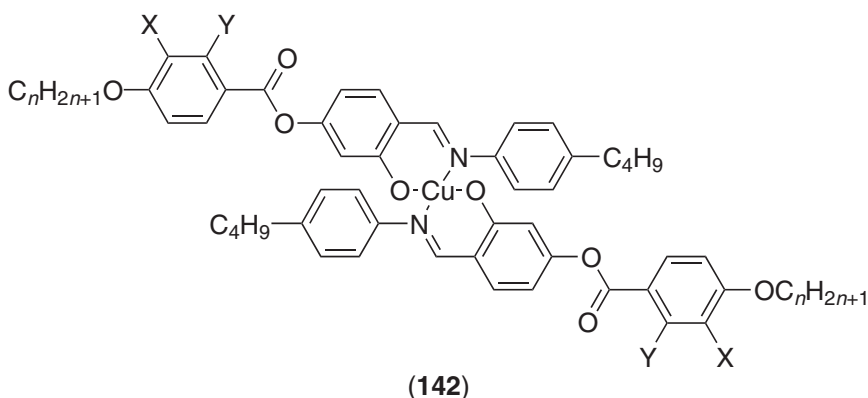
(140)



Lee and co-workers<sup>634</sup> reported the mesomorphism of unusual palladium(II) complexes bound by an  $\eta^1$ -benzylideneaniline ligand ((141):  $n=6, 10$ ) which, despite their disk-like shape, showed a smectic phase. The free ligands themselves were not mesomorphic, but upon complexation (note without *ortho*-metallation) both metal complexes exhibited monotropic SmA phases ((141):  $n=6$ : Cr 92 (SmA 61) I;  $n=10$  Cr 80 (SmA 65) I). The single-crystal X-ray structure of a model compound confirmed the coordination arrangement around palladium.



Courtieu and co-workers<sup>635</sup> have investigated the effects on mesomorphism of the addition of several chains to copper complexes based on elongated salicylaldimines, (142). The position of grafting of the additional chains was varied systematically ((142): X, Y = H,  $\text{OC}_m\text{H}_{2m+1}$ ), as was the length, which could be elongated independently from the main chain ( $n \neq m$ ). The transition temperatures of the ligands were increased upon complexation whatever the chain-substitution pattern, and their tendency to form N phases diminished considerably. On one hand, when the chain was in the 2-position ((142): X = H; Y =  $\text{OC}_m\text{H}_{2m+1}$ ;  $n = m$ ), only a N phase was observed for the copper complexes (as for the ligands), monotropic for  $n = m = 4, 8$ , and 16 and enantiotropic for  $n = m = 12$ , although over a range of only a few degrees (Table 59). On the other hand, however, when the chain was attached at the extremity of the molecules in the 3-position ((142): Y = H; X =  $\text{OC}_m\text{H}_{2m+1}$ ), the complexes exhibited smectic phases (SmC and an unidentified phase, S), the N phase seen for the ligand being suppressed totally upon complexation (Table 59). Moreover, dissymmetry in the chain length provoked either the suppression of the mesomorphism ((142):  $n = 1$ ; X =  $\text{OC}_m\text{H}_{2m+1}$ ,  $m = 2, 12$ ) or a slight increase of the mesophase stability ((142):  $n = 6$ ; X =  $\text{OC}_m\text{H}_{2m+1}$ ,  $m = 2-16$ ), depending on the length of the chain in the 4-position; the effect of the dissymmetry was also strong for the ligands, resulting in the decreasing stability of the SmC phase at the expense of the N phase.



In the same paper, the effect of chlorination of some derivatives was also described (143). The introduction of the chlorine in either the 3- or 5-position suppressed the mesomorphic properties of the ligands, probably due to the slight deviation from the planarity (3-position) and to the steric hindrance (5-position). The effect on the copper complexes was more interesting (Table 60). The chlorine atom in the 3-position did not perturb the molecular geometry of the complex significantly, but there was still a slight reduction in the mesophase stability as well as the

**Table 59** Transition temperatures of compound (142).

		$n = m$		$n = 6 \neq m$
$n$	$m$	$X = H; Y = OC_mH_{2m+1}$	$Y = H; X = OC_mH_{2m+1}$	$Y = H; X = OC_mH_{2m+1}$
4	4	Cr 128 (N 59.5) I	Cr 171.5 SmC 177.5 I	Cr 163.5 N 179 I
8	8	Cr 93 (N 65) I	Cr 138 S 158.5 I	Cr 144 S 158 SmC 161 I
12	12	Cr 52.5 N 61.5 I	Cr 115 S 141 I	Cr 132.5 S 154 I
16	16	Cr 75 (N 57.5) I	Cr 109.5 S 140 I	Cr 125.5 S 149 I

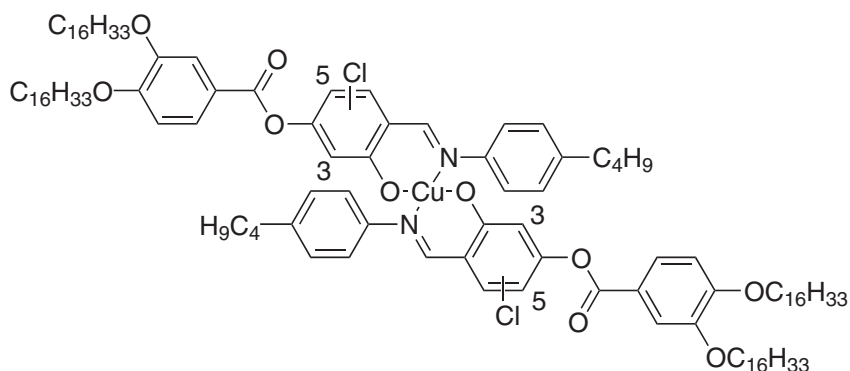
S: unidentified smectic mesophase.

**Table 60** Transition temperatures for ligands and complexes (143).

	$H$ in 3- and 5-position	$H$ in 5-position, $Cl$ in 3-position	$H$ in 3-position, $Cl$ in 5-position
Ligand	Cr 84.5 SmC 91 N 92.5 I	Cr 100.5 I	Cr 115 I
Complex	Cr 109.5 S 140 I	Cr 84 S 110 N 122 I	Cr 108.5 I

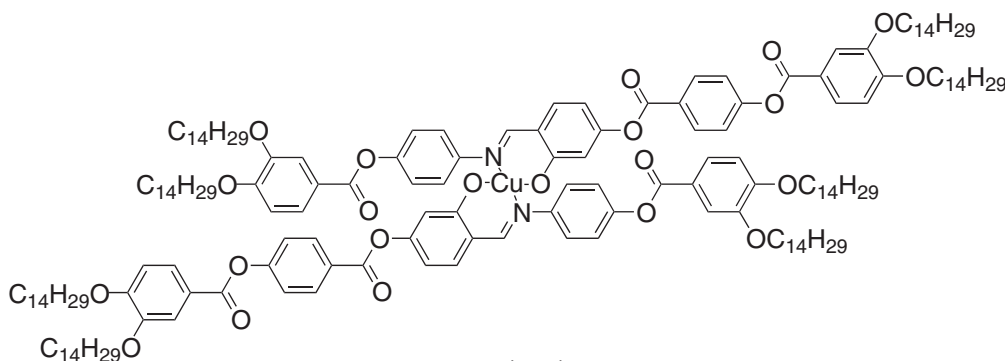
S: unidentified smectic mesophase.

induction of the N phase. However, the chlorine atom in the 5-position clearly affected the molecular geometry of the complex, and the mesomorphism was suppressed.



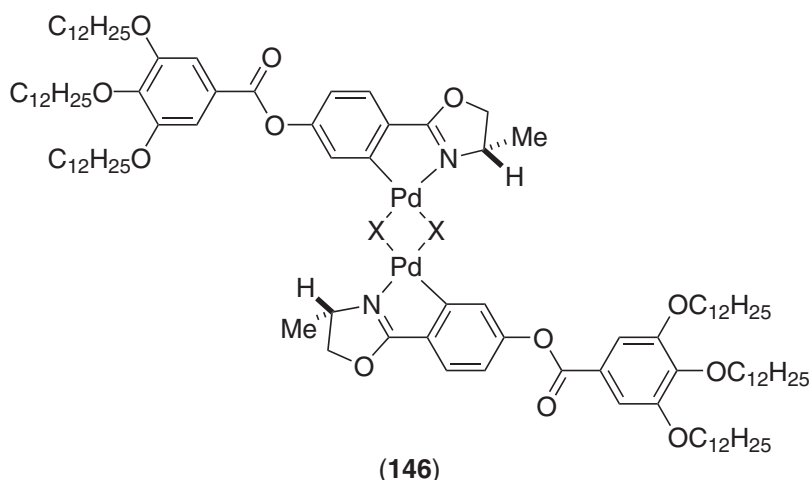
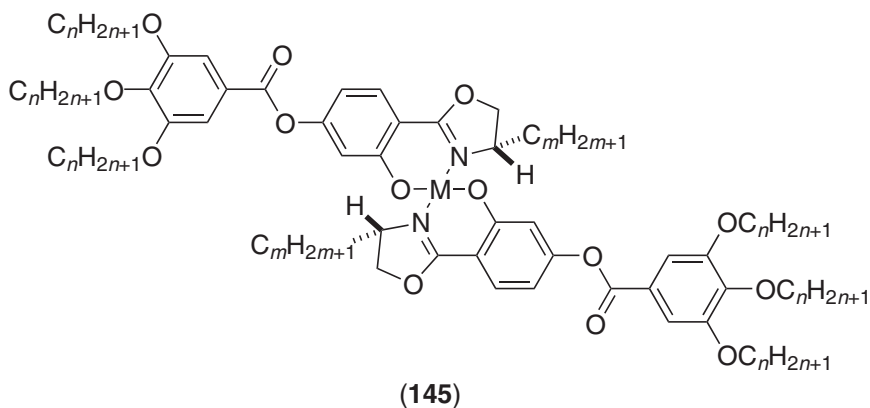
(143)

This series of compounds did not strictly behave as true polycatenar mesogens in the sense that no columnar mesomorphism was observed, despite their relatively low aspect ratio. Increasing the number of aromatic rings (144) to elongate the mesogenic core modified the thermal behavior quite drastically. Thus, complex (144) now displayed a Col<sub>o</sub> phase at high temperature (Cr 198 Col<sub>o</sub> 215 I).<sup>591</sup>



(144)

Serrano and co-workers have reported the synthesis of two interesting series of chiral, hexacatenar metal complexes, i.e., mono- and dinuclear derived from chiral oxazoline-based ligands.<sup>636</sup> None of the pure mononuclear complexes ((145): M = Pd, Ni, Cu, Zn;  $n = 6, 12$ ;  $m = 1, 4$ ) nor dinuclear compounds ((146): X = OAc, Cl) was mesomorphic and most were room-temperature oils or glassy materials. This is likely due to the sterically demanding central chiral unit preventing molecular stacking and, hence, mesophase formation.

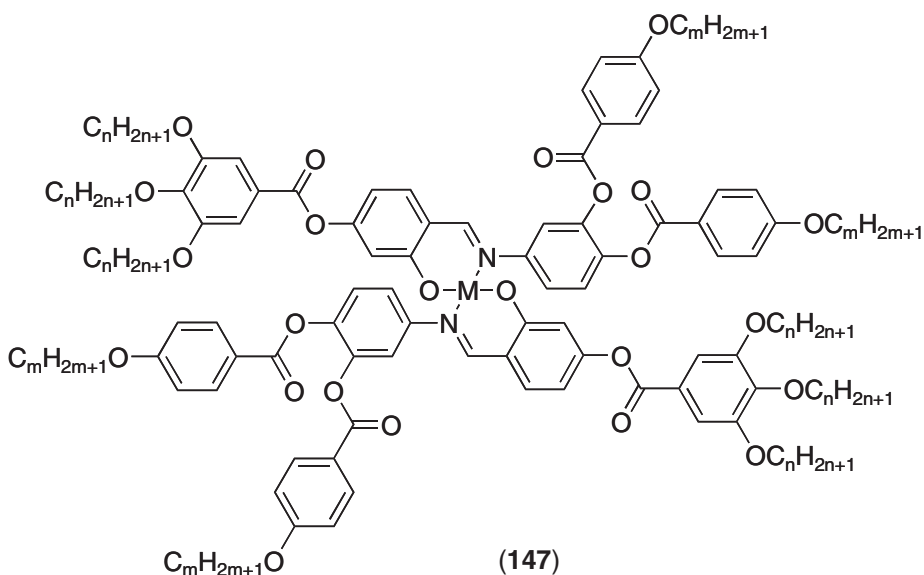


However, when mixed with TNF, they all formed charge-transfer complexes. At high TNF concentration ( $> 66\%$ ), demixing of the two components occurred, whereas below this concentration a mesophase was induced and surprisingly, despite the six peripheral chains, an SmA phase was identified. At lower TNF concentrations, the more sterically demanding materials exhibited SmA glasses on cooling, although in general the clearing temperatures increased with the TNF content. X-Ray investigations revealed that the structure of the mesophase consisted of the face-to-face arrangement of the complexes and TNF into layers, with an additional side-by-side organization, resembling the model proposed for the McMillan phase. These compounds have also been shown to act as chiral dopants with nematic hosts, and  $N^*$  phases have been induced.

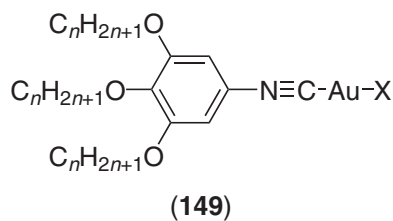
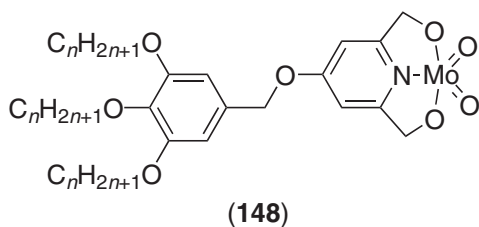
More recently, a series of polycatenar salicylaldimine complexes (147) has been reported with M = Pd, Cu, Ni and Fe—Cl.<sup>637</sup> For the two chain lengths reported ( $n = m = 10, 16$ ) it was found that neither of the Ni complexes, nor the shorter-chain Cu complex, was mesomorphic, but all the others showed a  $Col_h$  phase, identified from its characteristic optical texture. Clearing points were in the range  $102\text{--}11^\circ\text{C}$  for the mesomorphic Pd and Cu complexes, while the chloroiron(III) complexes cleared at  $172^\circ\text{C}$  ( $n = m = 10$ ) and  $160^\circ\text{C}$  ( $n = m = 16$ ).

#### 7.9.10.9 Wedge-shaped Complexes

A series of (pyridinediyl-2,6-dimethanolato)dioxomolybdenum(VI) complexes ((148):  $n = 8, 10, 12, 14, 16$ ), described by Swager *et al.*<sup>638</sup> were found to form  $Col_h$  mesophases, except the octyloxy



homolog which was not liquid crystalline. All the other complexes ((148):  $n = 10, 12, 14, 16$ ) melted from an unidentified, but disordered, phase into the mesophase at ca.  $100^\circ\text{C}$ , and cleared into the isotropic liquid between  $130^\circ\text{C}$  and  $140^\circ\text{C}$ , giving an average mesomorphic temperature range of  $25^\circ\text{C}$  to  $40^\circ\text{C}$ . The pyridinediyl-2,6-dimethanol ligands were not themselves mesomorphic. The formation of the columnar mesophase thus arose from complexation to the  $\text{MoO}_2$  fragment and its tendency to form polymeric chain structures both in the solid phase and mesophase containing weak  $(\cdots\text{Mo}=\text{O}\cdots\text{Mo}=\text{O}\cdots)$  interactions. From both infrared spectroscopy and X-ray diffraction, these complexes were regarded as being organized in such a way that the polar molybdenum head groups were located at the center of the columns, with the rest of the complexes extended radially from this "core." The flexibility of the ligand benzylic group will have helped the trialkoxyphenyl fragment to fill the free space arising from this arrangement.



The trialkoxyphenylisocyanatogold(I) complexes ((149):  $\text{M} = \text{Au}$ ,  $\text{X} = \text{Cl}$ ,  $n = 4, 6, 8, 10$ ;  $\text{X} = \text{Br}, \text{I}, \text{CN}, \text{SCN}$ ,  $n = 10$ ) were mesomorphic, forming a  $\text{Col}_h$  phase at room temperature despite being derived from non-mesomorphic ligands.<sup>639,640</sup>

In the halogold series, the clearing temperatures (Figure 65) decreased in accordance with the increasing size of the halide group, and X-ray diffraction revealed an intra-columnar separation of only  $4\text{ \AA}$ , supporting the existence of a basic dimeric arrangement arising from two molecules disposed in an antiparallel fashion. These dimers would then stack on top of each other, probably rotated by, on average,  $90^\circ$  from one to the next to generate an overall circular columnar core, in agreement with the hexagonal symmetry. The greater the size of the halide, the more perturbed was the stacking into columns, and the lower the clearing temperature.

This situation was slightly different for the cyano and the thiocyanato complexes, where the mesophase stability increased considerably compared to the halo compounds. In fact, X-ray diffraction suggested rather strong interactions between gold atoms ( $6.5\text{ \AA}$ ) in addition to a smaller stacking period of  $3.3\text{ \AA}$ , particularly for the  $\text{SCN}$  complex. Thus, the columnar structure remained basically the same, but was "tighter," consistent with the greater mesophase stability.

Related chloro(isocyanato)copper(I) complexes (150) have also been studied, and again, mesomorphic complexes were found even though the ligand was non-mesomorphic.<sup>641</sup> Two series were prepared, and most of the di-3,4- ((150):  $\text{R} = \text{H}$ ,  $n = 4, 6, 8, 10, 12$ ), and tri-3,4,5-alkoxyphenylisocyanatocopper(I) complexes ((150):  $\text{R} = \text{OC}_n\text{H}_{2n+1}$ ,  $n = 4, 6, 8, 10, 12$ ) exhibited  $\text{Col}_h$  phase, some of

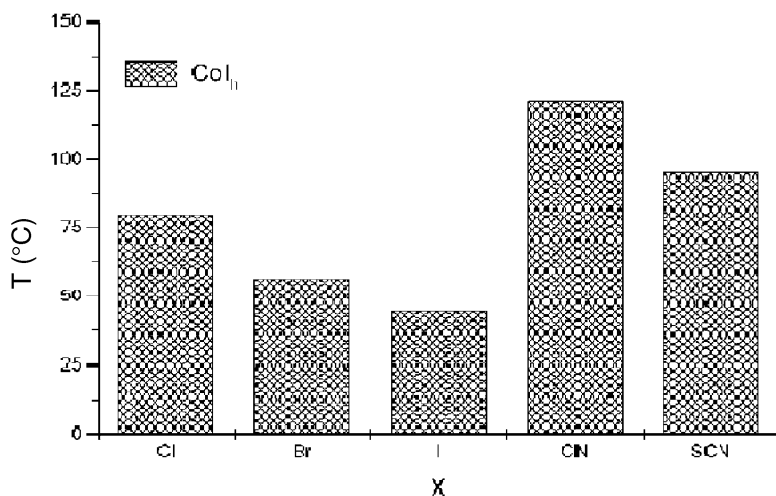
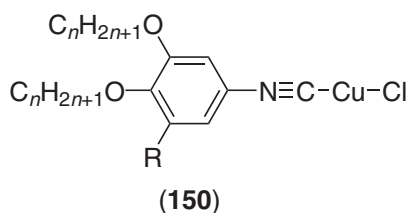


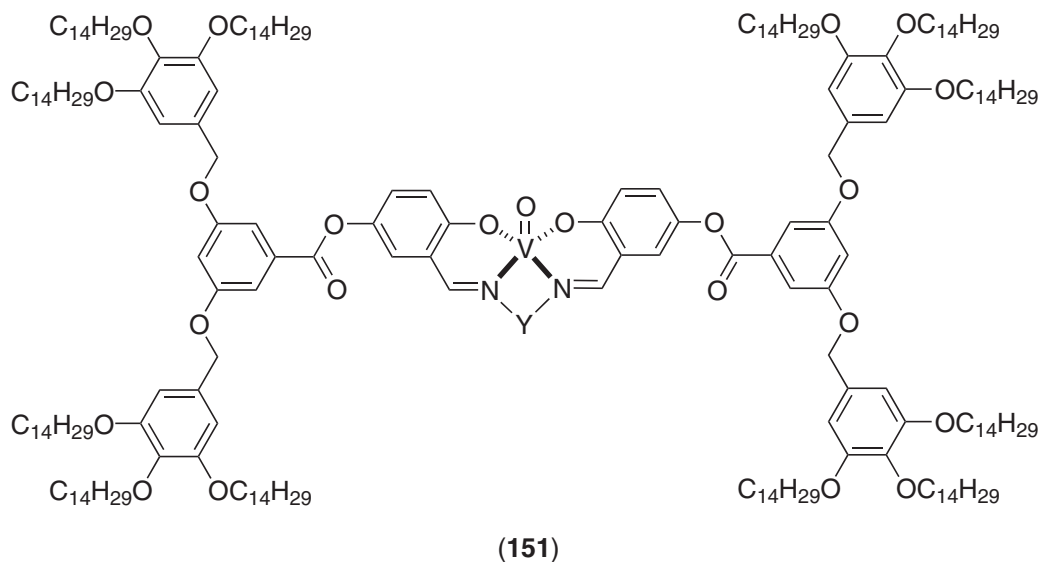
Figure 65 Mesomorphism of gold(I) complexes 149.



them at or near room temperature. Among the two-chained systems, the first two homologs of the series ( $n = 4, 6$ ) were not mesomorphic, clearing at ca.  $80^\circ\text{C}$ . The other derivatives exhibited a  $\text{Col}_h$  phase, with little influence of the chain length on the melting temperatures, ca.  $80\text{--}85^\circ\text{C}$ , but with an increase of the mesophase stability on lengthening the chains, with clearing temperatures at  $96.5^\circ\text{C}$ ,  $115^\circ\text{C}$ , and  $124^\circ\text{C}$  for  $n = 8, 10$ , and  $12$  respectively. Except the butyloxy derivative, which was not mesomorphic (Cr 99 I), all the other tri-alkoxy complexes displayed a  $\text{Col}_h$  phase from room temperature. The mesophase temperature range was substantially enhanced with respect to the dialkoxy compounds but with lower clearing temperatures, falling from  $105^\circ\text{C}$  to  $75^\circ\text{C}$  and then rising again to  $94^\circ\text{C}$  for the dodecyloxy homolog.

### 7.9.11 METALLODENDRIMERS

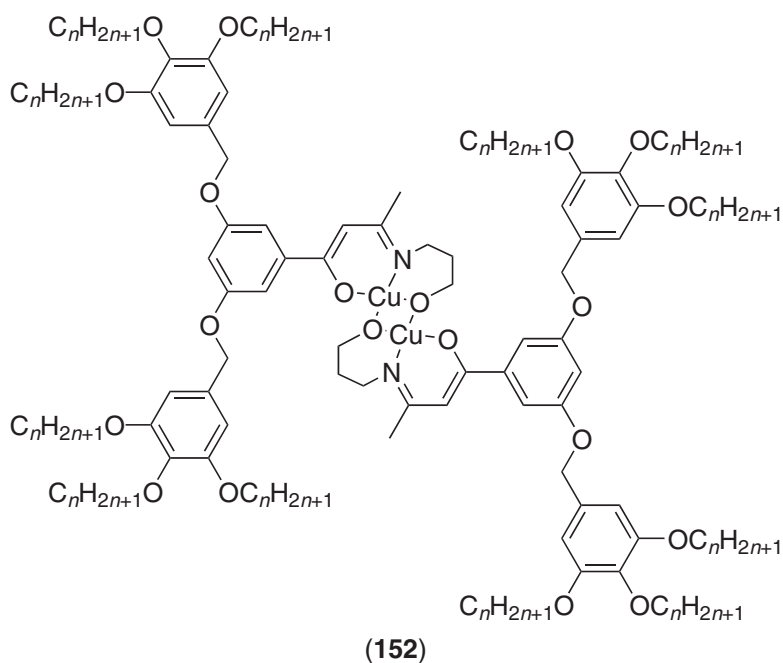
The field of liquid crystal dendrimers is a recent concept in the design of new molecular structures,<sup>642</sup> yet despite the relative youth of this topic, one can already observe the growth in this area with the emergence of few metallodendrimers with liquid-crystalline properties. The first report of a branched, metal complex showing columnar mesophases can be dated back to 1993, yet at this time, the term “dendrimer” was not used to describe it.<sup>627</sup> The complex consisted of first-generation vanadyl salen-type complexes. The spacer, Y, was varied ((151):  $\text{Y} = -\text{CH}_2\text{CH}_2-$ ,  $-\text{CH}_2\text{CH}_2\text{CH}_2-$ ,  $-\text{CH}_2\text{CMe}_2-\text{CH}_2-$ ), and the thermal behavior examined, and compared on the basis of the spacer length and the influence on the ability to form polymeric  $-\text{V}=\text{O}\cdots\text{V}=\text{O}-$  chains. The three complexes were mesomorphic at room temperature, showing columnar phases as expected due to their shape and number of chains; the free ligands were not mesomorphic (Table 61). Infrared spectroscopy further revealed the formation of linear chain structures for  $\text{Y} = \text{propyl}$  and  $\text{dimethylpropyl}$ , but when  $\text{Y} = -\text{CH}_2\text{CH}_2-$ , the complex was monomeric; the last nevertheless displayed the largest mesomorphic range. The high-temperature mesophase was identified as  $\text{Col}_r$  ( $c2mm$ ) in all cases, and two of the complexes exhibited the inverted the  $\text{Col}_h$ -to- $\text{Col}_r$  phase sequence. The destabilization of the hexagonal structure at the expense of the rectangular phase was thought to be due to the bulkiness of the terminal groups and to their spatial requirements, and the driving force for the  $\text{Col}_h$ -to- $\text{Col}_r$  transition may then be linked to the formation of linear chain structures. These could limit the lateral diffusion of the cores, and force the stacking of the core with limited conformational options.



**Table 61** Thermal behavior of (151).

<i>Y</i>	<i>Mesomorphism</i>
-CH <sub>2</sub> CH <sub>2</sub> -	Col <sub>r</sub> 119.5 Col <sub>r</sub> 156 I
-CH <sub>2</sub> -CH <sub>2</sub> -CH <sub>2</sub> -	Col <sub>h</sub> 36 Col <sub>h</sub> 97.5 Col <sub>r</sub> 151 I
-CH <sub>2</sub> -CMe <sub>2</sub> -CH <sub>2</sub> -	Col <sub>h</sub> 55 Col <sub>r</sub> 108 I

Another series of metallodendrimers with a closely related molecular structure to (152) has been reported.<sup>643</sup> The dendritic ligand was obtained by condensation of the corresponding 1,3-dione with aminopropanol, and the dicopper complex was then formed by the reaction with copper(II) acetate. The ligand itself was not mesomorphic, but upon complexation, mesophases were observed whose stability was found to be dependent on the number of chains, and their length.



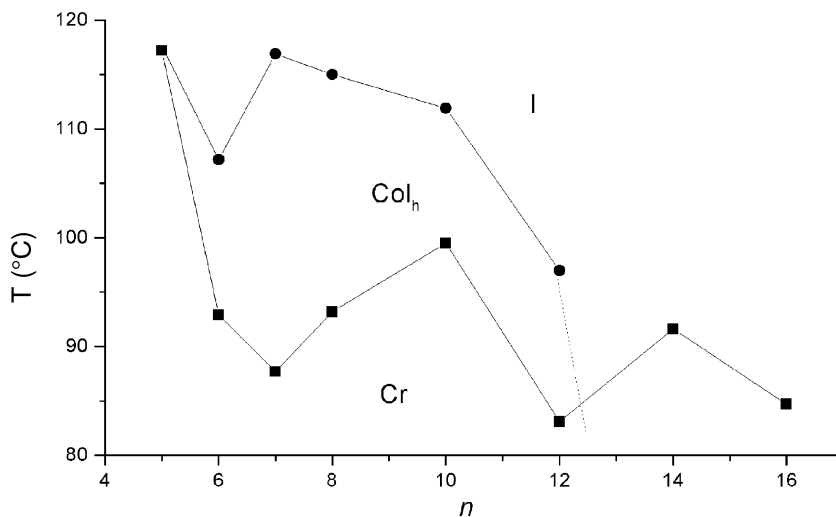
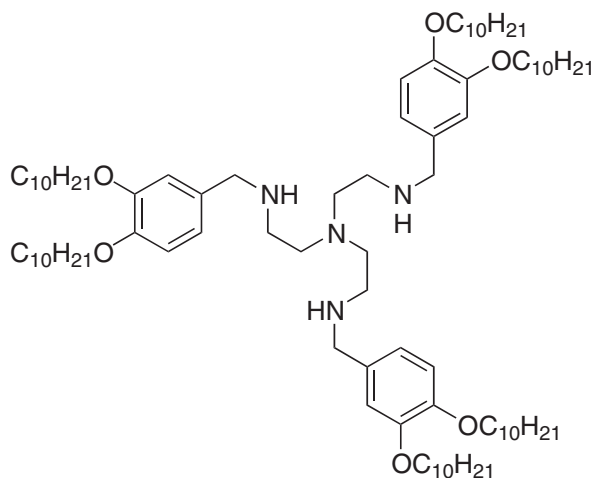


Figure 66 Mesomorphism of complexes (152).

The systems having one and two chains per terminal phenyl group were not mesomorphic, but those with three chains showed a Col<sub>h</sub> phase. However, the occurrence of the mesophase depended strongly on the chain length. Thus, short- and long-chain derivatives ((152):  $n = 5, 14$ , and 16) were not mesomorphic, whereas the intermediate-chain-length compounds ((152):  $n = 6-9, 10, 12$ ) displayed a Col<sub>h</sub> phase with transition temperatures being sensitive to the chain length (Figure 66). Compared to the previous dendrimer (151), the central core of (152) is kinked, giving rise to a more circular shape, which may explain the observation of only the Col<sub>h</sub> phase.

Complexation of first- (153) and second-generation (154) dendrimers derived from tris-(2-aminoethyl)amine to the metal salts CoCl<sub>2</sub>, NiCl<sub>2</sub>, CuX<sub>2</sub> (X = Cl, SCN and NO<sub>3</sub>), and ZnCl<sub>2</sub> allowed access to new type of metallomesogens of the type [MX<sub>2</sub>(L)], with two possible coordination geometries, i.e., trigonal bipyramidal giving rise to ionic complexes ([MXL]<sup>+</sup>[X]<sup>-</sup>) (Figure 67a) or octahedral leading to neutral complexes ([MX<sub>2</sub>L]) (Figure 67b).<sup>644</sup> On the basis of infrared and UV/vis spectroscopy, the cobalt(II) and copper(II) complexes were trigonal-bipyramidal ("azatran" geometry), the nickel(II) complexes octahedral, whereas the geometry around zinc could not be determined; all the first-generation complexes were mesomorphic (Table 62), except for [Ni(NO<sub>3</sub>)<sub>2</sub>(153)]. The melting temperatures of the metallomesogens were all very low, some of them being liquid crystals at room temperature ([CoCl(153)]Cl, [CuCl(153)]Cl, and [ZnCl<sub>2</sub>(153)]); the others melted at around 50 °C ([NiCl<sub>2</sub>(153)], [Cu(NO<sub>3</sub>)(153)](NO<sub>3</sub>), [Cu(SCN)(153)](SCN). Clearing temperatures were all found in the range 65–85 °C, except for



(153)

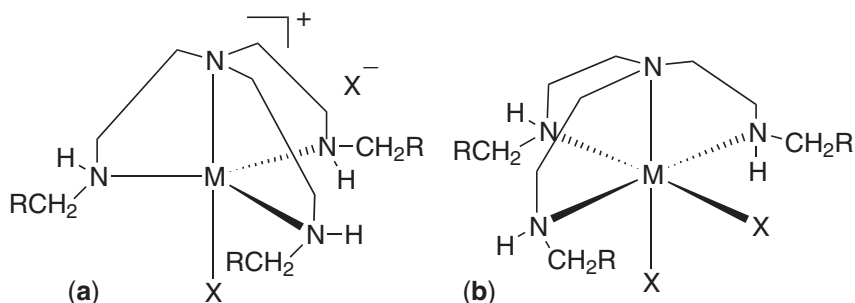
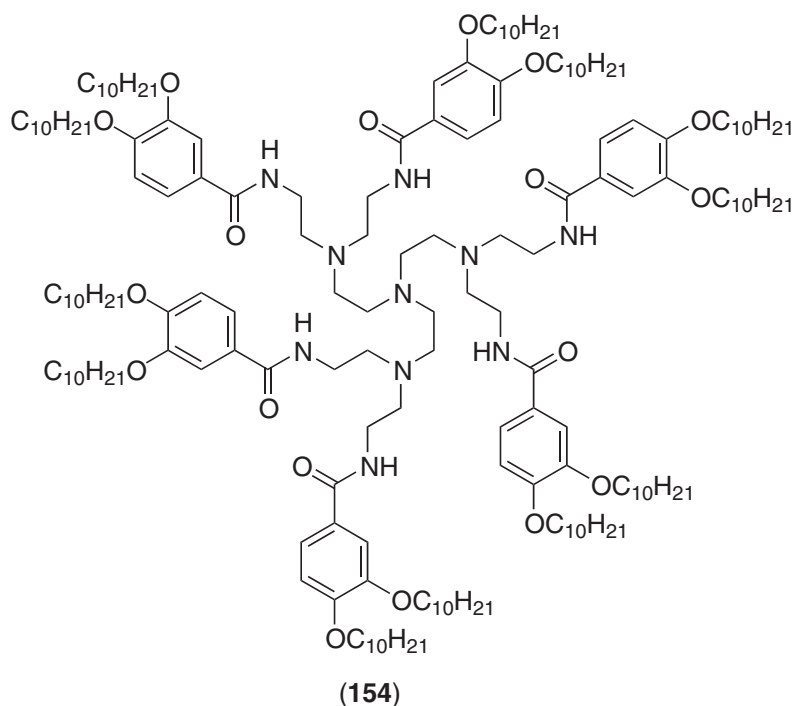


**Figure 67** The two possible coordination geometries (a) the ionic trigonal bipyramid geometry ( $[MX(L)]^+[X]^-$ ) and (b) the neutral octahedral geometry ( $[MX_2(L)]$ ).



the zinc(II) complex which cleared above 120 °C. X-Ray diffraction indicated that the mesophase exhibited by these systems was  $Col_h$ .

The second-generation dendrimer, **(154)**, was itself mesomorphic, having a monotropic  $Col_h$  phase below 98.5 °C.<sup>645</sup> Its complexation by  $CuCl_2$  did not alter the mesomorphic properties, and an enantiotropic  $Col_h$  phase was observed from room temperature to 140 °C. Thus, some sort of dendritic effect could be observed in that the mesophase stability was enhanced considerably

**Table 62** Mesomorphism of metal complexes of dendrimers **(153)** and **(154)**.

Dendrimer	$MX_2$	Transition temperatures
<b>(153)</b>	$CoCl_2$	g 56 $Col_h$ 85.5 I
	$NiCl_2$	g 40 Cr 47 $Col_h$ 64.5 I
	$Ni(NO_3)_2$	g 36 Cr 46.5 I
	$CuCl_2$	g 41 $Col_h$ 75 I
	$Cu(SCN)_2$	g 41 Cr 48.5 $Col_h$ 75 I
	$Cu(NO_3)_2$	g 36 Cr 47.5 $Col_h$ 79 I
	$ZnCl_2$	g 60 $Col_h$ 126 I
<b>(154)</b>	$CuCl_2$	g 49 $Col_h$ 140 I



**Table 63** Mesomorphic properties of tetrahedral Cu<sup>I</sup> complexes (**155**) and (**156**) and metallo-helicates (**157**) and (**158**).

<b>155</b>	<b>156</b>	<b>157</b>	<b>158</b>
Cr 48 Col <sub>h</sub> 75 I	Cr 49 Col <sub>h</sub> 117 I	Cr 25 Col <sub>r</sub> or Col <sub>o</sub> 181 I	Cr 115 Col <sub>L</sub> 187 I

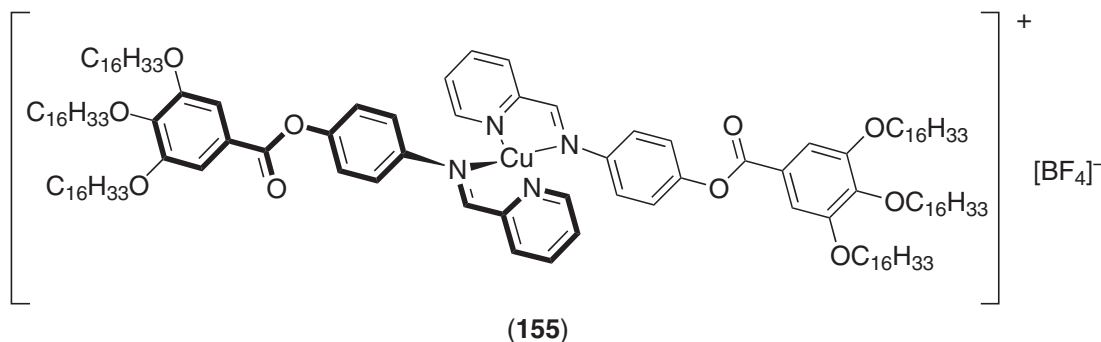
compared to the first-generation dendrimer [CuCl(**153**)]Cl. The UV/vis spectrum also suggested that the azatran geometry must be assumed for this complex.

In these three series of dendrimers, the metal is located as the central node of the macromolecule, and induction of mesomorphism was systematically observed on complexation of a metal ion. When coordinated to the metal, the dendritic core is likely to lose flexibility, its conformation being locked by the metal center, and the molecule adopts a molecular shape approximating that of a disk, or perhaps that of a cone.

### 7.9.12 TETRAHEDRAL COMPLEXES OF CU<sup>I</sup> AND METALLOHELICATES

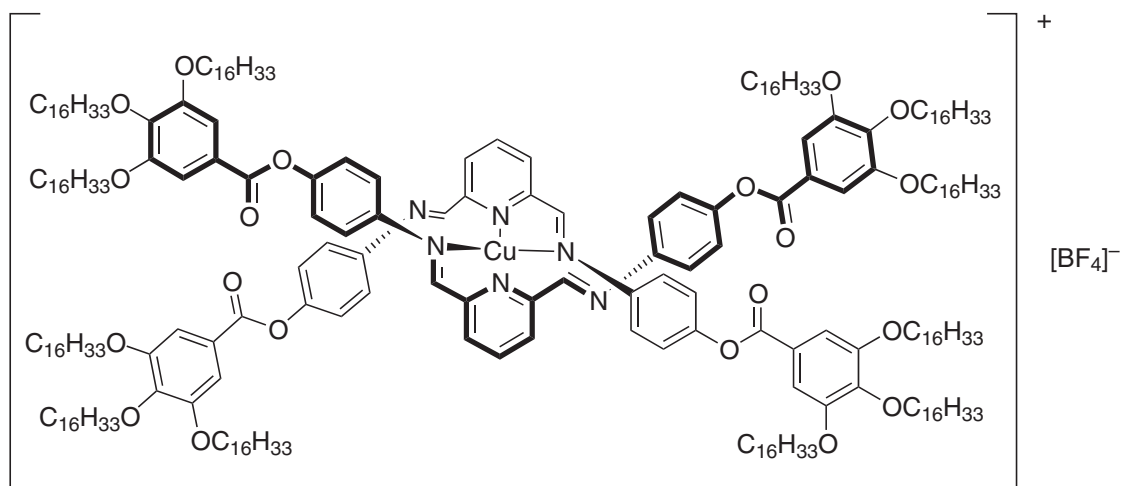
The discovery of mesomorphic metallohelicates formed by the selective complexation of non-mesomorphic, oligopyridine ligands represents an important development in the design of metallomesogens.<sup>646,647</sup> Oligopyridines such as 2,2'-bipyridines, 2,2':6',2''-terpyridines, and 1,10-phenanthrolines have long been known to be attractive building blocks for the construction of a wide range of complex three-dimensional structures such as, for example, catenanes, knots, grids,<sup>648</sup> and helicates,<sup>649</sup> due essentially to their ability to form specific chelates with a wide range of metals. The use of such building blocks has now also been found compatible with the formation of liquid crystals.<sup>650</sup>

Ziessel and co-workers<sup>651</sup> first reported tetrahedral complexes of Cu<sup>I</sup> based on imines derived from pyridine-2-carbaldehyde (**155**), and the related tetrahedral Cu<sup>I</sup> complexes based on pyridines which are 2,6-difunctionalized (**156**) suggests an *entrée* to helicates through the use of different pyridine building blocks, namely 2,2'-bipyridine-6,6-dicarbaldehyde (**157**),<sup>652</sup> and 2,2':6',2''-terpyridine-6,6'-dicarbaldehyde (**158**).<sup>653</sup> All of the complexes showed columnar mesophases at or near room temperature (Table 63). The symmetry of the columnar mesophase changes with the elongation of the rigid central core from hexagonal to lamello-columnar via a rectangular or oblique symmetry (phase symmetry not determined unequivocally). In the mesophases, the metal-pyridine unit forms the center of the column which is surrounded by molten alkyl chains, although in the case of (**156**), the chains are distributed homogeneously around the small polar core, hence the hexagonal symmetry. However, as the core increases in length, the chains become arranged along a preferential direction allowing for the central cores to interact with one other, leading to a lamellar organization for (**158**), or an intermediate situation as for (**157**).

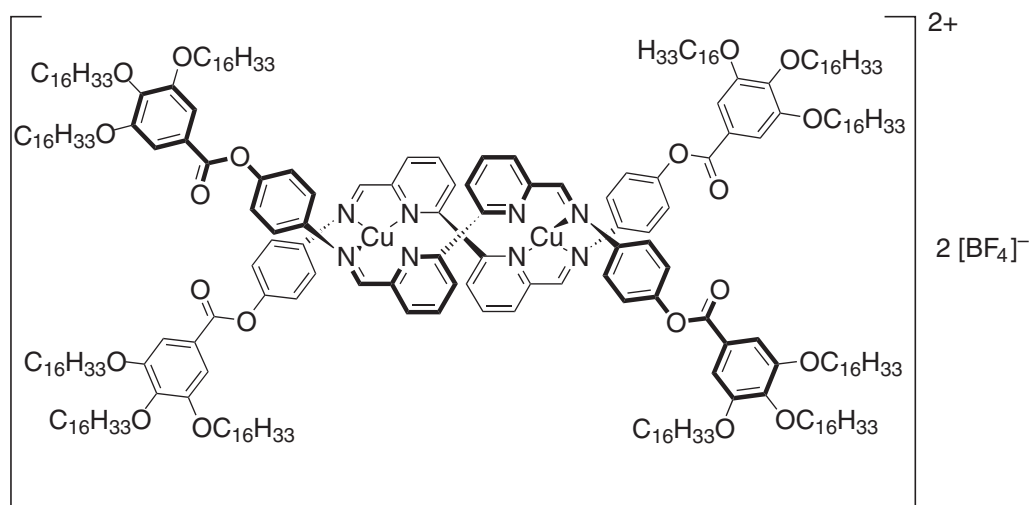


### 7.9.13 MISCELLANEOUS

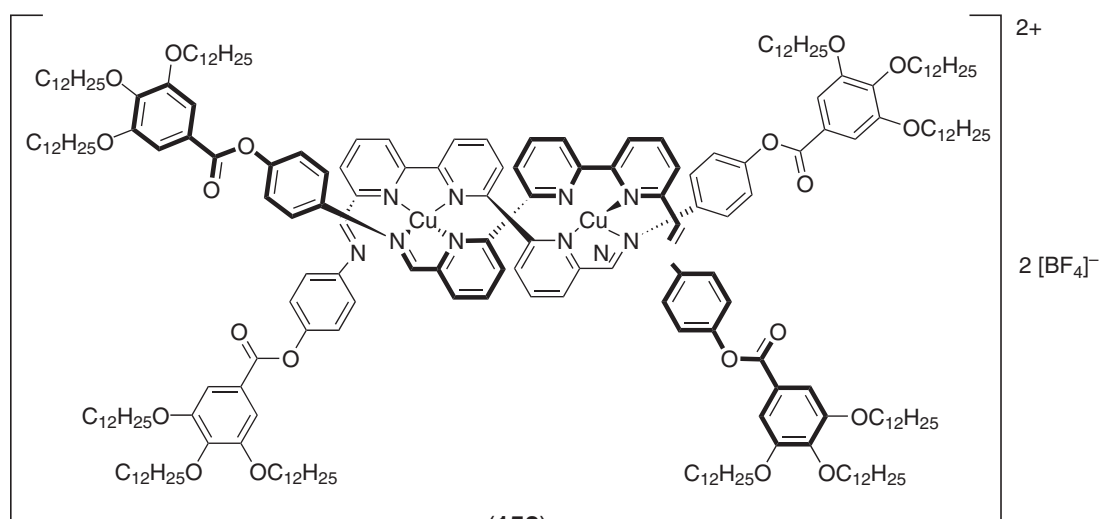
Several other, original molecular structures with apparently unfavorable geometries have also been found, quite surprisingly, to show mesomorphic properties.



(156)

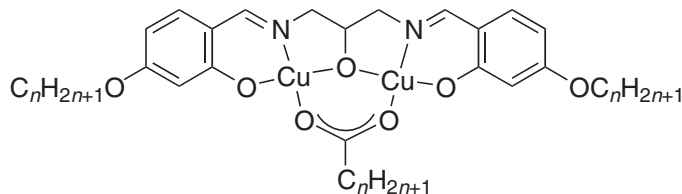


(157)

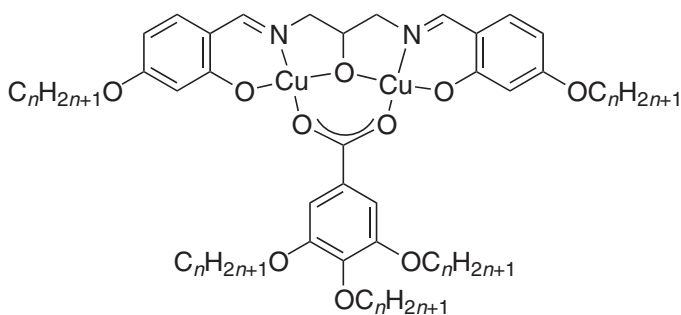


(158)

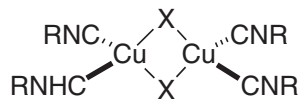
The dicopper(II) complexes derived from  $\mu$ -exogenous carboxylato- (**159**) and 3,4,5-trialkoxybenzoato-bridged (**160**)  $N,N'$ -(propan-2-ol)-bis-(4-alkoxysalicylaldehydes) were, despite their rather unusual shape, found to be mesomorphic.<sup>654</sup> The acetato-bridged compounds ((**159**):  $n = 10, 12, 14, 16, 18$ ) exhibited an enantiotropic SmA phase, melting around 172–143 °C and clearing between 177 °C and 159 °C. The SmA temperature range increased slightly with chain length, but overall remained narrow (<15 °C). The benzoato-bridged complexes ((**160**):  $n = 10, 14, 16$ ) all possessed a Col<sub>h</sub> phase from ca. 50–60 °C up to 145 °C.



(159)



(160)



(161)

Espinet *et al.* have reported binuclear mesogenic copper(I) isocyanide complexes<sup>655</sup> ((**161**):  $X = \text{Cl, Br, I}$ ;  $R = \text{C}_6\text{H}_4\text{C}_6\text{H}_4\text{OC}_{10}\text{H}_{21}$ ,  $\text{C}_6\text{H}_4\text{CO}_2\text{C}_6\text{H}_4\text{OC}_n\text{H}_{2n+1}$ ,  $\text{C}_6\text{H}_3(\text{OC}_n\text{H}_{2n+1})_3$ ) consisting of two tetrahedral  $[\text{CuX}_2(\text{CNR})_2]$  units sharing an edge that contains the two bridging halogens. With such a structure, the four coordination positions for the isocyanide ligands are co-planar and as such, mesomorphism might be anticipated. None of the complexes of the first series with the biphenylisocyanide ligands was mesomorphic ((**161**):  $X = \text{Cl, Br, I}$ ;  $R = \text{C}_6\text{H}_4\text{C}_6\text{H}_4\text{OC}_{10}\text{H}_{21}$ ) and all melted above 165 °C. However, with the other elongated isocyanide ligand ((**161**):  $X = \text{Cl, Br, I}$ ;  $R = \text{C}_6\text{H}_4\text{CO}_2\text{C}_6\text{H}_4\text{OC}_n\text{H}_{2n+1}$ ,  $n = 4, 6, 8, 10, 12$ ), the complexes showed an SmA phase, though at rather elevated temperatures (melting above 180 °C up to the point of decomposition). While the melting temperatures were kept constant, the clearing or decomposition temperatures decreased with increasing chain length or on substitution of Cl by Br or I, thus narrowing the range of the SmA phase. The complexes with 3,4,5-trialkoxyphenylisocyanides ((**161**):  $X = \text{Cl, Br, I}$ ;  $R = \text{C}_6\text{H}_3(\text{OC}_n\text{H}_{2n+1})_3$ ,  $n = 4, 6, 8, 10, 12$ ) displayed a Col<sub>h</sub> phase from room temperature up to 70 to 80 °C. The clearing temperature decreased in the order  $\text{I} > \text{Br} > \text{Cl}$  and those with short chain lengths displayed a monotropic Col<sub>h</sub> phase, with a mean stacking period of ca. 5 Å.

## 7.9.14 CALAMITIC MATERIALS

### 7.9.14.1 Introduction

This section will concentrate on rod-like complexes which typically form nematic and smectic phases. While the approach does not concentrate on design aspects, it may become apparent that in rod-like systems, design is not a simple matter and there are many factors to be taken into account to do with anisotropy, disposition of ligands and functional groups associated with the metal and introduced on complexation. Thus, while it has been said<sup>656</sup> (albeit with tongue slightly in cheek) that for discotic systems it is possible to realize liquid crystal systems by taking a

favorite disk-like molecule and adding six or more chains, calamitic systems are a little more “discerning” and design needs to be undertaken with a little more care and a greater appreciation of factors which influence mesomorphism. The section is, however, prefaced by a discussion of ionic materials whose mesomorphism is dominated by the formation of lamellar phases.

### 7.9.14.2 Ionic Metallomesogens

#### 7.9.14.2.1 Alkylammonium derivatives

Self-assembling organic–inorganic materials allow for a huge number of combinations of organic and inorganic components. In addition to the predominantly electrostatic interactions, different types of non-covalent interactions, such as hydrogen bonding, van der Waals’ interactions, and microsegregation effects may also play a major role in controlling the self-assembly process. For example,  $M-Cl\cdots H$  interactions have been shown to be of primary importance in the development of the chemistry of metal-containing ionic liquids.<sup>657</sup>

In this category, long-chain alkylammonium tetrachlorometallates,  $(C_nH_{2n+1}NH_3)_2[MCl_4]$ , were investigated in the mid 1970s,<sup>658,659</sup> and are known to form ordered and disordered lamellar structures depending on the temperature. For  $M = Mn, Cu, Fe,$  and  $Hg$  ( $n = 12, 16$ ), the structure is characterized by the presence of two-dimensional, extended anions of stoichiometry  $[MCl_4]^{2-}$  sandwiched between two alkylammonium layers in the low-temperature polymorph, the alkyl chains being tilted at an angle of about  $45^\circ$  with respect to the lamellar planes (Figure 68a). The solid-state structures of these anions remain practically unchanged when going to the higher-temperature, disordered phase which is built up of pronounced, disorganized aliphatic layers separated by thin, ionic layers (Figure 68c). In the case of  $M = Mn, Cu, Fe,$  and  $Hg$ , the coordination about the metal is octahedral, thus giving anions in which the area per metal atom is the key factor in the type of packing for the alkyl chains.

For  $M = Co$  and  $Zn$ , the structures are of the same type, but the alkyl chains ( $n = 9-17$ ) are perpendicular to the ionic layers with intercalation of chains between successive layers in the low-temperature, solid phase (Figure 68b).<sup>660</sup> However, in these cases, the coordination about the metal is tetrahedral so that extended anions are not formed and the chains of successive layers are able to intercalate. Note that the liquid-like order of the alkyl chains in the high-temperature phase of all these compounds has been proved by X-ray diffraction and infrared studies.<sup>661</sup>

Similar polymorphic behavior was observed for a series of bis(alkylammonium) tetrabromozincates ( $n = 10-16$ ).<sup>662</sup> It was shown by X-ray diffraction and infrared, NMR, and NQR techniques that the transition from the ordered solid to the disordered solid is accompanied by a conformational

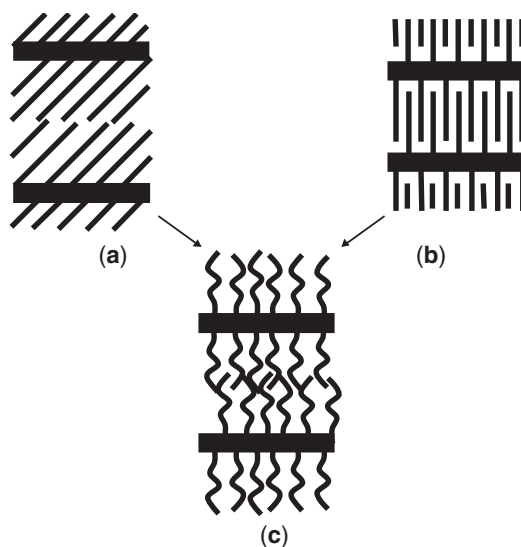


**Figure 68** Schematic representation of the lamellar structures of  $(C_nH_{2n+1}NH_3)_2[MCl_4]$ : (a)  $M = Mn, Cu, Fe, Hg$ ; (b)  $M = Co, Zn$ ; (c) structure of the high-temperature, disordered phase. Polar moieties represented by rectangles, alkyl chains by black lines.

melting of the hydrocarbon regions and that the ionic regions remain nearly unaltered after the transition. In fact, these stable, high-temperature phases are still crystalline solids despite the fact that the greatest part of the molar volume, occupied by the aliphatic chains, is in a liquid-like state. These features show a strong analogy to the smectic phase of rod-like molecules, as confirmed by spectroscopic studies on one tetrachlorocadmiate(II) derivative ( $n=10$ ).<sup>663</sup> In addition, at still higher temperatures, such tetrabromozincates exhibit a smectic phase where a two-dimensional melting of the inorganic regions has taken place, as evidenced by the total absence of any high-angle reflection in the X-ray diffraction pattern. In fact, the most dramatic change occurring in these systems as a function of the temperature is not the transition to the smectic phase, but rather that between the low-temperature to the high-temperature crystalline phases, where the aliphatic chains adopt suddenly a complete disordered conformation in the latter.

Mixtures of such compounds,  $(C_nH_{2n+1}NH_3)_2[MCl_4]$  with  $M = Mn$  and  $Zn$  and  $n = 12, 18$ , have shown long-range, anisotropic diffusion of the long-chain alkylammonium cations.<sup>664</sup> Annealing mixtures with compounds of different chain lengths results in the formation of mixed crystals in which bilayers of positionally and conformationally disordered alkylammonium cations alternate with crystalline halometallate layers. The macroanions are, at the same time, a support to the migrating alkylammonium cations and a hindrance to their demixing on crystallization.

The relationships between the thermal behavior and the crystal structure of long-chain,  $\alpha,\omega$ -alkylenediammonium tetrachlorozincates,  $(H_3N-(CH_2)_n-NH_3)[ZnCl_4]$ , ( $n=6-12$ ) is characterized by alternating  $[ZnCl_4]^{2-}$  tetrahedra and hydrocarbon layers as for the ammonium derivatives described above.<sup>665</sup> From the dimensions of the  $[ZnCl_4]^{2-}$  tetrahedra, the cross-section available for each alkylene diammonium group in a plane parallel to the ionic layers is found to be of the order of  $36.7 \text{ \AA}^2$ , indicating that the alkylene chains tilt at about  $55^\circ$ . On heating, the dodecylene salt gives rise to a smectic phase at  $237^\circ\text{C}$ , stable for more than  $40^\circ\text{C}$ . The mesomorphism of these systems is of interest as mesophases are observed in the apparent absence of what might be considered "classical" mesogenic groups. However, the alkyl chains and halometallate anions effectively phase separate in these systems, and dispersion forces are maximized in the observed bilayer structures in a situation similar to that found in the mesophases of the group 1 metal salts of carboxylic acids discussed earlier.

A new series of materials,  $(\{C_{18}H_{37}\}_n\{CH_3\}_3)_2[MCl_4]$  and  $(\{C_{18}H_{37}\}_2N\{CH_3\}_2)_2[MCl_4]$  with  $M = Co, Ni, Cu, Zn,$  and  $Cd$ , and quaternary nitrogen-containing cations, has been reported more recently.<sup>666</sup> These salts are thermotropic mesogens and, for instance, the tetrachlorocobaltate(II) salt,  $(\{C_{18}H_{37}\}_2N\{CH_3\}_2)_2[CoCl_4]$ , shows an SmA phase over a large temperature range from  $45^\circ\text{C}$  to  $155^\circ\text{C}$ . The mesophase formed by these complex salts is built up from alternating layers of ions and alkyl segments, similar to the salts described previously. Moreover, an SmA–SmA first-order DSC phase transition is observed for several tetrachlorometallate(II) salts, and has been interpreted as being due to changes in conformation of the melted alkyl segments.

#### 7.9.14.2.2 Complexes of long-chain amines

The formation of mesomorphic, lamellar structures by alternating polar and lipophilic sublayers has also been achieved by complexing long-chain primary or secondary amines to metal centers. For example, the zinc chloride complexes,  $[ZnCl_2(NH_2C_nH_{2n+1})_2]$  ( $6 \leq n \leq 16$ ) were shown to exhibit a mesophase over a short temperature range.<sup>667</sup> The dichlorocopper(II) complexes of the same type were found to melt with decomposition, and it was not clear whether a mesophase was formed.<sup>668</sup> However, the series of adducts employing the dibromozinc(II) moiety instead ( $n=4-18$ ) of the dichloro analog succeeded in generating a smectic mesophase as shown by X-ray diffraction.<sup>669</sup> Similarly, mesomorphic behavior of complexes obtained by reacting long-chain amines with copper(II) nitrate has been suggested by optical microscopy and DSC.<sup>670</sup>

The complexes  $[Ag(NH_2C_nH_{2n+1})_2][X]$  ( $n=6, 8, 10, 12, 14, X = NO_3, BF_4$ ) exhibit a fluid, birefringent phase identified as SmA by optical microscopy and X-ray diffraction.<sup>671</sup> The transition temperatures, and particularly the melting, increased with chain length for both salts, those of the nitrates being slightly higher than those of the tetrafluoroborates, from  $30^\circ\text{C}$  to  $70^\circ\text{C}$ , the clearing temperatures fluctuating between  $120^\circ\text{C}$  and  $140^\circ\text{C}$ . The SmA phase is characterized by a bilayer organization in which the silver cations adopt a U shape (Figure 69). The latter is deduced directly from the diffraction data which indicate that two  $[AgL_2][X]$  units occupy a tetragonal cell and are arranged in such a way that the chain-to-chain distance of about  $4.5 \text{ \AA}$  and the mean separation of  $6.4 \text{ \AA}$ , observed in the X-ray patterns, describe the ordering of the polar

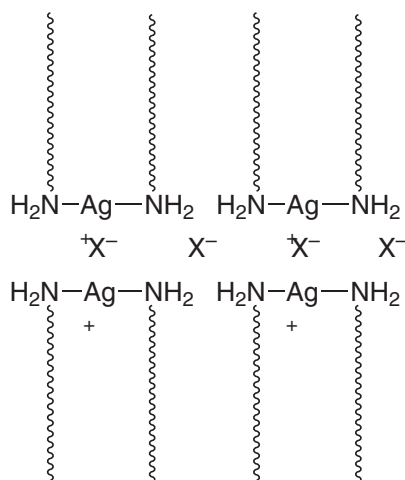


**Figure 69** U-shaped arrangement in the di(amino)silver(I) cations in the mesophases of  $[\text{Ag}(\text{NH}_2\text{C}_n\text{H}_{2n+1})_2][\text{X}]$ .

head groups (Figure 69). These requirements can only be fulfilled if the di(amino)silver(I) cations adopt a U shape. The silver atoms form a short-range, square array of 6.4 Å size, and the aliphatic chains extend on each side of a central slab containing the polar groups in such a way that the two hydrocarbon chains belonging to the same cation point in the same direction. This arrangement is adequate to fill space efficiently and accommodate the anions between these layers, where a good anion–cation electrostatic interaction can be obtained. In addition, the melting transition involves only disorder of the chains, whereas the clearing transition implies breaking of the anion–cation arrangement.

### 7.9.14.2.3 Pyridinium and imidazolium salts

Imidazolium (Figure 70a: mim,  $n = 12, 14, 16, 18$ ) and pyridinium (Figure 70b: py,  $n = 12, 14, 16, 18$ ) salts associated with tetrachlorocobaltate(II) ( $[\text{C}_n\text{-mim}]_2[\text{CoCl}_4]$  and  $[\text{C}_n\text{-py}]_2[\text{CoCl}_4]$ ) or tetrachloronickelate(II) counterions ( $[\text{C}_n\text{-mim}]_2[\text{NiCl}_4]$  and  $[\text{C}_n\text{-py}]_2[\text{NiCl}_4]$ ), exhibit liquid-crystalline behavior (Figure 72) and the thermal stability of the resultant SmA phase is related to the length of the alkyl chain, contrary to the free organic species.<sup>672</sup>

These salts may, therefore, be considered to be intermediate between “classical” molecular liquid crystals composed of a rigid and polarizable elongated core attached to one or two aliphatic chains, and those from the metal salts of carboxylic acids.<sup>464</sup> As already proposed for some other mesomorphic pyridinium derivatives,<sup>673</sup> it is suggested that in the mesophase the anions are positioned between the aromatic rings in an interdigitated structure, necessary to fill the space resulting from the large size of the tetrahedral chlorometallate(II) anions (Figure 71).

*N*-Alkylpyridinium tetrahalopalladate(II) salts of the type  $[\text{C}_n\text{-py}]_2[\text{PdX}_4]$  ( $n = 12, 14, 16, 18$ ;  $\text{X} = \text{Cl}, \text{Br}$ ) have also been deeply investigated. In a first step, the crystal structures of  $[\text{C}12\text{-py}]_2[\text{PdCl}_4]$ ,  $[\text{C}16\text{-py}]_2[\text{PdCl}_4]$ , and  $[\text{C}16\text{-py}]_2[\text{PdBr}_4]$  have been solved.<sup>674</sup> The crystal packing reveals layered structures with alternating polar and apolar sublayers where each  $[\text{PdX}_4]^{2-}$  anion, in a regular square–planar geometry, is sandwiched between two, antiparallel pyridinium cations. All of the halogen atoms of the anion are part of a three-dimensional hydrogen-bonding network, where hydrogen-bonded ring structures are formed within the ionic region. On increasing

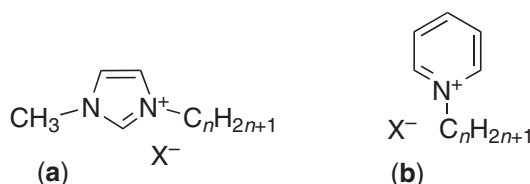


**Figure 70** (a) *N*-Alkyl-*N'*-methylimidazolium and (b) *N*-alkylpyridinium mesogens.

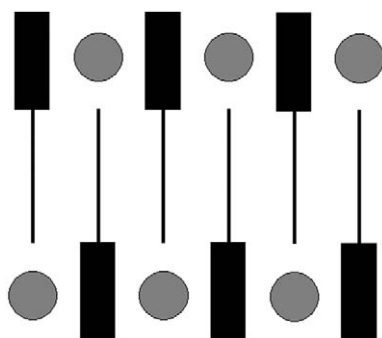


**Figure 71** The interdigitated structures proposed for the SmA of the various salts. Organic moieties are represented by rectangles, alkyl chains by black lines, and counterions by circles.

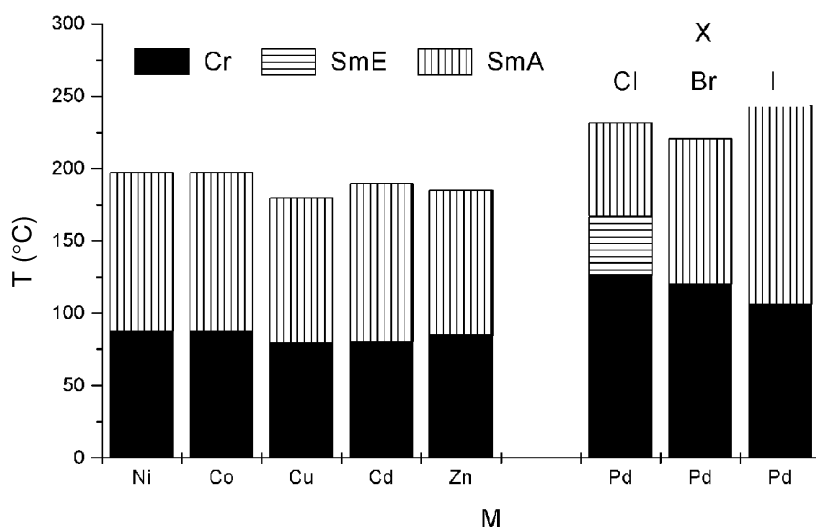


**Figure 72** Thermal behavior of  $[C_n\text{-py}]_2[\text{MCl}_4]$  ( $n = 16$ ) (left), and  $[C_n\text{-py}]_2[\text{PdX}_4]$  ( $n = 16$ ,  $X = \text{Cl}$ ,  $\text{Br}$ ,  $\text{I}$ ) (right).

the temperature, the  $[\text{PdCl}_4]^{2-}$  salts undergo transitions to a crystal smectic E phase and a smectic A phase, whereas the  $[\text{PdBr}_4]^{2-}$  salts undergo only a transition to a smectic A phase, where the ionic interactions are believed to remain similar (Figure 72).

The crystal architecture and mesophase structure of long-chain, *N*-alkylpyridinium tetrachlorometallates,  $[\text{C}_{16}\text{-py}]_2[\text{CdCl}_4]$ , have been determined by X-ray diffraction.<sup>675</sup> The single-crystal structure of the cadmium derivative revealed a layered arrangement with alternation of monolayers of interdigitated cations with layers of isolated  $[\text{CdCl}_4]^{2-}$  anions. Interionic  $\text{C}-\text{H}\cdots\text{Cl}-\text{Cd}$  interactions reinforce the association between anions and cations in the polar region of the supramolecular structure. In addition, an SmA phase is observed at high temperatures and is characterized by the melting of the alkyl chains, but with preservation of the parameters of the lamellar organization (Figure 72).

This work has been extended to the series of *N*-alkylpyridinium iodopalladate(II) salts,  $[C_n\text{-py}]_2[\text{PdI}_4]$  ( $n = 14, 16$ ).<sup>676</sup> The crystallographic structure of the  $n = 14$  homolog at room temperature is characterized by interdigitated bilayers where the aliphatic chains of the cations run almost parallel to the stacking direction and are fully stretched between polar planes built up on isolated  $[\text{PdI}_4]^{2-}$  anions and cation headgroups. Mesomorphic behavior is only observed for the  $n = 16$  compound between 106 °C and 138 °C where a smectic A phase is observed and characterized by a quasi-single layered arrangement with a strong interdigitation of the chains. Along the series  $[\text{C}_{14}\text{-py}]_2[\text{PdX}_4]$ , an enantiotropic mesophase is observed for the chloropalladate over a very narrow temperature range, a monotropic phase is seen for the bromopalladate, and no mesophase at all is found for the iodopalladate salt. Such a trend seems to parallel the decreasing strength of hydrogen-bonding interactions between the  $[\text{PdX}_4]^{2-}$  anions and the pyridinium cations.

More recently, a new series of tetrachlorocuprate(II) salts has been shown to exhibit an interesting mesomorphic behavior depending on the chain length attached to the pyridinium cation ( $n=6, 9-18$ ).<sup>677</sup> Most of these  $[Cn\text{-py}]_2[\text{CuCl}_4]$  salts show a crystalline state at room temperature where the ionic species give rise to layered structures. The organization is that of a monolayer with a strong interdigitation of the alkyl chains. With increasing temperature, all the homologs with  $n > 11$  show at least two different phases. For  $n=12-14$ , an enantiotropic columnar mesophase of hexagonal symmetry is observed, whereas for  $n=15$ , a cubic phase followed by an SmA phase has been found as a function of increasing temperature. For the higher members corresponding to  $n=16-18$ , only a smectic A phase is observed (Figure 73). Thermotropic columnar mesophases of single-tail amphiphiles are, in fact, very rare, and it is too early yet to know how the present mesogenic units self-assemble into a rigid core and how the cores are related to the columnar axis. In addition, it should be kept in mind that *N*-alkylpyridinium cations have a strong ability to promote extensive H bonding in the hydrophilic regions of the lamellar structure of such tetrahalometallates, which thus may play an important role in the thermal behavior of the corresponding salts.

#### 7.9.14.2.4 Thiolates

In the solid state, the silver(I) thiolates,  $\text{AgSC}_n\text{H}_{2n+1}$ , are known to show a crystalline phase characterized by a bilayer structure which consists of a central plane of silver atoms in a quasi-hexagonal arrangement,<sup>678</sup> connected by bridging  $\mu^3\text{-SR}$  groups extending perpendicular to the central slab on both sides.<sup>679</sup> This feature was the starting point for the preparation of the homologous series of long-chain silver thiolate compounds  $\text{AgSC}_n\text{H}_{2n+1}$  ( $n=4, 6, 8, 10, 12, 16, 18$ ).<sup>680</sup> On heating, the homologs with  $4 \leq n \leq 10$  display an SmA phase followed by a cubic phase at higher temperature. For  $n \geq 12$ , only a columnar hexagonal mesophase is observed, being constituted of cyclic structures of the type  $(\text{AgSR})_8$  which pile up on top of one other into columns. This has been interpreted as a change of the  $\mu^3$ -bridged bilayer structure in the solid state or in the lamellar mesophase, to a cyclic  $\mu^2$ -bridged structure in the columnar mesophase (in the same time, silver changes from trigonal-planar to linear coordination). The mesomorphism typically occurred between  $130^\circ\text{C}$  and  $170^\circ\text{C}$  ( $n=12, 16, 18$ ) and  $200^\circ\text{C}$  ( $n=4, 6, 8, 10$ ).

In the analogous series of copper(I) thiolates,  $\text{CuSC}_n\text{H}_{2n+1}$ , ( $n=4, 6, 8, 10, 12, 16, 18$ ), all the compounds melt at ca.  $150^\circ\text{C}$  directly into a columnar mesophase, characterized by disks formed of cyclic tetramers  $[\text{Cu}_4(\mu_2\text{-SC}_n\text{H}_{2n+1})_4]$ .<sup>681</sup> The mesophase was stable up to  $200^\circ\text{C}$ . This is not too surprising since copper(I) thiolate aggregates are known, not only with intramolecularly coordinating ligands and auxiliary donor ligands but also without donor ligands. In the present case, the sulfur atoms of the  $[\text{Cu}_4(\mu_2\text{-SC}_n\text{H}_{2n+1})_4]$  rings are believed to be bounded by their lone electron pairs to a Cu atom of another, adjacent  $[\text{Cu}_4(\mu_2\text{-SC}_n\text{H}_{2n+1})_4]$  ring. Thus, weak  $\text{S}\cdots\text{Cu}$  interactions could be

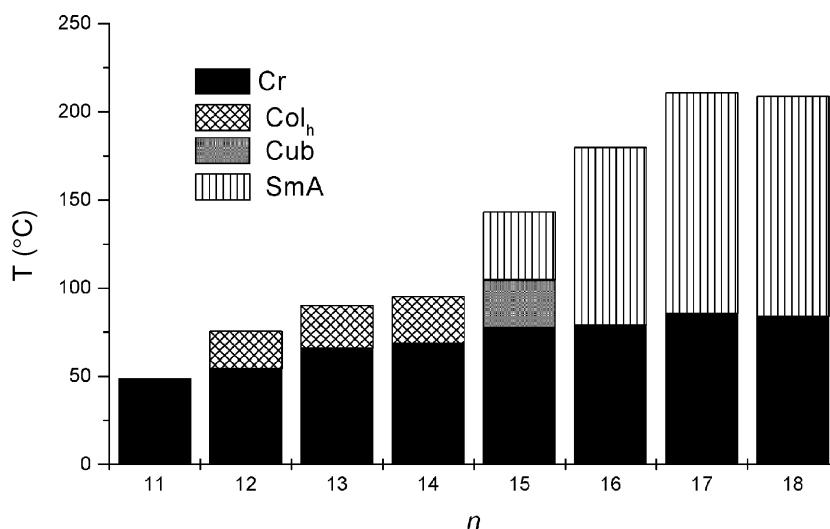


Figure 73 Thermal behavior of  $[Cn\text{-py}]_2[\text{CuCl}_4]$ .



established between the Cu atoms of one tetranuclear aggregate and the S atoms of the neighboring aggregates. Taking into account this additional interaction, the sulfur atoms would be  $\mu_3$ -bridging, connecting two Cu atoms of the central ring between them and also one Cu atom of the ring above or below, and the Cu atoms would be tricoordinate. The existence of these weak, additional interactions is presumably responsible for the excellent stability of the columnar mesophase in copper(I) thiolates.

#### 7.9.14.2.5 Dialkylphosphate salts

Lithium, sodium, potassium, rubidium, and caesium dihexadecylphosphates ( $\text{MO}_2\text{P}(\text{OC}_{16}\text{H}_{33})_2$ ), which are known to produce vesicles in the presence of water, were found to show thermotropic behavior.<sup>682,683</sup>

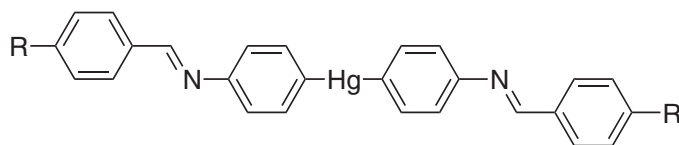
For Li and Na, only a two-dimensional columnar mesophase is observed, the structure of which involves the polar headgroups of the molecules, i.e., the metal phosphonate groups, superposed one over another in columns, surrounded by the alkyl chains in a disordered conformation. For K, Rb, and Cs, two mesophases were observed, namely a  $Ia\bar{3}d$  cubic phase between 100 °C and 130 °C, and a  $\text{Col}_h$  phase above. It is of interest to recall that the alkali metal alkanoates,<sup>471</sup> the molecules of which contain only one alkyl chain per ionic group, exhibit columnar mesophases in which the columnar cores, ribbon-like in shape, are arranged according to a two-dimensional centered rectangular lattice. Very presumably, the presence of two alkyl chains per ionic group in these phosphonate salts allows them to pack according to a more symmetric, hexagonal lattice.

The study of the homologous series of these potassium dialkylphosphates ( $(\text{KO}_2\text{P}(\text{OC}_n\text{H}_{2n+1})_2$ ),  $n = 8, 10, 12, 14, 16, 18$ ) shows that all the terms exhibit an  $Ia\bar{3}d$  cubic phase upon heating followed by a columnar mesophase of hexagonal symmetry.<sup>684</sup> Moreover, the temperature range of the cubic mesophase is found to narrow down as a function of increasing length of the alkyl chains. The X-ray diffraction experiments performed in the cubic and columnar mesophases show that both consist essentially of the same structural elements; that is, of short columns formed by a dense and rigid core of polar potassium phosphonate groups packed with a stacking period of 1.04 Å and surrounded by alkyl chains in a disordered conformation. The restricted length of the columns, of about 12–22 Å for the cubic and no more than 30–40 Å for the columnar phases, was interpreted as being due to steric and thermodynamic effects. In other words, the disordered alkyl chains need more space than is available at the surface of the polar core in order to develop their random conformation, and the interactions of the polar group may be insufficient to stabilize aggregates with a large number of molecules.

### 7.9.14.3 Complexes of Monodentate Ligands

#### 7.9.14.3.1 Complexes of organophenylenes

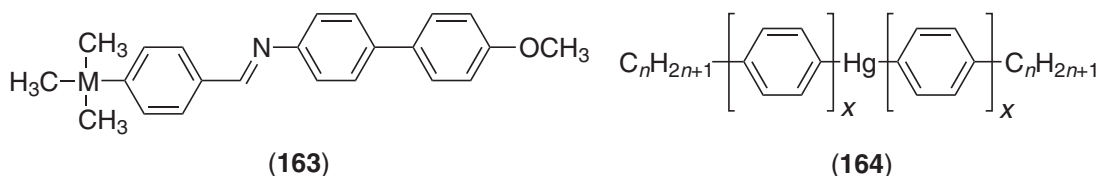
It is commonly accepted that one of the first publications on metallomesogens was one by Vorländer<sup>685</sup> in 1923, who reported a number of mercury-based mesomorphic materials,<sup>686</sup> such as the symmetrical Schiff-base complexes of diarylmercury(II) ((**162**):  $\text{R} = \text{H}, \text{NO}_2, \text{Me}, \text{OMe}, \text{OEt}$ ) and the related, asymmetric, monoaryl mercury chloride complexes. Both series of organometallic compounds exhibited high-temperature smectic phases.



(162)

It was only some fifty years later that the related benzylidene-(4'-methoxybiphenyl)amine bases were used again to form unsymmetrical complexes with a group 14 element such as  $\text{Si}^{\text{IV}}$ ,  $\text{Ge}^{\text{IV}}$ ,  $\text{Sn}^{\text{IV}}$ , and  $\text{Pb}^{\text{IV}}$  (**163**).<sup>687</sup> The bulky trimethyl substituents fixed at the termini of the organic moiety did not preclude mesophase formation in germanium and tin, providing the aspect ratio was large enough. The complexes ((**163**):  $\text{M} = \text{Ge}, \text{Sn}$ ) exhibited two, unidentified smectic phases

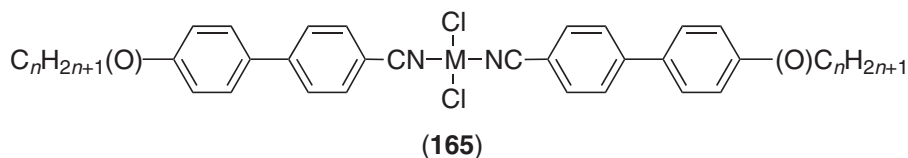
above 160 °C over narrow temperature ranges, at the expense of the broad temperature range nematic phase exhibited by the Schiff bases, substituted simply by alkoxy groups instead.



Organophenylene mercury complexes, such as *bis*(4-hexyloxy-4'-phenyl)mercury(II)<sup>688</sup> and some *bis*(4-alkoxy-4'-biphenyl)mercury(II)<sup>689</sup> ((164):  $x = 1, 2$ ) were also reported to be mesomorphic. The latter exhibited a monotropic SmA phase, as confirmed by an X-ray diffraction study (Cr 119 (SmA 97) I), whereas the strong thermal instability of the former complexes at elevated temperature hampered an accurate characterization of the mesomorphism.

#### 7.9.14.3.2 Complexes of organonitriles

Organonitriles<sup>690</sup> were central to the development of commercial LCDs<sup>691</sup> and viewed from the perspective of a coordination chemist, they are elaborate benzonitriles and, hence, might be expected to behave similarly. Thus, reaction with  $MCl_2$  equivalents ( $M = Pd, Pt$ )<sup>692-694</sup> led to the complexes (165), whose *trans* geometry was established by single-crystal X-ray structures,<sup>695,696</sup> and NMR studies.<sup>697</sup>



Four series of materials resulted:  $[PdCl_2(nCB)_2]$  (165a),  $[PdCl_2(nOCB)_2]$  (165b),  $[PtCl_2(nCB)_2]$  (165c) and  $[PtCl_2(nOCB)_2]$  (165d) (the ligands are abbreviated *nCB* and *nOCB*, depending on the absence or presence, respectively, of an oxygen between the chain and the biphenyl group). In each series, the predominant phase was nematic (in series (165a) this was always monotropic), although at longer chain lengths SmA and SmC phases were found; enantiotropic phases emerged at much shorter chain lengths in the complexes compared to the ligands. The melting points of the palladium complexes were typically in the range 100–120 °C, while for platinum that range was 160–190 °C. Clearing points were also quite different so that while most of the platinum complexes cleared in the range 190–230 °C (series (165d) higher than (165c)), the palladium analogs cleared between 90 °C and 140 °C (165b) and between 70 °C and 100 °C (165a). Observation of an SmC phase in some of these complexes showed that mesomorphism was modified on complexation.

Reaction of a similar organonitrile ligand with  $[Rh(\mu-Cl)(COD)]_2$  led to a *cis*-rhodium complex,  $[RhCl(CO)_2(nOCB)]$ , which was found to be mesomorphic over one degree only (Cr 78 N 79 dec.) above which it decomposed.

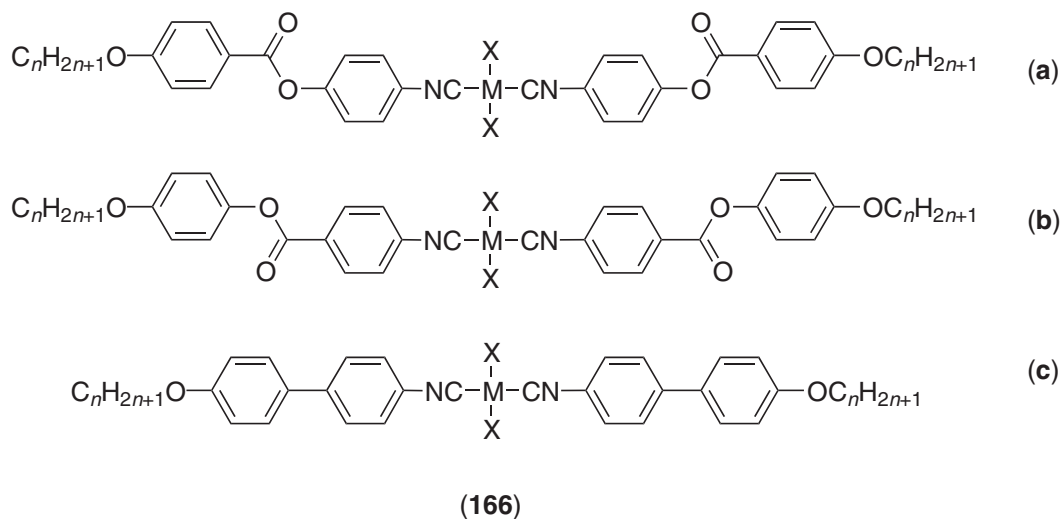
#### 7.9.14.3.3 Complexes of organoisonitriles

In a natural extension of the work with nitrile ligands, Takahashi, and later Espinet, began to examine complexes based on organoisonitriles.

##### (i) Palladium and platinum

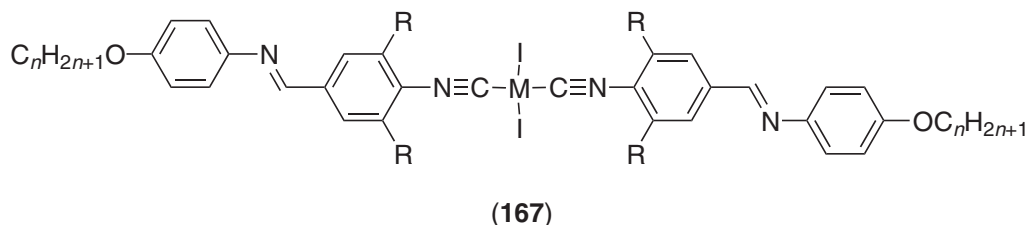
Takahashi studied<sup>698,699</sup> the dihalo- palladium(II) and platinum(II) systems ((166):  $M = Pd, Pt$ ;  $X = Cl, Br, I$ ), some of which (166c) are directly analogous to the nitrile complexes above (165). All the free alkoxy isonitrile ligands were mesomorphic (N and SmA phases below 85 °C). For  $M = Pd$ , both the bromo and iodo complexes were *trans* and gave mesomorphic complexes, while

for  $M = \text{Pt}$ , only the iodo complexes behaved in this way; the other *cis*-complexes were not mesomorphic. In general, the complexes melted at temperatures between  $120^\circ\text{C}$  and  $200^\circ\text{C}$  giving either N or SmC phases, depending on the particular ligand; clearing points were between  $200^\circ\text{C}$  and  $300^\circ\text{C}$ . Also, whereas in this case the melting and clearing points were *very* similar for the same combination of metal, halogen, and ligand, it is interesting to compare this with the corresponding *nitrile* complexes above where significant differences were found between the behavior of the palladium and platinum systems. This is attributed to the difference in the strength of the interaction between the ligands and the metal, with the weaker Pd–nitrile interactions leading to deviations from predicted behavior.



Chiral derivatives were reported by Omenat *et al.*<sup>700</sup> based on *trans*- $\text{PdI}_2$  complexes of some of the esters (**166b**), the chirality being introduced via the terminal chain ( $-\text{OC}^*\text{HMe}(\text{C}_6\text{H}_{13})$ ,  $-\text{O}(\text{CH}_2)_3\text{C}^*\text{HMeC}_2\text{H}_5$ ,  $\text{OC}^*\text{HMeCO}_2\text{C}_4\text{H}_9$ ). Chiral SmC\* and N\* phases were observed, at slightly reduced temperatures than the non-chiral homologs. Modest values for the spontaneous polarization of between about  $60 \text{ ncm}^{-2}$  and  $90 \text{ ncm}^{-2}$  were found. Chiral chlorogold(I) species were also made and SmC\* phases were observed there, too, although the spontaneous polarization could not be evaluated due to the inherent conductivity of the complexes.

Wang *et al.*<sup>701</sup> described some Pd and Pt iodide complexes of laterally substituted isonitrile ligands ((**167**):  $M = \text{Pd}, \text{Pt}$ ;  $R = \text{Me}, \text{CHMe}_2$ ) and while the ligands themselves were non-mesomorphic, the complexes ( $R = \text{Me}$ ) gave nematic phases at shorter chain length and SmC phases as the chains extended, with little difference on the transition temperatures between the palladium and platinum complexes. Typically, the complexes melted at temperatures between  $150^\circ\text{C}$  and  $260^\circ\text{C}$  and clearing points were between  $270^\circ\text{C}$  and  $300^\circ\text{C}$ . With the bulkier isopropyl side group ( $R = \text{CHMe}_2$ ), the mesomorphism was suppressed totally and the clearing temperatures depressed considerably.



### (ii) Gold and silver

Gold and silver isonitriles complexes were investigated recently ((**168**):  $M = \text{Au}, \text{Ag}$ ;  $X = \text{NO}_3, \text{PF}_6, \text{BF}_4$ ;  $n = 4, 8, 12$ ).<sup>702</sup> Overall, the phenyl and biphenyl gold derivatives showed an SmA phase, whereas the analogous silver complexes displayed an additional SmC phase (Figure 74). Electrostatic interactions thus seem to favor and stabilize lamellar arrangements, since phenyl isocyanides

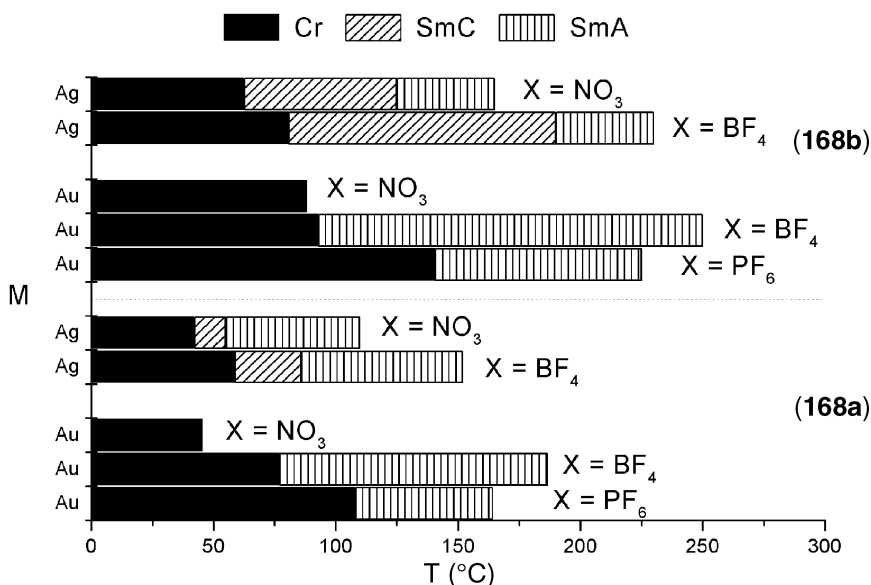
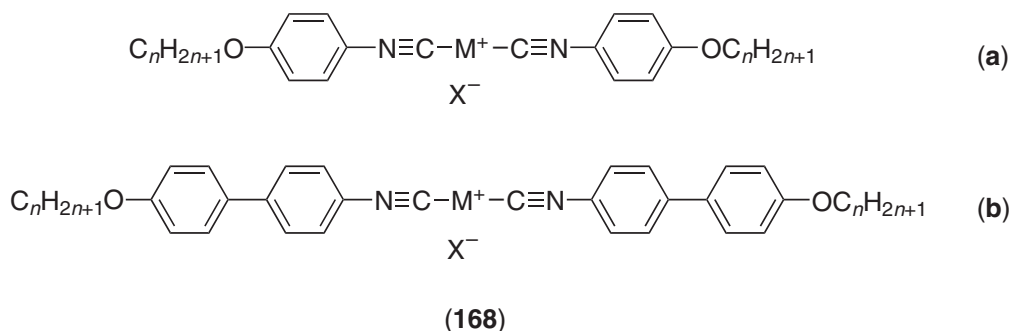


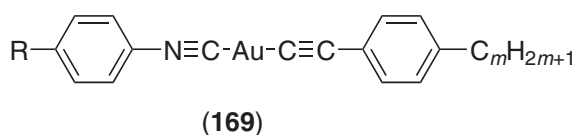
Figure 74 Influence of the metal and counter-anion on the mesophase stability of (168a) and (168b) ( $n=8$ ).

yield mesomorphic materials upon complexation to silver or gold. Elongation of the aromatic parts enhanced the mesophase stability, and that of the crystalline phase to a small degree. Irrespective of the isocyanide, the general trend of melting temperatures for the gold complexes is  $[\text{PF}_6]^- > [\text{BF}_4]^-$  and is opposite for the clearing temperatures. Note that the behavior of (168b) is markedly different to that of (166c) for which a nematic phase was observed, but no SmA phase.

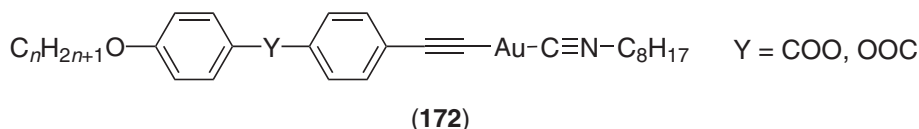
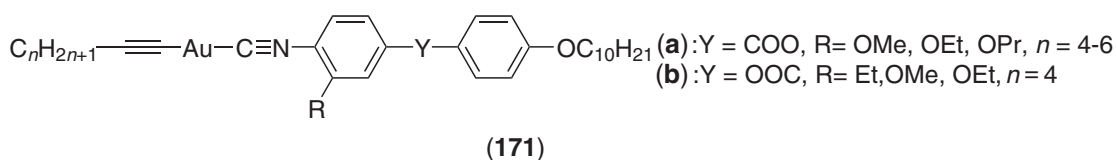
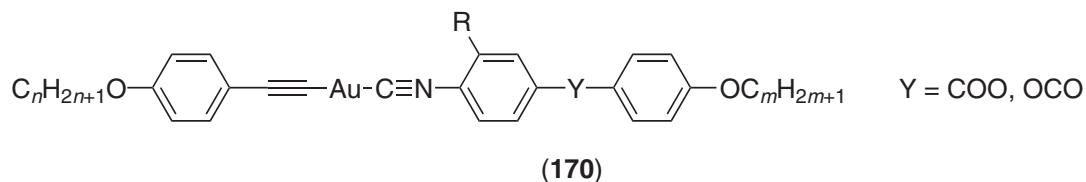


(iii) Mixed isonitrile-acetylide complexes

Espinet reported the gold complexes (169) ((169):  $\text{R} = \text{H}, \text{OC}_n\text{H}_{2n+1}$ ,  $n = 2, 4, 6, 8, 10$ ;  $m = 6, 8, 10, 12$ ) in which both an isonitrile and a substituted phenylacetylene were bound across the gold(I) center.<sup>703</sup> Despite the non-mesomorphic nature of both ligands, the complexes consistently gave rise to SmA phases, usually between 100 °C and 200 °C depending on both chain lengths ( $n$  and  $m$ ), although decomposition was a problem at high temperature; only the phenylisonitrile derivatives ( $\text{R} = \text{H}$ ) with chain length  $n \leq 10$  carbons on the acetylide side were not mesomorphic. Interestingly, the melting points were found to systematically decrease as the length of the acetylide ligands increase ( $m$ ), at the expense of the chain length of the isonitrile ( $n$ ).



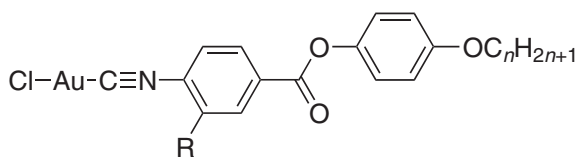
Takahashi<sup>704</sup> carried out an interesting systematic study of related liquid-crystalline isonitrile gold(I) acetylide complexes in order to lower transition temperatures and to avoid the decomposition processes usually associated with such compounds. When both the ligands contained at least one aromatic ring such as (170) ((170): Y = OCO, R = H), the complex was mesomorphic, showing mainly an SmA phase at 165 °C, with extensive decomposition. Introduction of a small lateral group ((170): Y = COO, R = OEt) resulted in the lowering of the melting of the crystal to the SmA (Cr 142 SmA dec.), but still with some decomposition. Larger side chains ((170): Y = COO, R = OC<sub>6</sub>H<sub>13</sub>) surprisingly suppressed the SmA phase, but a nematic was induced instead (Cr 87.5 N 130 I); this time, no decomposition was detected. Complexes resulting from either an aromatic isonitrile and an aliphatic acetylene, (171), or an aliphatic isonitrile and an aromatic acetylene, (172), were also prepared. Compounds (171) appeared thermally unstable compared to complexes (170), and showed SmA and N phases at low temperatures (below 130 °C). The type of phase and the mesophase stability were found to depend on the length of both the terminal and side chains. Thus, (171a) showed an enantiotropic SmA phase, which changed to a nematic phase for larger side groups; when both chains were elongated, the mesomorphism became metastable. (171b) showed a nematic phase, which was enantiotropic with a methoxy side group (Cr 78 N 108 I). Compounds (172) with linear chains showed enantiotropic nematic phases between 110 and 160 °C. Important reductions in clearing points (<100 °C), and to some extent in melting points (~80 °C to 100 °C) were obtained when the octylisonitrile chain was branched; in these cases, the nematic phase stability was also reduced. The complexes were thermally more stable than (171), and decomposition was observed less systematically.



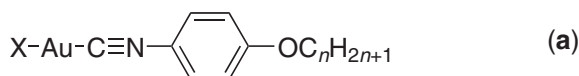
(iv) Halogold(I) isocyanide complexes

Takahashi reported the first halogold(I) isonitrile systems ((173): R = H, OC<sub>m</sub>H<sub>2m+1</sub>). Depending on the chain length, the ligands with R = H showed nematic and SmA mesophases between ca. 70 °C and 85 °C, while the complex showed SmA and SmC phases and at elevated temperatures (170–270 °C).<sup>705</sup> In order to perturb the strong intermolecular interactions and to depress the transition temperatures, systems with lateral chains were then prepared ((173): R = OC<sub>m</sub>H<sub>2m+1</sub>). The complexes showed nematic and SmA phases at reduced temperatures depending on *n* and *m* (90–190 °C) despite the non-mesomorphic nature of the ligands. However, increasing the size of the lateral substituent destabilized the mesophase.

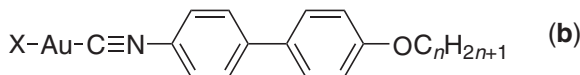
Alkoxyphenyl ((174a): X = Cl, Br, I, *n* = 2, 4, 6, 8, 10, 12)<sup>706</sup> and alkoxybiphenyl ((174b): X = Cl, Br, I, *n* = 4, 6, 8, 10, 12)<sup>707</sup> isonitrile ligands were also complexed to halogold(I) moieties to form thermally stable complexes. All the complexes (174a) again formed SmA phases between 120 °C and 170 °C for X = Cl, and 100 °C and 150 °C for X = Br, with the exception of the iodo derivatives where the SmA phase was found to be monotropic only for *n* = 12. Thus, the widest mesomorphic temperature range followed the trend Cl > Br > I (Figure 2). Biphenylisonitrile derivatives (174b)



(173)



(a)



(b)

(174)

were also mesomorphic and this time the iodo complexes also showed an SmA phase and transition temperatures were, in general, much higher in these materials (mesomorphic range between 120 °C and 300 °C, Figure 75). A nematic phase was also observed for the short-chain-length chloro- and bromogold(I) ( $n=4$ ). The trend in melting points of these materials ( $\text{Cl} < \text{Br} < \text{I}$ ), which is the opposite to what was observed for (174a), was interpreted according to polarizability arguments.<sup>708</sup> Lateral monofluorination of complexes (174a), in the *ortho* (3-F) or *meta* (2-F) position relative to the alkoxy chain, has also been investigated.<sup>709</sup> The 3-fluoro derivatives were mesomorphic, showing an SmA phase, although at much higher temperatures than in the non-fluorinated systems; the clearing temperatures of the former coincided with the melting temperatures of the latter. The 2-fluoro derivatives were very weakly mesomorphic in comparison, but a narrow nematic range was seen for the hexyloxy homolog and an SmA for the other members. The transition temperatures were found to decrease in the order 3-F > 2-F and in the order  $\text{Cl} > \text{Br} > \text{I}$ , the latter in accordance with the decrease in polarity of the Au—X bond, as above for complexes (174a). Complexes with pseudohalides were synthesized ((174a), (174b): X = CN, SCN,  $n=4, 6, 8, 10, 12$ ) with a number of simple ligands,<sup>710</sup> some monofluorinated, and in each case it was observed that lower transition temperatures resulted when thiocyanate was incorporated, rather than cyanide (Figure 75).

Note that chlorocopper(I) derivatives with the same biphenyl isonitrile ligand as (174b) were later reported,<sup>711</sup> which showed SmA and SmC phases (at longer chain length) between 100 °C and

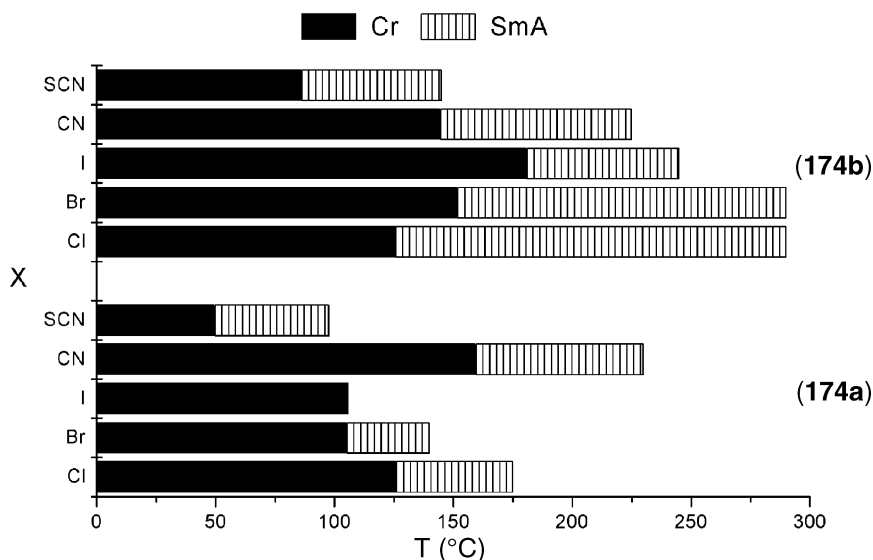
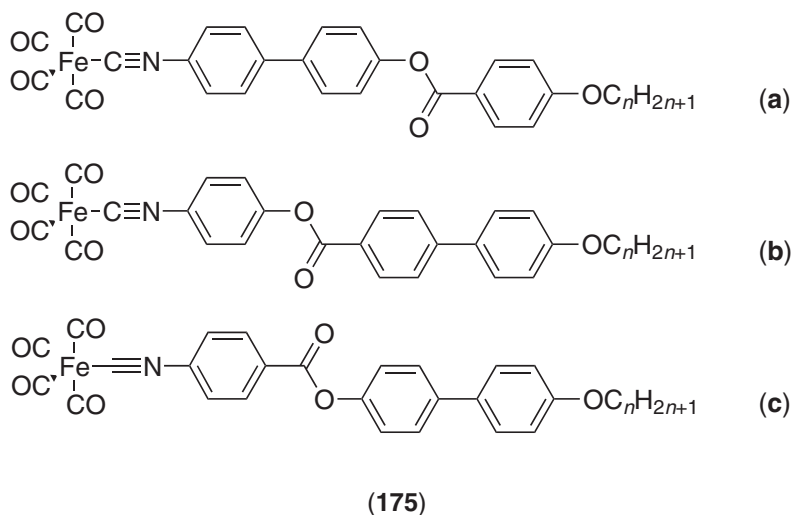


**Figure 75** Influence of the halogen or pseudo halogen X on the mesophases stability of the complexes (174a) and (174b) ( $n=8$ ).

200 °C, without apparent decomposition. Complexation to “CuCl” of isonitrile ligands based on phenyl benzoates considerably enhanced the mesophase stability, with mesophase temperatures well in excess of 200 °C and without decomposition.

A series of materials was synthesized in which isonitriles were also complexed to iron(0) and ((175):  $n = 6, 8, 10, 12$ ).<sup>712</sup> The free ligands from which complexes (175a) and (175b) were obtained showed a nematic phase at short chain length and the SmA phase as the chain grew longer, always decomposing on passing to the isotropic liquid. Free isonitriles used to form (175c) simply decomposed in the solid state before melting. However, all of the complexes melted at ca. 70–90 °C to show an SmC phase, although once more, decomposition was observed on clearing at 120 °C. The mesophase range was found to increase in the order (175c) < (175a) < (175b).



(v) Mixed phenylene–isonitrile gold complexes

The thermally stable, liquid crystalline mono- and dinuclear perhalophenylgold(I) isocyanide complexes (176, 177) have been thoroughly investigated by Espinet and co-workers.<sup>713</sup> Gold complexes (176a–c) (Figure 76) all showed a nematic phase at short chain lengths, a N and SmA phases for intermediate chain length and an SmA phase only for longer chain length. As observed

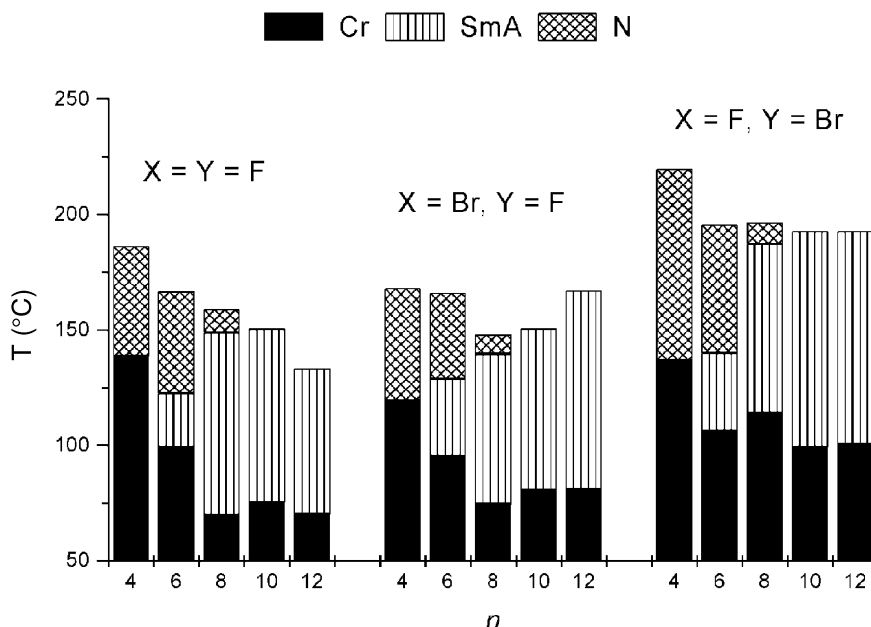
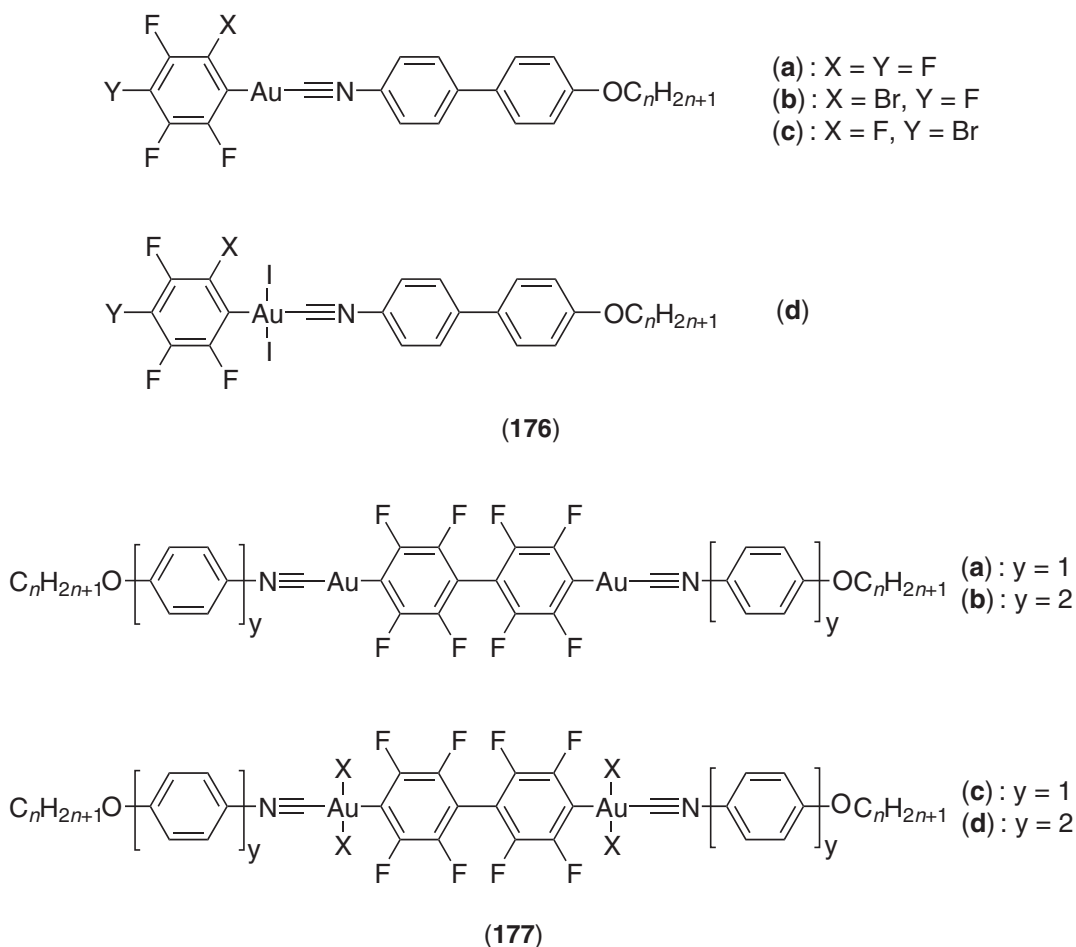


Figure 76 Mesomorphism of complexes (176a) to (176c).

by the authors, the variation in the thermal properties is regular, i.e., both the melting clearing transition temperatures decreased with increasing chain length to  $n \geq 8$  where they are roughly constant. Moreover, the decrease in the transition temperatures with increasing  $n$  is small for (176c), greater for (176b), and very strong for (176a). As a consequence, a change is produced in the sequence of melting and clearing temperature in the order (176c) > (176a) > (176b) for  $n \leq 6$  and (176c) > (176b) > (176a) for  $n \geq 8$  (Figure 76); these variations were explained in terms of polarization and polarizability arguments. The transition temperatures have been lowered, the mesomorphic range diminished, and the nematic phase enhanced when compared to the mesomorphic properties of the halogold complexes (174). The mononuclear gold(III) compounds (176d) were thermally unstable and not investigated further. The use of a chiral chain affected the mesomorphism quite drastically in compounds (176) ( $X = F$ ,  $Y = OC_mH_{2m+1}$ ).<sup>714</sup> With one chiral chain in the *para* position of the phenylene group, N\* and TGBA mesophases were induced (The TGBA, or twist-grain boundary A phase (a TGBC phase also exists), is found in highly chiral materials and is a variant on the SmA phase; blue phases are similarly found in highly chiral systems and are cubic in organization; both are discussed by Goodby<sup>18</sup>, Ch. V, Vol. I. In liquid crystals, the term "highly chiral" would apply to compounds with a very high ability to induce a helical twist in a liquid crystal solvent, or one which had a very short pitch as a pure material), whereas when both terminal chains were chiral, the three blue phases BPI, BPII, and BPIII were observed on cooling between the isotropic liquid and the N\* phase.



The dinuclear complexes (177a) and (177b) all displayed a single nematic phase at high temperatures (Figure 77). This is attributed to the symmetric nature of these digold complexes which means that the lateral, dipolar interactions (which normally stabilize smectic phases) cancel, favoring the nematic phase. As in the case of (176d), the dinuclear gold(III) species (177c) and (177d) ((177c):  $X = Br, I$ , (177d):  $X = Br, I$ ) decomposed upon thermal treatment to give the corresponding halogold(I) isocyanide complexes.



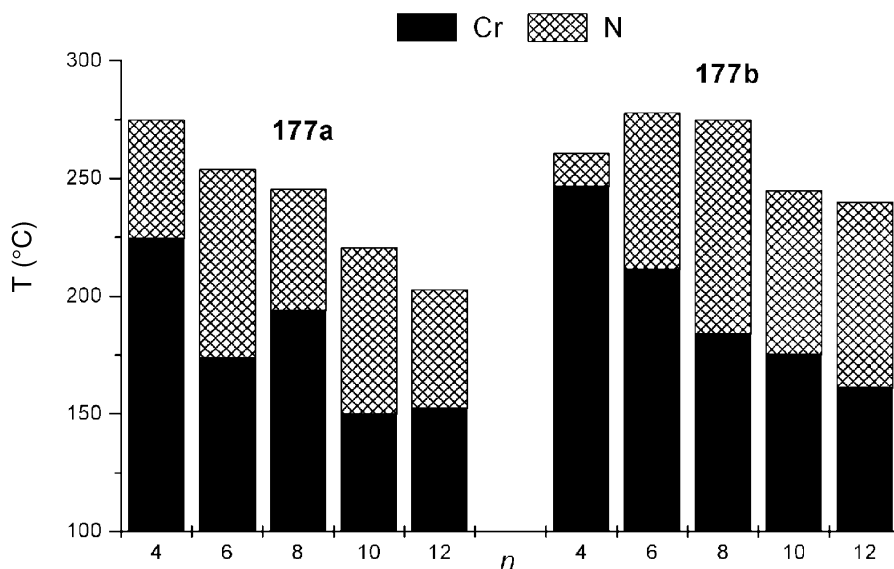
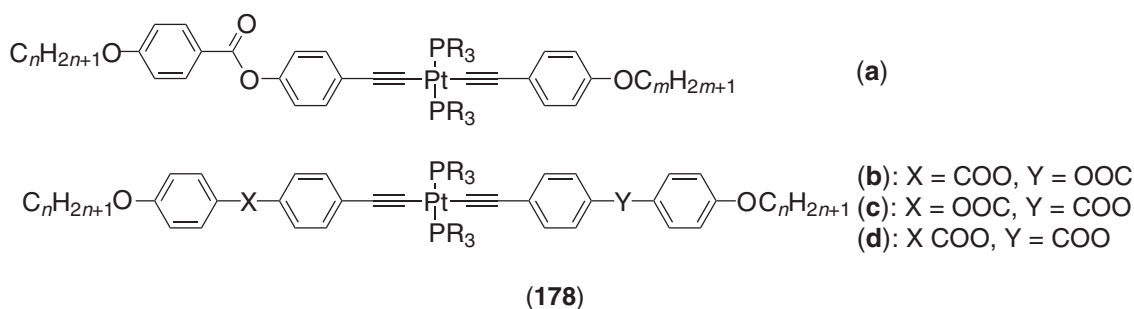


**Figure 77** Thermal behavior of dinuclear complexes (**177a**) and (**177b**). Temperature dependency with chain length.

#### 7.9.14.3.4 Acetylide complexes

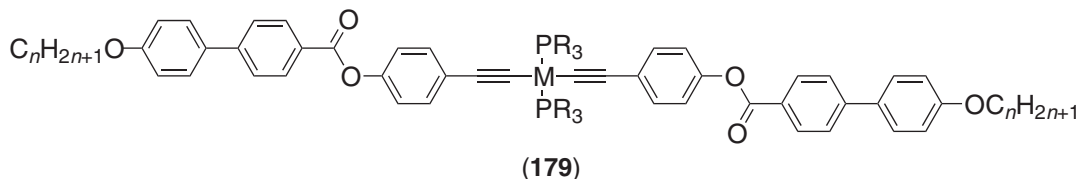
The platinum(II) complexes (**178**) were found to be mesomorphic, providing that the rigid core contains at least three aromatic rings.<sup>715,716</sup> The non-symmetrical compounds (**178a**) (R = Me) exhibited a nematic phase, in addition to an SmA phase for the complexes with  $m+n \geq 22$ . Melting points are typically around 170 °C (for  $m+n \geq 12$ ), and the clearing temperatures in the range 180–220 °C. This shows that the relative bulk of the two trimethylphosphine groups in the center of the complex does not have an adverse effect on the overall structural anisotropy of the complex, and indeed the high melting and clearing points suggest that the system may, in fact, tolerate slightly larger groups. This was shown to be the case when related, mesomorphic complexes bearing *triethyl*phosphine ligands were synthesized ((**178a**) to (**178d**): R = Et).<sup>717</sup> Now, all the compounds exhibited solely a nematic phase, monotropic for (**178a**) (R = Et), and enantiotropic for (**178b**) to (**178d**) (R = Et). Increasing the molecular structural anisotropy thus stabilized the nematic phase, and the enlargement of the side group contributed to a substantial depression of the transition temperatures (Table 64).



However, a later study with more anisotropic elongated acetylenes<sup>718</sup> ((**179**): M = Pt, Pd, R = Me, Et, Pr) indicated that larger phosphines were not well tolerated, mesomorphism being lost on the introduction of tripropylphosphine (Table 65).<sup>719</sup> Increasing the size of the phosphine substituents reduced considerably the melting transition temperatures. Mesomorphism was absent in the analogous palladium complexes, decomposing rapidly above 100 °C due to their lower thermal stability than their platinum congeners.

**Table 64** Transition temperatures of some derivatives of (178).

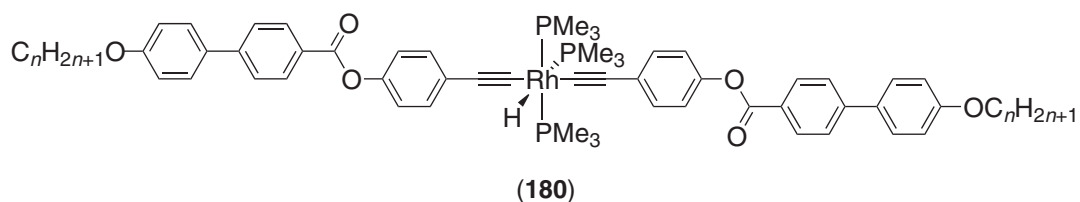
Complexes	$n$ ( $m$ )	$R$	Transition temperatures
(178a)	8 (8)	Me	Cr 173.5 N 205.5 I
(178a)	8 (8)	Et	Cr 93 (N 62) I
(178b)	8	Me	Cr ~ 200 N > dec.
(178b)	8	Et	Cr 134 N 156 I
(178c)	8	Et	Cr 124 N 142 I
(178d)	8	Et	Cr 114 N 156 I

**Table 65** Transition temperatures of some derivatives of (179) and (180).

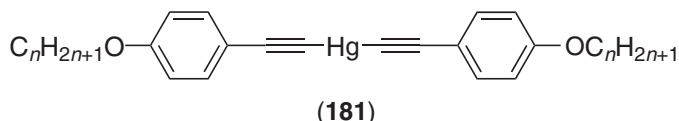
Complexes	$n$	$R$	Transition temperatures
(179)	8	Me	Cr 265 N 320 dec.
	10	Me	Cr 258 N 320 dec.
	8	Et	Cr 179 N 292 I
	10	Et	Cr 165 N 266 I
	8	Pr	Cr 111 I
	10	Pr	Cr 105 I
(180)	8		Cr 136 S 174 N 203 dec.
	10		Cr 142 S 172 N 202 dec.

S: unidentified smectic mesophase.

In contrast, some mesomorphic, octahedral rhodium(III) complexes having bulkier central metallic fragment<sup>720</sup> (180), were found to exhibit smectic (unidentified) and nematic phases up to the decomposition points, at ca. 200 °C (Table 65).



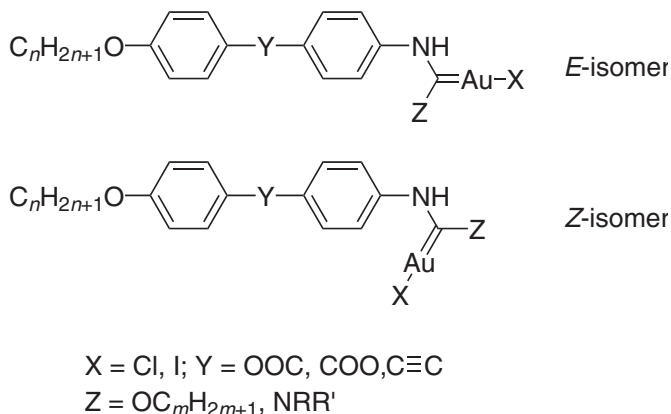
It is also worth noting the very simple mercury(II) acetylides reported by Yang and Wen (181).<sup>721</sup> These complexes showed N and/or SmA phases between 70 °C to 90 °C up to ca. 120 °C.



#### 7.9.14.3.5 Carbene complexes

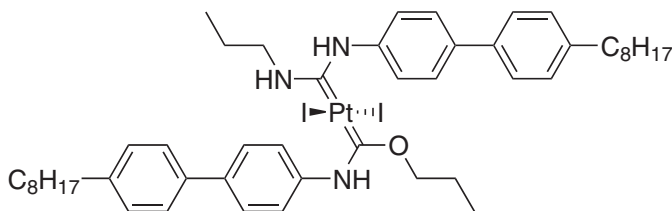
Takahashi and co-workers exploited the reactivity of bound isonitriles with aliphatic alcohol (ethanol, propanol, butanol, pentanol) and amines by synthesizing various gold(I) carbene complexes, (182).<sup>722,723</sup> The complexes existed as one of two geometric isomers which were separated in

some cases, and which interconverted in solution. Somewhat in common with the gold systems above bearing lateral alkoxy chains, these new carbenes also showed reduced transition temperatures (110–160 °C) with little difference between the two isomers. The mesomorphism was again dominated by the SmA phase, over a range of only around 15 °C. Within the series of carbene complexes having amino side groups, only those with a primary amine were mesomorphic ( $R = H$ ,  $R' = Pr$ ,  $Bu$ ), showing an SmA phase before decomposition. Note also the interesting case of a dinuclear gold–carbene complex, where the two carbene species are linked via a hexyldiamine bridge, which was mesomorphic but which decomposed below its clearing temperature (Cr 211 S dec.).



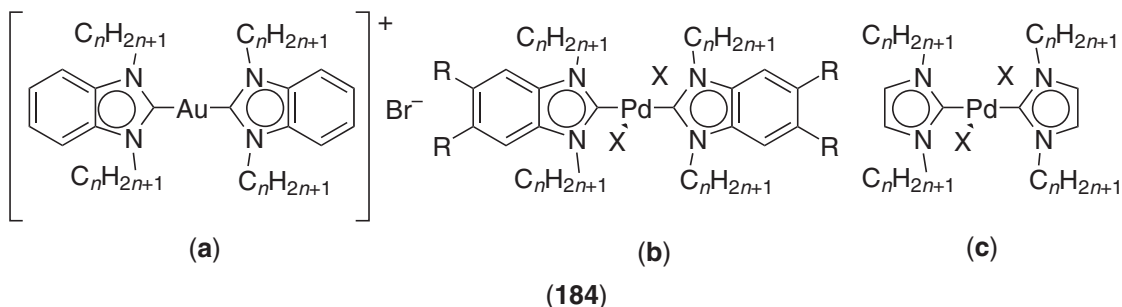
(182)

Using the same strategy, an unsymmetrically substituted bis(carbene)platinum(II) complex (**183**) was obtained by consecutive nucleophilic attack of propanol and then propylamine onto a *trans*-diiodo(bis-isocyanide)platinum(II) complex.<sup>724</sup> The stable complex gave rise to a nematic phase (Cr 142 N 173 I).



(183)

Smectic mesophases have been claimed for other gold(I) (**184a**)<sup>725</sup> and palladium(II) (**184b,c**)<sup>726</sup> carbene complexes based on 1,3-dialkylbenzimidazol-2-ylidene and 1,3-dialkylimidazol-2-ylidene. However, examination of the X-ray diffraction data in combination with the large clearing enthalpies suggest that these materials are highly ordered and may be better described as crystals.



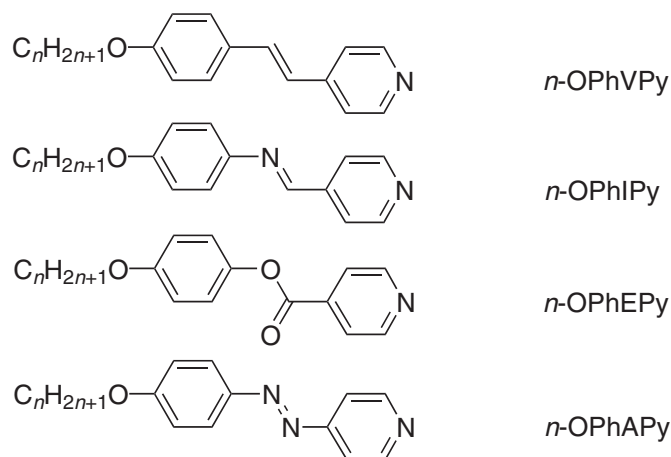


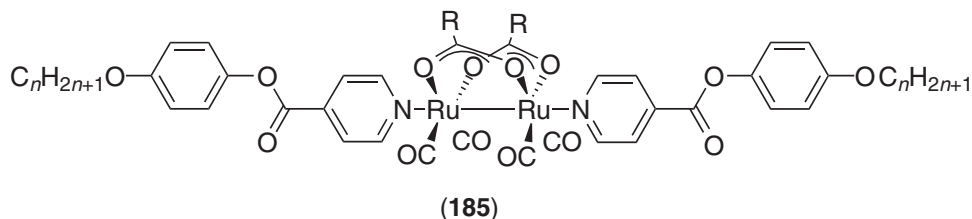
Figure 78 The most common substituted pyridines.

#### 7.9.14.3.6 Complexes of substituted pyridines

Pyridines are known to form a variety of stable metal complexes and so elaborated pyridines are neutral targets for ligands in metallomesogens. Various substituted pyridines have been used in this context and the greatest amount of work has been carried out with the *trans*-4-alkoxy-4'-stilbazoles (Figure 78, *n*-OPhVPy).<sup>727</sup> The materials chemistry of these stilbazoles has been reviewed recently.<sup>599,728</sup>

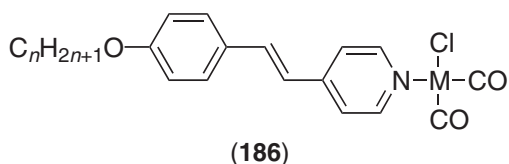
##### (i) Ruthenium complexes

Dimeric, ruthenium “saw-horse” complexes (**185**) were reported by Deschenaux *et al.*<sup>729</sup> A range of  $[Ru_2(CO)_4(\mu^2, \eta^2-O_2CR)_2L_2]$  complexes were synthesized with differing R groups ((**185**): R = H<sup>-</sup>, CF<sub>3</sub><sup>-</sup>, C<sub>6</sub>H<sub>5</sub><sup>-</sup>, 4-MeO-C<sub>6</sub>H<sub>4</sub><sup>-</sup>, 4-Me-C<sub>6</sub>H<sub>4</sub><sup>-</sup>) and different values of  $n$  ( $n = 6, 10, 12, 14, 16$ ). Despite the bulky central unit, induction of mesomorphism was achieved by introducing anisotropic pyridine-based ligands in the axial positions; all complexes were nematic, typically in the range 150–200 °C. The stability of the mesophase was found to be dependent upon the type of carboxylato bridges (decreasing order of stability: C<sub>6</sub>H<sub>5</sub> > C<sub>6</sub>H<sub>4</sub>-CH<sub>3</sub> > H, C<sub>6</sub>H<sub>4</sub>-OCH<sub>3</sub>). This class of metallomesogens represents a rare example of mesomorphic compounds containing covalent bonds between two metal atoms, and are of considerable interest due their structure and electronic properties, and also to their potential catalytic reactivity.<sup>730</sup>



##### (ii) Rhodium and iridium complexes

Reaction of the stilbazoles with  $[M_2(\mu-Cl)_2(COD)_2]$  (M = Rh, Ir; COD = 1,5-cyclooctadiene)<sup>731</sup> under CO led to a series of complexes ((**186**): M = Rh, Ir).



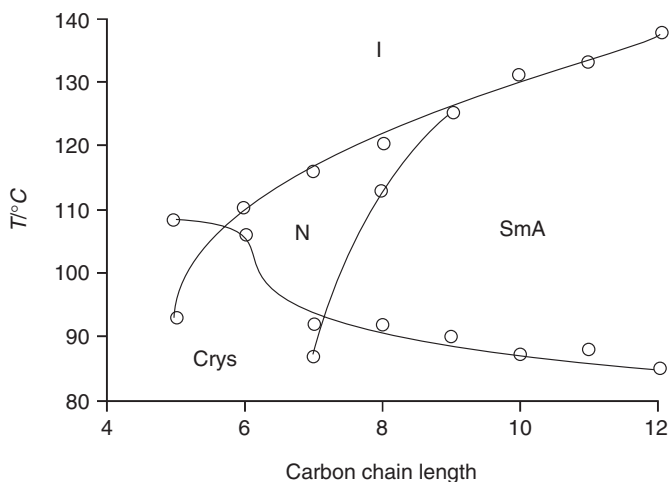


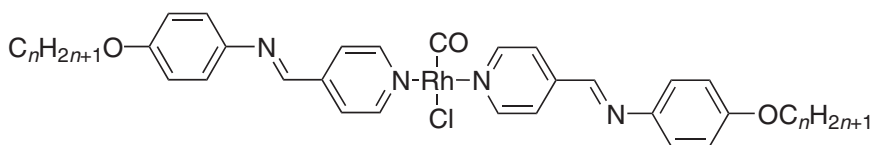
**Figure 79** Phase diagram for the complexes **(186)** ( $M = Ir$ ).

The rhodium(I) complexes were yellow/orange in the solid state, characteristic of mononuclear  $Rh^I$ , while the iridium(I) complexes were burgundy in the solid state and yellow in isotropic solution or in the melt. Infrared spectra suggested that the iridium complexes were associated in some way in the solid state, possibly in a stacking arrangement as found in  $[IrCl(CO)_2(py)]$ .<sup>732</sup> The phase diagram for the iridium complexes is shown in **Figure 79**.

The behavior is typical of relatively simple dipolar materials where a nematic phase was found at short chain lengths, giving way to an SmA phase in higher homologs. While the iridium complexes could be cycled in and out of the isotropic phase with few problems of decomposition, the rhodium complexes began to decompose rapidly on melting in air. Lateral fluorination of *cis*-iridium stilbazole complexes destabilized strongly the mesophase: the 2-fluorinated 4-alkoxystilbazole systems exhibited only monotropic N and SmA phase, whereas the structural isomeric 3-fluorinated compounds were not mesomorphic.<sup>733</sup>

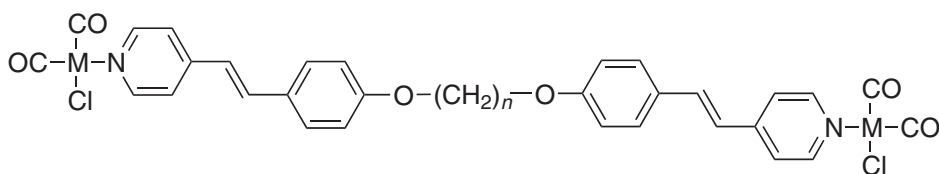
These complexes also formed stable Langmuir films, which could be transferred onto a range of various substrates to yield LB films.<sup>734,735</sup> A pyroelectric effect has been observed in alternate layers incorporating an iridium complex. Electronic hyperpolarizability of some chiral derivatives was also measured.<sup>736</sup>

Complexes related to these with *n*-OPhIPy ligands had previously been synthesized by Esteruelas *et al.*<sup>737,738</sup> The mesomorphism of these complexes was less extensive than in the related complexes with stilbazole ligands, and enantiotropic mesophases (N and SmA) were only established at the octyloxy homolog for both metals. Reaction of the rhodium derivatives with  $Me_3NO$  and an equivalent of ligand led to the *trans*-disubstituted derivatives, *trans*- $[MCl(CO)(n\text{-OPhIPy})_2]$  (**187**), which curiously were non-mesomorphic, decomposing above 300 °C.



**(187)**

Dimeric stilbazole complexes of  $Ir^I$  (**188**) were reported<sup>739</sup> and a very strong odd–even effect was noticed such that mesophases were observed when  $n = \text{odd}$ , but not when  $n = \text{even}$ .



**(188)**

It is worth mentioning tetrameric complexes synthesized by Lahoz *et al.* based on a pyridine imine derivative<sup>740</sup> and characterized by single-crystal X-ray methods. Unfortunately, none of these materials, despite their analogy to the Ru “saw-horse” compounds seen above (**185**), were mesomorphic.

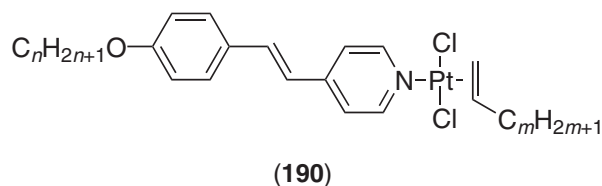
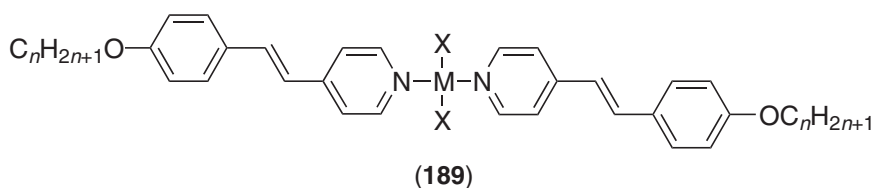
### (iii) Gold complexes

A related, non-centrosymmetric gold(I) complex ( $[\text{AuCl}(8\text{-OPhVPy})_2]$ ) was also synthesized, and was found to show a mesophase between 120 °C and 200 °C, the temperature at which it decomposed.<sup>692</sup>

### (iv) Palladium and platinum complexes

Complexation of 4-alkoxystilbazole to palladium(II) and platinum(II) led to simple, square-planar, *trans*- $[\text{MCl}_2\text{L}_2]$  complexes ((**189**): M = Pd, Pt, X = Cl), but few of them were mesomorphic so that only the longest-chain derivatives ((**189**):  $n > 9$ ) showed an SmC phase at elevated temperatures ( $>200$  °C) and only for M = Pt. However, replacement of the halides by aliphatic carboxylic acids to give the complexes (**189**) ((**189**): M = Pd, X =  $\text{O}_2\text{CC}_m\text{H}_{2m+1}$ ) and considerably improved the mesomorphic properties.<sup>741</sup> As might have been expected by comparison with studies of laterally substituted organic compounds, melting (between 140 °C and 150 °C) and clearing temperatures (between 160 °C and 170 °C) were dramatically reduced and nematic phases were preferred over smectic phases.

Derivatives were also obtained (**190**) where one of the stilbazoles was replaced with an alkene.<sup>741,742</sup> These materials now showed much reduced melting and clearing points and SmA phases were seen for most derivatives synthesized between 50 °C and 100 °C. It was also noted that, in general, the materials were non-mesomorphic when  $n + m \geq 8$ , showed monotropic mesomorphism when  $8 \leq n + m \leq 13$ , and gave enantiotropic mesophases for  $n + m \geq 14$ . The simultaneous increase of both  $m$  and  $n$  resulted in the decrease of the stability of the crystal phase (reflected by the low melting point) and in the increase of the clearing temperature, enhancing the temperature range of the SmA phase. Some of the complexes with  $m = 0$  were also mesomorphic ( $n \geq 8$ ), showing SmA phases, although at higher temperatures. Mixtures of some of these complexes were also carried out, and resulted in the enhancement of the SmA phase stability, essentially due to the depression of the melting points.



Finally here, the report of chiral platinum(II) complexes derived from asymmetric alkyl-methyl sulfoxides in place of the alkene chains (**190**) is noted. However, there exists some doubt over the claims made therein on account of the optical textures and large clearing enthalpies reported.<sup>743</sup>

Espinet *et al.*<sup>744</sup> reported a rather nice series of 2,6-dipicolinate derivatives whose structure is reminiscent of pincer-type complexes (Figure 80).<sup>745</sup> The first thing to note is that except in conjunction with the 3,4,5-tridecyloxyphenyl-based ligand (**191f**) where columnar phases were found in the approximate range of 75–110 °C, none of the complexes of dipicolinate ((**191**): X = O)

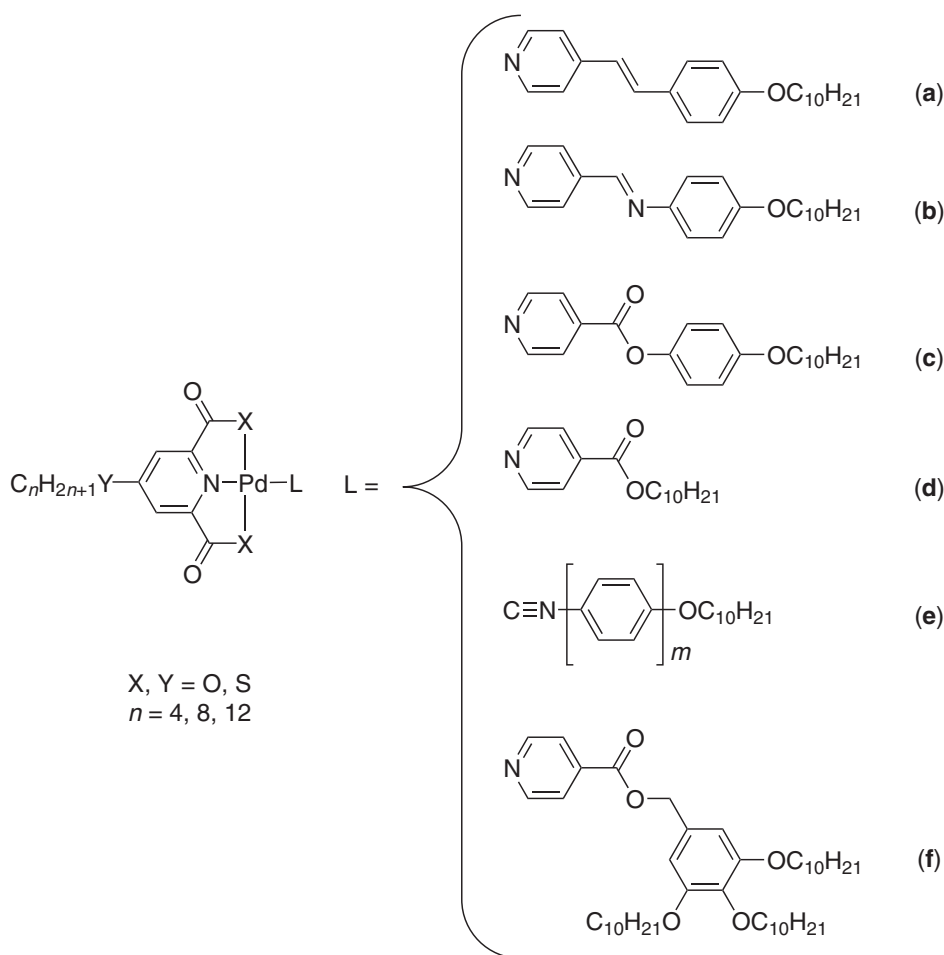
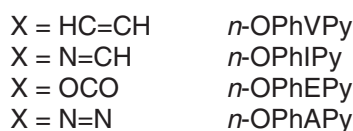
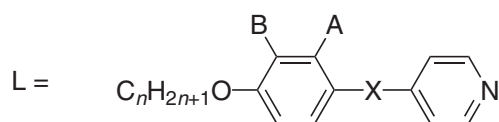


**Figure 80** Chemical structures of the pincer-type complexes (**191**).

was found to be mesomorphic. However, in the case of complexes derived from 2,6-bis(thiocarboxylato)pyridine ((**191**):  $X = S$ ), a different pattern emerged. Thus, complexed to ligands **c**, **d**, **e** ( $m = 1$ ) and (surprisingly perhaps) **f**, no liquid crystal properties were observed, while for ligands **a**, **b**, and **e** ( $m = 2$ ) the complexes exhibited mesomorphism showing predominantly SmC phases and, occasionally, a nematic phase. For complexes of ligands **a** and **b**, the mesophases were generally found above  $200^\circ\text{C}$  while melting points in the approximate range  $140\text{--}200^\circ\text{C}$  were found with ligand **e** ( $m = 2$ ). Moreover, when the pincer was substituted by thioalkyl chains ((**191**):  $Y = S$ ), instead of alkoxy chains ((**191**):  $Y = O$ ), the mesomorphic range was substantially enlarged, essentially due to an important reduction of the melting temperature.

#### (v) Silver complexes

Reaction of substituted pyridines with silver salts led to linear silver(I) complexes (**192**) according to **Figure 81**. The work of Bruce and co-workers in this area has been reviewed recently.<sup>609</sup> The mesomorphism of complexes of *n*-OPhIPy and *n*-OPhEPy with  $Y = \text{CF}_3\text{SO}_3$ ,  $\text{BF}_4$ ,  $\text{NO}_3$ , and  $\text{PF}_6$  has been systematically investigated.<sup>746</sup> All the silver salts exhibited a rich smectic mesomorphism, including unidentified smectic phases (**Table 66**), with an additional N phase at short chain length observed with the (pyridylmethylene)aniline  $\text{AgBF}_4$  complexes. Decomposition was observed for most of these complexes in the vicinity of the isotropic liquid. Novel azopyridine containing silver mesogens have recently been reported.<sup>747</sup> The AgDOS salts of *n*-OPhAPy exhibited nematic at short chain length ( $n = 4, 8$ ) and an SmA phase at longer chain length ( $n \geq 10$ ) between  $100^\circ\text{C}$  and  $120^\circ\text{C}$  on average (**Table 66**). Moreover, both chiral nematic and SmA phases were induced when a cholesteryl benzoate derivative was grafted at the extremity of the alkyl chain of the azopyridyl ligand.



A, B = H or F

Y = BF<sub>4</sub>, NO<sub>3</sub>, CF<sub>3</sub>SO<sub>3</sub> (OTf), C<sub>*m*</sub>H<sub>2*m*+1</sub>OSO<sub>3</sub> (*m* = 12, DOS; *m* = 8, OS)

**Figure 81** Schematic of the various mesomorphic silver(I) complexes (**192**) synthesized.

Complexes of alkoxy stilbazoles with AgBF<sub>4</sub> led to hygroscopic, light-sensitive materials forming SmC and SmA phases at long chain lengths and at very high temperatures where the materials decomposed (Table 66).<sup>748,749</sup> Similarly, high-melting and high-clearing materials were obtained for X = NO<sub>3</sub> and CF<sub>3</sub>SO<sub>3</sub> (OTf) with the same ligands (Table 66);<sup>750</sup> the phase diagram of the triflate salts of the alkoxy stilbazoles is shown in Figure 82. These were the first known ionic materials to show a nematic mesophase.<sup>751</sup>

The transition temperatures of these complexes were, however, significantly reduced when the small anions used above were replaced by alkylsulfates (dodecylsulfate—DOS;<sup>749</sup> octylsulfate—OS<sup>752</sup>);

**Table 66** Transition temperatures of some silver derivatives [AgL<sub>2</sub>][Y].

<i>L</i>	<i>Y</i>	Mesomorphism
8-OPhIPy	BF <sub>4</sub>	Cr 114.5 SmC 168 SmA 202 I
	CF <sub>3</sub> SO <sub>3</sub>	Cr 154 SmA 173 I
	NO <sub>3</sub>	Cr 84 SmC 154 SmA 186 dec.
	PF <sub>6</sub>	Cr 192 SmA 242 I
10-OPhIPy	BF <sub>4</sub>	Cr 103 SmC 188 SmA 206 I
	CF <sub>3</sub> SO <sub>3</sub>	Cr 142 SmA 183 I
10-OPhEPy	BF <sub>4</sub>	Cr 64 S1 162 SmC 203 SmA 217 I
	CF <sub>3</sub> SO <sub>3</sub>	Cr 111 S2 124 S3 142.5 SmA 181 I
8-OPhAPy	DOS	Cr 107 N 124 I
10-OPhAPy	DOS	Cr 108 S 127 I
8-OPhVPy	BF <sub>4</sub>	Cr 170 SmC 270 SmA 300 I
	CF <sub>3</sub> SO <sub>3</sub>	Cr 158 G 165 SmC 181 SmA 250 I
	NO <sub>3</sub>	Cr 152 SmC 221 SmA 250 I
	OS	Cr 135 SmC 144 SmA 181 I
10-OPhVPy	DOS	Cr 135 SmC 139 (S <sub>4</sub> 137) Cub 153 SmA 178 I
	CF <sub>3</sub> SO <sub>3</sub>	Cr 127 G 158 SmC 210 SmA 250 I
	NO <sub>3</sub>	Cr 141 SmC 220 SmA 243 I
	OS	Cr 120 SmC 142 SmA 183 I
8-3F-OPhVPy	DOS	Cr 108 [S <sub>4</sub> 113] SmC 123 [S <sub>4</sub> 136] Cub 153 SmA 168 I
	CF <sub>3</sub> SO <sub>3</sub>	Cr 130 (SmC 126) SmA 257 I
10-3F-OPhVPy	DOS	Cr 101 SmC 121 SmA 188 I
	CF <sub>3</sub> SO <sub>3</sub>	Cr 119 SmC 156 SmA 246 I
8-2F-OPhVPy	DOS	Cr 98 SmC 118 SmA 185 I
	CF <sub>3</sub> SO <sub>3</sub>	Cr 119 SmC 149 SmA 198 I
11-2F-OPhVPy	DOS	Cr 105 SmC 127 Cub 134 SmA 138 I
	CF <sub>3</sub> SO <sub>3</sub>	Cr 98 SmC 189 SmA 210 I
	DOS	Cr 84 SmC 130 Cub 140 SmA 145 I

S, S1, S2, S3: unidentified smectic mesophases.



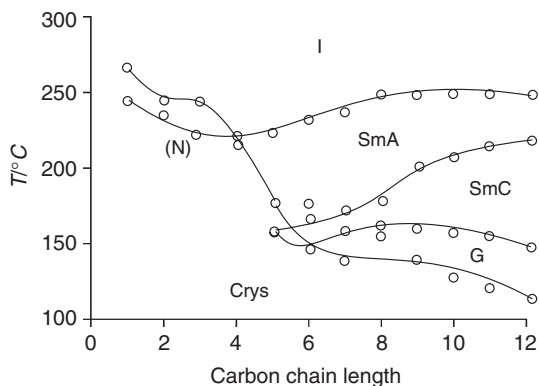


**Figure 82** Phase diagram for the complexes  $[\text{Ag}(n\text{-OPhVPy})_2][\text{OTf}]$ .

clearing points were now around  $180^\circ\text{C}$  and the materials were stable at these temperatures for periods long enough to allow their phase characterization by optical and X-ray methods (Figure 84, Table 66). Introduction of this anion chain is analogous to the addition of a covalent, lateral chain in organic mesogens<sup>753</sup> and this accounts for the observation of nematic phases as such chains prevent the association of the molecules into smectic layers. The disposition of the chain parallel to the molecule was indicated in the solid-state structure (Figure 83).<sup>752</sup>

However, more remarkable was the observation of SmA, SmC, and, in particular, cubic phases (Figure 84). In arguing that the lateral chains suppress smectic phases, it is then necessary to invoke intermolecular, electrostatic interactions between neighboring silver ions and alkylsulfate oxygens to stabilize the smectic phases.<sup>754</sup> The identification of the cubic phase in these materials

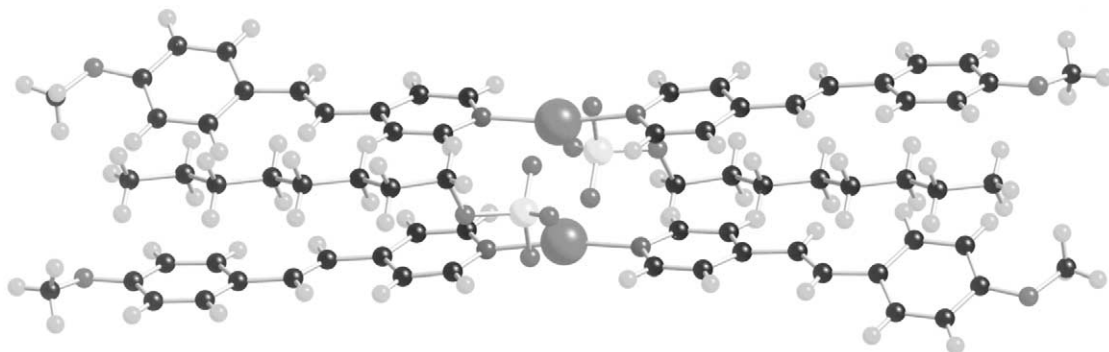


**Figure 83** Structure of one of the crystallographically independent dimers of  $[\text{Ag}(1\text{-OPhVPy})_2][\text{C}_8\text{H}_{17}\text{OSO}_3]$ .

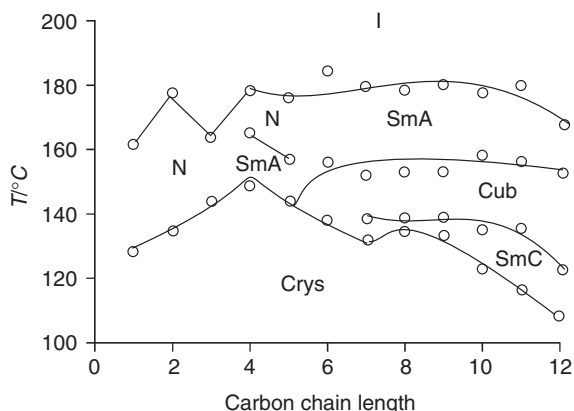


**Figure 84** Phase diagram for the complexes  $[\text{Ag}(n\text{-OPhVPy})_2][\text{DOS}]$ .

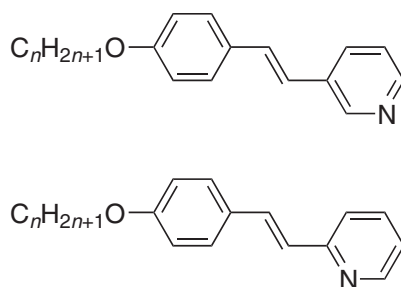
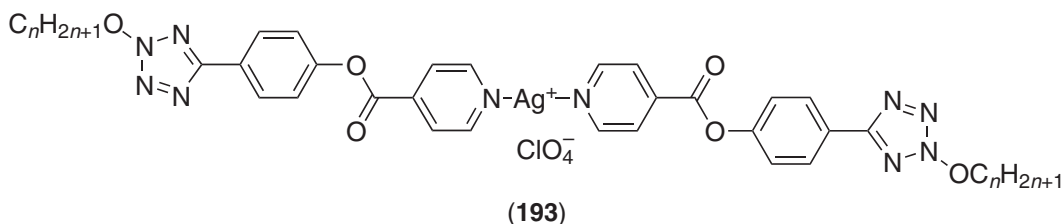


**Figure 85** 3- and 2-Stilbazoles.

was remarkable as at that time there were few examples known. Cubic phases are viscous, optically isotropic phases which normally occur, at least in calamitic materials, between the SmA and SmC phases. Small changes in the complex were able to destabilize the cubic phase, so that replacement of the DOS anion by octylsulfate (OS)<sup>752</sup> or a change to 4-alkoxy-3-fluoro-stilbazole suppressed its formation (promoting smectic phases instead), while it was retained in complexes using 4-alkoxy-2-fluorostilbazoles, in addition to the nematic phase.<sup>755</sup> The symmetry of the phase was identified as  $Ia\bar{3}d$  by X-ray methods<sup>754</sup> and freeze-fracture electron microscopy.<sup>756</sup> Note the presence of a rather unusual, metastable mesophase, known as the  $S_4$  mesophase, observed in the vicinity of the cubic phase, which has a three-dimensional tetragonal space group,  $I4_1/acd$ .<sup>757,758</sup>

More recently, 4-alkoxy-2- and 4-alkoxy-3-stilbazoles<sup>759</sup> have been reported (Figure 85) and their silver complexes with AgDOS and AgOTf have been synthesized.<sup>760</sup> While the ligands themselves are non-mesomorphic, the complexes show only SmA phases, although complexes of the 2-stilbazoles do not form readily. While the new complexes are liquid crystalline, the use of the isomeric stilbazoles suppresses the polymorphism of the 4-stilbazole isomers.

Two homologs of silver complexes of tetrazole-functionalized pyridines (**193**) were reported by Gallardo *et al.*<sup>761</sup> as perchlorate salts and a crystal structure was determined; from past experience, at least one author of this review regards them as brave to wish to heat a dry perchlorate salt at all. However, they found that the complexes where  $n=9$  and 14 both showed an SmA phase at temperatures above 150 °C.

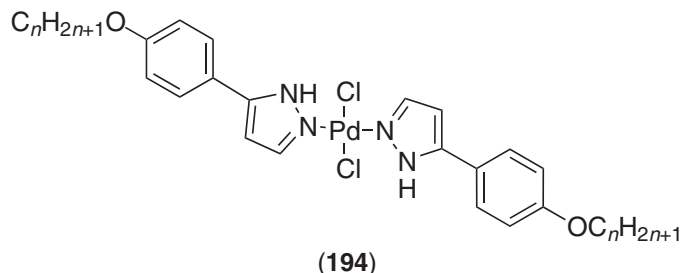


Several other metal complexes bearing stilbazoles or elongated pyridine-based ligands were also prepared as potentially new, octahedral metallomesogens. Thus, monosubstituted pentacarbonyl and *cis*-disubstituted tetracarbonyl tungsten<sup>762</sup> or *cis*-disubstituted dimethyldihaloplatinum<sup>763</sup> complexes were successfully synthesized and characterized. For short chain length, mesomorphism was not detected. However, at longer chain length ( $n \geq 8$ ), mesomorphism was observed, but owing to either extensive decomposition or their tendency to disproportionate, the mesophases could not be unequivocally identified. Finally, SmA mesomorphism has been claimed in metal-chain complexes based on dihalocopper(II) derivatized by monosubstituted pyridyl based ligands.<sup>764</sup>

#### 7.9.14.3.7 Pyrazole complexes

There have been only a few reports on metallomesogens based on 3-substituted pyrazole ligands. Non-centrosymmetric *cis*-dicarbonylchloro-rhodium(I) and -iridium(I) complexes were found to be poorly mesogenic (monotropic nematic phase), the existence of the mesophase being strongly influenced by the type of linking function between the pyrazole unit and the mesogenic group.<sup>765</sup>

Moreover, the mesomorphism of some di-3,5-alkoxyphenylpyrazoles was completely suppressed upon complexation to the same rhodium fragment.<sup>766</sup> Increasing the overall molecular length by complexing such ligands with PdCl<sub>2</sub> to yield (**194**) resulted in the improvement of the mesophase stability, and an enantiotropic SmC phase was observed for chain length greater than  $n = 10$ .<sup>767</sup> The temperature range of the SmC first increased with  $n$  (3 °C for  $n = 12$  to 12 °C for  $n = 16$ ), then decreased (7 °C for  $n = 18$ ).



#### 7.9.14.4 Physical Properties of Complexes of Monodentate Ligands

One of the properties likely to be affected by the inclusion of a metal center is the mean polarizability,  $\bar{\alpha}$ , due to the presence of a center of highly polarizable electron density, and Table 67 shows the results of some measurements reported on some of the complexes described above.<sup>768</sup> In each case, the increase is large and is probably best exemplified by the iridium complexes where the addition of the group *cis*-[IrCl(CO)<sub>2</sub>] virtually doubles the linear polarizability.

Polarizability is related to birefringence, and measurements were carried out in the nematic phases of [IrCl(CO)<sub>2</sub>(8-OPhVPy)], [PdCl<sub>2</sub>(*n*-OCB)<sub>2</sub>], and [Ag(*n*-OPhVPy)<sub>2</sub>][DOS]; the data are summarized in Table 68.

**Table 67** Polarizability data for some mesomorphic metal complexes.

Compound	$\alpha/10^{-40} \text{ J}^{-1} \text{ C}^2 \text{ m}^2$	$\Delta\alpha/10^{-40} \text{ J}^{-1} \text{ C}^2 \text{ m}^2$
<i>Trans</i> -[PdCl <sub>2</sub> (5CB) <sub>2</sub> ]	82 ± 8	45 ± 9
<i>Trans</i> -[PtCl <sub>2</sub> (5CB) <sub>2</sub> ]	90 ± 10	
5CB	37.5	19.4
<i>cis</i> -[IrCl(CO) <sub>2</sub> (7-OPhVPy)]	62 ± 6	59 ± 12
[Ag(8-OphVPy) <sub>2</sub> ][OTf]	92 ± 9	
[Ag(10-OphVPy) <sub>2</sub> ][DOS]	114 ± 14	
<i>n</i> -OphVPy	35 ± 4	28 ± 6

**Table 68** Birefringence data for some mesomorphic metal complexes.

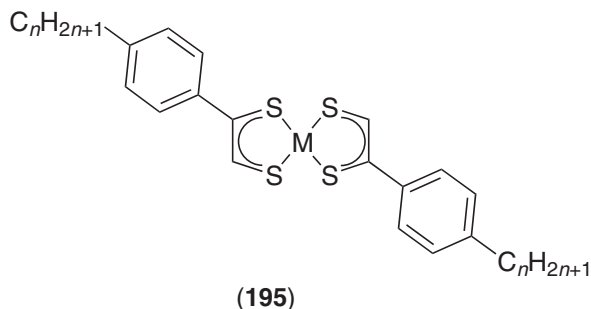
Compound	$\Delta n^a$
5OCB	0.1308
6OCB	0.1433
[PdCl <sub>2</sub> (5OCB) <sub>2</sub> ]	0.1608
[PdCl <sub>2</sub> (6OCB) <sub>2</sub> ]	0.1636
[PdCl <sub>2</sub> ( <i>x</i> OCB) <sub>2</sub> ] <sup>b</sup>	0.1730
[IrCl(CO) <sub>2</sub> (8-OPhVPy)]	0.1659
[Ag(1-OphVPy) <sub>2</sub> ][DOS]	0.1814
[Ag(2-OphVPy) <sub>2</sub> ][DOS]	0.1968

<sup>a</sup> Measured directly at a reduced temperature of 0.985 (i.e.,  $T/T_{NI} = 0.985$ ). <sup>b</sup> A preparation using equimolar amounts of 2OCB, 4OCB, and 6OCB; the mixture contains all eight possible complexes.

### 7.9.14.5 Mesomorphic Coordination Complexes of Bidentate Ligands

#### 7.9.14.5.1 Dithiolene complexes

The first complexes of this type were those of Giroud-Godquin and Mueller-Westerhoff ((**195**):  $M = \text{Ni, Pt, Pd}$ ) and their synthesis marked the beginning of interest in mesomorphic, metal-containing materials.<sup>769-772</sup>



In designing the complexes, it had been proposed that the two, fused five-membered rings would act in total like a phenyl ring, making the complexes analogous to 4,4''-dialkylterphenyls. This, however, turned out to be something of an oversimplification, given the profound effect of the metal on mesomorphism of these complexes (Table 69). Curiously, while the nickel and platinum derivatives were mesomorphic, those of palladium were not and no satisfactory explanation exists for this observation. A crystalline structure of one nickel complex ( $n = 8$ ) showed that the molecules adopt a zigzag conformation and arranged into layers, in agreement with the SmC mesomorphism observed on heating.<sup>773</sup>

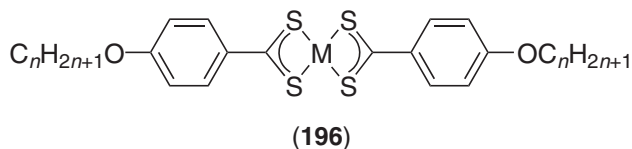
Introduction of branched terminal chains, providing that they are long enough, resulted in the reduction, as expected, of the temperature of the transition crystal-to-mesophase, as well as the thermal stability.<sup>774</sup> The nickel complex with the racemic 2-methyloctyl chains showed two mesophases, Cr 98 SmC 103 N 118 I, whereas that with the chiral *S*-5-methylheptyl chains presented an SmC\* between 119°C and 159°C.

#### 7.9.14.5.2 Dithiobenzoate complexes

Most of the work with calamitic dithiocarboxylates has centered on studies on metal complexes of 4-alkoxydithiobenzoic acids. Complexes of the empirical formula  $[M(n\text{-odtb})_2]$  were synthesized for  $M = \text{Ni, Pd, and Zn}$  (**196**) and square-planar gold(III) complexes showing SmA phases ( $[\text{AuX}_2(n\text{-odtb})]$ ;  $X = \text{Cl, Br, Me}$ ) were also described.<sup>775</sup>

**Table 69** Mesomorphism of some dithiolene complexes (**195**).

$M$	$n$	Transition temperatures
Ni	4	Cr 117 N 175 I
Ni	8	Cr 121 SmC 191 I
Ni	10	Cr 103 SmC 189 I
Pt	4	Cr 158 N 202 I
Pt	8	Cr 150 SmC 209 I
Pt	10	Cr 140 SmC 202 I
Pd	4	Cr 205 I
Pd	10	Cr 207 I



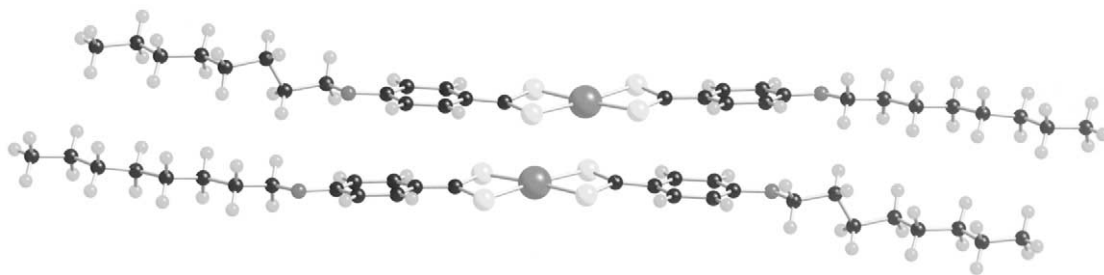


Figure 86 Molecular structure of  $[\text{Pd}(8\text{-odtb})_2]$ .

(i) Nickel and palladium dithiobenzoates

The palladium complex,  $[\text{Pd}(8\text{-odtb})_2]$ , was shown<sup>775</sup> by X-ray crystallography to have the expected square-planar structure about the metal with local  $D_{2h}$  symmetry (Figure 86), and the molecules associated in pairs with intermolecular Pd–S contacts of 3.38 Å.

These complexes showed a nematic phase at short chain length which was replaced by a smectic C phase at longer chain lengths; a crystal smectic phase existed below the SmC phase. The transition temperatures of the materials were high with melting typically occurring in the range 210–230 °C, with clearing (accompanied by extensive decomposition) at around 320 °C. As  $^1\text{H}$  NMR spectroscopy showed them to be diamagnetic, it was assumed that the nickel congeners were also square planar. Their mesomorphism was rather similar to that of the palladium complexes, except that melting and “clearing” points (see below) were reduced by some 30 °C and 80 °C, respectively. These materials also possessed the same ordered smectic phase found in the palladium complexes and this was proposed by Ohta (on the basis of X-ray evidence) to be a crystal smectic H phase.<sup>776</sup>

The palladium complexes were further studied using EXAFS.<sup>777</sup> In the solid state at room temperature, the data were readily fitted to the known crystal structure, which arrangement persisted through several crystalline modifications until the ordered smectic phase was entered. In this phase, the Pd–S distance increased to 3.8 Å where interaction must be precluded. Further heating into the SmC phase showed only four short Pd–S distances, confirming that the all significant intermolecular interactions had now disappeared.

The major difference in the nickel series was that at temperatures around 230 °C, the blue bis(dithiobenzoates) rearranged to form the red, mixed-ligand (alkoxydithiobenzoato)(alkoxytrithiobenzoato)nickel(II) species (Figure 87A) which were also mesomorphic. These complexes were identified by Ohta<sup>776</sup> by extracting and purifying a heated mixture, although it was found possible to synthesize them directly<sup>775</sup> using literature routes.<sup>778,779</sup>

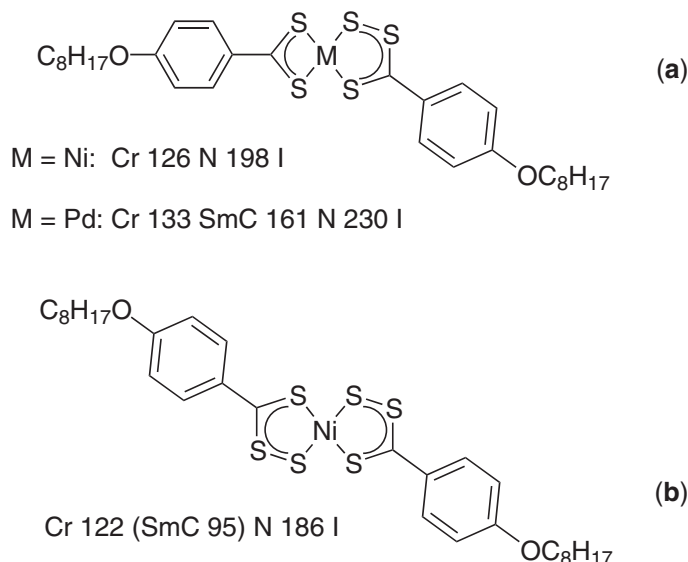


Figure 87 Mesomorphic trithiobenzoate complexes of  $\text{Ni}^{\text{II}}$  and  $\text{Pd}^{\text{II}}$ .

As might be expected from their reduced anisotropy, melting and clearing points were much lower than those of the symmetric bis(dithiobenzoato) compounds. While the symmetric bis(trithiobenzoato) complexes (Figure 87B) were not observed as a product of the thermal degradation, they could be synthesized independently, albeit in low yield, by reaction of the appropriate bis(alkoxytrithiobenzoato)zinc(II) complex with  $\text{NiCl}_2 \cdot 6\text{H}_2\text{O}$ .<sup>775</sup> The melting and clearing points of these materials were also lower than those of the bis(dithiobenzoato) complex and were in fact very similar to those found in the skeletally isostructural dithiolenes (**195**) described by Giroud.

Replacement of the alkoxy chains by chiral chains such as 1-ethylpentoxy or 2-ethylhexyloxy resulted in the significant decrease of the mesophase stability of the complexes with respect to those with linear chains.<sup>780</sup>

### (ii) Zinc dithiobenzoates

Reaction of a sodium alkoxydithiobenzoate with zinc acetate in dilute acetic acid led to complexes of the empirical formula  $[\text{Zn}(n\text{-odtb})_2]$ .<sup>775</sup> The as-obtained materials were analytically pure, orange powders which showed a complex mesomorphism, apparently involving more than one species. However, crystallization yielded red crystals which had a well-defined mesomorphism, giving mainly nematic and some smectic C mesophases.

Single-crystal X-ray studies of the butoxy and octyloxy homologs<sup>775</sup> showed that these crystalline materials were in fact dimers (Figure 88) containing an eight-membered ring. Such structures had been observed previously in dialkyldithiocarbamates of zinc(II),<sup>781–784</sup> although the unsubstituted dithiobenzoate of zinc(II) was, in fact, monomeric.<sup>785–787</sup>

The interesting feature of these materials was that while they were dimeric in the solid state, in solution in chloroform or toluene they were found to be monomeric.<sup>775</sup> What, then, was the species found in the nematic phase at elevated temperatures? The answer was provided by EXAFS studies which clearly showed that in the nematic phase of  $[\text{Zn}_2(8\text{-odtb})_4]$  at 160 °C, the dimer held together.

The mesomorphism of a series of 4-alkoxy-3-fluorodithiobenzoates of nickel, palladium, and zinc was studied.<sup>788</sup> Fluorination in the 3-position was found to promote SmC phase at the expense of the nematic phase with respect to the non-fluorinated analog. Moreover, while the mesomorphic temperature range of the nickel complexes was reduced slightly, it increased in the palladium complexes. Unidentified mesomorphic behavior was observed for the zinc complexes.

Zinc and a nickel complexes have been tested as stationary phases for ligand-exchange gas chromatography. Retention time and selectivity were affected greatly by simply coating about 5% of material on Chromosorb. These compounds were found suitable to separate efficiently polycyclic aromatic hydrocarbons and dialkylsulfides.<sup>789</sup>

#### 7.9.14.5.3 Dithiocarbamate complexes

The dithiocarbamate complexes (**197A**) (197A: M = Ni, Cu, Pd, Zn, n = 10, 18) were reported by Hoshino-Miyajima,<sup>790</sup> who found that derivatives bound to Ni, Cu, and Pd were mesomorphic, showing both nematic and SmC mesophases at elevated temperatures, i.e., above 260 °C up to 320 °C for the Ni and Pd complexes, between 200 °C and 250 °C for the Cu complexes; the zinc

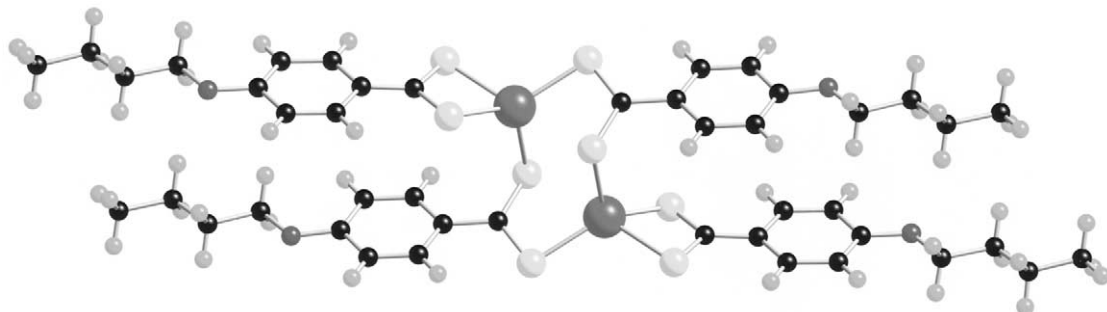
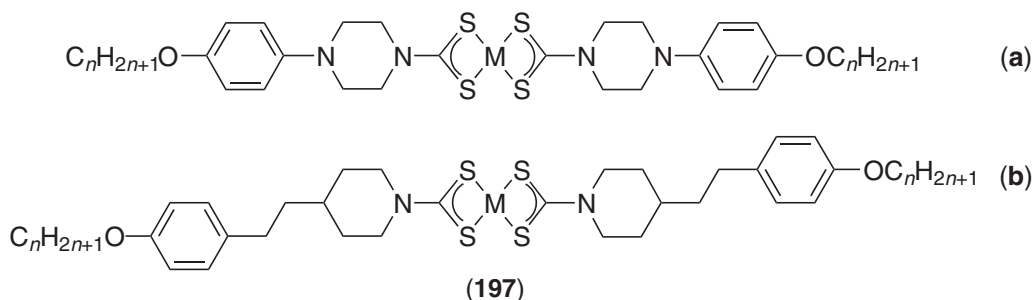


Figure 88 Single crystal structure of  $[\text{Zn}_2(8\text{-odtb})_4]$ .

complexes were not mesomorphic. Dithiocarbamate complexes ( $M = \text{Pd}, \text{Ni}, \text{Cu}, \text{Zn}$ ) based on partly hydrogenated stilbazoles were also reported (**197B**).<sup>791</sup> Again, only the Ni, Pd, and Cu complexes were mesomorphic (B and SmC phases), at high temperature ( $>200^\circ\text{C}$ ), accompanied by decomposition. The copper complexes were further studied by EPR spectroscopy in the mesophase.<sup>792</sup>



#### 7.9.14.5.4 Physical properties of mesogens with bidentate sulfur ligands

The mesogenic nickel dithiolenes were found<sup>793</sup> to have reduction potentials (against calomel) of  $+0.06\text{ V}$  and  $-0.76\text{ V}$  and as such were expected to form charge-transfer complexes with the mesomorphic, substituted tetrathiafulvalene (TTF) derivatives (Figure 89), which had oxidation potentials (also against calomel) of  $+0.43\text{ V}$  and  $+0.88\text{ V}$ .

Charge-transfer complexes were indeed formed and in a variety of stoichiometries; mixtures containing the decyl derivative of the nickel dithiolenes (Figure 89;  $R = \text{C}_{10}\text{H}_{21}$ ) were always smectic.

The butyl derivative of these nickel complexes was investigated as a dye in a guest–host system using 4-pentyl-4'-cyanobiphenyl (5CB) as the host.<sup>794</sup> The complex was found to have a large extinction coefficient of absorption ( $\epsilon = 28,000\text{ mol}^{-1}\text{ dm}^3\text{ cm}^{-1}$  at  $860\text{ nm}$ ) and dissolved in 5CB at concentrations up to 10% (w/w). At  $20^\circ\text{C}$ , such solutions showed a dichroic ratio ( $R_D$ , defined as  $A_{\parallel}/A_{\perp}$ ;  $A$  = absorbance) of 4.97 and a dye order parameter of 0.57.

Linear dichroism measurements were also made for the mesomorphic dithiobenzoates of nickel(II), palladium(II), and zinc(II).<sup>795</sup> They were made difficult by the very low solubility of the complexes in most solvents and data were typically obtained at dye concentrations of  $<0.5\text{ wt.}\%$ ; the solvents used were the commercial eutectic mixture of cyanobiphenyls and cyanoterphenyls, E7 (Merck) for the palladium complexes and the commercial mixture of cyanobicyclohexanes, ZLI2830 (Merck), for the nickel and zinc complexes. The nickel and palladium complexes both had two absorptions (Ni:  $\lambda_{\text{max}} = 595\text{ nm}$ , MLCT,  $\epsilon = 17,970\text{ mol}^{-1}\text{ dm}^3\text{ cm}^{-1}$  and  $\lambda_{\text{max}} = 375\text{ nm}$ , ligand-based,  $\epsilon = 127,220\text{ mol}^{-1}\text{ dm}^3\text{ cm}^{-1}$ ; Pd:  $\lambda_{\text{max}} = 432\text{ nm}$ , MLCT,  $\epsilon = 52,950\text{ mol}^{-1}\text{ dm}^3\text{ cm}^{-1}$  and  $\lambda_{\text{max}} = 335\text{ nm}$ , ligand-based,  $\epsilon = 55,530\text{ mol}^{-1}\text{ dm}^3\text{ cm}^{-1}$ ) while the zinc complex showed only the ligand-based absorption ( $\lambda_{\text{max}} = 372\text{ nm}$ ,  $66,020\text{ mol}^{-1}\text{ dm}^3\text{ cm}^{-1}$ ).

It was found that  $R_D$  increased according to  $\text{Zn}$  ( $4.2$  to  $4.7$ )  $<$   $\text{Ni}$  ( $5.1$  to  $6.0$ ) for the ligand-based absorption and according to  $\text{Ni}$  ( $7.0$  to  $10.12$ )  $<$   $\text{Pd}$  ( $8.7$  to  $12.8$ ) for the charge-transfer absorption; indeed, this latter absorption for palladium gave dye order parameters of up to 0.8.

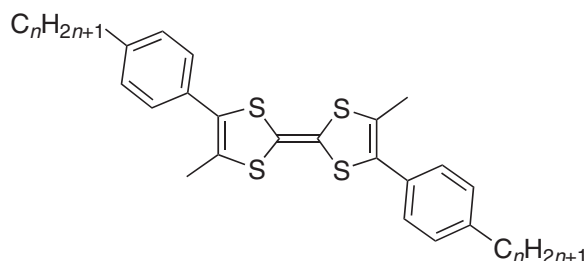
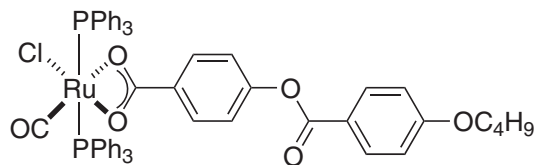


Figure 89 Structure of the mesomorphic TTF derivatives.

### 7.9.14.5.5 Benzoato complexes

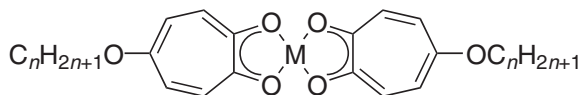
An octahedral metallomesogen, (**198**), containing a bulky ruthenium fragment and an elongated phenyl benzoate ligand was found to display an SmC phase above 225 °C.<sup>796</sup> However, on reaching the isotropic liquid, the complex started to sublime, and, thus, did not give rise to reproducible thermal behavior.



(198)

### 7.9.14.5.6 Tropolone complexes

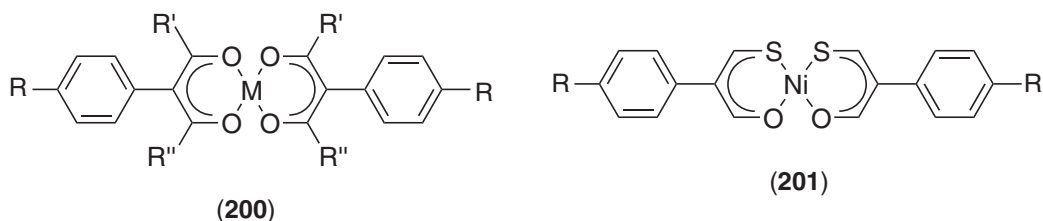
Recently, two groups concurrently reported a new class of calamitic metallomesogens based on 5-substituted tropolones.<sup>797–799</sup> The effects of the metal and of the chain (length, nature) were investigated thoroughly.<sup>800</sup> Thus, while none of the zinc(II), nickel(II), cobalt(II), and oxovanadium(IV) complexes of 5-alkoxytropolones (**199**) was mesomorphic, the copper compounds were, displaying smectic phases including SmB, SmC, crystal B, and crystal G/J phases, depending on the chain length. The mesophase temperature domain was not greatly affected by the chain length, ranging between 140 °C and 250 °C. The dioxouranium(VI) complex<sup>319</sup> ((**199**): M = *trans*-U(=O)<sub>2</sub>) displayed a narrow-temperature-range plastic phase (Cr 207 B/E 209 I). The nature of the chains also influenced the thermal behavior of these compounds in that none of the metal complexes of 5-alkylaminotropolone and 5-alkoxytropolone was mesomorphic.



(199)

### 7.9.14.5.7 Complexes $\alpha$ -substituted- $\beta$ -dialdehydes and $\alpha$ -substituted- $\beta$ -diketones

A number of  $\alpha$ -substituted- $\beta$ -diketone ((**200**): R' = R'' = Me),  $\alpha$ -substituted- $\beta$ -ketoaldehyde ((**200**): R' = Me, R'' = H), and  $\alpha$ -substituted- $\beta$ -dialdehyde ((**200**): R' = R'' = H) complexes were investigated to evaluate their liquid crystalline properties. Whereas none of the diketone and ketoaldehyde copper(II) complexes was mesomorphic,<sup>801</sup> bis(4-alkoxyphenylmalonaldehyde)copper and oxovanadium(IV) complexes<sup>802–804</sup> ((**200**): R' = R'' = H; R = OC<sub>n</sub>H<sub>2n+1</sub>, n ≥ 8 for M = Cu and n ≥ 10 for M = VO) and bis(4-alkoxyphenylmalonaldehyde)copper complexes ((**200**): M = Cu; R' = R'' = H; R = C<sub>n</sub>H<sub>2n+1</sub>, n ≥ 5) displayed a narrow-temperature-range (~10 °C) nematic phase above 200 °C. Some nickel complexes were also prepared but extensive decomposition hampered mesophase characterization.<sup>805</sup> Fluorination<sup>806</sup> and/or chlorination<sup>807</sup> at the 2- or 3-position was found to lower the transition temperature substantially in the copper complexes without destroying the nematic phase, but to inhibit mesophase formation in nickel and oxovanadium complexes.



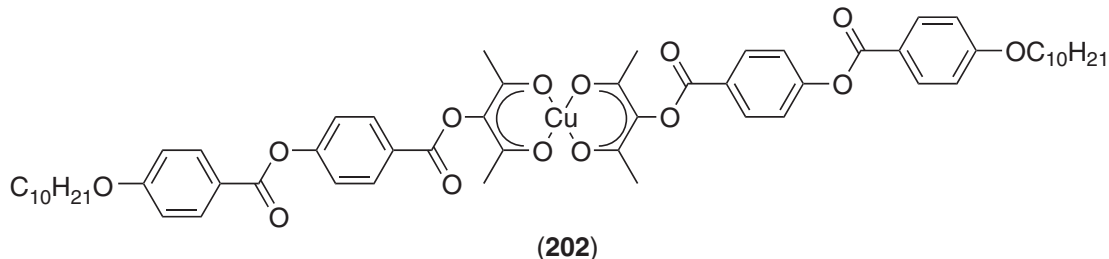
(200)

(201)

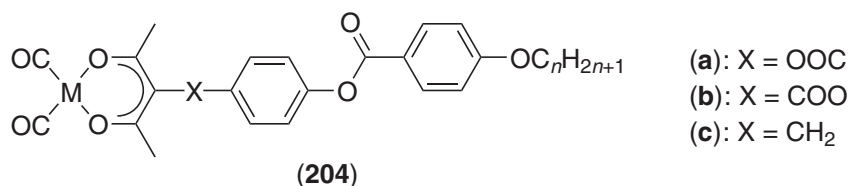
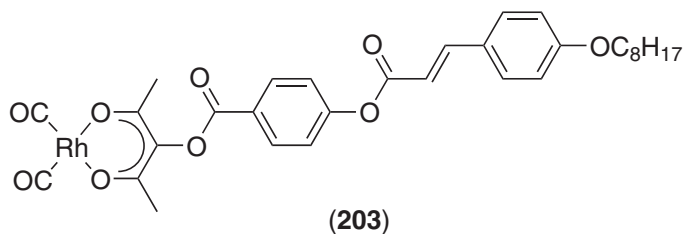


A great improvement in mesomorphic properties was achieved with the related bis[*cis*-2-(4'-alkylphenyl)-3-mercaptoacrylate]nickel(II) complexes ((**201**):  $R = C_nH_{2n+1}$ ,  $n \geq 2$ ), and related alkoxy derivatives ((**201**):  $R = OC_nH_{2n+1}$ ,  $n \geq 3$ ).<sup>808</sup> Both the alkyl and alkoxy complexes displayed wide nematic temperature ranges typically between about 100 °C and 200 °C; the alkyl derivatives possessing lower transition temperatures.

Only one such bis( $\alpha$ -substituted- $\beta$ -diketone) copper complex, with an elongated core, was found to be mesomorphic, showing a nematic phase ((**202**): Cr 222 N 226 I ).<sup>809</sup>

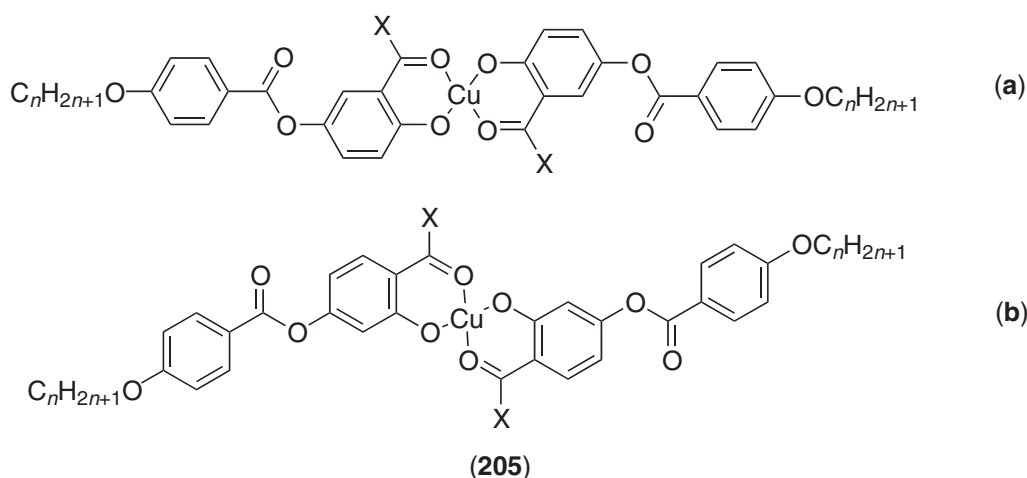


Such type of elongated  $\alpha$ -substituted- $\beta$ -diketone ligands also form rhodiumdicarbonyl and iridiumdicarbonyl complexes, which, when properly elaborated, can yield new metallomesogens. Thus, (**203**) exhibited a nematic phase between 84 °C and 132.5 °C,<sup>810</sup> whereas the existence of the mesomorphic properties in complexes (**204**) appeared to depend on the linking group, X. Wan *et al.* claimed SmC and N phases for the rhodium complexes (**204a**) ((**204a**): M = Rh;  $n = 7-12, 14$ )<sup>811,812</sup> between 150 °C and 170 °C; the nematic phase was monotropic and occurred for the dodecyloxy compound, all the other derivatives showing the SmC phase. However, contradictory results were reported by Barberá *et al.*<sup>813</sup> who did not observe mesomorphism for (**204a**): M = Rh, Ir;  $n = 10$ ; m.pt. 145 °C and 128 °C respectively) and (**204c**) ((**204c**): M = Rh, Ir;  $n = 10$ ; m. pt. 111 and 116 °C respectively), but a monotropic SmA phase for (**204b**) ((**204b**): M = Rh,  $n = 10$  Cr 101 (SmA 93) I; M = Ir,  $n = 10$  Cr 128 (SmA 96) I).



#### 7.9.14.5.8 Salicylaldehyde derivatives

Bis[5-(4'-alkoxybenzoyloxy)salicylaldehyde]copper(II) complexes ((**205a**): X = H;  $n = 6$  to 10, 12, 14) have been reported to show SmC phases for alkoxy chains containing eight or more methylene groups.<sup>814</sup> The SmC phase occurred at high temperatures (>240 °C), and over a narrow temperature range, essentially due to the decomposition of the complexes before clearing. In order to diminish the transition temperatures, several structural modifications were carried out. Thus, the slightly bent structure bis[4-(4'-alkoxybenzoyloxy)salicylaldehyde]copper(II) complexes ((**205b**): X = H), and the ketone derivatives ((**205a,b**): X = Me) were prepared, but none of them was mesomorphic, melting at high temperatures with decomposition (>200 °C).<sup>815</sup>



#### 7.9.14.5.9 Complexes of bipyridine ligands

2,2'-Bipyridines enjoy an extensive coordination chemistry, and as such are attractive candidates as ligands for thermotropic metal complexes. The first report of their use was by Hanabusa<sup>816</sup> who had made polymeric 5,5'-disubstituted systems (Figure 90); complexation to substantial amounts of six-coordinate metal centers suppressed the mesomorphism.

Araki and co-workers<sup>817</sup> reported some metal complexes of derivatized 6,6'-diamino-2,2'-bipyridines (M = Cu, Ni, Co, Pd), although the nature of the mesomorphism was not particularly clear.

More systematic work on bipyridines was published simultaneously by Bruce and Rowe<sup>818</sup> and by Douce *et al.*<sup>819,820</sup> Both groups looked at 5,5'-disubstituted-2,2'-bipyridines; Douce *et al.* looked at monosubstituted derivatives (Figure 91a) while Bruce and Rowe concentrated on diesters (Figure 91b). The bipyridines (a) showed SmA and SmB phases, while the diesters (b) showed N, SmA, and SmC phases, with a particularly wide SmC range. However, metal complexation to either system was rather unsuccessful in generating mesomorphic materials.<sup>821,822</sup>

Extension of this work showed that the use of six-ring ligands<sup>823</sup> led to metallomesogens on complexation to, for example, “[ReBr(CO)<sub>3</sub>]” (206).<sup>824,825</sup> These complexes ((206): X = Y = H and X = F, Y = H) showed N and SmC phases well above 200 °C, with clearing temperatures ranging between 300 °C and 360 °C.

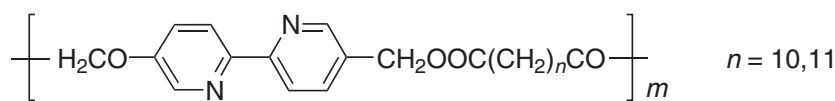
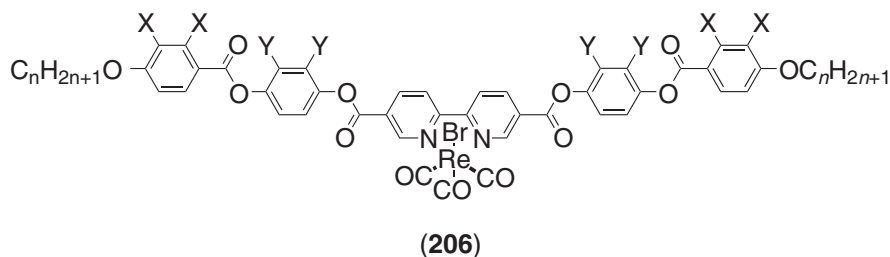
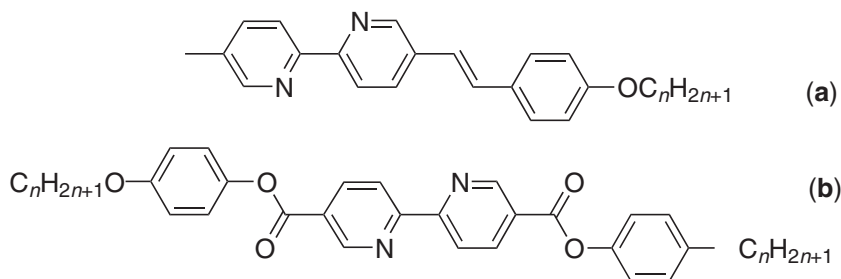


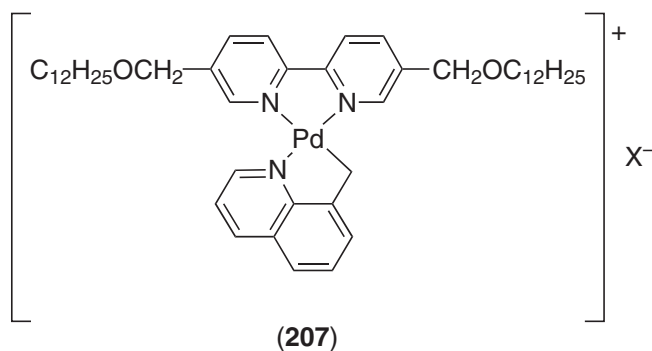
Figure 90 Polymeric 2,2'-bipyridines.



Another example was reported by El-ghayoury *et al.* and concerned some *ortho*-palladated quinolines coordinated to non-mesomorphic, 5,5'-disubstituted-2,2'-bipyridines ((207): X = BF<sub>4</sub>, C<sub>12</sub>H<sub>25</sub>OSO<sub>3</sub>).<sup>826</sup> Both complexes exhibited liquid crystallinity, but the thermal stability was much greater in the dodecylsulfate (DOS) salt compared to the tetrafluoroborate salt, which

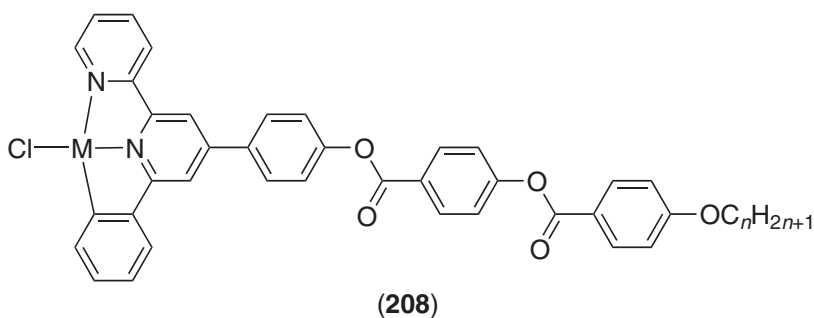


**Figure 91** Mesomorphic 2,2'-bipyridines.



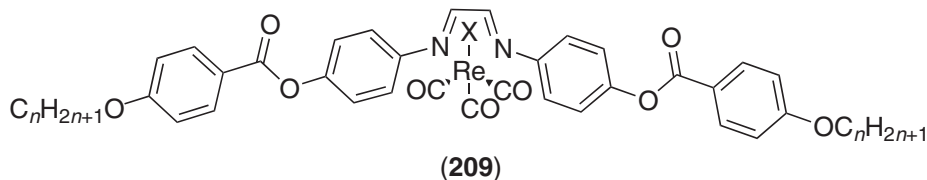
degraded rapidly on heating at high temperature. Two different liquid-crystalline mesophases were found for the DOS salt: Cr 131 Col<sub>r</sub> 168 SmA 216 I. At low temperature, the Col<sub>r</sub> phase was identified by X-ray diffraction, and resulted from the stacking of the nearly flat aromatic cores on top of each other. However, the columns were not completely surrounded by aliphatic chains, hence the polar centers of the columns were in lateral contact with one another, forming layers which are separated by layers of molten chains. The second mesophase was identified as SmA but with some local order of the columns still remaining.

Some elaborated 6'-phenyl-2,2'-bipyridine ligands and the corresponding *C,N,N*-cyclometalated chloropalladium(II) complexes, (**208**), were found to be mesomorphic.<sup>827</sup> The ligands showed a nematic phase between 140 °C and 170 °C for short chain lengths, and between 130 °C and 140 °C for the dodecyloxy homolog. The complexes, however, exhibited very high temperature mesophases, all monotropic, namely a nematic for the short-chain-length complexes, replaced by an SmA for  $n = 12$ . ((**208**):  $n = 6, 8, 12$ ).<sup>828</sup> These high temperatures result from the rather elongated anisometric part, but shorter ligand anisotropy led to materials deprived from mesomorphism. The interest in such compounds also arises from their potentially interesting photophysical properties, and particularly their electroluminescent properties.<sup>829</sup> Reaction of the same ligands with an iridium dimer followed by counterion exchange afforded a new series of cationic orthometalated iridium(III) complexes, unfortunately devoid of mesomorphism.<sup>830</sup>



### 7.9.14.5.10 Complexes of diazabutadiene ligands

A few *N,N'*-bis(4''-(4'-alkoxybenzoyloxy)phenyl)-1,4-diaza-1,3-butadiene ligands were complexed to various  $[\text{ReX}(\text{CO})_5]$  fragments to give new, mesomorphic, octahedral halotricarbonylrhenium(I) complexes ((**209**):  $\text{X} = \text{Cl}, \text{Br}, \text{I}, \text{CF}_3\text{SO}_3$ ;  $n = 8, 10, 12$ ).<sup>831,832</sup> The parent ligands showed large-temperature-range SmC and nematic phases from ca. 130 °C, with decomposition occurring systematically in the nematic phase (above 200 °C), making assignment of the clearing point difficult.



On complexation to many different metal fragments, i.e.,  $[\text{Mo}(\text{CO})_4]$ ,  $[\text{MnBr}(\text{CO})_3]$ ,  $\text{PdCl}_2$ ,  $\text{CuCl}$ ,  $\text{CuBr}$ ,  $\text{CuCN}$ , mesomorphism was not observed. The exception was when the ligands were bound to  $[\text{ReX}(\text{CO})_3]$  ((**209**):  $\text{X} = \text{Cl}, \text{Br}, \text{I}$ ), when materials with a nematic, and in two compounds with dodecyloxy chains ( $\text{X} = \text{Cl}, \text{Br}$ ), an additional SmC phase, resulted; no mesomorphism was detected for compounds with the bulkier triflate group. Clearing points were found to decrease in the order  $\text{Cl} > \text{Br} > \text{I} > \text{CF}_3\text{SO}_3$ , and with increasing  $n$  (Figure 92).

### 7.9.14.5.11 Complexes with *N,O* donor sets

Metal complexes derived from the salicylaldimines feature among the earliest and most widely studied class of metallomesogens.<sup>833</sup> Upon complexation, the two salicylaldiminato-based ligands arrange themselves in an antiparallel fashion giving rise to so-called “fused-twin” metallomesogens. In general, the advantages of incorporating an imine functionality lie in the versatility, structural variety, ease of preparation, and derivatization of such groups. Consequently, a large number of salicylaldimato complexes based on the ligand structures shown in Figure 93 have been synthesized using various metal ions such as copper(II), nickel(II), palladium(II), vanadium(IV), and iron, as well as the trivalent lanthanide ions.

The original work in this area was carried out by Galyametdinov and co-workers,<sup>834–841</sup> who synthesized several series of copper complexes based on dialkoxysalicylaldimines ((**210**)). Some of these copper complexes ((**210**):  $\text{M} = \text{Cu}$ ,  $m = 7$ ,  $\text{R} = \text{OC}_n\text{H}_{2n+1}$ ;  $\text{F}$ ) showed an SmA phase ( $n = 1$  to 4;  $\text{R} = \text{F}$ ), and both SmC and SmA ( $n = 5$ –12) typically between 130 °C and 140 °C, and 150 °C and

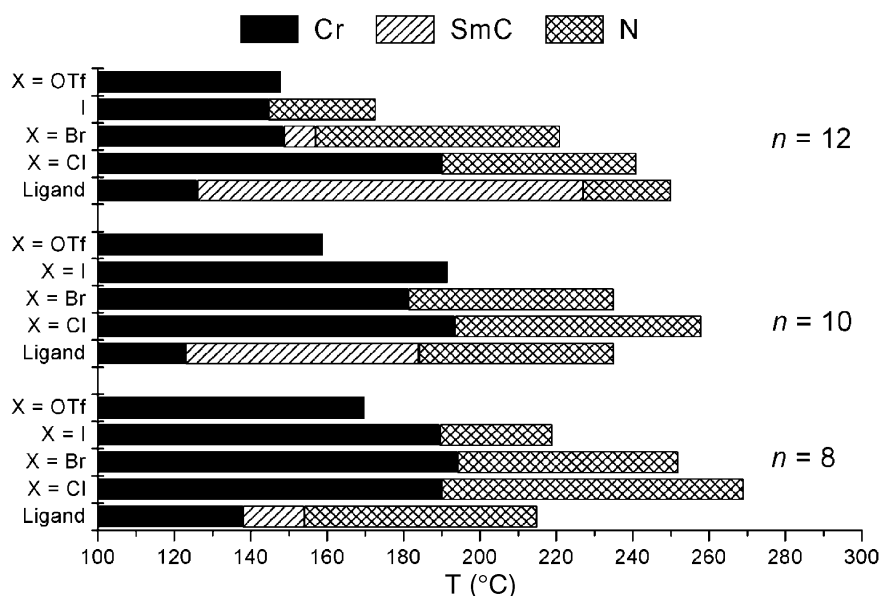
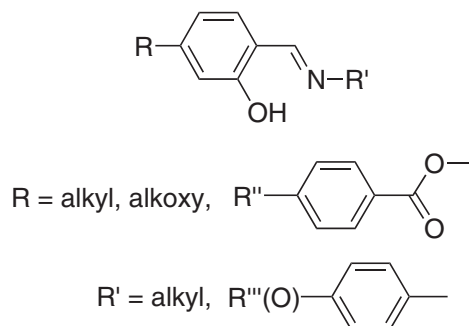
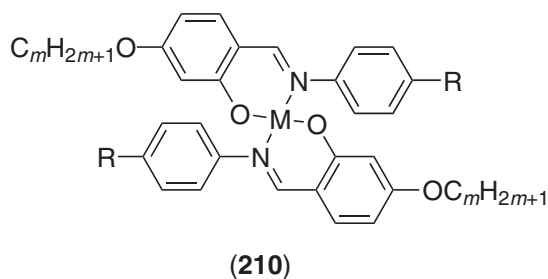


Figure 92 Mesomorphism of halotricarbonylrhenium(I) complexes, (**209**).



**Figure 93** Structure of the salicylidate ligands used to generate mesomorphic complexes.

170 °C, and, as such, were the first examples of materials with a paramagnetic nematic phase. Later, the same group reported an analogous (paramagnetic) complex of oxovanadium(IV) ((**210**):  $M = V=O$ ,  $m = 7$ ,  $R = OC_8H_{17}$ ),<sup>842</sup> although the exact nature of the mesophase was not reported by them until a few years later.<sup>843</sup> This paper was largely overlooked and a very important point was missed, namely that a mesomorphic metal-containing system containing a square-pyramidal center had been identified in a calamitic molecule. In the same paper, zinc(II), cobalt(II), nickel(II), and palladium(II) were also synthesized ( $m = 7$ ,  $R = OC_8H_{17}$ ). Only the  $Cu^{II}$ ,  $V^{IV}=O$ , and  $Pd^{II}$  were mesomorphic with the transition temperatures increasing from the copper (Cr 142 SmC 156 SmA 165 I) via the oxovanadium (Cr 152 SmC 170 SmA 180 I) to the palladium (Cr 164.5 SmC 198 SmA 209 I) complexes. X-Ray single-crystal structures of the copper(II) ((**210**):  $M = Cu$ ,  $m = 7$ ,  $R = OC_6H_{13}$ ),<sup>844</sup> and palladium(II) ((**210**):  $M = Pd$ ,  $m = 7$ ,  $R = OC_6H_{13}$ )<sup>845</sup> complexes showed that in both structures the molecules are packed into layers, with the terminal chains extended nearly parallel to each other; the aniline rings did not lie in the chelate plane.



Marcos and co-workers<sup>846</sup> examined several series of copper(II) complexes derived from Schiff-base ligands with one or two aromatic rings. None of the complexes derived from one-ring salicylaldehyde, salicylketone, and salicylidimine was mesomorphic. However, most of the other complexes ((**210**):  $M = Cu$ ,  $R = C_nH_{2n+1}$ ,  $OC_nH_{2n+1}$ ;  $n, m = 2, 6, 10, 14$ ) exhibited SmA and SmC phases. Other tetraalkoxy systems were then published with oxovanadium(IV) ((**210**):  $M = V=O$ ,  $m = 10$ ,  $R = OC_5H_{11}$ : Cr 135 SmC 156 SmA 178 I),<sup>847</sup> copper, and palladium(II) ((**210**):  $M = Cu, Pd$ ,  $m = 7$ ,  $R = OC_6H_{13}, OC_{10}H_{21}$ )<sup>848</sup> confirming smectic polymorphism. The copper complexes had the same SmA and SmC phases typically in the range 140–170 °C, while the palladium derivatives of the same ligands also showed the same mesophases; the melting point increased by between 20 °C and 60 °C and the mesophase range was extended greatly, being typically 20 °C wider. Investigations of the vanadyl and copper complexes by EPR techniques showed that the magnetic anisotropy was positive for the vanadyl complexes and negative for those of copper.<sup>849,850</sup>

Ghedini and co-workers investigated a series of *N*-(4-alkoxysalicylidene)-4'-alkylaniline copper complexes ((**210**):  $M = Cu$ ,  $m = 7, 12$ ;  $R = C_nH_{2n+1}$ ,  $n = 1-4$ ),<sup>851-853</sup> later extended to longer homologs ( $n = 6, 8$ ).<sup>854</sup> While the ligands showed SmC, SmA, and N phases, all of the copper complexes showed only an SmA phase with the exception of one which showed an SmB phase ( $m = 12$ ,  $n = 4$ : Cr 90 E 98 SmB 114 SmA 140 I) phase as well. The SmA is monotropic for short chain length ( $n = 1, 2$ ), and enantiotropic thereafter. Melting points for the ligands were typically between 50 °C and 70 °C, while clearing points were between 80 °C and 100 °C; for the

corresponding complexes the enantiotropic phases typically occurred between 100 °C and 120 °C and 140 °C and 150 °C.

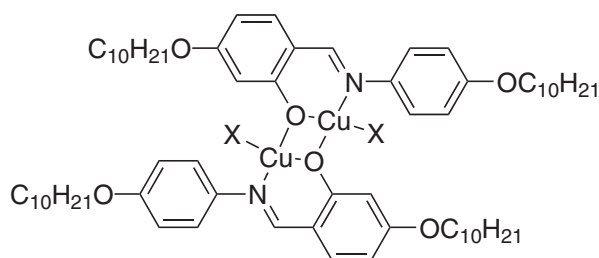
Low-angle X-ray diffraction experiments were carried out in the SmA and SmB mesophases of two of these copper complexes ( $m = 7, 12, n = 4$ ).<sup>855,856</sup> Results obtained in the SmA phase showed that the complexes had a negative diamagnetic anisotropy and that there was a weak, diffuse feature pointing to an in-layer Cu—Cu correlation at 8.5 Å corresponding to a side-to-side arrangement of the molecules. A ribbon-like structure was proposed for the SmB phase on the basis of the X-ray results and, again, a side-to-side correlation, this time of 8.6 Å, was found. Further studies of the SmB phase by EXAFS<sup>857</sup> revealed a Cu—Cu correlation at 3.85 Å showing the phase to have solid-like, translational order and therefore to be intrinsically biaxial, although macroscopic biaxiality has not yet been demonstrated in these systems. A crystalline structure of one homolog revealed that the molecular packing consisted of a layered structure containing interdigitated molecules, the molecules having a *trans* conformation around the metal center with the terminal chains being extended nearly parallel to each other ( $m = 12, n = 3$ ).<sup>858</sup> This structure seemed consistent with the model proposed for the SmA organization by X-ray diffraction and EPR. Other series of related copper complexes with different chain length ((**210**): M = Cu:  $m = 3-12, 14, 16, 18, R = C_2H_5$ ;  $m = 4; R = C_nH_{2n+1}, n = 6$  to 8;  $m = 8, 10, 16, 18, R = C_nH_{2n+1}, n = 6$ )<sup>859-861</sup> have been reported to show similar a smectic mesomorphism.

The influence of the metal has also been investigated, and the same ligands complexed to oxovanadium(IV) ((**210**): M = V=O,  $m = 12$ ; R =  $C_nH_{2n+1}, n = 1-4, 6, 8$ )<sup>862</sup> and palladium(II)<sup>863</sup> ((**210**): M = Pd,  $m = 12$ ; R =  $C_nH_{2n+1}, n = 1-4, 6, 8$ ) have been reported to be mesomorphic, too. As for the vanadyl complexes, the mesophase became destabilized with respect to that of the copper complexes, probably due to the distorted square-pyramidal geometry around the metal center. The first mesomorphic homolog ( $n = 4$ ) exhibited a monotropic SmA phase, whereas the hexyl homolog exhibited an enantiotropic SmA phase (Cr 153 SmA 160 I), and the octyl derivative both an SmA and a monotropic SmC phase (Cr 150 (SmC 142) SmA 161 I). For all the palladium complexes but one ( $n = 4$ ), an SmA phase was observed, monotropically for  $n = 1$  and 6, and enantiotropically for  $n = 2, 3$ , and 8; the phases appeared at higher temperatures than the copper and oxovanadium complexes, i.e., above 160 °C, and up to 200 °C.

As discussed above in the section on columnar systems, strong stabilization of the SmA phase was achieved in binary mixtures of copper<sup>864</sup> and palladium<sup>865</sup> complexes ((**210**):  $m = 10, M = Cu, Pd, R = C_{14}H_{29}$ ; M = Cu, R =  $OC_{14}H_{29}$ ) with the electron acceptor 2,4,7-trinitro-9-fluorenone (TNF). Indeed, for the three complexes, the mesophase was stabilized by nearly 60 °C, and this tendency was confirmed upon increasing TNF contents in the mixtures.

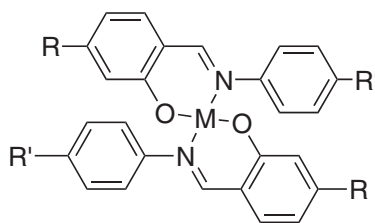
From this systematic study, it appeared that the tetra-alkoxy systems exhibited wider mesomorphic temperature ranges than the dialkoxy-dialkyl complexes and, since the melting points were similar, the mesophase stability was enhanced greatly in the former compared to the latter.

More recently, binuclear metallomesogens based on identical ligands have been reported to show an SmA phase between 91 °C and 125 °C for the chloro derivative ((**211**): X = Cl), and between 108 °C and 120 °C for the bromo analog ((**211**): X = Br).<sup>866</sup> These complexes (**211**) were obtained by the reaction of the mononuclear salicylaldimine ((**210**)) with metal halides. The temperature dependence of the magnetic properties indicated strong antiferromagnetic coupling between the metal atoms.



Several series of complexes substituted in the aldehyde, aniline, or both rings by alkanoyloxy chains have also been prepared and investigated. Sirigu<sup>848</sup> showed that the copper complexes ((**212**): M = Cu; R, R' =  $C_nH_{2n+1}CO_2, n = 5-11$ ) had SmC phases (and an additional SmA phase for one compound with  $n = 6$ ) typically in the range 180–210 °C; the palladium derivative of the

same ligands ( $n=7$ ) showed the same mesophases (Cr 238 SmC 247 SmA 250 I). Given that the copper and palladium complexes are largely isostructural in the solid state, it may be that at such elevated temperatures the copper complexes start to distort towards a tetrahedral arrangement thus reducing the molecular anisotropy and, with it, the clearing point. Complexes with an alkanoyloxy chain grafted onto the aldehyde rings, and a short alkoxy chain on the imine ring ((**212**):  $M = \text{Cu}$ ,  $R = \text{C}_n\text{H}_{2n+1}\text{CO}_2$ ,  $n = 4-11, 13, 15, 17$ ,  $R' = \text{OC}_2\text{H}_5$ ), were not mesomorphic,<sup>859</sup> melting into the isotropic liquid at ca. 180 to 220 °C. However, increasing the alkoxy chain length from the ethoxy to the hexyloxy ((**212**):  $M = \text{Cu}$ ,  $\text{Pd}$ ,  $V=O$ ,  $R = \text{C}_{17}\text{H}_{35}\text{CO}_2$ ,  $R' = \text{OC}_6\text{H}_{13}$ )<sup>867</sup> was found to be beneficial for mesomorphism in that an SmA phase was induced for all the complexes, monotropic for both the copper and palladium complexes, and enantiotropic for the oxovanadium complex (Cr 107.5 SmA 151.5 I). In contrast, all the complexes having the alkoxy and alkanoyl chains at the opposite ends of the imine ligand – that is, opposite to the situation just described ((**212**):  $M = \text{Cu}$ ,  $R = \text{OC}_n\text{H}_{2n+1}$ ,  $n = 2-12, 14, 16, 18$ ,  $R' = \text{MeCO}_2$ ,  $\text{C}_9\text{H}_{19}\text{CO}_2$ ,  $\text{C}_{17}\text{H}_{35}\text{CO}_2$ )<sup>868</sup> – exhibited a smectic mesomorphism, even those with short chain lengths. The acetoxy series exhibited a broad SmA phase between 130 °C and 190 °C; the nematic phase of the ligand was suppressed upon complexation. The other two series with long alkanoyl chains exhibited an SmC ( $n \geq 5$ ) and an SmA phase ( $2 \leq n \leq 6-7$ ) over narrower temperature ranges than in the acetoxy derivatives. Moreover, the transition temperatures were found to decrease from the decanoate to the octadecanoate series.



(212)

Copper, palladium, and oxovanadium complexes of this type have also been successfully exploited to generate ferroelectric materials by incorporating chiral chains in the *N*-aryl moiety. Marcos and co-workers used butyl lactate ( $R^* = \text{C}^*\text{HMeCO}_2\text{C}_4\text{H}_9$ ) as a source of chirality, linked to the mesogenic core through the aniline ring ((**210**):  $M = \text{Cu}$ ,  $\text{Pd}$ ,  $V=O$ ;  $m = 10$ ;  $R = \text{CH}=\text{CHCO}_2R^*$ ,  $\text{CO}_2R^*$ ,  $\text{OR}^*$ ).<sup>869-872</sup> Most of the resulting copper, palladium, and oxovanadium complexes exhibited a chiral SmC\* phase with, in addition, an SmA phase for the cinnamate derivatives or a N\* phase for the carbonyl compounds. A general lowering of the transition temperatures and of the mesophase stability was observed on going from the cinnamates, to the ester, to the ether derivatives, while they increased in the order  $\text{Cu} < V=O < \text{Pd}$ . In most cases, mesomorphism was induced upon complexation, particularly with the ester and ether compounds. Ghedini used other sources of chirality such as myrtilol, menthol, citronellol, and 2-octanol, but mesomorphism was observed only with citronellol ((**210**):  $M = \text{Pd}$ ,  $m = 12$ ,  $R = \text{S}(-)\beta\text{-citronellol}$ : Cr 123 SmC\* 131 SmA 134.5 I),<sup>873</sup> and 2-octanol ((**210**):  $M = \text{Pd}$ ,  $m = 12$ ,  $R = \text{R}(-)\text{OC}^*\text{HMeC}_6\text{H}_{13}$ : Cr 121 (Ch 103) I)<sup>874</sup> palladium complexes.

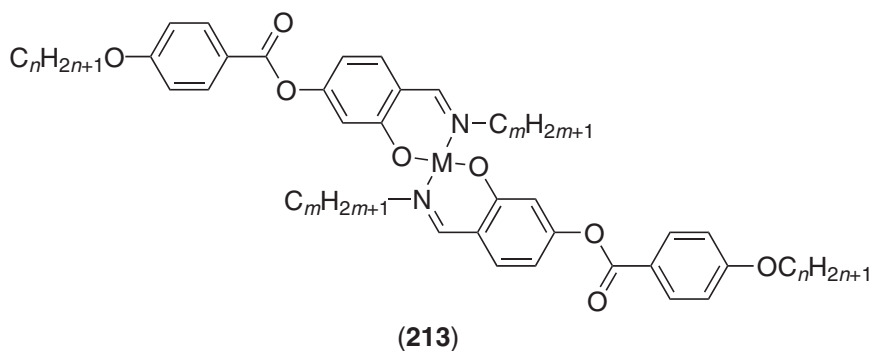
There have been very few examples of systems in which the chiral chains are attached to the aldehyde moiety. Tian *et al.*<sup>875</sup> employed the chiral 2-chloro-3-methylbutyryl group ((**212**):  $M = \text{Cu}$ ,  $R = \text{Me}_2\text{CHC}^*\text{HClCO}_2$ ,  $R' = \text{OC}_n\text{H}_{2n+1}$ ,  $n = 3-8, 10, 12$ ), and the resulting complexes showed an SmA phase ( $n \geq 4$ ), between ca. 150 °C and 160 °C (for  $n = 12$  the phase is stable between 112 and 163 °C), with two homologs showing an additional SmC\* phase ( $n = 8$ : Cr 126 SmC\* 133 SmA 163 I;  $n = 10$  Cr 138 SmC\* 152 SmA 164 I). Another such system was produced by Yelamaggad *et al.*<sup>876</sup> consisting of copper and palladium complexes containing a cholesteryl group bound to the ligand ((**212**):  $M = \text{Cu}$ ,  $\text{Pd}$ ,  $R = \text{O}(\text{CH}_2)_5\text{COOChol}$ ,  $R' = \text{C}_4\text{H}_9$ ,  $\text{C}_{10}\text{H}_{21}$ ,  $\text{OC}_2\text{H}_4\text{CHMeC}_3\text{H}_7\text{CHMe}_2$ ). Thus, the butyl complexes exhibited an enantiotropic SmA phase at elevated temperatures (above 150 °C), whereas the decyl and the citronellyloxy complexes exhibited a chiral nematic phase, enantiotropic over 5 to 10 °C for the former, and monotropic for the latter.

Thus, the formation of smectic phases (SmA and SmC) was favored over the nematic phase in this type of system ((**210**) and **212**). In order to enhance the tendency to form the nematic phase, several new series of complexes based on *N*-alkyl-[4-(4-alkoxybenzoyloxy)salicylaldehyde] ligands have been prepared. These complexes are still based on two-ring ligand systems, but owing to the

m	1	2	3	4	5	6	7	8	9	10	11	12	13	14	15	17
n																
4			N													
5			N													
6	N	(N)/N	N	N	N	N	N	N	N	N	N	N	N	N,SmC	N,SmC	N,SmC
7	N		N					N					N,[SmC]			
8	N		N					N					N,SmC			
9	N		N					N					N,SmC			
10	N,SmC	N	N	N	N	N	N	N	N	N	N,[SmC]	N,SmC	N,SmC	N,SmC	N,SmC	SmC
11	N,SmC		N					N					N,SmC			
12	N,SmC		N					N					N,SmC			
13	N,SmC							N					N,SmC			
14	SmC	Not LC	(N)/N LC	N LC	N	N	N	N	N	N	N,[SmC]	N,[SmC]	N,SmC	N,SmC	N,SmC	SmC
16			N													
18			N													

Figure 94 Mesomorphism of complexes (213) as a function of  $m$  and  $n$ .

terminal position of the metal chelate, the overall molecular anisotropy increased upon complexation. Several series of copper(II) ((213):  $M = Cu$ ,  $n = 10$ ,  $m = 1-10$ ; <sup>877-879</sup>  $n = 6$ ,  $m = 1, 2, 4-13$ ;  $m = 3$ ,  $n = 4-12, 14, 16, 18$ ; <sup>880,881</sup>  $m = 1$ ,  $n = 6-14$ ; <sup>882</sup>  $n = 14$ ,  $m = 1-15$ ; <sup>883</sup>  $m = 8, 13$ ,  $n = 6-14$ ;  $n = 6, 10$ ,  $m = 1-17$ ), <sup>884</sup> nickel ((213):  $M = Ni$ ,  $n = 10$ ,  $m = 1-10$ ; <sup>877</sup>  $m = 1$ ,  $n = 8, 11, 14$ ;  $n = 12$ ,  $m = 13$ ; <sup>884</sup>  $m = 3$ ,  $n = 4-12, 14, 16, 18$ ), <sup>885</sup> palladium ((213):  $M = Pd$ ,  $m = 1$ ,  $n = 8-11, 14$ ;  $m = 13$ ,  $n = 7, 8$ ;  $n = 14$ ,  $m = 3$ ;  $n = m = 8$ ), <sup>884</sup> and oxovanadium ((213):  $M = V=O$ ,  $n = 10$ ,  $m = 1, 5$ ; <sup>886-888</sup>  $m = 3$ ,  $n = 5-12, 14, 16, 18$ ), <sup>885</sup> have been found to be mesomorphic. They showed mainly the N phase and, for long-chain derivatives, an additional SmC phase; the SmA phase was, however, almost totally absent in this structural type. The essential part of this broad study was concerned mainly with copper complexes; the mesomorphic properties of the nickel, oxovanadium, and palladium complexes are in good general agreement with the overall mesomorphic tendency shown in the matrix (Figure 94), except for a few palladium or oxovanadium complexes only.



When one or both of  $n$  and  $m$  were short, only a nematic phase was seen and, indeed, for low values of  $n$ , only the nematic phase was seen up to  $m = 18$ ; both melting and clearing points decreased as  $n$  and  $m$  were increased (Figures 95 and 96). A significant difference is noted in the clearing temperatures of the nickel and oxovanadium derivatives where  $n = 3$  and  $m$  was varied, namely that the clearing temperatures of the vanadyl complexes are significantly lower by around  $25^\circ\text{C}$  (Figure 95). This was undoubtedly due to the lower symmetry (local  $D_{2h}$  for nickel and  $C_{2v}$  for vanadyl) which leads to a lower structural anisotropy and, hence, a lower clearing point. In fact, for the same ligand derivatives, Hoshino reported a general decrease in mesophase stability according to  $Ni > Cu > V=O$ , the lower position of copper being accounted for by its greater susceptibility to tetrahedral distortion which would reduce the structural anisotropy. The transition temperatures of the few palladium complexes that have been prepared were found to be intermediate between those of the copper and nickel complexes, and with narrower mesophase



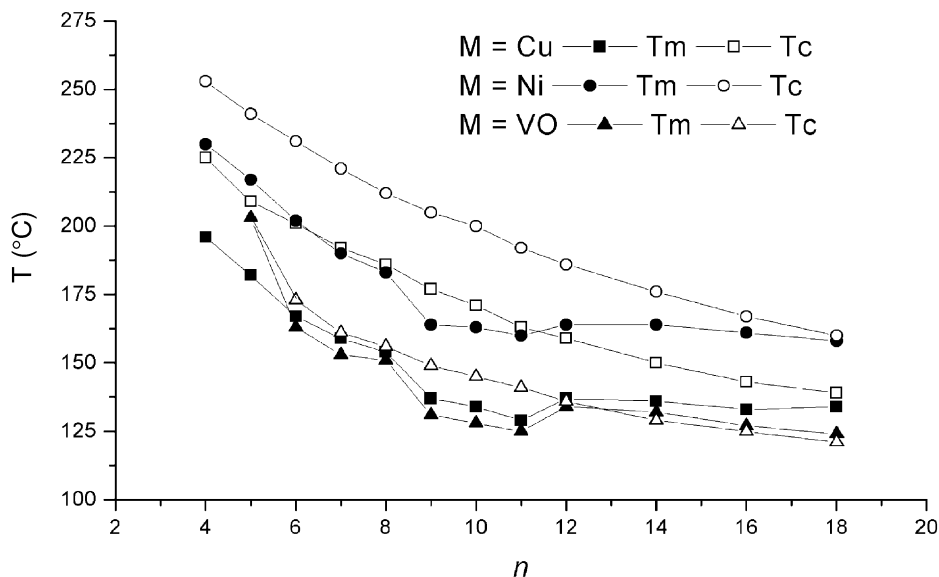


**Figure 95** Transition temperatures of the complexes (213) with M = copper (square), nickel (circle), and oxovanadium (triangle) complexes for  $m = 3$ . Tm: melting, Tc: clearing.

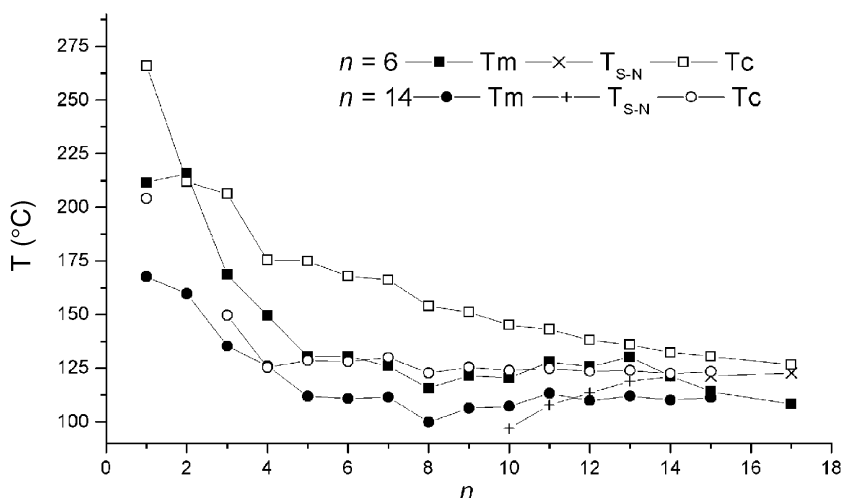


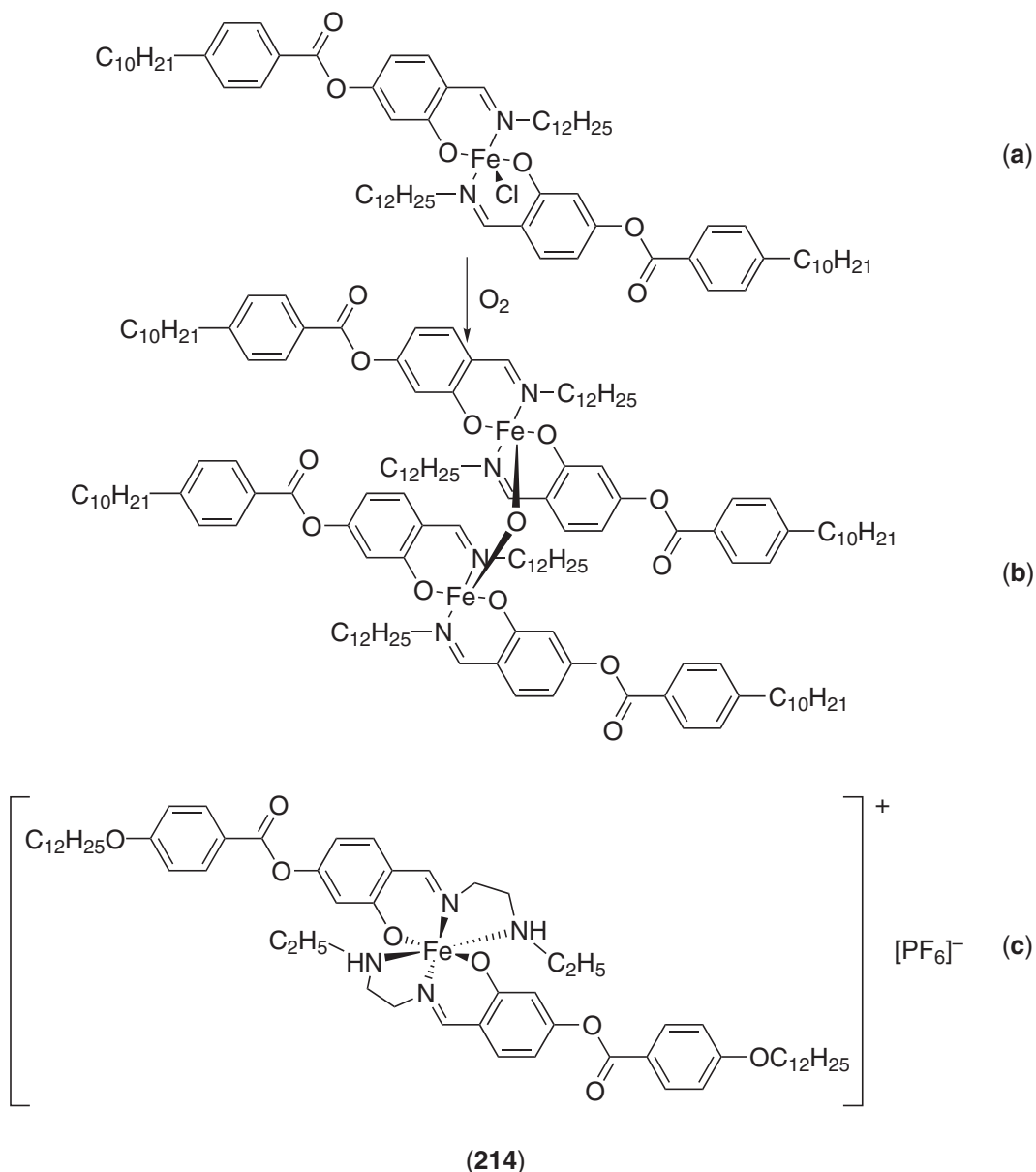
**Figure 96** Variation of the transition temperatures of complexes (213) with alkoxy and *N*-alkyl chain length. Tm: melting,  $T_{S-N}$ : SmC-to-N phase transition temperature, Tc: clearing.

temperature ranges i.e.,  $\approx 10^\circ\text{C}$  for  $m = 1$  and 13, or  $\approx 40^\circ\text{C}$  for  $m = 3$  and 8. Investigations of the vanadyl, nickel, and copper complexes by EPR techniques showed that the magnetic anisotropy was positive for the vanadyl and nickel complexes and negative for those of copper.

In the case of manganese(III) complexes ((213): M = MnCl,  $n = 10$ ,  $m = 1-10$ , 12, 14, 16),<sup>889</sup> the mesophases were destabilized considerably with respect to those of the divalent metal complexes, and a narrow-temperature-range (ca.  $20^\circ\text{C}$ ) SmC phase was seen (in the range  $100-140^\circ\text{C}$ ) on heating for  $n > 10$ . On cooling, additional monotropic SmC ( $n = 6-9$ ), SmA ( $n = 1$ ) and N ( $n = 3-9$ ) phases could be observed. This decrease in mesophase stability may be due to the peculiar geometry around the manganese ion, which can adopt a structure intermediate between a square pyramid (Cl in apical position) and a trigonal bipyramid (two apical nitrogen atoms), as observed for the oxovanadium complexes.

The chloroiron(III) complexes (214a),<sup>890,891</sup> however, exhibited an SmA phase between  $123^\circ\text{C}$  and  $154^\circ\text{C}$ , above an unidentified smectic phase (between  $70^\circ\text{C}$  and  $123^\circ\text{C}$ ). The original  $\mu$ -oxo-bridged diiron(III) complex (214b) obtained by oxidation of (214a) was also mesomorphic (Cr 105 SmA 115 N 159 I).<sup>892</sup> The pseudo-octahedral complex of iron(III) with related elongated ligands having

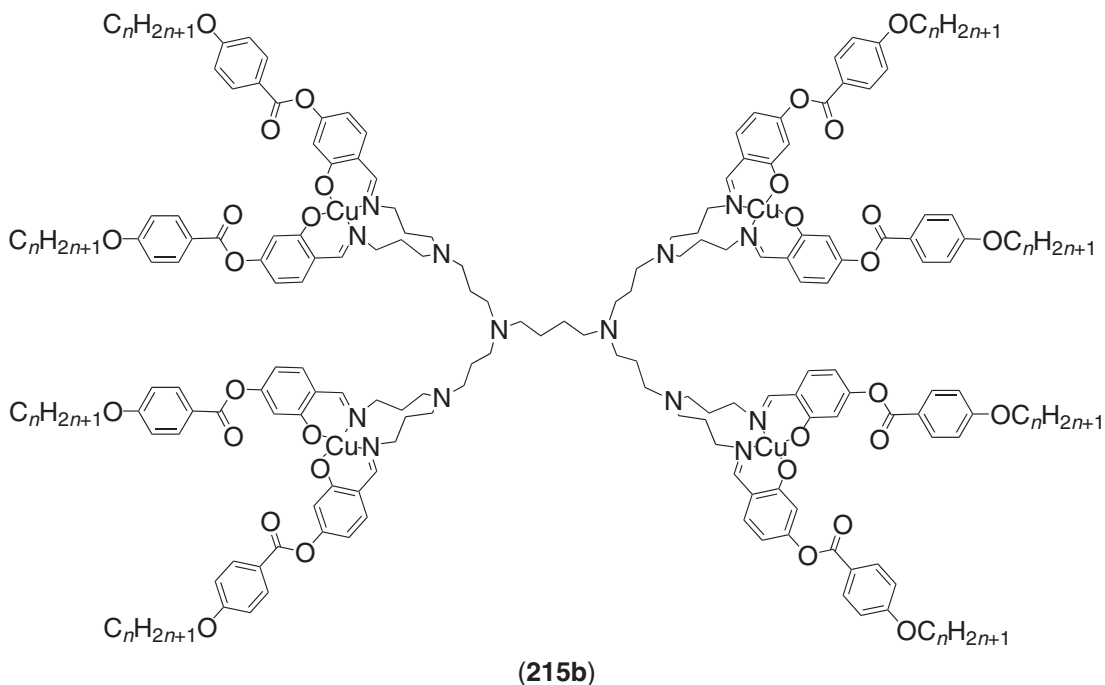
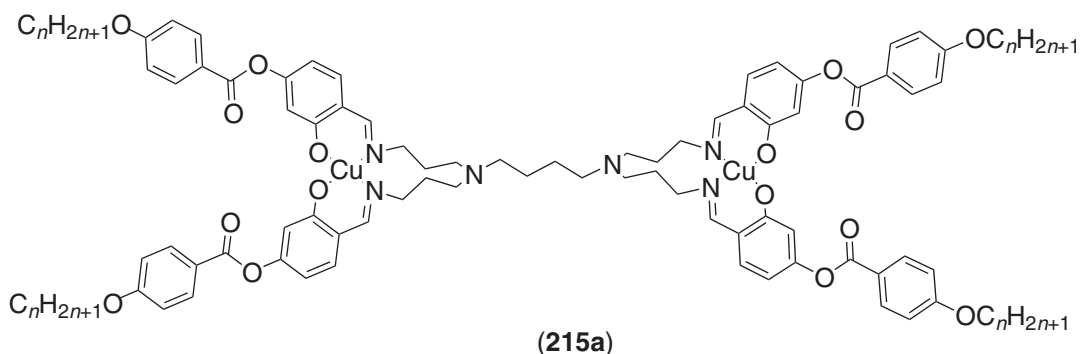
an  $\text{N}_4\text{O}_2$  coordination site (**214c**) was also mesomorphic, also showing an SmA phase between 115 °C and 146 °C; the nitrate salt, a precursor to (**214c**), was not investigated.<sup>893</sup> This is the first example of thermal spin transition in liquid crystals.



Chirality has been scarcely investigated in such complexes. A few complexes derived from (*S*)-(-)-2-methylbutylamine ((**213**):  $\text{C}_m\text{H}_{2m+1} = \text{CH}_2\text{C}^*\text{HMeC}_2\text{H}_5$ ,  $\text{M} = \text{Cu, Ni, V=O}$ ,  $n = 7$ ;  $\text{M} = \text{Pd, Ni}$ ,  $n = 12$ ) have been reported by Galyametdinov and Pyzuk<sup>894</sup> to show an enantiotropic chiral nematic phase with a small helical pitch, with in some cases one ((**213**):  $\text{M} = \text{Cu}$ : Cr 156 (BP 154)  $\text{N}^*$  157.9 I), or two blue phases ( $\text{M} = \text{Ni}$ : Cr 155 BPI 187.6 BPII 187.9  $\text{N}^*$  189 I). Similarly, the palladium and nickel complexes ( $n = 12$ ) also exhibited the chiral nematic phase and for the palladium what is recognized as the blue fog phase (the blue fog phase is one of the family of blue phases. Reference to further reading is found in Section 7.9.14.3.3(v)). Increasing the length of the chain bearing the chiral group ((**213**):  $\text{M} = \text{Ni}$ :  $m = 7$ ,  $\text{C}_m\text{H}_{2m+1} = \text{C}^*\text{HMeC}_{11}\text{H}_{23}$ ,  $\text{C}^*\text{HMeC}_6\text{H}_{13}$ ), or the alkoxy chain ( $n = 12$ ), has a destabilizing effect on the mesomorphism, and only monotropic phases were observed.<sup>895</sup> Other chiral sources were used such as (*S*)-(+)-1-amino-2-propanol ((**213**):  $\text{M} = \text{Pd}$ ,  $n = 10$ : Cr 198  $\text{N}^*$  226 I) or (*S*)-(+)-1-amino-2-propylhexanoate ((**213**):  $\text{M} = \text{Cu}$ ,  $n = 6$ : Cr 131 ( $\text{N}^*$  107) I).<sup>896</sup>

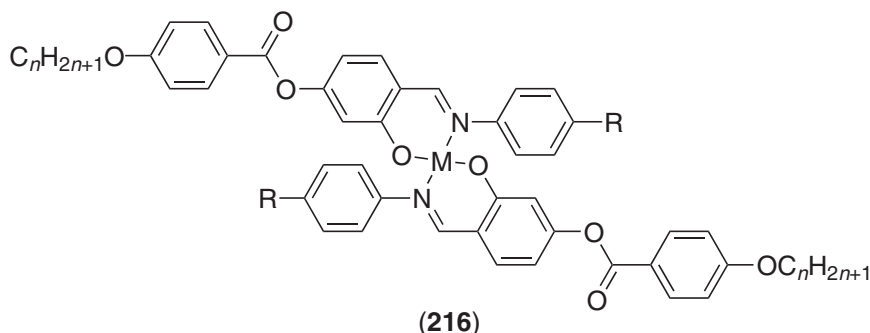
A few copper and nickel complexes based on *N*-alkyl[5-(4-decyloxybenzoyloxy)salicylaldimine] (alkoxybenzoate group *meta* to the ring position of the imine carbon) were also prepared and their mesomorphism compared to that of their isomers (**213**).<sup>897,898</sup> Except for the *N*-methyl derivatives which exhibited enantiotropic phases over large temperature ranges (M = Cu: Cr 188 SmC 243 N 267 I, M = Ni: Cr 240 SmC 267 N 281 I), the mesomorphism was in general suppressed. The range of the nematic phase diminished drastically for the *N*-ethyl derivative (M = Cu: Cr 164 N 170 I); the phase was suppressed or monotropic for longer alkylamine chains.

Dendromesogens based on first- and second-generation poly(propylene imine) dendrimers bearing four or eight 4-(alkoxybenzoyloxy)salicylaldimine peripheral units have been considered as organic ligands, and complexed to copper(II).<sup>899</sup> Whereas all the dendromesogens were found to possess a rich smectic mesomorphism,<sup>900</sup> their complexation to copper(II) prevented meso-phase formation in some of the corresponding metallodendrimers ((**215a,b**):  $n = 10, 14, 18$ ). Thus, only the long chain of the first ((**215a**):  $n = 14, 18$ ), and second generation ((**215b**):  $n = 18$ ) were mesomorphic, showing an SmC phase between 160 °C and 190 °C to 200 °C for the former and between 35 °C and 110 °C for the latter.



Bayle *et al.*<sup>901</sup> used the same basic framework to synthesize a number of Cu, Ni, and Pd complexes (**216**), as elongated derivatives of complexes (**213**) ((**216**): M = Cu, Ni, Pd;  $n = 1-12, 14, 16$ ; R = C<sub>4</sub>H<sub>9</sub> or OC<sub>m</sub>H<sub>2m+1</sub>). While none of the Ni complexes showed any mesomorphism, the Cu complexes with  $1 \leq n \leq 16$  and R = C<sub>4</sub>H<sub>9</sub> all showed only the nematic phase, with melting and clearing points in the range 220–158 °C and 233–264 °C, respectively. The palladium complex ((**216**): M = Pd,  $n = 16$ ,

R = C<sub>4</sub>H<sub>9</sub>) exhibited both an unidentified smectic and a nematic phase at temperatures similar to the copper complex. If, however,  $n$  was fixed at 16 and R was OC <sub>$m$</sub> H<sub>2 $m$ +1</sub> with  $m$  varying from 4 to 16, then an additional (unidentified) smectic phase was observed. Initial melting points were in the range 117–145 °C while clearing points varied from 215 °C to 252 °C, all temperatures decreasing with increasing  $m$ . The same copper complexes ((**216**): M = Cu,  $n = 4, 6, R = C_4H_9$ ) were later reported to show a nematic phase, but with clearing temperatures 20 °C higher.<sup>902</sup>



Both Marcos *et al.*<sup>903</sup> and Hoshino *et al.*<sup>904</sup> reported other copper complexes with the former varying  $m$  for  $n = 10$  ((**216**): M = Cu,  $n = 10, R = OC_mH_{2m+1}, m = 1-6, 8, 10, 14$ ), while the latter varied  $n$  for  $m = 2$  ((**216**): M = Cu, R = OC<sub>2</sub>H<sub>5</sub>,  $n = 6-12, 14, 16, 18$ ). Marcos reported that the complexes were mesomorphic for  $1 \leq m \leq 14$ , with a nematic phase observed from  $m = 1-10$  and an SmC phase seen for  $n = 3-10, 14$ ; melting points were around 155–180 °C with clearing points between 232 °C and 267 °C. For  $6 \leq n \leq 14$ , Hoshino reported a nematic phase with an SmC phase for  $11 \leq m \leq 18$ ; melting points were in the range 156–222 °C with clearing points between 251 °C and 275 °C. Marcos also synthesized the related nickel(II) ((**216**): M = Ni,  $n = 10, R = OC_mH_{2m+1}, m = 1-6, 8, 10, 14$ ) complexes and reported that at low values of  $m$ , a nematic phase was seen ( $m = 1-4$ ) with narrow mesomorphic ranges  $\approx 30$  °C and clearing points some 30–50 °C lower than those of the homologous copper complexes, whereas at larger  $m$ , only a crystal smectic phase was observed (see Table 70).

Other oxovanadium ((**216**): M = V=O,  $n = 10, R = OC_mH_{2m+1}, m = 1, 2, 5, 10$ )<sup>886</sup> and chloro-iron ((**216**): M = Fe—Cl,  $n = 10, R = OC_mH_{2m+1}, m = 1-10$ )<sup>905</sup> complexes were prepared. In common with their copper analogs, they showed both SmC and nematic phases, but the SmC appeared for larger values of  $m$  ( $m > 5$  for M = V=O, and  $m \geq 7$  for M = Fe—Cl) with the nematic phase being favored. The mesomorphic temperature ranges were considerably reduced in the square-pyramidal complex ( $\approx 80$  to 20 °C for M = V=O) and in the pseudo trigonal-bipyramid complex ( $\approx 40$  to 20 °C for M = Fe—Cl), compared to the 80 to 100 °C range observed for the copper complexes.

Only one chiral derivative has been reported ((**216**): M = Cu,  $n = 10, R = OCH_2C^*HClMe$ ). It showed a rich polymorphism, Cr 182 SmC\* 222 SmA 255 N\* 260.5 I, but the complex partly decomposed on successive heating-cooling cycles.<sup>906</sup>

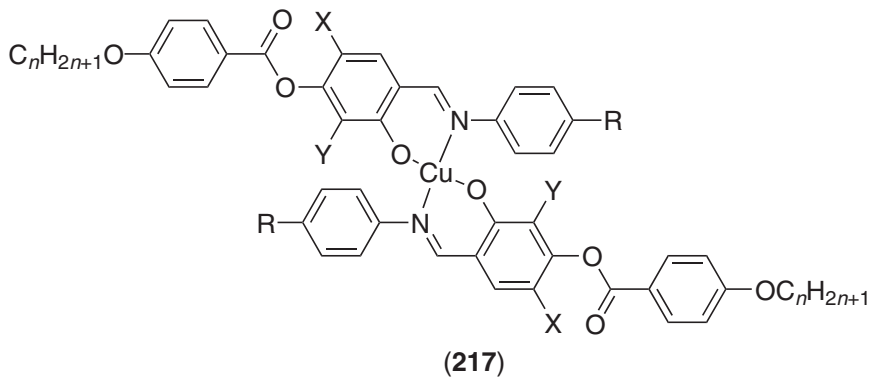
Bui *et al.* studied di-<sup>907</sup> and tetra-halogenated<sup>908</sup> derivatives of some of the Cu<sup>II</sup> complexes (**217**). The halogen was either Cl or Br and was situated in either the 3- (Y), the 5- (X) positions, or both, relative to the ring position bearing the imino carbon. In all cases the clearing temperatures of the nematic phase were reduced when compared to the non-halogenated analogs and these reductions were always greater for X = Br. For X = Cl, the reduction in clearing temperature was greatest for 5-substitution whereas for X = Br, no simple relationship was found (Table 71). The replacement of the butyl chain by a hexadecyloxy chain allowed the access to lower transition

**Table 70** Transition temperatures of some selected complexes (**216**) ( $n = 10, R = OC_mH_{2m+1}$ ).

$m$	$M = Cu$	$M = Ni$	$M = V=O$	$M = Fe-Cl$
1	Cr 167 N 267 I	Cr 183 N 213 I	Cr 209 N 282 I	Cr 209 N 233.5 I
2	Cr 161 N 255 I	Cr 219.5 N 230 I	Cr 207 N 281 I	Cr 202 N 253 I
5	Cr 174 SmC 230 N 266 I	Cr 204 I	Cr 225 N 266.5 I	Cr 210 N 226 I
10	Cr 164 SmC 248 N 248.5 I	Cr 197 I	Cr 227 SmC 240 N 247 I	Cr 180 SmC 190 N 210 I

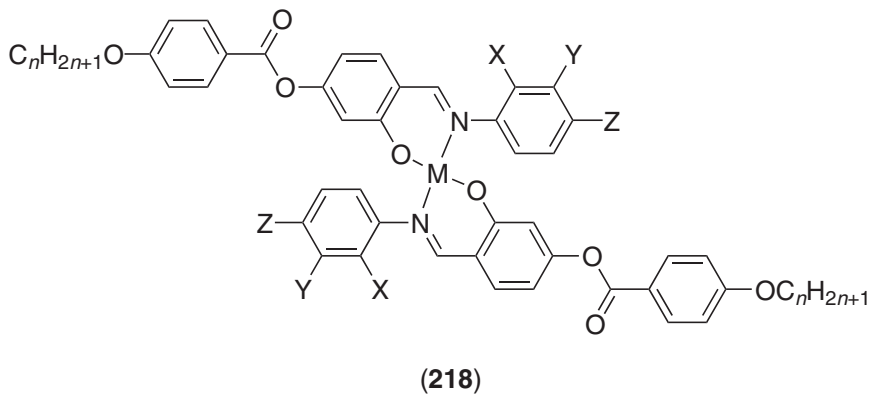
**Table 71** Effect of halogen substitution on mesomorphic properties of copper complexes (**217**).

<i>X</i>	<i>Y</i>	<i>R</i> = C <sub>4</sub> H <sub>9</sub> <i>n</i> = 4	<i>n</i> = 8	<i>n</i> = 12	<i>n</i> = 16	<i>R</i> = OC <sub>16</sub> H <sub>33</sub> <i>n</i> = 16
H	H	Cr 231 N 261 I	Cr 195 N 257 I	Cr 173 N 248 I	Cr 158 N 233 I	Cr 117 SmC 139 N 215 I
H	Cl	Cr 234 N 251 I	Cr 184 N 228 I	Cr 164 N 209 I	Cr 148 N 196 I	Cr 128 SmC 159 N 191 I
H	Br	Cr 227 N 240 I	Cr 188 N 200 I	Cr 179 N 185 I	Cr 174 N 179 I	Cr 176 N 181 I
Cl	H	Cr 238 N 245 I	Cr 197 N 221 I	Cr 172 N 201 I	Cr 158 N 183 I	Cr 104 SmC 119 N 179 I
Br	H	Cr 215 N 237 I	Cr 184 N 211 I	Cr 154 N 187 I	Cr 125 N 165 I	Cr 105 SmC 132 N 170 I
Cl	Cl	Cr 251 (N 241) I	Cr 176 (N 174) I	Cr 182 (N 159) I	Cr 144 (N 137) I	
Br	Cl	Cr 255 (N 244) I	Cr 171 (N 163) I	Cr 179 (N 157) I	Cr 142 (N 126) I	
Cl	Br	Cr 252 (N 241) I	Cr 182 (N 141) I	Cr 179 (N 111) I	Cr 146 (N 107) I	
Br	Br	Cr 256 (N 245) I	Cr 176 (N 128) I	Cr 179 (N 131) I	Cr 151 (N 107) I	



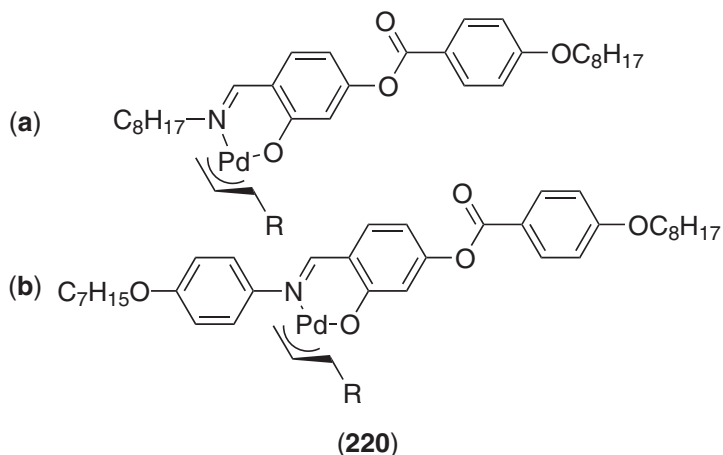
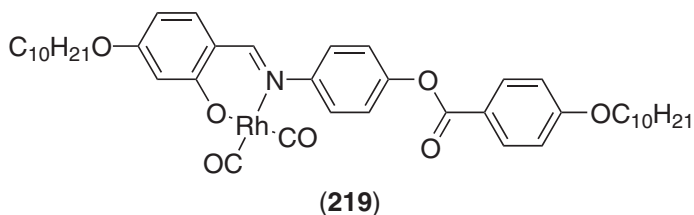
temperatures. For the dihalogenated compounds, the mesomorphism was suppressed considerably and only a monotropic nematic phase was observed (Table 71).

In a related piece of work, Campillos *et al.* investigated the effect on the mesomorphic properties of copper<sup>909</sup> and oxovanadium<sup>910</sup> complexes of polar substituents such as fluorine, trifluoromethane, and cyanide, and their position on the aniline ring ((**218**): M = Cu, V=O; *n* = 6, 10; X, Y, Z = H, F, CN, CF<sub>3</sub>, CH<sub>2</sub>CN). While the ligands exhibited a variety of mesophases, the mesophase stability was reduced considerably for the complexes, and the SmC phase totally suppressed. The results of this investigation were quite disappointing in that the transition temperatures were very high (especially for the copper complexes), and the mesomorphism of the free ligands, which consisted of SmA and N phases, was either suppressed upon complexation, particularly in the V=O complexes, or the mesophases became destabilized or existed over reduced temperature ranges.

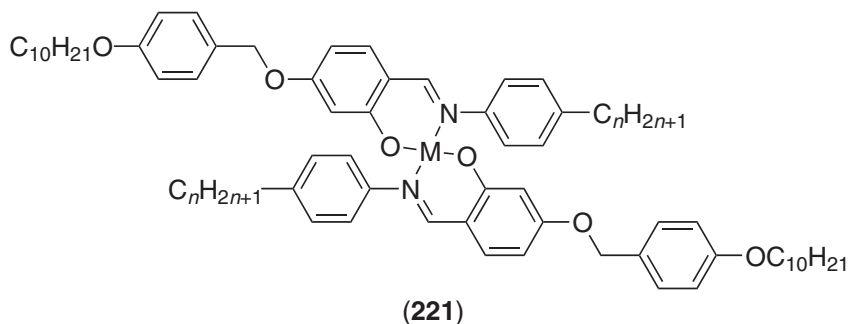


Appropriately designed salicylidimine ligands can form mesomorphic complexes when only one is bound to the metal center. For example, (**219**) shows a dicarbonylrhodium(I) moiety bound to a salicylidimine and SmA and N phases were observed (Cr 112 SmA 116.5 N 122 I).<sup>911</sup>

Related allylpalladium(II) complexes were realized<sup>912</sup> with similar ligands and in each case, perhaps surprisingly, the methallyl derivative led to the more stable nematic phase ((**220a**): R = H: Cr 89.5 I, R = Me: Cr 94 (N 40) I; (**220b**): R = H: Cr 138 (N 114.5) I, R = Me: Cr 148 (N 142.5) I).



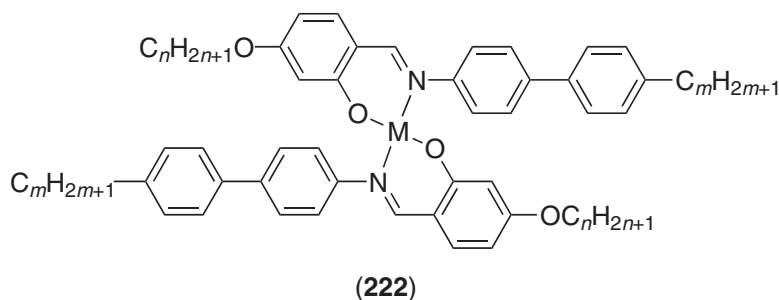
Interestingly, the replacement of the alkoxybenzoyloxy group by an alkoxybenzyloxy group led to materials ((**221**): M = Cu, V = O;  $n = 1-10$ ) showing SmA and SmC phases at the expense of the nematic phase which disappeared totally.<sup>913</sup> Thus, the copper complexes exhibited an SmA phase for  $1 \leq n \leq 6$ , and an SmC for  $5 \leq n \leq 10$  typically melting between 140 °C and 160 °C, and clearing between 200 °C and 230 °C. As for the oxovanadium complexes, the SmA was observed for  $1 \leq n \leq 7$ , and the SmC phase for  $6 \leq n \leq 10$ , at higher temperatures than their copper congeners, i.e., melting around 160–200 °C and similar clearing to the copper complexes. EPR spectroscopy revealed a positive anisotropy of the magnetic susceptibility,<sup>914</sup> as found for complexes (**216**).



Copper, palladium ((**222**): M = Cu, Pd,  $m = 12$ ,  $n = 1-12$ , 18),<sup>915</sup> platinum, oxovanadium ((**222**): M = Pt, V = O,  $m = 10$ ,  $n = 4-12$ , 18),<sup>916</sup> and nickel ((**222**): M = Ni,  $m = 12$ ,  $n = 1-12$ , 18)<sup>917</sup> have also been coordinated to *N*-4-(4''-alkylbiphenyl)-4'-alkoxysalicylaldehyde ligands, and high-temperature smectic phases were induced for all of them. For the Cu<sup>II</sup>, Pd<sup>II</sup>, Pt<sup>II</sup>, and V<sup>IV</sup>=O complexes, the SmA was present for all  $n$ , whereas for the Ni<sup>II</sup> complex, the SmA phase was lost for  $n > 9$ . The SmC phase appeared at longer chain length, i.e., for  $n > 6$  for Cu<sup>II</sup>, Pt<sup>II</sup>, and V<sup>IV</sup>=O,  $n > 5$  for Pd<sup>II</sup>, and  $n > 4$  for Ni<sup>II</sup>. Interestingly, a nematic phase was also observed in the decyl derivatives of V<sup>IV</sup>=O and Pt<sup>II</sup> when the alkoxy chain was removed, along with an SmC for the V=O compound (Cr 155 SmC 184 N 197 I), and both SmC and SmA phases for the platinum

**Table 72** Transition temperatures for complexes **(222)** ( $M = \text{Cu}, \text{Pd}, \text{Ni}; m = 12; M = \text{V}=\text{O}, \text{Pt}; m = 10$ ).

$n$	4	8	12	18
Cu	Cr 168 SmA 288 dec.	Cr 206 SmC 224 SmA 255 I	Cr 191 SmC 223 SmA 232 I	Cr 181 SmC 207 SmA 212 I
Pd	Cr 207.5 SmA 290 dec.	Cr 206 SmC 259 SmA 282 I	Cr 193 SmC 253 SmA 262 I	Cr 172 SmC 223 SmA 226 I
V=O	Cr 158 SmA 290 dec.	Cr 181 SmC 226 SmA 272 I	Cr 178 SmC 244 SmA 255 I	Cr 165 SmC 226 SmA 233 I
Pt	Cr 239 SmA 290 dec.	Cr 224 SmC 272 SmA 290 I	Cr 211 SmC 264 SmA 272 I	Cr 190 SmC 243 SmA 249 I
Ni	Cr 157 SmA 262 I	Cr 180 SmC 222 SmA 237 I	Cr 141 SmC 196 I	Cr 122 SmC 179 I



derivative (Cr 229 SmC 240 SmA 250 N 255 I). On average, the mesophase stability was found to follow the sequence  $\text{Pt} > \text{Pd} > \text{Cu} > \text{Ni}, \text{V}=\text{O}$ . Some selected data are given in Table 72.

SmC\* and N\* phases have also been reported for related copper derivatives bearing chiral chains, whereas the oxovanadium analogs only showed a single SmA phase.<sup>918,919</sup>

An interesting structural study was proposed by Reddy and Brown on modified alkoxysalicylaldehyde Schiff-base ligands in which the amino part was based on fluorene (**(223a)**:  $n = 4-10$ ), biphenyl (**(223b)**:  $n = 4-10$ ), or stilbene (**(223c)**:  $n = 4-10$ ).<sup>920</sup> Most of the free ligands exhibited SmA and N phases, whereas on complexation to copper only smectic phases were observed and over much narrower temperature ranges than found for the ligands. The SmA phase was enantiotropic for complexes **(223a)** ( $n > 6$ ) melting between 200 °C and 240 °C and clearing at 250 °C, and monotropic for all the derivatives **(223b)**, which cleared in the isotropic phase at around 260–280 °C; as for the complexes **(223c)**, an unidentified smectic phase was seen for all homologs between 200–250 °C and 280 °C. A lot of these complexes unfortunately decomposed in these high-temperature regions.

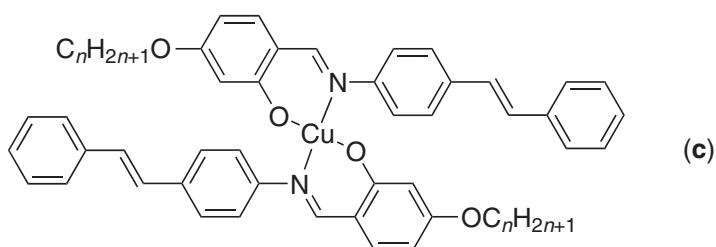
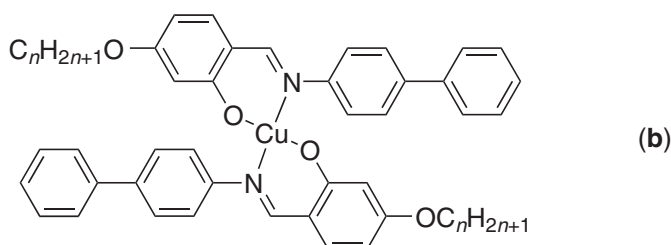
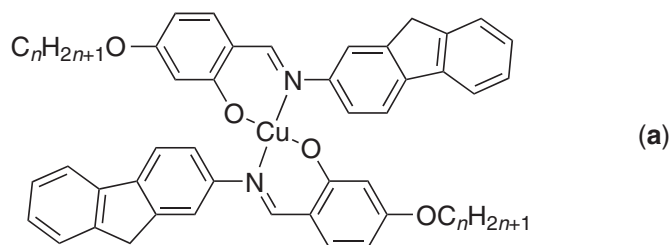
Heteronuclear complexes based on ferrocene-containing salicylaldehydes have also been reported to be mesomorphic **(224)**. The first investigation was carried out on the copper complexes, and for chain lengths equal to 10<sup>921</sup> and 12,<sup>922</sup> the trinuclear complexes exhibited a narrow-temperature-range nematic phase. This study was later extended to other metal ions (**(224)**: Ni, Pd, V=O, Fe—Cl,  $n = 12$ ), and for all of them, except the nickel derivative which decomposed before clearing, a nematic phase was found (Table 73).<sup>923</sup> Important reductions in

**Table 73** Transition temperatures of the complexes **(224)** ( $n = 12$ ).

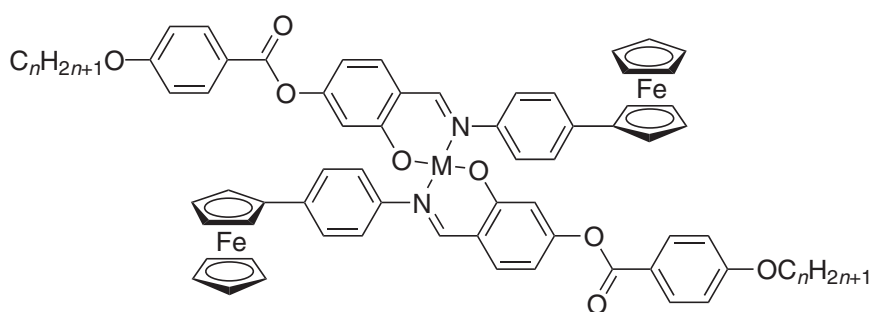
$M$	Transition temperatures
Cu	Cr 214 N 223 I
Ni	Cr 245 dec.
V=O	Cr 243 (N 240) I
Pd	Cr 271 N 275 I
Fe—Cl	Cr 195 S 205 I
ligand	Cr 154 N 165 I

S: unidentified smectic mesophase.

the transition temperatures, along with a considerable increase in the nematic temperature range, were achieved in the oxo-bridged hexa-iron complex ((225): Cr 155 N 232 I).



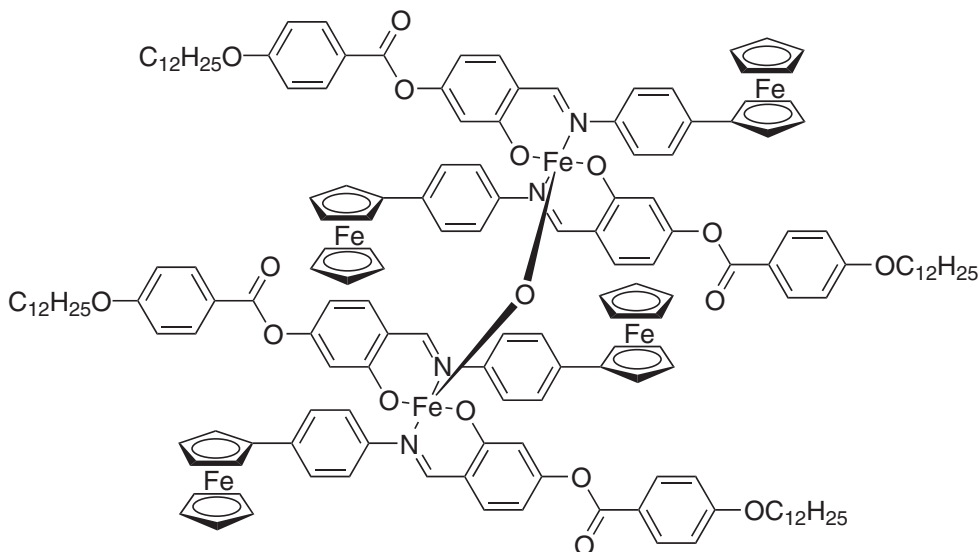
(223)



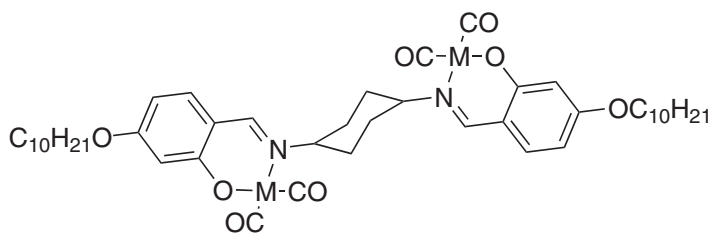
(224)

Two series of bimetallomesogens have been realized with various polyamine units used as a linker between different salicylaldehyde moieties. The first system was reported by Berdagué *et al.* who complexed dicarbonyl-rhodium(I) and -iridium(I) to a dimeric salicylaldehyde bridged by a 1,4-diaminocyclohexyl unit ((226): M = Rh, Ir).<sup>924</sup> Both complexes showed an SmA phase, that of the iridium (Cr 142 SmA 169 I) compound having a higher mesophase stability than the rhodium congener (Cr 141 SmA 145 I).





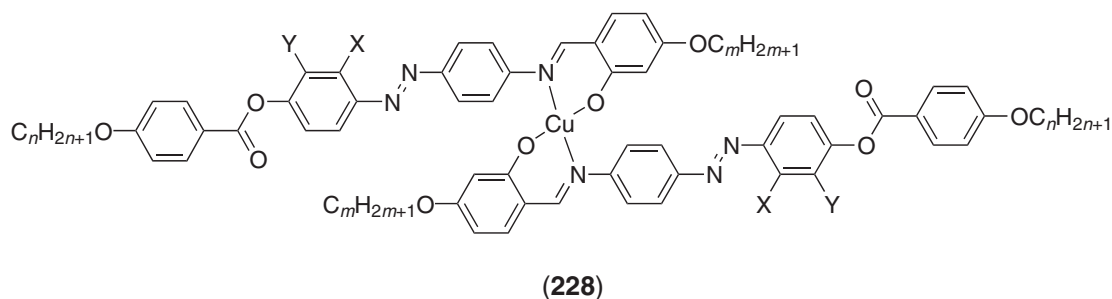
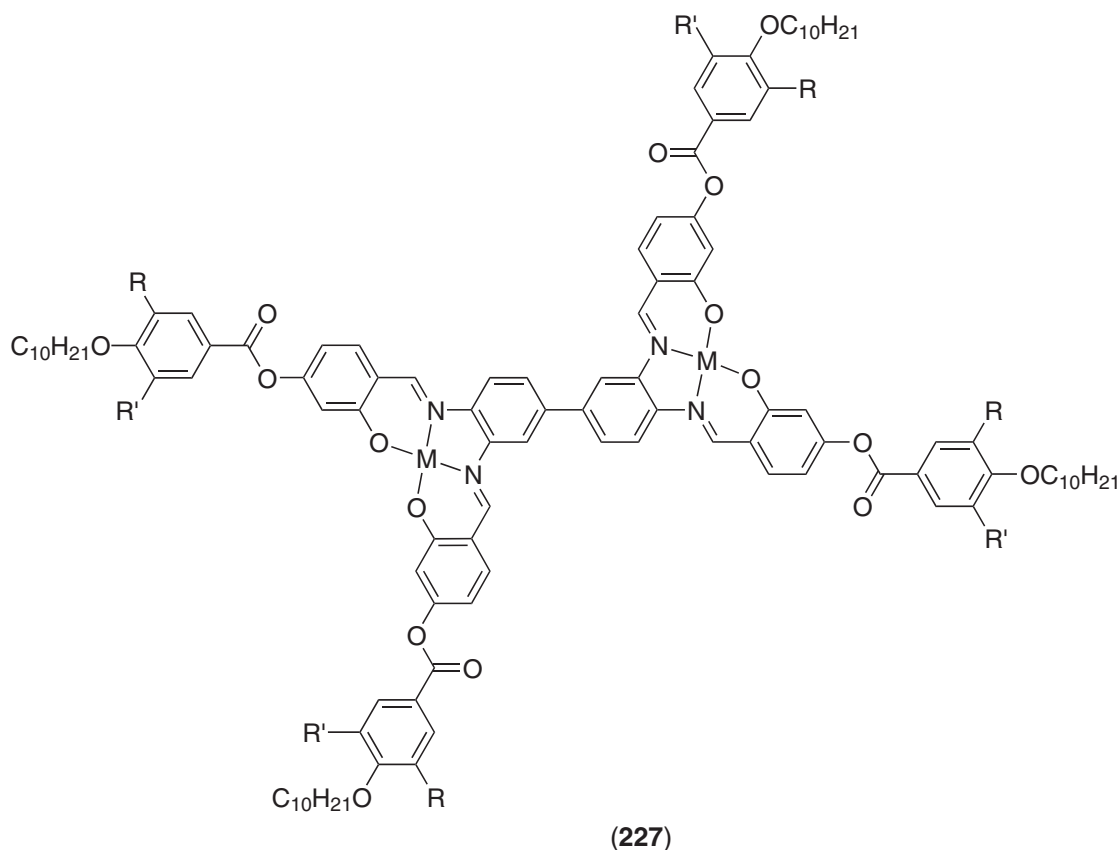
(225)



(226)

The other system is more recent and consisted of a central 3,3',4,4'-biphenyltetraamine from which a tetrameric salicylaldimine was formed.<sup>925</sup> These large ligands were mesomorphic as were the complexes with copper and oxovanadium ((227): M = Cu, V = O). With one terminal chain per branch (R = R' = H), the complexes and the ligands exhibited an SmC phase (M = Cu: Cr 190 SmC 230 dec.; M = V = O; Cr 215 SmC 293 dec.), whereas with two (R = OC<sub>10</sub>H<sub>21</sub>, R' = H) or three (R = R' = OC<sub>10</sub>H<sub>21</sub>), Col<sub>h</sub> mesophases were observed.

An interesting piece of work, carried out with salicylaldimato complexes of copper-containing four aromatic rings per ligand,<sup>926</sup> has shown that the nematic phase was largely promoted over smectic phases when alkoxy chains were added at the center of the molecule, despite the considerable length of the complexes ((228): Series I:  $m = 1$ , X = OC<sub>*m*</sub>H<sub>2*m*+1</sub>, Y = H,  $n = 4, 8, 12, 16$ ; Series II:  $m = 4$ , X = OC<sub>*m*</sub>H<sub>2*m*+1</sub>, Y = H,  $n = 2, 4, 6, 12, 16$ ; Series III:  $m = 12$ , X = OC<sub>*m*</sub>H<sub>2*m*+1</sub>, Y = H,  $n = 2, 4, 6, 8, 10, 12, 14, 16$ ). An evident decrease in the transition temperatures could also be observed when compared to non-substituted parents, or to the free ligand, if the lateral chains contain a sufficient number of carbon atoms: the longer the lateral chain, the wider the nematic temperature range (Table 74). The grafting of an additional chain in the terminal benzoate ring resulted in the decrease in the thermal stability of the nematic phase. When two lateral chains were grafted to the central core of the copper complexes ((228): Series IV: X = Y = OC<sub>*m*</sub>H<sub>2*m*+1</sub>,  $n = m = 4, 12$ ), liquid-crystalline properties were preserved, and fairly wide nematic domains were also seen (Table 74).<sup>927</sup> The clearing points, as well as the temperature range, were also very similar to those of the free ligand. It seems that the key to enlarging the nematic range was grafting lateral chains in the center of a rigid, rod-like core, which resulted in the decrease in lateral interactions.



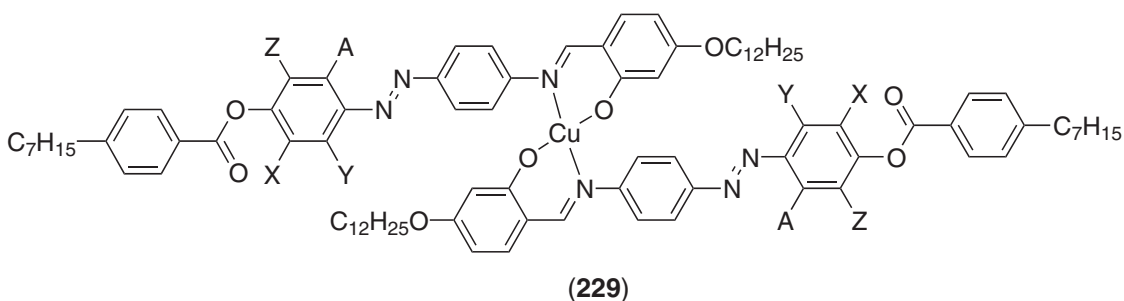
This study was extended to the effect of the number of lateral substituents, and stable SmC and extended nematic phases were obtained for compounds **(229)** for which small groups were introduced within the molecular core (Table 75).<sup>928</sup> The transition temperatures showed a weak dependency on the substituent positions, and the overall length of the molecules still dominated the mesomorphism.

**Table 74** Transition temperatures of complexes **(228)**.

<i>n</i>	Series I ( <i>m</i> = 1) <i>X</i> = OC <sub><i>m</i></sub> H <sub>2<i>m</i>+1</sub> <i>Y</i> = H	Series II ( <i>m</i> = 4) <i>X</i> = OC <sub><i>m</i></sub> H <sub>2<i>m</i>+1</sub> <i>Y</i> = H	Series III ( <i>m</i> = 12) <i>X</i> = OC <sub><i>m</i></sub> H <sub>2<i>m</i>+1</sub> <i>Y</i> = H	Series IV ( <i>n</i> = <i>m</i> ) <i>X</i> = <i>Y</i> = OC <sub><i>m</i></sub> H <sub>2<i>m</i>+1</sub>
4	Cr 239 N 265 dec.	Cr 188 N 267 dec.	Cr 107.5 N 198.5 I	Cr 229.5 N 266 dec.
8	Cr 207.5 N 250 I		Cr 94 N 181.5 I	
12	Cr 195.5 N 245 I	Cr 169 N 229 I	Cr 89 N 180 dec.	Cr 62.5 SmC 92.5 N 146 I
16	Cr 189 N 240 I	Cr 143.5 N 209 I	Cr 87 N 180 dec.	

**Table 75** Transition temperatures of complexes (229).

<i>X</i>	<i>Y</i>	<i>Z</i>	<i>A</i>	Transitions
H	Me	H	H	Cr 130 SmC 192.5 N 272.5 I
H	Me	H	Me	Cr 146.5 SmC 168.5 N 258.5 I
Me	H	Me	H	Cr 166.5 N 265.5 I
Me	Me	H	H	Cr 171.5 SmC 221 N 275.5 I
Me	Me	Me	Me	Cr 242.5 N 272.5 I



Several lanthanide complexes have been successfully coordinated with a wide range of salicylaldehyde ligands, and with appropriate ligand anisotropy and chain length, mesophases have been observed. This work has recently been collected into an excellent and most comprehensive review,<sup>15</sup> and also in a mini review<sup>929</sup> so that an overview is given here.

These are challenging materials as there is a need to reconcile the effectively contradictory requirements of structural anisotropy for mesophase formation, and high coordination numbers (normally CN = 9) around the lanthanide. The complexes were prepared by the reaction of the ligand with a lanthanide(III) salt in absolute ethanol or thf, and the lability of the complexes formed therein can offer difficulties in subsequent purification. The stoichiometry of the complexes has been the subject of debate and initial reports by Galyametdinov and co-workers suggested a formulation of  $[\text{Ln}(\text{LH})_2(\text{L})][\text{X}]_2$  where LH is the neutral salicylaldehyde (Figure 99), L its anionic form, and X the anion. However, such formulations have been based on the results of elemental analysis and yet <sup>1</sup>H NMR spectra of many complexes show only a single ligand environment. Some enhanced understanding was gained for nitrate complexes when X-ray single-crystal structures became available (e.g., Figure 97a) and showed the lanthanide ions to be nine-coordinate and ligated by three  $\kappa^2$ -O,O-nitrato anions and three neutral ligands bound in a monodentate fashion. The interesting aspect of this observation is that the ligands are coordinated through a deprotonated phenate oxygen which leaves the ligand in a zwitterionic form containing an iminium cation as demonstrated by selective NMR decoupling experiments.<sup>930,931</sup> The consequence of this is that being attached through only a single atom, the ligand is rather free to move around and so it becomes extremely difficult to determine what the organization might be in the mesophase as opposed to the solid state with over-riding lattice energy considerations governing the spatial arrangement. Of course, whether species other than nitrates arrange in this way is not yet clear. Nevertheless, it is possible to realize materials with reproducible stoichiometries.

The majority of complexes, prepared for the most part in elegant studies by Galyametdinov and co-workers and by Binnemans and co-workers, show only an SmA phase, and this was induced initially in lanthanide complexes based on ligand L<sup>1</sup>H (Figure 99) ( $[\text{Ln}(\text{L}^1\text{H})_2(\text{L}^1)][\text{X}]_2$  or  $[\text{Ln}(\text{L}^1\text{H})_3][\text{X}]_3$ ) whatever the length of the chains, and the counterion ( $\text{X} = \text{NO}_3$ ,<sup>930,932-940</sup> Cl,<sup>941,942</sup> DOS,<sup>943-945</sup> alkylsulfate<sup>946,947</sup>) was systematically varied. In general, the influence of the alkoxy chain length or the N-alkyl chain length is kept to a minimum, with a slight decrease in the transition temperatures with increasing  $n+m$ . In the nitrate series, the most studied, the lanthanide influenced considerably those mesomorphic properties, and while the melting point increased, the clearing temperatures decreased, resulting in an overall decrease in the mesophase range (Figure 98). Complexes with a chloride counterion showed higher transition temperatures than the analogous nitrate derivatives, whereas those with alkylsulfate<sup>943</sup> chains have much lower transition temperatures and narrow mesomorphic domains.

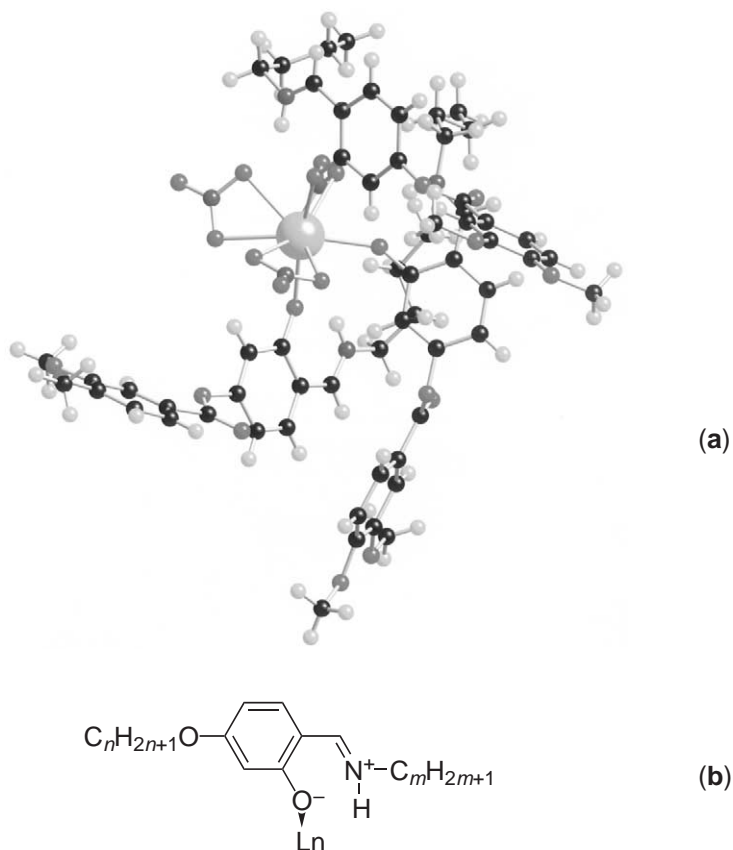


**Figure 97** (a) X-Ray single crystal structure of a salicyaldimine complex and (b) the zwitterionic form of the salicyaldimine ligand which binds to the lanthanide center.

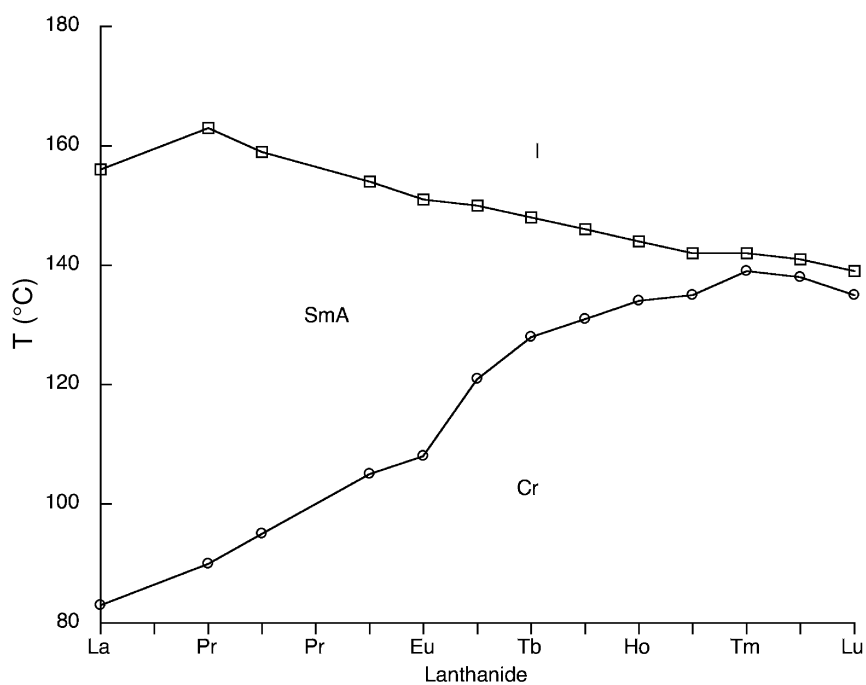


**Figure 98** Mesomorphism of a series of lanthanide nitrate complexes of ligand  $L^1H$ .

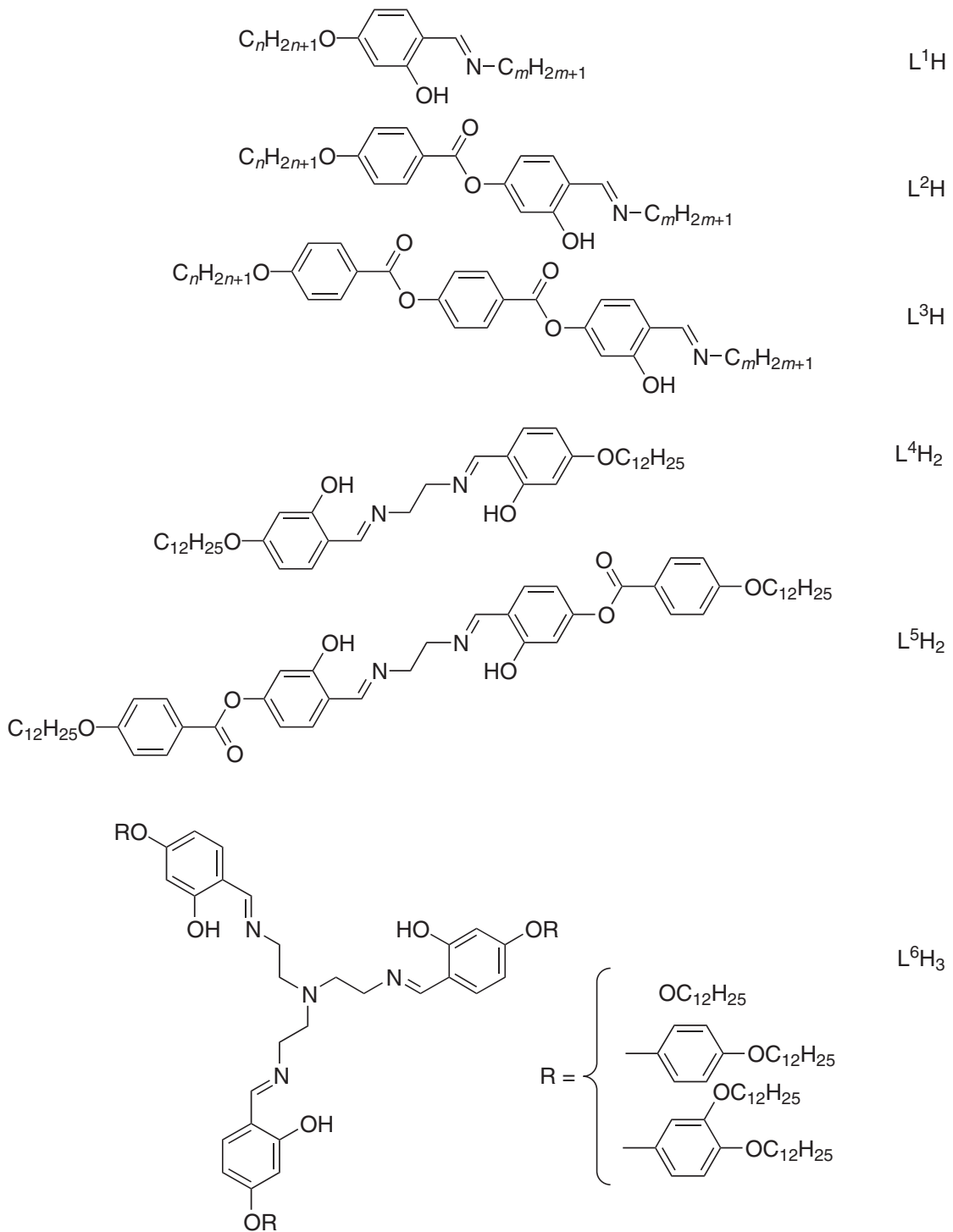


**Figure 99** Various Schiff-base ligands used to form lanthanide-containing liquid-crystals.

Liquid crystalline lanthanide complexes, essentially the nitrates, were also realized with ligands L<sup>2</sup>H<sup>948,949</sup> and L<sup>3</sup>H (Figure 99);<sup>950</sup> again, the complexes existed in one of the two possible stoichiometries. The complexes with L<sup>2</sup>H exhibited, again, an SmA phase, most of them decomposing at elevated temperatures; the transition temperatures of the nitrates were lower than those of the chlorides. Great reductions in both these temperatures and mesomorphic ranges were achieved when the counterion was dodecylsulfate.

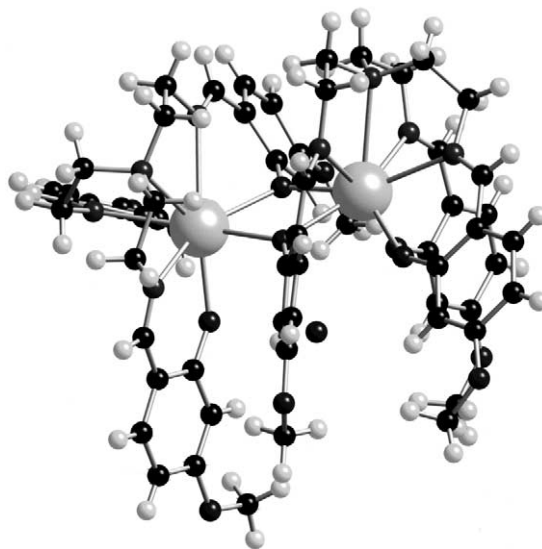


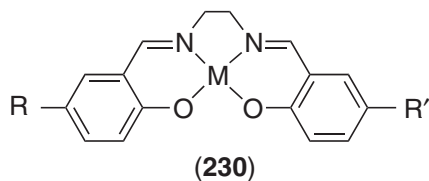
**Figure 100** X-Ray single crystal structure of a lanthanum complex of ligand  $L^6H$  ( $R = Me$ ).

With an additional chain grafted on ligand  $L^2H$ , a  $Col_h$  phase was formed for the nitrate and triflate lanthanide complexes, the latter having lower transition temperatures than the former.<sup>951</sup> Complexes formed with the elongated ligand  $L^3H$  showed an SmC phase, but were thermally unstable and decomposed before clearing. Lanthanide liquid crystalline systems have also been obtained with dimeric ( $L^4H_2$ ,  $L^5H_2$ )<sup>952</sup> and trimeric ( $L^6H_3$ )<sup>931</sup> ligands (Figure 99), though the mesophases have not yet been identified with any certainty. In the last of these, single-crystal X-ray crystallography revealed (Figure 100)<sup>931</sup> that the complex existed as a dimer. Thus, the ligand is bound in its triply deprotonated form to give a neutral “half” complex “ $Ln(L^6)$ ,” but even in this way, the ligand was insufficiently large to encapsulate the metal entirely and so the vacant surface on the metal ion was occupied by bridging oxygen atoms from another complex, giving a dimer.

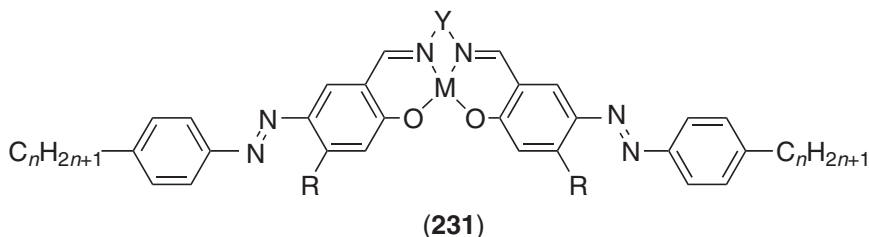
The magnetic anisotropy,  $\Delta\chi$ , of the SmA phase of some of these complexes has been measured and found to be orders of magnitude higher than those of organic liquid crystals.<sup>953–956</sup>

#### 7.9.14.5.12 *N,N'*-Disalicylidenealkylenediamine complexes

There were two reports<sup>957,958</sup> of the same *N,N'*-bis(5-alkoxysalicylidene)ethylenediamine complexes of nickel(II) and copper(II) ((230):  $M = Ni, Cu$ ;  $R = R' = OC_nH_{2n+1}$ ). In the earlier paper, the materials were reported to show SmA mesophases at elevated temperatures, while in the later report the mesophase was not identified beyond being smectic and the transition temperatures were quite different. A later re-investigation of these complexes revealed that these compounds were, in fact, unstable.<sup>959</sup> In the same paper, bis(5-alkyl)salen complexes of nickel and copper were described ((230):  $M = Ni, Cu$ ;  $R = R' = C_nH_{2n+1}$ ) which led again to controversial results. While Paschke *et al.* reported high-temperature SmA mesophases for the alkoxy derivatives (between 200 and 300 °C), Ohta *et al.* observed crystal smectic E and SmA phases with clearing temperatures being some 50 °C lower.<sup>960</sup> Such bis(alkoxy) and/or bis(alkyl) salen ligands were complexed to oxovanadium(IV)<sup>961</sup> and cobalt(II),<sup>962</sup> leading to similar mesomorphic behavior (i.e., ordered smectic and SmA phases), with an important depression in the transition temperatures in the  $V=O$  complexes, clearing at around 200 °C. In order to lower the transition temperatures, two other approaches were attempted. Ligand fluorination of some  $Ni^{II}$ ,  $Cu^{II}$ , and  $V^{IV}=O$  complexes resulted in the destruction or destabilization (monotropic phases) of the mesomorphic properties.<sup>963</sup> Unsymmetrically substituted copper(II) salen complexes ((230):  $M = Cu$ ;  $R \neq R'$ ) showed mesophases (crystal smectic E and/or SmA) with lower melting points, but still with high clearing temperatures (200 to 300 °C).<sup>964</sup> Crystal structures have been determined but only for the nickel complexes, and it was found that both the dialkoxy and dialkyl systems crystallized as face-to-face dimers; the existence of such dimers has also been proved by scanning tunneling microscopy.<sup>965,966</sup>



Enhancement of the molecular anisotropy of such salen complexes by the use of alkylphenylazo groups in place of the flexible chain ((231): M = Ni, Cu, V=O; R = H; Y = C<sub>2</sub>H<sub>4</sub>, C<sub>3</sub>H<sub>6</sub>) led to high-temperature mesomorphism.<sup>967</sup> The short-chain-length nickel and copper complexes showed a nematic phase (>220 °C) for (n = 6), and the oxovanadium complexes and the long-chain-length copper and nickel complexes (n = 14), an SmC phase. The SmC phase occurred also at high temperature but with a strong reduction in the melting point (nearly 100 °C) from Y = C<sub>2</sub>H<sub>4</sub> to Y = C<sub>3</sub>H<sub>6</sub>. None of the complexes with Y = CH<sub>2</sub>CMe<sub>2</sub>CH<sub>2</sub> was mesomorphic, nor were the ligands. The addition of two lateral alkoxy chains ((231): M = Ni; n = 14, R = OC<sub>m</sub>H<sub>2m+1</sub>; Y = C<sub>2</sub>H<sub>4</sub>, C<sub>3</sub>H<sub>6</sub>, CH<sub>2</sub>CMe<sub>2</sub>CH<sub>2</sub>) produced the correct molecular geometry to induce nematic and smectic (A and C) mesophases (Table 76).<sup>968</sup> The ligands with long chain length displayed SmC close to room temperature.



Related complexes, (232), were found to be stabilize smectic phases, particularly the SmA phase, on the introduction of various types of organosiloxane substituents.<sup>969–971</sup> The important step consisted of the preparation of the unsymmetrical ligand. Not only was the mesophase stabilized strongly by microsegregation, but also a wide variety of new molecular morphologies could be generated, particularly through the use of 1,3,5,7-tetramethylcyclotetrahydroxiloxane, and octakis(hydrodimethylsiloxy)octasilsequioxane (Figure 101).

#### 7.9.14.5.13 Bis(enaminoketonato) complexes

Another interesting family of square-planar metallomesogens is that constituted by complexes of enaminoketonates. Several copper complexes of type (233a) and (233b), with various n and m, have been synthesized, and when R is an alkoxy (OC<sub>n</sub>H<sub>2n+1</sub>), alkyl (C<sub>n</sub>H<sub>2n+1</sub>), or alkanoate (CO<sub>2</sub>C<sub>n</sub>H<sub>2n+1</sub>) group, the complexes are not liquid crystals, or exceptionally showed a monotropic SmA phase.<sup>972</sup>

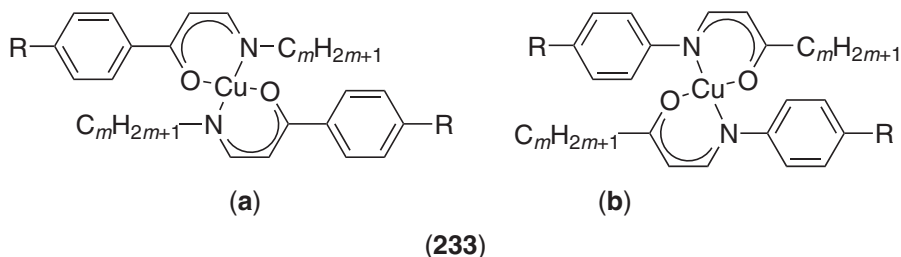


Table 76 Mesomorphism of the nickel complexes (231), n = 14.

R	Y = C <sub>2</sub> H <sub>4</sub>	Y = C <sub>3</sub> H <sub>6</sub>	Y = CH <sub>2</sub> CMe <sub>2</sub> CH <sub>2</sub>
H	Cr 263 SmC 312 dec.	Cr 173 SmC 302 dec.	Not LC
OC <sub>6</sub> H <sub>13</sub>	Cr 214 I	Cr 127 N 226 I	Cr 128 SmA 293 I
OC <sub>18</sub> H <sub>37</sub>	Cr 65.5 SmC 101 I	Cr 89.5 SmC 102 SmA 180 I	Cr 118 SmA 190 I

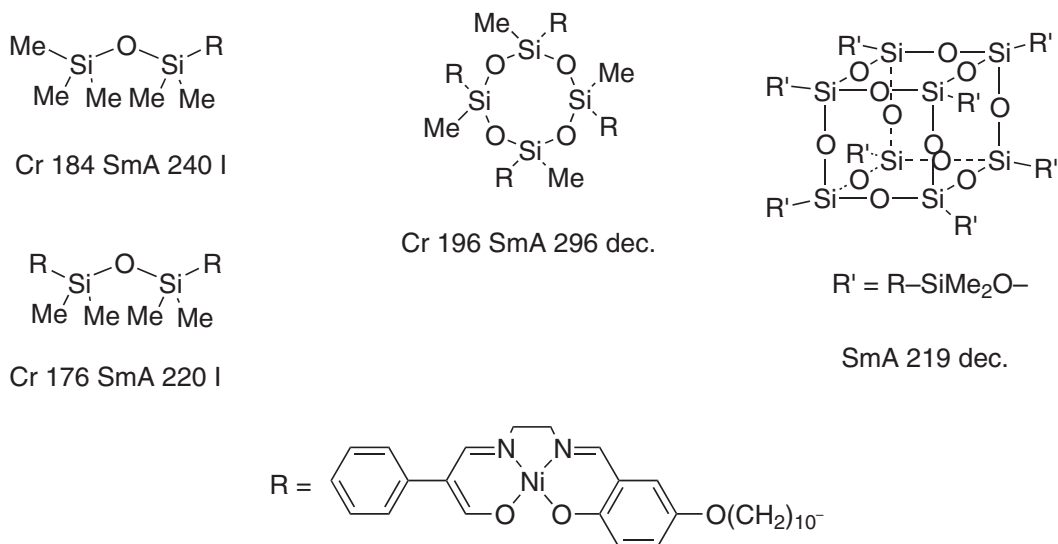
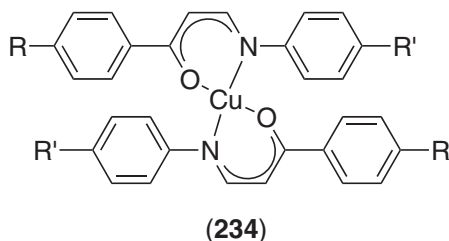


Figure 101 Various structures derived from complexes (232).

Elongation of the core of (233) by the incorporation of 4-alkyl-*trans*-cyclohexane ((233a,b):  $R = C_nH_{2n+1}C_6H_{10}^-$ ), helped to reduce transition temperatures. Thus, the elongated (233a) showed an enantiotropic nematic phase, which became monotropic as the chain length,  $m$ , increased.<sup>973,974</sup> On the other hand, the elongated (233b) showed nematic and SmA phases.<sup>975</sup>

Other enaminketone complexes of the type (234) were also prepared. It was found that when R was an alkoxy chain ( $R = OC_nH_{2n+1}$ ), and R' was a polar group ( $R' = F, CN, SCN, NO_2$ ) or a chain ( $R' = Me, Et, Bu, SEt, OC_6H_{13}, CO_2C_6H_{13}$ ), SmA ( $R' = F, Bu, SEt, OC_6H_{13}, CO_2C_6H_{13}$ ), N ( $R' = CN, NO_2, Me, Et, Bu$ ), and SmC ( $OC_6H_{13}, CO_2C_6H_{13}$ ) phases were observed but at high temperatures ( $>150^\circ C$ ), often accompanied by irreversible decomposition.<sup>976-978</sup>



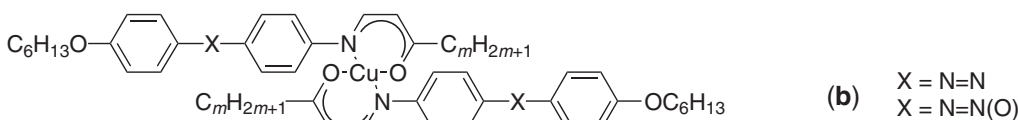
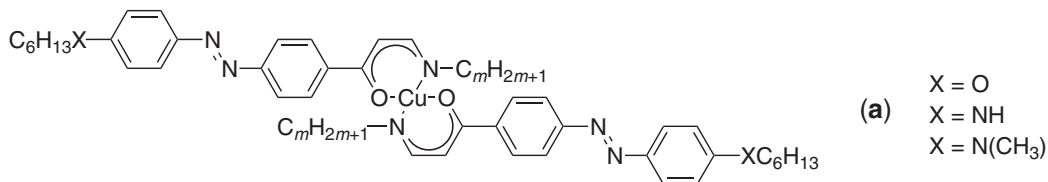
The copper complexes derived from more rigid and elongated enaminketone ligands having lateral chains attached to the nitrogen atom (235a) or on the carbonyl group (235b) were found to behave in a similar way to the complexes above (235); that is, in most cases the nematic phase was promoted over the smectic phases (Table 77).<sup>979</sup> In the first series ((235a):  $X = O; m = 3-13, 15, 18$ ), the nematic phase is present for all the complexes, in addition to an SmC phase for the longer homologs ( $m = 15$  and  $18$ , respectively). The ligand itself also showed both phases. The clearing temperatures decreased for all homologs, while the melting point first decreased and then rose for  $m = 11$ ; substitution by terminal alkylamino groups depressed both clearing and melting points significantly. For compounds, (235a)

Table 77 Selected data for complexes (235a) and (235b).

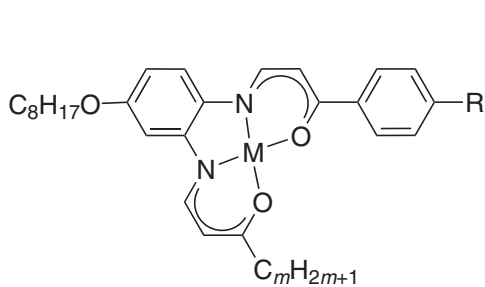
$X$	$n$	Mesomorphism	$X$	$n$	Mesomorphism
O	5	Cr 142 N 221.5 I	NH	6	Cr 104 N 125 I
	12	Cr 116 N 186 I		12	Cr 112 (SmA 105) I
	18	Cr 118.5 SmC 130 N 159 I		18	Cr 99 (SmC 93) SmA 101 I
N=N	5	Cr 143 N 181 dec.	NCH <sub>3</sub>	6	Cr 111 N 132 I
	11	Cr 156 (SmC 145.5 SmA 156) N 170 I		12	Cr 82 N 96 I
N=N(O)	11	Cr 141.5 (SmC 137) N 178 I	18	Cr 81.5 N 82.5 I	



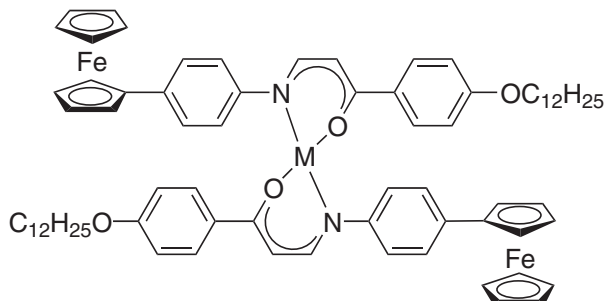
((235a): X = NH;  $m = 2$  to 6, 8, 10, 12, 18), layered structures were favored, while in the other series, ((235a): X = N(CH<sub>3</sub>);  $m = 6, 10-15, 18$ ), only nematic phases were observed, this difference being attributed to the stronger possibility of H-bonding formation in the former. In a second part of this study, the lateral chains were attached to the carbonyl groups, (235b). The complexes showed monotropic smectic and enantiotropic nematic phases. Overall, the nematic phase is largely promoted over the smectic phase in the azo compounds (Table 77).



(235)



(236)



(237)

More sophisticated ligand topologies were used for the enaminoketones in order to reduce the transition temperatures more efficiently and avoid problems of decomposition. In one series of materials (236),<sup>980</sup> the nickel complexes exhibited SmA and nematic phases, enantiotropic or monotropic depending on the structural parameters ((236): M = Ni,  $m = 1, 9, 11$ ; R = H, CN, OMe, OC<sub>8</sub>H<sub>17</sub>, OC<sub>11</sub>H<sub>23</sub>, OC<sub>12</sub>H<sub>25</sub>); poorer results were obtained for the corresponding oxovanadium complexes ((236): M = V=O,  $m = 1, 9$ ; R = CN, OMe, OC<sub>8</sub>H<sub>17</sub>). The heteropolynuclear complexes (237) ((237): M = Cu, Pd)<sup>981</sup> displayed only monotropic phases, Cr 144 (N 122) I for the copper complex and Cr 205 (SmC 195 N 198) I for the palladium analog.

The one-ring enaminoketones, 1-(4'-alkoxyphenyl)-3-alkylamino-2-propen-1-one (Figure 102, LH), can react with trivalent lanthanide nitrate or chloride ions to form metallomesogens having the general formula [Ln(LH)(L)<sub>2</sub>][X]<sub>2</sub>. The complexes Ln = La, Dy, Gd, Er, Eu, Tb, and X = NO<sub>3</sub>, Cl ( $n = 7, 12$ ;  $m = 12, 16, 18$ )<sup>982-984</sup> exhibited an SmA phase that can exist over a range of some 80 °C, that of the chlorides occurring at higher temperatures (ca. 160 °C), and over small temperature ranges.

#### 7.9.14.5.14 Other complexes with N,O donor sets

Despite their resemblance to the bis(hydroxyazomethine) complexes discussed above (216), bis(2-hydroxy-4-alkoxy-4'-butoxyazobenzene) complexes of copper(II) and palladium(II) ((238): M = Cu,

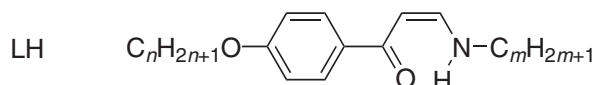
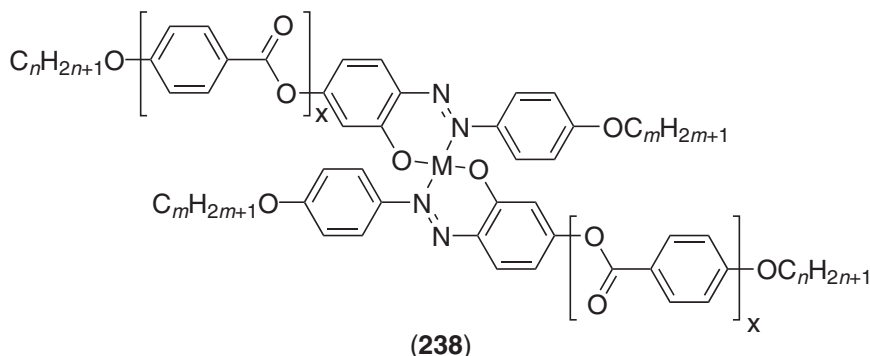
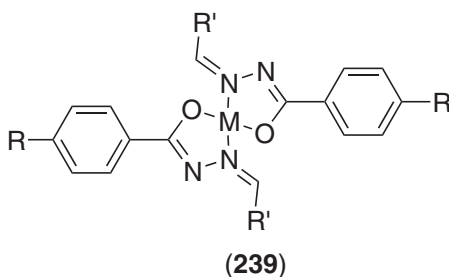


Figure 102 Enaminoketone ligand used to generate lanthanide-containing liquid crystals, [Ln(LH)(L)<sub>2</sub>][X]<sub>2</sub>.

Pd;  $x=0$ ,  $n=6, 12$ ;  $m=4$ ) were not mesomorphic, even though the ligands were themselves nematic.<sup>985</sup> Elongation of the ligand core did, however, eventually induce mesomorphism ((238):  $M = \text{Cu, Ni}$ ;  $x=1$ ,  $n=16$ ;  $m=1, 4$ ),<sup>986</sup> and the copper(II) and nickel(II) complexes displayed a nematic phase between *ca.* 180 °C up to 230 °C (*ca.* 100 °C and 180 °C for the ligands).



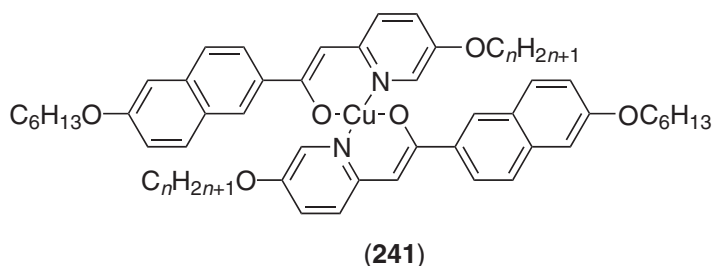
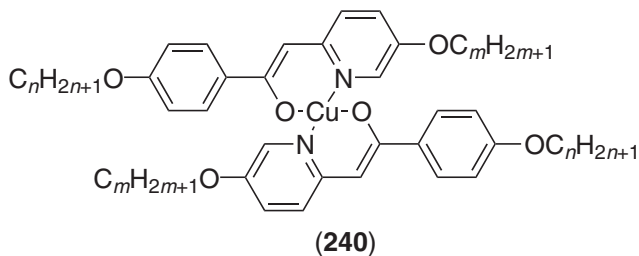
Bis(alkoxyarylhydrazinato)nickel(II) and copper(II) ((239):  $M = \text{Ni, Cu}$ ,  $R = \text{OC}_n\text{H}_{2n+1}$ ,  $R' = \text{H}$ )<sup>987</sup> were found to be mesomorphic, the copper derivatives being less thermally stable than those of nickel.<sup>988</sup> Thus, the nickel complexes showed a nematic phase ( $n=4-10$ ), and an SmC phase ( $n=10-22$ ) typically between 120 °C to 200 °C, and 130 °C to 210 °C (Table 78).<sup>989</sup> Mesophase formation was prevented in the larger *N*-alkylidene ((239):  $R' = \text{Me}$ ) or *N*-aralkylidene ((239):  $R' = \text{C}_6\text{H}_5, \text{C}_6\text{H}_5\text{OC}_{12}\text{H}_{25}$ ) complexes, probably due to the broadening of the molecule. Strangely, the bis(alkylarylhydrazinato)nickel derivatives<sup>990</sup> exhibited an SmA phase only, although the new mesophase existed over a much narrower temperature range than the mesophases of the alkoxy compounds (less than 10 °C). Fluorination in the meta position resulted in the suppression of the nematic phase (Table 78).



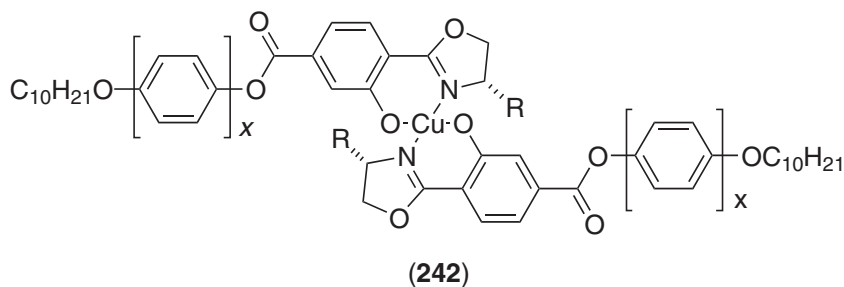
Copper complexes of bis(alkoxyphenacyl)pyridine (240)<sup>991</sup> and bis(alkoxynaphthylacyl)pyridine (241)<sup>992</sup> were found to show smectic mesomorphism. Complexes (240) ((240):  $n=m=2, 4, 6, 8, 11, 13$ ) exhibited an SmA mesophase for  $n \geq 6$ ; the melting point decreasing from 145 °C to 110 °C, and the clearing point from 166 °C to 142 °C on increasing chain length. Mesomorphism was suppressed in the non-symmetrically substituted isomeric compounds ((240):  $n=8, 13, m=2$ ). Elongation of the core of the phenacylpyridine ligand to the naphthalene derivative resulted in the stabilization of the mesomorphism, and enantiotropic N and SmC phases were induced. Upon complexation to copper(II), an SmA phase was seen between 150 °C and 170 °C for the homologs with  $n=4-8$ , whereas for greater  $n$ , ( $n=10, 11$ ), both SmB and SmC phases were formed typically between 100 °C and 150 °C. Thus, as for the ligands, the temperature range of the naphthylacylpyridine complexes (241) was broader than for the analogous phenacylpyridine complexes (240).

**Table 78** Transition temperatures of some selected nickel complexes (239) ( $R' = \text{H}$ ).

$n$	$R = \text{OC}_n\text{H}_{2n+1}$	$R = \text{C}_n\text{H}_{2n+1}$	<i>meta-F</i> , $R = \text{OC}_n\text{H}_{2n+1}$
6	Cr 161 N 187 I	Cr 146 (SmA 132) I	Cr 169 SmA 176 I
8	Cr 159 SmC 168 N 174 I	Cr 128 SmA 137 I	Cr 153 SmA 170 I
12	Cr 125 SmC 165 I	Cr 122 SmA 128 I	Cr 143 SmC 157 I

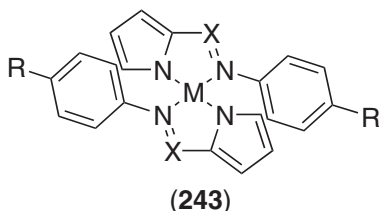


It was recently shown that copper complexes derived from (*S*)-2-(2-hydroxyaryl)oxazoline ligands ((**242**):  $x = 1$ :  $R = \text{CH}_3, \text{CHMe}_2, \text{CH}_2\text{CHMe}_2$ ;  $x = 1, 2$ :  $R = \text{C}^*\text{HCH}_3\text{CH}_2\text{CH}_3$ )<sup>993</sup> exhibited a very broad SmA phase, from 60 °C to around 150–190 °C. Used as chiral dopants (ca. 10 mol.%), a chiral nematic phase was induced systematically in all the systems, even those with  $x = 0$ , with, in some cases, an additional SmA phase being observed.

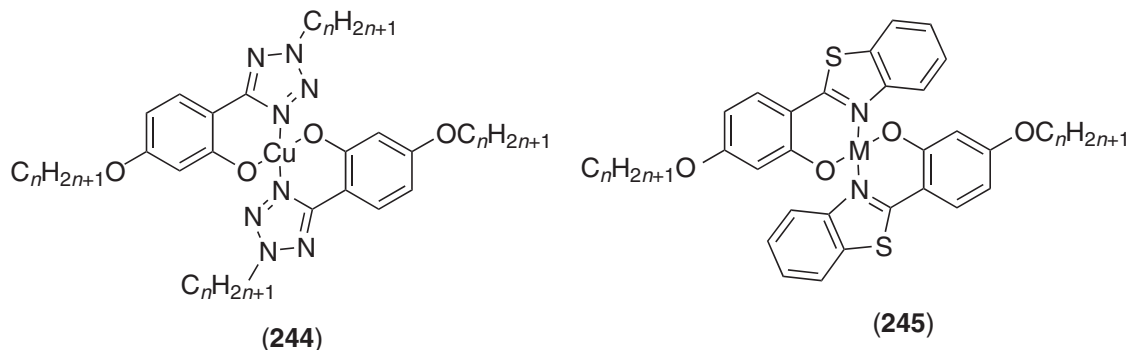


#### 7.9.14.5.15 Complexes with *N,N'* donor sets

Several other elongated, chelating bases have been used as ligands to form new metallomesogens. For instance, coordination of nickel(II) and copper(II) to 2-substituted pyrroles yielded new families of nematogenic metallomesogens.<sup>994</sup> Thus, the nickel complexes of 2-phenylazopyrrole ((**243**):  $M = \text{Ni}$ ,  $X = \text{N}$ ,  $R = \text{N}=\text{N}-\text{C}_6\text{H}_4\text{C}_6\text{H}_{13}$ ,  $\text{C}_6\text{H}_{10}\text{C}_6\text{H}_{13}$ ) and 2-phenylazomethine pyrrole ((**243**):  $M = \text{Ni}$ ,  $X = \text{CH}$ ,  $R = \text{C}_6\text{H}_{10}\text{C}_6\text{H}_{13}$ ) exhibited an enantiotropic nematic phase for the former materials (Cr 208 N 222 I and Cr 174 N 201 I, respectively), which became monotropic for the latter. As for the copper complexes, only those derived from the azomethine ligand ((**243**):  $M = \text{Cu}$ ,  $X = \text{CH}$ ,  $R = \text{C}_6\text{H}_{10}\text{C}_6\text{H}_{13}$ ) were mesomorphic (Cr 130 N 168 I), whereas the other bis(2-phenylazopyrrole) complexes of copper underwent an irreversible rearrangement upon heating; the newly formed binuclear species were not mesomorphic.



Note that the structurally related bis[5-(2-hydroxy-4-alkoxyphenyl)-2-alkyltetrazole]copper(II) ((**244**):  $n = 10, 12, 14$ ) were reported to exhibit monotropic SmA and SmC phases at around  $100^\circ\text{C}$ , whereas the bis[2-(2-hydroxy-4-decyloxyphenyl)benzothiazole]copper(II) and oxovanadium(IV) ((**245**):  $M = \text{Cu}, V = \text{O}$ ) melted directly into the isotropic liquid at ca.  $200^\circ\text{C}$ .<sup>995</sup>

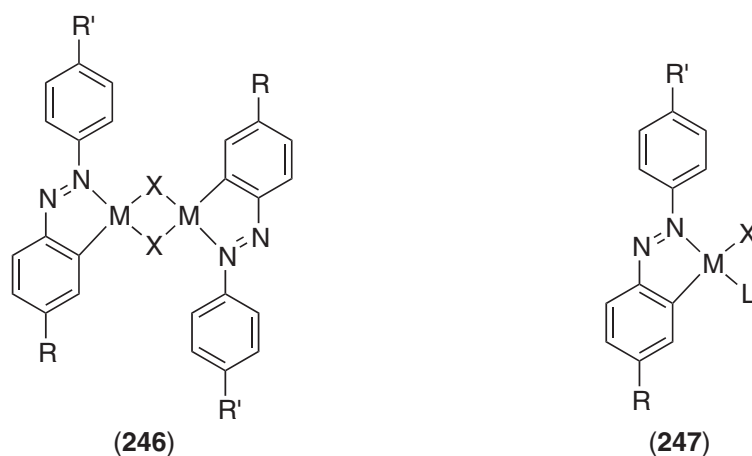


#### 7.9.14.5.16 *Ortho-metallated complexes*

*Ortho*-metallated complexes represent an interesting and broadly studied class of metallomesogens, and both dinuclear and mononuclear organometallic systems have been prepared. Many dinuclear *ortho*-metallated complexes consist of two ligands joined through a central bridge. In principal, such complexes exist as a mixture of two isomers (*anti* and *syn*), their proportion in the mixture depending both on the type of ligands and the intermetallic bridge.

##### (i) *Ortho-metallated azo complexes*

One of the earlier contributions to the revival of metal-containing liquid crystal systems was the synthesis of the *ortho*-metallated palladium complexes of mesogenic azobenzenes (**246**, **247**) by Ghedini and co-workers, which represented the first systematic attempt to coordinate metals to known liquid crystal systems.<sup>996</sup>



Initial studies<sup>997</sup> investigated the dipalladium complexes ((**246**):  $M = \text{Pd}, X = \text{Cl}, R = \text{OEt}$  and  $R' = \text{C}_4\text{H}_9\text{CO}_2, \text{C}_6\text{H}_{13}\text{CO}_2, \text{CH}_2=\text{CH}(\text{CH}_2)_8\text{CO}_2$ ) and the related mononuclear complexes ((**247**):  $X = \text{Cl}, L = \text{PPh}_3, \text{pyridine}, \text{quinoline}, \text{and aniline}$ ). All of the dinuclear complexes showed an enantiotropic nematic phase with melting points in the range  $165\text{--}210^\circ\text{C}$  and clearing points between  $185^\circ\text{C}$  and  $215^\circ\text{C}$ ; the free ligands typically melted in the range  $65\text{--}80^\circ\text{C}$  and cleared between  $105^\circ\text{C}$  and  $125^\circ\text{C}$ . The role of the bridging halogen in these systems was also investigated ((**246**):  $M = \text{Pd}, X = \text{Br}, \text{I}, R = \text{OEt}$  and  $R' = \text{C}_6\text{H}_{13}\text{CO}_2$ )<sup>998</sup> and it was found that the melting point increased in the order  $\text{Cl} < \text{Br} < \text{I}$  and that the temperature at which the nematic phase first

appeared increased according to the same order. Clearing points, however, followed a different trend; namely,  $\text{Br} > \text{I} > \text{Cl}$  ( $\text{X} = \text{Cl}$ : Cr 190 N 205 I,  $\text{X} = \text{Br}$ : Cr 210 (SmB 205) SmA 215 N 250 I,  $\text{X} = \text{I}$ : Cr 220 SmA 225 N 230 I). The reasons for these various changes are unclear. While none of the related mononuclear complexes with triphenylphosphine or aniline was mesomorphic, those with  $\text{L} = \text{py}$  and quinoline gave materials with nematic and smectic phases. For the pyridine (*N,N-cis*) complex, the nematic phase stability was similar to that found in the parent dinuclear systems (Cr 180 SmB 198 N 235 I), while for the quinoline (*N,N-trans*) complex, melting points and clearing points were somewhat reduced (Cr 136 SmA 151 N 180 I).

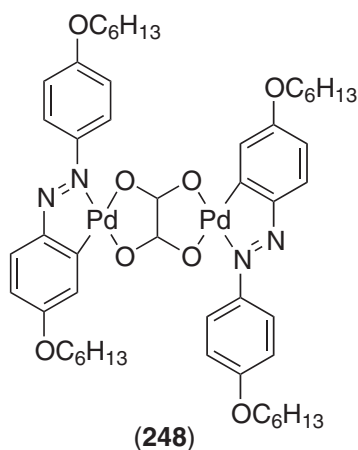
The fact that complexation of such systems enhances mesophase stability was further demonstrated in the azopalladium(II) complexes with 4-alkyl-4'-alkoxyazobenzenes for which induction and/or mesophase stabilization were observed ((**246**):  $\text{M} = \text{Pd}$ ,  $\text{R} = \text{H}$ ,  $\text{CH}_3$ ,  $\text{C}_2\text{H}_5$ ,  $\text{C}_3\text{H}_7$ ,  $\text{R}' = \text{OC}_n\text{H}_{2n+1}$ ,  $n = 1, 2, 7, 12, 18$ ).<sup>999-1001</sup> All the complexes were found to exist as equimolar mixtures of *cis* and *trans* isomers. Enantiotropic nematic phases, with in some cases additional smectic phases (SmA and SmC), were obtained; for short-chain-length complexes ( $n = 1, m = 1, 2, 7$ ), mesomorphism occurred above 200 °C, whereas for the derivatives with long alkoxy chains ( $n = 1, m = 12, 18$ ;  $m = 12, n = 2, 3$ ), mesophases appeared between melting points in the range 130–180 °C and clearing points around 160–200 °C. Molecular and macroscopic biaxiality have been claimed for these materials on the basis of order parameter measurements made by infrared techniques, calorimetry, and optical microscopy.<sup>1002</sup> Later investigations by neutron scattering and small-angle diffraction studies<sup>1003,1004</sup> suggested that the phases were uniaxial, although it is difficult to see how techniques which monitor rather short-range order could validate such a conclusion.

Several azopalladium(II) complexes of 4,4'-dialkoxyazobenzenes were also prepared. In one study, *ortho*-palladation of the 4,4'-di(tetradecyloxy)azobenzene ((**246**):  $\text{M} = \text{Pd}$ ,  $\text{R} = \text{R}' = \text{OC}_{14}\text{H}_{29}$ ) led to the formation of enantiotropic smectic phases, SmC for the acetato-bridged complex (Cr 92 SmC 104.5 I), and SmB for the chloro-bridged analog (Cr 150 SmB 180).<sup>1005</sup> Moreover, the use of a chiral acetate bridge ( $\text{CH}_3\text{ClCHCOO}$ ) gave rise to a ferroelectric smectic phase (Cr 67 SmC\* 84 SmA 91 I). Other means of inducing ferroelectric mesophases consisted of incorporating chiral alkoxy substituents such as (*R*)-(-)-2-octanol and (*S*)-(-)- $\beta$ -citronellol chains ((**246**):  $\text{M} = \text{Pd}$ ,  $\text{X} = \text{Cl}$ ,  $\text{I}$ ;  $\text{R} = \text{OC}_n\text{H}_{2n+1}$ ,  $n = 7, 10, 12, 14$ ;  $\text{R}' = \text{OCH}_2\text{CH}_2\text{C}^*\text{HMeCH}_2\text{CH}_2\text{CH}=\text{CMe}_2$ ,  $\text{OC}^*\text{HMeC}_6\text{H}_{13}$ ).<sup>1006</sup> Again, both benzene rings of the ligands underwent *ortho* palladation, and thus all the complexes existed as mixtures of isomers in various proportions. SmC\* and SmA phases were indeed induced (the free ligands with a citronellol chain exhibited N\* and/or SmA phases, while it was not mesomorphic with 2-octanol).

The series of cyclopalladated dimers obtained from the nematogen 4,4'-di(hexyloxy)azobenzene (Cr 108 N 116 I), with various bridging systems ((**246**):  $\text{M} = \text{Pd}$ ,  $\text{R} = \text{R}' = \text{OC}_6\text{H}_{13}$ ,  $\text{X} = \text{Cl}$ ,  $\text{Br}$ ,  $\text{I}$ ,  $\text{N}_3$ ,  $\text{SCN}$ ,  $\text{OAc}$ ; (**248**)) has been prepared, and the effectiveness of the bridging group in promoting mesophases evaluated.<sup>1007,1008</sup> From crystalline structures of homologous compounds, all the complexes except those containing the acetato-bridged are planar, and in their *trans* conformation; the latter possess a sort of "roof-shape", and exist as a *cis:trans* mixture.<sup>1009</sup> This study revealed that mesomorphism was favored for chloro-, bromo-, azido-, and oxalato complexes (**248**), but not for the iodo, thiocyanato, or acetato derivatives (Table 79). The presence of the nematic phase below the more ordered smectic phases is rather surprising. While such re-entrant behavior is known and possible, the authors tentatively explained this observation by the dissociation of molecular pairs into single molecular species of different mesomorphism. In the case of the oxalato complex, the nematic phase was transient and never reappeared on successive

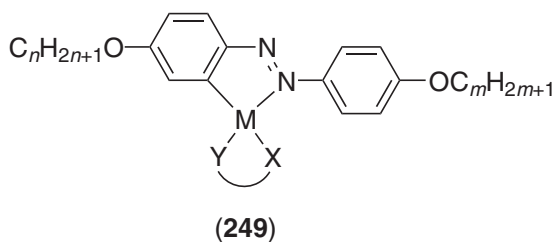
**Table 79** Thermal behavior of dinuclear complexes (**246**) ( $\text{M} = \text{Pd}$ ,  $\text{R} = \text{R}' = \text{OC}_6\text{H}_{13}$ ) and (**248**).

<b>246</b>	mesomorphism
$\text{X} = \text{Cl}$	Cr 213 N 221 SmE 235 dec.
$\text{X} = \text{Br}$	Cr 215 (N 196) I
$\text{X} = \text{I}$	Cr 211 I
$\text{X} = \text{N}_3$	Cr 186 SmA 190 dec.
$\text{X} = \text{SCN}$	Cr 220 I
$\text{X} = \text{OAc}$	Cr 140 I
<b>(248)</b>	Cr 238 N 246 SmA 290 dec.



heating-cooling runs; the extensive decomposition of the chloride did not allow such experiment to be carried out.

In order to obtain low-melting metallomesogens, several unsymmetric, mononuclear, *ortho*-metallated complexes combining 4,4'-bis(alkoxy)azobenzene and various types of simple chelating ligands have been prepared. Such dinuclear, chloro-bridged complexes may be reacted with anionic chelating ligand, and be converted to a stable, mononuclear species. Thus, complexes (249) ((249): M = Pd,  $n = m = 6$ ) with chelating ligand X–Y such as the *o,o*-monoanionic acac, hfac (hfac is the 1,1,1,5,5-hexafluoro-2,4-pentanedionato anion.), and tropolonate, the *N,o*2-amino-phenate and 2-amino-2-methyl-1-propanoate,<sup>1010</sup> as well as cyclopentadienyl<sup>1011</sup> ligands were prepared, but none of them was mesomorphic, probably due to the bulkiness of the co-ligands relative to the small anisotropy of the complex. Note that luminescence was induced by cyclopalladation.<sup>1012</sup> The related *ortho*-metallated gold<sup>1013</sup> and mercury<sup>1014</sup> complexes were not mesomorphic either. Low-temperature N\* and SmA phases were nevertheless observed at longer chain lengths in some related, chiral, palladium(II) complexes with an acac co-ligand Y–X ((249): M = Pd,  $n = 7, 10, 12, 14$ ,  $\text{OC}_m\text{H}_{2m+1} = (R)\text{-}(-)\text{-}2\text{-octanol}, (S)\text{-}(-)\text{-}\beta\text{-citronellol}$ ).<sup>1015</sup>



Other heteroligand palladium complexes (249) with Y–X being either a non-chiral *N*-[4'-(dodecyloxy)resorcyldiene]-4-alkylaniline or a chiral *N*-[4'-(dodecyloxy)resorcyldiene]-4-alkoxyanilines ((249): M = Pd,  $n = 14$ ,  $\text{OC}_m\text{H}_{2m+1} = (R)\text{-}(-)\text{-}2\text{-octanol}, (S)\text{-}(-)\text{-}\beta\text{-citronellol}$ ) have been prepared. They showed chiral mesophases over narrow temperature ranges.<sup>1016</sup>

In order to obtain reliable thermal behavior and to improve the mesomorphic properties of cyclometallated azobenzene complexes, the overall anisotropy of the complexes was enhanced by using elongated azobenzenes. Thus, Ghedini and co-workers prepared mesomorphic three- and four-ring azobenzene ligands and the corresponding *ortho*-metallated dinuclear and mononuclear complexes containing cyclopentadienyl,<sup>1011,1017</sup> acetylacetonate,<sup>1018</sup> tropolonate, and quinolate<sup>1019</sup> ligands. Most of these new organometallic species (250–253) were found to show mainly nematic phases with clearing temperatures lower than those of the parent ligands, except the chloro-bridged complexes for which mesophases occur at elevated temperatures (Table 80). Some are the first examples of mesomorphic complexes of octahedral Pt<sup>IV</sup> and were obtained from the oxidative addition to the square-planar platinum(II) complexes by I<sub>2</sub> and MeI.

**Table 80** Thermotropic behavior of the ortho-metallated complexes (250) to (253).

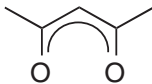
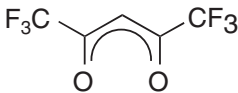
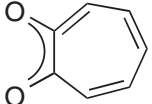


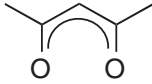
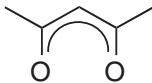
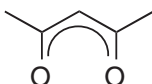


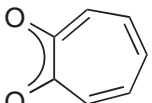
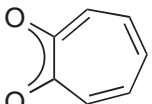
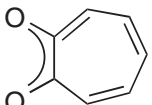
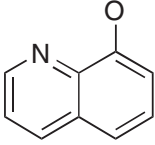
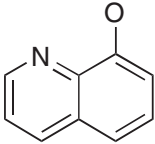
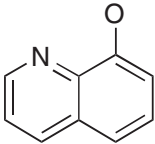
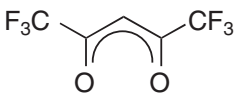
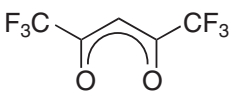
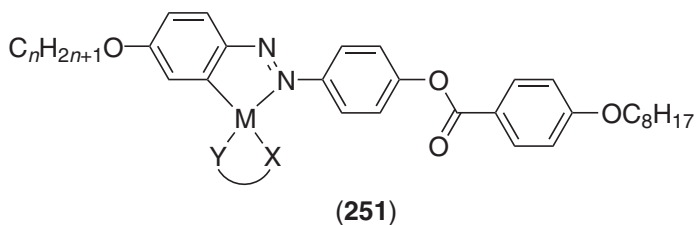
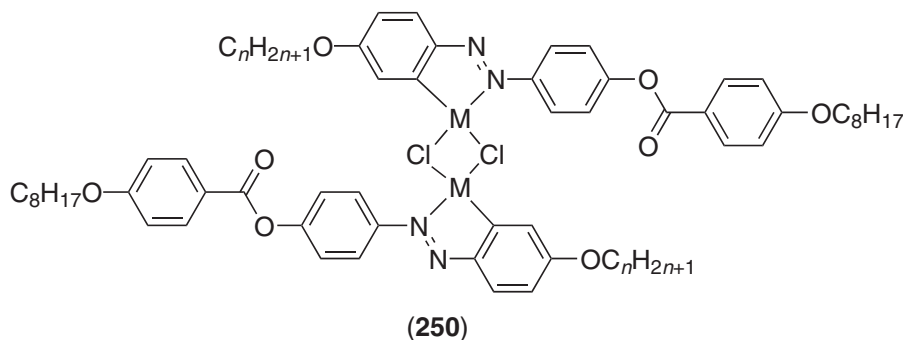
<i>Type</i>	<i>M</i>	<i>n</i>	<i>X-Y</i>	<i>Transition temperatures</i>
(250)	Pt	10		Cr 206 SmC 253 N 275 dec.
(251)	Pd	6		Cr 119 N 264 I
	Pd	6		Cr 110 N 167 I
	Pd	6		Cr 103 N 170 I
	Pd	6		Cr 117 N 144 I
	Pd	10		Cr 72.5 N 128.5 I
	Pt	10		Cr 131 N 196 I
	PtI <sub>2</sub>	10		Cr 125 (E 60) I
	PtMe <sub>2</sub>	10		Cr 108 N 230 dec.
(252)	Pd			Cr 250 SmC 331 dec.
	Pt			Cr 263 SmC 342 dec.
(253)	Pd			Cr 143 N 226 I
	Pt			Cr 160 N 250 dec.
	Pt			Cr 174 N 264 I
	PtI <sub>2</sub>			Cr 210 (N 209) I
	PtIMe			Cr 142 SmC 146 dec.

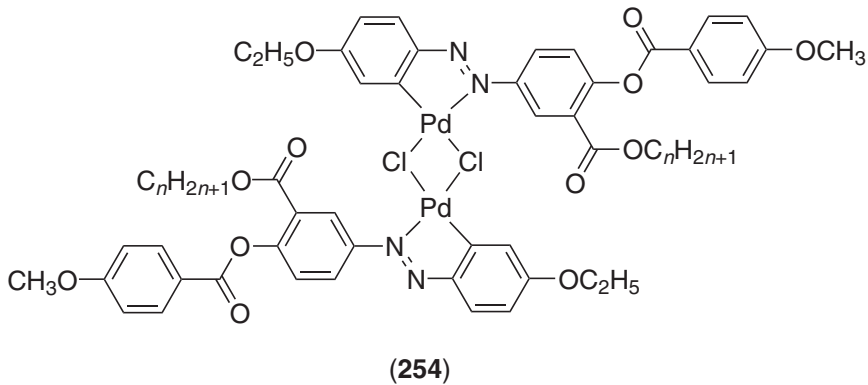
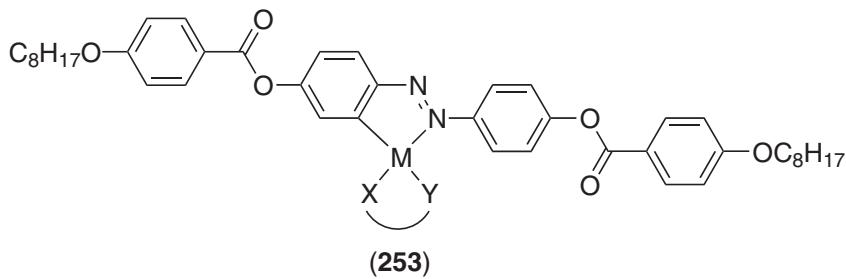
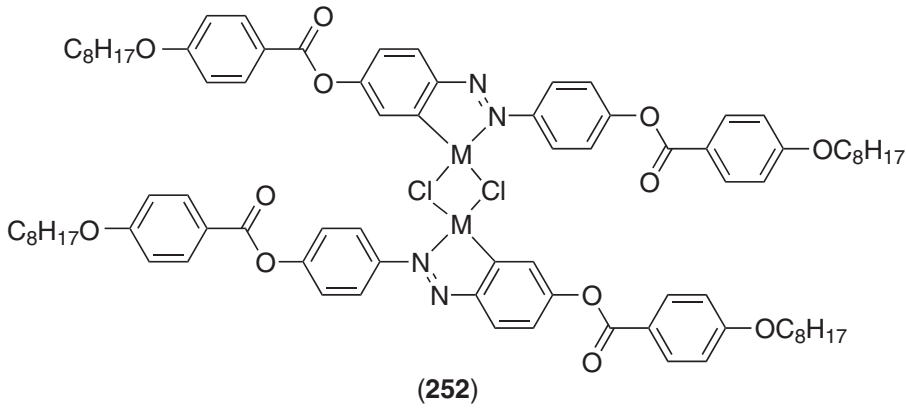
Table 80 continued

Type	M	n	X-Y	Transition temperatures
Pt				Cr 162 SmA 189 N 280 dec.
PtI <sub>2</sub>				Cr 211 SmC 218 N 255 dec.
PtIMe				Cr 147 SmC 154 dec.
Pt				Cr 165 N 209 dec.
PtI <sub>2</sub>				Cr 250 SmC 259 N 289 dec.



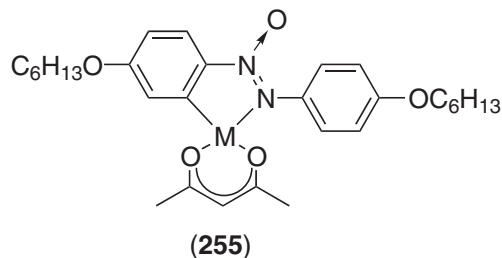
Note that a first example of such *ortho*-metallated complexes with elongated azobenzenes was reported by Hoshino *et al.* ((**254**):  $n = 1-10, 12, 14, 16, 18$ ).<sup>1020</sup> In common with the parent ligands, the complexes were nematic, although melting and clearing points were raised by 60 and 102 °C, respectively, on complexation giving the complexes a much wider nematic range. Variable-temperature <sup>1</sup>H NMR experiments using the  $n = 4$  derivative in isotropic solution in CDCl<sub>3</sub> confirmed the presence of dynamic processes which were interpreted on the basis of a model assuming that the lateral chain was, in fact, sitting in the central cleft of the molecule.



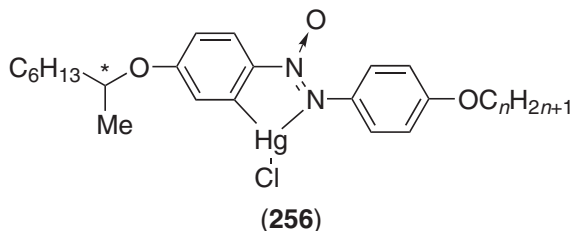


(ii) *Ortho-metallated azoxy complexes*

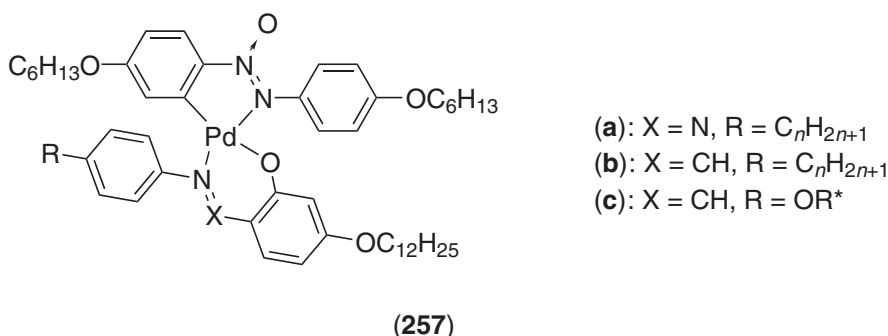
The mononuclear, *ortho*-palladated 4,4'-bis(hexyloxy)azoxybenzene acetylacetonate, (**255**), showed a nematic phase between 90 °C and 105 °C,<sup>1021</sup> with temperatures very comparable to that of the free azoxy ligand (Cr 80 N 126 I). This complex, dubbed Azpac, has been subjected to a vast number of studies in order to analyze some specific properties such as electric<sup>1022–1026</sup> and dielectric<sup>1027–1031</sup> properties, conductivity,<sup>1032</sup> viscoelasticity,<sup>1033</sup> and dynamics.<sup>1034–1036</sup>



Using azoxy ligands bearing chiral groups, Ghedini reported the formation of *ortho*-metallated complexes of mercury(II) ((256):  $n = 6, 10$ ), and demonstrated materials with a room-temperature SmC\* phase.<sup>1037</sup> These complexes existed as an equimolar mixture of two isomers due to the non-selective metallation. Prior to the metallation both ligands were room-temperature liquid crystals: N\* 34 I, and Cr 24.5 SmC\* 37 N\* 47 I for  $n = 6$  and 10, respectively. The mesophase stability was enhanced upon complexation, and both complexes exhibited a single SmC\* up to 56 °C and 63.5 °C, respectively.



Other mixed-ligand, mononuclear *ortho*-palladated complexes whose molecular structure consists of two different ligands, namely 4,4'-dihexyloxyazoxybenzene with 2-hydroxy-4-alkoxy-4'-alkylazobenzene ((257a):  $n = 1-4, 6, 8$ ),<sup>1038</sup> *N*-(4-dodecyloxysalicylidene)-4'-alkylaniline ((257b):  $n = 0-4, 6, 8$ ),<sup>1039</sup> and the chiral alkoxy analogs ((257c): R\* = (*S*)-(-)- $\beta$ -citronellyl, (*R*)-(-)-2-octyl)<sup>874</sup> ligands were studied. In the complexes of the series (257a), obtained as single *trans*-isomers only,<sup>1040</sup> monotropic nematic phases were most commonly observed. However, smectic behavior seemed promoted in series (257b) and (257c). For (257b), obtained as an isomeric mixture of *N,N-trans*/*N,N-cis* in a 5:1 ratio, both SmA and N phases were observed, monotropic for  $n = 0, 2$ , and 4 and enantiotropic for  $n = 1, 3, 6$ , and 8. In most cases, the mesophases occurred between 125 and 145 °C. Incorporation of chiral chains in the Schiff base ligand led to the formation of a chiral crystal smectic H\* phase for both complexes (257c) between 110 °C and 150 °C. In this case the *N,N-trans*/*N,N-cis* ratio was 9 to 1.

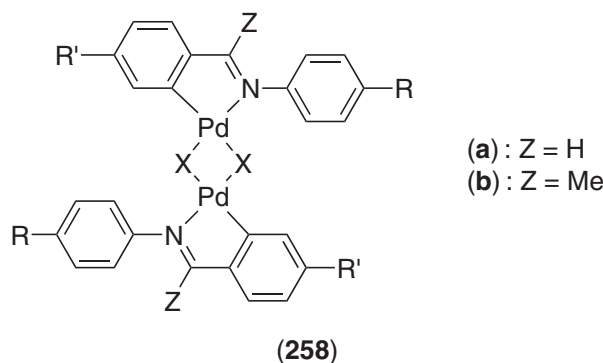


### (iii) *Ortho*-metallated imine complexes

As for the *ortho*-metallated azo compounds just described, a similar and broad systematic study has been carried out on the related imines and their corresponding dinuclear and mononuclear complexes.

Dinuclear *ortho*-palladated complexes based on three imine ligands, and various bridging groups, were initially investigated, namely (258a) ((258a): X = OAc, Cl, Br, SCN; R = C<sub>10</sub>H<sub>21</sub>, OC<sub>10</sub>H<sub>21</sub>, R' = OC<sub>10</sub>H<sub>21</sub>), and (258b) ((258b): X = OAc, Cl, Br, SCN; R = C<sub>10</sub>H<sub>21</sub>, R' = OC<sub>10</sub>H<sub>21</sub>).<sup>1041</sup> As for their azo analogs, mixtures of *cis/trans* complexes have to be considered. While the acetato- and halo-bridged systems were found to exist as single *trans* compounds, the thiocyanato compounds exist as a mixture of several isomers due to the different possibilities of coordination of the two unsymmetric thiocyanato groups.<sup>1042</sup> In general, the OAc bridge was found to be ineffective in promoting mesomorphism in these systems and the non-planar complex of only one ligand showed any mesomorphism (monotropic SmA). For the other bridging ligands, SmA phases were commonly observed along with an SmC phase for two examples where X = Cl. Mesomorphic ranges were typically 80–100 °C for X = Cl or Br, with clearing temperatures all above 200 °C. For X = SCN, 30 °C was the maximum range for the SmA phase, but the

mesophase occurred at much higher temperatures than that of the halo-bridged complexes. Interestingly, the lateral methyl group did not lead to any significant effects in the complexes even though it had suppressed mesomorphism in the parent ligand.



Two parallel systematic studies were later undertaken in order to determine the role of both the chain length and type, in addition to the nature of bridging group in determining the mesomorphism. In one study concentrating on the effect of the chain length ((258a): X = Cl, R = R' = OC<sub>n</sub>H<sub>2n+1</sub>, n = 2, 4, 6, 8, 10), results confirmed the absence of mesomorphism in the acetato-bridged complexes; previous mesophase assignments made on the chloro-bridged derivatives (SmA for all n, N for n = 2, and SmC for n = 8, 10) were also confirmed.<sup>1043</sup> Note that contradictory findings were reported by Zhang *et al.*<sup>1005</sup> who observed monotropic SmC for long-chain acetato-bridged palladated systems, and only the SmC phase for the chloro-bridged analogs ((258a): R = R' = OC<sub>n</sub>H<sub>2n+1</sub>, n = 6–12, 14).

Concerning the influence of the nature of the chains and bridges ((258a): X = Cl, Br; R/R' = C<sub>n</sub>H<sub>2n+1</sub>/OC<sub>m</sub>H<sub>2m+1</sub>, n = 1, 2, 6, 10 and m = 2, 6, 10), the overall trends can be summarized as follows.<sup>1044</sup> The longer the terminal chains, the lower are the melting points and the more ordered are the mesophases (smectic phase in place of the nematic phase). The complexes with solely alkoxy chains have more stable mesophases than those with both alkyl and alkoxy chains. Whereas SmC and SmA phases were seen for the chloro-bridged derivatives, those with bromine exhibited an SmA phase (and N for a few homologs), with the complete absence of any SmC phase. Finally, the mesophases existed at higher temperatures in the latter case (X = Br), compared to the former (X = Cl).

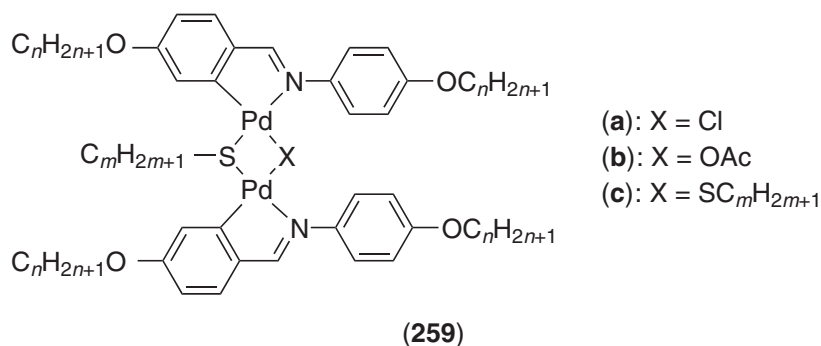
Studies of chloro- and acetato-bridged complexes derived from benzylidene ligands bearing polar groups either in the *para* position of the aldehyde ring ((258a): R = C<sub>8</sub>H<sub>17</sub>, OC<sub>8</sub>H<sub>17</sub>; R' = H, F, Cl, Br, CN, NO<sub>2</sub>, Me, OMe, CF<sub>3</sub>, OCOMe, OCOC<sub>6</sub>H<sub>5</sub>, CO<sub>2</sub>Me),<sup>1045</sup> or aniline ring ((258a): R = OC<sub>8</sub>H<sub>17</sub>; R' = H, Cl, CN, NO<sub>2</sub>, Me, OMe),<sup>1046</sup> and ((258a): R = C<sub>4</sub>H<sub>9</sub>, R' = OMe) were undertaken.<sup>1047</sup> None of the acetato-bridged complexes was mesomorphic, whereas all the chloro-bridged derivatives but one (R = H) exhibited an SmA phase above 140 °C, at which temperature most of them started to decompose; this behavior was observed regardless of the location of the polar group. Interestingly, those with a cyano group or with the shortest chain were the only complexes to show a nematic phase.

The introduction of one or two chiral 2-octanol chains<sup>1048</sup> in the benzylidene ligand led to new chloro-bridged *ortho*-palladated complexes exhibiting a ferroelectric SmC\* phase<sup>1049</sup> along with an SmA phase. The two chiral chain systems ((258a), X = Cl, R = OC<sub>n</sub>H<sub>2n+1</sub>, n = 6, 8, 10, 14; R' = OC\*HMeC<sub>6</sub>H<sub>13</sub>) and the isomeric analog ((258a), X = Cl, R = OC\*HMeC<sub>6</sub>H<sub>13</sub>, R' = OC<sub>8</sub>H<sub>17</sub>) exhibited both mesophases typically between 100 and 220–230 °C, the mesomorphic temperature range of the SmC\* increasing with elongation of the alkoxy chain. Interestingly, the SmC\* was more stable by 20 °C when the chiral chain was attached to the aniline ring. The mesophase stability of the SmC\* phase was reduced considerably in the complex containing four chiral chains ((258a), X = Cl, R = R' = OC\*HMeC<sub>6</sub>H<sub>13</sub>): Cr 114 (SmC 88) SmA 121 I).

Treatment of the chloro-bridged dimeric species with potassium 2-chloropropionate,<sup>1050</sup> or alternatively the acetato-bridged analogs with 2-bromopropionic acid<sup>1043</sup> led to new carboxylato-bridged dimers ((258a): X = CH<sub>3</sub>CHClCO<sub>2</sub>, CH<sub>3</sub>CHBrCO<sub>2</sub>; R = R' = OC<sub>n</sub>H<sub>2n+1</sub>) which were, against all expectations, mesomorphic, showing a broad-temperature-range SmA phase (ca. 100–150 °C), with some stable up to nearly 250 °C. Only small differences were observed in the transition temperatures between the chloro- and bromo-propionate derivatives, probably due to

the existence of the complexes as rich isomeric mixtures. Indeed, due to the chiral carboxylate group, in addition to the *cis* and *trans* isomers resulting from the arrangement of the two imines in the dimer, the chirality of the *trans* leads to two enantiomers,  $\Delta$  and  $\Lambda$ , the *cis* not being chiral. For both series, the thermal behavior was slightly complicated, and most of the complexes exhibited double melting behavior, i.e., the Cr SmA I' (or Cr') SmA I phase sequence was observed systematically. One dipalladium complex with tetradecyloxy chains and a bulkier carboxylate bridge ( $\text{Me}_2\text{CHCH}_2\text{C}^*\text{HCICO}_2$ ) was reported to show an SmC\* between 106 °C and 147 °C.<sup>1005</sup>

Another interesting part of this work was concerned with the study of dinuclear cyclopalladated complexes with mixed bridges (**259a,b**).<sup>1051</sup> Indeed, the reaction of the dichloro-bridged complexes (**259a**) with silver thiolate ( $\text{AgSC}_m\text{H}_{2m+1}$ ) led to dinuclear derivatives with mixed bridges  $\mu\text{-Cl}/\mu\text{-SC}_m\text{H}_{2m+1}$ , (**259a**) ((**259a**):  $n = 6, 8, 10$ ;  $m = 6, 8, 10, 18$ ). Likewise, treatment of the di- $\mu$ -acetato complexes with thiols ( $\text{HSC}_m\text{H}_{2m+1}$ ) or, alternatively, dinuclear (**259a**) with silver acetate, afforded the mixed-bridge complexes  $\mu\text{-OAc}/\mu\text{-SC}_m\text{H}_{2m+1}$ , (**259b**) ((**259b**):  $n = 6, 8, 10$ ;  $m = 6, 8, 10, 18$ ). Noteworthy, in addition to their mesomorphism, such mixed bridged complexes adopted a *cis*-geometry, as confirmed by NMR and X-ray studies. All the complexes (**259a**) displayed both SmC and SmA phases, at lower temperatures than their dichloro-predecessors, i.e., between 100 °C and 200 °C, with little influence of the chain length; the SmA phase existed over most of this temperature range. As for complexes (**259b**), the predominant phase was the SmA (N phase for  $n = 6$  only); the transition temperatures were also reduced, decreasing with  $m$  (from 160 °C to 70 °C for the melting point, and 170 to 140 °C for the clearing point). Recall that such mixed-bridge complexes were obtained initially by the reaction of alkylthiols to a chloropropionate bridge dinuclear complex ((**259a**):  $n = 6$ , X =  $\text{MeCHClCO}_2$ ,  $m = 6$ : Cr 140 N\* 157 I;  $m = 10$ : Cr 109.5 SmA 115 N\* 138 I;  $m = 18$ : Cr 92 SmA 128 N\* 132 I), to yield the first metallomesogens to show a chiral nematic phase.<sup>1050</sup> Recently, another such complex ((**259a**):  $n = 2$ , X =  $\text{MeCHClCO}_2$ ,  $m = 18$ ) was found to exhibit a monotropic blue phase (BPI) along with an N\* phase.<sup>1052</sup> (**259c**) exhibited a broad SmA phase above 150 °C.



The reactivity of di- $\mu$ -hydroxo complexes of *ortho*-palladated imines, obtained by the treatment of the di- $\mu$ -acetato complexes ((**258a**): X = OAc) with NaOH, has been exploited to extend the range of dinuclear complexes with double or mixed bridges, as well as produce some mononuclear examples. Thus, thermotropic, air-stable,  $\mu$ -amido- $\mu$ -hydroxo (**260a**),  $\mu$ -anilido- $\mu$ -hydroxo (**260b**), bis- $\mu$ -amido (**260c**),  $\mu$ -amido- $\mu$ -thiolato (**260d**), and  $\mu$ -amido- $\mu$ -carboxylato (**260e**) complexes, as well as the mononuclear complexes with mixed imine and *N,N*-dialkylthiocarbamate ligands (**260f**), were prepared (Figure 103).<sup>1053</sup> Most of the complexes (**260a**) were liquid crystals, showing a nematic phase at short chain length at elevated temperatures ( $n = 2$ ,  $m = 14, 18$ ), and an SmA phase at longer chain length ( $n = 6, 10$ ;  $m = 1, 6, 10, 14, 18$ ) from 60 °C to 120 °C up to 160–180 °C where they decomposed. Complexes (**260b**) behaved in a similar way to (**260a**) (slight increase in the transition temperatures), with a nematic phase for  $n = 2$  and an SmA phase for  $n = 6$  and 10. Replacement of the hydroxo bridge by an alkylthiol led to complexes (**260d**), which showed mainly an SmA phase for  $n = 6$  and 10 above 100 °C on average, but decomposing at the clearing point. Only a monotropic SmA phase was observed for the compounds with long amido and thiolato chains ( $m, q \geq 10$ ), and none of the complexes with  $n = 2$  was mesomorphic. The replacement of the  $\mu\text{-OH}$  by  $\mu$ -carboxylato gave slightly better results, and a stable SmA phase was seen between 76 °C and 107.5 °C for (**260e**) with  $n = 10$ . The complexes (**260c**) could not be studied because of their insolubility in organic solvents, and consequently it was impossible to isolate them as pure materials. Finally, the reaction of the  $\mu$ -dihydroxo complex with dialkylamine in  $\text{CS}_2$  led to the

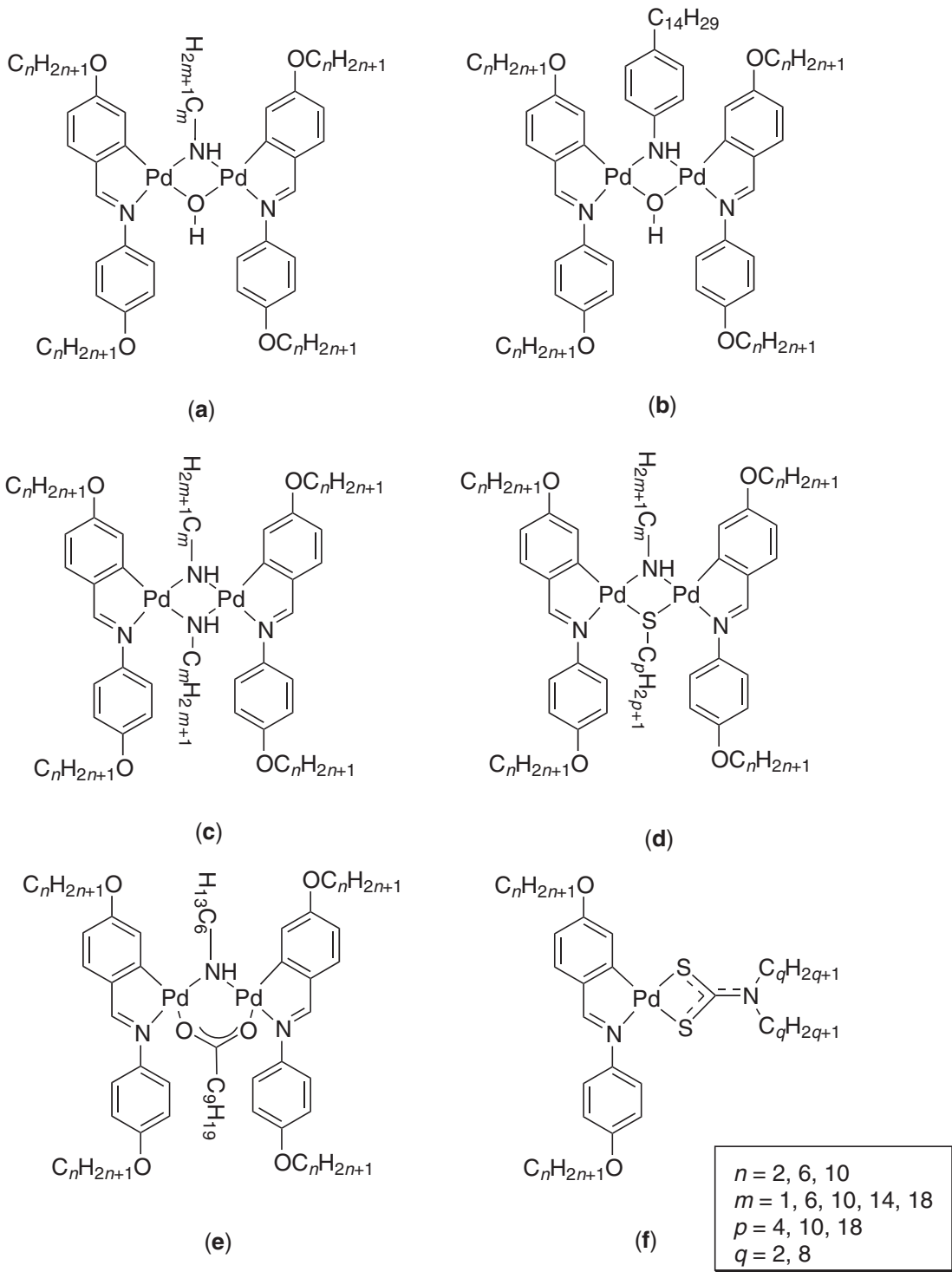
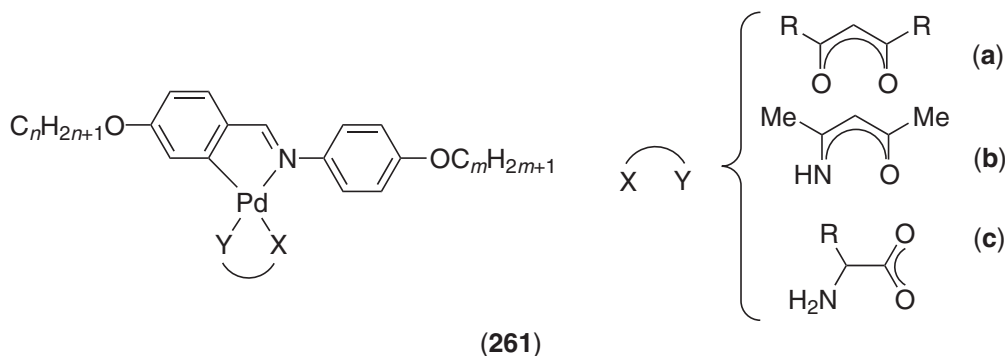


**Figure 103** Structures of the various mixed dinuclear complexes (**260a–e**), and of the mononuclear complex (**260f**).

mononuclear species (**260f**), which showed an enantiotropic SmA at very low temperatures for the derivatives with  $n = 10$  and  $q = 2$  (Cr 84 SmA 99.5 I) and 8 (Cr 56 SmA 73 I).

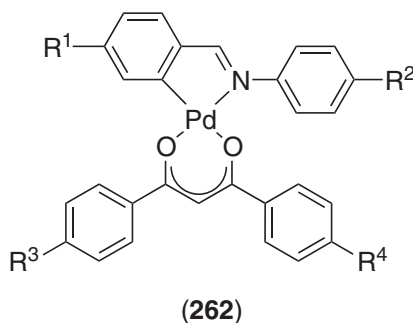
Cleavage of the dinuclear  $(\mu\text{-Cl})_2$  complexes (**258a**):  $X = \text{Cl}$ ) with  $\beta$ -diketones or  $\beta$ -enamino-ketones also led to various series of mononuclear derivatives (**261**). Thus, the new complexes with acetylacetonate co-ligand,<sup>1043,1054</sup> ((**261a**):  $R = \text{Me}$ ,  $n = m = 2, 4, 6, 8, 10$ ;  $n = 10 \neq m = 2, 6$ ) were

mesomorphic at much lower temperatures than their dichlorodipalladium predecessors, but more interestingly, the mesophases were more accessible and more stable in comparison to the parent complexes. A monotropic nematic phase was observed for the short-chain-length compounds, both enantiotropic SmA and N phases at intermediate chain length, and only the SmA phase for the derivative with two decyloxy chains. The lowering of the symmetry of the complex therefore appeared to be an excellent strategy for reducing the transition temperatures and preserving a large mesomorphic range simultaneously. However, some caution must be exercised in such an interpretation, as the mesophase stability of these complexes was found to be very sensitive to small, structural changes. The nematic phase became destabilized when the  $\beta$ -diketone used was trifluoroacetylacetonate, probably due both to the steric hindrance introduced by the  $\text{CF}_3$  group, and by the existence of an equimolar mixture of isomers.<sup>1055</sup> The use of aliphatic diketones ((261a):  $\text{R} = \text{C}_{10}\text{H}_{21}$ ;  $n = m = 10$ ) was correlated with a strong reduction in mesomorphic character.<sup>1056</sup>



The mononuclear complexes with  $\beta$ -aminoenonate ((261b):  $n = m = 2, 4, 6, 8, 10$ ), obtained as the *N,N-trans* isomer only, also yielded an accessible nematic phase (and an SmA for longer chains), over slightly narrower temperature ranges than in the acetylacetonate derivatives.<sup>1043</sup> Moreover, when the chain attached onto the fixed benzaldehyde ring was chiral (e.g., 2-octanol), the complex ((261b) ( $m = 8$ )) was found to exhibit monotropic BPII, BPI, and  $\text{N}^*$  phases at reasonably low temperatures.<sup>1052</sup> Using a similar approach, an  $\text{SmC}^*$  phase ((261c):  $\text{R} = \text{Me}$ ;  $n = m = 14$ ; Cr 81.5  $\text{SmC}^*$  174 I) and a broad SmA phase ((261c):  $\text{R} = \text{C}_6\text{H}_5\text{CH}_2, \text{Me}_2\text{CH}, \text{Me}_2\text{CHCH}_2$ ;  $n = m = 14$ ) were obtained in related mixed complexes with chiral amino acids, again at very accessible temperatures.<sup>1057</sup>

Espinet and co-workers have investigated in detail chiral derivatives of mononuclear *ortho*-palladated complexes incorporating a dialkoxybenzylidene and a di-4,4'-alkoxy-phenyl- $\beta$ -diketonate ligands,<sup>1058</sup> obtained from the cleavage of the dinuclear bridge by the thallium complex of the  $\beta$ -diketonate ((262):  $\text{R}^1 = \text{OC}^*\text{HMeC}_6\text{H}_{13}, \text{R}^2 = \text{OC}_{10}\text{H}_{21}, \text{OC}_{14}\text{H}_{29}, \text{R}^3, \text{R}^4 = \text{OC}_{10}\text{H}_{21}$ ). In both cases, monotropic  $\text{SmC}^*$  was observed. In an earlier publication, they described a material with a spontaneous polarization of  $206 \text{ nC cm}^{-2}$ , the highest value recorded for a metal-based system.<sup>1048</sup> In this case, although the  $\text{P}_s$  value was lower than recorded above ( $-22$  to  $-29 \text{ nC cm}^{-2}$ ), the switching time was now in the millisecond time regime, three orders of magnitude faster than the time reported for some dinuclear azine derivatives.<sup>1059</sup>



With a view to optimizing the system and finding an enantiotropic  $\text{SmC}^*$  phase, the effects of the position and number of chiral chains on the ferroelectric behavior of this system were investigated, and a series of twelve new materials was prepared ((262):  $\text{R}^1, \text{R}^2, \text{R}^3,$

**Table 81** Mesomorphism of complexes (262).

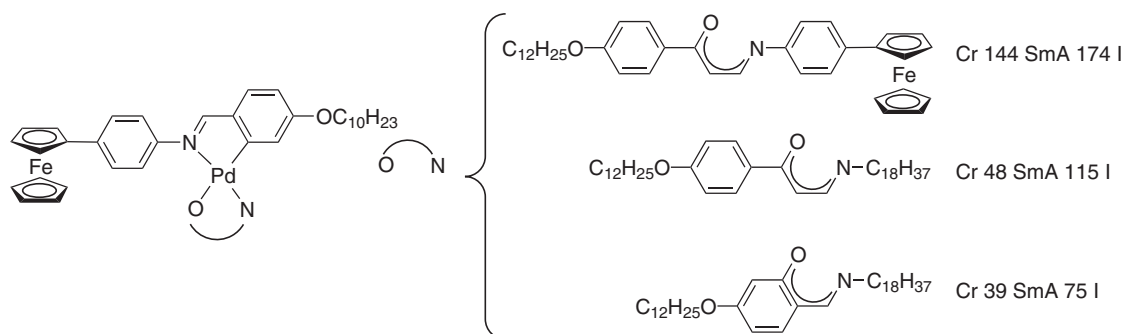
$R^1$	$R^2$	$R^3$	$R^4$	Transition temperatures
$OC_{10}H_{21}$	$OC_{10}H_{21}$	$OC_{10}H_{21}$	$OC_{10}H_{21}$	Cr 80 SmC 150 SmA 154 N 155 I
$OC^*HMeC_6H_{13}$	$OC_{10}H_{21}$	$OC_{10}H_{21}$	$OC_{10}H_{21}$	Cr 118 (SmC* 109 SmA 117) I
$OC_{10}H_{21}$	$OC^*HMeC_6H_{13}$	$OC_{10}H_{21}$	$OC_{10}H_{21}$	Cr 118 (SmC* 114) I
$OC_{10}H_{21}$	$OC_{10}H_{21}$	$OC^*HMeC_6H_{13}$	$OC_{10}H_{21}$	Cr 63 SmC* 104 N* 115 I
$OC^*HMeC_6H_{13}$	$OC^*HMeC_6H_{13}$	$OC_{10}H_{21}$	$OC_{10}H_{21}$	Cr 72 (SmC* 60) I
$OC^*HMeC_6H_{13}$	$OC_{10}H_{21}$	$OC^*HMeC_6H_{13}$	$OC_{10}H_{21}$	Cr 85 (SmA 77) I
$OC_{10}H_{21}$	$OC^*HMeC_6H_{13}$	$OC^*HMeC_6H_{13}$	$OC_{10}H_{21}$	Cr 93 (SmX' 60 smX 64) I
$OC_{10}H_{21}$	$OC_{10}H_{21}$	$OC^*HMeC_6H_{13}$	$OC^*HMeC_6H_{13}$	Cr 67 I
$OC^*HMeC_6H_{13}$	$OC^*HMeC_6H_{13}$	$OC^*HMeC_6H_{13}$	$OC_{10}H_{21}$	I
$OC^*HMeC_6H_{13}$	$OC_{10}H_{21}$	$OC^*HMeC_6H_{13}$	$OC^*HMeC_6H_{13}$	I
$OC_{10}H_{21}$	$OC^*HMeC_6H_{13}$	$OC^*HMeC_6H_{13}$	$OC^*HMeC_6H_{13}$	Cr 77 I
$OC^*HMeC_6H_{13}$	$OC^*HMeC_6H_{13}$	$OC^*HMeC_6H_{13}$	$OC^*HMeC_6H_{13}$	I

SmX', SmX: unidentified ordered smectic phases (SmX' SmI, SmF; SmX SmB)

$R^4 = OC^*HMeC_6H_{13}/OC_{10}H_{21}$ .<sup>1060</sup> Recall that the compounds with unsymmetrical diketone exist as a *cis/trans* isomeric mixture. The thermal behavior of these compounds is reported in Table 81, and several interesting observations were made. As the number of chiral chains increased, the transition temperatures decreased, and compounds having a chiral chain on the imine ligand exhibited monotropic behavior, whereas when this chain was on the diketone, the behavior was enantiotropic. All the compounds with two chiral chains exhibited only monotropic phases, the complex having the two chiral chains on the  $\beta$ -diketonate ligand being devoid of mesomorphism; none of the complexes with three and four chiral chains was liquid-crystalline. In addition, the number and position of these chains influenced the ferroelectric properties drastically, and particularly the spontaneous polarization, as well as the non-linear optical responses.<sup>1061</sup>

Similarly, smectic mesophases were obtained in heteronuclear *ortho*-palladated imine complexes based on various non-mesomorphic enaminketone ligands ((263) to (265), Figure 104). The precursor chloro-bridged complex was also mesomorphic, showing an SmA phase between 238 and 248 °C.<sup>1062</sup>

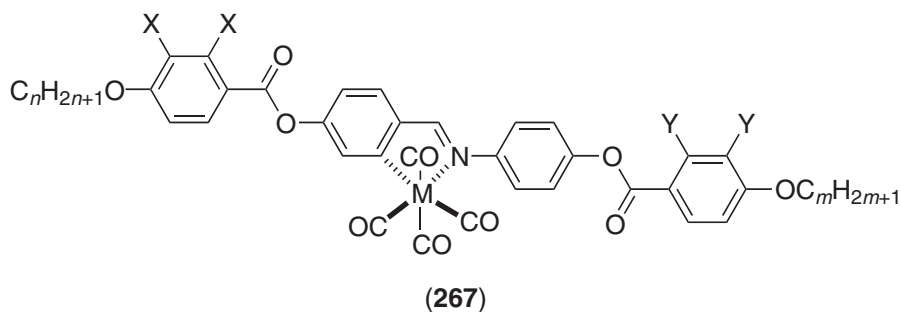
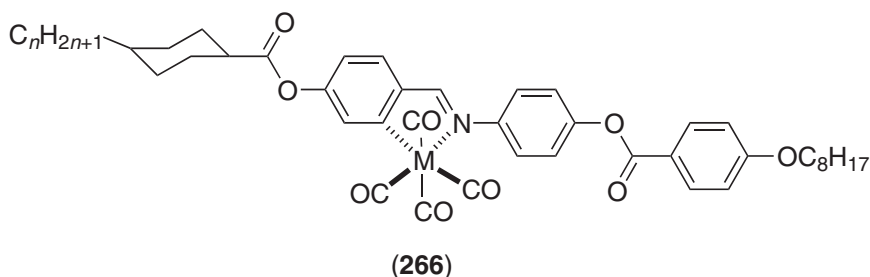
A similar, systematic study was also carried out with the platinum derivatives, and dinuclear cycloplatinated complexes of 4,4'-dialkoxybenzylidene with double ( $\mu$ -chloro $\mu$ -chloro,  $\mu$ -acetato  $\mu$ -acetato,  $\mu$ -thiolato  $\mu$ -thiolato,  $\mu$ -chloropropionato  $\mu$ -chloropropionato) or mixed ( $\mu$ -chloro  $\mu$ -thiolato,  $\mu$ -acetato  $\mu$ -thiolato, and  $\mu$ -chloropropionato  $\mu$ -thiolato) bridges.<sup>1063</sup> Mononuclear species with acetylacetonate and  $\beta$ -substituted-phenyldiketonate<sup>1065,1066</sup> co-ligands were also prepared. All the platinum complexes were mesomorphic, except the acetato-bridged material. They exhibited, in general, more ordered mesophases than their palladium analogs (e.g., an SmA phase was induced in place of the nematic phases) and overall, the transition temperatures, and particularly the clearing temperatures, were slightly higher for Pt compared to Pd. Note that in the platinum complexes existing as isomeric mixtures, the composition was different to that in the palladium congeners, explaining some discrepancy between the two series. The substitution of palladium by platinum thus resulted in an overall increase in the mesophase stability.

**Figure 104** Complexes (263) to (265).

Such metallomesogens possessing mixed bridges and non-centrosymmetric structures could represent interesting candidates for new molecular materials with non-linear optical properties, since they can easily be derivatized by the introduction of donor and acceptor groups.<sup>1067</sup>

Some of the chloro-bridged palladium (**258a**) ( $R = C_nH_{2n+1}$ ,  $R' = OC_mH_{2m+1}$ ), a mixed bridged  $\mu$ -acetato  $\mu$ -thiolato (**259b**) ( $n = m = 6$ ), and a mononuclear complex (**262**) ( $R^1, R^2, R^3, R^4 = OC_{10}H_{21}$ ) discussed above were also found to exhibit additional lyotropic mesophases in contact with apolar organic solvents such as linear alkanes (octane, decane, dodecane, and pentadecane), cycloocta-1,5-diene, and the chiral limonene.<sup>1068,1069</sup> A lyotropic lamellar phase was induced for the dichloro complexes with symmetrical chain length ( $n = m = 6, 10$ ) in linear alkanes; the transition temperatures were found to decrease from pentadecane to octane. Contact preparations of complexes (**259b**) and (**262**) with alkanes revealed the induction of a nematic phase, with the complete destabilization of the thermotropic smectic phases. For both complexes, mixing with solvents resulted in the substantial depression of both melting and clearing temperatures. In the case of (**259b**), the nematic range increased concomitantly with the length of the solvent chain. While mixtures with cyclooctadiene did not yield a mesophase, mixtures with the limonene gave unexpected results, depending strongly on the metal complexes. Mesomorphism was suppressed or destabilized for complexes (**258a**), and a chiral nematic phase was induced for (**259b**) and (**262**) over a large temperature range (Cr 93 N\* 147 I; Cr 65 N\* 136 I). This is the first case of chiral induction in binary systems between calamitic complexes and a chiral, apolar solvent.

Bruce and co-workers demonstrated mesomorphism in benzylideneaniline complexes bound to octahedral  $Mn^I$  and  $Re^I$ , providing that the imine ligand was sufficiently anisotropic; these complexes were the first simple octahedral complexes to show N and lamellar phases.<sup>1070</sup> They were formed by *ortho*-metallation reaction of the imine with  $[MMe(CO)_5]$  ( $M = Mn, Re$ ). The parent ligands showed smectic and nematic phases at temperatures up to 300 °C, whereas on complexation to  $Mn^I$ , only a nematic phase was seen for (**266**) ((**266**):  $M = Mn, n = 5, 7$ ) and (**267**) ((**267**):  $M = Mn, X = Y = H; n = m = 8$ ) which cleared below 190 °C with decomposition.<sup>1071</sup> The related  $Re^I$  complexes yielded materials with very similar transition temperatures and with enhanced thermal stability, so that decomposition was not observed at the clearing point.<sup>1072</sup> In the following part of this study, therefore, only the rhenium complexes were studied.



Both terminal chain lengths have been varied in a systematic way,<sup>1073</sup> and lateral ligand fluorination was employed,<sup>1074</sup> and the mesomorphism of the resulting complexes compared. In broad terms, the mesomorphism of the rhenium complexes was the same, and not influenced to a great extent by the chain length, melting into the nematic phase between ca. 130 °C and 155 °C, and clearing between 140 °C and 200 °C. Fluorination, however, had a more dramatic effect on the mesophase stability ((**267**):  $M = Re, X, Y = H, F$ ). Thus, while the phase remained unchanged as nematic, its mesophase stability reduced considerably with increasing fluorine substitution (Table 82). This systematic study



**Table 82** mesomorphism of octahedral complexes (266) to (267).

Complex	Transition temperatures
(266)	$n=5$ $n=7$ M = Mn: Cr 135 N 184 dec. M = Re: Cr 147 N 177 I
(267)	M = Mn: Cr 122 N 180 dec. M = Re: Cr 129 N 171 I
	X = Y = H, $n=m=8$ M = Mn: Cr 154 N 190 dec. M = Re: Cr 154 N 176 I
	X = Y = H, $n=12, m=8$ M = Re: Cr 130 N 164 I
	X = Y = H, $n=m=12$ M = Re: Cr 131 N 145 I
	X = F, Y = H, $n=m=8$ M = Re: Cr 153 N 164 I
	X = F, Y = H, $n=12, m=8$ M = Re: Cr 143 N 149 I
	X = F, Y = H, $n=m=12$ M = Re: Cr 141 I
	X = Y = F, $n=m=8$ M = Re: Cr 137 N 160 I
	X = Y = F, $n=12, m=8$ M = Re: Cr 125 N 138 I
	X = Y = F, $n=m=12$ M = Re: Cr 131 (N 125) I

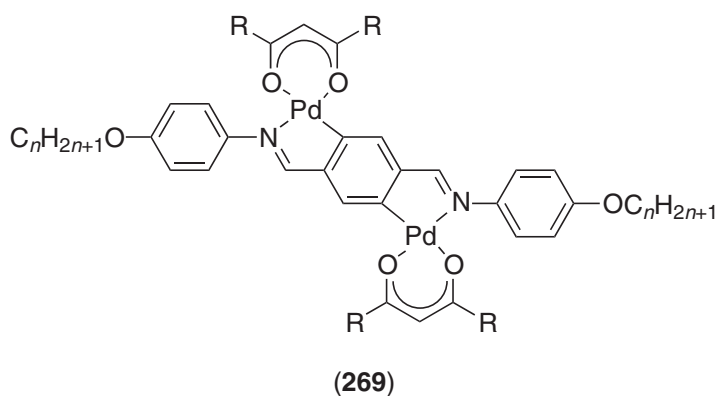
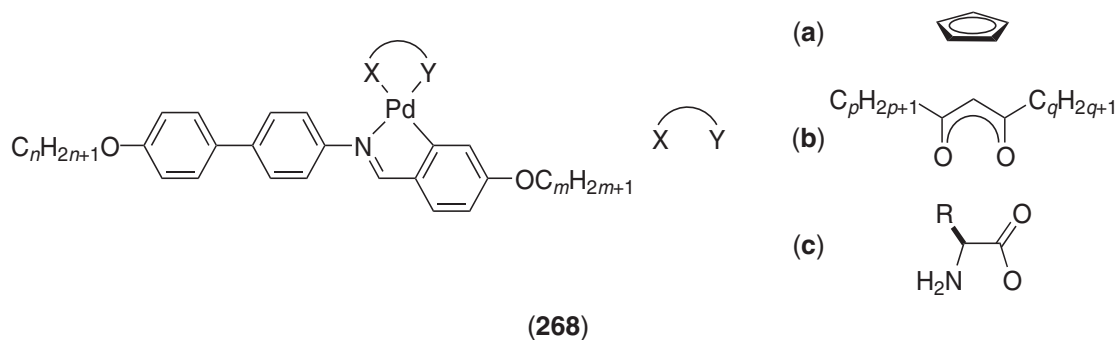
further revealed that complexes based on two-ring ligands were not mesomorphic, while monotropic nematic phases were observed for complexes of three-ring ligands, thus showing the need for ligands of sufficient anisotropy to generate mesomorphic systems with octahedral metal centers.<sup>1075</sup>

The effect of the nature of the terminal group and the position of the imine link have also been investigated. Thus, when hexyl chains are substituted at each end of the rhenium complex having the same motif as (267), a nematic phase was observed (Cr 129 N 167 I). Moreover, when one of the two hexyl chains were replaced by one or two perfluorinated chains, the mesophase was changed to SmA phase, and occurred at higher temperatures, with decomposition taking place in the mesophase.<sup>1076,1077</sup> Similar structural modifications using chiral aliphatic chains (citronellyloxy and its hydrogenated analog) were performed,<sup>1078</sup> and yielded complexes with a chiral nematic phase, though when *both* terminal chains were chiral, mesomorphism was suppressed. The phases typically occurred between 120 °C and 160 °C. Siting the bulky rhenium fragment in one extremity of the molecule resulted in the destabilization of the mesomorphism, but not its suppression.

Four- and five-ring systems diimine ligands and their corresponding dinuclear rhenium complexes were also prepared.<sup>1079</sup> However, while the diimines exhibited smectic and nematic phases between 100 °C and 400 °C, none of the dirhenium complexes was mesomorphic.

Rourke and co-workers demonstrated some years ago that cyclopalladated 4-alkoxy-*N*-(4'-alkoxybiphenyl)benzylidenes with various types of co-ligand, such as cyclopentadienyl ((268a):  $n, m$ : (4, 4), (4, 7), (7, 4), (7, 7)),<sup>1080</sup>  $\beta$ -diketonates ((268b):  $n, m$ : (4, 4), (4, 7), (7, 4), (7, 7);  $p, q$ : 1, 4, 6, 8),<sup>1081</sup> and amino acids ((268c):  $n, m$ : (4, 4), (4, 7), (7, 7), (10, 10); R = Me (alanine), <sup>1</sup>Pr (valine), <sup>1</sup>Bu (leucine), <sup>3</sup>Bu (isoleucine))<sup>1082</sup> led to several new series of mononuclear, *ortho*-palladated mesogens. The free ligands displayed SmF, SmC, and nematic phases between 150 °C and 250 °C, the nematic phase occurring at ca. 200 °C. The derivatives containing the cyclopentadienyl ring, (268a), exhibited mainly a nematic phase, while that with the longer chain (7, 7) showed an additional SmA phase. In this series, an important depression in transition temperatures with respect to free ligands was obtained, the mesophases occurring between ca. 100 °C and 180 °C, the temperature above which they decomposed. In the series with the amino acids, (268c), the SmA phase was the only mesophase observed, but at temperatures greater than 200 °C, where extensive decomposition took place. The thermal behavior of the  $\beta$ -diketonates (268b) was intermediate between that of (268a) and (268c). All the complexes were mesomorphic, showing for the majority both SmA and nematic phases, typically in the range 70–250 °C depending on the chain lengths  $n, m, p$ , and  $q$ . The transition temperatures of the acetylacetonate derivatives ((268b):  $p = q = 1$ ) mirrored perfectly those of the free ligands. The derivatives with  $n = m = 4$ , except for the acetylacetonates, all showed similar melting points at ca. 130 °C, and then the chain length of the imine ligand had little influence on the mesomorphic temperature ranges. The nematic phase disappeared at the expense of the SmA phase when both  $p$  and  $q$  increased.

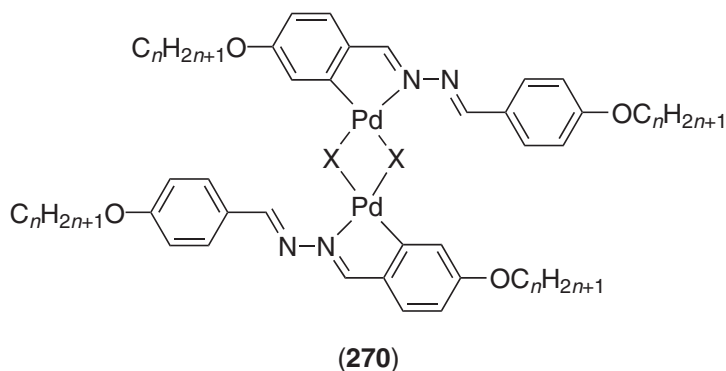
Di-cyclopalladation of ligands containing two imine groups, followed by the reaction with some  $\beta$ -diketonates, led to a novel family of dinuclear complexes, showing a nematic phase.<sup>1083</sup> For the acetylacetonate derivatives ((269): R = Me,  $n = 4-8$ ), the transition temperatures were too high (greater than 200 °C), and the complexes decomposed in the mesophase or in the isotropic liquid, except for the decyloxy homolog (Cr 187 N 246 I). However, a great reduction in transition temperatures was achieved by increasing the lateral chain length ((269):  $n = 8$ , R = butyl, hexyl) so that a nematic phase was seen between 100 °C and 150 °C; the nematic became monotropic or was suppressed totally when R was longer ((269):  $n = 8$ , R = octyl) or bulkier ((269):  $n = 8$ , R = Bu<sup>t</sup>), respectively.



(iv) *Ortho-palladated azine complexes*

Several series of dinuclear *ortho*-palladated complexes of symmetric azines were prepared with various bridges, and the mesomorphism analyzed accordingly ((270): X = OAc, Cl, Br, SCN,  $n = 10$ ).<sup>1084</sup> In the complexes where X = Cl and Br, only the *trans* isomer was observed (1H NMR spectroscopy), while for X = SCN, two isomers were observed in a 60:40 ratio and it was assumed that these were *cis* and *trans*.<sup>1085</sup> In each of these examples the complex was assumed to be planar by comparison with related structures in the literature. However, where X = OAc, the situation was more complex and *trans* and *cis* isomers in the ratio 3:1 were produced consistently. 1H NMR studies went on to show that the *trans* isomer was optically active and hence the structure had to be that of an “open book” (Figure 105, R = Me), although in the synthesis a racemic mixture was produced.

For the non-acetato-bridged dimers, the only mesophase seen was SmC which was typically in the range 100–250 °C (for  $n = 10$ ) while for the acetato-bridged complexes, a nematic phase was seen for  $6 \leq n \leq 8$  and for  $n \geq 7$ , an SmC phase was seen in addition (between ca. 100 °C and 160 °C). Mesophase ranges were very much larger in the planar materials.



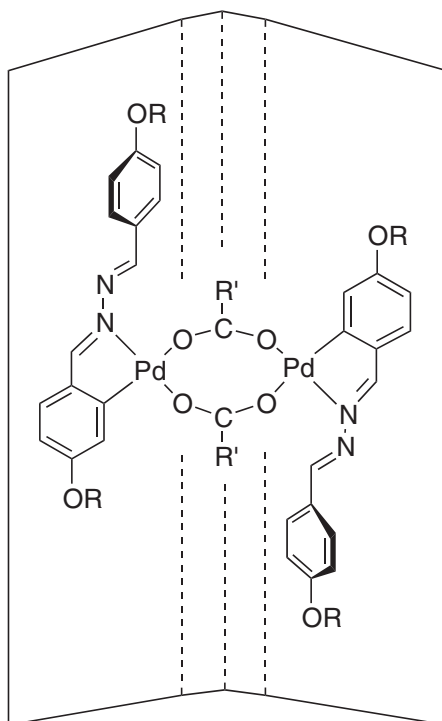


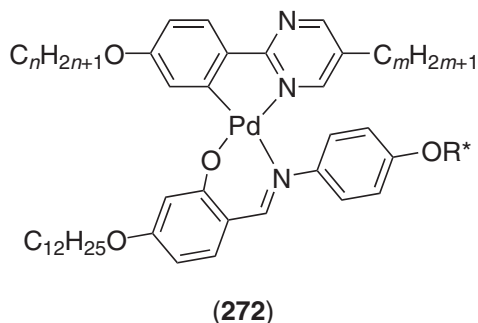
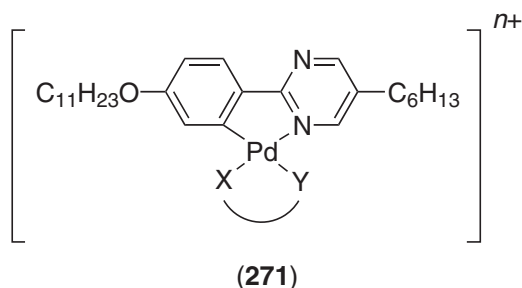
**Figure 105** Schematic structure of the chiral *trans*-isomer of the  $\mu$ -carboxylato palladium azines.

Using the fact that the *trans* isomer was chiral, a derivative was synthesized where the bridging carboxylate group was the optically pure (*R*)-2-chloropropionate ((**270**):  $X = \text{CHMeClCOO}$ ,  $n = 10$ ).<sup>1059</sup> Synthesized from the  $\mu\text{-Cl}_2$  species by reaction with the sodium salt of the acid, a mixture was produced which was shown by  $^1\text{H}$  NMR spectroscopy to have the following composition: *trans*- $\Delta R,R$  (34%), *trans*- $\Delta R,R$  (34%), *cis*-*R,R* (32%). Thus, while the *trans* components described a pair of diastereoisomers, the *cis* isomer was optically pure by virtue of the chiral acid groups. The mixture so produced had the phase sequence Cr 102 SmC\* 119 SmA 149 I and physical measurements showed that the SmC\* phase was ferroelectric, with a rise time of around 330 ms at a square wave voltage of  $\pm 17$  V and 0.5 Hz and a cell thickness of 11  $\mu\text{m}$ . Such response times were some three orders of magnitude longer than those found in calamitic SmC\* phases, something which was probably due to the greater viscosity of the palladium SmC\* phase which in turn resulted from the molecular shape. The full series of (*S*)-chloropropionate from  $n = 6$ –16 was later published by another group, and revealed an important mesophase stabilization, essentially due to the depression of the melting point.<sup>1005,1086</sup> One complex with the larger, chiral carboxylate ( $X = (\text{S})\text{-Me}_2\text{CHCH}_2\text{CHClCOO}$ ,  $n = 14$ ) also yielded an SmC\* phase but at much lower temperatures (between 45 °C and 58 °C).

The effect of the length of the bridging carboxylate was also studied ((**270**):  $X = \text{OOC}_m\text{H}_{2m+1}$ ,  $m = 0$ –11, 13, 15, 17  $n = 10$ ).<sup>1087,1088</sup> Thus, the shortest ( $m = 0$  to 3) and longest ( $m \geq 10$ ) carboxylates gave rise to an SmC phase, enantiotropic only for  $m = 0$ –2, whereas a nematic phase was seen for  $m \geq 3$ , both enantiotropic ( $2 \leq m \leq 6$ , and  $m = 10, 13, 17$ ) and monotropic ( $7 \geq n \geq 9$ , and  $m = 11, 15$ ). The mesomorphic range decreased rapidly as the chain length was increased, dropping from ca. 40 °C to almost nothing, although the transition temperatures became stabilized at around 100 °C, revealing the important perturbation brought to the lateral molecular packing by the carboxylate.

#### (v) *Ortho*-metallated pyrimidine complexes

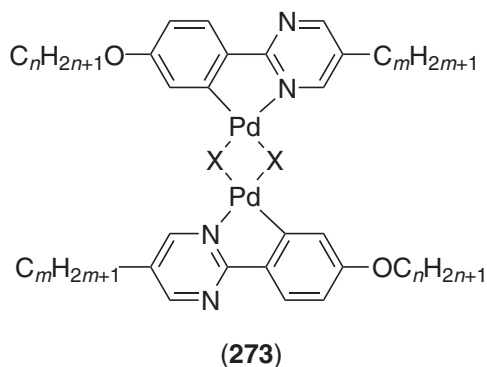
Other work in this area by Ghedini considered the products of the cyclopalladation of the well-known liquid crystals, the 2-phenyl-pyrimidines.<sup>1089</sup> Initially, dimeric products were obtained and then they were reacted further with species able to cleave the  $(\mu\text{-Cl})_2$  bridge to give a series of mononuclear derivatives (**271**).



For X–Y = 8-hydroxyquinolato ( $n=0$ ) and X–Y = 1,10-phenanthroline ( $n=1$ ), the complexes were non-mesomorphic. However, when X–Y = acac ( $n=0$ ), a material with a monotropic SmA phase resulted (Cr 83 (SmA 68) I) and when X–Y = 2,2'-bipyridine ( $n=1$  [BF<sub>4</sub>]<sup>−</sup> counterion), a material with an enantiotropic nematic phase was produced (Cr 146 N 158 I); related complexes with PF<sub>6</sub> or SbF<sub>6</sub> anions were non-mesomorphic. These are further, rare examples of ionic materials showing a thermotropic nematic phase.

Similarly, other mononuclear *ortho*-palladated phenylpyrimidines were obtained with  $\beta$ -diketonate ligands (see also Section 7.9.8.3)<sup>403</sup> or imines (272).<sup>874</sup>

Further studies of the same system looked at the dimeric precursors to such monomeric species and considered the *trans*-dinuclear complexes (273) ((273): X = Cl, Br, I, OAc).<sup>1090</sup>

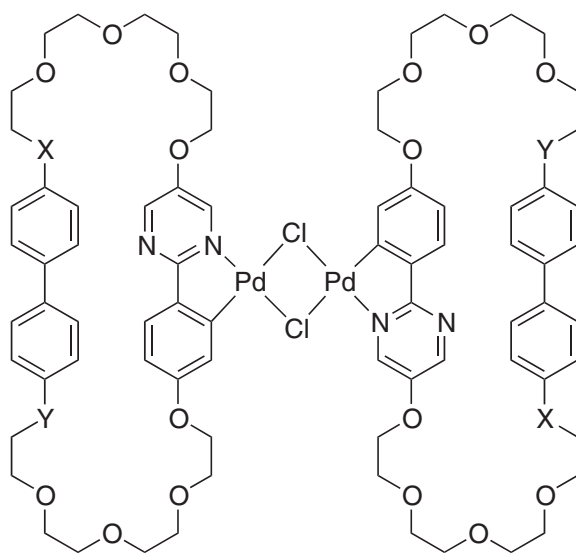


Four series of complexes were studied with the ligands ( $n, m$ ) = (6, 1), (9, 1), (6, 11), (9, 9). None of the complexes with X = OAc and no derivatives with ( $n, m$ ) = (6, 1) was mesomorphic; other non-mesomorphic combinations were ( $n, m$ ) = (9, 1) with X = I, and ( $n, m$ ) = (9, 9) with X = Cl. Of the remaining materials, all had a broad SmA phase (the parent ligands showed a nematic phase only) typically between 100 °C and 200 °C, while two materials (( $n, m$ ) = (9, 1) with X = Cl and ( $n, m$ ) = (9, 9) with X = I) were reported to have another smectic phase (SmX) above the SmA phase. Later studies<sup>1091</sup> showed that what had been identified as SmX was in fact SmA, while the phase identified as SmA was in fact an ordered smectic phase.

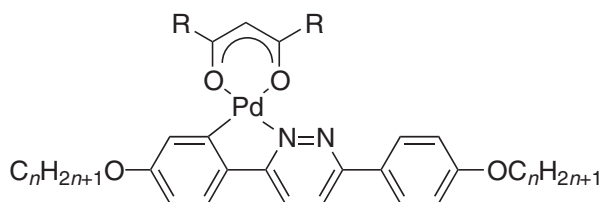
Mesophase stabilization and induction were observed by the cyclopalladation of the macrocyclic 2-phenylpyrimidine derivatives. Indeed, enantiotropic SmA and N phases were observed in the dipalladium complex ((274): X = Y = O, Cr 168 SmA 208 N 226 I), whereas the other dinuclear complex exhibited a nematic phase only ((274): X = Y = CH<sub>2</sub>O, Cr 118 (SmA 91) I).<sup>1092</sup>

#### (vi) Other *ortho*-metallated complexes

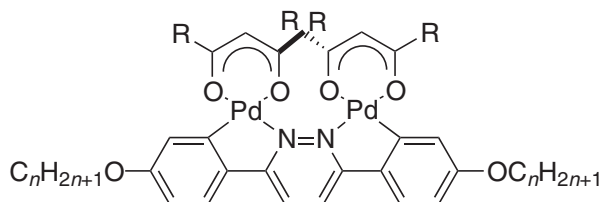
New, mesomorphic mono- ((275): R = Me, Bu,  $n=4-10$ ) and di-cyclopalladated ((276): R = Me, Bu,  $n=4-10$ ) pyridazine complexes have been reported.<sup>1093</sup> They were obtained by the mono- and di-cyclopalladation of elongated pyridazines, followed by the reaction with various  $\beta$ -diketones. The mononuclear complexes (275) exhibited a single SmA phase between 180 °C and ca. 300 °C for R = Me, except the first homolog of the series ( $n=4$ ) which showed an additional SmB phase (Cr 156 SmB 183 SmA 276). For those with the bulkier ketonate ((275): R = Bu), a significant depression in



(274)



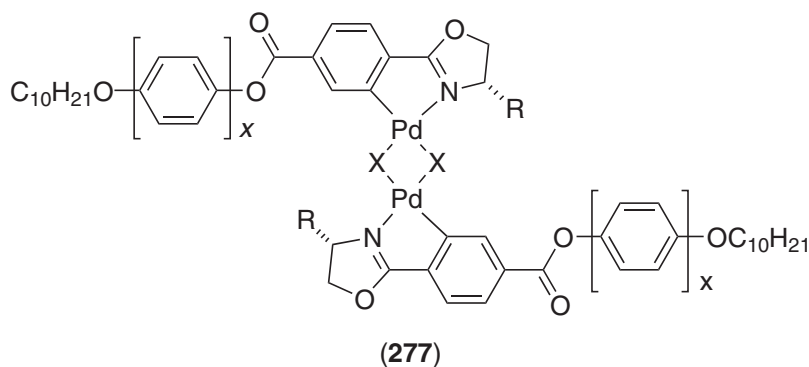
(275)



(276)

clearing temperatures of about 100 °C was observed, and a stable SmA phase was seen for all the homologs between 100 °C and 150 °C up to 190 °C. Amongst the dinuclear complexes, only the *cis*-dicyclopalladated acetylacetonate derivatives ((276): R = Me) showed an SmA phase, well above 200 °C for the short-chain-length homologs with extensive decomposition. Note that these dimetallated complexes have a sterically induced twist in the molecule that render them chiral. The related platinum species could not be isolated as their acetylacetonate derivatives.<sup>1094</sup>

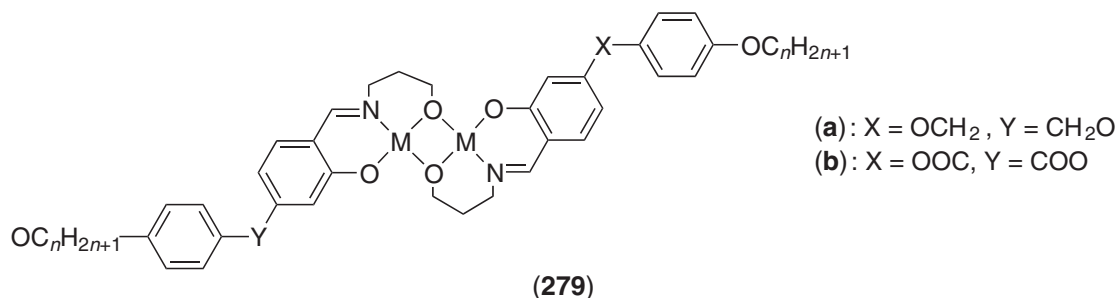
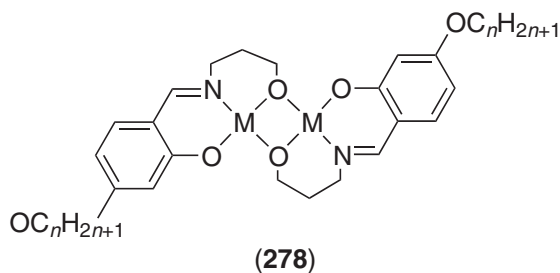
As above (242),<sup>993</sup> the dinuclear *ortho*-palladated complexes derived from (*S*)-2-(2-hydroxyaryl) oxazoline Schiff-base ligands ((277): X = OAc, Cl;  $x = 1$ ; R = CHMe<sub>2</sub>;  $x = 1, 2$ ; R = C\*HCH<sub>3</sub>CH<sub>2</sub>CH<sub>3</sub>) showed a broad SmA phase. In the planar, chloro-bridged complexes (*cis:trans* mixture 1:2), the phase existed from 50 °C to 170 °C, and up to 250 °C for the biphenyl derivative; as far as the non-planar acetato-bridged complexes (only *trans* isomer) were concerned, only the biphenyl derivative was mesomorphic (g 71 SmA 121 Cr 179 SmA 232 I). Used as chiral dopants (ca. 10 mol.%), a chiral nematic phase was induced systematically in both the chloro- and acetato-bridged series, with the suppression of the SmA phase in the chloro-bridged systems ( $x = 1$ ).



#### 7.9.14.5.17 Oxo-bridged complexes

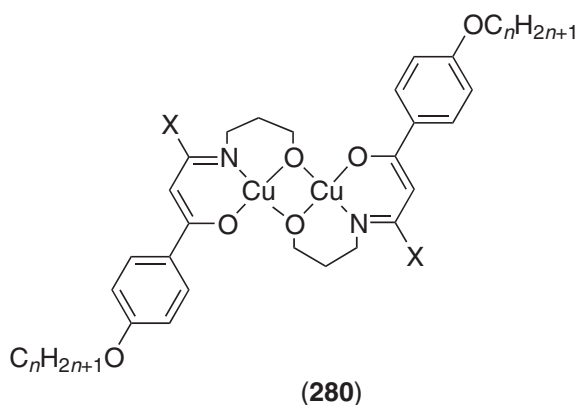
##### (i) O-bridged salicylaldimato complexes

Very recently, new oxygen-bridged bimetallic complexes based on salicylaldehyde ligands were reported, namely *N*-(3-hydroxypropyl)-4-alkoxysalicylaldehyde ((278): M = Cu, V=O, Pd, Fe—Cl;  $n = 8, 10, 12, 14, 16, 18$ ), *N*-(3-hydroxypropyl)-4-(4'-alkoxybenzoyloxy)salicylaldehyde ((279a): M = Cu, Pd;  $n = 8, 10, 12, 14, 16, 18$ ),<sup>1095,1096</sup> and *N*-(3-hydroxyalkyl)-4-(4'-alkoxybenzoyloxy)salicylaldehyde ((279b): M = Cu;  $n = 3, 4, 6, 8, 16, 18$ ).<sup>1097</sup> Dicopper and dipalladium complexes of the series (278) exhibited only a monotropic SmA phase, whereas none of the divanadyl and diiron complexes was mesomorphic. However, a slight improvement in the mesophase stability was achieved in the more elongated series (279a), where a small-temperature-range, enantiotropic SmA mesophase was observed for the dicopper ( $n = 12, 14$ ) and dipalladium complexes ( $n = 12, 14$ ). The melting points of the palladium complexes (160 to 180 °C) were lower than those of the copper compounds (190–210 °C), and the mesophase range more extended in the former ( $\approx 10$ –30 °C) than in the latter ( $\approx 10$ –20 °C). Strangely, none of the bimetallic complexes (279b) was mesomorphic.



##### (ii) O-bridged enaminketonato complexes

The closely related oxygen-bridged dicopper complexes based on  $\beta$ -enaminketonates were also studied ((280): X = H,  $n = 12, 14, 16, 18$ ).<sup>1098</sup> They exhibited an enantiotropic SmA phase typically between the melting point in the range 145–150 °C and the clearing point in the range 160–180 °C.

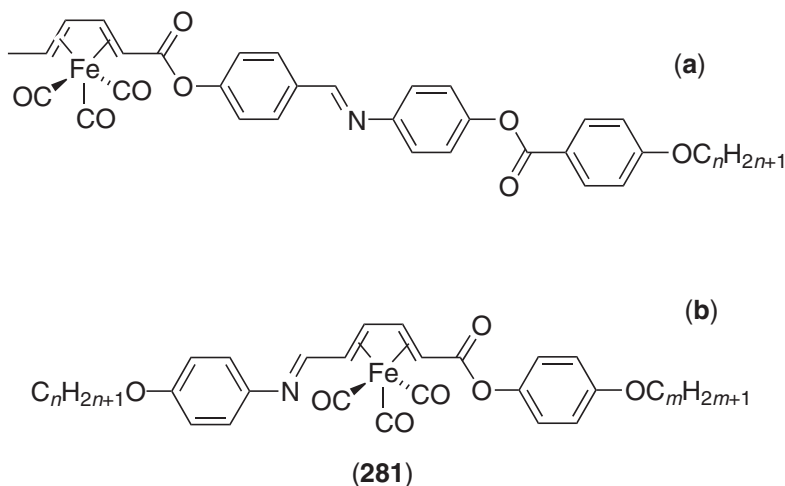


The mesophase was suppressed totally in the iminopropyl- $\beta$ -ketone derivatives ((280): X = Me,  $n = 8, 12, 16$ ), probably due to the steric hindrance of the bulky methyl groups closed to the core.

### 7.9.14.6 Organometallic Complexes

#### 7.9.14.6.1 Tricarbonyliron(0) derivatives

A most interesting group of complexes were the mesomorphic butadienetricarbonyliron(0) materials reported by Malthête and co-workers ((281)).<sup>1099,1100</sup>



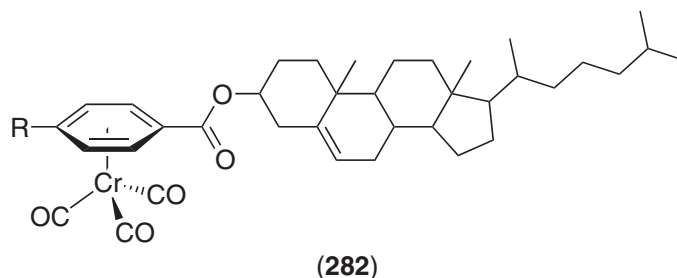
All of the terminally substituted complexes (281a) showed wide-range nematic phases (range  $>100^\circ\text{C}$ , between  $120^\circ\text{C}$  and  $220\text{--}250^\circ\text{C}$ ), while the disubstituted complexes ((281b):  $n = m$ ) displayed nematic phases at short-to-medium chain lengths ( $n = m = 6\text{--}10$ ) and SmA phases as the chains grew longer ( $n = m = 9\text{--}12$ ), though over narrow temperature ranges ( $<10^\circ\text{C}$ , below  $100^\circ\text{C}$ ). These compounds are interesting in that they possess a potentially chiral rigid unit (axial chirality if substituted unsymmetrically) with a rather large transverse dipole, making them good candidates as new ferroelectric liquid crystals. The resolution of the racemic mixture was successfully achieved, and the pure enantiomer (281b) exhibited SmA\* and N\*.

Other metallomesogens containing the optically active butadienetricarbonyliron(0) moiety, incorporated into promesogenic chiral nematic ligands derived from cholesteryl, have been reported.<sup>1101,1102</sup> Both the diastereoisomers exhibited a chiral nematic phase and a monotropic smectic phase, the chiral nematic phase being monotropic for the (+)-isomer (Cr 193 (S 93 N\*131) I), and enantiotropic for the (–)-isomer (Cr 117 (S 99) N\* 133 I).

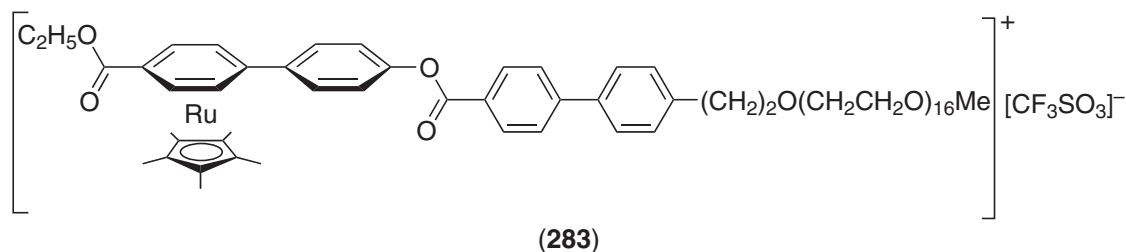
The results reported above clearly indicate that the butadiene iron tricarbonyl moiety can be inserted into mesogenic structures to give, when suitably designed, ferroelectric properties.

### 7.9.14.6.2 $\eta^6$ -Benzene complexes

A series of tricarbonylchromium complexes derived from cholesteryl 4-alkoxybenzoate ((**282**):  $R = OC_nH_{2n+1}$ ;  $n = 1-12$ ) ligands has been reported to show broad-temperature-range chiral nematic phases ( $\approx 40-100^\circ\text{C}$ ).<sup>1103</sup> The complexes are unsymmetrical, and due to the bulkiness of the metallic fragments, an important decrease in both the melting (ca.  $100^\circ\text{C}$ ) and clearing ( $150-200^\circ\text{C}$ ) temperatures as compared to the metal-free ligand was observed, as well as the complete disappearance of the smectic phase present in the free ligand.



Interestingly, Choi *et al.*<sup>1104</sup> reported an example of mesophase stabilization through the formation of a rod-coil ruthenium complex, (**283**). Whereas the organic moiety exhibited an SmB phase between  $120^\circ\text{C}$  and  $123^\circ\text{C}$ , the ruthenium species displayed the same SmB phase, but over a much wider temperature range, i.e., between  $44^\circ\text{C}$  and  $108^\circ\text{C}$ .



### 7.9.14.6.3 Ferrocene-containing thermotropic liquid crystals

#### (i) Introduction

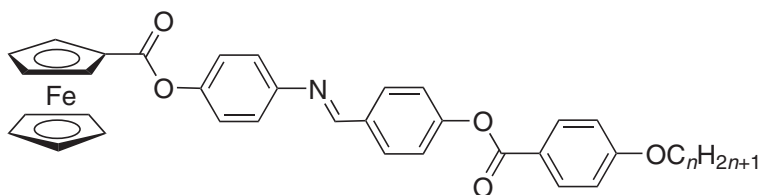
The purpose of this section is not to report all the ferrocene-containing liquid crystals that have been published and discuss their thermal and mesomorphic properties in detail. The aim is, therefore, to highlight, with *selected* examples, the most important results related to the three-dimensional structure and redox properties of ferrocene, which may give clues for the design of novel metallomesogens with specific properties.

The section commences with monosubstituted ferrocene derivatives, after which the influence of the substitution pattern on the formation and stability of liquid-crystalline phases for disubstituted ferrocene derivatives will be discussed. Next, the influence of the three-dimensional structure of ferrocene on the mesomorphic properties will be highlighted, optically active ferrocene materials will be described and, finally, ferrocene-containing liquid-crystalline dendrimers will be introduced; ferrocene-containing liquid-crystalline polymers will not be reported. Note that a review devoted to ferrocene-containing thermotropic liquid crystals has already been published.<sup>8</sup>

#### (ii) Monosubstituted ferrocenes

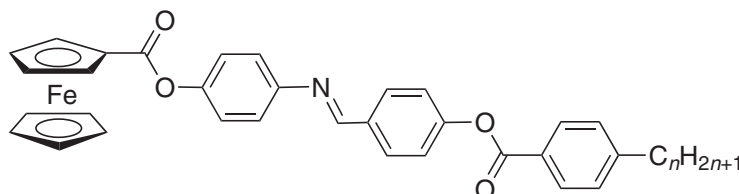
The first ferrocene-containing thermotropic liquid-crystals, i.e., compounds (**284**) to (**286**), were reported by Malthête and Billard in 1976,<sup>1105</sup> with enantiotropic (for (**284**)) or monotropic (for (**285**) and (**286**)) nematic phases being observed. Compounds (**284**) to (**286**) were designed specially to





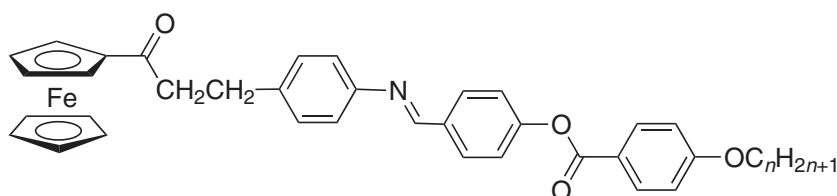
$n = 8$  Cr 153 N 167 I  
 $n = 10$  Cr 143 N 159 I

(284)



$n = 8$  Cr 152 (N 135) I

(285)



$n = 8$  Cr 137 (N 112) I

(286)

undertake Mössbauer studies in mesomorphic medium and represent the first, well-characterized organotransition metallomesogens.

Since these results were published, many monosubstituted ferrocene derivatives have been prepared,<sup>1106–1114</sup> and they have been reviewed by Imrie *et al.*<sup>1115</sup> With a few exceptions, for which (unidentified) smectic phases were observed, monosubstituted ferrocenomesogens gave rise to nematic phases. This behavior was attributed to steric effects induced by the ferrocene unit, so that the organic rod located on the ferrocene compensates only poorly for the influence of the bulky organometallic nucleus. As a consequence, the latter prevents significant intermolecular interactions.

Ferrocene undergoes fast and reversible one-electron transfer with the view to designing switchable liquid crystals based on the ferrocene–ferrocenium redox couple, the peralkylated ferrocenes (287) (Figure 106) were synthesized.<sup>1116,1117</sup> The peralkylated ferrocene moiety was selected as the redox-active center in order to utilize the ease of oxidation of this unit in comparison with less alkylated ferrocenes. Compounds (287) were readily oxidized with silver tosylate into the corresponding ferrocenium derivatives (288) (Figure 106). While compounds (287) were not mesomorphic, the ferrocenium derivatives (288) exhibited liquid-crystalline behavior and a monotropic smectic A phase was observed for (288a) and a monotropic columnar rectangular phase was obtained for (288b). The fact that the oxidized species (288) gave rise to mesomorphism is an indication that the formation of liquid-crystalline phases depends on both structural factors and ionic interactions, the latter helping the molecules to organize. This observation is in agreement with literature data obtained from ionic liquid crystals, such as liquid-crystalline pyridinium derivatives.<sup>1118</sup>

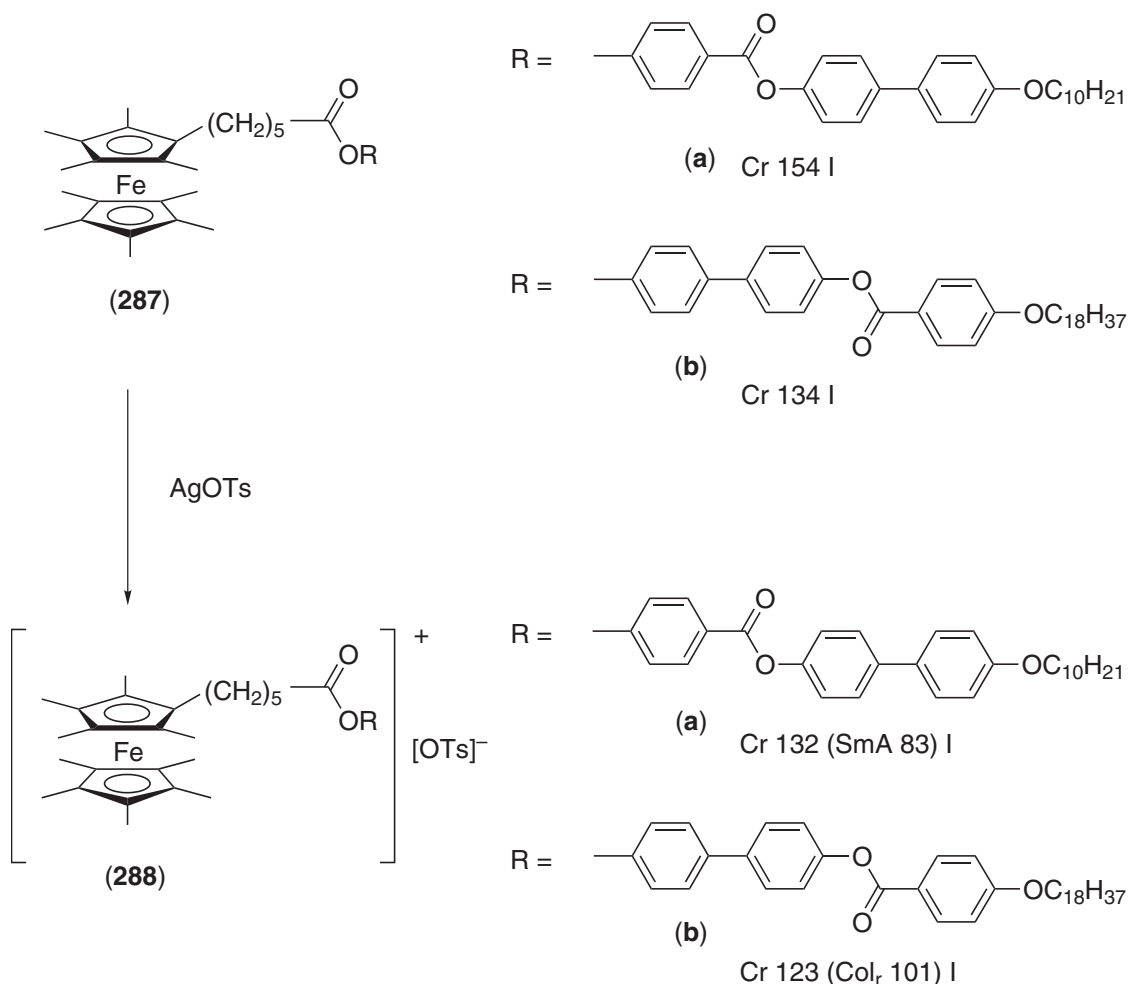


**Figure 106** Ferrocenes (287) and the related ferrocenium salts (288).

The smectic A (monomolecular organization) nature of the mesophase displayed by (288a) is due to a head-to-tail orientation of the molecules within the mesophase. The columnar phase obtained for (288b) was found to have a centered rectangular symmetry, the discrepancy between the molecular volume of the flexible tail and that of the rigid rod being responsible for the formation of the columnar phase.

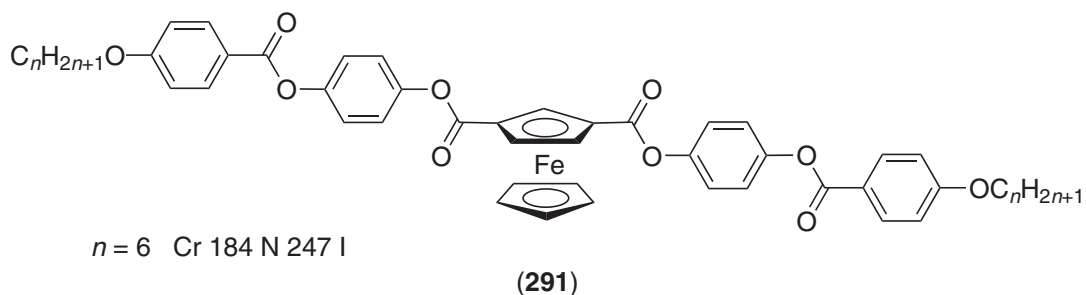
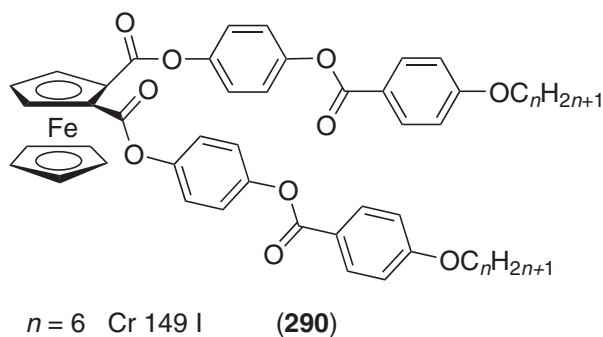
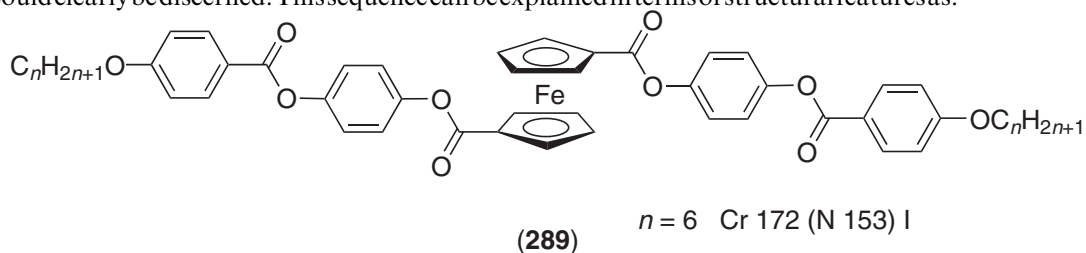
The redox properties of the ferrocene unit were also used to control the liquid-crystalline organization of side-chain liquid-crystalline poly(methacrylates): the reduced polymer gave rise to smectic C and smectic A phases whereas the oxidized polymer showed a nematic phase.<sup>1119</sup>

A detailed understanding of the influence of the structure, charge, and counter-ion on the thermal and mesomorphic properties requires the preparation and study of further ferrocenium materials. The above-reported results prove that liquid-crystalline switches should, in principle, be available by incorporation of ferrocene/ferrocenium into mesogenic materials.

### (iii) Disubstituted liquid-crystalline ferrocenes

During the early stage devoted to the design of ferrocene-containing liquid crystals, ferrocenes substituted at the 1,1'-positions<sup>1120–1128</sup> attracted considerable attention as they exhibited enhanced mesomorphic tendency in comparison with mono-substituted derivatives. Indeed, two substituents located on the organometallic core generate stronger intermolecular interactions than monofunctionalized systems. Various organic rods and functional groups (e.g., cyanobiphenyl, phenylbenzoates, cholesterols) have been attached to the ferrocene, and SmB, SmC, SmA, and N phases were obtained from those materials.

The three-dimensional structure of ferrocene offers multiple possibilities for the preparation of derivatives. To explore *structure-property* relationships, isomeric families of 1,1',<sup>1129,1130</sup> 1,2- and 1,3-disubstituted<sup>1131-1133</sup> ferrocene derivatives were prepared. Representative examples are illustrated by compounds (289) (1,1'-disubstituted ferrocenes), (290) (1,2-disubstituted ferrocenes), and (291) (1,3-disubstituted ferrocenes) and the following liquid crystal tendency: 1,3- > 1,1'- > 1,2-isomeric structures could clearly be discerned. This sequence can be explained in terms of structural features as:



the 1,3-disubstituted ferrocenes possess the highest molecular anisotropy among the isomeric structures;

the substituents located at the 1,1'-positions generate a step in the structure (S- or U-shape), the consequence of which is a reduction of the molecular anisotropy and a loss of co-linearity of the mesogenic substituents;

the substituents located at the 1,2-positions give rise to a hairpin structure which lacks molecular anisotropy.

#### (iv) Trisubstituted ferrocenes

However, Deschenaux and co-workers also reported the first 1,1',3-trisubstituted ferrocene-containing systems (Figure 107) which make for an interesting comparison.<sup>1136</sup> The first series of materials (Figure 107a), showed monotropic SmA and SmC phases ( $n = 12, 14$ ), and monotropic SmC phases ( $n = 16, 18$ ), all the complexes melting to the isotropic liquid at ca. 100 °C. However, the incorporation of an additional aromatic ring in each of the three pendant side groups yielded the complex shown as Figure 107b, which exhibited enantiotropic mesophases, although at rather elevated temperatures. These results are of fundamental importance since they show that the 1,1',3-trisubstitution pattern enhances the mesomorphic properties considerably over di- and mono-substitution.<sup>8</sup> Indeed, one aromatic ring per pendant group is sufficient to promote liquid

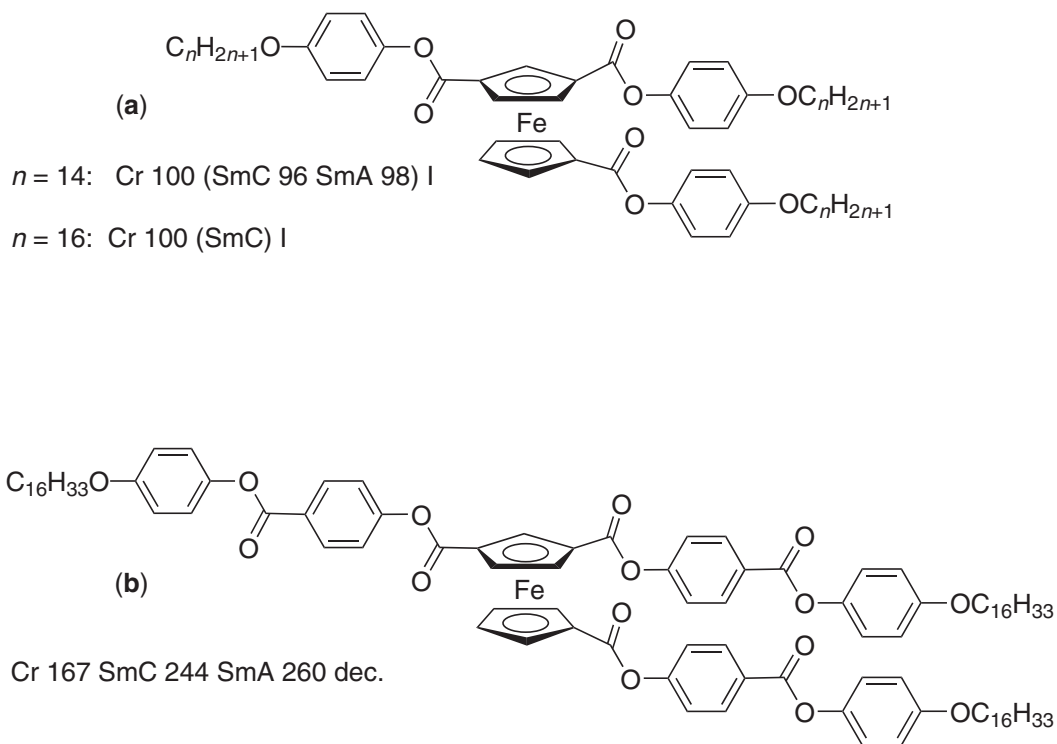
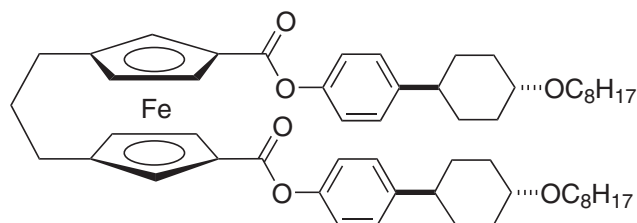


**Figure 107** 1,1',3-Trisubstituted ferrocenes.

crystallinity in these systems on the one hand, and the mesomorphic range is increased on the other hand. A structure–property relationship can, therefore, be formulated in which the liquid-crystal tendency varies as: 1,1',3-trisubstitution > 1,3-disubstitution > 1,1'-disubstitution > monosubstitution.

(v) *Ferrocenophanes*

[3]-Ferrocenophanes (**292**) and (**293**) (Figure 108) carrying mesogenic groups at the 2,2'- or 3,3'-positions were prepared.<sup>1134</sup> Though the 3,3'-isomer (**293**) displayed smectic C and nematic phases, the 2,2'-isomer (**292**) was found to be non-mesomorphic. Because of the bridge between the Cp rings, ferrocenophanes cannot give rise to different conformations about the ferrocene core (contrary to (**289**)). Therefore, (**293**) adopts a U-shape, and confirms that this conformation can also produce mesomorphism for ferrocenes in which rotation around the Cp rings is allowed (as in (**289**)). Obviously, from those results, the S-shape for compounds such as (**289**) cannot be excluded as the one that is formed within the mesomorphic state. For materials where rotation is permitted,

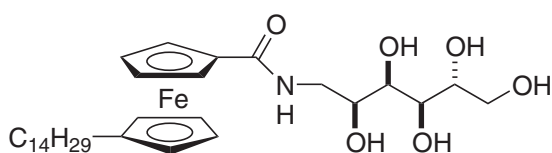


(**292**): 2,2'-disubstituted Cr 135.5 I  
 (**293**): 3,3'-disubstituted Cr 100 SmC 139.5 N 158 I

**Figure 108** Mesogenic [3]-ferrocenophanes.

several conformations should be present within the mesomorphic state among which are the S- and U-shapes. The non-mesomorphic behavior of (292) is, most likely, the consequence of lack of structural anisotropy.

To obtain lyotropic properties, ferrocene was functionalized at the 1,1'-positions by a sugar moiety (1-amino-1-deoxy-D-sorbitol) and a long alkyl chain, i.e., (294).<sup>1135</sup> The substituents, in particular the sugar framework, were selected in view of successful investigations performed with organic-type amphiphilic carbohydrate surfactants. Compound (294) showed both thermotropic and lyotropic mesophases, and the anhydrous material showed a smectic A phase from 98 °C to 137 °C. When (294) was dissolved in an excess of water, a fluid  $L_\alpha$  phase was obtained. For the thermotropic smectic A phase, a layer  $d$ -spacing of 37.7 Å was determined, while for the lyotropic lamellar phase, a layer  $d$ -spacing of 50 Å was found. Therefore, a 12.3 Å difference in layer thickness was obtained between the thermotropic and lyotropic mesophases, and this increase in the layer thickness was attributed to the incorporation of water molecules between the layers of (294). Ferrocene-containing lyotropic liquid crystals are of interest for the development of redox-active organized media for catalytic purposes; careful derivatization of ferrocene will lead to other lyotropic mesophases.



Thermotropic behavior: Cr 98 SmA 137 I

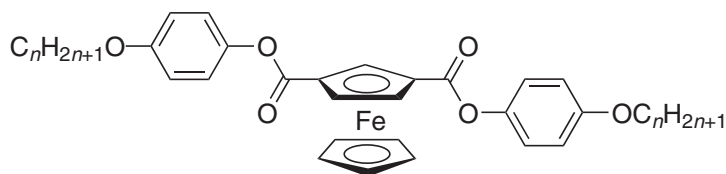
Lyotropic behavior:  $L_a$  at 60 °C (excess of water)

(294)

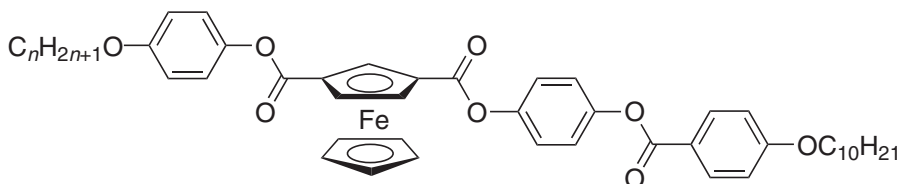
(vi) Influence of the ferrocene unit on thermal and mesomorphic properties

For the design of ferrocene-based liquid crystals, the main structural feature that has to be taken into account is the three-dimensional structure of ferrocene. Interestingly, depending on the groups that are located on the ferrocene, the latter unit can either reduce or enhance the stability of the liquid-crystalline state (*vide infra*).

It has been mentioned already that among the disubstituted ferrocene derivatives, the 1,3-disubstitution pattern induces the highest mesomorphic tendency. The fact that (295) and (296),<sup>1132,1137</sup> which contain either two or three aromatic rings (not including the ferrocene unit), did not exhibit liquid-crystalline properties supports the observation that the ferrocene unit usually reduces the liquid-crystalline tendency of materials to which it is bound.



(295)



(296)

These results were confirmed by Goodby *et al.* who investigated the thermal and mesomorphic behavior of a series of materials in which the ferrocene unit was replaced by a benzene ring or a

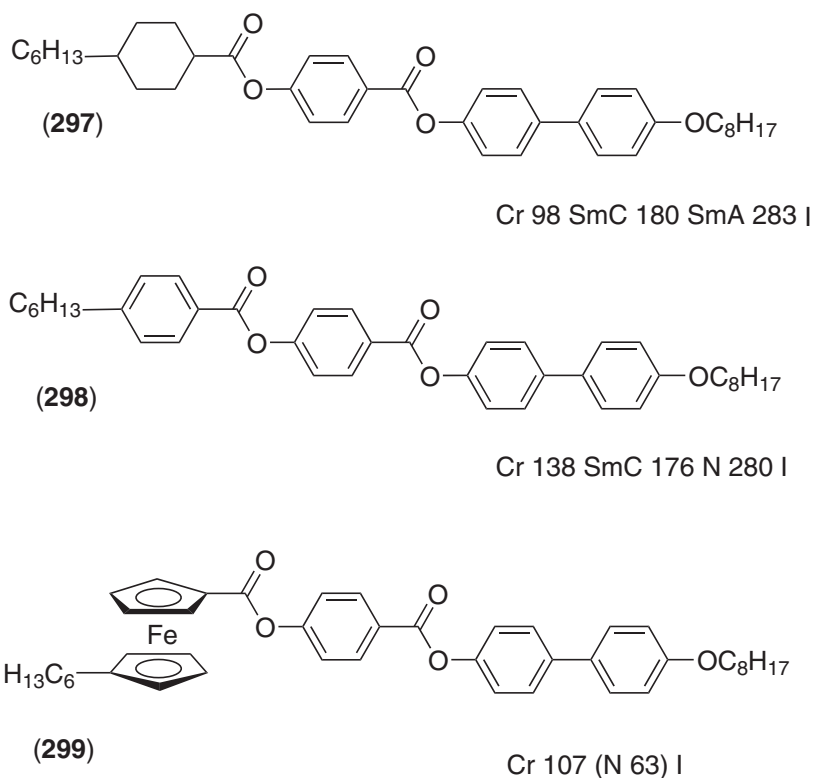


**Figure 109** Evaluation of ferrocene as a component of liquid crystals.

cyclohexane ring, seem for example, (297) to (299) (Figure 109).<sup>1137</sup> They observed that the ferrocene destabilized the liquid-crystalline state, indicating that ferrocene plays the role of a bulky unit, again as a consequence of its three-dimensional structure.

Twin liquid crystals containing either ferrocene (300), (301), or terephthalate (302), (303) as the connecting unit between mesomorphic rods were reported by Tschierske *et al.* (Figure 110).<sup>1138</sup> Comparison of their thermal and liquid-crystalline properties revealed that the ferrocene-based material had comparable or higher clearing temperatures and lower melting points than the structurally related terephthalates. Thus, broader liquid-crystalline domains were obtained for the ferrocene materials. The stabilization of the liquid-crystalline state when the ferrocene was used as the linking group was unexpected in view of literature data (*vide supra*). The authors explained this behavior by suggesting that the rotational flexibility of the ferrocene unit could lead to an improved arrangement of the individual molecules within the layers, the consequence of which was a greater stability of the mesophases.

#### (vii) *Optically active systems*

Only a few examples of optically active ferrocene-containing thermotropic liquid crystals have been reported. Compounds (304) and (305) have been prepared by functionalizing ferrocene with a chiral fragment bearing an asymmetric carbon atom. Ferrocene derivative (304) showed an SmC\* phase,<sup>1139</sup> while for (305), SmC\*, SmA, TGBA, N\*, and blue phases (blue phases are referred to in Section 7.9.4.3.3) were obtained.<sup>1140</sup> Ferrocene has also been substituted with a cholesterol derivative but the mesophases were not identified.<sup>1107</sup>

Deschenaux and co-workers designed optically active, ferrocene-containing thermotropic liquid crystals by introducing two different substituents at the 1,3-positions of a Cp ring,<sup>1141</sup> generating ferrocenes with planar chirality. Thus, ferrocene (306) (Figure 111) was obtained with an enantiomeric excess of 98%.<sup>1142</sup> The absolute configuration of the ferrocene has not yet been determined and, therefore, structure (306) has been drawn arbitrarily. SmC\* and SmA phases were observed for (306), and its spontaneous polarization was determined as  $2.8 \text{ nC cm}^{-2}$ . This low value is consistent with the structure of (306) which carries two organic fragments that are

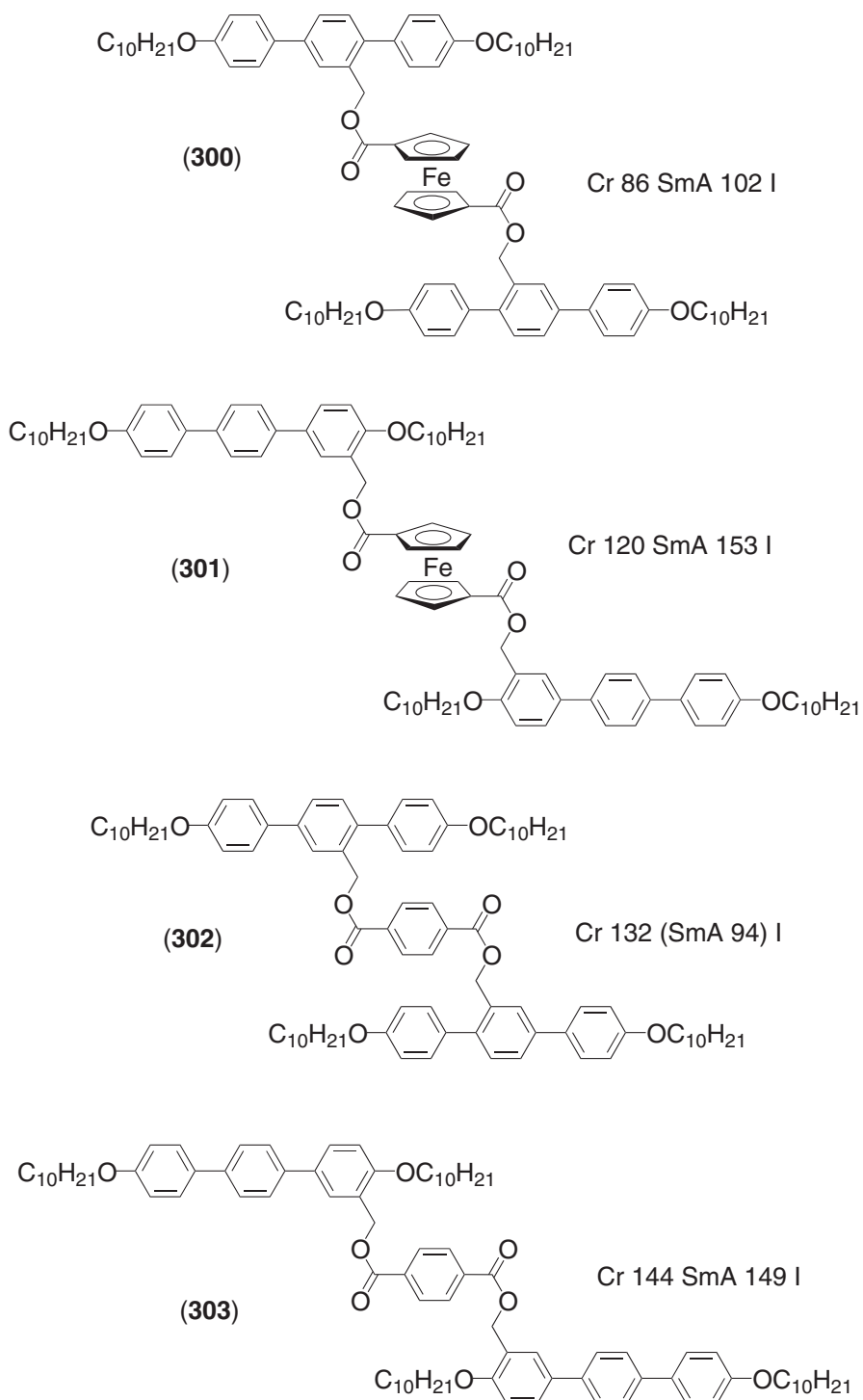


**Figure 110** Further evaluation of ferrocene as a component of liquid crystals.

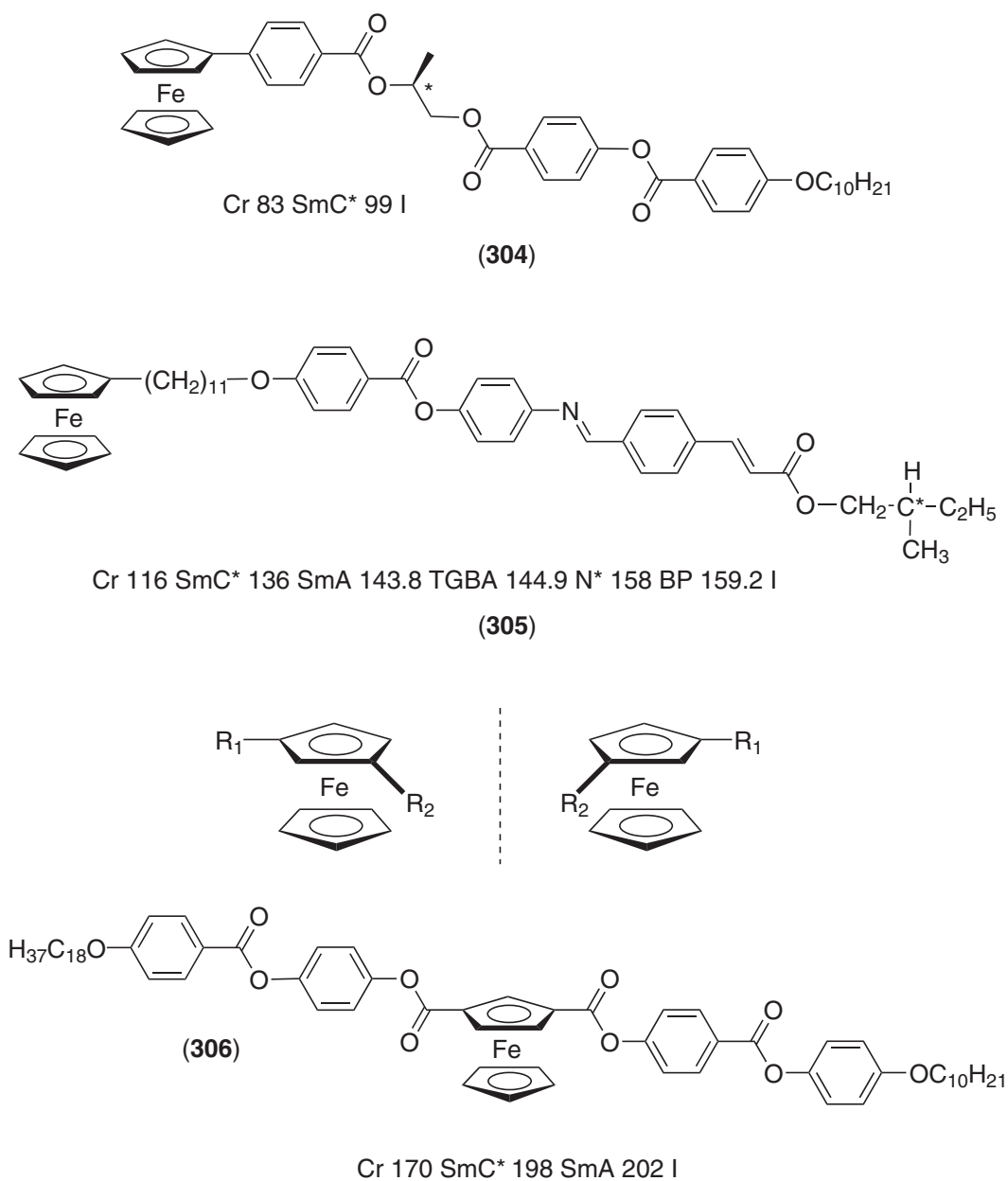


**Figure 111** The planar chirality of unsymmetric 1,3-disubstituted ferrocenes as exemplified by **306**.

differentiated only by the length of the terminal alkyl chains and the orientation of the external ester functions. Planar chirality is of interest as the chiral center is located at the ferrocene itself (Figure 111), and such structures might further help our understanding of the role of ferrocene on the formation, nature, and stability of liquid-crystalline phases. Also, as most of the studies on chiral liquid crystals are developed with compounds having point chirality, planar chirality is an alternative and elegant way to obtain optically active materials. For example, Malthête *et al.* used planar chirality to design ferroelectric butadiene–tricarboxyliron complexes (Section 7.9.14.6.1).<sup>1099,1100</sup>

(viii) *Ferrocene-containing dendrimers*

Dendrimers represent a class of materials which combine unique features (well-defined macromolecular structure, monodispersity, low viscosity) with remarkable properties (encapsulation, catalysis,



chiroptical properties).<sup>1143,1144</sup> Functionalized dendrimers, i.e., dendrimers incorporating active or reactive functions, are considered as new materials with high potential for application.

Deschenaux and co-workers have designed liquid-crystalline dendrimers containing ferrocene and/or fullerene,<sup>1145,1146</sup> all of which are prepared by a convergent and iterative synthetic methodology<sup>1147</sup> leading to precisely monodisperse macromolecules.

Second-generation dendrimer (307) gave rise to a smectic A phase from 52 °C to 169 °C.<sup>1148</sup> The mixed fullerene–ferrocene (308) of second generation showed a smectic A phase which cleared at 157 °C (the glass transition temperature was not detected).<sup>1149</sup> The association of fullerene (electron-acceptor unit) and ferrocene (electron-donor unit) within the same structure is of interest to elaborate liquid-crystalline switches<sup>1150</sup> based on the photo-induced electron transfer occurring from ferrocene to fullerene.<sup>1151</sup> Finally, (307) and (308) are stable materials, soluble in common organic solvents.

### (ix) Conclusions

Despite the three-dimensional structure of ferrocene which behaves as a bulky unit, a great variety of ferrocene-containing liquid crystals displaying rich mesomorphism have been prepared, providing lessons on how to accommodate non-ideal units into a mesogenic structure. It is anticipated, then, that the studies developed with ferrocene, and the results that have been obtained, will help in the design of other types of metallomesogens. For example, based on studies on ferrocene-containing thermotropic liquid crystals, successful preparations of mesomorphic ruthenocene<sup>1152</sup> and ( $\eta^6$ -arene)tricarbonylchromium(0)<sup>(621)</sup> (Section 7.9.12.6.2) materials have been reported. Further, the Fe<sup>III</sup> state is readily accessible giving an entry not only to colored materials, but also those with a spin–orbit-coupled magnetic response, and the notion of switchable metallomesogens has been explored above.

### 7.9.14.7 Metalloporphyrins

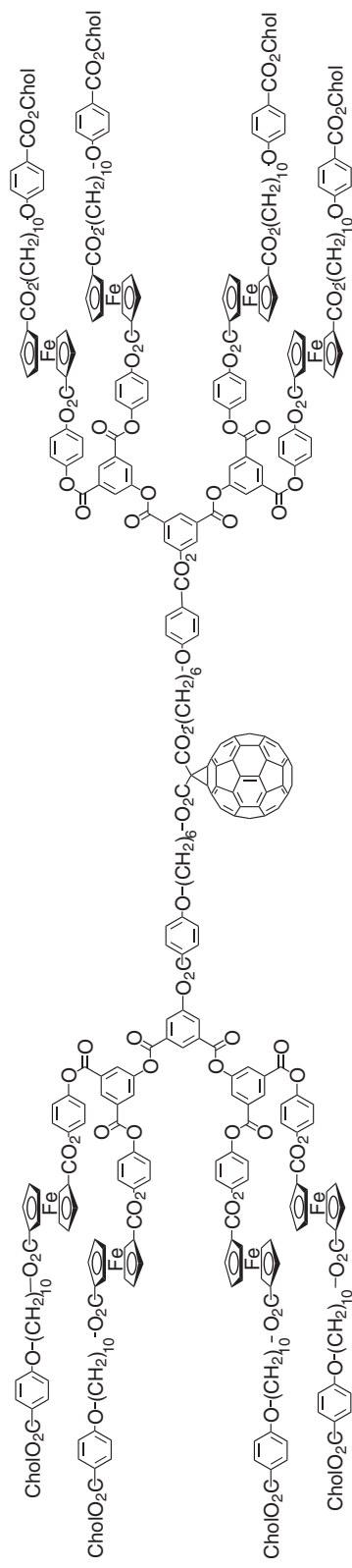
There have been only a few reports on the design of mesomorphic calamitic porphyrins, quite probably due to the great synthetic effort which has to be expended. Some 5,15-disubstituted copper(II) octamethylporphyrin derivatives were first reported ((309): R' = Me, n = 12, 22, M = Cu) and while none of the pure materials was mesomorphic, a monotropic schlieren texture was reported for mixtures of certain porphyrins with long-chain alkyl chlorides; the “phase” was never identified.<sup>1153</sup> Some related zinc porphyrins ((309): R' = C<sub>4</sub>H<sub>9</sub>, n = 8–10, M = Zn) were also prepared, but were not mesomorphic either.<sup>1154</sup>

The first examples of calamitic metalloporphyrins showing smectic mesophases, namely smectic crystal B and E phases were reported by Bruce *et al.* in 1992 ((310): R = OC<sub>n</sub>H<sub>2n+1</sub>, M = Zn).<sup>1155</sup> The mesophases occurred at high temperatures, with the clearing taking place well above 200 °C. By elongation of the groups bound in the 5- and 15- positions ((310): M = Zn, R = –OCO–C<sub>6</sub>H<sub>10</sub>–C<sub>n</sub>H<sub>2n+1</sub>, –OCO–C<sub>6</sub>H<sub>4</sub>–OC<sub>n</sub>H<sub>2n+1</sub>), it was then possible to show that fluid mesophases, SmA and N phases respectively, could be formed, but with elevated melting points (>300 °C).<sup>(625)</sup> Using “fly-over,”<sup>(624)</sup> or strapped<sup>1156</sup> chains nematic phases were observed with greatly reduced transition temperatures, on average by 200 °C, compared to the parent porphyrins.

### 7.9.14.8 Crown-ether Complexes

Complexation of metallic salts to the non-mesomorphic 1,10-bis[(4-alkyloxy)benzoyl]-1,10-diaza-4,7,13,16-tetrathiacyclooctadecane, [18]aneN<sub>2</sub>S<sub>4</sub> ((311)) resulted in the formation of a new family of host–guest macrocyclic liquid crystals. For instance, palladium (M = Pd, X = BF<sub>4</sub>; n = 12),<sup>1157</sup> copper (M = Cu, X = PF<sub>6</sub>; n = 6, 10–12, 14),<sup>1158</sup> and silver salts (M = Ag, X = CF<sub>3</sub>SO<sub>3</sub>, PF<sub>6</sub>; n = 12) all exhibited a thermotropic smectic A phase (Table 83).<sup>1159</sup> The related palladium complexes with [18]aneN<sub>2</sub>O<sub>4</sub> were, however, not mesomorphic. Mesomorphism was attributed to the stiffening of the azacrown core moieties through metal-to-ligand coordination. For the palladium and copper systems, the mesophase possessed an undulating ribbon structure, whereas for the tetrahedral silver complexes, the mesophase





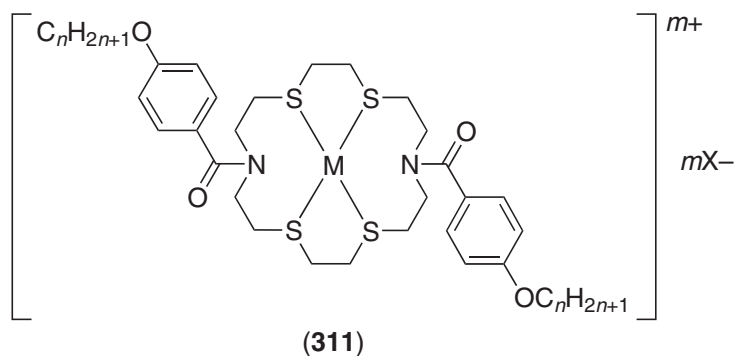
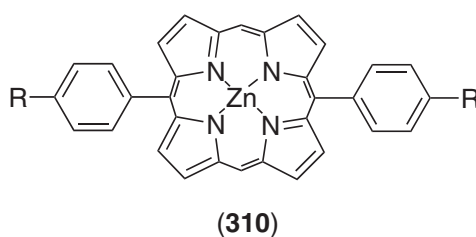
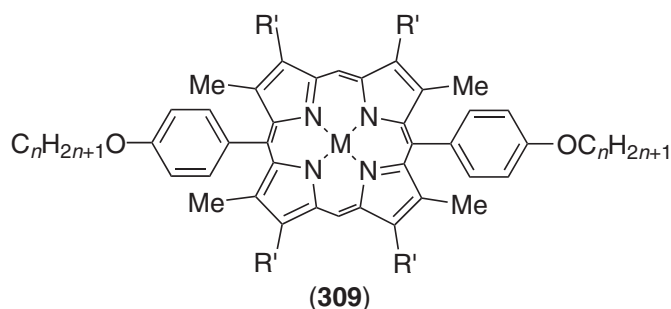
SmA 157 I

(308)

**Table 83** Mesomorphism of some of the macrocyclic systems (311) with  $n = 12$ .

$M$	$M$	$X$	Transition temperatures
Pd	2	$\text{BF}_4$	Cr 160 SmA 188 I
Cu	1	$\text{PF}_6$	Cr 123 SmA 190 I
Ag	1	$\text{CF}_3\text{SO}_3$	Cr 50 SmA 124 I
Ag	1	$\text{PF}_6$	Cr 70 SmA 160 I

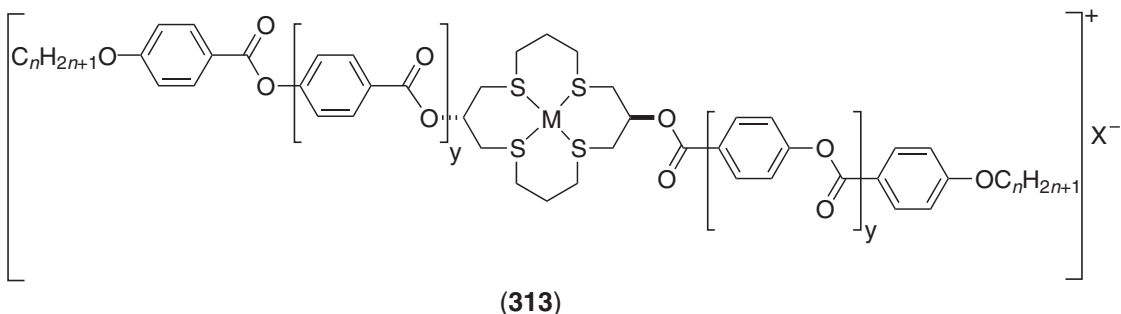
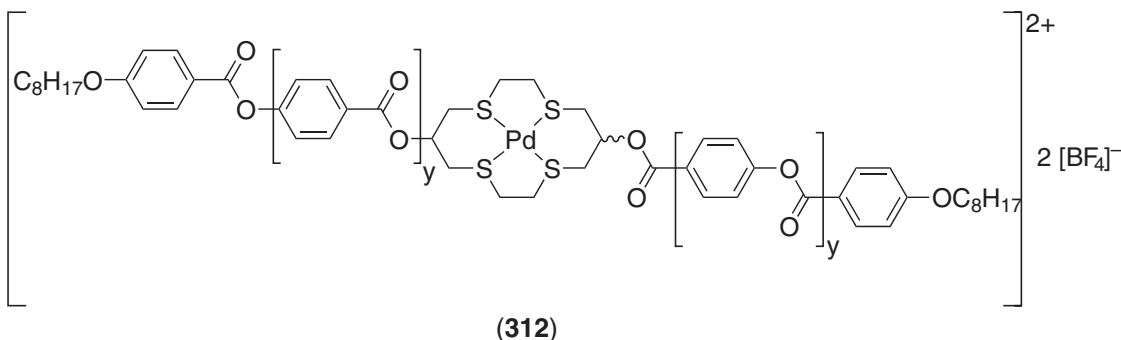
consisted of an undulating bilayer, consistent with the U-shaped molecular structure. Moreover, a lamellar phase was induced at room temperature in concentrated solutions of acetonitrile (13–35 wt.% acetonitrile). Four different mixtures of the  $\text{PF}_6$  salt in acetonitrile were prepared and studied in detail by X-ray diffraction. It showed an increase of both the lamellar periodicity and the surface area with increasing solvent content. The swelling of the lamellar phase compared to that of the anhydrous neat phase was associated with intralayer modulations induced by the insertion of solvent. Above 20% (w/w), the mesophase coexists with the isotropic liquid. The amphiphilic character is thought to be enhanced by the U-shape conformation of the complex. Indeed, the tetrahedral mode of coordination of silver to the macrocycle and the parallel arrangement of the chains was revealed by a single-crystal structure of the  $\text{PF}_6$  salt. Such favorable facial conformation, providing that it still remains in the mesophase, supported the idea of a bilayer organization. This assumption is confirmed



by the fact that the related linear palladium and copper complexes did not form a lyotropic mesophase.

Complexation of silver(I) triflate and tosylate salts to the related *N,N'*-bis(hexadecanoyl)-1,10-diaza-4,7,13,16-tetrathiacyclooctadecane also formed smectic A phase, between 74 °C and 107 °C for the triflate compound, and between 125 °C and 173 °C for the tosylate.<sup>1160</sup>

Finally, some work on macrocyclic thioethers was able to show that while a metal-free tetraester of a functionalised [14]aneS<sub>4</sub> diol was non-mesomorphic as either its *cis* or *trans* isomer, complexation to palladium(II) stiffened the whole molecular unit and allowed differentiation between the non-mesomorphic, nonlinear *cis* complex ((**312**):  $y=1$ : Cr 258 I), and the mesomorphic, linear *trans* complex ((**312**):  $y=1$ : Cr 312 (N 272) I).<sup>1161</sup> Substituted with shorter lateral arms, the palladium salts (Pd(BF<sub>4</sub>)<sub>2</sub>) exhibited monotropic SmC phases ((**312**):  $y=0$ : Cr 222 (SmC 164) I). Difunctionalised *trans*-[16]aneS<sub>4</sub> diol palladium ((**313**): MX = Pd(BF<sub>4</sub>)<sub>1</sub>,  $y=0,1$ ) also exhibited monotropic phase (SmC and N, respectively for  $y=0$  and 1),<sup>1162</sup> whereas the copper derivative ((**313**):  $y=0$ , MX = Cu(PF<sub>6</sub>)) was surprisingly devoid of mesomorphism.<sup>1163</sup> Note that some related aza macrocyclic metal complexes as potential metallomesogens were also studied, but it appeared that none of them were found to be mesomorphic.<sup>1164,1165</sup>



## 7.9.15 LYOTROPIC METALLOMESOGENS

### 7.9.15.1 Polymeric Systems

The mesophases formed by polymeric systems are largely nematic or hexagonal phases. Here, long, normally rigid rods are considered which dissolve in a solvent. These can then be arranged in a fashion analogous to a thermotropic nematic phase, except that the individual rods are solvent-separated. If the concentration of these rods is increased, then they can pack to give a more regular structure, namely the hexagonal phase. An example of a polymeric, lyotropic system is the nematic mesophase of Kevlar in oleum (Figure 112).

Takahashi *et al.*<sup>1166</sup> reported the synthesis of polymeric acetylides of platinum(II) (Figure 113) from 1,4-butadiyne or 1,4-diethynylbenzene. Molecular weight average ( $\overline{M}_w$ ) degrees of polymerization of up to  $7 \times 10^4 \text{ g mol}^{-1}$  (corresponding to a number average ( $\overline{M}_n$ ) of 108) were obtained. For polymers with ( $\overline{M}_w$ )  $\approx 10^5 \text{ g mol}^{-1}$  lyotropic nematic phases were observed at around 36 wt.% in trichloroethene.<sup>1167</sup>

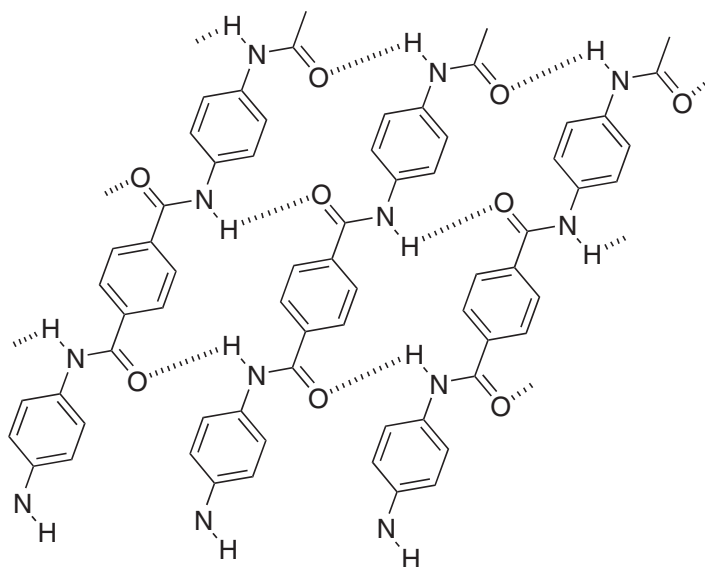


**Figure 112** The molecular organization within the mechanically aligned nematic phase of Kevlar.

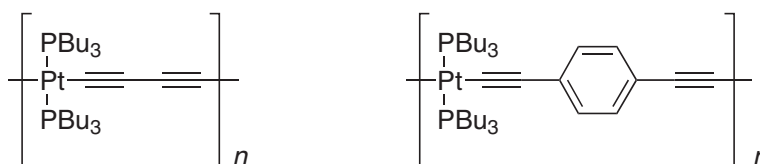


**Figure 113** Polymeric Pt acetylide complexes described by Takahashi.

Homo- (Figure 114;  $M = M'$ ) and hetero-metallic (Figure 114;  $M = \text{Pt}$ ,  $M' = \text{Pd}$  or  $\text{Ni}$ ;  $M = \text{Pd}$ ,  $M' = \text{Ni}$ ) polymers of 1,4-butadiyne were studied by  $^{31}\text{P}$  NMR spectroscopy which showed that all possessed a negative diamagnetic anisotropy ( $\Delta\chi < 0$ ); that is, they aligned with their long molecular axes perpendicular to the applied magnetic field. This was interpreted largely in terms of the negative diamagnetic anisotropy of the carbon-carbon triple bond.<sup>1168</sup>

However, subsequent studies<sup>1169</sup> of related materials showed that, in fact, the magnetic anisotropy was a more complex balance of ligand and metal. Thus, while the butadiyne homopolymer of palladium(II) (Figure 114);  $M = M' = \text{Pd}$  had  $\Delta\chi < 0$ , the block copolymer (Figure 115) had  $\Delta\chi > 0$  due to the fine balance of the opposite magnetic anisotropies of benzene and carbon-carbon triple bonds in the complexes, which may well be enhanced by conjugation.

A second noteworthy series is that of the dirhodium tetraalkanoates and tetrabenzoates which have been studied extensively as thermotropic mesogens (*vide supra*). In solution in alkane, columnar nematic phases were formed as evidenced by the schlieren textures observed.

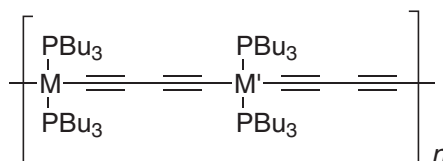


**Figure 114** Structure of the mixed-metal butadiyne polymers.

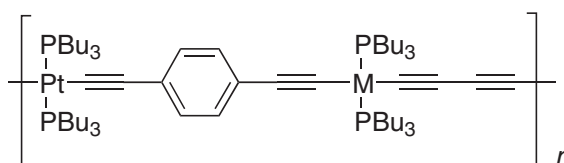


**Figure 115** Homometallic block copolymer with  $\Delta\chi > 0$ .

## 7.9.15.2 Amphiphilic Systems

### 7.9.15.2.1 Simple salts

Lytotropic behavior of simple metal carboxylates has been described earlier (Section 7.9.9). However, many alkaline earth metal salts of dodecylbenzenesulfonates<sup>1170–1173</sup> ( $\text{Mg}^{\text{II}}$ ,  $\text{Ba}^{\text{II}}$ , and  $\text{Ca}^{\text{II}}$ ), as well as those of  $\text{Hg}^{\text{II}}$ ,  $\text{Pb}^{\text{II}}$ ,  $\text{Al}^{\text{III}}$ ,  $\text{Mn}^{\text{II}}$ ,  $\text{Co}^{\text{II}}$ ,  $\text{Ni}^{\text{II}}$ ,  $\text{Cu}^{\text{II}}$ ,  $\text{Cr}^{\text{III}}$ , and  $\text{Fe}^{\text{III}}$ , have also been reported to form  $L_\alpha$  phases in water. At higher surfactant concentrations, another mesophase, with a poorly defined structure, was induced for some salts.

Lytotropic mesophases were reported for some trivalent, rare-earth dodecylsulfates,  $\text{Ln}(\text{C}_{12}\text{H}_{25}\text{OSO}_3)_3$  with  $\text{Ln} = \text{La}$  to  $\text{Lu}$  (except  $\text{Pm}$ ), and yttrium in the presence of ethylene glycol, water, and mixtures of both solvents.<sup>1174</sup> None of the compounds was thermotropic in the anhydrous state. The lyotropic mesomorphism of these complexes was investigated between ambient temperature and  $70^\circ\text{C}$  by polarized optical microscopy using contact preparations. In ethylene glycol, all formed a hexagonal  $H_1$  phase, recognized on the basis of its fan-like texture. At higher surfactant concentrations, between the solid and the hexagonal phases, an optically isotropic region, characteristic of a cubic phase, was seen. At these concentrations, the structure of the cubic phase is probably bicontinuous ( $V_1$ ), although its exact nature has not yet been determined. Although less soluble, mesophases were also observed in contact preparations between the lanthanide dodecylsulfates and water. Thus, in addition to the hexagonal  $H_1$  phase, a lamellar  $L_\alpha$  phase was seen at higher surfactant concentration, with no evidence of a cubic phase. Finally, the behavior in ethylene glycol–water mixture (50:50 v/v) was identical to that observed in pure ethylene glycol.

The  $\alpha,\omega$ -alkylenedisulfate salts of lithium, sodium, and potassium,  $\text{M}(\text{O}_3\text{SO}(\text{CH}_2)_n\text{OSO}_3)\text{M}$  with  $n = 12, 14, 16,$  and  $18$ , were reported to possess lyotropic properties in water, with the supposed existence of two critical micelle concentrations.<sup>1175</sup> The second *cmc* was explained by the existence of a rearrangement of the existing aggregates into another type of aggregate.

### 7.9.15.2.2 Amphiphilic metal complexes

Probably the first studies of materials of this type were those of Le Moigne and Simon who synthesized what they termed *annelides*, of which they reported an example on cobalt(III) showing a room-temperature, lamellar phase.<sup>1176</sup> Interestingly, these complexes ((**314a**)), can be thought of as amphiphilic in two ways, as they possess a hydrophobic octadecyl chain and *two* hydrophilic fragments, i.e., the cationic cobalt center *and* the ethylene oxide chains. The related dichlorocopper(II) complex (**314b**) exhibited an  $L_\alpha$  phase, which remained stable in the presence of up to 25% (v/v) of water, alkane (hexane, decane), or benzene.<sup>1177</sup>

Other amphiphilic cobalt(III) complexes were reported by Yashiro *et al.*<sup>1178</sup> (Figure 116a) who measured the *cmc* to be at very low concentrations ( $3.3 \times 10^{-5} \text{ mol dm}^{-3}$ ) in water but did not report any mesophase formation, while Bruce *et al.* demonstrated lyotropic mesophases in surfactant ethylenediamine-based complexes including examples on chromium(III) (Figure 116b).<sup>1179</sup>

A series of surfactant *tris*(bipyridyl)ruthenium(II) complexes first reported by Seddon and Yousif,<sup>1180</sup> was shown to be mesomorphic in water.<sup>1181,1182</sup> Thus, consistent with the packing

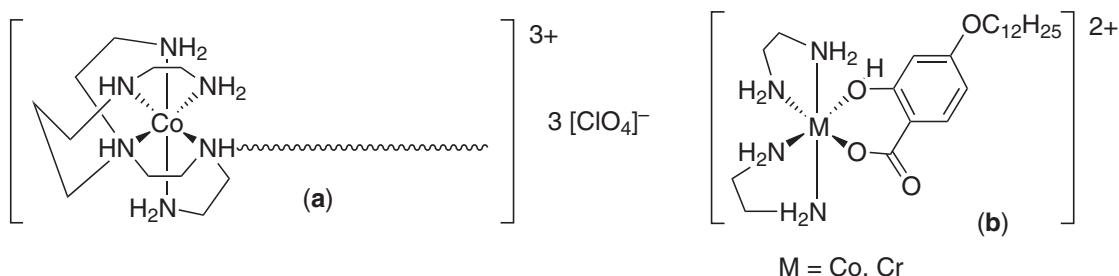
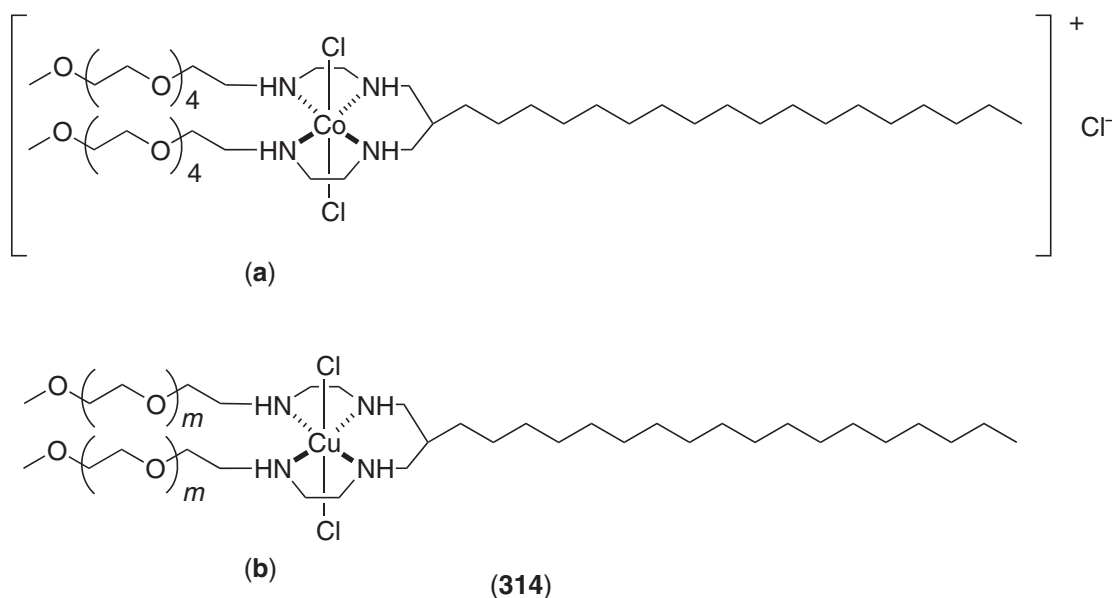
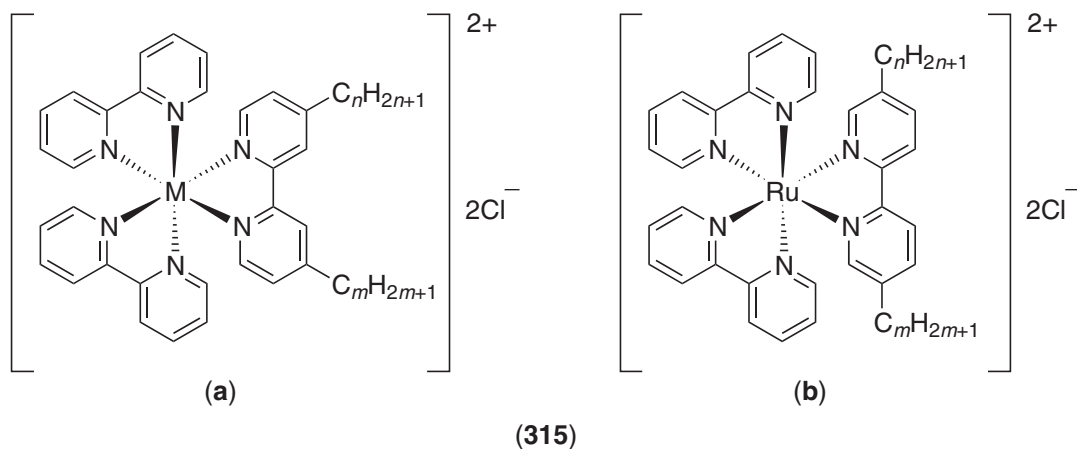


Figure 116 Amphiphilic complexes of  $\text{Co}^{\text{III}}$  and  $\text{Cr}^{\text{III}}$ .



constraint ideas of Israelachvili<sup>1183</sup> developed above, single-chained derivatives ((315a):  $m=1$ ,  $n=12-31$ ) showed  $I_1$  cubic mesophases, while double-chained derivatives ((315a):  $n=12$ ,  $m=12$ , 19) showed  $H_1$  hexagonal phases. The hexagonal phase of the double-chained complexes has been used to template the formation of mesoporous silicates using the true liquid crystal templating approach developed by Attard.<sup>1184</sup> On calcination of the initially formed gels, the ruthenium is left behind (as  $RuO_2$ ) on the porous silicate and shows catalytic activity in hydrogenation reactions following *in situ* reduction.<sup>1185</sup> Exceedingly high rates of hydrogenation are then realized if calcination conditions are controlled to give 20 Å particles of  $RuO_2$ .<sup>1186</sup>

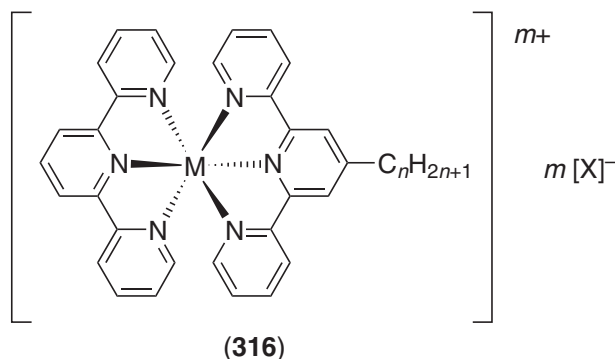


For the mono-chained material with  $m=1$  and  $n=12$ , the *cmc* was measured and found to be between  $5 \times 10^{-3} \text{ mol dm}^{-3}$  and  $9.5 \times 10^{-3} \text{ mol dm}^{-3}$  depending on whether it was measured by NMR spectroscopy or surface tension methods. Acquisition of similar data for the 4,4'-dialkylated complexes was restricted to shorter-chain-length examples ((315a):  $n=m=12-14$ ) due to the Krafft point being above room temperature; values of  $1 \times 10^{-4} \text{ mol dm}^{-3}$  were found and appeared reasonably independent of chain length for these three examples.<sup>1182,1189</sup> It was also found that these complexes would form Y-type Langmuir-Blodgett films and that in alternate layer preparations with long-chain alkanolic acids, pyroelectric response could be generated.<sup>1188</sup> Related osmium complexes were synthesized subsequently and were shown to behave in a very similar way.<sup>1189</sup>

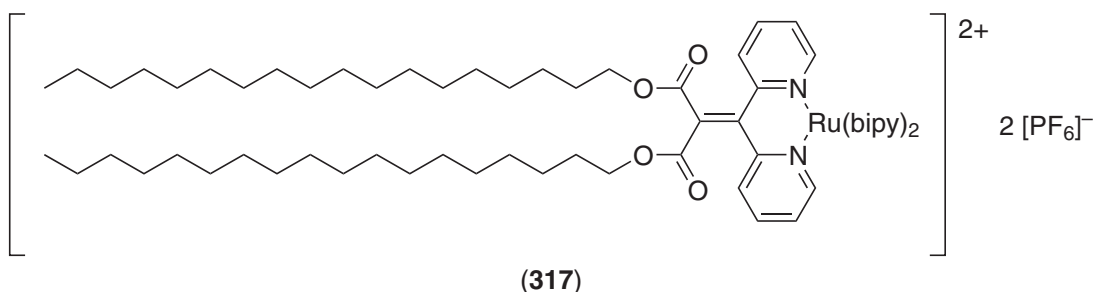


More recently, related complexes using bipyridines alkylated in the 5- or 5,5'-positions (**315b**) have been synthesized and compared with the 4,4'-analogs. Once more, cubic  $I_1$  phases were seen for the single-chained complexes, while hexagonal  $H_1$  phases were found for the double-chained materials.<sup>1182</sup> However, it appears that for the double-chained complexes, the first one or two methylene groups ought to be considered as part of the head group making it effectively larger and less hydrophilic. Hence, cubic phases were seen at shorter chain lengths, not disappearing until  $n = m = 17$ . The surface behavior of the 5,5'-dialkylated complexes was, however, less simple and measured by surface tension it appeared that the *cmc* first decreased with chain length and then increased once more. However, using conductivity and small-angle neutron scattering,<sup>1190</sup> it was found that there was indeed a monotonic decrease in *cmc* with chain length. It was subsequently shown by neutron reflectivity that the aberrant behavior in the surface tension experiment was due to slow kinetics of surface monolayer formation.<sup>1191</sup> Such behavior has been observed previously<sup>1192,1193</sup> with so-called *Gemini* surfactants which these 5,5'-disubstituted Ru complexes resemble.

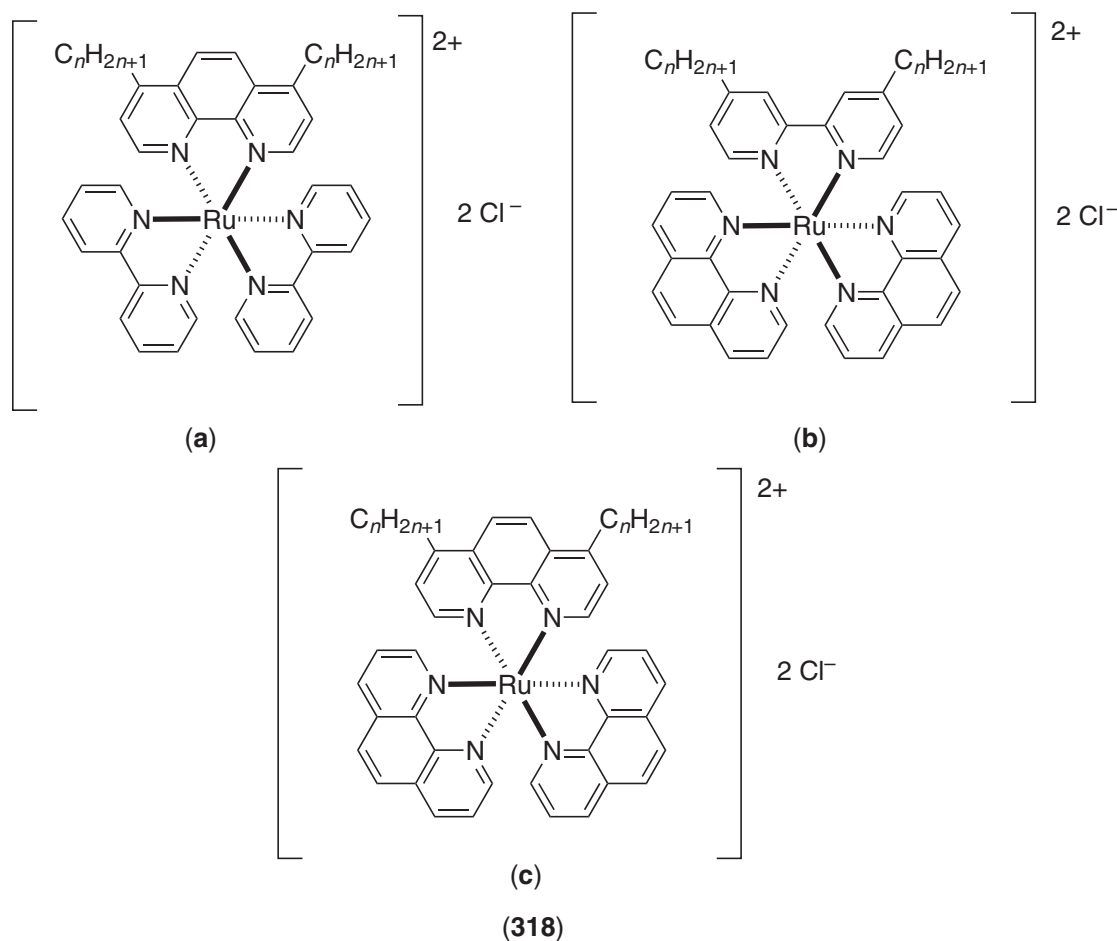
Related tris(bipyridine) complexes of  $Rh^{III}$  were not so stable and so in order to generate mesomorphic materials, it was necessary to use terpyridines which bind more strongly ((**316**):  $M = Ru^{II}$  ( $m = 2$ ),  $Rh^{III}$  ( $m = 3$ ),  $X = Cl, PF_6$ ). In this case, mesomorphic materials were obtained for both  $Ru^{II}$  and  $Rh^{III}$ , although in some cases it was necessary to use ethylene glycol as the solvent rather than water.<sup>1194</sup>



A structurally related amphiphilic ruthenium complex of bis(bipyridine) dipyrindylmethylene distearyl ester (**317**) was prepared and isolated as its hexafluorophosphate or perchlorate salt. In particular, the  $PF_6$  salt shows a lamellar mesophase in water which, however, quickly rearranges into the more stable multilayer vesicles.<sup>1195</sup>



Surfactant phenanthroline and mixed phenanthroline–bipyridine ruthenium(II) complexes have been reported (**318a** to **c**).<sup>1196</sup> The approach consisted in controlling the size of the surfactant polar head by varying the ligands used, i.e., beginning with the two-chain, tris(bipyridine) complex ((**315a**):  $n = m$ ) to the tris(phenanthroline) complex analog (**318c**), via the two mixed intermediates ( $[Ru(bipy)_2(phen)]^{2+}$ ) (**318a**) and ( $[Ru(bipy)(phen)_2]^{2+}$ ) (**318b**) complexes, and to relate the variations in such structural modification to the mesomorphic properties. The idea was then to control the pore size of resulting mesoporous silicates. The chloride salts systematically exhibit the hexagonal  $H_1$  mesophase in water. Only the Krafft temperature seemed to be affected by this structural modification, which was found to increase concomitantly with i) the increasing number of phenanthroline ligands and ii) the lengthening of the aliphatic chains. This approach confirmed previous results in that subtle modifications of the core–chain ratio modify the mesomorphic



properties, and proved the synthetic versatility of these materials. The authors were able to synthesize mesoporous silicates of variable pore sizes using the true liquid-crystal templating approach.

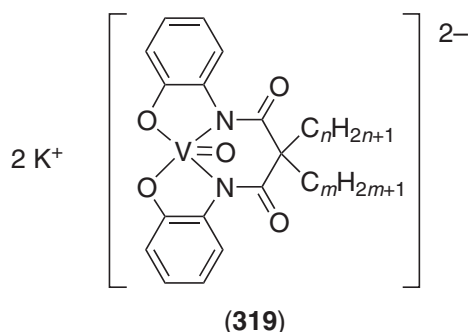
### 7.9.15.2.3 Schiff-base complexes

Swager<sup>1197</sup> reported one- and two-chained amphiphilic complexes of oxovanadium(IV) (**319**); none of the ligands was mesomorphic, and the metal complexes were not thermotropic. However, both of the double-chained vanadyl complexes exhibited a lamellar phase in water, and only slight differences with chain length were noted. For example, the longer-chain system ( $n=m=18$ ) displayed a narrow-range lamellar phase at concentrations greater than 12 wt.%, and above 38 °C (Krafft point), while the shorter homolog ( $n=m=10$ ) showed a much wider stability concentration range (14–50%) and at ambient temperature. Addition of decanol as co-surfactant into these binary systems stabilized the mesophase to concentrations as low as 6% of metallosurfactant. The one-chain systems did not show mesomorphism in binary mixtures with water only, but depending on the concentration and chain length, exhibited a lamellar ( $n=16$ ,  $m=1$ ) or both lamellar and hexagonal mesophases ( $n=12$ ,  $m=1$ ) in ternary phase diagrams with decanol. The domain of stability of the lamellar phase for the short-chain-length homolog was very large and extended up to 45% decanol content. The metal affects the stability of the complex under these conditions in that one- and double-chained copper homologs decomposed in ternary phased systems.

### 7.9.15.2.4 Concluding remarks

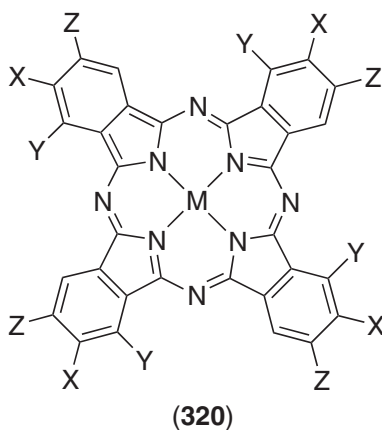
We can learn several things from the above observations. First, it is amply demonstrated that it is entirely possible to make surfactants based around metal complexes where the complex is an

integral part of the polar head group and, therefore, the amphiphile itself. Both cationic and anionic surfactants have been realized and in some cases, critical micelle concentrations have been measured; standard packing constraint ideas are also found to be applicable. These observations alone show that surfactant metal complexes are no different in their behavior from the more traditional organic surfactants.



### 7.9.15.3 Columnar Systems

The first reports of metallomesogens capable of forming lyotropic columnar phases were reported by Gaspard, who described mesomorphism in peripherally carboxylated copper(II) phthalocyanines,<sup>1198</sup> although their phase behavior was never properly defined ((**320**): M = Cu, X, Z = H; Y = CO<sub>2</sub><sup>-</sup>). He later reported other derivatives ((**320**): M = Co, Ni, Pd and Pt) which were not mesomorphic.<sup>1199</sup>



These systems and several other were later re-investigated by Usol'tseva through intensive research, mainly on metal complexes of phthalocyanines (**320**) and porphyrins ((**321**), (**322**) (Tables 84 and 85).<sup>1200-1204</sup> One of her aims was to understand the influence of structural modifications on the lyomesophase formation. In general, these substances are weakly soluble in water, but their solubility is enhanced substantially in alkaline solution (H<sub>2</sub>O-NaOH, H<sub>2</sub>O-NH<sub>3</sub>). The aggregation of the disk-like complexes into columns was confirmed systematically for complexes of divalent metal ions by spectral studies, while for the trivalent ions, the formation of  $\mu$ -oxo dimers was preferred, disfavoring stacking into columns. Thus, phthalocyanine and porphyrin complexes of copper(II), cobalt(II), zinc(II), nickel(II), and iron(II) form lyomesophases at very low dilution and under basic conditions. Due to the formation of  $\mu$ -oxo dimers with Al<sup>III</sup> and Co<sup>III</sup>, the possibility of intermolecular packing along the columns was precluded, and so was the induction of a mesophase. The metal-free macrocyclic compounds (**320**) to (**322**) behave exactly as the divalent systems in solvents. On the basis of optical texture observations and X-ray diffraction studies, columnar hexagonal and nematic phases were generally present. They appeared at different temperatures and concentrations with the columnar nematic phase being seen at higher solvent content. In both phases, the intramolecular stacking corresponding to the separation between the

**Table 84** Lyotropic properties of the phthalocyanines (320).

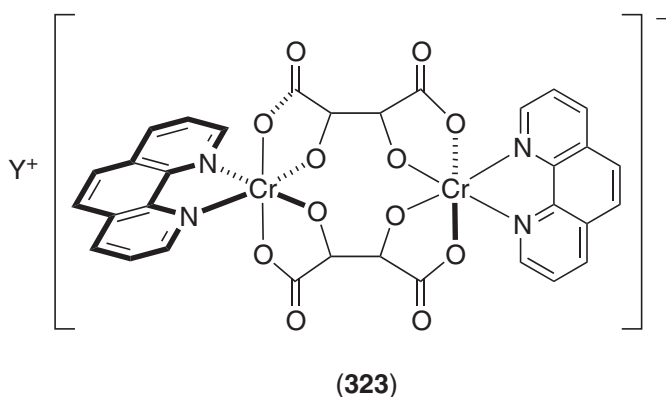
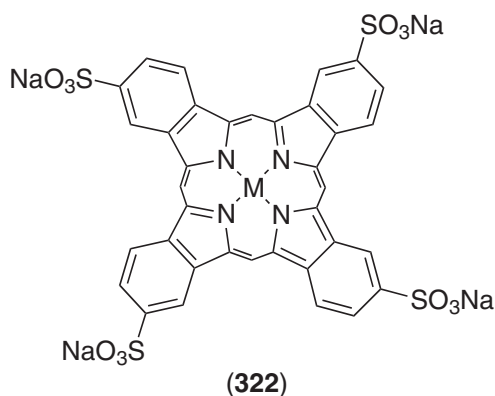
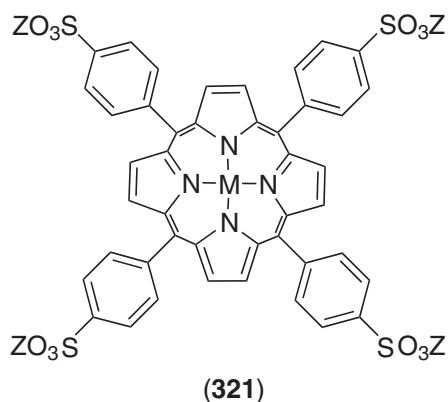
<i>M</i>	<i>Substituents</i>			<i>Lyomesophases in aqueous solutions</i>
	<i>X</i>	<i>Y</i>	<i>Z</i>	
Cu <sup>2+</sup>	-CO <sub>2</sub> H	-H	-H	H, N
Cu <sup>2+</sup>	-CO <sub>2</sub> Na	-H	-H	H, N
Cu <sup>2+</sup>	-CO <sub>2</sub> H	-H	-CO <sub>2</sub> H	H, N
Cu <sup>2+</sup>	-H	-CO <sub>2</sub> H	-H	H, N
Co <sup>2+</sup>	-CO <sub>2</sub> H	-H	-H	H, N
Co <sup>2+</sup>	-H	-CO <sub>2</sub> H	-H	No mesophase
Al <sup>3+</sup>	-CO <sub>2</sub> H	-H	-H	No mesophase
Al <sup>3+</sup>	-H	-CO <sub>2</sub> H	-H	No mesophase
Zn <sup>2+</sup>	-CO <sub>2</sub> H	-H	-CO <sub>2</sub> H	H, N
Zn <sup>2+</sup>	-CO <sub>2</sub> H	-H	-H	H, N
2H <sup>+</sup>	-CO <sub>2</sub> H		-CO <sub>2</sub> H	H, N
Co <sup>3+</sup>	-SO <sub>3</sub> H	-H	-H	No mesophase
Cu <sup>2+</sup>	-SO <sub>3</sub> H	-H	-H	H, N
Ni <sup>2+</sup>	-SO <sub>3</sub> H	-H	-H	H, N
Fe <sup>2+</sup>	-SO <sub>3</sub> H	-H	-H	H, N

**Table 85** Lyotropic properties of porphyrins (321) and (322).

	<i>M</i>	<i>Z</i>	<i>Mesomorphism in water</i>
(321)	2H <sup>+</sup>	-H	H, N
	Ni <sup>2+</sup>	-H	H, N
	Cu <sup>2+</sup>	-H	H, N
	Co <sup>3+</sup>	-H	No mesophase
	2H <sup>+</sup>	-Na	H, N
	Ni <sup>2+</sup>	-Na	H, N
(322)	Co <sup>3+</sup>	-Na	No mesophase
	2H <sup>+</sup>		H, N
	Zn <sup>2+</sup>		H, N
	Co <sup>3+</sup>		No mesophase

macrocycles in the solid state (3.5 Å) is retained, and thus the arrangement into columns is conditioned by these intermolecular  $\pi$ -interactions, with a possible contribution from hydrogen bonds between the carboxyl or sulfonyl groups due to the location of the polar solvents in the hydrophilic regions. The position and number of the polar groups seemed to influence the mesomorphism, too, and recall that complexes of type (320) and (322) exist as mixtures of isomers. Increasing the number of peripheral carboxyl and sulfonyl groups leads to an increase in the stability of the columns (and, thus, of the mesophases) presumably by the formation of a more dense, inter-molecular H-bonding network; a minimum of four solubilizing groups is necessary to get these properties. The nature of these solubilizing groups does not affect the mesophase type, but affects the temperature-concentration region for lyomesophase existence. For example, the carboxylate derivatives (320) form mesophases from 3 wt.% of complexes and at basic pH (9–11), while for the sulfonate homologous derivatives, mesophases appear at higher complex content (13 to 30 wt.%) and over a wider pH range (6–13). The lyotropic behavior of some of these compounds is summarized in the tables below.

The most uncommon molecular structure known so far to produce lyotropic mesophases is that of the chiral, dinuclear chromium(II) complex of phenanthroline and tartaric acid, (323).<sup>1205</sup> The complex does not possess an amphiphilic structure, i.e., no polar headgroup nor aliphatic tail, does not belong to the columnar type, and does not show thermotropic properties. Thus, the phenanthroline ligands must play the role of the hydrophobic part, while the central tartrate link must act as the hydrophilic one. A room-temperature, lyotropic mesophase was induced at low concentration in water (0.006 mol dm<sup>-3</sup>). Moreover, in the concentration range of 0.06 to 0.1 mol dm<sup>-3</sup> the mesophase was still observed and remained stable up to 100 °C. The self-aggregation of the complex into a birefringent mesophase was proved by the use of several techniques including polarized optical microscopy, viscosity, and electrical conductivity measurements, as well as <sup>23</sup>Na



and  $^2\text{H}$  NMR spectroscopy.<sup>1206</sup> Circular dichroism spectra of the mesophase indicates the presence of large chiral domains, with a macroscopic helical pitch. A ribbon-like assembly consisting of a lamellar structure with monolayers of metals separated by water layers was proposed on the basis of microscopy and scattering/diffraction methods.<sup>1207</sup> Owing to the chirality of the tartrate groups, and thus to the non-planarity of the complex, the molecules interact with each other by  $\pi$ - $\pi$  stacking between the phenanthroline rings, resulting in the formation of a helix along the molecular axes (as defined by the metal-metal bond). The tartrate species interact by hydrogen bonding in a direction normal to the layers. The mesophase is thought to be nematic-like, corresponding to the anisotropic spatial ordering of these assemblies in solutions. Extension of this work by exchanging sodium with potassium, ammonium and  $[\text{Co}(\text{en})_3]^{3+}$  counter-cations showed, under similar conditions of concentration and temperature, that the same type of lyotropic phase was formed for the sodium, potassium, and ammonium salts, but not for  $[\text{Co}(\text{en})_3]^{3+}$ .<sup>1208</sup>

### 7.9.16 CONCLUSIONS AND ACKNOWLEDGMENTS

In reality, the subject of metal-containing liquid crystals is nearly 150 years old, yet it is only since the 1980s that research in the area has begun apace. This has coincided with a period in the development of liquid crystal science which has been pure joy for the synthetic chemist as many new and interesting motifs have become recognized as components in liquid crystal design, and certain design factors which previously were thought to be detrimental have turned out to be of great interest. However, alongside all this synthesis, applications of liquid crystals have also developed and since the commercialization of the twisted nematic display in the early 1970s which revolutionized cheap, low-power displays, there have been many developments in display geometries and modes and non-display applications, too, such as in telecoms and, of course, thermography. This draws attention to the fact that while LCDs are the most common and well-understood manifestation of the liquid crystal state, they are ubiquitous and, for example, the compounds which make up the very cell membranes of our body have liquid crystal properties.

So where does this leave metallomesogens? At present, at least to the authors' knowledge, there are no commercial applications thereof and we suspect that any such applications may be a long way off in the sphere of conventional displays. However, metals have any attractive properties and we suspect that application will come in other fields. For example, large, well-defined three-dimensional structures are possible using dendrimers as a scaffold and metals can be incorporated therein giving rise to a variety of effects. Certain metallomesogens (e.g., ferrocenes) are redox active which may preview sensors applications, while redox activity in certain phthalocyanine systems has led to electrochromic behavior. In addition, lyotropic metallomesogens have been employed as templates for the formation of mesoporous silicates and have been shown to be precursors for highly active heterogeneous catalysts in such a mechanism.

However, perhaps the greatest joy is found in the sheer diversity of structures containing metal centers which show liquid crystal properties. We feel privileged that in this review we have been able to take an overview of the fruits of the creative minds of many talented individuals who make up the warm, friendly community that characterizes metallomesogen research and we thank them for providing us with such inspiration for our labors.

Finally, DG, RD, and DWB would like to pay tribute to BD not only for providing most of the original writing in this review, but also for allowing us access to his most comprehensive collection of literature. Yes, all 1208 references are catalogued and this made all of our lives so very much easier as I'm sure you can imagine

## 7.9.17 REFERENCES

1. Giroud-Godquin, A.-M.; Maitlis, P. M. *Angew. Chem. Int. Ed. Engl.* **1991**, *30*, 375–402.
2. Ohta, K.; Yamamoto, I. *J. Synth. Org. Chem.* **1991**, *49*, 486–496.
3. Espinet, P.; Esteruelas, M. A.; Oro, L. A.; Serrano, J. L.; Sola, E. *Coord. Chem. Rev.* **1992**, *117*, 215–274.
4. Bruce, D. W. Metal-Containing Liquid Crystals. In *Inorganic Materials*, 1st ed.; Bruce, D. W.; O'Hare, D. Eds.; Wiley, 1992; Chapter 8, pp 405–490; 2nd ed.; Bruce, D. W.; O'Hare, D. Eds.; Wiley, 1996; Chapter 8, pp 429–522.
5. Hudson, S. A.; Maitlis, P. M. *Chem. Rev.* **1993**, *93*, 861–885.
6. Polishchuk, A.; Timofeeva, T. V. *Russ. Chem. Rev.* **1993**, *62*, 291–321.
7. Bruce, D. W. *J. Chem. Soc., Dalton Trans.* **1993**, 2983–2989.
8. Deschenaux, R.; Goodby, J. W. Ferrocene-Containing Thermotropic Liquid Crystals. In *Ferrocene: Homogeneous Catalysis, Organic Synthesis, Materials Science*; Togni, A.; Hayashi, T. Eds.; VCH: Weinheim, 1995; Chapter 9, pp 471–495.
9. Zhang, L. F.; Huang, S. D. *Huaxue Tongbao* **1995**, *2*, 7–16.
10. Neve, F. *Adv. Mater.* **1996**, *8*, 277–289.
11. Giroud-Godquin, A.-M. Metal-Containing Liquid Crystals. In *Handbook of Liquid Crystals*; Demus, D.; Goodby, J.; Gray, G. W.; Spiess, H.-W.; Vill, V. Eds.; Wiley-VCH: Weinheim, 1998; Chapter XIV, pp 901–932.
12. Donnio, B.; Bruce, D. W. *Struct. Bond.* **1999**, *95*, 193–247.
13. Collinson, S. R.; Bruce, D. W. Metallomesogens-Supramolecular Organization of Metal Complexes in Fluid Phases. In *Transition Metals in Supramolecular Chemistry*; Sauvage, J. P. Eds.; Wiley, 1999; Chapter 7, pp 285–369.
14. Molochko, V. A.; Rukk, N. S. *Russ. J. Coord. Chem.* **2000**, *26*, 829–846.
15. Binnemans, K.; Görrler-Walrand, C. *Chem. Rev.* **2002**, *102*, 2303–2345.
16. Donnio, B. *Curr. Opin. Colloid Interface Sci.* **2002**, *7*, 371–394.
17. Serrano, J. L. *Metallomesogens: Synthesis, Properties and Applications* **1995**, VCH: Weinheim.
18. Demus, D.; Goodby, J.; Gray, G. W.; Spiess, H.-W.; Vill, V. Eds.; *Handbook of Liquid Crystals*; Wiley-VCH: Weinheim, 1998.
19. Sonin, A. S. *J. Mater. Chem.* **1998**, *8*, 2557–2574.
20. Sonin, A. S. *Colloid J.* **1998**, *60*, 129–151.
21. Davidson, P.; Batail, P.; Gabriel, J. C. P.; Livage, J.; Sanchez, C.; Bourgaux, C. *Prog. Polym. Sci.* **1997**, *22*, 913–936.
22. Oriol, L.; Serrano, J. L. *Adv. Mater.* **1995**, *7*, 348–369.
23. Oriol, L.; Piñol, M.; Serrano, J. L. *Prog. Polym. Sci.* **1997**, *22*, 873–911.
24. Reinitzer, F. *Monatsch. Chem.* **1888**, *9*, 421.
25. Virchow, R. *Virchows Arch.* **1854**, *6*, 571; see also Vill, V. *Mol. Cryst., Liq. Cryst.* **1992**, *213*, 67–71 for an appreciation of some of this early work.
26. Heintz, W. *J. Prakt. Chem.* **1855**, *66*, 1.
27. Toyne, K. J. Liquid Crystal Behavior in Relation to Molecular Structure. In *Thermotropic Liquid Crystals*; Gray, G. W. Eds.; Wiley: Chichester 1987; Chapter 2, pp 28–63.
28. Vill, V. *Liqcryst 2.0 – Database of Liquid Crystalline Compounds*, LCI, Hamburg; see also: <http://liqcryst.chemie.uni-hamburg.de/>
29. Hird, M.; Toyne, K. J. *Mol. Cryst., Liq. Cryst.* **1998**, *323*, 1–67.
30. Peltz, G.; Diele, S.; Weissflog, W. *Adv. Mater.* **1999**, *11*, 707–724.
31. Tschierscke, C. *J. Mater. Chem.* **1998**, *8*, 1845–1508.
32. Tschierscke, C. *J. Mater. Chem.* **2001**, *11*, 2647–2671.
33. Tschierscke, C. *Annu. Rep. Prog. Chem., Sect. C* **2001**, *97*, 191–267.
34. Goodby, J. W. *Science* **1986**, *231*, 350.
35. McDonnell, D. G. Thermochromic Cholesteric Liquid Crystals. In *Thermotropic Liquid Crystals*; Gray, G. W. Eds.; Wiley: Chichester **1987**; Chapter 5, pp 120–144.

36. This classification was proposed in: Leadbetter, A. J. Structural Classification of Liquid Crystals. In *Thermotropic Liquid Crystals*; Gray, G. W. Eds.; Wiley: Chichester 1987; Chapter 1, pp 1–27.
37. Gray, G. W.; Goodby, J. W. *Smectic Liquid Crystals; Textures and Structures*. Leonard Hill, Glasgow 1984.
38. Cladis, P. E. In *Handbook of Liquid Crystals*; Demus, D.; Goodby, J.; Gray, G. W.; Spiess, H.-W.; Vill, V. Eds.; Wiley-VCH: Weinheim, 1998; Chapter X.
39. Chandrasekhar, S.; Sadashiva, B. K.; Suresh, K. A. *Pramana* **1977**, *9*, 471.
40. Skoulios, A. *Adv. Coll. Interface Sci.* **1967**, *1*, 79–110.
41. Levelut, A. M. *J. Chim. Phys.* **1983**, *80*, 149–161.
42. Praefcke, K.; Singer, D.; Kohne, B.; Ebert, M.; Liebmann, M.; Wendorff, J. H. *Liq. Cryst.* **1991**, *10*, 147.
43. Bengs, H.; Karthaus, O.; Ringsdorf, H.; Baehr, C.; Ebert, M.; Wendorff, J. H. *Liq. Cryst.* **1991**, *10*, 161.
44. Tiddy, G. J. T. *Modern Trends of Colloid Science in Chemistry and Biology*, 148, Birkhauser Verlag, Basel, 1985; *idem. Phys. Rep.* **1980**, *57*, 1.
45. Tanford, C. *The Hydrophobic Effect*, 2nd ed.; Wiley, New York 1980.
46. Israelachvili, J. N.; Mitchell, D. J.; Ninham, B. W. *J. Chem. Soc., Faraday Trans. II* **1976**, *72*, 1525–1568.
47. Seddon, J. M.; Templer, R. H. *Phil. Trans. R. Soc. A* **1993**, *344*, 377–401.
48. Luzzati, V.; Spert, P. A. *Nature* **1967**, *215*, 701.
49. Charvolin, J.; Sadoc, J. F. *J. Phys.* **1988**, *49*, 521–526; *Idem, Phil. Trans. R. Soc. Lond. A* **1996**, *354*, 2173–2192.
50. Hyde, S. T. Identification of Lyotropic Liquid Crystalline Mesophases. In *Handbook of Applied Surface and Colloid Chemistry*; Holmberg, K. Eds.; Wiley, 2001; Chapter 16, pp 299–332.
51. Valenti, R.; Sartirania, M. L. *Nuovo. Chim. D* **1984**, *3*, 104.
52. Livolant, F.; Leforestier, A. *Prog. Polym. Sci.* **1996**, *21*, 1115–1164.
53. Attwood, T. K.; Lydon, J. E.; Hall, C.; Tiddy, G. J. T. *Liq. Cryst.* **1990**, *7*, 657–668.
54. Lydon, J. Chromonics. In *Handbook of Liquid Crystals*; Demus, D.; Goodby, J.; Gray, G. W.; Spiess, H.-W.; Vill, V. Eds.; Wiley-VCH: Weinheim, 1998; Chapter XVIII, pp 981–1007.
55. Praefcke, K.; Holbrey, J. D.; Usol'tseva, N. *Mol. Cryst., Liq. Cryst.* **1996**, *288*, 189–200.
56. Sage, I. Materials Requirements for Nematic and Chiral Nematic Electrooptical Displays. In *Thermotropic Liquid Crystals*; Gray, G. W. Eds.; Wiley: Chichester 1987; Chapter 3, pp 64–98.
57. Diele, S.; Grande, S.; Kain, J.; Pelzl, G.; Weissflog, W. *Mol. Cryst., Liq. Cryst.* **2001**, *362*, 111–132.
58. Dalcaneale, E. In *Comprehensive Supramolecular Chemistry*; Atwood, J. L.; Davies, J. E. D.; MacNicol, D. D.; Vögtle, F. Eds.; Pergamon : Elmsford, NY 1996; Vol. 10, pp 583–635.
59. Simon, J.; Sirlin, C. *Pure Appl. Chem.* **1989**, *61*, 1625–1629.
60. Simon, J.; Bassoul, P. In *Phthalocyanines: Properties and Applications*; Leznoff, C. C.; Lever, B. P. Eds.; Vol. 2, VCH, Weinheim, **1993**, pp 224–299.
61. Hanack, M.; Lang, M. *Adv. Mater.* **1994**, *6*, 819–833.
62. van Nostrum, C. F.; Nolte, R. J. M. *Chem. Commun.* **1996**, 2385–2392.
63. Eichhorn, H. *J. Porphyrins Phthalocyanines* **2000**, *4*, 88–102.
64. Reichert, A.; Ringsdorf, H.; Schuhmacher, P.; Baumeister, W.; Scheybani, T. In *Comprehensive Supramolecular Chemistry*; Atwood, J. L.; Davies, J. E. D.; MacNicol, D. D.; Vögtle, F. Eds.; Pergamon : Elmsford, NY 1996; Vol. 9, Chap. 20.
65. van Nostrum, C. F. *Adv. Mater.* **1996**, *8*, 1027–1030.
66. Piechocki, G.; Simon, J.; Skoulios, A.; Guillon, D.; Weber, P. *J. Am. Chem. Soc.* **1982**, *104*, 5245–5247.
67. Guillon, D.; Skoulios, A.; Piechocki, G.; Simon, J.; Weber, P. *Mol. Cryst. Liq. Cryst.* **1983**, *100*, 275–284.
68. Piechocki, C.; Simon, J. *Nouv. J. Chim.* **1985**, *9*, 159–166.
69. Weber, P.; Guillon, D.; Skoulios, A. *Liq. Cryst.* **1991**, *9*, 369–382.
70. Markovitsi, D.; Tran-Thi, T. H.; Briois, V.; Simon, J.; Ohta, K. *J. Am. Chem. Soc.* **1988**, *110*, 2001–2002.
71. Guillon, D.; Weber, P.; Skoulios, A.; Piechocki, C.; Simon, J. *Mol. Cryst. Liq. Cryst.* **1985**, *130*, 223–229.
72. Hanack, M.; Beck, A.; Lehmann, H. *Synthesis* **1987**, 703–705.
73. Knawby, D. M.; Swager, T. M. *Chem. Mater.* **1997**, *9*, 535–538.
74. Steven, J. *PhD thesis*, K.U. Leuven, 2002, Belgium.
75. Piechocki, C.; Boulou, J. C.; Simon, J. *Mol. Cryst. Liq. Cryst.* **1987**, *149*, 115–120.
76. Weber, P.; Guillon, D.; Skoulios, A. *J. Phys. Chem.* **1987**, *91*, 2242–2243.
77. Sirlin, C.; Bosio, L.; Simon, J. *J. Chem. Soc., Chem. Commun.* **1987**, 379–380.
78. Sirlin, C.; Bosio, L.; Simon, J. *J. Chem. Soc., Chem. Commun.* **1988**, 236–237.
79. Sirlin, C.; Bosio, L.; Simon, J. *Mol. Cryst. Liq. Cryst.* **1988**, *155*, 231–238.
80. Sakamoto, K.; Ohno-Okumura, E. *J. Porphyrins Phthalocyanines* **1999**, *3*, 634–642.
81. André, J. J.; Bernard, M.; Piechocki, C.; Simon, J. *J. Phys. Chem.* **1986**, *90*, 1327–1330.
82. Blanzat, B.; Barthou, C.; Tercier, N.; André, J. J.; Simon, J. *J. Am. Chem. Soc.* **1987**, *109*, 6193–6194.
83. Markovitsi, D.; Lécuyer, I. *Chem. Phys. Lett.* **1988**, *149*, 330–333.
84. Markovitsi, D.; Lécuyer, I.; Simon, J. *Chem. Phys. Lett.* **1990**, *167*, 467–470.
85. Markovitsi, D.; Lécuyer, I.; Simon, J. *J. Phys. Chem.* **1991**, *95*, 3620–3626.
86. Nishi, H.; Ueno, S. *Nippon Kagaku Kaishi* **1989**, 983–987.
87. Nishi, H.; Azuma, N.; Kitahara, K. *J. Heterocyclic Chem.* **1992**, *29*, 475–477.
88. Engel, M. K.; Bassoul, P.; Bosio, L.; Lehmann, H.; Hanack, M.; Simon, J. *Liq. Cryst.* **1993**, *15*, 709–722.
89. Haisch, P.; Winter, G.; Hanack, M.; Lüer, L.; Egelhaaf, H. J.; Oelkrug, D. *Adv. Mater.* **1997**, *9*, 316–321.
90. Henari, F.; Davey, A.; Blau, W.; Haisch, P.; Hanack, M. *J. Porphyrins Phthalocyanines* **1999**, *3*, 331–338.
91. Masurel, D.; Sirlin, C.; Simon, J. *New J. Chem.* **1987**, *11*, 455–456.
92. Ohta, K.; Jacquemin, C.; Sirlin, C.; Bosio, L.; Simon, J. *New J. Chem.* **1988**, *12*, 751–754.
93. van der Pol, J. F.; Neeleman, E.; Zwikker, J. W.; Nolte, R. J. M.; Drenth, W. *Recl. Trav. Chim. Pays Bas* **1988**, *107*, 615–620.
94. van der Pol, J. F.; Neeleman, E.; Zwikker, J. W.; Nolte, R. J. M.; Drenth, W.; Aerts, J.; Visser, R.; Picken, S. J. *Liq. Cryst.* **1989**, *6*, 577–592.
95. Vacus, J.; Doppelt, P.; Simon, J.; Memetzidis, G. *J. Mater. Chem.* **1992**, *2*, 1065–1068.
96. Severs, L. M.; Underhill, A. E.; Edwards, D.; Wight, P.; Thetford, D. *Mol. Cryst. Liq. Cryst.* **1993**, *234*, 235–240.

97. Haish, P.; Knecht, S.; Schlick, U.; Subramanian, L. R.; Hanack, M. *Mol. Cryst. Liq. Cryst.* **1995**, *270*, 7–16.
98. Zagal, J. H.; Gulppi, M. A.; Depretz, C.; Lelièvre, D. *J. Porphyrins Phthalocyanines* **1999**, *3*, 355–363.
99. Sleven, J.; Cardinaels, T.; Binnemans, K.; Guillon, D.; Donnio, B. *Liq. Cryst.* **2002**, *29*, 1425–1433.
100. Lelièvre, D.; Petit, M. A.; Simon, J. *Liq. Cryst.* **1989**, *6*, 707–710.
101. Otha, K.; Watanabe, H.; Hasebe, H.; Morizumi, Y.; Fujimoto, T.; Yamamoto, I.; Lelièvre, D.; Simon, J. *Mol. Cryst. Liq. Cryst.* **1991**, *196*, 13–26.
102. Ford, W. T.; Sumner, L.; Zhu, W.; Chang, Y. H.; Um, P. J.; Choi, K. H.; Heiney, P. A.; Maliszewskyj, N. C. *New J. Chem.* **1994**, *18*, 495–505.
103. Chang, Y. H.; Choi, K. H.; Ford, W. T.; Cho, S. J.; Ryoo, R. *J. Chem. Soc., Chem. Commun.* **1994**, 785–787.
104. Caseri, W.; Sauer, T.; Wegner, G. *Makromol. Chem., Rapid Commun.* **1988**, *9*, 651–657.
105. Sauer, T.; Wegner, G. *Mol. Cryst. Liq. Cryst.* **1988**, *162B*, 97–118.
106. Schouten, P. G.; Warman, J. M.; deHaas, M. P.; van der Pol, J. F.; Zwicker, J. W. *J. Am. Chem. Soc.* **1992**, *114*, 9028–9034.
107. van Nostrum, C. F.; Bosman, A. W.; Gelinck, G. H.; Schouten, P. G.; Warman, J. H.; Kentgens, A. P. M.; Devillers, M. A. C.; Meijerink, A.; C. F.; Picken, S. J.; Sohling, U.; Schouten, A. J.; Nolte, R. J. M. *Chem. Eur. J.* **1995**, *1*, 171–182.
108. Engelkamp, H.; van Nostrum, C. F.; Picken, S. J.; Nolte, R. J. M. *Chem. Commun.* **1998**, 979–980.
109. Usolt'seva, N.; Bykova, V.; Semeikin, A.; Ananjeva, G.; Smirnova, A.; Negrimovski, V. *Mol. Cryst. Liq. Cryst.* **1997**, *304*, 201–206.
110. Schouten, P. G.; Warman, J. M.; de Haas, M. P.; van Nostrum, C. F.; Gelinck, G. H.; Nolte, R. J. M.; Copyn, M. J.; Zwicker, J. W.; Engel, M. K.; Hanack, M.; Chang, Y. H.; Ford, W. T. *J. Am. Chem. Soc.* **1994**, *116*, 6880–6894.
111. van der Pol, J. F.; de Haas, M. J.; Warman, J. M.; Drenth, W. *Mol. Cryst. Liq. Cryst.* **1990**, *183*, 411–420.
112. Eichhorn, H.; Wöhrle, D.; Pressner, D. *Liq. Cryst.* **1997**, *22*, 643–653.
113. Ban, K.; Nishizawa, K.; Ohta, K.; Shirai, H. *J. Mater. Chem.* **2000**, *10*, 1083–1090.
114. Lux, A.; Rozenberg, G. G.; Petritsch, K.; Moratti, S. C.; Holmes, A. B.; Friend, R. H. *Synth. Met.* **1999**, *102*, 1527–1528.
115. Basova, T. V.; Gürek, A. G.; Ahsen, V. *Mater. Sci. Eng. C* **2002**, *22*, 99–104.
116. Gürek, A. G.; Bekaroglu, O. *J. Chem. Soc., Dalton Trans.* **1994**, 1419–1423.
117. Santiago, J.; Sugino, T.; Shimizu, Y. *Chem. Lett.* **1998**, 661–662.
118. Santiago, J.; Sugino, T.; Shimizu, Y. *Mol. Cryst. Liq. Cryst.* **1999**, *332*, 497–504.
119. Tantrawong, S.; Sugino, T.; Shimizu, Y.; Takeuchi, A.; Kimura, S.; Mori, T.; Takezoe, H. *Liq. Cryst.* **1998**, *24*, 783–785.
120. Eichhorn, H.; Bruce, D. W.; Wöhrle, D. *Adv. Mater.* **1998**, *10*, 419–422.
121. Usolt'seva, N. *Mol. Cryst. Liq. Cryst.* **1996**, *288*, 201–210.
122. Gürek, A. G.; Ahsen, V.; Heinemann, F.; Zugenmaier, P. *Mol. Cryst. Liq. Cryst.* **2000**, *338*, 75–97.
123. Basova, T. V.; Kolesov, B. A.; Gürek, A. G.; Ahsen, V. *Thin Solid Films* **2001**, *385*, 246–251.
124. Dulog, L.; Gittinger, A. *Mol. Cryst. Liq. Cryst.* **1993**, *237*, 235–242.
125. Dulog, L.; Gittinger, A.; Rosh, I.; Wagner, T. *Makromol. Chem.* **1993**, *194*, 493–500.
126. Dulog, L.; Gittinger, A. *Mol. Cryst. Liq. Cryst.* **1992**, *213*, 31–42.
127. Osburn, E. J.; Chau, L. K.; Chen, S. Y.; Collins, N.; O'Brien, D. F.; Armstrong, N. R. *Langmuir* **1996**, *12*, 4784–4796.
128. Usolt'seva, N.; Bykova, V.; Ananjeva, G.; Smirnova, A.; Shaposhnikov, G.; Maizlish, V.; Kudrik, E.; Shirokov, A. *Mol. Cryst. Liq. Cryst.* **2000**, *352*, 45–57.
129. Duro, J. A.; de la Torre, G.; Barberá, J.; Serrano, J. L.; Torres, T. *Chem. Mater.* **1996**, *8*, 1061–1066.
130. Cho, I. *LimY. Mol. Cryst. Liq. Cryst.* **1988**, *154*, 9–26.
131. Schouten, P. G.; van der Pol, J. F.; Zwicker, J. W.; Drenth, W.; Picken, S. J. *Mol. Cryst. Liq. Cryst.* **1991**, *195*, 291–305. *Erratum Ibid.* **1991**, *208*, 109.
132. van Nostrum, C. F.; Bosman, A. W.; Gelinck, G. H.; Picken, S. J.; Schouten, P. G.; Warman, J. M.; Schouten, A. J.; Nolte, R. J. M. *J. Chem. Soc., Chem. Commun.* **1993**, 1120–1121.
133. van der Pol, J. F.; Neeleman, E.; Nolte, R. J. M.; Zwicker, J. W.; Drenth, W. *Makromol. Chem.* **1989**, *190*, 2727–2745.
134. van der Pol, J. F.; Neeleman, E.; van Miltenburg, J. C.; Zwicker, J. W.; Nolte, R. J. M.; Drenth, W. *Macromolecules* **1990**, *23*, 155–162.
135. McKeown, N. B.; Painter, J. *J. Mater. Chem.* **1994**, *4*, 1153–1156.
136. Clarkson, G. J.; McKeown, N. B.; Treacher, K. E. *J. Chem. Soc., Perkin Trans. 1*, **1995**, , 1817–1823.
137. Clarkson, G. J.; Hassan, B. M.; Maloney, D. R.; McKeown, N. B. *Macromolecules* **1996**, *29*, 1854–1856.
138. Kroon, J. M.; Koehorst, R. B. M.; van Dijk, M.; Sanders, G. M.; Sudhölter, E. J. R. *J. Mater. Chem.* **1997**, *7*, 615–624.
139. Kimura, M.; Wada, K.; Ohta, K.; Hanabusa, K.; Shirai, H.; Kobayashi, N. *J. Am. Chem. Soc.* **2001**, *123*, 2438–2439.
140. Kobayashi, N.; Higashi, R.; Ishii, K.; Hatsusaka, K. Ohta K. *Bull. Chem. Soc. Jpn* **1999**, *72*, 1263–1271.
141. Dabak, S.; Ahsen, V.; Heinemann, F.; Zugenmaier, P. *Mol. Cryst. Liq. Cryst.* **2000**, *348*, 111–127.
142. Toupance, T.; Bassoul, P.; Mineau, L.; Simon, J. *J. Phys. Chem.* **1996**, *100*, 11704–11710.
143. Vacus, J.; Simon, J. *Adv. Mater.* **1995**, *7*, 797–800.
144. Osburn, E. J.; Schmidt, A.; Chau, L. K.; Chen, S. Y.; Smolenyak, P.; Armstrong, N. R.; O'Brien, D. F. *Adv. Mater.* **1996**, *8*, 926–928.
145. Smolenyak, P.; Osburn, E. J.; Chen, S. Y.; Chau, L. K.; O'Brien, D. F.; Armstrong, N. R. *Langmuir* **1997**, *13*, 6568–6576.
146. Smolenyak, P.; Peterson, R.; Nebesny, K.; Törker, M.; O'Brien, D. F.; Armstrong, N. R. *J. Am. Chem. Soc.* **1999**, *121*, 8628–8636.
147. Kobayashi, N. *Coord. Chem. Rev.* **2001**, *219–221*, 99–123.
148. Kimura, M.; Muto, T.; Takimoto, H.; Wada, K.; Ohta, K.; Hanabusa, K.; Shirai, H.; Kobayashi, N. *Langmuir* **2000**, *16*, 2078–2082.
149. Engelkamp, H.; Nolte, R. J. M. *J. Porphyrins Phthalocyanines* **2000**, *4*, 454–459.



150. Ahsen, V.; Yilmazer, E.; Ertas, M.; Bekâroglu, Ö. *J. Chem. Soc., Dalton Trans.* **1988**, 401–406.
151. Sielcken, O. E.; van Tilborg, M. M.; Roks, M. F. M.; Hendriks, R.; Drenth, W.; Nolte, J. M. *J. Am. Chem. Soc.* **1987**, *109*, 4261–4265.
152. Kobayashi, N.; Lever, A. B. P. *J. Am. Chem. Soc.* **1987**, *109*, 7433–7441.
153. Sirlin, C.; Bosio, L.; Simon, J.; Ahsen, V.; Yilmazer, E.; Bekâroglu, Ö. *Chem. Phys. Lett.* **1987**, *139*, 362–364.
154. Gürek, A.; Ahsen, V.; Gul, A.; Bekaroglu, O. *J. Chem. Soc., Dalton Trans.* **1991**, 3367–3371.
155. Ohta, K.; Watanabe, T.; Tanaka, S.; Fujimoto, T.; Yamamoto, I.; Bassoul, P.; Kucharczyk, N.; Simon, J. *Liq. Cryst.* **1991**, *10*, 357–368.
156. Ohta, K.; Azumane, S.; Watanabe, T.; Tsukada, S.; Yamamoto, I. *Appl. Organomet. Chem.* **1996**, *10*, 623–635.
157. Cammidge, A. N.; Gopee, H. *Chem. Commun.* **2002**, 966–967.
158. Hatsusaka, K.; Ohta, K.; Yamamoto, I.; Shirai, H. *J. Mater. Chem.* **2001**, *11*, 423–433.
159. Kimura, M.; Narikawa, H.; Ohta, K.; Hanabusa, K.; Shirai, H.; Kobayashi, N. *J. Mater. Chem.* **2002**, *14*, 2711–2717.
160. Lelièvre, D.; Bosio, L.; Simon, J.; André, J. J.; Bensebaa, F. *J. Am. Chem. Soc.* **1992**, *114*, 4475–4479.
161. Lelièvre, D.; Damette, O.; Simon, J. *J. Chem. Soc., Chem. Commun.* **1993**, 939–940.
162. Kobayashi, N.; Fukuda, T.; Lelièvre, D. *Inorg. Chem.* **2000**, *39*, 3632–3637.
163. Kobayashi, N. *Coord. Chem. Rev.* **2002**, *227*, 129–152.
164. Piechocki, C.; Simon, J.; André, J. J.; Guillon, D.; Petit, P.; Skoulios, A.; Weber, P. *Chem. Phys. Lett.* **1985**, *122*, 124–128.
165. Castaneda, F.; Piechocki, C.; Plichon, V.; Simon, J.; Vaxivière, J. *Electrochimica Acta* **1986**, *31*, 131–133.
166. Belarbi, Z.; Maitrot, M.; Ohta, K.; Simon, J.; André, J. J.; Petit, P. *Chem. Phys. Lett.* **1988**, *143*, 400–403.
167. Belarbi, Z.; Sirlin, C.; Simon, J.; André, J. J. *J. Phys. Chem.* **1989**, *93*, 8105–8110.
168. van de Craats, A. M.; Warman, J. M.; Hasebe, H.; Naito, R.; Ohta, K. *J. Phys. Chem. B* **1997**, *101*, 9224–9232.
169. Naito, R.; Ohta, K.; Shirai, H. *J. Porphyrins Phthalocyanines* **2001**, *5*, 44–50.
170. Sleven, J.; Görrler-Walrand, C.; Binnemans, K. *Mater. Sci. Eng. C* **2001**, *18*, 229–238.
171. Jiang, J.; Liu, R. C. W.; Mak, T. C. W.; Chan, T. W. D.; Ng, D. K. P. *Polyhedron* **1997**, *16*, 515–520.
172. Jiang, J.; Xie, J.; Choi, M. T.; Yan, Y.; Sun, S.; Ng, D. K. P. *J. Porphyrins Phthalocyanines* **1999**, *3*, 322–328.
173. Jiang, J.; Xie, J.; Ng, D. K.; Yan, Y. *Mol. Cryst. Liq. Cryst.* **1999**, *337*, 385–388.
174. Komatsu, T.; Ohta, K.; Fujimoto, T.; Yamamoto, I. *J. Mater. Chem.* **1994**, *4*, 533–536.
175. Komatsu, T.; Ohta, K.; Watanabe, T.; Ikemoto, H.; Fujimoto, T.; Yamamoto, I. *J. Mater. Chem.* **1994**, *4*, 537–540.
176. Toupance, T.; Ahsen, V.; Simon, J. *J. Am. Chem. Soc.* **1994**, *116*, 5352–5361.
177. Toupance, T.; Plichon, V.; Simon, J. *New J. Chem.* **1999**, *23*, 1001–1006.
178. Lapkina, L. A.; Niskanen, E.; Rönkkömäki, H.; Larchenkov, V. E.; Popov, K. I.; Tsvivadze, A. Y. *J. Porphyrins Phthalocyanines* **2000**, *4*, 588–590.
179. Ban, K.; Nishizawa, K.; Ohta, K.; van de Craats, A. M.; Warman, J. M.; Yamamoto, I.; Shirai, H. *J. Mater. Chem.* **2001**, *11*, 321–331.
180. Gürek, A. G.; Ahsen, V.; Luneau, D.; Pécaut, J. *Inorg. Chem.* **2001**, *40*, 4793–4797.
181. Yoshino, K.; Lee, S. B.; Sonoda, T.; Kawagishi, H.; Hidayat, R.; Nakayama, K.; Ozaki, M.; Ban, K.; Nishizawa, K.; Ohta, K. Shirai H. *J. Appl. Phys.* **2000**, *88*, 7137–7143.
182. Cook, M. J.; Daniel, M. F.; Harrison, K. J.; McKeown, N. B.; Thomson, A. J. *J. Chem. Soc., Chem. Commun.* **1987**, 1086–1088.
183. Cherodian, A. S.; Davies, A. N.; Richardson, R. M.; Cook, M. J.; McKeown, N. B.; Thomson, A. J.; Feijoo, J.; Ungar, G.; Harrison, K. J. *Mol. Cryst. Liq. Cryst.* **1991**, *196*, 103–114.
184. Cook, M. J.; Cracknell, S. J.; Harrison, K. J. *J. Mater. Chem.* **1991**, *1*, 703–704.
185. Critchley, S. M.; Willis, M. R.; Maruyama, Y.; Bandow, S.; Cook, M. J.; McMurdo, J. *Mol. Cryst. Liq. Cryst.* **1993**, *229*, 47–51.
186. Cook, M. J. *J. Mater. Sci., Mater. Electronics* **1994**, *5*, 117–128.
187. Swarts, J. C.; Langner, E. H. G.; Krokeide-Hove, N.; Cook, M. J. *J. Mater. Chem.* **2001**, *11*, 434–443.
188. Helliwell, M.; Deacon, A.; Moon, K. J.; Powell, A. K.; Cook, M. J. *Acta Cryst. B* **1997**, *53*, 231–240.
189. Chambrier, I.; Cook, M. J.; Helliwell, M.; Powell, A. K. *J. Chem. Soc., Chem. Commun.* **1992**, 444–445.
190. Hunter, C. A.; Sanders, J. K. M. *J. Am. Chem. Soc.* **1990**, *112*, 5525–5534.
191. Cammidge, A. N.; Cook, M. J.; Harrison, K. J.; McKeown, N. B. *J. Chem. Soc., Perkin Trans. 1* **1991**, 3053–3058.
192. Cammidge, A. N.; Cook, M. J.; Haslam, S. D.; Richardson, R. M.; Harrison, K. J. *Liq. Cryst.* **1993**, *14*, 1847–1862.
193. Cook, M. J.; Dunn, A. J.; Howe, S. D.; Thomson, A. J.; Harrison, K. J. *J. Chem. Soc., Perkin Trans.* **1988**, 2453–2458.
194. Usol'tseva, N.; Bykova, V.; Kudrik, E.; Shaposhnikov, G.; Smirnova, A.; Anajeva, G.; Nikolaev, I. *Mol. Cryst. Liq. Cryst.* **2001**, *367*, 509–516.
195. Cook, M. J. *J. Mater. Chem.* **1996**, *6*, 677–689.
196. Laschewsky, A. *Angew. Chem. Int. Ed. Engl.* **1989**, *28*, 1574–1577.
197. Chesters, M. A.; Cook, M. J.; Gallivan, S. L.; Simmons, J. M.; Slater, D. A. *Thin Solid Films.* **1992**, *210–211*, 538–541.
198. Poynter, R. H.; Cook, M. J.; Chesters, M. A.; Slater, D. A.; McMurdo, J.; Welford, K. *Thin Solid Films.* **1994**, *243*, 346–350.
199. Chambrier, I.; Cook, M. J.; Cracknell, S. J.; McMurdo, J. *J. Mater. Chem.* **1993**, *3*, 841–849.
200. Cook, M. J.; McMurdo, J.; Miles, D. A.; Poynter, R. H.; Simmons, J. M.; Haslam, S. D.; Richardson, R. M.; Welford, K. *J. Mater. Chem.* **1994**, *4*, 1205–1213.
201. Bryant, G. C.; Cook, M. J.; Ryan, T. G.; Thorne, A. J. *Tetrahedron* **1996**, *52*, 809–824.
202. Cook, M. J.; Cooke, G.; Jafari-Fini, A. *J. Chem. Soc., Chem. Commun.* **1995**, 1715–1716.
203. Bryant, G. C.; Cook, M. J.; Haslam, S. D.; Richardson, R. M.; Ryan, T. G.; Thorne, A. J. *J. Mater. Chem.* **1994**, *4*, 209–216.
204. Cook, M. J.; Heeney, M. J. *Chem. Eur. J.* **2000**, *6*, 3958–3967.
205. Bryant, G. C.; Cook, M. J.; Ryan, T. G.; Thorne, A. J. *J. Chem. Soc., Chem. Commun.* **1995**, 467–468.
206. Cook, M. J. *Adv. Mater.* **1995**, *7*, 877–880.
207. McKeown, N. B. *J. Mater. Chem.* **2000**, *10*, 1979–1995.

208. Cook, M. J.; Jafari-Fini, A. *J. Mater. Chem.* **1997**, *7*, 5–7.
209. Cook, M. J.; Jafari-Fini, A. *J. Mater. Chem.* **1997**, *7*, 2327–2329.
210. Ng, D. K. P.; Yeung, Y. O.; Chan, W. K.; Yu, S. C. *Tetrahedron Lett.* **1997**, *38*, 6701–6704.
211. Cammidge, A. N.; Chambrier, I.; Cook, M. J.; Garland, A. D.; Heeney, M. J.; Welford, K. *J. Porphyrins Phthalocyanines* **1997**, *1*, 77–86.
212. Polley, R.; Golo Linssen, T.; Stihler, P.; Hanack, M. *J. Porphyrins Phthalocyanines* **1997**, *1*, 169–179.
213. Nyokong, T.; Furuya, F.; Kobayashi, N.; Du, D.; Liu, W.; Jiang, J. *Inorg. Chem.* **2000**, *39*, 128–135.
214. Ohta, K.; Watanabe, T.; Fujimoto, T.; Yamamoto, I. *J. Chem. Soc., Chem. Commun.* **1989**, 1611–1613.
215. Ohta, K.; Azumane, S.; Kawahara, W.; Kobayashi, N.; Yamamoto, I. *J. Mater. Chem.* **1999**, *9*, 2313–2320.
216. Mohr, B. A.; Wegner, G.; Ohta, K. *J. Chem. Soc., Chem. Commun.* **1995**, 995–996.
217. Goodby, J. W.; Robinson, P. S.; Teo, B. K.; Cladis, E. *Mol. Cryst. Liq. Cryst., Lett. Sect.* **1980**, *56*, 303–309.
218. Gregg, B. A.; Fox, M. A.; Bard, A. J. *J. Chem. Soc., Chem. Commun.* **1987**, 1134–1135.
219. Paganuzzi, V.; Guatterri, P.; Riccardi, P.; Sacchelli, T.; Barberá, J.; Costa, M.; Dalcanale, E. *Eur. J. Org. Chem.* **1999**, 1527–1539.
220. Sartori, E.; Fontana, M. P.; Dalcanale, E.; Costa, M. *Mol. Cryst. Liq. Cryst.* **1996**, *290*, 31–39.
221. Sartori, E.; Fontana, M. P.; Costa, M.; Dalcanale, E.; Paganuzzi, V. *Thin Solid Films* **1996**, *284–285*, 204–207.
222. Facci, P.; Fontana, M.; P. Dalcanale, E.; Costa, M.; Sacchelli, T. *Langmuir* **2000**, *16*, 7726–7730.
223. Gregg, B. A.; Fox, M. A.; Bard, A. J. *J. Am. Chem. Soc.* **1989**, *111*, 3024–3029.
224. Liu, C. Y.; Pan, H. L.; Fox, M. A.; Bard, A. J. *J. Phys. Chem.* **1995**, *99*, 7632–7636.
225. Schouten, P. G.; Warman, J. M.; de Haas, M. P.; Fox, M. A.; Pan, H. L. *Nature* **1991**, *353*, 736–737.
226. Liu, C. Y.; Pan, H. L.; Fox, M. A.; Bard, A. J. *Science* **1993**, *261*, 897–899.
227. Liu, C. Y.; Pan, H. L.; Fox, M. A.; Bard, A. J. *J. Chem. Mater.* **1997**, *9*, 1422–1429.
228. Gregg, B. A.; Fox, M. A.; Bard, A. J. *J. Phys. Chem.* **1989**, *93*, 4227–4234.
229. Gregg, B. A. *Mol. Cryst. Liq. Cryst.* **1994**, *257*, 219–227.
230. Gregg, B. A.; Fox, M. A.; Bard, A. J. *J. Phys. Chem.* **1990**, *94*, 1586–1598.
231. Fox, M. A.; Grant, J. V.; Melamed, D.; Torimoto, T.; Liu, C. Y.; Bard, A. J. *J. Chem. Mater.* **1998**, *10*, 1771–1776.
232. Murashima, T.; Wakamori, N.; Uchihara, Y.; Ogawa, T.; Uno, H.; Ono, N. *Mol. Cryst. Liq. Cryst.* **1996**, *278*, 165–171.
233. Kugimiya, S. I.; Takemura, M. *Tetrahedron Lett.* **1990**, *31*, 3157–3160.
234. Griessar, K.; Athanassopoulou, M. A.; Soto-Bustamante, E. A.; Tomkowicz, Z.; Zaleski, A. J.; Haase, W. *Adv. Mater.* **1997**, *9*, 45–48.
235. Shimizu, Y.; Miya, M.; Nagata, A.; Ohta, K.; Matsumura, A.; Yamamoto, I.; Kusabayashi, S. *Chem. Lett.* **1991**, 25–28.
236. Shimizu, Y.; Miya, M.; Nagata, A.; Ohta, K.; Yamamoto, I.; Kusabayashi, S. *Liq. Cryst.* **1993**, *14*, 795–805.
237. Shimizu, Y.; Matsumo, J. Y.; Miya, M.; Nagata, A. *J. Chem. Soc., Chem. Commun.* **1994**, 2411–2412.
238. Nagata, A.; Shimizu, Y.; Nagamoto, H.; Miya, M. *Inorg. Chim. Acta* **1995**, *238*, 169–171.
239. Hill, J.; Sugino, T.; Shimizu, Y. *Mol. Cryst. Liq. Cryst.* **1999**, *332*, 119–125.
240. Shimizu, Y.; Santiago, J.; Sugino, T.; Monobe, H. *Mol. Cryst. Liq. Cryst.* **2001**, *364*, 235–242.
241. Sugino, T.; Santiago, J.; Shimizu, Y.; Heinrich, B.; Guillon, D. *Mol. Cryst. Liq. Cryst.* **1999**, *330*, 15–22.
242. Shimizu, Y.; Matsuno, J. Y.; Nakao, K.; Ohta, K.; Miya, M.; Nagata, A. *Mol. Cryst. Liq. Cryst.* **1995**, *260*, 491–497.
243. Shimizu, Y.; Ishikawa, A.; Kusabayashi, S.; Miya, M.; Nagata, A. *J. Chem. Soc., Chem. Commun.* **1993**, 656–658.
244. Shimizu, Y.; Higashiyama, T.; Fuchita, T. *Thin Solid Films* **1998**, *331*, 279–284.
245. Monobe, H.; Mima, S.; Shimizu, Y. *Chem. Lett.* **2000**, 1004–1005.
246. Monobe, H.; Mima, S.; Sugino, T.; Shimizu, Y. *J. Mater. Chem.* **2001**, *11*, 1383–1392.
247. Monobe, H.; Miyagawa, Y.; Mima, S.; Sugino, T.; Uchida, K.; Shimizu, Y. *Thin Solid Films* **2001**, *393*, 217–224.
248. Shimizu, Y. *Mol. Cryst. Liq. Cryst.* **2001**, *370*, 83–91.
249. Kroon, J. M.; Schenkels, P. S.; van Dijk, M.; Sudhölter, E. J. R. *J. Mater. Chem.* **1995**, *5*, 1309–1316.
250. Ramasseul, R.; Maldivi, P.; Marchon, J. C.; Taylor, M.; Guillon, D. *Liq. Cryst.* **1993**, *13*, 729–733.
251. Patel, B. R.; Suslick, K. S. *J. Am. Chem. Soc.* **1998**, *120*, 11802–11803.
252. Ohta, K.; Ando, N.; Yamamoto, I. *Liq. Cryst.* **1999**, *26*, 663–668.
253. Ohta, K.; Ando, N.; Yamamoto, I. *J. Porphyrins Phthalocyanines* **1999**, *3*, 249–258.
254. Ohta, K.; Yamaguchi, N.; Yamamoto, I. *J. Mater. Chem.* **1998**, *8*, 2637–2650.
255. Milgrom, L. R.; Yahioğlu, G.; Bruce, D. W.; Morrone, S.; Henari, F. Z.; Blau, W. J. *Adv. Mater.* **1997**, *9*, 313–316.
256. Milgrom, L. R.; Yahioğlu, G. *Tetrahedron Lett.* **1995**, *36*, 9061–9064.
257. Henari, F. Z.; Blau, W. J.; Milgrom, L. R.; Yahioğlu, G.; Phillips, D.; Lacey, J. A. *Chem. Phys. Lett.* **1997**, *267*, 229–233.
258. Miwa, H.; Kobayashi, N.; Ban, K.; Ohta, K. *Bull. Chem. Soc. Jpn* **1999**, *72*, 2719–2728.
259. Nakai, T.; Ban, K.; Ohta, K.; Kimura, M. *J. Mater. Chem.* **2002**, *12*, 844–850.
260. Zhao, Z.; Liu, G. *Liq. Cryst.* **2002**, *29*, 1335–1337.
261. Wang, X. Q.; Cao, C. S.; Gao, S.; Shi, T. S.; Yu, L. X.; Cao, X. Z. *Gaodeng Xuexia Huaxue Xuebao* **1996**, *17*, 684–686.
262. Wang, X. Q.; Gao, S.; Cao, C. S.; Shi, T. S.; Yu, L. X.; Cao, X. Z. *Gaodeng Xuexia Huaxue Xuebao* **1996**, *17*, 843–848.
263. Doppelt, P.; Huille, S. *New J. Chem.* **1990**, *14*, 607–609.
264. Morelli, G.; Ricciardi, G.; Roviello, A. *Chem. Phys. Lett.* **1991**, *185*, 468–472.
265. Lelj, F.; Morelli, G.; Ricciardi, G.; Roviello, A.; Sirigu, A. *Liq. Cryst.* **1992**, *12*, 941–960.
266. Pate, B. D.; Choi, S. M.; Werner-Zwanziger, U.; Baxter, D. V.; Zaleski, J. M.; Chisholm, M. H. *Chem. Mater.* **2002**, *14*, 1930–1936.
267. Belviso, S.; Ricciardi, G.; Lelj, F. *J. Mater. Chem.* **2000**, *10*, 297–304.
268. Eichhorn, S. H.; Bruce, D. W.; Guillon, D.; Gallani, J. L.; Fischer, T.; Stumpe, J.; Geue, T. *J. Mater. Chem.* **2001**, *11*, 1576–1584.
269. Fernández, O.; de la Torre, G.; Fernández-Lázaro, F.; Barberá, J.; Torres, T. *Chem. Mater.* **1997**, *9*, 3017–3022.
270. Cabezón, B.; Nicolau, M.; Barberá, J.; Torres, T. *Chem. Mater.* **2000**, *12*, 776–781.

271. Nicolau, M.; Cabezon, B.; Torres, T. *Coord. Chem. Rev.* **1999**, 190-192, 231-243.
272. Hunziker, M. *Eur. Pat.* **1985**, 162 804.
273. Forget, S.; Veber, M. *Mol. Cryst. Liq. Cryst.* **1997**, 300, 229-243.
274. Forget, S.; Veber, M.; Strzelecka, H. *Mol. Cryst. Liq. Cryst.* **1995**, 258, 263-275.
275. Forget, S.; Veber, M. *Mol. Cryst. Liq. Cryst.* **1997**, 308, 27-42.
276. Forget, S.; Veber, M. *New J. Chem.* **1997**, 21, 409-411.
277. Forget, S.; Kitzerow, H. S. *Liq. Cryst.* **1997**, 23, 919-922.
278. Kang, S. H.; Kim, M.; Lee, H. K.; Kang, Y. S.; Zin, W. C.; Kim, K. *Chem. Commun.* **1999**, 93-94.
279. Wu, H. C.; Sung, J. H.; Yang, C. D.; Lai, C. K. *Liq. Cryst.* **2001**, 28, 411-415.
280. Pecoraro, V. L.; Stemmler, A. J.; Gibney, B. R.; Bodwin, J. J.; Wang, H.; Kampf, J. W.; Barwinski, A. *Prog. Inorg. Chem.* **1997**, 45, 83-177.
281. Barberá, J.; Elduque, A.; Giménez, R.; Oro, L. A.; Serrano, J. L. *Angew. Chem. Int. Ed. Engl.* **1996**, 35, 2832-2835.
282. Barberá, J.; Elduque, A.; Giménez, R.; Lahoz, F. J.; López, J. A.; Oro, L. A.; Serrano, J. L. *Inorg. Chem.* **1998**, 37, 2960-2967.
283. Kim, S. J.; Kang, S. H.; Park, K. M.; Kim, H.; Zin, W. C.; Choi, M. G.; Kim, K. *Chem. Mater.* **1998**, 10, 1889-1893.
284. Praefcke, K.; Singer, D.; Gündo ğan, B. *Mol. Cryst. Liq. Cryst.* **1992**, 223, 181-195.
285. Praefcke, K.; Singer, D.; Gündo ğan, B.; Gutbier, K.; Langner, M. *Ber. Bunsenges. Phys. Chem.* **1994**, 98, 118-121. *Corrigendum Ibid* **1993**, 97, 1358-1361.
286. Praefcke, K.; Holbrey, J. D.; Usolt'seva, N. *Mol. Cryst. Liq. Cryst.* **1996**, 288, 189-200.
287. Praefcke, K.; Bilgin, B.; Usolt'seva, N.; Heinrich, B.; Guillon, D. *J. Mater. Chem.* **1995**, 5, 2257-2264.
288. Bilgin-Eran, B.; Singer, D.; Pickardt, J.; Praefcke, K. *J. Organomet. Chem.* **2001**, 620, 249-255.
289. Gündo ğan, B.; Praefcke, K. *Chem. Ber.* **1993**, 126, 1253-1255.
290. Heinrich, B.; Praefcke, K.; Guillon, D. *J. Mater. Chem.* **1997**, 7, 1363-1372.
291. Praefcke, K.; Diele, S.; Pickardt, J.; Gündo ğan, B.; Nütz, U.; Singer, D. *Liq. Cryst.* **1995**, 18, 857-865.
292. Usolt'seva, N.; Praefcke, K.; Singer, D.; Gündo ğan, B. *Mol. Mat.* **1994**, 4, 253-263.
293. Usolt'seva, N.; Praefcke, K.; Singer, D.; Gündo ğan, B. *Liq. Cryst.* **1994**, 16, 601-616.
294. Praefcke, K.; Holbrey, J. D.; Usolt'seva, N.; Blunk, D. *Mol. Cryst. Liq. Cryst.* **1997**, 292, 123-139.
295. Nesrullajev, A.; Bilgin-Eran, B.; Kazanci, N. *Mat. Chem. Phys.* **2002**, 76, 7-14.
296. Usolt'seva, N.; Hauck, G.; Koswig, H. D.; Praefcke, K.; Heinrich, B. *Liq. Cryst.* **1996**, 20, 731-739.
297. Galerne, Y. *Mol. Cryst. Liq. Cryst.* **1988**, 165, 131-149.
298. Yu, L. J.; Saupe, A. *Phys. Rev. Lett.* **1980**, 45, 1000-1003.
299. Praefcke, K.; Holbrey, J. D. *J. Incl. Phenom. Mol. Recogn. Chem.* **1996**, 24, 19-41.
300. Usolt'seva, N.; Praefcke, K.; Singer, D.; Gündo ğan, B. *Liq. Cryst.* **1994**, 16, 617-623.
301. Hegmann, T.; Neumann, B.; Kain, J.; Diele, S.; Tschierske, C. *J. Mater. Chem.* **2000**, 10, 2244-2248.
302. Lehn, J. M.; Malthête, J.; Levelut, A. M. *J. Chem. Soc., Chem. Commun.* **1985**, 1794-1796.
303. Malthête, J.; Levelut, A. M.; Lehn, J. M. *J. Chem. Soc., Chem. Commun.* **1992**, 1434-1436.
304. Liebmann, A.; Mertesdorf, C.; Plesnivý, T.; Ringsdorf, H.; Wendorff, J. H. *Angew. Chem. Int. Ed. Engl.* **1991**, 30, 1375-1377.
305. Bauer, S.; Plesnivý, T.; Ringsdorf, H.; Schumacher, P. *Makromol. Chem., Macromol. Symp.* **1992**, 64, 19-32.
306. Neve, F.; Ghedini, M.; Francescangeli, O. *Liq. Cryst.* **1996**, 21, 625-630.
307. Lattermann, G.; Schmidt, S.; Kleppinger, R.; Wendorff, J. H. *Adv. Mater.* **1992**, 4, 30-33.
308. Schmidt, S.; Lattermann, G.; Kleppinger, R.; Wendorff, J. H. *Liq. Cryst.* **1994**, 16, 693-702.
309. Walf, G. H.; Benda, R.; Litterst, F. J.; Stebani, U.; Schmidt, S.; Lattermann, G. *Chem. Eur. J.* **1998**, 4, 93-99.
310. Malthête, J. *Adv. Mater.* **1994**, 6, 315.
311. Xu, B.; Swager, T. M. *J. Am. Chem. Soc.* **1993**, 115, 1159-1160.
312. Swager, T. M.; Xu, B. *J. Incl. Phenom. Mol. Recogn. Chem.* **1994**, 19, 389-398.
313. Bulkin, B. J.; Rose, R. K.; Santoro, A. *Mol. Cryst. Liq. Cryst.* **1977**, 43, 53-58.
314. Ohta, K.; Yokoyama, M.; Kusabayashi, S.; Mikawa, H. *J. Chem. Soc., Chem. Commun.* **1980**, 392-393.
315. Ohta, K.; Jiang, G. J.; Yokoyama, M.; Kusabayashi, S.; Mikawa, H. *Mol. Cryst. Liq. Cryst.* **1981**, 66, 283-294.
316. Ohta, K.; Yokoyama, M.; Kusabayashi, S.; Mikawa, H. *Mol. Cryst. Liq. Cryst.* **1981**, 69, 131-142.
317. Ohta, K.; Yokoyama, M.; Mikawa, H. *Mol. Cryst. Liq. Cryst.* **1981**, 73, 205-221.
318. Tantrawong, S.; Styring, P. *Mol. Cryst. Liq. Cryst.* **1997**, 302, 309-314.
319. Clark, S.; Elliott, J. M.; Chipperfield, J. R.; Styring, P. M.; Sinn, E. *Inorg. Chem. Commun.* **2002**, 5, 249-251.
320. Zhanmei, L.; Haixia, S.; Tong, N.; Zhanpeng, W.; Xishan, L. *Chin. J. Appl. Chem.* **1997**, 14, 101-103.
321. Ohta, K.; Takenaka, O.; Hasebe, H.; Morizumi, Y.; Fujimoto, T.; Yamamoto, I. *Mol. Cryst. Liq. Cryst.* **1991**, 195, 135-148.
322. Praefcke, K.; Blunk, D.; Singer, D.; Goodby, J. W.; Toyne, K. J.; Hird, M.; Styring, P.; Norbert, W. D. *J. A. Mol. Cryst. Liq. Cryst.* **1998**, 323, 231-259.
323. Ohta, K.; Takenaka, O.; Hasebe, H.; Morizumi, Y.; Fujimoto, T.; Yamamoto, I. *Mol. Cryst. Liq. Cryst.* **1991**, 195, 123-133.
324. Ohta, K.; Akimoto, H.; Fujimoto, T.; Yamamoto, I. *J. Mater. Chem.* **1994**, 4, 61-69.
325. Zhang, H.; Yuan, X.; Fu, R.; Li, F.; Zhang, J.; Guo, B.; Wang, Z. *J. Chromatography A* **1998**, 809, 65-73.
326. Ohta, K.; Morizumi, Y.; Akimoto, H.; Takenaka, O.; Fujimoto, T.; Yamamoto, I. *Mol. Cryst. Liq. Cryst.* **1992**, 214, 143-149.
327. Tantrawong, S.; Styring, P. *Liq. Cryst.* **1997**, 22, 17-22.
328. Sadshiva, B. K.; Rao, P. R.; Srikanta, B. S. *Mol. Cryst. Liq. Cryst.* **1989**, 168, 103-109.
329. Chandrasekhar, S.; Sadshiva, B. K.; Ramesha, S.; Srikanta, B. S. *Pramana, J. Phys.* **1986**, 27, 713-715.
330. Chandrasekhar, S.; Sadshiva, B. K.; Srikanta, B. S. *Mol. Cryst. Liq. Cryst.* **1987**, 151, 93-107. *Erratum ibid.* **1989**, 166, 231.
331. Sadashiva, B. K.; Ghode, A.; Rao, P. R. *Mol. Cryst. Liq. Cryst.* **1991**, 200, 187-196.
332. Prasad, V.; Sadashiva, B. K. *Mol. Cryst. Liq. Cryst.* **1995**, 268, 89-100.
333. Thompson, N. J.; Gray, G. W.; Goodby, J. W.; Toyne, K. J. *Mol. Cryst. Liq. Cryst.* **1991**, 200, 109-131.
334. Chandrasekhar, S.; Sadshiva, B. K.; Ratna, B. R.; Raja, V. N. *Pramana, J. Phys.* **1988**, 30, 491.

335. Chandrasekhar, S.; Ratna, B. R.; Sadashiva, B. K.; Raja, V. N. *Mol. Cryst. Liq. Cryst.* **1988**, *165*, 123–130.
336. Chandrasekhar, S.; Nair, G. G.; Praefcke, K.; Singer, D. *Mol. Cryst. Liq. Cryst.* **1996**, *288*, 7–14.
337. Chandrasekhar, S. *Mol. Cryst. Liq. Cryst.* **1994**, *243*, 1–9.
338. Chandrasekhar, S.; Raja, V. N.; Sadshiva, B. K. *Mol. Cryst. Liq. Cryst. Lett.* **1990**, *7*, 65–71.
339. Thompson, N. J.; Goodby, J. W.; Toyne, K. J. *Mol. Cryst. Liq. Cryst.* **1992**, *213*, 187–205.
340. Thompson, N. J.; Goodby, J. W.; Toyne, K. J. *Mol. Cryst. Liq. Cryst.* **1992**, *214*, 81–95.
341. Giroud-Godquin, A.; Billard, J. *Mol. Cryst. Liq. Cryst.* **1981**, *66*, 147–150.
342. Godquin-Giroud, A.; Billard, J. *Mol. Cryst. Liq. Cryst.* **1983**, *97*, 287–295.
343. Usha, K.; Vijayan, K.; Sadashiva, B. K.; Rao, P. R. *Mol. Cryst. Liq. Cryst.* **1990**, *185*, 1–11.
344. Ohta, K.; Muroki, H.; Takagi, A.; Yamamoto, I.; Matsuzaki, K. *Mol. Cryst. Liq. Cryst.* **1986**, *135*, 247–264.
345. Usha, K.; Vijayan, K.; Sadashiva, B. K. *Mol. Cryst. Liq. Cryst.* **1991**, *201*, 13–21.
346. Usha, K.; Vijayan, K. *Mol. Cryst. Liq. Cryst.* **1992**, *220*, 77–86.
347. Usha, K.; Vijayan, K.; Chandrasekhar, S. *Liq. Cryst.* **1993**, *15*, 575–589.
348. Bose, M.; Ohta, K.; Sakurai, T.; Majumdar, C. K. *Mol. Cryst. Liq. Cryst.* **1999**, *326*, 229–247.
349. Usha, K.; Sadashiva, B. K.; Vijayan, K. *Mol. Cryst. Liq. Cryst.* **1994**, *241*, 91–102.
350. Bose, M.; Majumdar, C. K.; Sadashiva, B. K. *Mol. Cryst. Liq. Cryst.* **1997**, *307*, 57–68.
351. Eastman, M. P.; Horng, M. L.; Freiha, B.; Sheu, K. W. *Liq. Cryst.* **1987**, *2*, 223–228.
352. RIBEIRO, A. C.; MARTINS, A. F.; GODEQUIN-GIROUD, A. *Mol. Cryst. Liq. Cryst. Lett.* **1988**, *5*, 133–139.
353. Billard, J. C. R. *Acad. Sc. Paris, Ser. II* **1984**, *299*, 905–908.
354. Levelut, A. M. *J. Chim. Phys.* **1983**, *80*, 149–161.
355. Ohta, K.; Ishii, A.; Yamamoto, I.; Matsuzaki, K. *J. Chem. Soc., Chem. Commun.* **1984**, 1099–1101.
356. Ohta, K.; Ishii, A.; Yamamoto, I.; Matsuzaki, K. *Mol. Cryst. Liq. Cryst.* **1985**, *116*, 299–307.
357. Ohta, K.; Muroki, H.; Takagi, A.; Hatada, K. I.; Ema, H.; Yamamoto, I.; Matsuzaki, K. *Mol. Cryst. Liq. Cryst.* **1986**, *140*, 131–152.
358. Yang, X.; Lu, Q.; Dong, S.; Liu, D.; Zhu, S.; Wu, F.; Zhang, R. *J. Phys. Chem.* **1993**, *97*, 6726–6730.
359. Poelsma, S. N.; Servante, A. H.; Fanizzi, F. P.; Maitlis, P. M. *Liq. Cryst.* **1994**, *16*, 675–685.
360. Ohta, K.; Muroki, H.; Hatada, K. I.; Takagi, A.; Ema, H.; Yamamoto, I.; Matsuzaki, K. *Mol. Cryst. Liq. Cryst.* **1986**, *140*, 163–177.
361. Usha, K.; Vijayan, K.; Sadashiva, B. K. *Mol. Cryst. Liq. Cryst. Lett.* **1987**, *5*, 67–71.
362. Usha, K.; Vijayan, K. *Mol. Cryst. Liq. Cryst.* **1989**, *174*, 39–48.
363. Campo, J. A.; Cano, M.; Heras, J. V.; Lagunas, M. C.; Perles, J.; Pinilla, E.; Torres, M. R. *Helv. Chim. Acta* **2001**, *84*, 2316–2329.
364. Sakashita, H.; Nishitani, A.; Sumiya, Y.; Terauchi, H.; Ohta, K.; Yamamoto, I. *Mol. Cryst. Liq. Cryst.* **1988**, *163*, 211–219.
365. Bose, M.; Sadashiva, B. K. *Mol. Cryst. Liq. Cryst. Lett.* **1991**, *8*, 59–65.
366. Bose, M.; Sadashiva, B. K. *Mol. Cryst. Liq. Cryst. Lett.* **1992**, *8*, 137–143.
367. Haase, W.; Gehring, S.; Borchers, B. *Mat. Res. Soc. Symp. Proc.* **1990**, *175*, 249–255.
368. Lai, C. K.; Pan, H. B.; Yang, L. F.; Liu, K. T. *Liq. Cryst.* **2001**, *28*, 97–101.
369. Sadashiva, B. K.; Ramesha, S. *Mol. Cryst. Liq. Cryst.* **1986**, *141*, 19–24.
370. Prasad, V.; Sadashiva, B. K. *Mol. Cryst. Liq. Cryst.* **1991**, *195*, 161–167.
371. Usha, K.; Vijayan, K. *Liq. Cryst.* **1992**, *12*, 137–145.
372. Bose, M.; Saha, J.; Majumdar, C. K.; Sadashiva, B. K. *Mol. Cryst. Liq. Cryst.* **1997**, *307*, 43–55.
373. Ohta, K.; Muroki, H.; Hatada, K. I.; Yamamoto, I.; Matsuzaki, K. *Mol. Cryst. Liq. Cryst.* **1985**, *130*, 249–263.
374. Liu, Y.; Liu, C.; Ciu, L.; Fan, Z.; Xie, P.; Zhang, R. *Liq. Cryst.* **2000**, *27*, 5–10.
375. Styring, P.; Tantrawong, S.; Beattie, D. R.; Goodby, J. W. *Liq. Cryst.* **1991**, *10*, 581–584.
376. Tantrawong, S.; Styring, P.; Goodby, J. W. *J. Mater. Chem.* **1993**, *3*, 1209–1216.
377. Venkataraman, S.; Varghese, B.; Sadashiva, B. K.; Subramanian, S. *Mol. Cryst. Liq. Cryst.* **2001**, *357*, 199–219.
378. Godquin-Giroud, A. M.; Sigaud, G.; Achard, M. F.; Hardouin, F. *J. Phys. Lett.* **1984**, *45*, 387–392.
379. Terech, P.; Chachaty, C.; Gaillard, J.; Giroud-Godquin, A. M. *J. Phys.* **1987**, *48*, 663–671.
380. Giroud-Godquin, A. M.; Gauthier, M. M.; Sigaud, G.; Hardouin, F.; Achard, M. F. *Mol. Cryst. Liq. Cryst.* **1986**, *132*, 35–44.
381. Ohta, K.; Ema, H.; Muroki, H.; Yamamoto, I.; Matsuzaki, K. *Mol. Cryst. Liq. Cryst.* **1987**, *147*, 61–78.
382. Zheng, H.; Carroll, P. J.; Swager, T. M. *Liq. Cryst.* **1993**, *14*, 1421–1429.
383. Fan, P. C.; Lai, C. K. *J. Chin. Chem. Soc.* **1996**, *43*, 337–343.
384. Su, C.; Shu, C. R.; Wu, C. C. *Liq. Cryst.* **2002**, *29*, 1169–1176.
385. Valdebenito, N.; Oriol, L.; Barberá, J.; Díaz, F.; Serrano, J. L. *Macromol. Chem. Phys.* **2000**, *201*, 2573–2580.
386. Zheng, H.; Lai, C. K.; Swager, T. M. *Chem. Mater.* **1995**, *7*, 2067–2077.
387. Barberá, J.; Iglesias, R.; Serrano, J. L.; Sierra, T.; de la Fuente, M. R.; Palacios, B.; Pérez-Jubindo, M. A.; Vázquez, J. T. *J. Am. Chem. Soc.* **1998**, *120*, 2908–2918.
388. Palacios, B.; de la Fuente, M. R.; Pérez-Jubindo, M. A.; Iglesias, R.; Serrano, J. L.; Sierra, T. *Liq. Cryst.* **1998**, *25*, 481–485.
389. Serrano, J. L.; Sierra, T. *Chem. Eur. J.* **2000**, *6*, 759–766.
390. Zheng, H.; Xu, B.; Swager, T. M. *Chem. Mater.* **1996**, *8*, 907–911.
391. Barberá, J.; Cativiela, C.; Serrano, J. L.; Zurbano, M. M. *Adv. Mater.* **1991**, *3*, 602–605.
392. Atencio, R.; Barberá, J.; Cativiela, C.; Lahoz, F. J.; Serrano, J. L.; Zurbano, M. M. *J. Am. Chem. Soc.* **1994**, *116*, 11558–11559.
393. Trzaska, S. T.; Swager, T. M. *Chem. Mater.* **1998**, *10*, 438–443.
394. Poelsma, N. S.; Maitlis, P. M. *J. Organomet. Chem.* **1993**, *451*, 15–17.
395. Giroud-Godquin, A. M.; Rassat, A. C. R. *Acad. Sc. Paris Ser. II* **1982**, *294*, 241–243.
396. Zheng, H.; Swager, T. M. *J. Am. Chem. Soc.* **1994**, *116*, 761–762.
397. Swager, T. M.; Zheng, H. *Mol. Cryst. Liq. Cryst.* **1995**, *260*, 301–306.
398. Trzaska, S. T.; Hsu, H. F.; Swager, T. M. *J. Am. Chem. Soc.* **1999**, *121*, 4518–4519. Corrigendum, *ibid.* 4544.
399. Trzaska, S. T.; Zheng, H.; Swager, T. M. *Chem. Mater.* **1999**, *11*, 130–134.

400. Kumar, S.; Naidu, J. J. *Liq. Cryst.* **2002**, *29*, 1369–1371.
401. Kumar, S.; Naidu, J. J. *Mol. Cryst. Liq. Cryst.* **2002**, *378*, 123–128.
402. Hegmann, T.; Peidis, F.; Diele, S.; Tschierske, C. *Liq. Cryst.* **2000**, *27*, 1261–1265.
403. Hegmann, T.; Kain, J.; Diele, S.; Pelzl, G.; Tschierske, C. *Angew. Chem. Int. Ed.* **2001**, *40*, 887–890.
404. Lai, C. K.; Serrette, A. G.; Swager, T. M. *J. Am. Chem. Soc.* **1992**, *114*, 7948–7949.
405. Serrette, A. G.; Lai, C. K.; Swager, T. M. *Chem. Mater.* **1994**, *6*, 2252–2268.
406. Lai, C. K.; Lin, F. J. *J. Chem. Soc., Dalton Trans.* **1997**, 17–19.
407. Lai, C. K.; Chen, F. G.; Ku, Y. J.; Tsai, C. H.; Lin, R. *J. Chem. Soc., Dalton Trans.* **1997**, 4683–4687.
408. Lin, R.; Tsai, C. H.; Chao, M. Q.; Lai, C. K. *J. Mater. Chem.* **2001**, *11*, 359–363.
409. Veber, M.; Fugnitto, R.; Strzelecka, H. *Mol. Cryst. Liq. Cryst.* **1983**, *96*, 221–227.
410. Ohta, K.; Takagi, A.; Muroki, H.; Yamamoto, I.; Matsuzaki, K.; Inabe, T.; Maruyama, Y. *J. Chem. Soc., Chem. Commun.* **1986**, *ibid.*, 883–885. Corrigendum, *ibid.* 1744.
411. Ohta, K.; Takagi, A.; Muroki, H.; Yamamoto, I.; Matsuzaki, K.; Inabe, T.; Maruyama, Y. *Mol. Cryst. Liq. Cryst.* **1987**, *147*, 15–24.
412. Veber, M.; Davidson, P.; Jallabert, C.; Levelut, A. M.; Strzelecka, H. *Mol. Cryst. Liq. Cryst. Lett.* **1988**, *5*, 1–7.
413. Horie, H.; Takagi, A.; Hasebe, H.; Ozawa, T.; Ohta, K. *J. Mater. Chem.* **2001**, *11*, 1063–1071.
414. Ohta, K.; Hasebe, H.; Ema, H.; Fujimoto, T.; Yamamoto, I. *J. Chem. Soc., Chem. Commun.* **1989**, 1610–1611.
415. Ohta, K.; Hasebe, H.; Ema, H.; Moriya, M.; Fujimoto, T.; Yamamoto, I. *Mol. Cryst. Liq. Cryst.* **1991**, *208*, 21–32.
416. Ohta, K.; Hasebe, H.; Moriya, M.; Fujimoto, T.; Yamamoto, I. *Mol. Cryst. Liq. Cryst.* **1991**, *208*, 33–41.
417. Ohta, K.; Inagaki-Oka, Y.; Hasebe, H.; Yamamoto, I. *Polyhedron* **2000**, *19*, 267–274.
418. Ohta, K.; Hasebe, H.; Moriya, M.; Fujimoto, T.; Yamamoto, I. *Mol. Cryst. Liq. Cryst.* **1991**, *208*, 43–54.
419. Ohta, K.; Moriya, M.; Ikejima, M.; Hasebe, H.; Fujimoto, T.; Yamamoto, I. *Bull. Chem. Soc. Jpn* **1993**, *66*, 3553–3558.
420. Ohta, K.; Ikejima, M.; Moriya, M.; Hasebe, H.; Yamamoto, I. *J. Mater. Chem.* **1998**, *8*, 1971–1977.
421. Ohta, K.; Hasebe, H.; Moriya, M.; Fujimoto, T.; Yamamoto, I. *J. Mater. Chem.* **1991**, *1*, 831–834.
422. Ohta, K.; Moriya, M.; Ikejima, M.; Hasebe, H.; Fujimoto, T.; Yamamoto, I. *Bull. Chem. Soc. Jpn* **1993**, *66*, 3559–3564.
423. Ohta, K.; Moriya, M.; Ikejima, M.; Hasebe, H.; Kobayashi, N.; Yamamoto, I. *Bull. Chem. Soc. Jpn* **1997**, *70*, 1199–1203.
424. Ohta, K.; Higashi, R.; Ikejima, M.; Yamamoto, I.; Kobayashi, N. *J. Mater. Chem.* **1998**, *8*, 1979–1991.
425. Mohr, B.; Enkelmann, V.; Wegner, G. *Mol. Cryst. Liq. Cryst.* **1996**, *281*, 215–228.
426. Mohr, B.; Enkelmann, V.; Wegner, G. *J. Org. Chem.* **1994**, *59*, 635–638.
427. Mohr, B.; Pressner, D.; Spiess, H. W.; Wegner, G. 23<sup>rd</sup> Freiburger Arbeitstagung Flüssikristalle, **1994**.
428. Gümüs, G.; Ahsen, V. *Mol. Cryst. Liq. Cryst.* **2000**, *348*, 167–178.
429. Aversa, M. C.; Bonaccorsi, P.; Bruce, D. W.; Caruso, F.; Giannetto, P.; Lanza, S.; Morrone, S. *Inorg. Chim. Acta* **1997**, *256*, 23–2415.
430. Aversa, M. C.; Bonaccorsi, P.; Bruce, D. W.; Caruso, F.; Donnio, B.; Giannetto, P.; Guillon, D.; Lanza, S.; Morrone, S. *Mol. Cryst. Liq. Cryst.* **2000**, *348*, 53–64.
431. Lai, C. K.; Tsai, C. H.; Pang, Y. S. *J. Mater. Chem.* **1998**, *8*, 1355–1360.
432. Bacchi, A.; Carcelli, M.; Francescangeli, O.; Neve, F.; Pelagatti, P.; Pelizzi, C. *Inorg. Chem. Commun.* **1999**, *2*, 255–257.
433. Battistini, P.; Carcelli, M.; Dalcanale, E.; Pelizzi, C.; Pelizzi, G.; Righini, L. *Mol. Cryst. Liq. Cryst.* **1998**, *309*, 167–188.
434. Praefcke, K.; Singer, D.; Gündo an, B. *Mol. Cryst. Liq. Cryst.* **1992**, *223*, 181–195.
435. Praefcke, K.; Bilgin, B.; Pickardt, J.; Borowski, M. *Chem. Ber.* **1994**, *127*, 1543–1545.
436. Bilgin-Eran, B.; Singer, D.; Pickardt, J.; Praefcke, K. *J. Organomet. Chem.* **2001**, *620*, 249–255.
437. Praefcke, K.; Bilgin, B.; Pickardt, J.; Borowski, M. *J. Organomet. Chem.* **1999**, *592*, 155–161.
438. Singer, D.; Liebmann, A.; Praefcke, K.; Wendorff, J. H. *Liq. Cryst.* **1993**, *14*, 785–794.
439. Praefcke, K.; Singer, D. *Mol. Mat.* **1994**, *3*, 265–270.
440. Bilgin Eran, B.; Singer, D.; Praefcke, K. *Eur. J. Inorg. Chem.* **2001**, 111–116.
441. Zheng, H.; Lai, C. K.; Swager, T. M. *Chem. Mater.* **1994**, *6*, 101–103.
442. Lai, C. K.; Pang, Y. S.; Tsai, C. H. *J. Mater. Chem.* **1998**, *8*, 2605–2610.
443. Yang, C. D.; Pang, Y. S.; Lai, C. K. *Liq. Cryst.* **2001**, *28*, 191–195.
444. Pyzuk, W.; Krowczynski, A.; Chen, L.; Gorecka, E.; Biczaktaev, I. *Liq. Cryst.* **1995**, *9*, 675–677.
445. Krowczynski, A.; Pocięcha, D.; Szydłowska, J.; Przedmojski, J.; Górecka, E. *Chem. Commun.* **1996**, 2731–2732.
446. Szydłowska, J.; Krowczynski, A.; Górecka, E.; Pocięcha, D. *Inorg. Chem.* **2000**, *39*, 4879–4885.
447. Krowczynski, A.; Szydłowska, J.; Pocięcha, D.; Przedmojski, J.; Górecka, E. *Liq. Cryst.* **1998**, *25*, 117–121.
448. Pietrasik, U.; Szydłowska, J.; Krowczynski, A.; Pocięcha, D.; Górecka, E.; Guillon, D. *J. Am. Chem. Soc.* **2002**, *124*, 8884–8890.
449. Lin, H. D.; Lai, C. K. *J. Chem. Soc., Dalton Trans.* **2001**, 2383–2387.
450. Schulte, J. L.; Laschat, S.; Schulte-Ladbeck, R.; von Armin, V.; Schneider, A.; Finkelmann, H. *J. Organomet. Chem.* **1998**, *552*, 171–176.
451. Kumar, S.; Varshney, S. K. *Liq. Cryst.* **2001**, *28*, 161–163.
452. Heintz, W. *J. Prakt. Chem.* **1855**, *66*, 1.
453. Vorländer, D. *Ber. Dtsch. Chem. Ges.* **1910**, *43*, 3120–3135.
454. Skoulios, A.; Luzzati, V. *Nature* **1959**, *183*, 1310–1312.
455. Skoulios, A. E.; Luzzati, V. *Acta Cryst.* **1961**, *14*, 278–286.
456. Gallot, B.; Skoulios, A. E. *C. R. Acad. Sci. Paris* **1965**, *260*, 3033–3036.
457. Gallot, B.; Skoulios, A. E. *Acta Cryst.* **1962**, *15*, 826–831.
458. Gallot, B.; Skoulios, A. *Kolloid Z., Z. Polym.* **1966**, *209*, 164–169.
459. Gallot, B.; Skoulios, A. *Kolloid Z., Z. Polym.* **1966**, *210*, 143–149.
460. Gallot, B.; Skoulios, A. *Kolloid Z., Z. Polym.* **1966**, *222*, 51–55.
461. Gallot, B.; Skoulios, A. *C. R. Acad. Sci. Paris* **1961**, *252*, 142–144.

462. Gallot, B.; Skoulios, A. *Mol. Cryst. Liq. Cryst.* **1966**, *1*, 263–292.
463. Sanesi, M.; Ferloni, P.; Franzosini, P. *Z. Naturforsch. A* **1977**, *32*, 1173.
464. Gallot, B.; Skoulios, A. *Kolloid Z., Z. Polym.* **1966**, *213*, 143–150.
465. Sanesi, M.; Ferloni, P.; Zangen, M.; Franzosini, P. *Z. Naturforsch. A* **1977**, *32*, 627.
466. Busico, V.; Ferraro, A.; Vacatello, M. *J. Phys. Chem.* **1984**, *88*, 4055–4058.
467. Ubbelohde, A. R.; Michels, H. I.; Duruz, J. J. *Nature* **1970**, *228*, 50–52.
468. Mirnaya, T. A.; Prisyazhnyi, V. D.; Shcherbakov, V. A. *Russ. Chem. Rev.* **1989**, *58*, 821–834.
469. Mirnaya, T. A.; Yaremchuk, G. G.; Prisyazhnyi, V. D. *Liq. Cryst.* **1990**, *8*, 701–705.
470. Skoulios, A. *Adv. Colloid Interface Sci.* **1967**, *1*, 79–110.
471. Skoulios, A. *Ann. Phys.* **1978**, *3*, 421–450.
472. Luzzati, V.; Mustacchi, H.; Skoulios, A. *Nature* **1957**, *180*, 600–601.
473. Vincent, J. M.; Skoulios, A. *Acta Cryst.* **1966**, *20*, 432–440.
474. Luzzati, V.; Mustacchi, H.; Skoulios, A.; Husson, F. *Acta Cryst.* **1960**, *13*, 660–667.
475. Luzzati, V.; Mustacchi, H.; Skoulios, A. *Faraday Soc. Discussions* **1958**, *25*, 43–50.
476. Husson, F.; Mustacchi, H.; Luzzati, V. *Acta Cryst.* **1960**, *13*, 668–677.
477. Vincent, J. M.; Skoulios, A. *Acta Cryst.* **1966**, *20*, 441–447.
478. Gallot, B.; Skoulios, A. *Kolloid Z., Z. Polym.* **1966**, *208*, 37–43.
479. Skoulios, A. E. *Acta Cryst.* **1961**, *14*, 419–424.
480. Reiss-Husson, F.; Luzzati, V. *Nature* **1966**, *210*, 1351–1352.
481. Boden, N.; Jackson, P. H.; McMullen, K.; Holmes, M. C. *Chem. Phys. Lett.* **1979**, *65*, 476–479.
482. Boden, N.; Corne, S. A.; Jolley, K. W. *J. Phys. Chem.* **1987**, *91*, 4092–4105.
483. Holmes, M. C.; Reynolds, D. J.; Boden, N. *J. Phys. Chem.* **1987**, *91*, 5257–5262.
484. Morris, P. G.; Mansfield, P.; Tiddy, G. J. T. *Faraday Symp. Chem. Soc.* **1979**, *13*, 38–48.
485. Lindau, J.; Diele, S.; Krüger, H.; Dörfler, H. D. *Z. Phys. Chem.* **1981**, *262*, 775.
486. Cheda, J. A. R.; Ugarelli, P.; López de la Fuente, F. L.; Fernández-Martin, F.; Xu, Y.; Ijdo, W. L.; Westrum, E. F., Jr. *Thermochimica Acta* **1995**, *266*, 163–173.
487. Lindau, J.; Hillmann, W.; Dörfler, H. D.; Sackmann, H. *Mol. Cryst. Liq. Cryst.* **1986**, *133*, 259–266.
488. Fernández-García, M.; García, M. V.; Redondo, M. I.; Cheda, J. A.; Fernández-García, M. A.; Westrum, E. F., Jr.; Fernández-Martin, F. *J. Lipid Res.* **1997**, *38*, 361–372.
489. Fernández-García, M.; Cheda, J. A. R.; Westrum, E. F., Jr.; Fernández-Martin, F. *J. Colloid. Interface Sci.* **1997**, *185*, 371–381.
490. Cheda, J. A. R.; Fernández-García, M.; Ungarelli, P.; Ferloni, P.; Fernández-Martin, F. L. *Langmuir* **2000**, *16*, 5825–5830.
491. Spegt, P. A.; Skoulios, A. E. *C. R. Acad. Sci. Paris* **1962**, *254*, 4316–4318.
492. Spegt, P. A.; Skoulios, A. E. *Acta Cryst.* **1963**, *16*, 301–306.
493. Spegt, P. A.; Skoulios, A. E. *Acta Cryst.* **1964**, *17*, 198–207.
494. Spegt, P.; Skoulios, A. C. R. *Acad. Sci. Paris* **1962**, *251*, 2199–2201.
495. Spegt, P. A.; Skoulios, A. E. *Acta Cryst.* **1966**, *21*, 892–897.
496. Montmitonnet, P.; Monasse, B.; Haudin, J. M.; Delamare, F. *Mater. Lett.* **1985**, *3*, 98–102.
497. Spegt, P. A.; Skoulios, A. E. *J. Chim. Phys.* **1965**, *62*, 377–381.
498. Spegt, P. A.; Skoulios, A. E. *J. Chim. Phys.* **1965**, *62*, 418–422.
499. Ellis, H. A. *Mol. Cryst. Liq. Cryst.* **1986**, *138*, 321–326.
500. Luzzati, V.; Spegt, P. A. *Nature* **1967**, *215*, 701–704.
501. Mirnaya, T. A.; Berezniński, Y. V.; Volkov, S. V. *Z. Naturforsch.* **1996**, *51a*, 867–870.
502. Mirnaya, T. A.; Polishchuk, A. P.; Beretnitski, Y. V. *J. Chem. Eng. Data* **1996**, *41*, 1337–1339.
503. Mirnaya, T. A.; Yaremchuk, G. G.; Dradrakh, V. S.; Volkov, S. V. *Russ. J. Inorg. Chem.* **1999**, *44*, 775–778.
504. Ellis, H. A. *Mol. Cryst. Liq. Cryst.* **1986**, *139*, 281–290.
505. Amorim da Costa, A. M.; Burrows, H. D.; Geraldès, C. F. G. C.; Teixeira-Dias, J. J. C.; Bazuin, C. G.; Guillon, D.; Skoulios, A.; Blackmore, E.; Tiddy, G. J. T.; Turner, D. L. *Liq. Cryst.* **1986**, *1*, 215–226.
506. Bazuin, C. G.; Guillon, D.; Skoulios, A.; Amorim da Costa, A. M.; Burrows, H. D.; Geraldès, C. F. G. C.; Teixeira-Dias, J. J. C.; Blackmore, E.; Tiddy, G. J. T. *Liq. Cryst.* **1988**, *3*, 1655–1670.
507. Schwede, J.; Köhler, L.; Grossmann, H. P.; Pietralla, M.; Burrows, H. D. *Liq. Cryst.* **1994**, *16*, 267–276.
508. Burrows, H. D.; Geraldès, C. F. G. C.; Pinheiro, T. J. T.; Harris, R. K.; Sebald, A. *Liq. Cryst.* **1988**, *3*, 853–860.
509. Feio, G.; Burrows, H. D.; Geraldès, C. F. G. C.; Pinheiro, T. J. T. *Liq. Cryst.* **1991**, *9*, 417–432.
510. Adeosun, S. O.; Sime, S. J. *Thermochim. Acta* **1976**, *17*, 351.
511. Sanchez Arenas, A.; Garcia, V. M.; Redondo, M. I.; Cheda, J. A. R.; Roux, M. V.; Turrión, C. *Liq. Cryst.* **1995**, *18*, 431–441.
512. Ellis, H. A.; De Vries, A. *Mol. Cryst. Liq. Cryst.* **1988**, *163*, 133–138.
513. Ellis, A. *Mol. Cryst. Liq. Cryst.* **1997**, *308*, 111–120.
514. Attard, G. S.; West, Y. D. *Liq. Cryst.* **1990**, *7*, 484–494.
515. Akanni, M. S.; Burrows, H. D.; Ellis, H. A.; Ngu Asongwed, D.; Babatunde Babalola, H.; Ojo, P. O. *J. Chem. Tech. Biotechnol. A* **1984**, *34*, 127–135.
516. Akanni, M. S.; Abass, N. A. *Liq. Cryst.* **1989**, *6*, 597–608.
517. Cheda, J. A. R.; Ortega, F.; Sánchez-Arenas, A.; Cosío, A.; Fernández-García, M.; Fernández-Martin, F.; Roux, M. V.; Turrión, C. *Pure Appl. Chem.* **1992**, *64*, 65–71.
518. Roux, M. V.; Turrión, C.; Sánchez-Arenas, A.; Cheda, J. A. R. *Langmuir* **1996**, *12*, 2367–2370.
519. Bird, M. J.; Lomer, T. R. *Acta Cryst. B* **1972**, *28*, 242–246.
520. Lomer, T. R.; Perera, K. *Acta Cryst. B* **1974**, *30*, 2912–2913.
521. Lomer, T. R.; Perera, K. *Acta Cryst. B* **1974**, *30*, 2913–2915.
522. Ghermani, N. E.; Lecomte, C.; Rapin, C.; Steimetz, P.; Steimetz, J.; Malaman, B. *Acta Cryst. B* **1994**, *50*, 157–160.
523. Madivi, P.; Bonnet, L.; Giroud-Godquin, A. M.; Ibn-Elhaj, M.; Guillon, D.; Skoulios, A. *Adv. Mater.* **1993**, *5*, 909–912.
524. Attard, G. S.; Cullum, P. R. *Liq. Cryst.* **1990**, *8*, 299–309.

525. Takekoshi, M.; Watanabe, N.; Tamamushi, B. *Coll. Polym. Sci.* **1978**, *256*, 588–590.
526. Abied, H.; Guillon, D.; Skoulios, A.; Dexpert, H.; Giroud-Godquin, A. M.; Marchon, J. C. *J. Phys. France* **1988**, *49*, 345–352.
527. Maldivi, P.; Giroud-Godquin, A. M.; Marchon, J. C.; Guillon, D.; Skoulios, A. *Physica B* **1989**, *158*, 234–236.
528. Maldivi, P.; Guillon, D.; Giroud-Godquin, A. M.; Marchon, J. C.; Abied, H.; Dexpert, H.; Skoulios, A. *J. Chim. Phys.* **1989**, *86*, 1651–1664.
529. Guillon, D.; Skoulios, A. *J. Phys. IV* **1996**, *C4*, 41–48.
530. Giroud-Godquin, A. M.; Marchon, J. C.; Guillon, D.; Skoulios, A. *J. Phys. Lett.* **1984**, *45*, 681–684.
531. Abied, H.; Guillon, D.; Skoulios, A.; Weber, P.; Giroud-Godquin, A. M.; Marchon, J. C. *Liq. Cryst.* **1987**, *2*, 269–279.
532. Ibn-Elhaj, M.; Guillon, D.; Skoulios, A.; Giroud-Godquin, A. M.; Maldivi, P. *Liq. Cryst.* **1992**, *11*, 731–744.
533. Marchon, J. C.; Maldivi, P.; Giroud-Godquin, A. M.; Guillon, D.; Skoulios, A.; Strommen, D. P. *Phil. Trans. R. Soc. Lond. A* **1990**, *330*, 109–116.
534. Giroud-Godquin, A. M.; Maldivi, P.; Marchon, J. C.; Aldebert, P.; Péguy, A.; Guillon, D.; Skoulios, A. *J. Phys. France* **1989**, *50*, 513–519.
535. Ibn-Elhaj, M.; Guillon, D.; Skoulios, A. *Phys. Rev. A* **1992**, *46*, 7643–7651.
536. Attard, G. S.; Templer, R. H. *J. Mater. Chem.* **1993**, *3*, 207–213.
537. Liu, C. Y.; Yang, S. H.; Chau, M. H.; Shiue, C. C. *J. Chromatogr. A* **2001**, *933*, 117–128.
538. Liu, C. Y.; Chen, J. L.; Shiue, C. C.; Liu, K. T. *J. Chromatogr. A* **1999**, *862*, 65–83.
539. Petricek, S.; Kozlevcar, B. *Thermochimica Acta* **2002**, *386*, 59–64.
540. Rusjan, M.; Chaia, Z.; Piro, O. E.; Guillon, D.; Cukiernik, F. D. *Acta Cryst. B* **2000**, *56*, 666–676.
541. Akopova, O. B.; Shabyshv, L. S.; Bobrov, V. I. *Russ. Chem. Bull.* **1995**, *44*, 1210–1214.
542. Marcot, L.; Maldivi, P.; Marchon, J. C.; Guillon, D.; Ibn-Elhaj, M.; Broer, D. J.; Mol, G. N. *Chem. Mater.* **1997**, *9*, 2051–2058.
543. Ibn-Elhaj, M.; Guillon, D.; Skoulios, A.; Giroud-Godquin, A. M.; Marchon, J. C. *J. Phys. II France* **1992**, *2*, 2197–2206.
544. Seghrouchni, R.; Skoulios, A. *J. Phys. II France* **1995**, *5*, 1385–1405.
545. Seghrouchni, R.; Skoulios, A. *J. Phys. II France* **1995**, *5*, 1547–1565.
546. Terech, P.; Schaffhauser, V.; Maldivi, P.; Guenet, J. M. *Europhys. Lett.* **1992**, *17*, 515–521.
547. Giroud-Godquin, A. M.; Latour, J. M.; Marchon, J. C. *Inorg. Chem.* **1985**, *24*, 4452–4454.
548. Strommen, D. P.; Giroud-Godquin, A. M.; Maldivi, P.; Marchon, J. C.; Marchon, B. *Liq. Cryst.* **1987**, *2*, 689–699.
549. Redondo, M. I.; Garcia, M. V.; González-Tejera, M. J.; Cheda, J. A. R. *Spectrochimica Acta* **1995**, *51A*, 341–347.
550. Abied, H.; Guillon, D.; Skoulios, A.; Giroud-Godquin, A. M.; Maldivi, P.; Marchon, J. C. *Coll. Polym. Sci.* **1988**, *266*, 579–582.
551. Giroud-Godquin, A. M.; Maldivi, P.; Marchon, J. C.; Bée, M.; Carpentier, L. *Mol. Phys.* **1989**, *68*, 1353–1365.
552. Carpentier, L.; Bée, M.; Giroud-Godquin, A. M.; Maldivi, P.; Marchon, J. C. *Mol. Phys.* **1989**, *68*, 1367–1378.
553. Bée, M.; Giroud-Godquin, A. M.; Maldivi, P.; Williams, J. *Mol. Phys.* **1994**, *81*, 57–68.
554. Giroud-Godquin, A. M.; Marchon, J. C.; Guillon, D.; Skoulios, A. *J. Phys. Chem.* **1986**, *90*, 5502–5503.
555. Poizat, O.; Strommen, D. P.; Maldivi, P.; Giroud-Godquin, A. M.; Marchon, J. C. *Inorg. Chem.* **1990**, *29*, 4853–4854.
556. Ibn-Elhaj, M.; Guillon, D.; Skoulios, A.; Maldivi, P.; Giroud-Godquin, A. M.; Marchon, J. C. *J. Phys. II France* **1992**, *2*, 2237–2253.
557. Bardet, M.; Maldivi, P.; Giroud-Godquin, A. M.; Marchon, J. C. *Langmuir* **1995**, *11*, 2306–2311.
558. Maldivi, P.; Giroud-Godquin, A. M.; Marchon, J. C.; Guillon, D.; Skoulios, A. *Chem. Phys. Lett.* **1989**, *157*, 552–555.
559. Cukiernik, F. D.; Maldivi, P.; Giroud-Godquin, A. M.; Marchon, J. C.; Ibn-Elhaj, M.; Guillon, D.; Skoulios, A. *Liq. Cryst.* **1991**, *9*, 903–906.
560. Bonnet, L.; Cukiernik, F. D.; Maldivi, P.; Giroud-Godquin, A. M.; Marchon, J. C.; Ibn-Elhaj, M.; Guillon, D.; Skoulios, A. *Chem. Mater.* **1994**, *6*, 31–38.
561. Aquino, M. A. S. *Coord. Chem. Rev.* **1998**, *170*, 141–202.
562. Cukiernik, F. D.; Ibn-Elhaj, M.; Chaia, Z. D.; Marchon, J. C.; Giroud-Godquin, A. M.; Guillon, D.; Skoulios, A.; Maldivi, P. *Chem. Mater.* **1998**, *10*, 83–91.
563. Rusjan, M. C.; Sileo, E. E.; Cukiernik, F. D. *Sol. State Ionics* **1999**, *124*, 143–147.
564. Caplan, J. F.; Murphy, C. A.; Swansburg, S.; Lemieux, R. P.; Cameron, T. S.; Aquino, M. A. S. *Can. J. Chem.* **1998**, *76*, 1520–1523.
565. Cotton, F. A.; Matusz, M.; Zhong, B. *Inorg. Chem.* **1998**, *27*, 4368.
566. Cukiernik, F. D.; Luneau, D.; Marchon, J. C.; Maldivi, P. *Inorg. Chem.* **1998**, *37*, 3698–3704.
567. Estiú, G.; Cukiernik, F. D.; Maldivi, P.; Poizat, O. *Inorg. Chem.* **1999**, *38*, 3030–3039.
568. Clayton, R. H.; Chisholm, M. H.; Darrington, F. D. *Angew. Chem. Int. Ed. Engl.* **1990**, *29*, 1481–1483.
569. Baxter, D. V.; Clayton, R. H.; Chisholm, M. H.; Huffman, J. C.; Putilina, E. F.; Tagg, S. L.; Wesemann, J. L.; Zwanziger, J. W.; Darrington, F. D. *J. Am. Chem. Soc.* **1994**, *116*, 4551–4556.
570. Chisholm, M. H. *Acc. Chem. Res.* **2000**, *33*, 53–61.
571. Chisholm, M. H.; Mackley, M. R.; Marshall, R. T.; Putilina, E. F. *Chem. Mater.* **1995**, *7*, 1938–1941.
572. Baxter, D. V.; Chisholm, M. H.; Lynn, M. A.; Putilina, E. F.; Trzaska, S. T.; Swager, T. *Chem. Mater.* **1998**, *10*, 1758–1763.
573. Barberá, J.; Esteruelas, M. A.; Levelut, A. M.; Oro, L. A.; Serrano, J. L. *Inorg. Chem.* **1992**, *31*, 732–737.
574. Rusjan, M.; Donnio, B.; Guillon, D.; Cukiernik, F. D. *Chem. Mater.* **2002**, *14*, 1564–1575.
575. Chaia, Z.; Heinrich, B.; Cukiernik, F.; Guillon, D. *Mol. Cryst. Liq. Cryst.* **1999**, *330*, 213–220.
576. Rusjan, M.; Donnio, B.; Heinrich, B.; Cukiernik, F. D.; Guillon, D. *Langmuir* **2002**, *18*, 10116–10121.
577. Binnemans, K.; Görlner-Walrand, C. *Chem. Rev.* **2002**, *102*, 2303–2345.
578. Jongen, L.; Meyer, G.; Binnemans, K. *J. Alloys Comp.* **2001**, *323–324*, 142–146.
579. Mehrotra, K. N.; Shukla, R. K.; Chauhan, M. *Bull. Chem. Soc. Jpn* **1995**, *68*, 1825–1831.
580. Marques, E. F.; Burrows, H. D.; da Graça Miguel, M. *J. Chem. Soc., Faraday Trans.* **1998**, *94*, 1729–1736.
581. Jongen, L.; Binnemans, K.; Hinz, D.; Meyer, G. *Mater. Sci. Eng. C* **2001**, *18*, 199–204.

582. Binnemans, K.; Heinrich, B.; Guillon, D.; Bruce, D. W. *Liq. Cryst.* **1999**, *26*, 1717–1721.
583. Binnemans, K.; Jongen, L.; Görler-Walrand, C.; D'Olieslager, W.; Hinz, D.; Meyer, G. *Eur. J. Inorg. Chem.* **2000**, 1429–1436.
584. Binnemans, K.; Jongen, L.; Bromant, C.; Hinz, D.; Meyer, G. *Inorg. Chem.* **2000**, *39*, 5938–5945.
585. Jongen, L.; Binnemans, K.; Hinz, D.; Meyer, G. *Liq. Cryst.* **2001**, *28*, 1727–1733.
586. Jongen, L.; Binnemans, K.; Hinz, D.; Meyer, G. *Liq. Cryst.* **2001**, *28*, 819–825.
587. Jongen, L.; Hinz, D.; Meyer, G.; Binnemans, K. *Chem. Mater.* **2001**, *13*, 2243–2246.
588. Ohta, K.; Ema, H.; Yamamoto, I.; Matsuzaki, K. *Liq. Cryst.* **1988**, *12*, 1671–1687.
589. Ohta, K.; Morizumi, Y.; Ema, H.; Fujimoto, T.; Yamamoto, I. *Mol. Cryst. Liq. Cryst.* **1991**, *208*, 55–63.
590. Malthête, J.; Nguyen, H. T.; Destrade, C. *Liq. Cryst.* **1993**, *13*, 171–187.
591. Nguyen, H. T.; Destrade, C.; Malthête, J. *Adv. Mater.* **1997**, *9*, 375–388.
592. Guillon, D.; Heinrich, B.; Ribeiro, A. C.; Cruz, C.; Nguyen, H. T. *Mol. Cryst. Liq. Cryst.* **1998**, *317*, 51–64.
593. Fazio, D.; Mongin, C.; Donnio, B.; Galerne, Y.; Guillon, D.; Bruce, D. W. *J. Mater. Chem.* **2001**, *11*, 2852–2863.
594. Lee, M.; Yoo, Y. S.; Choi, M. G. *Bull. Korean Chem. Soc.* **1997**, *18*, 1067–1070.
595. Bruce, D. W.; Lalinde, E.; Styling, P.; Dunmur, D. A.; Maitlis, P. M. *J. Chem. Soc., Chem. Commun.* **1986**, 581–582.
596. Coco, S.; Diez-Expósito, F.; Espinet, P.; Fernández-Mayordomo, C.; Martín-Alvarez, J. M.; Levelut, A. M. *Chem. Mater.* **1998**, *10*, 3666–3671.
597. Benouazzane, M.; Coco, S.; Espinet, P.; Martín-Alvarez, J. M.; Barberá, J. J. *J. Mater. Chem.* **2002**, *12*, 691–696.
598. Varshney, S. K.; Shankar Rao, D. S.; Kumar, S. *Mol. Cryst., Liq. Cryst.* **2001**, *357*, 55–65.
599. Bruce, D. W. *Adv. Inorg. Chem.* **2001**, *52*, 151–204.
600. Donnio, B.; Bruce, D. W. *J. Chem. Soc., Dalton Trans.* **1997**, 2745–2755.
601. Donnio, B.; Heinrich, B.; Bruce, D. W.; Guillon, D. unpublished results.
602. Plasseraud, L.; Gonzalez-Cuervo, L.; Guillon, D.; Süß-Fink, G.; Deschenaux, R.; Bruce, D. W.; Donnio, B. *J. Mater. Chem.* **2002**, *12*, 2653–2658.
603. Eckert, J. F.; Maciejczuk, U.; Guillon, D.; Nierengarten, J. F. *Chem. Commun.* **2001**, 1278–1279.
604. Roll, C. P.; Donnio, B.; Weigand, W.; Bruce, D. W. *Chem. Commun.* **2000**, 709–710.
605. Rourke, J. P.; Fanizzi, F. P.; Salt, N. J. S.; Bruce, D. W.; Dunmur, D. A.; Maitlis, P. M. *J. Chem. Soc., Chem. Commun.* **1990**, 229–231.
606. Donnio, B.; Rowe, K. E.; Roll, C. P.; Bruce, D. W. *Mol. Cryst., Liq. Cryst.* **1999**, *332*, 383–390.
607. Mongin, C.; Donnio, B.; Bruce, D. W. *J. Am. Chem. Soc.* **2001**, *123*, 8426–8427.
608. Weissflog, W.; In *Handbook of Liquid Crystals*, eds. Demus, D.; Goodby, J.; Gray, G. W., Spiess, H.-W., Vill, V.; Wiley-VCH, Weinheim 1998, Vol. 2B, Chapter XI.
609. Bruce, D. W. *Acc. Chem. Res.* **2000**, *33*, 831–840.
610. Bruce, D. W.; Donnio, B.; Guillon, D.; Heinrich, B.; Ibn-Elhaj, M. *Liq. Cryst.* **1995**, *19*, 537–539.
611. Donnio, B.; Bruce, D. W.; Delacroix, H.; Gulik-Krzywicki, T. *Liq. Cryst.* **1997**, *23*, 147–153.
612. Donnio, B.; Bruce, D. W.; Heinrich, B.; Guillon, D.; Delacroix, H.; Gulik-Krzywicki, T. *Chem. Mater.* **1997**, *9*, 2951–2965.
613. Donnio, B.; Bruce, D. W. *J. Mater. Chem.* **1998**, *8*, 1993–1997.
614. Saito, K.; Shinhara, T.; Sorai, M. *Liq. Cryst.* **2000**, *27*, 1555–1559.
615. Donnio, B.; Bruce, D. W. *New J. Chem.* **1999**, *23*, 275–286.
616. Smirnova, A.; Bruce, D. W. *Chem. Commun.* **2002**, 176–177.
617. Elliott, J. M.; Chipperfield, J. R.; Clark, S.; Sinn, E. *Inorg. Chem.* **2001**, *40*, 6390–6396.
618. Elliott, J. M.; Chipperfield, J. R.; Clark, S.; Sinn, E. *Inorg. Chem. Commun.* **2002**, *5*, 99–101.
619. Nakazono, T.; Nakano, M.; Tamura, H.; Matsubayashi, G. E. *J. Mater. Chem.* **1999**, *9*, 2413–2417.
620. Jacq, P.; Malthête, J. *Liq. Cryst.* **1996**, *21*, 291–293.
621. Campillos, E.; Deschenaux, R.; Levelut, A. M.; Ziessel, R. *J. Chem. Soc., Dalton Trans.* **1996**, 2533–2536.
622. Seo, J. S.; Yoo, Y. S.; Choi, M. G. *J. Mater. Chem.* **2001**, *11*, 1332–1338.
623. Deschenaux, R.; Monnet, F.; Serrano, E.; Turpin, F.; Levelut, A. M. *Helv. Chim. Acta* **1998**, *81*, 2072–2077.
624. Wang, Q. M.; Bruce, D. W. *Chem. Commun.* **1996**, 2505–2506.
625. Bruce, D. W.; Wali, M. A.; Wang, Q. M. *J. Chem. Soc., Chem. Commun.* **1994**, 2089–2090.
626. Wang, Q. M.; Bruce, D. W. *Angew. Chem. Int. Edn. Engl.* **1997**, *36*, 150–152.
627. Serrette, A. G.; Swager, T. M. *Chem. Mater.* **1993**, *115*, 8879–8880.
628. Killian, D.; Knawby, D.; Athanassopoulou, M. A.; Trzaska, S. T.; Swager, T. M.; Wróbel, S.; Haase, W. *Liq. Cryst.* **2000**, *27*, 509–521.
629. Haase, W.; Killian, D.; Athanassopoulou, M. A.; Knawby, D.; Swager, T. M.; Wróbel, S. *Liq. Cryst.* **2002**, *29*, 133–139.
630. Binnemans, K.; Lodewyckx, K.; Donnio, B.; Guillon, D. *Chem. Eur. J.* **2002**, *8*, 1101–1105.
631. Krówczynski, A.; Szydłowska, J.; Pocięcha, D.; Górecka, E. *Polish. J. Chem.* **1996**, *70*, 32–35.
632. Lai, C. K.; Chang, C. H.; Tsai, C. H. *J. Mater. Chem.* **1998**, *8*, 599–602.
633. Lai, C. K.; Wang, K. W.; Lin, R. *J. Mater. Chem.* **1998**, *8*, 2379–2383.
634. Lee, M.; Yoo, Y. S.; Choi, M. G.; Chang, H. Y. *J. Mater. Chem.* **1998**, *8*, 277–278.
635. Berdagué, P.; Perez, F.; Courtieu, J.; Bayle, J. P. *Bull. Soc. Chim. Fr.* **1994**, *131*, 335–343.
636. Lehmann, M.; Sierra, T.; Barberá, J.; Serrano, J. L.; Parker, R. *J. Mater. Chem.* **2002**, *12*, 1342–1350.
637. Date, R. W.; Fernandez Iglesias, E.; Rowe, K. E.; Elliott, J. M.; Bruce, D. W. *Dalton Trans.* **2003**, 1914–1931.
638. Serrette, A. G.; Swager, T. M. *Angew. Chem. Int. Ed. Engl.* **1994**, *33*, 2342–2345.
639. Coco, S.; Espinet, P.; Martín-Alvarez, J. M.; Levelut, A. M. *J. Mater. Chem.* **1997**, *7*, 19–23.
640. Benouazzane, M.; Coco, S.; Espinet, P.; Martín-Alvarez, J. M. *J. Mater. Chem.* **1999**, *9*, 2327–2332.
641. Benouazzane, M.; Coco, S.; Espinet, P.; Barberá, J. *J. Mater. Chem.* **2001**, *11*, 1740–1744.
642. Chow, H. F.; Mong, T. K.; Nongrum, M. F.; Wan, C. W. *Tetrahedron* **1998**, *54*, 8543–8660.
643. Lai, C.; K. Lu, M. Y.; Lin, F. *J. Liq. Cryst.* **1997**, *23*, 313–315.
644. Stebani, U.; Lattermann, G.; Wittenbger, M.; Wendorff, J. H. *Angew. Chem. Int. Ed. Engl.* **1996**, *35*, 1858–1861.
645. Stebani, U.; Lattermann, G. *Adv. Mater.* **1995**, *7*, 578–581.
646. Douce, L.; Ziessel, R. *Mol. Cryst. Liq. Cryst.* **2001**, *362*, 133–145.



647. Ziessel, R. *Coord. Chem. Rev.* **2001**, 216–217, 195–223.
648. Lehn, J. M. *Supramolecular Chemistry: Concepts and Perspectives*. VCH: Weinheim, 1995.
649. Piguet, C.; Bernardinelli, G.; Hopfgartner, G. *Chem. Rev.* **1997**, 97, 2005–2062.
650. Tschierske, C. *Angew. Chem. Int. Ed.* **2000**, 39, 2454–2458.
651. Douce, L.; El-ghayoury, A.; Skoulios, A.; Ziessel, R. *Chem. Commun.* **1999**, 2033–2034.
652. El-ghayoury, A.; Douce, L.; Skoulios, A.; Ziessel, R. *Angew. Chem. Int. Ed.* **1998**, 37, 2205–2208.
653. Ziessel, R.; Douce, L.; El-ghayoury, A.; Harriman, A.; Skoulios, A. *Angew. Chem. Int. Ed.* **2000**, 39, 1489–1493.
654. Ku, S. M.; Wu, C. Y.; Lai, C. K. *J. Chem. Soc., Dalton Trans.* **2000**, 3491–3492.
655. Benouazzane, M.; Coco, S.; Espinet, P.; Barberá, J. *Inorg. Chem.* **2002**, 41, 5754–5759.
656. Bruce, D. W. *J. Chem. Soc., Dalton Trans.* **1993**, 2983–2989.
657. Hasan, M.; Kozhevnikov, I. V.; Siddiqui, M. R. H.; Femoni, C.; Steiner, A.; Winterton, N. *Inorg. Chem.* **2001**, 40, 795–800.
658. Landi, E.; Vacatello, M. *Thermochim. Acta* **1975**, 13, 441–447.
659. Landi, E.; Salerno, V.; Vacatello, M. *Gazz. Chem. Ital.* **1977**, 107, 27–30.
660. Ciajolo, M. R.; Corradini, P.; Pavone, V. *Acta Cryst. B* **1977**, 33, 553.
661. Carfagna, C.; Vacatello, M.; Corradini, P. *Gazz. Chem. Ital.* **1977**, 107, 131–133.
662. Busico, V.; Castaldo, D.; Vacatello, M. *Mol. Cryst. Liq. Cryst.* **1981**, 78, 221–226.
663. Casal, H. L.; Cameron, D. G.; Mantsch, H. H. *J. Phys. Chem.* **1985**, 89, 5557–5565.
664. Busico, V.; Vacatello, M. *Mol. Cryst. Liq. Cryst.* **1983**, 95, 251–269.
665. Busico, V.; Vacatello, M. *Gazz. Chim. Acta* **1981**, 111, 13–17.
666. Kanazawa, A.; Ikeda, T.; Nagase, Y. *Chem. Mater.* **2000**, 12, 3776–3782.
667. Salerno, V.; Landi, E.; Vacatello, M. *Thermochim. Acta* **1977**, 20, 407–415.
668. Busico, V.; Carfagna, C.; Salerno, V.; Vacatello, M. *Thermochim. Acta* **1980**, 39, 1–5.
669. Kurihara, K.; Matsunaga, Y. *Mol. Cryst. Liq. Cryst.* **1996**, 289, 207–220.
670. Paleos, C. M.; Margomenou-Leonidopoulou, G.; Anastassopoulou, J. D.; Papaconstantinou, E. *Mol. Cryst. Liq. Cryst.* **1988**, 161, 373–383.
671. Albéniz, A. C.; Barberá, J.; Espinet, P.; Lequernica, M. C.; Levelut, A. M.; López-Marcos, F. J.; Serrano, J. L. *Eur. J. Inorg. Chem.* **2000**, 133–138.
672. Bowlas, C. J.; Bruce, D. W.; Seddon, K. R. *Chem. Commun.* **1996**, 1625–1626.
673. Bazuin, C. G.; Guillon, D.; Skoulios, A.; Nicoud, J. F. *Liq. Cryst.* **1986**, 1, 181–188.
674. Neve, F.; Crispini, A.; Armentano, S.; Francescangeli, O. *Chem. Mater.* **1998**, 10, 1904–1913.
675. Neve, F.; Francescangeli, O.; Crispini, A. *Inorg. Chem. Acta* **2002**, 338, 51–58.
676. Neve, F.; Crispini, A.; Francescangeli, O. *Inorg. Chem.* **2000**, 39, 1187–1194.
677. Neve, F.; Francescangeli, O.; Crispini, A.; Charmant, J. *Chem. Mater.* **2001**, 13, 2032–2041.
678. Bensebaa, F.; Ellis, T. H.; Kruus, E.; Voicu, R.; Zhou, Y., *Can. J. Chem.* **1998**, 76, 1654–1659.
679. Dance, I. G.; Fisher, K. J.; Herath Banda, R. M.; Scudder, M. L. *Inorg. Chem.* **1991**, 30, 183–187.
680. Baena, M. J.; Lequerica, M. C.; Levelut, A. M. *J. Am. Chem. Soc.* **1992**, 114, 4182–4185.
681. Espinet, P.; Lequerica, M. C.; Martin-Alvarez, J. M. *Chem. Eur. J.* **1999**, 5, 1982–1986.
682. Tsiourvas, D.; Kardassi, D.; Paleos, C. M.; Gehant, S.; Skoulios, A. *Liq. Cryst.* **1997**, 23, 269–274.
683. Kardassi, D.; Tsiourvas, D.; Paleos, C. M.; Heinrich, B.; Skoulios, A. *Mol. Cryst. Liq. Cryst.* **1999**, 326, 49–54.
684. Paleos, C. M.; Kardassi, D.; Tsiourvas, D.; Skoulios, A. *Liq. Cryst.* **1998**, 25, 267–275.
685. Vorländer, D. *Z. Phys. Chem.* **1923**, 105, 211–254.
686. Bruce, D. W.; Heyns, K.; Vill, V. *Liq. Cryst.* **1997**, 23, 813–819.
687. Young, W. R.; Haller, I.; Green, D. C. *Mol. Cryst. Liq. Cryst.* **1971**, 13, 305–321.
688. Krigbaum, W. R.; Poirier, J. C.; Costello, M. J. *Mol. Cryst. Liq. Cryst.* **1973**, 20, 133–163.
689. Chandrasekhar, S. *Curr. Sci.* **1978**, 47, 523–525.
690. Gray, G. W.; Harrison, K. J.; Nash, J. A. *Electron. Lett.* **1973**, 9, 130.
691. Scheffer, T.; Nehring, J. In *Liquid Crystals, Applications and Uses*, Vol I, Bahadur, B. Eds.; World Scientific, Singapore, 1990.
692. Bruce, D. W.; Lalinde, E.; Styring, P.; Dunmur, D. A.; Maitlis, P. M. *J. Chem. Soc., Chem. Commun.* **1986**, 581–582.
693. Maitlis, P. M.; Bruce, D. W.; Dhillon, R.; Dunmur, D. A.; Fanizzi, F. P.; Hunt, S. E.; Le Lagadec, R.; Lalinde, E.; Orr, R.; Rourke, J. P.; Salt, N. J. S.; Stacey, J. P.; Styring, P. *New J. Chem.* **1990**, 14, 549–551.
694. Bruce, D. W.; Donnio, B.; Maggs, A. A.; Marsden, J. R. *Inorg. Chim. Acta* **1991**, 188, 41–43.
695. Adams, H.; Bailey, N. A.; Bruce, D. W.; Dunmur, D. A.; Lalinde, E.; Marcos, M.; Ridgway, C.; Smith, A. J.; Styring, P.; Maitlis, P. M. *Liq. Cryst.* **1987**, 2, 381–393.
696. Adams, H.; Bailey, N. A.; Bruce, D. W.; Dhillon, R.; Dunmur, D. A.; Hunt, S. E.; Lalinde, E.; Maggs, A. A.; Orr, R.; Styring, P.; Wragg, M. S.; Maitlis, P. M. *Polyhedron* **1988**, 7, 1861–1867.
697. Bruce, D. W.; Fan, S. M.; Luckhurst, G. R. *Liq. Cryst.* **1994**, 16, 1093–1099.
698. Kaharu, T.; Takahashi, S. *Chem. Lett.* **1992**, 1515–1516.
699. Kaharu, T.; Tanaka, T.; Sawada, M.; Takahashi, S. *J. Mater. Chem.* **1994**, 4, 859–865.
700. Omenat, A.; Serrano, J. L.; Sierra, T.; Amabilino, D. B.; Minguet, M.; Ramos, E.; Veciana, J. *J. Mater. Chem.* **1999**, 9, 2301–2305.
701. Wang, S.; Mayr, A.; Cheung, K. K. *J. Mater. Chem.* **1998**, 8, 1561–1565.
702. Benouazzane, M.; Coco, S.; Espinet, P.; Martín-Alvarez, J. M.; Barberá, J. *J. Mater. Chem.* **2002**, 12, 691–696.
703. Alejos, P.; Coco, S.; Espinet, P. *New J. Chem.* **1995**, 19, 799–805.
704. Kaharu, T.; Ishii, R.; Adachi, T.; Yoshida, T.; Takahashi, S. *J. Mater. Chem.* **1995**, 5, 687–692.
705. Kaharu, T.; Ishii, R.; Takahashi, S. *J. Chem. Soc., Chem. Commun.* **1994**, 1349–1350.
706. Coco, S.; Espinet, P.; Falagán, S.; Martín-Alvarez, J. M. *New J. Chem.* **1995**, 19, 959–964.
707. Benouazzane, M.; Coco, S.; Espinet, P.; Martín-Alvarez, J. M. *J. Mater. Chem.* **1995**, 5, 441–445.
708. Espinet, P. *Gold Bull.* **1999**, 32, 127–134.
709. Coco, S.; Espinet, P.; Martín-Alvarez, J. M.; Levelut, A. M. *J. Mater. Chem.* **1997**, 7, 19–23.
710. Benouazzane, M.; Coco, S.; Espinet, P.; Martín-Alvarez, J. M. *J. Mater. Chem.* **1999**, 9, 2327–2332.
711. Benouazzane, M.; Coco, S.; Espinet, P.; Barberá, J. *J. Mater. Chem.* **2001**, 11, 1740–1744.

712. Coco, S.; Espinet, P.; Marcos, E. *J. Mater. Chem.* **2000**, *10*, 1297–1302.
713. Bayón, R.; Coco, S.; Espinet, P.; Fernandez-Mayordomo, C.; Martin-Alvarez, J. *Inorg. Chem.* **1997**, *36*, 2329–2334.
714. Bayón, R.; Coco, S.; Espinet, P. *Chem. Mater.* **2002**, *14*, 3515–3518.
715. Kaharu, T.; Matsubara, H.; Takahashi, S. *J. Mater. Chem.* **1991**, *1*, 145–146.
716. Kaharu, T.; Matsubara, H.; Takahashi, S. *J. Mater. Chem.* **1992**, *2*, 43–47.
717. Kaharu, T.; Matsubara, H.; Takahashi, S. *Mol. Cryst., Liq. Cryst.* **1992**, *220*, 191–199.
718. Bruce, D. W.; Lea, M. S.; Marsden, J. R.; Rourke, J. P.; Tajbakhsh, A. R. *J. Mater. Chem.* **1994**, *4*, 1017–1020.
719. Bruce, D. W.; Lea, M. S.; Marsden, J. R. *Mol. Cryst., Liq. Cryst.* **1996**, *275*, 183–194.
720. Rourke, J. P.; Bruce, D. W.; Marder, T. B. *J. Chem. Soc., Dalton Trans.* **1995**, 317–318.
721. Yang, Y. G.; Wen, J. X. *Liq. Cryst.* **1998**, *25*, 765–766.
722. Ishii, R.; Kaharu, T.; Pirio, N.; Zhang, S. W.; Takahashi, S. *J. Chem. Soc., Chem. Commun.* **1995**, 1215–1216.
723. Zhang, S. W.; Ishii, R.; Takahashi, S. *Organometallics* **1997**, *16*, 20–26.
724. Zhang, S. W.; Motoori, F.; Takahashi, S. *J. Organomet. Chem.* **1999**, *574*, 163–170.
725. Lee, K. M.; Lee, C. K.; Lin, I. J. B. *Angew. Chem. Int. Ed. Engl.* **1997**, *36*, 1850–1852.
726. Lee, C. K.; Chen, J. C. C.; Lee, K. M.; Liu, C. W.; Lin, I. J. B. *Chem. Mater.* **1999**, *11*, 1237–1242.
727. Bruce, D. W.; Dunmur, D. A.; Lalinde, E.; Maitlis, P. M.; Styring, P. *Liq. Cryst.* **1988**, *3*, 385–395.
728. Bruce, D. W.; Davis, S. C.; Dunmur, D. A.; Hudson, S. A.; Maitlis, P. M.; Styring, P. *Mol. Cryst., Liq. Cryst.* **1992**, *215*, 1–11.
729. Deschenaux, R.; Donnio, B.; Rheinwald, G.; Stauffer, F.; Suss-Fink, G.; Velker, J. *J. Chem. Soc., Dalton Trans.* **1997**, 4351–4355.
730. Bruneau, C.; Dixneuf, P. H. *Chem. Commun.* **1997**, 507–512.
731. Bruce, D. W.; Dunmur, D. A.; Esteruelas, M. A.; Hunt, S. E.; Le Lagadec, R.; Maitlis, P. M.; Marsden, J. R.; Sola, E.; Stacey, J. M. *J. Mater. Chem.* **1991**, *1*, 251–254.
732. Jeter, D. Y.; Fleischer, E. B. *J. Coord. Chem.* **1974**, *4*, 107.
733. Adams, H.; Bailey, N. A.; Bruce, D. W.; Hudson, S. A.; Marsden, J. R. *Liq. Cryst.* **1994**, *16*, 643–653.
734. Richardson, T.; Topaçlı, A.; Majid, W. H. A.; Greenwood, M. B.; Bruce, D. W.; Thornton, A.; Marsden, J. R. *Adv. Mater. Opt. Electron.* **1994**, *4*, 243–251.
735. Greenwood, M. B.; Richardson, T.; Bruce, D. W.; Taylor, D. M.; Lacey, D.; Yarwood, J. *Thin Sol. Films* **1996**, *284–285*, 46–48.
736. Bruce, D. W.; Thornton, A. *Mol. Cryst. Liq. Cryst.* **1993**, *231*, 253–256.
737. Esteruelas, M. A.; Sola, E.; Oro, L. A.; Ros, M. B.; Serrano, J. L. *J. Chem. Soc., Chem. Commun.* **1989**, 55–56.
738. Esteruelas, M. A.; Sola, E.; Oro, L. A.; Ros, M. B.; Marcos, M.; Serrano, J. L. *J. Organomet. Chem.* **1990**, *387*, 103–111.
739. Bruce, D. W.; Hall, M. D. *Mol. Cryst., Liq. Cryst.* **1994**, *250*, 373–375.
740. Lahoz, F. J.; Martin, A.; Esteruelas, M. A.; Sola, E.; Serrano, J. L.; Oro, L. A. *Organometallics* **1991**, *10*, 1794–1799.
741. Rourke, J. P.; Fanizzi, F. P.; Salt, N. J. S.; Bruce, D. W.; Dunmur, D. A.; Maitlis, P. M. *J. Chem. Soc., Chem. Commun.* **1990**, 229–231.
742. Rourke, J. P.; Fanizzi, F. P.; Bruce, D. W.; Dunmur, D. A.; Maitlis, P. M. *J. Chem. Soc., Dalton Trans.* **1992**, 3009–3014.
743. Fanizzi, F. P.; Alicino, V.; Cardellicchio, C.; Tortorella, P.; Rourke, J. P. *Chem. Commun.* **2000**, 673–674.
744. Espinet, P.; Garcia-Orodea, E.; Miguel, J. *Inorg. Chem.* **2000**, *39*, 3645–3651.
745. Espinet, P.; Miguel, J. A.; Garcia-Granda, S.; Miguel, D. *Inorg. Chem.* **1996**, *35*, 2287–2291.
746. Marcos, M.; Ros, M. B.; Serrano, J. L.; Esteruelas, M. A.; Sola, E.; Oro, L. A.; Barbera, J. *Chem. Mater.* **1990**, *2*, 748–758.
747. Sudhadevi Antharjanam, P. K.; Ajay Mallia, V.; Das, S. *Chem. Mater.* **2002**, *14*, 2687–2692.
748. Bruce, D. W.; Dunmur, D. A.; Lalinde, E.; Maitlis, P. M.; Styring, P. *Nature* **1986**, *323*, 791–792.
749. Bruce, D. W.; Dunmur, D. A.; Hudson, S. A.; Lalinde, E.; Maitlis, P. M.; McDonald, M. P.; Orr, R.; Styring, P.; Cherodian, A. S.; Richardson, R. M.; Feijoo, J. L.; Ungar, G. *Mol. Cryst., Liq. Cryst.* **1991**, *206*, 79–92.
750. Bruce, D. W.; Dunmur, D. A.; Hudson, S. A.; Maitlis, P. M.; Styring, P. *Adv. Mater. Opt. Electron.* **1992**, *1*, 37–42.
751. Bruce, D. W.; Dunmur, D. A.; Maitlis, P. M.; Styring, P.; Esteruelas, M. A.; Oro, L. A.; Ros, M. B.; Serrano, J. L.; Sola, E. *Chem. Mater.* **1991**, *1*, 479–481 *Corrigendum* **1991**, *3*, 378.
752. Adams, H.; Bailey, N. A.; Bruce, D. W.; Davis, S. C.; Dunmur, D. A.; Hempstead, P. D.; Hudson, S. A.; Thorpe, S. J. *J. Mater. Chem.* **1992**, *2*, 395–400.
753. Weissflog, W. In *Handbook of Liquid Crystals*, eds. Demus, D.; Goodby, J.; Gray, G. W.; Spiess, H.-W.; Vill, V. Wiley-VCH, Weinheim 1998, Vol. 2B, Chapter XI.
754. Bruce, D. W.; Donnio, B.; Hudson, S. A.; Levelut, A. M.; Megtert, S.; Petermann, D.; Veber, M. *J. Phys. II France* **1995**, *5*, 289–302.
755. Bruce, D. W.; Hudson, S. A. *J. Mater. Chem.* **1994**, *4*, 479–486.
756. Donnio, B.; Bruce, D. W.; Delacroix, H. Gulik-Krzywicki T. *Liq. Cryst.* **1997**, *23*, 147–153.
757. Levelut, A. M.; Donnio, B.; Bruce, D. W. *Liq. Cryst.* **1997**, *22*, 753–756.
758. Levelut, A. M.; Clerc, M. *Liq. Cryst.* **1998**, *24*, 105–115.
759. Lin, H. C.; Lai, L. L.; Lin, Y.-S.; Tsai, C.; Chen, R.-C. *Mol. Cryst. Liq. Cryst.* **2000**, *339*, 55–71.
760. Huck, D. M.; Nguyen, H.-L.; Coles, S. J.; Hursthouse, M. B.; Donnio, B.; Bruce, D. W. *J. Mater. Chem.* **2002**, *12*, 2879–2886.
761. Gallardo, H.; Magnago, R.; Bortoluzzi, A. J. *Liq. Cryst.* **2001**, *28*, 1343–1352.
762. Bruce, D. W.; Rourke, J. P. *Polyhedron* **1995**, *14*, 1915–1922.
763. Beagley, P.; Starr, E. J.; Bacsa, J.; Moss, J. R.; Hutton, A. T. *J. Organomet. Chem.* **2002**, *645*, 206–211.
764. Park, L. Y.; Rowe, J. M. *Chem. Mater.* **1998**, *10*, 1069–1075.
765. Torralba, M. C.; Cano, M.; Campo, J. A.; Heras, J. V.; Pinilla, E.; Torres, M. R. *J. Organomet. Chem.* **2001**, *633*, 91–104.
766. Torralba, M. C.; Cano, M.; Campo, J. A.; Heras, J. V.; Pinilla, E.; Torres, M. R. *J. Organomet. Chem.* **2002**, *654*, 150–161.

767. Torralba, M. C.; Cano, M.; Campo, J. A.; Heras, J. V.; Pinilla, E.; Torres, M. R. *Inorg. Chem. Comm.* **2002**, *5*, 887–890.
768. Bertram, C.; Bruce, D. W.; Dunmur, D. A.; Hunt, S. E.; Maitlis, P. M.; McCann, M. *J. Chem. Soc., Chem. Commun.* **1991**, 69–70.
769. Giroud, A. M.; Mueller-Westerhoff, U. T. *Mol. Cryst., Liq. Cryst. Lett.* **1977**, *41*, 11–13.
770. Giroud, A. M. *Ann. Phys.* **1978**, *3*, 147–150.
771. Giroud, A. M.; Nazzal, A.; Mueller-Westerhoff, U. T. *Mol. Cryst., Liq. Cryst. Lett.* **1980**, *56*, 225–228.
772. Mueller-Westerhoff, U. T.; Nazzal, A.; Cox, R. J.; Giroud, A. M. *Mol. Cryst., Liq. Cryst. Lett.* **1980**, *56*, 249–255.
773. Cotrait, M.; Gaultier, J.; Polycarpe, C.; Giroud, A. M.; Mueller-Westerhoff, U. T. *Acta Cryst. C* **1983**, *39*, 833–835.
774. McCabe, R. W.; Llyr Parri, O.; Price, A. H. *J. Mater. Chem.* **1993**, *3*, 609–613.
775. Adams, H.; Albeniz, A. C.; Bailey, N. A.; Bruce, D. W.; Cherodian, A. S.; Dhillon, R.; Dunmur, D. A.; Espinet, P.; Feijoo, J. L.; Lalinde, E.; Maitlis, P. M.; Richardson, R. M.; Ungar, G. *J. Mater. Chem.* **1991**, *1*, 843–855.
776. Ohta, K.; Ema, H.; Morizumi, Y.; Watanabe, T.; Fujimoto, T.; Yamamoto, I. *Liq. Cryst.* **1990**, *8*, 311–330.
777. Guillon, D.; Bruce, D. W.; Maldivi, P.; Ibn-Elhaj, M.; Dhillon, R. *Chem. Mater.* **1994**, *6*, 182–189.
778. Fackler, Jr, J. P.; Fetchin, J. A.; Fries, D. C. *J. Am. Chem. Soc.* **1972**, *94*, 7323.
779. Fackler, Jr, J. P.; Coucouvanis, D.; Fetchin, J. A.; Seidel, W. C. *J. Am. Chem. Soc.* **1968**, *90*, 2784.
780. Ohta, K.; Morizumi, Y.; Ema, H.; Fujimoto, T.; Yamamoto, I.; Sakurai, T. *Mol. Cryst. Liq. Cryst.* **1992**, *214*, 151–159.
781. Bonamico, M.; Mazzone, G.; Vaciago, A.; Zambonelli, L. *Acta Cryst.* **1965**, *19*, 898.
782. Iwasaki, H. *Acta Cryst. B* **1973**, *29*, 2115.
783. Iwasaki, H.; Ito, M.; Kobayashi, K. *Chem. Lett.* **1978**, 1399.
784. Domenicano, A.; Torelli, L.; Vaciago, A.; Zambonelli, L. *J. Chem. Soc. A* **1968**, 1351.
785. Bellitto, C.; Flamini, A.; Piovesana, O.; Zanazzi, P. F. *Inorg. Chem.* **1980**, *19*, 3632.
786. Bellitto, C.; Dessy, G.; Fares, V.; Flamini, A. *J. Chem. Soc., Chem. Commun.* **1981**, 4096.
787. Bellitto, C.; Bonamico, M.; Dessy, G.; Fares, V.; Flamini, A. *J. Chem. Soc., Dalton Trans.* **1987**, 35.
788. Bruce, D. W.; Dhillon, R.; Dunmur, D. A.; Maitlis, P. M. *J. Mater. Chem.* **1992**, *2*, 65–69.
789. Hu, C. C.; Liu, C. Y. *Analytica Chim. Acta* **1996**, *332*, 23–30.
790. Hoshino-Miyajima, N. *J. Chem. Soc., Chem. Commun.* **1993**, 1442–1444.
791. Price, D. J.; Wali, M. A.; Bruce, D. W. *Polyhedron* **1997**, *16*, 315–320.
792. Martínez, J. L.; Bruce, D. W.; Price, D. J.; Alonso, P. *J. Liq. Cryst.* **1995**, *19*, 127–132.
793. Mueller-Westerhoff, U. T.; Nazzal, A.; Cox, R. J.; Giroud, A. M. *J. Chem. Soc., Chem. Commun.* **1980**, 497–498.
794. Marshall, K. L.; Jacobs, S. D. *Mol. Cryst. Liq. Cryst.* **1988**, *159*, 181–196.
795. Bruce, D. W.; Dunmur, D. A.; Hunt, S. E.; Maitlis, P. M.; Orr, R. *J. Mater. Chem.* **1991**, *1*, 857–861.
796. Barral, M. C.; Jiménez-Aparicio, R.; Priego, J. L.; Royer, E. C.; Torres, M. R.; Urbanos, F. A. *Inorg. Chem. Commun.* **1999**, *2*, 153–155.
797. Chipperfield, J. R.; Clark, S.; Elliot, J.; Sinn, E. *Chem. Commun.* **1998**, 195–196.
798. Mori, A.; Takemoto, M.; Mori, R.; Takeshita, H.; Ujiie, S.; Vill, V. *Chem. Lett.* **1998**, 601–602.
799. Mori, A.; Takemoto, M.; Mori, R.; Takeshita, H.; Ujiie, S.; Vill, V. *Mol. Cryst., Liq. Cryst.* **1999**, *332*, 127–134.
800. Elliott, J. M.; Chipperfield, J. R.; Clark, S.; Teat, S. J.; Sinn, E. *Inorg. Chem.* **2002**, *41*, 293–299.
801. Blake, A. J.; Chipperfield, J. R.; Clark, S.; Nelson, P. G. *J. Chem. Soc., Dalton Trans.* **1991**, 1159–1160.
802. Salas-Reyes, V.; Soto-Garrido, G.; Aguilera, C.; Griesar, K.; Athanassopoulou, M.; Finkelmann, H.; Haase, W. *Mol. Mat.* **1994**, *3*, 297–303.
803. Blake, A. J.; Chipperfield, J. R.; Clark, S. *Inorg. Chim. Acta* **1995**, *231*, 187–190.
804. Haase, W.; Salas-Reyes, V.; Athanassopoulou, M.; Soto-Garrido, G.; Griesar, K.; Schumacher, E. *Mol. Eng.* **1994**, *3*, 321.
805. Salas-Reyes, V.; Aguilera, C. *Z. Naturforsch. B* **1995**, *50*, 205–208.
806. Blake, A. J.; Chipperfield, J. R.; Clark, S. *Mol. Cryst. Liq. Cryst.* **1996**, *275*, 305–308.
807. Salas-Reyes, V.; Soto-Garrido, G.; Aguilera, C. *Z. Naturforsch. B* **1996**, *51*, 1679–1682.
808. Paschke, R.; Balkow, D.; Letko, I.; Pezls, G. *Liq. Cryst.* **1994**, *16*, 1105–1107.
809. Cativiela, C.; Serrano, J. L.; Zurbarano, M. M. *J. Org. Chem.* **1995**, *60*, 3074–3083.
810. Wan, W.; Zhao, K.; Guan, W.; Wang, C.; Zhang, L. *Chin. J. Appl. Chem.* **1997**, *14*, 81–83.
811. Wan, W.; Zhao, K. Q.; Guan, W. J.; Yang, L. M.; Zhang, L. F. *Acta. Chim. Sinica* **1998**, *56*, 278–283.
812. Wan, W.; Guan, W. J.; Zhao, K. Q.; Zheng, W. Z.; Zhang, L. F. *J. Organomet. Chem.* **1998**, *557*, 157–161.
813. Barberá, J.; Elduque, A.; Giménez, R.; Lahoz, F. J.; López, J. A.; Oro, L. A.; Serrano, J. L.; Villacampa, B.; Villalba, J. *Inorg. Chem.* **1999**, *38*, 3085–3092.
814. Campillos, E.; Marcos, M.; Serrano, J. L.; Alonso, P. J. *J. Mater. Chem.* **1991**, *1*, 197–199.
815. Marcos, M.; Romero, P.; Serrano, J. L.; Barberá, J.; Levelut, A. M. *Liq. Cryst.* **1990**, *7*, 251–259.
816. Hanabusa, K.; Higashi, J. I.; Koyama, T.; Shira, H.; Hojo, N.; Kurose, N. *Makromol. Chem.* **1989**, *190*, 1.
817. Kuboki, T.; Araki, K.; Yamada, M.; Shiraiishi, S. *Bull. Chem. Soc. Jpn* **1994**, *67*, 948–955.
818. Bruce, D. W.; Rowe, K. E. *Liq. Cryst.* **1995**, *18*, 161–163.
819. Douce, L.; Ziessel, R.; Seghrouchni, R.; Skoulios, A.; Campillos, E.; Deschenaux, R. *Liq. Cryst.* **1995**, *18*, 157–159.
820. Douce, L.; Ziessel, R.; Seghrouchni, R.; Campillos, E.; Skoulios, A.; Deschenaux, R. *Liq. Cryst.* **1996**, *20*, 235–242.
821. Rowe, K. E.; Bruce, D. W. *Liq. Cryst.* **1996**, *20*, 183–193.
822. Okamoto, K.; Matsuoka, Y.; Wakabayashi, N.; Yamagishi, A.; Hoshino, N. *Chem. Commun.* **2002**, 282–283.
823. Rowe, K. E.; Bruce, D. W. *J. Mater. Chem.* **1998**, *8*, 331–341.
824. Rowe, K. E.; Bruce, D. W. *J. Chem. Soc., Dalton Trans.* **1996**, 3913–3915.
825. Rowe, K. E.; Bruce, D. W. *Mol. Cryst. Liq. Cryst.* **1999**, *326*, 15–40.
826. El-ghayoury, A.; Douce, L.; Skoulios, A.; Ziessel, R. *Angew. Chem. Int. Ed.* **1998**, *37*, 1255–1258.
827. Neve, F.; Ghedini, M.; Crispini, A. *Chem. Commun.* **1996**, 2463–2464.
828. Neve, F.; Ghedini, M.; Francescangeli, O.; Campagna, S. *Liq. Cryst.* **1998**, *24*, 673–680.
829. Neve, F.; Crispini, A.; Campagna, S. *Inorg. Chem.* **1997**, *36*, 6150–6156.
830. Neve, F.; Crispini, A. *Eur. J. Inorg. Chem.* **2000**, 1039–1043.
831. Morrone, S.; Harrison, G.; Bruce, D. W. *Adv. Mater.* **1995**, *7*, 665–667.

832. Morrone, S.; Guillon, D.; Bruce, D. W. *Inorg. Chem.* **1996**, *35*, 7041–7048.
833. Hoshino, N. *Coord. Chem. Rev.* **1998**, *174*, 77–108.
834. Ovchinnikov, I. V.; Galyametdinov, Yu. G.; Ivanova, G. I.; Yagfarova, L. M. *Dokl. Akad. Nauk. SSSR* **1984**, *276*, 126–128.
835. Galyametdinov, Yu. G.; Ovchinnikov, I. V.; Bolotin, B. M.; Etingen, N. B.; Ivanova, G. I.; Yagarova, L. M. *Izv. Akad. Nauk. SSSR, Ser. Khim.* **1984**, 2379.
836. Galyametdinov, Yu. G.; Ivanova, G. I.; Ovchinnikov, I. V. *Zh. Obshch. Khim.* **1984**, *54*, 2796.
837. Galyametdinov, Yu. G.; Zakieva, D. Z.; Ovchinnikov, I. V. *Izv. Akad. Nauk. SSSR Ser. Khim.* **1986**, 491.
838. Bikchantaev, I. G.; Galyametdinov, Yu. G.; Ovchinnikov, I. V. *Zh. Strukt. Khim.* **1987**, *28*, 61–67 (*J. Struct. Chem* **1988**, 685–691).
839. Galimov, R. M.; Bikchantaev, I. G.; Ovchinnikov, I. V. *Zh. Strukt. Khim.* **1989**, *30*, 65.
840. Galyametdinov, Yu. G.; Ivanova, G. I.; Bikchantaev, I. G.; Tinchurina, L. M.; Ovchinnikov, I. V. *Izv. Akad. Nauk. SSSR, Ser. Khim.* **1989**, 2833–2838 (*Bull. Acad. Sci. USSR Div. Chem. Sci.* **1989**, *38*, 2597–2602).
841. Ovchinnikov, I. V.; Galyametdinov, Yu. G.; Bikchantaev, I. G. *Izv. Akad. Nauk. SSSR, Ser. Fiz.* **1989**, *53*, 1870–1879.
842. Galyametdinov, Yu. G.; Ivanova, G. I.; Ovchinnikov, I. V. *Zh. Obshch. Khim.* **1984**, *54*, 2796.
843. Galyametdinov, Yu. G.; Bikchantaev, I. G.; Ovchinnikov, I. V. *Zh. Obshch. Khim.* **1988**, *58*, 1326–1331 (*J. Gen. Chem. USSR* **1988**, *58*, 1180–1184).
844. Roviello, A.; Sirigu, A.; Iannelli, P.; Immirzi, A. *Liq. Cryst.* **1988**, *3*, 115–122.
845. Iannelli, P.; Immirzi, A.; Caruso, U.; Roviello, A.; Sirigu, A. *Acta Cryst. C* **1989**, *45*, 879–882.
846. Marcos, M.; Romero, P.; Serrano, J. L.; Bueno, C.; Cabeza, J. A.; Oro, L. A. *Mol. Cryst. Liq. Cryst.* **1989**, *167*, 123–134.
847. Pérez-Jubindo, M. A.; De La Fuente, M. R.; Marcos, M. *Adv. Mater.* **1994**, *6*, 941–944.
848. Caruso, U.; Roviello, A.; Sirigu, A. *Liq. Cryst.* **1988**, *3*, 1515–1523.
849. Alonso, P. J.; Marcos, M.; Martínez, J. I.; Orera, V. M.; Sanjuán, M. L.; Serrano, J. L. *Liq. Cryst.* **1993**, *13*, 585–596.
850. Alonso, P. J.; Martínez, J. I.; Orera, V. M. *Liq. Cryst.* **1999**, *26*, 649–655.
851. Ghedini, M.; Armentano, S.; Bartolino, R.; Kirov, N.; Petrov, M.; Nenova, S. *J. Mol. Liq.*, **1988**, *38*, 207–213.
852. Torquati, G.; Francescangeli, O.; Ghedini, M.; Armentano, S.; Nicoletta, F. P.; Bartolino, R. *Il Nuovo Cim.* **1990**, *12*, 1363–1376.
853. Bartolino, R.; Rustichelli, F.; Scaramuzza, N.; Versace, C. C.; Ghedini, M.; Pagnotta, M. C.; Armentano, S.; Ricci, M. A.; Benassi, P. *Sol. State Commun.* **1991**, *80*, 587–590.
854. Ghedini, M.; Morrone, S.; Gatteschi, D.; Znachini, C. *Chem. Mater.* **1991**, *3*, 752–758.
855. Ghedini, M.; Armentano, S.; Bartolino, R.; Torquati, G.; Rustichelli, F. *Solid State Commun.* **1987**, *64*, 1191–1194.
856. Levelut, A. M.; Ghedini, M.; Bartolino, R.; Nicoletta, F. P.; Rustichelli, F. *J. Phys. France.* **1989**, *50*, 113–119.
857. Albertini, G.; Guido, A.; Mancini, G.; Stizza, S.; Ghedini, M.; Bartolino, R. *Europhys. Lett.* **1990**, *12*, 629–633.
858. Armentano, S.; De Munno, G.; Ghedini, M.; Morrone, S. *Inorg. Chim. Acta* **1993**, *210*, 125–127.
859. Hoshino, N.; Takahashi, K.; Sekiuchi, T.; Tanaka, H.; Matsunaga, Y. *Inorg. Chem.* **1998**, *37*, 882–889.
860. Rao, N. V. S.; Singha, D.; Das, M.; Paul, M. K. *Mol. Cryst. Liq. Cryst.* **2002**, *373*, 105–117.
861. Bilgin-Eran, B.; Yörür, Ç.; Uzman, S. *J. Organomet. Chem.* **2002**, *655*, 105–110.
862. Ghedini, M.; Morrone, S.; Bartolino, R.; Formoso, V.; Francescangeli, O.; Yang, B.; Gatteschi, D.; Znachini, C. *Chem. Mater.* **1993**, *5*, 876–882.
863. Ghedini, M.; Morrone, S.; Francescangeli, O.; Bartolino, R. *Mol. Cryst. Liq. Cryst.* **1994**, *250*, 323–332.
864. Fletcher, I. D.; Omenat, A.; Serrano, J. L. *Anal. Quim. Int. Ed.* **1998**, *94*, 226–230.
865. Fletcher, I. D.; Guillon, D.; Heinrich, B.; Omenat, A.; Serrano, J. L. *Liq. Cryst.* **1997**, *23*, 51–58.
866. Liebsch, S.; Oakley, M. A.; Paschke, R.; Sinn, E. *Inorg. Chem. Commun.* **2002**, *5*, 525–526.
867. Diaz, F. R.; Valdebenito, N.; Serrano, J. L.; Marcos, M.; Martínez, J. I.; Alonso, P. J. *Liq. Cryst.* **1998**, *25*, 217–223.
868. Hoshino-Miyajima, N.; Sekiuchi, T.; Yamazaki, W.; Sasaki, T.; Matsunaga, Y. *Mol. Cryst. Liq. Cryst.* **1996**, *286*, 311–316.
869. Marcos, M.; Serrano, J. L.; Sierra, T.; Giménez, M. J. *Angew. Chem. Int. Ed. Engl.* **1992**, *31*, 1471–1472.
870. Marcos, M.; Serrano, J. L.; Sierra, T.; Giménez, M. J. *Chem. Mater.* **1993**, *5*, 1332–1337.
871. Merino, S.; de Daran, F.; de la Fuente, M. R.; Pérez-Jubindo, M. A.; Iglesias, R.; Marcos, M. *Adv. Mater.* **1996**, *8*, 644–647.
872. Iglesias, R.; Marcos, M.; Serrano, J. L.; Sierra, T.; Pérez-Jubindo, M. A. *Chem. Mater.* **1996**, *8*, 2611–2617.
873. Ghedini, M.; Pucci, D.; Scaramuzza, N.; Komitov, L.; Lagerwall, S. T. *Adv. Mater.* **1995**, *7*, 659–662.
874. Ghedini, M.; Pucci, D.; Cesarotti, E.; Francescangeli, O.; Bartolino, R. *Liq. Cryst.* **1993**, *15*, 331–344.
875. Tian, Y.; Su, F.; Xing, P.; Zhao, Y.; Tang, X.; Zhao, X.; Zhou, E. *Liq. Cryst.* **1996**, *20*, 139–145.
876. Yelamaggad, C. V.; Hiremath, U. S.; Shankar Rao, D. S. *Liq. Cryst.* **2001**, *28*, 351–355.
877. Marcos, M.; Romero, P.; Serrano, J. L. *J. Chem. Soc., Chem. Commun.* **1989**, 1641–1643.
878. Barberá, J.; Levelut, A. M.; Marcos, M.; Romero, P.; Serrano, J. L. *Liq. Cryst.* **1991**, *10*, 119–126.
879. Martínez, J. I.; Marcos, M.; Serrano, J. L.; Orera, V. M.; Alonso, P. J. *Liq. Cryst.* **1995**, *19*, 603–613.
880. Hoshino, N.; Hayakawa, R.; Shibuya, T.; Matsunaga, Y. *Inorg. Chem.* **1990**, *29*, 5129–5131.
881. Carotenuto, M.; Iannelli, P.; Immirzi, A.; Caruso, U.; Roviello, A.; Sirigu, A. *Acta Cryst. C* **1990**, *46*, 2031–2033.
882. Caruso, U.; Roviello, A.; Sirigu, A. *Liq. Cryst.* **1990**, *7*, 421–430.
883. Caruso, U.; Roviello, A.; Sirigu, A. *Liq. Cryst.* **1990**, *7*, 431–438.
884. Caruso, U.; Roviello, A.; Sirigu, A. *Liq. Cryst.* **1991**, *10*, 85–93.
885. Hoshino, N.; Kodama, A.; Shibuya, T.; Matsunaga, Y.; Miyajima, S. *Inorg. Chem.* **1991**, *30*, 3091–3096.
886. Serrano, J. L.; Romero, P.; Marcos, M.; Alonso, P. J. *J. Chem. Soc., Chem. Commun.* **1990**, 859–861.
887. Marcos, M.; Serrano, J. L. *Adv. Mater.* **1991**, *3*, 256–257.
888. Alonso, P. J.; Sanjuan, M. L.; Romero, P.; Marcos, M.; Serrano, J. L. *J. Phys. Condens. Mater.* **1990**, *2*, 9173–9182.
889. Barberá, J.; Castel, E.; Giménez, R.; Marcos, M.; Serrano, J. L. *Mol. Cryst. Liq. Cryst.* **2001**, *362*, 89–99.
890. Galyametdinov, Yu. G.; Ivanova, G. I.; Ovchinnikov, I. V. *Izv. Akad. Nauk. SSSR, Ser. Khim.* **1989**, 1931.
891. Haase, W.; Griesar, K.; Iskander, M. F.; Galyametdinov, Yu. *Mol. Mat.* **1993**, *3*, 115–130.

892. Galyametdinov, Y.; Ivanova, G.; Griesar, K.; Prosvirin, A.; Ovchinnikov, I.; Haase, W. *Adv. Mater.* **1992**, *4*, 739–741.
893. Galyametdinov, Y.; Ksenofontov, V.; Prosvirin, A.; Ovchinnikov, I.; Ivanova, G.; Gütlich, P.; Haase, W. *Angew. Chem. Int. Ed.* **2001**, *40*, 4269–4271.
894. Pyżuk, W.; Galyametdinov, Yu. *Liq. Cryst.* **1993**, *15*, 265–268.
895. Griesar, K.; Galyametdinov, Yu.; Athanassopoulou, Ovchinnikov, I.; Haase, W. *Adv. Mater.* **1994**, *6*, 381–384.
896. Bacilieri, A.; Caruso, U.; Panunzi, B.; Roviello, A.; Sirigu, A. *Polymer* **2000**, *41*, 6423–6430.
897. Marcos, M.; Romero, P.; Serrano, J. L.; Barberá, J.; Levelut, A. M. *Liq. Cryst.* **1990**, *7*, 251–259.
898. Campillos, E.; Marcos, M.; Serrano, J. L. *J. Mater. Chem.* **1993**, *3*, 1049–1052.
899. Barberá, J.; Marcos, M.; Omenat, A.; Serrano, J. L.; Martínez, J. I.; Alonso, P. J. *Liq. Cryst.* **2000**, *27*, 255–262.
900. Donnio, B.; Barberá, J.; Giménez, R.; Guillon, D.; Marcos, M.; Serrano, J. L. *Macromolecules* **2002**, *35*, 370–381.
901. Bayle, J. P.; Bui, E.; Perez, F.; Courtieu, J. *Bull. Soc. Chim. Fr.* **1989**, *4*, 532–536.
902. Borchers, B.; Haase, W. *Mol. Cryst. Liq. Cryst.* **1991**, *209*, 319–328.
903. Marcos, M.; Romero, P.; Serrano, J. L. *Chem. Mater.* **1990**, *2*, 495–498.
904. Hoshino, N.; Murakami, H.; Matsunaga, Y.; Inabe, T.; Maruyama, Y. *Inorg. Chem.* **1990**, *29*, 1177–1181.
905. Marcos, M.; Serrano, J. L.; Alonso, P. J.; Martínez, J. I. *Adv. Mater.* **1995**, *7*, 173–176.
906. Alonso, P. J.; Marcos, M.; Martínez, J. I.; Serrano, J. L.; Sierra, T. *Adv. Mater.* **1994**, *6*, 667–670.
907. Bui, E.; Bayle, J. P.; Perez, F.; Liebert, L.; Courtieu, J. *Liq. Cryst.* **1990**, *4*, 513–526.
908. Bui, E.; Bayle, J. P.; Perez, F.; Courtieu, J. *Bull. Soc. Chim. Fr.* **1991**, *127*, 61–70.
909. Campillos, E.; Marcos, M.; Oriol, L. T.; Serrano, J. L. *Mol. Cryst. Liq. Cryst.* **1992**, *215*, 127–135.
910. Campillos, E.; Marcos, M.; Omenat, A.; Serrano, J. L. *J. Mater. Chem.* **1996**, *6*, 349–355.
911. Oriol, L.; Piñol, M.; Poelsma, S.; Serrano, J. L.; Viñuales, A. J. *Polym. Sci. A, Polym. Chem.* **2000**, *38*, 4466–4477.
912. Ghedini, M.; Panunzi, B.; Roviello, A. *Liq. Cryst.* **1998**, *25*, 225–233.
913. Campillos, E.; Marcos, M.; Serrano, J. L.; Barberá, J.; Alonso, P. J.; Martínez, J. I. *Chem. Mater.* **1993**, *5*, 1518–1525.
914. Alonso, P. J.; Martínez, J. I. *Liq. Cryst.* **1996**, *21*, 597–601.
915. Prasad, V.; Sadashiva, B. K. *Mol. Cryst. Liq. Cryst.* **1993**, *225*, 303–312.
916. Sadashiva, B. K.; Ghode, A. *Liq. Cryst.* **1994**, *16*, 33–42.
917. Prasad, V.; Sadashiva, B. K. *Mol. Cryst. Liq. Cryst.* **1994**, *241*, 167–174.
918. Athanassopoulou, M. A.; Hiller, S.; Beresnev, L. A.; Galyametdinov, Yu. G.; Schweissguth, M.; Haase, W. *Mol. Cryst. Liq. Cryst.* **1995**, *261*, 29–39.
919. Bikhantaev, I.; Galyametdinov, Yu.; Prosvirin, A.; Griesar, K.; Soto-Bustamante, E. A.; Haase, W. *Liq. Cryst.* **1995**, *18*, 231–237.
920. Reddy, K. P.; Brown, T. L. *J. Mater. Chem.* **1991**, *1*, 757–764.
921. Galyametdinov, Yu. G.; Kadkin, O. N.; Ovchinnikov, I. V. *Bull. Acad. Sci. USSR, Div. Chem. Sci.* **1990**, *39*, 2235 (*Izv. Akad. Nauk. SSSR, Ser. Khim* **1990**, 2462–2463).
922. Galyametdinov, Yu. G.; Kadkin, O. N.; Ovchinnikov, I. V. *Bull. Acad. Sci. USSR, Div. Chem. Sci.* **1992**, *41*, 316–321 (*Izv. Akad. Nauk. SSSR, Ser. Khim* **1992**, 402–407).
923. Galyametdinov, Yu. G.; Kadkin, O. N.; Prosvirin, A. V. *Russ. Chem. Bull.* **1994**, *43*, 887–891 (*Izv. Akad. Nauk. SSSR, Ser. Khim* **1990**, 941–945).
924. Berdagué, P.; Courtieu, J.; Maitlis, P. M. *J. Chem. Soc., Chem. Commun.* **1994**, 1313–1314.
925. Barberá, J.; Giménez, R.; Serrano, J. L.; Alonso, P. J.; Martínez, J. I. *Chem. Mater.* **2003**, *15*, 958–964.
926. Berdagué, P.; Perez, F.; Judeinstein, P.; Bayle, J. P. *New J. Chem.* **1995**, *19*, 293–302.
927. Perez, F.; Judeinstein, P.; Bayle, J. P. *New J. Chem.* **1995**, *19*, 1015–1017.
928. Lesot, P.; Perez, F.; Judeinstein, P.; Bayle, J. P.; Allouchi, H.; Cotrait, M. *J. Chim. Phys.* **1997**, *94*, 1695–1714.
929. Binnemans, K. *Mat. Sci. Forum* **1999**, *315–315*, 169–174.
930. Binnemans, K.; Galyametdinov, Yu. G.; Van Deun, R.; Bruce, D. W.; Collinson, S. R.; Polishchuk, A. P.; Bikhantaev, I.; Haase, W.; Prosvirin, A. V.; Tinchurina, L.; Litvinov, I.; Gubajdullin, A.; Rakhmatullin, A.; Uytterhoeven, K.; Van Meervelt, L. *J. Am. Chem. Soc.* **2000**, *122*, 4335–4344.
931. Binnemans, K.; Bruce, D. W.; Collinson, S. R.; Van Deun, R.; Galyametdinov, Yu. G.; Martin, F. *Phil. Trans. R. Soc. Lond. A* **1999**, *357*, 3063–3077.
932. Martin, F. *PhD Thesis*, University of Exeter, 2000.
933. Galyametdinov, Yu. G.; Ivanova, G. I.; Prosvirin, A. V.; Kadkin, O. *Russ. Chem. Bull.* **1994**, *43*, 938–940 (*Izv. Akad. Nauk. Ser. Khim* **1994**, 1003–1005).
934. Galyametdinov, Yu. G.; Athanassopoulou, M.; Khaaze, V.; Ovchinnikov, I. V. *Russ. J. Coord. Chem.* **21**, **1995**, 718–719 (*Koord. Khim* **1995**, *21*, 751–752).
935. Ovchinnikov, I. V.; Galyametdinov, Yu. G.; Prosvirin, A. V. *Russ. Chem. Bull.* **1995**, *44*, 768–769 (*Izv. Akad. Nauk. Ser. Khim* **1995**, 787–788).
936. Galyametdinov, Yu. G.; Ivanova, G.; Ovchinnikov, I.; Prosvirin, A.; Guillon, D.; Heinrich, B.; Dunmur, D. A.; Bruce, D. W. *Liq. Cryst.* **1996**, *20*, 831–833.
937. Turanov, A. N.; Ovchinnikov, I. V.; Galyametdinov, Yu. G.; Ivanova, G. I.; Goncharov, V. A. *Russ. Chem. Bull.* **1999**, *48*, 690–693 (*Izv. Akad. Nauk. Ser. Khim* **1999**, 694–697).
938. Binnemans, K.; Van Deun, R.; Bruce, D. W.; Galyametdinov, Yu. G. *Chem. Phys. Lett.* **1999**, *300*, 509–514.
939. Van Deun, R.; Binnemans, K. *J. Alloys Comp.* **2000**, *303–304*, 146–150.
940. Galyametdinov, Yu. G.; Athanassopoulou, M. A.; Griesar, K.; Kharitonova, O.; Soto Bustamante, E. A.; Tinchurina, L.; Ovchinnikov, I.; Haase, W. *Chem. Mater.* **1996**, *8*, 922–926.
941. Van Deun, R.; Binnemans, K. *Mater. Sci. Eng. C* **2001**, *18*, 211–215.
942. Binnemans, K.; Moors, D.; Parac-Vogt, T. N.; van Deun, R.; Hinz-Hübner, Meyer G. *Liq. Cryst.* **2002**, *29*, 1209–1216.
943. Binnemans, K.; Galyametdinov, Yu. G.; Collinson, S. R.; Bruce, D. W. *J. Mater. Chem.* **1998**, *8*, 1551–1553.
944. Galyametdinov, Yu. G.; Ivanova, G. I.; Ovchinnikov, I. V.; Binnemans, K.; Bruce, D. W. *Russ. Chem. Bull.* **1999**, *48*, 385–387 (*Izv. Akad. Nauk. Ser. Khim* **1999**, 387–389).
945. Van Deun, R.; Binnemans, K. *Liq. Cryst.* **2001**, *28*, 621–627.

946. Malykhina, L. V.; Prosvirin, A. V.; Haase, W.; Galyametdinov, Yu. G. *Russ. Chem. Bull., Int. Ed.* **2001**, *50*, 488–493 (*Izv. Akad. Nauk. Ser. Khim* **2001**, 469–474).
947. Galyametdinov, Yu. G.; Haase, W.; Malykhina, L.; Prosvirin, A.; Bikchantaev, I.; Rakmatullin, A.; Binnemans, K. *Chem. Eur. J.* **2001**, *7*, 99–105.
948. Galyametdinov, Yu. G.; Ivanova, G. I.; Ovchinnikov, I. V. *Bull. Acad. Sci. USSR, Div. Chem. Sci.* **1991**, *40*, 1109 (*Izv. Akad. Nauk. Ser. Khim* **1991**, 1232).
949. Binnemans, K.; Lodewyckx, K.; Van Deun, R.; Galyametdinov, Yu. G.; Hinz, D.; Meyer, G. *Liq. Cryst.* **2001**, *28*, 279–285.
950. Lodewyckx, K.; Van Deun, R.; Binnemans, K. *Mater. Sci. Eng. C* **2001**, *18*, 217–221.
951. Martin, F.; Collinson, S. R.; Bruce, D. W. *Liq. Cryst.* **2000**, *27*, 859–863.
952. Collinson, S. R.; Martin, F.; Binnemans, K.; Van Deun, R.; Bruce, D. W. *Mol. Cryst. Liq. Cryst.* **2001**, *364*, 745–752.
953. Mironov, V. S.; Galyametdinov, Yu. G.; Ceulemans, A.; Binnemans, K. *J. Chem. Phys.* **2000**, *113*, 10293–10303.
954. Turanov, A.; Ovchinnikov, I. V.; Galyametdinov, Yu. G.; Bruce, D. W. *Liq. Cryst.* **2001**, *28*, 845–850.
955. Binnemans, K.; Van Deun, R.; Görrler-Walrand, C.; Haase, W.; Bruce, D. W.; Malykhina, L.; Galyametdinov, Yu. G. *Mater. Sci. Eng. C* **2001**, *18*, 247–254.
956. Binnemans, K.; Malykhina, L.; Mironov, V. S.; Haase, W.; Driesen, K.; van Deun, R.; Fluyt, L.; Görrler-Walrand, C.; Galyametdinov, Yu. G. *Chem. Phys. Chem.* **2001**, 680–683.
957. Paschke, R.; Zschke, H.; Mädicke, A.; Chipperfield, J. R.; Blake, A. B.; Nelson, P. G.; Gray, G. W. *Mol. Cryst. Liq. Cryst. Lett.* **1988**, *6*, 81–85.
958. Shaffer, T. D.; Sheth, K. A. *Mol. Cryst. Liq. Cryst.* **1989**, *172*, 27–39.
959. Paschke, R.; Balkow, D.; Baumeister, U.; Hartung, H.; Chipperfield, J. R.; Blake, A. B.; Nelson, P. G.; Gray, G. W. *Mol. Cryst. Liq. Cryst.* **1990**, *188*, 105–118.
960. Ohta, K.; Morizumi, Y.; Fujimoto, T.; Yamamoto, I.; Miyamura, K.; Gohshi, Y. *Mol. Cryst. Liq. Cryst.* **1992**, *214*, 161–169.
961. Serrette, A.; Carroll, P. J.; Swager, T. M. *J. Am. Chem. Soc.* **1992**, *114*, 1887–1889. Corrigendum *J. Am. Chem. Soc.* **1993**, *115*, 11656.
962. Paschke, R.; Diele, S.; Letko, I.; Wiegeleben, A.; Pelzl, G.; Griesar, K.; Athanassopoulou, M.; Haase, W. *Liq. Cryst.* **1995**, *18*, 451–456.
963. Blake, A. B.; Chipperfield, J. R.; Hussain, W.; Paschke, R.; Sinn, E. *Inorg. Chem.* **1995**, *34*, 1125–1129.
964. Paschke, R.; Balkow, D.; Sinn, E. *Inorg. Chem.* **2002**, *41*, 1949–1953.
965. Miyamura, K.; Sato, K.; Gohshi, Y. *Bull. Chem. Soc. Jpn* **1989**, *62*, 45.
966. Sakata, I.; Miyamura, K. *Chem. Commun.* **2003**, 156–157.
967. Aiello, I.; Ghedini, M.; Neve, F.; Pucci, D. *Chem. Mater.* **1997**, *9*, 2107–2112.
968. Aiello, I.; Ghedini, M.; La Deda, M.; Pucci, D.; Francescangeli, O. *Eur. J. Inorg. Chem.* **1999**, 1367–1372.
969. Saez, I. M.; Styring, P. *Adv. Mater.* **1996**, *8*, 1001–1005.
970. Saez, I. M.; Mehl, G. H.; Sinn, E.; Styring, P. *J. Organomet. Chem.* **1998**, *551*, 299–311.
971. Mehl, G. H.; Saez, I. M. *Appl. Organometal. Chem.* **1999**, *13*, 261–272.
972. Galyametdinov, Yu. G.; Ivanova, G. I.; Ovchinnikov, I. V. *Zh. Obshch. Khim.* **1991**, *61*, 234–238.
973. Pyzuk, W.; Gorecka, E.; Krowczynski, A. *Liq. Cryst.* **1992**, *11*, 797–802.
974. Pyzuk, W.; Gorecka, E.; Krowczynski, A.; Przedmojki, J. *Liq. Cryst.* **1993**, *14*, 773–784.
975. Pyzuk, W.; Gorecka, E.; Krowczynski, A. *Mol. Cryst., Liq. Cryst.* **1994**, *249*, 17–25.
976. Galyametdinov, Yu. G.; Polishchuk, A. P.; Bikchantaev, I. G.; Ovchinnikov, I. V. *J. Struct. Chem.* **1993**, *34*, 872–878 (*Zh. Struk. Khim* **1993**, *34*, 49–55).
977. Bikchantaev, I.; Galyametdinov, Yu. G.; Prosvirin, A.; Griesar, K.; Soto-Bustamante, E. A.; Haase, W. *Liq. Cryst.* **1995**, *18*, 231–237.
978. Turanova, O. A.; Galyametdinov, Yu. G.; Ovchinnikov, I. V. *Russ. Chem. Bull., Int. Ed.* **2001**, *50*, 805–808 (*Izv. Akad. Nauk. Ser. Khim* **2001**, 771–773).
979. Szydłowska, J.; Pyzuk, W.; Krowczynski, A.; Bikchantaev, I. *J. Mater. Chem.* **1996**, *6*, 733–738.
980. Krowczynski, A.; Szydłowska, J.; Górecka, E. *Liq. Cryst.* **1999**, *26*, 685–689.
981. Kadkin, O. N.; Galyametdinov, Yu. G.; Rakmatullin, A. I.; Mavrin, V. Yu. *Russ. Chem. Bull.* **1999**, *48*, 379–381 (*Izv. Akad. Nauk., Ser. Khim* **1999**, 381–383).
982. Galyametdinov, Yu. G.; Kharitonova, O. A.; Kadkin, O. N.; Ovchinnikov, I. V. *Russ. Chem. Bull.* **1994**, *43*, 1595 (*Izv. Akad. Nauk. Ser. Khim* **1994**, 1685).
983. Kharitonova, O. A.; Prosvirin, A. V.; Galyametdinov, Yu. G.; Ovchinnikov, I. V. *Russ. Chem. Bull.* **1996**, *45*, 2213–2215 (*Izv. Akad. Nauk. Ser. Khim* **1996**, 2331–2333).
984. Bikchantaev, I.; Galyametdinov, Yu. G.; Kharitonova, O. A.; Ovchinnikov, I. V.; Bruce, D. W.; Dunmur, D. A.; Guillon, D.; Heinrich, B. *Liq. Cryst.* **1996**, *20*, 489–492.
985. Galyametdinov, Yu. G.; Yagin, P. V.; Ovchinnikov, I. V. *Bull. Acad. Sci. USSR, Div. Chem. Sci.* **1991**, *45*, 2505–2508 (*Izv. Akad. Nauk. SSSR, Ser. Khim* **1991**, 2871–2874).
986. Prajapati, A. K.; Shah, G. R. *Mol. Cryst. Liq. Cryst.* **2000**, *350*, 19–27.
987. Abser, M. N.; Bellwood, M.; Holmes, M. C.; McCabe, R. W. *J. Chem. Soc., Chem. Commun.* **1993**, 1062–1063.
988. Abser, M. N.; Bellwood, M.; Buckley, C. M.; Holmes, M. C.; McCabe, R. W. *J. Mater. Chem.* **1994**, *4*, 1173–1180.
989. Bellwood, M.; Buckley, C. M.; Holmes, M. C.; McCabe, R. W.; Cookson, P. D. *Liq. Cryst.* **1998**, *25*, 13–22.
990. Abser, M. N.; Bellwood, M.; Buckley, C. M.; Holmes, M. C.; McCabe, R. W. *Mol. Cryst. Liq. Cryst.* **1995**, *260*, 333–337.
991. Šuste, A.; Šunjic, V. *Liq. Cryst.* **1996**, *20*, 219–224.
992. Šuste, A.; Moslavac, D.; Šunjić, V. *Liq. Cryst.* **1996**, *21*, 383–388.
993. Lehmann, M.; Marcos, M.; Serrano, J. L.; Sierra, T.; Bolm, C.; Weickhardt, K.; Magnus, A.; Moll, G. *Chem. Mater.* **2001**, *13*, 4374–4381.
994. Krówczynski, A.; Pyzuk, W.; Górecka, E. *Polish. J. Chem.* **1994**, *68*, 281–285.
995. Meyer, E.; Zucco, C.; Gallardo, H. *J. Mater. Chem.* **1998**, *8*, 1351–1354.
996. Ghedini, M.; Armentano, S.; Bartolino, R.; Rustichelli, F.; Torquati, G.; Kirov, N.; Petrov, M. *Mol. Cryst. Liq. Cryst.* **1987**, *151*, 75–91.

997. Ghedini, M.; Longeri, M.; Bartolino, R. *Mol. Cryst. Liq. Cryst.* **1982**, *84*, 207–211.
998. Ghedini, M.; Licocchia, S.; Armentano, S.; Bartolino, R. *Mol. Cryst. Liq. Cryst.* **1984**, *108*, 269–275.
999. Ghedini, M.; Armentano, S.; Neve, F. *Inorg Chim Acta* **1987**, *134*, 23–24.
1000. Ghedini, M.; Armentano, S.; Neve, F. *J. Chem. Soc., Dalton Trans.* **1988**, 1565–1567.
1001. Levelut, A.; M. Veber, M.; Francescangeli, O.; Melone, S.; Ghedini, M.; Neve, F.; Nicoletta, F. P.; Bartolino, R. *Liq. Cryst.* **1995**, *19*, 241–249.
1002. Versace, C. C.; Bartolino, R.; Ghedini, M.; Neve, F.; Armentano, S.; Petrov, M.; Kirov, N. *Liq. Cryst.* **1990**, *8*, 481–487.
1003. Bartolino, R.; Coddens, G.; Rustichelli, F.; Pagnotta, M. C.; Versace, C.; Ghedini, M.; Neve, F. *Mol. Cryst. Liq. Cryst.* **1992**, *221*, 101–108.
1004. Formoso, V.; Pagnotta, M. C.; Mariani, P.; Ghedini, M.; Neve, F.; Bartolino, R.; More, M.; Pépy, G. *Liq. Cryst.* **199**, *11*, 639–654.
1005. Zhang, L.; Huang, D.; Xiong, N.; Yang, J.; Li, G.; Shu, N. *Mol. Cryst. Liq. Cryst.* **1993**, *237*, 285–297.
1006. Ghedini, M.; Pucci, D.; Cesarotti, E.; Antogniazza, P.; Francescangeli, O.; Bartolino, R. *Chem. Mater.* **1993**, *5*, 883–890.
1007. Crispini, A.; Ghedini, M.; Morrone, S.; Pucci, D.; Francescangeli, O. *Liq. Cryst.* **1996**, *20*, 67–76.
1008. Ghedini, M.; Pucci, D.; Crispini, A.; Aiello, I.; Barigelletti, F.; Gessi, A.; Francescangeli, O. *Appl. Organomet. Chem.* **1999**, *13*, 565–581.
1009. Ghedini, M.; Crispini, A. *Comments Inorg. Chem.* **1999**, *21*, 53–68.
1010. Ghedini, M.; Morrone, S.; Neve, F.; Pucci, D. *Gazz. Chim. It.* **1996**, *126*, 511–515.
1011. Ghedini, M.; Pucci, D.; Neve, F. *Chem. Commun.* **1996**, 137–138.
1012. Ghedini, M.; Pucci, D.; Calogero, G.; Barigelletti, F. *Chem. Phys. Lett.* **1997**, *267*, 341–344.
1013. Vicente, J.; Bermúdez, M. D.; Carrión, F. J.; Martínez-Nicolás, G. *J. Organomet. Chem.* **1994**, *480*, 103–109.
1014. Barigelletti, F.; Ghedini, M.; Pucci, D.; La Deda, M. *Chem. Lett.* **1999**, 297–298.
1015. Ghedini, M.; Pucci, D.; Cesarotti, E.; Francescangeli, O.; Bartolino, R. *Liq. Cryst.* **1994**, *16*, 373–380.
1016. Pucci, D.; Francescangeli, O.; Ghedini, M. *Mol. Cryst. Liq. Cryst.* **2001**, *372*, 51–68.
1017. Ghedini, M.; Neve, F.; Pucci, D. *Eur. J. Inorg. Chem.* **1998**, 501–504.
1018. Ghedini, M.; Pucci, D.; Crispini, A.; Barberio, G. *Organometallics* **1999**, *18*, 2116–2124.
1019. Ghedini, M.; Pucci, D.; Barberio, G. *Liq. Cryst.* **2000**, *27*, 1277–1283.
1020. Hoshino, N.; Hasegawa, H.; Matsunaga, Y. *Liq. Cryst.* **1991**, *9*, 267–276.
1021. Ghedini, M.; Pucci, D.; Armentano, S.; Bartolino, R.; Versace, C.; Cipparrone, G.; Scaramuzza, N. *It. Pat.* **1992**, No VE92,000,003.
1022. Cipparrone, G.; Versace, C.; Duca, D.; Pucci, D.; Ghedini, M.; Umeton, C. *Mol. Cryst. Liq. Cryst.* **1992**, *212*, 217–224.
1023. Versace, C.; Cipparrone, G.; Lucchetta, D.; Pucci, D.; Ghedini, M. *Mol. Cryst. Liq. Cryst.* **1992**, *212*, 313–318.
1024. Scaramuzza, N.; Pagnotta, M. C. *Mol. Cryst. Liq. Cryst.* **1994**, *239*, 263–267.
1025. Petrov, A. G.; Ionescu, A. T.; Versace, C.; Scaramuzza, N. *Liq. Cryst.* **1995**, *19*, 169–178.
1026. Scaramuzza, N.; Pagnotta, M. C.; Pucci, D. *Mol. Cryst. Liq. Cryst.* **1994**, *239*, 195–202.
1027. Beica, T.; Alexe-Ionescu, A. L.; Ionescu, A. T.; Miraldi, E.; Pucci, D.; Rajteri, M. *Mol. Cryst. Liq. Cryst.* **1995**, *270*, 91–100.
1028. Ionescu, A. T.; Scaramuzza, N.; Versace, C. *J. Phys. Chem. B* **1997**, *101*, 8438–8442.
1029. Ionescu, A. T.; Pucci, D.; Scaramuzza, N.; Versace, C.; Petrov, A. G.; Bartolino, R. *J. Chem. Phys.* **1995**, *103*, 5144–5148.
1030. Scaramuzza, N.; Pagnotta, M. C.; Lucchetta, D. E.; Strangi, G.; Versace, C.; Ionescu, A. T. *Mol. Cryst. Liq. Cryst.* **2000**, *339*, 83–94.
1031. Francescangeli, O.; Ferrero, C.; Pucci, D.; Ghedini, M. *Mol. Cryst. Liq. Cryst.* **2002**, *378*, 77–88.
1032. Amoddeo, A.; Bartolino, R.; Caputi, L. S.; Colavita, E.; Formoso, V.; Ghedini, M.; Oliva, A.; Pucci, D.; Versace, C. *Mol. Cryst. Liq. Cryst.* **1992**, *221*, 93–99.
1033. Versace, C.; Formoso, V.; Lucchetta, D.; Pucci, D.; Ferrero, C.; Ghedini, M.; Bartolino, R. *J. Chem. Phys.* **1993**, *98*, 8507–8513.
1034. Calucci, L.; Catalano, D.; Ghedini, M.; Jones, N. L.; Pucci, D.; Veracini, C. A. *Mol. Cryst. Liq. Cryst.* **1996**, *290*, 87–98.
1035. Calucci, L.; Forte, C.; Geppi, M.; Veracini, C. A. *Z. Naturforsch. A* **1998**, *53*, 427–435.
1036. Dong, R. Y.; Morcombe, C. R.; Calucci, L.; Geppi, M.; Veracini, C. A. *Phys. Rev. E* **2000**, *61*, 1559–1566.
1037. Omenat, A.; Ghedini, M. *J. Chem. Soc., Chem. Commun.* **1994**, 1309–1310.
1038. Ghedini, M.; Morrone, S.; Francescangeli, O.; Bartolino, R. *Chem. Mater.* **1994**, *6*, 1971–1977.
1039. Ghedini, M.; Morrone, S.; Francescangeli, O.; Bartolino, R. *Chem. Mater.* **1992**, *4*, 1119–1123.
1040. Ghedini, M.; Morrone, S.; De Munno, G.; Crispini, A. *J. Organomet. Chem.* **1991**, *415*, 281–291.
1041. Barberá, J.; Espinet, P.; Lalinde, E.; Marcos, M.; Serrano, J. L. *Liq. Cryst.* **1987**, *2*, 833–842.
1042. Ciriano, M. A.; Espinet, P.; Lalinde, E.; Ros, M. B.; Serrano, J. L. *J. Mol. Struct.* **1989**, *196*, 327–341.
1043. Buey, J.; Espinet, P. *J. Organomet. Chem.* **1996**, *507*, 137–145.
1044. Baena, M. J.; Espinet, P.; Ros, M. B.; Serrano, J. L. *J. Mater. Chem.* **1996**, *6*, 1291–1296.
1045. Marcos, M.; Ros, M. B.; Serrano, J. L. *Liq. Cryst.* **1988**, *3*, 1129–1136.
1046. Ros, M. B.; Ruiz, N.; Serrano, J. L.; Espinet, P. *Liq. Cryst.* **1991**, *9*, 77–86.
1047. Ghedini, M.; Armentano, S.; De Munno, G.; Crispini, A.; Neve, F. *Liq. Cryst.* **1990**, *8*, 739–744.
1048. Barberá, J.; Espinet, P.; Ezcurra, A.; Ros, M. B.; Serrano, J. L. *J. Am. Chem. Soc.* **1994**, *116*, 1899–1906.
1049. Castro, M.; De La Fuente, M. R.; Ros, B.; Perez Jubindo, M. A.; Serrano, J. L.; Puertolas, J. A. *Mol. Cryst. Liq. Cryst.* **1995**, *265*, 521–525.
1050. Baena, M. J.; Buey, J.; Espinet, P.; Kitzerow, H. S.; Heppke, G. *Angew. Chem. Int. Ed. Engl.* **1993**, *32*, 1201–1203.
1051. Buey, J.; Diez, G. A.; Espinet, P.; García-Granda, S.; Pérez-Carreño, E. *Eur. J. Inorg. Chem.* **1998**, 1235–1241.
1052. Buey, J.; Espinet, P.; Kitzerow, H. S.; Strauss, J. *Chem. Commun.* **1999**, 441–442.
1053. Diez, L.; Espinet, P.; Miguel, J. A. *J. Chem. Soc., Dalton Trans.* **2001**, 1189–1195.
1054. Baena, M. J.; Espinet, P.; Ros, M. B.; Serrano, J. L. *Angew. Chem. Int. Ed. Engl.* **1991**, *30*, 711–712.

1055. Omnès, L.; Timimi, B. A.; Gelbrich, T.; Hursthouse, M. B.; Luckhurst, G. R.; Bruce, D. W. *Chem. Commun.* **2001**, 2248–2249.
1056. Thompson, N. J.; Iglesias, R.; Serrano, J. L.; Baena, M. J.; Espinet, P. *J. Mater. Chem.* **1996**, *6*, 1741–1744.
1057. Huang, D. J.; Xiong, N. Y.; Yang, J.; Wang, S. M.; Li, G. N.; Zhang, L. F. *Mol. Cryst. Liq. Cryst.* **1993**, *231*, 191–198.
1058. Baena, M. J.; Espinet, P.; Ros, M. B.; Serrano, J. L.; Ezcurra, A. *Angew. Chem. Int. Ed. Engl.* **1993**, *32*, 1203–1205.
1059. Espinet, P.; Etxebarria, J.; Marcos, M.; Pérez, J.; Remon, A.; Serrano, J. L. *Angew. Chem. Int. Ed. Engl.* **1989**, *28*, 1065–1066.
1060. Thompson, N. J.; Serrano, J. L.; Baena, M. J.; Espinet, P. *Chem. Eur. J.* **1996**, *2*, 214–220.
1061. Espinet, P.; Etxebarria, J.; Folcia, C. L.; Ortega, J.; Ros, M. B.; Serrano, J. L. *Adv. Mater.* **1996**, *8*, 745–748.
1062. Kadkin, O.; Galyametdinov, Y.; Rakhmatullin, A. *Mol. Cryst. Liq. Cryst.* **1999**, *332*, 109–118.
1063. Buey, J.; Diez, L.; Espinet, P.; Kitzerow, H. S.; Miguel, J. A. *Appl. Phys. B* **1998**, *66*, 355–358.
1064. Buey, J.; Diez, L.; Espinet, P.; Kitzerow, H. S.; Miguel, J. A. *Chem. Mater.* **1996**, *8*, 2375–2381.
1065. Ortega, J.; Folcia, C. L.; Etxebarria, J.; Ros, M. B.; Miguel, J. A. *Liq. Cryst.* **1997**, *23*, 285–291.
1066. Diez, L.; Espinet, P.; Miguel, J. A.; Ros, M. B. *J. Mater. Chem.* **2002**, *12*, 3694–3698.
1067. Buey, J.; Coco, S.; Diez, L.; Espinet, P.; Martín-Alvarez, J. M.; Miguel, J. A.; García-Granda, S.; Tesouro, A.; Ledoux, I.; Zyss, J. *Organometallics* **1998**, *17*, 1750–1755.
1068. Usol'tseva, N.; Espinet, P.; Buey, J.; Serrano, J. L. *J. Mater. Chem.* **1997**, *7*, 215–219.
1069. Usol'tseva, N.; Espinet, P.; Buey, J.; Praefcke, K.; Blunk, D. *Mol. Cryst. Liq. Cryst.* **1997**, *299*, 457–465.
1070. Bruce, D. W. *Adv. Mater.* **1994**, *6*, 699–701.
1071. Bruce, D. W.; Liu, X. H. *J. Chem. Soc., Chem. Commun.* **1994**, 729–730.
1072. Bruce, D. W.; Liu, X. H. *Liq. Cryst.* **1995**, *18*, 165–166.
1073. Liu, X. H.; Heinrich, B.; Manners, I.; Guillon, D.; Bruce, D. W. *J. Mater. Chem.* **2000**, *10*, 637–644.
1074. Liu, X. H.; Manners, I.; Bruce, D. W. *J. Mater. Chem.* **1998**, *8*, 1555–1560.
1075. Liu, X. H.; Abser, M. N.; Bruce, D. W. *J. Organomet. Chem.* **1998**, *551*, 271–280. *Publisher's erratum* **1999**, *577*, 150–152.
1076. Guillevic, M. A.; Bruce, D. W. *Liq. Cryst.* **2000**, *27*, 153–156.
1077. Guillevic, M. A.; Gelbrich, T.; Hursthouse, M. B.; Bruce, D. W. *Mol. Cryst. Liq. Cryst.* **2001**, *362*, 147–170.
1078. Guillevic, M. A.; Danks, M. J.; Harries, S. K.; Collinson, S. R.; Pidwell, A. D.; Bruce, D. W. *Polyhedron* **2000**, *19*, 249–257.
1079. Guillevic, M. A.; Light, M. E.; Coles, S. J.; Gelbrich, T.; Hursthouse, M. B.; Bruce, D. W. *J. Chem. Soc., Dalton Trans.* **2000**, 1437–1445.
1080. Lydon, D. P.; Cave, G. W. V.; Rourke, J. P. *J. Mater. Chem.* **1997**, *7*, 403–406.
1081. Cave, G. W. V.; Lydon, D. P.; Rourke, J. P. *J. Organomet. Chem.* **1998**, *555*, 81–88.
1082. Saccomando, D. J.; Black, C.; Cave, G. W. V.; Lydon, D. P.; Rourke, J. P. *J. Organomet. Chem.* **2000**, *601*, 305–310.
1083. Lydon, D. P.; Rourke, J. P. *Chem. Commun.* **1997**, 1741–1742.
1084. Espinet, P.; Lalinde, E.; Marcos, M.; Perez, J.; Serrano, J. L. *Organometallics* **1990**, *9*, 555–560.
1085. Elder, R. C.; Cruca, R. D. P.; Morrison, R. F. *Inorg. Chem.* **1976**, *15*, 1623.
1086. Zhang, L.; Huang, D.; Xiong, N.; Li, G. *Chin. Chem. Lett.* **1992**, *3*, 805–806.
1087. Espinet, P.; Perez, J.; Marcos, M.; Ros, M. B.; Serrano, J. L.; Barberá, J.; Levelut, A. M. *Organometallics* **1990**, *9*, 2028–2033.
1088. Levelut, A. M. *Mol. Cryst. Liq. Cryst.* **1992**, *215*, 31–46.
1089. Ghedini, M.; Pucci, D. *J. Organomet. Chem.* **1990**, *395*, 105–112.
1090. Ghedini, M.; Pucci, D.; De Munno, G.; Viterbo, D.; Neve, F.; Armentano, S. *Chem. Mater.* **1991**, *3*, 65–72.
1091. Ghedini, M.; Pucci, D.; Bartolino, R.; Francescangeli, O. *Liq. Cryst.* **1993**, *13*, 255–263.
1092. Neumann, B.; Hegmann, T.; Wolf, R.; Tschierske, C. *Chem. Commun.* **1998**, 105–106.
1093. Slater, J. W.; Lydon, D. P.; Rourke, J. P. *J. Organomet. Chem.* **2002**, *645*, 246–255.
1094. Slater, J. W.; Lydon, D. P.; Alcock, N. W.; Rourke, J. P. *Organometallics* **2001**, *20*, 4418–4423.
1095. Leu, Y. F.; Lai, C. K. *J. Chin. Chem. Soc.* **1997**, *44*, 89–91.
1096. Lai, C. K.; Leu, Y. F. *Liq. Cryst.* **1998**, *25*, 689–698.
1097. Eguchia, S.; Nozaki, T.; Miyasaka, H.; Matsumoto, N.; Okawa, H.; Kohata, S.; Hoshino-Miyajima, N. *J. Chem. Soc., Dalton Trans.* **1996**, 1761–1766.
1098. Lai, C. K.; Lin, R.; Lu, M. Y.; Kao, K. W. *J. Chem. Soc., Dalton Trans.* **1998**, 1857–1862.
1099. Ziminski, L.; Malthête, J. *J. Chem. Soc., Chem. Commun.* **1990**, 1495–1496.
1100. Jacq, P.; Malthête, J. *Liq. Cryst.* **1996**, *21*, 291–293.
1101. Huang, D. J.; Yang, J.; Zhang, L. F.; Liu, Y.; Xiang, S. P. *Hecheng Huaxue* **1994**, *2*, 1–3.
1102. Huang, D.; Yang, J.; Wan, W.; Ding, F.; Zhang, L. *Mol. Cryst., Liq. Cryst.* **1996**, *281*, 43–49.
1103. Yang, J.; Huang, D.; Ding, F.; Zhao, W.; Zhang, L. *Mol. Cryst., Liq. Cryst.* **1996**, *281*, 51–56.
1104. Kim, D. J.; Oh, N. K.; Lee, M.; Choi, M. G. *Mol. Cryst. Liq. Cryst.* **1996**, *280*, 129–134.
1105. Malthête, J.; Billard, J. *Mol. Cryst. Liq. Cryst.* **1976**, *34*, 117–121.
1106. Loubser, C.; Imrie, C.; van Rooyen, P. H. *Adv. Mater.* **1993**, *5*, 45–47.
1107. Nakamura, N.; Hanasaki, T.; Onoi, H.; Oida, T. *Chem. Express* **1993**, *8*, 467–470.
1108. Hanasaki, T.; Ueda, M.; Nakamura, N. *Mol. Cryst. Liq. Cryst.* **1993**, *237*, 329–336.
1109. Nakamura, N.; Onoi, H.; Hanasaki, T. *Mol. Cryst. Liq. Cryst.* **1994**, *257*, 43–48.
1110. Loubser, C.; Imrie, C. *J. Chem. Soc., Perkin Trans 2* **1997**, 399–409.
1111. Seshadri, T.; Haupt, H.-J. *J. Mater. Chem.* **1998**, *8*, 1345–1350.
1112. Nakamura, N.; Setodoi, S.; Hanasaki, T. *Mol. Cryst. Liq. Cryst.* **2000**, *350*, 93–101.
1113. Nakamura, N.; Maekawahara, H.; Hanasaki, T.; Yamaguchi, T. *Mol. Cryst. Liq. Cryst.* **2000**, *352*, 125–132.
1114. Zhao, K.-Q.; Hu, P.; Xu, H.-B.; Wan, W.; Zhou, Z.-Y.; Zhang, L.-F. *Mol. Cryst. Liq. Cryst.* **2001**, *364*, 759–768.
1115. Imrie, C.; Engelbrecht, P.; Loubser, C.; McClelland, C. W. *Appl. Organomet. Chem.* **2001**, *15*, 1–15.
1116. Deschenaux, R.; Schweissguth, M.; Levelut, A.-M. *Chem. Commun.* **1996**, 1275–1276.



1117. Deschenaux, R.; Schweissguth, M.; Vilches, M.-T.; Levelut, A.-M.; Hautot, D.; Long, G. J. *Organometallics* **1998**, *18*, 5553–5559.
1118. Cruz, C.; Heinrich, B.; Ribeiro, A. C.; Bruce, D. W.; Guillon, D. *Liq. Cryst.* **2000**, *27*, 1625–1631.
1119. Turpin, F.; Guillon, D.; Deschenaux, R. *Mol. Cryst. Liq. Cryst.* **2001**, *362*, 171–175.
1120. Bhatt, J.; Fung, B. M.; Nicholas, K. M.; Poon, C.-D. *J. Chem. Soc., Chem. Commun.* **1988**, 1439–1440.
1121. Khan, M. A.; Bhatt, J. C.; Fung, B. M.; Nicholas, K. M. *Liq. Cryst.* **1989**, *5*, 285–290.
1122. Bhatt, J.; Fung, B. M.; Nicholas, K. M. *J. Organomet. Chem.* **1991**, *413*, 263–268.
1123. Singh, P.; Rausch, M. D.; Lenz, R. W. *Liq. Cryst.* **1991**, *9*, 19–26.
1124. Bhatt, J.; Fung, B. M.; Nicholas, K. M. *Liq. Cryst.* **1992**, *12*, 263–272.
1125. Reddy, K. P.; Brown, T. L. *Liq. Cryst.* **1992**, *12*, 369–376.
1126. Hanasaki, T.; Ueda, M.; Nakamura, N. *Mol. Cryst. Liq. Cryst.* **1994**, *250*, 257–267.
1127. Nakamura, N.; Mizoguchi, R.; Ueda, M.; Hanasaki, T. *Mol. Cryst. Liq. Cryst.* **1998**, *312*, 127–136.
1128. Hanasaki, T.; Matsushita, K.; Wanatabe, T.; Enomoto, S.; Sato, Y. *Mol. Cryst. Liq. Cryst.* **2000**, *351*, 103–110.
1129. Deschenaux, R.; Marendaz, J.-L.; Santiago, J. *Helv. Chim. Acta* **1993**, *76*, 865–876.
1130. Deschenaux, R.; Rama, M.; Santiago, J. *Tetrahedron Lett.* **1993**, *34*, 3293–3296.
1131. Deschenaux, R.; Marendaz, J.-L. *J. Chem. Soc., Chem. Commun.* **1991**, 909–910.
1132. Deschenaux, R.; Kosztics, I.; Marendaz, J.-L.; Stoeckli-Evans, H. *Chimia* **1993**, *47*, 206–210.
1133. Deschenaux, R.; Santiago, J.; Guillon, D.; Heinrich, B. *J. Mater. Chem.* **1994**, *4*, 679–682.
1134. Werner, A.; Friedrichsen, W. *J. Chem. Soc., Chem. Commun.* **1994**, 365–366.
1135. Donnio, B.; Seddon, J. M.; Deschenaux, R. *Organometallics* **2000**, *19*, 3077–3081.
1136. Deschenaux, R.; Kosztics, I.; Nicolet, B. *J. Mater. Chem.* **1995**, *5*, 2291–2295.
1137. Thompson, A. J.; Goodby, J. W.; Toyne, K. J. *Liq. Cryst.* **1993**, *13*, 381–402.
1138. Andersch, J.; Diele, S.; Tschierke, C. *J. Mater. Chem.* **1996**, *6*, 1465–1468.
1139. Imrie, C.; Loubser, C. *J. Chem. Soc., Chem. Commun.* **1994**, 2159–2160.
1140. Seshadri, T.; Haupt, H.-J. *Chem. Commun.* **1998**, 735–736.
1141. Deschenaux, R.; Santiago, J. *Tetrahedron Lett.* **1994**, *35*, 2169–2172.
1142. Chuard, T.; Cowling, S. J.; Fernandez-Ciurleo, M.; Jauslin, I.; Goodby, J. W.; Deschenaux, R. *Chem. Commun.* **2000**, 2109–2110.
1143. Fréchet, J. M. J.; Tomalia, D. A., Eds. *Dendrimers and Other Dendritic Polymers*; John Wiley and Sons Ltd, Chichester: UK, 2001.
1144. Newkome, G. R.; Moorefield, C. N.; Vögtle, F., Eds. *Dendrimers and Dendrons: Concepts, Syntheses, Applications*, Wiley-VCH, Weinheim: Germany, 2001.
1145. Deschenaux, R.; Serrano, E.; Levelut, A.-M. *Chem. Commun.* **1997**, 1577–1578.
1146. Chuard, T.; Deschenaux, R. *J. Mater. Chem.* **2002**, *12*, 1944–1951.
1147. Grayson, S. M.; Fréchet, J. M. J. *Chem. Rev.* **2001**, *101*, 3819–3867.
1148. Chuard, T.; Deschenaux, R. *Chimia* **2001**, *55*, 139–142.
1149. Dardel, B.; Deschenaux, R.; Even, M.; Serrano, E. *Macromolecules* **1999**, *32*, 5193–5198.
1150. Even, M.; Heinrich, B.; Guillon, D.; Guldi, D. M.; Prato, M.; Deschenaux, R. *Chem. Eur. J.* **2001**, *7*, 2595–2604.
1151. Guldi, D. M.; Maggini, M.; Scorrano, G.; Prato, M. *J. Am. Chem. Soc.* **1997**, *119*, 974–980.
1152. Deschenaux, R.; Santiago, J. *J. Mater. Chem.* **1993**, *3*, 219–220.
1153. Gaspard, S.; Maillard, P.; Billard, J. *Mol. Cryst. Liq. Cryst.* **1985**, *123*, 369–375.
1154. Sudhölter, E. J. R.; van Dijk, M.; Teunis, C. J.; Sanders, G. M.; Harkema, S.; van de Velde, G. M. H.; Schouten, P. G.; Warman, J. M. *J. Mater. Chem.* **1996**, *6*, 357–363.
1155. Bruce, D. W.; Dunmur, D. A.; Santa, L. S.; Wali, M. *J. Mater. Chem.* **1992**, *2*, 363–364.
1156. Wang, Q. M.; Bruce, D. W. *Tetrahedron Lett.* **1996**, *37*, 7641–7644.
1157. Neve, F.; Ghedini, M. *J. Incl. Phenom. Mol. Recogn. Chem.* **1993**, *15*, 259–272.
1158. Neve, F.; Ghedini, M.; Levelut, A. M.; Francescangeli, O. *Chem. Mater.* **1994**, *6*, 70–76.
1159. Neve, F.; Ghedini, M.; De Munno, G.; Levelut, A. M. *Chem. Mater.* **1995**, *7*, 688–693.
1160. Neve, F.; Ghedini, M.; Francescangeli, O. *J. Mater. Chem.* **1995**, *5*, 931–932.
1161. Blake, A. J.; Bruce, D. W.; Fallis, I. A.; Parsons, S.; Richtzenhain, H.; Ross, S. A.; Schröder, M. *Phil. Trans. R. Soc. Lond. A* **1996**, *354*, 395–414.
1162. Richtzenhain, H.; Blake, A. J.; Bruce, D. W.; Fallis, I. A.; Li, W. S.; Schröder, M. *Chem. Commun.* **2001**, 2580–2581.
1163. Neve, F.; Ghedini, M. *Inorg. Chim. Acta* **1994**, *217*, 1–2.
1164. McGregor, A.; Crayston, J. A. *Mol. Cryst. Liq. Cryst.* **1993**, *235*, 147–153.
1165. Jejurkar, C. R.; Dave, J. S.; Patel, P. R.; Menon, M. R. *Mol. Cryst. Liq. Cryst.* **2001**, *364*, 753–758.
1166. Takahashi, S.; Kariya, M.; Yakate, T.; Sonogashira, K.; Hagihara, N. *Macromolecules* **1978**, *11*, 1063.
1167. Takahashi, S.; Murata, E.; Kariya, M.; Sonogashira, K.; Hagihara, N. *Macromolecules* **1979**, *12*, 1016.
1168. Takahashi, S.; Takai, Y.; Morimoto, H.; Sonogashira, K.; Hagihara, N. *Mol. Cryst., Liq. Cryst.* **1982**, *82*, 139.
1169. Takahashi, S.; Takai, Y.; Morimoto, H.; Sonogashira, K. *J. Chem. Soc., Chem. Commun.* **1984**, 3.
1170. Težak, D.; Strajnar, F.; Milat, O.; Stubicar, M. *Prog. Coll. Polym. Sci.* **1984**, *69*, 100–105.
1171. Težak, D.; Popovic, S.; Heimer, S.; Strajnar, F. *Prog. Coll. Polym. Sci.* **1989**, *79*, 293–296.
1172. Težak, D.; Babčić, O.; Derek, V.; Galešić, M.; Heimer, S.; Hrust, V.; Ivezić, Z.; Jurković, D.; Rupčić, S.; Zelović, V. *Coll. Surf. A Phys.-chem. Eng. Aspects* **1994**, *90*, 261–270.
1173. Težak, D.; Martinis, M.; Puncec, S.; Fischer-Palkovic, I.; Strajnar, F. *Liq. Cryst.* **1995**, *19*, 159–167.
1174. Galyametdinov, Y. G.; Jervis, H. B.; Bruce, D. W.; Ginnemans, K. *Liq. Cryst.* **2001**, *28*, 1877–1879.
1175. Ueno, M.; Yamamoto, S.; Meguro, K. *J. Am. Oil Chem. Soc.* **1974**, *51*, 373–376.
1176. Le Moigne, J.; Simon, J. *J. Phys. Chem.*, **1980**, *84*, 170–177.
1177. Bassoul, P.; Simon, J. *New J. Chem.* **1996**, *20*, 1131–1136.
1178. Yashiro, M.; Matsumoto, K.; Yoshikawa, S. *Chem. Lett.* **1989**, 985–988.
1179. Bruce, D. W.; Denby, I. R.; Tiddy, G. J. T.; Watkins, J. M. *J. Mater. Chem.* **1993**, *3*, 911–916.
1180. Seddon, K. R.; Yousif, Y. Z. *Tran. Met. Chem.* **1986**, *11*, 443.
1181. Bruce, D. W.; Holbrey, J. D.; Tajbakhsh, A. R.; Tiddy, G. J. T. *J. Mater. Chem.* **1993**, *3*, 905–906.
1182. Jervis, H. B. *PhD Thesis, University of Exeter*, 1999.

1183. Israelachvili, J. N.; Mitchell, D. J.; Ninham, B. W. *J. Chem. Soc., Faraday Trans.2* **1976**, *72*, 1525–1568.
1184. Attard, G.; Glyde, J. C.; Goltner, C. G. *Nature (London)* **1995**, *378*, 366.
1185. Jervis, H. B.; Raimondi, M.; Raja, R.; Maschmeyer, T.; Seddon, J. M.; Bruce, D. W. *Chem. Commun.* **1999**, 2031–2032.
1186. Danks, M. J.; Jervis, H. B.; Nowotny, M.; Zhou, W.; Maschmeyer, T. A.; Bruce, D. W. *Catal. Lett.* **2002**, *82*, 95–98.
1187. Jervis, H. B.; Holbrey, J. D.; Pidwell, A. D.; Tiddy G. J. T. ; Bruce, D. W. in preparation.
1188. Holbrey, J. D.; Grieve, M. B.; Richardson T.; Bruce, D.W. unpublished work.
1189. Pidwell, A. D.; Jervis, H. B.; Bruce, D. W. unpublished work.
1190. Bowers, J.; Danks, M. J.; Bruce, D. W.; Heenan, R. K. *Langmuir* **2003**, *19*, 292–298.
1191. Bowers, J.; Danks, M. J.; Bruce, D. W.; Webster, J. R. P. *Langmuir* **2003**, *19*, 299–305.
1192. Menger, F. M.; Keiper, J. S. *Angew. Chem., Int. Ed.* **2000**, *39*, 1906- and references therein.
1193. Rosen, M. J.; Mathias, J. H.; Davenport, L. *Langmuir* **1999**, *15*, 7340.
1194. Holbrey, J. D.; Tiddy, G. J. T.; Bruce, D. W. *J. Chem. Soc., Dalton Trans.* **1995**, 1769–1774.
1195. Draeger, C.; Böttcher, C.; Messerschmidt, C.; Schulz, A.; Ruhlmann, L.; Siggel, U.; Hammarström, L.; Berglund-Baudin, H.; Fuhrhop, J. H. *Langmuir* **2000**, *16*, 2068–2077.
1196. Yam, V. W. W.; Li, B.; Zhu, N. *Adv. Mater.* **2002**, *14*, 719–722.
1197. Zhu, S. S.; Swager, T. M. *Adv. Mater.* **1995**, *7*, 280–283.
1198. Gaspard, S.; Hochapfel, A. R.; Viovy, R. *C. R. Acad. Sci. Ser. C* **1979**, *289*, 387–390.
1199. Gaspard, S.; Hochapfel, A.; Viovy, R. *Springer Ser. Chem. Phys.* **1980**, *11*, 298.
1200. Usol'tseva, N. V.; Bykova, V. V.; Kormilitsyn, N. M.; Ananieva, G. A.; Maizlish, V. E. *Il Nuovo Cim. D* **1990**, *12*, 1237–1242.
1201. Usol'tseva, N.; Bykova, V. V. *Mol. Cryst., Liq. Cryst.* **1992**, *215*, 89–100.
1202. eBykova, V.; Usol'tseva, N.; Ananjeva, G.; Semeikin, A.; Karmanova, T. *Mol. Cryst., Liq. Cryst.* **1995**, *265*, 651–657.
1203. Kashitsin, A.; Usol'tseva, N.; Bykova, V.; Anajeva, G.; Zhukova, L. *Mol. Cryst., Liq. Cryst.* **1995**, *260*, 595–603.
1204. Usol'tseva, N. *Mol. Cryst., Liq. Cryst.* **1996**, *288*, 201–210.
1205. Koine, N.; Iida, M.; Sakai, T.; Sakagami, N.; Kaizaki, S. *J. Chem. Soc., Chem. Commun.* **1992**, 1714–1716.
1206. Iida, M.; Sakai, T.; Koine, N.; Kaizaki, S. *J. Chem. Soc., Faraday Trans.* **1993**, *89*, 1773–1778.
1207. Imae, T.; Ikeda, T.; Iida, M.; Koine, N.; Kaizaki, S. *Langmuir* **1998**, *14*, 5631–5635.
1208. Ikeda, T.; Imae, T.; Iida, M.; Koine, N.; Kaizaki, S. *Langmuir* **2001**, *17*, 361–368.

# 7.10

## Sol–Gel Processing of Metal Compounds

U. SCHUBERT

*Technische Universität Wien, Austria*

---

7.10.1	INTRODUCTION	629
7.10.2	SOL–GEL PROCESSING OF METAL SALTS	630
7.10.2.1	Hydrolysis	631
7.10.2.2	Condensation	632
7.10.2.2.1	<i>Polycations and polyanions</i>	634
7.10.2.3	Precipitation vs. Gelation	634
7.10.2.4	Influence of the Counteranion	635
7.10.3	SOL–GEL PROCESSING OF METAL ALKOXIDES	636
7.10.3.1	Synthesis of Metal Alkoxides	636
7.10.3.1.1	<i>Synthesis from metals and alcohols</i>	636
7.10.3.1.2	<i>Synthesis from metal chlorides and alcohols or alcoholates</i>	637
7.10.3.1.3	<i>Alkoxy group interchange</i>	638
7.10.3.1.4	<i>Exchange of amido groups with alkoxy groups</i>	638
7.10.3.1.5	<i>Formation of heterometallic alkoxides</i>	638
7.10.3.2	Structures of Metal Alkoxides in Solution and the Solid State	639
7.10.3.3	Sol–Gel Processing of Metal Alkoxides	641
7.10.3.3.1	<i>Metal oxo-alkoxides</i>	643
7.10.3.3.2	<i>Nonhydrolytic sol–gel processing</i>	644
7.10.3.4	Organically Substituted Metal Alkoxides	644
7.10.3.4.1	<i>Inorganic–organic hybrid materials</i>	647
7.10.4	REFERENCES	647

---

### 7.10.1 INTRODUCTION

Sol–gel processing makes possible the synthesis of solid products by gelation rather than by crystallization or precipitation. This process can be described as the creation of an oxide network by progressive polycondensation reactions of molecular precursors in a liquid medium, or as a process to form materials via a sol, gelation of the sol, and finally removal of the solvent. Publications dealing with sol–gel processing have appeared.<sup>1–3</sup>

The terms “sol” and “gel” are defined as follows. A sol is a stable suspension of colloidal solid particles or polymers in a liquid. The particles can be amorphous or crystalline. A gel consists of a porous, three-dimensionally continuous solid network surrounding and supporting a continuous liquid phase (“wet gel”). In “colloidal” (“particulate”) gels, the network is made by agglomeration of dense colloidal particles, whereas in “polymeric” gels the particles have a polymeric substructure resulting from the aggregation of subcolloidal chemical units. In general, the sol particles can be connected by covalent bonds, van der Waals forces, or hydrogen bonds. Gels can also be formed by entanglement of polymer chains. In most sol–gel systems used for materials syntheses, gelation (formation of the gels) is due to the formation of covalent bonds and is irreversible.

Sol–gel processing proceeds in several steps: (i) hydrolysis and condensation of the molecular precursors and formation of sols; (ii) gelation (sol–gel transition); (iii) aging; and (iv) drying. There are different processing options leading from the sol to various materials. Powders can be obtained by spray-drying of a sol. Gel fibers can be drawn directly from the sol, or thin films can be prepared by standard coating technologies such as dip- or spin-coating, spraying, etc. In the latter two cases, gelation occurs during the preparation of the film or fiber due to rapid evaporation of the solvent. Gelation can also occur after a sol is cast into a mold, in which case it is possible to make monoliths of a desired shape. Drying by evaporation of the pore liquid gives rise to capillary pressure that causes shrinkage of the gel network. The resulting dried gel is called a xerogel. Compared to the original wet gel its volume is often reduced by a factor of 5 to 10. Due to the drying stress, the monolithic gel body is often destroyed and powders are obtained. When the wet gel is dried in a way that the pore and network structure of the gel is maintained even after drying, the resulting dried gel is called an “aerogel.” Aerogels are usually obtained after supercritical drying processes, in which the interface between liquid and vapor is avoided during drying, and therefore no capillary pressure exists. Dense ceramics or glasses can be obtained after heat treatment of xerogels or aerogels to a temperature high enough to cause sintering.

The advantages of sol–gel processing compared with other methods to prepare oxide-based materials are the mild reaction conditions, especially the low processing temperatures (“chimie douce”), the employment of easy to purify molecular or soluble precursors, the easy modification of the chemical composition and the texture of the final materials, and the simple processing technologies (often more similar to polymer processing than ceramic processing). A unique advantage is that, due to the low processing temperatures, organic groups can be incorporated into the final materials. The resulting materials, consisting of both organic and inorganic entities or building blocks, are called inorganic–organic hybrid materials.<sup>4–9</sup> The blending of organic and inorganic components in one material on a molecular or nanoscale level allows the development of materials with new combinations of properties. There are two types of hybrid inorganic–organic materials. Organic molecules can simply be entrapped in the inorganic gel network. Alternatively, the organic and inorganic groupings can be linked by stable chemical bonds.

The fundamental issues pertaining to sol–gel processing have been extensively investigated for silica-based systems. One reason is that network structures based on Si–O–Si bonds with no long-range order form easily because the network is only formed from corner-sharing  $[\text{SiO}_4]$  tetrahedrons. Nevertheless, any metal oxide can, in principle, be prepared by sol–gel processing. Although the overall principles of sol–gel processing are constant, there will be differences in the chemistry of the respective precursors.

There are two types of precursors:<sup>10,11</sup> inorganic precursors (metal salts) or metal–organic (alkoxide) precursors. It is not the aim of this chapter to give an overview on all materials made by sol–gel processing, but instead to discuss the chemistry of the precursors, including ways to influence their reactivity, and the basic chemistry of sol–gel processes.

### 7.10.2 SOL–GEL PROCESSING OF METAL SALTS

Compared to metal alkoxides (see Section 7.10.3), metal salts are more readily available and cheaper precursors for sol–gel processing. Metal cations,  $\text{M}^{z+}$ , in aqueous solutions are solvated by water molecules, i.e., aquo complexes  $[\text{M}(\text{H}_2\text{O})_n]^{z+}$  are formed ( $n$  = coordination number of water molecules).<sup>12</sup> To obtain gels, the aquo ligands have to be converted to M–OH (hydroxo) and eventually to M–O–M (oxo) groups. This is usually achieved by pH changes (see below), i.e., gelation is restricted to a certain pH range for a given system. This limits the control on the texture of the gels compared with alkoxide precursors. Problems can also be encountered arising from the counterions of the metal salts used (see Section 7.10.2.4).

When two heteroatoms form a bond the electronegativity difference of the atoms causes each to acquire a partial positive or negative charge,  $\delta_i$ . Livage *et al.* have developed the so-called partial charge model that makes it possible to calculate, at least qualitatively, the partial charge,  $\delta_i$ , of each atom  $\text{X}_i$  in a given molecule.<sup>11</sup> After formation of the new bond, the electronegativities of all the atoms involved have the same value, called the mean electronegativity,  $\chi_m$ . For a molecule ( $p_1\text{X}_1 \cdot p_2\text{X}_2 \cdots p_i\text{X}_i$ )  $\chi_m$  is given by

$$\chi_m = \left( \sum_i p_i \sqrt{\chi_i^0} \right) / \left( \sum_i p_i / \sqrt{\chi_i^0} \right) \quad (1)$$

where  $\chi_i^\circ$  is the electronegativity of the neutral atom  $X_i$ . The partial charge  $\delta_i$  of each atom is then given by

$$\delta_i = (\chi_m - \chi_i^\circ) / k\sqrt{\chi_i^\circ} \quad (2)$$

where  $k$  is a constant that depends on the electronegativity scale ( $k = 1.36$  for Pauling's scale).

In substitution reactions, the species with the largest partial negative charge ( $\delta^-$ ) is the nucleophile and the substituent with the largest partial positive charge ( $\delta^+$ ) is the leaving group. Nucleophilic reactions cease when the strongest nucleophile acquires a partial charge  $\delta \geq 0$ . The partial charge model does not account for the precise electronic structures, steric effects, or changes in the coordination numbers of the reactants. However, it is possible to make a reasonable estimate of the enthalpy changes involved in hydrolysis and condensation reactions.

### 7.10.2.1 Hydrolysis

Coordination of the water molecules to a metal center is a Lewis acid/base reaction in which charge is transferred from the ligands (water) to the metal. This makes a coordinated water molecule more acidic than a noncoordinated one, i.e., dissociation of a proton from a coordinated water is easier than from a noncoordinated water. Depending on the magnitude of the charge transfer, the equilibrium concentrations of aquo complexes, hydroxo species, and oxo species (Equation (3)) are different. The formation of metal hydroxide species from aquo complexes is called hydrolysis.



The general formula of any aquo/hydroxo/oxo species in Equation (3) is  $[MO_nH_{2n-h}]^{(z-h)+}$ , where  $h$  is the molar ratio of hydrolysis. For aquo complexes  $[M(H_2O)_n]^{z+}$   $h = 0$ , whereas  $h = 2n$  for metallate ions,  $[MO_n]^{(2n-z)-}$ . If  $0 < h < 2n$ , the precursor can be an oxo-hydroxo complex,  $[MO_x(OH)_{n-x}]^{(n+x-z)-}$  ( $h > n$ ), a hydroxo-aquo complex,  $[M(OH)_x(H_2O)_{n-x}]^{(z-x)+}$  ( $h < n$ ), or a hydroxo complex,  $[M(OH)_n]^{(n-z)-}$  ( $h = n$ ). The precise nature of the complex depends on the pH of the solution (a higher  $H^+$  concentration, i.e., a lower pH, shifts the equilibria in Equation (3) to the left) as well as on the charge ( $z$ ), coordination number ( $n$ ), and electronegativity ( $\chi^\circ$ ) of the metal.<sup>11</sup> All parameters that increase the electron density at the metal (e.g., low  $z$ , high  $n$ , high  $\chi^\circ$ , strongly electron-donating coligands) inhibit hydrolysis, and vice versa.

The typical effects of metal charge ( $z$ ) and pH are shown schematically in Figure 1.<sup>13</sup> The diagram can be calculated by the partial charge model and explains in a qualitative manner why the hydrolysis of low-valent cations ( $z < 4$ ) yields aquo, hydroxo, or aquo-hydroxo complexes

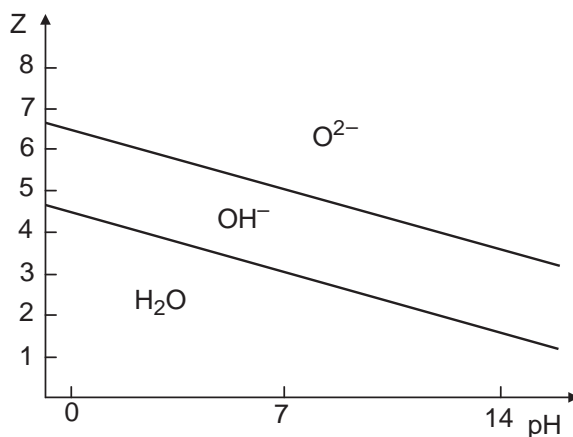


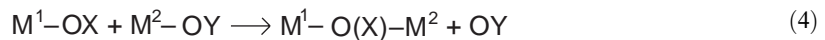
**Figure 1** Charge/pH diagram indicating the domains of aquo, hydroxo, and oxo species (reproduced by permission from *Inorganic Complexes*; Academic Press: London, 1963).

over the complete pH scale, whereas high-valent cations ( $z > 5$ ) form oxo or oxo–hydroxo complexes in the same pH range. Tetravalent metals can form any of the possible species depending on the pH.

For example, for Cr<sup>VI</sup> and V<sup>V</sup> the most acidic species are [CrO(OH)<sub>3</sub>]<sup>+</sup> and [VO(OH)(H<sub>2</sub>O)<sub>4</sub>]<sup>2+</sup>, respectively, while for Zr<sup>IV</sup> and Fe<sup>III</sup> the most acidic species are [Zr(H<sub>2</sub>O)<sub>8</sub>]<sup>4+</sup> and [Fe(H<sub>2</sub>O)<sub>6</sub>]<sup>3+</sup>. The most basic (i.e., the most deprotonated) form of Cr<sup>VI</sup> and V<sup>V</sup> is [CrO<sub>4</sub>]<sup>2-</sup> and [VO<sub>3</sub>(OH)]<sup>2-</sup>, respectively, but only [ZrO(OH)<sub>4</sub>]<sup>2-</sup> and [FeO(OH)<sub>3</sub>]<sup>2-</sup> for Zr<sup>IV</sup> and Fe<sup>III</sup> (Figure 1). Another example for the influence of  $z$ ,  $n$ , and  $\chi^\circ$  is that [Mn(H<sub>2</sub>O)<sub>6</sub>]<sup>2+</sup> ( $z = 2$ ,  $n = 6$ ) does not exhibit any acidic behavior (i.e., Equation (3) is on the left side), while HMnO<sub>4</sub> (= MnO<sub>3</sub>(OH) for  $z = 7$ ,  $n = 4$ ) is a strong acid (i.e., Equation (3) is on the right side).

### 7.10.2.2 Condensation

Condensation is initiated by nucleophilic substitution (Equation (4)) or nucleophilic addition (Equation (5)) of one of the species shown in Equation (3) to another. Nucleophilic addition requires an empty coordination site at M<sup>2</sup>. When both metals are coordinatively saturated, condensation occurs by nucleophilic substitution:



The oxygen atom in aquo ligands has no nucleophilic properties. Therefore, OX in Equations (4) and (5) can be O<sup>2-</sup> or OH<sup>-</sup>. However, O<sup>2-</sup> is a poor leaving group; therefore OY in Equation (4) will be OH<sup>-</sup> or H<sub>2</sub>O. Hydroxo complexes present at intermediate pH and intermediate  $z$  (Figure 1) contain both groups with good nucleophilic properties (O<sup>2-</sup> or OH<sup>-</sup>) as well as good leaving groups (H<sub>2</sub>O or OH<sup>-</sup>). Therefore, it is generally necessary to be in the hydroxo domain to generate condensed species. This domain can be reached from both sides, either by changing the oxidation state of the metal ( $z$ ) or the pH, i.e., by adding a base or oxidizing agent to aquo complexes [M(H<sub>2</sub>O) <sub>$n$</sub> ] <sup>$z+$</sup> , or an acid or reducing agent to metallate ions [MO <sub>$n$</sub> ]<sup>(2 $n$ - $z$ )<sup>-</sup></sup>.

The following examples illustrate the different possibilities. Nickel and cobalt hydroxide gels can be synthesized by dissolving the freshly prepared hydroxides in tartaric acid and adding KOH or NaOH.<sup>14</sup> Similar results are obtained through neutralization of Ni<sup>II</sup> acetate dissolved in glycerol with alcoholic KOH.<sup>15</sup> In the case of Co(OH)<sub>2</sub> gelation is slower, and partial oxidation to Co<sup>III</sup> takes place. Copper(II) hydroxide gels can be obtained through neutralization of copper acetate with diluted ammonia solution<sup>16,17</sup> or of CuCl<sub>2</sub> with NaOH.<sup>18</sup> ZrO<sub>2</sub>,<sup>19</sup> Nb<sub>2</sub>O<sub>5</sub>, or Ta<sub>2</sub>O<sub>5</sub> gels<sup>20</sup> can be synthesized by hydrolysis of the chlorides with ammonia. Careful washing or dialysis is sometimes necessary in order to remove the alkali metal or ammonium salts that form.

MnO<sub>2</sub> sols, colloids, and even gels are readily obtained through the reduction of KMnO<sub>4</sub> with various reducing agents.<sup>21–26</sup> Titania,<sup>27–29</sup> vanadia,<sup>30,31</sup> Nb<sub>2</sub>O<sub>5</sub>, Ta<sub>2</sub>O<sub>5</sub>,<sup>20</sup> WO<sub>3</sub>,<sup>32–37</sup> or Au<sub>2</sub>O<sub>3</sub> gels<sup>38</sup> can be made by acidifying alkali or ammonium titanate, vanadate, niobate, tantalate, tungstate, or NaAu(OH)<sub>4</sub> solutions. Acidification with a proton exchange resin is a particularly useful and easy method because it results in pure sols without washing or dialysis.<sup>30–34</sup> After protonation, and over certain concentration ranges, the solutions turn into gels mostly within a few hours.

Depending on the kind of bridging group initially formed between the metal centers, two condensation processes can be distinguished:

(i) *Olation* is a condensation process in which a *hydroxo* bridge is formed. For coordinatively saturated precursor species, olation proceeds by nucleophilic substitution. Since water is the leaving group, the kinetics of olation is related to the lability of the aquo ligand. The ability to dissociate from the metal center depends on the coordination number, electron configuration, and Lewis acidity of the metal ion (Figure 2).<sup>39–41</sup> Several types of OH bridges can be formed by olation, as shown in Equation (6).<sup>42</sup>

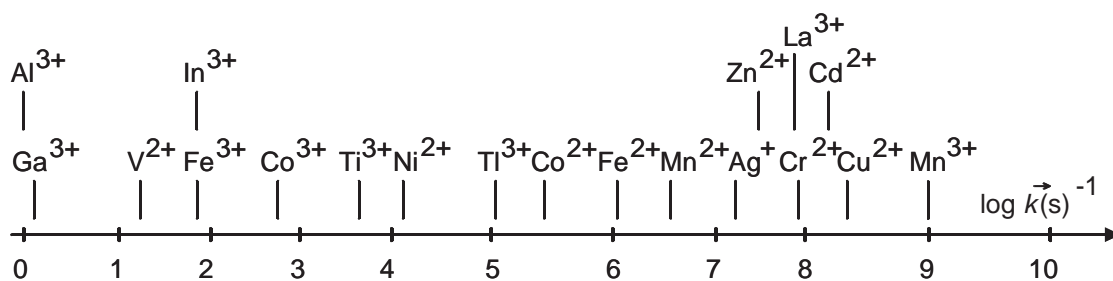
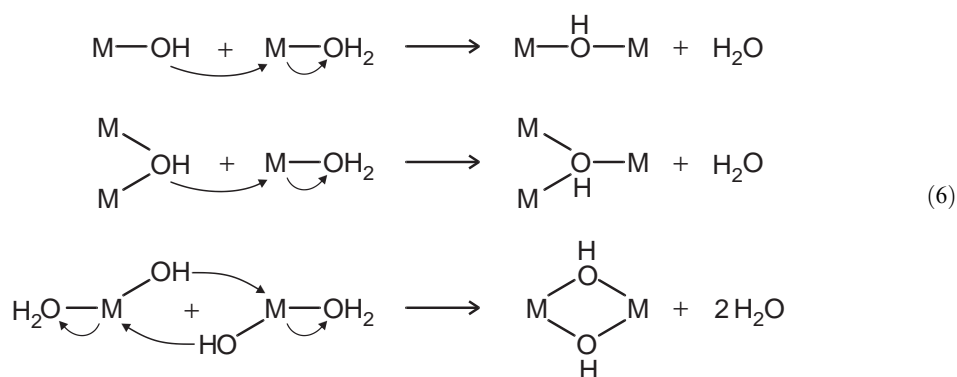
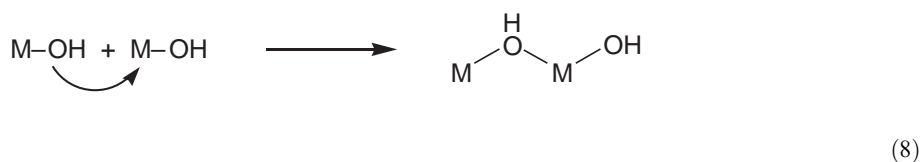
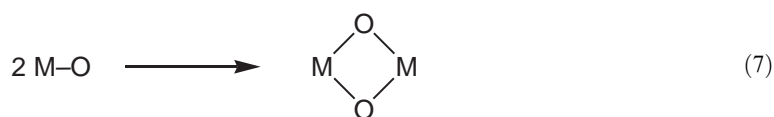


**Figure 2** Rate constants for the dissociation of an aquo ligand from complexes  $[\text{M}(\text{H}_2\text{O})_n]^{z+}$  (after Livage *et al.*<sup>11</sup>).



(ii) *Oxolation* is a condensation process in which an *oxo* bridge is formed. Such a condensation process is observed when no aquo ligand is available in the coordination sphere of the metal, i.e., for oxo-hydroxo species. There are two basic mechanisms. If the metal is coordinatively unsaturated, oxolation occurs by rapid nucleophilic addition (Equation (7)),<sup>43-46</sup> leading to chains or cycles of edge- or face-sharing polyhedrons without the removal of ligands. Otherwise, oxolation is a two-step addition/elimination process (Equation (8)). Under basic conditions, the first step is catalyzed, because a MOH group is deprotonated and the resulting  $\text{MO}^-$  is a stronger nucleophile. In the presence of an acid, the second step is catalyzed, because protonation of a terminal MOH group creates  $\text{MOH}_2^+$ , and water is a good leaving group. Thus, the rate of oxolation reactions is smallest at the isoelectric point. Owing to catalysis by both  $\text{H}^+$  and  $\text{OH}^-$ , oxolation occurs over a wider pH range than ololation.



### 7.10.2.2.1 Polycations and polyanions

Olation and oxolation reactions may stop at the stage of charged oligomers when the partial charge of the OH ligands ( $\delta_{\text{OH}}$ ) becomes zero or even positive with the extent of condensation.<sup>11</sup> As electron donating aquo ligands are removed during olation between cationic precursors  $[\text{MO}_n\text{H}_{2n-h}]^{(z-h)+}$  ( $z - h \geq 1$ ),  $\delta_{\text{OH}}$  becomes progressively less negative. Depending on the nucleophilicity of the starting compound, condensation in certain pH regimes may stop at the stage of dimers, such as  $[\text{M}_2(\text{OH})(\text{H}_2\text{O})_x]^{(2z-1)+}$  ( $\text{M} = \text{Cr}^{3+}, \text{Mn}^{2+}, \text{Co}^{2+}, \text{Ni}^{2+}$ ) or  $[\text{M}_2(\text{OH})_2(\text{H}_2\text{O})_x]^{(2z-2)+}$  ( $\text{M} = \text{Al}^{3+}, 47,48 \text{ Ga}^{3+}, 49 \text{ Ti}^{3+}, \text{VO}^{2+}, \text{Cr}^{3+}, \text{Fe}^{3+}, \text{Cu}^{2+}, 47$ ), trimers, such as  $[\text{M}_3(\text{OH})_4(\text{H}_2\text{O})_9]^{5+}$  ( $\text{M} = \text{Al}, \text{Ga}, 49 \text{ Fe}^{50-53}$ ), or tetramers, such as  $[\text{M}_4(\text{OH})_8(\text{H}_2\text{O})_{16}]^{8+}$  ( $\text{M} = \text{Zr}, \text{Hf}$ ),<sup>54,55</sup>  $[\text{Cr}_4(\text{OH})_6(\text{H}_2\text{O})_{12}]^{6+}$ ,<sup>56</sup> or  $[\text{M}_4(\text{OH})_4(\text{H}_2\text{O})_4]^{4+}$  ( $\text{M} = \text{Co}, \text{Ni}$ ).<sup>57</sup> The polycations thus formed are the products of hydrolysis and condensation in a given pH range. Further reaction can be achieved by a change of  $z$  or pH.

The polycations are often intermediates in the growth of extended structures from smaller units and their structures shed light on how condensation proceeds. One of the best studied and most stable polycations is the Keggin ion  $[\text{M}_{13}\text{O}_4(\text{OH})_{24}(\text{H}_2\text{O})_{12}]^{7+}$  ( $\text{M} = \text{Al}, 49,58-66 \text{ Ga}^{67,68}$ ). Several formation mechanisms have been proposed, all of which have the common feature that the Keggin structure is built up from smaller units such as  $[\text{M}_2(\text{OH})_2(\text{H}_2\text{O})_x]^{4+}$ ,  $[\text{M}_3(\text{OH})_4(\text{H}_2\text{O})_9]^{5+}$ , and possibly tetramers.<sup>1,69,70</sup> The ion  $[\text{Al}_{13}\text{O}_4(\text{OH})_{24}(\text{H}_2\text{O})_{12}]^{7+}$  may even condense to larger units, such as  $[\text{Al}_{30}\text{O}_8(\text{OH})_{56}(\text{H}_2\text{O})_{24}]^{18+}$ .<sup>71</sup>

*Polyanions* may be formed from oxo–hydroxo species via oxolation reactions, followed by deprotonation. The initially formed oligomers are also called polyacids. It depends on the metal at which stage of oligomerization  $\delta_{\text{OH}}$  becomes positive. For example, polycondensation of  $\text{VO}(\text{OH})_3$  ( $\delta_{\text{OH}} = -0.09$ ) stops at the stage of  $\text{V}_{10}\text{O}_{22}(\text{OH})_6$  ( $\delta_{\text{OH}} = +0.003$ ), which is spontaneously deprotonated to  $[\text{V}_{10}\text{O}_{28-x}(\text{OH})_x]^{(6-x)-}$  ( $x = 0-2$ ) in the pH range 2–6,<sup>47</sup> i.e., 10 vanadium atoms are required to make  $\delta_{\text{OH}}$  positive.

The investigation of polyacids has developed into its own branch of chemistry with considerable impact on both academic and applied research.<sup>72-74</sup> A discussion of all known polyanions would be beyond the scope of this chapter, but the reader is also directed to Chapter 7.1. Their structures are the result of balancing charges and coordination numbers.<sup>75</sup> For example, the structure of  $[\text{M}_6\text{O}_{19}]^{2-}$  ( $\text{M} = \text{Mo}, 76,77 \text{ W}^{78}$ ) consists of an octahedral arrangement of six edge-sharing  $[\text{MO}_6]$  octahedrons. The total metal charge of the six metal atoms in the +6 oxidation state is balanced by 19 oxygen atoms (oxidation state –2), resulting in a total overall charge of –2 for the polyanion. The 19 oxygen atoms must also balance 36 coordination sites as each metal atom is octahedrally coordinated. This is achieved by one  $\mu_6$ -oxygen (in the center of the polyanion), twelve  $\mu_2$ -oxygens, and six  $\mu_1$ -oxygens.

### 7.10.2.3 Precipitation vs. Gelation

Near the isoelectric point, neutral precursors ( $h = z$ ) are able to condense indefinitely via olation and/or oxolation reactions to form metal hydroxo or oxo–hydroxo species, depending on  $\delta_{\text{H}_2\text{O}}$ . When  $\delta_{\text{H}_2\text{O}} < 0$ , hydroxide products are isolated, and oxyhydroxides are formed as metastable intermediates to fully condensed metal oxides,  $\text{MO}_{z/2}$ , when  $\delta_{\text{H}_2\text{O}} > 0$ .

Whether gelation or precipitation eventually occurs is a question of the overall reaction kinetics. Whereas gels are kinetically controlled solids, crystalline precipitates form under thermodynamic control. Formation of gels therefore not only depends on the intrinsic thermodynamic and kinetic properties of a given system, but also on the reaction conditions (such as pH gradients, relative concentrations of the reactants, temperature, and speed and order of mixing the reactants). Gelation is found to be favored by slower reaction conditions.

As an example, gelation of vanadate systems depends on the solution concentration.<sup>31,79,80</sup> Decavanadic acid,  $[\text{V}_{10}\text{O}_{28-x}(\text{OH})_x]^{(6-x)-}$ , predominates below  $10^{-3} \text{ mol L}^{-1}$ . At higher concentrations, polymeric species are observed ( $M_w = 2 \times 10^6$ ), and gelation occurs if the vanadium concentration exceeds  $0.1 \text{ mol L}^{-1}$ . Decavanadic acid and fibrous polymeric species coexist at the gel point.<sup>11</sup>

The influence of reaction rates is demonstrated by the comparison of the hydrolysis and condensation behavior of  $\text{Cr}^{\text{III}}$  and  $\text{Fe}^{\text{III}}$  salts in aqueous solution. Both metals have similar electronegativities and the same coordination numbers. While green or blue-gray gels are formed when a base is added to solutions of  $\text{Cr}^{\text{III}}$  chloride, nitrate, sulfate, or acetate,<sup>81-84</sup> gelatinous precipitates are instead obtained from  $\text{Fe}^{\text{III}}$  salts.<sup>85</sup> In the case of iron, olation (nucleophilic



substitution) is much faster than in the case of  $\text{Cr}^{\text{III}}$  salts. As monolithic gels are more easily formed when the rate of condensation is slow, gels are easily formed with  $\text{Cr}^{\text{III}}$  but not with  $\text{Fe}^{\text{III}}$ .

Propylene oxide (and other epoxides) were used to promote gelation of metal salts in alcoholic solutions. It was postulated that a proton from the  $[\text{M}(\text{H}_2\text{O})]^{z+}$  ions is transferred to the epoxide, which then undergoes an irreversible ring-opening reaction with the anion of the metal salt used. The net effect is to add HX to the epoxide and thus to raise the pH of the solution slowly.<sup>86</sup> It was found that this method only applies to metal ions with  $z \geq 3$ ; the reason for this may be the lower acidity of the aquo complexes of mono- and divalent metals. Monolithic gels were obtained from lanthanide,<sup>87</sup> Al,<sup>86,88</sup> In, Ga, Zr, Hf, Ta, Nb,  $\text{Fe}^{\text{III}}$ ,  $\text{Cr}^{\text{III}}$ , and  $\text{W}^{\text{VI}}$  salts.<sup>86</sup>

There is an important structural difference between silicate systems and most transition metal systems. When a silica network grows, tetrahedral units are connected by shared corners. The question that decides on the morphology of the gels obtained is whether condensation of the tetrahedral units occurs preferentially at the end of a chain or at a central atom. In the former case, polymeric gels are obtained, and in the latter case particulate gels. For transition metal systems this issue is more complicated with the details not well understood in most cases. First, the charges of transition metals are higher than their coordination numbers (i.e.,  $z > n$ ). As a result, the polyhedrons (octahedrons, square antiprisms, etc.) must also share edges and faces to satisfy the coordination requirements of the metal (see above). This results in more compact structures and a higher tendency towards crystallization. Second, hydroxo or aquo ligands coordinated to the same metal may be chemically nonequivalent due to the effect of different *trans* ligands. For example, an aquo ligand *trans* to a  $\text{M}=\text{O}$  unit is a better leaving group than *trans* to a MOH group. The nucleophilicity of OH groups or the acidity of hydroxo and aquo ligands are also influenced by the *trans* ligands.

The gels formed from transition metal systems are not necessarily completely amorphous and can be formed from ordered substructures. For example, the polycation  $[\text{Zr}_4(\text{OH})_8(\text{OH}_2)_{16}]^{8+}$ , formed spontaneously above  $\text{pH} \approx 0$  from  $\text{Zr}^{\text{IV}}$  salts, may aggregate to produce nuclei consisting of 12–24 tetramers. Further aging can result in larger crystallites, which can themselves aggregate to give even bigger particles.<sup>89,90</sup> The growth model,<sup>90</sup> i.e., (i) generation of discrete oligomeric species, (ii) slow aggregation of these species to form stable nuclei and subsequently primary crystallites, and (iii) secondary aggregation of primary crystallites, may be common to a variety of metal oxide sols including  $\text{TiO}_2$ ,<sup>91,92</sup>  $\text{V}_2\text{O}_5$ ,<sup>79,80</sup> and  $\text{FeOOH}$ .<sup>93–95</sup>

#### 7.10.2.4 Influence of the Counteranion

The discussion up to this point has been somewhat simplistic since it has been assumed that the counteranion (X) of the metal salt precursor ( $\text{MX}_n$ ) does not interact with the metal center during hydrolysis and condensation reactions. In reality, the counterion can compete with the aquo, hydroxo, and oxo ligands for coordination to the metal center and, in many cases, strongly affects the evolving particle morphology and stability.<sup>96–100</sup> As will be discussed later for the modification of metal alkoxides with carboxylate ligands, an anionic ligand (X) may remain coordinated to the metal through all stages of the overall process and even be present in the final product.

The stability of a  $\text{M}-\text{X}$  bond in a metal complex depends on several electronic and steric factors. The complex must be stable with respect to both ionic dissociation and hydrolysis. Highly ionic bonds, prone to dissociation, are formed when the electronegativity difference  $\Delta\chi$  between M and X is high, e.g., for  $\text{X}^- = \text{ClO}_4^-$  ( $\chi_m = 2.86$ ). However, if the bond becomes more covalent (less ionic), i.e., if  $\Delta\chi$  becomes smaller, the susceptibility toward hydrolysis increases. For example, while  $\text{NiCl}_2$  (ionic  $\text{M}-\text{Cl}$  bond) dissociates in aqueous solution to give  $[\text{Ni}(\text{H}_2\text{O})_6]^{2+}$  plus  $2\text{Cl}^-$ ,  $\text{TiCl}_4$ , with covalent  $\text{M}-\text{Cl}$  bonds, readily reacts with water to give  $\text{TiO}_{2-0.5x}(\text{OH})_x$ . The latter reaction is of course a consequence of the hydrolytic instability of titanium aquo complexes, as discussed above. Only anions with mean electronegativities close to that of  $\text{H}_2\text{O}$  ( $\chi_m = 2.49$ ), such as sulfate, are able to form stable complexes over a wide pH range. Such anions strongly influence the morphology of colloids and precipitates. The stability range of the complexes can be calculated by the partial charge model.

For example, the stability range of  $\text{Ti}_x\text{X}_y$  species in aqueous solution was calculated to be  $\text{pH} < 2$  for  $\text{X} = \text{NO}_3^-$ ,  $\text{pH} < 4.5$  for  $\text{X} = \text{HSO}_4^-$ ,  $\text{pH} < 9.5$  for  $\text{X} = \text{SO}_4^{2-}$ ,  $\text{pH} 2.5\text{--}12$  for  $\text{X} = \text{HPO}_4^{2-}$ ,  $\text{pH} > 2.5$  for  $\text{X} = \text{PO}_4^{3-}$ ,  $\text{pH} > 7.5$  for  $\text{X} = \text{Cl}^-$ , or  $\text{pH} = 6.5\text{--}10.5$  for  $\text{X} = \text{acetate}$ , while  $\text{X} = \text{ClO}_4^-$  does not form stable complexes at all.<sup>101</sup> The calculations are in accordance with

the experimental observation that some anions, such as  $\text{SO}_4^{2-}$  or  $\text{PO}_4^{3-}$ , favor the formation of oligomeric metal complexes and thus lead to amorphous materials.<sup>102</sup>

Additional stabilization of M—X bonds is provided by entropic and resonance effects. Particularly stable complexes are formed with chelating multidentate ligands X (see Section 7.10.3.4). Multidentate ligands can remain coordinated to the metal in the final condensation product or can serve as network forming ligands.

Strong metal–anion interactions (coordination) can influence sol–gel processing in several ways: (i) the hydrolysis and condensation reactions may proceed differently when different salts of the same metal are employed; (ii) strong coordination of a counterion blocks coordination sites and leads to a smaller degree of condensation (fewer M—O—M links per metal atom can be formed); (iii) coordinated counterions can direct the site of nucleophilic attack (*cis* or *trans* to the coordinated X, for example) during hydrolysis and condensation reactions and thus influence the microstructure and morphology of the gels or precipitates; (iv) noncoordinated counterions may influence the electrostatic double layer of the sol particles and the ionic strength of the solution, and hence the aggregation of the sol particles; and (v) the counterions may (partially) stay in the material, and their (complete) removal may be difficult and may require special postsynthesis procedures.

An example of the influence of the counterion on the gelation behavior is the preparation of copper(II) hydroxide gels. Stable, blue gels can be obtained by neutralization of copper acetate with diluted ammonia solution in the presence of a small amount of sulfate ions. The use of the nitrate, chloride, or sulfate instead of the acetate results in gelatinous precipitates rather than gels.<sup>16,17</sup>

### 7.10.3 SOL-GEL PROCESSING OF METAL ALKOXIDES

Metal alkoxides are the second important class of precursors for the preparation of metal oxide materials by sol–gel processing. The most important differences between metal alkoxide precursors and the previously discussed metal salt precursors is that here water is only a reactant and not also a solvent. The MOH groups necessary for the condensation reactions are formed by hydrolysis of MOR groups rather than pH changes as in aqueous metal salt solutions. For sol–gel processing, the metal alkoxides are employed either neat (if they are liquids) or dissolved in an organic solvent (mostly an alcohol). Gelation is initiated by addition of a defined portion of water to the precursor solution. Alkoxide-based systems are more complex because a larger set of parameters influences the hydrolysis and condensation reactions. This gives more possibilities for controlling the morphology and properties of the obtained materials, but also requires careful optimization of the reaction conditions. Another advantage of metal alkoxides is that they can be modified by organic substituents (see below).

Since a discussion of the properties and structures of metal alkoxides is essential for an understanding of the chemical processes during hydrolytic polycondensation, a short introduction to the chemistry of metal alkoxides is given first. This overview is restricted to the alkoxides of the network forming elements relevant to sol–gel processing (i.e., alkali and alkaline earth alkoxides, organometallic alkoxides, or alkoxides with metal–metal multiple bonds are not treated) excluding silicon. Three comprehensive books on metal alkoxides have appeared.<sup>103–105</sup>

#### 7.10.3.1 Synthesis of Metal Alkoxides

It is not the intention here to discuss methods for the synthesis of metal alkoxides exhaustively but rather to give an overview of the more common procedures. All metal alkoxides are highly moisture sensitive (see Section 7.10.3.3) and care must be taken to exclude any source of water during preparation and handling of these compounds to avoid uncontrolled hydrolysis reactions.

##### 7.10.3.1.1 Synthesis from metals and alcohols

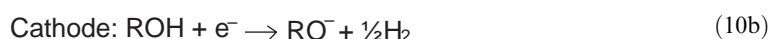
Direct reaction of metals with alcohols (Equation (9)) is restricted to the highly electropositive metals (alkali metals, alkaline earth metals, aluminum, lanthanides). An activator ( $\text{I}_2$ ,  $\text{HgCl}_2$ ,  $\text{SnCl}_4$ ) is sometimes needed, especially for less reactive metals. The facility of this reaction depends also on the acidity of the alcohol. Therefore, branched aliphatic alcohols, being less

acidic, react more slowly than their unbranched counterparts. The reactivity sequence is  $\text{MeOH} > \text{EtOH} > \text{Pr}^i\text{OH} > \text{Bu}^t\text{OH}$ . Related fluorinated alcohols are more acidic and therefore react more readily.



$\text{Al}(\text{OR})_3$ ,<sup>106–111</sup>  $\text{Ln}(\text{OPr}^i)_3$  (Ln = lanthanides),<sup>112–115</sup>  $\text{Ln}_5\text{O}(\text{OPr}^i)_{13}$  (Ln = Sc, Y, Nd, Yb),<sup>116–118</sup> and  $\text{Ta}(\text{OR})_5$  (R = Me, Et, Bu<sup>n</sup>, Pr<sup>i</sup>)<sup>119</sup> were prepared by this route.

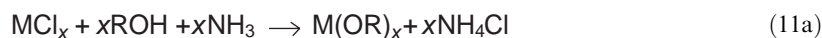
The reaction of metals with alcohols can be achieved using electrochemical methods. While the overall reaction is the same as in Equation (9), the formation of the metal alkoxides is the result of two separate electrode processes, i.e., the anodic oxidation (and dissolution) of the metal (Equation (10a)) and the cathodic formation of alkoxide ions and hydrogen (Equation (10b)).



A wide range of homoleptic alkoxides and oxo-alkoxides is accessible by this method such as  $\text{M}(\text{OR})_x$  (R = Me, Et, Bu, Pr<sup>i</sup>; M = Sc, Ln ( $x=3$ ),<sup>120</sup> Ti, Zr, Hf ( $x=4$ ), Nb,<sup>121</sup> Ta ( $x=5$ )<sup>119</sup>),  $\text{MO}(\text{OR})_4$  (R = Me, Et, Pr<sup>i</sup>; M = Mo, W),<sup>122–126</sup>  $\text{M}(\text{OCH}_2\text{CH}_2\text{OMe})_x$  (M = Ln, Zr, Hf, Nb, Ta, Fe<sup>III</sup>, Co, Ni, Sn<sup>II</sup>),<sup>127</sup>  $\text{Bi}(\text{OMe})_3$ ,<sup>128</sup>  $\text{V}(\text{OR})_3$ ,<sup>126</sup>  $\text{M}(\text{OR})_2$  (M = Fe, Co, Ni),<sup>129,130</sup>  $\text{Cu}(\text{OR})_2$  (R = Bu,  $\text{OCH}_2\text{CH}_2\text{OMe}$ ),<sup>131–133</sup>  $\text{Re}_4\text{O}_2(\text{OMe})_{16}$ ,<sup>134</sup> and  $\text{Hg}(\text{OR})_2$  (R = *n*-alkyl).<sup>135</sup>

### 7.10.3.1.2 Synthesis from metal chlorides and alcohols or alcoholates

Most metal chlorides undergo only partial metathetical halide/alkoxide exchange upon reaction with alcohols or no reaction at all even at elevated temperatures. The metal alkoxide chlorides thus obtained,  $\text{MCl}_x(\text{OR})_y$ , have not been used in sol-gel processing (see, however, Section 7.10.3.3.2). In order to achieve the preparation of homoleptic metal alkoxides from metal chlorides basic conditions are essential in order to trap the liberated HCl. This can be achieved by reaction of metal chlorides with alcohols in the presence of a base such as ammonia or, less often, trialkylamines or pyridine (Equation (11a)). The base also increases the equilibrium concentration of alkoxide ions, which are a more powerful nucleophile for reaction with the metal chloride than the parent alcohol. For this reason the use of alkali alkoxides (M'OR), mostly lithium, sodium, or potassium alkoxides, proves to be more successful (Equation (11b)). The use of LiOR has advantages for the preparation of insoluble metal methoxides because LiCl is soluble in methanol and is thus easily separated from insoluble metal alkoxides.

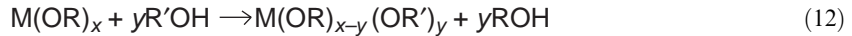


Metal alkoxides prepared by the ammonia method (Equation 11a) include  $\text{Ce}(\text{OPr}^i)_4$ ,<sup>136</sup>  $\text{Ln}[\text{OCH}(\text{CF}_3)_2]_3$ ,<sup>137</sup>  $\text{Ti}(\text{OEt})_4$ ,<sup>136,138</sup>  $\text{Zr}(\text{OR})_4$  (R = Et, Pr<sup>i</sup>, Bu, Bu<sup>s</sup>, Pr, Am),<sup>139,140</sup>  $\text{Hf}(\text{OR})_4$  (R = Et, Pr<sup>i</sup>),<sup>141,142</sup>  $\text{M}(\text{OR})_5$  (M = Nb, Ta; R = Me, Et, Pr, C<sub>4</sub>H<sub>9</sub>, C<sub>5</sub>H<sub>11</sub>),<sup>143–149</sup>  $\text{Se}(\text{OR})_4$  (R = Me, Et, CH<sub>2</sub>CF<sub>3</sub>),<sup>150,151</sup>  $\text{Te}(\text{OCH}_2\text{CF}_3)_4$ ,<sup>151</sup>  $\text{U}(\text{OCH}_2\text{CF}_3)_4$ ,<sup>152</sup> and  $\text{Pu}(\text{OPr}^i)_4$ .<sup>153</sup>

The transmetallation reaction (Equation (3b)) with alkali metal alkoxides is by far the most versatile preparative method for a wide range of metal alkoxides. Metal alkoxides of Ga,<sup>154–158</sup> In,<sup>116,154,159</sup> Ge,<sup>160,161</sup> Sn,<sup>162–164</sup> Pb,<sup>165–167</sup> As,<sup>168</sup> Sb,<sup>168–170</sup> Bi,<sup>171–177</sup> Se,<sup>150</sup> Te,<sup>151,178</sup> Ln,<sup>116,142,179–191</sup> Th,<sup>192</sup> U,<sup>193–196</sup> Np,<sup>197</sup> Ti,<sup>198</sup> V,<sup>199–201</sup> Cr,<sup>202–204</sup> Mo,<sup>205</sup> Re,<sup>206,207</sup> Fe,<sup>208,209</sup> Ni,<sup>209–211</sup> Pt,<sup>212–215</sup> and Cu<sup>216–221</sup> with different OR groups were prepared by this method. A restriction of this method is that stable heterobimetallic alkoxides of the type  $\text{M}'[\text{M}(\text{OR})_{x+1}]$  may be formed, especially when an excess of alkali metal alkoxide is used (see Section 7.10.3.1.5). For example, while  $\text{Ti}(\text{OEt})_4$  is obtained from  $\text{TiCl}_4$  and  $\text{NaOEt}$ ,<sup>198</sup>  $\text{Na}[\text{Sn}_2(\text{OEt})_9]$  is formed in the analogous reactions of  $\text{SnCl}_4$ .<sup>222</sup>

### 7.10.3.1.3 Alkoxo group interchange

An important chemical feature with high relevance to sol–gel processing is the ability of metal alkoxides to exchange alkoxo groups with alcohols (Equation (12)). This opens up the possibility of modifying the reactivity of the metal alkoxides in hydrolytic condensation reactions (see Section 7.10.3.3) starting from common precursors.



The alkoxo substituents of a variety of metal alkoxides were varied by this method, such as Al,<sup>223–225</sup> Ga,<sup>158</sup> In,<sup>159</sup> Ge,<sup>226,227</sup> Sn,<sup>228–231</sup> Sb,<sup>232</sup> Te,<sup>178</sup> Ln,<sup>136,179,185,186,191,233,234</sup> Ti,<sup>235–237</sup> Zr,<sup>238–241</sup> Hf,<sup>141</sup> V,<sup>242</sup> Nb,<sup>143,144,243–245</sup> Ta,<sup>144–147</sup> Fe,<sup>246</sup> Co,<sup>247</sup> Cu,<sup>248,249</sup> Zn,<sup>250</sup> Th,<sup>136,192,233</sup> and U.<sup>152,251,252</sup>

The alkoxo group exchange is an equilibrium reaction which can be shifted to the right side in Equation (12) by a large excess of R'OH and/or by removal of ROH by fractional distillation. Nevertheless, metal alkoxides with two different alkoxo groups ( $y \neq x$  in Equation (4)) are sometimes obtained. For example, Al(OBu<sup>1</sup>)<sub>2</sub>(OPr<sup>1</sup>) is obtained from Al(OPr<sup>1</sup>)<sub>3</sub> and Bu<sup>1</sup>OH even after fractional distillation.<sup>223</sup>

The exchange equilibrium is also shifted to the right side if the product is insoluble or less soluble than the starting alkoxide. Many methoxides are less soluble than their higher homologues; for example, when Ti(OEt)<sub>4</sub> or Ti(OPr<sup>1</sup>)<sub>4</sub> is treated with MeOH, insoluble Ti(OMe)<sub>4</sub> precipitates instantaneously.<sup>235</sup> The formation of insoluble precursors is normally an unwanted reaction in sol–gel processing. Therefore, care has to be taken in selecting the proper solvent. Solubility of the metal alkoxides is decreased with an increasing degree of association, which in turn is influenced by the size of the OR groups (see Section 7.10.3.3) and also by the solvent.

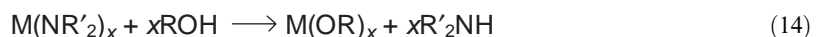
The ease of alkoxo group exchange also depends on the respective M–O and O–H bond strengths and steric factors. Alkoxo group exchange proceeds by nucleophilic attack of R'OH to the Lewis acidic metal center. Therefore, any electronic effect that increases the Lewis acidity of the metal or the Lewis basicity of the entering alcohol (relative to the leaving alcohol) facilitates the reaction.

A reaction related to the exchange of alkoxo groups by alcohols is the exchange of alkoxo groups by esters (Equation (13)), mainly acetates (R'' = Me). This is also an equilibrium reaction and is influenced by the same chemical and experimental parameters as discussed above. This method is particularly useful for the preparation of higher alkoxides due to the lower boiling point of the esters with a smaller R group. Alkoxides of Al,<sup>253</sup> Ga,<sup>158</sup> Ln,<sup>139,196,254</sup> Ti, Zr, Hf,<sup>253,255</sup> V,<sup>256</sup> Nb,<sup>257</sup> and Ta<sup>258</sup> were prepared by this method.



#### 7.10.3.1.4 Exchange of amido groups with alkoxo groups

This method is also related to the alkoxo group interchange, except than an amine is eliminated instead of an alcohol (Equation (14)). Mainly dialkylamido and bis(trimethylsilyl) amido groups have been employed. This method is particularly useful for metals with stronger M–O than M–N bonds, where the exchange equilibrium is strongly shifted to the metal alkoxide side. If necessary, the amine can be distilled off, as discussed for the alkoxo group interchange (Section 7.10.3.1.3). This method is mainly used for the synthesis of metal alkoxides that are otherwise difficult to prepare. Metal oxides of Al,<sup>259,260</sup> In,<sup>261</sup> Ge,<sup>262</sup> Sn,<sup>162,262</sup> Pb,<sup>166,263</sup> Bi,<sup>175,177</sup> Ln,<sup>114,264–277</sup> U,<sup>195,278</sup> Zr,<sup>142,199</sup> V, Nb, Ta,<sup>199,202</sup> Cr,<sup>199,202,279–281</sup> Mo,<sup>282</sup> W,<sup>283,284</sup> Mn,<sup>204,285,286</sup> Co,<sup>286,287</sup> Pt,<sup>288</sup> Zn,<sup>289</sup> and Cd<sup>290</sup> were prepared by this route.

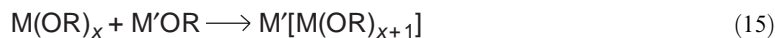


#### 7.10.3.1.5 Formation of heterometallic alkoxides

When two different metal alkoxides are mixed, two different reactions may occur: (i) formation of heterometallic alkoxides (also called polymetallic alkoxides (bi-, tri-, etc.), double alkoxides, or

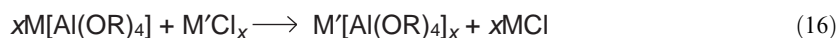
mixed alkoxides) in which the different metal atoms are bridged by alkoxo groups, or (ii) exchange of the alkoxo groups. The latter reaction involves the intermediate formation of heterometallic alkoxides. Heterometallic alkoxides may be divided in three classes: (i) those existing only in solution where they are appreciably dissociated, (ii) those being stable but that dissociate when heated under reduced pressure, and (iii) those that can be distilled or sublimed without dissociation. The latter class is subject to particular interest as single-source precursors for sol-gel-derived ceramic materials. Several review articles on heterometallic alkoxides have been published.<sup>291–295</sup>

For the simplest case, an alkali alkoxide (M'OR) is reacted with an alkoxide of a less electro-positive metal (M(OR)<sub>x</sub>) to give the compounds M'[M(OR)<sub>x+1</sub>] (Equation (15)) or, less often, M'[M<sub>2</sub>(OR)<sub>2x+1</sub>] (M = B,<sup>296</sup> Al,<sup>297–299</sup> Sn,<sup>300–303</sup> Sb,<sup>304,305</sup> Bi,<sup>305</sup> Ti,<sup>306,307</sup> Zr,<sup>142,306,308–310</sup> Ta,<sup>311</sup> Nb,<sup>311–316</sup> Cu,<sup>317</sup> Zn<sup>250</sup>).

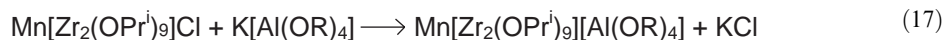


In place of alkaline metal alkoxides, alkoxides of other metals can be employed, e.g., the heterometallic alkoxides of the type M(OPr<sup>i</sup>)<sub>x-y</sub>[Al(OPr<sup>i</sup>)<sub>4</sub>]<sub>y</sub> (M = In,<sup>154</sup> Ln,<sup>318–320</sup> Hf,<sup>321,322</sup> Nb, Ta<sup>323</sup>) or M(OBu<sup>t</sup>)<sub>2</sub> (M = Ge, Sn, Pb).<sup>300</sup>

Mixed alkoxides of sodium and potassium can be used to prepare other bimetallic alkoxides by transmetallation with metal chlorides. In particular, M[Al(OR)<sub>4</sub>] (Equation (16), M' = In,<sup>154</sup> Ga,<sup>324</sup> Sn,<sup>325,326</sup> Ln,<sup>318–320</sup> Cr,<sup>327</sup> Mn,<sup>328</sup> Fe,<sup>329–331</sup> Co,<sup>332–334</sup> Ni,<sup>333–335</sup> Cu,<sup>333,334,336</sup> U,<sup>337</sup> Zn,<sup>338,339</sup> Cd, Hg<sup>338</sup>), M[Nb/Ta(OPr<sup>i</sup>)<sub>6</sub>] (M' = Cr,<sup>340</sup> Mn,<sup>328</sup> Fe,<sup>341,342</sup> Co,<sup>343</sup> Ni,<sup>344</sup> Cu<sup>345</sup>), and M[Zr<sub>2</sub>(OPr<sup>i</sup>)<sub>9</sub>] (M' = Fe,<sup>346,347</sup> Co,<sup>348</sup> Ni,<sup>349</sup> Cu<sup>350</sup>) (M = Na, K) were used for this purpose.



Tri- and even tetrametallic alkoxides can be prepared by the stepwise substitution of chloride ions by two different [M(OR)<sub>x</sub>]<sup>-</sup> anions.<sup>338,351–360</sup> An example is given in Equation (17).



### 7.10.3.2 Structures of Metal Alkoxides in Solution and the Solid State

An important structural feature of metal alkoxides [M(OR)<sub>x</sub>]<sub>n</sub> is the degree of aggregation (*n*), also called “molecular complexity.” Many physical properties as well as the chemical reactivity of the metal alkoxides are influenced by the degree of aggregation. The reason for aggregation is that the preferred coordination number (c.n.) of a particular metal is higher than its valency (*x*), which results in unoccupied coordination sites in the nonaggregated monomers. Because of the high Lewis acidity of the metal centers and the Lewis basicity of the alkoxo groups, alkoxo bridges may form between two or three metal centers. The degree of aggregation increases (i) as the metal becomes more Lewis acidic, (ii) with increasing coordination number of the metal, (iii) with decreasing size of the alkoxo ligands, i.e., smaller alkyl substituents,<sup>226,227,240,361</sup> and, sometimes, (iv) with increasing concentration. For example, the average degree of association of the isomeric OC<sub>5</sub>H<sub>11</sub> derivatives of Ti(OR)<sub>4</sub> (preferred c.n. of Ti is 6), Zr(OR)<sub>4</sub> (c.n. 7 or 8),<sup>240</sup> and Al(OR)<sub>3</sub> (c.n. 4 or 6)<sup>224</sup> was investigated. For Al(OC<sub>5</sub>H<sub>11</sub>)<sub>3</sub>, *n* decreases from 4 to ~2 as the branching increases, for Ti(OC<sub>5</sub>H<sub>11</sub>)<sub>4</sub> from 1.4 to 1, and for Zr(OC<sub>5</sub>H<sub>11</sub>)<sub>4</sub> from ~3.5 to 1. The low volatility and solubility of most metal methoxides is to a large extent due to the small size of the methyl groups resulting in high *n*. A donor functionality incorporated into the alkoxo group (e.g., OCH<sub>2</sub>CH<sub>2</sub>OR) may also increase *n*.

If the alkoxo groups are not too bulky, the preferred coordination number of the metal is satisfied by formation of a sufficient number of μ<sub>2</sub> or μ<sub>3</sub> alkoxo bridges. For example, in a monomeric Ti(OR)<sub>4</sub> (preferred c.n. of Ti is 6), only four coordination sites would be occupied by monodentate alkoxo ligands. All titanium atoms reach their optimal c.n. by formation of a tetrameric structure with two μ<sub>3</sub>-OEt and four μ<sub>2</sub>-OEt ligands, as found in the seminal structure of [Ti(OR)<sub>4</sub>]<sub>4</sub> (R = Me, Et,<sup>362</sup> Figure 3).

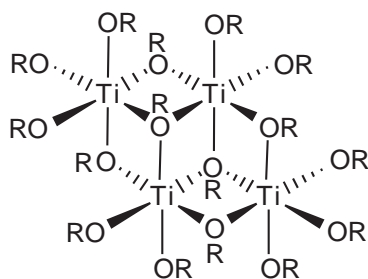


Figure 3 Structure of  $[\text{Ti}(\text{OR})_4]_4$ .

As will be discussed in more detail below, the reactivity of metal alkoxides towards water is influenced by  $n$ . It must be pointed out, however, that the degree of association found in the solid-state structures does not necessarily correspond to that in solution. In solution, equilibria between differently associated species may exist and, more importantly, polar solvents may interact with the metal atoms and thus reduce the degree of association. For example,  $\text{M}(\text{OPr}^i)_4$  ( $\text{M} = \text{Ce}$ ,<sup>233</sup>  $\text{Zr}$ ,<sup>142</sup>  $\text{Hf}$ <sup>363</sup>) crystallizes from isopropanol as  $[\text{Zr}(\text{OPr}^i)_4(\text{Pr}^i\text{OH})]_2$ , where each zirconium atom is six-coordinate and contains a coordinated propanol molecule (Figure 4). The stability of the solvent adducts increases with the positive charge at the metal atom and with increasing c.n. Therefore,  $\text{Ti}(\text{OEt})_4(\text{EtOH})$  can only be observed in solution at low temperature,<sup>364</sup> and no solvates are known for  $\text{Si}(\text{OR})_4$ . The degree of association is also lowered by the addition of strong bases, such as pyridine, which coordinate to the metal. However, such base adducts do not play a role in sol-gel chemistry.

In the following, some experimentally determined average degrees of association ( $n$ ) in solution are given and compared with X-ray structure determinations, where these are available.

*Trivalent metals.*  $\text{Al}(\text{OR})_3$ : freshly distilled  $\text{Al}(\text{OPr}^i)_3$  is trimeric in benzene, but it becomes tetrameric on aging;  $\text{Al}(\text{O}i\text{Bu})_3$  is dimeric.<sup>223,225,365-367</sup> Crystalline  $\text{Al}(\text{OPr}^i)_3$  is tetrameric with 4- and 6-coordinate aluminum atoms.<sup>111,368</sup>  $\text{Ga}(\text{OR})_3$  (in benzene): the methoxide is an insoluble polymer;  $n = 4$  for  $\text{R} = \text{Et}$  and higher  $n$ -alkyl;<sup>158</sup>  $n = 2$  for  $\text{R} = \text{Pr}^i$  and  $\text{Bu}^t$ .<sup>158,369</sup>  $\text{Sb}(\text{OMe})_3$ <sup>370</sup> and  $\text{Bi}(\text{OCH}_2\text{CH}_2\text{OMe})_3$ <sup>175,177</sup> have polymeric structures in the solid state, while  $\text{Bi}_2(\text{OCH}_2\text{Bu}^t)_6$  ( $\text{Bu}^t\text{OH}$ )<sub>2</sub> is dimeric.<sup>371</sup>  $\text{Ln}(\text{OR})_3$ :  $\text{Ln}(\text{OPr}^i)_3$ :  $n > 4$ ;<sup>185,186,191</sup>  $\text{Ln}(\text{OCH}_2\text{Bu}^t)_3$  ( $\text{Ln} = \text{La}, \text{Nd}$ ) is tetrameric in the solid state,<sup>273</sup>  $\text{La}(\text{O}i\text{Bu})_3$  and  $\text{Ce}(\text{OPr}^i)_3$  are solvated oligomers ( $\text{La}_3(\text{O}i\text{Bu})_9$  ( $\text{Bu}^t\text{OH}$ )<sub>2</sub> and  $\text{Ce}_2(\text{OPr}^i)_8(\text{Pr}^i\text{OH})_2$ <sup>372</sup>),  $\text{La}(\text{OCPh}_3)_3$ ,<sup>273</sup>  $\text{Ce}(\text{OCHBu}^t)_3$ ,<sup>274</sup> and  $\text{Lu}(\text{OCH}_2\text{CH}_2\text{OMe})_3$ <sup>275</sup> are dimers, and  $\text{Y}(\text{OCH}_2\text{CH}_2\text{OMe})_3$  forms a decameric ring.<sup>115</sup> Crystalline  $\text{Cr}(\text{OCH}_2\text{CH}_2\text{OMe})_3$  is monomeric.<sup>373</sup>

*Tetravalent metals.*  $\text{Sn}(\text{OR})_4$  (in benzene):  $n = 3$  for  $\text{R} = \text{Et}$ ;  $n = 1.5$  for  $\text{R} = \text{Pr}^i$ ;  $n = 1$  for  $\text{R} = \text{Bu}^t$ .<sup>374</sup>  $\text{Sn}(\text{O}i\text{Bu})_4$  is also monomeric in the solid state, while  $\text{Sn}_2(\text{OR})_8(\text{ROH})_2$  ( $\text{R} = \text{Pr}^i, \text{Bu}^t$ ) has the same structure as the  $\text{Zr}$  derivative shown in Figure 4.<sup>162,375</sup>  $\text{Ti}(\text{OR})_4$  (in benzene):  $n = 4$  for  $\text{R} = \text{Me}$ ;<sup>235</sup>  $n = 2.5-3$  for  $\text{R} = n$ -alkyl;<sup>361,376-378</sup>  $n = 1.4$  for  $\text{R} = \text{Pr}^i$ ;  $n = 1$  for  $\text{R} = t$ -alkyl.<sup>240,241,361</sup> Crystalline  $\text{Ti}(\text{OR})_4$  ( $\text{R} = \text{Me}, \text{Et}$ ) is tetrameric,<sup>362</sup> while  $\text{Ti}(\text{OCH}_2\text{Bu}^t)_4$  is dimeric.<sup>379</sup>  $\text{Zr}(\text{OR})_4$  ( $\text{Hf}(\text{OR})_4$ ) derivatives are similar: the methoxide is an insoluble polymer;  $n \approx 3.5$  for  $\text{R} = \text{Et}$  and higher  $n$ -alkyl;  $n = 3$  for  $\text{R} = \text{Pr}^i$ ;  $n = 1-3$  (depending on the chain length) for  $\text{R} = s$ -alkyl.<sup>361</sup>  $\text{Zr}[\text{OCMe}(\text{CF}_3)_2]_4$  is monomeric in the solid state.<sup>380</sup> The degree of association of  $\text{Zr}(\text{OR})_4$  is decreased in their parent alcohols due to coordination of alcohol molecules to the metal (see Figure 4).  $\text{M}(\text{OR})_4$  ( $\text{M} = \text{Ce}, \text{Th}$ ): the methoxides and ethoxides are insoluble polymers;<sup>136,381</sup>  $n \approx 4.2$  for  $\text{Ce}(\text{OPr}^n)_4$  and  $n \approx 6.5$  for  $\text{Th}(\text{O}i\text{Bu})_4$  and higher  $n$ -alkyl (in benzene).<sup>136</sup> Crystalline  $\text{Th}(\text{OCHPr}^i)_4$  is a dimer.<sup>382</sup>  $\text{V}(\text{OR})_4$ :  $n = 3$  for  $\text{R} = \text{Me}$ ;  $n = 2$  for  $\text{R} = \text{Et}$ ;  $n < 1.4$  for

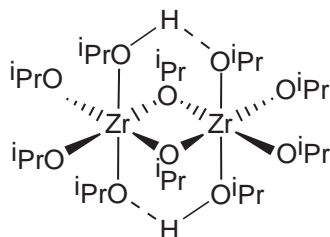


Figure 4 Structure of  $[\text{Zr}(\text{OPr}^i)_4(\text{Pr}^i\text{OH})]_2$ .

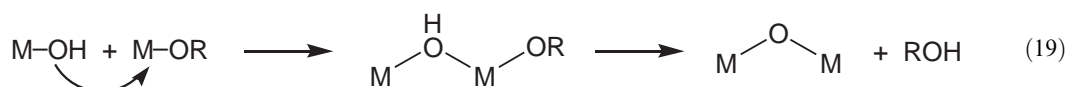
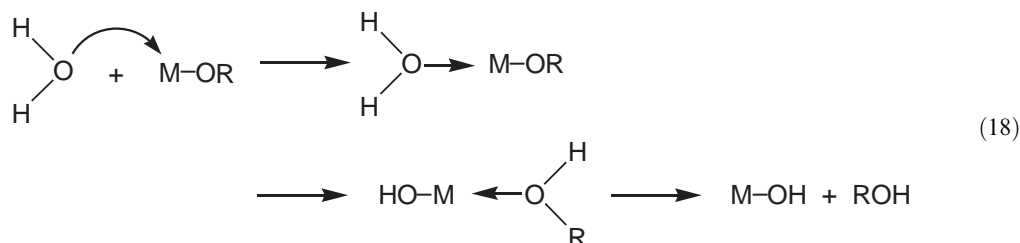
R = higher *n*-alkyl; *n* = 1 for *s*-alkyl and *t*-alkyl (in benzene).<sup>200</sup> Cr(OBu<sup>t</sup>)<sub>4</sub>; *n* = 1.<sup>280,281</sup> W(OR)<sub>4</sub>; *n* = 4 for R = Me and Et.<sup>284,383</sup>

*Pentavalent metals.* Crystalline Sb(OMe)<sub>5</sub><sup>384</sup> and U(OPr<sup>i</sup>)<sub>5</sub><sup>385</sup> are dimers. M(OR)<sub>5</sub> (M = Nb, Ta); *n* = 2 for R = methyl and higher *n*-alkyl (in benzene);<sup>143,145</sup> *n* = 1 for R = Pr<sup>i</sup> (at room temperature).<sup>147,386</sup> Crystalline Nb(OMe)<sub>5</sub><sup>149</sup> and Re(OMe)<sub>5</sub><sup>387</sup> are dimeric.

### 7.10.3.3 Sol-Gel Processing of Metal Alkoxides

The basic chemical principle behind sol-gel processing of metal alkoxides is the transformation of M—OR groups to M—O—M units via M—OH species. The direct formation of M—O—M units from metal alkoxides by ether cleavage is possible, but is only rarely observed under sol-gel conditions (see Section 7.10.3.3.1). Thus, the alkoxy ligands first have to be converted into hydroxo ligands (hydrolysis reaction), which can then undergo condensation reactions.

Metal alkoxides are very reactive due to the presence of highly electronegative OR groups that stabilize the metals in their highest oxidation states and render the metal very susceptible to nucleophilic attack. Hydrolysis of metal alkoxides occurs by an addition/elimination mechanism (Equation (18)). Water, as a Lewis base, is added to the Lewis acidic metal center in the first step. A proton is then transferred to the alkoxide ligand, and ROH is eliminated. The mechanisms of the condensation reactions are very similar to what was discussed in Section 7.10.2 for inorganic precursors. Both oxolation (Equation (8)) and ololation (Equation (6)) are possible; a ROH molecule may be the leaving group instead of H<sub>2</sub>O. Oxolation with elimination of an alcohol is also called alcoxolation (Equation (19)). The partial charge model<sup>11</sup> again makes it possible to predict the course of the reactions.



The water needed for hydrolysis is normally added to the metal alkoxide or the alkoxide solution, but may also be generated *in situ* by a chemical reaction, such as the aldol condensation of acetone<sup>388,389</sup> or ester formation between a carboxylic acid and an alcohol (see Section 7.10.3.3.1).

There are some important differences between metal alkoxides and Si(OR)<sub>4</sub>. (i) Owing to their lower electronegativity, metal alkoxides are stronger Lewis acids than silicon alkoxides. Nucleophilic attack at the metal is thus facilitated, and the hydrolysis rates are strongly increased. For example, the hydrolysis rate of Ti(OR)<sub>4</sub> is about 10<sup>5</sup> times faster than that of Si(OR)<sub>4</sub> with the same alkoxide substituents. (ii) Most metals have several stable coordination numbers, or the expansion of the coordination sphere in transition states is easier. Owing to both effects, the reactivity of some tetravalent isopropoxides in hydrolysis reactions increases in the order: Si(OPr<sup>i</sup>)<sub>4</sub> <<< Sn(OPr<sup>i</sup>)<sub>4</sub>, Ti(OPr<sup>i</sup>)<sub>4</sub> < Zr(OPr<sup>i</sup>)<sub>4</sub> < Ce(OPr<sup>i</sup>)<sub>4</sub>.

The reactivity of many metal alkoxides towards water is so high that precipitates are formed spontaneously. While the reactivity of alkoxy silanes has to be promoted by catalysts, the reactions of metal alkoxides must be moderated to obtain gels instead of precipitates. The most general method is to replace one or more alkoxide ligands by groups that are less easily hydrolyzed (i.e., that are more strongly bonded to the metal) and additionally block coordination sites

at the metal. The most common ligands used for this purpose are carboxylate or  $\beta$ -diketonate groups (see Section 7.10.3.4).

Important parameters that influence the hydrolysis and condensation reactions are the kind of precursor(s), the degree of association of the precursor, the alkoxy group to water ratio ( $R_w$ ), the kind of catalyst, the kind of solvent, the temperature, the pH, and the relative and absolute concentration of the components in the precursor mixtures.

(i) The kinetics of hydrolysis and condensation is influenced by steric factors. Any branching of the alkoxy group or increasing of the chain length lowers the hydrolysis rate of the alkoxides. For example, when 2 equivalents of water are added to  $\text{Ti}(\text{OPr}^i)_4$ , titania precipitates very quickly. When the same experiment is done with  $\text{Ti}(\text{OAm}^i)_4$ , a colloidal solution is obtained that is stable for months.<sup>240,241</sup> Inductive effects exerted by the organic groups of the OR ligands are very important, because they stabilize or destabilize the transition states during hydrolysis and condensation. Inductive effects of other groups attached to the same metal atom are even more important. For example, the electron density at the titanium atom increases in the following order:  $(\equiv\text{Ti}-\text{O})_3\text{Ti}-\text{OR} \ll (\equiv\text{Ti}-\text{O})_2\text{Ti}(\text{OR})_2 < \equiv\text{Ti}-\text{O}-\text{Ti}(\text{OH})(\text{OR})_2 < \equiv\text{Ti}-\text{O}-\text{Ti}(\text{OR})_3$ .<sup>11</sup> This order reflects the different electronic influence of oxo, hydroxo, and alkoxy ligands on the metal center.

(ii) A lower degree of association results in a higher reactivity in hydrolysis and condensation reactions. For example,  $\text{Ti}(\text{OPr}^i)_4$  dissolved in isopropanol is monomeric and therefore coordinatively unsaturated. It is hydrolyzed more rapidly than trimeric  $\text{Ti}(\text{OEt})_4$  dissolved in ethanol despite the bigger alkoxide groups. When the degree of oligomerization of two metal alkoxides  $\text{M}(\text{OR})_n$  with different R groups is the same, then the reaction kinetics are influenced by the size of R. The reaction rates decrease with bigger R groups.

(iii) When the alkoxides are dissolved in polar solvents such as alcohols, addition of solvent molecules competes with association. For example, hydrolysis of  $\text{Zr}(\text{OPr}^n)_4$  in  $\text{PrOH}$  is very fast and results in a precipitate, while hydrolysis of the same alkoxide in cyclohexane gives a homogeneous gel. The explanation of this difference is that OR-bridged oligomeric species are formed in cyclohexane solution, while an alcohol molecule is coordinated to  $\text{Zr}(\text{OPr}^n)_4$  in propanol solution.<sup>11</sup> Upon hydrolysis, the coordinated ROH is more easily cleaved than the OR bridge. Thus, starting from a particular metal alkoxide precursor, the reaction kinetics and the texture of the resulting gels can be controlled by the choice of the solvent.<sup>390</sup>

(iv) The overall reaction for sol-gel processing of  $\text{M}(\text{OR})_x$  requires  $x/2$  equivalents of water (alkoxy group/ $\text{H}_2\text{O}$  ratio  $R_w = 2$ ) to convert  $\text{M}(\text{OR})_x$  to  $\text{MO}_{x/2}$ . Increasing the water portion (i.e., lowering  $R_w$ ) generally favors the formation of  $\text{M}-\text{OH}$  groups over  $\text{M}-\text{O}-\text{M}$  groups.

(v) The solvent is important to homogenize the reaction mixture, especially at the beginning of the reaction. The polarity, dipole moment, viscosity, and protic or nonprotic behavior of the solvent influence the reaction rate and thus the structure of the final material. Polar and particularly protic solvents ( $\text{H}_2\text{O}$ , alcohols, formamide) stabilize polar species such as partially hydrolyzed alkoxides by hydrogen bridges.

(vi) Acid or base catalysis influences both the hydrolysis and condensation rates, and the structure of the gels. Acids protonate the alkoxy or hydroxy ligands producing the good leaving groups ROH or  $\text{H}_2\text{O}$  and eliminating the requirement for proton transfer in the transition state (see Equations (18) and (19)). According to the sequence of reactivity given in (i), OR groups at the end of a chain, i.e.,  $\equiv\text{Ti}-\text{O}-\text{Ti}(\text{OR})_3$ , are preferentially protonated. Therefore, acid catalysis results in more extended, less highly branched oligomers and polymers. This tendency is consistent with the observation that acid catalysis combined with high  $R_w$  values often result in monolithic gels<sup>391,392</sup> or spinnable sols.<sup>393,394</sup> Alkaline conditions produce strong nucleophiles by deprotonation of  $\text{M}-\text{OH}$  groups. Contrary to acid-catalyzed systems, base catalysis leads to more compact, highly branched species because a negatively charged transition state is better stabilized in a more highly branched unit such as  $(\equiv\text{Ti}-\text{O})_3\text{Ti}-\text{OR}$ .

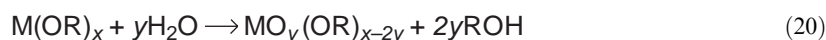
Many technically important materials prepared by sol-gel processing, such as perovskites, contain more than one kind of metal atom. The first approach is to employ precursor mixtures, which can be either mixtures of metal alkoxides or mixtures of one or more metal alkoxides and metal salts. The co-hydrolysis and co-condensation of different precursors may result in inhomogeneous materials because of their different reaction rates and the fact that the formation of a gel is a kinetically controlled process. The inhomogeneity can be on any length scale from the nanometer range up to macroscopic phase separation. Common methods to solve this problem and to obtain homogeneous (mixed on a nanometer scale) heterometallic gels from precursor



mixtures are to prehydrolyze the slower reacting component<sup>395</sup> or to lower the reactivity of the faster reacting metal alkoxide by chemical modifications (see Section 7.10.3.4). A third possibility is to employ single-source precursors. The disadvantage of the latter method is that suitable precursors are often difficult to prepare, especially with the desired stoichiometric ratio of the different metal atoms. The heterometallic alkoxides discussed in Section 7.10.3.1.5 can be used as single-source precursors. In another kind of precursor, the different metal atoms are linked by organic groups, which are removed by calcination after sol-gel processing. Examples are  $(\text{MeO})_3\text{SiCH}_2\text{CH}_2\text{CH}_2\text{C}[\text{C}(\text{Me})\text{O}]_2\text{Ti}(\text{OPr}^i)_3$  and  $\{(\text{MeO})_3\text{SiCH}_2\text{CH}_2\text{CH}_2\text{C}[\text{C}(\text{Me})\text{O}]_2\}\text{Ti}(\text{OPr}^i)_2$  which give  $\text{SiO}_2/\text{TiO}_2$  mixed oxides after sol-gel processing and calcination.<sup>396</sup>

### 7.10.3.3.1 Metal oxo-alkoxides

Metal oxo-alkoxides,<sup>397</sup>  $\text{MO}_y(\text{OR})_{x-2y}$ , may be considered intermediates between metal alkoxides  $\text{M}(\text{OR})_x$  and the corresponding metal oxide, and are the counterparts of the polyanions and polycations in aqueous systems. Controlled partial hydrolysis of  $\text{M}(\text{OR})_x$  (Equation (20)) does indeed sometimes result in structurally well-defined metal oxo-alkoxo oligomers (clusters) where  $\mu_2$ – $\mu_4$  oxo ligands connect the metal polyhedrons from which the clusters are constructed.



Although hydrolysis/condensation is the “normal” route leading to metal oxo-alkoxides, ether cleavage (Equation (21)) is another possibility for the formation of such species.



There are several substantiated examples that ether cleavage may occur during the preparation of alkoxides. Processes of this kind are typical for penta- and hexacoordinate alkoxides, particularly when bulky OR groups are involved. For example, when  $\text{W}(\text{NMe}_2)_6$  is reacted with ROH, the hexaalkoxides  $\text{W}(\text{OR})_6$  are formed for  $\text{R} = \text{Me}, \text{Et}, \text{Pr}^i$ , or allyl, while  $\text{Bu}^i\text{OH}$  gave  $\text{WO}(\text{OBu}^i)_4$ .<sup>398</sup> For molybdenum, only  $\text{Mo}(\text{OMe})_6$  was isolated;<sup>399,400</sup> otherwise the  $\text{MoO}(\text{OR})_4$  compounds which form have a high tendency to yield  $\text{MoO}_2(\text{OR})_2$  by ether elimination.<sup>122–125,401,402</sup> The binuclear complex  $\text{Ta}_2\text{O}(\text{O}^i\text{Pr})_9(\text{Pr}^i\text{OH})$  crystallizes from a solution of  $\text{Ta}(\text{OPr}^i)_5$  in  $\text{Pr}^i\text{OH}$  on refluxing.<sup>119</sup> Lead(II) alkoxides were reported to decompose on alcoholysis to form  $\text{Pb}_4\text{O}(\text{OR})_6$  and  $\text{Pb}_6\text{O}_4(\text{OR})_4$ .<sup>166</sup> The lanthanides are also known often to yield oxo-alkoxo derivatives instead of the oxo-free alkoxides. Some compounds originally formulated as homoleptic alkoxides turned out to be oxo-alkoxo derivatives; for example, “ $\text{Y}(\text{OPr}^i)_3$ ” is in fact  $\text{Y}_5\text{O}(\text{OPr}^i)_{13}$ .<sup>117</sup>

Due to the high reaction rates of hydrolysis and condensation reactions of metal alkoxides, information on the progressive structural evolution in transition metal systems is difficult to obtain. The oxo-alkoxo clusters are therefore interesting models to assist in understanding the growth of three-dimensional oxide structures from the alkoxides. Some oxo-alkoxo oligomers may even be intermediates in the formation of the gel networks.

Many mixed-metal oxo-alkoxo compounds have been isolated and structurally characterized. They are also interesting single-source precursors for bimetallic materials.<sup>294,295</sup> For example, crystalline  $\text{Ba}_2\text{Ti}_{13}\text{O}_{18}(\text{OR})_{24}$  ( $\text{R} = \text{CH}_2\text{CH}_2\text{OMe}$ ) was obtained by partial hydrolysis of  $\text{BaTi}(\text{OR})_6$ .<sup>403</sup>

A particularly impressive series of oxo-alkoxo compounds was structurally characterized for titanium. The series comprises  $\text{Ti}_3\text{O}(\text{OR})_{10}$ ,<sup>389,404,405</sup>  $\text{Ti}_7\text{O}_4(\text{OEt})_{20}$ ,<sup>406,407</sup>  $\text{Ti}_8\text{O}_6(\text{OCH}_2\text{Ph})_{20}$ ,<sup>408</sup>  $\text{Ti}_{10}\text{O}_8(\text{OEt})_{24}$ ,<sup>408</sup>  $\text{Ti}_{11}\text{O}_{13}(\text{OR})_{18}$ ,<sup>409</sup>  $\text{Ti}_{12}\text{O}_{16}(\text{OR})_{16}$ ,<sup>406,409,410</sup>  $\text{Ti}_{16}\text{O}_{16}(\text{OEt})_{32}$ ,<sup>411</sup>  $\text{Ti}_{17}\text{O}_{24}(\text{OPr}^i)_{20}$ ,<sup>412</sup> and  $\text{Ti}_{18}\text{O}_{27}(\text{OH})(\text{OBu}^i)_{17}$ .<sup>413</sup> The cluster  $\text{Ti}_3\text{O}_2(\text{OPr}^i)_5(\text{OCMe} = \text{CH}_2)_3(\text{Pr}^i\text{OH})$  was obtained by reaction of  $\text{Ti}(\text{OPr}^i)_4$  with acetone.<sup>414</sup> The  $\mu_3$ -oxo groups originate from water which is formed *in situ* by an aldol condensation.

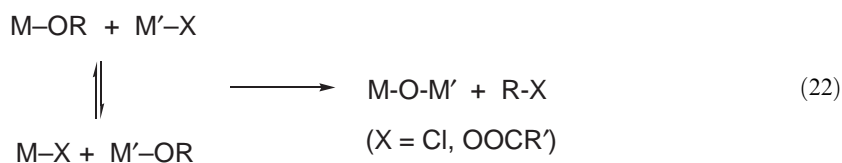
In the case of zirconium, only  $\text{Zr}_3\text{O}(\text{OH})(\text{OBu}^i)_9$  has a similar structure to the corresponding titanium complex ( $\text{Ti}_3\text{O}(\text{OR})_{10}$ ) with a c.n. of 6 for the metal.<sup>415</sup> Although fewer oxo-alkoxo compounds were isolated than for titanium, different structures are to be expected, because zirconium generally favors higher coordination numbers (>7). An example is  $\text{Zr}_{13}\text{O}_8(\text{OMe})_{36}$  with 7- and 8-coordinate Zr.<sup>416</sup>

The vanadium group has also a rich (structural) chemistry of neutral or anionic oxo-alkoxo compounds. Simple examples (without other ligands) are  $\text{V}_6\text{O}_7(\text{OEt})_{12}$  (V(IV,V)),<sup>417</sup>

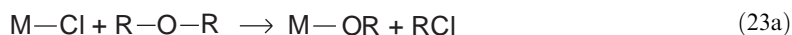
$M_8O_{10}(OEt)_{20}$  ( $M = Nb$ ,<sup>418–420</sup>  $Ta$ <sup>421</sup>), and  $Ta_7O_9(OPr^i)_{17}$ .<sup>120,422</sup> Structurally characterized examples of aluminum oxo-alkoxo compounds are  $Al_4O(OBu^i)_{10}(^iBuOH)^{423}$  and  $Al_{10}O_4(OEt)_{22}$ .<sup>424</sup>

### 7.10.3.3.2 Nonhydrolytic sol-gel processing

The conventional sol-gel process is based on the hydrolysis and condensation of molecular precursors leading to oxide networks. The oxo ions originate from water—which can be used as a solvent (Section 7.10.2), can be added as a reagent (Section 7.10.3), or may be formed *in situ* by water-producing reactions (Section 7.10.3.4)—and are formed by condensation reactions involving M—OH groups (Equations (6), (8), and (19)). Since the early 1990s, variations of these reactions have been developed, in which the oxo groups are formed by alkyl chloride or, less often, ester elimination instead of water or alcohol elimination in the traditional sol-gel process.<sup>425,426</sup> These reactions have been termed “nonhydrolytic sol-gel processes” because no water is involved. The basic reactions are given in Equation (22).



Condensation occurs at temperatures between 20 °C and 100 °C sometimes in the presence of a catalyst,  $FeCl_3$  being most commonly used. Redistribution between the OR and Cl ligands can take place before the reaction proceeds, i.e., the actual precursors may be chloro-alkoxo or carboxylate-alkoxo species. The metal alkoxide species may be generated *in situ* by reaction of metal chlorides with ethers (Equation (23a)) or alcohol (Equation (23b)).



The kinetics of nonhydrolytic sol-gel processes depend on the nature of the metal, the nature of the oxygen donor, electronic effects of the R group, and the composition of the initial metal alkoxide/metal chloride (carboxylate) mixture.<sup>427</sup>

Both single metal oxides such as  $Al_2O_3$ ,<sup>428–435</sup>  $TiO_2$ ,<sup>427,433–437</sup>  $ZrO_2$ ,<sup>438–440</sup>  $WO_3$ ,<sup>438,439</sup>  $Nb_2O_5$ ,<sup>438</sup> or  $Fe_2O_3$ ,<sup>438</sup> as well as mixed oxides such as  $SiO_2/Al_2O_3$ ,<sup>432,441–443</sup>  $SiO_2/SnO_2$ ,<sup>444</sup>  $SiO_2/TiO_2$ ,<sup>425,426,443,445</sup>  $SiO_2/ZrO_2$ ,<sup>445</sup>  $TiO_2/Al_2O_3$ ,<sup>446,447</sup>  $TiO_2/ZrO_2$ ,<sup>448,449</sup>  $TiO_2/V_2O_5$ ,<sup>450</sup>  $ZrO_2/WO_3$ ,<sup>439</sup>  $V_2O_5/Nb_2O_5$ ,<sup>451</sup> or  $SiO_2/V_2O_5/Nb_2O_5$ <sup>451</sup> have been prepared by nonhydrolytic routes. It has been postulated that nonhydrolytic routes lead to better control over the distribution of the elements in mixed-oxide systems. A noteworthy feature of this method is that nonhydrated oxides without residual hydroxyl groups are obtained.

### 7.10.3.4 Organically Substituted Metal Alkoxides

The mild reaction conditions of sol-gel processing, particularly the low reaction temperatures, make it possible to incorporate organic moieties in inorganic materials. Organic groups in sol-gel materials can serve different purposes. (i) They can control the reaction rates of the inorganic precursors, the rheology of the sols, or the homogeneity and microstructure of the derived gels. When used for this purpose, the organic groups are degraded during calcination to give purely inorganic materials. (ii) The organic groups can be retained to modify, functionalize, or cross-link the oxidic gel structures. The final materials are therefore composed of inorganic (oxidic) structures and organic entities and are called inorganic-organic hybrid materials.

In sol-gel processing of transition metal alkoxides, organically substituted metal alkoxides are used for both purposes. A crucial issue is to get a hydrolytically stable bond between the metal

alkoxide moiety and the organic group. Contrary to silicon chemistry, a direct metal-carbon bond is not possible because such bonds would be hydrolyzed during sol-gel processing.

Complexing ligands (CLs) have often been reported in the sol-gel literature as chemical additives to moderate the reactivity of nonsilicate metal alkoxides.<sup>11,452-454</sup> Acetic acid or acetylacetone were mainly used for this purpose. Both are bidentate ligands; in general  $\beta$ -diketonate ligands predominantly form chelates, while carboxylate ligands have a strong propensity to bridge metal centers. When a metal alkoxide  $M(OR)_x$  is reacted with acetic acid or acetylacetone, some of the alkoxide groups are substituted by acetate or acetylacetonate groups. A new molecular precursor  $M(OR)_{x-y}(CL)_y$  is obtained (Equation (24)) with a different structure and a lower reactivity. Bidentate ligands are more strongly bonded than comparable monodentate ligands and are therefore less readily hydrolyzed than the remaining OR groups upon sol-gel processing. This observation is supported by partial charge calculations.<sup>452-454</sup>



For example, when  $Ti(OBu^n)_4$  is reacted with one molar equivalent of acetic acid, an exothermic reaction takes place and the acetate-substituted titanium alkoxide  $(CH_3COO)Ti(OBu^n)_3$  is formed with a six-coordinate titanium atom.<sup>455</sup> While addition of water to  $Ti(OBu^n)_4$  results in immediate precipitation of titania, stable transparent gels are obtained from acetate-substituted titanium alkoxides with gelation times of several days or months. Similar observations were made for the reaction of  $Ti(OPr^i)_4$  with acetylacetone (acac-H).<sup>455</sup> The X-ray structure analyses of  $Ti(OR)_3(\beta\text{-diketonate})$  ( $\beta\text{-diketonate} = \text{acac}$ ,  $R = \text{Me, Et, Pr}^i$ ;  $\beta\text{-diketonate} = \text{Bu}^t\text{C}(\text{O})\text{CHC}(\text{O})\text{Bu}^t$ ,  $R = \text{Me, Pr, Pr}^i$ )<sup>456,457</sup> and  $Ti(OR)_2(\beta\text{-diketonate})_2$  ( $\beta\text{-diketonate} = \text{acac}$ ,  $R = \text{Pr}^i$ ,<sup>458</sup>  $\beta\text{-diketonate} = \text{benzoylacetate}$ ,  $R = \text{Bu}^t$ ,<sup>459</sup>  $\beta\text{-diketonate} = \text{PhC}(\text{O})\text{CHC}(\text{O})\text{CF}_3$ ,  $R = \text{Et}$ )<sup>460</sup> show that the former compound is dimeric and the latter monomeric; in both cases the titanium reaches its preferred c.n. of six.

CL-substituted metal alkoxide derivatives can, in principle, also be obtained by ligand exchange reactions between different metal complexes. For example, reaction of  $Y(\text{OCH}_2\text{CH}_2\text{OMe})_3$  with  $\text{Cu}(\text{acac})_2$  resulted in a variety of species, from which  $Y_3(\text{OCH}_2\text{CH}_2\text{OMe})_5(\text{acac})_4$  was isolated.<sup>461</sup> Depending on the combination of metal complexes, heterometallic compounds may also be formed in such reactions.<sup>462</sup>

The replacement of one or more OR groups by CL has several chemical and structural consequences for sol-gel processing. (i) The organically substituted precursor  $M(OR)_{x-y}(CL)_y$  has a different reactivity in the hydrolysis and condensation reactions because of the electronic and steric effects of CL. (ii) The degree of cross-linking of the inorganic network formed during sol-gel processing is decreased because fewer hydrolysable groups are available. (iii) The substitution of monodentate alkoxy group by bi- or multidentate CL blocks coordination sites. This additionally reduces the reactivity in hydrolysis and condensation reactions and furthermore lowers the connectivity of the molecular building blocks. The lower connectivity favors the formation of gels instead of crystalline precipitates. (iv) Since hydrogen bonds play a very important role in the network formation process, the polarity change by the organic groups has probably a similar effect on the network structure to changing the polarity of the solvent. (v) The complexing ligand may stereochemically direct the preferred hydrolysis or condensation site because the site *trans* to an organic group has a different reactivity from the *cis* sites. This effect is similar to what was discussed before for metal salt precursors, when counterions remain coordinated to the metal.

In principle, nearly any CL can be chosen to modify metal alkoxides, the most common ones being carboxylates,  $\beta$ -diketonates, glycols (or polyols), and aminoalcohols. Hydroxycarboxylic ( $\text{RCH}(\text{OH})\text{COOH}$ ),  $\alpha$ -aminocarboxylic ( $\text{RCH}(\text{NH}_2)\text{COOH}$ ), sulfonic ( $\text{RSO}_3\text{H}$ ), phosphonic ( $\text{RPO}_3\text{H}_2$ ), or hydroxamic ( $\text{RC}(\text{O})\text{NHOH}$ ) acids were also used, as well as Schiff bases, oximes, etc. The number of substituted OR groups depends to a large extent on steric factors (bulkier CL and OR ligands result in a smaller degree of substitution) and on the c.n. of the metal. The metal must not necessarily reach its optimum c.n. upon substitution of part of the alkoxide ligands by CL, and the obtained compounds may then be oligomeric as was discussed before for the parent alkoxides. The degree of association has not been determined in most cases.

Structurally characterized compounds of the type  $M(OR)_{x-y}(CL)_y$  (see below for related oxo-alkoxo derivatives) include carboxylate derivatives  $M_2(\text{OR})_6(\text{OOCR})_2$  ( $M = \text{Ti}$ ,<sup>405</sup>  $\text{Zr}$ ,<sup>548</sup>),  $\beta$ -diketonate derivatives  $\text{Al}_3(\text{OPr}^i)_6(\text{acac})$ ,<sup>463</sup>  $\text{Y}_3(\text{OCH}_2\text{CH}_2\text{OMe})_5(\text{acac})_4$ ,<sup>461</sup>  $\text{M}_2(\text{OR})_6(\text{acac})_2$  ( $M = \text{Ti}$ ,<sup>456,457</sup>  $\text{Sn}$ ,<sup>464</sup>  $\text{Ce}$ ,<sup>465</sup>),  $\text{Mn}_3(\text{OMe})_4(\text{MeOH})(\beta\text{-diketonate})_4$ ,<sup>466</sup> and  $\text{Fe}_2(\text{OR})_2(\beta\text{-diketonate})_2$ ,<sup>467</sup>

hydroxycarboxylate derivatives of Al,<sup>468</sup> Pb,<sup>469–471</sup> Zr,<sup>472</sup> and Nb alkoxides,<sup>245</sup> [Ti(OEt)<sub>3</sub>-(glycinate)]<sub>2</sub>,<sup>473</sup> Ti<sub>4</sub>(OPr<sup>i</sup>)<sub>8</sub>(O<sub>3</sub>PBu<sup>t</sup>)<sub>4</sub>,<sup>474,475</sup> and [Zr(OPr)(O<sub>3</sub>SMe)<sub>3</sub>]<sub>∞</sub>.<sup>476</sup> Particularly interesting oligomeric structures (molecular wheels) were found for [Fe(OMe)<sub>2</sub>(OOCCH<sub>2</sub>Cl)]<sub>10</sub><sup>477</sup> and [Co(OMe)(OAc)]<sub>8</sub>.<sup>478</sup>

Aminoalcohols with both OH and NH groups are always preferentially deprotonated at the OH group upon reaction with metal alkoxides. Other than —OCH<sub>2</sub>CH<sub>2</sub>OR ligands, where the OR group is normally noncoordinating, monoaminoalcoholate ligands such as —OCH<sub>2</sub>CH<sub>2</sub>NR<sub>2</sub> (R = H, alkyl) or —OCH<sub>2</sub>CH(Me)NR<sub>2</sub> are mostly chelating or bridging with coordination of the NR<sub>2</sub> group.<sup>479–493</sup> A simple example is Cu(OCH(Me)CH<sub>2</sub>NMe<sub>2</sub>)<sub>2</sub> where the copper atom is four-coordinate due to the coordination of nitrogen atoms.<sup>493</sup> A smaller number of cases is known in which both the OH and the NH<sub>2</sub> group of monoaminoalcohols is deprotonated to form dianionic chelating ligands.<sup>490–492,494–498</sup> Reaction of di-<sup>490–492,499,500</sup> and triaminoalcohols<sup>490–492,501–506</sup> mostly results in the deprotonation of all OH groups, although a few derivatives with dangling CH<sub>2</sub>CH<sub>2</sub>OH groups were also obtained. In particular, metal alkoxide derivatives derived from N(CH<sub>2</sub>CH<sub>2</sub>OH)<sub>3</sub> have gained some interest as precursors in sol-gel processing.<sup>507–512</sup> The solid-state structures of numerous derivatives have been determined.<sup>103–105</sup>

Glycolate are highly reactive towards metal alkoxides to form homoleptic and mixed alkoxo-glycolate derivatives.<sup>185,186,191,232,513–536</sup> This alcohol exchange reaction (see Section 7.10.3.1.3) is driven by the formation of chelated or bridged structures with both (dianionic) —OCR<sub>2</sub>CR<sub>2</sub>O— and/or (monoanionic) —OCR<sub>2</sub>CR<sub>2</sub>OH ligands. The ability to bridge two metal atoms and the reduced steric demand of a glycolate ligand compared to two alkoxo ligands leads to a high tendency to form aggregated structures. However, only a few glycolate derivatives have been structurally characterized, such as [Ti(OCH<sub>2</sub>CH<sub>2</sub>O)<sub>3</sub>]<sub>2</sub><sup>2-</sup>,<sup>537,538</sup> Ti<sub>5</sub>(OCH<sub>2</sub>CH<sub>2</sub>O)<sub>5</sub>(OPr<sup>i</sup>)<sub>10</sub>,<sup>539</sup> and M(OCR<sub>2</sub>CR<sub>2</sub>O)<sub>3</sub> (M = Mo, W; R = H, Me).<sup>540,541</sup> Several derivatives have been prepared with EtC(CH<sub>2</sub>OH)<sub>3</sub> (1,1,1-tris(hydroxymethyl)propane).<sup>245,542</sup> When the glycolate acts as a monodentate ligand, the dangling —OCR<sub>2</sub>CR<sub>2</sub>OH group can be used for alcohol exchange reactions with another metal alkoxide. For example, reaction of Zr<sub>2</sub>(OCMe<sub>2</sub>CMe<sub>2</sub>O)<sub>2</sub>(OCMe<sub>2</sub>CMe<sub>2</sub>OH)<sub>4</sub> with Ti(OPr<sup>i</sup>)<sub>4</sub> in 1:1 or 1:2 molar ratios results in the heterometallic complexes (HOCMe<sub>2</sub>CMe<sub>2</sub>O)<sub>2</sub>-(OCMe<sub>2</sub>CMe<sub>2</sub>O)<sub>2</sub>Zr<sub>2</sub>[(OCMe<sub>2</sub>CMe<sub>2</sub>O)<sub>2</sub>Ti(OPr<sup>i</sup>)<sub>2</sub>] and (OCMe<sub>2</sub>CMe<sub>2</sub>O)<sub>2</sub>Zr<sub>2</sub>[(OCMe<sub>2</sub>CMe<sub>2</sub>O)<sub>2</sub>-Ti(OPr<sup>i</sup>)<sub>2</sub>]<sub>2</sub>, respectively, in which the two metals are bridged by —OCMe<sub>2</sub>CMe<sub>2</sub>O— ligands.<sup>543</sup>

When metal alkoxides are reacted with an excess of carboxylic acids, oxo-alkoxo clusters of the general composition M<sub>a</sub>O<sub>b</sub>(OH/OR)<sub>c</sub>(OOCR)<sub>d</sub> are often formed instead of the substitution products M(OR)<sub>x-y</sub>(OOCR)<sub>y</sub>. The reason for the formation of the oxo clusters is that the alcohol liberated by the substitution reaction can react with the acid to give an ester and water and this slowly produced water hydrolyzes part or all of the remaining alkoxide groups. The substituted oxo-alkoxo clusters are themselves interesting building blocks for sol-gel materials. A variety of M<sub>a</sub>O<sub>b</sub>(OH/OR)<sub>c</sub>(OOCR)<sub>d</sub> clusters have been structurally characterized and make it possible to study the structural evolution of similar to the metal oxo-alkoxides, MO<sub>y</sub>(OR)<sub>x-2y</sub>, mentioned above. The greatest structural variety was again found for the group 4 metals. For M = Ti, the cluster types observed include Ti<sub>3</sub>O(OR)<sub>10</sub>(OOCR')<sub>2</sub>,<sup>405,544</sup> Ti<sub>4</sub>O<sub>2</sub>(OR)<sub>6</sub>(OOCR')<sub>6</sub>,<sup>545</sup> Ti<sub>4</sub>O<sub>4</sub>(OR)<sub>10</sub>(OOCR')<sub>2</sub>,<sup>546</sup> Ti<sub>4</sub>O<sub>4</sub>(OR)<sub>4</sub>(OOCR')<sub>4</sub>,<sup>547,548</sup> Ti<sub>6</sub>O<sub>2</sub>(OR)<sub>12</sub>(OOCR')<sub>4</sub>,<sup>410,547–549</sup> Ti<sub>6</sub>O<sub>4</sub>(OR)<sub>8</sub>(OOCR')<sub>8</sub>,<sup>545,550–554</sup> Ti<sub>6</sub>O<sub>6</sub>(OR)<sub>6</sub>(OOCR')<sub>6</sub>,<sup>405,546,555</sup> and Ti<sub>9</sub>O<sub>8</sub>(OR)<sub>4</sub>(OOCR')<sub>16</sub>.<sup>556,557</sup> Due to the higher coordination number of Zr, a higher degree of substitution is possible, and different structures are obtained, such as Zr<sub>4</sub>O<sub>2</sub>(OOCR)<sub>12</sub>,<sup>558,559</sup> Zr<sub>5</sub>O<sub>4</sub>(OR)<sub>2</sub>(OOCR)<sub>10</sub>(ROH)<sub>4</sub>,<sup>554</sup> Zr<sub>6</sub>(OH)<sub>4</sub>O<sub>4</sub>(OOCR)<sub>12</sub>,<sup>557,558</sup> Zr<sub>6</sub>O<sub>2</sub>(OR)<sub>10</sub>(OOCR')<sub>10</sub>, and Zr<sub>6</sub>O<sub>2</sub>(OR)<sub>6</sub>-(OOCR')<sub>14</sub>.<sup>560</sup> Carboxylate-substituted oxoniobium and oxotantalum clusters M<sub>4</sub>O<sub>4</sub>(OR)<sub>8</sub>(OOCR)<sub>4</sub> (M = Nb,<sup>561,562</sup> Ta<sup>563</sup>) as well as an oxovanadium cluster V<sub>3</sub>O<sub>3</sub>(OOCR)<sub>6</sub>(ROH),<sup>554</sup> were also obtained by *in situ* hydrolysis from M(OR)<sub>5</sub> and carboxylic acids. A series of methacrylate-substituted Ti/Zr mixed-metal clusters was similarly prepared from Ti(OR)<sub>4</sub>/Zr(OR)<sub>4</sub>/methacrylate acid mixtures.<sup>564</sup> Fe<sub>12</sub>O<sub>2</sub>(OMe)<sub>18</sub>(OAc)<sub>6</sub>(MeOH)<sub>4</sub> was prepared through the controlled oxidation of a methanolic solution of ferrous acetate and LiOMe.<sup>565</sup>

The use of other acids may also result in the formation of oxo-alkoxo clusters by *in situ* generation of water. The phosphonate- and phosphinate-substituted oxotitanium clusters Ti<sub>4</sub>O(OPr<sup>i</sup>)<sub>8</sub>(O<sub>3</sub>PR)<sub>3</sub> and Ti<sub>4</sub>O<sub>4</sub>(OPr<sup>i</sup>)<sub>4</sub>(O<sub>2</sub>PPh<sub>2</sub>)<sub>4</sub> were obtained by reaction of Ti(OR)<sub>4</sub> with the corresponding phosphonic or phosphinic acid.<sup>474,475,566,567</sup>

In the examples mentioned above, the water was produced by an *in situ* reaction. The water needed for the (partial) hydrolysis of the alkoxo groups can of course also be externally added as a reactant. For example, the clusters Ce<sub>6</sub>O<sub>4</sub>(OH)<sub>4</sub>(acac)<sub>12</sub>,<sup>568</sup> Ti<sub>18</sub>O<sub>22</sub>(OBu)<sub>26</sub>(acac)<sub>2</sub>,<sup>569</sup> Zr<sub>4</sub>O(OPr)<sub>10</sub>(acac)<sub>4</sub>,<sup>570</sup> and Zr<sub>10</sub>O<sub>6</sub>(OH)<sub>4</sub>(OPr)<sub>18</sub>(allylacetoacetate)<sub>6</sub><sup>571</sup> were prepared by adding water to a solution of M(OR)<sub>4</sub> and different portions of the corresponding β-diketone. Part or all of the

metal alkoxide is first substituted by the  $\beta$ -diketonate, and the resulting substituted derivative then reacts with water to give the metal oxide cluster.

The CL-substituted clusters have in common that the organic groups cap the cluster core. It was shown that, as a consequence, the CLs can also be used to influence the size of metal oxide particles obtained by sol-gel processing. When the particle size increases, the percentage of surface atoms decreases, i.e., fewer CLs are needed to saturate the surface atoms. The size of zirconia particles increased from 2 nm to 15 nm when the  $\text{Zr}(\text{OPr})_4/\text{acac-H}$  ratio was increased from 1 to 10.<sup>572</sup>

#### 7.10.3.4.1 Inorganic-organic hybrid materials

In one type of inorganic-organic hybrid material, organic molecules are physically entrapped in the inorganic gel network. Such materials are restricted to silica gels as the matrix. In the second type of inorganic-organic hybrid material, the organic and inorganic entities are linked by stable chemical bonds. This approach requires precursors in which the organic group is bonded to the oxide-forming element in a hydrolytically stable manner. When organically substituted metal alkoxides are used to control the reactivity of the precursors, the gels obtained are initially inorganic-organic hybrids. However, the properties originating from the presence of the organic groups in the as-synthesized gels are rarely noticed since the goal is usually to prepare metal oxide gels and the organic groups are removed by calcination.

It is becoming increasingly evident that CLs are also suited to introduce organic functionalities into metal oxide-based hybrid materials. The CL then has to be of the sort  $(\text{RO})_{x-y}\text{M}[\text{CG-X-A}]_y$ , where CG represents the complexing group, A the functional organic group, and X an inert spacer. Compared with the corresponding organofunctional alkoxy silanes, the chemistry and the use of such metal alkoxide precursors is still at an early stage. The most often used functional CLs are carboxylates, which are available with a variety of functional groups A.

Most examples of metal alkoxides substituted by functional CL are those in which the functional organic group is a polymerizable C=C bond. Polymerization of the unsaturated group after sol-gel processing affords dual network hybrid polymers. Methacrylic or acrylic acid are most often employed for this purpose,<sup>553,556-560,563,564</sup> but several other CLs with unsaturated groups in the side chain are also employed, such as methacrylamidosalicylic acid,<sup>573</sup> oleic acid,<sup>414</sup>  $\beta$ -diketones (allylacetoacetone,<sup>571</sup> 2-(methacryloyloxy)ethyl acetoacetone<sup>414,573-575</sup>), diols (*cis*-but-2-ene-1,4-diol, 3-allyloxypropane-1,2-diol),<sup>575</sup> and isoeugenol.<sup>576</sup> In practice, these compounds are often reacted *in situ* with the metal alkoxide, and polymerization is carried out without isolation of the  $(\text{CL})_x\text{M}(\text{OR})_y$  derivative. It should be noted again that cluster compounds are often formed especially when carboxylic acid derivatives are used.

2-Bromopropionate-substituted metal oxo clusters have been used as macroinitiators for atom transfer polymerizations.<sup>554</sup>

Another group of functional CLs are those capable of coordinating metal ions or metal complexes. In  $\text{M}(\text{OR})_3(\text{lysinate})$  ( $\text{M} = \text{Ti}, \text{Zr}$ ; lysinate =  $\text{OOC}-\text{CH}(\text{NH}_2)(\text{CH}_2)_4\text{NH}_2$ ), the dangling  $\omega$ -amino group is capable of forming amine complexes with metal ions.<sup>473,577</sup> Low-valent metal complexes bind better to metal alkoxide moieties via a phosphino group.  $\text{PPh}_2$ -substituted carboxylic, sulfonic, and hydroxamic acids were prepared for this purpose and used as functional CLs.<sup>476,578</sup> An even simpler way of heterogenizing metal complexes was found for sulfonated cobalt phthalocyanine (CoPc). When  $\text{CoPc}(4-\text{SO}_3\text{H})_4$ , was reacted with  $\text{M}(\text{OR})_4$  ( $\text{M} = \text{Ti}, \text{Zr}$ ), all  $-\text{SO}_3\text{H}$  groups were converted into  $-\text{SO}_3[\text{M}(\text{OR})_3]$  groups. Sol-gel processing of the thus formed sulfonyl alkoxide derivatives gave heterogenized catalysts with a high activity and stability in the reaction media.<sup>579,580</sup>

The reaction of 4-[6-amino(1-ferrocenyl)hexyl]salicylic acid with  $\text{Zr}(\text{OPr})_4$  introduces the ferrocenyl moiety into zirconia gels as an electroactive probe to study the polycondensation process.<sup>581</sup>

Polypyrrole-zirconia hybrid materials were prepared by first reacting  $\text{C}_4\text{H}_4\text{N}-(\text{CH}_2)_n-\text{X}$  ( $\text{X} = \text{COOH}$  or  $\text{RC}(\text{O})-\text{CH}-\text{C}(\text{O})\text{R}$ ) with  $\text{Zr}(\text{OPr})_4$ , where the carboxylate or  $\beta$ -diketonate moiety served to establish a stable link between the pyrrole and the zirconium alkoxide moiety, followed by sol-gel processing and electropolymerization of the pyrrole groups.<sup>582</sup>

## 7.10.4 REFERENCES

1. Brinker, C. J.; Scherer, G. W. *Sol-Gel Science: The Physics and Chemistry of Sol-Gel Processing*; Academic Press: San Diego, CA 1990.
2. Pierre, A. C. *Introduction to Sol-Gel Chemistry*; Kluwer: Boston, MA 1998.

3. Wright, J. D.; Sommerdijk, N. A. J. M. *Sol–Gel Materials—Chemistry and Applications*; Gordon and Breach: Amsterdam, 2001.
4. Sanchez, C.; Ribot, F. *New J. Chem.* **1994**, *18*, 1007.
5. Novak, B. M. *Adv. Mater.* **1993**, *5*, 422.
6. Schubert, U.; Hüsing, N.; Lorenz, A. *Chem. Mater.* **1995**, *7*, 2010.
7. Wen, J.; Wilkes, G. L. *Chem. Mater.* **1996**, *8*, 1667.
8. Avnir, D.; Klein, L. C.; Levy, D.; Schubert, U.; Wojcik, A. B. In *The Chemistry of Organic Silicon Compounds*; Rappoport, Z., Apeloig, Y., Eds.; Wiley: New York, 1998; Vol. 2, Part 3, p 2317.
9. Haas, K.-H. *Adv. Eng. Mater.* **2000**, *2*, 571.
10. Guglielmi, M.; Carturan, G. J. *Non-Cryst. Solids* **1988**, *100*, 16.
11. Livage, J.; Henry, C.; Sanchez, M. *Progr. Solid State Chem.* **1988**, *18*, 259.
12. Richens, D. T. *The Chemistry of Aqua Ions. Synthesis, Structure and Reactivity*; Wiley: New York, 1997.
13. Kepert, D. L. *The Early Transition Metals*; Academic Press: London, 1970.
14. Tower, O. F.; Cooke, M. C. J. *Phys. Chem.* **1922**, *26*, 728.
15. Tower, O. F. J. *Phys. Chem.* **1924**, *28*, 176.
16. Finch, L. S. J. *Phys. Chem.* **1914**, *18*, 26.
17. Weiser, H. B. J. *Phys. Chem.* **1923**, *27*, 685.
18. Kopaczewski, W. *Bull. Soc. Chim. Fr.* **1950**, 149.
19. Woodhead, J. L. J. *Phys.* **1986**, *C1–47*, 1.
20. Alquier, C.; Vandenborre, M. T.; Henry, M. J. *Non-Cryst. Solids* **1986**, *79*, 383.
21. Gelo, M. *Bull. Soc. Chim. Fr.* **1925**, 37, 491.
22. Ganguly, P. B.; Dhar, N. R. J. *Phys. Chem.* **1922**, *26*, 701.
23. Cuy, E. J. J. *Phys. Chem.* **1921**, *25*, 415.
24. Selwood, P. W.; Ellis, M.; Davis, C. F. J. *Am. Chem. Soc.* **1950**, *72*, 3549.
25. Lume-Pereira, C.; Baral, A.; Henglein, A.; Janatra, E. J. *Phys. Chem.* **1985**, *89*, 5772.
26. Buss, D. H.; Schaumberg, G.; Glemser, O. *Angew. Chem., Int. Ed. Engl.* **1985**, *24*, 1057.
27. Klosky, S.; Marzano, C. J. *Phys. Chem.* **1925**, *29*, 1125.
28. Klosky, S. J. *Phys. Chem.* **1930**, *34*, 2621.
29. Hurd, C. B.; Jacober, W. J.; Godfrey, D. W. J. *Am. Chem. Soc.* **1941**, *63*, 723.
30. Hazel, J. F.; McNabb, W. M.; Santini, R. J. *Phys. Chem.* **1953**, *57*, 681.
31. Gharbi, N.; Sanchez, C.; Livage, J.; Lemerle, J.; Nejem, L.; Levebre, J. *Inorg. Chem.* **1982**, *21*, 2758.
32. Richardson, E. J. *Inorg. Nucl. Chem.* **1959**, *12*, 79.
33. Chemseddine, A.; Henry, M.; Livage, J. *Rev. Chim. Mineral.* **1984**, *21*, 487.
34. Chemseddine, A.; Babonneau, F.; Livage, J. J. *Non-Cryst. Solids* **1987**, *91*, 271.
35. Kepert, D. L.; Kyle, J. M. J. *Chem. Soc., Dalton Trans. II* **1978**, 133.
36. Chatterjee, S. N. J. *Colloid Sci.* **1958**, *13*, 61.
37. El Wakkad, S. E. S.; Rizk, H. A. J. *Am. Chem. Soc.* **1957**, *61*, 494.
38. Jander, G.; Krien, G. Z. *Anorg. Allg. Chem.* **1960**, *304*, 154.
39. Pearson, R. G. J. *Chem. Educ.* **1961**, *38*, 164.
40. Eigen, M. *Pure Appl. Chem.* **1963**, *6*, 97.
41. Kruger, H. *Chem. Soc. Rev.* **1982**, *11*, 227.
42. Baran, V. *Coord. Chem. Rev.* **1971**, *6*, 65.
43. Freedman, M. L. J. *Am. Chem. Soc.* **1958**, *80*, 2072.
44. Kepert, D. L. *Prog. Inorg. Chem.* **1962**, *4*, 199.
45. Tytko, R. H.; Glemser, O. *Adv. Inorg. Chem. Radiochem.* **1976**, *19*, 239.
46. Schwarzenbach, G.; Maier, J. J. *Inorg. Chem. Radiochem.* **1976**, *19*, 239.
47. Baes, C. F.; Mesmer, R. E. *The Hydrolysis of Cations*; Wiley: New York, 1976.
48. Mesmer, R. E.; Baes, C. F. *Inorg. Chem.* **1971**, *10*, 2290.
49. Johansson, G. *Acta Chem. Scand.* **1962**, *16*, 403.
50. Bottero, J. Y.; Manceau, A.; Villéras, F.; Tchoubar, D. *Langmuir* **1994**, *10*, 316.
51. Rose, J.; Manceau, A.; Bottero, J. Y.; Masion, A.; Garcia, F. *Langmuir* **1996**, *12*, 6701.
52. Rose, J.; Flank, A. M.; Masion, A.; Bottero, J. Y.; Elmerich, P. *Langmuir* **1997**, *13*, 1827.
53. Rose, J.; Manceau, A.; Masion, A.; Bottero, J. Y. *Langmuir* **1997**, *13*, 3240.
54. Clearfield, A.; Vaughan, P. A. *Acta Crystallogr.* **1956**, *9*, 555.
55. Mak, T. C. W. *Can. J. Chem.* **1968**, *46*, 3491.
56. Stünzi, H.; Marty, W. *Inorg. Chem.* **1983**, *22*, 2145.
57. Kolski, G. B.; Kildahl, N. K.; Margerum, D. W. *Inorg. Chem.* **1969**, *8*, 1211.
58. Johansson, G. *Acta Chem. Scand.* **1960**, *16*, 771.
59. Johansson, G.; Lundgren, L. G.; Sillén, L. G.; Söderquist, R. *Acta Chem. Scand.* **1960**, *14*, 769.
60. Akitt, J. W.; Farthing, A. J. *Magn. Res.* **1972**, *32*, 345.
61. Akitt, J. W.; Farthing, A. J. *Chem. Soc., Dalton Trans.* **1981**, 1617.
62. Akitt, J. W.; Mann, B. E. J. *Magn. Res.* **1981**, *44*, 684.
63. Bottero, J. Y.; Cases, J. M.; Fissinger, F.; Poirier, J. E. J. *Phys. Chem.* **1980**, *84*, 2933.
64. Bottero, J. Y.; Tchoubar, D.; Cases, J. M.; Fissinger, F. J. *Phys. Chem.* **1982**, *86*, 3667.
65. Bottero, J. Y.; Alexos, M.; Tchoubar, D.; Cases, J. M.; Fripiat, J.; Fissinger, F. J. *Colloid Interf. Sci.* **1987**, *117*, 47.
66. Akitt, J. W.; Elders, J. M. J. *Chem. Soc., Dalton Trans.* **1988**, 1347.
67. Bradley, S. M.; Kydd, R. A.; Yamdagni, R. J. *Chem. Soc., Dalton Trans.* **1990**, *413*, 2653.
68. Bradley, S. M.; Kydd, R. A. J. *Chem. Soc., Dalton Trans.* **1993**, 2407.
69. Klopogge, J. T.; Seykens, D.; Jansen, J. B. H.; Geus, J. W. J. *Non-Cryst. Solids* **1992**, *142*, 94, **1993**, *160*, 144.
70. Michot, L. J.; Montargès-Pelletier, E.; Lartiges, B. S.; d'Espinose de la Caillerie, J.-B.; Briosis, V. J. *Am. Chem. Soc.* **2000**, *122*, 6048.
71. Allouche, L.; Gérardin, C.; Loiseau, T.; Férey, G.; Tailleur, F. *Angew. Chem. Int. Ed. Engl.* **2000**, *112*, 511.
72. See, for example special issue of. *Chem. Rev.* **1998**, *98*(1).

73. Pope, M. T. *Heteropoly and Isopoly Oxometallates* **1983**, Springer: Berlin.
74. Souchay, P. *Polyanions et Polycations*; Gauthier-Villars: Paris, 1963, and references therein.
75. Schubert, U. J. *Sol-Gel Sci. Technol.* **2003**, *26*, 47.
76. Allcock, H. R.; Bissel, E. C.; Shawl, E. T. *Inorg. Chem.* **1973**, *12*, 2963.
77. Nagano, O.; Sasaki, Y. *Acta Crystallogr.* **1979**, *B25*, 2387.
78. Fuchs, V. J.; Freiwald, W.; Hartl, H. *Acta Crystallogr.* **1978**, *B34*, 1764.
79. Livage, J. *Coord. Chem. Rev.* **1998**, *178-180*, 999.
80. Livage, J. *Chem. Mater.* **1991**, *3*, 578.
81. Nagel, C. F. *J. Phys. Chem.* **1914**, *18*, 331.
82. Bunce, E. H.; Finch, L. S. *J. Phys. Chem.* **1913**, *17*, 769.
83. Singh, K. K.; Sarode, P. R.; Ganguly, P. *J. Chem. Soc., Dalton Trans.* **1983**, 1895.
84. Saraswat, I. P.; Vajpei, A. C. *J. Mater. Sci. Lett.* **1984**, *3*, 515.
85. Rajendran, S.; Rao, V. S.; Maiti, H. S. *J. Mater. Sci.* **1982**, *17*, 2709.
86. Gash, A. E.; Tillotson, T. M.; Sacher, J. H.; Hrubesh, L. W.; Simpson, R. L. *J. Non-Cryst. Solids* **2001**, *285*, 22.
87. Tillotson, T. M.; Sunderland, W. E.; Thomas, I. M.; Hrubesh, L. W. *J. Sol-Gel Sci. Technol.* **1994**, *1*, 241.
88. Itoh, H.; Tabata, T.; Kokitsu, M.; Okazaki, N.; Imizu, Y.; Tada, A. *J. Ceram. Soc. Jpn.* **1993**, *101*, 1081.
89. Witten, T. A.; Sanders, I. M. *Phys. Rev. Lett.* **1981**, *47*, 1400.
90. Bleier, A.; Cannon, R. M. *Mat. Res. Soc. Symp. Proc.* **1986**, *73*, 71.
91. Pickles, D. E.; Lilley, E. *J. Am. Ceram. Soc.* **1985**, *68*, C222.
92. Edelson, L. H.; Gaugler, K.; Glaeser, A. M. *Am. Ceram. Soc. Bull.* **1986**, *65*, 504.
93. van der Woode, J. H. A.; DeBryn, P. L.; Pieters, J. *Colloid Surf.* **1984**, *9*, 173.
94. van der Woode, J. H. A.; DeBryn, P. L. *Colloid Surf.* **1984**, *12*, 179.
95. Flynn, C. M., Jr. *Chem. Rev.* **1984**, *84*, 31.
96. Matijevic, E.; Sapiessko, R. S.; Melville, J. B. *J. Colloid Interf. Sci.* **1975**, *50*, 567.
97. Matijevic, E.; Scheiner, P. *J. Colloid Interf. Sci.* **1978**, *63*, 509.
98. Hamada, S.; Matijevic, E. *J. Chem. Soc., Faraday Trans. I* **1982**, *78*, 2147.
99. Matijevic, E. *Acc. Chem. Res.* **1981**, *14*, 22.
100. Matijevic, E. *Ann. Rev. Mater. Sci.* **1985**, *15*, 483.
101. Livage, J.; Henry, M.; Jolivet, J. P.; Sanchez, C. *Mater. Res. Soc. Bull.* **1990**, *1*, 18.
102. Matijevic, E. *Ann. Rev. Mater. Sci.* **1985**, *15*, 483.
103. Bradley, D. C.; Mehrotra, R. C.; Gaur, D. P. *Metal Alkoxides*; Academic Press: London, 1978.
104. Bradley, D. C.; Mehrotra, R. C.; Rothwell, I. P.; Singh, A. *Alkoxo and Aryloxo Derivatives of Metals*; Academic Press: London, 2001.
105. Turova, N. Ya.; Turevskaya, E. P.; Kessler, V. G.; Yanovskaya, M. I. *The Chemistry of Metal Alkoxides*; Kluwer: Boston, MA, 2002.
106. Bradley, D. C. *Adv. Inorg. Chem. Radiochem.* **1972**, *15*, 259.
107. Young, W. G.; Harting, W. H.; Crossley, F. S. *J. Am. Chem. Soc.* **1936**, *58*, 100.
108. Adkins, H.; Cox, F. W. *J. Am. Chem. Soc.* **1938**, *60*, 1151.
109. Teichner, S. J. *Compt. Rend.* **1953**, *237*, 810.
110. Coffey, S.; Boyd, V. J. *J. Chem. Soc.* **1954**, 2468.
111. Turova, N. Ya.; Kozunov, V. A.; Yanovskii, A. I.; Bokii, N. G.; Struchkov, Yu. T.; Tarnopol'skii, B. I. *J. Inorg. Nucl. Chem.* **1979**, *41*, 5.
112. Mazdiyasn, K. S.; Lynch, C. T.; Smith, J. S. *Inorg. Chem.* **1966**, *5*, 342.
113. Brown, L. S.; Mazdiyasn, K. S. *Inorg. Chem.* **1970**, *9*, 2783.
114. Poncelet, O.; Hubert-Pfalzgraf, L. G.; Daran, J. C.; Astier, R. *J. Chem. Soc., Chem. Commun.* **1989**, 1846.
115. Poncelet, O.; Hubert-Pfalzgraf, L. G. *Polyhedron* **1989**, *8*, 2183.
116. Bradley, D. C.; Chudzynska, H.; Frigo, D. M.; Hammond, M. E.; Hursthouse, M. B.; Mazid, M. A. *Polyhedron* **1990**, *9*, 719.
117. Poncelet, O.; Sartain, W. J.; Hubert-Pfalzgraf, L. G.; Foltling, K.; Caulton, K. G. *Inorg. Chem.* **1989**, *28*, 263.
118. Helgesson, G.; Jagner, S.; Poncelet, O.; Hubert-Pfalzgraf, L. G. *Polyhedron* **1991**, *10*, 1559.
119. Turova, N. Ya.; Korolev, A. V.; Tschebukov, D. E.; Belokon', A. I.; Yanovsky, A. I.; Struchkov, Yu. T. *Polyhedron* **1996**, *15*, 3869.
120. Kozlova, N. I.; Turova, N. Ya.; Turevskaya, E. *Sov. J. Coord. Chem.* **1982**, *8*, 339.
121. Shreider, V. A.; Turevskaya, E. P.; Kozlova, N. I.; Turova, N. Ya. *Inorg. Chim. Acta* **1981**, *13*, L73.
122. Kucheiko, S. I.; Turova, N. Ya.; Schreider, V. A. *Russ. J. Gen. Chem.* **1985**, *55*, 2396.
123. Turova, N. Ya.; Kessler, V. G. *Russ. J. Gen. Chem.* **1990**, *60*, 113.
124. Turova, N. Ya.; Kessler, V. G.; Kucheiko, S. I. *Polyhedron* **1991**, *10*, 2617.
125. Kessler, V. G.; Mironov, A. V.; Turova, N. Ya.; Yanovsky, A. I.; Struchkov, Yu. T. *Polyhedron* **1993**, *12*, 1573.
126. Kessler, V. G.; Turevskaya, E. P.; Kucheiko, S. I. *Mater. Res. Soc. Symp. Proc.* **1994**, *346*, 3.
127. Turova, N. Ya.; Turevskaya, E. P.; Kessler, V. G.; Kozlova, N. I.; Belokon, A. I. *Russ. J. Inorg. Chem.* **1992**, *37*, 26.
128. Kucheiko, S. I.; Kessler, V. G.; Turova, N. Ya. *Sov. J. Coord. Chem.* **1987**, *13*, 586.
129. Lehmkuhl, H.; Eisenbach, W. *Ann. Chem.* **1975**, 672.
130. Rogova, T. V.; Turova, N. Ya. *Sov. J. Coord. Chem.* **1985**, *11*, 448.
131. Turevskaya, E. P.; Kozlova, N. I.; Turova, N. Ya.; Popovkin, B. A.; Yanovskaya, M. I. *Phys. Chem. Technol.* **1989**, *2*, 925.
132. Banait, J. S.; Pahil, P. K. *Synth. React. Inorg. Met.-Org. Chem.* **1986**, *16*, 1217.
133. Banait, J. S.; Pahil, P. K. *Polyhedron* **1986**, *5*, 1865.
134. Kessler, V. G.; Shevel'kov, A. V.; Khvorykh, G. V. *Russ. J. Inorg. Chem.* **1995**, *40*, 1424.
135. Banait, J. S.; Deol, S. K.; Singh, B. *Synth. React. Inorg. Met.-Org. Chem.* **1990**, *20*, 1331.
136. Bradley, D. C.; Chatterjee, A. K.; Wardlaw, W. *J. Chem. Soc.* **1956**, 2260.
137. Merbach, M.; Carrard, U. P. *Helv. Chim. Acta* **1971**, *54*, 2771.
138. Bradley, D. C.; Holloway, C. E. *J. Chem. Soc. A* **1968**, 1316.
139. Bradley, D. C.; Wardlaw, W. *J. Chem. Soc.* **1951**, 280.

140. Bradley, D. C.; Abd El-Harlm, F. M.; Sadek, W. E. A.; Wardlaw, W. J. *Chem. Soc.* **1952**, 2032.
141. Bradley, D. C.; Mehrotra, R. C.; Wardlaw, W. J. *Chem. Soc.* **1953**, 1634.
142. Vaarstra, B. A.; Huffman, J. C.; Gradeff, P. S.; Hubert-Pfalzgraf, L. G.; Daran, J. C.; Parraud, S.; Yunlu, K.; Caulton, K. G. *Inorg. Chem.* **1990**, *29*, 3126.
143. Bradley, D. C.; Chakravarti, B. N.; Wardlaw, W. J. *Chem. Soc.* **1956**, 2381.
144. Bradley, D. C.; Chakravarti, B. N.; Wardlaw, W. J. *Chem. Soc.* **1956**, 4439.
145. Bradley, D. C.; Wardlaw, W.; Whitley, A. J. *Chem. Soc.* **1955**, 726.
146. Bradley, D. C.; Wardlaw, W.; Whitley, A. J. *Chem. Soc.* **1956**, 1139.
147. Bradley, D. C.; Chakravarti, B. N.; Chatterjee, A. K.; Wardlaw, W.; Whitley, A. J. *Chem. Soc.* **1958**, 99.
148. Yanovsky, A. I.; Turevskaya, E. P.; Turova, N. Ya.; Dolgushin, F. M.; Pisarevsky, A. P.; Batsanov, A. S.; Struchkov, Yu.T. *Russ. J. Inorg. Chem.* **1994**, *39*, 1246.
149. Pinkerton, A. A.; Schwarzbach, D.; Hubert-Pfalzgraf, L. G.; Riess, J. G. *Inorg. Chem.* **1976**, *15*, 1196.
150. Denny, D. B.; Denny, D. Z.; Hammond, P. T.; Hsu, Y. F. *J. Am. Chem. Soc.* **1981**, *103*, 2340.
151. Tupuy, G. *Compt. Rend.* **1955**, *240*, 2238.
152. Jones, R. G.; Bindschadler, E.; Karmas, G.; Martin, G. A., Jr.; Thirtle, J. R.; Yoeman, F. A.; Gilman, H. *J. Am. Chem. Soc.* **1956**, *78*, 4289.
153. Bradley, D. C.; Harder, B.; Hudswell, F. J. *Chem. Soc.* **1957**, 3318.
154. Mehrotra, A.; Mehrotra, R. C. *Inorg. Chem.* **1972**, *11*, 2170.
155. Mehrotra, A.; Mehrotra, R. C. *Curr. Sci. (India)* **1964**, 241.
156. Reimann, R.; Tanner, A. Z. *Naturforsch. B* **1965**, *20*, 524.
157. Moegele, L. Z. *Anorg. Allg. Chem.* **1968**, *363*, 166.
158. Bindal, S. R.; Mathur, V. K.; Mehrotra, R. C. *J. Chem. Soc. A* **1969**, 863.
159. Chatterjee, S.; Bindal, S. R.; Mehrotra, R. C. *J. Indian Chem. Soc.* **1976**, *53*, 867.
160. Tabern, D. L.; Orndorff, W. R.; Dennis, L. M. *J. Am. Chem. Soc.* **1925**, *47*, 2039.
161. Sidgwick, N. V.; Laubengayer, A. W. *J. Am. Chem. Soc.* **1932**, *54*, 948.
162. Hampden-Smith, M. J.; Wark, T. A.; Rheingold, A. L.; Huffman, J. C. *Can. J. Chem.* **1991**, *69*, 121.
163. Athar, T.; Bohra, R.; Mehrotra, R. C. *Synth. React. Inorg. Metal-Org. Chem.* **1989**, *19*, 195.
164. Reuter, H.; Kremser, M. Z. *Anorg. Allg. Chem.* **1991**, 259, 598.
165. Mehrotra, R. C.; Rai, A. K.; Jain, N. C. *Polyhedron* **1991**, *10*, 1103.
166. Papiernik, R.; Hubert-Pfalzgraf, L. G.; Massiani, M. C. *Inorg. Chim. Acta* **1989**, *165*, 1.
167. Papiernik, R.; Hubert-Pfalzgraf, L. G.; Massiani, M. C. *Polyhedron* **1991**, *10*, 1657.
168. Moedritzer, K. *Inorg. Synth.* **1968**, *11*, 181.
169. Russias, C.; Damm, F.; Deluzarche, A.; Maillard, A. *Bull. Soc. Chim. France* **1966**, 2275.
170. Killard, A.; Deluzarche, A.; Marie, J. C.; Havas, I. *Bull. Soc. Chim. France* **1965**, 2962.
171. Mehrotra, R. C.; Rai, A. K. *Indian J. Chem.* **1966**, *4*, 537.
172. Evans, W. J.; Hains, J. H., Jr.; Ziller, J. W. *J. Chem. Soc., Chem. Commun.* **1989**, 1628.
173. Whitmire, K. H.; Jones, C. M.; Burkart, M. D.; Hutchison, J. C.; McKnight, A. L. *Mater. Res. Soc. Symp. Proc.* **1992**, *271*, 149.
174. Jones, C. M.; Burkart, M. D.; Bachmann, R. E.; Serra, D. L.; Hwu, S. J.; Whitmire, K. H. *Inorg. Chem.* **1993**, *32*, 5136.
175. Massiani, M. C.; Papiernik, R.; Hubert-Pfalzgraf, L. G.; Daran, J. C. *J. Chem. Soc., Chem. Commun.* **1990**, 301.
176. Massiani, M. C.; Papiernik, R.; Hubert-Pfalzgraf, L. G.; Daran, J. C. *Polyhedron* **1991**, *10*, 437.
177. Matchett, M. A.; Chiang, M. Y.; Buhro, W. E. *Inorg. Chem.* **1990**, *29*, 358.
178. Mehrotra, R. C.; Mathur, S. N. *J. Indian Chem. Soc.* **1965**, *42*, 1.
179. Misra, S. N.; Misra, T. N.; Mehrotra, R. C. *Aust. J. Chem.* **1968**, *21*, 797.
180. Evans, W. J.; Deming, T. J.; Olofson, J. F.; Ziller, J. W. *Inorg. Chem.* **1989**, *28*, 4027.
181. Bradley, D. C.; Faktor, M. M. *Chem. Ind.* **1958**, 1332.
182. Evans, W. J.; Sollberger, M. S.; Hanusa, T. P. *J. Am. Chem. Soc.* **1988**, *110*, 1841.
183. Gradeff, P. S.; Schreiber, F. G.; Brooks, K. C.; Sievers, R. E. *Inorg. Chem.* **1985**, *24*, 1110.
184. Gradeff, P. S.; Schreiber, F. G.; Mauermann, H. *J. Less-Common Met.* **1986**, *126*, 335.
185. Batwara, J. M.; Tripathi, U. D.; Mehrotra, R. K.; Mehrotra, R. C. *Chem. Ind.* **1966**, 1379.
186. Misra, S. N.; Misra, T. N.; Kapoor, R. N.; Mehrotra, R. C. *Chem. Ind.* **1963**, 120.
187. Mehrotra, A.; Mehrotra, R. C. *Indian J. Chem.* **1972**, *10*, 532.
188. Batwara, J. M.; Tripathi, U. D.; Mehrotra, R. C. *J. Chem. Soc. A* **1967**, 991.
189. Sankhla, B. S.; Misra, S. N.; Kapoor, R. N. *Chem. Ind.* **1965**, 382.
190. Mehrotra, R. C.; Batwara, J. M. *Inorg. Chem.* **1970**, *9*, 2505.
191. Sankhla, B. S.; Misra, S. N.; Kapoor, R. N. *Aust. J. Chem.* **1967**, *20*, 2013.
192. Bradley, D. C.; Saad, M. A.; Wardlaw, W. J. *Chem. Soc.* **1954**, 1091.
193. Andersen, R. A. *Inorg. Nucl. Chem. Lett.* **1979**, *15*, 57.
194. Lubben, T. V.; Wolczanski, P. T.; van Duyne, G. D. *Organometallics* **1984**, *3*, 977.
195. Jones, R. G.; Karmas, G.; Martin, G. A., Jr.; Gilman, H. *J. Am. Chem. Soc.* **1965**, *78*, 4285.
196. Bradley, D. C.; Chakravarti, B. N.; Chatterjee, A. K. *J. Inorg. Nucl. Chem.* **1957**, *3*, 367.
197. Samulski, E. T.; Karraker, D. G. *J. Inorg. Nucl. Chem.* **1967**, *29*, 993.
198. Bischoff, F.; Adkins, H. *J. Am. Chem. Soc.* **1924**, *46*, 256.
199. Thomas, I. M. *Can. J. Chem.* **1961**, *39*, 1386.
200. Bradley, D. C.; Mehta, M. I. *Can. J. Chem.* **1962**, *40*, 1183.
201. Choukroun, R.; Dia, A.; Gervais, D. *Inorg. Chim. Acta* **1979**, *34*, 211.
202. Bochmann, M.; Wilkinson, G.; Young, G. B.; Hursthouse, M. B.; Malik, K. M. A. *J. Chem. Soc., Dalton Trans.* **1980**, 901.
203. Kraus, H. L.; Munster, G. Z. *Anorg. Allg. Chem.* **1967**, *352*, 24.
204. Murray, B. D.; Hope, H.; Power, P. P. *J. Am. Chem. Soc.* **1985**, *107*, 169.
205. Gilbert, T. M.; Landes, A. M.; Rogers, R. D. *Inorg. Chem.* **1992**, *31*, 3438.
206. Hoffmann, D. M.; Lappas, D.; Wierda, D. A. *J. Am. Chem. Soc.* **1989**, *111*, 1531.



207. Hoffmann, D. M.; Lappas, D.; Wierda, D. A. *J. Am. Chem. Soc.* **1993**, *115*, 10538.
208. Kakos, G. A.; Winter, G. *Aust. J. Chem.* **1969**, *22*, 97.
209. Adams, R. W.; Bishop, E.; Martin, R. L.; Winter, G. *Aust. J. Chem.* **1966**, *19*, 207.
210. McWham, D. B.; Lundgren, G. *Acta Crystallogr. A* **1963**, *16*, 36.
211. Baetsle, L.; Pelsmaekers, J. *J. Inorg. Nucl. Chem.* **1962**, *21*, 124.
212. Bryndza, H. N.; Calabrese, J. C.; Marsi, M.; Roc, D. C.; Tam, W.; Bercaw, J. E. *J. Am. Chem. Soc.* **1986**, *108*, 4805.
213. Bryndza, H. N.; Kretschmar, S. A.; Tulip, T. H. *J. Chem. Soc. Chem. Comm.* **1985**, 977.
214. Alcock, N. W.; Platt, A. W. G.; Pringle, P. G. *J. Chem. Soc., Dalton Trans.* **1989**, 139.
215. Alcock, N. W.; Platt, A. W. G.; Pringle, P. G. *Inorg. Chim. Acta* **1987**, *128*, 215.
216. Purdy, A. P.; George, C. F.; Callahan, J. H. *Inorg. Chem.* **1991**, *30*, 2812.
217. Jones, G. E. M.; Hughes, O. L. *J. Chem. Soc.* **1934**, 1197.
218. Greiser, T.; Weiss, E. *Chem. Ber.* **1976**, *104*, 3142.
219. Tsuda, T.; Hashimoto, T.; Saegusa, T. *J. Am. Chem. Soc.* **1972**, *94*, 658.
220. Lemmen, T. H.; Goeden, G. V.; Huffman, J. C.; Geerts, R. L.; Caulton, K. G. *Inorg. Chem.* **1990**, *29*, 3680.
221. Brubaker, C. H., Jr.; Wicholas, M. *J. Inorg. Chem. Nucl. Chem.* **1965**, *27*, 59.
222. Bradley, D. C.; Caldwell, E. V.; Wardlaw, W. *J. Chem. Soc.* **1957**, 4775.
223. Mehrotra, R. C. *J. Indian Chem. Soc.* **1953**, *30*, 585.
224. Mehrotra, R. C. *J. Indian Chem. Soc.* **1954**, *31*, 85.
225. Oliver, J. G.; Worrall, I. J. *J. Chem. Soc. A* **1970**, 845.
226. Bradley, D. C.; Mehrotra, R. C.; Wardlaw, W. *J. Chem. Soc.* **1952**, 5020.
227. Bradley, D. C.; Kay, L.; Wardlaw, W. *Chem. Ind.* **1953**, 746.
228. Sasin, G. S.; Sadin, R. *J. Org. Chem.* **1955**, *20*, 770.
229. Marie, J. C. *Ann. Chem.* **1961**, *6*, 969.
230. Mehrotra, R. C.; Gupta, V. D. *J. Indian Chem. Soc.* **1964**, *41*, 537.
231. Shostakovskii, M. F.; Mirskov, R. G.; Vleasov, V. M. *Khim. Atsetilena* **1968**, 171.
232. Mehrotra, R. C.; Bhatnagar, D. D. *J. Indian Chem. Soc.* **1965**, *42*, 327.
233. Bradley, D. C.; Chatterjee, A. K.; Wardlaw, W. *J. Chem. Soc.* **1956**, 3469.
234. Bradley, D. C.; Chatterjee, A. K.; Wardlaw, W. *J. Chem. Soc.* **1957**, 2600.
235. Verma, I. D.; Mehrotra, R. C. *J. Chem. Soc.* **1960**, 2966.
236. Shihava, I.; Schwartz, Jr., W. T.; Post, H. W. *Chem. Rev.* **1961**, *61*, 1.
237. Campell, C.; Bott, S. G.; Larsen, R.; van der Sluys, W. G. *Inorg. Chem.* **1994**, *33*, 4950.
238. Bradley, D. C.; Faktor, M. M. *Nature* **1959**, *184*, 55.
239. Mehrotra, R. C.; Verma, I. D. *J. Indian Chem. Soc.* **1961**, *38*, 147.
240. Bradley, D. C.; Mehrotra, R. C.; Wardlaw, W. *J. Chem. Soc.* **1952**, 2027.
241. Bradley, D. C.; Mehrotra, R. C.; Wardlaw, W. *J. Chem. Soc.* **1952**, 4204.
242. Mittal, R. K.; Mehrotra, R. C. *Z. Anorg. Allg. Chem.* **1964**, *327*, 111.
243. Mehrotra, R. C.; Kapoor, P. N. *J. Less-Common Met.* **1966**, *10*, 354.
244. Bradley, D. C.; Holloway, C. E. *J. Chem. Soc. A* **1968**, 219.
245. Boyle, T. J.; Alam, T. M.; Dimos, D.; Moore, G. J.; Buchheit, C. D.; Al-Shareef, H. N.; Mechenbier, E. R.; Bear, B. R.; Ziller, J. W. *Chem. Mater.* **1997**, *9*, 3187.
246. Bradley, D. C.; Multani, R. K.; Wardlaw, W. *J. Chem. Soc.* **1958**, 126.
247. Goel, S. C.; Kramer, K. S.; Gibbons, P. C.; Buhro, W. E. *Inorg. Chem.* **1989**, *28*, 3619.
248. Purdy, A. P.; George, C. F.; Brewer, G. A. *Inorg. Chem.* **1992**, *31*, 2633.
249. Jeffris, P. M.; Wilson, S. R.; Girolami, G. S. *Inorg. Chem.* **1992**, *31*, 4503.
250. Mehrotra, R. C.; Arora, M. Z. *Anorg. Allg. Chem.* **1969**, *370*, 300.
251. Bradley, D. C.; Kapoor, R. N.; Smith, B. C. *J. Inorg. Nucl. Chem.* **1962**, *24*, 863.
252. Bradley, D. C.; Kapoor, R. N.; Smith, B. C. *J. Chem. Soc.* **1963**, 1034.
253. Baker, R. H. *J. Am. Chem. Soc.* **1938**, *60*, 2673.
254. Bradley, D. C.; Sinha, R. P. N.; Wardlaw, W. *J. Chem. Soc.* **1958**, 4651.
255. Mehrotra, R. C. *J. Am. Chem. Soc.* **1954**, *76*, 2266.
256. Mittal, R. K.; Mehrotra, R. C. *Z. Anorg. Allg. Chem.* **1964**, *331*, 89.
257. Mehrotra, R. C.; Kapoor, P. N. *J. Less-Common Met.* **1964**, *7*, 98.
258. Kapoor, P. N.; Mehrotra, R. C. *J. Less-Common Met.* **1966**, *10*, 66.
259. Chisholm, M. H.; Distasi, V. F.; Streib, W. E. *Polyhedron* **1990**, *9*, 253.
260. Cayton, R. H.; Chisholm, M. H.; Davidson, D. R.; Distasi, V. F.; Du, P.; Huffman, J. C. *Inorg. Chem.* **1991**, *30*, 1020.
261. Mlinea, L. A.; Suh, S.; Hoffman, D. M. *Inorg. Chem.* **1999**, *38*, 4447.
262. Fieldberg, T.; Hitchcock, P. B.; Lappert, M. F.; Smith, S. J.; Thorne, A. J. *J. Chem. Soc., Chem. Commun.* **1985**, 939.
263. Oliver, J. G.; Worrall, I. J. *J. Chem. Soc. A* **1970**, 2347.
264. Wedler, M.; Gilje, J. W.; Pieper, U.; Stalke, D.; Noltemeyer, M.; Edelmann, F. T. *Chem. Ber.* **1991**, *124*, 1163.
265. Bradley, D. C.; Chudzynska, H.; Hammond, M. E.; Hursthouse, M. B.; Motevalli, M.; Ruowen, W. *Polyhedron* **1992**, *11*, 375.
266. Herrmann, W. A.; Anwander, R.; Denk, M. *Chem. Ber.* **1992**, *125*, 2399.
267. Barnhart, D. M.; Clark, D. L.; Huffman, J. C.; Vincent, R. L.; Watkin, J. G. *Inorg. Chem.* **1993**, *32*, 4077.
268. Bradley, D. C.; Chudzynska, H.; Hursthouse, M. B.; Motevalli, M. *Polyhedron* **1993**, *12*, 1907.
269. Bradley, D. C.; Chudzynska, H.; Hursthouse, M. B.; Motevalli, M. *Polyhedron* **1994**, *13*, 7.
270. Bradley, D. C.; Chudzynska, H.; Hursthouse, M. B.; Motevalli, M.; Wu, R. *Polyhedron* **1994**, *13*, 1.
271. Evans, W. J.; Anwander, R.; Berlekamp, U. H.; Ziller, J. W. *Inorg. Chem.* **1995**, *34*, 3583.
272. Anwander, R. *Top. Curr. Chem.* **1996**, *179*, 149.
273. Evans, W. J.; Golden, R. E.; Ziller, J. W. *Inorg. Chem.* **1991**, *30*, 4963.
274. Stecher, H. A.; Sen, A.; Rheingold, A. *Inorg. Chem.* **1989**, *28*, 3280.
275. Anwander, R.; Munck, F. C.; Priermeier, T.; Scherer, W.; Runte, O.; Herrmann, W. A. *Inorg. Chem.* **1997**, *36*, 3545.

276. Barnhart, D. B.; Clark, D. L.; Gordon, J. C.; Huffman, J. C.; Watkin, J. G.; Zwick, B. D. *J. Am. Chem. Soc.* **1993**, *115*, 8461.
277. Bradley, D. C.; Chudzynska, H.; Hursthouse, M. B.; Motevalli, M. *Polyhedron* **1991**, *10*, 1049.
278. van der Sluys, W. G.; Sattelberger, A. P.; McElfresh, M. *Polyhedron* **1990**, *9*, 1843.
279. Bradley, D. C.; Hillyer, M. J. *Trans. Faraday Soc.* **1966**, *62*, 2382.
280. Aleya, E. C.; Basi, J. S.; Bradley, D. C.; Chisholm, M. H. *J. Chem. Soc. A* **1971**, 772.
281. Basi, J. S.; Bradley, D. C.; Chisholm, M. H. *J. Chem. Soc. A* **1971**, 1433.
282. Chisholm, M. H.; Reichert, W. W.; Thornton, P. *J. Am. Chem. Soc.* **1978**, *100*, 2744.
283. Akiyama, A.; Chisholm, M. H.; Cotton, F. A.; Extine, M. W.; Haitko, D. A.; Little, D.; Fanwick, P. E. *Inorg. Chem.* **1979**, *18*, 2266.
284. Chisholm, M. H.; Huffman, J. C.; Leonelli, J. *J. Chem. Soc., Chem. Commun.* **1981**, 270.
285. Horvath, B.; Moseler, R.; Horvath, E. G. *Z. Anorg. Allg. Chem.* **1979**, *449*, 41.
286. Bochmann, M.; Wilkinson, G.; Young, G. B.; Hursthouse, M. B.; Malik, K. M. A. *J. Chem. Soc., Dalton Trans.* **1980**, 1863.
287. Sigel, G. A.; Bartlett, R. A.; Decker, D.; Olmstead, M. M.; Power, P. P. *Inorg. Chem.* **1987**, *26*, 1773.
288. Alcock, N. W.; Platt, A. W. G.; Pringle, P. G. *J. Chem. Soc., Dalton Trans.* **1987**, 2273.
289. Goel, S. C.; Chiang, M. Y.; Buhro, W. E. *Inorg. Chem.* **1990**, *29*, 4646.
290. Boulmaaz, S.; Papiernik, R.; Hubert-Pfalzgraf, L. G.; Vaissermann, J.; Daran, J. C. *Polyhedron* **1992**, *11*, 1331.
291. Mehrotra, R. C.; Singh, A. *Progr. Inorg. Chem.* **1997**, *46*, 239.
292. Veith, M.; Mathur, S.; Mathur, C. *Polyhedron* **1998**, *17*, 1005.
293. Veith, M. *J. Chem. Soc., Dalton Trans.* **2002**, 2405.
294. Chandler, C. D.; Roger, C.; Hampden-Smith, M. J. *Chem. Rev.* **1993**, *93*, 1205.
295. Caulton, K. G.; Hubert-Pfalzgraf, L. G. *Chem. Rev.* **1990**, *90*, 969.
296. Vavilkin, A. S.; Dmitrieva, Z. T. *Zh. Obshch. Kim.* **1989**, *59*, 1970.
297. Meerwein, H.; Bersin, T. *Ann.* **1929**, *476*, 113.
298. v. Schloder, R.; Protzer, H. *Z. Anorg. Allg. Chem.* **1965**, *340*, 23.
299. Jain, N. C.; Rai, A. K.; Mehrotra, R. C. *Proc. Indian Acad. Sci. A* **1976**, *84*, 98.
300. Veith, M. *Chem. Rev.* **1990**, *90*, 3.
301. Veith, M.; Roesler, R. *Z. Naturforsch. B* **1986**, *41*, 1071.
302. Hampden-Smith, M. J.; Smith, D. E.; Duesler, E. N. *Inorg. Chem.* **1989**, *28*, 3399.
303. Veith, M.; Reimers, M. *Chem. Ber.* **1990**, *123*, 1941.
304. Athar, T.; Bohra, R.; Mehrotra, R. C. *Main Group Met. Chem.* **1987**, *10*, 399.
305. Veith, M.; Yu, E.-C.; Huch, V. *Chem. Eur. J.* **1995**, *1*, 26.
306. Mehrotra, R. C.; Agrawal, M. M. *J. Chem. Soc.* **1967**, 1026.
307. Hampden-Smith, M. J.; Williams, D. S.; Rheingold, A. L. *Inorg. Chem.* **1990**, *29*, 4076.
308. Bartley, W. G.; Wardlaw, W. *J. Chem. Soc.* **1958**, 421.
309. Sharma, C. K.; Goel, S.; Mehrotra, R. C. *Indian J. Chem. A* **1979**, *14*, 878.
310. Vaarstra, B. A.; Streib, W. E.; Caulton, K. G. *J. Am. Chem. Soc.* **1990**, *112*, 8593.
311. Mehrotra, R. C.; Agrawal, M. M.; Kapoor, P. N. *J. Chem. Soc. A* **1968**, 2673.
312. Weis, R. S.; Gaylord, T. K. *Appl. Phys. A* **1985**, *37*, 191.
313. Eichorst, D. J.; Payne, D. A. *Mater. Res. Soc. Symp. Proc.* **1988**, *121*, 773.
314. Cotton, F. A.; Diebold, M. P.; Roth, W. J. *Inorg. Chem.* **1988**, *27*, 3596.
315. Nazeri-Esghi, A.; Kuang, A. X.; Mackenzie, J. D. *J. Mater. Sci.* **1990**, *K*, 3333.
316. Goel, S. C.; Hollingsworth, J. A.; Beatty, A. M.; Robinson, K. D.; Buhro, W. E. *Polyhedron* **1998**, *17*, 781.
317. Purdy, A. P.; George, C. F. *Inorg. Chem.* **1994**, *33*, 761.
318. Mehrotra, R. C.; Agrawal, M. M.; Mehrotra, A. *Synth. React. Inorg. Met.-Org. Chem.* **1973**, *3*, 181, 407.
319. Mehrotra, R. C.; Batwara, J. M.; Kapoor, P. N. *Coord. Chem. Rev.* **1980**, *31*, 67.
320. Veith, M.; Mathur, S.; Shen, H.; Lecerf, N.; Hüfner, S.; Jilavi, M. H. *Chem. Mater.* **2001**, *13*, 4041.
321. Mehrotra, R. C.; Mehrotra, A. *J. Chem. Soc., Dalton Trans.* **1972**, 1203.
322. Turevskaya, E. P.; Berdyev, D. V.; Turova, N. Ya.; Starikova, Z. A.; Yanovsky, A. I.; Struchkov, Yu. T.; Belokon, A. I. *Polyhedron* **1997**, *16*, 663.
323. Govil, S.; Kapoor, P. N.; Mehrotra, R. C. *Inorg. Chim. Acta* **1975**, *15*, 43.
324. Mehrotra, R. C.; Singh, A. *J. Indian Chem. Soc.* **1993**, *70*, 885.
325. Mehrotra, R. C.; Rai, A. K.; Jain, N. C. *J. Inorg. Nucl. Chem.* **1977**, *40*, 349.
326. Mehrotra, R. C.; Jain, N. C.; Goel, R. R. *Synth. React. Inorg. Met.-Org. Chem.* **1981**, *11*, 345.
327. Singh, J.; Mehrotra, R. C. *Inorg. Chem.* **1984**, *23*, 1046.
328. Dubey, R. K.; Singh, A.; Mehrotra, R. C. *Indian J. Chem. A* **1992**, *31*, 156.
329. Mehrotra, R. C. *Coord. Chem.* **1981**, *21*, 113.
330. Shah, A.; Singh, J.; Singh, A.; Mehrotra, R. C. *Indian J. Chem. A* **1991**, *30*, 1018.
331. Gupta, R.; Singh, A.; Mehrotra, R. C. *Indian J. Chem. A* **1991**, *30*, 592.
332. Singh, A.; Mehrotra, R. C. *J. Coord. Chem.* **1984**, *13*, 273.
333. Stumpp, E.; Hillebrand, U. *Z. Naturforsch. B* **1979**, *34*, 262.
334. Garg, G.; Dubey, R. K.; Singh, A.; Mehrotra, R. C. *Polyhedron* **1991**, *10*, 1733.
335. Mehrotra, R. C.; Singh, J. V. *Can. J. Chem.* **1984**, *62*, 1003.
336. Singh, J.; Mehrotra, R. C. *Z. Anorg. Allg. Chem.* **1984**, *522*, 211.
337. Albers, H.; Deutsch, M.; Krastinat, W.; v. Asten, H. *Chem. Ber.* **1952**, *85*, 267.
338. Agrawal, M.; Sharma, C. K.; Mehrotra, R. C. *Synth. React. Inorg. Met.-Org. Chem.* **1983**, *13*, 571.
339. Sogani, S.; Singh, A.; Mehrotra, R. C. *Main Group Met. Chem.* **1992**, *15*, 197.
340. Agrawal, S. K.; Mehrotra, R. C. *Inorg. Chim. Acta* **1986**, *112*, 117.
341. Shah, A.; Singh, A.; Mehrotra, R. C. *Indian J. Chem. A* **1989**, *28*, 392.
342. Shah, A.; Singh, A.; Mehrotra, R. C. *Indian J. Chem. A* **1991**, *30*, 1018.
343. Dubey, R. K.; Singh, A.; Mehrotra, R. C. *Bull. Chem. Soc. Jpn.* **1988**, *61*, 983.
344. Jain, R.; Rai, A. K.; Mehrotra, R. C. *Z. Naturforsch. B* **1985**, *40*, 1371.

345. Dubey, R. K.; Singh, A.; Mehrotra, R. C. *Transition Met. Chem.* **1985**, *10*, 473.
346. Shah, A.; Singh, A.; Mehrotra, R. C. *Inorg. Chim. Acta* **1986**, *118*, 151.
347. Shah, A.; Singh, A.; Mehrotra, R. C. *Indian J. Chem. A* **1987**, *26*, 485.
348. Dubey, R. K.; Singh, A.; Mehrotra, R. C. *Inorg. Chim. Acta* **1988**, *143*, 169.
349. Jain, R.; Rai, A. K.; Mehrotra, R. C. *J. Inorg. Chem.* **1987**, *3*, 96.
350. Dubey, R. K.; Singh, A.; Mehrotra, R. C. *Polyhedron* **1987**, *6*, 427.
351. Mehrotra, R. C.; Agarwal, M. *Polyhedron* **1985**, *4*, 845, 1141.
352. Chiba, R. C.; Singh, A.; Mehrotra, R. C. *Synth. React. Inorg. Met.-Org. Chem.* **1990**, *20*, 989.
353. Garg, G.; Singh, A.; Mehrotra, R. C. *Indian J. Chem. A* **1991**, *30*, 688, 866.
354. Mehrotra, R. C.; Singh, A.; Tripathi, U. D. *Chem. Rev.* **1991**, *91*, 1287.
355. Mathur, S.; Singh, A.; Mehrotra, R. C. *Polyhedron* **1992**, *11*, 341.
356. Gupta, R.; Singh, A.; Mehrotra, R. C. *New J. Chem.* **1991**, *15*, 65.
357. Gupta, R.; Singh, A.; Mehrotra, R. C. *Indian J. Chem. A* **1993**, *32*, 310.
358. Sogani, S.; Singh, A.; Mehrotra, R. C. *Indian J. Chem. A* **1993**, *32*, 345, 449.
359. Mehrotra, R. C.; Singh, A.; Sogani, S. *Chem. Soc. Rev.* **1994**, *23*, 215.
360. Veith, M.; Mathur, S.; Huch, V. *Inorg. Chem.* **1996**, *7295 J. Chem. Soc., Dalton Trans* **1996**, 2485.
361. Bradley, D. C.; Mehrotra, R. C.; Swanwick, J. D.; Wardlaw, W. J. *Chem. Soc.* **1953**, 2025.
362. Ibers, J. A. *Nature* **1963**, *197*, 686; Wright, D. A.; Williams, D. A. *Acta Crystallogr. B* **1968**, *24*, 1107.
363. Veith, M.; Mathur, S.; Huch, V. *J. Chem. Soc., Dalton Trans.* **1997**, 2101.
364. Turevskaya, E. P.; Turova, N. Ya. *Bull. Acad. Sci. USSR Div. Chem. Sci.* **1977**, 1463.
365. Shiner, V. J.; Whittaker, D.; Fernandez, V. P. *J. Am. Chem. Soc.* **1963**, *85*, 2318.
366. Oliver, J. G.; Phillips, P. K.; Worrall, I. J. *J. Inorg. Nucl. Chem.* **1969**, *31*, 1609.
367. Huckerby, T. N.; Oliver, J. G.; Worrall, I. J. *Inorg. Nucl. Chem. Lett.* **1969**, *5*, 749.
368. Foltling, K.; Streib, W. E.; Caulton, K. G.; Poncelet, O.; Hubert-Pfalzgraf, L. G. *Polyhedron* **1991**, *10*, 1639.
369. Oliver, J. G.; Worrall, I. J. *Inorg. Nucl. Chem. Lett.* **1969**, *5*, 455.
370. Ensinger, V.; Schwarz, W.; Schrutz, B.; Sommer, K.; Schmidt, A. Z. *Anorg. Allg. Chem.* **1987**, *544*, 181.
371. Boyle, T. J.; Pedrotty, D. M.; Scott, B.; Ziller, J. W. *J. Am. Chem. Soc.* **1999**, *121*, 12104.
372. Toledano, P.; Ribot, F.; Sanchez, C. *Acta Crystallogr. C* **1990**, *46*, 1419.
373. Herrmann, W. A.; Nuber, N. W.; Anwender, R.; Priermeier, T. *Chem. Ber.* **1993**, *126*, 1127.
374. Gaur, D. P.; Srivastava, G.; Mehrotra, R. C. *J. Organomet. Chem.* **1973**, *63*, 221.
375. Chandler, C. D.; Caruso, J.; Hampden-Smith, M.; Rheingold, A. L. *Polyhedron* **1995**, *14*, 2491.
376. Caughlan, C. N.; Smith, H. S.; Katz, W.; Hodgson, W.; Crowe, R. W. *J. Am. Chem. Soc.* **1951**, *73*, 5652.
377. Martin, R. L.; Winter, G. *J. Chem. Soc.* **1961**, 2947.
378. Bradley, D. C.; Holloway, C. E. *Inorg. Chem.* **1964**, *3*, 1163.
379. Boyle, T. J.; Alam, T. M.; Mechenbier, E. R.; Scott, B. L.; Ziller, J. W. *Inorg. Chem.* **1997**, *36*, 3293.
380. Samuels, J. A.; Lobkovsky, E. B.; Streib, W. E.; Foltling, K.; Hufmann, J. C.; Zwanzinger, J. W.; Caulton, K. G. *J. Am. Chem. Soc.* **1993**, *115*, 5093.
381. Bradley, D. C.; Chatterjee, A. K.; Wardlaw, W. J. *Chem. Soc.* **1954**, 1091.
382. Clark, D. L.; Huffman, J. C.; Watkin, J. G. *J. Chem. Soc., Chem. Commun.* **1992**, 266.
383. Chisholm, M. H.; Huffman, J. C.; Kirkpatrick, C. C.; Leonelli, J.; Foltling, K. *J. Am. Chem. Soc.* **1981**, *103*, 6093.
384. Tempel, N.; Schwarz, W.; Weidlein, J. Z. *Anorg. Allg. Chem.* **1981**, *474*, 157.
385. Cotton, F. A.; Marler, D. O.; Schwotzer, W. *Inorg. Chem.* **1984**, *23*, 4211.
386. Akiyama, A.; Chisholm, M. H.; Cotton, F. A.; Extine, M. W.; Haitko, D. A.; Leonelli, J.; Little, D. *J. Am. Chem. Soc.* **1981**, *103*, 779.
387. Bryan, J. C.; Wheeler, D. R.; Clark, D. L.; Huffman, J. C.; Sattelberger, A. P. *J. Am. Chem. Soc.* **1991**, *113*, 3184.
388. Examples: Goel, S. C.; Chiang, M. Y.; Gibbons, P. C.; Buhro, W. E. *Mater. Res. Soc. Symp. Proc.* **1992**, *271*, 3.
389. Barkley, J. V.; Cannadine, J. C.; Hannaford, I.; Harding, M. M.; Steiner, A.; Tallon, J.; Whyman, R. *J. Chem. Soc., Chem. Commun.* **1997**, 1653.
390. Kunu, D.; Ganguli, D. *J. Mater. Sci. Lett.* **1986**, *5*, 293.
391. Prassas, M.; Hench, L. L. In *Ultrastructure Processing of Glasses, Ceramics and Composites*; Hench, L. L., Ulrich, D. R., Eds.; Wiley: New York, 1984; p 464.
392. Yoldas, B. E. *J. Mater. Sci.* **1986**, *21*, 1087.
393. Sakka, S.; Kamiya, K. *J. Non-Cryst. Solids* **1980**, *42*, 403.
394. Kamiya, K.; Tanimoto, K.; Yoko, T. *J. Mater. Sci. Lett.* **1986**, *5*, 402.
395. Yoldas, B. E. *J. Non-Cryst. Solids* **1980**, *38*, 81.
396. Rupp, W.; Hüsing, N.; Schubert, U. *J. Mater. Chem.* **2002**, *12*, 2594.
397. Review: Mehrotra, M. C.; Singh, A. *Chem. Soc. Rev.* **1996**, *25*, 1.
398. Bradley, D. C.; Chisholm, M. H.; Extine, M. W.; Stager, M. E. *Inorg. Chem.* **1977**, *16*, 1794.
399. Jacob, E. *Angew. Chem., Int. Ed. Engl.* **1982**, *21*, 142.
400. Tatzel, G.; Greune, M.; Weidlein, J.; Jacob, E. Z. *Anorg. Allg. Chem.* **1986**, *533*, 83.
401. Kessler, V. G.; Turova, N. Ya.; Panov, A. *Polyhedron* **1996**, *15*, 335.
402. Kessler, V. G.; Shevelkov, A. V.; Bengtsson-Klöö, L. A. *Polyhedron* **1998**, *17*, 965.
403. Champion, J.-F.; Payne, D. A.; Chae, H. K.; Maurin, J. K.; Wilson, J. R. *Inorg. Chem.* **1991**, *30*, 3244.
404. Day, V. W.; Eberspacher, T. A.; Chen, Y.; Hao, J.; Klemperer, W. G. *Inorg. Chim. Acta* **1995**, *229*, 391.
405. Boyle, T. J.; Tyner, R. P.; Alam, T. M.; Scott, B. L.; Ziller, J. W.; Potter, B. G., Jr. *J. Am. Chem. Soc.* **1999**, *121*, 12104.
406. Schmid, R.; Mosset, A.; Galy, J. *J. Chem. Soc., Dalton Trans.* **1991**, 1999.
407. Stenou, N.; Dromzee, Y.; Robert, F.; Sanchez, C. *Mater. Res. Soc. Symp. Proc.* **1996**, *435*, 487.
408. Day, V. W.; Eberspacher, T. A.; Klemperer, W. G.; Park, C. W.; Rosenberg, F. S. *J. Am. Chem. Soc.* **1991**, *113*, 8190.
409. Day, V. W.; Eberspacher, T. A.; Klemperer, W. G.; Park, C. W. *J. Am. Chem. Soc.* **1993**, *115*, 8469.
410. Steunou, N.; Robert, F.; Boubekeur, K.; Ribot, F.; Sanchez, C. *Inorg. Chim. Acta* **1998**, *279*, 144.
411. Mosset, A.; Galy, J. *Comp. Rend. Ser. 1* **1988**, *301*, 1747.

412. Stenou, N.; Kickelbick, G.; Boubekeur, F.; Sanchez, C. *J. Chem. Soc., Dalton Trans.* **1999**, 3653.
413. Campana, C. F.; Chen, Y.; Day, V. W.; Klemperer, W. G.; Sparks, R. A. *J. Chem. Soc., Dalton Trans.* **1996**, 691.
414. Hubert-Pfalzgraf, L. G.; Pajot, N.; Papiernik, P.; Parraud, S. *Mater. Res. Soc. Symp. Proc.* **1996**, 435, 137.
415. Evans, W. J.; Ansari, M. A.; Ziller, J. W. *Polyhedron* **1998**, 17, 869.
416. Morosin, B. *Acta Crystallogr.* **1977**, B33, 303.
417. Kessler, V. G.; Seisenbaeva, G. A. *Inorg. Chem. Comm.* **2000**, 3, 203.
418. Bradley, D. C.; Hursthouse, B. C.; Rodesiler, P. F. *J. Chem. Soc., Chem. Commun.* **1968**, 1112.
419. Bradley, D. C.; Hursthouse, B. C.; Rodesiler, P. F. *Can. J. Chem.* **1962**, 40, 62.
420. Kessler, V. G.; Turova, N. Ya.; Yanovsky, A. I.; Belokon', A. I.; Struchkov, Yu.T. *Russ. J. Inorg. Chem.* **1991**, 36, 938.
421. Turevskaya, E. P.; Turova, N. Ya.; Belokon', A. I.; Tschebukov, D. E. *Russ. J. Inorg. Chem.* **1998**, 43, 975.
422. Yanovsky, A. I.; Turova, N. Ya.; Korolev, A. V.; Tschebukov, D. E.; Struchkov, Yu.T. *Russ. Chem. Bull.* **1996**, 115.
423. Sinclair, R. A.; Brostrom, M. L.; Gleason, W. B.; Newmark, R. A. *Mater. Res. Soc. Symp. Proc.* **1992**, 271, 27.
424. Yanovsky, A. I.; Turova, N. Ya.; Kozlova, N. I.; Struchkov, Yu.T. *Koord. Khim.* **1987**, 13, 242.
425. Hay, J. N.; Raval, H. M. *Chem. Mater.* **2001**, 13, 3396.
426. Lafond, V.; Mutin, P. H.; Vioux, A. *J. Molec. Catal.* **2002**, 182-183, 81.
427. Arnal, P.; Corriu, R. J. P.; Leclercq, D.; Mutin, P. H.; Vioux, A. *Chem. Mater.* **1997**, 9, 694.
428. Acosta, S.; Corriu, R. J. P.; Leclercq, D.; Lefevre, P.; Mutin, P. H.; Vioux, A. *J. Non-Cryst. Solids* **1994**, 170, 234.
429. De Hazan, Y.; Shter, G. E.; Cohen, Y.; Rottmann, C.; Avnir, D.; Grader, G. S. *J. Sol-Gel Sci. Technol.* **1999**, 14, 233.
430. Grader, G. S.; Shter, G. E.; De Hazan, Y. *J. Mater. Res.* **1999**, 14, 1485.
431. Ciuffi, K. J.; de Lima, O. J.; Sacco, H. C.; Nassar, E. J. *J. Non-Cryst. Solids* **2002**, 304, 126.
432. Acosta, S.; Corriu, R. J. P.; Leclercq, D.; Mutin, P. H.; Vioux, A. *J. Sol-Gel Sci. Technol.* **1994**, 2, 25.
433. Corriu, R. J. P.; Leclercq, D.; Lefevre, P.; Mutin, P. H.; Vioux, A. *J. Mater. Chem.* **1992**, 2, 673.
434. Corriu, R. J. P.; Leclercq, D.; Lefevre, P.; Mutin, P. H.; Vioux, A. *Chem. Mater.* **1992**, 4, 961.
435. Hay, J. N.; Raval, H. M. *J. Sol-Gel Sci. Technol.* **1998**, 13, 109.
436. Arnal, P.; Corriu, R.; Leclercq, D.; Mutin, P. H.; Vioux, A. *J. Mater. Chem.* **1996**, 6, 1925.
437. Trentler, T. J.; Denler, T. E.; Bertone, J. F.; Agrawal, A.; Colvin, V. L. *J. Am. Chem. Soc.* **1999**, 121, 1613.
438. Arnal, P.; Corriu, R. J. P.; Leclercq, D.; Mutin, P. H.; Vioux, A. *Mater. Res. Soc. Symp. Proc.* **1994**, 346, 339.
439. Wilkinson, A. P.; Lind, C.; Pattanaik, S. *Chem. Mater.* **1999**, 11, 101.
440. Jansen, M.; Guenther, E. *Chem. Mater.* **1995**, 7, 2100.
441. Acosta, S.; Corriu, R. J. P.; Leclercq, D.; Mutin, P. H.; Vioux, A. *Mater. Res. Soc. Symp. Proc.* **1994**, 346, 345.
442. Janackovic, D.; Orlovic, A.; Skala, D.; Drmanic, S.; Kostic-Gvozdenovic, L. K.; Jokanovic, V.; Uskokovic, D. *Nanostruct. Mater.* **1999**, 12, 147.
443. Hay, J. N.; Raval, H. M. *J. Mater. Chem.* **1998**, 8, 1233.
444. Caruso, J.; Hampden-Smith, M. J. *J. Sol-Gel Sci. Technol.* **1997**, 8, 35.
445. Andrianainarivelo, M.; Corriu, R.; Leclercq, D.; Mutin, P. H.; Vioux, A. *J. Mater. Chem.* **1996**, 6, 1665.
446. Andrianainarivelo, M.; Corriu, R.; Leclercq, D.; Mutin, P. H.; Vioux, A. *Chem. Mater.* **1997**, 9, 1098.
447. Linacero, R.; Rojas-Cervantes, M. L.; Lopez-Gonzalez, J. D. *J. Mater. Sci.* **2000**, 35, 3269.
448. Andrianainarivelo, M.; Corriu, R.; Leclercq, D.; Mutin, P. H.; Vioux, A. *J. Mater. Chem.* **1997**, 7, 279.
449. Xu, J.; Lind, C.; Wilkinson, A. P.; Pattanaik, S. *Chem. Mater.* **2000**, 12, 3347.
450. Rice, L. G.; Scott, S. L. *Chem. Mater.* **1998**, 10, 620.
451. Barbieri, F.; Cauzzi, D.; De Smet, F.; Devillers, M.; Moggi, P.; Predieri, G.; Ruiz, P. *Catal. Today* **2000**, 61, 353.
452. Sanchez, C.; Livage, J.; Henry, M.; Babonneau, F. *J. Non-Cryst. Solids* **1988**, 100, 65.
453. Leaustic, A.; Babonneau, F.; Livage, J. *Chem. Mater.* **1989**, 1, 240.
454. Sanchez, C.; Livage, J. *New J. Chem.* **1990**, 14, 413.
455. Sanchez, C.; Babonneau, F.; Doeuff, S.; Leaustic, A. In *Ultrastructure Processing of Ceramics, Glasses and Composites*; Mackenzie, J. D., Ulrich, D. R., Eds.; Wiley: San Diego, CA, 1988; p 77.
456. Chisholm, M. H.; Budzichowski, T. A.; Feher, F. J.; Ziller, J. W. *Polyhedron* **1992**, 11, 1575.
457. Errington, R. J.; Ridland, J.; Clegg, W.; Coxall, R. A.; Sherwood, J. M. *Polyhedron* **1998**, 17, 659.
458. Bradley, D. C.; Howes, A. J.; Hursthouse, M. B.; Runnacles, J. D. *Polyhedron* **1991**, 10, 477.
459. Schubert, U.; Buhler, H.; Hirle, B. *Chem. Ber.* **1992**, 125, 999.
460. Wang, J. L.; Miao, F. M.; Fan, X. J.; Feng, X.; Wang, T. J. *Acta Crystallogr. C* **1990**, 46, 1633.
461. Poncelet, O.; Hubert-Pfalzgraf, L. G.; Daran, J. C. *Inorg. Chem.* **1990**, 2882.
462. Sauer, N. N.; Garcia, E.; Salazar, K. V.; Ryan, R. R.; Martin, J. A. *J. Am. Chem. Soc.* **1990**, 112, 1524.
463. Garbauskus, M. F.; Wengrovius, J. H.; Going, R. C.; Kasper, J. S. *Acta Crystallogr. C* **1984**, 40, 1536.
464. Chandler, C. D.; Fallon, G. D.; Koplick, A. J.; West, B. O. *Aust. J. Chem.* **1987**, 40, 1427.
465. Ribot, F.; Toledano, P.; Sanchez, C. *Chem. Mater.* **1991**, 3, 759.
466. Pence, L. E.; Caneshi, A.; Lippard, S. J. *Inorg. Chem.* **1996**, 35, 3069.
467. Le Gall, F.; de Biani, F. F.; Caneschi, A.; Cinelli, P.; Cornia, A.; Fabretti, A. C.; Gatteschi, D. *Inorg. Chim. Acta* **1997**, 262, 123.
468. Lewinski, J.; Zachara, J.; Grabska, E. *J. Am. Chem. Soc.* **1996**, 118, 6794.
469. Chandler, C. D.; Hampden-Smith, M. J. *Chem. Mater.* **1992**, 4, 1137.
470. Chandler, C. D.; Hampden-Smith, M. J.; Brinker, C. J. *Mater. Res. Soc. Symp. Proc.* **1992**, 271, 89.
471. Chandler, C. D.; Hampden-Smith, M. J.; Duesler, E. N. *Inorg. Chem.* **1992**, 31, 4891.
472. Kickelbick, G.; Schubert, U. *J. Chem. Soc., Dalton Trans.* **1999**, 1301.
473. Schubert, U.; Tewinkel, S.; Möller, F. *Inorg. Chem.* **1995**, 34, 995.
474. Mutin, P. H.; Mehring, M.; Guerrero, G.; Vioux, A. *Mater. Res. Soc. Symp. Ser.* **2001**, 628CC2.4.1.
475. Mehring, M.; guerro, G.; Dahan, F.; Mutin, P.; Vioux, A. *Inorg. Chem.* **2000**, 39, 3325.
476. Lorenz, A.; Kickelbick, G.; Schubert, U. *Chem. Mater.* **1997**, 9, 2551.
477. Taft, K. L.; Delfs, C. D.; Papaefthymiou, G. C.; Foner, S.; Gatteschi, D.; Lippard, S. J. *J. Am. Chem. Soc.* **1994**, 116, 823.
478. Beattie, J. K.; Hambley, T. W.; Klepetko, J. A.; Masters, A. F.; Turner, P. *J. Chem. Soc., Chem. Commun.* **1998**, 45.
479. Puri, D. M.; Mehrotra, R. C. *J. Indian Chem. Soc.* **1962**, 39, 447.

480. Mehrotra, R. C.; Srivastava, G. J. *Indian Chem. Soc.* **1962**, *39*, 521.
481. Sankhla, B. S.; Kapoor, R. N. *Bull. Chem. Soc. Jpn.* **1967**, *40*, 1381.
482. Mittal, R. K. *Z. Anorg. Allg. Chem.* **1969**, *351*, 309.
483. Mehrotra, R. C.; Bajaj, P. J. *Organomet. Chem.* **1970**, *24*, 611.
484. Bharara, P. C.; Gupta, V. D.; Mehrotra, R. C. *Z. Anorg. Allg. Chem.* **1973**, *403*, 337.
485. Bharara, P. C.; Gupta, V. D.; Mehrotra, R. C. *J. Indian Chem. Soc.* **1974**, *51*, 849.
486. Baranwal, B. P.; Bharara, P. C.; Mehrotra, R. C. *Transition Met. Chem.* **1977**, *2*, 204.
487. Bharara, P. C.; Gupta, V. D.; Mehrotra, R. C. *Synth. React. Inorg. Met.-Org. Chem.* **1977**, *7*, 537.
488. Goel, S. C.; Buhro, W. E. *Inorg. Synth.* **1997**, *31*, 294.
489. Duggal, R.; Mehrotra, R. C. *Inorg. Chim. Acta* **1985**, *98*, 121.
490. Mehrotra, R. C.; Mehrotra, R. K. *J. Indian Chem. Soc.* **1962**, *39*, 677.
491. Mehrotra, R. C.; Kapoor, P. N. *J. Indian Chem. Soc.* **1967**, *44*, 468.
492. Mehrotra, R. C.; Kapoor, P. N. *Indian J. Chem.* **1967**, *5*, 505.
493. Goel, S. C.; Kramer, K. S.; Chiang, M. Y.; Buhro, W. E. *Polyhedron* **1990**, *9*, 611.
494. Tanaka, T. *Bull. Chem. Soc. Jpn.* **1960**, *33*, 446.
495. Bills, J. L.; Cotton, F. A. *J. Phys. Chem.* **1964**, *68*, 802.
496. Mehrotra, R. C.; Chandra, G. *Indian J. Chem.* **1965**, *11*, 497.
497. Breezer, A. E.; Mortimer, C. T. *J. Chem. Soc. A* **1966**, 514.
498. Mehrotra, R. C.; Bajaj, P. J. *Organomet. Chem.* **1970**, *25*, 359.
499. Kuznetsov, E. V.; Ignatieva, E. K.; Emikh, L. A. *Zh. Obshch. Khim.* **1969**, *39*, 1816, 1820.
500. Mironov, V. F. *Main Group Met. Chem.* **1989**, *12*, 355.
501. Hein, F.; Albert, P. W. *Z. Anorg. Allg. Chem.* **1952**, *269*, 67.
502. Cohen, H. J. *J. Organomet. Chem.* **1967**, *9*, 177.
503. Lacy, M. J.; McDonald, C. G. *Aust. J. Chem.* **1976**, *29*, 1119.
504. Zeldin, M.; Ochs, J. *J. Organomet. Chem.* **1975**, *86*, 369.
505. Menge, W. M. P. B.; Verkade, J. G. *Inorg. Chem.* **1991**, *30*, 4628.
506. Kessler, V. G.; Hubert-Pfalzgraf, L. G.; Halut, S.; Daran, J. C. *J. Chem. Soc., Chem. Commun.* **1994**, 705.
507. Yoon, K. H.; Park, J. H.; Kang, D. H. *J. Amer. Ceram. Soc.* **1995**, *78*, 2267.
508. Tadanaga, K.; Ito, S.; Minami, T.; Tohge, N. *J. Non-Cryst. Solids* **1996**, *201*, 231.
509. Park, Y.-I.; Kim, C. E.; Lee, H. W. *J. Sol-Gel. Sci. Technol.* **1999**, *14*, 149.
510. Sharma, P. K.; Varadan, V. V.; Varadan, V. K. *Chem. Mater.* **2000**, *12*, 2590.
511. Jung, M. *Int. J. Inorg. Mater.* **2000**, *3*, 471.
512. Park, Y.-I.; Nagai, M.; Miyayama, M.; Kudo, T. *J. Mater. Sci.* **2001**, *36*, 1995.
513. Reeves, R. E.; Mazzeno, L. W. *J. Am. Chem. Soc.* **1954**, *76*, 2533.
514. Yamamoto, Y.; Kambara, S. *J. Am. Chem. Soc.* **1959**, *81*, 2663.
515. Mehrotra, R. C.; Kapoor, P. N. *J. Less-Common Met.* **1965**, *8*, 419.
516. Kapoor, R. N.; Prakash, S.; Kapoor, P. N. *Z. Anorg. Allg. Chem.* **1967**, *351*, 219.
517. Puri, D. M.; Mehrotra, R. C. *Indian J. Chem.* **1967**, *5*, 448.
518. Mehrotra, R. C.; Srivastava, G. J. *Chem. Soc.* **1962**, 1032, 3819, 4045.
519. Mehrotra, R. C.; Srivastava, G. J. *Indian Chem. Soc.* **1962**, *39*, 203.
520. Mehrotra, R. C.; Mehrotra, R. K. *J. Indian Chem. Soc.* **1962**, *39*, 635.
521. Mehrotra, R. C.; Chandra, G. *J. Chem. Soc.* **1963**, 2804.
522. Mehrotra, R. C.; Gupta, V. D. *J. Indian Chem. Soc.* **1966**, *32*, 727.
523. Mehrotra, R. C.; Mathur, S. N. *J. Indian Chem. Soc.* **1965**, *42*, 814.
524. Mehrotra, R. C.; Mathur, S. N. *J. Indian Chem. Soc.* **1965**, *42*, 749.
525. Mehrotra, R. C.; Narain, R. P. *Indian J. Chem.* **1967**, *5*, 444.
526. Mehrotra, R. C. *Pure Appl. Chem.* **1966**, *13*, 111.
527. Emblem, H. G.; Hargreaves, K. J. *Inorg. Nucl. Chem.* **1968**, *30*, 721.
528. Sharma, P. P.; Mehrotra, R. C. *J. Indian Chem. Soc.* **1969**, *46*, 123.
529. Dubey, S.; Bhandari, A. M.; Misra, S. N.; Kapoor, R. N. *Indian J. Chem.* **1970**, *8*, 97.
530. Puri, D. M. *J. Indian Chem. Soc.* **1970**, *47*, 535.
531. Saxena, U. B.; Rai, A. K.; Mehrotra, R. C. *Inorg. Chim. Acta.* **1973**, *7*, 681.
532. Mehrotra, R. C.; Singh, A. *Phosphorus, Sulfur, Silicon* **1997**, *124-125*, 153.
533. Turova, N. Va.; Tureuskaya, E. P.; Kessler, V. G.; Yanovsky, A. I.; Struchkov, Yu.T. *J. Chem. Soc., Chem. Commun.* **1993**, 21.
534. Mehrotra, R. C.; Singh, A.; Bhagat, M.; Godhwani, J. J. *Sol-Gel. Sci. Technol.* **1998**, *13*, 45.
535. Singh, A.; Mehrotra, R. C. *Chemtracts* **1999**, *12*, 607.
536. Crans, D. C.; Felty, R. A.; Chen, H.; Eckert, H.; Das, N. *Inorg. Chem.* **1994**, *33*, 2427.
537. Gainsford, G. J.; Kemmitt, T.; Lensink, C.; Milestone, M. B. *Inorg. Chem.* **1995**, *34*, 746.
538. Day, V. W.; Eberspacher, T. A.; Frey, M. H.; Klempner, W. G.; Liang, S.; Payne, D. A. *Chem. Mater.* **1996**, *8*, 330.
539. Pajot, N.; Papiernik, R.; Hubert-Pfalzgraf, L. G.; Vaissrman, J.; Parraud, S. *J. Chem. Soc., Chem. Commun.* **1995**, 1817.
540. Buth, S.; Wocadlo, S.; Neumüller, B.; Weller, F.; Dehnicke, K. *Z. Naturforsch. B* **1992**, *47*, 706.
541. Lehtonen, A.; Sillanpää, R. *Polyhedron* **1995**, *14*, 1831.
542. Boyle, T. J.; Schwatz, R. W.; Doedens, R. J.; Ziller, J. W. *Inorg. Chem.* **1995**, *34*, 1110.
543. Zechmann, C. A.; Huffman, J. C.; Folting, K.; Caulton, K. G. *Inorg. Chem.* **1998**, *37*, 5886.
544. Mijatovic, I.; Kickelbick, G.; Puchberger, M.; Schubert, U. *New. J. Chem.* **2003**, in press.
545. Moraru, B.; Hüsing, N.; Kickelbick, G.; Schubert, U.; Fratzl, P.; Peterlik, H. *Chem. Mater.* **2002**, *14*, 2732.
546. Boyle, T. J.; Alam, T. M.; Tafuya, C. J. *Inorg. Chem.* **1998**, *37*, 5588.
547. Lei, X.; Shang, M.; Fehlner, T. P. *Organometallics* **1996**, *15*, 3779.
548. Lei, X.; Shang, M.; Fehlner, T. P. *Organometallics* **1997**, *16*, 5289.
549. Doeuff, S.; Dromzee, Y.; Sanchez, C. C. *R. Acad. Sci. Ser. 2* **1989**, *308*, 1409.
550. Gautier-Luneau, I.; Mosset, A.; Galy, J. *Z. Kristallogr.* **1987**, *180*, 83.

551. Doeuff, S.; Dromzee, Y.; Taulelle, F.; Sanchez, C. *Inorg. Chem.* **1989**, *28*, 4439.
552. Laaziz, I.; Larbot, A.; Guizard, C.; Durand, J.; Cot, L. *Acta Crystallogr. C* **1990**, *46*, 2332.
553. Schubert, U.; Arpac, E.; Glaubitt, W.; Helmerich, A.; Chau, C. *Chem. Mater.* **1992**, *4*, 291.
554. Kickelbick, G.; Holzinger, D.; Brick, C.; Trimmel, G.; Moons, E. *Chem. Mater.* **2002**, *14*, 4382.
555. Papiernik, P.; Hubert-Pfalzgraf, L. G.; Vaissermann, J.; Goncalves, M. C. H. B. *J. Chem. Soc., Dalton Trans.* **1998**, 2285.
556. Kickelbick, G.; Schubert, U. *Eur. J. Inorg. Chem.* **1998**, 159.
557. Kickelbick, G.; Wiede, P.; Schubert, U. *Inorg. Chim. Acta* **1999**, *284*, 1.
558. Kickelbick, G.; Schubert, U. *Chem. Ber.* **1997**, *130*, 473.
559. Trimmel, G.; Gross, S.; Kickelbick, G.; Schubert, U. *Appl. Organomet. Chem.* **2001**, *15*, 401.
560. Moraru, B.; Gross, S.; Kickelbick, G.; Trimmel, G.; Schubert, U. *Monatsh. Chem.* **2001**, *132*, 993.
561. Hubert-Pfalzgraf, L. G.; Abada, V.; Halut, S.; Roziere, J. *Polyhedron* **1997**, *16*, 581.
562. Stenou, N.; Bonhomme, C.; Sanchez, C.; Vaissermann, J.; Hubert-Pfalzgraf, L. G. *Inorg. Chem.* **1998**, *37*, 901.
563. Gross, S.; Di Noto, V.; Kickelbick, G.; Schubert, U. *Mater. Res. Soc. Symp. Proc.* **2002**, *726*, Q4.1.1.
564. Moraru, B.; Kickelbick, G.; Schubert, U. *Eur. J. Inorg. Chem.* **2001**, 1295.
565. Taft, K. L.; Papaefthymiou, G. C.; Lippard, S. J. *Inorg. Chem.* **1994**, *33*, 1510.
566. Guerrero, G.; Mehring, M.; Mutin, P. H.; Dahan, F.; Vioux, A. *J. Chem. Soc., Dalton Trans.* **1999**, 1537.
567. Mehring, M.; Schurmann, M.; Mutin, P. H.; Vioux, A. *Z. Kristallogr.* **2000**, *215*, 591.
568. Toledano, P.; Ribot, F.; Sanchez, C. *C. R. Acad. Sci. Ser. II* **1990**, *311*, 1315.
569. Toledano, P.; In, M.; Sanchez, C. *C. R. Acad. Sci. Ser. II* **1991**, *313*, 1247.
570. Toledano, P.; In, M.; Sanchez, C. *C. R. Acad. Sci. Ser. II* **1990**, *311*, 1161.
571. Sanchez, C.; In, M.; Toledano, P.; Griesmar, P. *Mater. Res. Soc. Symp. Proc.* **1992**, *271*, 669.
572. Chatry, M.; Henry, M.; In M.; Sanchez, C.; Livage, J. *J. Sol-Gel Sci. Technol.* **1994**, *1*, 233.
573. Sanchez, C.; In, M. *J. Non-Cryst. Solids* **1992**, *147,148*, 1.
574. Di Maggio, R.; Fambri, L.; Guerriero, A. *Chem. Mater.* **1998**, *10*, 1777.
575. Miele-Pajot, N.; Hubert-Pfalzgraf, L. G.; Papiernik, R.; Vaissermann, J.; Collier, R. *J. Mater. Chem.* **1999**, *9*, 3027.
576. Barglik-Chory, C.; Schubert, U. *J. Sol-Gel Sci. Technol.* **1995**, *5*, 135.
577. Schubert, U.; Tewinkel, S.; Lamber, R. *Chem. Mater.* **1996**, *8*, 2047.
578. Lorenz, A.; Schubert, U. *Mater. Res. Soc. Symp. Proc.* **1996**, *435*, 333.
579. Schubert, U.; Lorenz, A.; Kundo, N.; Stuchinskaya, T.; Gogina, L.; Salanov, A.; Zaikovskii, V.; Maizlish, V.; Shaposhnikov, G. P. *Chem. Ber.* **1997**, *130*, 1585.
580. Stuchinskaya, T.; Kundo, N.; Gogina, L.; Schubert, U.; Lorenz, A.; Maizlish, V. *J. Mol. Catal. A* **1999**, *140*, 235.
581. Cattet, H.; Audebert, P.; Sanchez, C.; Hapiot, P. *J. Mater. Chem.* **1997**, *7*, 1461.
582. Roux, S.; Audebert, P.; Pagetti, J.; Roche, M. *New J. Chem.* **2000**, *24*, 877, 885.

# 7.11

## Molecular Electron Transfer

J. F. ENDICOTT

Wayne State University, Detroit, MI, USA

---

7.11.1	INTRODUCTION	658
7.11.1.1	Overview	658
7.11.2	MATTERS OF PRINCIPLE AND PERSPECTIVE	660
7.11.2.1	Molecular Properties that Contribute to the Efficiency of Electron Transfer and their Experimental Determination	661
7.11.2.1.1	<i>The free energy of the electron transfer step, <math>\Delta G_{\text{DA}}^0</math></i>	661
7.11.2.1.2	<i>The solvent reorganizational energy, <math>\lambda_s</math></i>	661
7.11.2.1.3	<i>The reorganizational energy associated with differences in molecular geometry, <math>\lambda_M</math></i>	661
7.11.2.1.4	<i>The pre-exponential nuclear frequency term</i>	662
7.11.2.1.5	<i>Electronic contributions</i>	662
7.11.2.1.6	<i>Experimental determinations of the contributions to electron transfer rate constants</i>	662
7.11.2.2	General Logic for Discussion of Thermal and Optical Electron Transfer	663
7.11.2.3	The Franck–Condon Factor	667
7.11.2.4	The Electronic Factor	668
7.11.2.5	Perturbation Theory Corrections for the Alteration of the Free Energy of Reaction Terms as a Consequence of D/A Configurational Mixing	670
7.11.2.6	Corrections to the Reorganizational Energy Terms that Result from D/A Configurational Mixing	671
7.11.2.7	The Temperature Dependence of Electron Transfer Rates	672
7.11.2.8	Special Features of Covalently Linked D/A Complexes	673
7.11.3	OBSERVATIONS IN THE LIMIT OF WEAK ELECTRONIC COUPLING: OUTER-SPHERE ELECTRON TRANSFER	675
7.11.3.1	The $[\text{Fe}(\text{CN})_6]^{4-3-}$ Self-exchange Reaction as a Case Study	676
7.11.3.2	General Considerations: The Significance of $\kappa_{\text{el}}$ in Outer-sphere Electron Transfer Reactions of Transition Metal Complexes	676
7.11.3.3	Observations on Cobalt(III)–(II) Systems	677
7.11.3.4	Franck–Condon Factors	683
7.11.3.4.1	<i>The solvent reorganizational free energy contributions (<math>\chi_s</math>)</i>	684
7.11.3.4.2	<i>Inner-sphere or molecular reorganizational contributions</i>	684
7.11.3.5	Gas-phase Solution-phase Comparisons	687
7.11.3.6	Coupling to Vibrational Modes: Gated Electron Transfer and Vibronic Issues	688
7.11.3.6.1	<i>Electron transfer coupled to large-amplitude changes in low-frequency vibrational modes, intermediates, and gated electron transfer</i>	689
7.11.3.6.2	<i>The response of outer-sphere electron transfer rates to specific vibrational excitation: vibronic coupling</i>	692
7.11.3.7	Optical–Thermal Comparisons in Outer-sphere Electron Transfer Systems	692
7.11.3.8	Overview and Summary	692
7.11.4	COVALENTLY LINKED $d\pi$ DONORS AND ACCEPTORS	693
7.11.4.1	Approaches to Interpreting the Properties of Covalently Linked Donor–Acceptor Complexes	697
7.11.4.1.1	<i>Mono-atomic bridging moieties</i>	697
7.11.4.1.2	<i>Diatomic bridging moieties</i>	697
7.11.4.1.3	<i>Polyatomic bridging ligands</i>	698
7.11.4.2	Some General Considerations Regarding Linked Donor–Acceptor Complexes when there is no Mixing of the Nuclear and Electronic Coordinates	698
7.11.4.3	Time Frames for Electron Transfer	699
7.11.4.4	The Mixing of the Nuclear and Electronic Coordinates in Linked Donor–Acceptor Complexes; Vibronic Coupling	700

7.11.4.4.1	<i>Concerted D–B and B–A nuclear motions and the PKS/Piepho vibronic coupling models</i>	703
7.11.4.5	Classification Schemes for Bridged Complexes	703
7.11.4.6	Experimental Observations in the Limit of Weak Electronic Coupling; Simple, Aromatic Bridging Ligands	704
7.11.4.7	Electron Transfer Systems in the Intermediate Regime	705
7.11.4.8	Experimental Observations in the Limit of Very Strong Electronic Coupling	706
7.11.4.8.1	<i>Pyrazine-bridged complexes</i>	707
7.11.4.8.2	<i>Polypyridyl ligand-bridged complexes in which coupling appears to be promoted by ligand-to-metal charge transfer (hole transfer systems)</i>	712
7.11.4.8.3	<i>Complexes with two-atom bridging moieties</i>	712
7.11.4.9	Covalently Linked, Sigma Donor–Acceptor Systems	717
7.11.4.10	Overview and Summary	719
7.11.5	ELECTRON TRANSFER IN LARGER-SCALE SYSTEMS	719
7.11.5.1	Systems Related to Biological Electron Transport	720
7.11.5.2	Complexes Containing Multiple Donors and/or Acceptors	721
7.11.5.3	Heterogeneous Electron Transfer Systems	723
7.11.6	REFERENCES	723

---

## 7.11.1 INTRODUCTION

Electron transfer is a ubiquitous type of fundamental chemical reaction. These reactions are important in all of chemistry and in applications as varied as the transduction of energy in biological systems and solar cells to the design of molecular-level electronic devices. Consequently, thermal electron transfer rates and optical electron transfer spectroscopy have been extensively studied and their general features are well understood. Studies have proliferated in the areas of science that might be classified as “molecular electron transfer” since the Meyer and Taube chapter on electron transfer reactions<sup>1</sup> in the first edition of *Comprehensive Coordination Chemistry (CCC)* in 1987. A sense of the vast amount of work in these areas is conveyed by the recent publication of a five-volume handbook, *Electron Transfer in Chemistry*.<sup>2</sup> Several other books have also been published; Astruc has published a general book emphasizing odd electron species,<sup>3</sup> Kuznetsov<sup>4,5</sup> has published two books and Kuznetsov and Ulstrup<sup>6</sup> a third book that emphasize the theoretical aspects of electron transfer, two volumes of *Advances in Chemical Physics*<sup>7,8</sup> have been devoted largely to theoretical aspects, and Kavarnos<sup>9</sup> has published a book and Fox and Channon<sup>10</sup> have edited a four-volume series on photo-induced electron transfer. Specialized monographs and special issues of journals, sometimes based on symposia, have been published spanning a broad range of electron transfer topics,<sup>11–15</sup> on heterogeneous photochemical electron transfer,<sup>16</sup> on photochemical and radiation chemical methods for study of electron transfer,<sup>17</sup> on aspects of the theoretical chemistry<sup>18</sup> and on biological and biophysical aspects of electron transfer.<sup>19–21</sup> Many of the relevant review articles since the early 1980s will be cited in the context of discussions below. This chapter cannot be truly representative of this mass and range of material. Its principal focus is on the evolution of understanding of electron transfer processes in coordination complexes. Of course, the basic principles and the basic theories are not substrate dependent. However, different classes of substrates require different levels of approximation for appropriate theoretical description and interpretation. Transition metal complexes have the advantage of a wide range of possible reactants with different electronic structures and of the relative ease of achieving systematic variations of critical parameters by means of changes in ligands, coordination geometry, etc. An important characteristic of these heavy metal complexes is that several different electronic states can have very similar energies. This feature may be important in facilitating electron transfer and, thus, in the key role of transition metal complexes in biological electron transport systems. However, this proximity of electronic states leads to a great deal of configurational mixing, and often makes the detailed interpretation of electron transfer parameters difficult. The interplay between various theoretical models and the observations on complex experimental systems has continued to provide much stimulus for research on electron transfer.

### 7.11.1.1 Overview

The chapter by Meyer and Taube<sup>1</sup> very nicely describes the evolution of electron transfer studies of coordination complexes and the experimental bases for distinguishing between classes of



electron transfer reactions. Most of those concepts are incorporated into this chapter, but there are some differences of emphasis. For example, the traditional outer-sphere/inner-sphere mechanistic distinction, still useful in many contexts, is often not so useful in the discussion of issues such as donor–acceptor electronic coupling. This is because the outer-sphere reaction rate constant is an average over the geometries and the separation distances of all possible encounter complexes while the inner-sphere reaction rate constant generally represents a relatively well-defined transition-state geometry. In fact, transition-state geometry is a major concern when issues of orbital overlap are important, as in discussions of electronic coupling.<sup>22</sup> Much of the material in this chapter is organized around concepts of weak and strong electronic coupling. It is initially convenient to discuss these concepts with respect to a semi-classical expression for the electron transfer rate constant, Equation (1),<sup>23</sup>

$$k_{\text{et}} = \kappa_{\text{el}} \nu_{\text{nu}} \kappa_{\text{nu}} \quad (1)$$

where  $\kappa_{\text{el}}$  is the electronic transmission coefficient (the probability of forming products once the nuclear configuration of the transition state is achieved),  $\nu_{\text{nu}}$  is the effective nuclear frequency along the reaction coordinate in the neighborhood of the transition state, and the nuclear transmission coefficient,  $\kappa_{\text{nu}}$ , is the classical exponential function of the activation energy. Then, the weak coupling limit corresponds to the limit in which  $\kappa_{\text{el}} \ll 1$  and the electronic mixing between reactants and products approaches zero, and the strong coupling limit for  $\kappa_{\text{nu}} = 1$ . In some contexts it is useful to express these limits in terms of the relative magnitudes of  $\nu_{\text{nu}}$  and the maximum frequency at which the electron moves between reactant and product configurations,  $\nu_{\text{el}}^*$ :  $\nu_{\text{el}}^* < \nu_{\text{nu}}$  for weak coupling and  $\nu_{\text{el}}^* > \nu_{\text{nu}}$  for strong coupling.

In practice, the weak electronic coupling limit includes most conventional outer-sphere electron transfer reactions, but it also includes some reactions in which the reactants are covalently linked. The limit in which the electronic mixing between the reactants and products approaches zero is the diabatic (or nonadiabatic) limit in which  $H_{\text{DA}} \rightarrow 0$  in Figure 1, where  $H_{\text{DA}} = \langle \psi_{\text{D}}^{\text{el}} | H | \psi_{\text{A}}^{\text{el}} \rangle$  represents the electronic matrix element,  $\psi_{\text{X}}^{\text{el}}$  (X = D or A) are the donor and acceptor electronic wave functions and  $H$  is a Hamiltonian operator. Clearly, there must be some electronic mixing in order that the electron does transfer. From the point of view adopted in this chapter, it is important to establish experimental criteria for the weak coupling/strong coupling distinction. The weak coupling limit is operationally defined here as the limit in which the electronic mixing does not significantly ( $\leq \sim 5\%$ ) alter the parameters (such as the reorganizational energy and the driving force) contributing to  $\kappa_{\text{nu}}$ . In the strong coupling limit,  $\kappa_{\text{el}} = 1$  and the associated electronic

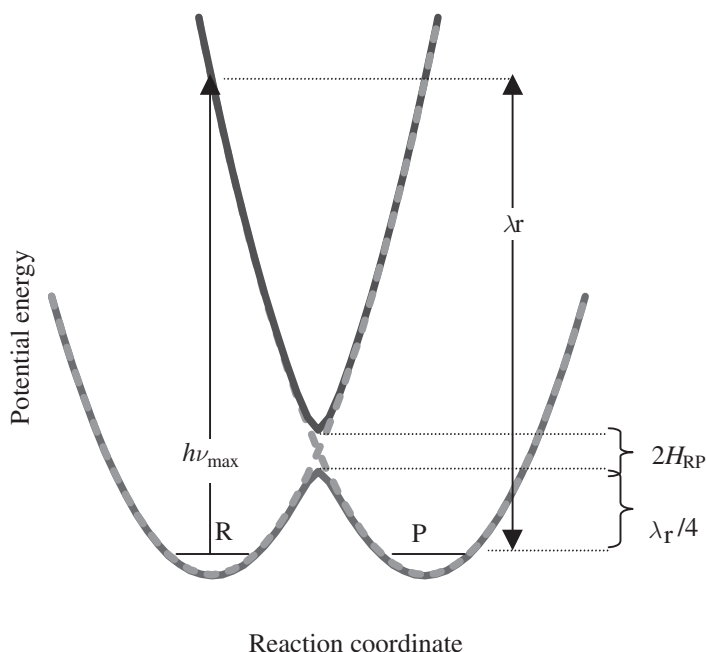


**Figure 1** PE surface for a self-exchange reaction.

mixing alters the parameters that contribute to  $\kappa_{\text{nu}}$ , relative to their values for the corresponding weak coupling limit. The extent of electronic coupling can affect reaction rates in both the weak and strong coupling limits. However, the way in which the kinetic parameters are affected is different in these limits.

The important experimentally accessible parameters are reaction rate constants ( $k_{\text{et}}$ ), activation free energies (proportional to  $RT \ln(k_{\text{et}})$ ), equilibrium constants of reactions and/or electrochemical potentials of the component couples, and electron transfer absorption (or emission) energies (e.g.,  $h\nu_{\text{abs}}$  in Figure 1), fine structure and bandwidths. The perturbations of these parameters by temperature variations, magnetic or electric fields and isotopic substitution can also provide relevant information. The experimental procedures used to evaluate these parameters are not the focus of this chapter. There are many sources dealing with general<sup>24–28</sup> or specific<sup>17,29–31</sup> techniques.

Reaction rate constants are rarely sufficient to classify an electron transfer reaction as belonging to the weakly or to the strongly coupled limit. Rate constant data are sometimes complemented by spectroscopic data, the study of magnetic and electric field effects, comparisons of the rate behavior of series of related reactions, etc. in order to probe the electronic coupling contributions to reaction rates. Computational approaches have evolved rapidly, and they are contributing to resolution of the issues involved. Photochemical techniques are commonly used to displace electron transfer equilibria in order to examine the electron transfer behavior of linked donor/acceptor complexes; some of these displacements result in recombination reactions with very large driving forces and some permit the probing of the evolution of the electron transfer system at various points along the reaction coordinate.

The material in this chapter is largely organized around the molecular properties that contribute to electron transfer processes in simple transition metal complexes. To some degree these molecular properties can be classified as functions of either: (i) the nuclear coordinates (i.e., properties that depend on the spatial orientation and separation, and the vibrational characteristics) of the electron transfer system; or (ii) the electronic coordinates of the system (orbital and spin properties). This partitioning of the physical parameters of the system into nuclear and electronic contributions, based on the Born–Oppenheimer approximation, is not rigorous and even in this approximation the electronic coordinates are a function of the nuclear coordinates. The types of systems that conform to expectation at the weak coupling limit will be discussed after some necessary preliminaries and discussion of formalisms. Applications to more complex, extended systems are mentioned at the end of the chapter.

### 7.11.2 MATTERS OF PRINCIPLE AND PERSPECTIVE

This section will selectively summarize concepts and principles governing electron transfer. The selectivity is an obvious necessity in view of the vast amount of material, some of it cited in the preceding section, and the author's experience and bias. The perspective of this chapter is phenomenological. Theoretical studies and concepts will be used as a framework for the consideration of experimental studies. The emphasis is on those theoretical issues and concepts that relate to experimental studies of coordination complexes. A good overview of the theory can be found in a recent chapter by Newton.<sup>32</sup>

The ubiquity of electron transfer processes make them a familiar subject for all chemists and a consequence of that familiarity is a general feeling that they are well understood. There is justification for that "feeling" in broad, general terms. General or large-scale patterns of electron transfer behavior can usually be predicted with considerable confidence. On the other hand, the continuing flow of basic experimental and theoretical work is a clear indication that there are fundamental aspects of electron transfer behavior that are not well understood.

Electron transfer processes are conveniently divided into two experimentally distinct categories: (i) nonradiative processes in which an initial state, with a particular electronic configuration, relaxes to a state with an electronic configuration that differs, at least in part, in the distribution of electrons over the atoms of the system; and (ii) processes in which the redistribution of electrons over the atoms of the system is accompanied by the absorption or emission of light. These two categories differ in their means of investigation, and in the theoretical description of the kind of operators that promote the processes, but the molecular properties that govern them are very similar. The relationships are so close that information from one category of processes can be used to resolve issues in the other. These relationships are extensively employed in this chapter.

### 7.11.2.1 Molecular Properties that Contribute to the Efficiency of Electron Transfer and their Experimental Determination

The measurement of the rate of change in the amount of a reactant and/or product species is the most basic experimental characterization of nonradiative electron transfer processes. The electron transfer step itself is first order in the concentration or number of reactant configurations, and it is characterized by a first order rate constant,  $k_{\text{et}} = \tau_{\text{nr}}^{-1}$  ( $\tau_{\text{nr}}$  the mean, nonradiative relaxation time) as in Equation (1). The rate constant can be interpreted as an expression of the probability of the reacting system crossing from a potential energy (PE) surface describing the reactants to a PE surface describing the products. These PE surfaces differ at least in the nuclear coordinates of their PE minima. In a transition-state approach, the nuclear transmission coefficient in Equation (1) has the form ( $N_{\text{A}}$  = Avagadro's number;  $k_{\text{B}}$  = Boltzman's constant and  $T$  = absolute temperature),<sup>1,23,33,34</sup>

$$N_{\text{A}}k_{\text{B}}T \ln \kappa_{\text{nu}} = -\Delta G_{\text{DA}}^{\ddagger} \quad (2)$$

A Marcus-type of approach leads (when only one high-frequency vibrational mode contributes) to an expression for the activation free energy such as,<sup>1,23,32-39</sup>

$$\Delta G_{\text{DA}}^{\ddagger} = (\Delta G_{\text{DA}}^0 + \chi_{\text{s}} + jh\nu_{\text{h}})^2 / 4\chi_{\text{s}} \quad (3)$$

In Equation (3),  $\Delta G_{\text{DA}}^0$  is the free energy change associated with the electron transfer step,  $\chi_{\text{s}}$  is the solvent reorganizational free energy (that reflects the difference in solvation of reactants and products),  $h$  is Planck's constant, and  $h\nu_{\text{h}}$  is the energy of a high-frequency vibrational mode ( $h\nu_{\text{h}} > k_{\text{B}}T$ ) that contributes to the difference in molecular geometry of the reactants and products. Equation (3) is written for contributions of one high-frequency distortion mode for simplicity; in an actual system, there could be many or no high-frequency vibrational mode contributions.

In terms of Equations (1) and (3), the fundamental physical properties of a reacting system that contribute to the electron transfer rate constant (or transition probability) are described below.

#### 7.11.2.1.1 The free energy of the electron transfer step, $\Delta G_{\text{DA}}^0$

For a discussion formulated in terms of PE surfaces, the equivalent parameter is the energy difference between the zeroth vibrational levels of the reactants' and products' PE surfaces.

#### 7.11.2.1.2 The solvent reorganizational energy, $\lambda_{\text{s}}$

Equation (3) is written in terms of free energies, for consistency, rather than in terms of reorganizational energies ( $\lambda_{\text{s}}$ ) as is common practice. One should use the solvent reorganizational free energy,  $\chi_{\text{s}}$ , since entropy contributions can be important.<sup>40,41</sup> This can be defined as the free energy required to rearrange solvent molecules so that the solvent environment of the product electronic configuration is identical to that of the reactant electronic configuration.

#### 7.11.2.1.3 The reorganizational energy associated with differences in molecular geometry, $\lambda_{\text{M}}$

The differences in bond lengths, bond angles, etc. between the reactants and the products,  $\lambda_{\text{M}}$ , can lead to both low-frequency and high-frequency contributions to  $\lambda_{\text{M}}$ , so that  $\lambda_{\text{M}} = \lambda_{\text{l}} + \lambda_{\text{h}}$  (for  $\lambda_{\text{h}}$  the reorganizational energy associated with  $\nu_{\text{h}}$ ). Since the effective reorganizational energy is  $\lambda_{\text{r}} = (\lambda_{\text{s}} + \lambda_{\text{M}}) = (\lambda_{\text{s}} + \lambda_{\text{l}} + \lambda_{\text{h}})$ , any contribution  $\lambda_{\text{l}}$  for which  $h\nu_{\text{l}} < k_{\text{B}}T$  is indistinguishable from  $\lambda_{\text{s}}$  in its contributions to theoretical expressions and to experimental measurements of rate parameters. However,  $\lambda_{\text{s}}$  (or  $\chi_{\text{s}}$ ) does enter the rate expression in different ways<sup>32</sup> and there may be some ambiguity in assigning the origin of the observed contributions.

### 7.11.2.1.4 The pre-exponential nuclear frequency term

In a transition-state formalism, the pre-exponential frequency term,  $\nu_{\text{nu}}$ , in Equation (1) is the frequency of the effective nuclear motion along the reaction coordinate at the transition state. The lowest frequency modes, typically solvent modes, are expected to be the dominant contribution, effectively limiting the rate of crossing through the transition state. However, this contribution should only be important when  $\kappa_{\text{el}} \sim 1$ .<sup>23</sup>

### 7.11.2.1.5 Electronic contributions

The contributions of donor–acceptor electronic coupling,  $H_{\text{DA}}$ , enter Equation (1) overtly through  $\kappa_{\text{el}}$  when the electronic coupling is weak. When  $H_{\text{DA}}$  is very large,  $\kappa_{\text{el}} \rightarrow 1$ , but the effects of variations in donor–acceptor coupling will be manifested in differences between  $\Delta G_{\text{DA}}^0$ ,  $\chi_{\text{s}}$  ( $\lambda_{\text{s}}$ ) and  $\chi_{\text{h}}$  ( $\lambda_{\text{h}}$ ) in the limit that  $H_{\text{DA}} \rightarrow 0$  and in the experimental system; this can also be expressed in terms of the differences in the shapes of the PE surfaces for the diabatic limit and for the adiabatic, experimental situation.

### 7.11.2.1.6 Experimental determinations of the contributions to electron transfer rate constants

There are many issues involved in the experimental determination of each of the above parameters. Many of the issues involved in these determinations are discussed later in this chapter. Only the general and ideal basis for the experimental measurements that permit the evaluation of the key parameters are mentioned here.

#### (i) The reaction driving force

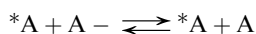
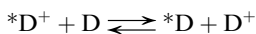
Determinations of  $\Delta G_{\text{DA}}^0$  are usually based on half-wave (or electrode) potentials of the component couples. Thus, for a bimolecular process,



The free energy change is given by ( $\Delta G^0 = -F\Delta E_{1/2}$ , where  $F$  is Faraday's constant,  $\Delta E_{1/2} = [E_{1/2}(\text{A}|\text{A}^-) - E_{1/2}(\text{D}|\text{D}^-)]$ ). When donor–acceptor electronic coupling is strong,  $F\Delta E_{1/2}$  may not be an accurate measure of  $\Delta G_{\text{DA}}^0$ .<sup>42,43</sup>

#### (ii) Self-exchange electron transfer reactions

The rate constants from electron transfer reactions in which reactant and products are chemically indistinguishable, self-exchange electron transfer reactions,



can be combined with Equations (1)–(3) (see ref. 1) to obtain  $\chi_{\text{r}} = 4\Delta G_{\text{DA}}^{\ddagger} = (\chi_{\text{s}} + \chi_{\text{h}})$ ; see also Figure 1.<sup>23,33,34,38</sup>

#### (iii) Absorption and emission bandwidths

The bandwidth, usually defined as the full width at half-height, of the corresponding electron transfer (or charge transfer) absorption or emission is, in principle, a measure of  $(\lambda_{\text{l}} + \lambda_{\text{s}})$ .<sup>44,45</sup>

*(iv) Vibronic fine structure*

In some cases the electron transfer absorption is composed of a sequence, or a progression of resolved components, rather than a single band. Such vibronic fine structure in electron transfer absorptions or emissions is, in principle, a direct measure of  $\nu_h$  and  $\lambda_h$ .<sup>36,42,46,47</sup>

*(v) The oscillator strength of electron transfer absorptions*

The oscillator strength, the integrated intensity of the absorption band, of the corresponding electron transfer absorption is, in principle, a direct measure of  $H_{DA}$ .<sup>2,22,44</sup>

*(vi) Absorption and emission band energies*

The energy of the corresponding electron transfer absorption band maximum is, in the simplest limit, equal to the sum of  $\Delta G_{DA}^0$  and  $\chi_r$ . The energy of the band maximum for the corresponding electron transfer emission is, in the simplest limit, equal to the difference between  $\Delta G_{DA}^0$  and  $\chi_r$  (e.g., see Figure 2).

The interrelationships between the classical, thermally activated electron transfer processes and optical electron transfer spectroscopy are clear from this brief list. Most of the points noted on this list need some modification in the application to real systems. Most of these modifications can be based on simple perturbation theory or elaborate computational arguments.<sup>32</sup> The physical models on which the above statements are based and their necessary modifications are dealt with below.

**7.11.2.2 General Logic for Discussion of Thermal and Optical Electron Transfer**

The classical Marcus model for electron transfer, and variations thereof, have been extensively discussed by many authors,<sup>23,32–35,38,39,44,45,48–50</sup> including Meyer and Taube.<sup>1</sup> This model constitutes a major element of the discussion in this chapter and a few general points, specifically about this model, will be mentioned here. This transition-state theory model assumes that the electron jumps (with frequency  $\nu_{el}$ ) only after the reactant nuclei (including the solvent) are rearranged in such a way that the electron has the same PE at both the donor and acceptor center. The transition state is constructed as the lowest energy nuclear arrangement that meets this condition. In terms of the concepts employed in this chapter, this is a model for the weak-coupling limit. At the other extreme, the assumption that the electronic distribution is in equilibrium with the nuclear arrangements (or coordinates) for all configurations across the reaction coordinate leads to models appropriate for the strong-coupling limit. The physical properties of systems at the weak- and strong-coupling limits are different. *Those differences are an important aspect of the discussion of material in this chapter.* The evaluation of the differences depends on proper referencing of the experimental observations to the weak-coupling limit.

Discussions of radiative and nonradiative electron transfer behavior are conveniently formulated in terms of Equations (5) and (6),<sup>36,37,47,51</sup>

$$P_{if}(\nu_{obs}) \propto \frac{H_{if}^2 f(\nu_{eff})}{(4\pi\chi_s k_B T)^{1/2}} (FC)_r \quad (5)$$

$$(FC)_r = \sum_j F_{j,h} [e^{-(G_j)^2/4RT\chi_s}] \quad (6a)$$

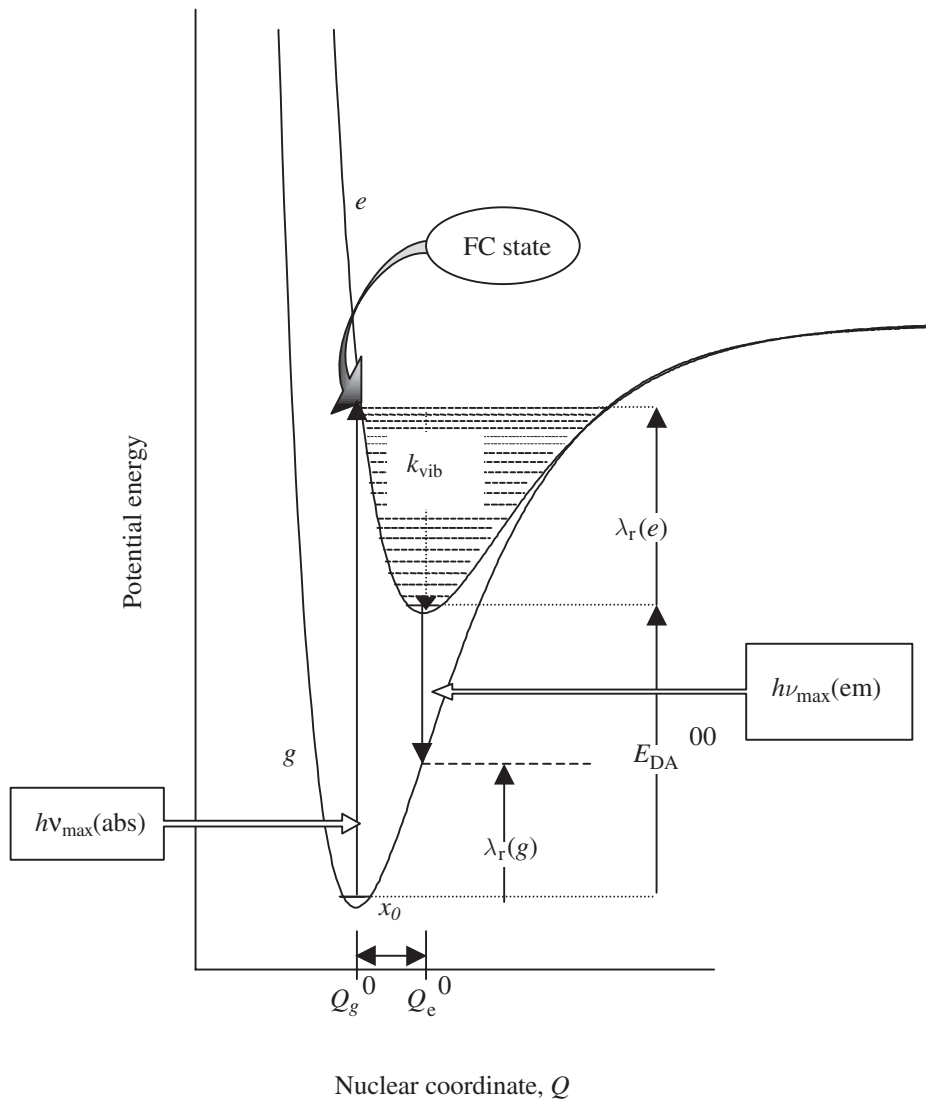


**Figure 2** PE surfaces for two states of very different energies.

$$F_{j,h} = S_h^j [\exp(-S_h)] / j! \quad (6b)$$

$$S_h = \lambda_h / h\nu_h$$

In this formulation,  $P_{if}$  is the probability for a transition (radiative or nonradiative) between the initial and final states and  $f(\nu_{\text{eff}})$  is an algebraic function, different for light absorption, light emission, and nonradiative relaxation (details below); the free energy notation is used here for the solvent reorganizational energy,  $\chi_s$ , for consistency with  $\Delta G_{\text{DA}}^0$ , the high-frequency contribution is usually evaluated in terms of an energy contribution. Note that the “Franck–Condon factor,” (FC factor), defined here differs from the commonly used<sup>32</sup> Franck–Condon-weighted density of states,  $(\text{FCWD}) = (\text{FC}) / (4\pi\lambda_s k_B T)^{1/2}$ . This equation differs only in detail from Equation (1), and the detailed differences have been kept to a minimum: this equation allows for only one high-frequency vibrational mode ( $\nu_H$ ) and it treats only the limit that  $\kappa_{\text{el}} \ll 1$ . The transition probability is exponential in  $G_j^2$ , where,

$$G_j(r) = \Delta G_{\text{if}}^0 + \chi_s + jh\nu_H + rh\nu_{\text{obsd}} \quad (7)$$

Light absorption, light emission, and nonradiative electron transfer rate constants differ in the last term (as well as in  $f(\nu_{\text{eff}})$ ),

$$r = -1 \text{ (light absorption)}$$

$$r = 0 \text{ (nonradiative)}$$

$$r = +1 \text{ (light emission)} \quad (8)$$

Since the exponential factor of (FC) dominates Equation (5), several features are very easily discussed. First, this exponential function is in Gaussian form, and is the basis for a Gaussian analysis of absorption or emission spectra.<sup>36,51</sup> A second point is that Equations (5)–(8) provide the basis for analyzing the absorption or emission spectral envelope by considering some range of values of light frequencies ( $\nu_{\text{obsd}}$ ), but the nonradiative rate constant corresponds to the zero-photon limit<sup>35,36</sup> (a point, not a spectrum).

The exponential term will usually dominate Equation (5), and this is the basis for several of the relationships mentioned above. In the simplest case, for very weak electronic coupling and when high-frequency modes do not contribute, the energy of the absorption maximum corresponds to the maximum value of this term (note that the nuclei do not move during the optical transition),

$$h\nu_{\text{max}}(\text{abs}) = \Delta G_{\text{DA}}^0 + \chi_s + \dots \quad (9)$$

The emission maximum is given by,

$$h\nu_{\text{max}}(\text{emis}) = \Delta G_{\text{DA}}^0 - \chi_s + \dots \quad (10)$$

The full widths at half-maximum height of the Gaussian-shaped absorption and emission peaks in this limit are both given by,

$$\Delta\nu_{1/2} = 4(k_{\text{B}}T\chi_s \ln 2)^{1/2} \quad (11)$$

However, this relationship is only rigorous if the parameters contributing to  $G_j$  are unique and well defined. Species in solution will typically be some ensemble of species having different solvent environments. Since  $\Delta G_{\text{DA}}^0$  and  $\chi_s$  vary with the solvent environment, one expects the bandwidth to also reflect some contribution from the distribution of solvates.<sup>52,53</sup> For the variations of  $(\Delta G_{\text{DA}}^0 + \chi_s)$  (i.e., for  $[\Delta G_{\text{DA}}^0 \pm \sigma_{\Delta G}]$  and  $[\chi_{\text{reorg}} \pm \sigma_{\chi}]$ ) given by<sup>54</sup>  $\sigma = [\sigma_{\Delta G}^2 + \sigma_{\chi}^2]^{1/2}$ , a term in  $\sigma$  should be added to Equation (11). This is clearly an issue of importance in rigid media, but it is generally ignored in fluid solutions.

When high-frequency vibrational modes contribute to the difference in excited-state and ground-state geometry, then the absorption (or emission) envelope will include a series of peaks (a vibronic progression), differing in intensity (an effect of  $F_j$ , an expression based on the vibrational overlap integral), but each with a bandwidth given by Equation (11). For a single contributing high-frequency vibrational mode, the energies of the maxima in the absorption and emission spectra are given by ( $j=0, 1, 2, \dots$ ),

$$h\nu_{\text{max}}(\text{abs})_j = \Delta G_{\text{DA}}^0 + \chi_s + jh\nu_{\text{H}} \dots \quad (12)$$

$$h\nu_{\text{max}}(\text{emis})_j = \Delta G_{\text{DA}}^0 - \chi_s - jh\nu_{\text{H}} \dots \quad (13)$$

These peaks will only be resolved when  $2\Delta\nu_{1/2} < h\nu_{\text{H}}$ ; when  $2\Delta\nu_{1/2} > h\nu_{\text{H}}$ , the vibronic components will be unresolved, but the spectral band may not have a Gaussian shape.

The high-frequency vibrational modes enter differently into spectroscopic and kinetic observations. For the electron transfer rate constant,  $G_j(r=0)$  is evaluated at the transition state ( $[G_j(O)]^2/4\chi_s = \Delta G^\ddagger$ ) and the contribution of high-frequency vibrational modes is restricted by their Boltzmann populations. If there are significant differences in reactant and product molecular geometries that correlate

with modes for which  $h\nu_H > 4k_B T$ , then the rate constant is small relative to expectation based on the unbiased population of all modes and nuclear tunneling factors become important.<sup>23,32,55,56</sup>

Several additional aspects of representing the observations in terms of Equation (5) need to be considered. This type of representation is based on the harmonic oscillator approximation, and, if large-amplitude nuclear displacements are required to describe the differences between the reactants and products (excited state and ground state), then a more complicated functional form is required. This representation also assumes similar vibrational frequencies in the reactants and products; this may not be the case when the reactants and products are chemically distinguishable.

An actual electron transfer process may be characterized by contributions from several high-frequency vibrational modes, and, when this is the case, Equation (5) should include a sum over these modes. Since the contributions of the high-frequency modes occur in the sums of differently weighted exponential terms, fitting Equation (5) to an average high-frequency mode has little physical meaning and such fittings are useless when these modes are actually resolved. In fact, Equation (5) has far more parameters than can be determined in ordinary kinetic studies, and the kinetic data generally must be supplemented by other types of measurement. It is often most useful for low-temperature spectroscopic studies.

Equation (5) is a necessary point of departure for any general discussion of electron transfer phenomena. Specific applications may require specific limiting forms, and some care with definitions. For example, if the  $n$ th vibronic component in absorption is associated with a transition moment  $M_{g0 \rightarrow en} = \langle M_{ge} \rangle S_{g0,en}$ , ( $\langle M_{ge} \rangle$  is a mean value of  $M_{ge}$  assumed to be independent of the nuclear coordinates,  $S_{g0,en} = \langle \phi_{g0} | \phi_{en} \rangle$  is the vibrational overlap integral and the  $\phi_{im}$  are the vibrational wavefunctions for the  $m$ th vibrational mode of the  $i$ th electronic state and  $g$  is a multiplicity factor),<sup>57</sup> then the oscillator strength for the  $g0 \rightarrow en$  vibronic absorption ( $\nu_{g0} - \nu_{en}$  in  $\text{cm}^{-1}$ ) is given by

$$f_{g0 \rightarrow en} = \frac{8\pi^2 g m_e c \nu_{g0 \rightarrow en}}{3 h e^2} |\langle M_{ge} \rangle|^2 |S_{g0,en}|^2 = 4.70 \times 10^{29} \nu_{g0 \rightarrow en} |\langle M_{ge} \rangle|^2 |S_{g0,en}|^2 \quad (14)$$

Summation of  $f_{g0 \rightarrow en}$  over all the allowed vibronic transitions,  $n$ , gives the theoretical absorption band envelope. This summation is generally expressed in terms of the molar absorptivity,  $\epsilon(\nu_m)$ , for light of energy  $h\nu_m$ , which is given approximately by<sup>51,58,59</sup>

$$\epsilon(\nu_m) = \frac{4\pi^2 |\langle M_{ge} \rangle|^2 \eta \nu_m N}{(3 \times 10^{10} \ln 10) h c} \sum_j \frac{\Gamma \langle \phi_{g0} | \phi_{ej} \rangle^2}{4\pi^2 (\nu_m - \nu_0 - \nu_j)^2 + \Gamma^2} \quad (15)$$

In Equation (15),  $\eta$  is the index of refraction,  $c$  is the speed of light,  $N$  is Avagadro's number,  $h\nu_0 = E_{ge}^{00}$ ,  $h\nu_j$  is the correlated excited state vibrational quantum and  $\Gamma$  is the lifetime-limited line width. The summation of Equation (15), over all the allowed vibronic transitions,  $j$ , gives the theoretical band envelope. The energy dependence of the transition moment is often explicitly represented by  $M_{ge}^2 \cong (H_{DA}/\nu_m)^2 (\Delta\mu_{DA})^2$  rather than the averaged parameter in Equations (14) and (15) ( $\Delta\mu_{DA}$  is the difference in ground state and excited state dipole moments; see also Equation (23), below). The resulting expression can be simplified using a time-dependent wave packet argument. The argument can be qualitatively summarized by noting that the ground state harmonic oscillator, vibrational wave functions are Gaussian functions of the nuclear displacements from the PE minimum. Then the probability of finding a system (or the fraction of an ensemble of molecules) with some specific nuclear displacement is a Gaussian function of the displacement. The effect of light absorption can then be described in terms of projecting this Gaussian function onto the excited state PE surface. Thus, Equation (15) can be put into the form,<sup>36,51,60</sup>

$$\epsilon_{\nu_m} = \frac{8N\pi^3}{3,000h^2c\nu_m \ln 10} \frac{\eta H_{DA}^2 (\Delta\mu_{DA})^2}{(4\pi\chi_s k_B T)^{1/2}} (\text{FC})_{r=-1} \quad (16)$$

The use of Equation (16) implies that  $\Delta\mu_{DA}$  and  $H_{DA}$  are constant over the absorption band (Condon approximation). A closely related expression can be used for the intensity of an electron transfer emission.<sup>36,47,61,62</sup>

$$I_{\nu_m} = \frac{64\pi^4}{3h^3 c^3 \ln 10} \frac{\nu_m \eta^3 H_{DA}^2 (\Delta\mu_{DA})^2}{(4\pi\chi_s k_B T)^{1/2}} (\text{FC})_{r=+1} \quad (17)$$



The related expression for the electron transfer rate constant is,<sup>35–37,47,57,61,63,64</sup>

$$k_{\text{et}} = \frac{2\pi^2}{h} \frac{H_{\text{DA}}^2}{(\pi\chi_s k_{\text{B}}T)^{1/2}} (\text{FC})_{r=0} \quad (18)$$

Equation (18) is for the weakly coupled,  $\kappa_{\text{el}} < 1$ , or “nonadiabatic” limit of Equation (1). A transparent connection to Equation (1) is obtained by setting  $\kappa_{\text{nu}} = (\text{FC})$  and,

$$\kappa_{\text{el}} \cong [1 + h\nu_{\text{nu}}(\pi\chi_s k_{\text{B}}T)^{1/2} / 2\pi^2 H_{\text{DA}}^2]^{-1} = (1 + \nu_{\text{nu}}/\nu_{\text{el}})^{-1} \quad (19)$$

More elaborate expressions are possible for  $\kappa_{\text{el}}$ , for example, based on Landau–Zener approaches,<sup>23,32,65</sup> but Equation (19) is usually adequate. In Equation (19),  $\nu_{\text{el}}$  is the frequency of electronic motion across the reaction coordinate.

The experimental approaches to most of the parameters discussed in this section were briefly mentioned in Section 7.11.1.1. These will be further discussed and illustrated below. There have been extensive theoretical discussions of most of these parameters, and some of the theoretical models will be discussed below. Some general features of this material warrant comment here.

From Equation (19), it is clear that whether a reaction is “adiabatic” ( $\kappa_{\text{el}} \approx 1$ ) or “nonadiabatic” ( $\kappa_{\text{el}} < 1$ ) depends on a ratio of molecular ( $H_{\text{DA}}$  and any molecular contributions to  $\chi_s$  and  $\nu_{\text{nu}}$ ) and experimental ( $T$  and solvent contributions to  $\chi_s$  and  $\nu_{\text{nu}}$ ) parameters, not simply on the magnitude of  $H_{\text{DA}}$ . The interpretation of rate constant data, as in the discussion of whether a reaction is adiabatic or nonadiabatic, is further complicated by the alteration of parameters contributing to the Franck–Condon factor, (FC), when  $H_{\text{DA}}$  is large. At a fundamental level, this is a consequence of the dependence of the electronic wavefunction on the nuclear coordinates, even in the Born–Oppenheimer approximation. The electronic mixing results in anharmonicities in the PE surface, and this changes the values of  $\Delta G_{\text{DA}}^0$ ,  $\chi_s$ , etc. relative to the limit for which  $H_{\text{DA}} \rightarrow 0$ . Since these parameters enter into the rate constant exponentially through (FC), the evaluation of  $\kappa_{\text{el}}$  is very sensitive to the model used for the Franck–Condon factor. Partly for these reasons, the material in this chapter is organized around electronic coupling: the approaches to evaluation of parameters in the limit that the coupling is very weak and how the coupling affects (FC).

### 7.11.2.3 The Franck–Condon Factor

Two classes of nuclear coordinates are generally considered in discussions of the FC factor for electron transfer processes:

- (i) those corresponding to the changes in the orientation and position of solvent molecules that occur in solution in response to the change of dipole moment that must occur when an electron is transferred.
- (ii) those corresponding to the differences, if any, in the internal nuclear coordinates (bond lengths and bond angles) of the donor and acceptor before and after electron transfer.

The classical, Marcus/Hush, limit corresponds to Equation (1) with  $\kappa_{\text{el}} = 1$  and  $\kappa_{\text{nu}} = (\text{FC})_{r=0}$ . This condition is achieved if either: (i) the structural differences between the reactants and products do not implicate high-frequency vibrational modes; or (ii) the exchange of energy (heat) between the high-frequency vibrational modes and the solvent is fast on the time scale for electron transfer. Statement (ii) is equivalent to the equilibrium assumption of transition-state theory. That this assumption is not always correct for reactions in solution has been demonstrated in ultrafast kinetic studies of reactions that vary:

- (i) from the competition between vibrational relaxation and predissociation of electronically excited  $\text{I}_2$  and the generation of electronic and vibrational excited states in the recombination of iodine atoms;<sup>66</sup>

- (ii) to faster back electron transfer than vibrational relaxation in photoinduced electron transfer in some cyanide-bridged bimetallic complexes.<sup>67–70</sup>

The great majority of transition metal electron transfer reactions are well described by the classical limit.<sup>1</sup> This is probably a consequence of the fact that the most important differences in the molecular geometries of the reactants and products involve changes in the lengths of metal–ligand bonds for which  $h\nu_{\text{H}}$  is typically less than or equal to  $3k_{\text{B}}T$  in ambient solutions, and the corresponding nuclear tunneling corrections are relatively small for thermally activated processes with  $(|\Delta G_{\text{DA}}^0|/\chi_{\text{r}}) < 1$ .<sup>55,71</sup> The classical limit is rarely appropriate for electron transfer processes when  $(|\Delta G_{\text{DA}}^0|/\chi_{\text{r}}) > 1$ , a condition for the “Marcus inverted region” and for many electronic excited states. For this condition, one should use Equation (6) ( $j=0, 1, 2, \dots$ ) for the FC factor.

The vibrational relaxation processes that accompany electron transfer range from some that are very fast (sub-picosecond) to some that are very slow (for some systems and some conditions, days). The rates of vibrational relaxation depend on heat flow from the molecule to the bulk solvent, the amplitude (or number of quanta) for the nuclear motion involved, the molecular and solvent vibrations that couple strongly to the nuclear motion, etc. Some aspects of the relevance of these relaxation times to the analytical expression describing the rate constant have been noted above. Apart from the general structure of the analytical expression, these relaxation times can affect the electron transfer rate constant through their effect on  $\Delta G_{\text{DA}}^0$ ,  $\chi_{\text{r}}$  and the pre-exponential  $\nu_{\text{nu}}$  factor.<sup>32</sup>

The free energy of reaction and reorganizational energy terms are most significantly altered when the vibrational relaxation times are slow compared to the frequency of electron transfer. In this limit, the vibrationally excited products (or reactants) are intermediates (at thermal equilibrium in the other nuclear degrees of freedom) with respect to the electron transfer process, and the free energy quantities have values appropriate to these “intermediates” rather than to the vibrationally equilibrated products (or reactants).<sup>72</sup> Electron transfer behavior in this limit can be observed when large-amplitude motions involving several nuclei are involved (as in ligand conformational changes),<sup>73–75</sup> when the effective barrier to electron transfer is very small, in the gas phase or sometimes in rigid media.

When  $\kappa_{\text{el}} = 1$ , and when the electron transfer process is intrinsically fast (small barrier), it can be coupled with some slower vibrational relaxation processes, usually in the solvent. When this is important, the retardation can be treated as a frictional effect ( $\kappa_{\text{r}}$ ), retarding the motion of the reactant system through the transition state,<sup>32,76</sup> and it results in a relatively small value of  $\nu_{\text{nu}}$ ; i.e., for (FC)  $\rightarrow 1$ ,  $k_{\text{el}} \cong \nu_{\text{nu}}\kappa_{\text{el}}$ .

### 7.11.2.4 The Electronic Factor

In a sense, the “chemistry” of electron transfer is contained in the electronic factor; it is here that the issues related to the nature and the occupation of the electronic orbitals—those of the donor, acceptor, the bridge, the surrounding medium, etc.—appear overtly. However, the elucidation of the influence of electronic factors on electron transfer reactivity has been difficult and controversial. The exponential free energy quantities contributing to Equation (18) are rarely known with sufficient accuracy that the pre-exponential quantities ( $H_{\text{DA}}$  or  $\kappa_{\text{el}}$ ) can be determined with certainty when  $|\Delta G_{\text{DA}}^\ddagger|$  is large. The evaluation of these quantities when  $|\Delta G_{\text{DA}}^\ddagger|$  approaches zero is less subject to experimental uncertainties, but it is model dependent. On the other hand, the electronic contributions to electron transfer absorption bands are qualitatively manifested in the band intensity.

In order to discuss electronic coupling, one must assume that the total wavefunction,  $\Psi_{\text{I}}(q_{\text{el}}, Q_{\text{nu}})$  where  $q_{\text{el}}$  represents electronic and  $Q_{\text{nu}}$  nuclear coordinates, associated with the properties of a specified state can be factored into electronic,  $\psi_{\text{I}}(q_{\text{el}}, Q_{\text{nu}})$ , and nuclear,  $\varphi_{\text{I}}(Q_{\text{nu}})$ , wavefunctions (the Born–Oppenheimer approximation),<sup>22,77</sup>

$$\Psi_{\text{I}}(q_{\text{el}}, Q_{\text{nu}}) = \psi_{\text{I}}(q_{\text{el}}, Q_{\text{nu}}) \times \varphi_{\text{I}}(Q_{\text{nu}}) \quad (20)$$

The electronic coupling between the donor and the acceptor can then be described in terms of Equations (21) [ $\alpha_{\text{DA}} = H_{\text{DA}}/E_{\text{DA}}$ ].

$$\psi_G = [\psi_D^0 + \alpha_{DA}\psi_A^0]/[1 + (\alpha_{DA})^2]^{1/2} \quad (21a)$$

$$\psi_E = [\psi_A^0 - \alpha_{AD}\psi_D^0]/[1 + (\alpha_{AD})^2]^{1/2} \quad (21b)$$

The wavefunctions,  $\psi_I^0$ , are chosen to describe some appropriate reference state in which there is no donor/acceptor mixing; the subscripts correspond to states in which the exchanging electron is localized on the donor (D) or the acceptor (A). The electronic coupling is formally defined as a matrix element of the secular determinant, in terms of the reference wave functions and a perturbation Hamiltonian that mixes them,  $H_{DA} = \langle \psi_A^0 | H' | \psi_D^0 \rangle$ . It is usually assumed that  $H_{DA}$  is independent of the nuclear coordinates or that the nuclear coordinate dependence can be factored out (Condon approximation).<sup>32,78–80</sup> Differences in molecular properties between the D/A complex and the reference systems can be interpreted in terms of the fraction of charge delocalized,  $\alpha_{DA}^2/(1 + \alpha_{DA}^2)^{1/2}$ , between the donor and acceptor. (Note: elsewhere in this chapter the  $\alpha_{IJ}$  and  $H_{IJ}$  parameters are understood to be normalized.) The mixing will alter the coulomb and the exchange integral terms.<sup>81,82</sup>

Models that allow for the variation of  $H_{DA}$  with variations of the nuclear coordinates have been developed. Piepho, Krausz, and Schatz (PKS) developed a model for symmetric (mixed valence) complexes in which  $H_{DA}$  varies with metal–ligand vibrations.<sup>83,84</sup> A molecular orbital version of this model employs Jahn–Teller formalisms for the interdependence of the nuclear motions and electronic coupling.<sup>85</sup> The PKS model has been found to be very useful in interpreting the electronic coupling in some mixed valence complexes in which the bridging units were atoms (M–X–M') and the vibrations of the bridging atoms resulted in variations of the metal/metal electronic coupling.<sup>86</sup> An interesting feature of this type of vibronic model is that it can lead to striking, symmetry-dependent interference effects in the electronic coupling in multi-metal complexes.<sup>87,88</sup> Weber and Reimers<sup>89</sup> have presented an elegant overview of vibronic coupling theory in the course of a discussion of pyrazine spectra.

The vibrations within the ligands that link the donor and acceptor may also be important in determining the magnitude of  $H_{DA}$ . This possibility has been considered theoretically by Ondrechen and co-workers;<sup>90,91</sup> and Endicott and co-workers<sup>92–96</sup> have found experimental evidence for such vibronic coupling. This aspect of bridging-ligand-mediated D/A coupling is discussed further in Sections 7.11.2.7 and 7.11.4.8.

The electronic matrix element can be interpreted in terms of overlap integrals,  $S_{DA}$ , and the vertical ionization energies of the diabatic donor,  $E_D$ , and acceptor,  $E_A$ , states.<sup>22,77,97</sup> One of the simplest interpretations, at the extended Hückel level, is the Wolfsberg–Helmholtz approximation:  $H_{DA} = K_{WH} S_{DA}^2 (E_A + E_D)/2$ , where  $K_{WH}$  is a constant, usually taken to be between 1 and 2. The interpretation, or the analytical expression relating  $H_{DA}$  to molecular parameters, depends on the choice of reference state, the kind and quality of the wavefunctions, or the Franck–Condon model used in describing the electronic states. Insofar as possible, the interpretation used in this chapter will define the reference state as the separated, equivalent metal complexes, for which  $H_{DA} \cong 0$ , under the same conditions as the system of interest. The changes in properties that are observed when the donor and acceptor complexes are brought together will be used to evaluate  $H_{DA}$ .

It is well known that the oscillator strengths of electronic absorption bands are directly proportional to  $H_{DA}^2$ , and that factors such as selection rules and the distance separating the donor and acceptor (through the overlap integral), etc. affect these band intensities.<sup>22,44,45,57</sup> The relationship of the experimental parameters and the electronic coupling matrix element for a Gaussian shaped absorption band is usually described as in Equation (22),<sup>22,44,45,78</sup>

$$H_{DA} = \frac{0.0206}{r_{DA}} \left[ \frac{(\varepsilon_{\max} \Delta\nu_{1/2}) \nu_{\max}}{g} \right]^{1/2} \quad (22)$$

The energies and frequencies in this equation are in units of  $\text{cm}^{-1}$ ,  $g$  is a degeneracy factor, and  $r_{DA}$  is in Å. In principle, Equation (22) gives the mean electronic matrix element per orbital (or electron). In practice,  $g$  is usually ignored because most physical measurements of most systems involve the same degeneracy and observed properties depend on the total electronic coupling of the implicated orbitals. The experimental quantities are the oscillator strength,  $\xi_{DA} = (4.61 \times 10^{-9}) \times (\varepsilon \Delta\nu_{1/2})$ , and the wavenumber of the absorption maximum,  $\nu_{\max}$ .

The distance parameter,  $r_{\text{DA}}$ , is the distance between the centers of electronic distribution in the donor and the acceptor orbitals, not a distance based on molecular geometry.<sup>22,32,78,98</sup> Since electron density in molecules is highly polarizable, Equation (22) often has only qualitative value in assessing electronic coupling.

An alternative means for the experimental evaluation of  $H_{\text{DA}}$  is by means of electroabsorption spectroscopy.<sup>98–106</sup> The electric field dependence of the absorption spectrum can be used to obtain the difference in the ground state and excited state dipole moments,  $|\Delta\mu_{\text{DA}}|$ .<sup>99</sup> This may be combined with the transition dipole moment (in Debyes),<sup>107</sup>  $|M_{\text{ge}}| = 16[\xi_{\text{DA}}/(1.08 \times 10^{-5} E_{\text{DA}})]^{1/2}$ , to obtain (neglecting vibronic and nonresonance overlap contributions),<sup>32,100</sup>

$$H_{\text{DA}} = \frac{|\vec{M}_{\text{ge}}|}{[4M_{\text{ge}}^2 + \Delta\mu_{\text{DA}}^2]^{1/2}} E_{\text{DA}} \quad (23)$$

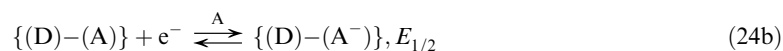
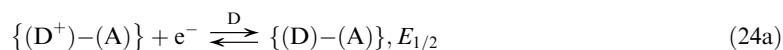
The comparison of the results of calculations based on Equations (22) and (23) have demonstrated that  $r_{\text{DA}}$  in Equation (22) is often much smaller than the geometrical distance between the donor and acceptor centers. This effect can be ascribed to an effect of mixing of the donor and acceptor orbitals, and it can be described in terms of the polarization of the electronic wavefunctions or in terms of the delocalization of electron density; either description results in a smaller than geometrical distance over which the electron is transferred. The discrepancy between  $r_{\text{DA}}$  and the separation between the donor and acceptor nuclei,  $d_{\text{DA}}$ , is expected to decrease as the amount of electron density delocalized decreases; however, the network of bridging atoms, solvent, etc., also act to polarize the wavefunctions and reduce  $r_{\text{DA}}$ .

Electroabsorption measurements to enable calculations based on Equation (23) have so far only been feasible for electron transfer systems with large transition dipole moments.<sup>100</sup> The corresponding thermally activated electron transfer process in these systems would have  $\kappa_{\text{el}} = 1$ , and one might wonder how such determinations of  $H_{\text{DA}}$  contribute to the understanding of actual electron transfer reactions. It is well known that donor/acceptor coupling alters the values of  $\Delta G_{\text{DA}}^0$ <sup>22</sup> and  $\chi_{\text{r}}$ .<sup>44,45,108–111</sup> and this has important consequences for the observed reaction rate constants. The evaluation of the effect of donor/acceptor coupling on these parameters requires their referencing to a system in which there is no effect of donor/acceptor coupling. This issue is addressed in Section 7.11.3. The present section treats the general structure of these alterations from a perturbation theory point of view: small energy corrections induced by the donor/acceptor coupling.

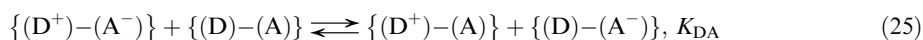
### 7.11.2.5 Perturbation Theory Corrections for the Alteration of the Free Energy of Reaction Terms as a Consequence of D/A Configurational Mixing

Differences of the half-wave potentials of the component couples are the most convenient experimental determination of  $\Delta G_{\text{DA}}^0$  in most transition metal donor/acceptor systems,

$$\Delta G_{\text{DA}}^0 = -F(E_{1/2}^{\text{D}} - E_{1/2}^{\text{A}}) = -F\Delta E_{1/2},$$



In addition to the usual solvational and electronic contributions,  $F\Delta E_{1/2} = (E_{1/2}^{\text{D}} - E_{1/2}^{\text{A}})$ , contains a contribution of  $2\varepsilon_{\text{s}} = 2H_{\text{DA}}^2/E_{\text{DA}}$  from the stabilization of the D/A pair that arises from the configurational mixing of the ground and excited electron transfer states.<sup>22</sup> When the donor and acceptor are covalently linked, the species involved in the electrochemical couples are different from those in Equations (9), (10), (12), or (13),<sup>81,112</sup> As a consequence, the electron transfer equilibrium in Equation (25)



is required to relate the electrochemical couples to those in the optical transitions.<sup>81,112</sup>

The combination of these equations leads to

$$-\Delta G_{\text{DA}}^0 = F\Delta E_{1/2}^{\text{D/A}} - RT \ln K_{\text{DA}} \quad (26)$$

where,  $(\Delta E_{1/2}^{\text{D/A}} = (E_{1/2}^{\text{A}} + E_{1/2}^{\text{D}}))$  and  $F$  is Faraday's constant). Substitution of Equation (26) into Equation (9) leads to Equation (27).

$$h\nu_{\text{max}} = -F\Delta E_{1/2}^{\text{D/A}} + RT \ln K_{\text{DA}} + \chi_{\text{r}} + \dots \quad (27)$$

Perturbation theory arguments can lead to useful estimates of  $K_{\text{DA}}$ . If the stabilization energy of the ground state that results from D/A mixing is<sup>22</sup>  $\varepsilon_{\text{s}} = H_{\text{DA}}^2/E_{\text{DA}}$ , the destabilization of the excited state is  $\varepsilon_{\text{d}} = H_{\text{AD}}^2/E_{\text{AD}}$ , if  $K_{\text{el}}$  represents the strictly electrostatic contribution to  $K_{\text{DA}}$ , and for  $\Delta K_{\text{exch}}$  the difference in exchange integral contributions then Equation (28) can be used:

$$RT \ln K_{\text{DA}} = -\varepsilon_{\text{s}} + \varepsilon_{\text{d}} + RT \ln K_{\text{el}} + \Delta K_{\text{exch}} \quad (28)$$

The equilibrium in Equation (25) refers to the PE minima, so  $h\nu_{\text{max}} = E_{\text{DA}} = (E_{\text{DA}}^{00} + \lambda_{\text{r}})$ ,  $E_{\text{AD}} = (E_{\text{DA}}^{00} - \lambda_{\text{r}})$ . Assume that  $H_{\text{DA}} = H_{\text{AD}}$  and allow for the effect of the shift in the PE minima that results from D/A mixing ( $\alpha_{\text{DA}}^2 x_0$  and  $-\alpha_{\text{AD}}^2 x_0$ , respectively, where  $x_0$  represents the separation of the reference reactant and product minima along the reaction coordinate) for the ground and excited states, to obtain Equation (29):<sup>43,113,114</sup>

$$\varepsilon_{\text{d}} \cong \varepsilon_{\text{s}} + 2\alpha_{\text{DA}}^2 \lambda_{\text{r}} + \dots \quad (29)$$

For a charge transfer absorption, Equation (27) may be rewritten as,

$$h\nu_{\text{max}} \cong -F\Delta E_{1/2}^{\text{D/A}} + \chi_{\text{r}}(1 + 2\alpha_{\text{DA}}^2) + RT \ln K_{\text{el}} + \Delta K_{\text{exch}} + \dots \quad (30)$$

It is assumed that free energy quantities may be substituted for energy quantities in the perturbational correction in Equation (30). The reorganizational parameter in Equation (30) has the same meaning as that in Equation (9), and the correction terms arise only because  $F\Delta E_{1/2}$  is not the same free energy quantity as  $\Delta G_{\text{DA}}^0$  in Equation (9).

The contributions of  $K_{\text{el}}$  may be important. These can be factored into intermolecular and intramolecular contributions. The former amounts to an ion-pair association constant and is expected to be small in high dielectric media. The intramolecular coulombic term is the largest term for the  $(\text{D}^+)-(\text{A}^-)$  species in Equation (25). Some additional considerations are required if the reaction free energy is referenced to the limit in which  $H_{\text{DA}} \rightarrow 0$ .

### 7.11.2.6 Corrections to the Reorganizational Energy Terms that Result from D/A Configurational Mixing

The configurational mixing between the donor and acceptor attenuates the reorganizational energy terms for the electron transfer process.<sup>49,56,109-111</sup> The dominant factor in the attenuation can be discussed in terms of electron delocalization and  $\alpha_{\text{DA}}^2$ ,<sup>110</sup>

$$\lambda_{\text{r}}(\text{obsd}) = \lambda_{\text{r}}^0(1 - 4\alpha_{\text{DA}}^2) \quad (31)$$

This corresponds to a very strong dependence of the reaction rate or the absorption or emission bandwidth on the D/A mixing. When the mixing becomes large, it is necessary to consider higher order terms. These can be readily generated from perturbation theory arguments. For  $E_{\text{DA}}^{00} \neq 0$ , the energy difference (of the zeroth vibrational levels) of the two PE minima,  $x_0$  and  $H_{\text{DA}}$  as defined above,  $\varepsilon_{\text{DA}}^0 = [H_{\text{DA}}^2/(E_{\text{DA}}^{00} + \lambda_{\text{r}}^0)]$  and  $k$  a force constant, the adiabatic excited state

( $V^+$ ) and ground state ( $V^-$ ) surfaces evaluated in the coordinate  $x$ , are most simply represented as Equation (32):

$$V^+(x) = E_{\text{DA}}^{00} + \frac{1}{2}k(x_0 - x)^2 + e_s(x) = E_{\text{DA}}^{00} + \frac{1}{2}k(x_0 - x)^2 + H_{\text{DA}}^2/[E_{\text{DA}}^{00} + \lambda_0 - kx_0x] \\ \cong E_{\text{DA}}^{00} + \lambda_0 - kx_0x + \frac{1}{2}kx^2 + \varepsilon_{\text{DA}}^0 \left(1 + kx_0x/E_{\text{DA}}^{00}\right) \quad (32)$$

$$V^-(x) = \frac{1}{2}k(x)^2 - H_{\text{DA}}^2/[E_{\text{DA}}^{00} + \lambda_0 - kx_0x] \cong \frac{1}{2}kx^2 - \varepsilon_{\text{DA}}^0(1 + kx_0x/E_{\text{DA}}^{00}) \quad (33)$$

The reorganizational energy appropriate to the vertical transition from the adiabatic ground state (absorption), is given by Equation (34):

$$\Delta V_a^+ = [V^+(\alpha_{\text{DA}}^2 x_0) - V^+(x_0 - \alpha_{\text{AD}}^2 x_0)] \quad \text{or} \quad (34)$$

$$\Delta V_a^+ = \lambda_r^0 [1 - 4\alpha_{\text{DA}}^2 + \alpha_{\text{DA}}^4 (3 + 2z^2 - z^4)] = \lambda_r(e)$$

where  $\alpha_{\text{AD}} = z\alpha_{\text{DA}}$  and  $z = (E_{\text{DA}}^{00} + \lambda_r^0)/(E_{\text{DA}}^{00} - \lambda_r^0)$ . It is necessary to define the reorganizational parameter for the emission with respect to the excited state PE minimum,  $x = (1 - \alpha_{\text{AD}}^2)x_0$  (with  $y = (\alpha_{\text{AD}}/\alpha_{\text{DA}}) \geq 1.0$ ), and on the ground state PE surface,

$$\Delta V_f^- = \lambda_r^0 [1 - 2\alpha_{\text{AD}}^2 (1 + y^2) + \alpha_{\text{AD}}^4 (1 + 2y^2 + y^4)] = \lambda_r(g) \quad (35)$$

Since  $\varepsilon_{\text{AD}} > \varepsilon_{\text{DA}}$  when  $E_{\text{DA}}^{00} > 0$ , the emission bandwidth is expected to be smaller than the absorption bandwidth. The reorganizational energy appropriate to the thermally activated electron transfer process is  $\lambda_r(g)$  not  $\lambda_r(e)$ .

### 7.11.2.7 The Temperature Dependence of Electron Transfer Rates

The semi-classical temperature dependence of electron transfer rate constants has been inferred from Equations (1)–(3).<sup>56,115</sup> However, it is frequently observed that these equations are more successful at describing the overall behavior of the activation free energy,  $\Delta G_{\text{DA}}^\ddagger$ , than that of the component activation enthalpy,  $\Delta H_{\text{DA}}^\ddagger$ , and entropy,  $\Delta S_{\text{DA}}^\ddagger$ , terms.<sup>32</sup> Newton<sup>32</sup> has suggested that some of the discrepancies may arise because  $\Delta H_{\text{DA}}^\ddagger$  and  $\Delta S_{\text{DA}}^\ddagger$  may be more sensitive to anharmonic contributions than is  $\Delta G_{\text{DA}}^\ddagger$ .

The description of the vertical energy difference (nuclei fixed) between the electron transfer states in terms of free energy quantities, Equation (9), has implications that do not seem to have been previously noted. This energy difference is defined in spectroscopic contexts as the sum of the difference in zero point energies of the two states,  $E_{\text{DA}}^{00}$ , and the vibrational reorganizational energy,  $\lambda_r$  (see Figure 2). As a result, in the harmonic oscillator limit (or in the absence of significant anharmonicities),<sup>43</sup>

$$|\Delta G_{\text{DA}}^0| + \chi_r = E_{\text{DA}}^{00} + \lambda_r \quad (36)$$

$$\text{If } |\Delta G_{\text{DA}}^0| = (E_{\text{DA}}^{00} - T\Delta S_{\text{DA}}^0) \text{ and } \chi_r = (\lambda_r - T\Delta S_r), \text{ then,} \quad (36)$$

$$(-T\Delta S_{\text{DA}}^0) = -(-T\Delta S_r) \quad (37)$$

and,

$$\Delta S_{\text{DA}} \cong -\Delta S_r \quad (38)$$

Then,

$$-\Delta S_{\text{DA}}^{\ddagger} = \frac{\partial(\Delta G_{\text{DA}}^{\ddagger})}{\partial T} \cong \left(\gamma + \frac{1}{4}\gamma^2\right)\Delta S_r \quad (39)$$

where  $\gamma = (|\Delta G_{\text{DA}}^0| - \chi_r)/\chi_r$ . For a self-exchange reaction,  $\Delta S_{\text{DA}}^{\ddagger}$  is expected to be small since  $\Delta S_{\text{DA}}^0 \cong -\Delta S_r = 0$  and  $h\nu_{\text{max}} = \chi_r$ . The experimental activation entropy would also contain contributions from  $R \ln(\kappa_{\text{el}})$ , and its evaluation is dependent on assumptions about the value of  $\nu_{\text{nu}}$  (and about  $K_A$  for bimolecular reactions).

Equations (39) and (40) reduce to the expected simple forms for self-exchange reactions; i.e., for the limit that  $h\nu_{\text{max}} = \chi_r = \lambda_r$  and  $\Delta S_{\text{DA}}^0 = 0$ . However, even in this limit  $\Delta S_{\text{DA}}^{\ddagger}$  is not identically zero. If one assumes that the entropy of solvation is the consequence of solvent ordering in the Coulombic field of the reactant ions, as in a Born charging model, then the entropy changes associated with the transfer between reactant centers is proportional to  $[(Z + \xi)^2/(r_{\text{eff}} + \delta)]F_{\text{coul}}$ , where  $Z$  is the ionic charge,  $\xi$  is the change in charge accompanying the processes,  $r_{\text{eff}}$  is the effective ionic radius,  $\delta$  is the change in radius that accompanies the electron transfer, and  $F_{\text{coul}}$  is a numerical constant that depends on solvent properties. Assuming that the transition state for a self-exchange reaction is solvated as if both centers have a charge of  $(Z + 0.5)$  and  $\delta = x_0/2$  (see Figure 1), the entropy change associated with formation of the transition state for exchange of an electron between +2 and +3 ions is  $\Delta S_{\text{DA}}^{\ddagger} \cong [(0.5 + 2.5x_0/r_{\text{eff}})F_{\text{coul}}]/r_{\text{eff}}$ ; i.e.,  $\Delta S_{\text{DA}}^{\ddagger} \geq 0.6 \text{ cm}^{-1} \text{ K}^{-1}$  ( $\sim 2$  e.u.) for reactions of hexaammine complexes.

The activation enthalpy in the limit considered here does not differ from the usual expression.<sup>56,115</sup> It can be expressed,

$$\Delta H_{\text{DA}}^{\ddagger} = \left( \frac{\partial \left( \frac{\Delta G_{\text{DA}}^{\ddagger}}{T} \right)}{\partial \left( \frac{1}{T} \right)} \right) = \frac{E_{\text{DA}}^{00}}{2} \gamma + \frac{\lambda_r}{4} [2 - \gamma] \gamma \quad (40)$$

When anharmonicities are large, i.e., when there is appreciable electron delocalization, each term in Equations (39) and (40) will be altered. The resulting corrections are algebraically complicated.

### 7.11.2.8 Special Features of Covalently Linked D/A Complexes

The covalent linking of a donor to an acceptor, D–B–A, can significantly influence their electron transfer properties. Some of these effects are strictly mechanical and derive from the geometric constraints imposed by the smaller number of degrees of freedom that result from the linkage. Thus, there is the possibility of controlling the mean separation distance and the orientation of the donor and acceptor in a series of related donors and acceptors by changes in the linker (B). These factors affect the donor/acceptor orbital overlap and should exert a corresponding influence on  $H_{\text{DA}}$ . The presence and the properties of the linker will also alter the values of  $\Delta G_{\text{DA}}^0$  and  $\chi_s$ . Some of these changes are the result of linker-induced changes in solvation. Some are the consequence of electronic mixing between the donor and acceptor orbital systems and those of the linker. The D/B and B/A electronic mixing provides a mechanism for extending the D/A electronic coupling over large distances, relative to atomic orbital radii, and the exploration of the related issues has attracted a great deal of attention.

Most of the studies of linked transition metal D/A complexes have employed bridging ligands that have relatively low energy  $\pi$ -type LUMOs and metals in which the electron transfer process involves  $d\pi$ -orbitals.<sup>109,116</sup> There are fewer studies of purely  $\sigma$  analogs, partly for reasons of complex instability. This section deals with some general issues that are presumably applicable to any type of substrate. Substrate-dependent issues are discussed in later sections.

The superexchange mechanism is most commonly employed to describe bridging-ligand-mediated D/A electronic coupling.<sup>78</sup> The basic concepts involved in this approach can be traced back to the theory of magnetic interactions,<sup>117</sup> and the first application to electron transfer processes is attributed to McConnell.<sup>118</sup> The approach can be most simply addressed in terms of a three-state system (see Figure 3): (i) ground state,  $\{(\text{D})-(\text{B})-(\text{A})\}$ ; (ii) bridge or metal-to-ligand charge transfer (MLCT) state,  $\{(\text{D}^+)-(\text{B}^-)-(\text{A})\}$ ; and (iii) acceptor or electron transfer

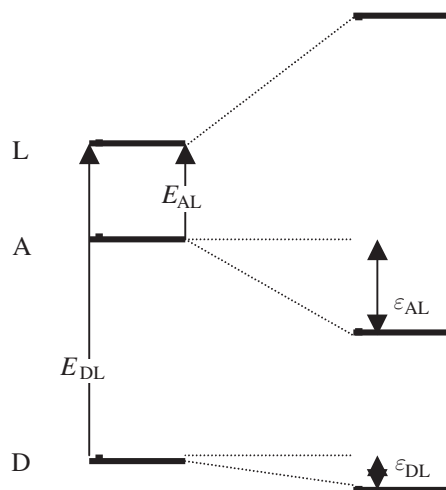


**Figure 3** Energy relations in a simple three-state system.

excited state,  $\{(D^+)-(B)-(A^-)\}$ . If  $H_{DA}$  is small or zero (no direct D/A overlap), then the bridge-mediated coupling will be dominant. The bridge-centered excited state is formulated as a MLCT state only because that is typical of the majority of linked transition metal systems. The bridging ligand state could also be a ligand-to-metal charge transfer (LMCT) state,  $\{(D)-(B^+)-(A^-)\}$ ; the formalisms are algebraically indistinguishable, except for a factor two that arises when the mixed bridging ligand orbital is unoccupied and the acceptor orbital is half occupied.<sup>107</sup> If the mixing coefficients for the donor and acceptor mixing with the bridging ligand are  $H_{DB}/E_{DB}$  and  $H_{BA}/E_{BA}$ , respectively (in two equations each, analogous to Equation (21)), then for MLCT mediation by a single bridging moiety,<sup>78,107</sup>

$$H_{DA}^{\text{spx}} = \frac{H_{DB}H_{BA}}{2E_{\text{av}}} \quad (41)$$

The related formulation for LMCT mediation of the coupling (“hole transfer”) for a single interacting bridging unit is,

$$H_{DA}^{\text{spx}'} = \frac{H_{AB}H_{BD}}{E_{\text{av}}} \quad (42)$$

In principle, the value of the energy parameter in the denominators of Equations (41) and (42) can be based on vertical energies from the charge transfer spectra of the metal complexes Equation (43),<sup>78</sup>

$$E_{\text{av}} = \frac{2E_{DB}E_{A-B}}{(E_{DB} + E_{A-B})} \quad (43)$$

These expressions can be generalized to a chain of linkers ( $B^{(1)}, B^{(2)}, \dots, B^{(n)}$ ). When only the interactions between nearest-neighbor moieties of the bridging ligand are considered, and for  $\gamma_{ij}$  the mixing coefficient between the  $i$ th and  $j$ th bridging ligand moieties, the D/A coupling matrix element becomes,<sup>32,78,79,118</sup>

$$H_{DA} = \frac{H_{DB^{(1)}}}{E_{DB^{(1)}}} \left[ \prod_{(i=1)}^{(i)=n-1} \gamma_{(i)(i+1)} \right] H_{B^{(n)}A} \quad (44)$$

In the limit of an infinite chain of identical bridging ligand moieties, Equation (44) takes the form of an exponential dependence on the geometrical distance between the donor and acceptor,  $d_{DA}$ ,<sup>32,78,79,118</sup>

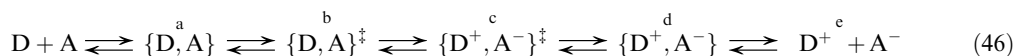
$$H_{DA} = H_{DA}(i=0)e^{-\beta d_{DA}} \quad (45)$$



An algebraically similar expression can be based on the overlap of spherical wavefunctions far from their nucleus of origin;<sup>119</sup> in this case  $\beta$  is an inverse orbital radius. The interpretation of  $\beta$  in a superexchange-based expression is more complicated.<sup>32</sup>

### 7.11.3 OBSERVATIONS IN THE LIMIT OF WEAK ELECTRONIC COUPLING: OUTER-SPHERE ELECTRON TRANSFER

In principle, outer-sphere electron transfer reactions can be defined as bimolecular reactions in which there is no significant covalent linkage between the donor and acceptor in the transition state. For some combinations of reactants, competing pathways are not important for electronic or stereochemical reasons. In many instances, the reactants can be designed to preclude any covalent linking, but in practice, weak linkages, such as hydrogen-bonded coupling of reactants through the solvent, are included. The donor and acceptor must diffuse to positions close to one another in order to optimize the product of  $\kappa_{\text{el}}$  and the effective reactant association constant,  $K_A$ . The outer-sphere reaction pathway can be represented as a series of discrete steps: (i) reactant association,  $K_A$ ; (ii) reactant activation,  $\kappa_{\text{nu}}$ ; (iii) electron transfer,  $\kappa_{\text{el}}\nu_{\text{nu}}$ ; (iv) vibrational relaxation of products,  $k_{\text{vib}}$ ; (v) dissociation of products,  $k_{\text{D}}$  and  $K_{\text{D}}$  (the brackets are used to designate species in van der Waals contact and  $\{\cdots\}^\ddagger$  designates a transition-state species).



The issues involved with this reaction pathway have been extensively discussed.<sup>1,4-6,23,32-35,37-39,44,45,48,49,55,64,120</sup> In terms of this representation, the classical limit corresponds to  $k_{\text{vib}} > \kappa_{\text{el}}\nu_{\text{nu}}$  and the overall reaction rate constant for the bimolecular reaction,  $k_{\text{biet}}$ , is given by Equation (47):

$$k_{\text{biet}} = K_A k_{\text{et}} \quad (47)$$

Estimates of  $K_A$  (and of  $K_{\text{D}}^{-1}$ ) are usually based on some variation of the Eigen–Fuoss equation (see also Equations (19), (20), and (33) in Meyer and Taube<sup>1</sup>). Equation (48) is usually a useful means of estimating  $K_A$  ( $d_{\text{DA}}$  in cm).<sup>121</sup>

$$K_A = \frac{4\pi N_A d_{\text{DA}}^3}{3000} e^{-(w_{\text{DA}}/kT)} \quad (48)$$

$$w_{\text{DA}} = \frac{Z_{\text{D}}Z_{\text{A}}e^2}{D_s} \left[ \frac{1}{d_{\text{DA}}'} - \frac{\beta_{\text{L}}\sqrt{I}}{1 + \beta_{\text{L}}d_{\text{DA}}'\sqrt{I}} \right] \quad (49)$$

$$\beta_{\text{L}} = \sqrt{\frac{8\pi N_A e^2}{1,000 D_s kT}} \quad (50)$$

In Equation (48)–(50),  $N_A$  is Avogadro's number,  $Z_I$  ( $I = \text{D}$  or  $\text{A}$ ) are the charges of the reactants,  $e$  is the charge on the electron,  $D_s$  is the static dielectric constant,  $I$  is the ionic strength, and  $d_{\text{DA}}'$  is the distance between the centers of charge of the reactants. In aqueous solutions of moderate ionic strength ( $0.1 \leq I \leq 1$ ), values of  $K_A$  for cationic reactants usually run in the range of  $10^{-2}$  to  $1 \text{ M}^{-1}$ .

It is the values of  $k_{\text{et}}$  that are important in the discussion of electron transfer processes, and corrections for variations in  $K_A$  must be made unless comparisons are based on systems in which size and charge are held constant. The reaction free energy (see Section 7.11.2),  $\Delta G_{\text{DA}}^0$ , refers to the electron transfer step, and the overall free energy change,  $\Delta G_{\text{DA}}^{0'}$ , must be corrected for the free energies of reactant association and product separation Equation (51),

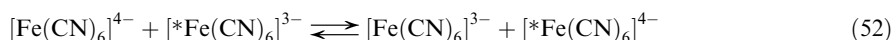
$$\Delta G_{\text{DA}}^{0'} = \Delta G_{\text{DA}}^0 - RT \ln(K_A \times K_{\text{D}}) \quad (51)$$

For a self-exchange electron transfer reaction, so that  $D^+$  and  $A$  are the same chemical species,  $K_A = K_D^{-1}$  and  $\Delta G_{DA}^{0'} = \Delta G_{DA}^0$ .

The basic features of the analysis of outer-sphere electron transfer systems have changed little since the mid 1980s. These features will be touched on here; the Meyer and Taube article<sup>1</sup> can be consulted for a more thorough discussion. This section will emphasize some relatively recent perspectives on these features, and it will explore the use of outer-sphere electron transfer reactions as an experimental approximation to the limit in which donor/acceptor coupling approaches zero. Electron transfer behavior in this limit forms an important reference with respect to which the behavior of more complex systems can be systematically evaluated.

### 7.11.3.1 The $[\text{Fe}(\text{CN})_6]^{4-}$ ,<sup>3-}</sup> Self-exchange Reaction as a Case Study

The following self-exchange reaction is a useful point of departure.



It has been extensively investigated, is strongly “catalyzed” by cations, and the uncatalyzed rate constant in aqueous solution (25 °C,  $I = 0.2 \text{ M}$ ) is  $k_{\text{biet}} = 2.2 \times 10^2 \text{ M}^{-1} \text{ s}^{-1}$ .<sup>122–124</sup> The  $\{[\text{Fe}(\text{CN})_6]^{4-}, [\text{Fe}(\text{CN})_6]^{3-}\}$  ion pair has been reported (in concentrated solutions, with  $[\text{K}^+] = 2.5 \text{ M}$ ,  $I \sim 10 \text{ M}$  and  $K_A$  determined as  $0.05 \text{ M}^{-1}$ ) to have an absorption maximum at  $12.2 \times 10^3 \text{ cm}^{-1}$  with  $\varepsilon_{\text{max}} = 28 \text{ cm}^{-1} \text{ M}^{-1}$  and  $\Delta\nu_{1/2} = 7.9 \times 10^3 \text{ cm}^{-1}$ .<sup>125</sup> Based on the ion-pair absorption spectrum and Equation (21) (neglecting  $g$ ),  $H_{\text{DA}} = 116 \text{ cm}^{-1}$ . Substitution into Equation (16) results in  $\kappa_{\text{el}} = 0.53$ . With this estimate of  $\kappa_{\text{el}}$  and (from Equation (48))  $K_A \cong 3.6 \times 10^{-2} \text{ M}^{-1}$ ,  $k_{\text{biet}}/K_A = k_{\text{et}} = 2.3 \times 10^4 \text{ s}^{-1}$ , or  $\Delta G_{\text{DA}}^\ddagger = \chi_r/4 \cong 3.64 \times 10^3 \text{ cm}^{-1}$  ( $45.1 \text{ kJ M}^{-1}$ ). For solvent reorganization the only contribution to  $\chi_r$  and  $\nu_{\text{nu}} \cong 2 \times 10^{12} \text{ s}^{-1}$ ,<sup>38</sup>  $\chi_s(\text{th}) \cong 14.6 \times 10^3 \text{ cm}^{-1}$ . Since  $\Delta G_{\text{DA}}^0 = 0$ , Equation (8) indicates that  $h\nu_{\text{max}} = \chi_r(\text{op}) = 12.2 \times 10^3 \text{ cm}^{-1}$ . Given the vast difference in conditions,  $\chi_r(\text{th})$  and  $\chi_r(\text{op})$  are in good agreement. In fact, the effect of  $[\text{K}^+]$  on the rate of this reaction has been estimated to be far larger than expected for solvent reorganization and to exceed the effect expected for ion pairing (e.g., as estimated by Meyer and Taube’s Equations (21) and (35))<sup>1</sup> by at least a factor of 10 for  $I = 0.2 \text{ M}$ .<sup>124,126</sup> An effect of this size would result in a smaller estimated value for  $\chi_r(\text{th})$  and account for most of the difference with  $\chi_r(\text{op})$ ; however, the arguments of Zahl *et al.*<sup>124</sup> imply that the presence of  $\text{K}^+$  alters the transmission coefficient. If this is correct, then  $\kappa_{\text{el}}$  is less than or equal to 0.05 for the “uncatalyzed” reaction.

The bandwidth reported for the  $\{[\text{Fe}(\text{CN})_6]^{4-}, [\text{Fe}(\text{CN})_6]^{3-}\}$  ion pair is about  $10^3 \text{ cm}^{-1}$  larger than expected based on the observed absorption maximum and Equation (10). This may indicate that the solutions used contain a distribution of ion-pair species, each with a slightly different (not necessarily symmetrical) solvation or distribution of associated cations, resulting in different values of  $\lambda_r$ ,  $\Delta G_{\text{DA}}^0$  and/or  $H_{\text{DA}}$ . This suggests a value of  $\sigma \cong 1 \times 10^3 \text{ cm}^{-1}$ .

These observations illustrate how the kinetic and the optical electron transfer behavior depend on the same parameters and how the different experiments provide complementary information. Finally, the parameters evaluated here indicate that  $\alpha_{\text{DA}}^2 \cong 10^{-4}$  and that there is very little delocalization of electron density in the ground state of the ion pair. Consequently, electronic configurational mixing in the ion pair does not significantly modify the properties of the donor and acceptor. This appears to be the general situation for transition metal outer-sphere electron transfer systems.

### 7.11.3.2 General Considerations: The Significance of $\kappa_{\text{el}}$ in Outer-sphere Electron Transfer Reactions of Transition Metal Complexes

The difficulty of determining the significance of electronic coupling from reaction rate studies has been noted above. There is a substantial body of evidence that the values of  $\kappa_{\text{el}}$  are generally a little less than unity for most reactions.

The self-exchange electron transfer rate constants,<sup>122–124,127–154</sup> redox potentials<sup>123,125,130,132,134,135,141,143–147,152,154–157</sup> and related parameters<sup>158,159</sup> for some representative

complex = couples are listed in Table 1. The reorganizational parameters,  $\chi_r$ , in Table 1 have been calculated based on Equations (1), (2), and (39)–(42), assuming that  $\kappa_{el} \cong 1$  and with  $\nu_{nu}$  based on Equation (48):<sup>38</sup>

$$\nu_{nu}^2 = \frac{\nu_s^2 \lambda_s + \nu_h \lambda_h}{\lambda_s + \lambda_h} \quad (53)$$

Observations for the ion-pair spectra in Table 2 are consistent with the assumption that  $\kappa_{el} \approx 1$  for these anion/cation cross-reactions. As noted in the discussion of the  $\{[\text{Fe}(\text{CN})_6]^{4-}, [\text{Fe}(\text{CN})_6]^{3-}\}$  ion pair, there are indications that  $\kappa_{el}$  may be less than 1 for some reactions. This is especially a concern for the  $\text{Co}^{\text{II}}/\text{Co}^{\text{III}}$  self-exchange reactions since many of the cobalt(II) complexes listed in Table 2 are high spin ( $t_2^5 e^2$   $d$ -orbital configuration) while the cobalt(III) complexes are all low spin ( $t_2^6$ ). The self-exchange reaction can be represented in terms of octahedral  $d$ -orbital configurations as,



This process is spin allowed, but it is technically a three-electron transition. In a corresponding ion pair, it would be strongly forbidden, and  $\kappa_{el}$  should be much less than 1. It is important to address the general behavior of outer-sphere electron transfer systems before this issue is considered in greater detail.

Almost all known ion-pair charge transfer systems involve anions associated with cations. Such ion pairs correlate with cross-reactions rather than with self-exchange reactions. Table 2 summarizes ion-pair charge transfer (IPCT) spectra for several cationic acceptors with anionic donors.<sup>125,160–178</sup> The IPCT absorptivities are small, less than  $50 \text{ M}^{-1} \text{ cm}^{-1}$  for  $\text{Ru}^{\text{III}}$  complexes with cyano-complex donors, and the calculated values of  $H_{\text{DA}}$  are large enough that  $\kappa_{el}$  is generally close to unity (a little smaller when based on Equation (18) above than when based on Equation (38) from Meyer and Taube<sup>1</sup>). Much of the absorptivity difference between the  $\text{Ru}^{\text{III}}$  ( $\varepsilon_{\text{max}} \sim 10\text{--}40 \text{ M}^{-1} \text{ cm}^{-1}$ ) and  $\text{Co}^{\text{III}}$  ( $\varepsilon_{\text{max}} \sim 100\text{--}300 \text{ M}^{-1} \text{ cm}^{-1}$ ) acceptors appears to arise from the differences in degeneracy ( $g$ ): three equivalent donor orbitals in the  $d\pi^6$  donors, in combination with one partly filled  $d\pi$  acceptor orbital in  $\text{Ru}^{\text{III}}$  and two unoccupied  $d\sigma$  acceptor orbitals in  $\text{Co}^{\text{III}}$ . Since these are spin-allowed transitions, the  $\text{Co}^{\text{II}}$  species in the Franck–Condon excited state generated by light absorption must be a low-spin species ( $t_2^6 e$  electronic configuration). Consequently, the inferred  $\kappa_{el}$  values may be appropriate to the corresponding cross-reactions, but they do not reflect on the  $\text{Co}^{\text{III}}/\text{Co}^{\text{II}}$  self-exchange reactions. One must also be cautious about inferring that other types of cross-reactions, for example, those involving the  $[\text{Ru}(\text{NH}_3)_6]^{3+,2+}$  couple, have similar values of  $\kappa_{el}$ . However, it does seem likely that the larger absorptivities observed for the halide-containing ion pairs are largely a consequence of a much smaller effective distance of separation,  $r_{\text{DA}}$  in Equation (21), and not a significantly larger value of  $H_{\text{DA}}$ . Since the ratios of  $H_{\text{DA}}$  to the energies of the IPCT absorption maxima are small, less than 0.15, and  $\alpha_{\text{DA}}^2 \leq 0.02$ , and D/A electronic mixing should not significantly alter the parameters ( $\Delta G_{\text{DA}}^0$  and  $\chi_r$ ) that contribute to the Franck–Condon factor. The parameters that contribute to (FC) for electron transfer reactions should be available from the spectroscopy of the corresponding, or closely related, ion pairs.

### 7.11.3.3 Observations on Cobalt(III)–(II) Systems

For reasons noted above, electron transfer reactions involving cobalt(III)/(II) couples have been the focus of much study and discussion. The experimental evaluation of  $\kappa_{el}$  from rate constant data has been complicated by the fact that  $\chi_r$  is large ( $\sim 36 \times 10^3 \text{ cm}^{-1}$ ) and reasonable uncertainties in this quantity will lead to very large uncertainties in  $\kappa_{el}$  (e.g., a 10% uncertainty in  $\chi_r$  for  $[\text{Co}(\text{NH}_3)_6]^{3+,2+}$  will lead to an uncertainty of a factor of  $\sim 10^2$  in  $\kappa_{el}$ ).

The  $[\text{Co}(\text{NH}_3)_6]^{3+,2+}$  couple has been a particular focus of attention because of its simplicity and because  $[\text{Co}(\text{NH}_3)_6]^{2+}$  has the high-spin electronic configuration. The self-exchange rate constant has been measured as  $6 \times 10^{-6} \text{ M}^{-1} \text{ s}^{-1}$  at  $40^\circ \text{C}$  in  $2.5 \text{ M NaCF}_3\text{SO}_3$ ;<sup>132</sup> thus,  $\chi_r \cong (32 \pm 4) \times 10^3 \text{ cm}^{-1}$ , assuming that  $\kappa_{el} \cong 1$ . *Ab initio* calculations<sup>179</sup> and semi-classical<sup>71</sup> calculations have estimated  $\chi_r$  to be approximately  $36 \times 10^3 \text{ cm}^{-1}$  for the three-electron process at  $25^\circ \text{C}$ . A commonly postulated, single electron transfer pathway involves the thermal population

**Table 1** Structural, electrochemical and self-exchange parameters for some simple coordination complexes.<sup>a</sup>

Couple	Electronic configuration <sup>b</sup>	$E^{0c}$ V vs. NHE	Bond lengths, $d_{ML}$ (pm)			Correlated vibrational mode	Mean size <sup>c</sup> (pm)	$k_{et}$ ( $M^{-1}s^{-1}$ ) ( $M^{-1}$ ) <sup>f</sup>	$\chi_{tr,g}$ ( $10^{-3} cm^{-1}$ )
			—A—	—D—	—D—				
[V(OH <sub>2</sub> ) <sub>6</sub> ] <sup>3+,2+</sup>	$t_2^2, t_2^3$	-0.226	201	216		325	$3 \times 10^{-3}$ (0.5) <sup>126</sup>	25.5	
[Cr(OH <sub>2</sub> ) <sub>6</sub> ] <sup>3+,2+</sup>	$t_2^3, t_2^3 e$	-0.41	198	207, 231 <sup>h</sup>		325	$\leq 2 \times 10^{-5}$ (1) <sup>127</sup>	$\geq 31.4$	
[Fe(OH <sub>2</sub> ) <sub>6</sub> ] <sup>3+,2+</sup>	$t_2^2 e^2, t_2^4 e^2$	0.77	197	210		322	4.2 (0.55) <sup>128</sup>	20.4	
[Ru(OH <sub>2</sub> ) <sub>6</sub> ] <sup>3+,2+</sup>	$t_2^5, t_2^6$	0.217 <sup>152</sup>	203	211		325	20 (5) <sup>152</sup>	20.4	
[Co(OH <sub>2</sub> ) <sub>6</sub> ] <sup>3+,2+</sup>	$t_2^6, t_2^5 e^2$	1.9	188	210		307	4 (1.0) <sup>130</sup>	22	
[Cu(OH <sub>2</sub> ) <sub>6</sub> ] <sup>2+,+</sup>	$t_2^6 e^3, t_2^6 e^4$	0.17 <sup>148</sup>				370, 380 <sup>71</sup>	$5 \times 10^{-7j}$		
[Co(NH <sub>3</sub> ) <sub>6</sub> ] <sup>3+,2+</sup>	$t_2^6, t_2^2 e^2$	-0.1 <sup>131,187</sup>	197	219		330	$6 \times 10^{-6}$ (2; 40 C) <sup>131</sup>	33	
[Co(en) <sub>3</sub> ] <sup>3+,2+</sup>	$t_2^6, t_2^5 e^2$	-0.24 <sup>132</sup>	197	217		365	$7.7 \times 10^{-5}$ <sup>132</sup>	31	
[Co(sep)] <sup>3+,2+</sup>	$t_2^6, t_2^5 e^2$	-0.30 <sup>133</sup>	199	2156		410	5.1 (0.1) <sup>133</sup>	20	
[Co(9laneN <sub>3</sub> ) <sub>2</sub> ] <sup>3+,2+</sup>	$t_2^6, t_2^5 e^2$	-0.40 <sup>134</sup>	197 <sup>158</sup>	212, 215, 219 <sup>134</sup>		440	4.08 (1) <sup>134</sup> 0.14 (0.1)	23.8	
[Co(9laneS <sub>3</sub> ) <sub>2</sub> ] <sup>3+,2+</sup>	$t_2^6, t_2^6 e$	0.45 <sup>134</sup>	225 <sup>134</sup>	224, 236, 237 <sup>159</sup>		450	$1.3 \times 10^4$ (0.1) <sup>134</sup>	14	
[Ru(NH <sub>3</sub> ) <sub>6</sub> ] <sup>3+,2+</sup>	$t_2^5, t_2^6$	0.06	212	214		335	$3.2 \times 10^3$ (0.1) <sup>136</sup>	13.4	
[Ru(en) <sub>3</sub> ] <sup>3+,2+</sup>	$t_2^5, t_2^6$				$a_{1g}$	370	$3.1 \times 10^4$ (0.75) <sup>137</sup>	12.8	
[Ru(9laneN <sub>3</sub> ) <sub>2</sub> ] <sup>3+,2+</sup>	$t_2^5, t_2^6$	0.366 <sup>129</sup>				445	$5.4 \times 10^4$ (0.1) <sup>129</sup>	11.7	
[Fe(sar)] <sup>3+,2+</sup>	$t_2^5, t_2^6$	0.093 <sup>129</sup>					$6 \times 10^3$ (0.1) <sup>j</sup> <sup>129</sup>		
[Ru(sar)] <sup>3+,2+</sup>	$t_2^5, t_2^6$	0.29 <sup>129</sup>					$1.2 \times 10^5$ (0.1) <sup>j</sup> <sup>129</sup>		
[Mn(sar)] <sup>3+,2+</sup>	$t_2^3, t_2^3 e^2$	0.519 <sup>129</sup>					17 (0.1) <sup>129</sup>		
[Fe(bpy) <sub>3</sub> ] <sup>3+,2+</sup>	$t_2^5, t_2^6$						$3.7 \times 10^6$ (0.07; AN) <sup>138</sup>	6.8	
[Fe(phen) <sub>3</sub> ] <sup>3+,2+</sup>	$t_2^5, t_2^6$						$6 \times 10^6$ (0.05; AN) <sup>138</sup>	21.5	
[Ru(bpy) <sub>3</sub> ] <sup>3+,2+</sup>	$t_2^5, t_2^6$						$4.2 \times 10^8$ <sup>139</sup>	22.1	
[Co(phen) <sub>3</sub> ] <sup>3+,2+</sup>	$t_2^6, t_2^5 e^2$	0.37 <sup>140</sup>					40 (0.1) <sup>140</sup>		
[Co(bpy) <sub>3</sub> ] <sup>3+,2+</sup>	$t_2^6, t_2^5 e^2$	0.315 <sup>140</sup>					20 (0.1) <sup>140</sup>		



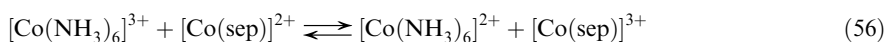
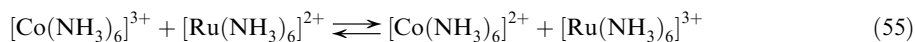


Co(en) <sub>3</sub> <sup>3+</sup>	NCS <sup>-</sup>	38.3				165			38.54
	Fe(CN) <sub>6</sub> <sup>4-</sup>	22.7	300			172		0.7-0.9	26.28
	Ru(CN) <sub>6</sub> <sup>4-</sup>	29.2	240					0.7-0.9	30.65
	I <sup>-</sup>	36.2	1150	8.2		171			34.91
	NCS <sup>-</sup>	38.3				165			37.32
	Fe(CN) <sub>6</sub> <sup>4-</sup>	24.2	195	9.0		164,173		0.7-0.9	25.1
	Ru(CN) <sub>6</sub> <sup>4-</sup>	28.6	260	10		165		0.9-1	29.39
	Os(CN) <sub>6</sub> <sup>4-</sup>	27.9	195	10.2		164		0.7-0.9	27.113
	Mo(CN) <sub>8</sub> <sup>4-</sup>	25.8	53	7.0		164			27.7
	W(CN) <sub>8</sub> <sup>4-</sup>	23.4	62	8.6		164			25.4
Co(sep) <sup>3+</sup>	Cl <sup>-</sup>	38.0				174			41.81
	Br <sup>-</sup>	36.8				174			37.85
	I <sup>-</sup>	33.8	2100	9.7		171			30.65
	NCS <sup>-</sup>	35.2				175			33.66
	Fe(CN) <sub>6</sub> <sup>4-</sup>	23	105			172		0.4-0.7	21.44
	Ru(CN) <sub>6</sub> <sup>4-</sup>	26.9				176			25.82
	Br <sup>-</sup>	36.8	150			177			40.79
Co([9]aneN <sub>4</sub> ) <sub>2</sub> <sup>3+</sup>	I <sup>-</sup>	34.2	220			177			33.58
	NCS <sup>-</sup>	35.1				175			36.60
	Fe(CN) <sub>6</sub> <sup>4-</sup>	20.2				177			24.37
	Ru(CN) <sub>6</sub> <sup>4-</sup>	27.2							28.9

<sup>a</sup> Calculated based on Equation (9) and parameters in Table 1. Most of the spectroscopic data has been collected previously in Table 1 of ref.<sup>113</sup>. Entries in the last column were recalculated and may differ from those in the previous report. <sup>b</sup> For IPCT spectra. <sup>c</sup> IPCT spectra and thermal parameters used for the value of  $\chi_r$ .

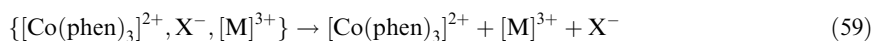
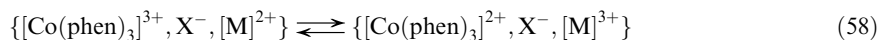
of the low-spin ( ${}^2E$ ) excited state of  $[\text{Co}(\text{NH}_3)_6]^{2+}$ .<sup>180</sup> Newton's higher level calculations<sup>179</sup> indicate that the PE surface involving the  ${}^2E$  state is about  $2,200\text{ cm}^{-1}$  higher in energy than the surface that represents the  $[({}^4T_1)\text{Co}(\text{NH}_3)_6]^{2+}$  reaction. The  ${}^2E$  pathway itself has a significant barrier to electron transfer; the Newton estimate<sup>179</sup> results in about  $\chi_r \cong 26 \times 10^3\text{ cm}^{-1}$  for the hexaamminecobalt system, and the low-spin  $[\text{Co}(\text{N}_4)(\text{OH}_2)_2]^{2+}/[\text{Co}(\text{N}_4)(\text{OH}_2)_2]^{3+}$  reactions ( $\text{N}_4$  = a tetraazamacrocyclic ligand) have been found to have  $\chi_r \cong 30 \times 10^3\text{ cm}^{-1}$ <sup>71</sup> (assuming that  $\kappa_{\text{el}} \cong 1$ ; see Table 1). It seems unlikely that the  $[\text{Co}(\text{NH}_3)_6]^{3+,2+}$  electron transfer proceeds by thermal population of an electronic excited state of one of the reactants. Newton has estimated  $\kappa_{\text{el}} \cong 1 \times 10^{-4}$  for the  ${}^4T_2/{}^1A_1$  electron transfer pathway,<sup>179</sup> a comparison of the semi-classical estimates of  $\chi_r$  to observed rate constant data resulted in an estimate of  $\kappa_{\text{el}} \approx 10^{-4 \pm 2}$ .<sup>71</sup> Turner and Schultz<sup>181,182</sup> have determined a very large positive entropy of activation ( $\Delta S_{\text{DA}}^\ddagger = 11 \pm 1\text{ cm}^{-1}$ ) for the electrochemical reaction of the closely related  $[\text{Co}(\text{9}]\text{aneN}_4)_2]^{3+,2+}$ . One might expect  $\Delta S_{\text{DA}}^\ddagger$  to be less than zero if there is a significant contribution from  $\kappa_{\text{el}} \ll 0$ , but the electron-transfer activation parameters are notoriously difficult to interpret as is discussion in Section 7.11.2.7, above.

There is evidence that some cross-reactions involving  $\text{Co}^{\text{III}}/\text{Co}^{\text{II}}$  couples have values of  $\kappa_{\text{el}} < 1$ . Rate constants for the simple electron transfer processes (only the electron transfer step is shown, not the subsequent substitution of the ligands) in Equations (55) and (56) are altered by intense magnetic fields:<sup>183</sup>



The magnetic field effects are complex (the rate constant initially decreases with magnetic field intensity, increases with higher fields and decreases again at very high fields) and temperature dependent. That the rate of the reaction in Equation (55) should be magnetic-field dependent is particularly interesting since both reactants are diamagnetic. These magnetic field effects have been attributed to a combination of the contributions of the electronic matrix element and a paramagnetic transition state to the reaction rate constant.<sup>183–185</sup> The matrix element contributions involve spin-orbit coupling perturbations to mix paramagnetic excited state components into the ground state reactant wave functions.<sup>183–185</sup> Similarly, complex magnetic field effects have been found for reactants with  $\{(t_2^5), (t_2^6)\}$  electronic configurations.<sup>184,185</sup>

It has also been observed that the rate constants for electron transfer in simple complexes can be perturbed by ion-pair formation in ways that depend on the energy of the IPCT transition and on the electronic structure of the reactants.<sup>161,186–190</sup> The observed effects can most simply be discussed with reference to Equations (52)–(54).



The overall electron transfer rate constant increased when the  $\text{X}/\text{X}^-$  reduction potential decreased (i.e., as the energy of the IPCT absorption maximum decreased; see above), and the effect was much larger when  $[\text{M}]^{2+}$  was  $[\text{Co}(\text{sep})]^{2+}$  than when it was  $[\text{Ru}(\text{NH}_3)_6]^{2+}$ . For example, for  $\text{X} = \text{CF}_3\text{SO}_3^-$  the respective rate constants were  $460\text{ M}^{-1}\text{ s}^{-1}$  and  $930\text{ M}^{-1}\text{ s}^{-1}$ , while for  $\text{X} = \text{ascorbate}$  the reduction by  $[\text{Co}(\text{sep})]^{2+}$  was 10 times faster than by  $[\text{Ru}(\text{NH}_3)_6]^{2+}$  ( $k_{\text{et}} = 23 \times 10^4\text{ M}^{-1}\text{ s}^{-1}$  and  $2.5 \times 10^4\text{ M}^{-1}\text{ s}^{-1}$ , respectively).<sup>186</sup> The correlation of the relative rate enhancements (e.g., the ratio of rate constants for reductions with  $[\text{Co}(\text{sep})]^{2+}$  to those for  $[\text{Ru}(\text{NH}_3)_6]^{2+}$ ) with the inverse of the  $([\text{Co}(\text{phen})_3]^{3+}, [\text{M}]^{3+})/\text{X}^-$  ion-pair charge-transfer absorption energies is essentially the behavior expected for the superexchange enhancement of the rate of a reaction in which  $\kappa_{\text{el}} < 1$  (see Section 7.11.2.7) relative to the rate of a reaction for which  $\kappa_{\text{el}}$  is close to one.

The  $[\text{Co}(\text{OH}_2)_6]^{3+,2+}$  couple presents a striking contrast to the electron transfer behavior of other self-exchange couples in Table 1. A useful comparison is to the  $[\text{Co}(\text{NH}_3)_6]^{3+,2+}$  couple. The reactants in these couples have about the same changes in metal-ligand bond lengths and the  $[\text{Co}(\text{OH}_2)_6]^{3+,2+}$  species are a little smaller (implying a larger solvent reorganizational barrier), yet the experimental self-exchange rate constant of the aquo complexes is at least a million times larger.<sup>131,132</sup> A further problem is that the acid-independent  $[\text{Co}(\text{OH}_2)_6]^{3+,2+}$  self-exchange



rate constant is inconsistent with outer-sphere cross-reaction rate data by many orders of magnitude.<sup>191</sup> This anomalous behavior has often been attributed to a change of mechanism. One possible mechanism is the thermal population of a  $[\text{Co}(\text{OH}_2)_6]^{3+}$  complex excited state.<sup>192</sup> This is feasible since the energy of the high-spin excited state of this complex may not be much above that of the ground state owing to the relatively small ligand field stabilization energy of  $\text{H}_2\text{O}$ .<sup>192</sup> The bond length changes that accompany the formation of the electron transfer transition state would further reduce the ligand field splitting. This excited state pathway corresponds to a one-electron process, and it is electronically allowed. Another proposed mechanistic pathway is inner-sphere, water-bridged electron transfer.<sup>191</sup> This possibility arises because  $\text{Co}^{\text{III}}$  is such a strong oxidant that the superexchange coupling contribution to  $H_{\text{DA}}$  is expected to be large for such a pathway due to a relatively small value of  $E_{\text{AB}}$  for Equation (42). This should at least partly compensate for the instability of the water bridge. One also expects the reorganizational barrier for the inner-sphere pathway to be significantly smaller than that for the outer-sphere pathway. Thus, the halide-bridged inner-sphere reaction rate constants of several  $\text{Co}^{\text{II}}/\text{Co}^{\text{III}}$  reactions have been found to be more than a million times larger than the corresponding outer-sphere rate constants,<sup>193–195</sup> and the reorganizational energies for the inner-sphere pathways have been found to be half those for the corresponding outer-sphere pathways.<sup>193,195</sup> Either of these mechanisms, or some combination of them, could account for the exceptional self-exchange properties of the  $[\text{Co}(\text{OH}_2)_6]^{3+,2+}$  couple. However, if the  $\text{Co}^{\text{III}}$  excited state mechanism is a factor in the self-exchange reaction, it appears that the excited state pathway is not available for the cross reactions.<sup>71</sup>

The  $[\text{Co}^{\text{III}}]^{3+}/[\text{Co}(\text{sep})]^{2+}$  reactions are formally three-electron processes, similar to those discussed above, while the  $[\text{Co}^{\text{III}}]^{3+}/[\text{Ru}(\text{NH}_3)_6]^{2+}$  reactions are two-electron processes. The magnetic field and IPCT perturbation studies indicate that  $\kappa_{\text{el}} < 1$  for both of these classes of electron transfer reaction, but smallest for the former. For a given coordination environment, outer-sphere electron transfer reactions involving cobalt(III) and high-spin cobalt(II) couples are likely to result in smaller values of  $\kappa_{\text{el}}$  than most other transition metal, one-electron transfer couples.

#### 7.11.3.4 Franck–Condon Factors

The Franck–Condon factor for an electron transfer reaction corresponds to the effect on the rate constant of the sum of all the energies required to change the potential energy of the exchanging electron from that of the system of reactants at equilibrium with the medium to that of the transition state. The transition state corresponds to the minimum-energy nuclear arrangement for which the exchanging electron has the same energy for the system of reactants and the system of products. When the electronic coupling between the electron donor and acceptor is sufficiently weak, the energy contributions of the nuclear displacements corresponding to different vibrational modes are additive, so that  $\chi_{\text{r}}^{(\text{D/A})} = 1/2(\chi_{\text{r}}^{(\text{D/D})} + \chi_{\text{r}}^{(\text{A/A})})$ . The  $\chi_{\text{r}}^{(\text{I/D})}$  (I = D, A) terms are the similarly defined reorganizational energies for self-exchange reactions, as illustrated by Equation (45), and they are not to be confused with individual reactant reorganizational energies. On the other hand, the additivity relations make it possible to relate the  $\chi_{\text{r}}^{(\text{I/D})}$  to the vertical ionization or affinity energies of the reactants (or products) in solution. These vertical energies are properly defined with respect to a standard initial and a standard final state. They are the classical barriers appropriate to the tunneling formulations of the electronic matrix element. Gorelsky *et al.*<sup>168</sup> obtained the vertical ionization and affinity energies for a number of inorganic complexes, and they have been able to extract reorganizational energies for the vertical processes that can be related to IPCT spectra. The vertical reorganizational energies of Gorelsky and Lever are very closely related to the  $\chi_{\text{r}}^{(\text{I/D})}$  terms discussed here.

The principle factors contributing to the Franck–Condon factor are the free energy of reaction ( $\Delta G_{\text{DA}}^0$ ), the contributions of low-frequency vibrational modes to the reorganizational free energy ( $\chi_{\text{s}}$ ), and the contributions of high-frequency vibrational modes and displacements ( $j h \nu_{\text{H}}$  and  $\lambda_{\text{H}}$ ). The contributions of these factors have been extensively discussed,<sup>1,2,4–7,18,33–39, 41,43–45,47,48,55,56,63,64,72,76,109–111,120,132,173,179,180,191,193,196–201</sup> and they are generally well understood. The general features of contributions to the Franck–Condon factor have been described in Section 7.11.2. This section contains some material selected to illustrate those contributions.

### 7.11.3.4.1 The solvent reorganizational free energy contributions ( $\chi_s$ )

A convenient choice for the illustration of the contributions of  $\chi_s$  are the self-exchange reactions of Ru<sup>II</sup>/Ru<sup>III</sup> complexes since the electron is exchanged between largely nonbonding orbitals and the accompanying changes in molecular geometry tend to be very small. The metal–ligand vibrational quanta are also small ( $300\text{--}600\text{ cm}^{-1} < 4k_{\text{B}}T$ ),<sup>202</sup> so that the contributions of high-frequency modes,  $\chi_{\text{M}}$ , to  $\chi_{\text{r}}$  are small. The self-exchange rate constants for these complexes are correspondingly large.<sup>196,203</sup> Since  $\chi_{\text{r}} = (\chi_{\text{s}} + \chi_{\text{M}})$ , values of  $\chi_{\text{s}}$  can be estimated from the experimental rate constants and  $\chi_{\text{r}} = 4\Delta G_{\text{DA}}^{\ddagger}$ , as discussed above, with corrections for the small contributions of  $\chi_{\text{M}}$ . These estimates of  $\chi_{\text{s}}$  for several ruthenium couples are summarized in Table 3. They correlate well ( $r^2 = 0.99$  for the ammine–polypyridine complexes) with the reciprocal of the estimates of the mean external radius<sup>196</sup> of the complexes (Figure 4). The least squares fit ( $\chi_{\text{s}}$  in units of  $10^5\text{ cm}^{-1}$  and  $r_{\text{mean}}$  in  $\text{pm}^{-1}$ ) of the observations for the ammine–polypyridine complexes is,

$$\chi_{\text{s}} = (4570 \pm 2)/r_{\text{mean}} + (0.1 \pm 0.4) \quad (60)$$

We have included data for the  $[\text{Ru}(\text{OH}_2)_6]^{3+,2+}$  and the  $[\text{Fe}(\text{CN})_6]^{3-,4-}$  couples in this comparison. The aquo complex seems to deviate slightly,  $2,000\text{ cm}^{-1}$  ( $\sim 25\%$ ), from the correlation line. This may be a consequence of stronger ligand–solvent (water) interaction for the aquo species than for the ammine or polypyridine complexes. On the other hand,  $\chi_{\text{s}}$  for  $[\text{Ru}(\text{CN})_6]^{3-,4-}$  is comparable to that for an ammine–polypyridine complex of the same mean size.

Marcus has described the solvent reorganizational free energy ( $\chi_{\text{s}}$ ) in terms of the repolarization (following the transfer of a charge  $e$ ) of a dielectric continuum (with index of refraction  $\eta$  and static dielectric constant  $D_{\text{s}}$ ) around two spherical reactants with radii  $a$  and  $b$ , separated a distance  $d_{\text{DA}}$ ,<sup>23,33,34</sup>

$$\chi_{\text{s}} = e^2 \left( \frac{1}{2a} + \frac{1}{2b} - \frac{1}{d_{\text{DA}}} \right) \left( \frac{1}{\eta^2} + \frac{1}{D_{\text{s}}} \right) \quad (61)$$

For a self-exchange reaction,  $a = b$ , and the slope of a plot of  $\chi_{\text{s}}$  vs.  $a^{-1}$  is expected to be  $31.9 \times 10^5\text{ cm}^{-1}\text{ pm}^{-1}$  based on Equation (61) (see the dashed line in Figure 4). The observed slope is about 50% larger than this, but Equation (61) clearly gives a reasonable first order approximation to the solvent reorganizational energy. That Equation (61) should somewhat underestimate the solvent reorganizational energy is reasonable since the local solvation (the second and third “coordination shells”) must certainly be poorly approximated by a dielectric continuum and bulk solvent properties. Elliptical cavity models have been developed and applied to a number of systems,<sup>49,204</sup> and specific solvation effects, such as hydrogen bonding, have been found to play significant roles in determining many of the properties of donor–acceptor systems.<sup>50</sup> It is possible that systematic variations in such factors contribute difference in the slopes based on the experimental data from Table 3 (Equation (60)) and that based on Equation (61) (see Figure 4); however, there is no experimentally established variation that depends on the number of N–H moieties available for hydrogen bonding and this possibility will not be further considered. Equation (60) is used for estimates of  $\chi_{\text{s}}$  throughout this chapter. More elaborate solvation models, in which the solvent structure near to the reactants plays an important role, are being explored.<sup>205,206</sup>

### 7.11.3.4.2 Inner-sphere or molecular reorganizational contributions

Since  $\chi_{\text{r}} = (\chi_{\text{s}} + \chi_{\text{M}})$ , where  $\chi_{\text{M}}$  are all the reorganizational contributions that arise from the changes in molecular structure that accompany electron transfer, the experimental values of  $\chi_{\text{M}}$  can be readily obtained as the difference between  $\chi_{\text{r}}$  values from Table 1 and  $\chi_{\text{s}}$  values calculated from Equation (60). The inner-sphere reorganizational contributions for a self-exchange reaction can be approximated by,<sup>23,33,34,38</sup>

$$\chi_{\text{M}} = 2 \sum_i^{\text{bonds}} \frac{f_{\text{II}(i)} f_{\text{III}(i)}}{f_{\text{II}(i)} + f_{\text{III}(i)}} (\Delta d_{\text{ML}(i)})^2 \quad (62)$$

**Table 3** Electron transfer parameters for some couples that involve very small molecular reorganizational energies.

Couple	$k_{\text{exch}}^a$ ( $\text{M}^{-1}\text{s}^{-1}$ )	$K_A^b$ ( $\text{M}^{-1}$ )	Size <sup>c</sup> (pm)	$\sim\chi_M^d$ ( $\text{cm}^{-1}$ )	$\lambda_s^e$ ( $10^{-3}\text{cm}^{-1}$ )
$[\text{Ru}(\text{NH}_3)_6]^{3+,2+}$	$3.2 \times 10^3$	0.018	335	240	13.2
$[\text{Ru}(\text{en})_3]^{3+,2+}$	$3.1 \times 10^4$	0.09	370	320	12.5
$[\text{Ru}(\text{9}[\text{aneN}_3)_2]^{3+,2+}$	$5.4 \times 10^4$	0.04	445	320	11.4
$[\text{Ru}(\text{OH}_2)_6]^{3+,2+}$	20	0.22	325	1,000	16
$[\text{Ru}(\text{NH}_3)_5\text{py}]^{3+,2+}$	$4.8 \times 10^5$	0.04	380	320	12.1
$[\text{Ru}(\text{NH}_3)_4\text{bpy}]^{3+,2+}$	$3.2 \times 10^6$	0.09	440	160	10.5
$[\text{Ru}(\text{NH}_3)_2(\text{bpy})_2]^{3+,2+}$	$8.4 \times 10^7$	1.2	560	100	7.9
$[\text{Ru}(\text{bpy})_3]^{3+,2+}$	$4.2 \times 10^3$	1	680	0	6.8
$[\text{Fe}(\text{CN})_6]^{4-,4-}$	$2.2 \times 10^2$		400		12.2 <sup>f</sup>

<sup>a</sup> From Table 1 except as noted.

<sup>b</sup> Based on Equations (48)–(50).

<sup>c</sup> Based on<sup>196</sup> d

<sup>e</sup> Based on Equation (60).

<sup>f</sup> Spectroscopic value; see Section 7.11.3.1.

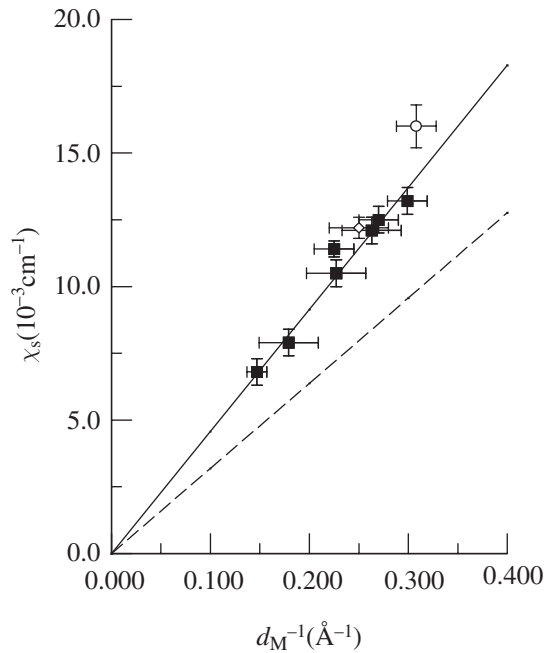


**Figure 4** The dependence of  $k_{\text{et}}$  on reactant size in water.

The summation is over all bonds, the  $f_{N(j)}$  ( $N = \text{II}$  or  $\text{III}$ ) are local bond force constants (not normal mode force constants) for the  $j$ th bond, and  $\Delta d_{\text{ML}(j)}$  is the bond length difference of the  $j$ th bond for the oxidant and reductant. The geometric changes tend to be large for  $\text{Co}^{\text{II}}/\text{Co}^{\text{III}}$  couples, so these have been selected for discussion of  $\chi_{\text{M}}$ . Since the pertinent force constant data is not available for all these complexes, it is convenient to modify the force constant ratio in Equation (62) in order to generate a simple, systematic comparison of several complexes. Molecular force constants depend on the molecular charge and very strongly on the metal–ligand bond length. This dependence can be expressed most simply by the Badger's rule<sup>207,208</sup> expression,<sup>143</sup>  $f_{\text{N}} = B_{\text{c}} Z_{\text{M}} / (d_{\text{ML}})^3$  ( $B_{\text{c}}$  is a constant of proportionality and  $Z_{\text{M}}$  is the charge on the complex). This simple expression has been found to correlate the force constant data very well for  $[\text{M}(\text{NH}_3)_6]^{n+}$  and  $[\text{M}(\text{OH}_2)_6]^{n+}$  complexes.<sup>143</sup> Since  $\text{Co}^{\text{II}}\text{L}$  bond lengths are usually longer than the  $\text{Co}^{\text{III}}$  analogs, it is convenient to set  $d_{\text{ML}}(\text{Co}^{\text{II}}) = [d_{\text{ML}}(\text{Co}^{\text{III}}) + \Delta d_{\text{ML}}]$ . After some additional algebra, Equation (62) becomes,

$$\chi_{\text{M}} = 2 \sum_j^{\text{bonds}} \frac{f_{\text{III}}}{1 + 1.5[1 + \Delta d_{\text{ML}(j)}/d_{\text{ML}}(\text{Co}^{\text{III}})]^3} (\Delta d_{\text{ML}(j)})^2 \quad (63)$$

Equation (63) assumes that one can use a common  $\text{Co}^{\text{III}}$  force constant and bond length for a given type of  $\text{Co}-\text{L}$  bond. Equation (63) forms the basis for a very good correlation of the values of  $(\chi_{\text{r}} - \chi_{\text{s}})$  for the cobalt couples in Table 1 with the reported crystallographic bond length differences, as illustrated in Figure 5 (the points for Figure 5 have been calculated using  $d_{\text{ML}}(\text{Co}^{\text{III}}) = 200$  pm). There are two exceptions among these complexes. The deviation from this correlation of the  $[\text{Co}(\text{OH}_2)_6]^{3+,2+}$  couple is expected in view of the discussion in Section 7.11.3.3. The  $[\text{Co}(\text{Me}_6[14]\text{dieneN}_4)(\text{OH}_2)]^{3+,2+}$  couple has the largest difference of cobalt(III)/(II) bond lengths reported (58 pm for each of the two axial water molecules).<sup>143</sup> It seems very unlikely that the discrepancy can have the same origin as that of the  $[\text{Co}(\text{OH}_2)_6]^{3+,2+}$  couple (e.g., a facile, water-bridged superexchange pathway can be ruled out based on stereochemical and energetic considerations). Possible sources of this discrepancy are that: (i) the very weak  $\text{Co}^{\text{II}}-\text{OH}_2$  bond force constant may not be well approximated by Badger's rule and Equation (63); (ii) the bond lengths may be different in the solid state and in solution; (iii) very long, weak bonds may not be well described by a harmonic oscillator model.

A wide variety of complexes and  $\text{Co}^{\text{III}}/\text{Co}^{\text{II}}$  structural differences are spanned by the correlation in Figure 5. The slope of the correlation (for points 1 and 3–8;  $r^2 = 0.94$ ) is

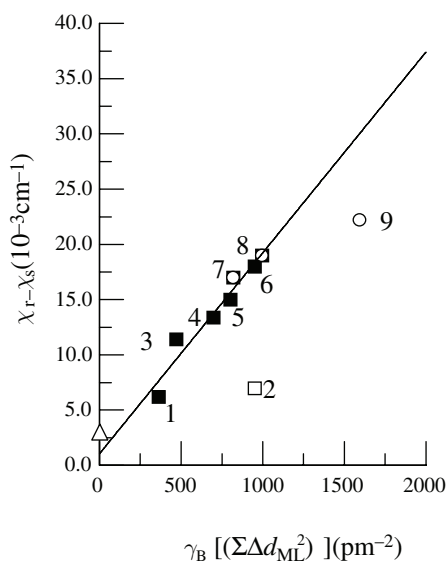


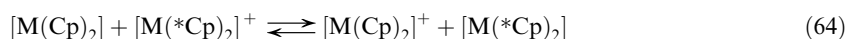
**Figure 5** Inner-sphere reorganizational energies.

$(0.018 \pm 0.002) \times 10^3 \text{ cm}^{-1} \text{ pm}^{-2}$ , and the intercept is  $(1.0 \pm 1.5) \times 10^3 \text{ cm}^{-1} \text{ pm}^{-2}$ . For a typical value of  $f_{\text{III}} = 200 \text{ N m}^{-1}$ ,<sup>143,202</sup> the calculated slope is  $(0.020) \times 10^3 \text{ cm}^{-1} \text{ pm}^{-2}$ . This is in excellent agreement with the experimental observations, especially considering the assumptions that  $f_{\text{III}}$  and  $d_{\text{ML}}(\text{Co}^{\text{III}})$  are constant, that all vibrations are harmonic (even for very large distortions), and that  $f_{\text{II}}$  can be approximated using Badger's rule. The quantity  $(\chi_r - \chi_s)$  may contain a contribution of  $4k_{\text{B}}T \ln \kappa_{\text{el}}$ , and the small positive intercept is consistent with values of  $\kappa_{\text{el}} < 1$ . Note that the intercept represents an averaged value, that both low-spin (points 7–9 and  $[\text{Co}(\text{9}]\text{aneS}_3)_2]^{3+,2+}$ ) and high-spin (points 4, 5, and 6)  $\text{Co}^{\text{II}}$  complexes are involved in the correlation and that  $\chi_{\text{M}}$  for  $\text{Co}(\text{NH}_3)_6]^{3+,2+}$  is the estimate for the inner-sphere reorganizational energy and should not contain uncompensated contributions from pre-exponential terms.<sup>71,179</sup> The uncertainty in the intercept is typical of the problem of determining pre-exponential quantities from experimental activation parameters. It is of interest that the largest and the smallest values of  $(\chi_r - \chi_s)$  are observed for  $\text{Co}^{\text{III}}/\text{Co}^{\text{II}}$  couples in which the cobalt(II) is low spin.

### 7.11.3.5 Gas-phase Solution-phase Comparisons

Gas phase electron transfer reactions provide some very useful contrasts and perspectives on the factors governing solution phase reactivity. The important differences are: (i) electrostatic interactions between reactants are far more important in the gas phase since solvent polarization tends to moderate these interactions in solution; (ii) the translational energy that the reactants bring into the collision complex must be distributed over the internal degrees of freedom during the lifetime of the reactive collision; (iii) in the absence of solvent, only the molecular geometry changes contribute to  $\chi_r$ . Owing to their very large Coulombic energies, simple gas-phase electron transfer between either similarly or oppositely charged ions are not readily compared to any solution study.<sup>200</sup> Ion molecule reactions are usefully compared, but studies of these reactions in crossed molecular beams involve large translational energies, short collision lifetimes and the results are not readily compared to solution studies. Several useful studies have employed ion cyclotron resonance (ICR) spectroscopic techniques.

For gas-phase ion-molecule reactions with small translational energies, the electrostatic attractions (e.g., ion-dipole) result in collision complexes with finite lifetimes,  $\tau_c$ , and a PE “well” in translational space that contains the electron transfer reaction coordinate (see Figure 6). In order for the comparison to solution studies to be meaningful,  $\tau_c$  must be longer than the lifetime required for vibrational relaxation and electron transfer. These criteria are satisfied for reactions of bis-cyclopentadienyl (Cp; Cp\* designates the pentamethyl-cyclopentadienyl ligand) complexes Equation (64),



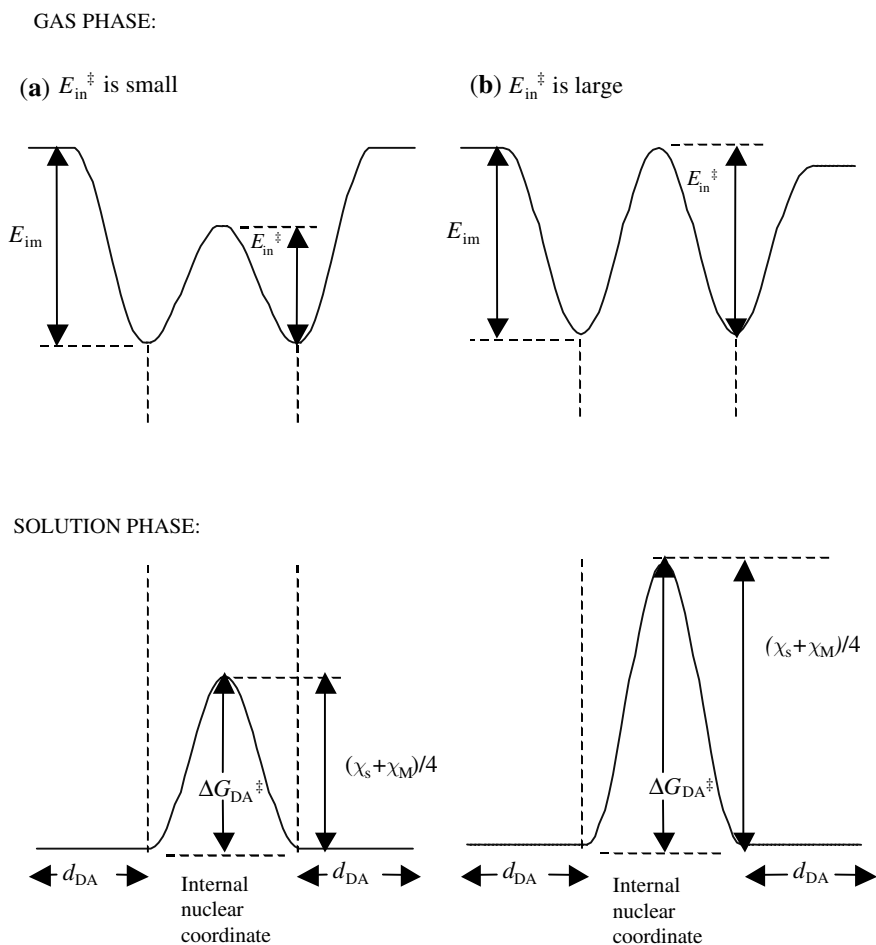


**Figure 6** PE curves for gas phase and solution phase electron transfer reactions.

Isotopic labeling of the Cp<sup>−</sup> rings enables the study of self-exchange reactions using the ICR technique. The observations for several [M(Cp)<sub>2</sub>]/[M(Cp)<sub>2</sub>]<sup>+</sup> complexes are summarized in Table 4.<sup>209–211</sup> The rate constants for the gas-phase reactions are close to the diffusion limit and about 10<sup>4</sup> times larger than their solution-phase equivalents. The slower solution reactions correspond to  $\chi_s \sim (12 \text{ to } 13) \times 10^3 \text{ cm}^{-1}$ . The variations in rate constants of the gas-phase reactions do correlate approximately with the differences in bond lengths of the donor and the acceptor, the couples that have the largest change in bond lengths, and, hence, the largest values of  $\chi_M$ , tend to have smaller rate constants. However, an opposite ordering occurs for the [Co(Cp)<sub>2</sub>]<sup>+0</sup> and [Fe(Cp)<sub>2</sub>]<sup>+0</sup> couples. The inverted order, with the cobalt exchange rate being larger, has been attributed to difference in electronic coupling, with an appreciably larger value of  $\kappa_{el}$  for [Co(Cp)<sub>2</sub>]<sup>+0</sup> than for [Fe(Cp)<sub>2</sub>]<sup>+0</sup>.<sup>211,212</sup>

The work summarized here demonstrates that electron transfer reactivity patterns are determined by the same parameters in the gas and solution phases and can be subjected to similar analyses, provided the obvious differences are taken into account.

### 7.11.3.6 Coupling to Vibrational Modes: Gated Electron Transfer and Vibronic Issues

The previous sections summarize and illustrate the detailed successes of a standard transition-state model for the electron transfer reaction coordinate when  $|\Delta G_{DA}^0| < \chi_r$ . The approaches employed above fundamentally assume that the nuclear coordinates of the reactants are in facile equilibrium with the medium all across the reaction coordinate, and that the donor–acceptor

**Table 4** Comparison of gas-phase and solution electron transfer self-exchange reactions of some cyclopentadienyl complexes.<sup>a</sup>

Couple	$\Delta r_{ML}$ (pm)	$f_{ave}$ (N m <sup>-1</sup> )	$k_{et}(M)/k_{et}(Co)$ gas phase <sup>a</sup>	$k_{et}(M)/k_{et}$ (Co)AN solution <sup>b</sup>
[Co(Cp) <sub>2</sub> ] <sup>+0</sup>	11	280	1	1
[Fe(Cp) <sub>2</sub> ] <sup>+0</sup>	4	300	0.33, 0.6 <sup>b</sup>	0.8 <sup>b</sup>
[Fe(Cp*) <sub>2</sub> ] <sup>+0</sup>			0.2 <sup>b</sup>	0.2 <sup>b</sup>
[Mn(Cp) <sub>2</sub> ] <sup>+0</sup>	25	195	0.017	
[Mn(Cp*) <sub>2</sub> ] <sup>+0</sup>	4	280	0.4	

<sup>a</sup> From<sup>208,209</sup> except as indicated. <sup>b</sup> From<sup>210</sup>.

electronic coupling is independent of the position along this coordinate. These assumptions are not always correct, even in simple, outer-sphere electron transfer systems. In several types of system, vibrational relaxation is demonstrably slow compared to the overall electron transfer process, and, in others, a closer, more detailed examination of the reaction coordinate has demonstrated that the coupling between the nuclear and electronic coordinates is significant.

#### 7.11.3.6.1 Electron transfer coupled to large-amplitude changes in low-frequency vibrational modes, intermediates, and gated electron transfer

When there is a large difference in molecular geometry between the reactants and products of a cross-reaction, then the electron transfer step may involve the formation of a product in a meta-stable geometry. This is only an issue when the relaxation (or equilibration) of the vibrational modes that correlate with the large geometry change occurs more slowly than electron transfer, and when the meta-stable product state is thermodynamically accessible and kinetically advantageous compared to direct generation of ground-state products from the reactants. It should be noted that the constraints on observation of such pathways are similar in principle to those that are involved in the intermediacy of electronic excited states in electron transfer pathways (e.g., see Sections 7.11.3.3 above). However, if the alternative pathways are selected only by the extent of nuclear reorganization, then such processes raise the possibility that protein conformational changes might enable the regulation of electron transfer in metallo-enzyme systems. Such “gated” electron transfer pathways have been explored theoretically.<sup>72,213</sup> The systematic experimental studies examining how this behavior is manifested in simple coordination complexes are largely those of Rorabacher and co-workers and are summarized briefly below.

Rorabacher and co-workers have found that the oxidations of Cu<sup>I</sup>(S<sub>n</sub>)<sub>(f)</sub> and reductions of Cu<sup>II</sup>(S<sub>n</sub>)<sub>(f)</sub> complexes, where (S<sub>n</sub>)<sub>(f)</sub> is a polythiaether ligand, often suggest that these processes occur by means of different pathways.<sup>73,74</sup> Since Cu<sup>II</sup>L and Cu<sup>I</sup>L generally have very different coordination geometries, these pathways have been associated with the generation of meta-stable Cu<sup>II</sup>L(Q) and Cu<sup>I</sup>L(P) intermediates, respectively, illustrated at the top of Figure 7. In principle, the reactivity associated with these pathways (A and B) can be interpreted in terms of self-exchange reactions that involve these intermediates: that is, the Cu<sup>II</sup>L(O)/Cu<sup>I</sup>L(P) and the Cu<sup>II</sup>L(Q)/Cu<sup>I</sup>L(R) self-exchange reactions, where Cu<sup>II</sup>L(O) and Cu<sup>I</sup>L(R) denote the equilibrium species.<sup>214</sup> It is simplest to first consider the self-exchange reactions of these complexes.

Self-exchange rate constants have been determined by NMR line-broadening for several of the Cu<sup>II</sup>L/Cu<sup>I</sup>L couples (e.g., see Table 1). These reactions may also proceed through meta-stable intermediates, although they need not be the same intermediates as in the cross-reactions. In the simplest limit, there is no direct electron exchange between Cu<sup>II</sup>L and Cu<sup>I</sup>L and the intermediates are in equilibrium with the reactants. This is illustrated in the scheme at the bottom of Figure 7. If the <sup>b\*</sup>Cu<sup>I</sup>L intermediate has the same coordination environment as Cu<sup>II</sup>L, and if <sup>a\*</sup>Cu<sup>II</sup>L has the same coordination environment as Cu<sup>I</sup>L, then  $k_{et(a)}$  and  $k_{et(b)}$  will be determined only by the solvent reorganizational energy,  $\chi_s$ . Yu *et al.*<sup>214</sup> have observed that the variations in the observed self-exchange rate constants are very nearly accounted for by the variations in the equilibrium constants for formation of the intermediates. If the complexes are all about the same size

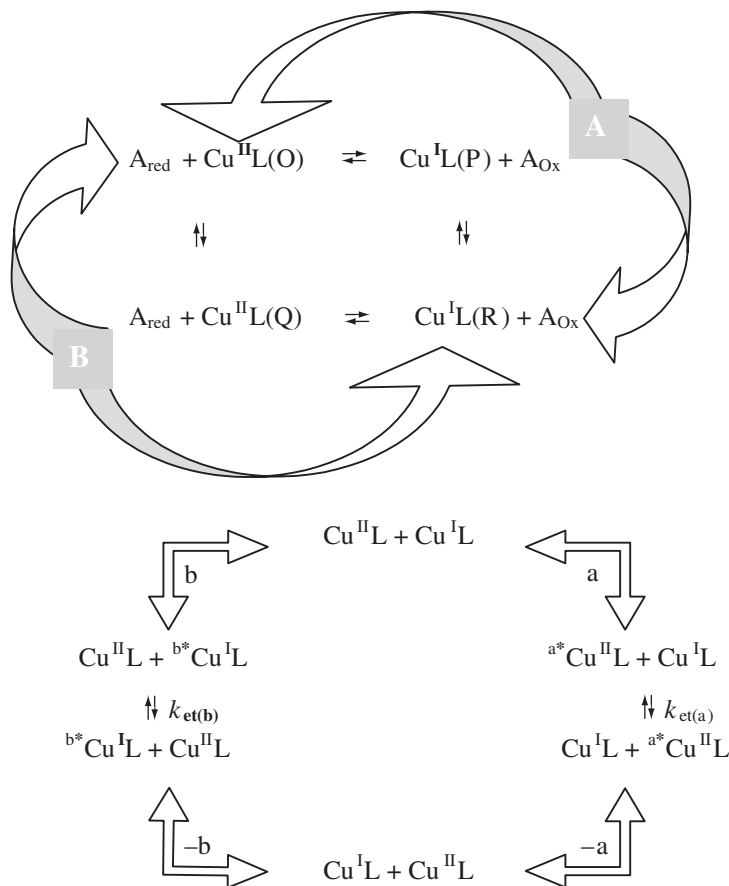


Figure 7 Square scheme.

( $\sim 440$  pm), then from Equation (60)  $\chi_s \cong 10.5 \times 10^3 \text{ cm}^{-1}$ , and the observed (second order) self-exchange rate constant is Equation (65),

$$K_A k_{\text{et}}(\text{obsd}) = K_A \left[ \frac{K_a}{1 + K_a} + \frac{K_b}{1 + K_b} \right] k_{\text{et}}(\text{solv}) \quad (65)$$

The value estimated for  $\chi_s$  corresponds to  $K_A k_{\text{et}}(\text{solv}) \cong 3 \times 10^5 \text{ M}^{-1} \text{ s}^{-1}$ . The values of  $\chi_r$  based on  $\nu_{\text{nu}} \cong k_B T/h = 2 \times 10^{12} \text{ s}^{-1}$  are very close to the estimated value of  $\chi_s$  (based on Equation (60)). Only the values for the  $[\text{Cu}([\text{14}] \text{aneS}_4)]^{2+,+}$  and the  $[\text{Cu}([\text{15}] \text{aneS}_4)]^{2+,+}$  couples are sufficiently different to infer an important contribution from the equilibria *a* and *b*. The equilibrium constants,  $K_a = 4 \times 10^{-5}$  and  $K_b = 0.02$ , have been determined from rapid-sweep cyclic voltammetry for  $[\text{Cu}([\text{14}] \text{aneS}_4)]^{2+,+}$ .<sup>214,215</sup> Substitution of these values into Equation (63) gives  $K_A k_{\text{et}}(\text{solv}) = 4 \times 10^5 \text{ M}^{-1} \text{ s}^{-1}$  in excellent agreement with the estimate based on the solvent reorganizational energy for complex ions of this size. These same pre-equilibrium processes have been implicated in cross-reactions of this class of Cu–thiaether complexes, and the transition region between the direct reaction of the equilibrium substrate to the reaction only of the intermediates has been examined by means of the suitable choice of counter-reagents.<sup>74,75,147,152,214,215</sup> This work clearly illustrates the modulation of electron transfer rates by ligand conformational changes.

The reactions of the  $[\text{Cu}(\text{S}_n)_{(j)}]$  complexes appear to involve well-defined chemical intermediates, and reaction pathways involving these intermediates are important because they are thermodynamically accessible and because the direct conversion of the equilibrium reactant species to the equilibrium product species would involve a substantial reorganizational energy. There is clearly a trade-off of the parameters contributing to Equations (4)–(6), but the reduction of the reorganizational energy must be greater than the reduction of the reaction free energy in these systems. For the classical limit with quadratic PE functions,  $|\Delta G_{\text{int}}^0| < (\chi_{\text{RP}} - \chi_{\text{int}})/4$  in



order for there to be any effect on the self-exchange reaction rate (see Figure 8). This necessarily means that the reorganizational energy,  $\chi_{\text{int}}$ , for the reaction pathway involving the intermediate must be smaller than that,  $\chi_{\text{RP}}$ , of the ground state surface when such an effect is observed; this is illustrated in Figure 8. In the  $[\text{Cu}(\text{S}_n)_{(j)}]$  systems, this constraint can be interpreted in terms of significant molecular distortions (bond breaking, conformational changes, etc.) along the ground state reaction coordinate, but only solvent reorganization along the reactant–intermediate reaction coordinate.

If the intermediates were only slightly higher in energy it would be very difficult to acquire direct evidence for their role in thermally activated electron transfer reactions. The constraints on the observation of intermediates in cross-reactions are somewhat more complex than those for self-exchange reactions. For the classical limit and quadratic potential surfaces, the condition for the observation of an intermediate (*int*) can be expressed as in Equation (66):

$$|\Delta G_{\text{int P}}^0| < \frac{(\chi_{\text{RP}} - \chi_{\text{int}})}{2} + \frac{(\Delta G_{\text{RP}}^0)^2}{2\chi_{\text{RP}}} - \frac{(\Delta G_{\text{Rint}}^0)^2}{2\chi_{\text{int}}} \quad (66)$$

The intervention of intermediates obviously becomes a more important issue for reactions with very large free energies of reaction, and it sometimes dominates the behavior of transition-metal excited states.

Conformational intermediates are described in this section as well-defined chemical species characterized by a local PE minimum. This does not always need to be the correct description, even when the conformational relaxation times are slow. If an unstable molecular conformation, or if a vibrational excited state is strongly coupled to the change of electronic configurations (i.e., large  $H_{\text{DA}}$  for the vibrational excited state), then electron transfer may occur in competition with relaxation to the PE minimum of the initial state. This corresponds to the behavior of many transition-metal excited states in which the crossing between different excited state PE surfaces (i.e., between states with different electronic configurations such as internal conversion, between states with the same spin multiplicity, or intersystem crossing, between states with different spin multiplicities) occurs in competition with vibrational relaxation within an initial PE surface. In such a situation, different counter reagents or different techniques may intercept the reacting system at different stages of its evolution along the nuclear reaction coordinate. Studies of the  $[\text{Cu}(\text{S}_n)_{(j)}]$  complexes seem to give results that are internally consistent with simple schemes involving well-defined intermediates, as in Figure 8.

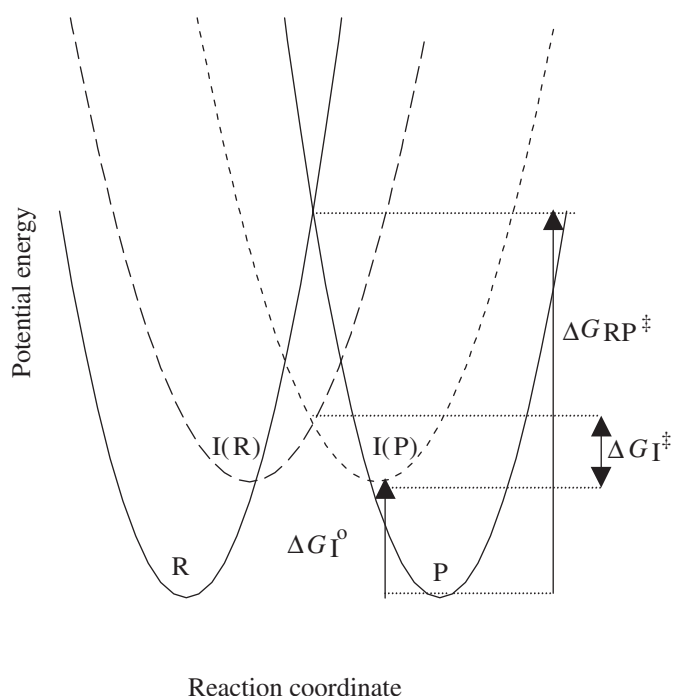
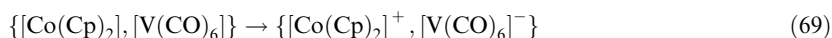
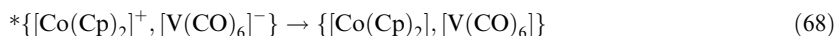
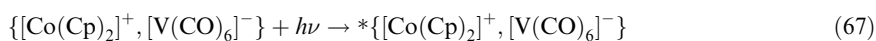


**Figure 8** Qualitative 2D PE curves illustrating the role of conformational Intermediates.

### 7.11.3.6.2 The response of outer-sphere electron transfer rates to specific vibrational excitation: vibronic coupling

The discussion so far has focused on reactions in the “Marcus-normal region”, for which  $|\Delta G_{\text{DA}}^0|/\chi_{\text{r}} < 1$ . The regime in which  $|\Delta G_{\text{DA}}^0|/\chi_{\text{r}} > 1$  is most readily accessed by means of photochemical or pulsed radiolysis techniques. Photochemical techniques are very powerful, but they usually involve an initial photo-induced electron transfer process, and this requires pre-assembly of the reactants. In the context of outer-sphere electron transfer processes, such pre-assembly involves ground state ion pairs.

Spears and co-workers<sup>216–219</sup> have performed very detailed, high-resolution studies of electron transfer following photo-excitation of the  $\{\text{[Co(Cp)}_2\text{]}^+, \text{[V(CO)}_6\text{]}^-\}$  ion pair in dichloromethane,



By using very short excitation pulses (75 fs) and infrared probing, these workers found two fast back electron transfer processes (Equation (69)) with lifetimes of  $\sim 700$  fs and  $\sim 5$  ps.<sup>219</sup> These correspond to species with slightly different absorption spectra and they are attributed to ion pairs with different geometries, one with the fivefold (Co(Cp)<sub>2</sub>) and threefold (V(CO)<sub>6</sub>) axes approximately aligned and one with the C<sub>2</sub> axes approximately aligned. The faster electron transfer rate was found to increase with increasing quanta of excitation of a non-totally symmetric stretching vibration of [V(CO)<sub>6</sub>]. This appears to indicate a breakdown of the Condon approximation ( $H_{\text{DA}}$  independent of the nuclear coordinates; based on Equation (10),  $H_{\text{DA}} = 417 \text{ cm}^{-1}$ ).<sup>219</sup>

### 7.11.3.7 Optical–Thermal Comparisons in Outer-sphere Electron Transfer Systems

The parameters in Tables 1 and 2 can be combined to illustrate the interrelationship between the optical and thermal parameters.<sup>113,114,204</sup> This is illustrated in Figure 9, in which the ion-pair charge transfer absorption (IPCT) band maxima in Table 2 are combined with the electrochemical and kinetic data from Table 1 as indicated in Equation (8).<sup>113,114</sup> The halide ion-pair data for  $\{\text{[Ru(NH}_3\text{)}_6\text{]}^{3+}, \text{X}^-\}$  ion pairs has been used to determine the halide  $\chi_{\text{r}}$  values for the correlation of the remaining ion pairs. These relative values clearly fall around the line of unit slope. On the other hand, most of the data for ion pairs with polycyanometallate donors fall below the line of unit slope. The exception is for the  $[\text{Fe(CN)}_6]^{3-}$  acceptor for which the contributions of  $\ln \kappa_{\text{el}}$  have been removed from  $\chi_{\text{r}}$  (see Section 7.11.3.1). Since the reorganizational parameters for the cationic acceptors in these ion pairs (except for those involving  $[\text{Co(NH}_3\text{)}_6]^{3+}$ ) have been derived from rate constant data, the resulting “reorganizational” parameters may contain a contribution from some additional factor such as  $2RT \ln \kappa_{\text{el}}$ ; this discrepancy averages about  $1,600 \text{ cm}^{-1}$  for Ru complexes and about  $2,700 \text{ cm}^{-1}$  for Co complexes. It is actually a little surprising that the cobalt ion pairs even come close to the line of unit slope since the spin-allowed IPCT transitions correlate with low-spin Co<sup>II</sup> and the self-exchange and electrochemical reactions involve the high-spin Co<sup>II</sup> complex. This suggests that the reorganizational energy is smaller and the free energy change is larger for the couples involving low spin than for those involving high spin Co<sup>II</sup>, and that the differences almost cancel one another.

While the details of the discrepancies from a 1:1 correlation of the optical and thermal parameters in Figure 9 are probably important, the overall correlation is very good considering that it combines data obtained independently in more than 40 different laboratories.

### 7.11.3.8 Overview and Summary

The observations summarized in this and the preceding subsection demonstrate that the magnitudes of solvational changes and geometrical differences dominate electron transfer reactivity, and that these contributions to the Franck–Condon factor are readily interpreted and analyzed in the

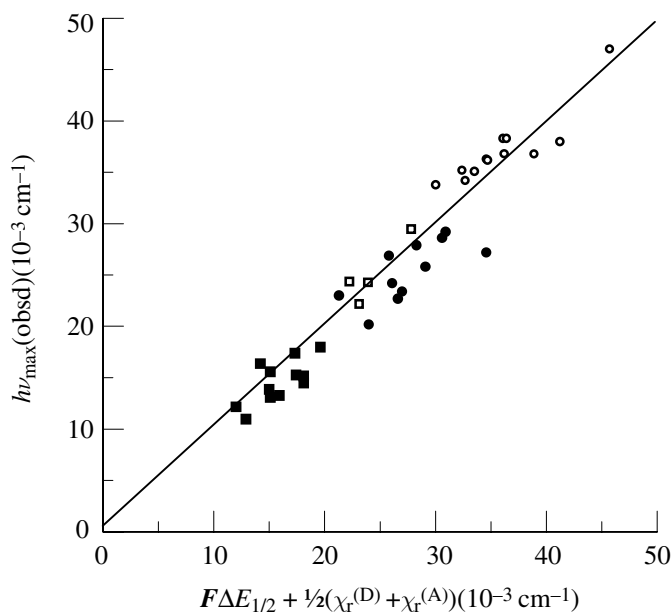


**Figure 9** Correlation of spectroscopic and thermo-chemical parameters for ion-pairs.

weak coupling limit. Electron transfer behavior in this limit is a useful point of reference for evaluating the behavior of more complex systems.

#### 7.11.4 COVALENTLY LINKED $d\pi$ DONORS AND ACCEPTORS

Even when the electron transfer agents are restricted to transition metals, the literature on covalently linked donors and acceptors is enormous.<sup>1,2,9,13,14,49,107,109,116,220–226</sup> In order to render it more approachable, this material is divided into somewhat arbitrary categories and subcategories. The principle categories for (formally) one-electron transfer systems are dictated by general types of orbitals involved in the electronic coupling of donor and acceptor:  $d\pi$  or  $d\sigma$  (formally nonbonding and bonding or anti-bonding metal-centered orbitals in most of the complexes considered). The principle subcategories are based on the strength of the electronic coupling, the type of study, etc. Various approaches to classifying bridged electron transfer systems are discussed in Section 7.11.4.5.

General matters of principle and the basic physics are the same for this class of electron transfer reactions as for the outer-sphere reactions summarized in the preceding sections. There are some important differences in details and in applications, and there are some issues that are much more important in bridged than in outer-sphere systems. One major difference is that simple two-state models can be very successfully employed to describe details of outer-sphere electron transfer reactions,<sup>56</sup> but the electronic structure of the bridging ligand can contribute profoundly to the properties of linked systems, and three-state models are generally more useful. In terms of the phenomenological approach employed in this chapter, linked, D–B–A, systems will be discussed in terms of idealized, limiting, noninteracting electronic configurations:  $\{(D)-(B)-(A)\}$ ,  $\{(D^+)-(B)-(A^-)\}$  and  $\{(D^+)-(B^-)-(A)\}$  (Figure 10; compare to Equation (44)). The properties of these limiting electronic configurations will be interpolated, insofar as possible, from the experimentally accessible properties of the equivalent outer-sphere complexes. The interpolation approaches will most often be based on standard perturbation theory. It is to be noted that these approaches are usually constructed in terms of stationary state wave functions of the system. Vertical energies, fixed nuclei, and large differences in the vibrational and electron transfer time scales are assumed in many of the conventional perturbation theory approaches. These assumptions are not always appropriate in the linked electron transfer systems.<sup>84,92,200,221,227–233</sup>

The presence of a ligand bridging the donor to the acceptor affects many properties of the resulting complex (see Sections 7.11.2.5–7.11.2.7). There are stereochemical constraints imposed

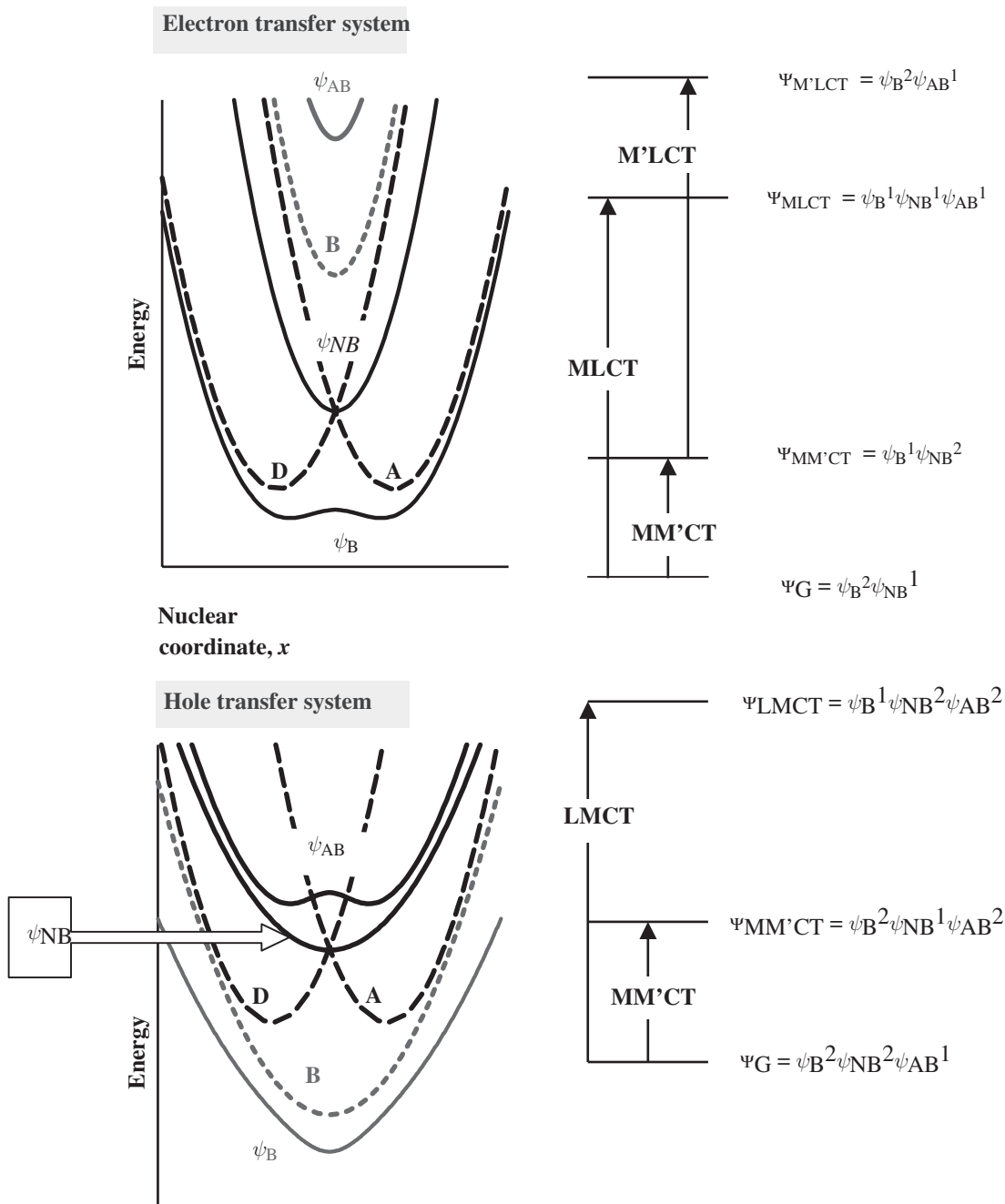


**Figure 10** Comparison of orbital and electronic state diagrams for three-state, bridged electron transfer systems.

by the bridge, there are changes in solvation and ion pairing, the bridge can mediate the electronic coupling or the bridge can more directly participate in the electron transfer. The most obvious function of the bridging ligand is to hold the donor and acceptor together. This enables the unique properties of the D/A complex to be determined, the photo-generation of electron transfer excited states of the complex or the exploitation of the unique physical or chemical properties of the complex. In the limit of weak electronic coupling between the donor and acceptor, the linked systems can model the electron transfer behavior of outer-sphere precursor and successor complexes. The properties of a representative selection of covalently linked complexes<sup>92,93,96,107,234–246</sup> are compared in Table 5.

**Table 5** Spectroscopic properties of some representative ligand-bridged, mixed-valence complexes:  $\{M(L)_2B\}^{m+}$ .

<i>M</i>	<i>L</i>	<i>B</i>	$h\nu_{\max}(MMCT)$ ( $\epsilon$ ) [ $\Delta\nu_{1/2}$ ]/Ru ( $10^{-3}$ cm $^{-1}$ )	$\sim\chi_r^a$ ( $10^{-3}$ cm $^{-1}$ )	$d_{DA}$ $\overset{b}{\text{\AA}}$	$h\nu_{\max}(MBCT)$ ( $\epsilon$ ) [ $\Delta\nu_{1/2}$ ] ( $10^{-3}$ cm $^{-1}$ )	$E_{1/2}^{Vc}$ *NHE, #SCE	
Ru	NH <sub>3</sub>	4,4'-bpy <sup>234,235</sup>	9.7 (920) [5.2]	13	11.3	19 (12.6) [5.1] <sup>107</sup>	0.41, 0.331	
		3,3'-bpy <sup>234,235</sup>	11.8 (60)	12.5	$\sim 10$			
Ru	NH <sub>3</sub>	Me <sub>2</sub> -4,4'-bpy <sup>234,235</sup>	11.2 (0.165) [6.2]	13	11.3		0.37, 0.31	
		NH(py) <sub>2</sub> <sup>234,235</sup>	10.9 (1.01) [6.4]	13	10.9		0.288, 0.20	
		CH <sub>3</sub> (py) <sub>2</sub> <sup>234,235</sup>	12.3 (0.030) [7.11]	13	10.5		0.36, 0.31	
		S(py) <sub>2</sub>	11.7 (0.070)	13	$\sim 11$			
		C <sub>2</sub> (py) <sub>2</sub> <sup>234,235</sup>	10.9 (0.640) [5.4]	14	14		0.43, 0.34	
		(CH <sub>3</sub> (py)) <sub>2</sub> <sup>234,235</sup>	10.4 (0.760) [5.3]	14	13.8		0.37, 0.30	
		<i>p</i> -DCB <sup>236</sup>	11.6 (0.507) [5.6]		11.8		22.8 (13) [4.6]	0.58, 0.512
		<i>m</i> -DCB <sup>236</sup>	13.3 (0.008) [5.86]		10.2		24.7 (8.7)	0.61, 0.55
		<i>o</i> -DCB <sup>236</sup>	9.45 (0.098) [5.4]		5.9		23.8 (4.6)	0.62, 0.53
		PZ <sup>237,238</sup>	6.37 (5.0)		12		17.7 (21) [3.23] <sup>272</sup>	0.376, 0.772
		<i>t</i> -pz[Ru(NH <sub>3</sub> ) <sub>4</sub> ]pz <sup>2+</sup> 245,246	6.0 (2.5) <sup>d,246</sup>		14		16.0 (23) [2.9] <sup>246</sup>	0.17, 0.28 <sup>239</sup>
		{ <i>t</i> -pz[Ru(NH <sub>3</sub> ) <sub>4</sub> ]pz <sup>2+</sup> }/2 <sup>g</sup>	9.8 (9.1) [4.6] <sup>g,246</sup>		10		0.72 <sup>h</sup>	0.72 <sup>h</sup>
		<i>t</i> -NC[Ru(py) <sub>4</sub> ]CN	10.0 (1.5) [6.2] <sup>96</sup>		13		14.3 ( $\sim 1.4$ )	0.05, 0.15 <sup>k,96</sup>
		{ <i>t</i> -NC[Ru(py) <sub>4</sub> ]CN}/2	14.3 ( $\sim 1.4$ ) <sup>302</sup>		12		1.29 <sup>96</sup>	1.29 <sup>96</sup>
		<i>c</i> -NC[Ru(bpy) <sub>2</sub> ]CN	9.5(0.35)[4.2] <sup>302</sup>		12		15.3(3.9)[5.0] <sup>93,302</sup>	-0.04 <sup>l,93</sup>
								-0.12, -0.06 <sup>k,232</sup>

Table 5 continued

<i>M</i>	<i>L</i>	<i>B</i>	$h\nu_{\max}(MMCT)$ ( $\epsilon$ ) [ $\Delta\nu_{1/2}$ ] / Ru ( $10^{-3} \text{ cm}^{-1}$ )	$\sim\chi_r^a$ ( $10^{-3} \text{ cm}^{-1}$ )	$d_{DA}$ , Å <sup>b</sup>	$h\nu_{\max}(MBCT)$ ( $\epsilon$ ) [ $\Delta\nu_{1/2}$ ] ( $10^{-3} \text{ cm}^{-1}$ )	$E_{1/2}V^c$ *NHE, #SCE
Os	NH <sub>3</sub>	NC[Cr(N <sub>4</sub> ) <sub>(1)</sub> ]CN <sup>+</sup>	10.0(0.18)[5.1] <sup>93</sup>	13	10.4	20.0(4.0)[4.9] <sup>93,302</sup>	0.32 <sup>k,93</sup>
		NC[Co(N <sub>4</sub> ) <sub>(2)</sub> ]CN <sup>+</sup>	11.2(0.14)[5.3] <sup>93</sup>	13	10.4	20.0(0.5)[7.0] <sup>93,302</sup>	0.36 <sup>k,93</sup>
		NC[Rh(N <sub>4</sub> ) <sub>(2)</sub> ]CN <sup>+</sup>	11.7(0.069)[6.1]	13	10.4	29.7(0.45)[5.9] <sup>93</sup>	0.31 <sup>k,93</sup>
		NC[Cr(N <sub>4</sub> ) <sub>(5)</sub> ]CN <sup>+</sup> pz <sup>240</sup>	11.9(0.15)[5.4] (note)	12	7.4	19.0(4.1)[5.1] <sup>93</sup>	0.34 <sup>k,93</sup>
Ru	(bpy) <sub>2</sub>	pz	7.4 (0.46)[ $\sim$ 5] <sup>241,244</sup>	8 <sup>l</sup>	6.8	12.9 (11,000)18.0 (29,000) ...	-0.4380.324 <sup>k</sup> 0.89, 1.01 <sup>k</sup>
Ru	CN <sup>-</sup>	pz					
Fe	CN <sup>-</sup>	pz	8.3 (22) [4800] $\sim$ 4 (3.9) <sup>242,243</sup>		6.8	19.7 (3,700)16.7 (7,300)13.4 (8000) <sup>243</sup>	
Ru	NH <sub>3</sub>	N <sub>2</sub>	9.8(1.5)[2.63] <sup>270</sup>	<12	5.5	38.2(21)	0.23, $\sim$ 1.2
Os	NH <sub>3</sub>	N <sub>2</sub>	8.5(0.72) <sup>270</sup> 5.7 ( $\sim$ 2.7) 5.4(3.9) 4.8(3.3)	<12	5.5	38.5(20)14.3(4)	-0.16, $\sim$ 1

<sup>a</sup> For the weakly coupled limit, based on outer-sphere self-exchange reactions or ion-pair spectra (see Tables 1 and 2). <sup>b</sup> Estimated metal-to-metal distance in contact ion pair.<sup>193</sup> <sup>c</sup> In water vs. S.H.E. except as indicated. <sup>d</sup> Formally a Ru<sup>II</sup>(NH<sub>3</sub>)<sub>5</sub>/Ru<sup>III</sup>(NH<sub>3</sub>)<sub>5</sub> (terminal/terminal) MMCT transition. There may not be a great deal of metal-metal charge-transfer character in this transition.<sup>239</sup> <sup>e</sup> Ru<sup>II</sup>/pz MLCT/Ru<sup>III</sup>(NH<sub>3</sub>)<sub>5</sub> in [Ru<sup>II</sup>(NH<sub>3</sub>)<sub>5</sub>]<sup>2+</sup>(pz)[Ru<sup>III</sup>(NH<sub>3</sub>)<sub>5</sub>]<sup>3+</sup>(pz)<sub>2</sub>. <sup>f</sup> In water vs. S.C.E. <sup>g</sup> Formally, a central-to-terminal transition in [Ru<sup>II</sup>(NH<sub>3</sub>)<sub>5</sub>]<sup>2+</sup>(pz)[Ru<sup>III</sup>(NH<sub>3</sub>)<sub>5</sub>]<sup>3+</sup>(pz)<sub>2</sub>. This is necessarily a transition from the symmetric combination of Ru<sup>II</sup>(NH<sub>3</sub>)<sub>5</sub> and Ru<sup>III</sup>(NH<sub>3</sub>)<sub>5</sub> moieties in the ground state to an antisymmetric combination in the MMCT excited state.<sup>239</sup> See the discussion of three-center-three-electron systems in Section 7.11.4.1.1. <sup>h</sup> Central metal reduction potential. <sup>i</sup> Formally a Ru<sup>II</sup>(NH<sub>3</sub>)<sub>5</sub>/Ru<sup>III</sup>(NH<sub>3</sub>)<sub>5</sub> (terminal/terminal) MMCT transition. <sup>j</sup> Formally, a central-to-terminal transition in [Ru<sup>II</sup>(NH<sub>3</sub>)<sub>5</sub>]<sup>2+</sup>(py)<sub>4</sub>[CN]<sup>+</sup>. <sup>k</sup> In acetonitrile vs. S.C.E. <sup>l</sup> Self-exchange rate measurements in acetonitrile;<sup>241</sup> probably convoluted with *K<sub>A</sub>*.

### 7.11.4.1 Approaches to Interpreting the Properties of Covalently Linked Donor–Acceptor Complexes

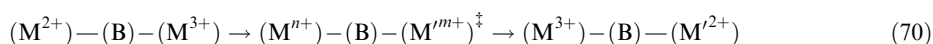
These are very complicated molecular systems. The three principle centers, donor, acceptor, and bridging ligand, each contributes to the resulting physical properties of the molecule. Many aspects of the standard perturbation theory approaches to describing the changes in physical and chemical properties that result from the linking of these three entities have been sketched in Section 7.11.2. Some of the variations in the structure of systematic treatments of these issues with the most basic structural elements of the bridging moiety are discussed in this section. Issues related to the coupling of the motions of the exchanging electron with the motions of nuclei in the molecule are developed in the following sections.

#### 7.11.4.1.1 Mono-atomic bridging moieties

The simplest conceptual limit is that in which a single atom bridges the donor and acceptor. Treatments that neglect the molecular and electronic structure of the bridging ligand are in essence presuming this limit. When the “spectator” (or nonbridging) ligands of the donor and acceptor are neglected, a perturbation theory treatment of the electronic interactions in this limit maps into a classical<sup>247</sup> three-center bonding treatment. This is illustrated in Figure 10 for the chemically degenerate limit (the donor and acceptor differ only in the exchanging electron and possibly the details of the positions of their ligands and solvent environment). The systems of interest here contain either three or five electrons in the three-center array of orbitals (i.e., ground state configurations of either  $\psi_B^2\psi_{NB}$  or  $\psi_B^2\psi_{NB}^2\psi_{AB}$ ). The three-center–three-electron system requires either an empty acceptor or an empty bridging ligand orbital. The three-center system with a vacant bridging ligand orbital is a useful limit for discussion of polypyridine-bridged D/A complexes with the  $\pi$ -antibonding orbital serving as the relevant bridging-ligand orbital, Figure 10a. In this limit both metal/bridging–ligand interactions would be described as a metal-to-ligand charge-transfer (MLCT) and the relevant mixing coefficients can be related to the corresponding MLCT spectroscopic parameters.

The two limits in which the bridging ligand contributes two electrons to the three-center bonding component have the inverted sequence of orbital energies illustrated in Figure 10b. The bridging ligands appropriately described by these limits are halide ions,  $O_2^{2-}$ , etc. In this situation, the ligand-to-metal charge-transfer excited states propagate the three-center mixing.

Figures 11a and 11b were constructed assuming that the one-electron orbital energies depend on the nuclear coordinates. Metal–ligand bond lengths tend to be different in different oxidation states of most transition metal complexes. As a result, the bridging ligand will tend to move in a concerted manner away from one metal towards the other as the electron is transferred,



Some of the consequences of this are discussed below. The energies of the different electronic states would be based on configurational wave functions, such as constructed in Figure 10, and the resulting energies of the two lowest energy states would result in PE surfaces resembling those in Figure 1. However, the three-center formulation implicates a third state in the description of the bridged electron transfer systems. Since the coupling to the bridging ligand is expected to be a strong function of the metal–ligand overlap integral,<sup>22,77</sup> since this overlap is strongly distance dependent and since the donor–acceptor electronic coupling in a single atom bridged system will be described by some variation of Equation (45),  $H_{DA}$  should typically depend on the nuclear coordinates for this type of system. Systems with single atom bridges have attracted relatively little attention.

#### 7.11.4.1.2 Diatomic bridging moieties

The most common diatomic bridging ligands are  $CN^-$ ,  $N_2$ ,  $C_2^{2-}$ ,  $O_2^-$  and  $O_2^{2-}$ . The diatomics are the simplest bridging ligands for which the molecular structure of the bridging moiety becomes an issue in the description of the electron transfer reaction coordinate. For example, bond length changes that accompany electron transfer, such as illustrated in Equation (70), must

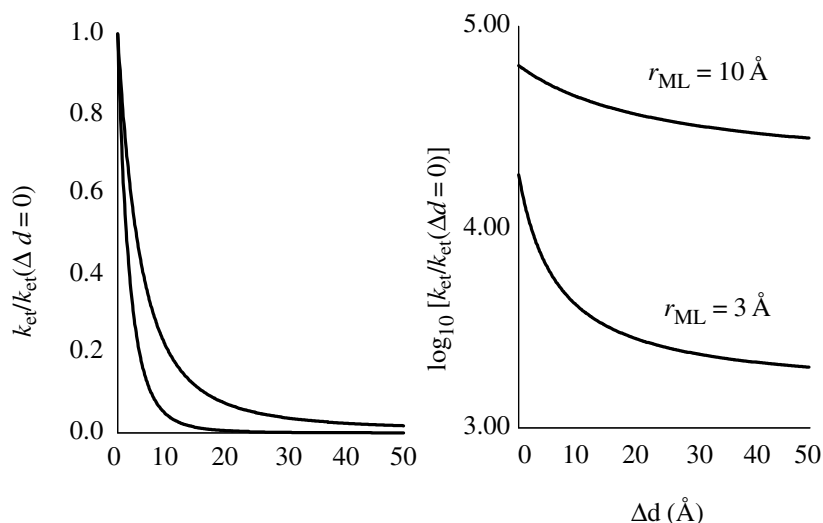


**Figure 11** The variations of rate constants with changes in solvent reorganizational energy with D/A separation.

be coupled to the bridging ligand vibrations, and changes of bond length within the diatomic ligand necessarily change the electronic overlap of the ligand atoms with the donor and acceptor. Representative systems are discussed in [Section 7.11.4.6](#).

#### 7.11.4.1.3 Polyatomic bridging ligands

The vast majority of studies of bridged electron transfer systems have employed polyatomic bridging ligands. This very important class of electron transfer systems is discussed in [Sections 7.11.4.4](#) and [7.11.4.5](#).

#### 7.11.4.2 Some General Considerations Regarding Linked Donor–Acceptor Complexes when there is no Mixing of the Nuclear and Electronic Coordinates

Several issues related to electron transfer in linked systems are covered in [Section 7.11.2](#), especially in sub-sections [7.11.2.4–7.11.2.7](#). Some additional issues are developed here. Some of these additional issues arise because the covalent linkage can function as a spacer, separating the donor and acceptor, and some arise because the linker can contribute to the electron transfer process.

[Equation \(62\)](#) suggests that the solvent reorganizational energy should increase as the linker increases in length (i.e., for the linker length,  $d_L = [d_{DA} - a - b]$ ). This can be a substantial effect, even if the linker does not otherwise affect the electron transfer rate constant.<sup>248,249</sup> The variations of the relative rate constant (in water) with increasing  $d_L$  are illustrated in [Figure 11](#) for donors and acceptors that differ only by an electron (“chemically symmetrical” D/A complexes) and which are the size of the  $[\text{Ru}(\text{NH}_3)_6]^{3+,2+}$  or the  $[\text{Ru}(\text{bpy})_3]^{3+,2+}$  couples. Since  $\alpha_{\text{DA}}^2$  decreases rapidly with  $d_L$  ([Section 7.11.2.4](#)), any attenuation of  $\chi_s$  due to the delocalization of electron density (see [Equation \(30\)](#)) will also decrease. This convolution of the distance dependencies of the electron transfer parameters, fundamentally of  $\chi_s$  and  $H_{\text{DA}}$ , can make it difficult to resolve the individual distance dependencies. This issue is further complicated by the fact the linker itself usually has dielectric parameters (e.g.,  $\eta$  and  $D_s$  in [Equation \(62\)](#)) that differ from those of the solvent. The increase of  $\chi_s$  with  $d_L$  implied in [Equation \(62\)](#) suggests that the bandwidth for absorption (or emission) should also increase with  $d_L$  (see [Equation \(11\)](#); the maximum increase in  $\Delta\nu_{1/2}$  is about 40%) and, consequently, that the electron transfer absorption maximum of the linked complexes should systematically shift to higher energies as  $d_L$  increases ([Equation \(9\)](#)).

In systems in which there is very strong electronic coupling, the ground and excited state (or reactant and product) PE surfaces can be very anharmonic. This can have large effects on  $\chi_r$ ,  $\Delta G_{\text{DA}}$ , and  $h\nu_{\text{max}}$ . Some aspects of the effects on  $\chi_r$  and  $\Delta G_{\text{DA}}$  were discussed in [Sections 7.11.2.5](#) and [7.11.2.6](#). A shift in the electronic absorption, with respect to a reference value, when the D/A



electronic coupling is mediated by a bridging ligand can provide useful information about the extent of configurational mixing between the donor (acceptor) and the bridging ligand.<sup>95,96</sup> For the simple limit in which the coupling between the donor and acceptor can be neglected ( $\alpha_{DA} \approx 0$ ), as when they are far apart in space, the effect of the bridging ligand in mediating the coupling can be formulated as,<sup>22,78</sup>

$$\psi_g = [\psi_D^0 + \alpha_{DB}\psi_B^0]/[1 + (\alpha_{DB})^2]^{1/2} \quad (71a)$$

$$\psi_e = [\psi_A^0 + \alpha_{AL}\psi_B^0]/[1 + (\alpha_{AB})^2]^{1/2} \quad (71b)$$

$$\psi_B = [\psi_B^0 - \alpha_{BD}\psi_D^0 - \alpha_{BA}\psi_A^0]/[1 + (\alpha_{BD})^2 + (\alpha_{BA})^2]^{1/2} \quad (71c)$$

The configurational mixing with the ligand reduces the energy of the ground state by  $\varepsilon_s(g) = H_{DB}^2/E_{DB}$ , and that of the electron transfer excited state by  $\varepsilon_s(e) = H_{AB}^2/E_{AB}$ . Since  $E_{DB} > E_{AB}$  (see Figure 3), the absorption maximum of the D  $\rightarrow$  A electronic transition is shifted to lower energy,

$$h\nu_{\max}(D/A) = h\nu_{\max}(\text{ref}) + \varepsilon_s(g) - \varepsilon_s(e) \quad (72)$$

The reference chosen for evaluating this shift should be a D/A complex in which there is no configurational mixing ( $H_{DB} = H_{AB} = 0$ ), and evaluated for general conditions as in the system investigated. Such a reference may be computationally accessible, in principle, but this is not a useful experimental definition. Relative values may be based on variations of absorption spectra within a homologous series of complexes, or more generally, the reference may be constructed using parameters from IPCT spectra or outer-sphere thermodynamic and kinetic data as discussed above. The shifts in the absorption maxima are a measure of the configurational mixing with the bridging ligand in strongly coupled systems; for a chemically symmetric system,  $H_{DB} = H_{AB}$ , and when no other factors contribute to the shifts in absorption maximum,

$$\Delta h\nu_{\max} = [h\nu_{\max}(D/A) - h\nu_{\max}(\text{ref})] = H_{DB}^2 \left( \frac{E_{DB} - E_{AB}}{E_{AB}E_{DB}} \right) \quad (73)$$

Comparison of Equations (36)–(38) with Equation (73) indicates that in a simple, chemically symmetrical system, (assuming one partly filled acceptor orbital, as in Ru<sup>II</sup>/Ru<sup>III</sup> couples) the shift of the absorption maximum should be closely related to the bridging-ligand-mediated superexchange coupling,<sup>95,96</sup> for a single, linker moiety that mediates D/A coupling by means of a MLCT excited state,

$$\Delta h\nu_{\max} \cong 4H_{DA}^{\text{spx}} \left[ \frac{E_{DA}}{E_{DB} + E_{AB}} \right] \quad (74)$$

Except for Equation (23), the treatment of the electronic contributions in Section 7.11.2.4 and elsewhere in this chapter are based on parameters determined for the nuclear coordinates in the absence of D/A electronic coupling; thus, diabatic, not adiabatic parameters are to be used in the perturbation theory expressions. This is a significant issue only when the  $H_{DA}$  and/or  $\alpha_{DA}$  are large. Appropriate parameters can often be inferred from the properties of related, but separate donor and acceptor complexes, or from the extrapolation of the properties of a closely related series of linked complexes to the limit that  $\alpha_{DA}^2 = 0$ .

The approaches to electron transfer described in previous sections are based on the assumptions: (i) that electronic motion occurs much faster than nuclear motion at the transition state (i.e., that  $\nu_{\text{el}} \ll \nu_{\text{nu}}$ ); and (ii) that stationary-state, or time-independent approaches to the electronic wave function provide appropriate descriptions of the reaction coordinate. These approaches are not always valid in covalently linked complexes.

#### 7.11.4.3 Time Frames for Electron Transfer

Franck–Condon factors tend to dominate electron transfer behavior and when this is the case the mean time required for reaction is relatively long, and the approaches outlined above have been very successful. When electronic mixing is large and the effective Franck–Condon factors are small, reaction rates can be very rapid and the relative time frames for electronic and nuclear motion along the reaction coordinate become important issues (see Section 7.11.3.6). This can be

especially important in covalently linked complexes. Based on a classical transition state theory/Landau–Zener analysis, the frequency of electronic motion along the reaction coordinate (evaluated at 298 K for energies in  $\text{cm}^{-1}$ ) is<sup>23,38,65</sup> (see also Equation (19)),

$$\nu_{\text{el}}(\text{LZ}) = \frac{2\pi^2 H_{\text{DA}}^2}{h(\pi\chi_s k_{\text{B}} T)^{1/2}} \cong 2.32 \times 10^{10} \frac{H_{\text{DA}}^2}{\sqrt{\chi_s}}, \text{s}^{-1} \quad (75)$$

In this equation,  $\nu_{\text{el}}$  can be interpreted as an upper limit of the frequency of hopping between the reactant and product configurations.<sup>250</sup> This frequency of the isoenergetic hopping between electronic configurations should not be confused with the vertical transition frequency at the transition state (analogous to Equation (9); energies in  $\text{cm}^{-1}$ ),

$$\nu_{\text{el}}(H) = H_{\text{DA}}/h = 3.0 \times 10^{10} H_{\text{DA}} \quad (76)$$

The introduction of an electron hopping frequency presumes a time-dependent electronic wave function, rather than the stationary state functions more often employed, and such an approach can facilitate the discussion of complexes with very large values of  $H_{\text{DA}}$ . The time-dependent and stationary state approaches should be equivalent when the time scales for electron transfer are long, such as for  $\kappa_{\text{el}} \ll 1$ . It is also important to observe that Equation (75) does not take into consideration any retardation effects that might arise due to coupling of the hopping frequency to relatively slow solvent relaxation times (“frictional” effects).<sup>76</sup> Thus, it may be interpreted as an estimate of the upper limit on the (barrier-less) electron hopping frequency. These estimates are compared for a range of complexes in Table 6.

It is useful to contrast calculated values of  $\nu_{\text{el}}$ , based on Equation (75) to the “actual” hopping frequency,  $\nu_{\text{el}}^*$ , that is appropriate (or, in principle, measurable) for a particular system in the absence of Franck–Condon restrictions. Equations (70) and (71) suggest that there are values of  $H_{\text{DA}}$  for which the frequency of electronic motion may be comparable to the vibrational frequencies for some nuclear motions. Under these circumstances, the nuclear and electronic frequencies should couple. A simple classical approach to the coupling between the frequencies of electron transfer and nuclear motions can be formulated in terms of a classical limit for the interaction of a vibration with the oscillating electric field of the hopping electron. For a vibration that involves a change of dipole,  $\Delta\mu_i = b\cos(2\pi\nu_i)$ , with frequencies  $\nu_{\text{d}}$  and  $\nu_{\text{a}}$  for the electron on the isolated donor and acceptor, respectively,  $\Delta\nu^0 = (\nu_{\text{d}} - \nu_{\text{a}})$  is the frequency difference in the limit that  $H_{\text{DA}} = 0$ . Two limiting models for the coupling are: (i) The change in vibrational frequency is exactly matched by a change in  $\nu_{\text{el}}$  (an idealized vibronic limit, or a “frictional” limit). (ii) The change in vibrational frequency is not accompanied by a change in  $\nu_{\text{el}}$  (i.e.,  $H_{\text{DA}}$  independent of the nuclear coordinates; this implies that the rate of exchange of excess energy with the bulk solvent is fast compared to  $\nu_{\text{el}}^{-1}$ ). The first limit is most easily treated, and a simple classical model of that limit is considered here. For the oscillating electric field induced by the hopping electron, the field intensity is  $F_{\text{el}} = a\cos(2\pi\nu_{\text{el}})$  and the interaction energy is given by Equation (77),

$$E_{i,\text{el}} = \Delta\mu_i \times F_{\text{el}} = ab\cos(2\pi\nu_i) \times \cos(2\pi\nu_{\text{el}}) \quad (77)$$

The limiting solutions of the resulting secular equation are: For  $\nu_{\text{el}} \ll \nu_i$ ,  $h\nu_{\text{nu}}(\text{obs}) = \frac{1}{2}h(\nu_{\text{d}} + \nu_{\text{a}}) \pm \frac{1}{2}\Delta h\nu^0$ ; and for  $\nu_{\text{el}} \gg \nu_i$ ,  $h\nu_{\text{nu}}(\text{obs}) = \frac{1}{2}h\nu_{\text{d}} + \nu_{\text{a}}$ .

In a stationary state formulation, the limit in which the electron is delocalized between a chemically equivalent donor and an acceptor corresponds to a time-dependent formulation with  $\nu_{\text{el}}^* > \nu_{\text{nc}}$  ( $\nu_{\text{nc}} = \nu_{\text{h}}$ ,  $\nu_{\text{s}}$ , etc. of Section 7.11.2) for all vibrations of the system. When  $\nu_{\text{el}}^*$  is less than any  $\nu_{\text{nc}}$ , the system is localized in the stationary state formulation. When  $\nu_{\text{el}}^*$  is roughly comparable to some  $\nu_{\text{nc}}$  that corresponds to nuclear distortions along the reaction coordinate, then these frequencies can mix, and a more complicated situation can result.

#### 7.11.4.4 The Mixing of the Nuclear and Electronic Coordinates in Linked Donor–Acceptor Complexes; Vibronic Coupling

The coupling of the nuclear and electronic coordinates is not a major issue in the discussion of most outer-sphere electron transfer reactions, partly because nuclear motions, or molecular

**Table 6** Electronic frequencies for some representative electron transfer systems.

<i>Electron transfer system</i>	$\chi_s^a$ ( $\text{cm}^{-1}$ )	$H_{\text{DA}}^a$ ( $\text{cm}^{-1}$ )	$\nu_{\text{el}}(\text{calc})_Z^b$ ( $\text{ps}^{-1}$ )	$\alpha_{\text{DA}}^2$	$\nu_{\text{el}}^*$ (method) <sup>c</sup> ( $\text{ps}^{-1}$ )	<i>Class</i>
$[\text{Co}(\text{NH}_3)_6]^{3+,2+}$	13,000					W
$[\text{Fe}(\text{CN})_6]^{3-,4-}$	12,000	120	1.2	0.0001	0.02 ( $\kappa_{\text{el}}\nu_{\text{nu}}$ )	W
$[\text{Ru}(\text{NH}_3)_6]^{3+,4+}$	13,000				0.15 ( $\kappa_{\text{el}}\nu_{\text{nu}}$ )	W
$\{[\text{Co}(\text{NH}_3)_6]^{3+}, [\text{Fe}(\text{CN})_6]^{4-}\}$	12,500	600	5.6	0.0007		W
$\{[\text{Ru}(\text{NH}_3)_6]^{3+}, [\text{Fe}(\text{CN})_6]^{4-}\}$	12,500	120	4	$8 \times 10^{-5}$		W
$[(\text{bpy})_2\text{Ru}(\text{bb})-\text{Co}(\text{bpy})_2]^{3+}$	4,100 <sup>249</sup>	40 ( $^2E$ Co <sup>II</sup> ) <sup>256</sup> 8 ( $^4T$ Co <sup>II</sup> ) <sup>256</sup>	0.58 0.02	$4 \times 10^{-6}$ $2 \times 10^{-7}$	$\sim 0.007$ ( $\kappa_{\text{el}}\nu_{\text{nu}}$ ) <sup>256</sup>	W
$[\text{Fe}(\text{bb})_3\text{Fe}]^{5+}$	7,500 <sup>257</sup>	19 <sup>257</sup>	0.1	$6 \times 10^{-6}$		W
$\{[\text{Ru}(\text{NH}_3)_5]_2(4,4'\text{-bpy})\}^{5+}$	13,000 <sup>d</sup>	750 <sup>102</sup>	110	0.058		I
$\{[\text{Ru}(\text{NH}_3)_5]_2\text{pz}\}^{5+}$	12,000 <sup>d</sup>	3,200 <sup>e</sup>	2,200	$\sim 0.5$	$< 10$ (IR) <sup>221</sup>	S
$[\text{NC}]_5\text{Ru}(\text{CNRu}(\text{NH}_3)_5)^-$	6,600 <sup>70</sup>	2,500 <sup>404</sup>	1,800		$\sim 10$ (TA) <sup>276,404</sup>	S
$[(\text{NH}_3)_5\text{Cr}(\text{CNRu}(\text{NH}_3)_5)]^{4+}$	6,000 <sup>93</sup>	3,900 <sup>93</sup>	4,600	0.038		S

<sup>a</sup> From Tables 1 and 2 except as noted. <sup>b</sup> Method of determination:  $\kappa_{\text{el}}\nu_{\text{nu}}$ , based on independent estimate of  $\kappa_{\text{el}}$  (Table 1 except as noted); IR, based on the narrowing of the MMCT absorption band, but the observation of ligand symmetric ring vibration in the IR;<sup>221</sup> TA, transient absorption measurements. <sup>c</sup> See text. <sup>d</sup> See text. <sup>e</sup> One half of the energy of the MMCT absorption maximum assuming that  $\Delta G_{\text{DA}}^{\ddagger} \sim 0$ .

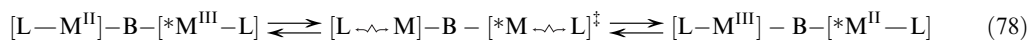
vibrations, at the donor and acceptor centers are independent of one another. It is concerted nuclear motions along the electron transfer reaction coordinate that lead to the largest effects of vibronic coupling. One perspective on the classical Marcus–Hush description of the electron transfer reaction coordinate (Section 7.11.2) is that it assumes that  $\kappa_{\text{el}}=0$  for all nuclear coordinates except for those of the transition state, and that  $\kappa_{\text{el}}=1$  at the transition state (a resonance condition). This description is useful since the nuclear motions are treated as random and independent at the donor and acceptor. As a result, when the reactant system is near to the transition state, a fluctuation in the positions of the nuclei that moves the system away from the product configuration is more probable than one that moves it towards that configuration. On the other hand, there may be some very probable nuclear motions of the reactant system near to the transition state that correspond to nuclear motion across the reaction coordinate and thus couple to the electronic distribution. This is especially possible for some bridging moieties that link the donor to the acceptor; for example, some vibrations of the bridge may be directly coupled to the electronic distribution between the donor and the acceptor.

The alterations of some key electron transfer parameters when there is appreciable delocalization of electron density are discussed in Section 7.11.2. These changes to the properties of the ground state can be described in terms of correlated increases in the anharmonicity of the ground state PE surface. Such anharmonicities imply that there are changes in the frequencies of some vibrational modes that are correlated with the reaction coordinate, and that the size of the anharmonic contribution correlates with increases in electron delocalization.

There are clearly several different ways in which the electronic and nuclear coordinates can mix in an electron transfer system: (i)  $H_{\text{DA}}$  may be different in ground and excited vibrational states (see the discussion in Section 7.11.3.6); (ii) a change in the nuclear coordinates of the ligands of one of the reactants may be directly coupled with a change in the nuclear coordinates of the other reactant; (iii) electron delocalization between the donor, the acceptor, and/or the bridging ligand may lead to significant anharmonicities along the reaction coordinate that alter the reactant–bridging ligand interaction; (iv) the time scale for electron transfer (i.e.,  $(\nu_{\text{el}}^*)^{-1}$ ) may be comparable to that for coupled nuclear vibrations ( $\nu_{\text{nc}}^{-1}$ ) or for the relaxation of vibrational excited states ( $k_{\text{vib}}^{-1}$  in Figure 2). Each of these effects is commonly referred to as “vibronic coupling” even though the underlying physics and/or the experimental manifestations are often different. The semantic confusion is exacerbated by the fact that the matrix elements in Equations (5) and (16)–(18) are correctly written as “vibronic” matrix elements in which  $H_{\text{DA}}$  is multiplied by a vibronic overlap factor<sup>32,249</sup> (omitted in the above).

Clearly, the issues related to vibronic coupling are very complicated. However, it is possible to get a general idea of some of these issues from the consideration of some oversimplified, limiting cases.

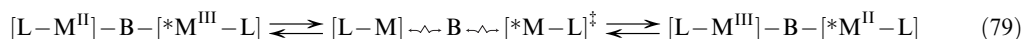
*Limit 1.* Consider a one-dimensional system in which the donor and acceptor differ only in the distances between metal and some nonbridging ligand(s), represented in Equation (78),



A lengthening of the M–L bond accompanies the transfer of charge between metal centers, while all other molecular parameters remain fixed. Vibronic models assume that the electron is equally distributed over the metals in the transition state, designated  $\{\dots\}^{\ddagger}$ , or, alternatively, that the “hopping frequency”  $\nu_{\text{el}}^* > \nu_{\text{ML}}, \nu_{*\text{ML}}$  (note that in the transition state,  $\nu_{\text{ML}}^{\ddagger} = \nu_{*\text{ML}}^{\ddagger}$  for the M–L stretches of the respective moieties of the symmetrical system). The asterisk is employed to distinguish the parameters of the different metal centers; to simplify the discussion, M and \*M are assumed to be identical. The classical, transition-state-based Marcus–Hush-type of models assume that the vibrations  $\nu_{\text{ML}}$  and  $\nu_{*\text{ML}}$  are completely independent. In a simple vibronic model it is assumed that the compression of [L–M] and the extension of [\*M–L] occur simultaneously (i.e., the  $\nu_{\text{ML}}$  and  $\nu_{*\text{ML}}$  stretches are out of phase) along the electron transfer coordinate. The transfer of electron density couples these vibrations of the donor and acceptor moieties. Symmetrical model systems, such as in Equation (78), are most simply discussed in terms of a reaction coordinate centered at the transition state, rather than one centered on the reactants. This simple vibronic model implicates only one of many nuclear coordinates and in an actual system the PE minima may correspond to charge localization at one or the other of the metal centers. If this is the case, then the system described here is obviously analogous to a Jahn–Teller system in which the transition state is electronically degenerate, but in which a nuclear distortion can stabilize one or the other of the two electronic configurations. The molecular motion that leads to this distortion, adapted to the transition-state coordinates, is the antisymmetric combination of

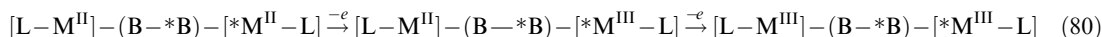
component stretching coordinates,<sup>88</sup>  $r_{\text{ML}}^{\{-\}} = (r_{\text{ML}} - r_{*\text{ML}})/2^{1/2}$ . The corresponding vibration is  $\nu_{\text{ML}}^- = \nu_{\text{ML}}^\ddagger - \delta_{\text{ML}}$ ; where  $\delta_{\text{ML}}$  is the coupling between the component stretches.

*Limit 2.* For a complex in which the donor and acceptor differ significantly in their distances to the bridging ligand, but not in the distances to the other ligands as in Equation (79), or



This has the same symmetry as *Limit 1*, but the coupled vibrational mode is different. The coupled nuclear motion is  $r_{\text{MB}}^- = (r_{\text{MB}} - r_{*\text{MB}})/2^{1/2}$ , and  $\nu_{\text{MB}}^- = \nu_{\text{MB}}^\ddagger - \delta_{\text{MB}}$ .

*Limit 3.* Consider a system in which the donor and acceptor have identical coordination environments, but the nuclear coordinates within the bridging ligand are different from those in the complexes with the metals in identical oxidation states,



The process that is considered in this limit and the symmetry of the system are both different from those of *Limits 1* and *2*. For the intramolecular electron transfer processes analogous to those described in Equations (78) and (79), in complexes with multi-atom bridges, the symmetry considerations are relatively complicated. Thus, when the bridging ligand distortion is in a totally symmetric mode and  $\text{M} = *\text{M}$ ,  $\nu_{\text{BB}}$  will not mix with  $\nu_{\text{ML}}^-$  or  $\nu_{\text{MB}}^-$ . This mixing can occur when the system is not symmetrical, as when  $\text{M} \neq *\text{M}$ ,  $\text{B} \neq *\text{B}$ , or when the bridging ligand is distorted in a nontotally symmetric mode. This limit corresponds to a system in which there is appreciable delocalization of electron density between the donor (acceptor) and the bridging ligand, the bridging ligand mediates donor-acceptor coupling and the bridging ligand distortion enhances the D/A coupling. The mixing with the bridging ligand suggests that this kind of system should be treated using a three- or possibly four-state model (including metal-ligand and ligand-metal CT states) in contrast to the two-state models commonly used for *Limits 1* and *2*.

A few more comments are included here about the models related to vibronic coupling mechanisms (b) and (c). The experimental observations are summarized in Section 7.11.4.4.

#### 7.11.4.4.1 Concerted D-B and B-A nuclear motions and the PKS/Piepho vibronic coupling models

These models were developed with respect to the metal-centered breathing modes (analogous to combining *Limits 1* and *2* so that  $r_a = (r_{\text{ML}} + r_{\text{MB}})$ ). The electron density delocalized, in an adiabatic description of the reaction coordinate, is a minimum at the PE minima and a maximum at the transition state, and consequently the electronic coupling matrix element in the adiabatic description is a function of the reaction coordinate ( $H_{\text{DA}} = \alpha r_a$ ). This description can be transformed into a diabatic description in which the electronic coupling,  $J_{\text{DA}}$ , is independent of the nuclear coordinates.<sup>89</sup> In the diabatic description, the PE is a linear (i.e.,  $\partial \text{PE} / \partial r_a \neq 0$ ), as well as quadratic function of the reaction coordinate and the diabatic potential can be written,

$$E_a = I(\Delta r_a) + \frac{1}{2}k_-(\Delta r_a)^2 \quad (81)$$

The solution of the resulting secular determinant gives a ground state potential function of the form,<sup>84,88</sup>

$$E_g = 1/2k_-(\Delta r_a)^2 - [J_{\text{DA}}^2 + I^2(\Delta r_a)^2]^{1/2} \quad (82)$$

The MO version of this model with an additional nuclear coordinate ( $r_{\text{M}*\text{M}}$ ) has been used to reproduce the band shape of the  $[(\text{NH}_3)_5\text{Ru}]_2\text{pz}]^{5+}$  ion.<sup>85</sup>

#### 7.11.4.5 Classification Schemes for Bridged Complexes

Many slightly different means have been used for classifying electron transfer systems, as, for example classifications based on: the reaction pathway (outer-sphere vs. inner-sphere); the fraction

of electron density delocalized; the electronic coupling matrix element (intensities of DACT absorptions); DACT absorption bandwidths; the Robin and Day classification scheme; comproportionation equilibrium constants. Each scheme is useful in some contexts and not in others. The difficulty in stating a useful and universal classification scheme is that electron transfer phenomena depend on several independent parameters; most notably the free energy of reaction, the reorganizational energy and the electronic coupling matrix element.

The Robin and Day scheme<sup>251</sup> has proved to be conceptually useful in many discussions of mixed-valence complexes. This scheme defines three classes of mixed-valence complexes. Class I is composed of complexes in which there is no significant electron delocalization. Class III is composed of complexes at the opposite limit in which the exchanging electron is completely delocalized. Class II contains all the intermediate situations. In practice, real systems fall into either class II or class III. This scheme is not very useful for nondegenerate systems since complete delocalization of the ground state is not possible when there is a net energy change for the electron transfer process. The limitations of this classification scheme, even for chemically degenerate D/A systems, have recently led several investigators to define an intermediate “Class II–III,” based on the mixed physical properties of some complexes in which electronic coupling is very large.<sup>221,229–231,252</sup>

A related scheme that discriminates more sensitively between related molecules might be based the fraction of charge delocalized,  $\alpha_{\text{DA}}^2$ . For example, the DACT absorption bandwidth is very sensitive to configurational mixing and Equation (31) might be used to set a lower limit on the range of systems appropriate to be considered strongly coupled. For more than a 10% reduction in bandwidth arising from configurational mixing,  $\lambda_{\text{r}}(\text{obsd})/\lambda_{\text{r}}^0 < 0.9$  and  $4\alpha_{\text{DA}}^2 > 0.025$ . For a symmetrical electron transfer system (i.e.,  $\Delta G_{\text{DA}}^0 = 0$ , as in a self-exchange reaction) with  $\chi_{\text{r}} = 10 \times 10^3 \text{ cm}^{-1}$ , this condition for a strongly coupled system leads to  $H_{\text{DA}} > 500 \text{ cm}^{-1}$ . However, since  $\alpha_{\text{DA}} = [H_{\text{DA}}/(\Delta G_{\text{DA}}^0 + \chi_{\text{r}})]$ , this parameter is a convolution of several more fundamental parameters and it also may not be useful in all contexts.

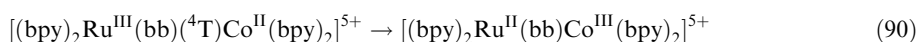
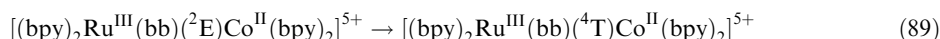
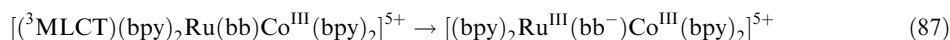
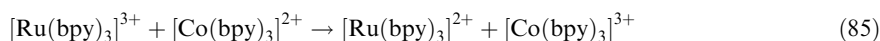
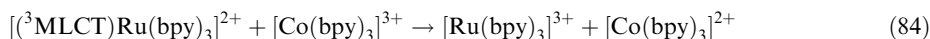
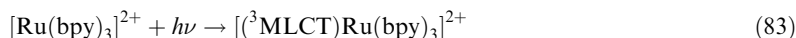
Several classification schemes based on the comparison of observed to limiting bandwidths have been proposed for weakly coupled systems.<sup>45,223,253</sup> When  $\alpha_{\text{DA}}^2 \sim 0.2$  (i.e., for a system that is 60% “localized”), Equation (11) combined with Equation (31) predicts very narrow absorption bands. For larger values of  $\alpha_{\text{DA}}^2$ , higher order perturbation theory expressions are necessary. Obviously, bandwidth criteria alone are not sufficient for distinguishing a valence “localized” ( $\alpha_{\text{DA}}^2 \ll 0.5$ ) from a “delocalized” ( $\alpha_{\text{DA}}^2 = 0.5$ ) system.

A parameter that is not considered much in the literature, but one that is convenient for the present discussion, is the electron hopping frequency,  $\nu_{\text{el}}^*$ . An upper limit for  $\nu_{\text{el}}^*$  is given by  $\nu_{\text{el}}(\text{LZ})$  (Equation (75)). For the “borderline” system with  $H_{\text{DA}} = 500 \text{ cm}^{-1}$  discussed above,  $\nu_{\text{el}} = 1.5 \times 10^{13} \text{ s}^{-1}$ , and  $\nu_{\text{el}}$  is similar in magnitude to metal–ligand vibrational frequencies (i.e.,  $\sim 1,600 \text{ cm}^{-1}$ ). This suggests a “natural” classification of electron transfer systems with respect to the calculated values of  $\nu_{\text{el}}$  such that a system is considered to be: (W) weakly coupled when  $\nu_{\text{el}}$  is smaller than vibrational frequencies of the reacting system, or approximately for  $\nu_{\text{el}} \leq 5 \times 10^{11} \text{ s}^{-1}$ ; and (S) very strongly coupled when  $\nu_{\text{el}}$  is significantly larger than any fundamentals of the molecular vibrational frequencies, or approximately when  $\nu_{\text{el}} \geq 10 \times 10^{13} \text{ s}^{-1}$ . For the intermediate regime (I),  $5 \times 10^{11} \text{ s}^{-1} < \nu_{\text{el}} < 10 \times 10^{13} \text{ s}^{-1}$ . Some representative examples of this classification scheme are presented in Table 6. It is important to note that each of the three categories is useful for known, real systems. The weakly coupled regime contains many outer-sphere electron transfer systems and many systems with aliphatic linkers. The intermediate regime contains many of  $d\pi/p\pi/d\pi$ -bridged systems and most of the ion-pair systems in Table 2. The very strongly coupled regime contains systems with very large DACT absorptivities such as those with pz or  $\text{CN}^-$  bridges, polypyridyl complexes, etc. The parameter  $\nu_{\text{el}}$  is used as a convenient basis for classification and for a sense of order of frequencies expected. These calculated values for  $\nu_{\text{el}}$  should not be interpreted literally since coupling to some low-frequency nuclear motions or to the polarizability of the medium may exert a retarding or frictional effect ( $\kappa_{\text{r}}$ ) on the observed rate constant,<sup>76</sup> and  $\nu_{\text{el}} \geq \nu_{\text{el}}^*$ .

#### 7.11.4.6 Experimental Observations in the Limit of Weak Electronic Coupling; Simple, Aromatic Bridging Ligands

Several studies of bimetallic complexes in which the donor and acceptor are linked across aliphatic chains have demonstrated that these are generally weakly coupled systems.<sup>254–259</sup> Very

detailed studies have been carried out employing the 1,2-bis(2,2'-bipyridyl-4'-yl)ethane (bb) linker. On balance, these studies seem to provide good models of the precursor complexes for outer-sphere electron transfer reactions of tris-polypyridyl complexes. Table 5 includes electron transfer parameters of the bimolecular back electron transfer reactions that follow the outer-sphere electron transfer quenching of  $[(^3\text{MLCT})\text{Ru}(\text{bpy})_3]^{2+}$  by  $[\text{Co}(\text{bpy})_3]^{3+}$ ,<sup>260</sup> Equations (78)–(80), to the back electron transfer process following photoexcitation of  $[(\text{bpy})_2\text{Ru}(\text{bb})\text{Co}(\text{bpy})_2]^{5+}$ ,<sup>256</sup> Equations (81)–(85):



Both of the back electron transfer reactions, Equations (85) and (90), are two to three orders of magnitude slower than expected based on comparison to the respective self-exchange reactions and free energy changes. This appears to be an electronic effect and  $\kappa_{\text{el}} \sim (10^{-2} \text{ to } 10^{-3})$  for both reactions;<sup>256,260</sup>  $H_{\text{DA}} \sim 8 \text{ cm}^{-1}$  for the spin-forbidden process in Equation (90) (additionally, a value of  $H_{\text{DA}} \sim 40 \text{ cm}^{-1}$  is estimated for  $[(\text{bpy})_2\text{Ru}^{\text{II}}(\text{bb})\text{Co}^{\text{III}}(\text{bpy})_2]^{5+}$ ).<sup>256</sup> A similarly small value of  $H_{\text{DA}} \cong 20 \text{ cm}^{-1}$  has been inferred from the spectroscopy of the mixed valence complex  $[\text{Fe}(\text{bb})_3\text{Fe}]^{5+}$ .<sup>257</sup> It should be observed that these values estimated for  $H_{\text{DA}}$  are appreciably smaller than those for the oppositely charged ion pairs in Table 2. A search for the  $\text{Ru}^{\text{II}}/\text{Ru}^{\text{III}}$  absorption of  $[(\text{bpy})_2\text{Ru}^{\text{II}}(\text{bb})\text{Ru}^{\text{III}}(\text{NH}_3)_4]^{5+}$  detected only a weak ( $\epsilon_{\text{max}} \leq 100 \text{ cm}^{-1} \text{ M}^{-1}$ ), broad and unresolved absorption near 900 nm.<sup>261</sup>

#### 7.11.4.7 Electron Transfer Systems in the Intermediate Regime

A large number of complexes has been prepared in which the donor and acceptor are bridged by 4,4'-bipyridine and closely related ligands.<sup>107,109,234,235,262–264</sup> The values for  $H_{\text{DA}}$  estimated for these complexes are more comparable to those of the ion pairs listed in Table 2 than for the *bb*-bridged complexes. However, the fraction of delocalized electron density,  $\alpha_{\text{DA}}^2$ , is small, and most of these complexes fit into the weakly coupled limit. Equations (68) and (69) can be used to estimate the value of  $h\nu_{\text{max}}$  expected in the limit that  $\alpha_{\text{DA}}^2 = 0$ . Thus, for complexes of the type  $[\{\text{Ru}(\text{NH}_3)_5\}_2\text{B}]^{5+}$ , plots of  $h\nu_{\text{max}}(D/A)$  vs.  $(\epsilon_{\text{max}}\Delta\nu_{\text{max}})$  extrapolate to  $h\nu_{\text{max}}(\text{ref}) = (13.0 \pm 0.5) \times 10^3 \text{ cm}^{-1}$  (Figure 12; various plots have  $r^2 \cong 0.8\text{--}0.9$ ). This is very similar to the value of  $\chi_r = 13.4 \times 10^3 \text{ cm}^{-1}$  estimated for the  $[\text{Ru}(\text{NH}_3)_6]^{3+,2+}$  couple in Table 1 and a little larger than the value ( $12.1 \times 10^3 \text{ cm}^{-1}$ ) estimated for  $[\text{Ru}(\text{NH}_3)_5\text{py}]^{3+,2+}$ ; however, the appropriate value of  $d_{\text{DA}}$  (Equation (61)) is probably larger for the 4,4'-bpy-bridged complex than the bimolecular reactions.

The value of  $h\nu_{\text{max}}(\text{ref}) = 13.0 \times 10^3 \text{ cm}^{-1}$  leads to  $\Delta h\nu_{\text{max}}(\text{obsd}) = 3.3 \times 10^3 \text{ cm}^{-1}$  for  $[\{\text{Ru}(\text{NH}_3)_5\}_2(4,4'\text{-bpy})]^{5+}$ . Electroabsorption measurements have been used to determine that  $H_{\text{DB}} = 5.5 \times 10^3 \text{ cm}^{-1}$  for  $[\text{Ru}(\text{NH}_3)_5(4,4'\text{-bpy})]^{2+}$ .<sup>104</sup> This value, combined with other spectroscopic parameters, implies that  $\Delta h\nu_{\text{max}}(\text{calcd}) = 3.4 \times 10^3 \text{ cm}^{-1}$  (Equation (73)). The use of these same parameters and Equation (74) suggests that  $H_{\text{DA}}^{\text{spX}} = 1.2 \times 10^3 \text{ cm}^{-1}$ . However, electroabsorption measurements indicate that  $d_{\text{DA}} \cong 2r_{\text{DA}}$  and  $H_{\text{DA}}^{\text{spX}}$  is actually about  $750 \text{ cm}^{-1}$ .<sup>101,102</sup> The discrepancy in values of  $H_{\text{DA}}^{\text{spX}}$  probably arises from treating 4,4'bpy as a single bridging moiety. If it is treated as a combination of two linked pyridines, then Equation (44) and the electroabsorption measurements imply that  $\gamma_{\text{py,py}} \cong 0.6$ . This analysis has neglected the effects of charge delocalization on  $\Delta h\nu_{\text{max}}$  (less than 17% for  $H_{\text{DA}}^{\text{spX}} < 1,000 \text{ cm}^{-1}$ ; Equations

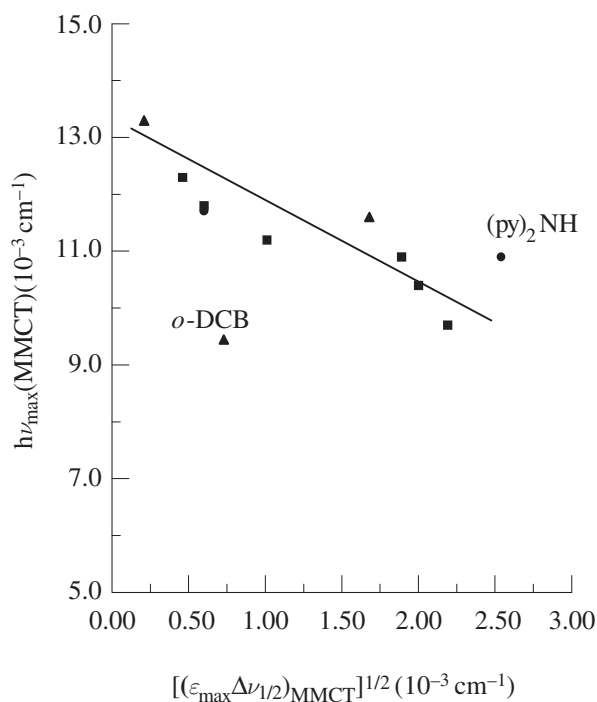


**Figure 12** Correlation of absorption maxima and oscillator strengths for bridged electron transfer systems based on the three state model.

(8) and (30)); there are also significant uncertainties in the small difference between the large numbers used to estimate  $\Delta h\nu_{\max}$ .

A related perspective on the most useful approach to treating bridging ligand mediation of metal–metal coupling is provided by dicyano–benzene (DCB) bridges.<sup>236,265</sup> The *p*-DCB bridge is about the same size,  $\Delta h\nu_{\max}$  is about half as large ( $\sim 1,400\text{ cm}^{-1}$ ), and the molar absorptivity of the Ru<sup>II</sup>/Ru<sup>III</sup> MMCT absorption band is about half as large as that for the 4,4'-bpy bridge. The mixed valence complex with the *m*-DCB bridge has  $\Delta h\nu_{\max} \approx 0$  and an absorptivity of about 1% that of the analogous 4,4'-bpy-bridged complex. These observations are in good agreement with expectation based on Equations (67)–(69). In contrast, the *o*-DCB bridged mixed valence complex has a relatively large value of  $\Delta h\nu_{\max}$  and a relatively small absorptivity. The much smaller metal–metal distance in the *ortho*- than in the *meta*-DCB-bridged complex is probably related to the appreciably larger absorptivity of the former and possibly to the smaller reorganizational energy of the latter. The qualitatively interesting point is that the absorptivities, and consequently the values of  $H_{\text{DA}}$ , are much smaller for the *meta*- and *ortho*- than for the *para*-dicyano-benzene bridged mixed valence complexes. The most notable features that are qualitatively similar in the *ortho*- and *meta*-DCB-bridged complexes, but different in the *para*-DCB-bridged complex are: (i) the MLCT and MMCT dipoles are aligned in the latter, but not in the former; and (ii) the LUMOs are in phase at the metal binding sites of the latter, but out of phase in the former (see Figure 13). Neither of these features was considered in the perturbation theory treatment described above. Richardson and Taube have discussed these systems in terms of a more detailed (one-electron) molecular orbital approach.<sup>236</sup> Phase contributions to  $H_{\text{DB}}$  and  $H_{\text{BA}}$  have been proposed as the origin of relatively weak metal–metal coupling in a few other bridged, mixed-valence systems in which superexchange coupling should determine  $H_{\text{DA}}$ .<sup>43,95,96</sup>

#### 7.11.4.8 Experimental Observations in the Limit of Very Strong Electronic Coupling

A wide range of range of electron transfer behavior is exhibited by D/A systems that are classified as very strongly coupled, and the properties of such systems have been extensively reviewed.<sup>109,116,221,222</sup> The prototype of a very strongly coupled D/A system has continued to be the Creutz–Taube ion,  $[\{\text{Ru}(\text{NH}_3)_5\}_2\text{pZ}]^{5+}$ .<sup>237,238,266</sup> This complex and related pyrazine-bridged



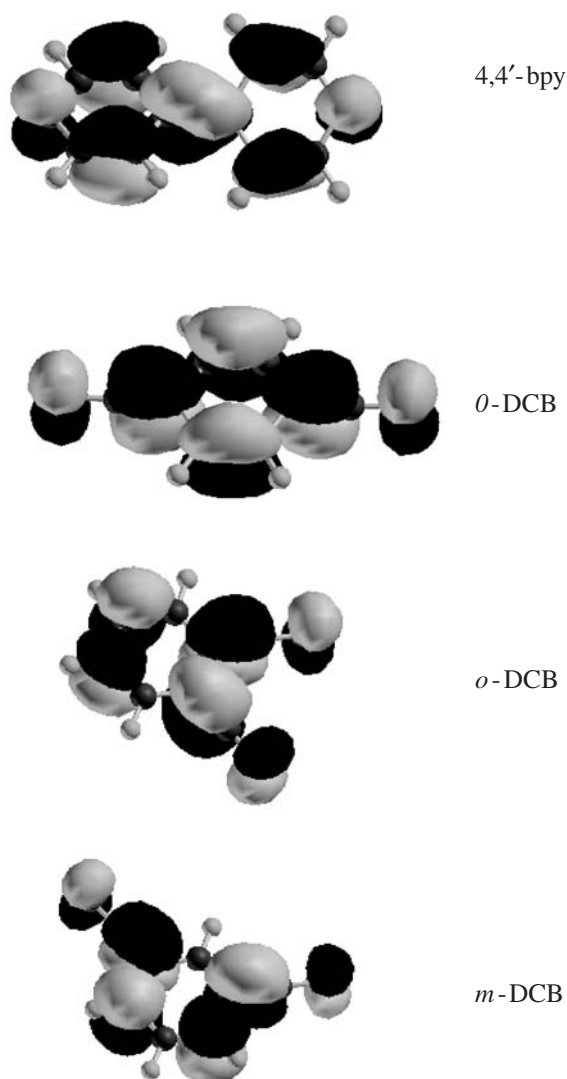


**Figure 13** LUMOs of dicyanobenzene and 4,4'-bipyridine bridging ligands.

complexes are employed in this section as the focus for examples of the issues and to develop the basic principles involved in this area. It is an area characterized by strong opinions and divergent interpretations of the same observations.

#### 7.11.4.8.1 Pyrazine-bridged complexes

Pyrazine-bridged, bimetallic complexes span an amazing range of physical properties. For example, the MMCT spectroscopy varies from that of  $[\{\text{Os}(\text{NH}_3)_5\}_2\text{pz}]^{5+}$  which does not exhibit a clearly defined  $\text{Os}^{\text{II}}/\text{Os}^{\text{III}}$  absorption band<sup>240,267</sup> to a pyrazine-bridged ( $\text{Ru}_3$ ) cluster complex ( $\text{Ru}_3 = [\text{Ru}_3(\mu_3\text{-O})(\mu\text{-CH}_3\text{CO}_2)_6(\text{CO})(\text{py})]^-$  for the  $\text{Ru}^{\text{II}}/\text{Ru}^{\text{II}}/\text{Ru}^{\text{III}}$ , “reduced” complex) in which a  $12 \times 10^3 \text{ cm}^{-1}$  absorption band with an absorptivity of  $12,200 \text{ M}^{-1} \text{ cm}^{-1}$  and bandwidth of  $3,760 \text{ cm}^{-1}$  has been assigned as an MMCT absorption.<sup>230,231</sup> The Creutz–Taube ion is intermediate in this spectroscopic range. The electronic coupling is clearly very strong in all three of these complexes, but the spectroscopic signatures of this coupling do not form a simple pattern that can be readily related to the discussions of the weak, intermediate, or strong coupling regimes as developed above. However, the basic physics of the donor–acceptor interactions must differ only in degree, not in kind from one coupling regime to another. This section will employ concepts sketched above to treat the strongly coupled systems.

From the perspectives developed above, and in the absence of any configurational mixing, the reorganizational energy,  $\lambda_r^0$ , for a weakly coupled  $[\{\text{Ru}(\text{NH}_3)_5\}_2\text{B}]^{5+,4+}$  electron transfer system (with  $d_{\text{DA}} \approx 7 \text{ \AA}$ ) is expected to be about  $12 \times 10^3 \text{ cm}^{-1}$  (i.e., comparable to that for  $[\text{Ru}(\text{NH}_3)_5\text{py}]^{3+,2+}$ ). In such a weakly coupled system this would be the energy of the MMCT absorption maximum and the absorptivity would be much less than  $10^3 \text{ M}^{-1} \text{ cm}^{-1}$ . However, the most intense MMCT absorption of  $[\{\text{Ru}(\text{NH}_3)_5\}_2\text{pz}]^{5+}$  occurs at  $h\nu_{\text{max}} = 6.25 \times 10^3 \text{ cm}^{-1}$ . The reported absorptivity is  $5 \times 10^3 \text{ cm}^{-1}$ ,  $\Delta\nu_{1/2} = 1,400 \text{ cm}^{-1}$  and the absorption band is asymmetric (Gaussian on the high-energy side and much narrower on the low-energy side).<sup>237,238,240</sup> A much weaker band has been reported<sup>240</sup> at  $13.0 \times 10^3 \text{ cm}^{-1}$ ; the energy difference is comparable to the energy difference between the pz LUMO and LUMO + 1.<sup>67,268</sup> The near-infrared band is usually considered to be the intervalence transition of this complex. This assignment implies that there is a great deal of MLCT/MMCT configurational mixing (e.g., see Equation (72) and Figures 3 and 11), and the prevailing view is that the exchanging electron is delocalized in the ground state of this complex in ambient solutions.<sup>1,83–85,91,101,102,116,200,222,240,269,270</sup> However, the spectroscopy of this complex is in dramatic contrast to that of the closely related  $[\{\text{Os}(\text{NH}_3)_5\}_2\text{pz}]^{5+}$ .<sup>240,267</sup> The electronic spectrum of the osmium complex contains several deep infrared absorptions ( $6,300\text{--}4,000 \text{ cm}^{-1}$ ), but many of these appear to be spin-orbit (or inter-configurational),  $d\pi/d\pi$  transitions, the most intense of them are at the lower end of the energy range, and none are classified as MMCT transitions.<sup>240</sup> There is also a curious band of significant intensity ( $\epsilon_{\text{max}} = 4,000 \text{ M}^{-1} \text{ cm}^{-1}$ ) at  $14.3 \times 10^3 \text{ cm}^{-1}$ .<sup>271</sup> To the extent that the properties of the  $[\text{M}(\text{NH}_3)_5\text{pz}]^{2+}$  and  $[\text{M}(\text{NH}_3)_5\text{pz}]^{3+}$  complexes may be taken as models for diabatic limit of the mixed-valence, bimetallic complexes, it is significant that  $\text{M}^{\text{II}}/\text{pz}$  MLCT transitions occur at  $21.2 \times 10^3$  and  $13.0 \times 10^3 \text{ cm}^{-1}$ , respectively for  $\text{M} = \text{Ru}$  and  $\text{Os}$ .<sup>272</sup> Thus, there is about a  $8,000 \text{ cm}^{-1}$  difference between the MLCT and MMCT excited states in the diabatic limit of  $[\{\text{Ru}(\text{NH}_3)_5\}_2\text{pz}]^{5+}$ , while these two excited states are degenerate in the diabatic limit of the osmium analog. As a consequence, the configurational mixing has to be much larger for the latter. The properties of  $[\{\text{Os}(\text{NH}_3)_5\}_2\text{pz}]^{5+}$  may be more representative of the delocalized limit than are those of  $[\{\text{Ru}(\text{NH}_3)_5\}_2\text{pz}]^{5+}$ . It has been argued that the latter is near to the delocalized limit, but that the exchanging electron is not completely delocalized in this complex.<sup>240</sup>

Meyer and co-workers have recently discussed the “residual” localization of the electron density in  $[\{\text{Ru}(\text{NH}_3)_5\}_2\text{pz}]^{5+}$ .<sup>221</sup> They have pointed out that some properties of this complex are characteristic of delocalization and others are characteristic of localization. The very small absorption bandwidth is often cited as evidence for electron delocalization, but this is not a good criterion for delocalization, as noted in Section 7.11.4.5. The MMCT absorption band characteristics are nearly solvent-independent, and this has also been cited as a criterion for electron delocalization.<sup>109</sup> However, the attenuation of the solvent reorganizational energy (Equation (31)) due to significant, but less than complete, electron delocalization would make the MMCT band relatively insensitive to changes of solvent. The observation of a symmetric pyrazine ring stretching vibration is cited as evidence for localization, and the concomitant loss of a center of symmetry.<sup>221</sup> In a stationary state, wave function approach, the delocalization of the exchanging electron in any orbital results in identical charges at the two centers and a centrosymmetric system. This approach cannot be used to describe a system that is delocalized in terms of some measurements and localized with respect to others. This type of intermediate situation can be interpreted as a proposal that either: (i) there is no barrier to electron transfer ( $\kappa_{\text{nu}} \approx 1$ ) and that the electron hopping frequency  $\nu_{\text{el}}^*$  of this complex is large compared to solvent vibrational frequencies, but small compared to many other molecular vibrational time scales (see Table 6 and Figure 14); or (ii) that there is a very small barrier to electron transfer ( $\kappa_{\text{nu}} < 1$ ). The values calculated for  $\nu_{\text{el}}$  in Table 6 easily span the appropriate frequency range. The interpretation in terms of Equation (1) (i.e., proposal (ii)) requires that  $k_{\text{et}} \approx \nu_{\text{nu}}$  (i.e.,  $\kappa_{\text{el}} = 1 \approx \kappa_{\text{nu}}$ ).<sup>109,221</sup>

There are several possible origins of the near-infrared absorption band asymmetry. In the simplest, idealized limit that the ground and excited state PE surfaces are parabolic and that the displacement of their minima is very small (i.e., for  $S_{\text{h}}$  in Equation (6b) approaching zero for all modes), then the absorption band will be very narrow and it will have a non-Gaussian shape because the band has a finite origin (the absorption maximum if  $S_{\text{h}} = 0$ ) the ground state/excited state vibrational overlap ( $F_{j,h}$  in Equation (6b)) is maximized for the coordinates of the PE minima ( $S_{\text{h}}$  and  $j = 0$ ).<sup>273</sup> The applicability of this limit to thermal electron transfer has been explored recently.<sup>223,253,274</sup> Possible sources of a non-Gaussian band shape when  $S_{\text{h}} > 0$  are: (i) an unresolved progression in coupled vibrational modes (see Equation (16)); (ii) a grossly anharmonic ground state or excited state PE surface; (iii) unresolved contributions from more than one

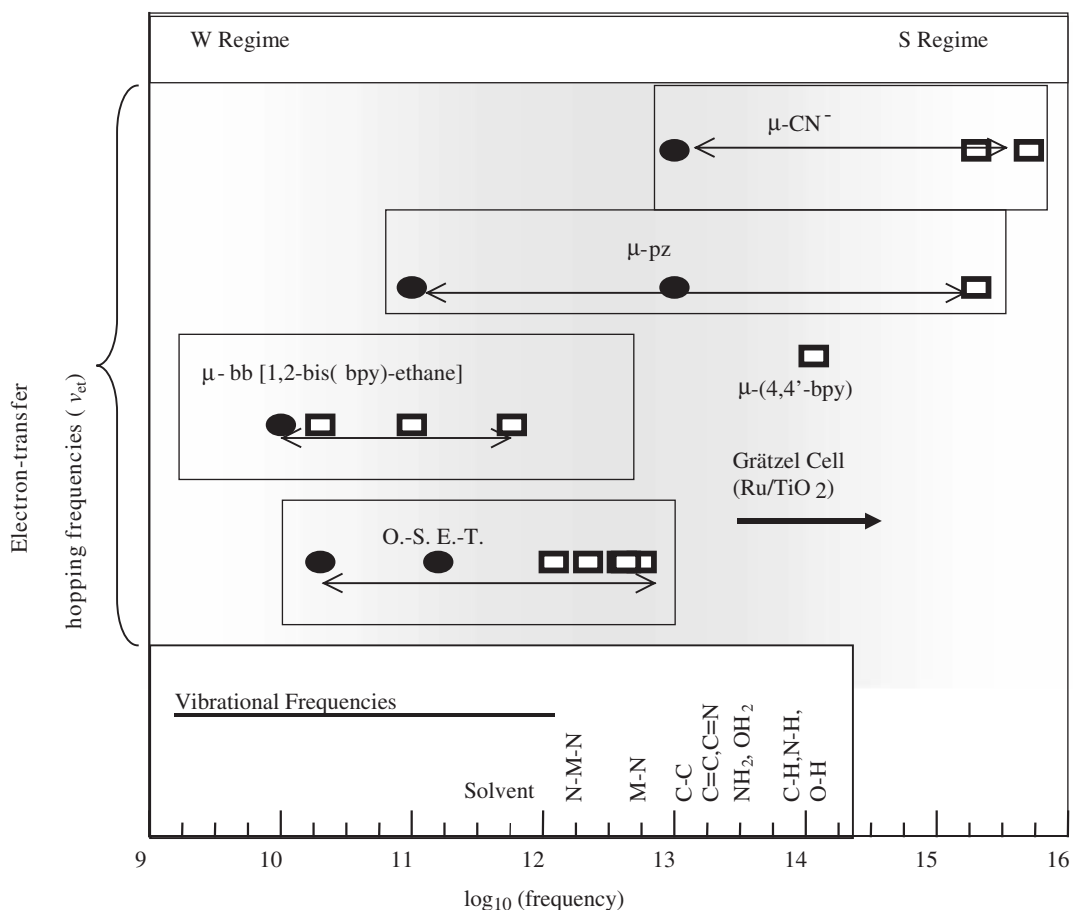


**Figure 14** Comparison of vibrational and electron transfer hopping frequencies. Closed ellipses based on kinetic data; open rectangles based on Equation (75). See Table 6.

electronic state; (iv) a dependence of  $H_{DA}$  on the nuclear coordinates. Vibronic models that involve the metal–ligand vibrations<sup>83–85</sup> or bridging ligand vibrations<sup>90,91,270</sup> have been employed to fit the spectrum. There is an intermediate range of electronic coupling for which the ground state distribution of nuclear coordinates is not Gaussian: when  $H_{DA}$  is large enough to eliminate all or most of the barrier to reaction, but not large enough that the ground state PE surface is parabolic (i.e., for  $H_{DA} \sim \lambda_r^0/4$ ). This intermediate situation has been referred to as the (Robin and Day) Class II/III transition. For  $[\{\text{Ru}(\text{NH}_3)_5\}_2\text{pz}]^{5+}$ ,  $\lambda_r^0/4 \cong (12 \times 10^3 \text{ cm}^{-1})/4 = 3,000 \text{ cm}^{-1}$  and  $H_{DA} \cong 3,100 \text{ cm}^{-1}$  (based on  $h\nu_{\text{max}} \approx 2H_{DA}$ ). It should also be observed that the MMCT/MLCT mixing is much larger for the ground state coordinates than for the coordinates of the diabatic surface crossing due to the smaller difference in excited state energies for the ground state coordinate system. This implies that  $H_{DA}$  is not constant along the reaction coordinate.

Coupling between nonbridging ligand vibrational and electron transfer frequencies has been demonstrated for some pyrazine-bridged, mono-carbonyl-tri-ruthenium cluster complexes (Figure 15) by Ito, Kubiak and co-workers.<sup>230,231,233</sup> The carbonyl stretches of the mixed-valence complexes broaden or coalesce into a single peak, with the broadening effect becoming more important as the absorptivity of the near-infrared “intervalence” band increases. The increase in absorptivity could correlate with an increase in  $H_{DA}$ , and, therefore, to an increase in the electron hopping frequency. This suggests that  $\nu_{el}^* < \nu_{vib}$  for these complexes, where  $\nu_{vib} \sim 6 \times 10^{13} \text{ s}^{-1}$  for the carbonyl stretch. Ito, Kubiak and co-workers have used an NMR-type of line-broadening analysis to find electron transfer frequencies in the  $(1-9) \times 10^{11} \text{ s}^{-1}$  range for these systems. The  $\nu_{vib}$  line broadening effects are also solvent dependent;  $k_{et}$  is roughly proportional to the fastest inertial solvent relaxation time, reasonably consistent with a frictional retardation,  $\kappa_f$ , of the electron hopping frequency;  $\nu_{el}^* = \kappa_f \nu_{el}$ .<sup>275</sup> In a related observation, sub-picosecond transient absorption studies have found the back electron transfer rates ( $k_{bet} \approx 10^{13} \text{ s}^{-1}$  in water) for  $[(\text{NH}_3)_5\text{Ru}(\text{CNM}(\text{CN})_5)]^-$  complexes to be retarded by increasing solvent viscosity (see also Section 7.11.4.8.3).<sup>69,276,404</sup>

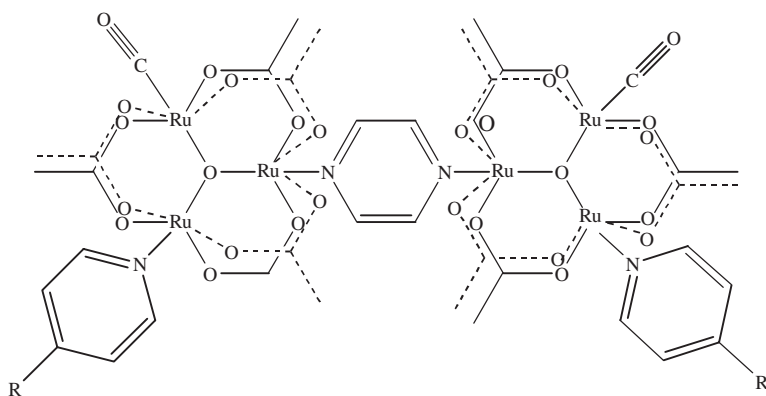


**Figure 15** Skeletal structure of a pyrazine-bridged  $\text{Ru}_3$ -cluster complex.

These studies of the pyrazine-bridged ( $\text{Ru}_3$ )-cluster complexes represent a striking and important perspective on electron transfer in strongly coupled systems. However, the interpretation of the observations remains challenging.

When the metal centers become more difficult to oxidize than  $[\text{Ru}(\text{NH}_3)_5\text{pz}]^{2+}$ , the  $\text{M}^{\text{II}}/\text{pz}$  MLCT absorption band shifts to higher energy<sup>81</sup> and the  $\text{M}^{\text{II}}/\text{M}^{\text{III}}$  coupling becomes smaller. This behavior is illustrated by the  $[\{\text{M}(\text{CN})_5\}_2\text{pz}]^{5-}$  complexes with  $\text{M} = \text{Fe}$ ,<sup>243</sup>  $\text{Ru}$ ,<sup>277</sup> and  $\text{Os}$ .<sup>278</sup> Thus, the  $[\text{Fe}(\text{CN})_5\text{pz}]^{3-}$  complex is more difficult to oxidize and the  $\text{M}^{\text{II}}/\text{pz}$  MLCT absorption maximum is higher in energy than found for  $[\text{Ru}(\text{NH}_3)_5\text{pz}]^{2+}$  in water, the MMCT transition is weaker ( $\varepsilon = 2,200 \text{ cm}^{-1}$ ), broader ( $\Delta\nu_{1/2} = 4,800 \text{ cm}^{-1}$ ) and at higher energy ( $8,300 \text{ cm}^{-1}$ ) in  $[\{\text{Fe}(\text{CN})_5\}_2\text{pz}]^{5-}$ <sup>243</sup> than in the Creutz-Taube ion. Qualitatively similar behavior has been observed for mixed-valence metal-polypyridine complexes with pyrazine bridges: the metals are relatively difficult to oxidize and the properties of the  $\text{M}^{\text{II}}/\text{M}^{\text{III}}$  complexes fall in the intermediate range rather than in the strongly coupled range. Since  $\chi_r^0$  is relatively small for the polypyridine complexes (see Table 2), the intervalence transitions are expected at relatively low energies (e.g., the MMCT transition of a  $\text{M}^{\text{II}}(\text{bpy})_2$  complex should occur at about half the energy of the comparable transition in an ammine complex, provided the MLCT coupling and energies are comparable). Unfortunately, the  $\text{M}^{\text{II}}/\text{polypyridine}$  MLCT transitions tend to obscure the  $\text{M}^{\text{II}}/\text{pz}$  transitions in these complexes.

In contrast to the observations for  $[\{\text{Ru}(\text{NH}_3)_5\}_2\text{pz}]^{5+}$ , the absorption bands of  $[\{\text{Fe}(\text{CN})_5\}_2\text{pz}]^{5-}$  are very strongly solvent-dependent: in acetonitrile the MLCT band occurs at  $13.4 \times 10^3 \text{ cm}^{-1}$  and the MMCT band is reported to be shifted to about  $4,000 \text{ cm}^{-1}$ .<sup>279</sup>

Mixed-valence complexes with multidentate polypyridine bridging ligands<sup>43,242,280–284</sup> are expected to follow the same general patterns, but the details are complicated by the variations in the basic properties of the systems, such as:  $\chi_s^0$ ; the bridging-ligand LUMOs; the energy differences and coupling between bridging-ligand  $\pi^*$  orbitals; metal-bridging ligand electronic coupling; etc.<sup>43</sup>

Overall, the variations in  $h\nu_{\text{max}}$  for the various optical transitions, and the patterns of differences of  $\Delta E_{1/2}$  for most of the pyrazine-bridged complexes, are most simply interpreted in terms of a perturbation theory treatment of the interactions between the metal moieties and the bridging ligand. For example, electroabsorption measurements show that the value of  $H_{\text{ML}}$  is about  $9 \times 10^3 \text{ cm}^{-1}$  for  $[\text{Ru}(\text{NH}_3)_5\text{pz}]^{2+}$ .<sup>104</sup> This value, combined with the estimate of  $\chi_r^0 \cong 12 \times 10^3 \text{ cm}^{-1}$  for  $[\{\text{Ru}(\text{NH}_3)_5\}_2\text{pz}]^{5+}$  and the observed  $21 \times 10^3 \text{ cm}^{-1}$  MLCT absorption of  $[\text{Ru}(\text{NH}_3)_5\text{pz}]^{2+}$ <sup>107</sup> suggests that the MLCT and electron transfer excited states are nearly completely mixed in the ground state coordinates (see Figure 16); i.e.,  $\alpha_{jk}^2 \approx 0.5$  for these two excited states. A clear distinction between MMCT and MLCT absorptions is not possible under these circumstances; some theoretical models have led to related conclusions.<sup>270</sup> The two-electron transfer states are degenerate for the nuclear coordinates of the transition state, and this suggests that important aspects of the electronic coupling change as the system moves from the coordinates of the diabatic ground state to those of the transition state. Just about any reasonable set of parameters for the diabatic states predicts that the MLCT/electron transfer state couplings in the symmetrical transition state would be sufficient to eliminate all or most of the (diabatic) transition-state barrier. However, the resulting ground-state PE surfaces are very anharmonic ( $H_{\text{DA}} \approx \chi_r^0/4$ ). Since the energy difference between the electron transfer states and the MLCT

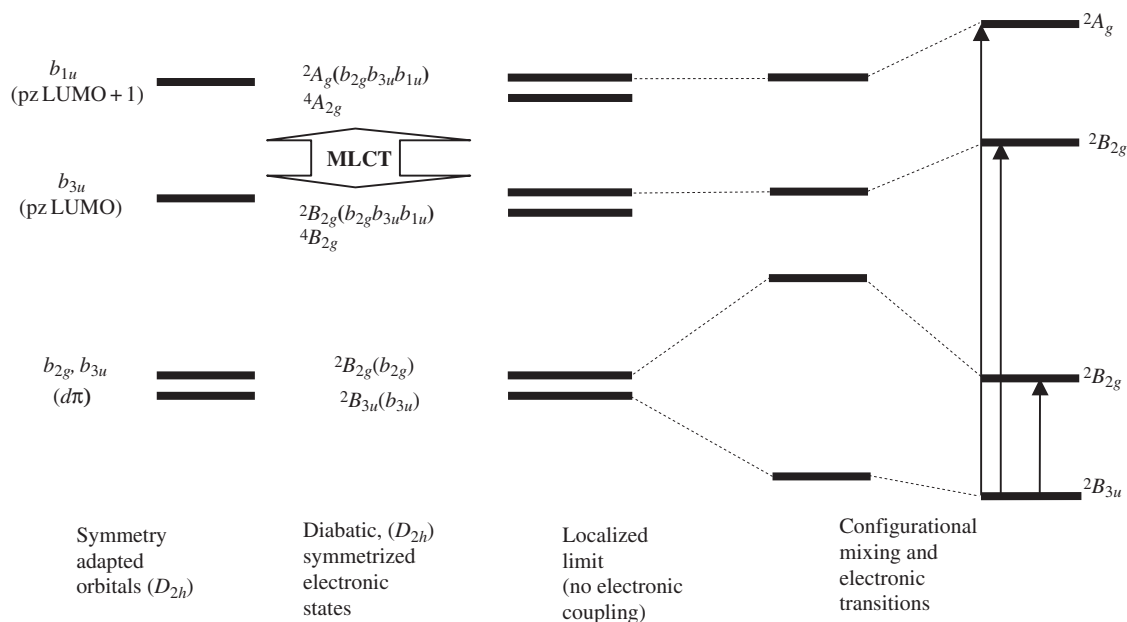


**Figure 16** Orbital and electronic state diagrams for a strongly coupled bimetallic complex.

state is about  $8,000\text{ cm}^{-1}$  smaller in the osmium analog of the Creutz–Taube ion, one expects these excited states to be nearly degenerate in the ground-state nuclear coordinates, and nearly degenerate with both electron-transfer states in the transition-state coordinates of the diabatic limit. In such a situation there is no meaningful distinction between the MMCT and MLCT electronic states.

Most discussions of the role of the pz bridge in mediating electronic coupling in mixed-valent systems treat the bridge as a simple, vacant orbital (analogous to the three-center, three-electron model). However, LUMO and LUMO + 1 of pyrazine are intrinsically coupled (the correlated orbitals are degenerate in benzene and are split about  $6,800\text{ cm}^{-1}$  by their coupling in pyrazine<sup>268,285</sup>), and a careful treatment of the pyrazine-bridged complexes should consider all four states. This is another reason for caution about simple comparisons and the simple assignment of observed spectroscopic transitions. The discussion in this section has attempted to treat a variety of ( $d\pi/p\pi/d\pi$ )-bridged D/A systems by means of variations in a (simple) three-state superexchange model. This approach has permitted a reasonably consistent discussion of the trends in the properties of these complexes, from those in which the electronic coupling is weak to those in which it is very strong. Thus, the difference between the observed MMCT transition and  $\chi_r^0$  is a measure of the metal–ligand mixing (Equation (72)), and this generally correlates with the other properties that are predicted to vary with  $H_{DL}$ . For example, the mixed-valence properties in pz-bridged complexes are generally proportional to  $(H_{MB}^2/E_{av})^2$  (i.e., by means of ligand-mediated superexchange coupling), and they tend to diminish as the M/pz MLCT absorption bands increase in energy and/or decrease in absorptivity. The simplest models that consider only orbital energies are often misleading, and simple configurational constructions of the electronic states, such as employed here, cannot quantitatively describe all the properties of all the complexes. For example, these constructions do not explicitly take account of the variations in the electron exchange energy contributions; the exchange energy can be considered to contribute to  $\Delta G_{DA}^0$  in many comparisons, but differences in this quantity can complicate electrochemical correlations (see Equation (30)) or arguments based on emission spectra. Even in some ruthenium complexes, especially am(m)ine complexes, the exchange energy can be a few thousand wavenumbers.<sup>43,82</sup> Some other problems with the simple three-state models become more obvious with the simpler, two-atom bridges, and these are discussed below.

Ito, Kubiak and co-workers have reported properties of their ruthenium cluster complexes that differ from this general pattern. For these complexes an absorption band, assigned as an intervalence absorbance, is reported at about  $12 \times 10^3\text{ cm}^{-1}$  (a larger energy than expected for  $\chi_r^0$  in dichloromethane) with  $\Delta\nu_{1/2} \cong (3\text{--}4) \times 10^3\text{ cm}^{-1}$  and  $\epsilon_{\max} \cong (10\text{--}16) \times 10^3\text{ cm}^{-1}$ . The arguments presented above predict such large oscillator strengths to be characteristic of MMCT absorption

bands that have a much smaller bandwidth and a much lower energy absorption maximum. However, these absorption bands of the  $[\{\text{Ru}_3\}_2\text{pz}]^-$  mixed-valence cluster complexes fall between other intense spectroscopic transitions, and they are probably complicated by a great deal of inter-configurational mixing. The nature of the observed transition is not clear. Furthermore, a value of  $k_{\text{et}} \approx 1 \times 10^{11} \text{ s}^{-1}$  together with Equations (1) and (9),  $\kappa_{\text{el}} = 1$  and  $\nu_{\text{nu}} \approx 10^{12} \text{ s}^{-1}$  suggests a value of  $h\nu_{\text{max}} \approx 2,000 \text{ cm}^{-1}$  for the intervalence MMCT transition,  $\text{cm}^{-1}$ . This is far lower energy than the band assigned as an intervalence MMCT transition, and it sufficiently close to the energy of the carbonyl stretching frequencies to raise questions about the quantitative interpretation of the line-broadening effects. An important feature of these complexes is that the reduction potentials are more than 1 V more negative than that of the  $[\{\text{Ru}(\text{NH}_3)_5\}_2\text{pz}]^{5+}$  complex.<sup>230,231</sup> Based on Equation (30), this should result in a very low energy MLCT excited state; the estimated (diabatic) transition energy would be roughly  $10 \times 10^3 \text{ cm}^{-1}$ , possibly lower energy than the diabatic intervalence transition. This suggests a possible reversal of the order of excited states from the one that is usually assumed, and as illustrated in Figure 10 and 16. For such a reversal of the ordering of the bridging ligand MLCT and the MMCT excited states, configurational mixing should result in an increased energy of the MMCT excited state. Whatever the ultimate interpretation of these interesting systems, they do nicely illustrate the coupling of electronic and nuclear motions in relatively simple molecules.

#### 7.11.4.8.2 Polypyridyl ligand-bridged complexes in which coupling appears to be promoted by ligand-to-metal charge transfer (hole transfer systems)

The lowest energy excited state that involves both the metal and ligand of the systems discussed above is a  $d\pi/p\pi$  MLCT state. The delocalization of electron density across the bridge can be described in terms of mixing between the ground and MLCT excited state. Many metal–ligand moieties have lower-energy LMCT states than MLCT states.<sup>113,286</sup> LMCT states can be just as effective as MLCT states in mediating D/A electronic coupling. Dicyanamide(2<sup>-</sup>) (dicyd<sup>2-</sup>) ligands, such as 1,4-dicyanamidobenzene, have relatively high-energy  $\pi$ -HOMOs that can contribute to low-energy LMCT transitions in their  $\text{Ru}^{\text{III}}$  complexes. Crutchley and co-workers<sup>116,252,287–292</sup> have documented the electron transfer properties of this class of bridging ligands. The LMCT absorptions tend to be in the visible region and the electronic coupling tends to be very strong in the  $[\{\text{Ru}(\text{NH}_3)_5\}_2\text{dicyd}]^{3+}$  complexes, and they have attributes similar to those of the most strongly coupled, pyrazine-bridged complexes.

#### 7.11.4.8.3 Complexes with two-atom bridging moieties

Many mixed-valence complexes with two-atom bridges have been investigated. Most of these studies have employed  $\text{N}_2$ , or  $\text{CN}^-$  bridging ligands. The cyanide bridge is by far the most versatile. These relatively simple ligands have cylindrical symmetry, they have a single, well-characterized vibrational mode, and they have general molecular orbital properties analogous to the more complicated polypyridyl bridging ligands. These two bridging ligands obviously differ in symmetry, and the cyanide-bridged complexes cannot be chemically degenerate with respect to electron transfer. One would expect many of the complex issues developed in the preceding section to be more clearly manifested in these complexes. Table 7 summarizes the properties of several such complexes.

The simplest of the  $\text{CN}^-$ -bridged complexes are of the type  $[(\text{NH}_3)_5\text{M}(\text{NCM}'(\text{CN})_5)]^{n-}$ . Hupp and Barbara and their co-workers have extensively examined complexes of his type with  $\text{M} = \text{Ru}$  or  $\text{Os}$  and  $\text{M}' = \text{Fe}$ ,  $\text{Ru}$ , or  $\text{Os}$ .<sup>67,69,70,104,120,261,280–283</sup> The electronic coupling in these complexes is very large,  $H_{\text{DA}}$  is of the order of  $2 \times 10^3 \text{ cm}^{-1}$ , and they typically exhibit an intense near-infrared  $\text{M}/\text{M}'$  absorption. A very remarkable feature of these complexes is the very fast back electron transfer relaxation of the excited state generated by irradiation of the  $\text{MM}'\text{CT}$  absorption band. The back electron transfer rate constant is of the order of  $10^{13} \text{ s}^{-1}$ , and faster than the  $\text{CN}^-$  vibrational relaxation rate. The back electron transfer apparently occurs from a vibrational excited state (largely  $\text{CN}^-$ -centered) of the electron transfer excited state to form a ground state with vibrationally excited cyanides.<sup>67–70,120,276</sup> Resonance-Raman studies indicate that nonbridging and bridging cyanide ligand vibrational modes contribute to the  $\text{MM}'\text{CT}$  absorption.<sup>293</sup>

**Table 7** Electron transfer parameters in some donor-acceptor complexes with two atom bridges.

Complex	$h\nu_{\text{max}}(\text{MMCT})^{\text{a}}$ ( $\epsilon_{\text{max}}$ ) [ $\Delta\nu_{1/2}$ ]	$h\nu_{\text{max}}(\text{MLCT})^{\text{a}}$ ( $\epsilon_{\text{max}}$ ) [ $\Delta\nu_{1/2}$ ]	$\chi^{\text{b}}$	$-\Delta G_{\text{DA}}^{0\text{c}}$	$H_{\text{DA}}^{\text{d}}$	$k_{\text{het}}(\text{obsd})^{\text{e}}$
$[(\text{bpy})_2\text{Ru}(\text{bb})\text{Co}(\text{bpy})_2]^{5+}$	{20} <sup>1256</sup>	22.1	12.3	7.7	0.008	$3 \times 10^{11}$
$[\{\text{Fc}\}_2(\text{bb}')_3]^{5+\text{g}}$	7.47 (0.24) [3.2] <sup>257</sup>	18.9, sh. (9700)	7.5	0	0.006	
$[(\text{NC})_5\text{Ru}(\text{CNRu}(\text{NH}_3)_5)]^{-}$	14.2 (~3000) [4.8] <sup>69,404</sup>		3.7	7.8		$1 \times 10^{13}$
$[(\text{NC})_5\text{Ru}(\text{CNOs}(\text{NH}_3)_5)]^{-}$	20.4 (1840) [4.5] <sup>176</sup>					
$[(\text{NC})_5\text{Fe}(\text{CNRu}(\text{NH}_3)_5)]^{-}$	9.6 <sup>69</sup>					
$[(\text{NC})_5\text{Fe}(\text{CNOs}(\text{NH}_3)_5)]^{-}$	15.9 (1640) [4.3] <sup>176</sup>					
$[(\text{NC})_5\text{Os}(\text{CNOs}(\text{NH}_3)_5)]^{-}$	17.9 (2090) [6.1] <sup>176</sup>					
$[(\text{NC})_5\text{Os}(\text{CNOs}(\text{NH}_3)_5)]^{-}$	26.6 (2400) [6.3] <sup>176</sup>					
$[(\text{NC})_5\text{Fe}(\text{CNCr}(\text{NH}_3)_5)]^{-}$	15.3 (6000) [5.65] <sup>302</sup>					
$[(\text{bpy})_2\text{Ru}(\text{CNRu}(\text{NH}_3)_5)]^{6+}$	12.1 (5800) [ $\sim$ 6]	25.3	11.2 <sup>299,302</sup>	4.5	3.4 <sup>93</sup>	$> 10^{11,297}$
$[(\text{bpy})_2\text{Os}(\text{CNRu}(\text{NH}_3)_5)]^{6+}$	14.9, sh ( $\sim$ 3500) <sup>96</sup>	25.1 (9100)			$\sim$ 2.5 <sup>96</sup>	
$[(\text{tpy})(\text{bpy})_2\text{Ru}(\text{CNRu}(\text{NH}_3)_5)]^{4+}$	14.2 (4100) [4.9] <sup>93,301</sup>	22.7	9.6 <sup>303</sup>	4.5	3.4 <sup>93</sup>	$> 10^{12,301}$
$[(\text{bpy})_2\text{Fe}(\text{CNRu}(\text{NH}_3)_5)]^{6+}$	10.5 (6580) [4.8] <sup>302</sup>	21.3	$\sim$ 11 <sup>303</sup>	4.5	2.7 <sup>93</sup>	
$[(\text{bpy})_2\text{Cr}(\text{CNRu}(\text{NH}_3)_5)]^{6+}$	15.3 (6000) [5.6] <sup>93,302</sup>				3.2 <sup>93</sup>	
$[(\text{bpy})_2\text{Rh}(\text{CNRu}(\text{NH}_3)_5)]^{6+}$	24.1 (1460) [9.25] <sup>93,302</sup>				$\sim$ 2.6 <sup>93</sup>	
$[(\text{NH}_3)_5\text{Ru}(\text{CNRu}(\text{NH}_3)_5)]^{4+}$	11.2 (4200) [5.6] <sup>h</sup>					
$[(\text{NH}_3)_5\text{Cr}(\text{CNRu}(\text{NH}_3)_5)]^{4+}$	21.6 (3100) [5.7] <sup>93</sup>				3.9 <sup>93</sup>	$3 \times 10^5$ (77 K) <sup>300</sup>
$[(\text{NH}_3)_5\text{Rh}(\text{CNRu}(\text{NH}_3)_5)]^{4+}$	25.6 (655) [6.4] <sup>93</sup>					
$tr-[(\text{N}_4)_{(1)}\text{Cr}(\text{CNRu}(\text{NH}_3)_5)]^{5+}$	20.0 (8000) [4.9] <sup>93</sup>		$\sim$ 14 <sup>92,303</sup>	4.5	3.9 <sup>93</sup>	$1.4 \times 10^{8,92}$
$tr-[(\text{N}_4)_{(2)}\text{Cr}(\text{CNRu}(\text{NH}_3)_5)]^{5+}$	19.4 (6400) [5.2] <sup>93</sup>					$1.2 \times 10^6$ (77 K) <sup>300</sup>
$tr-[(\text{N}_4)_{(1)}\text{Co}(\text{CNRu}(\text{NH}_3)_5)]^{5+}$	20.0 (1030) [7.0] <sup>93</sup>					$1.1 \times 10^6$ (77 K) <sup>300</sup>
$tr-[(\text{N}_4)_{(2)}\text{Co}(\text{CNRu}(\text{NH}_3)_5)]^{5+}$	19.5 (1400) [6.0] <sup>93</sup>					$2 \times 10^{9,299}$
$tr-[(\text{N}_4)_{(1)}\text{Rh}(\text{CNRu}(\text{NH}_3)_5)]^{5+}$	29.2 (800) [6.0] <sup>93</sup>					
$tr-[(\text{py})_4\text{Ru}(\text{CNRu}(\text{NH}_3)_5)]^{6+}$	14.6 (4200) [6.2] <sup>96</sup>	26.9 (16,500) [ $\sim$ 6] <sup>96</sup>				
$[(\text{NH}_3)_5\text{Ru}(\text{N}_2)]^{9+}$	9.8 (1400) [2.6] <sup>271</sup>					
$cis,cis-[\{(\text{bpy})_2(\text{Cl})\text{Os}\}_2\text{N}_2]^{3+}$	6.4 (370) [2.2]					
	11.3 (5200) [1.9]					
	13.4 (900) [2.4] <sup>221</sup>					
$tr, tr-[\{(\text{tpy})(\text{Cl})_2\text{Os}\}_2\text{N}_2]^{3+}$	5.2 (640) [0.85]					
	11.3 (700) [1.6]					
	11.7 (5100) [1.4] <sup>221</sup>					

<sup>a</sup> In aqueous solution at 25 °C except as noted. Energies in  $10^{-3} \text{ cm}^{-1}$ ; absorptivity in  $\text{cm}^{-1} \text{ M}^{-1}$ . <sup>b</sup> Reorganizational energy in  $\text{cm}^{-1}$ ; from reference noted in column 2 except as indicated. <sup>c</sup> Free energy change for back electron transfer; from reference noted in column 2 except as indicated. <sup>d</sup> Electronic matrix element in  $\text{cm}^{-1}/10^5$ ; from reference noted in column 2 except as indicated. <sup>e</sup> Back electron transfer rate constant observed after MMCT photoexcitation in  $\text{M}^{-1} \text{ s}^{-1}$ ; from reference noted in column 2 except as indicated. <sup>f</sup> Calculated from  $h\nu_{\text{max}} = \Delta G_{\text{DA}}^0 + \chi_{\text{r}}$ ; see also Table 2. <sup>g</sup>  $\text{bb}' = 1,4\text{-bis}[(4\text{-}(4\text{-methyl-}1,2,2\text{-bipyridyl)})\text{butane}]$ . <sup>h</sup> Watzky, M. A., Ph.D. Dissertation, Wayne State University, Detroit, 1994. <sup>i</sup> In  $\text{CD}_3\text{CN}$ .

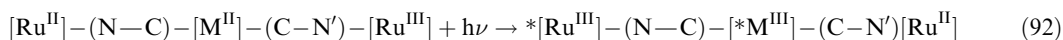
This vibrational state-to-vibrational state electron transfer is not properly described by the usual approaches to electron transfer problems (e.g., as represented in Section 7.11.2).

Complexes of the general stoichiometry  $[(L)_nM(CNRu(NH_3)_5)_{(6-n)}]^{m+}$  ( $n = 4$  or  $5$ ;  $L =$  a polypyridyl or am(m)ine nonbridging ligand;  $M = Fe, Ru, Os, Cr, Co, Rh$ ) exhibit a considerable range of donor–acceptor properties.<sup>92–96,239,294–303</sup> Some of the issues that have been raised above are relatively clearly manifested among these complexes. One very striking feature of the  $CN^-$ -bridged D/A complexes is that the  $CN$  stretch of a  $(L)_nM(CNRu)$  moiety is shifted to lower frequency relative to that of the monometallic  $[(L)_nM(CN)_{(6-n)}]^{p+}$  parent.<sup>92–94,296,298,302,303</sup> This is opposite to the direction of the shift expected (a “kinematic” shift) for a bridging cyanide.<sup>202</sup> For example,  $\nu_{CN} = 2,072$  and  $2,060\text{ cm}^{-1}$  for  $[Ru^{II}(bpy)_2(CN)_2]$  and  $2,057$  and  $2,011\text{ cm}^{-1}$  for  $[(bpy)_2Ru^{II}(CNRu^{III}(NH_3)_5)_2]^{6+}$ .<sup>298,302</sup> Reduction of the pentaammine moieties results in a complex with an expected kinematic shift,  $\nu_{CN} = 2,090$  and  $2,130\text{ cm}^{-1}$ , and the  $[(bpy)_2Ru^{II}(CNRh^{III}(NH_3)_5)_2]^{6+}$  complex exhibits similar kinematic shifts ( $\nu_{CN} = 2,105$  and  $2,124$ ).<sup>298,302,303</sup> The size of the shift of  $\nu_{CN}$  to lower frequencies in  $CN^-$ -bridged D/A complexes,  $\Delta\nu_{CN}$ , is proportional to the oscillator strength of the  $Ru^{II}/M^{III}$  MMCT absorption band,<sup>92,94,302,303</sup> and this suggests that the  $CN^-$  nuclear coordinates ( $Q_{CN}$ ) are a significant factor in determining the D/A electronic coupling. In centrosymmetric complexes,  $\Delta\nu_{CN}$  is 4–6 times larger for the symmetric combination of  $CN$  stretches than for the antisymmetric combination.<sup>94</sup> This is a clear demonstration of a symmetry-dependent molecular, not a local  $Ru^{II}(CN^-)Cr^{III}$ , coupling of electronic and nuclear properties. A vibronic model<sup>304,305</sup> has been proposed to account for this behavior,<sup>93,302</sup> with

$$H_{DA} = H_{DA^0} + bQ_{CN} \quad (91)$$

This model involves  $CN^-$ -mediated superexchange coupling of the bridged donor and acceptor with the concomitant delocalization of charge onto (by means of MLCT mixing) and/or from (by means of LMCT mixing)  $CN^-$  and weakening of the C–N bond (thus lowering the frequency of the  $CN$  stretch). The observed behavior corresponds to *vibronic coupling limit 3* discussed in Section 7.11.4.4.

Complexes with more than one cyanide, such as  $[(L)_4M(CN)_2]^{p+}$ , can function as bridging ligands. For a series of complexes of the type  $[(NH_3)_5Ru^{II}\{(NC)(N_4)_{(i)}M^{III}(CN)\}Ru^{III}(NH_3)_5]^{6+}$ , where  $(N_4)_{(i)}$  is a cyclic tetraamine, the  $Ru^{II}/Ru^{III}$  MMCT absorption band energies decrease in proportion to increasing absorptivity and decreasing energy of the  $Ru^{II}/M^{III}$  “MLCT” absorption, as expected (Equation (72)), but the MMCT band intensities are effectively constant, independent of the MMCT absorption properties and weak ( $\epsilon_{max} \cong 120\text{ M}^{-1}\text{ cm}^{-1}$ ). Since the simple superexchange coupling model requires that the MMCT band intensity increase with  $\Delta h\nu_{max}(\text{MMCT})$  (see Equation (74) and Figure 3), it appears that superexchange coupling is “turned off” for this type of bridging ligand.<sup>95</sup> This amounts to a vibronic selection rule for the electron transfer absorption. If one assumes that  $H_{DA}^0$  in Equation (91) is very small, then the  $Ru^{II}/M^{III}$  electronic coupling depends mostly on  $bQ_{CN}$ . If one uses the model described in the preceding paragraph, then the cyanide bridging  $Ru^{II}$  and  $M^{III}$  in the ground state of the  $[(N_4)_{(i)}M^{III}(CNRu^{II}(NH_3)_5)(CNRu^{III}(NH_3)_5)]^{6+}$  complex is configured for optimal electronic coupling ( $bQ_{CN}$  maximized) and the C–N bond is stretched; the cyanide bridging  $Ru^{III}$  and  $M^{III}$  is compressed (repulsive interaction or kinematic coupling). In the Franck–Condon excited state generated by MMCT excitation (i.e., with ground state nuclear coordinates), the cyanide bridging  $Ru^{II}$  to  $M^{III}$  is configured for a repulsive interaction ( $bQ_{CN}$  minimized),



This means that the two  $CN$  stretches are out of phase. This can conveniently be represented as  $H_{DB} \cong bQ_{CN} = y\cos\theta$  and  $H_{BA} \cong bQ_{CN'} = y\sin\theta$ . Then, setting  $\theta = 0$  and substituting into Equation (41) results in  $H_{DA}^{sp} \cong 0$ .<sup>95</sup> This vibronic phase restriction on the D/A coupling arises when the three states have appreciably different energies (Figure 3), because the properties of the electronic states are only perturbationally altered. If the MLCT and the MMCT excited states are degenerate (in the coordinates of the ground state), then the phase restriction should be relaxed. The  $Ru^{II}/Ru^{III}$  MMCT (central-to-terminal) transition in  $[(py)_4Ru^{II}(CNRu^{III}(NH_3)_5)_2]^{6+}$  occurs at  $14.6 \times 10^3\text{ cm}^{-1}$  ( $\epsilon_{max} = 4,200\text{ M}^{-1}\text{ cm}^{-1}$ ),<sup>96</sup> and this is very close to the diabatic reorganizational



energy ( $\approx(12-13) \times 10^3 \text{ cm}^{-1}$ ) expected for the terminal pentammine moieties. The  $\text{Ru}^{\text{II}}(\text{NH}_3)_5 \rightarrow \text{Ru}^{\text{III}}(\text{NH}_3)_5$  MMCT transition in  $[(\text{py})_4\text{Ru}^{\text{II}}(\text{CNRu}^{\text{II}}(\text{NH}_3)_5)_2(\text{CNRu}^{\text{III}}(\text{NH}_3)_5)_2]^{6+}$  is relatively intense ( $\epsilon_{\text{max}} = 1,500 \text{ M}^{-1} \text{ cm}^{-1}$ ),<sup>96</sup> consistent with the general argument developed here. This increased intensity of the MMCT transition is accompanied by a decrease in the intensity (per Ru) of the  $\text{Ru}^{\text{II}}/\text{Ru}^{\text{III}}$  (central-to-terminal) transition, and it is a nice example of intensity stealing. The degeneracy of the diabatic MLCT and MMCT excited states, proposed to be the origin of this increased intensity of the lowest energy CT band of  $[(\text{py})_4\text{Ru}(\text{CNRu}(\text{NH}_3)_5)_2]^{5+}$ , affects the properties of this mixed-valence system much differently than the effect of the very similar degeneracy in the  $[(\text{NH}_3)_5\text{Os}^{\text{II}}(\text{pz})\text{Os}^{\text{III}}(\text{NH}_3)_5)_2]^{5+}$  complex discussed in Section 7.11.4.8.1. The origin of this contrast is manifested in the absorptivities of the MLCT transitions ( $\text{Ru}_c^{\text{II}}/\text{Ru}_t^{\text{III}}$  and  $\text{Os}^{\text{II}}/\text{pz}$ , respectively) of the two complexes: about four times larger in the latter. Expressed in terms of perturbation theory mixing parameters,  $H_{\text{DB}}$  for the pyrazine-bridged osmium complex is 2–4 times larger than for the cyanide-bridged ruthenium complex. As a result, MLCT mixing has more than an order of magnitude greater effect on the pyrazine-bridged osmium complex than on the  $[(\text{py})_4\text{Ru}^{\text{II}}(\text{CN})_2]$ -bridged ruthenium complex. The stabilization energy that results from this mixing in the transition-state coordinates is greater than  $\chi_r^\ddagger$  for the osmium complex and much less than  $\chi_r^\ddagger$  for the ruthenium complex.

The irradiation of the  $\text{Ru}^{\text{II}}/\text{Cr}^{\text{III}}$  MMCT absorption band of the  $[(\text{Am})_n\text{Cr}(\text{CNRu}(\text{NH}_3)_5)_{(6-n)}]^{p+}$  complexes in 77 K DMSO/H<sub>2</sub>O glasses results in  $\text{Ru}^{\text{III}}/\text{Cr}^{\text{II}} \rightarrow \text{Ru}^{\text{II}}/\text{Cr}^{\text{III}}$  electron transfer emissions.<sup>300</sup> The emission bands have maxima at 850–775 nm (depending on L), are relatively broad ( $\Delta\nu_{1/2} \approx 1,000 \text{ cm}^{-1}$ ), broadened on the low energy side, and have roughly microsecond lifetimes. The emission energies are consistent with estimated electron transfer parameters. The emission bands are unstructured, but can be deconvoluted into vibronic progressions with  $h\nu_h \cong 400-500 \text{ cm}^{-1}$ ; these probably originate in Cr–N distortions. The emission lifetimes increase dramatically on am(m)ine perdeuteration. The ratio  $k_{\text{H}}/k_{\text{D}}$  is in the range of 20–30 depending on the number of coordinated N–H moieties, and the emission maxima shift approximately  $\pm 100 \text{ cm}^{-1}$  (*minus* if more N–H moieties are coordinated to Ru than to Cr; *positive* for the reverse). This suggests that the low-temperature back electron transfer is dominated by high-frequency (N–H) vibrational modes, apparently because these provide the most efficient means of disposing of energy in the Marcus-inverted region.<sup>35,306</sup> The shift of the absorption maxima on perdeuteration demonstrates a zero point energy difference between the electron transfer excited and ground states, and, therefore, a difference in (N–H) force constants in the ground and excited states. It is important to note that the excited state behavior of the  $[(\text{Am})_n\text{Cr}(\text{CNRu}(\text{NH}_3)_5)_{(6-n)}]^{p+}$  complexes is interpretable in terms of the standard electron transfer concepts outlined in Section 7.11.2, while that of the  $[(\text{NH}_3)_5\text{M}(\text{NCM}'(\text{CN})_5)]^{q-}$  complexes is not. This contrast has been ascribed to the generation of a lowest-energy doublet MM'CT excited state in the Cr/Ru systems whose back electron transfer to the ground state is spin-forbidden.<sup>300</sup>

Since there is no intrinsic bonding asymmetry of the dinitrogen bridge, ground state delocalization is bound to be more of an issue in the N<sub>2</sub>-bridged D/A complexes than in the CN<sup>−</sup>-bridged analogs. Perhaps a more important feature in the comparison of these complexes is that the  $\text{Ru}^{\text{II}}/\text{N}_2$  MLCT absorption bands<sup>271</sup> are at about the same energy and have more than ten times the absorptivity as the  $\text{Ru}^{\text{II}}/\text{CN}^-$  MLCT absorption bands.<sup>93</sup> This should lead to far greater D/A mixing in the N<sub>2</sub>-bridged complexes. The simplest of these are the  $[(\text{NH}_3)_5\text{M}]_2\text{N}_2]^{q+}$  complexes with M = Ru or Os.<sup>271,307–309</sup> The maximum symmetry of these complexes is  $D_{4h}$ , and Richardson, *et al.*<sup>271</sup> have based the simple molecular orbital scheme in Figure 17 on this symmetry. The mixed-valence complexes have a formal  $d\pi^{11}p\pi^4$  electronic structure and this gives rise to the set of electronic states for  $D_{4h}$  symmetry shown on the right-hand side of Figure 17 (the partly filled orbitals of each state are indicated in parenthesis). The  $\text{M}^{\text{II}}/\text{N}_2$  MLCT excited states tend to have relatively high energies ( $E_{\text{DB}} \cong h\nu_{\text{max}}(\text{MBCT})$ ; see Table 6). As a consequence, the MMCT absorption maximum is generally to be expected at higher energy for the dinitrogen than for the pyrazine-bridged complexes (see Equation (72)),

$$h\nu_{\text{max}}(\text{MMCT}) \cong h\nu_{\text{max}}(\text{diabatic}) + H_{\text{DB}}^2/E_{\text{DB}} - H_{\text{DB}}^2/E_{\text{AB}} \quad (93)$$

It is important to note that MMCT band characteristics are very similar for the homobimetallic, mixed-valence N<sub>2</sub>- and pz-bridged complexes of both Ru and Os.<sup>240,271</sup> Allowing for the excited state mixing described in Section 7.11.4.8.1 when B = pz, and giving equal weight to

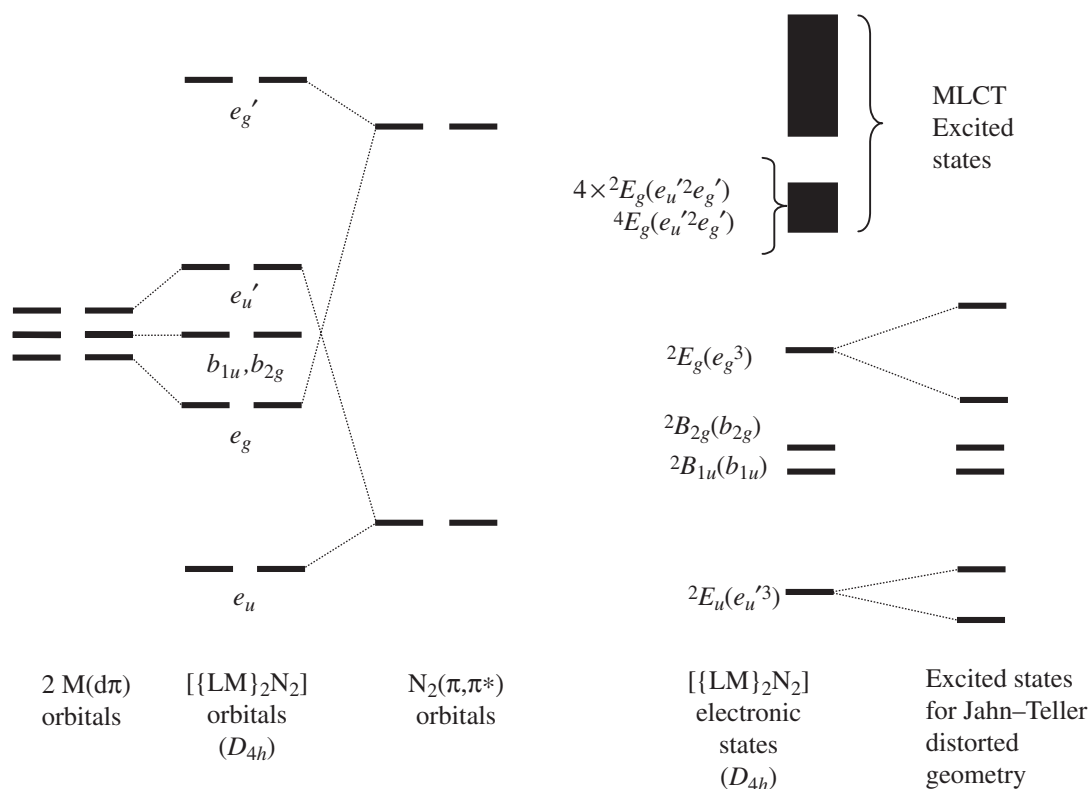


**Figure 17** Orbital and electronic state diagrams for dinitrogen-bridged D/A complexes. The solid blocks indicate a large number of similar-in-energy MLCT excited states.

both excited states, the simple perturbation theory argument suggests about  $2,000\text{ cm}^{-1}$  larger value for  $h\nu_{\text{max}}(\text{MMCT})$  in the  $[(\text{NH}_3)_5\text{Ru}]_2\text{N}_2^{5+}$  complex (with  $h\nu_{\text{max}}(\text{diabatic}) = 12,000\text{ cm}^{-1}$  (Section 7.11.4.8.1) and  $H_{\text{DB}} = 9,400\text{ cm}^{-1}$ , reported for B = pz,<sup>104</sup> for both complexes). Thus, the overall properties, if not all of the details, of the ruthenium complexes seem consistent with expectation for systems with very strong donor-bridge coupling.

However, there is a problem with the simple picture, and this is illustrated in Figure 17. The ground state,  ${}^2E_u$ , and the highest energy “MMCT” excited state,  ${}^2E_g$ , are both expected to be unstable with respect to a symmetry-lowering geometrical distortion (Jahn-Teller effect).<sup>28,97,286,304,305</sup> In order to remove the degeneracy of these electronic states, the nuclear distortion must be one that eliminates the fourfold rotational axis. This implicates a bending mode, either (H<sub>3</sub>N)-M-(NH<sub>3</sub>) or M-(N<sub>2</sub>)-M. The amplitude of the resulting splitting (corresponding to the population of orbitals in the *xz* and *yz* planes) of the electronic states depends on the strength of the coupling to the nuclear distortion. This coupling could be larger for Os than for Ru, leading to an incompletely resolved splitting for  $[(\text{NH}_3)_5\text{Ru}]_2\text{N}_2^{5+}$  (possibly contributing to the MMCT band shape), and very large splittings for  $[(\text{NH}_3)_5\text{Os}]_2\text{N}_2^{5+}$ , possibly accounting for the 700 nm absorption band. The relatively large spin-orbit coupling contributions are also bound to be an important factor in the spectroscopy of the osmium complexes and will contribute to the mixing of electronic states.<sup>221,271</sup>

The generally useful superexchange approach to D/A coupling, and the very large Ru<sup>II</sup>/N<sub>2</sub> absorptivities do lead to the expectation of very strong N<sub>2</sub>-mediated electronic coupling in these systems, perhaps even approaching the M=N=N- limit analogous to that proposed for mixed-valence, polyacetylide-bridged di-rhenium complexes.<sup>310,311</sup> Distortions along the M<sup>II</sup>-(N<sub>2</sub>)-M<sup>III</sup> axis (symmetric or antisymmetric stretches) may remove the center of symmetry, but they do not alter the degeneracy of the  ${}^2E$  electronic states. A Jahn-Teller distortion (a bending distortion with respect to the C<sub>4</sub> axis) should result in the maximum number of electronic transitions. Since a Jahn-Teller distortion need not result in an axial redistribution of electron density and electronic localization at one of the metal centers (e.g., the accompanying electronic redistribution could be

from the  $x,z$  to the  $y,z$  plane), the resolution of a large number of low-energy electronic transitions is not, of itself, demonstration of electronic localization.

The  $N_2$ -bridged complexes with symmetry lower than  $C_{4v}$ <sup>221,312,313</sup> will not usually have a fourfold symmetry axis, and will not have degenerate electronic states. Nevertheless, the energy differences between states and the number and intensities of the electronic transitions in these systems will largely depend on the same issues of vibronic coupling and spin-orbit coupling, as in the high-symmetry systems.

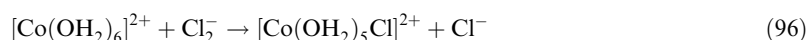
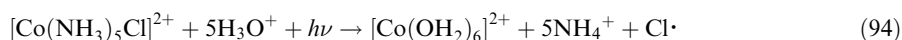
Resonance Raman data indicate only about a  $20\text{ cm}^{-1}$  shift of the  $N_2$ -stretch to lower frequency in the mixed-valence di-ruthenium complex,<sup>271</sup> compared to about  $50\text{ cm}^{-1}$  observed in strongly coupled, cyanide-bridged donor-acceptor complexes.<sup>94,302</sup> This is contrary to expectation based on the simplest stationary state assumption that all the mixed-valence properties are a function of  $\alpha_{DA}^2$ . Since the much larger MLCT absorbencies of the  $N_2$ -bridged complexes imply correspondingly larger values of  $H_{DB}$  (see Equations (22) and (23); the MLCT energies are about the same), and since the electron density delocalized should approximately increase with  $(H_{DB})^2$ , the bond distortion should be much larger in these complexes than in the  $CN^-$ -bridged complexes. The values inferred for  $\nu_{el}(H)$  (Equation (76)) are very different, and this discrepancy may be best addressed in terms of a time-dependent, or electron-hopping model. Based on Equation (76) for the MBCT transitions,  $\nu_{el} \approx 2.5 \times 10^{13}\text{ s}^{-1}$  for the  $CN^-$  bridge and about  $10 \times 10^{13}\text{ s}^{-1}$  for the  $N_2$  bridge. Since  $\nu_{CN} \cong \nu_{NN} \cong 6 \times 10^{13}\text{ s}^{-1}$ , the mean lifetime of the electron on the bridging ligand is greater than a mean vibrational lifetime for the former and somewhat less for the latter (note that in the few systems where information is available,  $\nu_{el}^* < \nu_{el}$ ). If such a contrast in the mean lifetime of the electron on the bridging ligand is correct, then it suggests that the alteration of bridging ligand vibrational frequencies that correlate with ligand mediation of strong D/A coupling will vary in amplitude as a function of the ratio of electronic-hopping frequency to the ligand vibrational frequency; large changes when  $\nu_{el}/\nu_h \leq 1$  and small changes when  $\nu_{el}/\nu_h \gg 1$ . Further studies are necessary to explore these ideas. There are some potentially significant implications about the proper description of bridged electron transfer systems and the use of theoretical descriptions in designing complex arrays of linked donors and acceptors.

#### 7.11.4.9 Covalently Linked, Sigma Donor-Acceptor Systems

The coupling of transition metal donor-acceptor complexes through  $\sigma$  networks has received much less attention than the coupling through  $\pi$  networks, discussed in the preceding section. The electronic coupling between  $d\sigma$  donor and  $d\sigma$  acceptor metal centers through a  $\sigma$  bond has long been presumed to be an element of inner-sphere electron transfer reactions.<sup>1,49,314,315</sup> The appropriate  $\sigma$  networks necessarily involve bonding orbitals and it has been difficult to develop simple complexes in which the electronic coupling may be probed by the means employed in the much more numerous  $\pi$  coupling networks. One issue in such systems has been to design complexes in which the transition metal donor and acceptor are in an appropriate geometry and in which the donor and acceptor orbitals can be relatively well defined with respect to the bridging ligand. A problem in such systems is that ligand substitution rates tend to be very large when the  $d\sigma$  orbitals are partly or fully occupied.<sup>316</sup>

The issues in thermal kinetic studies have generally related to the size and origin of the rate advantage of a  $\sigma$ -bridged, inner-sphere reaction pathway over the equivalent outer-sphere electron transfer pathway.<sup>1,49,71,315-318</sup> Thus, it has been shown that the inner-sphere, halide-bridged electron transfer self-exchange reactions are about  $10^6$  times faster than their outer-sphere equivalents when the reacting partners are tetraaza-macrocyclic ligand complexes of low-spin cobalt(II) and their cobalt(III) equivalents.<sup>145,193,317,319</sup> Most of this rate advantage appears to be in the reorganizational energy,<sup>193,195</sup> and diminution of the reorganizational barrier has been attributed, in part, to vibronic coupling<sup>195</sup> (Limit 2 in Section 7.11.4.4) since there must be a concerted motion of the bridging halide from donor to acceptor as the reacting system passes through the transition state.<sup>320</sup> The vibronic model employed involves the assumption that the electronic coupling depends on the overlap of donor, bridging ligand and acceptor orbitals, and, thus, the metal-halide bond length,  $H_{DA} = H_{DA}^0 + bQ_{MX}$ . Since this model involves the assumption that the electron density is in equilibrium with the nuclear coordinates across the reaction coordinate, the rate constant should reach a limiting, maximum value when  $|\Delta G_{DA}^0|$  is larger than  $\chi_r$ .<sup>195</sup>

The assumption that the electronic coupling in a  $\sigma$ -bridged pathway is a strong function of the donor orbital and the acceptor orbital overlap with some bridging-ligand orbital has also been examined in thermal kinetic studies.<sup>145,194</sup> Many tetraaza-macrocyclic ligands introduce constraints that result in unique directional distributions of electron density in the different metal complexes. Thus, the unpaired electron of the low-spin  $d^7$  metal complexes, such as those of cobalt(II) and nickel(III), can be constrained to be axial with respect to certain planar macrocyclic ligands ( $\sim 13$ – $15$  atoms comprising the inner ring of a tetra-coordinate ligand), while similar complexes of  $d^9$  metals, copper(II) and nickel(I), have the unpaired electron in the equatorial, macrocyclic ligand plane.<sup>321,322</sup> The strong metal–halide interactions are necessarily axial in these complexes, and these interactions are repulsive (antibonding) for low-spin  $d^8$  and  $d^9$  metals, weakly attractive for low-spin  $d^7$  and strongly attractive (bonding) for low-spin  $d^6$ . The inner-sphere rate advantage has been examined based on the kinetic comparison of the contrasts in reactivity for the  $[\text{Co}(\text{OH}_2)_6]^{3+}$  and  $[\text{Co}(\text{OH}_2)_5\text{Cl}]^{2+}$  oxidations of *trans*- $\text{M}^{\text{II}}(\text{N}_4)$  complexes ( $\text{N}_4$  = a tetraazamacrocyclic ligand).<sup>145,194</sup> The meta-stable  $[\text{Co}(\text{OH}_2)_5\text{Cl}]^{2+}$  complex was generated *in situ* photochemically Equation (94–96),<sup>194</sup>



The rate advantages (corrected for driving force differences),  $k^{(\text{IS})}/k^{(\text{OS})}$ , were  $>10^5$  for oxidations of low-spin  $[\text{Co}(\text{N}_4)(\text{OH}_2)_2]^{2+}$  complexes,  $\sim 10^{5\pm 1}$  for low-spin  $[\text{Ni}(\text{N}_4)]^{2+}$  complexes and  $\sim 3$  for  $[\text{Cu}(\text{N}_4)]^{2+}$  complexes.<sup>145</sup>

Bimetallic complexes with a  $\sigma$  bridging ligand between a transition metal donor and acceptor have been constructed by means of a xylene linkage between carbon atoms of two tetraaza macrocyclic ligands,<sup>323–326</sup> as in Figure 18. The  $[\text{L}\{\text{M}^{\text{II}}(\text{N}_4)\}_2]^{4+}$  complexes have large ion-pair association constants, they essentially act as chelates for halides,<sup>325</sup> Figure 18, and they are good models for  $\sigma$ -bridged donor–acceptor systems. Magnetic susceptibility measurements have demonstrated that the  $[\text{L}\{\text{Cu}^{\text{II}}(\text{N}_4)\}_2\text{X}]^{3+}$  complexes ( $\text{X} = \text{Cl}$  or  $\text{Br}$ ) are very weakly antiferromagnetic ( $|J| < 2 \text{ cm}^{-1}$ ).<sup>325</sup> The electrochemical oxidation of  $[\text{L}\{\text{Cu}^{\text{II}}(\text{N}_4)\}_2\text{Cl}]^{3+}$  consists of two unresolved steps ( $\Delta E_{1/2} \leq 30 \text{ mV}$ ).<sup>325</sup> This demonstrates that the halide bridge is not effective in mixing donor and acceptor orbitals that are largely orthogonal to the bridging axis. This is an issue of orbital overlap, and it supports the inferences from the kinetic study.<sup>145,194,325</sup> The high spin and low spin electronic configurations of nickel(II) in approximately planar, tetraaza-macrocyclic ligand complexes tend to be close in energy. The axial association with a halide ion tends to stabilize the high spin configuration relative to the low spin configuration, although it does not

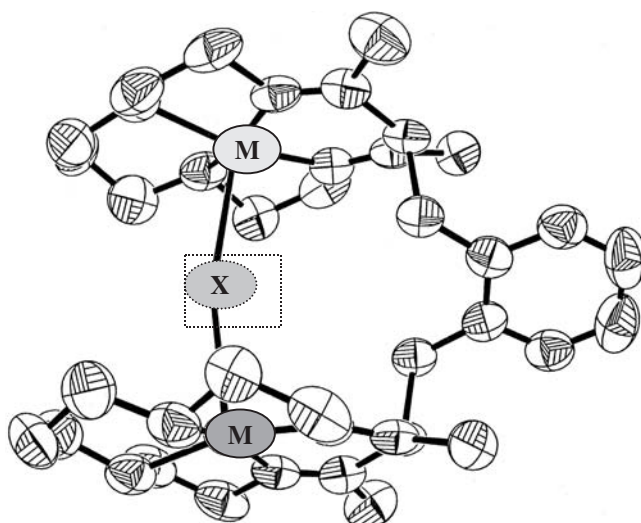


Figure 18 A halide-bridged bimetallic complex.

always result in a high spin ground state in solution. The oxidation of  $[\text{L}\{\text{Ni}^{\text{II}}(\text{N}_4)_2\text{Cl}\}]^{3+}$  occurs at a potential that is about 600 mV less positive than that of  $[\text{L}\{\text{Ni}^{\text{II}}(\text{N}_4)_2\}]^{4+}$ , but there is no resolvable splitting of the cyclic voltammograms.<sup>327</sup> The oxidations may correspond to removal of the relatively high energy, weakly coupled electrons from the macrocyclic plane; apparently,  $d\sigma/p\sigma/d\sigma$  coupling is weak in these complexes.

Gamelin, *et al.*<sup>86</sup> have thoroughly characterized the mixed-valence  $\{[(\text{Me}_3\text{N})_9\text{aneN}_3]\text{Fe}\}_2(\text{OH})_3]^{2+}$  complex using a variety of spectroscopic and computational techniques. The  $13.4 \times 10^3 \text{ cm}^{-1}$  absorption band has a non-Gaussian band shape and a  $3.7 \times 10^3 \text{ cm}^{-1}$  bandwidth (300 K in a propionitrile/butyronitrile solvent). The iron atoms lie along the molecular threefold rotational axis and resonance Raman probing of the near-infrared MMCT absorption demonstrated that the two totally symmetric vibrational modes,  $a_1'(1)$  and  $a_1'(2)$  (neglecting the aliphatic amine ligands and OH protons, these are the symmetric and antisymmetric combinations of Fe—Fe and  $\text{O}_3$  symmetric stretches), are most strongly coupled with the electronic transition. This demonstrates that the electron density is delocalized between the iron atoms in this complex. The non-Gaussian band shape was attributed to anharmonicities in the excited state PE surface. The Fe—Fe electronic coupling was inferred to be mediated by  $\text{Fe}(d\pi)\text{—O—Fe}(d\sigma)$  superexchange mechanism and  $H_{\text{DA}}$  was inferred to be a function of the Fe—Fe distance.

#### 7.11.4.10 Overview and Summary

The range of behavior and the complexities of bridged electron transfer systems is overwhelming. This section has attempted an internally consistent organization and treatment of the properties of these systems that encompasses the full range of the topic. Time, space, and personal bias have dictated appreciable selectivity in the systems discussed. It has not been possible to cite all the important contributions or even to do full justice to every aspect of the cited observations.

Overall, the properties of covalently linked electron transfer systems can be systematically addressed using the Franck–Condon parameters ( $\Delta G_{\text{DA}}^0$  and  $\chi_{\text{T}}$ ) and  $\nu_{\text{nu}}$  of the equivalent outer-sphere electron transfer systems as an experimentally accessible reference for the limit in which the electronic coupling approaches zero. The values of these parameters are altered in the linked systems, and in most cases the changes from the zero-coupling limit can be treated in terms of the electronic mixing of the donor and acceptor diabatic states with electronic states of the bridging ligand. In many cases this can be reduced to a three-state, perturbation theory problem involving only electronic mixing. The resulting superexchange model for the contributions to the electronic matrix element allow one to systematically address the contributions of the bridging ligand to the electronic coupling, and, therefore, to the ways in which the Franck–Condon parameters of the bridged system differ from those of the outer-sphere-limit reference. The observations summarized in this section do demonstrate that while the overall logic of the perturbation theory corrections of the Franck–Condon or rate constant parameters is generally useful, there are very important details that must often be considered in the perturbation theory approach. First among these is that when the electronic coupling becomes very large, the electronic and nuclear motions can be coupled and the perturbational correction terms are best based on vibronic models. The best formulation and the range of applicability of such models is still evolving. A second important detail is that variations in the spatial distribution of electron density in the donor, acceptor, and bridging ligand orbitals can give rise to very large spectroscopic and rate effects. Finally, there is the issue of what is meant by a “delocalized” electron transfer system. Quantum mechanical issues are demonstrably important in the molecular systems discussed here, and simple analogies to the properties of macroscopic wires are almost always misleading. To some degree the “localized vs. delocalized” discussion is reminiscent of the quantum problems of wave–particle duality and stationary-state vs. time-dependent solutions of the wave equation. The “correct” classification depends on the type of measurement being discussed, the type of question being asked. It is clear that there is much more to learn from the study of bridged-electron transfer systems.

### 7.11.5 ELECTRON TRANSFER IN LARGER-SCALE SYSTEMS

The interest in electron transfer in extended systems is expanding rapidly. These systems include the transfer of electrons from enzymes to substrates, across biological membranes, to (or from)

electrodes from (or to) substrates, between adsorbed molecular dyes and semiconductor particles, within synthetic films and nano-scale arrays, within “molecular wires,” etc. Most of these topics are treated in detail elsewhere in this volume. Only a few general comments will be offered here. The basic physics does not change with the scale of the system, but the nature of the properties observed, the experimental probes available, and the level of theoretical treatment that is useful may be very different.

### 7.11.5.1 Systems Related to Biological Electron Transport

The transport of electrons is an essential component of energy transduction in biological systems. The elementary electron transport steps often involve donors and acceptors separated by appreciable distances across cell membranes or through protein structure, multi-electron processes, etc. Electron transfer mechanisms in biological systems have provided challenges to the understanding of fundamental issues and inspirations for the design of efficient, synthetic catalytic systems. The mechanisms of efficient electron transfer processes in such systems have attracted a very great deal of interest.<sup>4,6-8,12,19-21,120,250,328-334</sup> The problems have been addressed by a combination of studies in synthetic “model systems” that attempt to isolate and mimic selected aspects of the more complicated biological systems and by chemical or genetic modification of key components of the biological systems.

Issues related to the preferred pathways and the distance dependence of electron transfer in biological systems have been addressed by covalently linking electron transfer donors or acceptors (e.g., a ruthenium complex) to specific sites (e.g., a histidine) of a protein or an enzyme.<sup>332,334-338</sup> The distance dependence of the electron transfer rate constants is generally fitted to Equation (45), with most values of  $\beta$  for proteins falling in the range of 1.0–1.3 Å<sup>-1</sup>.<sup>332</sup> In some general sense, the protein in these experiments can be regarded as a huge, largely aliphatic bridging ligand, and in most cases it is possible to identify several feasible  $\sigma$ -bonded pathways for the coupling of the donor to the acceptor. A variation on the superexchange coupling model (see Equation (44)), that assigns specific values for the electronic coupling between the different constituent moieties of the protein chain, has been used to identify the most likely of different possible pathways.<sup>332,339-343</sup> Similarly, these studies rarely attempt to make corrections for the distance dependence of the reorganizational energy (see Figure 11). The size and flexibility of the protein makes it difficult to accurately define either a precise distance between the donor and acceptor or a unique pathway.<sup>335,341,344</sup> In principle, both the distance dependence of electron transfer and the effectiveness of different kinds of bridging pathways can be addressed more systematically with well-designed, synthetic model systems in which an aliphatic linker is constrained to be relatively rigid.<sup>334,336,345-349</sup>

Isied and co-workers have examined photo-induced (or pulse-radiolytically initiated) electron transfer processes in which a polypyridine–ruthenium(II) complex is linked by means of a 4-carboxylato,4'-methyl,2,2'-bipyridine ligand and a polyproline chain to a [Co(NH<sub>3</sub>)<sub>5</sub>]<sup>3+</sup> or [(–NH-py)Ru<sup>III</sup>(NH<sub>3</sub>)<sub>5</sub>] acceptor.<sup>334,336,350</sup> Chains composed of from zero to six *cis*-prolines have been examined. The apparent distance dependence of the electron transfer rate constant, corrected for variations in the solvent reorganizational energy, seems to exhibit two types of distance dependence,  $\beta \approx 0.7-1$  for short chains and  $\beta \approx 0.3$  for long chains. A very detailed theoretical analysis of electron transfer in the complexes with four proline linkers has indicated that the electronic coupling is sensitive to conformational variations within the proline chain,<sup>32,351</sup> and the longer chains very likely have a higher probability of accessing conformations that provide strong inter-linker coupling than do the shorter chains. The temperature dependence of the electron transfer rates in these systems has been determined experimentally<sup>334,350</sup> and examined theoretically.<sup>32,351</sup> The activation free energy (or rate constant) variations are more amenable to simple theoretical analysis than are the activation enthalpy and entropy terms, possibly due to some cancellation of anharmonic contributions<sup>32,351</sup> (see also Section 7.11.2.7). In the evaluation of the activation entropy contributions, it is necessary to take account of the differences in the electronic configurations, in the density of the vibrational states, and in the zero-point energies of the reactants and products.<sup>32,351,352</sup>

When high-energy oxidants (or reductants) are employed, and when the bridge contains moieties that are relatively easily reduced (or oxidized), direct hole (or electron) transfer to bridge units may occur and the hole (or electron) may then hop from moiety to moiety (randomly) along

the bridge. In this limit the electron transfer rate will decrease only slowly with distance. This limit has been treated in terms of standard non-adiabatic electron transfer theory.<sup>250</sup>

Many metallo-enzymes function as multi-electron donors (or acceptors), and their function is to effect the oxidation or reduction of organic substrates or simple molecules such as H<sub>2</sub>O, N<sub>2</sub>, or O<sub>2</sub>. The enzymes involved often contain two or more metals at the active site.<sup>329–333,353,354</sup> The electronic coupling between the metals is often accompanied by electron spin–spin coupling and other unique spectroscopic features.<sup>86,355–358</sup> This electronic coupling may facilitate the multi-electron transfer reactions with the substrates. In simpler molecular systems, two-electron transfer processes most often require substrate “binding,” as in an inner-sphere group (or “atom”) transfer process.<sup>359,360</sup> Similar substrate binding is probably important in all facile multi-equivalent processes.

### 7.11.5.2 Complexes Containing Multiple Donors and/or Acceptors

The material in this chapter is primarily focused on bimetallic complexes. The few trimetallic complexes that are mentioned can be regarded as the first steps in the construction of nano-scale materials from simple molecular species. As the complex aggregates become larger, one might expect to find some features of the larger-scale complexes that are not observed in their bimetallic analogs. There are some hints of this, for example, in the vibronic phase effects observed in the dicyano-complex-bridged Ru(NH<sub>3</sub>)<sub>5</sub><sup>2+</sup>/Ru(NH<sub>3</sub>)<sub>5</sub><sup>3+</sup> complexes. The possibility of another such feature is suggested by the comparison of the spectra of [ {(NH<sub>3</sub>)<sub>5</sub>Ru<sup>II</sup> } B (Ru<sup>II</sup>L) B { Ru<sup>III</sup>(NH<sub>3</sub>)<sub>5</sub> } ]<sup>n+</sup> (B = pyrazine or cyanide; L = NH<sub>3</sub> or py). While the cyanide-bridged complex exhibits two nearly equal intensity, low-energy visible-infrared absorption bands ( $\lambda_{\max}$  at 700 and 1,000 nm) that are symmetric and antisymmetric components of the Ru<sub>t</sub><sup>II</sup>/Ru<sub>t</sub><sup>III</sup> and the Ru<sub>c</sub><sup>II</sup>/Ru<sub>t</sub><sup>III</sup> transitions,<sup>96</sup> the pyrazine-bridged complex exhibits a single band with  $\lambda_{\max} = 685$  nm.<sup>245,246</sup> There are several differences in the properties of these complexes: (i) the cyanide bridge has a smaller electron affinity than does the pz bridge (the MLCT transitions occur at about 350 and 550 nm, respectively); (ii) there is a larger difference in the potentials required for oxidation of the terminal and central metals in the cyanide-bridged than in the pyrazine-bridged complex; and (iii) the complexes differ in symmetry (See Figures 19 and 20). The striking effects that result from the mixing of the MLCT and MMCT excited states of pz-bridged, bimetallic complexes, when these excited states have similar energies, were discussed in the preceding

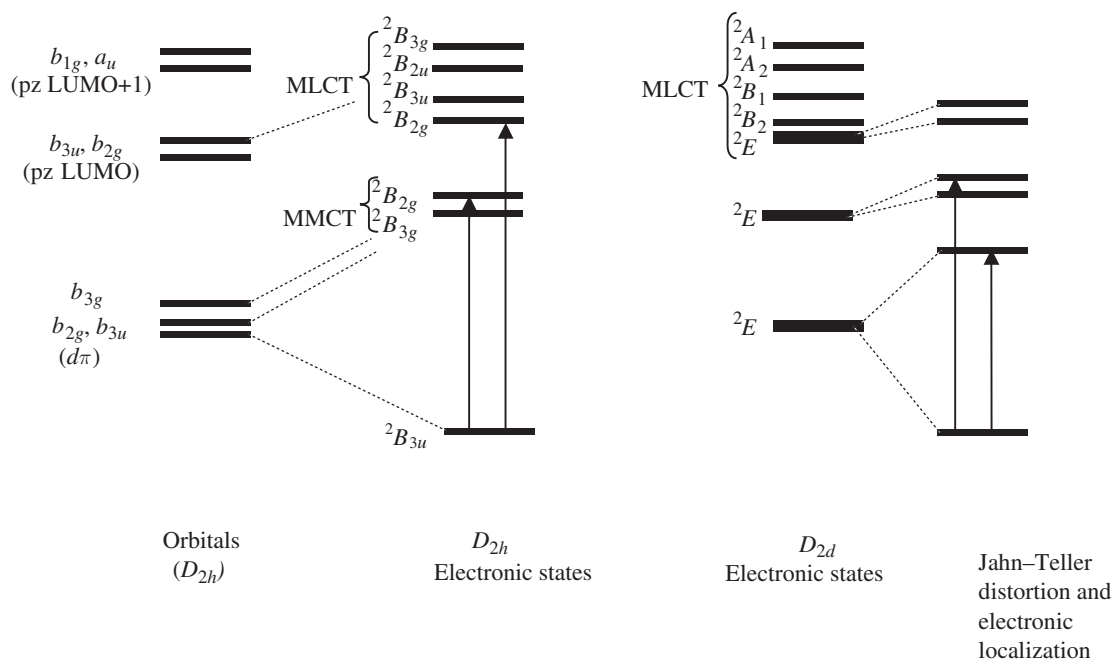


**Figure 19** Electronic structure diagrams for the  $D_{2h}$  and  $D_{2d}$  isomers of a pyrazine-bridged trimetallic complex.

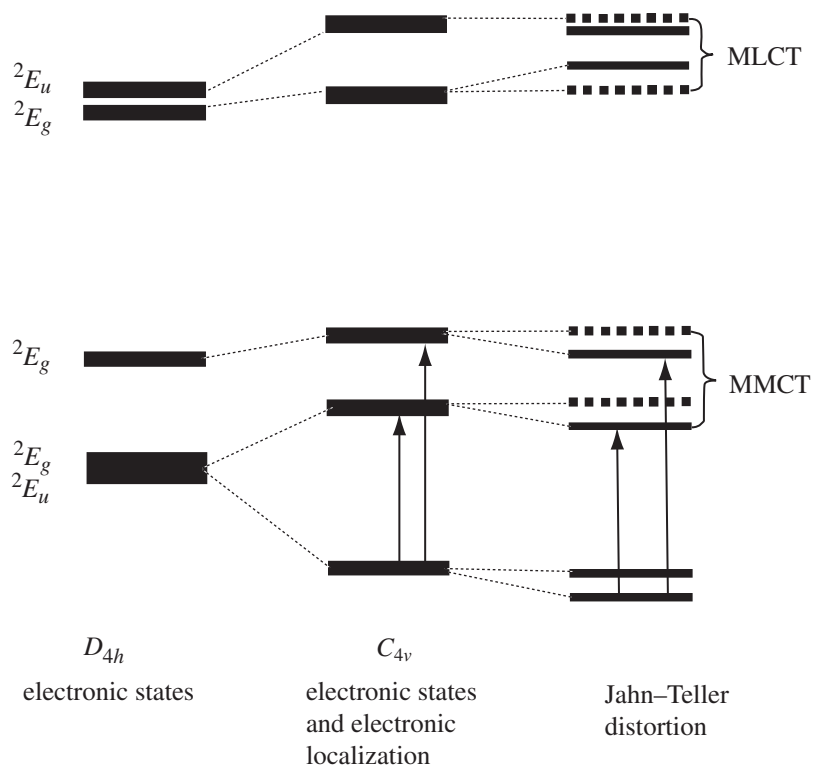


**Figure 20** Electronic structure diagrams for a cyanide-bridged trimetallic complex.

section. One problem in attempting a description of these trimetallic complexes is that, counting quartet (MLCT) as well as doublet (MLCT and MMCT) configurations, there are fourteen electronic configurations that differ from the ground state in the position of one electron, even assuming a single  $d\pi$  orbital at each ruthenium and a single  $\pi^*$  orbital on each pyrazine. This contrasts to three different excited electronic configurations for the Creutz–Taube ion based on the same assumptions.

In the pz-bridged trimetallic complex the MLCT excited states and two MMCT excited states have reasonably similar energies and there must be a great deal of mixing of the excited electronic configurations. The observed electronic transitions involving states with such mixed electronic configurations cannot be meaningfully assigned as MLCT or MMCT, as noted above and elsewhere.<sup>246</sup> However, the combination of the large number of electronic states, and the extensive configurational mixing, should lead to highly delocalized complexes with degenerate or nearly degenerate ground states. For example, a very approximate perturbation theory argument (based on the assumptions that  $(E_{DB} - E_{DA}) < H_{DB}$  and the electron transfer states have the same energy at their PE minima) indicates that for a linear complex with a large number of donor metals, the lowest energy MMCT excited state should approach approximately  $(E_{DB} - 2H_{DB})$  above the ground state. For a pyrazine-linked chain of ruthenium–ammine centers, such a state would be essentially degenerate with the ground state. This would not be the case for a cyanide-linked chain since the MLCT state energy is much higher. Molecular systems with highly degenerate ground states should exhibit high electron mobilities (i.e., very large hopping rates). This raises the possibility that further increases in the number of metals in the chain could increase the density of electronic states in the neighborhood of the ground state sufficiently that the linear chain begins to have metallic conduction properties.

It is also of interest that there are two possible isomers of the pz-bridged, trimetallic complex. These have limiting  $D_{2h}$  (pz rings coplanar) and  $D_{2d}$  (pz rings orthogonal) symmetries (see Figure 19). The configurational mixing and spectroscopy of these two isomers should be different. It is possible that the expected MMCT transitions have similar energies and to be unresolved in the experimental spectrum<sup>246</sup> (in  $D_{2d}$  this would imply no configurational mixing between the MMCT excited states; in  $D_{4h}$  a selection rule issue could be involved, see Figure 19) or their energy



differences could be large enough to fall outside the observation window (i.e., very large configurational mixing).

The issue of the “wire-like” properties of arrays of metal complexes has been of some interest, has been reviewed recently,<sup>361,362</sup> and is discussed in more detail elsewhere. More generally, Volume 5 of the series, “Electron Transfer in Chemistry,”<sup>2</sup> contains several chapters on the use of metals in molecular-level devices<sup>362–370</sup> and the topic has been reviewed elsewhere.<sup>371,372</sup>

### 7.11.5.3 Heterogeneous Electron Transfer Systems

There have also been many studies of electron transfer from (or to) molecular substrates within (or across) micelles and vesicles,<sup>373</sup> porous solid media,<sup>374,375</sup> layered materials<sup>376–378</sup> and to (or from) semiconductors and electrodes.<sup>181,379–384</sup> The studies of the electron transfer rates of small molecules at electrodes is, in principle, complementary to the homogeneous reactions discussed in this chapter.<sup>385,386</sup>

Schultz and co-workers have used the sweep rate dependence of cyclic voltammograms to determine the rate constants for electron transfer between several coordination complexes and an electrode.<sup>181,182,387–389</sup> When  $\kappa_{el} \cong 1$ , one expects  $\Delta S_{DA}^\ddagger \leq 11 \text{ J mol}^{-1} \text{ K}^{-1}$  for the electrochemical reaction<sup>181,182</sup> (see also Section 7.11.2.7). However, substantial positive values were found for reactions that involve a net change of spin multiplicity. The largest was  $\Delta S_{DA}^\ddagger = 137 \text{ J mol}^{-1} \text{ K}^{-1}$  for the  $[\text{Co}(\text{9}[\text{aneN}_3)_2]^{3+,2+}$  couple (see also Section 7.11.3.3).

The study of heterogeneous systems in which a donor or acceptor is linked to the surface of a conductor or semiconductor has been of considerable interest, especially when electron injection into the semiconductor or electrode can be induced by light absorption of the linked dye molecule.<sup>16,378–381,383,390–401</sup> Such systems have potential for the transduction of solar radiation into electrical energy. Grätzel and co-workers have used a ruthenium(II) complex linked to  $\text{TiO}_2$  by means of a *bis*-carboxylato-bipyridine ligand to construct a reasonably efficient photocell.<sup>16,381–383,390,402</sup> Many details of the functioning of this photocell are not well understood, but it is based on efficient ( $\sim 100\%$ ) injection of electrons from the MLCT excited state into the semiconductor. Femtosecond pump and probe experiments have demonstrated that at least some of the photoelectrons are injected within 50 ps of the MLCT excitation.<sup>394,403</sup> This is one of the fastest electron transfer rates yet measured.

## ACKNOWLEDGMENTS

Support from the Office of Basic Energy Sciences of the Department of Energy is gratefully acknowledged. Professor D. B. Rorabacher, Dr. Md. J. Uddin and Dr. K. Szacilowski have provided many useful comments on the manuscript and Dr. M. J. Heeg has provided some assistance with figures. Dr. C. Creutz and Professor C. Kubiak have generously provided pre-publication copies of manuscripts, and Dr. G. J. Ferraudi has provided some useful comments and discussion.

## 7.11.6 REFERENCES

1. Meyer, T. J.; Taube, H. Molecular electron transfer. In *Comprehensive Coordination Chemistry*; Wilkinson, G., Ed.; Pergamon: Oxford, England, 1987; p 331–384.
2. Balzani, V., Ed. *Electron Transfer in Chemistry*; Wiley-VCH: Weinheim, Germany, 2001, Vol. 1–5.
3. Astruc, D. *Electron Transfer and Radical Processes in Transition-Metal Chemistry*; Wiley: New York, 1995.
4. Kuznetsov, A. M. *Charge Transfer in Physics Chemistry and Biology: Physical Mechanisms of Elementary Processes and an Introduction to the Theory*; Gordon and Breach: New York, 1995.
5. Kuznetsov, A. M. *Charge Transfer in Chemical Reaction Kinetics*; Presses Polytechniques et Universitaires Romandes: Lausanne, Switzerland, 1997.
6. Kuznetsov, A. M.; Ulstrup, J. *Electron Transfer in Chemistry and Biology*; Wiley-VCH: New York, 1998.
7. Jortner, J., Bixon, M. Eds.; *Adv. Chem. Phys.* **1999**, *106*, 734 pp.
8. Jortner, J., Bixon, M. Eds.; *Adv. Chem. Phys.* **1999**, *107*, 735 pp.
9. Kavarnos, G. J. *Fundamentals of Photoinduced Electron Transfer*; VCH: New York, 1993.
10. Fox, M. A.; Channon, M., Eds. *Photoinduced Electron Transfer*; Elsevier: Amsterdam, 1988.
11. Johnson, M. K.; King, R. B.; Kurtz, D. M., Jr.; Kutal, C.; Norton, M. L.; Scott, R. A., Eds. *Electron Transfer in Biology and the Solid State*; A.C.S. Advances in Chemistry Vol. 226; American Chemical Society: Washington, 1989.

12. Bolton, J. R.; Mataga, N.; McLendon, G., Eds. *Electron Transfer in Inorganic, Organic and Biological Systems*; A.C.S. Advances in Chemistry Vol. 228; American Chemical Society: Washington, 1991.
13. Isied, S. S., Ed. *Electron Transfer Reactions*; A.C.S. Advances in Chemistry Series Vol. 253; American Chemical Society: Washington, 1997.
14. Jortner, J.; Ratner, M. A., Eds. *Molecular Electronics*; Blackwell Science Ltd: Oxford, 1997.
15. Meyer, T. J.; Newton, M. D., Ed. *Chem. Phys.* **1993**, *176*, 289–649.
16. Gratzel, M. *Heterogeneous Photochemical Electron Transfer*; CRC Press: Boca Raton, FL, 1989.
17. Wishart, J. N.; Nocera, D. G., Eds. *Photochemistry and Radiation Chemistry: Complementary Methods for the Study of Electron Transfer*; A.C.S. Advances in Chemistry Vol. 254; American Chemical Society: Washington, 1998.
18. Kornyshev, A. A.; Tosi, M.; Ulstrup, J., Eds. *Electron and Ion Transfer in Condensed Media*; World Scientific: Singapore, 1997.
19. Nicolini, C., Ed. *Biophysics of Electron Transfer and Molecular Bioelectronics*; Plenum Press: New York, 1998.
20. Canters, G. W.; Vijenboom, E., Eds. *Biological Electron Transfer Chains: Genetics, Composition and Mode of Operation*; Kluwer Academic Publishers: Dordrecht, Germany, 1998.
21. *Chem. Rev.* **1992**, *92*, 369–496.
22. Mulliken, R. S.; Person, W. B. *Molecular Complexes*; Wiley-Interscience: New York, 1967.
23. Newton, M. D.; Sutin, N. *Annu. Rev. Phys. Chem.* **1984**, *35*, 437.
24. Drago, R. S. *Physical Methods for Chemists*; Harcourt Brace Jovanovich: Orlando, 1992.
25. Zuman, P.; Patel, R. C. *Techniques in Organic Reaction Kinetics*; Wiley: New York, 1984.
26. Espenson, J. H. *Chemical Kinetics and Reaction Mechanisms*; McGraw-Hill: New York, 1981.
27. Rodgers, M. A. J., Ed. *Electron Transfer in Chemistry Vol. 1, Part 2. Methods and Techniques*; Wiley-VCH: Weinheim, Germany, 2001.
28. Solomon, E. I.; Lever, A. B. P., Eds. *Inorganic Electronic Structure and Spectroscopy Vols. I and II*; Wiley: New York, 1999.
29. Demas, J. N. *Excited State Lifetime Measurements*; Academic Press: New York, 1983.
30. Bard, A. J.; Faulkner, L. R. *Electrochemical Methods*; Wiley: New York, 1980.
31. Mirabella, F. M. *Modern Techniques in Applied Molecular Spectroscopy*; Wiley: New York, 1998.
32. Newton, M. D. In *Electron Transfer In Chemistry*; Balzani, V., Ed.; Wiley-VCH: Weinheim, Germany, 2001; Vol. 1, p 3.
33. Marcus, R. A. *Discuss. Faraday Soc.* **1960**, *29*, 21.
34. Marcus, R. A. *Annu. Rev. Phys. Chem.* **1964**, *15*, 155.
35. Englman, R.; Jortner, J. *Mol. Phys.* **1970**, *18*, 145.
36. Gould, I. R.; Noukakis, D.; Luis, G.-J.; Young, R. H.; Goodman, J. L.; Farid, S. *Chem. Phys.* **1993**, *176*, 439.
37. Kestner, N.; Logan, J.; Jortner, J. *J. Phys. Chem.* **1974**, *64*, 2148.
38. Sutin, N. *Progr. Inorg. Chem.* **1983**, *30*, 441.
39. Sutin, N. *Adv. Chem. Phys.* **1999**, *106*, 7.
40. Marcus, R. A.; Sutin, N. *Comments Inorg. Chem.* **1986**, *5*, 119.
41. Matyushov, D. *J. Phys. Chem. A* **1998**, *102*, 5027.
42. Lever, A. B. P.; Solomon, E. I. In *Inorganic Electronic Structure and Spectroscopy*; Solomon, E. I.; Lever, A. B. P. Eds.; Wiley: New York, 1999, Vol. I, p 1.
43. Seneviratne, D. S.; Uddin, M. J.; Swayambunathan, V.; Schlegel, H. B.; Endicott, J. F. *Inorg. Chem.* **2002**, *41*, 1502.
44. Hush, N. S. *Electrochim. Acta* **1968**, *13*, 1005.
45. Hush, N. S. *Prog. Inorg. Chem.* **1968**, *8*, 391.
46. Brunold, T. C.; Gudel, H. U. *Inorganic Electronic Structure and Spectroscopy*; Solomon, E. I.; Lever, A. B. P. Eds.; Wiley-Interscience: New York, 1999; Vol. 1, p 259.
47. Graff, D.; Claude, J. P.; Meyer, T. J. In *Electron Transfer in Organometallic and Biochemistry*; Isied, S. S., Ed.; A.C.S. Advances in Chemistry Vol. 253; American Chemical Society: Washington, 1997; p 183.
48. Sutin, N. *Acc. Chem. Res.* **1982**, *15*, 275.
49. Cannon, R. D. *Electron Transfer Reactions*; Butterworth: London, 1980.
50. Chen, P.; Meyer, T. J. *Chem. Rev.* **1998**, *98*, 1439.
51. Myers, A. B. *Acc. Chem. Res.* **1998**, *30*, 519.
52. Loring, R. F. *J. Phys. Chem.* **1990**, *94*, 513.
53. Rhodes, T. A.; Farid, S.; Goodman, J. L.; Gould, I. R.; Young, R. H. *J. Am. Chem. Soc.* **1999**, *121*, 5340.
54. Mark, H.; Workman, J., Jr. *Spectroscopy* **2000**, *15*, 20.
55. Marcus, R. A.; Sutin, N. *Biochem. Biophys. Acta* **1985**, *811*, 265.
56. Brunschwig, B. S.; Sutin, N. In *Electron Transfer in Chemistry*; Balzani, V., Ed.; Wiley-VCH: Weinheim, 2001; Vol. 2, p 583.
57. Birks, J. B. *Photophysics of Aromatic Molecules*; Wiley-Interscience: New York, 1970.
58. Myers, A. B. In *Laser Techniques in Chemistry*; Myers, A. B., Rizzo, T. R. Eds.; John Wiley, 1995; Vol. XXIII, p 325.
59. Myers, A. B.; Mathies, R. A. In *Biological Applications of Raman Spectroscopy*; Spiro, T. G., Ed.; Wiley: New York, 1982; Vol. 2, p1.
60. Casper, J. V.; Meyer, T. J. *Inorg. Chem.* **1983**, *22*, 2446.
61. Kober, E. M.; Casper, J. V.; Lumpkin, R. S.; Meyer, T. J. *J. Phys. Chem.* **1986**, *90*, 3722.
62. Murtaza, Z.; Graff, D.; Zipp, A. P.; Worl, L. A.; Jones, W. E. Jr.; Bates, W. D.; Meyer, T. J. *J. Phys. Chem.* **1994**, *98*, 10504.
63. Bixon, M.; Jortner, J.; Cortes, J.; Heilte, H.; Michel-Beyerle, M. E. *J. Phys. Chem.* **1994**, *98*, 7289.
64. Freed, K. F.; Jortner, J. *J. Chem. Phys.* **1970**, *52*, 6272.
65. Sumi, H. In *Electron Transfer in Chemistry*; Balzani, V., Ed.; Wiley-VCH: Weinheim, Germany, 2001; Vol. 1, p 65.
66. Harris, A. L.; Brown, J. K.; Harris, C. B. *Annu. Rev. Phys. Chem.* **1988**, *39*, 341.
67. Walker, G. I.; Barbara, P. F.; Doorn, S. K.; Hupp, J. T. *J. Phys. Chem.* **1991**, *95*, 5212.
68. Doorn, S. K.; Dyer, R. B.; Stoutland, P. O.; Woodruff, W. W. *J. Am. Chem. Soc.* **1993**, *115*, 6398.
69. Tominaga, D. A. V.; Kliner, A. E.; Johnson, A. E.; Levinger, N. E.; Barbara, P. F. *J. Chem. Phys.* **1993**, *98*, 1228.

70. Reid, P. J.; Silva, C.; Barbara, P. F.; Karki, L.; Hupp, J. T. *J. Phys. Chem.* **1995**, *99*.
71. Endicott, J. F.; Brubaker, G. R.; Ramasami, T.; Kumar, K.; Dwarakanath, K.; Cassel, J.; Johnson, D. *Inorg. Chem.* **1983**, *22*, 3754.
72. Brunshwig, B. S.; Sutin, N. *J. Am. Chem. Soc.* **1989**, *111*, 7454.
73. Bernardo, M. M.; Robandt, P. V.; Schroeder, R. R.; Rorabacher, D. B. *J. Am. Chem. Soc.* **1989**, *111*, 1224.
74. Martin, M. J.; Endicott, J. F.; Ochrymowycz, L. A.; Rorabacher, D. B. *Inorg. Chem.* **1987**, *26*, 3012.
75. Meagher, N. E.; Juntunen, K. L.; Sallhi, C. A.; Ochrymowycz, L. A.; Rorabacher, D. B. *J. Am. Chem. Soc.* **1992**, *114*, 10411.
76. Frauenfelder, H.; Wolynes, P. G. *Science* **1985**, *229*, 337.
77. Zahradnik, R.; Plolak, R. *Elements of Quantum Chemistry*; Plenum: New York, 1980.
78. Newton, M. D. *Chem. Rev.* **1991**, *91*, 767.
79. Newton, M. D. *J. Electroanal. Chem.* **1997**, *438*, 3.
80. Newton, M. D. *Adv. Chem. Phys.* **1999**, *106*, 303.
81. Lever, A. B. P.; Dodsworth, E. In *Electronic Structure and Spectroscopy of Inorganic Compounds*; Lever, A. B. P., Solomon, E. I. Eds.; Wiley: New York, 1999.
82. Lever, A. B. P.; Gorelsky, S. I. *Coord. Chem. Rev.* **2000**, *208*, 153.
83. Piepho, S. B.; Krausz, E. R.; Schatz, P. N. *J. Am. Chem. Soc.* **1978**, *100*, 2996.
84. Schatz, P. N. In *Inorganic Electronic Structure and Spectroscopy*; Solomon, E. I., Lever, A. B. P. Eds.; Wiley: New York, 1999; Vol. II, p 175.
85. Piepho, S. B. *J. Am. Chem. Soc.* **1990**, *112*, 4197.
86. Gamelin, D. R.; Bominaar, E. L.; Mathoniere, C.; Kirk, M. L.; Girerd, J.-J.; Solomon, E. I. *Inorg. Chem.* **1996**, *35*, 4323.
87. Bersuker, I. B.; Borshch, S. A. *Adv. Chem. Phys.* **1992**, *81*, 703.
88. Tsukerblat, B. S. *Group Theory in Chemistry and Spectroscopy*; Academic: London, 1994.
89. Weber, P.; Reimers, J. R. *J. Phys. Chem. A* **1999**, *103*, 9830.
90. Ondrechen, M. J.; Gozashiti, S.; Zhang, L.-T.; Zhou, F. In *Electron Transfer in Biology and the Solid State*; Johnson, M. K., King, R. B., Kurz, D. M., Kotal, C., Norton, M. L., Scott, R. A. Eds.; A.C.S Advances in chemistry Vol. 226; American Chemical Society: Washington, 1990; p 225.
91. Ferretti, A.; Lami, A.; Ondrechen, M. J.; Villani, G. *J. Phys. Chem.* **1995**, *99*, 10484.
92. Endicott, J. F.; Watzky, M. A.; Macatangay, A. V.; Mazzetto, S. E.; Song, X.; Buranda, T. In *Electron and Ion Transfer in Condensed Media*; Kornyshev, A. A., Tosi, M., Ulstrup, J. Eds.; World Scientific: Singapore, 1997; p 139.
93. Watzky, M. A.; Macatangay, A. V.; Van Camp, R. A.; Mazzetto, S. E.; Song, X.; Endicott, J. F.; Buranda, T. *J. Phys. Chem.* **1997**, *101*, 8441.
94. Macatangay, A. V.; Mazzetto, S. E.; Endicott, J. F. *Inorg. Chem.* **1999**, *38*, 5091.
95. Macatangay, A. V.; Song, X.; Endicott, J. F. *J. Phys. Chem.* **1998**, *102*, 7537.
96. Macatangay, A. V.; Endicott, J. F. *Inorg. Chem.* **2000**, *39*, 437.
97. Bersuker, I. B. *Electronic Structures and Properties of Transition Metal Compounds*; Wiley: New York, 1996.
98. Reimers, J. R.; Hush, N. S. *J. Phys. Chem.* **1991**, *95*, 9773.
99. Liptay, W. In *Excited States*; Lim, E. C., Ed.; Academic Press: New York, 1974, Vol. 1, p 129.
100. Brunshwig, B. S.; Creutz, C.; Sutin, N. *Coord. Chem. Rev.* **1998**, *177*, 61.
101. Oh, D. H.; Boxer, S. G. *J. Am. Chem. Soc.* **1990**, *112*, 8161.
102. Oh, D. H.; Sano, M.; Boxer, S. G. *J. Am. Chem. Soc.* **1991**, *113*, 6880.
103. Karki, L.; Lu, H. P.; Hupp, J. T. *J. Phys. Chem.* **1996**, *100*, 15637.
104. Shin, Y. K.; Brunshwig, B. S.; Creutz, C.; Sutin, N. *J. Phys. Chem.* **1996**, *100*, 8157.
105. Cave, R. J.; Newton, M. D. *Chem. Phys. Lett.* **1996**, *249*, 15.
106. Cave, R. J.; Newton, M. D. *J. Chem. Phys.* **1997**, *106*, 9213.
107. Creutz, C.; Newton, M. D.; Sutin, N. *Photochem. Photobiol. A: Chem.* **1994**, *82*, 47.
108. Cannon, R. D. *Adv. Inorg. Chem. Radiochem.* **1979**, *21*, 179.
109. Creutz, C. *Progr. Inorg. Chem.* **1983**, *30*, 1.
110. Matyushov, D. V.; Voth, G. A. *J. Phys. Chem. A* **2000**, *104*, 6470.
111. Matyushov, D. V.; Newton, M. D. *J. Phys. Chem. A* **2001**, *105*, 8516.
112. Curtis, J. C.; Sullivan, B. P.; Meyer, T. J. *Inorg. Chem.* **1983**, *22*, 224.
113. Endicott, J. F. In *Electron Transfer in Chemistry. Vol. 1*; Balzani, V., Ed.; Wiley-VCH: New York, 2001, Vol. 1, p 238.
114. Endicott, J. F.; Uddin, M. J. *Coord. Chem. Rev.* **2001**, *687*, 219–221.
115. Marcus, R. A.; Sutin, N. *Inorg. Chem.* **1975**, *14*, 213.
116. Crutchley, R. *Adv. Inorg. Chem.* **1994**, *41*, 273.
117. Anderson, P. W. In *Magnetism*; Rado, G. T., Suhl, H. Eds.; Academic Press: New York, 1963, Vol. 1, Chapter 2.
118. McConnell, H. M. *J. Chem. Phys.* **1961**, *35*, 508.
119. Dexter, D. L. *Phys. Rev.* **1962**, *126*, 1962.
120. Barbara, P. F.; Meyer, T. J.; Ratner, M. J. *J. Phys. Chem.* **1996**, *100*, 13148.
121. Astumian, R. D.; Schelly, Z. *J. Phys. Chem.* **1986**, *90*, 537.
122. Campion, R. J.; Deck, C. F.; King, P., Jr.; Wahl, A. C. *Inorg. Chem.* **1967**, *6*, 672.
123. Macartney, D. H. *Inorg. Chem.* **1991**, *30*, 3337.
124. Zahl, A.; van Eldik, R.; Swaddle, T. W. *Inorg. Chem.* **2002**, *41*, 757.
125. Billing, R.; Khoshitariya, D. E. *Inorg. Chem.* **1994**, *33*, 4038.
126. Khoshitariya, D. E.; Dolidze, T. D.; Neubrand, A.; van Eldik, R. *J. Mol. Liq.* **2000**, *89*, 127.
127. Krishnamurthy, K. V.; Wahl, A. C. *J. Am. Chem. Soc.* **1958**, *80*, 5921.
128. Anderson, A.; Bonner, N. A. *J. Am. Chem. Soc.* **1954**, *76*, 3826.
129. Silverman, J.; Dodson, R. W. *J. Phys. Chem.* **1952**, *56*, 846.
130. Bernhard, P.; Sargeson, A. M. *Inorg. Chem.* **1987**, *26*, 4122.
131. Habib, H. S.; Hunt, J. P. *J. Am. Chem. Soc.* **1966**, *88*, 1688.
132. Hammershoi, A.; Geselowitz, D.; Taube, H. *Inorg. Chem.* **1984**, *23*, 979.
133. Dwyer, F. P.; Sargeson, A. M. *J. Phys. Chem.* **1961**, *65*, 1892.

134. Creaser, I. I.; Gene, R. J.; Harrowfield, J. M. B.; Herlt, A. J.; Sargeson, A. M.; Snow, M. R.; Springborg, J. J. *Am. Chem. Soc.* **1982**, *104*, 6016.
135. Kueppers, H.-J.; Neves, A.; Pomp, C.; Ventur, D.; Weighardt, K.; Nuber, B.; Weiss, J. *Inorg. Chem.* **1986**, *25*, 2400.
136. Armstrong, G. D.; Sinclair-Day, J. D.; Sykes, A. G. *J. Phys. Chem.* **1986**, *70*, 3805.
137. Meyer, T. J.; Taube, H. *Inorg. Chem.* **1968**.
138. Beattie, J. K.; Smolenaers, P. J. *J. Phys. Chem.* **1986**, *90*, 3684.
139. Chan, M.-S.; Wahl, A. C. *J. Phys. Chem.* **1978**, *82*, 2542.
140. Young, R. C.; Keene, F. R.; Meyer, T. J. *J. Am. Chem. Soc.* **1977**, *99*, 2468.
141. Farina, R.; Wilkins, R. G. *Inorg. Chem.* **1968**, *7*, 514.
142. Macartney, D. H.; Sutin, N. *Inorg. Chem.* **1983**, *22*, 3530.
143. Endicott, J. F.; Durham, B.; Glick, M. D.; Anderson, T. J.; Kuszaj, J. M.; Schmonsees, W. G.; Balakrishnan, K. P. *J. Am. Chem. Soc.* **1981**, *103*, 1431.
144. Endicott, J. F.; Durham, B.; Kumar, K. *Inorg. Chem.* **1982**, *21*, 2437.
145. Kumar, K.; Rotzinger, F. P.; Endicott, J. F. *J. Am. Chem. Soc.* **1983**, *105*, 7064.
146. McAuley, A.; Norman, P. R.; Olubuyide, O. *Inorg. Chem.* **1984**, *23*, 1938.
147. Rorabacher, D. B.; Bernardo, M. M.; Vande Linde, A. M. Q.; Leggett, G. H.; Westerby, B. C.; Martin, M. J.; Ochrymowicz, L. A. *Pure Appl. Chem.* **1988**, *60*, 356.
148. McAuley, A.; Macartney, D. H. *J. Chem. Soc. Chem. Commun.* **1982**, 274.
149. Sisley, M. J.; Jordan, R. B. *Inorg. Chem.* **1992**, *31*, 2880.
150. Pett, V. B.; Diaddario, L. L., Jr.; Dockal, E. R.; Corfield, P. W.; Ceccarelli, C.; Glick, M. D.; Ochrymowicz, L. A.; Rorabacher, D. B. *Inorg. Chem.* **1983**, *22*, 3661.
151. Leggett, G. H.; Dunn, B. C.; Vande Linde, A. M. Q.; Ochrymowicz, L. A.; Rorabacher, D. B. *Inorg. Chem.* **1993**, *32*, 5911.
152. Krylova, K.; Kulatilleke, C. P.; Heeg, M. J.; Salhi, C. A.; Ochrymowicz, L. A.; Rorabacher, D. B. *Inorg. Chem.* **1999**, *38*, 4322.
153. Bernhard, P.; Helm, L.; Ludi, A.; Merbach, A. E. *J. Am. Chem. Soc.* **1985**, *107*, 312.
154. Corfield, P. W. R.; Ceccarelli, C.; Glick, M. D.; Moy, I. W.-Y.; Ochrymowicz, L. A.; Rorabacher, D. B. *J. Am. Chem. Soc.* **1985**, *107*, 2399.
155. Boettcher, W.; Brown, G. M.; Sutin, N. *Inorg. Chem.* **1979**, *18*, 1447.
156. Bernardo, M. M.; Schroeder, R. R.; Ochrymowicz, L. A.; Rorabacher, D. B. *Inorg. Chem.* **1991**, *30*, 1241.
157. Mohanty, J. G.; Chakravorty, J. G. *Inorg. Chem.* **1976**, *15*, 2912.
158. Glick, M. D.; Gavel, D. P.; Diaddario, L. L. Jr.; Rorabacher, D. B. *Inorg. Chem.* **1976**, 1190.
159. Mikanu, W.; Kuroda, R.; Konno, M.; Saito, Y. *Acta Crystallogr. Sect. B: Struct. Crystallogr. Cryst. Chem.* **1977**, *B33*, 1485.
160. Waysbort, D.; Evenor, M.; Navon, G. *Inorg. Chem.* **1975**, *14*, 514.
161. Ramasami, T.; Endicott, J. F. *Inorg. Chem.* **1984**, *23*, 3324.
162. Poupoulpoulou, V. G.; Taube, H. *Inorg. Chem.* **1997**, *36*, 2240.
163. Elsbernd, H.; Beattie, J. K. *Inorg. Chem.* **1968**, *7*, 2468.
164. Billing, R.; Vogler, A. *J. Photochem. Photobiol. A* **1997**, *103*, 239.
165. Yoneda, K. *Bull. Chem. Soc. Jpn.* **1955**, *28*, 125.
166. Curtis, J. C. *cited in ref. 168*.
167. Curtis, J. C.; Meyer, T. J. *Inorg. Chem.* **1982**, *21*, 239.
168. Gorelsky, S. I.; Kotov, V. Y.; Lever, A. B. P. *Inorg. Chem.* **1998**, *37*, 4584.
169. Vogler, A.; Kisslinger, A. *J. Am. Chem. Soc.* **1982**, *104*, 2311.
170. Linhard, M. Z. *Electrochem.* **1944**, *50*, 224.
171. Billing, R.; Benedix, R.; Hennig, H. Z. *Anorg. Allg. Chem.* **1991**, *600*, 21.
172. Haim, A. *Comments Inorg. Chem.* **1984**, *4*, 113.
173. Larsson, R. *Acta Chem. Scand.* **1967**, *21*, 257.
174. Pina, P.; Ciano, Q. C.; Mulazzani, V. M.; Balzani, V.; Moggi, L. *Sci. Papers I. P. C. R.*, **1984**, *78*, 166; *cited in ref. 168*.
175. Stich, G. *cited in ref. 168*.
176. Vogler, A.; Osman, A. H.; Kunkley, H. *Coord. Chem. Rev.* **1985**, *64*, 159.
177. Billing, R.; Stich, G.; Hennig, H. Z. *Chem.* **1990**, *30*, 377.
178. Toma, H. *J. Chem. Soc. Dalton Trans.* **1980**.
179. Newton, M. D. *J. Phys. Chem.* **1991**, *95*, 30.
180. Larsson, S.; Stahl, K.; Zerner, M. C. *Inorg. Chem.* **1986**, *25*, 3033.
181. Turner, J. W.; Schultz, F. A. *Coord. Chem. Rev.* **2001**, *219*, 81.
182. Turner, J. W.; Schultz, F. A. *J. Phys. Chem. B* **2001**, *106*, 2009.
183. Ronco, S.; Ferraudi, G. *Inorg. Chem.* **1990**, *29*, 3961.
184. Ferraudi, G. *Inorg. Chem.* **2000**, *39*, 2866.
185. Ferraudi, G. *Elements of Inorganic Photochemistry* **1988**, Wiley: New York.
186. Endicott, J. F.; Ramasami, T. *J. Am. Chem. Soc.* **1982**, *104*, 5252.
187. Endicott, J. F.; Ramasami, T.; Gaswick, D. C.; Tamilarasan, R.; Heeg, M. J.; Brubaker, G. R.; Pyke, S. C. *J. Am. Chem. Soc.* **1983**, *105*, 5301.
188. Endicott, J. F.; Ramasami, T. *J. Phys. Chem.* **1986**, *90*, 3740.
189. Endicott, J. F. *Acc. Chem. Res.* **1988**, *21*, 59.
190. Ramasami, T.; Endicott, J. F. *J. Am. Chem. Soc.* **1985**, *107*, 389.
191. Endicott, J. F.; Durham, B.; Kumar, K. *Inorg. Chem.* **1982**, *21*, 2437.
192. Winkler, J. R.; Rice, S. F.; Gray, H. B. *Comments Inorg. Chem.* **1981**, *1*, 47.
193. Durham, B.; Endicott, J. F.; Wong, C.-L.; Rillema, D. P. *J. Am. Chem. Soc.* **1979**, *101*, 847.
194. Rotzinger, F. P. K., K.; Endicott, J. F. *Inorg. Chem.* **1982**, *21*, 4111.
195. Schwarz, C. L.; Endicott, J. F. *Inorg. Chem.* **1995**, *34*, 4572.
196. Brown, G. M.; Sutin, N. *J. Am. Chem. Soc.* **1979**, *101*, 883.
197. Brunschwig, B. S.; Sutin, N. *Coord. Chem. Rev.* **1999**, *187*, 233.
198. Matyushov, D. V.; Ladanyi, B. M. *J. Phys. Chem. B* **1998**, *102*, 5027.

199. Richardson, D. E.; Taube, H. *Coord. Chem. Rev.* **1984**, *60*, 107.
200. Richardson, D. E. In *Inorganic Electronic Structure and Spectroscopy*; Solomon, E. I., Lever, A. B. P. Eds.; Wiley: New York, 1999; Vol. II, p 131.
201. Hendry, P.; Ludi, A. *Adv. Inorg. Chem.* **1990**, *35*, 117.
202. Nakamoto, K. *Infrared and Raman Spectra of Inorganic and Coordination Compounds. Part B*; Wiley: New York, 1997.
203. Brown, G. M.; Kreutzian, H. J.; Abe, M.; Taube, H. *Inorg. Chem.* **1979**, *18*, 3374.
204. Brunschwig, B. S.; Ehrenson, S.; Sutin, N. *J. Phys. Chem.* **1986**, *90*, 3657.
205. Levy, R. M.; Gallicchio, E. *Ann. Rev. Phys. Chem.* **1998**, *49*, 531.
206. Rotzinger, F. P. *private communication* **2001**.
207. Badger, R. M. *J. Chem. Phys.* **1935**, *3*, 710.
208. Badger, R. M. *J. Chem. Phys.* **1934**, *2*, 128.
209. Eyler, J. R.; Richardson, D. E. *J. Am. Chem. Soc.* **1985**, *107*, 6130.
210. Richardson, D. E. *J. Phys. Chem.* **1986**, *90*, 3697.
211. Phelps, D. K.; Gord, J. R.; Freiser, B. S.; Weaver, M. J. *J. Phys. Chem.* **1991**, *95*, 4338.
212. Newton, M. D.; Ohta, K.; Zhong, E. *J. Phys. Chem.* **1991**, *95*, 2317.
213. Hoffman, B. M.; Ratner, M. A. *J. Am. Chem. Soc.* **1987**, *109*, 6237.
214. Yu, Q.; Sallhi, C. A.; Ambundo, E. A.; Heeg, M. J.; Ochrymowycz, L. A.; Rorabacher, D. B. *J. Am. Chem. Soc.* **2001**, *123*, 5720.
215. Villeneuve, N. M.; Schroeder, R. R.; Ochrymowycz, L. A.; Rorabacher, D. B. *Inorg. Chem.* **1997**, *36*, 4475.
216. Sando, G. M.; Spears, K. G.; Hupp, J. T.; Ruhoff, P. T. *J. Phys. Chem.* **2001**, *105*, 5317.
217. Spears, K. G.; Shang, H. *J. Phys. Chem. A* **2000**, *104*, 2668.
218. Spears, K. G.; Wen, X.; Zhang, R. *J. Phys. Chem.* **1996**, *100*, 10206.
219. Marin, T. W.; Homoelle, B. J.; Spears, K. G. *J. Phys. Chem.* **2002**, *106*, 1152.
220. Piotrowiak, P. *Chem. Soc. Rev.* **1999**, *28*, 143.
221. Demadis, K. D.; Hartshorn, C. M.; Meyer, T. J. *Chem. Rev.* **2001**, *101*, 2655.
222. Kaim, W.; Klein, A.; Glockle, M. *Acc. Chem. Res.* **2000**, *33*, 755.
223. Brunschwig, B. S.; Creutz, C.; Sutin, N. *Chem. Soc. Rev.* **2002**, *31*, 168.
224. Scandola, F.; Chiorboli, C.; Indelli, M. T.; Rampi, M. A. In *Electron Transfer in Chemistry*; Balzani, V., Ed.; Wiley-VCH: Weinheim, 2001, Vol. 3, p 337.
225. Fabbri, L.; Licchelli, M.; Taglietti, A. In *Electron Transfer in Chemistry*; Balzani, V., Ed.; Wiley-VCH: Weinheim, 2001, Vol. 3, p 462.
226. Gust, D.; Moore, T. A.; Moore, A. L. *Acc. Chem. Res.* **2001**, *34*, 40.
227. Wu, R. W.; Arap Koske, S. K.; White, R. P.; Anson, C. E.; Jayasooriya, U. A.; Cannon, R. D. *J. Chem. Soc. Chem. Commun.* **1994**, 1657.
228. Wu, R. W.; Poyraz, M.; Sowrey, F. E.; Anson, C. E.; Wocadlo, S.; Powell, A. K.; Jayasooriya, U. A.; Cannon, R. D. *Inorg. Chem.* **1998**, *37*, 1913.
229. Stadler, C.; Daub, J.; Kohler, J.; Saalfrank, R. W.; Coropceanu, V.; Schunemann, V.; Ober, C.; Trautwein, A. X.; Parker, S. F.; Poyraz, M.; Inomata, T.; Cannon, R. D. *J. Chem. Soc. Dalton Trans.* **2001**, 3373.
230. Ito, T.; Hamaguchi, T.; Nagino, H.; Yamaguchi, T.; Kido, H.; Zavarine, I. S.; Richmond, T.; Washington, J.; Kubiak, C. P. *J. Am. Chem. Soc.* **1999**, *121*, 4625.
231. Ito, T.; Yamaguchi, T.; Kubiak, C. P. *Macromolecular Symposia* **2000**, *156*, 269.
232. Zavarine, I. S.; Kubiak, C. P.; Yamaguchi, T.; Ota, K.; Matsui, T.; Ito, T. *Inorg. Chem.* **2000**, *39*, 2696.
233. Yamaguchi, T.; Imai, N.; Ito, T.; Kubiak, C. P. *Bull. Chem. Soc. Jpn.* **2000**, *73*, 1205.
234. Sutton, J. E.; Sutton, P. M.; Taube, H. *Inorg. Chem.* **1979**, *18*, 1017.
235. Sutton, J. E.; Taube, H. *Inorg. Chem.* **1981**, *20*, 4021.
236. Richardson, D. E.; Taube, H. *J. Am. Chem. Soc.* **1983**, *105*, 40.
237. Creutz, C.; Taube, H. *J. Am. Chem. Soc.* **1969**, *91*, 3988.
238. Creutz, C.; Taube, H. *J. Am. Chem. Soc.* **1973**, *95*, 1086.
239. Bignozzi, C. A.; Paradisi, C.; Roffia, S.; Scandola, F. *Inorg. Chem.* **1988**, *27*, 408.
240. Lay, P. A.; Magnuson, R. H.; Taube, H. *Inorg. Chem.* **1988**, *27*, 2364.
241. Powers, M. J.; Meyer, T. J. *J. Am. Chem. Soc.* **1980**, *102*, 1289.
242. Ketterle, M.; Fiedler, J.; Kaim, W. *Chem. Commun.* **1998**, 1701.
243. Felix, F.; Ludi, A. *Inorg. Chem.* **1978**, *17*, 1782.
244. Callahan, R. W.; Keene, F. R.; Meyer, T. J.; Salmon, D. J. *J. Am. Chem. Soc.* **1977**, *99*, 1064.
245. Von Kameke, A.; Tom, G. M.; Taube, H. *Inorg. Chem.* **1978**, *17*, 1790.
246. Sommovigo, M.; Ferretti, A.; Venturi, M.; Ceroni, P.; Giardi, C.; Denti, G. *Inorg. Chem.* **2002**, *41*, 1263.
247. Cotton, F. A. *Chemical Applications of Group Theory*; 3rd ed.; Wiley: New York, 1990.
248. Sutin, N.; Brunschwig, B. S. In *Electron Transfer in Biology and the Solid State*; American Chemical Society Advances in Chemistry Series: Washington, 1990, Vol. 226, p 64.
249. Liu, Y.-P.; Newton, M. D. *J. Phys. Chem.* **1995**, *99*, 12382.
250. Bixon, M.; Giese, B.; Wessely, S.; Langenbacher, T.; Michel-Beyerle, M. E.; Jortner, J. *Proc. Natl. Acad. Sci. USA.* **1999**, *96*, 11713.
251. Robin, M. B.; Day, P. *Adv. Inorg. Chem. Radiochem.* **1967**, *10*, 247.
252. DeRosa, M. C.; White, C. A.; Evans, C. E. B.; Crutchley, R. J. *J. Am. Chem. Soc.* **2001**, *123*, 1396.
253. Nelson, S. F. *Chem. Eur. J.* **2000**, *6*, 581.
254. Cooley, L. F.; Headford, C. E. L.; Elliott, C. M.; Kelley, D. F. *J. Am. Chem. Soc.* **1988**, *110*, 6673.
255. Ryu, C. K.; Wang, R.; Schmehl, R. H.; Ferrere, S.; Ludwikow, M.; Merkert, J. W.; Headford, L. E.; Elliott, C. M. *J. Am. Chem. Soc.* **1992**, *114*, 430.
256. Song, X.; Lei, Y.; Van Wallendael, S.; Perkovic, M. W.; Jackman, D. C.; Endicott, J. F.; Rillema, D. P. *J. Phys. Chem.* **1993**, *97*, 3225.
257. Elliott, C. M.; Derr, D. L.; Matyushov, D. V.; Newton, M. D. *J. Am. Chem. Soc.* **1998**, *120*, 11714.
258. Schmehl, R. H.; Auerbach, R. A.; Wacholtz, W. F.; Elliott, C. M.; Freitag, R. A.; Merkert, J. W. *Inorg. Chem.* **1986**, *25*, 2440.

259. Tapolsky, G.; Duesing, R.; Meyer, T. J. *Inorg. Chem.* **1990**, *29*, 2285.
260. Berkhoff, R.; Krist, K.; Gafney, H. D. *Inorg. Chem.* **1980**, *19*, 1.
261. Seneviratne, D., Ph. D. Dissertation, Wayne State University, Detroit, MI, 1999.
262. Lavallo, D. K.; Fleischer, E. B. *J. Am. Chem. Soc.* **1972**, *94*, 2599.
263. Lavallo, D. K.; Fleischer, E. B. *J. Am. Chem. Soc.* **1972**, *94*, 2583.
264. Rieder, K.; Taube, H. *J. Am. Chem. Soc.* **1977**, *99*, 7891.
265. Richardson, D. E., Ph. D. Dissertation, Stanford Univ. Stanford, CA, 1981, cited in ref. 109.
266. Hush, N. S. In *Mechanistic Aspects of Inorganic Reactions*; Rorabacher, D. B., Endicott, J. F. Eds.; ACS Symposium Series 198; American Chemical Society: Washington, 1982; p 301.
267. Lay, P. A.; Magnuson, R. H.; Taube, H. *J. Am. Chem. Soc.* **1983**, *105*, 2507.
268. Weber, P.; Reimers, J. R. *J. Phys. Chem. A* **1999**, *103*, 9821.
269. Creutz, C.; Schwarz, H. A.; Wishart, J. F.; Fujita, E.; Sutin, N. *J. Am. Chem. Soc.* **1991**, *113*, 3361.
270. Ferretti, A.; Lami, A.; Villani, G. *Inorg. Chem.* **1998**, *37*, 2779.
271. Richardson, D. E.; Sen, J. P.; Taube, H. *Inorg. Chem.* **1982**, *21*, 3136.
272. Creutz, C.; Chou, M. H. *Inorg. Chem.* **1987**, *26*, 2995.
273. Solomon, E. I. *Comments Inorg. Chem.* **1984**, *3*, 227.
274. Lambert, C.; Noll, G. *J. Am. Chem. Soc.* **1999**, *121*, 8434.
275. Londergan, C. H.; Salsman, J. C.; Ronco, S.; Dolkas, L. M.; Kubiak, C. P. *J. Am. Chem. Soc.* **2002**, *124*, 6236.
276. Kambhampati, P.; Son, D. H.; Kee, T. W.; Barbara, P. F. *J. Phys. Chem. A* **2000**, *104*, 10637.
277. Scheiring, T.; Kaim, W.; Olabe, J. A.; Parise, A. R.; Fiedler, J. *Inorg. Chim. Acta* **2000**, *300*, 125.
278. Hornung, F. M.; Baumann, F.; Kaim, W.; Olabe, J. A.; Slep, L. D.; Fiedler, J. *Inorg. Chem.* **1998**, *37*, 5402.
279. Ketterle, M.; Kaim, W.; Olabe, J. A.; Parise, A. R.; Fiedler, J. *Inorg. Chim. Acta* **1999**, *291*, 66.
280. Ruminsky, R. R.; Serveiss, D.; Jacquez, M. *Inorg. Chem.* **1995**, *34*, 3358.
281. Poppe, J.; Moscherosch, M.; Kaim, W. *Inorg. Chem.* **1993**, *32*, 2640.
282. Glockle, M.; Kaim, W.; Katz, N. E.; Posse, M. G.; Cutin, E. H.; Fiedler, J. *Inorg. Chem.* **1999**, *38*, 3270.
283. Glockle, M.; Kaim, W.; Klein, A.; Roduner, E.; Hubner, G.; Zalis, S.; van Slageren, J.; Renz, F.; Gutlich, P. *Inorg. Chem.* **2001**, *40*, 2256.
284. Hartshorn, C. M.; Daire, N.; Tondreau, V.; Loeb, B.; Meyer, T. J. *J. Am. Chem. Soc.* **2002**, *124*, 000.
285. Walker, I. C.; Palmer, M. H. *Chem. Phys.* **1991**, *153*, 169.
286. Lever, A. B. P. *Inorganic Electronic Spectroscopy*; Elsevier: Amsterdam, 1984.
287. Naklicki, M. L.; Crutchley, R. J. *Inorg. Chim. Acta* **1994**, *225*, 123.
288. Evans, C. E. B.; Naklicki, M. L.; Rezvani, A. R.; White, C. A.; Kondratiev, V. V.; Crutchley, R. J. *J. Am. Chem. Soc.* **1998**, *120*, 13096.
289. Evans, C. E. B.; Yap, G. P. A.; Crutchley, R. J. *Inorg. Chem.* **1998**, *37*, 6161.
290. Mosher, P. J.; Yap, G. P. A.; Crutchley, R. J. *Inorg. Chem.* **2001**, *40*, 550.
291. Mosher, P. J.; Yap, G. P. A.; Crutchley, R. J. *Inorg. Chem.* **2001**, *40*, 1189.
292. DeRosa, M. C.; Al-mutlaq, F.; Crutchley, R. J. *Inorg. Chem.* **2001**, *40*, 1406.
293. Hupp, J. T.; Williams, R. T. *Acc. Chem. Res.* **2001**, *34*, 808.
294. Bignozzi, C. A.; Roffia, S.; Scandola, F. *J. Am. Chem. Soc.* **1985**, *107*, 1644.
295. Bignozzi, C. A.; Roffia, S.; Chiorboli, C.; Davila, J.; Indelli, M. T.; Scandola, F. *Inorg. Chem.* **1989**, *38*, 4350.
296. Bignozzi, C. A.; Bortolini, O.; Chiorboli, C.; Indelli, M. T.; Rampi, M. A.; Scandola, F. *Inorg. Chem.* **1992**, *31*, 172.
297. Buranda, T.; Lei, Y.; Endicott, J. F. *J. Am. Chem. Soc.* **1992**, *114*, 6916.
298. Endicott, J. F.; Song, X.; Watzky, M. A.; Buranda, T. *Chem. Phys.* **1993**, *176*, 427.
299. Endicott, J. F.; Song, X.; Watzky, M. A.; Buranda, T. *J. Photochem. Photobiol. A: Chem.* **1994**, *82*, 181.
300. Endicott, J. F.; McNamara, P. G.; Buranda, T.; Macatangay, A. V. *Coord. Chem. Rev.* **2000**, *208*, 61.
301. Ponce, A.; Bachrach, M.; Farmer, P. J.; Winkler, J. R. *Inorg. Chim. Acta* **1996**, *243*, 135.
302. Watzky, M. A.; Endicott, J. F.; Song, X.; Lei, Y.; Macatangay, A. V. *Inorg. Chem.* **1996**, *35*, 3463.
303. Endicott, J. F.; Watzky, M. A.; Song, X.; Buranda, T. *Coord. Chem. Rev.* **1997**, *159*, 295.
304. Ballhausen, C. J. In *Vibronic Processes in Inorganic Chemistry*; Flint, C. D., Ed.; Kluwer: Dordrecht, The Netherlands, 1989; p 53.
305. Bersuker, I. B. *The Jahn-Teller Effect and Vibronic Interactions in Modern Chemistry*; Plenum: New York, 1984.
306. Kenkre, V. M.; Tokmakoff, A.; Fayer, M. D. *J. Chem. Phys.* **1994**, *101*, 10618.
307. Harrison, D. E.; Weissberger, E.; Taube, H. *Science* **1968**, *159*, 320.
308. Treitel, I. M.; Flood, M. T.; Marsh, R. E.; Gray, H. B. *J. Am. Chem. Soc.* **1969**, *91*, 6512.
309. Magnuson, R. H.; Taube, H. *J. Am. Chem. Soc.* **1972**, *94*, 7213.
310. Brady, M.; Weng, W. Q.; Zhou, Y. L.; Seyler, J. W.; Amoroso, A. J.; Arif, A. M.; Bohme, M.; Frenking, G.; Gladysz, J. A. *J. Am. Chem. Soc.* **1997**, *119*, 775.
311. Seyler, J. W.; Weng, W.; Zhou, Y.; Gladysz, J. A. *Organomet.* **1993**, *12*, 3802.
312. Demadis, K. D.; El-Samanody, E.-S.; Cola, G. M.; Meyer, T. J. *J. Am. Chem. Soc.* **1999**, *121*, 535.
313. Dattelbaum, D. M.; Hartshorn, C. M.; Meyer, T. J. *J. Am. Chem. Soc.* **2002**, *124*, 4938.
314. Taube, H.; Myers, H.; Rich, R. L. *J. Am. Chem. Soc.* **1953**, *75*, 4118.
315. Taube, H. *Can. J. Chem.* **1959**, *37*, 129.
316. Wilkins, R. G. *Kinetics and Mechanisms of Transition Metal Complexes*; 2nd ed.; VCH: Weinheim Germany, 1991.
317. Endicott, J. F.; Durham, B. In *Coordination Chemistry of Macrocyclic Compounds*; Melson, G. A., Ed.; Plenum: New York, 1979.
318. Haim, A. *Progr. Inorg. Chem.* **1983**, *30*, 273.
319. Endicott, J. F.; Wong, C.-L.; Ciskowski, J. M.; Balakrishnan, K. P. *J. Am. Chem. Soc.* **1980**, *102*, 2100.
320. Stritar, J.; Taube, H. *Inorg. Chem.* **1969**, *8*, 2281.
321. Endicott, J. F.; Lilie, J.; Kuszaj, J. M.; Ramaswamy, B. S.; Schmonsees, W. G.; Simic, M. G.; Glick, M. D.; Rillema, D. P. *J. Am. Chem. Soc.* **1977**, *99*, 429.
322. Melson, G. A., Ed. *Coordination Chemistry of Macrocyclic Compounds*; Plenum: New York, **1979**.
323. Kajiwara, T.; Yamaguchi, T.; Kido, H.; Kawabata, S.; Kuroda, R.; Ito, T. *Inorg. Chem.* **1993**, *32*, 4990.

324. Kajiwaru, T.; Yamaguchi, T.; Oshio, H.; Ito, T. *Bull. Chem. Soc. Jpn.* **1994**, *67*, 2130.
325. Udugala-Ganeheneghe, M. Y.; Heeg, M. J.; Hyhroczyk, L. M.; Wenger, L. E.; Endicott, J. F. *Inorg. Chem.* **2001**, *40*, 1614.
326. Udugala-Ganeheneghe, M. Y., Ph. D. Dissertation, Wayne State University, Detroit, MI, 2000.
327. Udugala-Ganeheneghe, M. Y.; Szacilowski, K. *Work in progress*.
328. Lewis, F. D. In *Electron Transfer in Chemistry*; Balzani, V., Ed.; Wiley-VCH: Weinheim, 2001, Vol. 3, p 105.
329. Malmstrom, B. G. In *Electron Transfer in Chemistry*; Balzani, V., Ed.; Wiley-VCH: Weinheim, 2001, Vol. 3, p 39.
330. Pond, A. E.; Ledbetter, A. P.; Sono, M.; Goodin, D. B.; Dawson, J. H. In *Electron Transfer in Chemistry*; Balzani, V., Eds.; Wiley-VCH: Weinheim 2001, Vol. 3, p 56.
331. Moser, C. C.; Page, C. C.; Dutton, P. L. In *Electron Transfer in Chemistry*; Balzani, V., Ed., Wiley-VCH: Weinheim, 2001, Vol. 3, p 24.
332. Gray, H. B.; Winkler, J. B. In *Electron Transfer in Chemistry*; Balzani, V., Ed.; Wiley-VCH: Weinheim, 2001, Vol. 3, p 3.
333. Solomon, E. I.; Lowery, M. D.; Guckert, J. A. In *Electron Transfer Reactions*; Isied, S. S., Ed.; A.C.S. Advances in Chemistry Series Vol. 253; American Chemical Society: Washington, 1997; p 317.
334. Isied, S. S. In *Electron Transfer Reactions*; Isied, S. S., Ed.; A.C.S. Advances in Chemistry Series Vol. 253; American Chemical Society: Washington, 1997; p 349.
335. Durham, B.; Lian, P. P.; Hahm, S.; Long, L.; Millett, F. In *Electron Transfer in Biology and the Solid State*; Johnson, M. K., King, R. B., Kurtz, D. M., Jr. Kotal, C., Norton, M. L., Scott, R. A. Eds.; A.C.S. Symposium Series Vol. 226, American Chemical Society : Washington, 1990; p 181.
336. Isied, S. S. In *Electron Transfer in Biology and the Solid State*; Johnson, M. K., King, R. B., Kurtz, D. M., Jr. Kotal, C., Norton, M. L., Scott, R. A. Eds.; A.C.S. Symposium Series Vol. 226, American Chemical Society: Washington, 1990; p 91.
337. Winkler, J. R.; Gray, H. B. *Chem. Rev.* **1992**, *92*, 369.
338. Luo, J.; Reddy, K. B.; Salameh, A. S.; Wishart, J. F.; Isied, S. S. *Inorg. Chem.* **2000**, *39*, 2321.
339. Beratan, D. N.; Betts, J. N.; Onuchic, J. N. *Science* **1991**, *252*, 1285.
340. Skourtis, S. S.; Beratan, D. N. *Adv. Chem. Phys.* **1999**, *106*, 377.
341. Skourtis, S. S.; Beratan, D. N. In *Electron Transfer in Chemistry*; Balzani, V., Ed.; Wiley-VCH: Weinheim, 2001, Vol. 1, p 109.
342. Regen, J. J.; Onuchic, J. N. *Adv. Chem. Phys.* **1999**, *107*, 497.
343. Gray, H. B.; Winkler, J. R. *J. Electroanal. Chem.* **1997**, *438*, 43.
344. Warshel, A. *Acc. Chem. Res.* **2002**, *35*, 385.
345. Jones, G. A.; Carpenter, B. K.; Paddon-Row, M. N. *J. Am. Chem. Soc.* **1999**, *121*, 11171.
346. Jordan, K. D.; Paddon-Row, M. N. *Chem. Rev.* **1992**, *92*, 395.
347. Oevering, H.; Verhoeven, J. W.; Paddon-Row, M. N.; Warman, J. M. *Tetrahedron* **1989**, *45*, 4751.
348. Fernando, S. R. L.; Kozlov, G. V.; Ogawa, M. Y. *Inorg. Chem.* **1998**, *37*, 1900.
349. Kornilova, A. Y.; Wishart, J. F.; Xiao, W. Z.; Lasey, R. C.; Fedorova, A.; Shin, Y. K.; Ogawa, M. Y. *J. Am. Chem. Soc.* **2000**, *122*, 7999.
350. Ogawa, M. Y.; Wishart, J. F.; Young, Z.; Miller, J. R.; Isied, S. S. *J. Phys. Chem.* **1993**, *97*, 11456.
351. Ungar, L. W.; Newton, M. D.; Voth, G. A. *J. Phys. Chem. B* **1999**, *103*, 7367.
352. Richardson, D. E.; Sharpe, P. *Inorg. Chem.* **1993**, *32*, 1809.
353. Shilov, A. E. In *Electron Transfer in Chemistry*; Balzani, V., Ed.; Wiley-VCH: Weinheim, 2001, Vol. 2, p 878.
354. Forde, C. E.; Morris, R. H. In *Electron Transfer in Chemistry*; Balzani, V., Ed., Wiley-VCH: Weinheim, 2001, Vol. 2, p 905.
355. Vonseggern, I. V.; Tuzcek, F.; Bensch, W. *Inorg. Chem.* **1995**, *34*, 5530.
356. Solomon, E. I.; Tuzcek, F.; Root, D. E.; Brown, C. A. *Chem. Rev.* **1994**, *94*, 827.
357. Solomon, E. I.; Hanson, M. A. In *Inorganic Electronic Structure and Spectroscopy*; Solomon, E. I., Lever, A. B. P., Eds.; Wiley: New York, 1999; Vol. 2, p 1.
358. Brunold, T. C.; Gamelin, D. R.; Solomon, E. L. *J. Am. Chem. Soc.* **2000**, *122*, 8511.
359. Taube, H. In *Mechanistic Aspects of Inorganic Reactions*; Rorabacher, D. B. Endicott, J. F. Eds.; American Chemical Society Symposium Series 198; American Chemical Society: Washington, 1982; p 151.
360. Creutz, C. In *Electron Transfer Reactions*; Isied, S. S., Ed.; American Chemical Society Advances in Chemistry Series 253; Washington, 1997; p 151.
361. Launay, J.-P.; Coudret, C. In *Electron Transfer in Chemistry*; Balzani, V., Ed.; Wiley-VCH: Weinheim, 2001, Vol. 5, p 3.
362. De Cola, L.; Belsler, P. In *Electron Transfer in Chemistry*; Balzani, V., Ed.; Wiley-VCH: Weinheim, 2001, Vol. 5, p 97.
363. Lucas, A. S.; Wasielewski, M. R. In *Electron Transfer in Chemistry*; Balzani, V., Ed.; Wiley-VCH: Weinheim, 2001, Vol. 5, p 48.
364. de Silva, A. P.; McClenagh, N. D.; McCoy, C. P. In *Electron Transfer in Chemistry*; Balzani, V., Ed.; Wiley-VCH: Weinheim, 2001, Vol. 5, p 156.
365. Campagna, S.; Serroni, S.; Puntoriero, F.; Di Pietro, C.; Ricevuto, V. In *Electron Transfer in Chemistry*; Balzani, V., Ed.; Wiley-VCH: Weinheim, 2001, Vol. 5, p 186.
366. Houbrechts, S.; Hendricks, E.; Verbiest, T.; Clays, K.; Persoons, A. In *Electron Transfer in Chemistry*; Balzani, V., Ed.; Wiley-VCH: Weinheim, 2001, Vol. 5, p 243.
367. Venturi, M.; Credi, A.; Balzani, V. In *Electron Transfer in Chemistry*; Balzani, V., Ed.; Wiley-VCH: Wienheim, 2001, Vol. 3, p 501.
368. Ballardini, R. In *Electron Transfer in Chemistry*; Balzani, V., Ed.; Wiley-VCH: Weinheim, 2001, Vol. 3, p 539.
369. Armaroli, N.; Chambron, J.-C.; Collin, J.-P.; Dietrich-Buchecker, C.; Flamigini, L.; Kern, J.-M.; Sauvage, J.-P. In *Electron Transfer in Chemistry*; Balzani, V., Ed.; Wiley-VCH: Weinheim, 2001, Vol. 3, p 582.
370. Juris, A. In *Electron Transfer in Chemistry*; Balzani, V., Ed.; Wiley-VCH: Weinheim, 2001; p 655.
371. Sauvage, J.-P.; Dietrich-Buchecker, C. O., Eds. *Catenanes, Rotaxanes and Knots*; Wiley-VCH: Weinheim, 1999.
372. Ambabilino, D. B.; Stoddart, J. F. *Chem. Rev.* **1995**, *95*, 2725.
373. Hurst, J. K.; Khairutdinov, R. F. In *Electron Transfer in Chemistry*; Balzani, V., Ed.; Wiley-VCH: Weinheim, 2001, Vol. 4, p 578.

374. Vaidyalingam, A. S.; Coutant, M. A.; Dutta, P. K. In *Electron Transfer in Chemistry*; Balzani, V., Ed.; Wiley-VCH: Weinheim, 2001, Vol. 4, p 412.
375. Dutta, P. K.; Ledney, M. *Progr. Inorg. Chem.* **1997**, *44*, 209.
376. Vermeulen, L. A. *Progr. Inorg. Chem.* **1997**, *44*, 143.
377. Bhat, V.; Kazunari, D. In *Electron Transfer in Chemistry*; Balzani, V., Ed.; Wiley-VCH: Weinheim, 2001, Vol. 4, p 487.
378. Clegg, R. S.; Hutchison, J. E. In *Electron Transfer in Chemistry*; Balzani, V., Ed.; Wiley-VCH: Weinheim, 2001, Vol. 4, p 541.
379. Qu, P.; Meyer, G. J. In *Electron Transfer in Chemistry*; Balzani, V., Ed.; Wiley-VCH: Weinheim, 2001, Vol. 4, p 353.
380. Bignozzi, C. A.; Schoonover, J. R.; Scandola, F. *Progr. Inorg. Chem.* **1997**, *44*, 1.
381. Gerfin, T.; Gratzel, M.; Walder, L. *Progr. Inorg. Chem.* **1997**, *44*, 345.
382. Hagfeldt, A.; Gratzel, M. *Acc. Chem. Res.* **2000**, *33*, 269.
383. Gratzel, M.; Moser, J.-E. In *Electron Transfer in Chemistry*; Balzani, V., Ed.; Wiley-VCH: Weinheim, 2001, Vol. 5, p 589.
384. Zhu, X.-Y. *Ann. Rev. Phys. Chem.* **2002**, *53*.
385. Hush, N. S. *Trans. Faraday Soc.* **1961**, *57*, 557.
386. Marcus, R. A. *J. Chem. Phys.* **1965**, *43*, 670.
387. Crawford, P. W.; Schultz, F. A. *Inorg. Chem.* **1994**, *33*, 4344.
388. Gao, Y. D.; Lipkowitz, K. B.; Schultz, F. A. *J. Am. Chem. Soc.* **1995**, *117*, 11932.
389. Turner, J. W.; Schultz, F. A. *Inorg. Chem.* **1999**, *38*, 358.
390. Nazeeruddin, M. K.; Kay, A.; Rodicio, I.; Humphrybaker, R.; Muller, E.; Liska, P.; Vlachopoulos, N.; Gratzel, M. *J. Am. Chem. Soc.* **1993**, *115*, 6382.
391. Kamat, P. V. *Progr. Inorg. Chem.* **1997**, *44*, 273.
392. Rajeshwar, K. In *Electron Transfer in Chemistry*; Balzani, V., Ed.; Wiley-VCH: Weinheim, 2001, Vol. 5, p 279.
393. Lewis, N. S. *J. Electroanal. Chem.* **2001**, *508*, 1.
394. Hannappel, T.; Bernd, B.; Storck, W.; Willig, F. *J. Phys. Chem. B* **1997**, *101*, 6799.
395. Meier, A.; Selmarten, D. C.; Seimoneit, K.; Smith, B. B.; Nozik, A. J. *J. Phys. Chem. B* **1999**, *103*, 2122.
396. Asbury, J. B.; Ellingson, R. J.; Ghosh, H. N.; Ferrere, S.; Nozik, A. J.; Lian, T. Q. *J. Phys. Chem. B* **1999**, *103*, 3110.
397. Yang, M.; Thompson, D. W.; Meyer, G. J. *Inorg. Chem.* **2002**, *41*, 1254.
398. Kelly, C. A.; Meyer, G. J. *Coord. Chem. Rev.* **2001**, *211*, 295.
399. Galoppini, E.; Guo, W. Z.; Qu, P.; Meyer, G. J. *J. Am. Chem. Soc.* **2001**, *123*, 4342.
400. Oksam, G.; Bergeron, B. V.; Meyer, G. J.; Searson, P. C. *J. Phys. Chem. B* **2001**, *105*, 6867.
401. Qu, P.; Meyer, G. J. *Langmuir* **2001**, *17*, 6720.
402. Moser, J. E.; Gratzel, M. *Chimia* **1998**, *52*, 160.
403. Asbury, J. B.; Ellingson, R. J.; Ghosh, H. N.; Ferrere, S.; Nozik, A. J.; Lian, T. Q. *J. Phys. Chem. B* **1999**, *103*, 3110.
404. Son, D. H.; Kambhampati, P.; Kee, T. W.; Barbara, P. F. *J. Phys. Chem. A* **2002**, *106*, 4591.



# 7.12

## Electron Transfer from the Molecular to the Nanoscale

C. CREUTZ, B. S. BRUNSCHWIG,  
and N. SUTIN

*Brookhaven National Laboratory, Upton, NY, USA*

---

7.12.1	INTRODUCTION	732
7.12.1.1	Scope of Coordination Chemistry in Nanoscale Charge Transfer Systems	732
7.12.1.2	Scope of Charge Transfer Processes in Nanoscale Systems	734
7.12.1.3	Scope and Organization of this Chapter	734
7.12.2	SIZE EFFECTS IN NANOSCALE SYSTEMS FOR CHARGE TRANSFER: TOP DOWN AND BOTTOM UP	735
7.12.2.1	A Chemist's Perspective: A Molecular Orbital Approach	735
7.12.2.2	Clusters from Atoms	737
7.12.3	FROM MACROSTRUCTURES TO NANOSTRUCTURES	738
7.12.3.1	Classical Electrostatics for a Spherical Particle	738
7.12.3.2	Semiclassical Particle in a Sphere	740
7.12.3.2.1	<i>Polarization Energy for Semiclassical Particle in a Sphere</i>	740
7.12.3.3	Optical Excitation	742
7.12.3.4	Metal Clusters	744
7.12.3.5	Semiconductor Clusters	747
7.12.3.6	Soluble or Dispersed Nanoparticles: Coordination and Colloid Chemistry	749
7.12.4	FRAMEWORK AND MODELS	749
7.12.4.1	Energy Scales and Absolute Potentials	750
7.12.4.2	Relating Rate Constant and Conductance	751
7.12.4.3	Electronic Coupling Mechanisms in Nanostructures and Distance Dependences	753
7.12.4.4	Activation Barriers	754
7.12.4.4.1	<i>Inner-shell barrier</i>	754
7.12.4.4.2	<i>Medium reorganization barrier</i>	755
7.12.4.5	Molecular Electron Transfer in Solution	759
7.12.4.6	Electron Transfer through Monolayers on Metal Electrodes	759
7.12.4.7	Electron Transfer through Monolayers on Semiconductor Electrodes	760
7.12.4.8	Electron Transfer in Metal–Molecule–Metal Systems	761
7.12.5	EXPERIMENTAL STUDIES OF NANOSCALE SYSTEMS	763
7.12.5.1	Distance Dependence in Self-assembled Monolayers	763
7.12.5.2	Kinetic Dispersity	765
7.12.5.3	Electron Transfer and Coordination Chemistry in Cluster Synthesis	766
7.12.5.4	Electron Transfer at MPCs	766
7.12.5.4.1	<i>Solutions</i>	766
7.12.5.4.2	<i>Films</i>	767
7.12.5.5	Carrier Hopping between Semiconductor Nanoparticles	768
7.12.6	ORGANIZING STRATEGIES AND MEDIA	770
7.12.6.1	Polymers, Dendrimers	770
7.12.6.2	Self-assembled Monolayers on Solids	772
7.12.6.3	Porous Solids	773
7.12.7	CONCLUDING REMARKS	774
7.12.8	REFERENCES	774

---

## 7.12.1 INTRODUCTION

At present “nanoscale” is defined as a size/distance range of 1–100 nm. Charge transfer processes on the molecular and bulk scales are well characterized, while investigation of these processes on the nanoscale is at its beginning. Because the subject is intrinsic to the design of molecular electronics, the most comprehensive treatments of nanoscale charge transfer are found in the molecular electronics literature.<sup>1–3</sup> An extensive treatment of the full range of electron transfer in systems based on molecular units has been published.<sup>4</sup> Transport of charge through materials may occur via hopping between localized sites (as for molecular species in solution) or via spatially extended electronic bands (as in bulk metals and doped semiconductors). Thus a comprehensive description of nanoscale charge transfer can be expected to require the concepts of both chemical rate theory<sup>5,6</sup> and of solid-state physics.<sup>7,8</sup> Furthermore, nanoscale species—metal and semiconductor nanoparticles, carbon nanotubes—manifest size-dependent properties with both quantum and classical aspects that can influence charge transfer processes in which they engage.

Two issues need to be addressed at the outset. What is the role of coordination chemistry in nanoscale charge transfer systems? And what are the characteristics of these processes?

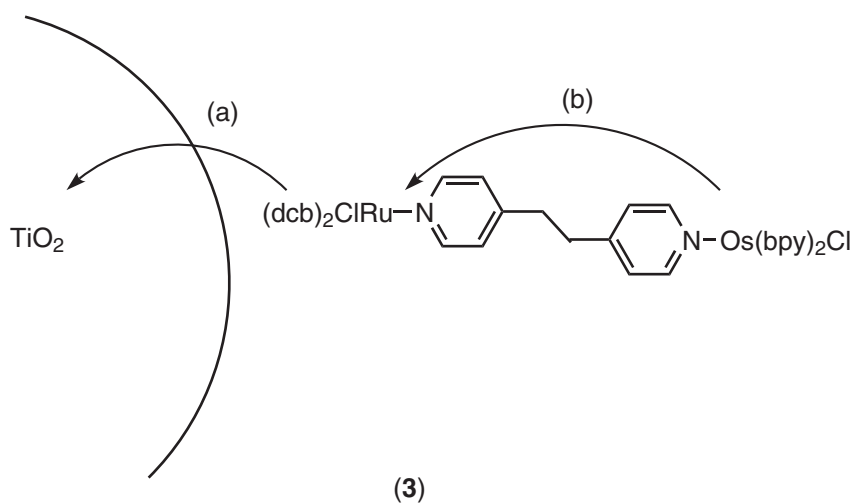
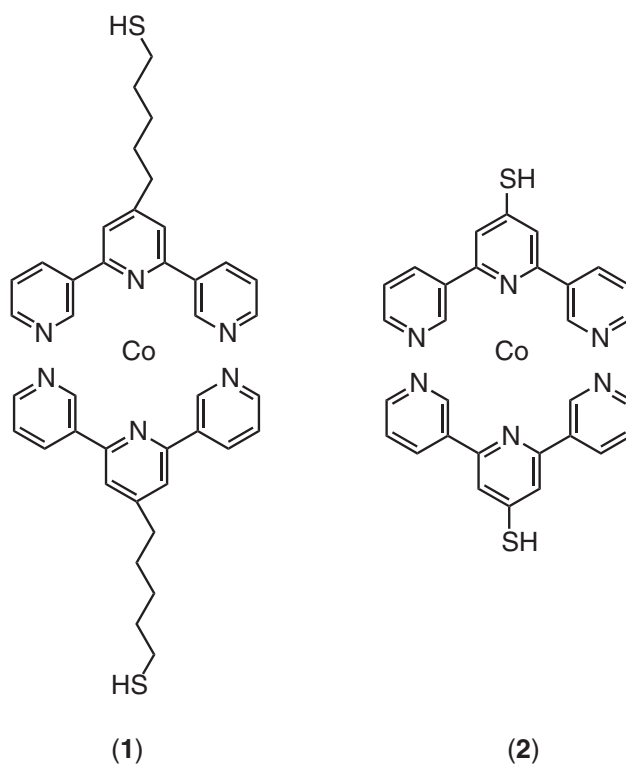
### 7.12.1.1 Scope of Coordination Chemistry in Nanoscale Charge Transfer Systems

Coordination complexes and coordination chemistry serve a range of roles in nanoscale charge transfer systems. Coordination complexes as small as monometallic species are being used as molecular probes of nanostructures. Thus  $\text{Fe}^{\text{II}}(\text{CN})_4\text{L}^{2-}$  has been attached to  $\text{TiO}_2$  nanoparticles to probe the energetics of charge transfer from the  $\text{Fe}^{\text{II}}$  to the particle.<sup>9</sup> Many serve as dyes for sensitized photoinduced electron injection into semiconductors.<sup>10</sup> Coordination complexes are used as building blocks of nanostructures, e.g., redox polymers<sup>11</sup> and dendrimers based on  $\text{M}(\text{bpy})_3$  complexes.<sup>12</sup> Utilization of metal-templated incorporation of redox-active metal-ligand units into the macrocycle framework of a host has demonstrated the possibility of using the host as an electrochemical sensor for guest substrate anions.<sup>13</sup> Hydrogen bonding interactions have been utilized to bind/detect neutral molecules.<sup>14</sup> Bis(dithiolate) complexes self-assembled in solids exhibit metallic conductivity<sup>15</sup> and superconductivity.<sup>16</sup> Metal complexes may serve as light collectors and electrical components in artificial photosynthetic polyelectrolyte assemblies.<sup>17</sup> Coordination chemistry is intimately involved in the growth of nanoparticles from mononuclear metal complexes in solution since rates of reduction of the cationic precursors are a function of their coordination state.<sup>18</sup> The term “molecular electronics”<sup>19</sup> is given to the multidisciplinary field that strives to use molecule-based systems to process optical, electrical, magnetic, or chemical signals.<sup>3,20</sup> “Wires” such as an organic or inorganic polymer connect the components.<sup>21</sup> (Wires that transport energy are also of great interest.<sup>22</sup>) An approximately octahedral cobalt complex consisting of a cobalt ion bonded to two terpyridine ligands with thiol end groups, sandwiched between nanoscopic gold electrodes on a  $\text{Si}/\text{SiO}_2$  gate, serves as a single-electron transistor when it contains insulating hydrocarbon side chains ((1), S-to-S distance 2.4 nm), but exhibits strong coupling when the side chains are not present ((2), S-to-S distance 1.3 nm).<sup>23</sup>

Rectification in an assembly designed to display diode-like behavior has been described for the binuclear complex (3)  $[\text{Ru}(\text{dcb})_2(\text{Cl})\text{-bpa-Os}(\text{bpy})_2(\text{Cl})](\text{PF}_6)_2$ , where dcb is 4,4'-( $\text{COOH}$ )<sub>2</sub>-2,2'-bipyridine and bpa is 1,2-bis(4-pyridyl)ethane, which is attached to nanocrystalline  $\text{TiO}_2$  through the carboxylate groups associated with the Ru center.<sup>24</sup>

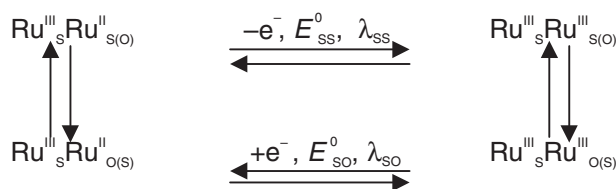
Following photoinduced electron injection (a) from the Ru or Os, the hole produced (b) resides on the distal Os so that the electron-hole recombination is five orders of magnitude slower than electron injection. Binuclear mixed-valence complexes have been proposed as components in quantum dot cellular automata computational schemes.<sup>25,26</sup>

The coordination chemistry of different metal centers is being exploited ingeniously to approach switching, gating, and machinery at the molecular level.<sup>27</sup> A substitution-labile dirhodium complex along with the axial ligand *trans*-1,2-bis(4-pyridyl)ethylene has been used in a layer-by-layer approach to build a metal-metal bonded film that bridges an 80 nm electrode gap, yielding an assembly that might find application as a switching or other device.<sup>28</sup> For a molecular switch or memory device, isomerization triggered by a redox event or light could also be utilized. Such hysteresis has been reported for a binuclear ruthenium complex containing S and S—O functions.  $\text{Ru}^{\text{II}}$  preferentially bonds to the S of the S—O moiety, while  $\text{Ru}^{\text{III}}$  has a higher affinity



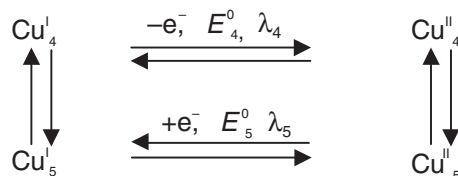
for the O.<sup>29</sup> This is illustrated in Scheme 1 where  $E^0$  is the redox potential of the  $\text{Ru}^{\text{III}}/\text{Ru}^{\text{II}}$  couple and  $\lambda$  is the (vertical) reorganization energy for the charge transfer. Due to the differences in these parameters the two electron transfer steps proceed at different rates (see Section 7.12.4.4).

Molecular motors<sup>30</sup> or machines<sup>31</sup> are inspired by biological molecules such as myosin which uses the chemical energy from hydrolysis of adenosine triphosphate to drive the linear push-pull motion of muscle. The different coordination demands of  $\text{Cu}^{\text{II}}$  and  $\text{Cu}^{\text{I}}$  are the basis of electrochemically induced molecular motion in a pseudorotaxane complex of copper.<sup>32,33</sup> As shown in Scheme 2,  $\text{Cu}^{\text{I}}$ , the stable, four-coordinate form is oxidized to unstable  $\text{Cu}^{\text{II}}$ , which rearranges to the stable five-coordinate form by sliding along the ligand. Reduction of the stable  $\text{Cu}^{\text{II}}$



Scheme 1

produces transient unstable  $\text{Cu}_5^{\text{I}}$  which rearranges to the original  $\text{Cu}_4^{\text{I}}$ . The redox processes for such systems are closely related to gated electron transfer and are inherently complex.<sup>34</sup>



Scheme 2

Finally, coordination chemistry is at the heart of the stabilization of nanoparticle solutions and solids; ligation of the surfaces of both metal and semiconductor particles prevents their agglomeration and can profoundly affect the electronic properties of the particles.

### 7.12.1.2 Scope of Charge Transfer Processes in Nanoscale Systems

Charge transfer processes involving nanoscale species in solution may, depending on reaction partner, involve outer- or inner-sphere electron transfer mechanisms, as discussed in Chapter 7.11. The charge transfer process will then be characterized by a bimolecular or unimolecular rate constant if the nanospecies is monodisperse. Electron transfer over distances of up to 4 nm has been extensively studied from a metal electrode to a molecular redox component (often ferrocene or a  $\text{Ru}(\text{NH}_3)_5\text{py}$  species) incorporated into a self-assembled monolayer; the experimental results can be expressed as first-order rate constants or conductances (see below). There is evidence for both tunneling and hopping processes in such long-distance processes, depending on the distance, the nature of the material separating the redox component from the electrode, and, in some cases, the temperature. The conductances of films of thiolate-protected gold clusters of 2–3 nm diameter core implicate an activated hopping mechanism.<sup>35</sup> Mixed-valent polymers exhibit hopping behavior at higher concentrations with a static percolation threshold around 40%.<sup>36</sup>

### 7.12.1.3 Scope and Organization of this Chapter

Unlike most of the articles in *Comprehensive Coordination Chemistry II* this chapter is not a review. Exploration of charge transfer on the nanoscale is just beginning. We anticipate that, over the first few years of the twenty-first century and beyond, coordination complexes and coordination chemistry approaches will be exploited extensively to create new materials of both fundamental and applied importance. Here we try to provide tools to assist coordination chemists who engage in this exciting new research area. We provide a broad overview of types of systems that may be important in the future, with lead-in references, and analyses of the energetics and electron transfer barriers from a dielectric continuum model for a range of conditions.

The size dependence of the properties of nanoscale species is treated in Sections 7.12.2 and 7.12.3. In Section 7.12.2 the point of departure is the properties of the atoms; in Section 7.12.3 it is the bulk material. Tools for predicting and modeling charge-transfer processes are developed in 7.12.4. In 7.12.5 examples are given of nanoscale charge-transfer systems that have been studied

experimentally. Approaches to the organization of molecular components into assemblies are outlined in 7.12.6.

### 7.12.2 SIZE EFFECTS IN NANOSCALE SYSTEMS FOR CHARGE TRANSFER: TOP DOWN AND BOTTOM UP

Some view nanoscale species as derived by making very small chunks of bulk materials—the so-called “top-down” approach and there are preparative methods, e.g., laser ablation, which are based on this strategy. By contrast, chemists tend to view nanoscale species as being built from atoms, molecules, and larger units of these successively—a “bottom-up” approach. Both philosophies find use as preparative strategies and both are valuable in predicting and understanding the properties of species in the nanoscale regime.

#### 7.12.2.1 A Chemist’s Perspective: A Molecular Orbital Approach

A range of nanoscale materials finds interest in the context of charge transfer. A number of these are built up from repeating polyatomic units, frequently with organic scaffolds, e.g., the *trans*-pyrazine-bridged ruthenium ammine polymer (4) (Figure 1) which should be a linear species assembled from mononuclear metal complexes, with properties predictable in terms of those of the  $(\text{NH}_3)_4\text{Ru}p_z^{2+/3+}$  building blocks. Two- and three-dimensional coordination polymers can be envisaged based on these and a wide range of other coordination complexes. Similarly, one-, two-, and three-dimensional redox materials can be based on catenation of an organic unit into which redox centers (e.g., metal complexes) are incorporated. These include dendrimers and block copolymer structures. In all such species, synthesis and properties are based on the monomeric repeat unit with the properties of this unit and the extended series described by molecular orbital theory.

In a complementary approach, the electronic structures of molecules and extended solids can be built up from constituent atoms with use of molecular orbital theory. The orbitals evolve into bands which provide a useful description when the number of atoms is large. To illustrate, consider the interaction of the  $p_z$  orbitals in a row of carbon atoms as the number of carbon sites  $N$  varies from small to very large (Figure 2).<sup>37</sup> For  $N=2$ , bonding and antibonding

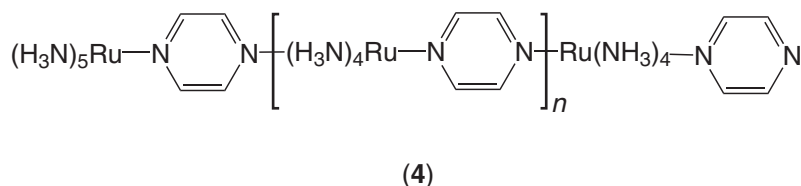


Figure 1 Coordination polymer with properties predictable from its building blocks.

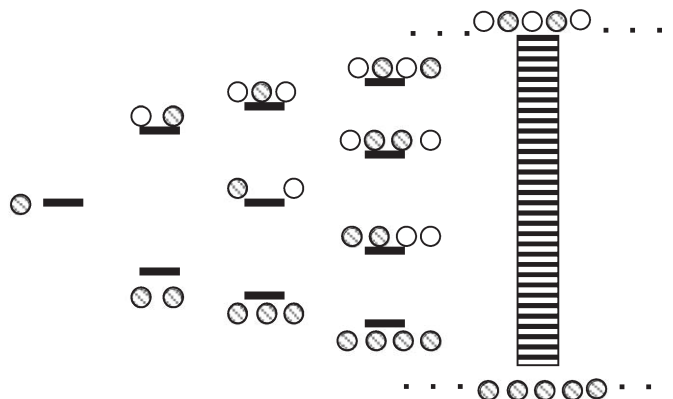


Figure 2 Orbitals of  $N$  atoms in a chain. The evolution depicted describes  $1s$  orbitals from H,  $2p_z$  orbitals providing the p bonding of a polyene chain (supported by s framework), or  $2s$  orbitals of Li. In each of these three cases each atom contributes one electron.

combinations are split by  $2H_{\text{BB}}$  (often denoted as  $\beta$ , the resonance integral). With one electron introduced with each  $p_z$  orbital, the lower molecular orbital (MO) will be doubly occupied (highest occupied molecular orbital, HOMO), while the upper antibonding molecular orbital is unoccupied (LUMO, lowest unoccupied molecular orbital). As the chain is extended to greater  $N$ , the number of molecular orbitals increases and the (equal numbers of) bonding and antibonding MOs grow closer and closer in energy, giving at very large  $N$  a band of molecular orbitals delocalized over the length of the chain with bandwidth  $4H_{\text{BB}}$ . (Bandwidth is the difference in energy between the lowest and the highest MO.) For the polyene, the band will be half-filled, and so the chain could exhibit metallic behavior if the level spacing is  $\ll k_{\text{B}}T$ . Similarly, each atom of an alkali metal contributes one electron from its highest occupied  $ns$  orbital ( $n=2$ , Li;  $n=3$ , Na, etc.). Because one  $ns$  electron is added with each atomic  $s$ -orbital, the band resulting at large  $N$  will again be half filled, and metallic behavior is expected when the intraband levels are separated by  $\ll k_{\text{B}}T$ . The density of states  $\rho(\varepsilon)$ , where  $N(\varepsilon)d\varepsilon$  is the number of energy levels in the range  $\varepsilon$  to  $\varepsilon + d\varepsilon$  per unit length goes to infinity at the edge of the band. Figure 3 depicts the evolution of bands when two types of atomic orbitals are included in a one-dimensional model.

These may arise from two atomic orbitals on one atom (e.g.,  $2s$  and  $2p$  on Mg) or on two different atoms. The separation between the top of the lower band and the bottom of the upper band is the band gap  $E_g$ . Denoting the energies of the atomic orbitals for  $N=1$  as  $E_1$  and  $E_2$  the condition for the bandgap to become zero at large  $N$  is

$$2H_{\text{BB},1} + 2H_{\text{BB},2} = E_2 - E_1 = E_{g,0} \quad (1)$$

At the left  $E_g$  is very large. When enough electrons are provided to exactly fill the lower energy band, depending upon the magnitude of the bandgap and the temperature, the material may be a semiconductor or an insulator. In general, the starting atomic ( $s$ ,  $p$ ,  $d$ ) orbitals are close enough in energy that including only one type does not provide a correct description of the metal. For example, for the alkaline metals, the  $np$  orbitals also need to be included. Figure 3(b) depicts the evolution of  $s$  and  $p$  bands when the  $ns$  and  $np_z$  orbitals are so close in energy that the resulting bands overlap. Thus, even though two electrons are added per atom and the  $s$ -band is filled, the gap between  $s$ - and  $p$ -bands, when  $\ll k_{\text{B}}T$ , is such that metallic behavior can still occur.

The evolution of bands from  $N$  atoms in three dimensions is analogous, but with interesting differences. The energy width of the bands in a cubic lattice (in which only nearest neighbor interactions are considered) is  $3 \times 4H_{\text{BB}}$ , rather than  $4H_{\text{BB}}$ . In contrast to the density of states for a one-dimensional band, which peaks at the edges, the density of states in three dimensions peaks at the center of the band.<sup>38</sup>

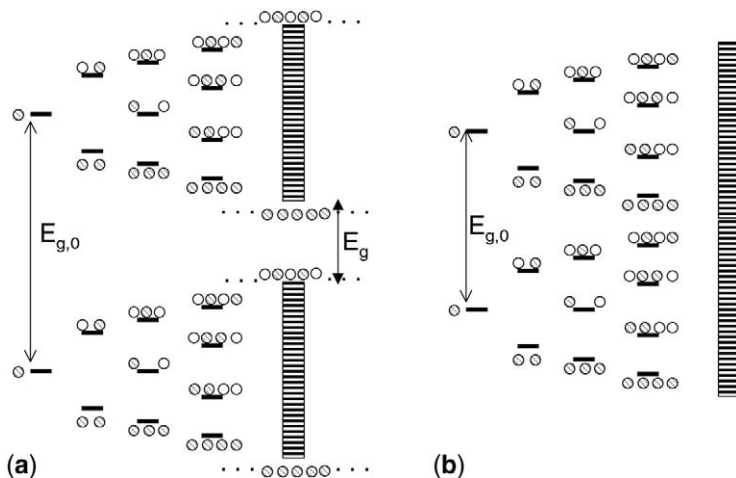


**Figure 3** One-dimensional evolution of  $s$  and  $p$  bands with increasing  $N$  with (a) interband gap  $\gg k_{\text{B}}T$  and (b)  $E_g \gg k_{\text{B}}T$ . The material shown in (a) is either a semiconductor or an insulator, while (b) is a metal.

### 7.12.2.2 Clusters from Atoms

As clusters are built up from atoms, size-dependent properties emerge.<sup>39–43</sup> Jortner has described the cluster size effects as the general expression  $X(N) = X(\infty) + AN^{-\beta}$ , where  $X$  is the property,  $A$  is a constant, and  $\beta$  lies between 0 and 1.<sup>3,44</sup> Size-dependent properties include

- (i) fraction of atoms on surface/at interior;
- (ii) shape/coordination number within a cluster;
- (iii) ensuing electronic structure—evolution of bands, size of band gap
  - (a) metal-like
  - (b) semiconductor-like;
- (iv) confinement;
- (v) absorption, emission energetics, dynamics;
- (vi) thermodynamic properties
  - (a) atom-atom binding energies
  - (b) melting points<sup>45</sup>
  - (c) electron affinity, ionization energy, reduction potential;
- (vii) reorganization energies for charge transfer.

An extremely important characteristic of nanoclusters is their high surface area. If a spherical model of the cluster is used and the bond distances within the cluster are assumed to be the same as in the bulk, the radius  $a$  (nm) of the cluster as a function of  $N$  can be calculated from the bulk density  $\rho$  ( $\text{g cm}^{-3}$ ) and the formula weight FW of the unit ( $\text{g mol}^{-1}$ ):

$$a_{\text{cluster}} = 0.0736 \left[ \frac{N(\text{FW})}{\rho} \right]^{1/3} \quad (2)$$

(Normally the diameter (not radius) of the sphere is reported in experimental papers.) For a spherical model, the fraction  $f_s$  of atoms on the surface is<sup>44</sup>

$$f_s = 4/N^{1/3} \quad (3)$$

For the bandgap shown in Figure 3(b) (also known as the Kubo gap):<sup>43</sup>

$$E_g = 4E_F/3N \quad (4)$$

where  $E_F$  is the Fermi level of the bulk metal, the energy of the highest occupied MO/level at 0 K. Values of the diameter, fraction of atoms on the surface, and  $E_g$  for metal particles (assuming  $E_F = 5.1 \text{ eV}$ ) are listed in Table 1. Thus the fraction of surface atoms, still 86% for a 1.5 nm particle, drops to 40% and 20% as  $N$  increases by a factor of 10 and 100. A 20 nm gold colloid particle, typical of that produced in the classical citrate synthesis,<sup>46,47</sup> contains  $2.5 \times 10^5$  atoms, with ~6% on the surface.

Real clusters are not expected to be spherical unless they are liquid and several structures have been inferred, e.g., cubooctahedra, in which each atom has 12 nearest neighbors. Then starting with one atom  $M$  and adding a shell of 12 more atoms gives  $M_{13}$ , in which 12 of the 13 atoms in

**Table 1** Spherical cluster model.

Number of atoms, $N$	$d$ (sphere)(nm)	$f_s$	$E_g$ (for $E_F = 5.1 \text{ eV}$ )(meV)
$10^1$	0.69	1.0	680
$10^2$	1.48	0.86	68
$10^3$	3.20	0.4	6.8
$10^4$	6.88	0.19	0.68
$2.5 \times 10^5$	20	0.063	0.027
$3.1 \times 10^7$	100	0.013	$2.2 \times 10^{-4}$
$6 \times 10^{23}$	2.7 cm	$5 \times 10^{-8}$	0

**Table 2** Filled cubooctahedral shell structures.

Number of atoms, $N$	Number of shells, $n$	$f_s$
1		1.0
13	1	0.92
55	2	0.76
147	3	0.63
309	4	0.52
561	5	0.45
1415	7	0.35

the cluster are on the surface. Continuing to add shells, with  $10n^2 + 2$  atoms added for the  $n$ th shell, gives the clusters shown in Table 2.<sup>39</sup>

Filled shells ( $N = 13, 55$ , etc.) have been associated with “magic numbers” associated with special cluster stability—an example of the special size effects that cause deviation of properties from a simple  $N^\beta$  dependence.

The size (diameter or radius) rises slowly with atom number, for the sphere, as  $N^{1/3}$ , the fraction of atoms on the surface falls as  $N^{-1/3}$ , while the increase in volume is directly proportional to  $N$ .

The cluster size-dependent properties of most direct importance for charge transfer studies are the electronic structure, the redox thermodynamics, and, for photoinduced charge transfer processes, absorption spectroscopy and excited state energy and lifetime. For metal nanoparticles, properties that depend on the energy level spacing—electronic conductivity and magnetic susceptibility—are proportional to  $N$  and particle volume, while diameter itself is proportional to  $N^{1/3}$ .

Equation (2) not only expresses a size dependence, it implies a temperature dependence. At room temperature,  $k_B T \sim 25$  meV; at 100 K,  $k_B T \sim 8$  meV. Thus the 100 atom, 1.48 nm nanoparticle in Table 1 should not exhibit bulk-like conductivity at room temperature or below, while the 1,000 atom, 3.2 nm particle should until very low temperature. As the number of atoms in a cluster increases, the cluster properties approach those of the bulk.

As will be developed below, the properties of nanoclusters differ from those of the bulk. However, having developed the idea of band structures from atomic and molecular orbitals, it is useful to use the bulk properties as a point of departure as considered in Section 7.12.3.

### 7.12.3 FROM MACROSTRUCTURES TO NANOSTRUCTURES

Despite the fact that building up nanostructures from the atomic level yields a useful intellectual framework, the physical properties of nanoclusters and other nanoscale structures are normally related to those of the bulk, with appropriate corrections for the nanoscale size. This approach is particularly useful for “larger” particles not subject to large specific quantum or other special effects (such as achieving a cluster magic number). When spheres of material are considered the bulk properties can be corrected for the finite size of the sphere.

#### 7.12.3.1 Classical Electrostatics for a Spherical Particle

The electrostatic or polarization energy  $P(r)$  of an electron, treated as a point charge, a distance  $r$  from the center of a spherical particle of radius  $a$  ( $r < a$ ), dielectric constant  $D_{in}$ , and in a medium of dielectric constant  $D_s$  (Figure 4(a)) is a function of the particle size:<sup>48–50</sup>

$$P(r) = \frac{e^2}{2a} \sum_{n=0}^{\infty} \frac{(D_{in} - D_s)(n+1)}{D_{in}[D_s + n(D_{in} + D_s)]} \left(\frac{r}{a}\right)^{2n} \quad (5)$$

$P(r)$  is plotted as a function of the radial coordinate in Figure 4(b). For  $D_{in} > D_s$  there is an image force pulling the charge toward the center of the particle. The dependence of the polarization energy on the particle size contributes to the size dependence of the ionization energy (IP), the electron affinity (EA), and the reduction potential of a nanoparticle.



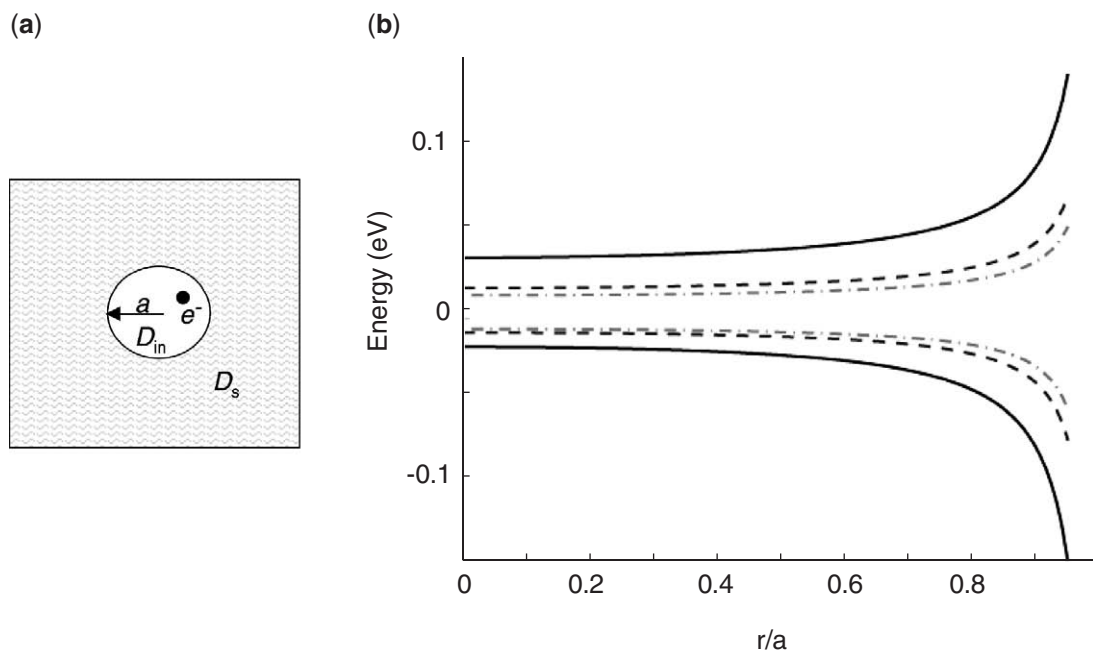


**Figure 4** (a) Spherical particle in a dielectric medium. (b) Top: energy (Equation (5)) of a point charge inside a dielectric sphere ( $D_{in}=10$ ), embedded in a dielectric medium of lower dielectric constant ( $D_s=4$ ), a model for silicon nanoparticles embedded in silica. Bottom: energy (Equation (5)) of a point charge inside a dielectric sphere ( $D_{in}=10$ ), embedded in a dielectric medium of higher dielectric constant ( $D_s=35$ ), a model for silicon nanoparticles in acetonitrile. The blue, red, and green curves are for 3 nm, 6 nm, and 8 nm particles, respectively.

Nanoparticles (radius  $a_1$ ) that are stabilized by a surface shell of radius  $a_2$  and thickness  $a_2 - a_1$  can be treated in terms of a core-shell-solvent model with three dielectric constants  $D_{in}$ ,  $D_{shell}$ , and  $D_s$ .<sup>51,52</sup> (Figure 5). Equation (5) is still applicable, but with  $P(r)$  given by

$$P(r) = \frac{e^2}{2a_1} \sum_{n=0}^{\infty} \frac{(A+B)(n+1)}{D_{in}(C+D)} \left(\frac{r}{a_1}\right)^{2n} \quad (6)$$

where

$$\begin{aligned} A &= (D_{shell} - D_s)[(n+1)D_{in} + nD_{shell}]a_1^{2n+1} \\ B &= (D_{in} - D_{shell})[(n+1)D_s + nD_{shell}]a_2^{2n+1} \\ C &= (D_{in} - D_{shell})(D_{shell} - D_s)n(n+1)a_1^{2n+1} \\ D &= [(n+1)D_{shell} + nD_{in}][(n+1)D_s + nD_{shell}]a_2^{2n+1} \end{aligned}$$

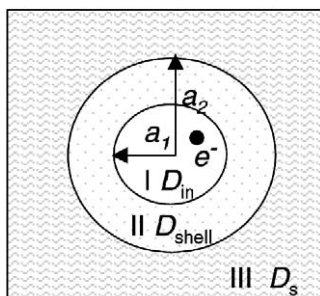


**Figure 5** Core-shell-solvent model.

and  $r < a_1$ . The above expression reduces to Equation (5) when  $a_2 = a_1$  or  $D_{\text{shell}} = D_s$ .<sup>51</sup> Solvatochromic shifts for stabilized CdSe particles are in good agreement with the above core-shell-solvent model.<sup>52</sup>

### 7.12.3.2 Semiclassical Particle in a Sphere

As discussed above, decreasing the size of a particle increases its bandgap, leading to shifts in the absorption and emission maxima. The size dependence of the bandgap is readily apparent for radii below  $\sim 5$  nm.<sup>53</sup> In addition, the energy levels become more molecular-like and the absorption and emission spectra of the nanoparticles exhibit a series of distinct transitions.

To treat the quantum size effect, an electron or hole inside a spherical particle is modeled as a “particle in a sphere.”<sup>41,54</sup> The electron is considered to be confined to a spherical potential well of radius  $a$  with potential energy  $V(r) = 0$  for  $r < a$  and  $V(r) = \infty$  for  $r > a$ . Solving the Schrödinger equation yields the wave functions<sup>41,54</sup>

$$\Psi = \frac{C j_l(\alpha_{n,l} \pi r / a) Y_l^m(\vartheta, \varphi)}{a} \quad (7a)$$

where  $C$  is a normalization constant,  $j_l(\alpha_{n,l} \pi r / a)$  is the  $l$ th-order spherical Bessel function,<sup>55,56</sup>  $\alpha_{n,l} \pi$  is the  $n$ th zero of  $j_l$ ,  $Y_l^m$  is a spherical harmonic, and  $n$  and  $l$  are atomic-like quantum numbers 1, 2, 3, ... and  $s, p, d, \dots$ , respectively. Note that although the wave functions have atomic-like quantum numbers, due to the difference in the boundary conditions the particle wave function for  $n = 1$  has 6  $l$  values, for  $n = 2$  has 4  $l$  values, and for  $n = 3$  has 1  $l$  value. For the first three levels  $\alpha_{n,l} = 1.00$  (1S), 1.43 (1P), and 1.82 (1D). The 1S wave function is spherically symmetric and is given by

$$\Psi_{1S} = C \sin(\pi r / a) / r \quad (7b)$$

for  $a \geq r$  and  $\Psi_{1S} = 0$  for  $r > a$ . The kinetic energy of the electron or hole confined within the potential well is given by

$$E_{n,l}^{\text{kin}} = \frac{\alpha_{n,l}^2 \hbar^2}{8m^* a^2} \quad (8)$$

where  $m^*$  is the effective mass of the electron or hole. For a 1S level  $E_{1,0}^{\text{kin}} = 0.376/m^* a^2$  eV ( $a$  in nm) where  $m^*$  is in units of the free electron mass.

#### 7.12.3.2.1 Polarization Energy for Semiclassical Particle in a Sphere

##### (i) Adiabatic process

The classical change in medium polarization energy is treated in Section 7.12.3.1. When an electron is removed or added to a very small nanoparticle the change in polarization energy can be considered as a perturbative correction to the kinetic energy (Equation (8)), using  $P(r)$  as the perturbation. The semiclassical shift in energy  $G_{\text{pol}}$  is<sup>48–50</sup>

$$G_{\text{pol}} = \int_0^a \Psi_{1S}^2 P(r) 4\pi r^2 dr \quad (9)$$

For a spherical nanoparticle in a dielectric medium (Figure 4(a)), the polarization energy is then

$$G_{\text{pol}} = \frac{e^2}{2a} \left( \frac{1}{D_s} - \frac{1}{D_{\text{in}}} \right) + \delta\Sigma \quad (10a)$$

When  $D_{\text{in}} \gg D_s$ ,  $\delta\Sigma$  is

$$\delta\Sigma = \frac{0.47e^2}{D_{\text{in}}a} \left( \frac{D_{\text{in}} - D_{\text{s}}}{D_{\text{in}} + D_{\text{s}}} \right) \quad (10b)$$

The  $n=0$  term in Equation (5) gives rise to the first term in Equation (10a) and the  $n>0$  terms give rise to the  $\delta\Sigma$  term. Similarly the polarization energy in the core-shell-solvent model (Figure 5) is

$$G_{\text{pol}} = \frac{e^2}{2} \left( \frac{1}{a_1} \left( \frac{1}{D_{\text{shell}}} - \frac{1}{D_{\text{in}}} \right) + \frac{1}{a_2} \left( \frac{1}{D_{\text{s}}} - \frac{1}{D_{\text{shell}}} \right) \right) + \text{additional terms} \quad (11a)$$

For a core with metallic properties,  $D_{\text{in}} = \infty$  and

$$G_{\text{pol}}^{\text{M}} = \frac{e^2}{2} \left( \left( \frac{1}{a_1} - \frac{1}{a_2} \right) \frac{1}{D_{\text{shell}}} + \frac{1}{a_2 D_{\text{s}}} \right) + \text{additional terms} \quad (11b)$$

When the kinetic energy term is neglected, as is justified at larger  $a$ , the adiabatic IP and EA of the spherical particle are related to those for the bulk material ( $a \rightarrow \infty$ ) in the same medium

$$M_{\text{s}} \rightarrow M_{\text{s}}^+ + e_{\text{vac}}^- \quad (\text{IP}) \quad (12a)$$

$$M_{\text{s}} + e_{\text{vac}}^- \rightarrow M_{\text{s}}^- \quad (\text{EA}) \quad (12b)$$

by

$$IP_r^0 = IP_{\infty} + G_{\text{pol}} \quad (13a)$$

$$EA_r^0 = EA_{\infty} - G_{\text{pol}} \quad (13b)$$

The difference in ionization energy and electron affinity is the band gap:

$$E_{g,r} = IP_r - EA_r \quad (14)$$

The repulsion resulting from addition or removal of a second 1S electron leads to a change in the electrostatic energy of the nanoparticle given by<sup>49</sup>

$$G_{\text{rep}} = \left( \frac{1}{D_{\text{s}}} + \frac{0.79}{D_{\text{in}}} \right) \frac{e^2}{a} \quad (15)$$

The above energy changes are illustrated in Figure 6. The energy shifts are equal but opposite for the case of electron and hole addition.<sup>49</sup>

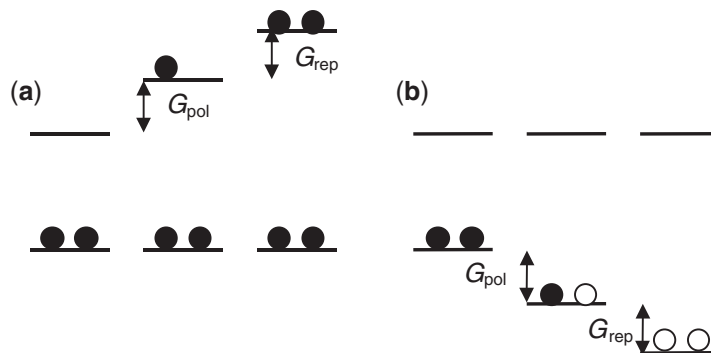


**Figure 6** Change in energy when one or two electrons are (a) added to or (b) removed from a spherical nanoparticle.

## (ii) Vertical processes

The vertical ionization energy and electron affinity of a spherical particle are related to the corresponding adiabatic values by the reorganization energy of the surrounding medium,  $\lambda_{\text{out}}$ :<sup>57</sup>

$$\lambda_{\text{out}}^{\infty} = \frac{e^2}{2a} \left( \frac{1}{D_{\text{op}}} - \frac{1}{D_s} \right) \quad (16)$$

where  $D_{\text{op}}$  is the optical dielectric constant of the medium (the square of the refractive index). The general expressions for the vertical ionization energy and electron affinity contain several terms; in the case of a spherical metal particle (Figure 4(a),  $D_{\text{in}} = \infty$ ) the expressions reduce to

$$IP_r^v = IP_{\infty} + \frac{e^2}{2aD_{\text{op}}} \quad (17)$$

$$EA_r^v = EA_{\infty} - \frac{e^2}{2aD_{\text{op}}} \quad (18)$$

The contributions to the vertical and adiabatic ionization energies and electron affinities are illustrated in Figure 7.

## 7.12.3.3 Optical Excitation

The energy required for optical excitation from a filled orbital or band to an unfilled orbital or band can be expressed as

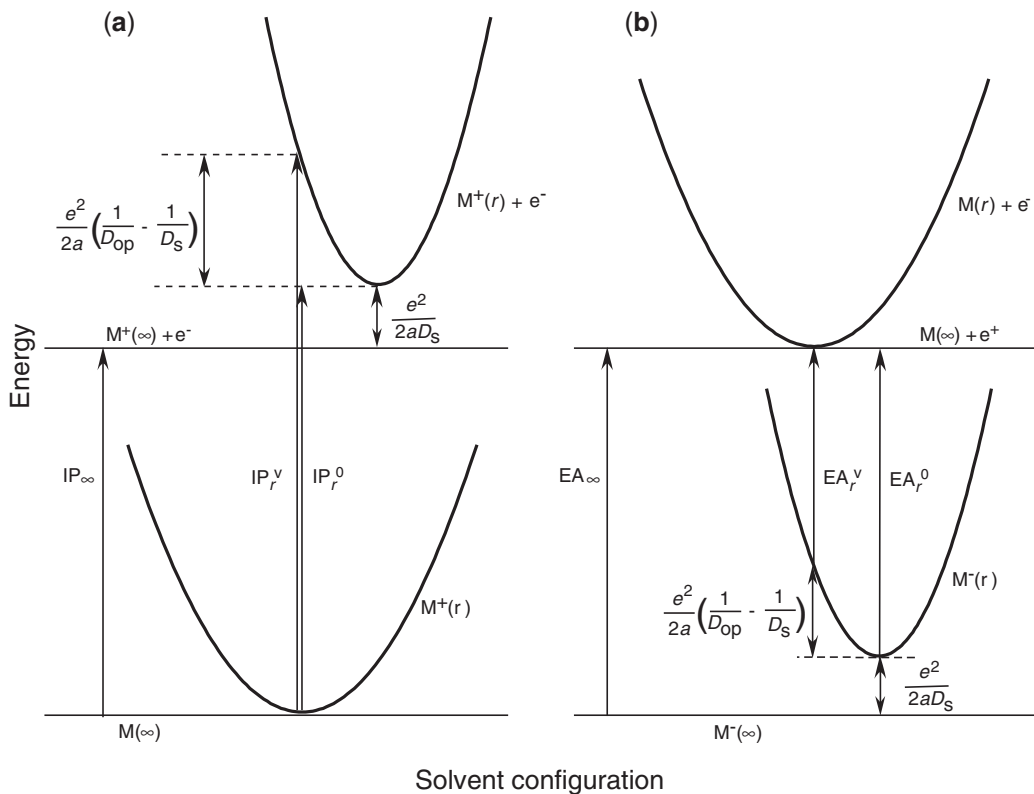


**Figure 7** Electrostatic contributions to (a) the ionization potential  $M_s \rightarrow M_s^+ + e_{\text{vac}}^-$  and (b) the electron affinity  $M_s + e_{\text{vac}}^- \rightarrow M_s^-$ .

$$E_{\text{op}} = h\nu = \lambda + \Delta G^0 \quad (19)$$

where  $E_{\text{op}}$  denotes the vertical nature of the transition,  $\Delta G^0$  is the free energy difference between the ground and equilibrated excited state formed, and  $\lambda$  is the reorganization energy. For semiconductors this optical transition commonly has ligand-to-metal charge transfer parentage and  $E_g$  is defined as  $\Delta G^0$ :

$$E_g^{\text{op}} = \lambda + \Delta G^0 = \lambda + E_g \quad (20)$$

Both  $\lambda$  and  $\Delta G^0$  depend on the nature and size of the particle. The reorganization energy includes “internal” energy changes, i.e., energy changes deriving from bond length and angle changes within the nanoparticle and the finite size of the particle and “external” energy changes deriving from structural changes in the surrounding medium:

$$\lambda = \lambda_{\text{in}} + \lambda_{\text{out}} \quad (21)$$

For metals and larger metal particles  $E_g$  is zero and the optical properties of the plasmon absorption are described in terms of Mie theory; published treatments address the influence of particle size, shape, and dielectric environment.<sup>58,59</sup>

For  $E_g \gg 0$  (nonmetal), the optical properties can generally be successfully modeled using the particle in a sphere model and its extensions.<sup>41,54</sup> Consideration of an electron and hole with negligible spatial correlation in a potential well, with neglect of polarization effects, leads to the following expression for the shift of the optical bandgap ( $1S_{\text{h}}1S_{\text{e}}$  excited state) with the radius of the sphere:

$$E_{g,r}^{\text{op}} - E_{g,\infty}^{\text{op}} = \text{KE} + G_{\text{coul}} + \delta G_{\text{pol}} + \delta \lambda_{\text{out}} \quad (22a)$$

$$\text{KE} = \frac{h^2}{8a^2} \left( \frac{1}{m_{\text{e}}^*} + \frac{1}{m_{\text{h}}^*} \right) = \frac{0.376}{a^2} \left( \frac{1}{m_{\text{e}}^*} + \frac{1}{m_{\text{h}}^*} \right) \text{ eV} \quad (a \text{ in nm}) \quad (22b)$$

$$G_{\text{coul}} = -\frac{1.8e^2}{D_{\text{in}}a} \text{ eV} \quad (a \text{ in nm}) \quad (22c)$$

where  $m_{\text{e}}^*$  and  $m_{\text{h}}^*$  are the effective masses of the electron and hole, respectively, in units of the free electron mass. The first term in Equation (22a) is the kinetic energy contribution that derives from the shift (in opposite directions) of the energy levels of an uncorrelated electron and hole upon confinement to the well, while the second term accounts for the electron–hole Coulomb interaction. The third term is the sum of three contributions: the polarization energies of the electron and the hole (each given by Equation (5)) and the interaction of the electron and the hole with the image charge of the other. The latter is equal to  $-(e^2/a)(1/D_{\text{s}} - 1/D_{\text{in}})$  and so exactly cancels the  $n=0$  terms in the polarization energies. Consequently  $\delta G_{\text{pol}}$  reduces to  $2\delta\Sigma$ .<sup>49,60</sup> The last term in Equation (22a) allows for the change in solvent reorganization energy. Detailed expressions for the solvent reorganization energy associated with charge transfer transitions are available.<sup>61</sup> In the limiting case that the optical transition produces a point dipole  $ed$  in the center of a sphere,  $\lambda_{\text{out}}$  is given by

$$\lambda_{\text{out}} = \frac{3e^2 d^2 (D_{\text{s}} - D_{\text{op}})}{a^3 (2D_{\text{s}} - D_{\text{op}})(2D_{\text{op}} - D_{\text{in}})} \quad (23)$$

Note that  $D_{\text{in}}$  decreases with decreasing particle size: its dependence on  $a$ , although smaller, is not negligible.<sup>49,50</sup> Expressions for the solvent reorganization energy associated with charge transfer between spheres or between a sphere and a “naked” planar or film-covered electrode are considered in Section 7.12.4.4.

As  $a$  decreases,  $\lambda_{\text{out}}$  and the quantum localization terms shift  $E_g$  to higher energy as  $1/a^3$  and  $1/a^2$ , respectively, while the Coulomb energy term shifts  $E_g$  to smaller values as  $1/a$ , so that for sufficiently small  $a$  the apparent bandgap will always increase with decreasing  $a$ . For 6 nm diameter CdS, the KE

and Coulomb energy terms are +0.27 eV and -0.15 eV, respectively.<sup>62</sup> Alternatively, the optical excitation may involve charge transfer between an adjacent donor and acceptor. For example, the optical transition in PbS has been described as charge transfer from  $S^{2-}$  to  $Pb^{2+}$ .<sup>63</sup> For the case of localized excitation the Coulomb interaction and solvent reorganization terms will be larger because of the smaller charge separation. Wang *et al.*<sup>63</sup> consider only the kinetic energy term and give the following expression for optical bandgaps in PbS nanoparticles:

$$E_{g,r} = \left[ E_{g,\infty}^2 + \frac{\hbar^2 E_g}{2a^2 m^*} \right]^{1/2} \quad (24)$$

Equation (24) yields bandgaps in good agreement with the experimental values for PbS particles larger than  $\sim 10$  nm. For smaller particles, the experimental values are in good agreement with shifts calculated including nearest-neighbor and next nearest-neighbor coupling.

### 7.12.3.4 Metal Clusters

We next consider the effect of cluster size on the adiabatic  $IP$  and  $EA$  of a “naked” metallic cluster. From Equation (10a),  $IP$  and  $EA$  for a spherical metallic cluster ( $a \sim$  nm) are related to those for the planar bulk metal ( $a \rightarrow \infty$ ) in the same medium by

$$IP_r = IP_\infty + \frac{(2z+1)e^2}{2D_s a} \quad (25)$$

$$EA_r = EA_\infty + \frac{(2z-1)e^2}{2D_s a} \quad (26)$$

where  $z$  is the initial charge of the metal cluster and  $D_s$  is the static dielectric constant of the medium.<sup>48</sup> Provided that  $IP_\infty = EA_\infty$ , the difference between  $IP(r)$  and  $EA(r)$ , the energy gap for a metal cluster, is simply equal to

$$IP_r - EA_r = \frac{e^2}{D_s a} = \frac{1.44}{D_s a} \text{ eV} (a \text{ in nm}) \quad (27)$$

Since the ionization energy and electron affinity of a bulk metal ( $z=0$ ) are both equal to the work function of the metal,  $IP_\infty = EA_\infty$  for a neutral cluster. Equation (27), with  $D_s = 1$  (vacuum), was also obtained from a detailed density functional treatment of a neutral cluster in vacuum.<sup>64</sup> By way of illustration,  $IP$  and  $EA$  of bulk gold are equal to 5.1 eV,<sup>65</sup> while  $IP$  and  $EA$  of an isolated gold atom are 9.23 eV and 2.32 eV, respectively. The density functional calculation (generalized gradient approximation) for a spherical 147-atom gold cluster,  $a=0.89$  nm, yields  $IP=5.80$  eV and  $EA=4.21$  eV corresponding to  $E_g=1.59$  eV, in excellent agreement with the value calculated from Equation (27). Equations (25) and (26) need to be used with caution: the value of the “constant” term may change depending upon the initial charge on the cluster ( $z \neq 0$ ).<sup>64</sup> An application of the INDO/S method to a 143-atom cylindrical gold cluster, parameterized to reproduce the ionization energy and electron affinity of a single gold atom, predicts  $IP=5.84$  eV and  $EA=4.61$  eV corresponding to  $E_g=1.23$  eV.<sup>66</sup>

In terms of the above model, the dependence of the reduction potential of a (bare) metal cluster on its radius is given by

$$E_r^0 = E_\infty^0 + \frac{(2z-1)e}{2D_s a} \quad (28)$$

where  $E_\infty^0$  is the potential of an uncharged metal surface (potential of zero charge) composed of the same material as the metal cluster in a given medium (Figure 8).<sup>67</sup> Thus the ionization energy of an uncharged cluster increases with decreasing cluster size, while the electron affinity and reduction potential decrease with decreasing cluster size.

For the case of a metallic particle of radius  $a_1$  enclosed in a ligand or other protective shell of radius  $a_2$  (Figure 5)

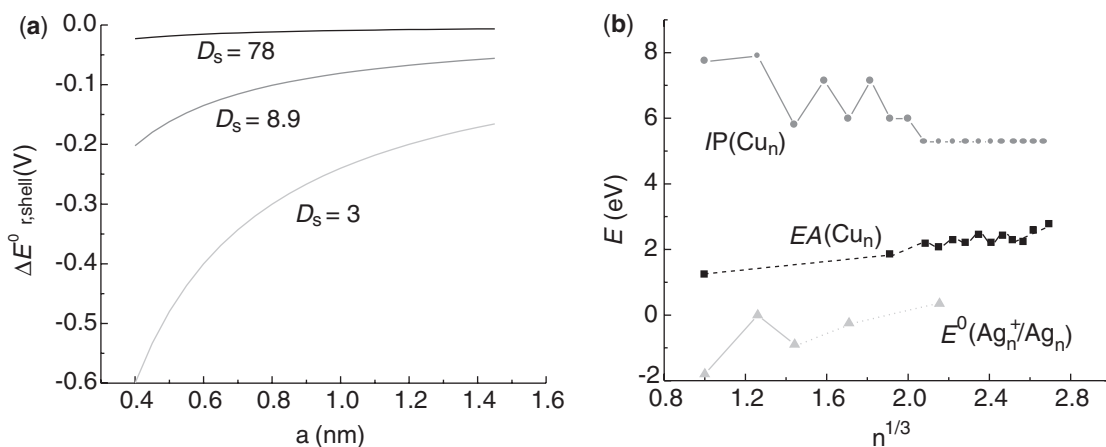


**Figure 8** (a) Charging of bare metal clusters (Equation (28)) in water, dichloromethane, and alkane solvents. (b) Experimental data for copper clusters in the gas phase<sup>68,69</sup> and silver clusters in water.<sup>70,71</sup>

$$E_{r,shell}^0 = E_{\infty}^0 + \frac{(2z-1)e}{2} \left( \left( \frac{1}{a_1} - \frac{1}{a_2} \right) \frac{1}{D_{shell}} + \frac{1}{a_2 D_s} \right) \quad (29a)$$

from a consideration of the change in electrostatic medium polarization accompanying the charging (Section 7.12.3.3, Equation (11b),  $D_{in} = \infty$ ), but neglecting confinement energy and the additional terms in Equation (22a). The “gap” between electrochemical oxidative and reductive processes is then

$$\Delta E_{r,shell}^0 = 0.72 \left( \left( \frac{1}{a_1} - \frac{1}{a_2} \right) \frac{1}{D_{shell}} + \frac{1}{a_2 D_s} \right) \text{ eV } (a \text{ in nm}) \quad (29b)$$

which is illustrated for specific ligand shell types and solvents in Figure 9.

The HOMO–LUMO gaps of metal nanoparticles can be evaluated experimentally from spectroscopy, electrochemistry, and scanning tunneling microscopy (STM). Data from spectroscopic and electrochemical studies of thiolate-encapsulated gold clusters studied in organic solvents are compared with calculated values in Table 3.<sup>72</sup> The experimental values from the two techniques and the calculated values from Equation (27) are in rather good agreement. By contrast STM data for “bare” clusters deposited onto highly oriented pyrolytic graphite in ultrahigh vacuum indicate much smaller gaps than expected from Equation (27) for a vacuum ( $D_s = 1$ ), possibly indicating some surface contamination.<sup>40</sup> The last two entries in Table 3 are  $\text{Au}_{11}$  clusters that lie at the coordination compound extreme of the nanocluster series. They exhibit bandgaps that depend significantly on the ligand shell, with  $E_g$  increasing from 1.4 eV to 1.8 eV when the chlorides and

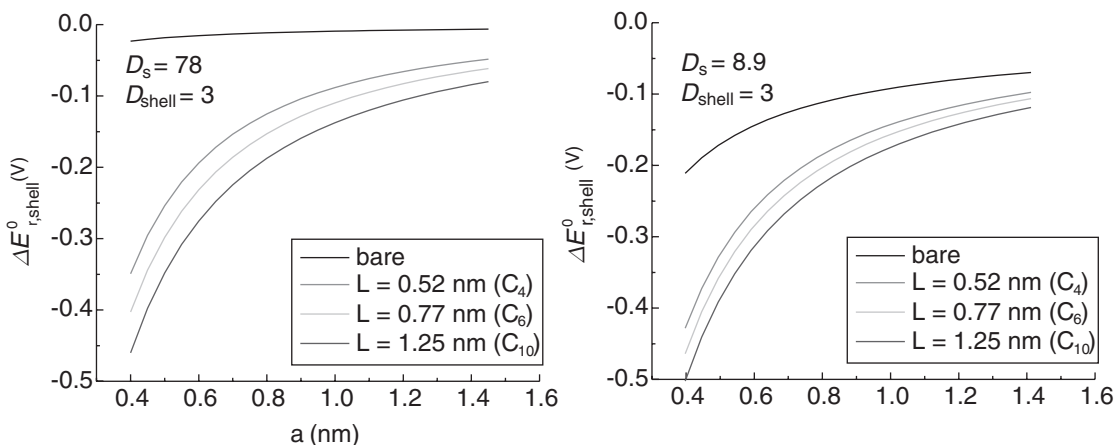


**Figure 9** Shift of particle redox potential from that of the bulk with size, ligand shell, and solvent (Equation (29)).

**Table 3** Energy gaps in thiolate-substituted gold clusters.<sup>72,74</sup>

Formula weight/formula	Number of atoms, <i>N</i>	<i>d</i> (nm)	<i>E<sub>g</sub></i> (spectr.) <sup>72</sup> (eV)	<i>E<sub>g</sub></i> (electro.) (eV)	<i>E<sub>g</sub></i> calcd. Equation (27) <sup>a</sup> (eV)
Bulk gold			0		
66 kD	342	22	<0.4		0.044
28 kD	145	1.65	<0.4		0.58
14 kD	75	1.35	0.6	0.74; <sup>72</sup> 0.42; <sup>74</sup>	0.74
8 kD	38	1.1	0.9	1.2; <sup>72</sup> 0.92; <sup>74</sup>	0.87
Au <sub>11</sub> Cl <sub>3</sub> (PPh <sub>3</sub> ) <sub>7</sub>	11	0.8		1.4; <sup>73</sup>	
Au <sub>11</sub> Cl <sub>3</sub> (PPh <sub>3</sub> ) <sub>7</sub> +L = HS(CH <sub>2</sub> ) <sub>11</sub> CH <sub>3</sub>	11	0.8	1.8 <sup>73</sup>	1.76 <sup>73</sup>	1.2

<sup>a</sup> *E<sub>g</sub>* calculated using *D<sub>s</sub>* = 3 for the alkanethiol cap.

phosphines are replaced by alkanethiolates.<sup>73</sup> This shift is qualitatively as expected from a core-shell-solvent model (Equation (29b)) since the phosphine ligands (*a*<sub>2</sub> ~ 0.7 nm) exclude much less of the (*D<sub>s</sub>* = 8.9) dichloromethane solvent than the much longer alkanethiolate (*a*<sub>2</sub> ~ 2 nm), but electronic effects arising from the different lead-in atoms are also expected to be significant for these small cluster that are near (or in) the molecular limit.

**Capacitive effects.** The presence of a protective layer on the surface of a metallic cluster decreases the capacity of the cluster. For a planar metal electrode, the electrical double layer comprised of the charge on the surface of the electrode and the ions of opposite charge in the solution (or the solvent dipoles) can be modeled as a parallel plate capacitor with capacity *C<sub>PP</sub>* in Farads (F) given by

$$C_{PP} = AD_{in}\epsilon_0/L \quad (30)$$

where *A* is the area of the electrode, *D<sub>in</sub>* (= *D<sub>s</sub>*) is the dielectric constant of the medium between the plates,  $\epsilon_0$  is the permittivity of free space ( $8.85 \times 10^{-12} \text{ F m}^{-1}$ ), and *L* is the thickness of the double layer (the distance separating the plates). For *L* ~ 1 nm the above expression yields a double-layer capacity of ~100 μF cm<sup>-2</sup> for a planar electrode in an aqueous medium (typical experimental values are in the range 10–40 μF cm<sup>-2</sup>). Reducing the area of the planar electrode to 10 nm<sup>2</sup> decreases its capacity to 10<sup>-17</sup> F. Similarly, the capacity of a spherical metal particle *C<sub>SP</sub>* with a spherical double layer of thickness *L* (Figure 5, *L* = *a*<sub>2</sub> – *a*<sub>1</sub>) and dielectric constant *D<sub>shell</sub>* modeled as two concentric spheres is<sup>74</sup>

$$C_{SP} = 4\pi\epsilon_0 D_{shell} a_1 a_2 / (a_2 - a_1) \quad (31)$$

where *a*<sub>1</sub> is the radius of the metal core. For *a*<sub>1</sub> ~ *L* ~ 1 nm, *C<sub>SP</sub>* ~ 2 × 10<sup>-17</sup> F in an aqueous medium. (For *a*<sub>2</sub> ≫ *a*<sub>1</sub> Equation (31) reduces to the expression for the capacity of a sphere in a medium of dielectric constant *D<sub>shell</sub>* = *D<sub>s</sub>*, while for *L* ≪ *a*<sub>1</sub> Equation (31) reduces to that for the capacity of a planar electrode.) Because of their very small capacities, double-layer charging or discharging of a planar or spherical metal nanoparticle produces relatively large potential changes. As a consequence, transfer of an electron to or from the nanoparticle can only occur at voltage intervals. For a spherical particle with *C<sub>SP</sub>* ~ 2 × 10<sup>-17</sup> F this voltage interval, Δ*V* = *e*/*C<sub>SP</sub>*, is ~10 mV. For *a*<sub>1</sub> ~ *L* ~ 1 nm, and *D<sub>shell</sub>* ~ 3, *C<sub>SP</sub>* ~ 10<sup>-18</sup> F and *e*/*C<sub>SP</sub>* is about 200 mV. The voltage quantization leads to the so-called Coulomb blockade and Coulomb staircase effects for metal particles. The dependence of the particle capacitance on radius shown in Figure 10 is very similar to that obtained from the core-shell-solvent model (Equation (29), Figure 9).

Murray and co-workers apply the term “monolayer protected clusters” (MPCs) to metal clusters of diameter less than ~10 nm stabilized by a monolayer of alkanethiolates and other thiolates.<sup>75</sup> According to a model,<sup>74</sup> the potential of a MPC in solution is related to its charge by

$$E_P = E_{PZC} + ze/C_{MPC} \quad (32a)$$



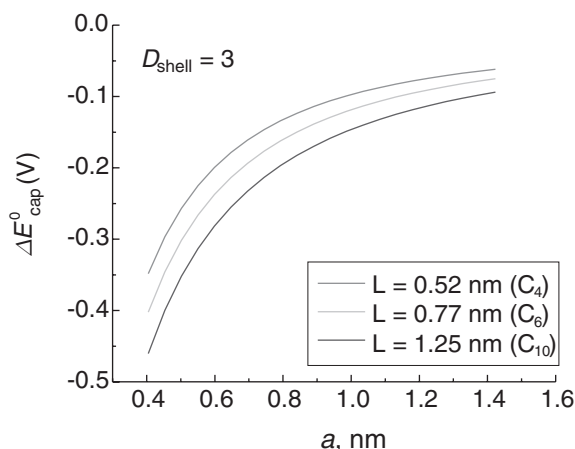


**Figure 10** Dependence of the particle capacitance on radius (Equation (30)).

where  $z$  is the number of charges on the cluster and  $E_{PZC}$  is the potential of zero charge of the cluster (i.e.,  $z = 0$ ).  $E_P$  is size dependent through the medium polarization contribution as in Equation (29). To the extent that  $E_{PZC}$  is independent of size it can be identified with  $E_{\infty}^0$  (Equation (28)).<sup>67</sup> MPCs can exhibit a range of one-electron redox processes; stepwise oxidation/reduction has been observed for  $z = 0$  to  $+7$  and  $z = 0$  to  $-6$ .<sup>76</sup> From the electrostatic work required to charge the MPC to potential  $E_P$ , the formal potential  $E^0(z, z - 1)$  of a mixture of MPC particles having charges  $z$  and  $z - 1$  in equal number is

$$E^0(z, z - 1) = E_{PZC} + (2z - 1)e/2C_{MPC} \quad (32b)$$

Substituting for  $C_{MPC}$  in Equation (32b) gives

$$\Delta E^0 = \frac{0.72}{D_{shell}} \left[ \frac{1}{a_1} - \frac{1}{a_2} \right] \text{eV} \quad (a \text{ in nm}) \quad (32c)$$

which is the first term in Equation (29b). The second term is absent because, in the capacitance model, the charge on the MPC is neutralized by a layer of counterions so that there is no net charge experienced by the external medium. The mixture of MPCs can thus be viewed as a multivalent redox system with the spacing between redox potentials remaining equal to  $e/C_{MPC}$  provided  $C_{MPC}$  is independent of the charge state of the MPC. A further transition from the above quantized double-layer capacitance charging to molecule-like redox charging occurs as the core size is decreased further ( $\square 100$  atoms).<sup>72,77</sup>

Before the onset of specific size-dependent properties, the reduction potentials of the metal clusters can be estimated from considerations given in Section 7.12.4.1. The (absolute) potential of zero charge of the particle (Equation (32)) is identified with or approximated as the work function of the metal<sup>67</sup> (cf. p 1151 of Bockris and Reddy<sup>78</sup>) and then polarization/capacitive effects are included. It should be noted that  $E_{\infty}^0$  differs from the reduction potential for the  $M/M^+$  couple because the latter refers to  $M^+$  in solution;  $E_{\infty}^0$  refers to  $M^+$  formed/reduced within the metal. Because of the relatively small range of metal work functions, the  $E_{\infty}^0$  values obtained through this approach (Table 4) exhibit a surprisingly small range.

### 7.12.3.5 Semiconductor Clusters

Additional issues arise when reduction of the size of a semiconductor is considered. In bulk semiconductors the valence and conduction bands bend. Because of the low carrier concentration, the electrical double layer in a bulk semiconductor/solution system extends into the interior of the semiconductor rather than into the solution. In terms of the Gouy–Chapman model,<sup>79</sup> the width of a diffuse double layer is inversely proportional to the square root of the carrier concentration: for a typical semiconductor carrier concentration of  $10^{15} \text{cm}^{-3}$  the band bending is calculated to occur over several hundred nanometers (in which region there is about one carrier).

**Table 4** Work function values<sup>a</sup> and particle reduction potential estimates as a function of metal.

<i>Metal</i>	$E_{\text{vac}}(\text{eV})$	$E_{\text{s}}^0(\text{V vs. NHE})$	<i>Metal</i>	$E_{\text{vac}}(\text{eV})$	$E_{\text{s}}^0(\text{V vs. NHE})$
Ag	4.3	-0.2	Ge	4.1	-0.4
Al	4.2	-0.3	Hg	4.5	0
Au	5.1	0.6	Ir	4.6	0.1
Au	5.4	0.9	Mn	3.8	-0.7
C	4.8	0.3	Ni	5.2	0.7
Cd	4.1	-0.4	Os	5.9	1.4
Ce	2.8	-1.7	Pd	4.6	0.1
Co	4.1	-0.4	Pt	4.8	0.3
Cr	4.4	-0.1	Re	4.8	0.3
Cs	1.8	-2.7	Rh	4.9	0.4
Cu	4.5	0	Ru	4.5	0.0
Fe	4.2	-0.3	Ti	4.2	-0.3
Ga	3.8	-0.7	V	4.4	-0.1

<sup>a</sup> Work function values from Haas.<sup>65</sup>

Consequently, negligible band bending takes place over nanoparticle dimensions, and the valence and conduction bands in a semiconductor nanoparticle can be considered as flat for all practical purposes: an electron injected into the conduction band of a semiconductor nanoparticle is not subjected to any *intrinsic* energy gradients driving it to or from the surface. In this respect, the manifestations of size reduction are observed much sooner (at much larger size) for semiconductors than for metals.

In the intermediate size regime the expressions for the size dependence of the electrostatic properties of semiconductor particles in a polar medium ( $D_{\text{in}} \ll D_{\text{s}}$ ) bear some resemblance to those of metals. For simplicity we assume the charge  $ze$  to be localized at the center of the particle of radius  $a$  in a sphere of radius  $\delta$  ( $\delta \ll a$ ). The electrostatic energy of the dielectric sphere is (see Equation (10a))<sup>80</sup>

$$G^{\text{D}} = \frac{(ze)^2}{2D_{\text{in}}\delta} + \frac{(ze)^2}{2a} \left( \frac{1}{D_{\text{s}}} - \frac{1}{D_{\text{in}}} \right) \quad (33a)$$

and when  $D_{\text{s}} \gg D_{\text{in}}$ , Equation (33a) reduces to

$$G^{\text{D}} = \frac{(ze)^2}{2D_{\text{in}}} \left( \frac{1}{\delta} - \frac{1}{a} \right) \quad (33b)$$

Equation (33a) leads to the following expressions for the ionization energy, electron affinity, and reduction potential for a neutral semiconductor particle in a polar medium provided that  $\delta$  is not a function of  $a$ :

$$IP_r = IP_{\infty} + \frac{(2z+1)e^2}{2a} \left[ \frac{1}{D_{\text{s}}} - \frac{1}{D_{\text{in}}} \right] \quad (34a)$$

$$EA_r = EA_{\infty} + \frac{(2z-1)e^2}{2a} \left[ \frac{1}{D_{\text{s}}} - \frac{1}{D_{\text{in}}} \right] \quad (34b)$$

$$E_r^0 = E_{\infty}^0 + \frac{(2z-1)e}{2a} \left[ \frac{1}{D_{\text{s}}} - \frac{1}{D_{\text{in}}} \right] \quad (34c)$$

Equations (34a) and (34b) correspond to Equations (25) and (26) for a metal particle. The same result is obtained for a spherically symmetric (1S) charge distribution (Equation (10) with neglect of  $\delta\Sigma$ ). Evidently the expressions for a metal particle reduce to those for a semiconductor when  $1/D_{\text{s}}$  for the outer medium is replaced by  $1/D_{\text{s}} - 1/D_{\text{in}}$  for the semiconductor particle. For a bulk

semiconductor, in contrast to bulk metal,  $IP_{\infty} \neq EA_{\infty}$ . Depending on its charge and the relative magnitudes of  $D_s$  and  $D_{in}$ , the particle may be more or less electron accepting or donating than the bulk material. Also, the direction of the size dependence will depend on the sign of  $(1/D_s - 1/D_{in})$ .

Reductions of polyoxometallates exhibit the linear dependence on  $z$  predicted by Equation (34c) in both  $M = Mo$  and  $W$ ,  $XM_{12}O_4^{n-}$  ( $X = P, Si, Ge, Zn$ , etc.) Keggin systems in water and organic solvents with slopes ranging from  $-0.2$  V per unit charge in water<sup>81</sup> to ca.  $-0.4$  V per unit charge in organic solvents<sup>82</sup> consistent with a  $D_{in}$  value of  $\sim 7$ . The size-dependent bandgap has been observed electrochemically for 4 nm, thioglycerol-capped CdS particles and the position of the one-electron reduction shifts ca.  $-0.25$  V on going from a 4.5 nm particle (bandgap of 3.06 eV) to a 3.9 nm particle (bandgap of 3.23 eV).<sup>83</sup>

The change in electron affinity or energy gap of a semiconductor (or metal cluster) with particle size can be used to modify the driving force for electron transfer. For example, electron transfer between large photoexcited CdS and TiO<sub>2</sub> particles proceeds quite rapidly since the bottom of the conduction band of nonquantized TiO<sub>2</sub> lies  $\sim 0.5$  eV below that of CdS. However, the conduction band of TiO<sub>2</sub> can be raised above that of CdS by decreasing the TiO<sub>2</sub> particle size. Thus, while electron transfer from photoexcited 3.6 nm diameter CdS nanoparticles to 1.2 nm diameter TiO<sub>2</sub> particles proceeds competitively with emission from the excited CdS, the electron transfer to smaller ( $\leq 1.0$  nm diameter) TiO<sub>2</sub> particles is uphill and does not occur (i.e., no emission quenching is observed).<sup>84</sup>

### 7.12.3.6 Soluble or Dispersed Nanoparticles: Coordination and Colloid Chemistry

To study solutions of either metal or semiconductor particles in the nanometric regime the particles must be coated by a protective layer to prevent their aggregation to the bulk material. Thiolate- or selenate-enveloped metal and semiconductor particles can be thought of as stabilized by a coordination shell, e.g.,  $Au^+S-R$ ,  $Cd^+Se-R$ . For Au, the shell appears to be stable with respect to thiol loss as the particles are charged with up to five electrons or holes (although there is evidence that displacement of one thiol by another is accelerated by cluster oxidation<sup>85</sup>). Similarly, the capping of II-VI (e.g., CdSe, CdS) semiconductor particles by R-Se groups confers molecule-like properties on the assemblies such that they (like MPCs) can be isolated from solution, subjected to chromatography, etc.<sup>41,86,87</sup> By contrast, at the weak adsorbate extreme, "bare" semiconductor nanoparticles in solution are stabilized in the colloidal state by a charged double layer or by the adsorption of a polymer. For the classical (10–20 nm) gold citrate particles<sup>46</sup> the protective layer of citrate is considered not to be very specifically bound, but rather to be stabilized by double-layer effects. The metal core is positively charged and adsorbs the citrate by electrostatic and van der Waals forces so that the particle acquires an overall negative charge. This negative charge attracts a layer of cations so that the metal core is surrounded by a double layer of ions. The kinetic stability of such particles arises from the activation barrier associated with interpenetration of the double layers of different particles.<sup>88</sup> This activation barrier decreases with the attractive force between particles (the Hamaker constant  $A$ ), with increasing ionic strength, and with decreasing surface potential.

The electrostatic work associated with bringing freely diffusing particles with charges  $z_1e$  and  $z_2e$  together (to aggregate or to undergo a charge transfer reaction) to a center-to-center separation of  $d_{12}$  in a medium of dielectric constant  $D_s$  and ionic strength  $\mu$  is<sup>89</sup>

$$W = \frac{z_1 z_2 e^2}{2D_s d_{12}} \left( \frac{\exp(\beta\sigma_1\sqrt{\mu})}{1 + \beta\sigma_1\sqrt{\mu}} + \frac{\exp(\beta\sigma_2\sqrt{\mu})}{1 + \beta\sigma_2\sqrt{\mu}} \right) \exp(-\beta d_{12}\sqrt{\mu}) \quad (35)$$

where  $\beta = (8\pi N_A e^2 / 1000 D_s k_B T)^{1/2} = 3.29 \text{ nm}^{-1}$  for water at 298 K and  $\sigma_i$  is the radius of the particle including its protective shell ( $a_{\text{core}} + L$ ), which is assumed to be impenetrable. More detailed expressions have been given.<sup>88</sup>

### 7.12.4 FRAMEWORK AND MODELS

The subject of molecular electron transfer is covered in Chapter 7.11 and the reader is referred there for background and detailed theoretical treatment. The purpose of this section is to develop a notation and set of expressions that will provide a framework for discussing charge transfer

processes in the range of settings needed for a coherent treatment of charge transfer on the nanoscale.

### 7.12.4.1 Energy Scales and Absolute Potentials

When considering the energy changes associated with electron transfer across a phase boundary it is necessary to refer the energy levels on either side of the boundary to the same reference state.<sup>79</sup> The potentials of redox couples in solution are generally expressed relative to the normal hydrogen electrode (NHE):



In terms of the Nernst equation:

$$E = E^0 + \frac{RT}{nF} \ln \frac{[A]}{[A^{n-}]} \quad (37)$$

The free energy change for the addition of  $n$  electrons to  $A$  vs. NHE is then

$$\Delta G^0 = -nE^0 \text{ eV molecule}^{-1} = -neE^0 \text{ J molecule}^{-1} \quad (38a)$$

$$= -nN_A E^0 \text{ eV mol}^{-1} = -nFE^0 \text{ J mol}^{-1} \quad (38b)$$

where  $F$  is the Faraday constant,  $e = F/N_A$ , with  $F = 96,500 \text{ C mol}^{-1}$ ,  $e$  is the absolute value of the charge on the electron and 1 eV is the energy needed to accelerate one electron through a potential of 1 V. For solids it is more convenient to take the free electron in vacuum as the reference state. Integrating these two reference scales continues to provide a challenge.<sup>67,90,91</sup> Here we take the redox potential of the NHE on the vacuum scale as +4.5 V.<sup>79</sup> This value can be rationalized in a cycle involving the standard hydrogen electrode (standard states 1 M  $\text{H}^+$ , 1 atm  $\text{H}_2$ ) and ionization of the “equilibrated” Pt electrode.

The potential of the couple on the vacuum scale is related to that of the NHE by the amount of work required to transfer an electron from the NHE to vacuum:

$$e^-(\text{Pt}) = \text{Pt} + e^-(\text{vac}) \quad \Delta G^0 = 4.5 \text{ eV} \quad (39a)$$

$$\text{H}^+_{\text{aq}} + e^-(\text{Pt}) = 1/2\text{H}_{2\text{g}} + \text{Pt} \quad \Delta G^0 = 0 \text{ eV} \quad (39b)$$

$$\text{H}^+_{\text{aq}} + e^-(\text{vac}) = 1/2\text{H}_{2\text{g}} \quad \Delta G^0 = -4.5 \text{ eV} \quad (39c)$$

More generally, the “absolute” energy of the transferring electron of a redox couple on the vacuum-level scale (denoted here by a prime) is given by

$$E'(\text{in eV}) = -[4.5 + E^0(\text{V vs. NHE})] \quad (40)$$

These quantities are illustrated in [Figure 11](#). Also shown is the distribution of occupied levels in a metal electrode in equilibrium with a redox couple (equimolar oxidized and reduced forms) of  $E^0 = 0.6 \text{ V}$  calculated from the Fermi-Dirac distribution function

$$f(\varepsilon) = \frac{1}{1 + \exp[\varepsilon/k_B T]} \quad (41)$$

where  $\varepsilon$  is the energy of the electrode level relative to its Fermi level. Since the metal and redox couples are in equilibrium their Fermi levels are each equal to  $-5.1 \text{ eV}$ .

How is this equilibration of the Fermi levels of metal and redox couple achieved? Consider a platinum electrode that is not connected to a power supply and an aqueous solution containing the electron acceptor  $A$  in [Figure 11](#) at a concentration of 1 mM and  $0.4 \mu\text{M}$  of its singly reduced

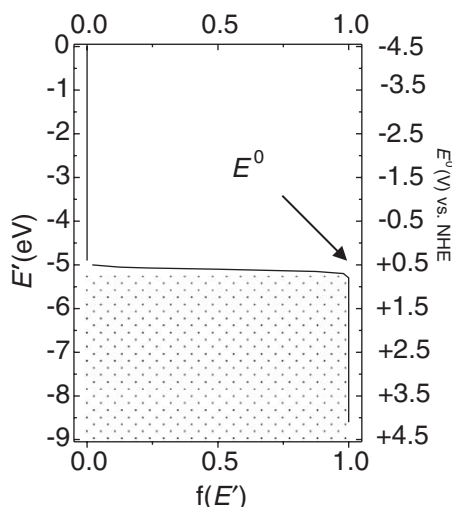


**Figure 11** Relationship between energy levels relative to an electron in vacuum and electrode potentials vs. the normal hydrogen electrode.

form  $A^-$ . Using the estimated potential of zero charge given in Table 4, the initial  $E_F$  of the platinum is +0.3 V. As soon as the platinum is immersed in the solution it will transfer electrons to the acceptor and acquire a positive charge. At the same time the solution near the electrode will acquire a negative charge, thereby creating a double layer of charge and its associated capacitance (Equation (42)). The resulting electric field across the interface serves to oppose the electron transfer from the platinum to  $A$  and promote the slower reverse electron transfer from  $A^-$  to the platinum. The forward and reverse electron transfers continue until their rates become equal and equilibrium is established. Once equilibrium is established the charge on the metal remains constant, as does the potential difference  $E_{eq}$  across the interface. Although no net current is flowing, the system is in dynamic equilibrium, with the electrochemical potential of the electron being the same in the platinum and in solution (equal to  $E_F$ , the Fermi energy). Further, the equality of the forward and reverse rates requires that

$$k_0[A]_{eq} \exp[-(E_{eq} - E^0)F/2RT] = k_0[A^-]_{eq} \exp[(E_{eq} - E^0)F/2RT] \quad (43a)$$

or

$$[A]_{eq}/[A^-]_{eq} = \exp[(E_{eq} - E^0)F/RT] \quad (43b)$$

where  $k_0$  is the exchange rate constant. This is a statement of the Nernst equation, derived here from kinetic considerations. In practice, only an infinitesimal amount of charge needs be transferred for the metal to acquire the Nernst potential of the  $A/A^-$  couple: for a typical double-layer capacity of  $20 \times 10^6 \text{ F cm}^{-2}$  only  $\sim 10^{14}$  electrons  $\text{cm}^{-2}$  are required for a 0.5 V potential difference.<sup>78,79</sup> For  $1 \text{ cm}^2$  Pt in contact with the solution above, the  $10^{-10}$  mol of electrons released to the solution increase  $[A^-]$  by 20% when the Pt is immersed in 1 mL of solution, thereby shifting the solution potential  $-9 \text{ mV}$  from the initial 0.80 V vs. NHE.

#### 7.12.4.2 Relating Rate Constant and Conductance

In studies of molecular charge transfer systems a transient method is generally used to determine an electron transfer rate constant from the variation of the concentration of a reactant or product as a function of time. By contrast, in characterizing charge transfer processes in electrochemical cells or at metal–molecule–metal junctions the parameter of interest is usually the resistance or conductance (reciprocal of resistance) of the cell or junction. The conductance of the cell or junction is generally determined from the variation of the current through the system as a function of applied voltage. Here we briefly consider the relationship between electron transfer rate constants and conductances.

Consider a cell consisting of two bulk metal electrodes connected by a molecular wire.<sup>92</sup> The current flowing from the donor to the acceptor electrode is obtained by summing the processes occurring through all of the wire states that lie between the Fermi energies of the two electrodes:

$$I = \int_{-eV}^0 g(\varepsilon) f_D(\varepsilon) [1 - f_A(\varepsilon + eV)] d\varepsilon / e \quad (44a)$$

where  $g(\varepsilon)$  is the conductance at energy  $\varepsilon$ ,  $V$  is the applied voltage (the Fermi level of the donor electrode defines the zero of energy), and the electron distribution functions  $f_D$  and  $f_A$  are given by Equation (41).<sup>92</sup> The net current flowing, the difference between currents in the forward and reverse directions, is given by the following equation when the system is close to equilibrium:

$$I = \int_{-eV}^0 g(\varepsilon) [f_D(\varepsilon) - f_A(\varepsilon + eV)] d\varepsilon / e \quad (44b)$$

Further, when the applied voltage is small the electron distribution functions can be expanded and a linear relationship between current and applied voltage obtains. This is the Ohm's law regime. In this regime the conductance is

$$g(E_F) = I/V \quad (44c)$$

For systems with more complex  $I$ - $V$  relationships,  $g$  at a particular voltage is calculated from  $dI/dV$ . The conductance of the above cell near equilibrium is related to the equilibrium (exchange) current by<sup>8</sup>

$$g^0 = eI_0/k_B T \quad (45a)$$

where  $g^0 = (dI/dV)_{V=0}$ . The exchange current  $I_0$  (per molecule) is related to the standard first-order rate constant<sup>79</sup>  $k^0$  by  $I_0 = ek^0$ , so that the equilibrium conductance  $g^0$  is simply

$$g^0 = e^2 k^0 / k_B T \quad (45b)$$

The conductance of a metal-molecule-metal junction is also given by the Landauer formula which relates the linear conductance to the electron transmission coefficient  $T_n$ <sup>8</sup>

$$g = \frac{2e^2}{h} T_n(E_F) \quad (46a)$$

where  $E_F$  is the Fermi level of the contacts at zero voltage bias. For  $T_n = 1$ ,  $g = 2e^2/h = (12.8 \text{ k}\Omega)^{-1}$ , the maximum conductance per molecule. Comparison of Equations (45b) and (46a) shows that the transmission coefficient is

$$T_n(E_F) = \frac{h}{2k_B T} k^0 \quad (46b)$$

The Landauer expression, which was derived for elastic transmission, can be extended to accommodate inelastic processes for the limiting case of a junction characterized by a small overall voltage bias, and an energy for charge injection into the wire small compared to  $k_B T$ .<sup>93,94</sup>

The use of metal–molecule–metal junctions as gates in circuits has generated much interest; it appears that either chemical or electrical tuning of the molecule energy levels may be used to control the current in molecular junctions.<sup>95</sup>

Finally, it should be noted that Equation (45a) also follows from the linearized Butler–Volmer equation<sup>79</sup> for an electrode in contact with a redox couple in solution. If the solution is well stirred or the currents are so low that the surface concentrations do not differ much from their bulk values then the net current is given by

$$I = I_0 \left[ \exp\left(-\frac{\alpha e(E - E_{\text{eq}})}{k_B T}\right) - \exp\left(\frac{(1 - \alpha)e(E - E_{\text{eq}})}{k_B T}\right) \right] \quad (46c)$$

where  $\alpha$  is the transfer coefficient. For  $E \sim E_{\text{eq}}$  the exponentials can be expanded to give

$$I = I_0 \left[ \left(1 - \frac{\alpha e(E - E_{\text{eq}})}{k_B T}\right) - \left(1 + \frac{(1 - \alpha)e(E - E_{\text{eq}})}{k_B T}\right) \right] \quad (46d)$$

$$I = -\frac{eI_0(E - E_{\text{eq}})}{k_B T} \quad (46e)$$

The negative of the derivative of the net current with respect to  $(E - E_{\text{eq}})$  at  $E \sim E_{\text{eq}}$  then gives Equation (45a). It is apparent from Equation (46d) that the slopes of the forward and reverse currents at  $E \sim E_{\text{eq}}$  depend upon the value of  $\alpha$  and are of opposite sign; when  $\alpha \sim 1/2$  the slopes are equal to one-half the slope of the net current at  $E \sim E_{\text{eq}}$ .

Analogous considerations show that the charge transfer resistance of an isolated DBA molecule is  $e^2 k_{\text{ex}}/k_B T$  ohms, where  $k_{\text{ex}}$  is the first-order electron exchange rate constant for the  $\Delta G^0 = 0$  system.

#### 7.12.4.3 Electronic Coupling Mechanisms in Nanostructures and Distance Dependences

In a D–B–A system in which direct interaction of donor and acceptor is negligible, the interaction between donor (D) and acceptor (A) orbitals through a molecular bridge (B) can determine the magnitude of the electronic coupling and the electron transfer mechanism. The donor HOMO and acceptor LUMO are located in the gap between the bridge HOMO and LUMO. The nature, magnitude, and energetics of the electronic interaction of the separated donor-acceptor sites determine whether the electron transfer proceeds by a coherent tunneling process (superexchange; exponential dependence on the separation distance), in which the electron never resides on the bridge, or involves thermally activated (or nonactivated) reduction of the bridge. Superexchange is mediated by the virtual charge transfer states  $D^+B^-A$  or  $DB^+A^-$  (for electron and hole transfer, respectively) although these states are not actually populated in a superexchange mechanism.

The exponential dependence of the superexchange (semiclassical, “sc”) rate constant  $k_{\text{sc}}$  on separation distance  $d_{\text{DA}}$  is commonly expressed as

$$k_{\text{ct}} = k_{\text{sc}} = k_0 \exp(-\beta_r d_{\text{DA}}) \quad (47)$$

where  $k_0$  contains the distance dependence of the nuclear factor.<sup>96</sup> In a superexchange model

$$\beta_r = -(2/a) \ln(H_{\text{BB}}/\Delta E_{\text{DB}}) \quad (48)$$

where  $H_{\text{BB}}$  is the internal bridge unit/bridge unit coupling energy,  $a$  is the bridge unit length, and  $\Delta E_{\text{DB}}$  is the energy of the mediating state ( $D^+B^-A$  or  $DB^+A^-$ ) above the ground state (Figure 12).

In the second mechanism the electron (or hole) actually resides on the bridge and may be delocalized over the entire bridge or diffuse by hopping between bridge sites. This is the so-called “chemical” mechanism. The charge transfer states  $D^+B^-A$  or  $DB^+A^-$  are real, rather than virtual. When diffusive hopping between bridge sites becomes rate limiting, the distance dependence of the electron transfer is Ohmic, i.e.<sup>93</sup>

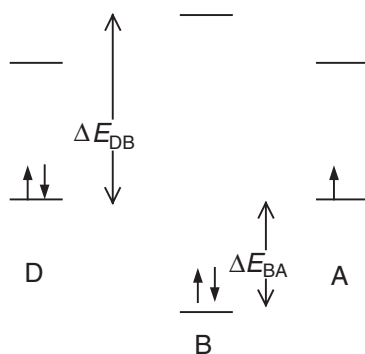


**Figure 12** Energy gaps relevant for electron- and hole-mediated superexchange.

$$k_{\text{et}} = k_{\text{hop}} \propto 1N \quad (49a)$$

When  $\Delta E_{\text{DB}}$  is positive, the rate depends on this energy gap:

$$k_{\text{et}} \propto (1N)\exp(-\Delta E_{\text{DB}}/k_{\text{B}}T) \quad (49b)$$

In general, the two pathways operate in parallel:

$$k_{\text{et}} = k_{\text{sc}} + k_{\text{hop}} \quad (50)$$

When both contribute significantly to the rate, a region of distance independence of the rate may occur. The different temperature dependences of the two pathways can be used to clarify the relative importance of each.

#### 7.12.4.4 Activation Barriers

The activation barrier for electron transfer  $\Delta G^*_{\text{DA}}$  is

$$\Delta G^*_{\text{DA}} = (\lambda_{\text{DA}} + \Delta G^0)^2/4\lambda_{\text{DA}} \quad (51)$$

where  $\lambda_{\text{DA}}$  is comprised of outer-shell or solvent contributions and inner-shell contributions:

$$\lambda_{\text{DA}} = \lambda_{\text{in}} + \lambda_{\text{out}} \quad (21)$$

Outer- and inner-sphere reorganization requirements for molecular electron transfer are described in detail in Chapter 7.11.

##### 7.12.4.4.1 Inner-shell barrier

Inner-shell or molecular reorganization  $\lambda_{\text{in}}$  or  $\chi_{\text{M}}$  derive from the changes in molecular structure that occur upon electron transfer. In terms of metal complexes as reactants, changes in metal–ligand distances ( $\Delta d_{\text{ML}}$ ), force constants ( $f_{\text{ML}}$ ), and angles must be included; for example

$$\lambda_{\text{in}} = \chi_{\text{M}} = 2 \sum_{\text{bonds}} \frac{f_{\text{ML}}^{\text{A}} f_{\text{ML}}^{\text{D}}}{f_{\text{ML}}^{\text{A}} + f_{\text{ML}}^{\text{D}}} (\Delta d_{\text{ML}})^2 \quad (52)$$

for a self-exchange reaction. In general, for nanoscale redox systems based on metal complexes  $\lambda_{\text{in}}$  for the molecular components will provide a useful estimate of  $\lambda_{\text{in}}$  in the larger system. At this juncture there is a dearth of structural information for estimation of  $\lambda_{\text{in}}$  for nanoparticles, with the exception of silicon nanoparticles (see Section 7.12.5.5).



### 7.12.4.4.2 Medium reorganization barrier

The outer-sphere contribution to the reorganization energy arises from the reorientation of charge in the medium. Its magnitude depends on the radii of the donor and acceptor sites, on their separation, and on the dielectric properties of the donor, the acceptor, and the medium.

#### (i) Conducting spheres in a dielectric medium

For spherical reactants of radii  $a_D$ ,  $a_A$ , separated by  $d_{DA}$  in a solvent of static dielectric constant  $D_s$  and optical dielectric constant  $D_{op}$  (= square of index of refraction  $n$ ), when  $d_{DA} \gg a_D + a_A$ , Marcus has given for conducting spheres

$$\lambda_{out} = \chi_s = (\Delta q)^2 \left( \frac{1}{2a_A} + \frac{1}{2a_D} - \frac{1}{d_{DA}} \right) \left( \frac{1}{D_{op}} - \frac{1}{D_s} \right) \quad (54a)$$

When the mutual polarization of the spheres is included in a uniform field approximation, sphere A induces an image dipole  $q_A a_D^3 / d_{DA}^2$  within sphere D (charge  $+q_A a_D / d_{DA}$  at the center and charge  $-q_A r_D / d_{DA}$  a distance  $r_D^2 / d_{DA}$  away) and vice versa. Even neglecting higher multipole effects, 12 integrals over the surface of each sphere need to be calculated.<sup>97</sup> Provided that  $d_{DA} \gg a_D$ ,  $a_A$ , the rather cumbersome expression for  $\lambda_{out}$  reduces to

$$\lambda_{out} = (\Delta q)^2 \left( \frac{1}{2a_A} + \frac{1}{2a_D} - \frac{(1+\gamma)}{d_{DA}} \right) \left( \frac{1}{D_{op}} - \frac{1}{D_s} \right) \quad (54b)$$

with  $\gamma = \gamma^c$  for two conducting spheres given by<sup>98,99</sup>

$$\gamma^c = (a_A^3 + a_D^3) / 2d_{DA}^3 \quad (54c)$$

Within this approximation

$$\lambda_{out}^C = 0.79 \left[ \frac{1}{2a_A} + \frac{1}{2a_D} - \frac{1}{d_{DA}} - \frac{(a_A^3 + a_D^3)}{2d_{DA}^4} \right] \text{eV in H}_2\text{O, 298 K, } \Delta q = 1e \quad (54d)$$

Exact expressions for conducting spheres, including multipole effects at separations down to  $(a_A + a_D)$ , are available.<sup>99</sup>

#### (ii) Dielectric spheres in a dielectric medium

In the case of two dielectric spheres with dielectric constants  $D_{in,A}$  and  $D_{in,D} \neq \infty$ , the image dipole moment induced at the center of sphere D by sphere A is  $q_A a_D^3 (D_{in,D} - D_s) / d_{DA}^2 (2D_s + D_{in,D})$  and vice versa.<sup>98,100</sup> Again neglecting multipole effects,  $\gamma$  is given by

$$\gamma^D = \frac{1}{2d_{DA}^3} \left[ (a_A^3 + a_D^3) - \frac{6D_s^2 a_A^3}{(2D_s + D_{in,A})^2} - \frac{6D_s^2 a_D^3}{(2D_s + D_{in,D})^2} \right] \quad (55a)$$

When  $D_{in,A} = D_{in,D} = D_{in} \neq \infty$ , the solvent reorganization energy reduces to<sup>98,100</sup>

$$\lambda_{out}^D = (\Delta q)^2 \left[ \frac{1}{2a_A} + \frac{1}{2a_D} - \frac{1}{d_{DA}} - \frac{(a_A^3 + a_D^3)}{d_{DA}^4} \left[ \frac{1}{2} - \frac{3D_s^2}{(2D_s + D_{in})^2} \right] \right] \left( \frac{1}{D_{op}} - \frac{1}{D_s} \right) \quad (55b)$$

When  $D_s \gg D_{in}$ , as is the case in a polar liquid, Equation (55b) reduces to

$$\lambda_{out}^D = (\Delta q)^2 \left[ \frac{1}{2a_A} + \frac{1}{2a_D} - \frac{1}{d_{DA}} + \frac{(a_A^3 + a_D^3)}{4d_{DA}^4} \right] \left( \frac{1}{D_{op}} - \frac{1}{D_s} \right) \quad (55c)$$

Comparison of Equations (54d) and (55c) shows that, for polar solvents, the solvent reorganization energy is always smaller for a conducting sphere than for a dielectric sphere. Exact expressions for dielectric spheres have been published.<sup>101</sup>

(iii) *A conducting sphere and a dielectric sphere in a dielectric medium*

It follows from Equations (54d) and (55b) that, within the above framework, the solvent reorganization energy for charge transfer from a conducting sphere D to a dielectric sphere A is given by

$$\lambda_{\text{out}}^{\text{C,D}} = (\Delta q)^2 \left( \frac{1}{2a_A} + \frac{1}{2a_D} - \frac{1}{d_{DA}} - \frac{1}{d_{DA}^4} \left[ \frac{(a_A^3 + a_D^3)}{2} - \frac{3D_s^2 a_A^3}{(2D_s + D_{\text{in,A}})^2} \right] \right) \left( \frac{1}{D_{\text{op}}} - \frac{1}{D_s} \right) \quad (56)$$

(iv) *Two conducting spheres in different dielectric media*

Next is considered the more general case of two conducting spheres in different dielectric media separated by a planar interface: sphere 1 with charge  $q_1$ , radius  $a_1$ , in medium  $D_1$  a distance  $d_1$  from the interface and sphere 2 in medium  $D_2$  a distance  $d_{12}$  from sphere 1 (Figure 13). The image charge induced by one sphere on the other is ignored since the field produced by a charged sphere is the same as that produced by a point charge at its center, the charged spheres are replaced by point charges.

The existence of the interface introduces further image charge effects. The electrostatic potential  $\Phi_1$  in region 1 can be approximated as the sum of three terms: the potential due to charge  $q_1$ ; the potential due to the image charge  $q'_1 = -q_1(D_2 - D_1)/(D_1 + D_2)$  induced by  $q_1$  and located in medium 2 a distance  $d_1$  from the interface; and the potential due to the effective charge  $2q_2D_1/(D_1 + D_2)$  located at the center of sphere 2.<sup>102</sup> (The latter can be viewed as the difference of two contributions: the real charge  $q_2$  and its image charge  $q'_2 = -q_2(D_1 - D_2)/(D_1 + D_2)$ ; in effect,  $q_2$  induces a pair of charges  $= +q'_2$  and  $-q'_2$  (i.e., a dipole) a distance  $2d_2$  apart.) The potential at the surface of sphere 1 is then given by

$$\Phi_1 = \frac{q_1}{a_1 D_1} - \frac{q_1}{2d_1 D_1} \left[ \frac{D_2 - D_1}{D_1 + D_2} \right] + \frac{2q_2}{d_{12}(D_1 + D_2)} \quad (57a)$$

where  $d_1 \gg a_1$ . Similarly, the potential at the surface of sphere 2 is

$$\Phi_2 = \frac{q_2}{a_2 D_2} - \frac{q_2}{2d_2 D_2} \left[ \frac{D_1 - D_2}{D_1 + D_2} \right] + \frac{2q_1}{d_{12}(D_1 + D_2)} \quad (57b)$$

where  $d_2 \gg a_2$ . The electrostatic free energy of the pair is equal to the work required to charge sphere 1 from 0 to  $q_1$  and sphere 2 from 0 to  $q_2$ :

$$G_s = \int_0^{q_1} \Phi_1 dq_1 + \int_0^{q_2} \Phi_2 dq_2 \quad (58a)$$

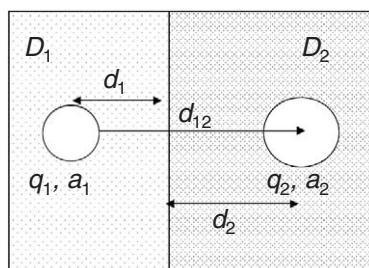


Figure 13 Conducting spheres in different dielectric media.

Setting  $q_1 = \gamma q_1$  and  $q = \gamma q_2$  and integrating over  $\gamma$  from 0 to 1 gives<sup>102</sup>

$$G_s = \frac{q_1^2}{2a_1 D_1} + \frac{q_2^2}{2a_2 D_2} + \left( \frac{q_1^2}{4d_1 D_1} - \frac{q_2^2}{4d_2 D_2} \right) \left[ \frac{D_1 - D_2}{D_1 + D_2} \right] + \frac{2q_1 q_2}{d_{12}(D_1 + D_2)} \quad (58b)$$

The corresponding medium reorganization energy, obtained from Equation (58) in the usual manner,<sup>102</sup> is given by

$$\lambda_{\text{out}} = \frac{(\Delta q)^2}{2a_1} \left( \frac{1}{D_1^{\text{op}}} - \frac{1}{D_1^{\text{s}}} \right) + \frac{(\Delta q)^2}{2a_2} \left( \frac{1}{D_2^{\text{op}}} - \frac{1}{D_2^{\text{s}}} \right) - \frac{2(\Delta q)^2}{d_{12}} \left( \frac{1}{D_1^{\text{op}} + D_2^{\text{op}}} - \frac{1}{D_1^{\text{s}} + D_2^{\text{s}}} \right) + \frac{(\Delta q)^2}{4d_1} \left( \frac{D_1^{\text{op}} - D_2^{\text{op}}}{D_1^{\text{op}}(D_1^{\text{op}} + D_2^{\text{op}})} - \frac{D_1^{\text{s}} - D_2^{\text{s}}}{D_1^{\text{s}}(D_1^{\text{s}} + D_2^{\text{s}})} \right) - \frac{(\Delta q)^2}{4d_2} \left( \frac{D_1^{\text{op}} - D_2^{\text{op}}}{D_2^{\text{op}}(D_1^{\text{op}} + D_2^{\text{op}})} - \frac{D_1^{\text{s}} - D_2^{\text{s}}}{D_2^{\text{s}}(D_1^{\text{s}} + D_2^{\text{s}})} \right) \quad (59)$$

For a one-electron transfer  $\Delta q = e$ . Equation (59) reduces to Equation (54a) for conducting spheres in a single dielectric medium where  $D_1^{\text{op}} = D_2^{\text{op}}$  and  $D_1^{\text{s}} = D_2^{\text{s}}$ .

A useful limiting form of Equation (57a) for the potential of a conducting sphere with charge  $q_1$  at a distance  $d_1$  from a (grounded) planar metal surface is obtained for  $q_2 = 0$  and  $D_2 = \infty$ :

$$\phi_1 = \frac{q_1}{D_1} \left( \frac{1}{a_1} - \frac{1}{2d_1} \right) \quad (60a)$$

The energy of the charged sphere is obtained by integrating  $\phi_1 dq_1$  from 0 to  $q_1$ :

$$G_s = \frac{q_1^2}{D_1} \left( \frac{1}{2a_1} - \frac{1}{4d_1} \right) \quad (60b)$$

The customary procedure then yields

$$\lambda_{\text{out}}^{\text{el}} = (\Delta q)^2 \left( \frac{1}{2a} - \frac{1}{4d} \right) \left( \frac{1}{D_{\text{op}}} - \frac{1}{D_{\text{s}}} \right) \quad (60c)$$

for the solvent reorganization energy associated with transfer of charge  $\Delta q$  between a spherical reactant and a metal electrode.<sup>102</sup> More generally, Equation (60c) is written as

$$\lambda_{\text{out}}^{\text{el}} = (\Delta q)^2 \left( \frac{1}{2a} - \frac{\alpha}{4d} \right) \left( \frac{1}{D_{\text{op}}} - \frac{1}{D_{\text{s}}} \right) \quad (60d)$$

where  $\alpha = 1$  for an ideal metal ( $D_{\text{in}} = \infty$ ) while  $\alpha = 0$  when the metallic screening is quenched (no image correction).<sup>102</sup>

#### (v) One reactant embedded in a dielectric shell

Next we consider two conducting spheres a distance  $d_{12}$  apart in medium  $D_1$ , but with one sphere ( $a_2, q_2$ ) surrounded by a larger dielectric sphere ( $R, D_2$ )<sup>103,104</sup> (see Figure 14). The electrostatic

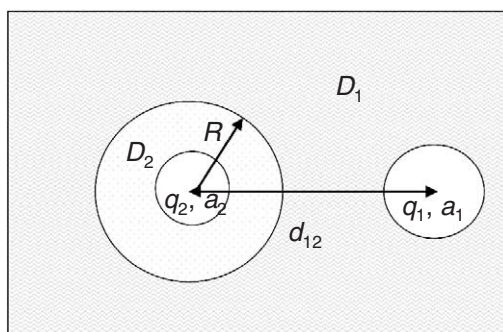


**Figure 14** Two conducting spheres in medium  $D_1$ , with one sphere in a dielectric sphere of  $D_2$ .

potential at the surface of sphere 1,  $\Phi_1$ , is the sum of three terms:  $\phi_1$  due to the charge of sphere 1,  $\phi'_{1,1}$  due to the image charge of sphere 1, and  $\phi_{1,2}$  due to  $q_2$  screened by the dielectrics. The image charge contribution has components due to a discrete charge  $q_1 b_1/R$  located between spheres 1 and 2 at a distance  $b_1 = R^2/d_{12}$  from the center of sphere 2 and higher order image charges between 0 and  $b_1$ :

$$\phi_1 = \frac{q_1}{D_1 a_1} \quad (61a)$$

$$\phi'_{1,1} = \frac{q_1(D_1 - D_2)}{RD_1(D_1 + D_2)} \left( \frac{b_1}{|d_{12} - b_1|} - \frac{D_1}{D_1 + D_2} \int_0^{b_1} \frac{(b_1/x)^{D_2/(D_1+D_2)}}{|d_{12} - x|} dx \right) \quad (61b)$$

$$\phi_{1,2} = \frac{2q_2}{d_{12}(D_1 + D_2)} \quad (61c)$$

$\Phi_2$ , the electrostatic potential at the surface of sphere 2, is the sum of terms:  $\phi_2$  due to charge  $q_2$  on sphere 2,  $\phi_{2,2}$  due to the charge of the sphere,  $\phi'_{2,2}$  due to its own image charge,  $\phi_{2,1}$  due to  $q_1$ , and  $\phi'_{2,1}$  due to the image charge of  $q_1$ :

$$\phi_2 = \frac{q_2}{D_2 a_2} \quad (62a)$$

$$\phi'_{2,2} = -\frac{q_2(D_1 - D_2)}{RD_2(D_1 + D_2)} \quad (62b)$$

$$\phi_{2,1} = \frac{2q_1}{d_{12}(D_1 + D_2)} \quad (62c)$$

$$\phi'_{2,1} = -\frac{q_1(D_1 - D_2)}{(D_1 + D_2)^2} \int_{d_{12}}^{\infty} \frac{(x/d_{12})^{D_2/(D_1+D_2)}}{x^2} dx \quad (62d)$$

The electrostatic free energy of the spheres is obtained by integration of  $\phi dq$  from 0 to  $q$ , as before

$$G_s = \frac{q_1}{2} \phi_1 + \frac{q_2}{2} \phi_2 \quad (63)$$

leading to the following expression for the solvent reorganization energy:

$$\begin{aligned} \lambda_{\text{out}} = & \frac{(\Delta q)^2}{2a_1} \left( \frac{1}{D_1^{\text{op}}} - \frac{1}{D_1^{\text{s}}} \right) + \frac{(\Delta q)^2}{2a_2} \left( \frac{1}{D_2^{\text{op}}} - \frac{1}{D_2^{\text{s}}} \right) - \frac{2(\Delta q)^2}{d_{12}} \left( \frac{1}{D_1^{\text{op}} + D_2^{\text{op}}} - \frac{1}{D_1^{\text{s}} + D_2^{\text{s}}} \right) \\ & - \frac{(\Delta q)^2}{2R} \left( \frac{(D_1^{\text{op}} - D_2^{\text{op}})^2}{D_1^{\text{op}} D_2^{\text{op}} (D_1^{\text{op}} + D_2^{\text{op}})} - \frac{(D_1^{\text{s}} - D_2^{\text{s}})^2}{D_1^{\text{s}} D_2^{\text{s}} (D_1^{\text{s}} + D_2^{\text{s}})} \right) + \frac{(\Delta q)^2}{2} \left[ \left( \frac{\phi'_{1,1}}{q_1} \right)^{\text{op}} - \left( \frac{\phi'_{1,1}}{q_1} \right)^{\text{s}} \right] \\ & + \frac{(\Delta q)^2}{2} \left[ \left( \frac{\phi'_{2,2}}{q_2} \right)^{\text{op}} - \left( \frac{\phi'_{2,2}}{q_2} \right)^{\text{s}} \right] \end{aligned} \quad (64)$$

The above expression reduces to the two-sphere expression when  $D_1^{\text{op}} = D_2^{\text{op}}$  and  $D_1^{\text{s}} = D_2^{\text{s}}$ .

#### (vi) Model for a self-assembled monolayer

In studies of self-assembled monolayers, a redox active group (to be modeled as a conducting sphere of radius  $a$ ) is positioned at the interface of the organic film (of thickness  $L$ ) and aqueous solution. Electron transfer is between the redox active group and a metal electrode. The three dielectric zones are the aqueous phase 1, the organic film 2, and the electrode 3 (Figure 15).

With use of cylindrical symmetry, the solvent reorganization barrier is given by the summation in Equation (65):<sup>105</sup>

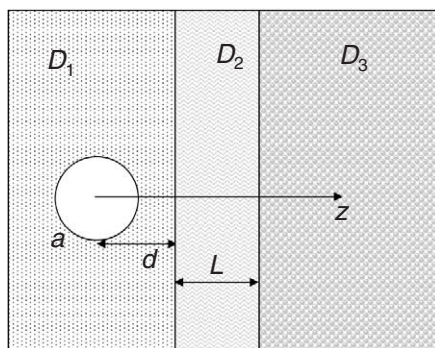


**Figure 15** Model for electron transfer between a redox-active group of radius  $a$  to a planar electrode through a SAM of thickness  $L$ .

$$\lambda_{\text{out}} = \frac{(\Delta q)^2}{2a} \left( \frac{1}{D_1^{\text{op}}} - \frac{1}{D_1^{\text{s}}} \right) - \frac{(\Delta q)^2}{4d} \left( \frac{D_1^{\text{op}} - D_2^{\text{op}}}{D_1^{\text{op}}(D_1^{\text{op}} + D_2^{\text{op}})} - \frac{D_1^{\text{s}} - D_2^{\text{s}}}{D_1^{\text{s}}(D_1^{\text{s}} + D_2^{\text{s}})} \right) + \sum_{n=1}^{\infty} \frac{(\Delta q)^2}{d + nL} \left( \frac{D_2^{\text{op}} \left( \frac{D_1^{\text{op}} - D_2^{\text{op}}}{D_1^{\text{op}} + D_2^{\text{op}}} \right)^{n-1} \left( \frac{D_2^{\text{op}} - D_3^{\text{op}}}{D_2^{\text{op}} + D_3^{\text{op}}} \right)^n}{(D_1^{\text{op}} + D_2^{\text{op}})^2} - \frac{D_2^{\text{s}} \left( \frac{D_1^{\text{s}} - D_2^{\text{s}}}{D_1^{\text{s}} + D_2^{\text{s}}} \right)^{n-1} \left( \frac{D_2^{\text{s}} - D_3^{\text{s}}}{D_2^{\text{s}} + D_3^{\text{s}}} \right)^n}{(D_1^{\text{s}} + D_2^{\text{s}})^2} \right) \quad (65)$$

Truncation of the sum at  $n = 1$ , consistent with the dominance of a single image charge contribution (that associated with the 2–3, film–electrode, interface), gives results very similar to those from the full expression<sup>105</sup> (see Section 7.12.5).

#### 7.12.4.5 Molecular Electron Transfer in Solution

Solution electron transfer reactions can generally be regarded as occurring via a molecule–space/bridge–molecule assembly. For bimolecular reactions, one considers the first-order rate constant for electron transfer within the D–B–A assembly (“precursor complex”).<sup>106</sup>

In the case of an outer-sphere reaction the so-called bridging material is simply the material between the redox centers—solvent molecules and, in the case of metal complexes, ligands surrounding the metal centers. Electron transfer between donor and acceptor sites connected by a molecular bridge is now fairly well understood.<sup>107,108</sup> The rates decrease with increasing separation of the donor and acceptor and can generally be interpreted in terms of a first-order rate constant  $k_{\text{et}}$ :

$$-d[\text{D}]/dt = k_{\text{et}}[\text{D}] \quad (66)$$

that is a function of a combination of electronic and nuclear factors:

$$k_{\text{et}} = \frac{2\pi H_{\text{DA}}^2}{h} \left[ \frac{\pi}{\lambda k_{\text{B}} T} \right]^{1/2} \exp \left[ -\frac{(\lambda + \Delta G^0)^2}{4\lambda k_{\text{B}} T} \right] \quad (67)$$

where  $H_{\text{DA}}$  is the electronic coupling between the donor and acceptor sites,  $\lambda$  is the nuclear reorganization parameter,  $h$  is Planck’s constant, and  $\Delta G^0$ , the standard free energy change for the electron transfer, is  $[E^0(\text{D}/\text{D}^+) - E^0(\text{A}/\text{A}^-)]e$ . For molecular species these parameters may be evaluated through spectroscopic studies of charge transfer band intensities and energies ( $H_{\text{DA}}$ ,  $\lambda$ ), structural and vibrational frequency differences ( $\lambda$ ), and electrochemical or other thermodynamic measurements ( $\Delta G^0$ ).

#### 7.12.4.6 Electron Transfer through Monolayers on Metal Electrodes

For molecular redox reagents such as ferrocene attached to metal electrodes through hydrocarbon chains electronic interaction between the metal and redox center is weak and a nonadiabatic formalism is appropriate. Specifically, it is necessary to consider the density of electronic states in the metal and the coupling between each state and the attached redox center. Under these

conditions the rate constant for electron transfer from the metal to an attached redox group is given by<sup>5,109–114</sup>

$$k_m = \frac{2\pi\rho_{m,\text{eff}}}{h} \left[ \frac{\pi}{\lambda k_B T} \right]^{1/2} \int_{-\infty}^{\infty} [H_{\text{DA}}(\varepsilon)]^2 \exp \left[ -\frac{(\lambda + [E_{\text{app}} - E^0(A/A^-)]e - \varepsilon)^2}{4\lambda k_B T} \right] f(\varepsilon) d\varepsilon \quad (68)$$

where  $\rho_{\text{eff}}$  is the effective density of electronic states in the electrode (assumed independent of energy; 0.3 per atom per eV for Au<sup>111</sup>);  $E_{\text{app}}$  is the applied potential,  $E^0$  is the reduction potential of the redox species vs. NHE, and  $\varepsilon = (\varepsilon_i - \varepsilon_{\text{F}})$  where  $\varepsilon_{\text{F}} = -E_{\text{app}}e$ . Equation (68) is analogous to Equation (67). Both express the non-adiabatic, electron transfer rate constant in terms of the reorganization barrier, the driving force (here  $(E_{\text{app}} - E^0)e$ ), and the electronic coupling element. Note, however, that for a given couple, e.g., ferrocene/ferrocinium (Fc/Fc<sup>+</sup>), the numerical value of  $\lambda$  in Equation (68) is half that in Equation (67). In homogeneous solution, one Fc and one Fc<sup>+</sup> are involved in each self-exchange; however, in the interfacial process only one Fc or Fc<sup>+</sup> undergoes electron transfer with the reaction partner being the metal electrode.

In an analogous manner the rate constant for electron transfer toward the metal electrode is

$$k_{m,r} = \frac{2\pi\rho_{m,\text{eff}}}{h} \left[ \frac{\pi}{\lambda k_B T} \right]^{1/2} \int_{-\infty}^{\infty} [H_{\text{DA}}(\varepsilon)]^2 \exp \left[ -\frac{(\lambda - [E_{\text{app}} - E^0(D/D^+)]e + \varepsilon)^2}{4\lambda k_B T} \right] [1 - f(\varepsilon)] d\varepsilon \quad (69)$$

where  $[1 - f(\varepsilon)]$  is the distribution of unoccupied levels in the electrode.

The electron transfer rate constant under equilibrium conditions is obtained from the above equations by setting  $E_{\text{app}} = E^0$  to yield<sup>113</sup>

$$k_m^0 = \frac{2\pi H_{\text{DA}}^2 \rho_{m,\text{eff}}}{h} \left[ \frac{\pi}{\lambda k_B T} \right]^{1/2} \int_{-\infty}^{+\infty} \left[ \frac{1}{1 + \exp(\varepsilon/k_B T)} \right] \exp \left[ -\frac{(\lambda - \varepsilon)^2}{4\lambda k_B T} \right] d\varepsilon \quad (70a)$$

where the electronic coupling element has been assumed to be independent of energy. Since  $\lambda \gg \varepsilon$  the quadratic term in the exponential can be dropped yielding

$$k_m^0 = \frac{2\pi H_{\text{DA}}^2 \rho_{m,\text{eff}}}{h} \left[ \frac{\pi}{\lambda k_B T} \right]^{1/2} \exp \left[ -\frac{\lambda}{4k_B T} \right] \int_{-\infty}^{+\infty} \frac{1}{\exp(-\varepsilon/2k_B T) + \exp(\varepsilon/2k_B T)} d\varepsilon \quad (70b)$$

The integral is  $\sim \pi k_B T$ <sup>112</sup> so that the expression for the exchange rate constant reduces to

$$k_m^0 = \frac{2\pi^2 H_{\text{DA}}^2}{h} \rho_{m,\text{eff}} \left[ \frac{\pi k_B T}{\lambda} \right]^{1/2} \exp \left[ -\frac{\lambda}{4k_B T} \right] \quad (71)$$

Evidently electron exchange at room temperature primarily involves a half-filled band of width  $2\pi k_B T$  (0.16 eV), centered at the Fermi level of the electrode.

#### 7.12.4.7 Electron Transfer through Monolayers on Semiconductor Electrodes

There is intense interest in semiconductor electrodes for both practical and fundamental reasons.<sup>10,115</sup> In an intrinsic semiconductor the Fermi level lies midway between the conduction band (CB) and the valence band (VB). There are no nearby filled or vacant energy levels. Electrons are thermally excited from the VB to the CB and the populations of CB electrons and (positively charged) VB holes remain equal. The populations are low for large-bandgap materials, which are consequently poor electrical conductors at room temperature. When the semiconductor is doped with an electron donor, electrons are transferred from the donor sites into the CB, and the Fermi level moves upward to just below the CB. Electrons are now the majority carriers, and the material is called an *n*-type semiconductor. When the semiconductor is doped with an electron acceptor, the

acceptor sites withdraw electrons from the VB. Holes are now the majority carriers and the material is called a *p*-type semiconductor.

When a semiconductor electrode is placed in a solution containing a redox couple there is electron transfer between the phases until their Fermi levels become equal. Consider an *n*-type semiconductor. If the Fermi level of the semiconductor lies above that of the redox couple in solution, electrons will flow from the semiconductor to the solution phase and a positively charged space-charge region is created in the region of the semiconductor close to the surface. The space-charge region leads to bending of the conduction and valence bands. The positions of the bands remain fixed (pinned) at the surface and the bands in the bulk of the semiconductor, and the Fermi level, move downward until equilibrium is established. Moderately doped *n*-type semiconductors thus generally carry out reductions. The opposite situation obtains in typical *p*-type semiconductor: holes are transferred from the semiconductor to the solution phase (oxidations), the space-charge region becomes negatively charged, and the bands in the bulk and the relatively low lying Fermi level move upward until equilibrium is established.

A space-charge region is also formed, and the bands bent, when a potential is applied to the electrode. As above, the band edges remain pinned at the electrode/solution interface, which arises because the potential drop between the bulk semiconductor and the solution is essentially entirely across the space-charge region rather than at the semiconductor interface. As a consequence, the intrinsic electron transfer rate constant is independent of applied potential. Nevertheless the current (and hence the effective rate constant) does depend on the applied potential because the concentration of electrons (the majority carriers) at the electrode surface relative to its bulk concentration has a Boltzmann dependence on the energy difference between the band edge and the interior of the electrode. (The Fermi–Dirac distribution reduces to a Boltzmann distribution when  $E \gg E_F$ .)

Formally, the treatments of electron transfer at a metal and at a semiconductor electrode are quite similar. However, as noted above, two modifications are needed for semiconductors. The first is simplifying—because the electron transfer occurs at a narrow band of energies at the bottom of the conduction band edge, the reorganization barrier remains essentially constant and can be factored out of the integral in the rate constant expression. Second, because of the dependence of the rates on the carrier density at the surface (which is much lower for semiconductors than for metal electrodes, since the electrons are essentially uniformly distributed throughout a metal) the density of states is no longer independent of energy. These considerations are embodied in the following expression<sup>116,117</sup> for the first-order rate constant for electron transfer from a semiconductor electrode to an attached acceptor:

$$k_{sc} = \frac{2\pi}{h} \left[ \frac{\pi}{\lambda k_B T} \right]^{1/2} H_{DA}^2 \exp \left[ -\frac{(\lambda + E^0(A, A^-)e - \varepsilon_{CB})^2}{4\lambda k_B T} \right] \int_{\varepsilon_{CB}}^{\infty} \rho_{sc,eff}(\varepsilon) f(\varepsilon) d\varepsilon \quad (72a)$$

As before, the electronic coupling is assumed to be independent of energy. The integral in Equation (72a) is

$$\int_{\varepsilon_{CB}}^{\infty} \rho_{sc,eff}(\varepsilon) f(\varepsilon) d\varepsilon = \frac{l_{sc} N_c}{d_{sc}^{2/3} (6/\pi)^{1/3}} \exp \left[ -\frac{(\varepsilon_{CB} - E^0(A, A^-)e + E_{app})^2}{k_B T} \right] \quad (72b)$$

where  $l_{sc}$  is an effective coupling length into the electrode (in cm),  $N_c$  is the effective density of states in the conduction band (in states  $\text{cm}^{-3}$ ), and  $d_{sc}$  is the atomic density of the semiconductor (in atoms  $\text{cm}^{-3}$ ). The exponential in Equation (72b) is simply the Boltzmann population of states at the conduction band edge, while the pre-exponential factor is the number of states at the Fermi level of the electrode.

#### 7.12.4.8 Electron Transfer in Metal–Molecule–Metal Systems

We next consider electron transfer between two metal electrodes (reservoirs of one-electron states) connected by a molecular bridge (wire). The expression for the rate constant derived from a scattering formalism is

$$k = (4\pi^2/h) \sum (T_{if})^2 f(E_i) [1 - f(E_f + eE_{\text{app}})] \delta(E_i - E_f) \quad (73a)$$

where the subscripts i and f refer to the initial and final states of the electron,  $T_{if}$  is the coupling element from scattering theory, the summation is over all the electronic states in the reservoirs, and the delta function ensures energy conservation.<sup>118</sup> If the applied voltage  $E_{\text{app}}$  is not too large, the Fermi–Dirac occupation functions are expanded (i.e., the low-temperature limit obtains), and it is assumed that the interaction of the states of the bridge is the same with each of the states in the reservoirs then the above expression reduces to

$$k = eE_{\text{app}}(4\pi^2/h) T_{LR}^2 \rho_L(E_F) \rho_R(E_F) \quad (73b)$$

where the subscripts L and R refer to the left and right metal electrodes, respectively,  $T_{LR}$  is the effective matrix element coupling the two reservoirs, and  $\rho_i$  are the density of states in the two electrodes.<sup>119</sup>

Consider the case in which a DBA assembly acts as the molecular wire. There are two mechanisms for the current to pass from one electrode to the other.<sup>93,120</sup> In the “chemical mechanism” D transfers an electron to A through the bridge. The newly formed  $D^+$  and  $A^-$  are then rapidly reduced and oxidized, respectively, at the electrodes, giving rise to a steady-state situation in which the current is determined by the rate of intramolecular electron transfer from D to A. The conductance via this pathway may be estimated from

$$g = e^2 k_{\text{ct}}^{\text{ss}} \rho_i(E_F) \quad (74a)$$

where  $\rho_i$  is the density of states of the initial metal manifold.<sup>93,120</sup> For typical situations  $\rho_i \sim 0.27 \text{ eV}^{-1}$ , so that the conductance may be estimated as

$$g(\Omega^{-1}) \sim 4 \times 10^{-20} k_{\text{ct}}^{\text{ss}} (\text{s}^{-1}) \quad (74b)$$

where  $\Omega$  and s denote ohms and seconds.<sup>93,119,120</sup> For a molecule (“bridge”) with a steady-state rate constant of  $5 \times 10^{11} \text{ s}^{-1}$ , the conductance is  $(50 \text{ M}\Omega)^{-1}$ . A similar expression for conductance of a bridging DBA assembly has been given on the basis of similar considerations.<sup>120</sup>

The alternative, parallel pathway involves tunneling. No oxidation or reduction of D and A is involved: D and A are considered to be chemisorbed (strongly coupled) on the left and right electrodes, respectively. Essentially the electron transfer is concerted, with the entire DBA molecule acting as the bridging group. Equation (50a) has been presented<sup>94</sup> for this pathway:

$$g \cong \frac{8e^2}{\pi^2 \Gamma_D^{(L)} \Gamma_A^{(R)}} k_{D \rightarrow A} \mathcal{F} \quad (75a)$$

where  $\mathcal{F}$  is the Franck–Condon factor

$$\mathcal{F} = \left[ \frac{1}{4\pi\lambda k_B T} \right]^{1/2} \exp \left[ -\frac{\lambda}{4k_B T} \right] \quad (75b)$$

and  $\Gamma_D$  and  $\Gamma_A$  are the widths deriving from the finite lifetimes of the electron on the chemisorbed donor and acceptor lead-in groups. Substituting Equation (67) into Equation (75a) yields

$$g \cong \frac{8e^2}{\pi^2 \Gamma_D^{(L)} \Gamma_A^{(R)}} k_{\text{ct}} = \frac{32e^2 H_{DA}^2}{h \Gamma_D^{(L)} \Gamma_A^{(R)}} \quad (76a)$$

With  $\Gamma_D^{(L)} = \Gamma_A^{(R)} \sim 0.5 \text{ eV}$  and  $\lambda = 0.5 \text{ eV}$  ( $\mathcal{F} = 0.02 \text{ eV}^{-1}$ ) Equation (76a) yields<sup>94</sup>

$$g(\Omega^{-1}) \sim 10^{-17} k_{\text{ct}} (\text{s}^{-1}) \quad (76b)$$

and conductances several orders of magnitude greater than obtained from Equation (74b).

Finally, the conductance of the DBA bridged system can also be estimated from Equation (46a) using a “traditional” electron transfer model.<sup>5,106</sup> Within this model the transmission coefficient



of the bridge is  $\tau_D/\tau_{el}$ , where  $\tau_D$  is the lifetime of the electron on the chemisorbed donor ( $h/2\pi\Gamma_D$ ) and  $\tau_{el}$  is the electron hopping time in DBA. Since D and A are considered part of the bridge and do not undergo oxidation or reduction, the nuclear configuration of DBA may be assumed constant upon electron transfer from the left to the right electrode. In other words,  $\{M(e^-)\}DBA\{M\}$  and  $\{M\}DBA\{M(e^-)\}$  may be regarded as two resonance forms of the system. The electron hopping time within such a degenerate system is of the order of  $h/2H_{DA}$ .<sup>121</sup> Assuming that  $H_{DA}$  for bridging by DBA is not very different from  $H_{DA}$  for electron transfer within an isolated DBA molecule in solution leads to the following expression for the electron hopping frequency:

$$\tau_{el} = \left( \frac{h\pi^2\bar{\mathcal{F}}}{k_{et}} \right)^{1/2} \quad (77a)$$

Substitution into Equation (46a) yields

$$g = \frac{e^2}{\pi^2\Gamma_D} \left( \frac{k_{et}}{h\bar{\mathcal{F}}} \right)^{1/2} = \frac{2e^2H_{DA}}{h\pi\Gamma_D} \quad (77b)$$

With  $\Gamma_D \sim 0.5$  eV and  $k_{et}/\bar{\mathcal{F}} \sim 10^{12}$  eV s<sup>-1</sup>, Equation (77b) yields  $g$  values very similar to those given by Equation (76a). For smaller values of  $k_{et}/\bar{\mathcal{F}}$  Equation (77b) yields larger values of  $g$  than Equation (76a).

## 7.12.5 EXPERIMENTAL STUDIES OF NANOSCALE SYSTEMS

### 7.12.5.1 Distance Dependence in Self-assembled Monolayers

Self-assembled monolayers (SAMs), e.g., alkanethiolates attached through sulfur to metal (Figure 16),<sup>109,122</sup> have played an important role in investigations of the distance dependence of electron transfer rates and conductances in the nanometer range. (It should be noted, however, that the exact nature of the site(s) to which the S is bound is not yet known.<sup>123</sup>) The adsorbate forms an ordered array on the electrode surface so that it is possible to define the distance from a point on the thiolate to the electrode surface (either through space or through bond) in a meaningful way (even for normally “floppy” alkane chains). A SAM comprised of only a hydrocarbon chain is an insulator. However, redox active groups, Ru(NH<sub>3</sub>)<sub>5</sub>py or ferrocene, can be covalently attached to the ends of the chains and introduced at low mole fraction into nonfunctionalized SAMs so that electron transfer between the redox active group and the electrode can be probed. In some cases

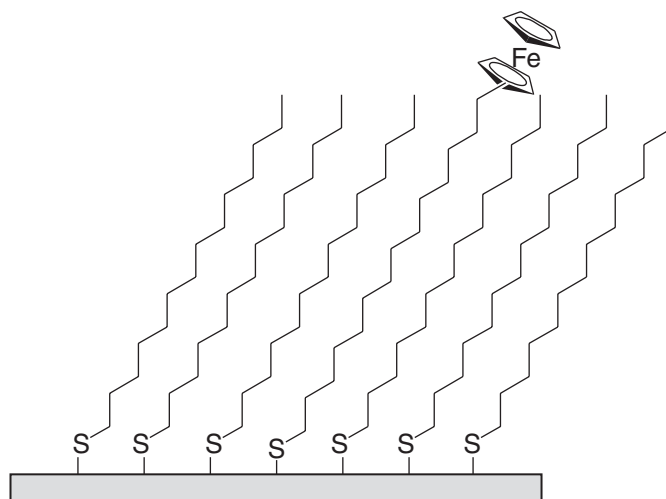


**Figure 16** Self-assembled monolayer of S-(CH<sub>2</sub>)<sub>n</sub>CH<sub>3</sub> on gold,  $n = 13$ , with a small fraction of the sites substituted by S-(CH<sub>2</sub>)<sub>n</sub>Fc (Fc = ferrocene/ferrocinium).

the redox moiety is attached directly to a carbon atom of the bridge; in others the linkage is through an ester or amide function, i.e., electrode-S(bridge)-NHC(O)-D/A or electrode-S(bridge)-OC(O)-D/A. An alternative approach used for the study of both metal and Si<sup>124</sup> electrodes is to study charge transfer from a redox solute through the SAM into the electrode.

The value of the exchange current (see Section 7.12.4.6) for the hybrid SAMs can then be determined as a function of bridge length, distance, and the nature of the bridging material. In systems studied to date the distance dependence of the exchange current is exponential in chain length, consistent with electron tunneling via a superexchange mechanism. Values of  $\beta$  (see Equation (47)) obtained from exchange current measurements are summarized in Table 5.<sup>113,125–128</sup> Also included are values determined from conductance measurements using conducting AFM in which the molecular redox group is replaced by the tip of the AFM.<sup>129</sup>

These are quite comparable to distance dependences of charge transfer rates for molecules in homogeneous solution from, for example,  $\sim 2 \text{ nm}^{-1}$  for unsaturated hydrocarbon bridges<sup>130,131</sup> to  $\sim 10 \text{ nm}^{-1}$  for saturated hydrocarbon bridges.<sup>132,133</sup>

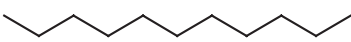
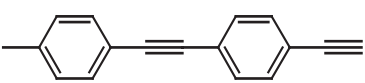
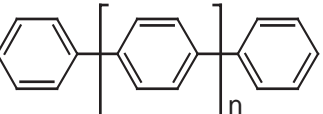
For SAMs of the conjugated oligophenylenevinylene ( $-(\text{C}_6\text{H}_4\text{CH}=\text{CH}-)_n-$ ) bridge, the temperature dependence of the electron transfer rate constant has been taken to indicate that the rates are not limited by electronic coupling for bridges out to 2.8 nm in length.<sup>134</sup>

A complication in the interpretation of the distance attenuation of the rates is that both the nuclear and electronic factors decrease with distance. (Inner-shell contributions to the reorganization barriers have been estimated as 0.03 eV and 0.17 eV for Fc<sup>113</sup> and Ru<sup>126</sup> complexes, respectively.) Thus interpretation of the electronic factor requires correction for  $\lambda_{\text{out}}$  as a function of  $n$  or  $d$ . Liu and Newton<sup>105</sup> have modeled  $\lambda_{\text{out}}$  for the ferrocene (radius  $a = 0.34 \text{ nm}$ ) SAM-electrode assembly in terms of three zones (aqueous phase “1”, SAM film “2”, electrode “3”) of different dielectric properties (see Section 7.12.4.4, Equation (64)). The solvent barrier is considerable and very sensitive to film thickness ( $L$ ) increasing from 0.75 eV to 0.86 eV when the thickness is increased from 0.5 nm to 1.5 nm. For  $\Delta G_{\text{DA}}^0 = 0$ , variation of  $\lambda_{\text{out}}$  with distance contributes  $\sim 1 \text{ nm}^{-1}$  to  $\beta$ . The simplified expression

$$\lambda_{\text{out}} = s/(L+a) \quad s = \left( \frac{D_2^s}{(D_2^s + D_1^s)^2} - \frac{D_2^{\text{op}}}{(D_2^{\text{op}} + D_1^{\text{op}})^2} \right) (\Delta q)^2 \quad (78)$$

( $D_1^s = 78$ ,  $D_1^{\text{op}} = 1.8$  and  $D_2^s = D_2^{\text{op}} = 2.25$  ( $D_3 = \infty$ )) which includes only the contribution of a single image charge (Fc assumed to be in contact with the film), with  $s = -0.137$ , gives values within 1% of those obtained from the full expression. Interestingly, moving the redox site to the

**Table 5** Distance dependence of electron transfer rate or conductance through hydrocarbon bridges with ferrocene/ferrocinium and gold electrodes.

Bridge	Assembly type/medium	$\beta_r$ ( $\text{nm}^{-1}$ )	$\beta_n$ (per unit)
	Fc-C(O)N-B, SAM, H <sub>2</sub> O, $-(\text{CH}_2)_n-$ , $n = 7-15$	8.5 <sup>125</sup>	1.1 per CH <sub>2</sub>
	Fc-C(O)O-B, H <sub>2</sub> O, $-(\text{CH}_2)_n-$ , $n = 5-9$	10 <sup>113</sup>	1.21 per CH <sub>2</sub>
	(NH <sub>3</sub> ) <sub>5</sub> Rupy-NHC(O)-B, CH <sub>3</sub> CN; $-(\text{CH}_2)_n-$ , $n = 10, 11, 15$	9.7 <sup>126</sup>	1.06 per CH <sub>2</sub>
	SAM, conducting AFM	9.4 <sup>129</sup>	
 phenyleneethynylene	Fc-C(O)O-B, H <sub>2</sub> O, $-(\text{C}_6\text{H}_4\text{C}\equiv\text{C}-)_n-$ , $n = 2-3$	5.7 <sup>127</sup>	
	Fc, H <sub>2</sub> O, $-(\text{C}_6\text{H}_4\text{C}\equiv\text{C}-)_n-$ , $n = 3-6$	3.6 <sup>128</sup>	11.7 per $-(\text{C}_6\text{H}_4\text{C}\equiv\text{C}-)$
	SAM conducting AFM	4.2 <sup>129</sup>	1.76 per C <sub>6</sub> H <sub>4</sub>

interior of the SAM can dramatically reduce the observed rate because of the inaccessibility to counterions.<sup>135</sup>

In parallel studies of metal–molecule–metal assemblies,  $\beta$  has been calculated using complex band structures. For alkane, alkene, and benzene chains the results shown in Figure 17 were obtained,<sup>136</sup> providing agreement with experiment. The HOMO–LUMO gaps obtained were 4.5 eV (alkane), 1.9 eV (alkene), and 2.1 eV.

In the SAM experiments the molecular redox group transfers an electron to/from a metal electrode. How does the rate depend upon the metal? Equation (71), the expression for the rate constant for this process, is based on the assumption that the electron transfer process is nonadiabatic and that all electronic levels near the Fermi level (represented in the metal density of states near  $E_F$ ) contribute equally to the rate. If the reaction is adiabatic, it should not depend on the nature of the metal. If it is nonadiabatic and all electronic levels near  $E_F$  contribute equally to the rate, then  $k_{et}/\rho(E_F)$  should be independent of the metal. Gosavi and Marcus<sup>112</sup> calculated rate constants for gold ( $\rho(E_F) = 0.29 \text{ eV}^{-1} \text{ atom}^{-1}$ ) and platinum ( $\rho(E_F) = 2.2 \text{ eV}^{-1} \text{ atom}^{-1}$ ) and found that the Pd d bands contribute little to the rate. This was confirmed experimentally<sup>137</sup> in a study of  $(\text{NH}_3)_5\text{RuNC}_5\text{H}_4\text{NHC}(\text{O})(\text{CH}_2)_{15}\text{S}$ — in monolayers of  $\text{HOC}(\text{O})(\text{CH}_2)_{15}\text{S}$ — on different metals. The rate constants were  $1.0 \pm 0.3 \text{ s}^{-1}$ ,  $1.7 \pm 0.4 \text{ s}^{-1}$ , and  $0.6 \pm 0.2 \text{ s}^{-1}$  for Au, Pt, and Ag;  $\lambda$  was  $0.8 \pm 0.1 \text{ eV}$ .

### 7.12.5.2 Kinetic Dispersity

Few nanosystems—nanoparticles, dendrimers, etc.—are monodisperse, that is, consist of species of a single size and composition. Thus nanoparticle samples typically display a range of core sizes and for a single core size may exhibit different degrees of coverage of the stabilizing organic layer. Even if both core and shell compositions should be of constant composition from one particle to another, there remains the possibility of a distribution of chemical and physical sites on and within the particle. While this situation is relatively uncommon in solution work, it arises in glasses and in solid-state redox melts<sup>36</sup> where a dispersion of redox hopping rates may arise from varying local environments and varying charge transfer distances. As discussed below, it is also likely to be a factor in the complex, slow recombination processes reported for  $\text{TiO}_2$  in the Grätzel cell.<sup>138</sup> Thus, it can be anticipated that even for a potentially simple first-order process involving a nanosystem, the kinetics observed may be complex.

Murray and colleagues have considered this issue for self-assembled thiol monolayers on Au(111) in the anticipation that a range of binding sites may arise either because of the nature of the surface or because of flaws in the coverage. Ferrocene-terminated monolayers on gold electrodes do exhibit broadened cyclic voltammetric waves and curved  $\log(i)$  versus time plots in potential-step experiments.<sup>139</sup> The departure from ideal behavior was modeled in terms of a Gaussian<sup>140</sup> distribution of formal potentials, a Gaussian distribution of reorganization energies, or a Gaussian distribution of tunneling distances resulting from the postulated range of different ferrocene sites. Although the Gaussian distribution of formal potentials is consistent with the observed wave broadening in the cyclic voltammetric experiments and the curved  $\log(i)$  versus time plots in the potential-step experiments, analyzing the kinetic data with this assumption can give erroneously low values of  $\lambda$  and high values of  $k^0$ . Similar results are obtained assuming a Gaussian distribution of reorganization energies. By contrast, analyzing the data assuming a Gaussian distribution of tunneling




	$\beta, \text{ nm}^{-1}$	$\beta, \text{ per C}$
	7.9	~1
	2.7	0.34
	2.7	

Figure 17 Distance dependence calculated for metal–molecule–metal assemblies.<sup>136</sup>

distances leads to undistorted  $\lambda$  values but a charge segment-dependent  $k^0$ . Overall, a Gaussian distribution of formal potentials is favored as the likely cause of the apparent kinetic heterogeneity.

Solar cells consisting of porous, dye-coated nanocrystalline  $\text{TiO}_2$  films in contact with an electrolyte generally exhibit very slow, nonexponential charge recombination kinetics and response times that depend on the incident light intensity. The complex kinetic behavior has been attributed to the presence of a high density of intrabandgap traps with the photoinjected electron undergoing a random walk between the traps prior to recombining with the oxidized dye.<sup>138,141,142</sup> An exponential density of trap states is assumed in this model:

$$g(E) = (aN_t/k_B T)\exp[-\alpha(E_c - E)/k_B T] \quad (79)$$

where  $N_t$  is the density of trap states per unit volume,  $E_c$  is the energy of the conduction band edge, and  $\alpha$  is the dispersion parameter ( $0 < \alpha < 1$ ). Experimental support for this type of model has been obtained.<sup>141–143</sup> Depending on the nature and proximity of the dye to the  $\text{TiO}_2$  surface, either rapid nonexponential recombination or slow exponential recombination is observed. The nonexponential kinetics is ascribed to electron transport between trap sites being rate determining while the slower exponential kinetics is ascribed to electron transport across the dye–semiconductor surface being rate determining. When electron transfer across the interface is sufficiently slow the injected electrons have time to equilibrate over the available trap sites resulting in the collapse of the distribution of recombination times into a single exponential decay.<sup>143</sup>

### 7.12.5.3 Electron Transfer and Coordination Chemistry in Cluster Synthesis

The mechanisms of cluster growth in silver and gold systems has been extensively studied in the laboratories of Henglein<sup>144–146</sup> and Belloni,<sup>147</sup> with reduction of  $M^+$  to  $M^0$  ( $M = \text{Ag}$ ) and  $M^{3+}$  to  $M^0$  ( $M = \text{Au}$ ) effected by photochemical or radiation chemical methods. For silver, the reduction potential ranges from  $-1.8$  V for monatomic silver to  $+0.79$  V for the bulk metal. Thus the smaller the cluster, the more reducing the cluster (with exceptions for  $n = 1–5$  associated with particularly stable cluster structures). From Equation (29), this might be expected to be a fairly general growth mechanism. Cluster growth proceeds via reduction of a larger cluster, followed by addition of a silver ion to the reduced cluster (Equations (80b)).<sup>148,149</sup> Such reactions are intrinsic to the silver halide photographic process.<sup>150</sup> The thermodynamics and kinetics are influenced by the complexation of  $\text{Ag}^+$ , as well as complexation/stabilization of the clusters. Analogous reactions have been observed for dendrimer-encapsulated metal clusters. Encapsulated copper(0),  $\text{Cu}_{55}$ , was oxidized to  $\text{Cu}^{2+}$  by the addition of  $\text{Ag}^+$ ,  $\text{Au}^{3+}$ ,  $\text{Pt}^{2+}$ , or  $\text{Pd}^{2+}$  with formation of encapsulated clusters of Ag, Au, etc. as long as  $E^0$  for the corresponding half-reactions was more positive than that for  $\text{Cu}^{2+}/\text{Cu}$ .<sup>151</sup>



### 7.12.5.4 Electron Transfer at MPCs

Monolayer protected clusters of gold have lent themselves to charge transfer studies in a variety of environments including solids, solutions, and as adsorbed monolayers. MPC reactivity can be probed as a function of metal core size and the nature and length of the protecting thiol ligand. In addition bifunctional thiols can be used to attach the cluster to a surface or to form a network of linked clusters.<sup>152</sup> In interpreting conductivity or kinetics data, an important issue is the distance separating metal cores when MPCs are in contact. For alkanethiolates intercalation of ligands on MPCs at contact has been inferred, such that for a ligand of length  $L$  the core edge–core edge separation is closer to  $L$  than to  $2L$ .<sup>75</sup>

#### 7.12.5.4.1 Solutions

MPCs exhibit capacitive electron and hole charging in solution, evident in cyclic voltammograms and differential pulse voltammograms.<sup>77</sup> When metal core size is held constant, the capacitance decreases with increasing ligand length (see Section 7.12.3.4, Equation (31)). Solutions of charged

MPCs act as conventional, molecular redox reagents;<sup>153</sup> they manifest Nernstian behavior and react with molecular redox agents such as ethylferrocene. Furthermore the charged solutions (with electrolyte) can be dried and stored. In addition to their intrinsic redox ability associated with core charging, their redox capacity can be altered and extended by incorporating ligands containing redox active molecular species, such as viologens, ferrocene, or quinones. Up to 15 Fc per MPC have been incorporated; the different Fc sites act independently manifesting one 15-electron redox process at a gold electrode.<sup>154</sup> MPC diffusion in solution has been studied<sup>155</sup> and shown to be consistent with the outer reaches of the ligand shell being permeable to solvent; ~2 nm core cluster capped with  $n=10$  or 12  $C_n$  alkanethiols exhibit diffusion coefficients of  $2 \times 10^{-6}$ – $3 \times 10^{-6}$  cm<sup>2</sup> s<sup>-1</sup> in toluene, about 1/10 that of ferrocene.

#### 7.12.5.4.2 Films

Films of MPCs of ~10 μm thickness are cast onto electrodes from toluene solution and conductivities measured using an interdigitated array electrode. Both alkanethiolate- and arenethiolate-capped gold clusters have been studied as a function of temperature and thiolate chain length, with values of  $\beta_r = 7.7^{156}$  nm<sup>-1</sup> and  $\sim 8^{35}$  nm<sup>-1</sup>. Electron hopping rates are calculated from conductivity measurements:

$$k_{\text{hop}}(\text{s}^{-1}) = \frac{6RT\sigma_{\text{el}}}{10^{-3}F^2\delta^2[\text{MPC}]} \quad (81)$$

where  $\sigma_{\text{el}}$  is the conductivity and  $\delta$  is the center-to-center core separation. The MPC concentration is calculated from

$$[\text{MPC}] = \frac{0.7 \times 10^3}{4\pi(r_{\text{core}} + l')^3 N_A/3} \quad (82)$$

where 0.7 is the fill factor of the film and  $l'$  is the effective ligand length. In the series  $\text{Au}_{309}(\text{S}(\text{CH}_2)_n\text{CH}_3)_{92}$   $n=3$ –15, conductivities decrease over six orders of magnitude as  $n$  increases. The electron hopping rates implicated for solid-state films of arenethiolate Au-core MPCs,  $\text{Au}_{309}(\text{S}(\text{CH}_2)_n\text{C}_6\text{H}_5)_{98}$ , are very high, ranging from  $10^8$  s<sup>-1</sup> to  $10^{11}$  s<sup>-1</sup> for  $n=4$  to 0.<sup>35</sup> Not surprisingly, these rates exceed the hopping rates in solid-state alkanethiolate MPC films.<sup>157</sup>

Charge transport in the films presumably occurs via an exchange reaction such as  $\text{Au}_{140}(\text{S}(\text{CH}_2)_5\text{CH}_3)_{53}^- + \text{Au}_{140}(\text{S}(\text{CH}_2)_5\text{CH}_3)_{53}^0 \rightarrow \text{Au}_{140}(\text{S}(\text{CH}_2)_5\text{CH}_3)_{53}^0 + \text{Au}_{140}(\text{S}(\text{CH}_2)_5\text{CH}_3)_{53}^-$ . Second-order rate constants for electron exchange in mixed-valent MPC films can be calculated from an expression analogous to Equation (82), but with the MPC concentration replaced by the product of the oxidized and reduced MPC concentrations. The bimolecular rate constants can only be evaluated when the concentrations of the relevant oxidation states are both known. Thus raw conductivity data and first-order rate constants are not as reliable as data for the  $\text{Au}_{140}$  species<sup>156</sup> which were measured as a function of potential so that the distribution of species (in the solution, prior to film formation) can be known; the latter are in the range  $(2\text{--}4) \times 10^{10}$  M<sup>-1</sup> s<sup>-1</sup>.

The rate of electron hopping in a multilayer film consisting of Au-core MPCs containing hexanethiolate and mercaptoundecanoic ligands linked to each other and to a Au electrode through carboxylate–Zn<sup>2+</sup>–carboxylate bridges in dichloromethane has been determined using a potential step method.<sup>158</sup> The change in electrical potential at the electrode–nanoparticle interface is followed by series of electron hops between nearest neighbors until the film reaches equilibrium with the applied potential. The current–time response yields the electron diffusion coefficient which is related to the electron hopping rate constant between nearest neighbor MPCs in a cubic lattice by

$$D_{\text{el}} = k_{\text{hop}}\delta^2/6 \quad (83)$$

Using a center-to-center core separation  $\delta = 5.14$  nm yields  $k_{\text{hop}} = 2.5 \times 10^6$  s<sup>-1</sup>, a surprisingly large rate constant for such a large hopping distance.

### 7.12.5.5 Carrier Hopping between Semiconductor Nanoparticles

The kinetics of carrier hopping between silicon nanoparticles in contact in wet and dry porous thin films has been examined in some detail and provides an application of several of the expressions presented earlier. The point of departure is Equation (21) with  $\lambda$  now given by

$$\lambda_{12} = \lambda_1 + \lambda_2 + \lambda_{\text{out}} \quad (84)$$

where  $\lambda_{12}$  is the vertical reorganization energy for carrier hopping,  $\lambda_1$  and  $\lambda_2$  are the reorganization energies ( $\lambda_{\text{in}}$ ) of the donor and acceptor nanoparticles, respectively, and, as before,  $\lambda_{\text{out}}$  is the solvent reorganization energy. For concreteness, electron transfer from a 1 nm radius silicon nanoparticle to silicon nanoparticles of varying size is considered.

The activation energy for the electron transfer is given by (cf. Equation (51))

$$\Delta G_{12}^* = (\lambda_{12} + \Delta G_{12}^0)^2 / 4\lambda_{12}$$

where  $\Delta G_{12}^0$  is the driving force for electron transfer from particle 1 to particle 2. There is evidence that the inner-shell reorganization energy of the nanoparticle varies as  $1/a^3$  and accordingly we calculate  $\lambda_{\text{in}}$  from the relation

$$\lambda_{\text{in}} = 0.012/a^3 \text{ eV} \quad (85)$$

where  $a$  is in nm and 0.012 eV is the value of  $\lambda_{\text{in}}$  for a 1 nm radius silicon particle.<sup>50</sup> The resulting  $\lambda_{\text{in}}$  values are 0.024 eV, 0.0135 eV, and 0.0124 eV for transfer to 1 nm, 2 nm, and 3 nm particles, respectively. The particle reorganization energies are quite small, consistent with the view that there is very little structural change upon the gain or loss of an electron or hole. If induced dipole moment effects are included, the solvent reorganization energy for two dielectric spheres is given by Equations (54b) and (54d).<sup>98</sup> The value of  $\lambda_{\text{out}}$  in an aqueous medium, where<sup>49</sup>

$$D_{\text{in}} = 1 + (11.4 - 1)[1 + (0.92/a)^{1.18}] \quad (86)$$

and 11.4 is the static dielectric constant of bulk silicon, is 0.369 eV, 0.306 eV, and 0.306 eV for electron transfer from  $a_1 = 1$  nm to  $a_2 = 1$  nm, 2 nm, and 3 nm, respectively (Figure 18). Clearly  $\lambda_1 + \lambda_2$  is much smaller than  $\lambda_{\text{out}}$  for electron transfer in an aqueous medium. The same does not hold for electron transfer in vacuum where  $\lambda_{\text{out}} = 0$ .

The value of  $\Delta G_{12}^0$  can be evaluated from  $\Delta(\text{KE}) + \Delta(G_{\text{pol}})$  where the first term is the change in the kinetic energy of the charge carrier (electron or hole) and the second is the change in the self-energies of the nanoparticles upon carrier gain and loss:

$$\Delta G_{12}^0 = [\text{KE}(2) + G_{\text{pol}}(2)] - [\text{KE}(1) + G_{\text{pol}}(1)] \quad (87)$$

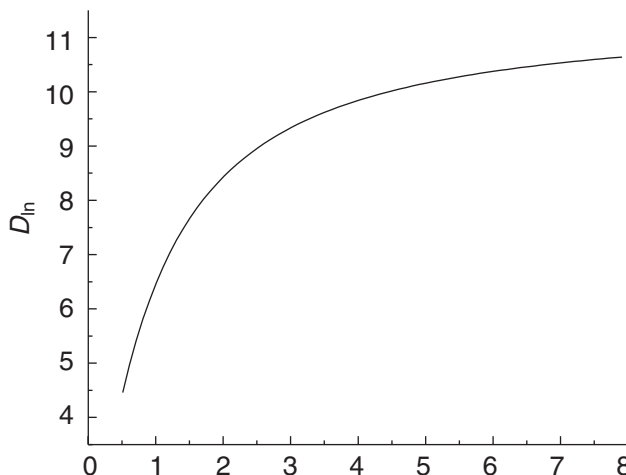


Figure 18 Dielectric constant of Si nanoparticles as a function of size.

According to Equation (22b) the KE term scales as  $a^{-2}$  but a better fit to the experimental bandgaps of silicon nanoparticles is obtained with an  $a^{-1.4}$  dependence. We therefore use KE values given by

$$\text{KE} = 0.390/a^{1.4} \text{ eV} \quad (88)$$

where 0.390 eV is the value of KE (averaged between the hole and electron) for a 1 nm radius particle.<sup>50</sup> These and  $G_{\text{pol}}$  values calculated from Equation (10) are included in Figure 19.

The resulting  $\log[\exp - (\Delta G_{12}^*/k_B T)]$  values for electron transfer from a 1 nm radius donor particle are plotted vs. the radius of the acceptor particle in Figure 20. The electron transfer in vacuum is in the inverted region and the rate decreases dramatically with increasing size of the acceptor particle. By contrast, because of the solvent reorganization, the electron transfer in the aqueous medium remains in the normal region and electron transfer to larger particles proceeds rapidly. Evidently the polar medium is very effective in promoting electron transfer between nanoparticles which would otherwise be in the inverted regime.

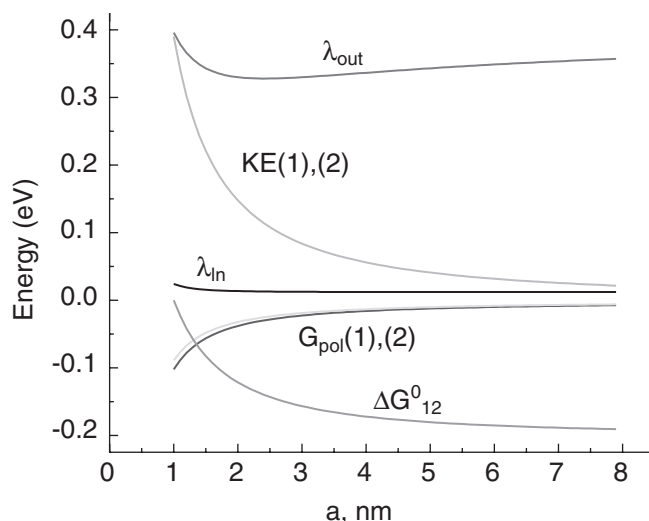


**Figure 19** Contributions to the energetics of  $E_g$  as a function of particle radius  $a$  for the kinetic energy and electrostatic terms of Equations (22b) and (22c) and polarization terms of Equation (10). Also shown is the driving force for electron transfer from a 1 nm particle to particles of radius  $a$  in water at 298 K.

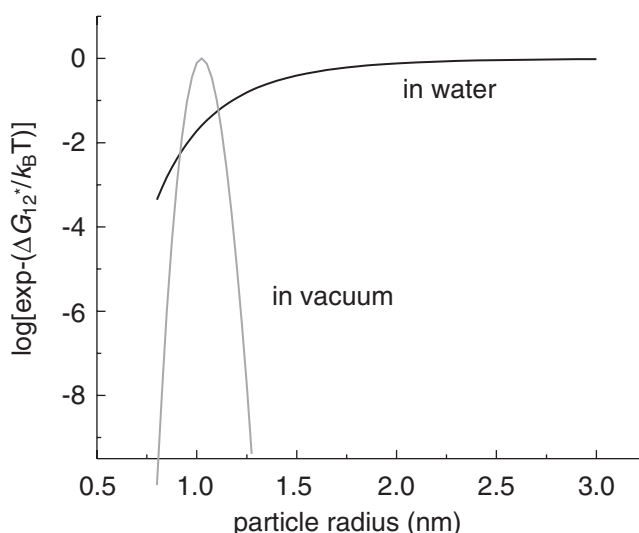


**Figure 20** Rate factors for electron transfer from a particle of 1 nm radius to acceptor particles of radius  $a$ .

### 7.12.6 ORGANIZING STRATEGIES AND MEDIA

There is great interest in organizing select functional molecular components into assemblies for applications such as sensors and solar energy conversion. For solar energy conversion a number of functions need to be accomplished efficiently: light collection, vectorial energy and electron transfer, and conversion of the energy to electricity or desired chemical products.<sup>159</sup> Knowledge gained from homogeneous solution studies guides the selection of the molecular components, which are then incorporated into supramolecular structures or anchored on or in different transparent solid materials. We divide the approaches used into three broad categories: “soft assemblies” such as polymers, Langmuir–Blodgett films, lipid bilayers, vesicles, micelles, and lipid bilayer membranes; self-assembled monolayers on solids; and assemblies in porous inorganic solids. The resulting assemblies may derive from covalent and/or coordinate bonding as in dyad D–B–A where D and A are polypyridyl metal complexes and B is a bridge such as 4,4'-bipyridine<sup>160,161</sup> or from hydrogen bonding, electrostatic, or hydrophobic/hydrophilic interactions between components. The most complex and elegant synthetic architectures are those of Gust *et al.*<sup>162,163</sup> in which the required components and assembly forces are deployed to assemble devices capable of converting the energy from light into a proton gradient. In this section we provide a brief overview of the approaches taken, with some (but not exclusive) emphasis on systems incorporating coordination complexes since the bulk of the approaches are adaptable to inclusion of coordination complexes.

#### 7.12.6.1 Polymers, Dendrimers

Polymers are of interest for assembling multiple charge or light collecting units when control of the exact three-dimensional environment of the unit is not crucial. As media for assembly they offer moderate control of environment with not too demanding synthetic chemistry. Large amounts of charge have been collected in polystyrene polymers loaded with Ru<sup>II</sup> and Os<sup>II</sup> polypyridyl complexes (see structure 5).<sup>164</sup> In these polymers metal centers on adjacent strands are separated by  $\sim 0.4$  nm and next-nearest neighbors are believed to be  $\sim 1.8$  nm apart.

The charge was introduced through oxidation of the excited polypyridyl complexes by an irreversible oxidant, 4-methoxybenzenediazonium tetrafluoroborate in acetonitrile solvent. Remarkably, the Ru<sup>II</sup> excited states in the mixed-valent polymer were found not to be quenched by Ru<sup>III</sup> or Os<sup>III</sup>. This was attributed to the fact that these electron transfer reactions lie in the inverted region. This behavior differs from that found in homogeneous aqueous solution where excited state quenching is near diffusion controlled.<sup>165</sup> Possibly the relative immobilization of the reactants on the polymer, along with the smaller value for  $\lambda_{\text{out}}$  in acetonitrile, prevents their reaction at the separations and orientations at which electron transfer occurs in homogeneous solution.

Polymers containing light-harvesting units have received particular attention as potential antennas in artificial photosynthetic assemblies. The dynamics of a 20-mer polystyrene unit containing Ru<sup>II</sup> and Os<sup>II</sup> polypyridyl complexes have been studied through transient absorption and emission and Monte Carlo calculations.<sup>166</sup> The energy migration process was initiated by the photoexcitation of the metal-to-ligand charge transfer (MLCT) transition in one of the Ru<sup>II</sup> complexes and terminated by energy transfer to a lower energy Os<sup>II</sup> trap. The energy transfer to Os<sup>II</sup> can occur in a single step if the excited state is formed adjacent to the Os<sup>II</sup>, or after a series of hops between isoenergetic rutheniums prior to reaching a Os<sup>II</sup> trap. Kinetic complexity arises from the presence of a distribution of donor-acceptor separations which is responsible for the generation of Os<sup>II</sup> emission over a range of timescales. Monte Carlo simulations indicate that the most probable Ru\*  $\rightarrow$  Os energy transfer time is  $\sim 400$  ps while the timescale for Ru\*  $\rightarrow$  Ru hopping is 1–4 ns.

Dendrimers possess a unique polymer architecture; they are well-defined, highly branched macromolecules emanating from a central core to a periphery that becomes more dense with increasing generation number. While in conventional organic polymers the repeat unit is linked to two nearest neighbors, in dendrimers the repeat unit is linked to two or three nearest neighbors. Dendrimers based on transition metal complexes such as ferrocene<sup>167</sup> and M(bpy)<sub>3</sub><sup>2+</sup> (M = Ru, Os)<sup>168</sup> are of interest because of their redox properties and/or light-harvesting properties; in these the interaction between units is small enough that absorption, emission, and redox properties are simply a sum of the individual units, but interaction between sites is sufficient for rapid intradendrimer electron and energy transfer. A dendrimer made of 10 Ru<sup>II</sup>-based units,



$[\text{Ru}\{(\mu\text{-}2,3\text{-dpp})\text{Ru}[(\mu\text{-}2,3\text{-dpp})\text{Ru}(\text{bpy})_2]_2\}_3]^{20+}$  is illustrated in Figure 21<sup>169</sup> (the building blocks are shown in structure 6).

Depending upon the nature of the branching the lifetime of the MLCT states may increase or decrease with generation number; quenching of the emission by oxygen and other oxidants slows as generation number increases, consistent with the smaller diffusion coefficients of the larger dendrimers.<sup>169</sup>

While several dendrimers based on redox active organic units or coordination complexes have been synthesized, their dynamical behavior is only beginning to be characterized.<sup>12,170</sup>

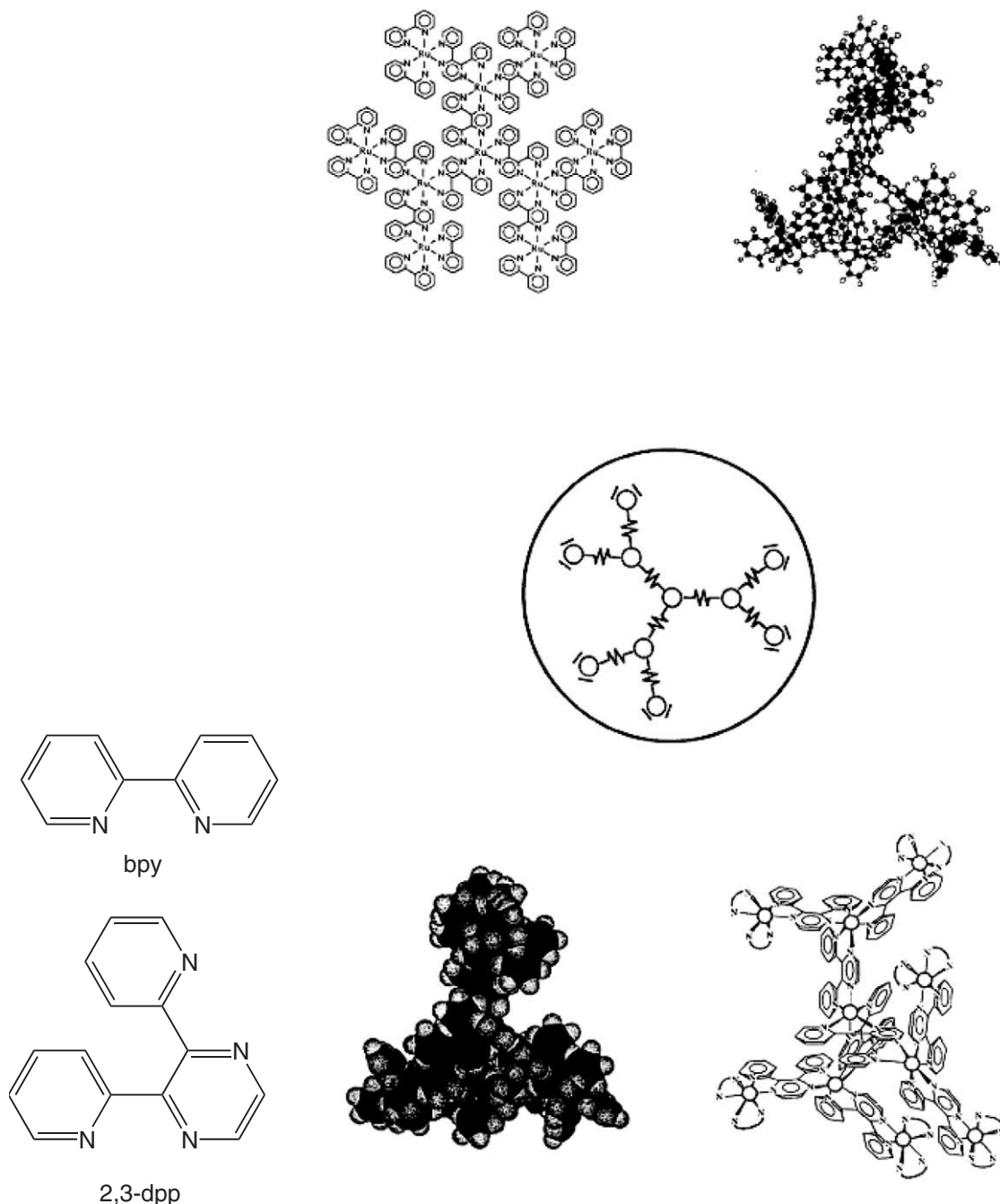


**Figure 21** Dendrimer containing 10 units (reproduced from *Coord. Chem. Rev.* **2001**, 219–221, 545–572).

Abruna's group has compared diffusion coefficients ( $D_0$ ,  $\text{cm}^2 \text{s}^{-1}$ ) for redox dendrimers from a pulsed field gradient spin echo (PFGSE) NMR method to those obtained from several electrochemical methods.<sup>171</sup> As expected, the diffusion coefficients measured for the dendrimers decrease with increasing size of the molecule. According to the Stokes–Einstein equation the diffusion coefficient of a spherical particle is

$$D = k_B T / 6\pi a \eta$$

where  $\eta$  is the viscosity of the solution. However,  $D$  values obtained from cyclic voltammetry and rotating disk electrochemistry were significantly smaller than those determined by the NMR method (by factors of 4–10 for the larger species). The electrochemical methods monitor the current due to  $\text{Ru}^{\text{II}}$  at the electrode surface and this current is limited by mass transport. For a large molecule with pendent redox groups, not all groups can simultaneously interact with the electrode; the molecule needs to turn (rotate) to accomplish this. However, during the time needed for the rotation, the molecule may diffuse away from contact with the electrode. Thus the apparent diffusion coefficient generated from the current is smaller.

The implications of the nature of dendrimer intraconnectivity for electronic coupling in charge transport have been considered.<sup>172</sup> The dendrimer architecture has also been exploited for the synthesis of small, robust catalytic metal nanoparticle arrays.<sup>151</sup>

### 7.12.6.2 Self-assembled Monolayers on Solids

Mixed self-assembled monolayers on gold exhibit light harvesting and photocurrent generation.<sup>173</sup> A ferrocene (Fc)–porphyrin (P)–fullerene ( $\text{C}_{60}$ ) triad thiol mixed with boron dipyrin thiol (B) exhibits 50% quantum efficiency. It is believed that light is collected both through direct porphyrin excitation and through energy transfer to the porphyrin from the excited boron–dipyrin dye. The porphyrin excited state transfers an electron to  $\text{C}_{60}$  and charge shifts from Fc to  $\text{P}^+$  to give  $\text{Fc}^+ - \text{P} - \text{C}_{60}^-$ .  $\text{C}_{60}^-$  then transfers an electron to an oxidant in solution ( $\text{O}_2$  or methyl viologen) and  $\text{Fc}^+$  is reduced back to Fc by an electron from the gold electrode resulting in cathodic photocurrent generation. Although the triad and B components are separated from the Au electrode by  $(\text{CH}_2)_{11}$  chains, the porphyrin singlet excited state is still quenched significantly by the metal electrode. By contrast, no significant quenching of the porphyrin excited state is observed in related assemblies on 2.4 nm gold nanoparticles.<sup>174</sup>

The conversion of solar energy into electricity has been accomplished primarily by semiconductor photovoltaic devices. However, liquid junction photovoltaic cells have been developed.<sup>175,176</sup> Dye-sensitized  $\text{TiO}_2$  nanoparticles and films are particularly important because of their potential application in liquid junction photovoltaic cells (Figure 22).<sup>177,178</sup> In these the dye is bound to the surface of a semiconductor nanoparticle. The high surface area of the nanoparticle makes possible the adsorption of sufficient dye for efficient light collection. Dye sensitization can involve direct photoinjection of an electron from the dye to the nanoparticle

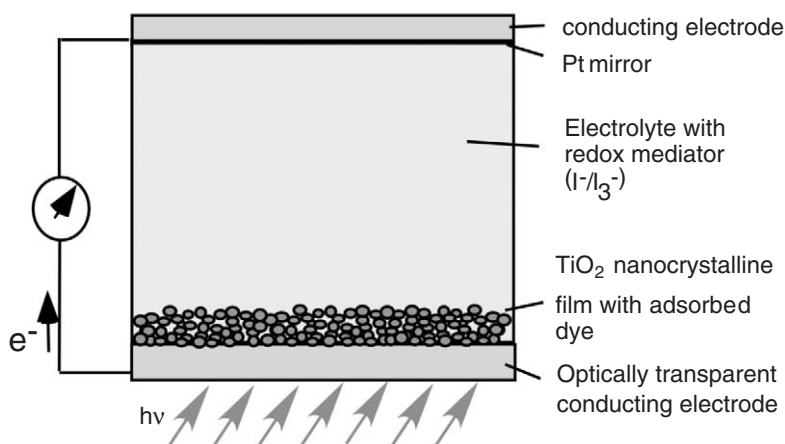


Figure 22 Grätzel cell based on nanoparticulate  $\text{TiO}_2$ .

as for  $\text{Fe}(\text{CN})_6^{4-}\text{-TiO}_2(\text{p})$ <sup>9,179</sup> or injection by a dye excited state as for  $\text{Ru}(\text{bpy})_2(\text{bpyCOOH})\text{-TiO}_2(\text{p})$ .<sup>178,180</sup> Indirect electron injection can be very rapid, often occurring from vibrationally excited modes of the charge transfer excited state.<sup>181–183</sup> In contrast to the very rapid charge injection step,<sup>184</sup> the subsequent conduction of the charge through the  $\text{TiO}_2$  is much slower. This charge transport involves electron diffusion between immobile trapping sites within the individual  $\text{TiO}_2$  particles and diffusion between particles.<sup>178,185</sup> Both can be viewed as percolation<sup>186</sup> phenomena. If the electronic interaction between individual particles is strong, an entire film can be viewed as a single entity. However, when the coupling is weak the interparticle percolation becomes important.

The back-electron transfer kinetics has been compared<sup>187</sup> for two sensitizers, “black dye” ( $\text{L}_1 = 4,4',4''\text{-tricarboxy-2,2':6',2''-terpyridine}$ ),  $\text{RuL}_1(\text{NCS})_3^-$ , and “red dye” ( $\text{L}_2 = 4,4'\text{-dicarboxy-2,2'-bipyridine}$ ),  $\text{Ru}(\text{L}_2)_2(\text{NCS})_2^{2-}$ . The back-electron transfer kinetics are similar for the two systems. The reduction potentials  $E_{\text{D}^+/\text{D}}^0$  are +0.69 V and +0.84 V vs. SCE for the black and red dye, respectively. Taking the  $\text{TiO}_2$  conduction band as  $-0.75$  eV vs. SCE, the driving force is 1.44 eV and 1.59 eV for the black and red dyes, respectively. Assuming a reorganization energy  $\lambda = 0.3$  eV, both the black dye/ $\text{TiO}_2$  and red dye/ $\text{TiO}_2$  systems fall deeply in the inverted region. Because of the difference of 150 mV in  $\Delta G^0$  between the two systems, a lower back-electron transfer rate is expected for the red dye. The observation of comparable back-electron transfer kinetics for the two systems at low light intensity then suggests that the back reaction is controlled by the probability for injected electrons to encounter oxidized dye molecules adsorbed on the mesoporous  $\text{TiO}_2$  film. Similarly, with  $\text{Re}^{\text{I}}$  “dyes” (*fac*- $\text{Re}(\text{deeb})(\text{CO})_3(\text{X})$ , *deeb* = 4,4'-( $\text{COOEt}$ )<sub>2</sub>-2,2'-bipyridine and  $\text{X} = \text{I}^-$ ,  $\text{Br}^-$ ,  $\text{Cl}^-$ ,  $\text{CN}^-$ , and [*fac*- $\text{Re}(\text{deeb})(\text{CO})_3(\text{py})$ ](OTf), OTf<sup>-</sup> is triflate anion and py is pyridine), thermodynamically favorable recombination of the injected electron in  $\text{TiO}_2$  with the oxidized sensitizer requires milliseconds for completion and the charge recombination kinetics are insensitive to the Re sensitizer employed.<sup>188</sup> The charge recombination kinetics have been contrasted with other sensitized  $\text{TiO}_2$  materials and are insensitive to a  $\sim 960$  mV change in apparent driving force. The results thus also suggest that the charge recombination rate is limited by diffusional encounters of the injected electron with the oxidized sensitizer.

### 7.12.6.3 Porous Solids

Porous solids are classified by pore diameter as microporous (<2 nm), mesoporous (2–50 nm), and macroporous (>50 nm). There is great interest in immobilizing catalytic, photo-, and redox active moieties in such media, especially for applications such as sensors and solar energy conversion.<sup>189</sup> For sensing or catalysis the need to deliver (reactant) and remove (product) small molecules can be met by the use of mesoporous oxides with interior spaces of 2–50 nm that are “wired” to the exterior.<sup>190</sup> This is an area where chemistry and materials chemistry come together.<sup>191</sup> The range of media considered and explored is broad and the media include layered intercalates,<sup>192,193</sup> gels,<sup>194</sup> layered metal oxides,<sup>195</sup> and zeolites.<sup>196,197</sup> Such components as catalysts, light collectors, and electron or energy shuttles can be separated by structural features of the solid, including adsorption onto the surface of a semiconductor as in the Grätzel cell (Section 7.12.6.2); in more complex architectures they may be encapsulated in specific cavities in a zeolite or layers responsible for the different functions may be separated by layers of inorganic oxide. Mallouk’s group assembled lamellar polyanion/polycation thin films which manifested some of the characteristics of an “artificial leaf,” including directional energy and electron transfer. With  $\text{HTiNbO}_5$  as the inorganic spacer a particularly long-lived, charge-separated state was obtained and it was inferred that the semiconducting oxide sheet plays an active role in relaying the electron from the photoexcited Pd–porphyrin layer to the viologen electron acceptor layer.<sup>17</sup>

Zeolite membranes have been proposed for use in photoconversion assemblies designed to separate the sites where oxidized and reduced products (e.g., oxygen and hydrogen) are generated.<sup>198</sup> The membrane pores are charged with a viologen, with essentially one confined to each supercage. Electron transport across the membrane occurs by a self-exchange mechanism. By analogy with diffusion in organic polymers the diffusion coefficient for such a process is

$$D_{\text{app}} = k_{\text{ex}} \delta^2 C / 6$$

where  $k_{\text{ex}}$  is the self-exchange rate for the viologen couple,  $\delta$  is the distance between immobilized viologen sites, and  $C$  is the concentration of the sites.

### 7.12.7 CONCLUDING REMARKS

Despite the disappointment of discovering<sup>199,200</sup> fabricated<sup>201,202</sup> results, nanoscale charge transfer is an exciting field of inquiry that is beginning to address important, fundamental questions.<sup>203</sup> Coordination compounds and coordination chemistry are playing an increasingly important role. Fundamental discoveries, such as photoinjection of electrons through a metal layer into a semiconductor, may lead to new nanodevices for electricity generation.<sup>204</sup> The development of the field will prove especially challenging in development of integrated theory that is applicable to a range of size scales and in the areas of materials synthesis and characterization. Furthermore methods for obtaining statistically significant measures of conductance in nanoassemblies need to be developed.

### ACKNOWLEDGMENTS

This research was carried out at Brookhaven National Laboratory under contract DE-AC02-98CH10886 with the US Department of Energy and supported by its Division of Chemical Sciences, Office of Basic Energy Sciences. We thank S. Feldberg for helpful discussions.

### 7.12.8 REFERENCES

1. Jortner, J.; Ratner, M. *Chemistry for the 21st Century* **1997**, 5–72. Blackwell: Oxford.
2. Aviram, A.; Ratner, M., Eds. *Molecular Electronics: Science and Technology (Annals of the New York Academy of Sciences)*; New York Academy of Sciences: New York, 1998; Vol. 852.
3. Ratner, M. A.; Jortner, J. In *Molecular Electronics*; Ratner, M. A., Jortner, J., Eds.; Blackwell: Oxford, UK, 1997; pp 5–72 and references therein.
4. Balzani, V., Ed., *Electron Transfer in Chemistry* **2001**, Wiley-VCH: New York.
5. Marcus, R. A.; Sutin, N. *Biochim. Biophys. Acta* **1985**, *811*, 265–322.
6. Hush, N. S. *Electrochim. Acta* **1968**, *13*, 1005–1023.
7. Kittel, C. *Introduction to Solid State Physics*; 7th ed.; **1996**, Wiley: New York.
8. Datta, S. *Electronic Transport in Mesoscopic Systems* **1995**, Cambridge University Press: Cambridge.
9. Yang, M.; Thompson, D. W.; Meyer, G. J. *Inorg. Chem.* **2002**, *41*, 1254–1262.
10. Qu, P.; Meyer, G. J. In *Electron Transfer in Chemistry*; Balzani, V., Ed.; Wiley-VCH: New York, 2001; Vol. 4, Part 2, pp 354–411 and references therein.
11. Williams, M. E.; Masui, H.; Long, J. W.; Malik, J.; Murray, R. W. *J. Am. Chem. Soc.* **1997**, *119*, 1997–2005.
12. Ghaddar, T. H.; Wishart, J. F.; Kirby, J. P.; Whitesell, J. K.; Fox, M. A. *J. Am. Chem. Soc.* **2001**, *123*, 12832–12836.
13. Beer, P. D.; Berry, N.; Drew, M. G. B.; Fox, O. D.; Padilla-Tosta, M. E.; Patell, S. *Chem. Commun.* **2001**, 199–200.
14. Bernhardt, P. V.; Hayes, E. J. *Inorg. Chem.* **2003**, *42*, 1371–1377.
15. Canadell, E. *Coord. Chem. Rev.* **1999**, *185–186*, 629–651.
16. Cassoux, P. *Coord. Chem. Rev.* **1999**, *185–186*, 213–232.
17. Kaschak, D. M.; Lean, J. T.; Waraksa, C. C.; Saupe, G. B.; Usami, H.; Mallouk, T. E. *J. Am. Chem. Soc.* **1999**, *121*, 3435–3445.
18. Goia, D. V.; Matijevic, E. *New J. Chem.* **1998**, 1203–1215.
19. Carroll, R. L.; Gorman, C. B. *Angew. Chem., Int. Ed.* **2002**, *41*, 4378–4400 and references therein.
20. de Silva, P., Ed., *Molecular-level Electronics, Imaging and Information, Energy and Environment*; Wiley-VCH: New York, 2001; Vol. 5, Part 1.
21. Launay, J.-P.; Coudret, C. In *Electron Transfer in Chemistry*; Balzani, V., Ed.; Wiley-VCH: New York, 2001; Vol. 5, Part 1, pp 3–47 and references therein.
22. Cola, L. D.; Belser, P. In *Electron Transfer in Chemistry*; Balzani, V., Ed.; Wiley-VCH: New York, 2001; Vol. 5, Part 1, pp 97–136 and references therein.
23. Park, J.; Pasupathy, A. N.; Goldsmith, J. I.; Chang, C.; Yaish, Y.; Petta, J. R.; Rinkoski, M.; Sethna, J. P.; Abruña, H. D.; McEuen, P. L.; Ralph, D. C. *Nature* **2002**, *417*, 722–725.
24. Kleverlaan, C.; Alebbi, M.; Argazzi, R.; Bignozzi, C. A.; Hasselmann, G. M.; Meyer, G. J. *Inorg. Chem.* **2000**, *39*, 1342–1343.
25. Lent, C. S.; Isaksen, B.; Lieberman, M. *J. Am. Chem. Soc.* **2003**, *125*, 1056–1063.
26. Lent, C. S.; Tougaw, P. D. *Proc. IEEE* **1997**, *85*, 541–557.
27. Fabbri, L.; Licchelli, M.; Pallavicini, P. *Acc. Chem. Res.* **1999**, *32*, 846–853.
28. Lin, C.; Kagan, C. R. *J. Am. Chem. Soc.* **2003**, *125*, 336–337.
29. Sano, M.; Taube, H. *Inorg. Chem.* **1994**, *33*, 705–709.
30. Ward, M. D. *Chem. Ind.* **2000**, 22.
31. Balzani, V.; Gomex-Lopez, M.; Stoddart, J. F. *Acc. Chem. Res.* **1998**, *31*, 405–414.
32. Sauvage, J.-P. *Acc. Chem. Res.* **1998**, *31*, 611–619.
33. Armadori, N.; Balzani, V.; Collin, J.-P.; Gavina, P.; Sauvage, J.-P.; Ventura, B. *J. Am. Chem. Soc.* **1999**, *121*, 4397–4408.
34. Brunshwig, B. S.; Sutin, N. *J. Am. Chem. Soc.* **1989**, *111*, 7454–7465.
35. Wuelfing, W. P.; Murray, R. W. *J. Phys. Chem. B* **2002**, *106*, 3139–3145.

36. Terrill, R. H.; Murray, R. W. In *Molecular Electronics*; Ratner, M. A., Jortner, J., Eds.; Blackwell: Oxford, UK, 1997; pp 215–239.
37. Hoffman, R.; Wijeyesekera, S. D.; Sung, S.-s. *Pure Appl. Chem.* **1986**, *58*, 481–494.
38. Cox, P. A. *The Electronic Structure and Chemistry of Solids* **1987**, Oxford University Press: New York.
39. Schmid, G. In *Nanoscale Materials in Chemistry*; Klabunde, K. J., Ed.; Wiley: New York, 2001.
40. Rao, C. N. R.; Kulkarni, G. U.; Thomas, P. J.; Edwards, P. P. *Chem. Soc. Rev.* **2000**, *29*, 27–35.
41. Brus, L. *J. Phys. Chem.* **1986**, *90*, 2555–2560.
42. Edwards, P. P.; Johnston, R. L.; Rao, C. N. R. In *Metal Clusters in Chemistry*; Braunstein, P., Oro, L. A., Raithby, P. R., Eds.; Wiley-VCH: New York, 1999; Vol. 3.
43. Johnston, R. L. *Phil. Trans. R. Soc. Lond. A* **1998**, *356*, 211–230.
44. Jortner, J. *Z. Phys.* **1992**, *D24*, 247–275.
45. Buffat, P.; Borel, J.-P. *Phys. Rev. A* **1976**, *13*, 2287–2298.
46. Enustun, B. V.; Turkevich, J. *J. Am. Chem. Soc.* **1963**, *85*, 3317–3328.
47. Demirci, S.; Enustun, B. V.; Turkevich, J. *J. Phys. Chem.* **1978**, *82*, 2710–2711.
48. Makov, G.; Nitzan, A.; Brus, L. E. *J. Chem. Phys.* **1988**, *88*, 5076.
49. Lannoo, M.; Delerue, C.; Allan, G. *Phys. Rev Lett.* **1995**, *74*, 3415–3418.
50. Brus, L. *Phys. Rev. B* **1996**, *53*, 4649–4656.
51. Iwamatsu, M.; Fujiwara, M.; Happo, N.; Horii, K. *J. Phys.: Condens. Matter* **1997**, *9*, 9881–9892.
52. Leatherdale, C. A.; Bawendi, M. G. *Phys. Rev. B* **2001**, *63*, 165315–165311.
53. Gorer, S.; Hodes, G. In *Semiconductor Nanoclusters—Physical, Chemical and Catalytic Aspects*; Kamat, P. V., Meisel, D., Eds.; Elsevier: Amsterdam, 1997; p 297.
54. Norris, D. J.; Bawendi, M. G.; Brus, L. E. In *Molecular Electronics*; Ratner, M. A., Jortner, J., Eds.; Blackwell: Oxford, UK, 1997; pp 281–323.
55. Flugge, S. *Practical Quantum Mechanics*; Springer: Berlin, 1971; Vol. 1.
56. Branson, J. “Quantum Physics 130,” UCSD, [http://heppc16.ucsd.edu/ph130b/130\\_notes/node225.html](http://heppc16.ucsd.edu/ph130b/130_notes/node225.html), 2002.
57. Marcus, R. A.; Sutin, N. *Comments Inorg. Chem.* **1986**, *5*, 119–133.
58. Kelly, K. L.; Coronado, E.; Zhao, L. L.; Schatz, G. C. *J. Phys. Chem. B* **2003**, *107*, 668–677 and references therein.
59. Mulvaney, P. *Langmuir* **1996**, *12*, 788–800 and references therein.
60. Allan, G.; Delerue, C.; Lannoo, M.; Martin, E. *Phys. Rev. B* **1995**, *52*, 11982–11988.
61. Brunschwig, B. S.; Ehrenson, S.; Sutin, N. *J. Phys. Chem.* **1987**, *91*, 4714–4723.
62. Brus, L. E. *J. Chem. Phys.* **1984**, *80*, 4403–4409.
63. Wang, Y.; Suna, A.; Mahler, W.; Kasowski, R. *J. Chem. Phys.* **1987**, *87*, 7315–7322.
64. Häberlen, O. D.; Chung, S.-C.; Stener, M.; Rösch, N. *J. Chem. Phys.* **1997**, *106*, 5189–5201.
65. Haas, G. A. *AIP Handbook of Physics* **1972**, Gray, D. E., Ed.; McGraw-Hill: New York.
66. Reimers, J. R.; Shapley, W. A.; Lambropoulos, N.; Hush, N. S. *Ann. NY Acad. Sci.* **2002**, *960*, 100–130.
67. Weaver, M. J.; Gao, X. *J. Phys. Chem.* **1993**, *97*, 332–338.
68. Zheng, L.-S.; Karner, C. M.; Brucato, P. J.; Yang, S. H.; Pettiette, C. L.; Craycraft, M. J.; Smalley, R. E. *J. Chem. Phys.* **1986**, *85*, 1681–1688.
69. Morse, M. D. *Chem. Rev.* **1986**, *1986*, 1049–1109.
70. Mostafavi, M.; Marignier, J. L.; Amblard, J.; Belloni, J. *Radiat. Phys. Chem.* **1989**, *34*, 605–617.
71. Henglein, A. *Isr. J. Chem.* **1993**, *33*, 77–88.
72. Chen, S.; Ingram, R. S.; Hostetler, M. J.; Pietron, J. J.; Murray, R. W.; Schaaff, T. G.; Khoury, J. T.; Alvarez, M. M.; Whetten, R. L. *Science* **1998**, *280*, 2098–2101.
73. Yang, Y.; Chen, S. *Nano Lett.* **2003**, *3*, 75–79.
74. Chen, S.; Murray, R. W.; Feldberg, S. W. *J. Phys. Chem. B* **1998**, *102*, 9898–9907.
75. Templeton, A. C.; Wuefling, W. P.; Murray, R. W. *Acc. Chem. Res.* **2000**, *33*, 27–36.
76. Hicks, J. F.; Miles, D. T.; Murray, R. W. *J. Am. Chem. Soc.* **2002**, *124*, 13322–13328.
77. Hicks, J. F.; Templeton, A. C.; Chen, S.; Sheran, K. M.; Jasti, R.; Murray, R. W.; Debord, J.; Schaaff, T. G.; Whetten, R. L. *Anal. Chem.* **1999**, *71*, 3703–3711.
78. Bockris, J. O. M.; Reddy, A. K. N. *Modern Electrochemistry 2* **1973**, Plenum Press: London.
79. Bard, A. J.; Faulkner, L. R. *Electrochemical Methods*, 2nd ed. **2001**, Wiley: New York.
80. Brus, L. *J. Chem. Phys.* **1988**, *88*, 5076.
81. Sadakane, M.; Steckhan, E. *Chem. Rev.* **1998**, *98*, 219–237.
82. Maeda, K.; Katano, H.; Osakai, T.; Himeno, S.; Saito, A. *J. Electroanal. Chem.* **1995**, *389*, 167–173.
83. Haram, S. K.; Quinn, B. M.; Bard, A. J. *J. Am. Chem. Soc.* **2001**, *123*, 8860–8861.
84. Sant, P. A.; Kamat, P. V. *Phys. Chem. Chem. Phys.* **2002**, *4*, 198–203.
85. Song, Y.; Murray, R. W. *J. Am. Chem. Soc.* **2002**, *124*, 7096–7102.
86. Steigerwald, M. L.; Alivisatos, A. P.; Gibson, J. M.; Harris, T. D.; Kortan, R.; Muller, A. J.; Thayer, A. M.; Duncan, T. M.; Douglass, D. C.; Brus, L. E. *J. Am. Chem. Soc.* **1988**, *110*, 3046–3050.
87. Kamat, P. V.; Murakoshi, K.; Wada, Y.; Yanagida, S. In *Nanostructured Materials and Nanotechnology*; Nalwa, H. S., Ed.; Academic Press: New York, 2002; pp 130–182.
88. Hiemenz, P. C.; Rajagopalan, R. *Principles of Colloid and Surface Chemistry*, 3rd ed. **1997**, Marcel Dekker: New York.
89. Debye, P. *Trans. Electrochem. Soc.* **1942**, *82*, 265.
90. Richardson, D. E. *Inorg. Chem.* **1990**, *29*, 3213–3217.
91. Scudiero, L.; Barlow, D. E.; Mazur, U.; Hipps, K. W. *J. Am. Chem. Soc.* **2001**, *123*, 4073–4080.
92. Ratner, M. A.; Davis, B.; Kemp, M.; Mujica, V.; Roitberg, A.; Yaliraki, S. *Ann. NY Acad. Sci.* **1998**, *852*, 22–37.
93. Segal, D.; Nitzan, A.; Ratner, M.; Davis, W. B. *J. Phys. Chem. B* **2000**, *104*, 2790–2793.
94. Nitzan, A. *J. Phys. Chem. B* **2001**, *105*, 2677–2679.
95. Mujica, V.; Nitzan, A.; Datta, S.; Ratner, M. A.; Kubiak, C. P. *J. Phys. Chem. B* **2003**, *107*, 91–95.
96. Brunschwig, B. S.; Ehrenson, S.; Sutin, N. *J. Am. Chem. Soc.* **1984**, *106*, 6858–6859.
97. Kharkats, Y. I. *Sov. Electrochem.* **1973**, *9*, 845–847.
98. German, E. D.; Kuznetsov, A. M. *Electrochim. Acta* **1981**, *26*, 1595–1608.
99. Kharkats, Y. I. *Sov. Electrochem.* **1983**, *19*, 1165–1169.

100. Kharkats, Y. I. *Sov. Electrochem.* **1976**, *12*, 566–569.
101. Kharkats, Y. I.; Chudin, N. I. *Sov. Electrochem.* **1984**, *20*, 826–832.
102. Marcus, R. A. *J. Phys. Chem.* **1990**, *94*, 1050–1055.
103. Kharkats, Y. I.; Ulstrup, J. *Chem. Phys. Lett.* **1999**, *303*, 320–324.
104. Iversen, G.; Kharkats, Y. I.; Ulstrup, J. *Mol. Phys.* **1998**, *94*, 297–306.
105. Liu, Y.-P.; Newton, M. D. *J. Phys. Chem.* **1994**, *98*, 7162–7169.
106. Sutin, N. *Prog. Inorg. Chem.* **1983**, *30*, 441–498.
107. Newton, M. D. *Chem. Rev.* **1991**, *91*, 767–792.
108. Davis, W. B.; Wasielewski, M. R.; Ratner, M. A.; Mujica, V.; Nitzan, A. *J. Phys. Chem. A* **1997**, *101*, 6158–6164.
109. Chidsey, C. E. D. *Science* **1991**, *251*, 919–922.
110. Levich, V. G. In *Advances in Electrochemistry and Electrochemical Engineering*; Delahay, P., Tobias, C. W., Eds.; Interscience: New York, 1966; Vol. 4.
111. Royea, W. J.; Fajardo, A. M.; Lewis, N. S. *J. Phys. Chem. B* **1997**, *105*, 11152–11159.
112. Gosavi, S.; Marcus, R. A. *J. Phys. Chem. B* **2000**, *104*, 2067–2072.
113. Smalley, J. F.; Feldberg, S. W.; Chidsey, C. E. D.; Linford, M. R.; Newton, M. D.; Liu, Y.-P. *J. Phys. Chem.* **1995**, *99*, 13141.
114. Smalley, J. F.; Finklea, H. O.; Chidsey, C. E. D.; Linford, M. R. C.; Ferraris, J. P.; Chalfant, K.; Zawodzinski, T.; Feldberg, S. W.; Newton, M. D. *J. Am. Chem. Soc.* **2003**, *125*, 2004–2013.
115. Rajeshwar, K. In *Electron Transfer in Chemistry*; Balzani, V., Ed.; Wiley-VCH: New York, 2001; Vol. 4, Part 2, pp 279–352 and references therein.
116. Royea, W. J.; Fajardo, A. M.; Lewis, N. S. *J. Phys. Chem. B* **1997**, *101*, 11152–11159.
117. Lewis, N. S. *J. Phys. Chem. B* **1998**, *102*, 4843–4855.
118. Mujica, V.; Kemp, M.; Ratner, M. A. *J. Chem. Phys.* **1994**, *101*, 6849.
119. Kerqueris, C.; Bourgoin, J.-P.; Palacin, S.; Esteve, D.; Urbina, C.; Magoga, M.; Joachim, C. *Phys. Rev. B* **1999**, *59*, 12505–12513.
120. Segal, D.; Nitzan, A.; Davis, W. B.; Wasielewski, M. R.; Ratner, M. A. *J. Phys. Chem. B* **2000**, *104*, 3817–3829.
121. Sutin, N. In *Bioinorganic Chemistry*; Gunther, G. L., Ed.; Elsevier: New York, 1973; Vol. 2, pp 611–653.
122. Chidsey, C. E. D.; Bertozzi, C. R.; Putvinski, T. M.; Mujica, A. M. *J. Am. Chem. Soc.* **1990**, *112*, 4301–4306.
123. Tachibana, M.; Yoshizawa, K.; Ogawa, A.; Fujimoto, H.; Hoffmann, R. *J. Phys. Chem. B* **2002**, *106*, 12727–12736 and references therein.
124. Cheng, J.; Robinson, D. B.; Cicero, R. L.; Eberspacher, T. B.; Chidsey, C. E. D. *J. Phys. Chem. B* **2001**, *105*, 10900–10904.
125. Weber, K.; Hockett, L.; Creager, S. *J. Phys. Chem. B* **1997**, *101*, 8286.
126. Finklea, H. O.; Hanshew, D. D. *J. Am. Chem. Soc.* **1992**, *114*, 3173–3181.
127. Sachs, S. B.; Dudeck, S. P.; Hsung, R. P.; Sita, S. R.; Smalley, J. F.; Newton, M. D.; Feldberg, S. W.; Chidsey, C. E. D. *J. Am. Chem. Soc.* **1997**, *119*, 10563–10564.
128. Creager, S.; Yu, C. J.; Bamdad, C.; O'Connor, S.; MacLean, T.; Lam, E.; Chong, Y.; Olsen, G. T.; Luo, J.; Gozin, M.; Kayyem, J. F. *J. Am. Chem. Soc.* **1999**, *121*, 1059–1064.
129. Wold, D. J.; Haag, R.; Rampi, M. A.; Frisbie, C. D. *J. Phys. Chem. B* **2002**, *106*, 2813–2816.
130. Woitellier, S.; Launay, J. P.; Spangler, C. W. *Inorg. Chem.* **1989**, *28*, 273.
131. Reimers, J. R.; Hush, N. S. *Electron Ion Transfer Condens. Media: Theor. Phys. React. Kinet.*, Proceedings of the Conference; Kornyshev, A. A., Ed.; World Scientific: Singapore, 1997; pp 326–346.
132. Closs, G. L.; Johnson, M. D.; Miller, J. R.; Piotrowiak, P. *J. Am. Chem. Soc.* **1989**, *111*, 3751–3753.
133. Shephard, M. J.; Paddon-Row, M. N.; Jordan, K. D. *Chem. Phys.* **1993**, *176*, 289–304.
134. Sikes, H. D.; Smalley, J. F.; Dudeck, S. P.; Cook, A. R.; Newton, M. D.; Chidsey, C. E. D.; Feldberg, S. W. *Science* **2001**, *291*, 1519–1523.
135. Sumner, J. J.; Creager, S. E. *J. Phys. Chem. B* **2001**, *105*, 8739–8745.
136. Tomfohr, J. K.; Sankey, O. F. *Phys. Rev. B* **2002**, *65*, 245105–245112.
137. Finklea, H. O.; Yoon, K.; Chamberlain, E.; Allen, J.; Haddox, R. *J. Phys. Chem. B* **2001**, *105*, 3088–3092.
138. Nelson, J. *Phys. Rev. B* **1999**, *59*, 15374–15380.
139. Rowe, G. K.; Carter, M. T.; Richardson, J. N.; Murray, R. W. *Langmuir* **1995**, *11*, 1797–1806.
140. Bäessler, H. *Mol. Cryst. Liq. Cryst.* **1994**, *252*, 11–21.
141. Nelson, J.; Hague, S. A.; Klug, D. R.; Durrant, J. R. *Phys. Rev. B* **2001**, *63*, 205321.
142. van de Lagemaat, J.; Frank, A. J. *J. Phys. Chem. B* **2001**, *105*, 11194–11205.
143. Clifford, J. N.; Yahioğlu, G.; Milgrom, L. R.; Durrant, J. R. *Chem. Commun.* **2002**, 1260–1261.
144. Spanhel, L.; Weller, H.; Henglein, A. *J. Am. Chem. Soc.* **1987**, *109*, 6632–6635.
145. Henglein, A. *Ber. Bunsenges. Phys. Chem.* **1995**, *99*, 903–913.
146. Henglein, A.; Giersig, M. *J. Phys. Chem. B* **1999**, *103*, 9533–9539.
147. Gachard, E.; Remita, H.; Khatouri, J.; Keita, B.; Nadjó, L.; Belloni, J. *New J. Chem.* **1998**, 1257–1265.
148. Henglein, A. *Chem. Rev.* **1989**, *89*, 1861–1873.
149. Henglein, A.; Mulvaney, P.; Linnert, T. *Faraday Discuss.* **1991**, *92*, 31–34.
150. Fyson, J. R.; Twist, P. J.; Gould, I. R. In *Electron Transfer in Chemistry*; Balzani, V., Ed.; Wiley-VCH: New York, 2001; Vol. 5, Part 2, pp 285–378 and references therein.
151. Crooks, R. M.; Zhao, M.; Sun, L.; Chechik, V.; Yeung, L. K. *Acc. Chem. Res.* **2001**, *34*, 181–190.
152. Brust, M.; Bethell, D.; Kiely, C. J.; Schiffrin, D. J. *Langmuir* **1998**, *14*, 5425–5429.
153. Pietron, J. J.; Hicks, J. F.; Murray, R. W. *J. Am. Chem. Soc.* **1999**, *121*, 5565–5570.
154. Hostetler, M. J.; Green, S. J.; Stokes, J. J.; Murray, R. W. *J. Am. Chem. Soc.* **1996**, *118*, 4212–4213.
155. Wuelfing, W. P.; Templeton, A. C.; Hicks, J. F.; Murray, R. W. *Anal. Chem.* **1999**, *71*, 4069–4074.
156. Wuelfing, W. P.; Green, S. J.; Pietron, J. J.; Cliffel, D. E.; Murray, R. W. *J. Am. Chem. Soc.* **2000**, *122*, 11465–11472.
157. Terrill, R. H.; Postlethwaite, T. A.; Chen, C.-h.; Poon, C.-D.; Terzis, A.; Chen, A.; Hutchison, J. E.; Clark, M. R.; Wignall, G.; Londono, J. D.; Superfine, R.; Falvo, M., Jr.; Samulski, E. T. *J. Am. Chem. Soc.* **1995**, *117*, 12537–12548.
158. Hicks, J. F.; Zamborini, F. P.; Osisek, A.; Murray, R. W. *J. Am. Chem. Soc.* **2001**, *123*, 7048–7053.

159. Bignozzi, C. A.; Schoonover, J. R.; Scandola, F. *Prog. Inorg. Chem.* **1997**, *44*, 1–95.
160. Scandola, F.; Chiorbelli, C.; Indelli, M. T.; Rampi, M. A. In *Electron Transfer in Chemistry*; Balzani, V., Ed.; Wiley-VCH: New York, 2001; Vol. 3, Part 2, pp 337–408 and references therein.
161. Balzani, V.; Ballardini, R.; Bolletta, F.; Gandolfi, M. T.; Juris, A.; Maestri, M.; Manfrin, M. F.; Moggi, L.; Sabbatini, N. *Coord. Chem. Rev.* **1993**, *125*, 75–88.
162. Gust, D.; Moore, T. A.; Moore, A. L. *Pure Appl. Chem.* **1998**, *70*, 2189–2200.
163. Gust, D.; Moore, T. A.; Moore, A. L. *Acc. Chem. Res.* **2001**, *34*, 40–48.
164. Worl, L. A.; Strouse, G. F.; Younathan, J. N.; Baxter, S. M.; Meyer, T. J. *J. Am. Chem. Soc.* **1990**, *112*, 7571–7578.
165. Creutz, C.; Sutin, N. *J. Am. Chem. Soc.* **1977**, *99*, 241–243.
166. Fleming, C. N.; Maxwell, K. A.; DeSimone, J. M.; Meyer, T. J.; Papanikolas, J. M. *J. Am. Chem. Soc.* **2001**, *123*, 10336–10347.
167. Casado, C. M.; Cuadrado, I.; Morán, M.; Alonso, B.; García, B.; González, B.; Losada, J. *Coord. Chem. Rev.* **1999**, *185–186*, 53–59.
168. Balzani, V. C. S.; Denti, G.; Juris, A.; Serroni, S.; Venturi, M. *Acc. Chem. Res.* **1998**, *31*, 26–34.
169. Balzani, V.; Ceroni, P.; Juris, A.; Venturi, M.; Campagna, S. *Coord. Chem. Rev.* **2001**, *219–221*, 545–572.
170. Ghaddar, T. H.; Wishart, J. F.; Thompson, D. W.; Whitesell, J. K.; Fox, M. A. *J. Am. Chem. Soc.* **2002**, *124*, 8285–8289.
171. Goldsmith, J. I.; Takada, K.; Abruna, H. *J. Phys. Chem. B* **2002**, *106*, 8504–8513.
172. Onuchic, J. N.; Risser, S. M.; Skourtis, S. S.; Beratan, D. N. In *Molecular Electronics*; Ratner, M. A., Jortner, J., Eds.; Blackwell: Oxford, UK 1997; pp 369–379 and references therein.
173. Imahori, H.; Norieda, H.; Yamada, H.; Nishimura, Y.; Yamazaki, I.; Sakata, Y.; Fukuzumi, S. *J. Am. Chem. Soc.* **2001**, *123*, 100–110.
174. Imahori, H.; Arimura, M.; Hanada, T.; Nishimura, Y.; Yamazaki, I.; Sakata, Y.; Fukuzumi, S. *J. Am. Chem. Soc.* **2001**, *123*, 335–336.
175. Frank, A. J.; Gregg, B. A.; Grätzel, M.; Nozik, A. J.; Zaban, A.; Ferrere, S.; Schlichthorl, G.; Huang, S. Y. *AIP Conf. Proc.* **1997**, *404*, 145–153.
176. Miller, R. J. D.; McLendon, G. L.; Nozik, A. J.; Schmickler, W.; Willing, F. *Surface Electron-Transfer Processes* **1995**, Wiley-VCH: New York.
177. Gerfin, T.; Grätzel, M.; Walder, L. *Prog. Inorg. Chem.* **1997**, *44*, 345–389.
178. Hagfeldt, A.; Grätzel, M. *Acc. Chem. Res.* **2000**, *33*, 269–277.
179. Yang, M.; Thompson, D. W.; Meyer, G. J. *Inorg. Chem.* **2000**, *39*, 3738–3739.
180. Kalyanasundaram, K.; Grätzel, M. *Coord. Chem. Rev.* **1998**, *77*, 347–414.
181. Hannappel, T.; Burfeindt, B.; Storck, W.; Willig, W. *J. Phys. Chem. B* **1997**, *101*, 6799–6802.
182. Asbury, J. B.; Hao, E.; Wang, Y.; Ghosh, H. N.; Lian, T. *J. Phys. Chem. B* **2001**, *105*, 4545–4557.
183. Asbury, J. B.; Hao, E.; Wang, Y.; Lian, T. *J. Phys. Chem. B* **2000**, *104*, 11957–11964.
184. Asbury, J. B.; Ellingson, R. J.; Ghosh, H. N.; Ferrere, S.; Nozik, A. J.; Lian, T. *J. Phys. Chem. B* **1999**, *103*, 3110–3119.
185. Tachibana, Y.; Moser, J. E.; Grätzel, M.; Klug, D. R.; Durrant, J. R. *J. Phys. Chem.* **1996**, *102*, 6455.
186. Blauch, D. N.; Saveant, J.-M. *J. Am. Chem. Soc.* **1992**, *114*, 3323–3332.
187. Bauer, C.; Boschloo, G.; Mukhtar, E.; Hagfeldt, A. *J. Phys. Chem. B* **2002**, *106*, 12693–12704.
188. Hasselmann, G. M.; Meyer, G. J. *J. Phys. Chem. B* **1999**, *103*, 7671–7675.
189. Mallouk, T. E., Ed., *Catalysis of Electron Transfer, Heterogeneous and Gas-Phase Systems*; Wiley-VCH: New York, 2001; Vol. 4, Part 2.
190. Ryan, J. V.; Berry, A. D.; Anderson, M. L.; Long, J. W.; Stroud, R. M.; Cepak, V. M.; Browning, V. M.; Rolison, D. R.; Merzbacher, C. I. *Nature* **2000**, *406*, 169–172.
191. Meyer, G. J., Ed., *Molecular Level Artificial Photosynthetic Materials* **1997**, 44Wiley: New York.
192. Ogawa, M.; Kuroda, K. *Chem. Rev.* **1995**, *95*, 399–438.
193. Kaschak, D. M.; Johnson, S. A.; Waraksa, C. C.; Pogue, J.; Mallouk, T. E. *Coord. Chem. Rev.* **1999**, *185*, 403–416.
194. Castellano, F. N.; Meyer, G. J. *Prog. Inorg. Chem.* **1997**, *44*, 167–208.
195. Bhat, V.; Domen, K. In *Electron Transfer in Chemistry*; Balzani, V., Ed.; Wiley-VCH: New York, 2001; Vol. 4, Part 2, pp 487–540.
196. Dutta, P. K.; Ledney, M. *Prog. Inorg. Chem.* **1997**, *44*, 209–271.
197. Vaidyalingham, A. S.; Coutant, M. A.; Dutta, P. K. In *Electron Transfer in Chemistry*; Balzani, V., Ed.; Wiley-VCH: New York, 2001; Vol. 4, Part 2, pp 412–486 and references therein.
198. Lee, H.; Dutta, P. K. *J. Phys. Chem. B* **2002**, *106*, 11898–11904.
199. Lee, J.-O.; Lientschnig, G.; Wiertz, F.; Martin Struijk, R. A. J. J.; Egberink, R.; Reinhoudt, D. N.; Hadley, P.; Dekker, C. *Nano Lett.* **2003**, *3*, 113–117.
200. Kagan, C. R.; Afzali, A.; Martel, R.; Gignac, L. M.; Solomon, P. M.; Schrott, A. G.; Ek, B. *Nano Lett.* **2003**, *3*, 119–124.
201. Beasley, M. R. C.; Datta, S.; Kogelnik, H.; Kroemer, H.; Monroe, D. *Report of the Investigation Committee on the Possibility of Scientific Misconduct in the Work of Hendrik Schön and Coauthors* (September 2002) ([http://www.lucent.com/news\\_events/pdf/researchreview.pdf](http://www.lucent.com/news_events/pdf/researchreview.pdf)).
202. Schön, J. H.; Meng, H.; Bao, Z. *Nature* **2003**, *422*, doi:10.1038/nature01464.
203. Adams, D.; Brus, L.; Chidsey, C. E. D.; Creager, S.; Creutz, C.; Kagan, C. R.; Kamat, P. V.; Lieberman, M. Lindsay, S.; Marcus, R. A.; Metzger, R. M.; Michel-Beyerle, M. E.; Miller, J. R.; Newton, M. D.; Rolison, D. R.; Sankey, O.; Schanze, K. S.; Yardley, J.; Zhu, X. *J. Phys. Chem. B* **2003**, *6668–6697*.
204. McFarland, E. W.; Tang, J. *Nature* **2003**, *421*, 616–618.

# 7.13

## Magnetism from the Molecular to the Nanoscale

D. GATTESCHI and R. SESSOLI

*University of Florence, Italy*

and

A. CORNIA

*University of Modena and Reggio Emilia, Italy*

---

7.13.1	FUNDAMENTAL ASPECTS	779
7.13.2	MAGNETIC COUPLING	780
7.13.2.1	Polarized Neutron Diffraction	785
7.13.3	ZERO-DIMENSIONAL SYSTEMS	786
7.13.3.1	Oligonuclear Systems	786
7.13.3.2	Mixed-valence Species	787
7.13.3.3	Valence Tautomeric Species	790
7.13.3.4	Antiferromagnetic Rings	791
7.13.3.5	Single-molecule Magnets	794
7.13.4	ONE-DIMENSIONAL SYSTEMS	802
7.13.4.1	Haldane Gap Systems	802
7.13.4.2	Azide-bridged One-dimensional Systems	803
7.13.4.3	Metal Radical Chains	805
7.13.4.3.1	<i>Metal nitroxide chains</i>	805
7.13.4.4	Oxalato Derivatives	807
7.13.5	REFERENCES	809

---

### 7.13.1 FUNDAMENTAL ASPECTS

The basic theory of magnetism in transition metal compounds is covered in several excellent books<sup>1-3</sup> and the interested reader is referred to them. Here we will briefly discuss some key points which may be needed later for understanding the language used throughout this section.

An isolated transition metal ion with one or more unpaired electrons behaves as a paramagnet, i.e., it has a non-zero magnetization only in the presence of an applied magnetic field. Of course, isolated transition metal ions are not frequently met in a chemical laboratory and in general they are found in a crystal or in a powder where large collections of ions are contained separated by a few Å from one another. Under these conditions the approximation of isolated ions is still valid, at least at relatively high temperature ( $T$ ), and the molar magnetic susceptibility  $\chi_m$  of the compound can be described by the Curie law:

$$\chi_m = C/T \quad (1)$$



where  $C$  is a constant, which depends on the spin and orbital magnetic moment of the metal ion. For orbitally non-degenerate ground states, as is generally true due to the low symmetry of the compounds and Jahn–Teller effects,  $C$  is given by:

$$C = \frac{N_A \mu_B^2 g^2 S(S+1)}{3k_B} \quad (2)$$

where  $S$  is the spin quantum number,  $N_A$  is Avogadro's number,  $k_B$  is Boltzmann constant,  $\mu_B$  is Bohr magneton, and  $g$  is the Landé factor which for a free electron, takes the value  $g_e = 2.0023$ .

The Curie law is followed by many transition-metal compounds, but deviations can be observed at low temperatures due to different reasons. One is that the approximation of isolated ions may break down at low temperatures. In fact, the ions may interact with each other both through space and through bonds. The former is the magnetic dipolar interaction, which is expected to depend on the inverse third power of the distance  $r$  between the paramagnetic centers. The latter is the so-called exchange interaction, which is due to the formation of very weak chemical bonds between neighboring ions. More details on this point will be provided in the following paragraphs.

A way of taking care of the interaction is to modify the Curie law introducing the so-called Weiss correction to yield the Curie–Weiss law:

$$\chi_m = \frac{C}{T - \theta} \quad (3)$$

The presence of interactions determines the passage from isolated magnetism (paramagnetism) to cooperative magnetism. At low temperature the interactions can take over on thermal agitation and a transition to a magnetically ordered state can occur. If the individual spins preferentially orient parallel to each other the ordered state is *ferromagnetic*. The critical temperature at which the transition to the ordered state is observed is called the Curie temperature,  $T_C$ . If the spins prefer to orient antiparallel to each other two cases can be observed: if the spins are all identical to each other the ordered state is *antiferromagnetic* and has no spontaneous magnetization. If, on the other hand, there are two sets of different spins then the individual moments will not compensate and the ordered state, characterized by spontaneous magnetization, is called *ferrimagnetic*. The critical temperature is called the Néel temperature,  $T_N$ . It must be stressed that in order to observe a magnetic transition it is necessary that a three-dimensional network of interactions be established. If the interactions are limited to a plane or to a chain, then low-dimensional magnetism is observed. Finite size clusters are often referred to as zero-dimensional magnets.

Deviations from the simple Curie law are also observed in the absence of cooperative phenomena. In a low-symmetry environment, as is often found in transition metal ion compounds, a spin multiplet characterized by quantum number  $S > 1/2$  removes its  $(2S+1)$ -fold degeneracy, corresponding to the different  $M$  components, as a result of the dipolar interactions between the unpaired electrons and of spin–orbit coupling. This phenomenon is called *zero-field splitting* (*ZFS*) and it determines deviations from the simple Curie law at low temperatures. In axial symmetry the energies of the zero-field-split levels are given by:

$$E(M) = DM^2 \quad (4)$$

where  $D$  is a constant which may be either positive or negative. If  $D$  is positive the levels with the minimum  $M$  components ( $\pm 1/2$  or 0 for half integer and integer  $S$ , respectively) lie lowest, while for  $D < 0$  the  $\pm S$  components lie lowest. In the former case, at low temperature the spins will tend to be orthogonal to the symmetry axis, while in the latter they will orient parallel to it. Positive  $D$  corresponds to an easy-plane magnetic anisotropy, while negative  $D$  corresponds to an easy-axis type (Ising) magnetic anisotropy.

### 7.13.2 MAGNETIC COUPLING

If two paramagnetic centers, characterized by spins  $S_1$  and  $S_2$ , are close to each other they may interact in such a way that their spins are no longer independent. The simplest way of

describing the interaction is through a spin Hamiltonian which, in rather general form, can be written as:

$$\mathbf{H} = \mathbf{S}_1 \cdot J_{12} \cdot \mathbf{S}_2 \quad (5)$$

where  $J_{12}$  is a matrix. Under some conditions, which are usually referred to as the “strong exchange limit” Equation (5) reduces to:

$$\mathbf{H} = J\mathbf{S}_1 \cdot \mathbf{S}_2 \quad (6)$$

where  $J$  is a constant, usually termed the Heisenberg–Dirac–van Vleck coupling constant.<sup>4</sup> A total spin may be introduced:

$$\mathbf{S} = \mathbf{S}_1 + \mathbf{S}_2 \quad (7)$$

When applied to a basis of  $(2S_1 + 1)(2S_2 + 1)$  functions the spin Hamiltonian Equation (6) gives rise to a ladder of levels labeled using the total spin  $S$ :

$$|S_1 - S_2| \leq S \leq S_1 + S_2 \quad (8)$$

with a separation following the Landé interval rule:

$$E(S) = (J/2)[S(S+1) - S_1(S_1+1) - S_2(S_2+1)] \quad (9)$$

In this convention  $J > 0$  puts the lowest  $S$  value at lower energy, therefore it corresponds to antiferromagnetic coupling, while  $J < 0$  corresponds to ferromagnetic coupling. It should be noted here that in the literature there are at least three other different conventions, corresponding to the Hamiltonians:

$$\mathbf{H} = -J\mathbf{S}_1 \cdot \mathbf{S}_2 \quad (10)$$

$$\mathbf{H} = -2J\mathbf{S}_1 \cdot \mathbf{S}_2 \quad (11)$$

$$\mathbf{H} = 2J\mathbf{S}_1 \cdot \mathbf{S}_2 \quad (12)$$

Equation (10) is more common in Europe, while Equation (11) is more common in the USA. It is apparent that all of the forms are theoretically equivalent, but in order to compare reported values of the coupling constants it is necessary to check the convention used.

The origin of the interaction is essentially the formation of a weak chemical bond,<sup>5</sup> analogous to that of two hydrogen atoms separated by a distance much larger than the equilibrium bond distance. In the following we will focus on pairs of transition metal ions, with some occasional inclusion of organic radicals in the treatment. The requirement that the two metal ions be “close” to each other is certainly a qualitative one. In fact it is not necessary that the metal orbitals have a significant direct overlap in order to observe magnetic coupling. In fact, the presence of suitable, formally diamagnetic ligands between the two metal ions may provide significant indirect overlap to ensure sizeable coupling. Copper(II) dinuclear species bridged by oxalate ions are particularly instructive. The two metal ions are separated by more than 5.5 Å and the antiferromagnetic coupling corresponds to  $J > 500 \text{ cm}^{-1}$ .<sup>6</sup>

A qualitative explanation of magnetic coupling was presented in the 1950s by Anderson<sup>7,8</sup> with a model that is reminiscent of the Heitler–London treatment of the bond in the hydrogen molecule. A first set of simple rules was suggested by Goodenough and Kanamori,<sup>9,10</sup> which helped in predicting or rationalizing the observed magnetic coupling in metal ion pairs. The rapid development of the molecular orbital (MO) techniques in chemistry after the 1960s required a translation of the Goodenough Kanamori rules into a more MO-oriented language. The main contributions in this direction were made by Hay, Thibault, and Hoffman (HTH)<sup>11</sup> on one side and by Kahn on the other.<sup>12</sup> The problem was also tackled experimentally by trying to establish empirical correlations between the structures of the metal pairs and the observed coupling constants. In the last few years Density Functional Theory (DFT)<sup>13,14</sup> has been applied to the calculation of coupling constants in dimers and more complex clusters.<sup>15</sup>

The semi-quantitative approaches of HTH<sup>11</sup> and Kahn<sup>12</sup> considered at the simplest level the case of a metal-ion pair containing only one unpaired electron per metal center. The main difference between the two approaches is that the former starts from orthogonal combinations  $\varphi_a$  and  $\varphi_b$  of magnetic orbitals, while the latter uses natural, non-orthogonal magnetic orbitals. Both approaches express the coupling constant  $J$  as the sum of two contributions, a ferromagnetic and an antiferromagnetic one. In the HTH approach  $J$ , in the formalism of Equation (6), is given by:

$$J = -2K_{ab} + \frac{(\varepsilon_1 - \varepsilon_2)^2}{J_{aa} - J_{ab}} \quad (13)$$

where the first term, corresponding to the exchange integral involving  $\varphi_a$  and  $\varphi_b$ , gives the ferromagnetic contribution, while the second gives the antiferromagnetic contribution.  $(\varepsilon_1 - \varepsilon_2)$  corresponds to the energy difference between the molecular orbitals, and  $J_{aa}$  and  $J_{ab}$  are Coulomb integrals. The advantage of this model is that it correlates the coupling constant  $J$  with some quantities which have become familiar to chemists who now extensively use MO language to discuss the stability and the reactivity of compounds. Equation (13) clearly states that if  $\varphi_a$  and  $\varphi_b$  are significantly split in the formation of the bonding and antibonding molecular orbitals the coupling is antiferromagnetic. Therefore, ferromagnetic coupling requires a vanishingly small splitting, but also the presence of regions where the spin densities associated with the two centers are large, in order to have a large exchange integral.

A limitation of the HTH approach is that it uses orthogonal magnetic orbitals, which are better suited for calculations but are more difficult to visualize. The Kahn approach overcomes this problem by using natural orbitals. The pair is arbitrarily cut into two fragments, in which the bridging ligands are considered twice. This procedure makes the approach unsuitable for calculations, but does allow the development of a simpler qualitative description of the magnetic coupling. In Kahn's formalism the coupling constant is expressed as:

$$J = 2k + 4h_{ab}S_{ab} \quad (14)$$

where  $k$  is the exchange integral between the natural orbitals,  $S_{ab}$  is the corresponding overlap integral, and  $h_{ab}$  is the one-electron Hamiltonian taking into account the kinetic energy of the electrons and their interactions with the nuclei and with all the passive electrons. The key role in Kahn's model is played by the overlap integral. If the integral is zero the antiferromagnetic contribution is zero and the system must display a ferromagnetic coupling, if it is different from zero an antiferromagnetic interaction is expected. In order to have a significant ferromagnetic coupling it is necessary that, even if  $S_{ab}$  is globally zero, there are regions in which the overlap densities differ from zero.

Neither method allows quantitative calculations although both have been successfully used to justify experimentally observed trends. In general, an Extended Hückel approach was used to calculate the splitting between the highest molecular orbitals as a function of some structural parameters, such as metal-bridge-metal angle, and useful conclusions were reached concerning the observed coupling constants.<sup>2,15-18</sup> A somewhat similar approach was used by Güdel *et al.*<sup>19</sup>

The difficulty for quantitative MO-based calculations is that small quantities like the  $J$  coupling constants are calculated as differences between much larger quantities. The  $J$  coupling constants are typically of the order  $10^0$ – $10^3$   $\text{cm}^{-1}$  to be compared with total energies that may be seven orders of magnitude larger. Furthermore, the systems are by definition open shell ones and large problems are encountered to properly account for electron correlation. Therefore, *ab initio* calculations are extremely difficult to perform as they involve large numbers of atoms. However, the rapid developments of the past few years in both hardware and software have drastically changed the landscape, and since the mid-1990s it has become possible to tackle molecules of increasing complexity, obtaining extremely accurate values of the coupling constants which compare quite well with the experimental ones.<sup>20,21</sup>

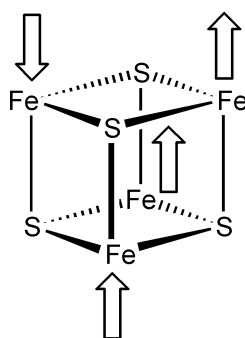
The current calculations, which are not yet routine, but which can now be performed on relatively simple computers, are based on DFT models for the description of the MOs of magnetic molecules, and on the so-called broken-symmetry approach, first suggested by Noodleman in 1981.<sup>22</sup>

The broken-symmetry approach was developed within the framework of unrestricted Hartree-Fock theory or spin-polarized density functional theory, i.e.,  $X\alpha$  theory.<sup>23,24</sup> It is based on the assumption that the energy difference between the singlet and triplet states resulting from the interaction between two  $S = 1/2$  spin centers is given by:

$$J = -2(E_{BS} - E_T) \quad (15)$$

where  $E_T$  is the energy of the triplet state and  $E_{BS}$  is the energy of the so-called broken-symmetry state. This is a state which corresponds to putting one electron in the magnetic orbital  $\varphi_a$  with spin  $\alpha$  and the other in the magnetic orbital  $\varphi_b$  with spin  $\beta$ . This is not a true singlet spin state, because a complete description involves a linear combination of this state with the symmetrical one where the  $\alpha$  spin is associated with  $\varphi_b$  and the  $\beta$  spin with  $\varphi_a$ . Therefore, the broken-symmetry state is a mixed-spin state (it is a mixture of singlet and triplet) with a lowered spatial symmetry. The approach can be easily generalized to the case where more than one unpaired electron is present on each center.

The Noodleman approach was first used to calculate the coupling constants in sulfur-bridged iron complexes relevant to iron-sulfur proteins.<sup>25–27</sup> More recently, detailed DFT calculations have been performed on the five known oxidation states  $[\text{Fe}_4\text{S}_4(\text{SCH}_3)_4]^{n-}$  ( $n=0, 1, 2, 3,$  and  $4$ ) clusters that model the active sites of iron-sulfur proteins.<sup>28</sup> The geometries of the clusters were optimized, giving in general good agreement with experiment, although the calculated bond lengths tend to be slightly larger than experimentally observed. A good correlation was also found between calculated and experimental reduction potentials. The spin density was also calculated and  $[\text{Fe}_4\text{S}_4]$  (all ferrous) system was found to have an  $S=4$  ground state as experimentally observed. This corresponds to the rather unusual spin alignment in Scheme 1.



Scheme 1

The method has been extended also to heterodinuclear species,<sup>29</sup> i.e., systems in which two different metal ions are magnetically coupled, and to polynuclear compounds.<sup>30–33</sup>

Beyond these quantitative approaches, another qualitative approach must be mentioned, namely that based on spin polarization effects. Neglecting electron correlation, the spin density on a given atom can only be positive, i.e., parallel to the external field. However, if electron correlation is correctly taken into account, zones of positive and negative spin density can be achieved. This is best understood in the allyl radical,  $\text{CH}_2\text{CHCH}_2$ , depicted in Figure 1. At the elementary level the unpaired electron is in an  $a_2$  orbital, giving rise to positive spin density on C1 and C3, while there is no spin density on C2 because the wavefunction has a node there. However, if the mixing of the excited configuration depicted in Figure 1 is taken into account, the unpaired spin density on C1 and C3 becomes larger, and a negative spin density is induced on C2.

Spin polarization effects are particularly apparent in the coupling of organic radicals.<sup>34</sup> For instance, it is believed that the weak ferromagnetic coupling responsible for the bulk ferromagnetic order observed at low temperature for  $\text{NITpNO}_2\text{Ph}$ , the radical shown in Figure 2, where  $\text{NITpNO}_2\text{Ph}$  is 2-(4-nitrophenyl)-4,4,5,5-tetramethyl-4,5-dihydro-1H-imidazol-1-oxyl-3-oxide occurs through the short intermolecular contacts between the NO group and the  $\text{NO}_2$  group, where a small spin density is delocalized.

In transition metal ions this approach has been systematically used in the rationalization of the magnetic coupling between ions bridged by aromatic ligands. The theory of exchange coupling was developed by Longuet-Higgins for alternant hydrocarbons. In Figure 3 is depicted a simple scheme for the case of two molybdenum(V) ions bridged by 4,4'-bipyridine and 4,5'-bipyridine.<sup>36–38</sup> In both cases it is assumed that the magnetic orbitals of the molybdenum ions are orthogonal to the  $\pi$  orbitals of the aromatic rings. In this case the spin density carried by neighboring atoms is opposite in sign. In the former case the molybdenum ions are separated by an even number of atoms, resulting in antiferromagnetic coupling, while in the latter the number of intervening atoms is odd, thus determining ferromagnetic coupling. Experimentally, it was found that the coupling constant is antiferromagnetic,  $J=33\text{ cm}^{-1}$ , for 4,4'-bipyridine, while for

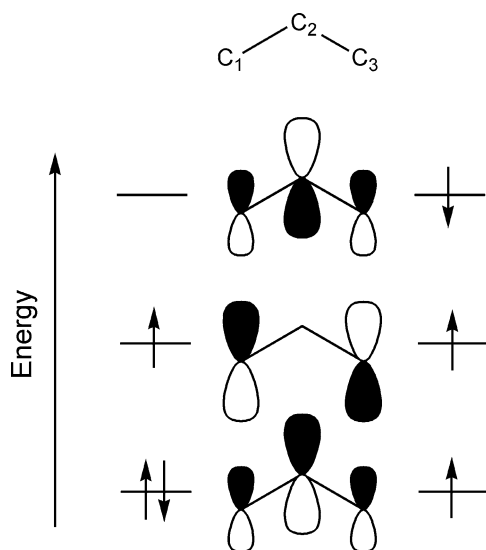


**Figure 1** Sketch of the molecular orbitals of the allyl radical  $\text{CH}_2\text{CHCH}_2$ . On the left is the ground configuration based on a SCF calculation, on the right an excited state configuration responsible for the spin polarization effect.

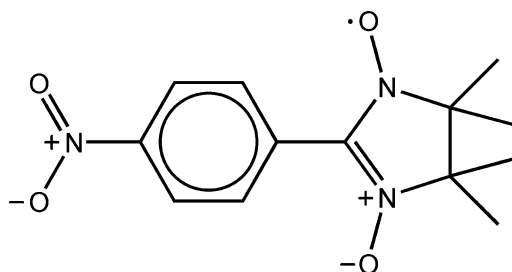


**Figure 2** Sketch of  $\text{NITpNO}_2\text{Ph}$ .

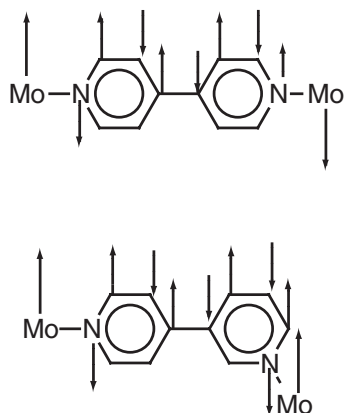


**Figure 3** Spin polarization mechanism of the exchange interaction between two molybdenum(V) ions bridged by 4,4'- and 4,5'-bipyridine.

4,5'-bipyridine it is weakly ferromagnetic,  $J = -0.8 \text{ cm}^{-1}$ . Of course, these are simplified schemes, which implicitly assume that the aromatic ring planes are parallel to each other. Experimentally, it was found that a variation of the twist angle from  $26^\circ$  to  $90^\circ$  reduced  $J$  by approximately 90%. DFT calculations have confirmed this view,<sup>39</sup> showing that there can be large deviations from these simple predictions if the planes are no longer parallel.

### 7.13.2.1 Polarized Neutron Diffraction

The nature of the magnetic coupling between transition metal ions can be investigated through several different experimental techniques, among which the measurement of the magnetic susceptibility as a function of temperature has certainly a very important, if not determinant, role. In recent years several new sophisticated tools have been added to those commonly used (see Chapter 2.36). We want here to briefly mention how polarized neutron diffraction techniques can provide a detailed map of the unpaired spin density in the ground state, therefore visualizing the nature of exchange interactions between the two metal ions.

Neutrons, which are characterized by a spin quantum number  $I = 1/2$ , are well known to interact both with the nuclei of a crystal and with the magnetic moments.<sup>40,41</sup> Diffraction techniques are used to determine the structures by taking advantage of the neutron–nucleus interaction. If the crystal is magnetized it is possible to determine a map of the magnetization density using spin-polarized neutrons, which interact in a different way with the positive and negative magnetization density areas. While in the case of permanent magnets the experiment can be performed in zero magnetic field, paramagnets like the dinuclear complexes considered here require the application of an external magnetic field in order to sufficiently polarize the electronic spins. The experiments are usually performed at liquid helium temperature or below, with applied fields of a few tesla. Analysis of the experimental data is far from simple, but with sophisticated techniques, like the maximum entropy approach, it is now possible to reconstruct a detached map of the magnetization density in the crystal.

The polarized neutron diffraction technique has been recently applied to several dinuclear transition metal derivatives. In  $[\text{Mn}(\text{CTH})\text{Cu}(\text{oxpn})](\text{CF}_3\text{SO}_3)_2$ , where  $\text{CTH} = \text{Me}_6\text{-[14]ane-N}_4$  and  $\text{oxpn} = N,N'$ -bis(3-aminopropyl)oxamidate, the manganese(II) ion ( $S = 5/2$ ), is bridged to a copper(II) ion  $S_2 = 1/2$  through an oxamidate bridge, with the two nitrogen atoms coordinated to copper and the two oxygen atoms to manganese.<sup>42,43</sup> Although the distance between the two ions is as large as 5.44 Å, the antiferromagnetic coupling is significant ( $J = 31.3 \text{ cm}^{-1}$ ), and gives rise to a ground state with  $S = 2$  and an excited state with  $S = 3$  separated by  $93.9 \text{ cm}^{-1}$ . The diffraction experiments were performed at 2 K in a field of 5 T. The results are depicted in Figure 4. It is apparent that the magnetization density is positive on manganese(II), while it is negative on copper(II). Further, the magnetization density is essentially isotropic on manganese(II), in accord with the  $d^5$  configuration corresponding to a  ${}^6A_{1g}$  ground state in octahedral symmetry, while it corresponds to that expected for a  $x^2 - y^2$  orbital in copper(II), again in accord with the square planar coordination around the  $d^9$  ion. Although most of the magnetization density is centered on the two metal ions, the role of the ligand in transmitting the interaction is apparent from the non-zero density observed on the atoms of the oxamidate moiety. In particular, the negative density present on the nearest neighbors of copper amounts to ca. 30% of the total, while the positive spin density on the manganese ions is only 7% of the total. This is a clear indication that the bonds around copper have a higher covalency than those around manganese.

Beyond these elegant qualitative considerations it is possible to reproduce the magnetization density map using DFT calculations. The agreement is rather good as shown by the values reported in Table 1.

The PND technique has now been widely applied to many dinuclear, oligonuclear, and one-dimensional magnetic systems involving transition metal ions.

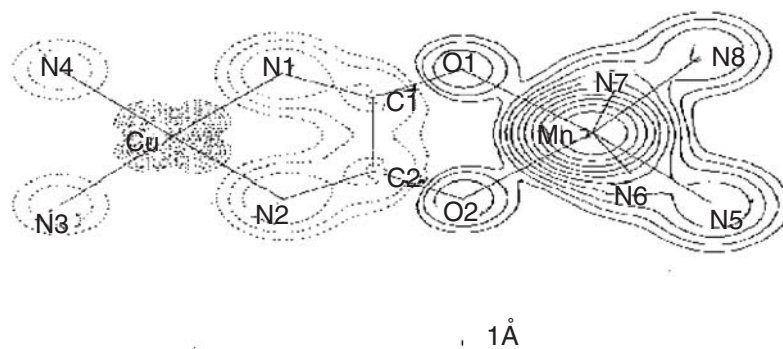


**Figure 4** Spin density map for  $[\text{Mn}(\text{CTH})\text{Cu}(\text{oxpn})](\text{CF}_3\text{SO}_3)_2$  at 2 K in a 5 T magnetic field. Dot contour lines are for negative spin density. After ref. 42.

**Table 1** PND and calculated atomic spin population ( $\mu_B$ ) for  $[\text{Mn}(\text{CTH})\text{Cu}(\text{oxpn})](\text{CF}_3\text{SO}_3)_2$ ,  $S = 2$ .

Atom	PND Data	DFT Data
$N_{\text{ax}}$	0.07(1)	0.03
$N_{\text{eq}}$	0.07(1)	0.02
Mn	4.32(2)	4.41
O	0.03(1)	0.02
C	-0.03(1)	0.00
$N_{\text{bridge}}$	-0.05(1)	-0.08
Cu	-0.47(1)	-0.27
N	-0.02(1)	-0.06

### 7.13.3 ZERO-DIMENSIONAL SYSTEMS

#### 7.13.3.1 Oligonuclear Systems

The simplest case is that of pairs. The nature of the magnetic interaction can be obtained from the analysis of the temperature dependence of the effective magnetic moment,  $\mu_{\text{eff}}$ , or of the  $\chi_m T$  product. The two quantities are related to each other by  $\mu_{\text{eff}} = \sqrt{8\chi_m T}$ .

In the older literature  $\mu_{\text{eff}}$  was more commonly reported, while in the more recent literature  $\chi_m T$  is generally used.

In the case of homonuclear pairs, antiferromagnetic coupling gives rise to a maximum in the temperature plot of susceptibility. The position of the maximum provides direct information on the value of  $J$ , as shown in Table 2 for homonuclear pairs with different individual spin  $S_i$ .

In the assumption of dominant exchange, i.e., if the total spin  $S$ , is a good quantum number, then the individual spins can be easily projected on the total spin, and the related observables in the total spin multiplets are linear combinations of the analogous observables of the individual spins.<sup>44</sup> The relations between the Zeeman factor, the hyperfine coupling constants, and the  $ZFS$  parameters of the coupled pair and those of the individual ions are given below:

$$g_S = c_1 g_1 + c_2 g_2 \quad (16)$$

$$A_S^k = c_1 A_1^k + c_2 A_2^k \quad (17)$$

$$D_S = d_1 D_1 + d_2 D_2 + d_{12} D_{12} \quad (18)$$

where

$$\begin{aligned} c_1 &= (1 + c)/2; & c_2 &= (1 - c)/2 \\ d_1 &= (c_+ + c_-)/2; & d_2 &= (c_+ - c_-)/2 \\ d_{12} &= (1 - c_+)/2 \end{aligned} \quad (19)$$

**Table 2** The relation between  $T_{\text{max}}$  and  $J$  for antiferromagnetically coupled pairs of  $S_i$  spins.

$S_i$	$k_B T_{\text{max}} J$
1/2	0.60
1	1.01
3/2	1.54
2	2.14
5/2	2.86

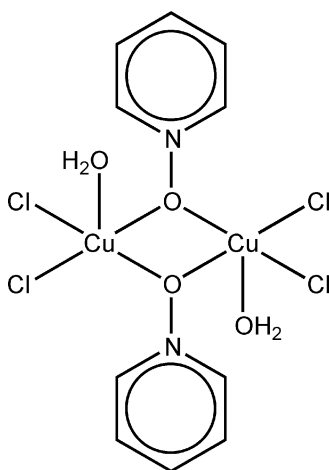
and

$$c = \frac{S_1(S_1 + 1) - S_2(S_2 + 1)}{S(S + 1)}$$

$$c_+ = \frac{3[S_1(S_1 + 1) - S_2(S_2 + 1)]^2 + S(S + 1)[3S(S + 1) - 3 - 2S_1(S_1 + 1) - 2S_2(S_2 + 1)]}{(2S + 3)(2S - 1)S(S + 1)} \quad (20)$$

$$c_- = \frac{4S(S + 1)[S_1(S_1 + 1) - S_2(S_2 + 1)] - 3[S_1(S_1 + 1) - S_2(S_2 + 1)]}{(2S + 3)(2S - 1)S(S + 1)}$$

In Equation (18)  $D_{12}$  is a tensor which describes the anisotropic interaction between the two spins. It has a through-space (magnetic dipolar) and through-bond (exchange determined) component. The validity of Equations (16)–(20) has been checked experimentally in many cases. McPherson *et al.* have provided an elegant example concerning the  $g$  and  $A$  tensors.<sup>45</sup> They investigated the EPR spectra of manganese(II)-doped dichloroquo(pyridine *N*-oxide)copper(II), whose structure is shown in Scheme 2.



Scheme 2

Since the copper(II) ions are antiferromagnetically coupled with a moderate coupling constant, at low temperature the host lattice becomes diamagnetic and the spectra of the copper(II)–manganese(II) pairs are easily observed. The spectra correspond to quintets ( $S = 2$ ), indicating antiferromagnetic coupling. The  $g$  and  $A$  values of the copper(II) centers were independently obtained from the spectra of zinc(II) doped species, while for manganese(II) it was assumed  $g = 2.002$ . Equations (16)–(20) require:

$$g_2 = (7/6)g_{\text{Mn}} - (1/6)g_{\text{Cu}}; \quad A_2^{\text{Cu}} = -(1/6)A^{\text{Cu}} \quad (21)$$

It must be recalled that the above relations are tensorial ones, which means that the comparison must be performed taking into account the relative orientations of the tensors. If this is done, the data shown in Table 3 are obtained.

The agreement is almost perfect. It should be stressed that the  $g$  values of the pairs are smaller than 2 due to the antiparallel orientation of the copper spin which is characterized by a  $g$  larger than 2.

A good agreement was also obtained between calculated and observed  $D$  tensors, although it was more difficult to obtain all the necessary information.

### 7.13.3.2 Mixed-valence Species

In the above treatment of exchange interactions we have considered the magnetic electrons, i.e., the ones involved in the interaction, as essentially localized on a given magnetic center. Although this is usually a good approximation for systems formed either by identical or by completely



**Table 3** Experimental and calculated spin Hamiltonian parameters for copper(II)–manganese(II) pairs in  $[\text{Cu}(\text{PyO})\text{Cl}_2\cdot\text{H}_2\text{O}]_2$ .<sup>a</sup>

	Experimental $S = 2$	Experimental copper (II)	Calculated $S = 2$
$g_x$	1.991	2.056	1.993
$g_y$	1.986	2.083	1.988
$g_z$	1.952	2.306	1.951
$A^{\text{Cu}}$	0.0023	0.0139	0.0023

<sup>a</sup> Hyperfine values in  $\text{cm}^{-1}$ .

different magnetic centers, like the copper(II)–manganese(II) pairs described above, there is a class of materials, namely mixed-valence species, where this simple description breaks down.

Mixed-valence systems contain the same metal ion in formally different oxidation states.<sup>46</sup> An accepted classification of mixed-valence compounds was given by Robin and Day,<sup>47</sup> who suggested three different classes of behavior, which can be best illustrated by referring to the potential energy diagrams depicted in Figure 5. In fact, it must be kept in mind that in a mixed-valence species there is a condition of electronic energy degeneracy, which determines the conditions for strong vibronic coupling. Class I corresponds to systems where the valences are localized, i.e., the two ions have well-defined, different oxidation states characterized, for instance, by different bond distances. Class I is rather unexciting, because the magnetic properties of the mixed-valence dinuclear species simply correspond to what can be expected using Equations (5) and (16)–(20). Several examples have been reported of dinuclear manganese compounds, with manganese(II)–manganese(III) and manganese(III)–manganese(IV) pairs. In this case the valence localization occurs because the  $d^4$  electronic structure of manganese(III) gives rise to strong Jahn–Teller effects.

At the opposite limit is class III, in which there is complete delocalization of the electrons on the two centers in such a way that related oxidation states have no meaning. The mobility of the electrons in this case introduces new types of magnetic phenomena, which can have spectacular effects on the behavior of the dinuclear species. Class II corresponds to an intermediate state where electron delocalization is fast but not infinitely fast.

A nice example of important magnetic effects in a mixed-valence dinuclear species is provided by the cation  $[\text{Ni}_2(\text{napy})_4\text{X}_2]^+$ , where  $\text{napy} = 1,8\text{-naphthiridine}$ ,  $\text{X} = \text{Cl}, \text{Br}, \text{I}$ .<sup>48</sup> Assuming for the halides the charge  $-1$ , the two nickel ions have a total charge  $+3$ , which suggests the presence of a nickel(II) and a nickel(I). Structural determinations on the bromide and iodide derivatives do not show any difference in the coordination environments of the two metal ions, suggesting either a Class II or a Class III Robin and Day classification. The two metal ions are separated by 2.6 Å and 2.4 Å in the bromide and iodide derivative, respectively.

The magnetic properties and the EPR spectra of  $[\text{Ni}_2(\text{napy})_4\text{X}_2]^+$  provide a clear indication of a ground  $S = 3/2$  state, with no evidence of thermal population of excited states. In particular, the EPR spectra show only one transition within the  $M = \pm 1/2$  components of  $S = 3/2$ . The corresponding  $g$  values are  $g_{\parallel} = 2.18$ ,  $g_{\perp} = 4.18$ . Polycrystalline powder spectra recorded at 245 GHz, shown in Figure 6, allowed a direct determination of the ZFS, i.e., the energy separation between the  $\pm 1/2$  and  $\pm 3/2$  states in zero field, together with the sign. It was found that the  $\pm 3/2$  components lie lower, with the  $\pm 1/2$  states at  $5.4 \text{ cm}^{-1}$ .

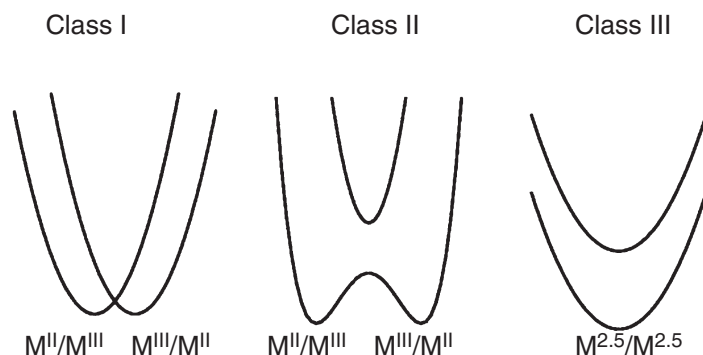


**Figure 5** Potential energy curves for mixed-valence  $\text{M}^{\text{II}}/\text{M}^{\text{III}}$  compounds corresponding to Class I, Class II, and Class III in the Robin and Day classification.

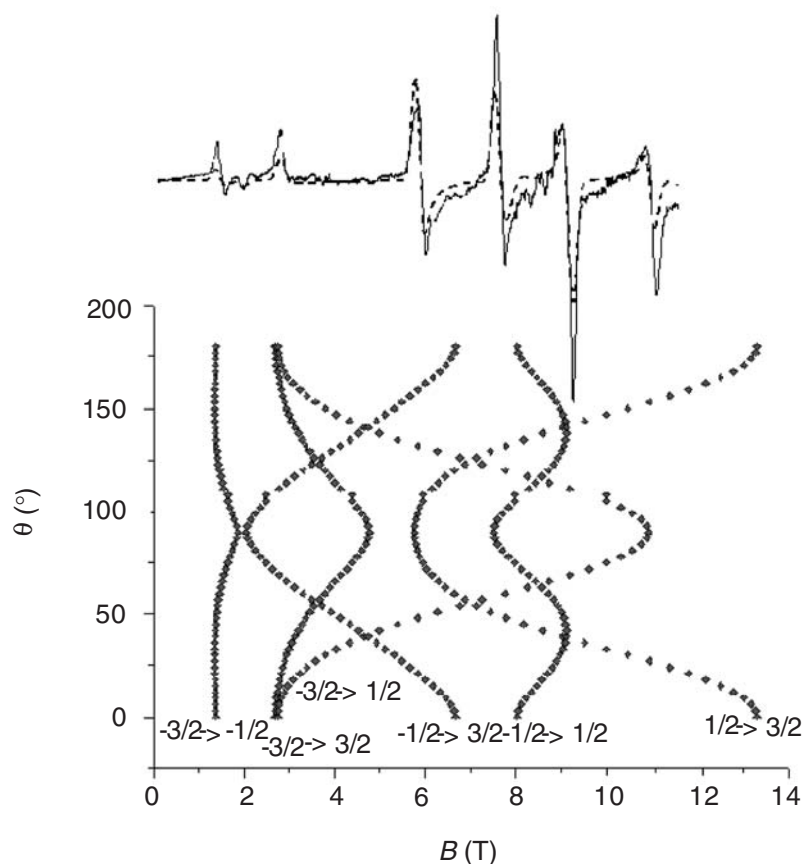


**Figure 6** Polycrystalline powder HF-EPR spectra (245 GHz) of  $[\text{Ni}_2(\text{napy})_4\text{I}_2]^+$  at 4.2 K. Experimental spectrum (solid line) and simulated spectrum (dashed line) with a  $S=3/2$  spin Hamiltonian with  $g_{\parallel}=2.18$ ,  $g_{\perp}=2.12$ , and  $D=-2.7\text{ cm}^{-1}$ . Bottom: Computed angular dependence of the transition fields in the  $xz$  plane. Replotted from data reported in ref. 48.

In a static description of  $[\text{Ni}_2(\text{napy})_4\text{X}_2]^+$  the ground  $S=3/2$  state is explained assuming a strong ferromagnetic coupling between the  $S_i=1/2$  nickel(I) and the  $S_i=1$  nickel(II). In fact,  $J$  was estimated to be larger than  $500\text{ cm}^{-1}$  using the spin Hamiltonian Equation (6). This value appears to be too large for a static mechanism, because the ferromagnetic pathway involving the  $z^2$  magnetic orbital on nickel(I) and the  $x^2-y^2$  magnetic orbital on nickel(II) does not seem to be very effective. Further, the interaction between the  $z^2$  magnetic orbitals is expected to be fairly strongly antiferromagnetic.

This contradiction was overcome by Girerd<sup>49</sup> who suggested that the observed effective ferromagnetic coupling is actually a consequence of the spin delocalization in the mixed-valence species. In fact, an electron passing from the nickel(I) center to the nickel(II) center must keep its spin “down”, as shown in Figure 7. In this way the spins of the two centers are effectively

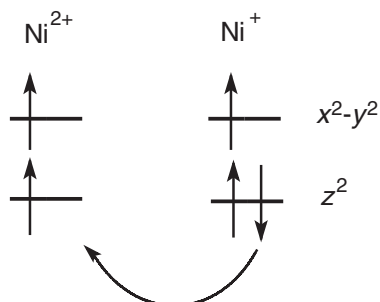


**Figure 7** Magnetic orbitals for  $\text{Ni}^{2+}$  and  $\text{Ni}^+$  ions.

polarized to remain parallel to each other. This mechanism has been named “double exchange”<sup>50</sup> and has been introduced to justify the observed ferromagnetic coupling in mixed-valence manganites. More recently it has been exploited for the development of colossal magneto-resistance in the same class of compounds.<sup>51,52</sup>

In the spin Hamiltonian description, the presence of double exchange can be described by the introduction of a new parameter:

$$B = \frac{t_{ab}}{2S_0 + 1} \quad (22)$$

where  $t_{ab}$  is the so-called transfer integral which determines the kinetic constant for the transfer of one electron from magnetic orbital  $a$  to  $b$ , and  $S_0$  is the spin of the magnetic center in the absence of the extra electron, i.e., of the electron responsible for the mixed valence nature of the pair.

Using Equations (6) and (22) the energy levels of the pair are given by:

$$E_{\pm} = (J/2)S(S+1) \pm B(S+1/2) \quad (23)$$

Equation (23) shows that the double exchange interaction doubles the number of spin levels. If  $B=0$  the pairs of levels remain degenerate and the double exchange does not produce any effect. If  $B$  is different from zero the levels with large spin  $S$  are stabilized, i.e., double exchange is effective in promoting ferromagnetic coupling. Therefore, the nature of the real ground state depends on the relative values of  $J$  and  $B$  when the former is antiferromagnetic.

The  $[\text{Ni}_2\text{X}_2(\text{napy})_4]^+$  compounds were also investigated using DFT approaches. It was found that the exchange coupling between the two metal ions is strongly antiferromagnetic, but the ground state is predicted to be ferromagnetic, as experimentally observed, due to the large value of  $B$ .

A thorough treatment of mixed-valence dimers and oligomers for various configurations of  $d$  electrons has been developed by Tsukerblat *et al.*<sup>53</sup> They also developed computer programs which can be used to calculate the magnetic properties of mixed-valence clusters.

### 7.13.3.3 Valence Tautomeric Species

Valence tautomeric species are conceptually akin to spin cross-over systems,<sup>54–58</sup> in the sense that their spin state changes under the effect of external stimuli such as temperature, pressure, or light as a consequence of entropy-driven transformations. However, they are also similar to mixed-valence species because valence tautomers differ in charge distribution. These conditions are found in complexes of transition metal ions with non-innocent ligands, i.e., ligands whose frontier orbitals are comparable in energy to the  $d$  metal orbitals. A typical example is provided by dioxolene ligands, which can bind to transition metal ions in three different oxidation states<sup>59–62</sup> as sketched in Figure 8. The catecholate,  $\text{Cat}^{2-}$ , and the quinone,  $\text{Q}$ , oxidation states are non-magnetic, while the intermediate semiquinonate,  $\text{SQ}^-$ , has one unpaired electron. With most transition metal ions it is possible to describe the charge distribution in metal–dioxolene complexes in a straightforward way, i.e., a well-defined oxidation state can be assigned to both the metal ion and the ligand. In some cases, as for manganese,<sup>63–68</sup> rhodium and iridium<sup>69,70</sup> complexes the charge distribution is more subtle. For cobalt it is possible to have stable tautomers formulated as  $[\text{Co}^{\text{III}}(\text{Cat})(\text{SQ})]$  and  $[\text{Co}^{\text{II}}(\text{SQ})_2]$ , respectively. The energies of the two forms are rather close to each other, as depicted in Figure 9. The bond lengths in  $[\text{Co}^{\text{II}}(\text{SQ})_2]$  are larger than in  $[\text{Co}^{\text{III}}(\text{Cat})(\text{SQ})]$ , and as a consequence the density of vibronic levels is much greater in the former than in the latter, thus giving rise to a strong entropic stabilization of the  $[\text{Co}^{\text{II}}(\text{SQ})_2]$  form

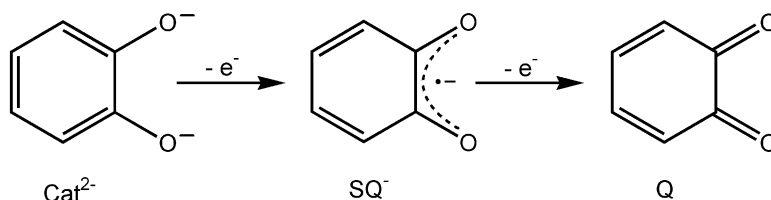
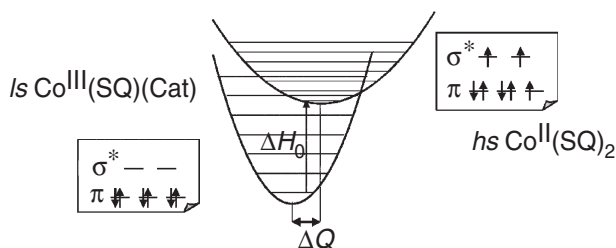


Figure 8 Stable oxidation states of dioxolene molecules.



**Figure 9** Relative energies and electronic configuration of the ground and first excited state in valence tautomeric molecules based on cobalt-dioxolene species.  $\Delta Q$  is the Co-O distance and  $\Delta H_0$  is the enthalpy difference between the two species.

at high temperature. The actual species showing valence tautomeric behavior contain ancillary diamine ligands.<sup>71–73</sup>

In  $[\text{Co}^{\text{III}}(\text{Cat})(\text{SQ})]$  both the cobalt ion and the catecholate ligand are diamagnetic, thus giving rise to a species with one unpaired electron. In  $[\text{Co}^{\text{II}}(\text{SQ})_2]$  the SQ and the cobalt(II) ions are magnetic thus giving rise to magnetic coupling. In fact, the  $\chi_m T$  value for  $[\text{Co}^{\text{III}}(\text{Cat})(\text{SQ})]$  is ca.  $0.4 \text{ emu mol}^{-1} \text{ K}$ , while for  $[\text{Co}^{\text{II}}(\text{SQ})_2]$  it ranges between  $2.4 \text{ emu mol}^{-1} \text{ K}$  and  $3.8 \text{ emu mol}^{-1} \text{ K}$ .<sup>54</sup>

The marked shortening of the metal bond distances which accompanies the transition from  $[\text{Co}^{\text{II}}(\text{SQ})_2]$  to  $[\text{Co}^{\text{III}}(\text{Cat})(\text{SQ})]$  may give rise to cooperative structural transformations which result in hysteretic behavior. It must be recalled here that this kind of magnetic hysteresis is paramagnetic in nature, and is not associated with domain wall motion as in ferro- or ferri-magnets, but rather to structural deformations. In any event, magnetic hysteresis is a very attractive property because it is associated with bistability i.e., the magnetization can have two different values depending on the history of the sample. Many groups have attempted to design and synthesize valence tautomeric species which may serve for information storage. So far, the best results have been obtained by Pierpont *et al.*<sup>74</sup> who reported that  $[\text{Co}^{\text{III}}(3,6\text{-DBCat})(3,6\text{-DBSQ})(\text{py}_2\text{O})]$ , where 3,6-DBCat = 3,6-di-tertbutyl-catecholate, undergoes a transition to  $[\text{Co}^{\text{II}}(3,6\text{-DBSQ})_2(\text{py}_2\text{O})]$ , with a critical temperature which shifts from 340 K on warming to 100 K on cooling! The width of the hysteresis loop is too large for application purposes, but it can be expected that by suitably choosing the co-ligands and the magnetically active dioxolene ligands a better-suited hysteresis loop may be designed, as in the case of spin cross-over systems.

Transition metal complexes with dioxolene ligands may also give rise to interesting magneto-optical properties. Dei *et al.* reported<sup>75</sup> that in  $[\text{Cr}(\text{TMC})\text{SQ}]$ , where TMC = 1,4,8,11-tetramethyl-1,4,8,11-tetraazacyclotetradecane, the forbidden transition  ${}^4T_{1g} \rightarrow {}^2E_g$ , which is responsible for the intense red color of ruby, has a dramatically increased intensity compared to simple chromium(III) complexes. The origin of this behavior is associated with the magnetic interaction between chromium(III) and the radical ( $S_i = 1/2$ ). In fact, in the ground  $S_i = 3/2$  state of chromium(III) the coupling is antiferromagnetic, yielding a ground  $S = 1$  and an excited  $S = 2$  state. A similar coupling must be expected in the  $S_i = 1/2$  excited state of chromium(III), yielding a singlet  $S = 0$ , and a triplet,  $S = 1$ . Consequently, the transition is no longer spin forbidden because now it occurs between two states with the same spin multiplicity. A quantitative treatment showed that the mechanism for intensity enhancement is the coupling with a charge transfer state at low energy.

#### 7.13.3.4 Antiferromagnetic Rings

The formation of cyclic architectures provides an impressive example of metal-directed assembly which, starting from smaller oligonuclear fragments or even simple transition-metal salts, directly affords objects of esthetic beauty and fascinating structural complexity.<sup>76</sup> The principles underlying ring formation are not yet fully understood and most cyclic clusters are the result of serendipitous synthesis,<sup>77</sup> although some control can be exerted, exploiting, for instance, host-guest interactions.<sup>78–83</sup> For example, a 12-membered cycle can be quantitatively converted into six-membered rings in solution by addition of lithium or sodium ions.<sup>82</sup>

In this section we will focus on chromium(III) and iron(III) rings, which have been magnetically investigated in greatest detail since the early 1990s.  $\text{Fe}_6$ ,<sup>78–80,83</sup>  $\text{Fe}_8$ ,<sup>84</sup>  $\text{Cr}_8$ ,<sup>85,86</sup>  $\text{Cr}_{10}$ ,<sup>87</sup>  $\text{Fe}_{10}$ ,<sup>88,89</sup>  $\text{Fe}_{12}$ ,<sup>81,82</sup> and  $\text{Fe}_{18}$ <sup>90</sup> cycles are known which feature essentially coplanar arrangements of metal

ions (for a twisted-ring structure, see Refs. 81, 82). Cyclic structures are usually supported by bridging ligands such as carboxylates,<sup>84–90</sup> halides,<sup>84,85</sup> alkoxides,<sup>78–83,87–90</sup> and hydroxides,<sup>86,90</sup> which provide effective superexchange pathways between paramagnetic metal ions. Antiferromagnetic nearest-neighbor (n.n.) interactions are generally observed which lead to an  $S=0$  ground state with complete cancellation of the local spins  $S_i$ . Low-lying excited states with  $S=1, 2, 3, \dots$  are found at energies roughly given by

$$\Delta_S = \frac{J}{N} S(S+1) \quad (24)$$

In Equation (24),  $2N$  is the number of spins in the ring and  $J$  is the n.n. exchange-coupling constant (see Section 2.36.4.1). The spin levels described by Equation (24) form a so-called “Landé band” ( $L$ -band),<sup>91,92</sup> as they follow the same pattern Equation (9) expected in a simple dimer of two interacting spins coupled by  $J' = 2J/N$ . In fact, the leading contribution to the lowest-lying states is provided by the spin configuration depicted in Figure 10, featuring parallel spin vectors within the two “sublattices” of odd and even sites. The  $L$ -band can then be generated by coupling two spins  $NS_i$  in an antiferromagnetic fashion. When a magnetic field is applied, the  $L$ -band naturally leads to multiple ground-state level crossings (LCs) at evenly spaced values of the magnetic field. At low temperature and close to each LC, the ring provides a simple realization of a two-level model system and exhibits abrupt variations in its static and dynamic properties, such as magnetization, magnetic torque, and proton spin-lattice relaxation rate.<sup>93–95</sup> Recently, hysteretic behavior at LC due to thermal nonequilibrium conditions (“phonon bottleneck effect”) has been observed in a  $\text{Fe}_6$  ring, suggesting the unusual possibility of cooling by adiabatic magnetization.<sup>96</sup> Theoretical investigations of the coherent dynamics of the Néel vector have drawn additional interest to magnetic rings as finite-size models for 1-D systems.<sup>97,98</sup>

With rare exceptions,<sup>81,82</sup> the magnetic rings exhibit either crystallographically dictated or idealized axial symmetry which greatly reduces the number of independent spin-Hamiltonian parameters.<sup>99</sup> As a result, magnetic rings provide a unique opportunity to investigate subtle aspects of magnetic interactions in nanoscale systems, such as those responsible for magnetic anisotropy.<sup>100</sup> Detailed studies by inelastic neutron scattering, EPR spectroscopy, torque magnetometry, and magnetic susceptibility measurements have evidenced a hard-axis type molecular anisotropy ( $D_S > 0$ ) in the lowest-lying  $S$ -multiplets of the  $L$ -band (see Section 2.36.5.2).<sup>79,85,101–106</sup>

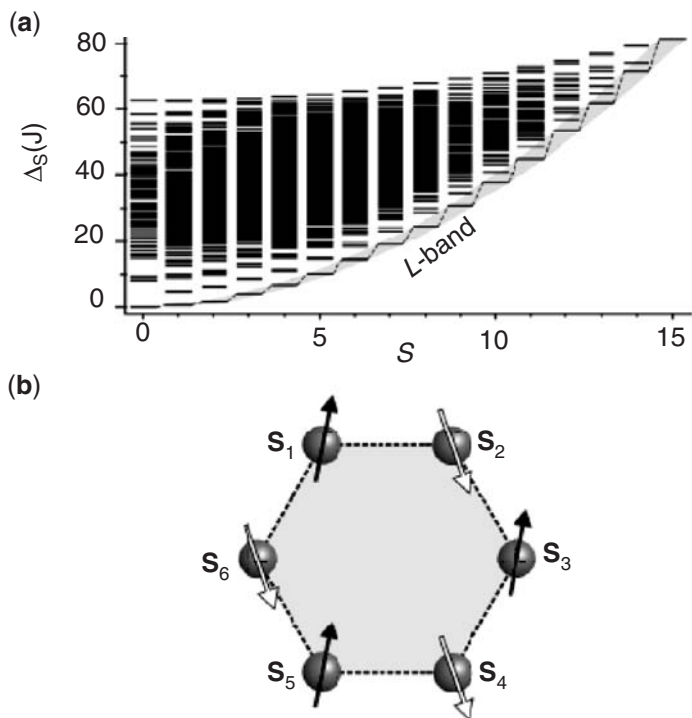


**Figure 10** (a) Energy spectrum of the  $2N=6$ ,  $S_i=5/2$  ring. The spin levels of the  $L$ -band are highlighted in gray (adapted from ref. 91). (b) Dominant spin configuration in the  $L$ -band.

For a quantitative analysis, the *ZFS* parameters  $D_S$  can be expressed as the sum of single-ion ( $D_S^{\text{si}}$ ), dipolar ( $D_S^{\text{dip}}$ ), and anisotropic exchange ( $D_S^{\text{ex}}$ ) terms, according to Equation (25).

$$D_S = D_S^{\text{si}} + D_S^{\text{dip}} + D_S^{\text{ex}} \quad (25)$$

Point–dipolar interactions favor a perpendicular arrangement of the spins with respect to the ring plane and thus provide a hard-axis type contribution ( $D_S^{\text{dip}} > 0$ ).<sup>94</sup> However, with few exceptions,<sup>102,103</sup> the observed anisotropy largely exceeds the calculated dipolar term. For instance, in the clusters  $[\text{NaFe}_6(\text{OCH}_3)_{12}(\text{pmdbm})_6]\text{ClO}_4$  (pmdbm = di(4-methoxybenzoyl)methanide) and  $[\text{Cr}_8\text{F}_8(\text{Bu}^t\text{CO}_2)_{16}]$ , dipolar interactions account for only about 30% of the measured triplet *ZFS* parameter ( $D_1$ ).<sup>85,102,106</sup> In the  $\text{Fe}_6$  cluster, single-ion terms have been identified as the source of the residual anisotropy by investigating an isostructural gallium(III) compound doped with iron(III) ions.<sup>106</sup> By contrast, anisotropic exchange contributions are likely to play a minor role, as expected considering the very weak *g*-factor anisotropy of high-spin iron(III).

Quantitative correlations between spin-Hamiltonian and geometric parameters have been established in a homogeneous family of  $\text{Fe}_6$  and  $\text{Fe}_8$  rings featuring bis(alkoxo) ligands. The *J* constant displays a remarkable linear dependence upon the  $\text{FeOFe}$  angle ( $\alpha$ ) subtended by the set of alkoxo ligands closer to the ring axis, as shown in Figure 11.<sup>105</sup> Since the  $\alpha$  angle is strongly affected by the presence of an alkali–metal ion in the center of the cluster (Li, Na, or Cs), magnetic rings provide a nice example of exchange-coupling modulation through host–guest interactions.<sup>80</sup> The effect can be quite dramatic, as shown by the 40% decrease of the *J* value upon replacement of  $\text{Na}^+$  with  $\text{Li}^+$  in  $[\text{NaFe}_6(\text{OCH}_3)_{12}(\text{dbm})_6]^+$  (dbm = dibenzoylmethanide). The angular dependence of *J* is qualitatively similar to that observed in a series of centrosym-

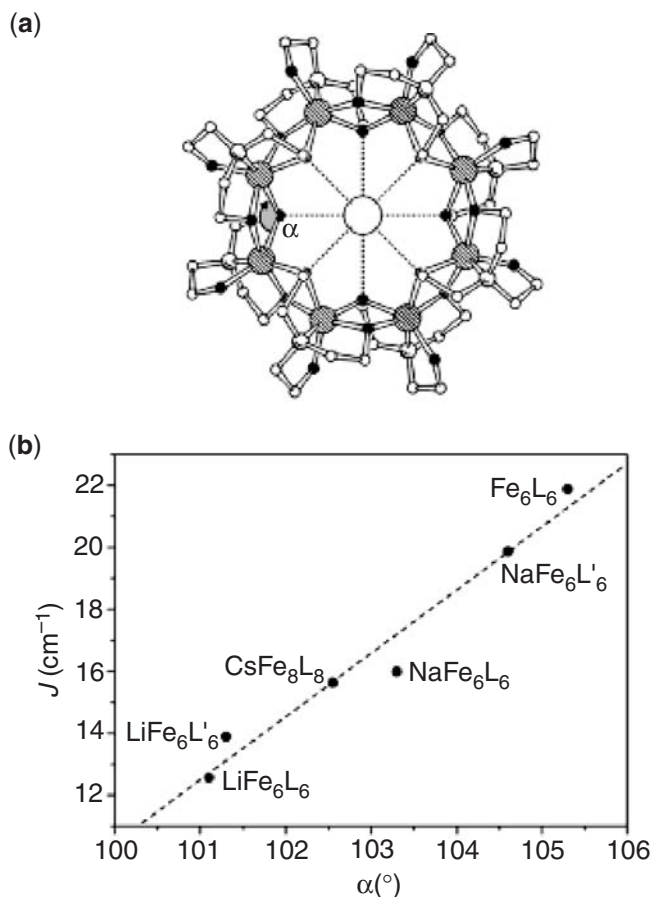


**Figure 11** (a) Molecular structure of  $[\text{CsFe}_8(\text{tea})_8]^+$ , with the definition of the  $\alpha$  angle. Atom code: large hatched circles = Fe; small black circles = O; small empty circles = C; medium-sized empty circles = N; large empty circle = Cs. (b) Coupling constant *J* versus the  $\alpha$  angle for selected ferric wheels (adapted from ref. 105). L = tea; L' = dbm; L'' = pmdbm.

metric di(alkoxo)-bridged  $\text{Fe}_2$  complexes, where a larger bridging angle leads to a stronger antiferromagnetic interaction.<sup>107</sup>

Turning now to magnetic anisotropy, the triplet ZFS parameter  $D_1$  exhibits an even more pronounced variability in the series, ranging from ca.  $1.2 \text{ cm}^{-1}$  in  $[\text{LiFe}_6(\text{OCH}_3)_{12}(\text{dbm})_6]\text{PF}_6$  to  $8.2 \text{ cm}^{-1}$  in  $[\text{Fe}_6(\text{tea})_6]$  ( $\text{H}_3\text{tea}$  = triethanolamine). The calculated point-dipolar contribution amounts to  $1.1\text{--}1.4 \text{ cm}^{-1}$  and is weakly structure dependent. If one neglects anisotropic exchange, the observed differences must then be ascribed to different single-ion anisotropies. In the homologous subset of compounds containing *tea* ligands, the effective ZFS parameters of the iron(III) ions ( $D^{\text{si}}$ ) have been successfully related to the position of the bridging oxygen donors closer to the ring axis (Figure 11).<sup>105</sup> Though more experimental and theoretical work is required in this area, it is clear that small variations in the coordination environment of the metal ions can have a big impact on the magnetic properties via the single-ion term, which is strongly influenced by the electronic properties of the ligands and by the geometrical distortions of the coordination sphere.<sup>85,108</sup> While a complete control of magnetic anisotropy at the synthetic level is currently out of reach, studies on high-symmetry systems may provide useful guidelines for the application-oriented design of new magnetic molecules like single-molecule magnets.

### 7.13.3.5 Single-molecule Magnets

A very fascinating class of zero-dimensional magnetic materials is characterized by an unusually large spin of the ground state, larger than the values observed in paramagnetic ions. The combination of the large spin and the magnetic anisotropy can give rise to a phenomenon which was observed for the first time at the beginning of the 1990s<sup>109,110</sup> on a molecule comprised of 12 manganese ions, characterized by a ground state with  $S=10$ ,  $[\text{Mn}_{12}\text{O}_{12}(\text{CH}_3\text{-COO})_{16}(\text{H}_2\text{O})_4]$ ,<sup>111</sup>  $\text{Mn}_{12}\text{ac}$ , whose structure is shown in Figure 12. This molecule exhibits slow relaxation of the magnetization at low temperature, which becomes of the order of months at 2 K.<sup>110</sup> Under these conditions a single molecule becomes like a tiny magnet, in the sense that if

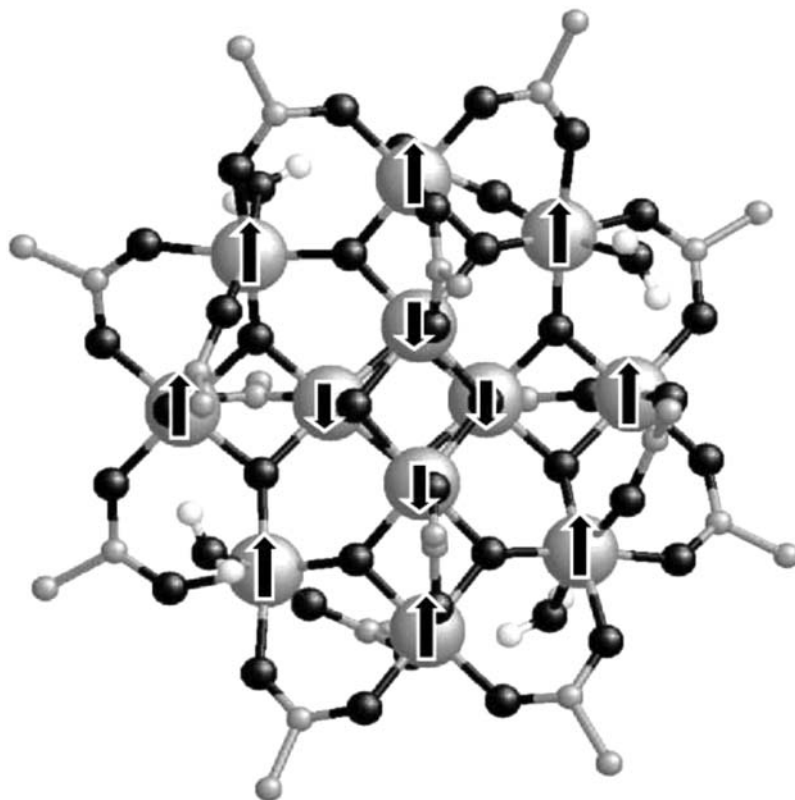


**Figure 12** Structure of  $\text{Mn}_{12}\text{ac}$ . The large spheres and the black small ones stand for manganese and oxygen atoms, respectively. The arrows schematically represent the spin structure of the ground  $S=10$  state.

magnetized by an applied field it retains the magnetization for days. In fact it gives rise to magnetic hysteresis, which is one condition for storing information in a particle. These molecules are now often called single-molecule magnets, SMMs.<sup>112</sup>

For slow relaxation to be observable in molecular clusters, a sizeable barrier for the reorientation of the magnetization must be present. This barrier can be introduced by the magnetic anisotropy which also splits the  $S$  manifold in zero field ( $ZFS$ ) according to the effective spin Hamiltonian of the form:

$$\mathbf{H} = DS_z^2 + E(S_x^2 - S_y^2) + g\mu_B\mathbf{S}\cdot\mathbf{H} \quad (26)$$

In the case that  $E$  is zero (no transverse anisotropy) and no magnetic field is applied, the energy of the  $M$  states, with  $M$  eigenvalue of  $S_z$ , is simply  $DM^2$ . If  $D$  is negative the two states characterized by  $M = \pm S$  are the most stable in energy. They correspond to the “spin up” and “spin down” configurations with respect to the z-axis of easy magnetization, as shown in Figure 13, and they are separated by an energy barrier  $\Delta E$  whose height is  $DS^2$  for integer  $S$  and  $D(S^2 - 1/4)$  for half-integers. This double-well potential is very similar to what is observed in single domain nanoparticles showing super-paramagnetism.<sup>113</sup> In order to reverse its magnetization, a molecule must cross this energy barrier and this occurs through a multi-Orbach type of process.<sup>114</sup> The intermediate states are the  $M$  states higher in the barrier. By taking into account the interaction of the phonons it has been shown that at low temperature the relaxation time follows the Arrhenius law characteristic of thermally activated mechanisms.<sup>114</sup>

$$\tau = \tau_0 \exp(\Delta E/kT) \quad (27)$$

with

$$\tau_0 = \frac{2\pi\hbar^4 \rho c^5}{3 |V_{10}|} \left[ \frac{S^2}{\Delta E} \right] \quad (28)$$

where  $\rho$  is the specific mass,  $c$  is the speed of sound in the material, and  $V_{10}$  is the spin-phonon matrix element of the last step in climbing the barrier, which is the slowest one of the process. At sufficiently low temperatures the relaxation time can become so long that a magnetized sample retains its magnetization. However, the phenomenon does not require any cooperativity and the magnetic hysteresis is a property of the molecule as nicely demonstrated by experiments on frozen dilute solutions of  $\text{Mn}_{12}\text{ac}$  in organic solvents.<sup>115–118</sup>

In order to behave as a SMM the system must satisfy three conditions: (i) the intra-cluster exchange interactions must stabilize a large spin ground state, (ii) the magnetic anisotropy must be of the easy-axis type, which corresponds to a negative  $D$ ; (iii) intercluster interactions must be vanishingly small compared to the barrier height and the related blocking temperature,  $T_B$ . The first requisite is very important because the barrier depends quadratically on the spin value.

The synthetic efforts of many groups now involved in the field of SMMs have led to new, interesting molecular clusters which are characterized by unusually large spins. Some of those characterized by ground state spin  $S > 6$  are listed in Table 4, where the barrier height, if known, is also reported.

As stated above, genuine ferromagnetic interactions are rare; however, the combination of more than two spins through the appropriate spin topology can also give rise to an unusually large spin state in the presence of antiferromagnetic interaction. A simple example is the case of

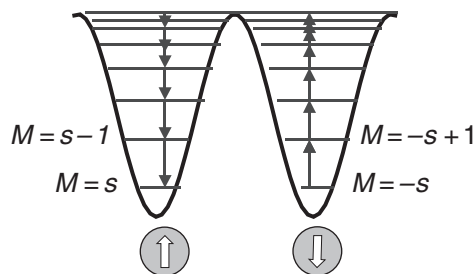


**Figure 13** Scheme of the energies of spin up and spin down configurations in a  $S = 10$  multiplet with easy-axis type magnetic anisotropy.



**Table 4** Spin of the ground state and experimentally determined barrier height for some high spin clusters.

Cluster	Ground state spin	Anisotropy barrier (K)	References
$[(\text{Me}_3\text{tacn})_6\text{MnCr}_6(\text{CN})_{18}]^{2+}$	13/2		119
$[\text{Mn}_{21}\text{O}_{24}(\text{OMe})_8(\text{O}_2\text{CCH}_2\text{tBu})_{16}(\text{H}_2\text{O})_{10}]$	13/2		120
$[\text{Mn}_{12}\text{O}_8\text{Cl}_4(\text{O}_2\text{CPh})_8(\text{hmp})_6]$	7	30	121
$[\text{Cr}\{\mu\text{-CN}\}\text{Ni}(\text{tetren})\}_6](\text{ClO}_4)_9$	15/2		122
$[\text{Mn}_4(\text{O}_2\text{CMe})_2(\text{Hpdm})_6](\text{ClO}_4)_2$	8	23*	123
$[\text{CuLGd}(\text{hfac})_2]_2$	8		124
$[\text{Mn}_9\text{O}_7(\text{OAc})_{11}(\text{thme})(\text{py})_3(\text{H}_2\text{O})_2]$	17/2	30	125
$[\text{Mn}_4(\text{hmp})_6\text{Br}_2(\text{H}_2\text{O})_2]\text{Br}_2$	9	40	126
$[\text{Mn}_{12}\text{O}_{12}(\text{O}_2\text{CPh})_{16}(\text{H}_2\text{O})_4] 8(\text{CH}_2\text{Cl}_2)$	19/2	57	127
$[\text{Mn}_{12}\text{O}_{12}(\text{CH}_3\text{COO})_{16}(\text{H}_2\text{O})_4]$	10	61	111,128
$[\text{PPh}_4]_2[\text{Mn}_{12}\text{O}_{12}(\text{O}_2\text{CCHCl}_2)_{16}(\text{H}_2\text{O})_4]$	10	44*	129
$[\text{Fe}_8\text{O}_2(\text{OH})_{12}(\text{tacn})_6]^{8+}$	10	24	130,131
$[\text{Fe}_{10}\text{Na}_2\text{O}_6(\text{OH})_4(\text{O}_2\text{CPh})_{10}(\text{chp})_6(\text{H}_2\text{O})_2(\text{Me}_2\text{CO})_2]$	11	5.5	132
$[\text{Mn}^{\text{II}}_4\text{Mn}^{\text{III}}_3(\text{teaH})_3(\text{tea})_3](\text{ClO}_4)_2$	11	19.6	133
$[\text{Mn}_6(\text{hfac})_{12}(\text{NITPh})_6]$	12		134
$[\text{NaMn}_6(\text{OMe})_{12}(\text{dbm})_6]^+$	12		135
$[\text{Ni}_{12}(\text{chp})_{12}(\text{O}_2\text{CMe})_{12}(\text{H}_2\text{O})_6(\text{THF})_6]$	12	9.6	136
$[\text{Ni}\{\text{Ni}(\text{MeOH})_3\}_8(\mu\text{-CN})_{30}(\text{M}(\text{CN})_3)_6] \text{M} = \text{Mo}, \text{W}$	12		137
$[\text{Mn}_{18}\text{O}_{14}(\text{O}_2\text{CMe})_{18}(\text{hep})_4(\text{hepH})_2(\text{H}_2\text{O})_2](\text{ClO}_4)_2$	13	21.3	138
$[\text{Cr}\{\mu\text{-CN}\}\text{Mn}(\text{trispicmeen})\}_6](\text{ClO}_4)_9$	27/2		139
$[\text{Fe}^{\text{III}}\text{Fe}^{\text{II}}_6(\text{MeO})_6(\text{HL}')_6]\text{Cl}_3$	29/2		140
$[\text{Fe}_{19}(\text{metheidi})_{10}(\text{OH})_{14}(\text{O})_6(\text{H}_2\text{O})_{12}]\text{Cl}$	33/2		141
$[\text{Mn}_9\{\text{W}(\text{CN})_8\}_6\text{24C}_2\text{H}_5\text{OH}]$	39/2		142
$[\text{Mn}\{\text{Mn}(\text{MeOH})_3\}_8(\mu\text{-CN})_{30}\{\text{Mo}(\text{CN})_3\}_6]$	51/2		143

\* not extracted from the Arrhenius plot. tacn = 1,4,7-triazacyclononane. hmpH = 2-hydroxymethylpyridine. tetren = 1,11-di-amino-3,6,9-triazaundecane.  $\text{H}_2\text{pdm}$  = pyridine-2,6-dimethanol.  $\text{H}_3\text{L}$  = 1-(2-hydroxybenzamido)-2-(2-hydroxy-3-methoxybenzylideneamino)ethane. Hhfac = hexafluoroacetylacetonate.  $\text{H}_3\text{thme}$  = 1,1,1-tris(hydroxymethyl)ethane. chp = 6-chloro-2-pyridonate.  $\text{H}_3\text{tea}$  = triethanolamine. NITPh = phenyl-4,4,5,5-tetramethylimidazole-1-oxyl-3-oxide. Hdbm = dibenzoylmethane. hepH = 2-(hydroxyethyl)-pyridine. trispicmeen =  $-\text{H}_2\text{L}' = 3$ -methoxy-2-salicylideneamino-1-ethanol.  $\text{H}_3\text{metheidi}$  = *N*-(1-hydroxymethylethyl)iminodiacetic acid.

the propeller-shaped tetranuclear cluster of formula  $\text{Fe}_4(\text{OCH}_3)_6(\text{dpm})_6$ ,<sup>144</sup> where Hdpm is dipivaloylmethane, shown in Figure 14. The ground spin state results from the parallel alignment of the outer spins, which are in turn antiparallel to the central one, resulting in a ground state  $S = 5$ . This compound and new ones of the same type indeed behave as SMMs even with  $T_B$  lower than in  $\text{Mn}_{12}\text{ac}$ . A large-spin ground state can result also from more complex spin connectivities as is the case of  $\text{Mn}_{12}\text{ac}$ . Here, at least four different exchange interactions can be envisaged (see Figure 12) and at least three of them are predicted to be antiferromagnetic on the basis of magneto-structural correlations extracted from the investigation of dimeric species.<sup>145–147</sup> The ground state is characterized by  $S = 10$  thanks to the spin arrangement of Figure 12. This spin arrangement has also been confirmed by a spin density map obtained through PND experiments,<sup>148,149</sup> however, this spin value results from a rather peculiar balance of the antiferromagnetic interactions in many triangles. Calculations have shown that relatively small modifications of the  $J$  ratios can lead to diamagnetic or low-spin ground states.<sup>145–147</sup>

At present, the highest spin state for a molecule is  $S = 51/2$  for the cluster of formula  $[\text{Mn}(\text{Mn}\{\text{MeOH}\}_3)_8(\mu\text{-CN})_{30}\{\text{Mo}(\text{CN})_3\}_6]$ , whose structure is reported in Figure 15.<sup>150</sup> The large spin state results from the ferromagnetic interaction of nine  $S_i = 5/2$  manganese(II) ions and six  $S_i = 1/2$  molybdenum(V) ions. Contrary to what could be expected from the dependence of the barrier on the square of the spin value, this type of molecular cluster exhibits a very low  $T_B$ . The reason is that the high symmetry of the cluster reduces the magnetic anisotropy significantly. Low  $T_B$  values due to high symmetry are also observed in another type of high-spin molecule, based on the hexacyanometalate building block and of general formula  $[\text{Cr}\{\mu\text{-CN}\}\text{M}^{\text{II}}\text{L}\}_6]^{n+}$ .<sup>150–153</sup> The largest spin ground state has been found for  $\text{M} = \text{Mn}$ , with  $S = 27/2$ , where the central  $\text{Cr}^{\text{III}}$  spin,  $S = 3/2$ , is antiferromagnetically coupled to six manganese spins,  $S = 5/2$ . More recently, magnetic anisotropy has been controlled by reducing the nuclearity and thereby breaking the octahedral symmetry.<sup>154</sup>

While the spin ground state can now be controlled at the synthetic level, the case is different for magnetic anisotropy. For Jahn–Teller distorted metal ions, like  $\text{Mn}^{\text{III}}$ , the magnetic anisotropy

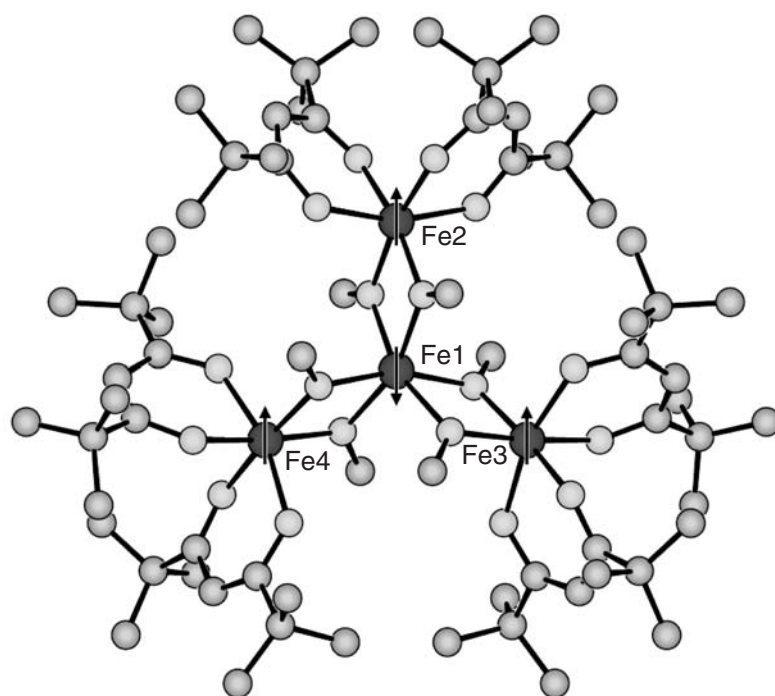


**Figure 14** Structure of  $\text{Fe}_4(\text{OCH}_3)_6(\text{dpm})_6$ .

can be predicted starting from the ligand field strength in the axial and equatorial positions,<sup>108,155</sup> but, for example, in the case of  $\text{Fe}^{\text{III}}$ , the magnetic anisotropy remains largely unpredictable and almost impossible to control.

Despite the difficulties in controlling the height of the barrier, molecular nanoclusters have attracted a great deal of interest because they exhibit other spectacular phenomena of

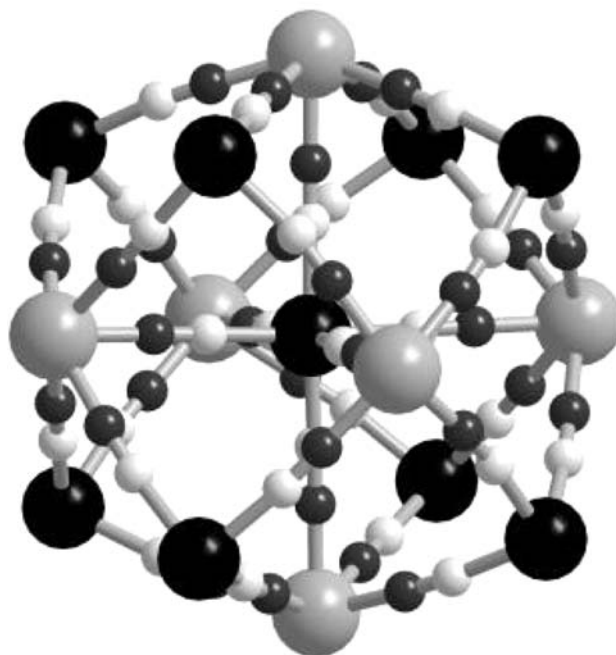


**Figure 15** Structure of the magnetic core of  $[\text{Mn}\{\text{Mn}(\text{MeOH})_3\}_8(\mu\text{-CN})_{30}\{\text{Mo}(\text{CN})_3\}_6]$ . The black and gray large spheres represent manganese and molybdenum atoms, respectively. Structure plotted with data available from ref. 143.

fundamental interest. In fact, SMMs are located at the interface of the classical and quantum domains and have provided a very nice example of the coexistence of quantum effects with the classical properties of magnets.<sup>128</sup> The main effect is the presence of under-barrier processes which allow the reversal of the magnetization through a tunneling mechanism.<sup>156,157</sup> In fact, the terms in the spin Hamiltonian that do not commute with  $S_z$  admix states which are on the opposite sides of the barrier. The transverse terms can be induced by the application of a transverse field or are intrinsic to the molecule if it has a symmetry lower than  $C_\infty$ .

If the tunneling mechanism involves the ground doublet with  $M = \pm S$ , the relaxation time becomes temperature independent as observed for another SMMs, the octanuclear cluster of formula  $[\text{Fe}_8\text{O}_2(\text{OH})_{12}(\text{tacn})_6]\text{Br}_8$ ,<sup>130</sup>  $\text{Fe}_8\text{Br}$ , shown in Figure 16. In this case the ground state is again  $S = 10$ <sup>131</sup> but the structural symmetry is rhombic and a stronger transverse anisotropy is active compared to  $\text{Mn}_{12}\text{ac}$ . The relaxation of the magnetization follows the Arrhenius law, but below 0.4 K the relaxation time becomes temperature independent, as shown in Figure 17.<sup>158</sup>

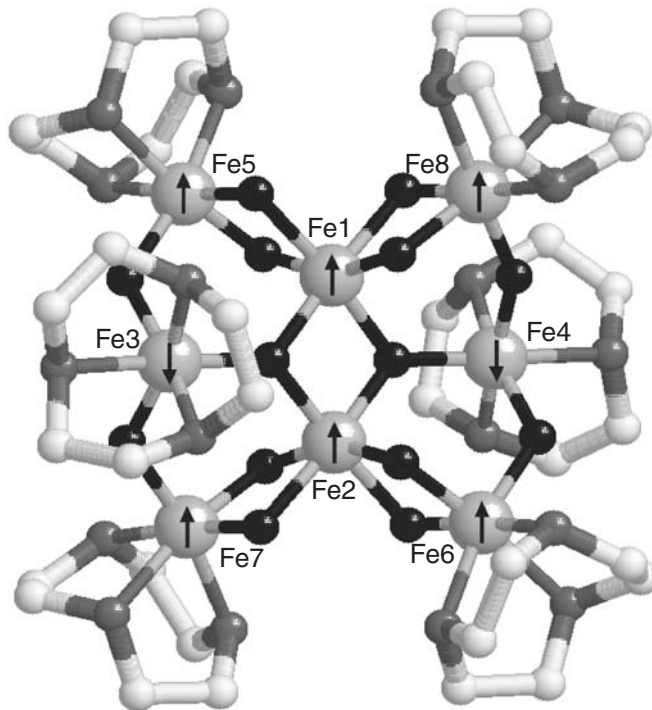


**Figure 16** Structure of  $[\text{Fe}_8\text{O}_2(\text{OH})_{12}(\text{tacn})_6]\text{Br}_8$ ,  $\text{Fe}_8\text{Br}$ . Oxygen, nitrogen, and carbon atoms are shown as black, gray, and pale gray spheres. The arrows schematically represent the spin structure of the ground  $S = 10$  state.

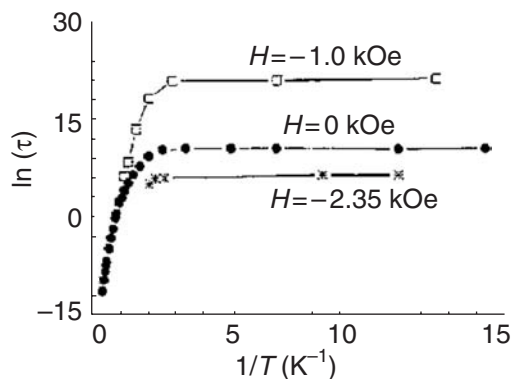


**Figure 17** Temperature dependence of the relaxation time of the magnetization of  $\text{Fe}_8\text{Br}$  measured at three different longitudinal fields. Plotted from data reported in ref. 158.

However, the tunneling effects are also evident at higher temperature in what has been called thermally activated quantum tunneling of the magnetization.<sup>93,159–162</sup> The states higher in the energy barrier are not significantly populated below  $T_B$ , however, they are more efficiently admixed by the transverse terms of the spin Hamiltonian, which act as a perturbation to the dominating easy-axis anisotropy. For instance, the transverse magnetic field only admixes the ground  $\pm 10$  doublet at the twentieth order of perturbation, and therefore is very inefficient. Much more effective are transverse anisotropy terms, especially the higher order terms, such as those depending on  $S_{\pm}^4$ , which in principle are present if the spin is larger than 2, or even higher terms for larger spin values. The tunneling mechanism represents a shortcut of the barrier thus inducing an acceleration of the relaxation compared to that expected from the Arrhenius law. However, the splitting induced by the transverse terms, also called tunnel splitting  $\Delta_t$ , is larger when the unperturbed energy levels are closer to each other. The unperturbed levels on opposite sides of the barrier are degenerate in zero field, as shown in Figure 18a, and tunneling is expected to be more efficient in zero field than in the presence of a longitudinal field. This goes against the classical picture of a reduction of the barrier induced by the field. A relative maximum of the relaxation rate in zero field is now considered a sort of fingerprint of the tunneling, even if experimental data must be rigorously analyzed since many other phenomena can mimic this behavior. The energy coincidence of the levels can, however, be re-established for critical values of the applied field, which in the simplest case of the spin Hamiltonian (Equation (26)) satisfies the condition  $H = nD/g\mu_B$ , with  $n$  integer, as shown in Figure 18b. Because of the resonant tunnel mechanism, accelerations are expected at regular field intervals, and indeed they are observed in many experiments; for instance, in the measurement of hysteresis loops that have a stepped shape,<sup>163,164</sup> as shown in Figure 19 for the  $\text{Fe}_8\text{Br}$  cluster. The flat regions of the hysteresis curve correspond to slow relaxation where tunneling is reduced by the presence of the field, while the vertical parts are the accelerations due to the resonant tunneling. Similar behavior can also be observed through different techniques, such as NMR spectroscopy<sup>165</sup> or specific heat measurements.<sup>166,167</sup>

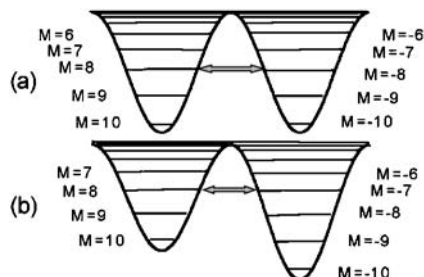


**Figure 18** Relative energies of the  $M$  levels of the ground  $S=10$  state of  $\text{Fe}_8\text{Br}$ . (a) Without an applied magnetic field; (b) with a field parallel to  $z$  and equal to  $D/g\mu_B$ .

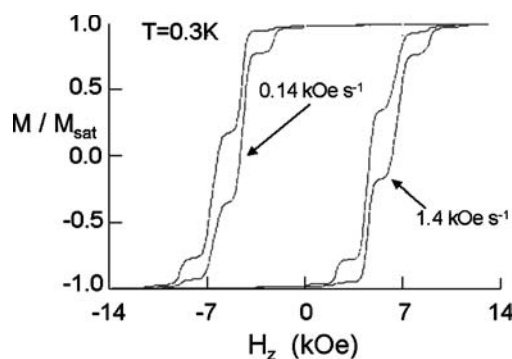


**Figure 19** Stepped hysteresis of  $\text{Fe}_8\text{Br}$  at 0.3 K. The curves were recorded at two scanning rates of the magnetic field. Plotted from data reported in ref. 163.

It is therefore possible not only to store information in one molecule, but the structured hysteresis cycle opens the possibility of a more powerful quantum bit. Of course, technological applications are not so straightforward. Several problems must first be solved: the low operative temperature, how to address a single molecule, or the intrinsically slow magnetization (writing) process of these materials. However, the field is relatively very young and contributions from neighboring areas (magneto-optics, quantum computing, nano electronics, etc.) are expected to become important in the future.

The tunneling mechanism in SMMs has been investigated using more sophisticated techniques. The good level of characterization that can be achieved in these materials has, however, played a crucial role, too. In contrast to the more classical nanoparticles, each cluster has a well-defined spin state, a well-defined magnetic anisotropy, etc.; furthermore, SMMs are often isolated as crystalline materials in which all the molecules are identical and with ordered orientation. Of course, this is true if defects are neglected, while their role can be important in the quantum dynamics of the magnetization.<sup>168–171</sup> Beyond bulk measurements of the thermodynamic properties—i.e., the magnetization—spectroscopic techniques can be used. Thanks to the interaction of the neutron spin with the magnetic moments of the sample, inelastic neutron spectroscopy (INS) can probe the energy of the magnetic excited states.<sup>172–177</sup> Electron paramagnetic resonance, especially the unconventional high field-high frequency version, HF-EPR,<sup>178</sup> provides the spin hamiltonian parameters, while magnetic circular dichroism measurements are a powerful tool to monitor the magnetization of dilute solutions of SMMs.<sup>116,118</sup> The magnetic techniques necessary for the investigation of these materials have also experienced a fast evolution. Due to the intrinsic anisotropy of SMMs, single crystal magnetic measurements are a must and high sensitivity techniques have been developed, like micro-Squid magnetometers, micro-Hall probes, and micro-capacitance torquemeters, already discussed in Vol I, Section 2.36. All of them use crystals of the same size as those employed for X-ray analysis, or even smaller.

HF-EPR<sup>179</sup> and INS<sup>180</sup> spectra have provided an accurate estimate of the  $D$  and  $E$  terms of Equation (26) for  $\text{Fe}_8\text{Br}$ ,  $D = -0.20 \text{ cm}^{-1}$ ,  $E = 0.03 \text{ cm}^{-1}$ , as well as sound evidence that higher order terms are present. Neglecting the higher order terms for the sake of simplicity, and using the above parameters, the energy separation of the ground  $M = \pm 10$  doublet, the so-called tunnel splitting  $\Delta_t$ , can be easily calculated. The result is of the order of  $10^{-8} \text{ K}$  and even including higher order terms, very effective for ground state tunneling,  $\Delta_t$  does not exceed  $10^{-7} \text{ K}$ . In order for tunneling to be efficient the energy bias of the unperturbed levels has to be smaller than this value. A longitudinal field as small as  $10^{-4} \text{ Oe}$  is thus already sufficient to suppress resonant tunneling. The distribution of internal dipolar fields expected in any magnetically concentrated sample has a width of the order of  $100 \text{ Oe}$ . Therefore most of the molecules in a macroscopic sample should not be able to tunnel. The internal field is, moreover, a static one at low temperature because the magnetic moments of the sample are frozen, at least as long as tunneling is not considered. Thus, something else must enter the scenario to solve the dilemma, and Prokofev and Stamp<sup>181</sup> have proposed that this new ingredient could be the field generated by the magnetic nuclei of the sample. The effect of the fluctuating hyperfine field is to broaden the levels, as shown schematically in Figure 20, bringing again into resonance a pair of levels within the  $\Delta_t$ . Confirmation of this hypothesis came from experiments on isotopically enriched samples of  $\text{Fe}_8\text{Br}$ , where field non-magnetic  $^{56}\text{Fe}$  nuclei ( $I = 0$ ) are replaced by  $^{57}\text{Fe}$  ( $I = 1/2$ ) to increase the hyperfine field or, on the contrary,  $^1\text{H}$  is partially replaced by  $^2\text{H}$  to decrease it. Significant differences in the relaxation rates are observed, with the  $^{57}\text{Fe}$  sample relaxing faster.<sup>182</sup> Further experiments are necessary to confirm and better characterize this unprecedented phenomenon, where the magnetization of the nuclei influences the electronic magnetization and not vice-versa.

The large efficiency of an oscillating field on promoting tunneling has been exploited to evaluate  $\Delta_t$  by sweeping the field back and forth on a resonance, which indeed in most cases represents an anti-crossing of levels as shown in Figure 21.<sup>183,184</sup> The tunnel splitting is related to the fraction of magnetization that reverses through the Landau–Zener–Stückelberg formula<sup>185–187</sup>

$$P_{M,M'} = 1 - \exp[-\pi\Delta_{M,M'}^2/(2hg\mu_B|M - M'|_0dH/dt)] \quad (29)$$

where  $dH/dt$  is the constant field sweeping rate and  $\Delta_{M,M'}$  is the tunnel splitting for the pair of levels in quasi-resonance involved in the tunnel transition.

This technique is now more widely used to investigate SMMs. In fact, the distribution of internal fields, which we have seen is crucial for the resonant tunneling mechanism, can be neglected in this type of experiment. A very interesting result obtained employing this technique

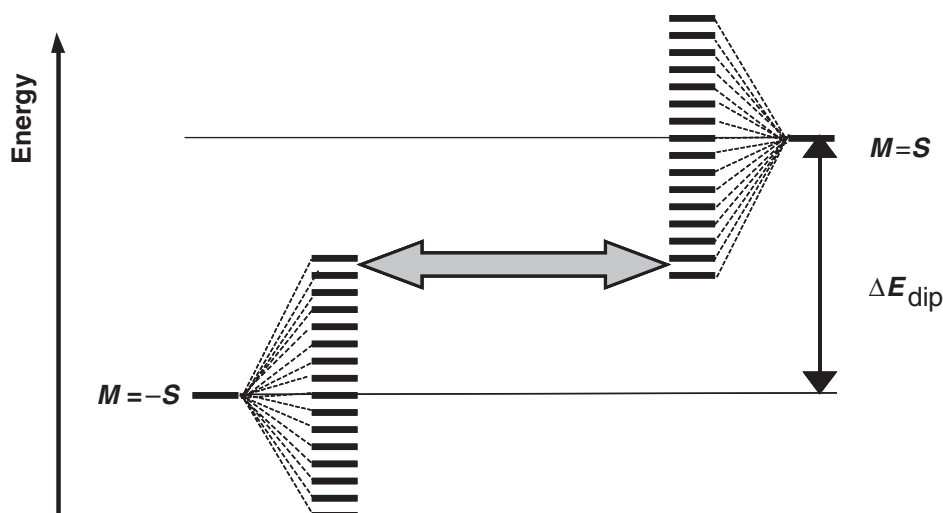


**Figure 20** Broadening of the  $M = \pm S$  levels due to the hyperfine coupling with magnetic nuclei.

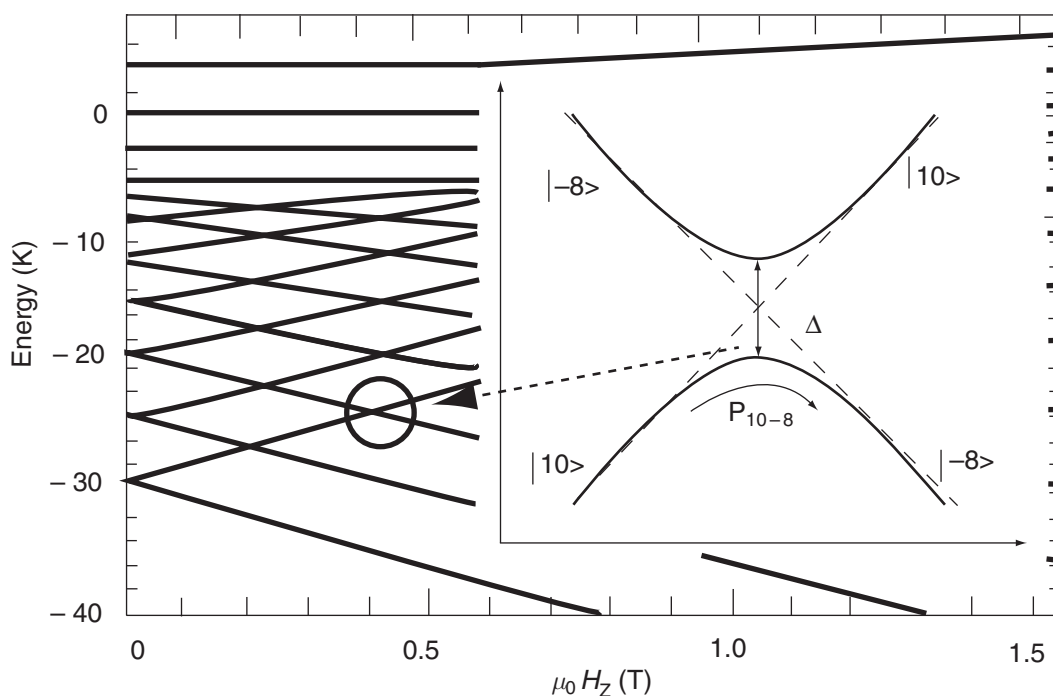


**Figure 21** Zeeman diagram for the  $S = 10$  ground spin state of Fe8 in a longitudinal applied magnetic field. In the inset, the anticrossing of the  $M = +10$  and  $M = -8$  levels.

is the first observation in magnetism of a phenomenon known as topological interference or Berry phase.<sup>188</sup> In this phenomenon the tunneling rate does not increase monotonically upon application of a transverse field, contrary to what could be expected starting from the intuition that a transverse field admixes states on opposite sides of the barrier. In particular conditions, an oscillation of the tunneling rate has been observed for Fe<sub>8</sub>,<sup>188</sup> and later for other SMMs,<sup>189</sup> with quenching of the tunnel splitting for critical values of the transverse field. These values are related again to the spin Hamiltonian parameters.<sup>190–192</sup> Starting from Equation (26) the magnetic field values at which  $\Delta_t$  is quenched not for symmetry reasons, (called “diabolical points”<sup>193–195</sup> because very uncommon in physics), occur at:

$$H_x(n) = 2n\sqrt{E'(E' + D')} \quad (30)$$

with  $n$  integer,  $E' = E/g_e\mu_B$ , and  $D' = D/g_e\mu_B$ . In addition to the fundamental interest, the observation of topological interference allows control of the dynamics of the magnetization through the application of a transverse field, a very important result that is unprecedented in magnetism.

Other factors can strongly influence the tunneling mechanism and therefore the dynamics of the magnetization in SMMs. It has recently been shown that interacting SMMs have very different dynamics, because the spin cross-relaxation can be an important pathway for the reversal of the magnetization.<sup>196,197</sup> Tunneling in zero field seems to be strongly reduced because it requires the contemporaneous tunneling of two magnetic moments. This is a very important aspect in the process of ultra miniaturization of magnetic memory. In fact, the stability of information stored in nanosized memories is expected to be strongly reduced by the tunnel effect. A mechanism of suppression of the tunnel effect is also an important achievement.

More recently, the interplay of tunnel dynamics with electromagnetic radiation has also attracted interest.<sup>198</sup> It has been shown theoretically that it is possible to observe the phenomenon of super-radiance in SMMs,<sup>199</sup> with population inversion caused by the application of a longitudinal field. The first experiments in this direction have now been performed.<sup>200,201</sup>

### 7.13.4 ONE-DIMENSIONAL SYSTEMS

One-dimensional systems are the simplest infinite assemblies of interacting spins for which a detailed understanding of the thermodynamic and dynamic properties can be achieved using the techniques of statistical mechanics.<sup>202</sup> The golden age of one-dimensional magnetic materials was in the 1970s, but recently there has been a revival, focusing especially on anisotropic systems like the Ising chains. In this section we will cover some aspects which we feel are relevant to show the fundamental role of molecular magnetism in order to develop new physics.

An important aspect of one-dimensional magnetism is the nature of the magnetic interaction between the spins. It can be isotropic, as described by the spin Hamiltonian Equation (6), or anisotropic. In the axial limit the anisotropy can be of the easy-axis type (Ising anisotropy) or of the easy-plane type (XY anisotropy). The former means that the spins tend to orient parallel to a preferential direction while for the latter they orient in a plane. The physical properties of the chains are strongly influenced by the nature of the anisotropy.<sup>203</sup>

#### 7.13.4.1 Haldane Gap Systems

The interest in one-dimensional antiferromagnets is still very high because they are expected to be very sensitive to quantum fluctuations, also currently a field of active research.<sup>204</sup> The common view of the magnetic behavior of one-dimensional isotropic antiferromagnets up to the 1980s was that the ladder of levels starting from the lowest-lying singlet is a continuous one, in accord with the infinite number of interacting spins. This is, in fact, known to be the case for systems of classical spins. It should be noted that the continuous nature of the levels is restricted to isotropic interactions because the presence of anisotropy opens a gap. However, in 1983, Haldane<sup>205</sup> suggested that, even in the case of isotropic interactions, systems with integer spin must have a gap, the so-called Haldane gap. This conjecture attracted much interest, and was confirmed by several numerical calculations.<sup>206,207</sup> It is now accepted that for a uniform Heisenberg  $S=1$  one-dimensional antiferromagnet there is a gap  $\Delta \approx 0.4$  J. The magnitude of the gap rapidly decreases with increasing  $S$ , in agreement with the fact that a chain of classical spins is gapless. The best calculations for  $S=2$  suggest  $\Delta \approx 0.09$  J.

Parallel to the development of suitable theories was the quest for suitable real systems on which to test the theoretical predictions.<sup>208,209</sup> The requirements for the ideal Haldane gap system are that: (i) it is effectively one-dimensional; (ii) it must be rather isotropic (Heisenberg exchange); (iii) the exchange coupling constant must not be too large or too small. Condition (i) requires that interactions between chains, reflected in the coupling constant  $J'$ , be small compared to intrachain interactions, monitored by  $J$ . Typical acceptable values of the  $J'/J$  ratio are smaller than  $10^{-4}$ . Condition (iii) is associated with the possibility of experimentally observing the gap. This can best be done using INS experiments or magnetic susceptibility measurements in the range of temperature  $T \ll \Delta/k_B$ . A very small value of  $\Delta$  requires the use of extremely low temperatures, while for larger  $\Delta$  values the onset of three-dimensional order triggered by interchain interactions may become too large.

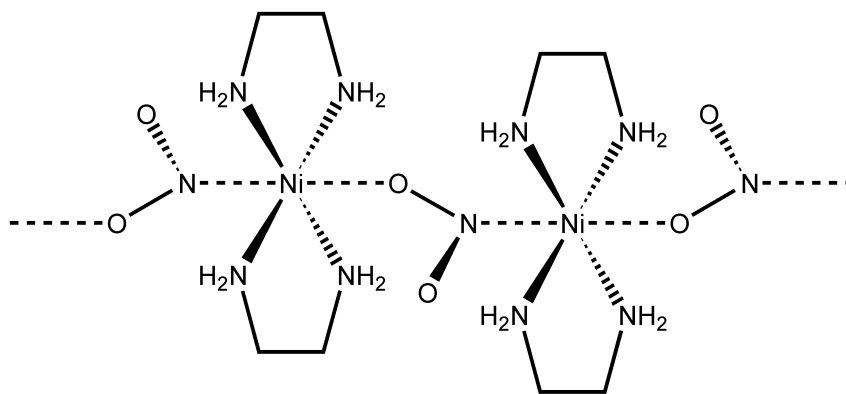


**Figure 22** Sketch of NENP.

A suitable  $S=1$  ion is octahedral nickel(II), which has a  ${}^3A_{2g}$  ground state, and is therefore rather isotropic, thus giving rise to Heisenberg-type magnetic interactions. However, nickel(II) is not completely isotropic because the  $S=1$  multiplet is split by spin-orbit coupling into a singlet and a doublet, separated by an energy gap that depends on the *ZFS* parameter  $D$  (see Chapter 2.36). Typical  $D$  values for nickel(II) are a few wavenumbers. Molecular derivatives of nickel(II) are also particularly well suited for forming well-isolated chains, taking advantage of the presence of organic moieties which cut suitable exchange pathways. In fact, the first real compound used for testing the existence of the Haldane gap was  $[\text{Ni}(\text{en})_2(\text{NO}_2)]\text{ClO}_4$ , where *en* = 1,2-diaminoethane,<sup>210,211</sup> NENP in the physical jargon, which has the structure shown in Figure 22. The nickel ions are coordinated by the four nitrogen atoms of *en* in a plane and are bridged by nitrate groups in axial positions. Characterization of the magnetic properties of NENP provided the values reported in Table 5.

Later, other systems were also synthesized, and their data are reported in Table 5. NINO<sup>212,213</sup> is the analog of NENP obtained by replacing *en* with 1,3-propanediamine. TMNIN<sup>214,215</sup> has the formula  $[\text{N}(\text{CH}_3)_4][\text{Ni}(\text{NO}_2)_3]$ . NINAZ,<sup>216</sup> is obtained by replacing the nitrate anion with the azide anion. This introduces us to the interesting world of one-dimensional systems containing azide bridges.

#### 7.13.4.2 Azide-bridged One-dimensional Systems

Azide has proved to be a very versatile bridging ligand, capable of transmitting both ferro- and antiferro-magnetic interactions, depending on the coordination mode.<sup>217</sup> In fact, there are two bridging modes of azide, end-to-end, (EE or 1,3) and end-on, (EO or 1,1), as sketched in Figure 23. With ions like nickel(II) and manganese(II) the EE mode yields antiferromagnetic coupling, while EO yields ferromagnetic coupling. The analysis of the factors determining the nature of the exchange has been a little controversial, but it seems now recognized that the EO mechanism involves a blend of spin delocalization and spin polarization.<sup>218,219</sup> The best results were obtained from the analysis of polarized neutron diffraction data of  $[\text{Cu}_2(t\text{-Bupy})_4(\mu\text{-N}_3)_2](\text{ClO}_4)_2$ , where *t*-Bupy is *p*-*tert*-butylpyridine.<sup>220</sup> The spin density map shown in Figure 24 shows that the spin density is mainly localized on copper(II), but positive spin density is also observed on the bridging and terminal nitrogen atoms of the bridging azide, thus ruling out the spin polarization mechanism.

**Table 5** Magnetic characteristics of Haldane gap systems based on molecular nickel(II) derivatives.

Compound	$J/k(\text{K})$	$D/k(\text{K})$	$\Delta_{xy}(\text{K})$	$\Delta_z(\text{K})$	References
NENP	48 44	12 9	14	30	210,211
NINO	52	18			212,213
TMNIN	12	4			214,215
NINAZ	145	44			216



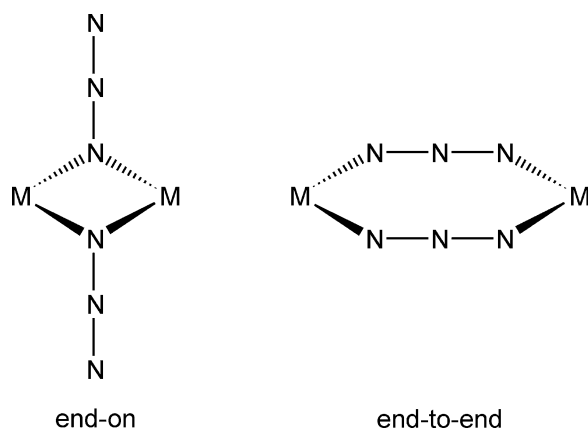


**Figure 23** Two bridging modes of azide: end-on, EO, and end-to-end, EE.

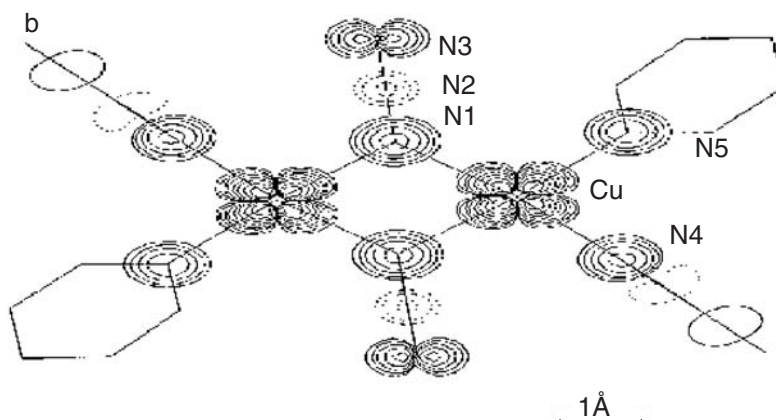


**Figure 24** Spin density in  $[\text{Cu}_2(t\text{-Bupy})_4(\mu\text{-N}_3)_2](\text{ClO}_4)_2$  at 1.6 K in a field of 4.6 T.

Using suitable co-ligands it has been found that zero-, one-, two-, and three-dimensional molecular magnets can be obtained.<sup>217</sup> In particular, the one-dimensional materials clearly show the incredible versatility of azide. In the EE mode, single azide bridges can be *trans* or *cis* while in the double bridge mode, only *cis* coordination is possible. It is also possible to observe alternating single and double bridges, while in the EO mode only double bridges are observed. Furthermore, it has been possible to obtain chains with mixed bridges, i.e., alternating EE and EO modes. In this case the EO bridges are always double, while the EE bridges can be either single or double. Finally, a complex alternation of one double EE bridge with three EO double bridges was also observed.

The nickel(II) derivatives with *trans* EE geometry are antiferromagnetically coupled, with  $J$  ranging from  $27\text{ cm}^{-1}$  to  $100\text{ cm}^{-1}$ .<sup>221</sup> Attempts have been made to correlate the observed magnetic coupling with structural features, such as the Ni–N–N angle and the dihedral angle between the coordination planes. The analogous compounds of *cis* EE geometry show, in general, a weaker antiferromagnetic coupling ( $J$  in the range  $3\text{--}33\text{ cm}^{-1}$ ). The only manganese(II) compound of *trans* EE geometry reported so far has a moderate antiferromagnetic coupling ( $J = 7\text{ cm}^{-1}$ ).<sup>222</sup>

The nickel(II) derivatives with double EO bridge are ferromagnetic, with  $J$  in the range  $-24\text{ cm}^{-1}$  to  $-57\text{ cm}^{-1}$ . One-dimensional ferromagnetic behavior was also observed in an analogous manganese(II) derivative.<sup>221</sup>

The systems with alternation of EE and EO bridges exhibit a dominant antiferromagnetic coupling, as expected.

### 7.13.4.3 Metal Radical Chains

Systems in which organic radical ligands are used in order to form one-dimensional materials have been found to have very peculiar and interesting physical properties. Essentially, two classes of radical have been used, taking advantage of their relative stability and ligating properties, namely the nitroxides and the TCNE-type radicals. The former are characterized by the presence of an NO group containing one unpaired electron. The radical state is stabilized by the presence of bulk substituents around the NO group. The oxygen atom can bind to a transition metal ion, although the nitroxides are rather weak Lewis bases, forming relatively weak complexes.

The TCNE-type radicals are much better ligands, and in fact these radicals have been used to form the molecular compound with the highest critical temperature to ferromagnetic order.<sup>223</sup> More recently, a very interesting class of one-dimensional compounds was reported comprising manganese(III) tetraphenylporphinato,  $[\text{Mn}(\text{TPP})]^+$  bridged by TCNE radicals.<sup>224,225</sup> The compounds behave as one-dimensional ferrimagnets, due to antiferromagnetic coupling between the  $S_i = 2$  spin of manganese(III) and the  $S = 1/2$  spin of the organic radical. The chains are rather well shielded from one another, therefore the behavior below 50 K is complicated by the interplay between weak dipolar interactions and the easy-axis type magnetic anisotropy associated with the manganese(III) ions. Spin glass behavior appears to compete with magnetic ordering.<sup>226</sup>

#### 7.13.4.3.1 Metal nitroxide chains

Nitronyl nitroxide derivatives, already shown in Figure 2, have often been used in molecular magnetism studies<sup>227–229</sup> because of their ability to bind transition metal ions and the fact that the two NO groups are completely equivalent. Since the unpaired electron is equally shared by the two NO groups the NIT radical behaves like a one-atom bridge and gives rise to strong coupling with different transition metal ions. Beyond the 1, 5 bridging mode, other types of extended one-dimensional structures have been obtained, as schematically shown in Figure 25. For transition metal ions, moderate ferromagnetic coupling is observed with copper(II), while a strong antiferromagnetic coupling is observed with manganese(II), cobalt(II), and nickel(II).<sup>228</sup> Ferromagnetic coupling is also observed for gadolinium(III).<sup>230</sup> However, the magnetic behavior of the gadolinium chains is rather peculiar, being dominated by next-nearest-neighbor antiferromagnetic interactions, which give rise to chiral order.<sup>231,232</sup>

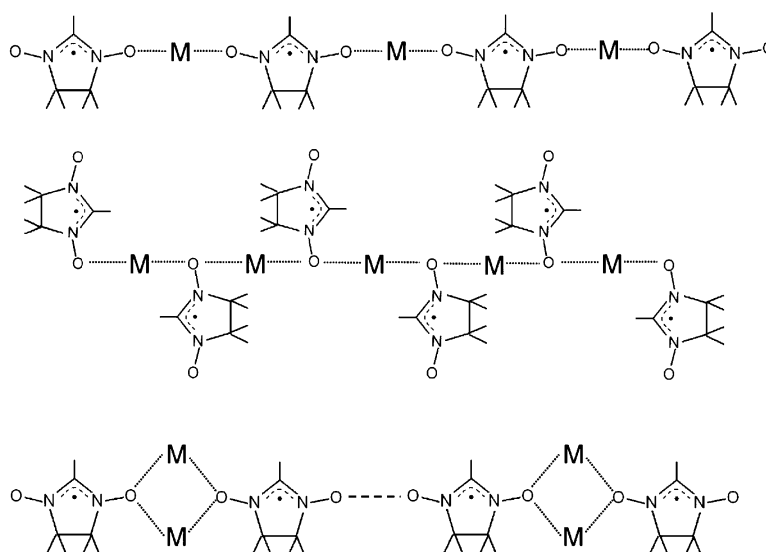


**Figure 25** Schematic view of three 1D magnetic structure obtained with nitronyl–nitroxide radicals and transition metal ions.

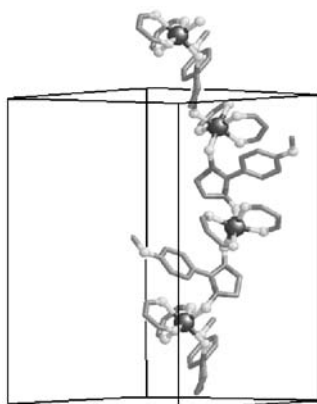


**Figure 26** Sketch of a trigonal helix formed by  $\text{Co}(\text{hfa})_2$  and NITR.

A typical structure for a metal–NITR chain is shown in Figure 26. The NITR radicals are very weak ligands, therefore they need relatively strong Lewis acids to form stable compounds. A very good acid is  $\text{M}(\text{hfac})_2$ , whose bulky  $\text{CF}_3$  groups keep the chains far from each other, minimizing their through-space (dipolar) magnetic interactions. Furthermore, the  $\text{CF}_3$  groups are magnetic insulators, in the sense that they give exceedingly weak superexchange couplings. Therefore, the metal–NITR chains are very good examples of one-dimensional magnetic materials, with large ratios between the intra- and inter-chain interaction. The relatively strong coupling between metal ions and radicals produces a rapid increase of the spin correlation length at low temperatures, and in some cases the weak dipolar interaction is sufficient to determine the cross-over to bulk three-dimensional magnetic order. For instance, the manganese(II) derivatives have been found to order as bulk ferrimagnets in the range 4–8 K.

Recently it has been discovered that the cobalt derivatives give rise to a novel magnetic behavior, analogous to that described above for SMMs. In  $[\text{Co}(\text{hfac})_2\text{NITPhOMe}]^{233}$  the coupling between the high-spin cobalt(II) ion and the radical is antiferromagnetic, giving rise to a ferrimagnetic chain. However, the interaction between the two spins is strongly anisotropic. The experiments performed on single crystals show that the anisotropy is of the easy-axis type, i.e., the spins are preferentially oriented parallel to a local anisotropy axis. If the dynamic susceptibility is measured at low temperature it is apparent that the relaxation time of the magnetization becomes long, and follows a thermally activated behavior, as shown in Figure 27. As in the SMM case there is no evidence of the onset of three-dimensional magnetic order, but rather a superparamagnetic-type behavior is evidenced. A qualitative explanation may rely on the idea that on

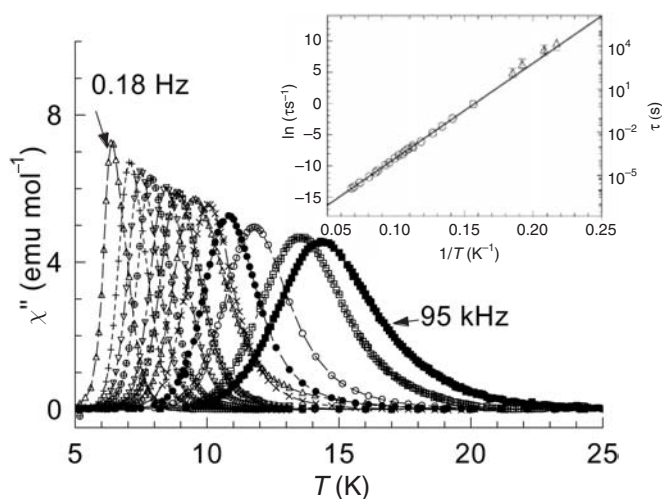


**Figure 27** ac frequency dependence of the out-of-phase component of the magnetic susceptibility of  $[\text{Co}(\text{hfac})_2\text{-NITPhOMe}]$ . In the inset is shown the temperature dependence of the relaxation time of the magnetization.

increasing the spin correlation length at low temperature the correlated spins give a larger effective  $S$  value, and it becomes more and more difficult to invert the magnetization.

A quantitative description of the relaxation of the magnetization in  $[\text{Co}(\text{hfac})_2\text{NITPhOMe}]$  has been achieved using the Glauber model.<sup>234</sup> This model was proposed in 1963 to describe the dynamic susceptibility of one-dimensional ferromagnets, but, although it has been widely used to describe different phenomena, including the spin cross-over transition, it had never been tested before on real magnetic systems.

The cobalt-radical chains, therefore, can be considered as magnetic nanowires, and in fact they give rise to magnetic hysteresis. In principle, these systems may be used to store information on a single chain (hence the name single-chain magnets, SCMs) magnetization, information storage in SCMs is possible at higher temperatures as compared with SMMs. Other systems have also been reported to have a similar behavior.<sup>235, 236</sup> In the particular case of  $[\text{Co}(\text{hfac})_2\text{NITPhOMe}]$ , the threefold symmetry of the crystalline space group causes a non-collinearity of the easy axis and a more complex behavior characterized by steps of the hysteresis loops, which, however, are not related to quantum tunneling.

#### 7.13.4.4 Oxalato Derivatives

Oxalato derivatives of transition metal ions are a wide class of materials which show a striking variety of magnetic behaviors.<sup>237–240</sup> First of all it must be stated that beyond oxalate it is possible to use several related ligands, like oxamide, or tioxalate. As a matter of fact, oxamido derivatives were the first examples of bulk molecular magnets.<sup>42</sup>

The first attractive property of oxalate bridges is that, although they connect metal ions through a minimum of three atoms, they are very efficient in transmitting an antiferromagnetic interaction. The best example is provided by copper(II) systems, shown in Figure 28. Although the two metal ions are separated by more than 5 Å, the two ions are antiferromagnetically coupled with  $J > 300 \text{ cm}^{-1}$ .<sup>261</sup> This is due to the favorable matching of the energies of the magnetic orbitals of the metal ions with the orbitals of the ligand.

From a chemical point of view, polynuclear oxalato derivatives can be considered to be formed starting from  $\text{M}(\text{ox})_3^{n-}$  building blocks, as shown in Figure 29. Being a tris-chelate derivative, the

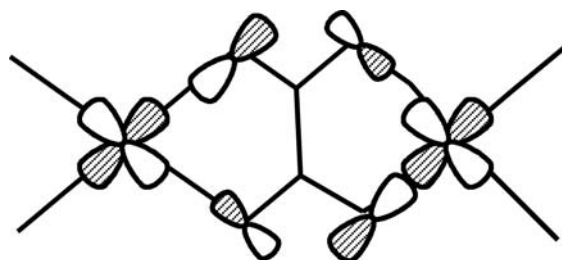


**Figure 28** Scheme of the magnetic orbitals responsible for the antiferromagnetic exchange in copper(II)-oxalato species.

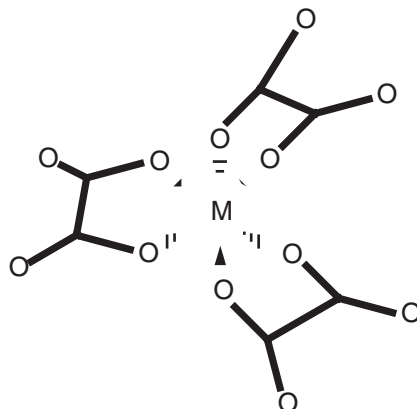


**Figure 29** Sketch of the building blocks of metal-oxalato derivatives.

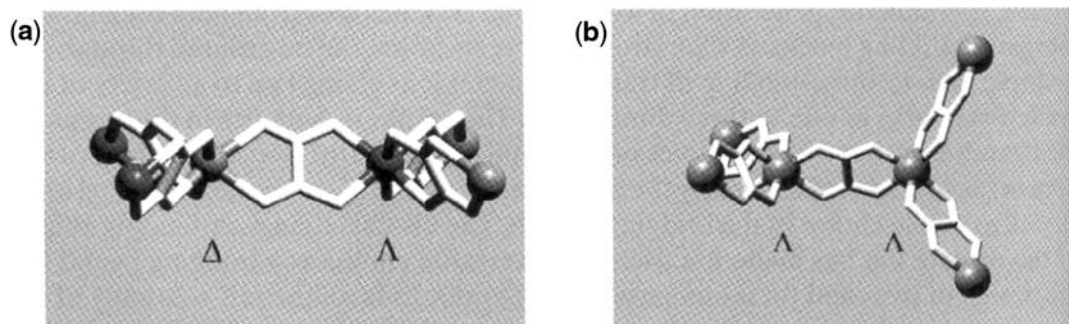


**Figure 30** Chiral  $M(\text{ox})_3$  building blocks assembled with: (a) alternating chiral configuration; (b) equal chiral configuration. After ref. 242.

metal center is dissymmetric and this must be taken into account when designing the structures of polymers. In fact, if the racemic mixture is used the polymer will display a two-dimensional honeycomb structure, while if a pure enantiomer is used then the structure will be three-dimensional as shown in Figure 30.

The actual structure of the polymers<sup>242</sup> will depend also on the nature of the cations which are needed to counterbalance the negative charges on the metal-oxalato framework.<sup>243,244</sup> The most investigated systems are the 2D ones, where an ordered array of  $M^{\text{III}}$  and  $M^{\text{II}}$  ions is observed as shown in Figure 31. An interesting example is provided<sup>245</sup> by  $A[\text{Fe}^{\text{II}}\text{Fe}^{\text{III}}(\text{ox})_3]$ ,

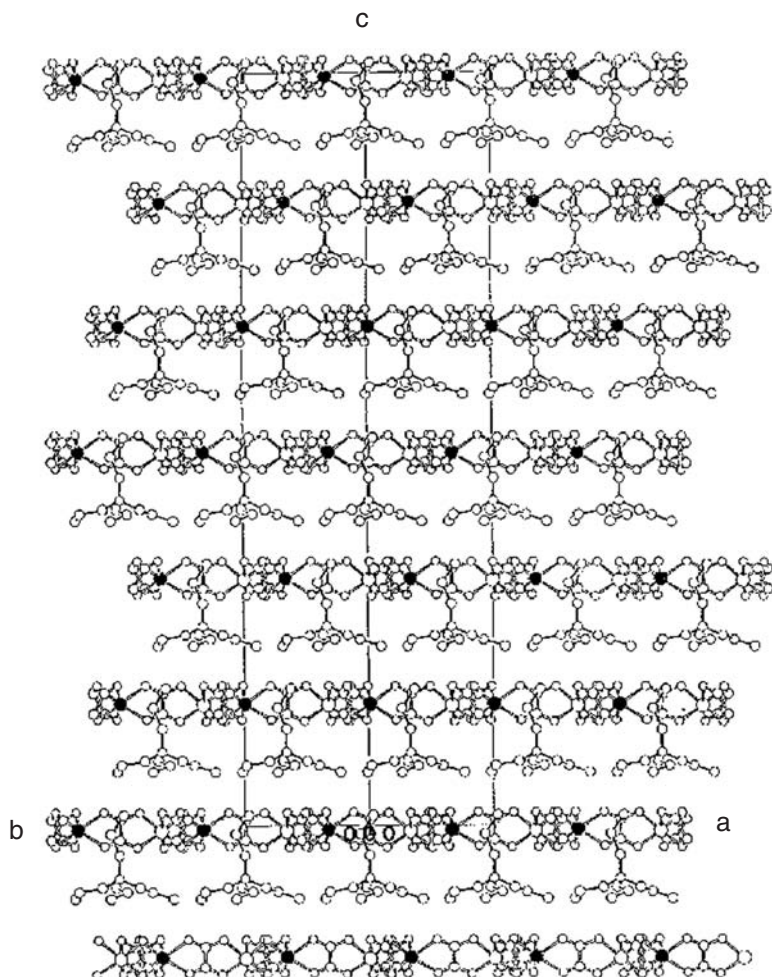


**Figure 31**  $[110]$  projection of  $[\text{N}(n\text{Pr})_4][\text{MnCr}(\text{ox})_3]$ . Black atoms indicate Mn ions. After ref. 242.

where  $A = \text{NBu}^n_4$ ,  $\text{NPr}^n_4$ . The antiferromagnetic coupling between  $\text{Fe}^{\text{II}}$  and  $\text{Fe}^{\text{III}}$  gives rise to a transition to ferromagnetic order. The interesting feature is that the magnetization at low temperature is negative, i.e., the preferred orientation is opposite to the applied magnetic field.<sup>246</sup> This is a nice demonstration of the validity of the Néel approach to ferrimagnets. The observed magnetization, in fact, in a ferrimagnet is due to the sum of the contributions of the two sublattices. However, the two magnetizations may have different temperature dependencies. The  $\text{Fe}^{\text{II}}$  sublattice has an initially steeper temperature dependence and it obviously follows the external field. However, on decreasing the temperature the magnetization of the  $\text{Fe}^{\text{III}}$  sublattice takes over and the magnetization becomes negative. It must also be noted that there is a temperature, called the compensation temperature, where the two magnetizations exactly cancel out.

An interesting application of molecular magnetism has been reported recently by Coronado *et al.*<sup>247</sup> They found that assembling in the same lattice BEDT–TTF cations and  $[\text{MnCr}(\text{C}_2\text{O}_4)_3]$  anions results in a novel material with coexistence of ferromagnetism and electric conductivity. Of course, inorganic conducting ferromagnets are well known, iron being an obvious example, but in this case the conducting electrons are different from the magnetic electrons. In fact, the former are localized on the organic radical part, while the latter are in the oxalato planes. This compound opens new, exciting perspectives and shows how it is possible to obtain novel combinations of properties using a molecular approach.

### 7.13.5 REFERENCES

1. Van Vleck, J. H. *The Theory of Electric and Magnetic Susceptibility*; Oxford University Press: Oxford, 1932.
2. Abraham, A.; Bleaney, B. *Electron Paramagnetic Resonance of Transition Ions*; Dover: New York, 1986.
3. Carlin, R. L. *Magnetochemistry*; Springer-Verlag: Berlin, 1986.
4. Kahn, O. *Molecular Magnetism*; VCH: Weinheim, 1993.
5. Goodenough, J. B. *Magnetism and the Chemical Bond*; Interscience: New York, 1963.
6. Julve, M.; Verdager, M.; Gleizes, A.; Philoche-Levisalles, M.; Kahn, O. *Inorg. Chem.* **1984**, *23*, 3808.
7. Anderson, P. W. *Phys. Rev.* **1959**, *115*, 2.
8. Anderson, P. W. *Magnetism*; Rado, G. T.; Suhl, H., Academic Press: New York, 1963; Vol. 1, p 25.
9. Goodenough, J. B. *J. Phys. Chem. Solids* **1958**, *6*, 287.
10. Kanamori, J. *J. Phys. Chem. Solids* **1959**, *10*, 87.
11. Hay, P. J.; Thibeault, J. C.; Hoffmann, R. H. *J. Am. Chem. Soc.* **1975**, *97*, 4884.
12. Kahn, O.; Briat, B. J. *J. Chem. Soc. Faraday Trans. II* **1976**, *72*, 268.
13. Parr, R. G.; Yang, W. *Density-Functional Theory of Atoms and Molecules*; Oxford University Press: New York, 1989.
14. Koch, W.; Holthausen, M. C. *A Chemist's Guide to Density Functional Theory*; Wiley VCH: Weinheim, 2000.
15. Miller, J. S.; Drillon, M. *Magnetism: Molecules to Materials: Models and Experiments*; Wiley-VCH: Weinheim, 2001.
16. Hatfield, W. A. *Inorg. Chem.* **1983**, *22*, 833.
17. Alvarez, S.; Julve, M.; Verdager, M. *Inorg. Chem.* **1990**, *29*, 4500.
18. Kahn, O. *Adv. Inorg. Chem.* **1995**, *43*, 179.
19. Weihe, H.; Guedel, H. U. *J. Am. Chem. Soc.* **1997**, 6539–6543.
20. De Loth, P.; Daudey, J. P.; Astheimer, H.; Walz, L.; Haase, W. *J. Chem. Phys.* **1985**, *82*, 5048.
21. Ceulemans, A.; Chibotaru, L. F.; Heylen, G. A.; Pierloot, K.; Vanquickenborne, L. G. *Chem. Rev.* **2000**, *100*, 787–806.
22. Noodleman, L. *J. Chem. Phys.* **1981**, *74*, 5737.
23. Noodleman, L.; Davidson, E. R. *Chem. Phys.* **1986**, *109*, 131.
24. Noodleman, L.; Post, D.; Baerens, E. J. *Chem. Phys.* **1982**, *64*, 159.
25. Noodleman, L.; Peng, C. Y.; Case, D. A.; Mouesca, J.-M. *Coord. Chem. Rev.* **1995**, *144*, 199–244.
26. Beinert, H.; Kennedy, M. C.; Stout, C. D. *Chem. Rev.* **1996**, *96*, 2335–2373.
27. Howard, J. B.; Rees, D. C. *Chem. Rev.* **1996**, *96*, 2965–2982.
28. Torres, R. A.; Lovell, T.; Noodleman, L.; Case, D. A. *J. Am. Chem. Soc.* **2003**, *125*, 1923–1936.
29. Cano, J.; Rodriguez-Fortea, A.; Alemany, P.; Alvarez, S.; Ruiz, E. *Chem. Eur. J.* **2000**, *6*, 327–333.
30. Kortus, J.; Baruah, T.; Bernstein, N.; Pederson, M. R. *Phys. Rev. B* **2002**, *66*, art. no. 092403.
31. Pederson, M. R.; Kortus, J.; Khanna, S. N. *J. Appl. Phys.* **2002**, *91*, 7149–7151.
32. Kortus, J.; Hellberg, C. S.; Pederson, M. R. *Phys. Rev. Lett.* **2001**, *86*, 3400–3403.
33. Kortus, J.; Pederson, M. R. *Phys. Rev. B* **2000**, *62*, 5755–5759.
34. Lahti, P. M., *Magnetic Properties of Organic Materials*; Marcel Dekker: New York, 1999.
35. Tamura, M.; Nakazawa, Y.; Shiomi, D.; Nozawa, Y.; Hosokoshi, M.; Ishikawa, M.; Takahashi, M.; Kinoshita, M. *Chem Phys. Lett.* **1991**, *186*, 401.
36. McCleverty, J. A.; Ward, M. D. *Acc. Chem. Res.* **1998**, *31*, 842–851.
37. Thompson, A. M. W. C.; Gatteschi, D.; McCleverty, J. A.; Navas, J. A.; Rentschler, E.; Ward, M. D. *Inorg. Chem.* **1996**, *35*, 2701–2703.
38. Ung, V. A.; Thompson, A. M. W. C.; Bardwell, D. A.; Gatteschi, D.; Jeffery, J. C.; McCleverty, J. A.; Totti, F.; Ward, M. D. *Inorg. Chem.* **1997**, *36*, 3447–3454.
39. Bencini, A.; Gatteschi, D.; Totti, F.; Sanz, D. N.; McCleverty, J. A.; Ward, M. D. *J. Phys. Chem. A* **1998**, *102*, 10545–10551.
40. Schweitzer, J.; Gillon, B. In: *Magnetic Properties of Organic Materials*; Lahti, P. M., Marcel Dekker: New York, 1999; Vol. pp 449–473.

41. Gillon, B. In: *Magnetism: Molecules to Materials*; Miller, J. S.; Drillon, M., Wiley-VCH: Weinheim, 2001; Vol. I, pp 357–378.
42. Kahn, O.; Pei, Y.; Verdager, M.; Renard, J.-P.; Sletten, J. J. *Am. Chem. Soc.* **1988**, *110*, 782.
43. Baron, V.; Gillon, B.; Plantevin, O.; Cousson, A.; Mathoniere, C.; Kahn, O.; Grand, A.; Öhrström, L.; Delley, B. *J. Am. Chem. Soc.* **1996**, *118*, 11822.
44. Bencini, A.; Gatteschi, D. *EPR of Exchange Coupled Systems*; Springer-Verlag: Berlin, 1990.
45. Paulson, J. A.; Krost, D. A.; McPherson, G. L.; Rogers, L. D.; Atwood, J. L. *Inorg. Chem.* **1980**, *19*, 2519.
46. Prassides, K., *Mixed Valence Systems: Applications in Chemistry, Physics, and Biology*; Kluwer: Dordrecht, 1991.
47. Robin, M. B.; Day, P. *Adv. Inorg. Chem. Radiochem.* **1967**, *10*, 247.
48. Bencini, A.; Berti, E.; Caneschi, A.; Gatteschi, D.; Giannasi, E.; Invernizzi, I. *Chem. Eur. J.* **2002**, *8*, 3660–3670.
49. Girerd, J.-J. *J. Chem. Phys.* **1983**, *79*, 1766.
50. Zener, C. *Phys. Rev.* **1951**, *82*, 403.
51. Rao, C. N. R. *Chem. Eur. J.* **1996**, *2*, 1499.
52. Anderson, P. W.; Hasegawa, H. *Phys. Rev.* **1955**, *100*, 675.
53. Borrás-Almenar, J. J.; Clemente-Juan, J. M.; Coronado, E.; Pali, A.; Tsukerblat, B. S.; Miller, J. S.; Drillon, M., Ed., In: *Magnetism: Molecules to Materials 2001*, Wiley-VCH: Weinheim, pp 156–210.
54. Shultz, D. A. *Magnetism: Molecules to Materials II*; Miller, J. S.; Drillon, M., Wiley-VCH: Weinheim, 2001; pp 281–306.
55. Hendrickson, D. N. In: *Mixed Valence Systems: Applications in Chemistry, Physics, and Biology*, Prassides, K. Ed. Kluwer: Dordrecht, 1991; p 67.
56. Creutz, C. In *Progress in Inorganic Chemistry*, Vol. 1; Lippard, S. J., Ed.; Wiley: New York, 1983; p 1.
57. Day, P. *Int. Rev. Phys. Chem.* **1981**, *1*, 149.
58. Gütlich, P.; Dei, A. *Angew. Chem. Int. Ed. Engl.* **1997**, *37*, 2734.
59. Pierpont, C. G.; Buchanan, R. M. *Coord. Chem. Rev.* **1981**, *38*, 45.
60. Pierpont, C. G.; Lange, C. W. *Progr. Inorg. Chem.* **1994**, *41*, 331.
61. Kaim, W. *Coord. Chem. Rev.* **1987**, *76*, 187.
62. Benelli, C.; Dei, A.; Gatteschi, D.; Pardi, L. *Inorg. Chim. Acta* **1989**, *163*, 99.
63. Caneschi, A.; Dei, A. *Angew. Chem. Int. Ed. Engl.* **1998**, *37*, 3005.
64. Attia, A. S.; Pierpont, C. G. *Inorg. Chem.* **1998**, *37*, 3051.
65. Attia, A. S.; Pierpont, G. C. *Inorg. Chem.* **1997**, *36*, 6184.
66. Attia, A. S.; Pierpont, G. C. *Inorg. Chem.* **1995**, *34*, 1172.
67. Lynch, M. W.; Hendrickson, D. N.; Fitzgerald, B. J.; Pierpont, G. C. *J. Am. Chem. Soc.* **1981**, *103*, 3961.
68. Lynch, M. W.; Hendrickson, D. N.; Fitzgerald, B. J.; Pierpont, G. C. *J. Am. Chem. Soc.* **1984**, *106*, 241.
69. Lange, C. W.; Földeaki, M.; Nevodchikov, V. I.; Cherkasov, V. K. *J. Organomet. Chem.* **1992**, *114*, 4220.
70. Abakumov, G. A.; Razuvaev, G. A.; Nevodchikov, V. I.; Cherkasov, V. K. *J. Organomet. Chem.* **1988**, *341*, 485.
71. Adams, D. M.; Dei, A.; Rheingold, A. L.; Hendrickson, D. N. *J. Am. Chem. Soc.* **1993**, *115*, 8221–8229.
72. Adams, D. M.; Hendrickson, D. N. *J. Am. Chem. Soc.* **1996**, *118*, 11515.
73. Jung, O. S.; Pierpont, C. G. *J. Am. Chem. Soc.* **1994**, *116*, 1127.
74. Jung, O.-S.; Jo, D. H.; Lee, J.-L.; Conklin, B. J.; Pierpont, C. G. *Inorg. Chem.* **1997**, *37*, 19.
75. Benelli, C.; Dei, A.; Gatteschi, D.; Güdel, H. U.; Pardi, L. *Inorg. Chem.* **1989**, *28*, 3089.
76. Lippard, S. J. *Nature* **2002**, *416*, 587.
77. Baxter, P. N. W. In *Comprehensive Supramolecular Chemistry*; Lehn, J.-M.; Atwood, J. L.; Davies, J. E. D.; MacNicol, D. D.; Voegtle, F., Pergamon Press: Oxford, 1996; Vol. 9, p 165.
78. Caneschi, A.; Cornia, A.; Lippard, S. J. *Angew. Chem. Int. Ed. Engl.* **1995**, *34*, 467–469.
79. Caneschi, A.; Cornia, A.; Fabretti, A. C.; Foner, S.; Gatteschi, D.; Grandi, R.; Schenetti, L. *Chem. Eur. J.* **1996**, *2*, 1379–1387.
80. Abbati, G. L.; Cornia, A.; Fabretti, A. C.; Malavasi, W.; Schenetti, L.; Caneschi, A.; Gatteschi, D. *Inorg. Chem.* **1997**, *36*, 6443–6446.
81. Caneschi, A.; Cornia, A.; Fabretti, A. C.; Gatteschi, D. *Angew. Chem. Int. Ed. Engl.* **1999**, *38*, 1295–1297.
82. Abbati, G. L.; Caneschi, A.; Cornia, A.; Fabretti, A. C.; Gatteschi, D. *Inorg. Chim. Acta* **2000**, *297*, 291–300.
83. Saalfrank, R. W.; Bernt, I.; Uller, E.; Hampel, F. *Angew. Chem. Int. Ed. Engl.* **1997**, *36*, 2482–2485.
84. Gerbeleu, N. V.; Struchkov, Y. T.; Manole, O. S.; Timko, G. A.; Batsanov, A. S. *Dokl. Akad. Nauk SSSR* **1993**, *331*, 184–187.
85. Van Slageren, J.; Sessoli, R.; Gatteschi, D.; Smith, A. A.; Helliwell, M.; Winpenny, R. E. P.; Cornia, A.; Barra, A. L.; Jansen, A. G. M.; Rentschler, E.; Timco, G. A. *Chem. Eur. J.* **2002**, *8*, 277–285.
86. Atkinson, I. M.; Benelli, C.; Murrie, M.; Parson, S.; Winpenny, R. E. P. *Chem. Commun.* **1999**, 285–286.
87. McInnes, E. J. L.; Anson, C.; Powell, A. K.; Thomson, A. J.; Poussereau, S.; Sessoli, R. *Chem. Commun.* **2001**, 89–90.
88. Taft, K. L.; Delfs, C. D.; Papaefthymiou, G. C.; Foner, S.; Gatteschi, D.; Lippard, S. J. *J. Am. Chem. Soc.* **1994**, *116*, 823–832.
89. Benelli, C.; Parsons, S.; Solan, G. A.; Winpenny, R. E. P. *Angew. Chem. Int. Ed. Engl.* **1996**, *35*, 1825–1828.
90. Watton, S. P.; Fuhrmann, P.; Pence, L. E.; Caneschi, A.; Cornia, A.; Abbati, G. L.; Lippard, S. J. *Angew. Chem. Int. Ed. Engl.* **1997**, *36*, 2774–2776.
91. Waldmann, O. *Phys. Rev. B* **2002**, *65*, art. no. 024424.
92. Schnack, J.; Luban, M. *Phys. Rev. B* **2001**, *63*, art. no. 014418.
93. Caneschi, A.; Gatteschi, D.; Sangregorio, C.; Sessoli, R.; Sorace, L.; Cornia, A.; Novak, M. A.; Paulsen, C.; Wernsdorfer, W. *J. Magn. Magn. Mater.* **1999**, *200*, 182–201.
94. Gatteschi, D.; Sessoli, R.; Cornia, A. *Chem. Commun.* **2000**, 725–732.
95. Affronte, M.; Cornia, A.; Lascialfari, A.; Borsa, F.; Gatteschi, D.; Hinderer, J.; Horvatic, M.; Jansen, A. G. M.; Julien, M. H. *Phys. Rev. Lett.* **2002**, *88*, art. no. 167201.
96. Waldmann, O.; Koch, R.; Schromm, S.; Müller, P.; Bernt, I.; Saalfrank, R. W. *Phys. Rev. Lett.* **2002**, *89*, art. no. 246401.
97. Honecker, A.; Meier, F.; Loss, D.; Normand, B. *Eur. Phys. J. B* **2002**, *27*, 487–495.
98. Affronte, M.; Lasjaunias, J. C.; Abbati, G. L. *Phys. Rev. B* **2002**, *66*, art. no. 180405.

99. Waldmann, O. *Phys. Rev. B* **2000**, *61*, 6138–6144.
100. Cornia, A.; Gatteschi, D.; Sessoli, R. *Coord. Chem. Rev.* **2001**, *219–221*, 573–604.
101. Pilawa, B.; Desquiotz, R.; Kelemen, M. T.; Weickenmeier, M.; Geisselmann, A. *J. Magn. Magn. Mat.* **1997**, *177–181*, 748–749.
102. Cornia, A.; Jansen, A. G. M.; Affronte, M. *Phys. Rev. B* **1999**, *60*, 12177–12183.
103. Cornia, A.; Affronte, M.; Jansen, A. G. M.; Abbati, G. L.; Gatteschi, D. *Angew. Chem. Int. Ed. Engl.* **1999**, *38*, 2264–2266.
104. Waldmann, O.; Schülein, J.; Koch, R.; Müller, P.; Bernt, I.; Saalfrank, R. W.; Andres, H. P.; Güdel, H. U.; Allenspach, P. *Inorg. Chem.* **1999**, *38*, 5879–5886.
105. Waldmann, O.; Koch, R.; Schromm, S.; Schülein, J.; Müller, P.; Bernt, I.; Saalfrank, R. W.; Hampel, F.; Balthes, E. *Inorg. Chem.* **2001**, *40*, 2986–2995.
106. Abbati, G. L.; Brunel, L. C.; Casalta, H.; Cornia, A.; Fabretti, A. C.; Gatteschi, D.; Hassan, A. K.; Jansen, A. G. M.; Maniero, A. L.; Pardi, L.; Paulsen, C. *Chem. Eur. J.* **2001**, *7*, 1796–1807.
107. Le Gall, F.; Fabrizi de Biani, F.; Caneschi, A.; Cinelli, P.; Cornia, A.; Fabretti, A. C.; Gatteschi, D. *Inorg. Chim. Acta* **1997**, *262*, 123–132.
108. Gatteschi, D.; Sorace, L. *J. Solid State Chem.* **2001**, *159*, 253–261.
109. Caneschi, A.; Gatteschi, D.; Sessoli, R.; Barra, A.-L.; Brunel, L. C.; Guillot, M. *J. Am. Chem. Soc.* **1991**, *113*, 5873–5874.
110. Sessoli, R.; Gatteschi, D.; Caneschi, A.; Novak, M. A. *Nature (London)* **1993**, *365*, 141–143.
111. Lis, T. *Acta Cryst.* **1980**, *B36*, 2042–2046.
112. Christou, G.; Gatteschi, D.; Hendrickson, D. N.; Sessoli, R. *Mrs Bulletin* **2000**, *25*, 66–71.
113. Morrish, A. H. *The Physical Principles of Magnetism*; John Wiley & Sons: New York, 1966.
114. Villain, J.; Hartman-Boutron, F.; Sessoli, R.; Rettori, A. *Europhys. Lett.* **1994**, *27*, 159–164.
115. Sessoli, R. *Mol. Cryst. Liquid Cryst.* **1995**, *274*, 145–157.
116. Cheesman, M. R.; Oganessian, V. S.; Sessoli, R.; Gatteschi, D.; Thomson, A. J. *Chem. Commun. (Cambridge)* **1997**, 1677–1678.
117. Caneschi, A.; Ohm, T.; Paulsen, C.; Rovai, D.; Sangregorio, C.; Sessoli, R. *J. Magn. Magn. Mater.* **1998**, *177*, 1330–1336.
118. McInnes, E. J. L.; Pidcock, E.; Oganessian, V. S.; Cheesman, M. R.; Powell, A. K.; Thomson, A. J. *J. Am. Chem. Soc.* **2002**, *124*, 9219–9228.
119. Sokol, J. J.; Hee, A. G.; Long, J. R. *J. Am. Chem. Soc.* **2002**, *124*, 7656–7657.
120. Brockman, J. T.; Huffman, J. C.; Christou, G. *Angew. Chem. Int. Ed. Engl.* **2002**, *41*, 2506.
121. Boskovic, C.; Brechin, E. K.; Streib, W. E.; Folting, K.; Hendrickson, D. N.; Christou, G. *Chem. Commun.* **2001**, 467–468.
122. Mallah, T.; Auberger, C.; Verdaguer, M.; Veillet, P. *Chem. Commun.* **1995**, 61.
123. Brechin, E. K.; Yoo, J.; Nakano, M.; Huffman, J. C.; Hendrickson, D. N.; Christou, G. *Chem. Commun.* **1999**, 783–784.
124. Kido, T.; Ikuta, Y.; Sunatsuki, Y.; Ogawa, Y.; Matsumoto, N. *Inorg. Chem.* **2003**, *42*, 398–408.
125. Brechin, E. K.; Soler, M.; Davidson, J.; Hendrickson, D. N.; Parsons, S.; Christou, G. *Chem. Commun.* **2002**, 2252–2253.
126. Yamaguchi, A.; Kusumi, N.; Ishimoto, H.; Mitamura, H.; Goto, T.; Mori, N.; Nakano, M.; Awaga, K.; Yoo, J.; Hendrickson, D. N.; Christou, G. *J. Phys. Soc. Jpn.* **2002**, *71*, 414–417.
127. Aubin, S. M. J.; Sun, Z.; Pardi, L.; Krzystek, J.; Folting, K.; Brunel, L.-C.; Rheingold, A. L.; Christou, G.; Hendrickson, D. N. *Inorg. Chem.* **1999**, *38*, 5329–5340.
128. Gatteschi, D.; Sessoli, R. *Angew. Chem. Int. Ed. Engl.* **2003**, *42*, 268–297.
129. Soler, M.; Chandra, S. K.; Ruiz, D.; Davidson, E. R.; Hendrickson, D. N.; Christou, G. *Chem. Commun.* **2000**, 2417–2418.
130. Wieghardt, K.; Pohl, K.; Jibril, I.; Huttner, G. *Angew. Chem. Int. Ed. Engl.* **1984**, *23*, 77–78.
131. Barra, A. L.; Debrunner, P.; Gatteschi, D.; Schulz, Ch.E.; Sessoli, R. *Europhys. Lett.* **1996**, *35*, 133–138.
132. Benelli, C.; Cano, J.; Journaux, Y.; Sessoli, R.; Solan, G. A.; Winpenny, R. E. P. *Inorg. Chem.* **2001**, *40*, 188.
133. Pilawa, B.; Kelemen, M. T.; Wanka, S.; Geisselmann, A.; Barra, A. L. *Europhys. Lett.* **1998**, *43*, 7–12.
134. Caneschi, A.; Gatteschi, D.; Laugier, J.; Rey, P.; Sessoli, R.; Zanchini, C. *J. Am. Chem. Soc.* **1988**, *110*, 2795.
135. Abbati, G. L.; Cornia, A.; Fabretti, A. C.; Caneschi, A.; Gatteschi, D. *Inorg. Chem.* **1998**, *37*, 1430–1431.
136. Cadiou, C.; Murrie, M.; Paulsen, C.; Villar, V.; Wernsdorfer, W.; Winpenny, R. E. P. *Chem. Commun.* **2001**, 2666–2667.
137. Bonadio, F.; Gross, M.; Stoekli-Evans, H.; Decurtins, S. *Inorg. Chem.* **2002**, *41*, 5891–5896.
138. Brechin, E. K.; Boskovic, C.; Wernsdorfer, W.; Yoo, J.; Yamaguchi, A.; Sanudo, E. C.; Concolino, T. R.; Rheingold, A. L.; Ishimoto, H.; Hendrickson, D. N.; Christou, G. *J. Am. Chem. Soc.* **2002**, *124*, 9710–9711.
139. Scuiller, A.; Mallah, T.; Verdaguer, M.; Nivorozhkin, A.; Tholence, J. L.; Veillet, P. *New J. Chem.* **1996**, *20*, 1–3.
140. Oshio, H.; Hoshino, N.; Ito, T.; Nakano, M.; Renz, F.; Gutlich, P. *Angew. Chem. Int. Ed. Engl.* **2003**, *42*, 223.
141. Goodwin, J. C.; Sessoli, R.; Gatteschi, D.; Wernsdorfer, W.; Powell, A. K.; Heath, S. L.; Barra, A. L. *J. Chem. Soc. Dalton. Trans.* **2000**, 4702.
142. Zhong, Z. J.; Seino, H.; Mizobe, Y.; Hidai, M.; Fujishima, A.; Ohkoshi, S.; Hashimoto, K. *J. Am. Chem. Soc.* **2000**, *122*, 2952–2953.
143. Larionova, J.; Gross, M.; Pilkington, M.; Andres, H.; Stoekli-Evans, H.; Güdel, H. U.; Decurtins, S. *Angew. Chem. Int. Ed. Engl.* **2000**, *39*, 1605.
144. Barra, A. L.; Caneschi, A.; Cornia, A.; De Biani, F. F.; Gatteschi, D.; Sangregorio, C.; Sessoli, R.; Sorace, L. *J. Am. Chem. Soc.* **1999**, *121*, 5302–5310.
145. Sessoli, R.; Tsai, H. L.; Schake, A. R.; Wang, S.; Vincent, J. B.; Folting, K.; Gatteschi, D.; Christou, G.; Hendrickson, D. N. *J. Am. Chem. Soc.* **1993**, *115*, 1804–1816.
146. Raghu, C.; Rudra, I.; Sen, D.; Ramasesha, S. *Phys. Rev. B* **2001**, *64*, 4419.
147. Regnault, N.; Jolicoeur, T.; Sessoli, R.; Gatteschi, D.; Verdaguer, M. *Phys. Rev. B* **2002**, *66*, art. no. 054409.
148. Langan, P.; Robinson, R.; Brown, P. J.; Argyriou, D.; Hendrickson, D.; Christou, G. *Acta Cryst.* **2001**, *C57*, 909–910.



149. Robinson, R. A.; Brown, P. J.; Argyriou, D. N.; Hendrickson, D. N.; Aubin, S. M. *J. Phys.: Condens. Matter* **2000**, *12*, 2805–2810.
150. Verdaguer, M.; Bleuzen, A.; Marvaud, V.; Vaissermann, J.; Seuleman, M.; Desplanches, C.; Sculler, A.; Train, C.; Garde, R.; Gelly, G.; Lomenech, C.; Rosenman, I. V. P.; Cartier, C.; Villain, F. *Coord. Chem. Rev.* **1999**, *190–192*, 1023–1047.
151. Mallah, T.; Marvilliers, A. In: *Magnetism: Molecules to Materials II*; Miller, J. S.; Drillon, M. Eds.; Wiley-VCH: Weinheim, **2001**, 189–227.
152. Marvaud, V.; Herrera, J. M.; Barilero, T.; Tuyeras, F.; Garde, R.; Sculler, A.; Decroix, C.; Cantuel, M.; Desplanches, C. *Monatsh. Chemie* **2003**, *134*, 149–163.
153. Marvaud, V.; Decroix, C.; Sculler, A.; Guyard-Duhayon, C.; Vaissermann, J.; Gonnet, F.; Verdaguer, M. *Chem. Eur. J.* **2003**, *9*, 1677–1691.
154. Marvaud, V.; Decroix, C.; Sculler, A.; Guyard-Duhayon, C.; Vaissermann, J.; Gonnet, F.; Verdaguer, M. *Chem. Eur. J.* **2003**, *9*, 1692–1705.
155. Barra, A. L.; Gatteschi, D.; Sessoli, R.; Abbati, G. L.; Cornia, A.; Fabretti, A. C.; Uytterhoeven, M. G. *Angew. Chem. Int. Ed. Engl.* **1997**, *36*, 2329–2331.
156. Stamp, P. C. P.; Chudnovsky, E. M.; Barbara, B. *J. Mod. Phys. B* **1992**, *6*, 1355.
157. Leggett, A. J. In: *Quantum Tunneling of Magnetization-QTM '94*; Gunther, L.; Barbara, B., Kluwer: Dordrecht, 1995; pp 1–18.
158. Sangregorio, C.; Ohm, T.; Paulsen, C.; Sessoli, R.; Gatteschi, D. *Phys. Rev. Lett.* **1997**, *78*, 4645–4648.
159. Fort, A.; Rettori, A.; Villain, J.; Gatteschi, D.; Sessoli, R. *Phys. Rev. Lett.* **1998**, *80*, 612–615.
160. Garanin, D. A.; Chudnovsky, E. M. *Phys. Rev. B* **1997**, *56*, 11102–11118.
161. Pohjola, T.; Schoeller, H. *Phys. Rev. B* **2000**, *62*, 15026–15041.
162. Leuenberger, M. N.; Loss, D. *Phys. Rev. B* **2000**, *61*, 1286–1302.
163. Friedman, J. R.; Sarachik, M. P.; Tejada, J.; Ziolo, R. *Phys. Rev. Lett.* **1996**, *76*, 3830–3833.
164. Thomas, L.; Lioni, F.; Ballou, R.; Gatteschi, D.; Sessoli, R.; Barbara, B. *Nature (London)* **1996**, *383*, 145–147.
165. Furukawa, Y.; Watanabe, K.; Kumagai, K.; Jang, Z. H.; Lascialfari, A.; Borsa, F.; Gatteschi, D. *Phys. Rev. B* **2000**, *62*, 14246–14251.
166. Fominaya, F.; Villain, J.; Fournier, T.; Gandit, P.; Chaussy, J.; Fort, A.; Caneschi, A. *Phys. Rev. B* **1999**, *59*, 519–528.
167. Fominaya, F.; Villain, J.; Gandit, P.; Chaussy, J.; Caneschi, A. *Phys. Rev. Lett.* **1997**, *79*, 1126–1129.
168. Chudnovsky, E. M.; Garanin, D. A. *Phys. Rev. Lett.* **2001**, *87*, art. no. 187203.
169. Garanin, D. A.; Chudnovsky, E. M. *Phys. Rev. B* **2002**, *65*, art. no. 094423.
170. Mertes, K. M.; Suzuki, Y.; Sarachik, M. P.; Paltiel, Y.; Strickman, H.; Zeldov, E.; Rumberger, E.; Hendrickson, D. N.; Christou, G. *Phys. Rev. Lett.* **2001**, *87*, art. no. 227205.
171. Cornia, A.; Sessoli, R.; Sorace, L.; Gatteschi, D.; Barra, A. L.; Daignebonne, C. *Phys. Rev. Lett.* **2002**, *89*, art. no. 257201.
172. Hennion, M.; Pardi, L.; Mirebeau, I.; Suard, E.; Sessoli, R.; Caneschi, A. *Phys. Rev. B* **1997**, *56*, 8819–8827.
173. Amoretti, G.; Caciuffo, R.; Combet, J.; Murani, A.; Caneschi, A. *Phys. Rev. B* **2000**, *62*, 3022–3024.
174. Zhong, Y. C.; Sarachik, M. P.; Friedman, J. R.; Robinson, R. A.; Kelley, T. M.; Nakotte, H.; Christianson, A. C.; Trouw, F.; Aubin, S. M. J.; Hendrickson, D. N. *J. Appl. Phys.* **1999**, *85*, 5636–5638.
175. Mirebeau, I.; Hennion, M.; Casalta, H.; Andres, H.; Güdel, H. U.; Irodova, A. V.; Caneschi, A. *Phys. Rev. Lett.* **1999**, *83*, 628–631.
176. Gatteschi, D. *J. Phys. Chem. B* **2000**, *104*, 9780–9787.
177. Barra, A. L.; Brunel, L. C.; Gatteschi, D.; Pardi, L.; Sessoli, R. *Acc. Chem. Res.* **1998**, *31*, 460–466.
178. Smith, G. M.; Riedi, P. C. In: *Electron Paramagnetic Resonance*, Vol. 18; Atherton, N. M., Davies, M. J., Gilbert, B. C. Eds., The Royal Soc. of Chem.: Cambridge, **2000**, pp 164–204.
179. Barra, A. L.; Gatteschi, D.; Sessoli, R. *Chem. Eur. J.* **2000**, *6*, 1608–1614.
180. Caciuffo, R.; Amoretti, G.; Murani, A.; Sessoli, R.; Caneschi, A.; Gatteschi, D. *Phys. Rev. Lett.* **1998**, *81*, 4744–4747.
181. Prokof'ev, N. V.; Stamp, P. C. E. *Phys. Rev. Lett.* **1998**, *80*, 5794–5797.
182. Wernsdorfer, W.; Sessoli, R.; Gatteschi, D. *Europhys. Lett.* **1999**, *47*, 254–259.
183. Gunther, L. *Europhys. Lett.* **1997**, *39*, 1–6.
184. Wernsdorfer, W. *Adv. Chem. Phys.* **2001**, *118*, 99–190.
185. Landau, L. *Phys.Z.Sowjetunion* **1932**, *4*, 46.
186. Zener, C. *Proc. R. Soc. London, Ser. A* **1932**, *137*, 696.
187. Stückelberg, E. C. G. *Helv. Phys. Acta* **1932**, *5*, 369.
188. Wernsdorfer, W.; Sessoli, R. *Science* **1999**, *284*, 133–135.
189. Wernsdorfer, W.; Soler, M.; Christou, G.; Hendrickson, D. N. *J. Appl. Phys.* **2002**, *91*, 7164–7166.
190. Garg, A. *Europhys. Lett.* **1993**, *22*, 205.
191. Garg, A. *Physica B* **2000**, *280*, 269–270.
192. Villain, J.; Fort, A. *Eur. Phys. J.* **2000**, *17*, 69–83.
193. Garg, A. *Phys. Rev. B* **2001**, *64*, art. no. 094414.
194. Garg, A. *Europhys. Lett.* **2000**, *50*, 382–388.
195. Kececioglu, E.; Garg, A. *Phys. Rev. B* **2001**, *63*, art. no. 064422.
196. Wernsdorfer, W.; Allaga-Alcalde, N.; Hendrickson, D. N.; Christou, G. *Nature* **2002**, *416*, 406–409.
197. Wernsdorfer, W.; Bhaduri, S.; Tiron, R.; Hendrickson, D. N.; Christou, G. *Phys. Rev. Lett.* **2002**, *89*, art. no. 197201.
198. Leuenberger, M. N.; Loss, D. *Nature* **2001**, *410*, 789–793.
199. Chudnovsky, E. M.; Garanin, D. A. *Phys. Rev. Lett.* **2002**, *89*, art. no. 157201.
200. Amigo, R.; Hernandez, J. M.; Garcia-Santiago, A.; Tejada, J. *Phys. Rev. B.* **2003**, *67*, art. no. 220402.
201. Sorace, L.; Wernsdorfer, W.; Thirion, C.; Barra, A.-L.; Pacchioni, M.; Maily, D.; Barbara, B. submitted for publication.
202. de Jongh, L. J.; Miedema, A. R. *Adv. Phys.* **1974**, *23*, 1.
203. Bonner, J. C. In: *Magneto-Structural Correlations in Exchange Coupled Systems*; Willett, R. D.; Gatteschi, D.; Kahn, O., Reidel: Dordrecht, 1985; Vol. C140, p 157.

204. Georges, R.; Borrás-Almenar, J. J.; Coronado, E.; Curély, J.; Drillon, M. In *Magnetism: Molecules to Materials*; Miller, J. S.; Drillon, M., Eds., Wiley-VCH: Weinheim, 2001, pp 1–47.
205. Haldane, F. D. M. *Phys. Rev. Lett.* **1983**, *50*, 1153.
206. Nightingale, M. P.; Blote, H. W. J. *Phys. Rev.* **1986**, *B33*, 659.
207. Sakai, T.; Takahashi, M. *Phys. Rev.* **1990**, *B42*, 1090.
208. Yamashita, M.; Ishii, T.; Matsuzaka, H. *Coord. Chem. Rev.* **2000**, *198*, 347–366.
209. Renard, J.-P.; Regnault, L.-P.; Verdaguer, M. *Magnetism: Molecules to Materials II*, Miller, J. S., Drillon, M., Eds., **2001**, Wiley-VCH: Weinheim, 49–93.
210. Renard, J.-P.; Verdaguer, M.; Regnault, L. P.; Erkelens, W. A. C.; Rossat-Mignod, J.; Stirling, W. J. *Europhys. Lett.* **1987**, *3*, 945–951.
211. Meyer, A.; Gleizes, A.; Girerd, J.-J.; Verdaguer, M.; Kahn, O. *Inorg. Chem.* **1982**, *21*, 1729–1739.
212. Renard, J.-P.; Verdaguer, L. P.; Regnault, L. P.; Erkelens, W. A. C.; Rossat-Mignod, J.; Ribas, J.; Stirling, W. G.; Vettier, C. *J. Appl. Phys.* **1988**, *63*, 5358–5342.
213. Yosida, T.; Fukui, M. *J. Phys. Soc. Jpn.* **1992**, *61*, 2304–2308.
214. Gadet, V.; Verdaguer, M.; Briois, V.; Gleizes, A.; Renard, J.-P.; Beauvillain, P.; Chappert, C.; Goto, T.; Le Dang, K.; Veillet, P. *Phys. Rev.* **1991**, *B44*, 705–712.
215. Chou, L. K.; Abboud, K. A.; Talham, D. R.; Kim, W. W.; Meisel, M. W. *Physica B* **1993**, *194–196*, 311–312.
216. Renard, J.-P.; Regnault, L. P.; Verdaguer, M. *J. Magn. Magn. Mater.* **1988**, *49*.
217. Ribas, J.; Escuer, A.; Monfort, M.; Vicente, R.; Cortés, R.; Lezama, L.; Rojo, T.; Goher, M. A. S. In: *Magnetism: Molecules to Materials II*; Miller, J. S.; Drillon, M., Eds., Wiley-VCH: Weinheim, 2001, 307–337.
218. Sikorav, S.; Bkouche-Waksman, I.; Kahn, O. *Inorg. Chem.* **1984**, *23*, 490.
219. Thomson, L. K.; Tandon, S. S.; Manuel, M. E. *Inorg. Chem.* **1995**, *34*, 2356.
220. Aebbersold, M. A.; Gillon, B.; Plantevin, O.; Pardi, L.; Kahn, O.; Bergerat, P.; Von Seggern, I.; Tuczec, F.; Ohrstrom, L.; Grand, A.; Lelievre-Berna, E. *J. Am. Chem. Soc.* **1998**, *120*, 5238–5245.
221. Ribas, J.; Escuer, A.; Monfort, M.; Vicente, R.; Cortés, R.; Lezama, L.; Rojo, T. *Coord. Chem. Rev.* **1999**, *193–195*, 1027.
222. Escuer, A.; Vicente, R.; Goher, M. A. S.; Mautner, F. A. *Inorg. Chem.* **1998**, *37*, 782.
223. Manriquez, J. M.; Yee, G. T.; McLean, R. S.; Epstein, A. J.; Miller, J. S. *Science* **1991**, *252*, 1415.
224. Miller, J. S.; Calabrese, J. C.; McLean, R. S.; Epstein, A. J. *Adv. Mater.* **1992**, *4*, 498.
225. Hibbs, W.; Rittenberg, D. K.; Sugiura, K. I.; Burkhart, B. M.; Morin, B. G.; Arif, A. M.; Liable-Sands, L.; Rheingold, A. L.; Sundaralingam, M.; Epstein, A. J.; Millers, J. S. *Inorg. Chem.* **2001**, *40*, 1915.
226. Girtu, M. A.; Wynn, C. M.; Sugiura, K.-I.; Miller, J. S.; Epstein, A. J. *J. Appl. Phys.* **1997**, *81*, 4410–4412.
227. Caneschi, A.; Gatteschi, D.; Sessoli, R.; Rey, P. *Acc. Chem. Res.* **1989**, *22*, 392–398.
228. Gatteschi, D.; Rey, P., In *Magnetic Properties of Organic Materials*; Lahti, P. M., Ed.; Dekker: New York, 1999; pp 601–627.
229. Iwamura, H.; Inoue, K. In: *Magnetism: Molecules to Materials II*; Miller, J. S.; Drillon, M., Eds., Wiley-VCH: Weinheim, 2001; pp 61–108.
230. Benelli, C.; Caneschi, A.; Gatteschi, D.; Pardi, L.; Rey, P. *Inorg. Chem.* **1989**, *28*, 275.
231. Benelli, C.; Gatteschi, D.; Sessoli, R.; Rettori, A.; Pini, M. G.; Bartolome, F.; Bartolome, J. *J. Magn. Magn. Mater.* **1995**, *140–144*, 1649–1650.
232. Affronte, M.; Caneschi, A.; Cucci, C.; Gatteschi, D.; Lasjaunias, J. C.; Paulsen, C.; Pini, M. G.; Rettori, A.; Sessoli, R. *Phys. Rev. B* **1999**, *59*, 6282–6293.
233. Caneschi, A.; Gatteschi, D.; Laloti, N.; Sangregorio, C.; Sessoli, R.; Venturi, G.; Vindigni, A.; Rettori, A.; Pini, M. G.; Novak, M. A. *Angew. Chem. Int. Ed. Engl.* **2001**, *40*, 1760–1763.
234. Glauber, R. J. *J. Math. Phys.* **1963**, *4*, 294–307.
235. Clerac, R.; Miyasaka, H.; Yamashita, M.; Coulon, C. *J. Am. Chem. Soc.* **2002**, *124*, 12837–12844.
236. Lescouezec, R.; Vaissermann, J.; Ruiz-Perez, C.; Lioret, F.; Carrasco, R.; Julve, M.; Verdaguer, M.; Dromzee, Y.; Gatteschi, D.; Wernsdorfer, W. *Angew. Chem. Int. Ed. Engl.* **2003**, *42*, 1843–1846.
237. Pilkington, M.; Decurtins, S. *Chimia* **2000**, *54*, 593–601.
238. Girerd, J.-J.; Kahn, O.; Verdaguer, M. *Inorg. Chem.* **1980**, *19*, 274–276.
239. Oshio, H.; Nagashima, U. *Inorg. Chem.* **1992**, *31*, 3295–3301.
240. Decurtins, S.; Schmalte, H. W.; Schnewly, P.; Oswald, H. R. *Inorg. Chem.* **1993**, *32*, 1888–1892.
241. Michalowicz, A.; Girerd, J.-J.; Goulon, J. *Inorg. Chem.* **1979**, *18*, 3004.
242. Oilkington, M.; Decurtins, S. In: *Magnetism: Molecules to Materials II*; Miller, J. S., Drillon, M. Eds., Wiley-VCH: Weinheim, **2001**, pp 339–356.
243. Tamaki, H.; Zhong, Z. J.; Matsumoto, N.; Kida, S.; Koikawa, M.; Achiwa, N.; Hashimoto, Y.; Okawa, H. *J. Am. Chem. Soc.* **1992**, *114*, 6974–6979.
244. Decurtins, S.; Schmalte, H. W.; Oswald, H. R.; Linden, A.; Enslin, J.; Gütllich, P. *Inorg. Chim. Acta* **1994**, *216*, 65–73.
245. Mathoniere, C.; Carling, S. G.; Yusheng, D.; Day, P. *J. Chem. Soc., Chem. Commun.* **1994**, 1551–1552.
246. Nuttall, C. J.; Carling, S. G.; Day, P. *Solid State Commun.* **1999**, *110*, 39–43.
247. Coronado, E.; Galan-Mascaros, J. R.; Gomez-Garcia, C. J.; Laukhin, V. *Nature* **2000**, *408*, 447–449.